DEVELOPMENTS IN SEDIMENTOLOGY 58

HEAVY MINERALS IN USE

EDITED BY
MARIA A. MANGE AND DAVID T. WRIGHT

SERIES EDITOR: A.J. VAN LOON

Developments in Sedimentology, 58

HEAVY MINERALS IN USE

This page intentionally left blank

Developments in Sedimentology, 58

HEAVY MINERALS IN USE

Edited by

MARIA A. MANGE

Department of Geology
University of California,
Davis, CA USA

DAVID T. WRIGHT

Department of Geology
University of Leicester
UK

ELSEVIER

Amsterdam ● Boston ● Heidelberg ● London ● New York ● Oxford
Paris ● San Diego ● San Francisco ● Singapore ● Sydney ● Tokyo

Elsevier
Radarweg 29, PO Box 211, 1000 AE Amsterdam, The Netherlands
Linacre House, Jordan Hill, Oxford OX2 8DP, UK

First edition 2007

Library of Congress Cataloging-in-Publication Data
A catalog record for this book is available from the Library of Congress

British Library Cataloguing in Publication Data
A catalogue record for this book is available from the British Library

ISBN: 978-0-444-51753-1
ISSN: 0070-4571

Printed and bound in Italy

07 08 09 10 11 10 9 8 7 6 5 4 3 2 1

LIST OF CONTENTS

1.3 Heavy Minerals and Grain Size

1.4 Miscellaneous Techniques

1.5 Numerical Data Analysis

PART II: PROVENANCE, TRANSPORT, DEPOSITION, EXHUMATION

2.1 Regional Studies—Modern and Ancient Environments

2.2 Tectonogenic Sediments: The Use of Heavy Minerals in Active Geodynamic Settings

PART III: INTEGRATED AND INTERDISCIPLINARY HEAVY MINERAL APPLICATIONS

3.1 Heavy Mineral Studies Integrated with Other Geoanalytical Techniques

3.2 The Use of Heavy Minerals in Interdisciplinary Research

3.2.1 Forensic Science—Evidence from Heavy Minerals in Criminal Investigation

3.2.2 Geoarchaeology

PART IV: INDUSTRIAL APPLICATIONS: RESERVOIR CHARACTERISATION, ECONOMIC HEAVY MINERAL DEPOSITS, DIAMOND PROSPECTING

4.1 Reservoir Characterisation

4.2 Mineral Exploration and Mining

4.3 The Role of Upper Mantle Derived Heavy Minerals in Diamond Exploration

This page intentionally left blank

CONTRIBUTING AUTHORS

S.H. AKHTER
Department of Geology, Dhaka University, Dhaka-1000, Bangladesh

D. ALJINOVIĆ
University of Zagreb, Faculty of Mining, Geology and Petroleum Engineering, Pierottijeva 6, HR-10000 Zagreb, Croatia

S. ANDÒ
Laboratorio di Petrografia del Sedimentario, Dipartimento di Scienze Geologiche e Geotecnologie, Università di Milano-Bicocca, Piazza della Scienza 4, 20126 Milano, Italy

R.M. BATEMAN
Jodrell Laboratory, Royal Botanic Gardens Kew, Richmond, Surrey TW9 3DS, UK

M.C. BAUMGARTNER
Mineral Services Canada, 205-930 Harbourside Drive, North Vancouver, B.C., Canada

T. BEZECZKY
Institute for Studies of Ancient Culture, Austrian Academy of Sciences, Bäckerstrasse 13, PF 8 1010 Vienna, Austria

R. BOGOCH
Geological Survey of Israel, 30 Malkhe Yisrael Street, Jerusalem 95501, Israel

R. BRUHN
Dong energy, Exploration and production, Agern Allé 24-26, DK-2970 Hørsholm, Denmark

G.L. BYNUM
761 Towhee Court, Fremont, CA 94539, USA (U.S. Geological Survey, retired)

J. CASCALHO
Centro de Geologia, Museu Nacional de História Natural da Universidade de Lisboa, Rua da Escola Politécnica, 58, 1250-102 Lisboa, Portugal

A. CARTER
Research School of Earth Sciences, University and Birkbeck College, London WC1E 6 BT, UK

J.A. CATT
Department of Geography, University College London, Gower Street, London WC1E 6BT, UK

W. CAVAZZA
Dipartimento di Scienze della Terra e Geologico-Ambientali, Universitá di Bologna, Piazza di Porta San Donato, 1-40127 Bologna, Italy

Z. CHEN
State Key Laboratory for Estuarine and Coastal Research, East China Normal University, Shanghai 200062, China

M. CRNJAKOVIĆ
Croatian Natural History Museum, Demetrova 1, HR-10000 Zagreb, Croatia

A.N. DERKACHEV
V.I. Il'ichev's Pacific Oceanological Institute, Far Eastern Branch, Russian Academy of Sciences, Vladivostok, 43 Baltiyskaya Street, Vladivostok, 690041, Russia

J.F. DEWEY
Department of Geology, UC Davis, One Shields Avenue, Davis, CA 95616, USA

G. DURN
University of Zagreb, Faculty of Mining, Geology and Petroleum Engineering, Pierottijeva 6, HR-10000 Zagreb, Croatia

W.R. DICKINSON
Department of Geosciences, University of Arizona, Box 210077, Tucson, AZ 85721, USA

M. FANNING
Research School of Earth Sciences, The Australian National University, Canberra, ACT 0200, Australia

P. FAUPL
Department of Geological Sciences, University of Vienna, Althanstrasse 14, A-1090 Vienna, Austria

C. FRADIQUE
Instituto Hidrográfico, Rua das Trinas, 49, 1249-093 Lisboa, Portugal

O.E. FRIHY
Coastal Research Institute, 15 El Pharaana Street, El Shallalat, 21514 Alexandria, Egypt

H. FRIIS
Department of Earth Sciences, University of Aarhus, Denmark

G. GANDOLFI
Dipartimento di Scienze della Terra e Geologico-Ambientali, Universitá di Bologna, Piazza di Porta San Donato, 1-40127 Bologna, Italy

E. GARZANTI
Laboratorio di Petrografia del Sedimentario, Dipartimento di Scienze Geologiche e Geotecnologie, Università di Milano-Bicocca, Piazza della Scienza 4, 20126 Milano, Italy

V.N. GRIGORYEV
Geological Institute of the Russian Academy of Sciences, 119017, Moskow, Pyzhevsky pereulok 7, Russia

J.J. GURNEY
Mineral Services South Africa, 42 Morningside, N'Dabeni, Cape Town, South Africa

C.R. HALLSWORTH
HM Research Associates West Mostard, Garsdale, Sedbergh, Cumbria LA10 5NT, UK

M.A. HANAN
Department of Geology and Geophysics, University of New Orleans, New Orleans, LA 70148, USA

D.J. HUISMAN
National Service for Archaeological Heritage, PO Box 1600 3800 Amersfoort, The Netherlands

R. HERRIES
Amerada Hess Malaysia, Level 9, Menara Tan and Tan, 207 Jalan Tun Razak, Kuala Lumpur 50400, Malaysia

D. INCE
Technical Geoscience Department, PCSB (Petronas Carigali Sdn Bhd) Level 16, Tower 2, Petronas Twin Towers KLCC 50088, Kuala Lumpur, Malaysia

W.C. ISPHORDING
Department of Earth Sciences, University of South Alabama, Mobile, AL 36688, USA

C.B. JENSEN
Department of Earth Sciences, Aarhus University, DK-8000 Århus C, Denmark

P.D. KOMAR
College of Oceanic and Atmospheric Sciences, Oregon State University, Corvallis, OR 97331, USA

L.Ó. KOVÁCS
Hungarian Geological Survey, Stefánia út 14, 1143 Budapest, Hungary

G.TH. KLAVER
TNO-NITG/National Geological Survey, PO Box 80015, 3508 TA, Utrecht, The Netherlands

P. KUMAR
Himalayan Research Laboratory, Department of Geology and Geography, Auburn University, Auburn, AL 36849, USA

B. LUGOVIĆ
University of Zagreb, Faculty of Mining, Geology and Petroleum Engineering, Pierottijeva 6, HR-10000 Zagreb, Croatia

A.S. MADDEN
Environmental Sciences Division, Oak Ridge National Laboratory, Oak Ridge, TN 37081-6036, USA

A.I. MALINOVSKY
Far East Geological Institute, Far-East Division, Russian Academy of Sciences, 690022, Vladivostok-22, Prospect 100-letyia Vladivostoka, 159, Russia

J. MALONE
John S. Herold 14 Westport Avenue Norwalk, CT 06851, USA

M.A. MANGE
Department of Geology, UC Davis, One Shields Ave., Davis, CA 95616, USA

P.V. MARKEVICH†
Far East Geological Institute, Far-East Division, Russian Academy of Sciences, 690022, Vladivostok-22, Prospect 100-letyia Vladivostoka, 159, Russia

J.T. MCGUIRE
Department of Geology and Geophysics, Texas A&M University, College Station, TX 77843-3115, USA

G. MIGIROS
Department of Sciences, Laboratory of Mineralogy-Geology, Agricultural University of Athens, Iera Odos 75, GR-11855 Athens, Greece

K.L. MILLIKEN
Department of Geological Sciences, Jackson School of Geosciences, The University of Texas at Austin, Austin, TX 78712, USA

R.O. MOORE
Mineral Services Canada, 205-930 Harbourside Drive, North Vancouver, B.C., Canada

A.C. MORTON
HM Research Associates, 2 Clive Road, Balsall Common, West Midlands CV7 7DW, UK
CASP, University of Cambridge, 181a Huntingdon Road, Cambridge CB3 0DH, UK

N.A. NIKOLAEVA
V.I. Il'ichev's Pacific Oceanological Institute, Far Eastern Branch, Russian Academy of Sciences, Vladivostok, 43 Baltiyskaya Street, Vladivostok, 690041, Russia

T.E. NOWICKI
Mineral Services Canada, 205-930 Harbourside Drive, North Vancouver, B.C., Canada

L. PAGANELLI
Dipartimento di Scienze della Terra e Geologico-Ambientali, Universitá di Bologna, Piazza di Porta San Donato, 1-40127 Bologna, Italy

S. PALENIK
Microtrace, 1750 Grandstand Place, Elgin, IL 60123, USA

S. PASSCHIER
Department of Earth and Environmental Studies, Mallory Hall 252, Montclair State University, Montclair, NJ 07043, USA

A. PAVLOPOULOS
Department of Sciences, Laboratory of Mineralogy-Geology, Agricultural University of Athens, Iera Odos 75, GR-11855 Athens, Greece

E.C. PIRKLE
Emeritus, Department of Geology, University of Florida, Gainesville, FL 32611, USA
Present address: 211 Boxwood Rd., Aiken, SC 29803, USA

F.L. PIRKLE
Gannett Fleming, Inc., 10751 Deerwood Park Blvd., Suite 140, Jacksonville, FL 32256, USA

W.A. PIRKLE
Department of Biology and Geology, University of South Carolina Aiken, Aiken, SC 29801, USA

M.L.K. POULSEN
Department of Earth Sciences, Aarhus University, DK-8000 Århus C, Denmark
Present address: Dong energy, Exploration and Production, Agern Allé 24-26, DK-2970 Hørsholm, Denmark

G.M.H. RUIZ
Geological Institute, Department of Earth Sciences, ETH-Zentrum, 8092 Zürich, Switzerland
Present address: Geological Institute, University of Neuchâtel, Rue Emile-Argand 11, 2009 Neuchâtel, Switzerland

P.D. RYAN
Department of Earth and Ocean Sciences, NUI, Galway, Ireland

J.N. SARMA
Department of Applied Geology, Dibrugarh University, Dibrugarh, Assam, India

J.S. SCHNEIDERMAN
Department of Earth Science and Geography, Vassar College, 124 Raymond Avenue, Poughkeepsie, NY 12604-0312, USA

F. SERRA
Dipartimento di Scienze della Terra e Geologico-Ambientali Università di Bologna, Via Zamboni, 67, 40127 Bologna, Italy

D. SEWARD
Geological Institute, Department of Earth Sciences, ETH-Zentrum, 8092 Zürich, Switzerland

D. SMALE
28 Bronte Street, Nelson, New Zealand (formerly of New Zealand Geological Survey and Institute of Geological and Nuclear Sciences)

S.D. SOKOLOV
Geological Institute of the Russian Academy of Sciences, 119017, Moskow, Pyzhevsky pereulok 7, Russia

J.B. SVENDSEN
Altinex Oil Denmark A/S, Kongevejen 100C, DK-2840 Holte, Denmark

E. THAMÓ-BOZSÓ
Geological Institute of Hungary, Stefánia út 14, 1143 Budapest, Hungary

A.R.A. THOMAS
Department of Earth Sciences, University of Oxford, Parks Road, Oxford, OX1 3PR and PADMAC Unit, Pitt Rivers Museum, University of Oxford, 60 Banbury Road, Oxford, OX2 6PN, UK
Present address: Neftex Petroleum Consultants Ltd., 115BD Milton Park, Abingdon, Oxfordshire, OX14 4SA, UK

M.W. TOTTEN
Department of Geology, Kansas State University, Manhattan, KS 66506, USA

M.I. TUCHKOVA
Geological Institute of the Russian Academy of Sciences, 119017, Moskow, Pyzhevsky pereulok 7, Russia

G. TURNER
British Geological Survey, Keyworth, Nottingham NG12 5GG, UK

P. TURNER
School of Geography, Earth and Environmental Sciences, The University of Birmingham, Birmingham B15 2TT, UK

A. UDDIN
Himalayan Research Laboratory, Department of Geology and Geography, Auburn University, Auburn, AL 36849, USA

A.J. VAN LOON
Geocom, Dillenburg 234, 6865 HR Doorwerth, The Netherlands

M.A. VELBEL
Department of Geological Sciences, 206 Natural Science Building, Michigan State University, East Lansing, MI 48824-1115, USA

H. VON EYNATTEN
Geowissenschaftliches Zentrum der Universität Göttingen, Abteilung Sedimentologie und Umweltgeologie, Goldschmidtstrasse 3, D-37077 Göttingen, Germany

R. WEIBEL
Department of Earth Sciences, University of Aarhus, Denmark

T. WEISSBROD
Geological Survey of Israel, 30 Malkhe Yisrael Street, Jerusalem 95501, Israel

W. WINKLER
Geological Institute, Department of Earth Sciences, ETH-Zentrum, 8092 Zürich, Switzerland

D.T. WRIGHT
Department of Geology, University of Leicester, University Road, Leicester LE1 7RH, UK

G.G. ZUFFA
Dipartimento di Scienze della Terra e Geologico-Ambientali Università di Bologna, Via Zamboni, 67, 40127 Bologna, Italy

† We record with great sadness the passing away of Professor Pavel V. Markevich, in October 2006; we wish to extend our sincere condolences to Pavel's family, friends and colleagues. Pavel Markevich was Head of the Sedimentology Laboratory of the Far East Geological Institute, Far East Branch of the Russian Academy of Sciences in Vladivostok, and was well known at international conferences, where he often chaired programme sessions. His contribution to this volume, together with his co-authors, provides a wide-ranging insight into the Mesozoic - Cenozoic sedimentary and volcano-sedimentary successions in the Russian Far East, and in some parts of the western Pacific Ocean, as studied and interpreted by Russian sedimentologists and mineralogists. Pavel has also helped to bring the valuable work of a number of Russian researchers, previously published mostly in Russian and not available or intelligible to non-Russian speakers, to the attention of an international audience.

It has been a pleasure to work with Pavel and we greatly regret that he will not see the appearance of his comprehensive work in this volume.

FOREWORD

The early "golden period" of heavy mineral analysis from 1870 to the Second World War was in stark contrast to the general scepticism towards their value thereafter as a result of the advent of glamorous, and supposedly better new techniques, which led many geologists to regard heavy mineral studies as uninteresting or useless. However, the technique was not completely neglected. Throughout the fifties and sixties, a number of researchers used heavy minerals successfully on a wide range of geological problems, which contributed to a better understanding of the factors that modify heavy mineral suites, and opened the way for more sophisticated interpretations. The expansion of heavy mineral studies into hitherto neglected fields, the application of advanced analytical techniques and of numerical data analysis have all been important advances, which have led to a rejuvenation of interest. Consequently, heavy mineral analyses are now more frequently employed and yield very important results.

Heavy mineral studies were kept alive in several places including Budapest, where Maria Mange was trained during the sixties to emerge as a first-rate practitioner. In Imperial College London during the 1970s and the University of Berne in the 1980s, she developed the techniques of high-resolution-heavy-mineral-analysis (HRHMA), which delves deeply into diagnostics through geochemistry, surface textures, and species varieties. HRHMA allows very specific conclusions to be drawn in many areas of sedimentology. Non-fossiliferous, commonly non-marine, sequences can be correlated very precisely at a level beyond the resolution of fossils, especially when used in conjunction with palaeomagnetic data, as shown by her work in the Triassic of the Irish Sea. Extremely precise statements can be made about the provenance of basin sequences and tectonic events in their source areas. In the Caledonides of western Ireland, her HRHMA analyses of Ordovician and Silurian sedimentary rocks demonstrated the progressive unroofing of a supra-subduction-zone ophiolite/juvenile arc and the sudden appearance of amphibolite-grade metamorphic detritus, which indicates the rapid extensional collapse of the Grampian Orogen. An interesting and instructive vignette attaches to the sudden appearance of Grampian detritus in the Ordovician rocks of the South Mayo Trough. During his Ph.D. work, the writer found two grains of staurolite in a thin section of an upper Derrylea turbidite (Llanvirn) in the South Mayo Trough, which led him to the conclusion that the Grampian Orogeny predated the Llanvirn. Subsequently, the thin section was lost, nobody could find staurolite in thin sections of Derrylea turbidites, and the opinion was that Dewey had mistakenly identified some other (unspecified) mineral as staurolite, much in the same way as prehnite and lawsonite were confused in the Olympic Peninsula. Maria Mange, using HRHMA in 1990, re-discovered staurolite

in the upper Derrylea. The simple message is that one cannot perform serious heavy mineral studies in thin section; HRHMA, a subtle and complicated technique, is the only viable course as shown in this book and in her book "Heavy Minerals in Colour".

Maria Mange has established herself as the world leader in heavy mineral studies and has undertaken many projects on behalf of the major hydrocarbon companies, in more recent years in association with her co-editor in this volume, David Wright. This practical application of heavy minerals has provided important information to decision-makers in reservoir characterization and exploitation. In editing this book, she, ably supported by David Wright and with the help of Tom van Loon, has done a truly prodigious amount of work over a 3-year period first by cajoling the best names in the field to contribute, and then doing an intensive job of reviewing, editing, and improving text, and redrawing figures. The result is a highly professional work, destined to become the definitive classic work in the field of heavy minerals. An especially valuable feature of this book is the eclectic coverage of the use of heavy minerals in a wide and diverse variety of applications including, provenance, correlation, diagenesis, geochemistry, forensics, and geoarchaeology.

John F. Dewey
30th October, 2006

PREFACE

Heavy mineral studies have been enriching earth sciences with informative data for well over a century. The methods employed are well-proven, and have stood the test of time, being both flexible and adaptable, with the potential for integration with applied geology and interdisciplinary research. The use of heavy minerals for constraining sediment provenance, source lithology and palaeotransport was recognised early on, while the range of heavy mineral applications increased progressively through the 20th century and up to the present day, in parallel with the growth of modern technology.

Modern research in earth sciences is increasingly driven by new advances in technology. The development of sophisticated equipment has encouraged the adoption of single-mineral-based techniques that have become intensively used because of their easy operation and rapid production of data. However, research focusing on such a restricted analysis is subject to severe shortcomings. Heavy minerals are generally not found in isolation but form part of a population of detrital, and often also authigenic, grains that collectively provide many important indices of information, essential for the correct interpretation of the data obtained. Relying on a single line of geochemical evidence can yield only partial resolution, and results almost inevitably in the loss of—often vital—information and, therefore, in an incomplete or misleading interpretation. Evaluation of heavy mineral compositions should be based on the analysis of all relevant data in a given sediment, and should involve an examination of the impact of processes involved during their transport, deposition and diagenesis. Compared with thin-section-based sandstone petrography, the great advantage of the heavy mineral technique is that through concentration by heavy liquids, the rare but often highly diagnostic species (usually not encountered in thin sections) can be detected.

Integrating microscopy with complex methods gives refinement and precision, and analysing the properties of individual minerals of a given assemblage is an important phase of any mineralogical or relevant research. It is important to emphasise, however, that the now frequently used single grain techniques all rely on information from *heavy minerals*! Ultrastable heavy minerals are unique repositories of geodynamic events. They endure multiple recycling and may encode successive stages of geological episodes. For example, a detrital *zircon grain* provided evidence for the existence of continental crust, and oceans on the Earth, as early as 4.4 Ga ago (Mojzsis et al., 2001; Wilde et al., 2001; Valley et al., 2002; Iizuka et al. 2006). Zircon, garnet, monazite, apatite, sphene (titanite), just to mention a few, are widely used for their isotopic systems, inclusions (that are dominantly heavy minerals) and

chemistry. Furthermore, the geochemistry or isotopic composition of a sediment without heavy minerals would yield extremely limited information.

Despite the popularity of instrument-driven techniques, heavy mineral analysis has remained a useful method in the study of sediments and applied disciplines. Numerous key-note works and case studies have appeared over recent decades, now scattered in journals, periodicals and other texts that are often not easily accessible and are effectively unavailable to many. So when, in 2002 at the 16th International Sedimentological Congress, in Johannesburg, Republic of South Africa, A.J. (Tom) van Loon, Series Editor of 'Developments in Sedimentology', proposed compiling a book on heavy minerals, it appeared to be an opportunity to respond to the continuing demand for information about the practicalities, usefulness and validity of heavy minerals in the modern world, as well as recognising the value of past research. We therefore decided to attempt a collation of both seminal and innovative studies in pure and applied research that will, we hope, provide the researcher and practitioner alike with a valuable and authoritative resource. Such a publication is long overdue. It is also hoped that the book will form a companion volume to an updated version of 'Heavy Minerals in Colour' (Mange and Maurer, 1992) that provides full colour illustration of virtually all transparent heavy minerals, present in detrital sediments, together with guidance on the scope of heavy mineral analysis, and instruction in laboratory techniques.

We adopted the title '*Heavy Minerals in Use*' as such a short title would be easy to refer to, use as a prompt and, at the same time, predict the wide range of disciplines to which heavy mineral analysis can be applied. The title is thus intended to convey the dynamic nature of the technique, that heavy minerals are not only 'in use' today in a diversity of geological and interdisciplinary fields, but have proven relevance to future studies.

The book is structured thematically encompassing principles, processes and products, and a wide spectrum of applications. Studies using heavy minerals nearly always include a customary introduction with details on factors that can cause modification of a particular heavy mineral assemblage throughout the rock cycle. In this book such a summary section is omitted; instead, the introduction and discussion of processes are presented by leading experts. Their key-note works are followed by specialist case studies that demonstrate the broad range of applications of heavy minerals in modern and ancient sedimentary environments from a variety of geological settings. Each work also provides information on the geology of the study area, many including a review of past and current research in the particular country, with a range of techniques and data treatment best suited to their study. The book would not be comprehensive without encompassing the field of interdisciplinary heavy mineral applications, such as forensic geology, geoarchaeology, economic heavy mineral deposits, diamond exploration and hydrocarbon reservoir evaluation. The eclectic use of heavy minerals, shown by the high number of contributions in this volume, represent the collective experience and wisdom of generations of working

geologists, and provide an invaluable source of references to works carried out in many parts of the world.

REFERENCES

Iizuka, T., Horie, K., Komiya, T., Maruyama, S., Hirata, T., Hidaka, H., Windley, B.F., 2006. 4.2 Ga zircon xenocryst in an Acasta gneiss from northwestern Canada: evidence for early continental crust. Geology 34, 245–248.

Mojzsis, S., Harrison, M., Pidgeon, R., 2001. Oxygen-isotope evidence from ancient zircons for liquid water at the Earth's surface 4,300 Myr ago. Nature 409, 178–181.

Valley, J.W., Peck, J.W., King, E.M., Wilde, S.A., 2002. A cool early Earth. Geology 30, 351–354.

Wilde, S., Valley, J., Peck, W., Graham, C., 2001. Evidence from detrital zircons for the existence of continental crust and oceans on the Earth at 4.4 Gyr ago. Nature 409, 175–178.

Maria A. Mange
Department of Geology, University of California, Davis One Shields Avenue, Davis, CA 95616, USA

David T. Wright
Department of Geology, University of Leicester, University Road, Leicester LE1 7RH, UK

This page intentionally left blank

ACKNOWLEDGEMENTS

The vast majority of submitted papers have been reviewed by two independent external reviewers, selected from the ranks of knowledgeable scientists, so as to extend the breadth of expertise and to promote impartiality. A few of the authors have also committed their energy and time to review papers relevant to their field. We would like to extend our sincere gratitude and appreciation to them all; their expert advice and constructive criticism have been invaluable in ensuring that the manuscripts received the most careful scrutiny and comment in preparation for publication.

We wish to place on record our deep thanks to John F. Dewey, not only for his work as a reviewer, but also for his sustained encouragement, interest, support and valuable advice throughout the editorial process.

In addition, we wish to acknowledge the work of the Series Editor A. J. (Tom) van Loon who did an outstanding job of examining all the revised manuscripts and bringing them to a form acceptable for publication. Tom often went beyond what was required in sometimes difficult circumstances, and the book has benefited greatly from his efforts.

Publication of this book could not have been achieved without the commitment, support, guidance and understanding of the Publishing Editor in Geology at Elsevier, Tirza van Daalen, and her assistant, Linda Versteeg-Buschman. We acknowledge our indebtedness to them both, and thank them for the personal and professional support they have given over the many months of preparation for publication.

From the start of designing and organising the book to the final stages of editing our relatives and friends provided us with continuous personal encouragement. DW would like to thank his wife, Freya, who has been an endless well of unconditional support during often demanding endeavours. MM thanks sister Zsuzsa Rajetzky, friends Martha Amorocho Elinor Kollmann, Susanna Kovacova, Diane Virdee and John Enos. Their affection, interest and understanding played an important role to make this book a reality. We give our heartfelt thanks to them.

The reviewers are:

Philip Allen
Tjeerd van Andel
John Aspden
Peter Balance
Roberto Barragan
Abhijit Basu
Richard M. Bateman
Bob Berner
Matthias Bernet
Sam Boggs

Sue Bruce
John Collinson
Salvatore Critelli
Ian Dalziell
Sarah Davies
Peter R. DeForest
Alex Densmore
John F. Dewey
Alveirinho Dias
Bill Dickinson
Yehezkel Druckman
Richard Ellison
Martin Evans
Henrik Friis
Robert Garrison
Jon Gluyas
Steve Graham
Todd Greene
Lars Hamberg
Andrew Hanson
Dave Harper
Richard Howarth
Tony Hurford
Andrew Hurst
Mads Huuse
Ray Ingersoll
Wayne C. Isphording
Cees Kasse
Oliver Kempf
Keren Kolodner
Paul D. Komar
Dave Krinsley
Deborah Lawrence
Jason Lederer
Lidia Lonergan
Bill Mahaney
Albert Matter
Earle McBride
Ahmet Mermut
Kitty L. Milliken
Andrea Mindszenty
Andy Moffat
Béla Molnar
Isabel Montanez
Eldridge Moores
Andrew C. Morton
Peter Mozley
Richard Munroe
Ray Murray
Victor Nechaev
Ervin Otvos
John Parnell
Georgina Pe-Piper
Curt Peterson
Karl Ramseyer
Ian Reid
Sarah Roeske
Laurence Robb
Ron Rose
Paul D. Ryan
Jürgen Schieber
Fritz Schlunegger
Richard Shutler, Jr.
Rudy Slingerland
Jean-Daniel Stanley
Peter Turner
A.J. (Tom) van Loon
Henk Weerts
Jeff Wilson
Xiong Yingqian
Robert Zierenberg

INTRODUCTION AND OVERVIEW

Each heavy mineral grain is a unique messenger of coded data, carrying the details of its ancestry and the vicissitudes of its sedimentary history

Clastic sediment packages are geological archives that record and preserve signatures of past geological events in source provinces, during transit, and at the depocentre. Their high-density grains represent the detrital occurrence of essential rock-forming minerals (e.g. garnet, pyroxenes, micas) or accessories (e.g. zircon, tourmaline, apatite) with densities >2.8: thus they are termed 'heavy minerals' (Mange and Maurer, 1992). They typically comprise $\sim$1% of siliciclastic sediments, so to study them effectively, they must be concentrated. This is normally carried out after rock disaggregation by mineral separation, using 'heavy' liquids, for example bromoform or tetrabromoethane, with specific gravities of 2.89 and 2.97, respectively. Alternatively, non-toxic sodium polytungstate or other LST products with adjustable densities may be used. Heavy minerals sink in these liquids, which permits their complete segregation from the less dense framework components (Mange and Maurer, 1992).

The recognition of heavy minerals in sands probably dates back to the times when prospecting started for placer deposits, gold and minerals of economic importance. The first known publication was by Dick (1887), as a result of his heavy mineral explorations in North Wales, while Artini (1898) provided the first thorough descriptions of heavy minerals in quantitative analyses of River Po sands. From the late 19th century to the beginning of the Second World War, heavy mineral studies were de rigueur and always a critical part of any serious sedimentary petrographic analysis, as described in Milner's (1929, 1962) and Boswell's (1933) classic texts. However, a subsequent decline in popularity resulted from the recognition that hydraulic effects can cause selective sorting according to size, shape and density, compounded by the realisation that other phenomena, such as inherited grain size dependence and post-depositional dissolution, could also affect heavy mineral compositions.

Knowledge of the behaviour of heavy minerals in a wide range of sedimentary environments, both surficial and diagenetic, increased in parallel with the growing understanding of sedimentary processes and factors operating in depositional environments. This led to the re-emergence of heavy mineral studies as a valuable investigative tool. Insights into such processes explained the 'enigmatic' response of heavy minerals during the rock cycle in, for example, selective grain sorting in transit, dissolution of unstable minerals in the pedogenesis zone during alluvial storage and the post-burial effects of 'intrastratal dissolution'. A revival in heavy mineral studies followed rapidly, and the recognition of their value is reflected in the increasingly diverse range of problems to which they have been applied, not only within earth sciences but also in the cross-disciplinary areas of forensic and

soil sciences, and geoarchaeology. Moreover, heavy minerals are probably even more frequently used than in past decades, stimulated by cutting-edge, instrument-oriented technologies that exploit the unique properties of individual minerals.

The history of any mineral begins during the petrogenesis of its parent rock. Crystallisation is a highly complex and prolonged process that includes a series of phases during which minerals are generated in accordance with their stability fields, and inherit the parameters of their particular phase. This is manifested in the properties of crystal structure, morphology, colour, chemical and optical zoning, inclusions, twinning and many other characteristics. Parent rocks may pass through episodes of progressive crystallisation, instability, retrogression, metamorphic overprint and other geochemical processes which can either generate new minerals or leave an imprint on existing ones. Examples include pyroxenes rimmed by amphiboles, sodic amphiboles surrounded by calcic amphibole rims, tourmaline cores preserving a pre-existing phase, garnet zoning and, probably the most well-known, the complex internal structure and overgrowths of zircons. The effects of transport, climate, alluvial storage, re-entrainment, deposition, burial diagenesis and, not uncommonly, recycling are preserved within the inherited morphology, structural properties and surface textures of a particular heavy mineral grain. Recognising these chemical and physical signatures enables the researcher to critically assess and interpret the information encoded within the heavy mineral assemblage. It is, however, important to establish a link between the component heavy minerals of the host sediment, the geological setting of their origin and their sedimentary history. The analyst also needs to have a sound knowledge of igneous and metamorphic petrology and the geology of the study area!

Optical mineralogy provides an overview of the heavy mineral assemblages and will prompt the researcher to invoke, if necessary, other instrumental techniques for further information, higher resolution and clarification. With the widespread availability of increasingly sophisticated modern instruments (EDS–SEM electron microprobe, laser ablation multicollector MC–ICP–MS, sensitive high-resolution ion microprobe (SHRIMP) to mention only a few), the heavy mineral technique can reach the highest level of precision. In all cases, however, the whole assemblage must be considered before conclusions are drawn.

Heavy mineral assemblages yield unique information, not provided by any other means, but that information is held in coded form that only the right keys can unlock. In assembling this volume, we have tried to provide examples of the usefulness and validity of heavy minerals in an expanding field of applications. We hope that the collation of seminal and innovative studies in pure and applied research in this volume will reveal the debt that we owe to early workers, while recognising the importance of recent advances and providing a much-needed and authoritative resource for researcher and practitioner alike.

'*Heavy Minerals in Use*' comprises a series of contributions across a wide spectrum of geological and related disciplines in which heavy mineral analysis played a decisive role, either alone or as part of a holistic approach with other techniques. The book is subdivided into sections to reflect, thematically, the diverse applications in which heavy mineral analysis has been used.

PART I: HEAVY MINERALS IN THE STUDY OF SILICICLASTIC SEDIMENTS: PRINCIPLES, PROCESSES AND PRODUCTS

Part I deals with fundamental processes, the principal factors that control the nature and composition of heavy mineral suites. Chapters here provide an insight into the main physical and chemical controls on heavy mineral abundances and composition in sediments, and the means by which heavy minerals can be studied. From the moment when heavy minerals are liberated from their host rock, along with framework components and lithic fragments, they are subjected to a series of mechanical and chemical weathering processes that persist until the assemblages are extracted from a sediment for study. These processes make their first impact on mineral detritus that accumulates temporarily in close proximity to the parent rocks. Once entrainment commences, heavy minerals, either in pristine form or affected by a degree of dissolution, enter the sedimentary cycle and are subjected to the effects of sediment transport.

1.1. Entrainment, Transport and Deposition: Hydraulic Control

Transported sediments commonly exhibit spatial mineralogical trends resulting from *hydraulic processes*. Paul D. Komar reviews the contrasting hydrodynamic properties of heavy minerals and quartz and feldspar grains related to differences in the ranges of particle sizes and shapes. He shows how differential rates of transport are reflected in distinct patterns of deposition related to particle attributes. He concludes that a better understanding of the physical processes that bring about mineral sorting is necessary to assist in provenance interpretations of heavy mineral analyses.

Omran E. Frihy examines modern physical processes in which waves and currents sort and concentrate the heavy mineral grains according to their densities, sizes and shapes during transport of beach sand between eroding and accreting shores along the Nile Delta. These two environments have distinctive heavy mineral assemblages, with garnet and zircon decreasing exponentially with distance from the site of erosion at a river mouth, while augite and hornblende show an opposite trend. Distinctive cross-shore patterns are also detected, with the densest minerals being most concentrated in the inner surf zone, and decreasing in concentration towards winnowed sediment sinks offshore that may be almost entirely free of detrital heavy minerals. Thus the suite of heavy minerals found in delta coastal sands can be used as natural tracers of sand movement related to large-scale shoreline change.

The third case study dealing with the operating factors in dynamic aquatic regimes is by João Cascalho and Catarina Fradique, who discuss processes on the Portuguese continental margin. They identified a main association, comprising biotite, andalusite, tourmaline, amphibole, garnet, staurolite, zircon and apatite, and a second, subordinate, suite that includes orthopyroxene, clinopyroxene and olivine. The latter is present only in the outer shelf and upper slope south of Porto canyon. The distribution patterns of the mineral species in the main association indicate that these terrigenous assemblages were delivered to the shelf by rivers in a highly selective manner, constrained by the hydraulic behaviour of the different grains. They found that mobile grains, such as biotite and the most platy amphiboles, are excellent sedimentary tracers of the present shelf transport dynamics, whereas the

less mobile grains, such as coarse garnet, andalusite, tourmaline, staurolite and zircon, reach only the inner shelf. Polycyclic, rounded grains found in the middle shelf in coarse-grained deposits represent relict and palimpsest sediments.

1.2. From Surface Weathering to Burial Diagenesis

Chemical weathering is a fundamental process in the geological cycle that operates not only on exposed rocks in the source area, but also on mineral grains in transit, at the depositional site and in the environment of diagenesis. It is responsible for the formation of soils and, being highly selective in its effects, it ultimately controls the composition of heavy mineral suites, affecting especially those which experienced a long geological history under substantial burial. Weathering processes and their products are extensively studied in earth and soil sciences by chemists, soil scientists, sedimentologists, geochemists and heavy mineral specialists. Seven contributions are presented, with case studies from different geological settings and at different stages of the sedimentary cycle.

Michael A. Velbel describes the effects of the weathering process by examining the surface textures of pyroxenes and amphiboles at different stages of dissolution. He investigates all aspects of heavy mineral responses and chemically produced surface features. Velbel concludes that surface textures on detrital heavy mineral grains can be used to infer weathering processes in soils and weathered regoliths, provenance and sedimentary environments, and intrastratal dissolution during burial diagenesis. He shows that the significance of etch pits and other surface textures on heavy minerals in a soil or regolith depends on the rates at which they form in that regolith, and how long the grains have been subject to such reactions (i.e., the age of the soil) in the weathering environment. Comparison of ranges of dissolution textures on pyroxenes and amphiboles in modern sediments with those of intrastratally dissolved grains in clastic sedimentary rocks indicated that these features are similar.

Richard M. Bateman and John A. Catt cover a wide range of themes in their evaluation of weathering processes affecting surficial sediments. They identify five stages in the sedimentary cycle, with six processes that may potentially modify the original sediment composition. Their work suggests that the boundary between superficial pedochemical and deeper geochemical weathering is largely artificial, and that the effects of biotic processes may be underestimated. Their holistic approach integrates multivariate ordinations, mineral depletion curves and different data sources to interpret patterns of variation in heavy mineral assemblages that can then inform the reconstruction of provenance and palaeoenvironments. Bateman and Catt also make a number of excellent observations on mitigating the risks of applying new techniques to heavy mineral analysis by constructing a conceptual framework for data interpretation, and on the potential for the better exploitation of existing data through rigorous statistical analysis.

A.J. (Tom) van Loon and Maria A. Mange deal with the rarely discussed environment of extreme weathering and the 'in situ' dissolution of heavy minerals. Diverse processes during the sedimentary cycle and extreme weathering imparted an unusual bulk and heavy mineral composition to the Tertiary Dutch and German 'silver sands' (sands that consist almost exclusively of quartz) which are devoid of clear provenance signatures. The study provides a new insight into the impact of

'in situ' weathering on heavy mineral assemblages and shows that understanding its end-products may be helpful in drawing stratigraphic boundaries between units with originally comparable heavy mineral compositions.

Andrew C. Morton and Claire Hallsworth explore the environment of burial diagenesis, and apply their knowledge and experience to show how heavy mineral assemblages respond to increasing burial depth through the progressive dissolution of unstable components. Case studies from sedimentary basins worldwide show a uniform pattern of relative mineral stability. Increasing pore fluid temperatures, accompanied by changes in pore fluid composition, are responsible for progressive mineral dissolution. Morton and Hallsworth show that an indirect relationship exists between mineral diversity and burial depth in sedimentary basins worldwide. However, the depths at which individual minerals disappear vary markedly between basins, largely because of differences in pore fluid temperature gradients. Geological time is another significant factor in mineral depletion.

Kitty L. Milliken takes the reader to the Gulf of Mexico Basin which, because of the well-documented provenance and simple burial history, serves as a natural laboratory for research into the nature of processes by which provenance information is 'erased' and otherwise complicated by diagenesis. She proposes a generalised model for basinal diagenesis of heavy minerals, characterised first by acid hydrolysis or weathering processes. At depths that overlap the ultimate completion of the subsurface weathering process, authigenic minerals, including a number of high-density phases, form by reactions that can be described as acid-releasing or reverse weathering. Finally at depths near the limit of coring (>5 km), the surviving ultrastable detrital heavy mineral assemblage (mostly zircon, tourmaline and rutile) is accompanied by a variety of high-density authigenic minerals (including anatase and titanite).

Gian G. Zuffa and Francesca Serra's contribution deals with the behaviour and modification of heavy mineral assemblages in a 500 m-thick turbidite succession, deposited in the rift valley of the 3300 m deep Escanaba Trough of the Juan de Fuca Plate, and shows the effects of hydrothermal fluid circulation on heavy minerals in a highly active geochemical environment. Their results provide an insight into the environment of circulating hydrothermal pore fluids that cause severe etching and the dissolution of heavy minerals at various depths, especially the chemically highly unstable ortho- and clinopyroxenes. These specific geochemical conditions also generated new minerals, mainly titanite, iron-rich magnesite, barite and pyrite. The length of time during which the sediments were affected by pore fluid movements is constrained by the Late Pleistocene ($\sim$60 ka) age of the sediments.

This section concludes with the contribution by Rikke Weibel and Henrik Friis, presenting a case study on the alteration of opaque heavy minerals from different depositional and diagenetic environments and various geochemical regimes in Denmark and the island of Helgoland. These include Triassic red beds with early oxidising conditions, the weakly reducing conditions of the Miocene Odderup Formation and the strongly reducing environment of the Gassum Formation, where abundant iron and organic matter, and thus related sulphate reduction, have influenced the alteration products. Extreme sulphur-dominated local environments are represented by Holocene carbonate-cemented sandstone pillars.

1.3. Heavy Minerals and Grain Size

Sceptics argue that the effect of grain size may impart a strong bias to interpretation of heavy mineral data because it causes selective sorting by weight, size and shape. This influence can be alleviated, largely, by dense sampling and by the understanding of 'hard' rocks and the nature of their mineral phases. Grain size and shape is usually *inherited* because a number of heavy mineral species have an affinity to certain grain sizes and crystal forms, a factor controlled primarily by conditions of crystallisation. Therefore, many heavy minerals enter the sedimentary cycle with their 'inherited' size and shape. For example, zircon usually occurs as small, frequently, euhedral or subhedral grains, whereas staurolite, kyanite, sillimanite, andalusite, topaz, and in many deposits, garnet, tourmaline and pyroxenes appear as relatively large grains with a variable shape.

During the sedimentary cycle, a variety of processes modify the original grain size and shape, and, as a result, heavy minerals can have an '*acquired*' grain size and shape. Differentiating between inherited and acquired characteristics may be possible by analysing the imprint of the process(es) responsible for the grain's size and shape, while the surface texture of the grains may prove useful for environmental reconstruction.

In this section, Alice R.A. Thomas integrates heavy mineral analysis with systematic grain size measurements on Palaeocene sediments of the London Basin. Her analysis reveals that grain size and heavy mineral characteristics show variations between two end-members: a tourmaline-dominated sediment with a 3.5 phi grain size mode and a zircon-dominated sediment with a 3 phi grain size mode. Grain size trends also reflect reworking of older sediments into a younger formation, whereas other beds show signs of pedogenic modification, and/or strong bioturbation. Her contribution indicates that combined grain size and heavy mineral studies of outcrop and borehole-derived material can improve our stratigraphic understanding of poorly preserved and bioturbated strata, despite the restrictions of poor exposures, small sample size and limited borehole distribution.

Matthew W. Totten and Mark A. Hanan challenge some of the preconceptions about heavy minerals in shales, including hydraulic equivalency, and stress the importance of using the heavy mineral fraction to complement the geochemical study of shales, while acknowledging that we do not yet fully understand the mechanism by which they were deposited. Whereas the mineralogical source of most trace elements in shales is attributed typically to clays, the frequently reported correlation between clay–mineral percentage and trace elements in whole-rock analyses is not always borne out in studies, and the variation may be due to geochemical variations of certain trace elements in component heavy minerals. An alternative explanation offered is the dilution of trace elements and clay minerals by quartz.

1.4. Miscellaneous Techniques

This section is an overview of techniques that take heavy mineral analyses beyond the light microscope and broaden knowledge of the assemblages by adding geochemical and/or optical information. Maria A. Mange and Andrew C. Morton review the benefits of single-mineral geochemical (varietal) analysis conferred by continuing

technological advances that provide increasingly higher levels of analytical precision. Virtually all detrital heavy minerals can now be subjected to a range of sophisticated geoanalytical techniques that can determine their isotopic composition, map the distribution of major and trace elements and identify their crystal chemistry. Mange and Morton present case studies on garnet, tourmaline, chrome spinel, apatite, pyroxenes, amphiboles and ilmenite, from a wide variety of geological settings and brief references are given to those that have, so far, received only minor interest.

The sharp, high-resolution images of the scanning electron microscope (SEM) have attracted heavy mineral specialists for over 30 years. Equipped with energy dispersive X-ray spectrometer (EDS) the SEM also provides a quick and easy way to increase information on heavy mineral species besides revealing great details of their surface characteristics at various stages of corrosion. It is probably the most frequently used auxiliary instrument in heavy mineral studies. This is reflected by the two substantial contributions of Grenville Turner and Andrew Morton, and by Michael A. Velbel, Jennifer T. McGuire and Andrew S. Madden. Kitty L. Milliken, Richard M. Bateman and John A. Catt and David Smale also illustrate the interpretation of their case study by high-resolution SEM images.

Maria A. Mange and David T. Wright discuss the principles of high-resolution heavy mineral analysis (HRHMA). They emphasise the complexity of heavy mineral assemblages and caution against recording grains of a particular species with differing characteristics (reflected by their appearance, physical and optical properties) as one category. Different varieties of a species may have marked differences in petrogenesis and provenance; thus not categorising varietal characteristics which occur at species level can generate misleading information and incorrect interpretations, while the full history of a sediment and the accurate reconstruction of its provenance remains concealed.

1.5. Numerical Data Analysis

Although a visual inspection of tabulated data and figures allows the detection of the more obvious mineral trends, less marked differences can be overlooked; hence, using advanced numerical techniques is of considerable importance if data assessment is to be objective. Imbrie and Van Andel (1964) were the first to numerically evaluate heavy mineral data by Q-mode factor analysis. This analysis is most applicable in studies involving complex and remote source regions and far-travelled, mixed sands, enhanced by maps showing regional variability patterns to reveal the aerial distribution of mineral assemblages. This method continued to be used for large databases (e.g., Frihy and Lofty, 1997; Carriquiry and Sánchez, 1999; Wong, 2002). Principle Component Analysis (PCA) finds a wide application in geology and is successfully used to analyse and interpret complex heavy mineral data (Pirkle et al., 1985; Svendsen, 2002). Because heavy mineral studies are generally data-intensive, they are particularly suitable for numerical data analysis. In this volume three case studies focus on numerical analysis of large heavy mineral datasets. Several authors in other sections in this volume also include statistical evaluation of their data (e.g., Bateman and Catt, Frihy, Malone, Poulsen et al., and Smale).

Of the case studies presented in this section, Alexander N. Derkachev and Natalia A. Nikolaeva demonstrate the value of multivariate statistics using an extremely

large heavy mineral database generated by the analysis of samples from basins in the western Pacific (Bering, Okhotsk, Japan, East China, Philippine, Banda, etc.) and from the Tonga and Vanuatu Trenches. Results allowed identification of several mineralogical provinces, linked to distinct hinterland complexes and associated tectonic controls. Q-mode factor analysis differentiates four major groups of assemblages of distinctive provenance. R-mode factors help to define representative mineral associations, which best characterise the mineral composition of the sediments of the individual marginal seas, and lead to the delineation of eight provinces, tied to distinct source provinces and associated tectonic controls. Despite the large latitudinal and environmental range of the study basins, the complexity of source rocks and volcanic signatures is clearly reflected in the distribution of heavy mineral assemblages.

Paul D. Ryan, Maria A. Mange and John F. Dewey developed new statistical techniques for treating the substantial heavy mineral data, produced over a 10-year period, from Ordovician rocks of the South Mayo Trough, western Ireland. They aimed at providing an independent and objective way to elucidate the stratigraphy and tectonic history of the region. A new method is presented for plotting normalised scores to emphasise stratigraphic trends of heavy minerals and specific heavy mineral varieties, which are shown to be largely non-normally distributed, with significant variation between formations. Also, a method is developed for testing significance of variation within a formation using non-parametric tests. PCA is used to identify major source regions throughout the life of this basin.

Edit Thamó-Bozsó and Lajos Ó.Kovács introduce the thick Quaternary successions of the central part of the Hungarian Plain to the reader and discuss the evolution of the fluvial network during the Quaternary. They benefited from a large heavy mineral database, obtained on borehole and modern river samples. Cluster analysis and PCA reveal appreciable similarities between the heavy mineral compositions of modern river sediments and those from borehole samples, resulting in a more refined reconstruction of the Quaternary fluvial network and sediment provenance. PCA has provided a clear differentiation of the garnet-rich sediments of the two main modern rivers flowing from opposite directions (Danube and Tisza), but uncertainties remain with the older sands probably because of changing source areas and/or intermixing the loads of different palaeo-rivers with time. Using PCA, a comparison of the heavy mineral composition of modern river sands and those deposited by their ancestors has revealed some differences, interpreted as the impact of tectonic and erosional changes during the Pleistocene.

PART II: PROVENANCE, TRANSPORT, DEPOSITION, EXHUMATION

2.1. Regional Studies—Modern and Ancient Environments

This section encompasses a wide spectrum of research commencing with a comprehensive study on modern sediments. These provide analogues that lead to the better understanding and faithful reconstruction of the history of ancient successions. Authors from different countries and continents present their case

studies, ranging from the Alps to Antarctica, demonstrating the potential of heavy mineral analyses in a variety of cratonic and dynamic plate-tectonic settings.

Eduardo Garzanti and Sergio Andò point out the genetic link between heavy mineral concentrations in sediments and the chemistry and tectono-stratigraphic level of rocks in source terranes. However, although mantle peridotites, lower crustal gabbros and high-grade metamorphic rocks yield more abundant heavy minerals than igneous and sedimentary rocks of the upper crust, depleted heavy mineral assemblages may result from severe diagenetic dissolution in ancient sandstones, for example, in Alpine and Himalayan foreland basins. Conversely, hydraulic sorting in the sediment cycle can concentrate and segregate heavy minerals within distinct grain size fractions in different, high-energy sedimentary environments. Garzanti and Andò show that in modern sands, the concentration of heavy minerals from different geodynamic settings depends primarily on the chemical composition and density of the source rocks. A good example is where heavy mineral concentrations of sediments increase upsection in a basin during the unroofing of progressively deeper tectono-stratigraphic levels within a source terrane. By applying heavy mineral concentration indices in conjunction with heavy mineral density and stability ratios, they are able to assess the effect of hydraulic sorting in sedimentary environments or that of diagenetic dissolution in ancient sandstones.

John Malone compares the heavy mineral 'fingerprint' from sediments of local rivers with that of seabed sediments to determine whether seabed sands off southeastern Ireland were derived from the Irish land mass. Perhaps surprisingly, Malone found that both the beach sands and offshore suites were rich in augite, which is not found with any frequency in river sediment, indicating that beach sands are largely derived from offshore sources. Malone supports his observations with multivariate statistical analyses to quantify differences in sediment provenance. Garnets present in the rivers confirm that the offshore sediments in the Irish Sea were not derived from the Irish landmass, but were delivered from Northern Ireland and Scotland by glacial processes. Glaucophane in offshore and some beach sediments indicates the high-pressure-ophiolite subduction complex of Anglesey, northwestern Wales, as a possible source perhaps delivered by an ice lobe.

In New Zealand, David Smale similarly reports how evidence from heavy minerals indicates that the silting of the harbours was caused largely by sediments transported from offshore, rather than from discharging rivers. In his review, Smale demonstrates his experiences with a variety of heavy mineral applications, that range from tracing the onset of volcanism and forensics, and notes how an increasing diversity of heavy minerals can be tied to the inception of the modern plate boundary system in the Miocene. He argues that optical examination must continue to underpin any heavy mineral study, adding that "to attempt not to do so is like studying petrology without thin sections".

The discovery of the persistence of identical heavy mineral assemblages from Pleistocene through to the modern sands in Willapa Bay, Washington State, allows Gretchen Luepke Bynum to conclude that the pattern of estuarine sedimentation in Late Pleistocene deposits closely resembles that of the modern Bay, with the same sediment source areas. However, the presence of a heavy mineral suite enriched in epidote in a few older Pleistocene units, associated with southwest-directed foresets in cross-bedded gravel, indicates derivation from the northeast, perhaps from an

area of glacial outwash. The presence of this suite in ancient estuarine sands exposed on the northeast side of the bay suggests that input from this northerly source may have intermittently dominated Willapa Bay deposition in the past.

Jill S. Schneiderman and Zhongyuan Chen studied drill core samples to document the Quaternary tectonic and palaeoenvironmental history of the southern Yangtze delta in China and to integrate the data with other studies to predict sedimentation rates and patterns, following the construction of the Three Gorges Dam on the Yangtze River. Heavy mineral data indicate a southward migration of the Yangtze River channel and deltaic depocentre to its present position. During the Quaternary, the Yangtze River flowed only across the northern delta plain, so that the southern delta plain received heavy minerals from local sources delivered by proximal rivers. However, heavy mineral assemblages in the upper portion of the core indicate that with continued subsidence, the Yangtze River channel shifted south and deposited sediments transported from distal source areas. Future planning requires a comprehensive understanding of the history of the development of the Yangtze delta plain.

Giorgio Gandolfi, Luigi Paganelli and William Cavazza integrate old and new heavy mineral analyses from 567 turbidite sandstone samples to provide the first basin-wide stratigraphic and sedimentological framework of the Miocene Marnoso-arenacea Formation of the Northern Apennines, Italy. They conclude that the turbidites are the product of distinct detrital inputs from opposing directions and source areas, and that these were deflected along the main axis of the basin, flowing side by side with only minor mixing, as exemplified by marker beds traceable over long distances.

Tuvia Weissbrod and Ron Bogoch employ heavy minerals to break down the apparent homogeneity of the Nubian Sandstone of the Arabo-Nubian Shield (ANS) and its northern periphery. The Nubian Sandstone is one of the largest siliciclastic sediment bodies preserved on earth, long considered to be a single unit because of its lack of useful biostratigraphic data and its laterally continuous lithological markers. Sharp changes in the heavy mineral assemblages, indicating unconformities and shifts of provenance, contrast with the presence or disappearance of metastable heavy minerals that may reflect changes in climate. Combined with sedimentological and palaeogeographic data and detrital zircon geochronology, Weissbrod and Bogoch have identified three major depositional sequences in the Nubian Sandstone ranging from Neoproterozoic to Mesozoic. The Neoproterozoic sequences were derived largely from a Pan-African igneous/metamorphic terrain within the ANS, while Early Palaeozoic sequences were derived mostly from Pan-African and older crust outside the ANS in the Gondwana interior. An ultrastable heavy mineral assemblage of the Late Palaeozoic-Early Mesozoic reflects mature sands mostly sourced from reworked internal siliciclastics, but which also incorporate detritus from extensive exposures of the ANS basement.

Far from the Nubian Desert, Sandra Passchier records the value of heavy minerals in reconstructing ice-sheet drainage patterns of the East Antarctic ice-sheet and glacial events in the Transantarctic Mountains. These demonstrate that the glacial tills can be subdivided into at least two end-member petrofacies of Caenozoic-glaciogenic sediments of the Sirius Group that represent different ice-sheet drainage patterns, with the tills deposited during consecutive stages of denudation of a rift

margin. Heavy mineral assemblages also demonstrate that the Sirius Group resulted from multiple glacial events, and enable the determination of palaeo-ice flow direction through source rock signatures from outcrops several 100 km upstream.

Goran Durn, Dunja Aljinović, Marta Crnjaković and Boško Lugović tackle the long-standing problem of the nature and relationship of terra rossa in the Istrian peninsula, Croatia, to underlying carbonates, and test the theory that it has developed from the insoluble residue of the carbonate rocks. The heavy mineral assemblage of amphiboles, zircon, tourmaline, garnet, kyanite, clinopyroxene and orthopyroxene, present in both loess deposits and in the terra rossa, clearly establish a link with Late Pleistocene loess. Heavy mineral data indicate that material was also derived from Istrian flysch, and that air-fall of particles from the Roman-Campanian Volcanic Province may also have contributed. Durn et al. conclude that the external contributions to the terra rossa, predominantly Middle Pleistocene loess with some from flysch and tephra, may constitute up to 50% of the polygenetic sediment, the rest coming from insoluble residues of presumed limestone and dolomite source formations. Late Pleistocene loess may have become incorporated in the upper parts of already formed terra rossa.

2.2. Tectonogenic Sediments: The Use of Heavy Minerals in Active Geodynamic Settings

In their second contribution, Eduardo Garzanti and Sergio Andò build on the conceptual models developed by earlier researchers and apply high-resolution heavy mineral and petrographic analyses to detrital heavy mineral assemblages from contrasting modern terrigenous geodynamic settings to diagnose sediment provenance. Because statistical techniques cannot easily identify valid end-members of the wide variety of mineral species in the sands, Garzanti and Andò employ all the evidence and information provided by raw datasets. They define ten standard groups of heavy minerals from different tectonic settings with similar provenance implications, which may be combined into supergroups and plotted for general conclusions, or split into subgroups for more detailed work. This enables them to determine the relationships between plate-tectonic setting and both framework silicates and heavy mineral assemblages.

Commonly, heavy minerals are essential for deciphering the provenance signals of the sediments in orogenic belts, because the composition of the source terrain cannot always be reconstructed from the framework constituents. For example, ophiolitic complexes or blueschist belts in pre-existing source terrains can only be proved through their diagnostic heavy minerals. Peter Faupl, Andreas Pavlopoulos and George Migiros, working in mainland Greece and the Peloponnese, use heavy mineral studies to help track Maastrichtian-Miocene flysch sedimentation in the Hellenides synorogenic basin during the destruction of the Tethys Ocean, and synthesise the results to build a geodynamic model of the Hellenides.

Pavel V. Markevich, Alexander I. Malinovsky, Marianna I. Tuchkova, Sergei D. Sokolov and Vladimir N. Grigoryev translate and report the work of Russian researchers who have used heavy minerals to reconstruct the provenance and source lithologies of Mesozoic-Caenozoic sedimentary complexes of the Far East and the western Pacific Ocean, and to identify their plate-tectonic settings. Their overview

also documents important findings from several hundred samples obtained during numerous marine geological expeditions. Markevich et al. integrated heavy mineral analyses with framework components, volcanics (lava, tuffs and tephra) and bulk chemical compositions to identify source rocks and link them to the plate-tectonic setting of the depositional area. For example, magnetite and chromite compositions were used to identify, and differentiate between, assemblages sourced from different types of ophiolites, while the chemistry of detrital pyroxenes identified the main types of volcanic arc sources.

Working in the eastern segment of the Himalayas, Ashraf Uddin, Pranav Kumar, Jogen N. Sarma and Syed H. Akhter, report heavy mineral analyses of representative Oligocene to Pleistocene sandstones from the Assam Basin, and compare these with existing heavy mineral data from coeval Caenozoic sequences in the Bengal Basin to help constrain the unroofing history of the eastern Himalayas and the Indo-Burman Ranges. Uddin et al. conclude that during the Oligocene, heavy minerals in the Assam Basin were derived from incipient uplifts in the Himalayas, whereas in the Bengal Basin supply was from Indian cratonic sources. However, heavy mineral contents in Miocene and younger sequences suggest that both the Bengal and Assam Basins were sourced from the Himalayan and Indo-Burman orogenic hinterlands to the north and east. They conclude from distinct heavy mineral associations that the Assam Basin appears to represent an earlier and more proximal repository of detritus, shed from Himalayan convergence, whereas the Bengal Basin was a downstream and somewhat younger depocentre.

PART III: INTEGRATED AND INTERDISCIPLINARY HEAVY MINERAL APPLICATIONS

3.1. Heavy Mineral Studies Integrated with Other Geoanalytical Techniques

This chapter consists of two sections. The first includes studies that invoke a variety of geoanalytical techniques. The second demonstrates the potential of heavy minerals in interdisciplinary research. The first contribution in this section is by Andrew Carter who reviews the intimate links between data of heavy mineral studies and fission-track analysis. He emphasises the mutual benefits of the fission-track analysis; detrital apatite and zircon provide complementary information on timing and rates of source exhumation that helps place heavy mineral evidence within a temporal framework. While combined heavy mineral—fission-track analyses strengthen provenance studies, the effects of lithological bias, small datasets and non-uniqueness of fission-track ages (and thermochronometric ages in general) can limit or hinder interpretation. Carter discusses these issues and presents new approaches that link high-precision geochemical data from single detrital grains with sediment composition and detrital age structure. Combined geochemical and isotopic signatures extracted from single grains permit more detailed resolution of source composition and evolution that strengthen the role of heavy mineral studies and fission-track thermochronometry.

D. Johannes Huisman and Gerard Th. Klaver obtained data from an extensive database of an earlier large-scale work that used heavy mineral compositions to

systematically distinguish lithostratigraphic units in single boreholes or borehole transects in The Netherlands. Huisman and Klaver use sophisticated computer software and create multiple contour maps of heavy mineral concentrations, with stacked threshold maps and colouring codes for depths that give an effective overview of the temporal and spatial distributions of sediments derived from various sources to the area. They use spatial variations of single minerals, as opposed to mineral assemblages, to illustrate the geometry of sediments on a countrywide scale. Distributions of selected heavy minerals (zircon, augite, hornblende, garnet and topaz) reflect ancestral flow paths of the modern major rivers.

Hilmar Von Eynatten provides a brief review of heavy mineral research on the Swiss Molasse Basin and summarises the results of recent studies. His contribution integrates heavy mineral analysis with high-resolution single-grain chemistry and thermochronological studies ($^{40}Ar/^{39}Ar$ laser-probe dating of white mica, fission-track dating of zircon). These techniques are applied to Rupelian to Serravallian ($\sim$31–$\sim$13 Ma) sandstones from two composite sections of the Swiss Molasse Basin, one in the east (Honegg-Kronberg-Hörnli) and one in the central part (Honegg-Napf). Their data indicate that the east experienced a normal unroofing sequence of the Austroalpine-Penninic nappe stack, whereas in the central part, erosion of basement rocks started significantly earlier; sediments younger than $\sim$20 Ma document increasing cooling rates of their source rocks, reflecting accelerated exhumation in the hinterland.

Geoffrey M.H. Ruiz, Diane Seward and Wilfried Winkler apply an integrated heavy mineral and zircon fission-track analysis to unravel the evolution of the Amazon basin in Ecuador. Heavy mineral analysis of the proximal shallow marine and continental deposits in the Sub-Andean Zone reveals an overall trend from ultrastable zircon, tourmaline and rutile dominated assemblages, to more complex heavy mineral suites with metamorphic and mafic volcanic signatures. This reflects successive derivation from shallow to deep crustal rocks and, subsequently, from accreted oceanic terranes during formation of the proto-Andes. They measured lag times of the zircons, which range from 400 to 0 Ma. In their study, they combine zero lag times with lithological and mineralogical datasets that have been used to identify volcanic events in the hinterland, thus enabling establishment of the stratigraphic age of the enclosing sediments more precisely.

3.2. The Use of Heavy Minerals in Interdisciplinary Research

3.2.1. Forensic Science—Evidence from Heavy Minerals in Criminal Investigation

Heavy minerals yield vital clues in criminal investigations and are highly appreciated by the forensic scientist. Their potential has been proved numerous times in court when comparative analyses provided the missing evidence. Of the two contributors to this section, Skip Palenik is a forensic microscopist and Wayne C. Isphording uses his geological knowledge and expertise in criminal investigations. Both provide an insight into the principles and practicalities of evidence gathering, and also indicate precautions that must be observed when working under legal scrutiny. They conclude with examples that illustrate how a mineral component that commonly comprises less than 1% of a typical sample, can provide the geoscientist with information that is critical in a wide variety of forensic investigations.

Because often only traces of material are available for study, special techniques are necessary to recover the minute quantities of accessory minerals that may be used in evidence. In describing these special techniques, Palenik provides useful guidance for geoscientists who in special cases can obtain only limited, even minute, amounts of sample material (such as samples from deep boreholes/wells, cuttings contaminated by excessive drilling mud and archaeological material that may be available in minute pieces, etc.).

3.2.2. Geoarchaeology

Archaeology and geology have long enjoyed a mutual interdependence because archaeological raw materials have a predominantly geological origin. Therefore, artefacts made of stone or clay, the principal inorganic raw materials of ancient times, can be best analysed by techniques used in geological laboratories. Pottery sherds are amongst the most abundant artefacts at archaeological sites and are suitable for heavy mineral analysis because they always include a certain portion of sand, called 'temper'. This is added to the clay during manufacturing to improve cohesion during working and firing and to increase durability in use. Heavy minerals of the sandy temper can thus provide information on the source and location of the raw material, and manufracturing practices. Comparative studies of potteries from different sites may indicate trade and transport routes in ancient times. Two contributions demonstrate the use of heavy minerals in geoarchaeology.

William R. Dickinson analysed prehistoric ceramics from a series of islands in Pacific Oceania and discovered a diverse array of volcanic sand tempers used by the ancient potters. Their heavy mineral suites allowed their sources to be linked to beach placer sands that reflect the phenocryst mineralogy of bedrock on the islands where pottery was made. Island groups within the region of ceramic cultures were found to extend from western Micronesia to western Polynesia with the temper recording hotspot, arc, postarc and backarc geotectonic settings. Because the relative proportions of heavy mineral species in Oceanian placer tempers correlate with the nature of restricted bedrock sources on individual islands, they serve as diagnostic evidence for temper origins wherever pottery was transported between islands.

Maria A. Mange and Tamás Bezeczky analysed sherds of amphorae from the Roman period, excavated in pottery workshops, owned by the Roman Laecanius family, on the peninsula of Istria, Croatia. Their distinctive heavy mineral asemblages furthered the characterisation of the amphorae and pointed to the source of the raw material used for the clay and sandy temper. Heavy mineral signatures in amphorae produced in other workshops facilitated their distinction from the Laecanius sherds. Comparative heavy mineral analysis of terra rossa, taken from an outcrop close to the workshop, indicates that terra rossa was the major source of the paste. Modern Adriatic sponge spicules found in the majority of Laecanius amphora sherds and the temper-derived, generally immature, heavy mineral assemblages suggest that the sandy material for the temper was obtained largely from Adriatic deposits. Results of both contributions prove that the heavy mineral technique is a powerful archaeometric tool.

PART IV: INDUSTRIAL APPLICATION: RESERVOIR CHARACTERISATION, ECONOMIC HEAVY MINERAL DEPOSITS, DIAMOND PROSPECTING

4.1. Reservoir Characterisation

Contributions of heavy mineral studies to solve problems in basin analysis, petroleum exploration and reservoir management have long been appreciated. When allied with other sedimentological and/or stratigraphical and geochemical techniques, they have much to offer towards a better understanding of sediment provenance and the history of a given basin. Heavy mineral assemblages prove especially informative when used in lithologically uniform successions, which are devoid of lithological and/or biostratigraphical markers. Systematical changes in heavy mineral compositions can reveal heterogeneity, caused either by shift in transport, changes in tectonics, climate, depositional mechanism or basin configuration. These impart particular signatures to the assemblages that are usually reflected by distinct heavy mineral zones. Heavy mineral zones with similar characteristics in related sand packages permit well-to-well or basin-wide correlation.

Andrew C. Morton, Rob Herries and Mark Fanning apply heavy mineral analysis to the construction of a correlation framework for the Triassic succession in the Strathmore Field, west of Shetland. They describe how correlation is dependent on the identification and quantification of parameters that are sensitive to changes in provenance, but are unaffected by other processes of the sedimentary cycle. Care must therefore be exercised when considering provenance signals, which may be overprinted by the effects of hydrodynamic, weathering and diagenetic processes on heavy mineral suites. Ratios of abundances of stable minerals having similar density and hydraulic behaviour, in a limited size range, can provide an accurate provenance indicator. An alternative approach uses the range of varietal parameters within a single-mineral group (e.g., zircons) that thus reflects provenance characteristics without significant hydrodynamic or diagenetic modification. Morton and his co-authors use integrated heavy mineral, mineral chemical and zircon age data to show that Triassic sandstones in the Strathmore Field were derived from different sources. The Early Triassic Otter Bank Formation is linked to recycled Devonian-Carboniferous rocks of Upper Clair Group, with contributions from Lewisian orthogneisses, on the eastern (British) margin of the Faeroe-Shetland rift. The overlying Middle-Late Triassic Foula Formation is interpreted to have been derived from high-grade metasedimentary/charnockitic basement rocks, thought to be located in the Nagssuqtoqidian belt of southern East Greenland, on the western side of the rift.

Maria A. Mange, Peter Turner, David Ince and David T. Wright, in a combination of high-resolution heavy mineral and palaeomagnetic studies on onshore type sections and cored interbedded sandstone and mudstone samples from the Triassic Sherwood Sandstone Group, generated a heavy mineral magnetostratigraphy. Heavy mineral zones are identified and tied to specific magnetostratigraphic Chrons. A reference section, combined with data from surface exposures and cored wells, is used to interpolate the defined heavy mineral and magneto zones to uncored

successions of nine wells in the East Irish Sea. The combined technique has yielded vital information on sediment provenance and dispersal within the basin. The assignment of absolute ages to the identified heavy mineral zones generates a time-stratigraphic framework for the Triassic of the East Irish Sea Basin and adjacent areas, within which basin evolution may be better reconstructed. The significance of this combined approach is its potential for the dating, subdivision and correlation of uncored wells and sedimentary successions that are barren or stratigraphically poorly constrained.

Mette Lise K. Poulsen, Henrik Friis, Johan B. Svendsen and Christian B. Jensen explore Palaeocene reservoirs in the Siri Canyon (Danish North Sea), comprising sands interbedded with deep marine muds and remobilised and/or injection deposits. The sands are subdivided into a series of flow units by interpreting Zr, Th and TiO_2 trends on the geochemical logs, and by heavy mineral grain size sorting. Distinct cycles, interpreted as reflecting systematic heavy mineral variations, have been recognised in homogenous, massive sands on the basis of elemental trends, gamma ray and grain density logs, and in factor score depth plots calculated by PCA. Poulsen et al. argue that each cycle represents a single surge within a larger flow event, and that the sediments were sorted by suspension fallout during deposition. They suggest that suspension fallout sorting of heavy mineral grains may be a common feature in concentrated density flow deposits, allowing the recognition of individual flow units within thick massive sands.

Andrew C. Morton develops an application of heavy mineral analysis as a real-time geosteering and correlation tool for horizontal wells that can be considered as an alternative to biostratigraphic methods where these have inadequate resolution. Morton points out that heavy mineral-directed geosteering is dependent on discovering recognisable stratigraphically significant variations in provenance between the pay zone and overlying and underlying units of the target succession, and requires the establishment of a robust correlation scheme prior to drilling. The technique has been successfully applied in a variety of depositional environments, including fluvial/aeolian, shallow and deep marine, in the Clair, Ross and Hannay Fields of the UK Continental Shelf.

4.2. Mineral Exploration and Mining

Scientific analysis of heavy minerals grew out of the prospecting for alluvial deposits containing gold, other precious metals or precious stones, dominantly diamonds. Exploitable sands are usually placer deposits which are described as ‘‘a surficial mineral deposit, formed by mechanical concentration of mineral particles from weathering debris. The mechanical agent is usually alluvial, but can also be marine, aeolian, lacustrine or glacial, and the mineral is usually a heavy metal such as gold’’ (Gary et al., 1972). Placer minerals are all heavy minerals, with specific gravities greater than 2.58; this is slightly lower than that of bromoform (2.9), the standard liquid used for separating heavy minerals from a heterogeneous mixture (Els and Eriksson, 2006).

Several of the world’s important mineral commodities have been obtained from placers, for example, gold, diamond, cassiterite, etc. Certain indispensable industrial minerals occur in sandy placers informally known as ‘black sands’, ‘heavy mineral

sand deposits' or 'heavy mineral sands'. Valuable heavy minerals associated with sand deposits are rutile, zircon, ilmenite, leucoxene, cassiterite, monazite, kyanite, tourmaline, sillimanite and garnet. They are exploited from coastal sand deposits in many parts of the world, for example, in Australia, Canada, India, Kenya, Madagascar, Mozambique, South Africa. (Harben and Bates, 1990; Force, 1991). Worldwide interest in heavy mineral deposits and the potential of mining commodities from heavy mineral sand is reflected by international heavy mineral conferences and by the monthly reports and annual reviews issued by the Perth-based consulting group TZ Minerals International Pty. Ltd.

Fredric L. Pirkle, William A. Pirkle and E.C. Pirkle present a concise review of the heavy mineral sands of the Atlantic and Gulf Coastal Plains, USA. Their contribution includes the history of prospecting and mining which started in this region in 1916, when ilmenite was first mined from the heavy mineral sands (Frontispiece A and B: Chapter 46). Their contribution provides a detailed description of the properties and development of all major deposits. They also outline the problem that heavy mineral mining industry faces along both the Atlantic and Gulf coastal plains, due to demands for land uses, such as forestry, residential and resort development and environmental concerns.

4.3. The Role of Tracer Heavy Minerals in Diamond Exploration

This volume would not be complete without including a review on the significance of particular heavy minerals as pathfinders in searching for diamonds. Tom E. Nowicki, Rory O. Moore, John J. Gurney and Mike C. Baumgartner provide an overview of kimberlite, a variety of ultramafic- and sub-volcanic rock, which is the dominant source of diamonds worldwide. Diamonds were formed in the deep ancient lithospheric keels of Archaean cratons and kimberlites are the transporting agents that "sample" deep, occasionally diamond-bearing, mantle material and rapidly convey it to surface. Along with diamonds, kimberlites pick up large quantities of other mantle minerals, commonly referred to as kimberlitic indicator minerals. From an exploration point of view, the most important indicator minerals are garnet, chromite, ilmenite, Cr-diopside and olivine. Several of these minerals display diagnostic visual and compositional characteristics, making them ideal pathfinders for kimberlite. The more chemically resistant minerals (garnet, ilmenite and chromite) are particularly useful due to their greater ability to survive weathering in the surface environment. Thus, prospecting for surface materials to recover kimberlitic indicator minerals and tracing these back to their source is a key component of most diamond exploration programs.

REFERENCES

Artini, E., 1898. Intorno alla composizione mineralogical delle sabbie di alcuni fiumi del Veneto, con applicazione ai terreni di transporto. Riv. Miner. Crist. Italiana 19, 33–94.

Boswell, P.G.H., 1933. On the Mineralogy of Sedimentary Rocks. Murby & Co., London, 393pp.

Carriquiry, J.D., Sánchez, A., 1999. Sedimentation in the Colorado River delta and Upper Gulf of California after nearly a century of discharge loss. Marine Geology 158, 125–145.

Dick, A.B., 1887. On zircon and other minerals contained in sand. Nature 36, 1–92.
Els, G., Eriksson, P., 2006. Placer formation and placer minerals. Ore Geology Reviews 28, 373–375.
Force, E.R., 1991. Geology of Titanium-Mineral Deposits. Geological Society of America Special Paper 259, 112.
Frihy, O.E., Lofty, M.F., 1997. Shoreline changes and beach-sand sorting along the northern Sinai coast of Egypt. Geo-Marine Letters 17, 140–146.
Gary, M., McAfee, R. Jr., Wolf, C.L. (Eds.), 1972. Glossary of Geology. American Geological Institute, Washington DC.
Harben, P.W., Bates, R.L., 1990. Industrial Minerals Geology and World Deposits. Industrial Minerals Division, Metal Bulletin plc, Surrey, UK.
Imbrie, J., Van Andel, Tj.H., 1964. Vector analysis of heavy mineral data. Bulletin of the Geological Society of America 75, 11131–11156.
Mange, M.A., Maurer, H.F.W., 1992. Heavy Minerals in Colour. Chapman and Hall, London, 147pp.
Milner, H.B., 1929. Sedimentary Petrography, 2nd rev. ed. Murby, London, 521pp.
Milner, H.B., 1962. Sedimentary Petrography, Vol. 1, Methods in Sedimentary Petrography, 4th Edition. George Allen and Unwin, London, 643pp.
Pirkle, F.L., Pirkle, E.E., Pirkle, A., Dichs, S.E., 1985. Evaluation through correlation and principal component analyses of delta origin for the Hawthorne and Citronelle sediments of peninsular Florida. Journal of Geology 93, 493–501.
Svendsen, J.B., 2002. Sedimentology and High-Resolution Stratigraphy of Fluvial-Aeolian Sequences Using Integrated Elemental Whole Rock Geochemistry. Ph.D. thesis. University of Aarhus, Denmark.
Wong, F., 2002. Heavy mineral provinces of the Palos Verdes margin, southern California. Continental Shelf Research 22, 899–910.

Maria A. Mange and David T. Wright

PART I: HEAVY MINERALS IN THE STUDY OF SILICICLASTIC SEDIMENTS: PRINCIPLES, PROCESSES AND PRODUCTS

1.1 Entrainment, Transport and Deposition: Hydraulic Control

This page intentionally left blank

Chapter 1

THE ENTRAINMENT, TRANSPORT AND SORTING OF HEAVY MINERALS BY WAVES AND CURRENTS

PAUL D. KOMAR

College of Oceanic and Atmospheric Sciences, Oregon State University, Corvallis, OR 97331, USA

ABSTRACT

Heavy-mineral grains in a sediment have hydrodynamic properties that are distinct from the particles of quartz and feldspar. Differences also occur within the suite of heavy minerals due to their ranges of densities, diameters and shapes. The contrasting hydrodynamic properties of these sediment grains can give rise to differential rates of transport by flowing fluids that yield distinct patterns of deposition based on the particle attributes. The higher densities and generally finer grain sizes make the heavy minerals more resistant to entrainment by flowing water, and they then experience lower rates of transport when carried as part of the bedload or in suspension where differences in grain settling velocities are important. In the extreme this hydrodynamic sorting can lead to the formation of heavy-mineral concentrates, or a placer when the deposit contains economically valuable minerals. The processes of mineral sorting have been investigated mainly in the context of the formation of placers found in rivers, beaches and in continental shelf sands. That research is reviewed in application to the hydrodynamic sorting of sediment grains in general, with the focus being on the mechanisms of selective entrainment, shear sorting during bedload transport, sorting within the geometry of bedforms such as ripples, and the effects of differences in particle settling velocities on grain sorting during suspension transport and when the sediments are deposited. Each of these mechanisms depends on the particle density, diameter and shape, and collectively account for the observed patterns of mineral sorting found in sediment deposits.

Keywords: beach placers; continental shelf sediments; grain entrainment; grain settling velocities; placers; river placers; sediment sorting; sediment transport

1. INTRODUCTION

The grains of heavy minerals in a sediment can have markedly different hydrodynamic properties compared with the light minerals, quartz and feldspar. Due to

Developments in Sedimentology, Vol. 58, 3–48

ISSN: 0070-4571/doi:10.1016/S0070-4571(07)58001-5

their contrasting densities as well as grain sizes and shapes, the heavy minerals are generally more difficult to entrain by flowing water than the light minerals, and this can lead to the formation of a lag deposit of concentrated heavy minerals when the light minerals are selectively transported away. This sorting continues for the particles that are under transport; the heavy minerals may have higher settling velocities than the quartz and feldspar, so their transport takes place closer to the bottom where the current velocities are lower.

Selective sorting of particles by differential entrainment and transport can also take place within the suite of heavy minerals due to their ranges of densities, grain sizes and shapes. This sorting may result in problems in the interpretation of ancient sedimentary deposits, for example to establish the sources of the sediment and the paleoenvironment of deposition based on the heavy-mineral content. On the other hand, the separation of the heavy minerals from the light minerals and the sorting within the suite of heavy minerals can produce concentrations having economic significance—placer deposits. Placers can be found in alluvial, marine, aeolian and lacustrian deposits, and have been important sources of metals such as gold, platinum, tin and titanium (Hails, 1976; Komar, 1989).

In spite of the sorting of sediment grains during transport being common and important to the formation of valuable placers, surprisingly little research has focused on the details of the physical processes responsible for this sorting. It is important that this science be improved in order to support a better understanding of the general processes of sediment transport that accounts for the ranges of sizes and densities of particles found in a sediment, to provide a sounder basis for the effective discovery of placer deposits, and in order to improve the interpretation of ancient sedimentary deposits from their heavy-mineral contents.

This chapter reviews the present scientific understanding of the hydraulic behavior of heavy minerals in comparison with the transport of particles of quartz and feldspar, which has been thoroughly investigated over more than a century. The grain sorting mechanisms are first outlined in general, a summary that serves as the basis for the review of research that has attempted to document the roles of those mechanisms through laboratory experiments or in field studies of heavy-mineral concentrates and placers found in various environments.

2. GRAIN DENSITIES, DIAMETERS AND SHAPES

The hydrodynamic properties of sediment grains depend on their densities, sizes and shapes. Emery and Noakes (1968) divided minerals into three groups based on their densities: ''heavy–heavy minerals'' being those with exceptionally high densities (e.g., gold with a density of 18 g/cm^3), the ''light–heavy minerals'' which have more moderate densities that fall within the range of common heavy minerals and the ''light minerals'', mainly quartz and feldspars. Particularly important to their sorting by flowing water is the contrast in densities between the heavy and light minerals, and the large range of densities within the suite of common heavy minerals, especially if one includes particles of gold and platinum important in placer deposits. Even for the common heavy minerals the densities range widely from approximately 7.0 g/cm^3 for cassiterite to 3.2 g/cm^3 for hornblende.

Differences in ranges of available particle sizes and shapes are also important to the hydrodynamic properties. Within their primary source rocks, most heavy minerals occur in sizes comparable to the grains of quartz and feldspar (Feniak, 1944; Kretz, 1966), but it is generally observed that in sediments derived from those rocks the heavy-mineral grains tend to be significantly smaller. This in part is a product of selective sorting by density and size, as will be examined in this chapter, but the abrasion and propensity of the heavy-mineral particles to fracture along cleavage planes during transport must be an important factor as well, since the larger grains commonly disappear entirely from the depositional system. The more resistant grains retain their sizes and even crystal shapes inherited from their primary rock sources; prismatic zircon crystals and euhedral garnet found in sediments are obvious examples. However, it is not well-established how grain properties such as their hardness and cleavability determine the abrasion and thus size and shape changes of the less resistant mineral particles during transport. Most investigators have concluded that grain abrasion and rounding are significantly greater on beaches than in rivers (Kuenen, 1964; Clemens and Komar, 1988), so the degree of change likely depends on the environment. Therefore, abrasion processes can affect the sizes and shapes of the mineral grains, which in turn influences their hydrodynamic properties and ultimately the contents of heavy minerals found in sediment deposits.

The reviews below of grain entrainment and other mechanisms of sorting by flowing water demonstrate the importance of particle density and size, and also their shape although this has been less well-established experimentally. As a result of their controls on particle sorting during transport, the sorting patterns are generally represented by systematic variations in particle densities and grain sizes, which have been interpreted in terms of the ''hydraulic equivalence'' of the different minerals with the equivalence dependent on the sorting mechanism (Rubey, 1933).

3. PHYSICAL PROCESSES OF MINERAL SORTING

The summary presented here of the sorting mechanisms begins with an examination of the selective entrainment by flowing water of grains from a sediment consisting of different particle sizes and densities. This is the first step in the sorting of heavy and light minerals, and generally turns out in most cases to be the process most important to the formation of heavy-mineral concentrates and placers. The subsequent transport is characterized as being in part a bedload consisting of the coarser (heavier) grains that move along the bed by sliding and bouncing (saltation), and a suspended load of finer grains that are lifted above the bed by the turbulent eddies of the flowing fluid. Grain sorting within the moving bedload can occur as the particles of mixed sizes and densities are sheared to form laminations, or may occur locally within the geometry of bedforms such as ripples and sediment dunes. Most important to the suspended load are the settling velocities of the sediment grains, wherein differences in their densities and diameters can lead to contrasting settling rates that give rise to selective transport and particle sorting. These basic mechanisms are reviewed in this section, while research documenting their roles in various environments are presented later in this chapter.

3.1. Grain Entrainment by Flowing Water

Grain entrainment or the initiation of sediment motion by a flowing fluid has been investigated by a great number of studies spanning more than a century. Nearly all of those investigations focused on the simplest condition that predicts the first movement of grains from a flat bed of nearly uniform particles, uniform in their densities and sizes. Such ideal conditions are not generally found in Nature, but the experiments still have been relied upon to serve as the basis for our standard grain threshold curves. Those results will be reviewed first as they provide the basis for a comparison with grain entrainment from a more natural deposit consisting of a mixture of grain sizes and densities, the condition of interest in this chapter concerned with the selective entrainment of heavy versus light minerals.

The laboratory measurements of the threshold of uniform grains from a flat bed have been compiled by Miller et al. (1977) and Yalin and Karahan (1979) to yield up-dated versions of the threshold curves. Of particular significance is the graphical presentation developed in 1936 by the engineer A. Shields, important in that it offers a non-dimensional analysis which unifies the threshold data and can be employed to evaluate the entrainment of grains of any density by a flowing liquid (but not gases, such as air). It is, therefore, applicable to heavy minerals as well as quartz-density particles. The up-dated Shields curve is given in Fig. 1A, and compares two dimensionless parameters, the Shields entrainment function

$$\theta_t = \frac{\tau_t}{(\rho_s - \rho)gD} \tag{1}$$

and the grain Reynolds number

$$\mathrm{Re}_* = \frac{u_{*\mathrm{t}}D}{v} = \frac{\rho u_{*\mathrm{t}}D}{\mu} \tag{2}$$

where τ_t is the threshold mean bed stress exerted by the current (the force per unit bed area), $u_{*\mathrm{t}} = \sqrt{\tau_\mathrm{t}/\rho}$ the corresponding shear velocity, ρ_s and ρ are, respectively, the densities of the sediment grains and fluid, D is the diameter of the grains, g is the acceleration of gravity, and v and μ are, respectively, the fluid's dynamic and kinematic viscosities ($v = \mu/\rho$). The curve shown in Fig. 1A is based on experiments using uniform sediments that individually represent mean grain sizes from silts through pebbles, grain densities from quartz through those of heavy minerals, and employing various liquids that included oils and glycerin as well as water. The agreement of the data for this variety of grain sizes and densities, and for different liquids, on a dimensionless graph illustrates the "universality" of the Shields curve, although it does not extend in application to the case of aeolian grain entrainment. The primary limitation of this threshold curve is that it is based on experiments with uniform grains formed into an artificially smoothed deposits in laboratory flumes, and the potential cohesive effects of clays have also been excluded.

The Shields graph of Fig. 1A can be employed to determine the threshold flow stress τ_t for a grain of density ρ_s and diameter D in a liquid of density ρ and viscosity μ. However, such an evaluation requires an inconvenient convergence approach

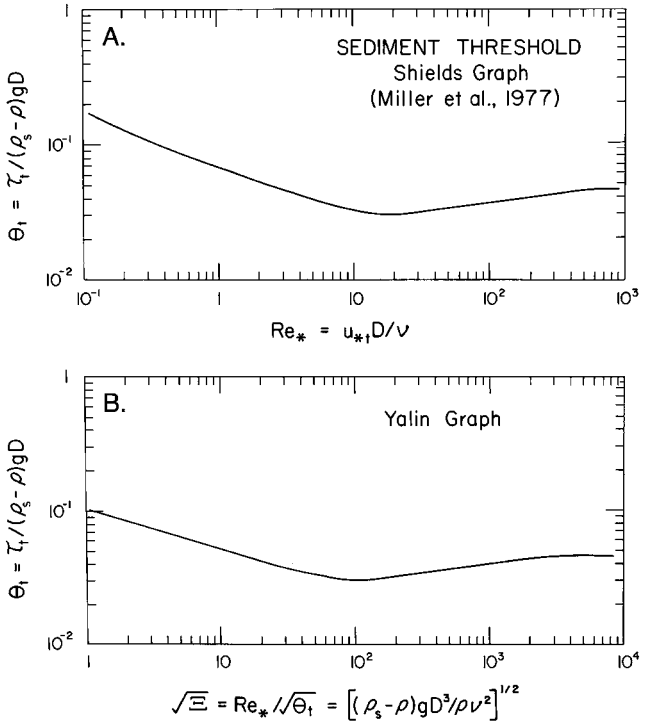

Fig. 1. (A) The standard Shields curve for the threshold of uniform grains. (B) The Yalin (1972) curve which is more convenient for threshold determinations. [After Miller et al. (1977).]

since τ_t is contained in both θ_t and Re_*, the two axes of the Shields graph. This problem induced Yalin (1972) to reformulate the presentation as θ_t versus

$$\Xi = \frac{Re_*^2}{\theta_t} = \frac{(\rho_s - \rho)gD^3}{\rho\nu^2} \tag{3}$$

yielding the curve in Fig. 1B based on the same data that established the Shields curve. The advantage of the Yalin approach is that Ξ can be calculated from known fluid and grain parameters so the threshold θ_t and τ_t can be determined directly without iterative calculations. Examples of derivative curves for the entrainment stress τ_t versus the grain diameter D are presented in Fig. 2 for the threshold of quartz-density grains and representative heavy minerals covering a range of densities. As expected, the curves are arranged in a vertical sequence according to the grain densities, with quartz at the bottom and gold at the top, the gold requiring the greatest entrainment flow stress for a given diameter. The results also demonstrate the significant range of entrainment stresses for the series of common heavy minerals, indicated by the curves for garnet and cassiterite.

The curves of Figs. 1 and 2 are based on experiments with unidirectional currents as found in a river. However, they have been shown to apply as well to grain threshold under the oscillatory water motions of waves. The primary difference is the

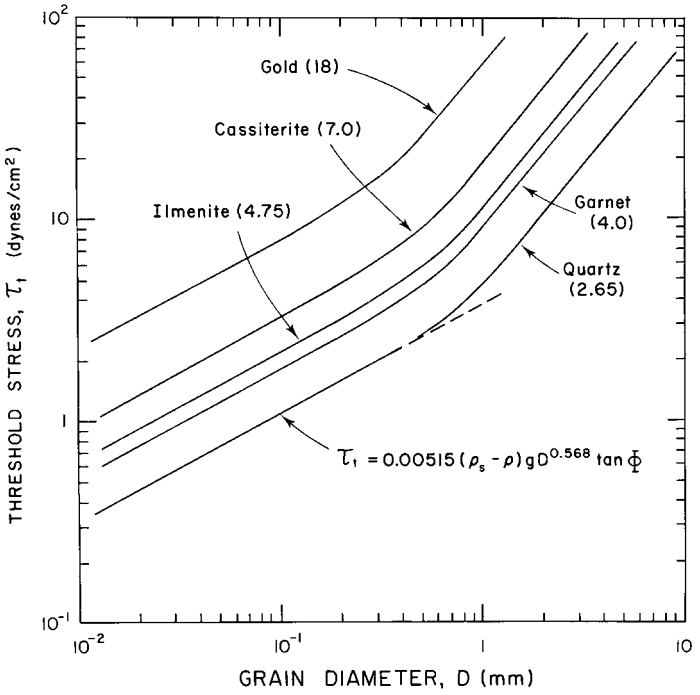

Fig. 2. Curves for the mean entrainment flow stress versus the grain diameter for quartz and representative heavy minerals (specific gravities in parentheses).

way in which the flow stress τ_t is evaluated. For a uniform flow in a river this stress can be calculated with the DuBoys equation $\tau_t = \rho ghS$ where h is the flow depth (or hydraulic radius) and S is the channel slope. For waves the mean stress (averaged over a wave cycle) is calculated with $\tau_t = 0.5 f u_m^2$ where u_m is the maximum orbital velocity of the waves at the bed and f is a friction coefficient appropriate for wave motions.

For most analyses of the sorting and concentration of heavy minerals, the threshold curves of Figs. 1 and 2 are not directly applicable since they represent conditions for sediment deposits consisting of only one mineral and effectively one grain size. For example, the curve for ilmenite in Fig. 2 applies strictly only to a deposit consisting of 100% of that mineral, a condition that might conceivably be achieved in a placer but is not relevant to the processes of sorting of the ilmenite mixed with other mineral grains during the concentration process. The curves of Figs. 1 and 2 mainly provide an assessment of the relative stabilities of heavy-mineral concentrates following their formation by the sorting processes.

The formation of a heavy-mineral concentrate involves the processes of selective entrainment governed by the contrasting densities and sizes of the grains, a condition that departs from the experiments used to establish the Shields and Yalin curves and their derivatives. The studies of Slingerland (1977) and Komar and Wang (1984) have examined the processes of selective entrainment in the formation of placers, with Komar (1989) providing a review. The factors important to the selective

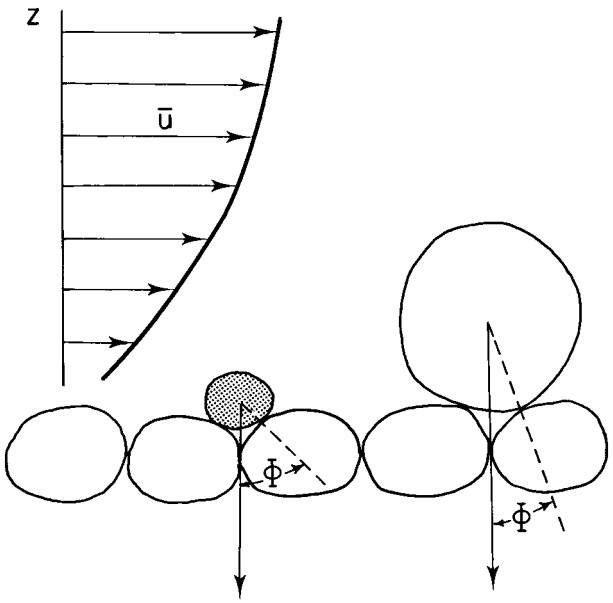

Fig. 3. Effects of relative exposure and variable pivoting angles on the selective entrainment of particles from a deposit of mixed grain sizes and densities, with the smaller heavy-mineral shaded. The velocity $\bar{u}$ is the local time average within the turbulent flow, this average increasing with distance above the sediment to define the flow's boundary layer.

entrainment processes are illustrated in Fig. 3, which contrasts the entrainment of a small heavy-mineral particle (shaded) with a larger quartz grain. The relative weights of the two particles are important to their entrainment, such that the higher density of the heavy mineral tends to offset its smaller size (the two particles illustrated might even have the same immersed weights). The smaller size of the heavy-mineral grain can also be a direct factor in reducing its mobility. Most obvious in Fig. 3 is its limited exposure to the profile of the flowing water, with the water's velocity increasing with distance above the sediment bed, in comparison with that of the larger quartz grain which projects further above the bed and hence experiences greater flow velocities and drag forces. In addition, the entrainment process generally involves the pivoting of the grain out of its resting position, and it is apparent in Fig. 3 that the smaller heavy-mineral particle has a larger pivoting angle Φ than does the quartz grain, a factor that will also increase its resistance to entrainment. Therefore, the increased exposure to the flow and smaller pivoting angles of the larger quartz grain both favor its entrainment in comparison with the heavy-mineral particle. In a deposit of mixed grains, a current may be able to entrain and transport the light minerals, leaving behind a lag of heavy minerals that are more resistant to movement by virtue of their higher densities, lower exposures to the flow and greater pivoting angles.

It is difficult to quantify these processes of selective entrainment, but Slingerland (1977) and Komar and Wang (1984) attempted to do this in connection with the formation of placers. Basic to their analyses are mechanical models that focus on

the forces of fluid drag and lift, which act to move the particle but are opposed by the immersed weight of the grain. This type of analysis was first undertaken by White (1940) for deposits of uniform grains, the results of which provide a process-based model that accounts for the success of the empirically based Shields graph (Fig. 1A). θ_t of Eq. (1) was found to be proportional to the ratio of the fluid-drag force responsible for the grain entrainment to the immersed weight of the particle resisting its entrainment, while the Reynolds number Re_* relates to the condition of fluid flow at the bed, its degree of turbulence. Slingerland (1977) and Komar and Wang (1984) expanded the analysis to account for the more natural condition where there is a distribution of grain sizes and densities.

Slingerland (1977) undertook analyses to examine how heavy-mineral enrichment is controlled by the boundary Reynolds number, Re_* of Eq. (2), and the ratio of the grain size in question to the average bottom roughness. He applied his analyses with some success to experiments undertaken in a wave tank and to natural heavy-mineral concentrations in beach sands. In a study of the formation of placers on Oregon beaches, Komar and Wang (1984) employed the threshold relationship

$$\tau_t = 0.00515(\rho_s - \rho)gD^{0.568} \tan\Phi \tag{4}$$

which was obtained empirically by Miller et al. (1977) for the entrainment of uniform grains of diameter $D < 0.1$ cm (see Fig. 2). With uniform grains there is an approximately constant $\Phi = 30^\circ$ [$\tan\Phi \approx 0.6$], but this pivoting angle varies with grain size within a deposit of mixed sizes as illustrated graphically in Fig. 3. Based on the experiments of Miller and Byrne (1966) and established further by Li and Komar (1986), such variations in the pivoting angle can be evaluated with

$$\Phi = e\left(\frac{D}{K}\right)^{-f} \tag{5}$$

where D is the diameter of the grain being entrained while K is the diameter of the grains over which it pivots, generally represented by the median grain size of the sediment. Values of the e and f coefficients are based on experiments, which demonstrated that they depend on grain shape (rollability and angularity) and on packing arrangements such as imbrication. From Eq. (5) it is seen that Φ decreases with increasing D/K as apparent geometrically in Fig. 3, so its use in Eq. (4) accounts in part for the grain sorting processes within a sediment of mixed sizes and densities. This selective grain entrainment model has been tested and verified by Li and Komar (1992a) in a series of laboratory flume experiments that showed excellent agreement between the predicted entrainment stress τ_t from the combined Eqs. (4) and (5) and those measured in the experiments covering a range of D/K from 0.59 to 1.4.

The combined Eqs. (4) and (5) were employed by Komar and Wang (1984) to generate the series of threshold curves given in Fig. 4, the selection of minerals included having been of specific interest to that study of the grain sorting processes leading to the formation of placers on Oregon beaches, to be reviewed later in this chapter. The curve from Eq. (4) with a fixed Φ is included for comparison, and is the same as that in Fig. 2 for uniform quartz grains. The other curves are for the selective entrainment by size and density where Φ varies according to Eq. (5). The selective

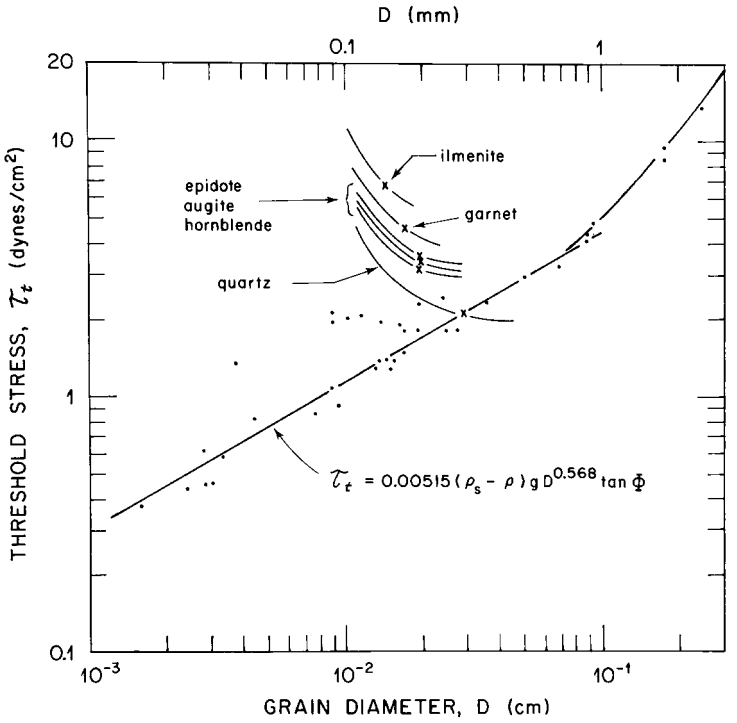

Fig. 4. Curves for the selective entrainment of particles from a deposit of mixed sizes for minerals important to placer formation on an Oregon beach, compared with the standard threshold curve for uniform quartz grains. [After Komar and Wang (1984).]

entrainment curve for quartz within a deposit of mixed sizes is seen to obliquely cross the standard threshold curve for beds of uniform quartz grains, with the crossing point being at the median grain size of the beach sand as a whole (indicated by the *x* on the curve), which initially is determined by the dominant quartz fraction. The curves for the other minerals were calculated on the basis of this same median grain size. Each selective entrainment curve slopes downward to the right; the calculations predict that the stress required for grain entrainment from a bed of mixed sizes of sand decreases with increasing grain diameter within that mixture. Of special interest to the formation of the Oregon beach placer, the series of curves shows that of the several minerals found in the sand, ilmenite would be most difficult to entrain due in part to its having the highest density, but also due to its being the finest grained. Of the several heavy minerals, hornblende is predicted to be most easily entrained, being the least dense and coarsest of the heavy minerals. As will be review in a later section, this predicted order of resistance to entrainment is matched by the degrees of concentration of these minerals in a placer on an Oregon beach, leading to the conclusion that selective entrainment was the primary sorting process important to the formation of that placer.

Analyses of the relative abundances of heavy minerals found in sediments have been presented in terms of their "hydraulic equivalence"—for example, best known is their settling equivalence as advocated by Rubey (1933), which will be discussed

below. There could be a comparable condition of "entrainment equivalence" found in sediments, but its development would be more complex. The selective entrainment curves shown in Fig. 4 for minerals found in Oregon beach sands is specific to that mixture, and for the mean grain size of the sand as a whole, dominated initially by the quartz–feldspar fraction. Other mixtures of minerals and grain sizes would yield a different series of entrainment curves. Furthermore, the curves would evolve as the sorting takes place, initially as the quartz and feldspar are preferentially transported away, affecting the mean grain size of the deposit as a whole, and then as the sorting affects the individual heavy minerals and alters their relative abundances. In the end there may be an approximate entrainment equivalence of the series of minerals remaining in the heavy-mineral concentrate, a condition that potentially could be evaluated employing Eqs. (4) and (5). For the minerals to be in entrainment equivalence, that is have the same τ_t entrainment stress, the combination of the two equations yields

$$(\rho_s - \rho)D^{0.568} \tan\left[e\left(\frac{D}{K}\right)^{-f}\right] = \text{constant} \tag{6}$$

which implies the establishment of an inverse relationship between the densities and grain sizes within the suite of heavy minerals. This relationship for the hydraulic threshold equivalence has not been directly tested employing laboratory or field data.

3.2. Shear Sorting of Mineral Grains

Once grain entrainment has occurred, the flowing fluid produces a transport of the sediment. The moving bedload in part involves the shearing of a thin layer of sand grains across the bed, within which there is a high gradient of the velocity of the concentrated fluid and sediment. This shearing can result in the formation of sediment laminations, which range up to approximately 20 mm in thickness. The laminations are most apparent when accompanied by a sorting of the grains to produce a layer of heavy-mineral concentration overlain by the light minerals, yielding a marked color contrast. Emery and Stevenson (1950), Clifton (1969) and Sallenger (1979) provide measurements of the grain-size and compositional sorting within individual laminations. Fig. 5 obtained by Clifton (1969) from a beach sand shows that a lamination consists of a basal fine layer of dark, heavy minerals and an upper coarser, light-mineral layer. Within an individual lamination the contrast between the heavy mineral and quartz-rich zones is gradual, but the interface between adjacent laminations is sharp.

On beaches the laminated sands are found primarily in the swash zone, produced by the alternating wave-swash runup and backwash across the beach face. The segregation between coarse and fine grains and between light and heavy minerals occurs quickly within the moving bedload layer of sand (Clifton, 1969). Thompson (1937) suggested that the laminations result from variations in the transporting power of the flowing water, the heavy-mineral concentration being produced by their settling out of suspension first to form the bottom of an individual lamination.

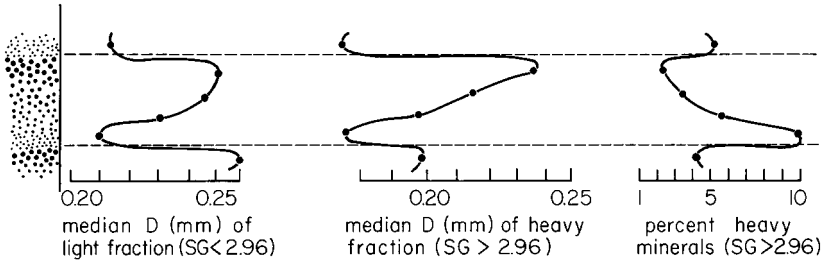

Fig. 5. Variations in grain sizes and heavy-mineral percentages through a single beach laminae. [After Clifton (1969).]

However, that mechanism cannot explain laminations found in coarse sands where there is a sorting by grain size but not necessarily by density, the coarser grains being at the top of each lamination. Most investigators have concluded that the laminations are produced instead by a shearing of the bedload layer and the action of the resulting dispersive pressure between the colliding grains. Bagnold (1954) demonstrated in detailed experiments that this dispersive pressure depends on the diameters and densities of the grains, on the total granular concentration, and on the local velocity gradient (the rate of shear). He went on to hypothesize that when grains of mixed sizes are sheared, the coarser grains tend to migrate upward to zones of lower shear while the finer grains move downward toward the bed where the shear is a maximum. The result is a layer having an inverse grading by size just as seen in Fig. 5, and since the heavy-mineral grains typically are smaller than the quartz, the grading will be accompanied by their concentration toward the base of the layer. Inman et al. (1966) coined the term "shear sorting" for this process, with his analysis having been for laminations formed in the slip face of aeolian sand dunes produced by the same mechanism.

Based on Bagnold's (1954) analyses of grain-dispersive pressures, Sallenger (1979) developed what can be termed the "grain-dispersive equivalence", the hypothesis being that at any single horizon within a sheared concentration particles of equal dispersive pressure will reside together. Employing Bagnold's dispersive-pressure equation, this balance yields

$$\rho_s^{1/2} D = \text{constant} \tag{7}$$

a simple inverse relationship between grain size and density such that a heavy-mineral particle will be smaller than an associated light mineral. Sallenger (1979) tested this relationship and found good agreement with shear laminations generated in the laboratory by subaerial grain flows and with the measurements of McIntyre (1959) of minerals within beach laminations. However, comparisons with other data sets showed poorer agreement.

Alternative hypotheses have been offered to explain the origin of laminations. It may be that some are formed by grain sorting during settling from suspension as suggested by Thompson (1937), even though this process cannot account for most laminated deposits. Middleton (1970) has argued that the sorting is produced by the smaller particles tending to fall into spaces between the larger particles, displacing

the larger upward toward the surface. Whatever the mechanism having produced the laminations, the sorting initially results only in a minor separation of heavy and light minerals, amounting to the few millimeters thickness of a single lamination. However, it is possible that by repeatedly shearing the sand as it is transported along a river or when a beach face is cut back by waves during a storm, the heavies will be driven progressively downward and concentrated while the larger quartz and feldspar grains rise to the surface of the shear zone to be transported away. Reid and Frostick (1985a) have emphasized this ancillary relationship between shear sorting and selective grain entrainment, with the shear sorting feeding the larger light minerals to the top of the mobile layer of sediment, where their preferential entrainment as treated above leaves behind a lag of smaller heavy minerals. It is conceivable that grains left behind in the heavy concentrate are dispersive equivalents as given by Eq. (7). This possibility was examined by Komar and Wang (1984) for the placer formed in the swash zone of an Oregon beach, and although it was found that the minerals are not in dispersive equivalence according to Eq. (7), it was still concluded that shear sorting likely played some role in the formation of the placer as suggested by Reid and Frostick (1985a), while being less important than selective entrainment.

3.3. Sediment Sorting within Bedforms

The transport of sediment can also give rise to a variety of bedforms such as ripples and dunes, and it has been observed that a local sorting of minerals by density and grain size can develop within their geometry. McQuivey and Keefer (1969) have shown that magnetite grains in a bed of predominantly quartz sand tend to concentrate just upstream of the ripple crests as diagrammed in Fig. 6, and Brady and Jobson (1973) found similar magnetite accumulations on dunes formed in streams.

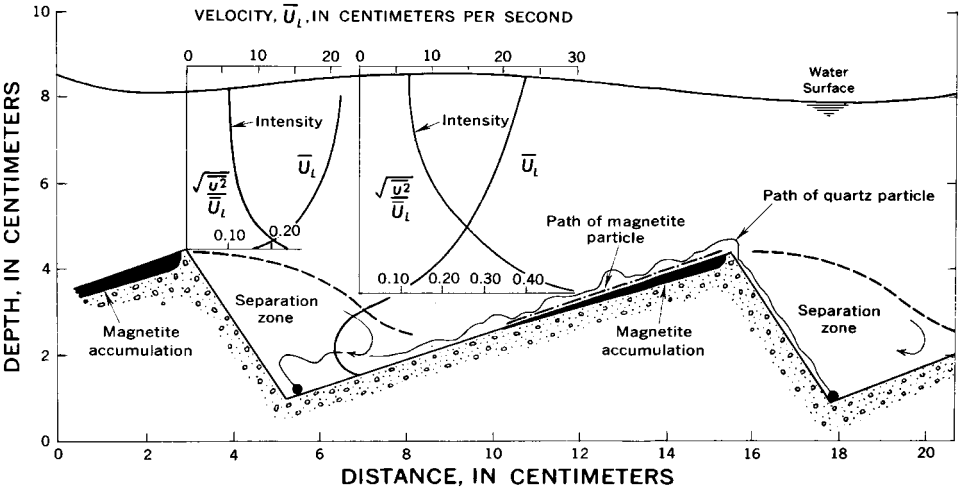

Fig. 6. The concentration of heavy minerals in the crests of ripples due to variations in the flow velocity and intensity of turbulence across the ripple profile. [After McQuivey and Keefer (1969).]

McQuivey and Keefer (1969) explained the pattern in terms of variations in the mean flow velocity and turbulence intensity over the ripple profiles as graphed in Fig. 6. Important is that the variation in the mean velocity is the inverse of the turbulence intensity, the velocity being greatest over the upstream-dipping stoss sides of the ripples, while the turbulence intensity is greatest in the separation zone of the boundary layer immediately downstream of the ripple's slip face. The resulting patterns of movement of the quartz versus magnetite grains are depicted in Fig. 6, with the quartz preferentially being carried over the crest of the ripples and then down the slip face, whereas the magnetite is deposited on top of the ripple.

Important to the resulting pattern of mineral sorting on the ripple, Fig. 6, is the occurrence of a zone of flow separation in the lee of the ripple crest, as it controls the distribution of eddy turbulence and also the pattern of mean bed stresses. The importance of flow separation to the concentration of heavy minerals was examined further by Best and Brayshaw (1985), including having undertaken laboratory flume experiments on the resulting patterns of heavy-mineral concentrations surrounding an isolated hemispherical obstacle clast placed on the bed, and the sorting associated with the confluence of two channels which results in a zone of flow separation that depends on the relative water discharges in the two channels. This points to the potential significance of flow separation to mineral sorting at a range of scales in rivers, including migrating bars, at the points of flow convergence within a braided channel, and at locations where the channel abruptly widens. Examples of sorting at these different scales in rivers will be presented later in this chapter.

3.4. Settling Velocities of Mineral Grains and their Sorting

Sediment transport as a suspended load is governed by the irregular motions of the flow, its turbulent eddies, compared with the settling velocities of the grains. If the grain-settling velocity is low then the eddy velocities are able to waft the grains above the bed where they can be carried along at high rates by the mean current. An understanding of grain settling is crucial to the evaluation of sediment transport in general, and can also be a factor in grain sorting where differences in densities and sizes produce contrasting settling rates. Most of the research into the settling behavior of sediment particles has focused on quartz grains of silt and sand, with some consideration given to the effects of their shapes on the rates of settling. The products of that research can be extended to the heavy minerals through known dependencies on the particle density as well as size.

Analyses of particle settling begin with a simple consideration of perfectly spherical grains for which theoretical relationships can be derived. Furthermore, there has been a considerable number of experiments undertaken to measure the forces of drag on a sphere moving relative to a fluid (''relative'' in the sense that either the sphere can be moving or the fluid is moving). It has been found experimentally that the frictional force is linearly proportional to the relative velocity so long as the particle is small, the velocity is low, or the viscosity of the fluid is large; more precisely, this condition is met when there is a low value for the dimensionless particle Reynolds number $\mathrm{Re} = \rho u_s D/\mu$, where D is the diameter of the particle, μ_s its relative velocity,

and μ the fluid's viscosity. For those conditions, in papers published in 1845 and 1851, Sir George Stokes theoretically derived the relationship

$$F_d = 3\pi\mu D u_s \tag{8}$$

for the drag force F_d, demonstrating its linear dependence on the relative velocity as well as the diameter of the sphere and fluid viscosity. His derivation involved a mathematical solution of the Navier–Stokes (momentum) equations, the basic relationships that govern fluid flow, but in order to solve those complex equations Stokes had to assume that the particle Reynolds number is less than approximately 0.5, indicating the limit of applicability of the simple relationship of Eq. (8).

With this relationship for the fluid drag it is simple to derive an equation for a sphere settling in a fluid, a relationship for the case where the grain is settling at a constant velocity, its "terminal velocity". At the terminal velocity there is a balance between the retarding drag force and the immersed weight of the particle that is pulling it downward. If there were no balance then the grain would either speed up or slow down until that balance is achieved. The immersed weight of the spherical particle is the difference between the force of gravity acting downward and the buoyancy force acting upward, and is given by

$$\text{immersed weight} = (\rho_s - \rho)g\left(\frac{1}{6}\pi D^3\right) \tag{9}$$

Equating this to the drag force of Eq. (8) and solving for the settling velocity yields

$$W_s = \frac{1}{18}\frac{1}{\mu}(\rho_s - \rho)gD^2 \tag{10}$$

(W_s is used to denote the settling velocity since the descent of the particle occurs in the vertical direction). It is seen that in the Stokes Range the settling velocity of a sphere is dependent on the square of its diameter, the density difference between the grain and fluid, and is inversely proportional to the viscosity of the fluid. This relationship is often referred to as the Stokes Equation for grain settling, in recognition of Stoke's contribution to its derivation. In being limited to the Stokes Range, $\mathrm{Re} < 0.5$, in applications to sediment grains its usefulness is limited to small particles, primarily to silt.

For larger grain sizes experiments have shown that the drag is proportional to the square of the velocity of the sphere relative to the fluid, empirically yielding

$$F_d = \left(\frac{1}{2}C_d\rho u_s^2\right)A \tag{11}$$

where C_d is a dimensionless drag coefficient that needs to be determined experimentally, with the measurements showing that it depends on the particle Reynolds number; u_s is again the relative velocity of movement between the grain and fluid and A the projected area of the particle in the direction of relative movement (equal to

$\pi D^2/4$ for a spherical grain). The balance between this drag relationship and the immersed weight of Eq. (9) yields

$$W_s = \left[\frac{4}{3}\frac{1}{C_d}\frac{\rho_s - \rho}{\rho} gD\right]^{1/2} \tag{12}$$

which can be applied to coarse grains settling at higher velocities. This relationship is sometimes referred to as the Impact Equation of grain settling in the mistaken impression that the drag is due to the impacts of water molecules against the cross-sectional area of the moving grain. For these coarser grain sizes the prediction is that the settling velocity is proportional to $D^{1/2}$, a weaker dependence than found in the Stokes Range. The application of this relationship is difficult due to the presence of the frictional drag coefficient, C_d that depends on the Reynolds number, which in turn depends on the settling velocity.

Empirical equations have been found that are easier to employ than Eq. (12) in routine computations of grain settling velocities. One in common use is that of Gibbs et al. (1971),

$$W_s = \frac{-3\mu + \sqrt{9\mu^2 + gr^2\rho(\rho_s - \rho)(0.015476 + 0.19841r)}}{\rho(0.011607 + 0.14881r)} \tag{13}$$

where $r = D/2$ is the radius of the spherical grain. This equation is not dimensionally homogeneous (i.e., the units do not balance), and therefore it is necessary that all parameters be in their cgs units (μ = g cm/sec; r = cm; g = cm/sec^2; ρ and ρ_s = g/cm^3). Gibbs et al. (1971) also provide the inverse relationship whereby the grain size (r) can be calculated for a known settling rate. Although this relationship is messy in appearance, its use is straightforward in that an evaluation of a drag coefficient is not required. Its chief limitation was that it applies only to quartz-density spheres settling in water. However, Komar (1981) found that while there is an increasing systematic error introduced as the density departs from that of quartz, a simple correction factor can be included that reduces the error so the relationship can be applied to the full range of common heavy minerals. As an alternative approach, Warg (1973) has derived empirical equations that accurately cover the full range of grain densities; his relationships are more complex than Eq. (13), but can be included in computer routines to calculate settling velocities of spherical grains having any density.

As well as establishing the expected dependence of the settling velocity on the diameter D of the spherical particle, Eqs. (10) and (12) predict the dependence on the grain's density relative to the density of water. This dependence is seen in the series of curves graphed in Fig. 7 for the settling velocities of spherical grains ranging in diameters from 0.01 to 10 mm (silt, sand and granules), and for grain densities from quartz through a range of heavy minerals to cassiterite (7.0 g/cm^3), and also a curve for gold (18 g/cm^3). In calculating these curves, values $\rho = 1.02$ g/cm^3 and $\mu = 0.01$ g · cm/sec for sea water were used. The Stokes Region is delineated in the graph by the Reynolds number limit $\mathrm{Re} = \rho u_s D/\mu < 0.5$. The curves are seen in Fig. 7 to be steepest for the small particle diameters in the Stokes Range, having a slope of 2 on this log–log graph in conformity with the Stokes settling Eq. (10). Similarly, the

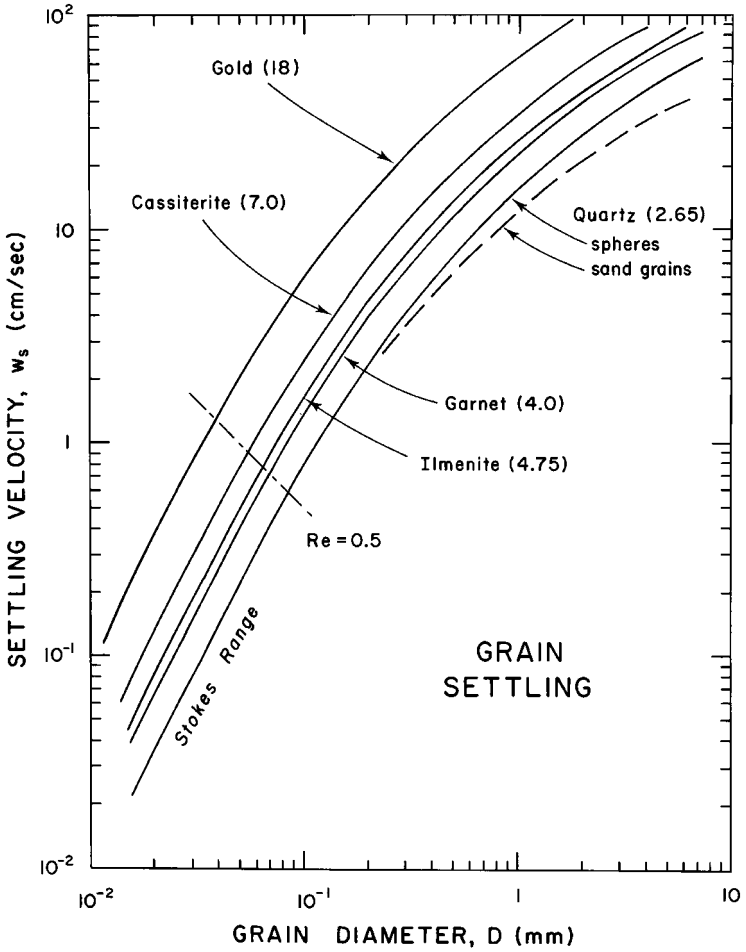

Fig. 7. Curves for the settling velocities of quartz and representative heavy minerals (specific gravities in parentheses). The dashed curve is for the settling velocity of natural quartz sand grains. [After Baba and Komar (1981).]

Impact Eq. (12) predicts a slope of 1/2 once the drag coefficient C_d has become essentially constant for large particle diameters; Fig. 7 indicates that this does not occur until the grains have diameters greater than approximately 5 mm. It is unfortunate that sand-size grains, the range of particular interest, falls between the Stokes and Impact relationships (with a constant C_d), so that direct determinations of the settling velocities of sand are the most difficult.

The primary series of curves in Fig. 7 are for the settling of perfect spheres, and therefore do not account for the irregularities typical of natural sediment particles. It is well established that grain non-sphericity and angularity act to decrease the particle's settling rate from that of a sphere having the same weight and volume (McNown and Malaika, 1950; Albertson, 1953; Williams, 1966; Komar and Reimers, 1978). The dashed curve in Fig. 7 is that obtained by Baba and Komar

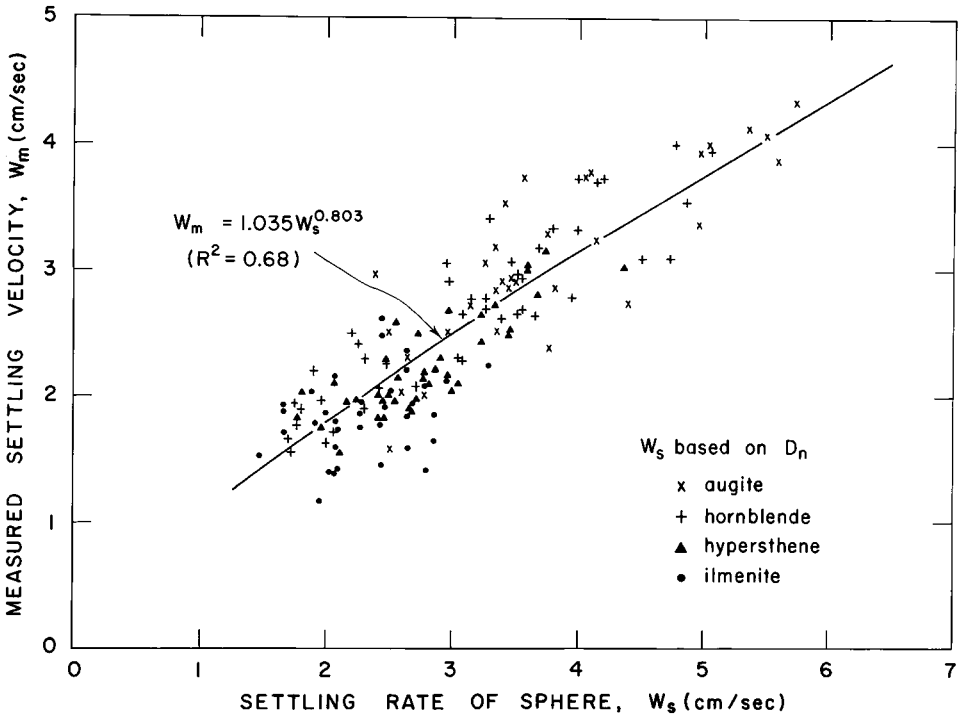

Fig. 8. Measured settling velocities of heavy minerals versus the settling rate of an equivalent spherical grain having the same mass and volume. [After Komar and Wang (1984).]

(1981) based on measured settling velocities of natural quartz grains obtained from beaches. Its departure from the curve for quartz-density spheres is small in the Stokes Range, but increases for the coarser grain sizes, a departure that Baba and Komar (1981) demonstrated was due primarily to the non-sphericity of the grains, with some reduction also due to the particle angularity. A similar decrease in the settling rates of heavy-mineral grains occurs due to their irregular shapes. Figure 8 shows the curve of measured settling velocities obtained for the placer minerals in the study of Komar and Wang (1984), compared with the settling rate of an equivalent sphere with the same density, calculated using the nominal diameter $D_n = \sqrt[3]{D_a D_b D_c}$, assuming that the heavy mineral is a triaxial ellipsoid having the measured axial diameters D_a, D_b and D_c of the actual particle (a similar correlation, but with somewhat greater scatter, is found if the settling velocity of the equivalent sphere is based only on the grain's intermediate diameter). Briggs et al. (1962) have undertaken the most extensive measurement study of the grain settling velocities of 15 common heavy minerals, demonstrating that the C_d drag coefficient in Eq. (12) depends on the grain's sphericity, the value of C_d increasing as the sphericity decreases, thereby in part accounting for the decrease in settling velocity.

The most extreme case of the effect of particle shape on grain settling is that of flat mica plates (Komar et al., 1984). Several investigators have stressed the importance of the effects of the flattened shapes of gold particles on their settling velocities, and hence on the sorting processes responsible for its accumulation in a placer (Tourtelot

and Riley, 1973; Kolesov, 1975a, b; Saks, 1976). Calculations indicate that with the flatness values typically found for gold particles, their settling rates would be decreased by some 30–50% from the rates they would have as spheres (Komar, 1989), an estimate that is supported by the limited measurements of gold settling velocities obtained by Shumilov and Shumovskiy (1975). Such a reduction in settling rates for gold particles yields values that are comparable to those of other heavy minerals, so shape effects may act to reduce the contrast in settling-equivalent sizes between gold and the lower density minerals.

Settling rates of individual grains in a suspension can also be reduced by the overall volumetric concentration of particles (Richardson and Zaki, 1954). Slingerland and Smith (1986) suggested that hindered settling may play a role in the separation of light and heavy minerals. Suspension concentrations would have to exceed roughly 5% in order for the settling rates of individual grains to be hindered by grain-to-grain interactions and by the generation of an upward counterflow of suspending fluid. Slingerland and Smith (1986) base their hypothesis on experiments undertaken by Richardson and Meikle (1961) where mixtures of equal volumes of two species of sand-sized spheres having contrasting densities and diameters were settled together. The densities and sizes were off-setting such that the two species of spheres had equal unhindered settling velocities. It was found that if the total concentration is less than 8%, the two species settled with equal (but reduced) velocities and produced a single mixed layer. If the total concentration was increased to between 8 and 10%, settling was found to produce three layers of sediment, the lower consisting solely of the denser grains, the upper entirely of the lighter grains, with the intermediate layer being a mixture. At concentrations above 10% settling produced two layers with complete segregation of the separate species. Richardson and Meikle (1961) explained these results in terms of the buoyant forces on the large light grains created by the mixture of fluid and small dense grains. As pointed out by Slingerland and Smith (1986), such a process might occur where natural flows rapidly decelerate and drop their suspended sediments at high concentrations. They suggested that this could occur in overwash flows on beaches or points of flow expansion in streams.

While such effects of sorting might occur locally due to differences in grain settling, a large-scale cumulative sorting could take place during prolonged transport. As noted above, the coarser particles with high settling velocities remain on the bed and are transported along as a bedload, while the smaller grains with low settling velocities are carried up into the water and are transported more rapidly in suspension. This division between bedload and suspension transport is generally defined by the limit $W_{sc}/u_* \approx 0.8$ to 1.5 where W_{sc} is the critical particle settling velocity for this division and u_* is the shear velocity of the flow that indirectly governs the intensities of the irregular velocities within the turbulent eddies that are actually responsible for suspending the grains. For a fixed u_* determined by the flow, grains having settling velocities greater than this W_{sc} cut-off are part of the bedload while grains having lower settling velocities are in the suspended load. The division is somewhat arbitrary, and this accounts for the range of values that have been used by various investigators.

Important to grain sorting is that within the suspended load particles having lower settling velocities tend to be carried higher above the bottom and at higher concentrations, up into the region of flow experiencing greater current velocities

(Brush, 1965). This vertical distribution of suspended grains is predicted by the Rouse equation

$$C \propto C_a z^{-w_s/u_*} \tag{14}$$

where C is the concentration of grains at the distance z above the bed and C_a a reference concentration of that particle size in close proximity to the bed. This relationship shows that the concentration decreases exponentially with distance z upward into the flow, with the rate of decrease depending on the ratio W_s/u_*; for a fixed value of u_* as might occur for example in a stretch of river, the higher the settling velocity of the particles the more rapid their decrease in concentration above the bed. The grain sorting itself is produced by the action of the current on this vertical distribution of suspension concentrations, being given by $C\bar{u}$ where $\bar{u}$ is the mean velocity of the flow at the elevation z where the grain concentration C occurs. Since this local flow velocity $\bar{u}$ increases with distance above the bed, the grains having lower settling velocities will be transported at greater rates than those having higher settling rates that remain close to the bed.

With the moving suspended load being finer grained than the sediments generally found on the bed, there is the potential for entrapment of some suspended grains within a coarser and largely immobile bed deposit. In this manner the heavy minerals having higher settling velocities might preferentially be trapped, reducing further their rates of transport. Such a process has been offered as an explanation for the presence of fine gold particles found within the matrix of gravels, a common association in both streams and gravel beaches (Smith and Minter, 1980; Vorob'yev, 1979). Kolesov (1975b) has analyzed the process of small grains "subsiding" through the pore spaces of an otherwise stationary bed of coarser grains. In a series of flume experiments, Minter and Toens (1970) demonstrated that gold can move into the interstices of a simulated river gravel. Frostick et al. (1984) experimented with compartments containing different simulated armor frameworks placed within a stream, while Reid and Frostick (1985a) discuss the results in the context of gold placer formation. They concluded that there is greater potential for placer development by entrapment where gravels fine upward, since the pore spaces tend to become uniformly packed. With a coarsening-up sequence the sub-surface pores are smaller than those of the armor layer, and this can lead to clogging the upper pores while leaving a considerable amount of unfilled space below the matrix plug. Although such processes have not been examined in the context of the preferential entrapment of heavy minerals other than gold, in some instances this might be significant to their selective sorting and concentration.

While there is a considerable potential for the extensive sorting of heavy and light mineral grains during transport and deposition due to their contrasting settling velocities, geologists and sedimentologists have been interested primarily in the relationship between the minerals in terms of their potential equivalence once the sediment has been deposited. This interest appeared early as the concept of a settling equivalence as formulated and advocated by Rubey (1933). His concept of hydraulic settling equivalence was stated as: "…whatever the conditions may have been which permitted the deposition of quartz grains of a certain size, these conditions would also permit the deposition of magnetite grains that had the same settling velocity"

(Rubey, 1933, p. 5). According to this concept, in a given sample the dominant size (mean grain size) of the magnetite grains would be smaller than the mean size of the quartz grains since the denser but smaller magnetite particles would have the same settling rate as the larger but low-density quartz. If one applies the Stokes Eq. (10) to examine this equivalence, the respective densities of magnetite (5.1 g/cm^3) and quartz (2.65 g/cm^3) require that the ratio of their diameters be 1.6 in order to have the same settling rates—the quartz must be a factor 1.6 larger in diameter.

Settling equivalence can be established in Fig. 7 by any horizontal line of constant settling velocity, crossing the series of curves for the several minerals at what would be their respective mean diameters found in a sediment deposited on that basis. The curves diverge somewhat as their grain sizes and settling velocities increase, so differences in sizes of settling-equivalent grains would be greater for coarser sands than for silts in the Stokes Range. Hyperdense gold has such an extreme density that its curve is displaced from those of other minerals, so it would be considerably finer grained if deposited in a condition of settling equivalence. The grain-settling Eqs. (10) and (12), respectively for the Stokes and Impact Regions, yield the following settling-equivalence relationships based on the condition $W_s = \text{constant}$:

$$\text{Stokes settling equivalence } (\rho_s - \rho)D^2 = \text{constant} \tag{15a}$$

$$\text{Impact settling equivalence } (\rho_s - \rho)D = \text{constant} \tag{15b}$$

Both show the expected inverse relationship such that an increase in particle density requires a decrease in grain diameter for the minerals to have the same settling velocities. Since sand is intermediate between the Stokes and Impact Ranges, the exponent for the grain diameter might be expected to be somewhere between 1 and 2.

Although seemingly sound in principle, the proposal by Rubey (1933) of the equivalence of settling velocities of simultaneously deposited grains has not generally been found in sediments according to measurements of actual distributions of heavy minerals and quartz grains (von Engelhardt, 1940; Rittenhouse, 1943; Briggs, 1965; Hand, 1967; Lowright et al., 1972; Slingerland, 1977; Komar et al., 1984). Explanations for this deviation from settling equivalence have followed two lines: (1) the distributions are affected by the inherited size restrictions from the source rocks, or (2) differential transport of the various minerals in a sand governs their relative size distributions. This second explanation involves grain sorting by the other processes discussed here, for example, that the equivalence has been controlled by selective entrainment rather than by settling equivalence. Although it appears that grains found together in close association within sediments rarely have equivalent settling velocities, it does not follow that settling velocities play little or no role in the sorting of sediments during transport and deposition, at times leading to the formation of heavy-mineral concentrates and placers. As will become apparent in the following section, multiple processes generally act to bring about the sorting of mineral grains according to their contrasting densities and diameters, with grain shape at times also being a factor.

4. ENVIRONMENTS OF MINERAL SORTING

The previous section presented a summary of the principal mechanisms involved in the sorting of sediments leading to concentrations of heavy minerals. Only passing reference was given to research that has examined the importance of those processes in various environments. The objective of this section is to more closely examine studies that have either undertaken direct experiments in the laboratory to test the grain-sorting models, or have documented sorting patterns found in rivers and marine environments, analyzing them in terms of the sorting processes. Here I have had to be selective in deciding which studies to review, not having the space to produce a full summary; other chapters of this volume fortunately provide additional coverage.

This presentation is organized into research undertaken with unidirectional currents as occur in rivers and ocean currents (including tides), versus the short-period oscillatory motions of waves which dominate sediment transport on beaches and offshore to water depths of 100 m or more on most continental shelves. In each case the research has involved both the controlled conditions of laboratory flumes or wave tanks, and the more complex conditions found in the natural environments of rivers and the ocean.

4.1. Mineral Sorting by Unidirectional Currents

Research of sediment sorting by unidirectional currents has included experiments in laboratory flumes, permitting an idealization and simplification of the processes in contrast to rivers, which can be exceedingly complex. The idealized conditions of the laboratory flume are illustrated in experiments undertaken by Meland and Norrman (1966, 1969) and Steidtmann (1982).

The experiments of Meland and Norrman (1966) examined the transport velocities of glass spheres measured over fixed beds of ideally packed, uniform spheres. Diameters of both the transported spheres and those in the fixed bed (which determine the boundary roughness) were varied to examine the effects of the relative roughness on the transport rates. For a fixed roughness size, larger grains moved faster than smaller ones, likely a result of the larger particles projecting higher into the velocity profile of the flowing water, and because the larger transported grains roll more easily over the comparatively small bed roughness, factors discussed earlier in the context of selective grain entrainment and depicted in Fig. 3. Meland and Norrman (1966) did not vary grain densities in their experiments, but Steidtmann (1982) did in experiments that were otherwise similar. Results from two experiments with different u_* shear-stress values are shown in Fig. 9 where the grain's transport velocity is related to both its diameter D and to the ratio D/K where $K = 0.35$ mm is the diameter of the grains forming the fixed bed in Steidtmann's experiments. The limit of grain movement occurred at approximately $D/K = 0.6$, apparently in response to the high pivoting angles and limited exposure of the particles to the flow. Transport velocities of the grains are seen in Fig. 9 to increase with D/K for a fixed u_*, and with increasing u_* for a fixed D/K. Transport velocities of the light minerals (L) are greater than the heavy minerals (H), the difference being small for low values of D/K but increasing for higher D/K.

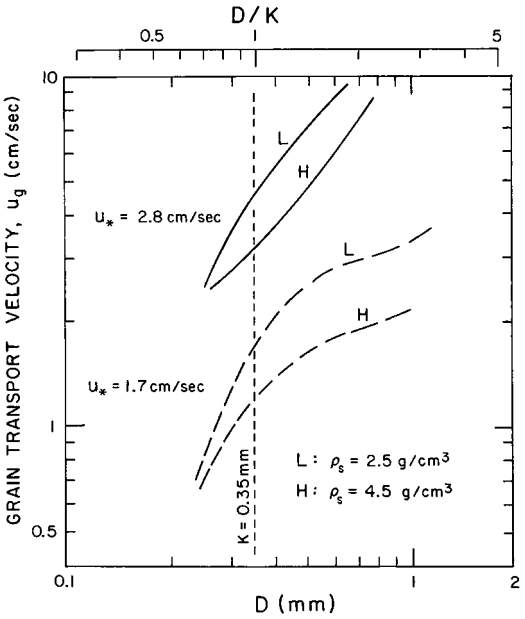

Fig. 9. Selective transport measurements of Steidtmann (1982) in a flume, showing that the relative transport rates of heavy (H) versus light minerals (L) depend on the shear velocity of the flow and the diameter D of the transported grain relative to the fixed bottom roughness K. [After Steidtmann (1982).]

Meland and Norrman (1969) and Steidtmann (1982) also undertook experiments with mobile beds, the moving sediment defining its own mean bed roughness. Meland and Norrman (1969) used glass beads and natural sand in different experiment series. They found that the maximum transport velocities occurred for intermediate sizes within the distributions, the smallest grains having lower rates just as found in the fixed-bed experiments, but there also was some reduction in transport velocities for the coarsest grains in the size distribution. They explained this reduced transport of the largest particles as resulting from their tendency to roll to the lowest positions on the lee surfaces of transverse bed forms as found by McQuivey and Keefer (1969) and illustrated in Fig. 6. Steidtmann (1982) experimented with a mixture of spherical glass beads having densities of 2.5 and 4.5 g/cm^3, the denser grains forming 5% of the mixture but having the same size range as the low-density grains. With plane-bed conditions he obtained results that are similar to those for a fixed bed, but for rippled beds no systematic difference could be found in transport rates of the heavy versus the light grains.

By having idealized the transport conditions to varying degrees, the flume experiments of Meland and Norrman (1966, 1969) and Steidtmann (1982) were able to reveal some of the grain-sorting mechanisms discussed earlier, but even under those simplified conditions it is apparent that multiple mechanisms are involved so the results are already becoming complex. The transport of bedload includes the repeated entrainment of grains, causing them to roll and saltate with the grains making repeated contacts with the bed, and in the case of completely mobile

sediments the grains are organized into ripples with their accompanying sorting. The grain sorting found in those studies, therefore, resulted from the mechanisms of grain entrainment and bedload transport, but did not extend to sufficiently intense flows to have included sorting during suspension transport. The dependence of the transport and sorting on D/K, the diameter of the moving grain D relative to the bed roughness or mean grain size of the sediment over which the movement occurs, in part verifies the significance of selective entrainment as illustrated in Fig. 3 and contained in Eqs. (4) and (5) derived for the entrainment model. However, the dependence on D/K in the flume experiments also resulted from the subsequent rollability of the grains during transport, with the grains rolling faster and probably for greater distances if D/K is large. This would enhance the transport of quartz grains relative to the smaller heavy minerals, the light minerals being more easily entrained and then rolling at faster rates once they become part of the bedload. The density difference itself is also important, apparent in Fig. 9 for the higher transport rates of the low-density grains (L) versus the high-density grains (H) for the same grain size D. Finally, the experiments documented the tendency of the largest particles to roll to the lowest positions on the lee surfaces of transverse bed forms. While that sorting tended to offset the higher rates of transport of the larger grains by rolling, decreasing the degree of size sorting, in application to the sorting of light versus heavy minerals where the heavy minerals generally have smaller diameters, this sorting within the bedforms would concur with that found by McQuivey and Keefer (1969) as depicted in Fig. 6, contributing to the lag of the heavy minerals during transport.

The observations and conclusions based on these laboratory flume experiments agree with the application of general sediment transport calculations based on formulations that include many of the grain sorting mechanisms. This is shown by analyses undertaken by Slingerland (1984) in his study of placer formation. He employed the bedload evaluation approach of Einstein, a model that simultaneously considers processes of selective entrainment and transport, and permits considerations of grain-sheltering effects. Similar to his 1977 study, which focused only on entrainment, Slingerland (1984) examined the effects of Re_* and the boundary roughness on the differential movement and segregation of minerals. Fig. 10 shows his results for a hypothetical mixture of 90% quartz and 10% magnetite sand with initial size distributions having nearly equal settling velocities. Slingerland (1984) found that for a given u_*, transport rates for all sizes and both minerals decrease with increasing bed roughness (which can be considered as being proportional to the coarseness of the average bed material). Also seen in Fig. 10 is that Slingerland (1984) determined that the relative proportion of magnetite in the moving bedload increases with increasing u_* for a certain bed roughness, and decreases with increasing roughness for a given flow u_*.

More advanced and generalized sediment transport formulations are being developed that include the conditions of dealing with a natural sediment having a mixture of grain sizes and densities. Vogel et al. (1992) in particular developed analysis procedures that include most of the grain sorting mechanisms discussed here, and tested their model versus several data sets of measured transport rates and their grain-size distributions measured in both flumes and streams. Of particular interest here, they also simulated the formation of a gold bearing placer deposit

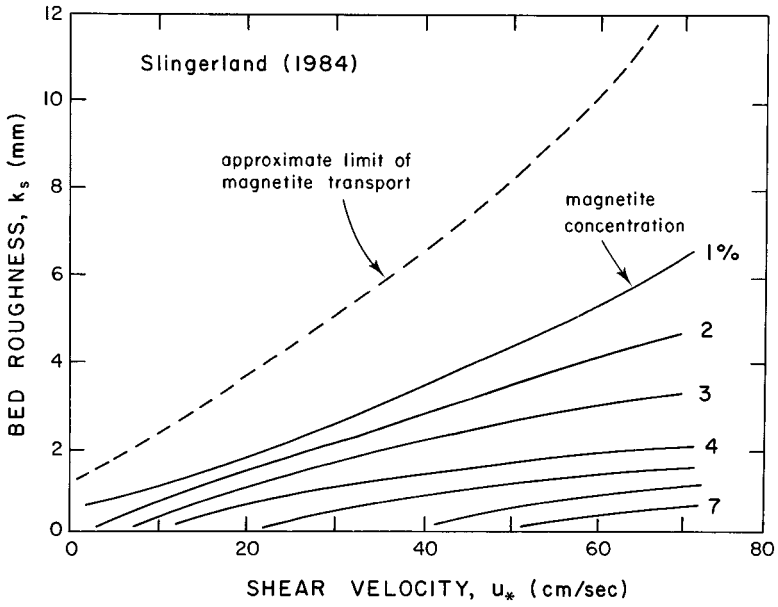

Fig. 10. Theoretical transport curves from Slingerland (1984) showing the effects of the bed roughness and shear velocity on the resulting concentration of magnetite in a deposit with quartz sand. [After Slingerland (1984).]

found in the Precambrian Witwatersrand of South Africa, with their model yielding reasonable results.

Beyond the highly idealized flume experiments like those of Meland and Norrman (1966, 1969) and Steidtmann (1982), flume studies by various investigators have attempted to simulate more realistically the transport and mineral sorting in what amounts to a small stream, the laboratory permitting controls of the flow discharge and sediment characteristics. One of the earliest studies of this type was that of Wertz (1949), who undertook experiments using a mixture of quartz and magnetite with the objective of improving the understanding of placer distributions found in South African rivers. While small scale and rather crude by modern standards, his experiments demonstrated the coincidence of the heavy-mineral concentrations with localized areas of erosion, while the barren zones corresponded to the areas of bulk sand accumulation. From the spatial distributions of mineral concentrations produced in his experiments and his discussions of the concentrations related to eddies, it is apparent that the patterns were associated with small-scale fluid motions and associated bedforms. Although he attempted to do so, his flume results should not be extrapolated to the large-scale sorting patterns of placer concentrations found in the South African rivers, which appear to be associated with pool-and-riffle sequences, with flow convergence zones in meander bends, and with sites where tributaries join the main channel (Wertz, 1949, Fig. 15).

Shepherd and Schumm (1974) undertook a series of flume experiments of channel incision into resistant "bedrock" materials (a mixture of kaolinite and sand), which also yielded information pertinent to mineral sorting found in natural rivers.

A sediment containing a small percentage of magnetite was transported along the experimental channel to simulate the erosion followed by aggradation during a major flood. It was found that the coarsest particles plus the magnetite formed a lag on the channel floor, that is, atop the "bedrock". As the post-flood aggradation continued, the magnetite was buried and preserved. The experiments, therefore, explained the common occurrence of heavy-mineral concentrations found atop or near bedrock in natural rivers, first documented by Cheney and Patton (1967). The concentrations of magnetite found in the experiments of Shepherd and Schumm (1974) were not uniformly distributed over the bedrock floor, but instead achieved maxima on both low and high points of the irregular topography. In the pools the heavy minerals were trapped within the voids of the coarsest material, while on the highs in reaches where the channel widths were also the greatest, the locally reduced flow velocities resulted in the deposition of heavy minerals.

Mosley and Schumm (1977) expanded the flume experiments of Shepherd and Schumm (1974) to examine heavy-mineral concentrations and placer occurrences at stream junctions, where the combined discharges and sediment inputs led to mineral sorting and accumulation. Their experiment series included variations in the tributary confluence angles, the ratio of their discharges, tributary widths and sediment loads. Important to the mineral concentration was the development of a localized scour hole within the zone of otherwise general sediment deposition. Dye injections demonstrated the existence of complex flow patterns in the convergence zone, but important was the shear along the boundary between the two converging flows that set up vertical vortices. Similar experiments with tributary channels were conducted by Best and Brayshaw (1985) in their documentation of the significance of flow separation and mineral sorting, with their study providing greater details of the patterns of heavy-mineral concentration percentages under different flow conditions.

Field studies of heavy-mineral sorting in rivers have focused primarily on recording occurrences of concentrated deposits related to the channel hydraulics and morphology. While this has included sorting within ripples and dunes, discussed above as one of the mineral sorting mechanisms, it has included large-scale sorting as observed with respect to the migrations of bars, concentrations found at points of flow convergence in channel junctions, and at locations where the channel abruptly widens. Much of this research concerns the formation and occurrence of gold-bearing deposits, generally within gravel bed material, but the results are relevant to the general patterns of heavy-mineral sorting in rivers and in most cases actually involved a documentation of easily sampled minerals such as magnetite.

Smith and Beukes (1983) investigated the occurrence of heavy-mineral concentrates within three flow reaches of two mixed sand and gravel rivers in South Africa, the interest being to document modern counterparts to gold-bearing sands found in the Witwatersrand Leader reef of that country. Of special interest were deposits extending for tens of meters along the length of the channel, formed in the convergent zones of sluiceways confined between a stable bank and a parallel margin of a bar that was migrating toward the bank. The patterns of mineral concentration were based on the magnetite contents, the primary heavy mineral in those rivers and easily extracted from bed sediments collected spatially through the channel reach. One example is shown in Fig. 11, a map view of the sampling locations and

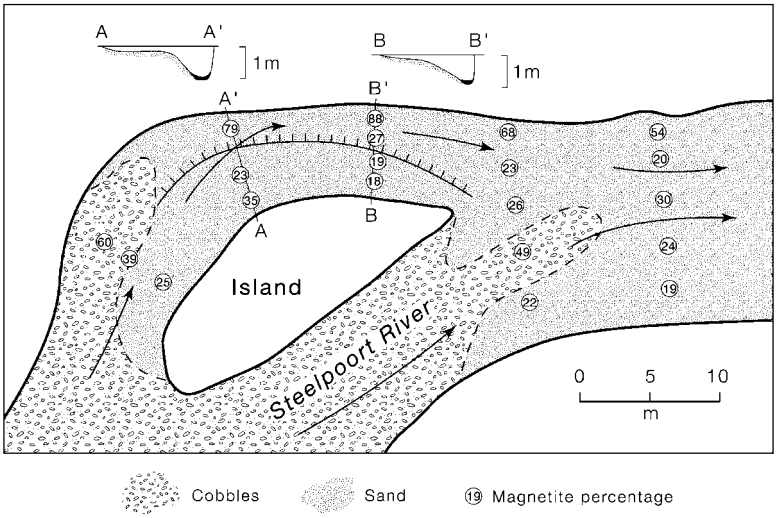

Fig. 11. Concentrations of magnetite grains as percentages of the sand fraction bed material, sampled in the Steelpoort River of South Africa, showing the highest concentrations in the zone of flow convergence in a sluiceway. [After Smith and Beukes (1983).]

magnetite percentages of the sand fractions in the Steelpoort River. The vectors included in the diagram depict the flow paths, with the convergence zone located along the stable outer bank of the river. The highest magnetite contents, reaching 88% of the sand, were found where the sluiceway currents were strongest, close to the outer bank. Five-fold magnetite enrichments were found in two of the three sluiceways investigated, those that had achieved an equilibrium geometry so the bars were no longer migrating toward the opposite bank, while sand was still being transported by oblique currents flowing across the bar toward the sluiceway; this provided a continuous supply of sand to be "processed" by the strong currents within the sluiceway. Enhanced concentrations of magnetite were not found in the third sluiceway studied, one that had not reached an equilibrium width so the bar was still migrating toward the opposite bank; the sand crossing the bar was instead deposited in bulk as foresets, without the processing that leads to the concentration of the magnetite. A small degree of magnetite concentration was found in the convergent zone immediately downstream from the island, corresponding to the sorting investigated by Mosley and Schumm (1977) and Best and Brayshaw (1985) in flume experiments. However, the degree of concentration found by Smith and Beukes (1983) in the South African river was relatively minor and varied in position with time as flow discharges and the bed morphologies changed, such that significant volumes of heavy minerals could not accumulate.

Smith and Beukes (1983) did not investigate in detail the actual mechanisms important to the concentration of the magnetite in the suiceway convergent zones, though it was clearly related to the locally increased intensity of the flow and the selective removal of the light minerals, leaving the magnetite as a lag. They did document that the settling velocities of the magnetite grains differ from the associated feldspar, so the concentration did not produce a grain-settling equivalence.

They suggested instead that selective particle entrainment was the most important sorting mechanism, a reasonable conclusion.

As seen in Fig. 11, much of the channel in the Steelpoort River studied by Smith and Beukes (1983) consisted of a cobble pavement (armor layer). They noted the enhanced accumulation of magnetite sand captured in the voids between the cobbles, achieving 60% magnetite in one sample, but this occurrence was not the focus of their study. Day and Fletcher (1989, 1991) investigated the sorting and distributions of magnetite and gold particles, compared with quartz, along a 5-km stretch of Harris Creek, a gravel-bed stream in British Columbia, Canada, where heavy-mineral entrapment within the pavement was shown to be important. Harris Creek has a pool and riffle sequence typical of many gravel-bed streams, and on a larger scale the creek changes from meandering to braided within their study area. The mean annual flood is approximately $19\,m^3$/sec, determined by the seasonal snowmelt. Following the peak of the spring-melt flood in 1986, bed sediment samples were collected along the study reach, at positions related to channel bars/riffles and low-energy eddy zones. With the sampling having occurred immediately after the spring flood, it recorded the deposits following the movement of the gravel bed material and its re-establishment as a pavement (armor) layer, and then the entrapment of the sand containing the magnetite and gold within the gravel voids and in the eddy zones where the deposits were entirely sand.

Following the classification of Slingerland (1984) developed for placer deposits at different scales, Day and Fletcher (1991) identified magnetite and gold concentrations in Harris Creek at three scales: the <1 m scale where the heavy mineral deposits formed by entrapment by the pavement voids; at the 10–100 m scale related to the preferential accumulation of heavies in the bar-head gravels of riffle-pool sequences; and at the >1000 m scale related to the average channel slope, with the highest concentrations found where the slope reduced from 0.04 to 0.02. The primary interest of their study was relating these observed variations in mineral concentrations, contrasting those of magnetite versus gold, to a model based on the processes of erosion and redeposition of the bed following a flood event. The model analyses employed applications of Einstein's bedload transport function, extending those of Slingerland (1984), with the flow and channel parameters chosen to represent the study reach of Harris Creek. In the model analyses the transported sediments included mixtures of magnetite, gold and quartz sand, with the series of model runs varying the diameter of the bed roughness (ranging from a 10-mm pavement to a sand bed) and for bottom slopes of 0.01, 0.02 and 0.04. In each model run the analysis yielded the ratio of the transport rate of quartz to the transport rate of magnetite or gold. The model results were compared with those measured in Harris Creek, showing good agreement. Both the model and field data demonstrated the importance of the pavement voids to the preferential entrapment of the heavy minerals, influenced by the particle size and density as this determined the frequency with which the minerals contacted the bottom permitting their capture within the voids, increasing the concentration of the gold relative to the magnetite, with both significantly increased relative to the quartz sand. The decrease in channel slope similarly led to the accumulation of sand-sized sediment, again with the preferential deposition of the high-density minerals, magnetite and gold. On the other hand, both the model and field data demonstrated that the sandy sediments in back-bar and

counter-current eddy pools are unfavorable sites for the preferential accumulation of the heavy minerals, their concentrations instead reflecting the bulk composition of sediments being transported along the river.

The research of mineral sorting by unidirectional currents undertaken in laboratory flumes and in natural rivers has led to a better understanding of the concentrating mechanisms and the resulting patterns of heavy-mineral concentrations and placer occurrences in rivers. The research products are being integrated into sediment transport models, which can serve in the quantitative analysis of mineral sorting that includes the major mechanisms, tools that will be useful in the interpretation of heavy-mineral deposits found in rivers, in both modern and ancient fluvial deposits.

4.2. Mineral Sorting by Waves (Beaches and Continental Shelves)

Concentrations of heavy minerals on sandy beaches are readily apparent, ranging in scale from the local sorting in backwash ripples and laminations to profile-scale sorting where the heavy minerals have accumulated in large volumes at the landward edge of the beach, the light minerals having been preferentially transported offshore. In the extreme the backshore deposit may consist of effectively a 100% black-sand mineral concentrate, potentially containing valuable placer minerals such as ilmenite, chromite, rutile and sometimes gold and platinum. Being readily visible, the heavy-mineral concentrates on beaches have received significant research attention, with a few studies having had the objective to establish which of the grain-sorting mechanisms were important to their formation.

Within the beach environment, the foreshore or swash zone is most conducive to the processes of heavy-mineral enrichment leading to black sand deposits and placers. Such occurrences has been documented by a number of studies, with the investigations by Rao (1957), Cordes (1966), Woolsey et al. (1975) and Komar and Wang (1984) having examined the conditions under which the heavy minerals were concentrated. Each study pointed to the importance of beach erosion, either a brief episode of recession leaving a thin layer or lens of black sand, or continued erosion over a long period forming an extensive deposit. Fig. 12 from Rao (1957) illustrates the role of beach erosion on the coast of India during a typhoon on the Bay of Bengal, the erosion having produced an extensive concentration of heavy minerals. The observations by Woolsey et al. (1975) on a Georgia beach and by

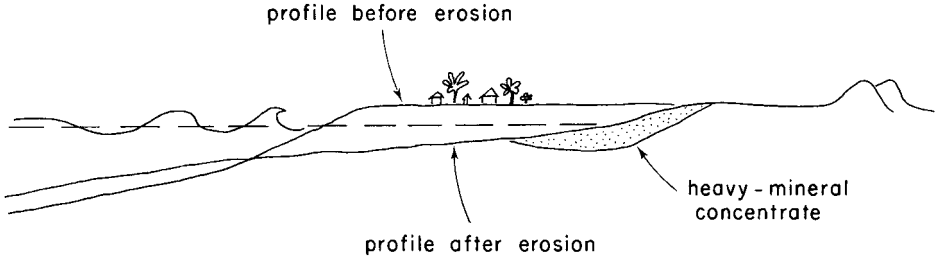

Fig. 12. The formation of a black-sand placer due to beach recession on the east coast of India during a typhoon. [After Rao (1957).]

Komar and Wang (1984) on the Oregon coast documented the development of smaller black-sand deposits during single storm events, the concentrating processes taking place within the zone of wave swash on the beach face. The heavy-mineral deposit investigated by Cordes (1966) at Skagen, Denmark, was unusual in that it formed in an area of erosion downdrift from harbor jetties.

Swash zone processes are ideal for the development of heavy-mineral concentrates by the selective winnowing of low-density quartz and feldspar, leaving behind the heavy minerals. The action of the swash is similar to the water motions induced by a prospector panning for gold. Measurements of the swash runup on the beach face have yielded the surprising result that when a storm occurs and breaking wave heights increase, the runup of the wave bores themselves at the shore do not necessarily increase. This unexpected result is attributed to the fact that doubling the offshore wave height doubles the depth at which the waves break, and the bores must then travel roughly twice as far from the breaker zone to the swash zone. However, there is a marked enhancement of swash motions having periods > 20 sec, the approximate upper limit of wave periods directly attributable to the storm. This long-period swash action, referred to as the "infragravity motions", must obtain its energy indirectly from the storm since it does increase with storm intensity and offshore wave heights. These long-period swash motions are a major factor in producing erosion of the beach face, and with the motion being comparable to the water oscillations in panning for gold, this increase in the long-period infragravity swash on beaches during storms is ideal for carrying away the quartz and feldspar, while leaving behind the concentrated heavy minerals.

The grain-sorting mechanisms that actually occur on the beach face have been investigated by Hand (1967), Trask and Hand (1985) and Komar and Wang (1984). Hand (1967) found that heavy minerals in beach sands settle more slowly than predicted by settling equivalence with the associated quartz. He attributed this difference to the difficulty of entraining the small heavy minerals in comparison with the larger quartz grains. Trask and Hand (1985) investigated sorting patterns on a beach along the eastern shore of Lake Ontario where the predominant direction of the waves resulted in a net northward longshore transport of the beach sand. From each sample they separated a fraction of grains, which had the same settling velocity, and then examined the longshore sorting of the minerals within that settling-equivalent fraction. It was found that the heavy minerals decrease in abundance in the direction of transport, and Trask and Hand (1985) were able to establish that the degree to which any mineral lags behind another lighter mineral is a function of the ratio of their effective densities. The sorting itself was attributed to differential entrainment and transport, the sampling procedure having eliminated sorting due to differences in settling velocities.

A more direct assessment of the roles of the potential sorting mechanisms was provided by the study of Komar and Wang (1984) of a heavy-mineral black sand on an Oregon beach. A series of sand samples was collected along a profile across the beach during an erosion event, at a time when the wave swash was removing sand from the beach face in the swash zone and transporting it offshore. This permitted a documentation of the minerals that were preferentially being left behind to form the black-sand concentrate, versus those that were selectively transported offshore, and permitted detailed analyses of which sorting processes were responsible. It was found

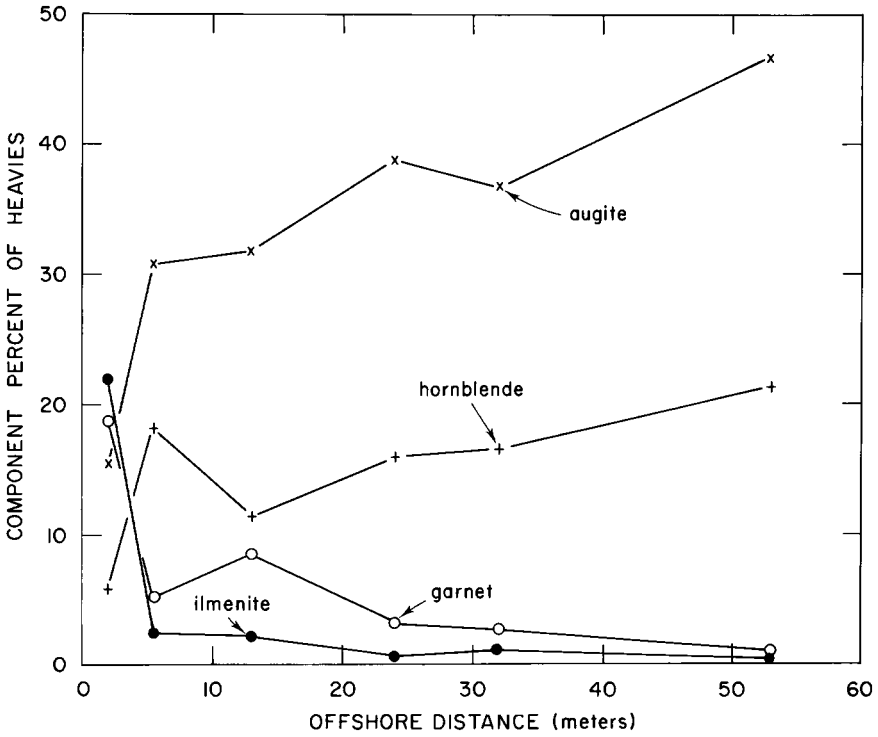

Fig. 13. Along-profile variations in heavy-mineral percentages in the swash zone of an Oregon beach. [After Komar and Wang (1984).]

that the overall concentration of heavy minerals systematically decreased across the width of the swash zone, being 96% heavies in the landward-most sample while 54 m down the beach face (but still within the swash zone) the sample contained only 6% heavies. Cross-shore changes in percentages within the heavy fraction of four of the principal minerals are graphed in Fig. 13, demonstrating that the efficiencies of the concentrating processes were not the same for each mineral. Nearly all of the ilmenite and garnet remained at the back of the beach in the most concentrated heavy-mineral deposit, while a greater proportion of the hornblende and augite moved offshore along with the quartz and feldspar. These cross-shore trends are clearer if expressed as a concentration factor for each mineral, its percentage in the accumulated black sand divided by its percentage in the offshore sample—here the light minerals were included so the ratio became a direct evaluation of the degree to which a mineral had been concentrated in the placer as opposed to having moved offshore with the quartz and feldspar. The results are shown in Fig. 14 as a graph of mineral densities versus their median diameters, the concentration factors being printed adjacent to the data symbols. The highest concentration factor is that of ilmenite (1 4 0 3) with zircon a close second (1 1 7 5), signifying that both remained in the concentrated deposit at the top of the beach and virtually none was carried offshore. Of the heavy minerals, hornblende has the lowest concentration factor (5), indicating that it did tend to remain in the placer but the concentrating processes

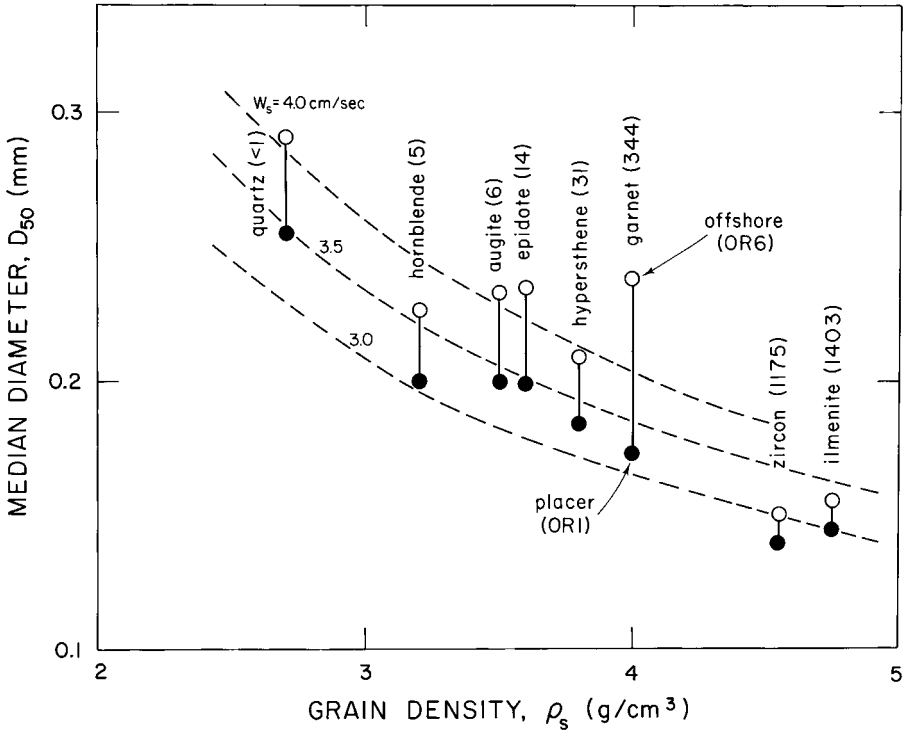

Fig. 14. The median grain diameters versus densities of the minerals in an Oregon beach, with the closed data symbols being for the concentrated black sand formed at the back of the beach while the open symbols are for a sample obtained 53 m down the beach face. The ratios of the mineral concentrations in the black sand to the offshore sample are shown in parentheses. The dashed lines represent constant grain settling velocities. [After Komar and Wang (1984).]

were less efficient so much of it moved offshore. Quartz has a concentration factor less than 1 since it preferentially moved offshore rather than remaining in the black sand.

The data of Komar and Wang (1984) in Fig. 14 demonstrate that for the several minerals found in the Oregon beach sand, the higher the density of the mineral the lower its median grain size within both the concentrated black sand and in the offshore sample. The concentration factor of the mineral in the black sand accordingly increased with increasing grain density and decreasing diameter. Ilmenite was most efficiently concentrated in the black sand because it is the densest of the minerals and is the finest grained, while the processes were least efficient in concentrating the hornblende because it has the lowest density and the largest diameter within the suite of heavy minerals. The graph of Fig. 14 also shows that for any given mineral, the median diameter is greater in the offshore sample than in the black sand. The pattern of sorting leading to the formation of the placer is, therefore, one where the processes have selectively removed the grains of lower density and coarser size, leaving grains of high density and small diameters in the black sand.

This inverse relationship between grain density and diameter suggested that there might be a settling equivalence between the several minerals (Komar and Wang, 1984). Direct measurements of their settling velocities demonstrated such a near equivalence, and this is also indicated in Fig. 14 where the dashed curves are for constant settling velocities depending on the combinations of grain diameter and density; a settling velocity of 3.5 cm/sec yields the curve most central to the minerals. It is apparent from this that no relationship can be found between the grain settling velocity and the respective concentration factors for the individual minerals. It was concluded that over the thousands of years of beach development, the waves and currents had sorted the minerals so the sediment particles have a relatively narrow range of settling velocities. However, this settling equivalence of all minerals in the beach sand largely precluded any further role of that parameter in producing grain sorting, leading to the formation of the black-sand concentrate. The analyses instead led to the conclusion that selective grain entrainment and transport were responsible for the sorting and mineral concentration. Fig. 4 presented earlier in the context of mineral sorting is from the study of Komar and Wang (1984), and includes curves for the entrainment stresses of the several heavy minerals present in the Oregon beach sand. In that graph it is seen that ilmenite is most difficult to entrain due to its high density and smaller diameters, while hornblende is most easily entrained of the heavy minerals. The sequence of curves given in Fig. 4 corresponds exactly to the order of concentration factors for the minerals, with the values being directly compared in Fig. 15. The uniform trend suggests that selective entrainment has been the

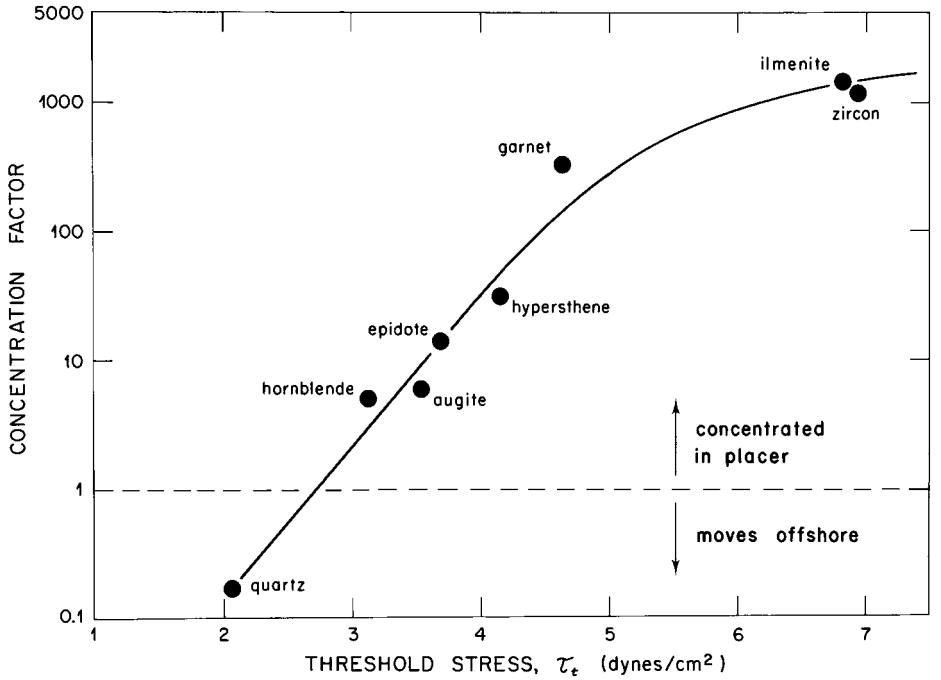

Fig. 15. Concentration factors of minerals in the Oregon-beach black sand versus the flow stresses required for their entrainment. [After Komar and Wang (1954).]

most important sorting process leading to the black-sand concentration on that Oregon beach. Both the high density and small diameters of the ilmenite grains increased their entrainment stress, and this accounted for its extreme concentration within the deposit. Hornblende is the other extreme in the suite of heavy minerals, it having the lowest density and largest median grain size, and therefore has the lowest entrainment stress so it tended to be carried away into the offshore with the light minerals. Quartz continues this trend, Fig. 15, being most easily entrained so it was readily transported offshore, leaving almost no quartz in the black sand deposit.

Further analyses indicated that relative transport rates of the different minerals also played a role in the formation of the black sand on that Oregon beach (Komar and Wang, 1984). The significance of different transport rates of the minerals toward the offshore was readily apparent thanks to the contrasting colors of the minerals. During offshore transport across the beach profile it is common to see the tan-colored quartz and feldspar move at the fastest rates and outdistance the other minerals, followed by the green augite, in turn followed by pink garnet, leaving the black ilmenite as a lag. Following the analysis approach of Slingerland (1984), Komar and Wang (1984) used the relationships of Einstein to calculate the relative transport rates of the different minerals, with the results providing further confirmation.

It is well-established that heavy-mineral concentrates tend to form in the swash zone of beaches during erosion events with offshore transport, and the dominant processes appear to have been identified. The interesting experiments by Saks (1978) indicate that sorting can also occur as a result of differential rates of transport in the onshore direction. He injected steel shot and lead filings into the mid-swash zone of a beach, and 45 min later measured concentrations along a cross-shore profile. Concentrations shoreward of the injection site were found to be 10 times those of an equivalent distance seaward, demonstrating that there was an active shoreward transport of those high-density grains, presumably due to the asymmetry of the swash motions with the landward uprush being stronger than the backwash.

When waves break at an angle to the shore they produce a longshore transport of the beach sand, and this can result in the sorting of mineral grains spanning many kilometers of shoreline length. A study comparable to that of Komar and Wang (1984), but of mineral sorting in the longshore direction, was undertaken by Li and Komar (1992b) adjacent to the mouth of the Columbia River. Beach-face sand samples were collected along a 70-km length of shore both to the north and south of the river mouth, and as graphed in Fig. 16 a marked longshore variation in the concentration of heavy minerals was found, the highest concentrations reaching 60–70% in the summer beach closest to the river mouth (approximately 100% in the eroded winter beach). There is a rapid decrease in concentrations both to the north and south, reduced to $<2\%$ after approximately 20 km of longshore transport away from the river source. The median grain sizes of the sand also varied with distance from the river, Fig. 16, initially decreasing to the north, the predominant direction of sand movement, but with a coarsening beyond the 25-km distance north of the river. Important to the development of this black-sand beach deposit was the construction of the jetties at the mouth of the Columbia River beginning in 1885 and extending into the early 20th century (Komar and Li, 1991). Their construction initially resulted in the formation of Peacock Beach to the immediate north of the jetties, and the small Clatsop Spit to the south (Fig. 16). However, the subsequent erosion of

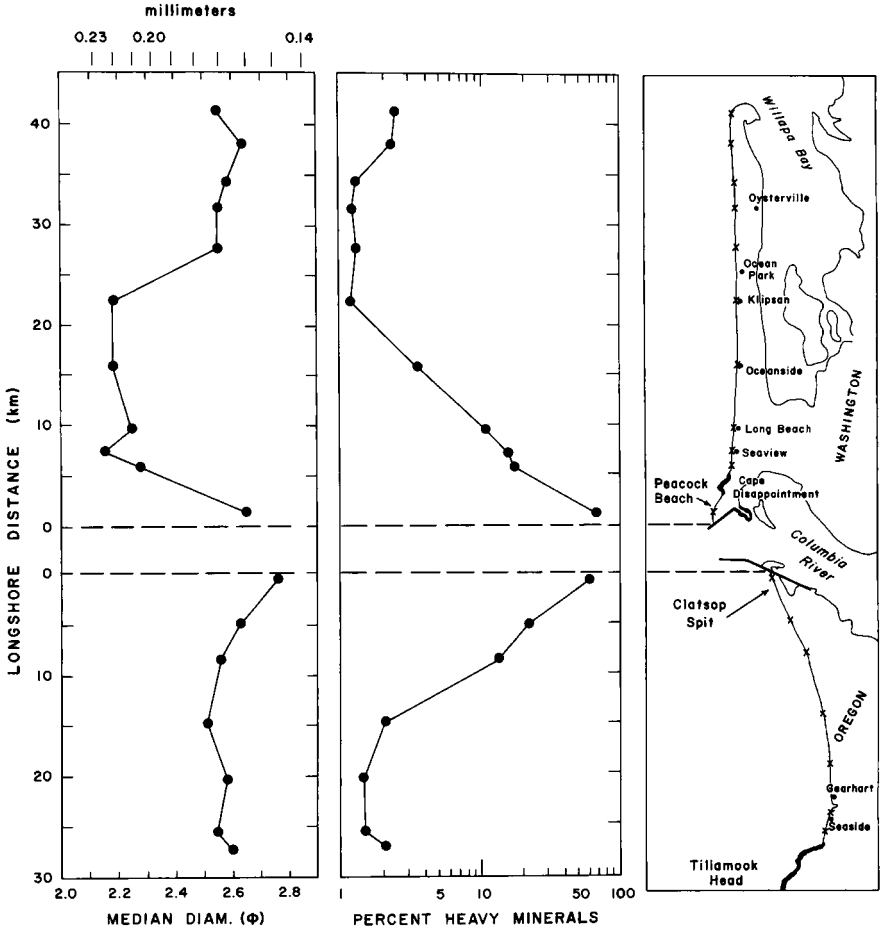

Fig. 16. Longshore variations in beach sand median diameters and percentages of heavy minerals north and south of the Columbia River. [After Li and Komar (1992b).]

these beaches, continuing up to the present, has led to the development of the concentrated black-sand placers in those areas and their progressive expansion alongshore to the north and south.

The objectives and analyses of the Li and Komar (1992b) study at the Columbia River mouth were much the same as those of Komar and Wang (1984), only directed along the length of shore rather than in the cross-shore direction along a beach profile. The mineralogies of the sands in the two studies differed due to having had significantly different sources. The study of Li and Komar (1992b) focused on the opaques (mainly magnetite), hypersthene, augite and hornblende, derived mainly from the volcanics that dominate the Columbia River watershed. An inverse relationship was again found between the grain densities and their sizes, with the concentrations in the placers adjacent to the river being greatest for the opaques and least for the hornblende, the same pattern found by Komar and Wang (1984) with the highest density and smallest diameter grains preferentially remaining in the

heavy-mineral deposit. The longshore decreases in mineral concentrations also depended systematically on the grain density and diameter, shown in Fig. 17 which contrasts the northward decrease of hornblende and the opaques, with the rates of decrease reflected in their respective exponents $k = -0.117$ and -0.205 in the relationship $C = C_o e^{kd}$, where C_o is the mineral concentration at the river mouth and C its concentration at the longshore distance d. The lower graph in Fig. 17 plots

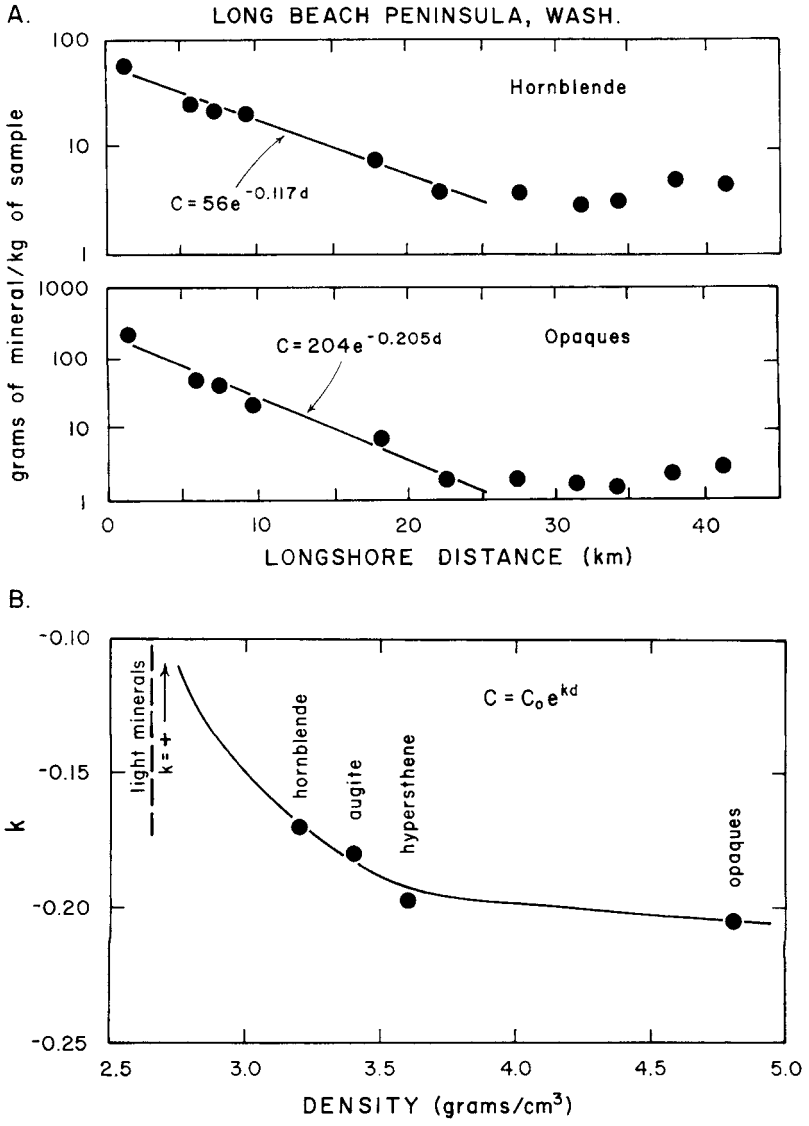

Fig. 17. The decreases in concentrations of hornblende and the opaque minerals in beach sands along the Long Beach Peninsula north of the Columbia River. The value of k reflects the exponential rate of mineral concentration decrease to the north as a function of the mineral's density. [After Li and Komar (1992b).]

the values of the k exponent as a function of mineral density for the five minerals (including quartz, which has a positive exponent since it increases in concentration with longshore distance). Measurements of grain settling velocities indicated that sorting by that mechanism may again explain the bulk characteristics of the beach sand, but cannot account for the enrichment of the dense minerals in the concentrated placer. Instead, minerals requiring higher selective entrainment stresses and having lower bedload transport rates were again found to be those most concentrated in the placer. This was the case for settling-equivalent fractions within the deposits, as well as for the entire samples. This is shown by the comparisons in Fig. 18, with the two graphs, respectively, comparing the mineral concentration factors with their entrainment stresses and calculated transport rates.

From this review it is seen that heavy-mineral concentrates commonly form in the swash zones of beaches, and based on the studies reviewed a reasonable understanding of the sorting mechanisms has been achieved. There is less evidence for similar processes operating within the surf and breaker zones, on the offshore bars and in the troughs eroded by longshore currents and rip currents. Black sands are sometimes found in those environments, but it is unclear whether they formed in situ

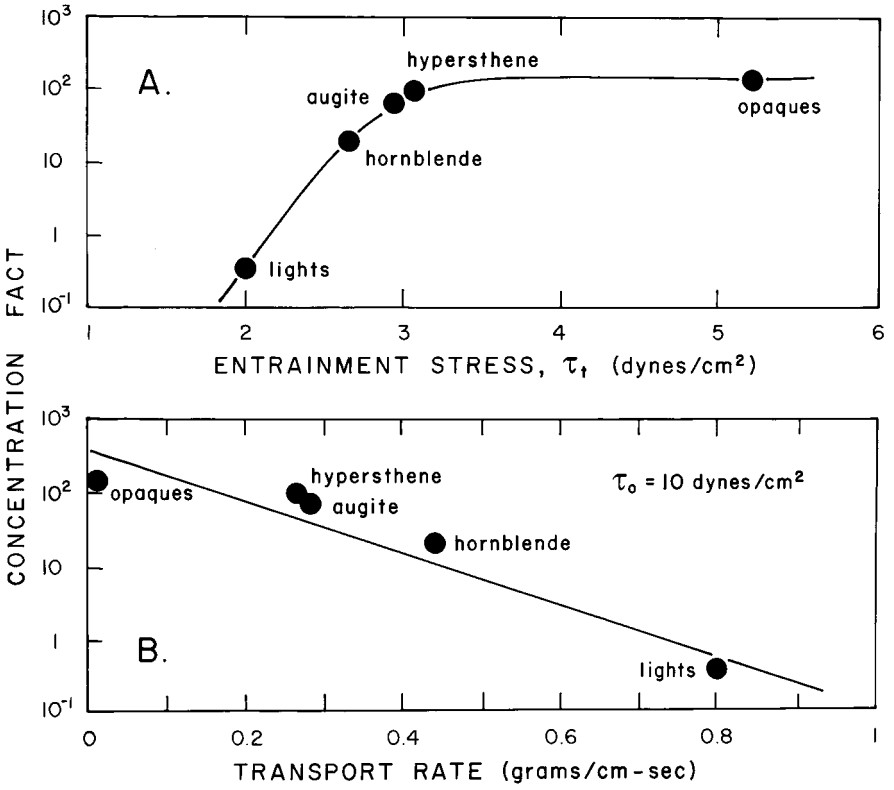

Fig. 18. The concentration factors of minerals in the black sand placer immediately north of the Columbia River versus (A) the flow stresses required for their entrainment and (B) their subsequent transport rates. [After Li and Komar (1992b).]

or resulted from processes operating in the swash zone followed by the offshore dispersal of the concentrated heavy minerals. The waves and currents in the outer portions of beaches are not as conducive to mineral sorting as in the swash zone. The breaker zone is characterized by high levels of turbulence, which carry sand in suspension, this having the effect of mixing of the sediments rather than sorting them according to their densities. Particles having low settling rates will tend to drift offshore from the breaker zone, and this may result in some degree of concentration of heavy minerals on the beach as a whole. This sorting would narrow the range of settling velocities of grains remaining on the beach, as found by Komar and Wang (1984) on Oregon beaches.

Reid and Frostick (1985b) documented the formation of heavy-mineral (ilmenite) concentrates on sand bars of beaches in Lake Turkana, Kenya. However, these were not submerged bars typical of breaker zones, but instead were swash bars that actively migrate onshore during rising lake levels and come under the action of the wave swash. The processes of mineral concentration were therefore likely similar to those discussed above for deposits formed in the swash zone. Two types of bars were recognized by Reid and Frostick (1985b) that differed in their cross-sectional shapes, their occurrence depending on the wave periods and energy levels. The bar shapes were in turn found to be important to the concentrating processes, with higher concentrations found on swash bars that have significant vertical reliefs, limiting the degree of overtopping by the waves. A pattern of increasing concentrations of heavy minerals from the break point up the swash slope was found, with peak concentrations occurring at and just over the bar crest. With lower wave periods and energies dune-like bars formed, their crests being approximately at the water level so wave overwash was frequent. Reid and Frostick (1985b) provided sedimentological evidence that grain suspension was more important on the dune-like bars, resulting in a less effective concentration of the heavy minerals.

Many beaches are characterized by having a longshore trough between the breaker zone and swash zone, an area of complex sediment transport brought about by the interplay of shoreward-moving wave bores and currents flowing in the longshore direction. Erosion can be significant in the troughs, at times leading to the development of a gravel lag. There may be some entrapment of heavy minerals and gold in the trough gravel, as well as in the gravel of the swash zone. The nearshore currents become strongest where they turn seaward to form rip currents, which transport sand offshore and deposit it beyond the breaker zone, often eroding embayments into the beach face. Bogdanov et al. (1986) found localized concentrations of heavy minerals on beaches along the Baltic Sea coast, which corresponded to the rhythmic topography of the beach produced by nearshore currents. The concentrations at the sediment surface were greatest over the tops of bars, and may represent erosional lags. There were also concentrations within seaward-trending troughs, but these were buried beneath several centimetres of overburden; it may have been that the troughs were eroded by strong rips at the time of a major storm, concentrating the heavy minerals, but later were buried during post-storm beach accretion.

Bogdanov et al. (1986) also found that when waves break obliquely to the beach and produce a longshore sand transport, the patterns of localized mineral concentrations tend to be erased. Under such conditions it is likely that the rip currents would migrate alongshore or disappear altogether, accounting for the disappearance

or burial of the local mineral concentrations they had produced. However, the longshore directed currents then become more important in the transport of sand, so it is possible that the processes of heavy-mineral concentration within longshore troughs are enhanced. This is speculation, and needs to be examined by field studies. There are cases where along-coast variations in placer development have been attributed to large-scale longshore sand movements. On the beaches of the east coast of Australia the net sand transport is to the north, and it has been found that the highest mineral concentrations are located to the south of headlands (Hails, 1976), an occurrence that has been attributed to the enhanced erosion caused by the deflection of northward flowing longshore currents to form a seaward flow similar to a very strong rip current. The heavy-mineral concentrates on the Oregon coast achieve their maximum developments to the south of headlands, but those beaches form isolated pockets with headlands at each end, within which seasonal reversals in the directions of longshore sand movement occur but with a long-term net zero transport. Peterson et al. (1986) formulated a model to explain this mineral concentration south of headlands, suggesting that strong winter storms from the southwest cause the northward transport of all minerals and grain sizes, whereas the weaker summer waves from the northwest preferentially return the light minerals to the south, leaving behind the heavies concentrated at the north ends of the beaches, that is to the south of the headlands. Furthermore, the northward movement of the sand during the winter occurs when the beach face is cut back exposing the concentrated heavy minerals, while the southward movement of the summer occurs when the black-sand concentrates are covered by quartz-rich sand.

Numerous exploration studies have been undertaken in the search for placer deposits offshore in continental shelf sands, but only limited research has been devoted to analyzing the processes of waves and currents at those depths that potentially could concentrate the heavy minerals. The long glacial period of lowered sea levels permitted the transport of river sands and their reworking as beach deposits in areas that are now covered by the sea. Following the depletion of high-grade mineral reserves on beaches, attention shifted to the adjacent offshore with the expectation that there would be a continuation of the placer deposits in sands of the continental shelf. However, in most cases this search has been disappointing. For example, the beaches of southeast Australia have been a rich source of rutile, zircon, monazite and ilmenite, but are now largely exhausted with mining activities continuing only in the low-grade accumulations of coastal dunes (Komar, 1989). This induced explorations of the adjacent continental shelf (Jones et al., 1982; Riech et al., 1982; Kudrass, 1987), but comparable offshore placers have not been found. The modern beaches contain some 10 times more heavy minerals than the offshore sands, and as shown in Fig. 19, there is a trend of decreasing percentages of heavy minerals with depth across the continental shelf.

This trend of decreasing concentrations offshore continues that found on beaches, as seen in Fig. 13 from the Oregon beach studied by Komar and Wang (1984). This suggests that the shelf trends are an extension of the sorting processes and patterns found in the nearshore. High-density minerals such as ilmenite and magnetite are concentrated within placers of the swash zone, whereas less-dense minerals such as augite are not as efficiently concentrated and tend to follow the quartz offshore during beach-erosion events. This makes the less-dense heavy minerals better

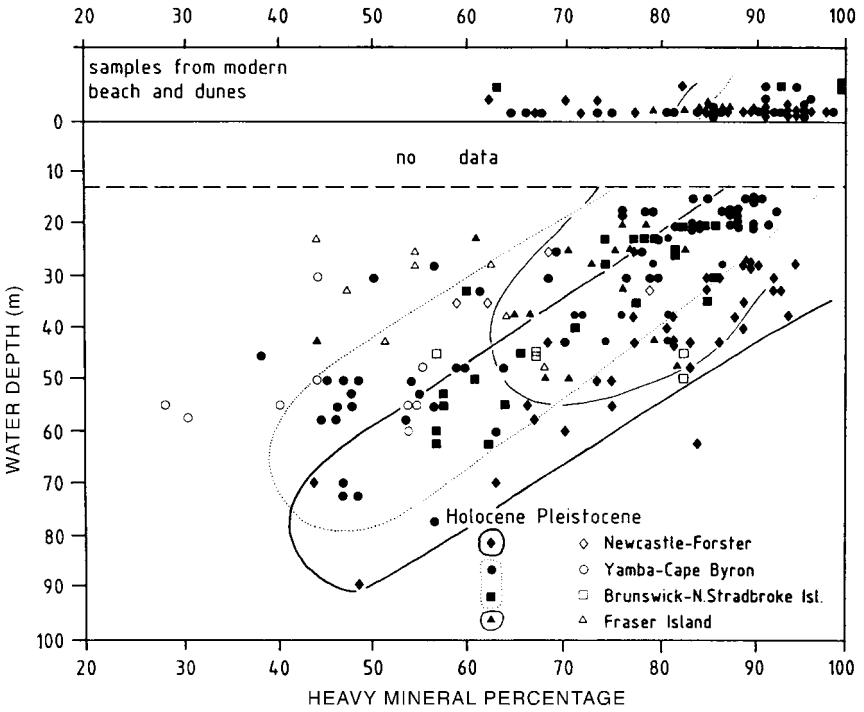

Fig. 19. The offshore decrease in the denser heavy minerals (rutile, ilmenite, zircon, magnetite and tourmaline) in the total heavy-mineral fractions found in various areas of the Australian continental shelf. Open symbols are for Holocene surface sediments, closed symbols for Pleistocene deposits in cores. [After Kudrass (1987).]

represented in the shelf sands. Jones and Davies (1979) and Jones et al. (1982) have invoked such sorting processes, together with considerations of sea-level transgressions, to explain the enrichment of heavy minerals in Australian beaches and their depletion in the adjacent shelf sands. Kudrass (1987) used this explanation as the basis of his "Australian model" for the search of shelf placers. Accordingly, with a rise in sea level the valuable minerals (ilmenite, magnetite, etc.) were progressively carried landward, remaining within the nearshore to accumulate in the modern beaches, whereas the low-density minerals were predominantly deposited in the trailing sand sheet left behind on the shelf.

Kudrass (1987) indicated that his "Australian model" applies mainly to high wave-energy coasts with narrow shelves and a low to moderate supply of terrigenous material. He also proposed a "Zambezi model" for coasts having a broad shelf and moderate to high terrigenous supply, based on the Mozambique shelf off the Zambezi Delta studied by Beiersdorf et al. (1980). In the Zambezi model the placers are envisioned to form along the delta during lowered sea levels, but the large quantities of sediment prevented complete reworking during the subsequent transgression. The result is a disseminated placer deposit like that found on the middle Zambezi shelf, rather than the depletion of the shelf sand of heavy minerals as off the coast of Australia.

The models proposed by Kudrass (1987) invoke something of a "sweeping" action of the waves, selectively pushing the heavy-minerals landward to concentrate them in the beach sands, depleting their concentrations in the offshore shelf sands. Part of this sweeping action may result from the orbital motions of the waves acting on the seafloor sand in the offshore. At intermediate to shallow water depths, ocean waves are characterized by crests that are narrow compared with the broad intervening troughs as depicted in Fig. 20. This asymmetry in the surface form of the waves is reflected in the orbital water motions at the bottom, also shown in the diagram. The water movement under a wave crest is directed shoreward and achieves a high velocity but with a short duration, whereas the offshore return flow under a trough is slower and of longer duration. This asymmetry can result in sediment sorting in the cross-shore direction, with the heavier grains being entrained during the higher velocities under the wave crests and thus moved onshore, but not by the lower velocities under the troughs that would return them to the offshore. At the same time, low-weight grains would readily move under both the landward and seaward orbital velocities, and so would not experience a net displacement unless simultaneously acted upon by a superimposed unidirectional current. The waves themselves can induce a net shoreward current, the Stokes Drift, but in general other ocean currents will be stronger so the low-weight grains would generally follow different transport paths than the heavier grains which tend to move onshore.

There are dramatic examples of the onshore transport of coarse debris that can be attributed to asymmetries in the wave-orbital velocities. Ballast dropped offshore by ships has washed up on beaches, and there is even a case where pig iron from a wrecked ship migrated 2 km to a beach. A number of field studies have established that offshore sources can contribute sediments to beaches, but few controlled experiments have been performed to test this mechanism of onshore sediment transport and sorting by wave orbit asymmetries. Of most direct interest, May (1973) performed a series of wave-tank tests on the relative shoreward movements of heavy versus light minerals, finding that under certain wave conditions the heavy minerals moved shoreward at faster rates than the light minerals, which he attributed to the asymmetries in the wave-orbital motions as depicted in Fig. 20.

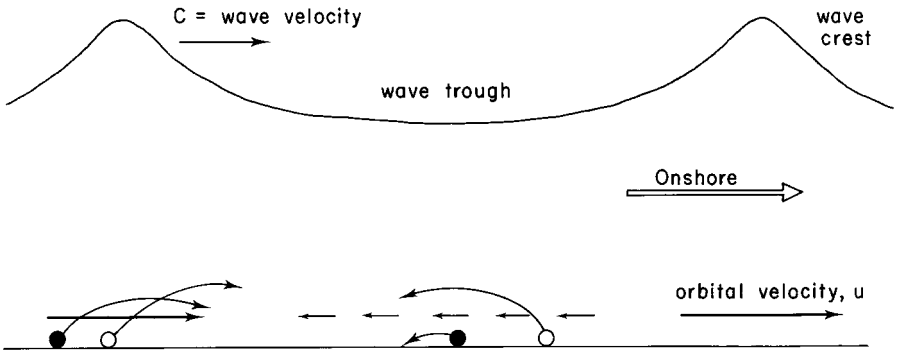

Fig. 20. The selective grain transport under the asymmetrical orbital motions of waves, the heavier grains (dark) moving shoreward a greater distance under the wave crests than seaward under the troughs, while the low-weight grains (light) move equal distances.

5. SUMMARY AND DISCUSSION

The flow of water in a river or the oscillatory motions of waves can bring about a sorting of sediment grains due to their contrasting densities, grain sizes and shapes. This hydrodynamic sorting visibly separates the heavy minerals from the light, producing heavy-mineral black-sand concentrates and in some cases valuable placers. Sorting can also occur within the suite of heavy minerals due to their differences in hydrodynamic properties. This chapter has reviewed the various processes or mechanisms through which this sorting can occur: this included differences in flow velocities and stresses required to entrain grains from a deposit of mixed sizes and densities; their further separation when transported as a bedload with the grain-dispersive pressure (shear sorting) forming laminations or with local sorting occurring in bedforms such as ripples and dunes; and the potential for large-scale sorting in the suspended load due to differences in grain setting velocities.

When one turns to an examination of the roles of these mechanisms in the sorting of mineral grains in rivers, beaches and in continental shelf sands, it is found in general that more than one mechanism is involved so it is difficult to establish any hydraulic equivalence of the deposited grains based on a single process such as an equality of their settling velocities. However, in more general terms an understanding of the grain-sorting processes provides explanations for the observed sorting patterns of minerals in natural environments. In the case of rivers researchers have investigated the occurrence of heavy-mineral concentrates in migrating bars, at points of flow convergence in channel junctions, and at locations where the channel abruptly widens. Particular attention has been given to the entrapment of transported heavy-mineral grains in the matrix of gravel-bed material, this being important to the formation of fluvial gold placers. Significant advances have been made in understanding the formation of black-sand mineral concentrates on beaches, demonstrating that occurrences in the swash zone are due primarily to selective entrainment and bedload transport, while grain suspension by the surf and breaking waves can have a counter effect of acting to homogenize the different minerals. The processes of waves and currents in these marine environments can also account for large-scale sorting patterns, as where the longshore transport of the sand leads to a concentration of heavy minerals adjacent to a river-mouth source or next to a headland, or the tendency for the waves to "sweep" the heavy minerals from continental shelf sands and concentrate them in landward beaches.

A practical product of this research into the processes of mineral sorting has been an improved understanding of the origin of placers, a scientific understanding that aids in the search for those valuable deposits, complementing the guidance previously based on the cumulative experience of prospectors and mining engineers. For example, we now know that the existence of valuable heavy-mineral sands found on a modern beach may not represent evidence that similar deposits exist on the adjacent shelf—to the contrary, the abundance of minerals in the beach may indicate that the shelf sands have been depleted. The improved understanding of mineral sorting may also assist in the analysis and interpretation of ancient sedimentary deposits based on their contents of heavy minerals. The dependence of the sorting patterns on processes of waves and currents can support an interpretation of the paleoenvironment of deposition, and provide an explanation for the patterns of

large-scale sediment movements where there are areas of erosion versus accretion. This is illustrated in modern environments, for example along the shores of river deltas. Deltas are conducive to the formation of heavy-mineral concentrates because they provide a major source of terrigenous sand and may undergo episodes of shore retreat and mineral concentration when attacked by storms or when the river mouth shifts position. In contrast, the stretches of shore experiencing accretion tend to be enriched in the light minerals. Such patterns related to shoreline erosion versus accretion are well-illustrated by the Nile Delta, reviewed in the following chapter.

A better understanding of the mineral-sorting processes can also assist in interpretations of analyses of the heavy-mineral contents of sediments, modern or ancient, to determine their sources. As an example, Clemens and Komar (1988) applied factor analysis to the heavy-mineral contents of beach sands collected along the Oregon coast, yielding three factors which established that the beach sands are mixtures of metamorphic minerals derived from the Klamath Mountains in southern Oregon and northern California, a limited suite of minerals from volcanic rocks in the Coast Range mountains, and from the Columbia River to the north. The proportions of minerals in the beach sand derived from these three sources depended on the relative proximity of the beach to those three sources. The Oregon beach containing the black-sand deposit whose origin was investigated by Komar and Wang (1984) consists mainly of Coast Range derived sand, but with a significant contribution from the Klamath Mountains. The multiple sand samples collected by that study from a single beach were subjected to a factor analysis which yielded two dominant factors (Komar et al., 1989), one containing the densest heavy minerals (mainly garnet and zircon), while the second included the lower density minerals (hornblende, augite and epidote). These two factors obviously reflected the cross-shore mineral sorting patterns found by Komar and Wang (1984), providing direct evidence that grain sorting can affect factor analyses and interpretations of sediment sources from their heavy-mineral contents.

In spite of the sorting of sediment grains during transport being of common occurrence and important to applications such as those noted above, relatively little research has focused on the details of the physical processes that actually bring about the sorting. It is important that this science be further improved in order to support the many applications of heavy-mineral analyses discussed in the other chapters of this volume.

ACKNOWLEDGMENTS

I would like to take this opportunity to belatedly acknowledge Professor Louis I. Briggs, my Masters thesis advisor in Geology at the University of Michigan during the 1960s, for his having initiated my interest in sediment sorting processes and for having guided my research into the concentration of heavy-mineral deposits on Lake Michigan beaches. I retain a fascination with this subject, which he inspired some 40 years ago. Thanks also to Ian Reid and Rudy Slingerland for their careful reviews of this chapter and helpful suggestions.

REFERENCES

Albertson, M., 1953. Effects of shape on the fall velocity of gravel particles. Proceedings of the 5th Iowa Hydraulic Conference, Iowa City, pp. 243–261.

Baba, J., Komar, P.D., 1981. Measurements and analysis of settling velocities of natural quartz sand grains. Journal of Sedimentary Petrology 51, 631–640.

Bagnold, R.A., 1954. Experiments on a gravity-free dispersion of large solid spheres in a Newtonian fluid under shear. Proceedings of the Royal Society of London, Series A 225, 49–63.

Beiersdorf, H., Kudrass, H.R., von Stackelberg, U., 1980. Placer deposits of ilmenite and zircon on the Zambezi shelf. Geologisches Jahrbuch D36, 5–85.

Best, J.L., Brayshaw, A.C., 1985. Flow separation—a physical process for the concentration of heavy minerals within alluvial channels. Journal of the Geological Society of London 142, 747–755.

Bogdanov, N.A., Aibulatov, N.A., Sharakov, V.P., 1986. Stability level of a modern placer in the outer part of the marine shore zone. Lithology and Mineral Resources 20 (4), 335–344 [translation from Litologiya i Poleznye Iskopaemye, July–August 1985].

Brady, L.L., Jobson, H.E., 1973. An experimental study of heavy-mineral segregation under alluvial-flow conditions. U.S. Geological Survey, Professional Paper 562-K, 38pp.

Briggs, L.I., 1965. Heavy mineral correlations and provenances. Journal of Sedimentary Petrology 35, 939–955.

Briggs, L.I., McCulloch, D.S., Moser, F., 1962. The hydraulic shape of sand particles. Journal of Sedimentary Petrology 32, 645–656.

Brush, L.M., Jr., 1965. Sediment sorting in alluvial channels: In: Middleton, G.V. (Ed.), Primary Sedimentary Structures and their Hydrodynamic Interpretation. Society of Economic Paleontologists and Mineralogists Special Publication No., vol. 12, pp. 25–33.

Cheney, E.S., Patton, T.C., 1967. Origin of bedrock values of placer deposits. Economic Geology 62, 852–860.

Clemens, K.E., Komar, P.D., 1988. Oregon beach sand compositions produced by the mxing of sediments under a transgressing sea. Journal of Sedimentary Petrology 58, 519–529.

Clifton, H.E., 1969. Beach lamination: nature and origin. Marine Geology 7, 553–559.

Cordes, E., 1966. Aufbau und Bildungsbedingungen der Schwermineralseifen bei Skagen (Danemark). Meyniana 16, 1–35.

Day, S.J., Fletcher, W.K., 1989. Effects of valley and local channel morphology on the distribution of gold in stream sediments from Harris Creek, British Columbia, Canada. Journal of Geochemical Exploration 32, 1–16.

Day, S.J., Fletcher, W.K., 1991. Concentration of magnetite and gold at bar and reach scales in a gravel-bed stream, British Columbia, Canada. Journal of Sedimentary Petrology 61, 871–882.

Emery, K.O., Noakes, L.C., 1968. Economic Placer Deposits on the Continental Shelf: U.N. Committee to Coordinate Joint Prospecting for Mineral Resources in Asian Offshore Areas, Technical Bulletin 1, 95pp.

Emery, K.O., Stevenson, R.E., 1950. Laminated beach sand. Journal of Sedimentary Petrology 20, 220–223.

von Engelhardt, W., 1940. Die Unterscheidung wasser-und windsortierter Sande auf Grund der Korngrossenverteilung ihrer leichten und schweren Gemengteile. Chemie der Erde 12, 445–465.

Feniak, M.W., 1944. Grain sizes and shapes of various minerals in igneous rocks. American Mineralogist 29, 415–421.

Frostick, L.E., Lucas, P.M., Reid, I., 1984. The infiltration of fine matrices into coarse-grained alluvial sediments and its implications for stratigraphical interpretation. Journal of the Geological Society of London 141, 955–965.

Gibbs, R.J., Matthews, M.D., Link, D.A., 1971. The relationship between sphere size and settling velocity. Journal of Sedimentary Petrology 41, 7–18.

Hails, J.R., 1976. Placer deposits. In: Wolf, K.H. (Ed.), Handbook of Strata-Bound and Stratiform Ore Deposits, vol. 3, pp. 213–244.

Hand, B.M., 1967. Differentiation of beach and dune sands, using settling velocities of light and heavy minerals. Journal of Sedimentary Petrology 37, 514–520.

Inman, D.L., Ewing, D.C., Corliss, J.B., 1966. Coastal sand dunes of Guerrero Negro, Baja California, Mexico. Bulletin of the Geologic Society of America 77, 787–802.

Jones, H.A., Davies, P.J., 1979. Preliminary studies of offshore placer deposits, eastern Australia. Marine Geology 30, 243–268.

Jones, H.A., Kudrass, H.R., Schluter, H.U., von Stackelberg, U., 1982. Geological and geophysical work on the east Australian shelf between Newcastle and Fraser Island—a summary of results from the SONNE cruise SO-15, 1980. Geologisches Jahrbuch D56, 197–215.

Kolesov, S.V., 1975a. Flattening and hydrodynamic sorting of placer gold. International Geologic Review 17, 940–944.

Kolesov, S.V., 1975b. Subsidence of gold grains in allocthonous alluvial and coastal-marine placers. International Geologic Review 17, 951–953.

Komar, P.D., 1981. The applicability of the Gibbs equation for grain settling velocities to conditions other than quartz grains in water. Journal of Sedimentary Petrology 51, 1125–1132.

Komar, P.D., 1989. Physical processes of waves and currents and the formation of marine placers. CRC Critical Reviews in Aquatic Sciences 1, 393–423.

Komar, P.D., Baba, J., Cui, B., 1984. Grain-size analyses of mica within sediments and the hydfraulic equivalence of mica and quartz. Journal of Sedimentary Petrology 54, 1379–1391.

Komar, P.D., Clemens, K.E., Li, M.Z., Shih, S.M., 1989. The effects of selective sorting on factor analysis of heavy mineral assemblages. Journal of Sedimentary Petrology 59, 590–596.

Komar, P.D., Li, M.Z., 1991. Beach placers at the mouth of the Columbia River, Oregon and Washington. Marine Mining 10, 171–187.

Komar, P.D., Reimers, C.C., 1978. Grain shape effects on settling rates. Journal of Geology 86, 193–209.

Komar, P.D., Wang, C., 1984. Processes of selective grain transport and the formation of placers on beaches. Journal of Geology 92, 637–655.

Kretz, R., 1966. Grain-size distribution for certain metamorphic minerals in relation to nucleation and growth. Journal of Geology 74, 147–173.

Kudrass, H.R., 1987. Sedimentary models to estimate the heavy-mineral potential of shelf sediments. In: Teleki, P.G., et al. (Eds.), Marine Minerals: Advances in Research and Resource Assessment. NATO Advanced Study Institutes Series, Series C, Mathematical and Physical Sciences, 588pp.

Kuenen, Ph.H., 1964. Experimental abrasion: 6. Surf action. Sedimentology, 3, 29–43.

Li, M.Z., Komar, P.D., 1986. Laboratory measurements of pivoting angles for applications to selective entrainment of gravel in a current. Sedimentology 33, 413–423.

Li, M.Z., Komar, P.D., 1992a. Selective entrainment and transport of mixed size and density sands: experiments simulating the formation of black-sand placers. Journal of Sedimentary Petrology 62, 584–590.

Li, M.Z., Komar, P.D., 1992b. Longshore grain sorting and beach placer formation adjacent to the Columbia River. Journal of Sedimentary Petrology 62, 429–441.

Lowright, R., Williams, E.G., Dachille, F., 1972. An analysis of factors controlling deviations in hydraulic equivalence in some modern sands. Journal of Sedimentary Petrology 42, 635–645.

May, J.P., 1973. Selective transport of heavy minerals by shoaling waves. Sedimentology 20, 203–211.

McIntyre, D.D., 1959. The hydraulic equivalence and size distributions of some heavy mineral grains from a beach. Journal of Geology 67, 278–301.

McNown, J.S., Malaika, J., 1950. Effects of particle shape on settling velocity at low Reynolds numbers. Transactions of the American Geophysical Union 31, 74–82.

McQuivey, R.S., Keefer, T.N., 1969. The relation of turbulence to deposition of magnetite over ripples. U.S. Geologic Survey, Professional Paper 650-D, pp. D244–D247.

Meland, N., Norrman, J.O., 1966. Transport velocities of single particles in bed-load motion. Geografiska Annaler 48, 165–182.

Meland, N., Norrman, J.O., 1969. Transport velocities of individual size fractions in heterogeneous bed load. Geografiska Annaler 51, 127–143.

Middleton, G.V., 1970. Experimental studies related to problems of flysch sedimentation. In: Lajoie, J. (Ed.), Flysch Sedimentology in North America. Geologic Association of Canada, Special Paper No. 7, 253–272.

Miller, M.C., McCave, I.N., Komar, P.D., 1977. Threshold of sediment motion under unidirectional currents. Sedimentology 24, 507–527.

Miller, R.L., Byrne, R.J., 1966. The angle of repose of a single grain on a fixed rough bed. Sedimentology 6, 303–314.

Minter, W.E.L., Toens, P.D., 1970. Experimental simulation of gold deposition in gravel beds. Transactions of the Geologic Society of South Africa 73, 89–99.

Mosley, M.P., Schumm, S.A., 1977. Stream junctions—a probable location for bed-rock placers. Economic Geology 72, 691–694.

Peterson, C.D., Komar, P.D., Scheidegger, K.F., 1986. Distribution, geometry, and origin of heavy mineral placer deposits on Oregon beaches. Journal of Sedimentary Petrology 56, 67–77.

Rao, C.B., 1957. Beach erosion and concentration of heavy mineral sands. Journal of Sedimentary Petrology 27, 143–147.

Reid, I., Frostick, L.E., 1985a. Role of settling, entrainment and dispersive equivalence and of interstice trapping in placer formation. Journal of the Geological Society of London 142, 739–746.

Reid, I., Frostick, L.E., 1985b. Beach orientation, bar morphology and the concentration of metalliferous placer deposits: a case study, Lake Turkana, N Kenya. Journal of the Geological Society of London, 142, 837–848.

Richardson, J.F., Meikle, R.A., 1961. Sedimentation and fluidization. Part III. The sedimentation of uniform fine particles of two-component mixtures of solids. Transactions of the Institute of Chemical Engineers 39, 348–356.

Richardson, J.F., Zaki, W.N., 1954. Sedimentation and fluidization. Part I. Transactions of the Institute of Chemical Engineers 32, 35–53.

Riech, V., Kudrass, H.R., Wiedicke, M., 1982. Heavy minerals of the east Australian shelf sediments between Newcastle and Fraser Island. Geologisches Jahrbuch D.56, 179–195.

Rittenhouse, G., 1943. Transportation and deposition of heavy minerals. Geologic Society of America Bulletin 54, 1725–1780.

Rubey, W.W., 1933. The size distribution of heavy minerals within a water-laid sandstone. Journal of Sedimentary Petrology 3, 3–29.

Saks, S.Ye., 1976. Principle of hydrodynamic equivalence of clastic particles. International Geological Review 18, 553–562.
Saks, S.Ye., 1978. Experimental study of the processes of beach placer formation. Litologiya i Poleznye Iskopaemye 13, 101–107 [translated in Lithol. Miner. Resour., vol. 15 (1979), pp. 595–600].
Sallenger, A.H. Jr., 1979. Inverse grading and hydraulic equivalence in grain-flow deposits. Journal of Sedimentary Petrology 49, 443–562.
Shepherd, R.G., Schumm, S.A., 1974. Experimental study of river incision. Geologic Society of America Bulletin 85, 257–268.
Shumilov, Y.V., Shumovskiy, A.G., 1975. Experimental data on the hydraulic size of some placer minerals in the northeast USSR. Doklady Akademii Nauk SSSR 225, 1174–1176.
Slingerland, R.L., 1977. The effects of entrainment on the hydraulic equivalence relationships of light and heavy minerals in sand. Journal of Sedimentary Petrology 47, 753–770.
Slingerland, R.L., 1984. Role of hydraulic sorting in the origin of fluvial placers. Journal of Sedimentary Petrology 54, 137–150.
Slingerland, R., Smith, N.D., 1986. Occurrence and formation of water-laid placers. Annual Review of Earth and Planetary Sciences 14, 113–147.
Smith, N.D., Beukes, N.J., 1983. Bar to bank convergence zones: a contribution to the origin of alluvial placers. Economic Geology 78, 1342–1349.
Smith, N.D., Minter, W.E.L., 1980. Sedimentological controls of gold and uranium in two Witwatersand palaeoplacers. Economic Geology 75, 1–14.
Steidtmann, J.R., 1982. Size-density sorting of sand-size spheres during deposition from bed-load transport and implications concerning hydraulic equivalence. Sedimentology 29, 877–883.
Thompson, W.O., 1937. Original structures of beaches, bars and dunes. Geologic Society of America Bulletin 48, 723–752.
Tourtelot, H.A., Riley, L.B., 1973. Sizes and shape of gold and platinum grains. In: Amstutz, G.L., Bernard, A.J. (Eds.), Ores in Sediments. Springer-Verlag, New York, NY, pp. 307–319.
Trask, C.B., Hand, B.M., 1985. Differential transport of fall-equivalent sand grains, Lake Ontario, New York. Journal of Sedimentary Petrology 55, 226–234.
Vogel, K.R., van Niekerk, A., Bridge, J.S., 1992. Routing of heterogeneous size density sediments over a moveable stream bed: model verification and testing. Journal of Hydraulic Engineering, American Society of Civil Engineers 118 (2), 263–279.
Vorob'yev, V.B., 1979. Mineral distribution in a gold beach placer. International Geologic Review 21, 72–78.
Warg, J.B., 1973. An analysis of methods for calculating constant terminal-settling velocities of spheres in liquids. Mathematical Geology 5, 59–72.
Wertz, J.B., 1949. Logarithmic pattern in river placer deposits. Economic Geology 44, 193–209.
White, C.M., 1940. The equilibrium of grains on the bed of a stream. Proceedings of the Royal Society of London, Series A 174, 332–338.
Williams, G.P., 1966. Particle roundness and surface texture effects on fall velocity. Journal of Sedimentary Petrology 36, 255–259.
Woolsey, J.R., Henry, V.J., Hunt, J.J., 1975. Backshore heavy-mineral concentration on Sapelo Island, Georgia. Journal of Sedimentary Petrology 45, 280–284.
Yalin, M.S., 1972. Mechanics of Sediment Transport. Pergamon Press, New York, NY.
Yalin, M.S., Karahan, E., 1979. Inception of sediment transport. Journal of the Hydraulics Division, American Society of Civil Engineers 105, 1433–1443.

Chapter 2

THE NILE DELTA: PROCESSES OF HEAVY MINERAL SORTING AND DEPOSITIONAL PATTERNS

OMRAN E. FRIHY

Coastal Research Institute, 15 El Pharaana Street, El Shallalat, 21514 Alexandria, Egypt

ABSTRACT

The Nile Delta has a long history of shoreline change. Multiple distributary channels supplied large quantities of sand to the shore, producing beach accretion with extensive black-sand deposits found on the beaches and in continental shelf sands. However, erosion increased as discharges of the river began to decrease in the late 19th century as a result of climate change and construction of dams. The shift from beach accretion to erosion induced a concentration of heavy minerals on stretches of the receding shore, as light minerals were selectively displaced to accretional areas. In this review the physical processes are examined by which waves and currents sort and concentrate the heavy mineral grains according to their densities, sizes and shapes during transport of the beach sand between eroding and accreting shores. As such, the suite of heavy minerals found in delta coastal sands are used as natural tracers of sand movement related to large-scale shoreline change. Results, obtained from several studies undertaken along the length of the Nile Littoral Cell from Alexandria (Egypt) to the northern coast of the northern Israeli and Lebanese margin, are synthesised. These studies illustrate the importance of heavy minerals in identifying sediment point sources, tracing sand transport paths, grain sorting processes, energy levels of transporting agents and sediment provenance (both modern and relict). This contribution also evaluates the potential of applying heavy minerals to discriminate between accreting and eroding beaches and to distinguish a variety of fluvio-marine environments such as river, lagoons, coastal dunes, accretion ridges and continental shelf.

Keywords: heavy mineral sorting; coastal processes; beach erosion; Nile Delta littoral-cell; black-sand placers

1. INTRODUCTION

Coastal deltas are environments where a river supplies large quantities of sediment to the shore, which is then reworked by waves and currents. Part of the sand may be

Developments in Sedimentology, Vol. 58, 49–74

ISSN: 0070-4571/doi:10.1016/S0070-4571(07)58002-7

carried offshore and deposited on the continental shelf, while the bulk is redistributed alongshore in beaches adjacent to deltas. As sand is transported from one area to another by waves, tides and currents, the suite of minerals it carries experiences sorting due to differences in particle densities, diameters and shapes (Komar, 2007, this volume). On river deltas, where large quantities of sands are delivered, the sands, after reaching the coast, are subjected to considerable sorting, often leading to extensive heavy mineral deposits (Pirkle et al., 2007, this volume). Such a sorting process is illustrated by the Nile Delta of Egypt where, for thousands of years, the River Nile has carried vast quantities of sediment (25% sand; 75% mud) from equatorial east Africa, leading to delta progradation seaward into the Mediterranean Sea (Fig. 1). At least seven distributary channels flowed across the Nile Delta and discharged into the Mediterranean at various times during the Middle to Late Holocene (Toussoun, 1922; Stanley and Warne, 1993). Five of these distributaries became silted up and are no longer active, leaving two presently active branches (the Damietta and Rosetta).

There has been a prolonged period of decrease in sediment discharge from the Nile since the late 19th century, initially caused by climate change and later augmented by a dramatic drop following the construction of the Aswan High Dam in the 1960s. The decreased sand supply led to major shoreline realignments along the delta coast, generally with extensive erosion occurring near the river mouths, with some accretion between the mouths. Along-coast redistribution of sand has been accompanied by considerable grain sorting, resulting in the concentration of heavy minerals in eroded areas near the river mouths.

Many studies have focused on Nile Delta erosion problems, beach-sand movement and mineral sorting patterns. The primary objective of the present contribution is to review these studies because they provide an actualistic model of sorting processes and highlight variations in mineral concentrations controlled by large-scale patterns of sand movement. In addition to the beaches, for completeness, this review also considers other delta environments, including lagoons, coastal dunes and others. Finally, studies that examined heavy minerals in sands on the continental shelf off the Nile Delta are also discussed.

2. THE RIVER NILE AND ITS COASTAL LITTORAL CELL

The River Nile has a length of 6825 km from the source of the Luvironza River in Tanzania to the shore of the Mediterranean Sea and follows generally a south to north path (Fig. 1). The Nile is the dominant source of sediment in the southeastern Mediterranean basin (Hassan, 1976; Said, 1981; Stanley, 1989). The main channel, which passes through Egypt, contains water derived from three major tributaries: the White Nile, Blue Nile and Atbara River (Fig. 1). On average, 84% of the flow in the lower Nile during summer floods is derived from the Ethiopian Plateau (a dominantly volcanic province), while 16% is introduced from the central/east African Lake Plateau (a dominantly argillaceous metamorphic province). The mineral suite of the volcanic Ethiopian Plateau is transported by the northern tributaries including the Blue Nile and the Atbara River, whereas the mineral suite of the central/east African Lake Plateau is transported by the southern tributaries (Sobat, Bahr El Ghazal and

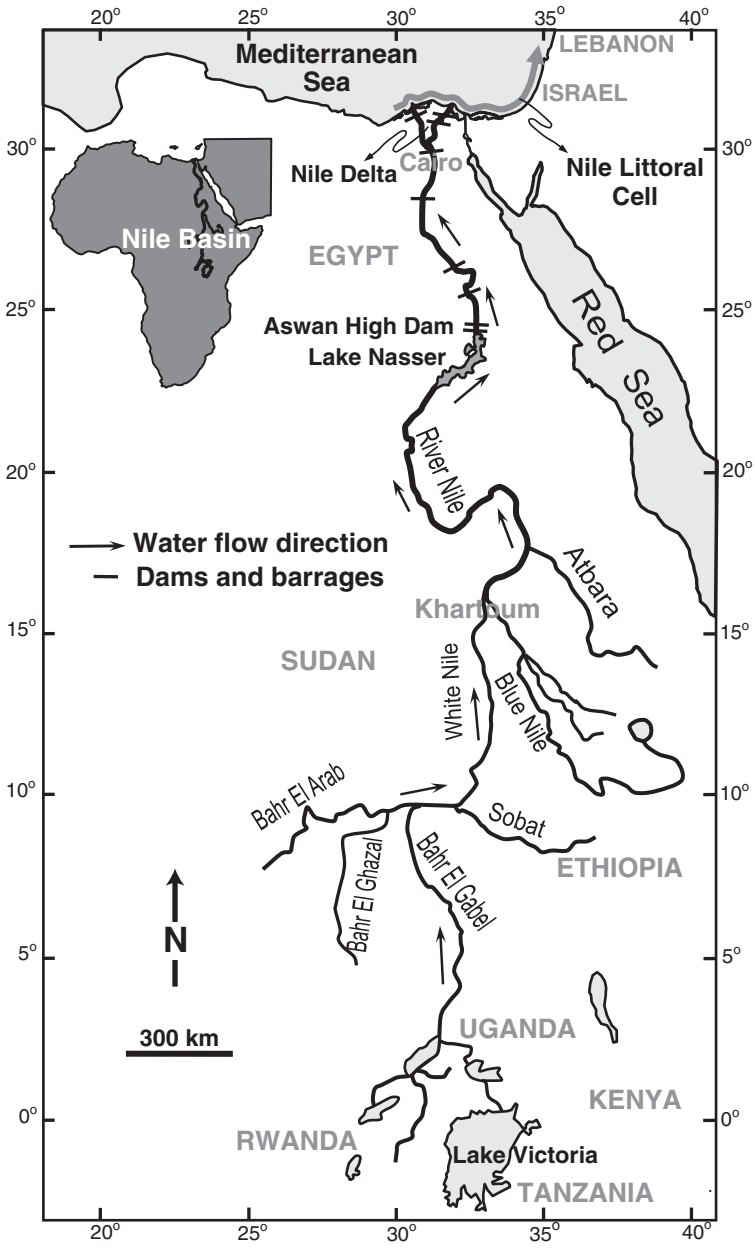

Fig. 1. General location of the Nile Basin in central East Africa and positions of the dams and barrages constructed on the Nile River since the late 19th century.

Bahr El Gabel) (Fig. 1). Sediments of the Blue Nile and Atbara River are rich in clinopyroxenes (augite), which are absent or scarce in the southern tributaries that are characterised by an abundance of metamorphic minerals such as sillimanite, staurolite, andalusite, kyanite and garnet (Shukri, 1950). Essentially, heavy mineral

assemblages record the major influence of transport to the delta coast from the Blue Nile and Atbara River sources, which contribute the highest volume of sediments. The dominant influence of basaltic volcanic rocks in the Ethiopian Plateau source terrain is preserved by the heavy mineral suites, identified in cores from Pleistocene and Holocene sediments of the Nile Delta (El Askary and Frihy, 1987) and offshore samples on the delta shelf (Stanley et al., 1979). Moreover, heavy minerals in modern coastal sands along the delta are also characterised by the Ethiopian components (Hilmy, 1951; El Fishawi and Molnár, 1985). In contrast, metamorphic minerals appear not to be preserved well in the beach and shelf sediments as can be deduced from their relatively minor to small proportions in the total heavy mineral budget. Having undergone transport by the Nile for a distance of ~4000 km, the mineral assortment has received minor additions from other rocks along the course of the river (Hilmy, 1951).

Mineralogical studies demonstrate that once Nile sands reach the coast, they are distributed along the shore of the southeastern Mediterranean Sea for a distance of ~670 km from Alexandria, Egypt, in the southwest to Akko, Israel, in the northeast (Goldsmith and Golik, 1980; Inman and Jenkins, 1984). This stretch of coast is part of the sedimentation system called the "Nile Littoral Cell" (Fig. 2), because it includes the river source, transport paths and sinks for Nile sediments. The continental shelf of this cell extends to ~70 km off the Nile Delta, and narrows to <10 km near Israel and Lebanon. Within this cell, the Nile has been the overwhelmingly dominant source of

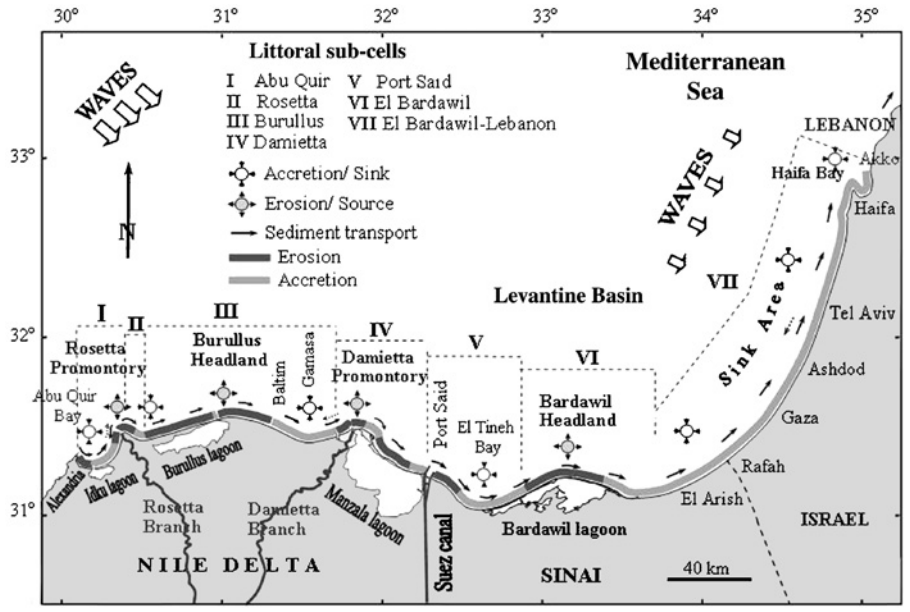

Fig. 2. The Nile Delta littoral cell in the southeastern Mediterranean, comprising a series of sub-cells (I–VII), extending from Abu Quir headland west of the Nile Delta of Egypt to Akko on Haifa Bay, Israel. The figure shows major sources (erosion) and sinks (accretion) separated by nodal points (after Goldsmith and Golik, 1980; Inman and Jenkins, 1984; Frihy et al., 1991).

sediment for beaches, coastal dunes and the continental shelf (Shukri, 1950; Emery and Neev, 1960; Pomerancblum, 1966; Azmon and Golik, 1995; Levin and Ben-Dor, 2004). An estimated total volume of $10 \times 10^9 \, m^3$ of sand has been deposited in the major sink off the Israeli coastline since the last glaciation (Pomerancblum, 1966).

The processes responsible for the transport of the Nile sediments include wind- and wave-driven currents associated with the eastern Mediterranean gyre (Goldsmith and Golik, 1980; Inman and Jenkins, 1984). On the delta shore, waves generated to the west by storms passing eastward along the length of the Mediterranean produce a generally eastward-directed transport of beach sand that, except for that trapped by jetties and breakwaters, is carried to the shores of the Sinai and then further north along the coast of Israel.

The advance or retreat of the delta shore has depended on the balance between the rate of sand supply from the Nile versus the rate at which the sand is removed and transported to the east by the waves and nearshore currents. Mud is also contributing to this balance, where it is deposited offshore on the continental shelf in which it is actively affected by the cross-shore transport processes. This interplay between deposition and removal is best seen near the mouths of the two Nile distributary branches, the Rosetta and Damietta. Over centuries the large supply of river sand has built out sand promontories on the delta, but during the past century these promontories have experienced much erosion as river discharges and sand yields have decreased.

Analyses of historical maps spanning the 19th and 20th centuries indicate that during the 1800s, delta promontories progressively extended into the Mediterranean Sea in response to the large quantities of sediment delivered to the coast by both the Rosetta and Damietta branches (UNESCO/UNDP, 1978; Fanos et al., 1991; Frihy and Lawrence, 2004). This general accretion reverted to erosion at the beginning of the 20th century, and rapid rates of shoreline retreat have been experienced since that time (UNESCO/UNDP, 1978; Frihy and Khafagy, 1991). This change from accretion to erosion is attributed primarily to the loss of sand supply after construction of two dams at Aswan on the upper river, and barrages on both the upper and lower Nile (Fig. 1). Prior to damming the river, an estimated 19 million tonnes of sand was discharged annually from the Nile, accounting for prevailing shoreline accretion (Hammad et al., 1979). The Aswan Low Dam was completed in 1907, and seven barrages were emplaced between 1881 and 1965. The Aswan Low Dam was designed to bypass the transported sediment, but the completion of the Aswan High Dam in 1964 created Lake Nasser. This lake has trapped the river sediment since that time, virtually eliminating sediment delivery to the coast and accounting, in large part, for the reversal from accretion to erosion.

However, there are also other factors involved in the reversal to erosion that began prior to the construction of the dams and barrages. Measurements of water discharges show that there was an abrupt decrease in the annual water yields at the beginning of the 20th century, attributable to low rainfall within the river's catchment in the Ethiopian Plateau and central Africa, reducing the sediment delivery to the delta shore even prior to dam construction (UNESCO/UNDP, 1978; Frihy and Khafagy, 1991). At the same time, an average sea-level rise of 2.2 mm per year (El Fishawi and Fanos, 1989) and local subsidence of the delta coast by up to 5 mm per year (Stanley, 1990; Stanley and Warne, 1993) also contributed to shoreline retreat.

Following virtual cessation of sand delivery to the coast from the Nile, the action of wave-driven longshore currents continued to transport beach sand to the east, resulting in a major adjustment of the delta coastline (UNESCO/UNDP, 1978; Blodget et al., 1991; Fanos et al., 1991; Inman et al., 1992). Maximum rates of erosion occurred adjacent to the Rosetta and Damietta promontories, with highest rates of erosion at the Rosetta promontory where, at present, the average shoreline retreat rate is −15 m per year. The eroded sand from this promontory is carried to the east, where it is deposited resulting in beach accretion just to the east of the promontory; this effectively smoothes the shoreline configuration. Erosion also occurs on the Damietta Promontory and along the Burullus region of the central delta (a location of the Sebennitic channel, a former third river distributary that dried up ~2000 B.P.) although it is occurring at lower rates (−10 and −6 m per year, respectively). Accretion areas form mainly in the "saddles" or embayments between the promontories, with rates of shoreline advance ranging up to 13 m per year, resulting in an overall smoothing of the coastline. A portion of the eroded material has accreted in the form of spits or shoals near the inlets (Frihy et al., 2003; Frihy and Lawrence, 2004).

Most recently, intensive intervention in the form of constructed protective engineering structures (revetments, jetties, groynes, detached breakwaters and seawalls) has occurred along the delta shore. This construction in most cases has blocked or retarded the eastward transport of the beach sand and, as a result, there has been locally induced marked shoreline change, particularly downdrift of the structures where enhanced erosion has occurred.

The full 670 km length of the Nile Littoral Cell from Alexandria to the coast of Israel can be divided into a series of sub-cells representing discrete sedimentation compartments, with each recording a complete cycle of sand source, littoral transport and deposition (Inman and Brush, 1973). On the delta itself, from west of the large jetties at Port Said at the entrance to the Suez Canal as far as Alexandria, four sub-cells have been identified by Orlova and Zenkovitch (1974) and Frihy et al. (1991). In these sub-cells, sand eroded from a promontory is transported to the east and is either deposited naturally in the next embayment, or trapped by an artificial structure, resulting in shoreline accretion (Fig. 2). Based on sand mineralogy, and the curvilinear coastline of Israel, two additional sub-cells have been identified by Frihy and Lotfy (1997) further east along the north Sinai coast of Egypt. These form a major convergence zone that act as a sediment sink for northward transported sand derived from the Sinai sub-cells (Goldsmith and Golik, 1980; Nir, 1982).

3. MINERAL SORTING ON DELTA BEACHES

The alternating patterns of erosion and accretion along the delta shore within the sub-cells are apparent by observing variations in concentrations of heavy minerals in the beach sands (Frihy and Komar, 1993; Frihy et al., 1995); these variations have been utilised as one aspect for defining the sub-cells. The presence of the highest concentrations of heavy minerals, forming black-sand placers in the zones of maximum erosion along the beaches of the Rosetta and Damietta promontories, was recognised in the 20th century. In the 1950s and 1960s these were mined for their zircon, garnet, rutile and ilmenite content.

Sorting of minerals in the beach sands has been induced by natural processes of waves and longshore currents responsible for transport of the sand generally towards the east. As reviewed by Komar (2007, this volume), selective transport of different minerals depends on their densities and grain sizes. The rapid changes in the positions of the Nile Delta shorelines have encouraged researchers to define patterns of erosion versus accretion according to heavy mineral contents. Differences in densities and mean grain sizes determine the fraction of beach sands that remain in areas of erosion as a lag, while other grains are preferentially transported to areas of accretion. A series of studies have been undertaken, ranging from local sorting patterns (Stanley, 1989; Frihy and Dewidar, 1993; Frihy and Lotfy, 1994a, b; Frihy et al., 1994) to a regional scale (Frihy and Komar, 1991, 1993; Frihy and Dewidar, 2003), and the results of this broad research are reviewed here.

On a delta-wide scale, Frihy and Komar (1993) found that variations in heavy mineral concentrations depict a trend of a series of saw-tooth peaks, in which the highest concentrations correspond to areas of shoreline erosion. Heavy minerals decrease alongshore having been reworked towards areas of shoreline accretion (Fig. 3B, C). These marked longshore variations in heavy mineral concentrations are also consistent with mean grain sizes of beach sands, which are coarsest in areas of beach accretion (Fig. 3B–D). This is further confirmed from a statistical correlation between concentrations of heavy minerals versus mean grain sizes for all beach-sand samples collected along the delta shore; this indicates a definite trend of increasing heavy mineral concentration with decreasing grain size. Such a relationship is expected from patterns of selective grain entrainment and transport, with sorting of grains according to their contrasting densities and sizes (e.g., Komar, 2007, this volume). Correlations also exist between long-term rates of erosion or accretion, established from beach profile data, and concentrations of heavy minerals and mean grain sizes for a series of beach-sand samples from the Damietta sub-cell. Similar correlations are found for the other sub-cells, but differ from sub-cell to sub-cell. As expected, the greater the rate of erosion, the higher is the concentration of heavy minerals and the finer is the mean grain size of sand. In areas of heavy mineral concentrations, coastal processes have selectively removed the grains of lower density and coarser size, leaving behind, as lag, grains of high density and small diameters; the end result of such processes is the formation of black-sand placer deposits. Data from Lotfy (1997), used in Fig. 4, demonstrate that for the suite of minerals found in Nile Delta environments, including the river, the higher the density of the mineral, the lower is its median grain size. Accordingly, opaque minerals concentrate preferentially because they are the finest grained and the most dense of the heavy minerals.

At a more local scale, a study was undertaken by Frihy and Lotfy (1994a) along the shore of the Rosetta promontory, where marked longshore variations in mineral concentrations and sorting are found. The large-scale pattern of shoreline change along the Rosetta promontory records the existence of sediment transport divergence: in the area of greatest erosion centred on the promontory tip (Fig. 5A), erosion diminishes along both the eastern and western promontory flanks, ultimately reverting to accretion. Two nodal points separate shorelines experiencing erosion or accretion, which are positioned at 6 and 8 km, respectively, west and east of the river mouth. Relationships between rates of beach change and both heavy mineral

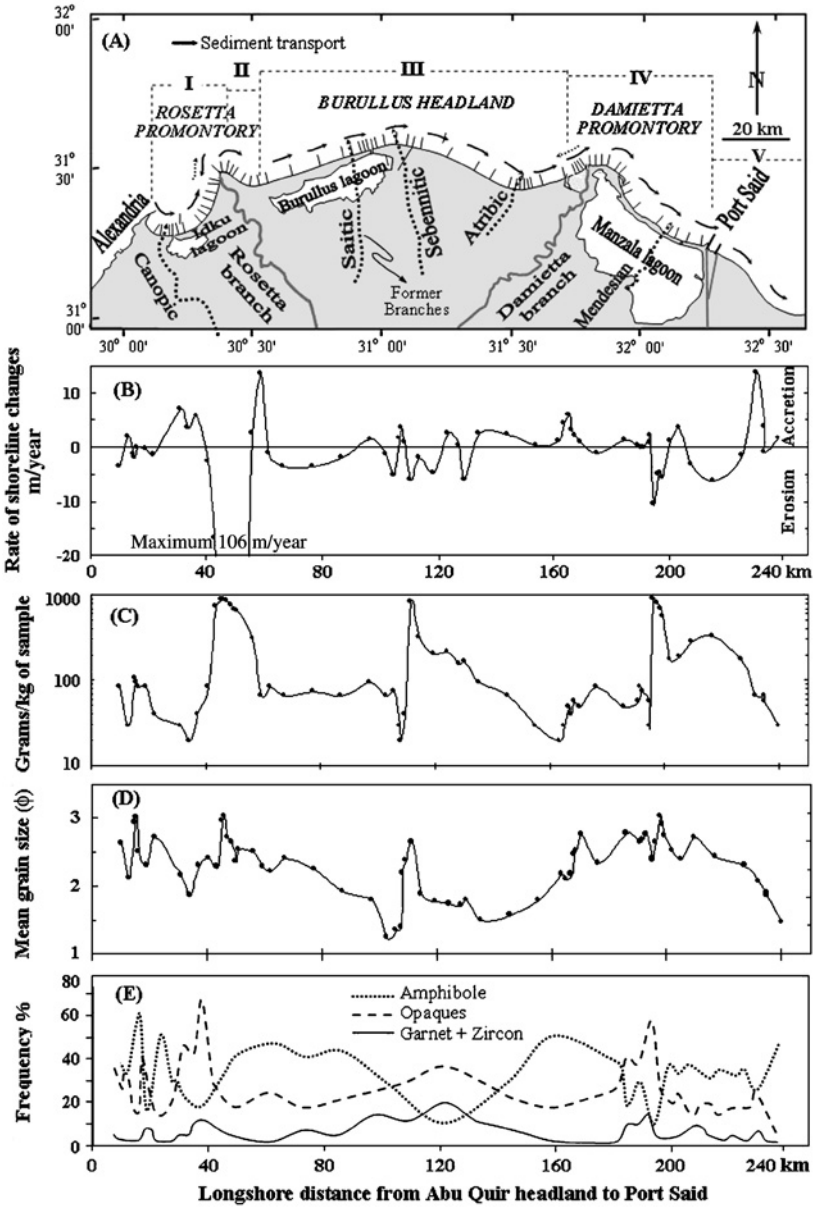

Fig. 3. Physiography of the Nile Delta region and sediment characteristics. A–D after Frihy and Komar (1993) and E after Frihy and Komar (1991). (A) Positions of beach-profile lines analysed to determine rates of beach changes. Dashed lines show the former positions of extinct branches of the Nile. (B) Alongshore variations in rates of shoreline change, alternating between erosion and accretion. (C) Alongshore variations in heavy mineral concentrations of beach samples collected at profile locations. (D) Alongshore variations in mean grain sizes of beach samples. (E) Alongshore mineral variations in beach samples. Opaques are plotted as percentages of total sample, whereas the other minerals are number-count percentages of non-opaque fractions.

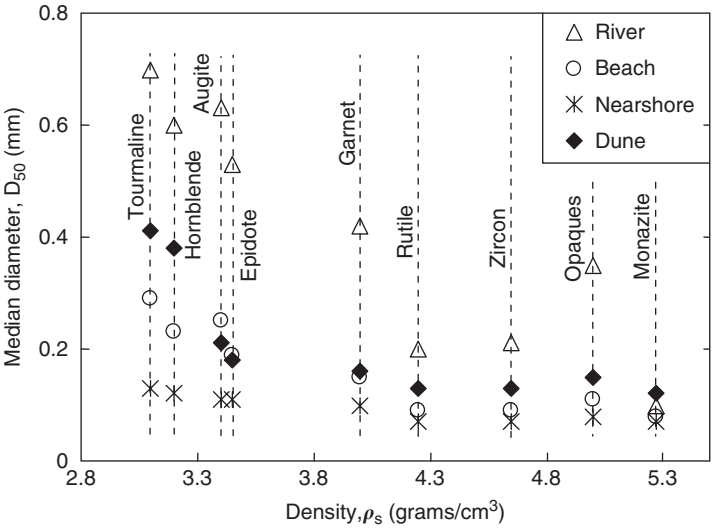

Fig. 4. Plot of median diameters versus densities of significant minerals in Nile Delta sands, showing an inverse relationship (data from Lotfy, 1997).

concentrations and mean grain sizes are also found along the Rosetta promontory (Frihy and Lotfy, 1994a). As indicated in Fig. 5B, C, there is a marked longshore variation in concentrations of heavy minerals, which are highly concentrated in beach sands close to the river (80–92%) where maximum erosion has occurred at this divergence point, but which decrease dramatically with longshore distance and annual values of erosion or accretion. To the east and west of the promontory flanks, heavy mineral concentrations range from 7 to 50%, where erosion reverses to accretion. The decrease in the percentage of heavy minerals with longshore distance from the Rosetta mouth results from their becoming progressively diluted by the light minerals, quartz and feldspars. Mean grain sizes of beach sand also vary with distance from the river, tending to be finer close to the Rosetta mouth, and coarser to both the east and southwest along accreting stretches of the shore (Fig. 5C). Therefore, on the local scale along the Rosetta promontory, just as in the delta scale analyses, an intimate relationship exists between shoreline erosion, mean grain size and concentration of heavy minerals. It appears that the finest grains concentrated in highly eroded areas, while the coarsest grains are associated with accreted coastal stretches.

A similar pattern was found by Frihy and Dewidar (1993) along the Burullus "bulge" on the central part of the Nile Delta, where beach erosion resulted from blocking the longshore sand transport by the jetties constructed on the Burullus lagoon inlet (see Fig. 2 for location). A sorting pattern was also found by El Asmar and White (2002) on both sides of the updrift (accretion) and downdrift beaches (erosion) of the Damietta harbour jetties.

A detailed analysis of mineral sorting was undertaken by Frihy and Komar (1991) with beach samples from Abu Quir Bay at the western end of the delta. This sector stretches from the Rosetta promontory to the Abu Quir headland east of Alexandria,

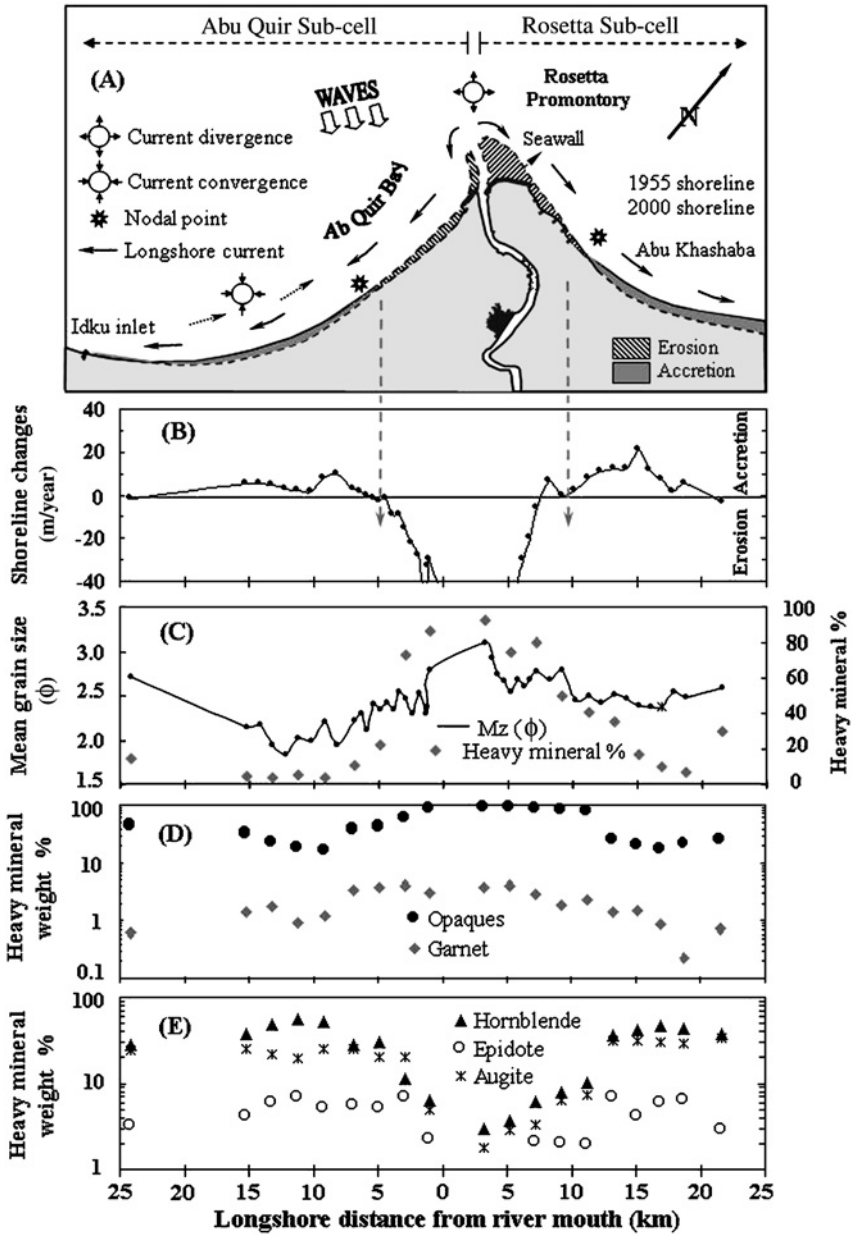

Fig. 5. Shoreline changes within the Rosetta promontory and longshore variations in general grain size and heavy mineral distributions. (A) Rosetta promontory showing Nile Delta subcells and general shoreline change, with 1955 and 2000 shorelines superimposed (after Frihy et al., 2003). Predominant wave directions, littoral currents and position of nodal points are indicated. (B) Annual rate of alongshore erosion and accretion pattern. (C) Longshore variations in mean grain size (Mz ϕ) and heavy minerals percent. (D) Longshore variations of opaques and garnet weight percentages. (E) Longshore variations in hornblende, augite and epidote in beach samples (after Frihy and Lotfy, 1994a).

the sector that represents the western end of the delta (see Fig. 2 for location). It was found that concentrations of opaques, zircon, rutile and garnet decrease exponentially with longshore distance from the Rosetta river mouth, while augite and hornblende increase exponentially in shoreline areas that are accreting. The coefficient in the exponential equation appeared to be a function of mineral density, demonstrating the control of this mineral property in grain sorting. Similar sorting patterns have been documented on an Oregon beach by Komar and Wang (1984), where selective transport is cross-shore, and by Li and Komar (1992) for longshore transport away from the Columbia River (see also Komar, 2007, this volume).

On a delta-wide scale, distributions of major heavy minerals, reported by Frihy and Komar (1991), show that the opaque mineral contents are greatest at the Rosetta and Damietta promontories, reaching ~70 and 60% of beach-sand compositions (Fig. 3E). A broad peak of opaque accumulations crosses the central delta, corresponding to the subdued promontory and the ancient location of the former Sebennitic branch of the Nile. Another maximum in opaque contents occurs within Abu Quir Bay, one that has been interpreted to be the former location of the now defunct Canopic branch. The distributions of garnet plus zircon matches closely to that found for the opaques, while amphiboles (principally hornblende) form an inverse pattern (Fig. 3E). The inverse correlation between percentages of opaque minerals and amphibole and pyroxene contents was noted on Nile Delta beaches by Hassan (1976), and also in shelf sands off the coast of Israel by Pomerancblum (1966). It is apparent that such delta-wide distributions of beach-sand compositions mirror patterns of shoreline erosion versus accretion: opaques and garnet plus zircon are significantly concentrated in areas of shoreline erosion while a decline in amphibole abundance in areas of erosion signals that they are selectively removed and transported alongshore to stretches of coast that are accreting or are relatively stable, but where active longshore transport still takes place.

Further east along the Sinai coast, two sub-cells were defined by Frihy and Lotfy (1997) on the basis of the heavy mineral composition of beach sands. Two discrete minerals groups, determined from factor analysis, correspond to alongshore variations in the pattern of shoreline erosion versus accretion and grain sizes of beach sands. Factor 1 consists of minerals that are coarse grained and have lower densities (augite, hornblende and epidote), whereas factor 2 includes minerals that are finer grained and have higher densities (opaques, zircon, rutile and monazite).

Grain sorting patterns of heavy minerals established alongshore on the delta coastline are also comparable to those distributed along the Rosetta promontory. They also provide a statistical relationship between the heavy mineral weight per cent and rate of shoreline change (Frihy and Lotfy, 1994a). Two heavy mineral groups are found: one group that is associated with the high-density minerals (4–5 g/cm^3) and a second group comprising lower density minerals (3.2–3.45 g/cm^3). The first group, represented by opaques and garnet (Fig. 5D), systematically decreases with distance from the distributary mouth, having a low concentration near nodal points close to accreted stretches, and then increases slightly at a point of erosion east of Abu Khashaba and southwest along the Abu Quir coastline. Longshore variations of this group are much the same as found for the total heavy mineral suite. The second group (augite, hornblende and epidote), comprising the least dense heavy minerals in the study sediments, increases in the longshore direction to the east

and southwest along accreted stretches (Fig. 5E). This increase continues along the eastern and southwestern flanks away from the mouth, where there is a slight reduction. The trend of this group is the inverse of that seen for the first group. Accordingly, within the heavy mineral assemblage the most dense opaques and garnet have the finest grain size whereas the least dense hornblende is the coarsest. Results obtained from a correlation coefficient analysis indicated that the greater the rate of shoreline erosion, the more concentrated is the first mineral group (garnet and opaques). The second group (augite, hornblende and epidote) is more concentrated with increased accretion rate. A similar pattern was found by Anwar et al. (1981) further east along the coastal-lagoon barrier between the Damietta mouth and Port Said, involving the same mineral suite (see Fig. 2 for location). Along this eroding coastal stretch, the higher the density of a particular mineral and the smaller its median diameter, the more concentrated it becomes close to the river mouth and decreases systematically with longshore distance towards Port Said to the east.

Because waves and currents affect mineral sorting, heavy mineral compositions serve to differentiate between eroded and accreted beaches. Based on the heavy mineral content, Frihy (1994) differentiated between sands from eroded and accreted beaches along the Nile Delta coastline, collecting samples from areas associated with erosion and accretion patterns (shown in Fig. 2) and using bivariate plots of raw weight-percentage data and factor analysis. Results of factor analysis yielded two dominant mineral factors, one that included lower density minerals (augite, hornblende and epidote), while the second contained the densest heavy minerals (opaque minerals, garnet, zircon, rutile and monazite). Discrimination between eroded and accreted sands was most efficient when cross plots were made using the two factor loadings (Fig. 6). The inverse relationship between the two factors, which is not related to differing sand provenance, suggests that it was the result of mineral sorting processes during entrainment and transport. Factor 2 represents concentrations of the densest minerals (those that remain in eroded areas), while factor 1 contains minerals with lower densities (that are more easily entrained by waves and currents, and transported alongshore to areas of accretion). The overlap of some samples from eroding and accreting areas in this plot suggests that they are located in transitional zones between eroded and accreted shores, probably in areas near nodal points that represent zones where the sediment regime changes from erosion to deposition, or vice versa. Samples from such areas have an intermediate mineral composition that signals both erosion and accretion.

With regard to mean grain sizes of the original samples, as mentioned earlier, accreted beach sands are coarser than the eroding ones due to grain size sorting processes for both the light and heavy minerals (Anwar et al., 1979; Frihy and Dewidar, 1993; Frihy and Komar, 1993). Results of the Rosetta promontory study are consistent with grain sorting processes, established worldwide for coasts where the beaches are undergoing erosion (Rao, 1957; Komar and Wang, 1984; Komar and Li, 1991; Li and Komar, 1992). Most of these studies demonstrated that waves and currents produce selective sorting, and the concentration of mineral grains according to their particular densities and sizes; these patterns operate in both longshore and cross-shore directions. Studies by Komar and Wang (1984) and Li and Komar (1992) for beach sands on the Oregon and Washington coasts showed that wave swash on the beach preferentially entrains and transports away coarser grains of

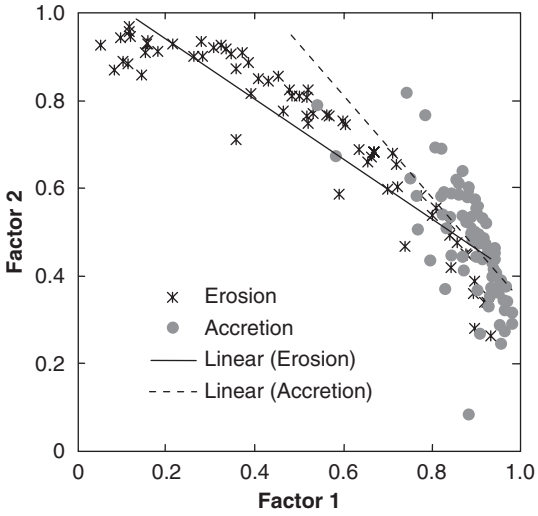

Fig. 6. Discrimination of eroded and accreted coasts. Plot of loadings of factor 1 (lower density minerals: augite, hornblende and epidote) versus factor 2 (higher density heavy minerals: opaque minerals, garnet, zircon, rutile and monazite), showing good discrimination between eroded and accreted sands. The plot also depicts the inverse relationship between the two factors (after Frihy, 1994).

light minerals (quartz and feldspars), tending to leave as a lag the dense, finer-grained heavy minerals, which was also revealed, in part, by the study of Frihy and Komar (1991) on the Nile Delta.

4. MINERAL SORTING AND DISCRIMINATION OF DELTA ENVIRONMENTS

The Nile Delta is a useful area in which to distinguish between individual heavy minerals in geographically related fluvio-marine environments, such as river, lagoon, coastal dune, accretion ridge, beach, nearshore and prodelta. Discrimination between these seven modern environments was carried out by Frihy et al. (1998) using combination plots of heavy mineral weight percentages. Degrees of discrimination ranged in scale from weak to good, with some overlap also occurring. However, using bivariate plots of heavy mineral species, it is possible to discriminate between either accretion sand ridges and/or lagoons from each of river, dune, beach, nearshore and prodelta environments. Discrimination is also possible between prodelta and each of river, beach and nearshore environments, and nearshore from river, dune and beach. Examples from these bivariate plots are shown in Fig. 7. Carried out as a test, these plots proved satisfactory in identifying and interpreting the origin of Holocene sediments from "unknown" environments collected from cores drilled at the Nile Delta coastal zone. In contrast, the plots fail to distinguish dune from beach or river, beach from river and ridge from lagoon. The wide range of discrimination between the seven environments is interpreted in terms of sediment provenance, selective

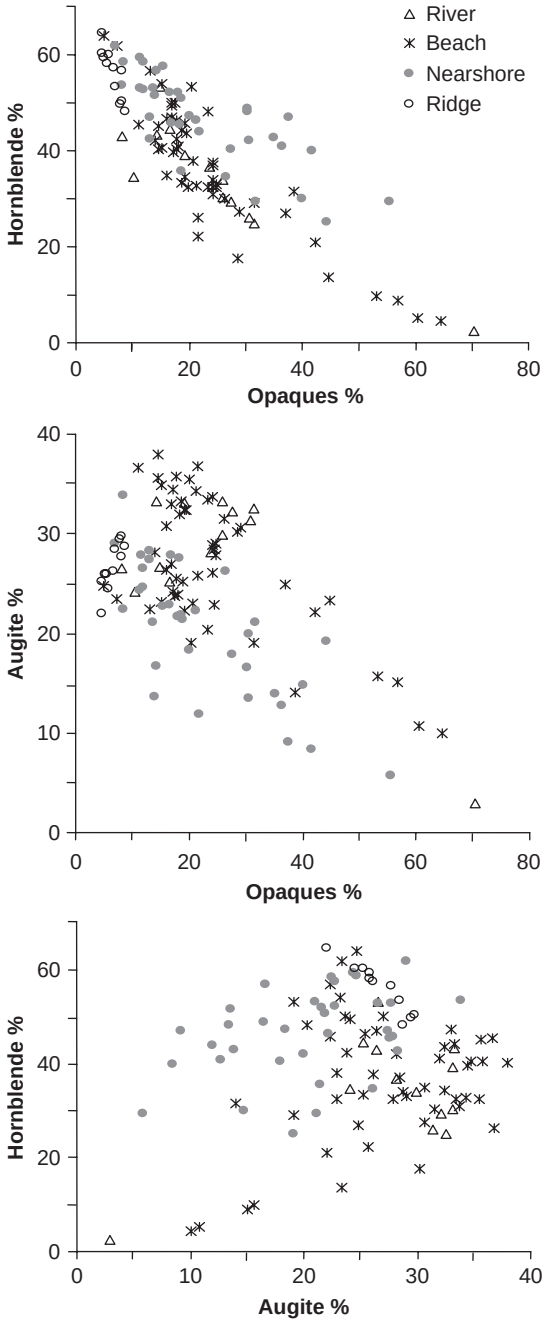

Fig. 7. Selected bivariate plots showing weak to good discrimination among fluvio-marine environments (river, beach, nearshore and accretion ridge samples) in the Nile Delta (after Frihy et al., 1998).

sorting by diverse dynamic processes and nature of the transporting agent (marine water, river or wind).

5. MINERAL SORTING IN CONTINENTAL SHELF SEDIMENTS

Similarly to studies of beaches investigations of heavy minerals in continental shelf sediments can provide useful information pertaining to source terrain, sand provenance, heavy mineral provinces and hydrodynamic processes. The objectives and analyses of shelf sand studies were much the same as those made on beaches, only directed spatially rather than in longshore direction. However, the mineralogy of continental shelf sands differed from that of the beaches as a result of intermixing modern and relict sediments of different provenance. In a series of publications, the mineralogies of continental shelf sands of the Nile Littoral Cell from Abu Quir Bay to Akko, northern Israel, were applied to interpret hydrodynamics and sediment provinces. Stanley (1989) refined the general sediment transport patterns across the entire cell; Frihy and Lotfy (1994b) located the former Sebennitic promontory at the central bulge of the Burullus coast; Frihy et al. (1994) outlined the major sediment sink at Abu Quir Bay; and Frihy and Dewidar (2003) interpreted the entire set of littoral sub-cells along the nearshore zone of the Nile Delta.

In a study of seabed level changes of bottom sediments in the nearshore zone of the delta Frihy and Dewidar (2003) used heavy minerals to interpret littoral sub-cells that developed during cross-shore and alongshore sediment transport. Rates of seabed changes were calculated from beach-nearshore profiles along the delta coast, surveyed over periods of 10–24 years (1971–1995). Areas of erosion that occur off delta promontories (maximum rate of −40 cm per year) are interpreted as a sediment source, while zones of accretion exist off saddles and embayment between these promontories (maximum rate of 40 cm per year) as sediment accumulations (Fig. 8A). The spatial dispersion of heavy mineral concentrations (g/kg of sample) across the study area show distinctive, delta-wide patterns, suggestive of both cross-shore and alongshore grain sorting during transport (Fig. 8B, C). It was found that concentrations of heavy minerals are highest near the delta promontories (200–900 g/kg), and diluted progressively to the offshore. The dispersion of heavy minerals showed the same tendency to alternate in the longshore direction, with low concentrations (0–200 g/kg) distributed within sinks between promontories. Variations of heavy minerals form a series of sectors, with the highest concentrations in areas of seabed erosion alternating with areas of decreasing concentrations where accretion prevails (Fig. 8A, B). The onshore-offshore heavy mineral pattern indicates that there is a cross-shore component to sediment movement, with erosion of the beach face and inner surf zone and transport of eroded sand towards the offshore as well as in the longshore direction. The lack of correlation between mean grain size and both rate of seabed modification and heavy mineral concentration indicated that erosional and accretional zones do not correlate with certain sediment sizes, i.e. the rate of seabed changes is independent of grain size (Fig. 8C). This relationship differs from that previously investigated on some adjacent beaches in the Nile Delta region (Anwar et al., 1979; Frihy and Dewidar, 1993; Frihy and Komar, 1993), in which it has been established that accreted beach sands are coarser than eroding ones due to grain size sorting

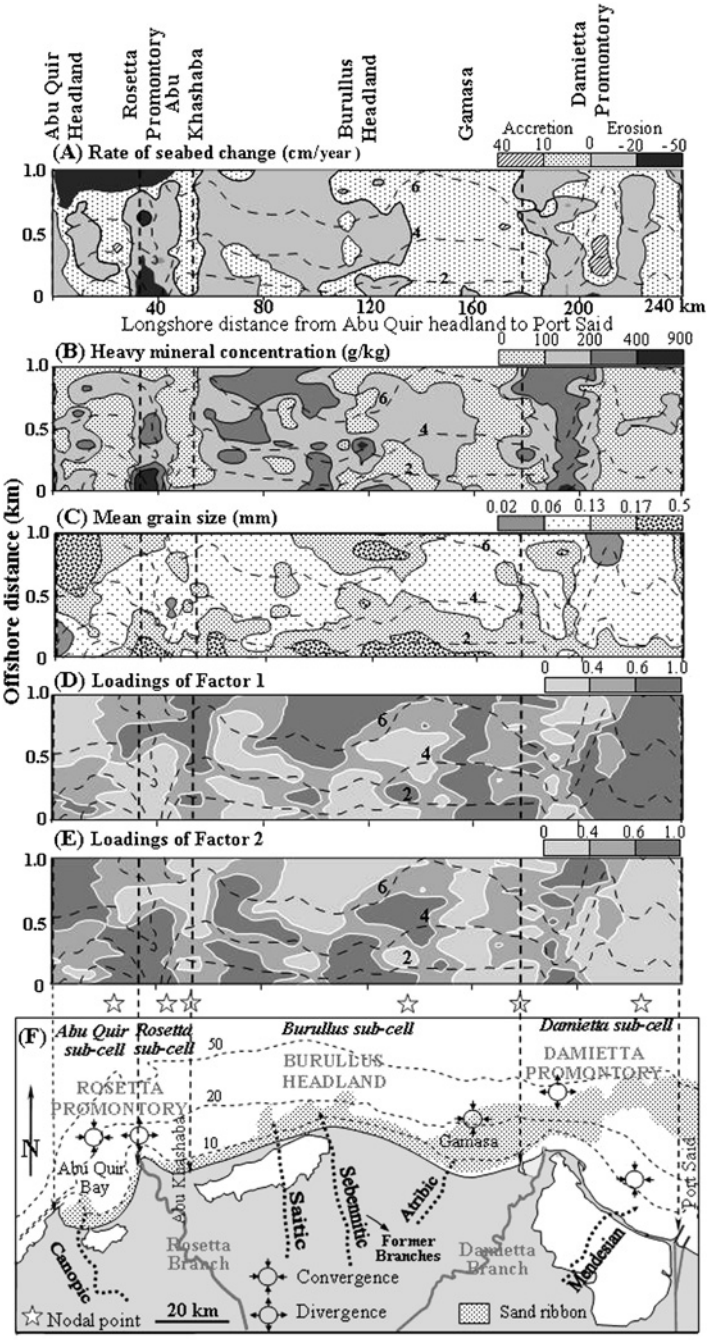
Abu Quir Headland
Rosetta Promontory
Abu Khashaba
Burullus Headland
Gamasa
Damietta Promontory
(A) Rate of seabed change (cm/year)
Accretion
Erosion
40 10 0 -20 -50
1.0
0.5
0
40 80 120 160 200 240 km
Longshore distance from Abu Quir headland to Port Said
(B) Heavy mineral concentration (g/kg)
0 100 200 400 900
(C) Mean grain size (mm)
0.02 0.06 0.13 0.17 0.5
(D) Loadings of Factor 1
0 0.4 0.6 1.0
(E) Loadings of Factor 2
Offshore distance (km)
(F)
Abu Quir sub-cell
Rosetta sub-cell
Burullus sub-cell
Damietta sub-cell
BURULLUS HEADLAND
DAMIETTA PROMONTORY
ROSETTA PROMONTORY
Abu Quir Bay
Abu Khashaba
Gamasa
Port Said
Saitic
Sebennitic
Former Branches
Atribic
Rosetta Branch
Damietta Branch
Mendesian
Canopic
Convergence
Divergence
Nodal point
20 km
Sand ribbon

processes. This disparity is attributed to intensive reworking process of both modern (fine-grained sand) and coarse-grained relict (palimpsest) sediments, leading to a mixed size distribution. Such mixed groups exist in the form of easterly-swept, shore-parallel blankets or ribbons that border the delta shoreline (El Bouseily and Frihy, 1984; Inman et al., 1992). These coarse-grained sediments are related to relict (palimpsest) sediment dispersed off the Nile Delta between the coast and the continental shelf break (Summerhayes et al., 1978; Stanley and Bernasconi, 1998). The relict sediments, originally fluvial, began to accumulate shortly after the maximum eustatic low-stand when the coastline had advanced northward to the outer edge of the continental shelf as early as latest Pleistocene (Stanley and Bernasconi, 1998). Other relatively younger relict sediments are related to the extinct seven Nile branches which flowed across the inner shelf during the Middle to Late Holocene.

In the nearshore zone of the delta area, Frihy et al. (1995) applied factor analysis to heavy mineral contents to determine the sorting of heavy minerals that develop during cross-shore and alongshore sediment transport (Fig. 8D, E). Factor analysis of the heavy mineral contents of samples, selected from the nearshore zone, shows that, comparable to the beach samples, two factors, representing mineral groups, result from sorting controlled by contrasting densities and sizes of the grains. One factor is dominated by augite, hornblende and epidote, whereas the second factor consists of opaques, garnet, zircon, rutile and monazite. Minerals of factor 1 are of lower densities and coarser sizes, and represent the grains that are selectively entrained by waves and currents in areas of seabed erosion and transported preferentially to zones of beach accretion where they are deposited. High-density and small-diameter minerals of factor 2 tend to become concentrated in areas of beach erosion, accounting for the formation of black-sand placers where erosion has been greatest. Again, the spatial distributions of these two factors (Fig. 8D, E) reflect grain-sorting patterns of heavy minerals which coincide with both rate of seabed changes (Fig. 8A) and with general trends of shoreline erosion versus accretion that exist along the length of the delta (Fig. 2). Spatial patterns of the two factors (Fig. 8D, E) show an alongshore rhythmic cycle between factors 1 and 2, with maximum loadings of factor 2 corresponding to three delta promontories (Rosetta, Burullus and Damietta) where shoreline erosion has been greater, and factor 1 having maximum weightings within the embayments where accretion has prevailed between promontories. Cross-shore grain-sorting is further revealed in factor

Fig. 8. Spatial distributions in the nearshore zone of the Nile Delta. (A–C after Frihy and Dewidar, 2003; D, E modified from Frihy et al., 1995) (contours in metres). (A) Annual rates of seabed changes. (B) Heavy mineral concentration. (C) Mean grain size. (D) Factor 1 loadings, the lower density heavy minerals, showing maximum weightings in areas of beach accretion. (E) Factor 2 loadings, depicting the higher density minerals accumulated in areas of delta erosion. (F) Nile Delta continental shelf, showing sediment transport divergence (source) and convergence (sink) trends, inferred from grain sorting patterns and rate of seabed changes. Positions of major extinct branches of the Nile that contributed to the sediment regime in the area are traced from Toussoun (1922). Spatial distribution of the offshore sand ribbon "blanket", relict and recent sand, migrating eastwards by littoral and coastal currents are modified after Coleman et al. (1981) and Inman et al. (1992). Vertical dashed lines indicate the limits of approximate positions between littoral sub-cells.

weightings along individual profiles. These show strong trends of offshore decrease in factor 2 in areas where long-term erosion has prevailed, with proportions of factors reflecting the bathymetry configuration, i.e. by distinguishing between bars (accretion) and troughs (erosion).

The correspondence among patterns of seabed depth variations, heavy mineral concentration (shown by mineral factor loadings) and, to some extent, texture of seabed sediments, serves to refine boundaries of littoral sub-cells of the Nile. These indicate sediment paths, sources, sinks, nodal points and zones of convergence and/or divergence of sediment transport (Fig. 8F). The general congruence of the rate of seabed change patterns and heavy mineral concentration (factor weightings) outline the operating sub-cells identified by Frihy et al. (1991). In their study they took into account blockage of sediment transport by jetties, deflection of inlets and variations in mineralogy and beach-sand grain sizes. Correspondence of these processes is not strongly correlated, as might be expected in this deltaic system where the sediment that has been recycled between recent and relict seabed settings is transported in long-shore and cross-shore directions. Displacement, intermixing and reworking of relict and modern sediments generate a shore-parallel blanket ''ribbon'', trending easterly along the delta coast by a high-speed circulation jet that could contaminate the existing recent sediment layer. This would produce sediments of low heavy mineral concentration resembling accreted near-shore areas (Fig. 8F). Nevertheless, examples given in this contribution show that the relationship between seabed-level changes, heavy mineral concentrations and, to some extent, sediment mean grain size in the littoral zone can be applied to other deltaic settings to facilitate interpretation of sediment transport pathways. This approach can provide particularly good resolution in areas where relict sediments are not abundant.

In a study of heavy mineral compositions of shelf sediments off the Burullus-Baltim coast to delineate relict beach sediments of the former Sebennitic branch of the Nile (Fig. 9A), Frihy and Lotfy (1994b) obtained similar mineral assemblage ''factors'' to those discussed above. The distinct mineral pattern, corresponding to sorting patterns found on the modern Rosetta promontory by Frihy and Komar (1991), provides partial confirmation of the hypothesis that the shelf sediments reflect the former geometry of the Nile promontory. It is postulated that sorting patterns of heavy minerals formed along the shoreline record the configuration of the Sebennitic promontory during its erosion. Such patterns in the shelf sediments provide evidence for the past extent of this promontory and position of the mouth of the Sebennitic branch. This mouth, which existed from ~6000 to 2000 B.P., is one of the oldest of the seven branches, and was located on what is now the inner to middle shelf off the north-central Nile Delta (Arbouille and Stanley, 1991). Mineral factors 1 and 2 in Nile shelf sediments off the central part of the delta indicate, respectively, mineral grains that are most easily entrained and transported versus those that tend to remain as a lag. Relative loadings of the two factors in the examined samples pinpointed three localised areas, deduced from long-term dispersal trends of heavy minerals (Fig. 9B, C). These small areas have lower loadings (high dilution) of factor 1 (augite and hornblende) and higher loadings (high concentration) of factor 2 (opaques, garnet, zircon, monazite, rutile and epidote). Such an inverse spatial distribution corresponds closely to selective sorting patterns near the modern river mouths: one mineral suite tends to concentrate near the mouth (densest minerals), while the other is transported

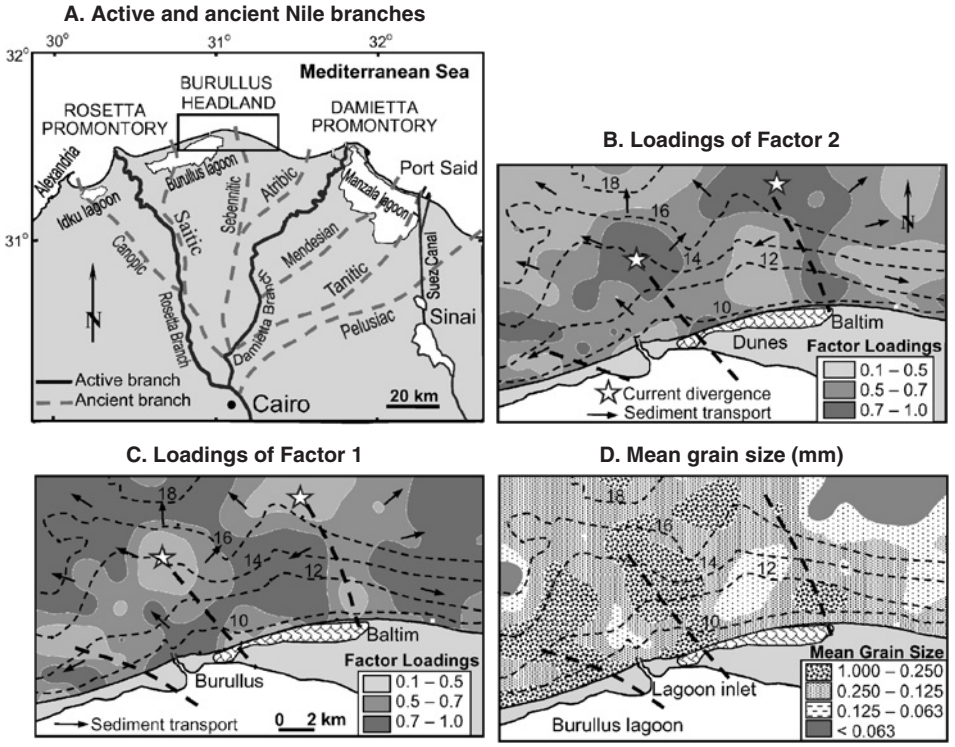

Fig. 9. Nile distributaries and spatial distribution of grain parameters. B–D are modified from Frihy and Lotfy (1994b) (depth in metres). (A) Positions of former Nile distributaries and present-day Rosetta and Damietta branches across the Nile Delta (modified after Toussoun, 1922). (B) and (C) Spatial distribution of the two factor loadings based on heavy mineral data of bottom and beach samples. Divergence trends are shown by arrows oriented in the direction of increasing or decreasing values of factor loadings. Dashed dendritic lines depict tentative paths of the former Sebennitic branches. (D) Spatial distribution of mean grain size. Sand-size sediment pattern, coinciding with higher and lower factor loadings established in B and C, reveals the submerged relict Sebennitic channel.

alongshore away from the mouth. As expected, high loadings of factor 2 exist near identified river mouths, indicating areas of maximum erosion. Sediment transport divergence is thus recorded with sediment that moves away from eroded point sources, interpreted as river mouths, towards depositional sites. These patterns characterise the ancient hydrodynamic regime in this region. It is worthy of note that in Fig. 9D the pattern of localised sand-size sediments closely coincides with the position and trend of areas that have the lowest loading of factor 1 and the highest loading of factor 2 (Fig. 9B, C). Additional evidence for the Sebennitic branch promontory was recently reported by Farid (2005), deduced from the higher concentration of heavy minerals in the coastal dune sand belt between Burullus and Baltim (10 km long by 2 km average width; see Fig. 9B for location). This dune belt borders the backshore of the continental shelf of the ancient Sebennitic promontory, now termed the ''Burullus headland''. As mentioned earlier, heavy mineral patterns related to the Sebennitic beach

sediments have been delineated on that shelf by Frihy and Lotfy (1994b). Farid (2005) found that heavy mineral content increased progressively from top of the dune downward to the base in the core sections, having a maximum of 8% by weight of sample. The enrichment of heavy minerals in the middle and lower parts of this dune belt most likely originated through aeolian processes that prevailed over the subaerially exposed beach and coastal flat of the Sebennitic promontory during the last Holocene low sea-level stand. Further evidence to support this conclusion is provided by numerous dune core samples (up to 30 m in length) drilled during exploration for economic mineral placers in this region.

It has been established that the dispersal of sediment including heavy minerals is primarily directed eastward from the Nile Delta region towards in what is termed the "Nile littoral cell" including the Sinai and Gaza shelves, and then to the north along the Israel margin (Goldsmith and Golik, 1980; Inman and Jenkins, 1984). Eroded sediments within this cell are moved primarily by wave-induced longshore currents and the counter-clockwise geostrophic East Mediterranean current (Fig. 2). As a result, beaches, dunes and continental shelf sediments of Israel are derived mainly from the Nile (Emery and Neev, 1960; Pomerancblum, 1966; Azmon and Golik, 1995; Levin and Ben-Dor, 2004). Stanley (1989) has compiled the data on heavy mineral contents of the shelf and coastal sands of Egypt and Israel in a regional study of transport paths, deduced from ratios of the pyroxenes, amphiboles and epidote. Two indices, termed "*i*Pyr" and "*i*Amph", proved useful in that they emphasise the variability of all three dominant transparent heavy mineral groups (pyroxenes, amphiboles and epidotes) that occur throughout this area. The two indices were computed as follows:

$$i\text{Pyrindex} = (\text{frequency of pyroxenes}/\text{frequency of pyroxenes} + \text{epidotes}) \times 100$$

$$i\text{Amphindex} = (\text{frequency of amphiboles}/\text{frequency of amphiboles} + \text{pyroxenes} \times 100$$

The results of Stanley (1989) were based on numerous surface samples and cores collected from coastal areas, rivers, and from the continental shelves off Egypt, Sinai, Gaza and Israel. Among these indices the *i*Pyr is perhaps the most useful marker of the Nile source and is thus a valuable criterion to identify transport trends away from the delta. Accordingly, the mineralogical difference between coast and shelf samples is depicted graphically by plotting regional variations of the *i*Pyr index (Fig. 10, top panel). Marked divergence of coastal (solid line) and shelf (dashed line) *i*Pyr values is recorded east of Bardawil Lagoon (C). On the other hand, high *i*Pyr index values (67–82) occur on shelves, from Nile Delta sources (B) to as far as the northern Israeli margin (E), while *i*Pyr values decrease (38–45) in the same direction (to D off Israel) along the major coastal transport path. The decrease of the index values on the Sinai coast east of Bardawil and on the Israeli coast is most likely caused by influx of locally supplied heavy mineral assemblages from wadis (Wadi El Arish) and rivers (Quishon River).

Changes in the paths of net sediment transport (i.e., particularly fluctuations of longshore currents and of geostrophic current flow) would best explain the progressively increasing divergence between the proportions of transparent heavy minerals on the coasts and shelves off eastern Sinai, Gaza and Israel. Longshore currents are

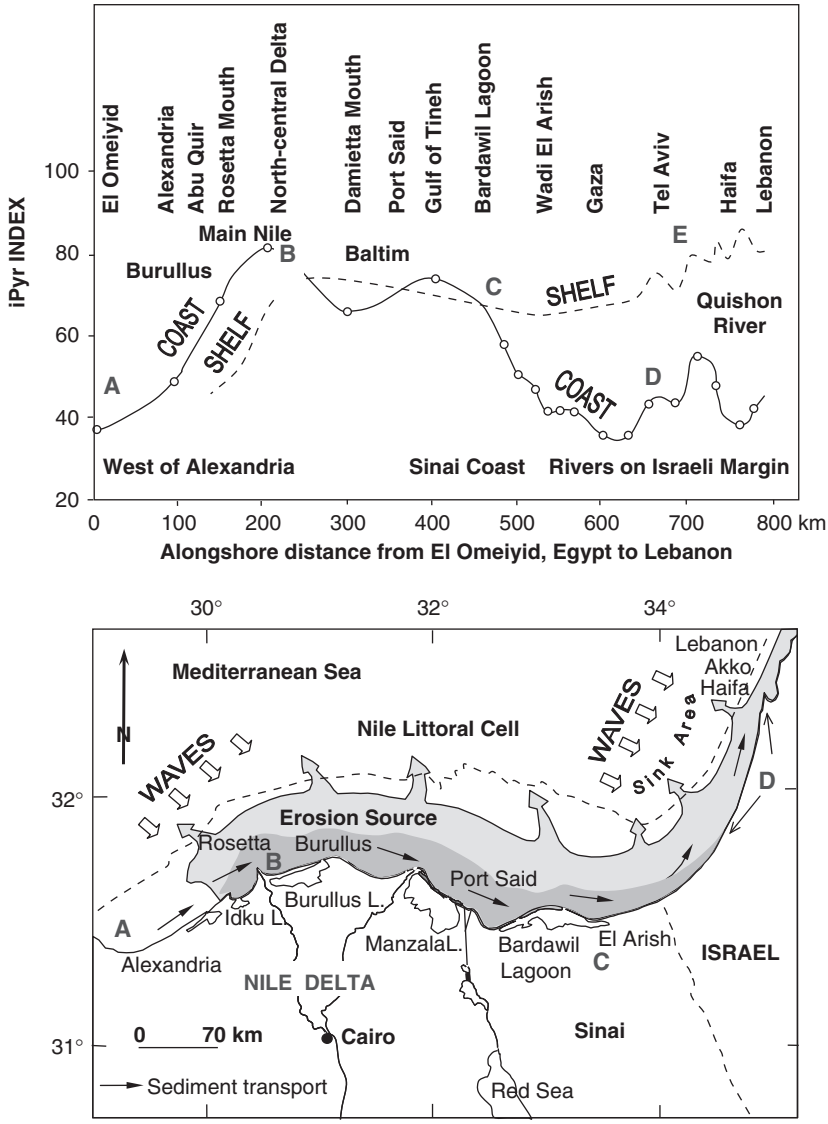

Fig. 10. Trend of *i*Pyr index between the Nile Delta and the Lebanese margin (top) and dominant sediment depositional pattern within the Nile littoral cell (bottom). Top: Diagram showing regional variations of the *i*Pyr index from Nile Delta sources (B) to the northern Israeli and Lebanese margin (E). The distribution pattern indicates that heavy mineral suites on coasts east of the Bardawil lagoon differ from Nile suites progressively in a direction away from the Nile Delta. Bottom: Map of the Nile littoral cell showing the dominant southeast Mediterranean depositional trend. The main supply of sediment from Nile sources (B) is introduced east of the carbonate margin (A) that lies west of Alexandria. The proportions of heavy minerals in sediment transported largely by wave-driven longshore transport to eastern Sinai, Gaza and Egyptian coasts (D) differ from those west of Bardawil (C). Heavy minerals on shelves in relict and reworked relict deposits may be displaced by currents driven by storm-wave activity in conjunction with the flow of the East Mediterranean Current (modified from Stanley, 1989).

believed to carry heavy minerals along the coast from the delta at least as far north as Haifa Bay, interpreted as a major "sediment sink" (Goldsmith and Golik, 1980; Stanley, 1989). Both modern and relict (palimpsest) sediments on the shelf are winnowed and displaced along broad zones, whereas some sediment near the shelf edge is probably transported onto the slope (Fig. 10, bottom panel) and deeper parts of the Levantine Basin (Stanley, 1988).

6. SUMMARY AND CONCLUSIONS

Examples of sediment sorting processes and dispersal patterns along the Nile Delta coast of Egypt are reviewed. To some extent, similar processes operate in the adjacent downdrift areas, east of the delta on the Sinai and Gaza shelves to the Israel margin, all within the Nile Littoral Cell. Grain sorting patterns in beach and shelf sediments are strongly influenced by the dynamic action and energy of waves and currents. Heavy minerals are used as signatures of grain sorting patterns in both longshore and cross-shore transport directions on both local and regional scales. A correct evaluation of mineral-sorting processes results in a fuller understanding of the hydrodynamics of coastal and shelf areas that, in turn, leads to better defined littoral cells. Such information, together with other field measurements, is important in planning and designing engineering structures, undertaking beach nourishment projects and in the exploration, discovery and evaluation of placer deposits. Moreover, improved understanding of mineral sorting helps to identify sedimentary provinces and the extent of incorporation of reworked relict (palimpsest) sediments in beach and shelf areas, originating mostly from sediment reworking during the Holocene transgression.

Nile Delta promontories, and major engineering structures between them, create a series of nearshore littoral sub-cells. The principal sources of sediment for each cell are the promontories that, through erosion, supply large quantities of sand to sink areas. These sinks occupy bays, embayments and saddles that generally lie to the east. The alongshore transport of sand by waves and littoral currents produces heavy mineral concentrations adjacent to delta promontories (divergence source areas), with a dilution tendency towards accreted coasts within convergence sink areas near a nodal point where erosion is replaced by accretion.

Heavy mineral analysis and factor analysis of heavy mineral data of beach and continental shelf sands of the Nile Delta and north Sinai were carried out in a series of studies. All have revealed the existence of two major heavy mineral groups, characterised by contrasting densities: one containing lower density minerals (augite, hornblende and epidote) and the other high-density minerals (opaques, garnet, zircon and monazite), both being generated by selective sorting processes. As a result of hydrodynamic sorting, the heavier heavy minerals concentrate in areas of erosion, but become progressively diluted with lighter heavy minerals with distance from the points of erosion. Lighter heavy minerals accumulate in areas of sand accretion. The resulting heavy mineral trends generally follow the hydrodynamic processes of shoreline and seabed erosion, or accretion, at the length of the delta that extends along the coast to the north of Sinai. Offshore, there is a general decrease in the higher density group relative to the lower density minerals, implying that the accumulation of black-sand concentrates has taken place mainly within the swash zone.

Sorting processes give rise to linear statistical relationships between rates of beach and seabed changes (erosion or accretion), where the extent of concentrations of heavy minerals is reflected by the weight percentages of total heavy mineral fractions. As expected, the greater the rate of erosion, the more concentrated are the higher density heavy minerals (factor group 2), while the lower density heavy minerals (factor group 1) accumulate in areas with increased rates of accretion. This simple relationship within heavy mineral suites allowed Frihy (1994) to discriminate between sands of eroded versus accreted beaches. Similarly, Anwar et al. (1979) determined that in the central delta, sectors of accreted sands are coarser-grained and less well sorted than in areas of sand erosion caused by grain sorting. On the other hand, Frihy et al. (1998) found a wide range of overlap of heavy minerals from different fluvio-marine environments along the Nile Delta, and attributed this to the interplay of diverse transport mechanisms that control sediment sorting. These include fluvial processes, forces of waves and currents in the marine environment and aeolian transport.

Distribution patterns of heavy minerals provided additional evidence for the delineation of the large ancient Sebennitic channel that formed the remnant Sebennitic promontory, now the Burullus bulge in the central delta. Channel flow occurred across the subaerially exposed continental shelf during the last Holocene low sea-level stand (Frihy and Lotfy, 1994b), and also at the Canopic branch in Abu Quir Bay (El Bouseily and Frihy, 1984; Frihy and Komar, 1991; Stanley, et al., 2004). The regional distribution of transparent heavy mineral suites also assisted in the tracing of the boundaries of the Nile Littoral Cell (Goldsmith and Golik, 1980; Inman and Jenkins, 1984; Stanley, 1989).

Heavy minerals in the Nile Delta and adjacent regions find a wide range of practical applications that can be applied in many other deltaic settings. However, caution is necessary in areas where coarse-grained relict sediments (palimpsest) are present because they can interfere with the grain sorting patterns of modern sediments. The use of heavy minerals in the evaluation of hydrodynamic conditions can yield especially valuable information in areas where relict sediments are absent or are of minor importance.

ACKNOWLEDGMENTS

Most of the studies cited in the review were undertaken by the Coastal Research Institute, National Water Research Centre, as part of the programme initiated to monitor beach changes along the Mediterranean coast of Egypt. I express my deep appreciation to Professors Paul Komar, Oregon State University, Daniel Stanley, Smithsonian Institutions, Washington D.C. and Dr. Deborah Lawrence, University of Reading, UK, for their constructive reviewing of the first version of the manuscript.

REFERENCES

Anwar, Y.M., El Askary, M.A., Lotfy, M.F., 1981. Mineralogy of sediments of Damietta-Port Said district. Journal of Jeddah Marine Research, Saudi Arabia 1, 47–63.

Anwar, Y.M., Gindy, A.R., El Askary, M.A., El Fishawi, N.M., 1979. Beach accretion and erosion, Burullus-Gamasa coast, Egypt. Marine Geology, Letter Section 30, M1–M7.

Arbouille, D., Stanley, D.J., 1991. Late Quaternary evolution of the Burullus lagoon region, north-central Nile Delta, Egypt. Marine Geology 99, 45–66.

Azmon, E., Golik, A., 1995. Provenance of heavy minerals on the Eastern Mediterranean Shelf: from the Nile or from the north? Marine Geology, Letter Section 122, 277–279.

Blodget, H.W., Taylor, P.T., Roark, J.H., 1991. Shoreline changes along the Rosetta-Nile Promontory: monitoring with satellite observations. Marine Geology 99, 67–77.

Coleman, J.M., Robert, H.H., Murray, S.P., Salama, M., 1981. Morphology and dynamic sedimentology of the eastern Nile Delta shelf. Journal of Geology 42, 301–312.

El Askary, M.A., Frihy, O.E., 1987. Mineralogy of the subsurface sediments at Rosetta and Damietta promontories, Egypt. Bulletin of the Institute of Oceanography and Fishery, Egypt 2, 111–120.

El Asmar, H., White, K., 2002. Changes in coastal sediment transport processes due to construction of New Damietta Harbour, Nile Delta, Egypt. Journal of Coastal Engineering 46, 127–138.

El Bouseily, A.M., Frihy, O.E., 1984. Textural and mineralogical evidence denoting the position of the mouth of the old Canopic Nile branch on the Mediterranean coast, Egypt. Journal of African Earth Science 2, 103–107.

El Fishawi, N.M., Fanos, A.M., 1989. Prediction of sea-level rise by 2100, Nile Delta coast. INQUA Commission on Quaternary Shorelines, Newsletter 11, 43–47.

El Fishawi, N.M., Molnár, B., 1985. Mineralogical relationships between the Nile Delta coastal sands. Acta Mineralogica Petrographica, Szeged 27, 89–100.

Emery, K.O., Neev, D., 1960. Mediterranean beaches of Israel. Israel Geological Survey Bulletin 26, 25–41.

Fanos, A.M., Frihy, O.E., Khafagy, A.A., Komar, P.D., 1991. Processes of shoreline change along the Nile Delta coast of Egypt. Coastal Sediments '91 Conference, Seattle, Washington, vol. 2, pp. 1547–1557.

Farid, A.H., 2005. Evaluation and mineral processing of some economic minerals in Burullus-Baltim sand dunes, Nile Delta, Egypt. Ph.D. thesis, Mansoura University, Egypt, 205pp.

Frihy, O.E., 1994. Discrimination of accreted and eroded coasts using heavy mineral composition of the Nile Delta beach sands, Egypt. Sedimentology 41, 905–912.

Frihy, O.E., Debes, E., El Sayed, W., 2003. Processes reshaping the Nile Delta promontories of Egypt: pre- and post-protection. Journal of Geomorphology 53, 263–279.

Frihy, O.E., Dewidar, K.M., 1993. Influence of shoreline erosion and accretion on texture and heavy mineral compositions of beach sands of the Burullus coast, north-central Nile Delta, Egypt. Marine Geology 114, 91–104.

Frihy, O.E., Dewidar, K.M., 2003. Patterns of erosion/sedimentation, heavy mineral concentration and grain size to interpret boundaries of littoral sub-cells of the Nile Delta. Marine Geology 199, 27–43.

Frihy, O.E., El Askary, M.A., Deghidy, E.M., Moufaddal, W.M., 1998. Distinguishing fluvio-marine environments in the Nile Delta using heavy minerals. Journal of Coastal Research 14, 970–980.

Frihy, O.E., Fanos, M.A., Khafagy, A.A., Komar, P.D., 1991. Nearshore sediment transport patterns along the Nile Delta, Egypt. Journal of Coastal Engineering 15, 409–429.

Frihy, O.E., Khafagy, A.A., 1991. Climatic and human induced changes in relation to shoreline migration trends in the Nile Delta promontories, Egypt. Catena 18, 197–211.

Frihy, O.E., Komar, P.D., 1991. Patterns of beach-sand sorting and shoreline erosion on the Nile Delta. Journal of Sedimentary Petrology 61, 544–550.

Frihy, O.E., Komar, P.D., 1993. Long-term shoreline changes and the concentration of heavy minerals in beach sands of the Nile Delta, Egypt. Marine Geology 115, 253–261.
Frihy, O.E., Lawrence, D., 2004. Evolution of the modern Nile Delta promontories: development of accretional features during shoreline retreat. Environmental Geology 46, 914–931.
Frihy, O.E., Lotfy, M.F., 1994a. Mineralogy and texture of beach sands in relation to erosion and accretion along the Rosetta Promontory of the Nile Delta, Egypt. Journal of Coastal Research 10, 588–599.
Frihy, O.E., Lotfy, M.F., 1994b. Mineralogic evidence for the Sebennitic promontory on the continental shelf off the central Nile Delta. Marine Geology 117, 187–194.
Frihy, O.E., Lotfy, M.F., Komar, P.D., 1995. Spatial variations in heavy minerals and patterns of sediment sorting along the Nile Delta, Egypt. Sedimentary Geology 97, 33–41.
Frihy, O.E., Lotfy, M.F., 1997. Shoreline changes and beach-sand sorting along the northern Sinai coast of Egypt. Geo-Marine Letters 17, 140–146.
Frihy, O.E., Moussa, A.A., Stanley, D.J., 1994. Abu Quir Bay, a sediment sink off the northern Nile Delta, Egypt. Marine Geology 121, 199–211.
Goldsmith, V., Golik, A., 1980. Sediment transport model of the southeastern Mediterranean coast. Marine Geology 37, 146–175.
Hammad, H.Y., Mobark, O., Khafagy, A.A., Sidky, S., 1979. A short note on the sediment regime of the River Nile. Bulletin of the Institute of Oceanography and Fishery (Egypt) 7, 314–322.
Hassan, F.A., 1976. Heavy minerals and the evolution of the modern Nile. Journal of Quaternary Research 6, 425–444.
Hilmy, M.E., 1951. Beach sands of the Mediterranean coast of Egypt. Journal of Sedimentary Petrology 21, 109–120.
Inman, D.L., Brush, B., 1973. The coastal challenge, fragile ribbons, which border our land, require more understanding, new technology, and resolute planning. Science 181, 20–31.
Inman, D.L., Elwany, H.S., Khafagy, A.A., Golik, A., 1992. Nile Delta profiles and migration sand blankets. Proceeding at the 23rd International Conference on Coastal Engineering (American Society of Civil Engineering), vol. 2, pp. 3273–3284.
Inman, D.L., Jenkins, S.A., 1984. The Nile littoral cell and man's impact on the coastal zone of the southeastern Mediterranean. Scripps Institution of Oceanography, Reference Series 84–31, University of California, La Jolla, 43pp.
Komar, P.D., 2007. The entrainment, transport and sorting of heavy minerals by waves and currents. In: Mange, M.A., Wright, D.T. (Eds.), Heavy Minerals in Use. Developments in Sedimentology (this volume).
Komar, P.D., Li, M.Z., 1991. Beach placers at the mouth of the Columbia River, Oregon and Washington. Marine Mining 10, 171–187.
Komar, P.D., Wang, C., 1984. Processes of selective grain transport and the formation of placers on beaches. Journal of Geology 92, 637–655.
Levin, L., Ben-Dor, E., 2004. Monitoring sand dune stabilization along the coastal dunes of Ashdod-Nizanim, Israel, 1945–1999. Journal of Arid Environments 58, 335–355.
Lotfy, M.F., 1997. Distribution of heavy mineral grains by granulometric fractions in some modern Nile Delta coastal sands, Egypt. INQUA Commission on Quaternary Shorelines, Newsletter 19, 33–41.
Li, Z., Komar, P.D., 1992. Longshore grain sorting and beach placer formation adjacent to the Columbia River. Journal of Sedimentary Petrology 62, 429–441.
Nir, Y., 1982. Offshore artificial structures and their influence on the Israel and Sinai Mediterranean beaches. 18th Coastal Engineering Conference, Cape Town, Republic of South Africa, vol. 3, pp. 1837–1856.
Orlova, G., Zenkovitch, V., 1974. Erosion of the shores of the Nile Delta. Geoforum 18, 68–72.

Pirkle, F.L., Pirkle, W.A., Pirkle, E.C., 2007. Heavy-mineral sands of the Atlantic and Gulf coastal plains, USA. In: Mange, M.A., Wright, D.T. (Eds.), Heavy Minerals in Use. Developments in Sedimentology (this volume).

Pomerancblum, M., 1966. The distribution of heavy minerals and their hydraulic equivalents in sediments of the Mediterranean continental shelf off Israel. Journal of Sedimentary Petrology 36, 162–174.

Rao, C.B., 1957. Beach erosion and concentration of heavy mineral sands. Journal of Sedimentary Petrology 27, 143–147.

Said, R., 1981. The geological evolution of the River Nile. Springer, New York, 151pp.

Shukri, N.M., 1950. The mineralogy of some Nile sediments. Quaternary Journal of the Geological Society of London 105, 511–534.

Stanley, D.J., 1988. Low sediment accumulation rates and erosion on the middle and outer Nile Delta shelf off Egypt. Marine Geology 84, 111–117.

Stanley, D.J., 1989. Sediment transport on the coast and shelf between the Nile Delta and Israeli margin as determined by heavy minerals. Journal of Coastal Research 5, 813–828.

Stanley, D.J., 1990. Recent subsidence and northeast tilting of the Nile Delta, Egypt. Marine Geology 94, 147–154.

Stanley, D.J., Bernasconi, M.P., 1998. Relict and palimpsest depositional patterns on the Nile Shelf recorded by molluscan faunas. Palaios 13, 79–86.

Stanley, J.D., Goddio, F., Jorstad, T.F., Schnepp, G., 2004. Submergence of ancient Greek cities off Egypt's Nile Delta: a cautionary tale. GSA Today 14 (1), 4–10.

Stanley, D.J., Sheng, H., Kholief, M.M., 1979. Sand on the southern Mediterranean Ridge: proximal basement and distal African Nile provenance. Nature 279, 594–598.

Stanley, D.J., Warne, A.G., 1993. Nile Delta: recent geological evolution and human impact. Science 260, 628–634.

Summerhayes, C.P., Sestini, G., Misdorp, R., Marks, N., 1978. Nile Delta: nature and evolution of continental shelf sediments. Marine Geology 27, 43–65.

Toussoun, O., 1922. Mémoires sur les anciennes branches du Nil, Epoque Ancienne. Mémoire de I'Institut d' Egypte 4, 212pp.

UNESCO/UNDP, 1978. Coastal protection studies of the Nile Delta. Final Technical Report, Paris 1, 155pp.

Chapter 3

THE SOURCES AND HYDRAULIC SORTING OF HEAVY MINERALS ON THE NORTHERN PORTUGUESE CONTINENTAL MARGIN

JOÃO CASCALHO[a] AND CATARINA FRADIQUE[b]

[a]*Centro de Geologia, Museu Nacional de História Natural da Universidade de Lisboa, Rua da Escola Politécnica, 58, 1250-102 Lisboa, Portugal*
[b]*Instituto Hidrográfico, Rua das Trinas, 49, 1249-093 Lisboa, Portugal*

ABSTRACT

Knowledge of the transparent heavy minerals present in the sand fraction of sediments on the northern Portuguese continental margin rests on the study of 504 samples, obtained from the shelf and upper slope (358), and from the major rivers (146). Results show the main association comprising biotite, andalusite, tourmaline, amphibole, garnet, staurolite, zircon and apatite. A second, subordinate, suite includes orthopyroxene, clinopyroxene and olivine and is present only in the outer shelf and upper slope south of Porto canyon. These two distinctive assemblages indicate derivation from different primary sources: the main heavy mineral suite is sourced from metamorphic and igneous rocks, widespread in the drainage basins of all northern Portuguese rivers, whereas the minor one is of different origin and points to a basic igneous source, located probably elsewhere in the outer shelf or upper slope, south of Porto canyon. The distribution patterns of the mineral species in the major association indicate that these terrigenous assemblages were delivered to the shelf by rivers in a highly selective manner. Only biotite and other platy grains are able to reach the middle shelf that is constrained by the analysis of the hydraulic behaviour of the different grains. Mobile grains, such as biotite and the most platy amphiboles, are excellent sedimentary tracers of the present shelf transport dynamics. Their distribution patterns suggest the influence of a downwelling oceanographic regime, which predominantly affects the inner and middle shelves. Corresponding distribution patterns between the most mobile heavy mineral grains and fine-grained sediments (muddy patches) may indicate the similarity of their hydraulic behaviour. In contrast, the less mobile grains, such as coarse garnet, andalusite, tourmaline, staurolite and zircon, reach only the inner shelf. Polycyclic, rounded grains found in the middle shelf in coarse-grained deposits represent relict and palimpsest sediments and contrast with the angular forms characteristic of the modern river and inner-shelf sediments.

Keywords: heavy minerals; sources; sorting; Portugal; continental margin

Developments in Sedimentology, Vol. 58, 75–110

ISSN: 0070-4571/doi:10.1016/S0070-4571(07)58003-9

1. INTRODUCTION

The first reference to the nature of sediments on the Portuguese continental shelf can be found in Murray and Renard (1891). However, it was only in the 1980s that the sedimentary dynamics of this shelf were addressed (Dias et al., 1980/1981; Dias and Nittrouer, 1984; Dias, 1987). As research continued through numerous programmes and projects on behalf of national and international institutions, several papers were published. Some of these focused on issues related to the sedimentary dynamics of the western Iberian continental shelf, namely sediment distribution patterns (Magalhães and Dias, 1992; Magalhães, 1999; Dias et al., 2002a), sedimentary processes (Dias et al., 2002b), sediment accumulation rates (Carvalho and Ramos, 1990), the stratigraphy and post-glacial evolution of the shelf (Rodrigues et al., 1991; Dias et al., 2000; Rodrigues, 2003), the Douro mud patch evolution (Drago et al., 1994, 1998), the use of clay minerals as an indicator of sedimentary dynamics (Oliveira et al., 2002a), nepheloid layer dynamics (Oliveira et al., 2002b) and the fine-grained sediment budget (Jouanneau et al., 2002).

Heavy minerals are particularly valuable in sedimentary studies of the shelf and littoral zones. The first study on the occurrence of heavy minerals in the sand fraction of the northern Portuguese shelf was carried out by Cascalho and Carvalho (1989, 1990). The provenance of heavy minerals in the northern and south-western shelves was discussed later by Cascalho and Carvalho (1993), Cascalho et al. (1994), Cascalho (1998) and Pombo et al. (2006). Most recent publications include studies dealing with heavy mineral occurrences in the sediment fill of the Douro estuary (Fradique and Cascalho, 2004; Fradique et al., 2006).

This paper demonstrates the use of heavy minerals in constraining the sedimentary dynamics of the Portuguese northern continental margin between the Minho River and Mondego Cape (Fig. 1). It is based on an analysis of 504 samples collected from the shelf, upper slope and main NW Portuguese rivers. Special attention is given to the hydraulic behaviour of the different heavy minerals, in view of the existing knowledge on the oceanographic regimes of the west Iberian margin.

2. REGIONAL SETTING

2.1. Oceanographic Processes

Tides along the Portuguese coast have periods of about 12 h 30 min. This mesotidal tidal regime has a maximum average high tide of 3.45 m and a minimum average low tide of 0.58 m at the Leixões seaport located near Porto town (Instituto Hidrográfico, 2004). According to Carvalho and Barceló (1966), the most frequent wave regime is characterised by a period (T_0) of 9–11 s and a significant height (H_s) of 1–2 m. The most frequent wave direction is between W10°N and W20°N (during ~100 days per year), with observed waves coming from W and S during a 75-day period per year. Pires and Pessanha (1986) note that the most common wave regime has $T_0 = 8$ s and $H_s = 2$ m and a direction of W20°N.

Between July 1996 and July 1999 the monthly statistics of wave parameters obtained by Vitorino et al. (2002) show a mean T_0 from 6 to 8.5 s and H_s between

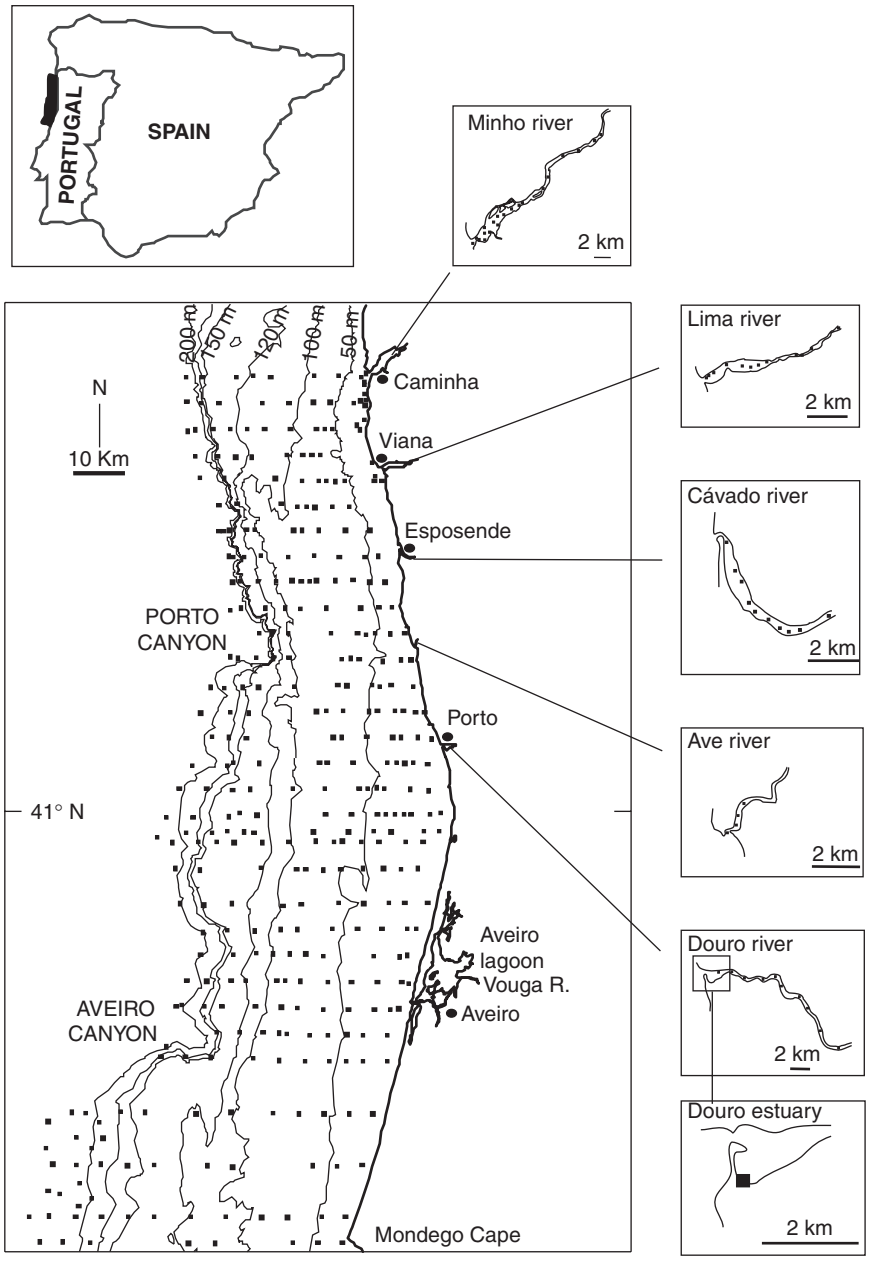

Fig. 1. Map showing sample locations.

1.4 m and 3.5 m. The most frequent high-energy wave conditions observed during winter and transitional periods (November to January) are characterised by NW swells with mean H_s above 3 m and T_0 above 8 s. This winter wave regime is generated by eastward-moving atmospheric low-pressure systems and their associated frontal systems that cross the north Atlantic. However, it should be noted that

during winter there are few occasions with swells from the SW, generated by low-pressure systems centred at SW of the Iberian Peninsula, or by the approach of a frontal system, associated with a low-pressure cell centred in the Atlantic.

According to Vitorino et al. (2002), the storms are characterised by $H_s > 5$ m and $T_0 = 10$ sec, resulting from strong NW or SW swells affecting the western margin of Iberia during one or two days or in some cases during one or two weeks. In extreme situations, the H_s can be up to 7.5 m or 8.7 m with corresponding T_0 equal to 16.5 or 20 sec.

The western continental margin of Portugal is characterised by two fundamental wind regimes generated by the relative position of the principal pressure cell systems over the North Atlantic. During the autumn and winter months the Azores high-pressure cell occupies a relatively southern position. In consequence, the Iceland low cell is reinforced and in turn the west Portuguese margin is very often affected by eastward-moving low-pressure cells and associated fronts. This situation causes the development of generally persistent winds with a southerly component (downwelling favourable) during December and January (Vitorino et al., 2002). Also, during these months (especially in December and February) the wind speed can be very strong, reaching in 3–5% of observation velocities above 50 km/h (Carvalho et al., 1991). During spring and summer the reinforcement and northward migration of the Azores High and the simultaneous development of a thermal low over the central Iberian Peninsula create a northerly wind regime (upwelling favourable), which can be especially constant during the summer months (Ribeiro et al., 1997).

2.2. *Geomorphology and Geology*

The northern Portuguese shelf (between the Minho river mouth and Mondego cape) has an average width of 44 km with a minimum of 35 km between Minho and Esposende and a maximum of 60 km at Mondego Cape parallel. The shelf break occurs at about 150 m depth. Two important canyons (Porto and Aveiro canyons) indent the shelf break at different latitudes (Fig. 2).

Palaeozoic metamorphic and igneous plutonic rocks emerging from the unconsolidated sedimentary cover are present in the northernmost inner shelf. The Late Cretaceous to Pleistocene sedimentary cover consists of limestones and sandstones. This succession has a general monoclinal structure, deepening to the west and fills the faulted basement structures (horsts and grabens). In the outer shelf areas, there are several outcrops composed mainly of these sedimentary rocks, for example the Beiral de Viana (located off Lima river mouth), Pontal da Cartola and Pontal da Galega (located south of Porto canyon) and Morraceiros (south of Aveiro canyon) (Rodrigues and Drago, 1990; Vanney and Mougenot, 1991; Rodrigues, 2003; Fig. 2). In the NW Iberian rivers' drainage basins, Precambrian and Palaeozoic, igneous (mainly granites) and metamorphic rocks (mainly schists, gneisses and greywackes) are found, covered by Mesozoic and Cenozoic sedimentary strata of the Portuguese Occidental sedimentary basin and the Douro basin (Fig. 3).

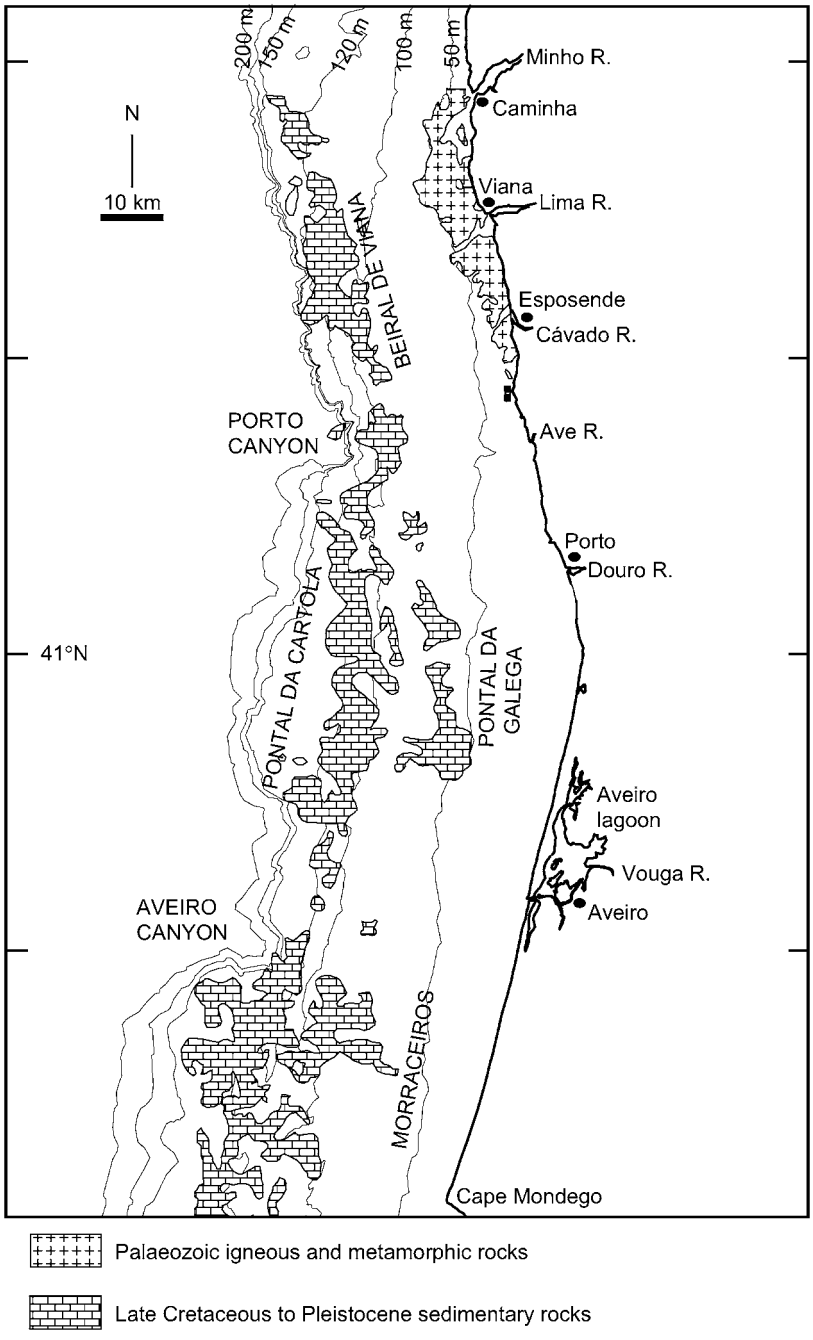

Fig. 2. Geological outline of the NW Portuguese continental shelf and upper slope.

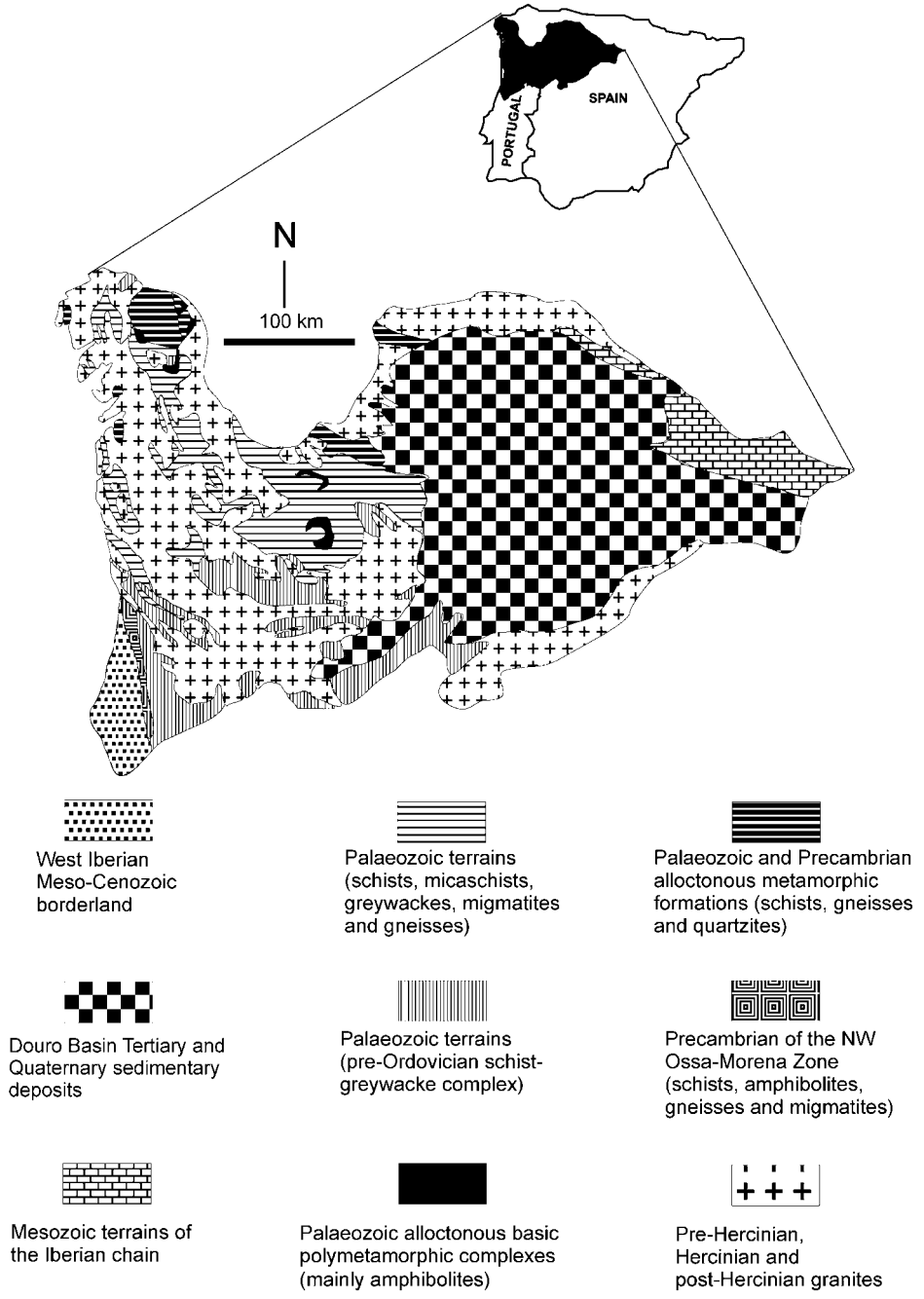

Fig. 3. Geological features of the NW Iberian river basins (adapted from Cascalho, 2000a).

2.3. Evolution of the Northern Portuguese Shelf

On the northern Portuguese shelf, sea level was approximately −130 to −140 m below present mean sea level during the Last Glacial Maximum (ca. 18 ka BP), and then rose to −100 m (ca. 16 ka BP). Following this rapid rise, sea level rose progressively and reached −40 m between 12 and 11 ka BP, then lowered to −60 m during the Younger Dryas. Between 10 ka and 8 ka BP it experienced a very fast rise to –20 m and achieved the present-day sea level at ca. 3500 ka BP (Dias, 1985; Rodrigues et al., 1991; Dias et al., 2000). These evolutionary stages have left strong imprints on the morphology and sedimentary aspects of the shelf, including the presence of various deposits located on the outer and middle shelves with relict and palimpsest characteristics (Dias and Nittrouer, 1984).

Shelf and upper slope surface sediments are generally sandy, the southern area (south of 41°N parallel) being richer in gravely sand, particularly in the mid shelf region, around the 11–10 ka BP ancient shoreline. Sediments north of the 41°N parallel are on average much finer grained (Magalhães, 1999; Fig. 4).

The major rivers contribute sediments to the shelf at times of major flood discharges, with finer-grained sands being carried further offshore while the coarser sediments are deposited in estuaries (Dias et al., 2002a). The two most important drainage basins in the region are those of the Douro (catchment area of 95,682 km^2) and the Minho (catchment area of 17,081 km^2). In these basins extensive outcrops of igneous and metamorphic rocks are present, mainly granites, schists, gneisses and greywackes, belonging to the Old Iberian Massif (Ribeiro et al., 1979, 1987).

3. METHODS

The present work is based on the study of 504 samples, collected from the unconsolidated sedimentary cover of the northern Portuguese continental shelf and upper slope (358 samples), from the major supplier rivers (Minho, Lima, Cávado, Ave and Douro—56 samples) and from the Douro estuary sedimentary infill (90 samples) (Fig. 1). Sampling of shelf and upper slope sediments was carried out during several cruises between 1986 and 1993, using Smith-McIntyre and Shipeck grabs on board hydrographical vessels (*Almeida Carvalho, Andromeda* and *Auriga*) within the scope of the Portuguese Instituto Hidrográfico SEPLAT programme and DISEPLA II project. Surface river sediments were sampled in 1993 using a *Petit Ponar* grab from a small boat, Zebro III, as part of the SEPLAT programme and PETDS project. Sampling of the sediment fill of the Douro estuary was undertaken during 1999 by rotary drilling, within the ENVI-CHANGES project.

Samples were first washed using hydrogen peroxide and distilled water. They were then wet sieved using 2 and 0.063 mm sieves. The sand fraction was oven dried and sieved to obtain five principal grain-size classes. Heavy minerals present in the fine sand (0.125–0.25 mm) and very fine sand (0.063–0.125 mm) were separated using bromoform and then mounted in Canada balsam on glass slides. The required amount of grains for each slide was obtained using a micro-splitter. About 300 heavy minerals per slide were identified and counted under the petrographic microscope in each grain size interval according to the ribbon method (Galehouse, 1971 cited in

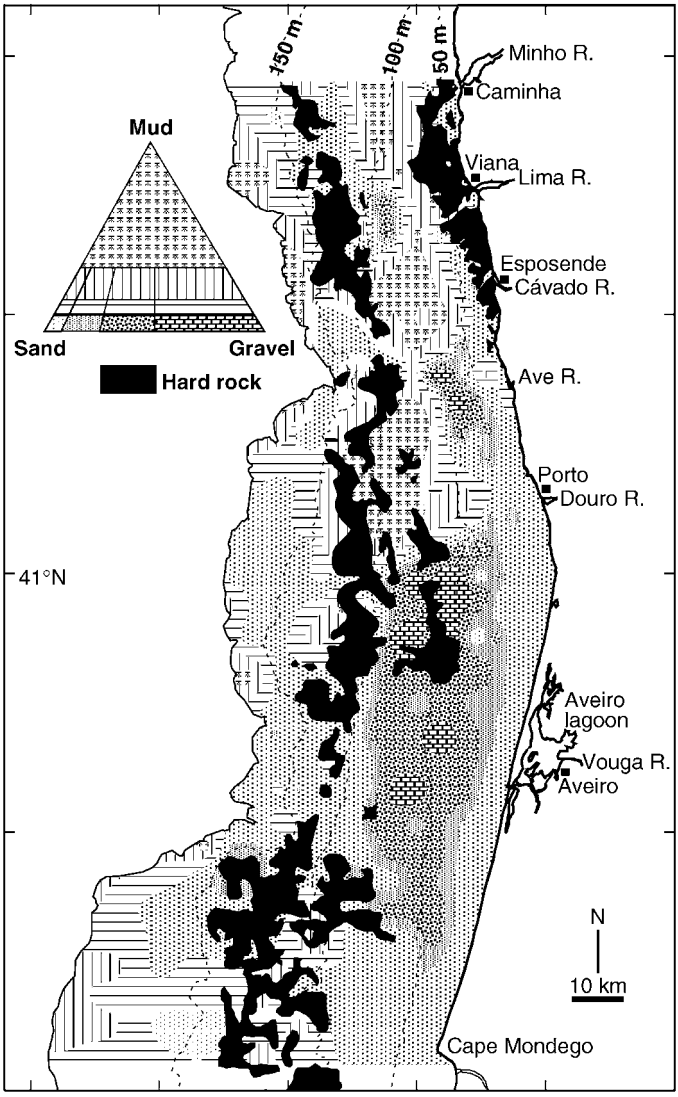

Fig. 4. Textural characteristics of the NW Portuguese unconsolidated sedimentary cover (adapted from Magalhães, 1999).

Mange and Maurer, 1992). The counting results were then converted to numeric percentages.

Some mineral species (e.g., garnet, pyroxenes, amphiboles and olivine) were also analysed by an electron microprobe, and for this purpose the minerals were mounted in specific grain mounts (mounted using 2 Part Epoxy Resin and then polished using *175 emery* for coarser polishing and *alumina optical 220* for finer polishing). Laboratory procedure was identical for the Douro estuary samples, but in this case the heavy minerals were separated using sodium polytungstate (Callahan, 1987) in three grain-size brackets: medium, fine and very fine sand.

4. RESULTS

4.1. Heavy Mineral Content

Biotite, andalusite, tourmaline, amphibole, garnet, staurolite, zircon and apatite form the major components of the transparent heavy mineral spectrum. Sillimanite, kyanite and rutile occur rarely and only in scattered locations. Epidote, anatase, brookite, monazite, orthopyroxene, clinopyroxene and olivine are generally very rare, the last three species being sometimes locally important (Cascalho, 1998; Fradique and Cascalho, 2004; Fradique et al., 2006, Appendix A, B and C). Figs. 5 and 6 and Table 1 illustrate the relative abundance of the main transparent heavy minerals in the shelf/upper slope and river sediments, and in the Douro estuary cores.

High *biotite* contents (more than 50%) are detected in all main river sediments with extreme maximum values of more than 80% in the Cávado River (Fig. 5 and Table 1). In shelf and upper slope environments, the average values are smaller (15%), but in some specific areas of the middle shelf north of 41°N, it is detected in high percentages (>31%). South of 41°N, biotite is almost absent, with the exception of a narrow area near shore and in some outer shelf and upper slope restricted areas (Fig. 7).

Andalusite is well represented in the river sands, especially in those from the Minho and Lima, whose sediments have average contents of, respectively, 12 and 15% (Fig. 5 and Table 1). This mineral is generally common in the shelf and upper slope sediments (Fig. 8), and in some middle and outer shelf zones andalusite is the main transparent heavy mineral (>31%).

The *garnet* percentage shows contrasting values in the sample groups, being more frequent in the shelf and upper slope (average of 19%) than in the rivers (average of 3%) and Douro cores (average of 7%—Fig. 5 and Table 1). The distribution pattern in the shelf is asymmetrical (Fig. 9). Garnet is poorly represented north of the Porto canyon (<25%) while being abundant south of this morphological feature (>33%).

Tourmaline shows relatively lower frequency values in the northern river surface sediments and Douro cores (average of 5%—Fig. 5 and Table 1). However, it is fairly common in the continental shelf and upper slope, with an average content of 15% (Fig. 5 and Table 1). The higher values are found in some outer shelf restricted areas north of Porto canyon (>31%) and in the middle shelf, south of Douro river mouth (>19% – Fig. 10).

In the northern rivers, *amphibole* is only significant in the Douro River surface and core sediments (7 and 17%, respectively), and is nearly absent in all others (⩽3%—Fig. 5 and Table 1). In the shelf and upper slope, the average values are identical to those in the Douro core samples (14%—Fig. 5). Fig. 11 shows a preferential occurrence of amphibole in the inner shelf domain south of the Douro river mouth (>21%). Significant amounts of amphibole grains (>21%) are also detected in the middle shelf off the Douro River mouth.

Zircon is uncommon in river and shelf/upper slope sediments (7%) and is nearly absent in the Douro cores (1%—Fig. 5 and Table 1) but it is more abundant in restricted areas north of the Porto canyon (>21%—Fig. 12). High zircon quantities were found in samples, collected from the inner shelf south of the mouth of the

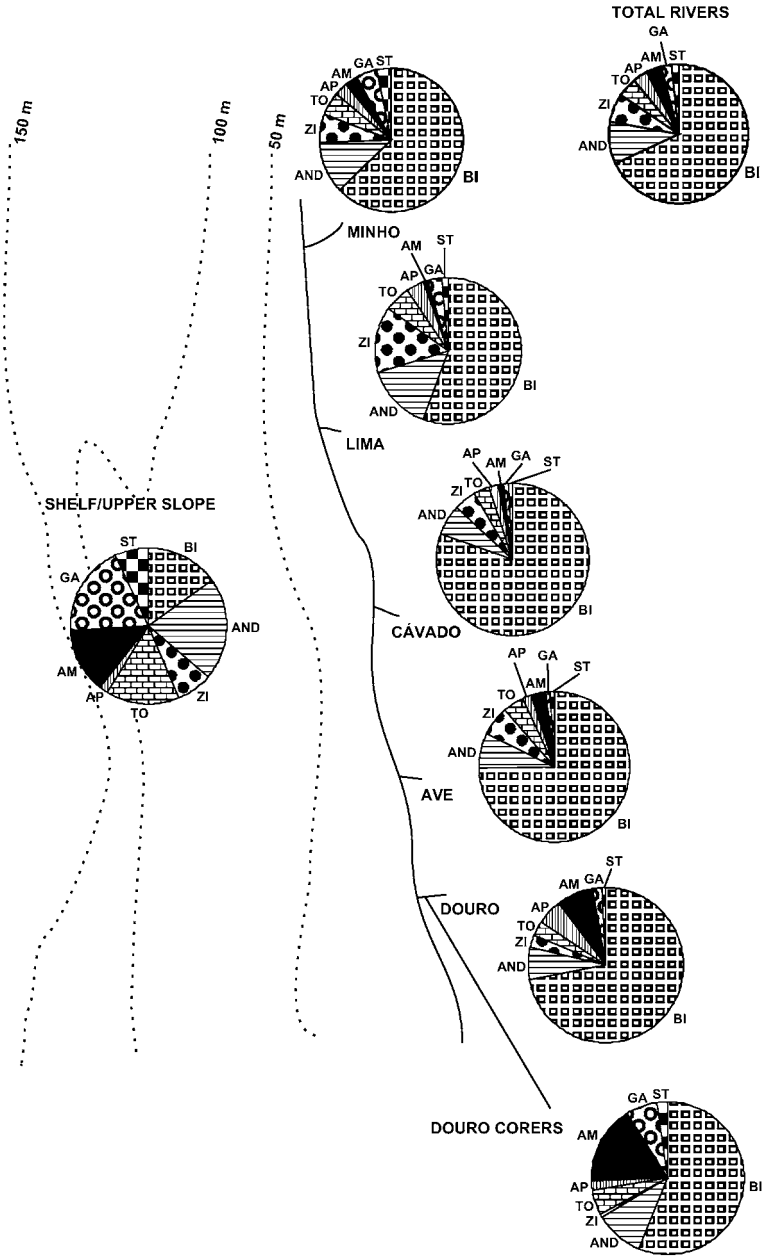

Fig. 5. Occurrence of the main transparent heavy minerals in the major NW Portuguese rivers and NW shelf/upper slope. BI – biotite; AND – andalusite; ZI – zircon; TO – tourmaline; AP – apatite; AM – amphibole; GA – garnet; ST – staurolite.

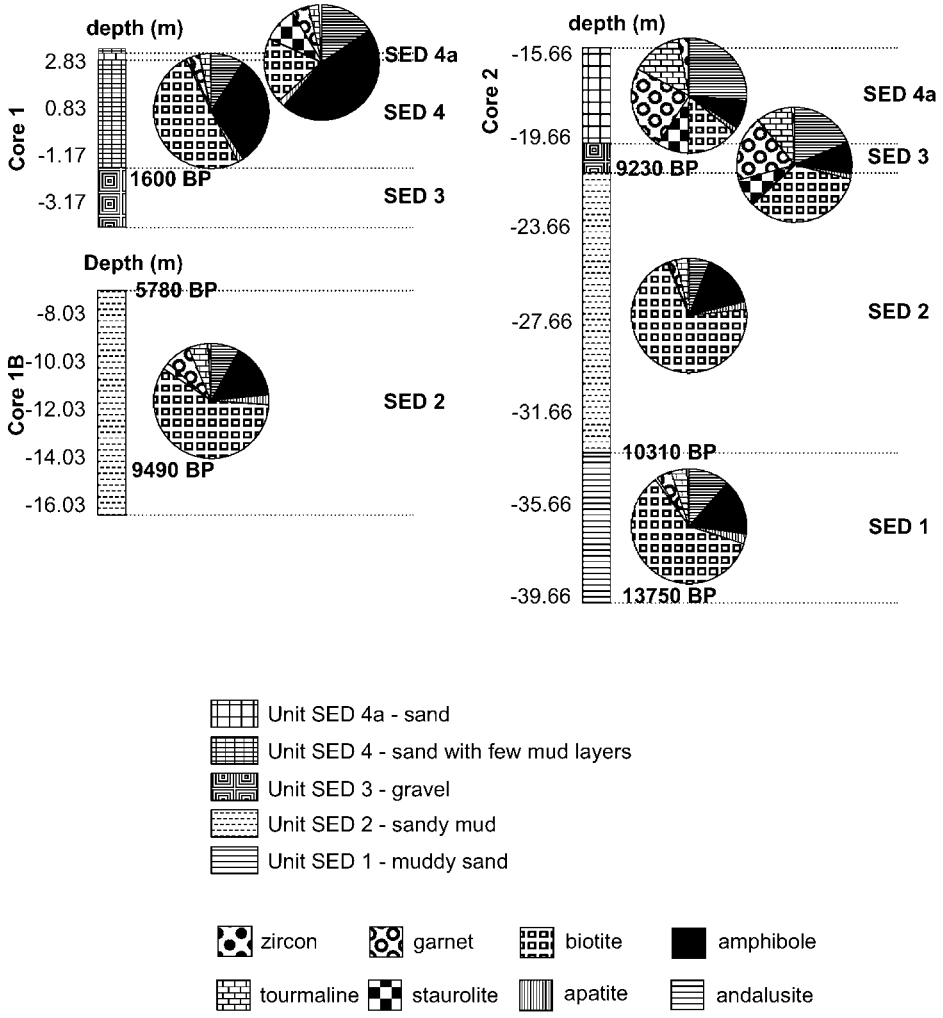

Fig. 6. Distribution of the main transparent heavy minerals in the sedimentary fill of the Douro estuary.

Minho River. These values are similar to that of zircon-rich surface sediments of the Lima River (Fig. 5 and Table 1).

Staurolite shows significant variations in the sample groups considered, being more frequent in the shelf and upper slope (average of 7%) than in northern rivers and Douro cores (average of 2%—Fig. 5 and Table 1). The distribution pattern in the shelf and upper slope is remarkably asymmetrical north and south of the Porto canyon. The greatest contents (>9%) are detected south of this morphological feature particularly in the middle shelf (Fig. 13).

Apatite is present in all sample groups (Fig. 5 and Table 1). In shelf and upper slope it has a uniform distribution pattern, while some middle and outer shelf and upper slope restricted areas have somewhat higher concentrations (>3%, Fig. 14).

Table 1. Average percentages of main non-opaque heavy minerals plotted in Fig. 5

	Minho river	Lima river	Cávado river	Ave river	Douro river	Total rivers	Douro corers	Shelf/upper slope
Biotite	62	56	81	75	72	67	56	15
Andalusite	12	15	6	7	7	10	10	21
Zircon	6	14	5	7	3	7	1	7
Tourmaline	6	6	3	4	3	5	5	15
Apatite	3	4	2	2	5	3	2	2
Amphibole	3	1	1	3	7	3	17	14
Garnet	5	3	1	1	2	3	7	19
Staurolite	3	1	1	1	1	2	2	7

4.2. Heavy Minerals of Local Occurrence

Pyroxenes and olivine are absent in the river sediments. In the shelf and upper slope they are present in a small area south of the Porto canyon. The maximum frequency values for orthopyroxene, clinopyroxene and also for olivine are detected near the Aveiro canyon (Figs. 15–17).

5. DISCUSSION

5.1. Heavy Mineral Provenance

The heavy mineral signatures of river sediments help to identify fluvial sediment flux to the shelf and indicate that they were sourced from the Old Iberian Massif (Table 2). The fluvial heavy mineral spectrum is characterised by a biotite, andalusite, zircon, tourmaline, amphibole, garnet, apatite and staurolite assemblage (Fig. 5 and Table 1). However, there are significant differences in the heavy mineral proportions between the five principal rivers. The northernmost rivers (Minho and Lima) have a relatively low biotite and high andalusite content. In the catchments of these two rivers extensive andalusite-rich metamorphic rocks exposed in the Caminha region (Teixeira and Assunção, 1961; Teixeira et al., 1965) are the likely source for the high quantities of andalusite in the loads of these rivers. Another important aspect is the relatively high amphibole content of the Douro River sediments, indicating derivation from amphibolite-facies rocks in the Douro metamorphic complex (Noronha and Leterrier, 1995). The results from the Douro estuary cores support derivation from this source, as expressed by the dominance of biotite, followed by amphibole, andalusite, garnet, tourmaline, staurolite, apatite and zircon (Fig. 5 and Table 1).

Data from the shelf and upper slope show andalusite as the main mineral, followed by, in decreasing abundance, garnet, biotite, tourmaline, amphibole, zircon and staurolite and apatite. This mineral association is different from the mineral spectra of the northern rivers and that of the sedimentary succession of the Douro estuary. Such differences can be ascribed to hydraulic sorting processes that

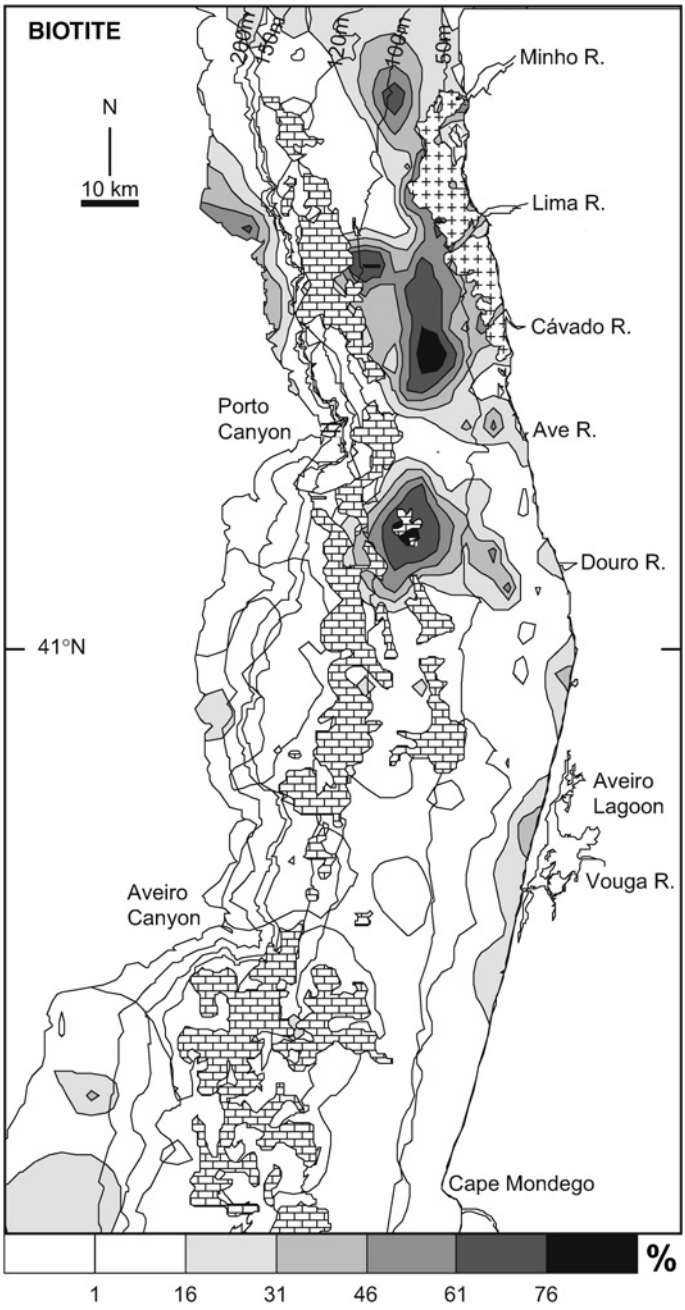

Fig. 7. Biotite distribution in shelf and upper slope. The percentage values are expressed in the total of non-opaque heavy minerals in the 0.063–0.250 mm grain-size interval.

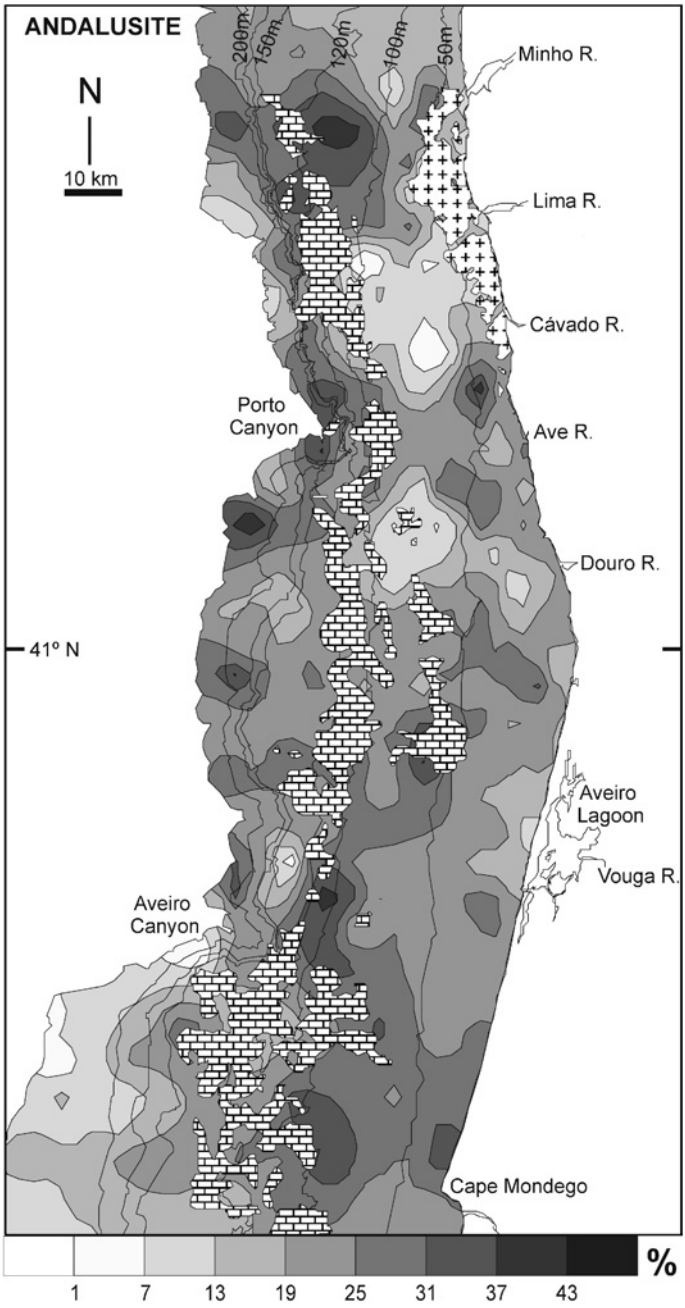

Fig. 8. Andalusite distribution in shelf and upper slope. The percentage values are expressed in the total of non-opaque heavy minerals in the 0.063–0.250 mm grain-size interval.

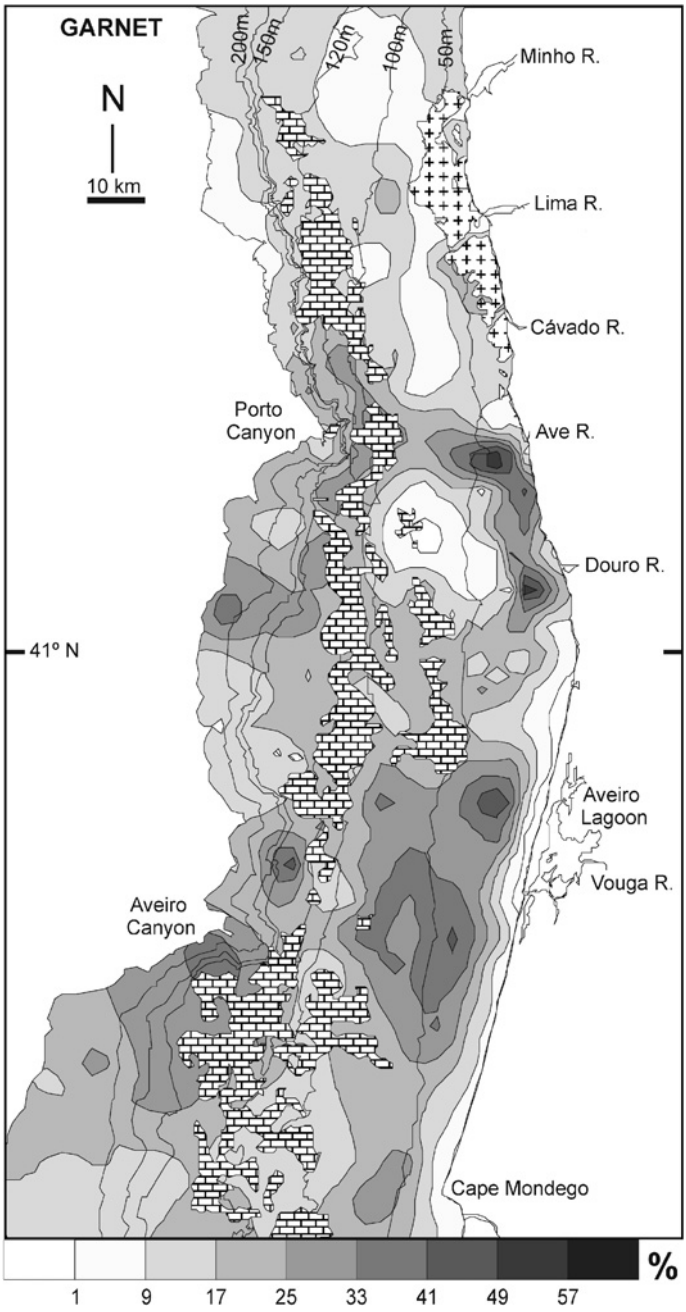

Fig. 9. Garnet distribution in shelf and upper slope. The percentage values are expressed in the total of non-opaque heavy minerals in the 0.063–0.250 mm grain-size interval.

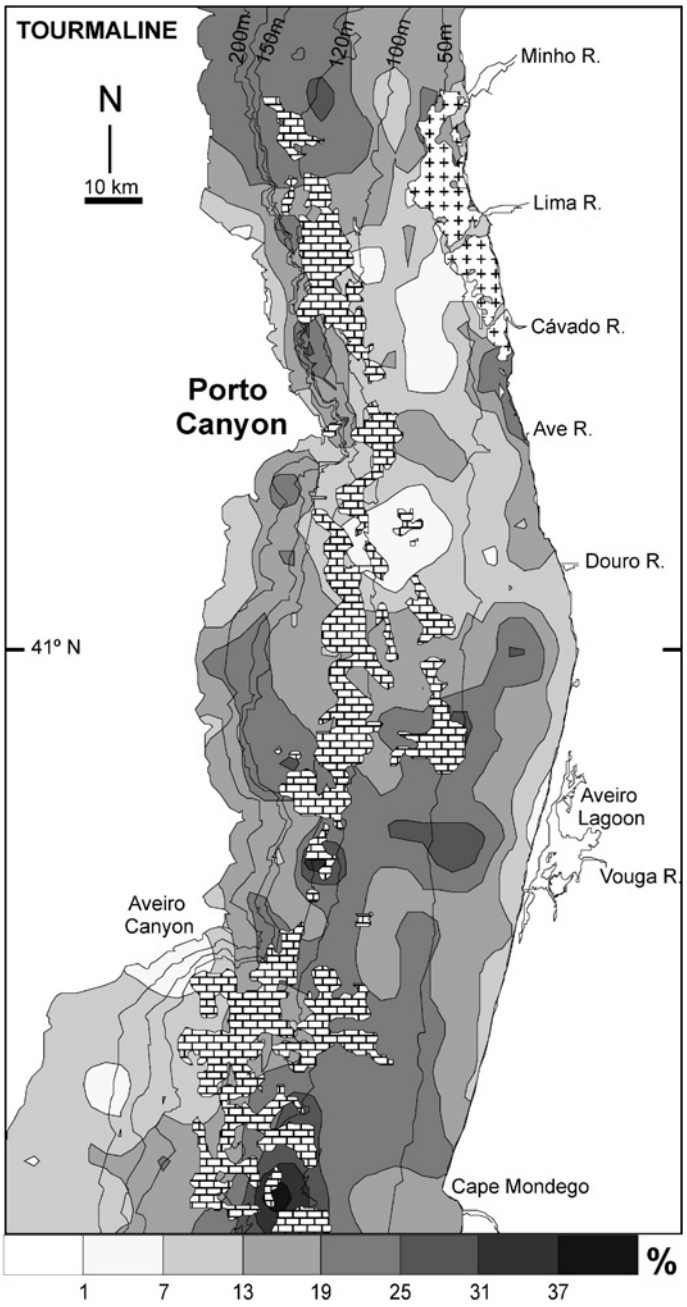

Fig. 10. Tourmaline distribution in shelf and upper slope. The percentage values are expressed in the total of non-opaque heavy minerals in the 0.063–0.250 mm grain-size interval.

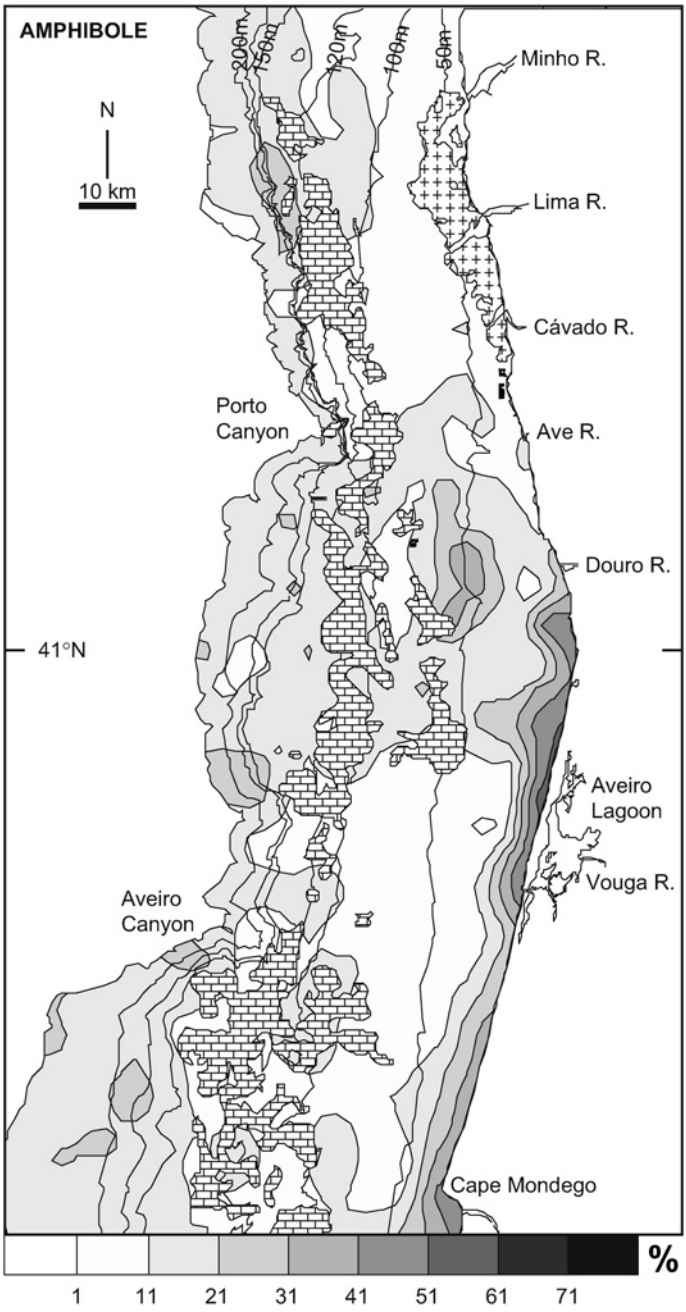

Fig. 11. Amphibole distribution in shelf and upper slope. The percentage values are expressed in the total of non-opaque heavy minerals in the 0.063–0.250 mm grain-size interval.

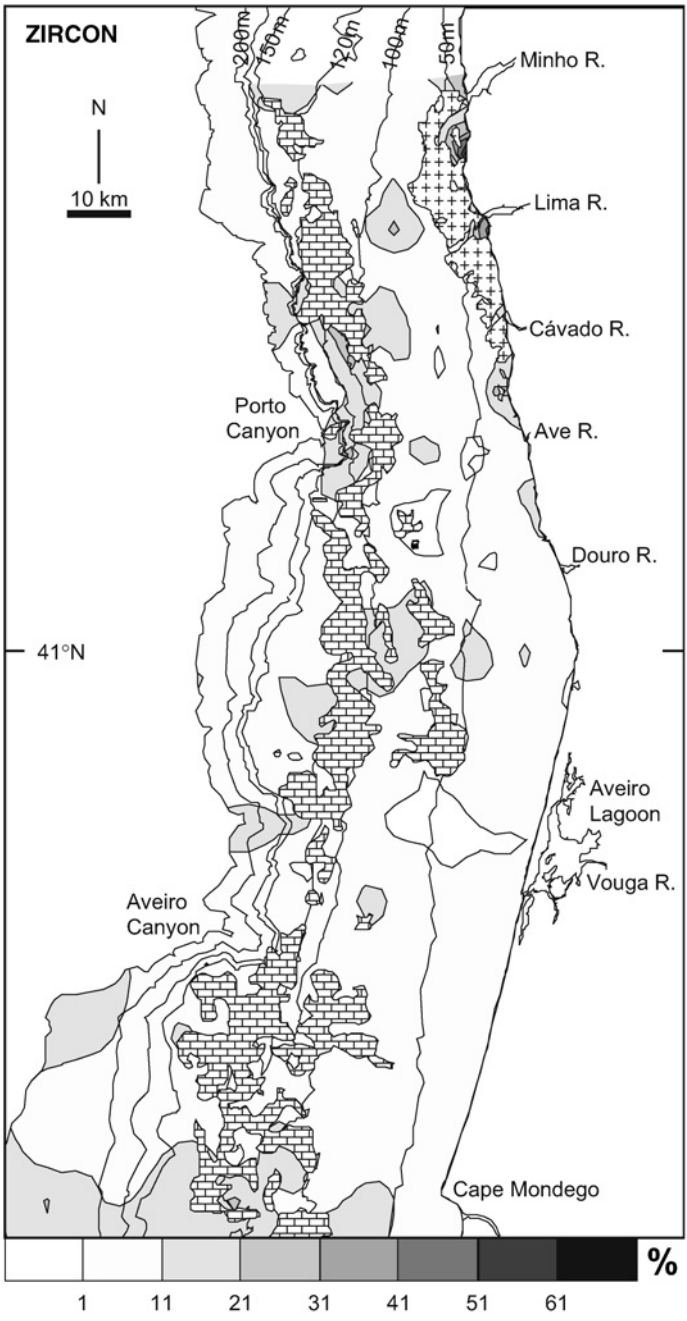

Fig. 12. Zircon distribution in shelf and upper slope. The percentage values are expressed in the total of non-opaque heavy minerals in the 0.063–0.250 mm grain-size interval.

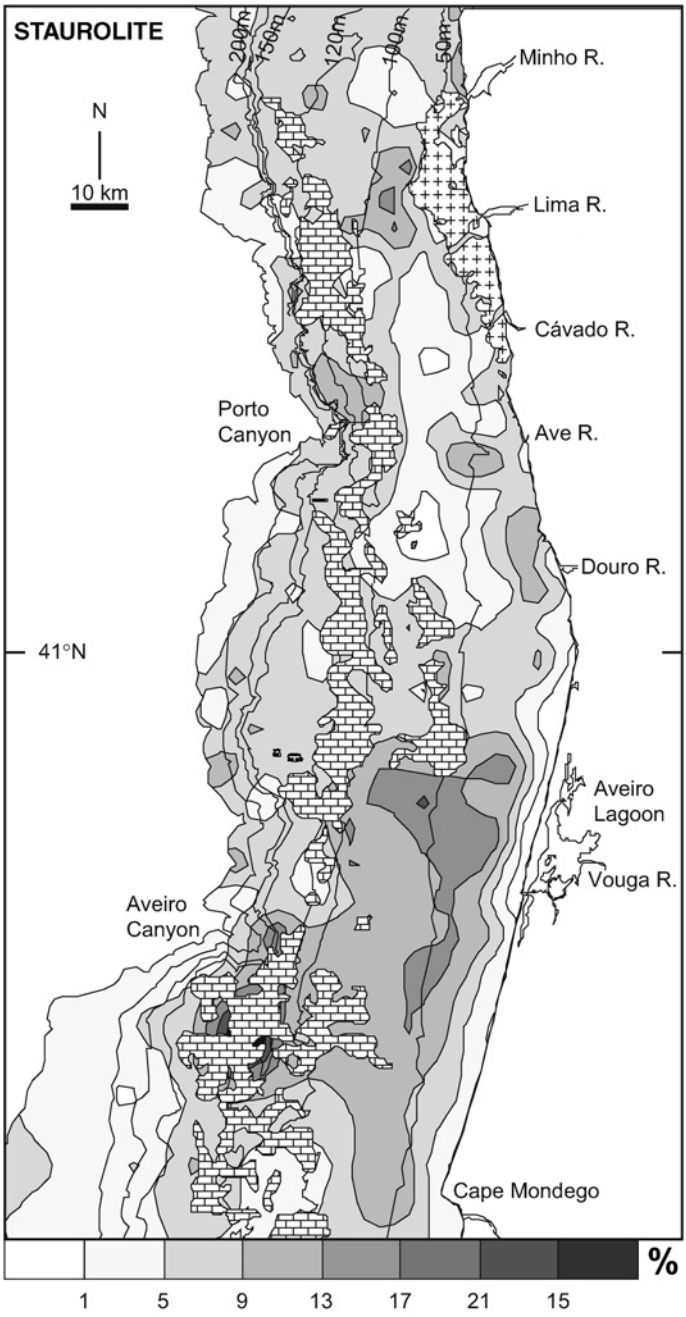

Fig. 13. Staurolite distribution in shelf and upper slope. The percentage values are expressed in the total of non-opaque heavy minerals in the 0.063–0.250 mm grain-size interval.

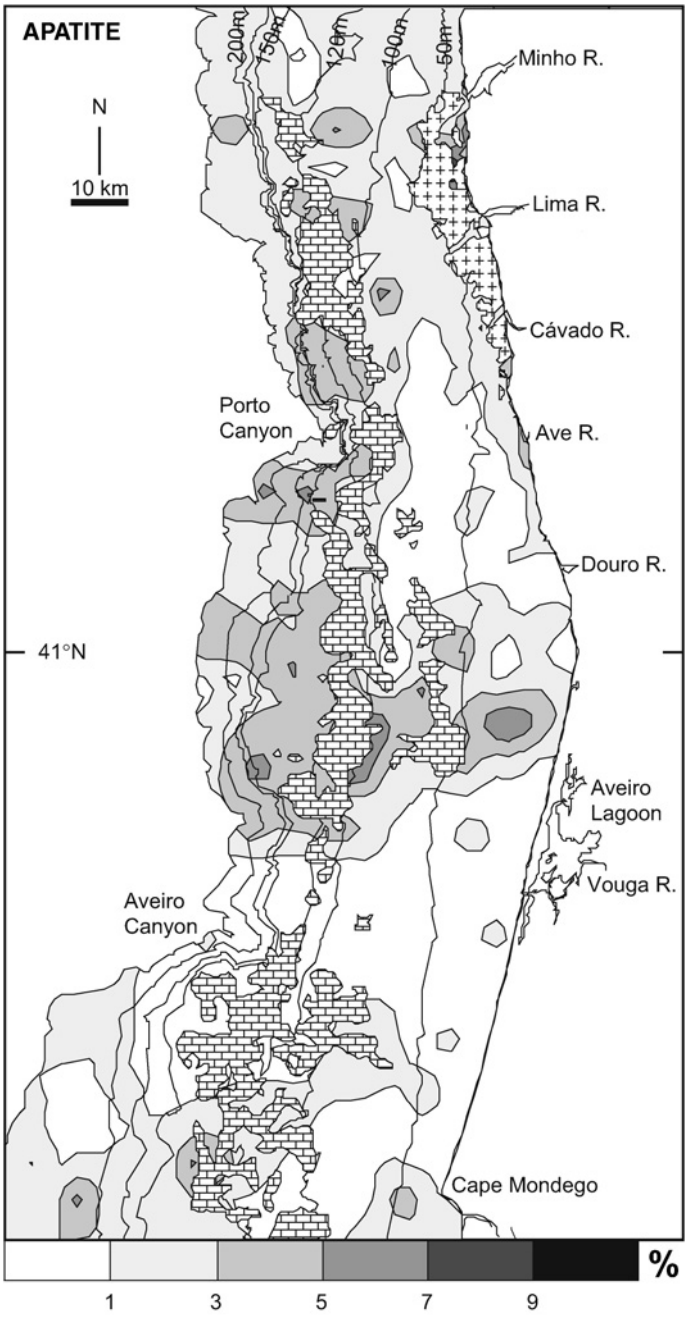

Fig. 14. Apatite distribution in shelf and upper slope. The percentage values are expressed in the total of non-opaque heavy minerals in the 0.063–0.250 mm grain-size interval.

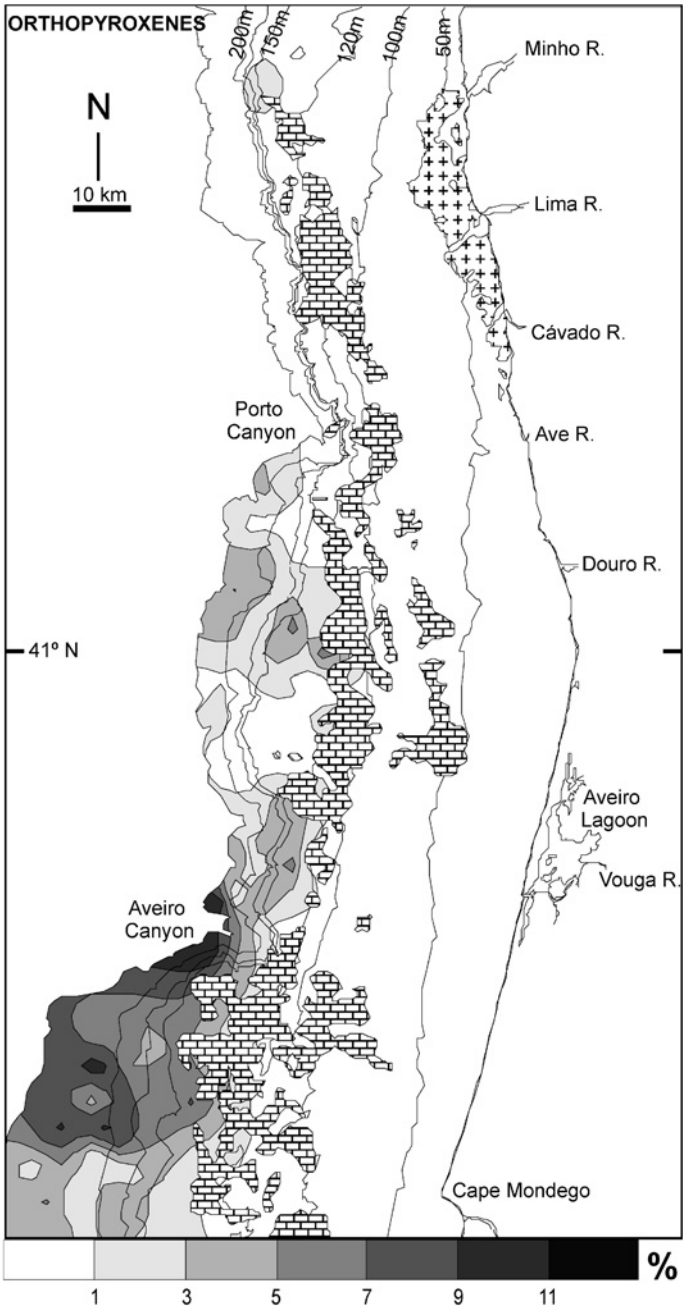

Fig. 15. Orthopyroxene distribution in shelf and upper slope. The percentage values are expressed in the total of non-opaque heavy minerals in the 0.063–0.250 mm grain-size interval.

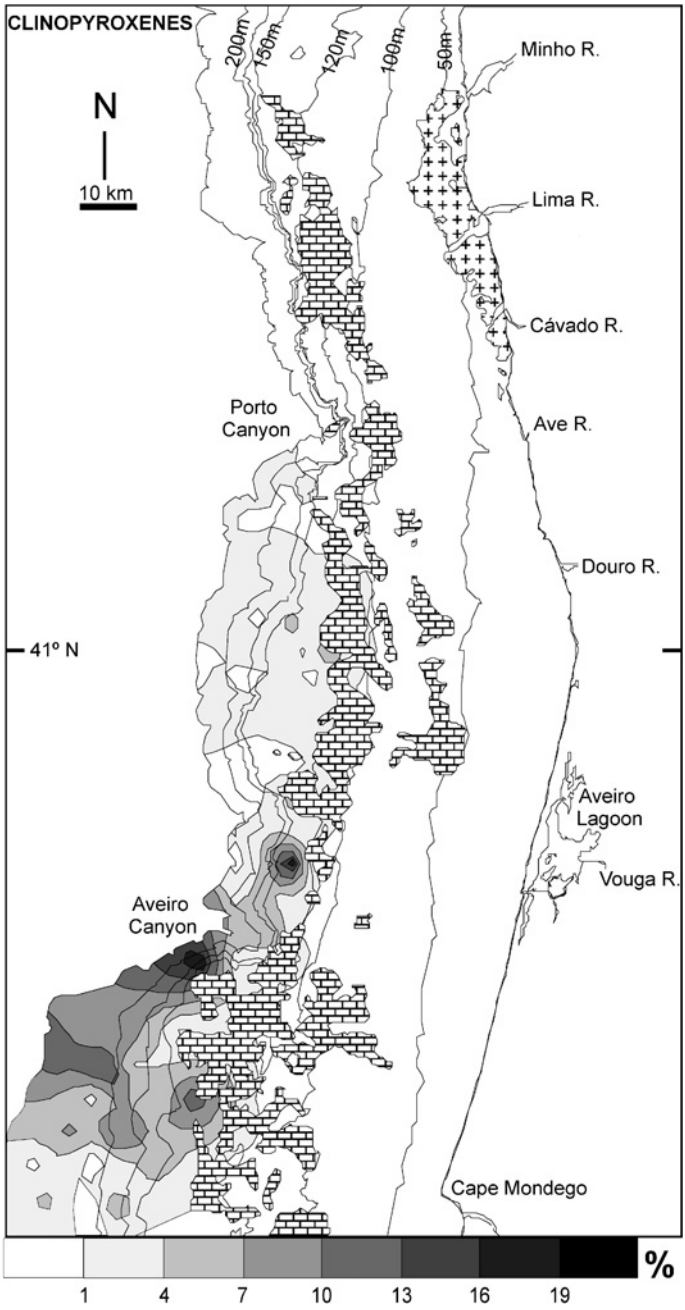

Fig. 16. Clinopyroxene distribution in shelf and upper slope. The percentage values are expressed in the total of non-opaque heavy minerals in the 0.063–0.250 mm grain-size interval.

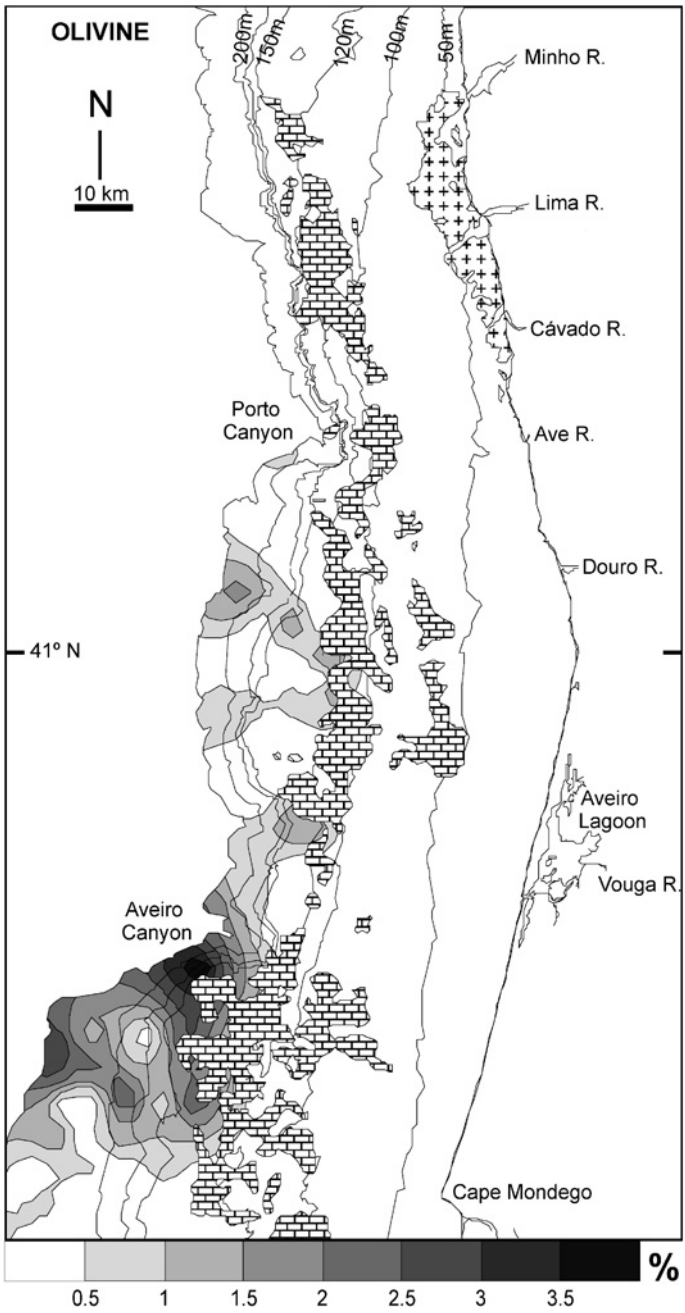

Fig. 17. Olivine distribution in shelf and upper slope. The percentage values are expressed in the total of non-opaque heavy minerals in the 0.063–0.250 mm grain-size interval.

Table 2. Principal source rocks of the main heavy mineral species, tabulated according to their occurrences in the Portuguese northern river basins (modified from Cascalho, 2000a)

Source rocks	Location (river basin)	Heavy minerals
Granites	Outcropping in the five Portuguese northern river basins. Main outcrops are present in Minho, Lima, Ave and Cávado river basins	Biotite, tourmaline, apatite, zircon, rutile, amphibole and iron, titanium oxides and occasionally garnet
Micaschists, gneisses and migmatites	Outcropping in the SW of Douro basin (Douro River mouth) and near the coastal zone south of the Douro River	Biotite, garnet, sillimanite, apatite and zircon
Amphibolites and amphibolitic schists	Outcropping in the SW of Douro basin (Douro River mouth) and near the coastal zone south of the Douro River	Amphibole (abundant), apatite (accessory)
Porphyroblastic schists	Outcropping in the SW limit of Douro basin and in the littoral south of the Douro River	Garnet, staurolite and biotite (abundant), zircon, tourmaline, apatite, sillimanite and magnetite (accessories)
Schist–greywacke complex	Outcropping mainly in the Douro River basin	Andalusite, garnet and staurolite (abundant in some schists and greywackes. Kyanite occasionally present
Schists, greywacke quartzites, hornfels and metasediments	Outcropping mainly north of the Douro River, and present in all river basins. There are several important outcrops which are crossed by the Lima and Minho rivers	Biotite, andalusite (chiastolite) in hornfels. Garnet and andalusite (chiastolite) in schists. Apatite, tourmaline, silimanite, amphibole, pyrite, ilmenite and zircon are also present

operate during transport and depositional stages. Some shelf areas appear to be representative of ancient littoral zones, being characterised by abundant coarse sediments (from medium sand to gravel grain size) occurring mainly in the middle shelf, south of the Cávado River mouth (Magalhães and Dias, 1992; Magalhães, 1999). In these areas hydraulic sorting processes have imparted significant changes to the provenance signal and have led to the formation of a heavy mineral association dominated largely by equant grains such as garnet, andalusite, tourmaline and staurolite. In other areas (as in the middle shelf area between the Douro and Minho rivers) that are characterised by high proportions of finer sediments (fine sand to mud) the heavy mineral suite is mostly composed of biotite and other platy grains such as amphiboles. In these two contrasting situations, sorting processes have substantially changed the primary source signal in specific shelf areas.

The presence of pyroxenes and olivine in some limited areas of the shelf and upper slope (Figs. 15–17) cannot be linked to fluvial input because basic igneous rocks that contribute pyroxenes and olivine (e.g., gabbros, dolerites, andesites and basalts) are not present in the drainage basin of the northern rivers. Moreover, pyroxene and

olivine distribution patterns do not match any of the presently known terrigenous source rocks, indicating that their origin is not related to the provenance of the modern river sediments. Electron microprobe analysis of several grains (Cascalho, 2000a) has identified clinopyroxenes belonging to the diopside–hedenbergite solid solution series and some of augite composition. A different pyroxene was allocated to the enstatite–ferrosilite series. Olivine grains were identified as forsterite.

Basic to ultra basic igneous rocks are unknown in the northern Portuguese margin. Nevertheless, Rodrigues et al. (1995) detected a morphological feature near the Porto canyon that can be recognised as a dyke, probably related to intrusive igneous activity (these observations were supported by remote operated vehicle images—ROV). Such intrusive episodes may be related to the earlier evolution of the Iberian margin, when the kinetic movements were followed by the rising of magma through deep crustal fractures (Rodrigues, 2003). Based on these results, and considering the distribution patterns of minerals with basic—ultra basic affinities, their source is probably located in the outer shelf/upper slope south of Porto canyon.

5.2. *Hydraulic Behaviour of the Heavy Minerals*

Of the principal factors that control the occurrence and distribution of heavy minerals in sediments, hydraulic processes may considerably mask the original provenance signal (Morton and Hallsworth, 1999). Four basic sorting mechanisms operate: suspension, entrainment, transport and shear (Slingerland, 1977; Sallenger, 1979; Komar and Wang, 1984; Komar, 1989, 2007, this volume), and their efficiency in promoting grain sorting is dependent on the grain's physical properties such as density, grain size and shape.

The hydraulic behaviour of heavy minerals in the Portuguese northern shelf was evaluated by Cascalho (2000a, 2000b), using the TRANSED programme developed by Taborda (1999). This programme enables the estimation of sediment transport in a non-cohesive sedimentary environment and the estimation of the influence of a grain's physical properties (density, shape and size) on their hydraulic behaviour.

The estimation of a particle's entrainment susceptibility is dependent on the transport mode. For finer grains that are transported as suspended load, the settling velocity is a good estimator of their hydraulic behaviour. For the coarser particles, transported as bed load, the shear critical velocity is the best estimator of their hydraulic behaviour. The settling velocity (W_s) and shear critical velocity (u^*_{cr}) were computed for several grain types in order to quantify the mobility of the heavy particles. The entrainment susceptibility of a grain was quantified, based on its shear critical velocity and settling velocity. The computation of these physical parameters for different sedimentary particles involved specific procedures. The shear critical velocity was obtained using the results by Wilberg and Smith (1987) and Taborda (1999) that estimates the particle entrainment considering different densities and shapes in a heterogeneous sedimentary environment. The settling velocity was obtained using the equation proposed by Gibbs et al. (1971), modified by Komar (1981) for application to heavy minerals. Fourteen heavy minerals were selected as representative grain types of the major heavy mineral species in the shelf and upper slope sandy sediments (Table 1). For each grain its density and nominal diameter were used (Table 3). The nominal diameter calculation considered that the generality

Table 3. Heavy mineral grains used on the TRANSED programme

Heavy grain	ρ	D_N	Mob
Ga1	4.3	0.2125	0.5
Ga2	4.3	0.1004	1.5
St1	3.8	0.1995	0.6
St2	3.8	0.1054	1.6
Zi1	4.7	0.1293	0.9
Zi2	4.7	0.0991	1.4
And1	3.2	0.1862	0.8
And2	3.2	0.1562	2.1
To1	3.2	0.2289	0.6
To2	3.2	0.1592	1.7
Am1	3.0	0.2392	0.7
Am2	3.0	0.1589	2.6
Bi1	2.9	0.0836	6.9
Bi2	2.9	0.0492	14.6

ρ is the density; D_N is the nominal diameter (mm) and Mob is the mobility parameter. Ga (garnet), St (staurolite), Zi (zircon), And (andalusite), To (tourmaline), Am (amphibole), Bi (biotite) (adapted from Cascalho, 2000a, 2000b).

of the sediment particles could be described as a three axes ellipsoid (Cui and Komar, 1984). Based on this assumption the nominal diameter (D_N) was obtained by the equation:

$$D_N = \sqrt[3]{D_L D_I D_S} \tag{1}$$

where D_L is the long diameter, D_I is the intermediate diameter and D_S is the small diameter. If the grain has a shape similar to a tetragonal prism, the relationship

$$D_N = \sqrt[3]{\frac{6 D_L D_I D_S}{\pi}} \tag{2}$$

was applied.

The critical shear and settling velocities obtained for each grain type, shown in Table 3, enable the evaluation of grain mobility with respect to their affinity to be transported as bed load or in suspension. The likelihood of each grain being transported under a specific mode was estimated through the mobility parameter (Mob), which was defined as the ratio between shear critical velocity and settling velocity (Cascalho, 2000a, 2000b):

$$\text{Mob} = \frac{u^*_{cr}}{W_s} \tag{3}$$

This parameter can be considered as a Rouse-type parameter (Dyer, 1986). The Mob < 1 grains are capable of being transported as bed load while the Mob > 1 grains are mainly transported as suspended load. Values for D_N and Mob for all grain types are presented in Table 3.

Considering the results obtained for the Mob parameter, the different hydraulic behaviour for the study of grains can be deduced. Thus, heavy minerals with higher Mob values occur in the most mobile sediment load. In turn, they can easily be remobilised and frequently transported by waves and currents. The susceptibility of the different heavy mineral grains to wave remobilisation potential was tested in the context of the TRANSED programme, according to the following wave regimes (Pires, 1989): $H_s = 2.5$ m and $T = 9$ sec (typical NW wave regime); $H_s = 4$ m and $T = 10$ s (typical SW wave regime); $H_s = 8$ m and $T = 16$ sec (West high-energy storm); $H_s = 10$ m and $T = 18$ sec (West extreme high energy storm). Inner shelf Mob > 1 grains are likely to be remobilised under the action of the prevailing wave regimes, whereas Mob < 1 grains are only remobilised under wave regimes of higher energy (storms).

Biotite and other grains with Mob > 1 values, for example Am2 (Table 3), are the most mobile species and tend to be transported as suspended load. On the other hand, the coarsest grains of garnet, staurolite, zircon, tourmaline and andalusite show the opposite behaviour and tend to be transported as bed load.

5.3. Heavy Mineral Distribution

The conjectures about the hydraulic behaviour of heavy minerals are very useful in interpreting their distribution patterns within the dynamic sedimentary regime of the northern Portuguese shelf and upper slope. Regarding the higher mobility grains (biotite—Bi1, Bi2 and amphibole—Am2), it is possible to assume that they are conveyed via rivers and estuaries to the shelf because, in general, they are transported as suspended load. Thus, they prove reliable tracers of suspended load transport paths in the shelf domain.

Biotite distribution patterns signal processes of river flux (Fig. 7). Areas of higher biotite concentration are located in the middle shelf north of the Douro River mouth. Biotite particles are probably carried to the inner and sometimes to the middle shelf when floods supply large amounts of sediment to the shelf. This occurs especially in the winter when river runoff is high. In winter, wave energy is so high that it can put these micas into suspension and, consequently, currents can transport them further offshore. The distribution pattern of the biotite in Fig. 7 illustrates the result of these mechanisms, revealing that high quantities of biotite are found in the inner and middle shelves, west and northward of the Douro River mouth.

This interpretation is consistent with the fate of the fine sediment particles that enter the shelf domain (Dias et al., 1984, 2002a, 2002b; Drago et al., 1998; Oliveira et al., 2002a). Furthermore, the sedimentary succession of the Douro estuary shows a remarkable correlation of the higher frequency peaks of biotite with the higher contents of finer sediments (Fradique et al., 2006). In fact, sedimentary units SED 1 (muddy sand) and SED 2 (sandy mud) are the richest units in biotite (Fig. 6). Our observations confirm the mutual relationship in hydraulic behaviour between sand-sized mica particles and fine sediments (silt and clay), known since the 1960s (Neiheisel, 1965; Pomerancblun, 1966; Doyle et al., 1968, 1983; Adegoke and Stanley, 1972).

The distribution of amphiboles is illustrative of the Douro sediment supply to the shelf with abundant amphibole in the inner-shelf sediments south of the Douro River mouth, and in the middle shelf west of the Douro estuary (Fig. 11). This pattern

appears to be consistent with the amphibole content of the Douro estuary and river sands. The following scenario can be considered for the unravelling of the transport paths of amphiboles: grains reaching the shelf through the Douro fluvial discharge are temporarily deposited close to the estuary. Some are then transported southward through the inner shelf, having hydraulic behaviour similar to that of the finer-grained sand particles (Dias et al., 2002a), while others are exported into the deepest areas and deposited in the middle shelf adjacent to the Douro estuary.

Heavy mineral grains with lower mobility values, such as coarsest garnet, staurolite, zircon, andalusite and tourmaline are very often incorporated into a coarser sediment, especially into middle-shelf sand-gravel deposits, south of 41°N parallel (Dias and Nittrouer, 1984; Magalhães, 1999). Some of these grains were found in the shelf sediments near the Douro and Ave River mouths, as reflected by the garnet and staurolite distribution patterns (Figs. 9 and 13). Although this evidence suggests a modern river input into the shelf, the morphological features of garnet and staurolite grains in the shelf sediments differ from those in the rivers and are more indicative of an ancient source. For example, garnet and staurolite grains present in the Ave and Douro River sediments are predominantly angular, indicating their derivation from primary sources. In contrast, garnet and staurolite in the coarser shelf sediments have predominantly rounded to sub-rounded forms, which suggest either a polycyclic origin or a long exposure to dynamic processes prior to deposition. Similarly contrasting shapes are also displayed by the coarser grains of andalusite, tourmaline and zircon in rivers and shelf sediments (Fig. 18). The coarse grain size and high degree of rounding indicate that these assemblages have preserved characteristics of sediments of the Pleistocene shoreline during low-sea level stand and are to be considered as relict or palimpsest deposits.

Heavy minerals with differing morphologies were also detected in the Douro estuary succession. It is important to note that the most rounded forms of garnet, andalusite, tourmaline and staurolite are present in the coarser sandy units, especially in sub-unit 4a of core 2 (Fradique and Cascalho, 2004) (Fig. 6). Their occurrence is similar to that observed in the shelf sediments. Factors controlling heavy mineral distribution and morphological features were perhaps very similar in both situations.

6. CONCLUSIONS

The results of the study of heavy minerals in the northern Portuguese continental margin sediments have broadened our understanding of the major sediment sources and transport paths. The provenance of the assemblages is linked to igneous and metamorphic rocks (mainly granites, gneisses and schists), outcropping in the drainage basins of all northern Portuguese rivers. However, the presence of pyroxenes and olivine is enigmatic. They were probably eroded from basic igneous rocks located offshore in the outer shelf or upper slope south of Porto canyon.

The existence of selective transport processes is well documented by the heavy mineral spectra of the surface sediments. The most mobile heavy mineral grains, such as biotite and amphibole, are likely to be frequently remobilised and transported to

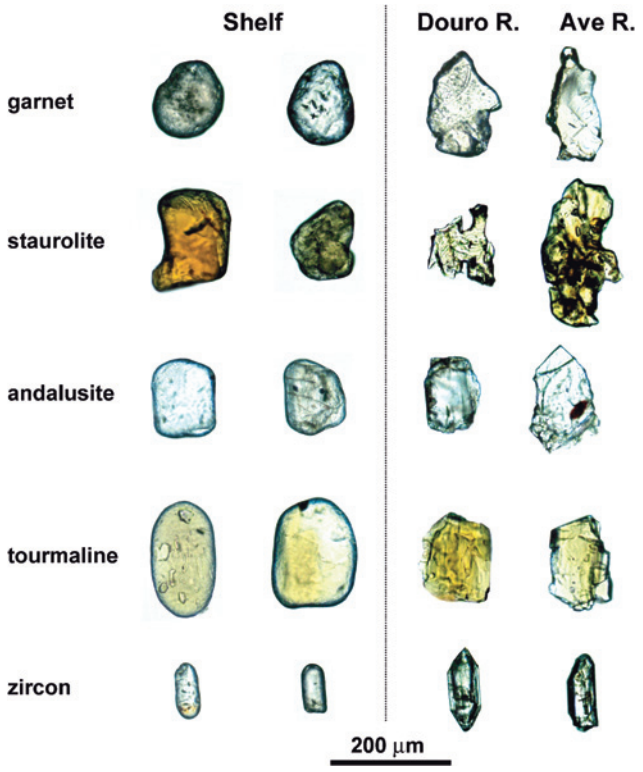

Fig. 18. Main transparent heavy grains with high values of mobility parameter (Mob). The two columns to the left show rounded grains collected from the shelf (SW of Douro River mouth at 50 m depth). They are from medium to coarse sands, which mark an ancient shoreline (relict to palimpsest deposits). The two columns to the right illustrate angular grains collected from the sediments of the Douro and Ave rivers.

both inner- and middle-shelf areas; therefore, they can be used as natural tracers of sediment transport paths. Their abundance in fluvial sands suggests that they are supplied during winter flood discharges. Once deposited in the inner-shelf domain they can be re-entrained and transported into deeper water, especially during winter storms, and this possibility was confirmed by the mobility evaluations of these grains.

Heavy mineral grains with lower mobility tend to remain relatively close to their input sources, and are found only in the inner-shelf zones, near estuaries. The evident morphological difference between the dominantly rounded heavy minerals present in some middle-shelf areas contrasts with their high angularity in river sediments, suggesting a complex sedimentary evolution. Rounded to sub-rounded grains found in some shelf areas and in coarser intervals in Douro cores are signatures of relict and/or palimpsest sediments, and indicate a long sedimentary history, while the predominantly angular to sub-angular forms found in river sediments suggest contemporary derivation from primary sources and an incipient mechanical abrasion.

ACKNOWLEDGEMENTS

We are grateful to Professor João A. Dias for helpful discussions and for reading an earlier version of the manuscript. The reviewing and useful comments of Professor Paul Komar, Dr. Maria Mange and Dr. David Wright are also acknowledged. We are particularly grateful to our colleagues Rui Taborda, Fernando Magalhães, Aurora Bizarro and Raul Fonseca for their comments and helpful discussions. This work was supported by the following projects: DISEPLA II Dinâmica Sedimentar da Plataforma e Vertente Continental Portuguesa—Junta Nacional de Investigação Científica e Tecnológica (JNICT) no. PMCT/C/MAR/692/90, BEVICAP O Beiral de Viana e o Canhão Submarino do Porto na Evolução da Margem Continental Portuguesa—JNICT no.° PMCT/C/MAR/683/90, PETDS Pesquisa e Caracterizaç ão de Elementos Traçadores da Dinâmica Sedimentar da Margem Setentrional Portuguesa—JNICT PMCT/C/MAR/706/90, ENVICHANGES Alterações Ambientais Durante o Quaternário Recente Deduzidas a Partir do Registo Sedimentar dos Estuários e da Plataforma Continental—Fundação para a Ciência e a Tecnologia (FCT) ARIPIPI/PLE/12/00. Special thanks are due to the Instituto Hidrográfico in the scope of the Sedimentos da Plataforma (SEPLAT) programme, which provided the samples from the northern Portuguese shelf. C. Fradique was funded by the ENVICHANGES project (FCT contract ARIPIPI/PLE/12/00).

REFERENCES

Adegoke, O.S., Stanley, D.J., 1972. Mica and shell as indicators of energy level and depositional regime on the Nigerian shelf. Marine Geology 13, M61–M66.

Callahan, J., 1987. A nontoxic heavy liquid and inexpensive filters for separation of mineral grains. Journal of Sedimentary Petrology 57, 765–766.

Carvalho, J.J.R., Barceló, J.P., 1966. Agitação marítima na costa oeste de Portugal metropolitano. Memórias do LNEC 290, 34.

Carvalho, R.A.C., Prior, V.M.S., Lamelas, M.H., 1991. Vento forte nas regiões costeiras de Portugal: frequência, duração e suas causas: Seminário Eurocoast—A zona costeira e os problemas ambientais, Aveiro, pp. 184–210.

Carvalho, F. P., Ramos, L. A., 1990. Lead 210 chronology in marine sediments from the northern margin of Portugal. 2 Congresso sobre a qualidade do ambiente, Lisboa, pp. A143–A151.

Cascalho, J., 1998. Associações de minerais pesados da cobertura arenosa da plataforma continental setentrional portuguesa. Comunicações do Instituto Geológico e Mineiro 84 (1), C11–C14.

Cascalho, J., 2000a. Mineralogia dos sedimentos arenosos da Margem Continental Setentrional Portuguesa. Ph.D. thesis, Lisbon University, (unpublished), 400pp.

Cascalho, J., 2000b. Heavy mineral hydrodynamic behaviour—the example of the Portuguese north shelf. Extended abstracts book of the 3rd Symposium on the Iberian Atlantic Margin, Faro, Portugal, pp. 253–254.

Cascalho, J., Carvalho, A.M.G., 1989. Estudo dos minerais pesados da plataforma continental portuguesa a norte da foz do rio Lima. Gaia 1, 15–17.

Cascalho, J., Carvalho, A.M.G., 1990. Distribuição dos minerais pesados da plataforma setentrional do Minho. Actas de la II Reunión del Cuaternário Ibérico (Madrid) 1, 1–7.

Cascalho, J., Carvalho, A.M.G., 1993. Proveniência dos minerais pesados da plataforma continental portuguesa a norte do paralelo de Espinho. Gaia 6, 10–25.

Cascalho, J., Magalhães, F., Dias, J.M.A., Carvalho, A.M.G., 1994. Sedimentary unconsolidated cover of the Alentejo continental shelf (first results). Gaia 8, 113–118.

Cui, B., Komar, P., 1984. Size measures and the ellipsoidal form of clastic sediment particles. Journal of Sedimentary Petrology 54 (3), 783–797.

Dias, J.M.A., 1985. Registos da migração da linha de costa nos últimos 18.000 anos na plataforma continental portuguesa setentrional. Actas da 1.ª Reunião do Quaternário Ibérico, pp. 281–295.

Dias, J.M.A., 1987. Dinâmica sedimentar e evolução recente da plataforma continental portuguesa setentrional. Ph.D. thesis, Lisbon University (unpublished), 500pp.

Dias, J.M.A., Boski, T., Rodrigues, A., Magalhães, F., 2000. Coast line evolution in Portugal since the Last Glacial Maximum until present—a synthesis. Marine Geology 170, 177–186.

Dias, J.M.A., Gaspar, L.C., Monteiro, J.H., 1980/81. Sedimentos recentes da plataforma continental portuguesa a norte do Canhão Submarino da Nazaré. Boletim da Sociedade Geológica de Portugal 22, 181–195.

Dias, J.M.A., Gonzalez, R., Garcia, C., Diaz del Rio, V., 2002a. Sediment distribution patterns on the Galicia-Minho continental shelf. Progress in Oceanography 52, 215–231.

Dias, J.M.A., Jouanneau, J.M., Gonzalez, R., Araújo, M.F., Drago, T., Garcia, C., Oliveira, A., Rodrigues, A., Vitorino, J., Weber, O., 2002b. Present day sedimentary processes on the northern Iberian shelf. Progress in Oceanography 52, 249–259.

Dias, J.M.A., Nittrouer, C.A., 1984. Continental shelf sediments of northern Portugal. Continental Shelf Research 3 (2), 147–165.

Doyle, L.J., Carder, K.L., Steward, R.G., 1983. The hydraulic equivalence of mica. Journal of Sedimentary Petrology 53, 643–648.

Doyle, L.J., Clearly, W.J., Pilkey, O.H., 1968. Mica: its use in determining shelf depositional regimes. Marine Geology 6, 381–389.

Drago, T., Jouanneau, J.M., Dias, J.M.A., Prud'homme, R., Kuel, S., Soares, A.M., 1994. La vasière Ouest-Douro et le piegeage des sediments estuariens récents. Gaia 9, 53–58.

Drago, T., Oliveira, A., Magalhães, F., Cascalho, J., Jouanneau, J.M., Vitorino, J., 1998. Some evidences of northward fine sediment transport in the northern Portuguese continental shelf. Oceanological Acta 21, 223–231.

Dyer, K.R., 1986. Coastal and estuarine dynamics. Wiley, Chichester, 342pp.

Fradique, C., Cascalho, J., 2004. Sedimentary processes in Douro estuary (Portugal)—A heavy mineral study. Thalassas 20 (2), 61–68.

Fradique, C., Cascalho, J., Drago, T., Rocha, F., Silveira, T., 2006. The meaning of heavy minerals in the recent sedimentary record of the Douro estuary (Portugal). Journal of Coastal Research SI 39, 165–169.

Gibbs, R., Mathews, D., Link, D., 1971. The relationship between sphere size and settling velocity. Journal of Sedimentary Petrology 41, 7–18.

Instituto Hidrográfico, 2004. Tabela de marés v. 1, Portugal, 186pp.

Jouanneau, J.M., Weber, O., Drago, T., Rodrigues, A., Oliveira, A., Dias, J.M.A., Garcia, C., Schmidt, S., Reyss, J.L., 2002. Recent sedimentation and sedimentary budgets on the western Iberian shelf. Progress in Oceanography 52, 261–275.

Komar, P.D., 1981. The applicability of the Gibbs equation for grain settling velocities to conditions other than quartz grains in water. Journal of Sedimentary Petrology 51, 1125–1132.

Komar, P.D., 1989. Physical processes of waves and currents and the formation of marine placers. Reviews in Aquatic Sciences 1–3, 393–423.

Komar, P.D. 2007. The entrainment, transport and sorting of heavy minerals by waves and currents. In: Mange, M.A., Wright, D.T. (Eds.), Heavy Minerals in Use. Developments in Sedimentology (this volume).

Komar, P.D., Wang, C., 1984. Processes of selective grain transport and the formation of placers on beaches. Journal of Geology 92, 637–656.

Magalhães, F., 1999. A cobertura sedimentar da plataforma continental portuguesa. Distribuição espacial. Contrastes temporais. Potencialidades económicas. Ph.D. Thesis, Lisbon University, (unpublished), 287pp.

Magalhães, F., Dias, J.M.A., 1992. Depósitos sedimentares da plataforma continental a norte de Espinho. Gaia 5, 6–17.

Mange, M.A., Maurer, H.F.W., 1992. Heavy minerals in colour. Chapman and Hall, London, 147pp.

Morton, A.C., Hallsworth, C.R., 1999. Processes controlling the composition of heavy minerals assemblages in sandstones. Sedimentary Geology 124, 3–29.

Murray, J., Renard, A.F., 1891. Report on deep-sea deposits based on the specimens collected during the voyage of H.M.S. Challenger in the years 1872 to 1876. Rep. Sci. Res. Voy. H.M.S. Challenger, nr. 9, 525pp.

Neiheisel, J., 1965. Source and distribution of sediments at Brunswick Harbour and vicinity, Georgia. U.S. Army Coastal Engineering Center, Technical Memorandum, 12, 21pp.

Noronha, F., Leterrier, J., 1995. Complexo Metamórfico da Foz do Douro. Geoquímica e geocronologia. Resultados preliminares. Memórias n. 4 do Museu e Laboratório Mineralógico e Geológico da Faculdade de Ciências da Universidade do Porto, pp. 769–774.

Oliveira, A., Rocha, F., Rodrigues, A., Jouanneau, J.M., Dias, J.M.A., Weber, O., Gomes, C., 2002a. Clay minerals from the sedimentary cover from the Northwest Iberian shelf. Progress in Oceanography 52, 233–247.

Oliveira, A., Vitorino, J., Rodrigues, A., Jouanneau, J.M., Dias, J.M.A., Weber, O., 2002b. Nepheloid layer dynamics in the northern Portuguese shelf. Progress in Oceanography 52, 195–213.

Pires, H., 1989. Alguns aspectos do clima de agitação marítima de interesse para a navegação na costa de Portugal. O clima de Portugal 37 (2), 34.

Pires, O., Pessanha, L., 1986. Wave power climate of Portugal. In: Evans, D., Falcão, A. (Eds.), Hydrodynamics of ocean wave-energy utilization. IUTAM symposium, Lisboa, 1985, Springer, Dordrecht, The Netherlands, pp. 157–167.

Pombo, J., Cascalho, J., Rodrigues, A., Taborda, R., Oliveira, A., 2006. The Sines subvolcanic intrusive complex: imprint on the inner shelf sedimentary cover (Sines, Portugal). Journal of Coastal Research SI 39, 250–254.

Pomerancblun, M., 1966. The distribution of heavy minerals and their hydraulic equivalence in sediments of the Mediterranean continental slope of Israel. Journal of Sedimentary Petrology 36, 162–174.

Ribeiro, A., Antunes, M.T., Ferreira, M.P., Rocha, R.B., Soares, A.F., Zbyszewski, G., Almeida, F.M., Carvalho, D., Monteiro, J.H., 1979. Introduction à la géologie générale du Portugal, Lisboa, 114pp.

Ribeiro, O., Lautensach, H., Daveau, S., 1987. Geografia de Portugal. I A posição geográfica e o território. Edições João Sá da Costa, Lisboa, 1.ª ed. 334pp.

Ribeiro, O., Lautensach, H., Daveau, S., 1997. Geografia de Portugal. II O ritmo climático e a paisagem. Edições João Sá da Costa, Lisboa, 3.ª ed. 288pp.

Rodrigues, A., 2003. Tectono-estratigrafia da plataforma continental setentrional portuguesa. Documentos técnicos do Instituto Hidrográfico (Portugal) 35, 226pp.

Rodrigues, A., Cascalho, J.P., Ribeiro, A., Dias, J.M.A., 1995. Evidências de actividade vulcânica nas cabeceiras do canhão submarino do Porto. Memórias no. 4 do Museu e Laboratório Mineralógico e Geológico da Faculdade de Ciências da Universidade do Porto, pp. 305–309.

Rodrigues, A., Drago, T., 1990. A relação relevo-estrutura no Beiral de Viana. Anais Inst. Hidrográfico 11, 19–29.

Rodrigues, A., Magalhães, F., Dias, J.M.A., 1991. Evolution of the north Portuguese coast in the last 18,000 years. Quaternary International 9, 67–74.

Sallenger, A.H. Jr., 1979. Inverse grading and hydraulic equivalence in grain-flow deposits. Journal of Sedimentary Petrology 49, 553–562.

Slingerland, R.L., 1977. The effects of entrainment on the hydraulic relationships of light and heavy minerals in sands. Journal of Sedimentary Petrology 47, 753–770.

Taborda, R., 1999. Modelação da dinâmica sedimentar da plataforma continental portuguesa. Ph.D. thesis, Lisbon University (unpublished), 366pp.

Teixeira, C., Assunção, C.T., 1961. Notícia explicativa da folha 1-C (Caminha) da Carta Geológica de Portugal na escala 1:50,000. Serviços Geológicos de Portugal, Lisboa, 41pp.

Teixeira, C., Medeiros, A.C., Assunção, C.T., 1965. Notícia explicativa da folha 9-A (Póvoa de Varzim) da Carta Geológica de Portugal na escala 1:50,000. Serviços Geológicos de Portugal, Lisboa, 50pp.

Vanney, J.R., Mougenot, D., 1991. La plate-forme continental du Portugal et les provinces adjacentes: analyse geomorphologique. Memórias dos Serviços Geológicos de Portugal, Lisboa 28, 86pp.

Vitorino, J., Oliveira, A., Jouanneau, J.M., Drago, T., 2002. Winter dynamics on the northern Portuguese shelf. Part 1: physical processes. Progress in Oceanography 52, 129–153.

Wilberg, P.L., Smith, J.D., 1987. A theoretical model for salting grains in water. Journal of Geophysical Research 94, 5011–5016.

APPENDIX A

	Shelf/upper slope			Minho river			Lima river			Cávado river		
	Average	Max.	Min.	Average	Max.	Min.	Average	Max.	Min.	Average	Max.	Min.
Amphibole	5.7	26.5	0.2	1.1	2.7	0.2	0.5	1.4	0.0	0.6	1.6	0.0
Andalusite	8.9	22.1	0.0	4.7	10.6	1.4	6.4	13.7	0.3	3.9	7.2	0.5
Garnet	7.9	32.1	0.2	1.9	6.6	0.3	1.3	2.5	0.0	0.7	2.1	0.0
Staurolite	2.9	11.8	0.0	1.3	2.9	0.2	0.6	2.4	0.0	0.5	2.0	0.0
Tourmaline	6.4	24.0	0.5	2.2	6.7	0.6	2.5	7.0	0.0	2.0	4.0	0.0
Apatite	0.7	3.7	0.0	1.2	2.9	0.0	1.7	4.1	0.0	1.3	4.1	0.0
Biotite	6.3	64.4	0.0	25.0	68.1	2.6	24.0	83.9	3.3	49.3	85.3	5.4
Zircon	3.1	21.7	0.0	2.5	5.4	0.3	6.2	11.1	1.0	2.8	4.3	1.9
Kyanite	0.7	5.2	0.0	0.1	0.3	0.0	0.0	0.2	0.0	0.0	0.0	0.0
Rutile	0.3	1.6	0.0	0.0	0.3	0.0	0.0	0.1	0.0	0.0	0.2	0.0
Sillimanite	0.2	1.6	0.0	0.8	3.0	0.0	1.0	1.9	0.1	0.5	0.8	0.0
Clinopyroxene	0.4	10.1	0.0	0.0	0.0	0.0	0.0	0.0	0.0	0.0	0.0	0.0
Orthopyroxene	0.3	5.8	0.0	0.0	0.0	0.0	0.0	0.0	0.0	0.0	0.0	0.0
Olivine	0.1	2.2	0.0	0.0	0.0	0.0	0.0	0.0	0.0	0.0	0.0	0.0
Others	0.7	4.7	0.0	0.2	0.3	0.0	0.4	1.1	0.0	0.5	1.5	0.2
Glaucony	3.8	50.2	0.0	0.0	0.0	0.0	0.0	0.1	0.0	0.0	0.0	0.0
Opaques	49.4	86.1	24.3	56.6	82.2	18.7	50.2	72.0	8.6	37.1	72.4	5.4
Non-identified	2.3	10.7	0.0	2.4	3.8	1.4	0.6	1.2	0.1	0.8	1.5	0.2

Average, maximum and minimum values for the main heavy minerals identified in the different samples groups. The item "others" includes the very rare species identified such as epidote, anatase, brookite and monazite.

APPENDIX B

	Ave river			Douro river			Total rivers		
	Average	Max.	Min.	Average	Max.	Min.	Average	Max.	Min.
Amphibole	1.5	4.8	0.6	4.8	13.9	0.2	1.7	4.8	0.5
Andalusite	3.9	5.8	2.5	4.3	7.1	0.6	4.6	6.4	3.9
Garnet	0.7	2.3	0.0	1.2	2.8	0.2	1.2	1.9	0.7
Staurolite	0.4	1.1	0.0	0.6	1.3	0.0	0.7	1.3	0.4
Tourmaline	2.3	3.0	1.2	2.1	5.7	0.6	2.2	2.5	2.0
Apatite	1.1	2.1	0.0	3.4	6.1	0.4	1.7	3.4	1.1
Biotite	39.7	62.2	8.8	46.5	71.5	23.9	36.9	49.3	24.0
Zircon	3.5	4.8	1.3	1.8	4.3	0.5	3.4	6.2	1.8
Kyanite	0.1	0.6	0.0	0.4	1.3	0.0	0.1	0.4	0.0
Rutile	0.0	0.0	0.0	0.2	0.6	0.0	0.1	0.2	0.0
Sillimanite	0.2	0.8	0.0	0.3	0.6	0.0	0.6	1.0	0.2
Clinopyroxene	0.0	0.0	0.0	0.0	0.0	0.0	0.0	0.0	0.0
Orthopyroxene	0.0	0.0	0.0	0.0	0.0	0.0	0.0	0.0	0.0
Olivine	0.0	0.0	0.0	0.0	0.0	0.0	0.0	0.0	0.0
Others	0.5	1.1	0.0	0.2	1.0	0.0	0.3	0.5	0.2
Glaucony	0.0	0.0	0.0	0.0	0.0	0.0	0.0	0.0	0.0
Opaques	45.6	69.6	27.3	33.3	46.7	23.1	44.6	56.6	33.3
Non-identified	0.4	0.7	0.0	0.8	1.8	0.0	1.0	2.4	0.4

Average, maximum and minimum values for the main heavy minerals identified in the different samples groups. The item "others" includes the very rare species identified such as epidote, anatase, brookite and monazite.

APPENDIX C

	SED 4			SED 4A			SED 3			SED 2			SED 1		
	Average	Max.	Min.	Average	Max.	Min.	Average	Max.	Min.	Average	Max.	Min.	Average	Max.	Min.
Amphibole	17.3	25.8	6.5	5.8	22.7	0.7	5.2	6.7	3.7	10.0	28.1	0.3	10.1	18.4	0.1
Andalusite	4.8	12.4	0.8	13.9	26.7	6.8	11.0	16.8	4.2	4.2	12.9	0.3	7.0	26.5	1.2
Garnet	1.3	3.3	0.1	12.6	23.1	2.4	10.9	12.5	9.5	2.7	13.4	0.0	2.3	7.6	0.0
Staurolite	0.4	1.2	0.0	5.0	7.4	0.0	4.5	5.2	3.7	0.6	3.0	0.0	0.5	1.4	0.0
Tourmaline	1.8	2.7	0.5	8.0	14.2	0.0	5.9	8.5	0.9	2.6	5.4	0.0	2.7	6.3	0.0
Apatite	1.1	2.1	0.0	0.8	1.7	0.0	0.8	1.4	0.4	1.6	4.5	0.0	1.7	5.5	0.0
Biotite	31.4	62.4	8.4	9.0	25.4	0.0	21.0	38.6	8.8	47.3	95.6	8.3	41.4	84.6	14.9
Zircon	0.1	0.7	0.0	0.8	9.3	0.0	0.5	0.8	0.2	0.4	2.0	0.0	0.3	1.1	0.0
Kyanite	0.1	0.3	0.0	0.6	2.5	0.0	0.6	1.0	0.0	0.2	1.2	0.0	0.2	0.9	0.0
Rutile	0.0	0.2	0.0	0.1	0.4	0.0	0.0	0.0	0.0	0.0	0.3	0.0	0.1	0.2	0.0
Sillimanite	0.2	1.0	0.0	1.5	18.3	0.0	0.1	0.2	0.0	0.3	4.3	0.0	0.2	1.8	0.0
Clinopyroxene	0.0	0.0	0.0	0.0	0.0	0.0	0.0	0.0	0.0	0.0	0.0	0.0	0.0	0.0	0.0
Orthopyroxene	0.0	0.0	0.0	0.0	0.0	0.0	0.0	0.0	0.0	0.0	0.0	0.0	0.0	0.0	0.0
Olivine	0.0	0.0	0.0	0.0	0.0	0.0	0.0	0.0	0.0	0.0	0.0	0.0	0.0	0.0	0.0
Others	0.2	2.4	0.0	1.8	7.0	0.0	0.7	1.8	0.0	0.7	4.8	0.0	0.7	3.7	0.0
Glaucony	0.0	0.0	0.0	0.0	0.0	0.0	0.0	0.0	0.0	0.0	0.0	0.0	0.0	0.0	0.0
Opaques	40.4	57.3	21.2	40.0	50.0	28.1	38.7	41.0	34.9	28.8	60.6	3.8	31.7	52.8	10.1
Non-identified	0.9	4.9	0.0	0.2	2.2	0.0	0.2	0.5	0.0	0.7	3.3	0.0	1.0	3.6	0.0

Average, maximum and minimum values for the main heavy minerals identified in the different samples groups. The item "others" includes the very rare species identified such as epidote, anatase, brookite and monazite.

1.2 From Surface Weathering to Burial Diagenesis

This page intentionally left blank

Chapter 4

SURFACE TEXTURES AND DISSOLUTION PROCESSES OF HEAVY MINERALS IN THE SEDIMENTARY CYCLE: EXAMPLES FROM PYROXENES AND AMPHIBOLES

MICHAEL ANTHONY VELBEL

Department of Geological Sciences, 206 Natural Science Building, Michigan State University, East Lansing, MI 48824-1115, USA

ABSTRACT

Natural weathering of pyroxenes and amphiboles corrodes them in a crystallographically controlled manner, resulting in ubiquitous etch pits on grain surfaces and eventually denticulated margins. Most denticles originate at fractures, but others form without fractures, along arrays of laterally adjacent dislocations. The range of corrosion morphologies is identical between pyroxenes and amphiboles. Weathered pyroxenes and amphiboles at numerous locations and in a wide variety of weathering environments exhibit the same types and ranges of weathering morphologies across a wide range of mineral compositions, regolith types and pedogenic/geochemical environments. Similar ranges of dissolution textures also occur on pyriboles (a short single term for single- and double-chain silicates) in modern sediments and on intrastratally dissolved pyriboles in clastic sedimentary rocks.

Mineral grains are exposed to varying physical and chemical conditions as they move through the sedimentary cycle. Grain surfaces respond to these changing conditions; thus, surface textures on detrital heavy-mineral grains are used to infer weathering processes in soils and weathered regoliths, provenance and sedimentary environments, and intrastratal dissolution during burial diagenesis. The ability to arrive at useful interpretations from sand grain morphology and/or grain-surface textures is based on specific relationships (which differ among different heavy minerals) between rates of surface-texture modification in a given environment and the length of time that the grain is exposed to modifying processes in that part of the sedimentary cycle. For chemically produced features, the timescale for the development of new grain-surface textures depends on the geochemical kinetics of the chemical texture-modifying reactions, which are in turn related to the persistence of each mineral in weathering and the sedimentary cycle. Pyroxenes and amphiboles are minerals with intermediate rates of dissolution and intermediate persistence among heavy minerals; they corrode gradually and survive long enough for the degree of corrosion to be a scientifically useful soil relative-age and environmental indicator. The significance of etch pits and other surface textures on heavy minerals in a soil or regolith depends on

Developments in Sedimentology, Vol. 58, 113–150

ISSN: 0070-4571/doi:10.1016/S0070-4571(07)58004-0

the rates at which they form in that regolith, and how long the grains have been subject to such reactions (i.e., the age of the soil) in the weathering environment. Similar relationships are to be expected in other compartments of the sedimentary cycle.

Keywords: amphibole; chain silicates; corrosion; etching; etch pits; hornblende; inosilicates; dissolution kinetics; pyribole; pyroxene; scanning electron microscopy

1. INTRODUCTION

Morphological and surface-textural attributes of minerals are employed in many ways across the geosciences. Surface textures on alluvial heavy-mineral grains are used to infer provenance and dispersal patterns in support of exploration for economic concentrations of durable gem and industrial heavy minerals (Berg and Dahy, 2002; Berg, 2004; Berg and Equall, 2004). The morphology of zircon (Callender and Folk, 1958; Pupin, 1980; Vavra, 1993; Corfu et al., 2003) has been used in a variety of investigations including tephrostratigraphic correlation (Winter, 1981) to such an extent that objective classification schemes have been developed to quantitatively describe zircon morphology (Matsuura and Aoki, 1989). Such petrogenetic and provenance applications presuppose that primary morphological attributes survive passage of zircon grains from one compartment of the sedimentary cycle to another, a reasonable assumption for a persistent heavy mineral.

Etching characteristics of less-persistent heavy silicate minerals are investigated for other purposes. For example, etching of hornblende during weathering has been used as a relative-age indicator of glacial deposits (e.g., Locke, 1979, 1986; Hall and Martin, 1986; Hall and Michaud, 1988; Hall and Horn, 1993), and as a measure of soil development on glacial parent materials (e.g., Mikesell et al., 2004; Schaetzl et al., 2006). Such applications of surface textures, as chronologic or environmental indicators, assume that dissolution-related morphological attributes of these less-persistent minerals adjust progressively (rather than instantly) to exposure to a new (in this case, weathering) environment.

In the case of zircon, it is the preservation and inheritance of morphological attributes from elsewhere in the rock cycle that allows petrogenesis of its primary source rock and/or provenance to be inferred. In the case of hornblende, it is the relatively rapid overprinting of "up-cycle" textures by characteristic textures in the new environment that allows corrosion features to be used as relative-age or environmental indicators. In both cases, the ability to arrive at useful interpretations from sand grain morphology and/or grain-surface textures is based on specific relationships between rates of surface-texture modification and the length of time the grain is exposed to modifying processes in each environment prior to sampling. Thus, the geochemical kinetics of surface-modifying reactions must be taken into account when studying the distribution and surface textures of those heavy minerals that survive weathering and occur in sediments and sedimentary rocks.

This contribution reviews the origin, distribution and occurrence of chemically produced grain-surface textures on pyroxenes and amphiboles during weathering and diagenesis. For the purposes of this volume, the relationship between surface textures on mineral grains and the geochemical kinetics of surface-modifying

reactions is especially important. At the temperatures characteristic of the Earth's surface, systems of silicate minerals and aqueous solutions seldom attain thermodynamic equilibrium between the solution and more than a very few of the solid phases present (if any). Rates of weathering reactions are slow compared with the time available for silicate-mineral reactions with the solutions percolating through the weathering profile (e.g., Velbel, 1989b). Thus, the emphasis in this contribution is on the kinetics of dissolution as they apply to natural weathering (specifically, etching during dissolution), and the consequences of reaction processes and mechanisms that might be observable and interpretable from microscopic observation of surface textures on naturally weathered mineral grains.

There is a large literature on the dissolution kinetics of silicate minerals in the laboratory that offers considerable insight into dissolution rates and relative persistence of different silicates, but much of this literature does not illustrate the resulting surface textures. In emphasising only those aspects of geochemical kinetics that have textural consequences, and in focusing on only chain silicates, this contribution is narrower in scope than most other recent papers. Readers interested in a more detailed discussion of the geochemical kinetics of silicate-mineral dissolution are directed to the many fine papers in the outstanding volume edited by White and Brantley (1995), and the more recent thorough reviews by Wilson (2004), Brantley (2005) and White (2005).

By virtue of the author's experience, and because (as will be shown below) there are many similarities between textures produced by dissolution during weathering and those produced by intrastratal dissolution during burial diagenesis, weathering is emphasised. After briefly introducing a framework linking dissolution kinetics with surface textures, this review concentrates on textures observed with conventional scanning electron microscopy (SEM) using secondary electron imaging (Welton, 1984; England, 1991), although transmitted polarised-light microscopy, SEM using backscattered electron imaging, field-emission SEM (FE-SEM) and transmission electron microscopy (TEM) will also be mentioned. All SEM images presented here are selected from a number of case studies on pyribole weathering by the present author, his colleagues and his students at Michigan State University (MSU). Study areas represented include the following two National Science Foundation Long Term Ecological Research (LTER) sites, and several others.

(1) Clinopyroxene from weathered pyroxenite, Koua Bocca, Ivory Coast, Africa. Optical petrography and compositions of pyroxenes and their weathering products at this locality were described by Delvigne (1983, 1990, 1998); Velbel and Barker (accepted) describe weathering of the same pyroxenes using SEM and FE-SEM.
(2) Hornblende from weathered amphibolite of the Carroll Knob (metamorphosed mafic-ultramafic) Complex, near Otto, North Carolina, U.S.A. Hornblende weathering at this locality (the Coweeta Hydrologic Laboratory southern hardwood forest ecosystem LTER site) was described by Velbel (1989a).
(3) Hornblende from weathered amphibolites of the Laurel Creek (metamorphosed mafic-ultramafic) Complex, Georgia, U.S.A.
(4) Pyriboles (mostly hornblende) in heavy-mineral separates from agricultural and forest soils on glacial parent material at the MSU Kellogg Biological Station (KBS; the LTER agroecosystems site), Hickory Corners, Michigan, U.S.A., and soil under forest on glacial parent material, Sanford Natural Area, MSU campus,

East Lansing, Michigan, U.S.A. Soil and garnet weathering at these sampling sites are described by Velbel et al. (2007, this volume).

(5) Hornblende grains in heavy-mineral separates from soil on glacial parent material, Grayling Fingers area, Michigan, U.S.A. Hornblende etching in this study area was reported by Mikesell et al. (2004) and Schaetzl et al. (2006).

Most images presented here are similar to, and representative of, large numbers of images in the references cited throughout this paper.

2. BACKGROUND: FORMATION OF ETCHING FEATURES ON MAJOR ROCK-FORMING SILICATES

Velbel (2000) discusses the interplay of transport and reaction processes for mineral-solution reactions (e.g., crystal growth from aqueous solutions, and crystal dissolution during rock and mineral weathering). Any heterogeneous (multiphase) reaction (e.g., a mineral/water reaction, for example, dissolution of halite; hydrolysis of silicate minerals during rock weathering) requires a sequence of steps for the reaction to proceed. Assuming all reactants are available in excess, the following steps must occur (in series) during crystal growth from, or dissolution into, aqueous solution (Berner, 1980, 1981).

(1) Aqueous reactants (e.g., hydrogen ions or hydronium), or solvent of appropriate composition (supersaturated with respect to the mineral for growth and undersaturated for dissolution), must arrive at the mineral/solution interface.

(2) The reaction must occur at the interface; a variety of specific kinds of reactions and processes can take place at the surface (Berner, 1980, 1981; Lasaga, 1998).

(3) Dissolved products (e.g., alkali or alkaline earth cations, aqueous silica) must leave the site of the interfacial reaction (lest they accumulate to the extent that equilibrium is attained or the reaction is otherwise kinetically suppressed).

If the 1st or 3rd step (transport) is slow (rate-determining), the reaction is said to be *transport limited*. If the 2nd process (reaction) is rate-determining, the reaction is said to be *reaction limited*, or *kinetically controlled*, or, in the case of heterogeneous (multiphase) reactions, *interface limited* (because the rate-limiting reaction takes place at the interface), also widely termed *surface-reaction controlled*. Velbel (2000) discusses these concepts in greater detail.

Following Berner (1978, 1980, 1981) and Lasaga (1998, p. 583), Velbel (2004) summarises four tests that can be used to distinguish transport-limited kinetics from interface-limited kinetics in crystal growth and mineral dissolution. The magnitude of the measured rate relative to the theoretical rate for diffusion, the effect of advective transport on the measured rate, the Arrhenius activation energy and the surface morphology of the reacting crystal can all be used to distinguish interface-limited and transport-limited kinetics in any individual set of experimental conditions. Only one of these four tests—surface morphology—applies to the case of naturally altered mineral grains, if detailed data on solution chemistry of the altering fluid are not available. Transport-limited and interface-limited reaction mechanisms each have different consequences for surface morphology of weathered mineral grains; therefore, microscopic examination of mineral surfaces and their morphologies and compositions helps reveal which of the two mechanisms dominates in any

individual instance (Berner, 1978, 1981), even in the absence of experimental constraints.

Surfaces of minerals dissolving by transport control should have smooth, rounded, featureless surfaces, reflecting the uniformity of attack on the surface (Berner, 1978, 1981). Diffusion is the slowest form of transport; the medium through which diffusion occurs may be the surrounding fluid, or a layer of residual or secondary solids (a "protective surface layer", PSL) on the surface of the dissolving mineral. Diffusion through aqueous solutions is rapid compared with diffusion through solids, so aqueous diffusion is rate-limiting only for rapidly dissolving, highly soluble reactants (Berner, 1978, 1981; Velbel, 2004). Measured dissolution rates of less-soluble substances, including silicate minerals, are too slow to be accounted for by aqueous diffusion (Berner, 1978, 1981), but diffusion through a diffusion inhibiting surface layer (PSL) could be rate-determining if such a layer with appropriate properties could be formed (Velbel, 1993a). Necessary conditions for the formation of PSLs are discussed by Velbel (1993a). Because such occurrences are likely to be uncommon (restricted to only certain reactant–product assemblages: Velbel, 1993a), and because other factors intervene such that even some permissible reactant–product assemblages do not actually form PSLs (Velbel et al., 1996), details of PSL formation will not be reviewed further here. Compositionally modified surface layers have been reported on naturally weathered pyriboles by some workers (e.g., Mogk and Locke, 1988), but micromorphological techniques have not revealed compositions and/or morphologies consistent with the "protective surface layer" hypothesis on most silicate minerals. Instead, etch pits (crystallographically controlled dissolution voids) are ubiquitous on naturally weathered feldspars, pyroxenes, amphiboles and olivines (e.g., Velbel, 1993a).

3. DISSOLUTION TEXTURES OF CHAIN SILICATES

The most abundant naturally occurring chain silicates belong to the pyroxenes (single-chain silicates) and amphiboles (double-chain silicates); together, the chain silicates make up 16% of Earth's crust (Klein, 2002). Pyroxenes and amphiboles are two closely related groups of minerals. The pyroxene structure consists of chains or "I-beams" of a pair of tetrahedral ("T") chains of corner-linked silica separated by an octahedral ("O") chain, forming "T-O-T" chains. Pyroxene I-beams are single-chain wide. Amphibole I-beams are made up of double-width T-O-T chains. In addition to tetrahedral and octahedral cations within the T-O-T chains, pyroxenes and especially amphiboles have other crystal-chemical sites between T-O-T I-beams. A broad range of crystal-chemical substitutions occurs in pyroxenes and amphiboles; as a consequence, many structurally similar but compositionally different minerals occur in the pyroxene and amphibole groups (e.g., Klein, 2002). However, the abundant pyroxene and amphibole minerals in Earth's crust are Mg- and Fe-species (with or without Ca). This brief review will emphasise the weathering and dissolution behaviour of common pyroxenes and amphiboles. Where phenomena are being discussed that are common to both pyroxenes and amphiboles, the term *pyriboles* will be used as a short single term for single- and double-chain silicates.

Among ferromagnesian silicates, chain silicates generally weather faster than micas and other sheet silicates, and more slowly than olivine (e.g., Goldich, 1938; Lasaga, 1984; Eggleton, 1986; Brantley, 2005). This relative susceptibility to weathering scales with the extent to which corners of silicate tetrahedra are shared (connected) with other silicate tetrahedra in the mineral structure; the greater the degree of connectedness, the slower is the weathering rate (Brantley and Chen, 1995; Brantley, 2005). Common pyroxenes weather faster than common amphiboles in both nature (Goldich, 1938; Hay, 1959) and the laboratory (Brantley and Chen, 1995; Brantley, 2005). Additional details regarding compositional influences on pyribole weathering are summarised by Brantley and Chen (1995) and Brantley (2005).

3.1. Dissolution (Corrosion) Features of Naturally Weathered Chain Silicates

The many different mineral species of the two major chain-silicate groups (pyroxenes and amphiboles) exhibit many similarities in dissolution textures. Natural weathering of chain silicates forms etch pits on their surfaces and eventually "sawtooth" or "denticulated" margins. Site-selective dissolution at dislocation outcrops on silicate minerals (nucleation of etch pits at dislocation outcrops on the reacting mineral surface; the role of strain energy in the locally distorted crystal structure around a screw or edge dislocation in both the dissolution kinetics of silicate-minerals and etch-pit morphology; the influence of the degree of undersaturation of the solution with respect to the dissolving mineral on the angular or rounded nature of the etch-pit edges etc.) is well understood (Berner, 1980, 1981; Wegner and Christie, 1985a, b; Brantley et al., 1986; Lasaga and Blum, 1986; Blum and Lasaga, 1987; Schott and Petit, 1987; Blum et al., 1990; Gratz et al., 1991a, b; Lasaga, 1998; Brantley, 2005). Etch pits on chain silicates, their occurrence and relationships to other weathering textures are discussed in detail in this section.

Etch pits on pyriboles form preferentially at sites where dislocations intersect mineral surfaces (Berner et al., 1980; Berner and Schott, 1982). Individual etch pits on pyriboles are elongate parallel to the crystallographic *z*-axis (parallel to the tetrahedral chains), producing lenticular (almond-shaped) depressions on their surfaces (Figs. 1A–D: Berner et al., 1980; Berner and Schott, 1982). Differences in etch-pit shape (e.g., aspect ratio, curvature of walls) may be related to the parent-mineral structure and composition and/or the chemistry of the solution into which the pyribole is dissolving; further investigation of controls on pyribole etch-pit shape (e.g., Cremeens et al., 1988, 1992) is required. Dislocations, and the etch pits formed from them, may be randomly distributed (Fig. 1A) or spatially organised (Fig. 1B). Some pyribole grains have both randomly distributed and spatially organised etch pits (Figs. 1C, D).

Etch pits on chain silicates progress through a sequence of stages. Progressive weathering causes the dissolution voids to increase gradually and systematically in size (both depth and cross-sectional area) on the usually well defined pre-weathering surface of the mineral grain. Where multiple etch pits grow and eventually coalesce, larger—more complex—surface textures result (Locke, 1979, 1986; Berner et al., 1980; Berner and Schott, 1982; Cremeens et al., 1992; Velbel, 1993a; Lang, 2000). The topography of the surfaces depends on whether the etch pits coalesce end to end (coalescence and overlap parallel to the crystallographic *z*-axis) or side by side; this in

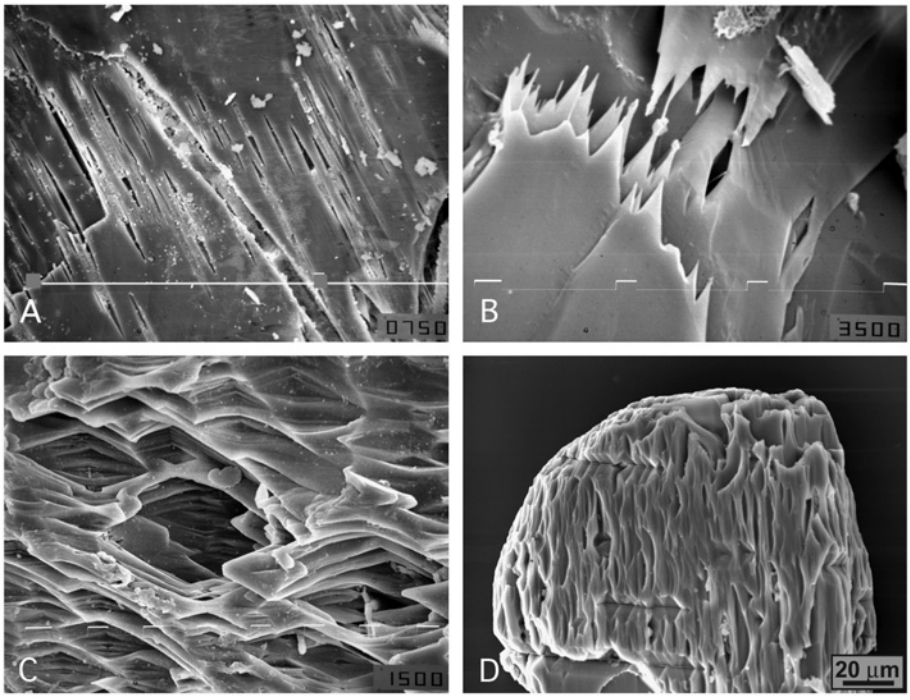

Fig. 1. Etch pits on various pyriboles weathered in different environments. (A) Large, high etch pit aspect (length/width) ratio lenticular etch pits on amphibole grain from weathered Laurel Creek Complex, Georgia, U.S.A. No treatment to remove alteration products was used. Scale marks are 100 µm apart. (B) *En echelon* lenticular etch pits and denticles formed by enlargement and coalescence of laterally adjacent lenticular etch pits. These etch pits and denticles did not originate at a fracture, but along an array of laterally adjacent dislocations. Clinopyroxene from weathered pyroxenite, Koua Bocca, Ivory Coast, Africa. No treatment to remove alteration products was used. Scale marks are 10 µm apart. (C) Large, low etch-pit aspect (length/width) ratio lenticular etch pits on ~0.2 mm-long pyribole grain from soil on glacial parent material, Sanford Natural Area, MSU campus, U.S.A. This sample was treated to remove soil organic matter and clay. Scale marks are 100 µm apart. (D) High etch-pit aspect (length/width) ratio lenticular etch pits on fine-sand sized hornblende grain from soil on glacial parent material, Grayling Fingers area, Michigan, U.S.A. This sample was treated to remove soil organic matter and clay.

turn is determined by the distribution of dislocations in the parent mineral. End-to-end coalescence results in the formation of longitudinal grooves or striations. Growth and coalescence of *en echelon* (side-by-side) lenticular etch pits on pyriboles (Figs. 1B–D and 2) form arrays of etch pits separated from one another by "pillars" consisting of undissolved pyribole. Continued dissolution eventually removes the thinnest parts of the "pillars", forming "sawtooth-lined microcracks" and "micro-caves" (Fig. 3). These are the so-called "cave features" of Berner et al. (1980), Berner and Schott (1982), Argast (1991) and Cremeens et al. (1992). Tooth-like denticles (the "sawteeth", superficially resembling stalactites and stalagmites) are the remnants of pyribole walls and pillars between the etch pits (Berner and Schott, 1982). Symmetrical

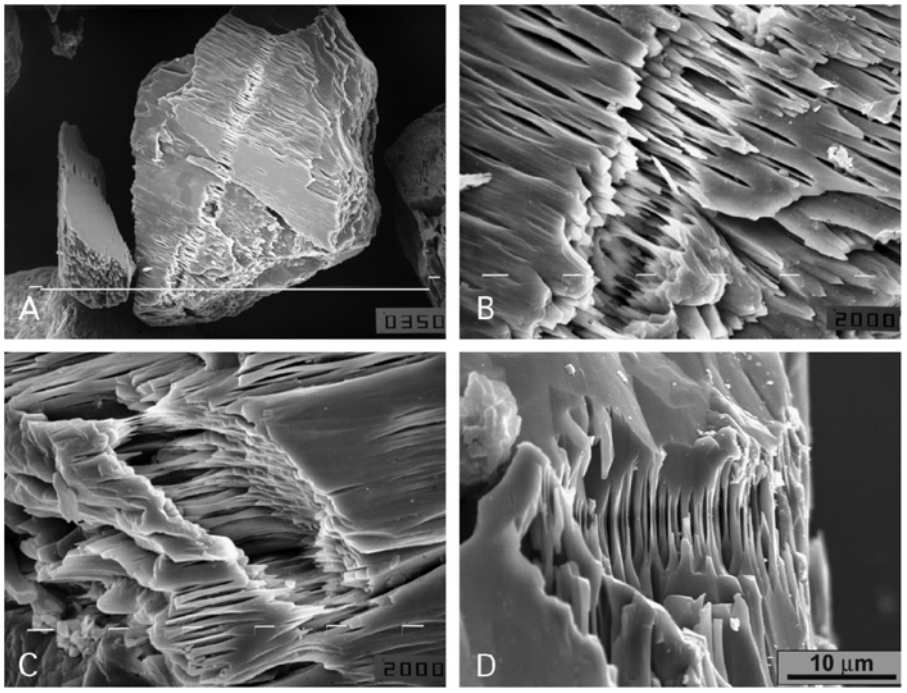

Fig. 2. *En echelon* lenticular etch pits (and randomly distributed lenticular etch pits), "stalactite/stalagmite-like" pillars left behind during intermediate stages of enlargement and coalescence of laterally adjacent lenticular etch pits, and denticles formed by further reduction of pillars, on pyribole grains from soils on glacial parent material. These etch pits and denticles did not originate at a fracture, but along an array of laterally adjacent dislocations. All these samples were treated to remove soil organic matter and clay. (A) Sample from soil under forest, MSU KBS, Michigan, U.S.A. Scale marks are 100 µm apart. (B) Close-up of bottom part of Fig. 2A. Scale marks are 10 µm apart. (C) Sample from soil under forest, MSU KBS, Michigan, U.S.A. Scale marks are 10 µm apart. (D) Hornblende grain from soil on glacial parent material, Grayling Fingers area, Michigan, U.S.A.

("mirror-image") arrays of denticles occur on opposite sides of the dislocation array (e.g., Figs. 1B–D, 2 and 3), so that a single pyribole crystal transected (at some high angle to the *z*-axis) by an array of dislocations is divided by weathering into smaller denticulated remnants (e.g., Wilson, 1986), separated from one another by sawtooth-lined voids (Fig. 3).

Symmetrical denticulation patterns also commonly occur on opposite sides of fractures transecting pyribole crystals at high angles to the *z*-axis (e.g., Delvigne, 1983, 1998). Occurrences in which multiple pyribole grains are optically aligned and have corresponding symmetrical denticulation patterns imply an origin of the ensemble by subdivision of a single pyribole crystal along (1) trans-mineral cleavage or other fractures (e.g., Delvigne, 1983, 1998) and/or (2) arrays of aligned dislocations (e.g., Figs. 1B–D, 2 and 3). In the former case, weathering products often persist where the fracture used to be (Berner and Schott, 1982; Velbel, 1989a) (Fig. 4), allowing the two origins to be distinguished. It is not possible to distinguish the two

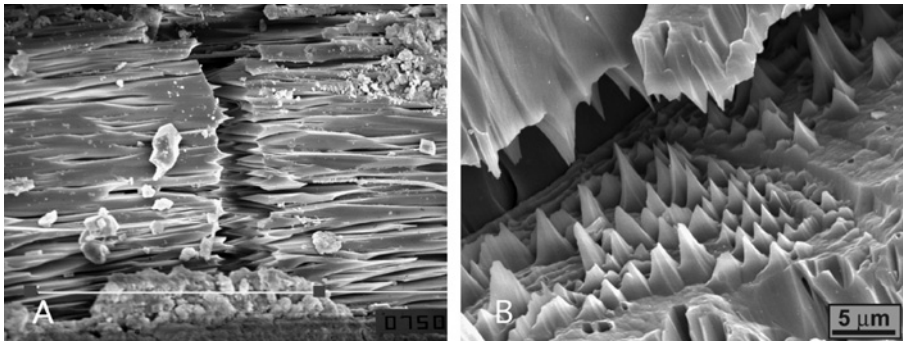

Fig. 3. Etch "caves" with "stalactite/stalagmite-like" denticles left behind during advanced stages of enlargement and coalescence of *en echelon* lenticular etch pits on hornblende in two different regoliths. These denticles did not originate at a fracture, but along an array of laterally adjacent dislocations. (A) Weathered Carroll Knob Complex, North Carolina, U.S.A. No treatment to remove alteration products was used. Scale marks are 100 µm apart. (B) Soil on glacial parent material, Grayling Fingers area, Michigan, U.S.A. This sample was treated to remove soil organic matter and clay.

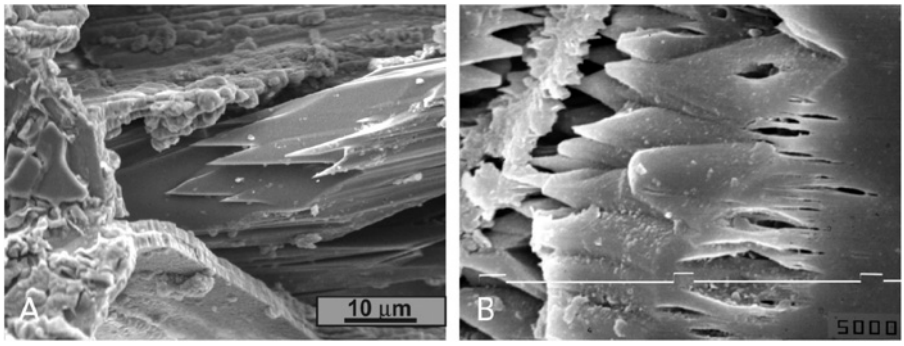

Fig. 4. Weathering products (boxwork) separated from denticulated pyribole remnant by space, implying removal of pyribole in solution. (A) Weathering products (kaolinite, gibbsite and goethite) constitute boxwork (with central parting) separated from denticulated hornblende remnant by space, implying removal of hornblende in solution. Weathered Carroll Knob Complex, North Carolina, U.S.A. No treatment to remove alteration products was used. (B) Pyribole from soil under forest on glacial parent material, Sanford Natural Area, MSU campus, Michigan, U.S.A. This sample was treated to remove soil organic matter and clay. Scale marks are 10 µm apart.

origins in samples from which weathering products have been removed in nature or during sample treatment. Denticles also form by penetration (preferentially along the *z*-axis) of etch pits into the ends of elongate pyribole crystals; in such occurrences, no corresponding denticles occur symmetrically on the other side of the grain boundary.

Coalescence of *en echelon* lenticular etch pits in any of the settings described above forms "sawtooth" or "denticulated" terminations (Fig. 5) (Berner et al., 1980; Berner and Schott, 1982; Velbel, 1989a; Argast, 1991; Moore, 1996). Denticulated margins (also known in older literature as "cockscomb terminations" or "hacksaw

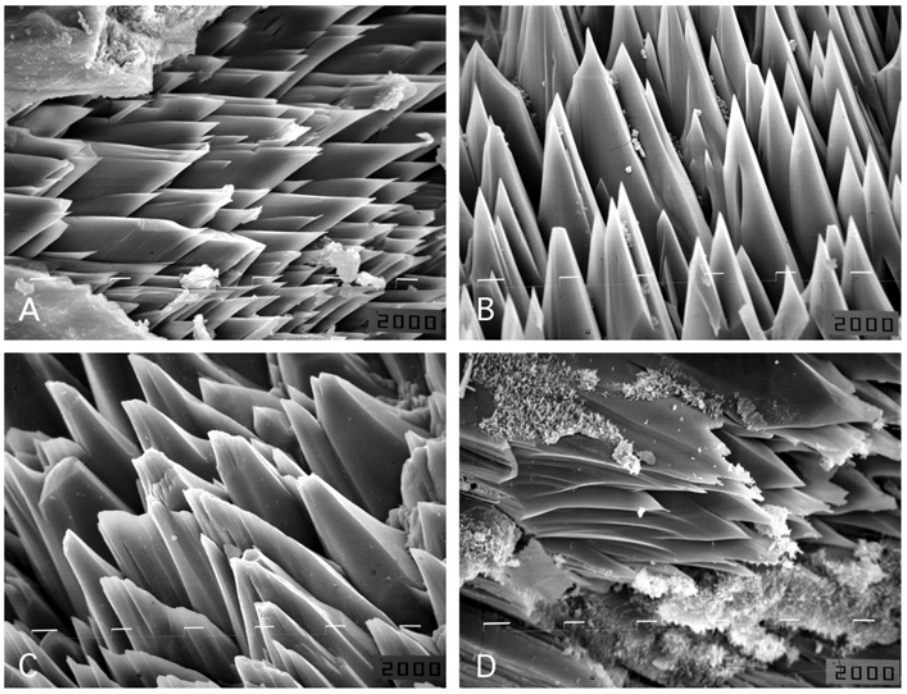

Fig. 5. Classic denticles formed by enlargement and coalescence of laterally adjacent lenticular etch pits on pyroxenes and amphiboles, in a variety of weathered rocks and soils. (A) Pyroxene from weathered pyroxenite, Koua Bocca, Ivory Coast, Africa. Delvigne (1998) presented colour photomicrographs from petrographic thin-sections illustrating identical features from near-identical depths in the same weathering profile. No treatment to remove alteration products was used. Scale marks are 10 μm apart. (B) Hornblende of weathered Carroll Knob Complex, North Carolina, U.S.A. No treatment to remove alteration products was used. Scale marks are 10 μm apart. (C) Pyribole grain from agricultural soil on glacial parent material, MSU KBS, Michigan, U.S.A. This sample was treated to remove soil organic matter and clay. Scale marks are 10 μm apart. (D) Weathering products distributed locally near tips of denticles on weathered amphibole, weathered Laurel Creek Complex, Georgia, U.S.A. The form and size of these denticles is similar to denticles devoid of weathering products (Figs. A, B, same magnification), suggesting that the presence of weathering products has no effect on etching and the formation of denticulated margins. Colin (1994) and Colin et al. (1990) illustrated identical distributions of products on naturally weathered pyroxene, suggesting no difference in this effect between hornblendes and pyroxenes. No treatment to remove alteration products was used. Scale marks are 10 μm apart.

terminations'') are easily visible by optical microscopy of grain mounts or in thin-section (e.g., Bradley, 1957; Hay, 1959; Cleaves, 1974; Delvigne, 1983, 1998; Colin, 1984; Pevear et al., 1984; Mange and Maurer, 1992) and can appear quite dramatic in scanning electron microscope images (Fig. 5) (e.g., Müller and Schwaighofer, 1979; Berner et al., 1980; Berner and Schott, 1982; Glasmann, 1982; Boulangé, 1984; Colin, 1984; Bateman and Catt, 1985; Colin et al., 1985; Ohse et al., 1985; Velbel, 1989a, 1993a). Figs. 5A–D are a series of images, all acquired at the same magnification, illustrating the similarity of denticles on pyroxenes and amphiboles, in a

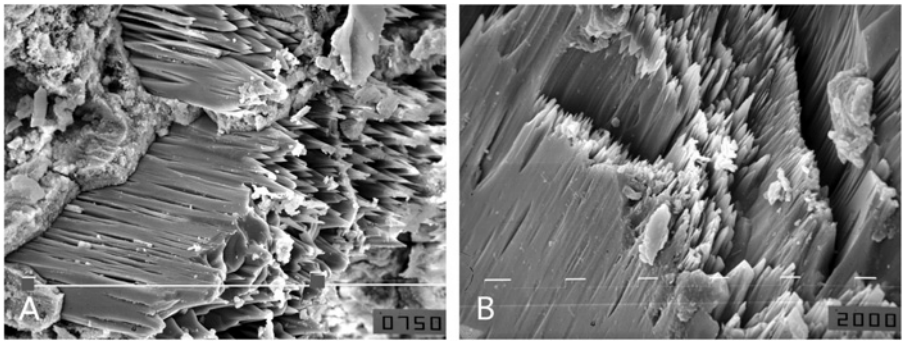

Fig. 6. Coexisting lenticular etch pits and denticles on pyriboles. These images illustrate the similarity of lenticular etch pits and associated denticles on pyroxenes and amphiboles, in a variety of weathered rocks, regoliths and soils. (A) Hornblende of weathered Carroll Knob Complex, North Carolina, U.S.A. No treatment to remove alteration products was used. Scale marks are 100 μm apart. (B) Pyribole grain from agricultural soil on glacial parent material, MSU KBS, Michigan, U.S.A. This sample was treated to remove soil organic matter and clay. Scale marks are 10 μm apart.

variety of weathered rocks and soils. Fig. 6 shows the coexistence of denticulated terminations with isolated etch pits, all elongate parallel to the crystallographic *z*-axis, on pyriboles from various weathering environments. However, in some occurrences denticulated terminations form on the ends of pyribole grains without development of lenticular etch pits on other surfaces of the same pyribole grain (Singh and Gilkes, 1993). Fig. 7 shows doubly terminated denticulated pyribole remnants from several different weathering environments (see also Berner et al., 1980; Delvigne, 1983, 1998; Boulangé, 1984; Colin, 1984), including saprolitic regoliths on crystalline parent rock and soils under different vegetation types on glacial parent material.

Pyribole dissolution voids (lenticular etch pits and denticles) are often empty (devoid of weathering products) in nature (Figs. 1B, 3A, 4, 5A, B, D and 7A) (Hay, 1959; Cleaves, 1974; Glasmann, 1982; Anand and Gilkes, 1984; Velbel, 1989a) but not always (Hay, 1959; Nahon and Colin, 1982; Chitale and Guven, 1989). The full range of surface textures, from minimally modified surfaces with a few small etch pits, to tiny remnants bounded entirely by denticles, occur in naturally weathered materials (e.g., Hay, 1959; Berner et al., 1980; Berner and Schott, 1982; Delvigne, 1998), although the range observed in any individual sample or weathering profile is commonly a subset of the full range known for these mineral groups.

The surface morphology of weathered pyriboles can be strongly influenced by the distribution of more- and less-weathering-resistant volumes of pyribole (Berner et al., 1980; Berner and Schott, 1982; Wilson and Jones, 1983; Argast, 1991; Wilson, 2004). In some occurrences, the ideal form of elongate lenticular etch pits is modified by apparent variations in the resistance of the adjacent material to corrosion. Some naturally weathered pyriboles exhibit etch pits with squared-off ends (Fig. 8A) rather than the more common sharp-pointed ends. Other naturally weathered pyriboles exhibit elongate etch pits in which corrosion of the walls is interrupted by planar discontinuities at high angles to the *z*-axis (Fig. 8B). (Denticles may be truncated

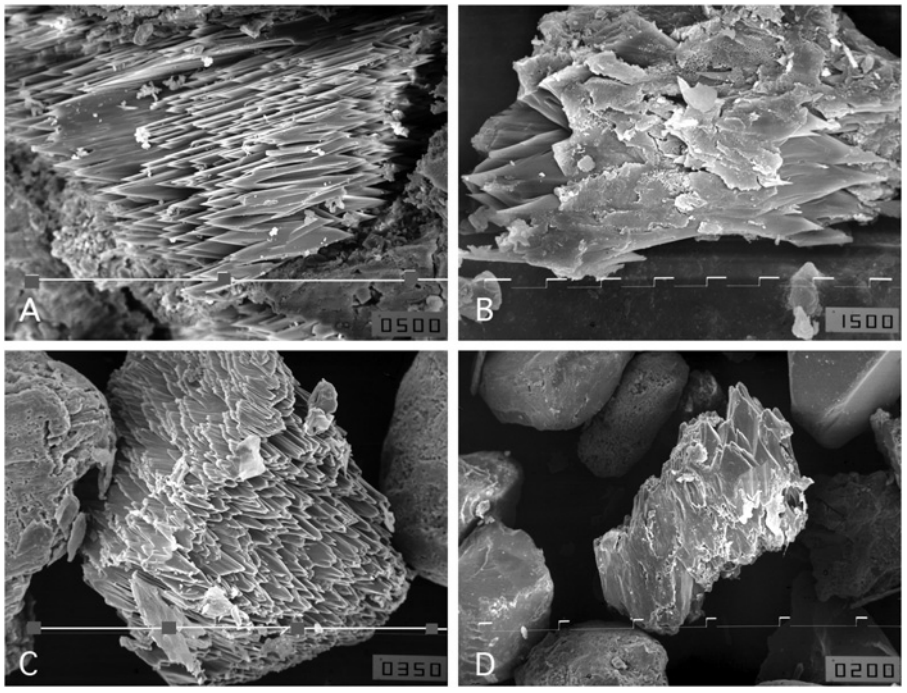

Fig. 7. Doubly terminated denticulated pyribole remnants from different weathering environments. (A) Hornblende from weathered Carroll Knob Complex, North Carolina, U.S.A. No treatment to remove alteration products was used. Scale marks are 100 μm apart. (B) Pyroxene from weathered pyroxenite, Koua Bocca, Ivory Coast, Africa. Delvigne (1998) presented colour photomicrographs from petrographic thin-sections illustrating identical features from near-identical depths in the same weathering profile. No treatment to remove alteration products was used. Scale marks are 10 μm apart. (C) Pyribole from agricultural soil on glacial parent material, MSU KBS, Michigan, U.S.A. This sample was treated to remove soil organic matter and clay. Scale marks are 100 μm apart. (D) Pyribole in soil under forest on glacial parent material, Sanford Natural Area, MSU campus, Michigan, U.S.A. This sample was treated to remove soil organic matter and clay. Scale marks are 100 μm apart.

similarly, but this might be due to either natural causes or breakage during sample handling.) In still other naturally weathered pyriboles, denticles are "capped" by tabular bodies of corrosion-resistant mineral material oriented at a high angle to the pyribole *z*-axis (Fig. 8C). These and other (Figs. 1D and 8D) similarly oriented discontinuities in the corrosion of pyriboles are referred to here as resistant planar features. Resistant planar features as described here are most likely consequences of differential dissolution of multiple exsolved pyribole phases. Exsolution lamellae comprising pyriboles of different compositions are primary features of many pyriboles (e.g., Veblen et al., 1993). These lamellae have different resistance to weathering that has been documented at TEM scales (Banfield and Barker, 1994).

Future studies of the simultaneous weathering of two or more pyriboles in the same sample could shed additional light on the influence of composition on relative weathering rates of pyriboles of different compositions, a subject currently unresolved

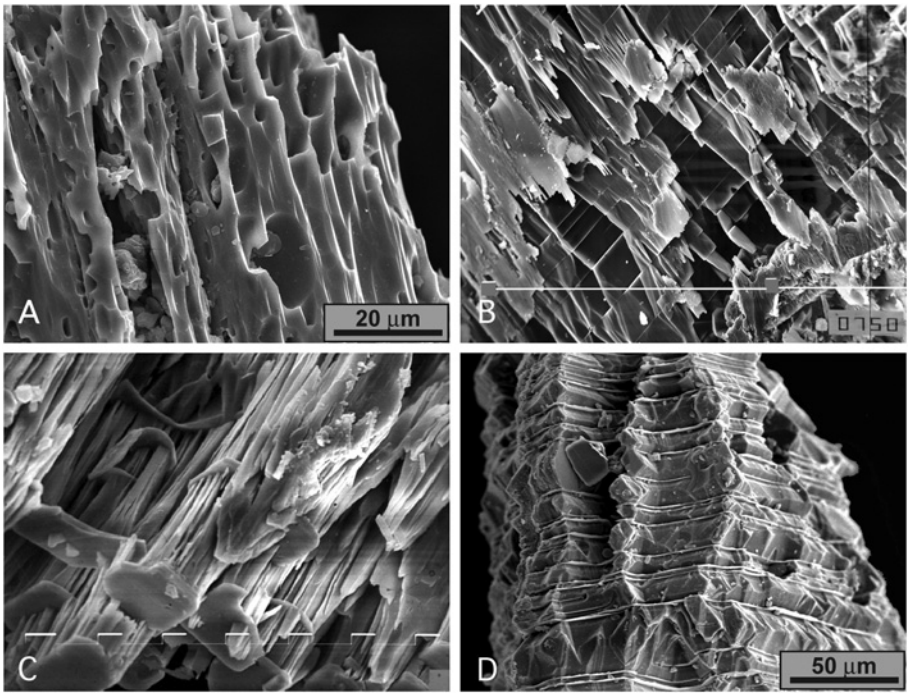

Fig. 8. Modification of ideal lenticular etch pit form by planar discontinuities. (A) While some simple lenticular etch pits (centre) and proto-denticles (upper left) occur on this hornblende grain, most etch pits are truncated at their ends rather than coming to a point. Hornblende grain from soil on glacial parent material, Grayling Fingers area, Michigan, U.S.A. This sample was treated to remove soil organic matter and clay. (B) Elongate lenticular etch pits with walls interrupted by planar discontinuities at a high angle to the pit elongation direction. Some denticles also appear to be truncated by the same discontinuities. Weathered hornblende, Laurel Creek Complex, Georgia, U.S.A. No treatment to remove alteration products was used. Scale marks are 100 μm apart. (C) Resistant tabular-planar features at high angle to denticles, some of which appear to penetrate the resistant material. Pyribole from agricultural soil on glacial parent material, MSU KBS, Michigan, U.S.A. This sample was treated to remove soil organic matter and clay. Scale marks are 100 μm apart. (D) Abundant closely spaced tabular-planar resistant features modulate etch-pit pattern. Hornblende grain from soil on glacial parent material, Grayling Fingers area, Michigan, U.S.A. This sample was treated to remove soil organic matter and clay.

by the very complex results from laboratory experiments (Brantley and Chen, 1995; Brantley, 2005). Even simple studies of coexisting large pyribole crystals of different compositions in the same weathered sample would shed new light on compositional controls and factors other than composition (e.g., nature and distribution of defects) that can influence weathering rates. For example, Delvigne (1983, 1990, 1998) reports that, contrary to expectations from experience elsewhere and from crystal-chemical considerations, Ca-poor orthopyroxene weathers more quickly than Ca-rich clinopyroxene in weathering profiles on ultramafic rocks in the Ivory Coast. Especially interesting would be studies of multiple pyribole phases that coexist at microscopic

scales as exsolution lamellae (Veblen et al., 1993) like that of Banfield and Barker (1994), who demonstrated the differential resistance to natural weathering of exsolved amphiboles of different compositions using TEM. Combined optical, SEM and TEM studies of naturally weathered defective, exsolved and coexisting pyriboles of different compositions would be very informative and are highly desirable.

3.2. Formation of Weathering Products

There are two grain-scale mechanisms by which primary silicate minerals in general, and chain silicates in particular, weather to secondary minerals—transformation and neoformation (Duchaufour, 1982; Eslinger and Pevear, 1988; Nahon, 1991).

3.2.1. Transformation

In transformation, the bonds linking the apical oxygens of the silica tetrahedra in the chains of the chain silicates are locally broken and remade, allowing single- and double-width chains to rearrange and reattach themselves laterally into extensive tetrahedral-octahedral-tetrahedral (T-O-T) sheets, the basic structural unit of 2:1 clay minerals. Products of transformation reactions are often pseudomorphic (Nahon, 1991) or—in the case of anhedral primary minerals—alteromorphic in the terminology of Delvigne (1998) after the primary reactant mineral. Products of transformation often (but not always: Singh and Gilkes, 1993) have regular crystallographic and orientation relations with the structure of the primary reactant mineral (Basham, 1974; Delvigne, 1983). The structural significance of this systematic orientation relationship was initially recognised from astute crystallographic interpretation (Eggleton, 1975; Cole and Lancucki, 1976) and where it occurs is readily observed by optical petrography (Delvigne, 1998) or TEM (Eggleton and Boland, 1982; Eggleton, 1986; Banfield and Barker, 1994; Taylor and Eggleton, 2001).

3.2.2. Neoformation

In neoformation, destruction of primary-mineral bonding is more complete, and secondary minerals are formed (often at some distance from the site of primary-mineral destruction) by crystal growth of secondary minerals from solutes. Because secondary-mineral formation by precipitation does not require any specific structural relationship with the primary reactant-mineral surface (from which precipitation may be separated by considerable distance), there is no necessary orientation relationship between primary (reactant) minerals and their neoformation products (Velbel, 1989a; Singh and Gilkes, 1993).

3.2.3. Petrographic distribution of chain silicate weathering products

Weathering commonly begins at grain boundaries and along cleavages, and that is where weathering products are observed at the earliest petrographically discernable stages of pyribole weathering (Figs. 4 and 6A) (Basham, 1974; Cleaves, 1974; Colman, 1982; Proust, 1982, 1985; Delvigne, 1983, 1998; Colin et al., 1990). These products often exhibit some kind of preferred optical-crystallographic orientation with respect to the reactant mineral (Basham, 1974; Wilson, 1975; Delvigne, 1983, 1998; Abreu and

Vairinho, 1990; Banfield and Barker, 1994) but are not always structurally controlled by the parent mineral (Wilson and Farmer, 1970; Berner and Schott, 1982; Singh and Gilkes, 1993). Continued weathering produces either pseudomorphs/alteromorphs of clay after pyroxene or amphibole (Hay, 1959; Eggleton, 1975; Cole and Lancucki, 1976; Ildefonse, 1980; Delvigne, 1983, 1990, 1998; Meunier, 1983; Smith et al., 1987; Abreu and Vairinho, 1990; Robertson, 1995; Robertson and Butt, 1997) or a "boxwork" structure (Fig. 4A; terminology of Stoops et al., 1979) in which fracture linings/fillings are preserved while the remainder of the reactant pyribole is dissolved congruently (Hay, 1959; Basham, 1974; Cleaves, 1974; Eswaran, 1979; Glasmann, 1982; Delvigne, 1983; Velbel, 1989a; Taylor and Eggleton, 2001). The boxwork preserves the original fracture and/or cleavage pattern, whereas the mineral has been "replaced" by voids. The location of the original grain-transecting fracture along which replacement began is marked by a central parting in the boxwork material (Fig. 4A), as discussed by Velbel (1989a). Complete removal of pyribole leaves a septoalteromorph in the terminology of Delvigne (1998), previously referred to as a "negative pseudomorph" by Velbel (1987, 1989a).

Secondary minerals vary among different geochemical and leaching environments; regolith geoscientists use a classification based on the major clay minerals formed (e.g., Taylor and Eggleton, 2001). At early stages of weathering and/or under conditions of minimal leaching of dissolved products, 2:1 clay minerals form as weathering products; such weathering, forming products comprising two tetrahedral silicate sheets per octahedral sheet, is termed *bisiallitic*. At intermediate degrees of weathering and/or leaching intensity, 1:1 clay minerals form; such weathering, forming products comprising one tetrahedral silicate sheet per octahedral sheet, is termed *monosiallitic*. When weathering has been so extensive or intense that silica has been essentially completely leached from the weathering profile, hydroxides and oxyhydroxides of Fe and Al are the dominant weathering products; such weathering is termed *ferrallitic*.

All varieties of clay mineral and (oxy-)hydroxide weathering products have been observed to form from naturally weathered pyriboles. Surface textures on the underlying chain silicates appear not to vary with differences in environment or the specific nature of the clay just above the corroded surface. For example, the etching textures illustrated in Figs. 1B, 5A and 7B are associated with smectite in an early stage of weathering in a poorly leached regolith setting (Delvigne, 1983, 1998) whereas those illustrated in Figs. 3A, 4A, 5B, 6A and 7A are associated with kaolinite, gibbsite and goethite in a thoroughly leached environment of more advanced weathering (Velbel, 1989a). Both these examples are from the weathering of broadly similar (metamorphosed mafic-ultramafic) parent bedrock. Similar chain silicates weathering from different parent rock types would form similar secondary minerals; however, the stage of weathering and/or climatic/environmental conditions under which a given product forms commonly differ systematically on different parent rocks (Nahon, 1991; Delvigne, 1998; Taylor and Eggleton, 2001). Denticle morphology within—or completely or partially superposed by—a mass of product appears indistinguishable from denticle morphology on product-free denticles in cross-section views in petrographic thin-sections (Delvigne, 1998). Detailed examination of reactant–product interfaces in SEM and TEM (Banfield and Barker, 1994) would be useful to establish whether pyribole corrosion morphology is

influenced at smaller scales by direct contact with weathering products and, if so, whether different weathering products are associated with different effects.

3.3. Biotic Influences on Textures

There is a large literature on possible biotic influences on mineral growth and dissolution, but most of this literature involves experimental rather than natural weathering; little involves silicates in general or chain silicates in particular, and very few papers present images of naturally weathered chain silicates. Frankel (1977) reported on the distribution of diatoms and algae on naturally weathered hornblende, but reported no association between the microorganisms and crystallographically controlled etch pits or related corrosion features. Jones et al. (1980, 1981) illustrate augite corrosion during basalt weathering by lichens. A number of experimental papers examine possible influences of microbes on hornblende dissolution kinetics (Kalinowski et al., 2000a, b; Liermann et al., 2000a, b; Brantley et al., 2001), but none report SEM imagery of unpolished surfaces of experimentally weathered pyribole minerals. TEM work on natural weathering of pyriboles in biotically dominated environments (Barker and Banfield, 1996, 1998; Banfield et al., 1999) is beyond the scope of the present review. The influence of biota on SEM-scale natural weathering textures of pyriboles, and how biotic effects differ from abiotic weathering, remains to be demonstrated.

3.4. Natural Weathering Textures of Chain Silicates and Soil-Forming Factors

Weathered chain-silicate minerals at numerous locations exhibit the same types and ranges of weathering morphologies, despite differences in parent material, geomorphic and regolith history, presence/absence and identity of secondary minerals, vegetation and land use. Pyriboles sampled from soils on glacial parent materials (Figs. 1C, D, 2A–D, 3B, 4B, 5C, 6B and 7C, D) resemble those sampled from weathering rinds (Figs. 1A, 3A, 4A, 5B, D, 6A and 7A) and various levels of deep saprolites (Figs. 1B, 5A and 7B) on mafic-ultramafic bedrock. Pyriboles sampled from agricultural soils (Figs. 5C, 6B and 7C) resemble those sampled from forest soils (Figs. 1C, 2A–C, 3A, 4A, B, 5B, 6A and 7A, C, D). Pyroxene and amphibole etching features appear identical in different weathering environments (Moore, 1996; Velbel et al., 1998a, b), despite the geochemical differences that result in formation of very different weathering products. Pyroxenes weathering by transformation or dissolution and reprecipitation (neoformation) to bisiallitic products (e.g., Figs. 5A and 7B), amphiboles weathering (by the same mechanisms) to monosiallitic and ferrallitic products (e.g., Figs. 1A, 5B and 6A), pyriboles dissolving congruently (Velbel, 1989a) without local formation of products (e.g., Figs. 1B, 3A, 4A, 7A and 8B) and pyriboles from which naturally occurring soil coatings have been removed (Figs. 1C, D, 2A–D, 3B, 5C, 6B, 7C, D and 8A, C, D) all exhibit similar etching and denticulation morphologies. Similarity of chain silicate weathering mechanism and textures in a wide variety of environments allows textures to be used as a basis for quantitative comparisons between different profiles.

Time and climate are related to variations in several measures of pyribole etching. The (quantitative) dimensions of various corrosion textures vary systematically with

the duration of natural weathering (Locke, 1979, 1986; Hall and Martin, 1986; Hall and Michaud, 1988; Hall and Horn, 1993), and the intensity of weathering in natural weathering profiles (e.g., Mikesell et al., 2004); however, dimensional differences are all variations on a single (qualitatively identical) theme of pyribole etching morphology. Other environmental factors appear not to vary sufficiently among sites to produce different surface textures, although future research may establish possible environmental influences on etch-pit aspect (length/width) ratio or wall curvature. If there were qualitative differences in weathering textures between weathering profiles, and if such qualitative differences were responses to environmental factors, quantitative comparisons for soil/landform relative-age dating and other applications would be much more difficult.

No morphological evidence has been yet presented of a PSL on any naturally weathered chain silicate. Ubiquitous etch pits and related features (denticles) suggest that chain silicate weathering in natural weathering profiles is interface controlled (Velbel, 1993a). Chain silicate weathering is texturally very conservative; this textural conservatism may be characteristic of interface-limited reactions, and is a necessary condition for the successful use of chain silicate etching as a tool for relative-age, soil-development and paleoclimate studies in glacial landscapes (see Applications, Section 5).

3.5. Comparison of Natural and Experimental Weathering Textures

Experimental dissolution of pyriboles at temperature and pH conditions similar to the conditions of natural weathering does not create familiar etch features (Nickel, 1973; Brantley and Chen, 1995; Werner et al., 1995; Chen and Brantley, 1998). Although the pHs are similar in nature and in the laboratory experiments at near-neutral pHs, even the longest of these experiments fail to form familiar etch pits. This suggests that either longer-duration experiments are required to remove enough reactant mass to form visible pits, or the near-neutral-pH experiments may not reproduce the mechanisms of natural weathering. Similarly, experiments involving biota have not yet produced natural-looking etching on chain silicates (see Section 3.3).

Nickel (1973) observed that experimentally etched mineral grains show etching features generally similar to those of naturally etched grains; however, he noted that there do not seem to be clear causal relationships between etching morphology and chemical environment. Furthermore, the experimentally produced surface features that resembled natural features were not generated during experiments to measure dissolution kinetics at normal pH conditions for weathering, but during separate experiments using mixtures of strong acids. Numerous experiments using strong acids (e.g., combinations of sulphuric, nitric and hydrofluoric acids) at higher-than-ambient temperatures (Brantley and Chen, 1995; Chen and Brantley, 1998) or extreme pHs (Nickel, 1973; Berner et al., 1980; Berner and Schott, 1982) produce etch pits resembling those widely observed on naturally weathered pyriboles. Although the pHs are significantly different in nature and in the laboratory experiments that form etch pits, the corrosion mechanisms may be similar. If corrosion reaction mechanisms are similar (and produce the same textural consequences) over a broad pH range, reaction may be fast enough at more acidic pHs (Brantley and Chen, 1995; Chen and Brantley, 1998) to create SEM-scale pits on experimental time-scales.

Failure of experiments at near-neutral pHs to produce natural-looking textures may merely reflect how slow the reactions are at those pHs. While important aspects of reaction mechanisms vary with pH, some insights relevant to natural pHs may be retrieved from experiments conducted at extreme pHs (Casey et al., 1993).

In addition to many similarities, there are some differences between natural and artificial etch pits. However, since it is commonly the case that the pyriboles being etched in the laboratory are not the same as those examined from natural weathering profiles, it is possible that differences are due to differences in the pyriboles being etched (e.g., defect/dislocation distribution; nature, composition and scale of exsolution lamellae) and not due to differences between natural and artificial corrosion processes. However, more research is required.

3.6. Diagenetic and Higher-Temperature Alteration Textures

Dissolution textures similar to the natural weathering textures described above also occur on sedimentary pyriboles (Mange and Maurer, 1992) in modern coastal (Lin et al., 1974; Mange and Otvos, 2005) and fluvial sediments (Milliken and Mack, 1990; Morton and Johnsson, 1993) and on intrastratally dissolved pyriboles in clastic sedimentary rocks [Edelman and Doeglas, 1932; Hay, 1959; Rahmani, 1973; Friis, 1974; Walker et al., 1978; Waugh, 1978; Morton, 1979, 1984; Berner et al., 1980; Milliken, 1988, 2007 (this volume); Milliken and Mack, 1990; Turner and Morton, 2007 (this volume)], suggesting that pyribole etching is similar in diagenetic and weathering environments. If weathering products or diagenetic cements or replacement minerals are masked photographically in petrographic images of altered pyribole, corrosion textures (e.g., denticulated terminations) are indistinguishable in kind or degree on pyriboles weathered in thoroughly leached or poorly leached weathering environments, and on pyriboles diagenetically altered in closed- or open-system diagenetic environments (Berner et al., 1980). Even though weathering and diagenetic environments differ in solution chemistry (pH, Eh, concentrations of various ions) and hydrology (mostly unsaturated pores and usually fast-flowing fluids in weathering, fully saturated pores and slow-moving fluids in diagenesis), chain silicates respond to the attack of corrosive agents in a similar manner. This suggests that the same mechanisms operate in similar ways in the burial diagenetic environment as in a wide variety of weathering environments (although almost certainly at different rates).

The similarity of pyribole corrosion textures and associated reaction mechanisms between weathering and diagenesis probably does not extend to higher-temperature pyribole/water reactions. At the same magnifications at which denticles are clearly visible in petrographic thin-sections, pyroxene partially replaced by products of natural high-temperature aqueous alteration (e.g., talc) does not exhibit denticles (Delvigne, 1998). Velde (1988) experimentally replaced diopside by talc and serpentine under conditions intended to simulate high-temperature aqueous alteration such as serpentinisation. Smooth rounded interfaces characterised the reactant–product interface in low-magnification SEM images (Fig. 1a in Velde, 1988), and no denticle-like features were observed on the diopside beneath the interface with the product (Velde, 1988). These observations suggest that pyribole/water reaction mechanisms at high temperatures are different from etching mechanisms that appear to be ubiquitous in weathering and diagenetic environments. The range of temperature,

fluid/rock ratio, fluid composition and pyribole composition over which pyribole/water reaction mechanisms and textures change, from those characteristic of weathering and diagenesis to those characteristic of high-temperature serpentinisation, remains to be established.

4. MINERAL SURFACE TEXTURES IN DIFFERENT COMPARTMENTS OF THE SEDIMENTARY CYCLE

Mineral surfaces can be modified throughout the sedimentary cycle (Stieglitz and Rothwell, 1978; Morton and Hallsworth, 1999). Mineral surface textures can be inherited (unmodified) from parent materials. Primary surface textures can be modified or even completely destroyed and replaced by new surface textures during weathering. Erosion of weathered grains from soils and regoliths, followed by transport and deposition, can change the surfaces of weathered grains (e.g., by abrasion), superimposing new textures. Burial diagenesis can further alter grain surface textures. Those formed in one part of the sedimentary cycle can be inherited in subsequent environments, incorporated into sedimentary rocks, and upon erosion of their sedimentary parent rocks may even survive into the next sedimentary cycle (Stieglitz and Rothwell, 1978).

4.1. Primary Features

Consider the grain-surface textures of a primary rock-forming silicate mineral exhumed from the parent rock (by natural physical weathering or during the course of study) but not otherwise weathered or modified. The grain outline, its crystal forms, the degree of perfection of the crystal-growth faces, "compromise" textures (e.g., impressions of adjacent grains on grain surfaces that are not crystallographic faces) and pitting resulting from the physical separation of exposed inclusions are just some of the primary textures that might occur on the surface of a newly exposed primary-mineral grain. If the exhumation of the grain from its parent rock exposes new interior surface (e.g., fracture or cleavage surfaces), characteristic internal features (e.g., morphological expression of twin lamellae or exsolution features, inclusions) can form the loci of weaknesses and avenues for the onset of chemical weathering.

4.2. Weathering Features

As minerals are released from the parent rock, chemical weathering can modify the grain surfaces (chemical weathering at grain boundaries may itself be a mechanism for disintegrating the rock). The discussions here emphasise the morphological features produced on naturally weathered heavy silicates by the common phenomenon of interface-controlled reaction (e.g., individual etch pits) and the more complex textures resulting from the coalescence and overlap of individual into more elaborate forms (e.g., denticulated margins on pyribole grains and sub-grain remnants, and imbricate wedge marks on garnet: Velbel et al., 2007, this volume). Similar features occur on grains of other rock-forming silicates as well (e.g., feldspars: Velbel, 1986;

and olivine: Velbel, 1993a). The less-common textures (smooth rounded primary-mineral surfaces and associated PSLs) produced during transport-limited weathering of garnet (Velbel, 1984, 1993a) are not discussed here. All these features are "superposed" by chemical weathering upon the surfaces of first-cycle silicate grains.

4.3. Mechanical Textures of Erosion, Transport and Deposition

Mineral grains exhumed from their parent rock and exposed to some degree of chemical weathering become the coarse (for our purposes, usually coarser-than-clay-size) fraction of clastic sediment. Mechanical processes during erosion, transport and/or deposition can subdue or even completely remove some surface textures.

Some mechanical modification of a grain's surface can occur before the grain enters the sedimentary cycle in a traditionally understood sense. For example, grain/grain interactions during mass-wasting and debris-avalanche processes have been suggested as being capable of producing extensive abrasion (Goudie and Bull, 1984) and fracturing (Komorowski et al., 1991) of quartz, plagioclase and heavy-mineral grains over even short length-scales of downslope movement (Mahaney, 2002). Such mechanically formed surfaces in the resulting slope deposits (e.g., colluvium, debris-flow lobes) might then have chemical weathering features imposed upon them before being exhumed as individual sand-size grains and transported as bedload downstream.

PSLs are widely observed on naturally weathered almandine garnet in a variety of weathered regoliths. The saprolitic regolith of the Coweeta Hydrologic Laboratory of North Carolina was investigated by Velbel (1984, 1993a), who found that PSLs are not observed at all only a few kilometres downstream of the Coweeta source regolith. Instead, smooth rounded grains, some with shallow etch pits, occur in the sand-size sediment of Coweeta Creek (Velbel, 1984). The rounded outlines may be primary, but may also include surfaces rounded by diffusion-limited weathering beneath PSLs in the source regolith.

The advent of "commodity" scanning electron microscopes in the 1970s stimulated a very large literature attempting to determine depositional environment from SEM-scale grain surface textures. The vast majority of this literature examined grains of the most abundant sand-size mineral in clastic sediments, quartz (Stieglitz, 1969; Margolis and Krinsley, 1974), but some examined heavy minerals as well (e.g., Setlow and Karpovich, 1972). In the end, the "SEM of sand grain surfaces" literature taken as a body arrived at two conclusions: (1) discrimination of depositional environments through the use of silicate grain-surface textures works only if the grains were subjected to the processes of a single depositional environment, long enough for the surface-texture assemblage to achieve "equilibrium" with the environment (short exposure to depositional processes often left intact surface textures, formed earlier in the grain's history—in other words, surface textures could be inherited from up-cycle); (2) environments could not be distinguished, but given sufficient time of exposure to transport-deposition processes, three categories of transport- and deposition-related surface processes could be identified. These are: (a) large-scale conchoidal fractures on quartz, formed by glacial comminution and mechanical interactions between grains in mass movements; (b) fine-scale abrasion features ("frosting") on quartz resulting from energetic grain/grain collisions during aeolian transport; (c) larger scale and different mechanical surface features on quartz formed

by the less energetic grain/grain collisions during transport in water. Different heavy minerals developed different textures in response to similar processes (Setlow and Karpovich, 1972).

4.4. Burial Diagenesis

Cements, overgrowths and intrastratal dissolution are just some of the widespread and common chemical modifications of clastic grains known to operate during burial diagenesis. Intrastratal dissolution of heavy minerals has been demonstrated and discussed in the literature for many decades. This literature is well represented by several contributions to this volume. A complete review is beyond the scope of this contribution, but several observations deserve mention here.

The burial diagenesis literature contains many transmitted light and SEM images of heavy minerals that suggest that surface textures formed during burial diagenesis (e.g., imbricate wedge marks on intrastratally dissolved garnets: Salvino and Velbel, 1989) are different from those produced by weathering (e.g., dodecahedral etch pits on weathered garnets: Velbel, 1984). However, recent experience suggests that these are differences of degree, not kind, of etching and that the intrastratal dissolution features on some of these minerals are merely larger, more complexly coalesced variants of the same etch features formed (to a lesser degree) during weathering. Velbel et al. (2007, this volume) demonstrate this for garnet.

Intrastratal dissolution textures on chain silicates examined by optical petrography or SEM appear identical with etching textures produced by weathering, as noted above. Microscopic imagery of individual heavy-mineral grains commonly shows grains isolated from their host sediment (e.g., transmitted-light images of heavy mineral grain mounts; SEM images of isolated grains from the heavy fractions of sediments and sedimentary rocks; see Turner and Morton, 2007, this volume). This means that the origin of such textures (inherited weathering textures or diagenetic corrosion) cannot be determined from surface textures alone. However, intrastratal dissolution of chain silicates can be distinguished from inherited dissolution textures from up-cycle if early-formed cements preserve the detrital, pre-diagenetic outline of the grain in thin-section (Walker et al., 1978; Scholle, 1979; Mathisen, 1984; Surdam et al., 1989). Similar relationships can be observed (albeit with greater difficulty because of the low abundance of heavy minerals) in SEM images of whole-sample chips (rather than heavy-mineral separates) from sandstones (e.g., hornblende: Walker et al., 1978; and garnet: Salvino and Velbel, 1989).

4.5. Interpreting Textures: Disequilibrium, Inheritance and Recycling

4.5.1. Disequilibrium

As with bulk sediments and their granulometric properties, the interpretation of textural properties of individual grains (including shape and surface textures) is made difficult by the fact that textural properties do not adjust instantaneously to new environments. For example, it takes a finite amount of reworking of sediment derived from a glacial till in a coastal environment for the grain-size distribution to become indistinguishable from other beach deposits; while fines are winnowed out fairly quickly, a coarse tail to the distribution may persist. Bulk-sediment- and grain-textures

take a finite amount of exposure to processes in an environment before they are completely adjusted to the environment; this might be referred to as *textural disequilibrium.* Until "textural equilibrium" is achieved, textures preserve at least part of the textural character of their predecessor material; such textural attributes that are not adjusted to the present environment are inherited from the predecessor material. Such inheritance of textures permits some textural attributes to survive one or more episodes of sediment recycling. Where inheritance of features is helpful to unravelling the natural history of the sedimentary material, textural disequilibrium is an asset to scientific understanding of the sediments rather than a liability. Textural equilibrium and disequilibrium, inheritance and recycling as they pertain specifically to grain surface textures are discussed in more detail further on.

4.5.2. Recycling

When a clastic sedimentary rock is uplifted and weathered, any grain-surface features that persist can be the initial surface for the next cycle of weathering and reintroduction to the sedimentary cycle. Consequently, the interpretation of weathering textures on mineral grains from weathered sedimentary rocks is extremely difficult. For this reason, most of the microscopic imagery of weathering textures on silicate minerals is from sample suites subjected to first-cycle weathering of primary (igneous or metamorphic) crystalline rocks. Mineral grains persistent enough to survive multiple passes through the sedimentary cycle are persistent by virtue of their slow reaction kinetics (Velbel, 1999). An additional consequence of this is that such grains have surfaces that do not respond quickly to most changes in chemical (and even physical) conditions. Consequently, inheritance of surface textures from upcycle or even from previous cycles is common on the most persistent heavy minerals (those most likely to constitute the heavy-mineral fraction of multicycle clastic sediments). Surface textures on polycyclic grains are interpretable if the resilience of the mineral results in negligible modification in the sedimentary cycle. In such instances, primary features may survive even multiple passes through the sedimentary cycle, allowing the "ultimate" provenance of such mineral grains to be established (e.g., zircon).

4.5.3. Equilibrium and inheritance

Stieglitz and Rothwell (1978) analysed how the full range of conditions to which a mineral grain might be exposed in the sedimentary cycle can influence, and must be taken into account in the interpretation of, surface textures on silicate mineral grains. Their analysis directly raises the matter of inheritance of grain surface textures and indirectly raises the matter of "textural equilibrium". For a specific grain-surface feature or texture to be indicative of a physical or chemical process or environment, that surface texture must form quickly once the grain is introduced to that environment. If it takes a long time to form a new surface texture in a specific environment in the sedimentary cycle, grains with exposure times to the environment shorter than the timescale for developing the surface feature specific to its conditions will exhibit surfaces that reflect textures inherited from the previous history of the grain. In this instance, the grain-surface textures preserve part of the history of the grain, but are not diagnostic of the physical/chemical environment in which the grains are currently found.

Persistence of surface textures on grains during their passage through the sedimentary cycle is known from the literature on heavy minerals. For example, elongate etch pits and denticles identical to those formed by weathering occur on pyriboles in modern fluvial sands (Milliken and Mack, 1990; Morton and Johnsson, 1993). Elongate etch pits on hornblende, identical in form and distribution to those formed by weathering, persist on hornblende grains in the swash zones of modern beach environments (Lin et al., 1974; Mange and Otvos, 2005). Evidently, it takes a finite amount of time for abrasion in a river or swash zone to erase pyribole surface textures formed in soils of the sediment source area.

4.6. Heavy Mineral Surface Textures in the Sedimentary Cycle: Closing Remarks

Silicate minerals with low persistence in weathering (e.g., olivine) rarely survive as detrital grains under most common circumstances. For minerals that are highly resistant to chemical weathering and mechanical abrasion (e.g., widespread persistent heavy minerals like zircon, tourmaline and rutile, and locally significant minerals of comparable persistence such as corundum), primary morphological features (Pupin, 1980; Vavra, 1993; Berg and Dahy, 2002; Corfu et al., 2003; Berg, 2004; Berg and Equall, 2004) survive down the sedimentary cycle, often with minimal physical or chemical modification. There is an extensive literature on using the morphology of zircon to infer the ultimate provenance of the zircon grains (Winter, 1981; Matsuura and Aoki, 1989); this is only possible because non-metamict zircon is almost unreactive in most weathering and diagenetic environments.

Surface textures of minerals with intermediate persistence in weathering and diagenesis can be either the most difficult to interpret or the most useful, depending on the purpose of the investigation undertaken using them. The grains themselves may survive multiple passes through the sedimentary cycle, but because their surfaces are modified readily, grain-surface textures at any stage can be a combination of inherited surface textures from one or more previous segments of the sedimentary cycle, and features added to the pre-existing surface by processes in the environment from which the grain is sampled.

For each mineral and each type of grain-surface feature, there is a range of timescales for the development of new surface textures. Velbel et al. (2007, this volume) quantitatively explore this concept for the case of chemical weathering of garnet. If the timescale for forming new surface features is long relative to the duration of exposure of the grain to processes in an environment, then inherited features dominate, and surface textures preserve information about provenance and history rather than information about the current environment (Velbel et al., 2007, this volume). Conversely, if the timescale for development of a particular surface texture is short relative to the duration of exposure of the grain to processes in the present environment or compartment of the sedimentary cycle, then surface textures adjust rapidly to surface-modifying conditions, and may accurately reflect those conditions. However, in this latter case, rapidly adjusting surface textures may not survive the next change in environmental conditions experienced by the grain, which might promptly impose a new assemblage of surface textures. Surface textures in instances of rapid adjustment will not preserve information about grain history. Preservation of grain-history information in cases of slow adjustment, and obliteration of grain-history information

in cases of rapid adjustment, depend upon the rate processes that produce surface textures and the residence time of grains in individual sedimentary and/or geochemical environments in the sedimentary cycle (Velbel et al., 2007, this volume).

If, in a given environment, the timescale of grain exposure to a specific set of conditions is only somewhat shorter than the timescale for complete resurfacing of a mineral grain, quantification of the degree or extent of resurfacing in a given environment is possible. Several applications of hornblende etching to understanding rate, timescale and climatic and pedogenic environmental factors of weathering have met with some success, and are described in Section 5.

5. APPLICATIONS

5.1. *Naturally Weathered Hornblende and Relative-Age Dating of Soils and Glacial Regolith*

Where the ages of multiple weathered regolith surfaces are unknown but parent material and post-exposure climate can be inferred to be uniform, the progressive development of etch pits and denticles (e.g., Figs. 1D, 3B, 7C, D and 8A) on naturally weathered hornblende can be used to determine the relative ages of the different regolith surfaces. In these studies, the general approach involves relating measures of hornblende denticulation (e.g., mean–maximum etching depth of Locke, 1979; denticulation amplitude of Mikesell et al., 2004), to surface age or exposure age (Locke, 1979). This approach assumes that changes in hornblende are sufficiently rapid to show measurable differences over the exposure timescale of interest, but not so rapid as to approach total resurfacing of the grains on that timescale. Relative-age dating by hornblende etching has been applied to Arctic and alpine glacial and periglacial deposits by several research teams (Locke, 1979; Hall and Martin, 1986; Hall and Michaud, 1988). Hornblende etching has been most commonly applied to soils and surfaces that are younger than 150–200 ka (Locke, 1979; Hall and Michaud, 1988), suggesting that it is a sensitive weathering indicator on relatively young surfaces but less discriminating than other surface exposure dating methods on much older surfaces (Mikesell et al., 2004).

5.2. *Determination of Weathering Rates from Naturally Weathered Hornblende*

Where the age of a weathered regolith surface is known, the progressive development of etch pits and denticles on naturally weathered amphiboles can be used to determine the rates of etching and/or denticulation. Locke (1979, 1986), Hall and Martin (1986), and Hall and Horn (1993) inferred from their data that the rate of hornblende weathering decreased exponentially with increasing age of the deposits being weathered. Using the methods of Cremeens et al. (1988, 1992), Brantley et al. (1993) calculated etching rates of hornblende from etch-pit size distributions in a soil catena on Pleistocene loess. They noted that etching rates calculated in this way are lower than bulk dissolution rates measured in laboratory experiments. This is consistent with other findings that experimentally determined dissolution rates are commonly up to three orders of magnitude faster than natural weathering rates for silicate minerals

(Velbel, 1985, 1986, 1989b, 1993b; White and Brantley, 2003; Brantley, 2005; Bricker et al., 2005; White, 2005). Lang (2000) used grain surface textures of hornblende to place constraints on the contributions of hornblende weathering to natural neutralisation of soil acidification.

5.3. Naturally Weathered Hornblende, Climate and Soil Development

Climate is known to affect many properties of soils, including hornblende etching (Locke, 1979; Hall and Martin, 1986; Hall and Horn, 1993; Mikesell et al., 2004). Locke (1979) determined that hornblende etching in soils of the Canadian Arctic was influenced by the effective precipitation and the amount of unfrozen water, and inferred a five-part sequence of pre-glacial to Neoglacial climate fluctuations from variations in hornblende etching in soils on glacial landforms of ages up to 200 ka in his study area. Working on alpine surficial deposits in the Tobacco Root Mountains of Montana, Hall and Martin (1986) were able to discern a likely confounding influence of precipitation gradients on hornblende-etching/age relations; Hall and Horn (1993) made similar observations over a larger range of study areas. Hall and Michaud (1988) showed that such confounding influences can be minimised in certain study areas in which all studied sites are geographically near one another, making age relationships more easily discernable.

Mikesell et al. (2004) examined depth trends of hornblende denticulation in four different soils on 13 ka glacial deposits of northern Michigan (Figs. 1D, 3B, 7C, D and 8A are from their study area and nearby). Their results support Hall and Horn's (1993) conclusion that etching, particularly at shallow soil depths, is rapid within the first 10,000–15,000 years of soil formation. The hornblende etching data of Mikesell et al. (2004) and Schaetzl et al. (2006) generally parallel their data for the degree of soil development in the soils they studied. The largest hornblende denticulation amplitudes occur in the most developed soil, whereas the smallest amount of etching is observed in the most weakly developed soil. The geographic distribution of hornblende etching parallels the geographic pattern of snowfall and infiltration in the study area, supporting the inferences of Locke (1979, 1986), Hall and Horn (1993), and Lang (2000), that, after the effect of age, soil moisture and depth of wetting are the most important factors in determining etching rates (Mikesell et al., 2004; Schaetzl et al., 2006). The literature that consistently shows this pattern is based on studies of soils on Arctic, alpine and continental glacial deposits, suggesting that similar processes operate on similar parent materials in all such environments.

5.4. Extraterrestrial Etching of Pyriboles in Meteorites from Mars and Etching of Terrestrial Pyribole Analogues

Wentworth et al. (2005) compared a variety of features, including pyribole etching, of soils from the Dry Valleys of Antarctica with counterpart features in a number of meteorites known to originate from Mars. The specific Antarctic soils they studied are on a regolith surface that was submerged by ancient Lake Wright prior to ~8 ka, so the weathering features reflect less exposure time and simpler exposure history than other recently studied regolith surfaces in Antarctica. By virtue of the "textural conservatism" of pyribole etching noted elsewhere in this contribution, the Antarctic

denticles are indistinguishable from denticles on pyriboles weathered (presumably more vigorously over shorter timescales) in other terrestrial weathering environments. While the pyribole etching features observed (by FE-SEM) in meteorites from Mars are smaller in scale than terrestrial counterparts, there is sufficient similarity in etch forms between Martian and terrestrial examples to permit the preliminary interpretation that the pyriboles in the Martian meteorites were slightly etched by aqueous solutions on Mars (although the similarity in the features is not yet sufficiently well understood to exclude other possibilities). The pyribole denticles figured by Wentworth et al. (2005) are from one of the youngest Mars meteorites (igneous crystallisation age ~165 Ma: Meyer, 2005), suggesting that, if aqueous alteration was responsible for forming the Martian denticles, aqueous activity persisted in at least small amounts relatively recently on Mars, where the preponderance of evidence suggests that most aqueous activity occurred very early in the history of Mars.

6. DISCUSSION: RELEVANT INSIGHTS FROM STUDIES OF OTHER MINERALS

Numerous workers using optical petrography and SEM have noted the ubiquity of etch pits (suggestive of interface-limited kinetics) on naturally weathered feldspars and chain silicates (e.g., Velbel, 1993a). Etch pits and related features (e.g., denticulated margins on weathered chain silicates), similar or identical to those on naturally weathered feldspars and chain silicates, are easily produced in the laboratory (Nickel, 1973; Berner and Holdren, 1977, 1979; Berner et al., 1980; Berner and Schott, 1982; Zhang et al., 1990; Lee and Parsons, 1995; Lee et al., 1998). Such features occur on these minerals in a wide variety of weathering environments regardless of the presence or identity of specific secondary minerals (e.g., Hay, 1959; Delvigne, 1998; Velbel et al., 1998a, b). This may be due in part to the fact that major rock-forming minerals contain insufficient abundances of "immobile" elements (e.g., Fe, Al) to form non-porous secondary-mineral coatings (Velbel, 1993a); coatings form during weathering, but may not have properties that allow them to be diffusion limiting. The ubiquity of etch features on naturally weathered feldspars, pyroxenes and amphiboles was one major line of evidence (and the only line of evidence readily available from naturally weathered materials: Velbel, 2004) that pointed the geochemical-kinetics community in the late 1970s and 1980s toward acceptance of interface-controlled kinetics for silicate-mineral weathering. This textural conservatism of major rock-forming silicates in general, and chain silicates in particular, during weathering is the main reason why hornblende etching can be used as a relative-age indicator and/or paleoclimate indicator in weathered glacial deposits; hornblende etching varies in extent—but not in style—with variations in environmental conditions. However, this same textural conservatism of feldspars and hornblende during weathering presently renders them undesirable research targets for textural investigations of natural rate processes; for these minerals, variations in weathering mechanisms and/or textural responses in different weathering environments are too small to allow detection of differences in mechanism through differences in alteration textures at optical or SEM scales.

In sharp contrast to the major rock-forming silicates, which have not exhibited discernable qualitative environmentally dependent textural variation during natural weathering (always etched and interface limited), textures consistent with diffusion-limited weathering (product layers of uniform thickness on smooth, rounded remnant-garnet surfaces lacking etch pits) from naturally weathered almandine and spessartine garnet have been known for more than two decades (Velbel, 1984, 1987, 1993a). Furthermore, unlike weathering textures on feldspars and chain silicates (which are the same regardless of environment or product), garnet weathering textures vary widely among environments. For example, PSLs on almandine and spessartine form only in oxidising saprolitic environments largely devoid of direct biological influence. In the rooting zone where biological/biogeochemical factors dominate, the coatings are absent, and weathered almandine surfaces directly exposed to soil solutions are densely covered with etch pits (Velbel, 1984, 1987, 1993a). In addition to the literature on garnet weathering, garnet surface textures in sedimentary deposits have been reported in the sedimentology/sedimentary-petrology literature (Morton et al., 1989; Salvino and Velbel, 1989; Hansley and Briggs, 1994, and references therein). Another large literature (in materials science and crystal growth) exists on growth and dissolution forms of garnets (because a number of synthetic crystals of economic importance to the materials science community have the garnet crystal structure) and can be used to assist in interpreting the surface textures of naturally weathered garnets. Garnet is an orthosilicate; because their silica tetrahedra are unpolymerised, orthosilicates have relatively simple crystal-chemical controls on their weathering rates (Eggleton, 1986; Velbel, 1999). Finally, garnet is the only common isometric rock-forming silicate that permits use of rate equations for the case of spherical symmetry to be applied more directly and with fewer qualifications and assumptions than for any other common silicate mineral. Thus, minerals of the garnet group offer the best hope of being able to detect different rate-determining mechanisms (e.g., interface-controlled, diffusion-controlled) from alteration textures of naturally weathered silicate mineral grains.

Velbel et al. (2007, this volume) show that, for garnet (a silicate mineral of intermediate persistence in weathering and the sedimentary cycle; Velbel, 1999) in a common regolith type and weathering environment (soil on Pleistocene glacial parent material), surface textures inherited from source rocks (e.g., imbricate wedge marks) and from the transport and depositional history of the parent regolith (e.g., conchoidal fractures) dominate garnet grain surfaces in several Michigan soils, even after more than ten thousand years of post-glacial weathering. Inherited grain-surface textures dominate in these and similar examples because the response time for surface textures is long relative to the time actually available for weathering to modify the garnet surfaces.

Pyribole etching features (e.g., denticles) might similarly survive glacial/glaciofluvial transport. If so, there exists a possible alternative reason for the common observation in studies of relative-age dating and soil development using hornblende etching, that even in the ostensibly fresh parent material, a small finite amount of hornblende modification is commonly observed (e.g., Locke, 1979, 1986; Hall and Martin, 1986; Hall and Michaud, 1988; Hall and Horn, 1993; Mikesell et al., 2004). Denticles (saw-tooth or "cockscomb" terminations) on hornblende grains in weathered regoliths or sediments may be better able to survive transport, reworking and recycling than some

older literature suggested. While such survival and inheritance of delicate surface textures from up-cycle would have little effect on commonly used methods for relative-age dating using hornblende etching because these are statistical studies using average values properties on large numbers of grains, it would render more difficult the interpretation of hornblende surface textures in SEM images of individual grains from a soil developed on a transported parent material.

The possibility that pyribole denticles survive transport implies that some instances of denticulated pyriboles in sedimentary rocks may not have been formed by intrastratal dissolution but may be inherited from weathered regolith in the source area of the sediment. Morton and Johnsson (1993) suggested that pyroxene (and to a lesser extent amphibole) abundances in fluvial sands may decrease as a result of weathering during temporary alluvial storage of the sand in fluvial systems, and they illustrate both fresh angular and denticulated amphibole grains from their fluvial sediments. Denticulated amphibole in fluvial sediments may have been weathered in the regoliths of the sediment source area, and/or in soils in the fluvial basin during temporary alluvial storage (Morton and Johnsson, 1993). Further supporting the possibility of inheritance are multiple reports of denticulated pyriboles in modern sediments that have not yet undergone burial diagenesis and intrastratal dissolution (e.g., Milliken and Mack, 1990; Morton and Johnsson, 1993; Mange and Otvos, 2005). Better understanding of the extent to which pyribole denticles survive fluvial and littoral transport would greatly advance their interpretation. This would aid evaluation of the corrosion rates of individual pyriboles during alluvial storage and the duration of mineral-grain exposure to flood-plain weathering conditions (possibly following a response-time approach like that applied to garnet by Velbel et al., 2007, this volume). Developing criteria for distinguishing possible inherited occurrences from genuinely diagenetic occurrences may improve interpretation of the latter, either by enabling filtering of data from cases with inherited features or by demonstrating that possible inheritance is not actually a concern in any category of case studies.

7. SUMMARY

Weathered pyroxenes and amphiboles at numerous locations and in a wide variety of weathering environments exhibit the same types and ranges of weathering morphologies (e.g., etch pits, denticulated margins), despite differences in parent material, geomorphic history, vegetation, land use, presence/absence of secondary minerals and geochemical differences that result in formation of very different weathering products. The dimensions of various corrosion textures vary systematically with the duration and intensity of weathering in natural weathering profiles; dimensional differences are all variations on a single theme of pyribole etching morphology. Similar ranges of dissolution textures also occur on pyriboles in modern sediments and on intrastratally dissolved pyriboles in clastic sedimentary rocks, suggesting that pyribole etching is similar in diagenetic and weathering environments.

The response time of mineral surface textures likely differs with the reactivity (geochemical kinetics) of the mineral in the environment, which is in turn related to the persistence of each mineral in weathering and the sedimentary cycle. Persistent minerals (with slow dissolution-weathering reaction kinetics, e.g., zircon) are largely

unmodified, and their inherited surface textures and grain morphologies reflect their provenance. Minerals of low persistence (that react rapidly, e.g., olivine) quickly and readily tend to take on surface textures characteristic of their new environment, but do not survive long enough for inherited surface textures to be of scientific value under common circumstances. Minerals with intermediate rates of dissolution and intermediate persistence (e.g., pyroxenes, amphiboles) gradually corrode and survive long enough for the degree of corrosion to be a scientifically useful soil relative-age and environmental indicator.

The significance of etch pits and other surface textures in a soil or regolith depends on the "response time" of those surface textures to weathering in that regolith, and the relationship of that timescale to the age of the soil and/or the residence time of soil grains in the weathering environment. Geomorphic dynamics, regolith history and landscape evolution affect the genesis and interpretation of grain-surface textures formed during mineral weathering. Similar considerations of (1) response time, (2) inheritance of surface textures, (3) recycling of mineral grains and their surface textures and (4) equilibrium/disequilibrium between grain-surface textures and the environmental conditions from which they are sampled collectively influence the interpretation of heavy mineral surface textures throughout the sedimentary cycle.

ACKNOWLEDGEMENTS

Numerous mentors, colleagues and students have accompanied me along parts of my journey through the world of silicate-mineral mechanical and dissolution textures, mechanisms and rates. They include Robert A. Berner, Daniel Nahon, Dave McKay, Tony Eggleton, Jeff Wilson, Jean Delvigne, Fabrice Colin, Bruno Boulangé, Graham Taylor, Sue Wentworth, Bill Barker, Jill Banfield, Bill Casey, Roland Hellmann, Ian Parsons, Ron Stieglitz, Robert D. Hall, Eric Tonui, Donald C. Rhoads, Randy Schaetzl, Joe McKee, Steve Nordeng, Gary Icopini, Jason Price, Leslie Mikesell, John Salvino, Deb Bryan, Jenn Wade, Charles Basso, Michael Zieg, Jennifer McGuire, Andrew Madden, Nathan Mellott, Michael Formolo, Mike Ranck and Jill Schlanser. I am especially grateful to the late Jean Delvigne for informative exchanges and providing a sample of weathered Koua Bocca pyroxenite.

Many of the SEM images in this paper were acquired by Jen McGuire (from her samples: Figs. 1C, 2A–C, 4A, 5C, 6B, 7C, D and 8C), Nathan Mellott (from my samples: Figs. 3A, 5B, 6A and 7A) and Mike Formolo (from my samples: Figs. 1A, 5D and 8B) during a Research Experience for Undergraduates project and subsequent work, and Leslie Mikesell acquired others (Figs. 1D, 2D, 3B, 8A and 8D) following up on her thesis results; I am grateful for their enthusiasm and excellent work during several stages of a larger project on chain silicate weathering. The assistance of Alan Pooley (Yale Peabody Museum) and Ewa Danielewicz (Michigan State University Center for Advanced Microscopy) has been invaluable in acquiring some of the SEM images that contributed to this review, and Harley Seeley ably prepared the images for publication. I thank Angela Donatelle, Ryan Currier and Leslie Mikesell for helpful discussions during the writing of this contribution, and Jeff Wilson, Kitty Milliken and Maria Mange for their helpful reviews of the manuscript.

My early studies of hornblende weathering at the Coweeta LTER site were supported by NSF grant NSF EAR 80-07815 (R.A. Berner, P.I.) and Coweeta LTER grant NSF BSR 85-14328 (D.A. Crossley, Jr., P.I.). Comparative microscopic studies of North American and African chain silicate weathering were supported by a grant from the Michigan State University Office of International Studies and Programs. Microscopic studies of chain silicate weathering at the Michigan State University Kellogg Biological Station were supported by an NSF REU Supplement to (LTER) grant NSF DEB 92-11771, and DEB 98-10220 (G.P. Robertson, Michigan State University Kellogg Biological Station, P.I.). This review was prepared with support from NASA Grant NNG05GL77G.

REFERENCES

Abreu, M.M., Vairinho, M., 1990. Amphibole alteration to vermiculite in a weathering profile of gabbro-diorite. In: Douglas, L.A. (Ed.), Soil Micromorphology: A Basic and Applied Science. Developments in Soil Science, vol. 19, pp. 493–500.

Anand, R.R., Gilkes, R.J., 1984. Weathering of hornblende, plagioclase, and chlorite in metadolerite, Australia. Geoderma 34, 261–280.

Argast, S., 1991. Chlorite vermiculitization and pyroxene etching in an aeolian periglacial sand dune, Allen County, Indiana. Clays and Clay Minerals 39, 622–633.

Banfield, J.F., Barker, W.W., 1994. Direct observation of reactant–product interfaces formed in natural weathering of exsolved, defective amphibole to smectite: evidence for episodic, isovolumetric reactions involving structural inheritance. Geochimica et Cosmochimica Acta 58, 1419–1429.

Banfield, J.F., Barker, W.W., Welch, S.A., Taunton, A., 1999. Biological impact on mineral dissolution: application of the lichen model to understanding mineral weathering in the rhizosphere. Proceedings of the National Academy of Science 96, 3404–3411.

Barker, W.W., Banfield, J.F., 1996. Biologically versus inorganically mediated weathering reactions: relationships between minerals and extracellular microbial polymers in lithobiontic communities. Chemical Geology 132, 55–69.

Barker, W.W., Banfield, J.F., 1998. Zones of chemical and physical interaction at interfaces between microbial communities and minerals: a model. Geomicrobiology 15, 223–244.

Basham, I.R., 1974. Mineralogical changes associated with deep weathering of gabbro in Aberdeenshire. Clay Minerals 10, 189–202.

Bateman, R.M., Catt, J.A., 1985. Modification of heavy mineral assemblages in English coversands by acid pedochemical weathering. Catena 12, 1–21.

Berg, R.B., 2004. Probable bedrock source of sapphires in alluvial deposits North of Butte, Montana. In: Castor, S.B., Papke, K.G., Meeuwig, R.O. (Eds.), Betting on Industrial Minerals. Proceedings of the 39th Forum on the Geology of Industrial Minerals: Nevada Bureau of Mines and Geology Special Publication, vol. 33, pp. 23–30.

Berg, R.B., Dahy, J.P., 2002. Montana sapphires and speculation on their origin. In: Scott, P.W., Bristow, C.M. (Eds.), Industrial Minerals and Extractive Industry Geology. Geological Society, London, pp. 199–204.

Berg, R.B., Equall, N., 2004. Scanning-Electron Micrographs of Sapphires from Alluvial Deposits in Southwestern Montana: Montana Bureau of Mines and Geology, Report 491, CD-ROM.

Berner, R.A., 1978. Rate control of mineral dissolution under earth surface conditions. American Journal of Science 278, 1235–1252.

Berner, R.A., 1980. Early Diagenesis: A Theoretical Approach. Princeton University Press, Princeton, NJ, 241pp.

Berner, R.A., 1981. Kinetics of weathering and diagenesis. In: Lasaga, A.C., Kirkpatrick, R.J. (Eds.), Kinetics of Geochemical Processes. Reviews in Mineralogy, vol. 8, pp. 111–134.

Berner, R.A., Holdren, G.R., 1977. Mechanism of feldspar weathering: some observational evidence. Geology 5, 369–372.

Berner, R.A., Holdren, G.R., 1979. Mechanism of feldspar weathering—II: observations of feldspars from soils. Geochimica et Cosmochimica Acta 43, 1173–1186.

Berner, R.A., Schott, J., 1982. Mechanism of pyroxene and amphibole weathering—II: observations of soil grains. American Journal of Science 282, 1214–1231.

Berner, R.A., Sjöberg, E.L., Velbel, M.A., Krom, M.D., 1980. Dissolution of pyroxenes and amphiboles during weathering. Science 207, 1205–1206.

Blum, A.E., Lasaga, A.C., 1987. Monte Carlo simulations of surface reaction rate laws. In: Stumm, W. (Ed.), Aquatic Surface Chemistry: Chemical Processes at the Particle-Water Interface. Wiley, New York, pp. 255–292.

Blum, A.E., Yund, R.A., Lasaga, A.C., 1990. The effect of dislocation density on the dissolution rate of quartz. Geochimica et Cosmochimica Acta 54, 283–297.

Boulangé, B., 1984. Les formations bauxitiques latéritiques de Côte-d'Ivoire: Travaux et Documents de l'ORSTOM, no. 175, 363pp.

Bradley, W.C., 1957. Origin of marine-terrace deposits in the Santa Cruz area, California. Geological Society of America Bulletin 68, 421–444.

Brantley, S.L., 2005. Reaction kinetics of primary rock-forming minerals under ambient conditions. In: Drever, J.I. (Ed.), Surface and Ground Water, Weathering, and Soils, Treatise on Geochemistry, vol. 5. Elsevier-Pergamon, Oxford, pp. 73–117.

Brantley, S.L., Blai, A.C., Cremeens, D.L., MacInnis, I., Darmody, R.G., 1993. Natural etching rates of feldspar and hornblende. Aquatic Sciences 55, 262–272.

Brantley, S.L., Chen, Y., 1995. Chemical weathering rates of pyroxenes and amphiboles. In: White, A.F., Brantley, S.L. (Eds.), Chemical Weathering Rates of Silicate Minerals. Reviews in Mineralogy, vol. 31, pp. 119–172.

Brantley, S.L., Crane, S.R., Crerar, D.A., Hellmann, R., Stallard, R., 1986. Dissolution at dislocation etch pits in quartz. Geochimica et Cosmochimica Acta 50, 2349–2361.

Brantley, S.L., Liermann, L., Bau, M., Wu, S., 2001. Uptake of trace metals and rare earth elements from hornblende by a soil bacterium. Geomicrobiology Journal 18, 37–61.

Bricker, O.P., Jones, B.F., Bowser, C.J., 2005. Mass-balance approach to interpreting weathering reactions in watershed systems. In: Drever, J.I. (Ed.), Surface and Ground Water, Weathering, and Soils, vol. 5, Treatise on Geochemistry. Elsevier-Pergamon, Oxford, pp. 119–132.

Callender, D.L., Folk, R.L., 1958. Idiomorphic zircon, key to volcanism in the lower Tertiary sands of central Texas. American Journal of Science 256, 257–269.

Casey, W.H., Banfield, J.F., Westrich, H.R., McLaughlin, L., 1993. What do dissolution experiments tell us about natural weathering? Chemical Geology 105, 1–15.

Chen, Y., Brantley, S.L., 1998. Diopside and anthophyllite dissolution at 25° and 90°C and acid pH. Chemical Geology 147, 233–248.

Chitale, D.V., Guven, N., 1989. Weathering of Deccan Trap basalts in western India. Clay Research 8, 67–83.

Cleaves, E.T., 1974. Petrologic and chemical investigation of chemical weathering in mafic rocks, eastern piedmont of Maryland. Maryland Geological Survey, Report of Investigations 25, 28pp.

Cole, W.F., Lancucki, C.J., 1976. Montmorillonite pseudomorphs after amphibole from Melbourne, Australia. Clays and Clay Minerals 24, 79–83.

Colin, F., 1984. Étude pétrologique des altérations de pyroxénite du gisement nickélifère de Niquelandia (Brésil). Thèse, Université Paris VII, 137pp.

Colin, F., Nahon, D., Trescases, J.J., Melfi, A.J., 1990. Lateritic weathering of pyroxenites at Niquelandia, Goias, Brazil: the supergene behavior of nickel. Economic Geology 85, 1010–1023.

Colin, F., Noack, Y., Trescases, J.J., Nahon, D., 1985. L'altération latérique débutante des pyroxénites de Jacuba, Niquelandia, Brésil. Clay Minerals 20, 93–113.

Colman, S.M., 1982. Chemical weathering of basalts and andesites: evidence from weathering rinds. U.S. Geological Survey Professional Paper, no. 1246.

Corfu, F., Hanchar, J.M., Hoskin, P.W.O., Kinny, P., 2003. Atlas of zircon textures. In: Hanchar, J.M., Hoskin, P.W.O. (Eds.), Zircon: Reviews in Mineralogy, vol. 53. pp. 469–500.

Cremeens, D.L., Darmody, R.G., Norton, L.D., 1992. Etch-pit size and shape distribution on orthoclase and pyriboles in a loess catena. Geochimica et Cosmochimica Acta 56, 3423–3434.

Cremeens, D.L., Norton, L.D., Darmody, R.G., Jansen, I.J., 1988. Etch-pit measurements on scanning electron micrographs of weathered grain surfaces. Soil Science Society of America Journal 52, 883–885.

Delvigne, J., 1983. Micromorphology of the alteration and weathering of pyroxenes in the Koua Bocca ultramafic intrusion, Ivory Coast, West Africa. In: Nahon, D., Noack, Y. (Eds.), Pétrologie des Altérations et des Sols, vol. II. Sciences Géologiques, Mémoires, vol. 72, pp. 57–68.

Delvigne, J., 1990. Hypogene and supergene alterations of orthopyroxene in the Koua Bocca ultramafic intrusion, Ivory Coast. Chemical Geology 84, 49–53.

Delvigne, J., 1998. Atlas of micromorphology of mineral alteration and weathering: the Canadian mineralogist. Special Publication 3, 495pp.

Duchaufour, P., 1982. Pedology, (T. R. Paton, Trans.). George Allen and Unwin, London, 448pp.

Edelman, C.H., Doeglas, D.J., 1932. Reliktstrukturen detritischer Pyroxene und Amphibole. Tschermaks Mineralogische und Petrographische Mitteilungen 42, 482–490.

Eggleton, R.A., 1975. Nontronite topotaxial after hedenbergite. American Mineralogist 60, 1063–1068.

Eggleton, R.A., 1986. The relation between crystal structure and silicate weathering rates. In: Colman, S.M., Dethier, D.P. (Eds.), Rates of Chemical Weathering of Rocks and Minerals. Academic Press, Orlando, FL, pp. 21–40.

Eggleton, R.A., Boland, J.N., 1982. Weathering of enstatite to talc through a sequence of transitional phases. Clays and Clay Minerals 30, 11–20.

England, B.M., 1991. The state of the science: scanning electron microscopy. The Mineralogical Records 22, 123–132.

Eslinger, E., Pevear, D., 1988. Clay minerals for petroleum geologists and engineers: Society of Economic Paleontologists and Mineralogists, Short Course Notes 22, 422pp.

Eswaran, H., 1979. The alteration of plagioclases and augites under differing pedo-environmental conditions. Journal of Soil Science 30, 547–555.

Frankel, L., 1977. Microorganism induced weathering of biotite and hornblende grains in estuarine sands. Journal of Sedimentary Petrology 47, 849–854.

Friis, H., 1974. Weathered heavy-mineral associations from the young-Tertiary deposits of Jutland, Denmark. Sedimentary Geology 12, 199–213.

Glasmann, J.R., 1982. Alteration of andesite in wet, unstable soils of Oregon's western Cascades. Clays and Clay Minerals 30, 253–263.

Goldich, S.S., 1938. A study in rock weathering. Journal of Geology 46, 17–58.

Goudie, A., Bull, P.A., 1984. Slope process change and colluvium deposition in Swaziland: an SEM analysis. Earth Surface Processes and Landforms 9, 289–299.

Gratz, A.J., Manne, S., Hansma, P.K., 1991a. Atomic force microscopy of atomic-scale ledges and etch pits formed during dissolution of quartz. Science 251, 1343–1346.

Gratz, A.J., Bird, P., Quiro, G.B., 1991b. Dissolution of quartz in aqueous basic solution, 106–236 °C: surface kinetics of "perfect" crystallographic faces. Geochimica et Cosmochimica Acta 54, 2911–2922.

Hall, R.D., Horn, L.L., 1993. Rates of hornblende etching in soils in glacial deposits of the northern Rocky Mountains (Wyoming Montana, U.S.A.): influence of climate and characteristics of the parent material. In: Brantley, S.L., Velbel, M.A. (Eds.), Geochemical Kinetics of Mineral-Water Reactions in the Field and the Laboratory, Chemical Geology, vol. 105, pp. 17–29.

Hall, R.D., Martin, R.E., 1986. The etching of hornblende grains in the matrix of alpine tills and periglacial deposits. In: Colman, S.M., Dethier, D.P. (Eds.), Rates of Chemical Weathering of Rocks and Minerals. Academic Press, Orlando, FL, pp. 101–128.

Hall, R.D., Michaud, D., 1988. The use of hornblende etching, clast weathering, and soils to date alpine glacial and periglacial deposits: a study from southwestern Montana. Geological Society of America Bulletin 100, 458–467.

Hansley, P.L., Briggs, P.H., 1994. Garnet dissolution in oxalic acid: a possible analog for natural etching of garnet by dissolved organic matter. U.S. Geological Survey Bulletin, Report B2106, 14pp.

Hay, R.L., 1959. Origin and weathering of late Pleistocene ash deposits of St. Vincent, B.W.I. Journal of Geology 67, 65–87.

Ildefonse, P., 1980. Mineral facies developed by weathering of a meta-gabbro, Loire-Atlantique (France). Geoderma 24, 257–273.

Jones, D., Wilson, M.J., McHardy, W.J., 1981. Lichen weathering of rock-forming minerals: application of scanning electron microscopy and microprobe analysis. Journal of Microscopy 124, 95–104.

Jones, D., Wilson, M.J., Tait, J.M., 1980. Weathering of a basalt by *Pertusaria corallina*. The Lichenologist 12, 277–289.

Kalinowski, B.E., Liermann, L.J., Brantley, S.L., Barnes, A., Pantano, C.G., 2000a. X-ray photoelectron evidence for bacteria-enhanced dissolution of hornblende. Geochimica et Cosmochimica Acta 64, 1331–1343.

Kalinowski, B.E., Liermann, L.J., Givens, S., Brantley, S.L., 2000b. Rates of bacteria-promoted solubilization of Fe from minerals: a review of problems and approaches. Chemical Geology 169, 357–370.

Klein, C., 2002. Manual of Mineral Science, 22nd ed.. Wiley, New York, 641pp.

Komorowski, J.-C., Glicken, H.X., Sheridan, M.F., 1991. Secondary electron imagery of microcracks and hackly fracture surfaces in sand-size clasts from the 1980 Mount St. Helens debris-avalanche deposits: implications for particle-particle interactions. Geology 19, 261–264.

Lang, L.-O., 2000. Heavy mineral weathering under acidic soil conditions. Applied Geochemistry 15, 415–423.

Lasaga, A.C., 1984. Chemical kinetics of water-rock interactions. Journal of Geophysical Research 89B, 4009–4025.

Lasaga, A.C., 1998. Kinetic Theory in the Earth Sciences. Princeton University Press, Princeton, NJ, 811pp.

Lasaga, A.C., Blum, A.E., 1986. Surface chemistry, etch pits, and mineral-water interactions. Geochimica et Cosmochimica Acta 50, 2363–2379.

Lee, M.R., Hodson, M.E., Parsons, I., 1998. The role of intragranular microtextures and microstructures in chemical and mechanical weathering: direct comparisons of

experimentally and naturally weathered alkali feldspars. Geochimica et Cosmochimica Acta 62, 2771–2778.
Lee, M.R., Parsons, I., 1995. Microtextural controls of weathering of perthitic alkali feldspars. Geochimica et Cosmochimica Acta 59, 4465–4488.
Liermann, L.J., Barnes, A.S., Kalinowski, B.E., Zhou, X., Brantley, S.L., 2000a. Microenvironments of pH in biofilms grown on dissolving silicate surface. Chemical Geology 171, 1–16.
Liermann, L.J., Kalinowski, B.E., Brantley, S.L., Ferry, J.G., 2000b. Role of bacterial siderophores in dissolution of hornblende. Geochimica et Cosmochimica Acta 64, 587–602.
Lin, J.I., Rohrlich, V., Slatkine, A., 1974. Surface microtextures of heavy minerals from the Mediterranean coast of Israel. Journal of Sedimentary Petrology 44, 1281–1295.
Locke III, W.W., 1979. Etching of hornblende grains in Arctic soils: an indicator of relative age and paleoclimate. Quaternary Research 11, 197–212.
Locke III, W.W., 1986. Rates of hornblende etching in soils on glacial deposits, Baffin Island, Canada. In: Colman, S.N., Dethier, D.P. (Eds.), Rates of Chemical Weathering of Rocks and Minerals. Academic Press, Orlando, FL, pp. 129–145.
Mahaney, W.C., 2002. Atlas of Sand Grain Surface Textures and Applications. University Press, Oxford, 237pp.
Mange, M.A., Maurer, H.F.W., 1992. Heavy Minerals in Colour. Chapman and Hall, London, 147pp.
Mange, M.A., Otvos, E.G., 2005. Gulf coastal plain evolution in West Louisiana: heavy mineral provenance and Pleistocene alluvial chronology. Sedimentary Geology 182, 29–57.
Margolis, S.V., Krinsley, D.H., 1974. Processes of formation and environmental occurrence of microfeatures on detrital quartz grains. American Journal of Science 274, 449–464.
Mathisen, M.E., 1984. Diagenesis of Plio-Pleistocene nonmarine sandstones, Cagayan Basin, Philippines: early development of secondary porosity in volcanic sandstones. In: McDonaldd, D.A., Surdam, R.C. (Eds.), Clastic Diagenesis, American Association of Petroleum Geologists Memoir, vol. 37, pp. 177–193.
Matsuura, A., Aoki, Y., 1989. A new method for quantitative representation of zircon morphology. Neues Jahrbuch für Mineralogie, Monatshefte 1989, pp. 309–319.
Meunier, A., 1983. Micromorphological advances in rock weathering studies. In: Bullock, P., Murphy, C.P. (Eds.), Soil Micromorphology: A.B. Academic Publishers, Dordrecht, pp. 467–483.
Meyer, C. 2005. Mars Meteorite Compendium: http://www-curator.jsc.nasa.gov/curator/antmet/mmc/mmc.htm
Mikesell, L.R., Schaetzl, R.J., Velbel, M.A., 2004. Hornblende etching and quartz/feldspar ratios as weathering and soil development indicators in some Michigan soils. Quaternary Research 62, 162–171.
Milliken, K.L., 1988. Loss of provenance information through subsurface diagenesis in Plio-Pleistocene sandstones, northern Gulf of Mexico. Journal of Sedimentary Petrology 58, 992–1002.
Milliken, K.L., 2007. Provenance and diagenesis of heavy minerals, Cenozoic units of the Northwestern Gulf of Mexico sedimentary basin. In: Mange, M., Wright, D.T. (Eds.), Heavy Minerals in Use. Developments in Sedimentology (this volume).
Milliken, K.L., Mack, L.E., 1990. Subsurface dissolution of heavy minerals, Frio Formation sandstones of the ancestral Rio Grande Province, South Texas. Sedimentary Geology 68, 187–199.
Mogk, D.W., Locke III, W.W., 1988. Application of Auger electron spectroscopy (AES) to naturally weathered hornblende. Geochimica et Cosmochimica Acta 52, 2537–2542.
Moore, C.L., 1996. Processes of Chemical Weathering of Selected Cainozoic Eastern Australian Basalts: Unpublished Ph.D. thesis, The Australian National University, 448pp.

Morton, A.C., 1979. Surface features of heavy mineral grains from Paleocene sands of the central North Sea. Scottish Journal of Geology 15, 293–300.

Morton, A.C., 1984. Stability of detrital heavy minerals in Tertiary sandstones from the North Sea Basin. Clay Minerals 19, 287–308.

Morton, A.C., Borg, G., Hansley, P.L., Haughton, P.D.W., Krinsley, D.H., Trusty, P., 1989. The origin of faceted garnets in sandstones: dissolution or overgrowth? Sedimentology 36, 927–942.

Morton, A.C., Hallsworth, C.R., 1999. Processes controlling the composition of heavy minerals in sandstones. Sedimentary Geology 124, 3–29.

Morton, A.C., Johnsson, M.J., 1993. Factors influencing the composition of detrital heavy mineral suites in Holocene sands of the Apure River drainage basin Venezuela. In: Johnsson, M.J., Basu, A. (Eds.), Processes Controlling the Composition of Clastic Sediments. Geological Society of America Special Paper, no. 284, pp. 171–185.

Müller, H.W., Schwaighofer, B., 1979. Frittung oder Tertiäre Verwitterung: Zur Frage der Rotfarbung in den Tertiären Liegend-sedimenten des Basalts von Stoob (Brugenland, österreich). Verhandlungen der Geologischen Bundesanstalt (Austria), Jahrgang 1979, pp. 133–160.

Nahon, D.B., 1991. Introduction to the Petrology of Soils and Chemical Weathering. Wiley, 313pp.

Nahon, D.B., Colin, F., 1982. Chemical weathering of orthopyroxenes under lateritic conditions. American Journal of Science 282, 1232–1243.

Nickel, E., 1973. Experimental dissolution of light and heavy minerals in comparison with weathering and intrastratal dissolution. Contributions to Sedimentology 1, 1–68.

Ohse, W., Matthess, G., Pekdeger, A., 1985. Equilibrium and disequilibrium between pore waters and minerals in the weathering environment. In: Drever, J.I. (Ed.), The Chemistry of Weathering. Reidel, Dordrecht, pp. 211–229.

Pevear, D.R., Goldin, A., Sprague, J.W., 1984. Mineral transformations in soils formed in glacialmarine drift, northwestern Washington. Soil Science Society of America Journal 48, 208–216.

Proust, D., 1982. Supergene alteration of hornblende in an amphibolite from Massif Central, France. In: van Olphen, H., Veniale, F. (Eds.), International Clay Conference, Bologna, Pavia, 1981. Developments in Sedimentology, vol. 35, pp. 357–364.

Proust, D., 1985. Amphibole weathering in a glaucophane-schist (Ile de Groix, Morbihan, France). Clay Minerals 20, 161–170.

Pupin, J.P., 1980. Zircon and granite petrology. Contributions to Mineralogy and Petrology 73, 207–220.

Rahmani, R.A., 1973. Grain surface etching features of some heavy minerals. Journal of Sedimentary Petrology 43, 882–888.

Robertson, I.D.M., 1995. Interpretation of fabrics in ferruginous lags. Australian Geological Survey Organization Journal of Australian Geology & Geophysics 16, 263–270.

Robertson, I.D.M., Butt, C.R.M., 1997. Atlas of Weather Rocks: Cooperative Research Centre for Landscape Evolution and Mineral Exploration, Open File Report 1.

Salvino, J.F., Velbel, M.A., 1989. Faceted garnets from sandstones of the Munising Formation (Cambrian), northern Michigan: petrographic evidence for origin by intrastratal dissolution. Sedimentology 36, 371–379.

Schaetzl, R.J., Mikesell, L.R., Velbel, M.A., 2006. Soil characteristics, related to weathering and pedogenesis, across a geomorphic surface of uniform age in Michigan. Physical Geography 27, 170–188.

Scholle, P.A., 1979. A Color Illustrated Guide to Constituents, Textures, Cements and Porosities of Sandstones and Associated Rocks. American Association of Petroleum Geologists Memoir 28, 201pp.

Schott, J., Petit, J.-C., 1987. New evidence for the mechanisms of dissolution of silicate minerals. In: Stumm, W. (Ed.), Aquatic Surface Chemistry: Chemical Processes at the Particle-Water Interface. Wiley, New York, pp. 293–315.

Setlow, L.W., Karpovich, R.P., 1972. "Glacial" micro-textures on quartz and heavy mineral sand grains from the littoral environment. Journal of Sedimentary Petrology 42, 864–875.

Singh, B., Gilkes, R.J., 1993. Weathering of spodumene to smectite in a lateritic environment. Clays and Clay Minerals 41, 624–630.

Smith, K.L., Milnes, A.R., Eggleton, R.A., 1987. Weathering of basalt: formation of iddingsite. Clays and Clay Minerals 35, 418–428.

Stieglitz, R.D., 1969. Surface textures of quartz and heavy-mineral grains from fresh-water environments: an application of scanning electron microscopy. Geological Society of America Bulletin 80, 2091–2094.

Stieglitz, R.D., Rothwell, B., 1978. Surface microtextures of freshwater heavy mineral grains. Geoscience Wisconsin 3, 21–34.

Stoops, G., Altemuller, H.-J., Bisdom, E.B.A., Delvigne, J., Dobrovolsky, V.V., Fitzpatrick, E.A., Paneque, G., Sleeman, J., 1979. Guidelines for the description of mineral alterations in soil micromorphology. Pedologie 29, 121–135.

Surdam, R.C., Dunn, T.L., MacGowan, D.B., Heasler, H.P., 1989. Conceptual models for the prediction of porosity evolution with an example from the Frontier Sandstone, Bighorn Basin, Wyoming. In: Coalson, E.B., Kaplan, S.S., Keighin, C.W., Oglesby, C.A., Robinson, J.W. (Eds.), Petrogenesis and Petrophysics of Selected Sandstone Reservoirs of the Rocky Mountain Region, Rocky Mountain Association of Geologists, pp. 7–28 (plates pp. 300–303).

Taylor, G., Eggleton, R.A., 2001. Regolith Geology and Geomorphology. Wiley, New York, 375pp.

Turner, G., Morton, A.C., 2007. The effects of burial diagenesis on detrital heavy mineral grain surface textures. In: Mange, M., Wright, D.T. (Eds.), Heavy Minerals in Use. Developments in Sedimentology (this volume).

Vavra, G., 1993. A guide to quantitative morphology of accessory zircon. Chemical Geology 110, 15–28.

Veblen, D.R., Banfield, J.F., Guthrie, G.D. Jr., Heaney, P.J., Ilton, E.S., Livi, K.J.T., Smelik, E.A., 1993. High-resolution and analytical transmission electron microscopy of mineral disorder and reactions. Science 260, 1465–1472.

Velbel, M.A., 1984. Natural weathering mechanisms of almandine garnet. Geology 12, 631–634.

Velbel, M.A., 1985. Geochemical mass balances and weathering rates in forested watersheds of the southern Blue Ridge. American Journal of Science 285, 904–930.

Velbel, M.A., 1986. Influence of surface area, surface characteristics, and solution composition on feldspar weathering rates. In: Davis, J.A., Hayes, K.F. (Eds.), Geochemical Processes at Mineral Surfaces, American Chemical Society, Symposium Series, no. 323, pp. 615–634.

Velbel, M.A., 1987. Rate-controlling factors in the weathering of some ferromagnesian silicate minerals: Transactions, 13th Congress of the International Society of Soil Science, Hamburg, FRG, vol. 6, pp. 1107–1118.

Velbel, M.A., 1989a. Weathering of hornblende to ferruginous products by a dissolution-reprecipitation mechanism: petrography and stoichiometry. Clays and Clay Minerals 37, 515–524.

Velbel, M.A., 1989b. Effect of chemical affinity on feldspar hydrolysis rates in two natural weathering systems. Chemical Geology 78, 245–253.

Velbel, M.A., 1993a. Formation of protective surface layers during silicate-mineral weathering under well-leached, oxidizing conditions. American Mineralogist 78, 408–417.

Velbel, M.A., 1993b. Constancy of silicate-mineral weathering-rate ratios between natural and experimental weathering: implications for hydrologic control of differences in absolute rates. Chemical Geology 105, 89–99.

Velbel, M.A., 1999. Bond strength and the relative weathering rates of simple orthosilicates. American Journal of Science 299, 679–696.

Velbel, M.A., 2000. Classroom index-card simulation of crystal growth. Journal of Geoscience Education 48, 261–266.

Velbel, M.A., 2004. Laboratory and homework exercises in the geochemical kinetics of mineral-water reaction: rate law, Arrhenius activation energy, and the rate-determining step in the dissolution of halite. Journal of Geoscience Education 52, 52–59.

Velbel, M.A., Barker, W.W., accepted. Conventional and low-voltage cryo-field emission scanning electron microscopy of pyroxene weathering to smectite, Koua Bocca ultramafic complex, Ivory Coast.

Velbel, M.A., Basso, C.L. Jr., Zieg, M.J., 1996. The natural weathering of staurolite: crystal-surface textures, relative stability, and the rate-determining step. American Journal of Science 296, 453–472.

Velbel, M.A., McGuire, J.T., Madden, A.S., 2007. Scanning electron microscopy of garnet from southern Michigan soils: etching rates and inheritance of pre-glacial and pre-pedogenic grain-surface textures. In: Mange, M., Wright, D.T. (Eds.), Heavy Minerals in Use. Developments in Sedimentology (this volume).

Velbel, M.A., McGuire, J.T., Mellott, N.P., Formolo, M.J., 1998a. Weathering of garnet and chain-silicates in forest and agricultural soils at the Kellogg Biological Station and Coweeta Hydrologic Laboratory LTER sites, and other Great Lakes and Southern Blue Ridge regional localities: Abstract, KBS LTER Site All Investigators Meeting, KBS, 21–22 July, 1998, pp. 44–45.

Velbel, M.A., Mellott, N.P., Formolo, M.J., 1998b. Reactant–product interfaces on naturally weathered chain-silicates from West Africa and the Southern Blue Ridge: Abstract, Clay Minerals Society Annual Meeting, 92pp.

Velde, B., 1988. Experimental pseudomorphism of diopside by talc and serpentine in $(Ni,Mg)Cl_2$ aqueous solutions. Geochimica et Cosmochimica Acta 52, 415–424.

Walker, T.R., Waugh, B., Crone, A.J., 1978. Diagenesis in first-cycle alluvium of Cenozoic Age, southwestern United States and northwestern Mexico. Geological Society of America Bulletin 89, 19–32.

Waugh, B., 1978. Diagenesis in continental red beds as revealed by scanning electron microscopy—a review. In: Whalley, W.B. (Ed.), Scanning Electron Microscopy in the Study of Sediments. Geological Abstracts, Norwich, pp. 329–346.

Wegner, M.W., Christie, J.M., 1985a. Chemical etching of amphiboles and pyroxenes. Physics and Chemistry of Minerals 12, 86–89.

Wegner, M.W., Christie, J.M., 1985b. General chemical etchants for microstructures and defects in silicates. Physics and Chemistry of Minerals 12, 90–92.

Welton, J.E., 1984. SEM petrology atlas: methods in exploration series, American Association of Petroleum Geologists, 237pp.

Wentworth, S.J., Gibson, E.K., Velbel, M.A., McKay, D.S., 2005. Antarctic Dry Valleys and indigenous weathering in Mars meteorites: implications for water and life on Mars. Icarus 174, 382–395.

Werner, A.J., Hochella, M.F. Jr., Guthrie, G.D. Jr., Hardy, J.A., Aust, A.E., Rimstidt, J.D., 1995. Asbestiform riebeckite (crocidolite) dissolution in the presence of Fe chelators. Implications for mineral-induced diseases. American Mineralogist 80, 1093–1103.

White, A.F., 2005. Natural weathering rates of silicate minerals. In: Drever, J.I. (Ed.), Surface and Ground Water, Weathering, and Soils, vol. 5, Treatise on Geochemistry. Elsevier-Pergamon, Oxford, pp. 133–168.

White, A.F., Brantley, S.L. (Eds.), 1995. Chemical Weathering Rates of Silicate Minerals. Mineralogical Society of America, Reviews in Mineralogy, v. 31, 583pp.

White, A.F., Brantley, S.L., 2003. The effect of time on the weathering of silicate minerals: why do weathering rates differ in the laboratory and field? Chemical Geology 202, 479–506.

Wilson, M.J., 1975. Chemical weathering of some primary rock-forming minerals. Soil Science 119, 349–355.

Wilson, M.J., 1986. Mineral weathering processes in podzolic soils on granitic materials and their implications for surface water acidification. Journal of the Geological Society, London 143, 691–697.

Wilson, M.J., 2004. Weathering of the primary rock-forming minerals; processes, products and rates. Clay Minerals 39, 233–266.

Wilson, M.J., Farmer, V.C., 1970. A study of weathering in a soil derived from a biotite-hornblende rock II. The weathering of hornblende. Clay Minerals 8, 435–444.

Wilson, M.J., Jones, D., 1983. Lichen weathering of minerals: implications for pedogenesis. In: Wilson, R.C.L. (Ed.), Residual Deposits: Surface Related Weathering Processes and Materials, vol. 11. Geological Society Special Publication, pp. 5–12.

Winter, J., 1981. Exakte tephrostratigraphische Korrelation mit morphologisch differenzierten Zirkonpopulationen (Grenzbereich Unter-Mitteldevon, Eifel-Ardennen). Neues Jahrbuch für Geologie und Paläontologie, Abhandlungen 162, 97–136.

Zhang, H., Bloom, P.R., Nater, E.A., 1990. Morphology and chemistry of hornblende dissolution products in acid solutions. In: Douglas, L.A. (Ed.), Soil Micromorphology: A Basic and Applied Science. Developments in Soil Science, vol. 19, pp. 551–556.

Chapter 5

PROVENANCE AND PALAEOENVIRONMENTAL INTERPRETATION OF SUPERFICIAL DEPOSITS, WITH PARTICULAR REFERENCE TO POST-DEPOSITIONAL MODIFICATION OF HEAVY MINERAL ASSEMBLAGES

RICHARD M. BATEMAN[a] AND JOHN A. CATT[b]

[a]*Jodrell Laboratory, Royal Botanic Gardens Kew, Richmond, Surrey TW9 3DS, UK*
[b]*Department of Geography, University College London, Gower Street, London WC1E 6BT, UK*

ABSTRACT

A typical complete sedimentary cycle involves five phases (pre-erosional, in transit, post-depositional pre-burial, post-burial, exhumation) and six processes potentially modifying the original composition of the sediment. Some processes add mineral species to an assemblage, others subtract minerals, and yet others can both add and subtract minerals; moreover, some can operate in only one of the five phases, whereas others can affect up to three phases. Authigenic growth and anthropogenic addition are relatively easy to recognise and compensate for, occurring in predictable and limited environmental conditions. Although mechanical weathering can substantially alter heavy mineral assemblages, its effects also are predictable, and prolonged or intense abrasion is required. In contrast, differential sorting of minerals during transport can have a rapid and profound modifying effect on a heavy mineral assemblage that is less readily compensated for but does broadly follow the laws of physics. In an analogous effect, any contrasts between heavy mineral studies in the size fraction selected by each analyst can seriously undermine data comparison. The widely recognised boundary between superficial pedochemical weathering and deeper geochemical weathering is largely artificial. Both phenomena frequently and often profoundly modify heavy mineral assemblages, but the resulting patterns of depletion vary considerably. For example, intrinsic properties of minerals conferring vulnerability to acid pedochemical weathering include well-developed multiple cleavage planes and/or inclusions, high-energy lattices and high Fe^{2+} content. However, these properties are insufficient to accurately predict a stability series in any particular heavy mineral assemblage, as both relative and absolute depletion rates are strongly influenced in the post-depositional environment by both abiotic factors (e.g., pH, redox potential) and under-researched biotic factors. Five case-studies of heavy mineral assemblages in British Tertiary and Quaternary deposits are used to illustrate these principles and to demonstrate the benefits of (a) using multivariate methods to elucidate patterns of variation in heavy mineral assemblages, (b) characterising a weathering front using 90% depletion (D^{90}) values

Developments in Sedimentology, Vol. 58, 151–188

ISSN: 0070-4571/doi:10.1016/S0070-4571(07)58005-2

and (c) integrating heavy mineral data with those derived from other geoanalytical and field-based techniques. This approach allows not only more accurate reconstruction of provenance but also of palaeoenvironments; both can then usefully inform correlation.

Keywords: archaeology; automated analysis; D^{90} value; heavy minerals; mineral stability; multivariate ordination; palaeoenvironment; pedology; provenance; Quaternary; sorting; Tertiary; weathering

1. INTRODUCTION

The second half of the 20th century witnessed a substantial decrease in heavy mineral studies across the earth sciences. Students of "superficial" deposits—notably Quaternary sedimentologists, soil scientists, forensic scientists and archaeologists—remain perhaps the most frequent users of heavy mineral analysis.

Although heavy mineral analysis can in theory be performed on virtually any sediment, standard petrological identification is most readily achieved on all, or a selected narrower portion of, the fine-sand fraction (63–250 μm, 4–2 ϕ). It requires disaggregation of the rock into its component particles followed by concentration of the heavy mineral grains. Physical and/or chemical extraction of heavy minerals from well-consolidated sediments inevitably damages those minerals most vulnerable to whichever physical or chemical extraction techniques are employed by the analyst. In practice, medium grained, poorly consolidated sediments are optimal for analysis. Poor consolidation in particular typifies most relatively recent superficial deposits, making them especially amenable for study.

As in investigations of older sediments, the main purpose of most heavy mineral studies of superficial deposits is to determine the provenance of each deposit present at a study site and to find its correlates in other recorded sections. However, the heavy mineral assemblages present in such deposits are subject to a wide range of processes that have the potential to radically modify the composition of the assemblages, thereby obscuring provenance. At least six such processes can be identified: sorting, mechanical weathering, pedochemical weathering, geochemical weathering, authigenesis and anthropogenic addition (Bateman, 1989; Morton and Hallsworth, 1999). Fortunately, surface and near-surface processes can often be observed directly in later Quaternary deposits, increasing the probability of correctly distinguishing the effects of each modifying process on the heavy mineral assemblages under scrutiny.

The consequences of these modifying processes are ignored in many publications, bewailed in some, but in a few more enlightened cases they have been used to add to, rather than detract from, the original goals of the study. Specifically, they can generate much useful palaeoenvironmental data, which if correctly interpreted can enhance rather than undermine attempts at correlation. Although the various modifying processes unquestionably complicate attempts to determine provenance, the most constructive response to this challenge is to develop an approach designed to compensate for the sedimentary history inferred for the assemblage, in order to estimate its original composition. This objective in turn requires understanding of the characteristic effects of each modifying process that is believed to have been active during the sedimentary history of the material (Bateman, 1989).

These modifying processes are the primary focus of this paper. Two important secondary objectives are: (a) to emphasise the value of applying appropriate

multivariate statistical techniques to identify trends in fully quantified heavy mineral data, and (b) to demonstrate that, as in any scientific discipline, the value of heavy mineral data is greatly enhanced if they are integrated with other types of compositional and/or (palaeo)environmental data. Examples of such data sources (the majority of which are discussed in this paper) include coarse clast orientation and lithology, anthropogenic artefact analysis, clay mineral XRD, microprobe analysis, detailed particle size analysis (often summarised statistically), geochemistry (major, minor and trace elements determined using mass spectrometry, plus carbon-influenced measures such as pH, loss-on-ignition, organic carbon and carbonate), SEM scrutiny of quartz (e.g., Mahaney, 2002) and other mineral grains, plant (e.g., pollen/spores, seeds, opaline phytoliths, wood fragments) and animal (e.g., beetles, diatoms, foraminifera) remains. Field relations and dating methods (e.g., radiometric, fission track, thermoluminescence, dendrochronology) are also critical to success (cf. Wilson et al., 1981; Bateman and Moffat, 1987; Farrington and Bateman, 1992). The paper unashamedly draws primarily on our own research in these areas, thereby allowing us to feature those case-studies that we can discuss with greatest authority.

2. CASE-STUDIES

In order to elucidate the relevance of the sedimentary cycle and the relative importance of the six main categories of modifying processes, we will first explore their implications in an overlapping series of five case-studies that were aimed primarily at determining provenance and/or palaeoenvironments in several Tertiary and Quaternary deposits of the British Isles. Dates of Quaternary deposits are given in years BP, adjusted to AD 1950. The geographical and stratigraphical coverage of these studies are outlined in Figs. 1A and B, respectively.

Most of the samples discussed in this paper have been analysed for 800–1000 grains each of the light, opaque heavy and non-opaque heavy fractions. This count range considerably exceeds the asymptote of 300–400 grains estimated theoretically as providing acceptable accuracy for quantifying the more common minerals in an assemblage, reflecting our desire to achieve acceptably small sampling errors for minerals of all but the lowest frequencies.

Mineral categories were delimited primarily on optical properties. Where an optical category encompassed a wide range of chemical compositions, such as those found in substitution series, that category is referred to in the plural (e.g., garnets, tourmalines), whereas more chemically restricted mineral species that consequently have more predictable properties are referred to in the singular (e.g., zircon, kyanite).

Four of the five case-studies presented here used a similar approach in summarising the fully quantified mineralogy of the samples analysed; similarities of samples were gauged using Gower's (1971) similarity coefficient, and the resulting values were used to generate principal coordinates plots (Gower, 1966), as programmed in *GENSTAT 7* (2004, VSN International). The purpose of such plots is to summarise the effects of many variables (in this case, optically delimited mineral categories) in a single, readily interpreted diagram. The quantified assemblages are arranged in multivariate hyperspace and then projected perpendicularly onto the plane that encompasses the greatest proportion of the observed variation (Fig. 2). This method simultaneously identifies

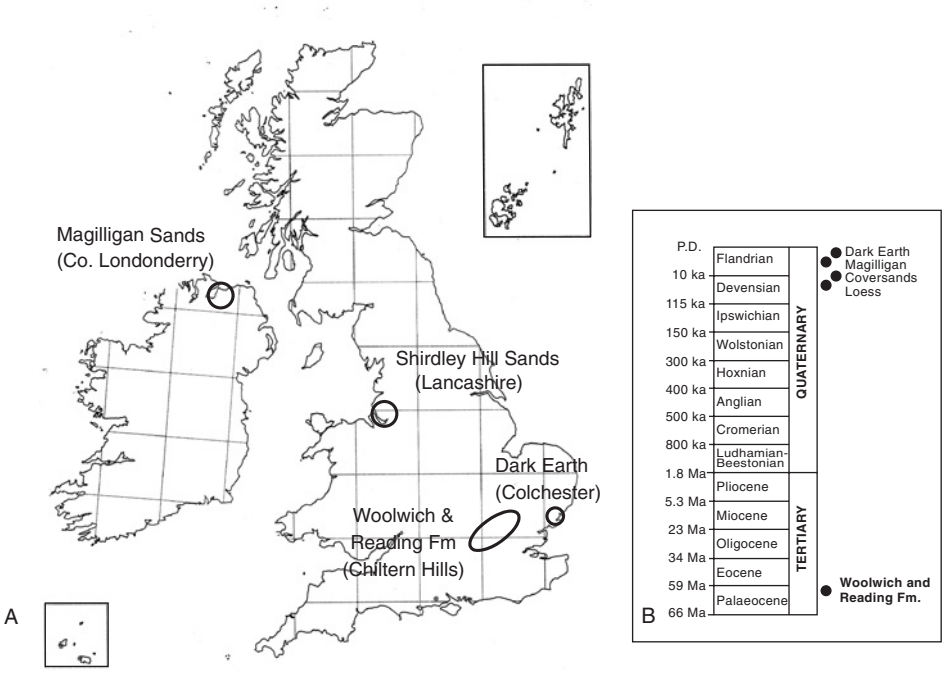

Fig. 1. Geographical locations in the British Isles (A) and stratigraphical spectrum (B) of the five case-studies of superficial heavy mineral assemblages reviewed in this paper. Tertiary stratigraphy follows Curry et al. (1978); Quaternary stratigraphy follows Mitchell et al. (1973), as modified by Bowen (1999).

which of the many variables interact together through positive or negative correlation (or covariance) to best represent the relative similarities of the sampled mineral assemblages.

In the case of the Dark Earth case-study, the Gower similarity coefficients generated during the ordination procedure were also used to generate an unrooted minimum spanning tree linking samples of greatest similarity (Gower and Ross, 1969), which is superimposed onto the ordinations. Each plot also shows the variables contributing most to each coordinate, indicating the direction of increase in frequency of each variable listed.

2.1. Palaeocene Woolwich and Reading Formation in the Chiltern Hills

The late Palaeocene Woolwich and Reading Formation (WRF: basally incorporating the ''Upnor Formation'' of Ellison et al., 1994) consists of a broadly fining-up sequence of conglomerates (the thin but especially lithologically complex and stratigraphically controversial ''Bottom Bed''), sands and silty clays that were deposited mainly in shallow marine environments and vary laterally in facies according to local depositional environments. These mostly poorly consolidated sediments are relatively thick in the centres of the London and Hampshire basins, and correlate with

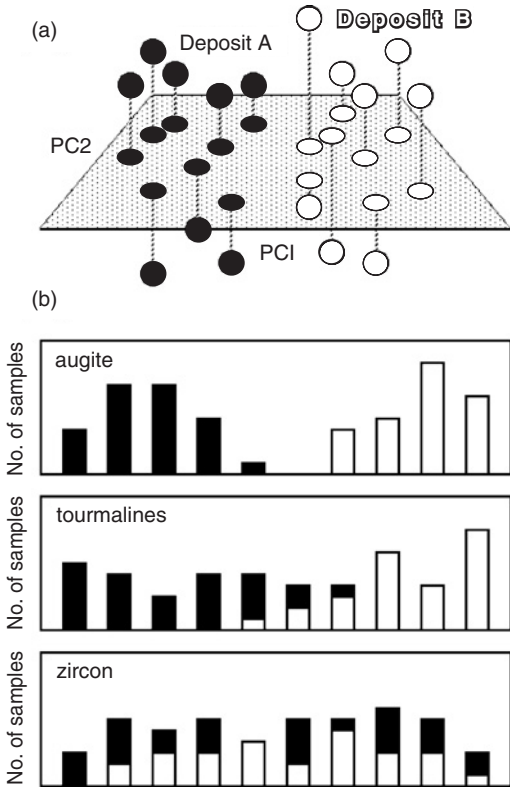

Fig. 2. (a) Hypothetical ordination of samples of eight mineral assemblages from each of two deposits, A and B, showing the samples ordinated in multivariate hyperspace and the way in which their respective positions are then projected by the computer algorithm perpendicularly onto the plane of maximum variation, which is delimited by two axes, PC1 and PC2. In this case, PC2 does not distinguish between the two deposits (perhaps reflecting a contrast in the degrees of weathering they have experienced), whereas PC1 reliably separates individual samples taken from the two deposits. (b) Hypothetical histograms of three minerals, each histogram plotting relative frequency in the assemblage (horizontal axis) against numbers of samples falling into that category of frequency (vertical axis). Augite is clearly highly diagnostic, being much less frequent in deposit A than deposit B, tourmaline appears partially diagnostic, but zircon varies randomly with respect to the two deposits.

even thicker, deeper-water deposits in the North Sea Basin to the east and northeast (e.g., Blondeau and Pomerol, 1968; Knox et al., 1981). However, they thin northwestwards in the London Basin until only a highly fragmented residue of outliers is found along the WSW–ENE-oriented chalk dipslope of the Chiltern Hills, reflecting both the marginal location in the depositional basin and subsequent Plio-Pleistocene erosional dissection (Hester, 1965; Ellison, 1983; Bateman and Moffat, 1987). These outliers are crucial to understanding the overall depositional history of the Formation but they also represent an unusually serious interpretational challenge that has engendered considerable controversy regarding both provenance and depositional

environments (cf. Morton, 1982, 1983; Moffat and Bateman, 1983; Bateman, 1984, unpublished manuscript; Bateman and Moffat, 1987).

Considerable variation was detected in the 55 heavy mineral assemblages analysed in the 63–250 μm size range from 25 localities in the Chiltern Hills. The majority of samples consisted of the three minerals most strongly resistant to both mechanical and chemical weathering: tourmalines, zircon and rutile. Also often present were considerable amounts of the metamorphically generated minerals staurolite and kyanite. More variable were garnets and epidotes, which each constituted up to 20% of some heavy mineral samples (especially of the Bottom Bed, often coinciding with an unusually high total heavy mineral content), but were virtually absent from others; a similar pattern of strong contrasts among samples characterised the glauconite content of the light fraction (Bateman and Moffat, 1987).

Patterns of variation became much clearer when subjected to principal coordinates analysis (Fig. 3). The first three coordinates together accounted for 48% of the total variance. The first coordinate primarily separated Bottom Bed samples from the overlying sands and clays according to the greater proportions of andalusite, epidotes and garnets in the former and of rutile and anatase in the latter. The second coordinate represented an inverse relationship between tourmalines and zircon, their relative proportions varying mainly according to the texture of the deposits (tourmalines are inherently large, zircons inherently small; Table 1); the second coordinate was thus less informative regarding provenance and correlation than the first and third coordinates. The third coordinate was dominated by kyanite, which when plotted separately mainly showed a geographic trend along the strike of the Chilterns from WSW to ENE (Fig. 4).

Seeking to infer provenance, Bateman and Moffat (1987) supported several previous studies in arguing that the bulk of the zircon, rutile and tourmalines originated from the same area as the staurolite and kyanite, which was most probably Armorica. In contrast, they were unable to support the existence of a previously suggested association, finding that these minerals apparently varied independently of each other.

The sudden increase in kyanite content evident about halfway along the WSW–ENE strike occurs about 12 km further west in the Bottom Bed relative to the overlying sands. Nonetheless, the similar direction of increase in kyanite in both units challenged previous assertions that the Bottom Bed represented a marine transgression to the northwest whereas the overlying sands and silty clays dominantly represented southward fluviatile deposition. Rather, a similar ENE direction of transport is envisaged throughout deposition of the WRF across the dipslope, and during the early stages of deposition fluviatile input may have been confined to a small area in the west.

The origin of the Bottom Bed is especially contentious, the most likely sources being the Late Cretaceous chalk (through syn-depositional erosion and/or post-depositional dissolution) or reworking of the Palaeogene Thanet Formation, perhaps supplemented from more distant primary sources, most likely via the North Sea Basin (e.g., Morton, 1982). The fact that the Bottom Bed is the most mineralogically heterogeneous of the depositional units suggests local reworking of pre-existing deposits, but the uniform rarity of hornblende and only very local occurrence of epidotes militate against large inputs from the Thanet Formation, which is rich in both of these heavy minerals. It also undermines the more recent suggestion of Hopson et al. (1996)

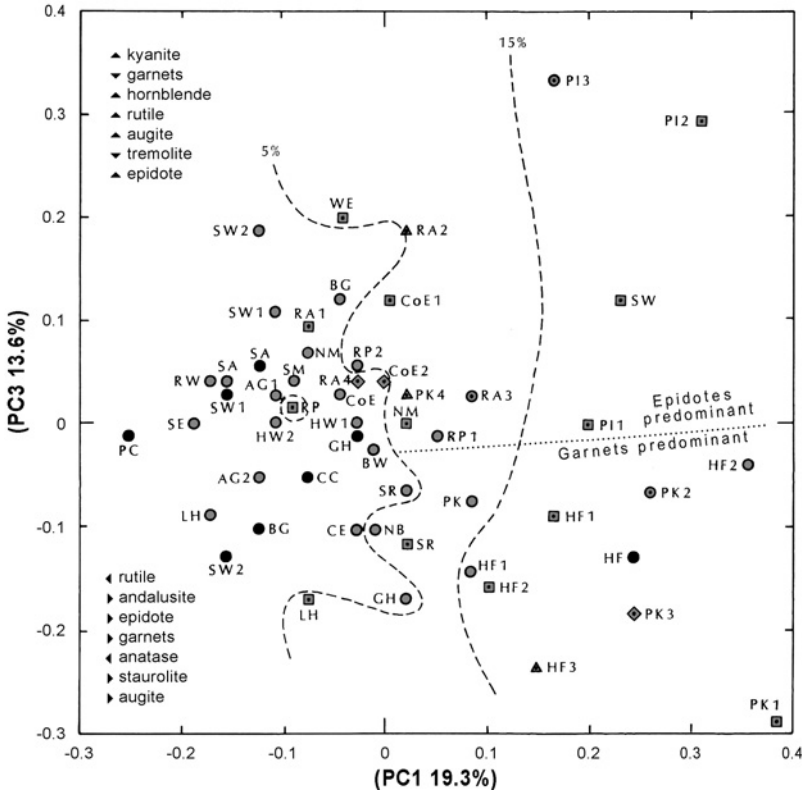

Fig. 3. Plot of the first and third principal coordinates for non-opaque heavy mineral data from the late Palaeocene Woolwich and Reading Formation of the Chiltern Hills, southeast England. The first coordinate accounted for 19.3% of the total variance and reflected variation in rutile (−), andalusite (+), epidote (+), garnets (+), anatase (−), staurolite (+) and augite (+). The third coordinate accounted for 13.6% of the total variance and was dominated by variation in kyanite (+), with subsidiary contributions from garnets (−), hornblende (+), rutile (+), augite (+), tremolite/actinolite (−) and epidote (+). Dashed isopleths are the combined frequency of garnets plus epidotes, which increases from left to right. The second coordinate, not shown but accounting for 14.7% of the total variance, mainly reflected size differences within the fine-sand fraction, being dictated by an antagonistic relationship between tourmalines (+: dominantly large grains) and zircon (−: dominantly small grains). (Modified after Bateman and Moffat, 1987, Fig. 8, Table 9).

that the WRF Bottom Bed was partially reworked from the Bullhead Bed, which constitutes the basal conglomerate of the earlier Thanet Sand Formation. [Note that Ellison et al. (1994) chose to lithostratigraphically redefine the traditional Woolwich and Reading Formation more narrowly, including the upper sands, silts and clays of earlier authors but excluding the Bottom Bed (basal conglomerate and associated heterogeneous deposits) which was designated the Upnor Formation; the entire ensemble was then designated the Lambeth Group.]

The failure of any subsequent marine or fluvial incursions to wholly erode the Bottom Bed basal conglomerates at any locality suggests that it could have formed

Table 1. Mean sizes of non-opaque heavy minerals within the 4–2 ϕ (63–250 μm) size range, based on data for 18 samples of three late Pleistocene coversand profiles located to the east of the British Pennine Hills

Mineral(s)	Mean size, Mz (ϕ)	Intrinsic size class
Andalusite	2.80	I
Staurolite	2.87	I
Tourmalines	2.88	I
Garnets	2.96	II
Augite	2.98	II
Kyanite	3.04	II
Hypersthene	3.06	II
Hornblende	3.13	II
Tremolite	3.25	III
Epidote	3.27	III
Rutile	3.40	IV
Sphene	3.43	IV
Apatite	3.48	IV
Zircon	3.60	IV

Notes: The more frequent minerals that consequently generate the most robust data are shown in boldface. Thresholds between the four size categories (I–IV) are arbitrary: I is the coarsest and IV the finest. (Modified after Bateman and Rose, 1994, Table 4).

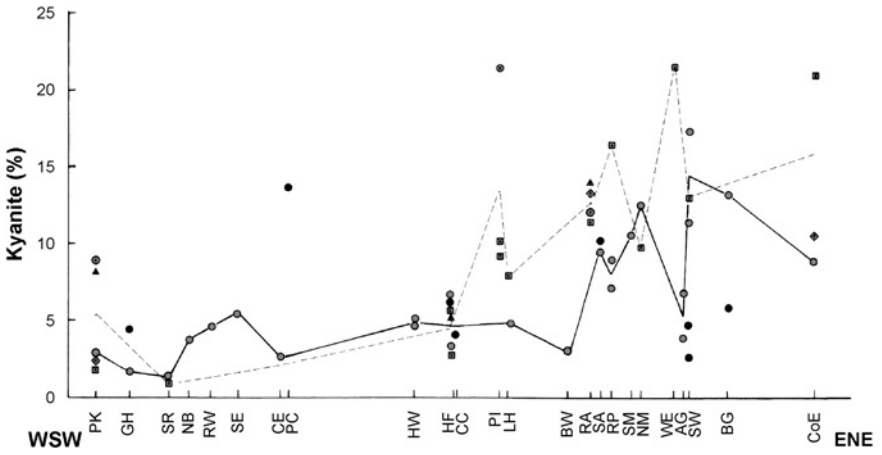

Fig. 4. Variation along the WSW–ENE strike of the Chiltern Hills in the kyanite content (percentage of the 63–250 μm non-opaque heavy mineral fraction) of the late Palaeocene Woolwich and Reading Formation s.l. The dashed line links mean values for the Bottom Bed, whereas the solid line links mean values for the overlying sands plus clays. (After Bateman and Moffat, 1987, Fig. 7.)

by dissolution of the immediately underlying chalk by percolating fluids. Some input from the Chalk is certain, but the relative concentration in the Bottom Bed of minerals moderately vulnerable to pedochemical weathering, such as epidotes and garnets, argues against extensive post-burial dissolution. Also, the amount of chalk

that would have to be dissolved to generate the Bottom Bed deposits is vast (on average only one non-opaque heavy mineral sand grain is recovered from every 20 g of chalk: Bateman, 1988). The presence of silcretes within the lower part of the Woolwich and Reading Formation indicates syn-depositional subaerial (pedochemical) weathering, but this was insufficient to eliminate vulnerable minerals only a few decimetres below. Admittedly, mineralogical evidence for subaerial weathering increases up the Chiltern dipslope, but this is more likely to reflect progressive exhumation during the later Tertiary and Quaternary (Bateman, 1988).

Thus, the most important factor hindering more precise interpretation of provenance and palaeoenvironments using heavy minerals in this sequence of deposits is uncertainty over the timing and degree of syn- and post-depositional weathering. The greatest strength of the study was being able to integrate heavy mineral data with many other kinds of sedimentological information, giving greater credence to the conclusion that the succession represents a marine incursion that was followed by lower energy fine sands and silts deposited in a marshy lagoon.

2.2. *Late Pleistocene Coversands in Northwest England*

Significant areas of the central British counties of Lancashire, Yorkshire, Lincolnshire and Norfolk are blanketed in distinctive coversands—well-sorted, homogeneous, poorly consolidated sands typically 0.5–3 m thick. The sands (which sustain important agriculture, forestry and glass-making activities) were deposited by multidirectional winds in the periglacial landscape that briefly dominated northwest Europe during the Younger Dryas, following the final Pleistocene glaciation (approximately 10,800–10,000 BP = 12,650–11,500 calendar years BP). Both their depositional environments and especially their provenance have been highly controversial (e.g., Bateman and Catt, 1985). Wilson et al. (1981) applied heavy mineral analysis and several other geoanalytical techniques to the 63–250 μm fractions of 30 samples of the Shirdley Hill Sand (SHS) of southwest Lancashire and 40 samples representing all the likely sources of the reworked sediments from the region: six other Quaternary deposits from contrasting depositional environments and three lithological categories of Carboniferous (Lower Coal Measures) and Triassic (Keuper/Bunter) sandstones.

The resulting principal coordinates plot (Fig. 5) revealed three main groups. The first group encompasses the marine Irish Sea sands, beach sands, coastal and inland dune sands, whereas the second group comprises the glaciofluvial sands, heterogeneous terrestrial tills and most SHS samples, which form a strikingly compact group. However, a few SHS samples fall within the bedrock Triassic sandstone sector, characterised by being dominated by tourmalines but impoverished in augite and hornblende (the apparent position of the Carboniferous sandstones in Fig. 5 is misleading; rich in garnets, rutile and zircon, they are strongly separated from the other sandstone sector samples on the third coordinate, which is not shown here. Two clusters of Quaternary samples representing the third group had broadly similar, diverse but augite-dominated assemblages that were separated on the second axis according to whether they were relatively rich in the metamorphic minerals staurolite and kyanite (probably ultimately derived from Scotland and/or Armorica) or in hypersthene.

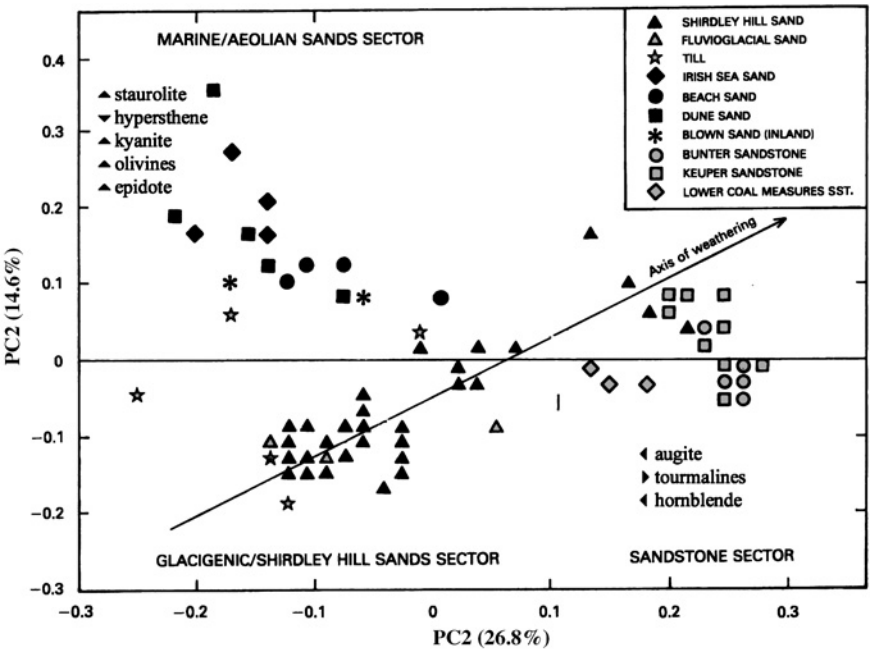

Fig. 5. Plot of the first and second principal coordinates for non-opaque heavy mineral data (63–250 μm) from the late Pleistocene SHS formation and several potential sources of the formation in southwest Lancashire, England. The first coordinate accounted for 26.8% of the total variance and reflected variation in augite (−), tourmalines (+) and hornblende (−). The second coordinate accounted for 14.6% of the total variance and reflected variation in staurolite (+), hypersthene (−), kyanite (+), olivine (+) and epidote (+). (After Wilson et al., 1981, Fig. 5, Table 2.)

Given this result, the temptation was to infer multiple sources for the SHS, albeit discounting the marine, dune and Carboniferous sands. However, it became apparent that samples of SHS occurring in the right-hand (i.e., low diversity) sector were invariably situated higher in the sampled successions than other deeper samples from the same localities, suggesting that the low diversity assemblages in the SHS had developed post-depositionally as a result of acid pedochemical weathering. This placed the emphasis for determining provenance on the cohesive main cluster of SHS samples in the bottom left of the ordination, which strongly indicate an origin by aeolian reworking of earlier glaciofluvial sands and, to a lesser degree, tills; in other words, they were derived from outwash of the Late Devensian ice sheet.

2.3. Pleistocene Loess in Southern England

Loess is the most widespread Quaternary deposit on Earth. Nonetheless, its origin remains controversial, partly because it is composed almost entirely of silt (2–63 μm, 9–4 ϕ), which is finer than the size fractions commonly used for provenance studies by heavy mineral analysts. The most frequently suggested origin of loess involves

long-distance (10^2–10^3 km) aeolian transportation of the silt. Although many loesses also contain a small amount of fine sand (63–250 μm), this is likely to be much more local in origin and so is a relatively poor indicator of the provenance of the predominant silt. Fortunately, heavy minerals can be separated from silt-sized fractions by centrifugation in a heavy liquid, and at least the coarser grains can usually be identified optically in a standard immersion liquid using conventional properties such as relief, colour, pleochroism, interference colours, extinction angle, crystal shape and cleavage patterns.

Earlier work on the origin of surface soils in England and Wales showed that many have upper horizons containing much more silt and a lower base saturation than would be predicted from the bedrock or the Quaternary formation on which, according to maps of the British Geological Survey, they have developed (Coombe et al., 1956; Perrin, 1956; Pigott, 1962). The particle size distribution of these superficial horizons often resembles that of loess, with a mode in the coarse silt, usually between 25 and 45 μm. The widespread occurrence of loess deposits on a broad range of physiographic surfaces also strongly suggests wind deposition. To confirm this hypothesised origin, we sampled topsoils from numerous parts of the country for granulometric and mineralogical analyses, and compared them with samples of undoubted loess from sites such as Pegwell Bay, Kent (Pitcher et al., 1954). Soils of 55 formal associations in England and Wales were found to be derived wholly or partly from loess; indeed, the distribution of these associations, as mapped by the National Soil Resources Institute (formerly Soil Survey of England and Wales, 1983), indicates the extent of loess in Britain (Catt, 1985) (Fig. 6A).

In eastern England, from the Yorkshire Wolds (Catt et al., 1974) southward to North Norfolk (Catt et al., 1971) and East Kent (Weir et al., 1971), the mineralogical composition of the coarse silt (16–63 μm) strongly resembles that of the late Devensian Skipsea Till of Holderness, Lincolnshire and North Norfolk (Madgett and Catt, 1978), suggesting that the loess was derived from outwash deposits of the late Devensian ice sheet spread over the then dry floor of the North Sea. A late Devensian age (18,000–14,000 BP) for the loess has since been confirmed by thermoluminescence dating (Wintle, 1981; Parks and Rendell, 1992).

From Yorkshire and Kent westward to East Devon, there is a progressive increase in the amounts of platy phyllosilicate minerals, such as muscovite in the light fraction of the coarse silt and chlorite (Fig. 6B) and biotite in the heavy fraction (Catt, 1978). The diverse suite of other metamorphic, igneous and sedimentary minerals in the loess remains almost unchanged, apart from ubiquitous proportionate decreases in response to the increasing abundance of platy minerals. However, a progressive westward decrease in the modal size of the silt is also evident (Fig. 6C). Together with the mineralogical changes, this cline suggests winnowing by anticyclonic easterly winds around the southern margin of the ice sheet. However, the loess on the Lizard Peninsula and in other parts of Cornwall (Catt and Staines, 1982) has a coarser modal size and contrasting silt mineralogy from that in East Devon, suggesting that it was derived from a different source, possibly the late Devensian glacial deposits of the Irish Sea Basin (cf. the coversands case-study outlined above, though the Cornubian loess deposits are older than the SHS). An Irish Sea source has also been suggested for loess in other parts of western England and North Wales (Vincent and Lee, 1981).

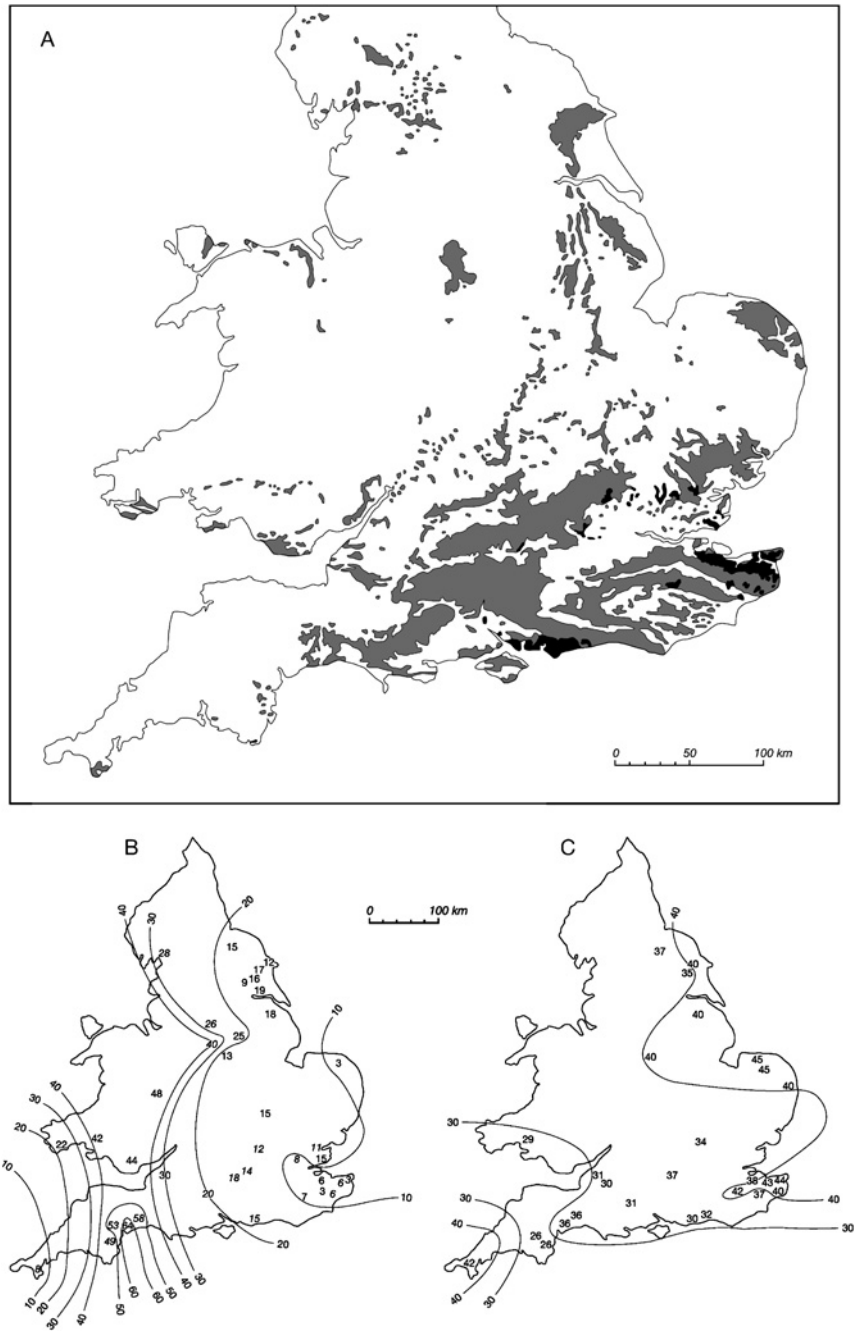

Fig. 6. Loess in England and Wales. (A) Distribution of loesses over 1 m thick (black) and 0.3–1 m thick (stippled). (B) Percent chlorite in non-opaque heavy fraction of coarse silt (16–63 μm) from late Devensian loess samples. (C) Modal size (μm) of silt from late Devensian loess samples. (A based on Soil Survey of England and Wales (1983); B and C modified, with later additions, from Catt (1978).)

The only effects of post-depositional pedogenetic modification of the coarse silt mineral assemblage detected in the late Devensian loess are diminution of calcite (mainly chalk fragments) and some largely biogenic phosphates (apatite and collophane), and oxidation of glauconite pellets to brown "limonitic" aggregates, which are then sometimes disaggregated to produce clay (Weir et al., 1971). The abundance of carbonate in the original loess and the relatively high pH (>6.0) of almost all the profiles studied have precluded changes in other minerals, such as those found in the podzols developed on coversands discussed below. Lastly, the study of a complex succession of silts at Borden, Kent by Catt et al. (1987) demonstrated that the potential for using multivariate ordinations to help interpret mineral assemblages is just as great for coarse silts as for fine sands.

2.4. Genesis of a Holocene Dune System in Northern Ireland

Magilligan Foreland, Ireland's largest coastal accumulation feature (32 km^2), is a triangular beach-ridge plain at the mouth of Lough Foyle, Co. Londonderry, that has evolved in response to land/sea-level changes during the Holocene (Wilson and Bateman, 1986, 1987; Bateman and Wilson, 1989; Wilson and Farrington, 1989). It consists of approximately 150 north/northeast-facing, swash-aligned beach ridges that are overlain by more localised, predominantly aeolian sediments. Most of the evidence for the evolution of Magilligan has been obtained from 12 vertical profiles sampled at five locations along low, actively eroding cliffs to the west. These provide a 3 km-long composite section perpendicular to the beach ridges (Fig. 7).

Magilligan has been the subject of a detailed interdisciplinary study designed to reconstruct its event stratigraphy and palaeoenvironments. Field studies involving topographic survey and soil profile description preceded laboratory analyses for particle size, fine-sand mineralogy (29 samples of the 63–250 μm range) and 12 chemical parameters. Nineteen high-precision radiocarbon dates obtained from wood, charcoal, peat, soil organic matter, freshwater marl and marine shell (Wilson and Bateman, 1986) were supplemented with nine low-precision dates of molluscs sampled from within the beach ridge sand (Wilson and Farrington, 1989).

Three main phases of deposition (Units I–III) terminate in palaeotopographies (termed palaeocatenas) that are delimited primarily by soil development and/or peat accumulation and represent periods of landscape stability. All three deposits are composed of texturally and mineralogically similar material; they are typically unconsolidated, very well-sorted fine sands, mostly eroded from extensive outcrops of Palaeocene–Eocene (61–58 Ma) Antrim basalts nearby (Wilson and Bateman, 1990). Thus, heavy mineral fractions are dominated by augite with subordinate hornblende and significant quantities of hypersthene/bronzite, chrysolite olivine, apatite, epidotes and garnets. Remarkably, the classic resistant suite of zircon, rutile, tourmalines, staurolite and kyanite constitutes on average only 5% of the overall assemblage. What makes the succession of particular interest is that, despite the multiple phases of deposition, the supply of marine sediment was constant. Hence, most of the textural and mineralogical heterogeneities in the succession reflect post-depositional modification, though its effects were at most modest; consequently, mineralogical variation was judged insufficient to justify use of multivariate analytical methods. Pedogenesis

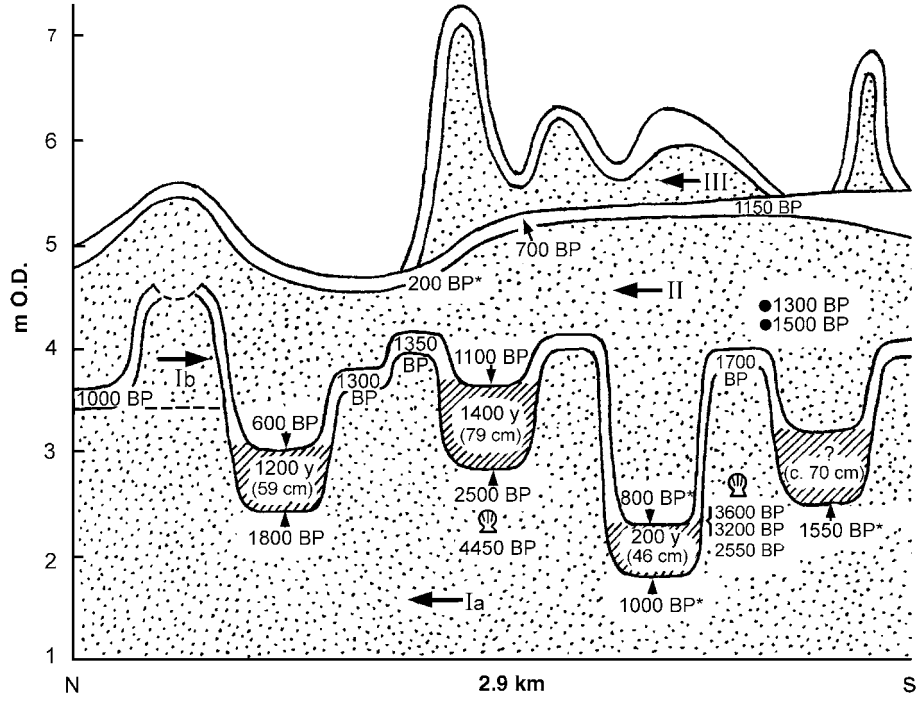

Fig. 7. Schematic topographic reconstruction of coastal section at Magilligan Foreland, Co. Londonderry, Northern Ireland, showing the direction of accumulation of the four main depositional units (Ia, Ib, II, III) and the locations of soil organic materials, peats (cross-hatched) and bivalve shells used for radiocarbon dating. The relative thicknesses and periods of accumulation of the dune-slack peats are indicated. Note that the vertical scale is enormously exaggerated. Asterisked radiocarbon dates were obtained in Belfast, the remainder in East Kilbride. (Summarises information from Wilson and Bateman (1986, Fig. 6), Wilson and Bateman (1987, Fig. 2) and Wilson and Farrington (1989).)

can be linked to field observations and radiocarbon dates to reconstruct with remarkable precision an event stratigraphy for the Foreland.

Development of the Foreland was initiated by the deposition of a west–east-oriented gravel barrier during the acme of the Early Holocene transgression (approximately 7000 BP). Many subsequent beach ridges of approximately equal amplitude accreted diachronously northward from the gravel nucleus, each marking the declining intertidal/supratidal boundary that reflected isostatic rise and/or eustatic regression. The younger, northern half of the beach-ridge plain accreted between approximately 3500 and 2500 BP. Exposure to subaerial weathering resulted in pedogenesis on the freely drained beach-ridge crests and slopes, while marine incursions persisted in the intervening depressions. Continuing gradual decline in sea level exposed the shallower depressions first, so that peat formation began earliest (approximately 2450 BP) in the shallowest depression studied and latest (approximately 1000 BP) in the deepest; thus, shallower depressions experienced longer peat-forming intervals and therefore contain thicker peats (Fig. 7). As accretion of the beach-ridge plain neared completion, more prominent

features formed on the seaward side of the beach ridges, representing southward-accreting aeolian deposition.

Pedochemical weathering and biotic colonisation of the beach ridges soon caused decalcification and associated destratification of up to 2 m of sand below soils and up to 0.6 m below peats, and those few minerals most vulnerable to acid pedochemical weathering (volcanic glass and glauconites in the light fraction, olivines and apatite in the heavy fraction) were substantially depleted. Observed degrees of weathering and humus translocation are unusually small relative to other podzol soils, indicating a comparatively short pedogenic interval, and soils developed on the palaeodunes to the north are even more immature. Radiocarbon dates of soil organic matter (1700–1000 BP) are considerably younger than the earliest date for peat formation, demonstrating that the dates provide only a minimum estimate for the onset of pedogenesis. However, progressive decreases in age confirm the northward accretion of the beach ridges.

Following minimal erosion of the beach-ridge topography, the Lough Foyle margin of the beach ridge/palaeodune topography was subsequently buried by aeolian sands of Unit II, which were derived by erosion and redistribution of the beach-ridge sands from the area now occupied by the intertidal sands of Lough Foyle. Dates of 1100 and 600 BP from the uppermost horizons of the peat lenses suggest that the dunes mirrored the earlier beach ridges in accreting diachronously northward. They were then eroded to a remarkably planar surface that increases in height from north to south by only 1.1 m over a distance of 2.6 km (Fig. 7). The degree of weathering in soils that characterise this surface indicates less severe (and thus presumably less prolonged) weathering than in those developed on the earlier landscapes. Radiocarbon dates for the soil vary between 1100 and 200 BP; the older dates are considered suspect, as the planation of the dunes is likely to reflect a single event after sand deposition had ceased in historical times, at approximately 600 BP.

Unit III is a discontinuous cover of undulating dunes close to the present Lough Foyle shoreline. They resemble the older, continuous dunes in lithology, northward direction of accretion, and degree of weathering. Their development could have begun as early as approximately 700 BP, but they are more likely to reflect erosion caused by the historically documented proliferation of rabbit warrens on the Foreland at approximately 300 BP.

2.5. Late Roman/Post-Roman Urban Archaeological Deposits at Colchester

Rescue excavations prompted by recent urban redevelopment in western Europe have revealed a dramatic and ubiquitous change in urban stratigraphy that approximates the contraction of the Roman Empire, early in the fifth century AD. Particularly in northwest Europe, the latest Roman buildings and roadways (notably excluding the city walls and, in the case of Colchester, the recently discovered circus) are blanketed with a thick (typically 0.5–3 m), apparently homogeneous, poorly sorted, unusually dark grey deposit termed Dark Earth. This enigmatic material, presumed to have been at least partly reworked from earlier archaeological strata, is the main physical evidence from about three centuries of the late Roman–early Anglo-Saxon period known colloquially as the ''Dark Ages'', and hence has been the subject of many speculative interpretations (e.g., Jones, 1991).

Farrington and Bateman (1992) presented an outline of an "holistic" archaeology protocol that placed unusual emphasis on properties of the matrix relative to those of the artefacts that it contains. They took advantage of urban regeneration in the 1980s to sample 24 sections from seven urban centres in England and France, though they published results from just one relatively simple section, at Culver Street, Colchester, Essex. The stratigraphy consists of a natural substratum of brickearth ultimately derived from Eocene London Clay Formation (one sample) overlain by two Roman construction–destruction cycles (successive phases of building and demolition: six samples) and finally a thicker (approximately 1 m) truncated layer of Dark Earth (nine samples). This focused study was designed to illustrate the value of integrating several geoanalytical techniques to determine for Dark Earth provenance, mode and environment of deposition, periods of deposition and of burial, and processes of post-depositional modification, in order to answer a higher level question: what is the true historical significance of Dark Earth?

All 16 samples (63–250 μm) were dominated by a non-opaque heavy mineral suite typical of the Palaeogene of the London Basin: mainly tourmalines and zircon, with subordinate rutile, staurolite and kyanite. Also present, particularly in the Dark Earths, were modest amounts of apatite, hornblende, augite and fayalite olivine. On the resulting principal coordinates plot (Fig. 8A) the natural substratum and various construction and destruction layers formed a tight cluster, whereas the Dark Earth samples, despite their similar appearance, formed three separate and less cohesive clusters according to stratigraphic position. The two lowest Dark Earth samples were richest in apatite and (in the light fraction) calcite, representing enrichment in bone and shell fragments respectively. The four upper samples were poorest in bone and shell, but shared with the three stratigraphically intermediate samples the possession of significant quantities of augite, fayalite and (in the light fraction) synthetic glass. Indeed, microprobe data from selected grains of these minerals (Farrington, 1992) supported optical evidence that they were formed anthropogenically rather than naturally, as a result of contemporaneous light industry.

These results suggest that the underlying brickearths provided the dominant sand component of the bricks, tiles and mortar that constituted the Roman buildings. Superimposed on this basic mineral suite are calcareous mineral components and especially foodstuff-derived household refuse, most prevalent in the lower Dark Earth samples, and materials produced during glass, enamel and/or metal processing, which particularly characterise higher levels of the Dark Earth.

A remarkable contrast is evident when these results are compared with an ordination of geochemical data obtained from the same 16 samples (Fig. 8B). Here, it is the Dark Earth samples (excluding the lowermost) that form a tight, cohesive cluster at the right-hand end of the first coordinate, distinguished by their high values for organic carbon, zinc and manganese (both readily bound to organic matter). In contrast, the non-Dark Earth deposits (together with the lowermost Dark Earth sample, suggesting that it contains materials from the underlying construction layer) are far less cohesive, being distributed largely along the second coordinate according to increases in pH, cobalt and nickel at the expense of chromium, perhaps indicating increasing proportions of mortar and/or cement. Interestingly, these changes coincide with increasingly high stratigraphic positions rather than deposit type or depositional environment. Similarly, lead content increased to remarkably high levels through the Dark Earth,

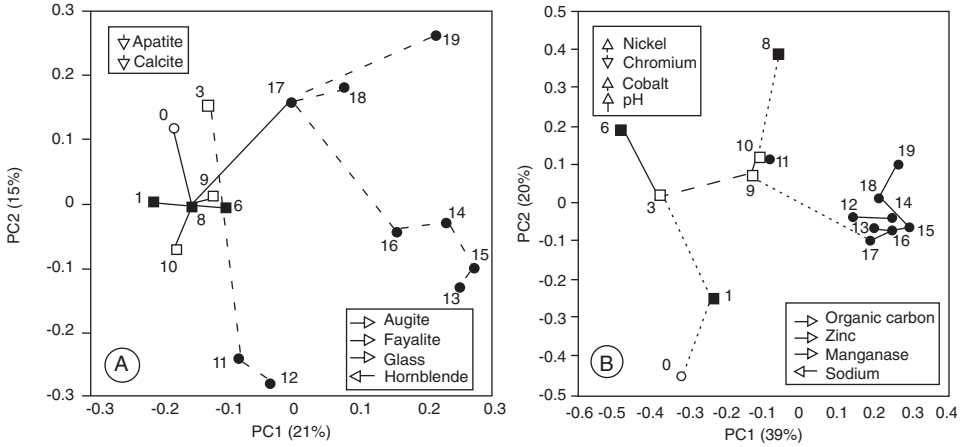

Fig. 8. Plots of the first two principal coordinates of two kinds of physical data from the Roman–Post-Roman urban stratigraphy of Colchester, eastern England. (A) Fine sand (63–250 μm) heavy plus light mineral data. The first coordinate accounted for 21% of the total variance and reflected variation in augite (+), fayalite olivine (+), anthropogenic glass (+) and hornblende (−). The second coordinate accounted for 15% of the total variance and reflected variation in apatite (−) and calcite (−). (B) Geochemical data (<2 mm fraction) obtained by ICP-MS plus organic carbon, carbonate and pH measurements. The first coordinate accounted for 39% of the total variance and reflected variation in organic carbon (+), zinc (+), manganese (+) and sodium (−). The second coordinate accounted for 20% of the total variance and reflected variation in nickel (+), chromium (−), cobalt (+) and pH (+). The 16 samples analysed are listed from stratigraphically lowest to stratigraphically highest: 0, natural substratum (Quaternary "brickearths" reworked from early Eocene London Clay Formation); 1, Colonium construction layer; 3, Boudiccan destruction layer; 6, Flavian reconstruction layer; 8, Opus Signinum floor; 9, 10, Flavian destruction layer; 11–19, post-Roman Dark Earth. Open circle = natural substratum, closed squares = construction layers, open squares = destruction layers, closed circles = Dark Earth. (A and B modified after Farrington and Bateman (1992, Figs. 6 and 4, respectively).)

peaking in the middle of the deposit at approximately 700 ppm (20 times the natural background level). Thus, the unusually dark colour of the deposit was attributed not to organic carbon content per se but rather to organic complexes with metallic ions.

In contrast with the other four case-studies described in this paper, there is remarkably little evidence in the Dark Earth of post-depositional weathering or translocation. Also, evidence of bioturbation is equivocal, making it especially difficult to separate potential syn-depositional and post-exhumation phases. The Dark Earth is too thick, and too rich in various anthropogenic materials, to have accumulated naturally. The upper occupation levels preceding the Dark Earth show gradual accumulation of urban waste in the environment, and some of this material was incorporated into the lowermost portion of the Dark Earth. The remainder of the Dark Earth shows a gradual transition in anthropogenic input away from household waste and toward small-scale industrial waste. This suggests that Dark Earth was deliberately deposited by man, utilising first more proximal sources of household waste and then more distal or concentrated sources of manufacturing

waste. It seems highly likely that this event signalled organised depopulation of this and probably all other urban centres across northwest Europe, a historically profound event.

3. NATURE OF A SEDIMENTARY CYCLE

We will now alter our emphasis from the specifics of our case-studies to more general issues that they raise. One of our key aims is to demonstrate that the interpretation of heavy mineral data initially requires careful consideration of several common forms of analytical error. Once these have been minimised, the potential history of a heavy mineral assemblage should be projected backward through time (i.e., from Phase E to Phase A in the sequence of events summarised below) in an attempt to estimate its unmodified composition at its original source. Such interpretation requires knowledge of the probable effects of the six modifying processes in the full range of environments likely to be encountered by a particular heavy mineral grain.

The potentially complex history of a heavy mineral assemblage can be summarised in the following idealised sedimentary cycle of phases A–E, which together entail modifying events 1–10:

A. Pre-erosional phase
   1. *Pedochemical weathering, at source*
B. In transit phase
   2. *Hydraulic sorting*
   3. *Mechanical weathering*
C. Post-depositional, pre-burial phase
   4. *Pedochemical weathering, at sink*
   5. *Authigenic growth*
D. Post-burial phase
   6. *Geochemical weathering*
   7. *Authigenic growth*
E. Exhumation phase
   8. *Pedochemical weathering, at (re)exposure*
   9. *Authigenic growth*
   10. *Anthropogenic addition*

Thus, of the six processes potentially modifying the mineral assemblage of a superficial deposit, four generally operate during only a single phase of a sedimentary cycle (hydraulic sorting, mechanical weathering, geochemical weathering and, except in very recent deposits, anthropogenic addition) but the remaining two can be active during up to three of the five phases of a cycle: the first, pedochemical weathering, can eliminate mineral species from an assemblage whereas the second, authigenesis, can add species to an assemblage. Moreover, reworking can, in theory, allow any grain to pass through more than one sedimentary cycle.

The following two sections separate processes that do not involve chemical weathering from those that do, which are a particular focus of this paper. In making this analysis it becomes evident that boundaries between the five phases outlined above, especially C and D, can in some circumstances become blurred.

4. NON-CHEMICAL MODIFICATION

4.1. Hydraulic Sorting (and Inherent Size Differences)

Most of the processes discussed under "Non-chemical modification" can either add mineral species to, or subtract mineral species from, an assemblage. The exception is sorting, which generally alters only the relative proportions of species present. Nonetheless, small differences in grain size can generate profound quantitative differences in heavy mineral assemblages (e.g., Friis, 1974, Fig. 2). Bateman (in Bateman and Rose, 1994) used the remarkable textural homogeneity of the Yorkshire, Lincolnshire and Brecklands coversands to investigate the distributions of heavy mineral species among a sequence of four 0.5 ϕ size classes (63–90, 90–125, 125–180 and 180–250 μm), and found differences of an order of magnitude in the frequencies of some species (their contrasting mean sizes are summarised in Table 1). These are considered to primarily reflect inherently different grain sizes at source; zircon, rutile and sphene typically form as small crystals in igneous rocks whereas garnets, staurolite and kyanite are larger crystals that characterise medium- to high-grade metamorphic rocks. Tourmalines too are inherently larger because they can form during hydrothermal activity.

Hydraulic equivalence during transportation has a lesser, though still significant, modifying effect on relative frequencies of heavy minerals (e.g., Komar, 2007, this volume). Although the hydrodynamic properties of a particular grain primarily reflect its weight (density × volume) they are also influenced by its shape; for example, tabular sheets of the readily cleaved mineral kyanite tend to associate with smaller grains of more equidimensional minerals such as zircon, which are less readily entrained in water or air currents.

We strongly suspect that grain size differences are a major contributor to the differences in heavy mineral assemblages documented in our case-studies, particularly those where samples differing greatly in texture and depositional environment are compared (WRF, SHS and its potential sources). This difficulty was exacerbated by our original decision to routinely analyse the broad size range of 63–250 μm. Our subsequent detailed exploration of the various coversands suggests that narrowing analysis to the 90–125 μm range offers the best compromise between maximising the spectrum of well-represented mineral species and obtaining sufficient numbers of grains for meaningful statistical analysis. However, it should be noted that variation in hydraulic equivalence means that, even within this narrow size range, grains of different species can respond differently to hydraulic conditions.

It is also important to note that for various reasons sediments differ greatly in total heavy mineral content, and that the heavy fractions in turn vary greatly in the relative proportions of low-diversity opaque and higher diversity non-opaque minerals. Consequently, the dominant provenance of a non-opaque heavy mineral assemblage (usually $<5\%$ and often $<1\%$) can be highly unrepresentative of the dominant provenance of the deposit as a whole, which is in most cases at least 90% quartz. For example, the range of non-opaque heavy mineral contents of the WRF (<0.01–0.45%, mean 0.08%) does not even overlap with that of the Magilligan deposits (0.8–12.4%, mean 4.5%), which benefit from their close proximity to the rich source of augite, hornblende and olivines in the Antrim basalts (R. Bateman and

P. Wilson, unpublished manuscript, 1990). A hypothetical 50:50 mix of typical sediments from these two formations would yield a non-opaque heavy mineral assemblage 98% dominated by the Magilligan Sands. This factor is a particular threat to conclusions reached in the Shirdley Hill Sands study, where the local Quaternary deposits interpreted as the main source of the SHS were far richer in non-opaque heavy minerals than the other potential contributors to the SHS, the much older Carboniferous and Triassic sandstones.

4.2. Mechanical Weathering

Natural mechanical weathering occurs primarily during transportation of grains. The degree of resistance of particular mineral species to mechanical weathering is determined primarily by its hardness (as traditionally classified on Moh's scale of 1–10) and by the number and degree of development of any cleavage planes. Thus, hard, poorly cleaved minerals such as zircon (Moh = 7.5) can survive many sedimentary cycles, whereas apatite is vulnerable due to its softness (Moh = 5) and amphiboles and pyroxenes are vulnerable due to the two well-developed sets of cleavage planes that parallel the *c*-axis. Well-cleaved minerals are especially vulnerable when recycled, because between periods of transportation, chemical weathering often penetrates the cleavage, further weakening the physical integrity of the grains. In addition to natural mechanical weathering, artificial mechanical weathering can occur during sample preparation. For example, if ultrasonic cleaning is attempted prior to grain counting, chemically weathered amphiboles and pyroxenes can literally be shaken apart and are in effect translated from the sand fraction into the silt fraction.

However, mechanical weathering has been only a modest cause of compositional modifications in our case-studies. There is little opportunity for mechanical damage during anthropogenic deposition in archaeological contexts such as Dark Earth. In aqueous environments represented by the WRF and the various beach/shallow marine sediments analysed for the Magilligan and SHS studies, mechanically vulnerable minerals persisted at high frequencies and typically with only modest rounding of the grains as a result of inter-grain abrasion during transport. Moreover, in the presumed higher-energy transgressive event represented by the WRF Bottom Bed, mechanically vulnerable minerals persist in considerably higher frequencies than in the overlying, lower energy deposits. Interestingly, greater rounding of mechanically vulnerable minerals helped us to distinguish marine from aeolian deposits in the Magilligan and Shirdley Hill studies, but despite this evident abrasion the relative frequencies of vulnerable minerals were not substantially reduced. We therefore conclude that mechanical weathering requires prolonged high-energy conditions to radically alter the composition of a heavy mineral assemblage.

4.3. Authigenic Growth

Thus far, we have discussed only destructive processes that have the capability of removing mineral species from an assemblage. We will now consider two categories of process that can add mineral species to an assemblage: authigenic growth and anthropogenic addition.

Authigenesis is characterised by euhedral crystals or crystal aggregates, often of relatively small and chemically simple minerals and reflecting in situ growth. In our case-studies, authigenesis typically occurred where chemical weathering had released selected ions into solution. Examples include pyrite (FeS_2) cubes/octahedra and jarosite ($KFe_3(SO_4)_2(OH)_6$) euhedra (e.g., Mange and Maurer, 1992) formed within the WRF Bottom Bed immediately above the contact with the chalk (Weir and Catt, 1969; Thorez et al., 1971; Bateman and Moffat, 1987; Bateman, 1988). However, quantities of crystals generated are much less and generally peak in the silt fraction. Modest amounts of anatase and brookite (polymorphs of TiO_2) characterise the WRF and are traditionally viewed as being authigenic, but they show sufficient abrasion to suggest that they were in fact recycled into the WRF from pre-existing deposits.

Overall, the effects of authigenesis on the heavy mineral assemblages studied by us have typically been negligible and were at most modest. Nonetheless, we recognise that in extreme cases post-depositional authigenesis can flood the syn-depositional heavy mineral assemblage (e.g., barytes in some North Sea evaporites and baryte-cemented sandstones).

4.4. Anthropogenic Addition

Because they constitute much of the present landscape and soils, superficial deposits are especially prone to anthropogenic addition of both biotic and abiotic minerals. Most of the biotic additions fall into the light rather than the heavy fractions; those appearing in the fine sands include fragments of calcite/aragonite mollusc shells and of phosphatic teeth and bones. Although not obligatorily anthropogenic, concentrations of such minerals around physical evidence of human habitation are indicative. These materials can in turn form nuclei for the precipitation from solution of chemically simple minerals such as calcite on invertebrate shells and vivianite on vertebrate bones. Opaline phytoliths, derived from degradation of the remains of species from many vascular plant families (e.g., Piperno, 1988), also commonly occur in soils.

The products of human industry also include light minerals, notably glass droplets, but metalworking in particular can add substantially to both the opaque (e.g., iron oxides) and non-opaque heavy suites, the latter including euhedral crystals of minerals such as iron-rich olivines and augites. Although such minerals occur primarily in relatively recent archaeological deposits, such as the Late Roman Dark Earths investigated by Farrington and Bateman (1992), the possibility of finding them in other kinds of Holocene deposit cannot be wholly discounted.

5. CHEMICAL WEATHERING

In a much-cited early review of geochemical weathering (also termed intrastratal dissolution), Pettijohn (1941) simply gathered a large body of observational data from the literature in order to assess the relative diminution of heavy minerals through geological time, noting in passing that coarse, porous rocks facilitated such diminution, especially where they overlay less permeable rocks. The overall result

was a now familiar stability series which suggested that zircon and tourmalines are more resistant than garnets, which in turn are more resistant than hornblendes, sphene and augite/hypersthene. However, it was not clear whether this series, largely reflecting deep-seated geochemical weathering, also applied to pedochemical (subaerial) weathering, which occurs at shallower depths than geochemical weathering, generally in a more open system subject to a greater diversity of biotic activities (compare Pettijohn, 1941; Dryden and Dryden, 1946; Allen, 1948; Sindowski, 1949; Raeside, 1959; Blatt and Sutherland, 1969; Mitchell, 1975; Morton, 1979, 1985; Bateman and Catt, 1985; Morton and Hallsworth, 1999, 2007, this volume). Both categories of weathering operate in wide ranges of environmental conditions (e.g., pressure, temperature, pH, redox potential, pore-water solute composition) and their time-scales overlap, suggesting that the boundary between pedochemical and geochemical weathering may in fact be largely artificial.

5.1. *Method for Assessing Variation in Within-Profile and Between-Profile Weathering Rates*

It rapidly became clear to us that the bulk of the post-depositional modification of heavy mineral assemblages investigated by us in each of the non-archaeological case-studies outlined above reflected pedochemical weathering. In order to explore this phenomenon in greater detail, we needed both a suitable "model" deposit and a suitable methodology that exploited the fact that heavy mineral assemblages are readily quantified. We judged Pleistocene loess and coversands especially suitable for the task, as intense and repeated sorting by multidirectional winds are especially effective in generating a soil parent material that is initially both texturally and compositionally homogeneous. Moreover, assuming an absence of post-depositional erosion of the surface, the period of weathering represented in the profile can be assessed from radiocarbon dating of organic materials immediately underlying, or included within, the aeolian deposit. We preferred coversands to loess because identification of grains in their modal fine-sand fractions is more straightforward than the modal coarse silt fractions of the loess, and because it was evident that the relatively coarse, non-calcareous porous coversands weather most rapidly. Thus, five profiles from four British coversands were analysed for the four 0.5 ϕ size fractions that together constitute the 63–250 μm (4–2 ϕ) range.

In order to better quantify mineral diminution, we devised a novel analytical method that we termed the D^{90} value (for a more detailed explanation, see Bateman and Catt, 1985). The frequency (in parts per thousand) of each mineral in each sample was plotted as a depth function. Sample points were then linked by computer-generated curves termed exact-fitting cubic splines. Each curve provided an estimate of the maximum frequency of that mineral in that sampled profile, which in turn provided an estimate of the depth in the profile to which that mineral had been reduced to 10% of its original frequency (i.e., the 90% depletion, or D^{90}, value). The deepest point at which a mineral has been wholly depleted (D^{100}) might intuitively seem more useful, but this value is subject to greater estimation errors due to the persistence of the occasional rare grain of otherwise eliminated species. Counts per fraction were large (typically 800 grains) to gain credible frequency distributions for all but the rarest heavy mineral species. The few mineral species whose frequency

increased upward through the profile were assumed to have been relatively enriched due to the depletion of other more vulnerable minerals, and thus were judged to show negligible depletion.

Depth functions for augite in the five profiles (Fig. 9) show that pedochemical weathering was most intense at Stockton and Messingham (D^{90} = approximately –30 cm) and least intense at Bickerstaffe (D^{90} = approximately +30 cm), where post-depositional erosion of the uppermost portion of the deposit is suspected. The depletion curves are typically sigmoidal. The steepest portion of the curve (termed by us the weathering front) varies in depth and gradient, but surprisingly does not coincide with the zones of redeposition of iron and/or humus that help define a podzol, suggesting that these components migrate down-profile at a different rate from the heavy mineral weathering front (this tended to coincide with peaks in Al rather than high Fe or low pH). Another insight gained from this approach was that in the Messingham and especially the Stockton profiles the least weathered sands (i.e., those richest in vulnerable minerals) occurred in the central portion of the profiles; weathering increased again toward the bottom of the profile, possibly reflecting pooling of groundwater immediately above less permeable underlying strata.

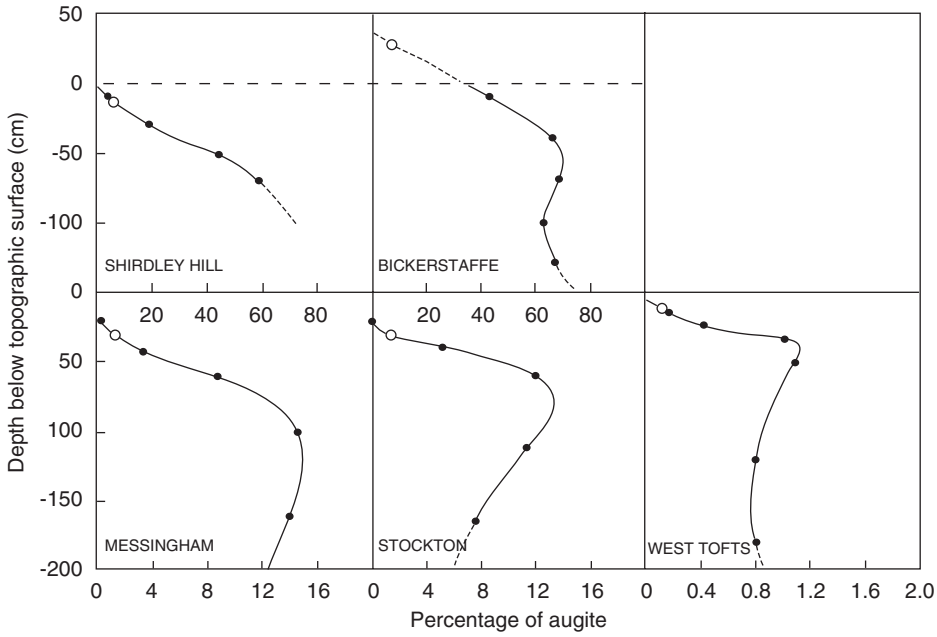

Fig. 9. Frequency of augite (percentage of non-opaque heavy mineral fraction as mean of four 0.5 ϕ fractions within the range 4–2 ϕ, 63–250 μm) within five profiles of four to six samples each, excavated through four late Pleistocene periglacial coversands from northwestern (Bickerstaffe, Shirdley Hill), northeastern (Stockton, Messingham) and eastern (West Tofts) England. Curves are exact-fitting cubic splines. Open circles indicate the depth at which 90% of the maximum amount of augite observed in each profile has been weathered out (here termed the D^{90} value). Note the contrasting horizontal scales. (After Bateman and Catt, 1985, Fig. 4.)

Setting aside these differences, general insights emerge when results from the five profiles are compared (Table 2). Very similar sequences of mineral depletion are evident in all profiles; the phosphatic mineral apatite is by far the most vulnerable, followed by amphiboles and pyroxenes, which are in turn followed by epidotes and then garnets. At any particular depth, the more vulnerable class is more or less eliminated before depletion of the next-most vulnerable class becomes evident, allowing the recognition of virtually discrete stages of mineral depletion. Minerals more resistant than garnets (notably staurolite, the kyanite group, the rutile group, tourmalines and zircon) had not been depleted in any of the profiles studied by us (Bateman and Catt, 1985). When this pattern was compared with those from other, less rigorous but broadly comparable studies, most studies reported depletion sequences that matched our own (Fig. 10) (Chandler, 1941; Richard and Chandler, 1944; Matelski and Turk, 1947; Marel, 1949; von Weyl, 1951; McCaleb, 1953; Krebs and Tedrow, 1957; Pawluk, 1960; Alias, 1961; Alias, 1964; Bosse, 1964; Franzmeier et al., 1964). Where mismatches occurred, careful re-examination of the available data suggested that evidence of ''depletion'' of minerals considered by us relatively resistant was in fact confined to etch features on grains of that species rather than to a demonstrably decreased frequency of the mineral upward through the profile. Thus, in our view, evidence of pedochemical weathering of minerals judged more resistant than garnets is, at best, equivocal.

The next obvious step was to seek shared intrinsic features of the depleted minerals that could help explain their relative vulnerability. With regard to mineral composition, the vulnerability in even mildly acid conditions of carbonates such as calcite and phosphates such as apatite is widely recognised. Most of the vulnerable silicates contain the Fe^{2+} ion whereas most resistant minerals do not, but there are awkward exceptions; epidotes lack Fe^{2+} but are vulnerable, whereas staurolite and schorlite tourmaline are rich in Fe^{2+} but are resistant. The two well-developed cleavage planes in pyroxenes and amphiboles undoubtedly contribute to their vulnerability to chemical weathering, yet kyanite is relatively resistant despite possessing three well-developed cleavage planes. There is also some evidence that compositional zoning or the presence of inclusions of other minerals (e.g., Figs. 11j–l) similarly reduce physical integrity and thus increase vulnerability. Large surface/volume ratios may also render grains more susceptible, as in phyllosilicates (Bateman and Catt, 1985); vulnerability is also enhanced by chemical etching of grain surfaces, thus providing a positive feedback mechanism that hastens the eventual demise of the grain.

Moving on to experimental and theoretical approaches, Nickel (1973) performed detailed laboratory experiments, immersing contrasting heavy minerals in corrosive solutions together spanning a wide range of pHs and observing the resulting rates of dissolution. The sequence of dissolution varied considerably between these pHs, hornblende being particularly vulnerable at 5.6, and epidote, tourmalines and sphene at 10.6, whereas apatite was far less vulnerable at 10.6 than at lower pHs (Table 3). The stability series obtained at pH 5.6 matched our results and Pettijohn's (1941) field-based results most closely, but the chosen species of garnet appeared improbably vulnerable (admittedly, this was almandine garnet rich in Fe^{2+}). We note, however, that the time-span allocated to the experiments was unrealistically short, so that the physico-chemical conditions created in order to achieve meaningful degrees of dissolution were of necessity unnaturally harsh.

Table 2. Depletion of non-opaque heavy minerals by acid pedochemical weathering in five English coversand profiles

Bickerstaffe Lancashire		Shirdley Hill Lancashire		West Tofts Norfolk		Messingham Lincolnshire		Stockton Yorkshire	
GROUP 3									
								Garnet (colourless)	−14.3
								Garnet (pink)	−14.5
				Zoisite/clinozoisite	+6.5	**Epidote**	−21.0	**Epidote**	−18.1
				Epidote	+4.5			Zoisite/ clinozoisite	−20.4
GROUP 2									
Hornblende (green)	c. +80	Tremolite/ actinolite	+3.0	Tremolite/ actinolite	+3.5	**Hypersthene/ bronzite**	−21.6	**Hornblende (green)**	−27.8
Augite	+28	**Hypersthene/ bronzite**	−5.8	**Hornblende (green)**	−10.1	**Hornblende (green)**	−22.2	**Hypersthene/ bronzite**	−28.1
Hypersthene/bronzite	+24	**Hornblende (green)**	−7.6	**Augite**	−10.3	Hornblende (brown)	−23.9	**Hornblende (brown)**	−30.6
Tremolite/actinolite	+19	**Augite**	−9.9	**Hornblende (brown)**	−13.0	**Augite**	−26.0	Tremolite/ actinolite	−31.1
Hornblende (brown)	−6.0	**Hornblende (brown)**	−33.9	Hypersthene/ bronzite	−14.7	Tremolite/ actinolite	−40.1	**Augite**	−32.2
GROUP 1									
Apatite	−26.4			Apatite	−36.0	**Apatite**	−109.5	**Apatite**	−41.5

Notes: Minerals are listed from top to bottom in order of decreasing 90% depletion (D^{90}) values (cm above (+) or below (−) the current soil surface); profiles are listed from left to right in order of increasing severity of pedochemical weathering. Bold letters indicate a mean frequency greater than 1.0% within the profile; all other values carry a greater percentage sampling error as they have mean frequencies of only 0.2–1.0%. (Modified after Bateman and Catt, 1985, Table 4.)

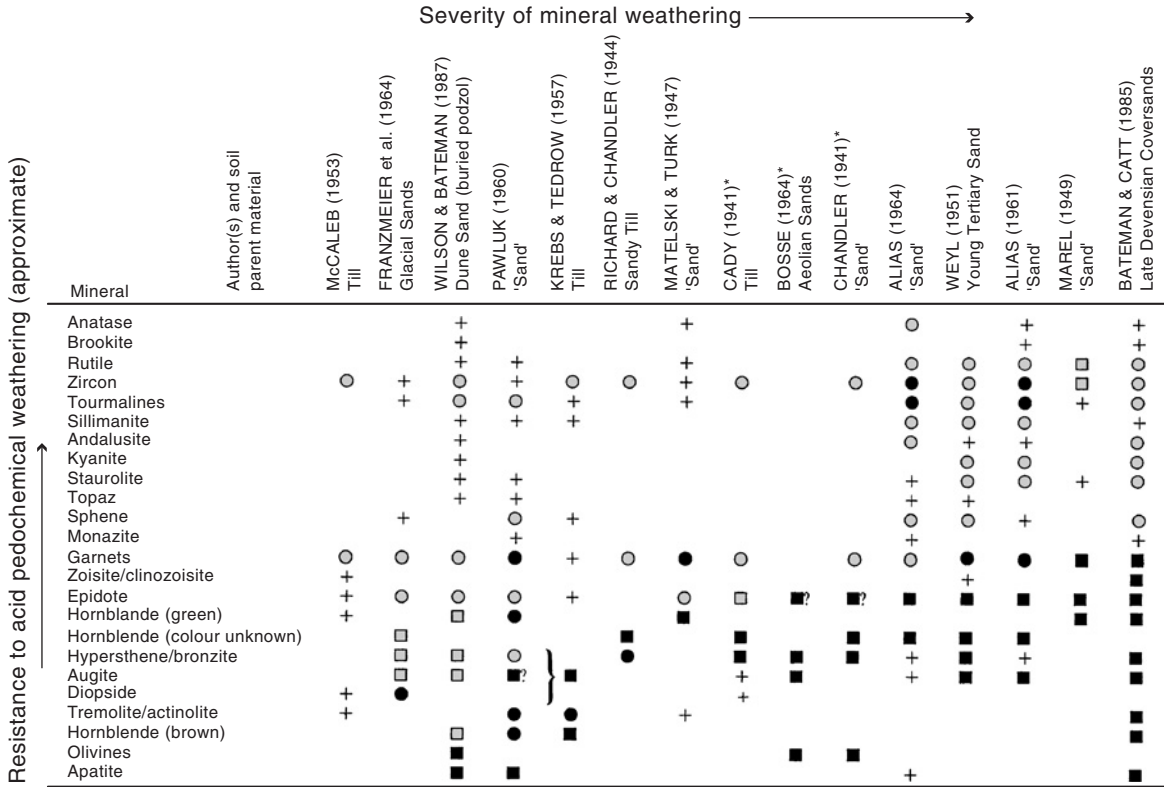

Fig. 10. Review of published data on depletion of non-opaque heavy minerals in superficial sediments subject to acid pedochemical weathering. Most profiles had modal sizes in the fine sand range, but the size range sampled for heavy minerals, the number of grains counted, and the method of data presentation varied considerably among the studies. Evidence of weathering has been reinterpreted by us, except in those papers lacking quantitative data (asterisked). When papers described more than one profile, only the most severely weathered is summarised here. Plus sign = mineral present in insufficient quantity to determine whether depletion had occurred, open circle = no depletion or etch features, closed circle = no depletion, but etch features indicative of pedochemical weathering reported, open square = depletion suggested by the author but not supported by the data presented, closed square = depletion clearly shown by the data provided. (After Bateman and Catt, 1985, Table 5.)

Gruner's (1950) theoretical approach involved calculating the energy indices of each crystal structure, and assuming that those of higher energy are inherently more unstable and thus more vulnerable to dissolution. His inferred stability series resembled that of Nickel (1973) but contrasted starkly with our empirical results in suggesting that garnet and sphene are more vulnerable to chemical weathering than is hornblende (Table 3).

Lastly, weathering of individual grains can be explored with greater subtlety under the SEM (compare Rahmani, 1973; Simpson, 1976; Gravenor, 1979; Gravenor and Gostin, 1979; Bateman and Catt, 1985; Milliken, 2007, this volume; Turner and Morton, 2007, this volume; Velbel, 2007, this volume); compare, for example, the slightly weathered with the heavily weathered grains of augite, epidote and garnets shown in Figs. 11a–l. Quantitative assessment of statistically valid samples usefully identifies shifts from less to more weathered morphological categories in progressively shallower samples (Fig. 12), demonstrating the potential to reveal chemical weathering before diminution of grains into smaller size categories (i.e., bona fide depletion) has become evident in mineral frequency data.

5.2. Causes of Variation in Within-Profile and Between-Profile Weathering Rates

Thus far, we have considered patterns of depletion in deposits chosen as ideal for the weathering studies. These rocks are highly permeable, poorly consolidated sands experiencing moderate rainfall regimes, which offer considerable potential for acid hydration reactions but are also sufficiently permeated by atmospheric gases to allow high redox potentials.

In order to test its broader relevance, the D^{90} approach to assessing mineral depletion was then applied to several weathering profiles (some composite) through the rather similarly textured Magilligan sands (Wilson and Bateman, 1987, Fig. 3, Table 3) and to four soils developed on chalk-rich glacial tills in southeastern England (R. Bateman and J. Catt, unpublished data; see also Sturdy et al., 1979). Both case-studies revealed much less weathering than was observed in any of the coversands. Although the Magilligan sands are similar in texture to the coversands, they have suffered much shorter periods of subaerial exposure (less than 1300 years versus 10,000 years). Consequently, only apatite and olivines showed substantial depletion in any profile (usefully demonstrating that olivines, which were wholly absent from the coversands, are the silicate minerals most vulnerable to acid pedochemical weathering). Weathering was even less evident in the glacial tills, where the only depletion evident was of apatite in the top few centimetres of the sediment, despite supposedly representing approximately 450,000 years of weathering elapsed since deposition of the tills during the Anglian glaciation. We suspect that the finer texture and much poorer sorting of these glacial deposits, compounded by their high carbonate content, considerably reduced permeability and thus greatly decreased the rate of weathering, though relatively recent erosion of previously weathered upper layers at each study site cannot be ruled out.

We thus return for the last time to the model system of the four coeval coversands. These were deposited in similar environments during the same brief periglacial period of the Younger Dryas, are similar in texture, have experienced similar climatic regimes since deposition, and have generated similar podzolised soils supporting broadly

similar chemistries and pH values. If we once again assume no surface erosion, the strong contrasts in degrees of weathering between the five study profiles are most likely to reflect contrasting periods of podzolisation, which is believed to have been initiated by clearance of the natural post-glacial vegetation by mankind. Thus, differing dates of clearance constitute one credible explanation for the disparity in weathering (compare Cady, 1941; Burges and Drover, 1953; Mackney, 1961; Dacey et al., 1981; Bateman and Catt, 1985).

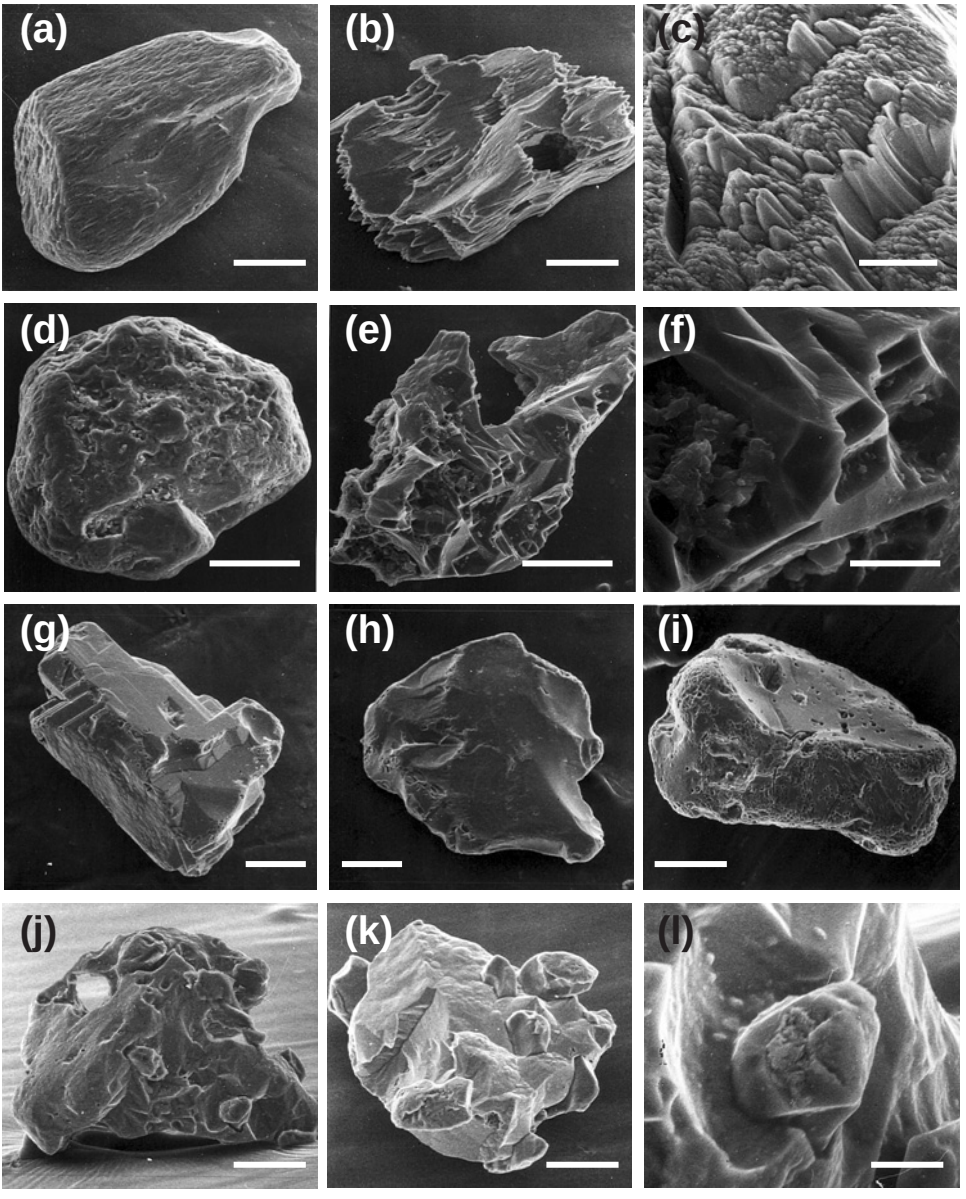

In summary, post-depositional chemical weathering is, along with in-transit sorting, the most important process modifying heavy mineral assemblages. It is also the least predictable, due to the unusually wide spectrum of factors that can influence both relative and absolute rates of mineral decay.

6. GENERAL CONCLUSIONS

6.1. Conceptual Recommendations

Although heavy minerals are a near-ubiquitous component of sediments, their study is now perceived by many applied mineralogists as inferior to increasingly sophisticated (and frequently automated) thin-section and geochemical techniques.

We believe that more effective exploitation of the often substantial volumes of heavy mineral data by rigorous statistical analysis, conducted within a sound conceptual framework, would help remedy this unwarranted decline. We further suggest that the most useful conceptual framework is to infer the history of a heavy mineral assemblage backward through time, from its current status to its original source(s), considering the likely effects of each potential modifying processes at each stage of the preceding sedimentary cycle (Bateman, 1989). Interpreting heavy mineral data within this framework provides invaluable palaeoenvironmental and stratigraphic data that are often casually dismissed as irritating "noise" obscuring the holy grail of provenance.

The effects of authigenic growth and anthropogenic addition are relatively easy to predict, as are the limited range of contexts in which they are likely to occur. Although mechanical weathering can substantially alter heavy mineral assemblages, its effects also are predictable, as prolonged or intense abrasion is required. In contrast, differential sorting of minerals during transportation can have a rapid and profound modifying effect on a heavy mineral assemblage that is less readily compensated for but does broadly follow the laws of physics.

Fig. 11. Scanning electron micrographs of grains of augite (a–c), epidotes (d–f) and garnets (g–l) showing contrasting degrees of pedochemical dissolution, selected from the 90 – 125 μm fraction of the Stockton coversand profile: (a) Augite showing mechanical rounding during transport and subsequent slight dissolution (category 6 of histogram in Fig. 12). (b) Augite showing severe etching, approaching the skeletal condition (borderline of categories 8 and 9). (c) Detail of augite grain similar to that in (b), featuring hacksaw terminations. (d) Epidote showing slight surface dissolution. (e) Severely etched epidote. (f) Detail of severely etched epidote (e), featuring angular etch features. (g) Garnet showing large scale facets, subsequent slight dissolution and rounding of edges (category 1). (h) Garnet showing conchoidal fracture and minimal dissolution (category 2). (i) Garnet showing abundant etch pits (category 4). (j, k) Severely etched garnets (category 5) showing perforations and exposure of more resistant inclusions. (l) Detail of relatively resistant inclusion within highly weathered garnet. Some photos reproduced from Bateman and Catt (1985), Plate 1. (Scale bar = 50 μm except (c) = 20 μm, (f) and (l) = 10 μm.)

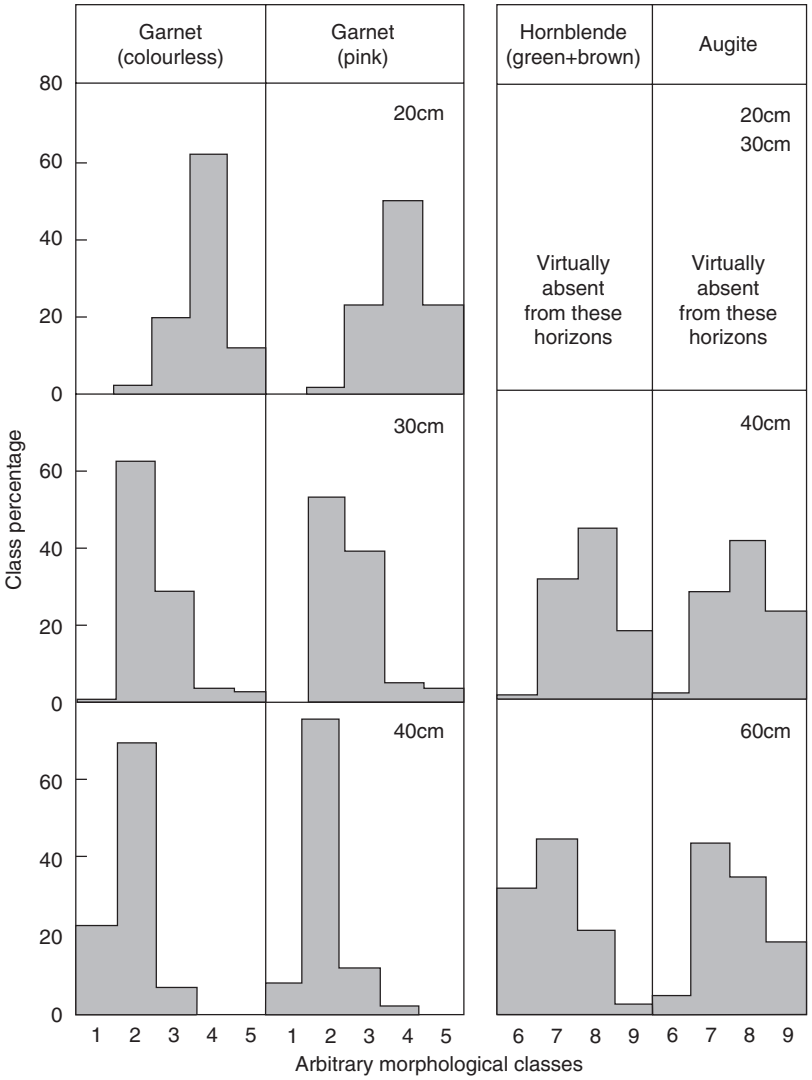

Fig. 12. Categorisation of the external morphology of garnet (colourless and pink), hornblende and augite grains from the 90–125 μm fraction of the shallowest horizons of the Stockton coversand profile. Morphological classes: (1) euhedral rhombic facets, (2) unmarked/mamillated/fractured grains, (3) few angular projections and/or etch pits, (4) many angular projections and/or etch pits, (5) very irregular/perforated (skeletal) grains, (6) hacksaw terminations absent, (7) short hacksaw terminations, (8) long hacksaw terminations, outline fairly regular, (9) long hacksaw terminations, outline highly irregular (skeletal). (After Bateman and Catt, 1985, Fig. 3; see also present Fig. 11.)

The boundary between superficial pedochemical weathering and deeper geochemical weathering is largely artificial and thus is challenging to define, either spatially or temporally. Both categories of chemical weathering frequently and often profoundly modify heavy mineral assemblages, but the resulting patterns of depletion vary considerably.

Table 3. Resistance to chemical weathering of common non-opaque heavy minerals, inferred using contrasting methods

	Pettijohn (1941)	Bateman and Catt (1985)*	Nickel (1973)			Gruner (1950)
	Persistence through geological time	Persistence in weathered cover-sands	Experimental dissolution at pH 3.6	Experimental dissolution at pH 5.6	Experimental dissolution at pH 10.6	Theoretical energy indices
Most	Zircon	Zircon + rutile + tourmalines	Zircon + rutile + hornblende	Zircon + rutile + sphene	Zircon + rutile	Zircon
	Tourmalines	Staurolite	Sphene	Tourmalines + staurolite	Staurolite + garnet†	Tourmalines
	Hornblende	Kyanite	Staurolite	Epidote	Hornblende	Hornblende
Order of resistance to chemical weathering	Garnets	Garnets	Tourmalines	Hornblende	Apatite	Garnets
	Sphene	Epidotes	Epidote	Garnet†	Sphene	Sphene
	Augite	Hornblende + hypersthene	Garnet†	Apatite	Tourmalines	Augite
	Hypersthene	Augite	Apatite		Epidote	
		Olivines**				
Least		Apatite				

*For more details see Table 2.
†Fe^{2+}-rich almandine garnet.
**Added by Wilson and Bateman (1987).

For example, intrinsic properties of minerals apparently conferring vulnerability to acid pedochemical weathering include well-developed multiple cleavage planes and/or inclusions, high-energy lattices and high Fe^{2+} content. However, these properties are insufficient to accurately predict a stability series in any particular heavy mineral assemblage, as both relative and absolute depletion rates are strongly influenced by interactions between intrinsic (compositional) and extrinsic (environmental) factors.

Some field-based research has been conducted to explore abiotic factors that are frequently (and justifiably) implicated in mineral weathering, notably pH and redox potential. Nonetheless, further laboratory experimentation (e.g., Nickel, 1973) is highly desirable to document the reaction of specific minerals to specific environmental phenomena. Such experiments need to reproduce natural conditions as accurately and as realistically as possible, within the inevitable constraint of operating on a timescale that is human rather than geological.

Lastly, the most under-researched factors operating in the post-depositional environment are biotic. As noted by Bateman and Catt (1985), field experiments are needed to compare profiles developed on similar soil parent materials with strongly contrasting and carefully recorded vegetation histories. The limited evidence currently available suggests that vegetation shifts, such as the widespread planting in the temperate zones of acid-generating conifers in permeable sediments previously occupied by broadleaf trees, can have a rapid and radical effect on pedochemical weathering rates and patterns. Deeper "geochemical" weathering has traditionally been viewed as a purely physico-chemical phenomenon, but even this assumption should now be revised, following the relatively recent demonstration of long-term habitation of rocks at depths of over a kilometre by bacteria and fungi (e.g., Frederickson and Onstott, 1996; Frederickson and Fletcher, 2001; Friedman, 2002).

6.2. Technical Recommendations

Given that even small textural differences can profoundly affect the perceived composition of a heavy mineral assemblage, we recommend confining analysis to narrow size fractions. In sandstones, a good compromise between the desires for extracting a reasonable quantity of non-opaque heavy mineral grains (facilitated by a wide size fraction), inter-sample comparability (facilitated by a narrow size fraction), ease of identification (facilitated by larger grains), and good representation of a diversity of minerals (facilitated by smaller grains) is the 90–125 μm fraction. Moreover, it is especially important to seek to standardise not only data collection but also data presentation, in order to allow meaningful comparison of quantitative data among studies published by different research groups. Only then will we be able to compare data matrices directly, rather than being obliged to reduce them to little more than presence or absence data prior to comparison.

We have demonstrated that computers can usefully be employed on quantitative heavy mineral data to smooth depth functions for individual minerals. More importantly, multivariate algorithms, such as principal coordinates analysis based on the Gower similarity coefficients emphasised here, are clearly extremely valuable for identifying trends in large matrices of heavy mineral frequency data. We believe that this approach could now be taken forward at least one further step. Specifically, mineral frequency data could be simultaneously ordinated with any other

quantitative data that might shed light on processes influencing those heavy mineral assemblages; geochemical data are an obvious example, though the approach could even be extended to ecological data representing biotic associates.

Far from being disadvantageous, the simplicity of manual heavy mineral identification means that this technique can be practiced successfully by any operator who possesses a petrological microscope and has acquired through experience sufficient skills; this discipline is as much an art as a science. However, given the decreasing number of experienced practitioners and the increasing predilection among scientists for automated data collection, it is worth briefly considering the potential for automated heavy mineral analysis.

Several automated systems have been developed during the last quarter century, though surprisingly few have led to detailed publications (Grant et al., 1989; Robinson et al., 2000; T. Williams and A. Kearsley, pers. comm., 2004). They typically rely on using backscattered electron images on a low-vacuum SEM to locate individual grains, mounted either as natural grains or as polished sections, and then X-ray spectra to categorise the grains, simultaneously gathering data on several statistical parameters representing shape and size (e.g., Robinson and Nickel, 1979; Robinson et al., 2000) for automatic deposition in files of programs such as MS Access. Relative to optical analysis, precision of identification is increased for some mineral groups but decreased for others (Grant et al., 1989). Rather, the main advantage of such systems is the volume of data generated; they can operate at a maximum rate of between 2000 (Grant et al., 1989) and 5000 (Robinson et al., 2000) grains per hour (an order of magnitude faster than a competent petrological microscopist), and can analyse overnight up to 36 mounts placed simultaneously in the SEM chamber.

Several difficulties with current automated analytical methods are noteworthy. Particularly in the early stages of a project, there is a high risk of encountering mineral species that have not been provided with an a priori X-ray identification category; such grains necessitate recording and subsequent manual checking via semi-quantitative EDX analysis. The systems are not yet able to distinguish among polymorphs such as the frequently encountered aluminosilicate triumvirate of kyanite, andalusite and sillimanite, and they are easily misled by composite grains, heavily included grains, and grains naturally coated with contrasting mineralogies such as iron oxides. Further problems are encountered with the operating software packages provided by manufacturers of SEM and EDX systems.

Nonetheless, widespread mineral genera that encompass chemical substitution series, such as pyroxenes, amphiboles, olivines, epidotes, garnets and tourmalines, can increasingly be further divided into compositionally delimited species by the more sophisticated of these analytical systems. Also, the probability of radical misidentifications should decrease, especially in more challenging fractions finer than the fine sands (i.e., $<63\,\mu m$). Moreover, the technique can be applied to the less mineralogically diverse light fractions, subdividing genera such as feldspars and micas and so providing a better test of whether patterns in the heavy fraction are mirrored in the light fraction (and thus are truly indicative of the history of the sediment as a whole). Also, thresholds of backscattered electron reflectance can be specified that allow some mineral categories to be emphasised while others are ignored (e.g., Robinson et al., 2000) so that, for example, frequency estimates of rarer minerals could be improved by continued counting until an acceptable percentage sampling error is achieved for each.

6.3. *A "New Synthesis"?*

It is especially ironic that developers of automated heavy mineral identification systems are currently being hampered by a dearth of "known" assemblages previously identified optically by competent operators. We are rapidly approaching a time when large bodies of heavy mineral data will be generated overnight by automated systems and fed directly into computer programs that convert the grain counts to percentages, estimate sampling errors, and even generate the resulting multivariate ordinations of assemblages, thereby freeing the researcher to focus on interpreting more rigorously the relationships among the samples. At this point, the only remaining constraint on heavy mineral analysis would be the quality of the scientific questions selected by the analyst for serious consideration.

ACKNOWLEDGEMENTS

We welcome this opportunity to thank the many collaborators who have, over the past 35 years, contributed data, concepts or simply timely encouragement to our studies. They include, in alphabetical order, the late Norman D'Cruz (to whom this paper is dedicated), Orpah Farrington, Rob Kemp, Paul Madgett, Maria Mange, Andy Moffat, Brin Roberts, Jim Rose, Alan Weir and Peter Wilson. We are also grateful to John Gower, the late James Rayner and Dick Webster for past statistical guidance, Paul Grant, Terry Williams and Anton Kearsley for advice on automated analysis of heavy mineral assemblages, Bob Norrish for logistical support, and Natalie Bell and Angela Watts for assisting in the preparation of this manuscript. Isabel Montanez and Maria Mange kindly provided constructive reviews.

REFERENCES

Alias, L.J., 1961. Weathering process in a humic podzol profile. Agrochimica 5, 338–351.

Alias, L.J., 1964. Mineralogia de un podsol humico ferrico. Anales de Edafologia y Agrobiologia 23, 225–241.

Allen, V.T., 1948. Weathering and heavy minerals. Journal of Sedimentary Petrology 18, 38–42.

Bateman, R.M., 1984. A Petrographic Study of Some Tertiary and Quaternary Sediments of the Chiltern Hills, with Particular Reference to the Ayot Palaeogene Outlier. B.Sc. thesis. Birkbeck College, London University, 132 pp.

Bateman, R.M., 1988. Relationship of the Woolwich and Reading Formation (Late Palaeocene) to the Upper Chalk (Late Cretaceous) and Clay-with-flints *sensu lato* (Quaternary) in the Chiltern Hills, southern England. Tertiary Research 10, 53–63.

Bateman, R.M., 1989. Interpretation of heavy mineral assemblages: outmoded art or undervalued science? 28th International Geological Congress, Washington, DC, Abstracts 1, pp. 97–98.

Bateman, R.M., Catt, J.A., 1985. Modification of heavy mineral assemblages in English coversands by acid pedochemical weathering. Catena 12, 1–21.

Bateman, R.M., Moffat, A.J., 1987. Petrography of the Woolwich and Reading Formation (late Palaeocene) of the Chiltern Hills, southern England. Tertiary Research 8, 75–103.

Bateman, R.M., Rose, J., 1994. Fine sand mineralogy of the early and middle Pleistocene Bytham Sands and Gravels of Midland England and East Anglia. Proceedings of the Geologists' Association 105, 33–39.

Bateman, R.M., Wilson, P., 1989. Geomorphic evolution of a large coastal accretionary complex in Northern Ireland. 28th International Geological Congress, Washington, DC, Abstracts 1, pp. 98–99.

Blatt, H., Sutherland, B., 1969. Intrastratal solution and non-opaque heavy minerals in shales. Journal of Sedimentary Petrology 39, 591–600.

Blondeau, A., Pomerol, C., 1968. A contribution to the sedimentological study of the Palaeogene of England. Proceedings of the Geologists' Association 79, 441–455.

Bosse, I., 1964. Verwitterungs-Bilanzen von characteristischen Bodentypen aus Flugsanden der nordwestdeutschen Geest (Mittelweser-Gebiet). Thesis. Georg-August-Universität, Göttingen, 75 pp.

Bowen, D.Q. (Ed.), 1999. A Revised Correlation of Quaternary Deposits in the British Isles. Geological Society of London Special Report 23.

Burges, A., Drover, D.P., 1953. The rate of podzol development in sands of the Woy Woy District, NSW. Australian Journal of Botany 1, 83–94.

Cady, J.G., 1941. Soil analyses significant in forest soils investigations and methods of determination. 3. Some mineralogical characteristics of podzols and brown podzolic soil profiles. Soil Science Society of America Proceedings 5, 352–354.

Catt, J.A., 1978. The contribution of loess to soils in lowland Britain. In: Limbrey, S., Evans, J.G. (Eds.), The Effects of Man on the Landscape: The Lowland Zone. Council for British Archaeology Research Report, vol. 21, pp. 12–20.

Catt, J.A., 1985. Soil particle size distribution and mineralogy as indicators of pedogenic and geomorphic history: examples from the loessial soils of England and Wales. In: Richards, K.S., Arnett, R.R., Ellis, S. (Eds.), Geomorphology and Soils. Allen and Unwin, London, pp. 202–218.

Catt, J.A., Bateman, R.M., Wintle, A., Murphy, C.P., 1987. The 'loess' section at Borden, Kent, SE England. Journal of Quaternary Science 2, 141–147.

Catt, J.A., Corbett, W.M., Hodge, C.A.H., Madgett, P.A., Tatler, W., Weir, A.H., 1971. Loess in the soils of north Norfolk. Journal of Soil Science 22, 444–452.

Catt, J.A., Staines, S.J., 1982. Loess in Cornwall. Proceedings of the Ussher Society 5, 368–375.

Catt, J.A., Weir, A.H., Madgett, P.A., 1974. The loess of eastern Yorkshire and Lincolnshire. Proceedings of the Yorkshire Geological Society 40, 23–39.

Chandler, R.F. Jr., 1941. The Relation of Soil Character to Forest Growth in the Adirondack Region. New York (Cornell) Agricultural Experimental Station Annual Report 54, 93–94.

Coombe, D.E., Frost, L.C., Le Bas, M., Watters, W., 1956. The nature and origin of the soils over the Cornish serpentine. Journal of Ecology 44, 605–615.

Curry, D., Adams, C.G., Boulter, M.C., Dilley, F.C., Eames, F.E., Funnell, B.M., Wells, M.K., 1978. A Correlation of the Tertiary Rocks of the British Isles. Geological Society of London Special Report, vol. 12.

Dacey, P.W., Wakerley, D.S., Le Roux, N.W., 1981. The Biodegradation of Rocks and Minerals with Particular Reference to Silicate Minerals: A Literature Survey. Warren Springs Laboratory Report LR 380, 44 pp.

Dryden, L., Dryden, C., 1946. Comparative rates of weathering of some common heavy minerals. Journal of Sedimentary Petrology 16, 91–95.

Ellison, R.A., 1983. Facies distribution in the Woolwich and Reading Beds of the London Basin, England. Proceedings of the Geologists' Association 94, 311–319.

Ellison, R.A., Knox, R.W.O'B., Jolley, D.W., King, C., 1994. A revision of the stratigraphical classification of the early Palaeogene strata of the London Basin and East Anglia. Proceedings of the Geologists' Association 105, 187–197.

Farrington, O.S., 1992. Microprobe analysis of sand-sized anthropogenic mineral grains from late Roman archaeological deposits in northwest Europe. In: Vandiver, P.B., Druzik, J.R.,

Wheeler, G.S., Freestone, I.C. (Eds.), Materials Issues in Art and Archaeology III. Materials Research Society Symposium Proceedings, vol. 267.
Farrington, O.S., Bateman, R.M., 1992. A holistic approach to the analysis of archaeological deposits, illustrated using a Late Roman urban sequence from northwest Europe. In: Vandiver, P.B., Druzik, J.R., Wheeler, G.S., Freestone, I.C. (Eds.), Materials Issues in Art and Archaeology III. Materials Research Society Symposium Proceedings, vol. 267, pp. 179–192.
Franzmeier, D.P., Whiteside, E.P., Mortland, M.M., 1964. A chronosequence of podzols in northern Michigan. III. Mineralogy, micromorphology, and net changes occurring during soil formation. Michigan Agricultural Station Quarterly Bulletin 46, 37–57.
Frederickson, J.K., Fletcher, M. (Eds.), 2001. Subsurface Microbiology and Biogeochemistry. Wiley, New York.
Frederickson, J.K., Onstott, T.C., 1996. Microbes deep inside the Earth. Scientific American 275, 42–47.
Friedman, R., 2002. Bugs from hell. European Astrobiology Magazine.
Friis, H., 1974. Weathered heavy mineral associations from the Young-Tertiary deposits of Jutland, Denmark. Sedimentary Geology 12, 199–213.
GENSTAT 7.0, 2004. VSN International. http://www.vsn-intl.com/.
Gower, J.C., 1966. Some distance properties of latent root and vector methods in multivariate analysis. Biometrika 53, 325–338.
Gower, J.C., 1971. A general coefficient of similarity and some of its properties. Biometrics 27, 857–872.
Gower, J.C., Ross, G.J.S., 1969. Minimum spanning trees and single linkage cluster analysis. Applied Statistics 18, 54–64.
Grant, P., Cramer, R., Bateman, R.M., 1989. Heavy mineral analysis by Combined Automated Chemical and Image Analysis (CACIA). 28th International Geological Congress, Washington, DC, Abstracts 1, pp. 578–579.
Gravenor, C.P., 1979. The nature of the Late Palaeozoic glaciation in Gondwana as determined from an analysis of garnets and other heavy minerals. Canadian Journal of Earth Sciences 16, 1137–1153.
Gravenor, C.P., Gostin, V.A., 1979. Mechanisms to explain the loss of heavy minerals from the Upper Palaeozoic tillites of South Africa and late Precambrian tillites of Australia. Sedimentology 26, 707–717.
Gruner, J.W., 1950. An attempt to arrange silicates in the order of reaction energies at relatively low temperatures. American Mineralogist 35, 137–148.
Hester, S.W., 1965. Stratigraphy and palaeogeography of the Woolwich and Reading Beds. Bulletin of the Geological Survey of Great Britain 23, 117–137.
Hopson, P.M., Aldiss, D.T., Smith, A., 1996. Geology of the country around Hitchin (Memoir for 1:50,000 sheet 221). British Geological Survey/HMSO, Keyworth, Notts.
Jones, R.F.J. (Ed.), 1991. Roman Britain: Recent Trends. Collis, Sheffield.
Knox, R.W.O'B., Morton, A.C., Harland, R., 1981. Stratigraphical relationships of Palaeocene sands in the UK sector of the central North Sea. In: Illing, L.V., Hobson, G.D. (Eds.), Petroleum Geology of the Continental Shelf of NW Europe. Heyden, London, pp. 267–281.
Komar, P.D., 2007. The entrainment, transport and sorting of heavy minerals by waves and currents. In: Mange, M.A., Wright, D.T. (Eds.), Heavy Minerals in Use. Developments in Sedimentology, vol. 58, pp. 1–48.
Krebs, R.D., Tedrow, J.C.F., 1957. Genesis of three soils derived from Wisconsin Till in New Jersey. Soil Science 83, 207–218.
Mackney, D., 1961. A podzol development sequence in oakwoods and heath in central England. Journal of Soil Science 12, 23–40.

Madgett, P.A., Catt, J.A., 1978. Petrography, stratigraphy and weathering of Late Pleistocene tills in east Yorkshire, Lincolnshire and north Norfolk. Proceedings of the Yorkshire Geological Society 42, 55–108.

Mahaney, W.C., 2002. Atlas of Sand Grain Surface Textures and Applications. Oxford University Press, Oxford, 237 pp.

Mange, M.A., Maurer, H.F.W., 1992. Heavy Minerals in Colour. Chapman and Hall, London.

Marel, H.W. van der, 1949. Mineralogical composition of a heath podzol profile. Soil Science 67, 193–207.

Matelski, R.P., Turk, L.M., 1947. Heavy minerals in some podzol soil profiles in Michigan. Soil Science 64, 469–487.

McCaleb, S.B., 1953. Profile studies of normal soils of New York. IV. Mineralogical properties of the gray-brown podzolic–brown podzolic soil sequence. Soil Science 77, 319–333.

Milliken, K.L., 2007. Provenance and diagenesis of heavy minerals, Cenozoic units of the northwestern Gulf of Mexico Sedimentary Basin. In: Mange, M.A., Wright, D.T. (Eds.), Heavy Minerals in Use. Developments in Sedimentology, vol. 58, pp. 247–261.

Mitchell, W.A., 1975. Heavy minerals. In: Gieseking, J.E. (Ed.), Soil Components. II. Inorganic. Springer, New York, pp. 449–480.

Mitchell, G.F., Penny, L.F., Shotton, F.W., West, R.G., 1973. A Correlation of the Quaternary Deposits in the British Isles. Geological Society of London Special Report 4.

Moffat, A.J., Bateman, R.M., 1983. The mineralogy of Palaeogene sediments in southeast England. Proceedings of the Geologists' Association 94, 271–274.

Morton, A.C., 1979. Depth control of intrastratal solution of heavy minerals from the Palaeocene of the North Sea. Journal of Sedimentary Petrology 48, 1–286.

Morton, A.C., 1982. The provenance and diagenesis of Palaeogene sandstones of southeast England as indicated by heavy mineral analysis. Proceedings of the Geologists' Association 93, 263–274.

Morton, A.C., 1983. The mineralogy of Palaeogene sandstones in southeast England. Proceedings of the Geologists' Association 94, 274–278.

Morton, A.C., 1985. Heavy minerals in provenance studies. In: Zuffa, G.G. (Ed.), Provenance of Arenites. Reidel, Dordrecht, pp. 249–277.

Morton, A.C., Hallsworth, C.R., 1999. Processes controlling the composition of heavy mineral assemblages in sandstones. Sedimentary Geology 124, 3–29.

Morton, A.C., Hallsworth, C.R., 2007. Stability of detrital heavy minerals during burial diagenesis. In: Mange, M.A., Wright, D.T. (Eds.), Heavy Minerals in Use. Developments in Sedimentology, vol. 58, pp. 215–245.

Nickel, E., 1973. Experimental dissolution of light and heavy minerals in comparison with weathering and intrastratal solution. Contributions to Sedimentology 1, 1–68.

Parks, D.A., Rendell, H.M., 1992. Thermoluminescence dating and geochemistry of loessic deposits in southeast England. Journal of Quaternary Science 7, 99–107.

Pawluk, S., 1960. Some podzol soils of Alberta. Canadian Journal of Soil Science 40, 1–14.

Perrin, R.M.S., 1956. The nature of 'Chalk Heath' soils. Nature 178, 31–32.

Pettijohn, F.J., 1941. Persistence of heavy minerals and geologic age. Journal of Geology 49, 610–625.

Pigott, C.D., 1962. Soil formation and development on the Carboniferous limestone of Derbyshire. 1. Parent materials. Journal of Ecology 50, 145–156.

Piperno, D.R., 1988. Phytolith Analysis. Academic Press, New York.

Pitcher, W.S., Shearman, D.J., Pugh, D.C., 1954. The loess of Pegwell Bay and its associated frost soils. Geological Magazine 91, 308–314.

Raeside, J.D., 1959. Stability of index minerals in soils with particular reference to quartz, zircon, and garnet. Journal of Sedimentary Petrology 29, 493–502.

Rahmani, R.A., 1973. Grain surface etching features of some heavy minerals. Journal of Sedimentary Petrology 43, 882–888.

Richard, J.A., Chandler, R.F. Jr., 1944. Some physical and chemical properties of mature podzol profiles. Soil Science Society of America Proceedings 8, 379–383.

Robinson, B.W., Hitchen, G.J., Verrall, M.R., 2000. The AutoGeoSEM: a programmable fully-automatic SEM for rapid grain-counting and heavy mineral characterisation in exploration. In: Kojonen, K., Carlson, L., Hölttä, P., Lahti, S. (Eds.), Modern Approaches to Ore and Environmental Mineralogy, Extended Abstracts, Mineralogical Society of Finland Mini-symposium, pp. 71–74.

Robinson, B.W., Nickel, E.H., 1979. A useful new technique in mineralogy: the backscattered electron/low vacuum mode of SEM operation. American Mineralogist 64, 1322–1328.

Simpson, G.S., 1976. Evidence of overgrowths on, and intrastratal solution of, detrital garnets. Journal of Sedimentary Petrology 46, 689–693.

Sindowski, F.K.H., 1949. Results and problems of heavy mineral analysis in Germany: a review of sedimentary-petrological papers 1936–1948. Journal of Sedimentary Petrology 19, 3–25.

Soil Survey of England and Wales, 1983. Soil Map of England and Wales, Scale 1:250,000. Soil Survey of England and Wales, Harpenden.

Sturdy, R.G., Allen, R.H., Bullock, P., Catt, J.A., Greenfield, S., 1979. Paleosols developed on Chalky Boulder Clay in Essex. Journal of Soil Science 30, 117–137.

Thorez, J., Bullock, P., Catt, J.A., Weir, A.H., 1971. The petrography and origin of deposits filling solution pipes in the Chalk near South Mimms, Hertfordshire. Geological Magazine 108, 413–423.

Turner, G., Morton, A.C., 2007. The effects of burial diagenesis on detrital heavy mineral grain surface textures. In: Mange, M.A., Wright, D.T. (Eds.), Heavy Minerals in Use. Developments in Sedimentology, vol. 58, pp. 393–412.

Velbel, M.A., 2007. Surface textures and dissolution processes of heavy minerals in the sedimentary cycle: examples from pyroxenes and amphiboles. In: Mange, M.A., Wright, D.T. (Eds.), Heavy Minerals in Use. Developments in Sedimentology, vol. 58, pp. 111–150.

Vincent, P.J., Lee, M.P., 1981. Some observations on the loess around Morecombe Bay, north-west England. Proceedings of the Yorkshire Geological Society 43, 281–294.

von Weyl, R., 1951. Schwermineralverwitterung in Schleswig-Holsteinen Böden. Schriften Naturwissenschaftlichen Vereins für Schleswig-Holstein 25, 157–165.

Weir, A.H., Catt, J.A., 1969. The mineralogy of Palaeogene sediments in north-east Kent (Great Britain). Sedimentary Geology 3, 17–33.

Weir, A.H., Catt, J.A., Madgett, P.A., 1971. Postglacial soil formation in the loess of Pegwell Bay, Kent (England). Geoderma 5, 131–149.

Wilson, P., Bateman, R.M., 1986. Nature and palaeoenvironmental significance of a buried soil sequence at Magilligan Foreland, Northern Ireland. Boreas 15, 137–153.

Wilson, P., Bateman, R.M., 1987. Pedogenic and geomorphic evolution of a buried dune palaeocatena at Magilligan Foreland, Northern Ireland. Catena 14, 501–517.

Wilson, P., Bateman, R.M., 1990. Portrush: Dhu Varren. In: Wilson, P. (Ed.), North Antrim and Londonderry. Irish Association for Quaternary Studies Field Guide, vol. 13, pp. 39–45.

Wilson, P., Bateman, R.M., Catt, J.A., 1981. Petrography, origin and environment of deposition of the Shirdley Hill Sand of southwest Lancashire, England. Proceedings of the Geologists' Association 92, 211–229.

Wilson, P., Farrington, O.S., 1989. Radiocarbon dating of the Holocene evolution of Magilligan Foreland, Co. Londonderry. Proceedings of the Royal Irish Academy 89, 1–23.

Wintle, A., 1981. Thermoluminescence dating of Late Devensian loesses in southern England. Nature 289, 479–480.

Chapter 6

'IN SITU' DISSOLUTION OF HEAVY MINERALS THROUGH EXTREME WEATHERING, AND THE APPLICATION OF THE SURVIVING ASSEMBLAGES AND THEIR DISSOLUTION CHARACTERISTICS TO CORRELATION OF DUTCH AND GERMAN SILVER SANDS

A.J. (TOM) VAN LOON[a] AND MARIA A. MANGE[b]

[a]*Geocom, Dillenburg 234, 6865 HR Doorwerth, The Netherlands*
[b]*Department of Geology, UC Davis, One Shields Ave., Davis, CA 95616, USA*

ABSTRACT

Diverse processes during the sedimentary cycle may generate heavy mineral associations that are devoid of clear signatures of the source region, especially in sediments that experienced unusually severe environmental conditions, and thus their provenance reconstruction becomes problematical. This study provides a new insight into the impact of 'in situ' weathering on heavy mineral assemblages, rarely dealt with in recent years, by evaluating the effects of extreme weathering that imparted an unusual bulk and heavy mineral composition to the Tertiary Dutch and German 'silver sands' (sands that consist almost exclusively of quartz).

Specific findings of our heavy mineral study of these silver sands include: (1) tourmaline can be strongly weathered; (2) the chemical weathering of tourmaline is colour-related and therefore depends probably on its particular chemistry; (3) staurolite is a reliable indicator of the degree of chemical weathering; (4) the effects of extreme chemical weathering on a heavy mineral assemblage differ fundamentally from those of burial diagenesis as, for example, in the total disappearance of apatite; (5) the joint occurrence of fresh and strongly weathered grains (with the same chemical composition) of one heavy mineral species indicates that the degree of chemical weathering is a statistical rather than a fixed parameter; (6) no heavy mineral analysis is reliable if the degree and the effects of in situ weathering are not taken into account; (7) a reliable analysis of extremely weathered sediments requires sand samples of several kilograms.

Although regional or local differences in weathering may obscure original heavy mineral compositions and thus impede subdivision of, and correlation between, sedimentary units, understanding the end-products of in situ weathering may also be helpful in drawing stratigraphic boundaries between units with originally comparable heavy mineral compositions, as is proven for the silver sands.

Developments in Sedimentology, Vol. 58, 189–213

ISSN: 0070-4571/doi:10.1016/S0070-4571(07)58006-4

Keywords: grain characteristics; *in situ* weathering; stratigraphic correlation; silver sands; tourmaline colour varieties; staurolite weathering; heavy mineral dissolution

1. INTRODUCTION AND GENERAL CONSIDERATIONS

It is widely documented that heavy mineral assemblages do not necessarily reflect the original assemblages that were deposited at the sampling site: some of the heavy mineral species may have disappeared completely, while the ratios of others may have changed as a result of differential dissolution (Morton and Hallsworth, 2007, this volume). Mange and Maurer (1992) state in this context, 'The importance of post-depositional dissolution cannot be overemphasised.' Changes of heavy mineral compositions with time in outcrop and shallow subsurface are commonly the result of weathering (particularly if a soil was formed not far above a particular deposit) but other processes (almost always related to groundwater movements) may also play a role; corrosive pore fluids may affect—or even completely dissolve—unstable minerals (Morton, 1985; Morton and Hallsworth, 2007, this volume). Diagenetic processes, in addition to the progressive dissolution of the labile grains, cause changes in heavy mineral compositions of a different kind by the formation of new heavy minerals. Another important point also needs consideration: during disaggregation fine lithic fragments, present in some sandstones, especially lithic arenites in low-permeability intervals, may release fresh mineral grains. These, being protected from pore fluids, preserve important clues to the history of the sediment. To the authors' knowledge, no such occurrences have, apart from concretions and early carbonate cement-sealed sediments, ever been evaluated. Although diagenesis is, in the mineralogical context, commonly considered as a process that leads to authigenesis (the formation of new minerals, with or without grains of the same mineral as a nucleus), it should be realised that most of the authigenic minerals owe their origin to the entire or partial dissolution of previously present minerals (which may be either the same or other species). In soil horizons, and in the underlying sediments, both light and heavy mineral assemblages may become severely depleted, and many species may even disappear entirely. Under such conditions, heavy mineral composition in a specific unit progressively changes with depth in accordance with the decreasing influence of the zone of pedogenesis (Grimm, 1973; Friis, 1976; Milliken and Mack, 1990). Because the chemically highly stable species are most likely to survive, relatively high concentrations of ultrastable minerals such as zircon, rutile and tourmaline are commonly found in superficial deposits. Surprisingly, however, the presence of high concentrations of ultrastable minerals is often ascribed to another factor, viz. their resistance to attrition during prolonged transport and/or several depositional cycles of repeated erosion and transport.

One of the main reasons why early, pre-burial chemical weathering of heavy minerals is considered relatively rarely in geology, as opposed to burial diagenesis, is because not all heavy minerals react in the same way to specific conditions. The result is that some minerals are relatively easily dissolved under conditions that hardly affect others, whereas the situation may be the reverse under different conditions (e.g., Morton et al., 2003; Morton and Hallsworth, 2007, this volume). The behaviour of particular species during weathering is contrasted with its response to

burial and acid versus alkaline conditions. Climate also influences the dissolution response of heavy minerals during soil formation (Busacca and Cremaschi, 1998; Lång, 2000; Xiubin et al., 2002, 2004). It is important to recognise and evaluate the effects of climate, because understanding the response of heavy mineral assemblages to weathering in different climatic regimes may allow inferences to be drawn about particular ancient climatic conditions (Amireh, 1991).

Heavy mineral assemblages in modern sediments mirror primarily the effects of a single phase of post-depositional weathering that commonly involves a number of simultaneous and/or progressive processes affecting the individual grains (Hubert, 1971; Nickel, 1973; Morton, 1984, 1985, 2003). The nature of various factors controlling the weathering process may change overtime, giving rise to stepwise weathering of the same particular grains (Grimm, 1973). Stages of weathering may be diverse because minerals may undergo weathering during temporary alluvial storage or weathering may already start in the source area (Friis, 1978; Dill, 1995, 1998; Xiubin et al., 1997; Singh and Rajamani, 2001) marked by conditions that differ from those during transport (Morton and Smale, 1990; Weibel, 2003), or at the final depositional site. Other studies emphasise the influence of organic matter on chemical weathering (e.g., Olivia et al., 1999).

Recognition and understanding of the wide variety of processes that are encoded in the heavy mineral composition of a sediment sample help to reconstruct its history. The early literature on heavy mineral research, published in the middle of the twentieth century (Edelman and Doeglas, 1934; Bramlette, 1941; Dryden and Dryden, 1946; Blatt and Sutherland, 1969; Nickel, 1973), reflects this well. However, the results of experimental weathering (and comparisons with field data) were found strongly contradictory (Velbel, 2007, this volume and references therein). It is one of the reasons why assessment of weathering has often been neglected in heavy mineral studies, although this is particularly relevant when exploring for economically valuable ores (Peuraniemi and Heinänen, 1985). The heavy mineral composition of a given sediment may be so different from that of the parent rocks that the omission of weathering analysis may prevent recognition of the relationship between the sediment and its source area (Friis, 1974; Milliken, 1988; Lacassie et al., 2004).

A primary parent rock may be affected by strong subaerial weathering, or a pre-existing sedimentary source rock may have undergone advanced diagenesis (Sawyer, 1986; Morton et al., 1996, 2002). The consequences of intensive weathering of a parent rock are commonly overlooked. This aspect is, nevertheless, of utmost importance because detritus eroded from a source rock (or regolith) that has undergone deep weathering and, hence, comprises a low diversity heavy mineral suite, will produce sediments with an equally low-diversity heavy mineral composition (and an equally low or even lower heavy mineral content). This could erroneously be interpreted as a consequence of strong in situ weathering of the resulting sediments (or the effect of deep burial diagenesis). Advanced diagenesis in a pre-existing sedimentary source rock may also generate authigenic heavy minerals that will be transferred to the sediments derived from it. These 'detrital' diagenetic minerals may be erroneously interpreted as being authigenic, perhaps leading to false proof of deep burial of the derived sediment.

Although there are, obviously, important relationships between the heavy mineral assemblages of the parent and daughter sediments, a resemblance of the heavy

mineral assemblages of a given sediment to those of a lithified potential source rock does not, by definition, imply that the two units have a mother/daughter relationship. On the other hand, parent rocks whose heavy mineral suites include species that become easily weathered and eliminated may result in daughter sediments with a strongly diverging heavy mineral assemblage (Yang et al., 2003). This is an extremely important issue because there is an increasing tendency to reconstruct sediment provenance from rare-earth elements in the daughter sediments (Bhatia, 1985; Mongelli, 1993; Yang et al., 2002). The rare-earth signatures of a given sediment are generally provided by its heavy mineral composition, because a relatively large part of the rare-earth contents (commonly tens of percents) are found in the accessory heavy mineral fraction of a sediment (e.g., Yang et al., 2001; Totten and Hanan, 2007, this volume).

This does not imply that weathering has only negative consequences for establishing relationships between mother and daughter sediments, or for reconstructing provenance and palaeotransport. On the contrary, analyses of the extent of weathering may help to establish lithostratigraphic correlations (see also Mange-Rajetzky, 1995; Mange et al., 1999; Morton et al., 2002) and to define stratigraphic boundaries at locations where other techniques are not available, too expensive, or otherwise impracticable (Van Loon, 1972/1973).

2. HEAVY MINERALS IN EXTREMELY WEATHERED SEDIMENTS

The most intensive chemical weathering of source rocks and derived sediments occurs in the tropics. Pedogenesis in the tropics can, depending on the type of sediment, affect the surficial sediments to a considerable depth (tens of metres), with leaching of the labile components. A specific type of sediment may result, particularly if the parent material is a pre-existing sediment that yields already well sorted detritus. Examples are the white sands that, in many countries in Europe, are called 'silver sands' (the bright white colour is caused by the virtual leaching of nearly all mineral species—including iron oxide and iron hydroxide coatings—leaving a residue containing predominantly quartz). Their remaining heavy mineral percentages (in the 50–500 μm size fraction) may be as low as 0.003% (De Jong and Van der Waals, 1971).

2.1. Sampling Problems

The above-mentioned very low heavy mineral percentages present a problem, because relatively large bulk samples need to be prepared to obtain sufficient amounts of grains for a statistically acceptable grain counting. A further problem is that the high weathering rate generally results in the relative enrichment of opaque minerals (predominantly leucoxene, ilmenite and virtually opaque rutile); these constitute up to 80% of the heavy mineral fraction in the silver sands under study. In addition, the transparent to translucent suite comprises varying amounts of unidentifiable, strongly weathered grains. These are generally grouped into a category, termed 'alterites', which often make up 5–10% of the non-opaque grains. Statistically reliable heavy mineral data, i.e., an analysis with a 95% chance of a maximum

deviation of 10%, if a particular species makes up exactly 50% of the identifiable grains, requires that at least 100 identifiable grains are counted (Kalsbeek, 1969). Therefore, the size of a sample, collected at an outcrop, should be large enough to meet the prerequisite of a reliable heavy mineral analysis. The following principles need to be considered:

(1) A heavy mineral content of 0.003%, as sometimes found in the silver sands under study (De Jong and Van der Waals, 1971), implies that only 3 out of 100,000 grains are heavy mineral grains. To encounter 1 heavy mineral grain, a field sample containing approximately 33,000 grains is therefore needed.
(2) As mentioned above, up to 80% of the heavy mineral fraction is made up by opaque grains. To find 1 non-opaque grain, one thus needs a field sample of $5 \times 33{,}000 =$ (approximately) 165,000 grains.
(3) Up to some 10% of the non-opaque heavy mineral grains are alterites. Therefore, to find 1 non-opaque, non-alterite heavy mineral grain a field sample of $1.1 \times 165{,}000$ grains = (approximately) 183,000 grains need to be available.
(4) If 100 identifiable grains have to be counted per sample, one thus needs a field sample of $100 \times 183{,}000 = 18{,}300{,}000$ grains (roughly 20×10^6 grains).
(5) If these grains have average dimensions of $0.25 \times 0.25 \times 0.1$ mm ($= 0.00625\,mm^3$) and an average mass of $0.003\,g/mm^3$, one grain weights on the average $0.0000187\,g$ ($\sim 20 \times 10^{-6}\,g$).
(6) This implies that one reliable count needs a field sample of at least some $(20 \times 10^6) \times (20 \times 10^{-6})\,g = 400\,g$.
(7) It is generally necessary to have a sufficient amount of material available for a possible control; thus, taking into account 'laboratory losses', a sample should be at least 1 kg.

In general, a heavy mineral analysis should be based on the counting of more grains than described above. Reliable results need approximately 300 identifiable non-opaque grains. Consequently, the weight of each field sample should be at least 3 kg in the case of extremely weathered sediments. If the routine heavy mineral analysis is to be complemented by the investigation of particular mineral species, for instance for a weathering analysis (see below), a statistically reliable result requires the additional counting of approximately 100 grains of the selected specific mineral. If such a mineral makes up some 10% of the non-opaque, non-alterite heavy mineral fraction, the sample weight should be 10 times larger than the weight calculated above (3 kg), i.e., some 30 kg (10 kg if 'only' 100 specimens of the selected mineral type have to be analysed). Such unusually large samples are difficult to process, and this may explain why commonly insufficient grains of a specific mineral are available for weathering analysis. This also occurred in the present study but only in a few samples (indicated in the text or the figure captions).

3. METHODS

Material for the study was taken from two shafts (II and IV) of the previous Dutch coal mine Hendrik, from sandpit Beaujean, approximately 2–3 km north of the town of Heerlen (The Netherlands), and from sandpit Nievelstein (Germany), approximately 7 km east of Heerlen (Fig. 1). From the Hendrik-shaft II section, 56,

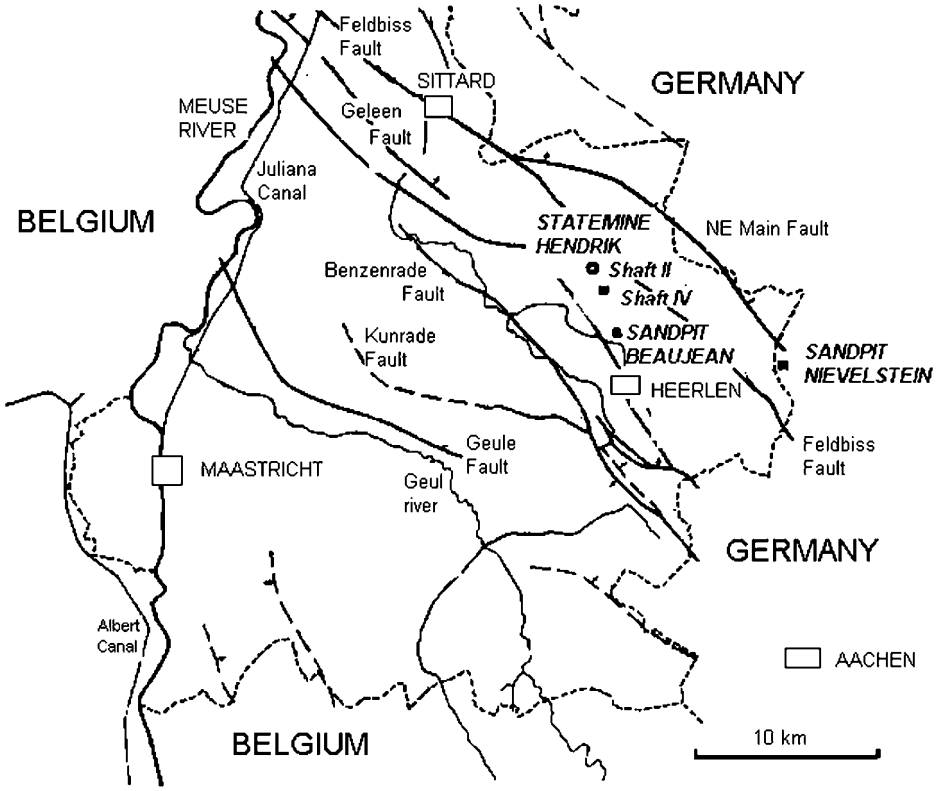

Fig. 1. Location map with the four sample areas (shafts II and IV of the Hendrik State Mine, Beaujean pit, Nievelstein pit).

and from shaft IV, 35 samples were collected. From the Beaujean surface profile 16 and from the Nievelstein pit 10 samples were taken. No material was sampled from the nearby silver sands at a possibly similar stratigraphic position in Belgium. Sample preparation for heavy mineral analyses focused on the 50–500 μm size range. For statistical reliability, explained above, 100 transparent heavy mineral grains were counted in each sample, except in sample L20 where, due to small sample size, only 65 identifiable heavy mineral grains were found. When specific heavy mineral species were investigated for their properties (shape, weathering and—in the case of tourmaline—colour), wherever possible, 100 grains of the particular species were counted in each sample, though this sum could not always be reached.

4. THE DUTCH/GERMAN SILVER SANDS

Characteristic examples of extremely weathered silver sands are represented by Tertiary deposits in the border area of The Netherlands, Germany and Belgium ('Dutch/German/Belgian silver sands') (Fig. 1). They are typically fine-grained, with well-rounded mineral grains, and are economically significant because they are often

Fig. 2. Browncoal seam (approximately 30 cm thick) of the Ville Formation overlying the silver sands (Heksenberg Member of the Breda Formation) in the Beaujean pit.

exploited for glass manufacturing or, as in the case of Southern Limburg (The Netherlands), for the production of fine-grained abrasives.

The origin and the age of these sands still remain enigmatic. In The Netherlands, they form the 5–50 m thick Heksenberg Member of the Breda Formation (De Mulder and Ritsema, 2003), previously known as the Heksenberg Formation (Kuyl, 1975). This is overlain by the Ville Formation (previously considered part of the then Heksenberg Formation; Kuyl, 1975), a browncoal unit (Fig. 2) of up to 300 m thick (although, in places, this brown coal has been entirely eroded).

4.1. Palaeogeography

The Heksenberg silver sands are considered as possibly beach sands by De Mulder and Ritsema (2003). Others argue that the occurrence of specific shell fragments points to tidal-flat conditions (Laban, 2004). One of the main problems in the interpretation of the depositional environment is that only a relatively thin part (some 20 m) of the Heksenberg Member is exposed. The original type section of the former Heksenberg Formation (now Heksenberg Member of the Breda Formation) was represented by a section in the Beaujean pit (which has disappeared through ongoing exploitation), combined with underlying strata, known only from a borehole (Kuyl, 1975). A further problem is that the scattered exposures (there are five isolated silver sand quarries in this area of The Netherlands) prevent an accurate palaeogeographical interpretation. The overall uniform grain size makes it, as a rule, difficult to recognise sedimentary structures and to analyse facies transitions. Schematic sketches of the palaeogeography during the Oligocene and Miocene are provided by Westerhoff et al. (2003), indicating that the area was roughly at the seashore at that time. The 'reference section' referred to in this contribution (shaft II of the Hendrik State Mine) contains by far the longest vertical section through the silver sands, however, a follow-up study of palaeogeographic developments and sedimentological

characteristics is prevented by the lack of surface exposures and the fact that the shaft is no longer accessible because the mine has been closed several decades ago.

4.2. Dating and Stratigraphic Correlations

Originally, the silver sands were probably 'normal' sediments, containing clay (typical of almost all shallow marine and coastal deposits), plant debris and iron components (which occur in almost all sands); this hypothesis is supported by such characteristics in the lateral, eastward, continuation of this unit. The sands in the Dutch/German border area, however, have lost all these components, and are strongly depleted in both labile light and heavy minerals. Their extreme weathering (a form of eogenesis) is attributed to a combination of tropical pedogenesis and subsequent long-lasting leaching caused by large volumes of percolating humic acids from the overlying—originally locally up to 300 m thick—browncoal seams of the Ville Formation.

The lack of any suitable component in the silver sands has prevented thus far a reliable dating. Muller (1943), on the basis of their heavy mineral content, which he compared with similar assemblages from dated stratigraphic units, considered them as possibly ranging from Early Oligocene to Middle Miocene. However, Muller did not take account of the significant post-depositional changes in the heavy mineral assemblages of the silver sands. The age of the overlying browncoal seams is not precisely known either, but is now assumed to be Oligocene and/or Miocene (De Mulder and Ritsema, 2003; Laban, 2004). This would imply that Muller's dating was probably—at least in part—incorrect. It is hoped that, as new techniques become available, exact dating of these sands may be achieved.

All silver sands in the Dutch/German/Belgian border region (Fig. 3) look macroscopically exactly the same, commonly without any traceable sedimentary structures, which makes it practically impossible to distinguish and subdivide them in the field. The former Netherlands State Geological Survey, nevertheless, considered it important to identify any characteristics that might help to establish their stratigraphic position for correlation purposes. This was one of the objectives of Muller's (1943) heavy

Fig. 3. Silver sands in the Nievelstein sandpit (Germany), closely resembling those in the nearby Beaujean pit (Netherlands). Height of the sand wall approximately 15 m.

mineral study. Later heavy mineral analysis by Van Loon (1972/1973) resulted in a more relevant approach, which facilitated recognition of either differences in sediment supply or non-deposition when pedogenesis and post-depositional weathering prevailed. As a result, units with different geological histories could be distinguished, and boundaries between them delineated. It is beyond the scope of this contribution to discuss the precise stratigraphy yielded by heavy mineral analysis. Instead, attention will be focused on the approach used and observations that resulted in the successful analysis of these extremely weathered sands.

4.3. Heavy Mineral Content

Following identification and point counting, the number-percentages of the identified detrital heavy mineral species were calculated. Samples from all four analysed sites (Fig. 1) show low-diversity assemblages, consisting mainly of tourmaline, zircon, rutile and minor quantities of anatase; high-grade metamorphic minerals such as andalusite, staurolite and kyanite occur in very low number, and sillimanite was found only in trace amounts. The metamorphic minerals showed similar physical appearance and identical optical properties in all samples, and were interpreted as having been derived from one single metamorphic source. Garnet was found only in the two mineshafts in almost each sample (commonly in relatively high abundance: 10–30%) (Fig. 4). Epidote occurs throughout the samples from both mineshafts but is rare in the Beaujean pit, and absent in the Nievelstein pit. Accessory minerals (brookite, hornblende, corundum, monazite, sphene, zoisite, spinel and topaz) were encountered only in samples from the mineshafts. Apatite is completely absent, which is interpreted by its sensitivity to tropical weathering and/or leaching by humic acids.

Similarities of the heav mineral associations and the presence/absence of epidote, garnet and accessories allowed us to reach the tentative conclusion that all four sites represent a similar—or at least partly similar—stratigraphic interval, and that the sands in the two sandpits had undergone a more intensive and continued weathering than those in the shafts.

4.4. Stratigraphic Subdivision Based on Heavy Mineral Assemblages

Based on changes in the ratios of the main heavy mineral components the ‘reference section’ can be subdivided into five units (Fig. 4A). Muller (1943) tentatively allocated them as Early Oligocene, Middle Oligocene, Middle Miocene + reworked Oligocene, distinguishing also a Middle Miocene garnet-bearing assemblage and a Middle Miocene, Limburg assemblage, respectively. The current study found similar changes in heavy mineral compositions but—because Muller’s dating had no precise constraints—in this study the five units are indicated by letter codes (A through E, from bottom to top) rather than by chronostratigraphic terms. The boundaries between the five units are based on the following changes in heavy mineral composition (Fig. 4A):

- A/B boundary: distinct increase in ultrastable minerals (zircon, rutile, anatase), decrease in epidote and garnet;
- B/C boundary: almost complete disappearance of epidote, increase in garnet; some increase in tourmaline. Muller (1943) considered this unit, which he called ‘Middle

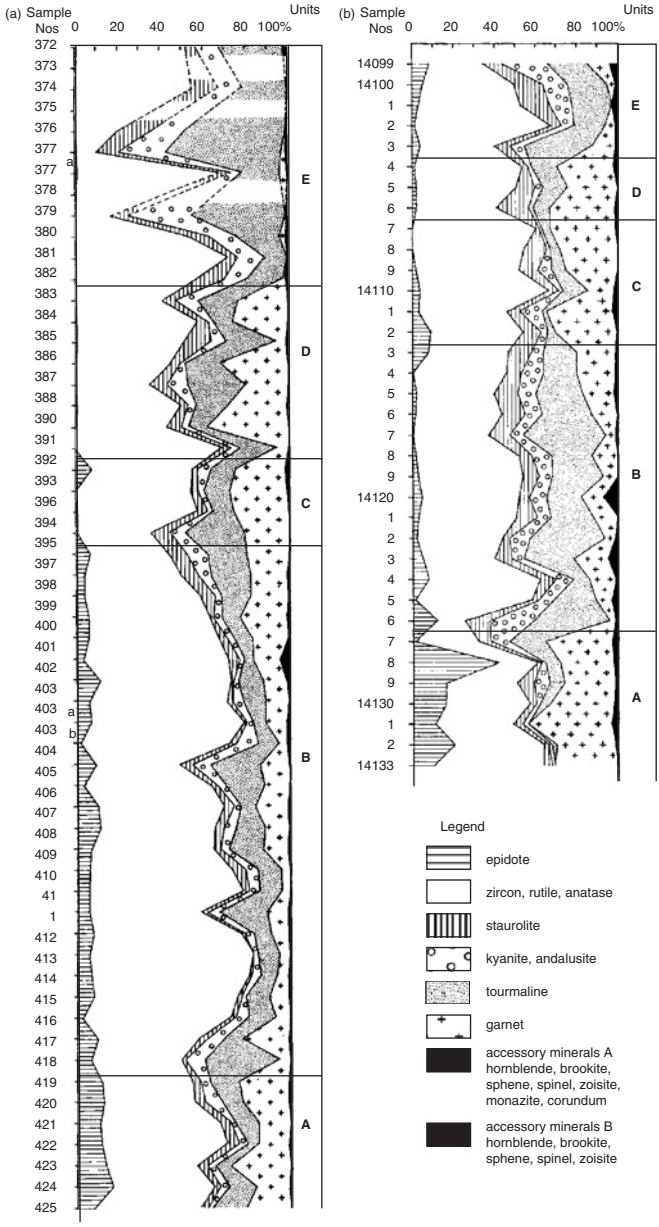

Fig. 4. Composition of the 50–500 μm heavy mineral fraction from the shafts of the Hendrik State Mine (based on 100 translucent grain counts per sample). Adapted after Van Loon (1972/1973). a (left): Shaft II. Stratigraphic interpretation according to Muller (1943). b (right): Shaft IV. Counting by the then Geological Survey of The Netherlands.

Miocene + reworked Oligocene' as a unit composed of newly supplied sediment, intermixed with reworked material from the top of the underlying unit. The present authors fully agree with this interpretation;

- C/D boundary: strong increase in garnet, mainly at the expense of the ultrastable species; further increase in tourmaline;
- D/E boundary (marks the most obvious change in composition): a sudden, almost complete, disappearance of garnet, accompanied by an increase of staurolite and a marked increase in tourmaline.

Garnet has not been encountered in any of the samples from the Beaujean pit, and was found only as a very minor component in the lowermost sample from the Nievelstein pit. The overall heavy mineral content gives the clear indication that the lower section (80%) of the Beaujean samples should be attributed to unit E (Fig. 5A). The upper part (20%) is marked by a sharp increase in the abundance of zircon, rutile and anatase from ~10 to ~30–50%, accompanied by a distinct decrease in tourmaline from ~50 to ~35%. The upper part of the Beaujean Pit is, therefore, tentatively allocated to a level above unit E, although no boundary between these two units can be observed in the field. The situation is less clear for the

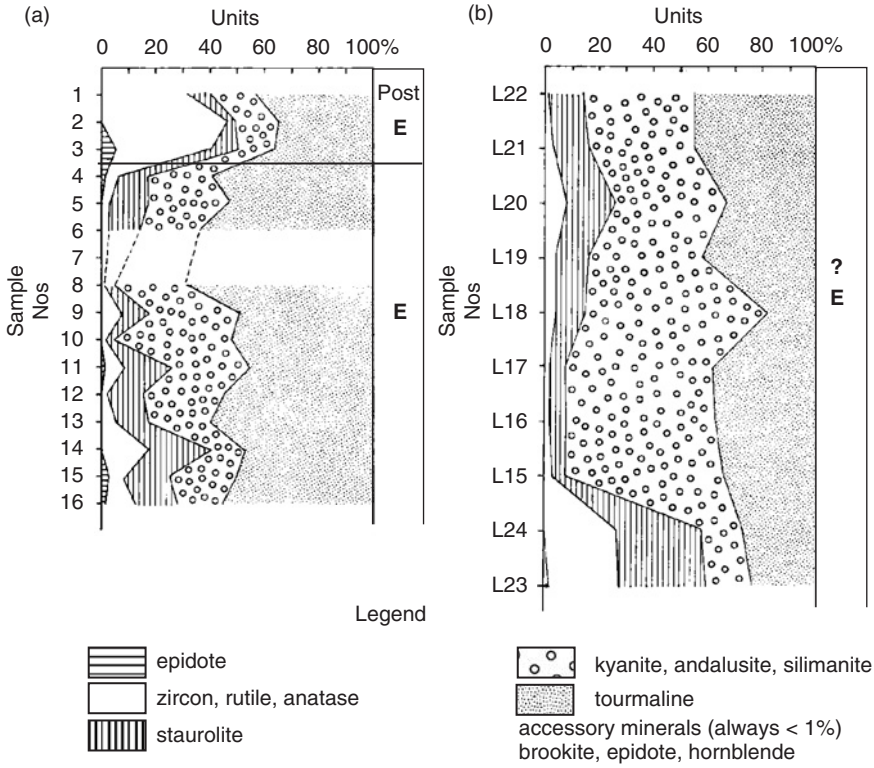

Fig. 5. Composition of the 50–500 μm heavy mineral fraction from the two investigated sandpits (based on 100 translucent grains counts per sample). Slightly modified after Van Loon (1972/1973). a (left): Sandpit Beaujean (The Netherlands). b (right): Nievelstein sandpit (only 65 translucent grains were found in sample L20).

Nievelstein pit (Fig. 5B), although the ratios between the various heavy minerals suggest that this section is correlatable with the lower part of unit D.

4.5. Tourmaline Colour Varieties

Tourmaline, overall the most abundant mineral, comprises a number of colour varieties, which were distinguished in eight groups:

1. Grains are pleochroic from dirty grey to entirely black. Sometimes a slight pink tint may glimmer through the grey colour.
2. Grains are mainly brown. The following pleochroism may be found: (a) colourless to brown; (b) light brown to dark brown; (c) brown to almost black; (d) faintly pleochroic, fairly dark brown; (e) brown to greenish; (f) yellow to brown.
3. Grains show both brown and greenish blue colours. This may be due to pleochroism when the grain is rotated over 90° but these colours may also exist simultaneously, usually showing brown streaks in a greenish blue field. Greenish blue, non-pleochroic grains are also considered to belong to this colour variety.
4. Grains are mainly green, sometimes with a brownish tint. Pleochroism may be: (a) from light to dark green; (b) from green to almost black; (c) almost absent in dark green grains.
5. Grains are blue, usually with a very bright hue, changing from light to darker, rarely from dark blue to almost black.
6. Grains have a typical wine red to brownish red colour, turning into very dark green (sometimes nearly black) when rotating them over 90°.
7. Grains show pleochroism from dirty pink to greenish blue.
8. Grains show pleochroism from light red to bright green.

None of these groups showed more than a vague relationship with the total mineralogical compositions and indicated no relationship at all with the total tourmaline percentage in a sample. However, some trends were detectable between the various colour varieties and one colour variety showed a distinct relationship with the staurolite percentage. This is noteworthy because, as will be shown later, staurolite abundance reflects the degree of weathering. This implies that the response of the various tourmaline colour varieties to the intensity of weathering may not be uniform, and this might explain the differences reported in the literature on the resistance of tourmaline to chemical weathering (see, amongst others, Makarov and Kondrateva, 1965; Varadachari et al., 1994; Morton and Hallsworth, 2007, this volume).

4.6. Grain Shapes

The original grain shape of minerals is affected primarily by weathering and attrition during transport/recycling and by weathering in situ. To augment information, the morphology of zircon (idiomorphic, rounded prisms, rounded) and tourmaline (idiomorphic, irregular, rounded) was also recorded. This revealed that the tourmaline colour varieties responded similarly to attrition. The effects of chemical weathering on tourmaline colour varieties will be evaluated in the next section.

5. CHEMICAL WEATHERING OF HEAVY MINERALS IN THE SILVER SANDS

Studies on weathering processes aim to assess the rate of weathering, to identify the chemical milieu and to reconstruct the time span over which grains were exposed to particular weathering conditions (Velbel, 2007, this volume). If the rate of weathering is not excessive many mineral species can be investigated. The highly weathered silver sands contain only three species (in sufficient quantities) that are suitable for a weathering analysis: garnet, staurolite and tourmaline. All three display clearly the different stages of weathering. This is remarkable because garnet is commonly considered as relatively prone to chemical weathering, while tourmaline is generally defined as an ultrastable, highly resistant species. However, unusual conditions in the silver sands (tropical pedogenesis, followed by the percolation of humic acids, probably in large amounts, during a prolonged period) indicate that weathering under extremely aggressive conditions differs considerably from common chemical weathering, even if it continues for a long time.

Garnet is present in suitable quantities in shaft IV (100 grains per sample) and shaft II (50 grains) of the Hendrik mine but is virtually absent in the two sandpits. Staurolite was successfully investigated from all four localities and its relative abundance allowed inspecting 50 grains per sample. Tourmaline was found in sufficient quantities in both the mineshafts and the Nievelstein pit sands, enabling inspection of 100 grains per slide.

5.1. Weathering of Garnet

It has been proved that garnet disappears at a geologically rapid rate in acidic soils (e.g., Velbel, 1984), which explains the paucity of garnet in the analysed samples. Where garnet was present, the grains could be subdivided into four dissolution stages (Fig. 6), ranging from fresh (no dissolution can be detected under the light microscope) to strongly corroded (either at one or several points, or the entire grain). Differing garnet chemical compositions and internal structure, such as zoning, can

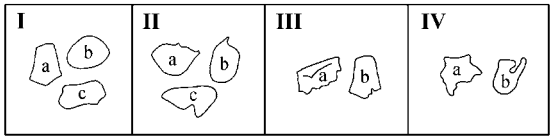

Fig. 6. Schematic representation of corrosion classes (dissolution stages) of garnet. I: The contours of the grains show no irregularities as a result of corrosion, but some etching may be found. Usually, the grains are angular (a), possibly due to frequent breakage; sometimes they are well rounded (b) or sub-rounded (c). II: The shape of the grain is difficult to explain by transport only. The grains may be rounded, but initial corrosion seems to have taken place (a). Selective corrosion may result in 'spines' at resistant parts (b) or in cavities at less resistant areas (c). III: The grains show distinct corrosion, usually only locally (b). One fresh surface (a) may originate from breakage shortly before deposition. IV: The grains indicate highly advanced dissolution. They may be entirely corroded (a), or dissolution occurs only in one particular area (b).

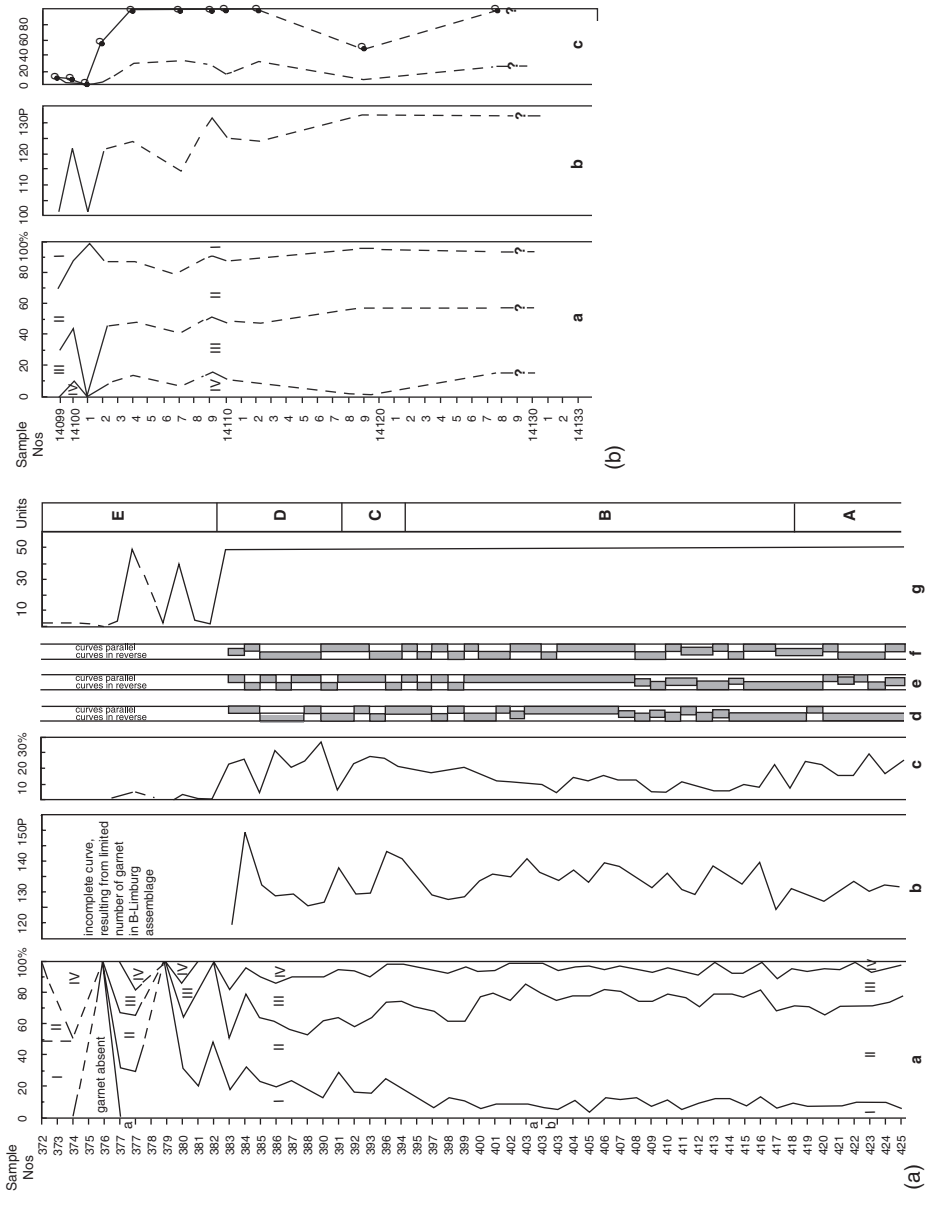
Sample Nos
Units
E
D
C
B
A
garnet absent
incomplete curve, resulting from limited number of garnet in B-Limburg assemblage
curves parallel
curves in reverse
(a)
(b)

cause differences in garnet behaviour during chemical weathering. It is therefore important to note that all garnets observed during these analyses had similar optical characteristics (colour, isotropism, inclusions, relief), even though their weathering degrees showed differences. It is, from a chemical/petrological/pedological point of view, interesting that all four dissolution stages (Fig. 6) were detected in almost all samples from the two mineshafts, presenting an association of strongly corroded and completely fresh grains in a single sample. Because all grains were extracted from relatively small size samples, this enigmatic behaviour cannot be explained with spatially different corrosive conditions.

The fragile form of the heavily corroded garnet grains indicates that they are not inherited because these would have been destroyed by the prolonged rigorous action of waves and currents in their depositional environment; therefore, dissolution must have taken place in situ (after deposition). Considering the fact that all garnet grains in these sands have similar properties, the logical conclusion is that chemical weathering affects minerals in a statistical way, with the implication that—if a realistic insight into the degree of post-depositional weathering is to be achieved—a statistically significant number of grains of a particular mineral species needs to be analysed. The sample size of extremely weathered sediments should therefore be larger than the 10 kg mentioned above, even if garnet is present in quantities of over 10% in the non-opaque suite.

Fig. 7 shows that no relationship exists between the degree of garnet weathering and garnet percentage in the samples. This may be due to the fact that extreme weathering causes the complete dissolution of many of the garnet grains, resulting in an unrealistic picture caused by the relative enrichment of the less affected grains. Concluding from the above, garnet is—in general—less suitable for the study of mineral weathering in highly weathered sediments; on the other hand, it can be used as a very good signature for the relative degree of weathering in less intensely weathered sediments.

5.2. Weathering of Staurolite

In the silver sands, staurolite appears to be resistant to acidic leaching, as indicated by an increase in its percentage in samples containing a relatively high number of weathered grains (Fig. 8) but, similarly to garnet, 'fresh' specimens coexist with strongly corroded ones. This finding is consistent with that of Ollier (1969), who

Fig. 7. Corrosion of the garnet in the shafts of the Hendrik State Mine. Adapted after Van Loon (1972/1973). a (left): Shaft II. (a) Relative proportions of corrosion classes (see Fig. 6 for details). (b) Simplified curve, constructed on the basis of weighed percentages of the corrosion classes. (c) Percentage of garnet in the 50–500 μm heavy mineral fraction. (d) Relationship between simplified corrosion curve (b) and percentage curve (c). (e) Relationship between simplified corrosion curve (b) and the corrosion of staurolite. (f) Relationship between simplified corrosion curve (b) and the corrosion of tourmaline. (g) Number of classified garnet grains. b (right): Shaft IV. (a) Relative proportions of corrosion classes (see Fig. 6 for details). (b) Simplified curve, constructed on the basis of weighed percentages of the corrosion classes. (c) Percentage of garnet in the 50–500 μm heavy mineral fraction (left) and number of classified garnet grains (right).

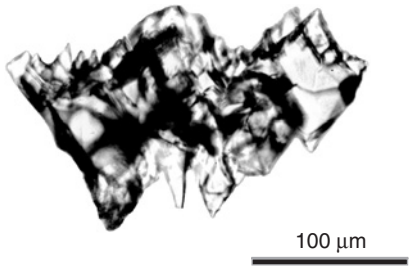

Fig. 8. Strongly corroded staurolite grain (plane polars).

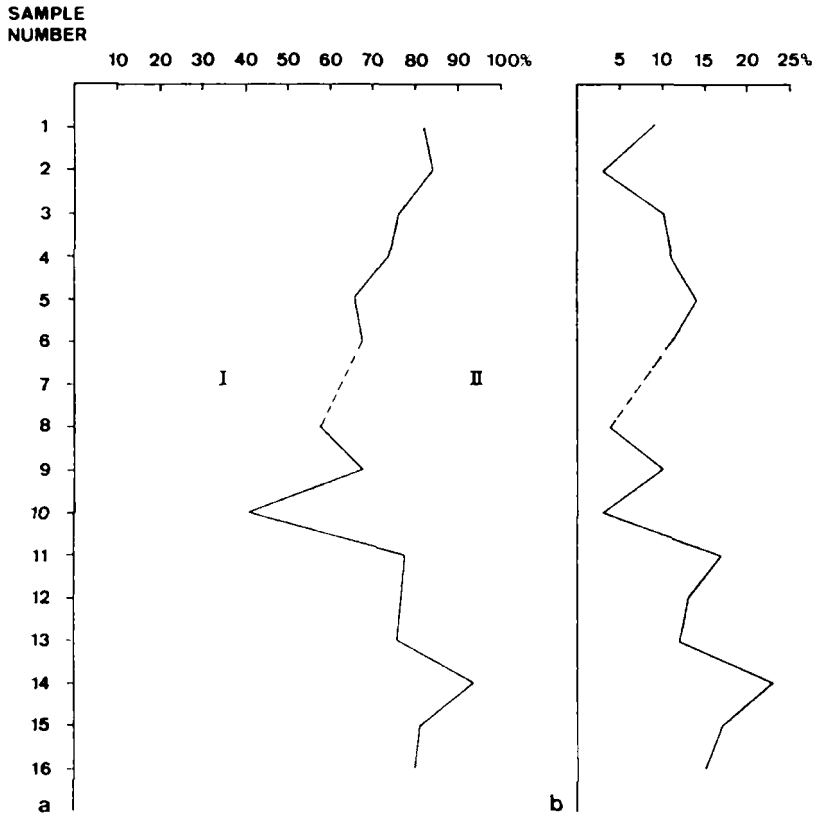

Fig. 9. Corrosion of the staurolite in the Beaujean sandpit. In each sample 50 grains were classified, except in samples 10 (34 grains) and 12 (30 grains). From Van Loon (1972/1973). (a, left) Corrosion curve, dividing type I grains (the grains are not or only slightly weathered) from those of type II (strongly corroded grains). (b, right) Percentage of staurolite in the heavy mineral fraction.

called staurolite a useful indicator mineral of weathering. There are some horizons, particularly in the upper part ('younger than unit E') in the Beaujean pit, however, where the weathering/corrosion curves and the percentage curves show distinctly opposite trends, contrasting with the 'normal', parallel, curves in the lower part of

the section (Fig. 9). The only explanation for this trend is that the quantity of staurolite was initially different in beds in the upper level. This observation is significant, because it indicates that, even in extremely weathered sediments, staurolite—if present—may be used for detecting changes in sediment supply.

5.3. Weathering of Tourmaline

A high number of tourmaline grains shows appreciable signs of corrosion in the reference section (Fig. 10). Although tourmaline is generally considered both mechanically and chemically resistant and has been shown that it is able to survive several deposition/erosion/transport cycles (e.g., Ollier, 1969; Nickel, 1973; Friis, 1974, 1976; Morton and Hallsworth, 1999), in most samples of the reference section some 10–20% of tourmaline grains show a certain extent of corrosion (Fig. 11), commonly in the form of etch pits, but sometimes as thin, fragile 'wings'. Idiomorphic grains appear to be corroded slightly more frequently than rounded ones (Fig. 12). The various colour varieties also display slight differences in their weathering susceptibility. The influences of both shape and, concluding from their colour, chemical composition make tourmaline less suitable for studies of weathering under extreme conditions. This is amplified by the fact that tourmaline cannot be

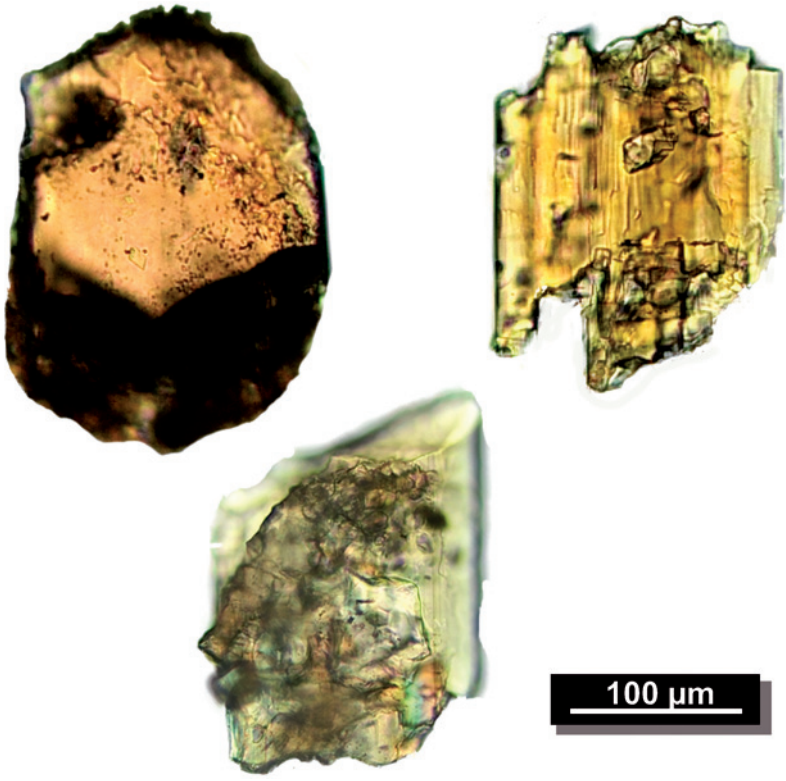

Fig. 10. Strongly corroded tourmaline grains.

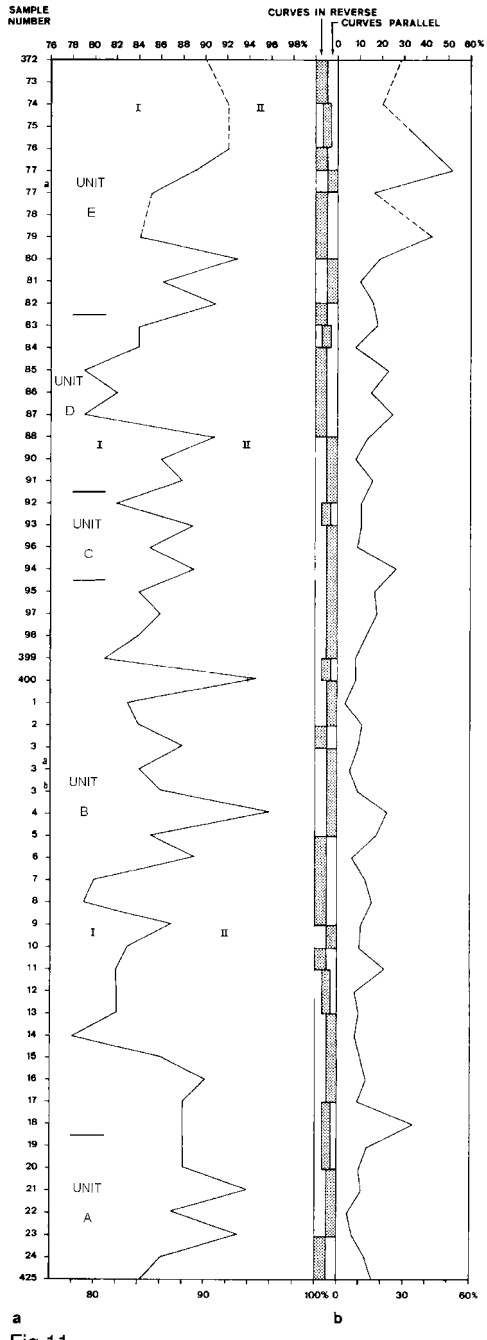
SAMPLE NUMBER
CURVES IN REVERSE
CURVES PARALLEL
76 78 80 82 84 86 88 90 92 94 96 98%
0 10 20 30 40 50 60%
UNIT E
UNIT D
UNIT C
UNIT B
UNIT A
I
II
80 90 100% 0 30 60%
a
b

Fig.11

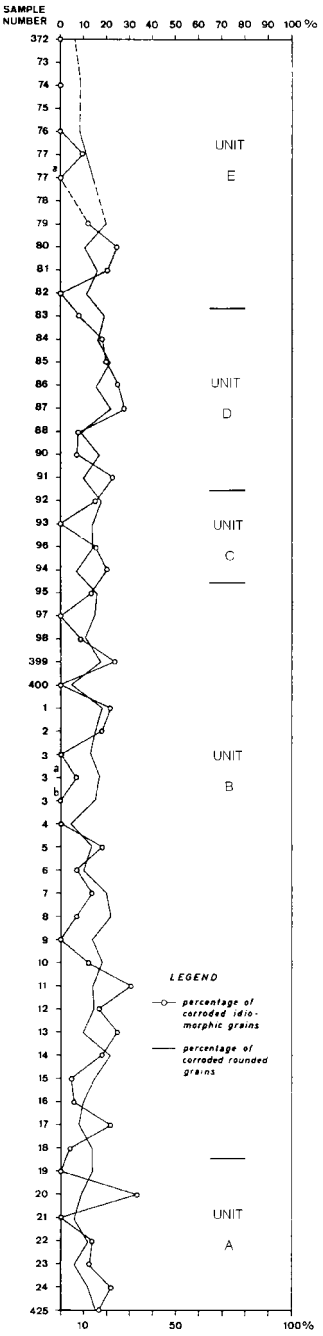
SAMPLE NUMBER
0 10 20 30 40 50 60 70 80 90 100 %
UNIT E
UNIT D
UNIT C
UNIT B
UNIT A
LEGEND
percentage of corroded idiomorphic grains
percentage of corroded rounded grains
10 50 100%

Fig.12

selectively enriched as a result of weathering but, as shown by this study, it can also become relatively impoverished with highly advanced weathering (see also Morton and Hallsworth, 2007, this volume). Our observations may contradict most findings thus far, including the well-established ZTR (zircon, tourmaline, rutile) maturity index (Hubert, 1962) but such extreme conditions that produced the silver sands are far less frequent than common chemical weathering.

6. CONCLUSIONS

Extremely weathered sands, exemplified by the Dutch/German silver sands, contain not only very low proportions of heavy minerals but, resulting from dissolution of the less stable minerals, also a limited number of species. The present-day heavy mineral content differs considerably from their original composition. On the basis of the remaining specific minerals, the degree of weathering can be estimated. Staurolite, when present, appears to be most suitable for assessing the intensity of weathering in extremely weathered sediments. This, in turn, may allow an assessment of the other minerals that may have been present initially. For instance, strongly weathered staurolite in a sample indicates that minerals that are more susceptible to weathering were eliminated. Moreover, the presence of staurolite, often associated with andalusite and kyanite in regionally metamorphosed rocks, suggests that they were probably present at the time of sedimentation, and provides information on sand provenance.

The Dutch/German silver sands present a prime example of dual episodes of intensive weathering that were presumably common in the geological past. This study also conveys a warning, and demonstrates that a low-diversity, stable-ultrastable species-dominated heavy mineral content should not be routinely ascribed to the causes of deep-burial diagenesis. Therefore, a low-diversity heavy mineral assemblage in surficial sediments may reflect in situ weathering, or deep weathering of the source rocks. The location (either source rock or derived sediment) of the weathering can be reconstructed from grain morphology. Because fragile grains cannot survive—at least not in large quantities—long transport or processes like wave action, their presence in a given sediment indicates that weathering has taken place in situ. On the other hand, if there are no signs of in situ corrosion in highly depleted assemblages, it is most likely that the dissolution took place in the sediment source area. Distinguishing between these possible sites of weathering is important for accurate provenance determination using heavy minerals, and for correlating sand units in reservoir successions.

Fig. 11. Corrosion of the tourmaline from shaft II of the Hendrik State Mine. In each sample 100 grains were classified, except in samples 372 (55 grains), 381 (59 grains) and 413 (69 grains). Slightly modified after Van Loon (1972/1973). (a) Corrosion curve, dividing type I grains (the grains are not or only slightly weathered) from those of type II (strongly corroded grains). (b) Percentage of tourmaline in the heavy mineral fraction.

Fig. 12. Corrosion curves for idiomorphic and rounded tourmaline grains from shaft II of the Hendrik State Mine. Slightly modified after Van Loon (1972/1973).

Grain shape also influences the susceptibility to post-depositional weathering, and should be taken into account, especially if a species is represented by different or contrasting morphologies, such as idiomorphic and rounded. This is especially applicable to mechanically highly resistant minerals such as zircon, rutile and tourmaline.

The simultaneous occurrence of highly corroded and apparently fresh grains of the same mineral species within one single sample indicates that corrosion has statistical significance; therefore, the degree of weathering cannot be determined on the basis of a few corroded grains alone. Weathered grains with fragile 'spines' cannot be transported far by running water without losing most of the fragile parts, as grains in the 50–500 μm size range are most commonly transported by saltation and as bedload; in both cases strain is exerted on the grains. This study shows that the combined presence of fresh and strongly weathered grains does not necessarily signal supply from dual or multiple sources.

It is essential to analyse a sufficient number of grains (at least 50–100 grains per species) to enable comparison and evaluation of the degree of weathering in different samples from a sediment package. Our study of the silver sands reveals that whereas slow, prolonged weathering produces grains with (for one mineral species) approximately similar degrees of weathering, aggressive weathering, even during a shorter time span (such as pedogenesis under tropical conditions; Horbe et al., 2004), may result in variably corroded grains. Such aggressive conditions were probably responsible for the extreme corrosion of the mineral components of the silver sands.

The response of minerals of a solid solution series between two (or more) chemical end members, such as tourmaline, to chemical weathering appears to be partly controlled by the chemistry of the individual members. In contrast to what is commonly stated in the literature, tourmaline content, though generally becoming higher with increasing degree of weathering, can also become relatively impoverished at some intervals. The relative proportions of tourmaline colour varieties (see Hawthorne and Henry, 1999 for an overview of minerals of the tourmaline group) in the current study most probably reflect their different chemistry-controlled reactions to the weathering agents. Unravelling the geological history of a sediment on the basis of varying grain shape and composition of the tourmaline colour varieties is a novel approach. For example, Willner (1987) and Jiang et al. (1999) demonstrated that a detailed analysis of changes in the ratios between the various colour varieties could provide information on different sediment source areas.

The greater is the diversity of a heavy mineral assemblage, especially if rare but diagnostic species are present, the more accurately the provenance of the sediments can be reconstructed. In cases of low-diversity assemblages high-resolution heavy mineral analysis (as demonstrated by Lihou and Mange-Rajetzky, 1996) may help with provenance reconstruction and correlation by focusing on the characteristic varieties of ultrastable minerals. The silver sands under study are poor in heavy mineral species and no provenance-diagnostic minerals occur. Their highly depleted heavy mineral assemblages have presented a particular challenge. However, distinguishing and combining corrosion and attrition signatures of the suitable heavy mineral species enabled, with great reliability, the correlation of the sample set from shaft IV of the Hendrik State Mine with a large part of the reference section (i.e., shaft II the Hendrik State Mine) (compare Fig. 4). Similarly, the silver sands from the Nievelstein sandpit in Germany could also be correlated with the reference

section, though with somewhat less certainty because the extreme weathering in the Nievelstein sandpit had progressed so far that almost all heavy mineral species have disappeared. Nevertheless, its lower profile seems to be comparable with the upper part of the reference section (compare Fig. 4).

Weathering signatures also proved useful in the case of the Beaujean silver sandpit. Sudden changes, both in heavy mineral composition (Fig. 5A) and in grain characteristics, permitted delineation of a distinct boundary, even though no boundary could be detected in the field. Concluding from differences in the degree of corrosion, the lower interval of the Beaujean section can be correlated with the top part of the reference section (compare Figs. 4A and 5A). This also indicates that the upper part of the Beaujean pit is younger (post-unit E) than the upper part of the reference section (units D and E).

Surficial sediments may show heavy mineral assemblages that have been modified in the course of time by dissolution during intensive weathering. They thus obscure the original heavy mineral composition and may also give misleading (or at least incomplete) information on sediment provenance. No heavy mineral study is therefore complete without a systematic analysis of the degree of weathering. This study introduces the environment of advanced weathering in surficial sediments, contrasting with that of deep burial (Morton and Hallsworth, 2007, this volume). Although both processes result in depleted heavy mineral suites that comprise the common ultrastable 'heavy mineral end-members', their geochemical environments (e.g., temperature, pressure, pore fluids, compaction) differ considerably. When analysing diagenetically affected, low-diversity assemblages (especially where a systematic analysis of progressive changes/depletion of heavy mineral suites is not possible), it is most important to consider whether all dissolution occurred during burial diagenesis, or whether the sediments experienced a longer period of surface weathering and mineral dissolution prior to burial, which then may have imparted little modification to the already depleted assemblages.

Finally, it is important to note that detailed analysis of the dissolution stages of specific heavy minerals in extremely weathered sands (such as the silver sands studied here) requires unusually large field samples (at least a few kg and for specific purposes even 10 kg). The difficulty of dealing with such large sample volumes may be one of the reasons why so few studies of this type have been carried out on sediments with very low heavy mineral content.

ACKNOWLEDGEMENTS

We express our sincere thanks to Albert Matter and an anonymous reviewer for their constructive criticism of an earlier version of the manuscript and to Cees Laban (Netherlands Institute of Applied Geosciences TNO), who kindly provided the photograph of figure 2.

REFERENCES

Amireh, B.S., 1991. Mineral composition of the Cambrian-Cretaceous Nubian series of Jordan: provenance, tectonic setting and climatological implications. Sedimentary Geology 71, 99–119.

Bhatia, M.R., 1985. Rare earth element geochemistry of Australian Paleozoic graywackes and mudrocks: provenance and tectonic control. Sedimentary Geology 45, 97–113.
Blatt, H., Sutherland, B., 1969. Intrastratal solution and non-opaque heavy minerals in shales. Journal of Sedimentary Petrology 39, 591–600.
Bramlette, M.N., 1941. The stability of minerals in sandstone. Journal of Sedimentary Petrology 11, 32–36.
Busacca, A., Cremaschi, M., 1998. The role of time versus climate in the formation of deep soils of the Apennine fringe of the Po valley, Italy. Quaternary International 51/52, 95–107.
De Jong, J.D., Van der Waals, L., 1971. Depositional environment and weathering phenomena of the white Miocene sands of Southern Limburg (The Netherlands). Geologie en Mijnbouw 50, 417–424.
De Mulder, F.J., Ritsema, I., 2003. Duurzaam gebruik en beheer van de ondergrond. In: De Mulder, F.J., Geluk, M.C., Ritsema, I., Westerhoff, W.E., Wong, Th.E. (Eds.), De Ondergrond van Nederland (Geologie van Nederland 7). Nederlands Instituut voor Toegepaste Geowetenschappen, Utrecht, pp. 11–64.
Dill, H.G., 1995. Heavy mineral response to the progradation of an alluvial fan: implications concerning unroofing of source area, chemical weathering and palaeo-relief (Upper Cretaceous Parkstein fan complex, SE Germany). Sedimentary Geology 95, 39–56.
Dill, H.G., 1998. A review of heavy minerals in clastic sediments with case studies from the alluvial-fan through the near-shore environments. Earth-Science Reviews 45, 103–132.
Dryden, A.L., Dryden, C., 1946. Comparative rates of weathering of some common heavy minerals. Journal of Sedimentary Petrology 16, 91–96.
Edelman, C.H., Doeglas, J.D., 1934. Über Umwandlungserscheinungen an detritischem Staurolith und anderen Mineralien. Tschermaks Mineralogische und Petrologische Mitteilungen 45, 225–234.
Friis, H., 1974. Weathered heavy mineral associations from the young-Tertiary deposits of Jutland, Denmark. Sedimentary Geology 12, 199–213.
Friis, H., 1976. Weathering of a Neogene fluviatile fining-upwards sequence at Voervadsbro, Denmark. Bulletin of the Geological Society of Denmark 25, 99–105.
Friis, H., 1978. Heavy mineral variability in Miocene marine sediments in Denmark: a combined effect of weathering and reworking. Sedimentary Geology 21, 169–188.
Grimm, W.-D., 1973. Stepwise heavy mineral weathering in the residual quartz gravel, Bavarian Molasse (Germany). Contributions to Sedimentology 1, 103–125.
Hawthorne, F.C., Henry, D.J., 1999. Classification of the minerals of the tourmaline group. Journal of Mineralogy 11, 201–215.
Horbe, A.M.C., Horbe, M.A., Seguio, K., 2004. Tropical spodosols in northeastern Amazonas State, Brazil. Geoderma 119, 55–68.
Hubert, J.F., 1962. A zircon-tourmaline-rutile maturity index and the interdependence of the composition of heavy mineral assemblages with the gross composition and texture of sandstones. Journal of Sedimentary Petrology 32, 440–450.
Hubert, J.F., 1971. Analysis of heavy mineral assemblages. In: Carver, R.E. (Ed.), Procedures in Sedimentary Petrology. Wiley, New York, pp. 453–478.
Jiang, S.Y., Yang, J.H., Palmer, M.R., 1999. Chemical compositions of tourmaline from the Inch Conglomerate Formation, Dingle Peninsula, SW Ireland, and their implications in provenance analysis. Chemie der Erde 59, 123–133.
Kalsbeek, F., 1969. Note on the reliability of point counter analyses. Neues Jahrbuch für Mineralogie, Monatshefte, Jahrgang, pp. 1–6.
Kuyl, O.A., 1975. Lithostratigrafie van de Mio-Oligocene afzettingen in Zuid-Limburg. In: Zagwijn, W.H., Van Staalduinen, C.J. (Eds.), Toelichting bij geologische overzichtskaarten van Nederland. Rijks Geologische Dienst, Haarlem, pp. 56–63.

Lacassie, J.P., Roser, B., Del Solar, J.R., Hervé, F., 2004. Discovering geochemical patterns using self-organizing neural networks: a new perspective for sedimentary provenance analysis. Sedimentary Geology 165, 175–191.

Laban, C., 2004. Wandelen over kanariezand. Mens & Wetenschap 31, 62–65.

Lång, L.-O., 2000. Heavy mineral weathering under acidic soil conditions. Applied Geochemistry 15, 415–423.

Lihou, J.C., Mange-Rajetzky, M.A., 1996. Provenance of the Sardona Flysch, eastern Swiss Alps: example of high-resolution heavy mineral analysis applied to an ultrastable assemblage. Sedimentary Geology 105, 141–157.

Makarov, V.N., Kondrateva, D.M., 1965. Alterations of tourmaline in weathering profile of the Yakovlev iron-ore deposits in the Kursk magnetic anomaly area. Akademiya Nauk Ukrainskoi SRS (Kiev) Dopovdi 1, 84–87.

Mange, M.A., Maurer, H.F.W., 1992. Heavy Minerals in Colour. Chapman and Hall, London, 147.

Mange, M.A., Turner, P., Ince, D., Pugh, J., Wright, D., 1999. A new perspective on the zonation and correlation of barren strata: an integrated heavy mineral and palaeomagnetic study of the Sherwood Sandstone Group, East Irish Sea Basin and surrounding areas. Journal of Petroleum Geology 22, 325–348.

Mange-Rajetzky, M.A., 1995. Subdivision and correlation of monotonous sandstone sequences using high-resolution heavy mineral analysis, a case study: the Triassic of the Central Graben. In: Dunay, R.E., Hailwood, E. (Eds.), Dating and Correlating Biostratigraphically-Barren Strata, 89. Geological Society of London Special Publication, pp. 23–30.

Milliken, K.L., 1988. Loss of provenance information through subsurface diagenesis in Plio-Pleistocene sandstones, northern Gulf of Mexico. Journal of Sedimentary Petrology 58, 992–1002.

Milliken, K.L., Mack, L.E., 1990. Subsurface dissolution of heavy minerals, Frio Formation sandstones of the ancestral Rio Grande Province, South Texas. Sedimentary Geology 68, 187–199.

Mongelli, G., 1993. REE and other trace elements in a granitic weathering profile from ''Serre'', southern Italy. Chemical Geology 103, 17–25.

Morton, A.C., 1984. Stability of detrital heavy minerals in Tertiary sandstones from the North Sea Basin. Clay Minerals 19, 287–308.

Morton, A.C., 1985. Heavy minerals in provenance studies. In: Zuffa, G.G. (Ed.), Provenance of Arenites. Reidel, Dordrecht, pp. 249–277.

Morton, A.C., 2003. Heavy minerals. In: Middleton, G.V. (Ed.), Encyclopedia of Sediments and Sedimentary Rocks. Kluwer, Deventer, pp. 356–358.

Morton, A.C., Allen, M., Simmons, M., Spathopoulos, F., Still, J., Hinds, D., Ismail-Zadeh, A., Kroonenberg, S., 2003. Provenance patterns in a neotectonic basin: Pliocene and Quaternary sediment supply to the South Caspian. Basin Research 15, 321–337.

Morton, A.C., Claoué-Long, Berge, C., 1996. SHRIMP constraints on sediment provenance and transport history in the Mesozoic Statfjord Formation, North Sea. Journal of the Geological Society 153, 915–929.

Morton, A.C., Hallsworth, C.R., 1999. Processes controlling the composition of heavy mineral assemblages in sandstones. Sedimentary Geology 124, 3–29.

Morton, A.C., Hallsworth, C.R., 2007. Stability of detrital heavy minerals during burial diagenesis. In: Mange, M.A., Wright, D.T. (Eds.), Heavy Minerals In Use. Developments in Sedimentology (this volume).

Morton, A., Knox, R.W.O.-B., Hallsworth, C., 2002. Correlation of reservoir sandstones using quantitative mineral analysis. Petroleum Geoscience 8, 251–262.

Morton, A.C., Smale, D., 1990. The effects of transport and weathering on heavy minerals from the Cascade River, New Zealand. Sedimentary Geology 68, 117–123.

Muller, J.E., 1943. Uitkomsten van nieuwe geologisch-paleontologische onderzoekingen van den ondergrond van Nederland. Sedimentpetrologie van het dekgebergte in Limburg. Mededelingen Geologische Stichting Serie C-II 2 (2), 1–78.

Nickel, E., 1973. Experimental dissolution of light and heavy minerals in comparison with weathering and intrastratal solutions. Contributions to Sedimentology 1, 1–68.

Olivia, P., Viers, J., Dupré, B., Fortuné, J.P., Martin, F., Braun, J.J., Nahon, D., Robain, H., 1999. The effect of organic matter on chemical weathering: study of a small tropical watershed: Nsimi–Zoétélé site, Cameroon. Geochimica et Cosmochimica Acta 63, 4013–4035.

Ollier, C.D., 1969. Weathering. Oliver & Boyd, Edinburgh, 304pp.

Peuraniemi, V., Heinänen, K., 1985. Mineralogical investigations in the interpretation of heavy mineral geochemical results of till. Journal of Geochemical Exploration 23, 315–328.

Sawyer, E.W., 1986. The influence of source rock type, chemical weathering and sorting on the geochemistry of clastic sediments from the Quetico metasedimentary belt, Superior Province, Canada. Chemical Geology 55, 77–95.

Singh, P., Rajamani, V., 2001. REE geochemistry of recent clastic sediments from the Kaveri floodplain, southern India: implication to source area weathering and sedimentary processes. Geochimica et Cosmochimica Acta 65, 3093–3108.

Totten, M.W., Hanan, M.A., 2007. Heavy minerals in shales. In: Mange, M.A., Wright, D.T. (Eds.), Heavy Minerals In Use. Developments in Sedimentology (this volume).

Varadachari, C., Barman, A.K., Ghosh, K., 1994. Weathering of silicate minerals by organic acids. 2. Nature of residual products. Geoderma 61, 251–258.

Van Loon, A.J., 1972/1973. "Habitus" of some heavy minerals from the Tertiary of Southern Limburg (The Netherlands). Mededelingen Rijks Geologische Dienst, Nieuwe Serie 23, 39–67.

Velbel, M.A., 1984. Natural weathering mechanisms of almandine garnet. Geology 12, 631–634.

Velbel, M.A., 2007. Surface textures and dissolution processes of heavy minerals in the sedimentary cycle: Examples from pyroxenes and amphiboles. In: Mange, M.A., Wright, D.T. (Eds.), Heavy Minerals In Use. Developments in Sedimentology (this volume).

Weibel, R., 2003. Alteration of detrital Fe-Ti oxides in Miocene fluvial deposits, central Jutland, Denmark. Bulletin of the Geological Society of Denmark 50, 171–183.

Westerhoff, W.E., Wong, Th.E., De Mulder, E.F.J., 2003. Geschiedenis van de ondergrond. In: De Mulder, F.J., Geluk, M.C., Ritsema, I., Westerhoff, W.E., Wong, Th.E. (Eds.), De Ondergrond van Nederland (Geologie van Nederland 7). Nederlands Instituut voor Toegepaste Geowetenschappen, Utrecht, pp. 119–246.

Willner, A.P., 1987. Detrital tourmalines as indicators for the source rocks of Late Precambrian—Lower Cambrian greywackes (Puncoviscana Formation) in NW Argentina. Zentralblatt für Geologie und Paläontologie 1987, 885–891.

Xiubin, H., Junliang, T., Keli, T., Jianzhong, S., Matthews, J.A., 2004. Bio-climatic imprints on a Holocene loess palaeosol from China. Journal of Asian Earth Sciences 22, 455–464.

Xiubin, H., Keli, T., Juanliang, T., Matthews, J.A., 2002. Paleopedological investigation of three agricultural loess soils on the Loess Plateau in China. Soil Science 167, 478–491.

Xiubin, H., Keli, T., Xiangyi, L., 1997. Heavy mineral record of the Holocene environment on the Loess Plateau in China and its pedogenetic significance. Catena 29, 323–332.

Yang, S.Y., Jung, H.S., Choi, M.S., Li, C.X., 2001. The rare earth element compositions of the Changjiang (Yangtze) and Huanghe (Yellow) river sediments. Earth and Planetary Science Letters 210, 407–419.

Yang, S.Y., Jung, H.S., Lim, D.I., Li, C.X., 2003. A review on the provenance discrimination of sediments in the Yellow Sea. Earth-Science Reviews 63, 93–120.

Yang, S.Y., Li, C.X., Jung, H.S., Lee, H.J., 2002. Discrimination of geochemical compositions between the Changjiang and the Huanghe sediments and its application for the identification of sediment source in the Juangsu coastal plain, China. Marine Geology 186, 229–241.

This page intentionally left blank

Chapter 7

STABILITY OF DETRITAL HEAVY MINERALS DURING BURIAL DIAGENESIS

ANDREW C. MORTON[a,b] AND CLAIRE HALLSWORTH[c]

[a]*HM Research Associates, 2 Clive Road, Balsall Common, West Midlands CV7 7DW, UK*
[b]*CASP, University of Cambridge, 181a Huntingdon Road, Cambridge CB3 0DH, UK*
[c]*HM Research Associates, West Mostard, Garsdale, Sedbergh, Cumbria LA10 5NT, UK*

ABSTRACT

Detrital heavy-mineral assemblages respond to increasing burial diagenesis by progressive dissolution of unstable components. Case studies from sedimentary basins worldwide show a uniform pattern of relative stability. The order of stability during burial diagenesis is olivine (least stable) < orthopyroxene, clinopyroxene < sodic pyroxene < calcic amphibole, andalusite, sillimanite < epidote < titanite < kyanite < sodic amphibole < staurolite < allanite < garnet, chloritoid < tourmaline, monazite, spinel < rutile, anatase, brookite, zircon, apatite (most stable). Mineral dissolution can be recognised by corrosion textures on grain surfaces and by preservation of unstable minerals in low-porosity zones adjacent to friable sandstones with less diverse assemblages. Increasing pore fluid temperatures, accompanied by changes in pore fluid composition, are responsible for progressive mineral dissolution. There is, therefore, an indirect relationship between mineral diversity and burial depth in sedimentary basins worldwide. However, the depths at which individual minerals disappear vary markedly between basins, largely due to differences in pore fluid temperature gradients. Geological time is another significant factor in mineral depletion.

Interpretation of provenance using heavy-mineral data from sandstones likely to have suffered burial diagenesis must carefully consider the possibility that some heavy-mineral species have been eliminated through dissolution. Evaluation of provenance under such circumstances must rely on parameters that are demonstrably unaffected by diagenesis. A combined approach, integrating provenance-sensitive ratio measurements with varietal data, either petrographic, geochemical or isotopic, is recommended.

Keywords: heavy minerals; diagenesis; stability; corrosion; provenance

Developments in Sedimentology, Vol. 58, 215–245

ISSN: 0070-4571/doi:10.1016/S0070-4571(07)58007-6

1. INTRODUCTION

Heavy-mineral analysis is one of the most widely used techniques in the determination of sandstone provenance. A large number of detrital heavy-mineral species have been identified in sandstones: over 50 translucent detrital minerals were described by Mange and Maurer (1992), many of which have specific and restricted parageneses, thereby providing crucial provenance information that cannot be acquired by any other means.

One of the problems encountered while using heavy-mineral data to interpret provenance is that heavy-mineral assemblages in sandstones do not solely reflect the composition of the parent rocks. This is because the original provenance signal is modified by a number of processes that operate at different stages during the sedimentation cycle (see review by Morton and Hallsworth, 1999, and references therein). Assemblages are modified by weathering at source, prior to sediment entering the transport system; by processes that operate during transport and deposition (hydrodynamic fractionation, mechanical abrasion and weathering during alluvial storage); and post-depositionally by diagenesis during burial. These processes can cause sandstones derived from a single source, possessing a common mineralogical signature at the time of origin, to now contain markedly heterogeneous heavy-mineral assemblages. Similarly, sandstones from different sources, with different suites at the time of origin, may now possess superficially similar assemblages. Therefore, it is crucial that the potential effects of these modifying factors are considered when using heavy-mineral data to characterise and differentiate provenance.

Arguably, the most profound modification of heavy-mineral assemblages takes place in the subsurface, during burial diagenesis. Heavy-mineral suites react to burial diagenesis by dissolution of unstable phases (a process known as intrastratal dissolution) and growth of secondary minerals, as documented in the accompanying chapters by Turner and Morton (2007, this volume) and Milliken (2007, this volume). Burial diagenesis has the potential to dramatically alter heavy-mineral assemblages, causing detrital suites that have high diversity at the time of deposition to become highly restricted at great burial depths. In this chapter, we (1) discuss the features that are diagnostic of dissolution in the subsurface, (2) consider, by means of case studies, the effects of burial diagenesis on heavy-mineral suites and (3) work towards the establishment of a comprehensive stability series for heavy minerals during burial. Finally, we briefly describe the heavy-mineral parameters that can be used to evaluate provenance in sandstones that have undergone extensive diagenetic modification.

2. DIAGNOSTIC CRITERIA FOR HEAVY-MINERAL DISSOLUTION

Mineral dissolution in the subsurface can be recognised in three ways: (1) by the presence of corroded surfaces on mineral grains, (2) by the co-existence of high-diversity and low-diversity assemblages in adjacent high- and low-permeability sandstones, and (3) by a decrease in mineral diversity with increasing burial depth

within the sedimentary basin. The presence of all three lines of evidence may be taken as proof of intrastratal dissolution, but caution is required if some of the evidence is missing. For instance, decreasing diversity with increasing depth might be a provenance effect, and the presence of corrosion textures on mineral grains may be the result of localised weathering processes (for example, in a non-marine depositional setting or below a subaerial unconformity).

2.1. Surface Textures

The most direct indication of heavy-mineral dissolution is the presence of corrosion textures on grain surfaces. Corrosion textures, which were first documented by Edelman and Doeglas (1932, 1934), include etch pits, surface mamillae, facets, ragged edges, hacksaw terminations and skeletal structures (Rahmani, 1973; Hemingway and Tamar-Agha, 1975; Morton, 1979; Milliken, 2007, this volume; Turner and Morton, 2007, this volume; Van Loon and Mange, 2007, this volume; Velbel, 2007, this volume). Differences in mineral composition and crystal structure yield different surface corrosion textures. It is also possible that differences in fluid composition may lead to variations in surface textures. Hubert (1971) urged caution in interpreting all corrosion textures as indicative of ongoing dissolution, arguing that they can be inherited from precursor diagenetically modified sandstones. For example, Palaeozoic sandstones of the Clair Field, west of Shetland (UK), contain etched staurolite and garnet in conjunction with unetched grains of epidote (Allen and Mange-Rajetzky, 1992). Since epidote is less stable than staurolite and garnet, the surface textures of these co-existing minerals indicate that the staurolite and garnet were recycled from pre-existing sandstones. However, such situations are comparatively rare, and we believe that grain surface corrosion should be regarded as indicative of in situ intrastratal dissolution unless it can be argued otherwise.

Corrosion textures similar to those observed on natural grain surfaces have been produced in laboratory experiments. Nickel (1973) used a variety of acids and alkalis to leach heavy minerals, Berner et al. (1980) simulated natural hacksaw terminations on clinopyroxene and amphibole by acid leaching at room temperature, and Hansley (1987) generated faceted surfaces on garnet using warm acids. There has been a debate over the origin of some surface textures, most notably facets on garnet grains, which have been attributed to both corrosion and overgrowth. Morton et al. (1989) and Salvino and Velbel (1989) used thermodynamic considerations, experimental studies, distribution of faceted garnets in the subsurface, textural relationships and compositional variations within faceted grains, to examine this question in detail, and concluded that the overgrowth hypothesis cannot be sustained.

Although the presence of corrosion textures on grain surfaces is strong evidence for the operation of dissolution processes, it has been argued that intrastratal dissolution is a local, rather than a widespread, phenomenon (Van Andel, 1959; Weissbrod and Nachmias, 1986). However, as Turner and Morton (2007, this volume) show, corrosion textures are commonplace in sedimentary basins worldwide. It is therefore becoming evident that heavy-mineral corrosion is a global feature, implying that intrastratal dissolution is likely to have operated in all deep sedimentary basins to some extent.

2.2. Preservation of High-Diversity Assemblages

Direct evidence for mineral dissolution in the subsurface is provided by the occurrence of high-diversity detrital heavy-mineral zones within sandstone successions otherwise typified by low-diversity assemblages. Examples include: higher-diversity assemblages in early calcite concretions compared with enclosing friable sandstones, as first identified by Bramlette (1941); higher-diversity assemblages in mudstones compared with interbedded sandstones (Blatt and Sutherland, 1966); and higher-diversity assemblages in oil-bearing sandstones compared with adjacent water-wet sandstones (Yurkova, 1970). Similar examples have been described in Palaeocene sandstones of the UK continental shelf (Morton, 1984; Morton et al., 2002), with higher-diversity heavy-mineral assemblages occurring in calcite concretions, in analcite-cemented zones, in mudstones, in sandstones with limited pore-fluid connectivity and in oil-bearing intervals, compared with adjacent sandstones with low-diversity assemblages (Fig. 1).

In such cases, it is unreasonable to argue for a difference in provenance between the high-diversity and adjacent low-diversity zones. Therefore, at the time of deposition, there was no significant difference between heavy-mineral assemblages in zones that now show marked differences in diversity. This implies that the high-diversity zones were protected from the corrosive action of pore waters that caused depletion of unstable heavy minerals in the adjacent low-diversity sandstones. Protection has been afforded by (1) poor initial permeability (as in the case of the mudstones), (2) early cementation, destroying initially good permeability and sealing the sandstone from circulating pore waters, (3) poor fluid connectivity, restricting the circulation of pore waters and (4) displacement of pore waters by oil during hydrocarbon emplacement. Identification of adjacent high- and low-diversity heavy-mineral zones is important not only because it proves that intrastratal dissolution has taken place, but also because the preserved assemblages give important provenance information, since they provide a record of the composition of the detrital assemblage prior to dissolution.

2.3. Relationships Between Burial Depth and Diversity

Patterns of decreasing mineral diversity with increasing burial depth are common in sedimentary basins worldwide. The most likely cause of such patterns is intrastratal dissolution during burial diagenesis. However, such patterns could also arise through an evolution in provenance, and this possibility should always be eliminated before diagnosing burial-related diagenesis as the cause. Evaluation of potential provenance variations can be achieved using parameters that are insensitive to diagenetic processes, as discussed by Morton and Hallsworth (1994, 1999) and summarised later in this contribution. The case studies described below come from sandstones known to have a common provenance, so that depth/diversity relationships can be confidently ascribed to intrastratal dissolution.

2.3.1. Palaeocene-Eocene, North Sea.

Palaeocene-Eocene sandstones of the Dornoch and Forties Formations in the central North Sea provide a well-constrained study of the effects of burial diagenesis on

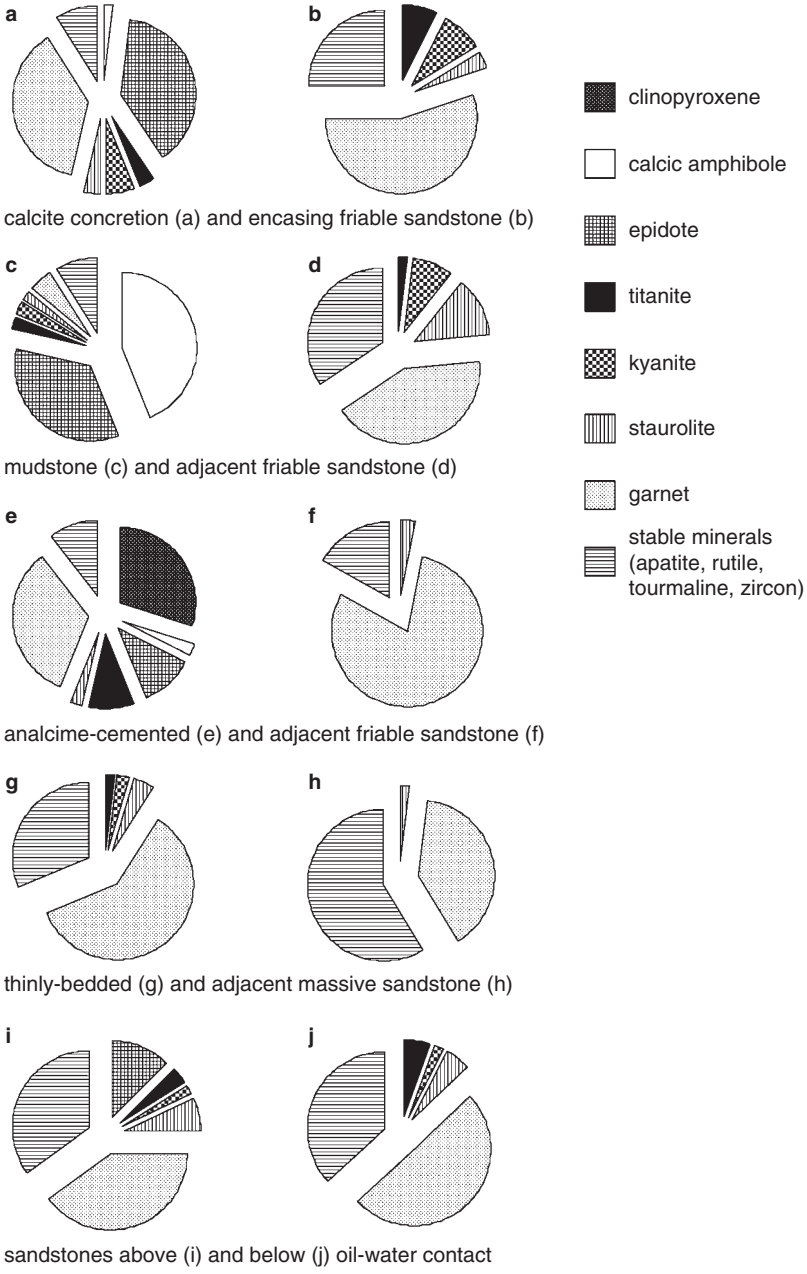

Fig. 1. Examples of preservation of heavy minerals from North Sea Palaeocene-Eocene successions. (a) Well 2/10-4, 1652 m; (b) Well 2/10-4, 1645 m; (c) Well 9/13-1, 1459 m; (d) Well 9/13-1, 1460 m; (e) Well 15/26-2, 1914 m; (f) Well 15/26-2, 1978 m; (g) Well 21/30-1, 2003 m; (h) Well 21/30-2, 1996 m; (i) Well 16/26-6, 1936 m; (j) Well 16/26-6, 1973 m.

heavy-mineral assemblages (Morton, 1984). The Dornoch Formation represents a prograding coastal-deltaic complex, shown, on the basis of seismic data, to be derived from a source area in the Scottish landmass to the northwest (Rochow, 1981; Bowman, 1998). The Forties sandstones were deposited in a submarine fan complex at the foot of a delta slope, basinward of the area where the Dornoch sandstones were deposited. The top of the succession is less than 200 m below seabed at the basin margin, but is nearly 3 km at the basin centre, and the thermal history is one of continued subsidence throughout the Tertiary. The Palaeocene-Eocene of the central North Sea thus forms an ideal case study of the effects of increased pore-fluid temperature on heavy-mineral suites.

Within this succession, suites become steadily less diverse as burial increases due to elimination of heavy-mineral species through dissolution (Fig. 2). Calcic amphibole is the first to disappear, at around 600 m below seabed. This is followed successively by epidote (~1100 m), titanite (~1400 m), kyanite (~1800 m) and staurolite (~2400 m). Each phase becomes more corroded as burial depth increases (Fig. 2). Although garnet declines markedly in abundance relative to the stable mineral zircon, in conjunction with increasing severity of surface corrosion textures, it does not disappear entirely. However, in the underlying Jurassic of the central North Sea, garnet is rarely present at burial depths in excess of 3500 m (Fig. 3). Other minerals present in the North Sea Palaeocene-Eocene (anatase, apatite, chrome spinel, monazite, rutile, tourmaline and zircon) rarely display signs of etching, and are apparently stable (Morton, 1979).

2.3.2. Palaeocene, Faeroe-Shetland Basin.

Palaeocene sandstones in the Foinaven Sub-basin (Faeroe-Shetland Basin) cover a wide range in burial depth, from approximately 1300 to 2400 m below seabed. Provenance variations within these sandstones are relatively muted, with all sandstones having a similar range of minerals in the shallow subsurface. However, there is evidence for differences in relative contributions from metamorphic basement and Palaeozoic-Mesozoic sediment, and also in the degree of weathering prior to sediment entering the transport system (Morton et al., 2002).

Burial depth/abundance plots for a number of minerals in Palaeocene sandstones from the Foinaven Sub-basin are shown in Fig. 4. Amphibole is the first mineral to disappear, being absent from virtually all samples over 1500 m below seabed. Epidote disappears at ~1620 m, titanite at ~1700 m and kyanite at ~1760 m. Staurolite and garnet are present throughout. Relative abundances of garnet become greater with increased burial between ~1400 and 1800 m burial, compensating for the disappearance of amphibole, epidote and titanite. Some samples below 2200 m have relatively low garnet abundances, but this is considered to be a provenance effect related to deep weathering of the Cretaceous land surface (Morton et al., 2002), rather than depletion during burial diagenesis. Other minerals in the Palaeocene of the Foinaven Sub-basin (apatite, chrome spinel, monazite, rutile, tourmaline and zircon) show no evidence for depletion with increasing burial depth, and are considered stable.

2.3.3. Plio-Pleistocene, US Gulf Coast.

Milliken (1988, 2007, this volume) examined dissolution of heavy minerals in the Plio-Pleistocene of the US Gulf Coast, using a combination of thin section

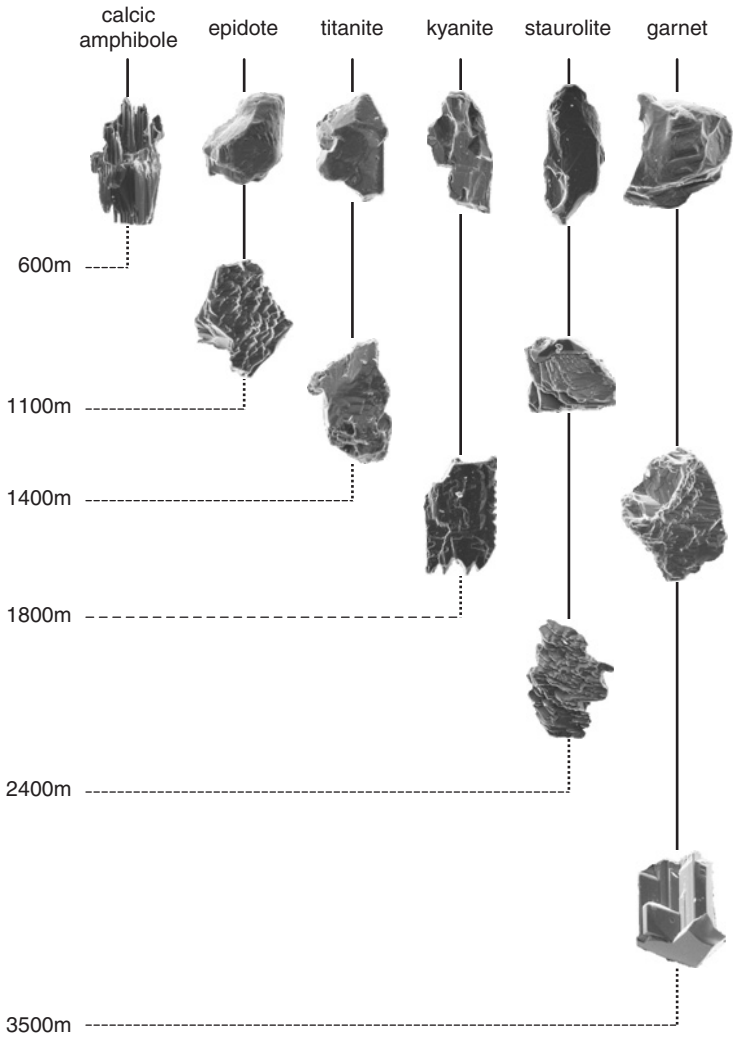

Fig. 2. Burial depth distribution of heavy minerals in Palaeocene-Eocene sandstones of the central North Sea, showing the decrease in mineral diversity with increasing burial caused by dissolution of unstable minerals (adapted from Morton, 1984, and Morton and Hallsworth, 1999).

petrography coupled with SEM examination to identify grain surface corrosion. These sediments were all transported by the Mississippi River system, and—because of extremely high sedimentation rates—are buried between ~450 m and 5 km. In these sandstones, pyroxene is least stable, followed by amphibole, kyanite, epidote, titanite and garnet. Oligocene sediments in the US Gulf Coast show a similar pattern (Milliken and Mack, 1990; Milliken, 2007, this volume). Stable heavy-mineral phases in the US Gulf Coast are considered to be apatite, chrome spinel, TiO_2 minerals, monazite, tourmaline and zircon. The pattern of mineral depletion in the US Gulf Coast is similar to that seen in the North Sea and Faeroe-Shetland Basins, except for

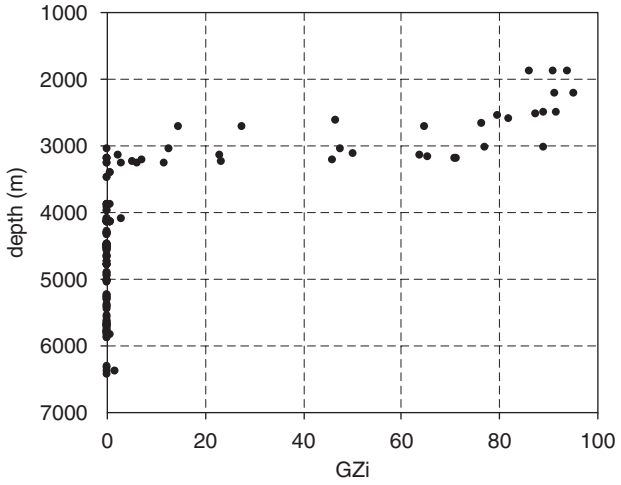

Fig. 3. Relationship between GZi and depth in Late Jurassic sandstones of the central North Sea, showing that complete garnet dissolution is commonplace in sandstones buried in excess of 3.5 km. GZi = % garnet in total garnet plus zircon (see Morton and Hallsworth, 1994, for definition).

kyanite, which disappears at shallower depths than epidote and titanite. However, the burial depths at which the heavy minerals disappear in the Gulf Coast succession are considerably greater than in the offshore UK area. For example, titanite persists to 3–4 km in the Plio-Pleistocene of the Gulf Coast, compared with just over 1 km in the North Sea.

2.3.4. Pliocene, Kura Basin, Azerbaijan.

Pliocene sediments from the Kura Basin of Azerbaijan were sourced from Mesozoic metamorphic, ophiolitic and volcanic rocks of the Lesser Caucasus and transported by the paleo-Kura River (Morton et al., 2003). Provenance-sensitive ratio and garnet geochemical data from paleo-Kura sandstones are closely comparable to those of the modern Kura, indicating little difference in source area characteristics between the Pliocene and the present day. Despite the uniform provenance, there are marked variations in the relative abundance of amphibole, epidote and clinopyroxene within the group of samples sourced from the Lesser Caucasus. Amphibole contents range from 3 to 40%, clinopyroxene from 0 to 70%, and epidote from 1 to 75%. A ternary plot of the relative abundances of the three minerals (Fig. 5) shows that the modern Kura River and Pliocene sandstones from the Aktapa Bridge outcrop have the highest clinopyroxene abundances. By contrast, sandstones from depths in excess of 4000 m from the Kursanga and Karabagli oilfields are epidote dominated, with scarce amphibole and clinopyroxene. Sandstones from relatively shallow burial depths (<3500 m) in the Kursanga and Karabagli oilfields, together with outcrop material from the Babazanan site, show a trend away from the clinopyroxene pole.

Sandstones from intermediate burial depths in Kursanga and Karabagli (3500–4000 m) show a second trend towards the epidote pole. Morton et al. (2003) explained this pattern as the result of progressive mineral dissolution, initially of

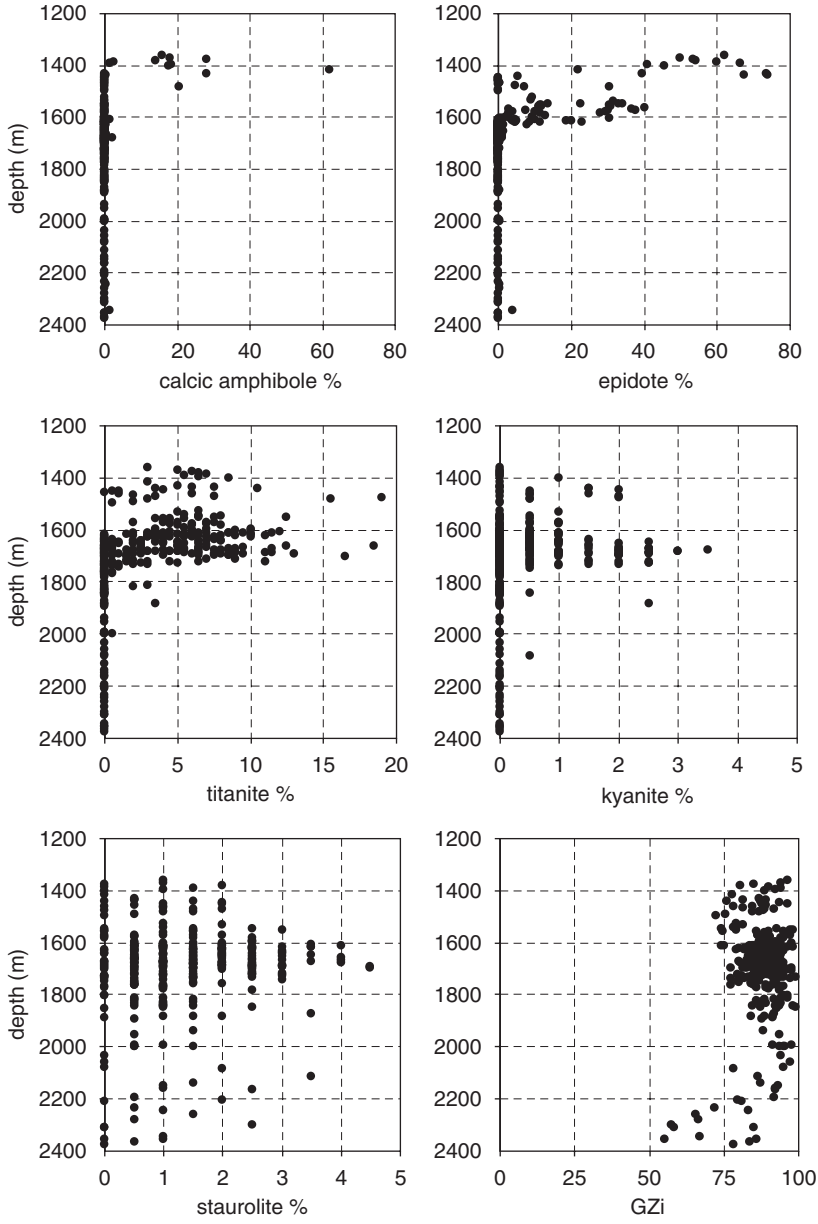

Fig. 4. Distribution of heavy minerals in subsurface Palaeocene sandstones of the Foinaven Sub-basin, Faeroe-Shetland Basin (adapted from Morton et al., 2002).

clinopyroxene and then of amphibole. The dissolution concept is supported by the presence of etched surfaces on clinopyroxene and amphibole grains, which diagnose ongoing corrosion in the subsurface (Turner and Morton, 2007, this volume). Other minerals in the sandstones (apatite, chrome spinel, garnet, rutile, titanite, tourmaline and zircon) show no evidence of corrosion, and are present at all burial depths.

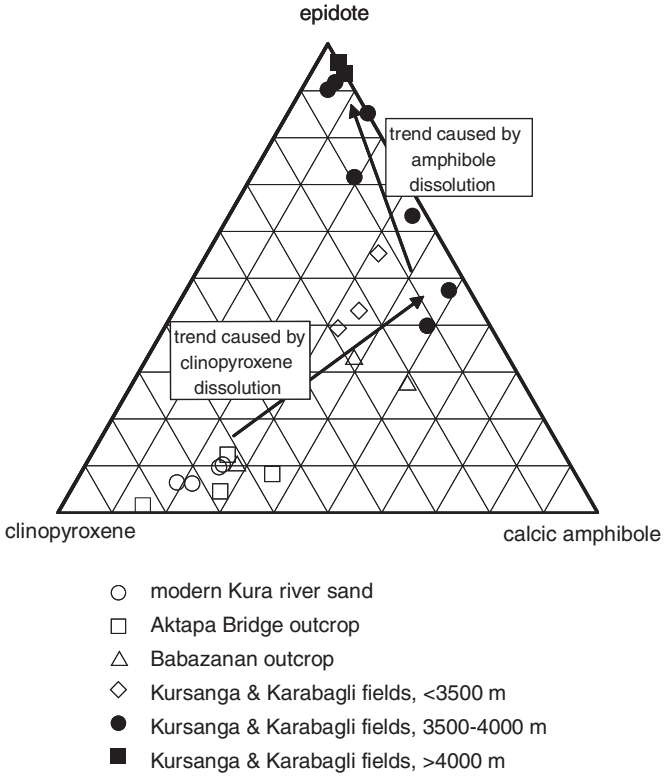

Fig. 5. Relative abundance of amphibole, clinopyroxene and epidote contents in sandstones deposited by the Kura River, Azerbaijan, and its late Miocene-Pliocene precursor, showing the modification to mineral assemblages caused by burial diagenesis (adapted from Morton et al., 2003).

These phases therefore appear to be stable in the Kura Basin over the investigated depth range.

2.3.5. Miocene, Bengal Basin.

Miocene sandstones of the Bengal Basin, Bangladesh, were deposited by a paleo-Brahmaputra river system that drained the nascent Himalayan mountain belt during uplift (Uddin and Lundberg, 1998a, 1999). Variations in provenance characteristics within the Miocene succession are comparatively limited, with an orogenic source identified throughout, although continued unroofing led to the exposure of granitic rocks in the Late Miocene and Pliocene (Uddin and Lundberg, 1998b).

Heavy-mineral assemblages in a 3000 m thick Miocene sandstone succession in the Bengal Basin show a marked decline in mineral diversity with depth. Calcic amphibole disappears at approximately 2 km depth, epidote (excepting the rare-earth epidote mineral allanite) at about 3 km depth, and kyanite and titanite at some 3.3 km depth (Fig. 6). Increasingly intense surface corrosion features accompany the downhole decrease in abundance of these minerals. Staurolite also shows a decline in abundance, and displays surface corrosion textures (Turner and Morton, 2007, this

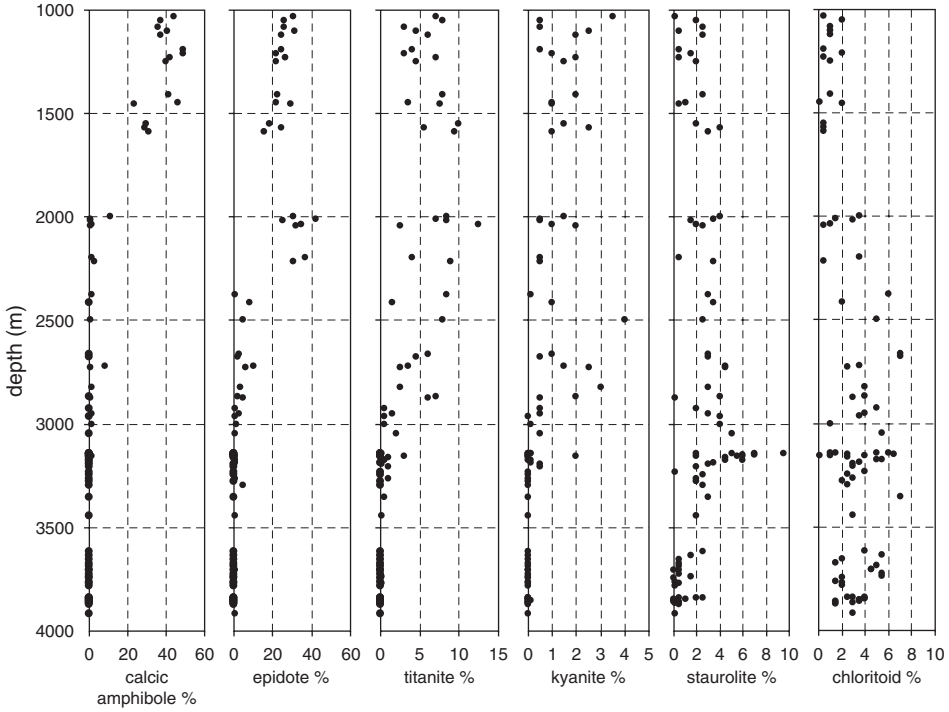

Fig. 6. Relationship between abundance of selected minerals and burial depth in Miocene sandstones of the Bengal Basin.

volume), but does not disappear entirely from the assemblages. The relationship between the decline in mineral abundance and increased surface corrosion texture indicates that the decreasing diversity is the result of intrastratal dissolution, rather than provenance. Other minerals (allanite, apatite, chloritoid, chrome spinel, garnet, monazite, rutile, tourmaline and zircon) do not decline in abundance with increasing depth, lack well-developed surface corrosion textures, and are considered stable in the analysed sandstones.

2.3.6. Eastern India.

Miocene sandstones derived from the Eastern Ghats of India have diverse heavy-mineral assemblages, including andalusite, anatase, apatite, calcic amphibole, chrome spinel, chloritoid, epidote, garnet, kyanite, monazite, rutile, sillimanite, staurolite, titanite, tourmaline, zinc spinel and zircon. Nevertheless, there is a well-defined pattern of decreasing calcic amphibole and sillimanite abundances with depth (Fig. 7), in both cases accompanied by an increase in severity of surface corrosion textures (Turner and Morton, 2007, this volume). None of the other heavy minerals show depletion with increasing depth, but this is because data are available only over a comparatively limited burial depth range (~1100–1600 m), precluding a comprehensive assessment of the diversity/depth relationship in this case study.

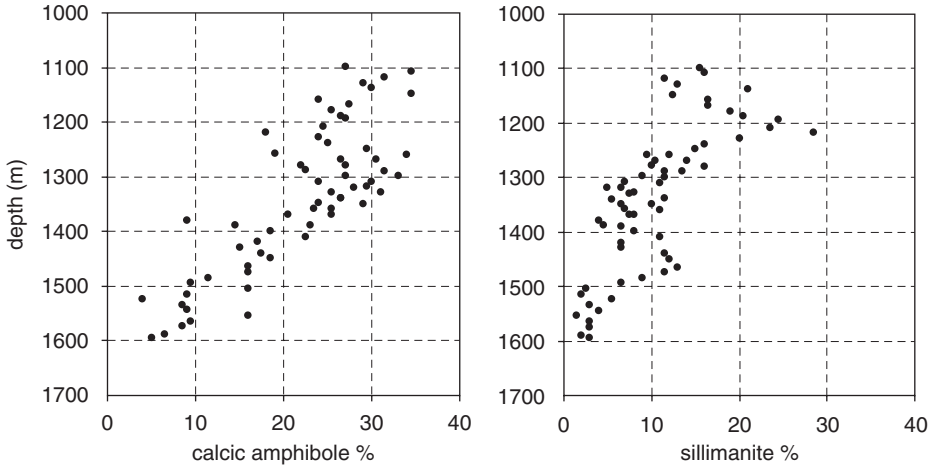

Fig. 7. Abundance of calcic amphibole and sillimanite with respect to burial depth in Miocene sandstones from eastern India, showing that the two minerals have very similar rates of depletion.

2.3.7. Eocene-Oligocene, New Zealand.

Heavy-mineral dissolution patterns in the Eocene-Oligocene McKee sandstones of New Zealand were discussed by Smale and Morton (1987) and Smale (2007, this volume). The McKee sandstones had a uniform provenance, comprising basement schists and granites, and have been subjected to burial depths in the range 2100–4100 m. However, the maximum burial depth is not known in all cases, since some of the area has been subject to uplift. All the suites in the McKee sandstones contain a relatively limited number of detrital heavy minerals, but they show a clear decrease in diversity with depth, staurolite disappearing at ~3100 m and garnet at ~3600 m. Both species show evidence of surface corrosion prior to their ultimate disappearance. Zircon, rutile, tourmaline, apatite, chloritoid and spinel are apparently stable.

2.3.8. Neogene, Yugoslavia.

Miocene and Pliocene sandstones of the Sava River Basin (Yugoslavia) show a decline in heavy-mineral diversity with depth (Scavnicar, 1979), interpreted as resulting from intrastratal dissolution. Kyanite disappears first, followed by epidote group minerals, titanite and finally staurolite. Garnet, chloritoid, rutile, tourmaline, zircon and apatite are present throughout. Apart from the disappearance of kyanite at comparatively shallow depths, the pattern of mineral disappearance matches those described elsewhere. The possibility that provenance variations may have been a factor in controlling some of the changes in mineralogy, notably the shallow disappearance of kyanite, cannot be entirely eliminated in this case study.

2.3.9. Contessa Megabed, Italy.

Cavazza and Gandolfi (1992) demonstrated that a sandstone unit with an essentially uniform provenance (the Contessa megabed in the northern Apennines of Italy)

shows mineralogical variations related to burial depth. Of the heavy minerals, zircon, monazite, rutile, spinel, garnet and chloritoid are ubiquitous over the area, and are considered to be stable under the conditions experienced by the megabed, but staurolite and titanite show variable distribution attributed to dissolution during burial. This study is particularly significant because it demonstrates that other mineralogical parameters also vary because of burial depth, notably the abundance of smectite and interstratified illite/smectite and the abundance of intrabasinal carbonate clasts.

3. RELATIVE MINERAL STABILITY

In addition to the case studies described above, there are a number of other areas where burial-related dissolution is interpreted to have taken place. These include the Northern Apennines of Italy (Gazzi, 1965), the Vienna Basin in Austria (Wieseneder and Maurer, 1958), the Cleveland Basin of Yorkshire, UK (Smithson, 1941), the Cretaceous-Tertiary of Alberta, Canada (Rahmani, 1973) and the North Sumatra Basin of Indonesia (Morton et al., 1994). There is, therefore, overwhelming evidence to show that there is a consistent pattern of declining mineral diversity with increasing burial depth in sedimentary basins worldwide.

The case studies described above have not established diversity/depth relationships for all detrital heavy minerals. This is partly due to the relative scarcity of some heavy-mineral species, such as corundum, lawsonite, pumpellyite and topaz, which precludes acquisition of meaningful abundance data across the range of burial depths in any individual sedimentary basin. Certain other minerals, such as andalusite or olivine, are relatively common in sediments derived from specific lithologies, but diversity/depth data are not presently available from sediments derived from such sources. The relative stability of such minerals can be judged only by the extent to which corrosion textures develop on their grain surfaces compared with minerals that have known stability relationships. The present status of knowledge on relative mineral stability is summarised below.

3.1. Olivine

Olivine is an exceptionally scarce detrital phase in sandstones, despite its abundance in certain source rocks (for example, basic and ultrabasic igneous rocks). The reason for its scarcity is almost certainly its instability. Olivines in a sand sample from the seabed on the west coast of Scotland show well-developed corrosion textures on their grain surfaces (Turner and Morton, 2007, this volume), indicating ongoing dissolution at ambient temperatures without any burial. Clinopyroxenes in the same sample show no evidence for dissolution, indicating that olivine is less stable than clinopyroxene. This supports previously published relative stability patterns, such as those of Pettijohn (1941, 1975) and Morton (1984), which also show olivine to be the least stable of all detrital heavy minerals.

3.2. Pyroxene

Clinopyroxene is known to be highly unstable in sandstones, being more stable only than olivine (Pettijohn, 1941, 1975; Morton, 1984). The instability of clinopyroxene is further verified by the Kura Basin data described above, where it becomes depleted more rapidly than calcic amphibole and epidote during burial, and by the advanced development of grain surface corrosion textures in the shallow subsurface (Turner and Morton, 2007, this volume). The relative stability of other pyroxenes is less well known, due to their general scarcity in sediments. Orthopyroxene is generally held to be as unstable as clinopyroxene (Pettijohn, 1941, 1975; Morton, 1984). Aegirine, by contrast, appears to be more stable than clinopyroxene, given that highly etched clinopyroxene co-exists with unetched or slightly etched aegirine in the same sample from the shallow subsurface in the Rockall Trough (Turner and Morton, 2007, this volume). The same sample also contains highly etched aenigmatite, a pyroxenoid mineral, indicating that aenigmatite and clinopyroxene have similar stabilities. At present, there is no information on the stability of other pyroxene or pyroxenoid minerals, such as jadeite or wollastonite, which are virtually unrecorded as detrital phases.

3.3. Amphibole

Calcic amphibole is highly unstable in the subsurface, being more stable only than olivine and pyroxene. Its instability is verified by its relatively early disappearance from heavy-mineral assemblages during burial in the central North Sea Basin, Faeroe-Shetland Basin, Bengal Basin, Kura Basin and US Gulf Coast, and by the widespread occurrence of well-developed grain surface corrosion textures in amphibole-bearing sandstones (Rahmani, 1973; Morton, 1979; Milliken, 2007, this volume; Turner and Morton, 2007, this volume). Calcic amphiboles have a wide range of compositions (Deer et al., 1997a), and it is likely that different varieties have different stabilities; however, to date there has been no systematic study on the relative stability of the calcic amphibole group.

There is much less information on the stability of the other amphibole group minerals. The iron-magnesium amphiboles (such as grunerite and cummingtonite) and the sodic-calcic amphiboles (such as kataphorite) are scarce as detrital phases. Sodic amphiboles (such as glaucophane and riebeckite) are more common, but despite their wider distribution their relative stability remains poorly known. The little available data suggest that they are considerably more stable than calcic amphiboles. In Miocene sandstones of the Mahakam delta area, offshore Borneo, highly etched sodic amphibole (glaucophane) co-exists with etched staurolite and slightly etched garnet (Turner and Morton, 2007, this volume); kyanite and titanite are scarce or absent. In this basin, therefore, sodic amphibole appears to be more stable than kyanite and titanite, and marginally less stable than staurolite.

3.4. Epidote

Case studies from the central North Sea Basin, Faeroe-Shetland Basin, Bengal Basin, Sava River Basin and US Gulf Coast demonstrate that epidote group minerals are

unstable during burial, although they are more stable than pyroxene and calcic amphibole. The instability of epidote is further demonstrated by increasingly intense surface corrosion textures with increasing burial depth (Morton, 1984; Turner and Morton, 2007, this volume). Epidote group minerals show a range of compositions (Deer et al., 1997b; Spiegel et al., 2002), with variations in both major elements (notably Ca, Fe, Mg, Mn and rare-earth elements) and trace elements. There is, however, little information on the effects of varying composition on epidote stability. The only piece of available evidence is from the rare-earth epidote mineral allanite, which appears to be significantly more stable than other epidote minerals. This is shown by the persistence of allanite to greater depths than the other epidote group minerals in the Bengal Basin, and by the minor development of corrosion textures on allanite grains in association with etched staurolite (Turner and Morton, 2007, this volume). Therefore, allanite appears to be more stable not only than the other epidote group minerals, but also than titanite, kyanite and staurolite.

3.5. Titanite

The relatively stability of titanite can be judged on the basis of several case studies, including the central North Sea Basin, Faeroe-Shetland Basin, Bengal Basin, Sava River Basin, US Gulf Coast and Contessa megabed. In most of these examples, titanite appears to be less stable than kyanite, staurolite and garnet, but more stable than epidote. However, in the Bengal Basin, titanite and kyanite disappear at similar depths, and in the US Gulf Coast and the Sava River Basin, kyanite depletion appears to take place before that of titanite. The reason for this inconsistency is unclear. It may be partly a provenance effect, rather than a diagenetic effect. However, it could also be due to differences in titanite composition, since the mineral shows compositional ranges in a number of elements, including Al, Fe and rare earths (Deer et al., 1997c).

3.6. Al_2SiO_5 Minerals (Kyanite, Sillimanite, Andalusite)

The three Al_2SiO_5 polymorphs (kyanite, sillimanite and andalusite) have markedly different stabilities during burial. Kyanite is the most common of the three minerals in detrital heavy-mineral assemblages, and therefore its relative stability is comparatively well known. The instability of kyanite in the subsurface is demonstrated by the widespread development of intense surface corrosion textures (Morton, 1984; Turner and Morton, 2007, this volume). In most case studies, kyanite depletion occurs after that of titanite and before that of staurolite. However, in the Faeroe-Shetland Basin, kyanite depletion appears to occur at depths similar to that in the case of titanite, and in the US Gulf Coast and the Sava River Basin, kyanite apparently disappears before titanite.

The only well-constrained data set on sillimanite stability is from eastern India, where sillimanite depletion occurs at a rate similar to that of calcic amphibole (Fig. 7). Grain surface corrosion textures are well developed on both minerals (Turner and Morton, 2007, this volume), indicating that the depletion trend is due to burial diagenesis. It therefore appears that sillimanite has a stability similar to that of calcic amphibole.

The only available evidence for the relative stability of andalusite is from surface textural information, because andalusite is comparatively rare in heavy-mineral suites from sandstones in the subsurface. Where present, andalusite is generally corroded (Turner and Morton, 2007, this volume) and therefore appears to be highly unstable, confirming conclusions reached by previous workers (Pettijohn, 1941, 1975; Morton, 1984).

3.7. Staurolite

Staurolite shows burial-related diagenetic depletion in many of the cases studies described above. In all cases, staurolite survives to greater depths than kyanite, titanite, epidote, calcic amphibole and pyroxene, and is therefore considered more stable than these species. However, it is less stable than garnet. Staurolite shows limited geochemical variation, mainly expressed in terms of Fe, Mg, Mn and Zn contents (Deer et al., 1997c); there is no information available on the effects of staurolite composition on its stability. The instability of staurolite in the subsurface is further demonstrated by the widespread development of spectacular grain surface corrosion textures (Morton, 1984; Turner and Morton, 2007, this volume).

3.8. Garnet

Garnet dissolution has been recognised in many deep basins, including the central North Sea (Morton, 1984), offshore New Zealand (Smale and Morton, 1987), the Cleveland Basin of Yorkshire (Smithson, 1941) and the Vøring Basin, offshore Norway (Morton et al., 2005a, b). In all cases, garnet survives at depths greater than those shown by staurolite, and is therefore considered more stable.

Compared with other heavy minerals, a comparatively large amount of data on detrital garnet compositions is available because garnet geochemistry is a highly sensitive guide to the discrimination and identification of provenance (Morton et al., 2004). The garnet compositional dataset can be used to examine the relationships between garnet composition and stability. Cretaceous-Palaeocene sandstones in the Vøring Basin, offshore Norway, can be categorised into a number of sandstone types based on heavy-mineral criteria (provenance-sensitive ratios, mineral chemistry and detrital zircon age data), each representing input from a different source region (Morton et al., 2005a, b). The effects of increasing burial diagenesis on garnet compositions in two of the sand types, MN1 (derived from northern mid-Norway) and MN2a (derived from northern East Greenland), are evaluated in Fig. 8. In both sandstone types, there is a clear relationship between Ca content and burial depth, with a marked decrease in Ca content of garnet with increasing burial. In compensation, there is a distinct increase in Fe content, with little perceptible effect on Mg or Mn. The data from the Vøring Basin are therefore entirely consistent with data from Palaeocene-Eocene sandstones of the central North Sea (Morton, 1987), Late Cretaceous sandstones of offshore Taranaki, New Zealand (Smale and Van der Lingen, 1989) and Oligocene sandstones of the US Gulf Coast (Milliken and Mack, 1990), which also suggested that Ca contents control garnet stability. Since Ca-rich garnets are less stable than Ca-poor garnets, increasing burial causes detrital garnet

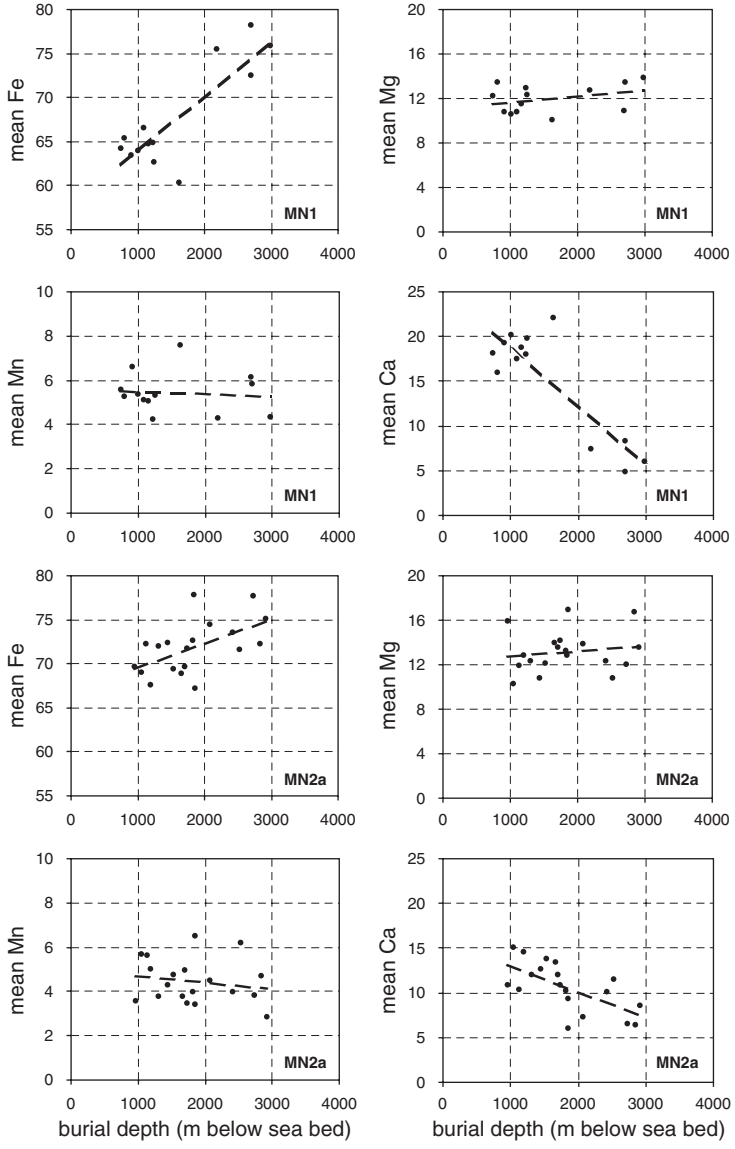

Fig. 8. Effects of burial depth on garnet compositions in Cretaceous-Palaeocene sandstones of the Vøring Basin, offshore Norway. Two examples are shown, relating to two different sand types (MN1 and MN2a, as defined by Morton et al., 2005a, b).

populations to decrease in diversity and become dominated by low-Ca types, prior to complete garnet dissolution.

Garnet also undergoes dissolution by acidic groundwater during weathering, and this process should always be considered as a possible cause of low garnet abundances, especially if low-garnet zones are found in association with high-garnet zones. For example, garnet depletion in specific zones within the

Rhaetian-Hettangian Statfjord Formation of the northern North Sea has been attributed to phases of intense surface weathering (Morton and Berge, 1995; Morton et al., 1996). Since garnet is more stable than apatite under weathering conditions (Morton, 1984), garnet depletion through weathering is likely to have taken place only if apatite depletion has also occurred.

3.9. Chloritoid

Chloritoid is a relatively stable heavy mineral, but is nevertheless susceptible to dissolution in very deeply buried sandstones, where it shows surface corrosion textures (Morton and Hallsworth, 1999; Turner and Morton, 2007, this volume). The data from the Bengal Basin (Fig. 6) show that chloritoid is more stable than staurolite, but provide no evidence for the relative stability of garnet and chloritoid. In Cretaceous sandstones in the Vøring Basin (offshore Norway), chloritoid depletion apparently occurs at similar depths to garnet, indicating that chloritoid has stability similar to that of Ca-poor garnet. Chloritoid shows variations in composition, mainly expressed by Fe, Mg and Mn but there is no information on the effects of compositional variations on chloritoid stability.

3.10. Tourmaline

Tourmaline is regarded as one of the most stable detrital minerals in sandstones (Hubert, 1962; Pettijohn, 1975). This is borne out by the various case studies described above, in which tourmaline contents show no relationship with burial depth. However, there is some evidence to suggest that tourmaline is unstable under some circumstances. Morton and Hallsworth (1999) figured an etched tourmaline from Jurassic sandstones in the Outer Moray Firth, North Sea, and suggested that one possible explanation is that tourmaline may be unstable in reservoirs where the hydrocarbons contain high H_2S contents. Since this first record of etched tourmaline, further instances have been noted, including Jurassic sandstones from the Norwegian Sea (Turner and Morton, 2007, this volume), and Palaeocene sandstones of the Faeroe-Shetland Basin. In all cases where tourmaline etching has been noted, burial depths are very high, close to or in excess of 4 km, and it therefore appears that tourmaline does become unstable in very deeply buried sandstones. However, tourmaline etching does not appear to be ubiquitous at great depth, and it may be that tourmaline dissolution requires the combination of depth and unusual fluid compositions, one possibility being high H_2S contents. Tourmaline etching has also been observed in silver sands (The Netherlands, Belgium and Germany), which have been subjected to extreme weathering (Van Loon and Mange, 2007, this volume).

Authigenic tourmaline has been observed to occur in evaporites, ironstones and carbonates (e.g., Henry et al., 1993, 1999). Although secondary tourmaline has been identified in sandstones (e.g., Stow, 1932), it is relatively uncommon, and does not appear to be specifically related to burial diagenesis. As with tourmaline dissolution, tourmaline growth probably requires special geochemical conditions to proceed.

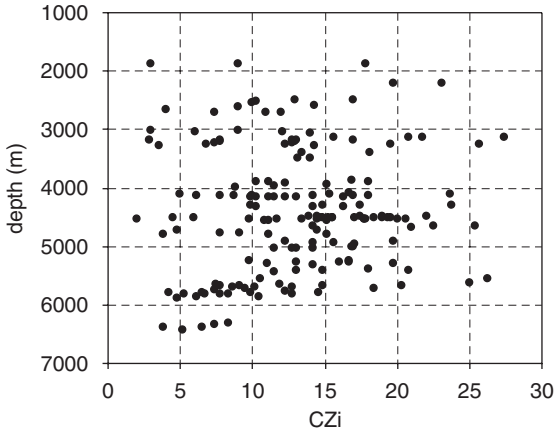

Fig. 9. Plot of chrome-spinel/zircon ratio (CZi) and burial depth in Late Jurassic sandstones of the central North Sea, showing that there is no evidence for loss of chrome spinel even at burial depths in excess of 6000 m.

3.11. Spinel

A wide range of natural spinel compositions are known, but comparatively few are commonly found as detrital heavy minerals. The most common translucent detrital spinels belong to the chromite series (chromite and magnesiochromite), collectively termed chrome spinel. Detrital chrome spinels are sufficiently common to enable an assessment of its stability during burial diagenesis. In the Upper Jurassic of the central North Sea, which is variably buried to depths from approximately 2000 m to in excess of 6000 m (Fig. 9), there is no evidence for a relationship between depth and the chrome–spinel/zircon index (CZi). In the same sandstones, complete garnet depletion occurs at ~3500 m (Fig. 3). In the most deeply buried North Sea Late Jurassic sandstones, there is some evidence for incipient grain surface corrosion (Turner and Morton, 2007, this volume), but this is of limited extent, and chrome spinel is therefore considered to be an exceptionally stable detrital phase.

The only other translucent spinel commonly found in sandstones is the zinc spinel, gahnite. However, it is much less common than chrome spinel, rarely forming more than 0.5% of heavy-mineral residues. It is therefore difficult to reliably ascertain depth/abundance relationships, and surface textural evidence provides the only basis for determining its stability. As Turner and Morton (2007, this volume) show, gahnite shows no evidence of corrosion textures as a result of burial diagenesis, and the phase is, therefore, considered stable.

3.12. Monazite

Monazite is also considered to be a stable phase during burial diagenesis, with no evidence for depletion with increasing depth in the case studies described above. Its stability is supported by surface texture data, with little or no evidence for corrosion at depth. Monazites in deeply buried (> 4400 m) Triassic sandstones from the central

North Sea are unetched (Morton and Hallsworth, 1999). Most monazites in Jurassic sandstones from the Norwegian Sea, buried to depths in excess of 5100 m are unetched, although minor incipient etch pitting was observed on a small number of grains (Turner and Morton, 2007, this volume). Monazite is therefore considered to be stable during burial. However, monazite frequently shows mechanically induced pitting owing to its relatively low hardness. Mechanical pitting, which is unoriented, is readily distinguished from etch pitting, which is crystallographically controlled (see Turner and Morton, 2007, this volume).

3.13. Rutile, Anatase and Brookite

Rutile is considered to be amongst the most stable detrital minerals in sandstones (Hubert, 1962; Pettijohn, 1975). In all the case studies described above, there is no evidence for depletion of rutile with increasing burial depth. Furthermore, there is no surface textural evidence to suggest that rutile grains become corroded in the subsurface (Morton, 1979; Turner and Morton, 2007, this volume). Detrital anatase and brookite are less common components of heavy-mineral assemblages, and consequently data on the relationship between abundance and burial depth are lacking. However, both minerals are common as authigenic phases, implying that they are stable under burial diagenetic conditions.

3.14. Zircon

Zircon is another member of the group of minerals considered to be stable in sandstones (Hubert, 1962; Pettijohn, 1975). It shows no evidence for depletion with increasing burial, and grains lack surface corrosion textures even under advanced diagenetic conditions (Morton, 1979; Turner and Morton, 2007, this volume). Therefore, although dissolution of zircon has been observed in isolated cases of specific weathering environments (Carroll, 1953; Oliva et al., 1999), zircon is considered to be an exceptionally stable phase during burial.

Metamict zircons (those that have suffered radiation damage to their crystal lattice) are known to be more soluble in weathering environments than crystalline zircons (Balan et al., 2001). It is reasonable to assume that they are also more susceptible to dissolution by high-temperature pore fluids during burial diagenesis, although direct evidence from the subsurface is presently lacking.

3.15. Xenotime

Since xenotime is generally scarce in detrital heavy-mineral assemblages, direct evidence for its stability during burial is scarce. However, sandstones that have been subjected to advanced burial diagenesis commonly contain zircons with xenotime 'outgrowths', described initially by Butterfield (1936) and Smithson (1937), and illustrated by Turner and Morton (2007, this volume). Development of xenotime outgrowths on zircon marks an advanced stage of burial diagenesis, since it generally occurs in sandstones that have undergone garnet depletion, an observation made originally by Smithson (1937). Xenotime is therefore considered to be stable during burial diagenesis. As discussed by Vallini et al. (2005), overgrowths on xenotime

offer possibilities for U-Pb radiometric dating of diagenetic events by the sensitive high-resolution ion microprobe (SHRIMP).

3.16. Apatite

In the 'order of persistence of heavy minerals' formulated by Pettijohn (1941), apatite appears to be less stable than zircon, rutile, tourmaline and garnet. However, apatite shows no evidence for dissolution during deep burial, either in the case studies discussed above or in the North Sea Jurassic as described by Morton (1986). Indeed, apatite grains commonly develop overgrowths during advanced stages of burial diagenesis (Morton and Hallsworth, 1999; Turner and Morton, 2007, this volume). Apatite is therefore considered to be exceptionally stable under burial diagenetic conditions. The extent to which apatite develops overgrowths in the subsurface presumably depends on the availability of phosphate, and is therefore more likely to take place in marine sediments rich in biogenic phosphate. Secondary apatite growth is believed to have important implications for the validity of whole-rock Sm-Nd model ages in sediments (Ehrenberg and Nadeau, 2002), and the widespread occurrence of apatite overgrowths therefore indicates that caution is required during interpretation of Sm-Nd isotopic data in diagenetically modified sandstones.

Nevertheless, apatite grains frequently show evidence of corrosion, indicating that they have been partially dissolved. An example of etched apatite is shown by Turner and Morton (2007, this volume). This etched apatite co-exists with pristine apatite grains that show no sign of corrosion, evidently indicating that the etching did not take place in situ. Apatite is known to be unstable under surficial weathering conditions, especially in humid environments (Morton, 1986), and the presence of etched apatite grains in subsurface sandstones therefore indicates that the sediment has undergone a phase of weathering under subaerial conditions. Apatite is less stable than garnet in surficial weathering environments, explaining why it appears below garnet in the 'order of persistence of heavy minerals' (Pettijohn, 1941), despite being more stable during burial diagenesis.

4. FACTORS INFLUENCING HEAVY-MINERAL DISSOLUTION IN THE SUBSURFACE

The order of stability of detrital heavy minerals gleaned from case studies and surface textural data is shown in Table 1. Several unknowns still remain, the main ones being the stability of generally scarce minerals such as cassiterite, corundum, pumpellyite and topaz, and variations in stability within complex mineral groups such as the amphiboles. However, it is unlikely that major alterations to the pattern shown in Table 1 will be necessary as further data from deep sedimentary basins will become available.

Although the order in which heavy minerals disappear during deep burial remains essentially uniform in sedimentary basins worldwide, there are major differences in the burial depths at which specific minerals become depleted. For example, amphibole depletion takes place at ca. 4000 m in the Kura Basin Pliocene, but only 600 m in the central North Sea Eocene. Garnet dissolution is complete at ~3500 m in the central

North Sea Jurassic, but shows only incipient signs of dissolution at the same depth in the Bengal Basin. Clearly, therefore, burial depth itself is not the only control, with other factors also playing an important role. The most important of these other factors are pore-fluid temperature and composition, rate of pore fluid movement, and time (Morton and Hallsworth, 1999).

4.1. Pore Fluid Temperature and Composition

Increasing pore fluid temperatures are an inevitable consequence of increased burial, and it would therefore appear that pore fluid temperature is the main driving mechanism behind heavy-mineral dissolution. The importance of elevated pore fluid temperatures, as opposed to increased burial depth, is illustrated by Karroo (Permian) sandstones in Zimbabwe. Bond (1943) noted that staurolite, present throughout the Karroo in the area of study, was etched only in a sandstone immediately below a basaltic lava flow, and he therefore considered that the etching was caused by flushing of the sandstones by high-temperature pore fluids introduced at the time of basalt emplacement. A similar situation occurs in the Pleistocene of the Escanaba Trough (Juan de Fuca Plate, NW Pacific), where dissolution of pyroxene and amphibole has taken place in sandstones affected by hydrothermal alteration (Zuffa et al., 2002; Zuffa and Serra, 2007, this volume).

As sandstones are buried and pore fluid temperatures rise, reactions take place to alter the composition of the pore waters, such as the transformation of smectite to illite (Hower et al., 1976) and the decarboxylation of organic matter to generate hydrocarbons (Tissot et al., 1974). The rising pore fluid temperatures and consequent changes in pore water composition cause heavy minerals to become unstable and start dissolving. The relative stability of the heavy minerals remains the same, but the

Table 1. Relative stability of detrital heavy minerals in deep burial conditions

Least stable
Olivine
Orthopyroxene, Clinopyroxene
Sodic pyroxene
Calcic amphibole, Andalusite, Sillimanite
Epidote
Titanite
Kyanite
Sodic amphibole
Staurolite
Allanite
Garnet, Chloritoid
Tourmaline, Monazite, Spinel
Rutile, Anatase, Brookite, Zircon, Apatite
Most stable

absolute depths at which they become unstable vary from basin to basin, dependent on the pore fluid temperature gradient, which is ultimately controlled by heat flow. One of the main reasons why heavy minerals are preserved to anomalously great depths in the Kura Basin is the suppressed thermal regime of the South Caspian Basin (Abrams and Narimanov, 1997), caused by low heat flow and rapid Mesozoic-Cenozoic sedimentation (Morton et al., 2003).

Comparatively little is known about the precise conditions under which burial-related mineral dissolution occurs, with only garnet having been studied in detail. Hansley (1987) documented the generation of etch facets on garnets by the action of warm dicarboxylic acid, and concluded that organic acids at temperatures exceeding 80 °C, generated through alteration of organic matter, cause garnet dissolution. In the Cleveland Basin of Yorkshire, sandstones showing intense garnet dissolution (Smithson, 1941) are associated with secondary sphalerite, which contain fluid inclusions that indicate crystal growth took place at temperatures of 79–82 °C (Shepherd, quoted in Hemingway and Riddler, 1982). In the same succession, vitrinite reflectance and spore colouration measurements indicate a maximum temperature of 95 °C (Cooper and Barnard, quoted in Hemingway and Riddler, 1982). In a series of mineral dissolution experiments using fluids with pHs of 3.6, 5.6 and 10.6 at room temperature, Nickel (1973) failed to simulate the pattern of relative mineral stability identified during burial. However, a limited series of experiments using a near-neutral fluid (pH of 8) simulated the relative stability of apatite, kyanite and garnet as seen in deep burial, with kyanite < garnet < apatite (Nickel, 1973). This suggests that near-neutral fluids best describe the conditions responsible for the subsurface dissolution patterns.

The only mineral to show significant differences in relative stability in sedimentary basins worldwide is kyanite. For example, kyanite is more stable than titanite in the central North Sea, but disappears at depths similar to that for titanite in the Faeroe-Shetland Basin, and is reported to be less stable than titanite in the US Gulf Coast. It is unclear why kyanite behaves more erratically than the other heavy minerals, but differences in pore fluid composition between the various basins discussed in this contribution are considered to be the most likely cause.

4.2. Rate of Pore Fluid Movement

The rate at which pore fluid moves through sandstones is another important factor in governing mineral distribution in the subsurface. Poor porosity and low permeability inhibit pore fluid movement, thereby decreasing the rate of mineral dissolution. Mineralogically immature sandstones may degrade rapidly during early burial, as in the case of the Kura Basin, where the sandstones have a predominantly volcanic provenance (Morton et al., 2003). Siltstones and mudstones also have poor porosity and permeability, and thus tend to preserve more diverse heavy-mineral assemblages than adjacent sandstones (Blatt and Sutherland, 1966). Early cementation, for example by carbonate minerals, causes a reduction in porosity and permeability, thereby preserving unstable heavy minerals compared with adjacent less cemented sandstones (Bramlette, 1941).

4.3. Geological Time

Pettijohn (1941) showed that, in general, older sandstones have less diverse heavy-mineral assemblages compared with younger sandstones, and proposed that the principal cause of heavy mineral loss was geological age. Turnau-Morawska (1984), however, presented an alternative relationship between heavy mineral diversity and age, in which only Quaternary sediments have significantly more heavy minerals than the remainder of the geological column. There are many examples of ancient sandstones with rich and diverse heavy-mineral assemblages: the Permo-Triassic of the pre-Urals foredeep (Ukraine) contains abundant amphibole and pyroxene (Sarksiyan, 1958), the upper Devonian of the Pyrenees (France and Spain) contains abundant amphibole and epidote (Stattegger, 1976), the Ordovician of the Southern Uplands (Scotland) contains abundant amphibole and pyroxene (Kelling, 1962; Styles et al., 1989), and the Ordovician of the South Mayo Trough contains abundant amphibole, pyroxene and sillimanite (Dewey and Mange, 1999). These ancient successions with anomalously diverse assemblages tend to be poorly sorted and contain high proportions of labile lithic material, which limited permeability prior to burial and underwent further rapid degradation of reservoir quality during diagenesis. Under such circumstances, the preservation of unstable heavy minerals is regarded as a consequence of the low permeabilities, which sealed the sediment from circulating pore fluids and thus protected the heavy-mineral grains from dissolution.

Therefore, although older sandstones tend to have low-diversity heavy-mineral assemblages, the presence of ancient sandstones with diverse heavy-mineral assemblages proves that geological age is not the main factor controlling intrastratal dissolution. Nevertheless, inevitably, the longer sandstones are subjected to circulating high-temperature pore fluids, the more depleted the assemblages will become. Geological age is therefore an important factor, albeit indirectly. A comparison of the Upper Jurassic and Palaeocene-Eocene of the central North Sea illustrates the effects of increasing age. In the Palaeocene-Eocene, as described above, staurolite is a common component of assemblages until burial depths of approximately 2400 m. However, staurolite is extremely scarce in the underlying Jurassic, even in the shallowest sandstones at less than 2000 m burial.

5. ASSESSMENT OF PROVENANCE IN DIAGENETICALLY MODIFIED SANDSTONES

Dissolution of unstable heavy minerals during diagenesis causes loss of valuable provenance information (Morton, 1984; Milliken, 1988), and the role of burial-related diagenetic processes on heavy-mineral assemblages must therefore be considered when assessing provenance. Nevertheless, despite the possibly profound impact of burial diagenesis on the detrital mineralogy, assemblages still retain fundamental information on provenance. It is therefore critical that the parameters used for interpretation of provenance reflect source area characteristics, rather than subsequent diagenetic processes. Two complementary approaches were recommended to assess provenance under such circumstances (Morton and Hallsworth,

1994, 1999), one that uses the entire heavy-mineral suite (conventional heavy-mineral analysis) and one that concentrates on the attributes of individual mineral species (varietal heavy-mineral analysis).

5.1. Conventional Heavy-Mineral Analysis

Ratios of stable minerals with similar hydrodynamic behaviour reflect source area characteristics, since they cannot be fractionated either by burial diagenesis or by hydraulic processes that operate during transport and sedimentation (Morton and Hallsworth, 1994, 1999) Of the provenance-sensitive parameters proposed by Morton and Hallsworth (1994), rutile/zircon (RuZi), monazite/zircon (MZi), chrome-spinel/zircon (CZi) and apatite/tourmaline (ATi) ratios are unaffected by burial diagenetic processes, since apatite, chrome spinel, monazite rutile, tourmaline and zircon are all stable. The garnet/zircon index (GZi) is, however, likely to be modified in sandstones that have suffered garnet dissolution, and care is therefore required in interpreting GZi values under such circumstances. Although ATi is a useful provenance-sensitive parameter, it may also be affected by loss of apatite during weathering at several stages in the sedimentation cycle, and therefore may provide information on sediment transport history. Prolonged or intense weathering may also result in lowered GZi, as in the Statfjord Formation of the northern North Sea (Morton and Berge, 1995).

5.2. Varietal Heavy-Mineral Analysis

The effects of diagenesis on heavy-mineral assemblages can be minimised by concentrating on properties displayed by a single stable mineral group. Varietal heavy-mineral methods fall into three main categories, petrographic, geochemical, and isotopic. Petrographic varietal data relate to optical properties such as colour, habit or zoning pattern. For example, zircon morphology has been used as a petrogenetic indicator (Pupin, 1976), and colour varieties of zircon (Mackie, 1923) and tourmaline (Krynine, 1946; Mange-Rajetzky, 1995) may be diagnostic of provenance. Textural data may also yield important information on sedimentation history. For example, changes in apatite morphology within the Devonian-Carboniferous succession of the Clair Field, UK continental shelf, are attributable to variable interplay between fluvial and aeolian transport processes (Allen and Mange-Rajetzky, 1992).

Mineral chemistry, as determined by electron microprobe methods, is a powerful tool in provenance reconstruction from diagenetically modified suites. The two most useful minerals are garnet and tourmaline, since both are relatively stable and show a wide range in compositions that can be related to specific source lithologies (Henry and Guidotti, 1985; Morton et al., 2004). The applicability of garnet geochemical analysis is restricted, since garnet undergoes dissolution in very deep burial conditions. The method can be used in sandstones in which garnet dissolution has been active, but caution is required in interpretation since Ca-rich garnets are less stable than Ca-poor varieties. Chrome spinel has variations in major element composition that have been used to infer provenance (Pober and Faupl, 1988; Cookenboo et al., 1997), although Power et al. (2000) suggest that characterisation of provenance using chrome spinel compositions may be unreliable. The other stable phases (apatite,

monazite, rutile, zircon) lack significant major element variation, but trace element data may prove useful in provenance reconstruction. For example, rare earth element variations in apatite (Fleischer and Altschuler, 1986; Morton and Yaxley, in press) and trace element abundances in rutile (Zack et al., 2004) appear to be dependent on their source rock composition.

Single-grain isotopic methods provide powerful constraints on provenance, since they give geochronological data that can be used to complement the mineralogical constraints provided by conventional heavy mineral and mineral chemical data. Single-grain U-Pb dating of zircon (Rainbird et al., 1992) and monazite (Evans et al., 2001), both of which are stable phases during diagenesis, is now relatively commonplace, and provides crucial information on the ages of major crust-forming events in the source area. Alternatively, $^{40}Ar-^{39}Ar$ laser probe dating of mica (Sherlock et al., 2000) and fission-track dating of minerals such as apatite or zircon (e.g., Carter, 1999) provide information on the metamorphic history and unroofing of the source terrain.

ACKNOWLEDGMENTS

We are grateful to Andrew Hurst, Maria Mange and Peter Mozley for their constructive comments on an earlier draft on this manuscript.

REFERENCES

Abrams, M.A., Narimanov, A.A., 1997. Geochemical evaluation of hydrocarbons and their potential sources in the western South Caspian depression, Republic of Azerbaijan. Marine and Petroleum Geology 14, 451–468.

Allen, P.A., Mange-Rajetzky, M.A., 1992. Devonian-Carboniferous sedimentary evolution of the Clair Area, offshore northwestern UK: impact of changing provenance. Marine and Petroleum Geology 9, 29–52.

Balan, E., Neuville, D.R., Trocellier, P., Fritsch, E., Muller, J.-P., Calas, G., 2001. Metamictization and chemical durability of detrital zircon. American Mineralogist 86, 1025–1033.

Berner, R.A., Sjöberg, E.L., Velbel, M.A., Krom, M.D., 1980. Dissolution of pyroxenes and amphiboles during weathering. Science 207, 1205–1206.

Blatt, H., Sutherland, B., 1966. Intrastratal solution and non-opaque heavy minerals in shales. Journal of Sedimentary Petrology 39, 591–600.

Bond, G., 1943. Solution etching of detrital staurolite. Geological Magazine 80, 155–156.

Bowman, M.B.J., 1998. Cenozoic. In: Glennie, K.W. (Ed.), Introduction to the Petroleum Geology of the North Sea. Blackwell, Oxford, pp. 350–375.

Bramlette, M.N., 1941. The stability of minerals in sandstone. Journal of Sedimentary Petrology 11, 32–36.

Butterfield, J.A., 1936. Outgrowths on zircon. Geological Magazine 73, 511–516.

Carroll, D.S., 1953. Weatherability of zircon. Journal of Sedimentary Petrology 23, 106–116.

Carter, A., 1999. Present status and future avenues of source region discrimination and characterization using fission track analysis. Sedimentary Geology 124, 31–45.

Cavazza, W., Gandolfi, G., 1992. Diagenetic processes along a basin-wide marker bed as a function of burial depth. Journal of Sedimentary Petrology 62, 261–272.

Cookenboo, H.O., Bustin, R.M., Wilks, K.R., 1997. Detrital chromian spinel compositions used to reconstruct the tectonic setting or provenance: implications for orogeny in the Canadian Cordillera. Journal of Sedimentary Research 67, 116–123.

Deer, W.A., Howie, R.A., Zussman, J., 1997a. , 2nd ed. Double-chain silicates. Rock-Forming Minerals, vol. 2B. Geological Society, London.

Deer, W.A., Howie, R.A., Zussman, J., 1997b. , 2nd ed. Disilicates and ring silicates. Rock-Forming Minerals, vol. 1B. Geological Society, London.

Deer, W.A., Howie, R.A., Zussman, J., 1997c. , 2nd ed. Orthosilicates. Rock-Forming Minerals, vol. 1A. Geological Society, London.

Dewey, J., Mange, M., 1999. Petrography of Ordovician and Silurian sediments in the western Irish Caledonides: tracers of a short-lived Ordovician continent-arc collision orogeny and the evolution of the Laurentian Appalachian-Caledonian margin. In: MacNiocaill, C., Ryan, P. D. (Eds.), Continental Tectonics. Geological Society of London, Special Publication 164, 55–107.

Edelman, C.H., Doeglas, D.J., 1932. Reliktstructuren detritischer Pyroxene und Amphibole. Tschermaks Mineralogische und Petrographische Mitteilungen 42, 482–490.

Edelman, C.H., Doeglas, D.J., 1934. Über Umwandlungserscheinungen an detritischem Staurolith und anderen Mineralien. Tschermaks Mineralogische und Petrographische Mitteilungen 44, 225–234.

Ehrenberg, S.N., Nadeau, P.H., 2002. Postdepositional Sm/Nd fractionation in sandstones: implications for neodymium-isotope stratigraphy. Journal of Sedimentary Research 72, 304–315.

Evans, J.A., Chisholm, J.I., Leng, M.J., 2001. How U-Pb detrital monazite ages contribute to the interpretation of the Pennine Basin infill. Journal of the Geological Society, London 158, 741–744.

Fleischer, M., Altschuler, Z.S., 1986. The lanthanides and yttrium in minerals of the apatite group—an analysis of the available data. Neues Jahrbuch für Mineralogie, Monatshefte 10, 467–480.

Gazzi, P., 1965. On the heavy mineral zones in the Geosyncline series. Recent studies in the northern Apennines, Italy. Journal of Sedimentary Petrology 35, 109–115.

Hansley, P.L., 1987. Petrologic and experimental evidence for the etching of garnets by organic acids in the Upper Jurassic Morrison Formation, northwestern New Mexico. Journal of Sedimentary Petrology 57, 666–681.

Hemingway, J.E., Tamar-Agha, M.Y., 1975. The effects of diagenesis on some heavy minerals from the sandstones of the Middle Limestone Group in Northumberland. Proceedings of the Yorkshire Geological Society 40, 537–546.

Hemingway, J.E., Riddler, G.P., 1982. Basin inversion in North Yorkshire. Transactions of the Institute of Mining and Metallurgy 91, 175–186.

Henry, D.J., Guidotti, C.V., 1985. Tourmaline as a petrogenetic indicator mineral: an example from the staurolite-grade metapelites of NW Maine. American Mineralogist 70, 1–15.

Henry, D.J., Lu, G., McCabe, C., 1993. Authigenic tourmaline growth in sedimentary iron-stones: an example from the Silurian Rose Hill Formation, Virginia. Transactions of the American Geophysical Union 74, 168.

Henry, D.J., Kirkland, B.L., Kirkland, D.W., 1999. Sector-zoned tourmaline from the cap rock of a salt dome. European Journal of Mineralogy 11, 263–280.

Hower, J., Eslinger, E.V., Hower, M.E., Perry, E.A., 1976. Mechanisms of burial and metamorphism of argillaceous sediment. I. Mineralogical and chemical evidence. Geological Society of America Bulletin 87, 725–737.

Hubert, J.F., 1962. A zircon-tourmaline-rutile maturity index and the interdependance of the composition of heavy mineral assemblages with the gross composition and texture of sandstones. Journal of Sedimentary Petrology 32, 440–450.

Hubert, J.F., 1971. Analysis of heavy mineral assemblages. In: Carver, R.E. (Ed.), Procedures in Sedimentary Petrology. Wiley, New York, pp. 453–478.

Kelling, G., 1962. The petrology and sedimentation of Upper Ordovician rocks in the Rhinns of Galloway, south-west Scotland. Transactions of the Royal Society of Edinburgh 65, 107–137.

Krynine, P.D., 1946. The tourmaline group in sediments. Journal of Geology 54, 65–87.

Mackie, W., 1923. The source of purple zircons in the sedimentary rocks of Scotland. Transactions of the Edinburgh Geological Society 11, 200–213.

Mange, M.A., Maurer, H.F.W., 1992. Heavy Minerals in Colour. Chapman and Hall, London, 147pp.

Mange-Rajetzky, M. A., 1995. Subdivision and correlation of monotonous sandstone sequences using high resolution heavy mineral analysis, a case study: The Triassic of the Central Graben. In: Dunay, R. E., Hailwood, E. A. (Eds.), Non-Biostratigraphical Methods of Dating and Correlation. Geological Society of London, Special Publication 89, 23–30.

Milliken, K.L., 1988. Loss of provenance information through subsurface diagenesis in Plio-Pleistocene sediments, northern Gulf of Mexico. Journal of Sedimentary Petrology 58, 992–1002.

Milliken, K. L., 2007. Provenance and diagenesis of heavy minerals, Cenozoic units of the northwestern Gulf of Mexico sedimentary basin. In: Mange, M. A., Wright, D. T. (Eds.), Heavy Minerals in Use. Developments in Sedimentology (this volume).

Milliken, K.L., Mack, L.E., 1990. Subsurface dissolution of heavy minerals, Frio Formation sandstones of the ancestral Rio Grande Province, South Texas. Sedimentary Geology 68, 187–199.

Morton, A.C., 1979. Surface textures of heavy mineral grains from the Palaeocene of the central North Sea. Scottish Journal of Geology 15, 293–300.

Morton, A.C., 1984. Stability of detrital heavy minerals in Tertiary sandstones of the North Sea Basin. Clay Minerals 19, 287–308.

Morton, A.C., 1986. Dissolution of apatite in North Sea Jurassic sandstones: implications for the generation of secondary porosity. Clay Minerals 21, 711–733.

Morton, A.C., 1987. Influences of provenance and diagenesis on detrital garnet suites in the Forties sandstone, Paleocene, central North Sea. Journal of Sedimentary Petrology 57, 1027–1032.

Morton, A.C., Berge, C., 1995. Heavy mineral suites in the Statfjord and Nansen Formations of the Brent Field, North Sea: a new tool for reservoir subdivision and correlation. Petroleum Geoscience 1, 355–364.

Morton, A.C., Hallsworth, C.R., 1994. Identifying provenance-specific features of detrital heavy mineral assemblages in sandstones. Sedimentary Geology 90, 241–256.

Morton, A.C., Hallsworth, C.R., 1999. Processes controlling the composition of heavy mineral assemblages in sandstones. Sedimentary Geology 124, 3–29.

Morton, A. C., Yaxley, G., (in press). Detrital apatite geochemistry and its application in provenance studies. Geological Society of America, Special Paper.

Morton, A.C., Borg, G., Hansley, P.L., Haughton, P.D.W., Krinsley, D.H., Trusty, P., 1989. The origin of faceted garnets in sandstones: dissolution or overgrowth. Sedimentology 36, 927–942.

Morton, A.C., Humphreys, B., Dharmayanti, D.A., Sundoro, 1994. Palaeogeographic implications of the heavy mineral distribution in Miocene sandstones of the North Sumatra Basin. Journal of Southeast Asian Earth Sciences 10, 177–190.

Morton, A.C., Claoué-Long, J., Berge, C., 1996. Factors influencing heavy mineral suites in the Statfjord Formation, Brent Field, North Sea: constraints provided by SHRIMP U-Pb dating of detrital zircons. Journal of the Geological Society of London 153, 911–929.

Morton, A. C., Boyd, J. D., Ewen, D. F., 2002. Evolution of Palaeocene sediment dispersal systems in the Foinaven Sub-Basin, West of Shetland. In: Jolley, D. W., Bell, B. R. (Eds.), The North Atlantic Igneous Province: Stratigraphy, Tectonics, Volcanic and Magmatic Processes. Geological Society, London, Special Publication 197, 69–93.

Morton, A.C., Allen, M.B., Simmons, M.D., Spathopoulos, F., Still, J., Ismail-Zadeh, A., Kroonenberg, S., 2003. Provenance patterns in a neotectonic basin: Pliocene and Quaternary sediment supply to the South Caspian. Basin Research 15, 321–337.

Morton, A.C., Hallsworth, C.R., Chalton, B., 2004. Garnet compositions in Scottish and Norwegian basement terrains: a framework for interpretation of North Sea sandstone provenance. Marine and Petroleum Geology 21, 393–410.

Morton, A. C., Whitham, A. G., Fanning, C. M., Claoué-Long, J. C., 2005a. The role of East Greenland as a source of sediment to the Vøring Basin during the Late Cretaceous. In: Wandås, B. T. G., Eide, E. A., Gradstein, F., Nystuen J. P. (Eds.), Onshore-Offshore Relationships on the North Atlantic Margin. NPF (Norsk Petroleumsforening). Special Publication 12, 83–110, Elsevier, Amsterdam.

Morton, A.C., Whitham, A.G., Fanning, C.M., 2005b. Provenance of Late Cretaceous-Paleocene submarine fan sandstones in the Norwegian Sea: integration of heavy mineral, mineral chemical and zircon age data. Sedimentary Geology 182, 3–28.

Nickel, E., 1973. Experimental dissolution of light and heavy minerals in comparison with weathering and intrastratal solution. Contributions to Sedimentology 1, 1–68.

Oliva, P., Viers, J., Dupré, B., Fortuné, J.-P., Martin, F., Braun, J.-J., Nahon, D., Robain, H., 1999. The effect of organic matter on chemical weathering: study of a small tropical watershed: Nsimi-Zoétélé site, Cameroon. Geochimica et Cosmochimica Acta 63, 4013–4035.

Pettijohn, F.J., 1941. Persistence of heavy minerals and geologic age. Journal of Geology 49, 610–625.

Pettijohn, F.J., 1975. Sedimentary Rocks, 3rd ed. Harper and Row, New York.

Pober, E., Faupl, P., 1988. The chemistry of detrital chromian spinels and its implications for the geodynamic evolution of the Eastern Alps. Geologische Rundschau 77, 641–670.

Power, M.R., Pirrie, D., Andersen, J.C.Ø., Wheeler, P.D., 2000. Testing the validity of chrome spinel chemistry as a provenance and petrogenetic indicator. Geology 28, 1027–1030.

Pupin, J. -P., 1976. Signification des caractères morphologiques du zircon commun des roches en pétrologie. Base de la méthode typologique—Applications. Ph.D. thesis. University of Nice.

Rahmani, R.A., 1973. Grain surface etching features of some heavy minerals. Journal of Sedimentary Petrology 43, 880–882.

Rainbird, R.H., Heaman, L.M., Young, G., 1992. Sampling Laurentia: detrital zircon geochronology offers evidence for an extensive Neoproterozoic river system originating from the Grenville orogen. Geology 20, 351–354.

Rochow, K.A., 1981. Seismic stratigraphy of the North Sea 'Palaeocene' deposits. In: Illing, L.V., Hobson, G.D. (Eds.), Petroleum Geology of the Continental Shelf of North-West Europe. Heyden and Son, London, pp. 255–266.

Salvino, J.F., Velbel, M.A., 1989. Faceted garnets from sandstones of the Munising Formation (Cambrian), northern Michigan: petrographic evidence for origin by intrastratal dissolution. Sedimentology 36, 371–379.

Sarksiyan, S.G., 1958. Upper Permian continental Molasses of the Pre-Urals. Eclogae Geologicae Helvetiae 51, 1043–1051.

Scavnicar, B., 1979. Pjescenjaci Pliocena i Miocena savske potoline. Zbornik Radova, Sekcija za Primljenu Geologiju, Geofiziku, Geokemiju, Serija A 6, 351–382.

Sherlock, S.C., Jones, K.A., Jones, J.A., 2000. A central European Variscide source for Upper Carboniferous sediments in SW England: $^{40}Ar/^{39}Ar$ detrital white mica ages from the Forest of Dean Basin. Journal of the Geological Society, London 157, 905–908.

Smale, D., 2007. Sediment trails in tectonically active islands: heavy minerals in use in New Zealand. In: Mange, M. A., Wright, D. T. (Eds.), Heavy Minerals In Use. Developments in Sedimentology (this volume).

Smale, D., Morton, A.C., 1987. Heavy mineral suites of core samples from the McKee Formation (Eocene-Lower Oligocene), Taranaki: implications for provenance and diagenesis. New Zealand Journal of Geology and Geophysics 30, 299–306.

Smale, D., Van der Lingen, G.J., 1989. Differential leaching of garnet grains at a depth of 3.5 km in Tane-1, Offshore Taranaki, New Zealand. New Zealand Geological Survey Record 40, 57–60.

Smithson, F., 1937. Outgrowths on zircon in the Middle Jurassic of Yorkshire. Geological Magazine 74, 281–283.

Smithson, F., 1941. The alteration of detrital minerals in the Mesozoic rocks of Yorkshire. Geological Magazine 78, 97–112.

Spiegel, C., Siebel, W., Frisch, W., Berner, Z., 2002. Nd and Sr isotopic ratios and trace element geochemistry of epidote from the Swiss Molasse Basin as provenance indicators: implications for the reconstruction of the exhumation history of the Central Alps. Chemical Geology 189, 231–250.

Stattegger, K., 1976. Schwermineraluntersuchungen in den klastischen Serien der variszischen Geosynklinale der Ost- und Zentral-Pyrenäen. Mitteilungen der Österreichischen geographischen Gesellschaft 69, 267–290.

Stow, M.H., 1932. Authigenic tourmaline in the Oriskany Sandstone. American Mineralogist 17, 150–152.

Styles, M.T., Stone, P., Floyd, J.D., 1989. Arc detritus in the Southern Uplands: mineralogical characterisation of a 'missing' terrain. Journal of the Geological Society, London 146, 397–400.

Tissot, B., Durand, B., Espitalic, J., Combaz, A., 1974. Influence of nature and diagenesis of organic matter in formation of petroleum. Bulletin of the American Association of Petroleum Geologists 58, 499–506.

Turner, G., Morton, A. C., 2007. The effects of burial diagenesis on detrital heavy mineral grain surface textures. In: Mange, M. A., Wright, D. T. (Eds.), Heavy Minerals In Use. Developments in Sedimentology (this volume).

Turnau-Morawska, M., 1984. Importance of heavy mineral analysis in solving geological problems. In: Luepke, G. (Ed.), Stability of Heavy Minerals in Sediments. Van Nostrand Reinhold, New York, pp. 280–287 (translated from the original 1955 article in Acta Geologica Polonica 5, 363–388).

Uddin, A., Lundberg, N., 1998a. Unroofing history of the eastern Himalaya and the Indo-Burman ranges: heavy-mineral study of Cenozoic sediments from the Bengal Basin, Bangladesh. Journal of Sedimentary Research 68, 465–472.

Uddin, A., Lundberg, N., 1998b. Cenozoic history of the Himalayan-Bengal system: sand composition in the Bengal Basin, Bangladesh. Bulletin of the Geological Society of America 110, 497–511.

Uddin, A., Lundberg, N., 1999. A paleo-Brahmaputra? Subsurface lithofacies analysis of Miocene deltaic sediments in the Himalayan-Bengal system, Bangladesh. Sedimentary Geology 123, 239–254.

Vallini, D.A., Rasmussen, B., Krapez, B., Fletcher, I.R., McNaughton, N.J., 2005. Microtextures, geochemistry and geochronology of authigenic xenotime: constraining the cementation history of a Palaeoproterozoic metasedimentary sequence. Sedimentology 52, 101–122.

Van Andel, T.H., 1959. Reflection on the interpretation of heavy mineral analyses. Journal of Sedimentary Petrology 29, 153–163.

Van Loon, A. J., Mange, M. A., 2007. Dutch/German silver sands and the application of heavy mineral weathering characteristics to the stratigraphy and correlation of sediments. In: Mange, M. A., Wright, D. T. (Eds.), Heavy Minerals in Use. Developments in Sedimentology (this volume).

Velbel, M. A., 2007. Surface textures and dissolution processes of heavy minerals in the sedimentary cycle: Examples from pyroxenes and amphiboles. In: Mange, M. A., Wright, D. T. (Eds.), Heavy Minerals in Use. Developments in Sedimentology (this volume).

Weissbrod, T., Nachmias, J., 1986. Stratigraphic significance of heavy minerals in the late Precambrian-Mesozoic clastic sequence ('Nubian Sandstone') in the Near East. Sedimentary Geology 47, 263–291.

Wieseneder, H., Maurer, J., 1958. Ursachen der räumlichen und zeitlichen Aenderung des Mineralbestandes der Sedimente des Wiener Beckens. Eclogae Geologicae Helvetiae 51, 1155–1172.

Yurkova, R.M., 1970. Comparison of postsedimentary alteration of oil-, gas- and water-bearing rocks. Sedimentology 15, 53–68.

Zack, T., von Eynatten, H., Kronz, A., 2004. Rutile geochemistry and its potential use in quantitative provenance studies. Sedimentary Geology 171, 37–58.

Zuffa, G.G., Normark, W.R., Serra, F., Brunner, C.A., 2002. Turbidite megabeds in an oceanic rift valley recording jökulhlaups of Late Pleistocene glacial lakes of the western United States. Journal of Geology 108, 253–274.

Zuffa, G. G., Serra, F., 2007. Effects of hydrothermal fluids on the heavy mineral assemblage of a late Pleistocene succession deposited in an oceanic ridge valley (Escanaba Trough, Juan De Fuca Plate). In: Mange, M. A., Wright, D. T. (Eds.), Heavy Minerals in Use. Developments in Sedimentology (this volume).

This page intentionally left blank

Chapter 8

PROVENANCE AND DIAGENESIS OF HEAVY MINERALS, CENOZOIC UNITS OF THE NORTHWESTERN GULF OF MEXICO SEDIMENTARY BASIN

KITTY L. MILLIKEN

Department of Geological Sciences, Jackson School of Geosciences, The University of Texas at Austin, Austin, TX 78712, USA

ABSTRACT

Heavy mineral studies in the post-Mesozoic units of the Gulf of Mexico (GOM) passive margin basin include numerous classic applications for deciphering sediment provenance and for stratigraphic correlation. Because of the well-documented provenance and simple burial history, this basin has also served as a natural laboratory for research into processes by which provenance information is 'erased' and otherwise complicated by diagenesis.

Based on observations in the GOM, a generalised model for basinal diagenesis of heavy minerals is proposed. From the surface to depths corresponding to around 80–100 °C, diagenesis of the heavy mineral assemblage is dominated by dissolution that is best characterised as an acid hydrolysis or weathering process. At depths that overlap the ultimate completion of the subsurface weathering process, precipitates, including a number of high-density phases, form by reactions that can be described as acid-releasing or reverse-weathering. At depths near the limit of coring (>5 km), the surviving ultrastable detrital heavy mineral assemblage (mostly zircon, tourmaline, and rutile) is accompanied by an intriguing variety of high-density authigenic minerals (including anatase and titanite). The provenance interpretation of heavy mineral extracts from rocks that have had a protracted history of burial must be evaluated cautiously and with an emphasis on the use of ultrastable species.

Keywords: diagenesis; mineral dissolution; provenance; Gulf of Mexico; scanning electron microscopy

1. THE NORTHWESTERN GULF OF MEXICO: A TYPICAL PASSIVE MARGIN BASIN

The post-Mesozoic sediment fill of the Gulf of Mexico (GOM) passive margin basin has been a target of petroleum exploration for over a century (Salvador, 1991a).

Developments in Sedimentology, Vol. 58, 247–261

ISSN: 0070-4571/doi:10.1016/S0070-4571(07)58008-8

Samples and data arising from this activity have been used to compile a detailed history of GOM sedimentation and depositional architecture that, in turn, allows this basin to be used as a natural laboratory for investigations into basinal chemical evolution through fluid/rock interactions. Heavy mineral studies in the GOM have addressed both 'classic' applications for deciphering provenance and stratigraphic correlation (Bornhauser, 1940; Cogen, 1940; Bullard, 1942; Hsu, 1960; Van Andel and Poole, 1960; Flores and Shideler, 1978), and also research into the nature of processes by which provenance information is 'erased' by diagenesis (e.g., Milliken, 1988; Milliken and Mack, 1990).

The history of tectonics and sedimentation in the GOM basin is reviewed in detail in Salvador (1991a). The GOM basin opened by rifting in the Triassic (Salvador, 1991b). During the Mesozoic, basin filling was dominated by basin-margin carbonate sedimentation with local siliciclastic incursions along the northern and western basin margins (Salvador, 1991b). Carbonate sedimentation ceased as a result of Laramide uplift that initiated a flood of siliciclastic sediment into the basin that continues to the present (Coleman et al., 1991; Galloway et al., 1991).

The extensive syn-depositional growth faulting of Cenozoic units allows observation of time-equivalent units across a range of depths ranging from the surface to ~6 km of burial (the approximate limit of drilling) (Galloway et al., 1991, 2000). Because it is reasonable to assume that present burial depth and temperature are near-maximum (Galloway et al., 1991, 2000) this basin is useful as a natural laboratory for the study of burial diagenesis.

2. PROVENANCE VARIATION IN THE GOM

Goldstein (1942) identified four heavy mineral provinces on the modern shelf of the northwestern GOM (Eastern Gulf, Mississippi, Western Gulf, and Rio Grande), a finding confirmed and refined by later workers (Hsu, 1960; Van Andel and Poole, 1960; Flores and Shideler, 1978) who noted the complication of long-shore drift in mixing the contributions of individual river systems. Heavy minerals in each GOM province are diverse and include minerals of widely variable stability. Notable trends are the prominent occurrence of the pelitic metamorphic minerals kyanite, sillimanite, and staurolite in the eastern Gulf and Mississippi River province, derived from the southern Appalachians and its proximate sediment cover; a hornblende/pyroxene assemblage in the Mississippi River province derived largely from reworking of glacial deposits of the upper mid-continent; an assemblage generally lacking pyroxenes with prominent occurrence of ultrastable phases such as zircon and tourmaline, along the western Gulf and Texas coast, generally derived by a combination of local river sources (relatively short distance of transport) and by long-shore drift; and finally, the Rio Grande province contains a prominent volcanogenic component including basaltic hornblende and titanaugite derived from northern Mexico and far west Texas (Bullard, 1942; Flores and Shideler, 1978).

During the Cenozoic, siliciclastic sediments shed from a large portion of North America, have been deposited in the GOM, as the principal depositional axes have shifted around the Gulf margin in response to remote tectonic events (Winker, 1981) (Fig. 1). The geography of temporal shifts in provenance around the

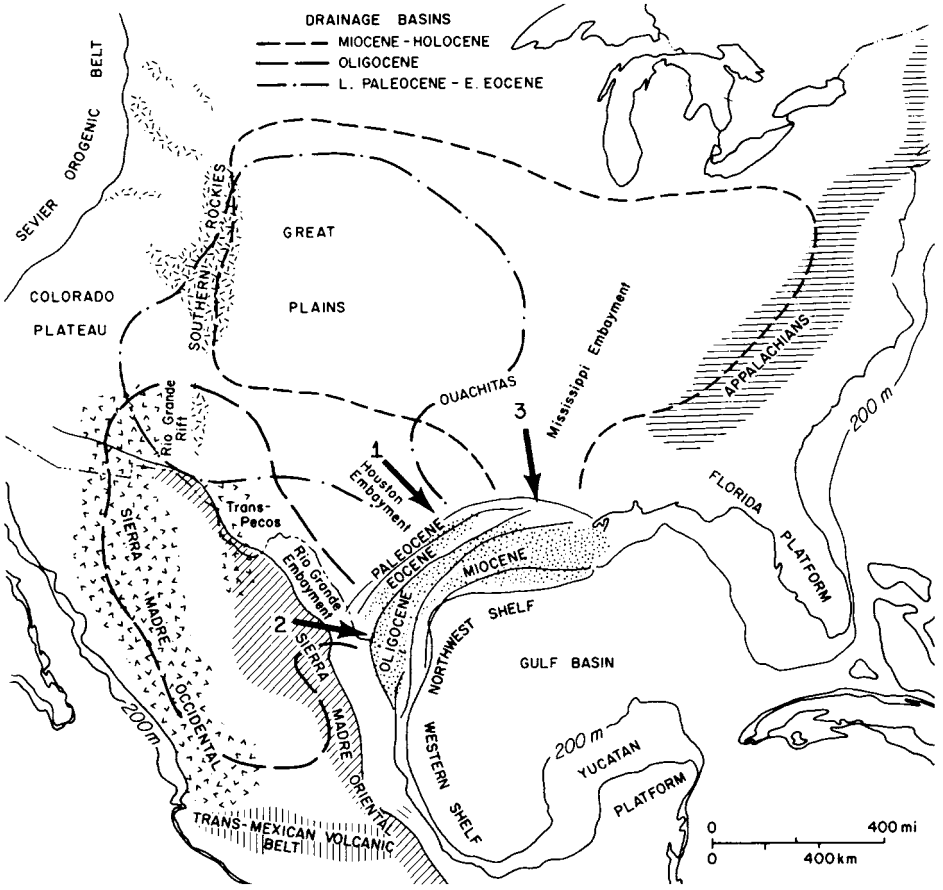

Fig. 1. Provenance of siliciclastic sediments in each of the four major Cenozoic depocentres in the Gulf of Mexico basin. (1) Eocene. (2) Oligocene. (3) Miocene and Plio-Pleistocene. From Galloway et al. (1991), modified from Winker (1981). With permission.

margin of the GOM is known largely from studies of sediment geometry that delineate the locations and sizes of the principal depositional centres and their associated fluvial axes (Winker, 1981; Galloway et al., 2000), but provenance trends are also consistently reflected by changes in detrital sand compositions (Loucks et al., 1984). Provenance variation in modern GOM sediments is one useful indicator of the initial compositions of heavy mineral assemblages that characterised the various Cenozoic depocentres, which, in broad outline, had drainage areas analogous to modern ones. For example, although sedimentation along the depositional axis of the Rio Grande is greatly diminished today in comparison with the Oligocene (Galloway et al., 2000), evidence from both light and heavy mineral assemblages in the modern Rio Grande and the adjacent shelf (Flores and Shideler, 1978; Milliken et al., 1989) provide insights into the likely composition of heavy mineral assemblages in the Oligocene (Loucks et al., 1984; Milliken et al., 1989; Milliken and Mack, 1990).

The volumetrically significant Eocene sedimentation in the GOM was centred along today's upper Texas coast, with sediments derived from a broad area of the central mid-continent (Galloway et al., 2000). In the Oligocene, the principal depocentres shifted far to the south in response to a period of enhanced volcanism in west Texas and northern Mexico (Galloway et al., 2000). Beginning in the Miocene, sedimentation shifted northward, dominated by sediment supplied by the ancestral Mississippi River. This initial shift in sedimentation was in response to localised uplift and erosion of Palaeozoic-age sediments in the southern Appalachians (Boettcher and Milliken, 1994; Galloway et al., 2000). Through the Pliocene, Pleistocene, and today, the sediments of the Mississippi drainage include volcanic materials from the northern Rocky Mountains, glacial sediments of the southern Canadian Shield, as well as continued contributions from the southern Appalachians (Russell, 1937; Milliken, 1988).

3. DIAGENETIC MODIFICATION OF HEAVY MINERAL ASSEMBLAGES IN THE GOM

3.1. Grain Dissolution and the Loss of Provenance Information: Early Observations

Trends in heavy minerals related to provenance variation in Cenozoic sediments of the GOM are at least partly obscured by diagenesis. It is interesting to revisit early stratigraphic studies of heavy minerals in this context, keeping in mind that these pre-date the seminal statement on intrastratal dissolution by Pettijohn (1941). A major effort by Shell Oil Company to apply heavy mineral zones to a stratigraphic understanding of the GOM was reported by Bornhauser (1940) and by Cogen (1940). Based on over 2000 samples from both outcrop and subsurface, this study documented heavy mineral zones that have prominent depth-related variations. Because the guiding paradigm of the study was application of heavy minerals to stratigraphic interpretation, the identified zones are not listed by Cogen in depth order, although he notes: "It is demonstrated that mineral-zone boundaries may transect formations and paleontologic horizons" (Cogen, 1940, Abstract).

In order of increasing average depth, the heavy mineral zones described by Cogen are:

- *Hornblende*: epidote, garnet, kyanite, staurolite, titanite (sphene), tourmaline, zircon, and locally, minor diopside-augite;
- *Kyanite*: staurolite, garnet (generally missing in outcrop samples);
- *Staurolite*: zircon, tourmaline, garnet, minor rutile;
- *Lower epidote*: staurolite, garnet, titanite, epidote.

In a prescient observation Cogen notes: "The mineral zones down to the Lower epidote zone show impoverishment in variety of mineral species successively with depth, …." (Cogen). He points out that the hornblende zone, similar in composition to the Mississippi River assemblage described by Russell (1937) is notably erratic in its occurrence and is only found in younger units nearer the coast. Cogen (1940, p. 2097) also observed that garnet is notably absent from the Kyanite zone in outcrop whereas equivalent zones in the subsurface are garnet-bearing), an observation that recalls the loss of garnet through meteoric exposure such as reported

by Morton (1987). In hindsight, it is easy to identify the overprint of dissolution that complicates the interpretation of heavy mineral assemblages described by Bornhauser and Cogen. The 'impoverishment' noted above also corresponds to progressive loss of unstable species and the consequent relative enrichment of the stable ZTR assemblage. In view of our present understanding of heavy mineral diagenesis, it is not surprising that this major study, fraught with multiple and largely unrecognised controls on heavy mineral occurrence, did not reveal patterns that proved useful in stratigraphic correlation. Later studies in the GOM benefited from deeper drilling and from sampling within a single provenance region of a single formation to document with greater clarity the progressive nature of subsurface heavy mineral loss.

3.2. *Grain Dissolution and the Loss of Provenance Information: Depth Trends and SEM Evidence*

Detrital heavy mineral assemblages in GOM sediments display evidence of diagenetic modification through dissolution at relatively shallow depths in the subsurface (1–2 km), and at greater depths are ultimately reduced to an assemblage dominated by zircon, tourmaline, and rutile (Milliken, 1988; Milliken and Mack, 1990). Evidence for this is twofold, including both the depth trends observed in sample sets that are well-constrained for provenance (Fig. 2) and direct petrographic evidence for in situ dissolution.

In general, the ultrastable minerals display surface textures related to the primary crystal form as variably modified by transport and abrasion. Zircons, for example, display surfaces that vary from highly smooth and euhedral (Fig. 3A) to highly rounded (Fig. 3C).

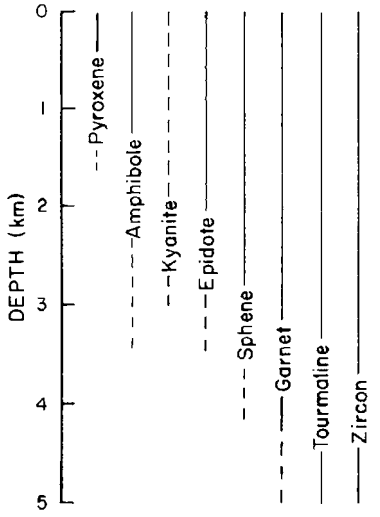

Fig. 2. Depth trends for heavy minerals in Plio-Pleistocene sediments beneath the Louisiana shelf. The average geothermal gradient in the region is 20°C/km. From Milliken (1988). With permission from the Society for Sedimentary Geology.

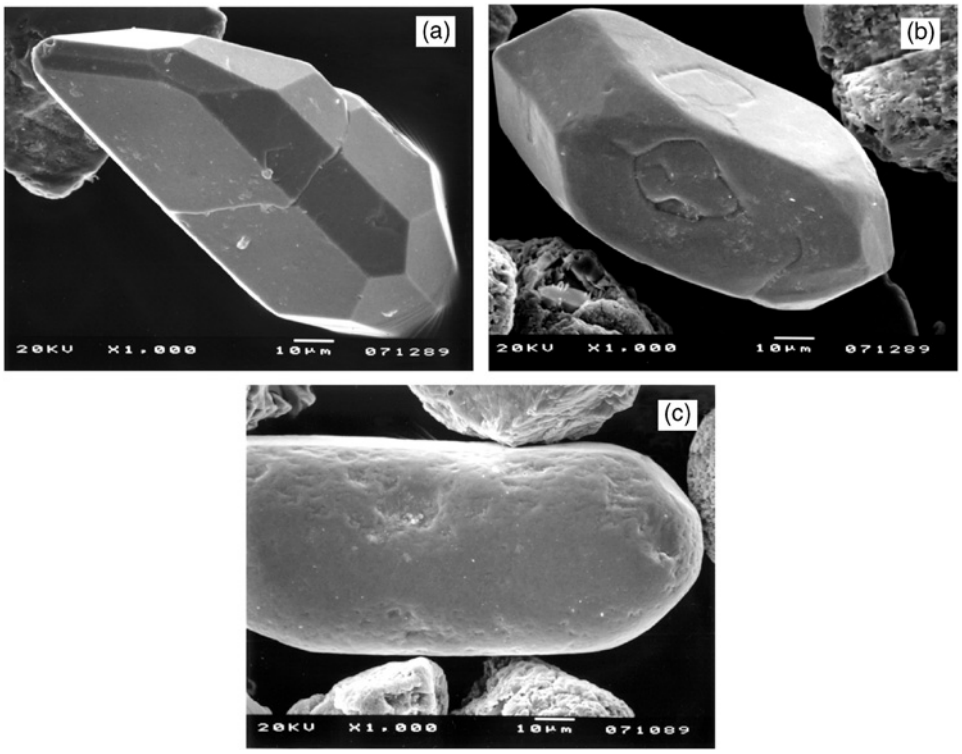

Fig. 3. Detrital zircons. (A) Euhedral zircon, Frio Formation, Oligocene, South Texas, depth 3095 m. (B) Subhedral zircon. Frio Formation, Oligocene, South Texas, depth 3095 m. (C) Highly rounded zircon. Frio Formation, Oligocene, South Texas, depth 1995 m.

Less stable species however, display a range of surface features that include those related to dissolution. Most pyroxenes (though not all) and many amphibole grains display prominent evidence of highly localised (surface-reaction-controlled) dissolution even in modern fluvial sands (Fig. 4). Dissolution fabrics for most other silicates, however, are less well-displayed in modern river sands than in samples from outcrop and the subsurface. Garnets in the subsurface are characterised by highly distinctive surface patterns related to dissolution (Fig. 5). The degree to which these features are developed on the surface of individual garnets varies widely, Fe and Fe–Mn garnets appearing to be somewhat less prone to dissolution (Fig. 5B) and displaying prominent crystallographically controlled dissolution patterns, whereas Ca-rich garnets display highly irregular pitting of the grain (Fig. 5C). Staurolite (Fig. 6A) and titanite (Fig. 6C) typically also show pronounced crystallographically controlled patterns of dissolution. Epidote is prone to dissolution that preserves extremely elongated, spiky crystal remnants (Fig. 6B).

Among opaque Fe/Ti oxides, the Fe- and Ti-rich end member species are relatively stable in comparison with ilmenite of intermediate composition (Fig. 7). Distinctive intergrowth patterns are revealed by the dissolution of ilmenite (Fig. 7C).

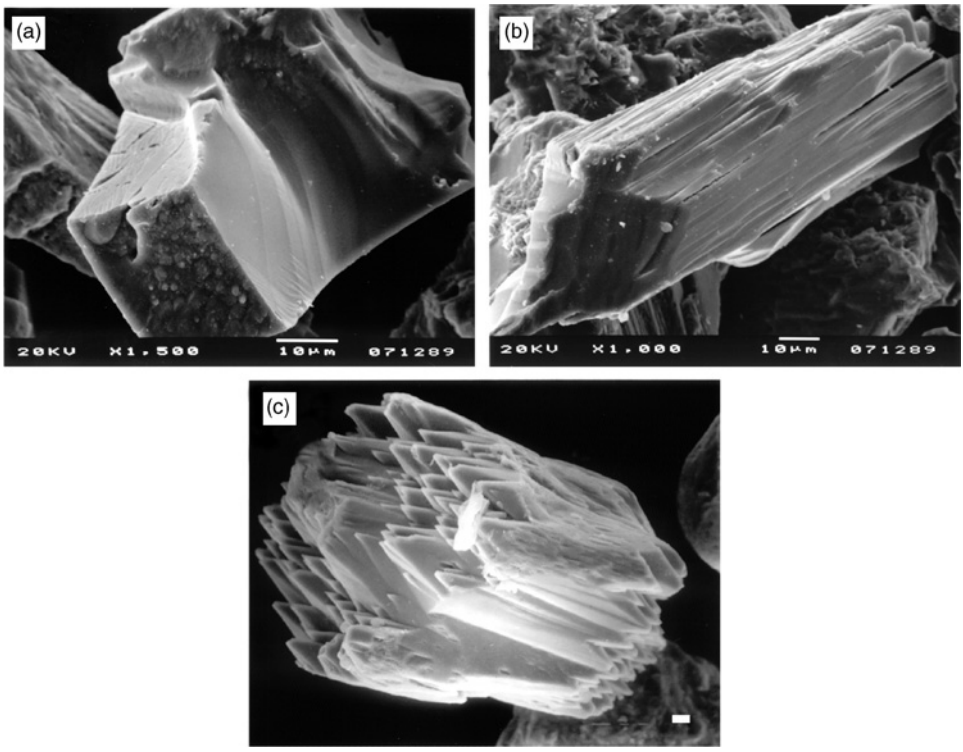

Fig. 4. Detrital pyroxenes and amphiboles. (A) Titanaugite. Modern Rio Grande, Lantry, Texas. (B) Amphibole. Modern Rio Grande, Langtry, Texas. (C) Pyroxene. Pleistocene, offshore Lousiana, depth 797 m. White bar is 10 µm.

3.3. Authigenic Heavy Minerals

An intriguing variety of authigenic minerals are extracted in heavy mineral separates, revealing phases that are not readily detected in conventional light microscopy (Fig. 8). Sphalerite (Tieh, 1987; Milliken, 1992; Taylor and Land, 1997), barite (Bornhauser, 1940; Taylor and Land, 1997; Enos and Kyle, 2002), fluorite, titanite (Richmann et al., 1980; Milliken, 1992), anatase (Milliken, 1992), and tourmaline (Henry et al., 1997) are some of the notable authigenic heavy minerals observed in the GOM sedimentary basin.

All of the authigenic minerals listed above (with the possible exception of tourmaline) display prominent spatial localisation as replacements of detrital grains, typically, detrital feldspars and carbonate rock fragments (Fig. 9). It is also seen in Fig. 9 that the precipitation of these minerals is not entirely circumscribed by the boundaries of the replaced grain, but also includes growth into the surrounding intergranular spaces. Thus, replacement of the detrital minerals by these authigenic phases is not a volume-for-volume process, but rather a case in which the nucleation of the replacement phase is preferentially localised at the site of a dissolving grain, but is not otherwise limited by the spatial extent of the material being dissolved.

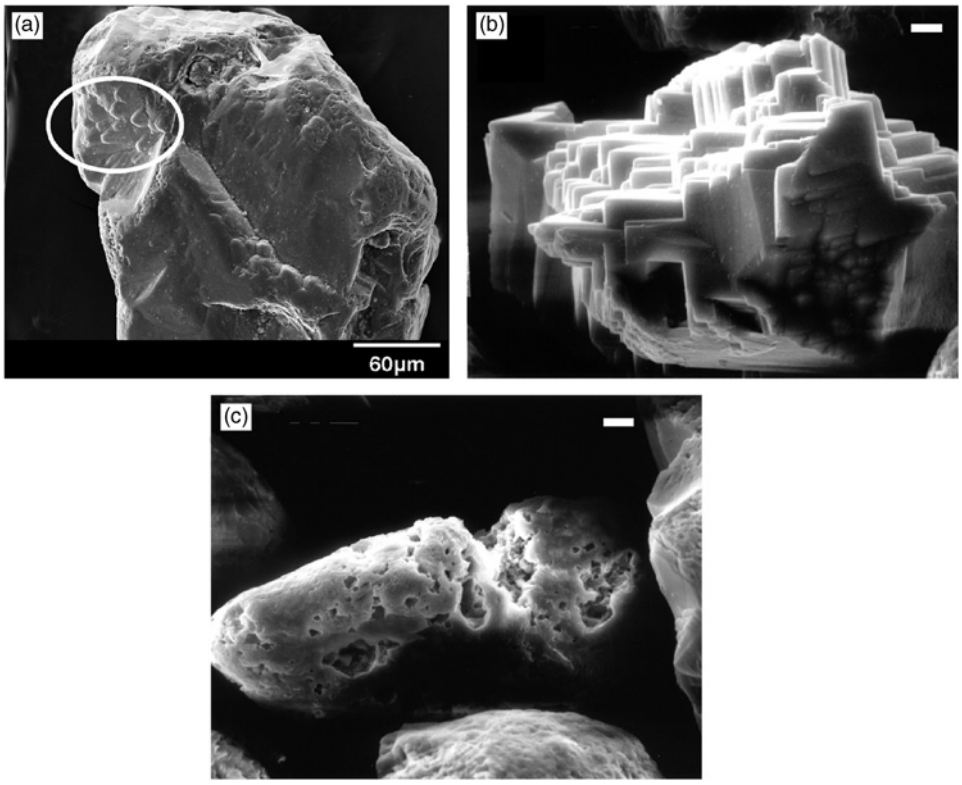

Fig. 5. Detrital garnets. White bars are 10 µm. (A) Fe (Ca, Mn) garnet (almandine or spessartine?). White circle indicates nascent dissolution features that are generally poorly developed on river garnets as compared with their subsurface counterparts. Modern, Red River. (B) Fe garnet (almandine), Miocene. South Louisiana, depth 4263 m. (C) Ca (Fe)-garnet (probable andradite), Plio-Pleistocene. Offshore Louisiana, depth 1421 m.

4. A MODEL FOR THE EVOLUTION OF HEAVY MINERALS IN BURIAL DIAGENESIS

Fig. 10 presents a conceptual model, based on observations in the GOM, for heavy mineral alteration and formation in burial diagenesis.

In the GOM, dissolution surface features observed on partially dissolved detrital heavy mineral grains are similar across modern sediments, unconsolidated sediments in the shallow subsurface, and lithified sandstones in the subsurface. In each setting, dissolution of detrital heavy minerals is clearly 'surface-reaction controlled', as described by Berner and colleagues (Berner, 1978; Berner and Schott, 1982). Like all silicate minerals prone to dissolution in aqueous solution at low temperatures, the dissolution is spatially localised at crystal defects. There is no evidence to suggest that reaction mechanisms in heavy mineral dissolution change in any way across the temperature range observed in the GOM.

Because silica and cations released from heavy mineral dissolution must be transferred into aqueous solution, it is reasonable to construe the reaction as acid

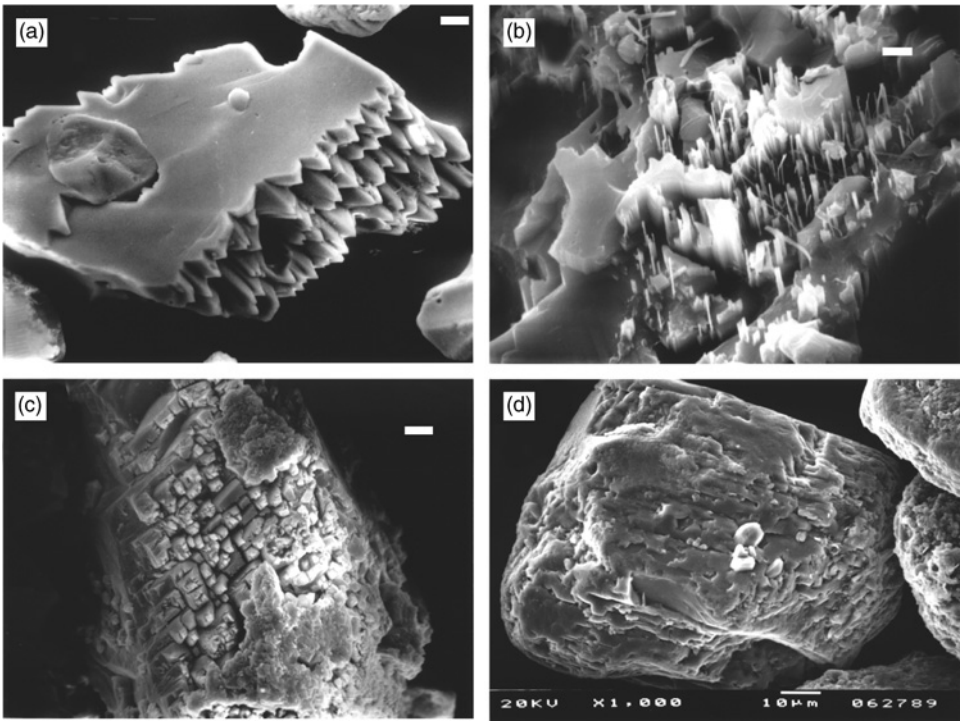

Fig. 6. Dissolution features on various detrital heavy minerals. White bars are 10 µm. (A) Staurolite. Miocene, South Louisiana, depth 2953 m. (B) Epidote. Plio-Pleistocene. Offshore Louisiana, depth 2236 m. (C) Titanite (sphene). Frio Formation, Oligocene, south Texas, 2176 m. (D) Apatite. Frio Formation, Oligocene, south Texas, 3362 m.

hydrolysis, or weathering reactions, for example for the pyroxene diopside:

$$CaMg(Si_2O_6) + 4H^+ + 2H_2O \rightarrow Ca^{2+} + Mg^{2+} + 2H_4SiO_4 \quad (1)$$

Conversely, reactions responsible for the wide variety of heavy minerals observed as authigenic phases (both silicates and non-silicates) in the GOM, can generally be written as acid-releasing, or reverse-weathering reactions, for example, for titanite:

$$Ti^{4+} + Ca^{2+} + H_4SiO_4 + H_2O \rightarrow CaTiSiO_5 + 6H^+ \quad (2)$$

The spatial patterns of authigenic heavy mineral growth (Fig. 9) support this interpretation, because the associated dissolving phases do not generally constitute adequate sources of elements required by the precipitation phase. Rather, the role of the detrital grain appears to be primarily as a site for nucleation, fostered perhaps by the local pH-buffering (acid-consumption) provided by reactions such as (1), above.

This is not to suggest that weathering and reverse-weathering (or acid-releasing) reactions, as represented in reactions (1) and (2), balance precisely among heavy mineral destruction and creation. Indeed, reactions involving heavy minerals are a miniscule portion of an overall reaction system in basinal diagenesis that is

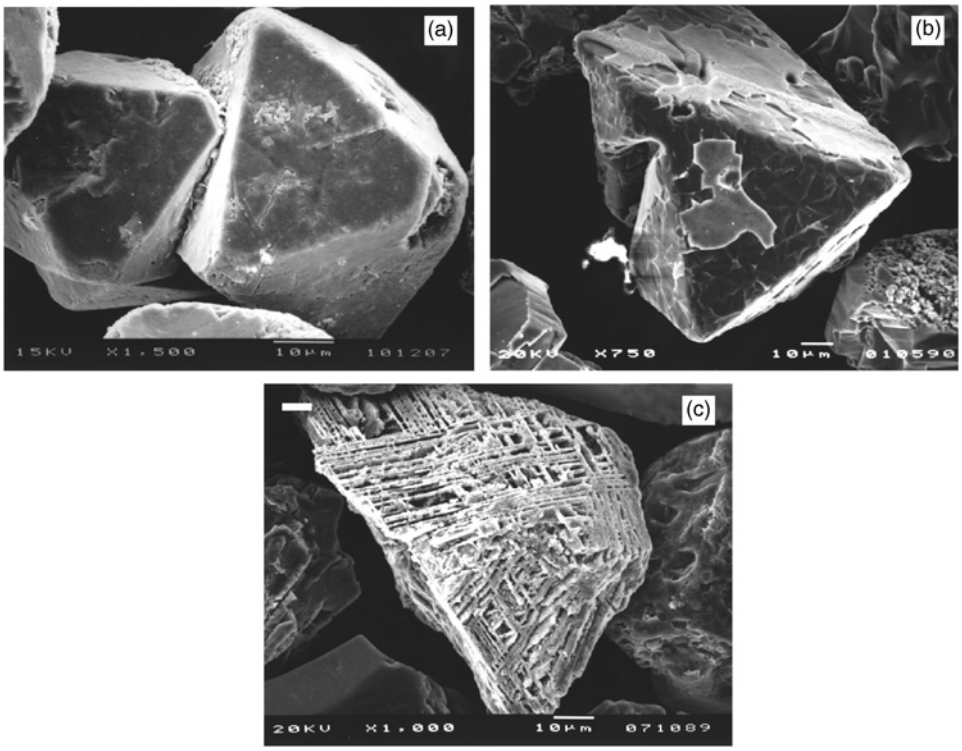

Fig. 7. Detrital Fe/Ti oxides. (A) Magnetite. Modern Rio Grande, Langtry, Texas. (B) Cr–Fe spinel. Frio Formation, Oligocene, south Texas, 2641 m. (C) Fe (Ti)-oxide (ilmenite). Frio Formation, Oligocene, south Texas, 1995 m.

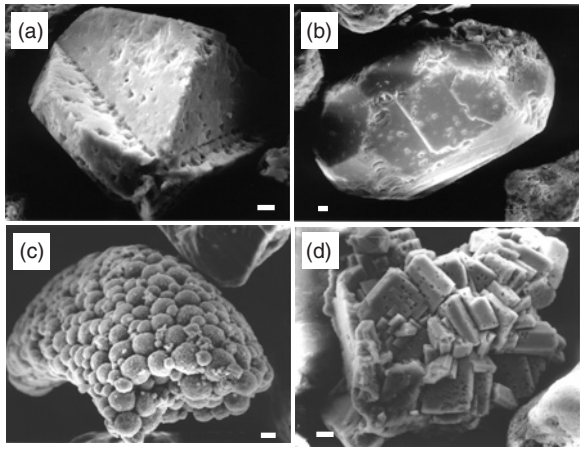

Fig. 8. Authigenic heavy minerals as they appear in heavy mineral separates. White bars are 10 µm. (A) Sphalerite. Wilcox Formation, Eocene, central Texas coast, depth 2788 m. (B) Barite. Miocene, South Louisiana, depth 4837 m. (C) Pyrite cast of foraminifer or small mollusk. Pleistocene. Offshore Louisiana, depth 434 m. (D) Anatase. Wilcox Formation, Eocene, central Texas coast, depth 1587 m.

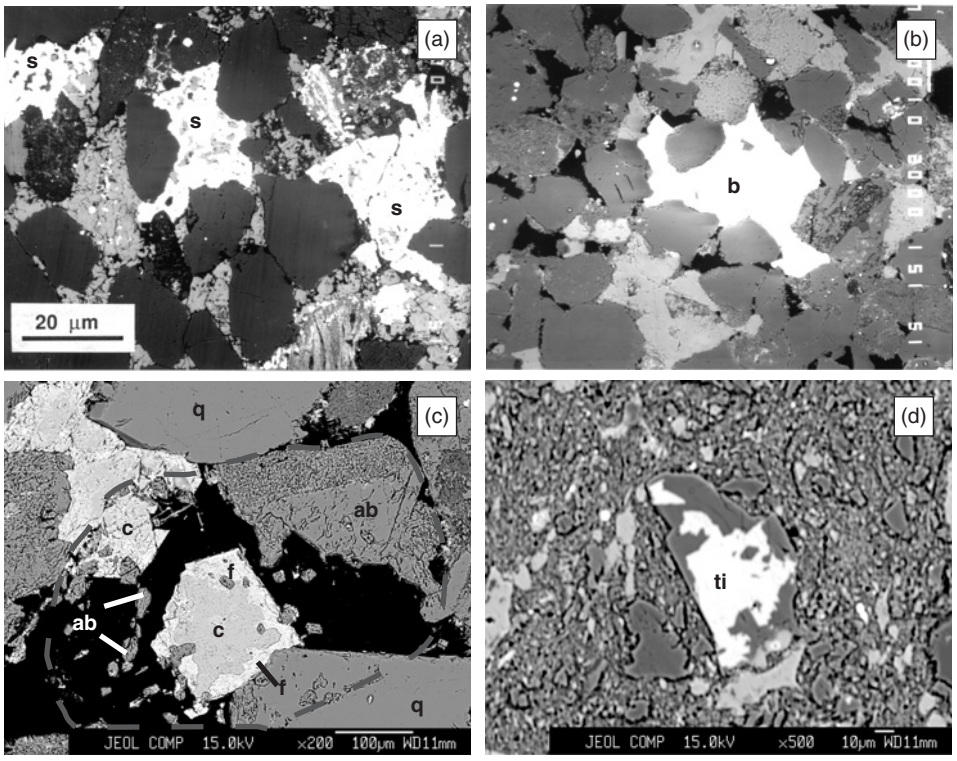

Fig. 9. Back-scattered electron images of authigenic heavy minerals, revealing their localisation as grain replacements. In all of these images porosity is black. (A) Nucleation of sphalerite (s) is highly localised on carbonate rock fragments (seen as small remnants surrounded by the sphalerite) but extends outward from these grains into the surrounding intergranular pore spaces. Wilcox Formation, Eocene, central Texas coast, depth 2788 m. (B) Similar to the sphalerite in A, the barite (b) is highly localised as a grain replacement (fills what would otherwise be an over-sized pore) but extends outward from these grains into the surrounding intergranular pore spaces. Frio Formation, Oligocene, south Texas, depth 4216 m. (C) Fluorite (f) is located within the volume of a leached replaced feldspar grain (outline) that is also replaced calcite (c), quartz (q), and albite (ab). Frio Formation, Oligocene, central Texas coast, depth 4776 m. (D) Titanite (sphene, Ti) together with albite replaces a detrital feldspar. Elsewhere in this rock, many such replaced grains preserve remnants of the original detrital K-feldspar (Milliken, 1992). Frio Formation, Oligocene, south Texas, depth 4769 m.

dominated by the volumetrically significant and highly reactive detrital clays and feldspars (Land et al., 1997; Milliken, 2004). Placement of the heavy minerals into this system however allows certain generalisations about the evolution of heavy mineral associations during basinal diagenesis (Fig. 10).

At deposition, heavy mineral populations reflect provenance, at least to the degree that weathering and depositional processes allow, and are characterised by associations of mineral species formed across a wide range of temperatures and having diverse histories of transport and recycling. As basinal diagenesis proceeds, this

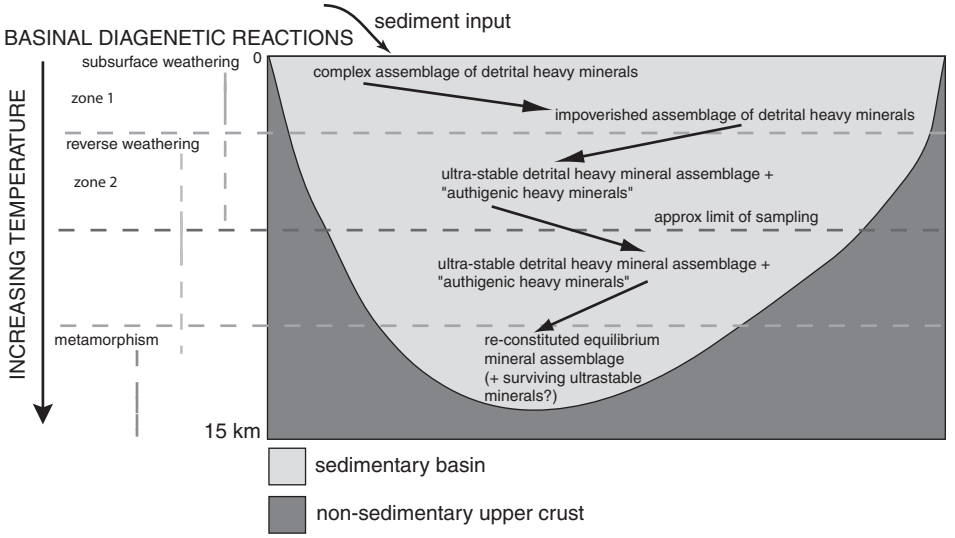

Fig. 10. A model for evolution of the sandstone heavy mineral fraction in basinal diagenesis.

primary assemblage is 'impoverished' through the progressive removal of less stable species by weathering-type reactions in the subsurface (zone 1 of Fig. 10).

At temperatures coinciding with substantial (though still not complete) removal of the reactive portion of the primary detrital assemblage ($>80^{\circ}C$), localised emplacement of a wide variety of 'new' heavy minerals begins (zone 2 of Fig. 10). Authigenic heavy minerals tend to occur as *both* cements (filling primary intergranular pore space) and as replacements of the surviving detrital grains. Spatial localisation as grain replacements (Fig. 9) is significant as evidence that these mineral precipitations serve to balance the acid requirements of the simultaneously occurring grain dissolution (subsurface weathering). In the deeper portions of the GOM subsurface weathering has reduced the detrital heavy mineral assemblage to zircon, tourmaline, rutile, and other ultrastable species. The association of ultrastable detrital heavy minerals with nascent, relatively low-temperature, reverse-weathering (or, at least, acid-releasing), grain-replacement phases is, indeed, one of the hallmarks of late diagenesis.

In ancient sandstones of poorly-known burial history, care must be taken to avoid interpreting mixed assemblages of ultrastable and authigenic heavy minerals as 'primary'. ZTR + anatase, titanite (e.g., Merino, 1975; Aldahan and Morad, 1986; Yau et al., 1987; Van Panhuys and Trewin, 1990; Milliken, 1992), epidote (Grapes et al., 2001), actinolite (e.g., De Ros et al., 1994; McKinley et al., 2001), and perhaps other 'low-rank metamorphic' phases may be the product of late burial diagenesis rather than a primary detrital association. Textural evidence on mineral habit can be used to discriminate these distinct origins. Microchemical techniques to extract provenance and stratigraphic information from ultrastable detrital heavy minerals (e.g., cathodoluminescence, back-scattered electron imaging, trace elements by electron microprobe or ICP-MS, and single-grain age determinations) are appealing avenues for research, in view of the manner in which diagenesis appears to compromise heavy mineral grain populations.

5. SUMMARY

Seven decades of heavy mineral studies in the GOM sedimentary basin have encompassed a broad range of approaches, including classic work for understanding provenance and stratigraphy as well as investigations into the diagenetic evolution of heavy mineral assemblages. At different times in the Cenozoic, GOM sediments bearing complex assemblages of heavy minerals were derived from various provenance regions across North America. At great depth however, all of these assemblages are reduced, essentially, to an ultrastable detrital assemblage of zircon, tourmaline, Ti-oxides, and a diverse group of authigenic heavy minerals. The GOM offers a dramatic case study for documenting the impact of simple burial diagenesis on heavy mineral assemblages.

ACKNOWLEDGEMENTS

Heavy mineral studies at the University of Texas at Austin have been supported by the Gulf Coast Association of Geological Societies, the Edwin Allday Chair in Subsurface Geology (L.S. Land), and the J. Nalle Gregory Chair in Sedimentary Geology (E.F. McBride) under the auspices of the Geology Foundation of the University of Texas at Austin, the National Science Foundation grant EAR-8904489, and graduate research fellowships from Texaco and Tenneco. I thank Joe Jaworski for making photographic prints of the SEM images and also Suk-Joo Choh for his assistance in creating high-quality digital scans of the prints. I greatly appreciate the encouragement from Maria Mange for the creation of this short review and also the helpful efforts of reviewers Bob Berner and Karl Ramseyer.

REFERENCES

Aldahan, A.A., Morad, S., 1986. Authigenic sphene in sandstones from the Brottum Formation (Norway) and the Dala Sandstone (Sweden). Neues Jahrbuch fuer Mineralogie, Monatshefte 1986, 135–144.

Berner, R.A., 1978. Rate control of mineral dissolution under earth surface conditions. American Journal of Science 278, 1235–1252.

Berner, R.A., Schott, O., 1982. Mechanism of pyroxene and amphibole weathering, II. Observations of soil grains. American Journal of Science 282, 1214–1231.

Boettcher, S.S., Milliken, K.L., 1994. Mesozoic–Cenozoic unroofing of the southern Appalachian Basin: apatite fission track evidence from middle Pennsylvanian sandstones. Journal of Geology 102, 655–663.

Bornhauser, M., 1940. Heavy mineral associations in quaternary and late tertiary sediments of the Gulf Coast of Louisiana and Texas. Journal of Sedimentary Petrology 10, 125–135.

Bullard, F.M., 1942. Source of beach and river sands on Gulf coast of Texas. Geological Society of America Bulletin 51, 1021–1044.

Cogen, W.M., 1940. Heavy-mineral zones of Louisiana and Texas gulf coast sediments. American Association of Petroleum Geologists Bulletin 24, 2069–2101.

Coleman, J.M., Roberts, H.H., Bryant, W.R., 1991. Late quaternary sedimentation. In: Salvador, A. (Ed.), The Gulf of Mexico Basin: The Geology of North America, v. J. Geological Society of America, Boulder, CO, pp. 325–352.

De Ros, L.F., Anjos, S.M.C., Morad, S., 1994. Authigenesis of amphibole and its relationship to the diagenetic evolution of Lower Cretaceous sandstones of the Potiguar rift basin, northeastern Brazil. Sedimentary Geology 88, 253–266.

Enos, J.S., Kyle, J.R., 2002. Diagenesis of the Carrizo sandstone at Butler Salt Dome, East Texas Basin, USA: Evidence for fluid-sediment interaction near halokinetic structures. Journal of Sedimentary Research 72, 68–81.

Flores, R.M., Shideler, G.L., 1978. Factors controlling heavy-mineral variations on the South Texas outer continental shelf, Gulf of Mexico. Journal of Sedimentary Petrology 48, 269–280.

Galloway, W.E., Bebout, D.G., Fisher, W.L., Dunlop, J.B. Jr., Cabrera-Castro, R., Lugo-Rivera, J.E., Scott, T.M., 1991. Cenozoic. In: Salvador, A. (Ed.), The Gulf of Mexico Basin: The Geology of North America, v. J. Geological Society of America, Boulder, CO, pp. 245–324.

Galloway, W.E., Ganey-Curry, P.E., Li, X., Buffler, R.T., 2000. Cenozoic depositional history of the Gulf of Mexico basin. American Association of Petroleum Geologists Bulletin 84, 1743–1774.

Goldstein, A. Jr., 1942. Sedimentary petrologic provinces of the northern Gulf of Mexico. Journal of Sedimentary Petrology 12, 77–84.

Grapes, R., Roser, B., Kashai, K., 2001. Composition of monocrystalline detrital and authigenic minerals, metamorphic grade, and provenance of Torlesse and Waipapa graywacke, central North Island, New Zealand. International Geology Review 43, 139–175.

Henry, D.J., Kirkland, B.L., Kirkland, D.W., 1997. Sector-zoned tourmaline from the cap rock of a salt dome. European Journal of Mineralogy 11, 263–280.

Hsu, K.J., 1960. Texture and mineralogy of the recent sands of the Gulf Coast. Journal of Sedimentary Petrology 30, 380–403.

Land, L.S., Mack, L.E., Milliken, K.L., Lynch, F.L., 1997. Burial diagenesis of argillaceous sediment, south Texas Gulf of Mexico sedimentary basin: a reexamination. Geological Society of America Bulletin 109, 2–15.

Loucks, R.G., Dodge, M.M., Galloway, W.E., 1984. Regional controls on diagenesis and reservoir quality in Lower Tertiary sandstones. In: McDonald, D.A., Surdam, R.C. (Eds.), Clastic Diagenesis: Memoir, v. 37. American Association of Petroleum Geologists, Tulsa, OK, pp. 15–45.

McKinley, J.M., Worden, R.H., Ruffell, A.H., 2001. Contact diagenesis; the effect of an intrusion on reservoir quality in the Triassic Sherwood Sandstone Group, Northern Ireland. Journal of Sedimentary Research 71, 484–495.

Merino, E., 1975. Diagenesis in tertiary sandstones from Kettleman North Dome, California, I. Diagenetic mineralogy. Journal of Sedimentary Petrology 45, 320–336.

Milliken, K.L., 1988. Loss of provenance information through subsurface diagenesis in Plio-Pleistocene sandstones, Gulf of Mexico. Journal of Sedimentary Petrology 58, 992–1002.

Milliken, K.L., 1992. Chemical behavior of detrital feldspars in mudrocks versus sandstones, Frio Formation (Oligocene), South Texas. Journal of Sedimentary Petrology 62, 790–801.

Milliken, K.L., 2004. Late diagenesis and mass transfer in sandstone-shale sequences. In: Mackenzie, F.T. (Ed.), Sediments, Diagenesis, and Sedimentary Rocks: Treatise on Geochemistry, Vol. 7. Elsevier-Pergamon, Oxford, pp. 159–190.

Milliken, K.L., Mack, L.E., 1990. Subsurface dissolution of heavy minerals, Frio Formation sandstones of the ancestral Rio Grande province, South Texas. Sedimentary Geology 68, 187–199.

Milliken, K.L., McBride, E.F., Land, L.S., 1989. Numerical assessment of dissolution versus replacement in the subsurface destruction of detrital feldspars, Oligocene Frio Formation, South Texas. Journal of Sedimentary Petrology 59, 740–757.

Morton, A.C., 1987. Influences of provenance and diagenesis on detrital garnet suites in Paleogene Forties Sandstone, Central North Sea. Journal of Sedimentary Petrology 57, 1027–1032.

Pettijohn, F.J., 1941. Persistence of heavy minerals with geologic age. Journal of Geology 49, 612–625.

Richmann, D.-L., Milliken, K.L., Loucks, R.G., Dodge, M.M., 1980. Mineralogy, diagenesis, and porosity in Vicksburg sandstones, McAllen Ranch Field, Hidalgo County, Texas. Gulf Coast Association of Geological Societies Transactions 30, 473–481.

Russell, R.-D., 1937. Mineral composition of Mississippi river sands. Geological Society of American Bulletin 48, 1307–1348.

Salvador, A., 1991a. Introduction. In: Salvador, A. (Ed.), The Gulf of Mexico Basin: The Geology of North America, v. J. Geological Society of America, Boulder, CO, pp. 1–12.

Salvador, A., 1991b. Origin and development of the Gulf of Mexico basin. In: Salvador, A. (Ed.), The Gulf of Mexico Basin: The Geology of North America, v. J. Geological Society of America, Boulder, CO, pp. 389–444.

Taylor, T.R., Land, L.S., 1997. Association of allochthonous waters and reservoir enhancement in deeply buried Miocene sandstones: Picaroon Field, Corsair Trend, Offshore Texas. In: Crossey, L.J., Loucks, R.G., Totten, M.W. (Eds.), Siliciclastic Diagenesis and Fluid Flow: Concepts and Applications: Special Publication, Vol. 55. Society for Sedimentary Geology, Tulsa, OK, pp. 37–48.

Tieh, T.T., 1987. Sphalerite in sandstone and limestones of the Gulf Coast and north Texas. Economic Geology 82, 1064–1069.

Van Andel, T.-H., Poole, D.M., 1960. Sources of recent sediments in the northern Gulf of Mexico. Journal of Sedimentary Petrology 30, 91–122.

Van Panhuys, M., Trewin, N.H., 1990. Authigenic sphene cement in Permian sandstones from Arran. Scottish Journal of Geology 26, 139–144.

Winker, C.D., 1981. Cenozoic shelf margins, northwestern Gulf of Mexico basin: recognition of shallow-water structure-affected formations of the Gulf Coast Basin. In: Perkins, B.F., Ventress, W.P.S., Edwards, M.B. (Eds.), Cenozoic Shelf Margins, Northwestern Gulf of Mexico Basin, Society of Economic Paleontologists and Mineralogists, Gulf Coast Section, Annual Research Conference, vol. 2, pp. 74–82.

Yau, Y.-C., Peacor, D.R., Essene, E.J., 1987. Authigenic anatase and titanite in shales from the Salton Sea geothermal field, California. Neues Jahrbuch für Mineralogie, Monatshefte 1987, 441–452.

This page intentionally left blank

Chapter 9

EFFECTS OF HYDROTHERMAL FLUIDS ON THE HEAVY MINERAL ASSEMBLAGE OF A LATE PLEISTOCENE SUCCESSION DEPOSITED IN AN OCEANIC RIDGE VALLEY (ESCANABA TROUGH, JUAN DE FUCA PLATE)

GIAN G. ZUFFA AND FRANCESCA SERRA

Dipartimento di Scienze della Terra e Geologico-Ambientali Università di Bologna, Via Zamboni, 67, 40127 Bologna, Italy

ABSTRACT

This short contribution deals with the behaviour and modification of heavy mineral assemblages in a 500 m-thick turbidite succession deposited in the rift valley of the 3300 m deep Escanaba Trough of the Juan de Fuca Plate. To our knowledge, there have been no previous studies on the effects of hydrothermal fluid circulation on heavy minerals in such an active geochemical environment.

The sediments were transported mainly from glacial lakes of the Columbia drainage basin by cataclysmic floods during the last 60 ka. Climatic and sediment transport conditions imply minor weathering of the source rocks, with little sorting and mechanical abrasion of heavy minerals during transit. Our results indicate that the heavy minerals experienced severe chemical etching and dissolution by circulating hydrothermal pore fluids that caused, at various depths, the complete loss of particular species, especially the chemically highly unstable ortho- and clinopyroxenes. These specific geochemical conditions also generated new minerals, mainly titanite, iron-rich magnesite, barite, and pyrite. However, at present there is insufficient data to fully constrain the kinetics of dissolution of the various minerals as a function of pH, temperature, composition of pore fluids, and sediment-permeability. The length of time during which the sediments were affected by pore fluid movements is constrained by the very young (Late Pleistocene, ~60 ka) age of the sediments.

Keywords: heavy minerals; hydrothermal fluids; Pleistocene; Escanaba Trough; turbidite

Developments in Sedimentology, Vol. 58, 263–276

ISSN: 0070-4571/doi:10.1016/S0070-4571(07)58009-X

1. INTRODUCTION

Adding data of heavy mineral analyses to the bulk composition of arenites may greatly augment the accuracy of provenance and palaeogeographic reconstructions (Zuffa, 1987; Zattin and Zuffa, 2004) if parameters controlling the final composition of sediments can be assessed.

Numerous studies have been conducted on a large variety of sedimentary systems in order to better understand the influence of processes known to mask or severely modify original heavy mineral assemblages (Zattin and Zuffa, 2004; and references therein). These studies have provided clues to the recognition of heavy mineral response to conditions in a particular sedimentary environment and contributed to increased knowledge by which heavy mineral data can be reliably evaluated. Nevertheless, more research remains to be conducted through selected case studies, including the exploration of heavy mineral behaviour in rarely studied, unusual geochemical environments.

The aim of this contribution is to show the effects of hydrothermal pore fluid circulation in Late Pleistocene turbidites deposited in an oceanic spreading centre. Importantly, in the present case, the influence of weathering in the source area, sorting and mechanical abrasion during transport, and burial diagenesis (the succession is only 500 m-thick), that may potentially influence the ultimate heavy mineral suite (Morton and Hallsworth, 1999; and references therein) is considered to be minor or absent. Bearing in mind that changes in bulk composition are minor or absent, only hydrothermal pore fluid circulation and compositional changes in the sediment supply can be considered responsible for the observed down-hole pattern of heavy mineral variations.

2. GEOLOGICAL SETTING

The Escanaba Trough, which forms the southeastern limit of the axial valley of the actively spreading Gorda Ridge (Juan De Fuca Plate) (Fig. 1), is filled by turbidite strata locally exceeding 500 m in thickness. Centres of igneous activity spaced approximately 15 km apart along the rift axis of Escanaba Trough (grey areas in Fig. 1b) are sites of hydrothermal discharge and formation of massive-sulphide deposits (Shipboard Scientific Party, 1998b). Hydrothermal fluids, driven by heat from these igneous centres, migrate vertically along faults toward the surface, and horizontally within the porous turbidite sands.

The turbidite deposits were drilled by DSDP and ODP in 1970 and 1996, during Legs 5, and 169; the first author was aboard as a sedimentologist during Leg 169. Drilling at Site 35 reached a hole depth of 390 m, with a poor recovery (Moore and Sharman, 1970). Hole 1037B, with a nearly complete recovery, was drilled as a "reference hole" to assess the stratigraphy and thermal evolution in an area further away from a hydrothermal upflow zone (Shipboard Scientific Party, 1998b). Basaltic rocks, that appear to be a thick ponded flow, were cored from 507.8 to 546 metres below sea floor (mbsf) (Zierenberg et al., 2000). By contrast, Hole 1038I (Fig. 1b) was drilled close to the centre of an upflow zone (Central Hills) (Shipboard Scientific Party, 1998c). At this site, the temperatures of fluids are far higher than in the other

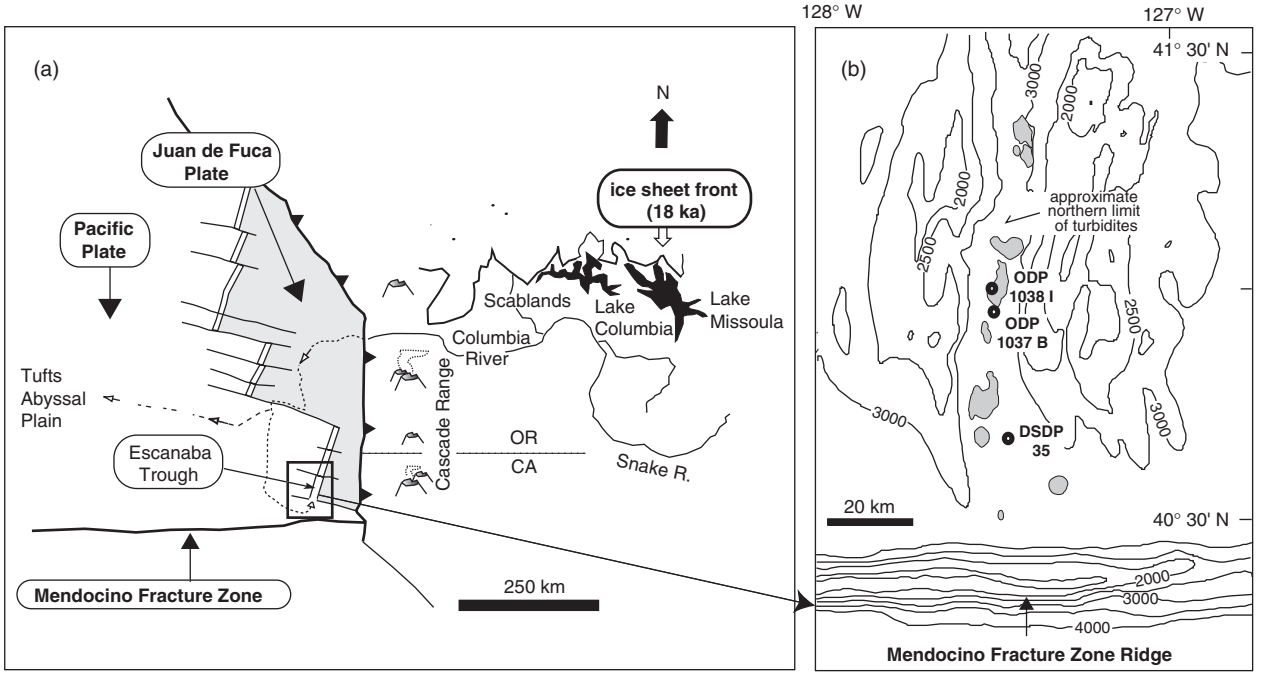

Fig. 1. (a) Schematic map showing glacial lakes (in black) and probable submarine pathway (heavy dashed line) to Escanaba Trough and Tufts abyssal plain of the sediment carried by cataclysmic floods from the glacial lakes passing through the Columbia River drainage basin. (b) Bathymetric map of Escanaba Trough showing igneous centres (grey areas) and location of ODP Sites 1038 and 1037, and DSDP Site 35 (see lithostratigraphic columns in Fig. 2).

two holes, and composition of pore-fluid chemistry shows prominent down-hole variations. The base of the cored section at 403 mbsf consists of a basaltic sill which was probably intruded near the base of the succession (Zierenberg et al., 2000).

Results of earlier studies on core stratigraphy, sand composition, and age dating for the sediments in the three holes have appeared in several publications (Zuffa et al., 1997, 2000; Brunner et al., 1999). The upper 317 m of the turbidite strata recovered in Hole 1037B (Fig. 2) were deposited during the last 32182 ± 200 year, and the bottom of the succession is likely to date back to the beginning of Marine Isotope Stage 3 ($\sim$60 ka) (Zuffa et al., 2000). Sediment, mainly derived from the Columbia River's drainage basin, reached the Escanaba Trough through the Cascadia Channel, running along the north flank of the Mendocino Fracture Zone and entering the oceanic rift valley flowing towards the north (Fig. 1a). Age, sediment composition, and the very high depositional rates indicate that most of the turbidite beds were derived from lake outbursts during deglaciation periods. The cataclysmic floods from the glacial lakes continued flowing as hyperpycnally generated turbidity currents on entering the sea at the mouth of the Columbia River, and were able to reach the Escanaba Trough resulting in a submarine transport path of >1100 km (Zuffa et al., 2000).

3. METHODS

Sands are generally very fine grained, in the average range of 62.5–125 μm; only a few samples are of medium grain size. The samples collected from the coarser-grained core intervals (Fig. 2) were processed by wet sieving to remove the <62 μm fraction in order to facilitate preparing thin sections of impregnated sands and heavy mineral grain mounts. Point-counting of 43 thin sections was performed using the criteria proposed by Gazzi (1966), Dickinson (1970), and Zuffa (1985, 1987) that minimise drawbacks arising from grain size variations. From 300 to 400 grains were counted in thin sections, stained for K-feldspar and used for sand-classifications (Fig. 3). Data for Holes 1038I and 1037B, dealt with earlier by Zuffa et al. (2000), are not presented here but, on request, are available from the Journal of Geology Office free of charge. Data for hole at Site 35 were published in Zuffa et al. (1997).

Heavy minerals were separated in tetrabromo-ethane (density 2.96 g/cm^3) using the 250–62.5 μm size range. Grain counts on 42 heavy mineral grain mounts were made by inspecting narrow bands on the slide and recording a number of mineral grain categories (i.e., transparent grains, opaques, turbids) as suggested by Gazzi et al. (1973, p. 26). In each sample, about 200 transparent grains were identified and point counted. Three samples, analysed earlier by Vallier et al. (1973), have also been included in Table 1 in order to collate the results as a complete set of the analysed samples published for Site 35 (McManus et al., 1970; Vallier, 1970; Vallier et al., 1973).

4. RESULTS

Results from the framework components, plotted in QFL diagrams (Dickinson and Suczek, 1979), indicate a provenance from a transitional/dissected magmatic arc. The composition of sands from the Columbia River, studied by Whetten et al.

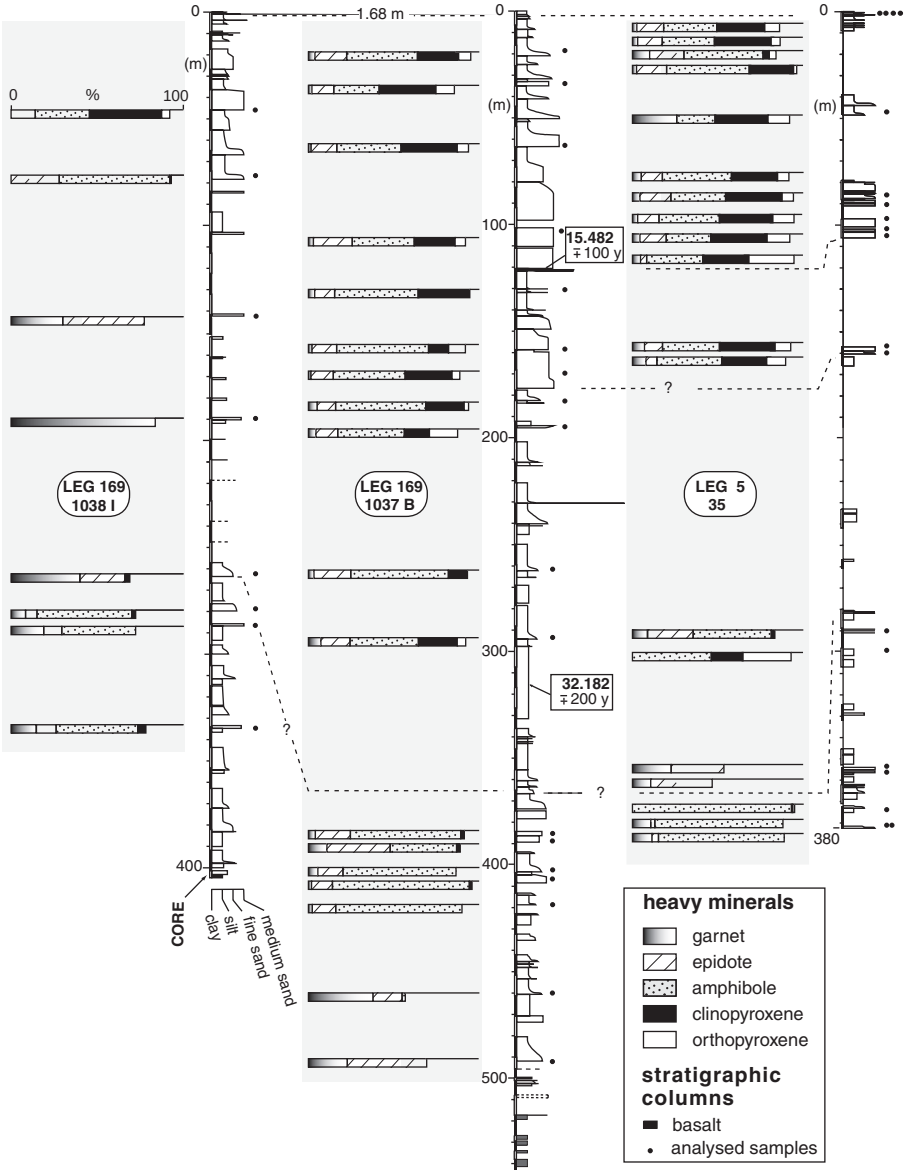

Fig. 2. Lithostratigraphic columns for the ODP Holes 1038I and 1037B, and DSDP Site 35. Dashed lines show probable correlation of the three holes. Stacked bar charts show the down-hole distribution of garnet, epidote (including pistacite, clinozoisite, and allanite), amphibole (including hornblende, oxy-hornblende, and actinolite), clino- and orthopyroxene. Data from Vallier et al. (1973), and Zuffa et al. (1997, 2000).

(1969), corresponds closely to that of the Escanaba sand, sampled during Legs 5 and 169. The bulk of the detritus was derived dominantly from volcanic sources (Cascade Range) and from minor dissected crystalline basement rocks of the Columbia drainage system (Fig. 1a).

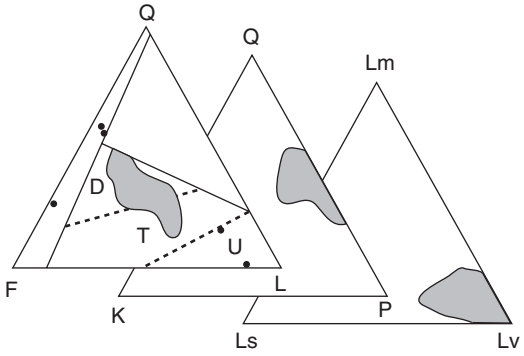

Fig. 3. Composition of the Late Quaternary Escanaba Trough sands (data from Zuffa et al. (1997, 2000)). Q, quartz; F, feldspar; L, lithic fragments, K, k-feldspar; P, plagioclase; Lm, lithic metamorphic; Ls, lithic sedimentary; Lv, lithic volcanic; D, dissected arc; T, transitional arc; U, undissected arc. Classification diagrams according to Dickinson and Suczek (1979).

The proportion of the heavy mineral contents of the 62.5–250 μm grain size fraction in Holes 35 and 1037B decreases down-hole, although locally unusually low abundances are present at intermediate depths. Hole 1038I shows almost constantly low values (Fig. 4).

The heavy mineral assemblage (Table 1) is characterised by abundant amphiboles (brown-green, green and blue-green hornblende, oxy-hornblende, and actinolite), clinopyroxene (augite and titanaugite), orthopyroxene (bronzite and hypersthene), and epidotes (clinozoisite/epidote) (Fig. 2). Garnet is present in almost all samples, but in highly variable quantities. Other characteristic minerals such as allanite, zoisite, olivine, chloritoid, staurolite, glaucophane, sillimanite, kyanite, andalusite, monazite, and spinel occur irregularly in small or trace amounts. Titanite, barite, and iron-rich magnesite are present locally, mostly as authigenic minerals. The down-hole heavy mineral distribution at sites 35 and 1037B shows a transition from an amphibole/clino- and orthopyroxene assemblage to an amphibole-rich suite.

Titanite, iron-rich magnesite, and barite (mostly formed by authigenesis) are particularly abundant in the lower interval of Hole 1037B and at Site 35 (Figs. 5 and 6A). In Hole 1038I, titanite occurs at various depths and iron-rich magnesite is abundant in the lower interval. Authigenic spherical grains and aggregates of pyrite laths are present in most of the analysed samples (Fig. 6d in Zuffa et al., 1997).

In Hole 1037B (reference site) the upper, amphibole/clino- and orthopyroxene assemblage changes gradually down-hole to an amphibole-rich clinopyroxene assemblage, and the deepest sediments—directly above the underlying basalts—are characterised by a garnet–epidote association. Ratios of stable/stable + unstable heavy minerals versus depth (Fig. 7) show that medium and high ratio values, caused by loss of unstable minerals, occur only below 389 mbsf. However, two samples at 406 and 418 mbsf display low ratio values compared to samples from the upper part of the hole. The pH values range between 7.1 and 7.9 without showing any trend. The measured geothermal gradient of about 0.16°C/m yields an estimated temperature of about 84°C at the base of the sedimentary succession (~508 mbsf) above the basaltic basement. The sediments below the deepest sample analysed in this study

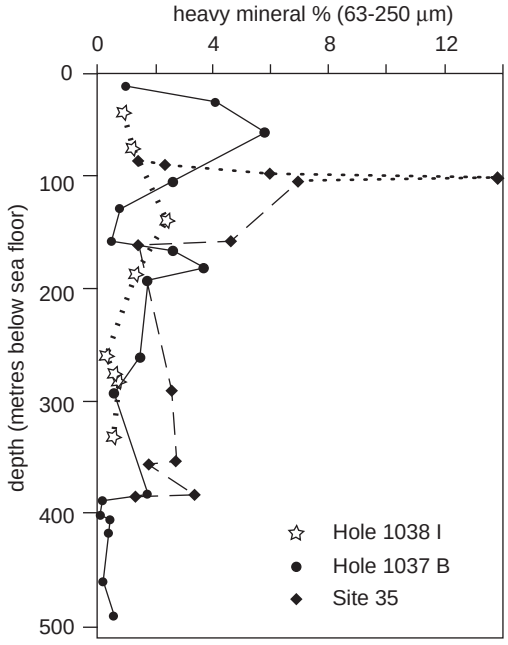

Fig. 4. Down-hole percentages of heavy mineral contents for ODP Holes 1038I and 1037B, and DSDP Site 35. Data from Vallier et al. (1973) and Zuffa et al. (1997, 2000). Heavy mineral percentages are calculated weight of the total heavy mineral (63–250 µm) fraction/weight of the bulk 63–250 µm sand fraction × 100.

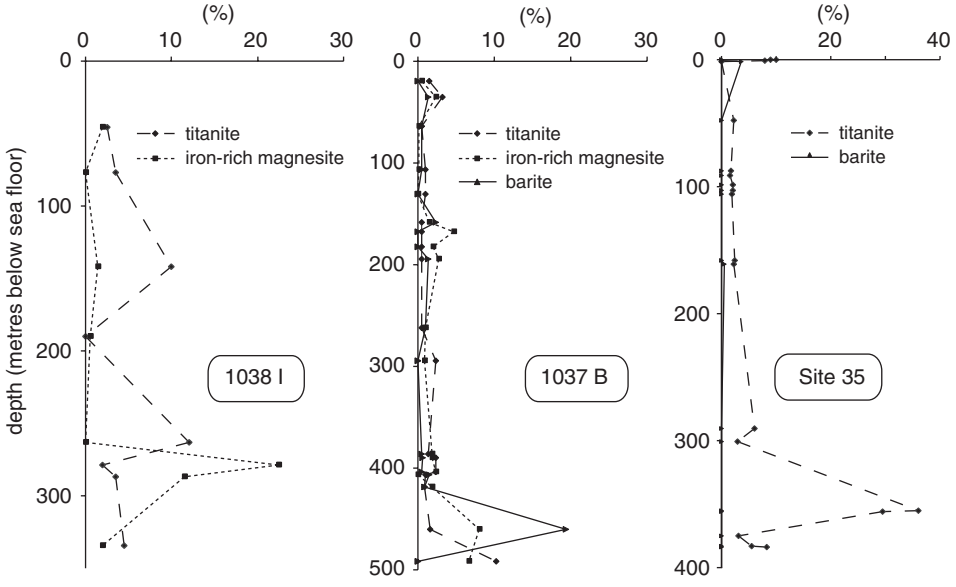

Fig. 5. Down-hole distribution of mostly authigenic heavy minerals for ODP Holes 1038I and 1037B, and DSDP Site 35. Data from Vallier et al. (1973) and Zuffa et al. (1997, 2000).

Table 1. Composition of the heavy mineral fraction of samples from ODP Holes 1038I, and 1037B, and DSDP Site 35

	Hole 1038 I								Hole 1037 B														
Samples	104	108	110	110a	111/111a	113/113a	114	119/119a	9	14	18	24	26	29/29a	30	33/33a	34	40/40a	40b	51a	52	53	
Depth (mbsf)	45.69	77.15	141.79	189.87	262.99	279.00	286.95	334.49	19.7	35.4	64.0	106.3	130.1	158.7	168.0	182.8	194.7	262.2	294.2	385.9	389.5	403.5	
Heavy minerals/(2–4 phi)%	0.9	1.1	2.3	1.1	0.1	0.5	0.7	0.4	1.0	4.0	5.8	2.6	0.9	0.4	2.6	3.7	1.7	1.5	0.5	1.7	0.1	0.1	
Opaques	7.9	9.8	31.9	17.0	NA	4.4	5.9	12.7	37.7	17.4	15.5	6.0	21.1	56.6	66.6	20.7	79.1	50.0	11.6	6.1	66.9	72.0	
Turbids	4.8	4.7	1.9	2.0	NA	7.1	2.7	3.0	3.8	1.9	2.3	5.2	0.8		1.6	4.1	0.6	4.9	3.6	13.7	3.0	0.8	
Transparents	87.3	85.5	66.2	81.0	NA	88.5	91.3	84.4	58.5	80.7	82.2	88.8	78.1	43.4	31.8	75.2	20.4	45.1	84.7	80.2	30.1	27.2	
Total	100.0	100.0	100.0	100.0		100.0	100.0	100.0	100.0	100.0	100.0	100.0	100.0	100.0	100.0	100.0	100.0	100.0	100.0	100.0	100.0	100.0	
Zircon	0.5		2.4	2.0	4.8			0.5		1.4			0.5	0.5	tr	1.5	0.9	1.0			1.2		
Tourmaline	0.5	0.5	1.0	1.5		0.5	0.5	0.5	1.0			1.9		0.5	1.9		2.3	0.5	0.5	0.9	0.6	0.9	
Rutile			0.5	1.5		tr	0.5	tr	0.5	0.5		0.5			0.5		0.5						
Garnet			30.0	83.5	39.8	8.0	18.5	14.5	3.0	1.4	0.5	1.9	2.9	1.4	0.9	4.4	3.7	2.5	6.6	3.3	10.5	4.7	
Titanite	2.5	3.5	10.0		12.0	2.0	3.5	4.5	1.5	3.2	0.5	1.0	1.0	0.5	0.5	0.5	0.5	0.5	2.4	1.4	2.3	2.4	
Allanite			2.9					0.5	1.5		0.5				0.5	0.5		0.5		0.9	0.6	0.5	
Epidote	14.5	28.0	47.6		26.5	6.5	10.5	11.5	18.5	12.4	15.6	19.9	11.3	12.9	13.0	11.3	12.4	19.3	16.6	20.9	37.4	14.7	
Zoisite						0.5	0.5		0.5	0.9	0.5	3.9	0.5	1.9			0.9	2.5	0.5	0.5		0.9	
Chloritoid		1.0		2.0	4.8	1.5	3.0	5.0									1.4	0.5				0.9	
Staurolite	0.5				3.6		4.0	3.5			0.5	0.5			0.5	0.5	0.5					0.9	
Kyanite					4.8		1.0	4.0	tr	0.9	0.5	0.5	0.5	0.5	1.9	0.5		0.5		0.9	1.2	0.5	
Andalusite	0.5																					0.5	
Sillimanite																					0.6		
Glaucophane								tr					1.5										
Actinolite	3.5	6.0				8.5	4.0	4.0	5.0	2.3	2.8	8.7	6.9	8.6	3.3	10.3	3.2	6.9	0.9	13.7	1.2	1.9	
Hornblende	26.0	57.5			2.4	46.0	39.0	42.0	34.5	23.5	34.0	25.7	42.2	44.5	37.7	40.9	35.5	50.0	38.3	50.3	36.9	63.0	
Oxy-hornblende	2.0	0.5						1.5	1.5		tr	1.0		tr	0.9	1.0	tr		0.9				
Clinopyroxene	42.0	1.5				2.0		5.0	25.0	34.1	33.0	24.3	29.9	12.4	27.9	23.2	14.7	11.4	23.2	1.9	2.3		
Orthopyroxene	4.5					0.5			6.5	10.6	6.6	5.8		9.6	4.2	2.0	16.6		4.7			0.5	
Olivine							0.5				0.5				0.9		1.4						
Spinel	0.5	0.5	0.5							0.5	0.9			0.5								0.5	
Apatite		0.5	3.8	7.5			3.0	1.0		2.3	1.4	1.0	1.0						1.9	0.5		0.5	
Corundum						0.5																	
Monazite	0.5	0.5			1.2	1.0			tr	1.8	0.9	0.5	1.5		0.5	1.0	0.5			0.5	2.3	2.4	
Iron-rich magnesite	2.0		1.4	0.5		22.5	11.5	2.0	0.5	2.3	tr	tr		1.4	4.7	2.0	2.8	1.0	0.9	1.9	1.8	2.4	
Anatase and brookite				1.5						0.5	0.9		0.5	1.0			0.5		1.4	0.9	0.6	0.9	
Barite										1.4	0.5	0.5		2.4			1.4	1.0		0.5	0.6	0.5	
Undetermined									0.5			2.4		1.4	0.5	0.5	0.5	2.0	0.9	0.9		0.5	
Total	100.0	100.0	100.1	100.0	99.9	100.0	100.0	100.0	100.0	100.0	100.0	100.0	100.0	100.0	100.0	100.0	100.0	100.1	100.0	99.9	100.1	100.0	

Note: NA, data not available; tr, trace. Data for the three samples in parentheses (2_6), (11_2), and (16_2) are from Vallier et al. (1973).

Hole 1037 B				DSDP Site 35																	
54	54a	57/57a	61/61a	28G	26G	27G	25G	(2_6)	3_6	4_2	5_1	5_4	5_6	6_1	6_3	10_1	(11_2)	14_1	14_2	(16_2)	17_1a	17_1b
406.4	418.6	460.6	491.2	0.12	0.34	0.71	1.18	87.2	90.9	98.5	99.9	102.9	104.3	105.9	158.1	158.7	161.3	290.2	354.9	355.9	383.2	383.5
0.4	0.4	0.1	0.5	NA	NA	NA	NA	NA	1.4	2.4	6.0	13.7	6.9	4.6	1.3	2.5	NA	2.7	1.8	NA	1.5	3.3
16.6	12.6	57.3	71.6	10.5	19.0	92.8	73.0	2.0	17.9	25.2	18.8	32.4	25.9	20.3	18.7	23.2	4.3	78.4	91.4	15.0	27.0	11.9
6.4	0.4	3.2	0.4	2.0	2.0	0.5	6.6		2.5	3.3	2.7	7.5	3.7	3.1	2.7	1.9		0.9	1.0		1.8	2.6
77.0	87.0	39.5	28.1	87.5	79.0	6.7	20.4	98.0	79.6	71.5	78.5	60.1	70.4	76.6	78.6	74.9	95.7	20.7	7.6	85.0	71.2	85.5
100.0	100.0	100.0	100.0	100.0	100.0	100.0	100.0	100.0	100.0	100.0	100.0	100.0	100.0	100.0	100.0	100.0	100.0	100.0	100.0	100.0	100.0	100.0
	0.5		0.9	0.5		2.0			0.9			1.0	1.4	1.5	1.3	1.0		5.0	5.9		1.5	2.0
0.5	1.4		1.3	1.5	1.0	1.0		0.5	1.4		0.5	0.5	tr		0.6	2.0	tr			tr		
		1.6	0.4	0.5	tr				0.4			0.5	tr	1.0	tr	1.5						
1.0	1.9	37.1	21.9	1.5	2.0	9.0	1.8	25.2	4.5	3.6	3.0	3.7	4.2	6.0	7.4	8.0	1.7	22.0	10.3		10.5	11.3
1.0	0.9	1.6	10.3	9.0	10.0	8.0		2.2	1.8	1.5	2.0	2.1	1.9	2.5	2.2	6.0	3.0	36.0	29.4	3.1	5.5	8.2
0.5	0.0		1.3	1.0	0.5						0.5	1.0		0.5		1.0		3.0	1.5		2.0	tr
13.2	14.0	17.7	46.4	13.0	12.5	20.0	17.8	0.5	10.6	16.4	11.5	14.5	2.8	10.0	6.8	27.0	0.6	25.0	36.7		2.5	3.6
	0.5			3.5	3.0	1.0			2.3	2.6	1.5	1.6	0.5	1.5	0.6	1.0		6.0				0.5
		8.1	0.4									0.5		tr		0.5						
								0.5	0.4				tr		tr		tr					
0.5					tr		tr		0.4	0.5	0.5	0.5	tr	0.5	0.6	0.5						
				0.5											1.1							
	0.5				0.5					0.5			0.5									
6.4	14.0			3.5	2.0	1.0	3.6		2.7	1.0	2.0	1.0	3.8	2.5	2.2	3.5					2.5	2.6
72.6	58.1	1.6		27.0	27.5	43.0	44.6	19.3	36.6	29.3	31.5	22.3	29.2	27.5	32.4	42.0	31.6	0.5		91.2	73.0	71.3
0.5	0.5			0.5	0.5	2.0		2.6	0.9	1.5	1.5	2.6	0.5	2.5	2.8	tr	12.4			2.2		
1.5	0.5			28.0	34.0	4.0	26.8	31.9	27.5	33.4	31.5	33.7	27.4	34.0	26.7	2.5	18.7			1.4		
				9.0	5.0	4.0	1.8	12.7	6.9	6.7	13.0	12.9	26.4	9.0	11.3		28.6			0.3		
				0.5				0.5	0.4	1.0	0.5	1.6	0.5				0.1			1.3		
				0.5	0.5	2.0			1.4	0.5				tr		0.5						
	3.7	4.8	9.4		0.5	1.0								1.0		2.5		2.0	16.2		2.5	
0.5	0.5		0.4																			
	1.9	8.1	6.7																			
0.5	tr		0.4																			
1.5	0.9	19.4					3.6								0.6							
	0.5				0.5	2.0		0.5	0.9	1.5	0.5		0.9		3.4	0.5	3.3	0.5		0.5		0.5
100.2	100.0	100.0	100.0	100.0	100.0	100.0	100.0	96.4	100.0	100.0	100.0	100.0	100.0	100.0	100.0	100.0	100.0	100.0	100.0	100.0	100.0	100.0

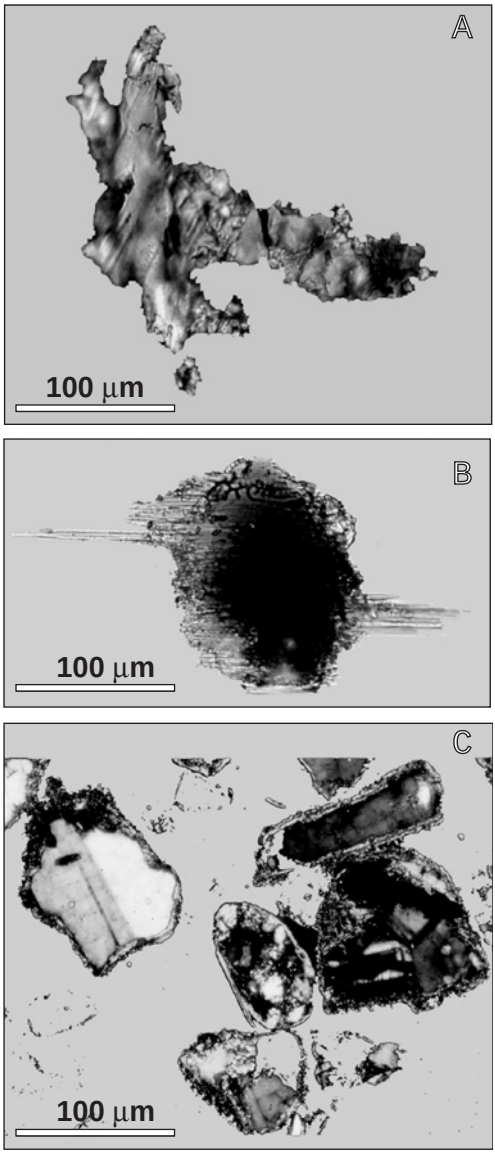

Fig. 6. Representative heavy mineral grains of the Escanaba Trough cores (see Fig. 2 for sample location). (A) Authigenic titanite from DSDP Site 35 sample depth: 354.9–355.9 mbsf (crossed-polars). (B) Etched blue amphibole from DSDP Site 35; sample depth: 383.2–393.2 mbsf. (C) Altered light minerals with clay rims from DSDP Site 35: sample depth 0.7 mbsf.

(silicified calcareous claystone) have been thermally altered and contain authigenic Mg-hornblende crystals formed in vugs by hot fluid circulation through extensional fractures. Below 450 mbsf, the organic matter is thermally altered (Shipboard Scientific Party, 1998a). Down-hole changes in pore-fluid geochemistry below

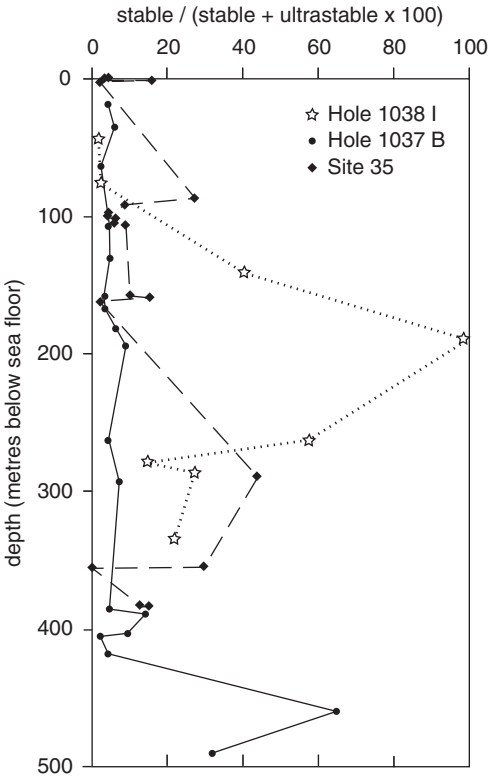

Fig. 7. Ratios of stable/(stable + unstable) × 100 heavy minerals versus depth. Unstable: allanite, epidote, zoisite, staurolite, kyanite, andalusite, sillimanite, glaucophane, actinolite, hornblende, oxy-hornblende, clinopyroxene, orthopyroxene, olivine, corundum, anatase, and brookite. Stable and ultrastable: zircon, tourmaline, rutile, garnet, chloritoid, spinel, monazite. Titanite, iron-rich magnesite, and barite are not included because of their diagenetic origin.

360 mbsf were first thought to be a signature of provenance change (Shipboard Scientific Party, 1998b) adopting the explanation of Vallier et al. (1973) and Zuffa et al. (1997). However, it has been reinterpreted later by Zuffa et al. (2000) as the impact of hot fluid circulation in the lower part of the succession. This conclusion is preferred here, based mainly on the absence of significant changes in gross composition, and the lack of evidence for renewed sediment flux to the Escanaba Trough from the rivers debouching to the south of the Columbia River mouth. Geochemical changes in pore water profile are thus related to the hydrothermal alteration of sediments in the bottom of the section coinciding with the loss of unstable heavy minerals.

Variations in the heavy mineral assemblage in Hole 1038I are somewhat similar to those described in Hole 1037B, but some samples contain only garnet and epidote, or garnet alone at intermediate depths (i.e., samples at 141.8, 189.9, 263.0 mbsf). Nonetheless, in the bottom sample at 334.5 mbsf, clinopyroxene is present whereas orthopyroxene appears only in the uppermost sample (45.7 mbsf). Ratios of stable/stable + unstable heavy minerals versus depth show high values at intermediate depth.

Medium values are clustered in the lower part of the succession, while pH ranges between 6.6 and 7.6 but no appreciable trend can be observed. The average geothermal gradient is about 2°C/m and shows that the estimated temperatures are much higher here than in Hole 1037B above the basalt at the base of the succession (403.2 mbsf). The organic matter is thermally altered and bitumen fluorescence indicates high maturation temperatures of 150–250°C (Shipboard Scientific Party, 1998c).

In the hole at Site 35, variations in the heavy mineral assemblage are once more comparable to those described in Hole 1037B. The garnet–epidote association is found at ~355 mbsf but the bottom samples from 374.5 and 383.5 mbsf are characterised by a garnet–amphibole association. Ratios of stable/stable + unstable heavy minerals versus depth are very irregular and show medium and high values at different depths.

The down-hole transition observed from an amphibole/clino- and orthopyroxene to an amphibole-rich assemblage or to a garnet–epidote dominated suite, could indicate a change in source area composition, but changes in the bulk composition do not support this interpretation (Fig. 3). The strong variations of the heavy mineral assemblage, and the anomalous distribution of authigenic minerals can be interpreted in terms of hydrothermal alteration affecting the sediments. This is also indicated by distinct corrosion on several pyroxene, amphibole, and epidote grains, also on volcanic rock fragments and feldspars in the light fraction, and by clay alteration rims around these grains (Figs. 6B, C). A depleted, garnet–epidote-dominated association occurs also in samples of the intermediate part of Hole 1038I (Fig. 2, samples at 141.8, 189.9, and 263.0 mbsf), which is known to have been affected by severe hydrothermal alteration (Shipboard Scientific Party, 1998c).

To summarise, the heavy minerals clearly show that they have experienced chemical etching by hydrothermal fluids. These fluids probably interacted with salty marine pore waters, circulating via fractures and permeable layers and caused the partial to complete loss of individual species (especially ortho- and clinopyroxenes). These processes also generated new minerals (titanite, iron-rich magnesite, barite, and pyrite). However, it still remains difficult to reconstruct the extent and kinetics of the dissolution of the various minerals as a function of pH, temperature, composition of pore fluids, and sandstone permeability. The sediments have been subjected to pore fluid circulation in this environment over a relatively short period, as indicated by the young age (60 ka) of the sediments.

5. CONCLUSIONS

The composition and trends displayed by heavy mineral suites down-hole in Holes 1038I, 1037B, and in the hole at Site 35, the absence of significant changes in gross composition, and the anomalous distribution of authigenic minerals indicate that the cause of partial to complete loss of heavy mineral species (especially ortho-and clinopyroxenes) and the growth of new minerals (titanite, iron-rich magnesite, barite, and pyrite) reflect the circulation of corrosive hydrothermal fluids, intermixing with salty marine pore waters and percolating through fractures and permeable layers in the turbidite succession that was deposited in the oceanic rift valley of the Escanaba Trough (Juan de Fuca Plate) during the last 60 ka.

This is a novel discovery and, because such processes have not been observed previously in heavy mineral assemblages, there is insufficient data to fully understand the dissolution rates of the various minerals and conditions of neoformation as a function of pH, temperature, chemistry of pore fluids, and sediment permeability. The length of time during which the sediments were affected by pore fluid movements is, however, constrained by the very young age of sediments.

ACKNOWLEDGEMENTS

The financial support for G.G. Zuffa was provided by the National Council for Research (CNR 96.00286 CT 05, 97.00268 CT 05). The manuscript was critically reviewed by Tom van Loon and Robert Zierenberg. The editorial help of Maria Mange and David Wright is gratefully acknowledged.

REFERENCES

Brunner, C.A., Normark, W.R., Zuffa, G.G., Serra, F., 1999. Deep-sea sedimentary record of the late Wisconsin cataclysmic floods from the Columbia River. Geology 27, 463–466.

Dickinson, W.R., 1970. Interpreting detrital modes of graywacke and arkose. Journal of Sedimentary Petrology 40, 695–707.

Dickinson, W.R., Suczek, C.A., 1979. Plate tectonics and sandstone compositions. American Association of Petroleum Geologists Bulletin 63, 2164–2182.

Gazzi, P., 1966. Le arenarie del flysch sopracretaceo dell'Appennino modenese: correlazioni con il flysch di Monghidoro. Mineralogica et Petrographica Acta 16, 69–97.

Gazzi, P., Zuffa, G.G., Gandolfi, G., Paganelli, P., 1973. Provenienza e dispersione litoranea della sabbie delle spiagge adriatiche fra le foci dell'Isonzo e del Foglia: inquadramento regionale. Memorie della Società Geologica Italiana 12, 1–37.

McManus, D.A., et al., 1970. Site 35. In: McManus, D.A., et al. (Eds.), Initial Reports of the Deep Sea Drilling Project, vol. 5. U.S. Government Printing Office, Washington, pp. 165–202.

Moore, G.W., Sharman, G.F., 1970. Summary of scan Site 4: Deep Sea Drilling Project Initial Reports 5, 761–773.

Morton, A.C., Hallsworth, C.R., 1999. Processes controlling the composition of heavy mineral assemblages in sandstones. Sedimentary Geology 124, 3–29.

Shipboard Scientific Party, 1998a. Introduction: investigation of hydrothermal circulation and genesis of massive sulphide deposits at sediment-covered spreading centers at Middle Valley and Escanaba Trough. In: Fouquet, Y., Zierenberg, R.A., Miller, D. J., et al. (Eds.), Proceedings of ODP, Initial Reports. vol. 169. College Station, TX (Ocean Drilling Program), pp. 253–298.

Shipboard Scientific Party, 1998b. Escanaba Trough: Reference Site (Site 1037). In: Fouquet, Y., Zierenberg, R.A., Miller, D.J., et al. (Eds.), Proceedings of ODP, Initial Reports, vol. 169. College Station, TX (Ocean Drilling Program), pp. 205–251.

Shipboard Scientific Party, 1998c. Escanaba Trough: Central Hill (Site 1038). In: Fouquet, Y., Zierenberg, R.A., Miller, D.J., et al. (Eds.), Proceedings of ODP, Initial Reports, vol. 169. College Station, TX (Ocean Drilling Program), pp. 253–298.

Vallier, T.L., 1970. The mineralogy of some turbidite sands from Sites 32 and 35. In: McManus, D.A., et al. (Eds.), Initial Reports of the Deep Sea Drilling Project, vol. 5. U.S. Government Printing Office, Washington, pp. 535–539.

Vallier, T.L., Harold, P.J., Girdley, W.A., 1973. Provenances and dispersal patterns of turbidite sand in Escanaba Trough, Northeastern Pacific Ocean. Marine Geology 15, 67–87.

Whetten, J.T., Kelley, J.C., Hanson, L.G., 1969. Characteristics of Columbia River sediment and sediment transport. Journal of Sedimentary Petrology 39, 1149–1166.

Zattin, M., Zuffa, G.G., 2004. Unravelling the source rocks of the Late Eocene–Miocene orogenic wedge and foredeep arenites of the northern Apennines and southern Alps. Bollettino della Società Geologica Italiana 123, 67–76.

Zierenberg, R.A., Fouquet, Y., Miller, D.J., Normark, W.R. (Eds.), 2000. Proceedings of ODP, Scientific Results, vol. 169 (CD-ROM). Available from: Ocean Drilling Program, Texas A&M University, College Station, TX 77845-9547, USA.

Zuffa, G.G., 1985. Optical analyses of arenites: influence of methodology on compositional results. In: Zuffa, G.G. (Ed.), Provenance of Arenites: NATO-ASI. Reidel Publ. Co., Dordrecht, pp. 165–189.

Zuffa, G.G., 1987. Unravelling hinterland and offshore palaeo-geography from deep-water arenites. In: Leggett, J.K., Zuffa, G.G. (Eds.), Marine Clastic Sedimentology, Models and Case Studies [a volume in memory of C. Tarquin Teale]. Graham and Trotman, London, pp. 39–61.

Zuffa, G.G., De Rosa, R., Normark, W.R., 1997. Shifting sources and transport paths for the late Quaternary Escanaba Trough sediment fill (northeast Pacific). Giornale di Geologia 59, 35–53.

Zuffa, G.G., Normark, W.R., Serra, F., Brunner, C.A., 2000. Turbidite megabeds in an oceanic rift valley recording jökulhlaups of late Pleistocene glacial lakes of the western United States. Journal of Geology 108, 253–274.

Chapter 10

ALTERATION OF OPAQUE HEAVY MINERALS AS A REFLECTION OF THE GEOCHEMICAL CONDITIONS IN DEPOSITIONAL AND DIAGENETIC ENVIRONMENTS

RIKKE WEIBEL AND HENRIK FRIIS

Department of Earth Sciences, University of Aarhus, Denmark

ABSTRACT

Detrital opaque heavy minerals are minor but common constituents of most detrital sediments. It is sometimes possible to map the diagenetic paths of those opaques that are readily altered through changing oxidising and reducing geochemical environments, both depositional, post-depositional and diagenetic. The alteration of opaque heavy minerals from different depositional and diagenetic environments, reflecting various geochemical regimes, is reviewed and evaluated. The investigated deposits span from Triassic red beds (Skagerrak and Bunter Sandstone Formations) with early oxidising conditions (including local reduction spots representing early reducing conditions) through weakly reducing conditions of the Miocene Odderup Formation to the strongly reducing environment of the Gassum Formation, where abundant iron and organic matter, and thus related sulphate reduction, have influenced the alteration products. Extreme sulphur-dominated local environments are represented by Holocene carbonate-cemented sandstone pillars.

When successive phases of oxidation and reduction occur, the resulting assemblage of primary detrital opaque heavy minerals and their alteration products converge; a detailed study can sometimes reveal the sequence of events. A comparison of the alteration sequence of detrital Fe–Ti oxides, together with identification of authigenic opaques, from red and drab parts of the succession in Triassic red beds (Skagerrak and Bunter Sandstone Formations), has enabled us to distinguish primarily oxidised horizons, primarily reduced areas, secondarily reduced originally oxidised areas, and secondarily oxidised originally reduced areas.

Keywords: opaque heavy minerals; alteration; ilmenite; magnetite; titanomagnetite; hematite; Fe-Ti oxides; geochemical conditions; oxidising conditions; reducing conditions; diagenetic environment.

Developments in Sedimentology, Vol. 58, 277–303

ISSN: 0070-4571/doi:10.1016/S0070-4571(07)58010-6

1. INTRODUCTION

Geochemical conditions in post-depositional environments determine the alteration pattern of detrital opaque heavy minerals. Some of the first studies of alteration of opaques under reducing and oxidising conditions were conducted on red beds and their in situ hosted reduction spots (e.g., Miller and Folk, 1955; Van Houten, 1968; Thompson, 1970). This was an ideal setup for comparative studies, as possible source area differences were avoided. For example, Force et al. (2001) described the perfect preservation of a volcanic-sourced magnetic ilmenite/hematite intergrowth which survived the alteration of most other Fe–Ti oxides in Mesozoic-Early Tertiary uranium deposits.

The complex textural and compositional variations of detrital opaque heavy minerals have commonly been used as an aid to determine the provenance of sedimentary rocks, and many studies of recent or sub-recent deposits have proved their potential (Riezebos, 1979; Darby and Tsang, 1987; Basu and Molinaroli, 1989, 1991; Grigsby, 1990, 1992; Schneiderman, 1995; Force et al., 2001), but they have also demonstrated the masking influence of the complex alteration pattern of these minerals on provenance evaluation. Weathering may drastically change the heavy mineral population (Van Loon and Mange, 2007, this volume), and many opaque minerals are altered or dissolved during diagenesis (Van Houten, 1973; Turner, 1980; Morad and Aldahan, 1986; Weibel, 1998, 2003; Weibel and Friis, 2004). Textural patterns can survive diagenetic alterations, but the mineralogy may change together with the chemical signature of the original detrital grain. While these changes may occur very early, as demonstrated by palaeomagnetic studies (Turner et al., 1999), others take place during late diagenesis (Weibel and Friis, 2004). The alteration of opaque heavy minerals is controlled by their post-depositional environment and this must be taken into account when they are used for provenance and palaeomagnetic studies.

This contribution describes and summarises the main alteration trends of detrital opaques in five geochemically different post-depositional environments: (1) oxidising diagenetic conditions (Skagerrak and Bunter Sandstone Formations); (2) reducing diagenetic conditions (reduced areas in Skagerrak and Bunter Sandstone Formations); (3) reducing diagenetic conditions with abundant Fe and S (Gassum Formation); (4) reducing conditions with abundant S (Holocene carbonate-cemented sandstone pillars); (5) weakly reducing weathering conditions (Odderup Formation). We present the main observations from these investigations that allowed us to evaluate the alteration of opaques as defined by their geochemical post-depositional environment, and discuss how their alteration sequence can help to unravel the diagenetic pathway of a given sediment.

2. DEPOSITIONAL ENVIRONMENTS

The investigated sediments include Triassic, Jurassic and Miocene deposits from onshore wells and outcrops in Denmark, outcrops of Triassic successions on Helgoland, and Holocene shallow marine deposits from Denmark (Fig. 1).

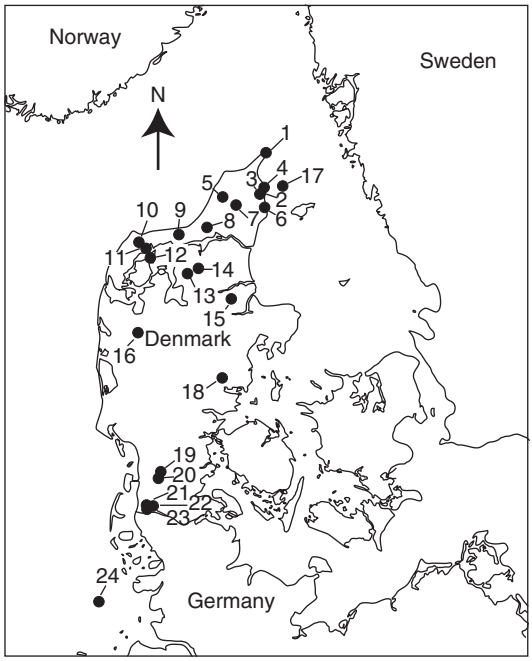

Fig. 1. Locality map with investigated outcrop and well locations. 1 = Skagen 2 (Skagerrak and Gassum Formations); 2 = Frederikshavn 1 (Gassum Formation); 3 = Frederikshavn 2 (Skagerrak and Gassum Formations); 4 = Frederikshavn 3 (Skagerrak Formation); 5 = Børglum 1 (Gassum Formation); 6 = Sæby 1 (Skagerrak Formation); 7 = Flyvbjerg 1 (Skagerrak and Gassum Formations); 8 = Vedsted 1 (Skagerrak and Gassum Formations); 9 = Fjerritslev 2 (Gassum Formation); 10 = Thisted 4 (Skagerrak Formation); 11 = Thisted 2 (Skagerrak Formation); 12 = Mors 1 (Skagerrak Formation); 13 = Farsø 1 (Gassum Formation); 14 = Aars 1A (Gassum Formation); 15 = Gassum 1 (Skagerrak and Gassum Formations); 16 = Vinding 1 (Skagerrak Formation); 17 = Marine Holocene carbonate cemented sandstone pillars; 18 = Voervadsbro open pit (Odderup Formation); 19 = Arnum 1 (Bunter Sandstone Formation); 20 = Hønning 1 (Bunter Sandstone Formation); 21 = Tønder 1 (Bunter Sandstone Formation); 22 = Tønder 4 (Bunter Sandstone Formation); 23 = Tønder 5 (Bunter Sandstone Formation); 24 = Helgoland coastal cliffs (Bunter Sandstone Formation).

2.1. Triassic Skagerrak Formation

The Early to Late Triassic Skagerrak Formation has been interpreted as having formed in an alluvial fan or braided fluvial depositional environment (Deegan and Scull, 1977; Bertelsen, 1980; Pedersen and Andersen, 1980; Priisholm, 1983). The study area forms a north-east to south-west belt from the Fennoscandian Border Zone to a deepening basin in the south-west—the Danish Sub-basin—which is part of the Triassic Central North Sea Basin (Fisher and Mudge, 1998). The Skagerrak Formation is the lateral equivalent of German-type facies (Buntsandstein, Muschelkalk and Keuper). At the time of deposition of the Skagerrak Formation, the climate was arid to semi-arid (Bertelsen, 1980), consistent with the occurrence of

the interfingering evaporitic deposits and of calcrete (Pedersen and Andersen, 1980; Weibel, 1998). In this climate, the interstitial water was generally oxidising but sparse reduction spots developed locally. These were most likely associated with organic matter where locally reducing conditions formed immediately after deposition and then remained reducing, unless the reducing agent was exhausted (Weibel, 1998).

2.2. Triassic Bunter Sandstone Formation

The studied Early Triassic Bunter Sandstone Formation consists of sandstone and mudstone intervals. The mudstone intervals are interpreted as having formed in sabkha, very shallow marine inland basin, playa-lake and lake depositional environments (Bruun-Petersen and Krumbein, 1975; Clemmensen, 1979, 1985, 1991; Bertelsen, 1980; Olsen, 1987; Binot and Röhling, 1988). The sandstone intervals have controversially been interpreted as fluvial (Wurster, 1960; Bertelsen, 1980; Binot and Röhling, 1988) or a mixture of ephemeral streams and aeolian sand sheets (Clemmensen, 1979, 1985, 1991; Olsen, 1987). The climate was arid to semi-arid with mega-monsoonal circulation, leading to strong seasonal rainfall (Clemmensen, 1979; Van der Zwan and Spaak, 1992). Oxidising conditions prevailed in this environment and the drab colour of the deposited sediment changed to red with the exception of local reducing areas. Locally formed algal mats may have created the large-scale reducing environments in the mudstones, whereas erosion by winds or ephemeral streams may have created isolated reduction spots around rip-up clasts containing carbonate and organic matter (Weibel and Friis, 2004).

2.3. Late Triassic-Early Jurassic Gassum Formation

The Gassum Formation comprises a basin–marginal complex forming the threshold of the eastern part of the Norwegian–Danish Basin. The depositional environment was originally inferred to represent a delta front with interdistributary swamps, submerged/drowned delta plain and limnic conditions (Larsen, 1966; Bertelsen, 1978). Nielsen (2003), on the other hand, interprets the sediments as fluvial/estuarine, shoreface and lagoonal. The climate became more humid during deposition of the Jurassic, and large amounts of organic matter were then preserved (Bertelsen, 1978).

2.4. Miocene Odderup Formation

The Middle Miocene Odderup Formation is characterised by braided fluvial and lacustrine sediments (Rasmussen, 1961; Hansen, 1985; Weibel, 1993). In the Miocene, the Baltic River System supplied material from the Fennoscandian Shield and the Baltic Platform to the North-west European Basin (Bijlsma, 1981). This basin was flanked to the north-east by the Fennoscandian Shield and the Baltic Platform, to the south by the Variscan Massif, and to the west by the Pennine Highs and the Scottish Highlands (Bijlsma, 1981; Ziegler, 1987, 1990). Climatic and botanic investigations of contemporaneous deltaic-coastal deposits in the western part of Denmark indicate a warm temperate to subtropical climate during the Miocene, resulting in deposits containing scattered organic matter and occasional lignite layers (Koch et al., 1973; Friis, 1975, 1979).

2.5. Holocene Methane-Generated, Dolomite-Cemented Sandstone Pillars

Migration of sand ridges has exposed large sandstone pillars on the sea bottom in Kattegat, east of Frederikshavn. The migrating sand was well sorted and contained only a small amount of organic matter. The sandstone pillars, cemented by Ca-rich dolomite, are up to 4 m high and 1 m in diameter, and were formed as methane was seeping through the sand ridges (Jørgensen, 1989). The geochemical environment was controlled by methane gas which forced an upward flow of interstitial water (Dando et al., 1994). Bacterial sulphate reduction may have been related to precipitation of dolomite cement in the sandstone pillars, similar to the dolomite formation associated with sulphate-reducing bacteria in ephemeral lakes in South Australia (Wright, 1999). Methane was biogenically oxidised by sea water sulphate, which was continuously supplied by the pore water flow. The sulphate reduction rate was high (Dando et al., 1994) and, although much H_2S escaped with the seeping methane, the concentration of dissolved sulphide may have reached high values.

3. GEOCHEMICAL CONDITIONS OF THE POST-DEPOSITIONAL ENVIRONMENTS

The post-depositional environments have been grouped according to differences in stability and transformation pattern of opaque heavy minerals (Table 1).

3.1. Reducing Conditions

Sparse organic matter in the Triassic Skagerrak and Bunter Sandstone Formations was associated with locally reducing conditions and resulted in reduction spots and occasionally large-scale reduced areas in the red bed host (Weibel, 1998; Weibel and Friis, 2004). Interfingering evaporitic deposits may have been important sources of sulphate.

In the Miocene Odderup Formation, scattered organic matter led to a post-depositional environment characterised by weakly reducing conditions. The activity of sulphur was low, due to the fluviatile depositional environment and a lack of associated evaporitic deposits.

The early diagenetic environment of the Late Triassic-Early Jurassic Gassum Formation was characterised by abundant sulphate (due to the marine influence on the depositional environment) and readily decomposable organic matter which promoted sulphate reduction and liberated abundant iron.

Table 1. Subdivision of studied post-depositional geochemical environments

Reducing conditions	
Weakly reducing	Odderup Fm.
Reducing	Reduction spots/areas in Skagerrak Fm. and Bunter Sandstone Fm.
Reducing with abundant S and Fe	Gassum Fm.
Reducing with abundant S	Holocene carbonate-cemented pillars
Oxidising conditions	Bunter Sandstone Fm. and Skagerrak Fm.

The Holocene host sand of the carbonate-cemented sandstone pillars is poor in organic matter and available iron. Both methane and sulphate were imported by unrestricted permanent flow systems (Dando et al., 1994) in a strongly reducing, sulphide-rich post-depositional environment in which insufficient iron was available for the mineralization of all the sulphide.

3.2. Oxidising Conditions

In the arid to semi-arid Triassic climate, the interstitial water was oxidising, and a widespread oxidising environment existed in the sediments shortly after deposition that continued during burial. Early diagenesis occurred under conditions generally similar to those existing at the surface today in arid to semi-arid climates. Investigations of modern analogues of red bed successions have shown that early diagenesis generally took place under alkaline and oxidising conditions (Walker, 1967, 1968; Walker and Honea, 1969; Zielinski et al., 1983; Walker and Runnels, 1984). Petrographical investigations of the Skagerrak and Bunter Sandstone Formations also suggest predominating oxidising interstitial conditions (Weibel, 1998; Weibel and Friis, 2004). Burial of red beds commonly results in formation waters becoming progressively more reducing and less alkaline (Metcalfe et al., 1994).

3.3. Secondary Oxidising Conditions

Secondary oxidising conditions may develop when the reducing agent is exhausted (and can occur as a transition zone around the original reduction spot) or by meteoric water flushing after uplift (Weibel, 1998; Weibel and Friis, 2004). Metcalfe et al. (1994) reported that formation waters in uplifted successions (telogenesis) generally become more oxidising and less saline as they become diluted with meteoric water.

3.4. Secondary Reducing Conditions

Large scale secondary reduction was probably associated with hydrocarbon migration, especially in highly porous sandstone units (Weibel and Friis, 2004) as seen in the Bunter Sandstone Formation outcrops on Helgoland. Highly reducing neutral-alkaline early diagenetic brines may also have occurred locally, originating from density-stratified saline lakes that had trapped organic matter in bottom brines (Metcalfe et al., 1994).

4. ALTERATION OF ILMENITE

4.1. Reducing Conditions (Reduction Spots/Areas in the Bunter Sandstone Fm. and the Skagerrak Fm.)

Ilmenite was typically altered to leucoxene, and only rarely dissolved in reduction spots in red beds, whereas authigenic anatase and occasionally framboidal pyrite precipitated in adjacent pore spaces (Fig. 2). Leucoxene is defined as a cryptocrystalline, titanium-rich (generally $> 70\%$ TiO_2) alteration product of titanium-bearing

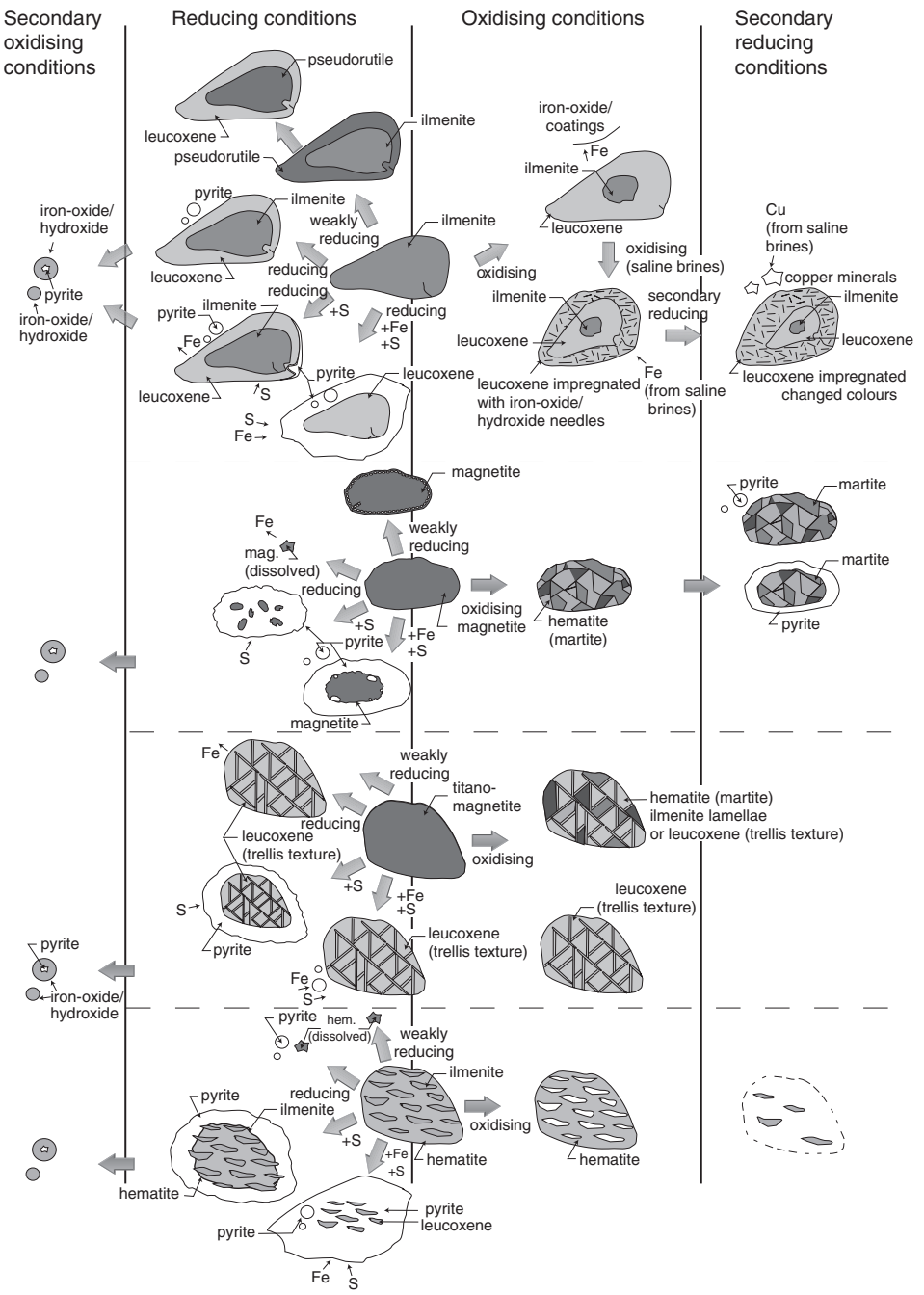

Fig. 2. Evolutionary pathway diagram explaining different alterations of the detrital opaque heavy minerals, ilmenite, hematite, magnetite and titanomagnetite, in relation to the geochemical environments.

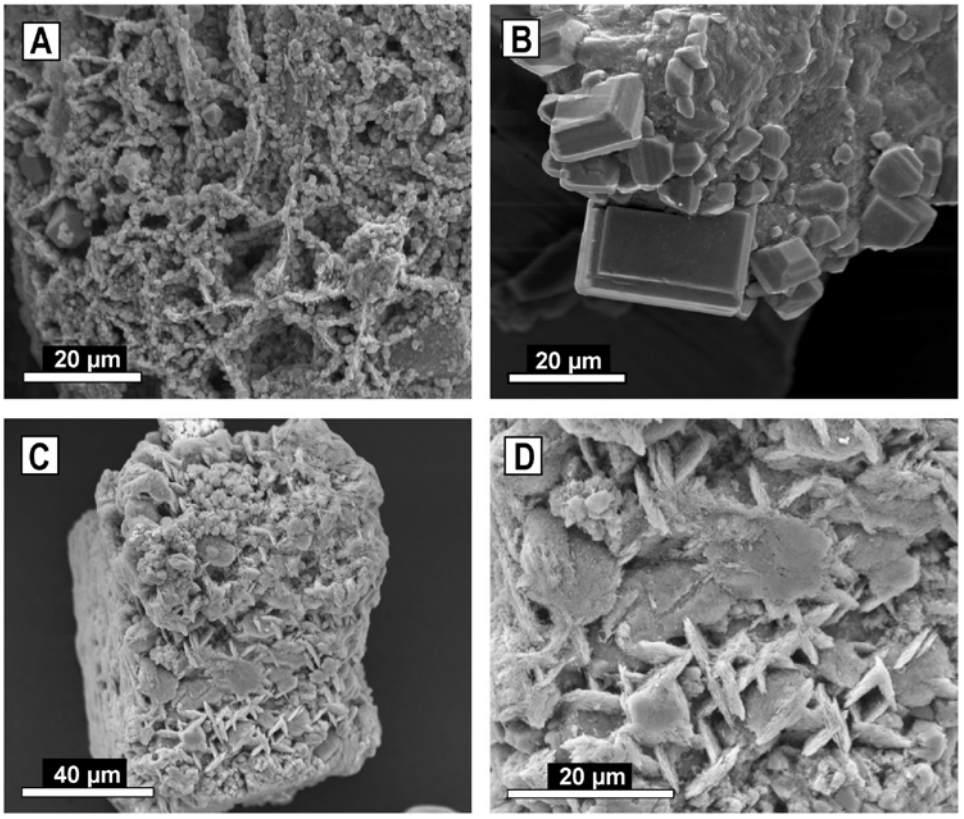

Fig. 3. Scanning electron micrographs of leucoxene. (A) Leucoxene meshwork of very small TiO_2 crystals and some euhedral anatase crystals. Bunter Sandstone Fm., Tønder 5 (TØ 5205), reducing conditions. (B) Leucoxene alteration of an ilmenite grain. Anatase crystal identified by its basal pinacoid and pyramidal crystal faces. Bunter Sandstone Fm., Tønder 5 (TØ 5205), reducing conditions. (C) Leucoxene alteration of titanomagnetite. Bunter Sandstone Fm., Tønder 4 (TØ 4505), oxidising conditions. (D) Close up of C showing the preferential orientation of leucoxene in three different directions. Bunter Sandstone Fm., Tønder 4 (TØ 4505), oxidising conditions.

minerals (Lynd et al., 1954; Bailey et al., 1956; Golding, 1961; Temple, 1966; Dimanche and Bartholomé, 1976; Riezebos et al., 1978; Morad and Aldahan, 1986; Hugo and Cornell, 1991; Mücke and Chaudhuri, 1991). In reflected light, leucoxene is mainly identified by its bright white, yellow, orange or red internal reflections which can commonly be observed without crossed polars in oil immersion. Anatase and rutile have occasionally been positively identified in reflected light microscope and/or scanning electron microscope (Figs. 3A, B) but it is commonly impossible to distinguish between the different TiO_2 polymorphs, rutile, brookite and anatase (Figs. 3C, D). The term "leucoxene" is therefore used for the titanium-oxide alteration products.

The earliest investigations of opaques in red beds led to the conclusion that ilmenite had been dissolved in the reduced areas (Miller and Folk, 1955; Van Houten,

1968). Miller and Folk (1955) pointed out that red beds of Silurian (Rose Hill shale and sandstone, eastern West Virginia) and Permo-Triassic age (Pierce Canyon red beds, west Texas and southeast New Mexico) contain detrital ilmenite, whereas reduced areas contain little or no detrital ilmenite. They suggested that ilmenite was dissolved under locally reducing conditions after deposition. Van Houten (1968) observed that ilmenite altered to leucoxene in oxidising areas, whereas it was dissolved in reducing environments.

Later investigations have revealed that ilmenite is altered to leucoxene under both reducing and oxidising conditions (Thompson, 1970; Adams et al., 1974; Dimanche and Bartholomé, 1976; Morad and Aldahan, 1986; Weibel, 1998; Weibel and Friis, 2004). This is consistent with the limited stability field of ilmenite and the broad stability field of titanium oxides (i.e., anatase under most environments) under both oxidising and reducing (non-alkaline) conditions (Adams et al., 1974). Iron, liberated during ilmenite alteration to leucoxene, commonly results in associated pyrite formation under reducing conditions when sulphide is present, but is precipitated as iron-oxide/hydroxide rims on detrital grains under oxidising conditions. This has been shown in investigations of the red host, and the locally reduced areas in the Skagerrak and Bunter Sandstone Formations, and is supported by other investigations of red beds by Dimanche and Bartholomé (1976) and Morad and Aldahan (1986). Dimanche and Bartholomé (1976) concluded that, under slightly reducing conditions, detrital ilmenites were altered to rutile and, in the presence of sulphide, ilmenites were altered into pyrite and rutile. Morad and Aldahan (1986) also considered that early diagenetic alteration of detrital Fe–Ti oxides (predominantly ilmenite) resulted in leucoxene and hematite under oxidising conditions and in leucoxene and pyrite under reducing conditions. Accordingly, the geochemical conditions in the diagenetic environment can be revealed by the nature of the authigenic iron phase accompanying the altered ilmenite grains.

4.2. Reducing Conditions with Abundant Sulphur and Iron (Gassum Fm.)

In the reducing environment of the Gassum Formation, ilmenite grains are altered to leucoxene and the liberated iron has promoted framboidal pyrite precipitation in adjacent pore space (Figs. 2 and 4A). Hematite lamellae in original ilmenite grains, now altered to leucoxene, are replaced by pyrite that may have initiated the concretionary precipitation of pyrite (Fig. 4B).

The Gassum Formation has a high pyrite content, both as pore-filling and concretionary cement, reflecting excess iron and sulphur concentrations during diagenesis. The early diagenetic pattern of the Gassum Formation is dominated by (biogenic) framboidal pyrite that formed close to an iron source—either ilmenite, magnetite, hematite or an iron-rich silicate mineral. This is similar to the chemical or biochemical reactions which took place in reduction spots/areas of the Bunter Sandstone and Skagerrak Formations. However, conditions changed during later diagenesis when pyrite precipitated in the form of concretions. Under such intense diagenetic conditions, it can be difficult to distinguish the original opaque phases.

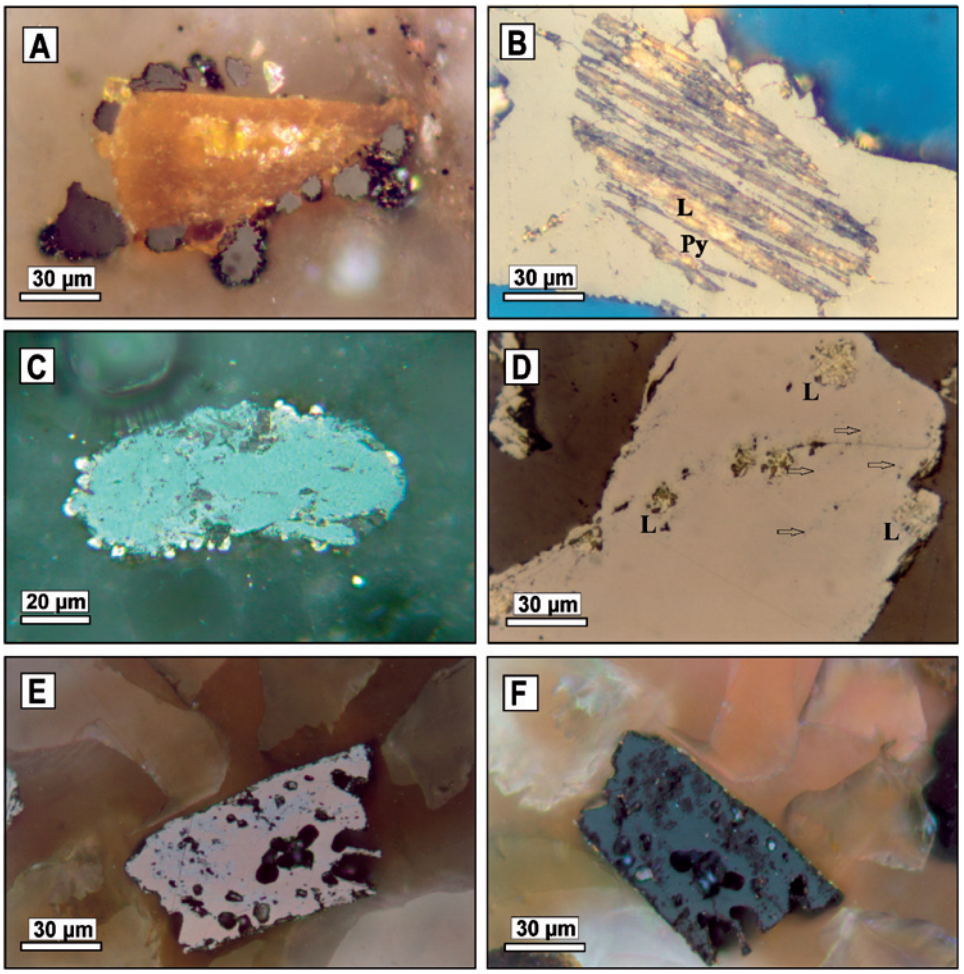

Fig. 4. (A) Former ilmenite grain, now completely replaced by leucoxene. It has provided a source for the formation of anatase crystals and framboidal pyrite as overgrowth or in the adjacent pore space. Gassum Fm., Børglum 1(BØ400G), reducing conditions. Reflected light, oil immersion, crossed polars. (B) Originally an ilmenite grain with hematite lamellae. The ilmenite has been replaced by leucoxene (L) and the hematite lamellae have been replaced by pyrite (Py), which locally occurs as a pore-filling mineral. Gassum Fm., Gassum 1 (G600G), reducing conditions. Reflected light, oil immersion, crossed polars. (C) Ilmenite with weak alteration to leucoxene in the centre and beginning alteration to pyrite along the rim. Holocene carbonate-cemented sandstone pillars (#3), reducing conditions. Reflected light, oil immersion. (D) Ilmenite grain partly altered to pseudorutile along the rim and fissures, and in spots (bright patches, L) altered to leucoxene. Note that the alteration to pseudorutile tends to progress along crystal planes (arrowed). Odderup Fm. (14A), weakly reducing conditions. Reflected light, oil immersion, crossed polars. (E) Ilmenite grain with spotted alteration to pseudorutile. Odderup Fm. (14A), weakly reducing conditions. Reflected light, oil immersion. (F) As in E, crossed polars.

4.3. Reducing Conditions with Abundant Sulphur (Holocene Sandstone Pillars)

In the Holocene carbonate-cemented sandstone pillars, the homogeneous ilmenite grains may be unaltered or have some framboidal pyrite around their rims. Ilmenite grains with twinning or initial alteration to leucoxene can be more or less replaced by pyrite (Fig. 4C), indicating that iron is more accessible from altered ilmenite grains and from those with crystallographic weaknesses.

Iron liberated within ilmenite grains during their alteration to leucoxene was immediately fixed as pyrite, even inside the original grain. This was also suggested by Dimanche and Bartholomé (1976) as an explanation for the origin of leucoxene skeletons containing pyrite in unconsolidated Belgian silver sands. The fixation of pyrite inside the ilmenite grain is strong evidence for the abundance of sulphide and the paucity of iron in this environment. Some iron, however, diffused outwards through the altered ilmenite grains and precipitated on their periphery. Continuation of this process could have led to the formation of thick pyrite replacement rims. Pyrite formation in relation to a methane-seep environment has been reported previously (Hovland et al., 1987) but it was not specified whether the detrital minerals were being replaced. Dimanche and Bartholomé (1976) also observed pyrite-mantled ilmenite grains in silver sands from Belgium, which they attributed to iron addition from other sources precipitating as pyrite on the detrital ilmenite grains, because the amount of pyrite was generally greater than would be expected from the altered ilmenite grains. Thick replacement rims may retard or inhibit further dissolution/replacement. It has also been suggested by Dimanche and Bartholomé (1976) and Canfield and Berner (1987) that pyrite replacement rims on detrital ilmenite or detrital magnetite grains may protect them from further alteration. This easily recognisable pyrite-replacement of ilmenite is a strong evidence for alteration taking place under reducing conditions with extremely high sulphide activity.

4.4. Weakly Reducing Conditions (Odderup Fm.)

Where alteration advanced slowly under weakly reducing conditions, as in the Odderup Formation, two successive alteration products of ilmenite can be distinguished: pseudorutile and leucoxene (Fig. 4D). Pseudorutile is defined by Temple (1966) and Grey and Reid (1975) as an intermediate alteration product of ilmenite with the chemical composition $Fe_2O_3 \cdot nTiO_2 \cdot mH_2O$ $(3 < n < 5;\ 1 < m < 2)$. In the Odderup Formation, pseudorutile can be recognised optically from its isotropic nature, grey appearance, low reflectivity, and the absence of both bi-reflectance and internal reflections. Homogeneous ilmenite grains are commonly rimmed by pseudorutile with equal constant alteration depth; other ilmenite grains are altered to pseudorutile along fissures, cleavage planes, twin planes or other crystallographic weaknesses (Figs. 4D–F).

The mechanism for alteration of ilmenite to pseudorutile may involve the oxidation and removal of iron by diffusion through the ilmenite lattice (Temple, 1966; Grey and Reid, 1975; Dimanche and Bartholomé, 1976). Scattered organic material in the Odderup Formation increased iron solubility due to complexing with organic acids, lowering both the pH and Eh of the groundwater (Weibel, 2003). This created the optimum conditions for alteration of ilmenite to pseudorutile, which is

assumed to take place in the zone of saturation under mildly reducing conditions in which iron is highly soluble (Temple, 1966; Grey and Reid, 1975; Dimache and Bartolomé, 1976).

The transformation of pseudorutile into leucoxene requires a complete rearrangement of the crystal structure, since both iron and oxygen must be removed. The morphological appearance of altered ilmenite with much smaller amounts of leucoxene suggests formation of leucoxene through a dissolution process (Figs. 3A, D). The fact that leucoxene is commonly arranged according to the crystallography of a former phase is an indication of an incongruent dissolution process, where some of the titanium remains in place. The remaining titanium will initially duplicate the crystallography of pseudorutile, but this lattice will become unstable as iron is continuously leached. Titanium is then organised into fine crystals of rutile or anatase. Transformation of pseudorutile into leucoxene during dissolution, followed by an epitactic reprecipitation of titanium oxide on the seed material, has also been suggested by Grey and Reid (1975), Dimanche and Bartholomé (1976) and Frost et al. (1983). Mücke and Chaudhuri (1991), on the other hand, have observed a continuous alteration of pseudorutile into leucoxene and suggest a process of leaching and hydrolysis.

Temple (1966) and Grey and Reid (1975) suggested that the alteration of pseudorutile into leucoxene occurred in the zone of oxidation (i.e., above the water table) and was related to the decomposition of organic material, which forms organic acids capable of dissolving pseudorutile. Mücke and Chaudhuri (1991) argued against the formation of pseudorutile and leucoxene in different environments because these alterations commonly occur in the same sediment and even in the same grains. The successive alteration of ilmenite into pseudorutile and finally leucoxene has typically been identified in young, relatively unmodified sediments. This alteration sequence has been observed in recent beach environments (Lynd et al., 1954; Bailey et al., 1956; Riezebos et al., 1978; Mücke and Chaudhuri, 1991), modern rivers (Riezebos et al., 1978; Mücke and Chaudhuri, 1991), Holocene dunes (Golding, 1955; Hugo and Cornell, 1991) and South African aeolian sands and fossil dunes (Dimanche, 1972; Dimanche and Bartholomé, 1976) and Miocene fluviatile sediments (Weibel, 2003). It can therefore be concluded that pseudorutile is an intermediate alteration product commonly occurring in the early stages of alteration (weathering or early diagenesis under weakly reducing conditions), and that pseudorutile alters to leucoxene during continued diagenesis.

4.5. Oxidising Conditions (Bunter Sandstone Fm. and Skagerrak Fm.)

Ilmenite is unstable under oxidising conditions in the Skagerrak and Bunter Sandstone Formations and is commonly altered to leucoxene or dissolved, thus promoting anatase and iron-oxide/hydroxide formation in the adjacent pore space (Figs. 5A, B).

Ubiquitous anatase crystals, occurring adjacent to altered ilmenite grains, indicate that titanium was locally mobilised and reprecipitated. This suggests that titanium variations in diagenetically modified sediments reflect their original pattern.

Compilation of investigations of sediments ranging from Proterozoic through Devonian to Triassic age consistently shows that ilmenite alteration under oxidising conditions results in two phases: titanium oxide and iron-oxide/hydroxide (Van Houten, 1968; Grey and Reid, 1975; Dimanche and Bartholomé, 1976; Turner, 1980;

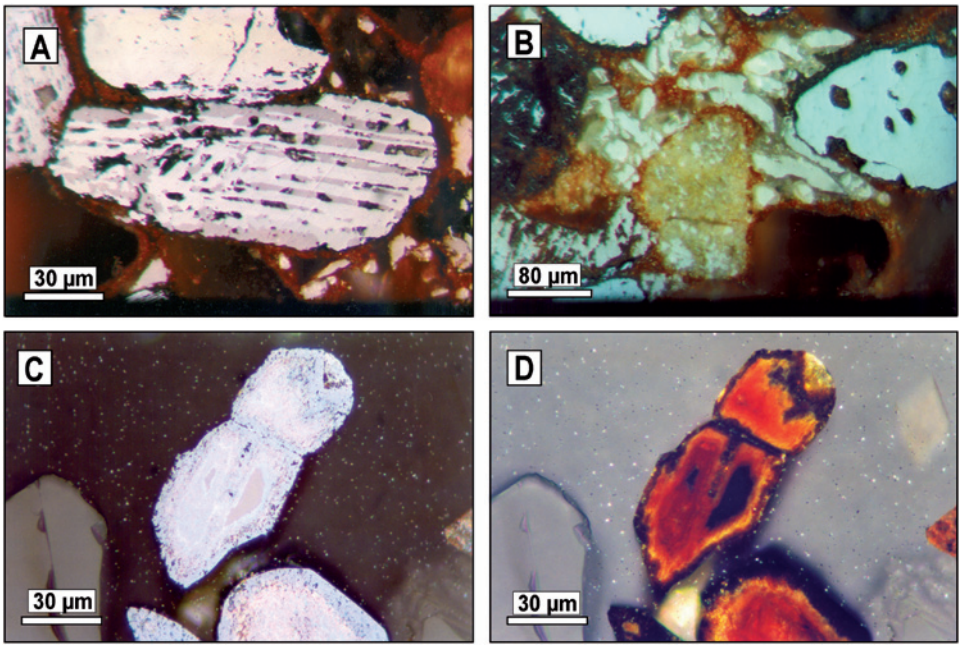

Fig. 5. (A) Originally an ilmenite grain with hematite lamellae, in which ilmenite has been partly dissolved, whereas the hematite part remains unaltered. Skagerrak Fm., Thisted 2 (TH350), oxidising conditions. Reflected light, oil immersion. (B) Ilmenite grain (centre) completely replaced by leucoxene. Anatase crystals are numerous in the pore space. Skagerrak Fm., Thisted 2 (TH350), oxidising conditions. Reflected light, oil immersion. (C) Two-stage alteration of ilmenite. The pinkish grey cores are the remnants of the original ilmenite grain, which outwards has been replaced by leucoxene. The outermost rim of the leucoxene has been impregnated by iron-oxide/hydroxide needles. Bunter Sandstone Fm., Tønder 4 (TØ 4500), oxidising conditions. Reflected light, oil immersion. (D) As in C, crossed polars.

Morad and Aldahan, 1986; Weibel, 1998; Weibel and Friis, 2004). A discrepancy, however, exists in the identification of the actual titanium oxide polymorph, as both rutile (Dimanche and Bartholomé, 1976; Turner, 1980) and anatase (Adams et al., 1974; Banfield and Veblen, 1992; Banfield et al., 1993) have been suggested. The iron-oxide/hydroxides are typically interpreted as hematite formed by direct precipitation or through a metastable phase of limonite—probably ferrihydrite (Walker, 1967, 1968) or goethite (Dimanche and Bartholomé, 1976; Walker, 1976; Ixer et al., 1979; Turner, 1980; Weibel and Grobety, 1999; Weibel and Friis, 2004). The nature of the iron phase accompanying the leucoxene-altered ilmenite grains reflects the diagenetic geochemical environment.

Ilmenite occurs with a characteristic two-stage alteration in the red parts of the Bunter Sandstone Formation (Figs. 5C, D; Weibel and Friis, 2004). In the first stage, ilmenite is replaced by leucoxene, which originally probably had a porous structure similar to leucoxenes in reduced areas. The second stage consists of a later growth of iron-oxide/hydroxide needles into this leucoxene mesh, beginning from the outer rim and penetrating into the grains along fractures (Figs. 6A, B). These needles resemble

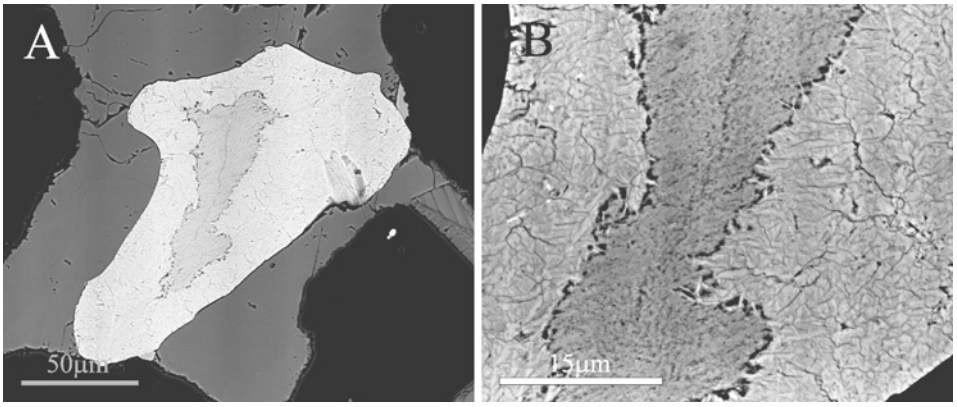

Fig. 6. Back-scatter electron images of iron-oxide/hydroxide needle impregnation of ilmenite altered to leucoxene. (A) Two-stage alteration of ilmenite. The innermost part consists of leucoxene, whereas the outer rim is impregnated with iron-oxide/hydroxide needles. Bunter Sandstone Fm., Tønder 4 (TØ 4505), oxidising conditions. (B) Close up of A where the iron-oxide/hydroxide needles can be observed at the transition between pure leucoxene and the impregnated leucoxene. Bunter Sandstone Fm., Tønder 4 (TØ 4505), oxidising conditions.

lepidocrocite more than goethite (Schwertmann and Taylor, 1989) and possibly indicate iron hydroxide precipitation from chloride-rich solutions (Weibel and Friis, 2004).

5. ALTERATION OF MAGNETITE

5.1. *Reducing and Weakly Reducing Conditions (Reduction Spots and Areas in Bunter Sandstone Fm., Skagerrak Fm. and Odderup Fm.)*

Magnetite grains were generally dissolved under reducing (acid to neutral) conditions in reduction spots of the Bunter Sandstone and Skagerrak Formations, with the exception of rare cases where they were protected by early cement (e.g., gypsum). Magnetite is also slightly altered under weakly reducing conditions in the Odderup Formation. Magnetite appears with several dissolution voids around the rim, along parting planes and fissures or in various parts of the grain.

Miller and Folk (1955) observed that red beds of Silurian (Rose Hill shale and sandstones, eastern West Virginia) and Permo-Triassic age (Pierce Canyon red beds, west Texas and southeast New Mexico) generally contain detrital magnetite and ilmenite as the most abundant heavy minerals, except in reduced areas which have few or none of them. They suggested that these minerals were dissolved under local reducing conditions after deposition. Van Houten (1968) investigated opaque minerals in red beds, ranging in age from Precambrian to Pleistocene and observed that magnetite was dissolved in most of the drab parts of red beds but volcanically derived magnetite persisted longer than magnetite from non-volcanic sources. This may have consequences when using opaques for provenance studies or when determining the geochemical weathering or diagenetic regime according to the degree of alteration of opaques. In their study of the Morrison Formation, New Mexico,

Adams et al. (1974) found that permeable sandstones, close to uranium deposits, were essentially devoid of black opaque minerals. They concluded that the cause was a selective dissolution of iron from magnetite and ilmenite that occurred in the presence of oxygen-deficient groundwater, possibly enhanced by dissolved organic matter. All these investigations agree that more or less intense dissolution of magnetite occurs under reducing conditions.

5.2. Reducing Conditions with Abundant Sulphur and Iron (Gassum Fm.) and Abundant Sulphur (Holocene Carbonate-Cemented Sandstone Pillars)

In the Holocene sandstone pillars, with abundant sulphur present, magnetite grains typically show intensive replacement by pyrite (Fig. 7A). In the Gassum Formation, with abundant sulphur and iron, magnetite typically occurs with abundant dissolution voids, often rimmed by framboidal pyrite that has partially filled the adjacent pore space.

Thus, the activity of iron has a strong influence on the mode of pyrite precipitation. Under high iron (and high sulphide) activity, pyrite precipitates as framboids and even as concretions, whereas pyrite replaces the iron-containing detrital minerals under low iron (and high sulphide) activity. Canfield and Berner (1987) investigated the alteration of magnetite in anoxic marine sediments and found that magnetite is dissolved when sulphide concentrations are low. When sulphide activity is high, extensive replacement of magnetite with pyrite takes place. This is identical to observations from the carbonate cemented-sandstone pillars. In the Gassum Formation, where pyrite replacement has not taken place, the activity of both iron and sulphide was high.

5.3. Oxidising Conditions (Bunter Sandstone Fm. and Skagerrak Fm.)

Magnetite is generally completely replaced by hematite under the oxidising conditions of the Bunter Sandstone and Skagerrak Formations. Hematite crystals grow along three different crystallographic orientations, parallel to the (1 1 1) plane of the original magnetite grain, thereby creating a texture called "martite" (Fig. 7B).

The mechanism of martitization (hematization of magnetite) could involve an intermediate phase of maghemite (γ-Fe_2O_3), or a compound intermediate in composition between Fe_3O_4 and Fe_2O_3 or the direct formation of hematite (α-Fe_2O_3) from magnetite (Fe_3O_4) (Turner, 1980). Experimental evidence, though, suggests that martitization most commonly proceeds without formation of an intermediate maghemite phase (Turner, 1980). Hematization of magnetite has been reported from various red bed successions, taking place under oxidising conditions (Van Houten, 1968; Thompson, 1970; Turner, 1980; Walker et al., 1981; Weibel, 1998; Weibel and Friis, 2004). This process most likely occurs at a very early stage, as indicated by palaeomagnetic data, and is supported by the fact that unaltered magnetite grains are unknown in ancient red beds where they only occur as relict cores within hematites, and always show extensive signs of oxidation (Turner, 1980; Turner et al., 1999). Hematite with martite texture is thus a characteristic alteration product of magnetite forming under oxidising diagenetic conditions.

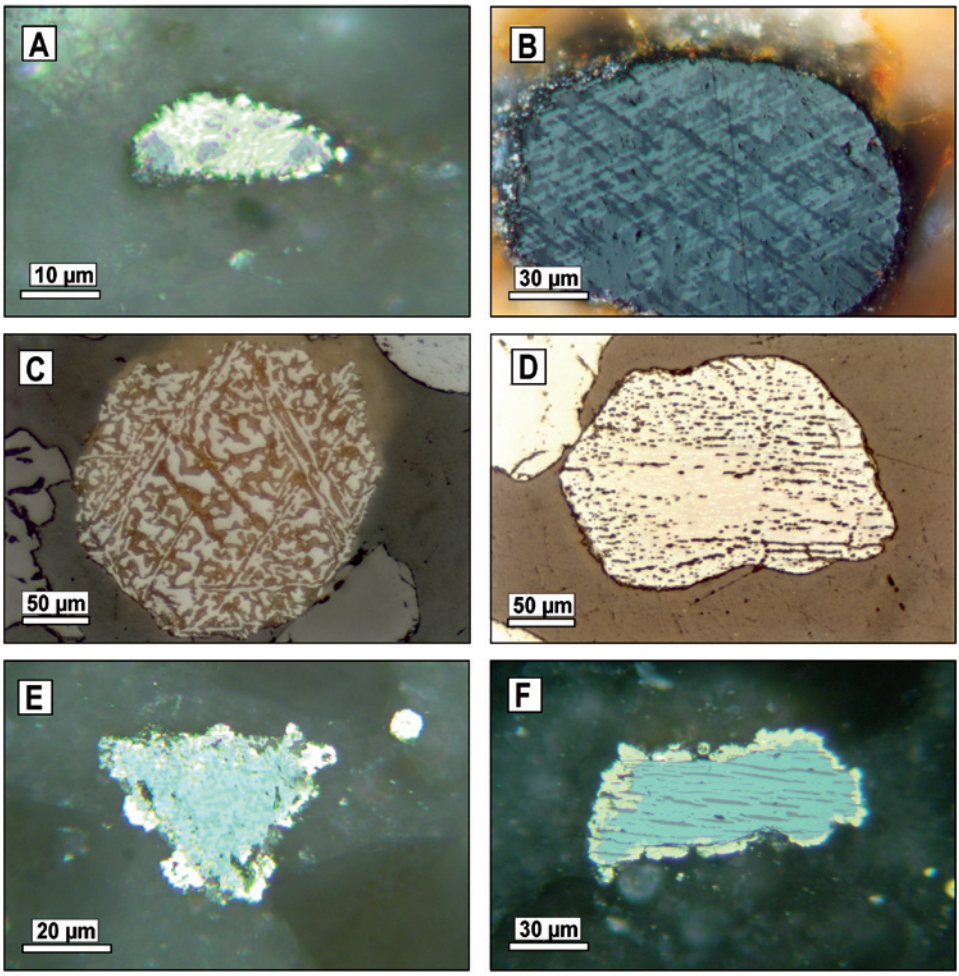

Fig. 7. (A) Magnetite grain extensively replaced by pyrite. Holocene carbonate-cemented sandstone pillars (#3), reducing conditions. Reflected light, oil immersion. (B) Magnetite grain completely altered to hematite. The hematite crystals are orientated in three different directions in a texture called martite, thereby reflecting the crystallography of the original magnetite. Skagerrak Fm., Gassum 1 (G805), oxidising conditions. Reflected light, oil immersion, crossed polars. (C) Titanomagnetite completely altered to leucoxene. The origin of the mineral is revealed by the orientation of leucoxene in trellis texture. Odderup Fm. (14B), weakly reducing conditions. Reflected light. (D) Preferential dissolution of hematite exsolution lamellae in ilmenite host. Along the rim, the hematite exsolution lamina have been dissolved and can now be observed as dissolution voids in the ilmenite host arranged parallel to the hematite exsolution lamina. Odderup Fm. (5C), weakly reducing conditions. Reflected light, oil immersion. (E) Polycrystalline hematite grain partly altered to pyrite along the rim. Holocene carbonate-cemented sandstone pillars (#3), reducing conditions. Reflected light, oil immersion. (F) Hematite grain with ilmenite exsolution lamellae in which the hematite part has been replaced by pyrite and the ilmenite lamellae have been left unaffected. Holocene carbonate-cemented sandstone pillars (#3), reducing conditions. Reflected light, oil immersion.

6. ALTERATION OF TITANOMAGNETITE

6.1. Various Reducing Conditions (Reduction Spots/Areas in Bunter Sandstone, Skagerrak, Odderup and Gassum Fms)

Under reducing (acid to neutral) conditions in the reduction spots in red beds, the magnetite host of titanomagnetite is dissolved and the ilmenite lamellae are replaced by orientated leucoxene with a trellis texture (Fig. 7C). In weakly reducing environments (such as in the Odderup Formation), titanomagnetite grains show similar alteration patterns, with the complete replacement of ilmenite lamellae by leucoxene, orientated in three directions, accompanied by dissolution of the magnetite host. The absence of the intermediate phase (pseudorutile) in the altered ilmenite lamellae in titanomagnetite from the Odderup Formation—where pseudorutile otherwise is relatively common—suggests that the alteration process reached completion in most titanomagnetite grains. The presence of several zones of weakness in the magnetite host of titanomagnetite allowed dissolution to proceeded more rapidly than in the more homogeneous magnetite. Alteration also proceeded more rapidly in the small unprotected ilmenite lamellae in the titanomagnetite than in larger homogeneous ilmenite grains, leading to the almost exclusive occurrence of the final alteration stage—leucoxene in a trellis texture (Weibel, 1998, 2003).

Reynolds and Goldhaber (1978) found pyrite replacement of detrital titanomagnetite in the reduced part of a roll-type uranium deposit. Even though pyrite precipitation is quite common in the Gassum Formation, and titanomagnetite is completely replaced by leucoxene, the dissolution of the magnetite host has resulted in pyrite precipitation in the adjacent pore space. Associated pyrite formation indicates reducing conditions during alteration of titanomagnetite, whereas weakly reducing conditions only result in leucoxene in a trellis texture.

6.2. Oxidising Conditions (Bunter Sandstone and Skagerrak Fms)

Titanomagnetite consists of a magnetite host with ilmenite lamellae arranged parallel to the (1 1 1) plane of the magnetite, i.e., in a trellis texture (Fig. 3C). The magnetite host of the titanomagnetite may appear dissolved, but is generally replaced by hematite in the Skagerrak and Bunter Sandstone Formations. Ilmenite lamellae are either unaltered, dissolved or altered to leucoxene in a trellis texture.

Turner (1980) investigated Recent and Cenozoic continental red beds, and found partially altered magnetite grains in which thin hematite plates had formed along the (1 1 1) planes of original magnetite grain, resulting in a triangular alteration pattern. In more ancient red beds (such as the Siluran Ringerike Group, Norway and the Triassic St. Bees Sandstones, UK), the original magnetite grains had been completely altered to hematite with a triangular martitization texture, and the ilmenite exsolution lamellae were commonly replaced by hematite and rutile or anatase. Consequently, hematite that formed with a martite texture, at the expense of the magnetite host, reflects an oxidising diagenetic environment. Alteration of ilmenite exsolution lamellae is, on the other hand, not indicative of the geochemical environment.

7. ALTERATION OF HEMATITE

7.1. Reducing and Weakly Reducing Conditions (Reduction Spots and Areas in Bunter Sandstone, Skagerrak and Odderup Fms)

Hematite only occurs as exsolution lamellae and intergrowths in ilmenite grains in the Odderup Formation (under weakly reducing conditions) and in the Skagerrak and Bunter Sandstone Formations (under reducing conditions). Hematite is always more intensively dissolved than the ilmenite host (Fig. 7D), though ilmenite lamellae can have a protective effect that usually delays dissolution. Occasionally, hematite is replaced by pyrite, as observed in some reduction spots of the Bunter Sandstone Formation, or by framboidal pyrite precipitate in the adjacent pore space, as seen in the Skagerrak Formation (Weibel, 1998; Weibel and Friis, 2004).

Dissolution of hematite grains in the reduction spots/areas of the Bunter Sandstone and Skagerrak Formations is consistent with the observations of Van Houten (1968) who investigated Precambrian to Pleistocene red beds and observed that hematite was absent in the older drab deposits but was abundant in the red beds. Thompson (1970), on the other hand, observed no differences in hematite content between the red and drab parts of Ordovician red beds in Pennsylvania. Machel (1995) concluded, on the basis of thermodynamic calculations, that hematite would be replaced by magnetite under reducing conditions with low sulphur activity. When replacement did not take place, he attributed it to thermodynamic disequilibrium. However, less alkaline and more neutral to acid porewaters may explain why hematite is dissolved in reducing conditions, and not replaced by magnetite (cf. Adams et al., 1974). Although some discrepancy exists between authors, the petrographic investigations in this study show that hematite is dissolved under reducing and weakly reducing conditions.

7.2. Reducing Conditions with Abundant Sulphur and Iron (Gassum Fm.)

Original ilmenite grains with hematite exsolution lamellae show a particular alteration pattern in the Gassum Formation. The ilmenite host has been replaced by leucoxene, whereas the hematite lamellae are replaced by pyrite that may have promoted, by forming nucleii, the concretionary precipitation of pyrite (Fig. 4B).

The Gassum Formation has a high content of pyrite, both as pore-filling and concretionary cement, reflecting excess iron and sulphur concentrations, especially during late diagenesis. The early diagenetic pattern of Gassum Formation is dominated by framboidal pyrite, forming close to an iron source, such as altered hematite grains. However, conditions changed during later diagenesis when pyrite precipitated as concretions, thereby making identification of the original grains difficult.

7.3. Reducing Conditions with Abundant Sulphur (Holocene Sandstone Pillars)

In the Holocene carbonate-cemented sandstone pillars homogeneous hematite grains are weakly altered, giving rise to formation of framboidal pyrite on their rims. More intensive alteration can be observed in grains with crystallographic weaknesses

which is manifested by more intensive pyrite replacement of polycrystalline hematite (Fig. 7E) than homogeneous hematite. The rim of hematite grains that contain ilmenite exsolution lamellae show pyrite replacement, whereas the ilmenite lamellae remain unaltered (Fig. 7F).

Intensive pyrite replacement of hematite indicates the prevalence of special post-depositional conditions with low iron availability and high sulphide activity. Such conditions appear similar to the replacement of detrital (titano) hematite by pyrite in the reduced part of a roll-type uranium deposit in Texas, described by Reynolds and Goldhaber (1978). The remarkable alteration pattern of hematite with a pyrite replacement rim is only obtained under reducing conditions and in the presence of excess sulphide and very low activity of iron. It is important to distinguish between pyrite replacements of the original hematite grain, indicating extreme geochemical conditions, and pyrite rims around the original hematite grain, indicating reducing conditions.

7.4. Oxidising Conditions (Bunter Sandstone Fm. and Skagerrak Fm.)

Hematite grains remain unaltered under the oxidising conditions of the investigated red beds, some hematite grains even having a syntaxial overgrowth (Fig. 8A). Other petrographic observations revealed hematite occurring as "doughnut-shaped" pore-filing arrangements and red coatings, or as intensive hematization of magnetite, mica and hornblende (Weibel, 1998; Weibel and Grobety, 1999; Weibel and Friis, 2004). Thus, the interstitial conditions are in equilibrium with hematite under the oxidising conditions in the Skagerrak and Bunter Sandstone Formations.

8. SECONDARY OXIDISING CONDITIONS (BUNTER SANDSTONE FM., SKAGERRAK FM.)

Under reducing conditions, alteration of ilmenite and magnetite grains may be followed by precipitation of framboidal pyrite in the pore space which may, in turn, be replaced by iron-oxides/hydroxides (limonite) under secondary oxidising conditions. A similar limonite replacement of pyrite, which originally had replaced titanomagnetite, has been observed by Reynolds and Goldhaber (1978) in the oxidised part of the roll-front of a uranium deposit. The effects of secondary oxidising conditions are also revealed by the occurrence of secondary copper minerals that replace the primary copper minerals (Weibel and Friis, 2004). These mineral alterations indicate exhaustion of the reducing agent (organic matter) and penetration of the oxidation front into the previously reduced part of the sediments. In other cases, secondary oxidisation occurs where reduced areas have been exposed to flushing of meteoric water.

9. SECONDARY REDUCING CONDITIONS (BUNTER SANDSTONE FM.)

Secondary reducing conditions in the Bunter Sandstone Formation are revealed by relicts of red coatings on detrital grains next to authigenic copper minerals (Weibel and Friis, 2004). It has been proposed that chloride complexes in

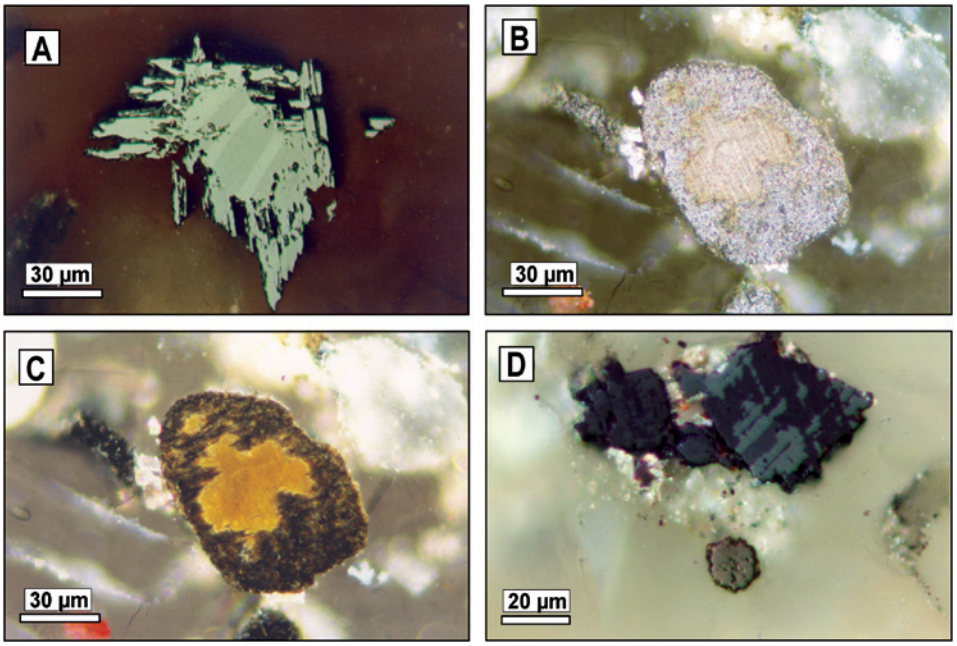

Fig. 8. (A) Twinned hematite grain with syntaxial overgrowth. Skagerrak Fm., Gassum 1 (G715), oxidising conditions. Reflected light, oil immersion, crossed polars. (B) Diluted two-stage alteration of ilmenite. The innermost part of the ilmenite has been completely altered to leucoxene, and the outermost rim has been impregnated by iron-oxide/hydroxide needles. As the leucoxene seems to be more diluted in this grain, the iron oxide/hydroxide needles are more easily seen. Bunter Sandstone Fm., Tønder 4 (TØ 5205), secondary reducing conditions. Reflected light, oil immersion. (C) As in B, crossed polars. (D) Magnetite grain completely replaced by hematite (martite) and pyrite in adjacent pore space. Skagerrak Fm., Gassum 1 (G100), secondary reducing conditions. Reflected light, oil immersion, crossed polars.

evaporative fluids, migrating through red beds, can transport copper to the reduction sites, where copper sulphides then precipitate (Rose, 1989; Hofmann, 1990; Lines et al., 1996). Additionally copper minerals typically occur in porous sandstone intervals, suggesting that the secondary reducing conditions were associated with migrating fluids.

The two-stage alteration of ilmenite, where the first stage alteration product leucoxene is impregnated by iron-oxide/hydroxide needles, appears less dense and with diluted colours of the internal reflections in the secondary reduced areas (Figs. 8B, C) compared with the originally oxidising areas (Figs. 5C, D). The change from reddish to yellowish internal reflections may be due to increased leaching of iron from the leucoxene (cf. Mücke and Chaudhuri, 1991). Another indicator of secondary reducing conditions is that magnetite grains are completely replaced by hematite (martite) next to framboidal pyrite that forms in the adjacent pore space (Fig. 8D). Reynolds et al. (1993) also described replacement of titanomagnetite and titanohematite by pyrite in areas where sulphide- and/or hydrocarbon-bearing brines entered along faults into sandstones that otherwise had oxidising conditions.

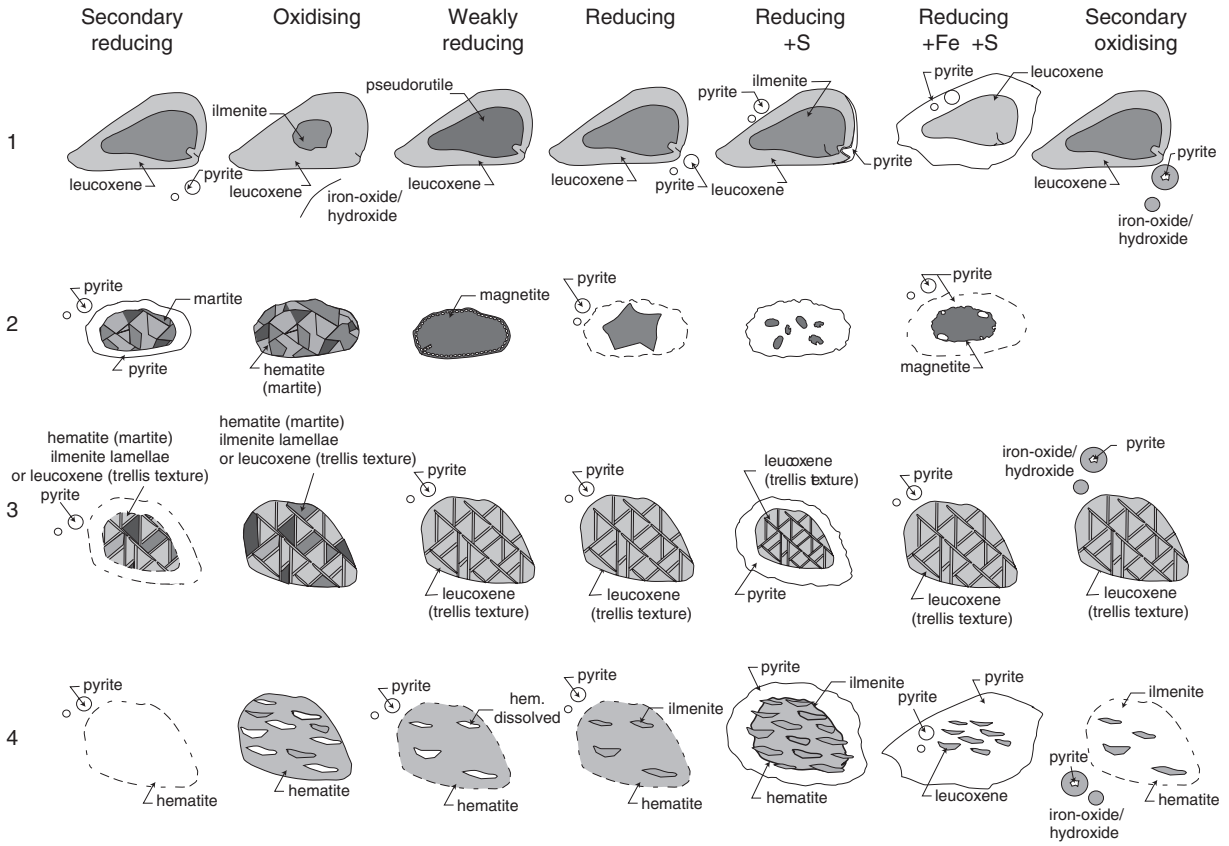

Fig. 9. Simplified schematic diagram showing the typical alteration of Fe–Ti oxides and their associated alteration product according to geochemical regime. (1) Ilmenite; (2) magnetite; (3) titanomagnetite; (4) hematite. Hem = hematite; mag = magnetite; ilm = ilmenite; py = pyrite; leu = leucoxene; pseu = pseudorutile; iron = iron-oxide/hydroxide. Note that magnetite alteration under secondary oxidising conditions has not been identified, and that magnetite and titanomagnetite have not been identified in concretions.

In the Bunter Sandstone Formation, large reduced areas have been detected which are believed to have formed during later migration of hydrocarbons (or reducing fluids) (Weibel and Friis, 2004). It is important to note that both secondary oxidising and secondary reducing conditions effectively change the Fe–Ti oxide-bearing population, and thus mask potential provenance fingerprints. Late diagenetic magnetic minerals may form which can be mistaken for original magnetic minerals.

10. CONCLUSIONS

The alteration products of ilmenite, magnetite, titanomagnetite and hematite are related to the Eh of the surrounding environment, and are influenced by the activity of Fe and S (Fig. 9). Identification of the specific iron phase precipitated in the pore space next to altered magnetite, hematite or ilmenite grains can also be used to assess whether alteration took place under oxidising or reducing conditions. However, a reliable conclusion on the nature of the geochemical regime will generally depend on the presence of more than one mineral phase, indicating alteration under similar geochemical conditions (Fig. 9).

Oxidising conditions result in unaltered hematite grains (some even develop an overgrowth), hematization of magnetite and titanomagnetite, alteration of ilmenite to leucoxene with iron-oxide/hydroxide (goethite or hematite) and anatase formation in the adjacent pore space. A special feature of the oxidising conditions of the Bunter Sandstone Formation is iron-oxide/hydroxide (most likely lepidocrocite) needle impregnation of the porous leucoxene, replacing ilmenite.

Reducing conditions are characterised by the dissolution of magnetite, hematite and the magnetite host of titanomagnetite, together with the alteration of ilmenite to leucoxene. Under weakly reducing conditions, ilmenite is altered to leucoxene through the metastable phase of pseudorutile. Occurrence of pseudorutile is associated with less intensive alterations under sub-aerial weathering or during early diagenesis. With progressive diagenesis, the alteration of ilmenite becomes complete when pseudorutile is replaced by leucoxene. Iron liberated under reducing conditions during the alteration and/or dissolution of Fe–Ti oxides is either transported away or precipitated as pyrite in adjacent pore spaces. When sulphide and iron are present in excess, pyrite commonly forms as poikilotopic cement or concretions. Pyrite replacement of Fe–Ti oxides can be observed under conditions where iron availability is limited but sulphide activity is extremely high.

This overall pattern may be disturbed under particular conditions, which include hydrocarbon movement through a sediment body, flushing by meteoric water, or exhaustion of the reducing agent in reduction spots or areas, with e.g., iron-oxide/hydroxide replacement of pyrite and hematized magnetite occurring alongside pyrite. A correct identification of these opaque heavy mineral phases provides clues for reconstruction of the geochemical history of a given succession. This will reveal changing palaeo-redox conditions, e.g., secondarily reduced after being originally oxidising, or secondarily oxidised after being originally reduced.

Fe–Ti oxides can thus be used as sensitive indicators of geochemical environments and as aids in the reconstruction of the diagenetic history of a specific sediment.

However, their application to geochemical provenance studies is generally limited because of their often complete alteration during diagenesis.

ACKNOWLEDGEMENTS

We are very grateful to reviewers Professors Peter Turner and John Parnell and to editors Maria Mange and Dave Wright for useful comments and suggestions which considerably improved the final manuscript. Grethe Nielsen is thanked for drawing the figures. Richard Wilson kindly improved the English text.

REFERENCES

Adams, S.S., Curtis, H.S., Hafen, P.L., 1974. Alteration of detrital magnetite-ilmenite in continental sandstones of the Morrison Formation, New Mexico. In: Symposium on the Formation of Uranium Ore Deposits. International Atomic Energy Agency, Vienna, pp. 219–253.

Bailey, S.W., Cameron, E.N., Spedden, H.R., Weege, R.J., 1956. The alteration of ilmenite in beach sands. Economic Geology 51, 263–279.

Banfield, J.F., Bischoff, B.L., Anderson, M.A., 1993. TiO_2 accessory minerals: coarsening, and transformation kinetics in pure and doped synthetic nanocrystalline materials. Chemical Geology 110, 211–231.

Banfield, J.F., Veblen, D.R., 1992. Conversion of perovskite to anatase and TiO_2 (B). A TEM study and the use of fundamental building blocks for understanding relationships among TiO_2 minerals. American Mineralogist 77, 545–557.

Basu, A., Molinaroli, E., 1989. Provenance characteristics of detrital opaque Fe–Ti oxide minerals. Journal of Sedimentary Petrology 59, 922–934.

Basu, A., Molinaroli, E., 1991. Reliability and application of detrital opaque Fe–Ti oxide minerals in provenance determination. In: Morton, A.C., Todd, S.P., Haughton, P.D.W. (Eds.), Developments in Sedimentary Provenance Studies. Geological Society of London Special Publication, vol. 57, pp. 55–65.

Bertelsen, F., 1978. The Upper Triassic—Lower Jurassic Vinding and Gassum Formations of the Norwegian-Danish Basin. Geological Survey of Denmark B 3, 25pp.

Bertelsen, F., 1980. Lithostratigraphy and depositional history of the Danish Triassic. Geological Survey of Denmark B 4, 59pp.

Bijlsma, S., 1981. Fluvial sedimentation from the Fennoscandian area into the North-west European Basin during the Late Cenozoic. Geologie en Mijnbouw 60, 337–345.

Binot, F., Röhling, H.-G., 1988. Lithostratigraphie und natürliche Gammastrahlung des Mittleren Buntsandsteins von Helgoland—Ein Vergleich mit der Nordseebohrung J/18-1. Zeitschrift der Deutschen Geologischen Gesellschaft 139, 33–49.

Bruun-Petersen, J., Krumbein, W.E., 1975. Rippelmarken, Trockenrisse und Seichtwassermerkmale im Buntsandstein von Helgoland. Geologische Rundschau 64, 126–143.

Canfield, D.E., Berner, R.A., 1987. Dissolution and pyritization of magnetite in anoxic marine sediments. Geochimica et Cosmochemica Acta 51, 645–659.

Clemmensen, L.B., 1979. Triassic lacustrine red-beds and palaeoclimate: The ''Buntsandstein'' of Helgoland and the Malmros Klint Member of East Greenland. Geologische Rundschau 68, 748–774.

Clemmensen, L.B., 1985. Desert plain and sabkha deposits from the Bunter Sandstone Formation (L. Triassic) at the northern margin of the German Basin. Geologische Rundschau 74, 519–536.

Clemmensen, L.B., 1991. Controls on aeolian sand sheet formation exemplified by the Lower Triassic of Helgoland. Acta Mechanica 2, 161–170.

Dando, P.R., Jensen, P., O'Hara, S.C.M., Niven, S.J., Schmaljohann, R., Schuster, U., Taylor, L.J., 1994. The effects of methane seepage at an intertidal/shallow subtidal site on the shore of the Kattegat, Vendsyssel, Denmark. Bulletin of the Geological Society of Denmark 41, 65–79.

Darby, D.A., Tsang, Y.W., 1987. Variation in ilmenite element composition within and among drainage basins: implications for provenance. Journal of Sedimentary Petrology 57, 831–838.

Deegan, C.E., Scull, B.J., 1977. A standard lithostratigraphic nomenclature for the Central and Northern North Sea. Institute of Geological Sciences and Norwegian Petroleum Directorate (Oljedirektoratet), Report 77/25, Bulletin 1, 36pp.

Dimanche, F., 1972. Évolution minéralogique de quelques sables titanifères d'Afrique du Sud. Annales de la Société Géologique de Belgique 95, 183–190.

Dimanche, F., Bartholomé, P., 1976. The alteration of ilmenite in sediments. Minerals, Science and Engineering 8, 187–201.

Fisher, M.J., Mudge, D.C., 1998. Triassic. In: Glennie, K.W. (Ed.), Petroleum Geology of the North Sea, 4th ed.. Blackwell Scientific Publications, Oxford, pp. 212–244.

Force, E.A., Butler, R.F., Raynolds, R.L., Houston, R.S., 2001. Magnetic ilmenite-hematite detritus in Mesozoic-early Tertiary placer and sandstone-hosted uranium deposits of the Rocky Mountains. Economic Geology 96, 1445–1454.

Friis, E.M., 1975. Climatic implications of microcarpological analyses of the Miocene Fasterholt flora, Denmark. Bulletin of the Geological Society of Denmark 24, 179–191.

Friis, E.M., 1979. The Damgaard flora: a new Middle Miocene flora from Denmark. Bulletin of the Geological Society of Denmark 27, 117–142.

Frost, M.T., Grey, I.E., Harrowfield, I.R., Mason, K., 1983. The dependence of alumina and silica contents on the extent of alteration of weathered ilmenites from Western Australia. Mineralogical Magazine 47, 201–208.

Golding, H.G., 1955. Leucoxenic grains in dune sands at North Stadbroke Island, Queensland. Journal of Royal Society of New South Wales 89, 217–231.

Golding, H.G., 1961. Leucoxene terminology and genesis. Economic Geology 56, 1138–1149.

Grey, I.E., Reid, A.F., 1975. The structure of pseudorutile and its role in the natural alteration of ilmenite. American Mineralogist 60, 898–906.

Grigsby, J.D., 1990. Detrital magnetite as provenance indicator. Journal of Sedimentary Petrology 60, 940–951.

Grigsby, J.D., 1992. Chemical fingerprinting in detrital ilmenite: a viable alternative in provenance research? Journal of Sedimentary Petrology 62, 331–337.

Hansen, J.Ø., 1985. En lithofaciesundersøgelse af nogle kvartssandsforekomster i Midtjylland. Unpublished M.Sc. thesis. University of Aarhus, 126pp.

Hofmann, B., 1990. Reduction spheroids from northern Switzerland: mineralogy, geochemistry and genetic models. Chemical Geology 81, 55–81.

Hovland, M., Talbot, M.R., Quale, H., Olaussen, S., Aasberg, L., 1987. Methane-related carbonate cements in pockmarks of the North Sea. Journal of Sedimentary Petrology 57, 881–892.

Hugo, V.E., Cornell, D.H., 1991. Altered ilmenites in Holocene dunes from Zululand, South Africa: petrographic evidence for multistage alteration. South African Journal of Geology 94, 365–378.

Ixer, R.A., Turner, P., Waugh, B., 1979. Authigenic iron titanium oxides in Triassic red beds: St. Bees Sandstone, Cumbria, Northern England. Geological Journal 14, 179–192.

Jørgensen, N.O., 1989. Holocene methane-derived, dolomite-cemented sandstone pillars from the Kattegat, Denmark. Marine Geology 88, 71–81.

Koch, B.E., Friedrich, W.L., Christensen, E.F., Friis, E.M., 1973. Den miocæne brunkulsflora og den geologiske miljø i Søby-Fasterholt området sydøst for Herning. Geological Society of Denmark. Årsskrift for 1972, 1–57.

Larsen, G., 1966. Rhaetic-Jurassic-Lower Cretaceous sediments in the Danish embayment (a heavy mineral study). Geological Survey of Denmark II, 91, 127pp.

Lines, A.W., Parnell, J., Mossman, D.J., 1996. Reduction speroids from the Upper Carboniferous Hopewell Group, Dorchestr Cape, New Brunswick: notes on the geochemistry, mineralogy and genesis. Atlantic Geology 32, 159–172.

Lynd, L.E., Sigurdson, H., North, C.H., Anderson, W.W., 1954. Characteristics of titaniferous concentrates. Mining Engineering 6, 817–824.

Machel, H.G., 1995. Magnetic mineral assemblages and magnetic contrasts in diagenetic environments—with implications for studies of palaeomagnetism, hydrocarbon migration and exploration. In: Turner, P., Turner, A. (Eds.), Palaeomagnetic Applications in Hydrocarbon Exploration and Production. Geological Society of London Special Publication, vol. 98, pp. 9–29.

Metcalfe, R., Rochelle, D., Savage, D., Higgo, J.W., 1994. Fluid-rock interactions during continental red bed diagnesis: implications for theoretical models of mineralizations in sedimentary basins. In: Parnell, J. (Ed.), Geofluids: Origin, Migration and Evolution of Fluids in Sedimentary Basins. Geological Society of London Special Publications, vol. 78, pp. 301–324.

Miller, D.N., Folk, R.L., 1955. Occurrence of detrital magnetite and ilmenite in red sediments: new approach to significance of redbeds. American Association of Petroleum Geologists Bulletin 39, 338–345.

Morad, S., Aldahan, A.A., 1986. Alteration of detrital Fe-Ti oxides in sedimentary rocks. Geological Society of America Bulletin 97, 567–578.

Mücke, A., Chaudhuri, B., 1991. The continuous alteration of ilmenite through pseudorutile to leucoxene. Ore Geology Reviews 6, 25–44.

Nielsen, L.H., 2003. Late Triassic-Jurassic development of the Danish Basin and the Fennoscandian Border Zone, southern Scandinavia. In: Ineson, J.R., Surlyk, F. (Eds.), The Jurassic of Denmark and Greenland. Geological Survey of Denmark and Greenland Bulletin 1, pp. 459–526.

Olsen, H., 1987. Ancient ephemeral stream deposits: a local terminal fan model from the Bunter Sandstone Formation (L. Triassic) in the Tønder-3, -4 and -5 wells, Denmark. In: Frostick, L., Reid, I. (Eds.), Desert Sediments: Ancient and Modern. Geological Society of London Special Publication, vol. 35, pp. 69–86.

Pedersen, G.K., Andersen, P.R., 1980. Depositional environments, diagenetic history and source areas of some Bunter Sandstones in northern Jutland. Geological Survey of Denmark, Årbog 1979, 69–93.

Priisholm, S., 1983. Geothermal reservoir rocks in Denmark. Geological Survey of Denmark, Årbog 1982, 73–86.

Rasmussen, L.B., 1961. De miocæne formationer i Danmark. Danmarks Geologiske Undersøgelse IV, Række 5, 45pp.

Reynolds, R.L., Goldhaber, M.B., 1978. Origin of a south Texas roll-type uranium deposit: I. Alteration of iron-titanium oxide minerals. Economic Geology 73, 1677–1689.

Reynolds, R.L., Goldhaber, M.B., Tuttle, M.L., 1993. Sulfidization and magnetization above hydrocarbon reservoirs. In: Aissaui, D.M., McNeill, D.D., Hurley, N.F. (Eds.), Application of Paleomagnetism to Sedimentary Geology. SEPM Special Publication, vol. 49, pp. 167–179.

Riezebos, P.A., 1979. Compositional downstream variation of opaque and translucent heavy residues in some modern Rio Magdalena sands (Colombia). Sedimentary Geology 24, 197–225.

Riezebos, P.A., Bisdom, E.B.A., Boersma, O., 1978. Composite grains in Maas (Meuse) sediments: a survey and a discussion of their opaque components. Geologie en Mijnbouw 57, 417–431.

Rose, A.W., 1989. Mobility of copper and other heavy metals in sedimentary environments. In: Boyle, R.W., Brown, A.C., Jefferson, C.W., Jowett, E.C., Kirkham, R.V. (Eds.), Sediment-Hosted Stratiform Copper Deposits. Geological Association of Canada Special Paper 36, 97–110.

Schneiderman, J.S., 1995. Detrital opaque oxides as provenance indicators in River Nile sediments. Journal of Sedimentary Research A65, 668–674.

Schwertmann, U., Taylor, R.M., 1989. Iron oxides. In: Dixon, J.B., Weed, S.B. (Eds.), Minerals in Soil Environments. Soil Science Society of America, Madison, pp. 379–438.

Temple, A.K., 1966. Alteration of ilmenite. Economic Geology 61, 695–714.

Thompson, A.M., 1970. Geochemistry of color genesis in red-bed sequence, Juniata and Bald Eagle Formations, Pennsylvania. Journal of Sedimentary Petrology 40, 599–615.

Turner, P., 1980. Continental red beds. Developments in Sedimentology, vol. 29, Elsevier Scientific Publishing Company, Amsterdam, 562pp.

Turner, P., Chandler, P., Ellis, D., Leveille, G.P., Heywood, M.L., 1999. Remanence acquisition and magnetostratigraphy of the Leman Sandstone Formation: Jupiter Fields, southern North Sea. In: Tarling, D.H., Turner, P. (Eds.), Palaeomagnetism and Diagenesis in Sediments. Geological Society of London Special Publication, vol. 151, pp. 109–124.

Van der Zwan, C.J., Spaak, P., 1992. Lower to Middle Triassic sequence stratigraphy and climatology of the Netherlands, a model. Palaeogeography, Palaeoclimatology, Palaeoecology 91, 277–290.

Van Houten, F.B., 1968. Iron oxides in red beds. Geological Society of America Bulletin 79, 399–416.

Van Houten, F.B., 1973. Origin of red beds. A review—1961–1972. Annual Review of Earth and Planetary Science 1, 39–61.

Van Loon, A.J., Mange, M.A., 2007. 'In situ' dissolution of heavy minerals through extreme weathering, and the application of the surviving assemblages and their dissolution characteristics to correlation of Dutch and German silver sands. In: Mange, M.A., Wright, D.T. (Eds.), Heavy Minerals in Use. Developments in Sedimentology (this volume).

Walker, T.R., 1967. Formations of red beds in modern and ancient deserts. Geological Society of America Bulletin 78, 353–368.

Walker, T.R., 1968. Formations of red beds in modern and ancient deserts: reply. Geological Society of America Bulletin 79, 281–282.

Walker, T.R., 1976. Diagenetic origin of continental red beds. In: Falke, H. (Ed.), The Continental Permian in Central, West, and South Europe. Reidel Publishing Company, Dordrecht, pp. 240–282.

Walker, T.R., Honea, R.M., 1969. Iron content of modern deposits in the Sonoran Desert: a contribution to the origin of red beds. Geological Society of America Bulletin 80, 535–544.

Walker, T.R., Larson, E.E., Hoblitt, R.P., 1981. Nature and origin of hematite in the Moenkopi Formation (Triassic), Colorado Plateau: a contribution to the origin of magnetism in red beds. Journal of Geophysical Research 86, 317–333.

Walker, T.R., Runnels, D.D., 1984. Potential role of smectite-illite conversion in the formation of hematite pigment in red beds. Abstract Geological Society of America Annual Convention, Reno, Nevada.

Weibel, R., 1993. Mineralogiske ændringer i miocænt, fluviatilt sand, Voervadsbro [Mineralogical alterations in Miocene fluviatile sand, Voervadsbro, Denmark]. Unpublished M.Sc. thesis. University of Aarhus (with English abstract), 162pp.

Weibel, R., 1998. Diagenesis in oxidising and locally reducing conditions—an example from the Triassic Skagerrak Formation, Denmark. Sedimentary Geology 121, 259–276.
Weibel, R., 2003. Alteration of detrital Fe-Ti oxides in Miocene fluvial deposits, central Jutland, Denmark. Bulletin of the Geological Society of Denmark 50, 171–183.
Weibel, R., Friis, H., 2004. Opaque minerals as keys for distinguishing oxidising and reducing diagnetic conditions in the Lower Triassic Bunter Sandstone, North German Basin. Sedimentary Geology 169, 129–149.
Weibel, R., Grobety, B., 1999. Pseudomorphous transformation of goethite needles into hematite in sediments of the Triassic Skagerrak Formation. Clay Minerals 34, 657–660.
Wright, D.T., 1999. The role of sulphate-reducing bacteria and cyanobacteria in dolomite formation in distal ephemeral lakes of the Coorong region, South Australia. Sedimentary Geology 126, 147–157.
Wurster, P., 1960. Kreuzschichtung im Buntsandstein von Helgoland. Geologisches Staatsinstitut, Hamburg, Mitteilung 29, 61–65.
Ziegler, P.A., 1987. Evolution of the Arctic-North Atlantic and the Western Tethys. AAPG Memoir 43, 198pp.
Ziegler, P.A., 1990. Geological Atlas of Western and Central Europe. Shell Internationale Petroleum Maatschappij, The Hague, 239pp.
Zielinski, R.A., Bloch, S., Walker, T.R., 1983. The mobility and distribution of heavy metals during the formation of first cycle red beds. Economic Geology 78, 1574–1589.

This page intentionally left blank

1.3 Heavy Minerals and Grain Size

This page intentionally left blank

Chapter 11

AN INTEGRATED GRAIN-SIZE AND HEAVY MINERAL ANALYSIS OF THE PALAEOCENE STRATA OF THE LONDON BASIN

ALICE R.A. THOMAS[a,1]

[a]*Department of Earth Sciences, University of Oxford, Parks Road, Oxford, OX1 3PR and PADMAC Unit, Pitt Rivers Museum, University of Oxford, 60 Banbury Road, Oxford, OX2 6PN, UK*
[1]*Present address: Neftex Petroleum Consultants Ltd., 115BD Milton Park, Abingdon, Oxfordshire, OX14 4SA, UK*

ABSTRACT

Grain-size and heavy mineral data are presented for the Palaeocene strata of the London Basin, southeastern England. This succession comprises four main sedimentary units: the Thanet Sand, Upnor, Woolwich and Reading formations. Samples from two borehole sections (Coppermills and Hadley Road) and one exposure (Herne Bay) have been analysed. The boundary between the Thanet Sand and Upnor formations is clearly defined lithologically at the base of a transgressive pebble bed, but is also recognised by a change from a tourmaline-dominated to a zircon-dominated heavy mineral assemblage and a shift in grain-size mode from 3.5 to 3 phi. At Herne Bay, strata close to the lower and upper boundaries of the Upnor Formation display atypical mineral assemblages, suggesting, at least at the upper boundary, that bioturbation has masked these contacts. Samples from the Lower Mottled Clay Member of the Reading Formation show clear evidence of multiple provenance. Grain-size and heavy mineral characteristics show variation between two end-members: a tourmaline-dominated sediment with a 3.5 phi grain-size mode and a second zircon-dominated sediment with a 3 phi grain-size mode. The former may represent fluvially reworked Thanet Sand sediment and the latter either reworked Upnor sediment or continued sedimentation from the same source area (s) as the Upnor Formation. The Reading Formation, particularly the Upper Mottled Clay Member, shows signs of pedogenic modification. The results presented in this contribution indicate that combined grain-size and heavy mineral studies of borehole-derived material can improve our stratigraphic understanding of poorly preserved and bioturbated strata, despite the restrictions of small sample size and limited borehole distribution.

Keywords: Palaeocene; London Basin; stratigraphy; heavy minerals; grain size

Developments in Sedimentology, Vol. 58, 307–322

ISSN: 0070-4571/doi:10.1016/S0070-4571(07)58011-8

1. INTRODUCTION

An integrated analysis of grain-size and heavy mineral characteristics can refine the stratigraphy of poorly exposed and preserved strata and help to resolve chronostratigraphic relationships that may be undetectable in separate lithostratigraphic, palaeontological and mineralogical studies. In the present study this approach is applied to the Palaeocene strata of the London Basin (southeastern England) which, together with the Hampshire Basin (south-central England), represents the only onshore record of Early Cenozoic sedimentation in Britain. A number of problems are encountered when applying classical stratigraphic methods to the Palaeocene of the London Basin: the sediments are poorly exposed and preserved, lithologically highly variable laterally (lacking good marker horizons), and often heavily bioturbated. The stratigraphy is also complicated by interdigitating and mixed lithologies and the recurrence of similar facies at various levels within the succession. Despite these problems a great deal of lithostratigraphic, palaeontological, palaeobotanical and mineralogical work has been published in the last century (e.g., Boswell, 1916; Groves, 1931; Hester, 1965; Blondeau and Pomerol, 1968; Weir and Catt, 1969; Morton, 1982; Aubry et al., 1986; Knox, 1990; Knox et al., 1990; Crane and Goldring, 1991; Jolley, 1992a, b; Ellison et al., 1994; Ellison, 1983). However, many of these studies are specific to a particular region or even a single site.

Direct comparisons between studies of the grain-size and heavy mineral characteristics of the British Palaeocene are restricted by methodological variations: different sample sizes and size fractions have been examined by different authors. Some workers (e.g., Morton, 1982) have chosen a narrow size bracket, such as 3–4 phi (125–63 μm, equivalent to the 'very fine sand' fraction on the Wentworth scale). This has the advantage of eliminating apparent variations in mineral proportions caused by differences in grain size, thus reducing the effect of hydraulic sorting. However, given that certain mineral species tend to be concentrated in particular grain-size ranges (Mange and Maurer, 1992, p. 6), such a strategy risks over-representing one or more species which have concentrated in the selected size bracket and/or missing a diagnostic species that is present outside the selected size range. Other authors use broad grain-size brackets or examine the entire sand fraction (−1 to +4 phi, 2000–63 μm, ranging from the 'very coarse sand' to 'very fine sand' of Wentworth). This technique ensures that all potentially diagnostic species are identified and characterises the entire mineral suite, but the hydraulic effects may be magnified. Furthermore, the presence of a wide range of grain sizes makes mounting and analysis difficult. Different workers also use heavy liquids of/at different densities for heavy mineral separation. This may impede comparisons between studies because identical samples separated at different densities are likely to yield assemblages with a different range, and different relative proportions, of heavy mineral species. The number of non-opaque grains counted by different authors also varies significantly. Morton (1982) counted 200 grains per sample, whereas Macdonald (1965) counted between 672 and 2439 per sample. However, Dryden (1931) demonstrated that the accuracy of the data increases rapidly with the increasing number of heavy mineral grains counted, up to a total of 300 grains. Above this number, accuracy increases very slowly.

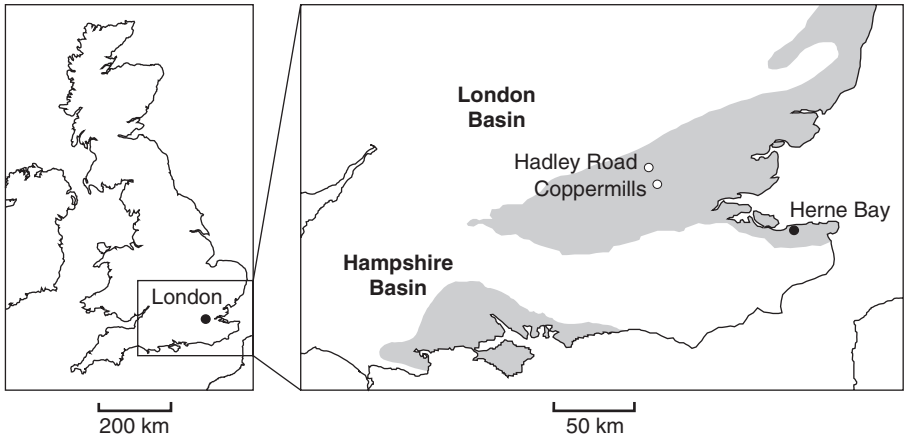

Fig. 1. Location of the Hadley Road, Coppermills and Herne Bay sample sites. The distribution of Palaeocene strata is shaded.

As has already been discussed, the British Palaeocene outcrops in both the London and Hampshire Basins (Fig. 1), but is largely covered by later Cenozoic sediments; Palaeocene strata are exposed only at the margins of the two basins. The Palaeocene successions represent the lowermost part of a complex transgressive–regressive sequence, which may be attributed to eustacy (Neal, 1996) or pulsed tectonism (Knox, 1996). The succession comprises four main sedimentary units: the basal Thanet Sand Fm., the overlying Upnor Fm. and the succeeding Reading and Woolwich formations. The latter two formations are considered lateral equivalents of each other and interdigitate in the London area.

The present study aims to demonstrate the advantages of an integrated method that utilises both grain-size and heavy mineral analyses to construct a high-resolution stratigraphy for the problematic strata of the London Basin. Grain-size and heavy mineral characteristics are used to identify and correlate strata. Changes in these characteristics can often be attributed to bioturbation, reworking, provenance or a combination thereof. This study also assesses the effect of restricted sample size and grain-size bracket on the heavy mineral assemblages of the Thanet Sand and Upnor Formations.

2. METHODS

The English Palaeocene currently lacks good onshore exposures. Fortunately, the British Geological Survey (BGS) has preserved extensive borehole material which is available for sampling, although samples extracted from boreholes are small (usually less than 100 g). To determine the effect that sample size exerts on grain-size and heavy mineral analyses, both small (~95 g) and large (~425 g) samples were selected from outcrop for comparison. These samples were taken from the same sample site (vertical and lateral positions are identical) at Herne Bay (Fig. 1), one of the few remaining good exposures of Palaeocene strata. As it is known that the use of different grain-size brackets can produce variability in heavy mineral results, both

2–4 phi (250–63 μm) and 3–4 phi (125–63 μm) fractions were separately mounted and counted for both large and small samples.

Grain-size and heavy mineral datasets were determined for samples extracted from two BGS boreholes: Hadley Road (BGS registration number: TQ39NW19) and Coppermills (BGS registration number: TQ38NE301), and were compared with those from the more distant Herne Bay exposure. The borehole sites are sufficiently close (~10 km) so that some shared lithostratigraphy was expected. Some facies differentiation was also expected because the Hadley Road borehole is situated near the northern edge of the existing outcrop, whereas the Coppermills borehole is sited further towards the basin centre (Fig. 1).

Cores and exposures were sampled at regular intervals (multiples and fractions of 300 cm) and immediately above every facies change. Samples were air dried (drying vessels were lightly covered by paper to avoid dust accumulation) and accurately weighed (in grams to 2 decimal places). Following disaggregation (using a pestle and mortar) and wet sieving, the sand fractions were oven dried and reweighed. A grain-size distribution was determined for the sand fractions using a sieve shaker with nested sieves (duration: 20 minutes, amplitude: 10, motion: continuous). The sand fractions were then reweighed and stored for later analysis. A grain-size distribution for the silt- and clay-grade fractions was determined by laser granulometry. LST Fastfloat (a solution of sodium heteropolytungstates) was then used to separate the heavy and light fractions of each sample. Heavy liquid density was maintained at 3 g/cm^3. Heavy fractions were then mounted in Canada balsam and mineral counts were made using the 'ribbon' technique (Galehouse, 1971). A count size of 300 non-opaque grains per sample was adopted for this study (Table 1).

The grain-size curves are expressed as smoothed line graphs, rather than cumulative frequency graphs or histograms, in order to more clearly display grain-size trends. Line graphs allow curves to be easily compared because they highlight subtle shifts in mode, modal breadth and curve shape, which are difficult to observe on cumulative frequency plots. No error bars have been displayed on the grain-size curves as high repeatability suggests uncertainties are insignificant.

In the following sections, samples are referred to by their sample depth. Data for each sample are also labelled by sample depth. For the Coppermills and Hadley Road samples this depth represents metres below ground level and for the Herne Bay samples metres below the overlying Harwich Formation basal pebble bed (the clearest and closest stratigraphic marker available at the site). The Harwich Formation generally disconformably overlies the Woolwich or Reading Formations, but at Herne Bay, rests directly on the Upnor Formation.

3. RESULTS AND DISCUSSION

3.1. Sample Size and Grain-Size Bracket Experiment

Mineralogical counts of 300 translucent grains appear largely independent of sample size for the study sediments (Fig. 2). The mineral counts differ little between bracket size (at least between 2–4 and 3–4 phi), although zircon does tend to be slightly over-represented in the finer fraction (3–4 phi), which may be significant in zircon-rich

Table 1. Heavy mineral abundance data for the Hadley Road and Coppermills boreholes. Borehole samples are described by sampling depth in metres below (existing) ground level. Herne Bay samples are named by sampling depth below the basal Harwich pebble bed. Mineral species with abundances less than 2% (six counted grains) are grouped as 'others'

Stratigraphy	Sample	Tourmaline	Zircon	Rutile	Garnet	Staurolite	Kyanite	Hornblende	Epidote	Sillimanite	Clinozoisite	Cassiterite	Apatite	Calcite	Others
UMC	H 15.14	157	64	30	–	26	12	–	–	–	–	–	–	–	11
LMC	H 17.60	68	69	28	22	34	14	–	–	–	–	–	6	44	15
	H 20.32	62	70	22	18	28	13	–	–	–	6	–	–	71	10
	H 21.96	51	120	26	27	24	9	–	6	–	–	–	–	30	7
U	H 23.04	106	88	8	26	40	13	–	–	–	–	–	–	14	5
	H 24.50	65	97	26	38	30	16	–	8	–	–	–	–	11	9
	H 24.81	110	32	15	22	26	26	–	–	–	–	–	–	62	7
	H 26.11	37	155	29	13	25	16	–	–	–	–	–	–	19	6
TS	H 29.02	137	64	16	26	19	9	–	19	–	–	–	6	–	4
	H 29.40	139	68	12	32	17	16	–	–	–	–	–	8	–	8
UMC	C 27.67	168	73	23	–	16	14	–	–	–	–	–	–	–	6
LMC	C 29.17	113	61	38	–	38	23	–	–	6	–	–	–	–	21
	C 31.42	65	140	54	–	13	17	–	–	–	–	–	–	–	11
	C 32.06	142	47	19	27	34	24	–	–	–	–	–	–	–	7
U	C 37.42	79	79	24	33	35	37	–	–	–	–	–	–	–	13
	C 37.91	36	159	30	19	23	9	–	11	–	7	–	–	–	6
	C 38.09	94	84	25	17	37	23	–	7	–	6	–		–	7
	C 38.73	53	103	30	18	30	18	–	–	–	–	–	6	37	5
	C 39.21	50	171	30	12	16	15	–	–	–	–	–	6	–	–
TS	C 48.90	143	48	11	19	37	15	–	14	–	7	–	–	–	6
	C 49.47	125	52	20	26	36	9	–	17	–	7	–	–	–	8
U/H	HB 1.50 small	129	59	35	21	31	11	9	–	–	–		–	–	5
U	HB 4.50 small	14	190	36	17	11	9	–	–	–	–		–	–	23
TS/U	HB 7.20 small	70	83	49	21	29	12	10	–	–	–	8	–	–	18

Note: Sample prefixes H, C and HB relate to the Hadley Road and Coppermills boreholes and the Herne Bay site, respectively. Stratigraphical formations are coded as follows: TS/U = (close to the) Thanet Sand/Upnor boundary; TS = Thanet Sand Formation; U = Upnor Formation; U/H = (close to the) Upnor/Harwich boundary; LMC = Lower Mottled Clay (Reading Formation); UMC = Upper Mottled Clay (Reading Formation).

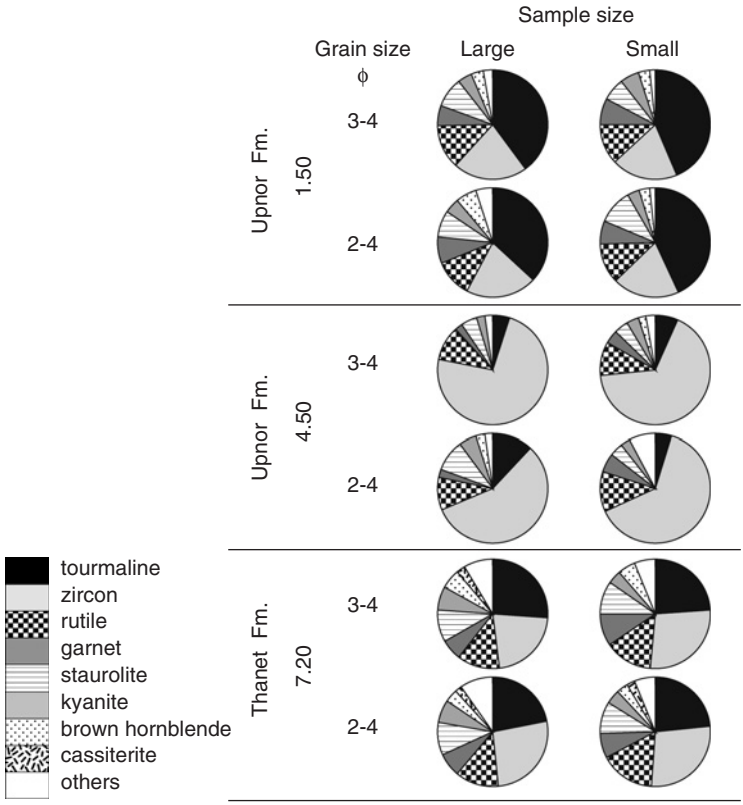

Fig. 2. Heavy mineral data for the Herne Bay samples (1.50, 4.50 and 7.20). Data for large (~425 g) and small (~95 g) sample sizes and 2–4 phi (250–63 μm) and 3–4 phi (125–63 μm) grain-size brackets are shown. Mineral species with abundances less than 2% (six counted grains) are grouped as 'others'.

assemblages. It is noted that the larger samples display greater (though still minor) variation in their modal species between different bracket sizes.

3.2. Stratigraphic Signatures of Grain-Size and Heavy Mineral Assemblages

3.2.1. Thanet Sand Formation

The basal conglomerate samples from Hadley Road (H 29.40) and Coppermills (C 49.47) boreholes show closely matched grain-size curves (modal peak at 3.5 phi) and heavy mineral assemblages (discussed below; Fig. 3); they clearly represent the same sediment body. The overlying sands display similar grain-size and heavy mineral characteristics to each other and to the underlying conglomerate samples. However,

Fig. 3. Grain-size and heavy mineral data for samples from the Hadley Road and Coppermills boreholes and the Herne Bay exposure site. Mineral species with abundances less than 2% (six counted grains) are grouped as 'others'. The Herne Bay samples shown are 1.50 small, 4.50 small and 7.20 small (as indicated by the 's' suffix).

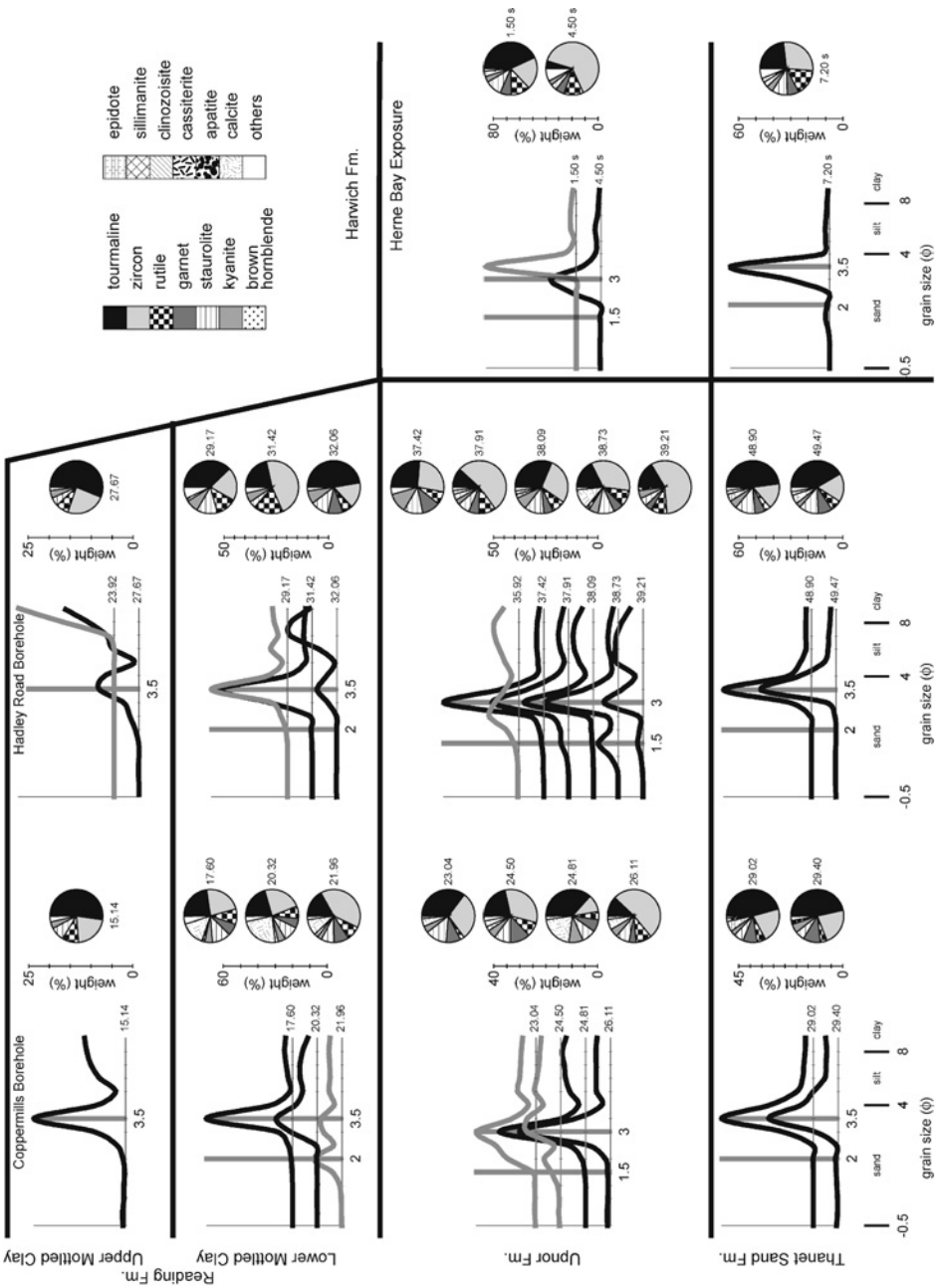
tourmaline
zircon
rutile
garnet
staurolite
kyanite
brown hornblende
epidote
sillimanite
clinozoisite
cassiterite
apatite
calcite
others
Harwich Fm.
Coppermills Borehole
Hadley Road Borehole
Herne Bay Exposure
Reading Fm.
Upper Mottled Clay
Lower Mottled Clay
Upnor Fm.
Thanet Sand Fm.
weight (%)
grain size (ϕ)
sand
silt
clay

the modal grain-size frequencies of these sand samples (H 29.02 and C 48.90) are 10% higher than those of the underlying pebble bed. The pebble bed samples also contain a greater proportion of sediment between 4 and 6 phi relative to the overlying sands. Weir and Catt (1969) suggest that this additional 4–6 phi sediment may reflect the incorporation of sediment from another source into the pebble bed matrix. Such sediment may have been derived from the weathering residuum which developed on the exposed Chalk landmass prior to submergence and deposition of the Thanet Sand Formation (Weir and Catt, 1969). Alternatively, silt-grade sediment may have been derived from in situ dissolution of the Chalk by acidic pore waters, via illuviation from the overlying strata or by some combination of these processes (Weir and Catt, 1969). The similarity of lithofacies, heavy mineral assemblages and grain-size curves between the two sites suggests that the strata have a common provenance, and have been deposited in the same palaeoenvironment. The abundance of glauconite in these samples indicates a marine environment with low rates of terrigenous input. Ellison et al. (1994) suggest an inner shelf setting above fair-weather wave base.

The Thanet Sand Formation assemblages from the Hadley Road and Coppermills boreholes are all dominated by tourmaline with subsidiary zircon, garnet, staurolite, rutile and kyanite; epidote and apatite are also present in some samples. This differs from Morton's (1982) study which reported a greater degree of mineralogical variation for the Thanet Sand Formation; he found some samples to be dominated by ultrastable zircon with low proportions of less stable minerals (such as garnet, epidote and apatite) and, at other sites and horizons, samples were found to be dominated by garnet, epidote and apatite. He noted a correlation between increasing etching intensity of these unstable species and their decreased abundance higher up in the succession and ascribed this mineralogical variability to acidic groundwater circulation associated with pre-Upnor Formation weathering. The Thanet Sand Formation samples from Hadley Road and Coppermills have a uniform mineralogy, and no stark depletion in, or dissolution of, unstable species was observed. Consequently, either any acidic weathering, as described by Morton (1982), did not take place at the Hadley Road and Coppermills sites or the acidic groundwater did not percolate to the basal Thanet Sand Formation strata at the two sites.

The lack of tourmaline in Morton's (1982) assemblages is puzzling as tourmaline is an ultrastable species and would be expected to be found even in assemblages intensively modified by acidic weathering. Further, relative proportions of tourmaline would be likely to increase as relative proportions of unstable minerals decreased. As the Thanet Sand Formation is understood to have been laid down in a series of onlapping sequences (Haq et al., 1987), the disparity between the two datasets could reflect sampling of different sequences characterised by different heavy mineral assemblages. As described earlier, such differences do not appear to be caused by variation in sample size or bracket size (Morton uses a 3–4 phi bracket, whereas a 2–4 phi bracket is used in the present study). However, Morton's (1982) count size (200 grains) is inherently more prone to error than the count size (300 grains) used in the present study.

The lowermost Herne Bay sample (HB 7.20 small) is interpreted as representing the uppermost Thanet Sand Formation. This concurs with Ward's (1978) study, although the lithological distinctions he describes from the foreshore exposures were

not observed in the cliff face. HB 7.20 small is interpreted in this way for two reasons: firstly, it displays the characteristic strong 3.5 phi modal peak; and secondly, the heavy mineral assemblage is intermediate in character between the tourmaline-dominated Thanet Sand assemblage discussed above and the zircon-dominated Upnor assemblage discussed below. This is consistent with the observations of Hester (1965) and Ellison et al. (1994), who reported that the Thanet Sand/Upnor boundary is gradational in the eastern London Basin due to bioturbation. Alternatively, HB 7.20 small could represent a depositional intermediate between the tourmaline-dominated Thanet Sand assemblage and zircon-dominated Upnor assemblage. If so, this succession of assemblages could reflect gradual changes in source rocks eroded from essentially the same source area (s), a change in source area or changing dominance in sediment supply between multiple source areas. Moffat and Bateman (1983) also suggested that mineralogical variation in the Thanet Sand Formation was more likely related to provenance. However, if source areas are changing through the succession, varietal types would also be expected to change, but brown tourmaline remains dominant, relative to other colours, throughout the Palaeocene succession. Multiple source areas could explain this phenomenon if the dominant tourmaline-supplying source remained constant throughout the Palaeocene, but, in addition, other source provinces and transport pathways became periodically active. The predominance of brown tourmaline, which is characteristic of Cornish source rocks (Brammal, 1928), and the presence of zoned zircons (possibly derived from the Cornish granites) in the assemblage suggest that Cornubia may have been a significant source area (M. Mange, personal communication, 2004). Other suggested source areas include Armorica (Groves, 1928; Blondeau and Pomerol, 1968; Weir and Catt, 1969), 'northern seas' (Blondeau and Pomerol, 1968), an amphibolite-facies metamorphic province (Weir and Catt, 1969), the Scottish Highlands (Morton, 1982) and the Cretaceous Greensand (M. Mange, personal communication, 2004). Some workers have also suggested that the formation may have multiple source areas (e.g., Blondeau and Pomerol, 1968; Weir and Catt, 1969). All of the proposed sources are plausible.

3.2.2. Upnor Formation

The Thanet Sand/Upnor Formation boundary is shown lithologically at the Hadley Road and Coppermills sites as a change from sand to conglomerate (Fig. 4). The boundary coincides with a shift in grain-size mode from 3.5 to 3 phi and a change from a tourmaline-dominated to a zircon-dominated heavy mineral assemblage. This slight coarsening of the sand-grade modal peak indicates an increase in hydraulic energy, implying that the Upnor Formation was deposited in shallower water than the Thanet Sand Formation. This is supported by Ellison et al.'s (1994) interpretation of shelf to coastal sedimentation in partially tidally influenced environments. The change in relative abundance of tourmaline and zircon between the Thanet Sand and Upnor Formations may reflect the difference in density between the two species (tourmaline 3.03–3.25 and zircon 4.6–4.7) which results in concentrations of one or the other in response to variations in current velocity. Consequently, the development from a tourmaline-rich assemblage to a zircon-rich assemblage also suggests increasing hydraulic energy through the Thanet Sand Formation into the Upnor Formation and possibly a shallowing-upwards succession. This concurs with Ellison

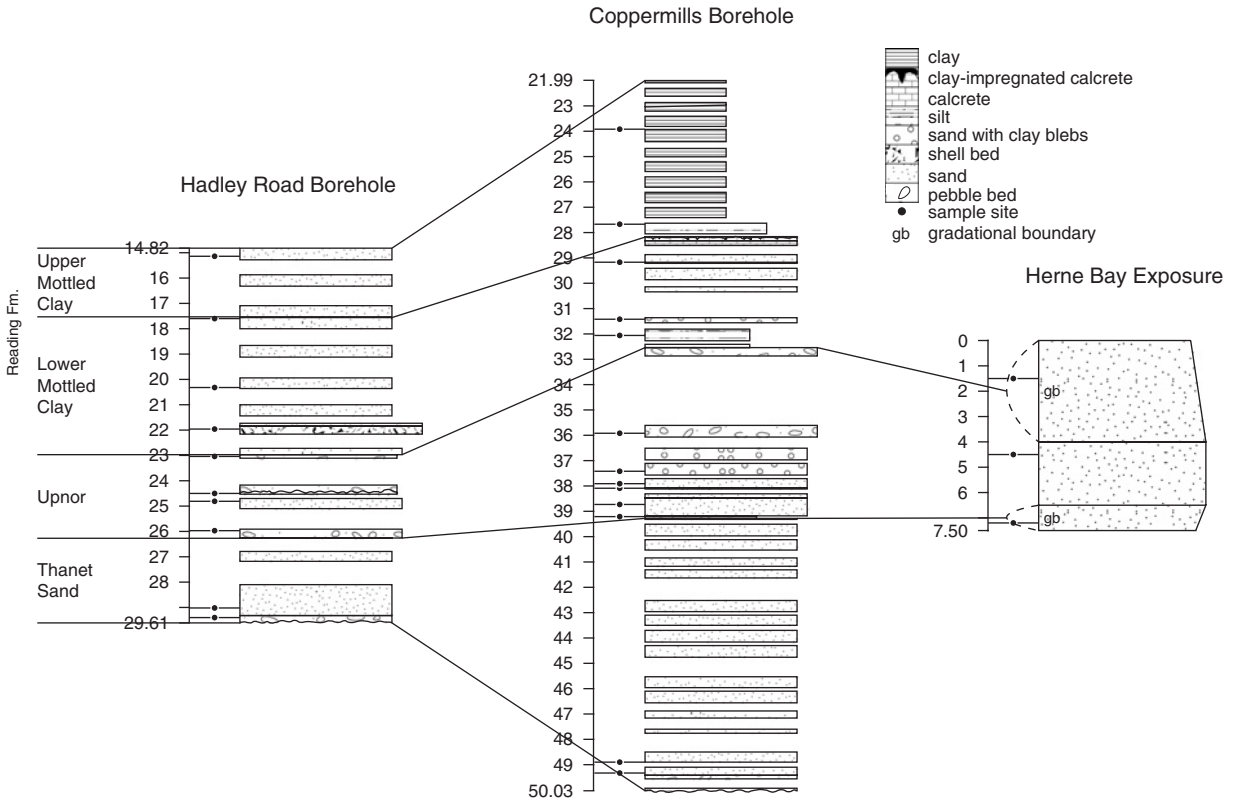

Fig. 4. Lithology logs for the Hadley Road and Coppermills boreholes and the Herne Bay site. Sample depth for the boreholes is given in metres below (existing) ground level and for Herne Bay samples as metres below the overlying Harwich Formation basal pebble bed.

et al.'s (2004) description of a coarsening-upwards Thanet Sand Formation. The overstep of the Thanet Sand Formation by the Upnor Formation in the west of the basin may suggest that the Upnor Formation represents a more extensive transgression than the Thanet Sand Formation. However, given that the Thanet Sand Formation may have been eroded prior to deposition of the Upnor Formation, overstep is not considered to be conclusive evidence of a larger transgression.

The samples of matrix from the basal Upnor Formation conglomerate (H 26.11 and C 39.21) correlate well in terms of grain-size and heavy mineral characteristics (Fig. 3). The overlying samples show more variable characteristics; Hadley Road sample H 24.81 and Coppermills samples C 38.73, C 38.09, C 37.91 and C 37.42 display characteristic 3 phi peaks, but all are asymmetrical (displaying more 3.5 phi sediment than 2.5 phi sediment). This asymmetry suggests the presence of contaminating Thanet Sand Formation or Reading Formation sediment. Coppermills sample C 35.92 shows an atypical grain-size distribution due to the distorting presence of glauconite. Samples C 24.50 and C 23.04 display grain-size characteristics of intermediate character between the Upnor Formation and the overlying Reading Formation (Lower Mottled Clay Member); this is interpreted as representing Reading Formation contamination, possibly driven by bioturbation. Sample H 24.50 was extracted from a shelly pebble bed; the presence of well-rounded flint pebbles, fractured pebbles and shell fragments suggests an increase in hydraulic energy relative to the underlying silty sands (represented by sample H 24.81). This may suggest progradation of the shoreline/regression that has allowed the transportation/accumulation of littoral pebbles further towards the centre of the basin than previously recorded by the underlying Upnor Formation strata.

All of the Hadley Road and Coppermills samples except for those extracted from the basal Upnor pebble bed (H 26.11 and C 39.21) show variable heavy mineral assemblages, either dominated by zircon or tourmaline or co-dominated by both species. This variation is attributed to the interplay of two sediment sources: a marine source (dominated by zircon) and a tourmaline-rich source which may represent Thanet Sand Formation sediment, fluvially reworked from the fringes of the basin.

Detrital calcite present in samples H 26.11, H 24.81, H 24.50, H 23.04 and C 38.73 suggests either an Upnor Formation transgression and erosion of the Chalk landmass or increased significance of coastal sediment sources (eroding and transporting calcite from the English Chalk landmass). The dominance of tourmaline in H 24.81 may be attributed to reworking of Thanet Sand Formation-derived material. Sample H 24.81 shows the greatest abundances of calcite and tourmaline compared to the other Upnor Formation samples; if these species do, respectively, indicate Chalk-derived and fluvially reworked Thanet Sand sediment, perhaps this stratum records a regression or localised progradation.

Samples HB 4.50 small and HB 1.50 small from Herne Bay (Fig. 3) are both interpreted as representing the Upnor Formation; HB 4.50 small displays the typical strong 3 phi modal peak and zircon-dominated assemblage. Conversely, HB 1.50 small shows a tourmaline-dominated mineralogy and 3.5 phi modal peak; it exhibits the characteristics of the Thanet Sand Formation. This seems stratigraphically confusing until the overlying Harwich Formation is investigated. Weir and Catt (1969) and Morton (1982) both describe the Harwich Formation as displaying similar

mineralogical characteristics to the Thanet Sand Formation; if this is the case at Herne Bay, HB 1.50 small may represent an infilled burrow, extending down from the Harwich Formation into the Upnor Formation. Such burrows have been recognised by several authors (e.g., Ellison et al., 1994). Weir and Catt (1969) also sampled the Upnor Formation (approx. 25 cm below sample HB 1.50 small, i.e. 1.75 m below the Harwich basal pebble bed) and interpreted the Upnor as having 'exactly the same mineral composition' as the underlying Thanet Sand Formation. This suggests that the authors, due to their use of a lower resolution sampling strategy than applied in the present study, may have missed the zircon-rich Upnor assemblage. This scenario again highlights the stratigraphic pitfalls presented by successions with recurring facies, provenance and mineral assemblages.

The presence of minor amounts of Cornubian detritus within the zircon-dominated Upnor assemblage has been noted by Groves (1931) and Macdonald (1965). Blondeau and Pomerol (1968), Weir and Catt (1969) and Morton (1982) suggested the granitic and metamorphic rocks of the Armorican massifs as the dominant source region due to the mixed igneous/metamorphic nature of the Upnor assemblages. Morton (1982) also suggested the Ardennes and Rhenish massifs as source areas based on the presence of allanite in his samples. The change from a tourmaline- to a zircon-dominated assemblage may reflect the increasing importance of one source region compared with others or, alternatively, the successive erosion of tourmaline-rich and then zircon-rich source lithologies.

3.2.3. Reading Formation: Lower Mottled Clay Member

Sample H 21.96 displays the characteristic Lower Mottled Clay peak at 2 phi in addition to a second sand-grade peak between 3 and 3.5 phi (Fig. 3). The latter peak is intermediate in character between the Upnor Formation 3 phi peak and the Reading Formation 3.5 phi peak and suggests the presence of Upnor Formation-derived sediment. Such sediment may have been reworked by the streams and rivers of the Reading Formation. Samples H 20.32 and H 17.60 have the characteristic Lower Mottled Clay peak at 3.5 phi; the asymmetry of the H 20.32 peak again suggests the presence of Upnor Formation-derived sediment (typified by a 3 phi peak; Fig. 3).

The heavy mineral assemblage of sample H 21.96 is zircon-dominated unlike the assemblages of H 20.32 and H 17.60 (which are co-dominated by zircon and tourmaline). Consequently, H 21.96 is interpreted as a sample contaminated by reworking of the underlying Upnor Formation. H 20.32 preserves a greater proportion of calcite and a smaller proportion of zircon than H 21.96; this suggests an increased importance of Chalk-derived sediment and/or decreased importance of Upnor-derived material away from the Upnor/Reading formation boundary.

The heavy mineral assemblages of H 20.32 and H 17.60 resemble that of HB 7.20 small, although the Hadley Road samples preserve calcite. If HB 7.20 small (Herne Bay site, Fig. 3) represents an assemblage largely produced by bioturbation-mediated mixing, H 20.32 and H 17.60 may represent reworking of both Upnor and Thanet Sand Formation sediments. However, if HB 7.20 small represents a depositional intermediate between the underlying and overlying assemblages, this could suggest that the sandy facies of the Lower Mottled Clay are largely reworking the uppermost strata of the Thanet Sand Formation from the fringes of the basin.

Coppermills samples C 32.06, C 31.42 and C 29.17 all display the generic Lower Mottled Clay sand-grade peak at 3.5 phi. The peak shown by C 31.42 is asymmetrical; this is attributed to the presence of Upnor Formation sediment (which is typified by a peak at 3 phi). C 31.42 is dominated by zircon and possesses large proportions of tourmaline and rutile; this is interpreted as a mixed assemblage produced by incorporation of Upnor Formation-derived sediment into the stratum. The increased levels of rutile and lack of garnet suggest pedogenically-mediated impoverishment of the assemblage.

Samples C 32.06 and C 29.17 are tourmaline-dominated; these samples may represent reworking of the tourmaline-dominated Thanet Sand Formation assemblage. C 29.17 displays higher proportions of zircon and rutile than C 32.06. If garnet was originally present and subsequently destroyed by palaeoweathering, these increased proportions may simply reflect the stability of zircon and rutile.

3.2.4. Reading Formation: Upper Mottled Clay Member

Samples H 15.14, C 27.67 and C 23.92 display grain-size characteristics which indicate progressively increased signs of pedogenesis. H 15.14 displays the typical Upper Mottled Clay peak at 3.5 phi. C 27.67 shows a peak between 3.5 and 4 phi, which is interpreted as pedogenically-mediated distortion of the characteristic Upper Mottled Clay 3.5 phi peak. C 27.67 also shows increasing proportions of silt- and clay-grade material from 5 to 9 phi. C 23.92 displays increasing proportions of silt and clay-grade material from 6 to 9 phi; this type of distribution is identified as the extreme end-product of pedogenic alteration.

H 15.14 and C 27.67 are both tourmaline-dominated and the assemblages closely resemble one another. Zircon, rutile, staurolite and kyanite are expected subsidiary minerals. The lack of garnet may reflect the effects of palaeoweathering, to which garnet is susceptible.

Morton (1982) proposes a Scottish provenance for the Reading and Woolwich Formations, envisaging deposition within a lagoon which stretched across both the London and Hampshire Basins. He also suggests that the Reading Formation sediments are the sub-aerially weathered remnants of Woolwich Formation clays. This interpretation is at odds with the depositional model of Hester (1965) and the lithostratigraphic model of Ellison et al. (1994), both of which argue that the Reading Formation sands and clays are predominantly fluviatile and pass eastwards into the estuarine/lagoonal facies of the Woolwich Formation. The latter interpretation is supported by the results shown in the present contribution. Data from the present study indicate that the recurrence of zircon-rich sand bodies higher in the Reading Formation can be attributed to varying sources of reworked sediments. Where reworked Upnor sources dominate, the mixed assemblages are zircon-rich (e.g., C 31.42), and where reworked Thanet Sand sources dominate (e.g., H 15.14 and C 27.67), assemblages are tourmaline-rich. Consequently, erosion and redeposition of the Upnor Formation, as suggested by Hester (1965) and Morton (1982), is locally important. If the tourmaline-dominated sediments reworked into the Reading Formation largely represent fluvially reworked Thanet Sand Formation sediment, the later Thanet Sand Formation transgressions must have exceeded the existing outcrop in size.

4. CONCLUSIONS

The constraint of restricted sample size has been shown in this study not to impede significantly the production of reliable heavy mineral abundance data. Mineral counts of $\geqslant 300$ translucent grains from core samples can be compared accurately with those extracted from larger surficial samples. Surprisingly, for the outcrop samples studied (HB 7.20 small, HB 4.50 small and HB 1.50 small) the variation in heavy mineral abundances between 2–4 phi and 3–4 phi grain-size brackets was minimal; this may reflect a concentration of heavy minerals in the 3–4 phi fraction. However, consistency in bracket size is essential in comparative studies as mineral abundances can vary widely relative to grain size.

The Palaeocene formations of the London Basin display distinct grain-size and heavy mineral signatures. At the sites examined, the Thanet Sand Formation is very homogenous and characterised by sand-grade peaks at 2 and/or 3.5 phi and a tourmaline-dominated assemblage. The Upnor Formation is typified throughout by peaks at 1.5 and/or 3 phi. The basal Upnor conglomerate is zircon-dominated, but succeeding strata are mineralogically more variable. This variation is probably due to the proximity of the studied Hadley Road and Coppermills sites to the oscillating shoreline and therefore to onshore sediment sources. The Lower Mottled Clay Member of the Reading Formation is characterised by peaks at 2 and/or 3.5 phi and displays an assemblage either co-dominated by tourmaline and zircon or tourmaline-dominated with subsidiary zircon. The Upper Mottled Clay Member of the Reading Formation is typified by a peak at 3.5 phi and a tourmaline-dominated assemblage. The Reading Formation may largely represent reworked Thanet Sand Formation sediment.

Results presented in this contribution indicate that integrated grain-size and heavy mineral studies of core-derived material can be a valuable tool for studying poorly preserved and bioturbated strata, despite small sample size and limited borehole distribution. This approach has the potential to distinguish bioturbation, reworking and provenance as causes of changing grain-size and/or mineralogical characteristics. An extended study (covering the entire London Basin) utilising the methodology outlined here, and complemented by tourmaline geochemistry, is currently in preparation.

ACKNOWLEDGEMENTS

The author wishes to thank Richard Ellison and Andy Moffat for valuable comments on the manuscript and Stephen Hesselbo for editing advice. She is also indebted to the British Geological Survey for access to borehole and survey material and to the 'C.S.A. Fund for Palaeolithic Archaeology' for funding this research.

REFERENCES

Aubry, M.P., Hailwood, E.A., Townsend, H.A., 1986. Magnetic and calcareous-nannofossil stratigraphy of the lower Palaeogene formations of the Hampshire and London Basins. Journal of the Geological Society London 143, 729–735.

Blondeau, A., Pomerol, C., 1968. A contribution to the sedimentological study of the Palaeogene of England. Proceedings of the Geologists' Association 79, 441–445.

Boswell, P.G.H., 1916. The stratigraphy and petrology of the Lower Eocene deposits of the north-eastern part of the London Basin. Quarterly Journal of the Geological Society London 71, 536–591.

Brammal, A., 1928. Dartmoor detritals: a study in provenance. Proceedings of the Geologists' Association 39, 27–48.

Crane, P.R., Goldring, R., 1991. The Reading formation (late Palaeocene to early Eocene) at Cold Ash and Pincent's Kiln (Berks.) in the western London Basin. Tertiary Research 12, 147–158.

Dryden, A.L., 1931. Accuracy in percentage representation of heavy mineral frequencies. Proceedings of the National Academy of Sciences of the U.S.A. 17 (5), 233–238.

Ellison, R.A., 1983. Facies distribution in the Woolwich and Reading Beds of the London Basin, England. Proceedings of the Geologists' Association 94, 311–319.

Ellison, R.A., Knox, R.W.O'B., Jolley, D.W., King, C., 1994. A revision of the lithostratigraphical classification of the early Palaeogene strata of the London Basin and East Anglia. Proceedings of the Geologists' Association 105, 187–197.

Ellison, R.A., Woods, M.A., Allen, D.J., Forster, A., Pharoah, T.C., King, C., 2004. Palaeogene-Palaeocene. In: Ellison, R.A. (Ed.), Geology of London. Memoir of the British Geological Survey, pp. 22–43, 114.

Galehouse, J.S., 1971. Point counting. In: Carver, R.E. (Ed.), Procedures in Sedimentary Petrology. Wiley, New York, pp. 385–407.

Groves, A.W., 1928. Eocene and Pliocene outliers between Chipstead and Headley, Surrey. Proceedings of the Geologists' Association 39, 471–485.

Groves, A.W., 1931. The unroofing of the Dartmoor granite and the distribution of its detritus in the sediments of southern England. Quarterly Journal of the Geological Society of London 87, 62–96.

Haq, B.U., Hardenbol, J., Vail, P.R., 1987. Chronology of fluctuating sea levels since the Triassic. Science 253, 1156–1167.

Hester, S.W., 1965. Stratigraphy and palaeogeography of the Woolwich and Reading Beds. Bulletin of the Geological Survey of Great Britain 23, 117–137.

Jolley, D.W., 1992a. Palynofloral association sequence stratigraphy of the Palaeocene Thanet Bed and equivalent sediments in eastern England. Review of Palaeobotany and Palynology 74, 207–237.

Jolley, D.W., 1992b. Spore-dominated assemblages from the lowermost Reading Beds (Palaeocene) of North Essex. Proceedings of the Yorkshire Geological Society 49, 149–153.

Knox, R.W.O'B., 1990. Thanetian and Ypresian chronostratigraphy in south-east England. Tertiary Research 11, 57–64.

Knox, R.W.O'B., 1996. Tectonic controls on sequence development in the Palaeocene and earliest Eocene of south-east England: implications for North Sea stratigraphy. In: Hesselbo, S.P., Parkinson, D.N. (Eds.), Sequence Stratigraphy in British Geology, vol. 103. Geological Society, London, Special Publications, pp. 209–230.

Knox, R.W.O'B., Morigi, A.N., Ali, J.R., Hailwood, E.A., Hallam, J.R., 1990. Early Palaeogene stratigraphy of a cored borehole at Hales, Norfolk. Proceedings of the Geologists' Association 101, 145–151.

MacDonald, H.A.H., 1965. Mineral analyses of four samples of sand from the Woolwich and Reading Beds. Bulletin of the Geological Survey of Great Britain 23, 139–143.

Mange, M.A., Maurer, H.F.W., 1992. Heavy Minerals in Colour. Chapman and Hall, London, 147pp.

Moffat, A.J., Bateman, R.M., 1983. The mineralogy of Palaeogene sediments in southeast England. Proceedings of the Geologists' Association 94, 271–273.

Morton, A.C., 1982. The provenance and diagenesis of Palaeogene sandstones of southeast England as indicated by heavy mineral analysis. Proceedings of the Geologists' Association 93, 263–274.

Neal, J.E., 1996. A summary of Palaeogene sequence stratigraphy in northwest Europe and the North Sea. In: Knox, R.W.O'B., Dunay, R.E. (Eds.), Correlation of the Early Palaeogene in Northwest Europe, vol. 13. Geological Society, London, Special Publications, pp. 15–42.

Ward, D.J., 1978. The Lower London Tertiary (Palaeocene) succession of Herne Bay, Kent. Report for the Institute of Geological Sciences 78/10, 12.

Weir, A.H., Catt, J.A., 1969. The mineralogy of Palaeogene sediments in northeast Kent (Great Britain). Sedimentary Geology 3, 17–33.

Chapter 12

HEAVY MINERALS IN SHALES

MATTHEW W. TOTTEN[a] AND MARK A. HANAN[b]

[a]*Department of Geology, Kansas State University, Manhattan, KS 66506, USA*
[b]*Department of Geology and Geophysics, University of New Orleans, New Orleans, LA 70148, USA*

ABSTRACT

Although shales dominate the sedimentary rock record, when compared to sandstones their heavy mineral fraction has received little attention. A principal reason for this disparity is the difficulty of density separations in rocks with high clay contents using organic liquids. These liquids work well for clean sandstones, but their effectiveness in clay-rich samples is limited by the adsorption of organic molecules onto clay minerals. Additionally, the small size of heavy mineral grains within shales demands advanced observational conditions, and considerable expertise that analysts must develop before undertaking these investigations.

In this study heavy minerals were separated from the clay and light-mineral matrices of over 100 shale samples using lithium metatungstate (LMT), a non-organic heavy liquid. The sample sets include sites from Ordovician through Mississippian shales from the Ouachita Mountains of Oklahoma and Arkansas, USA, and Miocene through Pleistocene shales from the subsurface Gulf of Mexico (GOM). Heavy minerals include variable amounts of zircon, tourmaline, rutile, apatite, baryte, monazite, and xenotime. Opaque minerals are Fe, Ti, Fe-Mn, Ba-Mn, and Cr-Fe oxides, as well as Fe-rich micas. Comparisons with heavy-mineral contents of interbedded sandstones with the surrounding deep-water shales show that heavy minerals are equally plentiful and diverse in the finer-grained clastics.

Tectonic and provenance interpretations based on trace-element geochemistry rely upon the assumption that signature elements are quantitatively transferred from the same source as the bulk of the sediments. Trace-element analyses of whole-rock and light-mineral separates indicate that heavy minerals are sometimes the dominant sites for some of the trace elements in shales. The potential control of signature trace elements by an accessory mineral phase, perhaps from a secondary, low-volume source terrain, needs to be addressed.

We stress the importance of using the heavy-mineral fraction to complement the geochemical study of shales. Heavy minerals in shales can be as effective in determining sediment provenance as they have proven to be in sandstones. A source of some of the heavy minerals within shales could be from resistate mineral inclusions within both light and heavy host minerals. This is

Developments in Sedimentology, Vol. 58, 323–341

ISSN: 0070-4571/doi:10.1016/S0070-4571(07)58012-X

particularly important for zircon, rutile, and monazite, based upon their observed size in shales. This should be considered when using heavy minerals in shales for provenance studies.

Keywords: heavy minerals; shale; Ouachita Mountains; Gulf of Mexico; trace-elements

1. INTRODUCTION

Shales comprise at least two-thirds of the sedimentary record and their low permeability is favourable for the preservation of heavy minerals. The potential of heavy mineral analyses of fine-grained rocks (shales) for broadening our understanding of sedimentary systems was first proposed by Blatt 35 years ago (Blatt and Sutherland, 1969) and was more recently outlined by Schieber and Zimmerle (1998). Their arguments are valid even today.

Some of our preconceptions regarding shales may impede their study. We learn in introductory-level sedimentation classes about hydraulic equivalency, and the association of silt-sized heavy minerals with sand-sized clastic sediments. When we make the transition to shales, which by definition have a mean grain size in the clay to silt range, the initial response is that there should not be any heavy minerals large enough to separate and work with, or they are so minor in abundance that they can be ignored. They certainly are rarely mentioned in chapters covering shales in sedimentary petrology texts, with the exception of Boggs (1992) who cites the presence of heavy minerals within shales but adds that little is known about their occurrence or abundance.

A number of previous studies hint at the potential utility of heavy minerals in shales, even though we do not yet fully understand the mechanism by which they were deposited. Of particular interest are studies that, while not directly looking for heavy minerals, attempted to explain whole-rock geochemical variations of certain trace elements by implicating heavy minerals. The most commonly used normalising constant for sedimentary geochemistry, the North American Shale Composite (NASC), is consistently not constant for certain elements. Gromet et al. (1984) reported significant heterogeneity in different aliquots of NASC for certain trace elements, and argues that this variability was controlled by variable amounts of heavy minerals such as zircon. Condie (1991) was more specific and used trace-element ratios, likely influenced by specific heavy minerals (e.g., La/P_2O_5 for apatite; Zr/Hf for zircon), to explain the observed whole-rock ratios. Comparative studies provide evidence for the concentration of some signature trace elements in heavy minerals (Preston et al., 1998, 2002). These studies are the exception, with the majority of sedimentary geochemists citing clays as the mineralogical source of most trace elements (Cullers et al., 1975). The reported correlation between clay-mineral percentage (or Al_2O_3 as a proxy) and many trace elements (e.g., TiO_2) seemingly supports this conclusion (Condie, 1991; Totten and Blatt, 1993). An alternative explanation for this observation is the dilution of trace elements and clay minerals primarily by quartz, the major framework component of siliciclastic sediments.

Shale heavy minerals are a robust source of potential insight into sediment provenance, in exactly the same way that sandstones have proven to be over the last 100+ years. Their study could solve significant stratigraphic problems in shales in a manner similar to Mange et al. (2003) for coarser-grained rocks. The potential of

individual heavy-mineral species in determining shale provenance (Morton, 1991; Schneiderman, 1995) is also untapped. The major goal of reviewing the findings of our previous work is to raise (excite) interest in the heavy-mineral fraction of mudstones, inviting especially colleagues who study heavy minerals in coarser-grained rocks.

2. UNITS OF STUDY

Heavy minerals have been separated from shales of two distinct depositional basins from formations ranging in age from Ordovician to Pleistocene. The initial sample set was collected from the Stanley Formation (Mississippian) of the Ouachita Mountains. Sample locations are described in Totten et al. (2000). Pre-Carboniferous shale samples from the same general area as the Stanley Formation include those from Arkansas, including the Novaculite Shale (Devonian), Missouri Mountain Shale (Silurian), and Polk Creek Shale, Big Fork Chert, Womble Shale, Blakely Shale (Ordovician). These shales are marine deep-water clastics.

The Cenozoic shale samples were collected from well cuttings offshore GOM from a single well in the Ship Shoal area. Their age was determined by comparison with published palaeontological markers.

3. METHODOLOGY

3.1. Heavy Minerals from Shales

The early work by Blatt and others—on separating the heavy-mineral fraction from fine-grained sediments—relied upon organic heavy liquids such as tetrabromethane and bromoform. Not only are these liquids toxic but are especially problematic when used with clay-rich rocks. The highly polar organic molecules strongly adsorb onto clay-mineral surfaces, often creating an almost gel-like substance that rafts other grains, and make it difficult to reclaim the liquid (Nelson, 1971). Blatt and Sutherland (1969) used bromoform to separate heavy minerals from Tertiary shales, although they decanted the smaller than 10 μm fraction before separation. Their method avoided the problems associated with the interaction of organic liquids and clays, but ignored the finer grained, <10 μm, heavy minerals. These studies are the exception, and the overall impression seems to be that organic heavy liquids do not work with well-indurated, clay-rich sedimentary rocks (Schieber and Zimmerle, 1998). Personal experience by the senior author, working in Blatt's sedimentation lab in the late 1970s (and early 1990s), confirmed this observation, and prompted us to test more suitable heavy liquids.

We have developed a technique that uses a non-toxic heavy liquid, LMT, which does not react with clay minerals. It is a water-soluble salt that has a working density range between 2.0 and 3.1 g/cm^3. The ability to adjust LMT to precise densities, its deflocculating behaviour with natural clays, and the ease with which it may be washed off of clay-mineral surfaces allowed us to separate the common species of clay minerals from one another and recover the liquid (Totten et al., 2002). It works extremely well in separating heavy minerals from shales. Details of the LMT separation technique are given in Hanan and Totten (1996).

3.2. The Challenge of Identifying Fine-Grained Heavy Minerals

Blatt and Sutherland (1969) reported the difficulty in identifying heavy-mineral grains finer than 10 μm using the petrographic microscope. Tourmaline, because of its strong pleochroism and prismatic morphology, is an exception and often is recognisable down to 5 μm. Because of these limitations, and because we were also interested in the opaque fraction, we relied upon micro-beam imaging to identify the mineralogy of the heavy fraction.

We have examined different shale sample sets for heavy minerals, and although there have been slight variations as the technique developed, we always relied on the scanning electron microscope (SEM) to identify and quantify the presence of the heavy minerals. SEM images combined with energy dispersive spectra (EDS) on grains (and grain areas within rock fragments) reveal details that would be difficult to see with an optical microscope, especially on grains less than 10 μm in size. The analytical techniques for mineral identification include EDS on individual grains, elemental X-ray maps, and backscattered electron imaging. Combinations of these techniques may be particularly effective for identifying opaque heavy minerals and for finding less abundant, but important, heavy minerals that are known to sequester specific trace elements.

The mineralogy of the heavy fraction was further refined using the SEM-EDS to identify the opaque heavy minerals. Photomicrographs of the plain-light grain images allowed comparison to backscattered images of grain areas at the SEM workstation. Backscattered X-ray intensity and EDS spectra of grains intersecting the polished surface of the grain mount were matched to opaque and non-opaque grains in the projected slide. Matching grains seen by the SEM with their opaque image on the slide was time-consuming. Although all of the grains are visible by the light microscope, only grains that intersect the polished surface can be imaged on the SEM. SEM grain images are the result not only of the grain size but also of the depth of the polished surfaces. Many grains are below the surface of the epoxy and not imaged by backscattered electrons or their outlines are very small.

Due to the fine-grained nature of shales it is important not to exclude the finest size fractions of heavy minerals as is routinely done in traditional heavy-mineral studies on sandstones. The reason for our focus on the entire population of heavy-mineral sizes is because of the fine-grained nature of shale samples, and a desire to overcome misconceptions about the presence of the heavy minerals in shales. Currently, we are still testing and assessing better methods for a complete extraction and identification of the entire population of heavy minerals present.

4. HEAVY-MINERAL SEPARATION FROM FINE-GRAINED TURBIDITES OF THE OUACHITA MOUNTAINS

4.1. Sandstone and Shale Pairs

Heavy minerals were separated from interbedded sandstone and shale pairs collected throughout the Mississippian Stanley Shale from the Ouachita Mountains of Oklahoma and Arkansas, USA (Totten and Hanan, 1998). The heavy minerals were as abundant in the shales as they were in the sandstones. A somewhat unexpected

result was that, on an average, the shales have a higher weight percentage of heavy minerals (0.95%) than the interbedded sandstones (0.65%). Fig. 1 shows the variation in the heavy-mineral yields from the sandstone/shale pairs and illustrates this relationship.

The overall median grain-size of the heavy minerals in the shales is approximately 25 μm less than that of the heavy minerals in the sandstones. Most shale samples show that the largest portion of the heavy minerals are concentrated in the finer than 10 μm size-fraction, grains that would have been lost using the method of Blatt and Sutherland (1969). Fig. 2 is a plot of the median grain-size of the sandstone and shale pairs.

More heavy minerals might be expected in the sandstones because of the higher energy of the depositional environment and hydraulic equivalency of the silt-sized heavy minerals with coarser-grained quartz and feldspar grains. The apparent hydrodynamic disequilibrium of the shale heavy minerals with primarily clay-sized light minerals might be explained by non-sphericity of the heavy (Fe-rich) micas, rafting of heavy-mineral grains on or within clay-mineral flocculants, and perhaps authigenesis of heavy minerals (mainly Fe-oxides). It is also possible that the sandstones had more heavy minerals initially but intrastratal dissolution has reduced their amount in the more permeable sandstones.

Rafting of heavy minerals by light minerals was certainly a problem during the heavy-mineral separation procedure. Although the amount of rafting of heavy minerals by clay floccules during transport and deposition of fine-grained sediments is unknown, it is possible that the tendency of the much more abundant light fraction to raft the sparse heavy fraction is as important to the understanding of the distribution of heavy minerals as is the hydrodynamic equivalency of grains in shales.

Fig. 3 shows a composite photomicrograph of the 20–30 μm size heavy minerals in a sandstone/shale pair from the Stanley Shale under the same magnification. Fig. 3 serves to reinforce the findings of Blatt and Sutherland (1969) for Texas Gulf Coast shales and

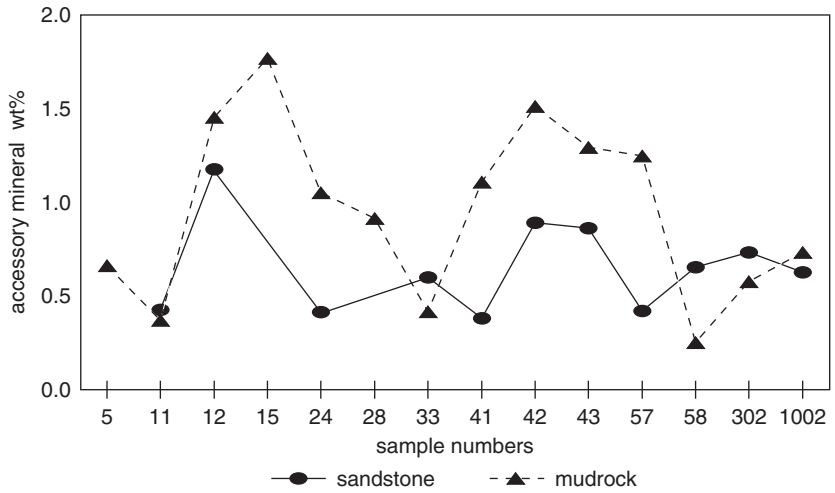

Fig. 1. Relative abundance of heavy minerals within interbedded sandstone–shale pairs from the Mississippian Stanley Formation of the Ouachita Mountain foldbelt.

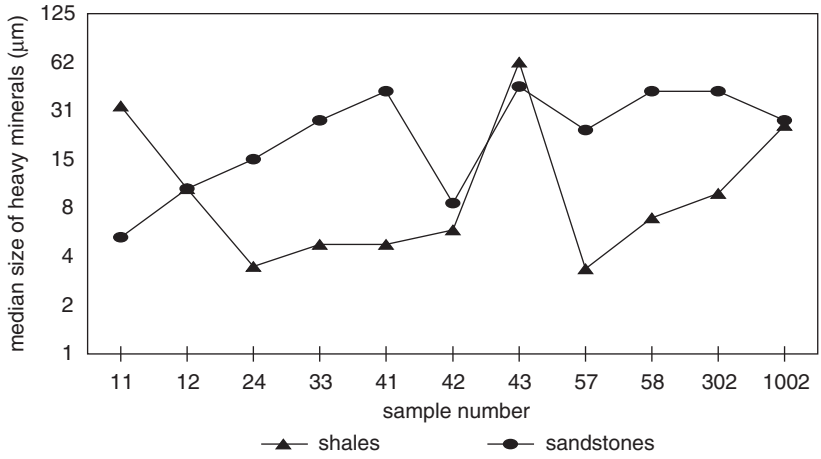

Fig. 2. Median grain-size of the heavy minerals in the interbedded sandstone–shale pairs from the Mississippian Stanley Formation of the Ouachita Mountain foldbelt.

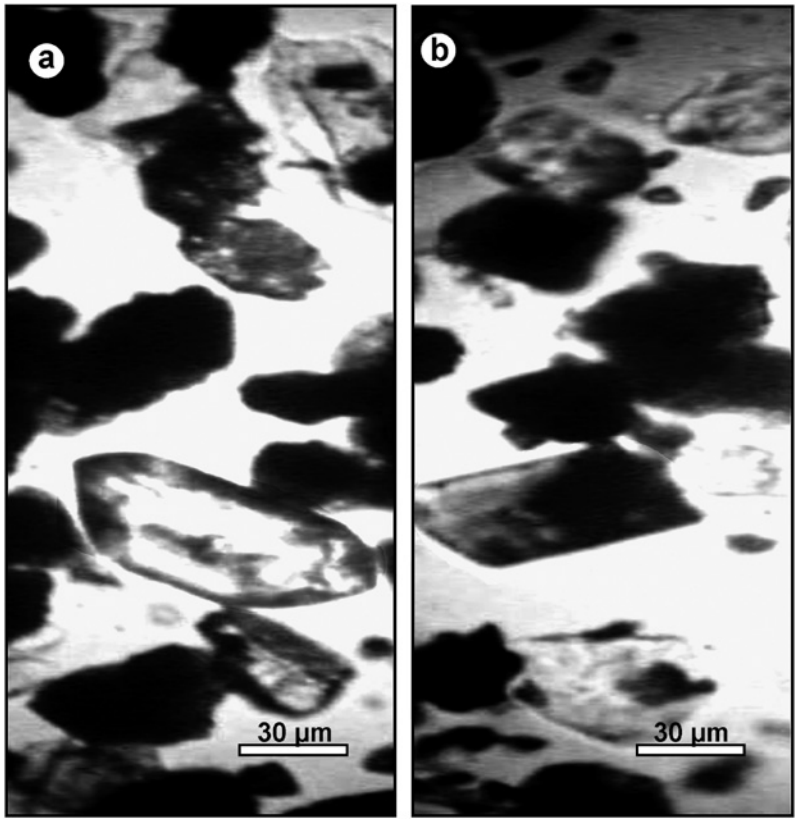

Fig. 3. Photomicrographs of heavy minerals in the 30–62 μm fractions of shale and interbedded sandstone from the Stanley formation of the Ouachita Mountain foldbelt. Both photos taken at 200 power.

illustrates that there are sufficient coarse-grained heavy minerals in these ancient shales to enable a 'classical' heavy-mineral approach to provenance determinations using the light microscope. The high percentage of finer-sized material and the widespread availability of SEM technology provides opportunities to go much farther.

4.2. Image Analyses of all Size Composites

The average mineralogy of the heavy fraction from 66 Stanley Shale samples is illustrated in Fig. 4. Data for the Stanley Formation in Arkansas and Oklahoma were collected from grain mounts that included the entire size fraction of the heavy-mineral separates. Each sample was examined using an Amray 1820 digital SEM equipped with an EDS. Heavy minerals were identified by comparing their EDS elemental spectra to EDS spectra obtained from known heavy minerals. The cross-sectional area of each grain was determined using the image analysis capabilities of the *Iridium IXRF* software. The relative proportions of heavy minerals present and their size distribution were calculated from these data.

Fe-oxides, Ti-oxides, and Fe-bearing biotites are the dominant minerals in the heavy-mineral fraction of the Stanley Shale samples. The common non-opaques include apatite, zircon, tourmaline, garnet, and monazite. Except for monazite this mineralogy is similar to the heavy minerals found in the Stanley interbedded sandstones reported by Bokman (1953).

The quantity and diversity of the finer-sized heavy minerals seen in grain mounts indicate that these are important constituents of the total heavy-mineral fraction. Even though these very fine-grained heavy minerals are abundant, it is not feasible to measure and count all of the small grains in the fields of view. Moreover, small grains

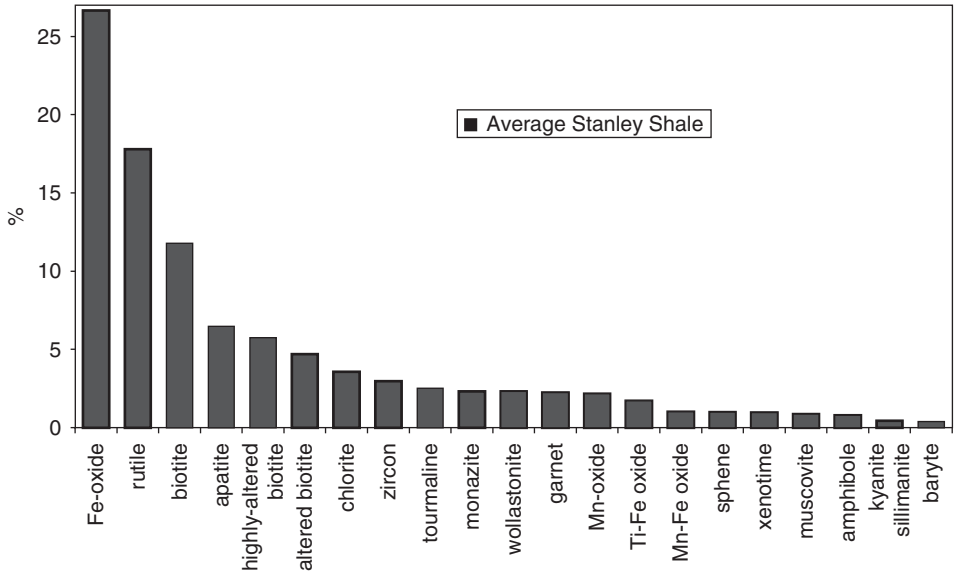

Fig. 4. Average distribution of specific minerals contained within the heavy mineral fraction of shales from the Stanley shale of the Ouachita Mountains.

are often observed within part of a larger rock fragment. In fact, monazite most often occurs intergrown with quartz as is shown in the composite grain in Fig. 5. Although the total cross-sectional area of the smaller grains does not comprise a major portion of the entire grain area, we are concerned that this method of determining mineral abundances might overlook significant minerals within the very fine-grained fraction.

The occurrence of small monazites in rock fragments is important and suggests that some portion, a sub-population, probably remains in the light fraction during separation (i.e., the small heavy-mineral grains become locked within light-mineral composite grains) and we need to modify our methods to ensure a more complete segregation of this heavy mineral sub-population. The work of Caggianelli et al. (1992) and Gromet et al. (1984) suggests that even intense disaggregation may not release all the heavy minerals because the extremely small (2 μm or less) grains stay locked up within the light-mineral rock fabric of shales.

4.3. Pre-Carboniferous Shale Samples from the Ouachita Mountain Flysch

There is also geochemical evidence that a portion of the heavy minerals remain in the light fraction, even after intense disaggregation. A suite of shale samples from the pre-Stanley Ouachita flysch (Ordovician to Mississippian) were analysed using standard XRF techniques. Fine-grained powders were prepared by milling in a SPEX shatter box for 30 min. According to information provided by SPEX, this produces a powder with grain sizes between 1 and 4 μm. Aliquots of these samples were processed using LMT and the powdered heavy-mineral fractions were then removed. The resulting heavy-mineral grains are too small to be identified; however, their chemistry may be indirectly determined by assessing the amount of each

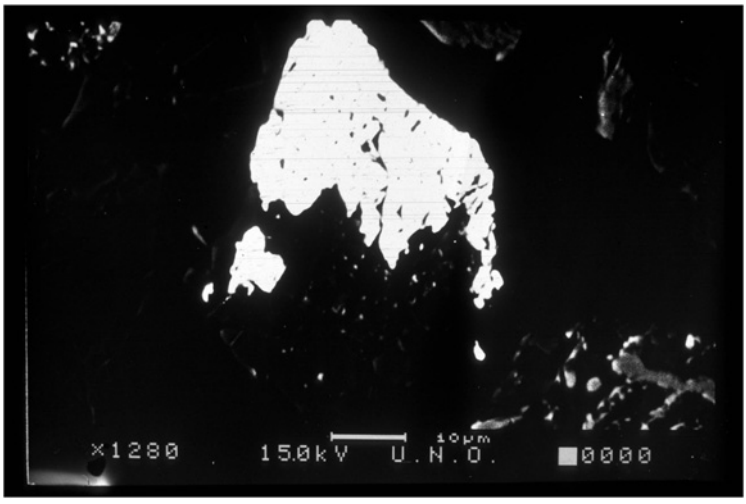

Fig. 5. Backscattered SEM image of composite monazite–quartz grain. Bright area of composite grain is caused by the high atomic number of monazite, which was further confirmed by its characteristic EDS spectra.

element removed with the heavy fraction. The light fractions of these powders were analysed by XRF using the same settings as used for the original whole-rock powders. Not surprisingly, the major element concentrations were nearly identical between the whole-rock and light-mineral fraction for each sample. Many trace elements, however, show a distinctly lower concentration in the light-mineral fraction when compared to the whole-rock concentrations. Figs. 6–8 show that the removal of heavy minerals reduced the concentrations of La, TiO_2, and Zr, in the XRF powders, respectively. Sample no. 25 is particularly interesting because of the large amounts of Zr, La, and TiO_2 related to the heavy-mineral fraction. Sample no. 25 contains approximately 50% La, 33% TiO_2, and 73% Zr, all associated with the heavy-mineral fraction. This suggests that there is a strong control of heavy minerals on the concentration of these elements, contained dominantly by monazite, rutile, zircon, and other heavy minerals in the pre-Carboniferous Ouachita shales.

For the pre-Carboniferous shale samples we prepared two sets of heavy-mineral separates. The SEM samples were prepared using extremely short milling times (20–30 sec) so as to leave relatively large heavy-mineral grains intact for identification and imaging. The XRF samples were prepared by long milling times (30 min) to produce homogeneous powders for the analyses. Inspection of the samples showed that the amounts of heavy minerals were generally higher in the separates than in the powdered material for XRF analyses.

In the heavy-mineral fraction of sample no. 25 from the Polk Creek Shale we expected that in the SEM analysis zircons would be common because of the high

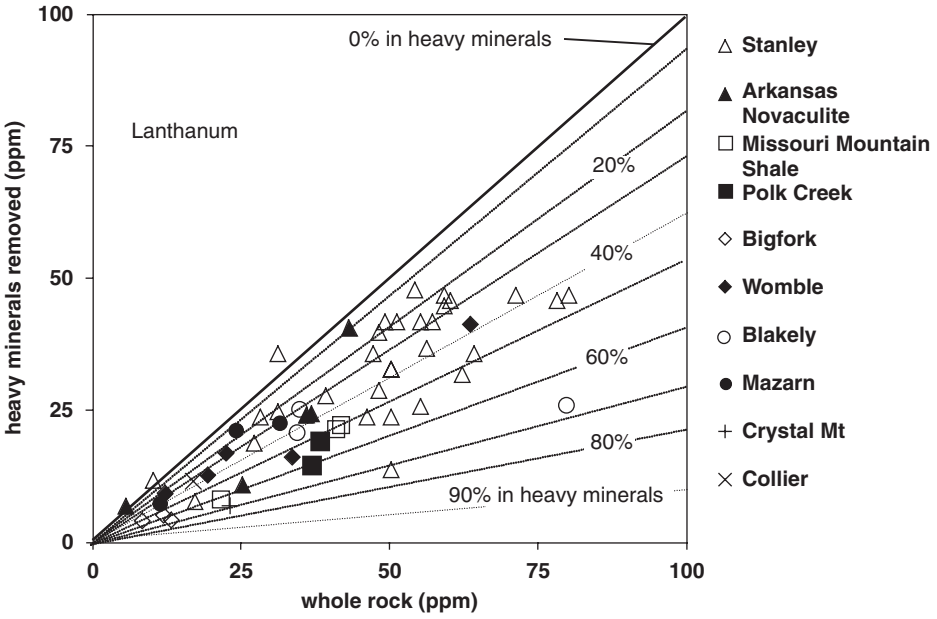

Fig. 6. Whole-rock Lanthanum concentrations versus Lanthanum concentrations in the light fraction after heavy-mineral separations from Ordovician–Mississippian shales of the Ouachita foldbelt. The difference between the two values is presumed to reside in the heavy-mineral fraction.

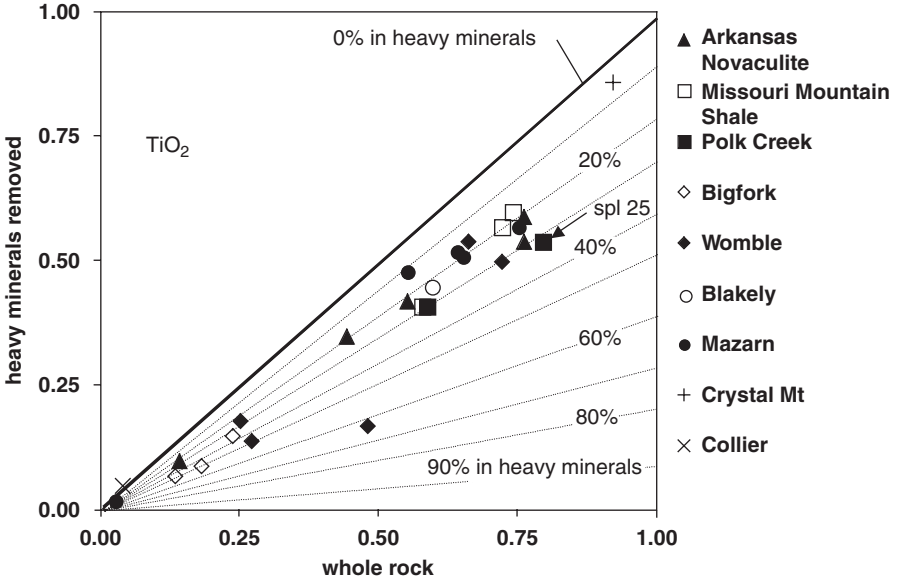

Fig. 7. Whole-rock TiO_2 concentrations versus TiO_2 concentrations in the light residue after heavy-mineral separations from Ordovician–Mississippian shales of the Ouachita foldbelt. The difference between the two values is presumed to reside in the heavy-mineral fraction.

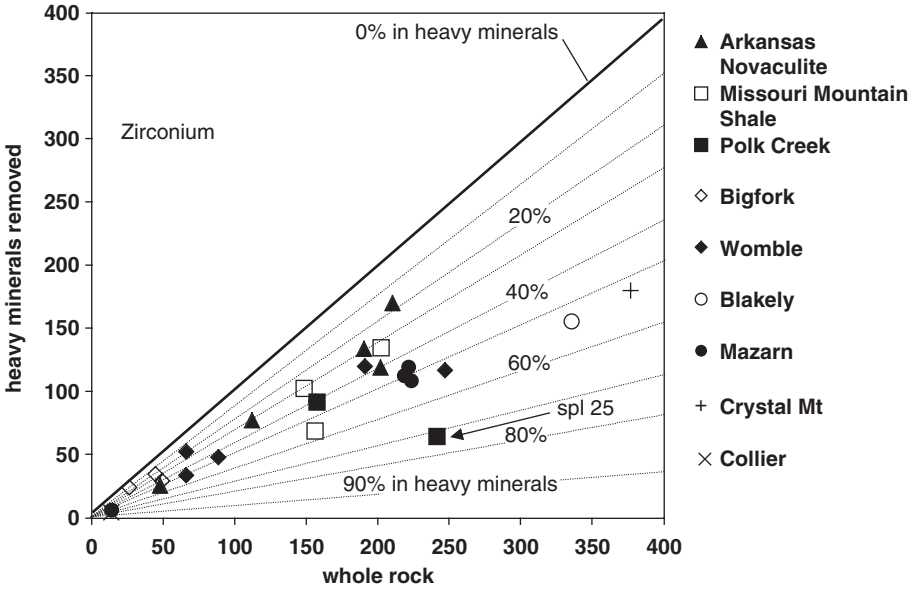

Fig. 8. Whole-rock Zirconium concentrations versus Zirconium concentrations in the light residue after heavy-mineral separations from Ordovician-Mississippian aged shales of the Ouachita foldbelt. The difference between the two values is presumed to reside in the heavy-mineral fraction.

amount of Zr, concentrated by the density separation (anticipated to be in zircons). However, we found zircons to be rare. This may be the result of the short milling times that were insufficient to free the small-sized zircon population from the rock fragments in this sample. To determine the abundance of zircon in the XRF powder we prepared a grain mount of the powdered heavy-mineral separate for X-ray mapping. The X-ray map of the Polk Creek Shale sample no. 25 revealed a significant and consistent occurrence of tiny zircons (near 1 μm) throughout the powder. Apparently, the longer milling times yielded higher amounts of zircon by crushing rock fragments containing zircon (or minerals with zircon inclusions) and releasing a population of tiny zircons. An analogous situation could arise with other heavy minerals that commonly occur as inclusions within other minerals (e.g., monazite).

The heavy-mineral control of important trace elements often used for provenance discrimination is illustrated in Fig. 9, which shows an element variation diagram from a sample of the Womble Shale. The whole-rock curve in Fig. 9 is plotted consistently above the light-mineral fraction in the right side of the chart and is typical of the pre-Carboniferous Ouachita Flysch samples. Significant portions of the high-field strength elements (HFSE) Zr, Hf, Ti, Nb, Ta, Hf, V are separated out with the heavy minerals. Petrogenetic discrimination schemes based on HFSE of whole-rock analyses of shales (e.g., Bhatia and Crook, 1986; Garver and Scott, 1995) might actually be measuring the presence of late-stage, highly evolved, resistate heavy minerals that sequester these HFSE.

The results of the heavy-mineral separations on powdered shale samples strongly imply that many heavy minerals are contained in rock fragments with lighter minerals, and have an average density lower than that of LMT. Fig. 5 clearly shows a

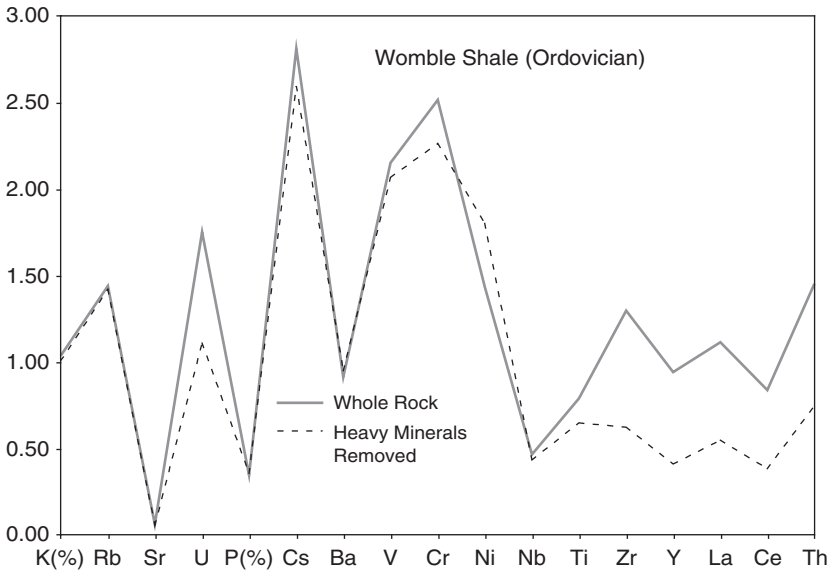

Fig. 9. (Spider) Diagrams showing elemental distribution of whole-rock and in the heavy-mineral-removed fraction in a shale sample from the Ordovician Womble Shale of the Ouachita foldbelt. Note the distinct shift of trace elements on the right side of the diagram, even though only less than 1% of the rock was removed during heavy mineral separation.

composite grain of monazite and quartz that sank with the heavy fraction. A more intense milling process for the XRF powders frees many more of these grains from the rock fragments, allowing them to be separated. Clearly, it is important to define the goal of each separation to determine the best method to use. Milling destroys the original petrographic information but is necessary for geochemical analyses. Producing a light fraction entirely free of heavy minerals will require long milling times before LMT separation but this will destroy the shape and grain size distribution of the heavy minerals. Because it is important to identify heavy-mineral contents and grain sizes, perhaps a better technique would be to perform LMT separation on samples subjected to both short and long milling times.

5. CENOZOIC SHALES FROM THE GULF OF MEXICO

Heavy minerals were separated from shale samples, collected from an oil well drilled in the GOM, offshore Louisiana. Our goal was to compare the results of heavy-mineral separations from these younger shales with the older Palaeozoic shales from the Ouachita Mountains. These two basins are often compared in the literature, especially for outcrop analogies to the deeply buried fine-grained turbidites in the Gulf (Slatt et al., 1994). Both are shale-rich successions, with intermittent interbedded sandstones and similar rates of deposition.

The drill cuttings used in this study are from a vertical well in the Ship Shoal protraction block. Sample collection began at 1500 m and continued to the total depth penetrated at 4146 m. These samples range in age from Pleistocene to late Miocene, based upon micropalaeontological picks. Ten samples were selected for heavy-mineral separation from an approximately 300 m interval. Shale sections were chosen using wire-line logs, recorded during drilling operations.

The weight percentages of heavy minerals separated from these shales range from 0.21 to 0.73%, comparable to the amounts recovered from the shales of the Ouachita Mountains. Fig. 10 compares the average heavy-mineral distribution in the $>10\,\mu m$ size fraction in the GOM samples to the Palaeozoic Stanley data. The heavy-mineral suite of the GOM shales was very similar to the heavy minerals found in the Stanley Shale. The major difference between the two basins is in the mineralogy of the iron-rich suite. The most abundant heavy mineral in the GOM shales is pyrite, in contrast to the abundant iron oxides and rare pyrite in the Stanley. Whether this is the result of different oxidation potentials in the depositional environment or diagenetic alteration is unknown at present. An additional contrast between the two basins is the presence of carbonate minerals in the GOM samples, represented by ankerite and dolomite. They were present at every sampled interval but both decreased in abundance with depth.

For provenance identification, the individual heavy-mineral species were grouped into mineral assemblages based upon the main rock suites in which they commonly occur: felsic igneous rocks are represented by tourmaline, biotite, muscovite, zircon, rutile, monazite, sphene, and apatite (Boggs, 1992). The metamorphic assemblage includes kyanite-andalusite-sillimanite, staurolite, wollastonite, and garnet.

The abundance of the metamorphic and the felsic igneous heavy-mineral group versus depth is shown in Fig. 11. The latter group shows a consistent increase with depth from less than 10% to nearly 40%. The metamorphic minerals show a more

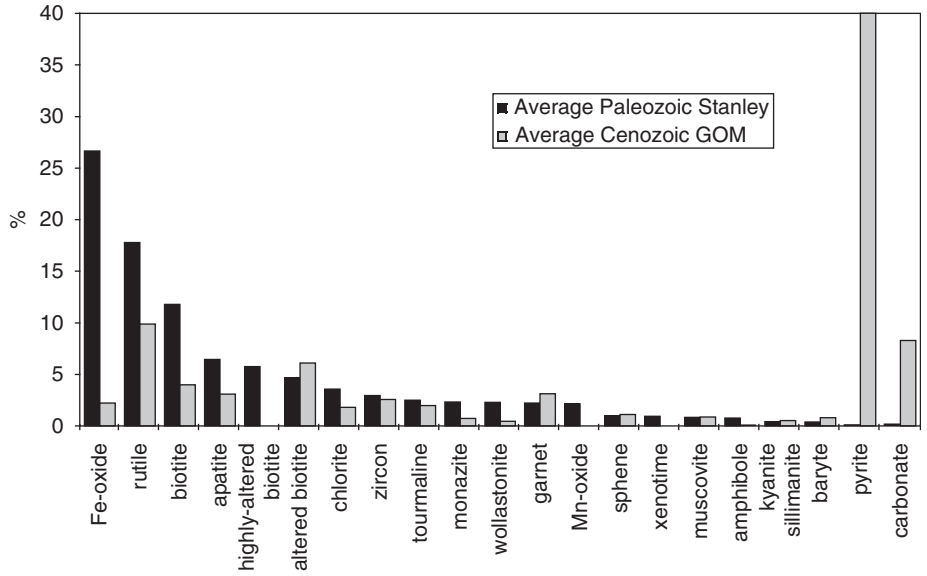

Fig. 10. Average distribution of heavy minerals contained within the heavy mineral fraction of late Miocene through Pleistocene shales from the Gulf of Mexico, compared to the average from the Mississippian Stanley Shale of the Ouachita Mountains. The major difference is seen in Fe-sulfides in place of Fe-oxides, and a significant carbonate component in the GOM samples.

moderate increase with depth. This dual provenance mirrors the lithology of source areas that provide sediment to the modern GOM, with a metamorphics-dominated Appalachian source and an igneous-rich western source. During Miocene time, the felsic igneous source was dominant but has gradually diminished relative to a metamorphic source during the Pliocene.

6. DISCUSSION

6.1. *The Occurrence of Heavy Minerals in Shales*

The results of our work to date confirm the presence of a significant heavy-mineral fraction in shales. The diversity of our set of sample shales over a wide age range and from multiple basins supports our conclusion that this is not an isolated occurrence. In fact, the quantity of heavy minerals in shales is comparable to that in many sandstones. The mineralogy of the heavy fraction is also comparable to those of sandstones. The major difference is the fine grain size of heavy minerals in the shales. Our results stress the importance of the $<10\,\mu m$ fraction, which however presents many challenging technical problems for separation, identification, and quantification.

6.2. *Are Heavy Minerals an Important Source of Trace Elements in Shales?*

Fig. 12 shows an example of the strong correlation between Al_2O_3 and TiO_2 from Stanley Shales of the Ouachita Mountains (Totten and Blatt, 1993). There are many

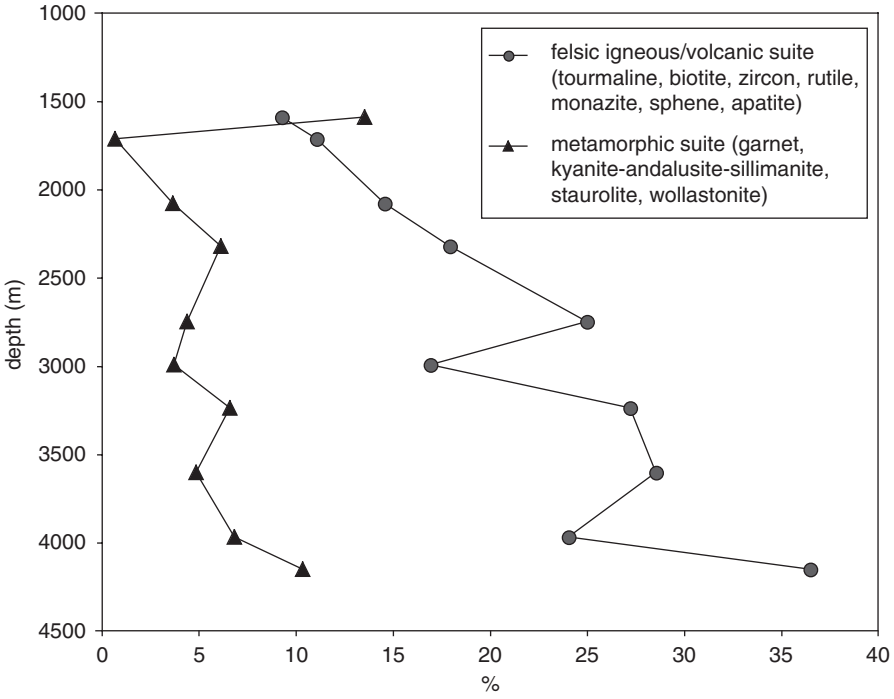

Fig. 11. Provenance-controlled variation of heavy mineral assemblages with depth from a well in Ship Shoal area of the Gulf of Mexico.

examples using similar comparisons that are generally used to conclude that specific trace elements must reside on clays. It is worth noting that the *y*-intercept of TiO_2 is non-zero, suggesting the presence of a titanium phase that is separate from the clay fraction, similar to what was reported by Condie (1991). The overwhelming impression, however, is that trace elements occur within the clay-mineral fraction of shales (Chaudhuri and Cullers, 1979).

The implications of this for the study of shales are vital. Because quartz contains extremely low concentrations of most trace elements, and because quartz dominates the silt-size range in both shales and sandstones (Charles and Blatt, 1978; Blatt and Totten, 1981), what these correlations might be testing is not whether trace elements reside in clays but, rather, that they do *not* reside in the quartz population. As the percentage of quartz increases, both the percentage of clay and the concentration of trace elements decrease. The two latter components appear to correlate, but the actual cause of this correlation is an equivalent variation in quartz percentage. An end-member of this reasoning would be a pure quartz-arenite, which would contain extremely low concentrations of trace elements. The opposite end-member, a very pure clay-mineral sample (which may be rare in nature) is often presumed to have significant trace-element concentrations adsorbed onto clay-mineral surfaces. However, we have consistently separated significant amounts of heavy minerals in clay-mineral standards available through the Clay Mineral Society's repository (Totten et al., 2002). Published chemical analyses of the clay-mineral standards are

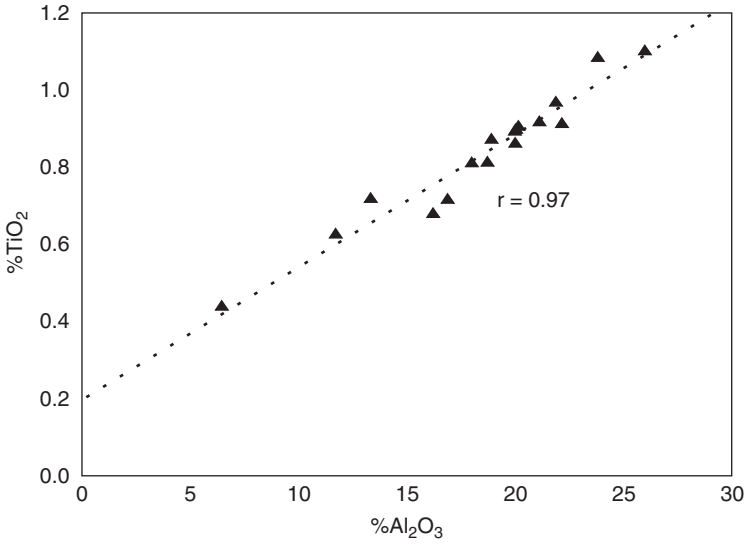

Fig. 12. TiO_2 versus Al_2O_3 for Stanley shales. Y-intercept greater than zero suggests a titanium mineral separate from the clay mineral fraction. assuming Al_2O_3 exists primarily within the clay-mineral fraction of these shales.

available, but these are whole-rock data and include the fraction we have removed. If not completely controlled by clays, and obviously not in quartz, where do the bulk of trace elements reside? Our results, and those of Preston et al. (2002), suggest that the heavy-mineral fraction is an important source. Specific heavy minerals can sequester specific trace elements in very high concentrations, easily influencing the overall whole-rock chemistry of shales. In this case, a little truly does go a long way!

6.3. *Implications for whole-rock shale geochemistry*

We have constructed a simple mixing model to illustrate the contribution of even minor amounts of heavy minerals to the whole-rock trace chemistry (Totten et al., 2000). In this model, monazite was used as a control on the overall rare earth element (REE) pattern of a hypothetical fine-grained sediment (Fig. 13). We intentionally chose two very different components, NASC and a mid-oceanic ridge basalt (MORB). As expected, a 50/50 mixture of these components results in an REE pattern intermediate between those of the two parents. The addition, however, of only 70 ppm of monazite to the 50/50 mix results in a calculated pattern that is indistinguishable from NASC. Monazites contain such a high percentage of light rare earth elements (LREE) that even a trivial amount of the mineral can greatly influence the whole-rock values of these elements that generally occur in trace amounts.

Gromet et al. (1984), while analysing the NASC, found HF-resistant zircon grains and surmised that the heterogeneity between aliquots of a homogenised and powdered sample involved these zircons. They also presumed another minor phase that concentrates LREE. Based on our finding monazites with the SEM in all of our shale samples, we believe that this presumed minor phase was monazite. Our results also confirm the

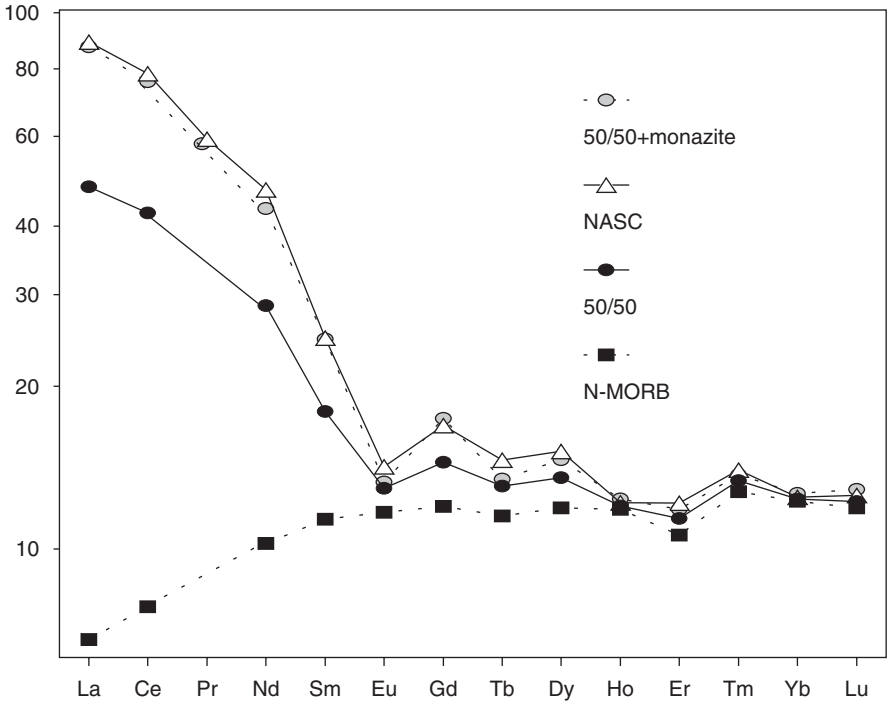

Fig. 13. Chondrite normalized REE distributions for N-MORB, NASC, a 50/50 mixture of N-MORB and NASC, and a mixture containing 70ppm monazite (0.007% monazite, 49.9965% N-MORB, and 49.9965% NASC by weight). Modified from Totten and Hanan, (1998).

control of certain trace-element concentrations by zircon. The REE contents of common heavy minerals range from one to several orders of magnitude greater than those of the average shale (Taylor and McLennan, 1995). One other implication involves the widespread use of whole-rock Sm/Nd isotopic signatures in determining provenance. These two isotopes are members of the LREE that can be dominantly controlled by variable amounts of specific heavy minerals such as monazite. In these cases, the isotopic signature would indicate the provenance of the monazite, and not necessarily the whole rock. Authigenic monazite growth, as reported by Evans and Zalasiewicz (1996), would further complicate whole-rock signatures.

The implications for determining provenance, based upon whole-rock trace-element geochemistry, are important. If minor phases can control overall chemistry out of proportion to their abundances, an understanding and consideration of this fact is vital to sedimentary petrologists. Consequently, it is essential to research and learn more about the distribution of heavy minerals in shales.

6.4. The Potential for Size Bias

The potential for size bias, associated with the disaggregation of rocks in preparation for heavy mineral separation can be problematic for coarse-grained sediments, and

the bias may be even more important to consider in fine-grained shales. Currently, we are experimenting to develop techniques that will allow to separate and quantify the entire grain-size population of heavy minerals in shales. Although very important for provenance studies and for textural information (e.g., the presence of reworked, rounded heavy minerals), the sub-population of coarser-grained ($>10\,\mu m$) heavy minerals in shales may not be representative of the entire heavy mineral population. The dilemma associated with shale heavy minerals, as mentioned earlier, is that light milling/disaggregation helps to preserve larger grains and facilitates identification, but it also has a drawback because more rock fragments will appear in the heavy mineral separations (e.g., intergrown heavy/light minerals, forming composite grains). With light milling (i.e., short times in the shatter box) some unknown proportion of heavy + light mineral-containing rock fragments, with densities lower than $2.85\,g/cm^3$, will float in the light fraction. This suggests that a significant proportion of very fine-grained heavy minerals may remain locked up with light minerals and/or rock fragments during separation. The geochemical data from whole-rock samples and from light-mineral fractions suggest that small heavy minerals, present as inclusions within other mineral phases, can easily escape settling in the heavy liquid. In either case, whether they are discrete heavy minerals that are separable from a rock, or inclusions within a mineral phase, heavy minerals are important components that sequester many trace elements and significantly influence whole-rock chemistry.

7. SUMMARY

Our ongoing research does not yet allow us to conclude firmly how increased understanding of the heavy mineral control on trace elements (especially the HFSE and REE) will effect future research, especially on clastic sediment provenance, or where exactly a further study of shale heavy minerals will take us. If important tectonic or provenance signatures in shales appear to be controlled largely by particular, resistant, heavy minerals, as we suspect, then the question arises how do these minerals, which are nearly insignificant by volume or weight, correlate in age and provenance with the bulk of clay minerals, quartz, and other light minerals? The pervading presence of trace amounts of monazites and zircons found in the analysed shale samples also raises the question whether Sm/Nd model ages, based on whole-rock shale samples, are merely measures of the composite ages of these minerals. A fundamental observation of our study on the occurrence of heavy minerals in shales is that for XRF analysis all whole-rock shale samples should be powdered as long as possible to avoid heterogeneity problems introduced by the resistant heavy-mineral suite.

REFERENCES

Bhatia, M.R., Crook, K.A.W., 1986. Trace element characteristics of greywackes and tectonic setting discrimination of sedimentary basins. Contributions to Mineralogy and Petrology 92, 181–193.

Blatt, H., Sutherland, B., 1969. Intrastratal solution and non-opaque heavy minerals in mudrocks. Journal of Sedimentary Petrology 39, 591–600.

Blatt, H., Totten, M.W., 1981. Detrital quartz as an indicator of distance from shore in marine mudrocks. Journal of Sedimentary Petrology 51, 1259–1266.

Boggs, S., 1992. Petrology of sedimentary rocks. Macmillan Publishing Company, New York, 707pp.

Bokman, J., 1953. Lithology and petrology of the Stanley and Jackfork Formations. Journal of Geology 61, 152–172.

Caggianelli, A., Fiore, S., Mongelli, G., Salvemini, A., 1992. REE distribution in the clay fraction of pelites from the southern Apennines, Italy. Chemical Geology 99, 253–263.

Charles, R.C., Blatt, H., 1978. Quartz, chert, and feldspars in modern fluvial muds and sands. Journal of Sedimentary Petrology 48, 427–432.

Chaudhuri, S., Cullers, R.L., 1979. The distribution of rare-earth elements in deeply buried Gulf Coast sediments. Chemical Geology 24, 327–338.

Condie, K.C., 1991. Another look at rare earth elements in mudrocks. Geochimica et Cosmochimica Acta 55, 2527–2531.

Cullers, R.L., Chaudhuri, S., Arnold, B., Lee, M., Wolf, W., 1975. Rare-earths in size fractions and sedimentary rocks of Pennsylvanian-Permian age from the mid-continent of the USA. Geochimica et Cosmochimica Acta 39, 1691–1703.

Evans, J., Zalasiewicz, J., 1996. U-Pb, Pb-Pb and Sm-Nd dating of authigenic monazite: implications for the diagenetic evolution of the Welsh Basin. Earth and Planetary Science Letters 144, 421–433.

Garver, J.I., Scott, T.J., 1995. Trace elements in shale as indicators of crustal provenance and terrane accretion in the southern Canadian Cordillera. Geological Society of America Bulletin 107, 440–453.

Gromet, L.P., Dymek, R.F., Haskin, L.A., Korotev, R.L., 1984. The "North American shale composite": its compilation, major and trace element characteristics. Geochimica et Cosmochimica Acta 48, 2469–2482.

Hanan, M.A., Totten, M.W., 1996. Analytical techniques for the separation and SEM identification of heavy minerals in mudrocks. Journal of Sedimentary Research 66, 1027–1030.

Mange, M.A., Dewey, J.F., Wright, D.T., 2003. Heavy minerals solve structural and stratigraphic problems in Ordovician strata of the western Irish Caledonides. Geological Magazine 140, 25–30.

Morton, A.C., 1991. Geochemical studies of detrital heavy minerals and their application to provenance research. In: Morton, A.C., Todd, S.P., Haughton, P.D.W. (Eds.), Developments in Sedimentary Provenance Studies. In: Geological Society of London Special Publication, vol. 57, pp. 31–45.

Nelson, T.A., 1971. Density separation of clay minerals. Unpublished M.S. thesis. Oregon State University, Corvallis, 59pp.

Preston, J., Hartley, A., Hole, M., Buck, S., Bond, J., Mange, M., Still, J., 1998. Integrated whole-rock trace element geochemistry and heavy mineral chemistry studies: the key to the correlation of continental red-bed successions. Petroleum Geoscience 4, 7–16.

Preston, R.J., Hartley, A.J., Mange-Rajetzky, M., Hole, M.J., May, G., Buck, S., Vaughan, L., 2002. The provenance of Triassic continental sandstones from the Beryl Field, Northern North Sea; mineralogical, geochemical and sedimentological constraints. Journal of Sedimentary Research 72, 18–29.

Schieber, J., Zimmerle, W., 1998. Petrography of shales: a survey of technics. In: Schieber, J., Zimmerle, W., Sethi, P. (Eds.), Shales and Mudstones. Petrography, Petrophysics, Geochemistry and Economic Geology, vol. II. Schweizerbart, Stuttgart, pp. 3–12.

Schneiderman, J.S., 1995. Detrital opaque oxides as provenance indicators in River Nile sediments. Journal of Sedimentary Research 65, 668–674.

Slatt, R.M., Jordan, D.W., Stone, C.G., Wilson, M.S., 1994. Stratigraphic and structural compartmentalization observed within a model turbidite reservoir, Pennsylvanian upper

Jackfork Formation, Hollywood Quarry, Arkansas. In: Wiemer, P., Bouma, A., Perkins, B.F. (Eds.), Submarine Fans and Turbidite Systems: Gulf Coast Section SEPM 15th Annual Research Conference Proceedings, pp. 349–356.

Taylor, S.R., McLennan, S.M., 1995. The geochemical evolution of the continental crust. Reviews of Geophysics 33, 241–265.

Totten, M.W., Blatt, H., 1993. Alteration in the non-clay-mineral fraction of pelitic rocks across the diagenetic to low-grade metamorphic transition, Ouachita Mountains, Oklahoma and Arkansas. Journal of Sedimentary Petrology 63, 899–908.

Totten, M.W., Hanan, M.A., 1998. The accessory mineral fraction of mudrocks and its significance for whole-rock trace-element geochemistry. In: Schieber, J., Zimmerle, W., Sethi, P. (Eds.), Shales and Mudstones. Petrography, Petrophysics, Geochemistry and Economic Geology, vol. II. Schweizerbart, Stuttgart, pp. 35–53.

Totten, M.W., Hanan, M.A., Mack, D., Borges, J., 2002. Characteristics of mixed-layer smectite/illite density separates during burial diagenesis. American Mineralogist 87, 1571–1579.

Totten, M.W., Hanan, M.A., Weaver, B.L., 2000. Beyond whole-rock geochemistry of shales: the importance of assessing mineralogic controls for revealing tectonic discriminants of multiple sediment sources for the Ouachita Mountain flysch deposits. Geological Society of America Bulletin 112, 1012–1022.

This page intentionally left blank

1.4 Miscellaneous Techniques

This page intentionally left blank

Chapter 13

GEOCHEMISTRY OF HEAVY MINERALS

MARIA A. MANGE[a] AND ANDREW C. MORTON[b,c]

[a]*Department of Geology, UC Davis, One Shields Avenue, Davis, CA 95616, USA*
[b]*HM Research Associates, 2 Clive Road, Balsall Common, West Midlands CV7 7DW, UK*
[c]*CASP, University of Cambridge, 181a Huntingdon Road, Cambridge CB3 0DH, UK*

ABSTRACT

This contribution provides an insight into the use of mineral chemistry in provenance research, and demonstrates how studies, by using microbeam techniques on several detrital heavy mineral species, benefit from continuing technological advances. Virtually all detrital heavy minerals can now be subjected to sophisticated geoanalytical techniques that can determine their major and trace element compositions and identify their crystal chemistry. Petrogenetic controls impart distinctive elemental signatures to mineral phases in igneous and metamorphic rocks that are preserved in mineral grains eroded from them, and can be used as a genetic tool to help decode their parageneses. Of particular interest are those heavy minerals that are widespread in sediments with compositions that are suitable for routine geochemical analysis. In this review, the geochemistry of garnet, tourmaline, chrome spinel, apatite, pyroxenes and amphiboles and its application to specific geological problems is discussed in detail; brief references are given to minerals that have not been used frequently in provenance studies. It is important to emphasise that a particular species, chosen for geochemistry, is generally associated with other minerals that are also carriers of information. Therefore, mineral chemical data need to be integrated with information from the whole assemblage to ensure that the conclusions are truly comprehensive.

Keywords: heavy mineral chemistry; single mineral (varietal) analysis; microbeam techniques; garnet; tourmaline; apatite; chrome spinel

1. INTRODUCTION

Quantifying the characteristics of a single mineral (single-mineral analysis) is now frequently applied to increase confidence in detrital mineral studies and to add detail

Developments in Sedimentology, Vol. 58, 345–391

ISSN: 0070-4571/doi:10.1016/S0070-4571(07)58013-1

unavailable from conventional heavy mineral analyses. Single-mineral (varietal) analytical methods are extremely diverse but fall into three main categories: petrographic, isotopic and geochemical.

Petrographic characteristics include parameters such as colour, shape, habit, and zoning patterns. For example, zircon morphology has long been regarded as a petrogenetic indicator (Pupin and Turco, 1981; Corfu, 2001; Corfu et al., 2003). Colour varieties of minerals such as zircon and tourmaline are known to be provenance-diagnostic (Mackie, 1923; Krynine, 1946; Mange-Rajetzky, 1995). Apatite morphology has been used to evaluate sediment transport history, for example in Devonian-Carboniferous sandstones of the Clair Field, west of Shetland (Allen and Mange-Rajetzky, 1992).

Radiogenic methods are being used with increasing frequency, including fission track dating of zircons and apatites and U-Pb dating of phases such as detrital zircon, monazite and titanite. The study of isotopic systems is beyond the scope of this chapter, however, zircon and apatite fission track analysis (ZFTA, AFTA), which has a long history of application in sedimentary basins, is outlined here by Carter (2007 – this volume). Isotopic analysis of zircon in provenance studies is reviewed by Fedo et al. (2003).

Geochemical analysis, using a variety of microbeam techniques, has been applied to a large range of detrital heavy mineral species, including garnet, chrome spinel, tourmaline, amphiboles, pyroxenes, zircon, apatite, ilmenite and rutile. The objective of this contribution is to provide an insight into the use of mineral chemistry in sedimentary research, and how this has benefited from continuing technological advances. Almost all detrital heavy minerals can now be subjected to a range of sophisticated geoanalytical techniques that can determine their major and trace element compositions and identify their crystal chemistry. Petrogenetic controls impart distinctive elemental signatures to mineral phases in igneous and metamorphic rocks. These are preserved in detrital mineral grains derived from them, and can be used as a genetic tool to help decode their paragenesis. Of particular interest are those heavy minerals that are most widespread in sediments with compositions suitable for routine geochemical analysis. In this review, garnet, tourmaline, chrome spinel, apatite, pyroxenes and amphiboles are discussed in detail, while brief references are given to minerals that have not been used frequently in provenance studies.

It is important to emphasise that heavy mineral assemblages are relatively diverse, and the particular species chosen for geochemistry is associated with other minerals that are also carriers of information. Therefore, the mineral chemical data need to be integrated with information from the whole assemblage to ensure that the conclusions are truly comprehensive.

2. HISTORICAL OVERVIEW

With the advent of increasingly sophisticated microanalytical techniques in the latter part of the last century, mineral chemical analysis has become an integral part of many heavy mineral provenance studies. The earliest mineral chemical provenance studies (e.g., Luepke, 1980) were undertaken by atomic absorption analysis.

Because this technique requires relatively large amounts of sample, analysis was conducted on bulk separates. Although such studies were pioneering in their day, the conclusions that can be drawn from them were limited, because the data represent an averaged signal from a wide variety of potential source rocks. Geochemical analysis of mineral separates, therefore, at best gives only an imprecise view of provenance, and can, at worst, be seriously misleading. This approach was rapidly superseded by single-grain microbeam methods, particularly electron microprobe analysis, which became widely available in the 1980s, spawning a series of works on the geochemistry of a variety of mineral species, such as amphibole (Mange-Rajetzky and Oberhänsli, 1982), clinopyroxene (Cawood, 1983), tourmaline (Henry and Guidotti, 1985), garnet (Morton, 1985), zircon (Owen, 1987) and chrome spinel (Press, 1986).

More recently, yet more sophisticated technology has been developed, such as the sensitive high-resolution ion microprobe (SHRIMP) and laser ablation inductively-coupled plasma mass spectrometry (LA-ICPMS), which enable high-precision determination of trace elements and isotopic compositions of single-mineral grains. Although the main application of such techniques has been in radiometric dating of detrital heavy minerals such as zircon and monazite, they have also been used for mineral-chemical studies, either to provide trace element data on minerals more commonly analysed by electron microprobe, such as garnet (Čopjaková et al., 2005), or on minerals that show little major element variation, such as zircon (Belousova et al., 2002a) and apatite (Morton and Yaxley, 2007).

3. HEAVY MINERALS USED FREQUENTLY FOR GEOCHEMICAL ANALYSIS

3.1. Garnet

Garnet geochemistry is the most widely used mineral-chemical tool for determination and discrimination of sediment provenance, for several reasons. Firstly, it is a common component of many heavy mineral assemblages. Secondly, garnet is a relatively stable mineral under both weathering and burial diagenetic conditions (Morton and Hallsworth, 1999; Morton and Hallsworth, 2007, this volume), and, most importantly, it shows a wide range in major element compositions, enabling easy acquisition of mineral-chemical data using readily available electron microprobe facilities. Garnet is especially interesting in that it varies not only by bulk composition (protolith), but also P and T of formation, in both igneous and metamorphic rocks. In the latter, it often preserves the metamorphic path, i.e., the growth during changing P-T conditions, which can be particularly diagnostic. Most naturally-occurring garnets correspond to the general formula $(Mg,Fe^{2+},Mn,Ca)_3(Al,Cr,Ti,Fe^{3+})_2Si_3O_{12}$, but there are several other possible substitutions (Deer et al., 1997). Garnets fall into two isomorphous series: pyralspite $[(Mg,Fe^{2+},Mn)_3Al_2Si_3O_{12}]$ and ugrandite $[Ca_3(Al,Cr,Ti,Fe^{3+})_2Si_3O_{12}]$. Variations within the individual series are fairly complete and continuous, but there is no evidence for continuous variation between the two series.

The first paper to show the potential of garnet geochemistry as a provenance indicator was by Morton (1985). Since then, garnet geochemical constraints on

sediment provenance have been included in a large number of papers dealing with sediments from the Palaeozoic to the Holocene in sedimentary basins worldwide, among them being the Devonian of the Midland Valley of Scotland (Haughton and Farrow, 1988), the Carboniferous of the Culm Basin, Czech Republic (Hartley and Otava, 2001), Permian to Jurassic sandstones of the southern Kitakami Terrane,

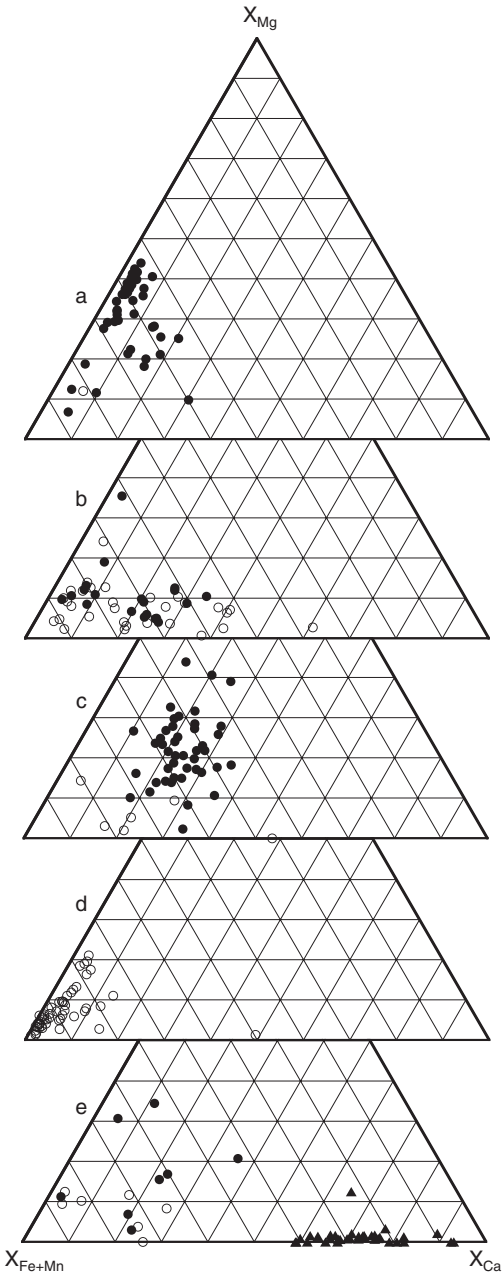

Japan (Takeuchi, 1994), the Triassic of the Barents Shelf, north of Norway (Mørk, 1999), Cretaceous to Palaeocene sandstones from the Polish Western Carpathians (Oszczypko and Salata, 2005), Jurassic to Cretaceous sandstones of Papua New Guinea (Morton et al., 2000), Cretaceous sandstones of the eastern Alps (Von Eynatten and Gaupp, 1999), Eocene to Oligocene sandstones from offshore New Zealand (Smale and Morton, 1987), Pliocene sandstones from the Southern Caspian Basin, Azerbaijan (Morton et al., 2003a), Miocene to Quaternary sandstones from the Bengal Fan (Yokoyama et al., 1990) and modern river sediments in the Netherlands (Tebbens et al., 1995).

The wide variety of garnet populations found in sandstones (Fig. 1) clearly illustrates how useful garnet assemblages are for distinguishing sandstones from different sources. However, using these data to reconstruct source area lithology is more problematic, since different parageneses may contain similar garnets. For instance, Wright (1938) showed that there is strong overlap between garnets from biotite schists and amphibolites, and between amphibolites and eclogites (Fig. 2). Morton et al. (2004) suggested that this problem could be overcome by using a deterministic approach that characterises the garnet assemblages from different potential sources by analysing assemblages from modern river sediment. They used these data to tie garnet assemblages in ancient sandstones back to specific source regions. One of the main outcomes of this work was to demonstrate that amphibolite facies metasedimentary terrains supply garnet assemblages with low Mg and variable Ca, which they termed Type B (Fig. 3). By contrast, high-grade mafic and ultramafic gneisses provide detrital garnet assemblages rich in high-Mg, high-Ca garnets, termed Type C (Fig. 3). Garnets from ultramafic rocks such as pyroxenites and peridotites have higher Mg contents than those from metabasic rocks (Morton et al., 2004). In western Norway, for example, garnets in pyroxenites and peridotites have $X_{Mg} > 50\%$, whereas most garnets from metabasic rocks have $X_{Mg} < 40\%$ (Fig. 4). A subdivision of Type C garnets into Ci ($X_{Mg} < 40\%$) and Cii ($X_{Mg} > 40\%$) may therefore be useful in assessing the relative contributions from mafic and ultramafic metamorphic sources (Fig. 5).

Fig. 1. Variations in garnet compositions illustrating the value of garnet geochemical analysis as a discriminator of sandstone provenance. (a) Triassic sandstone from the Strathmore Field, west of Shetland, UK (Well 205/26a-2, 2596.5 m), dominated by high-Mg, low-Ca garnets, derived from a high-grade (granulite facies) metasedimentary or charnockitic terrain (Morton et al., 2007, this volume). (b) Palaeocene sandstone from the Gannet area, central North Sea, UK (Well 21/30-13, 2279.6 m), containing low-Mg garnets with variable Ca, derived from amphibolite facies Dalradian metasediments of Scotland (Morton et al., 2004). (c) Palaeocene sandstone from the Ormen Lange area, Møre Basin, Norway (Well 6306/10-1, 1190.7 m), derived from high-grade metabasic rocks of western Norway (Morton et al., 2004). (d) Oligocene sandstone from the Georgian Republic, Asia (CASP sample WG95/1), containing high-Mn, low-Mg and low-Ca garnets, derived from granitoids in the Dzirhuli Massif. (e) Pliocene sandstone from Babazanan, Azerbaijan, containing Fe^{3+}-Ca-rich garnets derived from very low-grade metabasic rocks in the Lesser Caucasus (Morton et al., 2003a). X_{Fe}, X_{Mg}, X_{Ca}, X_{Mn} = ionic contents of Fe, Mg, Ca and Mn respectively, calculated on the basis of 24 oxygens, and normalised to total Fe + Mg + Ca + Mn, as recommended by Droop and Harte (1995). All Fe calculated as Fe^{2+}. Filled circles, garnets with $X_{Mn} < 5\%$; open circles, garnets with $X_{Mn} > 5\%$; triangles, garnets with $Fe^{3+}/Al > 0.10$.

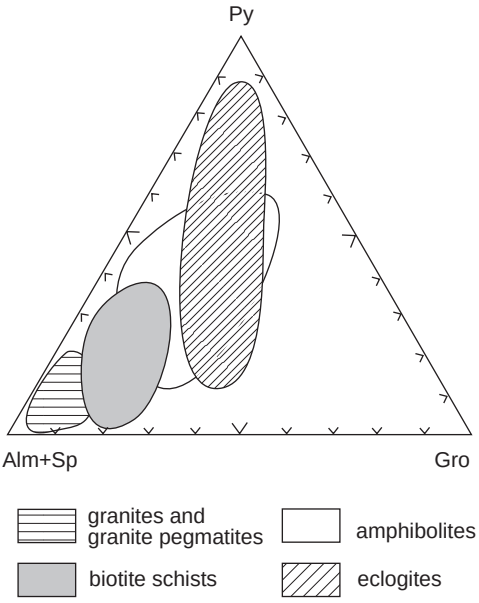

Fig. 2. Range of garnet compositions from granites and granite pegmatites, biotite schists, amphibolites and eclogites, adapted from Wright (1938) and Preston et al. (2002).

Type A garnet assemblages, which have high Mg and low Ca (Fig. 2) are generally attributed to high-grade (granulite facies) metasedimentary rocks or charnockites (Sabeen et al., 2002; Morton et al., 2004). However, Hamer and Moyes (1982) reported similar garnets from xenocrysts and in xenoliths in intermediate-acidic igneous rocks of the Antarctic Peninsula, where they represent metamorphic material incorporated into the magma at deep crustal levels. Type A garnets have also been recorded as phenocryst phases in intermediate-acidic igneous rocks (Green and Ringwood, 1968; Fitton, 1972), resulting from direct crystallisation from acid calc-alkaline magma at pressures of 0.9–1.8 $\times$ 10^9 Pa. Therefore, Type A garnets can be derived from intermediate-silicic igneous rocks that are the products of magmas emanating from deep crustal levels. Integrating heavy mineral data with garnet geochemical data would readily enable a distinction of the two alternative sources of Type A garnet, because assemblages derived from high-grade metasedimentary rocks or charnockites have markedly different characteristics to those derived from a predominantly igneous terrain.

Detrital garnet assemblages with low abundances of Types A, B and C have been found in a variety of circumstances, for example, in Pliocene to Holocene sediments from the South Caspian Basin, Azerbaijan (Fig. 1). Sediments transported by both the modern Kura and palaeo-Kura river systems, sourced from the Lesser Caucasus mountain range, are characterised by abundant Fe^{3+}-Ca (andradite-grossular) garnets (Fig. 1). Such garnets are here termed 'Type D'. The most typical occurrence of Type D garnets is in contact or thermally metamorphosed calcareous sediments, and especially in associated metasomatic skarns (Deer et al., 1997). However, such a provenance is unlikely in the case of the Kura and palaeo-Kura assemblages, since

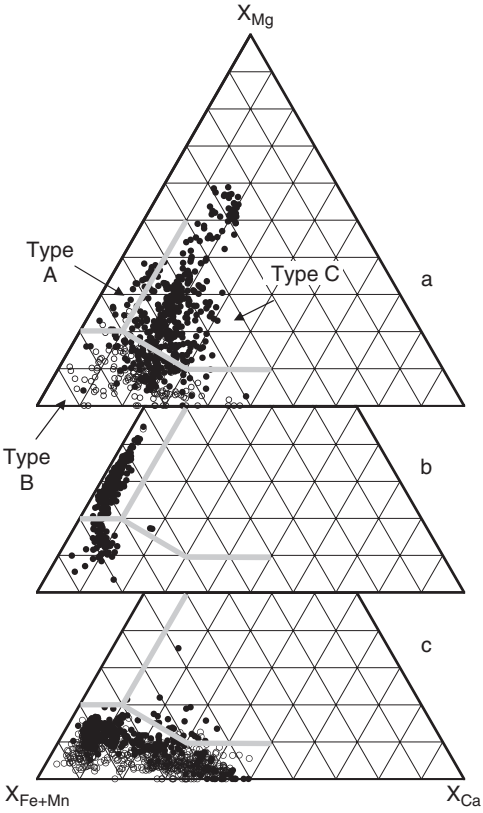

Fig. 3. Garnets in modern river and beach sediments, illustrating the close relationship between detrital garnet compositions and their source rocks. (a) Sediments from rivers draining the Western Gneiss Region of western Norway, an area with widespread high grade basic gneisses (from Morton et al., 2004). Note the abundance of garnets corresponding to Type C (high Ca, high Mg). (b) Sediments from beaches and rivers in southern India, an area comprising high grade (granulite facies) metasediments and charnockites (from Sabeen et al., 2002). Note the abundance of Type A garnet (low Ca, high Mg). (c) Sediments from rivers draining Moine metasediments of the Northern Highlands of Scotland, which are predominantly at amphibolite facies (from Morton et al., 2004). Note the predominance of Type B garnet (low Mg, variable Ca).

the Lesser Caucasus source region is dominated by basic volcanic rocks (Kazmin et al., 1986), and provides heavy mineral suites rich in clinopyroxene (Morton et al., 2003a). The association of Type D garnets with clinopyroxene-dominated assemblages suggests that they were derived from very low-grade metabasic rocks, similar to those found in New Zealand (Coombs et al., 1973). Dasgupta and Pal (2005) have indicated another possible origin for Type D garnets. They found that grandite garnets of variable composition occur in ultra-high temperature metamorphosed calc-silicate granulites as a result of a number of reactions involving, among other minerals, clinopyroxene, scapolite, plagioclase, wollastonite and calcite.

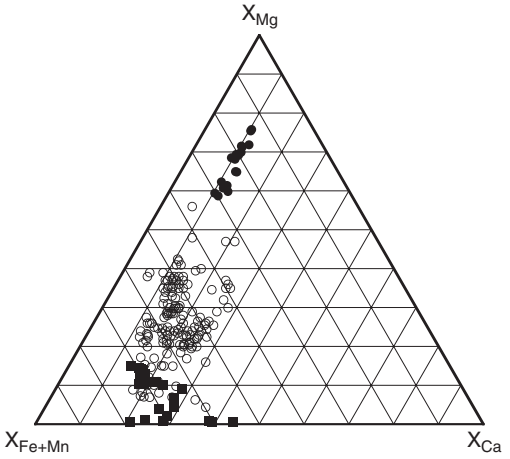

Fig. 4. Garnets in peridotites and pyroxenites (filled circles), in eclogites, other mafic gneisses, and quartz-biotite gneisses (open circles), and in granitic gneisses, tonalitic gneisses, hybridised gneisses and pegmatites (filled squares) from western Norway (Krogh, 1980; Medaris, 1980, 1984; Mysen and Heier, 1972). X_{Fe+Mn}, X_{Mg}, X_{Ca} are as in Fig. 1.

Although most detrital garnets have primary metamorphic sources, granitoids and associated pegmatites can also provide garnet-rich sediment. For example, garnet is common in the Dartmoor granite of SW England (Brammall, 1928) and in some Scottish granites (Mackie, 1926). Garnets from intermediate-acidic igneous rocks have distinctive low-Mg, low-Ca compositions and are frequently rich in Mn (Deer et al., 1997). Detrital garnets with these characteristics have been found in Oligocene sandstones of Georgia (Fig. 1), and were derived from granites located in the Dzirhuli Massif. Such garnets are classified as Type B using the terminology of Morton et al. (2004), but have a markedly different origin to the Type B garnets in Scottish river sediments (Fig. 3), which were derived from amphibolite facies metasediments. Subdivision of Type B garnets into Bi ($X_{Ca} < 10\%$) and Bii ($X_{Ca} > 10\%$) may therefore prove useful in differentiating sediment derived from granitoids, which supply assemblages dominated by Mn-rich Bi garnets (Fig. 1), and sediment derived from metasediments, which tend to have a wider range of compositions within the overall Type B spectrum. Integration of heavy mineral and mineral-chemical data provides further constraints on the origin of such detrital garnets.

A variety of other garnet types are known from igneous and metamorphic sources, including yamatoite ($Mn_3V_2Si_3O_{12}$), kimzeyite ($Ca_3(Zr,Ti)_2(Al,Si)_3O_{12}$) and yttrogarnet ($Y_3Al_2Al_3O_{12}$). Despite acquisition of a large amount of detrital garnet geochemical data, however, such garnets have yet to be recorded as detrital phases. The only exception to this is the vanadian garnet goldmanite ($Ca_3V_2Si_3O_{12}$), which was identified in Palaeocene sandstones in the northern North Sea by Hallsworth et al. (1992). Some garnets, in particular those containing high proportions of the pyrope (Mg) end member, also have high Cr contents: these are of special importance in diamond exploration, because chrome-rich pyrope garnet and/or chromite are important minor phases in many mantle-derived peridotites which appear as xenolits in kimberlites (McClenaghan and Kjarsgaard, 2001; Nowicki et al., 2007, this volume).

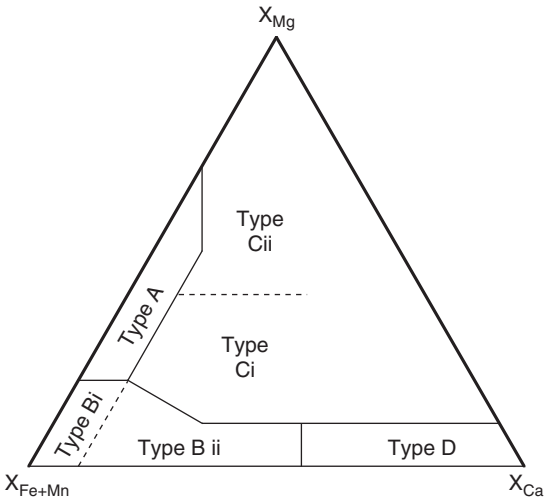

Fig. 5. Subdivision of the garnet Fe + Mn-Mg-Ca ternary plot showing definitions of garnet types A, Bi, Bii, Ci, Cii and D, as discussed in the text. Note that these types reflect natural sedimentary groupings, and are not intended to be diagnostic of particular garnet-bearing source rocks. Nevertheless, observations from modern and ancient sediments indicate the following: Type A garnets are mainly derived from high-grade granulite-facies metasediments or charnockites, but can also be supplied from intermediate-acidic igneous rocks sourced from deep in the crust. Type B garnets are derived from amphibolite-facies metasediments. However, garnet populations that plot exclusively in the Type Bi field suggest derivation from intermediate-acidic igneous rocks. Type C garnets are derived mainly from high-grade metabasic rocks. Within this group, garnets with very high Mg contents (Type Cii) imply sourcing from ultramafics such as pyroxenites and peridotites. Type D garnets are generally derived from metasomatic rocks such as skarns, from very low-grade metabasic rocks, or from ultrahigh temperature metamorphosed calc-silicate granulites.

The vast majority of garnet geochemical studies have concentrated on major elements variations, which are readily determined using conventional electron microprobe methods. However, Čopjaková et al. (2005) combined major electron analysis using the electron microprobe with trace element analysis using laser ablation ICP-MS to provide additional insight into garnet provenance in the Culm Basin of the Czech Republic. They showed that trace element patterns are useful for distinguishing garnets from different granulite sources. For example, garnets derived from the Miroslav Crystalline Unit (Fig. 6) show strong enrichment in heavy rare earth elements (HREE), whereas those derived from the Náměšť Granulite Massif have flat to negatively sloped chondrite-normalized HREE patterns. Although conventional electron microprobe methods are likely to remain at the forefront of detrital garnet studies, trace element analysis using laser ablation ICP-MS is likely to add significant sophistication to garnet provenance studies in the future.

Garnet geochemistry was used as a potential archaeometric tool by Mannerstrand and Lundqvist (2003) who traced the possible source rocks for the garnets found in the Slöinge excavation site in southwest Sweden and in Denmark to understand better Iron Age trade. Using SEM equipped with an EDS-detector they carried out

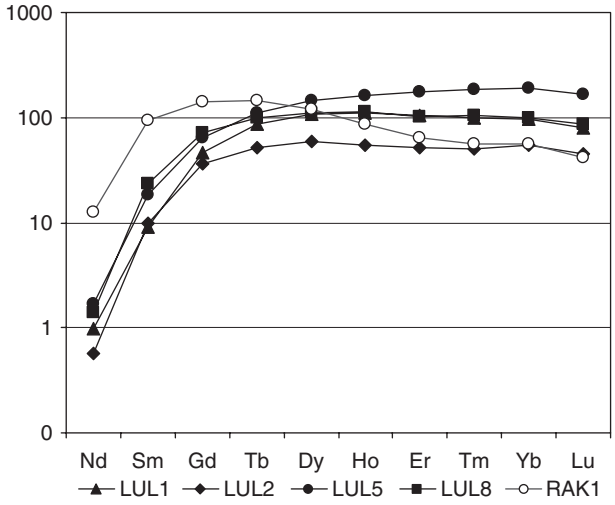

Fig. 6. Chondrite-normalised REE patterns of garnets derived from the Miroslav Crystalline Unit (samples LUL1, LUL2, LUL5 and LUL8) and the Náměšť Granulite Massif (sample RAK1), from Čopjaková et al. (2005). Normalisation values from Taylor and McLennan (1985).

comparative analyses on garnets from potential source rocks in Sweden and their results indicated that the probable source rocks are garnet amphibolites/mafic granulites, common in southwest Sweden, and that an important trade with garnet from a few mines occurred during the late Iron Age.

The use of garnet geochemical data to solve questions concerning sediment provenance is limited by the stability of garnet during burial diagenesis. Although garnet is relatively stable during burial, it undergoes dissolution by high-temperature porefluids (Morton, 1984; Morton and Hallsworth, 2007, this volume). Furthermore, the stability of garnet is controlled by its composition, with high-Ca garnets being less stable than low-Ca garnets (Morton, 1987; Smale and Van der Lingen, 1989; Morton and Hallsworth, 2007, this volume). Therefore, Type Bii, Type C and Type D garnets are less stable than Type A and Type Bi garnets. In consequence, sandstones that have undergone significant modification during burial diagenesis may contain garnet assemblages that are not entirely representative of their source region. Garnet populations that have been modified by dissolution during deep burial can be recognised by petrographic observation of their surface textures (see Turner and Morton, 2007, this volume).

3.2. *Chrome Spinel*

Chrome spinel $[(Mg,Fe^{2+})(Cr,Al,Fe^{3+})_2O_4]$ is a ubiquitous accessory mineral in ultramafic to mafic rocks. It owes its value as a petrogenetic indicator to its particular chemical character, being extremely sensitive to bulk rock composition and petrogenesis of the host rock. The principal constituents (Cr, Mg and Al) behave differently during fractional crystallisation or partial melting: Cr and Mg are

strongly partitioned into the solid, whereas Al is strongly partitioned into the melt. Partitioning of Mg and Fe^{2+} between spinel, silicate melts and minerals is strongly temperature dependent (Irvine, 1965, 1967; Dick and Bullen, 1984; Hisada and Arai, 1993). The ratios of these cations change according to physicochemical conditions and equilibrium temperature, and can thus reveal petrogenetic signatures of geodynamic settings in which chrome spinel-bearing complexes are formed.

An extensive literature exists on the paragenesis, crystal chemistry and geotectonic significance of chrome spinel in mafic and ultramafic bodies, predominantly ophiolites, meta-ophiolites and other types of ultramafic bodies. Irvine (1965, 1967) was one of the earliest to recognise the value of chrome spinel as a petrogenetic indicator. His publications raised much interest, prompting researchers to unravel the geochemical properties of chrome spinels in a variety of geological environments. Studies aimed to reconstruct the petrogenesis and plate tectonic settings of igneous complexes and sediments sourced from them, and the proliferation of publications has greatly enriched the geological literature. For example, Dick and Bullen (1984) refined the discrimination field and provided a comprehensive review of chrome spinel as a petrogenetic indicator in abyssal and alpine-type peridotites, while Barnes and Roeder (2001) collated a wide spectrum of spinel compositional fields from a variety of mafic and ultramafic igneous rock types and their tectonic environment. Arai (1992) showed that the composition of chrome spinel in volcanic rocks is a reliable guide to magma chemistry.

For graphical evaluation, cation ratios are calculated as $Cr\# = Cr/(Cr + Al)$ and $Mg\# = Mg/(Mg + Fe^{2+})$, and plotted as bivariate plots (Dick and Bullen, 1984; Pober and Faupl, 1988; Arai, 1992; Sciunnach and Garzanti, 1997; Barnes and Roeder, 2001). Chrome spinels derived from different ophiolite parageneses cluster in distinctive areas in these plots (Fig. 7). Other bivariate diagrams are constructed by using TiO_2 wt% versus Fe^{2+}/Mg (Ganssloser (1999), TiO_2 wt% versus $Cr/(Cr + Al)$ (Hisada et al., 1999) (Fig. 8), and/or other ratio combinations (Figs. 9 and 10). Ternary plots (Fig. 11) are constructed by plotting the major trivalent cations Cr^{3+}, Al^{3+} and Fe^{3+} (Cookenboo et al., 1997; Barnes and Roeder, 2001). They illustrate the fields delineating different types of ophiolites and other ultramafics.

The potential of detrital chrome spinel in fingerprinting sediment provenance and in reconstructing source rock composition and geotectonic setting has been demonstrated by numerous studies. Zimmerle (1984) was the first to recognise the geotectonic significance of "detrital brown spinel" (commonly referred to as chrome spinel), not only because its composition is a sensitive indicator of the parental melt but, also, because in detrital sediments its higher abundance correlates with orogenic episodes (e.g., Caledonian, Variscan and Alpine). He showed that a marked increase of "detrital brown spinel" in a succession marks the stratigraphical interval which records the beginning of processes that expose and progressively erode obducted ophiolitic mafic–ultramafic complexes. Evidence for such processes was demonstrated by Dewey and Mange (1999) in the western Irish Caledonides. Press (1986) was one of the first to use chrome spinel chemistry to trace the source of Middle Devonian sediments of the Rhenish Massif to alpine-type peridotites, and Pober and Faupl (1988) showed, in a comprehensive study, how chrome spinel chemistry helped understanding the geodynamic evolution of the eastern Alps. An increasing number of publications focus on chrome spinel chemistry, alone or combined with that of

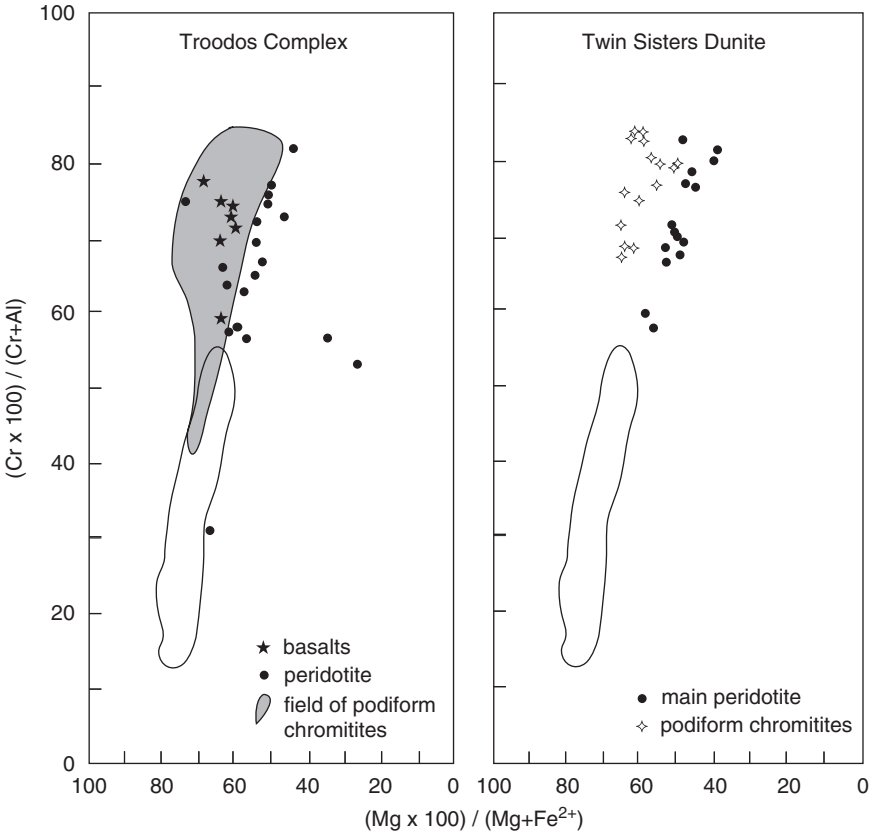

Fig. 7. Mg# versus Cr# bivariate plots, showing the compositional fields of chromian spinels for alpine-type peridotites. Solid circles are spinel peridotites, filled stars basalts, and open stars are chromitites or dunites (after Dick and Bullen, 1984).

other mineral phases present in the heavy mineral fractions. These include, amongst others, Arai and Okada (1991), Hisada and Arai (1993), Gieze et al. (1994), Árgyelán (1996), Arai et al. (1997, 2006), Cookenboo et al. (1997), Sciunnach and Garzanti (1997), Asiedu et al. (1998, 2000a), Hisada et al. (1998, 1999, 2004), Ganssloser (1999), Preston et al. (2002), Zhu et al. (2004), Mikes et al. (2005), Oszczypko and Salata (2005) and Grzebyk and Leszczyński (2006).

Lenaz and Kamenetsky (2000) were the first to analyse melt inclusions in detrital chromian spinels, extracted from Maastrichtian to Middle Eocene sandstones of sedimentary basins in the SE Alps. Based on their TiO_2 and Fe^{2+}/Fe^{3+} contents, they successfully discriminated two principal compositional groups which indicated one peridotite and one basaltic volcanics-sourced spinel population. Furthermore, heterogeneous geochemical characteristics within the latter group indicated that they were generated in different basaltic melts in different plate tectonic environments. Zhu et al. (2004) adopted this novel approach and included it in their study of the Middle-Late Cretaceous turbiditic sandstones of the Tianba Flysch series in southern Tibet.

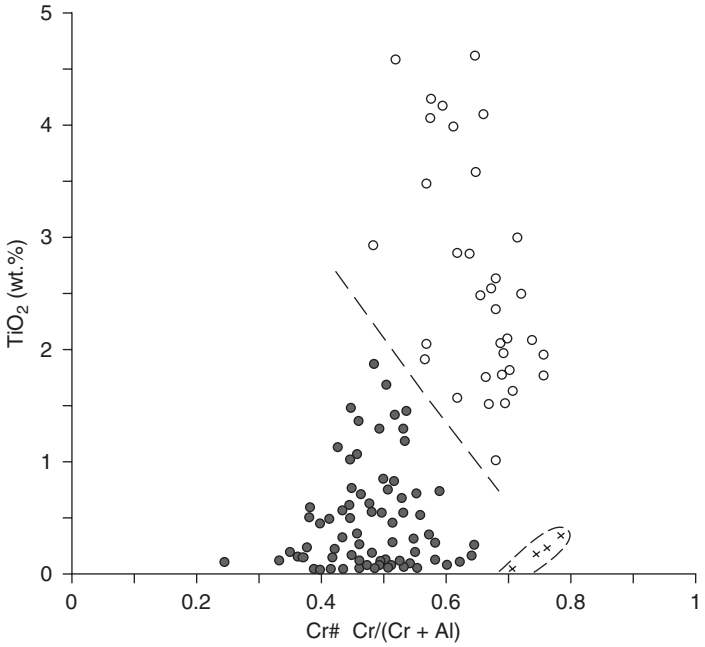

Fig. 8. Chrome spinel bivariate plot based on Cr# versus TiO2 wt%. Open circles show high-Ti spinels, solid circles low Ti spinels and crosses high-Cr spinels (after Hisada et al., 2004).

A brief review of the geotectonic significance of detrital chrome spinel was published by Lee (1999), however Power et al. (2000) challenged its validity as a petrogenetic indicator. The latter authors analysed the chemistry of chrome spinels from different parts of the Rum intrusion, a layered complex in the British Tertiary Volcanic Province, and from streams draining the Rum complex. They found that chrome spinels have diverse chemistry within individual megacyclic units and that disseminated detrital chrome spinels are chemically comparable but are different from the within-seam chrome spinels. Because the mechanism of formation and chemistry of parental magma of the within-seam chrome spinels are different to those of their disseminated counterparts, they generate chrome spinels with different chemistry. Power et al. (2000) argued that disseminated and within-seam spinels are, therefore, not equivalent, a finding that contrasts with Irvine's (1965, 1967) assumptions. Chrome spinels from stream samples were sourced from disseminated chrome spinels from the main body of the intrusion, rather than from chromitite seams, indicating that the latter contributed only minor amounts to the detritus. They also noted that hydrothermal alteration and serpentinisation causes changes in chrome spinel chemistry. During serpentinisation, chrome spinel grains lose Al and Mg and become enriched in Fe; this change particularly affects disseminated chrome spinels. They conclude that chrome spinels occur in much wider tectonic settings than the currently-used discrimination diagrams suggest. In this context, it is worthy of note that the Rum intrusion formed in a Palaeocene hotspot setting, different to that of other ultramafic complexes and oceanic lithosphere.

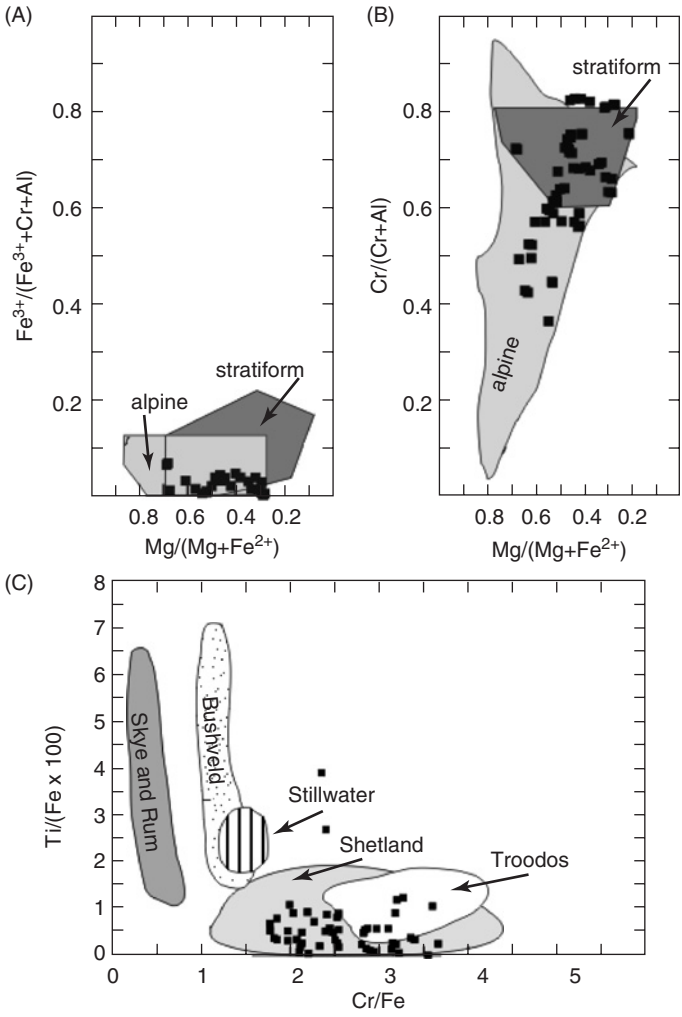

Fig. 9. Major-element composition of chrome spinels from Triassic red beds in the Beryl Field, North Sea, UK. (A) $Mg/(Mg+Fe^{2+})$ and $Fe^{3+}/(Fe^{3+}+Cr+Al)$ ratios are plotted from well 9/13-S48 and compared with chrome spinels from stratiform- and alpine-type ultramafic rocks (after Dick and Bullen, 1984; Cookenboo et al., 1997). (B) Major-element composition of chrome spinels from well 9/13-S48 plotted using $Mg/(Mg+Fe^{2+})$ and $Cr/(Cr+Al)$ ratios, which are compared with chrome spinels from stratiform- and alpine-type ultramafic rocks (after Dick and Bullen, 1984; Cookenboo et al., 1997). (C) Ti/Fe versus Cr/Fe ratio plot for chrome spinels from well 9/13-S48 compared with those from layered ultramafic intrusions (Skye, Rum, Bushveld and Stillwater), and with chrome spinels from ophiolitic sources (Shetland and Troodos) (after Prichard and Neary, 1985).

Detrital chrome spinel chemistry also serves as an important alluvial tracer for diamond in kimberlite terrains. This particular use is reported by Nowicki et al. (2007, this volume). Chrome spinel chemistry is a powerful tool in the evaluation of the ore quality in economic mineral deposits (Pownceby, 2005), and proved valuable

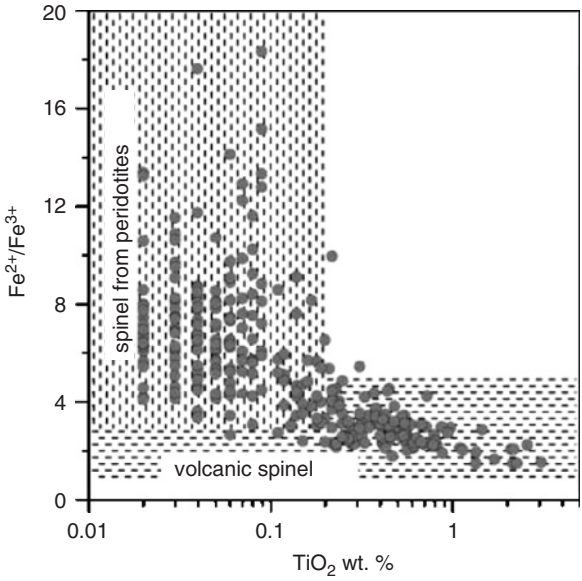

Fig. 10. Cross plot for discriminating volcanic and peridotite-derived chrome spinels, using TiO_2 wt% versus Fe^{2+}/Fe^{3+} (after Lenaz and Kamenetsky, 2000).

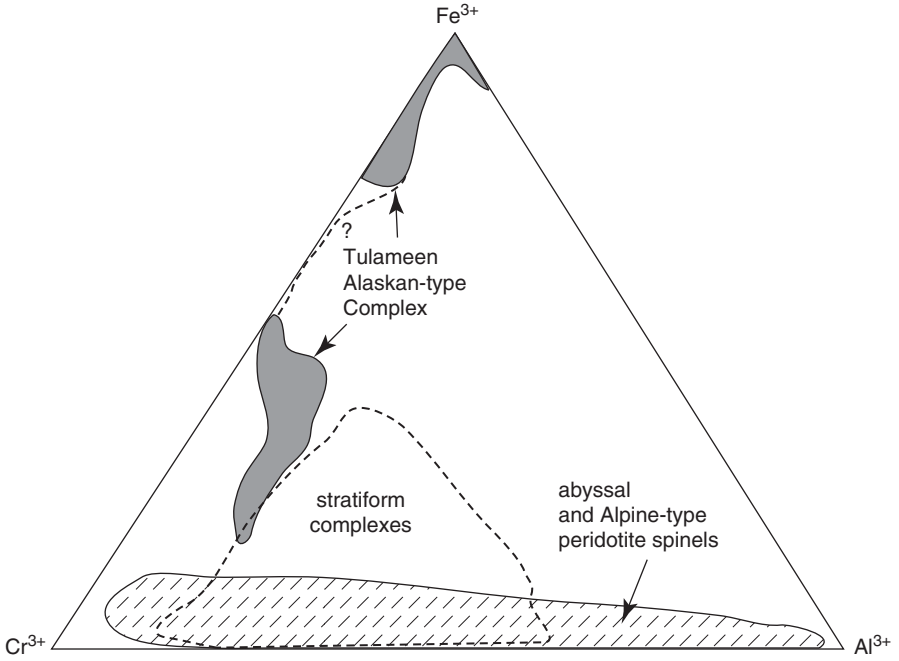

Fig. 11. Trivalent major cation plot, discriminating between different types of ultramafic complexes (after Cookenboo et al., 1997).

in solving a problem in commercially important Ti mineral deposits in southeastern Africa (Pownceby and Bourne, 2006). Because even minor Cr levels can downgrade the ilmenite concentrate, it was important to find the source of the Cr-bearing mineral phase. Chrome spinel analyses showed the presence of two distinctive compositional groups, denoting two chemically-different provenances. One group of spinels had a high magnetite component and these could be easily removed, thus increasing the value of the concentrates.

Chrome spinel is chemically more stable than all other minerals in ultramafic rocks, and preserves its compositional signature after burial. The minor disadvantage lies in the possibility of recycling, but this is generally negligible because most tectonogenic sediments are first cycle. If recycling is suspected, it can be easily ascertained by grain morphology and by the character of associated minerals. Chrome spinel is easily recognised both in transmitted light and reflected light petrography.

This review of studies using chrome spinel geochemistry is far from complete. However the examples cited above provide an insight into a repository of information to draw from, and to guide researchers in the field of sedimentology, tectonics and other disciplines.

3.3. Tourmaline

Tourmaline is a complex borosilicate with a considerable range of potential compositions. Its general formula is $XY_3(T_6O_{18})(BO_3)_3V_3W$ (Hawthorne and Henry, 1999). The X site may be occupied by Na, Ca or possibly K, but can be largely vacant. The Y site is usually occupied by Li^{1+}, Mg^{2+}, Fe^{2+}, Mn^{2+}, Al^{3+}, Cr^{3+}, V^{3+}, Fe^{3+} or Ti^{4+}. The T site is usually occupied by Si, occasionally Al, and possibly B. The V site contains OH^{1-} and O^{2-}, whereas the W site contains F^{1-}, OH^{1-} and O^{2-}. The wide range of potential compositions makes tourmaline an ideal mineral to use for geochemical discrimination of provenance. The application of tourmaline geochemistry in provenance studies has been enhanced by the work of Henry and Guidotti (1985) and Henry and Dutrow (1992), who demonstrated that tourmaline geochemistry reflects the local environment in which the mineral developed. They showed that the use of two ternary diagrams (Al-Fe_{total}-Mg and Ca-Fe_{total}-Mg) enabled discrimination of tourmalines from a wide range of rock types (Fig. 12). These provenance discrimination diagrams are very powerful, because they permit not only an evaluation of similarities and differences between detrital tourmaline populations, but they also put constraints on the nature of their source areas. Furthermore, because tourmaline is stable in both weathering and diagenetic environments (Morton and Hallsworth, 1999, 2007, this volume), tourmaline geochemistry can be applied to provenance analysis of any sandstone, irrespective of the extent to which it has been modified during the sedimentary cycle.

Despite the evident potential of tourmaline geochemistry for provenance analysis, the method has been applied only sporadically to date. Willner (1987) used the technique to evaluate the provenance of Precambrian/Cambrian sandstones in Argentina. Jeans et al. (1993) suggested that variations in tourmaline composition in the UK Triassic reflect differences in provenance. Tourmalines also proved useful to constrain the provenance of Early Jurassic sandstones in Slovakia (Aubrecht and

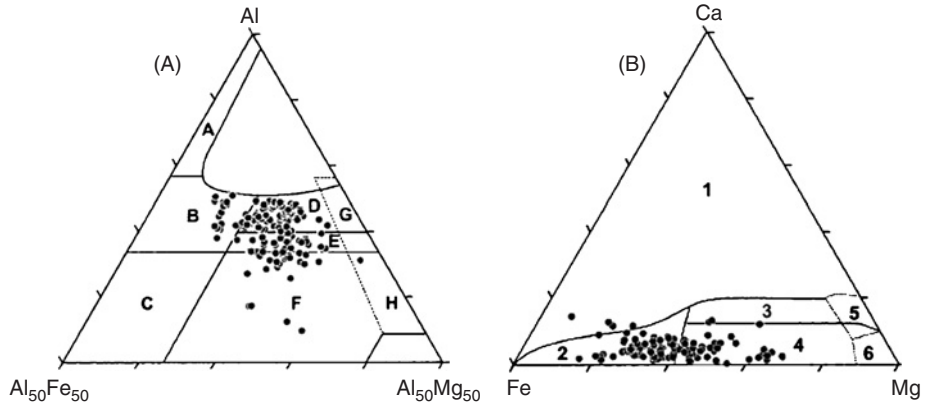

Fig. 12. Tourmalines from the Triassic of the Beryl Field, northern North Sea, plotted on the provenance-discriminant Al-Fe_{total}-Mg and Ca-Fe_{total}-Mg ternary diagrams of Henry and Guidotti (1985), adapted from Preston et al. (2002). Plot A: Field A, Li-rich granitoids, pegmatites and aplites. Field B, Li-poor granitoids, pegmatites and aplites. Field C, Hydrothermally-altered granitic rocks. Field D, Aluminous metapelites and metapsammites. Field E, Al-poor metapelites and metapsammites. Field F, Fe^{3+}-rich quartz-tourmaline rocks, calc-silicates and metapelites. Field G, Low-Ca ultramafics. Field H, Metacarbonates and metapyroxenites. Plot B: Field 1, Li-rich granitoids, pegmatites and aplites. Field 2, Li-poor granitoids, pegmatites and aplites. Field 3, Ca-rich metapelites, metapsammites and calc-silicates. Field 4, Ca-poor metapelites, metapsammites and quartz-tourmaline rocks. Field 5, Metacarbonates. Field 6, Metapyroxenites.

Kristin, 1995), of Jurassic to Cretaceous sandstones of Papua New Guinea (Morton et al., 2000), and of Triassic sandstones in the northern North Sea (Preston et al., 2002). Jiang et al. (1999) analysed tourmalines in clasts from Devonian conglomerates of SW Ireland, thereby establishing the nature of the metamorphic basement source and its affinity with other basement blocks in Ireland. Li et al. (2004) suggested that tourmaline compositions in Carboniferous sandstones of central China reflect an evolution in their source area with time. Morton et al. (2005a) showed that northerly- and southerly-derived Carboniferous sandstones of the southern North Sea contain different tourmaline geochemical populations, an observation that is particularly significant in view of the extensive diagenetic modification that has caused depletion of all but the most stable heavy minerals.

Tourmaline geochemistry proved to be a vital component of the multidisciplinary provenance study of Late Cretaceous sandstones in the Norwegian Sea (Morton et al., 2005b). Their study used a combination of heavy mineral data, provenance-sensitive ratio data, garnet geochemistry, tourmaline geochemistry and zircon geochronology to identify three main sources, each of which generated a distinctive sand type. Sand type MN1 was derived from northern Norway, sand type MN2 was derived from northern East Greenland and sand type MN3 was derived from western Norway. A total of 64 tourmaline populations were analysed during the course of this study, each of which was characterised by electron microprobe data from 50 individual tourmalines. The tourmaline populations consist mainly of

metasedimentary types (falling in fields D, E and F on the Al-Fe_{total}-Mg ternary diagram as defined by Henry and Guidotti, 1985), with minor numbers of grains derived from Li-poor granitoids (Field B), as shown by the typical tourmaline populations in Fig. 13. The relative abundances of Field B, Field D, Field E and Field F tourmalines vary systematically between the three sand types (Fig. 14), enabling distinction of their provenance and placing constraints on the tourmaline-bearing lithologies in the source regions.

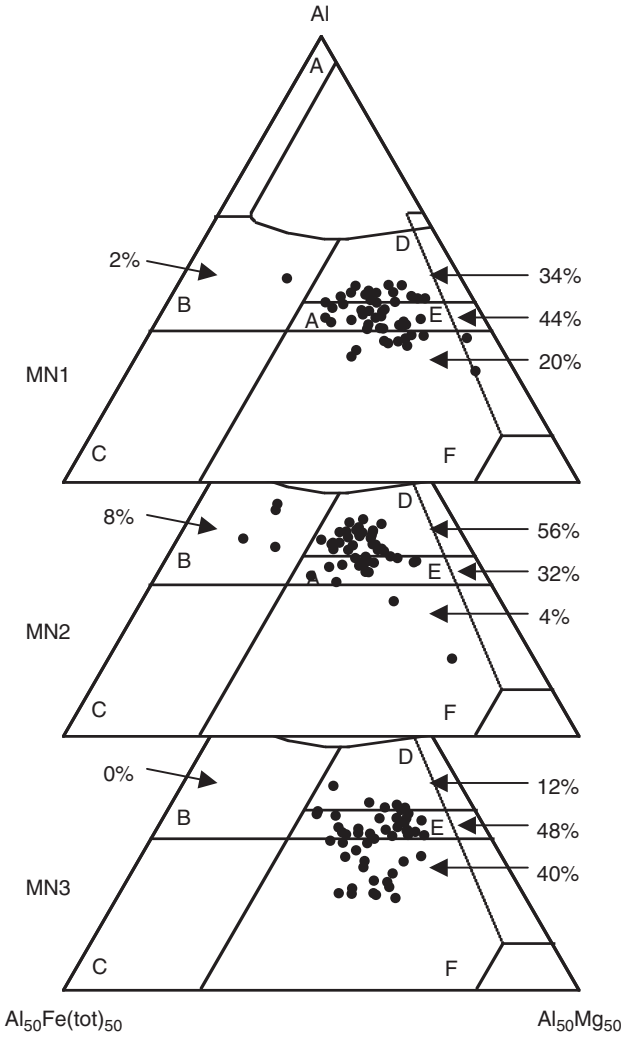

Fig. 13. Typical tourmaline assemblages from Late Cretaceous sandstone types MN1, MN2 and MN3 from the Norwegian Sea plotted on the provenance-discriminant Al-Fe_{total}-Mg ternary diagram devised by Henry and Guidotti (1985) (after Morton et al., 2005b). Figures denote percentage of grains falling into fields B, D, E and F. See Fig. 12 for definition of the fields illustrated. MN1, well 6507/2-2, depth 3338.5 m; MN2, well 6607/5-2, depth 4172.9 m; MN3, well 6305/7-1, depth 2959.0 m.

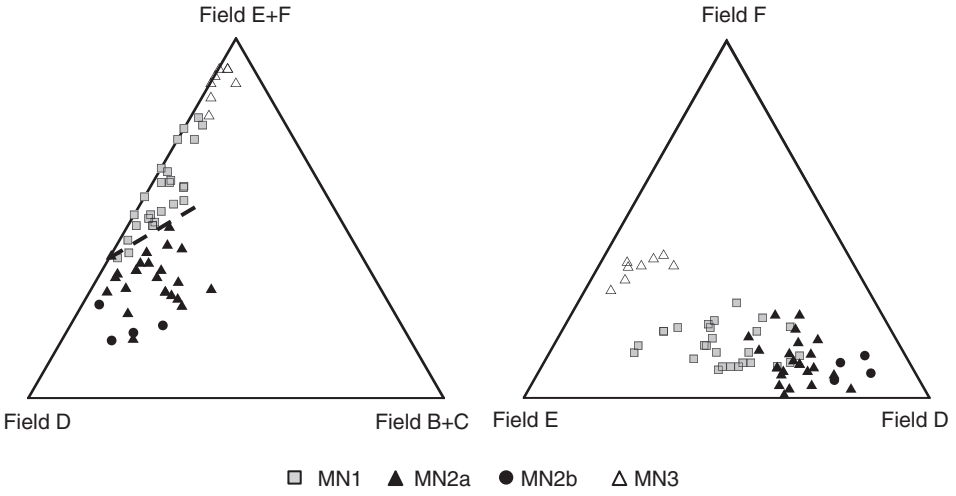

Fig. 14. Discrimination of provenance of Late Cretaceous sandstone types MN1, MN2 and MN3 from the Norwegian Sea using tourmaline geochemical data (from Morton et al., 2005b). Fields B, C, D, E and F as defined by Henry and Guidotti (1985).

3.4. *Pyroxenes*

Pyroxenes are the most important group of ferromagnesian rock-forming minerals. They occur in almost every type of igneous and metamorphic rocks, and crystallise under a range of different conditions (Deer et al., 1992). The pyroxene group includes orthorhombic [orthopyroxenes: $(Mg,Fe)SiO_3$] and monoclinic (clino) pyroxenes. The latter are members of the four-component system $CaMgSi_2O_6$-$CaFeSi_2O_6$-$Mg_3Si_2O_6$-$Fe_3Si_2O_6$.

Comprehensive studies of pyroxene compositions in sedimentary successions are considerably fewer than for garnet and chrome spinel, partly because of the unstable character of pyroxenes under weathering and diagenetic conditions. Chemical compositions of pyroxenes in their parent rocks are well-established for all parageneses, and this knowledge is an essential guide to the study of pyroxenes in derived sediments. General guides to pyroxene classification include the discrimination diagram of Poldervaart and Hess (1951) and the nomenclature of pyroxenes by Morimoto (1988). The work of Leterrier et al. (1982) on using clinopyroxene composition for the identification of palaeovolcanic magmatic affinities, and that of Nisbet and Pearce (1977) on clinopyroxene composition in mafic lavas from different tectonic settings are amongst the most frequently cited. Clinopyroxene data is traditionally plotted on the diagrams established by Poldervaart and Hess (1951), Nisbet and Pearce (1977) and Morimoto (1988). Important information is provided by Le Bas (1962) on the role of aluminium in igneous pyroxenes and their affinities to particular magma types.

Although many pyroxenes are removed from sediments by dissolution processes (weathering, diagenesis), they can be preserved in the sedimentary record. Geochemical analyses have highlighted their usefulness in the reconstruction of

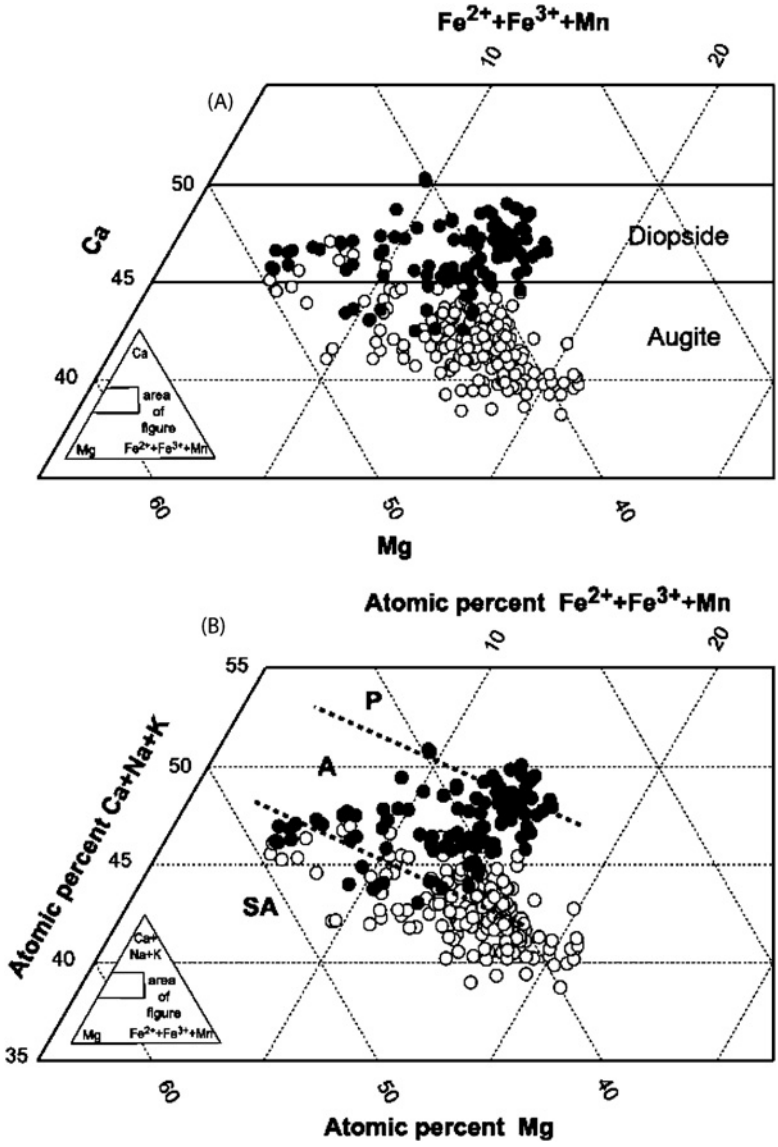

Fig. 15. Classification diagram for clinopyroxenes from sandstones in the Central Depression and Altiplano, Chile, using the scheme of Morimoto (1988). Open circles, Central Depression; filled circles, Altiplano (after Pinto et al., 2004). (A) Clinopyroxenes from the Central Depression (open circles) and Altiplano (filled circles). (B) Same data as in A, plotted on a discrimination diagram for subalkaline (SA), alkaline (A) and peralkaline (P) magma suites, using the discrimination scheme of Le Bas (1962).

geotectonic events, hinterland lithology and the provenance of the host sediment (e.g., Cawood, 1983, 1991a, b; Styles et al., 1989, 1995; Arai and Okada, 1991; Gieze et al., 1994; Acquafredda et al., 1997; Krawinkel et al., 1999; Lee and Lee, 2000; Pinto et al., 2004).

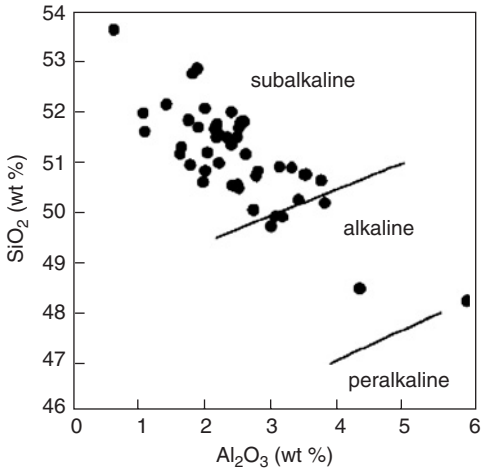

Fig. 16. Clinopyroxene compositions reflecting different tectonic settings. Plotting Al_2O_3 wt% against SiO_2 wt% enables clinopyroxenes from subalkaline, alkaline and peralkaline sources to be distinguished (after Lee and Lee, 2000).

Figs. 15 and 16 are examples of graphical presentations, drawn from publications by Pinto et al. (2004) and Lee and Lee (2000).

Determination of the crystal chemistry of pyroxenes is a fundamental part of the research on pyroxene-bearing rocks in a mosaic of plate boundary zones and in continental domains. Numerous publications provide templates for comparative work on pyroxenes in sedimentary basins. Cawood (1991a) shows a relevant example from the Tonga arc, where the geochemistry of pyroxenes in the volcaniclastic sediments furthered our understanding of the history of the New England Fold Belt complex in southeastern Australia. Cawood's petrographic and chemical analyses reveal that Miocene to Recent volcaniclastic sediments from the Tonga arc indicate derivation from a relatively uniform, low-K tholeiitic province. In the New England Fold Belt relict pyroxene compositions from the lower part of the stratigraphic pile suggest derivation from a transitional low-K to calc-alkaline source. By contrast volcaniclastic sediments deposited during the later stages of arc evolution indicate the emergence of a calc-alkaline to high-K tholeiite source.

Noda et al. (2004) integrated a range of methods, including sandstone petrography, modal analysis of conglomerate clasts and their major and trace element chemistry, chemical compositions of detrital pyroxene and garnet, and K-Ar geochronology to understand better the evolution of the Murihiku Terrane, New Zealand. This multi-method approach constrained its formation during the Middle Jurassic, while detrital clinopyroxene compositions indicated detritus from an island arc source.

Krawinkel et al. (1999) combined the techniques of sandstone petrography, heavy mineral analysis and clinopyroxene geochemistry of lithic sandstones in a comprehensive study of Middle Eocene to Late Neogene successions of the Azeuro-Soná Complex of NW Panama. The geochemistry of the pyroxenes enabled recognition of changing magma compositions of the clinopyroxene host rocks, thus adding further

constraints to sediment provenance and to palaeogeographic and plate tectonic reconstructions.

A similarly detailed and informative work is that of Pinto et al. (2004) on Neogene basins in the Central Andes. Clinopyroxene chemistry indicates that the volcanic sources of the successions in the Mauri and Corque basins of the Bolivian Altiplano had different degrees of magmatic differentiation and alkalinity, whereas the pyroxene-bearing host rocks which supplied sediments to the Central Depression in Chile were less differentiated. Markevich et al. (2007, this volume) showed how pyroxene geochemistry can illuminate discrimination, provenance and dispersal of tectonogenic sediments in the dynamic regimes surrounding the western Pacific subduction complexes. Schneiderman (1997) analysed detrital clinopyroxenes from the Nile and its delta, and was able to differentiate between clinopyroxenes shed from the Ethiopian highlands and those sourced by the Red Sea Hills on the basis of their chemistry. Pyroxene suites from the latter were identified by the presence of diopside, titaniferous augite and orogenic, high Ca, low Cr + Ti augite.

3.5. *Amphiboles*

Amphiboles constitute an extremely complex group of minerals that form in a variety of igneous and metamorphic rocks. They crystallise over a broad spectrum of P-T conditions, with a wide variation of chemical and physical properties (Leake, 1978; Deer et al., 1992; Mange and Maurer, 1992; Leake et al., 1997). The strong relationship between these properties and the conditions of crystallisation is displayed, in a limited way, by their optical properties but can be identified precisely by their chemistry. For allocation of individual members of the amphibole group, data are plotted on the diagrams defined in the amphibole nomenclature of the Subcommittee of Amphiboles (Leake, 1978; Leake et al., 1997). Preceding this nomenclature sodic amphibole analyses were plotted on the Miyashiro diagram (Miyashiro, 1957).

Members of the amphibole group are well represented in young detrital sediments and, being more stable than pyroxenes, are more frequently encountered in older strata. However, by contrast with pyroxenes, relatively few studies include a systematic, sequential analysis of the geochemistry of sedimentary amphiboles, especially calcic amphiboles. The standard optical practice relies on distinguishing orthorhombic amphiboles, the generally fibrous grains of the tremolite-ferroactinolite series, other amphiboles and, within the hornblende group colour varieties, such as green-brown, blue-green and deep-brown oxy-hornblende. More interest is paid to sodic amphiboles (blue amphiboles of the glaucophane-riebeckite series) because their paragenesis indicates high-pressure/low-temperature origin and exhumed subduction complexes.

The chemistry of detrital amphiboles from Palaeogene sediments in the southwest Rockall Plateau area (located south of Iceland and west of the British Isles) was determined by electron microprobe analysis by Morton (1991). These analyses permitted the differentiation of two distinct amphibole suites, associated with contrasting heavy mineral assemblages, signalling different source provinces. One suite that contains actinolite, actinolitic-hornblende and magnesio-hornblende, and is associated with epidote group minerals, including piemontite, points to a Greenland

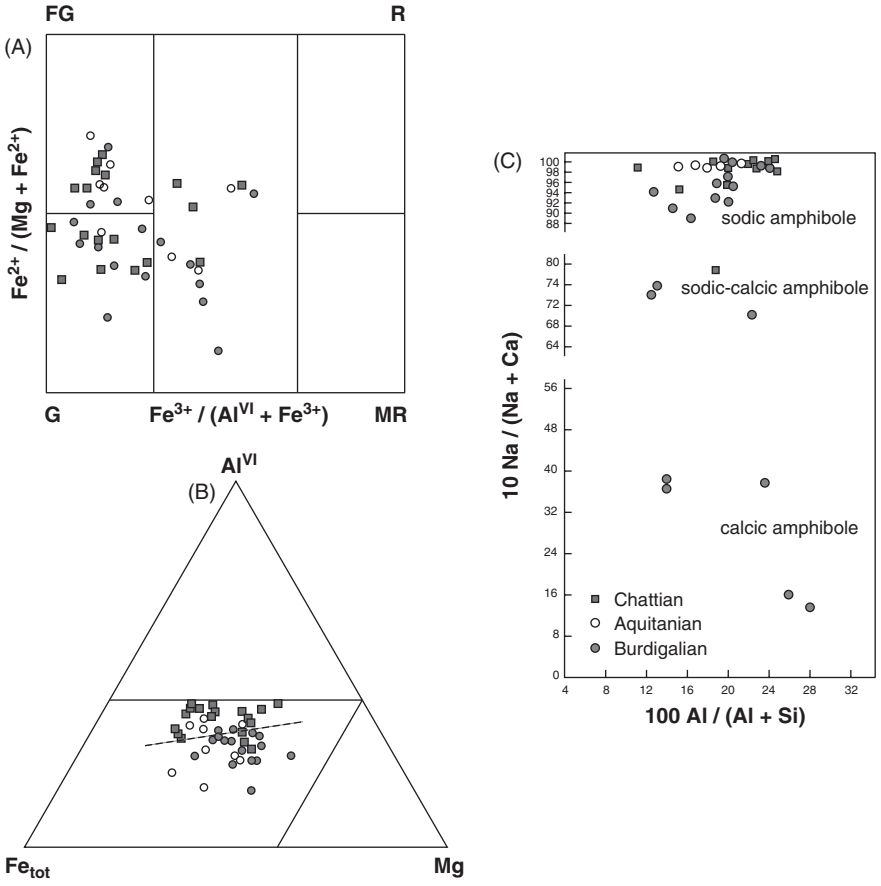

Fig. 17. Blue sodic amphibole, sodic-calcic amphibole and calcic amphibole compositions from the peri-Alpine Molasse Basin of France. Chattian blue amphiboles have dominantly glaucophane and ferroglaucophane compositions whereas Burdigalian amphiboles show sodic-calcic and calcic amphibole compositions (after Mange-Rajetzky and Oberhänsli, 1982). (A) Blue sodic amphibole compositions plotted on the Miyashiro diagram (FG = ferroglacophane, R = riebeckite, G = glaucophane, MR = magnesio-riebeckite). (B) Ternary plot showing the separation of blue sodic amphiboles from the Chattian and Burdigalian molasse. (C) Bivariate plot showing the age-related spread of blue sodic amphibole, sodic-calcic and calcic amphibole compositions.

provenance. The other suite contains an edenite and pargasite suite, and is found in association with clinopyroxene, garnet and apatite. Differences in geographical distribution suggest that the former suite was derived from southern Greenland, whereas the latter originated on the Rockall Plateau.

Schäfer (1996) and Schäfer et al. (1997) studied a large number of detrital amphiboles from Palaeozoic greywackes from the Erbendorf, Saxothuringian flysch, Germany. Integrated with other methods, their aim was to constrain exhumation at a Variscan active margin. The amphiboles, identified as magnesio- and tschermakitic hornblende, had a remarkably similar composition throughout. By comparing them

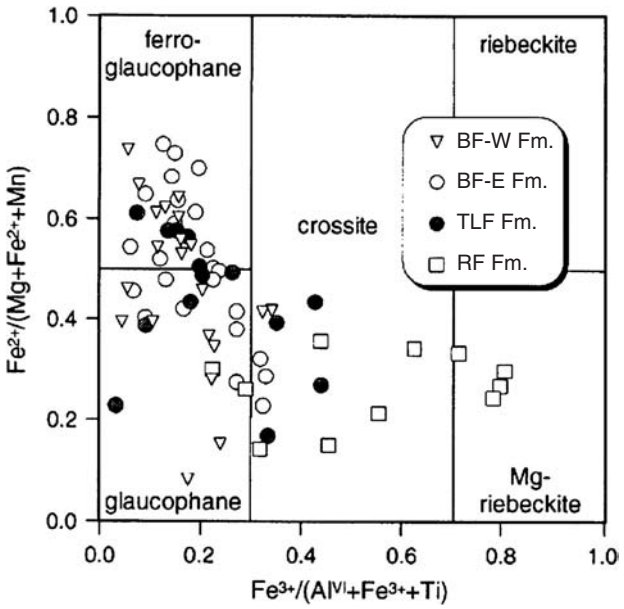

Fig. 18. Blue sodic amphiboles from Cretaceous synorogenic sandstones in the Eastern Alps plotted on the classification diagram of Leake (1978) (from Von Eynatten and Gaupp, 1999). BF-W, Branderfleck West Fm.; BF-E, Branderfleck East Fm.; TLF, Tannheim and Losenstein Fms; RF, Rossfeld Fm.

with amphiboles from neighbouring mafic rocks, they found a good correspondence with amphibolites of the Münchberg klippe to the northwest. These results were compatible with data achieved by other comparative geochemical methods (Schäfer, 1996).

Von Eynatten and Gaupp (1999), in a comprehensive study of the provenance of Cretaceous synorogenic successions in the Eastern Alps, determined the composition of several heavy mineral species, including green and brown calcic amphiboles whose chemistry reveals the presence of several members of the hornblende series and varying compositions within the tremolite-ferroactinolite series. Linking these amphibole suites to specific parent rocks greatly increased the resolution of provenance reconstruction. Durn et al. (2007, this volume; their Fig. 13) analysed calcic amphiboles from terra rossa in Istria, Croatia, to identify the different detrital input during terra rossa formation. Calcic amphibole chemistry also proved useful in geoarchaeology and helped to trace the source of temper in Roman ceramics (Freestone and Middleton, 1987).

Knowledge of the geotectonic evolution of the Hellenides is considerably augmented by studies of the detrital components of various tectonic units. Detrital blue sodic amphibole geochemistry from Palaeocene flysch in the western Othrys Mountain, Pelagonian Zone s.l. (Faupl et al., 2002), revealed that they were chemically comparable with blue amphiboles from the Cyclades. Their occurrence is consistent with the Cretaceous onset of blueschist facies metamorphism in parts of the Hellenides, especially in the Cycladic belt. Further details on the tectonic units of the Hellenides are provided by Faupl et al. (2007, this volume).

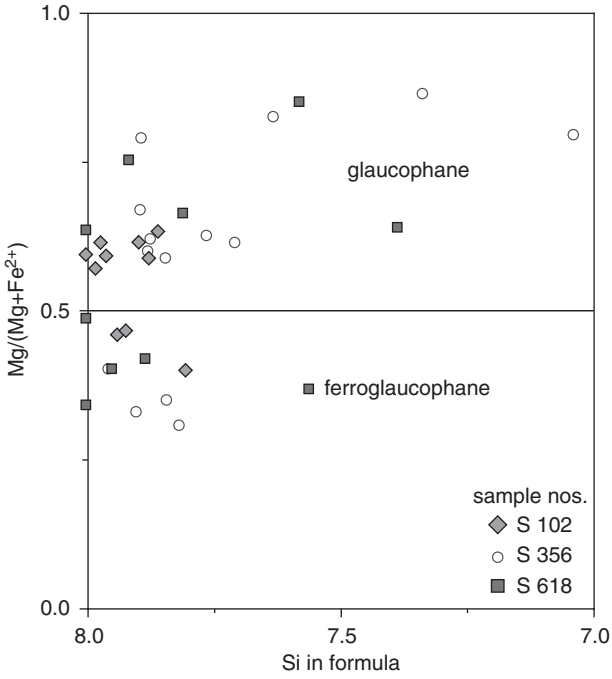

Fig. 19. Blue sodic amphibole compositions from the Ordovician Portpatrick Formation, Southern Uplands, Scotland, plotted on the classification diagram of Leake et al. (1997) (after Mange et al., 2005).

Acquafredda et al. (1997) analysed blue amphiboles from the southern Apennines, Ganssloser et al. (1996) from greywackes of the Harz Mountains and Mange-Rajetzky (1981) from southern Turkey. Mange-Rajetzky and Oberhänsli (1982) studied the chemistry of blue sodic amphiboles in the Peri-Alpine molasse, France. Systematic compositional changes of the blue amphiboles in successive Oligocene/Miocene lithostratigraphic units mirrored the exhumation and erosional unroofing of the products of different phases of high-pressure, low-temperature metamorphism in the Alpine internal zone. Al-rich glaucophane and ferro-glaucophane in Early Chattian sediments were formed during the eo-Alpine high-pressure phase, whereas Ca-bearing and Mg-rich crossite and glaucophane from the Burdigalian molasse were generated at a later stage, associated with more diverse metamorphic conditions. Changes in calcic amphibole compositions paralleled the trend of sodic amphiboles (Fig. 17).

Von Eynatten and Gaupp (1999) included analysis of blue sodic amphiboles from various stratigraphic units in their study of the Cretaceous sandstones in the Eastern Alps. Plots, using the classification scheme of Leake (1978), reveal the presence of a heterogeneous blue amphibole population (Fig. 18). Glaucophane, ferroglaucophane and crossite were well-represented and magnesio-riebeckite was also identified. The results shed new light on the exhumation of high-pressure rocks in the hinterland during, at least, Albian to Coniacian time. Von Eynatten and Gaupp (1999) also

concluded that blue amphiboles from the oldest formation were probably derived from different lithologies.

Amphibole geochemistry provided significant new data to the still imperfectly solved provenance of the Southern Uplands Terrane, Scotland (Mange et al., 2005). Blue amphiboles of glaucophane and ferroglaucophane composition, and newly discovered lawsonite in the Portpatrick Formation, defined blueschist derivation (Fig. 10 in Mange et al., 2005) (Fig. 19). Associated garnet in the same formation contains inclusions with sodic-calcic amphibole composition, prompting the authors to invoke a cryptic terrane for the provenance of these enigmatic detritus. The most likely source is Avalonia, which probably incorporated a Cadomian fragment, before collision with Laurentia.

3.6. *Apatite*

The value of apatite, $Ca_5(PO_4)_3(OH,F,Cl)$, as a provenance indicator has been relatively underplayed, for a variety of reasons. Firstly, apatite is a common accessory mineral in virtually all igneous and many metamorphic rocks (McConnell, 1973; Nash, 1984; Chang et al., 1998), and is therefore not an especially specific provenance indicator mineral. Secondly, its distribution in sandstones is commonly controlled by the extent of weathering during the sedimentary cycle, rather than provenance (Morton and Hallsworth, 1999). Thirdly, apatite shows only limited major element geochemical variations (Chang et al., 1998), confined to substitution of F (fluorapatite), Cl (chlorapatite) and OH (hydroxyapatite). This effectively precludes the use of conventional electron microprobe analysis in the acquisition of provenance-sensitive data. Consequently, until recently, the only varietal studies of apatite have dealt with its morphological properties. For instance, apatite morphology has proved useful as a tool for reservoir subdivision and correlation in Triassic sediments of the Irish Sea (Mange et al., 1999) and in Devonian to Carboniferous sandstones from the Clair oilfield, west of Shetland (Allen and Mange-Rajetzky, 1992; Morton et al., 2003b).

The recent advent of LA-ICPMS has enabled accurate determination of trace element abundances on single apatite grains. This has opened a new dimension to mineral-chemical provenance studies, because trace element abundances in apatite are known to be controlled by the composition of the host rock.

Several elements, such as Sr, Y, Mn, U, Th and the rare earth elements (REE), substitute for Ca in igneous apatite, usually in trace amounts (Nash, 1984; Ayers and Watson, 1993; Chang et al., 1998; Belousova et al., 2002b). Trace element abundances appear to be related to whole rock SiO_2 contents, indicating that the degree of host rock fractionation is a major control on apatite compositions in igneous rocks. For example, Y, Mn and the heavy rare earth elements (HREE) become relatively enriched during fractionation, whereas Sr becomes relatively depleted. Belousova et al. (2002b) proposed that apatite host rocks can be discriminated using binary plots of abundances of elements such as Sr-Y and Sr-Mn. The Th contents are also lower in highly fractionated rocks, possibly due to crystallisation of monazite, which removes Th and the light rare earth elements (LREE) from the melt (Belousova et al., 2002b). By contrast, U is more abundant in granites and granite pegmatites than in dolerites (Belousova et al., 2002b). Dill

(1994) suggested that the Th-U binary plot is a useful diagram for discrimination of provenance, and this may be partly due to the different behaviour of the two elements during fractionation.

The total REE abundances in apatite are controlled by the REE content of the host rock, the greatest REE contents being found in apatites from alkaline rocks (Chang et al., 1998; Belousova et al., 2002b). The shape of the chondrite-normalised REE pattern is also controlled by the host rock composition (Nash, 1984), in particular the degree of fractionation (Belousova et al., 2002b). Apatites from less-fractionated mafic rocks have strong relative LREE enrichment, whereas those from highly fractionated rocks, such as granite pegmatites, show relative LREE depletion. Belousova et al. (2002b) therefore proposed that $(Ce/Yb)_{cn}$ (where 'cn' denotes 'chondrite-normalised') is a useful index of host rock composition. Fleischer and Altschuler (1986) came to a similar conclusion, although they proposed the use of a different parameter $[(La + Ce + Pr)/\Sigma REE]$. Fleischer and Altschuler (1986) also showed that the gradient shown by the LREE is a useful discriminant of apatites from silicic and alkaline magmas. For example, apatites from granites and granite pegmatites have low La/Nd ratios, whereas those from alkaline rocks (including pegmatites) have high La/Nd ratios.

Many apatites have negative Eu anomalies on chondrite-normalised REE plots, being especially pronounced in more fractionated rocks. According to Budzinski and Tischendorf (1989), this is probably caused by feldspar crystallisation, which concentrates Eu^{2+} from the melt. Thus, Belousova et al. (2002b) propose that the magnitude of the Eu anomaly (Eu/Eu*) is another useful measure of host rock composition.

In two case studies investigating the application of apatite geochemistry in provenance studies, Morton and Yaxley (2007) show that the most useful discriminators of apatite provenance appear to be the La/Nd − $(La + Ce)/\Sigma REE$ plot proposed by Fleischer and Altschuler (1986) and the Th-U plot proposed by Dill (1994). The examples considered by Morton and Yaxley (2007) concern Pliocene sandstones of the South Caspian Basin and Devonian to Carboniferous sandstones of the Clair Oilfield, west of the Shetland Islands (off Scotland).

During the Pliocene, two major river systems, the palaeo-Kura and the palaeo-Volga, transported sediment into the western part of the South Caspian Basin (Baturin, 1947; Reynolds et al., 1998; Morton et al., 2003a). The palaeo-Kura drained the Lesser Caucasus mountain belt to the west, which mainly comprises mafic igneous (largely volcanic) rocks of both low-Ti (calc-alkaline) and high-Ti (alkaline) compositions, ophiolites and metamorphic rocks (Kazmin et al., 1986). The palaeo-Volga system had a much larger catchment area on the Russian Platform to the north, largely comprising Phanerozoic sediments that form the cover of the East European Craton, together with basement rocks, many of gneissic nature.

The apatite populations (Fig. 20) faithfully reflect the differences in lithology between these two source regions. The majority of palaeo-Kura apatites have moderate to high La/Nd and high $(La + Ce)/\Sigma REE$ ratios, falling in the fields defined by mafic/intermediate and alkaline host rocks, consistent with the widespread distribution of basic volcanic rocks of both alkaline and calc-alkaline compositions in the Lesser Caucasus. By contrast, the palaeo-Volga apatite populations include a large number of grains derived from silicic sources, characterised by low La/Nd and

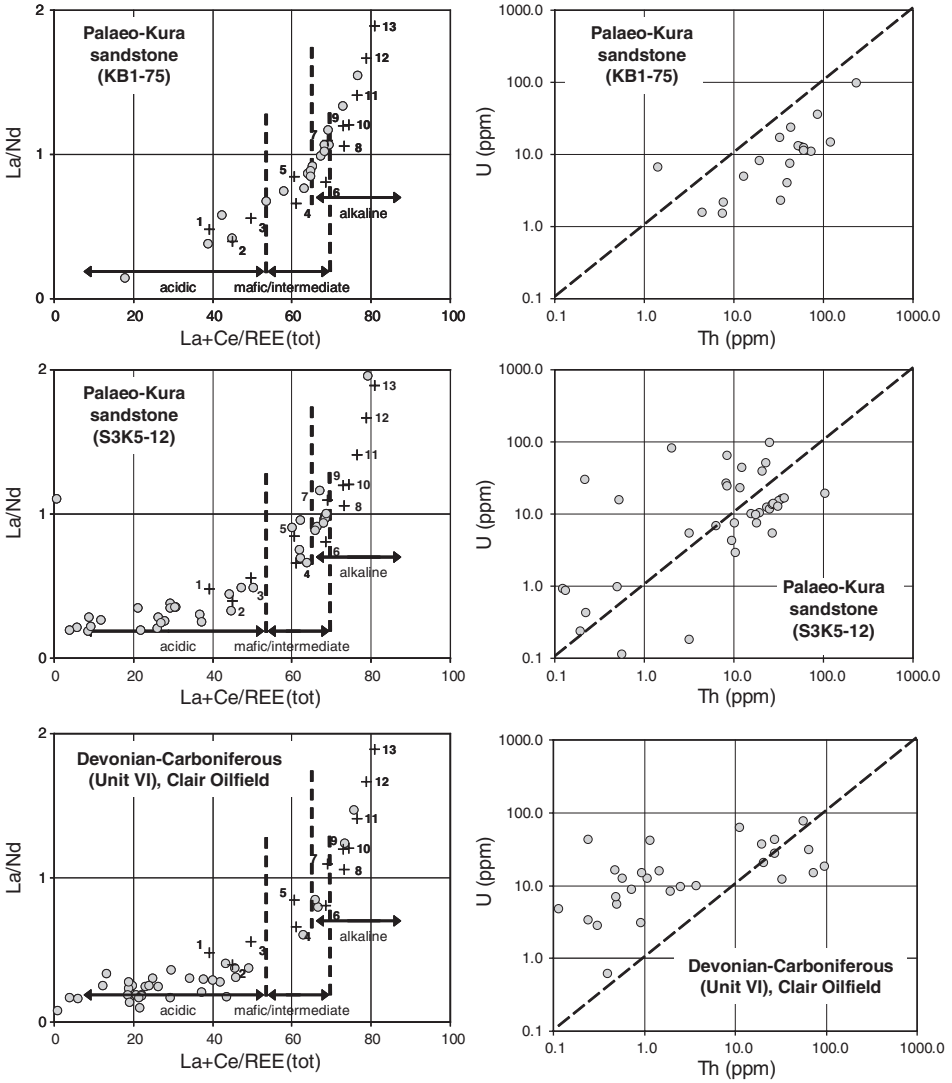

Fig. 20. Representative apatite populations in Pliocene sandstones of the South Caspian Basin and Devonian-Carboniferous sandstones of the Clair Oilfield plotted on the La/Nd – (La + Ce)/ΣREE classification diagram of Fleischer and Altschuler (1986) and the Th-U plot of Dill (1994), adapted from Morton and Yaxley (2007). 1, granite pegmatite; 2, gneiss/migmatite; 3, granite; 4, gabbro; 5, granodiorite; 6, kimberlite; 7, syenite; 8, alkali ultramafic; 9, carbonatite; 10, iron ores; 11, ultramafic; 12, alkaline; 13, alkaline pegmatite.

low (La + Ce)/ΣREE ratios. Apatites derived from alkaline host rocks (high La/Nd, high (La + Ce)/ΣREE ratios) are especially scarce in the palaeo-Volga sandstones. Virtually all the palaeo-Kura apatites have Th > U, consistent with the scarcity of highly-evolved rocks, such as granitoids, in the Lesser Caucasus. By contrast,

approximately 40–60% of the palaeo-Volga apatites have Th < U, indicating the widespread occurrence of acidic rocks, consistent with the evidence from the La/Nd – (La + Ce)/ΣREE plot. The greater diversity shown by the palaeo-Volga apatite populations reflects the larger size of the catchment area and the polycyclic nature of the sediment, which would inevitably have introduced sediment from a wide range of sources. The large number of apatites derived from highly evolved rocks indicates that the ultimate source of the palaeo-Volga sediment contained widespread granites and/or acidic gneisses, a typical feature of ancient cratonic basement terrains. The geochemistry of both the palaeo-Kura and the palaeo-Volga apatite populations contrasts markedly with that of the Devonian/Carboniferous sandstones from the Clair Oilfield. The great majority of Clair Field apatites have low La/Nd and low (La + Ce)/ΣREE ratios, thereby falling in the acidic field on the La/Nd – (La + Ce)/ΣREE plot (Fig. 20), with subsidiary intermediate/mafic apatites and very few of alkaline composition. Most of the apatites in Clair Field sandstones have U > Th (Fig. 20). These features combine to indicate that the source regions supplying sediment to the Clair Oilfield area during the Devonian and Carboniferous contained wide tracts of rocks with highly evolved (silicic) compositions.

Allen and Mange-Rajetzky (1992) and Nichols (2005) considered that Archaean gneisses of the Lewisian Complex (Hebridean Craton, Scotland) formed an important part of the source area for the Devonian to Carboniferous succession of the Clair Oilfield. The gneisses of the Lewisian Complex are predominantly tonalitic, trondhjemitic or granodioritic in composition, with subordinate granite gneiss sheets and lenses (Park et al., 2002). The apatite geochemical data are therefore consistent with derivation from Lewisian gneisses. However, it is also possible that the apatites were recycled from sediments ultimately derived from the Lewisian Complex, such as those forming the Proterozoic metasedimentary successions of northern Scotland (the Moine and Dalradian). These metasediments are also considered to be a potential source for the Clair succession (Allen and Mange-Rajetzky, 1992), and some contain a large amount of Archaean detritus (Cawood et al., 2003). It is also possible that younger (Proterozoic) basement complexes may also have been involved, either directly or indirectly.

Dill (1994), Belousova et al. (2002a) and Morton and Yaxley (2007) demonstrate that apatite geochemical data acquired by LA-ICPMS have considerable potential value for provenance reconstruction. The stability of apatite during deep burial (Morton and Hallsworth, 2007, this volume) makes the method applicable to diagenetically-modified sediment, which is a limiting factor for the large number of minerals that are unstable in the subsurface (notably pyroxene, amphibole and epidote). However, apatite is unstable under acid weathering conditions, and thus the method will be difficult to apply to sandstones that have undergone prolonged weathering during transport. The possible modification of the compositional range of apatite populations during weathering, by selective removal of the more unstable apatite varieties, may also be a factor. At present, unequivocal identification of provenance using apatite geochemistry is limited by the lack of a comprehensive database on apatite compositions in some of the potential source rocks, particularly those of metamorphic origin. Further work is therefore needed in order to improve the identification of prospective apatite source lithologies.

4. HEAVY MINERALS USED INFREQUENTLY FOR GEOCHEMICAL ANALYSIS

4.1. Chloritoid

Chloritoid [$(Fe^{2+},Mg,Mn)_2(Al,Fe^{3+})(OH)_4Al_3O_2(SiO_4)_2$] is an index mineral in two metamorphic parageneses, reflected in its crystal chemistry. It is most common in low-to-medium-grade metapelites which have a high Al and Fe content but occurs also in metasediments and metabasalts with ophiolitic affinities and in pelitic blueschists. Al-Fe chloritoid with additional Mn is characteristic of regionally-metamorphosed metapelites, whereas chloritoid appears in high-pressure rocks with a high Mg content (Chopin and Schreyer, 1983; Goffé and Bousquet, 1997). Such distinctive geochemistry implies that detrital chloritoid is a diagnostic provenance indicator. However, few heavy mineral studies include studies of chloritoid composition. Morton (1991) showed that chloritoids in the Early Jurassic Bridport Sands of Dorset, UK, have similar compositions to those from metapelites in the Ile de Groix in France, supporting the concept of a southerly source for these sediments (Davies, 1969). Nanayama (1997) included a small number of chloritoid analyses in a provenance study of Amazon fan sediments. Von Eynatten and Gaupp (1999), in their study of Cretaceous sandstones in the eastern Alps, used chloritoid geochemistry to infer derivation from blueschist facies rocks, and Lonergan and Mange-Rajetzky (1994) obtained evidence for the exhumation of the deepest part of the Internal Zone of the Betic Cordillera, Spain, from the appearance of high-Mg chloritoid in Langhian sediments (Fig. 21).

4.2. Epidote Group

Epidote minerals crystallise dominantly in regionally-metamorphosed rocks but also form in a wide variety of igneous parageneses, and they are also common in the sedimentary record. Compositionally they include zoisite and clinozoisite $[Ca_2Al_2O \cdot AlOH \cdot [Si_2O_7][SiO_4]$, epidote $[Ca_2Al_2O\ (Al,Fe^{3+})OH[Si_2O_7][SiO_4]$, piemontite $[Ca_2(Mn^{3+},Fe^{3+},Al)_3O \cdot OH[Si_2O_7][SiO_4]$ and allanite $[Ca,Mn,Ce,La,Y)_2$-$Fe^{2+},Fe^{3+},Ti)Al,\ Fe^{3+})_2O \cdot OH[Si_2O_7][SiO_4]$.

Because of their occurrence in a broad range of lithologies, they are not typically diagnostic of provenance. The stability of epidote minerals under burial diagenesis is higher than that of calcic amphiboles, andalusite and sillimanite but lower than that of titanite (Morton and Hallsworth, 2007, this volume).

Reports on the chemistry of epidote minerals in sediments appear only in few publications. Yokoyama et al. (1990) analysed epidotes from Neogene sediments of the Bengal fan, and detected limited compositional variations on the basis of $Fe^{3+}/(Al+Fe^{3+})$ ratios. However, they identified two distinctive zones, one characterised by the presence of zoisite, and another with a narrow range in $Fe^{3+}/(Al+Fe^{3+})$ ratios. These variations were ascribed to heterogeneity in the predominantly Himalayan source and to subordinate supply from the Indian subcontinent. Gieze et al. (1994) found that epidotes in Ordovician greywackes in the Rügen borehole on the Island of Rügen, Germany, have homogeneous compositions. Asiedu et al. (2000b) showed that epidotes in the Early Cretaceous Sasayama Group sandstones of SW

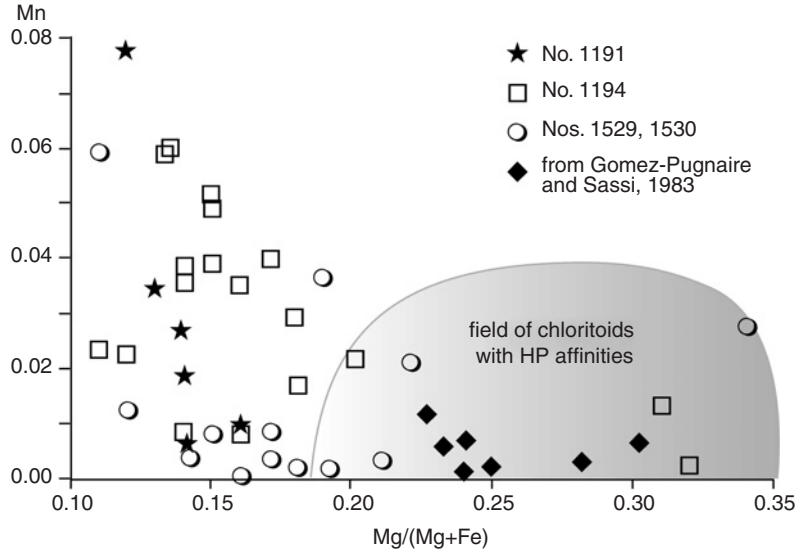

Fig. 21. Bivariate plot showing changing chloritoid compositions with the progressive exhumation of the internal zone of the Betic Cordillera, Spain. High-Mg chloritoids in the Burdigalian sandstones signal the exhumation of high-pressure rocks (after Lonergan and Mange-Rajetzky, 1994). Y axis shows ionic proportions on the basis of 14 O,OH. No. 1191, No. 1194, Nos. 1529, 1530 are sample numbers.

Japan have wide $Fe^{3+}/(Al+Fe^{3+})$ ratios and linked these to greenschist to epidote-amphibolite facies metamorphic rocks. Durn et al. (2007, this volume) analysed epidote group minerals from terra rossa on the island of Korčula (approximately 300 km SE of Istria, Croatia). These epidotes fall in a relatively narrow compositional range, with $Fe^{3+}/(Al+Fe^{3+})$ ratios ranging from 0.239 to 0.157, suggesting low-grade metamorphic source complexes.

Although traditional microprobe analyses yield informative data for the chemical characterisation of epidote minerals, tracing epidote assemblages to their potential parent rocks has limitations. Epidotes with similar compositions appear in a wide spectrum of rock types, and so may be delivered from geologically different source regions. When such sediments become intermixed, for example, in large fluvial systems or on continental shelves, they lose their provenance identity. This problem was addressed in a study of detrital epidotes from sandstones of the Swiss molasse basin by Spiegel et al. (2002), which integrated isotopic and trace element compositions of epidotes with zircon fission track data. This approach therefore combined information from zircon, which is generally sourced from silicic parentages, and from epidote, which is more common in basic lithologies that are difficult to date because they are generally poor in zircon and white mica. The study used Nd and Sr isotopic data to differentiate between different types of epidote-bearing source parageneses, and in particular to find out whether they were eroded from crust- or mantle-derived rocks. Spiegel et al. (2002) proved that crustal and mantle source rocks could be clearly distinguished by Nd and Sr data of detrital epidote grains,

which permitted the refinement of the exhumation history of the Oligo/Miocene Central Alps.

4.3. Staurolite

Staurolite $\{(Fe^{2+},Mg,Zn)_2(Al,Fe^{3+},Ti)_9O_6[(Si,Al)O_4]_4(O,OH)_2\}$ normally forms in Al-rich metapelites, but can occur also in metasediments of other compositions, such as metapsammites, under suitable conditions (Hoschek, 1967; Wallace, 1975; Deer et al., 1997). Kepezhinskas and Koryluk (1973) noted that there are variations in staurolite composition related to changing metamorphic environments, expressed by the ratio $(Fe^{2+} + Mn + Fe^{3+})/(Fe^{2+} + Mn + Fe^{3+} + Mg)$, which they termed 'ferruginosity'. Despite the evidence for compositional variations in staurolite related to metamorphic grade, detrital staurolite geochemistry has been rarely applied to provenance analysis. Morton (1991) reported regional and stratigraphic variations in staurolite chemistry, both in terms of Fe/Mg ratio and Zn contents, in North Sea sediments, reflecting changes in provenance. Nanayama (1997) included a small number of staurolite analyses in a provenance study of Amazon fan sediments. Acquafredda et al. (1997) analysed staurolite compositions in Plio/Pleistocene sediments of the southern Apennines, and showed that their compositions were comparable to those in their presumed source rocks.

4.4. Rutile

Rutile (TiO_2) is one of the ultrastable minerals and commonly occurs both in ancient and young sediments. In hard rocks it is widely distributed as an accessory mineral in magmatic and metamorphic parageneses. Zack et al. (2002) used electron microprobe and laser ablation microprobe data for a range of high-field strength and other trace elements in rutile from eclogites and garnet-mica schists from the Central Alps with the view of developing a useful provenance tracer. Their results indicate that trace element contents of detrital rutile grains have the potential to be used as a powerful tool for sedimentary provenance studies because they reflect the key element ratios (especially Nb/TiO_2 and Cr/TiO_2) of their source rocks. This may help to distinguish between sources of high-grade metamorphics, eclogites and high-pressure granulites from hydrothermal ore deposits and kimberlites.

In a follow-up study, Zack et al. (2004) discussed the use of rutile chemistry in quantitative provenance studies. Since rutile is one of the most stable detrital mineral, extracting geochemical information from it is of great importance, especially in the study of mature sediments that have been depleted in more diagnostic but less stable minerals. Zack et al. (2004) showed that input from the two principal sources of rutile (metapelites and metabasites) can be distinguished on the basis of their Nb and Cr contents. They also showed that Zr in metapelitic rutile, where it coexists with zircon and quartz, is extremely temperature dependent, indicating that the Zr content can be used to measure maximum metamorphic temperatures. This single-grain geothermometer is believed to be the first of its kind to be used in provenance studies.

Rutile compositions were analysed from hydrocarbon reservoirs in Triassic continental red-beds in the Beryl Field, North Sea, by Preston et al. (1998).

Combined with the geochemistry of garnet, chrome spinel and trace element data, they aimed at developing a method for subdividing and correlating biostratigraphically barren successions by geochemical fingerprinting. Detrital rutile compositions in the study well (Well 19/13a-S48) showed a considerable homogeneity (Fig. 22) being almost pure TiO_2 with only a small proportion containing appreciable Nb_2O_5 or FeO. The common presence of Nb-rich and Nb-poor rutiles in a single assemblage indicates that these grains are independent of size and/or hydraulic controls.

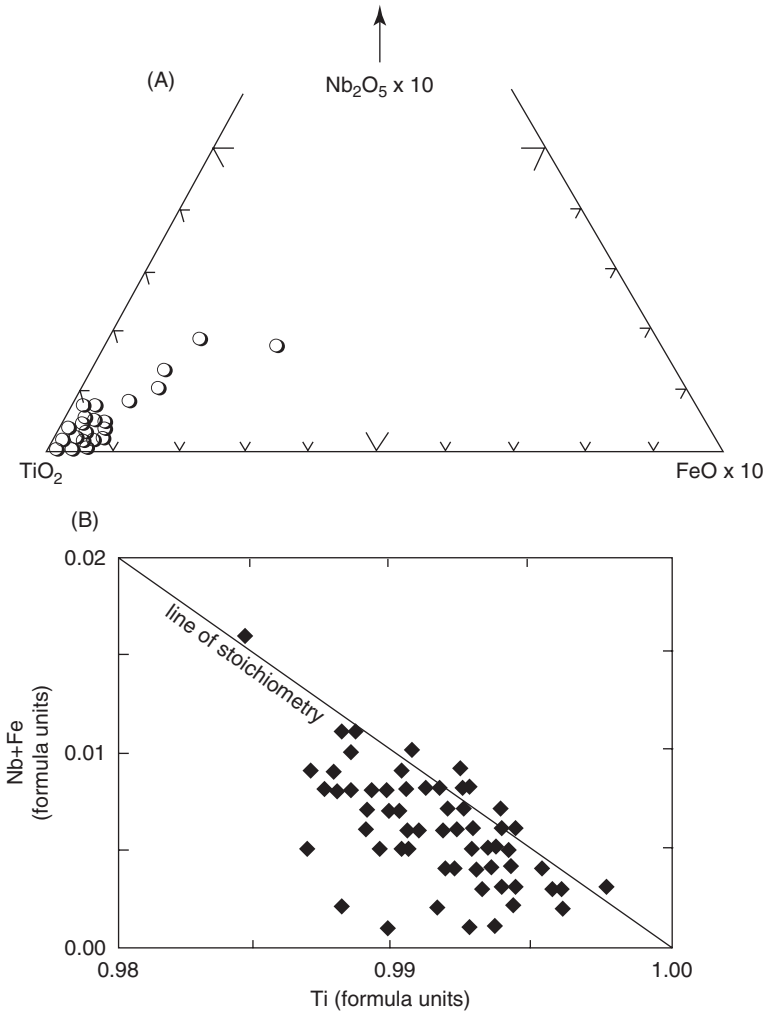

Fig. 22. Detrital rutile compositions from the Triassic red beds of the Beryl Field, North Sea, UK. (A) The majority of rutile grains fall into the almost pure TiO_2 field but a small portion shows higher Nb_2O_5 or FeO content. (B) Nb-poor rutile plotted along the line of stoichiometry, defined by the substitution scheme $3Ti^{4+} \rightleftharpoons 2NbO^{5+} + Fe^{2+}$. Deviation from this line indicates the presence of very small amounts of other trace elements such as Cr or Al (after Preston et al., 1998).

4.5. Monazite

Monazite [(Ce, Ld, Nd, Th)PO_4] occurs in silicic igneous rocks and in regionally metamorphosed argillaceous sediments (Overstreet, 1967; Nash, 1984; Chang et al., 1998), and compositional variations are reported to be related to paragenesis. Monazite crystals typically contain distinct compositional domains, many in the order of 5–10 μm, representing successive generations of mineral growth, which record details of the geological history of its host rocks. The electron microprobe can be used to characterise the geometry and quantitative composition of domains. In igneous rocks, the degree of LREE enrichment is related to host rock composition, with alkaline igneous rocks and carbonatites having much higher La/Nd ratios than granites and granite pegmatites (Fleischer and Altschuler, 1969). In metapelites, the ThO_2 content is generally related to metamorphic grade, the lowest values found in greenschist facies rocks, increasing through amphibolite facies, with the highest values found in the granulite facies (Overstreet, 1967). There may also be a relationship between temperature and Y content in monazite, with Y_2O_3 forming as much as 5% of high temperature monazites (Jonasson et al., 1988). However, these general observations are not always upheld: for instance, there is no relationship between metamorphic grade and Th content in metapelites of the eastern Mojave Desert, USA (Kingsbury et al., 1993).

Despite the evidence for variations in composition related to paragenesis, there have been remarkably few studies that relate detrital monazite composition to provenance. The obvious exception to this is the use of Th, U and Pb contents to date both detrital and secondary monazite in sediments using the CHIME (chemical Th-U-total Pb) method (e.g., Suzuki et al., 1991; Kusiak et al., 2006, and papers cited therein). However, geochronological methods (CHIME, together with conventional and microbeam U-Pb dating of monazite) are beyond the scope of this review.

4.6. Zircon

Zircon ($ZrSiO_4$) forms in a wide variety of igneous and metamorphic rocks, although it is most abundant in silicic igneous rocks such as granitoids. In provenance analysis, studies that concentrate on zircon almost exclusively concern single-grain U-Pb dating using techniques such as the SHRIMP or the LA-ICPMS. This geochronological approach is beyond the scope of this review: for further information, the reader is referred to Fedo et al. (2003). However, zircon displays variations in trace element contents that are believed to reflect host rock composition (Heaman et al., 1990; Hoskin and Ireland, 2000; Belousova et al., 2002a), and such variations have potential applications in provenance studies. The most significant variations are believed to be with the REE, but other trace elements such as U, Th, Y, Nb, Ta and Sc are also believed to have discriminatory potential. Owen (1987) proposed that Hf contents in detrital zircons could be used to discriminate provenance.

Heaman et al. (1990), in a study based on a relatively small data set, provided evidence that zircons from a variety of host rocks could be distinguished on the basis of Lu, Sc, Th/U, Lu/Sm and Hf. Belousova et al. (2002a) proposed that the total REE content increases from ultramafic, through mafic, to silicic whole rock

compositions. In addition, there are variations in the REE patterns: zircons from carbonatites and kimberlites have relatively flat chondrite-normalised REE patterns, whereas those from granites and pegmatites show strong LREE depletion. A similar relationship was observed by Hoskin and Ireland (2000), who showed that mantle-derived and crust-derived zircons have different REE contents and patterns. However, their work suggested that it is not possible to discriminate between zircons from different crustal rock types. Metamorphic zircons can be distinguished from those of igneous origin on the basis of Th/U ratios, since magmatic zircons have Th/U ratios between 0.2 and 1.5, much higher than in metamorphic rocks, where the Th/U ratio is in the range 0.001–0.1 (Vavra et al., 1999; Hartmann et al., 2000). In a study of detrital zircons sourced from the Brazilian Shield, however, Hartmann and Santos (2004) showed that zircons from metamorphic sources are strongly under-represented, a fact that they attributed to preferential loss through abrasion during transport. For a detailed review of the composition of zircon in igneous and metamorphic rocks, the reader is referred to Hoskin and Schaltegger (2003).

In a provenance study of Carboniferous sandstones in the Pennine Basin, UK, Hallsworth et al. (2000) observed that zircons in the westerly-derived Clifton Rock had significantly lower U and Th contents than sandstones shed from the south (Dalton Rock, Halesowen Formation) or from the north (Rough Rock, Ashover Grit and pre-Marsdenian sandstone), as shown in Fig. 23. Zircons with high U and Th contents are more liable to become metamict (i.e., to have their crystal structure compromised), since they suffer a higher radiation dose through the emission of α particles (Holland and Gottfried, 1955). Metamict zircons are much more liable to dissolution during weathering compared with non-metamict grains (Balan et al., 2001), and are also more likely to be mechanically unstable. Hallsworth et al. (2000) suggested that the low U and Th contents in the Clifton Rock resulted from a polycyclic history, with repeated episodes of weathering and transport, leading to loss of zircons with high U and Th contents. The possible relationship between zircon composition and sediment maturity is a topic worthy of further investigation.

4.7. Ilmenite

Ilmenite ($FeTiO_3$) has long been the focus of geochemical analyses because it is one of the most important constituents of economic heavy mineral deposits (Pownceby, 2005; Pownceby and Bourne, 2006; Pirkle et al., 2007, this volume, and references therein). The chemistry of ilmenite and its trace element compositions for decoding petrogenetic signatures and provenance fingerprinting have been tested by Darby (1984), Darby and Tsang (1987), Grigsby (1991) and Asiedu et al. (2000a). Basu and Molinaroli (1991) found that ilmenite grains with TiO_2 contents between 50 and 60 wt% are more prevalent in metamorphic rocks, but they also occur in igneous rocks ranging in between 40 and 50 wt%. Schneiderman (1995) noted that ilmenite from metamorphic sources is richer in TiO_2 than ilmenite in igneous rocks. She also used detrital pyroxenes and ilmenite as provenance and palaeoclimate indicators in Nile delta deposits.

Schroeder et al. (2002) carried out a detailed investigation of the phases of ilmenite weathering in weathering profiles on granite and ultramafic chlorite schist for evidence of morphological and chemical alteration. Ilmenite grains in the schist

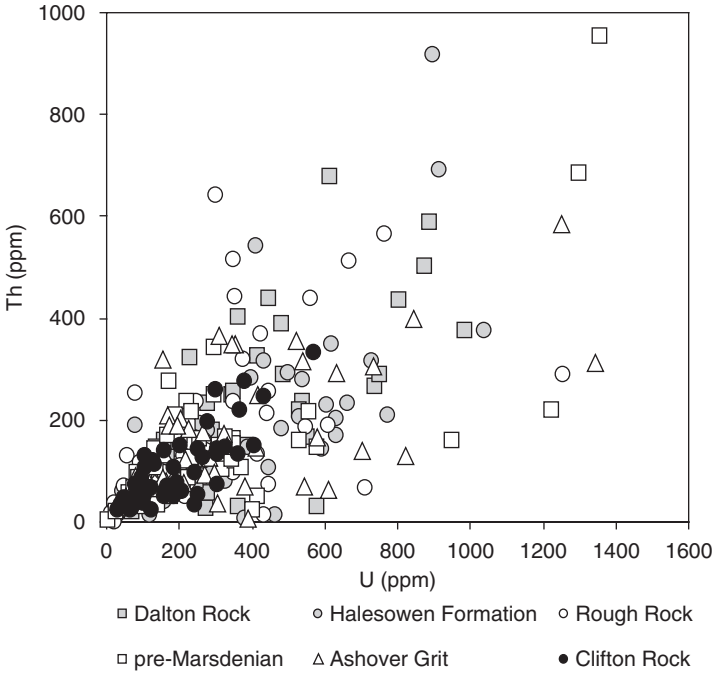

Fig. 23. U and Th contents of detrital zircons from Carboniferous sandstones of the Pennine Basin, UK (from Hallsworth et al., 2000).

profile occur as fractured anhedral grains with uncommon lamellae of rutile. Ilmenite from the granite profile is rich in Mn, which was also reported by Grigsby (1991) and Asiedu et al. (2000a). Ilmenite from the schist profile contained minor amounts of Mn. They recognised the development of two distinct grain populations, characteristic for each profile, and concluded that using ilmenite minor-element chemistry as a tracer for sediment provenance is a valid technique, but they also cautioned that textural features of ilmenite in colluvium may be distinct from those in the parent rock. Secondary phases, such as anatase, goethite and hematite in soil profiles form, in part, from the alteration of ilmenite. The significance of ilmenite chemistry in diamond exploration is reviewed by Nowicki et al. (2007, this volume).

ACKNOWLEDGEMENTS

We are grateful to CASP for permission to show garnet geochemical data from sample WG95/1. We extend our thanks to Sarah Roeske, John Dewey and Dave Wright for carefully reviewing and commenting on earlier versions of the manuscript.

REFERENCES

Acquafredda, P., Fornelli, A., Piccarreta, G., Summa, V., 1997. Provenance and tectonic implications of heavy minerals in Pliocene-Pleistocene siliciclastic sediments of the southern Apennines, Italy. Sedimentary Geology 113, 149–159.

Allen, P.A., Mange-Rajetzky, M.A., 1992. Sedimentary evolution of the Devonian-Carboniferous Clair Field, offshore northwestern UK: impact of changing provenance. Marine and Petroleum Geology 9, 29–52.

Arai, S., 1992. Chemistry of chromian spinel in volcanic rocks as a potential guide to magma chemistry. Mineralogical Magazine 56, 173–184.

Arai, S., Kadoshima, K., Manjoorsa, M.V., David, C.P., Kida, M., 1997. Chemistry of detrital chromian spinels as an insight into petrological characteristics of their source peridotites: an example from the Ilocos Norte ophiolite, northern Luzon, Philippines. Journal of Mineralogy, Petrology, Economic Geology 92, 137–141.

Arai, S., Kadoshima, K., Morishite, T., 2006. Widespread arc-related melting in the mantle section of the northern Oman ophiolite as inferred from detrital chromian spinels. Journal of the Geological Society of London 163, 869–879.

Arai, S., Okada, H., 1991. Petrology of serpentine sandstone as a key to tectonic development of serpentine belts. Tectonophysics 195, 65–81.

Árgyelán, G.B., 1996. Geochemical investigations of detrital chrome spinels as a tool to detect an ophiolitic source area (Gerecse Mountains, Hungary). Acta Geologica Hungarica 39, 341–368.

Asiedu, D.K., Suzuki, S., Shibata, T., 1998. Compositions of detrital spinels from Lower Cretaceous Sasayama Group Hyogo Prefecture, Japan: constraints on source lithology and tectonic setting. Journal of Mineralogy, Petrology, Economic Geology 93, 27–41.

Asiedu, D.K., Suzuki, S., Shibata, T., 2000a. Provenance of sandstones from the Wakino Subgroup of the Lower Cretaceous Kanmon Group, northern Kyushu, Japan. The Island Arc 9, 128–144.

Asiedu, D.K., Suzuki, S., Shibata, T., 2000b. Provenance of sandstones from the Lower Cretaceous Sasayama Group, Inner Zone of Southwest Japan. Sedimentary Geology 131, 9–24.

Aubrecht, R., Kristin, J., 1995. Provenance of detrital tourmaline in the Lower Jurassic of the Male Karpaty Mtns. Mineralia Slovaca 27, 37–44.

Ayers, J.C., Watson, E.B., 1993. Solubility of apatite, monazite, zircon, and rutile in supercritical aqueous fluids with implications for subduction zone geochemistry. Philosophical Transactions of the Royal Society, London, Series A 335, 365–375.

Balan, E., Neuville, D.R., Trocellier, P., Fritsch, E., Muller, J.-P., Calas, G., 2001. Metamictization and chemical durability of detrital zircon. American Mineralogist 86, 1025–1033.

Barnes, S.J., Roeder, P.L., 2001. The range of spinel compositions in terrestrial mafic and ultramafic rocks. Journal of Petrology 42, 2279–2302.

Basu, B., Molinaroli, E., 1991. Reliability and application of detrital opaque Fe-Ti oxide minerals in provenance determination. In: Morton, A.C., Todd, S.P., Haughton, P.D.W. (Eds.), Developments in Sedimentary Provenance Studies, vol. 57. Geological Society of London Special Publication, pp. 55–65.

Baturin, V.P., 1947. Petrographical analysis of the geological past using terrigene components. Academy of Science, USSR (in Russian).

Belousova, E.A., Griffin, W.L., O'Reilly, S.Y., Fisher, N.I., 2002a. Igneous zircon: trace element composition as an indicator of source rock type. Contributions to Mineralogy and Petrology 143, 602–622.

Belousova, E.A., Griffin, W.L., O'Reilly, S.Y., Fisher, N.I., 2002b. Apatite as an indicator mineral for mineral exploration: trace-element compositions and their relationship to host rock type. Journal of Geochemical Exploration 76, 45–69.

Brammall, A., 1928. Dartmoor detritals: a study in provenance. Proceedings of the Geologists Association 39, 27–48.

Budzinski, H., Tischendorf, G., 1989. Distribution of REE among minerals in the Hercynian postkinematic granites of Westerzgebirge-Vogtland, GDR. Zeitschrift für Geologische Wissenschaften 17, 1019–1031.

Carter, A., 2007. Heavy minerals and detrital fission-track thermochronology. In: Mange, M.A., Wright, D.T. (Eds.), Heavy Minerals in Use. Developments in Sedimentology (this volume).

Cawood, P.A., 1983. Modal composition of detrital clinopyroxene geochemistry of lithic sandstones from the New England Fold Belt (east Australia): a Palaeozoic terrane forearc. Geological Society of America Bulletin 94, 1199–1214.

Cawood, P.A., 1991a. Characterisation of intra-oceanic magmatic arc source terranes by provenance studies of derived sediments. New Zealand Journal of Geology and Geophysics 34, 347–358.

Cawood, P.A., 1991b. Nature and record of igneous activity in the Tonga arc, SW Pacific, deduced from the phase chemistry of derived detrital grains. In: Morton, A.C., Todd, S.P., Haughton, P.D.W. (Eds.), Developments in Sedimentary Provenance Studies, vol. 57. Geological Society of London Special Publication, pp. 305–321.

Cawood, P.A., Nemchin, A.A., Smith, M., Loewy, S., 2003. Source of the Dalradian Supergroup constrained by U-Pb dating of detrital zircon and implications for the East Laurentian margin. Journal of the Geological Society of London 160, 231–246.

Chang, L.L.Y., Howie, R.A., Zussman, J., 1998. Rock-forming minerals, volume 5B: Non-silicates: Sulphates, Carbonates, Phosphates and Halides, 2nd ed. Geological Society, London, 383pp.

Chopin, C., Schreyer, W., 1983. Magnesiocarpholite and magnesiochloritoid: two index minerals of pelitic blueschists and their preliminary phase relations in the model system MgO-Al_2O_3-SiO_2-H_2O. American Journal of Science 283-A (Orville volume), 72–96.

Cookenboo, H.O., Bustin, R.M., Wilks, K.R., 1997. Detrital chromian spinel compositions used to reconstruct the tectonic setting of provenance: implication for orogeny in the Canadian Cordillera. Journal of Sedimentary Research 67, 116–123.

Coombs, D.S., Kawachi, Y., Houghton, B.F., Hyden, G., Pringle, I.J., Williams, J.G., 1973. Andradite and andradite-grossular solid solutions in very low grade regionally metamorphosed rocks in southern New Zealand. Contributions to Mineralogy and Petrology 63, 229–246.

Čopjaková, R., Sulovský, P., Paterson, B.A., 2005. Major and trace elements in garnets from Variscan Moldanubian felsic granulites as sediment provenance indicators, Lithos 82, 51–70.

Corfu, F., 2001. Zircon, the petrogenetic messenger: how well do we understand its message? Eleventh Annual V.M. Goldschmidt Conference. Abstract.

Corfu, F., Hanchar, J.M., Hoskin, P.W.O., Kinny, P., 2003. Atlas of zircon textures. In: Hanchar, J.M., Hoskin, P.W.O. (Eds.), Zircon: Reviews in Mineralogy and Geochemistry, vol. 53. Mineralogical Society of America, pp. 469–500.

Darby, D.A., 1984. Trace elements in ilmenite: a way to discriminate provenance or age of coastal sands. Geological Society of America Bulletin 95, 1208–1218.

Darby, D.A., Tsang, Y.W., 1987. Variation in ilmenite element composition within and among drainage basins: implications for provenance. Journal of Sedimentary Petrology 57, 831–838.

Dasgupta, S., Pal, S., 2005. Origin of grandite garnet in calc-silicate granulites: mineral–fluid equilibria and petrogenetic grids. Journal of Petrology 46, 1045–1076.

Davies, D.K., 1969. Shelf sedimentation: an example from the Jurassic of Britain. Journal of Sedimentary Petrology 37, 1344–1370.

Deer, W.A., Howie, R.A., Zussman, J., 1992. The Rock-Forming Minerals. Longman, London, 696pp.

Deer, W.A., Howie, R.A., Zussman, J., 1997. Rock-forming minerals, volume 1A: Orthosilicates (2nd ed.). Geological Society, London, 919pp.

Dewey, J., Mange, M., 1999. Petrography of Ordovician and Silurian sediments in the Western Irish Caledonides: tracers of a short-lived Ordovician continent-arc collision orogeny and the evolution of the Laurentian Appalachian/Caledonian margin. In: Mac Niocaill, C., Ryan, P.D. (Eds.), Continental Tectonics, vol. 164. Geological Society of London Special Publication, pp. 55–107.

Dick, H.J.B., Bullen, T., 1984. Chromian spinel as a petrogenetic indicator in abyssal and alpine-type peridotites and spatially associated lavas. Contributions to Mineralogy and Petrology 86, 54–76.

Dill, H.G., 1994. Can REE patterns and U–Th variations be used as a tool to determine the origin of apatite in crustal rocks? Sedimentary Geology 92, 175–196.

Droop, G.T.R., Harte, B., 1995. The effect of Mn on the phase relations of medium grade pelites: constraints from natural assemblages on petrogenetic grid topology. Journal of Petrology 36, 1549–1578.

Durn, G., Aljinović, D., Crnjaković, M., Bocko Lugović, B., 2007. Heavy and light fractions indicate polygenesis of extensive terra rossa soils in Istria, Croatia. In: Mange, M.A., Wright, D.T. (Eds.), Heavy Minerals in Use. Developments in Sedimentology (this volume).

Faupl, P., Pavlopoulos, A., Migiros, G., 2007. Provenance of flysch sediments and the Palaeogene—Early Miocene geodynamic evolution of the Hellenides: a contribution from heavy mineral investigations. In: Mange, M.A., Wright, D.T. (Eds.), Heavy Minerals in Use. Developments in Sedimentology (this volume).

Faupl, P., Petrakakis, K., Migiros, G., Pavlopoulos, A., 2002. Detrital blue amphiboles from the western Othrys Mountain and their relationship to the blueschist terrains of the Hellenides (Greece). International Journal of Earth Sciences (Geologische Rundschau) 91, 433–444.

Fedo, C.M., Sircombe, K.N., Rainbird, R.H., 2003. Detrital zircon analysis of the sedimentary record. In: Hanchar, J.M., Hoskin, P.W.O. (Eds.), Zircon: Reviews in Mineralogy and Geochemistry, vol. 53. Mineralogical Society of America, pp. 277–303.

Fitton, J.G., 1972. The genetic significance of almandine-pyrope phenocrysts in the calc-alkaline Borrowdale Volcanic Group, northern England. Contributions to Mineralogy and Petrology 36, 231–248.

Fleischer, M., Altschuler, Z.S., 1969. The relationship of the rare-earth element composition of minerals to geological environment. Geochimica et Cosmochimica Acta 33, 725–732.

Fleischer, M., Altschuler, Z.S., 1986. The lanthanides and yttrium in minerals of the apatite group—an analysis of the available data. Neues Jahrbuch für Mineralogie, Monatshefte 10, 467–480.

Freestone, I.C., Middleton, A.P., 1987. Mineralogical applications of the analytical SEM in Archaeology. Mineralogical Magazine 51, 21–31.

Ganssloser, M., 1999. Detrital chromian spinels in Rhenohercynian greywackes and sandstones (Givetian-Visean, Variscides, Germany) as indicators of ultramafic source rocks. Geological Magazine 136, 437–451.

Ganssloser, M., Theye, T., Wachendorf, H., 1996. Detrital glaucophane in graywackes of the Rhenohercynian Harz Mountains and the geodynamic implications. Geologische Rundschau 85, 755–760.

Gieze, U., Katzung, G., Walter, R., 1994. Detrital composition of Ordovician sandstones from the Rügen boreholes: implications for the evolution of the Tornquist Ocean. Geologische Rundschau 83, 293–308.

Goffé, B., Bousquet, R., 1997. Ferrocarpholite, chloritoid and lawsonite in metapelites of the Versoyen and Petit St. Bernard units (Valaisan zone, Western Alps). Schweizerische Mineralogische und Petrographische Mitteilungen 77, 137–147.

Green, T.H., Ringwood, A.E., 1968. Origin of garnet phenocrysts in calc-alkaline rocks. Contributions to Mineralogy and Petrology 16, 59–67.

Grigsby, J.D., 1991. Chemical fingerprinting in detrital ilmenite: a viable alternative in provenance research? Journal of Sedimentary Petrology 62, 331–337.

Grzebyk, J., Leszczyński, S., 2006. New data on heavy minerals from the Upper Cretaceous-Paleogene flysch of the Beskid Slaski Mts. (Polish Carpathians). Geological Quarterly 50, 265–280.

Hallsworth, C.R., Livingstone, A., Morton, A.C., 1992. Detrital goldmanite from the Palaeocene of the North Sea. Mineralogical Magazine 56, 117–120.

Hallsworth, C.R., Morton, A.C., Claoué-Long, J.C., Fanning, C.M., 2000. Carboniferous sand provenance in the Pennine Basin, UK: constraints from heavy mineral and SHRIMP zircon age data. Sedimentary Geology 137, 147–185.

Hamer, R.D., Moyes, A.B., 1982. Composition and origin of garnet from the Antarctic Peninsula Volcanic Group of Trinity Peninsula. Journal of the Geological Society of London 139, 713–720.

Hartley, A.J., Otava, J., 2001. Sediment provenance and dispersal in a deep marine foreland basin: the Lower Carboniferous Culm Basin, Czech Republic. Journal of the Geological Society of London 158, 137–150.

Hartmann, L.A., Leite, J.A.D., Silva, I.C., Remus, M.V.D., McNaughton, N.J., Groves, D.J., Fletcher, I.R., Santos, J.O.S., Vasconce-Ilos, M.A.Z., 2000. Advances in SHRIMP geochronology and their impact on understanding the tectonic and metallogenic evolution of southern Brazil. Australian Journal of Earth Sciences 47, 829–844.

Hartmann, L.A., Santos, J.O.S., 2004. Predominance of high Th/U, magmatic zircon in Brazilian Shield sandstones. Geology 32, 73–76.

Haughton, P.D.W., Farrow, C.M., 1988. Compositional variation in Lower Old Red Sandstone detrital garnets from the Midland Valley of Scotland and the Anglo-Welsh Basin. Geological Magazine 126, 373–396.

Hawthorne, F.C., Henry, D.J., 1999. Classification of the minerals of the tourmaline group. European Journal of Mineralogy 11, 201–215.

Heaman, L.M., Bowins, R., Crocket, J., 1990. The chemical composition of igneous zircon suites: implications for geochemical tracer studies. Geochimica et Cosmochimica Acta 54, 1597–1607.

Henry, D.J., Dutrow, B., 1992. Tourmaline in a low grade clastic metasedimentary rock; an example of the petrogenetic potential of tourmaline. Contributions to Mineralogy and Petrology 112, 203–218.

Henry, D.J., Guidotti, C.V., 1985. Tourmaline as a petrogenetic indicator mineral: an example from the staurolite-grade metapelites of NW Maine. American Mineralogist 70, 1–15.

Hisada, K., Arai, S., 1993. Detrital chrome spinels in the Cretaceous Sanchu sandstone, central Japan: indicator of serpentinite protrusion into a fore-arc region. Palaeogeography, Palaeoclimatology, Palaeoecology 105, 95–109.

Hisada, K., Arai, S., Lee, Y.I., 1999. Tectonic implication of Lower Cretaceous chromian spinel-bearing sandstones in Japan and Korea. The Island Arc 8, 336–348.

Hisada, K., Arai, S., Yamaguchi, T., 1998. Detrital chromian spinels from Site 960 in the Côte d'Ivoire-Ghana transform margin. Proceedings of the Ocean Drilling Program, Scientific Results 150, 133–139.

Hisada, K., Sugiyama, M., Ueno, K., Charushiri, P., Arai, S., 2004. Missing ophiolitic rocks along the Mae Yuam Fault as the Gondwana-Tethys divide in north-west Thailand. The Island Arc 13, 119–127.

Holland, H.D., Gottfried, D., 1955. The effect of nuclear radiation on the structure of zircon. Acta Crystallographica 8, 291–300.

Hoschek, G., 1967. Untersuchungen zum Stabilitätsbereich von Chloritoid und Staurolith. Contributions to Mineralogy and Petrology 14, 123–162.

Hoskin, P.W.O., Ireland, T.R., 2000. Rare earth element chemistry of zircon and its use as a provenance indicator. Geology 28, 627–630.

Hoskin, P.W.O., Schaltegger, U., 2003. The composition of zircon and igneous and metamorphic petrogenesis. In: Hanchar, J.M., Hoskin, P.W.O. (Eds.), Zircon: Reviews in Mineralogy and Geochemistry, vol. 53. pp. 27–62.

Irvine, T.N., 1965. Chromian spinel as a petrogenetic indicator. Part 1. Theory. Canadian Journal of Earth Sciences 2, 648–672.

Irvine, T.N., 1967. Chromian spinel as a petrogenetic indicator. Part 2. Petrologic applications. Canadian Journal of Earth Sciences 4, 71–103.

Jeans, C.V., Reed, S.J.B., Xing, M., 1993. Heavy mineral stratigraphy in the UK Trias of the North Sea Basin. In: Parker, J.R. (Ed.), Petroleum Geology of NW Europe: Proceedings of the 4th Conference. Geological Society of London, pp. 609–624.

Jiang, S.Y., Yang, J.H., Palmer, M.R., 1999. Chemical compositions of tourmaline from the Inch Conglomerate Formation, Dingle Peninsula, SW Ireland and their implication in provenance analysis. Chemie Der Erde—Geochemistry 59, 123–133.

Jonasson, R.G., Bancroft, G.M., Boatner, L.A., 1988. Surface reactions of synthetic, end-member analogues of monazite, xenotime and rhabdophane, and evolution of natural waters. Geochimica et Cosmochimica Acta 52, 767–770.

Kazmin, V.G., Sborshchikov, I.M., Ricou, L.-E., Zonenshain, L.P., Boulin, J., Knipper, A.L., 1986. Volcanic belts as markers of the Mesozoic-Cenozoic active margin of Eurasia. Tectonophysics 123, 123–152.

Kepezhinskas, K.B., Koryluk, V.N., 1973. Range of variation in the composition of staurolite from typical metapelities with pressure and temperature of metamorphism. Doklady, Academy of Sciences of the USSR, Earth Science Section 212, 121–125.

Kingsbury, J.A., Miller, C.F., Wooden, J.L., Harrison, T.M., 1993. Monazite paragenesis and U–Pb systematics in rocks of the Mojave Desert, California, USA: implications for thermochronometry. Chemical Geology (including Isotope Geology) 110, 147–167.

Krawinkel, H., Wozazek, S., Krawinkel, J., Hellmann, W., 1999. Heavy-mineral analysis and clinopyroxene geochemistry applied to provenance analysis of lithic sandstones from the Azuero-Soná Complex (NW Panama). Sedimentary Geology 124, 149–168.

Krogh, E.J., 1980. Geochemistry and petrology of glaucophane bearing eclogites and associated rocks from Sunnfjord, western Norway. Lithos 13, 355–380.

Krynine, P.D., 1946. The tourmaline group in sediments. Journal of Geology 54, 65–87.

Kusiak, M.A., Kedzior, A., Paszkowski, M., Suzuki, K., Gonzalez-Alvarez, I., Wajsprych, B., Doktor, M., 2006. Provenance implications of Th–U–Pb electron microprobe ages from detrital monazite in the Carboniferous Upper Silesia Coal Basin, Poland. Lithos 88, 56–71.

Leake, B.E., 1978. Nomenclature of amphiboles. Mineralogical Magazine 42, 533–563.

Leake, B.E., Woolley, A.R., Arps, C.E.S., Birch, W.D., Gilbert, M.C., Grice, J.D., Hawthorne, F.C., Kato, A., Kisch, H.J., Krivovichev, V.G., Linthout, K., Laird, J., Mandarino, J., Maresch, W.V., Nickel, E.H., Rock, N.M.S., Schumacher, J.C., Smith, D.C., Stephenson, N.C.N., Ungaretti, L., Whittaker, E.J.W., Youzhi, G., 1997. Nomenclature of amphiboles: report of the Subcommittee on Amphiboles of the International Mineralogical Association, Commission on New Minerals and Mineral Names. The Canadian Mineralogist 35, 219–246.

Le Bas, M.J., 1962. The role of aluminium in igneous clinopyroxenes with relation to their parentage. American Journal of Science 260, 267–288.

Lee, J.L., Lee, Y.I., 2000. Provenance of the Lower Cretaceous Hayang Group, Gyeongsang Basin, southeastern Korea: implications for continental-arc volcanism. Journal of Sedimentary Research 70, 151–158.

Lee, Y.I., 1999. Geotectonic significance of detrital chromian spinel: a review. Geosciences Journal 1, 23–29.

Lenaz, D., Kamenetsky, V.S., 2000. Melt inclusions in detrital spinel from the SE Alps (Italy-Slovenia): a new approach to provenance studies of sedimentary basins. Contributions to Mineralogy and Petrology 139, 748–758.

Leterrier, J., Maury, R., Thonon, P., Girard, D., Marchal, M., 1982. Clinopyroxene composition as a method of identification of the magmatic affinities of paleo-volcanic series. Earth and Planetary Science Letters 59, 139–154.

Li, R., Li, S., Jin, F., Wan, Y., Zhang, S., 2004. Provenance of Carboniferous sedimentary rocks in the northern margin of Dabie Mountains, central China and the tectonic significance: constraints from trace elements, mineral chemistry and SHRIMP dating of zircons. Sedimentary Geology 166, 245–264.

Lonergan, L., Mange-Rajetzky, M.A., 1994. Evidence for the Internal Zone unroofing from foreland basin sediments, Betic Cordillera, SE Spain. Journal of the Geological Society of London 151, 515–529.

Luepke, G., 1980. Opaque minerals as aids in distinguishing between source and sorting effects on beach-sand mineralogy in southwestern Oregon. Journal of Sedimentary Petrology 50, 489–496.

Mackie, W., 1923. The source of purple zircons in the sedimentary rocks of Scotland. Transactions of the Edinburgh Geological Society 11, 200–213.

Mackie, W., 1926. The heavier accessory minerals in the granites of Scotland. Transactions of the Edinburgh Geological Society 12, 22–40.

Mange, M.A., Dewey, J.F., Floyd, J.D., 2005. The origin, evolution and provenance of the northern, Ordovician, belts of the Southern Uplands Terrane, Scotland: a heavy mineral perspective. Proceedings of the Geologists' Association, London 116, 251–280.

Mange, M.A., Maurer, H.F.W., 1992. Heavy Minerals in Colour. Chapman and Hall, London, 147pp.

Mange, M.A., Turner, P., Ince, D.M., Pugh, J.M., Wright, D.T., 1999. A new perspective on the zonation and correlation of barren strata: an integrated heavy mineral and palaeomagnetic study of the Sherwood Sandstone Group, East Irish Sea Basin and surrounding areas. Journal of Petroleum Geology 22, 325–348.

Mange-Rajetzky, M.A., 1981. Detrital blue sodic amphibole in Recent sediments, southern coast, Turkey. Journal of the Geological Society of London 138, 83–92.

Mange-Rajetzky, M.A., 1995. Subdivision and correlation of monotonous sandstone sequences using high resolution heavy mineral analysis, a case study: the Triassic of the Central Graben. In: Dunay, R.E., Hailwood, E.A. (Eds.), Non-Biostratigraphical Methods of Dating and Correlation, vol. 89. Geological Society of London Special Publication, pp. 23–30.

Mange-Rajetzky, M.A., Oberhänsli, R., 1982. Detrital lawsonite and blue sodic amphibole in the Molasse of Savoy, France and their significance in assessing Alpine evolution. Schweizerische Mineralalogische und Petrographische Mitteilungen 62, 415–436.

Mannerstrand, M., Lundqvist, L., 2003. Garnet chemistry from the Slöinge Excavation, Halland and additional Swedish and Danish excavations—comparisons with garnet occurring in a rock context. Journal of Archaeological Science 30, 169–183.

Markevich, P.V., Alexander, I., Malinovsky, A.I., Tuchkova, M.I., Sokolov, S.D., Grigoryev, V.N., 2007. The use of heavy minerals in determining the provenance and tectonic evolution of Mesozoic and Cenozoic sedimentary basins in the continent-Pacific Ocean

transition zone: examples from Sikhote-Alin and Koryak-Kamchatka regions (Russian Far East) and western Pacific. In: Mange, M.A., Wright, D.T. (Eds.), Heavy Minerals in Use. Developments in Sedimentology (this volume).

McClenaghan, M.B., Kjarsgaard, B.A., 2001. Indicator mineral and geochemical methods for diamond exploration in glaciated terrain in Canada. In: McClenaghan, M.B., Bobrowsky, P.T., Hall, G.E.M., Cook, S.J. (Eds.), Drift exploration in glaciated terrain, vol. 185. Geological Society of London Special Publication, pp. 85–123.

McConnell, D., 1973. Apatite—its crystal chemistry, mineralogy, utilization and geologic and biologic occurrences. Springer-Verlag, New York, 111 pp.

Medaris, L.G., 1980. Petrogenesis of the Lien peridotite and associated eclogites, Almklovdalen, western Norway. Lithos 13, 339–353.

Medaris, L.G., 1984. A geothermobarometric investigation of garnet peridotites in the Western Gneiss Region of Norway. Contributions to Mineralogy and Petrology 87, 72–86.

Mikes, T., Dunkl, I., Von Eynatten, H., 2005. Significance of ophiolitic and high-grade metamorphic detritus in the Tertiary External Dinaride Flysch Belt. 7th Alpine Workshop, Opatija. Abstract.

Miyashiro, A., 1957. The chemistry, optics and genesis of the alkali-amphiboles. Tokyo University, Faculty of Sciences Journal II 11, 51–83.

Morimoto, N., 1988. Nomenclature of pyroxenes. American Mineralogist 73, 1123–1133.

Mørk, M.B.E., 1999. Compositional variations and provenance of Triassic sandstones from the western Barents Shelf. Journal of Sedimentary Research 69, 690–710.

Morton, A.C., 1984. Stability of detrital heavy minerals in Tertiary sandstones of the North Sea Basin. Clay Minerals 19, 287–308.

Morton, A.C., 1985. A new approach to provenance studies: electron microprobe analysis of detrital garnets from Middle Jurassic sandstones of the northern North Sea. Sedimentology 32, 553–566.

Morton, A.C., 1987. Influences of provenance and diagenesis on detrital garnet suites in the Forties sandstone, Paleocene, central North Sea. Journal of Sedimentary Petrology 57, 1027–1032.

Morton, A.C., 1991. Geochemical studies of heavy minerals and their application to provenance research. In: Morton, A.C., Todd, S.P., Haughton, P.D.W. (Eds.), Developments in Sedimentary Provenance Studies, vol. 57. Geological Society of London Special Publication, pp. 31–45.

Morton, A.C., Allen, M.B., Simmons, M.D., Spathopoulos, F., Still, J., Ismail-Zadeh, A., Kroonenberg, S., 2003a. Provenance patterns in a neotectonic basin: Pliocene and Quaternary sediment supply to the South Caspian. Basin Research 15, 321–337.

Morton, A.C., Hallsworth, C.R., 1999. Processes controlling the composition of heavy mineral assemblages in sandstones. Sedimentary Geology 124, 3–29.

Morton, A.C., Hallsworth, C.R., 2007. Stability of detrital heavy minerals during burial diagenesis. In: Mange, M.A., Wright, D.T. (Eds.), Heavy Minerals in Use. Developments in Sedimentology (this volume).

Morton, A.C., Hallsworth, C.R., Chalton, B., 2004. Garnet compositions in Scottish and Norwegian basement terrains: a framework for interpretation of North Sea sandstone provenance. Marine and Petroleum Geology 21, 393–410.

Morton, A.C., Hallsworth, C.R., Moscariello, A., 2005a. Interplay between northern and southern sediment sources during Westphalian deposition in the Silverpit Basin, southern North Sea. In: Collinson, J.D., Evans, D.J., Holliday, D.S., Jones, N.S. (Eds.), Carboniferous Hydrocarbon Geology: The Southern North Sea and Surrounding Onshore Areas, vol. 7. Yorkshire Geological Society Occasional Publication, pp. 135–146.

Morton, A.C., Humphreys, B., Manggal, G., Fanning, C.M., 2000. Provenance and correlation of Upper Jurassic and Lower Cretaceous reservoir sandstones in Papua New Guinea using heavy mineral analysis. In: Buchanan, P.G., Grainge, A.M., Thornton, R.C.N. (Eds.), Petroleum Exploration and Development in Papua New Guinea: Proceedings of the Fourth PNG Petroleum Convention. PNG Chamber of Mines and Petroleum, Port Moresby, Papua New Guinea, pp. 187–203.

Morton, A.C., Spicer, P.J., Ewen, D.F., 2003b. Geosteering of high-angle wells using heavy-mineral analysis: the Clair Field, west of Shetland, UK. In: Carr, T.R., Mason, E.P., Feazel, C.T. (Eds.), Horizontal Wells: Focus on the Reservoir. American Association of Petroleum Geologists, Methods in Exploration 14, 249–260.

Morton, A.C., Whitham, A.G., Fanning, C.M., 2005b. Provenance of Late Cretaceous-Paleocene submarine fan sandstones in the Norwegian Sea: integration of heavy mineral, mineral chemical and zircon age data. Sedimentary Geology 182, 3–28.

Morton, A.C., Herries, R., Fanning, M., 2007. Correlation of Triassic sandstones in the Strathmore Field, west of Shetland, using heavy mineral provenance signatures. In: Mange, M.A., Wright, D.T. (Eds.), Heavy Minerals in Use. Developments in Sedimentology (this volume).

Morton, A.C., Yaxley G., 2007. Detrital apatite geochemistry and its application in provenance studies. In: Arribas, J., Critelli, S., Johnsson, M.J. (Eds.), Sediment Provenance and Petrogenesis: Perspectives from Petrography and Geochemistry, Geological Society of America, Special Paper 420, 319–344.

Mysen, B.D., Heier, K.S., 1972. Petrogenesis of eclogites in high grade metamorphic gneisses, exemplified by the Hareidland Eclogite, western Norway. Contributions to Mineralogy and Petrology 36, 73–94.

Nanayama, F., 1997. An electron microprobe study of the Amazon fan. Proceedings of the Ocean Drilling Program, Scientific Results 155, 147–158.

Nash, W.P., 1984. Phosphate minerals in terrestrial igneous and metamorphic rocks. In: Nriagu, J.O., Moore, P.B. (Eds.), Phosphate Minerals. Springer-Verlag, New York, pp. 215–241.

Nichols, G.J., 2005. Sedimentary evolution of the Lower Clair Group, Devonian, west of Shetland: climate and sediment supply controls on fluvial, aeolian and lacustrine deposition. In: Doré, A.G., Vining, B. (Eds.), Petroleum Geology: North-West Europe and Global Perspectives: Proceedings of the 6th Petroleum Geology Conference. Geological Society of London, pp. 957–967.

Nisbet, E.G., Pearce, J.A., 1977. Clinopyroxene compositions in mafic lavas from different tectonic settings. Contributions to Mineralogy and Petrology 63, 149–160.

Noda, A., Takeuchi, M., Adachi, M., 2004. Provenance of the Murihiku Terrane, New Zealand: evidence from the Jurassic conglomerates and sandstones in Southland. Sedimentary Geology 164, 203–222.

Nowicki, T.E., Moore, R.O., Gurney, J.J., Baumgartner, M.C., 2007. Diamonds and associated heavy minerals in kimberlite: A review of key concepts and applications. In: Mange, M.A., Wright, D.T. (Eds.), Heavy Minerals in Use. Developments in Sedimentology (this volume).

Oszczypko, N., Salata, D., 2005. Provenance analyses of the Late Cretaceous-Palaeocene deposits of the Magura Basin (Polish Western Carpathians)—evidence from a study of the heavy minerals. Acta Geologica Polonica 55, 237–267.

Overstreet, W., 1967. The geologic occurrence of monazite. US Geological Survey Professional Paper 530, 327pp.

Owen, M.R., 1987. Hafnium content of detrital zircons, a new tool for provenance study. Journal of Sedimentary Petrology 57, 824–830.

Park, R.G., Stewart, A.D., Wright, D.T., 2002. The Hebridean terrane. In: Trewin, N.H. (Ed.), The Geology of Scotland, 4th ed. Geological Society of London, Bath, UK, pp. 45–80.

Pinto, L., Herail, G., Moine, B., Fontan, F., Charrier, R., Dupre, B., 2004. Using geochemistry to establish the igneous provenances of the Neogene continental sedimentary rocks in the Central Depression and Altiplano, Central Andes. Sedimentary Geology 166, 157–183.

Pirkle, F.L., Pirkle, W.A., Pirkle, E.C., 2007. Heavy mineral sands of the Atlantic and Gulf Coastal Plains, USA. In: Mange, M.A., Wright, D.T. (Eds.), Heavy Minerals in Use. Developments in Sedimentology (this volume).

Pober, E., Faupl, P., 1988. The chemistry of detrital chrome spinels and its implications for the geodynamic evolution of the Eastern Alps. Geologische Rundschau 77, 641–670.

Poldervaart, A., Hess, H.H., 1951. Pyroxenes in the crystallization of basaltic magmas. Journal of Geology 59, 472–489.

Power, M.R., Pirrie, D., Andersen, J.C.Ø., Wheeler, P.D., 2000. Testing the validity of chrome spinel chemistry as a provenance and petrogenetic indicator. Geology 28, 1027–1030.

Pownceby, M.I., 2005. Compositioinal and textural variation in detrital chrome spinels from the Murray Basin, southeastern Australia. Mineralogical Magazine 69, 191–204.

Pownceby, M.I., Bourne, P., 2006. Detrital chrome-spinel grains in heavy-mineral sand deposits from southeast Africa. Mineralogical Magazine 70, 51–64.

Press, S., 1986. Detrital spinels from alpinotype source rocks in Middle Devonian sediments of the Rhenish Massif. Geologische Rundschau 75, 333–340.

Preston, J., Hartley, A., Hole, M., Buck, S., Bond, J., Mange, M., Still, J., 1998. Integrated whole-rock trace element geochemistry and heavy mineral studies: aids to correlation of continental red-bed reservoirs in the Beryl Field, UK North Sea. Petroleum Geoscience 4, 7–16.

Preston, J., Hartley, A., Mange-Rajetzky, M., Hole, M., May, G., Buck, S., Vaughan, L., 2002. The provenance of Triassic continental sandstones from the Beryl Field, northern North Sea: mineralogical, geochemical, and sedimentological constraints. Journal of Sedimentary Research 72, 18–29.

Pupin, J.P., Turco, G., 1981. Le zircon, minéral commun significatif des roches endogènes et exogènes. Bulletin Minéralogie 104, 724–731.

Reynolds, A.D., Simmons, M.D., Bowman, M.B.J., Henton, J., Brayshaw, A.C., Ali-Zade, A.A., Guliyev, I.S., Suleymanova, S.F., Ateava, E.Z., Mamedova, D.N., Koshkarly, R.O., 1998. Implications of outcrop geology for reservoirs in the Neogene Productive Series: Apsheron Peninsula, Azerbaijan. Bulletin of the American Association of Petroleum Geologists 82, 25–49.

Sabeen, H.M., Ramanujam, N., Morton, A.C., 2002. The provenance of garnet: constraints provided by studies of coastal sediments from Southern India. Sedimentary Geology 152, 279–287.

Schäfer, J., 1996. Mikrosondenuntersuchungen an Geröllen und detritischen Mineralen im Flysch des Saxothuringikums: Ein Beitrag zur Exhumierungsgeschichte des Liefergebietes. Ph.D. thesis. University of Giessen, 221pp.

Schäfer, J., Neuroth, H., Ahrendt, H., Dörr, W., 1997. Accretion and exhumation at a Variscan active margin, recorded in the Saxothuringian flysch. Geologische Rundschau 86, 599–611.

Schneiderman, J.S., 1995. Detrital opaque oxides as provenance indicators in River Nile sediments. Journal of Sedimentary Research 65, 668–674.

Schneiderman, J.S., 1997. Potential paleoclimate indicators: composition of detrital pyroxene and ilmenite in River Nile and Nile delta sediments. In: Proceedings of the 30th International Geological Congress Bejing, vol. 8, pp. 81–106.

Schroeder, P.A., Le Govan, J.F., Roden, M.F., 2002. Weathering of ilmenite from granite and chlorite schist in the Georgia Piedmont. American Mineralogist 87, 1616–1625.

Sciunnach, D., Garzanti, E., 1997. Detrital chromian spinels record tectono-magmatic evolution from Carboniferous rifting to Permian spreading in Neotethys (India, Nepal, Tibet). Ofioliti 22, 101–110.

Smale, D., Morton, A.C., 1987. Heavy mineral suites of core samples from the McKee Formation (Eocene-Lower Oligocene), Taranaki: implications for provenance and diagenesis. New Zealand Journal of Geology and Geophysics 30, 299–306.

Smale, D., Van der Lingen, G.J., 1989. Differential leaching of garnet grains at a depth of 3.5 km in Tane-1, Offshore Taranaki, New Zealand. New Zealand Geological Survey Record 40, 57–60.

Spiegel, C., Siebel, W., Frisch, W., Berner, Z., 2002. Nd and Sr isotopic ratios and trace element geochemistry of epidote from the Swiss Molasse Basin as provenance indicators: implications for the reconstruction of the exhumation history of the Central Alps. Chemical Geology 189, 231–250.

Styles, M.T., Perez-Alvarez, M., Floyd, J.D., 1995. Pyroxenous greywackes in the Southern Uplands of Scotland and their petrotectonic implications. Geological Magazine 132, 539–547.

Styles, M.T., Stone, P., Floyd, J.D., 1989. Arc detritus in the Southern Uplands: mineralogical charcterisation of a 'missing' terrain. Journal of the Geological Society of London 146, 397–400.

Suzuki, K., Adachi, M., Tanaka, T., 1991. Middle Precambrian provenance of Jurassic sandstone in the Mino Terrane, central Japan: Th-U-total Pb evidence from an electron microprobe monazite study. Sedimentary Geology 75, 141–147.

Takeuchi, M., 1994. Changes in garnet chemistry show a progressive denudation of the source areas for Permian-Jurassic sandstones, southern Kitakami Terrane, Japan. Sedimentary Geology 93, 85–105.

Taylor, S.R., McLennan, S.M., 1985. The Continental Crust: Its Composition and Evolution. Blackwell, Oxford, 312pp.

Tebbens, L.A., Kroonenberg, S.B., Vandenberghe, M.W., 1995. Compositional variation of detrital garnets in Quaternary Rhine, Meuse and Baltic river sediments in the Netherlands. Geologie en Mijnbouw 74, 213–224.

Turner, G., Morton, A.C., 2007. The effects of burial diagenesis on detrital heavy mineral grain surface textures. In: Mange, M.A., Wright, D.T. (Eds.), Heavy Minerals in Use. Developments in Sedimentology (this volume).

Vavra, G., Schmid, R., Gebauer, D., 1999. Internal morphology, habit and U-Th-Pb microanalysis of amphibolite-to-granulite facies zircons: geochronology of the Ivrea Zone (southern Alps). Contributions to Mineralogy and Petrology 97, 205–217.

Von Eynatten, H., Gaupp, R., 1999. Provenance of Cretaceous synorogenic sandstones in the Eastern Alps: constraints from framework petrography, heavy mineral analysis and mineral chemistry. Sedimentary Geology 124, 81–111.

Wallace, R.C., 1975. Staurolite from the Haast schists in South Westland, New Zealand. Journal of Geology and Geophysics 18, 343–348.

Willner, A.P., 1987. Detrital tourmalines as indicators for the source rocks of Late Precambrian—Lower Cambrian graywackes (Puncoviscana Formation) in NW Argentina. Zentralblatt für Geologie und Paläontologie 1987, 885–891.

Wright, W.I., 1938. The composition and occurrence of garnets. American Mineralogist 23, 436–449.

Yokoyama, K., Amano, K., Taira, A., Saito, Y., 1990. Mineralogy of silts from the Bengal Fan. Initial Reports of the Deep Sea Drilling Project 116, 59–73.

Zack, T., Kronz, A., Foley, S., Rivers, T., 2002. Trace element abundances in rutiles from eclogites and associated garnet mica schists. Chemical Geology 184, 97–122.

Zack, T., Von Eynatten, H., Kronz, A., 2004. Rutile geochemistry and its potential use in quantitative provenance studies. Sedimentary Geology 171, 37–58.

Zhu, B., Kidd, W.S.F., Rowley, D.B., Currie, B.S., 2004. Chemical compositions and tectonic significance of chrome-rich spinels in the Tianba Flysch, southern Tibet. The Journal of Geology 112, 417–434.

Zimmerle, W., 1984. The geotectonic significance of detrital brown spinel in sediments. Mitteilungen aus dem Geologisch-Paläontologischen Institut der Universität Hamburg 56, 337–360.

This page intentionally left blank

Chapter 14

THE EFFECTS OF BURIAL DIAGENESIS ON DETRITAL HEAVY MINERAL GRAIN SURFACE TEXTURES

GRENVILLE TURNER[a] AND ANDREW C. MORTON[b,c]

[a]*British Geological Survey, Keyworth, Nottingham NG12 5GG, UK*
[b]*HM Research Associates, 2 Clive Road, Balsall Common, West Midlands CV7 7DW, UK*
[c]*CASP, University of Cambridge, 181a Huntingdon Road, Cambridge CB3 0DH, UK*

ABSTRACT

A wide-ranging study of heavy mineral grain surface textures using the scanning electron microscope has demonstrated that heavy mineral dissolution is widespread in sedimentary basins worldwide. Many heavy mineral grains, including andalusite, amphibole, chloritoid, epidote, garnet, kyanite, olivine, pyroxene, sillimanite, staurolite and titanite show dissolution textures, which range from pits, mamillated surfaces, facets and deep parallel grooves and furrows, to hacksaw terminations and skeletal forms. Dissolution has been observed in sedimentary basins from the North Sea, Faeroe-Shetland Basin, Rockall Trough, Norwegian Sea, Germany, France, Ivory Coast, Nigeria, south Caspian Basin, Bengal Basin, India, Borneo, US Gulf Coast and Trinidad. Heavy mineral grain surface texture studies therefore testify to the fact that intrastratal dissolution is a global, rather than a local, phenomenon. Some heavy minerals (apatite, monazite, rutile, spinel, tourmaline and zircon) rarely display surface corrosion during deep burial, and are considered to be essentially stable. However, tourmalines have been observed to develop etch facets under some deep burial circumstances, and both monazite and chrome spinel show signs of incipient corrosion in extreme burial situations. Apatite shows both overgrowth and corrosion textures in the subsurface, with overgrowths tending to develop as burial proceeds. Etched apatite generally coexists with unetched grains irrespective of burial depth, and the corrosion is therefore not related to in-situ diagenetic processes. Dissolution of apatite is considered to occur through weathering in the source area and during periods of alluvial storage during transport, rather than in-situ corrosion in the subsurface. Evaluation of the extent to which heavy mineral assemblages have undergone post-depositional modification by dissolution processes is crucial when evaluating provenance, and the scanning electron microscope has an important role to play in this regard.

Keywords: heavy minerals; corrosion; etching; overgrowth; dissolution; burial; weathering

Developments in Sedimentology, Vol. 58, 393–412

ISSN: 0070-4571/doi:10.1016/S0070-4571(07)58014-3

1. INTRODUCTION

Despite the widespread application of scanning electron microscopy (SEM) in the study of sands and sandstones, comparatively few papers deal with detrital heavy minerals. Most SEM work on heavy minerals has concentrated on the effects of superficial processes on surface textures of detrital heavy mineral grains. For example, mechanical effects (such as unoriented V-shaped indentations, impact grooves, breakage blocks, striations and chattermark trails) caused by transport processes have been described by Steiglitz (1969), Setlow (1977), Setlow and Karpovich (1972), Lin et al. (1974), Mallik (1986), Mahaney and Milner (1998) and Mahaney (2002). Dissolution of amphibole and epidote during weathering of coastal dune sands has been illustrated by Setlow (1977). Berner et al. (1980), Berner and Schott (1982) and Velbel (1984, 1989, 1993, 2007: this volume) have presented SEM images of etched pyroxene, amphibole and garnet grains generated through weathering in soil profiles. The effects of weathering on heavy minerals in palaeosols have been described by Tejan-Kella et al. (1991), Mahaney (2002) and Van Loon and Mange (2007: this volume). Morton and Johnsson (1993) used the SEM to show corrosion on apatite and amphibole grain surfaces, caused by weathering during periods of alluvial storage. Dissolution of ferromagnesian minerals, such as pyroxene and amphibole, is considered a key process in the formation of red beds (Walker et al., 1978). Finally, the SEM atlas of Welton (1984) includes scanning electron micrographs of amphibole, pyroxene and titanite.

Relatively few papers, by contrast, have used the SEM to deal systematically with the effects of burial diagenesis on heavy mineral grain surfaces. Rahmani (1973) described corrosion textures on amphibole, epidote, titanite, staurolite and garnet from Cretaceous–Palaeocene sandstones of Alberta, Canada. Morton (1979, 1984) and Morton and Hallsworth (1999) examined the effects of burial diagenesis on apatite, amphibole, chloritoid, chrome spinel, epidote, garnet, kyanite, monazite, staurolite, tourmaline and zircon, in Palaeocene sandstones of the central North Sea. Milliken and Mack (1990) and Milliken (2007: this volume) used the SEM to illustrate etching of heavy minerals, including pyroxene, amphibole and garnet from Cenozoic–Recent sediments in the Gulf of Mexico sedimentary basin. Hemingway and Tamar-Agha (1975) and Robson (1984) documented garnet etching in Carboniferous sandstones of northern England. Other contributions dealing with garnet dissolution in the subsurface include diagenetic studies of Triassic sandstones in Germany (Werle and Schneider, 1977; Borg, 1986), a study of Late Precambrian and Late Palaeozoic tillites from Australia and South Africa (Gravenor and Gostin, 1979), and a diagenetic study of Jurassic sandstones in New Mexico (Hansley, 1986, 1987). Scanning electron micrographs of etched heavy mineral grains (garnet, pyroxene, amphibole and staurolite) were presented by Mange and Maurer (1992). On a related topic, a number of papers show scanning electron micrographs of heavy minerals etched in laboratory experiments in attempts to replicate natural corrosion textures (Nickel, 1973; Gravenor and Leavitt, 1981; Hansley, 1987; Hansley and Briggs, 1994).

Surface textures indicative of corrosion include pits, mamillated surfaces, facets, imbricate wedge markings, hacksaw or cockscomb terminations, ragged or frayed

edges and deep parallel grooves and furrows (Edelman and Doeglas, 1932, 1934; Rahmani, 1973; Hemingway and Tamar-Agha, 1975; Morton, 1979; Gravenor and Leavitt, 1981; Mange and Maurer, 1992). Although such features are visible under the petrographic microscope, as demonstrated, for example, by Mange and Maurer (1992) and Van Loon and Mange (2007: this volume), the SEM is the most appropriate tool for investigation of dissolution textures on heavy mineral grains, since it offers much greater imaging capacity and resolution.

This contribution presents scanning electron micrographs of heavy minerals from sedimentary basins of northwest Europe (North Sea, Faeroe-Shetland Basin, Rockall Trough, Norwegian Sea), Africa (offshore Ivory Coast and Nigeria), Asia (south Caspian Basin, Bengal Basin, eastern India, Mahakam delta) and South America (offshore Trinidad). A wide range of detrital heavy mineral surface textures (andalusite, amphibole, chloritoid, epidote group minerals, garnet, kyanite, monazite, olivine, pyroxene and related minerals, rutile, sillimanite, spinel, staurolite, titanite, tourmaline and zircon) were investigated in the course of the study, the main aim being to provide an overview of the effects of burial diagenetic processes on detrital heavy mineral surface textures from sedimentary basins worldwide. The implications of the surface textural data described herein are discussed in the accompanying chapter by Morton and Hallsworth (2007: this volume), particularly with regard to relative mineral stability and distribution of heavy minerals in sandstones.

2. ANALYTICAL METHODS

Representative heavy mineral grains were picked from heavy mineral residues under a polarising microscope, mounted on double-sided adhesive tape, and coated with a thin layer of carbon (~2 nm) in an Emitech K950 carbon evaporation coater. Heavy mineral residues were obtained by standard heavy liquid separation techniques (Mange and Maurer, 1992), in bromoform (density 2.8 g/cm$^{3)}$, following gentle disaggregation and cleaning using mortar and pestle and ultrasonic probe. No chemical treatment (such as acid digestion) was used, precluding the possibility that any of the dissolution features identified under the SEM could have been generated during the sample preparation process. The samples discussed here are mainly taken from cores drilled during hydrocarbon exploration activities, and their precise locations and depths are therefore confidential. Twenty to thirty grains were examined per sample, although this was not possible for less abundant phases.

The specimens were examined in a Leo435VP SEM in high-vacuum mode. The instrument was set to a routine accelerating voltage of 20 kV, and images were obtained using a secondary electron detector. Qualitative chemical analyses were obtained with an Oxford Instruments ISIS 300 energy-dispersive X-ray microanalysis system in order to verify the composition of the mineral grains. X-ray spectra are displayed as plots of energy (0–10 keV) versus X-ray intensity, which enable basic elemental chemistry to be deduced. This system cannot determine the presence of elements with an atomic number lower than carbon (atomic number 6). The images are shown in Figs. 1–11.

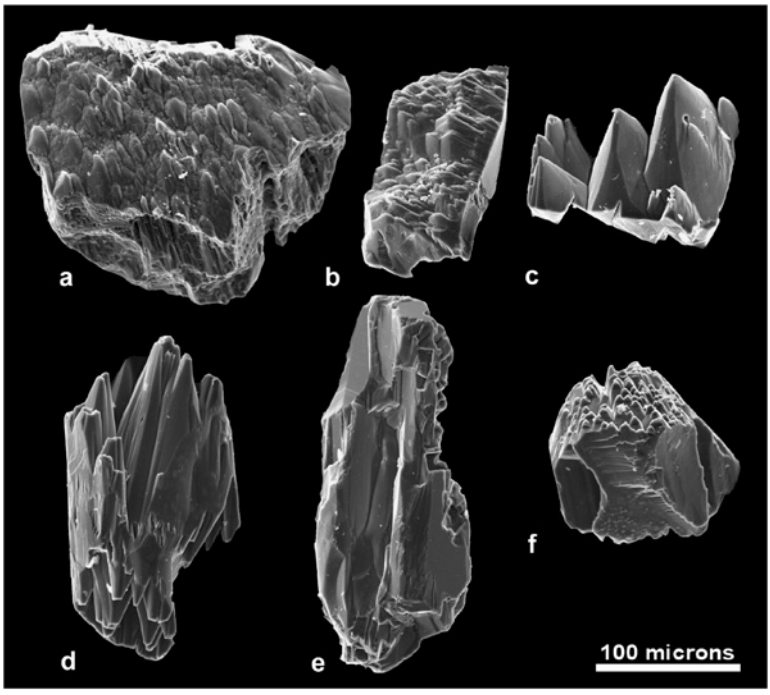

Fig. 1. Olivine and pyroxene etching. (a) and (b) Etched olivine, seabed sediment sample, offshore western Scotland. (c) Highly etched clinopyroxene, Pliocene sandstone, southern Caspian Basin, 3530 m depth. (d) Highly etched clinopyroxene, Eocene sandstone, Rockall Trough, 39 m depth. (e) Slightly etched sodic pyroxene (aegirine), Eocene sandstone, Rockall Trough, 39 m depth. (f) Highly etched aenigmatite, Eocene sandstone, Rockall Trough, 39 m depth.

3. SURFACE TEXTURES

3.1. Olivine

Olivines in a sand sample from the seabed on the west coast of Scotland show large scale etch facets on their grain surfaces (Figs. 1a, b), indicating an advanced level of corrosion. It is possible that these features have been inherited from a previous phase of corrosion (most likely during weathering of its inferred basic/ultrabasic igneous source material). However, this seems unlikely, since none of the olivines analysed from the sample show any evidence of mechanical abrasion, despite their shallow marine shelf depositional setting. The etching is therefore considered to have taken place in situ at the sea floor, indicating that olivine dissolution took place at ambient temperatures without any burial.

3.2. Pyroxene

Surface textures of clinopyroxene grains have been studied from deeply buried Pliocene sandstones from the south Caspian Sea Basin (Fig. 1c) and Eocene sandstones at shallow burial in the Rockall Trough (Fig. 1d). In both cases, the

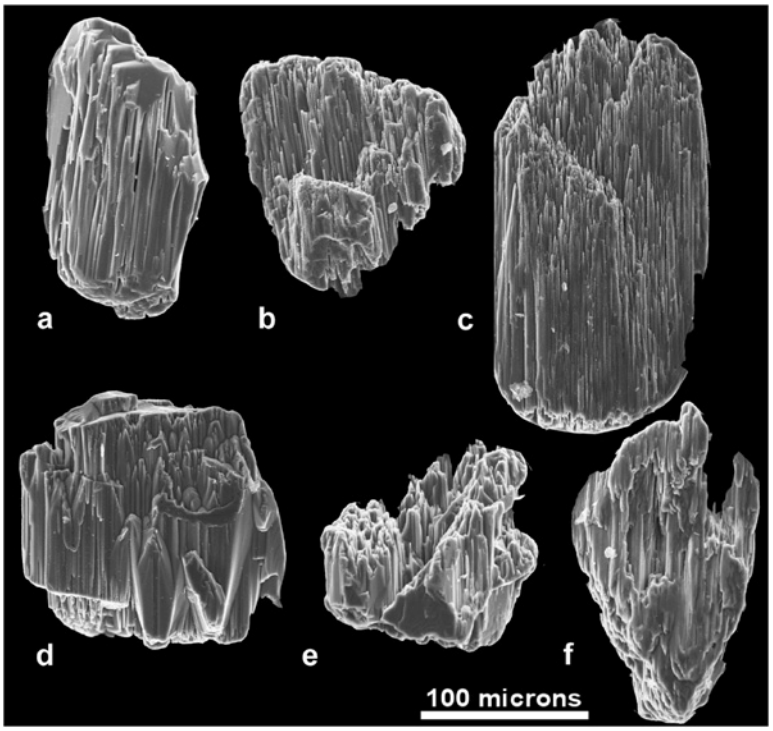

Fig. 2. Amphibole etching. (a) and (b) Etched calcic amphibole, Miocene sandstone, eastern India, 2210 m depth. (c) and (d) Etched calcic amphibole, Pliocene sandstone, southern Caspian Basin, 3220 m depth. (e) and (f) Etched sodic amphibole, Miocene sandstone, Mahakam delta, 2690 m depth.

clinopyroxenes show evidence for extreme corrosion, all grains displaying well-developed, large-scale hacksaw terminations. The textures seen on the clinopyroxenes in this study are similar to those seen in Rio Grande sediments from the US Gulf Coast (Milliken and Mack, 1990) and the Oligocene of the Barrême Basin of France (Mange and Maurer, 1992). Clinopyroxenes etched during weathering processes show similar surface textures (Berner et al., 1980; Berner and Schott, 1982). Surface textural data therefore indicate that clinopyroxene is highly unstable during burial. Sodic pyroxenes (aegirine) in the same Rockall Trough sample (Fig. 1e) show little evidence for dissolution, indicating that they are more stable than clinopyroxenes. However, the pyroxene-like mineral aenigmatite, which occurs in conjunction with clinopyroxene and sodic pyroxene in the Eocene of the Rockall Trough, shows advanced corrosion (hacksaw terminations) similar to those shown by clinopyroxene (Fig. 1f).

3.3. *Amphibole*

Amphibole grains from the subsurface commonly display evidence of corrosion. In this contribution, etched amphiboles are illustrated from Miocene sandstones from eastern India and the Mahakam delta (Indonesia), and from Pliocene sandstones of the south Caspian Sea Basin. Calcic amphibole corrosion is generally manifested

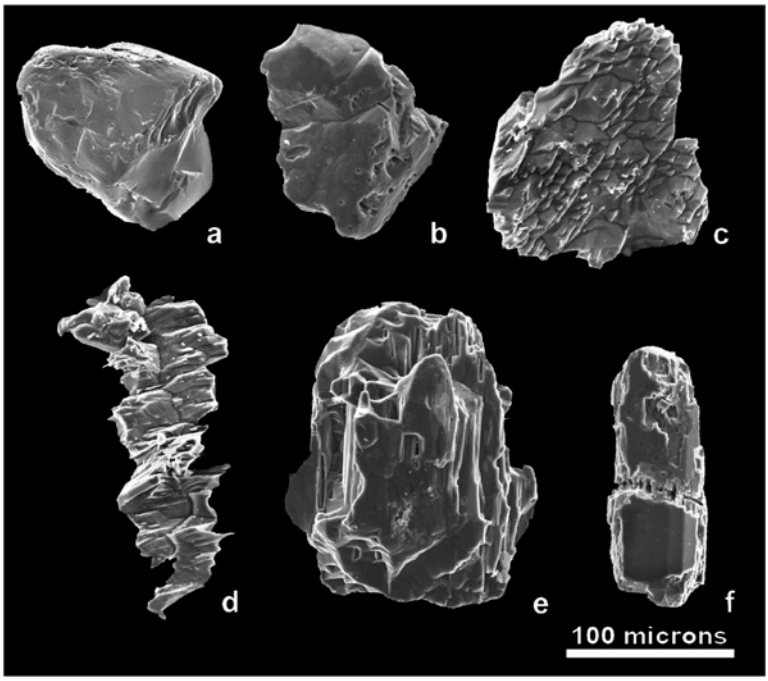

Fig. 3. Epidote etching. (a) Unetched epidote, Miocene sandstone, eastern India, 2210 m depth. (b) Epidote with minor etch pitting, Miocene sandstone, eastern India, 2210 m depth. (c) Etched epidote, Palaeocene sandstone, Faeroe-Shetland Basin, 3586 m depth. (d) Highly etched epidote, Palaeocene sandstone, Faeroe-Shetland Basin, 3586 m depth. (e) Slightly etched epidote, Pliocene sandstone, southern Caspian Basin, 3220 m depth. (f) Slightly etched allanite, Miocene sandstone, Bengal Basin, 3841 m depth.

by development of slender, needle-like terminations and hacksaw terminations (Figs. 2a–d). Similar features have been recognised on sodic amphibole grains from Miocene sandstones of the Mahakam delta (Figs. 2e, f). The surface textures illustrated here are comparable to those seen on amphiboles from burial environments in the North Sea Palaeocene (Morton, 1979), Cretaceous–Palaeocene sandstones of Alberta (Rahmani, 1973) and the Barrême Basin Oligocene (Mange and Maurer, 1992), as well as weathered amphiboles from soil profiles (Berner et al., 1980; Berner and Schott, 1982; Velbel, 1989, 1993, 2007: this volume).

3.4. Epidote Group

With increasing burial, the epidote group minerals generally show increasing intensity of surface-corrosion features. Grains from Miocene sandstones in the shallow subsurface of eastern India (Figs. 3a, b) show little modification by diagenetic processes, and retain features acquired during transport, such as rounding and fracturing. Some grains show evidence of incipient corrosion, with poorly defined mamillations and pitting. The etch pits shown on the epidote in Fig. 3b are unoriented, and probably result from leaching of inclusions rather than the epidote itself, since they lack crystallographic control. Grains from Pliocene sandstones of the south Caspian Sea Basin show more advanced corrosion, with development of deep parallel grooves

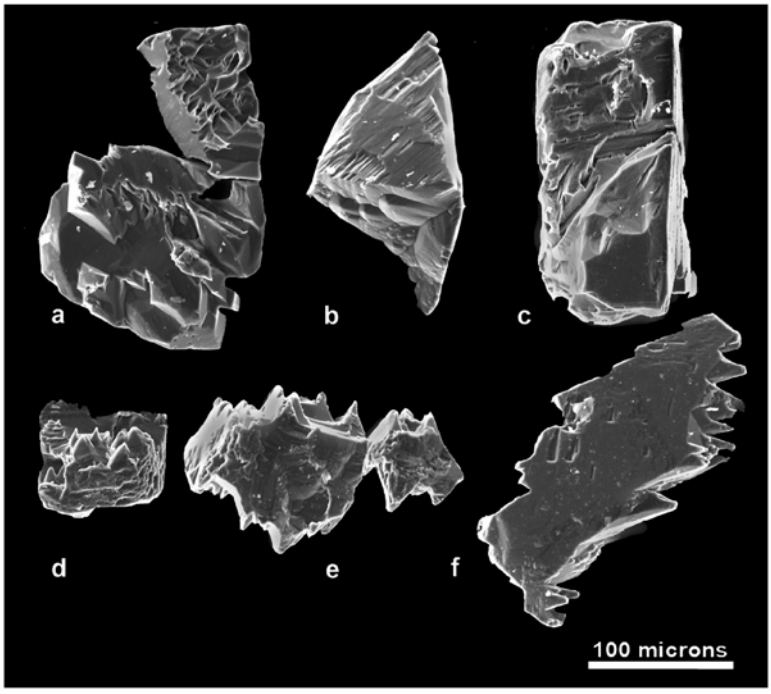

Fig. 4. Al_2SiO_5 polymorphs etching. (a) Highly etched andalusite, Cretaceous sandstone, offshore SW England, 4 m depth. (b) Etched sillimanite, Miocene sandstone, eastern India, 2210 m depth. (c) Kyanite with incipient etching, Palaeocene sandstone, Norwegian Sea, 1097 m depth. (d) Etched kyanite, Pliocene sandstone, southern Caspian Basin, 4585 m depth. (e) and (f) Highly etched kyanite, Jurassic sandstone, Norwegian Sea, 2259 m depth.

and oriented etch pits (Fig. 3e). Intensely etched epidote from the Palaeocene of the Faeroe-Shetland Basin (Figs. 3c, d) show well-developed, large-scale facets, and some grains display a skeletal character. The development of corrosion textures shown by epidote illustrated herein is similar to that described in the North Sea Palaeocene (Morton, 1979, 1984).

Allanite, the rare earth epidote mineral, also displays evidence of corrosion, although the extent of dissolution is significantly less than that with clinozoisite and epidote sensu stricto. Allanite from Miocene sandstones at considerable depth (below the limit of persistence of other epidote-group minerals in the Bengal Basin; see Morton and Hallsworth, 2007: this volume) are virtually unetched, except for incipient etching along a structural weakness running through the grain (Fig. 3f). Allanite is therefore interpreted as being more stable than other members of the epidote group.

3.5. *Kyanite, Andalusite, Sillimanite*

All three of the Al_2SiO_5 polymorphs display evidence of corrosion in the subsurface, although more data are available on kyanite than on andalusite and sillimanite, owing to its more widespread occurrence in sediments. Corrosion textures on andalusite (Fig. 4a) take the form of hacksaw terminations and facets, and many grains also display large pits or holes. However, the pitting is commonly unoriented, and is

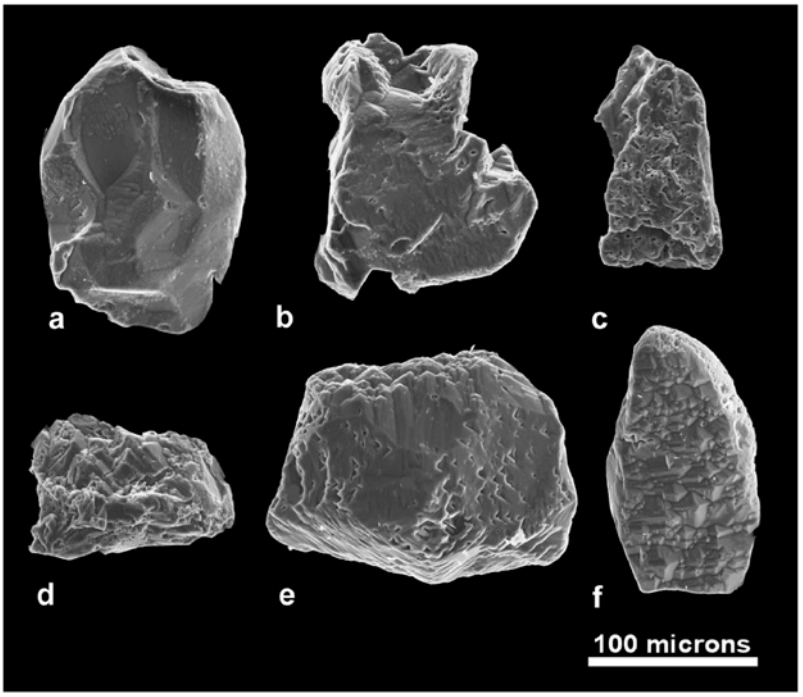

Fig. 5. Titanite etching. (a) Unetched titanite, Palaeocene sandstone, Norwegian Sea, 1097 m depth. (b) Titanite with incipient etching, Palaeocene sandstone, Norwegian Sea, 1097 m depth. (c) and (d) Highly etched titanite, Tertiary sandstone, offshore Ivory Coast, 2386 m depth. (e) and (f) Etched titanite, Palaeocene sandstone, Norwegian Sea, 1457 m depth.

therefore probably the result of leaching of inclusions, which are often present in andalusite grains. Sillimanite corrosion (Fig. 4b) is manifested as deep parallel grooves and facets, which develop into hacksaw terminations as dissolution proceeds.

In the shallow subsurface, kyanite lacks corrosion textures, with grains retaining the typical bladed or prismatic character with well-developed cleavage traces (Fig. 4c). Early stages of corrosion are manifested by oriented pits (Fig. 4c), but as dissolution proceeds, kyanite develops large-scale hacksaw terminations (Figs. 4d–f). The corrosion textures on kyanite described here (from the Pliocene of the south Caspian Sea Basin and from the Jurassic and Palaeocene of the Norwegian Sea) are closely comparable to those from the North Sea (Morton, 1979, 1984).

3.6. Titanite

At shallow depths, titanite grain surfaces show little modification by diagenetic processes, and retain features acquired during transport, such as rounding and fracturing (Fig. 5a). Some grains (Fig. 5b) show evidence of incipient corrosion, with local development of small-scale oriented pits. As dissolution proceeds, grains become more pitted and develop large-scale facets (Figs. 5c–f). The corrosion textures described in this paper (from the Palaeocene of the Norwegian Sea and the Tertiary offshore Ivory Coast) are similar to those described from the North Sea Palaeocene (Morton, 1984) and the Cretaceous–Palaeocene of Alberta (Rahmani, 1973).

3.7. Staurolite

In the central North Sea Palaeocene, staurolite shows a progressive increase in etching intensity with increasing burial (Morton, 1979, 1984). Grains at shallow depth have surfaces dominated by mechanically produced features, such as breakage blocks and conchoidal fractures, but with increasing depth small scale hacksaw terminations appear. These hacksaw terminations become larger as dissolution proceeds, until grains display skeletal characteristics. The pattern observed in the North Sea is

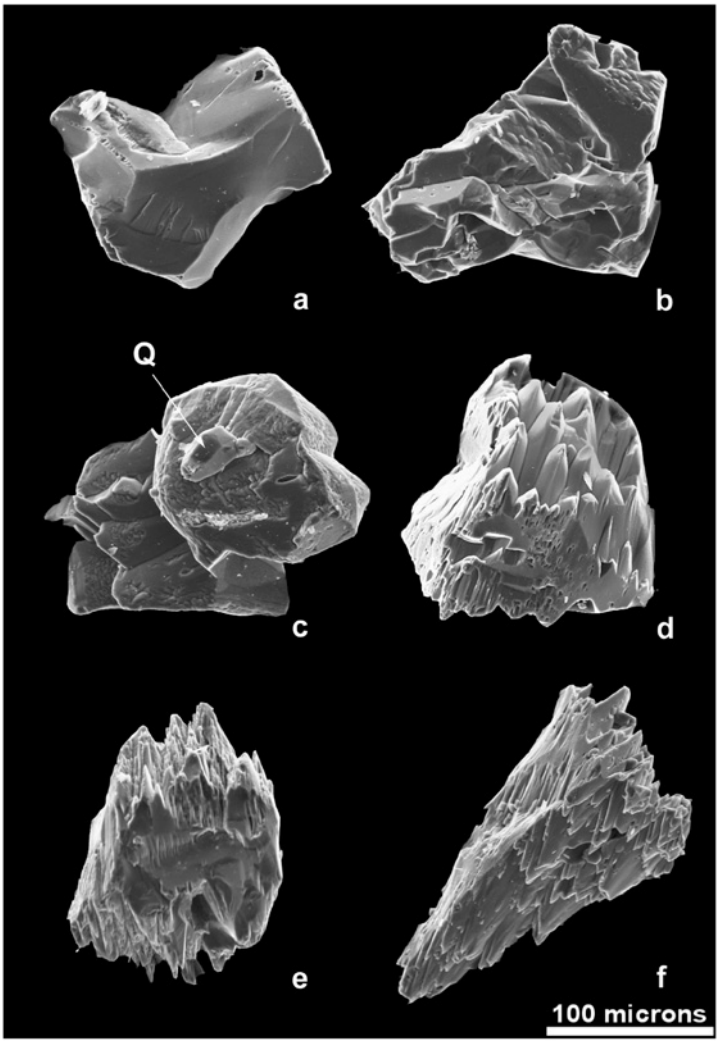

Fig. 6. Staurolite etching. (a) Unetched staurolite, Palaeocene sandstone, Norwegian Sea, 1097 m depth. (b) Staurolite with incipient etching, Palaeocene sandstone, Norwegian Sea, 1097 m depth. (c) Moderately etched staurolite exposing quartz inclusion (Q), Miocene, offshore Nigeria, 4440 m depth. (d) Highly etched staurolite, Cretaceous sandstone, Norwegian Sea, 2315 m depth. (e) Highly etched staurolite, Miocene sandstone, Bengal Basin, 3841 m depth. (f) Highly etched staurolite, Oligocene sandstone, offshore Trinidad, 1561 m depth.

repeated in sedimentary basins around the world, including the Norwegian Sea, offshore Nigeria, Bengal Basin and offshore Trinidad. Grains from shallow depths (such as the Palaeocene of the Norwegian Sea) have surfaces exclusively shaped by mechanical processes (Fig. 6a) or with slight modification by dissolution (Fig. 6b). By contrast, staurolite grains from sandstones that have undergone more advanced diagenesis display well developed hacksaw terminations (Figs. 6c–f). Evidence for dissolution is also afforded by quartz inclusions (Fig. 6c), which have been exhumed from the staurolite grains by continued etching. Staurolite etching has also been recorded during SEM study of Cretaceous–Palaeocene sandstones of Alberta (Rahmani, 1973) and Jurassic sandstones of New Mexico (Hansley, 1986).

3.8. Garnet

Of all diagenetically induced surface textures on detrital heavy minerals, those that develop on garnet grains have been the subject of maximum attention under the

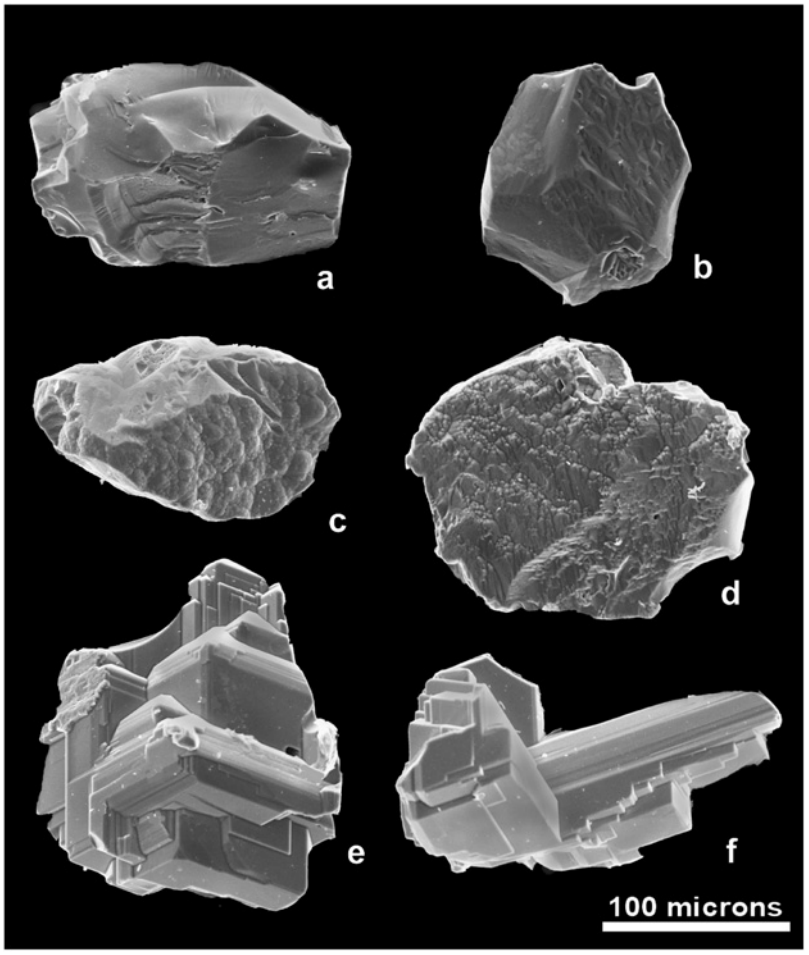

SEM. Rahmani (1973), Hemingway and Tamar-Agha (1975), Gravenor and Gostin (1979), Morton (1979, 1984), Borg (1986), Hansley (1986, 1987), Salvino and Velbel (1989) and Milliken and Mack (1990) all identify large-scale etch facets as the result of advanced garnet dissolution. Garnet dissolution proceeds initially by the appearance of mamillations and pits on surfaces otherwise generated by mechanical processes related to transport. Small-scale facets then appear, in some cases imparting a 'microscaly' appearance (Beveridge, 1960). In most cases, the scale of the facets increases with ongoing dissolution, although Hemingway and Tamar-Agha (1975) identified a phase of small-scale facets appearing on larger-scale facets. The same picture of increasing scale of faceting is evident from garnets in Jurassic, Cretaceous and Palaeocene sandstones of the Norwegian Sea, and from garnets in Miocene sandstones from the Mahakam delta (Figs. 7a–f).

One of the main reasons for the attention paid to garnet is that some authors have attributed the facets to overgrowth, rather than to corrosion. This question was considered in detail by Morton et al. (1989), who concluded, on the basis of thermodynamic considerations, experimental studies, distribution of faceted garnets in the subsurface, textural relationships and compositional variations within faceted grains, that the overgrowth hypothesis cannot be sustained.

3.9. *Apatite*

In contrast to the minerals described above, apatite does not appear to undergo dissolution in the subsurface. In fact, as shown in Fig. 8, apatite commonly develops secondary overgrowths with increasing burial. Grains at relatively shallow depth (Figs. 8a, b) retain their depositional morphology. As burial diagenesis proceeds, grains begin to develop small-scale apatite overgrowths (Figs. 8d, e) around recognisably detrital grains, until ultimately the detrital grain is entirely encased in a secondary overgrowth (Fig. 8f). Examples of overgrowth have been found in the Norwegian Sea and the North Sea, and Mange and Maurer (1992) illustrate well developed apatite overgrowths from the North German Basin. Further examples will probably emerge during studies of other deep basins.

Although most apatite grains in the subsurface lack corrosion features, occasional grains display evidence of dissolution, such as that shown in Fig. 8c. This etched apatite coexists with pristine apatite grains that show no sign of corrosion (Figs. 8a, b), therefore indicating that the corrosion did not take place in situ. Since apatite is unstable in weathering conditions, especially in humid environments (Morton, 1986), the presence of etched apatite indicates that the sediment has undergone a phase of weathering under subaerial conditions. SEM studies of apatite therefore have an important role to play in evaluating sediment transport history, in

Fig. 7. Garnet etching. (a) Unetched garnet, Palaeocene sandstone, Norwegian Sea, 1097 m depth. (b) Garnet with incipient etching, Palaeocene sandstone, Norwegian Sea, 1097 m depth. (c) Slightly etched garnet, Miocene sandstone, Mahakam delta, 2690 m depth. (d) Moderately etched garnet, Cretaceous sandstone, Norwegian Sea, 3261 m depth. (e) and (f) Highly etched garnet, Jurassic sandstone, Norwegian Sea, 4430 m depth.

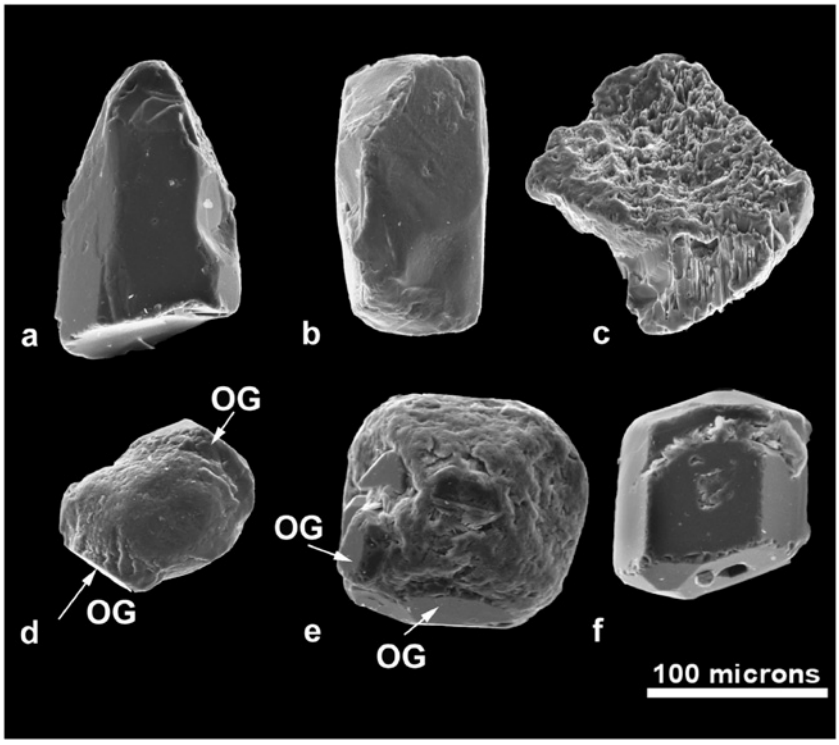

Fig. 8. Apatite etching. (a) and (b) Angular apatite, Tertiary sandstone, offshore Ivory Coast, 2386 m depth. (c) Etched apatite, Tertiary sandstone, offshore Ivory Coast, 2386 m depth. (d) Rounded apatite with secondary overgrowth (OG), Jurassic sandstone, North Sea, 2626 m depth. (e) Rounded apatite with secondary overgrowth (OG), Jurassic sandstone, Norwegian Sea, 4430 m depth. (f) Apatite entirely encased in euhedral secondary overgrowth, Jurassic sandstone, Norwegian Sea, 4430 m depth.

particular evaluating the extent of weathering, either in the regolith or during periods of alluvial storage.

3.10. Chloritoid

Although chloritoid is not an uncommon component of heavy-mineral assemblages, it is rarely present in abundance. Consequently, there have been very few SEM studies of chloritoid surface textures. New data from the Cretaceous of the Norwegian Sea and Miocene of the Mahakam delta (Figs. 9a–c), together with evidence from the Jurassic of the North Sea (Morton and Hallsworth, 1999), show that grains in the shallow subsurface are predominantly shaped by mechanical processes, with little modification by dissolution. Some grains display pitting (Fig. 9a), but these lack any preferred orientation, and are therefore the result of leaching of inclusions. Corrosion is recognised by the appearance of pits with triangular morphology (Fig. 9b), which develop into diamond-shaped pits (Fig. 9c) as dissolution proceeds.

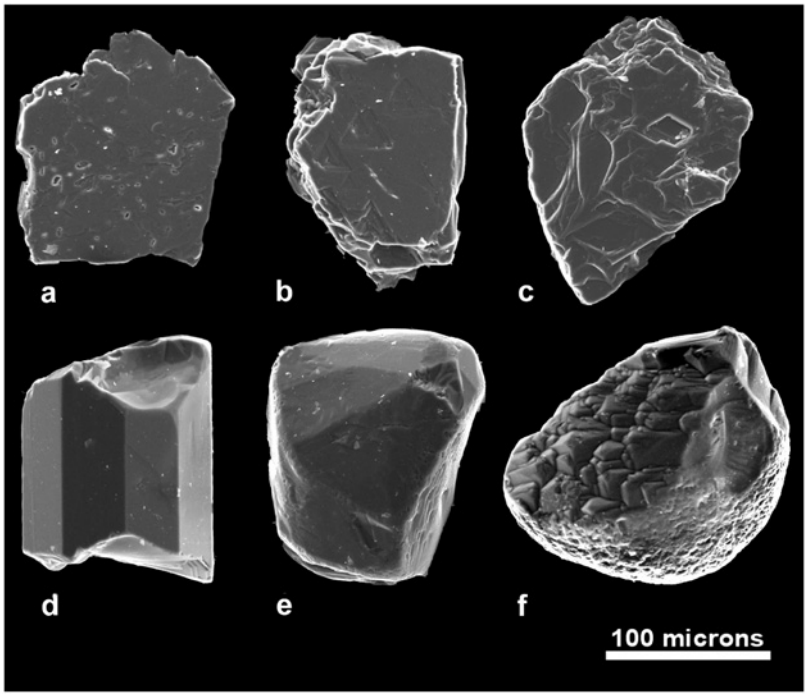

Fig. 9. Chloritoid and tourmaline etching. (a) Unetched chloritoid, Cretaceous sandstone, Norwegian Sea, 2315 m depth. (b) Chloritoid with incipient triangular-shaped etch pitting, Cretaceous sandstone, Norwegian Sea, 2315 m depth. (c) Etched chloritoid, Miocene sandstone, Mahakam delta, 2690 m depth. (d) Prismatic tourmaline, Jurassic sandstone, Norwegian Sea, 5167 m depth. (e) Subangular tourmaline, Jurassic sandstone, Norwegian Sea, 5167 m depth. (f) Etched rounded tourmaline, Jurassic sandstone, Norwegian Sea, 5167 m depth.

3.11. Tourmaline

Most tourmaline grains in sandstones from the subsurface retain their depositional morphology, which ranges from prismatic (Fig. 9d) to subrounded (Fig. 9e), and commonly show indentations resulting from grain–grain impact (Morton, 1979). However, in a small number of cases, tourmalines develop facets indicative of ongoing corrosion. These have been seen in the Jurassic, both of the Norwegian Sea (Fig. 9f) and of the North Sea (Morton and Hallsworth, 1999), and in Tertiary silver sands from Germany, The Netherlands and Belgium (Van Loon and Mange, 2007: this volume). Tourmaline etching is readily distinguished from tourmaline with overgrowths, which have been frequently recorded in heavy mineral assemblages in sandstones (e.g., Krynine, 1946). Tourmaline overgrowths are clearly recognisable under the petrographic microscope on the basis of a colour contrast with the host grain, as shown by Mange and Maurer (1992). However, tourmaline overgrowths can usually be attributed to growth during regional metamorphism in the protolith (e.g., Henry and Dutrow, 1992) rather than to authigenic growth in the

sandstone. The occurrence of etched tourmaline suggests that tourmaline is less stable than previous studies have suggested, although the precise conditions under which tourmaline etching proceeds have yet to be fully evaluated.

3.12. Rutile

Rutile grains display no sign of corrosion during burial diagenetic conditions, with no evidence for modification of depositional morphology. An example is shown in Fig. 10a, which is from a Jurassic sandstone buried to depths in excess of 5000 m in

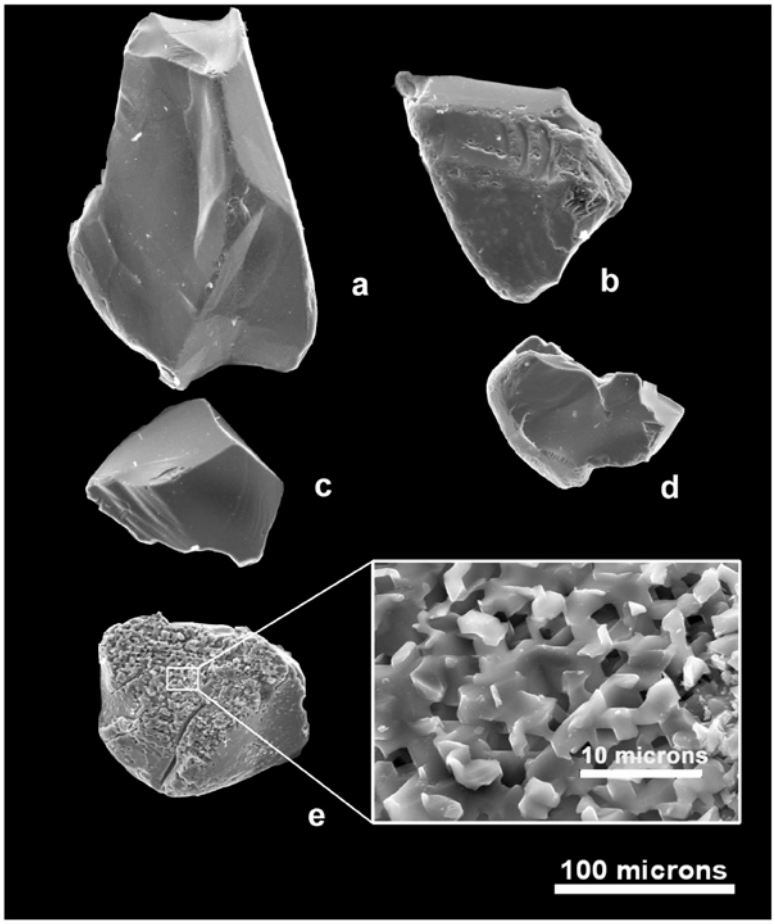

Fig. 10. Rutile and spinel surface textures. (a) Angular rutile, Jurassic sandstone, Norwegian Sea, 5167 m depth. (b) Angular gahnite (zinc spinel), Oligocene sandstone, offshore Trinidad, 1561 m depth. (c) Angular chrome spinel, Jurassic sandstone, Norwegian Sea, 1656 m depth. (d) Rounded chrome spinel, Jurassic sandstone, North Sea, 6325 m depth. (e) Chrome spinel with incipient etching, Jurassic sandstone, North Sea, 6325 m depth, with a magnified image of etched surface showing detail of etch pattern.

the Norwegian Sea. Similarly, surface textures on rutile grains from the North Sea Palaeocene (Morton, 1979) show only the effects of mechanical abrasion.

3.13. Spinel

The two most common detrital spinels are chrome spinel (chromite-magnesiochromite) and zinc spinel (gahnite). Both types of spinel rarely show any sign of corrosion. The zinc spinel in Fig. 10b (from the Oligocene, offshore Trinidad) is subangular, with a fractured surface showing indentations caused by mechanical processes. Zinc spinel grains from the North Sea Jurassic (Morton and Hallsworth, 1999) also lack any evidence for post-depositional corrosion. The vast majority of chrome spinels from the Jurassic of the Norwegian Sea and North Sea also reflect mechanical processes. The grain from relatively shallow burial (~1650 m) in the Norwegian Sea (Fig. 10c) is angular, and shows smooth fractured surfaces. A chrome spinel from considerable depth (in excess of 6000 m) in the North Sea (Fig. 10d) is subangular to subrounded, and again lacks any indication of corrosion. Chrome spinel grains from the southern North Sea Carboniferous, buried to a depth of ~3800 m (Morton and Hallsworth, 1999), are also unetched. However, another chrome spinel buried to over 6000 m in the North Sea Jurassic displays evidence of incipient dissolution, with a thin corroded surface layer. Detrital zinc and chrome spinels therefore appear to be highly stable in the subsurface, although there is evidence that chrome spinel undergoes slight corrosion at great depth.

3.14. Monazite

Monazite grains from Jurassic sandstones at depths over 5000 m in the Norwegian Sea (Figs. 11a, b) are subrounded to rounded, and most surface features are due to mechanical processes, rather than dissolution. This confirms previous observations of monazite from deeply buried Triassic (~4400 m) of the North Sea (Morton and Hallsworth, 1999). However, occasional grains show oriented etch pits (Fig. 11b), indicating incipient corrosion.

Under the petrographic microscope, many monazites in subsurface sandstones are seen to have brown surface coatings. SEM study has enabled the determination of the nature of this surface coat. The darker layer coating the top of the monazite grain in Fig. 11a was analysed using the energy-dispersive X-ray microanalysis system, which indicated that it consists essentially of carbon. Minor P and REE peaks are from the underlying monazite: these peaks are much more evident in the spectrum from the detrital grain. These coats are therefore interpreted to comprise solid bitumen, similar to those found coating monazite grains in Permo-Triassic sandstones of Western Australia (Rasmussen et al., 1989). The bitumen coats are believed to have formed by radiation-induced polymerisation of liquid hydrocarbons in contact with the detrital monazite grains (England et al., 2001). Recognition of the presence of such coats is important since they indicate the former presence of liquid hydrocarbons even in sandstones that no longer contain oil.

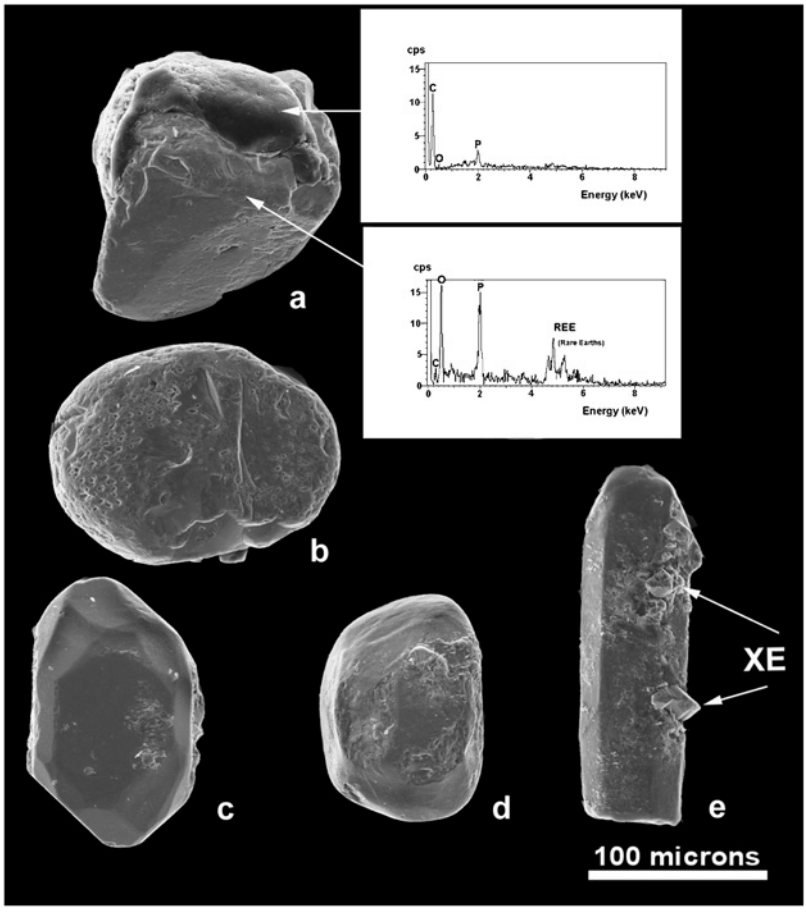

Fig. 11. Monazite etching and zircon morphology. (a) Monazite, Jurassic sandstone, Norwegian Sea, 5167 m depth, with bituminous surface layer, as verified by the ED spectrum of the coating (large C peak) and the underlying grain (REE, P, O peaks). (b) Monazite with incipient etching, Jurassic sandstone, Norwegian Sea, 5167 m depth. (c) Slightly rounded euhedral zircon, Jurassic sandstone, Norwegian Sea, 5167 m depth. (d) Rounded zircon, Jurassic sandstone, Norwegian Sea, 5167 m depth. (e) Prismatic zircon with xenotime (XE) outgrowths, Jurassic sandstone, Norwegian Sea, 5167 m depth.

3.15. Zircon

Zircon grains in the subsurface retain their depositional characteristics and have not been modified by dissolution processes. Examples shown in Figs. 11c–e are from the Jurassic of the Norwegian Sea, buried to depth in excess of 5000 m. These grains range from slightly rounded prismatic and euhedral to subrounded types, and display no signs of corrosion. Similar morphologies were described by Morton (1979) from the Palaeocene of the North Sea. Surface textural data therefore confirm the stability of zircon during burial diagenesis.

In very deeply buried sandstones, some zircons show development of small triangular-shaped crystals adhering to grain surfaces. These were originally described as 'outgrowths' by Butterfield (1936) and Smithson (1937). Energy-dispersive X-ray analysis of these outgrowths shows them to consist of xenotime. Development of xenotime outgrowths on zircon appears to mark an advanced stage of burial diagenesis, since it generally occurs in sandstones that have undergone garnet depletion, an observation made originally by Smithson (1937). Xenotime overgrowths offer possibilities for U-Pb radiometric dating of diagenetic events, for example by the sensitive high-resolution ion microprobe (SHRIMP), as discussed by Vallini et al. (2005).

4. SUMMARY

Although it is impossible to provide a comprehensive overview of the effects of burial diagenesis on heavy mineral surface textures in sedimentary basins worldwide, this contribution, in conjunction with previous systematic studies (Rahmani, 1973; Morton, 1979, 1984; Milliken and Mack, 1990), demonstrates that heavy mineral dissolution is widespread in the subsurface. A wide variety of heavy minerals show dissolution textures on grain surfaces, including andalusite, amphibole, chloritoid, epidote, garnet, kyanite, olivine, pyroxene, sillimanite, staurolite and titanite. Dissolution has been observed in sedimentary basins of Europe (North Sea, Faeroe-Shetland Basin, Rockall Trough, Norwegian Sea, Germany, France), Africa (offshore Ivory Coast and Nigeria), Asia (south Caspian Basin, Bengal Basin, eastern India, Mahakam delta) and America (US Gulf Coast, offshore Trinidad). SEM data from heavy mineral grain surfaces therefore indicate that intrastratal dissolution is a global, rather than a local, phenomenon. This aspect is considered further by Morton and Hallsworth (2007: this volume). Evaluation of the extent to which heavy mineral assemblages have undergone post-depositional modification is therefore crucial when evaluating provenance, and SEM has an important role to play in this regard.

Heavy minerals that do not display surface corrosion to any appreciable extent during deep burial are apatite, monazite, rutile, spinel (chrome and zinc varieties), tourmaline and zircon, and these minerals can be considered to be essentially stable. Nevertheless, under certain deep burial circumstances, tourmalines develop etch facets, and both monazite and chrome spinel show signs of incipient corrosion in extreme burial situations. By contrast, apatite tends to develop overgrowths during burial. Some sandstones contain both etched and unetched apatite, irrespective of burial depth: this is explained by variable apatite weathering in the source area and during periods of alluvial storage during transport, rather than in-situ corrosion in the subsurface.

ACKNOWLEDGEMENTS

We are grateful to Henrik Friis, David Krinsley and Maria Mange for their constructive comments on an earlier draft of this manuscript and for editing the figures. It is published by permission of the Executive Director, British Geological Survey, Natural Environment Research Council (NERC).

REFERENCES

Berner, R.A., Schott, J., 1982. Mechanism of pyroxene and amphibole weathering II: observations of soil grains. American Journal of Science 282, 1214–1231.

Berner, R.A., Sjöberg, E.L., Velbel, M.A., Krom, M.D., 1980. Dissolution of pyroxenes and amphiboles during weathering. Science 207, 1205–1206.

Beveridge, A.J., 1960. Heavy minerals in Lower Tertiary formations in the Santa Cruz Mountains, California. Journal of Sedimentary Petrology 30, 513–537.

Borg, G., 1986. Facetted garnets formed by etching: examples from sandstones of Late Triassic age, south Germany. Sedimentology 33, 141–146.

Butterfield, J.A., 1936. Outgrowths on zircon. Geological Magazine 73, 511–516.

Edelman, C.H., Doeglas, D.J., 1932. Reliktstructuren detritischer Pyroxene und Amphibole. Tschermaks Mineralogische und Petrographische Mitteilungen 42, 482–490.

Edelman, C.H., Doeglas, D.J., 1934. Über Umwandlungserscheinungen an detritischem Staurolith und anderen Mineralien. Tschermaks Mineralogische und Petrographische Mitteilungen 44, 225–234.

England, G.L., Rasmussen, B., Krapez, B., Groves, D.I., 2001. The origin of uraninite, bitumen nodules, and carbon seams in Witwatersrand gold-uranium-pyrite ore deposits, based on a Permo-Triassic analog. Economic Geology 96, 1907–1920.

Gravenor, C.P., Gostin, V.A., 1979. Mechanisms to explain the loss of heavy minerals from the Upper Palaeozoic tillites of South Africa and Australia and the late Precambrian tillites of Australia. Sedimentology 26, 707–717.

Gravenor, C.P., Leavitt, R.K., 1981. Experimental formation and significance of etch patterns on detrital garnets. Canadian Journal of Earth Sciences 18, 765–775.

Hansley, P.L., 1986. Relationship of detrital, non-opaque heavy minerals to diagenesis and provenance of the Morrison Formation, southwestern San Juan Basin, New Mexico. In: Turner-Petersen, C.E., Santos, E.S., Fishman, N.S. (Eds.), A Basin Analysis Case Study: The Morrison Formation, Grants Uranium Region. American Association of Petroleum Geologists, Studies in Geology, vol. 22, pp. 257–276.

Hansley, P.L., 1987. Petrologic and experimental evidence for the etching of garnets by organic acids in the Upper Jurassic Morrison Formation, northwestern New Mexico. Journal of Sedimentary Petrology 57, 666–681.

Hansley, P.L., Briggs, P.H., 1994. Garnet dissolution in oxalic acid: a possible analog for natural etching of garnet by dissolved organic matter. US Geological Survey Bulletin 1206, 1–14.

Hemingway, J.E., Tamar-Agha, M.Y., 1975. The effects of diagenesis on some heavy minerals from the sandstones of the Middle Limestone Group in Northumberland. Proceedings of the Yorkshire Geological Society 40, 537–546.

Henry, D.J., Dutrow, B.L., 1992. Tourmaline in a low grade clastic metasedimentary rock: an example of the petrogenetic potential of tourmaline. Contributions to Mineralogy and Petrology 112, 203–218.

Krynine, P.D., 1946. The tourmaline group in sediments. Journal of Geology 54, 65–87.

Lin, I.J., Kohrlich, V., Slatkine, A., 1974. Surface microtextures of heavy minerals from the Mediterranean coast of Israel. Journal of Sedimentary Petrology 44, 1281–1295.

Mahaney, W.C., 2002. Atlas of Sand Grain Surface Textures and Applications. Oxford University Press, New York.

Mahaney, W.C., Milner, M., 1998. Zircon microstriators in the sand of auriferous Andean tills: fine tools and noble metals. Boreas 27, 140–152.

Mallik, T.K., 1986. Micromorphology of some placer minerals from Kerala beach, India. Marine Geology 71, 371–381.

Mange, M.A., Maurer, H.F.W., 1992. Heavy minerals in colour. Chapman and Hall, London, 147pp.

Milliken, K.L., 2007. Provenance and diagenesis of heavy minerals, Cenozoic units of the northwestern Gulf of Mexico sedimentary basin. In: Mange, M.A., Wright, D.T. (Eds.), Heavy Minerals in Use. Developments in Sedimentology (this volume).

Milliken, K.L., Mack, L.E., 1990. Subsurface dissolution of heavy minerals: Frio Formation sandstones of the ancestral Rio Grande Province, South Texas. Sedimentary Geology 68, 187–199.

Morton, A.C., 1979. Surface textures of heavy mineral grains from the Palaeocene of the central North Sea. Scottish Journal of Geology 15, 293–300.

Morton, A.C., 1984. Stability of detrital heavy minerals in Tertiary sandstones of the North Sea Basin. Clay Minerals 19, 287–308.

Morton, A.C., 1986. Dissolution of apatite in North Sea Jurassic sandstones: implications for the generation of secondary porosity. Clay Minerals 21, 711–733.

Morton, A.C., Borg, G., Hansley, P.L., Haughton, P.D.W., Krinsley, D.H., Trusty, P., 1989. The origin of faceted garnets in sandstones: dissolution or overgrowth. Sedimentology 36, 927–942.

Morton, A.C., Hallsworth, C.R., 1999. Processes controlling the composition of heavy mineral assemblages in sandstones. Sedimentary Geology 124, 3–29.

Morton, A.C., Hallsworth, C.R., 2007. Stability of detrital heavy minerals during burial diagenesis. In: Mange, M.A. and Wright, D.T. (Eds.), Heavy Minerals in Use. Developments in Sedimentology (this volume).

Morton, A.C., Johnsson, M.J., 1993. Factors influencing the composition of detrital heavy mineral suites in Holocene sands of the Apure River drainage basin, Venezuela. In: Johnsson, M.J., Basu, A. (Eds.), Processes Controlling the Composition of Clastic Sediments. Geological Society of America Special Paper 284, 171–185.

Nickel, E., 1973. Experimental dissolution of light and heavy minerals in comparison with weathering and intrastratal solution. Contributions to Sedimentology 1, 1–68.

Rahmani, R.A., 1973. Grain surface etching features of some heavy minerals. Journal of Sedimentary Petrology, 43, 882–880.

Rasmussen, B., Glover, J.E., Alexander, R., 1989. Hydrocarbon rims on monazite in Permian-Triassic arenites, northern Perth Basin, Western Australia: pointers to the former presence of oil. Geology 17, 115–118.

Robson, D.A., 1984. Scanning electron micrographs of some common heavy minerals from the sandstones of the Northumberland Trough. Transactions of the Natural History Society of Northumbria 52, 27–34.

Salvino, J.F., Velbel, M.A., 1989. Faceted garnets from sandstones of the Munising Formation (Cambrian), northern Michigan: petrographic evidence for their origin by intrastratal solution. Sedimentology 36, 371–379.

Setlow, L.W., 1977. Age determination of reddened coastal dunes in northwest Florida, USA, by use of scanning electron microscope. In: Whalley, W.B. (Ed.), Scanning Electron Microscopy in the Study of Sediments. Geo Abstracts, Norwich, pp. 283–305.

Setlow, L.W., Karpovich, R.P., 1972. 'Glacial' micro-textures on quartz and heavy mineral sand grains from the littoral environment. Journal of Sedimentary Petrology 42, 864–875.

Smithson, F., 1937. Outgrowths on zircon in the Middle Jurassic of Yorkshire. Geological Magazine 74, 281–283.

Steiglitz, R.D., 1969. Surface textures of quartz and heavy-mineral grains from fresh-water environments: an application of scanning electron microscopy. Bulletin of the Geological Society of America 80, 2091–2094.

Tejan-Kella, M.S., Fitzpatrick, R.W., Chittleborough, D.J., 1991. Scanning electron microscope study of zircons and rutiles from a podsol chronosequence at Ycooloola, Queensland. Catena 18, 11–30.

Vallini, D.A., Rasmussen, B., Krapez, B., Fletcher, I.R., McNaughton, N.J., 2005. Microtextures, geochemistry and geochronology of authigenic xenotime: constraining the cementation history of a Palaeoproterozoic metasedimentary sequence. Sedimentology 52, 101–122.

Van Loon, A.J., Mange, M.A., 2007. 'In situ' dissolution of heavy minerals through extreme weathering, and the application of the surviving assemblages and their dissolution characteristics to correlation of Dutch and German silver sands. In: Mange, M.A., Wright, D.T. (Eds.), Heavy Minerals in Use. Developments in Sedimentology (this volume).

Velbel, M.A., 1984. Natural weathering mechanisms of almandine garnet. Geology 12, 631–634.

Velbel, M.A., 1989. Weathering of hornblende to ferruginous products by a dissolution-reprecipitation mechanism: petrography and stoichiometry. Clays and Clay Minerals 37, 515–524.

Velbel, M.A., 1993. Formation of protective layers during silicate-mineral weathering under well-leached, oxidizing conditions. American Mineralogist 78, 405–414.

Velbel, M.A., 2007. Surface textures and dissolution processes of heavy minerals in the sedimentary cycle: examples from pyroxenes and amphiboles. In: Mange, M.A., Wright, D.T. (Eds.), Heavy Minerals in Use. Developments in Sedimentology (this volume).

Walker, T.R., Waugh, B., Crone, A.J., 1978. Diagenesis in first-cycle desert alluvium of Cenozoic age, southwestern United States and northwestern Mexico. Bulletin of the Geological Society of America 89, 19–32.

Welton, J.E., 1984. SEM Petrology Atlas. American Association of Petroleum Geologists, Methods in Exploration Series, 4.

Werle, B., Schneider, H.E., 1977. Scanning electron microscope observations of diagenesis in the Triassic sediments of the Saar area, West Germany. In: Whalley, W.B. (Ed.), Scanning Electron Microscopy in the Study of Sediments. Geo Abstracts, Norwich, pp. 355–362.

Chapter 15

SCANNING ELECTRON MICROSCOPY OF GARNET FROM SOUTHERN MICHIGAN SOILS: ETCHING RATES AND INHERITANCE OF PRE-GLACIAL AND PRE-PEDOGENIC GRAIN-SURFACE TEXTURES

MICHAEL A. VELBEL[a], JENNIFER T. MCGUIRE[b] AND ANDREW S. MADDEN[c]

[a]*Department of Geological Sciences, 206 Natural Science Building, Michigan State University, East Lansing, MI 48824-1115, USA*
[b]*Department of Geology and Geophysics, Texas A&M University, College Station, TX 77843-3115, USA*
[c]*Environmental Sciences Division, Oak Ridge National Laboratory, Oak Ridge, TN 37081-6036, USA*

ABSTRACT

Garnet surface textures are known to be modified by processes in several portions of the sedimentary cycle: (1) weathering (first-cycle), (2) erosion, transportation, and deposition by moving water or ice, and (3) sandstone diagenesis. Previous studies have not assessed, however, the relative importance of inherited and newly formed grain-surface features of sand-size garnet grains. Garnets from soils developed by weathering of glacial (till and outwash) deposits at agricultural and forested sites in Michigan's Lower Peninsula were examined by scanning electron microscope to determine possible associations of grain-surface textures with parent material provenance and soil processes. All Michigan soil localities examined contain garnets that exhibit surface features apparently inherited from their pre-existing sedimentary source rocks, and/or features formed during glacial transport. Widespread preservation of inherited pre-pedogenic surface textures suggests that garnet in Michigan soils has undergone little weathering since deglaciation. Some garnet grains from both forested and agricultural soils, however, have well-formed 1–10 μm etch pits on their surfaces that may have formed either in garnet source-area regoliths or by weathering in the present soil.

At published garnet dissolution rates experimentally determined under weathering conditions, formation of 1–10 μm etch pits would take decades to centuries. Given that mineral weathering rates in nature are almost invariably one to three orders of magnitude slower than in the laboratory, the small size of the observed Michigan soil–garnet etch pits is broadly consistent with

Developments in Sedimentology, Vol. 58, 413–432

ISSN: 0070-4571/doi:10.1016/S0070-4571(07)58015-5

the age of the Michigan soils. This suggests that the "response time" of garnet surface textures to environmental perturbations is long relative to the time since the last deglaciation; the time required to develop large, extensive, and abundant weathering textures on garnet is longer than the age of Michigan soils. Even millennia under present weathering conditions are not sufficient to destroy pre-pedogenic and pre-glacial (e.g., source-rock) garnet surface textures and replace them with characteristic garnet weathering textures.

Keywords: etch pits; garnet; glacial deposits; imbricate wedge marks; Michigan; regolith; soil; weathering rates

1. INTRODUCTION

Morphological and surface-textural attributes of minerals are employed in many ways in geosciences. For example, provenance investigations can exploit objective classification schemes that have been developed to quantitatively describe zircon morphology (e.g., Pupin, 1980; Winter, 1981; Matsuura and Aoki, 1989; Vavra, 1993; Corfu et al., 2003). Such provenance applications presuppose that primary morphological attributes survive passage of zircon grains through the rock cycle, a reasonable assumption for a persistent heavy mineral.

Etching of less-persistent minerals, such as hornblende, during weathering has been used as a relative age indicator of glacial deposits (e.g., Locke, 1979, 1986; Hall and Martin, 1986; Hall and Michaud, 1988; Hall and Horn, 1993), and as a measure of soil development on glacial parent materials (e.g., Mikesell et al., 2004). Such applications of surface textures as chronologic or environmental indicators assume that dissolution-related morphological attributes of these less-persistent minerals adjust progressively (rather than instantly) to exposure to a new (in this case, weathering) environment.

In the case of zircon, it is the preservation and inheritance of morphological attributes from a previous compartment of the rock cycle that allows provenance to be inferred; in the case of hornblende, it is the relatively rapid overprinting of "up-cycle" textures in the new environment that allows corrosion features to be used as relative-age or environmental indicators. In both cases, the ability to arrive at useful interpretations from sand grain morphology and/or grain-surface textures is based on specific relationships between rates of surface-texture modification and the length of time the grain is exposed to modifying processes in the next stage of the sedimentary cycle. Surface textures of detrital mineral grains have been studied, catalogued, and used to interpret environments for some time. While it is intuitive that textures can be formed, modified, or destroyed at any place in the sedimentary cycle, quantification of modification rates and response time has not often been attempted.

This contribution examines the relationship between the rate of modification of inherited (up-cycle) surface textures on the heavy minerals and the timescale of exposure to new (down-cycle) environments, using the example of garnet weathered in a glacial parent regolith of complex provenance. Garnet (general formula $(Ca,Fe^{II},Mn,Mg)_3(Al,Fe^{III},Ti)_2Si_3O_{12}$) was selected for several reasons. Garnet-group minerals are relatively abundant in the heavy mineral fraction of many sediments (e.g., Morton and Hallsworth, 1999), intermediate in persistence among such minerals in

weathering and the sedimentary cycle in general (Velbel, 1999, and references therein), and in sediments and sedimentary rocks in particular (e.g., Morton and Hallsworth, 1999, and references therein), and highly symmetrical in crystal form.

Many previous studies of garnet weathering address weathering-related variations in abundances but not textures; most studies of garnet weathering textures examined garnets from saprolitic and lateritic deep-weathering profiles (Velbel, 1984, 1993a). Previous work on low-temperature mineral-solution reactions involving garnet (including weathering and burial diagenesis) has suggested that garnet grain-surface textures show more variation after alteration in different environments than other silicate minerals, possibly indicating that garnet surfaces and surface textures are more sensitive to variations in the geochemical environment of alteration than other silicates (Velbel, 1984, 1993a; Salvino and Velbel, 1989). Despite the importance of soils on glacial parent materials in many mid- and high-latitude landscapes, comparatively few studies have examined garnet weathering textures in soils on transported (e.g., glacial, glaciofluvial) parent materials (Ghabru et al., 1989); the present contribution extends studies of garnet surface textures to a larger range of glacially transported regolith types than previous work, in a region with well-studied glacial deposits and soils.

Interpretation of many surface features on garnet grains (e.g., etch pits, imbricate wedge marks (IWMs), and the relationships between them) requires attention to the morphological crystallography of garnet, because the dissolution features are euhedral (bounded by crystallographic planes) even if the grains themselves are not euhedral. Garnet has high crystallographic symmetry (isometric system, hexoctahedral class). While many minerals crystallize in this class, garnet is the only common rock-forming silicate in this crystal class, and it is the only common isometric silicate mineral with redox-sensitive elements (e.g., Fe, Mn) as major constituents.

On a well-developed euhedral garnet crystal, there may be many crystal faces. However, all the faces in the same form (related to one another by symmetry) are symmetrically identical, so that on crystals of high-symmetry compounds, even a large number of crystal faces represent only a small number of distinct unique surface properties. Most euhedral natural garnets have morphologies dominated by only a few crystallographic forms, commonly the dodecahedron {0 1 1} and the trapezohedron {1 1 2} (e.g., Pabst, 1943; Cherepanova et al., 1992; Boutz and Woensdregt, 1993). Similarly, the isotropy of garnet's structure means that there is less directional variation in bonding in garnet than in any other major rock-forming silicate mineral. For both euhedral crystals and fractured grains, the high symmetry of garnet minimizes variation in the crystallographic/crystal-chemical properties of different exposed surfaces, and thereby minimizes difficulties in interpreting surface textures.

Garnet surface textures have been previously studied from several parts of the sedimentary cycle: (1) weathered (first-cycle) garnets, (2) garnets eroded, transported, and deposited by moving water or ice, and (3) diagenetically modified garnets in sandstones. After reviewing salient previous works on garnet surface textures in different compartments of the sedimentary cycle, this contribution describes grain-surface features observed on garnets in several soils in southern Michigan. We then estimate the rate at which garnet grain surfaces are affected by etching during weathering, and discuss implications of the resulting rates and

time-scales that allow interpretation of grain-surface textures in the context of regolith history and the sedimentary cycle.

2. GARNET SURFACE TEXTURES IN THE SEDIMENTARY CYCLE

Mineral surfaces can be modified at any of a number of stages of the sedimentary cycle (e.g., Stieglitz and Rothwell, 1978; Morton and Hallsworth, 1999). Mineral surface textures can be inherited (unmodified) from parent materials. Primary surface textures can be modified or even completely destroyed and replaced by new surface textures during weathering. Erosion of weathered grains from soils and regoliths, followed by transport and deposition of the sediment, can modify the surfaces of weathered grains (e.g., by abrasion), superimposing new textures, while burial diagenesis can further modify grain-surface textures. Acquired grain-surface textures can be inherited in subsequent compartments, and may even survive into the next sedimentary cycle, as sedimentary parent rocks are weathered and eroded, and grains derived from them are redeposited (Stieglitz and Rothwell, 1978).

2.1. Weathering of Almandine and Spessartine Garnet

Biologically active soil and sub-soil regolith (e.g., saprolite) are both weathering environments, but chemical differences between them produce very different garnet surface textures. Almandine and spessartine garnets from the saprolitic interval of deep weathering profiles exhibit grain-surface features consistent with the "protective surface layer" (PSL) hypothesis, especially in weathering microenvironments in which Al, Fe, and Mn are essentially immobile (Velbel, 1984, 1993a).

In many lateritic and saprolitic regoliths, layers of ferruginous weathering products replace garnet. Replacement begins at grain boundaries and along internal fractures traversing the garnet, and the replacement front evolves from the original grain boundary toward the grain or fragment center, a texture known as "centripetal replacement" (Velbel, 1984). The resulting products occur as layers of uniform thickness (e.g., Stoops et al., 1979; Velbel, 1984). The contact between the garnet surface and the layer of weathering products is sharp and smooth, and garnet subgrain corners (e.g., at the junctions of fractures) are visibly rounded beneath the layers. PSLs are not observed on garnets in the soils studied here.

In many soils, almandine garnet surfaces are directly exposed to soil solutions (Velbel, 1984, 1993a; Ghabru et al., 1989; Graham et al., 1989). In the rooting zone of soils, PSLs do not form and pre-existing layers are dissolved, evidently due to biochemical processes (Embrechts and Stoops, 1982; Velbel, 1984). Such "unprotected" grains in soils (where Al, Fe, and Mn are mobile) exhibit numerous well-formed etch pits (Velbel, 1984, 1993a). Depending on the degree of development of the individual pits and the orientation of the grain surface relative to the crystallographic axes of garnet, etch pits take on a variety of appearances. Shallow etch pits include "nail-head" depressions (Ghabru et al., 1989) exhibiting triangular or tetragonal pyramidal outlines, and broader shallow pits with rhombic bottoms (Velbel, 1984). Deeper, more completely developed etch pits are depressions

bounded by dodecahedral faces (Velbel, 1984). The walls of garnet etch pits are all common (e.g., dodecahedral) faces that dominate as growth faces of garnet crystals.

2.2. Sedimentary (Transportational and Depositional) Modification of Pedogenic Surface Features

Chatter marks, conchoidal fractures, and other physical surface features have been reported from garnet sand grains in unconsolidated sediments (e.g., Folk, 1975; Bull et al., 1980; Gravenor, 1985). Mechanical fracturing is implied, but specific mechanical processes vary among different transport processes and have for the most part not been investigated in detail for garnet. Garnets from fluvial sediments from Coweeta Creek (near Otto, NC, USA) in the Southern Blue Ridge have etch pits apparently inherited from exposure in soil (Velbel, 1984); the grains themselves are rounded, which could be either due to abrasion, or natural physical or chemical removal of protective ferruginous layers exposing the rounded sub-PSL-surface.

2.3. Burial Diagenetic Modification of Surface Features

A complete review of the extensive literature on burial diagenetic surface textures of garnets is beyond the scope of this contribution, which examines modification of garnet grain-surface textures during weathering rather than diagenesis. However, as some diagenetic textures appear to be inherited on garnets eroded from sandstones and deposited in the glacial parent materials of Michigan soils, certain diagenetic textures and the literature discussing them are briefly summarized here.

IWMs, small faceted features of apparent positive relief and reminiscent of abundant small overgrowths, occur on garnets from numerous diagenetically altered sandstones (Morton et al., 1989; Salvino and Velbel, 1989). Despite Bramlette's (1929) correct inference that such features result from corrosion during intrastratal dissolution, there was considerable debate in the 1970s and 1980s between sedimentary petrologists over the authigenic or dissolution origin of IWMs (e.g., Simpson, 1976; Gravenor and Leavitt, 1981; Morton et al., 1989; Salvino and Velbel, 1989; Turner and Morton, 2007—this volume). Salvino and Velbel (1989) reviewed this literature and presented unequivocal textural evidence from Cambrian sandstones of northern Michigan for the origin of IWMs by intrastratal dissolution, strongly supporting the arguments of Morton et al. (1989) who arrived at the same conclusion based on their studies of garnets elsewhere. Hansley (1987) and Hansley and Briggs (1994) produced similar dissolution features experimentally under simulated diagenetic conditions.

2.4. Relationship of Etch Pits to IWMs

Etch pits are crystallographically controlled dissolution voids, produced by interface-limited weathering mechanisms (Velbel, 1984, 1993a, and references contained therein). Individual etch pits on almandine are depressions (''negative crystals'', voids with crystal faces) with dodecahedral faces. IWMs appear to form by overlap and coalescence of dodecahedral etch pits, and represent a more advanced stage of etching.

Being crystallographically controlled, all pits on any individual garnet grain have identical orientations. However, by virtue of garnet's high symmetry and easy conchoidal fracture, these crystallographically controlled etch pits can occur on any surface of a given garnet, regardless of the crystallographic orientation of that surface. As a result of dodecahedral pits occurring on a variety of surface orientations, the pits may present different appearances on different surfaces. Furthermore, the depth/width ratio of the etch pit can affect the relative importance of the floor and walls of the etch pit, resulting in different appearances even for etch pits with the same form on grain surfaces with similar crystallographic orientations (e.g., Velbel, 1984; Fig. 3 in Velbel, 1993a).

Dodecahedral pits on a surface oriented such that the bottom of the pit is the intersection of three dodecahedral faces will appear as small negative dodecahedra. Dodecahedral pits on a surface oriented such that the bottom of the pit is one of the dodecahedral faces can appear as a shallow diamond (rhombic) depression (so-called "nail-head" depressions of Ghabru et al., 1989). However, all such slightly different surface morphologies are merely identical etch pits "intersecting" surfaces that have different orientations relative to the garnet's crystal structure.

Etch pits on garnet progress through a sequence of stages. While each individual stage has been documented in individual case studies (e.g., Velbel, 1984, 1993a, and Ghabru et al., 1989 for weathering; Salvino and Velbel, 1989 for intrastratal dissolution during burial diagenesis) the sequence of stages and their relationship to one another have not been previously described. Progressive weathering causes the dissolution voids to gradually and systematically increase in size (both depth and cross-sectional area) on the pre-weathering surface of the mineral grain. The pre-weathering surfaces of garnets may have any of several surface textures. These include: relict crystal-growth features; smooth rounded surfaces exhumed from beneath PSLs; or (in altered sedimentary materials) mechanically abraded or conchoidally fractured surfaces.

Extensive weathering of multiple etch pits on an individual grain results in their coalescence. (This is well-established for dissolution of major rock-forming silicate minerals; see review by Velbel, 2007—this volume.) The topography of surfaces produced by coalescence of dodecahedral etch pits eventually (after all pre-etching surface has been removed by the lateral expansion of the euhedral pits) consists of only dodecahedral etch-pit walls. All prominences and depressions on the surface at this stage are intersections of crystal faces, which are themselves walls of enlarged etch pits. The overall array of multiple small areas with identically oriented crystal faces (that constitute IWMs) is easily visible in transmitted-light microscopy of grain mounts (e.g., Hamblin, 1958).

The threefold and fourfold symmetry axes of the garnet are readily apparent in the arrangements of the faces. The IWM surfaces resemble numerous small crystallographically aligned overgrowths (similar to quartz overgrowths on detrital quartz cores in early stages of sandstones cementation), and have been previously misinterpreted as such (see references in Salvino and Velbel, 1989). Unequivocal evidence of a dissolution (rather than growth) origin for IWMs on garnets has been published (e.g., Salvino and Velbel, 1989; Hansley and Briggs, 1994; Turner and Morton, 2007—this volume), and IWMs are now best understood not as a unique garnet surface feature but rather as a more advanced stage of garnet etching, the stage at which no pre-etching surface remains between the walls of euhedral etch pits.

It has been difficult to discern the relationship between garnet surfaces pocked with individual etch pits and surfaces dominated by IWMs because garnet seems to dissolve much more extensively during burial diagenesis than during weathering. Published reports of minimally modified surfaces with etch pits are all from weathered regoliths, whereas reports of IWMs are all from sedimentary rocks subjected to burial diagenesis (including intrastratal dissolution of garnet). It appears from comparing the weathering and diagenesis references cited above that only during burial diagenesis are garnet surfaces corroded long enough to reach the IWM stage of morphological development. It remains to be determined whether this is because geochemical conditions are more corrosive to garnet in the diagenetic environment than in the weathering environment, or because sand grains are subjected to similar geochemical conditions for much longer periods of time during burial diagenesis than during weathering (e.g., Velbel, 1989). However, regardless of the precise geochemical reason, it is now apparent that IWMs represent a greater degree or extent of garnet corrosion than euhedral etch pits, not a fundamentally different style of garnet corrosion. The faces of IWMs are the same crystallographic planes as the walls of etch pits. The style of garnet etching is similar in weathering and diagenesis; it is the extent that differs. Weathered garnet surfaces are partially covered with small euhedral etch pits, whereas intrastratally dissolved garnets in many sandstones have been completely resurfaced by corrosion, such that their surfaces are now consist entirely of walls of euhedral etch pits (IWMs).

3. TIMESCALES OF ETCH-PIT FORMATION ON GARNET DURING WEATHERING

Etch pits on garnet are small equant dodecahedral depressions (e.g., Velbel, 1984, 1993a), but for the purposes of simple calculations, a hemispherical shape can be assumed. The volume (V) of a hemispherical etch pit of radius r is

$$V = \frac{2}{3}\pi r^3$$

The internal surface area (A) of a hemispherical etch pit of radius r is

$$A = 2\pi r^2$$

The number of moles (M) of mineral removed when a volume V of mineral is dissolved is

$$M = \frac{V}{V^{\circ}}$$

where V° is the molar volume (cm^3/mol) of the specific mineral being dissolved. For almandine garnet $Fe_3Al_2(SiO_4)_3$, $V^{\circ} = 115.43\,cm^3$/mol.

The time required to dissolve a mass M is

$$t_d = \frac{M}{JA}$$

where J is the dissolution rate (mol/cm^2/sec). The dissolution rate (J) can be determined from laboratory experiments, or from geochemical mass-balance in natural systems where watershed-scale solute-flux data are available.

Substituting gives

$$t_{\mathrm{d}} = \frac{(2/3\pi r^3)/V^{\mathrm{o}}}{J2\pi r^2}$$

$$t_{\mathrm{d}} = \frac{r}{3V^{\mathrm{o}}J} = \frac{d/2}{3V^{\mathrm{o}}J} = \frac{d}{6V^{\mathrm{o}}J}$$

$$t_{\mathrm{d}} = \frac{r}{3V^{\mathrm{o}}J} = \frac{d}{6V^{\mathrm{o}}J}$$

If the dissolution rate of the mineral in a natural system can be estimated by adjusting experimentally determined dissolution rates for known differences between laboratory and field rates (e.g., Velbel, 1993b), or determined for the specific natural regolith being studied from geochemical mass-balance, the time required to form hemispherical etch pits of a measured diameter can be determined.

This approach assumes that all dissolution occurs at the walls of etch pits; in other words, that all reactive surface area on naturally corroded garnets is within etch pits, and that the garnet surface between etch pits is not reactive. Using optical interferometry Lüttge et al. (1999) and Lasaga and Lüttge (2001) observed that bulk dissolution of anorthite involves dissolution from both etch pits and retreat (lowering) of the surface between them. However, the surface textures of garnet suggest that the dissolution process may operate differently on different silicate minerals.

At advanced stages of garnet dissolution (manifested as IWMs on garnets subjected to prolonged intrastratal dissolution; Salvino and Velbel, 1989) the entire grain surface consists of facets on IWMs. These facets are the walls of coalesced euhedral (e.g., dodecahedral) etch pits. Consequently, from IWM development onward, the entire garnet surface consists of etch-pit walls, and there is no other surface. At earlier stages of garnet dissolution, there is unetched surface between the etch pits. However, the fact that such surface does not survive at more advanced stages of garnet dissolution suggests that etch-pit edges are consumed faster by lateral growth of etch pits (dissolution of etch-pit walls and edges) than by bulk-surface lowering, unlike feldspar dissolution. Given the great diversity of crystal structures, crystal chemistry, and dislocation distributions and characteristics of different silicate minerals, it is perhaps not surprising that different silicate minerals dissolve with different relative contributions to dissolution from different kinds of surfaces (e.g., dislocation-influenced vs. bulk surface). The preponderance of morphological evidence from naturally dissolved garnets suggests that enlargement of etch pits by preferential dissolution of etch pits walls is dominant relative to solutional lowering of surface between etch pits. The inferred dominance of solutional loss from etch-pit walls is embodied in the equations above.

4. MATERIALS AND METHODS

Samples were collected from three soils from Michigan's Lower Peninsula. All three soils are developed on Pleistocene glacial deposits (deglaciated approximately 14 ka: Robertson et al., 1993). Soils (Typic Haludalfs) of the Oshtemo and Kalamazoo soil series (USDA Soil Conservation Service, 1981) were sampled from a deciduous forest (Long Woods) and an agricultural soil, both developed on glacial outwash (Farrand and Bell, 1982; Robertson et al., 1993) at the Kellogg Biological Station (KBS) Long Term Ecological Research (LTER) site (near Battle Creek, MI). Soil pHs on uncultivated sites at KBS are approximately 6; cultivated sites have pHs approximately 7 due to agricultural practices such as liming (Robertson et al., 1993). Such practices affect modern soil properties, but the historical period of agriculture in this region is only the most recent few centuries of the regolith history, prior to which the sites were not differentiated from one another by difference in land-use practices. A deciduous forest soil of the Cohoctah soil series developed on glacial till (ground moraine; Farrand and Bell, 1982) was sampled at the Sanford Natural Area on the Michigan State University campus (East Lansing, MI). Soil pH for the Cohoctah soil series is typically 6–8 (USDA, 1979).

Possible provenances of sand-sized first-cycle garnets in glacial deposits of Michigan's Lower Peninsula include unweathered crystalline bedrock of the Canadian Shield (Dworkin et al., 1985) and pre-glacially weathered regolith on the Canadian Shield. Possible provenances of multicycle garnets in glacial deposits of southern Michigan include a variety of indurated Palaeozoic sedimentary rocks of the northern and central Michigan Basin. Sandstones of Cambrian age with heavy-mineral fractions including garnet are presently exposed on the northern shore of Michigan's Upper Peninsula (Hamblin, 1958). Closer to the areas of the present study, Carboniferous sandstones are widespread beneath a glacial cover, and crop out locally, in Michigan's Lower Peninsula. Mississippian sandstones are known from studies of subsurface material to contain a diverse heavy-mineral assemblage, including biotite mica, several varieties of amphibole, and garnet (Stearns, 1933). A sparse heavy-mineral assemblage dominated by highly resistant minerals is known from Pennsylvanian sandstones of Michigan (reviewed in Price, 1994).

The most likely source of multicycle garnet (recycled from sedimentary source rocks) in the glacial deposits of southern Michigan is the Cambrian sandstones exposed along the southern shore of Lake Superior, well to the north of, and along the glacial heavy-mineral dispersal path to (Dworkin et al., 1985), the study areas. In principle, it is possible that some garnets in glacial deposits of southern Michigan may have been exhumed from nearby Carboniferous sandstones. However, the following evidence suggests that such local sources are unlikely to have contributed garnet to the glacial deposits.

Price and Velbel (2000) reported extensive leaching by dilute, oxidizing solutions that produced groundwater ferricrete in now-exposed Pennsylvanian sandstones. Many less-resistant heavy minerals of shallow Carboniferous sandstones in Michigan may have been leached (along with other phases like early-diagenetic cements) from outcrops and shallow subcrops during such alteration. Along with the paucity of less-resistant heavy-mineral types in the Carboniferous sandstones near the top of the local Palaeozoic stratigraphic sections, this suggests that, even in Carboniferous

sandstones that may have originally contained garnet, near-surface occurrences (those most likely to have been eroded and incorporated into the glacial sediment load) may have been leached of all but their most resistant heavy minerals prior to glacial erosion. Consequently, the Carboniferous sandstones of the Michigan Basin are not likely to have been the source of much garnet in glacial deposits. In contrast, garnet is known to have persisted to the present even in outcrops of Cambrian sandstones of the northern Michigan Basin (Hamblin, 1958); these Cambrian sandstones are, therefore, plausible candidate sources for possible multicycle garnet in glacial deposits of southern Michigan. Diagenetically altered garnets in these prospective Palaeozoic sedimentary source rocks of the Pleistocene glacial deposits were previously examined from quartz arenite of the Cambrian Munising Formation in northern Michigan (Salvino and Velbel, 1989).

Matelski and Turk (1947) reported the presence and distribution of several optically different (color) varieties of garnet in a number of different podzolic (spodosolic) soil profiles on glacial parent materials in the northern part of Michigan's Lower Peninsula. They found that all other heavy minerals they examined (including opaque minerals and several color-varieties of hornblende) were less resistant to podzolic weathering than the garnets. Whether their results apply to the predominantly alfisolic soils that dominate the southern Lower Peninsula of Michigan remains to be established.

Garnets were extracted from heavy-mineral separates (concentrated using sodium polytungstate, density >2.89) from mechanically sieved fine-sand (0.125–0.250 mm) fractions. Heavy-mineral separates were mounted on sample stubs, coated with gold, and examined in secondary-electron imaging mode using a JEOL T-20 scanning electron microscope.

5. RESULTS

5.1. *Scanning Electron Microscopy*

Garnets from all Michigan localities exhibit a wide range of surface features. These include IWMs (Fig. 1) and conchoidally fractured surfaces (Fig. 2) formed during glacial transport. Some garnet grains from KBS (both forested and agricultural soils) have well-formed 1–10 μm etch pits on their otherwise facetted (Figs. 3 and 4), conchoidal (Fig. 5), or rounded (Fig. 6) surfaces. Several garnet grains (Figs. 4 and 6) also have even smaller-scale (submicron) surface roughness or scalloping.

5.2. *Etching Rates and Inheritance of Pre-Glacial and Pre-Pedogenic Grain-Surface Textures*

Natural weathering rates for garnet in the Michigan soils are not known from local mass-balance studies, and so must be estimated by other means. For many other common rock-forming silicate minerals, abundant experimentally determined dissolution rates under weathering conditions have been published (e.g., papers in White and Brantley, 1995). Dissolution rates of well-studied rock-forming silicate minerals are known to exhibit minima at circum-neutral to mildly acidic pH (papers

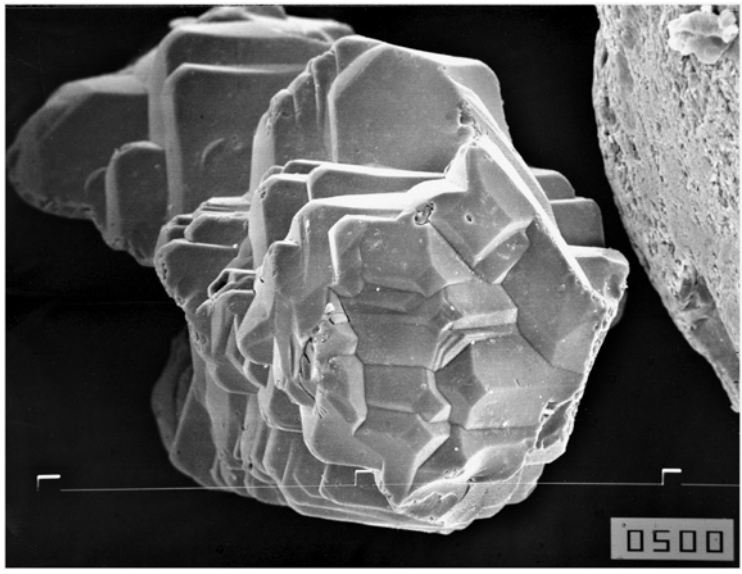

Fig. 1. Imbricate wedge marks (inherited from diagenetically altered Palaeozoic sandstones in the source area of the glacial deposits) on garnet from soil in the Sanford Natural Area on the campus of Michigan State University. Scale marks are 100 μm apart.

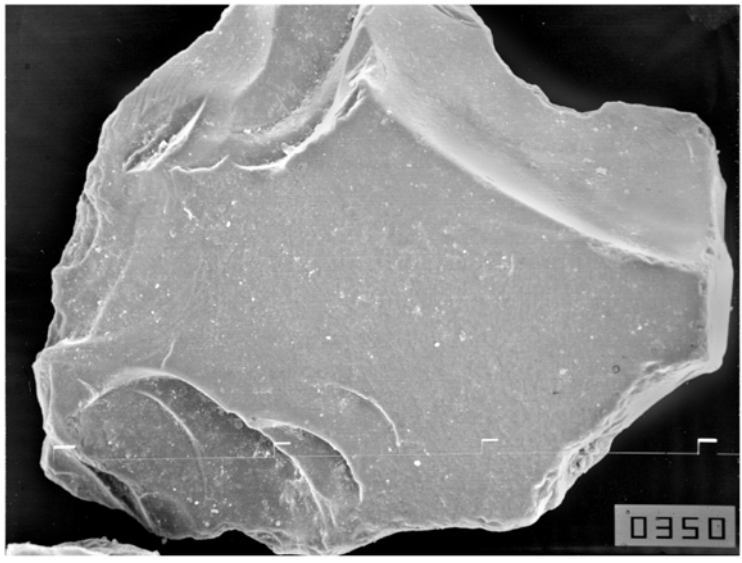

Fig. 2. Conchoidally fractured garnet (fracturing took place most likely during glacial transport) from soil in the Sanford Natural Area on the campus of Michigan State University. Scale marks are 100 μm apart.

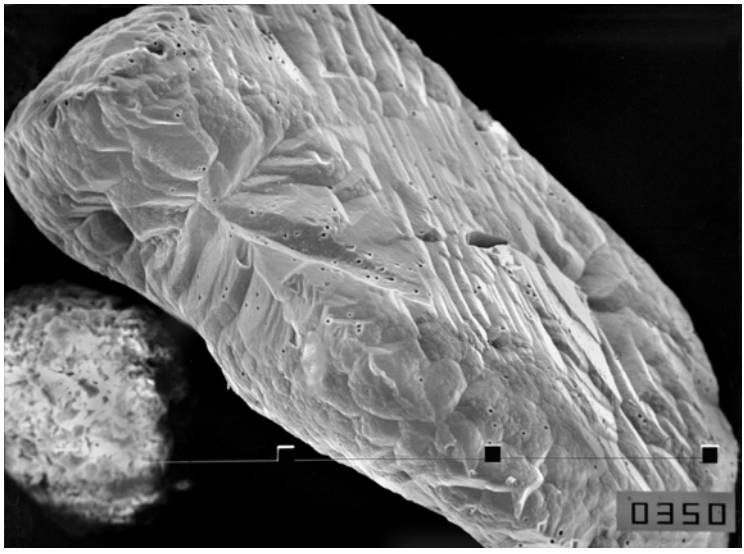

Fig. 3. Etch pits superimposed on imbricate wedge marks (inherited from diagenetically altered Palaeozoic sandstones in the source area of the glacial deposits) on garnet from agricultural soil at the Michigan State University Kellogg Biological Station. Scale marks are 100 μm apart.

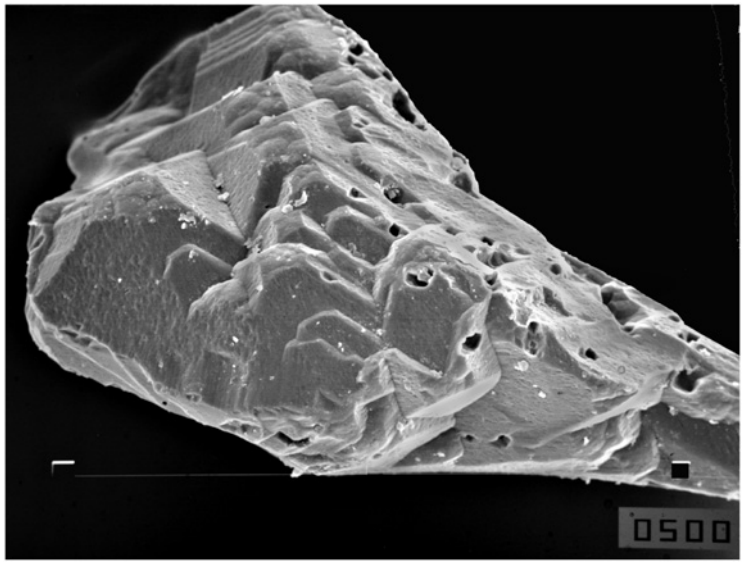

Fig. 4. Etch pits superimposed on imbricate wedge marks (inherited from diagenetically altered Palaeozoic sandstones in the source area of the glacial deposits) on garnet from forest soil in Long Woods at the Michigan State University Kellogg Biological Station. Scale marks are 100 μm apart.

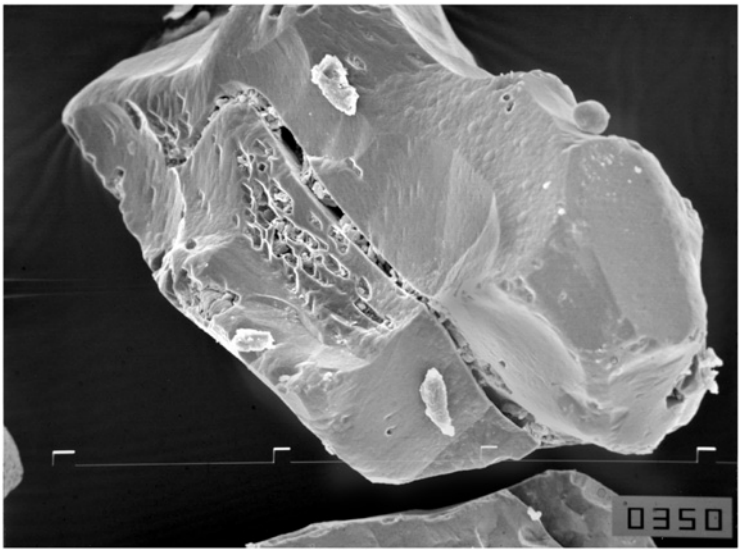

Fig. 5. Etch pits superimposed on conchoidally fractured surface on garnet from forest soil in Long Woods at the Michigan State University Kellogg Biological Station. Scale marks are 100 μm apart.

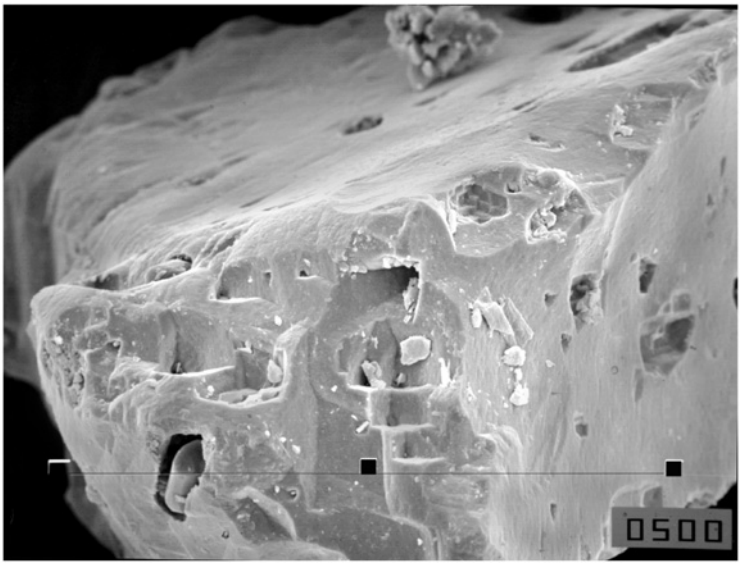

Fig. 6. Etch pits superimposed on rounded surface on garnet from agricultural soil at the Michigan State University Kellogg Biological Station. Scale marks are 100 μm apart.

in White and Brantley, 1995); for feldspars, the rate minimum is broad, and feldspar dissolution rates are lowest over a range of several pH units above and below pH 6–7, "a pattern common to all feldspars and many other silicates" (Blum and Stillings, 1995, p. 305). Experimental data for the rate of silica release from garnet at

pH conditions relevant to hydrolytic weathering in the circum-neutral pH range ($5 < pH < 9$; as distinct from acid weathering or dissolution under alkaline conditions) are available from only one published study (the pH 5.6 results of Nickel, 1973). The soil horizons sampled for this study are devoid of natural carbonate, and agricultural liming is a recent modification to the soils, so the use of dissolution-rate data from circum-neutral to mildly acidic pH conditions is preferable to the use of data from alkaline pH (e.g., > 10, the next highest pH for which experimental garnet dissolution-rate data are available: Nickel, 1973).

No studies exist that investigate the effects of variations in solution chemistry other than pH on garnet dissolution rates (e.g., different acids, organic acids, etc.). However, published experimental results for other silicate minerals suggest that dissolution rates usually vary by less than one order of magnitude (rarely up to two or more) as a consequence of using different organic acids (e.g., Mast and Drever, 1987; Drever and Stillings, 1997; Welch et al., 1999). While it is commonly expected that biotic (e.g., microbial) effects will accelerate silicate dissolution during weathering, in fact some microbes and their associated compounds actually suppress dissolution rates (e.g., Welch and Vandevivere, 1994; Welch et al., 1999). Santelli et al. (2001) and Welch and Banfield (2002) show etch pits from experimentally altered olivine that are very similar to those of naturally weathered olivine (Velbel, 1993a). Of particular note is the fact that such pits are formed only on olivine altered in abiotic experiments. Such features are not observed on olivine grains altered under biotically influenced conditions.

Given that (1) variation among inorganic rates for common silicates commonly does not exceed an order of magnitude at any given pH (especially in the circum-neutral to mildly acidic pH range) and (2) the effects of specific organic soil compounds and microbes might be to either enhance or suppress dissolution rates relative to rates under inorganic/abiotic conditions even for better-studied silicate minerals, there is no basis in the experimental dissolution-rate literature for rejecting the limited published data available for garnet dissolution rates. The pH 5.6 data of Nickel (1973) are used here to arrive at the best estimate for garnet weathering-rate/dissolution–time relationships that the present literature permits.

The dissolution rate of garnet at pH 5.6 is 1.1×10^{-15} mol/cm^2/sec (Nickel, 1973). For garnet, 3 mol silica are released per mole garnet dissolved, giving $J = 3.7 \times 10^{-16}$ mol/cm^2/sec. So, for almandine, using experimentally determined rates:

$$t_d(\text{sec}) = \frac{r(\text{cm})}{(3 \times 115.43\ \text{cm}^3/\text{mol} \times 3.7 \times 10^{-16}\ \text{mol/cm}^2/\text{sec})}$$

$$t_d(\text{sec}) = \frac{r(\text{cm})}{(1.3 \times 10^{-13}\ \text{cm/sec})}$$

$$= r(\text{cm}) \times (7.9 \times 10^{12}\ \text{sec/cm})$$

$$t_d(\text{year}) = r(\mu\text{m}) \times (7.9 \times 10^{12}\ \text{sec/cm}) \times (10^{-4}\ \text{cm/}\mu\text{m}) \times (1\ \text{year}/3.15 \times 10^{7}\ \text{sec})$$

$$t_d(\text{year}) = r(\mu\text{m}) \times 25\ \text{year/}\mu\text{m}$$

$$= d(\mu\text{m}) \times 12.5\ \text{year/}\mu\text{m}$$

thus, on the order of ~10 years/μm diameter.

At experimentally determined garnet dissolution rates under weathering conditions (25°C, pH = 5.6), formation of 1–10 μm etch pits (Figs. 3–6) would take decades to centuries. Given that mineral weathering rates in nature are almost invariably one to three orders of magnitude (10–1000 times) slower than in the laboratory (e.g., Velbel, 1993b), a timescale of centuries to tens of millennia may be required to produce etch pits of the observed size. Larger corrosion features (e.g., IWMs) could not have formed in the present weathering environment even on post-glacial timescales, and are almost certainly inherited from the pre-glacial histories of the grains on which they occur.

6. DISCUSSION

Surfaces of garnets in the Michigan soils studied here display three generations of textures: (1) inherited from the pre-glacial history of the grains; (2) textures modified by glacial transport and/or deposition during deglaciation; (3) small etch pits possibly formed during weathering after exposure of the glacial materials on deglaciation (14 ka). Some garnet grains examined here show clear evidence of mechanical modification during glacial transport, in the form of conchoidally fractured surfaces (Figs. 2 and 5) while others show IWMs (Figs. 1, 3 and 4) identical to IWMs in diagenetically modified Cambrian sandstones of northern Michigan (Salvino and Velbel, 1989). Mahaney (2002) noted that different glacial transport paths have different modifying effects on the surfaces of sand-sized quartz grains. Although physical modification by fracturing is common, grains can also be glacially transported without showing signs of crushing, resulting in sand grains in glacial deposits with inherited pre-glacial surface textures (Mahaney, 2002). Our observations suggest that heavy mineral grains can also retain surface characteristics formed in a previous environment, similar to the quartz sand studied by Mahaney (2002).

Small (1–10 μm) etch pits on facetted, fractured, and rounded surfaces (Figs. 3–6) may have formed either in garnet source-area regoliths (pre-glacially weathered regolith on crystalline rocks of the Canadian Shield; pre-glacially weathered Cambrian sandstone) or by weathering in the present soils. If the small etch pits formed in soils since deglaciation, their small size (1–10 μm) is broadly consistent with the age of the soils (developed on ~14 ka glacial deposits). In contrast the time required to extensively modify pre-existing facetted or conchoidal surfaces (Figs. 1–5), or to form facetted surfaces (IWMs) by coalescence of large dodecahedral etch pits, is longer than the deposition and exposure age of the parent material on which the soil is developed. This finding is consistent with the conclusion of Gravenor (1985) that etching features are inherited on garnets in soils developed on Wisconsin-age glacial parent materials, and that only older (Sangamon) soil profiles contain garnets with etch pits that formed in situ.

Garnets in Pleistocene glacial/glaciofluvial sediments, and in soils developed on Pleistocene glacial/glaciofluvial deposits, in Michigan, are multicycle. Widespread preservation of surface textures inherited from previous episodes in the grains' history, including IWMs (of intrastratal dissolution origin) that persist on garnets apparently derived from Cambrian quartz arenite and conchoidal fractures indicative of mechanical processing during transport (Figs. 1–6), suggests that garnets in

Michigan soils have undergone little weathering since deglaciation. Even centuries to millennia under present weathering conditions are not sufficient to destroy pre-pedogenic (Figs. 1–6) and pre-glacial (Figs. 1, 3, and 4) surface textures and completely replace them with weathering textures. Specific garnet surface textures are not associated with specific land-use (forest, agriculture) at KBS; the time required to create new assemblages of surface textures is much longer than the time available since anthropogenic differentiation of the studied localities.

Inheritance of heavy-mineral surface textures in glacial deposits and even in soils developed on such glacial materials has several implications. Textures formed by mechanical fracturing on a variety of minerals, including specifically garnet, have been long interpreted as consequences of vigorous physical transport, including glacial transport (e.g., Folk, 1975; Bull et al., 1980; Gravenor, 1985). However, our observations show that delicate surface textures from source rocks (e.g., IWMs) survive even on garnet grains transported by continental glaciers for hundreds of kilometres from their source areas. This implies that at least some mechanisms of subglacial/englacial transport can move sand-size grains great distances without creating supposedly characteristic mechanical surface textures.

Survival of delicate heavy-mineral surface textures in demonstrably glacially/glaciofluvially transported sediments also provides a possible alternative reason for the common observation in studies of relative age-dating and soil development using hornblende etching, that even in the ostensibly fresh parent material, a small finite amount of hornblende modification is commonly observed (e.g., Locke, 1979, 1986; Hall and Martin, 1986; Hall and Michaud, 1988; Hall and Horn, 1993; Mikesell et al., 2004). It has been suggested (e.g., Berner et al., 1980) that denticulations (sawtooth or ''cockscomb'' terminations) on hornblende grains in weathered regoliths are too delicate to survive transportation and therefore must have formed in situ. While this may well be true in residual, relict, or sedentary (untransported) regoliths, it may not be true in the case of a transported regolith. Our observations suggest that some heavy-mineral grains, even in glacial deposits, may retain corrosion features inherited from preglacial alteration (e.g., weathering of pre-glacial regoliths and/or diagenesis in sedimentary rocks in the source area of the glacial deposits). While this would have little effect on commonly used methods for relative-age dating using hornblende etching (Locke, 1979, 1986; Hall and Martin, 1986; Hall and Michaud, 1988; Hall and Horn, 1993; Mikesell et al., 2004, and references therein) because these are statistical studies using average values properties on large numbers of grains, it would render more difficult the interpretation of hornblende surface textures in SEM images of individual hornblende grains from a soil developed on a transported parent material.

7. CONCLUSIONS

At reasonable weathering rates for natural systems, the length of time required to dissolve the amount of garnet represented by the small etch pits observed on grains is broadly consistent with the age of deposition of glacial parent materials and the onset of weathering of the host soils by deglaciation in southern Michigan. Large-scale grain surface features (especially the larger etch pits, IWMs, and other surface

features) are too large to have been formed in the present weathering regime, and are interpreted to be inherited from the pre-pedogenic and pre-glacial history of the garnet grains.

Changes in physical and chemical processes (from one compartment or stage of the sedimentary cycle to another) result in new assemblages of grain-surface textures. However, the change is not instantaneous on introduction of the grain to the new environmental conditions; a finite amount of time (the ''response time'') is required for the grain-surface to acquire new surface textures characteristic of the new conditions. In the interim, grain-surfaces are dominated by inherited ''up-cycle'' textures.

Our results show that, for garnets in soils developed on Pleistocene glacial parent materials in a common weathering environment, inherited surface textures from source rocks (e.g., IWMs; Figs. 1, 3, and 4) and from the transport and depositional history of the parent regolith (e.g., conchoidal fractures; Figs. 2 and 5) are dominant in several Michigan soils, even after more than 10,000 years of post-glacial weathering. Inherited grain-surface textures dominate in these and similar examples because the response time for surface texture modification is long compared to the time actually available for weathering to modify the garnet surfaces.

The response may differ according to the reactivity of the mineral in a particular weathering environment. Highly resistant minerals have surfaces that are modified slowly, and inherited textures likely dominate whereas less-resistant minerals may quickly take on surface textures characteristic of their new environment. Labile minerals do not survive long enough to observe inherited or environment-dependent surface textures.

The significance of etch pits and other surface textures on grains in a soil or regolith depends on:

- the ''response time'' of the surface textures to weathering in that regolith (or soil) and
- the relationship of that timescale to the age of the soil and/or how long the grains remained in the weathering/soil environment.

Geomorphic dynamics, regolith history, and landscape evolution affect the genesis and interpretation of grain-surface textures formed during mineral weathering. Similar relationships are to be expected in other compartments of the sedimentary cycle.

ACKNOWLEDGMENTS

Samples were collected with the assistance of Stephanie Gillain. The first author thanks Roland Hellmann for thought-provoking conversations at the GES-6 meeting, and Ahmet Mermut, Karl Föllmi, and several anonymous reviewers of several versions of this paper. This project was supported by Long-Term Ecological Research (LTER) grants NSF DEB 92-11771 and DEB 98-10220 (G.P. Robertson, Michigan State University Kellogg Biological Station, P.I.) and an REU Supplement.

REFERENCES

Berner, R.A., Sjöberg, E.L., Velbel, M.A., Krom, M.D., 1980. Dissolution of pyroxenes and amphiboles during weathering. Science 207, 1205–1206.

Blum, A.E., Stillings, L.L., 1995. Feldspar dissolution kinetics. In: White, A.F., Brantley, S.L., (Eds.), Chemical Weathering Rates of Silicate Minerals, Mineralogical Society of America Reviews in Mineralogy, vol. 31. pp. 291–351.

Boutz, M.M.R., Woensdregt, C.F., 1993. Theoretical growth forms of natural garnets. Journal of Crystal Growth 134, 325–336.

Bramlette, M.N., 1929. Natural etching of detrital garnet. American Mineralogist 14, 336–337.

Bull, P.A., Culver, S.J., Gardner, R., 1980. Chattermark trails as paleoenvironmental indicators. Geology 8, 318–322.

Cherepanova, T.A., Bennema, P., Yanson, Y.A., Vogels, L.J.P., 1992. Morphology of synthetic and natural garnets: theory and observations. Journal of Crystal Growth 121, 17–32.

Corfu, F., Hanchar, J.M., Hoskin, P.W.O., Kinny, P., 2003. Atlas of zircon textures. In: Hanchar, J.M., Hoskin, P.W.O. (Eds.), Zircon: Mineralogical Society of America Reviews in Mineralogy. vol. 53, pp. 469–500.

Drever, J.I., Stillings, L.L., 1997. The role of organic acids in mineral weathering: colloids and surfaces A. Physicochemical and Engineering Aspects 120, 167–181.

Dworkin, S.I., Larson, G.J., Monaghan, G.W., 1985. Late Wisconsinan ice-flow reconstruction for the central Great Lakes region. Canadian Journal of Earth Sciences 22, 935–940.

Embrechts, J., Stoops, G., 1982. Microscopical aspects of garnet weathering in a humid tropical environment. Journal of Soil Science 33, 535–545.

Farrand, W.R., Bell, D.L., 1982. Quaternary geology of Southern Michigan: 1:500,000 scale map. Michigan Geological Survey, Lansing, MI.

Folk, R.L., 1975. Glacial deposits identified by chattermark trails in detrital garnets. Geology 3, 473–475.

Ghabru, S., Mermut, A., St. Arnaud, R., 1989. Characterization of garnets in a typic Cryoboralf (*Gray luvisol*) from Saskatchewan, Canada. Soil Science of America Journal 53, 575–582.

Graham, R.C., Weed, S.B., Bowen, L.H., Buol, S.W., 1989. Weathering of iron-bearing minerals in soils and saprolite on the North Carolina Blue Ridge Front: I. Sand-size primary minerals. Clays and Clay Minerals 37, 19–28.

Gravenor, C.P., 1985. Chattermarked garnets found in soil profiles and beach environments. Sedimentology 32, 295–306.

Gravenor, C.P., Leavitt, R.K., 1981. Experimental formation and significance of etch patterns on detrital garnets. Canadian Journal of Earth Sciences 18, 765–775.

Hall, R.D., Horn, L.L., 1993. Rates of hornblende etching in soils in glacial deposits of the northern Rocky Mountains (Wyoming–Montana, U.S.A.): Influence of climate and characteristics of the parent material. Chemical Geology 105, 17–29.

Hall, R.D., Martin, R.E., 1986. The etching of hornblende grains in the matrix of alpine tills and periglacial deposits. In: Colman, S.M., Dethier, D.P. (Eds.), Rates of Chemical Weathering of Rocks and Minerals. Academic Press, Orlando, FL, pp. 101–128.

Hall, R.D., Michaud, D., 1988. The use of hornblende etching, clast weathering, and soils to date alpine glacial and periglacial deposits: A study from southwestern Montana. Geological Society of America Bulletin 100, 458–467.

Hamblin, W.K., 1958. Cambrian Sandstones of Michigan: Publications of the Michigan Department of Conservation. Geological Survey Division 51, 146.

Hansley, P.L., 1987. Petrologic and experimental evidence for the etching of garnets by organic acids in the Upper Jurassic Morrison Formation, northwestern New Mexico. Journal of Sedimentary Petrology 57, 666–681.

Hansley, P.L., Briggs, P.H., 1994. Garnet dissolution in oxalic acid: a possible analog for natural etching of garnet by dissolved organic matter. U.S. Geological Survey Bulletin, Report B2106, 14pp.

Lasaga, A.C., Lüttge, A., 2001. Variation of crystal dissolution rate based on a dissolution stepwave Model. Science 291, 2400–2404.

Locke III, W.W., 1979. Etching of hornblende grains in Arctic soils: An indicator of relative age and paleoclimate. Quaternary Research 11, 197–212.

Locke III, W.W., 1986. Rates of hornblende etching in soils on glacial deposits, Baffin Island, Canada. In: Colman, S.M., Dethier, D.P. (Eds.), Rates of Chemical Weathering of Rocks and Minerals. Academic Press, Orlando, FL, pp. 129–145.

Lüttge, A., Bolton, E.W., Lasaga, A.C., 1999. An interferometric study of the dissolution kinetics of anorthite: the role of reactive surface area. American Journal of Science 299, 652–678.

Mahaney, W.C., 2002. Atlas of Sand Grain Surface Textures and Applications. Oxford University Press, New York, NY, 237pp.

Mast, M.A., Drever, J.I., 1987. The effect of oxalate on the dissolution rates of oligoclase and tremolite. Geochimica et Cosmochimica Acta 51, 2559–2568.

Matelski, R.P., Turk, L.M., 1947. Heavy minerals in some podzol profiles in Michigan. Soil Science 64, 469–487.

Matsuura, A., Aoki, Y., 1989. A new method for quantitative representation of zircon morphology. Neues Jahrbuch für Mineralogie, Monatshefte 1989, 309–319.

Mikesell, L.R., Schaetzl, R.J., Velbel, M.A., 2004. Hornblende etching and quartz/feldspar ratios as weathering and soil development indicators in some Michigan soils. Quaternary Research 62, 162–171.

Morton, A.C., Hallsworth, C.R., 1999. Processes controlling the composition of heavy minerals in sandstones. Sedimentary Geology 124, 3–29.

Morton, A.C., Borg, G., Hansley, P.L., Haughton, P.D.W., Krinsley, D.H., Trusty, P., 1989. The origin of faceted garnets in sandstones: Dissolution or overgrowth? Sedimentology 36, 927–942.

Nickel, E., 1973. Experimental dissolution of light and heavy minerals in comparison with weathering and intrastratal dissolution. Contributions to Sedimentology 1, 1–68.

Pabst, A., 1943. Large and small garnets from Fort Wrangell, Alaska. American Mineralogist 28, 233–245.

Price, J.R., 1994. Geochemical mass balance models of sandstone weathering in the Pennsylvanian recharge beds of south-central Michigan. Unpublished M.Sc. thesis. Michigan State University, 109pp.

Price, J.R., Velbel, M.A., 2000. Weathering of the Eaton Sandstone (Pennsylvanian), Grand Ledge, Michigan: geochemical mass-balance and implications for reservoir properties beneath unconformities. Journal of Sedimentary Research, A 70, 1118–1128.

Pupin, J.P., 1980. Zircon and granite petrology. Contributions to Mineralogy and Petrology 73, 207–220.

Robertson, G.P., Crum, J.R., Ellis, B.G., 1993. The spatial variability of soil resources following long-term disturbance. Oecologia 96, 451–456.

Salvino, J.F., Velbel, M.A., 1989. Faceted garnets from sandstones of the Munising Formation (Cambrian), northern Michigan: petrographic evidence for origin by intrastratal dissolution. Sedimentology 36, 371–379.

Santelli, C.M., Welch, S.A., Westrich, H.R., Banfield, J.F., 2001. The effect of Fe-oxidizing bacteria on Fe-silicate mineral dissolution. Chemical Geology 180, 99–115.

Simpson, G.S., 1976. Evidence of overgrowths on, and solution of, detrital garnets. Journal of Sedimentary Petrology 46, 689–693.

Stearns, M.D., 1933. The petrology of the Marshall Formation of Michigan. Journal of Sedimentary Petrology 3, 99–112.

Stieglitz, R.D., Rothwell, B., 1978. Surface microtextures of freshwater heavy mineral grains. Geoscience Wisconsin 3, 21–34.

Stoops, G., Altemuller, H.-J., Bisdom, E.B.A., Delvigne, J., Dobrovolsky, V.V., Fitzpatrick, E.A., Paneque, G., Sleeman, J., 1979. Guidelines for the description of mineral alterations in soil micromorphology. Pedologie 29, 121–135.

Turner, G., Morton, A., 2007. The effects of burial diagenesis on detrital heavy mineral grain surface textures. In: Mange, M.A., Wright, D.T. (Eds.), Heavy Minerals in Use. Developments in Sedimentology (this volume).

United States Department of Agriculture Soil Conservation Service, 1979. Soil Survey of Ingham County. Michigan, 142pp.

United States Department of Agriculture Soil Conservation Service, 1981. Soil Association Map of Michigan, Michigan State University Agricultural Experiment Station Cooperative Extension Service, Extension Bulletin E-1550.

Vavra, G., 1993. A guide to quantitative morphology of accessory zircon. Chemical Geology 110, 15–28.

Velbel, M.A., 1984. Natural weathering mechanisms of almandine garnet. Geology 12, 631–634.

Velbel, M.A., 1989. Effect of chemical affinity on feldspar hydrolysis rates in two natural weathering systems. Chemical Geology 78, 245–253.

Velbel, M.A., 1993a. Formation of protective surface layers during silicate-mineral weathering under well-leached, oxidizing conditions. American Mineralogist 78, 408–417.

Velbel, M.A., 1993b. Constancy of silicate-mineral weathering-rate ratios between natural and experimental weathering: implications for hydrologic control of differences in absolute rates. Chemical Geology 105, 89–99.

Velbel, M.A., 1999. Bond strength and the relative weathering rates of simple orthosilicates. American Journal of Science 299, 679–696.

Velbel, M.A., 2007. Surface textures and dissolution processes of heavy minerals in the sedimentary cycle: examples from pyroxenes and amphiboles. In: Mange, M.A., Wright, D.T. (Eds.), Heavy Minerals in Use. Developments in Sedimentology (this volume).

Welch, S.A., Banfield, J.F., 2002. Modification of olivine surface morphology and reactivity by microbial activity during chemical weathering. Geochimica et Cosmochimica Acta 66, 213–221.

Welch, S.A., Barker, W.W., Banfield, J.F., 1999. Microbial extracellular polysaccharides and plagioclase dissolution. Geochimica et Cosmochimica Acta 63, 1405–1419.

Welch, S.A., Vandevivere, P., 1994. Effect of microbial and other naturally occurring polymers on mineral dissolution. Geomicrobiology Journal 12, 227–238.

White, A.F., Brantley, S.L. (Eds.), 1995. Chemical weathering rates of silicate minerals. In: Mineralogical Society of America Reviews in Mineralogy, vol. 31, 583pp.

Winter, J., 1981. Exacte tephrostratigraphische Korrelation mit morphologisch differenzierten Zirkonpopulationen (Grenzbereich Unter-Mitteldevon, Eifel-Ardennen). Neues Jahrbuch für Geologie und Paläontologie, Abhandlungen 162, 97–136.

Chapter 16

HIGH-RESOLUTION HEAVY MINERAL ANALYSIS (HRHMA): A BRIEF SUMMARY

MARIA A. MANGE[a] AND DAVID T. WRIGHT[b]

[a]*Department of Geology, UC Davis, One Shields Avenue, Davis, CA 95616, USA*
[b]*Department of Geology, University of Leicester, University Road, Leicester LE1 7RH, UK*

ABSTRACT

High-resolution heavy mineral analysis (HRHMA) is the identification and categorisation of different varieties of individual heavy mineral species, based on the recognition that the majority of rock-forming and accessory minerals form in a diversity of size and habit and are represented by several chemical, structural, colour and optical varieties, controlled primarily by petrogenetic conditions. Because a wide range of lithologies provide detritus to siliciclastic sediments, their heavy mineral assemblages are complex and an individual species may comprise several kinds of varieties. Variables that prove most informative are grain morphology, colour and internal structure. These can be provenance-diagnostic, facies-independent or facies-sensitive. Failure to appreciate such information by grouping the diverse varieties of a particular species into one single mineral category can generate misleading information and often incorrect interpretations, while the full history of a sediment and accurate reconstruction of provenance remains concealed. HRHMA can be easily conducted under the polarising microscope, it is internally consistent and categories can easily be defined and kept without errors. Categorisation and point counting of the varieties of a single species also eliminates problems caused by density-controlled sorting during transport and dissolution processes that affect chemically unstable species.

Keywords: heavy mineral varieties; grain morphology; colour and morphological categories; zircon - tourmaline - apatite- varieties

1. EXPLOITING THE FULL POTENTIAL OF THE HEAVY MINERAL ASSEMBLAGES

The impact of processes which may cause marked changes to heavy mineral assemblages are now well understood and approaches that evaluate and mitigate

Developments in Sedimentology, Vol. 58, 433–436

ISSN: 0070-4571/doi:10.1016/S0070-4571(07)58016-7

their effects (e.g., geochemistry, provenance-sensitive parameters) have been proposed and tested. High-resolution heavy mineral analysis (HRHMA) has been applied successfully in many studies including sediments that are devoid of biological and lithological markers (Mange-Rajetzky, 1995; Lihou and Mange, 1996; Mange et al., 1999 and 2007, this volume). HRHMA extracts optimum information from the assemblages because it goes beyond the species level and categorises the varieties of a single species. This permits a more precise characterisation of mineral grains and avoids misinterpreting provenance indicators at the species level. For example, the origin and sedimentary history of a sharp euhedral zircon is in stark contrast with that of an old rounded purple grain (Fig. 1).

Although the term HRHMA is relatively new, the potential for using varieties was emphasised by Brammal (1928) who pointed out that 'the varietal features of a species in a detrital assemblage may be of greater significance than the mere presence of that species'. Indeed, during the history of heavy mineral analyses, numerous studies have proved that the value of results has increased considerably when the various types of a particular mineral or of a mineral group were distinguished and

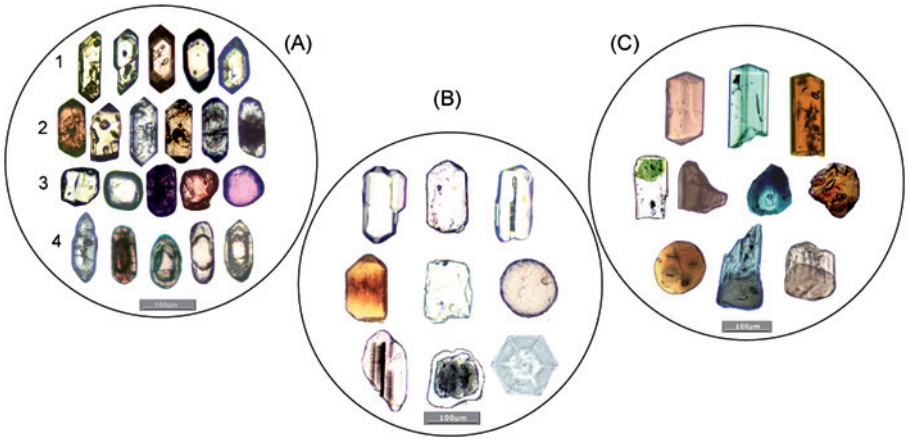

Fig. 1. Characteristic heavy mineral varieties. (A) Examples showing the diversity of zircon varieties. Row 1: Sharp euhedral, volcanogenic crystals (three grains on the left) and two lower-temperature euhedral crystals. Row 2: euhedral purple, pencil-shaped crystal with abundant microlite inclusions and zoned zircons from granitoids; grain to the far right shows an isotropic core. Row 3: rounded, recycled colourless and purple zircons. Row 4: grains showing a variety of overgrowths. (B) Apatite varieties. Top row: sharp euhedral volcanogenic crystal, prismatic grain with somewhat rounded edges and rounded prism with a microlite and opaque inclusions. Middle row: volcanogenic, reddish-brown pleochroic prism, angular and spherical grains. Bottom row: rounded prism with parallel inclusions of opaque dust, rounded overgrowth on a rounded, dusky pre-existing grain, hexagonal euhedral crystal developing over a spherical detrital grain. (C) Tourmaline varieties. Top row: sharp euhedral crystals. Middle row: rounded colourless prism preserving a pre-existing nucleus, irregular angular grain, sharp basal form and rounded grain with a zircon inclusion. Bottom row: spherical grain, large overgrowth on a rounded detrital tourmaline and grain showing rounded overgrowth on a rounded core.

recorded. For example, Todd and Folk (1957) distinguished different categories of zircon and tourmaline in the basal Clairborne Formation in Texas. Similarly, El-Hinnawi et al. (1973) recoded the different zircon and tourmaline varieties in the 'Nubian Sandstone' while Mange-Rajetzky (1995), by categorising tourmaline and apatite varieties in the barren Triassic red bed successions of the Central Graben, North Sea achieved recognition of high-quality reservoir sandstone intervals and their basin-wide correlation. Winter (1981) provided a precise tephra-stratigraphy and correlation by focusing on different zircon varieties. Understanding of the Quaternary evolution of the Gulf coastal plain and sediment provenance in West Louisiana was significantly enhanced by the recording of zircon varieties (Mange and Otvos, 2005). Allen and Mange-Rajetzky (1992), Morton (2007, this volume, and Mange et al. (2007, this volume) found that apatite morphology faithfully signals environmental changes, while Wozazek and Krawinkel (2002) recorded the roundness and colour of tourmaline in their study of the Côte d'Ivoire Basin. The editors have successfully applied HRHMA to a wide range of projects in the field of hydrocarbon exploration and reservoir characterisation over many years, but most of the reports are necessarily proprietary and the work remains unpublished.

Despite experiencing several episodes of recycling, many varieties remain provenance-diagnostic. Provenance-sensitive species and varieties inherit properties such as chemical composition, crystal form and colour from their parent lithologies. Subsequent sedimentary processes generate morphological types and dissolution features which are considered facies-sensitive. Consequently, a series of genetic and/or sedimentary histories are encoded in each variety. This supports the principle that, in reality, heavy mineral assemblages are more diverse and thus more informative than indicated by a simple species-level analysis that ignores all these characteristics. HRHMA can be used universally where ultrastable species are present: zircon, tourmaline and apatite are almost ubiquitous in detrital sediments, typically occur in significant quantities and are represented by several varieties. Categorisation and point counting of the varieties of a single species eliminates problems caused by density-controlled sorting during transport and dissolution processes that affect chemically unstable species (Morton and Hallsworth, 1999). Thus, observed changes in the heavy mineral spectrum are clear indications of a shift in provenance.

The principle of HRHMA is, therefore, the identification and categorisation of different varieties of individual heavy mineral species. Variables that prove most informative are grain morphology, colour and internal structure. Figs. 1A–C illustrate the many varieties of a single species (e.g., morphology from sharp euhedral to rounded, range of colours and internal structures, inclusions, zoning and many other). These can be provenance-diagnostic, facies-independent or facies-sensitive. Failure to appreciate the value of the information provided by diverse varieties of a particular mineral species can generate incomplete or biased information. In such cases, any discernible trends in heavy mineral populations may be misleading, or represent only a limited part of the history of a sediment, thereby calling into question attempts claiming to accurately predict sediment provenance.

HRHMA can be easily conducted under the polarising microscope, it is internally consistent and categories can easily defined and kept without errors.

REFERENCES

Allen, P.A., Mange-Rajetzky, M.A., 1992. Sedimentary evolution of the Devonian Carboniferous Clair Field, offshore northwestern UK: impact of changing provenance. Marine and Petroleum Geology 9, 29–52.

Brammal, A., 1928. Dartmoor detritals: a study in provenance. Proceedings of the Geologists Association 39, 27–48.

El-Hinnawi, E.E., Kabesh, M.L., Zahran, I., 1973. Mineralogy and chemistry of Nubian sandstones from the Central Eastern Desert of Egypt. Neues Jahrbuch Mineralogische Abhandlungen 118, 211-234

Lihou, J.C., Mange-Rajetzky, M.A., 1996. Provenance of the Sardona Flysch, eastern Swiss Alps: example of high-resolution heavy mineral analysis applied to an ultrastable assemblage. Sedimentary Geology 105, 141–157.

Mange, M.A., Otvos, E.G., 2005. Gulf Coastal Plain Evolution in West Louisiana–Heavy Mineral Provenance and Pleistocene Alluvial Chronology. In: Fanning, M., Mahoney, B., Link, P.K. (Eds.), Interdisciplinary and isotopic studies of sediment provenance. Sedimentary Geology 182, 29–57.

Mange, M.A., Turner, P., Ince, D., Wright, D., 2007. High-resolution heavy mineral- and magnetostratigraphy; a powerful tool for subdivision and correlation of barren successions: an example from the Sherwood Sandstone Group (Triassic of the East Irish Sea Basin and surrounding areas. In: Mange, M.A., Wright, D.T. (Eds.), Heavy Minerals In Use. Developments in Sedimentology (this volume).

Mange, M.A., Turner, P., Ince, D., Pugh, J., Wright, D., 1999. A new perspective on the zonation and correlation of barren strata: an integrated heavy mineral and palaeomagnetic study of the Sherwood Sandstone Group, East Irish Sea Basin and sorrounding areas. Journal of Petroleum Geology 22, 325–348.

Mange-Rajetzky, M.A., 1995. Subdivision and correlation of monotonous sandstone sequences using high resolution heavy mineral analysis, a case study: the Triassic of the Central Graben. In: Dunay, R.E., Hailwood, E.A. (Eds.), Non-Biostratigraphical Methods of Dating and Correlation, vol. 89. Geological Society of London Special Publication, pp. 23–30.

Morton, A., 2007. The role of heavy mineral analysis as a geosteering tool during drilling of high-angle wells. In: Mange, M.A., Wright, D.T. (Eds.), Heavy Minerals In Use. Developments in Sedimentology (this volume).

Morton, A.C., Hallsworth, C.R., 1999. Processes controlling the composition of heavy mineral assemblages in sandstones. Sedimentary Geology 124, 3–29.

Todd, T.W., Folk, R.L., 1957. Basal Clairborne of Texas, record of Appalachian tectonism during Eocene. Bulletin of the American Association of Petroleum Geologists 41, 2545–2566.

Winter, J., 1981. Exacte tephrostratigraphische Korrelation mit morphologisch differenzierten Zirkonpopulationen (Grenzbereich Unter-Mitteldevon, Eifel-Ardennen). Neues Jahrbuch für Geologie und Paläontologie, Abhandlungen 162, 97–136.

Wozazek, S., Krawinkel, H., 2002. Development of the Côte d'Ivoire Basin: reading provenance, sediment dispersal, and geodynamic implications from heavy minerals. International Journal of Earth Sciences (Geologische Rundschau) 91, 906–921.

1.5 Numerical Data Analysis

This page intentionally left blank

Chapter 17

MULTIVARIATE ANALYSIS OF HEAVY MINERAL ASSEMBLAGES OF SEDIMENTS FROM THE MARGINAL SEAS OF THE WESTERN PACIFIC

ALEXANDER N. DERKACHEV AND NATALIA A. NIKOLAEVA

V.I. Il'ichev's Pacific Oceanological Institute, Far Eastern Branch, Russian Academy of Sciences, Vladivostok, 43 Baltiyskaya Street, Vladivostok, 690041, Russia

ABSTRACT

Heavy mineral data of sediments from the marginal seas of the Western Pacific (Bering, Okhotsk, Japan, East China, Philippine, Banda, etc.), from the Tonga and Vanuatu Trenches and from adjacent areas have been evaluated using multivariate statistics and correlation, factor, cluster and discriminant analyses. The overall characteristics of heavy mineral assemblages and the regional variability of mineral associations are described and interpreted. Despite the large latitudinal and environmental range of the study basins, the complexity of source rocks and volcanic signatures are clearly reflected in the distribution of heavy mineral assemblages. Results allowed identification of several mineralogical provinces, linked to distinct hinterland complexes and associated tectonic controls. Q-mode factor analysis differentiated four major groups of assemblages of distinctive provenance. R-mode factors helped to define representative mineral associations, which best characterise the mineral composition of the sediments of the individual marginal seas, and led to the delineation of eight provinces.

Lithogeodynamic discriminant diagrams, based on average values of heavy mineral compositions, identify assemblages which are most typical of differing types of magmatic and metamorphic rocks, and discriminate between them and those associated with other crustal lithologies. Changing compositions of the heavy mineral assemblages indicate a clear trend from simple geodynamic environments to composite ones, including oceanic uplifts, young island arcs, evolved and mature island arcs, marginal-continental volcanic ranges, fold belts, ancient cratons and platforms.

Keywords: heavy mineral assemblages; marginal seas of the Western Pacific; multivariate statistics; indicators of sedimentary environments; lithogeodynamic diagrams.

Developments in Sedimentology, Vol. 58, 439–464

ISSN: 0070-4571/doi:10.1016/S0070-4571(07)58017-9

1. INTRODUCTION

Heavy mineral studies provide unique and essential information for determining sediment provenance and constraining the evolution of sedimentary basins, correlating sedimentary successions and mapping the distribution of mineral resources. An actualistic model, based on analysis and mapping of the distribution patterns of detrital heavy minerals in modern settings, and constrained by factors that control the formation and distribution of particular assemblages, is a prerequisite of basin analysis. Numerous studies on sedimentary mineralogy have indicated that the main factors determining the composition of mineral assemblages are the structural position of the sedimentary basin, the lithology of the supplying provinces, climate, processes occurring during sediment transport, the dynamics of the depositional environment and, finally, diagenesis (Baturin, 1947; Kukharenko, 1961; Strakhov, 1963; Van Andel, 1964; Grossgeim, 1972; Dickinson and Suczek, 1978; Pettijohn, 1981; Maynard et al., 1982; Kazansky, 1983; Viyding, 1984; Valloni, 1985; Berger, 1986; Morton and Hallsworth, 1999, etc.).

In this paper we consider the impact of factors that influence the distribution of heavy mineral assemblages in specific marine environments and, using the results of multivariate statistics, interpret the interrelationship of the assemblages with the tectonic setting of their depositional basins (see also Nechaev, 1991; Nechaev and Isphording, 1993). In particular, we have focused on the formation of modern heavy mineral suites in the marginal seas of an active continental margin within the Western Pacific, presenting data that hitherto was not available to many researchers.

2. MATERIALS AND METHODS

Heavy mineral analyses were performed on surface sediments (0–10 cm) collected from marginal seas of the Western Pacific, situated in different climatic belts and geodynamic environments (Fig. 1). Material (about 1200 analyses) was obtained by the authors from the Okhotsk, Japan, East China, Philippine and South China Seas. The Banda and Sulawesi Seas, Lau Basin and Tonga trench sediments were studied to a lesser degree (56 analyses). Published data on mineral compositions of sediments from the Bering, Okhotsk, Yellow and East China Seas were also included to obtain a representative database (Gershanovich, 1955; Petelin, 1957; Aleksina, 1962; Lisitsin, 1966; Suzuki, 1975a, 1975b; McManus et al., 1977; Murdmaa et al., 1979, 1980; Suzuki, 1985; Lee et al., 1988; Chen, 1989; Malinovsky et al., 1990; Derkachev et al., 1993, Qin et al., 1996; and others).

Heavy mineral analyses were carried out using the technique described by Petelin (1961) as 'immersion method': sediment samples were wet-sieved using 0.1 and 0.05 mm sieves. Heavy mineral fractions (density $> 2.89\ g/cm^3$) were extracted from the 0.1 to 0.05 mm fractions using bromoform ($CHBr_3$) and analysed under a polarising microscope, in an immersion liquid of 1.655 refractive index. Not less than 300 grains were identified and counted in each sample. Rock fragments, unidentifiable grains as well as authigenic and opaque minerals (glauconite, collophane, ilmenite, hematite, magnetite, leucoxene, iron and manganese hydroxides, etc.) were excluded from the total sum to obtain uniform, comparable data on transparent

assemblages for the characterisation of mineralogical provinces. The sum of transparent minerals was recalculated to a value of 100% and the abundance of each heavy mineral species was scaled accordingly. The mineralogical zones identified in the marginal seas in an earlier study were computed using Q-mode cluster analysis (Derkachev et al., 1989, 1993; Derkachev and Nikolaeva, 1995, 1999a; Nechaev and Derkachev, 1995; Derkachev, 1996).

The significance rating of the mineral assemblages as defining discrete heavy mineral provinces was evaluated by discriminant analysis (Afifi and Azen, 1982; Le Maitre, 1982). Results indicated rather high efficiency with $>85\%$ confidence levels. Multivariate statistical methods are widely used to estimate the principal patterns in the formation and distribution of mineral assemblages. Identification of the paragenetic relationships of the heavy mineral assemblages is based on methods of correlation analysis, Q- and R-mode cluster and factor analyses. Examples of the successful application of these methods to sedimentological and detrital heavy mineral studies are well known (Imbrie and Van Andel, 1964; Knebel and Creager, 1973; Egiazarov, 1981; Firek and Shideler, 1977; McManus et al., 1977; Chen et al., 1982; Wang and Liang, 1982; Chen et al., 1984; Carriquiry and Sánchez, 1999; Wong, 2002 and many others). In this study, programmes and algorithms, published by Davis (1977) and modified for an IBM PC by Utkin (2002), were used as the basic software.

3. RESULTS AND INTERPRETATION

3.1. Q-Mode Factor Analysis

Comparison of average values of heavy mineral compositions (147 mineral assemblages) in the mineral provinces, recognised on the basis of Q-mode factor analysis (Table 1), has allowed us to establish the regional variability in mineral distribution and ascertain the reasons causing this variability. The results indicated that 88.4% of all variability in the distribution of minerals could be attributed to five factors. A considerable percentage of the total dispersion is accounted for by the first two factors with a contribution of 33.8 and 31.6%, respectively. The loads of the next three factors are insignificant, and they range from 3.7 to 9.7%.

Fig. 1 shows that most of the mineralogical provinces are combined into two major groups.

Factor I (with a 33.8% contribution to the variance) defines the first group of provinces, which includes those next to the continental coast containing ancient cratons and orogens with granitic and metamorphic rocks (western coast of the Okhotsk Sea, Korean Peninsula, China and Indochina) (Table 2). The main heavy mineral assemblage in these provinces is represented by brown-green and green hornblende and epidote, with subsidiary actinolite, high-grade metamorphic minerals (kyanite, staurolite, andalusite, sillimanite), and stable minerals (zircon, sphene, tourmaline, garnet, rutile, anatase). Detrital calcites are also present, although their contents vary from province to province (Table 1).

Some heavy mineral assemblages, clearly different in origin from those considered above, also occur in this group. These are volcaniclastic assemblages, represented

mainly by hornblende (including brown hornblende and oxyhornblende). Apatite, hypersthene and clinopyroxene are present as an admixture. They typically occur in the West Philippine Province (Philippine Sea), in the central part of the Sulawesi and Sulu Seas, and in the northern part of the Coral Sea. The sediments of the Sanyin

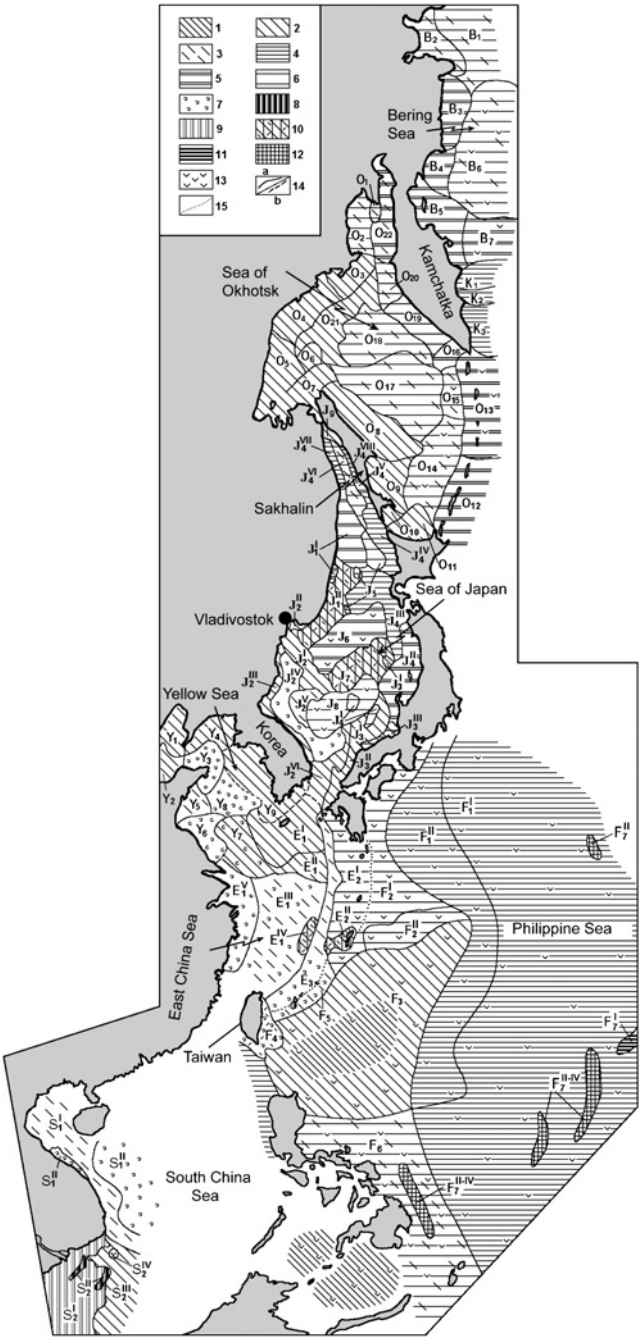

Province (south-eastern part of the Japan Sea) have a specific mineral composition typified by high concentrations of hornblende and hypersthene. The oxyhornblende–hypersthene association is characteristic of the products of volcanic eruptions from southwest Japan (Daysen Volcano, etc.) (Tsukui, 1984).

Factor II (with a 31.6% contribution to the variance) comprises the second group of provinces that contain heterogeneous assemblages of differing origin. Heavy minerals here are the products of intensive Neogene-Quaternary and contemporary volcanic activity. Mineral diversity is low, consisting mostly of clino- and orthopyroxenes with the prevalence of clinopyroxenes, often accompanied by high

Fig. 1. Heavy mineral provinces of the sediments in the marginal seas of the Western Pacific. Provinces and subprovinces: *Bering Sea Provinces* (Lisitsin, 1966; McManus et al., 1977): B_1, Eastern part of the Anadyr Gulf; B_2, Western part of the Anadyr Gulf; B_3, Koryakian; B_4, Olutor Gulf; B_5, South-western mixed; B_6. South-eastern; B_7, Komandor. *Eastern Kamchatka coast Provinces* (Aleksina, 1962): K_1, North Kronotsk; K_2, South Kronotsk; K_3, Avacha. *Okhotsk Sea Provinces* (Petelin, 1957): O_1, Taygonos; O_2, Shelikhov Gulf; O_3, Koni-Pyagina; O_4, Okhotsk-Chalomzhinsk; O_5, Ayan-Okhotsk; O_6, Iona Island; O_7, Sakhalin Bay; O_8, North Sakhalin; O_9, South Sakhalin; O_{10}, Aniva; O_{11}, Hokkaido; O_{12}, South Kuril; O_{13}, North Kuril; O_{14}, Southern deep-water basin; O_{15}, Eastern border of deep-water basin; O_{16}, First Kamchatka; O_{17}, First Central; O_{18}, Second Central; O_{19}, Second Kamchatka; O_{20}, Third Kamchatka; O_{21}, Northern; O_{22}, Fourth Kamchatka. *Japan Sea Provinces* (Derkachev, 1996): J_1^I, –Kuznetsovo; J_1^{II}, South-Eastern; J_2^I, Tumangan-South-Primorye; J_2^{II}, Ussuri Bay; J_2^{III}, –Eastern Korean; J_2^{IV}, –Mica; J_2^V, –East Korean Rise; J_2^{VI}, Korean Strait; J_3^I, –Oki; J_3^{II}, Eastern part of the Korean Strait; J_3^{III}, –Vakasa; J_4^I, Oki-Kita-Oki; J_4^{II}, Western Honshu; J_4^{III}, Oshima-Okusiri; J_4^{IV}, Moneron-Rebun; J_4^V, –Delangle; J_4^{VI}, Central part of the Tatar Strait; J_4^{VII}, –Sovgavan; J_4^{VIII}, Lamanon-Coastal; J_5, North-western submarine Rises; J_6, Central Japan Sea; J_7, Yamato; J_8, Ulreung-do; J_9, Aleksandrovsk. *East-China Sea Provinces* (Derkachev and Nikolaeva, 1995): E_1, East-China (E_1^I, E_1^{II}, E_1^{III}, E_1^{IV}, E_1^V subprovinces); E_2, Island-arc (E_2^I, E_2^{II} subprovinces); E_3, Okinawa Trough. *Yellow Sea Provinces* (Chen et al., 1982; Shen et al., 1984; Chen, 1989): Y_1, Northern part of the Bohai Gulf; Y_2, Southern part of the Bohai Gulf; Y_3, Pentsai-Haiyan; Y_4, Lyaodun; Y_5, Qingdao; Y_6, Huanghe River old delta; Y_7, Eastern part of the Yellow Sea; Y_8, Central part of the Yellow Sea (transitional); Y_9, South-western Korea. *Philippine Sea Provinces* (Nechaev and Derkachev, 1995): Eastern Island arcs (F_1^I, F_1^{II}, subprovinces); North-western Island arcs (F_2^I, F_2^{II}, subprovinces); F_3, West –Philippine; F_4, Taiwan; F_5, Sakishima; F_6, Philippine; deep-water trenches (F_7^I,– Mariana; $F_7^{II\text{-}IV}$,– Yap; Palau, Philippine—subprovinces). *South China Sea Provinces* (Derkachev and Nikolaeva, 1997): Annam-Hainan (S_1^I, S_1^{II}, subprovinces); Mekong (S_2^I, S_1^{II}, S_2^{III}, S_1^{IV}, subprovinces). Note: The mineral assemblages of the provinces were discriminated by cluster analysis. The mean values of mineral compositions in the provinces illustrated here are shown in Table 1. Provinces 1–9 as represented by factors: 1–3 *factor I* (epidote-hornblende* assemblage) with factor loadings: 1, 0.9–1.0; **2**, 0.75–0.9; 3, 0.5–0.75; 4–6 *factor II* (olivine-orthopyroxene-clinopyroxene assemblage) with factor loadings: 4, 0.9–1.0; 5, 0.75–0.9; 6, 0.5–0.75; **7**, *factor III* (hornblende-mica assemblage); 8–9, *factor IV* (hornblende-epidote-zircon assemblage with an increased background of the tourmaline, anatase, garnet) with factor loadings: 8, 0.75–1.00; 9, 0.5–0.75; 10, hornblende-clinopyroxene-epidote assemblage with an increased content of chlorite and actinolite; 11, olivine assemblage of the deep-water trenches; 12, epidote-actinolite-chlorite-hornblende assemblage of the deep-water trenches; 13, volcaniclastic assemblage; 14, boundaries of provinces and subprovinces (a, established; b, supposed); 15, boundary between provinces of the East China and Philippine Seas.
Note: * minerals are listed in order of increasing abundance.

Table 1. Mean percentages of provincial heavy mineral composition of surface sediments in the marginal seas of the Western Pacific

Provinces, subprovinces	cpx	opx	ol	npx	hb_1	hb_2	hb_3	hb_4	act	Nam	ep	gr	zr	ap	sph	tou	an	chl	mt	mi	ca	ba	Quantity of samples
Bering Sea																							
B_1	29.00	3.57			33.65				2.82		19.88	3.30	2.82	2.37	–	–	–	2.59	–	–	–		
B_2	32.47	9.14			27.35				2.71		17.05	2.48	4.51	2.03	–	–	–	2.26	–	–	–		
B_3	40.19	4.57			21.53				2.31		18.77	2.67	3.07	1.91	–	–	–	4.98	–	–	–		
B_4	48.43	3.31			16.13				2.94		19.33	1.38	2.30	2.30	–	–	–	3.88	–	–	–		
B_5	49.68	3.08			30.07				2.19		9.87	0.48	0.97	1.70	–	–	–	1.96	–	–	–		
B_6	33.63	5.33			32.53				2.04		14.19	1.22	2.04	3.29	–	–	–	5.73	–	–	–		
B_7	50.53	2.76			25.65				0.79		12.96	1.58	1.38	1.78	–	–	–	2.57	–	–	–		
Eastern Kamchatka coast																							
K_1	62.40	24.00			7.40	2.90		2.00			1.00	–	0.30	–	–	–			–		–		
K_2	62.00	24.30			10.90	1.19		1.20			0.40	–	0.01	–	–	–			–		–		
K_3	54.40	24.10			8.80	4.40		1.29			6.60	–	0.01	0.40	–	–			–		–		
Sea of Okhotsk																							
O_1	38.36	7.08			10.62		23.89	7.67			7.37	1.77	1.77		1.47						–		
O_2	35.78	7.57			12.16		14.22	6.19			18.58	0.92	3.44		1.14						–		
O_3	22.78	3.61			23.33		24.17	5.00			18.33	0.83	1.39		0.28						0.28		
O_4	12.44	3.34			13.04		36.06	3.33			25.14	2.12	3.02		1.51						–		
O_5	11.83	2.16			12.63		36.29	2.69			30.08	1.35	1.35		1.08						0.54		
O_6	17.07	8.04			22.20		21.71	4.86			20.73	1.96	1.96		1.47						–		
O_7	9.03	1.93			12.87		33.85	1.15			25.77	5.77	5.39		4.04						0.20		
O_8	7.68	1.73			7.67		34.41	1.25			35.38	3.72	3.96		3.46						0.74		
O_9	12.67	2.34			8.45		39.44	0.94			27.22	1.88	3.76		3.30						–		
O_{10}	20.11	5.32			20.74		20.71	1.18			20.11	4.16	5.92		1.75						–		
O_{11}	17.38	1.07			7.45		36.15	0.71			28.03	1.77	4.97		2.47						–		
O_{12}	50.41	35.23			5.31		1.52	1.52			2.67	0.19	0.37		0.11						2.67		
O_{13}	51.06	31.08			7.03		1.11	4.81			2.20	0.12	–		–						2.59		
O_{14}	30.03	13.8			7.15		21.90	1.90			19.99	0.95	1.43		0.95						1.90		
O_{15}	41.86	4.25			12.09		2.61	28.76			5.89	–	0.31		0.31						3.92		
O_{16}	41.12	9.44			13.86		6.11	5.56			12.25	0.54	0.54		–						10.58		
O_{17}	26.84	6.08			8.95		13.60	3.58			9.66	0.72	0.72		0.72						29.13		
O_{18}	33.05	5.50			18.22		16.10	8.05			10.60	2.12	1.26		0.43						4.67		
O_{19}	38.03	26.26			10.56		5.44	4.83			4.83	9.06	0.90		–						0.09		
O_{20}	33.26	24.38			11.96		7.42	7.66			8.84	4.31	1.45		0.72						–		
O_{21}	27.21	9.89			14.49		20.17	8.83			15.89	1.05	1.42		0.71						0.34		
O_{22}	42.85	10.17			13.46		7.14	11.26			9.08	3.58	2.19		0.27						–		
Japan Sea																							
J_1^I	50.23*		0.06		10.65				0.02	0.01	34.78	0.73	1.18	0.90	0.57	0.21	0.11	0.15	0.12	0.25	0.03		45
J_1^{II}	18.08	4.47	0.01		18.43	0.29	0.09	0.01	0.05		53.62	0.83	1.38	1.07	0.33	0.21	0.29	0.21	0.10	0.53			54
J_2^I	14.43	3.24	0.20	0.11	35.28	2.48	3.84	0.38	2.67	0.18	25.00	1.29	1.96	1.38	1.56	0.15	0.42	0.73	0.08	4.45	0.17	–	17
J_2^{II}	32.67*		0.02		49.98				0.01		12.04	2.61	0.96	0.65	0.38	0.05	0.01		0.53	0.09			50

J_2^{III}	10.25	3.29	0.17		30.56	1.12	16.08		6.33		12.09	3.59	1.62	1.47	3.15	1.24	0.36	0.57	0.98	6.45	0.68		158
J_2^{IV}	6.72	1.01	–	0.59	15.05	2.29	8.04	0.34	4.16	0.04	11.39	1.30	0.47	1.20	1.46	0.31	0.15	0.34	0.14	40.92	4.08	–	25
J_2^{V}	16.12	7.43	0.48	0.54	18.07	4.76	4.87	0.17	2.53	0.76	20.09	3.27	2.39	2.33	2.30	0.81	0.49	0.94	0.35	7.05	3.78	0.47	17
J_2^{VI}	3.09	4.65	0.04	0.01	22.77	2.33	17.68	0.53	3	–	27.90	5.13	3.44	2.21	1.56	1.04	0.83	0.49	0.11	2.04	1.15	–	14
J_3^{I}	12.53	8.57	0.48	0.05	40.98	3.26	2.93	3.60	1.25	0.03	14.62	0.76	1.39	1.56	0.24	0.17	0.34	0.36	0.11	6.26	0.38	0.13	19
J_3^{II}	4.79	5.33	0.06	–	33.06	2.34	7.62	2.25	1.02	0.07	26.09	2.61	2.85	2.69	1.11	0.47	0.51	0.65	0.16	5.90	0.42	–	11
J_3^{III}	10.65	26.82	0.07	–	22.84	5.57	3.72	6.45	0.38	–	10.97	1.25	4.66	1.98	0.68	0.04	0.28	0.88	0.01	2.63	0.12	–	16
J_4^{I}	30.38	26.26	0.50	–	12.28	10.62	2.62	2.97	0.45	–	6.89	0.42	1.11	1.43	0.40	0.14	0.07	–	–	3.33	0.08	0.05	7
J_4^{II}	33.84	25.79	0.15	0.30	11.27	3.6	0.28	1.69	0.5	0.39	13.63	0.58	1.06	2.91	0.42	0.06	0.43	0.59	0.02	2.01	0.24	0.24	12
J_4^{III}	55.56	5.56	4.14	1.80	7.51	4.44	0.84	2.34	0.43	1.42	7.37	0.26	0.36	1.50	0.18	0.07	0.02	0.43	–	5.34	0.10	0.33	17
J_4^{IV}	79.24*		0.52		10.26				0.08	0.08	5.65	1.21	1.55	0.47	0.13	0.06	0.18	0.46			0.11		11
J_4^{V}	36.59*		0.94		7.93				0.37	0.03	12.21	10.64	20.31	2.68	4.07	0.68	1.77	1.38	0.07		0.33		16
J_4^{VI}	36.31*		0.11		28.69				1.02	0.04	15.23	3.88	5.12	2.31	1.10	1.04	0.96	1.18	0.04	2.67	0.30		18
J_4^{VII}	67.29*		0.53		11.93						13.04	2.28	1.95	0.63	1.17	0.40	0.01	0.03	0.01	0.72	0.01		33
J_4^{VIII}	67.03*		–		9.75				0.05	0.01	6.51	5.48	3.31	1.46	2.20	0.15	0.91	0.84	0.01	1.78	0.51		7
J_5	27.26*		0.44		16.61				1.22	0.20	45.47	0.82	1.18	0.99	0.58	0.12	0.31	0.67	0.06	1.59	1.39	1.09	23
J_6	42.28	1.23	0.85	12.95	6.62	3.04	0.28	1.51	1.7	9.52	8.21	0.48	1.18	2.50	0.54	0.09	0.30	0.49	–	6.14	0.09	–	10
J_7	22.04	7.57	0.19	1.50	13.68	2.27	0.64	0.46	1.16	0.62	30.90	0.92	1.66	1.63	0.74	0.16	0.38	0.95	0.03	10.77	0.22	1.51	44
J_8	33.03	5.07	0.03	3.43	8.95	11.94	0.48	1.95	0.91	0.02	7.99	0.65	0.37	3.54	0.65	0.23	0.11	0.16	0.06	19.03	0.47	0.93	23
J_9	16.09*		–		41.97				–		22.30	7.76	4.42	0.91	4.04	0.75	0.43		–	1.33			12
East China Sea																							
E_1	5.69	2.79	–	0.02	23.43	0.21	4.19	0.09	6.89	0.04	24.57	4.59	2.35	2.48	3.22	1.02	0.52	4.79	0.57	11.07	1.47	–	92
E_1^{I}	5.29	2.30	–	0.02	23.14	0.23	6.33	0.07	6.19	0.05	29.85	5.46	2.78	2.66	3.30	1.03	0.52	5.56	0.51	3.86	0.85	–	36
E_1^{II}	5.71	3.44	–	–	27.03	0.20	3.18	0.10	8.00	0.03	19.39	4.17	2.05	2.82	3.34	1.09	0.46	4.21	0.62	12.59	1.57	–	26
E_1^{III}	4.70	1.49	–	–	23.46	0.20	1.49	0.09	7.41	0.05	18.81	3.61	1.82	2.00	2.98	1.07	0.46	4.53	0.66	22.67	2.50	–	25
E_1^{IV}	11.42	9.48	–	–	4.58	0.13	7.56	0.24	3.15	–	40.21	5.44	3.06	1.77	3.24	0.31	1.19	3.54	0.40	4.06	0.22		5
E_2	32.05	40.50	0.13	–	8.27	0.11	1.74	0.93	1.34	0.09	5.89	1.51	0.74	1.17	0.43	0.19	0.45	1.46	0.13	2.71	0.16	–	19
E_2^{I}	33.10	47.49	–	–	4.32	0.03	1.41	0.87	1.17	–	5.12	1.09	0.27	1.16	0.27	0.12	0.13	1.85	–	1.57	0.03	–	11
E_2^{II}	34.37	29.75	–	–	5.65	–	2.53	0.25	0.95	0.13	10.58	4.59	3.10	1.07	0.96	0.54	1.05	0.64	–	3.61	0.23	–	3
E_3	19.48	9.42	0.29	–	16.21	1.32	7.72	2.18	2.78	0.10	11.33	3.28	2.08	1.42	1.11	0.66	0.74	1.57	0.24	17.23	0.84	–	20
Yellow Sea																							
Y_1	1.13	–			37.51				1.34		31.03	12.02	7.71	0.72	5.24	0.72	0.73		1.34	0.51			120
Y_2	1.53	–			48.48				1.12		29.35	5.62	2.56	0.61	3.48	0.61	0.61		1.12	4.91			58
Y_3	0.40	–			17.30						5.70	2.10	0.10	0.20	0.70	0.20			0.10	68.20	5.00		34
Y_4	0.80	–			41.00						16.30	9.40	0.30	0.70	1.80	0.70			0.20	21.50	7.30		25
Y_5	0.30	–			35.75						28.60	6.65	0.40	0.90	2.60	0.40			0.10	17.30	7.00		15
Y_6	0.80	–			24.60						11.80	2.20	–	0.30	1.20	0.30			0.10	47.10	11.60		12
Y_7	0.90	–			40.35						22.75	3.90	0.20	0.60	1.50	0.50			0.50	20.50	8.30		27
Y_8	0.80	–			27.90						16.10	6.10	0.40	0.70	1.90	0.50			0.20	39.40	6.00		16
Y_9	1.20	1.70	1.50		47.60				5.70		17.00	14.00	3.80	–	0.80	1.20	0.40		5.10				38
Philippine Sea																							
F_1^{I}	63.32	27.13	0.57	–	2.86	0.39	–	1.05	0.22	–	1.28	0.21	0.05	1.57	0.05	–	–	0.22	0.44	0.43	0.03	0.18	20

Table 1 (*Continued*)

Provinces, subprovinces	cpx	opx	ol	npx	hb_1	hb_2	hb_3	hb_4	act	Nam	ep	gr	zr	ap	sph	tou	an	chl	mt	mi	ca	ba	Quantity of samples
F_1^{II}	76.32	6.63	2.56	–	5.81	0.88	0.06	0.99	0.42	0.01	2.84	0.33	0.16	1.27	–	–	0.03	0.47	0.15	0.59	0.09	0.39	40
F_2^{I}	32.39	49.65	–	–	5.90	–	1.29	0.46	1.14	–	3.71	0.56	0.45	0.66	0.39	0.14	0.55	1.72	0.12	0.83	0.04	–	17
F_2^{II}	26.78	32.03	0.03	–	17.31	2.02	4.71	1.81	1.03	–	4.44	1.14	1.34	1.16	0.50	0.45	1.08	1.12	–	3.02	–	0.03	13
F_3	32.02	5.62	0.34	–	43.40	2.06	0.40	6.50	0.43	–	2.71	0.11	0.21	1.33	0.07	0.21	0.13	1.35	0.04	3.02	0.03	0.02	36
F_4	4.74	0.23	0.07	–	5.83	1.23	–	1.95	0.47	–	6.82	0.40	0.55	–	–	0.16	0.24	52.80	0.08	23.13	1.30	–	4
F_5	11.79	5.48	0.04	–	14.50	1.48	2.50	3.09	1.73	0.18	9.04	0.25	0.40	1.37	0.29	0.89	0.28	4.70	0.14	40.48	1.37	–	8
F_6	43.76	2.55	0.01	–	18.10	1.40	0.90	1.10	6.00	–	22.25	–	–	0.70	0.01	–	0.01	2.80	–	0.41	–	0.0	4
F_7^{I}	26.50	3.10	46.70	–	1.90	–	8.80	0.50	2.20	–	10.30	–	–	–	–	–	–	–	–	–	–	–	3
F_7^{II}	7.10	–	1.50	–	69.27	–	–	–	–	–	22.10	0.01	0.01	–	0.01	–	–	–	–	–	–	–	3
F_7^{III}	11.25	3.40	3.30	–	8.44	1.10	–	0.20	12.80	–	55.10	0.30	0.50	0.50	0.40	0.01	0.10	1.70	0.10	0.60	0.10	0.10	5
F_7^{IV}	25.80	5.70	–	–	28.20	5.40	–	1.10	2.70	0.20	21.80	0.80	1.60	0.60	0.30	1.80	0.40	2.30	–	3.00	–	–	2
South-China Sea																							
S_1^{I}	1.64	0.59	0.27	–	26.74	–	–	–	7.74	0.24	33.57	1.98	5.44	0.62	1.52	3.34	2.42	3.83	0.83	7.69	1.54	–	44
S_1^{II}	1.64	0.90	0.52	–	16.61	–	–	–	3.58	–	10.43	0.37	1.11	0.26	0.39	2.76	0.62	2.36	0.13	51.76	6.56	–	13
S_2^{I}	2.26	1.36	–	–	14.12	–	–	–	0.14	–	20.51	1.51	22.50	1.95	0.93	12.40	3.81	0.32	7.82	4.22	6.15	–	17
S_2^{II}	1.10	0.96	0.07	–	13.66	–	–	–	1.66	0.17	22.06	3.38	34.66	0.66	2.14	6.67	3.57	0.72	1.28	4.98	2.26	–	31
S_2^{III}	1.96	0.53	–	–	29.27	–	–	–	–	–	39.91	0.66	11.35	1.00	0.32	7.63	1.25	–	2.46	3.24	0.42	–	21
S_2^{IV}	3.31	8.23	4.78	–	27.43	–	–	–	1.28	0.06	22.45	2.66	12.96	1.13	3.17	3.95	1.87	1.57	0.69	3.58	0.88	–	12

Abbreviations for minerals: cpx, clinopyroxene; opx, orthopyroxene; ol, olivine; npx, alkaline pyroxene; hb_1, brown-green hornblende; hb_2, brown hornblende; hb_3, green hornblende; hb_4, basaltic hornblende; act, actinolite; Nam, alkaline amphibole; ep, epidote group (epidote, clinozoisite and zoisite); gr, garnet; zr, zircon; ap, apatite; sph, sphene; tou, tourmaline; an, sum of anatase, brookite and rutile; chl, chlorite; mt, metamorphic minerals (staurolite, andalusite, kyanite, sillimanite); mi, sum of micas; ca, non-biogenic carbonate; ba, barite.

Notes: Dash, the mineral was not found; blank, the mineral was not determined. Full names of the provinces and subprovinces are given in the caption of Fig. 1.

*Sum of clinopyroxene and orthopyroxene.

Table 2. Q-mode factor loadings for mean provincial heavy mineralogical compositions of the surface sediments within the marginal seas of the Western Pacific

Provinces, subprovinces	Factor I (33.8%)	Factor II (31.6%)	Factor III (9.7%)	Factor IV (9.6%)	Factor V (3.7%)
Bering Sea					
B_1	0.69	0.56	0.08	0.16	0.05
B_2	0.59	0.66	0.07	0.18	0.08
B_3	0.47	0.75	0.06	0.15	0.04
B_4	0.34	0.88	0.05	0.13	0.03
B_5	0.49	0.78	0.06	0.06	0.03
B_6	0.64	0.64	0.08	0.12	0.05
B_7	0.44	0.87	0.06	0.08	0.02
Eastern Kamchatka coast					
K_1	0.17	0.95	0.02	0.02	0.12
K_2	0.18	0.95	0.03	0.01	0.12
K_3	0.23	0.92	0.03	0.04	0.13
Sea of Okhotsk					
O_1	0.67	0.63	0.07	0.07	0.06
O_2	0.62	0.65	0.07	0.15	0.06
O_3	0.84	0.37	0.09	0.11	0.05
O_4	0.87	0.22	0.09	0.16	0.06
O_5	0.86	0.20	0.09	0.16	0.05
O_6	0.85	0.31	0.09	0.14	0.08
O_7	0.86	0.17	0.09	0.21	0.05
O_8	0.82	0.15	0.09	0.23	0.05
O_9	0.86	0.23	0.09	0.18	0.05
O_{10}	0.81	0.38	0.08	0.20	0.06
O_{11}	0.82	0.31	0.09	0.21	0.04
O_{12}	0.13	0.87	0.02	0.04	0.19
O_{13}	0.20	0.89	0.03	0.03	0.17
O_{14}	0.64	0.59	0.08	0.14	0.11
O_{15}	0.65	0.65	0.08	0.05	0.04
O_{16}	0.48	0.75	0.08	0.11	0.07
O_{17}	0.51	0.53	0.12	0.18	0.06
O_{18}	0.72	0.57	0.09	0.09	0.05
O_{19}	0.38	0.73	0.04	0.07	0.18
O_{20}	0.51	0.67	0.06	0.09	0.18
O_{21}	0.76	0.49	0.08	0.11	0.08
O_{22}	0.54	0.74	0.06	0.09	0.07
Japan Sea					
J_1^{I}	0.29	0.74	0.04	0.16	0.01
J_1^{II}	0.49	0.29	0.07	0.25	0.05
J_2^{I}	0.82	0.28	0.16	0.17	0.06
J_2^{II}	0.77	0.50	0.08	0.08	0.02
J_2^{III}	0.86	0.21	0.20	0.12	0.06
J_2^{IV}	0.43	0.13	0.87	0.11	0.05
J_2^{V}	0.71	0.40	0.24	0.22	0.09

Table 2 (*Continued*)

Provinces, subprovinces	Factor I (33.8%)	Factor II (31.6%)	Factor III (9.7%)	Factor IV (9.6%)	Factor V (3.7%)
J_2^{VI}	0.85	0.09	0.13	0.22	0.07
J_3^{I}	0.86	0.25	0.18	0.11	0.09
J_3^{II}	0.85	0.12	0.18	0.19	0.08
J_3^{III}	0.72	0.28	0.12	0.15	0.21
J_4^{I}	0.52	0.62	0.11	0.07	0.19
J_4^{II}	0.37	0.71	0.08	0.11	0.19
J_4^{III}	0.25	0.94	0.11	0.04	0.03
J_4^{IV}	0.14	0.97	0.02	0.04	0.00
J_4^{V}	0.21	0.73	0.01	0.44	0.01
J_4^{VI}	0.58	0.68	0.11	0.18	0.01
J_4^{VII}	0.20	0.95	0.04	0.08	0.00
J_4^{VIII}	0.16	0.97	0.05	0.08	0.00
J_5	0.45	0.45	0.09	0.23	0.02
J_6	0.24	0.88	0.14	0.07	0.01
J_7	0.48	0.48	0.26	0.22	0.08
J_8	0.45	0.67	0.40	0.08	0.05
J_9	0.83	0.31	0.11	0.21	0.03
East China Sea					
E_1	0.73	0.15	0.32	0.24	0.06
E_1^{I}	0.75	0.13	0.17	0.26	0.06
E_1^{II}	0.75	0.15	0.36	0.21	0.07
E_1^{III}	0.61	0.12	0.55	0.21	0.05
E_1^{IV}	0.45	0.26	0.14	0.30	0.10
E_2	0.21	0.64	0.07	0.06	0.27
E_2^{I}	0.12	0.61	0.04	0.05	0.29
E_2^{II}	0.20	0.72	0.09	0.14	0.22
E_3	0.61	0.47	0.42	0.15	0.10
Yellow Sea					
Y_1	0.80	0.04	0.09	0.31	0.05
Y_2	0.86	0.05	0.16	0.19	0.05
Y_3	0.16	0.00	0.98	0.07	0.05
Y_4	0.76	0.03	0.45	0.16	0.05
Y_5	0.74	0.02	0.38	0.21	0.05
Y_6	0.37	0.02	0.91	0.13	0.04
Y_7	0.76	0.03	0.43	0.17	0.05
Y_8	0.49	0.02	0.69	0.15	0.05
Y_9	0.88	0.05	0.09	0.18	0.06
Philippine Sea					
F_1^{I}	0.07	0.95	0.02	0.02	0.13
F_1^{II}	0.11	0.98	0.03	0.02	0.03
F_2^{I}	0.13	0.59	0.03	0.04	0.29
F_2^{II}	0.47	0.58	0.10	0.07	0.24
F_3	0.75	0.50	0.12	0.03	0.06
F_4	0.14	0.08	0.40	0.05	0.04

Table 2 (*Continued*)

Provinces, subprovinces	Factor I (33.8%)	Factor II (31.6%)	Factor III (9.7%)	Factor IV (9.6%)	Factor V (3.7%)
F_5	0.36	0.23	0.88	0.09	0.07
F_6	0.45	0.75	0.07	0.11	0.03
F_7^{I}	0.21	0.42	0.03	0.06	0.03
F_7^{II}	0.91	0.11	0.09	0.09	0.04
F_7^{III}	0.38	0.18	0.07	0.25	0.05
F_7^{IV}	0.72	0.51	0.14	0.16	0.06
South China Sea					
S_1^{I}	0.68	0.05	0.23	0.33	0.05
S_1^{II}	0.23	0.03	0.96	0.13	0.05
S_2^{I}	0.41	0.07	0.12	0.79	0.05
S_2^{II}	0.34	0.04	0.10	0.85	0.05
S_2^{III}	0.66	0.05	0.12	0.41	0.05
S_2^{IV}	0.71	0.12	0.14	0.45	0.11

Note: Factor loadings only for mineralogical provinces/subprovinces listed in Table 1, are shown here.

concentrations of opaque minerals (magnetite, titanomagnetite, ilmenite) and, in some areas, olivine. The grains are fresh, idiomorphic, and are often enclosed by volcanic glass. Mineral assemblages of this type extend as a continuous belt along the system of island arcs and can be traced up to a few hundreds of kilometres in marginal seas, widening especially in bordering areas of the Pacific Ocean (Fig. 1). Assemblages with maximal values of factor loadings characterise provinces related to ensimatic (young) island arcs (Mariana, Izu-Bonin, Tonga, Vanuatu) where clinopyroxene-rich assemblages with subordinate olivine dominate. Assemblages with smaller factor loading values are peculiar to mature and evolved (Aleutian, Kurile-Kamchatka, Japanese, Nansey, Philippine, Sunda) island arcs with widespread occurrence of the calc-alkaline magmatic rocks (Kuno, 1959; Kovalenko, 1987). These assemblages are characterised by high orthopyroxene content. Explosive volcanic activity is the main source of clastic minerals here: the areal extent of the numerous ash-falls can be tracked in the sediments as pure inter-layers of pyroclastics or as dispersed volcaniclastics at distances of over 1000 km (Machida and Arai, 1976, 1978; Arai et al., 1981; Machida and Arai, 1983).

In addition to the volcaniclastic island-arc provinces described above, *Factor II* combines provinces that are derived from volcanic and volcaniclastic rocks of basic to intermediate composition (including plateau basalts) of Neogene-Quaternary age. Provinces of this type adjoin northern Sikhote-Alin, the western coast of Sakhalin, the coast of northern Kamchatka and Koryack (Fig. 1). They are characterised by heavy mineral assemblages dominated by clinopyroxenes and with comparatively increased content of hornblendes and epidote (Table 1).

Factors III and IV incorporate mineral assemblages that have sharply different hydraulic properties. *Factor III* makes a 9.7% contribution to the variance and characterises mineral assemblages with a high content of most hydraulically

susceptible minerals, mainly micas. Similar assemblages have been found in the Japan Sea near the eastern Korean coast (Mica Province), Yellow (Provinces Bohai Gulf, Pentsai-Haiyan; Shen et al., 1984; Likht, 1997) and East China Seas (Yangtze Province). Abundant mica serves as a good indicator of quiet or low energy hydrodynamic conditions in the depositional environment (Derkachev et al., 1983). In the Japan Sea, areas of high mica concentrations and sedimentary rates are found at the foot of the Korean continental slope extending into bathyal basins. Similar conditions occur in some coastal areas, at large river mouths and in halistatic zones (the central, slack-water, parts of the gyres formed by the currents, where fine-grained sediments accumulate) of the Yellow and East China Seas (Milliman and Meade, 1983; Shen et al., 1984; Chen, 1989; Derkachev and Nikolaeva, 1995; Derkachev, 1996).

A zircon/rutile/anatase/garnet assemblage is defined by *Factor IV* with a contribution to the variance of 9.6%, and is restricted to the wide shelves of large bays (East Korean, Peter the Great and Delangle in the Japan Sea), the Korean Strait, the East China outer shelf and the south-western part of the South China Sea (Mekong Shelf). It generally has a local distribution and belongs either to relict sediments of submarine coastal-slope facies, or to bottom areas that are subjected to the influence of strong tidal currents (Oki Strait in the Japan Sea, the area near Qingdao Peninsula in the Yellow Sea, etc.) (Shen et al., 1984; Yokota et al., 1990; Derkachev, 1996).

Factor V (with a contribution to the variance of 3.7%) defines volcaniclastic assemblages with orthopyroxene dominating over clinopyroxene. Typical examples of these assemblages are found in the provinces adjoining Kyushu Island and the northern part of Ryukyu island arc (Suzuki, 1975a; Derkachev and Nikolaeva, 1995).

When evaluating the regional variability in the distribution of mineral assemblages, it is necessary to note specific assemblages, which were not distinctly reflected by the Q-factor analysis (the values of factor loadings on each of the factors are lower than 0.5). These include hornblende/clinopyroxene/epidote assemblages with the dominance of epidote and rather high contents of chlorite and actinolite, formed mainly by the breakdown and erosion of greenschist facies metasedimentary and metavolcanic rocks. Such assemblages usually occupy areas adjacent to ancient marginal-continental volcanic belts of pre-Cenozoic age (Okhotsk-Chukotka, Sikhote-Alin, Honshu-Korean) (Belyiy, 1998). The south-eastern province of the Japan Sea, adjoining the Sikhote-Alin volcanic belt, is representative of such assemblages. A similar composition characterises assemblages in some Japan Sea rises (provinces of the north-western submarine rises and Yamato) (Fig. 1, Table 1).

Subaquaeous destruction of metabasites, ultrabasics, amphibolites, actinolite-chlorite-epidote schists, gabbros, etc., which form raised blocks on the oceanic crust, release mineral assemblages that are distributed in deep-water trenches within the Western Pacific (Mariana, Yap, Palau, Philippine, Tonga). These metaophiolite-derived assemblages are spatially disconnected and usually occupy small areas on the slopes and on the bottom of trenches. The proportions of the main minerals in these assemblages (clinopyroxenes, chlorite, green hornblende, actinolite, epidote) can vary in the various trenches, as a function of parent rock composition (Skornyakova et al., 1978; Murdmaa et al., 1980; Derkachev et al., 1989; Nechaev and Derkachev, 1995). Enstatite-bronzite, olivine, diopside, chromite and other diagnostic minerals

(with chlorite aggregates, serpentine and talc in the light fraction) are present as accessory minerals in assemblages of some trenches, especially where outcrops of ultrabasics are present (Mariana, Yap, Tonga).

Towards the central areas of the basins, the influence of coastal supply diminishes, with the formation of mixed mineral assemblages in the central deep-water areas of the Bering, Okhotsk and (to a lesser degree) Japan Seas. Fig. 1 shows that individual features of terrigenous-mineralogical provinces can be traced up to a few hundreds of kilometres (usually 150–250 km) from the coast. This distance is greater for the seas with wide shelves: the East China and southwest part of the South China (Sunda Shelf). The areal spread of minerals in the volcaniclastic provinces is much wider.

3.2. R-Factor Models

R-factor models help to define the main mineral associations, which best characterise the mineral composition of the sediments of the individual marginal seas. Analysis of several tens of R-factor diagrams of the mineral composition of sediments, plotted for individual mineralogical provinces, has revealed a regular combination of minerals with considerable statistical stability and consistent correlations (Derkachev and Nikolaeva, 1995, 1997; Nechaev and Derkachev, 1995; Derkachev, 1996). The make-up of these mineral associations, as will be seen below, is a function, primarily, of the lithology of their source rocks, the nature of volcanism (defined by the plate tectonic setting) and the hydrodynamics of the bottom waters. R-factor analysis of the integrated dataset was based on both regular sampling for all marginal seas (1200 analyses) and sampling of average values of mineral contents for separate provincial assemblages. Results have indicated a strong correspondence with the main features of the mineral assemblages in the source formations, thus proving the potential of the method. Mean values plotted in Fig. 2 show that *Factor I* reflects key differences in the nature of heavy mineral associations, caused by tectonic discontinuity in the continent-ocean transition zone. We interpret this factor as the *factor of geodynamic setting*.

The plot of factor values in Fig. 2 shows that mineral assemblages, associated with the geodynamic environments of island arcs, deep-water trenches and back-arc spreading, generally have $F1 > 0$. This clearly reflects a trend in the evolution of magmatism in a continent-ocean transition zone. Mineral assemblages reflecting features of both island arc magmatism on the oceanic basement (epioceanic or young island arcs) and associated deep-water trench environments show $F1 > 1$. The olivine/clinopyroxene suite with the dominance of clinopyroxene is most widespread in these environments.

Assemblages associated with island arcs, founded on more mature subcontinental or continental crust (epicontinental or mature and evolved island arcs), occupy an isolated position. Differentiated calc-alkaline igneous rocks with increased content of orthopyroxene and—for some areas (the back arcs)—of hornblende, are more widespread here in comparison with ensimatic island arcs. The two-pyroxene (orthopyroxene/clinopyroxene) assemblages and, to a lesser degree, clinopyroxene/orthopyroxene/hornblende suites (with dominant brown-green, brown hornblendes and oxyhornblende) are most typical for this geodynamic environment.

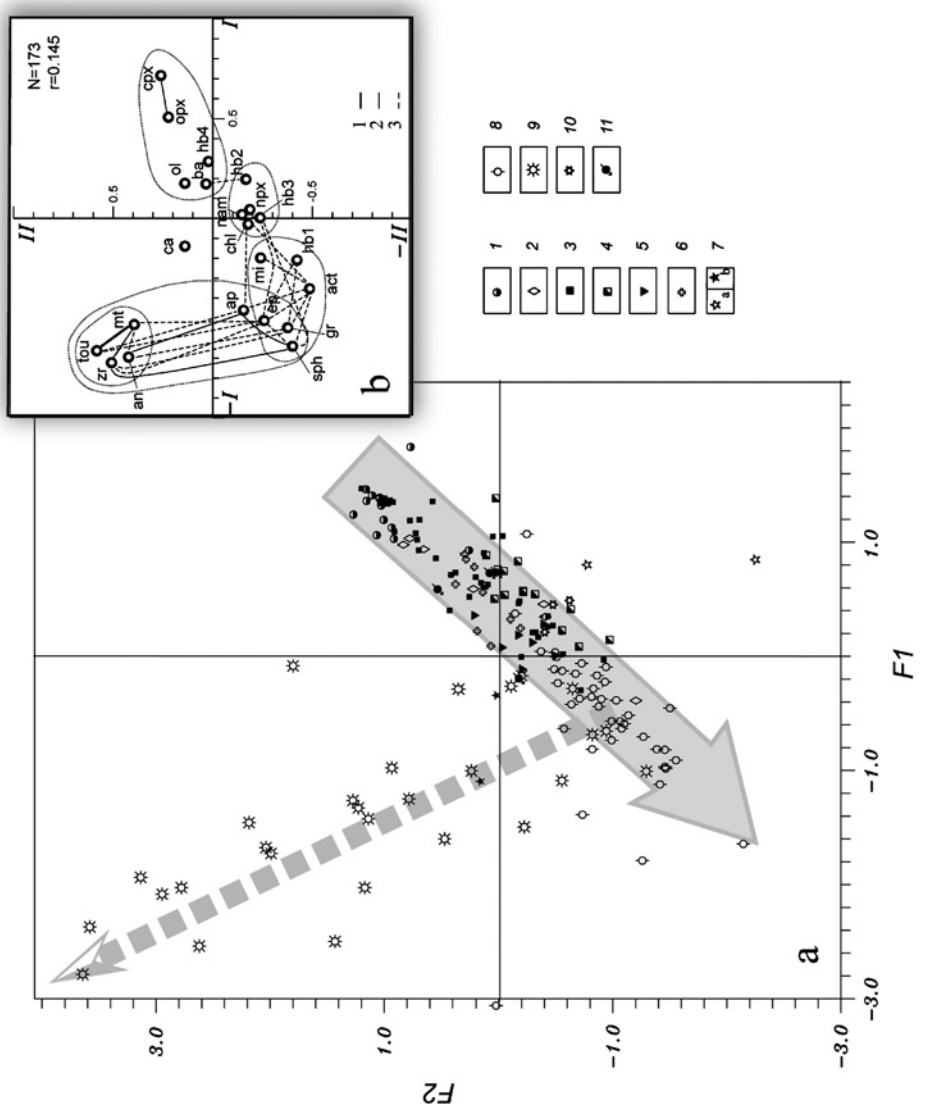
N=173
r=0.145
cpx
opx
ol
ba
hb4
hb2
nam
chl
npx
hb3
hb1
act
gr
sph
ap
ep
rml
ca
tou
zr
mt
an
b
a
F1
F2
3.0
1.0
-1.0
-3.0
0.5
-0.5
1 —
2 —
3 --
1
2
3
4
5
6
7
8
9
10
11

Mineral assemblages representing mature continental crust have $F1 < 0$ and are clustered in the left part of the plot (Fig. 2a). They define a clear trend in mineral density (dashed arrow), as a result of hydrodynamic differentiation of the clastic material by wave action and tidal currents. This process is highlighted by *Factor II* and is interpreted as *the factor of hydrodynamics*. This factor contrasts mineral associations with different hydraulic properties, for example: zircon/anatase (rutile)/tourmaline versus actinolite/hornblende/micas/apatite (Fig. 2b).

The other factors discriminate between mineral associations, reflecting the petrographic composition of particular rock complexes in the source areas. These associations are: (a) sphene/garnet/apatite; (b) epidote/green and brown-green hornblende; (c) various micas, etc. Mineral constituents of alkaline volcanic rocks from areas of active tectono-magmatic regimes form independent suites. The association of alkali pyroxene/alkali amphibole/brown hornblende (Fig. 2b) is the most clearly expressed and is reflected by *Factor III*. Its typical occurrences are the Central Japan Sea and Ulreung-do Provinces in the Japan Sea. The high contents of both alkali pyroxenes and alkali amphiboles (on an average 12.9 and 9.5%, respectively), together with a predominance of clinopyroxenes over orthopyroxenes, are distinctive features of the Central Japan Sea mineral assemblage. Alkali pyroxenes and alkali amphiboles are not found in such high amounts in any other area of the marginal seas within the Western Pacific. They are connected with activity of the Korean Baegdusan Volcano (Machida et al., 1981). The clinopyroxene/brown hornblende/oxyhornblende/biotite/apatite association, most typical for eruptions of the

Fig. 2. R-mode factor model of detrital mineral composition in the marginal seas of the Western Pacific, based on mean heavy mineral contents of the assemblages in the heavy mineral provinces. (a) The position of mineral assemblages on the plot of factor values: along the *X*-axis, values of the first factor (F_1); along the Y-axis, values of the second factor (F_2). 1–11, mineral assemblages with affinities to: 1, island arcs on the oceanic basement, or young island arcs (olivine-clinopyroxene assemblage); 2, deep-water trenches; 3, evolved and mature island arcs (predominantly orthopyroxene-clinopyroxene assemblage); 4, the same, but with the predominance of volcanogenic hornblende; 5–6, Meso-Cenozoic marginal-continental volcanic belts; 5, hornblende-epidote-pyroxene assemblage; 6, the same, but with the predominance of clinopyroxene; 7, the areas of renewed tectonics and magmatism with: a, acid alkaline magmatism (Baegdusan, Ullreung-do Volcanoes), b, basaltic magmatism (volcanoes of the Vietnamese Shelf); 8, ancient consolidated areas with the prevalence of sedimentary, granitic and metamorphic rocks; 9, the same, but within shelves with active hydrodynamics of near-bottom waters; 10, the areas of island arc-continent collision with the primary involvement of mica-chlorite assemblages (Taiwan Island); 11, mixed mineral suites of the Central Okhotsk Sea. *Solid arrow* indicates the evolutionary trend of detrital mineral distribution, controlled by the geodynamics of the sedimentary environment (a trend from simple geodynamic conditions for oceanic crust toward composite processes for consolidated continental crust). *Dashed arrow* shows a trend of evolving heavy mineral assemblages as a response to near-bottom water hydrodynamic processes causing mineralogical differentiation. (b) Main heavy mineral assemblages on the plot of factor loadings: *N*, quantity of data (based on mean values of provincial assemblages); *r*, significant (at 95%) correlation coefficient. Lines—significant positive correlations between minerals: 1, strong (>0.5); 2, moderate (0.3–0.5); 3, weak (<0.3). *Circles with dotted lines* outline main heavy mineral associations. Abbreviations for minerals are given in the Table 1.

Ullreung-do volcano (Japan Sea) (Machida et al., 1984), is expressed to a lesser degree.

3.3. *Influence of Grain Size, Mineral Stability and Climate*

For the marginal seas (Okhotsk, Japan, etc.), the common tendency of detrital mineral dispersal coincides with grain-size trends from coarse-grained sands and gravels to silty-clays and appears to be connected with mineralogical differentiation by hydraulic processes (Derkachev and Nikolaeva, 1993, 1997). Correlation analysis between grain size and heavy mineral content showed for the coarse suites a positive correlation between high-density heavy minerals (opaque minerals, zircon, garnet, sphene, anatase and metamorphic minerals). The opposite behaviour is characteristic for minerals with lower density and greater hydraulic mobility (micas, brown-green hornblende, actinolite and calcite), which concentrate in fine-grained deposits.

The large latitudinal extent of the Western Pacific marginal seas allows us to estimate whether the climatic factor essentially influences the behaviour of detrital mineral assemblages from north to south. For this purpose, we have taken mean values of mineral groups (stable, moderately stable and unstable to chemical weathering according to Berger, 1986) for the studied provinces. The interrelations of these mineral groups were considered for regions with different climate (Fig. 3). The comparative analysis has shown that immature mineral assemblages are characteristic for sediments in all studied seas. Tectonic activity in adjoining land and seabed along with volcanic processes are the main reasons for the presence of immature

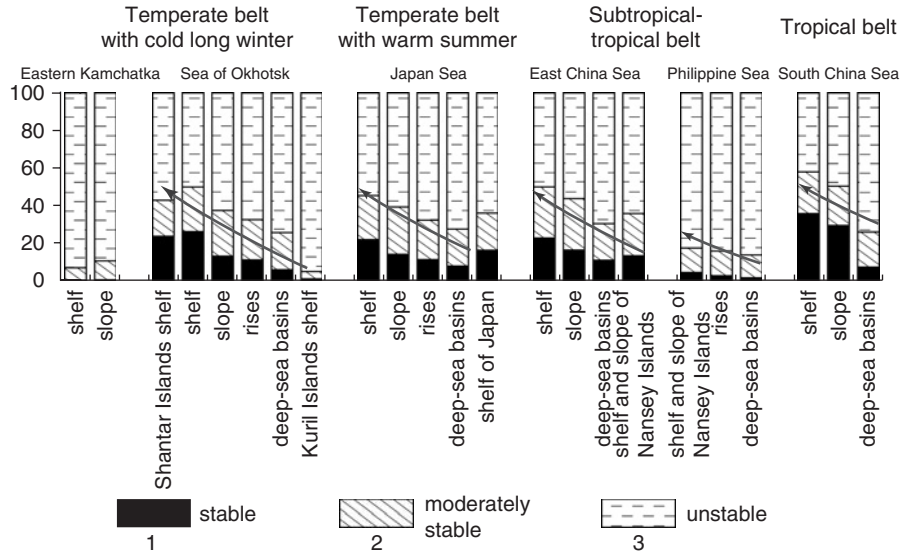

Fig. 3. Comparison of mean values for stable, moderately stable and unstable minerals within sedimentary basins grouped according to climatic belts and main structural elements of the seabed. 1–3, Percentage of mineral groups according to their stability under weathering. Arrows show a trend of the maturity increase for mineral assemblages within different climatic belts.

heavy mineral assemblages. Neotectonic movements on land with renewed activities on both ancient platform and folded areas have created significant topography. As a result, intensive erosion, exceeding the thickness of the weathering zone, ensured the delivery of fresh clastic material to the marginal seas. Increased erosion during tropical cyclones (typhoons) also exerted considerable influence on the character of the detrital mineral assemblages. Consequently, vast masses of clastic material were transported outside the coastal zone and bypassed it without any significant hydraulic sorting or mineralogical differentiation.

However, a small but noticeable increase in mineral maturity can be observed from the subarctic belt to the subequatorial zone. Derkachev and Nikolaeva (1993, 1999) discerned this tendency by mapping the distribution of the stability coefficient in the mineral assemblages, calculated as the ratio of stable minerals to moderately stable and unstable ones. They found that a considerable scatter of the stability coefficient values is characteristic for detrital mineral assemblages of a subequatorial belt. Overall, the values vary from high, as in sediments of shelves with an active hydrodynamic regime (e.g., the Mekong River shelf) to rather low, peculiar to continental slope environments and deep-water basins of the South China Sea (Fig. 3). The large transit rivers (Mekong, Red, etc.) draining strongly dissected mountains with high rates of erosion, cutting into unaltered bedrock, mask the influence of the climatic factor. However, the influence of the climatic factor is more strongly expressed in north-eastern areas of the Siam Gulf near the Cambodian coast and on northern coast of the Bakbo Gulf, where the land is drained by river systems flowing through a thick weathering zone (Chen and Zhang, 1986; Li and Ye, 1987; Derkachev and Nikolaeva, 1999a), but such areas have limited distribution.

The above indicates that climatic factor, even within the subequatorial belt, does not reflect the features of detrital mineral compositions of the Western Pacific marginal seas. The structural position of sedimentary basins, the petrography of source complexes and the hydrodynamics of the drainage systems exert greater influence on mineral compositions and formation of the sediments than climate. In our case, it is possible to conclude with confidence that the detrital mineral composition of the marine basins carries and maintains individual signatures of respective source rock lithologies despite some homogenisation and simplification resulting from environmental and hydrodynamic factors. Fig. 3 illustrates the proportions of heavy minerals with differing stabilities in a series of marine basins situated in different climatic zones. A trend with decreasing mineral maturity in a sequence of depositional environments from shelf-continental slope-submarine rises to deep-water basins is clearly noticeable in this figure. All these conclusions are supported by Q- and R-mode factor analyses.

Consequently, we have made an attempt to assess whether heavy mineral assemblages can be used as indicators of particular geodynamic environments within zones of near-continental depositional settings. Using data on individual heavy mineral abundances, heavy minerals were grouped into discrete suites according to their genetic affinities to particular magmatic and metamorphic rocks. Eight heavy mineral suites were recognised from four (A–D) distinct rock types:

A: mafic intrusive and effusive rocks of variable composition:

1. olivine/clinopyroxene,
2. orthopyroxene,

3. brown hornblende/oxyhornblende,
4. alkali pyroxene/alkali amphibole;

B: acid intrusive rocks of sialic type:

5. green hornblende/brown-green hornblende,
6. zircon/apatite/sphene (GM);

C: greenschist facies metamorphic rocks (MT_1):

7. epidote/actinolite/tremolite/chlorite;

D: high-grade metamorphic rocks (MT_2):

8. garnet/anatase/rutile/staurolite/andalusite/kyanite/sillimanite/tourmaline/calcite.

3.4. Discriminant Analysis

Variations in the detrital mineral spectra of sediments is best studied using comparative analysis of average values of both the provincial mineral assemblages and those in the individual areas of a particular basin. Therefore, to obtain fully representative heavy mineral compositions, we have analysed data not only from the marginal seas of the Western Pacific but also from other areas of the world's oceans, located in different climatic belts and different geodynamic environments (published data on detrital mineral assemblages from the Atlantic, Arctic and Indian Oceans, as well as from the Mediterranean, Baltic and North Sea, the Sea of Azov, and the Black, Aral and Kaspian Sea were used. However, references are too numerous to be listed here). The resultant representative dataset, comprising 320 mineral assemblages, was processed by discriminant analysis with the calculation of the equations of linear discriminant functions (df1, df2, df3) (see Fig. 4). This calculation was made with the use of the statistical software 'STATGRAPHICS':

$$
\begin{aligned}
df_1 = &-5.678x_1 - 5.703x_2 - 5.738x_3 - 5.659x_4 - 5.705x_5 \\
&- 5.78x_6 - 5.743x_7 - 5.742x_8 + 571.785 \\
df_2 = &-59.797x_1 - 59.714x_2 - 59.739x_3 - 59.717x_4 - 59.764x_5 \\
&- 59.825x_6 - 59.704x_7 - 59.674x_8 + 5976.46 \\
df_3 = &-30.154x_1 - 30.098x_2 - 30.147x_3 - 30.059x_4 - 30.206x_5 \\
&- 30.108x_6 - 30.149x_7 - 30.139x_8 + 3015.14,
\end{aligned}
$$

where x_1 = sum of clinopyroxene and olivine, x_2 = orthopyroxene, x_3 = brown-green and green hornblende, x_4 = brown hornblende and oxyhornblende, x_5 = sum of epidote, actinolite and chlorite, x_6 = sum of garnet, anatase, rutile, staurolite, andalusite, corundum, sillimanite, tourmaline and calcite, x_7 = sum of zircon, sphene and apatite, x_8 = sum of alkali pyroxene and alkali amphibole.

In calculating discriminant function values, the sum of minerals used in the equations was taken as 100%. Opaque and authigenic minerals, mica and rock fragments were excluded from the calculation. Discriminant analysis has revealed an intimate relationship between heavy mineral assemblages and the structural setting of the studied sedimentary basins. The points of discriminant function values were plotted on two diagrams to achieve the best characterisation of mineral assemblages.

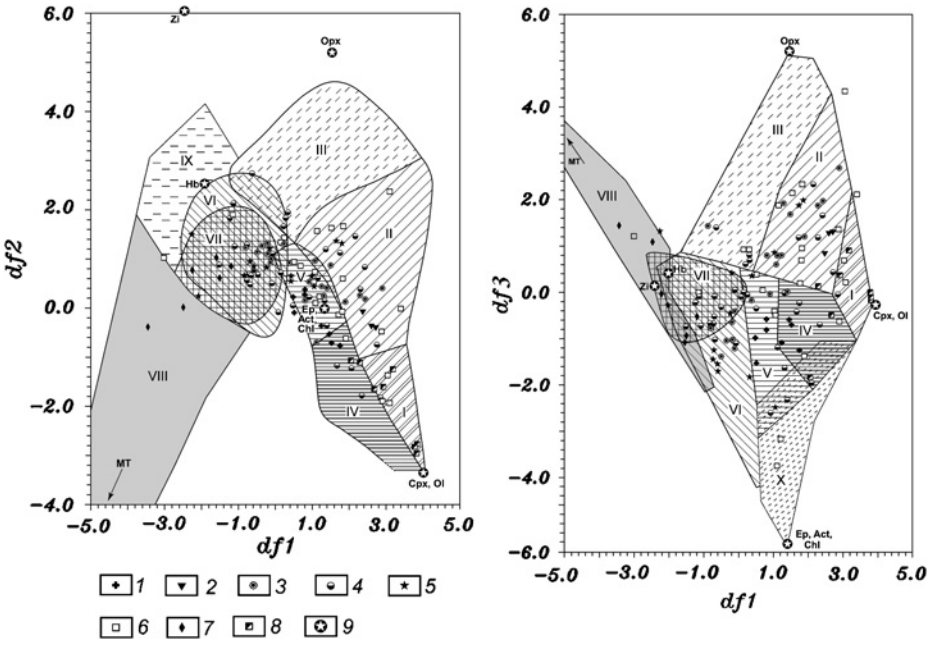

Fig. 4. Lithogeodynamic diagrams, reflecting the dependence of composition of heavy mineral assemblages on the geotectonic setting of sedimentary basins. I–VIII, fields of location of the imaging points for heavy mineral assemblages of different types of geodynamic environments: I, young island arcs on oceanic basement, evolved (II) and mature (III) island arcs; IV, young folded areas with evolving primary Cenozoic volcanogenic and volcanogenic-sedimentary rocks, along with areas of active tectonics and magmatism with Pliocene-Quaternary effusive basaltic volcanism, forming thick covers of plateau basalts; V, Meso-Cenozoic marginal-continental volcanic belts; VI, areas of ancient Precambrian fold belts with primary sedimentary, granitic and metamorphic rocks; VII, Precambrian cratons and intermediate massifs comprising granitic and metamorphic complexes; VIII, ancient platforms; IX, field of the mineral assemblages with high proportions of stable minerals (predominantly zircon) formed by hydraulic differentiation processes; X, field of mineral assemblages formed by destruction of altered ultrabasic rocks, including ophiolites. 1–9, assemblages in mineral provinces of the Seas: 1, Bering; 2, eastern coast of the Kamchatka; 3, Okhotsk; 4, Japan; 5, East China; 6, Philippine; 7, South China; 8, Tonga Trench; 9, the position of the hypothetical mineral assemblages with the 100% content of clinopyroxene and olivine (Cpx, Ol), orthopyroxene (Opx), brown-green and green hornblende (Hb), zircon, apatite, sphene (Zi), group of greenschist facies metamorphic minerals: epidote, chlorite, actinolite (Ep, Act, Chl), group of high-rank metamorphic minerals of: tourmaline, rutile, anatase, kyanite, staurolite, sillimanite, andalusite, calcite (MT).

The first diagram is plotted in a plane of the 1st and 2nd discriminant functions (Fig. 4a), and the second in a plane of the 1st and 3rd ones (Fig. 4b). The use of two diagrams has facilitated the recognition of details, which could be missed if only one diagram was used. Assemblages associated with deep-water trenches (*field X*) appear more clearly on the second diagram (Fig. 4b). Heavy mineral suites representing discrete crustal lithologies are easily recognized in the diagrams from a change in the

trend of mineral assemblages from oceanic to continental areas (Fig. 4). This is also confirmed by R-mode factor analysis (as discussed above).

In the search for signatures of particular geodynamic environments for sedimentary basins, Romanovsky (1991, 1998) introduced the term 'lithogeodynamics'. According to his suggestion, lithogeodynamics is the science studying lithological indicators of past geological regimes. It allows the identification of objective and reliable lithological features (in our case these are detrital mineral assemblages) of tectonic regimes in which sedimentary sequences are formed. The author uses this term for the diagrams shown in Fig. 4, because they essentially reflect the unique geotectonic features of the studied sedimentary basins. For example, detritus from intra-oceanic uplifts and young island arcs, comprising predominantly clinopyroxenes and to a lesser extent olivines, differ considerably in composition from all other environments (*field I*). The typical mineral assemblages in this case are the products of Mariana, Izu-Bonin, Tonga-Kermadek and Vanuatu island arcs. Higher amounts of olivine, in varying proportions, and the appearance of titaniferous clinopyroxene (Nechaev, 1991) is characteristic for mineral assemblages of intra-oceanic uplifts.

Mineral assemblages of evolved and mature island arcs scatter within well-defined areas (*fields II and III*), separate from other fields in the plot. The main sources of clastic material supply are the differentiated volcanic island-arc complexes of mainly calc-alkaline series, which are characterised by two-pyroxene {clinopyroxene-orthopyroxene (hypersthene)} assemblages (Kuno, 1959; Kovalenko 1987; Miyashi and Miyashi, 1988). Mature island arcs (Aleutian, Kurile-Kamchatka, Japanese, Ryukyu, Philippine, Sunda, New Zealand, etc.) are characterised by strong explosive volcanic activity and, as a result, pyroclastic material is scattered at considerable distances and becomes intermixed with sediments of the contiguous deep-water basins. Mineral assemblages, characteristic of the Japanese island arc (Suzuki, 1975a, 1975b, 1985; Yokota et al., 1990), cluster within the field of mature island arcs (*field III*) and those of pyroclastic flows of many volcanoes from Kyusyu and Honshu islands (Miyashi and Miyashi, 1988) tend towards the same field. Products of volcanism, associated with water-saturated magmas are widely distributed in back-arc zones of mature island arcs with rather thick continental crust. Accordingly, the influence of explosive volcanism of this type is reflected in the mineral compositions of sediments of the surrounding seas. Hydrous aluminosilicates are predominant as the ferromagnesian phase, including volcanogenic brown-green hornblendes with subordinate biotite, brown hornblende, oxyhornblende and hypersthene (Table 1). They are most common in areas adjoining southwest Japan, the northern part of the Philippine Arc (Luson, Batan, Babuyan Islands) and to the east of New Guinea. On the discriminant-functions diagrams they cluster in the far left part of *field III* (Fig. 4a). The virtual absence of metamorphic (MT_1 and MT_2) and sialic (GM) mineral groups distinguishes them from those hornblende-rich assemblages that define fold belts of continental areas (see below).

Detrital mineral assemblages derived from marginal-continental, volcano-plutonic belts (Sikhote-Alin, Okhotsk-Chukotka, Honshu-Korean, etc.) occupy a distinct position (*field V*) on the diagrams (Fig. 4a, b). Increased amounts of sialic minerals and rather high pyroxene content, combined with the presence of the epidote group (the latter are typical of greenschist facie metamorphics: MT_1), are

characteristic for these assemblages. The field in which they are located is partially overlapped by that of island-arc assemblages.

In mineral assemblages of source provinces, the amount of metamorphic minerals shed by greenschist facies (MT_1) rocks decreases with the emergence of more basic effusive rocks and the rejuvenation of magmatism within marginal-continental volcanic belts. Consequently, a definite trend towards primitive, olivine-clinopyroxene dominated, suites of young island arcs (Fig. 4a) is highlighted by the distribution of points signalling the mineral assemblages of these environments (*field IV*). The provinces, bordering the Olutor-Koryak coast of the Bering Sea and the northwest coast of the Japan Sea (Kuznetsovo and Sovgavan Provinces), are representative of this mineral suite. It should be noted that the mineral assemblages from areas adjacent to Pliocene-Quaternary plateau basalts occupy the same field, e.g., the Sovgavan (northern Sikhote-Alin), Orlov (western Sakhalin), Shkotovo (southern Primorye). Other plateau basalts are located outside the studied Western Pacific areas (Emelyanov, 1979; Kharin et al., 1979; Emelyanov and Kharin, 1982).

Mineral assemblages from deep-water trenches overlap *fields IV and V*, and form a trend along a line Ol, Cpx → Ep, Act, Chl. This geodynamic environment is enhanced in Fig. 4b, where the assemblages occupy a distinct field (*field X*). *Field X* is partially overlapped by the fields of marginal-continental volcanic belts (*field V*) and areas of renewed tectono-magmatic activity (*field IV*).

Detritus from mature continental crust differs in mineral composition (Fig. 4), being dominated by brown-green and green hornblende-rich assemblages, with subordinate epidote and accessory minerals from granitic and metamorphic rocks. The typical representatives of similar mineral assemblages are those of the Western Okhotsk Sea (including the Amur River Basin), and all assemblages along the coast of Korea, China and Indochina. On the diagrams of Fig. 4 they fall into fields, controlled by different mineral groups (GM and MT). The assemblages adjoining to ancient fold belts, with the predominance of granitic-metamorphic and sedimentary rocks, occupy *field VI*. Heavy minerals derived from pre-Cambrian cratons of ancient platforms trend towards *field VII*. These fields partially overlap, and are shown clearly only in Fig. 4b (in the direction of MT_1 mineral group) in the field defining VI, caused by the increase in contribution from metasedimentary rocks of ancient fold belts.

Highly mature polycyclic suites, derived from granitic and metamorphic rocks (GM and MT_2), characterise the cratonic cover sediments of ancient platforms (East European, North American, Australian etc.) and form two distinct fields (*VIII and IX*). *Field VIII* comprises assemblages of cover rocks on ancient platforms, while *field IX* depicts the most mature suite, dominated by zircon. Heavy mineral accumulations formed by hydraulic sorting, e.g., placer deposits, and those resulting from high-energy conditions on the shelves, also point towards *field IX*. As a rule, similar assemblages are conjugated with Recent and relict (Pleistocene) beach facies and with those on underwater coastal slopes. The typical locations of such assemblages are those on the Sunda Shelf (South China Sea), and some areas of the outer shelf of the East China and Japan Seas (Yokota et al., 1990; Derkachev and Nikolaeva, 1995, 1999; Derkachev, 1996). Heavy minerals released by the disintegration of weathering crust, and those eroded from microcontinents (Seychelles), also trend

towards *field IX*. Intensive weathering of granites (dominant type of rocks on the Seychelles) under wet tropical climate have resulted in the concentration of stable minerals with a predominance of zircon (Korotky and Raszhigaeva, 1992; Derkachev et al., 1997).

4. CONCLUSIONS

Multivariate and comparative analyses of the spatial distribution of heavy mineral assemblages, as presented in this paper, show that the detrital mineral composition of marginal seas within the Western Pacific is determined, primarily, by the structural position of these seas in the zone of continent to ocean transition. Hydrodynamic and, to a lesser extent, climatic factors have an appreciable influence.

Lithogeodynamic diagrams show a strong relationship between the composition of heavy mineral assemblages and the structural setting of the sedimentary basins. The evolutionary trends of geodynamic sedimentary environments, connected with an increase in maturity of the earth's crust, are clearly expressed. The increased frequency of both hornblendes and diagnostic minerals of granitic and metamorphic rocks in heavy mineral assemblages within sedimentary basins indicates an increasingly sialic continental crust with time in the study region. It is connected with structural processes and is reflected in oceanic uplifts, juvenile island arcs, evolved and mature island arcs, marginal-continental volcanic belts, fold belts of different age and ancient cratons and platforms.

Only the largest structural elements are outlined in this paper but they can be complemented and refined further with the availability of new data. The authors hope that the current study, based on heavy mineral compositions in modern settings, will provide a model that may be useful for the geodynamic reconstruction of ancient sedimentary basins. Such work can be integrated with QFL studies based on framework components. We recognise that our multivariate analysis and the diagrams presented herein reflect modern depositional conditions. Therefore, when using this approach on ancient successions, interpretation of results must be made with caution, especially for those that are known to be affected by post-depositional modification. In the latter case complementing the geodynamic study with geochronology, geochemistry and varietal studies of heavy minerals have a considerable potential for increasing resolution.

ACKNOWLEDGEMENTS

The authors would like to express their gratitude to the research workers of the sedimentology laboratory of the POI who, during numerous marine expeditions in different areas of the world's oceans (frequently together with the authors), have obtained vast amounts of sediment samples that were used by the authors for their mineralogical analysis. Thanks are due to Professors Viktor Nechaev and Paul Ryan for their critical review of the manuscript and for their valuable suggestions. We are grateful to the editors for improving the English.

REFERENCES

Afifi, A.A., Azen, S.P., 1982. Statistical Analysis—A Computer Oriented Approach, 2nd ed. Mir, Moscow, 488pp. (in Russian).

Aleksina, N.A., 1962. Mineralogy of coarse-aleuritic fractions of bottom sediments in Kronotsk and Avacha Gulfs. Proceedings of the Oceanological Institute of the USSR Academy of Sciences, Moscow 61, 104–154 (in Russian).

Arai, F., Oba, T., Kitazato, H., et al., 1981. Late Quaternary tephrochronology and palaeo-oceanography of the sediments of the Japan Sea. Quaternary Research of Japan 20, 209–230.

Baturin, V.P., 1947. Petrographic analysis of geologic past on terrigenous components. USSR Academy of Sciences, Moscow, 358pp. (in Russian).

Belyiy, V.F., 1998. Marginal-continental tectonic-magmatic belts of the Pacific segment of the Earth. Magadan, 58p. (in Russian).

Berger, M.G., 1986. Terrigenous Mineralogy. Nedra, Moscow, 226pp. (in Russian).

Carriquiry, J.D., Sánchez, A., 1999. Sedimentation in the Colorado River delta and upper Gulf of California after nearly a century of discharge loss. Marine Geology 158, 125–145.

Chen, L., 1989. A study of mineral assemblages in sediments of the Bohai Sea, the Huanghai Sea and the East China Sea. Marine Sciences 1, 1–13.

Chen, L., Fan, S., Mao, Y., 1984. The statistical analysis of the heavy mineral assemblages in the sediments of the East China Sea. Studia Marine Sinica 21, 291–296.

Chen, L., Luan, Z., Zhen, T., et al., 1982. Mineral assemblages and their distribution patterns in the sediments of the Gulf of Bohai Sea. Chinese Journal of Oceanology and Limnology 1, 82–103.

Chen, L.R., Zhang, X.R., 1986. Peculiarities of mineral distribution in sediments of northern part of the Bakbo Gulf. Acta Oceanologica Sinica 8, 340–346.

Davis, J., 1977. Statistics and Data Analysis in Geology. Mir, Moscow, 571pp. (in Russian).

Derkachev, A.N., 1996. Mineralogical Features of the Marginal-Sea Sedimentogenesis (Japan Sea as Example). Dalnauka, Vladivostok, 226pp. (in Russian).

Derkachev, A.N., Botsul, A.I., Nikolaeva, N.A., 1997. Quaternary deposits and peculiarities of their mineral composition. In: Lelikov, E.P. (Ed.), Geological Structure of the Amirante Arc in the Indian Ocean. Dalnauka, Vladivostok, pp. 129–147 (in Russian).

Derkachev, A.N., Botsul, A.I., Puschin, I.K., 1989. Quaternary sediments of the Tonga Trench. In: Likht, F.R. (Ed.), Perioceanic Sedimentogenesis. Dalnauka, Vladivostok, pp. 101–119 (in Russian).

Derkachev, A.N., Likht, F.R., Markov, Yu.D., et al., 1993. Structure and composition of Cretaceous deposits. In: Lelikov, E.P. (Ed.), Geological Structure of the Western Part of the Japan Sea and Adjacent Continent. Dalnauka, Vladivostok, pp. 149–195 (in Russian).

Derkachev, A.N., Nikolaeva, N.A., 1993. Mineralogical features of sediments from Eastern Asia marginal seas. Pacific Geology 6, 58–74 (in Russian).

Derkachev, A.N., Nikolaeva, N.A., 1995. Heavy mineral associations found in sediments of the East China Sea and adjacent Ryukyu and Taiwan areas. Terrestrial, Atmospheric and Oceanic Sciences, Taiwan 6, 75–90.

Derkachev, A.N., Nikolaeva, N.A., 1997. Mineralogical features. In: Likht, F.R. (Ed.), Recent Sediment Formation within Marginal Seas of the Asian East (Statistical Models). Dalnauka, Vladivostok, pp. 189–215 (in Russian).

Derkachev, A.N., Nikolaeva, N.A., 1999. Associations of heavy minerals in sediments of western part of the South China Sea. Geology of Pacific Ocean 14, 503–534.

Derkachev, A.N., Utkin, I.V., Gorbarenko, S.A., et al., 1983. Correlation and sedimentation rates for Japan Sea in late-postglacial period. Pacific Geology 4, 22–29 (in Russian).

Dickinson, W.R., Suczek, C.A., 1978. Plate tectonics and sandstone compositions. Bulletin of American Association of Petroleum Geologists Bulletin 63, 2164–2182.

Emelyanov, E.M., 1979. Mineral composition of Mediterranean Sea sediments. Oceanological Researches: Moscow, Soviet radio 26, 61–108 (in Russian).

Emelyanov, E.M., Kharin, G.S., 1982. Role of volcanism in the formation of mineral composition of modern and late Quaternary sediments within northern Atlantica. In: Udintsev, G.B. (Ed.), Bottom Geology of the World Ocean. Biostratigraphy and Tectonics, Moscow, Science, 66–116pp (in Russian).

Egiazarov, B.X. (Ed.), 1981. Formations and Sedimentogenesis of Continental Margin. Nedra, Leningrad, 196pp. (in Russian).

Firek, F., Shideler, G., 1977. Heavy mineral variability in bottom sediments of the lower Chesapeake Bay, Virginia. Marine Geology 23, 217–237.

Gershanovich, D.E., 1955. Bottom sediments of the Shantar area in the Sea of Okhotsk and conditions of their formation. Proceedings of the State Oceanographical Institute, Moscow 23, 58–110 (in Russian).

Grossgeim, V.A., 1972. Terrigenous Sedimentation in Mesozoic and Cenozoic of the USSR European part (in Connection with Searches of Lithological Reservoirs of Oil and Gas). Nedra, Leningrad, 245pp. (in Russian).

Imbrie, J., Van Andel, T., 1964. Vector analysis of heavy-mineral data. Bulletin of American Geological Society 75, 1131–1156.

Kazansky, Ju.P., 1983. Introduction to Theory of Sedimentation, Science. Novosibirsk, Russia, 223pp. (in Russian).

Kharin, G.S., Emelyanov, E.M., Vasilenko, V.M., et al., 1979. Mineralogical provinces of deep-sea sediments in the Atlantic ocean. Oceanological Researches, Moscow 26, 49–60 (in Russian).

Knebel, H., Creager, J., 1973. Sedimentary environments of the east-central Bering Sea continental shelf. Marine Geology 15, 25–49.

Korotky, A.M., Raszhigaeva, N.G., 1992. Relief and Sediments of the Seychelles. Dalnauka, Vladivostok, 137pp. (in Russian).

Kovalenko, V.I. (Ed.), 1987. Magmatic Rocks. Evolution of Magmatism in Earth History. Science, Moscow, 438pp (in Russian).

Kukharenko, A.A., 1961. Mineralogy of the Placer Deposits. State Geological Technical Publishing House, Moscow, 317pp. (in Russian).

Kuno, H., 1959. Origin of Cenozoic Petrographic provinces of Japan and surrounding areas. Bulletin Volcanologique, Series II 20, 38–76.

Lee, H.J., Jeong, K.S., Han, S.J., et al., 1988. Heavy minerals indicative of Holocene transgression in the southeastern Yellow Sea. Continental Shelf Research 8, 255–266.

Le Maitre, R.W., 1982. Numerical Petrology (Statistical Interpretation of Geochemical Data). Elsevier Science Publishing Company, Amsterdam, 281pp.

Li, P., Ye, W., 1987. A study on heavy minerals of the surface deposits in the shallow area of northern Beibu Gulf. Tropic Oceanology 6, 39–47 (in Chinese with English abstract).

Likht, F.R. (Ed.), 1997. Recent Sediment Formation within Marginal Seas of the Asian East (Statistical Models). Dalnauka, Vladivostok, 295pp (in Russian).

Lisitsin, A.P., 1966. Modern Sedimentary Processes in the Bering Sea. Science, Moscow, 574pp. (in Russian).

Machida, H., Arai, F., 1976. The discovery and significance of the very widespread tephra. The Aira-Th ash: Japan, Kagaku 46, 339–347.

Machida, H., Arai, F., 1978. Akahoya ash—a widespread marker erupted from the Kikai caldera, southern Kyushu, Japan. Quaternary Research of Japan 17, 143–163.

Machida, H., Arai, F., 1983. Extensive ash falls in and around the Sea of Japan from large late Quaternary eruptions. Journal of Volcanology and Geothermal Research 18, 151–164.

Machida, H., Arai, F., Lee, B., et al., 1984. Late Quaternary tephras in Ulreung-do Island, Korea. Journal of Geography of Japan 93, 1–14.

Machida, H., Arai, F., Moriwaki, H., 1981. Two Korean tephras, Holocene markers in the Sea of Japan and the Japan islands. Kagaku (Science), Japan 51, 562–569.

Malinovsky, S.A., Gorbarenko, S.A., Kulyamin, L.I., 1990. Lithology and genesis of sediments. In: Vasilyev, B.I. (Ed.), Geological-Geophysical Investigations in the New Hebrides Region. Dalnauka, Vladivostok, pp. 59–80 (in Russian).

Maynard, J.B., Valloni, R., Yu, H.S., 1982. Composition of modern deep-sea sands from arc-related basins. In: Leggett, J.K. (Ed.), Trench-Forearc Geology. Sedimentation and Tectonics of Modern and Ancient Plate Margins. Geological Society of London, pp. 551–561.

McManus, D., Venkatayathnam, K., Hopkins, D., et al., 1977. Distribution of Bottom Sediments on the Continental Shelf, Northern Bering Sea. US Geological Survey Professional Paper 759-C. US Government Printing Office, Washington, D.C., 31pp.

Milliman, J.D., Meade, R.H., 1983. World-wide delivery of river sediment to the oceans. Journal of Geology 91, 1–21.

Miyashi, M., Miyashi, M., 1988. Heavy minerals of the pyroclastic flow deposits in southern Kyushu, Japan. Kyushu daygaku keebu migaku kenkyu khokoku, Japan, pp. 5–15.

Morton, A.C., Hallsworth, C.R., 1999. Processes controlling the composition of heavy mineral assemblages in sandstones. Sedimentary Geology 123, 3–29.

Murdmaa, I., Grechin, V., Muzylev, N., et al., 1980. Sediments and sedimentary rocks. In: Peyve, A.V. (Ed.), Bottom Geology of the Philippine Sea. Moscow, Science, pp. 38–106 (in Russian).

Murdmaa, I., Lisitsin, A., Emelyanov, E., et al., 1979. Mineralogy of ocean sediments. In: Bezrukov, P.L. (Ed.), Ocean Geology. Sedimentation and Magnetism of Ocean. Science, Moscow, pp. 104–156 (in Russian).

Nechaev, V.P., 1991. Evolution of the Philippine and Japan Seas from the Clastic Sediment Record. Marine Geology 97, 167–190.

Nechaev, V.P., Derkachev, A.N., 1995. Heavy mineral assemblages in Quaternary sediments of the Philippine Sea as indicators of subduction/collision-related tectonics. In: Takuyama, H., Scheka, S.A. (Eds.), Geology and Geophysics of the Philippine Sea. Terra Scientific Publishing Company (TERRAPUB), Tokyo, pp. 215–233.

Nechaev, V.P., Isphording, W.C., 1993. Heavy-mineral assemblages of continental margins as indicators of plate-tectonic environments. Journal of Sedimentary Petrology 63, 1110–1117.

Petelin, V.P., 1957. Mineralogy of sandy-silt sediment fractions of the Sea of Okhotsk. Proceedings of the Oceanological Institute of the USSR Academy of Sciences 22, 77–138 (in Russian).

Petelin, V.P., 1961. About choice of a method of the mineralogical analysis for sandy-silt fractions of bottom sediments. Proceedings of the Oceanological Institute of the USSR Academy of Sciences 50, 170–173 (in Russian).

Pettijohn, F.D., 1981. Sedimentary Rocks. Science, Moscow, 751pp. (in Russian).

Qin, Y., Yiyang, Z., Chen, L., Songling, Z. (Eds.), 1996. Geology of the East China Sea. Beijing, China: Science Press, 358pp.

Romanovsky, S.I., 1991. Direct task of lithogeodynamics. Reports of USSR Academy of Sciences 319, 442–446 (in Russian).

Romanovsky, S.I., 1998. Lithogeodynamic grounds for classification of sedimentary basins. In: Shcheglov, A.D. (Ed.), Lithogeodynamics and Minerageny of Sedimentary Basins. VSEGEI Press, Saint-Peterburg, pp. 9–118 (in Russian).

Shen, S., Chen, L., Xu, W., 1984. Mineral composition and peculiarities of its distribution in sediments of the Huanghai Sea. Oceanologica et Limnologica sinica 15, 240–250.

Skornyakova, N.S., Gorbunova, Z.N., Kruglikova, S.B., et al., 1978. The sediments and sedimentary rocks of the Marian Trench. Lithology and Mineral Resources 5, 18–32 (in Russian).

Strakhov, N.M., 1963. Types of Lithogenesis and Their Evolution in Earth History. State Geological Technical Publishing House, Moscow, 534pp. (in Russian).

Suzuki, T., 1975a. Heavy mineral composition of the marine sediments on the continental shelf, western offshore areas of Kyushu, Japan. Geological Survey of Japan 255, 1–18.

Suzuki, T., 1975b. Heavy mineral composition of some deep-sea sediments near the Mariana Islands, northern Pacific Ocean. Geological Survey of Japan 255, 19–25.

Suzuki, T., 1985. Heavy mineral composition of marine sediments in Ishikari Bay, Hokkaido. Geological Survey of Japan 36, 395–413.

Tsukui, M., 1984. Geology of Daisen Volcano. Geological Society of Japan 90, 643–658.

Utkin, I.V., 2002. Computer statistical data processing on grain-size data of bottom sediments for the characterization of the recent sedimentary environments. In: Likht, F.R. (Ed.), Conditions of the Generation of Bottom Sediments and Related Mineral Deposits within Marginal Seas. Dalnauka, Vladivostok, pp. 96–113 (in Russian).

Valloni, R., 1985. Reading provenance from modern marine sands. In: Zuffa, G.G. (Ed.), Provenance of Arenites, NATO ASI, Dordrecht: Reidel Publishing Company, 148 (C), pp. 309–332.

Van Andel, Th.H., 1964. Recent marine sediments of Gulf of California. In: Van Andel, Th.H., Shor, G.G. (Eds.). Marine Geology of the Gulf of California: A Symposium, American Association of Petroleum Geologists Memoir 3, pp. 216–310.

Viyding, X.A., 1984. Role of the different factors in formation and evolution of sedimentary rocks on ancient platforms. In: Kazansky, Yu.L. (Ed.), Environments of Sedimentation and Their Evolution. Science, Moscow, pp. 94–103 (in Russian).

Wang, X., Liang, J., 1982. Study of the factors controlling heavy-mineral distribution on the East China Sea continental shelf by using statistical analysis. Acta Oceanologica Sinica 4, 65–77.

Wong, F.L., 2002. Heavy mineral provinces of the Palos Verdes margin, southern California. Continental Shelf Research 22, 899–910.

Yokota, M., Okada, H., Arita, M., et al., 1990. Distribution of heavy minerals in the bottom sediments of the Southern Sea of Japan, off the Shimane Peninsula, south-west Japan. Science Reports of Geology Department, Japan, Kyushu University, vol. 16, pp. 59–86.

Chapter 18

STATISTICAL ANALYSIS OF HIGH-RESOLUTION HEAVY MINERAL STRATIGRAPHIC DATA FROM THE ORDOVICIAN OF WESTERN IRELAND AND ITS TECTONIC CONSEQUENCES

PAUL D. RYAN[a], MARIA A. MANGE[b] AND JOHN F. DEWEY[b]

[a]*Department of Earth and Ocean Sciences, NUI, Galway, Ireland*
[b]*Department of Geology, UC Davis, One Shields Avenue, Davis, CA 95616, USA*

ABSTRACT

High-resolution heavy mineral data from the Ordovician of the South Mayo Trough, western Ireland is subject to a detailed statistical analysis. The aim of this study is to develop new techniques for treating such data thereby providing an independent and objective way to help elucidate the stratigraphy and tectonic history of the region. A new method is presented for plotting normalised scores to emphasise stratigraphic trends of heavy minerals and specific heavy mineral varieties, which are shown to be largely non-normally distributed, with significant variation between formations. A method is developed for testing significance of variation within a formation using non-parametric tests. Techniques are introduced for comparing and correlating formations on the basis of heavy mineral data even when sample sizes are small. The likely causes of correlations between heavy mineral distributions and zircon varieties are discussed, and principal components analysis is used to identify major source regions throughout the life of this basin. This analysis shows that there is a statistically significant change with early deposits dominated by arc-accretionary prism detritus, whereas juvenile metamorphic detritus becomes increasing more important up-section. The South Mayo Trough remained below sea-level during this progressive change in provenance. The generally accepted model for the evolution of this basin is that it represents a fore-arc basin that collided with the Laurentian margin during the Grampian orogeny. The problem of how a hanging wall basin remained below sea-level during and after arc-continent collision is discussed and explained.

Keywords: high-resolution heavy mineral data; statistical analysis; MANOVA; Spearman's; principal components analysis; preservation of anchimetamorphic terranes; South Mayo Trough

Developments in Sedimentology, Vol. 58, 465–489

ISSN: 0070-4571/doi:10.1016/S0070-4571(07)58018-0

1. INTRODUCTION

In this contribution, we investigate the use of statistical techniques to enhance tectonic interpretation and stratigraphic correlation using high-resolution heavy mineral data from the Ordovician succession of the South Mayo Trough (SMT) in western Ireland (Dewey and Mange, 1999; Mange et al., 2003). The SMT provides an excellent succession for such analysis. The stratigraphy is well understood and dominated by rapidly deposited clastic sediments. The succession is simply folded, of low metamorphic grade, and largely undisrupted by subsequent faults. There is a considerable body of stratigraphically controlled high-resolution heavy mineral data (Dewey and Mange, 1999; Mange et al., 2003) and there is a current consensus as to the basin's tectonic setting. We begin with a brief overview of the geology of South Mayo, then develop a statistical methodology for using high-resolution heavy mineral analysis (HRHMA) to monitor the evolution of the basin, and then show that the results of this analysis provide insights into the tectonic evolution of this region.

HRHMA is a powerful technique that provides more data than simple species-level mineral analysis because, in addition to the conventional point-counting of heavy minerals in a grain mount, it records the informative varieties of highly resistant species such as zircon, tourmaline and apatite in discrete categories (Mange-Rajetzky, 1995; Dewey and Mange, 1999). Results show that the assemblages are more diverse and more informative than those obtained by species-level analysis. It is especially rewarding in the study of mature sediments and in those of low mineralogical or biotic diversity. The method generates a complex database, particularly suitable for statistical analyses.

2. ORDOVICIAN OF THE SOUTH MAYO TROUGH

The SMT is a broadly simple syncline of Ordovician strata lying between strips of Silurian strata that conceal the contacts between Ordovician and Dalradian rocks. The southern limb of the syncline preserves a succession (~7.8 km) of Early Ordovician arc and proximal fore-arc strata, whereas the northern limb consists of a thicker (~9.0 km), steeply dipping, almost homoclinal, southward-younging, distal fore-arc succession (Fig. 1).

The Ordovician stratigraphy of the SMT in the western Irish Caledonides (Harper and Parkes, 2000) records the Tremadocian/Arenigian growth of a north-facing oceanic volcanic arc and supra-subduction-zone ophiolite, its collision with and northward obduction onto the rifted Laurentian continental margin to generate the Grampian Orogen, and the erosional and extensional unroofing of that orogen, all during an interval of ~11 million years from ~475 to 464 Ma (Dewey and Shackleton, 1984; Dewey and Ryan, 1990; Dewey and Mange, 1999; Clift et al., 2004). The beginning of arc collision is marked by a change from mafic (Lough Nafooey) to silicic (Glensaul) volcanism (Draut and Clift, 2001). A high-pressure (phengite, glaucophane) dextrally transpressive high strain zone marks the Clew Bay zone of Grampian collisional suturing, which separates Grampian Barrovian metamorphic assemblages of the Dalradian to the north from the anchimetamorphic accretionary

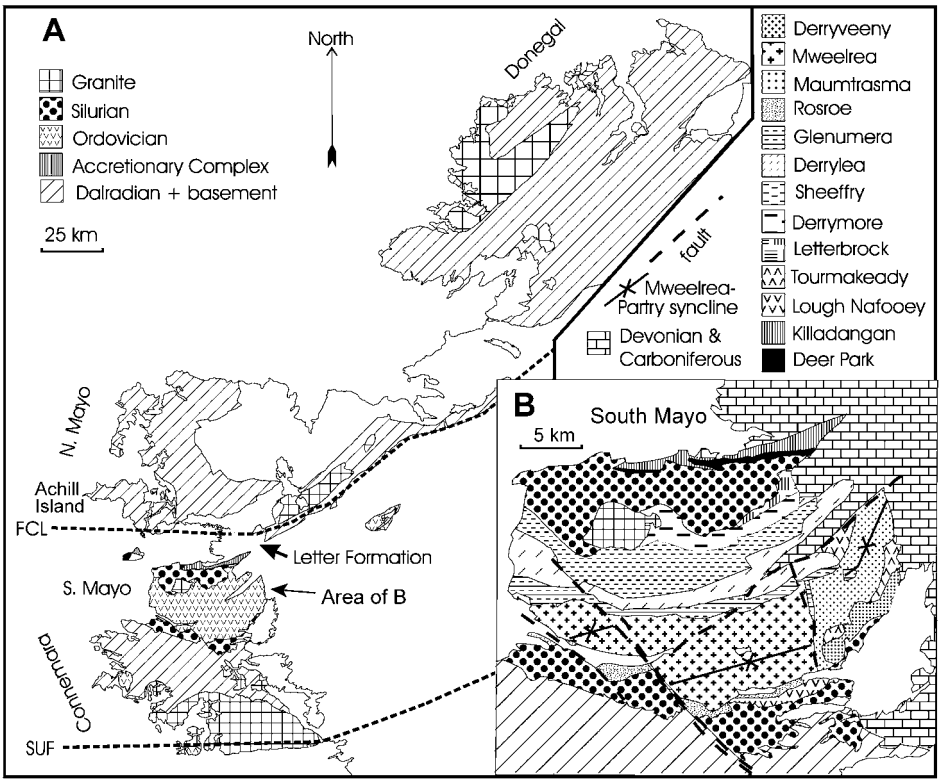

Fig. 1. Location map (A) and simplified geological map of the South Mayo Trough (B). The key to part B gives the names of the various formations within the South Mayo Trough. *FCL = Fair Head-Clew Bay Magnetic Line; SUF = Southern Uplands Fault.*

prism (Killadangan Formation, Ballytoohy Formation) of the pre-collisional arc. The stratigraphy of the SMT is shown in Fig. 2.

Heavy mineral suites, gross lithological assemblages, and quartz/feldspar/lithic ratios in the sediments of the SMT (Dewey and Mange, 1999) record tectonic events on the evolving Laurentian margin. The Letterbrock Formation was sourced from the north by the obducted Killadangan accretionary prism and the deformed ultramafic/mafic assemblage of the Deer Park Complex [part of the dismembered supra-subduction-zone ophiolite (Ryan et al., 1983) basement of the pre-collisional arc], and from the south by the early-obducted arc. The Sheeffry and lower Derrylea formations record the progressive erosional denudation of the obducted supra-subduction-zone ophiolite/arc nappe. The upper Derrylea and upper Rosroe Formations record the sudden appearance of garnet and staurolite, indicating the abrupt unroofing of a Grampian Barrovian amphibolite source to the north. This strongly suggests the beginning of a phase of extensional tectonic denudation. It is believed to coincide, during and just after subduction polarity flip, with the development of a free subduction face to the south (Clift et al., 2004) towards which the Grampian Orogen could collapse, perhaps aided by subduction roll-back, starting at ~466 Ma. The Glenummera Formation represents a period of low Grampian elevation during

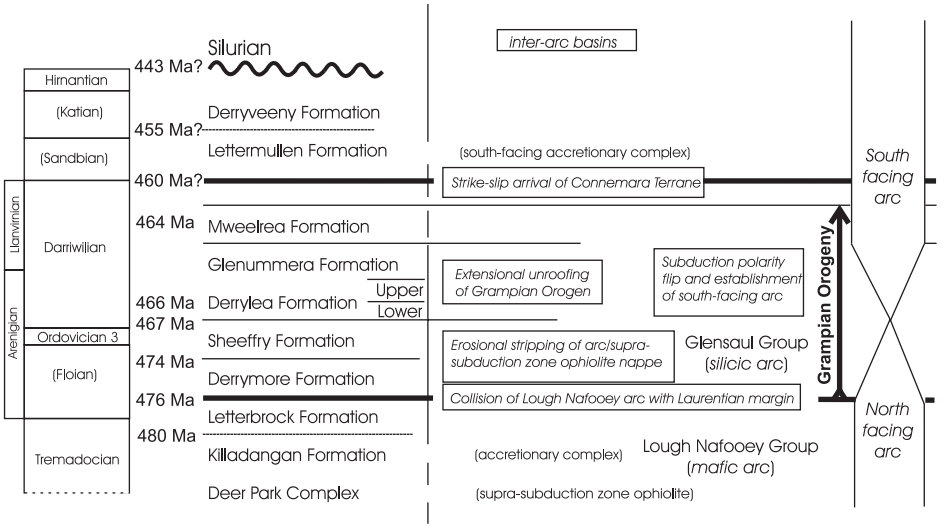

Fig. 2. Tectonostratigraphic evolution of the South Mayo Trough (see text for details; for complete stratigraphy see Dewey and Mange, 1999 and Mange et al., 2003). The naming system used for the Ordovician global stages follows Bergström et al. (2006).

waning collapse; the fluviatile Mweelrea Formation and its ignimbrite bands, with the 463 Ma quartz-diorites and the 462 Ma Oughterard Granite, record the establishment of the new silicic, post-flip arc and the final stages of erosional unroofing of the Grampian Orogen, during a renewed, Andean-style, shortening phase. Silurian clastic sediments and calc-alkaline volcanics accumulated in a series of intra-arc basins unconformably across, and sourced from the disrupted Grampian/arc terrane complex.

The tectonic setting of the SMT above, based upon more than 40 years of detailed investigation, requires that there should be a significant change in provenance through the sedimentary section. We develop below a statistical method to determine whether the expected significant variation is recorded in the heavy mineral data and, if so, provides a statistical validation of the HRHMA technique.

3. DESCRIPTIVE STATISTICS

Stratigraphic variation in heavy mineral species is commonly represented by a vertically stacked compound bar chart or frequency-polygon with stratigraphic interval on the vertical axis and relative proportion of individual mineral species on the horizontal axis (Fig. 3). Such figures are easily readable for the more common species.

However, the relative proportions of less common species are difficult to assess from such a plot and the stratigraphic variations of those species that plot within the body of the chart are distorted with respect to those occurring at either margin (compare 'zircon' with 'apatite' in Fig. 3). Thus, the impression of the figure is somewhat dependent on the order in which the samples are plotted. These difficulties

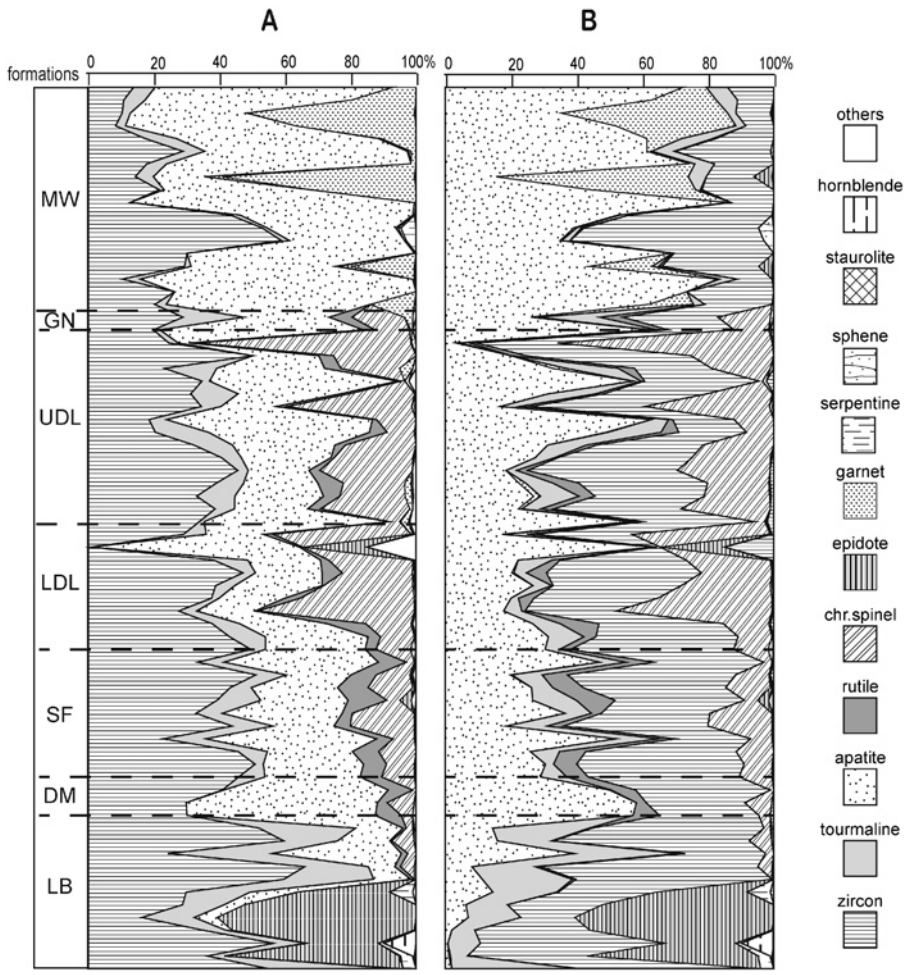

Fig. 3. Relative stratigraphic variation in heavy mineral species for the northern limb of the South Mayo Trough Ordovician succession (data from Dewey and Mange, 1999) shown as a compound, vertically stacked, frequency polygon. (A) Mineral species order (left to right) zircon, tourmaline, apatite, rutile, chrome-spinel, epidote, garnet, serpentine, sphene, staurolite, hornblende, others. (B) Mineral species order (left to right) apatite, garnet, tourmaline, rutile, zircon, chrome-spinel, epidote, serpentine, sphene, staurolite, hornblende, others.

are overcome by calculating standardised scores for each mineral species and plotting them against stratigraphic intervals (Fig. 4).

Such scores can be calculated as follows:

$$\text{score}_{i,z} = \frac{X_{i,z} - \text{mean}_\text{i}}{\text{sdev}_\text{i}}$$

where $X_{i,z}$ = the individual mineral count for the ith mineral at stratigraphic level z, mean_i = the mean mineral percentage for species i; and sdev_i = the standard

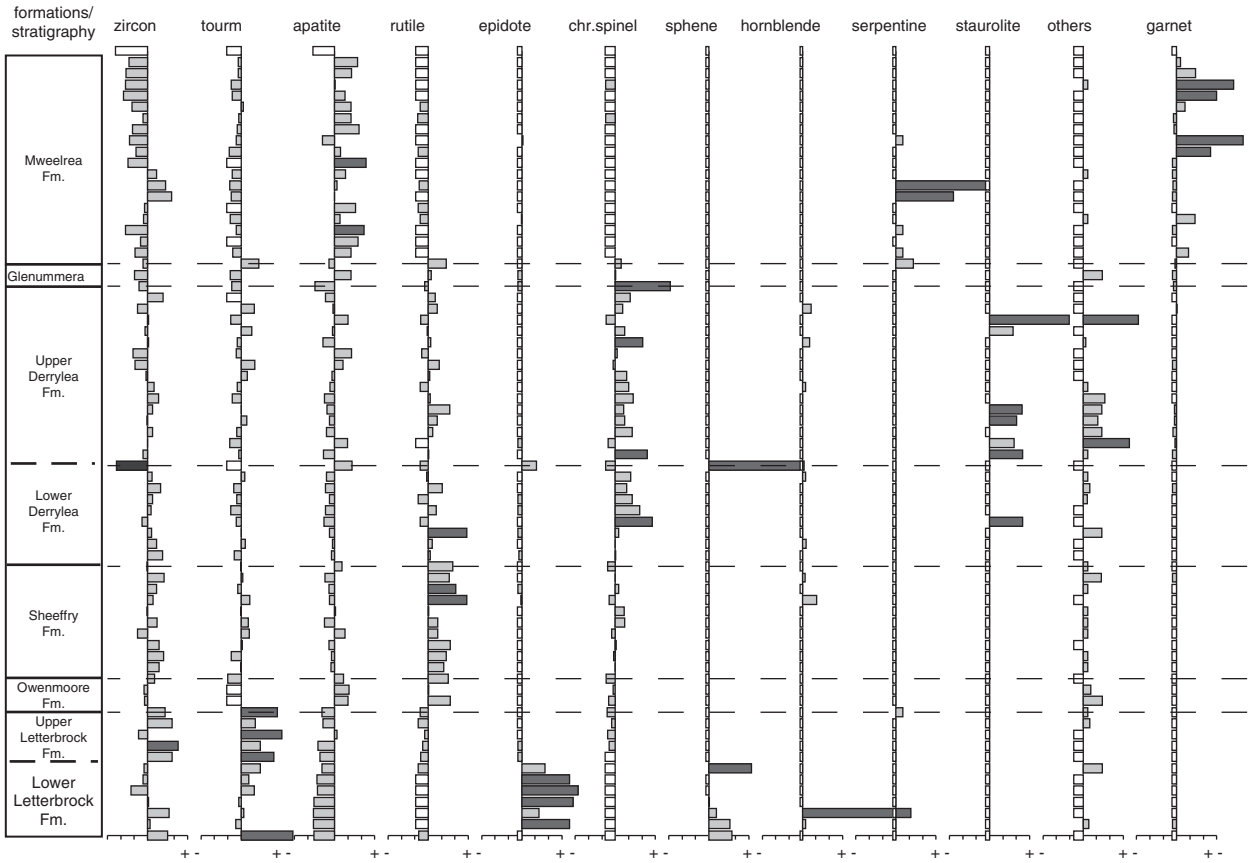

Fig. 4. Vertical bar chart of standardised percentage scores for each mineral species at each stratigraphic interval for the north limb succession of the South Mayo Trough Ordovician. Bars to the left of the central line are below the mean and to the right are above the mean. Unfilled bars represent absences. Darker shade means that the scores are ± 1.96 standard deviations away from the mean. It should be noted that varieties such as staurolite that are rare will tend to give distinct peaks as the standard deviation will be low.

Table 1. Mean and standard deviations for percentages of each mineral species within the South Mayo dataset for the north limb successions used in Fig. 3

Mineral species	Mean	Standard deviation	Number of samples with data
Zircon	33.79	14.15	70
Tourmaline	8.27	7.76	63
Apatite	35.27	21.71	70
Rutile	2.85	3.09	52
Chrome-spinel	10.37	13.37	46
Epidote	4.38	13.34	20
Garnet	3.86	10.95	29
Serpentine	0.15	0.67	7
Sphene	0.45	2.06	5
Staurolite	0.05	0.18	9
Hornblende	0.22	1.19	9
Others	0.33	0.47	30

deviation for species i. The mean and standard deviations for each mineral used in Fig. 3 are given in Table 1.

Fig. 4 shows that zircon generally increases, then decreases up-section. Tourmaline is highest in the Letterbrock Formation, apatite is lowest in the Letterbrock Formation and highest in the Mweelrea Formation. Rutile and chrome-spinel behave similarly with the former highest in the Sheeffry Formation and the latter in the Derrylea Formation. Staurolite, apart from a single grain, is only recorded in the upper Derrylea Formation. Epidote and sphene are highest at the base of the section, whereas garnet and serpentine are highest in the Mweelrea Formation. Hornblende and 'others' are dominated by a single sample. Such plots do not show the relative importance of a given species, so should be used in conjunction with the conventional plot (Fig. 3). A drawback of standardised plots occurs when absences are treated as real scores. A zero value produces a small negative score (e.g., sphene in the Mweelrea Formation). The standard scores can be calculated omitting the zero values. However, zero is a reasonable value, which in a relatively small sample does not imply the complete absence of a mineral. In point counting, the 95% upper bounds for a zero count for the samples sizes used in this analysis ($N = 271$–75) range from 1.10 to 3.95%, respectively (Howarth, 1998). Zero values are here distinguished from real scores below the mean by not colouring the relevant bar.

Such plots represent time series, and it is important to study variations in mineral species with time. However, the stratigraphic intervals may be only relative, not absolute, so that many methods commonly used in time series analysis may not be appropriate. It is important to note that, on these plots, we use stratigraphic rank order, not stratigraphic separation. Each successive sample is placed one standard increment above the previous sample. On sections with precise control, such as borehole data, an even clearer picture can be obtained by using absolute, not relative, stratigraphic separation.

A simple method that overcomes some of the disadvantages of the stacked compound frequency polygon is to use a moving average filter. Fig. 5 shows the same data as Fig. 3A, plotted with a rectangular filter averaging five (5) readings.

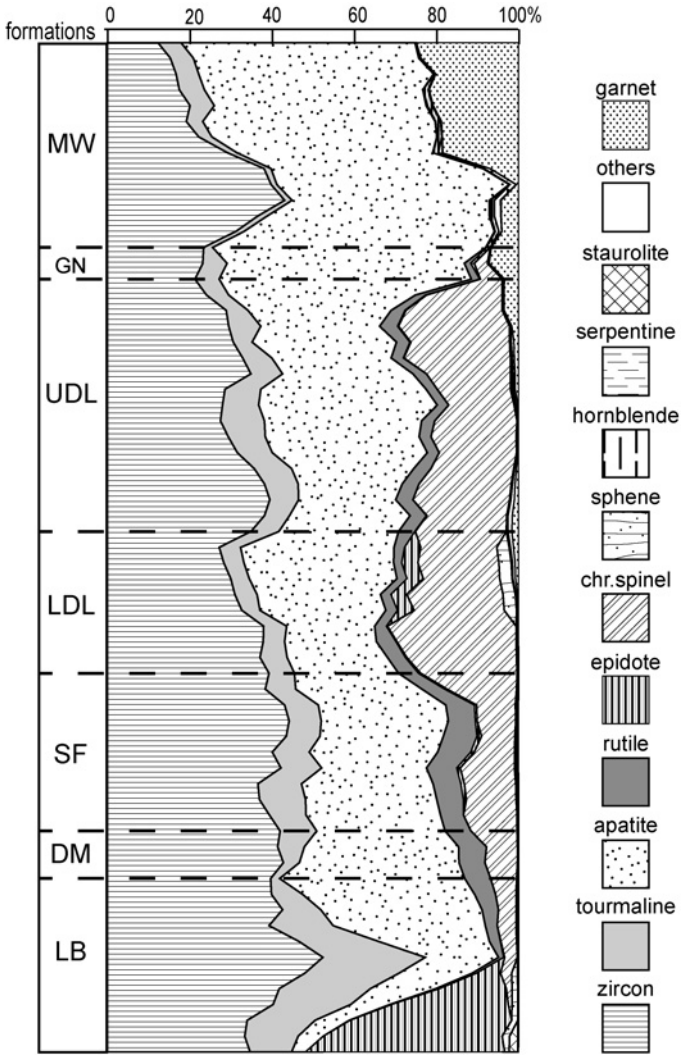

Fig. 5. Relative stratigraphic variation in mineral species shown in Fig. 3A, smoothed using a 5-point rectangular moving average.

The calculation of any score is:

$$\text{score}_{i,z} = \sum_{i=-2}^{i=+2} \frac{Xi}{5.0}$$

This diagram shows that garnet is a significant component in the Mweelrea Formation, whereas chrome-spinel is important in the Sheeffry and Derrylea formations, and that epidote dominates in the Letterbrock Formation. However, such filters smooth out values for a formation with only a few readings. The peak of apatite recorded in the Owenmore Formation (Figs. 3A or 5) is smoothed out. Also,

the stratigraphic ranges of species can be smeared beyond their actual range. These effects can be reduced by using a small smoothing window with respect to the sample size for each formation.

3.1. Testing Stratigraphic Variation

It is desirable to test whether these stratigraphic variations are statistically significant. Three approaches can be adopted. First, a simple univariate test can be used to determine whether the samples for a given mineral species within all formations could have been drawn from the same distribution. Before selecting such a test, it is advisable to determine whether the various mineral species are distributed normally. The Lilliefors test is used on the South Mayo data and the results are presented in Table 2.

This analysis shows that only three of the seven more common minerals might have been drawn from a normal distribution. Therefore, it is best to use a non-parametric test to detect stratigraphic variation. Kruskall–Wallace and Mann–Whitney 'U' are used to test the significance of stratigraphic variation. These are based on the rank order of individual scores in a given sample; they do not assume a normal distribution but that each value, in this case mineral proportion, is random and independent of the proportion for that mineral in other samples.

3.2. Testing the Entire Section

The Kruskall–Wallace test can be used to investigate whether the heavy mineral assemblages of each formation, within the northern limb succession, could have been drawn from the same underlying distribution. This implies a Null Hypothesis that,

Table 2. Lilliefors test statistic scores for the percentages of each mineral species within all formations

Mineral species	kD (Lilliefors)	*N*	Reject null hypothesis?
Zircon	0.0610	70	No
Tourmaline	0.1417	70	No
Apatite	0.1278	70	No
Rutile	0.1958	70	Yes
Chrome-spinel	0.2192	70	Yes
Epidote	0.4563	70	Yes
Garnet	0.4066	70	Yes
Serpentine	0.4905	70	Yes
Sphene	0.5074	70	Yes
Staurolite	0.5183	70	Yes
Hornblende	0.4465	70	Yes
Others	0.3196	70	Yes

Note: The Null Hypothesis is that they were all drawn from a normal distribution. The values for kD of 9 out of the 12 species are so high that the null hypothesis can be rejected.

Table 3. Results of Kruskall–Wallace analysis for the percentages of the 12 mineral species in the four 'formations' (the 3 samples from the Owenmore Formation are included in the Letterbrock Formation and the 2 from the Glenumera Formation in the Derrylea Formation for the purposes of this analysis) of the north limb succession of the South Mayo Trough

Mineral species	Degrees of freedom	Kruskall–Wallace '*K*'	Reject null hypothesis?
Zircon	3	18.72	Yes
Tourmaline	3	32.27	Yes
Apatite	3	31.45	Yes
Rutile	3	48.59	Yes
Chrome-spinel	3	51.76	Yes
Epidote	3	13.63	Yes
Garnet	3	30.11	Yes
Serpentine	3	3.89	No
Sphene	3	4.84	No
Staurolite	3	4.85	No
Hornblende	3	1.70	No
Others	3	9.89	Yes

Note: The following number of samples were analysed for each formation: Letterbrock = 15; Sheeffry = 10; Derrylea = 27; Mweelrea = 18.

'for each formation, a given mineral species is derived from the same population (or source?)'. In this analysis, the Derrymore Formation ($N = 3$) has been included in the Letterbrock Formation and the Glenumera Formation ($N = 2$) with the Derrylea Formation. This test yields a '*K*' statistic that has the distribution of χ^2 at $N-1$ degrees of freedom, where N is the number of formations. In this case, $N = 3$ and the critical value for χ^2 at the 95% confidence level is 7.81. The results of this analysis for the SMT succession are given in Table 3.

In the studied successions the six most common species could not have been drawn from a single population (or source?). This analysis implies a statistically significant stratigraphic variation in the zircon, tourmaline, apatite, rutile, chrome-spinel, epidote and garnet. The inability to reject the Null Hypothesis for the less-common mineral species is probably a result of their distribution being dominated by many absences (see Table 1), leading to a high number of ties in the ranks for each formation and an underlying distribution dominated by these absences. In the light of this variation it is desirable to compare the heavy mineral composition of one formation with the overlying formation.

3.3. Mann–Whitney 'U' on Individual Formations

The Mann–Whitney test can also be used to compare mineral species in each formation with that in the overlying formation. The results are given in Table 4.

The Sheeffry Formation has higher apatite, rutile and chrome-spinel than the Letterbrock Formation. The Derrylea Formation has lower rutile and zircon, but higher chrome-spinel than the Sheeffry Formation. The Mweelrea Formation has

Table 4. The results of a Mann–Whitney 'U' test comparing heavy mineral contents with those of the overlying formation

Formations compared	zr	tr	ap	ru	ch	ep	gt	se	sp	st	hbl	ot
Derrylea/Mweelrea	−1	−1	+1	−1	−1	0	+1	0	0	0	0	+1
Sheeffry/Derrylea	−1	0	0	−1	+1	0	0	0	0	0	0	0
Letterbrock/Sheeffry	0	0	+1	+1	+1	0	0	0	0	0	0	0

Note: A zero (0) represents no significant difference, whereas '−1' represents a significant (at the 95% level) decrease up-section, and '+1' represents a significant increase up-section. The following abbreviations are used for the columns: zr, zircon; tr, tourmaline; ap, apatite; ru, rutile; ch, chrome-spinel; ep, epidote; gt, garnet; se, serpentine; sp, sphene; st, staurolite; hb, hornblende; ot, others.

less zircon, tourmaline, rutile and chrome-spinel but more apatite and garnet than the Derrylea Formation. All other changes are not significant at the 95% level.

3.4. Testing for Variation Within Formations

The analyses used above can test only for changes at succession or formation level. Significant changes may occur within formations. For example, the incoming of staurolite in the upper Derrylea Formation of the SMT has been used as a signature of the arrival of juvenile orogenic material within this basin, and hence provide stratigraphic evidence for the timing of the Grampian Orogeny (Dewey and Mange, 1999; Soper et al., 1999). The Mann–Whitney 'U' test can be used to compare two samples with each having as few as five observations. However, such low sample numbers require a complete rank separation for the two samples to be statistically distinct, so a larger number of samples is desirable. The following strategy is adopted: a window of 16 values, starting at the base of the column is split into a lower and an upper block of 8 samples each. The Mann–Whitney 'U' test is used to test whether the upper block could have been drawn from the same distribution as the lower. The window is then moved upward by one sample and the analysis repeated until the top of the section is reached. The results are displayed in Fig. 6, where the Z score associated with each test is plotted against a stratigraphic interval.

This analysis indicates that the following changes are significant. The Letterbrock/Derrymore transition is marked by a decrease in tourmaline and by increases in apatite, rutile and chrome-spinel. The Derrymore/Sheeffry transition is marked by increases in rutile and chrome-spinel, whereas rutile decreases and chrome-spinel increases in the upper part of the Sheeffry Formation. The Sheeffry/Derrylea transition is marked by decreases in tourmaline and rutile and increased chrome-spinel. Rutile decreases throughout the Derrylea, sometimes significantly, whereas apatite and garnet tend to increase, also sometimes significantly. Chrome-spinel increases up-section in the lower Derrylea Formation, but decreases in the upper Derrylea Formation. The lower to upper Derrylea transition is characterised by the incoming of staurolite. The Derrylea/Mweelrea contact marks an increase in apatite accompanied by decreases in rutile, tourmaline and chrome-spinel. Higher in the section, zircon, rutile, and chrome-spinel decrease while garnet increases.

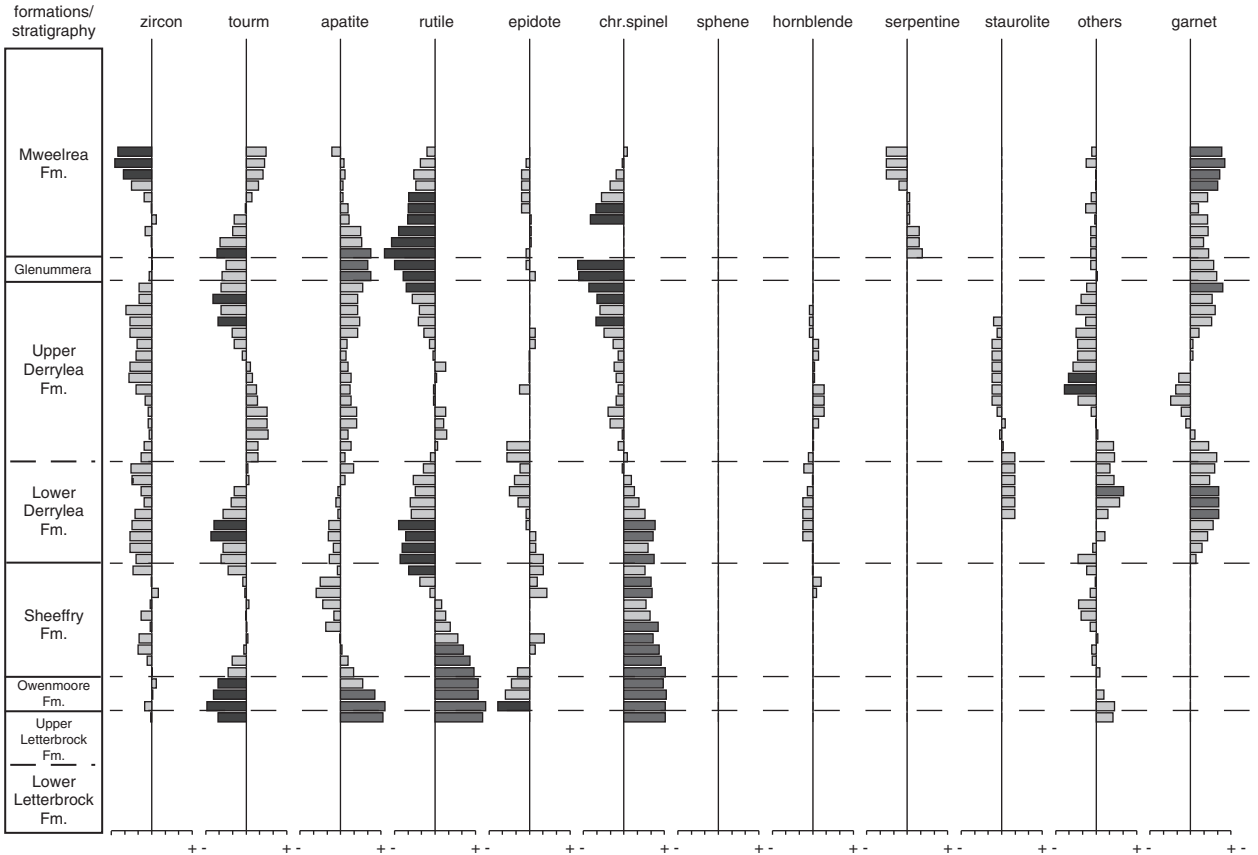

Fig. 6. Relative stratigraphic variation of mineral species percentage tested by using the Mann–Whitney 'U' Test on blocks of 16 data points split into an upper and lower sample of 8 data points. A score corresponding with a positive (i.e., upwards increase) value is shown to the right of the central bar, a score corresponding with a negative value (upwards decrease) is shown to the left of the bar. If the increase is statistically significant, the bar is filled with darker colour. An upward-moving filter is used, consequently the results will be smeared slightly downwards (see discussion on Fig. 5). As the size of the window decreases relative to the total number of stratigraphic levels, changes will be more accurately mapped to stratigraphic levels.

4. COMPARISON OF DATA FROM TWO FORMATIONS

4.1. Matching an Unknown Formation to a Succession

The Letter Formation occurs in a small inlier along strike to the east of the main outcrop of the SMT. It is, however, of extreme stratigraphic importance because it is of Ordovician age and unconformably overlain by Early Devonian strata (Graham and Smith, 1981) and, because most authors correlate it with South Mayo, it is used to place an upper limit on the timing of the deformation of this succession and, effectively, on the timing of the Caledonian Orogeny sensu stricto. Five heavy mineral samples were collected (Mange et al., 2003) and a correlation was suggested with the Derrylea Formation of South Mayo. Statistical tools for treating such a dataset with small samples sizes, univariate non-normal distributions and a large number of zero scores are not readily available. Multiple univariate tests on multivariate data ignore the correlations between minerals and can lead to a false rejection of the null hypothesis. Multivariate techniques such as multivariate analysis of variance (MANOVA) assume that the variables are continuous or discrete and normally distributed. This is unlikely to be the case for the individual mineral species (Table 2). However, the data for six zircon varieties (euhedral, subhedral, anhedral, rounded colourless, rounded purple and with overgrowths (see Dewey and Mange, 1999) do not significantly depart from a normal distribution when samples with zero scores were omitted. The results for comparisons of the Letter Formation with the Mweelrea, Rosroe, Derrylea and Maumtrasma Formations using MANOVA on these six zircon varieties are given in Table 5. This analysis suggests that the zircon varieties within the Letter Formation may have come from the same population as those in the Maumtrasma Formation. However, in view of the small sample sizes this analysis must be treated with extreme caution. It is, however, consistent with

Table 5. Results of the comparison of the zircon variety data from the Letter Formation with the Derrylea, Rosroe, Mweelrea and Mautrasma Formations of South Mayo using MANOVA

Formation	Wilk's λ	F	Hypothesis df	Error df	Signif.	Partial η^2
Maumtrasma	0.093	4.865	6.000	3.000	0.111	0.907
Derrylea	0.326	5.520	6.000	16.000	0.003	0.674
Rosroe	0.212	6.814	6.000	11.000	0.003	0.788
Mweelrea	0.324	4.859	6.000	14.000	0.007	0.676

Note: The analysis was performed using SPSS 14 following the method of Brace et al. (2003). The following varieties were used: 'euhedral'; 'subhedral'; 'anhedral'; 'rounded colourless'; 'rounded purple'; and 'with metamorphic overgrowths' (see Dewey and Mange, 1999, for details) and only those samples which had at least one of all of these varieties were used. The numbers of valid samples (N) for each formation are: Letter Formation, $N = 5$; Maumtrasma Formation, $N = 5$; Derrlea Formation, $N = 18$; Rosroe Formation, $N = 13$; Mweelrea Formation, $N = 16$. The table gives the value for Wilk's λ, the F score associated with that value (F) and its significance (signif.). As there are only two levels (formations) in each test, the F scores are identical for all other statistics. The degrees of freedom for the null hypothesis (Hypothesis df) and error (Error df) are given along with the partial η^2 value, which suggests that a large proportion of the variance occurs within the combined formations.

hornblende and pyroxene both being relatively more common in the Letter and Maumtrasma Formations than in the others. It should be noted that having similar heavy mineral varieties does not necessarily imply stratigraphic correlation. In arc-related basins, such as the SMT, adjacent coeval fans on the sea floor may have different sources.

4.2. Testing the Similarity of Two Formations

The Killadangan Formation occurs to the north of the SMT and is of disputed age. Palaeontological data suggests a range of ages from mid-Cambrian (sponges: Rushton and Phillips, 1973) to Ordovician (conodonts: Harper et al., 1989) to Silurian (trilete spores: Williams et al., 1994). It is generally interpreted as being part of an accretionary prism. This formation contains no primary metamorphic detritus (Dewey and Mange, 1999) and shows clear evidence of sedimentological linkage with the Early Ordovician Letterbrock Formation (Dewey and Ryan, 1990; Dewey and Mange, 1999). It is, therefore, thought to have formed prior to the Grampian event that affected the Laurentian margin. However, some authors accept the palynological data and construct tectonic models that require Silurian subduction along this margin (Williams et al., 1994). The contact of this formation with the Silurian strata south of Clew Bay is also in dispute. Most authors view it as lying beneath a tectonised unconformity, a view that supports an Ordovician or older age, whereas others suggest that this contact represents a major terrane boundary (Williams et al., 1994; Williams, 2002). Heavy mineral data can be used to test whether the combined total raw count of heavy minerals of the Silurian strata and the Killadangan Formation were derived from the same population. χ^2 is selected as an appropriate test. The total count is calculated for each mineral species for each formation (Table 6). This has the advantage of reducing the number of species—where less than five observations were made—to two (spinel in the Silurian and staurolite in the Killadangan). A high proportion of such scores will invalidate this test. Also, the

Table 6. Contingency table for the heavy mineral species from the Killadangan Formation and the Silurian of South Mayo

	zr	tr	ap	ru	ch	ep	gt	sp	st	hb	Row total
Observed (O)											
Silurian	781	191	1175	19	33	233	137	4	25	18	2616
Killadangan	1778	97	587	92	5	14	7	6	1	11	2598
Column total	2559	288	1762	111	38	247	144	10	26	29	5214
Expected (E)											
Silurian	1272	143.1	875.6	55.2	18.9	122.7	71.6	5.0	12.9	14.4	
Killadangan	1263	142.1	869.6	54.8	18.8	121.9	71.1	4.9	12.8	14.3	
$(O-E)^2/E$											
Silurian	189.4	16.0	102.3	23.7	10.6	99.0	59.8	0.2	11.3	0.9	513.2
Killadangan	210.0	14.3	91.8	25.3	10.1	95.5	57.8	0.2	10.9	0.8	516.8
										χ^2	1030.0

Note: Abbreviations for the columns are the same as in Table 4.

category 'others' has been eliminated because, in this analysis, an attempt was made to make the total count for each species equal to two hundred observations. Although there is a considerable variation from this value, many samples are close to it, which means that, if the values for the 11 other species are known, the value for 'others' can be predicted. It cannot, therefore, be considered a truly random variable. The resultant χ^2 value achieved is 1030 with nine degrees of freedom (Table 6). A value above 27.88 allows the Null Hypothesis to be rejected at the 99.9% confidence level. It is concluded that the bulk heavy mineral counts of the Killadangan Formation are unlikely to be drawn from the same population as those of the combined Silurian datasets.

5. CORRELATION

Correlation of one mineral species against another may yield useful information about sedimentary provenance. A positive correlation may arise for several reasons. The two minerals may come from the same source. If this is the case, such positive correlations occur along strike and at all stratigraphic levels deriving material from that source. The two mineral species may come from different sources whose importance is decreasing or increasing together at that particular place and time. If both sources do not have the same influence throughout the extent and life of a basin, such correlations will not be repeated along strike or at different stratigraphic levels. A third possibility is that two labile mineral species are selectively removed by diagenetic or anchimetamorphic processes. Negative correlations can occur when one source replaces another; thus the mineral species, typical of one source, decreases whereas those from the other increase. Such negative correlations can also occur when a labile mineral, which is selectively removed by geochemical processes at different stratigraphic or metamorphic levels, is correlated with a stable mineral. In all these cases, the nature of the mineral species will also give a clue to the reasons for the correlation.

Normally, correlation is calculated using Pearson's Product Moment Correlation Coefficient (PMCC), r; functions to calculate this are provided in modern spreadsheets. Problems exist with this approach. The PMCC (r) is a measure of whether the two variables are linearly related. There is no reason to assume that this is the case in heavy mineral analysis. For example, in the simple case where two minerals are derived from the same source, a linear relationship requires that the two minerals were in the same proportion throughout the source, and that transport, depositional and diagenetic processes acted in a linear manner on both. The second problem is that one must assume that both mineral species have a normal distribution; it has already been demonstrated that this is commonly not the case. An approach that avoids these difficulties is to use a rank correlation coefficient, such as Spearman's ρ. This non-parametric technique assumes that both variables are independent and compares their ranks, not the absolute values, of the two datasets. For example, the rank correlation coefficient of epidote versus garnet for all of the formations from the SMT that are thought to have had a significant input of juvenile orogenic material (the Rosroe, Derrylea, Maumtrasna and Mweelrea formations: data from Dewey and Mange, 1999) is significant at $\rho = 0.530$ with 15 samples where both are

present. However, the PMCC is not significant and almost zero ($r = 0.025$), implying no linear correlation; the reasons for this are evident from Fig. 7.

A further problem with any correlation of two variables is that a matrix of heavy mineral data from several localities within several formations normally contains, as mentioned above, many empty cells, where a particular mineral was not recorded in a given sample. The user must decide whether to include such cells in any analysis. In general, a larger number of paired cells, both containing zero, will increase the absolute value of the product moment correlation coefficient and, obviously, the number of pairs used in the computation. The more pairs, the lower the absolute value any correlation coefficient has to be considered significant. Thus, samples with many paired zero values will tend to yield significant correlations, even though there may be very few of those minerals present. In rank correlation, all such pairs will be tied at the same rank, which tends to bias the analysis towards a positive correlation unless the correction for tied ranks is used.

To illustrate these effects, a correlation matrix has been prepared for the Rosroe, Derrylea, Maumtrasna and Mweelrea formations. The analysis has been performed including all samples (Table 7A) and then only for those pairs within two samples that contain non-zero values (Table 7B). Both analyses are corrected for tied scores.

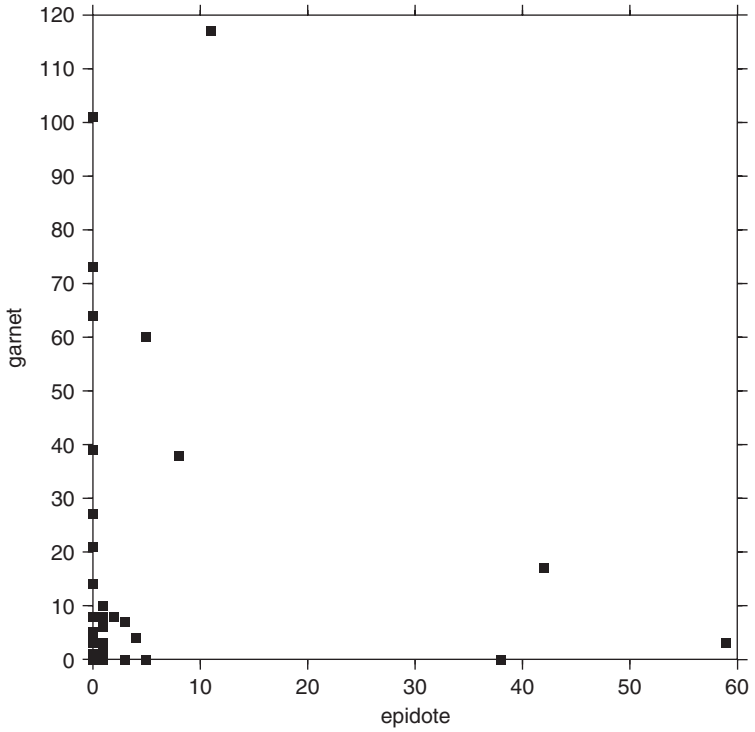

Fig. 7. XY plot of epidote against garnet from the upper successions of the South Mayo Trough. Note that there is a general increase in epidote (from 1 to 59) with garnet (from 1 to 117). However, two outliers exist, which have high epidote value for low garnet values. These outliers mean that there is almost no linear correlation, whereas the general pattern of the data ensures that there is a significant rank correlation.

Table 7. Correlation matrix using Spearman's ρ corrected for ties in the upper successions within the South Mayo Trough

	zr	tr	ap	ru	ch	ep	gt	sp	sn	st	hbl	ot
A: Correlation using all samples												
zr		0.02	**−0.36**	0.35	0.39	−0.04	**−0.35**	−0.07	−0.15	0.23	−0.02	0.19
tr	73		−0.19	0.36	0.50	**−0.30**	0.22	0.13	**−0.37**	0.27	−0.21	0.01
ap	73	73		**−0.63**	**−0.62**	−0.20	0.14	−0.09	−0.03	−0.15	−0.14	**−0.30**
ru	73	73	73		0.82	−0.07	−0.21	−0.11	−0.16	0.28	−0.09	0.24
ch	73	73	73	73		−0.14	**−0.34**	−0.14	**−0.25**	0.41	−0.18	0.19
ep	73	73	73	73	73		0.17	−0.09	0.40	−0.15	0.26	0.28
gt	73	73	73	73	73	73		0.22	0.03	−0.02	−0.04	0.08
sp	73	73	73	73	73	73	73		−0.11	−0.10	−0.19	**−0.24**
sn	73	73	73	73	73	73	73	73		−0.12	0.46	0.16
st	73	73	73	73	73	73	73	73	73		−0.20	0.24
hbl	73	73	73	73	73	73	73	73	73	73		0.30
ot	73	73	73	73	73	73	73	73	73	73	73	
B: Correlation using all non-zero samples; no correlation coefficient is recorded where there are less than five pairs												
zr		−0.13	**−0.36**	0.24	0.22	**−0.49**	−0.19	0.93	−0.06	−0.21	−0.33	−0.25
tr	56		−0.10	0.69	0.31	−0.09	0.12	−0.56	0.32	−0.51	**−0.67**	−0.19
ap	73	56		**−0.36**	**−0.67**	−0.29	−0.04	−0.28	−0.43	0.41	−0.22	0.10
ru	41	33	41		0.27	−0.25	−0.12			−0.53	−0.28	−0.03
ch	30	28	30	29		−0.55	−0.03			−0.61	0.22	**−0.51**
ep	25	17	25	14	9		0.53		0.13		0.11	0.08
gt	42	34	42	21	12	15		−0.62	−0.22		0.68	−0.08
sp	6	6	6	2	1	1	6					
sn	9	5	9	4	1	7	6	0			0.31	0.92
st	7	7	7	6	7	1	4	0	0			0.36
hbl	21	14	21	12	6	10	10	0	7	0		0.43
ot	30	25	30	22	17	14	18	0	5	5	13	

Note: The upper diagonal contains the correlation score. All correlations significant at the 95% level are shown with a leading zero and in bold if negative and underlined if positive. The lower diagonal contains the number of pairs used in the analysis. Abbreviations for the column and row labels are as in Table 4, plus sn = sphene.

As would be expected, the matrix for pairs with non-zero values (Table 7B) yields similar results but fewer significant correlations than the matrix in which all values are considered (Table 7A). However, the removal of pairs with one or more zero from the analysis introduces seven correlations (Table 8) that are significant in this matrix but not in that using all data. This is because, in each of these cases, there are a large number of pairs in which one value was zero and the other non-zero (e.g., epidote/zircon; hornblende/tourmaline). The effect of these pairs, where the other values must have had a range of ranks while zero will always have the lowest rank, is to reduce the absolute value of the correlation coefficient. The best analysis to use, therefore, is probably a rank correlation including all datasets, but to ensure that the correction for ties is made. Also, as discussed above, a zero score does not necessarily imply total absence of that mineral species.

Table 8. Correlations which are significant when only pairs with non-zero scores are used

Mineral 1	Mineral 2	*N* of non-zero pairs	*N* with only one zero value
Epidote	Zircon	25	48
Garnet	Epidote	15	37
Zircon	Serpentine	6	67
Hornblende	Tourmaline	14	49
Hornblende	Garnet	10	43
Others	Chrome-spinel	17	26
Others	Sphene	5	29

A final problem is that, if a fixed number of counts are taken, one of the columns of data will not be independent, because its value can be deduced by subtracting the total of all other counts from the grand total. This can be avoided by eliminating the column for 'other' unspecified mineral species from the analysis.

The majority of the significant correlations support the provenance model of Dewey and Mange (1999), which argues for primary arc material being sourced from the south and variable proportions of ophiolitic, basement and juvenile metamorphic detritus from the north. The positive zircon/chrome-spinel and zircon/rutile correlation may reflect metamorphic, basement and ophiolite-sourced zircons. The negative zircon/apatite correlation suggests their dilution by arc-sourced apatite. The positive correlations of rutile with both staurolite and tourmaline reflect derivation from a juvenile metamorphic source. The negative tourmaline/epidote correlation suggests juvenile metamorphic detritus diluted by ophiolitic material. The negative tourmaline/sphene, rutile/apatite and garnet/zircon may represent the decreasing importance of arc-derived over juvenile metamorphic materials-section. The negative apatite/chrome-spinel correlation implies arc-diluting ophiolitic detritus. Care should be exercised in considering correlations with total zircon, because this resistant mineral is derived, to some extent, from all sources (Dewey and Mange, 1999).

6. MULTIVARIATE ANALYSIS

Multivariate methods, either factor analysis or principal components analysis (PCA), are methods of re-displaying datasets containing several correlated variables so that the maximum variation is displayed. No decisions can be made from such analyses, but they assist in framing hypotheses. The PCA method is used here because it uses all available data and requires no factor weighting; data is plotted in hyperspace. In the case of the South Mayo samples, there are, potentially, 11 mutually orthogonal axes if the individual heavy minerals (zircon, tourmaline, rutile, apatite, chrome-spinel, epidote, garnet, serpentine, sphene, staurolite and hornblende) are plotted, and 11 axes if the stable mineral species, apatite, tourmaline and rutile are plotted against zircon varieties (euhedral, subhedral, anhedral, elongate, rounded colourless, rounded purple, zoned and with overgrowth) are analysed. New eigenvectors are then computed as simple linear combinations, or eigenvalues, of

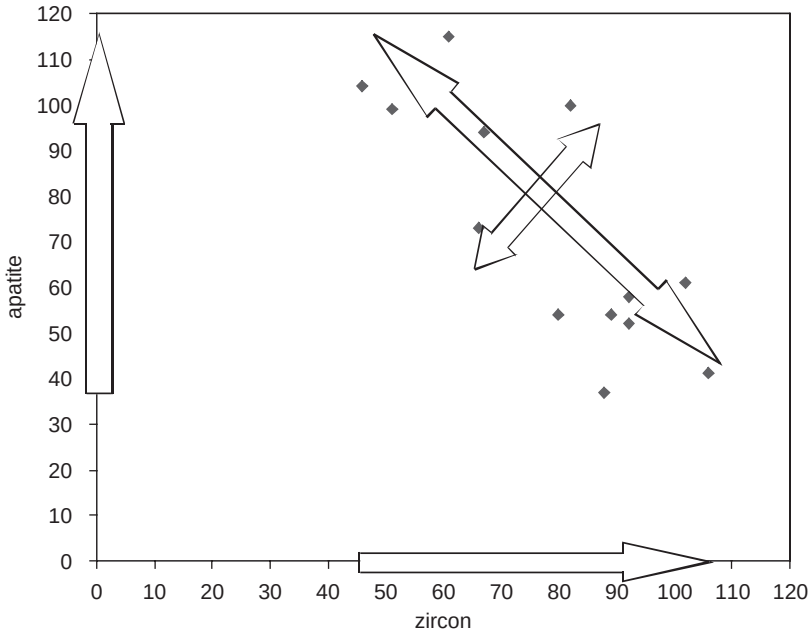

Fig. 8. Plot of zircon versus apatite for the Sheeffry Formation, South Mayo. The single headed arrows show the maximum range for the data on the Cartesian abscissa and ordinate axes. The double-headed arrows show the range when plotted on the axes calculated using the reduced major axis method (Ryan et al., 1995).

these 11 axes. The first eigenvector is the hyperspace axis that shows the greatest variation, then second the next greatest and so on until the eleventh eigenvector shows the least variation. In two dimensions, this is equivalent to plotting new axes, the first of which is a best fit line through the data and the second is the axis with least variation. Fig. 8 is a plot of apatite versus zircon for the Sheeffry Formation. The variables are negatively correlated (Table 7) with approximately 43% of the variability along the abscissa and 57% along the ordinate (single-headed arrows in Fig. 8). If a new axis is drawn that shows the maximum variation by the reduced major axis method, 73% of the variation occurs on this axis and only 27% on the orthogonal axis (double-headed arrows in Fig. 8). PCA works in a similar manner but uses either the variance–covariance or correlation matrix scores to define these new axes or principal components.

The results of a PCA analysis for South Mayo using the HRHMA of zircon varieties plus the stable minerals are presented in Fig. 9 and Table 9.

This suite is chosen over the total heavy mineral count because it contains few absences and relies only upon stable minerals. The variation in metamorphic grade from zeolite facies to biotite-greenschist facies (Ryan et al., 1980) plus the huge thickness (~8–9 km) of sediments within the SMT, implies that factors other than provenance, such as diagenesis, might influence the total heavy mineral population.

Table 9 shows that 76.93% of the variation occurs on the first eigenvector and 8.84% on the second, and gives the loadings on the individual axes. Simplifying,

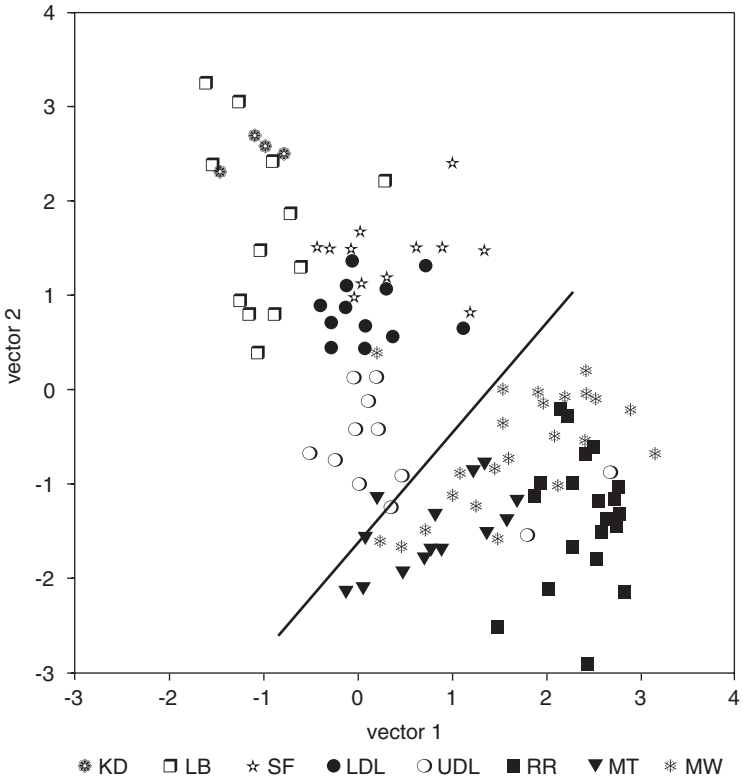

Fig. 9. Data from the various formations of the South Mayo Trough plotted on the first (abscissa) and second (ordinate) eigenvector after principal components analysis based upon the stable heavy mineral assemblages and zircon varieties. The following abbreviations are used: KD, Killadangan; LB, Letterbrock; SF, Sheeffry (including Owenmore); LDL, lower Derrylea; UDL, upper Derrylea; RR, Rosroe; MT, Maumtrasma; MW, Mweelrea Formations.

85.77% of the variation relies heavily upon the apatite components (eigenvector 1) and rounded purple zircon (eigenvector 2), suggesting that the two sources that have the most variation are basement (to the north) and arc (to the south, see above). Fig. 9 shows that the Killadangan, Letterbrock and Sheeffry (including Derrymore) Formations have a significant basement component, whereas the Rosroe, Maumtrasna and Mweelrea Formations have significant arc detritus. The Derrylea Formation, which is a lateral equivalent of the Rosroe Formation, spans these two groups. The different nature of the Rosroe and Derrylea Formations has led to considerable discussion about their stratigraphic equivalence (Dewey and Mange, 1999; Harper and Parkes, 2000; Williams, 2002; Clift et al., 2003; Mange et al., 2003). The results of the PCA analysis are consistent with a model where the Derrylea Formation is linked to a source dominated by the northerly ophiolite, basement and juvenile metamorphic sources, whereas the Rosroe Formation is dominated by the southerly arc source, which from time to time also comprises a significant component of the Derrylea Formation source—perhaps as a result of far run-out mass flows originating in the south (Dewey and Mange, 1999).

Table 9. Loadings on the individual axes for each eigen vector (columns 1–11) and the percentage variation along that vector (column 12)

	Heavy minerals			Zircon varieties							%var
	tr	ap	rt	eu	sub	an	el	rd_c	rd_p	zone	over	
v1	−0.09	0.96	−0.03	0.07	0.05	−0.01	−0.03	0.07	−0.24	0.00	−0.02	76.93
v2	0.39	0.28	0.13	−0.22	−0.19	0.03	0.15	−0.05	0.77	0.00	0.24	8.84
v3	−0.68	−0.01	0.04	0.02	0.05	0.00	0.10	−0.11	0.11	0.01	0.70	5.32
v4	0.52	−0.05	0.07	−0.18	−0.15	0.00	−0.09	0.04	−0.52	0.01	0.62	2.81
v5	−0.14	−0.05	−0.01	−0.19	−0.18	0.02	0.06	0.95	0.05	0.01	0.01	2.65
v6	0.29	−0.02	−0.17	0.57	0.63	−0.02	0.20	0.25	0.13	0.01	0.22	1.58
v7	−0.01	0.00	0.89	0.25	0.09	0.25	−0.24	0.08	0.00	0.01	−0.03	0.79
v8	−0.01	0.01	0.13	−0.69	0.66	0.16	0.19	−0.03	−0.07	−0.02	−0.07	0.50
v9	0.01	−0.01	0.23	0.11	−0.23	0.05	0.91	−0.06	−0.21	0.02	−0.10	0.45
v10	0.00	0.00	−0.28	0.07	−0.10	0.95	−0.01	−0.03	0.00	0.05	0.02	0.12
v11	0.00	0.00	0.00	−0.02	0.02	−0.05	−0.01	0.00	0.00	1.00	−0.02	0.02

Note: The following abbreviations are used: vN, eigen vector, N; tr, tourmaline; ap, apatite; rt, rutile; eu, euhedral; sub, subhedral; an, anhedral; el, elongate; rd_c, rounded colourless; rd_p, rounded purple; zone, zoned; over, with overgrowths; %var, percentage variation.

7. DISCUSSION OF STATISTICAL ANALYSIS

Statistical analysis of a comprehensive heavy mineral dataset assists in the interpretation of the stratigraphy of a complex basin such as the SMT. Normalised and smoothed stacked bar charts display broad stratigraphic trends. One sample testing shows that these stratigraphic changes are significant for half of the mineral species, but that many are not normally distributed. Non-parametric testing of entire formations reveals that different sources dominate different formations and that level-by-level analysis highlights the stratigraphic levels where these changes occur. For example, chrome-spinel generally decreases up-section as the ophiolite source becomes less important, whereas garnet increases up-section as a juvenile metamorphic source becomes more important. The initial pulse of staurolite, which may mark the local extensional removal of an ophiolite nappe cover to expose the metamorphic complex beneath, is marked by an upward decrease then an increase, perhaps as upper levels of this complex were eroded. Statistical analysis can be used to test various propositions concerning correlation of individual formations. Such analyses suggest that the unfossiliferous Letter Formation may share a common source of zircons with the Maumtrasma Formation. However, comparison of the heavy mineral assemblages of samples from the Silurian successions shows that it is extremely unlikely that they shared a common source with the Killadagan Formation. Correlations and multivariate analysis provide statistical support for the model proposed by Dewey and Mange (1999) for the evolution of the SMT. The greatest variation and, hence, the best discrimination, is given by basement-sourced zircon and arc-sourced apatite although other mineral groups, such as ophiolite-derived chrome-spinel and juvenile metamorphic garnets may be numerically more important

locally. Such analysis cautions that it is unwise to rely solely upon the more common heavy mineral species to characterise provenance in a complex tectonic setting.

8. TECTONIC CONSEQUENCES

The SMT is an anchimetamorphic to very low-grade zone preserved within an orogen, developed by mid-Ordovician arc-continent collision. The preservation of low-grade rocks in collisional orogens is an apparent paradox; in zones of collision, crustal thickening and mountain building, it might be supposed that erosion would strip the high-level low-grade rocks to expose deeper, higher-grade assemblages. The preservation of many Caledonian 'slate belt' successions such as the Southern Uplands accretionary prism can be explained by the ''soft'' sinistral transpressional, late Silurian/early Devonian collision between Laurentia and Avalonia that generated the paratectonic Caledonides of the British Isles (Dewey, 1969). There was scarcely any crustal thickening and very little erosion, yet granite plutons in sinistral pull-aparts with associated silicic volcanism are widespread as ''a sea of red ink''; Devonian strata rest unconformably upon both paratectonic and orthotectonic Caledonides and there has been little burial, erosion or change in crustal thickness, of the British Isles since then.

The evolution and preservation of the SMT presents a greater apparent problem. The SMT evolved as a fore-arc basin to an oceanic arc that collided with, and was obducted upon, the rifted Laurentian continental margin to generate the Grampian (= Taconic) orogeny (Dewey and Shackleton, 1984; Dewey and Ryan, 1990; Dewey, 2005). Throughout both its pre-collisional history and collisional development in the thrust hanging wall above the evolving Grampian orogen, the SMT and its oceanic basement not only escaped erosional removal but remained below or near sea-level throughout Tremadocian to Llanvirnian sedimentation and volcanism, while Grampian deformation and metamorphism were occurring immediately beneath the obducted sheet. HRHMA clearly documents this process (Dewey and Mange, 1999) and, at least in terms of the heavy mineral content, shows that the change from an arc/ophiolite-dominated source to that of a youthful orogen upsection is statistically significant.

A possible alternative is that the South Mayo arc was not obducted onto, but bull-dozed and thickened the Laurentian margin and remained depressed. We prefer the obduction model for four reasons. First, along strike in Newfoundland, the obducted sheet is preserved as the Bay of Islands Ophiolite Complex (Dewey and Shackleton, 1984). Secondly, heavy minerals in the Ordovician stratigraphy of the SMT record the progressive stripping of an ophiolite sheet (Dewey and Mange, 1999). Third, Ordovician sedimentation was continuous and the SMT was not folded until post-Mweelrea time; continuous sedimentation would be easier on an obducted piggy-back basin below or near sea-level. Fourth, the steep Clew Bay suture zone contains Ordovician blueschists and separates amphibolite-facies Dalradian rocks to the north from the anchimetamorphic rocks of the SMT to the south (Fig. 1). The blueschists indicate a substantial top-to-the-south displacement on the Clew Bay zone before it was steepened indicating, in turn, that the SMT was at least partly above the Dalradian rocks of north Mayo.

Only during late Llanvirnian, post-subduction-flip, shortening (Fig. 2) was the SMT folded into a broad syncline and eroded before the late Llandovery marine transgression by which time the crust was returned to normal thickness, mainly by extension, not erosion (Clift et al., 2004; Dewey, 2005). Excluding the bull-dozer model, the preservation of the SMT may have been the result of four factors. First, subduction systems commonly show a general subsidence of the over-riding lithosphere resulting from the colder negative buoyancy of the subducting slab(s) (Lambert and McKerrow, 1976; Zhong and Gurnis, 1994). Second, the subducting, thinned and stretched, Laurentian continental margin probably contained substantial amounts of mafic igneous rocks judging from the amount of mafic volcanics and sills in the Dalradian of Donegal (Pitcher and Berger, 1972). If these mafic rocks were converted to eclogite during Grampian continental thickening (Ryan, in press), it would contribute to depression of the orogen and reduce erosion. Third, the 12 km-thick obducted arc/supra-subduction-zone ophiolite had an average density of $\sim 3200\,\mathrm{kg \cdot m^{-3}}$, beneath which the evolving Grampian orogen was depressed; the Ordovician sediments of the SMT comprise only a small component of the obducted slab and at least two-thirds of these had a density of $\sim 3000\,\mathrm{kg \cdot m^{-3}}$ resulting from the large amount of detrital chrome-spinel and chromite (Dewey and Mange, 1999). Fourthly, the Grampian orogen in western Ireland enjoyed a period of extensional denudation, during late Derrylea time, when only recently generated staurolite-bearing garnet amphibolites were drawn up beneath an extensional detachment(s) to contribute a statistically significant pulse of detritus to the upper Derrylea, as the hanging wall, containing the SMT was drawn down. Subduction flip led to extensional collapse and, probably, delamination/detachment of the eclogitised Laurentian root, which would generate uplift of the Grampian core from which the high-level obducted sheet was withdrawn. Hence, erosional denudation was forestalled by extensional denudation; the SMT was in the hanging wall of a major extensional detachment before it could be eroded but the rising Grampian core rapidly provided staurolite/garnet metamorphic detritus. The principal detachment was within the Clew Bay Zone, the site of earlier collisional obduction: the collisional hanging wall became the extensional hanging wall (Clift et al. 2004; Dewey, 2005). In this model, we see the fine-grained Glenummera Formation as an expression of the last stage of extensional collapse before the onset of shortening and the deposition of the Mweelrea Formation (Dewey, 2005). Of these four preservational factors, it is as yet unclear which is the predominant; we lean towards extensional denudation and the high density of the obducted slab. We are investigating the role of the density of the obducted slab by numerical modelling.

9. CONCLUSIONS

We have presented a variety of simple statistical techniques that, we believe, are applicable to many HRHMA datasets. These methods promote the power of the data and offer an independent and objective way to highlight and test the statistical significance of stratigraphic trends, to identify and evaluate correlations within the dataset; and allow for statistical testing of correlation between formations. The statistically significant trends identified within the SMT permitted a refined

correlation of some critical formations and strengthened the conclusions of earlier studies on sedimentary and volcanic geochemistry (e.g., Clift and Ryan, 1994; Draut and Clift, 2001), regional tectonics (Dewey and Ryan, 1990) and heavy minerals (Dewey and Mange, 1999). In particular, they provide support for the contention that sedimentation continued in the SMT during primitive arc evolution, arc-continent collision and rapid orogenic unroofing and subduction flip. The statistically significant change in source up-section requires a mechanism for suppressing basin topography during collision. We suggest that this might be due to a combination of four dynamic and isostatic processes during the Grampian orogeny.

ACKNOWLEDGEMENTS

The authors acknowledge helpful reviews from Richard Howarth and David Harper which improved this analysis.

REFERENCES

Bergström, S.M., Finney, S.C., Chen, Xu., Goldman, D., Leslie, S.A., 2006. Proposed names for the three Ordovician global stages. Ordovician News 23, 10–11.

Brace, N., Kemp, R., Snelgar, R., 2003. SPSS for Psychologists. Palgrave MacMillan, Basingstoke, pp. 238–247.

Clift, P.D., Dewey, J.F., Draut, A.E., Chew, D.M., Mange, M., Ryan, P.D., 2004. Rapid tectonic exhumation, detachment faulting and orogenic collapse in the Caledonides of western Ireland. Tectonophysics 383, 91–113.

Clift, P.D., Dewey, J.F., Draut, A.E., Mange, M., 2003. Discussion of 'Buried oblique-slip faults in the Irish Caledonides' by D.M. Williams. Geological Journal 39, 99–100.

Clift, P.D., Ryan, P.D., 1994. Geochemical evolution of an Ordovician island arc, South Mayo, Ireland. Journal of the Geological Society, London 151, 329–342.

Dewey, J.F., 1969. Evolution of the Caledonian–Appalachian orogen. Nature 222, 124–129.

Dewey, J.F., 2005. Orogeny can be very short. Proceedings of the National Academy of Sciences of the USA 102, 15286–15293.

Dewey, J.F., Mange, M., 1999. Petrography of Ordovician and Silurian sediments in the western Ireland Caledonides: tracers of a short-lived Ordovician continent arc collision orogeny and the evolution of the Laurentian Appalachian Caledonian margin. In: MacNiocaill, C., Ryan, P.D. (Eds.), Continental Tectonics, vol. 164. Geological Society of London Special Publication, pp. 55–107.

Dewey, J.F., Ryan, P.D., 1990. The Ordovician evolution of the South Mayo Trough, western Ireland. Tectonics 9, 887–901.

Dewey, J.F., Shackleton, R.M., 1984. A model for the evolution of the Grampian tract in the early Caledonides and Appalachians. Nature 312, 115–121.

Draut, A.E., Clift, P.D., 2001. Geochemical evolution of arc magmatism during arc-continent collision, South Mayo, Ireland. Geology 29, 543–546.

Graham, J.R., Smith, D.G., 1981. The age and significance of a small Lower Palaeozoic inlier in County Mayo. Journal of Earth Sciences Royal Dublin Society 4, 1–5.

Harper, D.A.T., Parkes, M., 2000. Ireland. In: A revised correlation of Ordovician rocks in the British Isles. Geological Society of London Special Report on the Ordovician System, vol 24, 52–64.

Harper, D.A.T., Williams, D.M., Armstrong, H.A., 1989. Stratigraphical correlations adjacent to the Highland Boundary Fault in the west of Ireland. Journal of the Geological Society, London 146, 381–384.

Howarth, R.J., 1998. Improved estimators of uncertainty in proportions, point-counting and pass-fail test results. American Journal of Science 298, 594–607.

Lambert, R.St.J., McKerrow, W.S., 1976. The Grampian Orogeny. Scottish Journal of Geology 12, 271–292.

Mange, M.A., Dewey, J.F., Wright, D.T., 2003. Heavy minerals solve structural and stratigraphic problems in Ordovician strata of the Western Irish Caledonides. Geological Magazine 140, 25–30.

Mange-Rajetzky, M.A., 1995. Subdivision and correlation of monotonous sandstone sequences using high resolution heavy mineral analysis, a case study: the Triassic of the Central Graben. In: Dunay, R.E., Hailwood, E.A. (Eds.), Non-Biostratigraphic Methods of Dating and Correlation, vol. 89. Geological Society of London Special Publication, pp. 23–30.

Pitcher, W.S., Berger, A.R., 1972. The Geology of Donegal: A Study of granite Emplacement and Unroofing. Wiley, New York, 435 pp.

Rushton, A.W.A., Phillips, W.E.A., 1973. A *Protospongia* from the Dalradian of Clare Island, Co. Mayo, Ireland. Palaeontology 16, 231–237.

Ryan, P.D. (in press). The preservation of fore-arc basins during island arc-continent collision: some insights from the Ordovician of western Ireland. Bulletin of the Geological Society of America.

Ryan, P.D., Floyd, P.A., Archer, J.B., 1980. The stratigraphy and petrochemistry of the Lough Nafooey Group (Tremadocian), western Ireland. Journal of the Geological Society, London 137, 443–458.

Ryan, P.D., Harper, D.A.T., Whalley, J., 1995. PALSTAT: Statistics for Palaeontologists and Palaeobiologists. Chapman and Hall, London, 74 pp.

Ryan, P.D., Sawal, V.K., Rowlands, A.S., 1983. Ophiolitic melange separates ortho- and para-tectonic Caledonides in western Ireland. Nature 301, 50–52.

Soper, N.J., Ryan, P.D., Dewey, J.F., 1999. Age of the Grampian Orogeny in Scotland and Ireland. Journal of the Geological Society, London 156, 1231–1236.

Williams, D.M., 2002. Buried oblique-slip faults in the Irish Caledonides. Geological Journal 37, 135–142.

Williams, D.M., Harkin, J., Armstrong, H.A., Higgs, K.T., 1994. A late Caledonian melange in Ireland: implications for tectonic models. Journal of the Geological Society, London 151, 307–314.

Zhong, S., Gurnis, M., 1994. Controls on trench topography from dynamic models of subducted slabs. Journal of Geophysical Research 99, 15683–15695.

This page intentionally left blank

Chapter 19

EVOLUTION OF QUATERNARY TO MODERN FLUVIAL NETWORK IN THE MID-HUNGARIAN PLAIN, INDICATED BY HEAVY MINERAL DISTRIBUTIONS AND STATISTICAL ANALYSIS OF HEAVY MINERAL DATA

EDIT THAMÓ-BOZSÓ[a] AND LAJOS Ó.KOVÁCS[b]

[a]*Geological Institute of Hungary, Stefánia út 14, 1143 Budapest, Hungary*
[b]*Hungarian Geological Survey, Stefánia út 14, 1143 Budapest, Hungary*

ABSTRACT

Heavy mineral data of 590 samples from ten cored boreholes, penetrated into Quaternary fluvial successions in the central part of the Hungarian Plain, and complemented by data from modern river sediments, have been evaluated using numerical methods. Cluster analysis and principal component analysis (PCA) have revealed appreciable similarities between the heavy mineral composition of modern river sediments and those from borehole samples, resulting in a more refined reconstruction of the Quaternary fluvial network and sediment provenance. Interpretation relied on the presumption that Quaternary physiography and the geological settings of the source regions were comparable to those of today. Comparative analyses showed that the modern Tisza River and its tributaries, draining the Hungarian Plain, carry pyroxene, hornblende, chlorite or garnet-rich sediments from the Carpathian Belt, Apuseni Mountains and North Hungarian Range, while the River Danube and its tributaries transport garnet-dominated heavy mineral assemblages mainly from the Alps, western Carpathians and the Bohemian Massif.

During the Quaternary, sediments in the western part of the study area were deposited by the Palaeo-Danube, flowing then from the northwest and partly from the north. In the central part, the sediments of the Palaeo-Danube interfinger with deposits of the Palaeo-Tisza and its tributaries, arriving from the northeast or north. Closer to the Apuseni Mountains the direction of palaeodrainage changed frequently.

PCA has provided a clear differentiation of the garnet-rich sediments of the modern Danube and Tisza rivers, but uncertainties remain with the older sands due probably to changing source areas and/or intermixing the loads of different palaeo-rivers with time. Both cluster analysis and PCA identified metamorphics-derived chlorite and garnet as well as volcanogenic hornblende and pyroxene as the dominant minerals of the Quaternary sands. A comparison of the heavy mineral composition of modern river sands and those deposited by their ancestors using PCA has revealed some differences, interpreted as the impact of tectonic and erosional changes during the

Developments in Sedimentology, Vol. 58, 491–514

ISSN: 0070-4571/doi:10.1016/S0070-4571(07)58019-2

Pleistocene. For example, chlorite-rich sands that are abundant in the Early Quaternary become less frequent in Late Quaternary deposits and are uncommon in the modern rivers, suggesting that their low-grade parent rocks have been progressively eroded. Variations in heavy mineral distributions also reflect tectonics-controlled fluvial channel switching.

Keywords: detrital heavy minerals; cluster analysis; principal component analysis; Quaternary fluvial network; Hungary

1. INTRODUCTION

Quaternary fluvial sediments in the central part of the Hungarian Plain have been studied in ten cored boreholes (Fig. 1). The penetrated 40–700 m thick successions consist mostly of fluvial sand, silt and clay, underlain by Pliocene strata. Studies, including sedimentology, geomorphology, hydrogeology and mineralogy have shown that during the Quaternary the Palaeo-Danube and Palaeo-Tisza distributary systems transported sediments from contrasting directions into the Hungarian

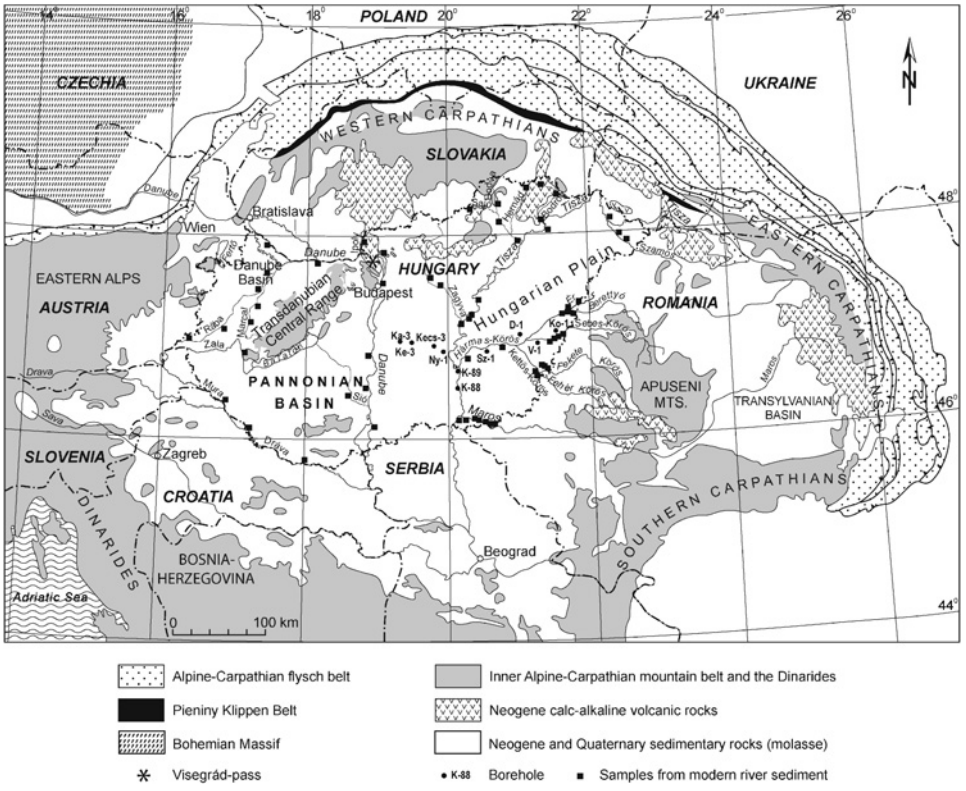

Fig. 1. Geological sketch map of the Carpathian–Pannonian region, with the locations of the studied boreholes and samples from modern river sediments.

Plain (Sümeghy, 1951, 1955; Urbancsek, 1960; Molnár, 1967; Gedeon-Rajetzky, 1973a, 1976a, 1976b; Borsy, 1992). The aim of our study was to reconstruct the evolving Quaternary fluvial network of the Hungarian Plain by evaluating a large set of existing heavy mineral data, using numerical methods.

Traditional heavy mineral analysis in Hungary started in the early 20th century, when Aladár Vendl separated the heavy minerals of sand by using a heavy liquid and magnetic separator, and examined them under binocular and polarising microscopes (Vendl, 1910). He also used microchemical reactions to enable positive mineral identification. However, heavy mineral analysis was used at that time only by a few researchers (Melczer, 1913; Lengyel, 1930; Sztrókay, 1935; Miháltz, 1937). Interest increased from the 1950s when several heavy mineral studies were undertaken (e.g. Hermann, 1954; Ravasz-Baranyai, 1962; Molnár, 1963, 1964; Csánk, 1969; Gedeon-Rajetzky, 1971, 1973a, 1973b, 1976a, 1976b; Radócz-Komáromy, 1971). The first results were qualitative, but following the introduction of point counting, percentage-based compositional data were generated. In the mid-1960s the heavy mineral technique flourished, as shown by the approximately 50–70 publications and reports per year that included heavy mineral data. During the following decades the popularity of this method gradually declined, although it was not abandoned. In the 1980s, conventional optical mineral identification was complemented by other analytical techniques (X-ray diffraction, X-ray fluorescence spectrometry, electron-probe microanalysis, scanning electron microscopy). Data collected by Sallay (1984) show that up to that time, about 20,000 heavy mineral compositions had been determined from Cenozoic sedimentary rocks, reflecting an intensive use of the technique.

Heavy mineral analyses were performed on a variety of sands and sandstones; sometimes the sand fractions of gravel, silt, clay, bauxite, loess and volcanic tuffs were analysed, traditionally, all in the 0.1–0.2 mm size fraction. Heavy minerals were distinguished and grouped according to their origin, such as metamorphic, magmatic and recycled sedimentary, and their provenance and source areas were evaluated (e.g. Molnár, 1964; Gedeon-Rajetzky, 1973a). Results of heavy mineral analysis helped to understand better depositional conditions and diagenesis, the extent of reworking older sedimentary rocks, identifying volcanic ash falls and the plate-tectonic setting of source areas. Occasionally the combined heavy and light mineral composition of clastic sediments proved useful to reconstruct palaeoclimate. The study of heavy minerals proved as a suitable tool to delineate heavy mineral provinces (Molnár, 1965) and to subdivide thick clastic successions by their distinctive heavy mineral associations (Gedeon-Rajetzky, 1973a, 1976a; Elek, 1979, 1980b). Several Hungarian handbooks provided useful information on the heavy mineral technique and its applications (Vendel, 1959; Molnár, 1971, 1981; Wallacher, 1989; Balogh and Hajdú-Molnár, 1991). Data generated by the high number of heavy mineral analyses over decades were thus ideal for statistical analysis.

2. STUDY AREA

The study area is situated in the central part of the Pannonian Basin, the largest intermontane basin in Europe, surrounded by the Alps, Carpathians and Dinarides.

(Fig. 1). The elevation of the basin is between 83 and 110 m above sea level, the western area being higher than the eastern and central parts. Major rivers draining the basin are the Danube and Tisza and their tributaries. The northern tributaries of the Tisza are the Szamos, Bodrog, Sajó (Bódva, Hernád) and Zagyva rivers, originating in the northeastern Carpathians and in the Northern Hungarian Mountain Range. The eastern tributaries include the Berettyó and Ér, while the Sebes (fast)-, Fekete (black)- and Fehér (white)- Körös rivers join downstream into the Hármas (triple)-Körös. These rivers, draining the Apuseni Mountains, display an approximately east–west transverse pattern. The confluence of Tisza and Danube, which are the major outflow, is in the southern part of the Pannonian Basin, in Serbia. Recent rivers in the Hungarian Plain carry mostly suspended load and there are marked differences in the size, geology and morphology of their catchment areas.

The fluvial sediments under study were deposited in the latest phase of Pannonian Basin evolution. The basin originated in the Early-Middle Miocene by back-arc style rifting, coeval with the late stages of thrusting in the Carpathian belt. During the Late Miocene and Pliocene, two independent extensional phases with post-rift thermal subsidence occurred (Horváth and Cloetingh, 1996; Csontos and Nagymarosy, 1999). The subsided basin was filled by the brackish Pannonian Lake that was in contact with the former Paratethys. After the complete isolation of the Pannonian Lake from the marine environment, it was gradually filled up by prograding delta systems flowing from the northwest and northeast during the Upper Miocene and Pliocene. This succession represents a time-transgressive facies change from offshore basin through basin slope and delta slope to delta front and then delta plain sediments, passing up into alluvial facies which represents the latest stage of the basin fill (e.g. Juhász, 1994).

During the Quaternary, a still active basin inversion, starting at about the end of the Late Miocene, characterised by northwest–southeast and north–east compressions, resulted in significant uplift of the marginal parts, with local subsidence of the basin centre (e.g. Horváth and Cloetingh, 1996; Csontos and Nagymarosy, 1999; Horváth and Tari, 1999). This complex morphology initiated the development of the modern radial fluvial network, with rivers transporting detritus towards the central part of the Pannonian Basin from the northwest, north, northeast, east and southeast.

In the Körös sub-basin, in the eastern part of the study area, where the Dévaványa (D-1) and Vésztő (V-1) boreholes were drilled (Fig. 2), subsidence was uninterrupted, resulting in the accumulation of a 420–460 m thick continuous Pleistocene fluvial succession of fine-grained sediments, comprising predominantly silt and clay with minor fine-sand intervals (Rónai, 1985). Paleomagnetic data obtained from these two boreholes provide a chronostratigraphic framework for this area (Cooke et al., 1979; Rónai, 1985). High-resolution cyclostratigraphical and palaeoclimate analyses of the Pleistocene fluvial sediments in the Körös sub-basin indicated that they represent Milankovitch cycles, 100 ka cyclicity for the upper section of the boreholes (younger than 1 Ma), and 40 ka for the older parts, consistent with the global palaeoclimate records (Nádor et al., 2003).

East of the Körös sub-basin in the Komádi borehole (Ko-1), fluvial siltstone, clay and sand build up the 450 m thick Quaternary succession. West and southwest of the Körös sub-basin in boreholes Szarvas (SZ-1), Csonrád (K-89) and Mindszent (K-88), palaeontological data suggest that the 450–690 m thick Pleistocene fluvial

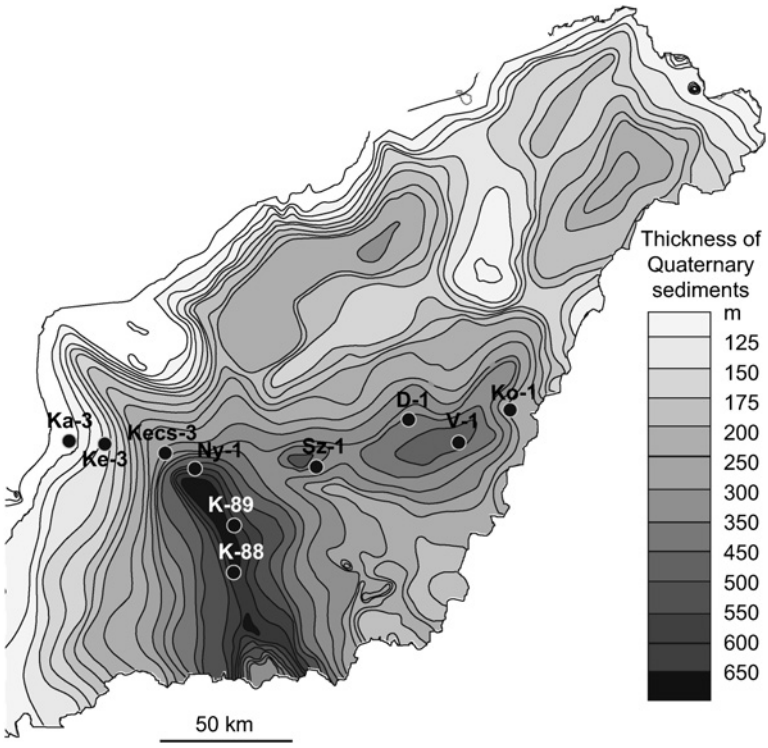

Fig. 2. Thickness of the Quaternary sediments (after Franyó, 1992), with the locations of the studied boreholes.

record is more or less continuous. It comprises frequently alternating sand, siltstone and clay layers. In the western part of the study area in boreholes Nyárlőrinc (NY-1), Kecskemét (Kecs-3), Kunadacs (Ka-3) and Kerekegyház (Ke-3) the Quaternary sediments attain a thickness between 40 and 370 m, with thickness increasing gradually towards the east. The fluvial sands contain fewer gravel, siltstone and clay beds and show intercalation of aeolian sand in the upper section (Rónai, 1985).

3. EVOLUTION OF THE FLUVIAL NETWORK OF THE HUNGARIAN PLAIN DURING THE QUATERNARY

It was recognised as early as 1809 that the ancestral river network in the Hungarian Plain was different from the present one, concluding from abandoned fluvial channels and alluvial fans with no connection to any active river system (Somogyi, 1961 and references therein). Contrasting with the present north–south path of the Danube, geologists and geographers, using sedimentology, terrace-morphology, hydrogeology and borehole electric logs, proved that the channels of the ancestral Danube had a northwest–southeast flow direction (Fig. 3), and built up a large alluvial fan in the western part of the study area (Treitz, 1903; Schafarzik, 1918;

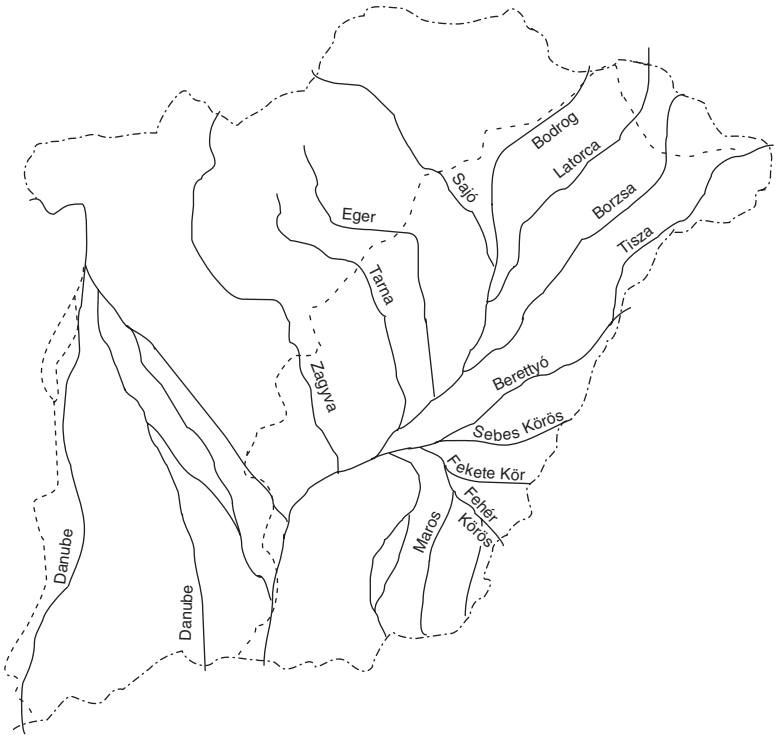

Fig. 3. Late Pleistocene palaeo-river network reconstruction (after Urbancsek, 1960), based on electrical logs and palaeontological data from boreholes. Dotted lines show the major modern rivers.

Scherf, 1935; Sümeghy, 1944, 1951; Bulla, 1953; Pécsi, 1959; Urbancsek, 1960; Rónai, 1985; Borsy, 1989, 1992; Gábris, 1994).

There is no uniform agreement about the time when the Palaeo-Danube changed its course to a west–east direction, cut across the Visegrád Pass and then turned towards the southeast (Fig. 1), or when the modern river network developed. Urbancsek (1960) and Borsy (1989) postulated that the Palaeo-Danube cut through the Visegrád Pass in the Late Pliocene and then flowed in a northwest–southeast direction until the Late Pleistocene. Later, the main channel of the Palaeo-Danube gradually shifted to a westerly direction, triggered by tectonic movements, and finally attained a north–south path (Urbancsek, 1960). Others argued that the Danube cut through the Visegrád Pass only at the end of the Günz-Mindel interglacial (Mike, 1991; Neppel, et al., 1999). It is, however, well established that after incising the Visegrád Gorge and developing a sharp bend, the Danube reached its recent north–south course during the Riss-Würm interglacial (Urbancsek, 1960), or in the Holocene (Somogyi, 1961; Rónai, 1985).

Sedimentological and hydrogeological investigations indicated that the Palaeo-Tisza flowed south of its present course, in the valley of the modern Ér River (Sümeghy, 1944, 1951, 1955; Urbancsek, 1960; Borsy, 1989). Urbancsek (1960) suggested the existence of a different large river that flowed from northeast to

southwest, more or less parallel with the Palaeo-Tisza, and collected the waters of rivers flowing from the north (Fig. 3). The Tisza and its tributaries may have occupied their recent course in the Günz-Mindel interglacial by shifting gradually towards the west (Molnár, 1997) or, as suggested by Somogyi (1961), during the Holocene, caused by Holocene tectonic movements. Borsy et al. (1989) argued that this happened only 4500 years ago.

In the debate on the palaeo-river network reconstructions (Sümeghy, 1951; Urbancsek, 1960; Somogyi, 1961; Borsy, 1989; Borsy et al., 1989; Mike, 1991; Gábris, 1994; Neppel, et al., 1999), Borsy (1989) proposed the most acceptable model (Figs. 4A, B). He argued that until the beginning of the Late Pleniglacial, sediments were transported principally by the Palaeo-Danube from a northwesterly direction to the western part of the study area. The sites of boreholes K-89 and K-88 were reached by both the Danube and Tisza. In the central and eastern parts of the study area, the Tisza and its tributaries carried sediments dominantly from the northeast and north.

Heavy mineral studies have contributed further evidence to the reconstruction of the provenance of the Quaternary fluvial deposits in the Mid-Hungarian Plain (e.g. Molnár, 1964, 1965, 1980; Gedeon-Rajetzky, 1973a, 1976a, 1976b; Elek, 1979, 1980a, 1980b; Gheith, 1982). Results indicated that in the western part of the study area (Ka-3, Ke-3, Kecs-3, NY-1) the sediments bear signatures of the Palaeo-Danube (Molnár, 1976; Elek, 1980b). Aeolian reworking during dry periods was occasionally observed. In the central part (K-89 and K-88) the deposits of the Palaeo-Danube and Palaeo-Tisza alternated. The precursors of Zagyva, Tarna and Sajó rivers delivered material from the north to the area of borehole K-89, while at the site of borehole K-88 the sediments of the ancestral Körös, Berettyó and Maros rivers were identified (Gedeon-Rajetzky, 1973a; Gheith, 1982). The succession penetrated by borehole SZ-1 was deposited by the Palaeo-Körös, Ér, Berettyó and Tisza, and it is likely that the Palaeo-Danube occasionally reached this region (Gedeon-Rajetzky, 1973a, 1976b). To the eastern part of the study area (D-1, V-1, Ko-1) the ancestral Körös, Berettyó and Tisza carried sediments, shifting their courses over the area in time and space (Elek, 1980a; Molnár, 1980).

4. STUDY METHODS

Heavy mineral data used in this study were generated during earlier projects (Szabó, 1955, 1967; Molnár, 1964, 1976, 1980; Gedeon-Rajetzky, 1973a, 1976a, 1976b; Elek, 1979, 1980a, 1980b; Kuti et al., 1987; Molnár et al., 1989, 1990) when around 530 samples were analysed from ten boreholes, and 57 sand samples from modern rivers. Microscopy included the identification and point counting of ~200 detrital grains in the 0.1–0.2 mm fraction. The frequencies of 27 detrital heavy mineral species, identified in the Quaternary samples, have been compared using cluster analysis and principal component analysis (PCA). Cluster analysis is a standard technique of numerical classification. It arranges samples into approximately homogeneous groups based on similarities in terms of multiple variables. After several tests of the different versions of cluster analysis, hierarchical classification was applied to the current case using Euclidean distance and the weighted pair-group

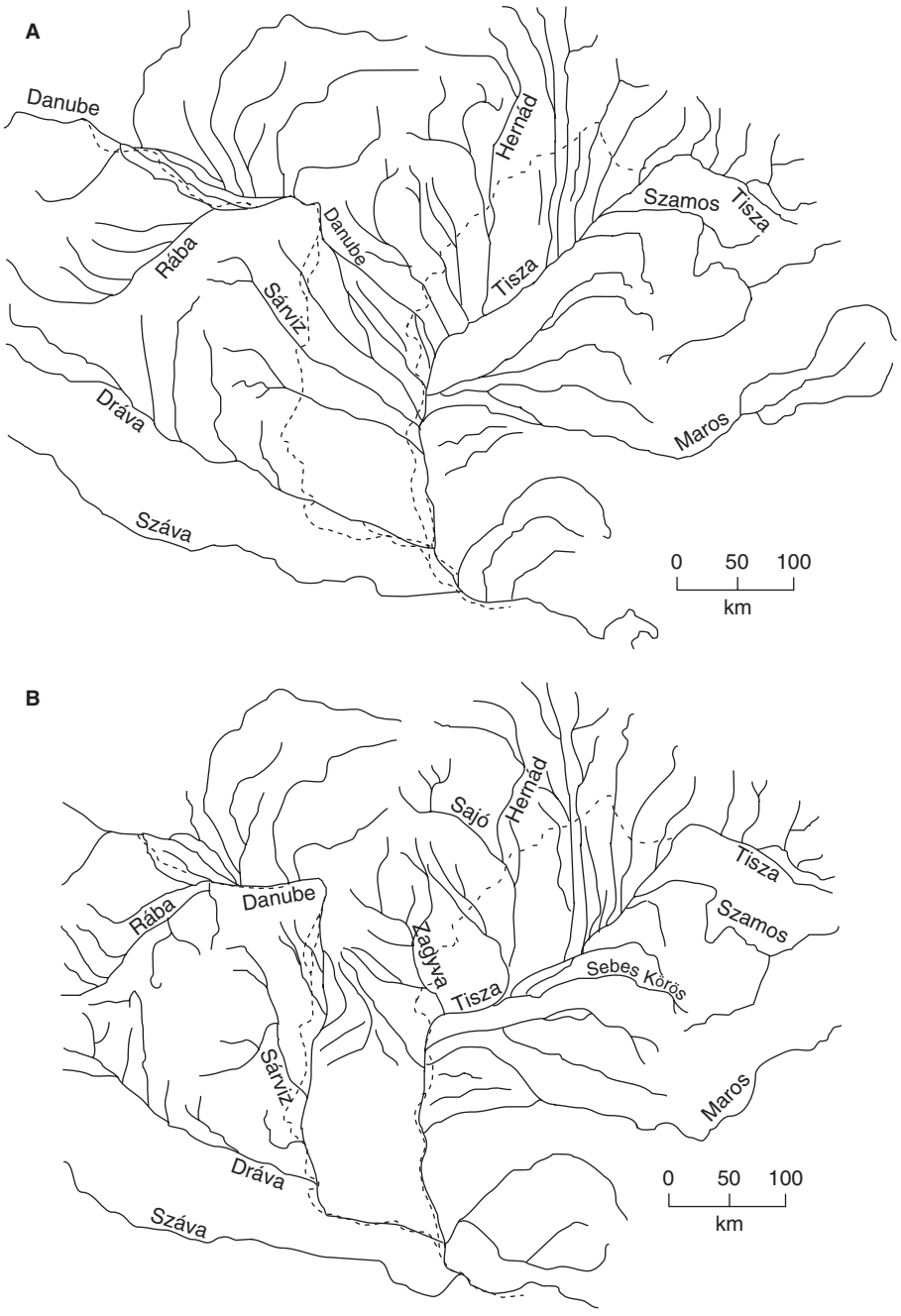

Fig. 4. Palaeo-river network reconstruction (after Borsy, 1989). Dotted lines show the major modern rivers. (A) At the beginning of the Pleistocene. (B) At the beginning of the Late Pleniglacial.

average method (Davis, 1986). This method was successful in tracing the provenance of Recent fluvial sediments in Italy (Ibbeken and Schleyer, 1991) and determining the palaeotransport directions of Quaternary sediments in the Körös sub-basin in Hungary (Thamó-Bozsó et al., 2002). In the present study each sample, characterised by the frequency of the 27 detrital heavy mineral constituents, represented a point in the 27-dimensional space. The Euclidian distance between the samples in this space was used as a measure of similarity. This type of cluster analysis was carried out using "Deli-Clus-Dend" in-house software of Ó.Kovács (1986). Samples within a particular group have a similar detrital heavy mineral composition, i.e. the major heavy mineral species are the same, suggesting that, given the geological and geographical constraints of the region, they originate from the same source area. As the number of the samples is limited in the usage of cluster analysis, only data of two nearest boreholes have been compared with the composition of the modern fluvial sediments.

PCA is one of the most frequently used multivariate statistical technique (Le Maitre, 1982). The calculated principal component coordinates, when plotted against each other, provide the optimum way of viewing the data, enabling both sample classification and variable interpretation. The principal component coordinates are derived from the principal components. Geometrically, if the set of samples is considered as a cloud of points, the first principal component is an axis through the cloud, along which there is the maximum amount of spread of the samples (the maximum of variance of the data). The second principal component defines the direction of maximum spread at right angles to the first, the third one has the maximum spread at right angles to the first and second, and so on. The principal component coordinates are obtained by projecting the sample points onto the axes representing the principal components. PCA was successfully used in numerical analysis of heavy mineral data by Pirkle et al. (1985), Stattegger (1982) and Ryan et al. 2007 (this volume). In the present study it was performed on all samples and on the same heavy mineral species used in the cluster analysis. The results clearly indicate the heavy mineral species that are the most significant in the differentiation of the sample groups. Plotting the samples in the plane of the two main components, the heavy mineral composition of samples that fall closer to each other have more similarities than those that are farther from them.

5. RESULTS

5.1. Characteristics of Heavy Mineral Suites

Heavy mineral composition of Quaternary sands in the ten study boreholes shows meaningful differences in their average heavy mineral proportions (Table 1). In the western part, in boreholes Ka-3, Ke-3, Kecs-3, Ny-1, K-88 and K-89, garnet is the most frequent component. These sands contain a large amount (about 30–40%) of heavy minerals of metamorphic origin (epidote, zoisite, clinozoisite, chlorite, chloritoid, andalusite, sillimanite, kyanite, staurolite and calcic amphiboles, mostly tremolite, actinolite and antophyllite). Moreover, assuming that the garnet is predominantly from metamorphic rocks the proportion of heavy minerals sourced from

Table 1. Average abundance values of heavy minerals (%) in samples from the study boreholes

Heavy minerals	Kunadacs Ka-3 (7 samples)		Kerekegyház Ke-3 (14 samples)		Kecskemét Kecs-3 (29 samples)		Nyárlőrinc Ny-1 (39 samples)		Csongrád K-89 (81 samples)		Mindszent K-88 (96 samples)		Szarvas SZ-1 (108 samples)		Dévaványa D-1 (43 samples)		Vésztő V-1 (80 samples)		Komádi Ko-1 (59 samples)	
Garnets		36.43		30.29		32.46		15.81		33.94		21.48		17.29		10.38		8.69		21.27
Hornblende	7.43		7.29		7.37		9.19		7.70		8.40		13.90		4.66		19.33		11.26	
Oxyhornblende	2.29	12.66	0.29	10.08	0.43	10.41	0.37	10.94	3.62	16.63	4.71	19.18	8.68	25.13	5.97	11.82	2.06	22.47	0.73	12.39
Other amphiboles	2.94		2.50		2.61		1.38		5.31		6.07		2.55		1.19		1.08		0.40	
Chlorite		3.43		6.21		3.89		13.67		7.99		17.00		15.65		22.61		16.36		12.39
Epidote		15.04		18.43		29.99		1.47		13.78		11.36		7.65		0.74		11.81		9.90
Magnetite-ilmenite		8.60		13.57		8.50		5.05		11.63		4.58		7.91		11.73		9.19		8.54
Orthopyroxene	5.15	6.01	1.46	2.32	1.79	2.06	3.42	7.68	2.33	2.80	4.56	6.14	8.47	10.85	3.34	7.62	3.37	4.63	0.34	0.59
Clinopyroxene	0.86		0.86		0.27		4.26		0.47		1.58		2.38		4.28		1.25		0.25	
Biotite		1.29		0.39		0.07		1.07		0.73		2.48		3.28		4.51		4.25		2.99
Apatite								0.77		0.65		1.55		0.09		1.42		0.01		
Tourmaline		2.43		2.50		1.79		0.77		1.51		1.35		3.36		1.01		2.62		3.02
Rutile		0.29		0.07		0.10		0.02		0.05		0.26		1.08		0.57		0.05		0.25
Clinozoisite		2.01		1.64		1.20		1.57		1.81		0.80		1.00		0.54		0.77		0.31
Kyanite		1.87		2.21		1.72		0.73		2.77		2.12		0.74		0.26		0.56		1.03
Staurolite				0.14		0.03		0.24		0.30		0.15		0.16		0.18				
Zoisite				0.14		0.36		0.19		0.69		0.68		0.23		0.11		0.14		0.02
Topaz																0.07				
Sphene						0.02				0.16		0.14		0.86		0.04		0.11		0.02
Zircon		0.29		0.43		0.04		0.03		0.85		0.45		0.24		0.03		0.31		0.64
Olivine																		0.02		
Piemontite		0.29		0.14		0.07				0.17		0.02		0.01				0.01		0.12
Andalusite										0.01		0.35		0.06						
Chloritoid						0.07				0.47		0.09		0.48						
Spinel														0.02						
Sphalerite														0.02						
Sillimanite										0.09										
Pyrite		0.85		1.93		0.90		0.55		0.70		0.54				3.03		1.76		1.10
Carbonate		0.29		0.14				8.47		0.53		5.95				1.25				0.01
Altered minerals		7.85		9.21		6.27		26.42		2.65		2.59		3.91		22.17		16.24		25.51
Total (%)		99.63		99.89		99.95		100.60		100.91		99.26		100.02		100.09		99.99		100.10

metamorphics reaches up to 60–70%. In samples from boreholes SZ-1, D-1 and V-1 amphibole and/or chlorite are more common, while in the easternmost borehole (Ko-1) the main heavy minerals are garnet, hornblende and chlorite. The amount of altered grains is the highest in boreholes Ny-1, D-1, V-1 and Ko-1.

5.2. Result of Cluster Analysis

Heavy mineral composition of paired nearest boreholes and modern river sediments, evaluated by cluster analysis, are illustrated by dendrograms (Fig. 5). They show that the samples group into two, three or four major clusters, and within these some sub-clusters can be distinguished. The labels of the clusters and sub-clusters (e.g. px-am) indicate which heavy minerals are the most common or most characteristic in the samples forming that particular cluster or sub-cluster. Table 2 shows the most frequent heavy minerals of the clusters and sub-clusters, including the sediments of modern rivers with similar heavy mineral composition. Their transport directions are also indicated. The distribution of different clusters and sub-clusters along the borehole logs can be seen in Figs. 7 and 8 where palaeotransport directions in the study boreholes were plotted on west–east and north–south profiles.

Garnet-rich sands (cluster ''gr'') occur in all boreholes but they are more common in the western part of the study area. Garnet is transported today mainly by the Danube and its tributaries, some of the northerly and eastern rivers (Zagyva, Sebes-Körös and, occasionally, the Tisza, Sajó and Berettyó). Thus, garnet-rich sands can arrive from the northwest and north in the western part of the study area, and also from the northeast in other parts. Pyroxene-rich sands (cluster ''px'' ''px-am'') occur only in the middle part of the study area (in boreholes SZ-1, D-1, V-1, K-88, K-89). The alluvium of the Tisza and most of its tributaries contain abundant pyroxene (transported from northeasterly sources by the Tisza, Szamos and Bodrog, from the north by the Sajó, Hernád and Bódva, and from the southeast by the Fekete-, Fehér-, Hármas-Körös and Maros). The River Ipoly, a tributary of the Danube, carries such detritus from the north. Sands with high hornblende, garnet and pyroxene contents (cluster ''am-gr-px'') are only found in borehole SZ-1. Because the Tisza and two of its tributaries (Bodrog and Bódva) carry similar heavy mineral assemblages, by analogy, the sands in borehole SZ-1 were probably derived from the northeast. Chlorite-rich sediments (cluster ''chl'') are frequently found in the majority of the boreholes, but they are absent in Ka-3, Ke-3 and Kecs-3 in the west. In contrast, modern, chlorite-rich fluvial sands are very rare in the study area. Only small amounts appear in the Tisza and Bodrog, which suggests a northeasterly transport for the chlorite-rich Quaternary sediments. Some of the samples in boreholes D-1, V-1 and Ko-1, in the eastern part of the study area, are characterised by hornblende, epidote and/or garnet suites (clusters ''am-e'', ''e-am'' and ''gr-e-am''). Of today's rivers only the Fekete-Körös carries similar heavy mineral suites, suggesting that these sands were derived from a southeasterly direction. Cluster ''am-px'' is defined by high quantities of hornblende and pyroxene and such composition is typical of the alluvium of the modern Tisza and its tributaries.

Cluster analysis of detrital heavy minerals permitted an almost full differentiation of the sediments of the various palaeo-rivers. Its limitations arise, however, in cases where different rivers carry similar heavy mineral suites. Thus, cluster analysis was

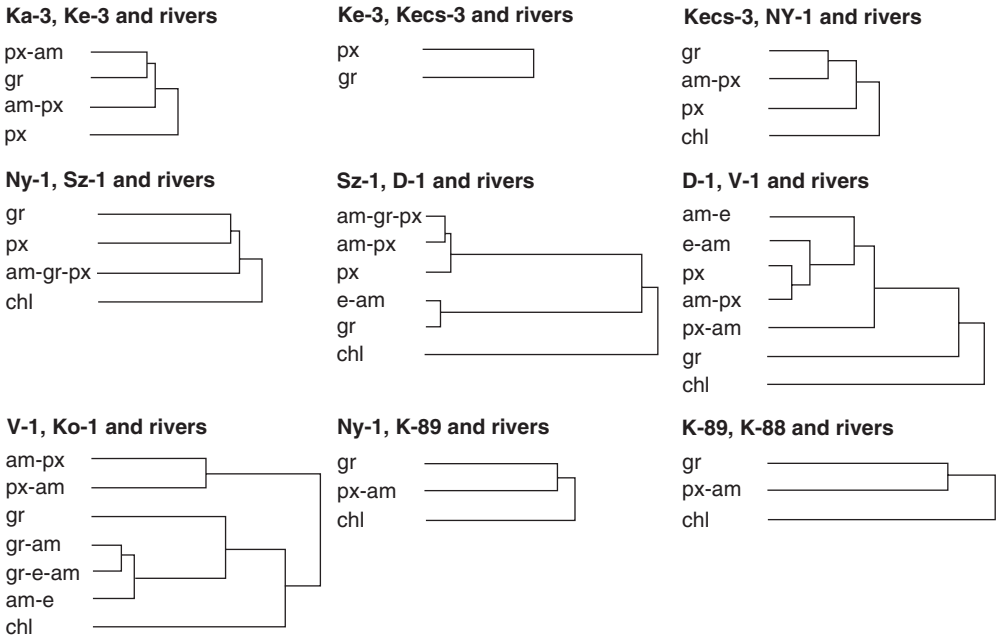

Fig. 5. Dendrograms showing simplified results of cluster analysis (V-1: borehole; am = amphibole; px = pyroxene; gr = garnet; chl = chlorite; e = epidote).

Table 2. Most frequent detrital heavy minerals of the clusters and sub-clusters, with similar heavy mineral suites of modern rivers, and their transport directions

Clusters and sub-clusters	Most frequent detrital heavy minerals of the clusters and sub-clusters	Modern river sediments	Transport directions from
Gr	Garnet + epidote, magnetite, hornblende, pyroxene	Danube*	NW
		Zagyva, Sajó	N
		Berettyó, Sebes-Körös, Tisza	NE
Gr-am	Garnet + hornblende, epidote, chlorite, magnetite	Tisza	NE
Gr-e-am	Garnet, epidote, hornblende, magnetite	Fekete-Körös	SE
Px	Orthopyroxene + clinopyroxene, hornblende	Tisza, Szamos, Bodrog	NE
		Sajó, Bódva, Hernád	N
		Fekete-, Fehér-, Hármas-Körös, Maros	SE
		Ipoly	NW
Px-am	Orthopyroxene + hornblende, epidote, magnetite	Tisza, Szamos, Bodrog	NE
		Bódva, Sajó, Hernád	N
		Fehér-, Fekete-, Hármas-Körös, Maros	SE
Am-px	Hornblende + pyroxene, epidote	Bodrog, Szamos, Tisza (Sajó)	NE
		Fekete-, Fehér-, Hármas-Körös, Maros	SE
Am-gr-px	Hornblende, garnet, pyroxene, chlorite, epidote	Tisza, Bodrog (Bódva)	NE
Chl	Chlorite + hornblende, pyroxene, biotite, magnetite	Tisza, Bodrog	NE
E-am	Epidote + hornblende, magnetite, garnet, chlorite	Fekete-Körös	SE
Am-e	Hornblende + epidote, magnetite, garnet, chlorite	Fekete-Körös	SE

*Danube River and its tributaries without Ipoly River.

not efficient enough to distinguish between the garnet-rich sands of the modern and ancient Danube and some tributaries of Tisza. This problem can be addressed by using another numerical method.

5.3. Results of Principal Component Analysis

Parallel with cluster analysis, PCA was also performed on all samples. Results identified garnet, chlorite, amphibole and pyroxene as the most important heavy minerals in the differentiation between the assemblages of the Danube and Tisza and their tributaries. The first two principal components represent 78% of the total variance, making their plots an acceptable representation of the whole data set (Fig. 6).

In the PCA plots of Fig. 6 the sediments of the modern Danube and its tributaries occupy a well-defined area ($x > -0.5$ and $y < 0.3$), with the exception of the alluvium of the northwesterly Ipoly, while the assemblages of the modern Tisza appear in a different field ($x > -0.5$ and $y > 0.3$). However, the Sebes-Körös, Zagyva, Sajó and some part of the Tisza sediments overlap the field of the "Danube sediment area". Many samples from the central and eastern boreholes (SZ-1, K-89, K-88, D-1, V-1,

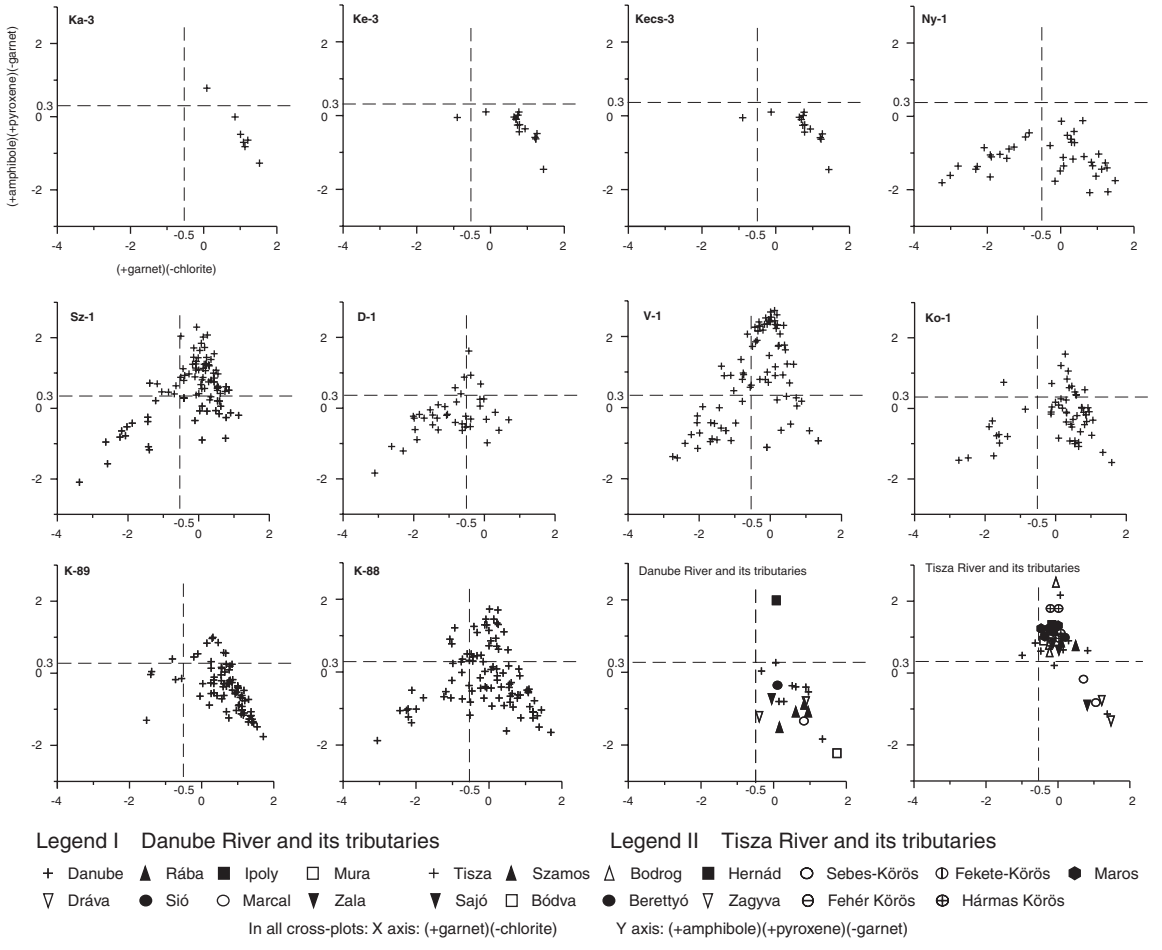

Fig. 6. PCA plots of the samples from the studied boreholes and modern river sediments.

Ko-1) plot in the "Tisza sediment area" ($x > -0.5$ and $y > 0.3$) as was expected, confirming that most of them are the deposits of the Palaeo-Tisza and its tributaries. The majority of borehole samples from the western and central parts of the study area (boreholes Ka-3, Ke-3, Kecs-3, Ny-1, K-89, K-88) appear in the "Danube sediment area" ($x > -0.5$ and $y < 0.3$) and thus define Palaeo-Danube deposits.

Comparison of the heavy mineral compositions of river sediments and borehole samples by PCA is particularly instructive (Fig. 6); the modern river samples cluster on the right side of the plots ($x > -1$), contrasting with the position of the borehole samples that commonly occur on the left ($x < -1$). The latter contains high quantities of chlorite and indicates that the Quaternary rivers carried chlorite-rich sediments, while the modern rivers are almost devoid of them. As mentioned earlier, the chlorite-rich sands were, most probably, derived from the northeast because they occur only in the central and eastern parts of the study area.

PCA clearly indicates that garnet, chlorite, hornblende and pyroxene are the most potential in the differentiation of the various sediment groups. It also suggests their most important numerical relations: hornblende positively correlates with pyroxene, both hornblende and pyroxene negatively correlate with garnet and garnet negatively correlates with chlorite. Composition of axis titles in Fig. 6 reflects these relationships. Results pinpointed three discrete source provinces for the sediments under study: one supplying garnet-rich, the other chlorite-rich detritus and one with high hornblende and pyroxene contents. It is worth mentioning that the well-defined distribution of the chlorite-rich sands indicates that the high chlorite content is not caused by selective sorting during transport and deposition because chlorite is abundant in both the coarse- and fine-grained sediments in the central and eastern areas. Transport directions, deduced from cluster analysis and PCA, complemented by palaeomagnetic, palaeontological and sedimentological data (Kretzoi and Krolopp, 1972; Rónai, 1985; Jámbor, 1998), are indicated in Figs. 7 and 8 where dotted lines show the correlation of sampled intervals in the boreholes.

The limitation of PCA in our study is shown by two examples: (i) Some assemblages from boreholes appear in the "Danube field"; however, their geographic location indicates that that they could not be carried by the Palaeo-Danube. In this case the presence of similar heavy mineral assemblages precludes a complete differentiation of Palaeo-Danube deposits from those of the Palaeo-Tisza and its tributaries. (ii) In the central part of the study area (boreholes K-89, K-88, SZ-1) where the sediments of the Danube and Tisza merged, heavy mineral assemblages share several common signatures (e.g. high garnet content), despite the different geological settings of the rivers catchment areas. Thus, differentiating between their deposits is beyond the capacity of both PCA and cluster analysis.

6. DISCUSSION

When attempting the reconstruction of Quaternary palaeotransport directions using heavy mineral data, we presume that Pleistocene physiography and the geology of potential source areas was comparable to that seen today. Consequently, heavy mineral compositions of modern river sediments, with well-constrained provenance, can be extrapolated to the borehole data. Then, by analogy, palaeocurrent directions

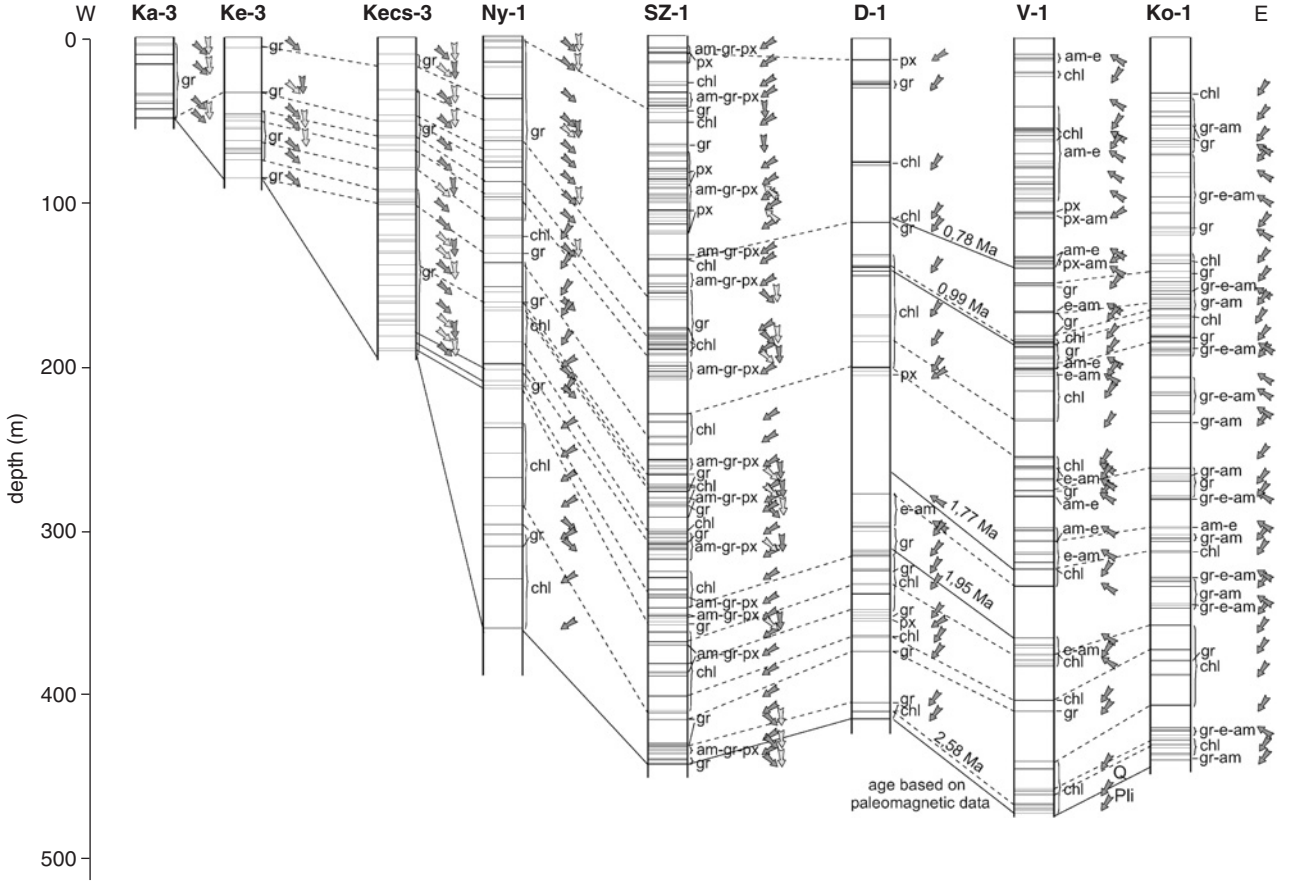

Fig. 7. Clusters and sub-clusters along the boreholes in a W–E section, with sediment transport directions plotted using the results of cluster analysis, PCA and sedimentological analysis (gr = garnet; chl = chlorite; px = pyroxene; am = amphibole; e = epidote; Q = Quaternary; Pli = Pliocene. Darker arrows show the dominant transport directions; dashed lines show correlation).

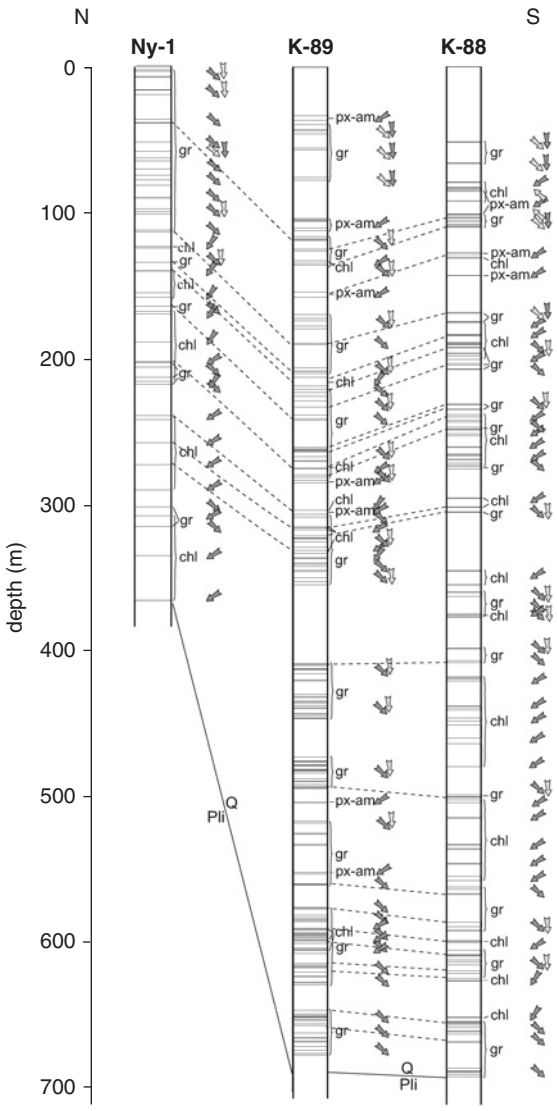

Fig. 8. Clusters and sub-clusters along the boreholes in a N–S section, with sediment transport directions using the results of cluster analysis, PCA and sedimentological analysis (gr = garnet; chl = chlorite; px = pyroxene; am = amphibole; Q = Quaternary; Pli = Pliocene. Darker arrows show the dominant transport directions; dashed lines show correlation).

and the distribution of Pleistocene sediments can be reconstructed by comparison with the modern ones.

Consistent with the lithology of the mountain belt surrounding the Pannonian Basin (Petrescu, 1966; Ianovici et al., 1976; Szepesházy, 1980; Brezsnyánszky, 1989; Fülöp, 1989), the modern Tisza and its tributaries carry pyroxene, hornblende, chlorite and/or garnet to the Hungarian Plain from the northeastern Carpathians, the Apuseni Mountains and the North-Hungarian Range from the northeast, east

and north (Fig. 1). In its catchment area the Tisza and some of its tributaries (Tisza, Szamos, Bodrog, Hernád, Fehér-Körös, Maros) cut through Neogene andesites, rhyolites and tuffs constituting the Inner Carpathian Volcanics. The Sajó and Zagyva drain Upper Miocene–Pliocene basalts in the north, in the east the Fehér-Körös erode Jurassic basalts, and the Fekete-Körös Permian acidic volcanics. Some tributaries of the Tisza (Szamos, Sebes-, Fehér-, Fekete-Körös, Maros) carry sediments from granitoids from the direction of the Apuseni Mountains, and from a variety of metamorphics (Szamos, Zagyva, Berettyó, Bodrog, Hernád, Sajó, Maros and the triple Körös). They also incorporate polycyclic detritus mainly from Neogene and older Quaternary molasse successions, from Cretaceous–Palaeogene flysch (Tisza, Bodrog, Hernád, Sajó, Maros) and from Permian and Mesozoic clastics (triple Körös) but carbonates are subordinate throughout.

Abundant garnet in the modern Danube is derived mainly from the Alps, western Carpathians, Bohemian Massif and the Transdanubian Central Range (Fig. 1). Major lithologies include Precambrian crystalline schists, flysch and molasse, Mesozoic carbonates, Hercynian granites of the Bohemian Massif, older granitoids of the eastern Alps and western Carpathians, Neogene andesites, rhyolites and some basalts of the Inner Carpathian Volcanics, including also minor low-grade metamorphics.

Fundamental differences thus characterise the catchment basins of the two principal rivers: the Tisza and its tributaries drain abundant volcanics, contrasting with those of the largely metamorphic and granitoid complexes of the Danube (Fig. 9). Statistical methods have served as an independent, objective measure for the

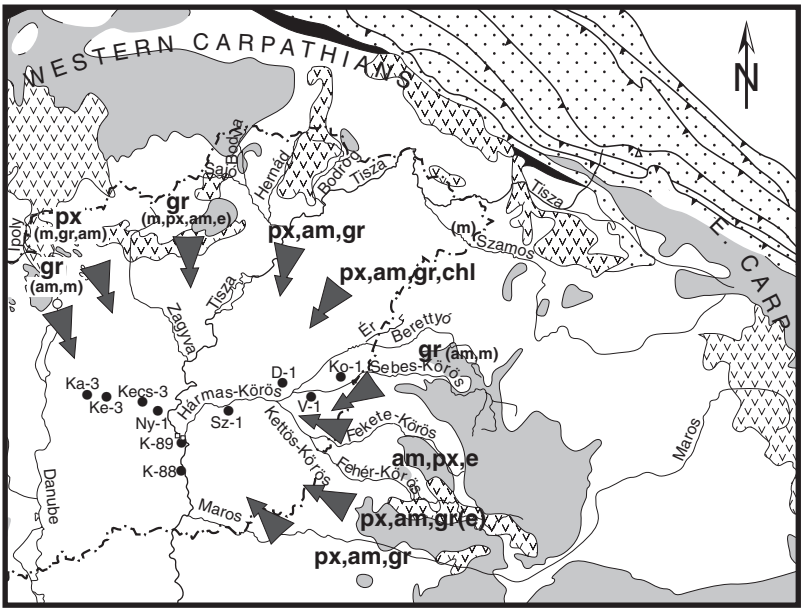

Fig. 9. Transport directions with the main heavy minerals (gr = garnet; chl = chlorite; px = pyroxene; am = amphibole; e = epidote; m = magnetite. Other explanations are in Fig. 1).

characterisation and differentiation of these two sediment groups. Because the Tisza River system also transports metamorphics-derived garnet, but devoid of associated, provenance-diagnostic minerals, statistical methods are not suitable to make distinction between the two garnet-bearing assemblages. Geochemical analysis of the garnets could be potentially useful for identifying the provenance of individual garnet grains and distinguishing between the easterly, northeasterly and westerly derived garnet-rich assemblages.

PCA has also revealed slight differences in the occurrence and proportions of some heavy mineral species between the modern rivers and their ancestors. Most significant is the distribution of the older chlorite-rich sediments that differ considerably from the overlying modern ones, suggesting that the source area underwent some changes, most probably erosional denudation with time.

7. SUMMARY AND CONCLUSION

Heavy mineral data of earlier analyses on modern river sediments and borehole successions from the Mid-Hungarian Plain were treated statistically using PCA and cluster analysis. Known catchment area geology and heavy mineral composition of the modern river sediments were extrapolated to borehole data from which sediment provenance and evolution of the intricate Quaternary palaeodrainage patterns have been reconstructed.

During the first part of the Early Pleistocene, rivers of the Palaeo-Tisza distributary system carried sediments with high chlorite and/or garnet content from metamorphic rocks in the northeastern Carpathians and Apuseni Mountains, situated northeast from the central and eastern parts of the study area (V-1, D-1, SZ-1, Ko-1). Because the Pliocene and Upper Miocene successions in this area are characterised by abundant chlorite and garnet (Thamó-Bozsó and Juhász, 2002) these sands are interpreted as representing a transitional interval between the Early Pleistocene and underlying Pliocene and Upper Miocene (Pannonian) sediments. The areas of boreholes K-89, K-88 and occasionally SZ-1 were drained by the Palaeo-Danube, carrying garnet-rich sands from the crystalline schists of the Alps and western Carpathians to the northwest. By contrast, volcanics, dominating the source areas of the Palaeo-Tisza distributary system to the northeast, furnished hornblende and/or pyroxene-rich detritus to the sites of boreholes SZ-1, K-89, K-88 and D-1. Because these assemblages are similar to those in the alluvium of the modern Tisza and its northern tributaries their appearance in the subsurface sequences signals the active erosion of the volcanics of the Inner Carpathians.

Pleistocene sands with garnet and/or epidote-amphibole suites in boreholes Ko-1, V-1 and D-1 are similar to those of the Fekete-Körös that transports detritus from the metamorphics of the Apuseni Mountains and older sedimentary rocks, and from Neogene volcanics from the southeast. Heavy mineral signatures indicate that the southeasterly derived sediments reached the area of boreholes Ko-1 and V-1, situated closer to the Apuseni Mountains, earlier than those in borehole D-1. Deposition at the former sites persisted only for a short period, reflecting a change from the earlier transverse drainage, parallel to the Apuseni Mountains, to a subsequent axial fluvial system as a response to a switch from the active tectonic uplift of

the Apuseni Mountains to isostatic uplift (Thamó-Bozsó et al., 2002). In the central part of the study area (boreholes K-89, K-88 and NY-1), Early Pleistocene sands with either high garnet or chlorite content interfinger and represent deposits of a complicated radial network flowing from the northwest, north and northeast. Sands in borehole D-1 are dominated by chlorite and occasionally pyroxene or garnet, defining transport from the northeast.

During the Middle and Late Pleistocene, sands characterised by abundant pyroxene, hornblende or chlorite in the central part of the study area (in boreholes K-88, K-89, SZ-1) indicate transport from the northeast, while the garnet-rich sediments here originate, most probably, from the north carried by the Palaeo-Zagyva. Meanwhile the Palaeo-Danube and/or subordinate Palaeo-Zagyva brought garnet-enriched sediments to the western part of the study area (boreholes Ka-3, Ke-3, Kecs-3, NY-1). These successions contain intervals of wind-blown sand with Danube characteristics, representing the aeolian reworking of Palaeo-Danube sediments during dry periods. The position and thickness of the Palaeo-Danube sediments with abundant garnet in these locations indicate that the Palaeo-Danube gradually reached its present course (i.e. the N–S direction) by that time.

Cluster analysis of heavy mineral data proved useful for the reconstruction of sediment transport directions but it failed differentiating positively the garnet-rich sediments of the different rivers. PCA resulted in the clear differentiation of the garnet-bearing sediments of the Danube and Tisza but uncertainties remained with the older sands due probably to changing source areas and/or intermixing the sediments of different palaeo-rivers with time. The results of PCA also highlighted some differences in the heavy mineral composition of modern river sands and those deposited by their ancestors, suggesting that the source regions have been affected by tectonic and erosional changes during the Quaternary. The best example for such changes is the distribution of chlorite. Chlorite is abundant in the Early Quaternary sands in the central and eastern parts of the study area, but is less common in the Late Quaternary deposits, appearing only in minor amounts in the modern rivers. This is interpreted by the progressive erosion of the low-grade parent rocks during the Pleistocene.

Both PCA and cluster analysis identified garnet, chlorite, hornblende and pyroxene as the most significant species in the differentiation of the analysed Quaternary sands. Metamorphics-derived garnets, contrasting with volcanogenic hornblende and pyroxenes, were eroded from discrete, lithologically different source provinces and were transported from opposing directions. Mapping the temporal and lateral shifting of genetically linked, provenance-diagnostic heavy mineral suites proved to be a powerful tool for the reconstruction of the intricate drainage network of the Mid-Hungarian Plain and its evolution from the Early Quaternary to present.

ACKNOWLEDGEMENTS

This research was funded by the Hungarian National Science Research Fund (OTKA T-32956 and T-46307). Help from Annamária Nádor and the reviews by Áron Jámbor and Béla Molnár and their valuable suggestions are gratefully acknowledged. We thank the editors, Maria A. Mange and David T. Wright for their

constructive criticism and correction of our English, and especially Maria A. Mange for her help in editing the text and figures for publication.

REFERENCES

Balogh, K., Hajdú-Molnár, K., 1991. Sands and sandstones. In: Balogh, K. (Ed.), Sedimentology II. (in Hungarian). Akadémiai Kiadó, Budapest, pp. 102–157.

Borsy, Z., 1989. Quaternary evolution of the alluvial fans of the Great Hungarian Plain (in Hungarian). Földrajzi Értesítő 38, 211–224.

Borsy, Z., 1992. Evolution of the alluvial fans of the Alföld. In: Rachocki, A.H., Church, M. (Eds.), Alluvial Fans: A Field Approach. Wiley, New York, pp. 229–246.

Borsy, Z., Félegyházi, E., Csongor, É., 1989. The development of the Bodrogköz and its fluvial network (in Hungarian). Alföldi Tanulmányok 13, 65–82.

Brezsnyánszky, K., 1989. Orogenic structures of Hungary and its environs 1: 2000000. Geological Institute of Hungary, Budapest.

Bulla, B., 1953. The evolution of the Great Hungarian Plain (in Hungarian). Alföld Congress, Hungarian Academy of Sciences, Geological Committee, pp. 59–67.

Cooke, H.B.S., Hall, J.M., Rónai, A., 1979. Paleomagnetic, sedimentary and climatic records from boreholes at Dévaványa and Vésztő, Hungary. Acta Geologica Academiae Scientiarum Hungaricae 22, 89–109.

Csánk, E., 1969. Mineralogical and petrological analysis of the Oligocene sediments of the Dorog Basin (in Hungarian). Annual Report of the Hungarian Geological Institute from 1967, pp. 83–133.

Csontos, L., Nagymarosy, A., 1999. Late Miocene inversion versus extension in the Pannonian Basin. Abstracts of the 4th Workshop on Alpine Geological Studies, Tübingen, Geowissenschaftlichte Arbeiten, Ser. A 52, 132.

Davis, J.C., 1986. Statistics and Data Analysis in Geology. Wiley, New York, 646pp.

Elek, I., 1979. Micromineralogical examination of rocks sampled by perspective exploration drillings of Kunadacs Ka-3, Kerekegyháza Ke-3 and Kecskemét Kecs-3 (in Hungarian). Annual Report of the Hungarian Geological Institute from 1977, pp. 113–120.

Elek, I., 1980a. Micromineralogical logging of borehole Vésztő V-1 (in Hungarian). Annual Report of the Hungarian Geological Institute from 1978, pp. 167–172.

Elek, I., 1980b. Summary evaluation of the results of micromineralogical analysis of Kunadacs, Kerekegyház, Kecskemét, Nyárlőrinc, Csongrád, Szarvas, Dévaványa, Vésztő and Komádi boreholes (in Hungarian). Manuscript, National Geological and Geophysical Archive, Budapest.

Franyó, F., 1992. Map of bottom depth of Quaternary strata in Hungary, 1:200 000 (in Hungarian). Manuscript, National Geological and Geophysical Archive, Budapest.

Fülöp, J., 1989. Introduction into the geology of Hungary (in Hungarian). Akadémiai Kiadó, Budapest, 246pp.

Gábris, Gy., 1994. Pleistocene evolution of the Danube in the Carpathian Basin. Terra Nova 6, 495–501.

Gedeon-Rajetzky, M., 1971. Post-Pannonian evolution of the area between Badacsony and Szigliget based on micromineralogical analysis (in Hungarian). Annual Report of the Hungarian Geological Institute from 1969, pp. 353–371.

Gedeon-Rajetzky, M., 1973a. Micromineralogical analysis of materials from exploratory drilling at Mindszent and Csongrád: determination of paleotransport directions (in Hungarian). Annual Report of the Hungarian Geological Institute of 1971, pp. 169–184.

Gedeon-Rajetzky, M., 1973b. Evaluation of the micromineralogical spectra of ancient fluvial sediments based on the analysis of Recent detritus (in Hungarian). Bulletin of the Hungarian Geological Society (Földtani Közlöny) 103, 285–293.

Gedeon-Rajetzky, M., 1976a. Contribution to the knowledge of the northern Great Hungarian Plain (in Hungarian). Annual Report of the Hungarian Geological Institute from 1973, pp. 181–194.

Gedeon-Rajetzky, M., 1976b. Micromineralogical characterization of Late Pliocene and Quaternary depositional cycles in the Szarvas-1 borehole (in Hungarian). Annual Report of the Hungarian Geological Institute from 1974, pp. 171–183.

Gheith, A., 1982. Mineralogical and geochemical variations in relation to sedimentation rates in the Hungarian Basin. Acta Geologica Hungarica 25, 365–393.

Hermann, M., 1954. Micromineralogy of the Pannonian sands from the foreland of the Bükk Mountains, eastern Hungary (in Hungarian). Bulletin of the Hungarian Geological Society (Földtani Közlöny) 84, 338–348.

Horváth, F., Cloetingh, S., 1996. Stress induced late-stage subsidence anomalies in the Pannonian Basin. In: Cloetingh, S., Ben Avraham, Z., Sassi, W., Horváth, F. (Eds.), Dynamics of extensional basins and inversion tectonics, vol. 266. Tectonophysics, pp. 287–300.

Horváth, F., Tari, G., 1999. IBS Pannonian Basin project: a review of the main results and their bearings on hydrocarbon exploration. In: Durand, B., Jolivet, L., Horváth, F., Sérrane, M. (Eds.), The Mediterranean Basins: Tertiary Extension within the Alpine Orogen. In: Geological Society of London, Special Publications, vol. 156, pp. 195–213.

Ianovici, V., Borcos, M., Bleahú, M., Patrulius, D., Lupu, M., Dimitrescu, R., Savu, H., 1976. Geologia Muntilor Apuseni. Academia Romania, Bucuresti, 631pp.

Ibbeken, H., Schleyer, R., 1991. Source and Sediment. A Case Study of Provenance and Mass Balance at an Active Plate Margin (Calabria, Southern Italy). Springer, Berlin, 286pp.

Jámbor, Á., 1998. A review of the stratigraphy of the Hungarian Quaternary (in Hungarian). In: Bérczi, I., Jámbor, Á. (Eds.), Stratigraphy of geological successions in Hungary. MOL Rt. and MÁFI, Budapest, pp. 495–517.

Juhász, Gy., 1994. Comparision of sedimentary sequences in the Late Neogene subbasins in the Pannonian Basin, Hungary (in Hungarian). Bulletin of the Hungarian Geological Society (Földtani Közlöny) 124, 341–365.

Kretzoi, M., Krolopp, E., 1972. Stratigraphy of Late Neogene and Quaternary in the Hungarian Plain based on paleontological data (in Hungarian). Földrajzi Értesítő 21, 133–158.

Kuti, L., Molnár, P., Elek, I., Vermes, J., Sallay, M., Gyuricza, Gy., 1987. Investigation of the Recent and fossil placer deposits in Hungary (in Hungarian). Manuscript, National Geological and Geophysical Archive, Budapest.

Le Maitre, R.W., 1982. Numerical Petrology: Developments in Petrology, vol. 8. Elsevier, Amsterdam, 281pp.

Lengyel, E., 1930. Mineralogical composition of different sands from the Hungarian Plain (in Hungarian). Bulletin of the Hungarian Geological Society (Földtani Közlöny) 60, 67–75.

Melczer, G., 1913. About the sands from the bottom layers of Lake Balaton (in Hungarian). Manuscript, National Geological and Geophysical Archive, Budapest.

Miháltz, I., 1937. Separation of minerals with different densities (in Hungarian). Bulletin of the Hungarian Geological Society (Földtani Közlöny) 67, 257–270.

Mike, K., 1991. The palaeoriver network of Hungary and the history of modern rivers (in Hungarian). AQUA kiadó, Budapest, 698pp.

Molnár, B., 1963. Sedimentgeologische Untersuchungen in pliozän und pleistozän Ablagerungen in Osten des Ungarischen Tiefebene. Geologische Rundschau 53, 848–866.

Molnár, B., 1964. Heavy mineral analysis of the sandy sediments of Hungarian rivers (in Hungarian). Hidrológiai Közlöny 44, 347–355.

Molnár, B., 1965. Lithologic and geologic study of the Quaternary deposits of the Great Hungarian Plain (Alföld). Acta Geologica Hungarica 9, 57–63.
Molnár, B., 1967. Evolution of Pleistocene strata on the South-Hungarian Plain and their hydrogeological relevance (in Hungarian). Hidrológiai Közlöny 47, 537–552.
Molnár, B., 1971. Application of micromineralogical analysis in geological research (in Hungarian). In: New results in sedimentary petrography, Geological Society of Hungary (Magyarhoni Földtani Társulat), Budapest, pp. 123–176.
Molnár, B., 1976. Results of micromineralogical and grain shape analysis of the Nyárlőrinc borehole (in Hungarian). Manuscript, National Geological and Geophysical Archive, Budapest.
Molnár, B., 1980. Changes of source areas as reflected by the depression of the Körös Rivers. Acta Universitatis Szegediensis, Acta Mineralogica-Petrographica 24, 339–353.
Molnár, B., 1981. Sedimentology I. Manuscript, József Attila University, Szeged, 291pp.
Molnár, B., 1997. The geological makeup and evolution of the Great Hungarian Plain. In: Hydro-Petro-Geology and Hungary, Geological Society of Hungary (Magyarhoni Földtani Társulat), Manuscript, Budapest, pp. 1–57.
Molnár, P., Gyuricza, Gy., Thamó-Bozsó, E., 1990. Progress Report on the program Investigation of Recent and fossil placer deposits in Hungary in 1989 (in Hungarian). Manuscript, National Geological and Geophysical Archive, Budapest.
Molnár, P., Thamó-Bozsó, E., Gyuricza, Gy., 1989. Progress Report on the program Investigation of Recent and fossil placer deposits in Hungary in 1988 (in Hungarian). Manuscript, National Geological and Geophysical Archive, Budapest.
Nádor, A., Lantos, M., Tóth-Makk, Á., Thamó-Bozsó, E., 2003. Milankovitch-scale multiproxy records from fluvial sediments of the last 2.6 Ma, Pannonian Basin, Hungary. Quaternary Science Reviews 22, 2157–2175.
Neppel, F., Somogyi, S., Domokos, M., 1999. Palaeogeography of the Danube and its catchment. A hydrographic monograph, vol. 5. Water Resources Research Plc. (VITUKI), Budapest, 62pp.
Ó.Kovács, L., 1986. Cluster analysis procedures for a TPA/L computer (in Hungarian). Annual Report of the Hungarian Geological Institute from 1985, pp. 571–582.
Pécsi, M., 1959. Evolution and morphology of the Danube Valley in Hungary (in Hungarian). Akadémiai Kiadó, Budapest, 346pp.
Petrescu, I., 1966. Romania harta geologica 1:1000000. Institutul Geologic al României, Bucuresti.
Pirkle, F.L., Pirkle, E.C., Pirkle, W.A., Dicks, S.E., 1985. Evaluation through correlation and principal component analyses of delta origin for the Hawthorne and Citronelle sediments of peninsular Florida. Journal of Geology 93, 493–501.
Radócz-Komáromy, E., 1971. Micromineralogical investigations of Eocene rocks in the Northern Bakony Mountain (in Hungarian). Annual Report of the Hungarian Geological Institute from 1969, pp. 133–139.
Ravasz-Baranyai, L., 1962. Petrological analysis of the Ellend-1 geological key borehole. Annual Report of the Hungarian Geological Institute from 1959, pp. 439–461.
Rónai, A., 1985. The Quaternary of the Great Hungarian Plain (in Hungarian). Geologica Hungarica, series Geologica 21, 446pp.
Ryan, P.D., Mange, M.A., Dewey, J.F.D., 2007. Statistical analysis of high resolution heavy mineral stratigraphic data from the Ordovician of western Ireland and its tectonic consequences. In: Mange, M., Wright, D.K. (Eds.), Heavy Minerals in Use. Developments in Sedimentology (this volume).
Sallay, M., 1984. Micromineralogical data of Neogene and Quaternary sedimentary rocks in Hungary I–IV (in Hungarian). Manuscript, National Geological and Geophysical Archive, Budapest.

Schafarzik, F., 1918. Paleohydrogeography of the Danube at Budapest (in Hungarian). Bulletin of the Hungarian Geological Society (Földtani Közlöny) 48, 184–200.

Scherf, E., 1935. Geology and geomorphology of Pleistocene and Holocene successions of the Hungarian Plain and their role in soil development (in Hungarian). Annual Report of the Hungarian Geological Institute from 1925–28, pp. 265–301.

Somogyi, S., 1961. Outline of the evolution of the river network in Hungary (in Hungarian). Földrajzi Közlöny 85, 25–50.

Stattegger, K., 1982. Schwermineraluntersuchungen in der östlichen Grauwackenzone (Steiermark/Oesterreich) und deren statistische Auswertung. Verhandlungen der Geologischen Bundesanstalt 2, 107–122.

Sümeghy, J., 1944. Tiszántúl. Geological Description of the Hungarian Regions VI (in Hungarian). Magyar Királyi Földtani Intézet, Budapest, 208pp.

Sümeghy, J., 1951. Some geological aspects of the regulation of the Tisza River (in Hungarian). Annual Report of the Hungarian Geological Institute from 1945–47, pp. 31–35.

Sümeghy, J., 1955. A review of the Hungarian Pleistocene (in Hungarian). Annual Report of the Hungarian Geological Institute from 1953 2, 395–403.

Szabó, P., 1955. Origin of the Late Pleistocene sandy strata on the Duna-Tisza Interfluve, based on their mineralogical composition (in Hungarian). Bulletin of the Hungarian Geological Society (Földtani Közlöny) 85, 442–456.

Szabó, D., 1967. Summary report and apprisal of the exploratory phase of the Biharkeresztes-Ártánd gravel research (in Hungarian). Manuscript, National Geological and Geophysical Archive, Budapest.

Szepesházy, K., 1980. Major tectonics of the Trans-Tisza Region as related to the Transylvanian Central Mountains (Muntii Apuseni) (in Hungarian). Annual Report of the Hungarian Geological Institute from 1978, pp. 173–186.

Sztrókay, K., 1935. Sedimentary petrography of Pontian sands in the Zala Valley (in Hungarian). Földtani Közlöny 65, 281–291.

Thamó-Bozsó, E., Juhász, Gy., 2002. Mineral composition of Upper-Miocene-Pliocene (Pannonian s. l.) sands and sandstones in the different sedimentary subbasins in Hungary. Geologica Carpathica, vol. 53, Special issue: XVIIth Congress of the Carpathian-Balkan Geological Association, CD-ROM.

Thamó-Bozsó, E., Kercsmár, Zs., Nádor, A., 2002. Tectonic control on changes in sediment supply on Quaternary alluvial systems, Körös sub-basin, SE Hungary. In: Jones, S.J., Frosrick, L.E. (Eds.), Sediment Flux to Basin: Causes, Controls and Consequences. In: Geological Society of London, Special Publications, vol. 191, pp. 37–53.

Treitz, P., 1903. Agrogeological description of the Duna-Tisza Interfluve (in Hungarian). Bulletin of the Hungarian Geological Society (Földtani Közlöny) 33, 297–316.

Urbancsek, J., 1960. Specific water output of the artesian wells on the Hungarian Plain and hydrogeological and paleogeographical conclusions drawn from them (in Hungarian). Hidrológiai Közlöny 40, 398–403.

Vendel, M., 1959. Methods in rock determination (in Hungarian). Akadémiai kiadó, Budapest, 754pp.

Vendl, A., 1910. Data to the knowledge of the sand of the Danube (in Hungarian). Manuscript, National Geological and Geophysical Archive, Budapest.

Wallacher, L., 1989. Sedimentary rocks and their rock forming minerals (in Hungarian). Manuscript, University of Miskolc, Faculty of Earth Sciences and Engineering (Bányamérnöki Kar), Budapest, 816pp.

PART II: PROVENANCE, TRANSPORT, DEPOSITION, EXHUMATION

2.1 Regional Studies—Modern and Ancient Environments

This page intentionally left blank

Chapter 20

HEAVY MINERAL CONCENTRATION IN MODERN SANDS: IMPLICATIONS FOR PROVENANCE INTERPRETATION

EDUARDO GARZANTI AND SERGIO ANDÒ

Laboratorio di Petrografia del Sedimentario, Dipartimento di Scienze Geologiche e Geotecnologie, Università di Milano-Bicocca, Piazza della Scienza 4, 20126 Milano, Italy

ABSTRACT

Heavy mineral concentration in sediments depends primarily on the chemistry and tectono-stratigraphic level of rocks eroded within continental-block, arc, or orogenic source terranes. Detritus derived from mantle peridotites and lower crustal gabbros, as well as from high-pressure (oceanic or continental eclogite) and high-temperature (amphibolite, granulite) metamorphic rocks contains one to two orders of magnitude more heavy minerals than detritus derived from upper crustal rocks including granites and sedimentary successions.

Concentrated heavy mineral assemblages, however, may result from density-sorting during erosion, transport, or deposition by tractive currents, which can very effectively segregate minerals with even small differences in density within distinct grain-size fractions and sedimentary environments (e.g., fluvial channel versus overbank, beach versus shelf). Conversely, depleted heavy mineral assemblages may result from severe diagenetic dissolution in ancient sandstones, a process that in Alpine and Himalayan foreland basins very extensively affected clastic wedges older than the Pleistocene.

Through a series of key modern examples from various geodynamic settings in arid to semi-arid climate, we stress the importance of giving full consideration to heavy mineral concentration while interpreting provenance of terrigenous sediments and sedimentary rocks. The concentration parameters introduced herein (Heavy Mineral Concentration index, Source Rock Density index), coupled with parameters based on heavy mineral species with either contrasting density (% opaque, % ultradense, % ZR) or chemical stability, allow us to reveal and quantify also the effects of hydraulic sorting in the depositional environment and of diagenetic dissolution in ancient terrigenous rocks. We document that in most modern sands, the relative abundance of chemically stable species (e.g., zircon, tourmaline, rutile, apatite, chrome spinel) is considerably less than the experience on ancient sandstones generally induces to believe, and show that the actualistic approach provides crucial insight for a correct interpretation of heavy mineral suites.

Developments in Sedimentology, Vol. 58, 517–545

ISSN: 0070-4571/doi:10.1016/S0070-4571(07)58020-9

Keywords: heavy minerals; oceanic lithosphere; arc crust; continental crust; orogens; diagenesis; hydraulic sorting; grain size.

1. INTRODUCTION

The concentration of heavy mineral grains in sand-sized terrigenous sediments may fluctuate considerably because of several factors, including provenance, sedimentary processes, and post-depositional dissolution (Mange and Maurer, 1992; Morton and Hallsworth, 1999). In modern beaches and deltaic cusps, for instance, their concentration is commonly observed to increase by an order of magnitude or more because of selective removal of lighter grains by wave erosion (Komar and Wang, 1984; Hughes et al., 2000). Conversely, in ancient sandstones it may be depleted by an order of magnitude or more because of selective leaching of unstable species during diagenesis (Gazzi, 1965; Morton, 1985). Such complex effects can modify both the original amount and spectrum of heavy mineral species conspicuously, and thus make provenance diagnoses difficult and uncertain, particularly for ancient clastic wedges.

The aim of the present contribution, which is based on a large set of data collected from modern sands in a variety of geodynamic settings, is to show how—in the absence of significant mechanical or chemical breakdown during transport, of hydraulic sorting during transport and deposition, and of dissolution during diagenesis—the overall percentage (and not just the spectrum) of heavy minerals found in a sedimentary deposit mirrors primarily the lithology of parent rocks, and specifically their composition, average density, and tectono-stratigraphic level. The concentration of heavy minerals (as well as their spectrum) is therefore *by itself* a crucial element that must be fully considered in provenance interpretations, and specifically while estimating sedimentary budgets from the integration of mineralogical and petrographic data. This contribution also shows how positive or negative anomalies in heavy mineral concentration can be related to hydraulic sorting or diagenetic dissolution, respectively.

2. HEAVY MINERAL CONCENTRATION IN SOURCE ROCKS

Sedimentary to very low-grade metasedimentary rocks and felsic plutonic rocks (e.g., sandstone, metasandstone, granite), which characterise upper tectono-stratigraphic levels of the Earth's crust, have relatively low density ($\delta \leqslant 2.70\,g/cm^3$; Daly et al., 1966). As a consequence they contain, and therefore can provide, only few heavy minerals.

By contrast, ultramafic and mafic igneous rocks (peridotite, gabbro), or high-temperature to high-pressure (amphibolite, granulite, eclogite) metamorphic rocks, that make up deeper tectono-stratigraphic levels of the lithosphere, are much denser ($\delta = 2.80$–$3.45\,g/cm^3$), and therefore include and can supply a wealth of heavy minerals (e.g., pyroxenes, amphiboles, garnet). Their contribution in heavy minerals will be, as a consequence, typically much more significant than the areal percentage

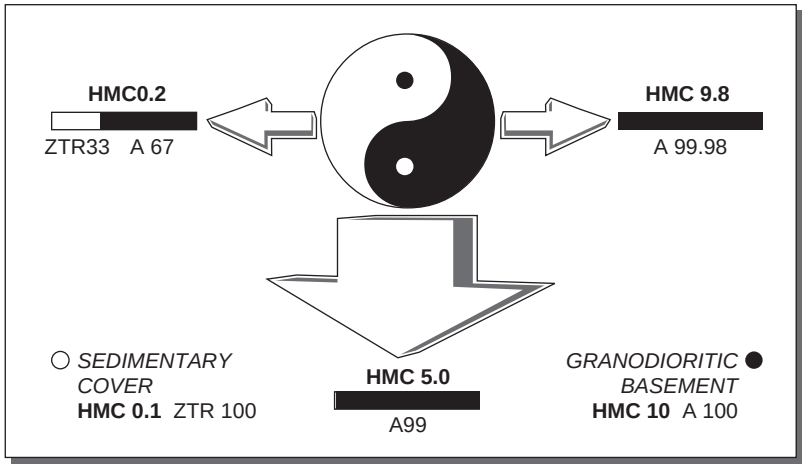

Fig. 1. Asymmetric effect of a two-order-of-magnitude difference in heavy mineral concentration in detritus from basement and cover rocks. Granodioritic batholiths (dark yin) supply dominant amphiboles (HMC 10; A 100), whereas sedimentary successions (bright yang) only supply few recycled ultrastable minerals (HMC 0.1; ZTR 100). Where cover strata are widespread (left side of the T'ai-chi T'u; e.g., "Undissected Craton subprovenance"), even a small basement high (black seed, representing 2% in outcrop area) is readily revealed by a low heavy mineral yield and an amphibole-rich assemblage. Instead, where basement is widespread (right side of the T'ai-chi T'u; e.g., "Dissected Craton subprovenance"), locally preserved sedimentary strata (white seed, representing 2% in outcrop area) have an insignificant dilution effect on the heavy mineral assemblage. Even in the intermediate case (whole of the T'ai-chi T'u; e.g., "Transitional Craton subprovenance"), the main effect of sedimentary covers (50% of outcrop area) is to halve the concentration of amphibole-dominated heavy mineral assemblages.

of their outcrops. In other words, wherever exposed they will impose their diagnostic mark on detrital heavy mineral suites. At the same time, the heavy mineral concentration in the derived sediments will increase (Fig. 1).

3. HEAVY MINERAL-RICH AND HEAVY MINERAL-POOR SEDIMENTS

The concentration of heavy minerals in sediments produced in various tectonic settings displays variations of up to two orders of magnitude, in close relationship with chemical composition and density of source rocks. This fact is usually given scarce consideration in provenance studies, even though it represents a fundamental aspect, which does not only provide crucial information for provenance diagnosis (e.g., heavy mineral-rich deposits are by themselves diagnostic of specific sources) but also helps us to avoid gross mistakes.

Heavy mineral-poor and heavy mineral-rich suites with the same mineralogical spectrum do not necessarily have the same meaning. A good example is provided by dune sands of Arabian deserts which, close to basement or ophiolitic outcrops, may be characterised by amphibole- or pyroxene-dominated assemblages, respectively (McClure, 1984, p. 102; El-Sayed, 1999). Heavy mineral concentration, however,

remains very low, indicating trivial bulk-sediment contribution from local heavy mineral-rich sources. Petrographic data testify in fact to long-distance transport and fundamentally polycyclic origin of quartzose desert sand (Garzanti et al., 2003).

The distortive effect related to the different potential of various lithotypes to generate sand-sized detritus must always be taken into full account in provenance diagnoses (Palomares and Arribas, 1993). This is particularly true for heavy mineral suites that tend to document aberrantly a limited number of sources (e.g., ultramafic and mafic igneous and metamorphic rocks), while several others are barely recorded (limestone, chert, shale, granite).

4. DATA BASE AND ANALYTICAL TECHNIQUES

Mineralogical data considered in the present contribution, unless differently specified, are derived from a series of case studies made by the authors and co-workers on modern Mediterranean, Arabian, and Himalayan sands (Fig. 2). In these largely semiarid to hyperarid climatic conditions, chemical weathering is negligible and detrital signatures can thus be held as primary and used as a reference for

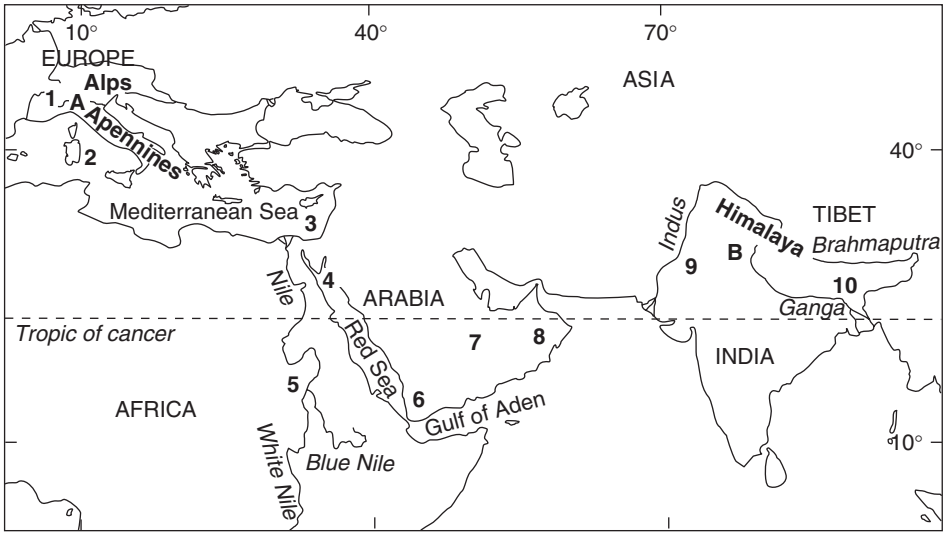

Fig. 2. Alpine, Mediterranean, Middle East, and Himalayan key regions revisited for the present work. The reader may refer to the modern and ancient case studies listed below for detailed information on geology of source terranes and analytical data. (1) Western, Central, and Southern Alps (Garzanti et al., 2004a, 2006a); (2) Apennines and Tyrrhenian Sea (Garzanti et al., 1998, 2002a); (3) Troodos and Kizildag ophiolites (Garzanti et al., 2000); (4) Levant margin and Northern Red Sea (unpublished data); (5) Nile River system (Garzanti et al., 2006b); (6) Southern Red Sea and Gulf of Aden (Garzanti et al., 2001); (7) Arabian deserts (Garzanti et al., 2003); (8) Sama'il and Masirah ophiolites (Garzanti et al., 2002b); (9) Indus River system (Garzanti et al., 2005); (10) Brahmaputra River system (Garzanti et al., 2004b). (A) Alpine foreland basin (Muttoni et al., 2003); (B) Himalayan foreland basin (Najman and Garzanti, 2000; White et al., 2002; Najman et al., 2003a, 2003b; Szulc et al., 2006).

provenance interpretation of ancient clastic suites deposited in comparable geodynamic settings. We give here specific attention to sediment samples from small streams draining single tectono-stratigraphic units, and not only to sediments of large rivers, beaches, and sand seas derived from composite source terranes (''1st versus 3rd order sampling scales'' of Ingersoll, 1990).

All of the analyses were carried out using the same analytical methods. For each sand or sandstone sample, 200–250 transparent heavy minerals were counted in grain mounts, according to the ''ribbon-counting'' or ''Fleet'' methods (Mange and Maurer, 1992). Heavy minerals were concentrated with sodium metatungstate (density 2.90 g/cm^3), using the 4–2 ϕ (63–250 μm) size fraction, treated with acetic and oxalic acids to eliminate carbonates and iron oxides, respectively (Parfenoff et al., 1970). Treatment in acetic acid was prolonged for 24 h only. This time is generally sufficient to eliminate only a fifth to half of the carbonate fraction, depending on several factors including the abundance of calcite and dolomite, and the amount and grain size of the treated material. Point-bar and levee deposits of Nile sediments from Ethiopia and Sudan were dry-sieved and split in grain-size subclasses at 0.5 ϕ intervals; each grain-size subclass was point-counted separately (Garzanti et al., 2006b).

5. PARAMETERS

In this section, we introduce a few parameters by which heavy mineral concentration in sediments and sedimentary rocks can be expressed quantitatively and related with average density of source rocks. We also define a set of simple ratio parameters, based on heavy mineral species with highest density or chemical stability, which are helpful in detecting anomalies of concentration parameters caused by either hydraulic sorting or diagenetic dissolution.

5.1. The HMC Index

The ''Heavy Mineral Concentration index'' (HMC) defines the abundance of heavy minerals (transparent, opaque, and unidentifiable turbid grains denser than 2.90 g/cm^3) contained in the 4–2 ϕ (very-fine to fine sand-size) fraction of terrigenous extrabasinal loose sediment or lithified sedimentary rock.

The weight percentage of total grains denser than ~2.9 g/cm^3 obtained by separation in sodium metatungstate is first converted into frequency percentage (H%), the correction factor being the ratio between the weighted average densities of total framework grains (Δ_{TOT}) and of total dense grains (Δ_H):

$$H\% = \left(\frac{W_H}{W_{TOT}}\right)\left(\frac{\Delta_{TOT}}{\Delta_H}\right)$$

where W_H is the weight of total grains denser than ~2.9 g/cm^3 and W_{TOT} the weight of the total sediment fraction considered. Simplifications used to calculate Δ_H are discussed below (Section 5.3); supplementary petrographic data are needed to calculate Δ_{TOT} with satisfactory approximation.

Next, two corrections must be made to calculate the HMC index. First, several dense grains are not considered as heavy minerals proper, even though they sink in a dense liquid (2.90 g/cm^3). These include phyllosilicates (chlorite, biotite), carbonates (mesitite), "light" minerals intergrown with oxides (e.g., quartz-opaque or serpentine-magnetite aggregates), and detrital grains of artificial origin locally found in modern sands (e.g., corundum and moissanite, used as industrial abrasives). Their relative abundance is thus subtracted:

$$\mathrm{HM}\% = H\% \times \left(1 - \frac{s}{h}\right)$$

where s is the total "spurious" grains counted in grain mounts, and h the total grains counted in grain mounts.

The second correction, which again requires supplementary petrographic data, is needed whenever the analysed sediment or sedimentary rock contains significant amounts of intrabasinal (e.g., bioclasts, ooids, mudclasts, glaucony) or authigenic components (e.g., quartzose cement, calcite), which dilute the original heavy mineral concentration. The HMC index is thus calculated as:

$$\mathrm{HMC} = \frac{\mathrm{HM}\%}{(1 - d/t)} \times 100$$

where d is the total diluting allochemical and orthochemical components determined by point-counting in thin section, and t the total components determined by point-counting in thin sections. In compiling data for ancient clastic units from the literature, where no detailed petrographic information was reported, we assumed $d/t = 0.25$ to account for cements and other authigenic components.

The HMC index of detritus derived entirely from a single rock unit, in absence of significant chemical weathering, hydraulic sorting, or diagenesis, expresses the capacity of that source to generate heavy mineral grains.

5.2. The tHMC Index

Heavy mineral analyses generally focus on transparent dense grains which can be identified under the microscope. However, altered grains which cannot be identified under the microscope (turbid grains) invariably occur in various proportions and cannot be simply disregarded, because alteration affects unstable species selectively and thus introduces a bias potentially leading to provenance misinterpretations. Opaque grains, which are best identified in reflected light, also occur. Because of their very high density, they are excellent indicators of hydraulic-sorting effects (see below).

The "transparent Heavy Mineral Concentration index" (tHMC) is calculated from the HMC index with the simple formula:

$$\mathrm{tHMC} = \mathrm{HMC}(1 - \%\mathrm{opaque} - \%\mathrm{turbid})$$

where % opaque and % turbid are the percentages of opaque and turbid heavy minerals over total heavy minerals, respectively.

The tHMC index is needed for calculating contributions from single sediment sources (i.e., tributaries, lithological units, tectonic units) to total sediment budgets, and more in general to integrate complementary provenance information from bulk-petrography and heavy mineral analyses (Garzanti et al., 2004b, 2005, 2006). HMC and tHMC values are generally close in detritus from high-grade metamorphic rocks, whereas in detritus from very low-grade and retrogressed metamorphic rocks, contributing abundant turbid and opaque grains, tHMC may be half than HMC or less.

5.3. The SRD Index

The "Source Rock Density index" (SRD), here defined as the weighted average density of extrabasinal terrigenous grains, is a proxy of the average density of source rocks (Fig. 3), and thus of their chemical composition and crustal level. The SRD index is also useful to demonstrate the hydraulic-sorting control on anomalous concentrations of heavy minerals (e.g., SRD $\geqslant$ 3.50 in heavy mineral placers, which is higher than the densest rock in outcrop; Daly et al., 1966).

In order to simplify calculations, we assume:

- an average density of 2.65 g/cm^3 (equal to density of quartz) for all "light" ($<$2.90 g/cm^3) extrabasinal terrigenous grains;
- an average density of 5.00 g/cm^3 (intermediate between magnetite and ilmenite) for opaque heavy minerals;
- an average density for non-identified turbid grains equal to the average density of identified transparent grains; and
- either the density of common chemical compositions or an average value for solid-solution series and complex mineral groups ($\delta = 3.20$ for amphiboles, $\delta = 3.30$ for clinopyroxenes and enstatite; $\delta = 3.35$ for olivine; $\delta = 3.40$ for hypersthene; $\delta = 3.45$ for epidote-group minerals; $\delta = 4.00$ for garnet).

The errors induced by these assumptions are considered as tolerable with respect to our primary aim, which is to compare heavy mineral suites derived from different source terranes.

The SRD index is thus calculated from the HMC index with the formula:

$$SRD = \frac{[\Delta_{tHM}(1 - \%\text{opaque}) + 5.00 \times \%\text{opaque})\text{HMC} + 2.65(100 - \text{HMC})]}{100}$$

where Δ_{tHM} is the weighted average density of transparent heavy minerals.

Because heavy minerals are concentrated in the fine tail of the grain-size distribution (Rittenhouse, 1943; Fletcher et al., 1992), the SRD index (calculated from the 63 to 250 μm size fraction) tends to overestimate the average density of source rocks for medium- and coarse-grained sands.

5.4. Ratio Parameters Based on Density Contrasts

There is a marked difference in density between lower density ($\delta \leqslant 3.20$: prehnite, carpholite, tremolite, lawsonite, tourmaline, andalusite, apatite) and ultradense ($\delta \geqslant 3.80$: garnet, anatase, brookite, rutile, barite, chrome spinel, zircon, xenotime,

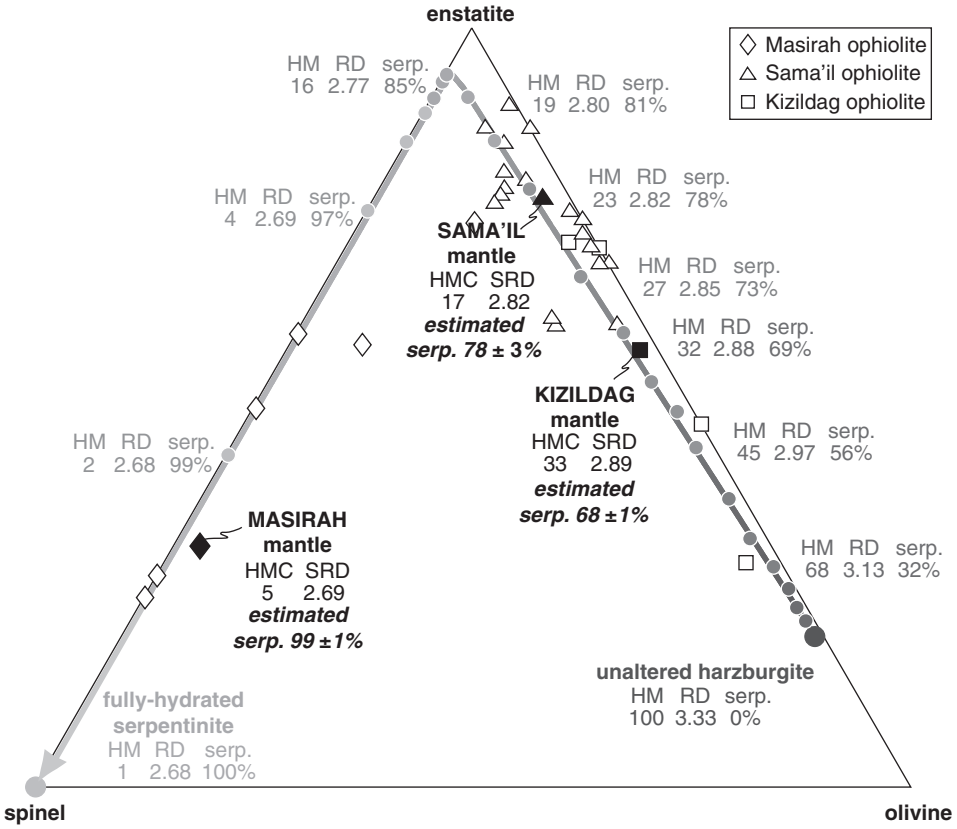

Fig. 3. Insights from mantle-derived heavy mineral suites. The triangular diagram highlights the strict relationships that exist between average degree of serpentinisation, rock density, and both absolute and relative abundance of heavy minerals in ultramafic source rocks. This is directly reflected by both heavy mineral concentration and heavy mineral suites in mantle-derived detritus (dark grey to light grey arrow). The trend is calculated theoretically by assuming different alteration functions for olivine and enstatite with respect to stable chrome spinel, calibrated after empirical data by Lippard et al. (1986, Fig. 3.16). The degree of serpentinisation of Tethyan peridotite sources can thus be assessed, independently and with consistent results, both from heavy mineral concentration (HMC and SRD indices) and from relative abundances of detrital olivine, enstatite, and chrome spinel (data after Garzanti et al., 2000, 2002b). Note that mantle-derived detritus cannot (and in fact usually does not) contain $\geqslant$10% spinel, unless $\geqslant$60% pyroxene and 100% olivine have been selectively destroyed, either before or after erosion. Parameters in grey (HM = heavy mineral abundance; RD = rock density; serp. = average degree of serpentinisation) refer to the harzburgitic source rock.

monazite, opaques) heavy minerals (Mange and Maurer, 1992). The density distribution of heavy minerals provides a key to assess hydraulic effects in the sedimentary environment. Three simple indices, apt to this purpose, are:

- % opaque = the percentage of opaque grains (δ 4.50 to 5.30: ilmenite, magnetite, hematite) over total heavy minerals;

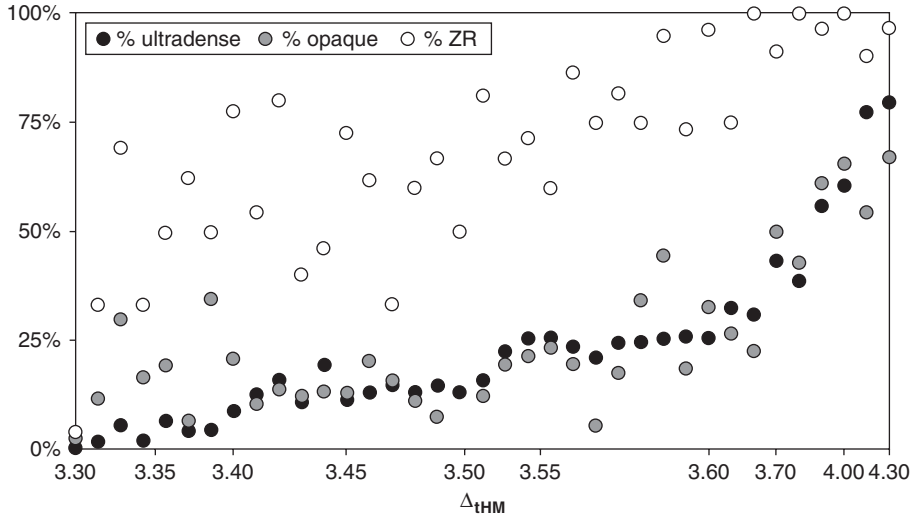

Fig. 4. Parameters based on heavy mineral species with contrasting densities (% opaque, % ultradense, % ZR, Δ_{tHM}) help to quantify sedimentary effects on heavy mineral assemblages. Good correlation ($r \geqslant 0.64$; significance level 0.1%) among all of the four parameters defined herein reveals locally varying degrees of hydraulic-sorting control in modern Arabian sands from the Gulf of Aden to the Persian Gulf. The 37 samples, all chiefly recycled from cover strata of the Arabian platform ("Undissected Rift Shoulder" to "Undissected Craton" sub-provenances: Garzanti et al., 2001, 2003), are ordered by increasing Δ_{tHM} from left to right.

- % ultradense = the percentage of ultradense transparent grains ($\delta \geqslant 3.80$) over total identified transparent heavy minerals;
- % ZR = the percentage of ultradense ultrastable grains (zircon and rutile) over total ultrastable grains (zircon, tourmaline, and rutile; Hubert, 1962).

Anomalously and concomitantly high HMC, SRD, % opaque, % ultradense, % ZR, and Δ_{tHM} indices (Fig. 4) indicate the effect of hydraulic sorting, as in placer deposits.

5.5. Ratio Parameters Based on Stability Contrasts

The ZTR index was defined by Hubert (1962) as the percentage of chemically ultrastable species (zircon, tourmaline, and rutile) among transparent detrital heavy minerals. In modern sands derived from collision orogens, magmatic arcs, volcanic rifted margins, and dissected rift shoulders and cratonic shields, the ZTR index is observed to be mostly <10 (Garzanti and Andò, 2007, this volume). Higher values are observed only in modern sands derived from undissected rift shoulders and cratonic shields, because of extensive recycling of ancient sedimentary successions coupled locally with hydraulic-sorting effects (in this latter case ZR tends to 100%). High ZTR values, instead, very commonly characterise ancient sandstones, because of extensive diagenetic dissolution of less stable species. Independent petrographic and morphological observations may help in distinguishing between ancient polycyclic sandstones and ancient diagenetically modified sandstones (McBride, 1985).

6. HEAVY MINERAL CONCENTRATION IN MODERN SANDS

Three primary sources of detritus are considered here: oceanic lithosphere, arc crust, and continental crust. Oceanic lithosphere at one extreme displays a relatively simple stratigraphy, whereas continental crust at the other extreme is characterised by a very complex and variable structure formed during its typically multistage geological evolution. Arc and continental crustal sources are given full consideration in current provenance models (''Magmatic Arc'' and ''Continental Block'' Provenances of Dickinson and Suczek, 1979), whereas oceanic lithospheric sources received less specific attention (Garzanti et al., 2002b). Orogenic belts, which incorporate largely metamorphosed remnants of oceanic, arc, and continental rock units, represent a distinct source of detritus (''Recycled Orogen Provenance'' of Dickinson, 1985). Heavy mineral concentration in sediments depends on the average density of source rocks, and therefore it tends to increase during unroofing of progressively deeper tectono-stratigraphic levels within most source terranes.

6.1. Oceanic Lithosphere

Oceanic lithosphere commonly includes harzburgitic mantle peridotites at the base. The lower crust consists of layered gabbroic rocks (including gabbronorites in supra-subduction-zone ophiolites), followed by isotropic amphibole gabbros and plagiogranite sills, crystallised at the top of the magma chamber. The upper crust includes sheeted diabase dikes, typically affected by extensive actinolite-facies oceanic metamorphism, tholeiitic pillow basalts, and a thin pelagic sediment cover (Malpas et al., 1990; Boudier and Juteau, 2000).

All along the Alpine-Himalayan convergent plate-boundary, complete lithospheric sections representing the floor of either truly oceanic or supra-subduction-zone basins are exposed in obducted ophiolite belts. These formed where and when, following an earlier stage of intraoceanic subduction, a continental margin has been dragged underneath oceanic lithosphere (Coleman, 1971; Searle and Stevens, 1984). The examples considered here include modern sands shed by Tethyan ophiolites from northern Italy to Pakistan (Table 1).

6.1.1. Heavy minerals from oceanic mantle

Fresh harzburgite consists entirely of heavy minerals (75–85% olivine, 15–25% orthopyroxene, $\leqslant 2\%$ spinel). Exposed mantle rocks, however, are extensively serpentinised (typically $\geqslant 60\%$; Lippard et al., 1986). Heavy mineral suites supplied even by mildly deformed oceanic nappes exposed in hyperarid regions are consequently dominated by enstatite rather than olivine, and have high but not extreme heavy mineral concentrations. Heavy mineral assemblages derived from ultramafic rocks cannot be dominated by chrome spinel unless alteration of ferromagnesian silicates is complete (degree of serpentinisation $>99\%$); quite low heavy mineral concentration (HMC <2) is expected in this case (Fig. 3). Because of the markedly different mineralogical stability of olivine and pyroxenes versus chrome spinel, the degree of serpentinisation of peridotite source rocks can be estimated independently from heavy mineral concentration and from relative abundance of heavy mineral species, if the original peridotite composition is known (Fig. 3).

Table 1. Heavy mineral concentration is invariably high in detritus from serpentinized ultramafic levels of obduction orogens (Tethyan ophiolites)

Level	Lithology	Unit	n°	HMC	tHMC	Δ_{tHM}	SRD	% op_{HM}	% ud_{HM}	% ZR	ZTR	T&	LgM	Gt	HgM	Hb	&A	CPX	OPX	OS	HCI	MMI
OBDUCTED OPHIOLITE NAPPE																						
Sediment cover	Remnant-ocean turbidites	Liguride flysches	35	2	1	3.66	2.67	18	34	74	8	5	15	30	2	11	6	12	5	6	28	11
Upper crust	Basalts	Bela	1	17	9	3.41	2.80	8	0	33	1	0	9	0	0	7	1	81	1	0	n.d.	n.d.
Middle crust	Sheeted dikes	Troodos	3	24	20	3.35	2.85	6	0	n.d.	0	0	45	0	0	4	7	40	3	0	31	n.d.
Middle crust	Sheeted dikes	Kizildag	1	33	31	3.30	2.86	0	0	n.d.	0	0	4	0	0	6	10	69	11	1	19	n.d.
Lower crust	Gabbros	Internal Liguride	1	17	15	3.32	2.79	1	2	n.d.	0	0	1	0	0	1	2	94	0	1	n.d.	n.d.
Mantle	Harzburgites	Sama'il	2	17	12	3.34	2.84	26	2	n.d.	0	0	3	0	0	1	1	6	70	19	n.d.	n.d.
Mantle	Harzburgites	Kizildag	3	33	31	3.34	2.89	2	2	n.d.	0	0	0	0	0	0	0	3	56	41	n.d.	n.d.
SUBDUCTED CONTINENTAL-MARGIN UNITS																						
Lawsonite-carpholite facies	Metasediments	Saih Hatat	1	0.4	0.1	3.44	2.65	15	8	92	9	0	46	0	0	5	11	22	8	0	n.d.	n.d.
Blueschist facies	Metasediments	Saih Hatat	2	14	5	3.40	2.82	30	2	70	3	0	72	0	0	4	10	7	4	0	n.d.	n.d.
Eclogite facies	Metasediments	Saih Hatat	1	37	22	3.51	3.14	30	26	100	4	1	42	22	0	1	17	6	7	0	n.d.	n.d.

Note: Invariably high heavy mineral concentration in detritus from serpentinised ultramafic and partly altered mafic rocks of the obducted oceanic lithosphere. For subducted continental-margin units, concentration increases sharply with depth reached during subduction beneath the ophiolite nappe. ZTR = ultrastable minerals (zircon, tourmaline, rutile); T& = other minerals (e.g., sphene, anatase, brookite, apatite, monazite, barite); LgM = low-grade metamorphic minerals (epidote-group, chloritoid, prehnite, pumpellyite, carpholite, lawsonite); Gt = garnet; HgM = high-grade metasedimentary minerals (staurolite, andalusite, kyanite, sillimanite); Hb = hornblende; &A = other amphiboles; CPX = clinopyroxenes; OPX = orthopyroxenes; OS = olivine and spinel. HCI (Hornblende Color Index of Garzanti et al., 2004a) = (1/3 green hornblende + 2/3 green-brown hornblende + brown hornblende)/total hornblende × 100. MMI (Metasedimentary Minerals Index of Garzanti and Andò, 2007, this volume) = (1/3 staurolite + 2/3 kyanite + sillimanite)/(chloritoid + staurolite + kyanite + sillimanite) × 100; n.d. = not determined.
%Opaque = % op_{HM}, % Ultradense = % ud_{HM}.

6.1.2. Heavy minerals from oceanic crust

Because hydrothermal circulation at mid-ocean ridges is mainly confined to the upper crustal section (Nicolas and Boudier, 1991), exposed lower-crustal gabbroic rocks are generally fresh, and supply very rich, clinopyroxene-dominated heavy mineral assemblages including green to brown hornblende (and hypersthene in supra-subduction-zone settings).

Heavy mineral concentration is also high in detritus from higher crustal levels, which are extensively affected by actinolite-facies to prehnite-pumpellyite-facies oceanic metamorphism (Pflumio, 1991). Sheeted dikes contribute pyroxenes (commonly altered or amphibolitised diopside, associated with significant hypersthene in supra-subduction settings), actinolitic amphibole, and abundant epidote where epidosite zones are extensively developed at the base of the complex (Robinson and Malpas, 1990; Juteau et al., 2000). Pillow lavas provide chiefly clinopyroxene (associated with orthopyroxene in detritus from boninites).

6.1.3. Heavy minerals from oceanic sediments

The thin pelagic covers, including chert or micritic limestone, are devoid of heavy minerals. An exception is represented by thick turbidite packages accumulated adjacent to collision zones (Ingersoll et al., 2003). Remnant-ocean turbidites, however, lose much of their heavy mineral content because of severe intrastratal dissolution during deep burial, tectonic accretion in trench settings, and subsequent orogenic anchimetamorphism (Gazzi, 1965). They thus chiefly supply depleted assemblages, enriched in stable and ultrastable recycled grains including chrome spinel.

6.2. Arc Crust

Magmatic arcs form above oceanic subduction zones. Arc crust includes gabbroic to granitic calc-alkaline batholiths at depth, and basaltic to rhyolitic lavas and pyroclastic deposits at the surface (Gill, 1981). The examples considered here include modern sands from Alpine to Himalayan active-margin batholiths as well as from Mediterranean volcanic arcs (Table 2, but see also Table 4).

6.2.1. Heavy minerals from dissected arc batholiths

The Transhimalayan belt, extending from Pakistan to Burma north of the Indus-Tsangpo ophiolitic suture, includes Andean-type batholiths locally dissected to their granulite-facies roots (Gansser, 1980). These plutonic to high-grade metaigneous rocks supply detritus rich in heavy minerals where assemblages are dominated by blue-green and subordinately green and brown hornblende, with epidote, minor clinopyroxenes and green-pink hypersthene. Alpine tonalites to granodiorites (Bregaglia, Adamello) contribute slightly less concentrated, hornblende-dominated assemblages with subordinate epidote, sphene, and zircon.

6.2.2. Heavy minerals from undissected volcanic arcs

Volcanic arcs shed heavy mineral assemblages dominated by green augite and yellow-green hypersthene, associated with either olivine or dark-brown to reddish-brown hornblende (oxyhornblende). Heavy mineral concentration, although fluctuating widely, is commonly high to extremely high.

Table 2. Heavy mineral concentration in modern sands from active and extinct Mediterranean volcanic arcs

Volcanic centre	Main volcanic products	Age	No.	HMC	tHMC	Δ_{tHM}	SRD	% op_{HM}	% ud_{HM}	% ZR	ZTR	T&	LgM	Gt	HgM	Hb	&A	CPX	OPX	OS	HCI	MMI
Active volcanic centers																						
Campi Flegrei	Tephrite	Holocene	1	20	19	3.31	2.79	3	1	n.d.	0	0	0	1	0	0	0	99	0	0	n.d.	n.d.
Vesuvio	Tephrite and phonolite	Holocene	1	58	54	3.32	3.05	6	2	n.d.	0	0	2	0	0	9	1	82	0	6	82	n.d.
Stromboli	High-K basalt to basaltic andesite	Holocene	3	59	53	3.31	3.05	9	0	n.d.	0	0	0	0	0	0	0	82	0	18	n.d.	n.d.
Panarea	Felsic andesite to rhyodacite	Holocene	1	53	44	3.32	3.02	17	0	n.d.	0	0	0	0	0	26	0	38	36	0	98	n.d.
Vulcano	Tephrite to rhyolite	Holocene	2	41	37	3.30	2.96	6	0	n.d.	0	0	0	0	0	0	0	94	0	6	n.d.	n.d.
Salina	High-Al basalt to dacite	Holocene	2	64	48	3.33	3.26	8	0	n.d.	0	0	0	0	0	1	0	64	27	8	72	n.d.
Lipari	Largely rhyolite	Holocene	3	16	15	3.31	2.76	6	0	n.d.	0	0	0	0	0	1	0	86	13	0	67	n.d.
Santorini	High-Al basalt to rhyolite	Holocene	1	21	18	3.35	2.80	13	0	n.d.	0	0	1	0	0	1	0	51	38	7	100	n.d.
Extinct Mesozoic to Cenozoic centers																						
Mt. Amiata	Rhyodacite	Quaternary	1	6	5	3.41	2.70	5	1	n.d.	0	0	0	1	0	0	0	3	96	0	n.d.	n.d.
Capraia	High-K andesite to rhyolite	Mio-Pliocene	1	5	4	3.33	2.69	17	0	n.d.	0	0	0	0	0	4	0	62	33	0	100	n.d.
S. Pietro	Peralkaline rhyolite	Miocene	1	3	1	3.43	2.69	15	12	100	1	10	10	3	0	6	36	21	12	0	64	n.d.
Lesvos	High-K basalt to rhyolite	Miocene	1	3	3	3.30	2.67	9	0	n.d.	0	0	0	0	0	4	0	94	2	0	92	n.d.
Dolomiti	Latite	Middle Triassic	1	34	32	3.30	2.89	2	0	n.d.	0	0	0	0	0	0	0	100	0	0	n.d.	n.d.

Note: Anomalously high HMC and SRD indices invariably characterise modern sands from active volcanoes, as well as detritus from Triassic volcanic rocks. Parameters same as in Table 1.
%Opaque = % op_{HM}, % Ultradense = % ud_{HM}.

In the case of non-holocrystalline, largely glassy source rocks, we expect a direct relationship with phenocryst abundance, and only an indirect one with magma chemistry and density. Orogenic andesites usually contain 20–50% phenocrysts in volume, typically two-thirds of which are plagioclase (Gill, 1981). Circum-Pacific basalts and andesites contain and thus can shed an average of $9 \pm 2\%$ heavy minerals (Ewart, 1976). This is far less than HMC indices commonly observed in modern sands. In detritus from volcanoes of the Aeolian and Aegean arcs, HMC ranges from a minimum of 5 for rhyolite-derived fluvial sand to mostly 50–60 in beach sand derived from basalt to dacite. SRD indices, as a consequence, range from a minimum of 2.70 to commonly > 3.00, which exceeds not only the typical densities of volcanic source rocks but even those of their plutonic equivalents (Daly et al., 1966). This anomaly may be ascribed to both grain-size effects (analysed sands are mostly medium-grained) and to selective breakdown and hydraulic removal of fragile, unstable, and light (i.e., pumice) volcanic glass in high-energy sedimentary environments. Hydraulic-sorting effects, including selective entrainment of lighter feldspar grains, are in fact spectacularly displayed by most erosional beaches made of volcaniclastic sand (Frihy et al., 1995; Dye and Dickinson, 1996; Garzanti et al., 2002a).

6.3. Continental Crust

The continental crust is the product of a multistep differentiation process which, through a series of plate-tectonic cycles, progressively concentrated less dense materials in the shallower levels of the lithosphere (Vielzeuf et al., 1990). Its complex stratigraphy, ideally including a granulite-facies lower crust with sill-like mafic intrusions, an amphibolite-facies middle crust with intermediate to felsic intrusions, and a weakly metamorphosed upper crust with sedimentary or volcanic cover rocks (Handy, 1990), is exposed in old cratonic shields, along young rifted-margin escarpments, and in external thrust belts of collision orogens. Complete sections through the whole crust, however, are never found in outcrop. Lower crustal levels are only known from a few localities, whereas uppermost crustal levels are largely stripped off during and after the orogenic events which determined cratonisation (Fountain et al., 1990).

The examples considered here include modern sands derived from Precambrian shields of Africa, Arabia, and India, as well as from both autochthonous (Red Sea-Gulf of Aden) and allochthonous (i.e., involved in orogenic deformation; Southern Alps) rifted-margin successions (Table 3).

6.3.1. Heavy minerals from the lower crust

One of the best-preserved lower crustal sections is the classic Ivrea-Verbano Zone of the Southern Alps, including gabbros intruded into a granulite-facies metasedimentary succession (Zingg et al., 1990). Detritus from these granulitic rocks is characterised by extremely concentrated heavy mineral assemblages, including hypersthene, brown hornblende, garnet, clinopyroxene, and sillimanite. SRD indices (gabbros 3.10 ± 0.16, kinzigites 2.94 ± 0.15) tend to overestimate the actual measured densities of source rocks (gabbros $\delta = 2.98 \pm 0.07$, kinzigites $\delta = 2.87 \pm 0.09$: Sinigoi et al., 1995). Extreme concentration indices (SRD 3.15) are reached in olivine-dominated

Table 3. Heavy mineral concentration in modern sands from distinct tectono-stratigraphic levels of continental crust (Arabian-Nubian and Indian shields)

Level	Lithology	Unit	No.	HMC	tHMC	Δ_{tHM}	SRD	% op_{HM}	% ud_{HM}	% ZR	ZTR	T&	LgM	Gt	HgM	Hb	&A	CPX	OPX	OS	HCI	MMI
Upper crust																						
Cover	Sediments	Orobie	5	0.7	0.4	3.51	2.66	24	26	33	5	4	25	22	8	30	3	3	1	0	32	40
Cover	Sediments	Levant/Nubia	17	0.8	0.4	3.60	2.66	31	23	61	30	4	28	6	8	17	1	5	1	0	11	40
Cover	Sediments	Gulf of Aden	19	0.9	0.6	3.58	2.66	27	28	77	14	1	38	15	1	22	2	4	2	1	32	31
Cover	Sediments	Indian Shield	2	1	0.8	3.73	2.67	20	38	51	45	7	26	5	2	13	2	0	0	0	11	67
Cover	Sediments + lavas	Dolomites	2	2	0.9	3.41	2.67	15	11	73	2	3	12	7	0	6	0	70	0	0	56	n.d.
Cover	Sediments + lavas	Levant/North Red Sea	26	1	0.7	3.52	2.67	23	12	68	15	3	13	2	2	16	0	45	0	3	15	36
Cover	Sediments + lavas	Gulf of Aden	6	2	1	3.40	2.67	12	7	61	4	1	19	3	1	25	2	33	7	4	32	39
Basement + cover		External Massifs	5	3	2	3.41	2.68	6	11	76	5	2	33	7	1	44	5	2	1	0	54	n.d.
Basement + cover		North Red Sea	22	4	2	3.42	2.69	23	8	73	7	3	22	3	2	42	1	20	0	0	14	37
Basement + cover		Gulf of Aden	8	3	3	3.41	2.68	13	9	87	5	1	43	4	0	35	3	6	2	0	28	32
Middle crust																						
Amphibolite facies	Metasediments	Serie dei Laghi	12	5	4	3.56	2.70	8	32	32	5	2	10	29	16	33	3	1	0	0	17	50
Amphibolite facies	Granitoids, metavolcanics	North Red Sea	11	9	5	3.39	2.76	27	6	77	6	9	12	1	1	53	1	16	0	0	11	39
Amphibolite facies	Granitoids, metavolcanics	South Red Sea	4	12	11	3.30	2.75	5	2	67	1	2	17	1	0	62	2	14	0	0	9	n.d.
Amphibolite facies	Granitoids, gneisses	Gulf of Aden	10	13	11	3.30	2.75	8	5	65	3	2	10	2	1	73	2	4	2	1	11	42
Amphibolite facies	Gneisses, granitoids	Indian Shield	5	7	6	3.39	2.71	8	15	84	2	3	9	13	2	61	1	7	1	0	18	59
Lower crust																						
Granulite facies	Kinzigites	Ivrea-Verbano	8	35	31	3.44	2.94	1	21	79	1	2	14	20	8	36	5	12	1	1	38	100
Granulite facies	Gabbros	Ivrea-Verbano	3	44	31	3.46	3.10	12	18	75	1	0	5	17	0	23	2	12	40	0	87	n.d.
Mantle	Peridotites	Ivrea-Verbano	1	70	57	3.33	3.15	2	2	n.d.	0	0	1	2	0	14	3	12	15	52	43	n.d.

Note: Heavy mineral concentration increases steadily with deeper tectono-stratigraphic level of source rocks. SRD indices of detritus from supracrustal basement and cover units compare with the estimated mean density of the upper continental crust (2.67 g/cm^3: Taylor and McLennan, 1985). Parameters same as in Table 1. %Opaque = % op_{HM}, % Ultradense = % ud_{HM}.

detritus from peridotites which may represent slivers of subcontinental mantle (Table 3; Rivalenti et al., 1981; Boriani and Giobbi, 2004).

6.3.2. Heavy minerals from the middle crust

Middle-crustal levels, chiefly consisting of granitoid and amphibolite-facies metamorphic rocks, are uplifted and widely exposed all along the shoulders of the Red Sea-Gulf of Aden rift system from Jordan to Oman, and on the Shillong Plateau in eastern India. In all of these cases, heavy minerals are abundant, with the dominance of blue-green to green-brown hornblende.

In the Southalpine section, middle-crustal levels largely consist of amphibolite-facies metasediments (“Serie dei Laghi”: Boriani and Giobbi, 2004), supplying slightly less concentrated assemblages with garnet, kyanite, and staurolite.

6.3.3. Heavy minerals from the upper crust

Upper-crustal low-grade rocks and cover strata of Precambrian to Tertiary age have survived erosion in vast areas of northern Africa, central Arabia, and northwestern India. In these regions, beach, fluvial, or aeolian sands have low heavy mineral abundance and include largely recycled assemblages with significant amounts of ultrastable minerals. Epidote is abundant, and locally dominant (e.g., in southern Yemen sands derived from greenschist-facies dikes, lavas and tuffs, representing the shallow roots of the Pan-African Mukalla arc terrane: Windley et al., 1996).

Only trivial amounts of heavy minerals are provided by sedimentary cover successions. In sharp contrast, rift-related basalts from Syria to Yemen yield abundant heavy minerals with the dominance of lilac-brown titanian augite, associated with olivine and minor brown hornblende.

6.4. Orogenic Metamorphic Sources

Alpine-type, thick-skinned collision orogens have a complex tectono-stratigraphy that includes slivers of oceanic and continental units, deformed and metamorphosed during initial subduction and subsequent indentation stages (Beaumont et al., 1996). Protolith rocks are progressively re-equilibrated during prograde or retrograde metamorphism. As pressure and temperature change during nappe stacking or exhumation, the more hydrated mineral assemblages are replaced by less hydrated ones or vice-versa, and rock density varies consequently. Each metamorphic facies is thus characterised by distinctive mineralogy, as well as by a typical range of rock densities and, therefore, by a given potential to supply heavy minerals. The examples considered here include modern sands from metamorphic complexes exposed in both collision (Alps, Himalaya) and obduction (Oman) orogens (Tables 1 and 4).

6.4.1. Heavy minerals from oceanic metamorphic nappes

Ophiolites, instead of being obducted or offscraped and incorporated in the shallow structural level of orogenic belts (Oman-type obduction orogens or Apennine-type accretionary prisms), can undergo subduction and high-pressure metamorphism, to be finally subcreted and exhumed in the axial part of Alpine-type collision orogens.

Mantle peridotites are extensively transformed into schistose antigorite-serpentinites, and thus contribute limited amounts of heavy minerals which commonly

Table 4. Heavy mineral concentration in modern sands from distinct tectono-stratigraphic levels of collision orogens (Alpine and Himalayan belts)

Level	Lithology	Unit	No.	HMC	tHMC	Δ_{tHM}	SRD	% op_{HM}	% ud_{HM}	% ZR	ZTR	T&	LgM	Gt	HgM	Hb	&A	CPX	OPX	OS	HCI	MMI
Alps																						
Oceanic units																						
Non-metamorphic	Sediments	San Remo	4	0.2	0.1	3.70	2.65	12	42	69	24	4	23	22	2	14	2	5	3	1	28	51
Very-low grade	Metasediments	Ubaye-Parpaillon	2	0.0	0.0	3.92	2.65	51	56	66	73	0	8	8	0	2	2	6	2	0	n.d.	n.d.
Blueschist (carpholite zone)	Metasediments	Calcschists	3	1	0.3	3.39	2.66	6	3	25	2	6	49	0	0	8	25	9	0	0	43	0
Blueschist	Metasediments	Calcschists	5	3	2	3.46	2.67	9	13	58	8	1	57	8	1	8	15	2	1	0	21	7
Eclogite facies	Metaophiolites	Zermatt-Voltri	7	29	24	3.35	2.86	1	6	100	1	1	44	5	1	15	25	6	1	1	6	60
Continental units																						
Blueschist → carpholite zone	Metasediments	Ligurian Brianconnais	4	1	0.3	3.50	2.66	9	16	60	12	2	55	8	2	12	4	3	1	0	15	33
Blueschist → greenschist facies	Metasediments	Brianconnais	3	3	1	3.46	2.68	15	14	35	13	3	54	10	1	9	8	1	1	0	30	0
Blueschist → greenschist facies	Basement	Brianconnais	4	4	2	3.51	2.69	11	21	57	3	6	44	18	0	19	7	1	1	0	20	2
Amphibolite facies	Basement	Lepontine Dome	25	9	8	3.43	2.72	3	21	69	2	1	14	20	4	49	5	3	1	0	25	60
Eclogite → greenschist facies	Basement	Internal Massifs	5	7	6	3.67	2.73	3	42	71	4	2	45	39	1	6	2	1	0	0	5	17
Eclogite facies → very low grade	Basement	Sesia-Lanzo	7	16	14	3.53	2.80	1	22	100	1	3	59	21	0	7	8	1	0	0	12	n.d.
Granulite → greenschist facies	Lower crust	Dent Blanche	2	21	14	3.63	2.87	3	44	n.d.	1	1	25	43	6	12	2	5	5	0	55	99
Batholiths	Tonalite-granodiorite	Periadriatic Zone	5	14	12	3.30	2.75	12	4	100	3	4	15	0	0	78	0	0	0	0	7	n.d.
Himalaya																						
Very-low grade	Metasediments	Tethys Himalaya	5	1	0.7	3.43	2.66	15	22	9	53	3	7	16	11	7	1	2	0	0	24	47
Very low grade	Metasediments	Outer Lesser Himalaya	6	1	0.4	3.41	2.66	17	14	23	31	3	36	7	2	13	3	5	0	0	4	60
Greenschist facies	Metasediments	Inner Lesser Himalaya	2	7	6	3.52	2.73	13	33	42	5	1	18	31	3	38	4	0	0	0	3	67
Greenschist facies	Metasediments	North Himalaya	1	8	2	3.52	2.72	5	12	35	20	5	56	3	0	11	1	4	0	0	2	0
Amphibolite facies	Metasediments	Greater Himalaya	14	10	9	3.61	2.76	6	41	42	5	2	7	38	13	22	1	11	0	0	26	75
Batholiths	Gabbro-granite	Transhimalaya	5	25	20	3.28	2.84	8	1	83	1	3	16	0	0	69	3	4	4	0	16	n.d.

Note: Orogenic sands are complex mixtures of detritus from several distinct tectono-metamorphic assemblages. Major sources of heavy minerals in the Alps include oceanic and outer-continental-margin units, which have undergone high-pressure metamorphism during attempted subduction in the early collisional stages and were later re-equilibrated at very low- to medium-grade conditions, as well as up to granulite-facies pre-Alpine basement slivers. Major sources of heavy minerals in the Himalaya include amphibolite-facies metasedimentary units and active-margin batholiths. Parameters same as in Table 1.
%Opaque = % op_{HM}, % Ultradense = % ud_{HM}.

include magnetite, produced during serpentinisation of Fe-bearing olivine (Wicks and Whittaker, 1977). Eclogitic metagabbros and metabasalts are extremely dense rocks that consist entirely of heavy minerals (omphacitic clinopyroxene, garnet, rutile), but they unavoidably undergo blueschist-facies to greenschist-facies retrogression during exhumation. Detrital heavy mineral assemblages contributed by them have very high but not extreme concentration, and comprise dominantly epidote and amphiboles (glaucophane, blue-green barroisitic hornblende, actinolite) with only minor clinopyroxene and garnet. Much less concentrated assemblages are supplied by metasedimentary deep-water cover rocks (e.g., calcschists).

6.4.2. Heavy minerals from continental metamorphic nappes

The thinned distal edge of continental margins is commonly involved in attempted subduction during the early stages of continent–continent collision (Dal Piaz, 1999; Guillot et al., 2003). Continental basements and their sedimentary covers are dragged down to depths of several tens of kilometres and undergo eclogite-facies metamorphism, followed by re-equilibration at lower pressures during exhumation. Mineralogy and rock density change in accord with the evolving P-T path.

Alpine continental eclogites shed heavy mineral-rich, epidote-dominated detritus, similarly to oceanic eclogites, but in significantly lower concentration, with more garnet, and less ferromagnesian silicates (e.g., glaucophane). Blueschist-facies continental-margin units retrogressed at greenschist facies or very low-grade conditions also supply epidote-rich assemblages, but with much lower heavy mineral concentrations. Abundant unidentifiable turbid grains from metasedimentary cover rocks, chloritoid, and a few ultrastable minerals also occur.

Comparable detrital signatures are observed in northern Oman, where concentration of epidote-dominated assemblages increases markedly and steadily from carpholite/lawsonite-grade, to blueschist facies, and finally to eclogite-facies source rocks, exposed from the periphery to the core of the Saih Hatat window.

Where metamorphic overprint, subsequent to the early subduction stage, reached amphibolite-facies, modern detritus consists of dominantly neoformed mineral grains. Hornblende-dominated heavy mineral assemblages are eroded from granitoid gneisses exposed in the Lepontine Dome of the Central Alps, whereas chiefly metasedimentary rocks of the Greater Himalaya contribute garnet-kyanite-sillimanite-diopside suites. Both display the high heavy mineral concentration (HMC $\sim$ 10) typical of detritus from middle-crustal levels.

Slivers of lower-continental crust may also occur within the axial metamorphic belt of collision orogens (e.g., Dent Blanche Nappe in the Alps). Because of widespread greenschist-facies retrogression, heavy mineral concentration is significantly reduced even though granulite-facies minerals (garnet, sillimanite, hypersthene, brown hornblende) predominate over epidote-group minerals.

7. HEAVY MINERAL CONCENTRATION IN ANCIENT SANDSTONES

It has long been known that diagenesis exerts a major control on heavy mineral assemblages (Bramlette, 1941; Pettijohn, 1941; Blatt and Sutherland, 1969; Morton and Hallsworth, 1999). By following an actualistic approach (Valloni et al., 1991),

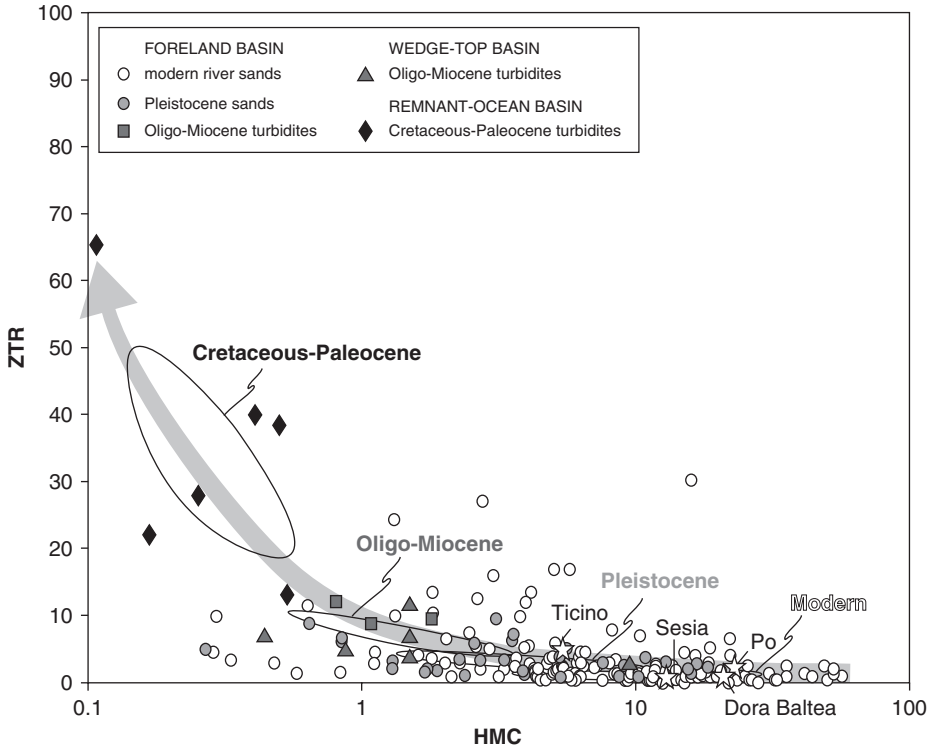

Fig. 5. Sharp discrepancy between heavy mineral suites in modern and ancient sediments derived from the Alps. Concentration (HMC index) steadily decreases, while chemical stability (ZTR index) progressively increases, from modern, to Pleistocene, to Oligo-Miocene, to Cretaceous-Palaeocene clastic wedges. This trend demonstrates the overwhelming effect of diagenetic dissolution in ancient sandstones. Data from Liguride remnant-ocean, Epiliguride wedge-top, and Apennine foredeep clastics after Gazzi (1965), Gandolfi et al. (1983), Valloni et al. (1991), Cibin et al. (1993), and Fontana et al. (1994). 90% confidence regions for the entire population calculated after Weltje (2002).

the post-depositional selective loss of unstable mineral species can be demonstrated and quantified with the help of concentration parameters. Large data sets from modern Alpine and Himalayan river sands are here compared with Pleistocene to Late Cretaceous clastic suites, deposited in Alpine and Himalayan remnant-ocean and foreland basins (Figs. 5 and 6).

7.1. *Alpine Foreland-Basin and Remnant-Ocean-Basin Sediments*

Modern to Pleistocene fluvial sands of the Po Plain, chiefly derived from the Alps, are rich in heavy minerals and include invariably abundant amphiboles, associated with epidote, garnet, and minor pyroxenes (Muttoni et al., 2003). Oligo-Miocene turbidites, also mostly derived from the Alps and deposited in Alpine and Apenninic foredeeps (Valloni et al., 1991; Di Giulio, 1999; Carrapa and Di Giulio, 2001) are, by contrast, low in heavy mineral abundance. They contain garnet-dominated

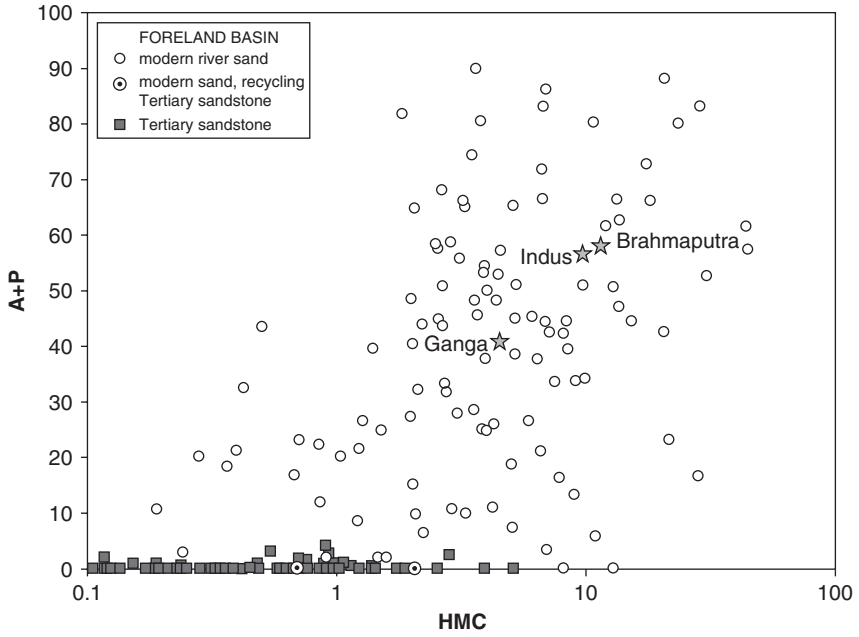

Fig. 6. Sharp discrepancy between heavy mineral suites in modern and ancient sediments derived from the Himalayas. Virtually all modern sands (115 major tributaries of the Indus, Ganga, and Brahmaputra rivers) are rich in heavy minerals with abundant amphiboles (A) and significant pyroxenes (P) (HMC 7 ± 8, A 32 ± 23, P 7 ± 10). Instead, Tertiary foreland basin sandstones (74 samples from 16 different stratigraphic units from Pakistan to Nepal) contain mostly poor to very poor assemblages virtually devoid of ferromagnesian silicates (HMC 0.8 ± 0.8, A 0.4 ± 0.4, P 0.1 ± 0.1). Tertiary sandstones have virtually no modern analogue (the only four modern sands that are free of ferromagnesian silicates, contain either abundant heavy minerals or are chiefly eroded from Miocene sandstones), testifying to widespread and invariably extensive diagenetic dissolution.

assemblages and lack ferromagnesian silicates (Gazzi, 1965; Gandolfi et al., 1983). Coeval sandstones of the Epiliguride succession, deposited stratigraphically on top of the Apenninic wedge, have slightly higher concentrations, and commonly include epidote or staurolite; amphiboles occur locally (Gazzi, 1965; Cibin et al., 1993). Late Cretaceous remnant-ocean turbidites yield low amounts of heavy minerals. Assemblages are dominated by ultrastable species and garnet; locally, they contain chrome spinel, staurolite, or epidote but are completely devoid of ferromagnesian silicates (Fig. 5; Gazzi, 1965; Fontana et al., 1994).

7.2. *Himalayan Foreland-Basin Sediments*

The Indus and Brahmaputra Rivers, which drain large areas north of the Indus-Tsangpo suture zone and cut impressive gorges into rapidly exhuming crustal antiforms at the western and eastern Himalayan syntaxes, carry heavy mineral-rich, hornblende-dominated sediment, containing epidote, garnet, and pyroxenes (Garzanti et al., 2004b, 2005). The Ganga, and other rivers draining only the Himalayan

belt south of the suture, carry assemblages with lower heavy mineral concentration that include amphiboles, garnet, epidote, kyanite, sillimanite, and pyroxenes. In sharp contrast, the Eocene to Miocene foreland-basin sandstones invariably comprise depleted to strongly depleted assemblages dominated by ultrastables and garnet; they are devoid of ferromagnesian silicates (Fig. 6).

7.3. Provenance versus Diagenesis

In the sands carried by large modern rivers derived from the Alps and the Himalayas, the HMC index is mostly much higher than 1. Amphiboles commonly dominate, and ultrastable minerals are minor (ZTR index mostly <10); some pyroxenes and traces of olivine also occur. By contrast, in ancient sandstones of the Alpine and Himalayan foreland basins, HMC is mostly <1 and ferromagnesian silicates are absent.

These differences may partly suggest causes other than diagenetic dissolution. Only the modern systems can be comprehensively studied. Drainage patterns are known and trunk rivers, representing the major avenues of sediment transport from the highly metamorphic core of the belt, can be fully investigated. Studies of ancient foreland-basin strata—in outcrop and in the subsurface—are focused on the best or more accessible sections. It is unlikely that many of these sections were deposited by a major river system, because the most accessible area—in outcrop and in the subsurface—is the proximal part of the foreland basin, fed by transverse supply from many short streams. These mostly drain sedimentary to low-grade metasedimentary sequences, as well as molasse units accreted along the front of the range. Trunk rivers carrying high-grade metamorphiclastic detritus can be intercepted along a small portion of the long mountain front. These rivers, occupying a relatively small area of the whole alluvial plain, mostly flow in distal position close to, or even beyond, the forebulge (Burbank, 1992).

Nevertheless, we do not believe that strata deposited by major fluvial systems during all of the time slices considered could be missed when accurate and systematic sampling of many selected stratigraphic sections was carried out. The striking discrepancies between heavy mineral suites of modern sands and ancient sandstones prove unequivocally the overwhelming effects of intrastratal dissolution, which progressively eliminates first the unstable and then the semi-stable heavy minerals during diagenesis.

7.4. The Incidence of Diagenetic Dissolution

A broad correspondence is observed between heavy mineral concentration and relative abundance of heavy mineral species in ancient sandstones of the Alpine and Himalayan foreland basins:

- where HMC is $\sim$1, garnet is associated with epidote-group minerals, high-grade metasedimentary minerals, and ultrastable minerals; a few amphiboles may locally occur (ZTR 10 ± 5);
- where HMC is 0.5–1, garnet dominates over ultrastable minerals, epidote-group minerals, and minor high-grade metasedimentary minerals (ZTR 25 ± 15);
- where HMC is 0.2–0.5, ultrastable minerals, garnet and locally chrome spinel become the only abundant species; minor epidote-group minerals and high-grade metasedimentary minerals occur (ZTR 50 ± 20);

- finally, where HMC is $\leqslant 0.2$, ultrastable minerals become dominant to exclusive (ZTR 90 ± 15).

Such distinct spectra are interpreted as diagenetic suites fundamentally controlled by the different chemical stability of mineral species (Gazzi, 1965; Morton, 1985). This implies that, in ancient sandstones with HMC index < 1, provenance diagnosis becomes qualitative and uncertain. Concentration indices must be given full consideration in order to avoid gross mistakes while interpreting heavy mineral data from ancient sandstones.

8. GRAIN SIZE AND HYDRAULIC-SORTING EFFECTS

Absolute and relative abundance of heavy mineral species in sediments depends significantly on grain size, and can be modified substantially by hydraulic sorting (Flores and Shideler, 1978; Komar and Wang, 1984; Frihy et al., 1995). The incidence of size, density, and shape fractionation during erosion, transport, and deposition can be revealed and quantified by the use of concentration and density parameters. Modern sediments from the Tonga islands (Dye and Dickinson, 1996), from the Arabian platform (Fig. 4), and from the Nile River (Fig. 7) are considered here as examples.

8.1. Beach Placers of Tonga

Along beaches around coral islands of the Tonga Archipelago (southern Pacific), the overwhelming allochemical fraction is locally removed selectively by strong ocean waves. The resulting lag deposit is a black sand, markedly enriched in pyroxenes and titanomagnetite, derived from basaltic-andesite to dacite tephra. Extreme concentration indices (HMC 91 ± 6, SRD 3.4 ± 0.3, opaque $11 \pm 13\%$ in pyroxene-rich placers; HMC 98 ± 2, SRD 4.8 ± 0.2, opaque $84 \pm 11\%$ in magnetite-rich placers: Dye and Dickinson, 1996) highlight the prominent effect of beach erosion on heavy mineral concentration.

8.2. Aeolian and Beach Sands of Arabia

In the southern Arabian peninsula from Yemen to the Persian Gulf, modern sands contain limited amount of heavy minerals with broadly homogeneous assemblages comprising epidote, amphiboles, pyroxenes, garnet, and ultrastables (HMC 1 ± 1, SRD 2.66, opaque $19 \pm 10\%$, ultradense $17 \pm 10\%$, ZR $72 \pm 17\%$), as expected for detritus from supracrustal strata.

Beach samples with high to extreme concentration and density indices, however, locally occur along the Gulf of Aden coast of Oman (up to HMC 12, SRD 2.88, opaque 65%, ultradense 60%, ZR 100%) and Yemen (up to HMC 91, SRD 4.58, opaque 67%, ultradense 80%, ZR 97%: Greenwood and Bleackley, 1967). Such markedly anomalous concentrations with concomitant enrichment in all ultradense species (opaques, zircon, rutile, garnet, locally chrome spinel; Fig. 4) are not associated with any significant provenance change, and are not characteristic of duplicate samples collected in nearby areas or in subsequent years. Virtually all of the observed

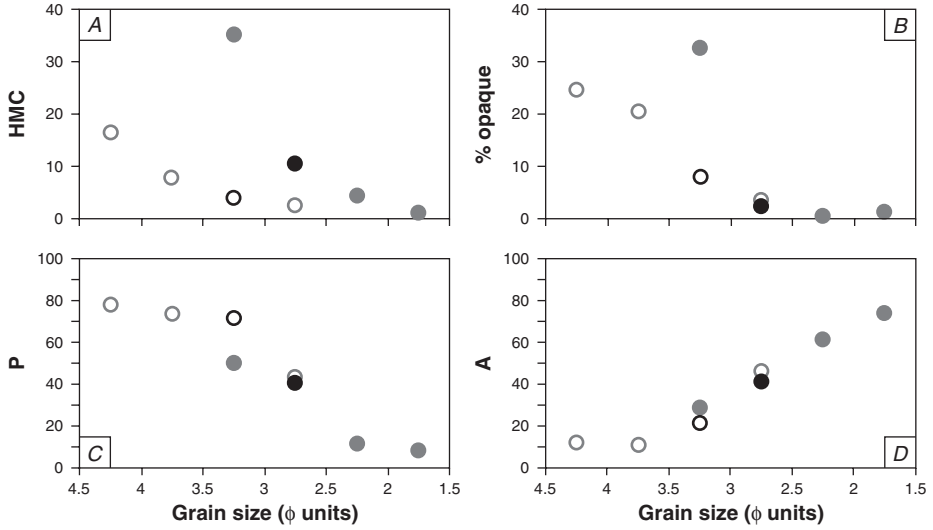

Fig. 7. Striking compositional fractionation in Blue Nile river sediments at Wad Medani, Sudan (data after Garzanti et al., 2006b). (A) Heavy minerals are markedly enriched in the finer grain-size fractions for each transport mode, and much more concentrated in the fine tail of the bedload (dots; modal class in black) than in the coarse tail of suspended load (circles; modal class in black). (B) For both transport modes, opaques and other ultradense grains (zircon, rutile, garnet) are concentrated in finer grain-size fractions with respect to less-dense heavy minerals. (C, D) Grain-size control causes a steady increase of denser clinopyroxenes (chiefly brown titanian augite) with respect to lighter amphiboles (chiefly blue-green hornblende) from medium-grained sand to coarse silt. A = amphiboles; P = pyroxenes.

compositional variance can be ascribed to sedimentary processes in the depositional environment (Fig. 8 of Garzanti et al., 2003).

8.3. River Sands of the Blue Nile

The Blue Nile in Sudan has a markedly seasonal discharge promoted by heavy summer rainfall on Ethiopian highlands (Foucault and Stanley, 1989). Compositional fractionation of its sediments is visible with the naked eye: longitudinal bars and point bars consist of clean white sand richer in quartz, whereas levee deposits are made of dark-grey silty sand enriched in volcanic grains. In the same sample site, heavy minerals display systematic variation in concentration and relative abundances with both grain size and transport mode (Fig. 7).

At Wad Medani southeast of Karthoum, point-bar sand (bedload) displays sharp and regular mineralogical changes. The medium sand fraction contains few heavy minerals, dominated by amphiboles. In contrast, the very-fine sand fraction is rich in heavy minerals, dominated by brown titanian augite and including ultradense grains (opaques, minor zircon, rutile, and garnet). A parallel increase of heavy mineral concentration with decreasing grain size is observed for levee deposits (suspended load). The heavy mineral yield of the fine-sand fraction is poor; assemblages are made up of subequal amounts of amphiboles and pyroxenes. The very-fine-sand and

coarse-silt fractions, instead, are enriched in heavy minerals, with a progressive increase—with decreasing grain size—of heavy mineral concentration, of opaques among total heavy minerals, and of pyroxenes among transparent heavy minerals. These steady trends indicate strong concentration of denser grains within finer grain-size classes for each transport mode, and overall concentration of denser minerals in the bedload with respect to the suspended load.

Grain-size-dependent fractionation results from the hydraulic equivalence of small dense grains with larger and lighter grains (Rubey, 1933; Rittenhouse, 1943; Reid and Frostick, 1985). As a consequence, ferromagnesian silicates in sandy fluvial bedload are expected to have their modal size up to half ϕ class, and ultradense grains up to one full ϕ class, finer than the bulk of the sediment (brown titanian augite up to a fifth of ϕ class finer than blue-green hornblende; Friedman, 1961). Mineralogical differentiation is expected to be somewhat less pronounced for suspended-load sediments. In fact, the observed variation of concentration indices is sharper for the bedload (from HMC 1 and SRD 2.66 in medium sand to HMC 35 and SRD 3.08 in very-fine sand) than for the suspended load (from HMC 2 and SRD 2.67 in fine sand to HMC 16 and SRD 2.82 in coarse silt).

The Blue Nile case demonstrates that tractive currents very effectively segregate minerals with even small differences in density within distinct grain-size fractions. Although partly averaged out when a broad size window is analysed (e.g., 4–2 ϕ), this effect must be given full consideration in heavy mineral studies of sands and sandstones.

9. SUMMARY

Compositional signatures of detrital sediments mirror the combined effects of, at least, three major groups of variables (geology of source terranes, sedimentary processes, diagenesis), each of which alone can cause variations by more than an order of magnitude in both the absolute and relative abundance of heavy mineral species. The superposed effects of these three groups of variables commonly generate considerable uncertainties in provenance interpretation of heavy mineral suites in ancient sediments. However, modern settings where diagenesis has not occurred and information is readily available on topography, climate, sedimentary processes, lithology, and tectonic structure of source areas, can provide suitable conditions in which the relative incidence of each controlling factor can be individually assessed and quantified.

In heavy mineral studies of both modern and ancient deposits, the first and simplest parameter to be taken into account is heavy mineral concentration (defined as HMC index). Not only because it is fundamental while examining (with no matter how much sophisticated technology) a minor component to consider its relative significance in relationship with the information provided by the framework components, but also because heavy mineral concentration *per se* provides us with the most fundamental evidence on provenance, hydraulic sorting, or diagenetic processes.

We have studied detritus eroded from oceanic lithosphere thrusted to the top of obduction orogens, from arc crust produced above subduction zones, from

continental crust exposed in old cratonic shields or young rift escarpments, and from their metamorphosed equivalents incorporated within orogenic belts. We have also documented how the concentration of heavy minerals in modern sands from such different geodynamic settings depends primarily on chemical composition and density of source rocks. As a consequence, heavy mineral concentrations tend, ideally, to increase during unroofing of progressively deeper tectono-stratigraphic levels within the source terrane. Finally, with a series of examples, we have illustrated how heavy mineral concentration indices can be effectively used, in conjunction with ratio parameters based on heavy mineral species with either contrasting density or chemical stability, to assess the effect of hydraulic sorting in sedimentary environments or that of diagenetic dissolution in ancient sandstones.

ACKNOWLEDGEMENTS

The manuscript benefited from careful reviews by Andy Morton and Ervin Otvos. This work has been made possible with the generous help of our colleagues and friends, including Ada Ali Abdel Megid, Paolo Paparella, Stefania Canclini, Giovanna Castiglioni, Andrea Coltura, Giulia Erbetta, Elisabetta Mauri, Stefano Monguzzi, and Cristian Vidimari, who painstakingly generated the numerous data upon which our ideas were based, and Bruno Lombardo, Francesca Serra, Luca Trombino, Renzo Valloni, and Gianni Zuffa, who provided valuable advice drawn from their long experience in the study of heavy minerals. Funding by FIRB 2002 and PRIN 2003 to E. Garzanti.

REFERENCES

Beaumont, C., Ellis, S., Hamilton, J., Fullsack, P., 1996. Mechanical model for subduction-collision tectonics of alpine-type compressional orogens. Geology 24, 675–678.

Blatt, H., Sutherland, B., 1969. Intrastratal solution and non-opaque heavy minerals in shales. Journal of Sedimentary Petrology 39, 591–600.

Boriani, A., Giobbi, E., 2004. Does the basement of Western Southern Alps display a tilted section through the continental crust? A review and discussion. Periodico di Mineralogia, 73, 5–23.

Boudier, F., Juteau, T., 2000. The ophiolite of Oman and United Arab Emirates. Marine Geophysical Researches 21, 145–407.

Bramlette, M.N., 1941. The stability of minerals in sandstone. Journal of Sedimentary Petrology 11, 32–36.

Burbank, D.W., 1992. Causes of recent Himalayan uplift deduced from deposited patterns in the Ganges basin. Nature 357, 680–683.

Carrapa, B., Di Giulio, A., 2001. The sedimentary record of the exhumation of a granitic intrusion into a collisional setting: the lower Gonfolite Group, Southern Alps, Italy. Sedimentary Geology 139, 217–228.

Cibin, U., Cavazza, W., Fontana, D., Milliken, K.L., McBride, E.F., 1993. Comparison of composition and texture of calcite-cemented concretions and host sandstones, Northern Apennines, Italy. Journal of Sedimentary Petrology 63, 945–954.

Coleman, R.G., 1971. Plate tectonic emplacement of upper mantle peridotites along continental edges. Journal of Geophysical Research 76, 1212–1222.

Dal Piaz, G.V., 1999. Austroalpine-Piedmont nappe stack and the puzzle of Alpine Tethys. Memorie della Società Geologica Italiana 51, 155–176.

Daly, R.A., Manger, G.E., Clark, S.P., 1966. Density of rocks, Section 4, Handbook of Physical Constants. Geological Society of America Memoirs, 19–26.

Di Giulio, A., 1999. Mass transfer from the Alps to the Apennines: volumetric constraints in the provenance study of the Macigno-Modino source-basin system, Chattian-Aquitanian, northwestern Italy. Sedimentary Geology 124, 69–80.

Dickinson, W.R., 1985. Interpreting provenance relations from detrital modes of sandstones. In: Zuffa, G.G. (Ed.), Provenance of Arenites. In: NATO ASI Series, vol. 148. Reidel, Dordrecht, pp. 333–361.

Dickinson, W.R., Suczek, C.A., 1979. Plate tectonics and sandstone composition. American Association of Petroleum Geologists Bulletin 63, 2164–2172.

Dye, T.S., Dickinson, W.R., 1996. Sources of sand tempers in prehistoric Tongan pottery. Geoarchaeology 11, 141–164.

El-Sayed, M.I., 1999. Sedimentological characteristics and morphology of the aeolian sand dunes in the eastern part of the U.A.E.: a case study from Ar Rub' Al Khali. Sedimentary Geology 123, 219–238.

Ewart, A., 1976. Mineralogy and chemistry of modern orogenic lavas—some statistics and implications. Earth and Planetary Science Letters 31, 417–432.

Fletcher, W.K., Church, M., Wolcott, J., 1992. Fluvial-transport equivalence of heavy minerals in the sand size range. Canadian Journal of Earth Sciences 29, 2017–2021.

Flores, R.M., Shideler, G.L., 1978. Factors controlling heavy mineral variations on the South Texas outer continental shelf, Gulf of Mexico. Journal of Sedimentary Petrology 48, 269–280.

Fontana, D., Spadafora, E., Stefani, C., Stocchi, S., Tateo, F., Villa, G., Zuffa, G.G., 1994. The Upper Cretaceous Helminthoid Flysch of the Northern Apennines: provenance and sedimentation. Memorie della Società Geologica Italiana 48, 237–250.

Foucault, A., Stanley, D.J., 1989. Late Quaternary palaeoclimatic oscillations in East Africa recorded by heavy minerals in the Nile delta. Nature 339, 44–46.

Fountain, D.M., Percival, J., Salisbury, M.H., 1990. Exposed cross-sections of the continental crust—synopsis. In: Salisbury, M.H., Fountain, D.M. (Eds.), Exposed Cross-Sections of the Continental Crust. In: NATO ASI Series, vol. 317. Kluwer, Dordrecht, pp. 653–662.

Friedman, G.M., 1961. Distinction between dune, beach, and river sands from their textural characteristics. Journal of Sedimentary Petrology 31, 514–529.

Frihy, O.E., Lotfy, M.F., Komar, P., 1995. Spatial variations in heavy minerals and patterns of sediment sorting along the Nile delta, Egypt. Sedimentary Geology 97, 33–41.

Gandolfi, G., Paganelli, L., Zuffa, G.G., 1983. Petrology and dispersal pattern in the Marnoso-Arenacea Formation (Miocene, Northern Apennines). Journal of Sedimentary Petrology 53, 493–507.

Gansser, A., 1980. The Peri-Indian suture zone. In: Auboin, J., Debelmas, J., Latreille, M. (Eds.), Géologie des Châines Alpines issues de la Téthys. Mémories du Bureau de Recherches Géologiques et Minières 115, 140–148.

Garzanti, E., Andò, S., 2007. Plate tectonics and heavy mineral suites of modern sands (this volume).

Garzanti, E., Andò, S., Scutellà, M., 2000. Actualistic ophiolite provenance: the Cyprus Case. Journal of Geology 108, 199–218.

Garzanti, E., Andò, S., Vezzoli, G., 2006a. The continental crust as a source of sand (Southern Alps cross-section, Northern Italy). Journal of Geology 114, 533–554.

Garzanti, E., Andó, S., Vezzoli, G., Ali Abdel Megid, A., El Kammar, A., 2006b. Petrology of Nile River sands (Ethiopia and Sudan): sediment budgets and erosion patterns. Earth and Planetary Science Letters 252, 327–341.

Garzanti, E., Andò, S., Vezzoli, G., Dell'Era, D., 2003. From rifted margins to foreland basins: investigating provenance and sediment dispersal across desert Arabia (Oman, UAE). Journal of Sedimentary Research 73, 572–588.

Garzanti, E., Canclini, S., Moretti Foggia, F., Petrella, N., 2002a. Unravelling magmatic and orogenic provenances in modern sands: the back-arc side of the Apennine thrust-belt (Italy). Journal of Sedimentary Research 72, 2–17.

Garzanti, E., Scutellà, M., Vidimari, C., 1998. Provenance from ophiolites and oceanic allochthons: modern beach and river sands from Liguria and the Northern Apennines (Italy). Ofioliti 23, 65–82.

Garzanti, E., Vezzoli, G., Andò, S., 2002b. Modern sand from obducted ophiolite belts (Oman, U.A.E.). Journal of Geology 110, 371–391.

Garzanti, E., Vezzoli, G., Andò, S., Castiglioni, G., 2001. Petrology of rifted-margin sand (Red Sea and Gulf of Aden, Yemen). Journal of Geology 109, 277–297.

Garzanti, E., Vezzoli, G., Andò, S., France-Lanord, C., Singh, S.K., Foster, G., 2004b. Sediment composition and focused erosion in collision orogens: the Brahmaputra case. Earth and Planetary Science Letters 220, 157–174.

Garzanti, E., Vezzoli, G., Andò, S., Paparella, P., Clift, P.D., 2005. Petrology of Indus River sands: a key to interpret erosion history of the Western Himalayan Syntaxis. Earth and Planetary Science Letters 229, 287–302.

Garzanti, E., Vezzoli, G., Lombardo, B., Andò, S., Mauri, E., Monguzzi, S., Russo, M., 2004a. Collision-orogen provenance (Western and Central Alps): detrital signatures and unroofing trends. Journal of Geology 112, 145–164.

Gazzi, P., 1965. On the heavy mineral zones in the geosyncline series, recent studies in the Northern Apennines, Italy. Journal of Sedimentary Petrology 35, 109–115.

Gill, J., 1981. Orogenic Andesites and Plate Tectonics. Springer-Verlag, Berlin, 390pp.

Greenwood, J.E.G.W., Bleackley, D., 1967. Geology of the Arabian Peninsula. Aden Protectorate. Geological Survey, Professional Paper 560-C, 96pp.

Guillot, S., Garzanti, E., Baratoux, D., Marquer, D., Mahéo, G., De Sigoyer, J., 2003. Reconstructing the total shortening history of the NW Himalaya. Geochemistry, Geophysics, Geosystems 4, 1064.

Handy, M.R., 1990. The exhumation of cross sections of the continental crust: structure, kinematics and rheology. In: Salisbury, M.H., Fountain, D.M. (Eds.), Exposed Cross-Sections of the Continental Crust. In: NATO ASI Series, vol. 317. Kluwer, Dordrecht, pp. 485–507.

Hubert, J.F., 1962. A zircon-tourmaline-rutile maturity index and the interdependence of the composition of heavy minerals assemblages with the gross composition and texture of sandstones. Journal of Sedimentary Petrology 32, 440–450.

Hughes, M.G., Keene, J.B., Joseph, R.G., 2000. Hydraulic sorting of heavy mineral grains by swash on a medium-sand beach. Journal of Sedimentary Research 70, 994–1004.

Ingersoll, R.V., 1990. Actualistic sandstone petrofacies: discriminating modern and ancient source rocks. Geology 18, 733–736.

Ingersoll, R.V., Dickinson, W.R., Graham, S.A., 2003. Remnant-ocean submarine fans: largest sedimentary systems on Earth. Geological Society of America Special Paper 370, 191–208.

Juteau, T., Manac'h, G., Moreau, O., Lécuyer, C., Ramboz, C., 2000. The high temperature reaction zone of the Oman ophiolite: new field data, microthermometry of fluid inclusions, PIXE analyses and oxygen isotopic ratios. In: Boudier, F., Juteau, T. (Eds.), The Ophiolite of Oman and United Arab Emirates, vol. 21. Marine Geophysical Research, pp. 351–385.

Komar, P.D., Wang, C., 1984. Processes of selective grain transport and the formation of placers in beaches. Journal of Geology 92, 637–655.

Lippard, S.J., Shelton, A.W., Gass, I.G., 1986. The Ophiolites of Northern Oman. Blackwell, London, 178pp.

Malpas, J., Moores, E., Panayiotou, A., Xenophontos, C., 1990. Oceanic crustal analogues. In: Proceedings of the Symposium "Troodos 1987", Geological Survey Department, Ministry of Agriculture and Natural Resources, Nicosia, 733pp.

Mange, M.A., Maurer, H.F.W., 1992. Heavy Minerals in Colour. Chapman and Hall, London, 147pp.

McBride, E.F., 1985. Diagenetic processes that affect provenance determinations in sandstones. In: Zuffa, G.G. (Ed.), Provenance of Arenites. In: NATO ASI Series, vol. 148. Reidel, Dordrecht, pp. 95–113.

McClure, H.A., 1984. Late Quaternary palaeoenvironments of the Rub' Al Khali. Ph.D. Thesis. University of London, 245pp.

Morton, A.C., 1985. Heavy minerals in provenance studies. In: Zuffa, G.G. (Ed.), Provenance of Arenites. In: NATO ASI Series, vol. 148. Reidel, Dordrecht, pp. 249–277.

Morton, A.C., Hallsworth, C.R., 1999. Processes controlling the composition of heavy mineral assemblages in sandstones. Sedimentary Geology 124, 3–29.

Muttoni, G., Carcano, C., Garzanti, E., Ghielmi, M., Piccin, A., Pini, R., Rogledi, S., Sciunnach, D., 2003. Onset of major Pleistocene glaciations in the Alps. Geology 31, 989–992.

Najman, Y., Garzanti, E., 2000. An integrated approach to provenance studies: reconstructing early Himalayan palaeogeography and tectonic evolution from Tertiary foredeep sediments (N. India). Geological Society of America Bulletin 112, 435–449.

Najman, Y., Garzanti, E., Pringle, M., Bickle, M., Stix, J., Khan, I., 2003a. Early-Middle Miocene paleodrainage and tectonics in the Pakistan Himalaya. Geological Society of America Bulletin 115, 1265–1277.

Najman, Y., Pringle, M., Bickle, M., Garzanti, E., Andò, S., Burbank, D., Brozovic, N., 2003b. Determining orogenic exhumation, steady state, and frontal accretion, using the sediment record: an example from the Himalayan foreland basin. Abstract, EGS-AGU-EUG Meeting, Nice.

Nicolas, A., Boudier, F., 1991. Rooting of the sheeted dike complex in the Oman ophiolite. In: Peters, T., Nicolas, A., Coleman, R.G. (Eds.), Ophiolite Genesis and Evolution of Oceanic Lithosphere. Kluwer, Dordrecht, pp. 39–54.

Palomares, M., Arribas, J., 1993. Modern stream sands from compound crystalline sources; composition and sand generation index. In: Johnsson, M.J., Basu, A. (Eds.), Processes Controlling the Composition of Clastic Sediments. Geological Society of America Special Paper 284, 313–322.

Parfenoff, A., Pomerol, C., Tourenq, J., 1970. Les minéraux en grains—méthodes d'étude et détermination. Masson, Paris, 578pp.

Pettijohn, F.J., 1941. The persistence of minerals and geologic age. Journal of Geology 49, 610–625.

Pflumio, C., 1991. Evidences for polyphased oceanic alteration of the extrusive sequence of the Semail Ophiolite from the Salahi Block (northern Oman). In: Peters, T., Nicolas, A., Coleman, R.G. (Eds.), Ophiolite Genesis and Evolution of Oceanic Lithosphere. Kluwer, Dordrecht, pp. 313–351.

Reid, I., Frostick, L.E., 1985. Role of settling, entrainment and dispersive equivalence and of interstice trapping in placer formation. Journal of the Geological Society of London 142, 739–746.

Rittenhouse, G., 1943. Transportation and deposition of heavy minerals. Geological Society of America Bulletin 54, 1725–1780.

Rivalenti, G., Garuti, G., Rossi, A., Siena, F., Sinigoi, S., 1981. Existence of different peridotite types and of a layered igneous complex in the Ivrea Zone of the Western Alps. Journal of Petrology 22, 127–153.

Robinson, P.T., Malpas, J., 1990. The Troodos ophiolite of Cyprus: new perspectives on its origin and emplacement. In: Malpas, J., Moores, E.M., Panayiotou, A., Xenophontos, C. (Eds.), Ophiolites, Oceanic Crustal Analogues. Geol. Surv. Dept. Nicosia, pp. 13–26.

Rubey, W.W., 1933. The size-distribution of heavy minerals within a water-laid sandstone. Journal of Sedimentary Petrology 3, 3–29.

Searle, M.P., Stevens, R.K., 1984. Obduction processes in ancient, modern and future ophiolites. In: Gass, I.G., Lippard, S.J., Shelton, A.W. (Eds.), Ophiolites and Oceanic Lithosphere. In: Geological Society of London Special Publication, vol. 13, pp. 303–319.

Sinigoi, S., Quick, J.E., Mayer, A., Demarchi, G., 1995. Density-controlled assimilation of underplated crust, Ivrea-Verbano Zone, Italy. Earth and Planetary Science Letters 129, 183–191.

Szulc, A.G., Najman, Y., Sinclair, H.D., Pringle, M., Bickle, M., Chapman, H., Garzanti, E., Andò, S., Huyghe, P., Mugnier, J-L., Ojha, T., DeCelles, P., 2006. Tectonic evolution of the Himalaya constrained by detrital ^{40}Ar-^{39}Ar, Sm-Nd and petrographic data from the Siwalik foreland basin succession, SW Nepal. Basin Research 18, 375–391.

Taylor, S.R., McLennan, S.M., 1985. The Continental Crust: Its Composition and Evolution. Blackwell, Oxford, 312pp.

Valloni, R., Lazzari, D., Calzolari, M.A., 1991. Selective alteration of arkose framework in Oligo-Miocene turbidites of the Northern Apennines foreland: impact on sedimentary provenance analysis. In: Morton, A.C., Todd, S.P., Haughton, P.D.W. (Eds.), Developments in Sedimentary Provenance Studies. In: Geological Society of London Special Publication, vol. 57, pp. 125–136.

Vielzeuf, D., Clemens, J.D., Pin, C., Moinet, E., 1990. Granites, granulites, and crustal differentiation. In: Vielzeuf, D., Vidal, Ph. (Eds.), Granulites and Crustal Evolution. In: NATO ASI Series, vol. C 311. Kluwer, Dordrecht, pp. 59–85.

Weltje, G.J., 2002. Quantitative analysis of detrital modes: statistically rigorous confidence methods in ternary diagrams and their use in sedimentary petrology. Earth-Science Reviews 57, 211–253.

White, N., Pringle, M., Garzanti, E., Bickle, M., Najman, Y., Chapman, H., Friend, P., 2002. Constraints on the exhumation and erosion of the High Himalayan slab, NW India, from foreland basin deposits. Earth and Planetary Science Letters 195, 29–44.

Wicks, F.J., Whittaker, E.J.W., 1977. Serpentine textures and serpentinization. Canadian Mineralogist 15, 459–488.

Windley, B.F., Whitehouse, M.J., Ba-Bttat, M.A.O., 1996. Early Precambrian gneiss terranes and Pan-African island arcs in Yemen: crustal accretion of the eastern Arabian Shield. Geology 24, 131–134.

Zingg, A., Handy, M.R., Hunziker, J.C., Smith, S.M., 1990. Tectonometamorphic history of the Ivrea-Verbano Zone and its relationship to the crustal evolution of the Southern Alps. Tectonophysics 182, 169–192.

This page intentionally left blank

Chapter 21

THE RIVERS OF SOUTHEAST IRELAND AND THE SANDS OF THE IRISH SEA: HEAVY MINERALS SHOW THAT PROXIMITY DOES NOT ALWAYS PREDETERMINE PROVENANCE

JOHN MALONE

John S. Herold 14 Westport Avenue Norwalk, CT 06851, USA

ABSTRACT

In an attempt to quantify the denudation rate of the highlands of southeastern Ireland, researchers at Trinity College Dublin conducted an analysis of the flux of sediment being carried by the region's rivers to the Irish and Celtic Seas. Mineralogical "fingerprints" were identified for the sediment from each of the major local rivers and compared to the mineralogy of seabed sediments to determine whether seabed sands were derived from southeastern Ireland.

The region's four main river catchments—the Slaney, Liffey, Avoca and Vartry and the Barrow—are made up of a wide range of bedrock types. Each river's basin encompasses bedrock of the Leinster Massif, characterised by a approximately 1500 km^2 Caledonian-age batholith, along with rocks of the surrounding metamorphic aureole and low metamorphic country rock. This bedrock variety is reflected in the heavy mineral assemblage of each river. The major sediment routing systems of southeastern Ireland in the vicinity of the Leinster Massif were examined and quantified.

The heavy mineral suite of each river is closely related to the river's catchment lithology. The heavy mineral suites of offshore sediments indicate that the sands of the Irish Sea are not derived from southeastern Ireland, as the offshore suites show a preponderance of the clinopyroxene augite, which is not found with any frequency in river sediment. The beaches of southeast Ireland also show large augite proportions, indicating that beach sands are largely derived from offshore sources.

Garnet chemistry reveals that the proportions of calcium, magnesium and manganese in each garnet vary according to source. Garnets from the Irish Sea and southeastern Irish rivers confirm that the offshore sediments in the Irish Sea are not derived from the nearby Irish landmass. The bulk of sediment was delivered by glacial processes from the direction of Northern Ireland and Scotland. Glaucophane in offshore and some beach sediments indicates a possible ice lobe that transported material from the high-pressure-ophiolite subduction complex of Anglesey, North Wales.

Keywords: Southeastern Ireland; Irish Sea; river sediment mineralogy; principal components analysis; Fenitian glaciation; provenance

Developments in Sedimentology, Vol. 58, 547–568

ISSN: 0070-4571/doi:10.1016/S0070-4571(07)58021-0

1. INTRODUCTION

In an attempt to quantify the denudation rate of the highlands of southeastern Ireland, researchers at Trinity College Dublin conducted an analysis of the flux of sediment being carried by the region's rivers to the Irish and Celtic Seas. The measurement of suspended sediment is a fairly straightforward process, essentially involving the measurement of the mass of material carried in a known volume of water. Measuring the flux bedload, the portion of material that is carried as sand, is a more difficult endeavour. Generally bedload is assumed to be a percentage of the total measured suspended sediment load (usually in the order of 10%: Gaillardet et al., 1995).

Establishing mineralogical "fingerprints" for river sediments can provide insight into the provenance of downstream sediment, and help determine whether or not a particular river is contributing bedload sediment to a downstream basin. Heavy mineral analysis is one of the most useful methods of establishing these fingerprints, since the composition of heavy mineral suites can indicate the nature of the sediment's source.

This contribution outlines the methodology and results of the analysis of sediment from the major rivers and beaches of southeastern Ireland, and the comparison of these sediments to sediment samples from the Irish Sea Basin offshore of Ireland, to determine whether the regional seabed sediment is derived from the nearby Irish landmass. The heavy mineral suites from each sample are isolated, analysed quantitatively and compared using multivariate statistical methods.

1.1. Regional Geology

The geology of southeast Ireland is dominated by the Leinster Massif, which comprises a variable Early Palaeozoic succession of marine sedimentary rocks (largely shales and greywackes) along with Ordovician alkaline volcanics. These country rocks has intruded a Caledonian batholith known as the Leinster Granite (O'Connor and Reimann, 1993). The intrusion generated a contact-metamorphic aureole of primarily phyllites and schists. Later marine deposition created a succession of carbonate rocks to the west and south of the granite, with exposure of limestones as young as the Carboniferous (Fig. 1).

1.2. Quaternary History of the Region

The most recent glaciation that affected the Irish landmass, termed the Fenitian, lasted approximately 63,000 years, commencing approximately 73,000 years B.P. and ending approximately 10,000 years B.P. (Warren, 1993). Two large ice sheet systems were active in the area of the Leinster during the Fenitian glaciation. The first moved to the east from the Midlands of central Ireland, developing from two large domes or ice spreading centres to the north and west (termed Midlands Ice) (Fig. 2). From the east, a second ice lobe from the Irish Sea (ultimately from Scotland) moved south/southeast and pushed up onto the eastern coastline, depositing seafloor material onto land. This Irish Sea lobe reached up onto the highlands of the Leinster Massif in the east. To the north of the Leinster Massif the Midland and Irish Sea lobes met in a line roughly parallel to the present day coastline; the Midlands lobe was diverted from its

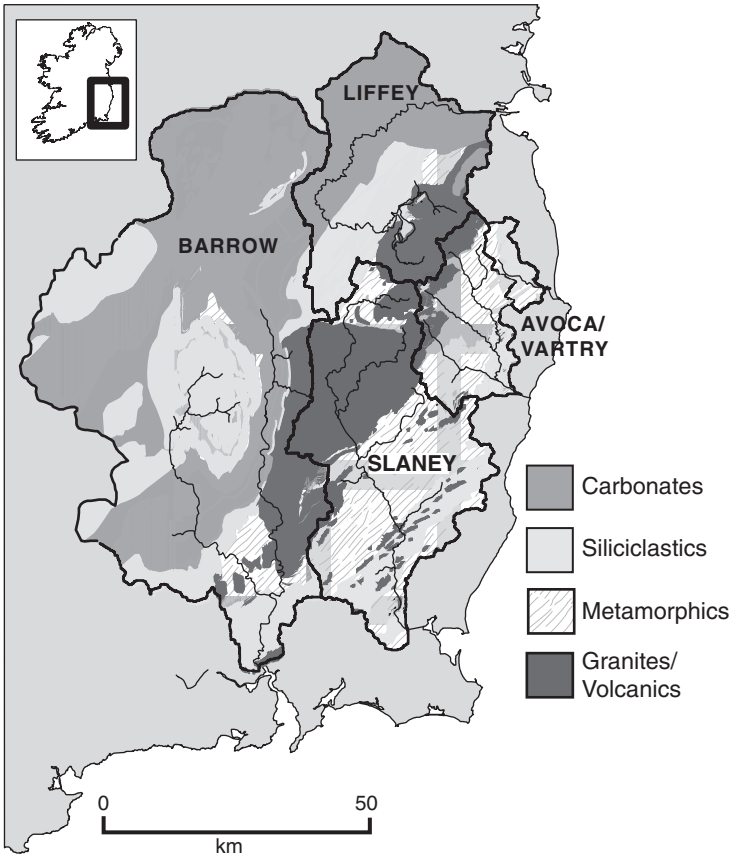

Fig. 1. Catchment bedrock lithologies for the Avoca, Vartry, Barrow, Liffey and Slaney river catchments. [After Tietzsch-Tyler and Sleeman (1994a, 1994b).]

southeasterly course by the highlands of the northern Leinster Massif, while the Irish Sea lobe ran parallel to the coast, east of the Massif. Concurrently, a number of smaller Alpine glaciers travelled down from the Leinster Massif highlands.

The glacially derived sands of the Irish Sea lobe blanket the seafloor of the western Irish Sea along the southeastern coast of Ireland. Surveys by the Geological Survey of Ireland (GSI) of the seabed of the western Irish Sea, off the coast of southeastern Ireland, show that seafloor sand and gravel deposits are in places over 100 m thick. Onshore, glacially derived tills cover much of the low-lying areas of the Leinster Massif. Along the Slaney Valley thicknesses are in the 10–20 m range, while deposits pushed onshore by Irish Sea ice along the eastern coast can be up to 50 m thick along the southern coast, and up to 100 m thick along the coast east of the Leinster Massif (Tietzsch-Tyler and Sleeman, 1994a, 1994b). While erratics from the Midlands and Irish Sea ice sheets are found in tills overlying bedrock composed of Leinster granites or metamorphic rocks of the contact aureole, the vast bulk of the tills in the area are locally derived.

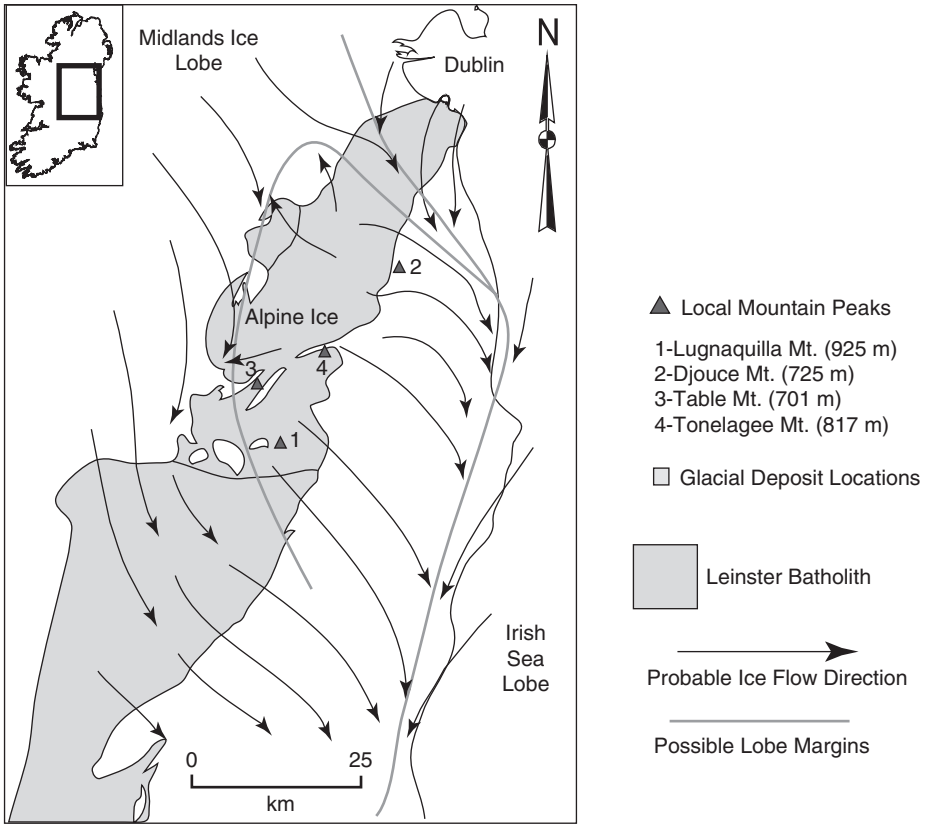

Fig. 2. Patterns of ice movement during the maximum of the Fenitian glaciation. [After Warren (1993).]

1.3. Catchment Lithologies

The River Liffey, with a drainage basin of 1480 km^2, drains the northern part of the Leinster Massif. The basin bedrock comprises (heading downriver) granites of the northern batholith; metamorphic rocks of the surrounding contact aureole; a series of Cambrian, Ordovician and Silurian greywackes and shales; and large areas of Carboniferous limestone. The Quaternary cover of the area is composed of units of two distinct provenances that blend into one another: in the upper catchment, the river incises through tills derived from Alpine ice from the Massif highlands, while downstream the river cuts through Midlands ice till.

For the purposes of this study, the contiguous Avoca and Vartry catchments are treated as one system, with a combined area of 740 km^2. The Avoca is fed by four major tributaries, all of which have their headwaters in the granitic rocks of the Leinster Massif. The bedrock in this area is mostly coarse microcline granites, with occasional pegmatites. Further downstream, the Avoca and its tributaries pass through phyllites, schists and slates. A series of lamprophyre sheets run roughly

parallel to the igneous/metamorphic bedrock contact. The upper reaches of the catchment are overlain with tills from Alpine glaciation, while close to the river mouth are deposits left by Irish Sea ice.

Of the rivers studied, the catchment of the River Vartry contains the fewest number of different bedrock lithologies. The bulk of the bedrock of the eastern and southern portions of the catchment is made up of greywackes, shales and quartzites. In the western and southern headwaters of the Vartry catchment the bedrock is composed of slates, phyllites and schists, while in the far south of the catchment outcrops of buff slate and silver micaceous schists are found.

With a catchment area of 1987 km^2, the River Slaney drains the largest portion of the Leinster Massif of all the rivers studied. From its source in the highlands of the Leinster granite, the river flows across the contact aureole surrounding the granite (a series of Cambrian and Ordovician metasediments) into a region of fine- to medium-grained mudstones and slates. The river then passes into a region of Cambrian turbidites interspersed with thin quartzites before debouching into the Irish Sea. Like the Liffey, Avoca and Vartry, the Slaney incises local Alpine glacier tills in its headwaters. Downstream, however, the river moves through tills deposited by both Midlands and Irish Sea ice left behind as the two lobes interacted south of the Massif.

The River Barrow has the largest total drainage area of the rivers examined here (5014 km^2), but it drains the smallest area of the Leinster Massif. The majority of the catchment is Carboniferous limestone, interspersed with occasional outcrops of metasedimentary rocks and andesitic/basaltic sheets. Most of these carbonates have undergone a process of dolomitisation. In the eastern part of the catchment, a series of small tributaries drain the western edge of the Leinster Massif and carry igneous and metamorphic material into the Barrow channel proper. Midlands ice covered most of the Barrow catchment during the last glaciation, with some Alpine ice flowing down from the highlands to the east.

2. METHODOLOGY

Sediments from four major river catchments in the region of the Leinster Massif—viz. those of the Liffey, Avoca and Vartry, Slaney and Barrow—and from local beaches were sampled for comparison with Irish Sea sands to determine the provenance of seabed sands (Fig. 1). A total of 119 samples were taken for laboratory analysis: 53 from the local rivers, 39 from the Irish and Celtic Sea seabeds and 27 from beaches (Fig. 3). Of the 53 river samples, 21 are from the Slaney, 15 from the Liffey, 8 from the Barrow, 6 from the Avoca and 3 from the Vartry (the Vartry and Avoca are, in this study, treated as 1 river system as their catchment lithologies are similar). River samples were taken whenever possible from within the active river channels; otherwise sampling was done on point or longitudinal bars. Beach samples are from the area of the high tide line, and were often taken from obvious heavy mineral lags in the beach sands (which may bias the total heavy mineral count).

Twenty-seven samples were taken along the coastline of southeastern Ireland, 23 from beaches and 4 from coastal bluffs composed of till. Each beach sample was taken in the region of the high tide line; in cases where heavy mineral lags were

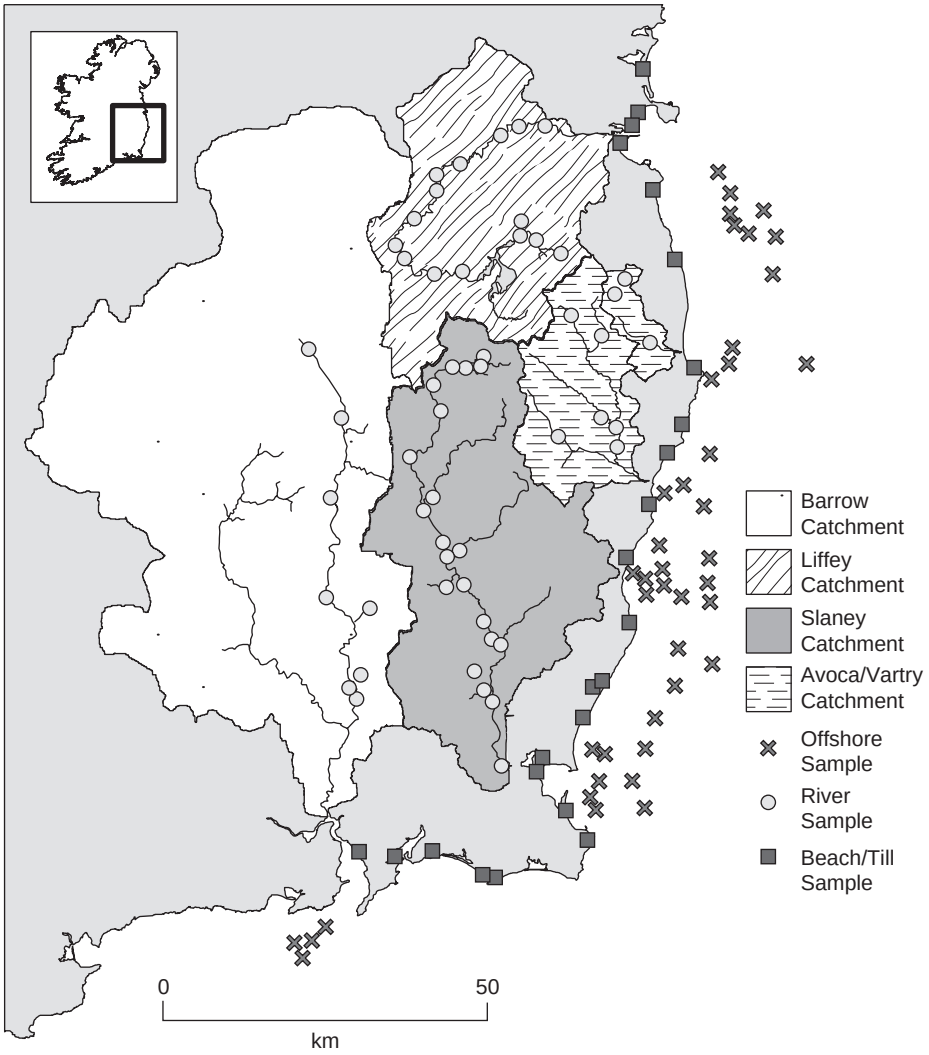

Fig. 3. Locations of river and seabed samples.

observed in the sand. Samples labelled as "beach" were also taken from bluffs composed of glacial till along the coastline. Offshore samples, 35 from the eastern Irish Sea and 4 from the Celtic Sea offshore of Waterford, were provided by the GSI (Fig. 3). All offshore samples are surficial and were taken by a grab sampler. Offshore samples were chosen from the GSI archives according to sand content, as the heavy minerals analysed in this study occur primarily in the sand sized fraction of sediments. The maximum water depth from which a sample was obtained was 46 m.

All sediment samples were analysed granulometrically. Each was divided into four subsamples by wet sieving: (i) larger than $-1\,\varphi$ (2 mm), (ii) between –1 and $1\,\varphi$ (2 mm–500 μm), (iii) between 1 and $4\,\varphi$ (500–63 μm) and (iv) smaller than $4\,\varphi$. The

mass of silt/mud/clay ($<4\,\varphi$) was calculated as the mass lost by washing each sample on a 63 μm mesh sieve. This procedure can lead to the exaggeration of the percentage of silt/mud/clay in offshore samples, as the presence of sea salt can add extra mass that will be lost in sieving (Grosz, 1993).

The gravel and coarse to medium sand fractions (all grains are larger than 500 μm in diameter) were weighed and discarded, and finer than 63 μm washed away. The finer silt fraction can also be rich in heavy minerals (Mange-Rajetzky, 1983). However in the present study, the finer fraction was discounted because the ease of transport of finer sediment in suspension can lead to a wider distribution of material of more distal provenance (Behrends et al., 1998), thus hindering any attempt to correlate offshore sand bodies with onshore input. Discounting this fraction can, however, lead to inaccurate counts of the total of particular heavy mineral species such as zircon. As the aim of the present study is to identify sediment fingerprints, not to establish resource potential, ignoring the finer fraction was considered acceptable.

Subsamples of approximately 100 g each of the 63–500 μm fraction were isolated and placed into glass funnels containing between 1 and 1.5 l of lithium heteropolytungstate solution (LST). LST is a non-toxic heavy liquid, with a maximum density of 2.96 g/cm^3. The liquid's density (ρ) and viscosity (μ) are largely temperature-dependent; in this study the liquid was kept at approximately 20 °C, which results in a density of approximately 2.88 g/cm^3 and a viscosity of approximately 13 cP.

Following a reconnaissance study of the first heavy mineral suites, it was decided to further separate the heavy mineral suites by grain size. A large number of "alterite" grains (unidentifiable polyminerallic grains) and rock fragments were encountered. These unidentifiable grains were on average larger than the heavy mineral grains. The samples were, therefore, subdivided into two subsamples: one of grain sizes between 250 and 500 μm, the other between 63 and 250 μm. The coarser-grained of these two subsamples was found to be almost exclusively alterites and rock fragments, and therefore all subsequent heavy mineral suites were similarly divided, with only the finer fraction used for later analysis. All heavy mineral suites referenced in this study, therefore, are taken from 63 to 250 μm fraction of the sediment under examination; it is important to note that any subsequent references to a sample's "heavy mineral suite" or "heavy mineral assemblage" refer to the proportions of mineral species identified within this particular grain size range. It should not be inferred that the assemblage identified for each sample necessarily represents the entire range of heavy minerals within that sample. To eliminate carbonate grains, all heavy mineral suites were placed in a 10% acetic acid solution for approximately 48 h each following liquid separation. Alterites, opaques and carbonates not removed by acid treatment were not counted. An estimate of their proportion in each sample was, however, calculated by counting the number of each in one ribbon during point counting, and multiplying these numbers by the total number of ribbons counted.

The separates were then washed, cleaned ultrasonically and dried. The heavy mineral fraction was then split according to the method described by Hutton (1950), which involves pouring the mineral grains into a cone and quartering them with a razor. This method precludes any bias by grain sorting. This subsample was mounted onto a glass slide using Canada balsam (index of refraction = 1.538). The

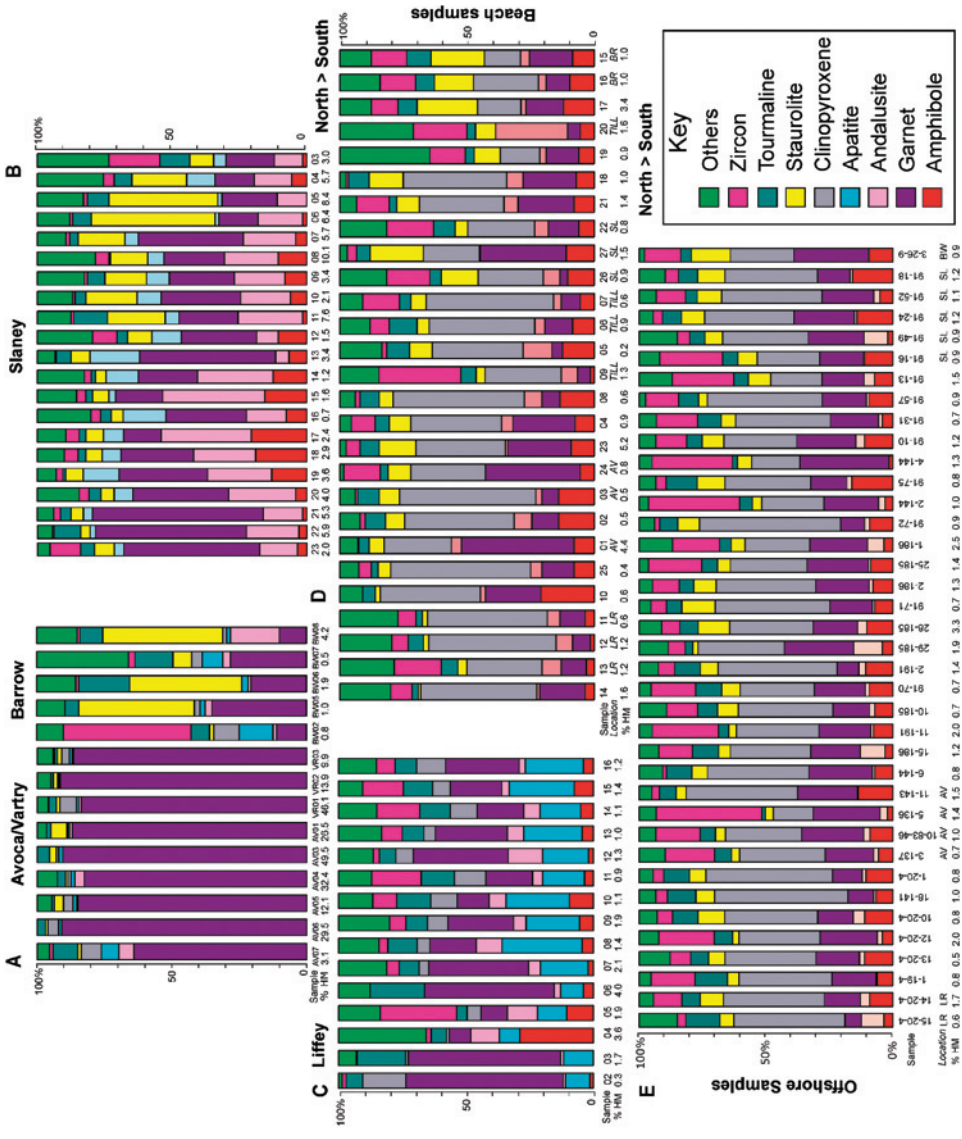
A
Avoca/Varty
Barrow
B
Slaney
C
Liffey
D
North > South
Beach samples
E
Offshore Samples
Key
Others
Zircon
Tourmaline
Staurolite
Clinopyroxene
Apatite
Andalusite
Garnet
Amphibole

mounts were examined optically using a Nikon E400 petrographic microscope, and 200 grains per mount were counted using the ribbon method (Galehouse, 1971).

3. ONSHORE HEAVY MINERAL RESULTS

It is important to note that the heavy mineral results described here are as percentages, so that a sample's heavy mineral suite can have a high percentage of a certain mineral, but the sand samples can have very little in the way of total heavy minerals. Two samples with the same percentage of a particular mineral species can have very different total counts for that species.

The heavy mineral suites found in each of the river catchments, the beaches and offshore are for the most part easily differentiated from one another, based on the proportions of certain diagnostic minerals that are largely related to bedrock lithology. In the following section, the heavy mineral assemblages of samples collected along each river are examined, and the resultant sedimentological signatures correlated to the catchment rocks.

3.1. Avoca and Vartry Catchment Heavy Mineralogy

Due to the small size of the Vartry catchment and its limited variety of bedrock lithologies (essentially higher grade metamorphics upstream and low grade to unmetamorphosed sedimentary rocks nearer to the mouth), only three samples were taken along its length (Fig. 4A). Garnets dominate the heavy mineral assemblage, and are for the most part rounded with dark cores; occasionally, however, they occur as clear anhedral fragments. Geochemical analysis (discussed later) showed them to be mostly almandine to an almandine-spessartine solid solution, which is characteristic of the metasedimentary bedrock source (Nesse, 1991).

High proportions of garnet are the defining characteristic of the Vartry samples. It is probable that the metamorphic bedrock provides the source of the garnets; an early study of the heavy mineralogy of the area (Smithson, 1923) showed that the local phyllites and schists contain numerous garnets, often rounded and with dark inclusions. Such garnets form the bulk of those found in sample VR02.

One of the Vartry samples (VR01) also includes grains of augite, a common constituent of ultramafic to intermediate igneous rocks (Deer et al., 1996). Augite

Fig. 4. (A–C) Representative heavy mineral suites of river samples, shown from upstream to downstream (= left to right). (D) Representative heavy mineral suites from local beaches arranged from north to south (= left to right). (E) Heavy mineral suites from offshore samples, arranged from north to south (= left to right). Location of beach samples indicates samples taken close to river mouths (AV = Avoca/Vartry, BW = Barrow, LR = Liffey, SL = Slaney) or from till bluffs (TILL). Location of offshore samples show samples taken close to river mouths (AV = Avoca/Vartry, BW = Barrow, LR = Liffey, SL = Slaney). Others include: amphibole, epidote, hornblende, kyanite, orthopyroxene, rutile, sillimanite, sphene. HM% denotes the percentages of each mineral in the total heavy mineral suite of each sample.

presents an interesting puzzle throughout this study, since (as will be shown later) Irish Sea and beach samples are defined by its abundance. Augite is also found with some frequency in the Liffey drainage basin, and in the suites of isolated samples from the Slaney and Avoca catchments. In addition to mafic sources, augite may be derived from more silicic rocks such as diorites or granodiorites (Nesse, 1991). Both of these rock types are found in the Leinster Massif.

The catchment of the Vartry, however, contains none of the bedrock types that would account for the presence of augite. Only two possibilities exist to explain its occurrence in the Vartry catchment. Firstly, augite grains could be found in the local greywackes and shales, and are being recycled into the present river systems. This is unlikely, however, because the morphology of the grains found in the Vartry (sub- to euhedral, with fairly distinct "hacksaw" terminations, Fig. 5: CPX) seems to preclude recycling, which would produce much more rounded grains.

A more likely explanation derives from the fact that, during the last glaciation, ice from the Irish Sea and the Midlands converged on the northeastern margin of the Leinster Massif in the area of the Vartry catchment. It is, therefore, possible that this "foreign" ice introduced grains from outside the Vartry catchment; this explanation

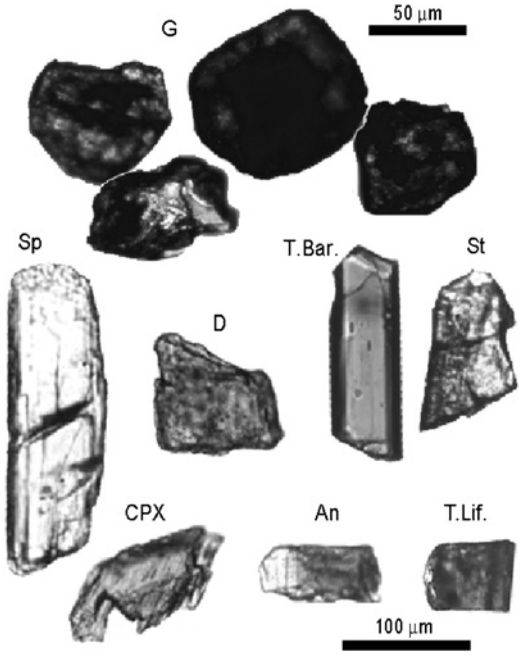

Fig. 5. Characteristic heavy minerals in the river sediments. G: Garnet from sample AV01. Garnets in the Avoca and Vartry catchments are generally anhedral or well-rounded, and often have dark cores. Sp: Clinopyroxene, presumed to be the lithium clinopyroxene spodumene. D: Dolomite rhomb from sample BW02. T.Bar.: Euhedral tourmaline from sample BW08. The dark color and pleochroism of this grain suggest it to be the Fe-bearing tourmaline schorl. St: staurolite from BW08. CPX: Augite from the Vartry River, exhibiting diagnostic "hacksaw" terminations at the edges. T.Lif.: Typical Liffey tourmaline in sample LR16. An: Andalusite from sample LR16.

becomes especially credible when it is considered that augite is found with some abundance in areas (the Liffey catchment, the Irish Sea) that are situated directly "up-ice" of the Vartry basin. Downstream Vartry samples are comparatively low in pyroxenes.

A single non-augite pyroxene grain was identified in the Vartry catchment. It is a clear clinopyroxene with a very small extinction angle (the augite identified in this study, in contrast, is almost universally honey-brown and has an extinction angle of approximately 40°). It is thought that this pyroxene is spodumene (Fig. 5: Sp), a lithium-rich mineral derived from lithium pegmatites (Deer et al., 1996). Such pegmatites do, in fact, outcrop in the area of the Leinster Granite (McArdle and Kennan, 1987; O'Connor et al., 1991); however, no pegmatite-bearing rocks are mapped in the Vartry catchment. Pegmatites have been described along the southeastern margin of the Leinster Granite, as well as among the smaller satellite granites in the eastern Massif. Spodumene-bearing pegmatites have also been mapped on the east coast of County Dublin in the area of Killiney. It is unclear how spodumene grains could be found in the catchment of the River Vartry, as any tills introduced from outside the catchment would have come from the north or east (the pegmatites are found to the southwest). It is possible that Alpine ice may have brought material into the catchment from the Avoca drainage basin.

Other than the minerals mentioned above, the three samples of the Vartry catchment contain minute amounts of lesser heavy minerals. Small amounts of epidote-clinozoisite are found, in keeping with a low- to medium-grade bedrock source (Mange and Maurer, 1992). Occasional grains of euhedral (but highly abraded) tourmaline also occur, as do well-weathered grains of hornblende and actinolite-amphiboles. Staurolite and sillimanite are also present in minute quantities.

Six samples were taken in the Avoca catchment; each tributary feeding the Avoca system was sampled at least once. As with the samples from the Vartry catchment, Avoca samples are very rich in garnet. Sample AV07 was taken at the Glenmacnass waterfall, an abrupt change in elevation that marks the contact between the microcline porphyritic granite of the Leinster Granite and the lower elevation metamorphic contact aureole rocks. AV07 is distinct from the other samples of the Avoca catchment in that it has a lower proportion of garnet, and elevated proportions of igneous heavy minerals. Tourmaline, apatite and clinopyroxene make up the bulk of the non-garnet fraction, along with the contact-metamorphic mineral andalusite (Fig. 5: An). Spodumene was also found; its presence is enigmatic as no lithium-bearing pegmatites are mapped in this section of the catchment. It is likely that these spodumene grains are derived from an as yet unmapped area of lithium-bearing pegmatite in the granites of the northern or eastern catchment. The remainder of the clinopyroxenes is augite, possibly derived from Type I granodiorites to the northeast of the granite/aureole contact.

The rest of the Avoca samples are dominated by garnet, mostly in the form of rounded grains (Fig. 5: G). AV01, from the northern Avonmore tributary channel in Maulin metamorphic rocks (phyllites and schists), contains small quantities of staurolite. Occasionally rutile also occurs, but it is entirely absent in Vartry samples. As with the Vartry, the presence of such high proportions of garnet is most likely due to incision through contact-metamorphic rocks, which comprise half of the total area of the Avoca and Vartry catchments.

3.2. Slaney Catchment Heavy Mineralogy

The Slaney catchment, although smaller than that of the Barrow, actually drains the largest area of the Leinster Massif of any of the rivers studied (Fig. 1). The samples, taken from the headwaters, have very high proportions of spessartine garnet and andalusite, derived from local coticules (metamorphic rocks composed of spessartine garnet, mica and quartz). Moderate proportions of euhedral tourmaline and zircon represent input from igneous sources. As with all other river samples from the highlands of the batholith, all grains are dominantly euhedral.

Farther downstream, as the river incises the schists and local andesites, its heavy mineral signature begins to change. Garnet counts decrease while the proportions of other metamorphic minerals increase, including hornblende (along with other amphiboles), sillimanite, staurolite and especially andalusite. Downstream, the Slaney heavy mineral suite is dominated by large grains of staurolite, interspersed with (on average) slightly smaller grains of andalusites and purplish etched garnet grains. Other mineral proportions vary widely. While the upper reaches of the Slaney show a variety of different signatures due to tributaries' inputs, the large expanse of the contact aureole in the Slaney catchment produces a metamorphic signature that characterises the sediment being carried to the sea (Fig. 4B).

3.3. Liffey Catchment Heavy Mineralogy

The Liffey, unlike the Avoca and Vartry, carries sediment that is relatively low in heavy mineral percentages (Fig. 4C). The upstream samples taken from the Liffey catchment came from an area of Leinster Granite, and thus have similar heavy mineral suites, that is enriched in garnets, with lesser igneous minerals such as tourmaline (possibly from the local Type I granodiorites) and apatite. The assemblage is similar to that found in upstream Avoca samples, also taken from a channel incising granite. The high garnet abundance is accounted by the presence of low-grade siltstone/slate and schist/quartzite/coticule rocks.

These samples also contain numerous spodumene grains along with lepidolite, a lithium-bearing mica, associated with spodumene in lithium-bearing pegmatites. The presence of both spodumene grains and detrital lepidolite suggest the occurrence, as in the Avoca catchment, of unmapped lithium pegmatites among the granites in the northern part of the Leinster Granite.

It is interesting to note that the signature of the King's River, a tributary of the Liffey that is characterised by amphibole and orthopyroxene, is lost quickly downstream from the river's confluence with the Liffey. The Pollaphuca Reservoir lake appears to act as a sink for upstream sediment because few of the defining characteristics of sediment from the batholith are in evidence downstream of the reservoir. LR06, taken from the Liffey channel approximately 5 km downstream of the outlet point from the reservoir, shows high garnet counts (more than 50% garnet), in keeping with the greywackes and shales that comprise the local bedrock. This high garnet proportion drops off rapidly in downstream samples, averaging approximately 25% in the nine samples taken between LR06 and the Liffey mouth.

While the proportions of mineral species vary as the Liffey channel moves downstream through siliciclastic and into carbonate bedrock, the overall pattern remains

relatively stable: progressively lower counts of amphibole, higher average proportions of apatite and lower proportions of garnet in samples lower downstream. The abundance of tourmaline (Fig. 5: T.Lif.) and zircon is most likely due to their stability and resistance to weathering. This is not to say, however, that the sediment of the Liffey is necessarily enriched in zircon or tourmaline with respect to other rivers in the area; the absence of a wide contact aureole in the area (which would contribute metamorphic heavy minerals) or large areas of metapelites (which would increase the garnet percentage) results in elevated proportions of the remaining heavy minerals. It is interesting to note that, while the Liffey has higher percentages of certain minerals than other rivers, the overall abundance of heavy minerals in Liffey sands is the lowest in the area studied.

In short, the Liffey is characterised by high proportions of (in decreasing order) garnet, apatite, tourmaline and zircon. The signature of the King's River tributary contributes the dominance of locally derived amphiboles and orthopyroxenes, but they are effectively filtered by the sediment sink of the Pollaphuca Reservoir. The heavy mineral suite reflects an igneous source, with the exception of abnormally high proportions of garnet. As the river flows across carbonate bedrock, the local lithology is reflected by an increase in dolomite rhombs.

3.4. Barrow Catchment Heavy Mineralogy

The Barrow carries a high proportion of fine-grained sediments that are not suitable for heavy mineral analysis. Therefore, only eight viable samples were obtained from the Barrow system, including both the main channel and minor tributaries draining the western margin of the Leinster Batholith (Fig. 4A). One of the defining characteristics of the Barrow catchment is the large proportion of dolomitised bedrock in the area. This is reflected by a high proportion of carbonate rhombs in the heavy mineral fractions (Fig. 5: D). Following acetic acid immersion the number of rhombs was not appreciably reduced, as would be expected with grains of calcite. This treatment, therefore, proved that the rhombs are dolomite. The high quantities of dolomite in Barrow samples precluded accurate counts of other heavy minerals in three of the eight samples, and these three are therefore not included in later statistical analyses.

Despite the masking effect of dolomite, several samples contain useful provenance information. Samples upstream of any Leinster Massif input contain rounded yellow rutile (denoting a low Fe content) and zircon, suggesting input from a mature sedimentary source. Closer to the outcrops of the Leinster Granite, sands are dominated by zircon, apatite, euhedral prisms of tourmaline (Fig. 5: T.Bar.) and clinopyroxene (especially diopside). The euhedral morphology of these grains suggests a nearby source.

Farther downstream igneous (granites and granodiorites) and metamorphic (schists, gneisses and coticules) rocks control the heavy mineral fraction, which includes staurolite (Fig. 5: St) and garnet. The mineralogy of samples from tributaries draining the highlands of the western batholith are largely controlled by their proximity to contact aureole rocks. Staurolite and garnet from local schists are found with hornblende and other amphiboles, reflecting amphibolite input.

Overall, high proportions of detrital dolomite characterise the sediment of the Barrow. Their predominance prohibits a statistical analysis of some heavy mineral

data but, because the source of the dolomite is identifiable, allows it to be used as a provenance signature. The samples taken from directly atop the batholith or contact aureole show mineral assemblages that would be expected from such bedrock lithologies.

4. COASTAL AND OFFSHORE HEAVY MINERAL RESULTS

4.1. Beach and Coastline Bluff Heavy Mineralogy

Samples were collected along the coastline of southeastern Ireland, from beaches and from coastal bluffs composed of till. Each beach sample was taken in the region of the high tide line; in cases where heavy mineral lags were observed in the sand. Although one would expect these lags to garner high percentages of heavy minerals, the proportions of total heavy minerals in the beach sands is not appreciably higher than the proportions in the offshore samples (Fig. 4D).

The beach samples appear to be more closely related to Irish Sea sands and not the local river sediment. This conclusion is supported by the high percentages of clinopyroxene, nearly all of which are augite, similar to that found offshore. The average percentage of clinopyroxene in all beach samples is extremely close to that of this mineral in offshore samples (34% for beaches vs. 35% for offshore). Along with augite, glaucophane (detected in offshore samples but not in any of the river catchments) is found in several beach samples.

Other mineral species show geographic variations in the beach and bluff samples that closely parallel the variations of these species in offshore samples. Clinopyroxene percentages decrease from north to south, just as they do offshore; staurolite percentages increase to the south, again mirroring the offshore pattern. Other minerals show no discernible geographic trends.

The modern river systems do, however, contribute some material to the beaches: spodumene grains were found in two beach samples (no spodumene was identified in offshore samples). The percentages of garnet in beach samples also seem to indicate some catchment input: garnet proportions are at their highest in beach samples taken directly south of the mouths of the Vartry and Avoca, both of which have overwhelmingly garnet-rich heavy mineral assemblages. Qualitatively, however, it appears that the majority of sediment found on the beaches along the southeastern coast is of Irish Sea derivation.

All of the samples taken from till bluffs along the Irish Sea coastline, except one, show the elevated clinopyroxene levels indicative of offshore sands. Sample BCH20, from a till bluff along the southern coast, is the only ''beach'' sample that is obviously not derived from an Irish Sea source, because it is the only coastline sample that contains virtually no clinopyroxene. It is dominated by amphiboles (including hornblende) and, to a lesser extent, epidote and staurolite. Such an assemblage mirrors the local bedrock lithology of paragneisses and other metamorphic rocks. The other tills sampled appear to have been deposited by Irish Sea Lobe ice, which moved along the southeastern coast during the maximum of the last glaciation. These tills (and the beach samples adjacent to them), therefore, show a signature virtually identical to that of Irish Sea sediment. Sample BCH20, however, is from a

till that is not from the Irish Sea Lobe (Carter and Orford, 1982). Because its mineralogy matches bedrock lithology to the north, this till must have been deposited by southwards-moving ice of terrestrial origin.

4.2. Irish Sea Heavy Mineralogy

All Irish Sea samples are enriched in clinopyroxene (Fig. 4E). Individual clinopyroxenes cannot be accurately differentiated by optical means alone, so they were counted as a single group for this study. Most of the clinopyroxenes analysed appear to be augite. Augite grains are found in a variety of forms, ranging from subhedral/euhedral elongate grains displaying characteristic "hacksaw" terminations to rounded, smooth grains. All have characteristic pleochroism (mostly green to brown, but with occasional grains showing purple pleochroism, denoting higher titanium content; Deer et al., 1996).

The source of these augite grains is enigmatic. Augites are some of the main constituents of basic or ultramafic rocks, being commonly found in basalts and gabbros (Deer et al., 1996). The presence of augite in some of the upstream reaches of the rivers in the present study shows that there are in fact augite-bearing rocks in the Leinster Granite. There is no obvious optical difference between the augites in the river catchments and those of the Irish Sea samples, other than perhaps a greater proportion of rounded grains in the offshore sands. However, the high proportions of augite in offshore samples compared to the relatively low percentages found in the river catchments are indicative of a source for the augite-bearing sediment other than the Leinster Massif. The offshore samples have an average of 35% augite; none of the rivers have augite proportions $>7\%$. Pyroxenes are unstable and their abundance cannot be ascribed to relative enrichment resulting from the elimination of other minerals carried out to sea (Mange and Maurer, 1992).

The amphibole group also includes high-pressure metamorphic index glaucophane. It is interesting to note that no glaucophane is found in any of the onshore samples, thus its presence is a powerful argument for a sediment source other than the Leinster Massif region, as glaucophane is generally the product of low-temperature, high-pressure metamorphism (Deer et al., 1996). A possible source terrain is the blueschist facies rocks in Anglesey, North Wales (Gibbons, 1981; Gibbons and Gyopari, 1986), across the Irish Sea from southeastern Ireland. Thus these glaucophane grains suggest input from the western coast of Britain to the seabed sediments along the Irish coastline.

There is no readily apparent geographical trend in the proportions of most of the minerals taken from offshore samples, at least along the southeast coast of the Irish landmass. Percentages of andalusite vary widely. Staurolite, along with andalusite diagnostic of the Slaney, also shows little geographic variation along the east coast. In the four Celtic Sea samples, both andalusite and staurolite are found in greater relative abundance than in Irish Sea samples. Staurolite is especially common in these samples; this indicates a definite Barrow River input, as staurolite is the defining heavy mineral of samples taken from the Barrow in the downstream regions of the Leinster Granite and surrounding aureole. The proportions of both augite and tourmaline are lower in the Celtic Sea samples. It is interesting to note that much of

the tourmaline identified is schorl, an Fe-rich variety that denotes a granitoid source (Mange and Maurer, 1992).

More importantly, the Celtic Sea samples contain large numbers of dolomite rhombs. The presence of dolomite, along with elevated levels of Barrow index minerals staurolite and andalusite, indicates a Barrow source for these Celtic Sea samples.

Garnet becomes more common to the south, reaching a peak in samples to the south of the Avoca river mouth. Garnet is also abundant in samples taken from directly offshore the mouth of the Vartry. Both rivers carry sediment strongly enriched in garnet. The four Celtic Sea samples also show high garnet percentages (although this could be due to their relative starvation of clinopyroxene and tourmaline). Amphibole is a minor constituent of all offshore heavy mineral suites.

In summary, samples from the seabed of the Irish and Celtic seas show a clinopyroxene/garnet assemblage. This fact, along with the presence of glaucophane, differentiates them from any of the river catchments.

5. GARNET GEOCHEMISTRY

As an adjunct to the heavy mineral analysis, a geochemical analysis of detrital garnet grains was undertaken to determine if any geographic variation within the garnets could be linked to provenance (heavy mineral provenance results can be independently confirmed using variations in the chemistry of a single mineral species (e.g., Morton, 1985; Malone, 1997)). Garnets were isolated from seven offshore samples, and from one sample in each river, then analysed using a scanning electron microscope fitted with an energy dispersive spectrometer (EDS).

Virtually all the garnets from the study area examined proved to be almandines. However, normalising the results for iron shows a considerable variation in the garnet grains' manganese chemistry. Offshore samples have a wide range of Mn percentages, with no apparent geographic pattern. River samples, on the other hand, are almost uniformly Mn-rich, and only the Liffey sample shows an appreciable amount of Mn-poor garnets. The results support the theory that the offshore samples are derived from a source other than the Leister Massif area; the presence of Mn-poor garnets in the Liffey catchment area can be explained by glacial input. (Analytical data can be obtained from the author.)

6. STATISTICAL ANALYSES

6.1. Background

In order to qualitatively and quantitatively determine the relationships between the mineral suites from the various rivers and the offshore, two different statistical methods were used: principal components analysis (PCA) and cluster analysis.

PCA allows for quantitative analysis of "closed" datasets; that is, data that are bounded, such as the percentages of heavy minerals in a sample. PCA is used to create linear combinations of the variables in each sample, called "principal components", that account for as much of the (original) total variation as possible. Each component is extracted in such a way as to be uncorrelated with each other, and so

that they account for successively smaller amounts of the total variation (Dillon and Goldstein, 1984). The aim of PCA is to describe as much of the variation as possible using the minimum number of these components (Jambu, 1991). It is especially useful in plotting data in a two-dimensional format, in which comparisons can be made between components that describe a majority of the total variance (Everitt, 1974). PCA is used in this study not to identify the correlations between variables, but to describe the differences between the heavy mineral assemblages of each locality and identify the variables responsible for those differences.

A more qualitative technique, cluster analysis, was also used to augment the PCA results. Cluster analysis is a method by which individual samples, each characterised by a series of variables, are placed in groups, or ''clusters'', based on the similarity of one sample to the next (Dillon and Goldstein, 1984). The relationships between these groups are graphically represented as two-dimensional dendrograms, which illustrate the fusions between groups at different points through the analysis. Clusters are linked together at varying ''heights'', or distances, from one another. These distances denote the mathematical difference between points. In cluster analysis they are the Cartesian distances between two points in *n*-space, *n* being the number if variables under examination (i.e., the number of different mineral species being counted). The greater the ''height'' of joining two clusters, the greater the difference between those clusters in *n*-space. It is important to note that these ''heights'' are dimensionless, and used here simply to compare qualitatively the relationships between samples. It is therefore, strictly speaking, not a statistical procedure. The results are somewhat subjective as different measures of similarity produce different dendrograms from the same data sets. The method chosen for this analysis (Ward's method) uses the error sum of squares for each cluster as the similarity criterion, and the mathematical distances between points are Euclidean.

6.2. Results

PCA, incorporating all samples collected and analysed (with the exception of Barrow and Celtic Sea samples overwhelmed by dolomite) was conducted, and components 1 and 2 are plotted in Fig. 6. PCA analysis reveals that each locality has its own signature, characterised by distinct mineral species. Component 1 explains 54% of the total variance within the samples; component 2 explains 20%. The Avoca and Vartry samples group together due to their proportions of garnet; garnet is the most heavily weighted variable of component 1. Clinopyroxene is the second most important variable. Slaney samples show a wide range of values in component 1, all of which (except SL03, taken at the river mouth) are <0 (denoting low clinopyroxene). In component 2, dominated by clinopyroxene and staurolite, the Slaney sediment again shows a wide spread. Liffey samples lie closer to the offshore samples than do those of the Slaney. Barrow samples show a wide spread of values, but for the most part group well with the Slaney samples due to both rivers' high proportions of staurolite and garnet. Beach samples group for the most part with those from the offshore; a few samples, notably those from the coast of the Celtic Sea, plot closer to samples from the Liffey and Slaney because of their low clinopyroxene content.

Overall, PCA results indicate that the sediment of the rivers and nearshore are distributed along three axes. The offshore and beach samples are on the opposite side

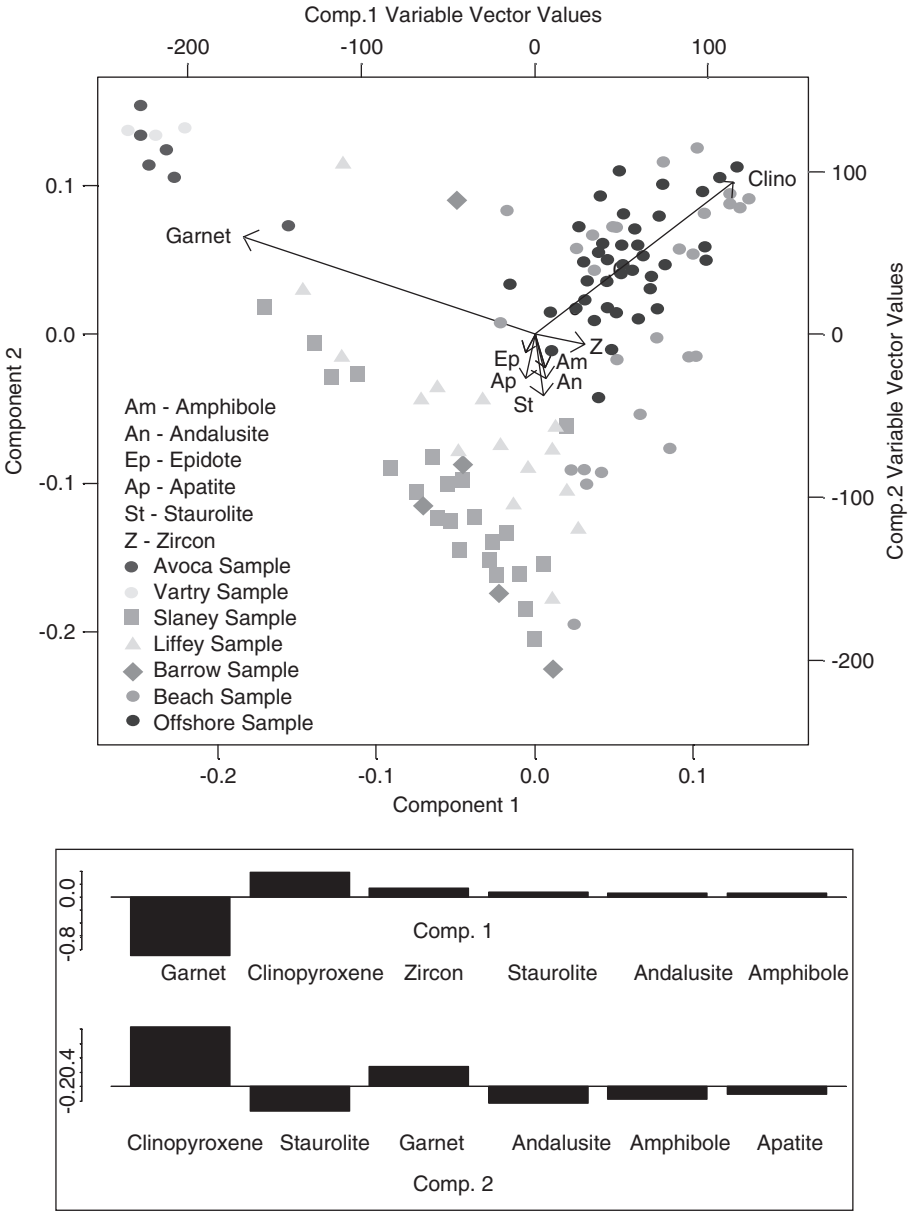

Fig. 6. Principal component analysis results and components 1 and 2 loadings (relative vector values of mineral species in each component) for all southeastern Ireland samples.

of all river samples along the axis defined by clinopyroxene; that is, the high proportion of augite in offshore and beach samples is what statistically differentiates these samples from the river sediment. The Avoca and Vartry samples lie at the end of an axis defined by garnet, in keeping with the anomalously high garnet proportions in these samples. The third axis, made up of a number of less common

species—amphibole, andalusite, staurolite, amphibole, zircon, apatite and epidote—differentiate the other river samples from both the offshore/beach assemblages and the Avoca and Vartry system.

In the cluster analysis, the river samples group together, although with considerable overlap between rivers (Fig. 7). For example, a number of Slaney (SL13, SL21, SL22, SL23), Liffey (LR2, LR3, LR6) and Avoca (AR07) samples cluster together; interestingly, all of these samples were taken at sites where their respective rivers were directly incising the Leinster Granite. These results show the strong correlation between bedrock type and heavy mineral assemblages. Barrow samples, due to the high variability within their mineral suites, cluster with a variety of different groups. Most importantly, there is a clear-cut divide between the offshore samples and those taken from the rivers. Only three river samples are grouped within the single "mega-cluster" that encompasses all of the offshore samples: (1) LR05, a Liffey sample anomalously rich in apatite, amphibole and zircon; (2) Barrow sample BW02, also high in zircon and apatite; and (3) SL03, the river mouth sample cited earlier, which is enriched in clinopyroxene.

7. DISCUSSION AND CONCLUSIONS

Statistical analyses of the heavy mineral data in this study have yielded unexpected and meaningful information on the nature and provenance of river and nearshore sediments of southeastern Ireland. Firstly, each of the local rivers contains a distinct heavy mineral assemblage, and these assemblages closely match the local bedrock lithologies, changing somewhat as the rivers incise different rock types. Secondly, the sediments of the beaches of southeastern Ireland and the adjacent seabed of the Irish Sea have similar, augite dominated, heavy mineral suites that are, in large part, not directly linked to fluxes from the modern rivers. Importantly, the mineral suites of the rivers and the beaches/offshore are sufficiently dissimilar that they can be distinguished statistically.

The differences between the river, beach and offshore assemblages can most probably be attributed to the effects of glaciation. As shown above, the influx of Irish Sea ice would have brought erratics from the north, including mafic rocks from the highlands of Northern Ireland and Scotland (Warren and Keary, 1988). This theory is supported by the fact that, of all the rivers, the heavy minerals from the Liffey correlate most closely with those of the beach and offshore sediments. Because of its geographic position, the Liffey catchment (Figs. 2 and 3) would be the most susceptible to an influx of material carried south by glaciers, whereas those of the other rivers lie more in the lee (to the south) of the highlands of the Leinster Massif. Liffey sediment would, therefore, be expected to carry material derived from the north, similar to the sands of the Irish Sea.

Results presented in this paper demonstrate that multivariate statistics, when applied to heavy mineral data, can quantify differences in sediment provenance. The application of these methods to southeast Ireland has revealed that the basinal sediments are not necessarily derived from the nearest highlands, even when the rivers of these highlands appear to be the closest sources of sediment. These observations show that modern processes can carry the overprint of the effects of

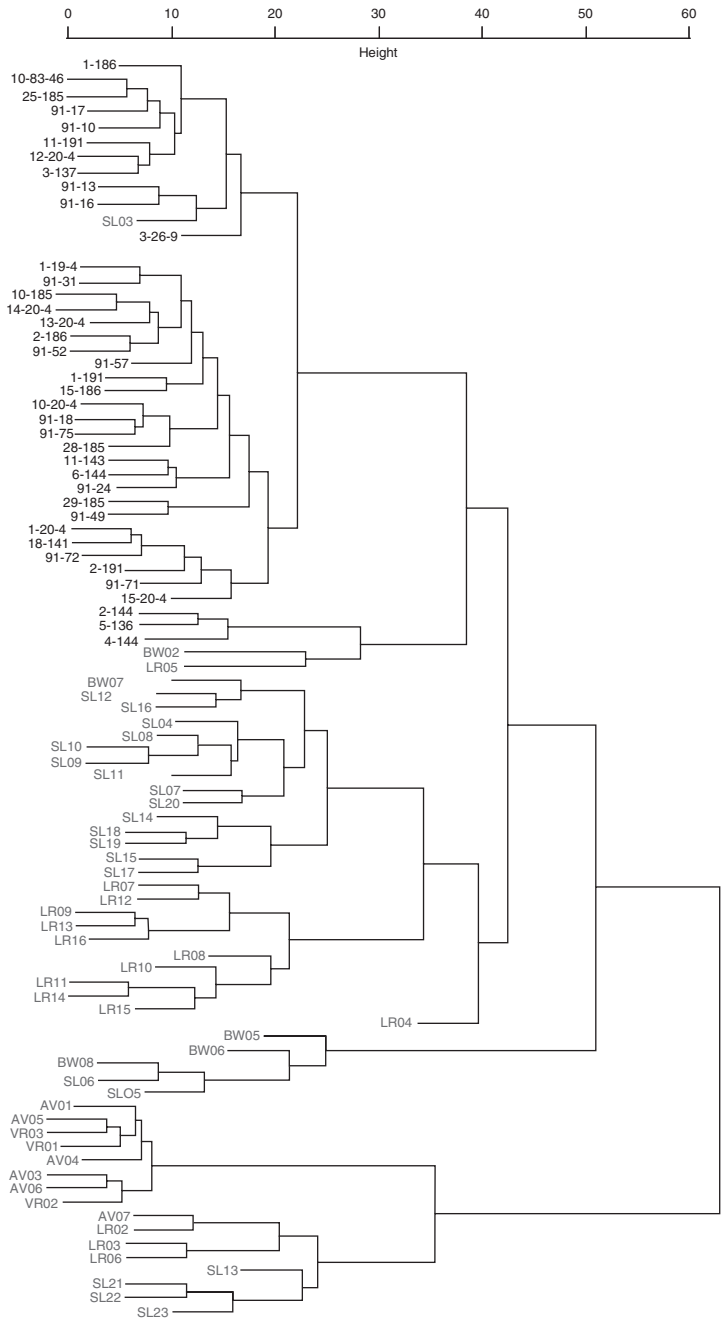

Fig. 7. Cluster analysis for all river catchment samples and offshore samples. Distance is Euclidian, method is Ward's error sum of squares. Note sample SL03, taken at the mouth of the Slaney River, which clusters closely with offshore samples.

previous glaciations. The presence of some anomalous mineral types also support this conclusion. Spodumene grains found in the river samples do not appear offshore, while glaucophane, found in Irish Sea sediment, cannot originate in the area of the Leinster Massif. The high percentages of augite found offshore also preclude provenance from the southeastern Irish landmass. Garnet geochemistry provides a useful tool in augmenting and confirming heavy mineral results.

The rapid disappearance of particular mineral signatures as the rivers flow towards the sea, whether caused by overwhelming flux from other species or by filtering through manmade reservoirs, emphasises the importance of collecting a number of samples systematically along a river's course to obtain a typical mineral signature.

ACKNOWLEDGEMENTS

My sincere thanks to Maria Mange for both including my work in this compilation, and for her invaluable assistance in the study itself. Thanks are also due to Philip Allen, who as my primary adviser made this study possible; and especially to Alex Densmore for his guidance on the project and his review of this manuscript. And, of course, my beautiful wife Maura for her patience and support.

REFERENCES

Behrends, M., Hoops, E., Peregovich, B., 1998. Distribution patterns of heavy minerals in Siberian rivers, the Laptev Sea and the eastern Arctic Ocean: an approach to identify sources, transport and pathways of terrigenous matter. In: Kassens, H. (Ed.), Land-Ocean Systems in the Siberian Arctic: Dynamics and History. Springer Lecture Notes on Earth Sciences, Berlin.

Carter, R.W.G., Orford, J.D., 1982. IAQS Field Guide No. 4: The South and East Coasts of Wexford. Irish Quaternary Association, Dublin, 36pp.

Deer, W.A., Howie, R.A., Zussman, J., 1996. An Introduction to the Rock-Forming Minerals. Longman, Essex, U.K, 696pp.

Dillon, W.R., Goldstein, M., 1984. Multivariate Analysis: Methods and Applications. Wiley, New York, NY, 587pp.

Everitt, B.S., 1974. Cluster Analysis. Heinemann Educational Books, London, 170pp.

Gaillardet, J., Dupre, B., Allegre, C.J., 1995. A global geochemical mass budget applied to the Congo Basin rivers: erosion rates and continental crust composition. Geochimica et Cosmochimica Acta 59, 3469–3485.

Galehouse, J.S., 1971. Point counting. In: Carver, R.E. (Ed.), Procedures in Sedimentary Petrology. Wiley, New York, NY, pp. 385–407.

Gibbons, W., 1981. Glaucophanic amphibole in a Monian shear zone on the mainland of N. Wales. Journal of the Geologic Society of London 138, 139–143.

Gibbons, W., Gyopari, M., 1986. A greenschist protolith for blueschist in Anglesey, U.K. In: Evans, B.W., Brown, E.H. (Eds.), Blueschists and Eclogites. Geological Society of America Memoir, vol. 164, pp. 217–228.

Grosz, A.E., 1993. Mineralogy and heavy mineral resource potential of surficial sediments of the Atlantic Continental Shelf offshore of Georgia. U.S. Geological Survey Project Report 19, U.S. Geological Survey, Reston, VA, 31pp.

Hutton, C.O., 1950. Studies of heavy detrital minerals. Bulletin of the Geological Society of America 61, 635–710.

Jambu, M., 1991. Exploratory and Multivariate Data Analysis. Academic Press, Boston, MA, 474pp.

Malone, J.T., 1997. Determining Provenance of River Sediment, Kennebec and Androscoggin Rivers, Maine. Unpublished M.Sc. thesis. University of Maine, Orono, Maine, 125pp.

Mange, M.A., Maurer, H.F.W., 1992. Heavy Minerals in Colour. Chapman & Hall, London, 147pp.

Mange-Rajetzky, M.A., 1983. Sediment dispersal from source to shelf on an active continental margin, S. Turkey. Marine Geology 52, 1–26.

McArdle, P., Kennan, P.S., 1987. The distribution, genesis and potential of tungsten, lithium and associated metal deposits on the southeast margin of the Leinster Granite. Geological Survey of Ireland Bulletin 4, 27–40.

Morton, A.C., 1985. A new approach to provenance studies: electron microprobe analysis of detrital garnets from Middle Jurassic sandstones of the northern North Sea. Sedimentology 32, 553–566.

Nesse, W.D., 1991. Introduction to Optical Mineralogy. Oxford University Press, New York, NY, 335pp.

O'Connor, P.J., Gallagher, V., Kennan, P.S., 1991. Genesis of lithium pegmatites from the Leinster Granite margin, southeast Ireland: geochemical constraints. Geological Journal 26, 295–305.

O'Connor, P.J., Reimann, C., 1993. Multielement regional geochemical reconnaissance as an aid to target selection in Irish Caledonian terrains. Journal of Geochemical Exploration 47, 63–87.

Smithson, F., 1923. Geological studies in the Dublin District: I. The heavy minerals of the granite and the contiguous rocks in the Ballycorus district. Proceedings of the Royal Irish Academy 28, 12–25.

Tietzsch-Tyler, D., Sleeman, A.G., 1994a. Geology of Carlow-Wexford. Geological Survey of Ireland, Dublin, 57pp.

Tietzsch-Tyler, D., Sleeman, A.G., 1994b. Geology of South Wexford. Geological Survey of Ireland, Dublin, 62pp.

Warren, W.P., 1993. Wicklow in the Ice Age. Geological Survey of Ireland, Dublin, 46pp.

Warren, W.P., Keary, R., 1988. The sand and gravel resources of the Irish Sea Basin. In: Geographical Society of Ireland Special Publication, vol. 3, pp. 63–67.

Chapter 22

SEDIMENT TRAILS IN TECTONICALLY ACTIVE ISLANDS: HEAVY MINERALS IN USE IN NEW ZEALAND

DAVID SMALE

28 Bronte Street, Nelson, New Zealand (formerly of New Zealand Geological Survey and Institute of Geological and Nuclear Sciences)

ABSTRACT

Several basement terranes in New Zealand are characterised by distinctive though varied heavy mineral assemblages. The Rakaia and Pahau Terranes of the Torlesse Superterrane contain prominent, granite-derived detrital biotite. Although there is a considerable overlap of heavy mineral suites in these two terranes they each show distinctive features both in Canterbury and in Wellington. Caples and Bay of Islands (Waipapa) Terrane rocks include heavy mineral suites that are typified by the dominance of pyroxene and hornblende, suggesting volcanic derivation.

The Cretaceous/Tertiary cover sediments are largely proximal and were deposited close to their basement source rocks. They are less indurated and have been affected by weathering and intrastratal dissolution. Acidic pore fluids in Cretaceous and Eocene coal measures have dissolved almost all heavy minerals except ilmenite and zircon. Intrastratal dissolution also reflects depth of burial. The Taranaki McKee Formation shows a well-defined pattern of heavy mineral dissolution with increasing burial.

Indications of the onset of volcanism are easier to detect in the younger sediments, but remain detectable in some older ones. From the Miocene, an increasing diversity of heavy minerals reflects the inception of the modern plate boundary system. Along the Alpine Fault, 480 km of dextral movement has left detectable traces in south Westland sediments from rock units passing on the other side of the fault.

Heavy minerals in modern sediments have been used in a variety of studies in New Zealand. For example, in Westport, Riverton, and Tauranga heavy mineral signatures indicated that the silting of the harbours was caused largely by sediments transported from offshore, rather than from discharging rivers. The extent of sediment mixing from different sources has been quantified at the mouth of the Wanganui River where four source areas have contributed to the sediment load (including the flux of titanomagnetite now mined from beaches and dunes), and in a major irrigation race.

The forensic use of heavy minerals has assisted several court cases. In one case soil from suspects' shoes indicated that they had been present at a crime scene they claimed not to have visited, while in another study heavy minerals on paua (abalone) shells offshore from the northwest coast of the South Island enabled the sources of a poacher's harvest to be identified.

Developments in Sedimentology, Vol. 58, 569–585

ISSN: 0070-4571/doi:10.1016/S0070-4571(07)58022-2

Keywords: Torlesse; Murihiku; Rakaia; Pahau; Waipapa; Taranaki; Alpine Fault; south Westland; Wanganui River; harbour siltation; geoforensics

1. INTRODUCTION

This chapter draws on the author's 30 years of experience (22 years in New Zealand) with heavy minerals. It summarises studies in three main areas: some New Zealand basement terranes (including indurated Mesozoic sediments), overlying Cretaceous-Tertiary sediments, and more diverse applications for recent sediments. The use of heavy minerals as a geological tool in New Zealand benefited from two classic studies in the 1950s. Hutton (1950) made a very detailed inventory of minerals occurring in modern river sediments on the West Coast of the South Island, and determined their sources. Brothers (1959a, 1959b) worked on Mesozoic indurated sedimentary basement rocks and overlying sediments in Southland. Following Hutton and Brothers, heavy mineral studies have mainly been used to characterise sediments and sedimentary rock formations, and reconstruct their provenance. Since the 1960s these studies have been assisted further by advances in electron microscopy, the electron microprobe, and X-ray diffraction (XRD) techniques. Problems relating to leaching and intrastratal dissolution have become better understood and evaluated. South Island studies have been summarised by Smale (1990b). Other studies, e.g. by Smale (1991b), assess mixing of sediment from different sources, whereas heavy mineral characteristics have been potentially useful in several forensic cases (e.g., Bremner and Clarke, 2004).

1.1. Techniques

Laboratory preparation and separation followed the standard techniques of Milner (1962), Smale (1990b), and Mange and Maurer (1992) in most heavy mineral studies. Heavy minerals from the 2–4 ϕ (0.06–0.25 mm) size fraction of disaggregated or crushed rocks are separated in funnels using tetrabromoethane or bromoform, and from the early 1980s in the non-toxic sodium polytungstate solution. Grains are examined in a 1.63 refractive index oil using a petrographic microscope. In quantitative studies, proportions are established by counting all the grains in random fields of view until a minimum of 300 grains has been reached. Doubtful identifications are confirmed using XRD on crushed single grains, or by analytical scanning electron microscope (SEM-EDX). The SEM-EDX is also used for single-mineral studies such as garnet compositions.

Interpretation of results has been carried out largely on raw data, but statistical analysis also proved helpful. Cluster analysis (Rohlf, 1988) groups similar samples, and indicates degrees of similarity by assembling samples on different branches of a dendrogram. Methods of factor analysis (Full et al., 1982) provide statistical estimates of different populations that might by mixing have produced the suites present. Both could be very useful guides, but, because they relate purely to statistics and not to geology, they should be applied with caution. For example, a population consisting of ilmenite and zircon is not so much a provenance indicator as a hydraulic effect and/or a reflection of their greater resistance to weathering and post-depositional intrastratal dissolution.

1.2. Key Indicators for the Identification of Heavy Minerals of Similar Optical Properties, with Particular Relevance in New Zealand

Epidote group minerals are widespread in the indurated, low-grade metasedimentary Mesozoic basement rocks of New Zealand. Although a distinction has been attempted between epidote and clinozoisite this is based largely on colour, which is not necessarily a reliable discriminator. Many sediments contain whitish, fine-grained aggregates of epidote or pumpellyite and quartz (Smale, 1988). Such aggregates are characteristic of the basement rocks, but almost impossible to identify without using XRD. Consequently, they have been classified as "alterite" (van der Linden, 1969), "composite granular epidote" (Brothers, 1959a, 1959b), or "semi-opaque debris" (Smale, 1988). Discriminating between pumpellyite aggregates and epidote aggregates is possible optically only if the mineral colour is detectable. If they are colourless (and many are), XRD is the only means of identification because their intimate intergrowth habit with quartz and their similar chemistry are confusing, even for SEM-EDX or microprobe.

The abundance of epidote in rocks of sedimentary provenance and of clinopyroxene in some volcanics makes the distinction between these two minerals critical, but some pyroxenes can easily be confused with epidote. One useful optical property for their distinction is that the optic axial plane is parallel with the cleavage in those clinopyroxenes most resembling epidote (diopside-hedenbergite and augite), but it is perpendicular to the cleavage in epidote and clinozoisite. The cleavage thus appears to run between the isogyres in the interference figure of epidote, and joins the isogyres in the clinopyroxene.

The characteristics of titanite (sphene) show distinct affinities to its particular host rock. In schists and in some sedimentary basement rocks, titanite is dark brown and appears with a sphenoidal shape, but in the granites it occurs typically as orange-coloured, six-sided euhedral crystals that are less resistant to abrasion. The two varieties almost appear as different minerals, but both have the high dispersion and incomplete extinction between crossed polars characteristic of titanite, and a typical low to moderate 2 V.

Many studies (e.g., Smale, 1990b and references therein) have recorded three types of opaque minerals: magnetite, ilmenite, and pyrite. The method of their distinction is to move a magnet near the grains in an oil mount: magnetite grains show movement whereas ilmenite is unaffected. Non-magnetic grains with a brassy appearance in oblique incident light are identified as pyrite. Although such identifications cannot be regarded as accurate, large-scale distinctions based on this three-fold division are valid. It can provide valuable information as in the case of the Tauranga Harbour (Smale, 1993) where the relative abundance of magnetite proved instrumental in the identification of fluxes.

2. BASEMENT TERRANES

2.1. Western Province and Median Batholith

Few heavy mineral studies have been undertaken on the rocks of the Western Province or the Median Batholith (Mortimer, 2004). However, some investigations

on the provenance of Cretaceous-Tertiary sediments have included basement samples, and these are summarised in Table 1.

The Western Province (Buller Terrane) and the Median Batholith samples are from very localised areas, and are by no means representative of these groups as a whole. Nevertheless, the data suggest certain characteristics. In Fiordland, granitoid samples contain prominent biotite and hornblende, with lower abundances of epidote. In the Karamea Batholith, biotite is even more prominent but hornblende is only a minor constituent. Locally, sillimanite can be a useful provenance indicator. The Greenland Group consists of low-grade metasediments, and heavy mineral suites are characterised by semi-opaque debris (fine-grained aggregates of epidote or pumpellyite and quartz: Smale, 1988). Biotite may suggest derivation from granitoid rocks. It is perhaps surprising that epidote is not more conspicuous.

2.2. *Palaeozoic-Mesozoic Sedimentary Terranes*

Terranes of indurated Palaeozoic-Mesozoic sedimentary rocks are very extensive in New Zealand (Fig. 1, Mortimer, 2004). Most terranes have distinctive average QFL modes (Dickinson, 1985), reflecting their particular plate tectonic setting, and bulk compositions ranging from basaltic to rhyolitic (Mackinnon, 1983; Roser and Korsch, 1986; Mortimer, 2004). Distinctive heavy mineral populations reflect these bulk compositional differences, and provide further insights into source area composition.

The Mesozoic rocks studied by Brothers (1959a) are from an area now considered mostly as Murihiku Terrane (but also including some from the Maitai and Caples Terranes). Brothers noted that the heavy mineral species were typically either those that survived intrastratal dissolution, or authigenic minerals produced during diagenesis or low-grade metamorphic alteration. Thus, the heavy mineral suites comprise stable assemblages with non-opaque constituents being zircon, apatite, and epidote, with sporadic biotite, hornblende, clinopyroxene, and titanite. The Murihiku samples are typically poor in biotite, but rich in hornblende and clinopyroxene (Table 1). Although 45 thin sections have been studied from the Caples Terrane in the Thomson Mountains (Turnbull, 1979), heavy minerals were not separated, and few have had quantitative estimates of mineral proportions. Caples Terrane suites, similarly to the Murihiku samples, contain greater proportions of hornblende and pyroxene than the Maitai or Caples samples from further east (Brothers, 1959a). Few samples have been studied from the Bay of Islands Terrane, and the studied samples were probably atypical (Hayward and Smale, 1992). The analysed sandstones southeast of Auckland City are greenish and clinopyroxene-rich, contrasting with more abundant grey sandstones in which heavy minerals are sparse. Nevertheless, the results confirm that sporadic mafic volcanism existed at the time of deposition of the Bay of Islands Terrane.

The diversity of heavy minerals present in many Mesozoic basement rocks suggests that they became indurated soon after deposition and, generally, the effects of intrastratal dissolution have been noticeably less severe than those in the Cretaceous and Palaeogene cover sediments. However, this has not prevented later leaching by fluids circulating from superjacent coal measures, causing impoverishment of the heavy mineral suites. Such depleted suites occur in north Canterbury in the top few

Table 1. Regional average compositions of heavy mineral suites in rocks of basement terranes

	Fiordland (Median Batholith)	Karamea Batholith (Buller)	Greenland Group (Buller)	Southland Murihiku*	Canterbury Rakaia	Canterbury & Wellington Rakaia	Marlborough Pahau	Wellington Pahau
N	25	20	4	10	33	18	65	3
Ilmenite	9	†1	†11		21	14	26	16
Magnetite	5				0	1	5	
Pyrite					2	4	6	40
Semi-opaque debris	1		23	0	24	14	28	7
Biotite	26	44	24	1	18	43	5	5
Chlorite	1	10	30	4	3	3	2	1
Garnet	1			1	2	0	3	6
Zircon		5	2	21	2	4	3	5
Titanite	2	10		1	5	3	3	1
Epidote	9	3		19	14	7	12	9
Clinozoisite	1				3	4	3	10
Tourmaline		2	3	0				
Sillimanite		1						
Pumpellyite					2	2	1	
Hornblende	39	4	1	18	1		0	
Clinopyroxene	4		1	9				
Rutile/anatase		1	1	0				
Apatite	2	19	4	24	3	1	2	0

Notes: Figures are to the nearest per cent; "0" indicates a value between 0.2% and 0.5%, and no value indicates absence (or <0.2%). Note that these compositions are not necessarily representative of the groups listed; they are simply a summary of samples examined by Smale (1985a, 1985b, 1990a): Fiordland (Median Batholith of Mortimer, 2003); Smale and Nathan (1980): Karamea Batholith and Greenland Group (Buller Terrane of Mortimer, 2003); Brothers (1959a): Southland (Murihiku Terrane); Smale (1990b): Canterbury (Rakaia Terrane); Smale and Laird (1993): Marlborough (Pahau Terrane); Smale (1997): Wellington (Rakaia and Pahau Terranes).

*Opaques are present but excluded in percentages, and semi-opaque debris is classified as epidote.

†Includes both ilmenite and magnetite.

metres of the basement below the unconformity at the base of the Cretaceous-Tertiary sediments (Smale, 1989).

2.3. Rakaia and Pahau Terranes in Canterbury, Marlborough, and Wellington

The Rakaia and Pahau Terranes are areally the most extensive. They are both turbidite-dominated, but differ in age and petrography; the Rakaia is Permian-Triassic (older Torlesse Superterrane), and the Pahau is Jurassic-Cretaceous (younger Torlesse). These terranes have been studied extensively using heavy minerals: representative suites are shown in Table 1.

Both Rakaia and Pahau heavy mineral suites are distinguished from those of other terranes by the abundance of low-grade metamorphic epidote (including "semi-opaque debris") and detrital biotite (Smale, 1990b). The prominence of biotite, titanite, and garnet reflects a granitic source. Pyroxene, hornblende, and magnetite, common indicators of contemporaneous volcanism, are sparse. In Canterbury biotite, apatite, and hornblende are more prominent in Rakaia Terrane samples than in Pahau, and possibly correspond to Permian rather than Triassic strata (Mackinnon, 1983). The hornblende is erratically distributed, but is present mainly in southwest Canterbury and north Otago. In the Pahau Terrane garnet is more dominant, while magnetite is prominent in some local areas (Smale, 1990b) possibly reflecting greater frequency of tuffs and juvenile volcanism in the Pahau Terrane (Mortimer, 2004). This distinction appears widespread, as it has also been noted in Wellington (Smale, 1997). In Wellington, as in Marlborough and Canterbury, rocks of the Pahau and Rakaia Terranes are separated by a melange zone (Esk Head Melange: Fig. 1). Only three definite Pahau samples were included in the Wellington study, and five samples were analysed from the Esk Head Melange. As shown in a cluster analysis (Fig. 2), three Esk Head samples showed strong affinity with Pahau samples, and two showed strong affinity with Rakaia, indicating that within the melange the parent rocks have maintained their compositional distinction.

It is inevitable that in samples spread over wide areas, as shown in Table 1, the distinctions between groups become more blurred than in local areas, as the variance within groups increases. In spite of this, the substantial difference in biotite contents between the two terranes, and the smaller distinction between garnet contents, are still recognisable.

3. CRETACEOUS-TERTIARY SEDIMENTS

3.1. Cretaceous-Palaeogene and Intrastratal Dissolution

Heavy minerals in many late Cretaceous and Tertiary cover sediments have not proved to be the useful provenance indicators that might have been expected because they have been affected by diagenesis and intrastratal dissolution. In the Cretaceous and lower Tertiary, most heavy mineral suites consist of little but ilmenite and zircon. Coal measures are abundant in these rocks, and it is likely that a vigorous weathering regime at the time of erosion and transport of the sediment has

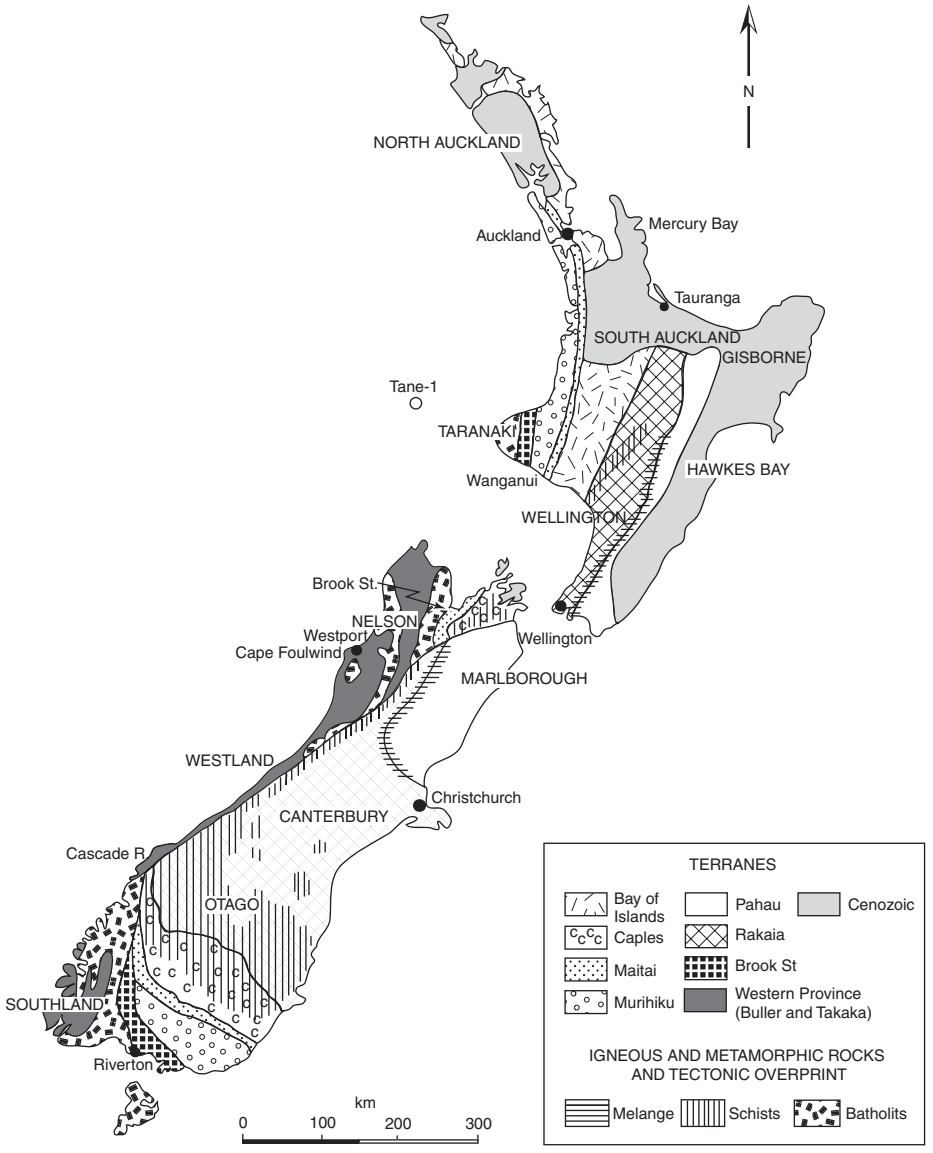

Fig. 1. Map of New Zealand showing basement terranes, geographic names, and land districts (after Mortimer, 2004). Shaded areas are those covered by younger sediments and volcanics.

eliminated nearly all the heavy minerals except the most resistant ilmenite and zircon (Nickel, 1973, and references therein).

Despite post-depositional alteration, some signals are sufficiently strong to be still recognised. Brothers (1959b) concluded that in Southland Cretaceous and Tertiary sediments were deposited in small local basins and that their heavy minerals were mostly derived from immediately adjacent older rocks. Later, with the widening of

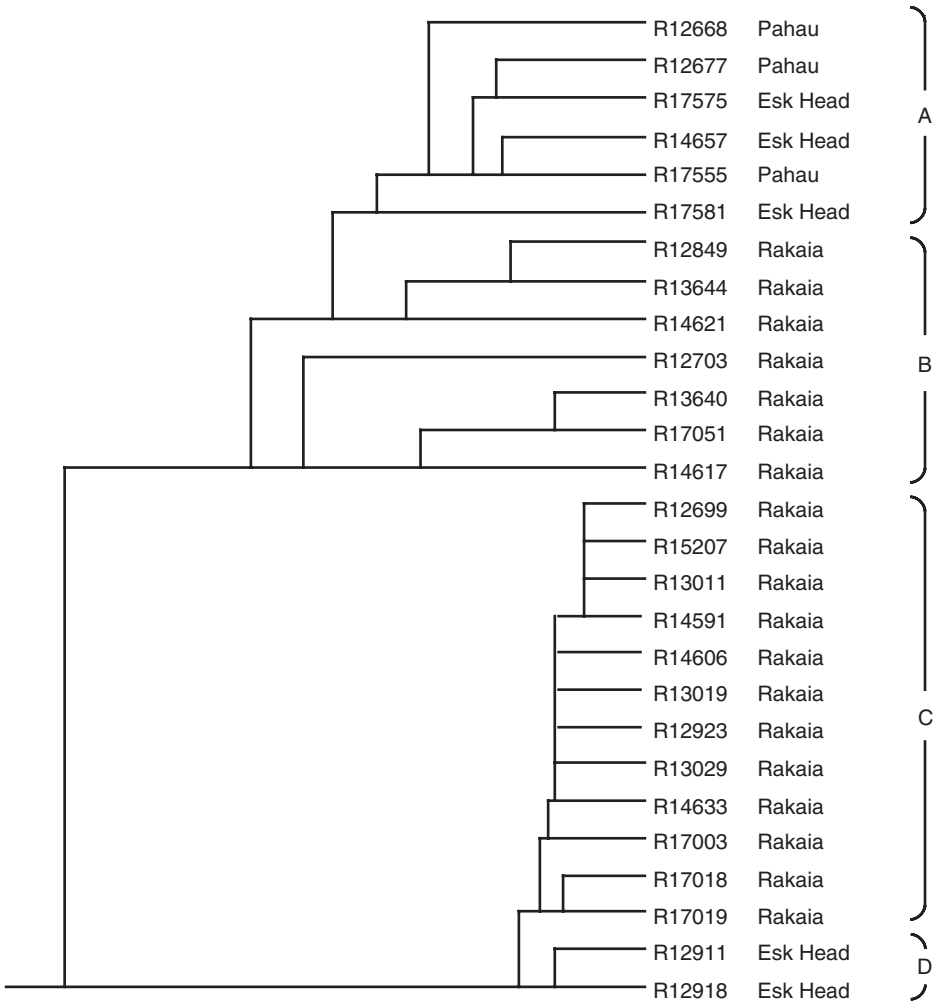

Fig. 2. Cluster analysis of Mesozoic basement heavy mineral suite from the Wellington area. Four clusters are distinguished. Samples from the Esk Head Melange show clear affinities with either Pahau or Rakaia. Cluster A is distinguished on high garnet and semi-opaque debris and epidote + clinozoisite; Cluster B on much higher semi-opaque debris, and not quite so high epidote + clinozoisite; Cluster C is rich in biotite; Cluster D is rich in biotite, but contains very little semi-opaque debris or garnet.

marine transgression, a more even spread and admixing of detritus occurred. Many other examples of Tertiary sediments containing distinctive minerals from underlying or adjacent rocks include (a) pyroxene in late Cretaceous sediments in Marlborough and the east coast of the North Island, derived from penecontemporaneous volcanics (Smale, 1993); (b) staurolite in Eocene sediments near Cape Foulwind, so localised as to indicate that it was derived from the contact aureole of adjacent granite (Smale and Nathan, 1980; Smale, 1990b); (c) a trail of aegerine in Eocene sediments near Lake Monowai in Southland derived from underlying granite (Smale, 1985b). The

transport distance of most sediments from source to deposition is perhaps no more than a few tens of kilometres. There are significant exceptions, however, as noted below for south Westland.

Patterns of intrastratal dissolution with burial depth in Taranaki sediments from onshore and offshore oil exploration boreholes parallel those described from the North Sea (Morton, 1984) and from the northern Gulf of Mexico (Milliken, 1988; Morton and Hallsworth, 2007). In the sandstones of the Eocene McKee Formation (Smale and Morton, 1987) amphibole, epidote, titanite, and kyanite are absent from a burial depth greater than 2745 m. Staurolite and garnet are absent at burial depths greater than 3100 and 3600 m, respectively. Dissolution in some Tertiary North Sea sediments occurred at significantly shallower depths (800–900 m), and in the northern Gulf of Mexico at about 2 km, but the sequence of mineral dissolution is the same.

Close to their depth stability limits mineral grains show strong solution effects. Garnets analysed by SEM-EDX from sediments from near 3.5 km depth in borehole Tane-1 (on the Western Platform off the coast of Taranaki) were of three types (Fig. 3): spessartine-rich, almandine-rich, and grossular (Smale and van der Lingen, 1989). These compositions are consistent with the lithology of potential parent rocks in nearby north-west Nelson: spessartine-rich garnet occurs in Rahu-Suite granites, while almandine-rich garnet is found in schists intruded by Separation Point granites. Grossular is present in contact aureoles around Separation Point granites, and occurs only rarely in Taranaki Basin sediments. Fig. 4 (A–F) illustrates the dissolution stages of garnets in accord with their differing chemistry: grossular grains are the most corroded, almandine grains are less so, and spessartine grains show only small solution pits on vertices.

The differences in solubility of certain minerals such as apatite and epidote at different pH (Morton, 1984) allow some assessment of the pH of pore fluids. Epidote tends to be soluble at a wide pH range, but apatite, though readily soluble at pH <7, is less soluble at pH >7. Most impoverished Cretaceous-Eocene heavy mineral suites

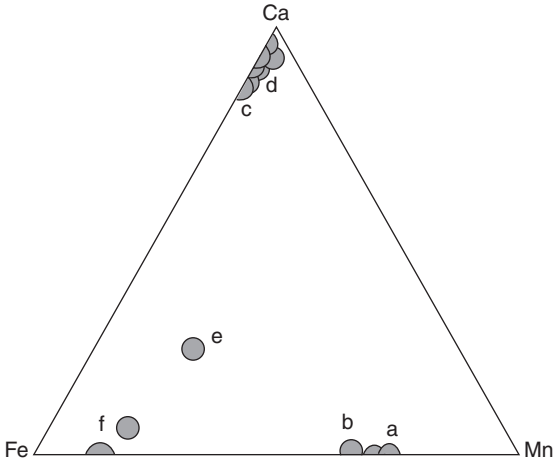

Fig. 3. Semi-quantitative (SEM-EDX) compositions (cation %) of garnet grains from 3515 m in Tane-1. Labelled grains correspond to those shown in Fig. 4.

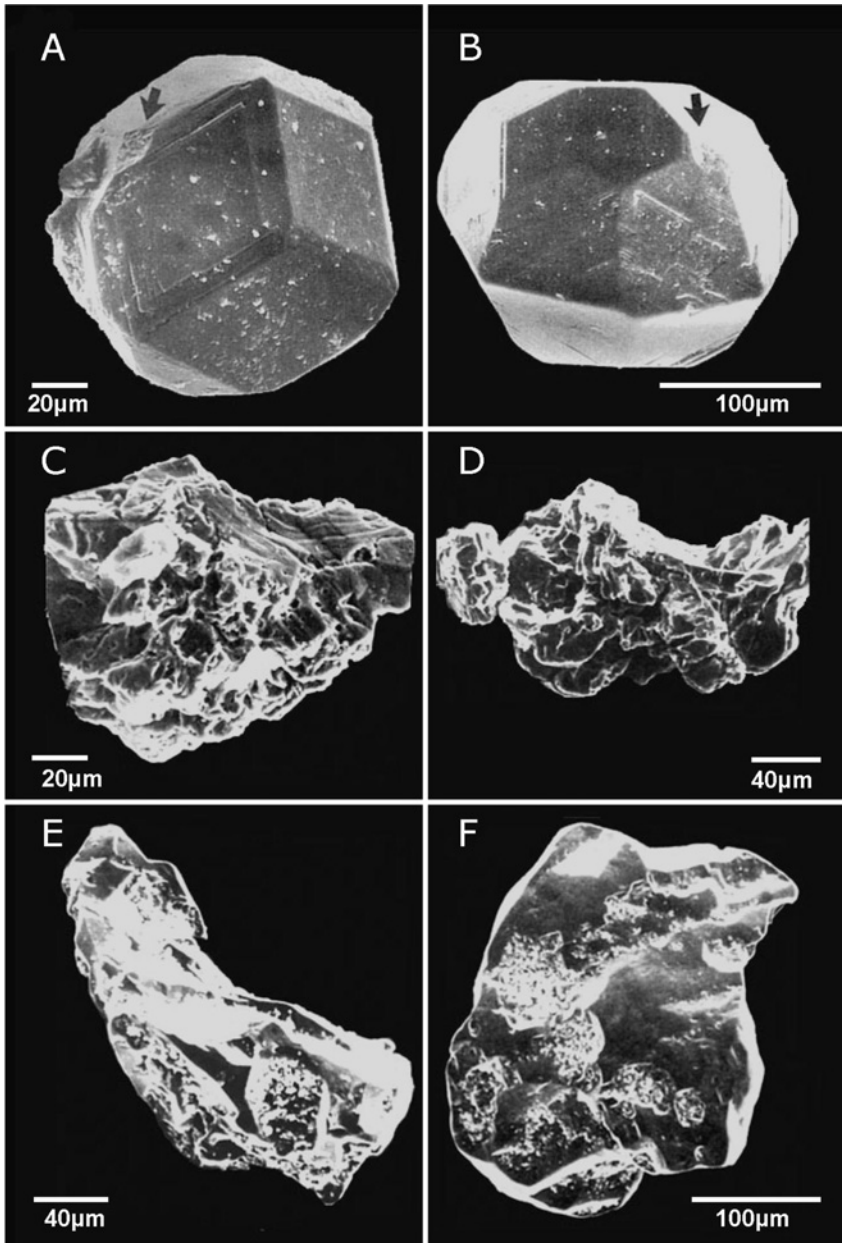

Fig. 4. Grains of spessartine (A–B), grossular (C–D), and almandine (E–F) garnets from 3515 m depth in Tane-1 offshore drillhole, showing different solution features. Chemical compositions are shown in Fig. 3 (after Smale and van der Lingen, 1989). Arrows show the incipient solution on the spessartine.

contain mostly zircon and ilmenite, and both epidote and apatite are seldom present, despite sediment derivation from the epidote-bearing Torlesse basement. In an SEM study of a Ngaterian (mid-Cretaceous) sample from Marlborough (Smale and Laird,

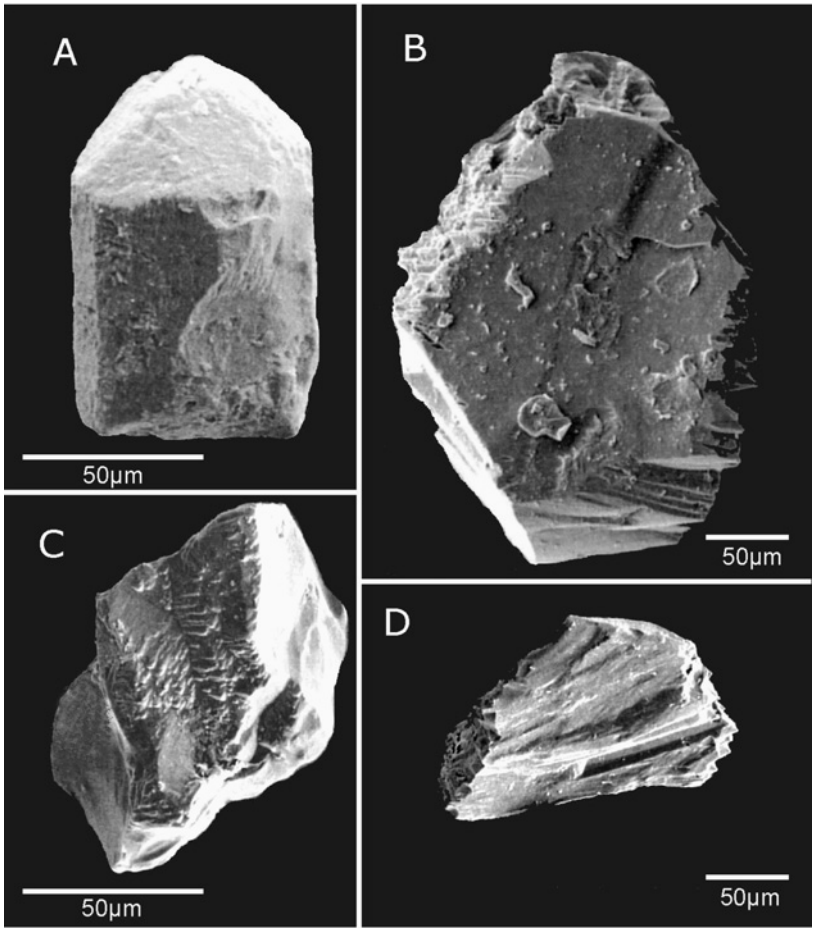

Fig. 5. Apatite (A), clinopyroxene (B), titanite (C), and staurolite (D) from a mid-Cretaceous (Ngaterian) sample from Mt Lookout in the Inland Kaikoura Range, Marlborough. (after Smale and Laird, 1995). Apatite shows no solution effects, other grains display various, solution-generated, surface textures.

1995), unetched apatite was present in association with partially etched pyroxene, titanite and staurolite, but epidote was absent (Fig. 5). This pattern occurs with pH > 7, and suggests that intrastratal alkaline fluids during burial were the most likely cause of dissolution rather than weathering (Morton, 1984; Morton and Hallsworth, 2007).

3.2. Neogene

In Miocene and younger sediments the diversity of heavy minerals is greater than in the older sediments. This may result from less advanced intrastratal dissolution, or it may reflect the inception of movement on the plate boundary between the Australian and Pacific plates with the flux of detritus richer in heavy minerals. The increase in

diversity is very evident in south Westland (Smale, 1991a), where the late Miocene saw the incoming of a flood of garnet from the Alpine Schist, adjacent to the western edge of the Pacific Plate. In early Pliocene sediments the suites are flooded abruptly by hornblende, probably derived from Fiordland on the Australian Plate, west of the Alpine Fault—a major plate boundary transform with a dextral displacement of around 480 km since the Miocene. In the overlying units the abundance of hornblende declines. It is later succeeded by olivine from the nearby Red Mountain Ultramafics and, finally, by pyroxene from the more serpentinised ultramafics north of Red Mountain. This sequence is consistent with Miocene-Recent dextral movement along the fault. The late Miocene flood of garnet seen in south Westland was not detected in Canterbury or Marlborough, and garnet is not prominent anywhere after the Palaeocene. In the latter location, garnet may have been derived from the garnet-bearing Cretaceous Mt Somers or Mt Misery Volcanics (Smale, 1990b).

4. RECENT SEDIMENTS

Heavy mineral studies in Recent sediments, where dissolution has had little or no effect, have been used in a wider field of studies than in older sediments. Examples are presented below from case studies where heavy mineral studies yielded potentially useful evidence to the solution of longstanding or controversial problems.

4.1. River Sands and Mixing Proportions

In 1989, a heavy mineral study of sand in the Wanganui River (Smale, 1991b) formed part of an investigation to assess the possible disturbing effects on river and estuarine sediments of the diversion of a tributary near the Wanganui headwaters to assist electricity generation. Variations in the proportions of orthopyroxene, clinopyroxene, hornblende, epidote, and garnet indicated four source regions: (a) the central North Island volcanoes (a suite dominated by orthopyroxene); (b) Taranaki volcanics (dominated by clinopyroxene); (3) Miocene-Pliocene marine sediments, with a higher proportion of recycled biotite, epidote, and garnet; and (4) Pleistocene marine sediments reflecting the onset of further volcanism, with hornblende and clinopyroxene.

The composition of the sand in the lower reaches of the Wanganui River is different from that of the adjacent coastal sediments, probably as a result of longshore drift, which had earlier allowed assessment of the contribution each source had made to the sand bar at the river mouth (Willett, 1959). Evaluation of samples collected on three other occasions between 1964 and 1989 were similarly based on the individual proportions of clinopyroxene, orthopyroxene, and hornblende from each sample. In 1959, the river sediment had a greater influence on the bar than in 1964 or 1983, when the sand was nearly all coast-derived. The influence of the river was greatest in 1989, when nearly half the bar was river-derived. This was probably the result of river floods, and suggested that the diversion of the headwaters had no discernible effect at the mouth.

In a study carried out for the Ministry of Works in Canterbury in 1979 (Smale, unpublished document), the extent of mixing of sediments was determined in a

substantial water irrigation race (the Rangitata Diversion Race). The object was to see if sediment was entering the race at siphon points where it crossed rivers. All heavy fractions were typical of the local Rakaia Terrane, but there was some variation, probably largely brought about by the nearby Mt Somers Volcanics. The variation was enough to show that very little sediment was entering the race via the siphons.

The effects of weathering, fluvial transport, and beach abrasion on heavy minerals were studied in the Cascade River of south Westland. This river system was chosen because it drained a distinctive region of ultramafic rocks, and the heavy minerals from such rocks were considered susceptible to these processes. It was also an area where longshore drift had limited influence on the beach sand composition. Results have indicated that the processes had little effect on the proportions or composition of the heavy minerals present: even olivine, shown experimentally to be susceptible to abrasion, showed negligible modification (Morton and Smale, 1990).

4.2. Iron-Ore Sands

The presence of ironsands on New Zealand beaches has long been known; they were noted by Captain Cook as "thrown upon the shore" in Mercury Bay (15th November 1769); he also noted (10th January 1770) "a black sandy bottom" in about 40 fathoms northwest of Woody Head, about 100 km south of Auckland. North Island volcanism, particularly in the Taupo Volcanic Zone and Taranaki, has produced most of these deposits, which are dominated by titanomagnetite and ilmenite. Large quantities have been carried to the coast by rivers, particularly the Wanganui and the Waikato, and transported long distances by longshore drift between Wanganui and Northland (Hamill and Ballance, 1985). Extreme sorting in beach and dune environments has concentrated the titanomagnetite and ilmenite in extensive areas, resulting in deposits with large reserves. However, only in the last 40 years has commercial mining proved feasible. Annual production of concentrate from beach sands is now around 1.7 million tonnes, worth about NZ$ 30 million (New Zealand—Crown Minerals; Ministry of Economic Development).

Ilmenite has been similarly concentrated on the west coast of the South Island, but as yet deposits have not proved commercial. Most of the beach sand ilmenite, which contains innumerable silicate inclusions, comes from the biotite- and garnet-bearing schists of the Southern Alps produced by metamorphism of Torlesse sediments. Ilmenite without silicate inclusions is present in the Buller River (which flows through Westport), and is distinct from that in the beach sands. Buller ilmenite is probably being derived from lamprophyres and dioritic rocks inland in the Paparoa Range (McPherson, 1978). Independent assessment of ratios of ilmenite and magnetite to rounded (Torlesse-derived) and euhedral (igneous-derived) zircon confirmed that most beach sand ilmenite came from the schists (Bradley et al., 1979).

4.3. Siltation in Harbours

In a study of siltation in the northern part of Tauranga harbour, a drowned estuary enclosed by a barrier island, Smale (1993) showed that the sediment was derived dominantly from the open sea rather than from the rivers draining into the harbour.

Much of the sediment may have passed through the harbour, but must then have been fed back from the sea after mixing with other sediment. While sand from the harbour had mineralogy very similar to that from the hinterland, the ratio of magnetite to ilmenite was much lower in the harbour and offshore (~1:10) than in the hinterland (~3:2). Results of private contract studies in 1984 and 1985 showed similar, offshore-derived sand (though with different mineralogy) in harbours at Riverton and Westport.

4.4. Forensic Studies

Various forensic studies in New Zealand criminal cases have linked suspects to the scene of a crime by comparing heavy minerals from soils at the crime scene with those in soil found on suspects' clothing or on items they used. The path of the campervan used by the French agents who sank the "Rainbow Warrior" in Auckland Harbour in 1985 was tracked by various geological comparisons. These were mostly lithological, but the presence of magnetite and orthopyroxene was instrumental in tracing the source of some of the sand on the van to Muriwai Beach (Skinner et al., 1988).

Off the northwest coast of the South Island heavy minerals in the sand adhering to paua shells (*Haliotis iris* or abalone), suspected of having been taken illegally (poached) from a reserve area adjacent to the licence (legal) area, were compared with those from carefully sampled in situ paua (Bremner and Clarke, 2004). The heavy mineral fractions were all very similar, but showed sufficient variation to allow a conviction. The verdict also drew information from a previous heavy mineral study (van der Linden, 1969), which had established that sediments were distributed by currents flowing northeast along the coast (Tortell, 1981). In the paua study (Richard Clarke, personal communication), trends in the direction of transport showed an increase in amphibole and epidote, and a decrease in mica and chlorite. This probably reflects a change in the coastal geology from granite in the south to Tertiary sediments in the north, with input of amphibole and epidote from the more northerly rivers, and attrition and dispersion of chlorite and mica. Comprehensive investigation included various scatter plots and histograms of suspect and control samples. For example, epidote/mica versus amphibole/chlorite plots revealed four distinct groups among the suspect samples. Two suspect groups resembled control samples from within the legal area of the fishery, but most of the suspect samples and control samples from the prohibited area at the southern end of the fishery formed one group. The suspect eventually pleaded guilty.

5. CONCLUDING REMARKS

Studies of heavy minerals have been and continue to be of considerable value in characterising regional formations and terranes, and determining the provenance of sediments. In New Zealand, studies of ferromagnesian minerals are routinely used to differentiate between ignimbrites and their associated tephras. Such studies involve methodical counting of grains and careful optical mineralogy. This skill is becoming less common as other methods of mineral identification are developed that are both

reliable and quantitative. However, optical examination must continue to underpin any heavy mineral study; to attempt not to do so is like studying petrology without thin sections. In older and more porous sediments it is important to have an understanding of the factors that are likely to cause post-depositional dissolution of chemically unstable minerals.

Preferred techniques change with time. Heavy mineral studies now benefit from techniques such as electron microprobe, SEM and quantitative XRD. As analytical techniques have advanced, studies of individual minerals have proved informative, and associated developments have led to independent techniques such as fission track dating of apatite and zircon and SHRIMP uranium-lead zircon ages.

ACKNOWLEDGEMENTS

I would like to acknowledge many colleagues, including the late Nick Brothers (who taught me at Auckland University), several at Amdel (Adelaide) and the National Institute for Metallurgy (Johannesburg) with whom I explored the heavy minerals repertoire, Simon Nathan (who pointed me towards heavy minerals studies in New Zealand), Nick Mortimer (who provided the terrane details on the map of New Zealand—Fig. 1), David Shelley (who could find an optical answer to any mineralogical problem), Andy Morton (who has probably seen and recognised the significance of more heavy minerals than I ever could have), and finally Maria Mange for her insistence and cooperation in stimulating this paper. I am very grateful to Nick Mortimer and Peter Ballance for reviewing the manuscript.

The Royal Society of New Zealand gave permission to reproduce Figs. 2 and 5 from the New Zealand Journal of Geology and Geophysics (Fig. 6 in Smale and Laird, 1995; and Fig. 2 in Smale, 1997). The Institute of Geological and Nuclear Sciences, which inherited the copyright for New Zealand Geological Survey Publications, gave permission to reproduce Figs. 3 and 4 from the New Zealand Geological Survey Record (Figs. 1 and 2 in Smale and van der Lingen, 1989).

REFERENCES

Bradley, J.P., Wilkins, C.J., Oldershaw, W., Smale, D., 1979. A study of detrital heavy minerals in the Taramakau catchment. Journal of the Royal Society of New Zealand 9, 233–251.

Bremner, G., Clarke, R., 2004. The use of heavy minerals to establish the provenance of suspect shellfish. Abstract for 17th International Symposium on the Forensic Sciences, March 28–April 2, 2004, Wellington, New Zealand.

Brothers, R.N., 1959a. Heavy minerals from Southland: Part 1—Permian-Jurassic sediments. New Zealand Journal of Geology and Geophysics 2, 622–633.

Brothers, R.N., 1959b. Heavy minerals from Southland: Part 2—Upper Cretaceous—Lower Tertiary coal measures. New Zealand Journal of Geology and Geophysics 2, 788–798.

Dickinson, W.R., 1985. Interpreting provenance relations from detrital modes of sandstones. In: Zuffa, G.G. (Ed.), Provenance of Arenites. In: NATO ASI Series, vol. 148. Reidel, Dordrecht, pp. 333–361.

Full, W.E., Ehrlich, R., Bezdek, J.C., 1982. FUZZY QMODEL—a new approach for linear unmixing. Mathematical Geology 14, 259–270.

Hamill, P.F., Ballance, P.F., 1985. Heavy mineral rich beach sands of the Waitakere coast, Auckland, New Zealand. New Zealand Journal of Geology and Geophysics 28, 503–511.
Hayward, B.W., Smale, D., 1992. Heavy minerals and the provenance history of Waitemata Basin sediments (early Miocene, Northland, New Zealand). New Zealand Journal of Geology and Geophysics 35, 223–242.
Hutton, C.O., 1950. Studies of heavy detrital minerals. Geological Society of America Bulletin 61, 635–710.
Mackinnon, T.C., 1983. Origin of the Torlesse terrane and coeval rocks, South Island, New Zealand. Geological Society of America Bulletin 94, 967–985.
Mange, M.A., Maurer, H., 1992. Heavy Minerals in Colour, Routledge. Chapman and Hall, New York, 147pp.
McPherson, R.I., 1978. Geology of Quaternary ilmenite-bearing coastal deposits at Westport. New Zealand Geological Survey Bulletin 87, 95pp.
Milliken, K.L., 1988. Loss of provenance information through sub-surface diagenesis in Plio-Pleistocene sandstone, northern Gulf of Mexico. Journal of Sedimentary Petrology 58, 992–1002.
Milner, H.B., 1962. Sedimentary Petrology, vol. 2 (4th ed.) George Allen and Unwin, London, 715pp.
Mortimer, N., 2004. New Zealand's geological foundations. Gondwana Research 7, 261–272.
Morton, A.C., 1984. Stability of detrital heavy minerals in Tertiary sandstones from the North Sea Basin. Clay Minerals 19, 287–308.
Morton, A.C., Hallsworth, C.R., 2007. Stability of detrital heavy minerals during burial diagenesis. In: Mange, M.A., Wright, D.T. (Eds.), Heavy Minerals in Use. Developments in Sedimentology (this volume).
Morton, A.C., Smale, D., 1990. The effects of transport and weathering on heavy minerals from the Cascade River, New Zealand. Sedimentary Geology 68, 117–123.
Nickel, E., 1973. Experimental dissolution of light and heavy minerals in comparison with weathering and intrastratal solution. Contributions to Sedimentology 1, 1–68.
Rohlf, F.J., 1988. NTSYS-pc, numerical analysis ands mulivariate analysis system. Exeter Software.
Roser, B.P., Korsch, R.J., 1986. Determination of tectonic setting of sandstone-mudstone suites using SiO_2 content and K_2O/Na_2O ratio. Journal of Geology 94, 635–650.
Skinner, D.N.B., Challis, G.A., Mildenhall, D.C., Watters, W.A., 1988. Of Rainbow Warriors, deer antlers, platinum, and other things: forensic science in New Zealand Geological Survey. New Zealand Geological Survey Report G130, 13pp.
Smale, D., 1985a. Waiau Basin Cretaceous-Tertiary heavy minerals. New Zealand Geological Survey Report SL 12, 23pp.
Smale, D., 1985b. Heavy minerals in Tertiary sandstones of the Te Anau Basin. New Zealand Geological Survey Report SL 13, 16pp.
Smale, D., 1988. Detrital pumpellyite and epidote group minerals in Cretaceous and Tertiary sandstones in the South Island, New Zealand. Journal of Sedimentary Petrology 58, 985–991.
Smale, D., 1989. Leaching of heavy minerals above and below the mid-Cretaceous unconformity in the Ohuriawa Gorge area of the Waipara River, north Canterbury. New Zealand. Journal of Sedimentary Petrology 59, 1011–1021.
Smale, D., 1990a. Heavy minerals from south-west Fiordland. New Zealand Geological Survey Report SL 22, 10pp.
Smale, D., 1990b. Distribution and provenance of heavy minerals in the South Island: a review. New Zealand Journal of Geology and Geophysics 33, 557–571.
Smale, D., 1991a. Provenance changes and movement on the Alpine Fault indicated by heavy minerals from Cretaceous-Cenozoic sediments in south Westland. Journal of the Royal Society of New Zealand 21, 151–160.

Smale, D., 1991b. Distribution and provenance of sand in the Wanganui River. New Zealand Geological Survey Record 43, 7–13.

Smale, D., 1993. Sediment source and movement in Tauranga Harbour and nearshore Bay of Plenty. Institute of Geological and Nuclear Sciences Science Report 93/25, 20pp.

Smale, D., 1997. Heavy minerals in the Torlesse Terrane of the Wellington area. New Zealand Journal of Geology and Geophysics 40, 499–506.

Smale, D., Laird, M.G., 1995. Relation of heavy mineral populations to stratigraphy of Cretaceous formations in Marlborough, New Zealand. New Zealand Journal of Geology and Geophysics 38, 211–222.

Smale, D., Morton, A.C., 1987. Heavy mineral suites of core samples from the McKee Formation (Eocene–Lower Oligocene), Taranaki: implications for provenance and diagenesis. New Zealand Journal of Geology and Geophysics 30, 299–306.

Smale, D., Nathan, S., 1980. Heavy minerals in the pre-Tertiary rocks of the Paparoa Range, West Coast, South Island. New Zealand Geological Survey Report G 36, 11pp.

Smale, D., van der Lingen, G.J., 1989. Differential leaching of garnet grains at a depth of 3.5 km in Tane-1, Western Platform, New Zealand. Research Notes, New Zealand Geological Survey Record 40, 57–60.

Tortell, P., 1981. New Zealand Atlas of Coastal Resources. Government Printer, Wellington, 28pp, (15 maps).

Turnbull, I.M., 1979. Petrography of the Caples Terrane of the Thomson Mountains, northern Southland, New Zealand. New Zealand Journal of Geology and Geophysics 22, 709–727.

van der Linden, W.J.M., 1969. Off-shore sediments, north-west Nelson, South Island, New Zealand. New Zealand Journal of Geology and Geophysics 12, 87–103.

Willett, R.W., 1959. Tongariro River power development: effects of diversions on Wanganui Harbour. Report from New Zealand Geological Survey to Sir Alexander Gibb and Partners, 12th March.

This page intentionally left blank

Chapter 23

HEAVY-MINERAL PROVENANCE IN AN ESTUARINE ENVIRONMENT, WILLAPA BAY, WASHINGTON, USA: PALAEOGEOGRAPHIC IMPLICATIONS AND ESTUARINE EVOLUTION

GRETCHEN LUEPKE BYNUM[1]

761 Towhee Court, Fremont, CA 94539, USA

ABSTRACT

Modern sediments from representative localities in Willapa Bay, Washington, comprise two principal heavy-mineral suites. One contains approximately equivalent amounts of hornblende, orthopyroxene, and clinopyroxene; this is derived from the Columbia River, which discharges into the Pacific Ocean a short distance south of the bay. The other suite, dominated by clinopyroxene, is restricted to sands of rivers flowing into the bay from the east. The heavy-mineral distributions within the bay suggest that sand discharged from the Columbia River, borne north by longshore transport and carried into the bay by tidal currents, accounts for nearly all of the sand within the interior of Willapa Bay today.

Pleistocene deposits on the east side of the bay contain three heavy-mineral assemblages, two of which are identical to the modern assemblages described above. These assemblages reflect the relative influence of tidal and fluvial processes on the Late Pleistocene deposits (100,000–200,000 BP. Amino acid racemization in Quaternary shell deposits at Willapa Bay, Washington. Geochimica et Cosmochimica Acta 43, 1505–1520). They are also consistent with those processes inferred on the basis of sedimentary structures and stratigraphic relations in about two-thirds of the samples examined. Anomalies can be explained by recycling of sand from older deposits. The persistence of the two heavy-mineral suites suggests that the pattern of estuarine sedimentation in Late Pleistocene deposits closely resembled that of the modern bay.

The third heavy-mineral suite is enriched in epidote and occurs in a few older Pleistocene units. On the north side of the bay, the association of this suite with southwest-directed foresets in cross-bedded gravel indicates derivation from the northeast, perhaps from an area of glacial outwash. The presence of this suite in ancient estuarine sands exposed on the northeast side of the bay suggests that input from this northerly source may have intermittently dominated Willapa Bay deposition in the past.

[1]U.S. Geological Survey (retired)

Developments in Sedimentology, Vol. 58, 587–605

ISSN: 0070-4571/doi:10.1016/S0070-4571(07)58023-4

Keywords: heavy-mineral provenance; estuarine; fluvial; palaeogeography; Pleistocene; Columbia River; Washington

1. INTRODUCTION

Results of heavy-mineral studies in modern estuaries help to identify where the greatest amount of interaction between oceanic and river influences takes place and thereby determine the extent of influence of the tidal prism within the estuary. The degree of fluvial influence in estuarine sediment, relative to other input mechanisms, depends on the location within the estuary and the mass and mode of fluvial sediment transport relative to other transport mechanisms (Guilcher, 1967). Streams with limited discharge relative to the tidal prism influence only their immediate areas of discharge within an estuary.

Van Andel (1955) was one of the first to recognize and quantify mineralogical variation in depositional environments of the Rhône River delta. He divided the identified heavy minerals into "marine" and "terrestrial" groups. More recent studies of heavy minerals in estuarine environments have concentrated on variations due to selective sorting (Al-Bakri, 1986) and differing sediment textures where mineralogical differences could not be discerned (Mohan, 1995).

On the West coast of the United States, Kulm and Byrne (1966) used relative abundances of heavy minerals to differentiate among the marine, fluviatile, and marine–fluviatile realms of depositions in Yaquina Bay, Oregon. Scheidegger and Phipps (1976) also identified marine, river and "mixed" sediments in Gray's Harbor, just north of Willapa Bay, based on heavy-mineral content. In similar studies in Tillamook Bay, Oregon (Glenn, 1978) and Alsea Bay, Oregon (Peterson et al., 1982), zones of dominant marine, shoreline, and river influence were identified. Peterson et al. (1984b) extended the earlier study of Alsea Bay by examining relative amounts of hypersthene as an indicator of the presence of beach sand in estuarine deposits as seen in sediment cores. In comparing six estuaries along the Oregon and Washington coasts, Peterson et al. (1984a) found that a normalized ratio of hypersthene to augite was sufficient to determine the relative amounts of beach and river sands in the modern sediments of four of the estuaries.

A few studies have used heavy minerals to interpret sediment-input mechanisms in pre-Pleistocene deposits. Derry (1933) showed that glacial tills and interglacial sediments in the Don Valley, near Toronto, Canada, contained similar heavy minerals, but different relative abundances. Zemstov (1974) deciphered an unfossiliferous succession on interglacial-alluvial, glacial-moraine, and marine Quaternary deposits of the West Siberian plain, using specific heavy-mineral associations.

Terrace deposits exposed around the margins of Willapa Bay, Washington, represent the filling of a succession of ancient estuarine bays that existed at this site during the Pleistocene (Clifton, 1983). In these deposits, faunal assemblages, trace fossils, sedimentary structures, textural characteristics, and geometric considerations provide a basis for developing criteria for identifying depositional facies within an estuary fill (Clifton and Phillips, 1980; Clifton, 1982, 1994; Anima et al., 1989; Clifton et al., 1989; Clifton and Leithold, 1991; Gingras et al., 1999; Clifton and Gingras, 2004). The mineralogy of these sediments is another source of information about the in-filling of this tidal basin (Luepke and Clifton, 1983). The present paper is a summary and update of that initial work.

The distribution of heavy minerals in bay deposits should reflect the proportions of sedimentary input from different sources. For most estuaries, the input is oceanic, through tidal transport, from drainage basins that feed the estuary through fluvial transport, or from sources within the estuary itself through wave or tidal-current erosion of bay cliffs.

2. MODERN BAY SETTING

The Willapa Bay tidal inlet lies 50 km north of the Columbia River on the southwestern coast of Washington (Fig. 1). Long Beach Peninsula, also known as the Willapa Barrier, separates the bay from the open ocean. This sand spit (38 km long by 2.0–3.5 km wide) is the most extensive along the Pacific coast (Smith et al., 1999). Extending from the headland at the mouth of the Columbia River, it is built by sediments from the river as they are swept northward by longshore currents. Several rivers drain directly into the bay from the north, south, and east sides; none of these rivers compare in size to the Columbia (see Table 1). Pleistocene terraces border the bay on the north, south, and east sides. When this study was undertaken, Willapa Bay was described as the last relatively unspoiled large estuary in the United States (Chasan, 1978). Estuaries are natural magnets for human settlement, and more development has occurred since the 1970s, particularly on Long Beach Peninsula. Nevertheless Willapa Bay itself remains relatively undisturbed (Vanderburgh et al., 2003).

Dominant directions of longshore transport along this part of the Washington coast are from south to north. Winds from extra-tropical cyclones approach the coast generally from the west and generate most of the larger waves that reach the coast (Ruggiero et al., 1997). Local winds range from northwest to southwest (Ballard, 1964; Ruggiero et al., 2005). Tides are mixed semi-diurnal and range from 2.5 m at the bay's entrance to 3.1 m at Nachotta on the bay's west side; the size of the tidal prism has been calculated at 0.72 km^3 (Andrews, 1965; Ruggiero et al., 2005).

The rivers that drain the south and east side of Willapa Bay flow through primarily Eocene volcanic terrane (Fig. 1), especially the Crescent Formation (Wagner, 1967a, b; Wells, 1979). Petrographic examinations of rocks of the Crescent Formation show them to contain 25–37% augite (Pease and Hoover, 1957; Wolfe and McKee, 1972). By contrast, the rivers on the north side drain an area covered mostly by Quaternary terraces and the Tertiary Lincoln Creek and Astoria Formations (Gower and Pease, 1965; Wagner, 1967a). A preliminary examination of several units within the terraces there indicates a varied mineralogy similar in many ways to that of the Columbia River (Luepke, 1982a).

Andrews (1965), who identified heavy minerals but did not study their distribution in detail, made the first survey of Willapa Bay sediments. Heavy-mineral studies on the sediments of the Columbia River and beaches adjacent to its mouth have been documented in numerous publications (Hodge, 1934; Ballard, 1964; Kelley and Whetten, 1969; Whetten et al., 1969; Scheidegger et al., 1971; Luepke, 1982b).

3. PLEISTOCENE DEPOSITS

Pleistocene terraces crop out extensively along the northern and eastern margins of the bay and around much of Long Island at the south end of the bay. Many of

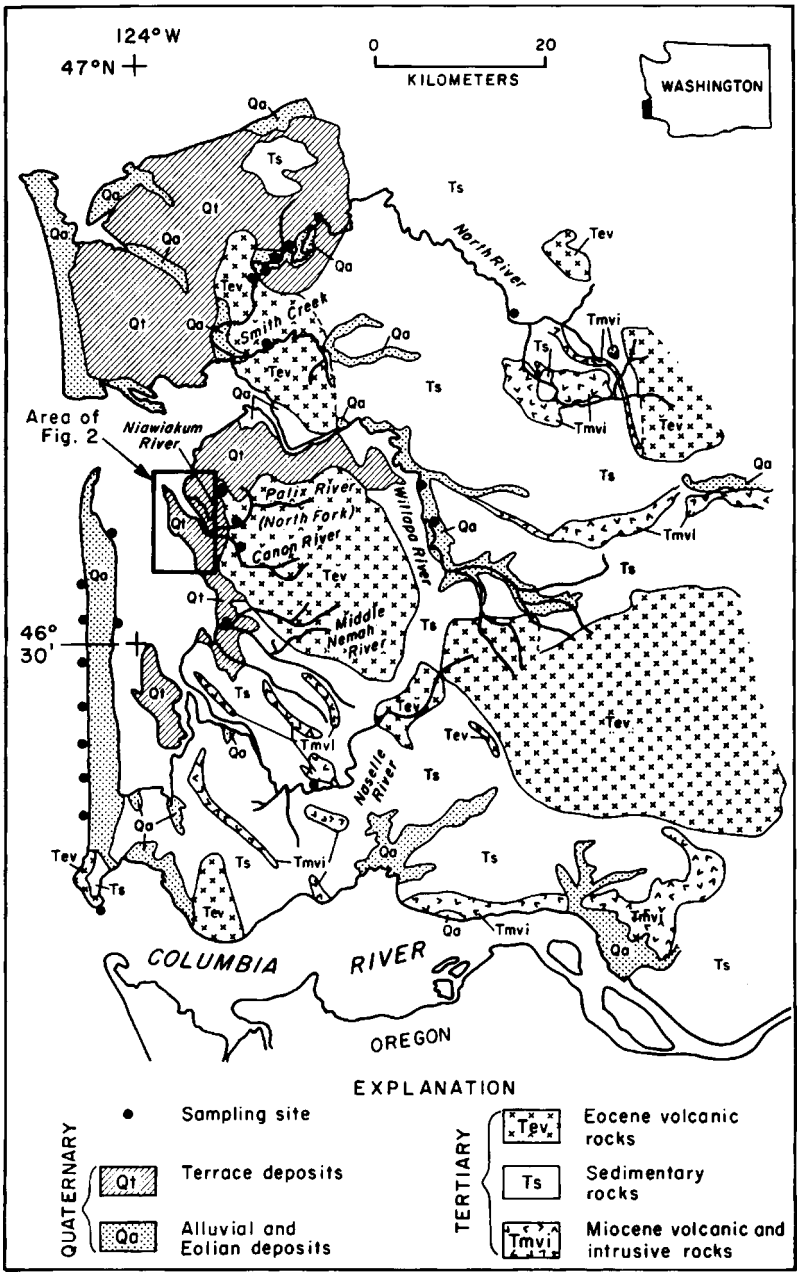

Fig. 1. Geological map showing location of samples collected on beaches and rivers in the Willapa Bay area. Geology modified from Pease and Hoover (1957), Wagner (1967a, b), Wolfe and McKee (1968, 1972), Wells (1979). From Luepke and Clifton (1983) with permission from Elsevier.

Table 1. Comparison of the Columbia River with rivers draining into Willapa Bay, Washington

River	Total length (km)	Drainage area (km^2)	Average annual discharge (m/sec)
Columbia	1931	670,810	5650
North	93	826	27
Willapa	67	668	18
Naselle	45	345	12
Smith Creek	23	174	–
Canon*	15	26	–
Middle Nemah	14	23	3
Palix, North Fork*	12	23	–
Niawiakum	11	10	–

Note: –, No data available.
*Lengths and drainage area measured directly from U.S. Geological Survey quadrangle maps. Other lengths and drainage area complied from Veirs (1969). Average yearly discharges compiled from U.S. Geological Survey (1972, 1974). Columbia River data from Rand McNally (1980).

these deposits contain sedimentary structures and fauna indigenous to the modern bay, and clearly represent transgressive-to-highstand estuary deposits. High-stand terrace surfaces related to these bayfills are evident around the margins of Willapa Bay, although the higher, older surfaces are much dissected and difficult to define. The best-defined, and apparently youngest, terrace surface lies at an elevation of ~13 m and can be traced from Goose Point to Pickernell Creek on the eastern side of the bay (Fig. 2).

Deposits underlying this terrace comprise a variety of intertidal and subtidal deposits (Clifton, 1983). Their ages, based on amino-acid racemization of shells, extend back ~100,000–200,000 years BP (Kvenvolden et al., 1979). The deposits beneath the 13 m terrace have been divided into five stratigraphic units (Fig. 3), four of which formed at substantially different relative positions of sea level (Clifton, 1983). Table 2 summarizes the sediment characteristics, ages, and depositional environments of the five units.

One suite of samples collected from Goose Point in the oldest unit (Unit I) contained diatoms filled with diagenetic pyrite. Two genera, *Camplyodiscus* and *Cosinodiscus*, are present. *Camplyodiscus* dominates the assemblage; it is a benthic diatom that attaches itself to brackish-water plants. *Cosinodiscus* is a marine-shelf to open-ocean planktonic form. Diatoms in Willapa Bay have been described in detail by Hemphill-Haley (1993a, b, 1995). Towards the southern end of the exposures, near Pickernell Creek, Unit I becomes somewhat sandier and contains angular pebbles of basalt, suggesting proximity to local sources.

Unit II represents subtidal deposition (Clifton, 1983). Unit III, which dissects both Units I and II, appears to be a valley fill formed during, or at the end of, a period of lowered sea level (Clifton, 1983). Unit IV is the most extensively exposed of the terrace units and directly underlies most of the 13 m terrace. Bimodally opposed foreset-bedding implies a strong tidal influence during the deposition of this unit. Channels filled to the 13 m terrace level with sandy and muddy sediments locally

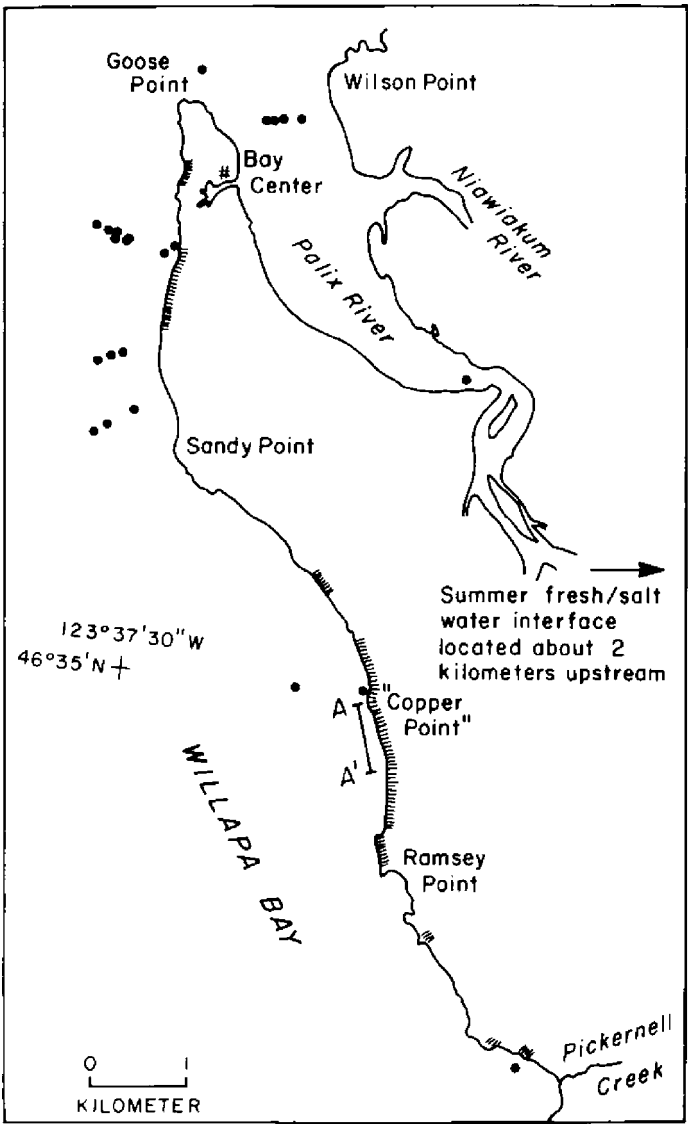

Fig. 2. Enlargement of area in Fig. 1, showing sampling sites on tidal flats and within the lowermost reach of the Palix River. Hachured area shows location of the 13 m terrace from Goose Point to Pickernell Creek. Sea-Cliff section A–A' shown in Fig. 3. From Luepke and Clifton (1983) with permission from Elsevier.

dissect this unit. The Unit V strata generally lack fauna and burrows and are therefore considered to represent a fluvially dominant episode deposited after, but at the same sea-level position as, Unit IV (Clifton, 1983).

Stratigraphic relations among the deposits that underlie the higher, older terraces are less clear. A number of units exist at elevations up to 150 m (Wagner, 1967b);

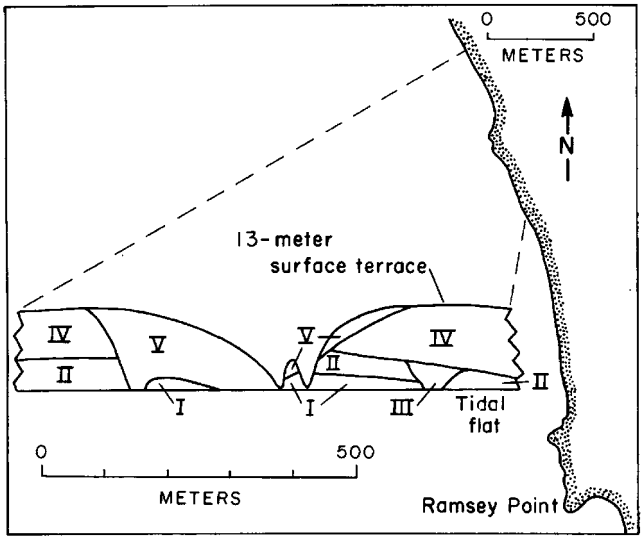

Fig. 3. Schematic diagram of relationships of the five units below the youngest (13 m) Pleistocene terrace, Willapa Bay. See Fig. 2 for location of section A–A'. From Luepke and Clifton (1983) with permission from Elsevier.

Table 2. Summary of information on the Pleistocene terrace units examined in Willapa Bay

Unit	Sediment texture	Age* (years BP)	Depositional environment†	Number of samples point-counted
I	Mud; locally sandy with angular pebbles	200,000	Intertidal and uppermost subtidal	27
II	Cross-bedded and bioturbated sand	200,000	Subtidal	24
III	Mud with root and rhizome structures	Dissects Units I and II	Valley fill	17
IV	Interbedded mud and sand	100,000	Subtidal to intertidal near terrace surface	18
V	Sand and mud, with local gravel and abundant logs and wood clasts	Locally dissects unit IV	Fluvial	12

Note: See Fig. 3 for schematic diagram of stratigraphic relationships.
*Amino-acid racemization dates on shells in unit, from Kvenvolden et al. (1979).
†As identified by Clifton (1983) with permission from Elsevier.

they are slightly deformed and generally less well exposed than the lower terrace units.

4. METHODS

Samples from the five Late Pleistocene units were taken between Goose Point and Pickernell Creek (see Fig. 2). To examine the potential for sediment input, beach samples were collected from both sides of the Long Beach Peninsula and fluvial samples from the following rivers: Middle Nemah, Naselle, Willapa, Palix (North Fork), Canon, Niawiakum, and North rivers, and from Smith Creek (see Fig. 1). Modern tidal-flat samples were confined to flats adjacent to the 13 m Pleistocene bay cliffs (see Fig. 2).

Modern beach samples of 300–500 g were collected in the upper swash zone of the Long Beach Peninsula by scraping the upper surface of the sand to a depth of 2 cm. Tidal-flat samples were similarly collected. River samples were taken in sandy areas near the banks, upstream from the zone of tidal influence. The five samples from the lowermost reaches of the Palix River (Fig. 2) were collected at depths from 1.8 to 5.5 m by SCUBA divers using coring equipment (Luepke and Clifton, 1983).

Only sand-sized material (2.0–0.062 mm) was analysed. Samples were washed with demineralised water, the water decanted to remove silt and clay, and then air-dried. Splits of samples were separated in tetrabromoethane (density = 2.96). The heavy minerals were then sieved and the 3–4 phi (0.125–0.062 mm) fraction microsplit for grain mounts. Lakeside 70 ($n = 1.54$) was used as the mounting medium.

The number of grains counted depended on their abundance and the prevalence of opaque minerals and mineral aggregates (grains containing more than one mineral). The average number of non-opaque grains counted was ~250. For some samples, a total of 300 grains sufficed to provide enough identifiable heavy minerals, but a few samples required a count of up to 600 grains. Total counts as low as 143 grains usually represented samples with very few heavy-mineral grains in the 0.125–0.062 mm fraction. Regardless of how many grains were actually counted, the entire slide was examined, and any mineral species seen but not encountered during the point-count was noted as present. In addition to the heavy-mineral samples point-counted from the five Late Pleistocene units (see Table 2), 18 samples were point-counted from tidal flats, 27 from rivers, 25 from beaches, and 14 from older Pleistocene units. A total of 200 samples were point-counted for the study.

Heavy minerals were counted using the line method. To ensure that all grains would be randomly encountered, half the total number of grains per slide was counted in left-right traverses, and the other half in up-down traverses. Care was taken that the two traverses never overlapped. Though this method gives a number frequency, which biases a sample towards the larger grains, counting a limited size range (Galehouse, 1969, p. 814) minimizes this problem. To check the method's accuracy, the heavy minerals from 16 beach samples were sieved at 1/4 phi (0.25 mm) intervals. Point counts of minerals in the 0.149–0.125 mm and 0.125–0.105 mm size ranges were compared with those in the 0.125–0.062 mm range. No significant differences in mineral frequencies were noted (Luepke and Clifton, 1983).

5. DISTRIBUTION OF HEAVY MINERALS

The heavy-mineral suites in both the modern and Pleistocene deposits in Willapa Bay contain a wide variety of minerals (Luepke, 1982a), attesting to the mineralogical immaturity of the sediments. The same mineral species identified in the Pleistocene terraces also appear in the modern estuary, beach, and river sands. Of the 200 samples point-counted for this study, 52 selected samples are presented in Table 3.

The most common groups are orthopyroxene (mostly hypersthene, with rare enstatite), clinopyroxene (mostly augite and titanaugite, with rare diopside and aegerine-augite), and hornblende (green, blue-green, brown, and basaltic hornblende). These three groups comprise more than 70% of the non-opaque heavy-mineral count. Various percentages of epidote group minerals, garnet, kyanite, sphene, zircon, and rutile occur in nearly all samples. Other minerals identified include apatite, staurolite, sillimanite, chloritoid, tourmaline, and glaucophane.

5.1. Modern Sediments

The percentages of orthopyroxene, clinopyroxene, and hornblende in samples from modern beaches, rivers, and tidal flats were normalized to 100% and plotted on ternary diagrams (Fig. 4). In the discussion to follow, samples that plot near the centre of the ternary diagram are said to have an hornblende-orthopyroxene-clinopyroxene (H–O–C) suite and those near the clinopyroxene end member are said to have a clinopyroxene suite.

Samples from the ocean side of Long Beach Peninsula tend to have approximately equal proportions of the three mineral species in the H–O–C suite, with either hornblende or orthopyroxene being the greatest of the three species (Fig. 4a). This H–O–C heavy-mineral suite resembles that described in samples taken from the Columbia River (Whetten et al., 1969), a clear reflection of the influence of northward longshore transport on the development of the Long Beach Peninsula. Two samples collected at the mouth of the Columbia River plot within the field of the ocean-Beach samples (Fig. 4a).

Samples collected on the tidal flats form a pattern on the ternary diagram (Fig. 4b) very similar to the ocean side beach-sand pattern of Fig. 4a. Two contrasting heavy-mineral assemblages were detected in samples from above the zone of tidal influence in rivers draining directly into Willapa Bay (Fig. 4a). The rivers draining from the north side of the bay (North River and Smith Creek) have a mixed assemblage of the three mineral groups, but much less orthopyroxene than in the Long Beach Peninsula samples. The heavy-mineral suite from rivers draining into the bay from the east, in contrast, is almost totally dominated by clinopyroxene. This reflects the dominance of basalt of the Crescent Formation on the Bay's east side (Wagner, 1967b). However, the samples taken from the east-side Palix River below the interface of fresh and saline water (see Fig. 2) contain the H–O–C suite (Fig. 4b).

5.2. Pleistocene Deposits

Samples from each of the five terrace units were also plotted on ternary diagrams (Fig. 5). The H–O–C suite dominates in all but a few samples from the Pleistocene

Table 3. Non-opaque heavy-mineral composition of selected samples collected in Willapa Bay, Washington

Sample no.	Collection site	OPX	CPX	HBL	EPI	GAR	Sphene	Zircon	Rutile	APA	KYA	STAR	UNK	Other
74Na-1	Naselle River	13.4	58.2	17.9	4.0	1.0	1.0			2.0		0.5	2.0	
74Nem-2	Nemah River	9.0	74.1	11.4	3.5	*	*	0.5			0.5		1.0	
74Wi-3	Willapa River	2.1	91.5	3.5	2.1		*							0.7
77NP-1	North Palix River	6.3	63.8	18.5	8.3	0.4	0.4	*			0.4	0.4	1.6	
77C-2	Canon River	6.8	88.9	1.8	1.8		0.7							
74No-1	North River	14.5	24.8	33.6	18.7	3.8	2.3	0.8	0.4		*	0.4	0.4	0.4
77No-1	North River	19.6	22.0	36.4	16.3	1.4	0.5	1.0	1.0		*	1.0	0.5	0.5
77No-2	North River	16.7	25.4	36.0	17.5	2.2	0.9	*	0.4		0.4			0.4
77S-1	Smith Creek	14.7	16.9	43.3	16.5	3.4	1.1	0.4	0.8	0.4	0.8	0.4	*	1.5
77S-2	Smith Creek	13.8	13.5	34.2	20.7	6.6	4.3	2.6	*	0.7	*	2.0	1.0	0.6
74WGL-51	LBP, bay side	39.4	18.9	14.4	14.4	9.1	0.8	*	1.5	0.8			0.8	
77WGL-53	LBP, bay side	24.6	19.6	36.3	15.9	1.4	0.4	*		*	1.4	0.4		
77WGL-54	LBP, bay side	25.0	16.8	41.4	13.1	0.4				*	1.2	0.4	0.4	1.2
74WGL-56	LBP, ocean side	45.8	22.2	20.4	5.1	3.2	0.9	*		0.9	*	*	0.5	1.0
77WGL-63	LBP, ocean side	26.2	11.5	52.7	9.0		0.4							0.4
77WGL-68	LBP, ocean side	29.9	15.2	44.3	10.2	*	*			*	0.4			*
Q823-12b	Palix R. mouth	20.9	15.0	41.4	15.0	5.1	*	*	0.4		0.4	*	0.4	0.8
Q824-6	Palix R. mouth	23.4	20.9	36.5	13.1	4.1	0.4	0.4		*	0.4		0.8	
Q824-10	Palix R. mouth	30.5	18.9	29.7	11.9	7.0	0.4	*	*	*	0.8	0.4	0.4	
74T1-8	Tidal flat	38.1	23.0	22.9	10.7	2.0	0.4		*	0.8	0.8	*	0.8	0.4
74T3-5	Tidal flat	31.0	23.0	19.4	14.2	7.1	1.3	0.4	*	0.4	1.8	0.9		0.4
74T4-4	Tidal flat	29.2	27.4	22.8	11.9	5.9	1.4	0.9		*	0.5	*		
S801-1	Tidal flat	20.5	37.7	20.5	19.7	0.8		*		0.8	*			*
P114-1	Unit I	16.5	27.8	42.1	9.4	1.9	0.4	*		0.4	*		0.4	1.1
R901-9	Unit I	12.3	51.8	20.9	11.8	1.8	*	*		*	*	0.5		1.0
R902-3	Unit I	5.9	59.2	19.2	13.5	0.8	*	*	0.4		0.8	*	0.4	*
S828-1	Unit I	19.8	16.4	39.2	19.4	3.4	0.4		*	*	0.4			1.1

77WGL-77	Unit I	24.2	13.5	42.5	14.3	2.7	0.4		0.4	0.2	0.4	0.2		1.2
77WGL-11	Unit II	41.7	9.9	33.4	9.1	2.3	1.2		0.4	*	1.2	*	0.4	
77WGL-12	Unit II	33.5	3.4	41.8	14.8	3.4	0.4			0.8	1.5	*	0.4	*
77WGL-47	Unit II	40.1	19.0	23.0	11.9	4.4	0.4	1.2	*	*	*			
P113-12	Unit II	36.0	22.7	15.6	10.0	13.3	0.5	*	0.5	*	0.5	*	0.9	
S825-2	Unit II	45.6	13.3	21.4	11.9	5.8	1.0	*	*		*	0.3		0.6
77WGL-13	Unit III	37.3	20.8	17.3	10.2	12.2	0.8	*			0.4	*	0.8	0.4
77WGL-35	Unit III	44.1	9.3	19.0	14.6	10.5	0.4	*		*	0.8	1.2		
77WGL-43	Unit III	37.4	11.3	27.8	13.5	8.7	0.4	0.4	*	*	*	*	0.4	
P113-6	Unit III	39.7	16.5	28.1	5.8	9.1	*	*		0.4	0.4	*		
R902-1	Unit III	8.1	71.1	13.4	6.9						0.4			
77WGL-9	Unit IV	24.1	37.9	21.4	8.5	4.9	1.3	0.4		*	0.4	*		*
77WGL-15	Unit IV	33.2	9.5	40.3	11.9	2.0	*	0.4		0.8	0.8	0.8		0.4
77WGL-18	Unit IV	26.2	31.3	32.5	7.1	2.0	0.8	*		*	*	*		
77WGL-29	Unit IV	32.8	17.0	26.3	11.2	10.4	0.8		*	*	*	1.2		0.4
S825-3	Unit IV	20.8	47.9	15.8	11.6	1.9	*	0.8		0.4	0.8			*
77WGL-51	Unit V	3.7	83.5	7.0	5.5	*	*	*					0.4	
77WGL-52	Unit V	3.3	89.2	3.0	3.0	0.7	0.4			*			0.4	
P113-5	Unit V	17.6	48.6	20.0	4.8	6.2	0.5	*	0.5	0.5	*	*	1.4	
R901-1	Unit V	4.0	87.6	4.0	2.0	1.5	*	0.5						0.5
U822-2	Unit V	6.6	72.1	6.2	13.6	0.8	0.4	*			*	0.4		
77WGL-80	Older terrace	6.2	3.7	23.0	59.7	4.1	1.2	0.4	*		0.8	0.8		
77WGL-82	Older terrace	17.1	6.0	26.7	43.0	6.0	0.4	0.4	*	0.4	*			
U824-4	Older terrace	7.8	76.4	4.3	11.6	*	*					*		
U827-6	Older terrace	9.3	0.8	35.5	45.6	1.6		0.8	2.0					0.8

Note: Data complied from Luepke (1982a). Key: LBP, Long Beach Peninsula; OPX, orthopyroxene; CPX, clinopyroxene; HBL, hornblende; EPI, epidote group; GAR, garnet; APA, apatite; KYA, kyanite; STA, staurolite; UNK, unknown. Samples beginning with numbers collected by the author; samples beginning with letters collected by H. E. Clifton with permission from Elsevier.

*Mineral is present in sample at <0.1percent.

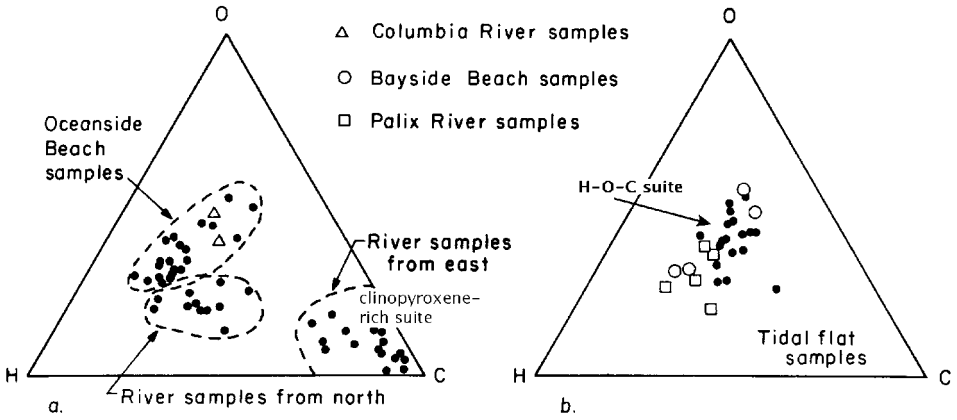

Fig. 4. Normalized distribution of orthopyroxene (O), clinopyroxene (C), and hornblende (H) in modern Willapa Bay sediments. (a) Ocean-side beach and river sands. Note similarity of samples from the Columbia River to ocean-side beach samples. (b) Bayside beach and tidal-flat sands. Note difference of samples at the mouth of the Palix River from other river samples in a. After Luepke and Clifton (1983) with permission from Elsevier.

units. Four samples from Unit II have the lowest clinopyroxene content of all five units (Fig. 5b). Four samples from Unit I and six from Unit V contain more than 60% orthopyroxene (Figs. 5a, e).

Another distinctive heavy-mineral suite appears in some of the terrace deposits older than those of the 13 m terrace. These samples, collected on both the north and east sides of Willapa Bay (Luepke, 1982a), contain a pronounced epidote-rich heavy-mineral suite (40–60% epidote). This heavy-mineral suite is anomalous here because none of the other Pleistocene deposits examined contain so much epidote. Two of the epidotiferous samples from the north side of the bay were taken from a gravely bed in which large-scale cross-bedding dips uniformly towards the southwest, suggesting a source to the north.

Epidote has been found to be susceptible to dissolution in acidic weathering conditions, which may be related to pyrite oxidation (Smale's personal communication with Crampton and Moore, 1990, cited on p. 336). In Unit I, the only unit to contain pyritized diatoms, no correlation exists between epidote percentages and the presence of the diatoms. In all five units the percentage of epidote ranges between 4 and 15%, with two samples from Unit V showing values lower than 4%. Again, no correlation exists between lower percentages of epidote and indications of environmental instability such as grain etching or iron-oxide encrustation, both of which were noted in some samples. It is therefore unlikely that effective acidic weathering conditions influenced the preservation of epidote group minerals in the Late Pleistocene terrace deposits.

6. MODERN INPUT MECHANISMS

Sediment enters Willapa Bay in three primary ways: (1) tidal transport of oceanic sand into the bay; (2) discharge from interior rivers; and (3) erosion of adjacent

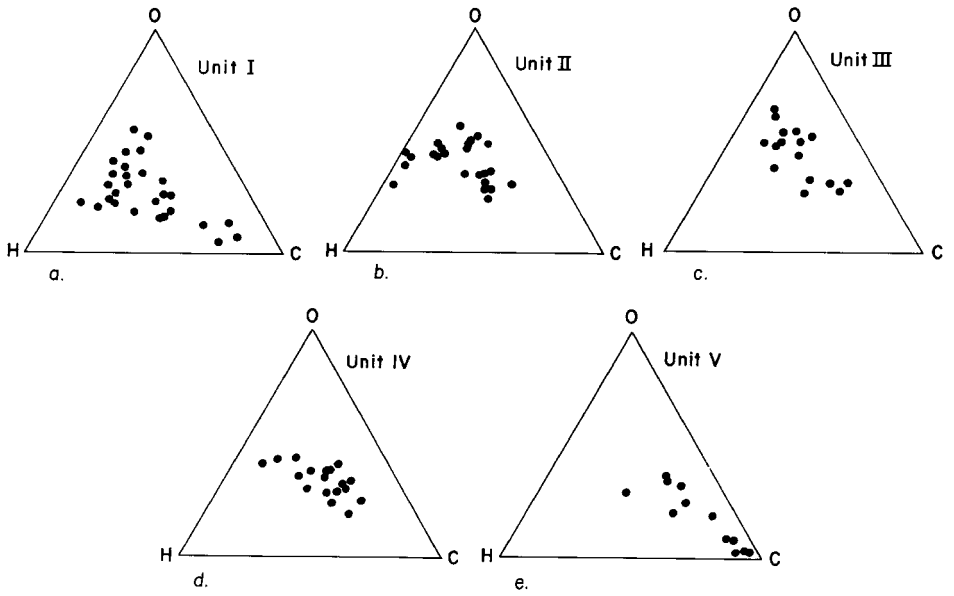

Fig. 5. Normalized distribution of hornblende (H), orthopyroxene (O), and clinopyroxene (C) in sediments of Pleistocene terrace units, Willapa Bay. From Luepke and Clifton (1983). (a) Unit I (oldest). Note the Pickenrell Creek samples near the C point. (b) Unit II. Note the four samples with very low percentages of clinopyroxene. (c) Unit III. (d) Unit IV. (e) Unit V (youngest) with permission from Elsevier.

Pleistocene terraces. The heavy-mineral assemblages do not permit a clear separation of oceanic input from that derived by erosion of the terraces: both would yield the H–O–C suite signature. Moreover, input from rivers draining from the north side of the bay cannot be accurately assessed because of their general similarity to Columbia River sediments.

In contrast, the rivers draining into the bay from the eastern side bear a heavy-mineral suite rich in clinopyroxene that reflects the widespread basaltic rocks in the drainage basins. This distinctive suite is also directly relevant to interpreting the heavy-mineral assemblages of the Pleistocene units examined in detail on the bay's east side.

The dominance of the H–O–C suite in the samples from the lower reaches of the Palix River implies that the clinopyroxene suite is highly restricted within the modern bay sediments. Although the number and distribution of river samples taken below the fresh/salt water interface are limited, the clinopyroxene suite most likely predominates today only above the zone of tidal transport.

7. PALAEOGEOGRAPHIC IMPLICATIONS

7.1. Unit I

The heavy minerals in most samples from Unit I reflect the H–O–C suite (Fig. 5a), which is consistent with the interpretation of this unit as an intertidal to uppermost

subtidal depositional environment (Clifton, 1983). A highland area underlain by Miocene and older rocks (Huntting et al., 1961) that ranges in elevation from 50 to over 1000 m separates the Columbia River from the Willapa Bay drainage basin. At the south end of the bay, where the divide is lowest (around 50 m), older Pleistocene terrace deposits show no evidence of a major, north-flowing fluvial system attributable to the Columbia River. Therefore the mineral assemblage probably reflects oceanic sand introduced by tidal transport. The presence of open-ocean diatoms locally within Unit I is also consistent with an oceanic input. Four samples from Unit I, however, plot within the clinopyroxene-rich field of the ternary diagram (Fig. 5a). These particular samples were collected near Pickernell Creek, a location where more abundant sand and basaltic pebbles suggest a stronger fluvial influence.

7.2. Unit II

Samples from Unit II also show an H–O–C heavy-mineral suite (Fig. 5b). Four samples contain the lowest clinopyroxene content of all five units. The reasons for this are not clear. Kittleman (1972, p. 173) noted a decrease in brown clinopyroxene with increasing age and weathering of sediments in the Wildcat Canyon Archaeological Site on the Columbia River. Intrastratal dissolution, where documented, has been found to affect the heavy-mineral suite of a sandstone far more than a corresponding shale, because the greater porosity of sandstone allows corrosive fluid circulation and the possibility of chemical attack (Blatt and Sutherland, 1969; Morton and Hallsworth, 2007, this volume). Unit II contains significant amounts of sand, and its porosity may have permitted intrastratal dissolution to occur. However, optical examination of the grains has shown no significant difference in the degree of grain etching present in this unit as compared with the other units in modern sediments.

7.3. Unit III

Unit III is a muddy channel-fill that has no evidence of tidal influence, although the samples show only the H–O–C suite (Fig. 5c). It is likely that the heavy-mineral suite reflects sediments eroded from the units (I and II) into which these ancient channels cut.

7.4. Unit IV

Samples from Unit IV contain an H–O–C suite (Fig. 5d), consistent with a stratigraphic interpretation as a tidally influenced estuarine fill.

7.5. Unit V

Unit V has been interpreted as a fluvially dominant unit with a suggestion of tidal influence. The heavy minerals of this unit support this interpretation, because about half of the samples contain the clinopyroxene-rich suite characteristic of the fluvially dominated sediments in this area (Fig. 5e). However, it is not clear whether samples characterized by an H–O–C suite reflect tidal influence or derivation from older

sediments, because Unit V cuts both Units II and IV, which contain an H–O–C heavy-mineral suite.

7.6. Older Pleistocene Deposits

The epidote-dominated heavy-mineral suite found in samples from two older Pleistocene units was at the time of its discovery somewhat enigmatic (Luepke and Clifton, 1983). This suite seems to be altogether absent from sediments in the modern Bay as well as from the Late Pleistocene deposits studied, suggesting that its source was available only intermittently during the Pleistocene. The apparent northerly derivation of this suite present in deposits on the Bay's north side suggests that it may have come from an area covered by glacial outwash. Significant epidote-bearing rocks are now known to be meta-sedimentary rocks in the Olympic Mountains in northwest Washington (C.D. Peterson, personal communication, 2003). The occurrence of the epidote-rich suite in estuarine sediments on the Bay's east side (Wilson Point, Fig. 2) indicates that during the time of their deposition, fluxes carrying abundant epidote may have dominated the central part of the estuary, similarly to that of the modern H–O–C suite.

A complete palaeogeographic reconstruction of Willapa Bay during the Pleistocene is beyond the scope of this study. However this heavy-mineral study suggests a possible outside sediment source and a different palaeotransport direction not obvious from the examination of modern sediments alone.

8. CONCLUSIONS

Pleistocene terrace deposits, exposed on the east side of Willapa Bay, comprise five units that contain three distinctive heavy-mineral suites, two of which are present in adjacent modern bay sediments. One is similar to the Columbia River suite and the other to the clinopyroxene-rich assemblage in sediments from rivers that currently drain into the east side of the estuary. The Columbia River suite, defined as H–O–C suite, is the most common in Late Pleistocene sediments, being present in samples from all five terrace units. It is, however, unlikely that the Columbia River ever discharged directly into this site of the bay. The H–O–C suite is interpreted to be the result of tidal currents carrying oceanic sand from discharges of the Columbia River, or from local erosion of older deposits in which this suite predominates. This interpretation is based on the distribution of the H–O–C suite in modern bay sediment. The clinopyroxene suite is particularly valuable for confirming the influence of fluvial influx in the Pleistocene sediments. The presence of this suite in Unit I, where it is restricted to the southernmost exposures, is consistent with textural changes and the occurrence of basaltic clasts at the same locality. This distribution aids reconstruction of the shape of the Bay at the time Unit I was deposited.

Unit III, although interpreted sedimentologically as a fluvial unit lacking evidence of tidal influence, nevertheless contains an H–O–C suite and is therefore re-interpreted as a channel-fill deposit. The dominance of the H–O–C suite here can readily be attributed to reworking of sands from Units I and II, into which the channels are incised. The predominance of the H–O–C suite in Units II and IV is consistent with

their interpretation as the result of deposition in large, tide-dominated bays that resemble the modern Bay in geometry and size of tidal prism. Unit I presents an interpretive problem. It is composed of more uniformly muddy sediments than either Unit II or IV. Evidence for tidal transport is cryptic, even though these deposits, from other criteria, clearly lay within the zone of tidal influence. However, the predominance of the H–O–C suite suggests that tidal transport was an important factor in the deposition of this unit, inasmuch as local sources for the H–O–C suite cannot clearly be identified. The clinopyroxene suite, dominating Unit V, supports the interpretation of fluvial activity based on other evidence, and suggests that tidal transport had little influence on sedimentation in this unit.

The presence of a different heavy-mineral suite, dominated by epidote, in some Pleistocene deposits older than the 13 m terrace, suggests that in earlier periods of deposition, the input mechanisms differed radically from those of the present day. The identification of epidote-bearing rocks in the Olympic Mountains far to the north of Willapa Bay confirms a potential source and direction of transport for these sediments. Other than the heavy mineralogy, there are few if any indications that sediment input within an ancient bay came predominantly from an external source such as glacial outwash.

No significant differences in the degree of grain etching have been noted in the Pleistocene sediments as compared to the modern ones. This indicates that, in general, intrastratal dissolution did not materially affect the heavy-mineral suites within the youngest Pleistocene sediments. In Willapa Bay, where sediment sources have not changed over the studied time-span, heavy-mineral analysis is a useful tool that, when integrated with stratigraphy and sedimentary structures, adds an extra—sometimes critical—dimension to the interpretation of ancient depositional environments.

ACKNOWLEDGEMENTS

I thank John Barron, U.S. Geological Survey, for identifying the diatoms. Curt Peterson of Portland State University, Portland, Oregon, and Bob Garrison of The University of California at Santa Cruz critically reviewed the manuscript, as did the editors of this volume.

REFERENCES

Al-Bakri, D., 1986. Provenance of the sediments in the Humber Estuary and the adjacent coasts, eastern England. Marine Geology 72, 171–186.

Andrews, R.S., 1965. Modern sediments of Willapa Bay, Washington—a coastal plain estuary. Department of Oceanography, University of Washington, Technical Report 118, 43pp.

Anima, R.J., Clifton, H.E., Phillips, R.L., 1989. Comparison of modern and Pleistocene estuarine facies in Willapa Bay, Washington. In: Reison, G.E. (Ed.), Modern and ancient examples of clastic tidal deposits—a core and peel workshop. Canadian Society of Petroleum Geologists, Calgary, Alberta, pp. 1–19.

Ballard, R.L., 1964. Distribution of beach sediments near the Columbia River. Department of Oceanography, University of Washington, Technical Report 98, 82pp.

Blatt, H., Sutherland, B., 1969. Intrastratal solution and non-opaque heavy minerals in shales. Journal of Sedimentary Petrology 39, 591–600.

Chasan, D.J., 1978. Willapa Bay—an end to dredging. Pacific Search 12, 9.

Crampton, J.S., Moore, P.R., 1990. Environment of deposition of the Maungataniwha Sandstone (Late Cretaceous), Te Hoe River area, western Hawke's Bay, New Zealand. New Zealand Journal of Geology and Geophysics 33, 333–348.

Clifton, H.E., 1982. Estuarine deposits. In: Scholle, P.A., Spearing, D. (Eds.), Sandstone Depositional Environments. American Association of Petroleum Geologists Memoir, vol. 31, pp. 179–189.

Clifton, H.E., 1983. Discrimination of subtidal and intertidal facies in Pleistocene deposits, Willapa Bay, Washington. Journal of Sedimentary Petrology 53, 353–369.

Clifton, H.E., 1994. Preservation of transgressive and highstand late Pleistocene valley-fill/estuary deposits, Willapa Bay. In: Dalrymple, R.A., Zaitlin, B.A., Boyd, R. (Eds.), Incised Valley Systems: Origin and Sedimentary Sequences. SEPM Special Publication No. 51, pp. 321–333.

Clifton, H.E., Gingras, M.K., 2004. Modern and Pleistocene Estuary and Valley-fill deposits, Willapa Bay Washington. Canadian Society of Petroleum Geologists Field Trip Guidebook, 89pp.

Clifton, H.E., Leithold, E.L., 1991. Quaternary coastal and shallow marine facies sequences, northern California and the Pacific Northwest. In: Morrison, R.B. (ed.), Quaternary Nonglacial Geology, Conterminous United States: Geological Society of America DNAG, vol. K-2, pp. 143–156.

Clifton, H.E., Phillips, R.L., 1980. Lateral trends and vertical sequences in estuarine sediments, Willapa Bay, Washington. In: Field, M.E., Bouma, A.H., Colburn, I.P., Douglas, R.G., Ingle, J.C. (Eds.), Pacific Coast Paleogeography Symposium 4, Quaternary Depositional Environments of the Pacific Coast, Pacific Section, Society of Economic Paleontologists and Mineralogists, pp. 55–71.

Clifton, H.E., Phillips, R.L., Anima, R.J., 1989. Sedimentary facies of Willapa Bay, Washington—a field guide: Canadian Society of Petroleum Geologists, Field Trip Guidebook, 2nd International Research Symposium on Clastic Field Deposits, 64pp.

Derry, D.R., 1933. Heavy minerals in the Pleistocene beds of the Don Valley, Toronto, Canada. Journal of Sedimentary Petrology 3, 113–118.

Galehouse, J.S., 1969. Counting grain mounts—number percentage vs. number frequency. Journal of Sedimentary Petrology 39, 812–815.

Gingras, M.K., Pemberton, S.G., Saunders, T., Clifton, H.E., 1999. The ichnology of modern and Pleistocene deposits at Willapa Bay, Washington: variability in estuarine settings. Palaios 14, 352–374.

Glenn, J.L., 1978. Sediment sources and Holocene sedimentation history in Tillamook Bay, Oregon: U.S. Geological Survey Open-File Report 78–680, 64pp.

Gower, H.D., Pease, M.H., 1965. Geology of the Montesano quadrangle, Washington: U.S. Geological Survey, Geologic Quadrangle Map GQ-374, scale 1: 62,500.

Guilcher, A., 1967. Origin of sediment in estuaries. In: Lauff, G.J. (Ed.), Estuaries, American Association for the Advancement of Science Publication, vol. 83, pp. 149–179.

Hemphill-Haley, E., 1993a. Occurrence of recent and Holocene intertidal diatoms (Bacillariophyta) in northern Willapa Bay, Washington: U.S. Geological Survey Open-File Report 93–284, 94pp.

Hemphill-Haley, E., 1993b. Taxonomy of recent and fossil Holocene intertidal diatoms (Bacillariophyta) in northern Willapa Bay, Washington: U.S. Geological Survey Open-File Report 93–289, 151pp.

Hemphill-Haley, E., 1995. Intertidal diatoms from Willapa Bay, Washington: application to studies of small-scale sea-level changes. Northwest Science 69 (1), 29–45.

Hodge, E.T., 1934. Geology of beaches adjacent to mouth of Columbia River and petrology of their sands: U.S. Army Corps Engineers, Portland, Oregon. Unpublished Report, 53pp.

Huntting, M.T., Bennett, W.A.G., Livingston, V.E., Moen, W.S., 1961. Geologic map of Washington: Washington Division of Mines and Geology, 2 sheets, 1:500,000.

Kelley, J.C., Whetten, J.T., 1969. Quantitative analysis of Columbia River sediment samples. Journal of Sedimentary Petrology 39, 1167–1173.

Kittleman, L.R., 1972. Heavy minerals, pyroclastic layers, and alluvial chronology—an example. Northwest Science 46, 165–176.

Kulm, L.D., Byrne, J.V., 1966. Sedimentary response to hydrography in an Oregon estuary. Marine Geology 4, 85–118.

Kvenvolden, K.A., Blunt, D.A., Clifton, H.E., 1979. Amino acid racemization in Quaternary shell deposits at Willapa Bay, Washington. Geochimica et Cosmochimica Acta 43, 1505–1520.

Luepke, G., 1982a. Heavy-mineral data from samples collected in Willapa Bay and vicinity, Washington: U.S. Geological Survey Open-File Report 82–739, 21pp.

Luepke, G., 1982b. Heavy-mineral variability in beach and dune sands in the vicinity of the mouth of the Columbia River: U.S. Geological Survey Open-File Report 82–1091, 18pp.

Luepke, G., Clifton, H.E., 1983. Heavy-mineral distribution in modern and ancient bay deposits, Willapa Bay, Washington, U.S.A. Sedimentary Geology 35, 233–247.

Mohan, P.M., 1995. Distribution of heavy minerals in Parangipettai (Porto Novo) Beach, Tamil Nadu. Journal of the Geological Society of India 46, 401–408.

Morton, A.C., Hallsworth, C., 2007. Stability of detrital heavy minerals during burial diagenesis. In: Mange, M.A., Wright, D.T. (Eds.), Heavy Minerals in Use. Elsevier, Amsterdam (this volume).

Pease, M.H., Hoover, L., 1957. Geology of the Doty-Minot Peak area, Washington: U.S. Geological Survey Oil and Gas Investigation Map OM-188, scale 1: 62,500.

Peterson, C., Scheidegger, K., Komar, P., 1982. Sand-dispersal patterns in an active-margin estuary of the northwestern United States as indicated by sand composition, texture and bedforms. Marine Geology 50, 77–96.

Peterson, C., Scheidegger, K., Komar, P., Niem, W., 1984a. Sediment composition and hydrography in six high-gradient estuaries of the northwestern United States. Journal of Sedimentary Petrology 54, 86–97.

Peterson, C.D., Scheidegger, K.F., Schrader, H.J., 1984b. Holocene depositional evolution of a small active-margin estuary of the northwestern United States. Marine Geology 59, 51–83.

Rand McNally, 1980. Encyclopedia of World Rivers. Rand McNally, Chicago, IL, 352pp.

Ruggiero, P., Kaminsky, G.M., Gelfenbaum, G., Voigt, B., 2005. Seasonal to interannual morphodynamics along a high-energy dissipative littoral cell. Journal of Coastal Research 21, 553–578.

Ruggiero, P., Kaminsky, G.M., Komar, P.D., McDougal, W.G., 1997. Extreme waves and coastal erosion in the Pacific Northwest. In: Ocean Wave Measurement and Analysis, Proceedings of the Conference American Society of Civil Engineers, Nov. 3–7, 1997, Virginia Beach, Virginia, pp. 947–961.

Scheidegger, K., Kulm, L.D., Runge, E.W., 1971. Sediment sources and dispersal patterns of Oregon continental shelf sands. Journal of Sedimentary Petrology 41, 1112–1120.

Scheidegger, K., Phipps, J.L., 1976. Dispersal of sands in Grays Harbor estuary, Washington. Journal of Sedimentary Petrology 46, 163–166.

Smith, D.G., Meyers, R.A., Jol, H.M., 1999. Sedimentology of an upper-mesotidal (3.7 m) Holocene barrier, Willapa Bay, southwestern Washington, U.S.A. Journal of Sedimentary Research 69, 1290–1296.

U.S. Geological Survey, 1972. Surface water supply of the United States, 1966–1970, Part 14. Pacific Slope Basins in Oregon and Lower Columbia River Basin: U.S. Geological Survey Water-Supply Paper 2135, 1036pp.

U.S. Geological Survey, 1974. Surface water supply of the United States, 1966–1970, Part 12, Vol. 1. Pacific Slope Basins in Washington except the Lower Columbia River Basin: U.S. Geological Survey Water-Supply Paper 2132, 640pp.

Van Andel, Tj.H., 1955. Sediments of the Rhône Delta II. Sources and deposition of heavy minerals. Geologie en Mijnbouw 15, 515–543.

Vanderburgh, S., Gelfenbaum, G., Jol, H., Kaminsky, G., Peterson, C., Phipps, J., 2003. Coastal erosion, dynamic shoreline, processes, and beach management controversies of the Columbia River littoral cell, southwest Washington and northwest Oregon: Geological Society of America Field Trip Guide no. 6, 2003 Annual Meeting, 77pp.

Veirs, C.E., 1969. River mile index—coastal tributaries, Pacific coast, Washington. Hydrology and Hydraulics Committee, Pacific Northwest River Basins Commission, 56pp.

Wagner, H.C., 1967a. Preliminary geologic map of the Raymond quadrangle, Pacific County, Washington: U.S. Geological Survey Open-File Report, scale 1: 62,500.

Wagner, H.C., 1967b. Preliminary geologic map of the South Bend quadrangle, Pacific County, Washington: U.S. Geological Survey Open-File Report, scale 1: 62,500.

Wells, R.E., 1979. Geologic map of the Cape Disappointment—Naselle River area, Pacific County, Washington: U.S. Geological Survey Open-File Report 79–389, scale 1: 48,000.

Whetten, J.T., Kelley, J.C., Hanson, L.G., 1969. Characteristics of Columbia River sediment and sediment transport. Journal of Sedimentary Petrology 39, 1149–1166.

Wolfe, E.W., McKee, E.H., 1968. Geology of the Grays River Quadrangle, Wahkiakum and Pacific Counties, Washington: Washington Division of Mines and Geology, Geologic Map GM-4, scale 1: 62,500.

Wolfe, E.W., McKee, E.H., 1972. Sedimentary and igneous rocks of the Grays River Quadrangle, Washington: U.S. Geological Survey Bulletin 1335, 70pp.

Zemstov, A.A., 1974. Mineral composition of Quaternary deposits and problems of paleogeography of the north of western Siberia. International Geology Review 16, 1162–1167.

This page intentionally left blank

Chapter 24

INTERPRETATION OF QUATERNARY TECTONIC AND ENVIRONMENTAL CHANGE USING HEAVY MINERALS OF THE YANGTZE DELTA PLAIN

JILL S. SCHNEIDERMAN[a] AND ZHONGYUAN CHEN[b]

[a]*Department of Earth Science and Geography, Vassar College, 124 Raymond Avenue, Poughkeepsie, NY 12604-0312, USA*
[b]*State Key Laboratory for Estuarine and Coastal Research, East China Normal University, Shanghai 200062, China*

ABSTRACT

A 20 m long core drilled into the southern Yangtze delta plain reveals temporal variations, and variations in the distribution of heavy minerals in late Quaternary stratigraphic horizons. The most abundant transparent heavy minerals observed in the core are amphibole, epidote, iron-titanium oxides, metamorphic minerals (garnet, sillimanite, kyanite, staurolite, chloritoid), pyroxene, zircon, tourmaline, rutile and apatite. Heavy minerals found in lower quantities are sphene, monazite, allanite and siderite. Also present in the heavy mineral separates are rock fragments, authigenic framboidal pyrite and pyritised foraminifera. Relative abundances of heavy minerals suggest one main source of sediment to the delta plain during the late Pleistocene to early Holocene and the addition of another source in the late Holocene.

Proximal sources west of the southern Yangtze delta plain, including bedrock of the southern delta plain itself (Jurassic to Cretaceous igneous rocks, Precambrian medium-grade metamorphic rocks and Palaeozoic to Mesozoic carbonate sequences) and the western Mao-shan and Tian-mu-shan highlands (Palaeozoic to Mesozoic clastics and carbonate rocks), most likely were the source of late Pleistocene to early Holocene fluvial sediments. These sediments were carried eastward in river channels originating in the highlands. A complex of fluvial channels that migrated southward across the delta plain during the late Holocene added an additional source of sediment to the delta plain. They originated from western and northern distal source areas similar to those exposed in the modern Yangtze drainage basin.

Evidence from heavy minerals supports previous studies of the core that document the tectonic and palaeoenvironmental history of the southern Yangtze delta plain. In particular, prior to 10,000 years B.P., the southern Yangtze delta plain supported the formation of an oxidising soil when sea level was low and heavy mineral influx came from proximal sources. During the period from 10,000 to 7000 years B.P., an open coastal setting characterised the southern delta plain

Developments in Sedimentology, Vol. 58, 607–620

ISSN: 0070-4571/doi:10.1016/S0070-4571(07)58024-6

region. Pyrite in heavy mineral separates, representing the period between 7000 and 4000 years B.P., supports evidence from other studies indicating that lagoons and freshwater marshes created reducing conditions during this time period. As sea level approached its present level 4000 years B.P., tectonically induced differential subsidence of the Yangtze delta plain progressed from north to south. Heavy mineral input to the delta plain reflects the resultant southward migration of the Yangtze river channel and deltaic depocentre to its present position.

Keywords: southern Yangtze delta plain; palaeoenvironmental history; Mao-shan and Tian-mu-shan highlands; provenance signature

1. INTRODUCTION

The tide-dominated Yangtze delta is home to more than 20 million people engaged in agricultural and industrial activities. With an average elevation of less than 5 m above mean sea level, people of the region are highly vulnerable to sea-level fluctuations, high tides, typhoons and flooding (Chen, 1999). Sediments of the delta plain are derived from a vast drainage basin that is more than 6300 km in length, has a catchment area of more than 1.9 million km^2 and produces suspended loads and water discharges among the highest on earth (Chen et al., 2001). The delta coast has been prograding rapidly at approximately 50 km per 1000 years during the last 5000 years (Hori et al., 2001). The rate increased abruptly from 38 to 80 km per 1000 years ~2000 years ago and the delta coast has subsequently grown in size by more than 500 km^2 in the last half century (Chen and Gupta, 2001; Hori et al., 2001). Such an increase in sediment production in the Yangtze drainage basin may be due to a relative decrease in sediment deposition in the middle section of the river related to river-channel stability combined with widespread human influence (Hori et al., 2001).

Construction of the Three Gorges Dam on the Yangtze is an attempt to control one of the earth's major rivers that operates as an essential lifeline in China. The dam will create a 600-km-long reservoir with a surface area of 1060 km^2 stretching from Yichang to Chongqing. Although it will control flooding on the river, the dam will trap behind it sediment, ordinarily destined for the Yangtze delta and its plain (Lu and Higgitt, 2001). Such a manipulation requires comprehensive understanding of the history of the development of the Yangtze delta plain in order to facilitate planning for and management of future land-use in the region. Heavy mineral studies of Yangtze delta sediments have added information that is critical to understanding Yangtze delta plain development.

This contribution reports on the integration of information derived from the study of heavy minerals in a core from the Yangtze delta, with that deduced from investigations of other petrological and biological indicators including clay mineralogy, micropalaeontology and palynology (Liu et al., 1992; Yu, 1994; Zhang et al., 1994; Stanley et al., 1999). Taken on the southern Yangtze delta plain, the core under investigation begins in the late Pleistocene and contains a nearly complete sedimentological record for the Holocene. The core site is located at 121°11′02″ longitude and 31°08′01″ latitude immediately at the lee side of a series of chenier ridges east of Taihu lake in the delta plain (Fig. 1). The elongate, linear, shelly ridges rise

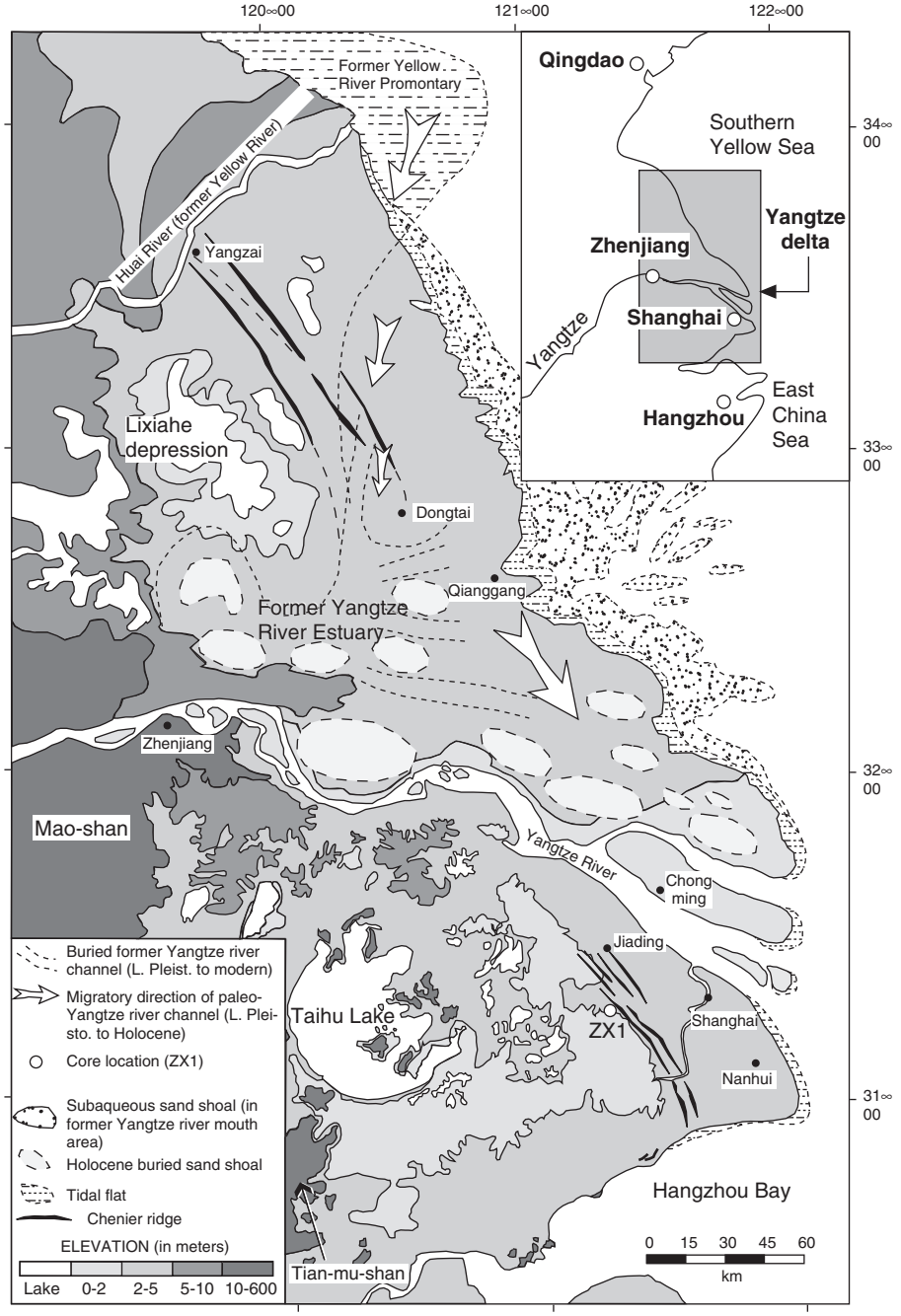

Fig. 1. Map showing morphological features of the Yangtze delta plain and location of core site (after Chen, 1999).

approximately one metre above mean sea level, are subparallel to the coastline and mark its previous location. Taihu lake, 60 km west of the core site, occupies a dish-like depression centred in the southern Yangtze delta plain. Highlands elevated up to 500 m above mean sea level occur to the west of the delta plain. Heavy minerals extracted from the core provide valuable information about shifting sediment sources, transport paths and environmental changes affecting the delta.

2. METHODS

Lithological, radiocarbon, faunal and floral data from previous investigations of more than 100 long cores (> 50 m) and numerous trenches dug throughout the Yangtze delta plain show that in general, 10–50 m thick, grey, silty, Holocene muds overlie dark green, stiff muds of Pleistocene age with little if any sand (Li et al., 1986; Yan and Xu, 1987; Yan and Hong, 1988; Liu et al., 1992; Chen and Stanley, 1995; Stanley et al., 1999). Core ZX1, obtained by rotary drilling, was taken on the southern Yangtze delta plain and used to obtain additional information and to examine the distribution of heavy minerals to track tectonic and environmental changes suggested by other data.

The 20 m long, 10 cm diameter core was recovered at the ground surface elevation of 2.67 m above mean sea level and consists mostly of clay and silt. The core penetrates the Holocene successions down to the uppermost late Pleistocene strata. The Pleistocene section, marked by a distinct unconformity at the base of the Holocene succession, was reached at a depth of ~15 m below ground elevation. As part of previous investigations, core ZX1 was split and logged by visual examination at ~30 cm intervals. The core has been interpreted on the basis of changes in lithology, grain size, magnetism, geochemistry and biogenic assemblages (foraminifers, pollen, spores) (Chen and Stanley, 1998). Also, samples composed of peat, organic matter and shell fragments were selected at different core depths for conventional and AMS (Accelerator Mass Spectrometry) radiocarbon dating by Beta-Analytic, Inc. (Table 1).

Fifty-one sediment samples were taken for heavy mineral examination at ~30 cm intervals along the length of the core (Schneiderman et al., 2003). All samples were wet-sieved to remove the silt- and clay-size fraction (< 63 μm). Clay-rich samples were cleaned ultrasonically to disaggregate the grains before wet-sieving. The

Table 1. Depths and ages of radiocarbon-dated samples from core ZX1

Depth (m)	Age (years B.P.)
1.1	2580 ± 60
4.5	4160 ± 40
8.8	6850 ± 80
12.5	7750 ± 50
14.08	7900 ± 35
14.1	7820 ± 35
14.9	13,070 ± 60

sand-size fraction (63–250 μm) was then dried at 50 °C. Heavy minerals were separated from the 63–250 μm fraction in sodium polytungstate (density 2.96 g/cm^3) using standard gravity separation procedures. The heavy mineral concentrate was washed with distilled water to remove sodium polytungstate coatings from the grains. Polished grain mounts were prepared for each of the 51 samples and these were examined petrographically. Modal abundances of heavy minerals in the core were determined for 20 thin sections at 1 m intervals by point-counting 300 grains per thin section.

Additionally, heavy minerals from 19 polished grain mounts were analysed with an electron microprobe to confirm identities of those heavy minerals more rarely observed and less easily identified with a standard petrographic microscope. Compositions of the major heavy minerals (amphibole, epidote, Fe-Ti oxides, garnet, staurolite, sillimanite, kyanite, chloritoid, pyroxene, zircon, tourmaline, rutile and apatite) were also examined for systematic geochemical variations along the cored interval. Mineral analyses were acquired on the JEOL JXA-8600 electron microprobe at Yale University. Data of electron microprobe analyses of heavy minerals are available from the first author.

3. RESULTS

The most abundant heavy mineral species in both the lower and upper portions of core ZX1 are iron-titanium oxides, epidote and amphibole. Less abundant but still readily identified and point-counted are pyroxene and metamorphic minerals such as garnet, staurolite, sillimanite, kyanite and chloritoid. Other species include zircon, tourmaline, rutile and apatite. Present throughout the core but in trace amounts are sphene, monazite, allanite and siderite.

Fig. 2 shows the vertical distribution of transparent and opaque heavy minerals along the length of the core determined by point-counting while Table 2 summarises these data. Reported percentages have been normalised to account for the substantial presence of rock fragments in heavy mineral separates in the upper and lower portions of the core. We recognise four distinct intervals, defined here as units based on the types and proportions of heavy minerals that each core section contains.

3.1. Unit A (20–14.9 m)

This unit has the highest content of amphibole (32.8%) and epidote (51.0%) in the core. It also contains substantial amounts of iron-titanium oxides (up to 31.1%) and metamorphic minerals (garnet + staurolite + sillimanite + kyanite; up to 9.0%). The highest content of amphibole corresponds with the highest content of iron-titanium oxides in this portion of the core and occurs at 15.9 m. The highest epidote content corresponds with the greatest metamorphic mineral content in the lower core section and occurs at 14.9 m. Also at this depth is a relatively high modal abundance of stable heavy minerals (zircon, tourmaline, rutile, apatite, ZTRA; 6.5%). Present in this unit, though in minor abundance, are the rare earth element-bearing minerals allanite and monazite as well as sphene and the iron carbonate, siderite. Pyroxene and authigenic framboidal pyrite and pyritised foraminifers are absent from this

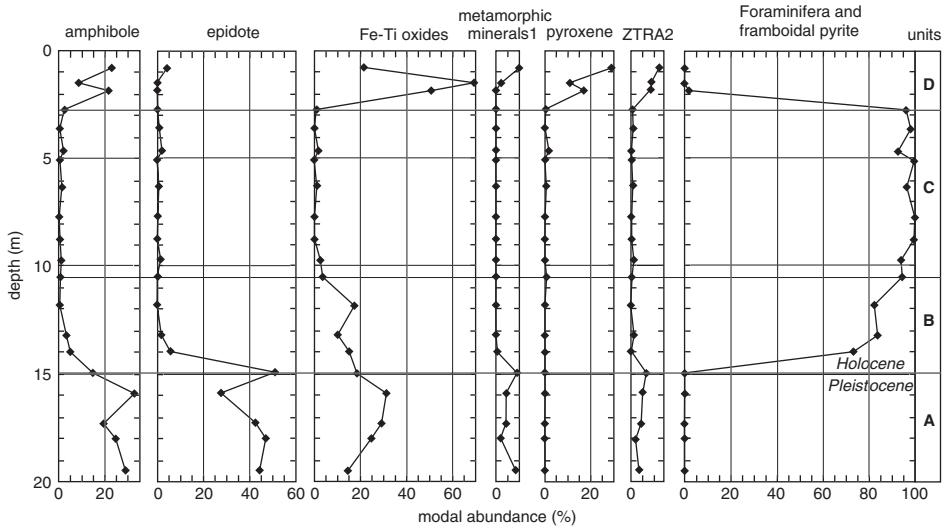

Fig. 2. Modal abundance and vertical distribution of heavy minerals in core ZX1 divided into units A (20.0–14.9 m), B (14.9–10.5 m), C (10.5–2.7 m) and D (2.7–0.5 m). Percentages have been normalised to account for the presence of rock fragments in the heavy mineral assemblages. (1) Metamorphic minerals are garnet, staurolite, sillimanite, kyanite and chloritoid; (2) ZTRA represents zircon, tourmaline, rutile and apatite.

unit. A radiocarbon-dated sample at 14.9 m indicates an age of 13,070 ± 60 years B.P. (Stanley et al., 1999).

3.2. Unit B (14.9–10.5 m)

This unit is marked by the appearance of framboidal authigenic pyrite and pyritised foraminifers at 14 m (73.5%) with increasing abundance to the boundary with unit C at 10.5 m (94.5%). Transparent heavy minerals, observed in unit A, are also present in this unit though in considerably lower proportions. The modal abundances of amphibole, epidote, iron-titanium oxides, metamorphic minerals and ZTRA decrease to low values at the top. Unit B yielded radiocarbon dates of 7820 ± 35 years B.P., 7900 ± 35 years B.P. and 7750 ± 50 years B.P. at approximately 14.10, 14.08 and 12.5 m, respectively (Stanley et al., 1999).

3.3. Unit C (10.5–2.7 m)

Heavy mineral separates from this unit contain almost exclusively authigenic framboidal pyrite and pyritised foraminifera (93–100%). One sample at 4.6 m yielded 1.9% amphibole, 1.9% epidote, 1.6% iron-titanium oxides, 0.3% ZTRA and 1.6% pyroxene. Two types of pyroxene, augite and pigeonite, were identified, the latter mineral being a particularly characteristic constituent of andesitic and dacitic volcanic rocks. A few grains of sphene were also detected. Unit C yielded two radiocarbon dates: 6850 ± 80 years B.P. at ~8.8 m and 4160 ± 40 years B.P. at ~4.5 m (Stanley et al., 1999).

Table 2. Modal abundance of detrital grains in core ZX1

Sample number	Sample depth (m)	Amphibole	Epidote	Fe-Ti oxide	Metamorphic minerals (garnet + staurolite + aluminosilicate + chloritoid)	Pyroxene	Zircon + tourmaline + rutile + apatite	Foraminifera and framboidal pyrite	Rock fragments
1–10	0.8	11.9	2.2	11.2	5.2	15.2	6.3	0	48
3–10	1.5	2	0	15.9	0.5	2.5	2	0	77.1
4–9	1.8	4.3	0	10.2	0	3.4	1.7	0.4	79.9
7–5	2.7	2.2	0	0.6	0	0.3	0.8	96.1	0
9–5	3.6	0.3	0.7	0	0	0	1	98	0
12–6	4.6	1.9	1.9	1.6	0	1.6	0.3	92.8	0
14–5	5.1	0.3	0	0	0	0	0.3	99.3	0
18–2	6.3	1.1	0.3	0.8	0	0.5	0.8	96.5	0
22–4,5	7.7	0	0	0	0	0	0.3	99.7	0
24–6	8.7	0.3	0	0	0	0	0.3	99.3	0
27–6,7	9.7	0.9	1.3	2.5	0	0	1.3	94	0
29–9	10.5	0.6	0	3.6	0	0.6	0.6	94.5	0
32B–9,10	11.8	0.3	0	17.3	0	0	0	82.4	0
36–1	13.2	3.2	1.6	10.2	0	0	1.3	83.7	0
38–3	14	4.9	5.5	15.1	0.6	0	0.3	73.5	0
40–6	14.9	4.6	15.8	5.7	2.8	0	2	0	69
43–5	15.9	5.9	5	5.6	0.8	0	0.9	0	82
46–5	17.3	16.4	35.9	24.6	3.6	0	3.6	0	15.8
49–1,2	18	13.2	25.2	13.2	1.1	0	1.1	0	46.3
51–9	19.5	19.6	30.2	10	5.7	0	2.3	0	32.2

Note: Data in this table have not been normalised to account for the presence of rock fragments in the heavy mineral assemblages.

3.4. Unit D (2.7–0.5 m)

This unit shows an upward increasing trend of amphibole, epidote, metamorphic minerals, pyroxene and ZTRA. This section of the core also contains the highest amounts of iron-titanium oxides observed (69.4%). In this unit maximum modal abundances of the minerals are 22.9% amphibole, 4.2% epidote, 69.4% iron-titanium oxides, 10.0% metamorphic minerals, 29.2% pyroxene and 12.1% ZTRA. Occasional grains of sphene and monazite were also observed. The reappearance of the heavy minerals that characterise units A and B and the abrupt disappearance of framboidal pyrite and pyritised foraminifera distinguishe this unit from the underlying one. Unit D produced a radiocarbon date of 2580 ± 60 years B.P. at ~1.1 m (Stanley et al., 1999).

4. DISCUSSION

4.1. Provenance of Heavy Minerals and Signatures of River Channel Migration

Bedrock of the southern delta plain consists largely of Jurassic to Cretaceous igneous rocks. Small, irregularly dispersed Precambrian high-grade metamorphic rocks and Palaeozoic to Mesozoic carbonate successions have also been mapped as part of the bedrock of the southern delta plain (Shanghai Seismological Bureau, 1984; Zhu et al., 1984). In the northern delta plain, Jurassic to Cretaceous igneous rocks that are equivalent to the bedrock of the southern delta plain surround to the north, west and south, the Subei Basin: a large, irregularly shaped depression that occupies the centre of the northern delta plain (Shanghai Seismological Bureau, 1984). Cretaceous igneous rocks also form a rise in the centre of the basin. The 400–550 m high Mao-shan and Tian-mu-shan highlands immediately west of the southern Yangtze delta plain consist of Palaeozoic to Mesozoic clastic and carbonate rocks (Nanjing Institute of Geography and Limnology, 1991).

The types of heavy minerals observed in the grain mounts are consistent with the bedrock geology of the southern and northern Yangtze delta plain and that of the Mao-shan and Tian-mu-shan western highlands. We interpret differences in heavy mineral assemblages along the length of core ZX1 as indicating an increase in sediment sources that furnished the southern Yangtze delta plain during the late Quaternary. Heavy mineral signatures indicate that late Pleistocene to earliest Holocene samples were derived from proximal source areas west of the core site, namely the Mao-shan and Tian-mu-shan western highlands, and the bedrock in the southern delta plain. Late Holocene samples have heavy mineral assemblages that suggest derivation not only from the western highlands and southern delta plain bedrock, but also from distant sources derived from a drainage basin similar to that of the modern Yangtze river.

Jurassic to Cretaceous igneous rocks that occur as bedrock in the Yangtze delta plain are petrologically tenable sources of the iron-titanium oxides, amphibole, zircon, tourmaline, rutile, apatite, allanite and sphene (Shanghai Seismological Bureau, 1984; Jiangsu No. 2 Hydrogeological and Geoengineering Team, 1985; Zhejiang Geological and Mineral Resources Bureau, 1987). The Precambrian metamorphic

rocks that have been mapped as part of the bedrock of the southern delta plain might also have supplied some of these minerals but most importantly are reasonable sources for the high-grade pelitic metamorphic minerals garnet, staurolite, kyanite, sillimanite and chloritoid. Epidote may have come from this metamorphic source. Thus, heavy minerals in unit A suggest that normal fluvial processes, including seasonal floods, caused influx of sediments from these regions.

The distribution of heavy mineral assemblages in unit B when compared with unit A reflects the continued influx of fluvial sediment that originated in the Mao-shan and Tian-mu-shan western highlands and Mesozoic and Precambrian bedrock exposed today in the southern delta plain. The similarity of heavy mineral assemblages between the two units may also suggest that surface sediments were reworked, perhaps by tidal action and coastal transport as a result of rising sea level and seawater incursion onto the plain.

The absence of detrital heavy minerals in unit C of the core reveals the cessation of terrigenous sediment input from either proximal or distal sediment sources by fluvial transport. Rather the presence of authigenic framboidal pyrite and pyritised foraminifera in the heavy mineral separates of this unit corresponds to a changed environment of deposition.

In unit D, the reappearance of amphibole, epidote, iron-titanium oxides, metamorphic minerals and ZTRA signals resumption of fluvial flux. As ascertained for units A and B, the presence of these minerals in unit D is consistent with derivation from southern delta plain bedrock and the Mao-shan and Tian-mu-shan western highlands. However, pyroxenes appear in substantial amounts in unit D. Their presence here, in contrast to their absence in the lower units, suggests fluvial input from a new source lithology. There is no evidence that pyroxene was once present in the lower units but was dissolved by the action of corrosive acids that would have been produced during pedogenesis and pyrite-oxidation. In fact, the presence in lower units of well-preserved apatite—there is no sign of dissolution, pitting or deep corrosion in the apatite grains—which would be similarly sensitive to acidic conditions, supports our interpretation of provenance change-related pyroxene in this unit. We suggest that the addition of pyroxene may be the signal of the appearance of the southward migrating Yangtze river channel.

Our observations are consistent with Chen and Stanley (1995) who documented the heavy mineral assemblages of fluvial sands from the northern and southern delta plains. They found that amphibole and epidote are ubiquitous among sands from both the northern and southern plains. Our results contrast, however, with those of Qin et al. (1996), who examined two cores from the Yangtze delta. They used the presence of hornblende in the cores as an indicator of Yangtze river input to the delta. Neither Chen and Stanley (1995), nor Qin et al. (1996), recognised pyroxene in heavy mineral assemblages from the core. This may be because pyroxene is easily mistaken for epidote without the benefit of electron microprobe analysis or BSE/SEM imaging. It is important to note, therefore, that simple binocular or standard petrographic analysis of heavy minerals alone may cause researchers to miss additional clues regarding sediment provenance.

Migration of the Yangtze river channels from north to south previously postulated and ascribed primarily to differential subsidence of the northern and southern plains (Chen and Stanley, 1995) can explain the distribution of heavy minerals in

core ZX1. At the beginning of the Quaternary, the Yangtze river was unable to flow across the southern delta plain because it was topographically higher than the northern delta plain and was also blocked by the Mao-shan and Tian-mu-shan highlands. Palaeochannels record that, at least from the early Quaternary, the Yangtze river flowed across the northern part of the northern delta plain into the Yellow Sea (Chen and Stanley, 1995).

Proximal river channels originating in the Mao-shan and Tian-mu-shan highlands would have been the local sources responsible for deposition of the heavy minerals seen in core ZX1 at depths below 10.5 m. The change of channel course occurred while the southern plain, though topographically higher than the northern plain, began to subside. The onset of differential subsidence with more rapid lowering of the southern delta plain would explain the progressive southward migration of the former Yangtze channels with time. Thicker Quaternary sections in the southern plain provide evidence for such differential tectonism (Chen and Stanley, 1995). As subsidence of the Yangtze delta plain progressed from north to south, the Yangtze river channel shifted over time to its present position. Thus, heavy minerals in the upper portion (unit D) of core ZX1 reflect additional input from distal source areas similar to those exposed in the modern Yangtze drainage basin.

4.2. Types of Heavy Minerals in Relation to Quaternary Environmental Change

Information derived from previous studies including sedimentology, geomorphology, palaeontology, palaeoclimatology and archaeology reveals that the depositional environment of the area now occupied by the Yangtze delta plain has evolved from fluvial to marine and to deltaic coast since the late Pleistocene. Fig. 3 provides a tabulation of the data and the associated palaeoenvironmental interpretation. Our study of core ZX1 showed that information from heavy minerals adds meaningful information to understand better palaeoenvironmental changes.

Unit A (20–14.9 m) consists of stiff muds (Chen and Stanley, 1993)—hard mottled silt and clay whose mean grain size ranges from 15 to 20 μm—and irregularly distributed organic matter. Previous studies indicate that this interval of the core was deposited in the late Pleistocene between 35,000 and 10,000 years B.P. (Chen and Stanley, 1993, 1998; Sun and Huang, 1993). The sediment composition, including the presence of the heavy minerals described previously, suggests pedogenesis on a fluvial plain during the late Pleistocene. Biostratigraphic evidence, including carbonate-cemented tree roots in the stiff muds and pollen, indicating a cold dry climate (Wang et al., 1984), suggests that unit A records the subaerial exposure of the former Yangtze delta plain during a period of lower global sea level stands (Pirazzoli, 1991).

Unit B (14.9–10.5 m) consists of yellowish grey to light grey silt and silty clay with mean grain size ranging from 8 to 12 μm. Radiocarbon dates obtained for this unit are consistent with an early Holocene age (10,000–7000 years B.P.). Thin peaty units (1–3 cm) are present in the lower portion of this core section; root traces prevail, but shell fragments are rare. The appearance of authigenic pyrite (framboids) and pyritised foraminifers in the heavy mineral assemblages, beginning at 14 m, records shallow marine to brackish water incursions. Reworked intraclastic mud pebbles that appear abruptly at a core depth of 14.5–15 m occur along the contact with the underlying stiff muds. They support the interpretation from silicates in the heavy

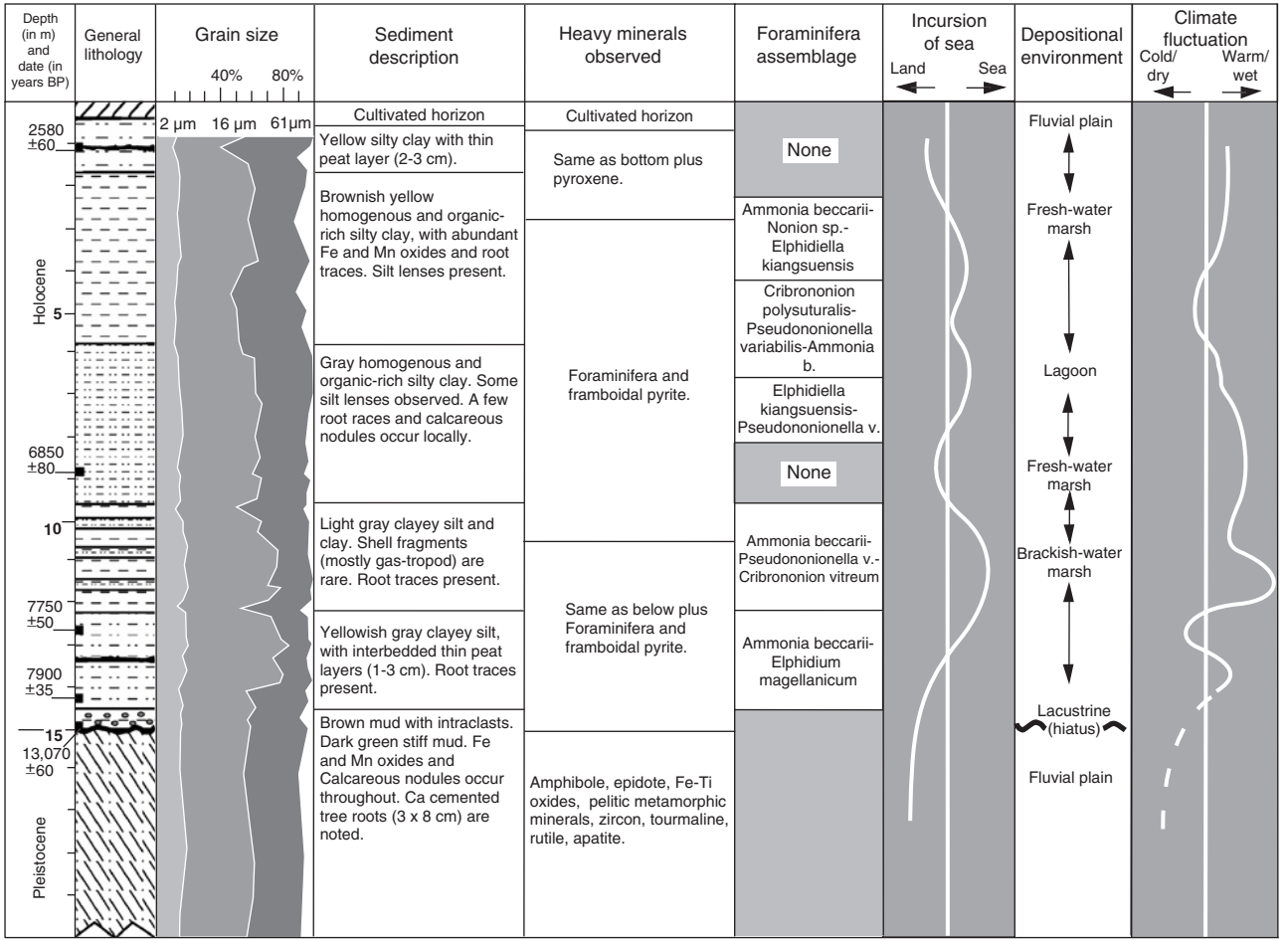

Fig. 3. Late Quaternary sediment log of core ZX1 showing general lithology, grain size, sediment description, heavy mineral and foraminifer assemblages in relation to sea-level change, depositional environment and climate fluctuation.

mineral suites of units A and B that rising sea level caused sediments to be reworked by tidal action and coastal transport. The combined sedimentological and mineralogical evidence for unit B suggests climate warming during the early Holocene and a brackish-water marsh environment.

Unit C (10.5–2.7 m) consists of homogenous yellowish and grey silty clay interspersed with silty lenses with mean grain size ranging from 14 to 25 μm. Radiocarbon dates yielded a middle Holocene age (7000–3000 years B.P.) for this unit. Organic patches in the sediment increase upward and only a few root traces and calcareous nodules occur. The predominance of authigenic framboidal pyrite and pyritised foraminifers compared to the dearth of oxide and silicate minerals in the heavy mineral separates suggests a fully marine depositional environment. The formation of such bacteriogenic pyrite requires organic matter in the sediment, sulphate in solution in the pore water and a locally anaerobic chemical environment, created by the decay of organic matter. Pollen and spore assemblages (Chen et al., 2005), the paucity of terrigenous detrital heavy minerals and, also, the overwhelming presence of pyrite and pyritised foraminifers in the heavy mineral assemblage of unit C suggest continued sea-level rise. Chenier ridges were formed east of the core site in response to sea-level rise and increased dynamism along the coast. They served ultimately as coastal barriers to incursion of the sea so that the delta plain, still influenced partially by seawater via tidal creeks, progressively changed from a brackish lagoon to a freshwater marsh. The area west of the core site that is now the Taihu depression was inundated first by brackish water and eventually became a reducing, calm water environment (Chen and Stanley, 1998; Sun and Huang, 1993). Evidence for such conditions comes from the pyritised microfossils in the core (i.e., *Ammonia beccarii, Pseudononionella variabilis, Elphidiella kiangsuensis, Cibrononion polysuturalis*). These events correspond to the megaclimate warming trend of the middle Holocene.

Unit D (2.7–0.5 m) consists principally of grey to brownish yellow silty clay with mean grain size ranging from 20 to 30 μm. Radiocarbon dates obtained for this unit are consistent with a late Holocene age (3000 years B.P. to the present). The virtual absence of pyrite and pyritised marine microfossils in the heavy mineral assemblage of this unit and the presence of abundant iron-titanium oxide and silicate minerals suggest the return of fluvial plain and upper tidal flat depositional environments to the delta. Thin peaty beds (2–3 cm) with characteristic pollen and spore assemblages (Chen et al., 2005) especially in the upper portion of this core section along with root traces and silty lenses support this interpretation. Unit D therefore corresponds with the stabilisation of sea level and a warm, wet climate recorded also in other Yangtze delta cores (Wang et al., 1984). An ~0.5 m thick interval of sediment at the top of the core indicates recent anthropogenic activity (Chen et al., 2005).

5. CONCLUSION

Examination of heavy minerals in core ZX1 from the southern Yangtze delta plain led to the following conclusions: Heavy minerals in the deepest unit of the core reflect fluvial input from the western highlands and bedrock of the southern delta plain by proximal channels during the late Pleistocene when the delta was subaerially

exposed. Framboidal pyrite and pyritised foraminifers in the heavy mineral assemblages from the middle units of the core reveal seawater incursion and the evolution of saltwater, brackish and freshwater environments from the early through middle Holocene. The appearance of pyroxenes in the heavy mineral assemblages from the upper unit of the core indicates the beginning of fluvial input from the ancestral Yangtze during the late Holocene.

Heavy mineral distributions in core ZX1 support the results of previous studies demonstrating the southward migration of the Yangtze river channel. During the Quaternary, the Yangtze river flowed only across the northern delta plain into the southern Yellow Sea. This is the result of two factors: (1) differential lowering of the northern plain relative to the southern plain from the late Tertiary to the late Pleistocene; and (2) a ''topographic barrier effect'' produced by the Mao-shan and Tian-mu-shan highlands west of the southern delta plain that prevented the river system from flowing to and across the southern plain. Consequently, heavy minerals from local sources were delivered by proximal river channels to the southern delta plain as it began to subside. With continued subsidence, the Yangtze river channel shifted south and, as reflected by heavy mineral assemblages in the upper portion of the core, deposited sediments derived from distal source areas similar to those exposed in the modern Yangtze drainage basin that include andesitic and dacitic volcanic rocks. As the channel progressively migrated southward, the river flowed into the East China Sea and reached its present position ~4000 years ago (Chen and Stanley, 1995). River channel migration, in association with frequent shifts of the deltaic depocentre, along with climatically induced sea level fluctuations inevitably affected the temporal and spatial distribution of the heavy minerals on the Yangtze delta plain.

ACKNOWLEDGMENTS

This project was supported by the Collins faculty research fund at Vassar College and the China Natural National Science Foundation (Grant No. 49971011). JSS thanks Meg E. Stewart for critical assistance with the figures. We appreciate very helpful reviews by Abhijit Basu, Maria Mange, Dave Wright and Xiong Yingqian.

REFERENCES

Chen, Z., 1999. Geomorphology and coastline change of the lower Yangtze delta plain, China. In: Miller, A.J., Gupta, A. (Eds.), Varieties of Fluvial Form. Wiley, New York, pp. 427–443.

Chen, Z., Gupta, A., 2001. The Yangtze River: an introduction. Geomorphology 41, 73–75.

Chen, Z., Li, J., Shen, H., Zhanghua, S., 2001. Yangtze River of China: historical analysis of discharge variability and sediment flux. Geomorphology 41, 77–91.

Chen, Z., Stanley, D.J., 1993. Alluvial stiff muds (late Pleistocene) underlying the lower Nile delta plain, Egypt: petrology, stratigraphy and origin. Journal of Coastal Research 9, 539–576.

Chen, Z., Stanley, D.J., 1995. Quaternary subsidence and river channel migration in the Yangtze delta plain, Eastern China. Journal of Coastal Research 11, 927–945.

Chen, Z., Stanley, D.J., 1998. Sea-level rise on eastern China's Yangtze delta. Journal of Coastal Research 14, 360–366.

Chen, Z., Wang, Z., Schneiderman, J., Tao, I., Cai, Y., 2005. Holocene climate fluctuations in the Yangtze delta of eastern China and the Neolithic response. The Holocene 15, 915–924.

Hori, K., Saito, Y., Zhao, Q., Cheng, X., Wang, P., Sato, Y., Li, C., 2001. Sedimentary facies and Holocene progradation rates of the Changjiang (Yangtze) delta, China. Geomorphology 41, 233–248.

Jiangsu No. 2 Hydrogeological and Geoengineering Team, 1985. Hydrogeological and Geoengineering Evaluation on Xu, Huai and Yan regions (in Chinese, unpublished). Internal Report, 306pp.

Li, C., Ming, Q.B., Sun, H.P., 1986. Holocene strata and transgression of southern Yangtze delta plain (in Chinese). Kexuetongbao 21, 1650–1653.

Liu, K.B., Shun, C.S., Xin, H.J., 1992. Environmental change in the Yangtze River delta since 12,000 years B.P. Quaternary Research 3, 23–45.

Lu, X.X., Higgitt, D.L., 2001. Sediment delivery to the Three Gorges 2: local response. Geomorphology 41, 157–169.

Nanjing Institute of Geography and Limnology, 1991. Atlas of Natural Resources of the Taihu Basin (in Chinese and English). Chinese Academy of Sciences, Taihu Basin Management Bureau, Ministry of Water Resources. Science Press, Beijing, 105pp.

Pirazzoli, P.A., 1991. World atlas of Holocene sea-level changes. Oceanographic Series 58. Elsevier, Amsterdam.

Qin, Y., Zhao, Y., Chen, L., Zhao, S., 1996. Geology of the East China Sea. Science Press, Beijing, 357pp.

Schneiderman, J.S., Chen, Z., Eckert, J.O. Jr., 2003. Heavy minerals and river channel migration in the Yangtze delta plain, eastern China. Journal of Coastal Research 19, 326–335.

Shanghai Seismological Bureau, (1984). Geological Tectonics in Shanghai Region (unpublished map collection). Tongji University, Shanghai Geological Survey, 40pp.

Stanley, D.J., Chen, Z., Song, J., 1999. Inundation, sea-level rise and transition from Neolithic to Bronze age cultures, Yangtze delta, China. Geoarcheology 14, 15–26.

Sun, S.C., Huang, Y.P., 1993. The Taihu Lake (in Chinese with English summary). China Ocean Press, Beijing, 271pp.

Wang, K.F., Zhang, Y.L., Jiang, H., Han, X.B., 1984. Palynological assemblages from the Holocene sediments of the Yangtze River delta and their geological significance (in Chinese with English summary). Marine Geology and Quaternary Geology 4 (3), 70–86.

Yan, Q., Hong, X., 1988. Issues of the Holocene transgression on the southern plain of the Changjiang delta. Acta Oceanologica Sinica 7, 578–590.

Yan, Q., Xu, S.Y., 1987. Recent Yangtze delta deposits (in Chinese with English summary). East China Normal University Press, Shanghai, 438pp.

Yu, L.Z., 1994. Paleoenvironmental implications of rock magnetic measurements on sediment core from Taihu lake in Yangtze delta, East China. Quaternary Research 33, 369–377.

Zhang, X., Zhang, W., Yu, L., Endo, K., 1994. Paleoenvironmental changes in southern Yangtze delta over the last 20,000 years. Quaternary Research 33, 379–384.

Zhejiang Geological and Mineral Resources Bureau, Jiangsu Geological Bureau, Shanghai Geological Survey and Shanghai Marine Geology Survey, 1987. Report on Hydrogeological and Geoengineering Evaluation, unnumbered pages (in Chinese, unpublished report).

Zhu, J., Zhu, L., Liu, Y., Su, W., 1984. Geological structure and seismic activity in Shanghai and its vicinity (in Chinese, with English summary). Journal of East China Normal University, Natural Science Edition 4, 81–90.

Chapter 25

HEAVY-MINERAL ASSOCIATIONS AS TRACERS OF LIMITED COMPOSITIONAL MIXING DURING TURBIDITIC SEDIMENTATION OF THE MARNOSO-ARENACEA FORMATION (MIOCENE, NORTHERN APENNINES, ITALY)

GIORGIO GANDOLFI, LUIGI PAGANELLI AND WILLIAM CAVAZZA

Dipartimento di Scienze della Terra e Geologico-Ambientali, Universitá di Bologna, Piazza di Porta San Donato, 1-40127 Bologna, Italy

ABSTRACT

Petrographic and mineralogical analyses of 567 sandstone samples indicate that the turbidite beds of the Marnoso-arenacea Formation (Miocene, Northern Apennines foredeep basin) are the product of distinct detrital inputs from different source areas. These inputs were deflected along the main axis of the basin and flowed side by side with only minor mixing, as shown by the detrital modes of discrete stratigraphic intervals and of multi-sourced marker beds traceable over long distances.

The bulk of the basin fill is made of sandstone turbidite beds with southeastward-directed palaeocurrents that can be subdivided into three petrofacies (A, B, and C) based on heavy-mineral and framework compositions: A is characterised by zircon, tourmaline and rutile (ZTR), garnet ± staurolite, and abundant plutonic rock fragments; B features ZTR, garnet, epidote-group minerals, sphene, staurolite, kyanite, glaucophane, and abundant metamorphic rock fragments; C contains ZTR, garnet, very abundant epidote-group minerals, hornblende, sphene, staurolite, kyanite, glaucophane, and abundant metamorphic rock fragments. Petrofacies A and B are time-equivalent (Langhian–Serravallian), while petrofacies C ranges from the late Serravallian to the late Tortonian. Petrofacies A occurs mainly in the thrust sheets closest to the Apenninic (SW) side of the basin, petrofacies B in the thrust sheets towards the Adriatic (NE) side, and petrofacies C comprises the late-stage deposits in the evolution of the basin, when the depocentre shifted further to the northeast. Petrofacies A is made of detritus derived from the Western Alps and/or from the Corsica–Sardinia massif, while petrofacies B and C were derived from the terrains of the Central Alps.

The southern portion of the basin is still volumetrically dominated by turbidite beds derived from the northwest, but is also characterised by detrital inputs derived from south and southwest

Developments in Sedimentology, Vol. 58, 621–645

ISSN: 0070-4571/doi:10.1016/S0070-4571(07)58025-8

(petrofacies D, E, and F). These produced turbidite beds which are interbedded with the predominant NW-derived beds and have a distinctive composition characterised by abundant bioclasts (D, including the Contessa megaturbidite marker bed) plus mudrock lithics and staurolite (E), or plus mudrock lithics, very abundant staurolite and chrome spinel (F).

Keywords: turbidite dispersal pattern; multi-sourced marker beds; Marnoso-arenacea formation; northern Apennines; intrastratal dissolution.

1. INTRODUCTION

The Marnoso-arenacea Formation (MAF; Langhian–Tortonian) is a succession of turbidites up to 3500 m thick which was deposited in the Apenninic foredeep basin of north-central Italy (Fig. 1). This basin was narrow and elongate in a northwest–southeast direction and experienced intense subsidence during Miocene time. Basin-fill deposits—including the MAF—were subsequently incorporated into the Apenninic orogen (Fig. 2) due to progressive northeastward thrusting accompanied by concomitant migration of depocentres in the same direction (see Argnani and Ricci Lucchi, 2001, for a review). The MAF crops out extensively over a distance of

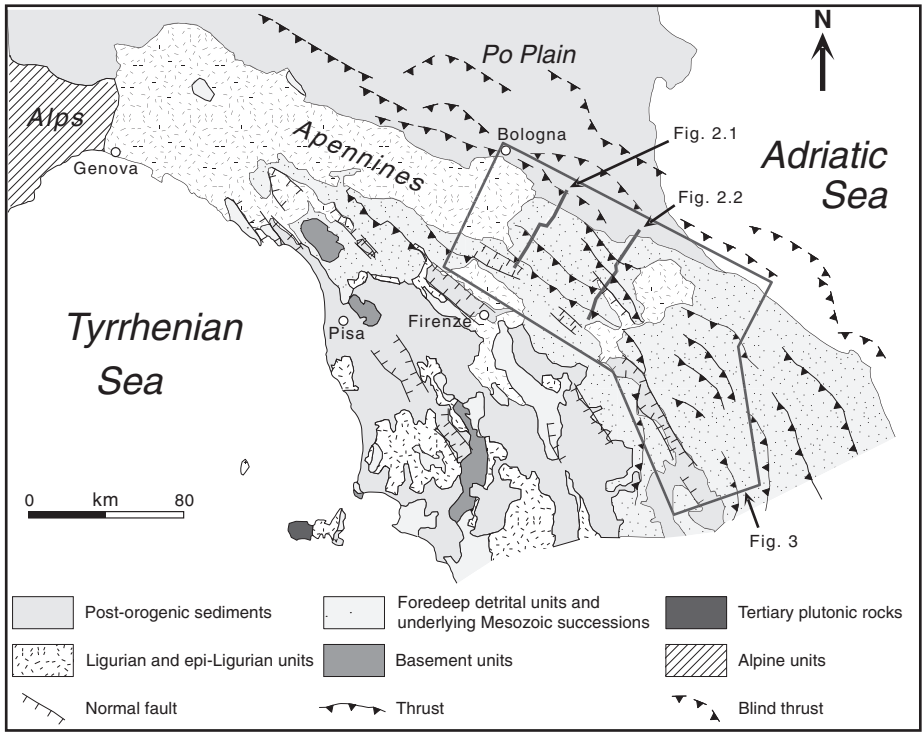

Fig. 1. Simplified geological map of the Northern Apennines (modified from Zattin et al., 2002). Arrows indicate geological cross sections of Fig. 2 and geological map of Fig. 3.

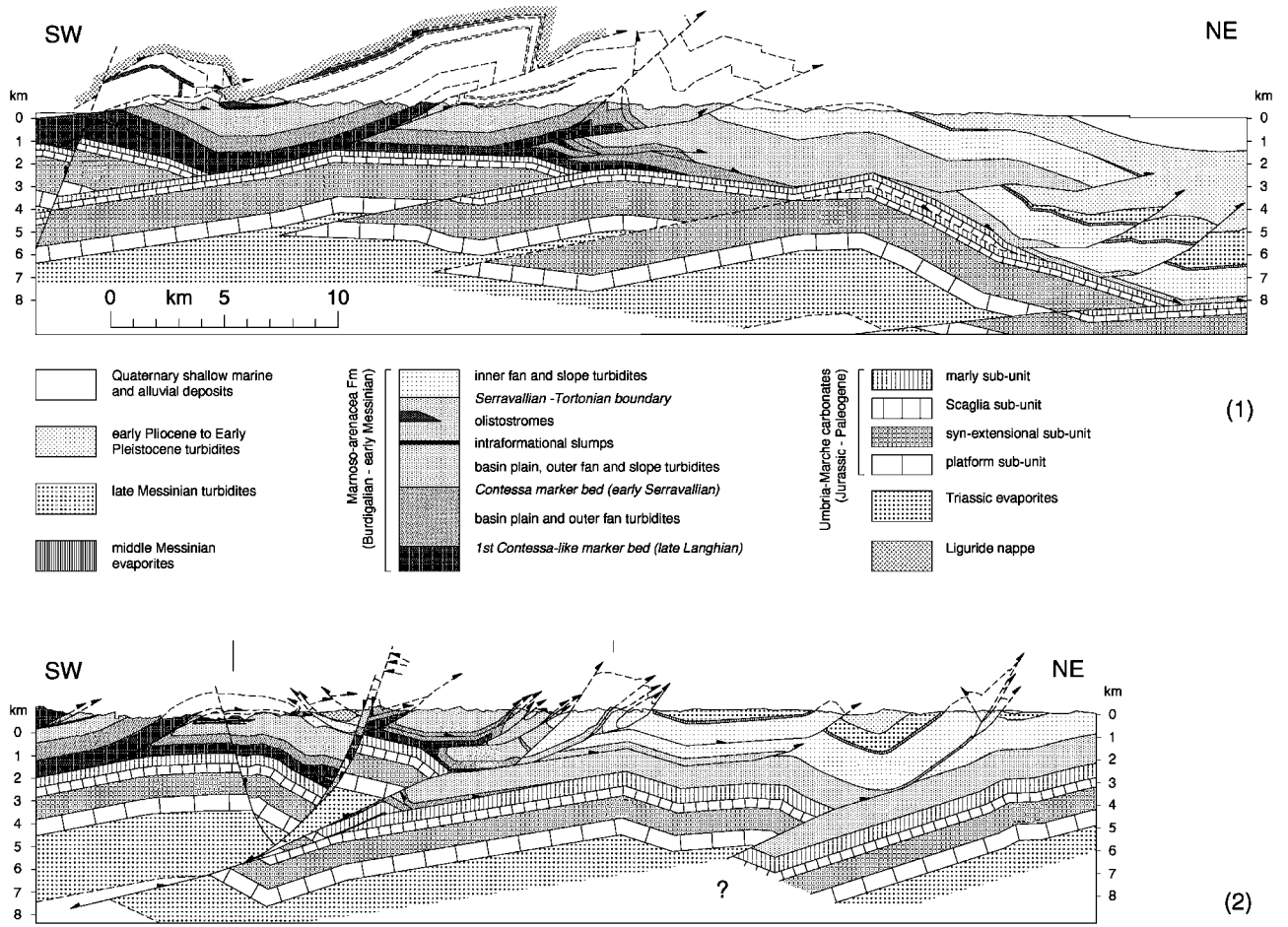

Fig. 2. Geological sections across the study area; see Fig. 1 for location (modified from Barchi et al., 2001).

some 180 km following the structural trend of the Apennines and is cut by several antecedent fluvial valleys (Fig. 3); the northwestern portion of the MAF is buried beneath younger sediments of the Po Plain.

In spite of being one of the better studied turbidite successions in the world, the framework composition (Cipriani and Malesani, 1963a, 1963b, 1963c; Chiocchini et al., 1986) and heavy-mineral content (Gazzi, 1961, 1965; Gandolfi and Gazzi, 1962, 1963) of the MAF have been mostly studied in local sections not easily related to a basin-wide stratigraphic and sedimentological framework. Gandolfi et al. (1983) carried out petrographic work on 11 stratigraphic sections distributed throughout the outcrop area, but only 48 samples were analysed. According to these workers, palaeocurrents, framework composition, rock fragments and heavy minerals suggested six source areas, of which five were primarily extrabasinal (Alpine I and II and Apenninic I, II, and III), and one intrabasinal. Petrofacies Alpine I and II and Apenninic I are associated with southeastward longitudinal dispersal, whereas the volumetrically subordinate petrofacies Apenninic II and III are associated with northwestward palaeocurrents.

Cavazza and Gandolfi (1992) collected 15 sandstone samples of the Contessa megaturbidite, a key bed derived from the southeast and present over the whole outcrop area of the MAF. At each location, a NW-derived sandstone layer, stratigraphically close to the Contessa bed, was also collected. A comparison of these paired samples revealed that as burial proceeded, $CaCO_3$ became more mobile, the illite/smectite ratio increased and the staurolite content decreased, the latter being interpreted as the result of intrastratal dissolution processes.

Gandolfi and Paganelli (1992, 1993) studied other Oligocene–Miocene Apenninic sandstones of the Macigno, Modino, Cervarola and Falterona Formations, showing the presence of directly superposed beds having different heavy-mineral suites. Such changes cannot be ascribed to post-depositional dissolution, and were explained as the result of sediment supply switching or of mixing of different detrital inputs.

Here, we present new petrographic data on the MAF, in order to better constrain the petrofacies, their distribution in the basin and their provenance. Extensive petrographic sampling (567 samples compared to 30 of Cavazza and Gandolfi, 1992, and 48 of Gandolfi et al., 1983) resolved compositional changes along the transport direction, transversally and vertically, within the successions and also within individual megaturbidite key beds.

2. GEOLOGICAL FRAMEWORK AND SAMPLING

The MAF was deposited in a laterally confined NW–SE elongated basin (Ricci Lucchi, 1978). A pulsating deep-sea fan system, alternately advancing and retreating and supplied by prevailing Alpine sources but also by transversal sediment sources, was active from the Langhian to the Tortonian. The turbidity currents bypassing the fan system deposited their load on the basin plain. Palaeocurrent directions are axial, with the main flows being southeastward and the subordinate ones northwestward (Fig. 4) (e.g., Lucente, 2004), thus indicating the absence of significant topographic gradients along the basin axis. Turbidity currents generated along the basin margins were deflected along the basin axis.

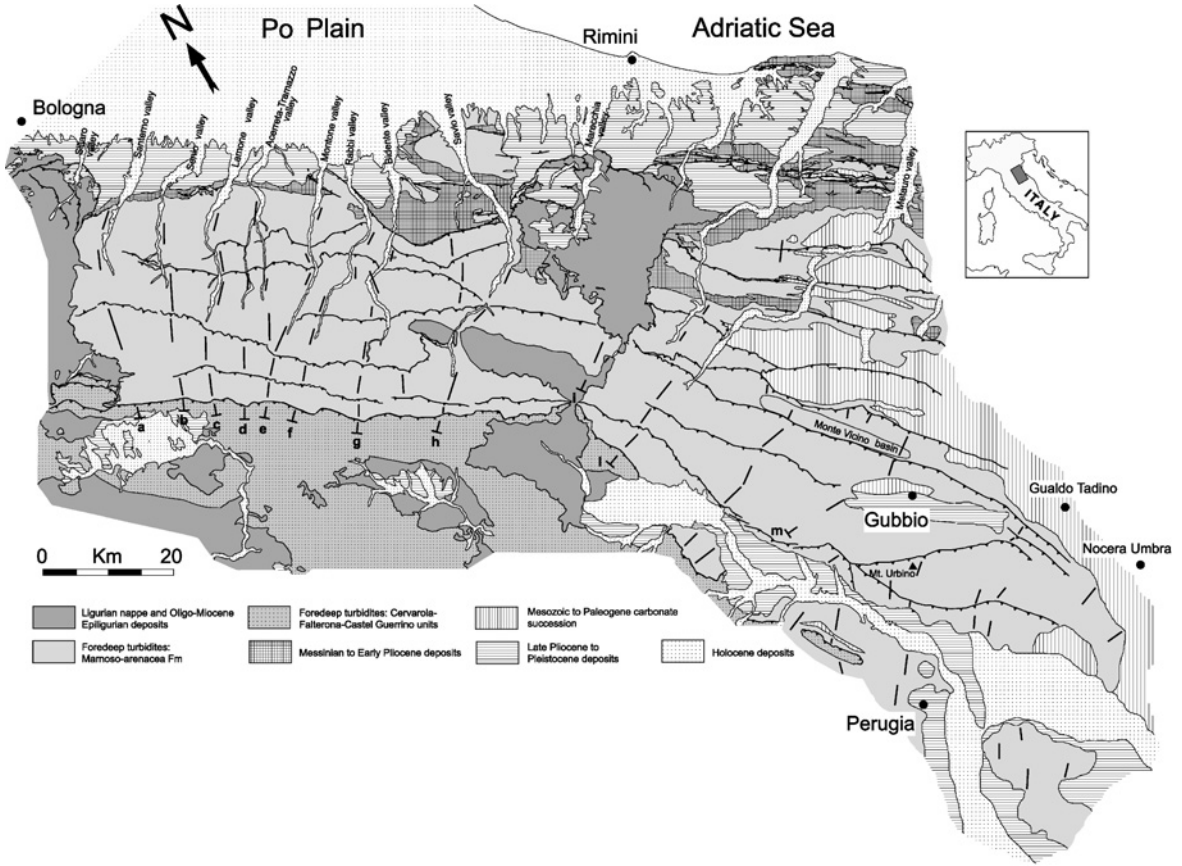

Fig. 3. Geological sketch map (modified from Capozzi et al., 1991) of the studied Marnoso-arenacea Formation. Traces of the main thrust faults affecting the Marnoso-arenacea Formation and location of the sample series (line segments) and of the cross sections, closely corresponding to fluvial valleys, are shown (a: Santerno, b: Senio, c: Lamone, d: Acerreta-Tramazzo, e: Montone, f: Rabbi, g: Bidente, h: Savio, i: Marecchia, l: Metauro, and m: Assino).

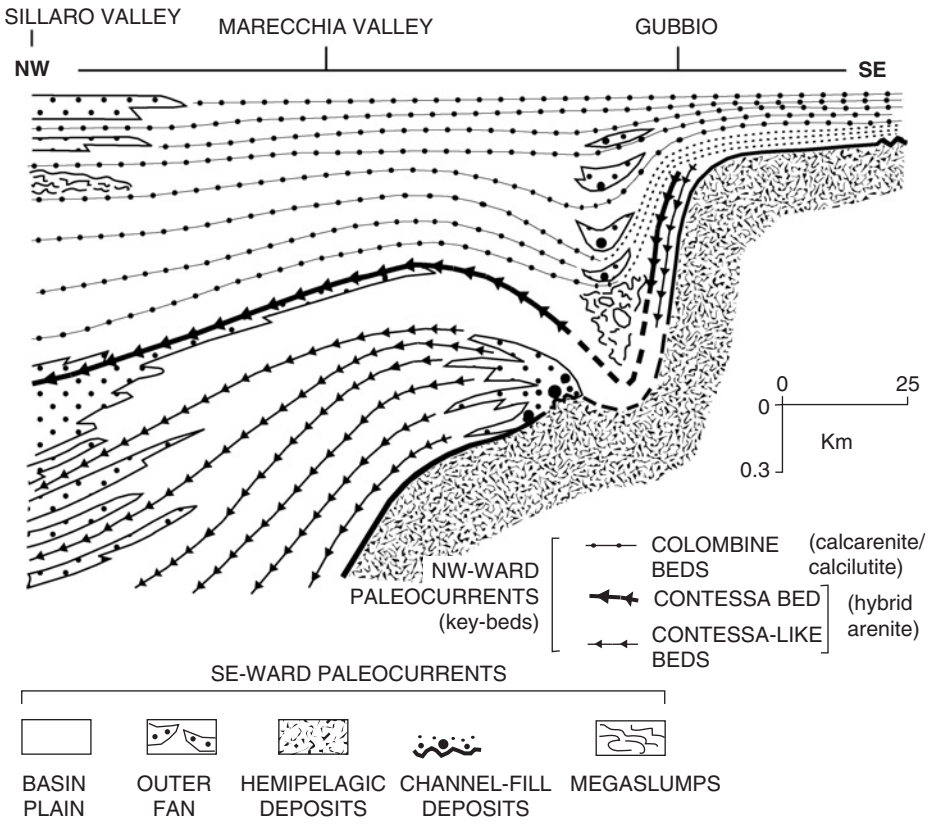

Fig. 4. Schematic longitudinal (NW–SE) cross section of the Marnoso-arenacea basin (modified from Ricci Lucchi and Valmori, 1980).

The MAF crops out for ~200 km along a NW–SE direction, parallel to the axis of the Northern Apenines foredeep basin, and for 50 km perpendicular to it (Ricci Lucchi, 1978). Apenninic thrusts faults parallel to the basin axis repeat the stratigraphy (Fig. 2) (Bonini et al., 1991; Capozzi et al., 1991; Delle Rose et al., 1991; De Donatis and Mazzoli, 1994; Deiana and Pialli, 1994; Barchi et al., 2001). Individual sedimentary sections can be up to ~2000 m thick (Gandolfi and Gazzi, 1963; Ricci Lucchi, 1975).

Stratigraphic correlation in the foredeep of the Northern Apennines is detailed (e.g., Ricci Lucchi and Valmori, 1980). Likewise, the structural setting of the basin is well understood (see Barchi et al., 2001, for a review). This allowed for detailed sampling throughout the main structural units (thrust sheets) and the entire stratigraphic thickness of the MAF. Samples were taken along the SW–NE-trending main valleys, orthogonal to the structural grain of the Apennines (Fig. 3).

3. SANDSTONE PETROGRAPHY AND MINERALOGY

Framework detrital modes of sandstone samples were determined through point counting with the Gazzi–Dickinson method. This procedure, proposed by Gazzi

(1966) and Dickinson (1970), and discussed by Gazzi et al. (1973), Ingersoll et al. (1984) and Zuffa (1985), minimises the variation of composition with grain size. Three hundred points per section were counted and assigned to nineteen categories. Sandstone point-count data were then recalculated to produce the grain parameters indicated in Table 1. Heavy-mineral concentrates were prepared following the procedures of Gazzi et al. (1973). Two hundred transparent heavy-mineral grains in the 2–4 phi range were counted using the petrographic microscope and heavy liquids of known refractive indices. Heavy-mineral raw counts were then recalculated to produce the fourteen categories included in Table 2. Further details on sample preparations and analytical techniques to determine the framework compositions and heavy-mineral assemblages of the sandstone samples can be found in previous papers (Gazzi et al., 1973; Zuffa, 1980; Gandolfi et al., 1983). Raw point-count data (framework composition) and the heavy-mineral data are available from the senior author upon request.

3.1. Framework Composition

Point-count data summarised here incorporate results from 48 samples of Gandolfi et al. (1983), 12 samples of Cavazza and Gandolfi (1992), as well as 39 new complete analyses and 38 partial analyses [(100.K/(K + P), see below]. From these data (137 samples) we calculated the ratio between K- and plagioclase-feldspars [100.K/(K + P)] and the ratio between plutonic and metamorphic rock fragments [100.P/(P + M)]. The composition of 191 additional samples was evaluated qualitatively in this section.

Sandstone samples contain quartz, feldspars, lithics (> 4 phi internal grain size), micas, chlorites, and carbonate components (clasts, cement, and micritic matrix). The sample set can be divided into two groups based on the amount of intrabasinal carbonate clasts (CI; Fig. 5): samples with a high percentage of CI grains are invariably from beds showing palaeocurrents towards the northwest, whereas turbidite beds with palaeocurrents towards the southeast are virtually devoid of CI clasts (Table 1). Beds with SE-directed palaeocurrents form the great majority of the volume of the MAF. Considering both framework composition and heavy-mineral composition (see discussion of heavy-mineral data below) the two groups of samples can be subdivided into six discrete petrofacies (A through F). The CI grains include intraclasts, fossils, and micritic grains. The intraclasts and the micritic grains were poorly lithified at the time of deposition as they are not veined and are deformed between more rigid framework grains.

Both mono and polycrystalline quartz grains show features that suggest a prevailing metamorphic and magmatic provenance, while evidence of a sedimentary source rock is rare. Plagioclase prevails among the feldspars in the main supply from the northwest, while K-feldspar prevails in the minor one from the southeast. Based on their composition, twinning laws, zoning, and the types of lithic grains in which they occur, the plagioclase-feldspars are derived mainly from plutonic and metamorphic rocks and less frequently from volcanic rocks. Plagioclase grains mainly range from albite to oligoclase. Zoned crystals and feldspar grains with andesine–labradorite compositions, derived from volcanic and mafic rocks, respectively, are scarce. The most abundant K-feldspar is microcline, perthitic to various degrees. There is also a more homogeneous and transparent K-feldspar phase with 2Vx

Table 1. Framework composition (mean and standard deviation) of sandstone petrofacies of the Marnoso-arenacea Formation

Sandstone samples	N-derived petrofacies						S-derived petrofacies					
	A ($n = 35$)		B ($n = 15$)		C ($n = 5$)		D ($n = 29$)		E ($n = 11$)		F ($n = 4$)	
	Mean	SD	Mean	SD	Mean	SD	Mean	SD	Mean	SD	Mean	SD
Quartz	32.5	4.0	34.8	3.8	34.1	4.2	21.8	8.8	18.0	5.6	22.6	5.6
K-feldspar	6.2	2.2	6.2	1.2	2.7	0.9	9.9	5.0	7.2	3.5	8.6	2.9
Plagioclase	11.0	3.2	12.6	3.4	10.0	2.8	7.7	4.0	4.7	2.3	6.1	1.3
Volcanic rock fragments	1.2	0.7	1.5	1.1	1.8	0.6	1.9	1.1	4.0	2.7	4.9	2.8
Metamorphic rock fragments	3.7	3.1	4.5	1.9	5.0	2.5	1.6	1.4	1.7	1.2	2.4	1.3
Sedimentary rock fragments	**1.3**	**1.6**	**0.9**	**1.1**	**1.6**	**1.3**	**3.4**	**5.0**	**10.4**	**7.2**	**12.6**	**3.1**
Micas	9.4	3.3	9.3	3.0	10.1	2.3	0.8	0.9	0.8	0.7	1.1	0.7
Accessory minerals	1.5	0.9	2.0	1.6	4.2	1.3	0.6	0.5	0.8	0.5	0.7	0.2
Extrabasinal carbonate grains (CE)	14.4	7.0	8.1	10.2	13.0	7.5	5.1	6.0	8.0	10.0	10.2	7.2
Intrabasinal carbonate grains (CI)	0.0	0.0	0.0	0.0	0.0	0.0	35.7	28.3	36.2	27.9	13.5	10.9
Carbonate cement	18.8	7.9	20.1	7.9	17.5	4.5	11.4	7.6	8.3	6.2	17.4	2.4
Others	0.0	0.0	0.0	0.0	0.0	0.0	0.0	0.1	0.1	0.2	0.0	0.0
Total	100.0	–	100.0	–	100.0	–	100.0	–	100.0	–	100.0	–
QF(R + C)%Q	46.8	6.7	51.3	5.9	51.0	5.8	45.0	7.6	37.9	11.8	33.6	6.2
QF(R + C)%F	24.7	5.5	27.9	7.0	19.5	4.6	34.6	7.5	22.6	6.6	21.6	3.2
QF(R + C)%R	8.2	4.1	10.1	4.0	12.4	2.4	13.0	7.8	29.0	11.3	30.3	8.5
QF(R + C)%C	20.3	8.5	10.7	12.3	17.1	9.2	7.4	7.7	10.5	12.6	14.5	11.1
NCE	82.3	7.9	90.5	10.9	87.1	7.7	55.4	24.8	52.7	19.9	71.3	9.1
CI	**0.0**	**0.0**	**0.0**	**0.0**	**0.0**	**0.0**	**38.8**	**28.9**	**38.5**	**28.1**	**16.2**	**12.8**
CE	17.7	7.9	9.5	10.9	12.9	7.7	5.8	6.7	8.8	11.2	12.5	9.0
$100 \times K/(K + P)$	**36.1**	**8.5**	**33.7**	**6.9**	**22.1**	**9.3**	**57.6**	**7.5**	**61.0**	**7.6**	**57.7**	**4.1**

Note: Variables most useful for the establishment of petrofacies A through F are shown in bold.

Table 2. Heavy-mineral composition (mean and standard deviation) of sandstone petrofacies of the Marnoso-arenacea Formation

Heavy-mineral species	N-derived petrofacies						S-derived petrofacies					
	A ($n = 223$)		B ($n = 95$)		C ($n = 47$)		D ($n = 26$)		E ($n = 60$)		F ($n = 17$)	
	Mean	SD	Mean	SD	Mean	SD	Mean	SD	Mean	SD	Mean	SD
ZTR	6.6	3.4	4.5	1.9	2.9	1.4	12.2	5.5	11.8	8.7	10.2	4.9
Garnet	87.1	6.7	72.9	8.7	46.4	8.1	77.6	8.0	69.3	9.9	63.1	7.6
Orthite	0.4	0.5	0.7	0.5	0.5	0.4	0.1	0.2	0.1	0.4	0.0	0.0
Sphene	**0.8**	**1.8**	**3.8**	**2.8**	**3.9**	**1.6**	**0.1**	**0.3**	**0.5**	**1.2**	**1.2**	**1.7**
Epidotes	**0.9**	**2.2**	**10.0**	**6.7**	**34.2**	**5.0**	**0.1**	**0.2**	**0.1**	**0.2**	**0.1**	**0.2**
Chloritoid	0.9	1.0	0.9	1.0	1.1	1.2	1.1	1.3	1.2	0.9	0.9	0.9
Staurolite	**2.6**	**3.0**	**5.5**	**2.9**	**3.8**	**1.8**	**1.7**	**2.2**	**9.9**	**5.0**	**17.9**	**5.3**
Kyanite	0.0	0.2	0.6	0.9	1.5	1.0	0.0	0.0	0.2	0.5	0.0	0.0
Glaucophane	0.0	0.2	0.4	0.6	1.1	1.3	0.0	0.0	0.0	0.1	0.0	0.0
Hornblende	**0.0**	**0.0**	**0.1**	**0.6**	**4.2**	**5.6**	**0.0**	**0.0**	**0.0**	**0.0**	**0.0**	**0.0**
Chrome spinel	**0.2**	**0.5**	**0.1**	**0.2**	**0.0**	**0.1**	**5.2**	**3.6**	**5.2**	**2.6**	**5.1**	**3.8**
Monazite	0.3	0.4	0.1	0.2	0.0	0.1	1.4	1.8	1.1	0.9	0.8	1.1
Xenotime	0.1	0.3	0.1	0.4	0.0	0.1	0.2	0.2	0.2	0.3	0.2	0.4
Others	0.1	0.5	0.3	1.1	0.4	2.4	0.3	0.7	0.4	1.7	0.5	0.6
Total	100.0	–	100.0	–	100.0	–	100.0	–	100.0	–	100.0	–

Note: Variables most useful for the establishment of petrofacies A through F are shown in bold.

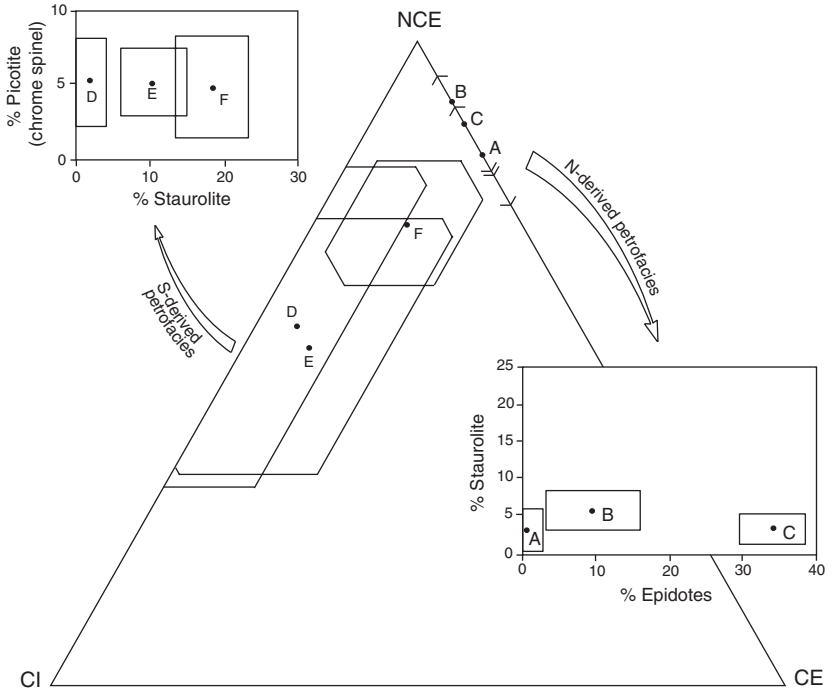

Fig. 5. NCE-CI-CE ternary diagram (sensu Zuffa, 1980) showing composition of sandstone samples from the Marnoso-arenacea Formation. NCE, CI, and CE indicate noncarbonate extrabasinal grains, carbonate intrabasinal grains, and total carbonate extrabasinal grains, respectively. Dots and polygons indicate mean and standard deviation, respectively, of petrofacies A through F. North- and south-derived petrofacies can be differentiated further on the basis of their heavy-mineral compositions (rectangular plots; see also Table 2).

between 30° and 50°, which we infer to be volcanic sanidine. Feldspar alteration is variable, with unaltered plagioclase and/or K-feldpars coexisting with partially or deeply altered grains of the same minerals, seemingly indicating mixing of discrete populations derived from differing sources and being either first cycle or recycled from older sedimentary rocks.

The most abundant aphanitic lithic fragments are noncarbonate extrabasinal grains derived from metamorphic rocks, mostly phyllite and subordinate chlorite-schist, serpentinite and serpentine-schist. Low-grade and high-pressure metamorphic rocks (with albite, epidote-group minerals, and glaucophane) are scarce and randomly distributed, but are well correlated to the distribution of epidote-group minerals in the heavy-mineral assemblages. Sedimentary rock fragments, mainly siltstone and shale, are randomly distributed in sediments supplied from the northwest, but dominate in those from the southeast.

Among the carbonate extrabasinal grains (CE), two categories were distinguished: limestone and dolostone. Limestone grains are mostly micritic and biomicritic, with subordinate arenaceous, silty, and cherty limestones. They may coexist with CI grains in the same sample. Dolostone grains have a saccharoidal texture.

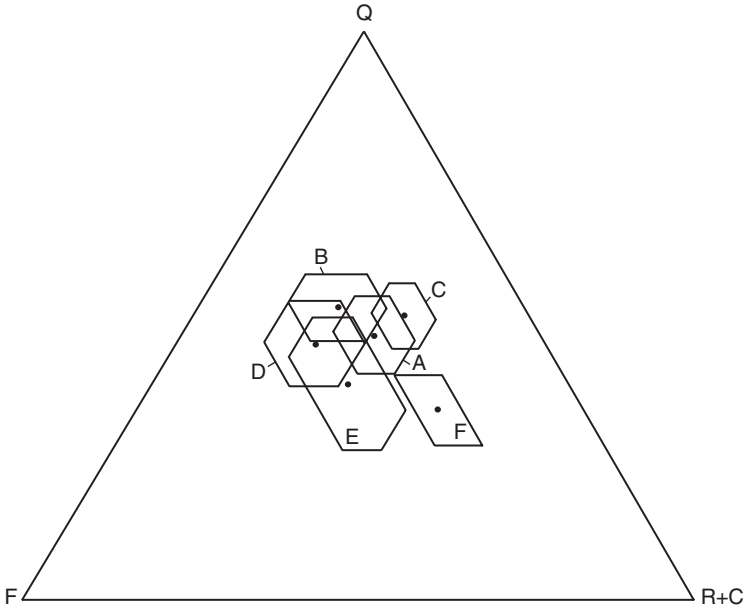

Fig. 6. QF(R + C) ternary diagram of sandstone composition of samples from the Marnoso-arenacea Formation. Q, F, and (R + C) indicate total quartz, total feldspars, and total aphanitic lithic fragments (including carbonate lithics), respectively. Dots and polygons indicate mean and standard deviation, respectively, of petrofacies A through F.

In medium- and coarse-grained sandstones samples, lithic fragments with an internal grain size coarser than 4 phi were counted separately. The most abundant rock fragment types are gneiss, micaschist, granite, and sandstone. A standard QF(R + C) ternary plot (Fig. 6) cannot discriminate adequately the north- and south-derived petrofacies.

3.2. Heavy Minerals

Four hundred and sixty-eight heavy-mineral analyses have been considered (Table 2), of which 99 are from previous papers (Gazzi, 1961; Gandolfi and Gazzi, 1963; Gandolfi et al., 1983; Cavazza and Gandolfi, 1992). Among the new analyses, 55 are from 5 key beds and 30 from profiles taken across single megaturbidite beds.

Garnet predominates in all samples. Zircon, tourmaline, and rutile (ZTR) occur in the range 2–10% for sediment derived from the northwest and in the range 10–20% (zircon from 4.5% to 18.5%) for sediment derived from the southeast. Monazite is virtually absent in the sediment derived from the northwest, but is present in the turbidites derived from the southeast. The minerals that show the most significant spatial variations are epidote-group minerals, sphene, staurolite and the high-pressure minerals kyanite and glaucophane; chrome spinel is abundant only in sediment supplied from the southeast.

The amount of epidote-group minerals and the 100.K/(K + P) ratio show a good inverse correlation: the samples with high epidote content have lower ratios (typically around 20), while the samples low in epidote have higher ratios (> 30).

The integration of framework compositional data (Table 1) and heavy-mineral data (Table 2) allow further discrimination of petrofacies within the two main provenances. Turbidites with palaeocurrents directed towards the SE include three petrofacies (A, B, and C).

Petrofacies A comprises ~50% of all samples and is characterised by a very simple heavy-mineral assemblage dominated (> 90%) by garnet and ZTR; all other mineral species are scarce (< 1%) with the only exception of staurolite (2.6 ± 3.0%). This petrofacies is also characterised by abundant plutonic rock fragments.

Petrofacies B contains significant amounts of epidote-group minerals (10.0 ± 6.7%) (these numbers indicate mean and standard deviation, respectively), staurolite (5.5 ± 2.9%), and sphene (3.8 ± 2.8%). The 95 samples having this composition define an assemblage with garnet, ZTR, epidote-group minerals, staurolite, and sphene. This petrofacies is also characterised by abundant metamorphic rock fragments.

A third group—**Petrofacies C**—is rich in epidote-group minerals (34.1 ± 5.0%) and shows a more varied heavy-mineral assemblage, including also hornblende (4.2 ± 5.6%) and kyanite (1.5 ± 1.0%). This petrofacies also contains abundant metamorphic rock fragments.

Turbidites with palaeocurrents flowing towards the NW are generally characterised by abundant garnet, ZTR, and by chrome spinel (> 5%). As to the framework composition, CI grains are characteristically abundant in all sandstone samples. In more detail, three petrofacies (D, E, and F) can be discriminated for turbidites with NW-directed palaeocurrents.

Petrofacies D is distinguished by abundant garnet (77.8 ± 8.0%) and ZTR (12.2 ± 5.5%), and by a significant amount of chrome spinel (5.2 ± 3.6%). This petrofacies is also typified by a low percentage of staurolite and sedimentary rock fragments compared to the other turbidites with north-westerly palaeocurrents.

Petrofacies E contains significant amounts of staurolite (9.9 ± 5.0%) and a much higher percentage of sedimentary lithic fragments (10.4 ± 7.2%), mostly siliciclastic mudrock.

Petrofacies F is rich in staurolite (17.9 ± 5.3%) and sedimentary lithic fragments (12.6 ± 3.1%), mostly siliciclastic mudrock grains.

3.3. Diagenesis

Data from modal analyses suggest that only minor diagenetic changes affected the MAF sandstones (see also Milliken et al., 1998). The widespread presence of feldspar and biotite grains having different degrees of alteration in the same samples points to provenance as the prevailing controlling factor of composition. Analogous conclusions concerning the limited effect of diagenesis on the composition are described in previous papers on the Apenninic formations of the Tuscan domain, southwest of our study area (Gandolfi and Paganelli, 1992, 1993).

Evidence of post-depositional modifications include (i) microcracks in the coarser grains, (ii) plastic deformation of pelitic grains, (iii) flexure and mashing of mica

grains, and (iv) the partial dissolution of the carbonate components with simultaneous recrystallisation in the form of cement (see also Fontana et al., 1986; Morton and Hallsworth, 1999). In fact, the presence of carbonate cement is conditioned by the occurrence of carbonate clasts. In samples devoid of carbonate clasts, cement is absent, while in samples with only a few carbonate clasts, cement occurs only in their immediate surroundings, thus suggesting a very localised dissolution–recrystallisation process (see also Cibin et al., 1993; McBride et al., 1995; Milliken et al., 1998). Analogous processes are absent for the terrigenous siliciclasts, but some feldspar grains were partially replaced by calcite (see, for instance, Fig. 9 in Cavazza and Gandolfi, 1992); such replacement could be related either to diagenesis or to alteration processes in the source area. Mainly in the coarser and monocrystalline grains, compaction processes caused fractures filled with siliciclastic matrix, cement, or deformed parts of more plastic grains.

The presence or absence of the most significant heavy-mineral species, as well as their abundance and distribution within the basin, is compatible with provenance and dispersal as the main factors controlling the detrital modes of the MAF, with diagenesis playing a subordinate role. This conclusion is supported by (i) the alternation, within the same stratigraphic section, of layers lacking dissolution-prone mineral species (e.g., epidote-group minerals) with layers rich in epidotes, (ii) the negative correlation between epidote and staurolite content, and (iii) the high content of stable minerals such as chrome spinel and zircon in thinner and less deeply buried (Zattin et al., 2000) successions of the southeastern part of the basin (minor sources), as opposed to their absence or low content in the thicker and more deeply buried successions in the northwestern part of the basin. More unstable mineral species are present in the latter region.

4. VERTICAL AND LATERAL DISTRIBUTION OF SANDSTONE PETROFACIES

The high level of stratigraphic and structural knowledge of the present-day geometry of the sedimentary fill of the Northern Apennines foredeep basin, the variety of source rocks, the large numbers of samples analysed, and the low degree of diagenetic modifications all allow for a detailed reconstruction of the vertical and lateral arrangement of the sandstone petrofacies of the MAF. In many cases, the presence of prominent marker beds makes it possible to follow the same stratigraphic horizon for a long distance, even across multiple structural discontinuities (mostly thrust faults). The MAF of northern Italy thus provides a unique opportunity for the mapping of sediment dispersal patterns within a foreland basin dominated by turbidite sedimentation. Our extensive dataset allows for a detailed delineation of the petrofacies, including their overall vertical and lateral arrangement. However, a thorough discussion would require more space and goes beyond the scope of this contribution.

The great bulk of the MAF ($>90\%$ of the total volume) is composed of turbidite beds showing palaeocurrents towards the southeast. Within this predominant provenance, Gandolfi et al. (1983) distinguished three provenance-defined sandstone petrofacies (Alpine I, Apenninic I, Alpine II), on the basis of the composition of 13,

17, and 5 samples, respectively. They correspond to petrofacies B, A, and C of the present contribution as distinguished by the composition of 95, 223, and 47 samples, respectively.

Petrofacies A and B are coeval (Langhian–Serravallian; Fig. 7), with A occurring in the structural units (thrust sheets) closer to the southwestern (inner) margin of the basin and B occurring in the more external structural units to the northeast. In terms of sandstone provenance, during the Langhian and the early Serravallian the basin was thus subdivided into two parts: a southwestern one (Apenninic side) in which flowed turbidity currents carrying sands of petrofacies A, and a northeastern one (Adriatic side) in which flowed turbidity currents carrying sands of petrofacies B. The two petrofacies are considerably interfingered.

Petrofacies C ranges from the late Serravallian to the late Tortonian and it is limited to the northeasternmost portion of the basin (Fig. 7). The distinctive heavy-mineral suite of petrofacies C, dominated by abundant epidote-group minerals ($34.1 \pm 5.0\%$) and including also hornblende ($4.2 \pm 5.6\%$) and kyanite ($1.5 \pm 1.0\%$) (Table 2), makes the recognition of its stratigraphic and areal extent relatively easy. Petrofacies C represents the vast majority of the basin fill during the Tortonian, when subsidence shifted towards the northeast (*foredeep phase* of Ricci Lucchi, 1975, 1978) due to flexural loading of the basin floor, induced by the encroaching Apenninic thrust sheets.

None of the three petrofacies (D, E, and F) with palaeocurrents from the southern margins of the basin can be described as coherent three-dimensional lithosomes like A, B, and C. They represent instead occasional, yet compositionally distinctive, pulses of turbiditic fluxes flowing towards the NW within a volumetrically predominant background of turbidite sedimentation towards the SE. From Ricci Lucchi and Valmori (1980) to Lucente (2004), such turbidites have been the object of much detailed sedimentological and stratigraphic research.

Forty-five samples were taken from the base of the Contessa key bed (belonging to petrofacies D) which crops out for ~130 km parallel to the longitudinal axis of the basin and for ~20 km transversally. The heavy-mineral assemblage of the Contessa bed is dominated by garnet and ZTR, with subordinate quantities of chrome spinel, staurolite, chloritoid ± sphene. Staurolite and, subordinately, sphene contents increase irregularly from SW to NE across the main structural units. This was interpreted by Cavazza and Gandolfi (1992) in terms of intrastratal dissolution during burial diagenesis in the deepest, southwestern portion of the basin. Results of this study point instead to a multi-sourced, multiple provenance for this catastrophic megaturbidite (over 30 km^3; Ricci Lucchi and Valmori, 1980): petrofacies fingerprinting leads to at least two main entry points in the southern portion of the basin through which detritus entered the basin, was deflected, and flowed side by side towards the NW (Fig. 8). Intrastratal dissolution cannot have been a factor in the present-day spatial distribution of heavy-mineral species because staurolite and sphene are present in turbidite layers just above and below the Contessa marker bed throughout the basin.

Several individual marker beds belonging to various petrofacies were sampled vertically in order to check for compositional variations. A decrease in the amount of the heavy-mineral fraction and a slight decrease of garnet from the base to the top of some beds was observed. These vertical trends within single beds reflect a typical

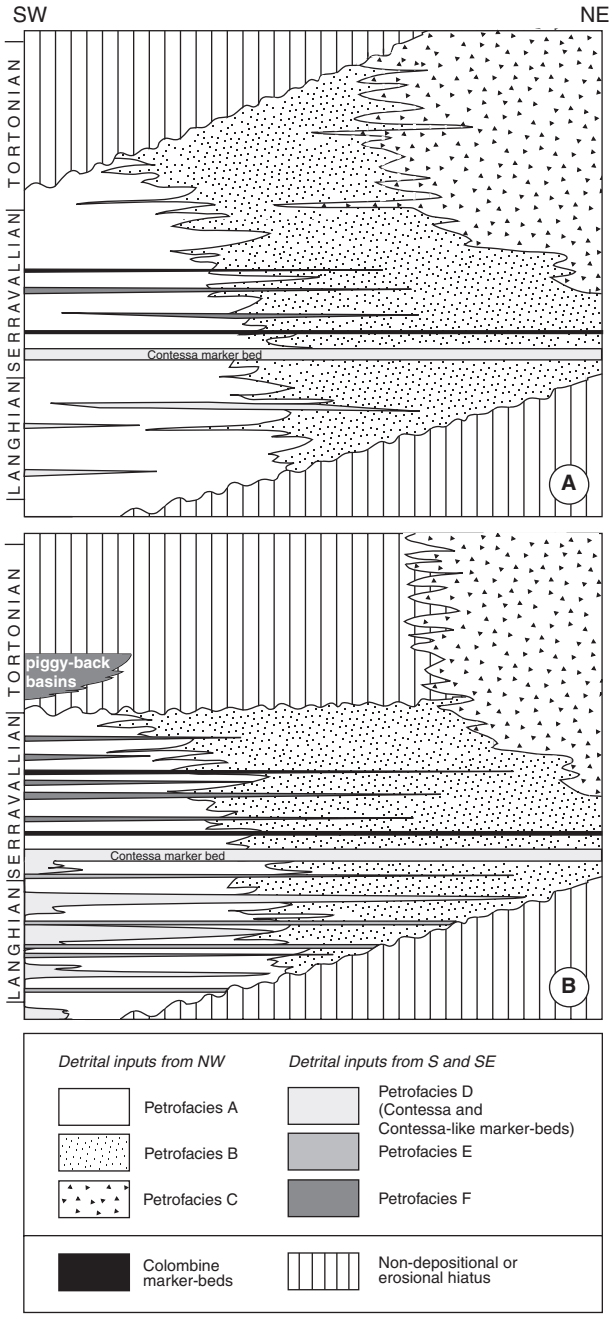

Fig. 7. Chronostratigraphic relationships among petrofacies A through F in the Marnoso-arenacea Formation north (A) and south (B) of the Marecchia Valley (see Fig. 3 for location).

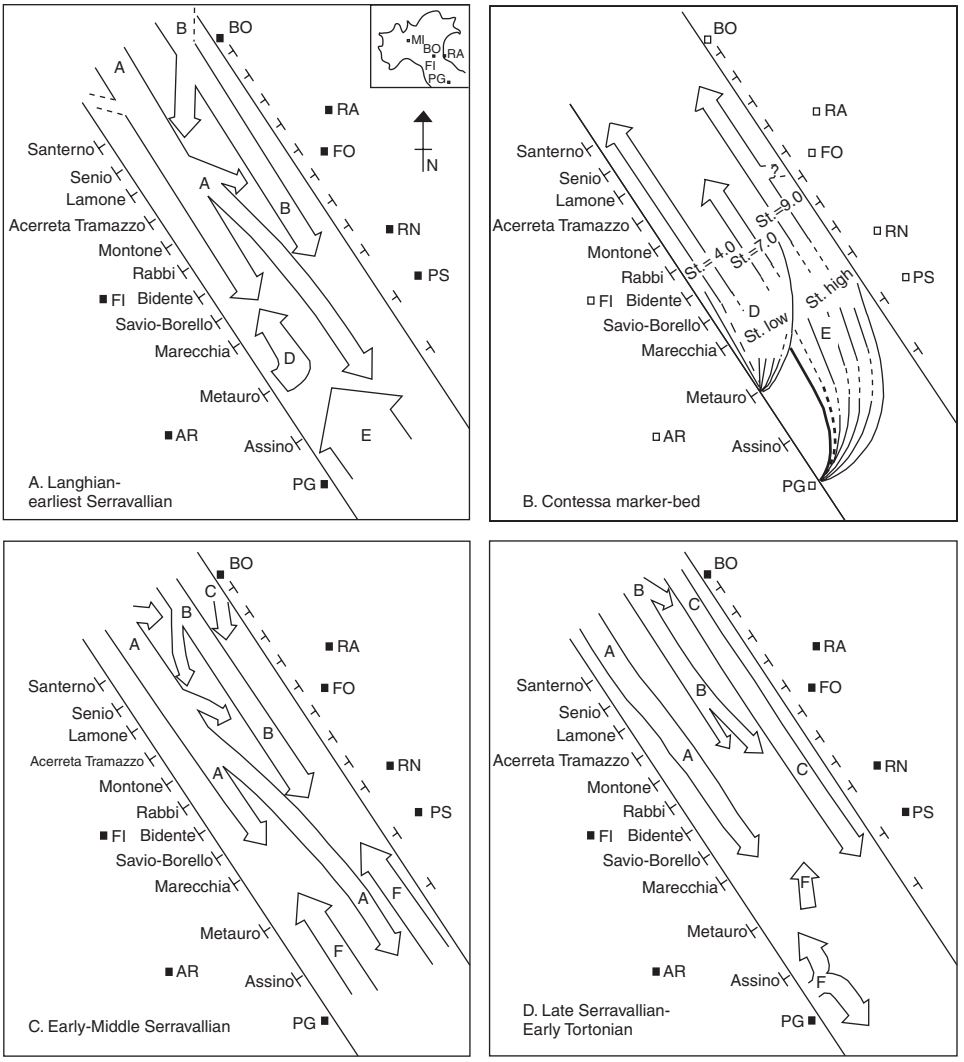

Fig. 8. Non-palinspastically restored sediment palaeodispersal patterns within the Apenninic foredeep during deposition of the Marnoso-arenacea Formation. A, B, C, D, E, and F indicate sandstone petrofacies as defined in the text. St: staurolite, AR: Arezzo, BO: Bologna, FI: Firenze, FO: Forlì, MI: Milan, RN: Rimini, PG: Perugia, PS: Pesaro, RA: Ravenna. For geographic location of river valleys see Fig. 3.

settling (fall out) sequence within a turbidite flow. Other minor vertical variations are irregularly distributed. Variations in the carbonate component are more significant, particularly in the sandstone division of the Contessa bed in which, from the base to the top, eight samples show the following percentages of carbonate: 44.3, 57.8, 67.2, 61.7, 67.5, 71.4, 83.9, and 84.6. This trend may be caused by the fine grain size of micrite and pelite particles, and by the porosity of the larger carbonate intraclasts (including bioclasts) which behave hydraulically like finer grained particles. The

same trend was observed in seven samples from the ''Masso Grosso'' bed, a distinctive marker bed with palaeocurrents towards the southeast.

The temporal evolution of the detrital modes and their palaeogeographic distribution can be summarised by subdividing the MAF into four chronostratigraphic intervals. The first interval comprises the lower portion (Langhian–early Serravallian) of the formation up to the Contessa key bed (Fig. 8A), including other key beds (A1, A24, A70 of Ricci Lucchi and Valmori, 1980). The second one is represented by the Contessa marker bed (Fig. 8B), the third one covers the early-middle Serravallian (Fig. 8C), and the fourth one the late Serravallian–Tortonian (Fig. 8D).

In the first time interval (Fig. 8A) petrofacies A and B are predominant. Petrofacies A dominates the first three internal (i.e., southwestern) structural units (thrust sheets), while towards the northeast only petrofacies B is present. In the first two thrust sheets, between the Senio and Rabbi sections (Sections b and f, Fig. 3), A and B are interbedded. Therefore, it is likely that turbidite sedimentation was supplied by different sources, Apenninic for petrofacies A and Alpine for petrofacies B. In view of their compositional differences, the turbidites could each maintain their composition during the course of the deposition, at times and in places alternating and mixing. Specific key beds can be tied to this peculiar, multi-sourced detrital supply. For example, key bed A1 (Ricci Lucchi and Valmori, 1980) belongs to petrofacies A in the Santerno section, to petrofacies B in the Senio section, again to A in the Montone and Savio sections. The A1 key bed in the Assino section is referred to petrofacies A in which siltite and sandstone grains are more abundant, thus suggesting a possible added supply. During this time interval the southern portion of the basin was volumetrically dominated by NW-derived petrofacies A and B (Fig. 7B), yet this area is characterised also by significant amounts of S- and SE-derived turbidites (petrofacies D and E) containing significant amounts of mudrock clasts and epidote-group mineral grains.

The early Serravallian Contessa megabed is characterised by CI grains, mixed with CE and noncarbonate grains (hybrid arenite; Zuffa, 1980). It shows variations—both parallel and perpendicular to the basin axis—in the abundance of some heavy minerals, particularly staurolite, sphene, and kyanite + glaucophane. To explain this areal distribution we must invoke two intrapenninic sources (Fig. 8B)—with low staurolite and high staurolite contents, respectively—which supplied heterogeneous detritus (biogenous and terrigenous), with entry points near Città di Castello and Gubbio, as indicated by the presence of deep-sea fans (Ricci Lucchi, 1978). The presence of quantitatively subordinate heavy-mineral species (sphene, kyanite, and glaucophane) in the more external (northeastern) portion of the basin is possibly the result of minor detrital inputs entering the basin from its Adriatic side. Burial diagenesis cannot be invoked as the same mineral species are present in areas that underwent much deeper burial. The emplacement of the huge volume of sediment ($> 30\,km^3$) of the Contessa megabed necessarily implies the contemporaneous mobilisation of sediment stored in different source areas, comprising a variety of contributing sediment source rocks. The fact that the provenance fingerprints of such source rocks have not been lost implies that only limited mixing occurred during transport.

The third chronostratigraphic interval (early-middle Serravallian) is still dominated by petrofacies A and B (Figs. 7 and 8C). Once again, considering the entire

stack of NE-verging thrust sheets in the study area, petrofacies A is most common in the southwestern thrust sheets, whereas petrofacies B is prevalent in the northeastern ones. Interfingering of petrofacies A and B can be proven within the same thrust sheet in some of the better exposed sections along the river valleys, for example, in the upper-middle reaches of the Senio, Lamone, and Rabbi valleys (Sections b, c, and f, Fig. 3). Compositional mixing seems instead very limited, thus pointing possibly to the existence of longitudinal structures (thrust tips and anticlines) which may have helped maintaining the compositional integrity of individual turbidity currents during flow, in agreement with Lucente (2004). Petrofacies C, characterised by high percentages of epidote-group minerals and hornblende, is present in the northeasternmost portions of the Lamone and Montone sections.

The composition of early-middle Serravallian turbidites with northwest-directed palaeocurrents is markedly different from that of their older counterparts. Reduced amounts of CI grains and high staurolite contents define a new, predominant petrofacies (F), whereas petrofacies D and E are no longer present. South-derived turbidites comprise also the distinctive, laterally extensive yet volumetrically insignificant, ''Colombine'' marker beds (Fig. 7), made almost entirely of intrabasinal micritic carbonate grains.

During the fourth interval (late Serravallian–early Tortonian) petrofacies A and B are still predominant (Fig. 8D) with significant interbedding between the Santerno and Senio sections and between the Lamone and Montone sections. The northeasternmost structural unit is dominated by petrofacies C, with an invasion of petrofacies B between the Santerno and Senio sections and between the Savio and Marecchia sections.

Middle-late Tortonian sedimentation (not shown in Fig. 8) was dominated by petrofacies C in a much narrower Apenninic foredeep while the detrital inputs of petrofacies A and B were no longer active. Similarly, there was no detrital input from the southern margin of the basin during this time interval.

5. SEDIMENT PROVENANCE AND DISPERSAL PATTERN

Petrofacies A (Apenninic I of Gandolfi et al., 1983) was possibly derived from the magmatic and metamorphic terranes of the Western Alps. The detritus entered the basin either directly from its northwestern terminus or from the Apenninic side with supplies of recycled detritus from the Alps or the European crust of the Corsica–Sardinia massif (Fig. 9). Petrofacies A has constant composition from the base to the top of the MAF and is coherently located along the southwestern (Apenninic) half of the basin. This petrofacies is volumetrically more important than postulated by Gandolfi et al. (1983).

The provenance of petrofacies B (Alpine I of Gandolfi et al., 1983) is ascribed to sediment supplies mainly from metamorphic Alpine terranes. Petrofacies B also has coherent detrital modes from the base to the top of the formation, and is present mainly in the northeastern half (Adriatic side) of the basin.

The provenance of petrofacies C (Alpine II of Gandolfi et al., 1983) might also be ascribed to chiefly metamorphic terranes in the central or eastern Alps entering into the basin either from its northwestern end or from its northeastern side. Petrofacies

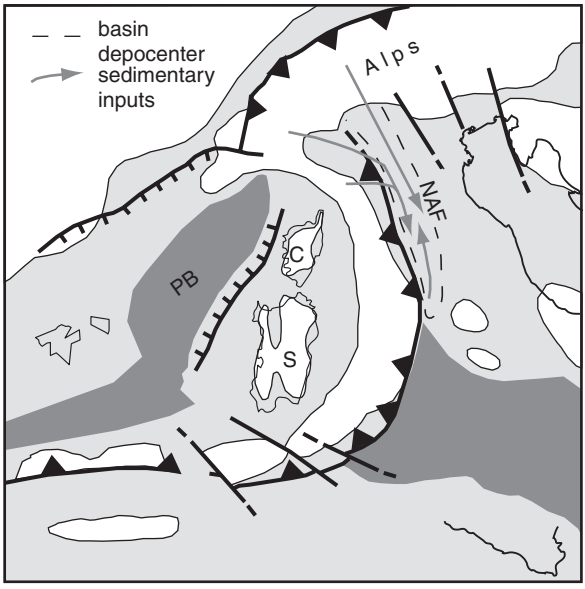

Fig. 9. Overall palaeogeographic–palaeotectonic setting of the Northern Apennines foredeep in Langhian time. Only active tectonic elements are shown. White, exposed land; light grey, epicontinental sea; darker grey, oceanic crust. C: Corsica; NAF: Northern Apennines foredeep; PB: Provençal Basin; and S: Sardinia. Modified from Cavazza and Wezel (2003).

C began later than A and B in the late-early Serravallian (Units 4 and 5) and became prominent in the Tortonian.

The inferred dispersal pattern was possibly promoted by basin topography. Modest anticlinal reliefs with longitudinal trends may have promoted the growth of sub-basins (De Donatis and Mazzoli, 1994) in which the flows of petrofacies A, B, and C were somehow confined. Transverse fault scarps with limited vertical throw may have allowed local flow diversion, causing their alternation or partial mixing.

Some of the main compositional characters of the subordinate northwest-directed detrital supplies (K-feldspar higher than plagiolase, granitic higher than metamorphic rock fragments, and the abundance of chrome spinel) raise critical questions about their sediment source areas. In the Apenninic domain the occurrence of granitic source rocks is unknown for the Miocene, although the existence of a granitic massif near the southeastern end of the basin and near the Ligurian tectonic units has been suggested by Chiocchini and Cipriani (1984). Alternatively, the arkosic detrital component can be the result of the recycling of feldspathic sandstones such as the Monghidoro (Late Cretaceous) and Loiano (Oligocene) Formations, present only in the Emilia and Tuscany regions. It is also difficult to explain the abundance of staurolite and especially chrome spinel. The latter derives characteristically from mafic and ultramafic rocks, which are lacking amongst the lithic grains of the sandstones having a southeastern provenance. However, the provenance of these minor supplies could be ascribed to (i) Apenninic source areas with parent rocks of unknown nature or (ii) sedimentary recycling.

Northwest-directed detrital inputs, albeit volumetrically subordinate, generated most of the thicker marker beds cropping out in the study area. This implies that the events triggering large turbidity flows (large magnitude earthquakes inducing shelf-edge and slope failures?) along the southern margin of the basin were more rare yet capable of mobilising large masses of sediment.

6. DISCUSSION ON INTRASTRATAL DISSOLUTION

Since Goldich (1938) various attempts have been made to quantify mineral stability in different sedimentary environments as a function of element mobility, the energy of the chemical bonds, and other factors (e.g., Reiche, 1950; Keller, 1954; see also Morton and Hallsworth, 2007, this volume; Velbel, 2007, this volume). Attempts to study experimentally mineral equilibria under conditions approximately reproducing those of natural systems—as it had been done for the magmatic and metamorphic processes—did not yield significant results. These attempts were then abandoned. Since Pettijohn (1941) mineral stability orders are mostly based on hypothetical orders of appearance in progressively younger sedimentary units where intrastratal dissolution had progressively less time to act.

Corroded heavy-mineral grains have been used as an important argument in favour of intrastratal dissolution (see also Van Loon and Mange, 2007, this volume). Such corroded grains were interpreted as indicators of significant heavy-mineral intrastratal dissolution also in the MAF by Gandolfi and Gazzi (1963) and Cavazza and Gandolfi (1992). Based on the data reported in the present contribution—probably the largest heavy-mineral dataset on a single rock unit—we cannot apply any longer the hypothesis that a significant heavy-mineral loss occurred due to intrastratal dissolution within the MAF. There are two main reasons:

(1) turbidite beds characterised by similar framework composition, porosity, and permeability but with "stable" and "unstable" heavy-mineral assemblages are commonly interbedded (e.g., Fig. 10) and
(2) the absence of dissolution features on unstable framework minerals (like sanidine and plagioclases of basic intermediate compositions) in beds containing also a "mature" heavy-mineral suite.

How to explain then the dissolution features sometimes found in heavy-mineral concentrates during this and other studies? Clearly, intrastratal dissolution is a viable and significant diagenetic process which affects the heavy-mineral assemblages in adequately documented case studies. However, in the specific case of the MAF dissolution features of either heavy or light minerals are rare in thin sections, in spite of the fact that several hundred samples were examined microscopically, whereas they are present in the separates (see, for instance, Fig. 7 in Cavazza and Gandolfi, 1992). Relatively few examples of heavy-mineral dissolution features in thin section have been imaged in the literature (e.g., Fig. 2 in Walker et al., 1978). Grains with delicate hacksaw terminations have been found mostly in heavy-mineral granular separates produced after mechanical disaggregation. It is our opinion that in several published examples the role of intrastratal dissolution may have been somehow overemphasised and that at least some of the features ascribed to intrastratal dissolution may be instead the result of artificial fracturing along mineral cleavage

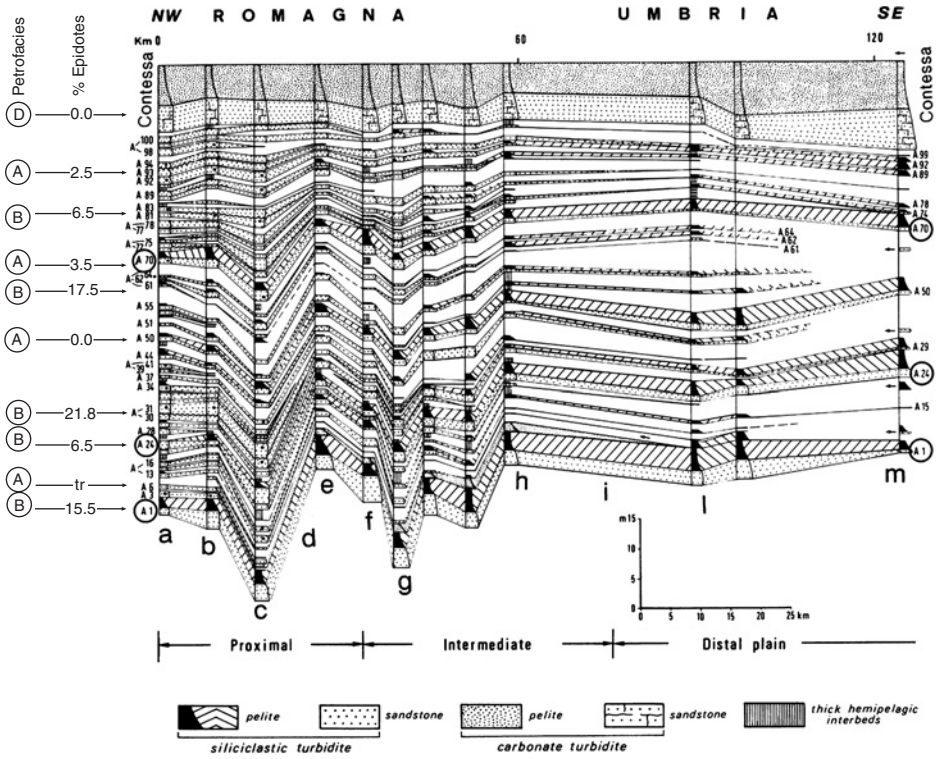

Fig. 10. Fence diagram showing intimately interbedded sandstone petrofacies of the Marnoso-arenacea Formation along a NW–SE transect in the Northern Apenninic foredeep (modified from Ricci Lucchi and Valmori, 1980). Stratigraphic columns show individual thick-bedded turbidites. Blank intervals represent thin-bedded, pelite-dominated portions with alternating fine-grained turbiditic and hemipelagic deposits. Letters a–m indicate the sample traverses shown in Fig. 3.

planes during sample preparation. In fact, if such delicate features were already present in the sample, they would hardly survive mechanical disaggregation without breaking.

7. CONCLUSIONS

The main results of this study can be summarised as follows. Turbidite beds within the Periadriatic basin are commonly the product of distinct yet contemporaneous detrital inputs derived from discrete sediment source areas; these inputs were deflected along the main axis of the basin and flowed side by side with only minor intermixing of their distinctive sedimentary components. This is particularly evident in the numerous prominent marker beds traceable in the basin over long distances, as the compositions of single marker beds vary coherently in the different portions of the basin.

Detrital modes of the opposing longitudinal supplies within the Apenninic foredeep during deposition of the MAF are different. The volumetrically predominant

turbidite layers with southeastward palaeocurrents are characterised by (i) minor content of carbonate rock fragments, among which intraclasts are absent, (ii) dolomite as abundant as 20% of total carbonate component, (iii) plagioclase more common than K-feldspar, and (iv) predominance of metamorphic versus plutonic rock fragments. Heavy-mineral assemblages define three petrofacies: A is characterised by ZTR, garnet ± staurolite, and abundant plutonic rock fragments; B features ZTR, garnet, epidote-group minerals, sphene, staurolite, kyanite, glaucophane, and abundant metamorphic rock fragments; C contains ZTR, garnet, very abundant epidote-group minerals, hornblende, sphene, staurolite, kyanite, glaucophane, and abundant metamorphic rock fragments.

The quantitatively subordinate turbidite layers with northwestward palaeocurrent directions are characterised by (i) abundant carbonate rock fragments, among which intraclasts are dominant, (ii) absence of dolomite, (iii) K-feldspar more abundant than plagioclase, and (iv) predominance of plutonic versus metamorphic rock fragments. Their heavy-mineral assemblages include abundant staurolite, chrome spinel, zircon, monazite, and xenotime, and lack epidote-group minerals. Within this group three petrofacies (D, E, and F), characterised by different amounts of sedimentary rock fragments (mostly siliciclastic siltstone and sandstone) and staurolite, can be discriminated. The relative abundance of siltstone and sandstone grains can be ascribed to increasing importance of intra-Apenninic sources (cannibalisation of the growing Apennines) related to lateral fans often linked to transverse faults (Ricci Lucchi, 1978).

The effects of burial diagenesis on the basin fill were minor and limited to the most labile constituents (i.e., carbonate grains and clay minerals). Had only a limited data set been available, the areal distribution of the petrographic compositions of sandstone layers shown above might have been considered erroneously the effect of burial diagenesis. Dense sampling is therefore imperative when studying the provenance/diagenesis of multi-sourced successions in sedimentary basins.

ACKNOWLEDGEMENTS

The authors would like to thank I. Cibin, W.R. Dickinson, A.C. Morton, and G.G. Zuffa for their comments on an earlier version of this manuscript. Some aspects of this paper were discussed with A. Landuzzi and M. Zattin. The submitted manuscript was reviewed by E. McBride and S. Critelli. This research was funded by the Italian Ministry of the University and Research (MIUR).

REFERENCES

Argnani, A., Ricci Lucchi, F., Vai, G.B., Martini, I.P. (Eds.), 2001. Anatomy of an Orogen—The Apennines and Adjacent Mediterranean Basins. Kluwer Academic Publishers, Dordrecht, Netherlands, pp. 327–350.

Barchi, M., Landuzzi, A., Minelli, G., Pialli, G., Vai, G.B., Martini, I.P. (Eds.), 2001. Anatomy of an Orogen—The Apennines and Adjacent Mediterranean Basins. Kluwer Academic Publishers, Dordrecht, Netherlands, pp. 215–254.

Bonini, M., Morelli, M.A., Sani, F., 1991. Rilevamento strutturale della catena appenninica nel settore Firenzuola-Bocca Trabaria. Memorie Descrittive della Carta Geologica d'Italia 46, 227–337.

Capozzi, R., Landuzzi, A., Negri, A., Vai, G.B., 1991. Stili deformativi ed evoluzione tettonica della successione neogenica romagnola. Studi Geologici Camerti special volume 1991/1, 261–278.

Cavazza, W., Gandolfi, G., 1992. Diagenetic processes along a basin-wide marker bed as a function of burial depth. Journal of Sedimentary Petrology 62, 261–272.

Cavazza, W., Wezel, F.C., 2003. The Mediterranean region—a geological primer. Episodes 26, 160–168.

Chiocchini, U., Cipriani, N., 1984. Petrografia delle arenarie torbiditiche del bacino di Monte Vicino (Marche settentrionali). Bollettino della Società Geologica Italiana 103, 579–589.

Chiocchini, U., Chiocchini, M., Cipriani, N., Torricini, F., 1986. Petrografia delle unità torbiditiche della Marnoso-arenacea nella Alta Valle tiberina. Memorie della Società Geologica Italiana 35, 57–73.

Cibin, U., Cavazza, W., Fontana, D., Milliken, K.L., McBride, E.F., 1993. Comparison of composition and texture of calcite-cemented concretions and host sandstones, Northern Apennines, Italy. Journal of Sedimentary Petrology 63, 945–954.

Cipriani, C., Malesani, P.G., 1963a. Ricerche sulle arenarie: VII La composizione mineralogica di una serie di rocce della formazione Marnoso-arenacea. Periodico di Mineralogia 32, 302–342.

Cipriani, C., Malesani, P.G., 1963b. Ricerche sulle arenarie: VIII Determinazioni microscopiche sulle arenarie delle formazioni del Macigno e Marnoso-arenacea. Periodico di Mineralogia 32, 343–385.

Cipriani, C., Malesani, P.G., 1963c. Ricerche sulle arenarie: IX Caratterizzazione e distribuzione geografica delle arenarie appenniniche oligoceniche e mioceniche. Memorie della Società Geologica Italiana 4, 339–375.

De Donatis, M., Mazzoli, S., 1994. Kinematic evolution of thrust-related structures in the Umbro-Romagnan parautochthon (Northern Apennines, Italy). Terra Nova 6, 563–574.

Delle Rose, M., Guerrera, F., Moretti, E., Rusciadelli, G., Corona, F., 1991. The Marnoso-arenacea Fm between Bocca Trabaria and Campigna (Northern Apennines): lithostratigraphy from the Schlier to the Verghereto Marls Fms in a new structural context. Giornale di Geologia 53, 131–142.

Deiana, G., Pialli, G., 1994. The structural provinces of the Umbro-Marchean Apennines. Memorie della Società Geologica Italiana 48, 473–484.

Dickinson, W.R., 1970. Interpreting detrital modes of graywacke and arkose. Journal of Sedimentary Petrology 40, 695–707.

Fontana, D., McBride, E.F., Kugler, R., 1986. Diagenesis and porosity evolution of submarine-fan and basin-plain sandstones, Marnoso-arenacea Formation, Northern Apennines, Italy. Bulletin of Canadian Petroleum Geology 34, 313–328.

Gandolfi, G., Gazzi, P., 1962. Sull'uniformità e sul significato della distribuzione dei minerali pesanti nel "Macigno". Acta Geologica Alpina 8, 433–442.

Gandolfi, G., Gazzi, P., 1963. Sulla distribuzione verticale dei minerali pesanti nella Formazione Marnoso-arenacea romagnola lungo la valle del Bidente. Mineralogica et Petrografica Acta 9, 273–288.

Gandolfi, G., Paganelli, L., 1992. Il Macigno costiero fra La Spezia e Grosseto. Giornale di Geologia 54 (1), 163–179.

Gandolfi, G., Paganelli, L., 1993. Le torbiditi arenacee oligo-mioceniche dell'Appennino settentrionale fra La Spezia ed Arezzo. Studio petrografico ed implicazioni paleogeografiche. Giornale di Geologia 55, 93–102.

Gandolfi, G., Paganelli, L., Zuffa, G.G., 1983. Petrology and dispersal pattern in the Marnoso-arenacea Formation (Miocene, Northern Apennines). Journal of Sedimentary Petrology 53, 493–507.

Gazzi, P., 1961. Ricerca sulle distribuzione dei minerali pesanti nei sedimenti arenacei dell'Appennino tosco-romagnolo. Acta Geologica Alpina 8, 379–422.

Gazzi, P., 1965. On the heavy mineral zone in the geosyncline series. Recent studies in the Northern Apennines, Northern Italy. Journal of Sedimentary Petrology 35, 109–115.

Gazzi, P., 1966. Le arenarie del flysch sopracretaceo dell'Appennino modenese; correlazioni con il flysch di Monghidoro. Mineralogica et Petrographica Acta 12, 69–97.

Gazzi, P., Zuffa, G.G., Gandolfi, G., Paganelli, L., 1973. Provenienza e dispersione litoranea delle sabbie delle spiagge adriatiche fra le foci dell'Isonzo e del Foglia: inquadramento regionale. Memorie della Società Geologica Italiana 12, 1–37.

Goldich, S.S., 1938. A study in rock weathering. Journal of Geology 46, 17–58.

Ingersoll, R.V., Bullard, T.F., Ford, R.L., Grimm, J.B., Pickle, J.D., Sares, S.W., 1984. The effect of grain size on detrital modes: a test of the Gazzi–Dickinson point-counting method. Journal of Sedimentary Petrology 54, 103–116 (Also, see discussions and replies: vol. 55, pp. 616–621.).

Keller, W.D., 1954. The binding energy of some silicate minerals. American Mineralogist 39, 783–793.

Lucente, C.C., 2004. Topography and palaeogeographic evolution of a middle Miocene foredeep basin plain, Northern Apennines, Italy. Sedimentary Geology 170, 107–134.

McBride, E.F., Milliken, K.L., Cavazza, W., Cibin, U., Fontana, D., Picard, M.D., Zuffa, G.G., 1995. Heterogeneous distribution of calcite cement at the outcrop scale in Tertiary sandstones, Northern Apennines, Italy. American Association of Petroleum Geologists Bulletin 79, 1044–1063.

Milliken, K.L., McBride, E.F., Cavazza, W., Cibin, U., Fontana, D., Zuffa, G.G., 1998. Geochemical history of calcite precipitation in Tertiary sandstones, Northern Apennines, Italy. In: Morad, S. (Ed.), Carbonate Cementation in Sandstones. International Association of Sedimentologists Special Publication no. 26, pp. 213–239.

Morton, C.A., Hallsworth, R.C., 1999. Processes controlling the composition of heavy mineral assemblage in sandstones. Sedimentary Geology 124, 3–29.

Morton, C. A., Hallsworth, R. C., 2007. Stability of detrital heavy minerals during burial diagenesis. In: Mange, M. A., Wright, D. T. (Eds.), Heavy Minerals in Use. Developments in Sedimentology (this volume).

Pettijohn, F.J., 1941. Persistence of heavy minerals and geologic age. Journal of Geology 49, 610–625.

Reiche, P., 1950. A survey of weathering processes and products. University of New Mexico Publications in Geology, New Mexico, vol. 3, pp. 1–95.

Ricci Lucchi, F., 1975. Miocene paleogeography and basin analysis in the Periadriatic Apennines. In: Squyres, C. (Ed.), Guidebook to the Geology of Italy. Geological Society of Libya, Tripoli, Libya, pp. 129–236.

Ricci Lucchi, F., 1978. Turbidite dispersal in a Miocene deep-see plain. Geologie en Mijnbouw 57, 559–576.

Ricci Lucchi, F., Valmori, E., 1980. Basin-wide turbidites in a Miocene, over-supplied deep-sea plain: a geometrical analysis. Sedimentology 27, 241–270.

Van Loon, A.J., Mange, M.A., 2007. 'In situ' dissolution of heavy minerals through extreme weathering, and the application of the surviving assemblages and their dissolution characteristics to correlation of Dutch and German silver sands. In: Mange, M.A., Wright, D.T. (Eds.), Heavy Minerals in Use. Developments in Sedimentology (this volume).

Velbel, M.A., 2007. Surface textures and dissolution processes of heavy minerals in the sedimentary cycle: examples from pyroxenes and amphiboles. In: Mange, M.A., Wright, D.T. (Eds.), Heavy Minerals in Use. Developments in Sedimentology (this volume).

Walker, T.R., Waugh, B., Grone, A.J., 1978. Diagenesis in first-cycle desert alluvium of Cenozoic age, southwestern United States and northwestern Mexico. Geological Society of America Bulletin 89, 19–32.

Zattin, M., Landuzzi, A., Picotti, V., Zuffa, G.G., 2000. Discriminating between tectonic and sedimentary burial in a foredeep succession, Northern Apennines. Journal of the Geological Society, London 157, 629–633.

Zattin, M., Picotti, V., Zuffa, G.G., 2002. Fission-track reconstruction of the front of the Northern Apennine thrust wedge and overlying Ligurian unit. American Journal of Science 302, 346–379.

Zuffa, G.G., 1980. Hybrid arenites: their composition and classification. Journal of Sedimentary Petrology 50, 21–29.

Zuffa, G.G., 1985. Provenance of Arenites. NATO ASI vol. C-148. Reidel Publishing Company, Dordrecht, Netherlands, pp. 1–408.

This page intentionally left blank

Chapter 26

DISTRIBUTION PATTERN AND PROVENANCE IMPLICATIONS OF THE HEAVY MINERALS IN NEOPROTEROZOIC TO MESOZOIC SILICICLASTIC SUCCESSIONS IN THE ARABO-NUBIAN SHIELD AND ITS NORTHERN PERIPHERY: A REVIEW

TUVIA WEISSBROD AND RON BOGOCH

Geological Survey of Israel, 30 Malkhe Yisrael Street, Jerusalem 95501, Israel

ABSTRACT

Following the consolidation and erosion of the Arabo-Nubian Shield (ANS) in the Neoproterozoic, extensive siliciclastics were deposited above it and along its northern margins. These sediments consist of two thick successions, which are separated by an erosional surface representing a regional peneplain. They comprise Neoproterozoic-Early Cambrian orogenic, molasse-type, immature conglomerates and arkoses, and a Palaeozoic to Early Mesozoic succession of platformal, mature sandstones. The heavy mineral contents generally parallel those of the major framework components, e.g., a prevalence of unstable species in the lower, and dominantly ultrastable minerals in the upper succession. This maturation is controlled by provenance and chemical weathering at the source, during transportation or both. Environmental and climate changes are indicated by the presence or absence of detrital apatite, which disappears in the Late Palaeozoic and onward, reacting to acidic weathering in a warm climate, and in the abundance of garnet in the Middle Ordovician to Early Silurian successions due to colder climatic conditions with limited weathering. Authigenic apatite is present locally and is formed at a later phase, as a result of fluid migration during the early stages of the Tertiary Dead Sea Rift.

The following three provenance-controlled heavy mineral suites may be distinguished. (1) An unstable heavy mineral assemblage of the Neoproterozoic immature, siliciclastic deposits, derived mostly from a Pan-African igneous/metamorphic terrain within the ANS. This records only mechanical abrasion and a short-distance of transport. (2) An ultrastable/stable heavy mineral assemblage of the Early Palaeozoic, mature, siliciclastic successions, derived mostly from Pan-African and older crust outside the ANS (interior of Gondwana), but with intermittent input from locally exposed basement rocks of the ANS. This assemblage underwent mainly chemical weathering over a long transport distance. (3) An ultrastable heavy mineral assemblage

Developments in Sedimentology, Vol. 58, 647–676

ISSN: 0070-4571/doi:10.1016/S0070-4571(07)58026-X

of the Late Palaeozoic-Early Mesozoic mature, siliciclastic sediments, sourced mostly from reworked older internal siliciclastics, and from beyond the ANS, but which also incorporate detritus from extensive exposures of the ANS basement. They were affected by chemical weathering and experienced long to moderate transport.

Keywords: heavy minerals; Arabo-Nubian Shield; Pan-African; Neoproterozoic; Palaeozoic; Early Cretaceous; provenance; authigenesis

1. INTRODUCTION

Neoproterozoic and Phanerozoic siliciclastic successions are widely exposed in northeastern Africa and the Arabian platform along the northern and eastern margins of the Arabo-Nubian Shield (ANS), and form one of the largest siliciclastic sediment bodies preserved on earth (Figs. 1 and 2). Because of the apparent monotony and uniformity of rock fabrics, the lack of laterally continuous lithological markers and the paucity of biostratigraphic data, early studies considered these clastics as a single unit termed 'Nubian Sandstone' and treated them as a regional magnafacies (lithosome) (Rüssegger, 1847; Picard, 1938; Pomeyrol, 1968). The search for reliable criteria to allow stratigraphic discrimination and correlation led investigators to conduct heavy mineral studies on the various successions and to reconstruct sediment provenance, parent rock composition, weathering and diagenetic processes (e.g., Shukri and Said, 1945; Bender, 1968; Weissbrod and Nachmias, 1986; Amireh, 1991, 1994). Most of these studies indicated that the heavy minerals are not sufficiently diagnostic to be used as a tool for stratigraphic differentiation since the heavy mineral spectra throughout the Palaeozoic to Mesozoic section are generally similar and only certain system-wide mineral variations can be delineated.

Since the Palaeozoic rocks became a primary target for oil exploration in the 1980s, extensive sedimentological and biostratigraphical studies on these deposits have revealed differences in rock parameters, such as grain size, texture, composition and sorting, a wide range of environments and biostratigraphical diversity. Early Palaeozoic graptolites, trilobites, chitinozoa and acritarch assemblages were identified along with Late Palaeozoic fossil plants and palynomorphs. These parameters were applied in establishing local stratigraphies, and to weld them into a solid stratigraphic scheme of regional validity (Fig. 3).

Although heavy minerals proved to be of limited use for stratigraphic applications, their role as provenance indicators is of greater significance, the more so since new methods of age determinations of relevant minerals (zircon, apatite) have been utilised. Sedimentological data have long suggested that the source area was located south of the depositional arena, but the question as to whether this was within the ANS or beyond it is still being discussed. The present contribution reviews the heavy mineral distribution and current understanding of the provenance of the 'Nubian Sandstone'.

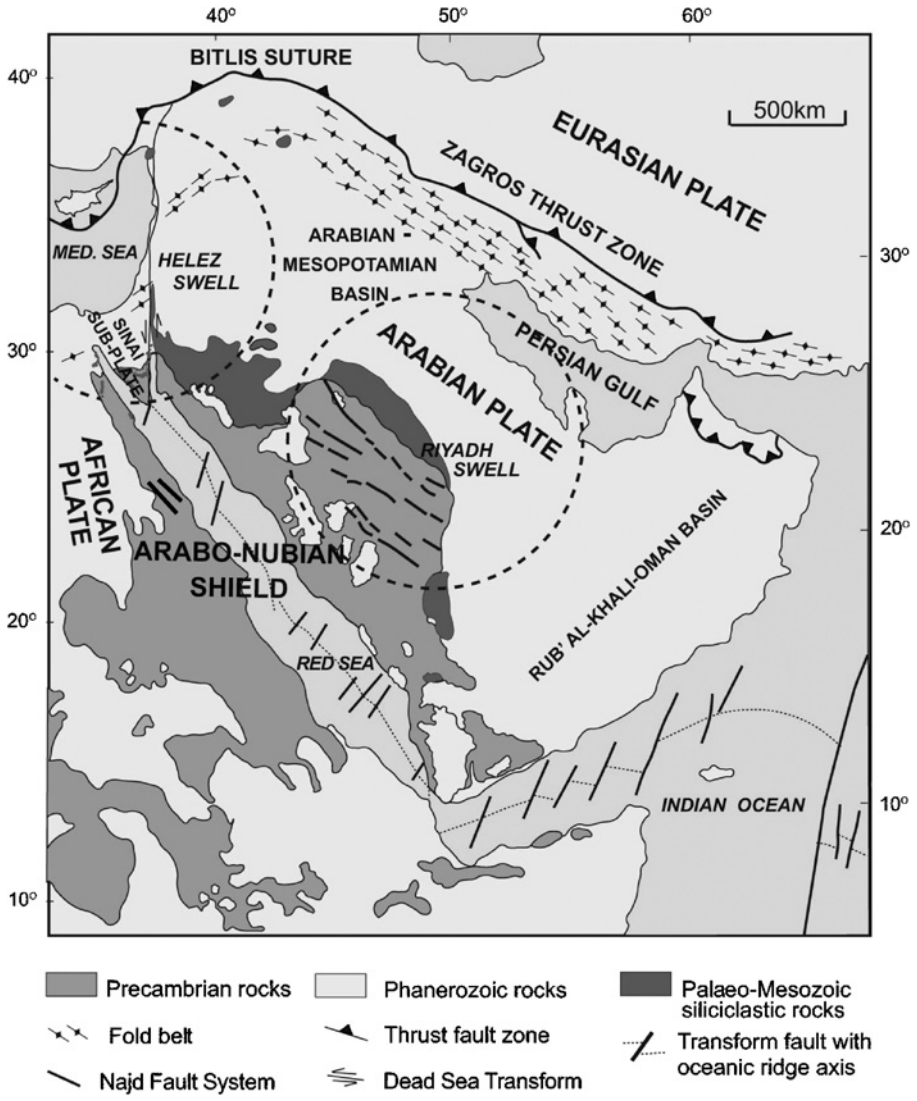

Fig. 1. Arabian and adjacent plates showing the Arabo-Nubian Shield, with outlines of the main tectonic features, exposures of Palaeozoic to Early Mesozoic siliciclastic successions, and the Late Palaeozoic swells. [Modified after Weissbrod and Sneh (2002) with permission from Geological Survey of Israel Bulletin.]

2. GEOLOGICAL OUTLINE

The ANS forms part of the northern margin of Gondwana and was formed by the collision and accretion of continental terrains and island arc complexes during the Neoproterozoic Pan-African event (~900–540 Ma; Stern, 1994). It consists mainly of juvenile Neoproterozoic crustal material added during this event, and remobilised,

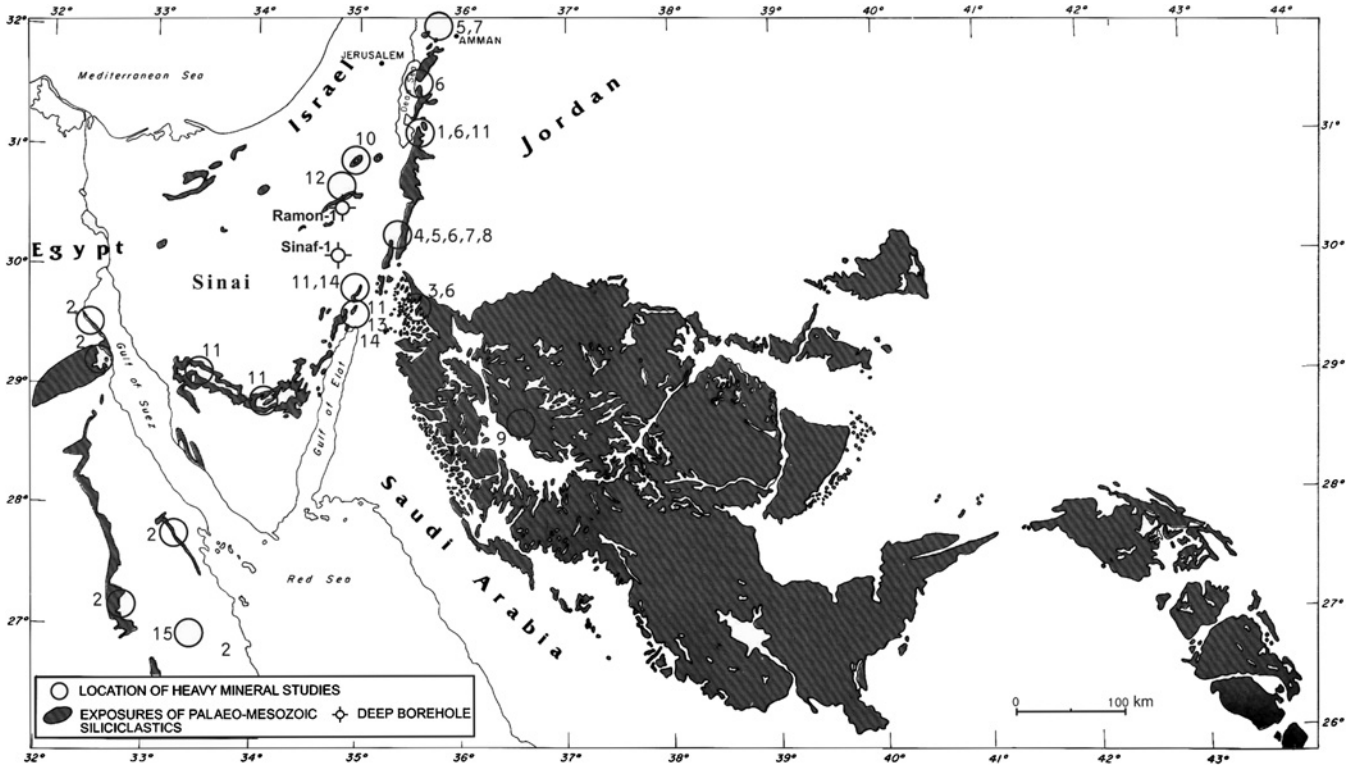

Fig. 2. Distribution of Palaeozoic to Early Mesozoic siliciclastic successions in the northern margin of the Arabo-Nubian Shield, showing location of studied sections for heavy minerals (plus two deep boreholes which penetrated the Neoproterozoic clastics). 1 = Vroman (1944); 2 = Shukri and Said (1945); 3 = Bender (1968); 4 = Lillich (1969); 5 = Nasir and Sadeddin (1989); 6 = Amireh (1991); 7 = Amireh (1992); 8 = Amireh (1994); 9 = Powers et al. (1966); 10 = Greenberg (1968); 11 = Weissbrod and Nachmias (1986); 12 = Becker and Becker (1997); 13 = Kohn and Weissbrod (1993); 14 = Avigad et al. (2003); 15 = Wilde and Yousssef (2002). The location of sections studied by Shukri and El Ayouti (1953), El-Hinnawi et al. (1973) and Bisewski (1982) in the central and southern Eastern Desert and the Dakhla basin are beyond the present map.

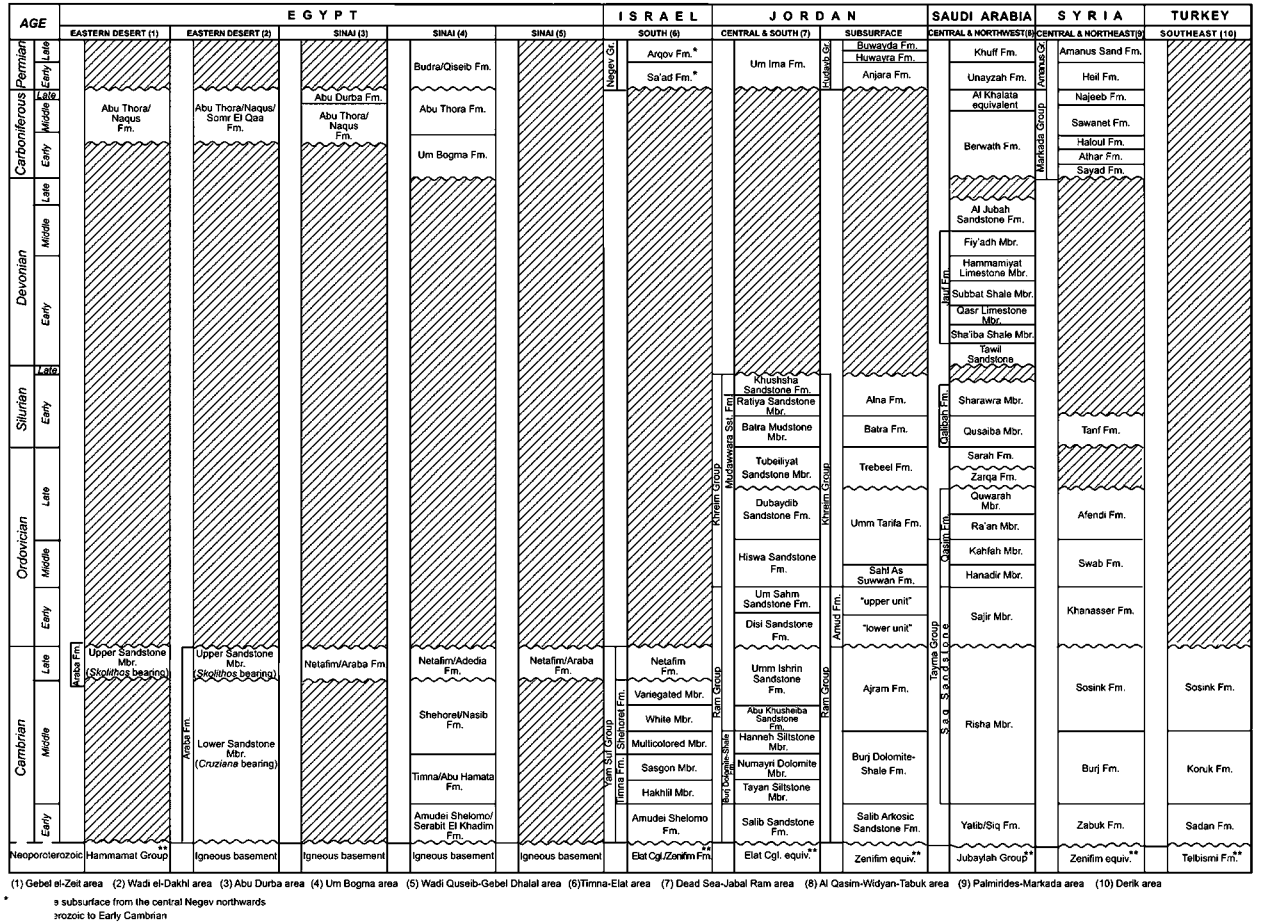

Fig. 3. Correlation chart of current nomenclature of Palaeozoic successions in Israel and adjacent areas (not to scale). The juxtaposition of sections is based on correlation and age (far left column) as proposed by Weissbrod (2005). Hatched areas represent stratigraphic gaps.

older uplifted and subsequently deeply denuded continental crust. Pan-African exposures in the ANS consist predominantly of metamorphic and plutonic (mostly granitoid) rocks, which suggest erosion of the orogen to shallow levels. The erosional depth is constrained by the metamorphic grade of the rocks which in the ANS were formed mostly under upper greenschist to lower amphibolite facies conditions, whereas in the older continental crust, amphibolite to even granulite facies conditions are recorded (Garfunkel, 1999). The rock pile was stripped off the ANS during almost 100 million years, across the Neoproterozoic-Phanerozoic boundary (620–525 Ma), mostly during and following the emplacement of widespread calc-alkaline granitic plutons at 620–580 Ma (Bentor, 1985). The exhumation is estimated to reach approximately down to 8–12 km depth in the lower grade terrains, and up to twice as much in the high-grade terrains. The relief was thus lowered and denudation reached a level close to that at present, as attested by the overlying Neoproterozoic conglomerates in which clast composition mirrors rock types now exposed in the region. In the later stages of the Pan-African event, erosion removed not much more than 1–2 km of rock (Garfunkel, 1999).

Most of the unroofed material is incorporated in the immature Neoproterozoic sediments, which display two broad lithofacies: conglomerates of exclusively igneous and metamorphic components, and arkosic sands. The conglomerates are primarily clast-supported and poorly sorted with round to sub-angular pebbles and boulders with interbedded sandstone layers. They were derived from nearby mountainous areas which underwent mainly mechanical weathering, short-distance transport, with deposition and rapid burial in intramontane basins and extensional fault-bounded depressions within the igneous terrain. They formed fault-scarp deposits and coalescing alluvial fan systems, attaining a thickness of up to several thousands of metres (Delfour, 1970; Grothaus et al., 1979; Hadley and Schmidt, 1980). Sedimentation was contemporaneous with alkaline granite intrusions, while extrusive rhyolitic flows and pyroclastics contributed to the thickness of the fill. The conglomeratic facies is believed to have been extensively distributed in the ANS, but most of it was removed during the last stages of the Pan-African event. Remnants are exposed today mainly in central and northern Saudi Arabia and the Eastern Desert of Egypt.

The sands and finer detritus (with occasional pebbles) of the arkosic facies were transported into a broad marginal basin (the Arabian-Mesopotamian basin) at the northern passive margin (Weissbrod and Sneh, 2002). The basin extended over the Arabian Peninsula and across the Levant and Mesopotamia to the Proto-Tethys in the north and northeast where it was terminated by the Taurus (Bitlis) and Zagros thrust belts (sutures) in Turkey and Iran (Weissbrod and Sneh, 2002) (Fig. 1). The sedimentology of this facies indicates a transgressive succession of alluvial fans and alluvial plains dominated by sand flats of braided streams in the southern part, merging northwards to more distal tracts of marginal tidal flats and shallow marine environments. These sediments and associated intrusive and extrusive rocks have been encountered in deep boreholes in Israel, Jordan and Sinai, and are exposed at several localities in southeastern Turkey (Ketin, 1966; Dean et al., 1997).

During the latest Neoproterozoic, the relief of the ANS was planed down to an elevation close to sea level, as shown by a marine episode that invaded the area from the east and north and deposited cherty and dolomitic limestone in fault-controlled depressions in Saudi Arabia and the gulf states (Delfour, 1970), and by the tidal flat

characteristics of the upper part of the arkosic succession in the pericratonic basin (Weissbrod and Sneh, 2002). Soon after marine retreat, further erosion affected the continental landscape, which developed into a vast peneplain. Positioned in low latitudes under tropical to sub-tropical conditions, its shaping was enhanced by chemical weathering. This peneplain marks a prominent change in the tectonic and sedimentary evolution of the ANS from an orogenic belt to a stable platform, as reflected by the gradual termination of the extensional tectonics and magmatic activity and by the changes in the grain size, composition and texture of the sediments and mode of transportation.

In the late Early Cambrian, extensive deposition resumed with a shift of provenance, probably in response to tectonic uplift in the interior of Gondwana. Subsequently, large amounts of detritus were deposited over the ANS and its margins in a system of alluvial fans grading to braided plains and deltas, and these basal and succeeding sediments covered most of the peneplain. Overlying the basement are Palaeozoic and Mesozoic siliciclastic successions that are widely distributed in North Africa and Arabia with extensive exposures now found fringing the ANS basement (Figs. 1 and 2). They consist mainly of platform-type mature, medium- to fine-grained and moderately to well-sorted subarkose and quartz-arenite, becoming more mature, finer-grained and better-sorted basinward and through time. Only a limited re-exposure of the basement took place in the Late Cambrian, and more extensively from the Late Devonian onward (Weissbrod and Gvirtzman, 1988; Al-Laboun, 1990; Weissbrod, 2003).

The Early Palaeozoic siliciclastic succession consists mostly of laterally homogeneous rock units with gradual thickness changes along the depositional slope, varying vertically from fluvio-deltaic to mid-shelf marine environments of recurrent transgressions and regressions (Bender, 1968; Al-Laboun, 1986; Powell, 1989; Konert et al., 2001; Garfunkel, 2002). Only occasionally was the uniform and continuous deposition interrupted. In the Late Ordovician, glaciation affected Arabia leading to the development of valleys, locally cutting down to the Cambrian succession, with glacial and periglacial sediments (Vaslet, 1990; Powell et al., 1994). Following the melting of the ice in the Early Silurian, a marine transgression occurred over the entire platform with deposition of organic-rich shale, whereas a global sea level drop in the Late Silurian resulted in a major hiatus (Al-Laboun, 1986; Lüning et al., 2000). In addition, limestone successions were deposited during the Middle Cambrian and Early to Middle Devonian. Throughout the Palaeozoic, the ANS and its periphery formed a slowly subsiding stable shelf accumulating a thick section (up to 5000 m) of mostly clastic sediments but substantial parts of these were later truncated. However, occasional epeirogenic movements formed dome-like swells (geanticlines), hundreds of kilometres in diameter that were truncated as they rose, while sedimentation continued almost uninterruptedly in the intervening basins. The most prominent of these movements involved two pulses of uplift/erosion and affected the Arabian and NE African terrains during the Late Palaeozoic forming the Helez and Riyadh swells (Gvirtzman and Weissbrod, 1984; Weissbrod and Gvirtzman, 1988) (Fig. 1).

Reconstruction of the Early Carboniferous eroded surface of the Helez swell (Fig. 4) shows successive concentric belts of increasing erosion from the flanks of the structure, which towards its culmination reached down to the Precambrian, with all Devonian, Silurian and Ordovician sediments removed from the regions of Israel,

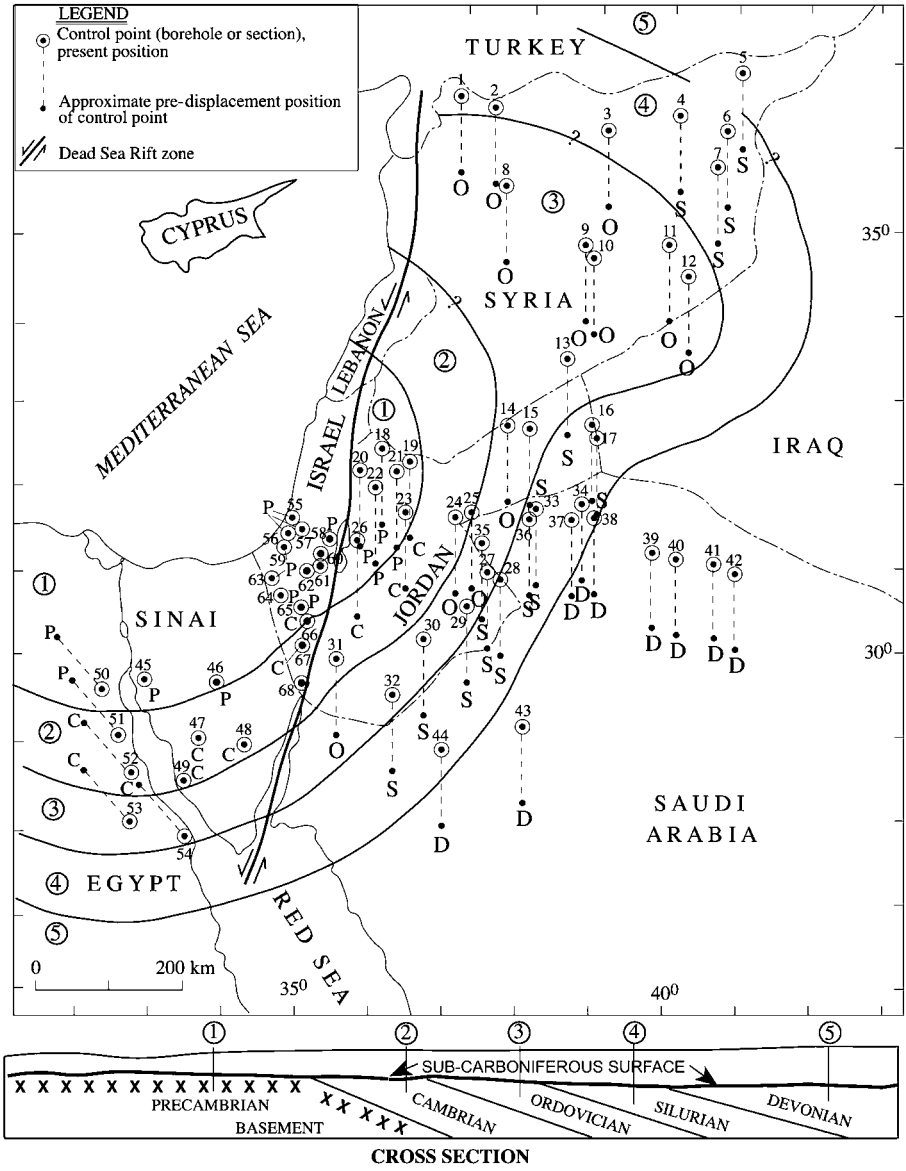

Fig. 4. Model of the truncated Helez Swell (geanticline) showing the sub-Carboniferous erosion surface and concentric subcrop belts of the Early Palaeozoic systems. The pre-Carboniferous eroded surface was mostly superseded by later, Early Permian erosion with relicts mostly in Syria, NW Saudi Arabia (Widyan basin) and the Egypt (Gulf of Suez area). It is mostly a virtual surface, as reconstructed for the areas of Israel, Jordan and northern Sinai. System units found below the erosion surface: P = Precambrian (belt no. 1); C = Cambrian (belt no. 2); O = Ordovician (belt no. 3); S = Silurian (belt no. 4); D = Devonian (belt no. 5). The data points (circled dots) east of the Dead Sea Rift were shifted 105 km northward (dashed lines) from their original Palaeozoic position by the late Tertiary left-lateral movement of this block, whereas data points west of the Gulf of Suez were shifted some 80 km to NNW or NW (dashed lines) to compensate for the post-Late Palaeozoic displacement of this block (Freund et al., 1970; Rybakov et al., 1996; Weissbrod, 2004). Schematic cross-section shows the (reconstructed) sub-Carboniferous erosion surface, still existing in southwestern Sinai and the Eastern Desert, most of Syria and apparently in northwestern Saudi Arabia (Widyan Basin).

Sinai, the Eastern Desert of Egypt and from parts of Jordan and Syria (Fig. 4). Similarly, Early Palaeozoic sediments were differentially removed from the Riyadh swell in the Arabian Peninsula. Overall, a sedimentary section of up to 2500–3000 m in thickness was removed from these areas in the first pulse, as demonstrated by the wide stratigraphic gaps in the local sections (Fig. 3).

Following erosion and subsequent subsidence, these terrains were again covered by a new cycle of sediments. The present distribution of Carboniferous sediments in several depocentres located in Syria, Egypt and NW Saudi Arabia, may imply an infill of a palaeorelief, though deposition could have occurred over the entire region; it may have been selectively removed during the Late Carboniferous-Early Permian transition in the second pulse of uplift-and-erosion (Weissbrod and Gvirtzman, 1988). The remaining Carboniferous succession is up to 700 m thick in Egypt (Abdallah and Adindani, 1965; Keeley, 1989) and consists mostly of continental to marginal marine sandstones, with local limestone intercalations; it is up to 2000 m thick in Syria where it occurs as marine shales (Al Youssef and Ayed, 1992). Late Carboniferous-Early Permian glaciation was reported in SE Arabia (McClure et al., 1988) and in the SW Desert of Egypt (Klitzsch and Wycisk, 1987; Klitzsch, 1990).

At the outset of the Permian, the uplifted swells in the region were eroded but the ANS remained relatively elevated. This was followed by deposition of sandstones and shales in fluvial to marginal tracts covering the sub-Carboniferous surface and locally filling relief. In the Late Permian, the sea level rose (melting of the Early Permian continental glaciers) and transgressed over the Arabian terrain partly covering the ANS core, with deposition of transgressive–regressive sequences dominated by limestone with inland mixed sand/shale wedges. The onlapping relations are expressed in exposures fringing the shield, by thinning and an increase of clastic components landward (Powers et al., 1966).

In the northern margin of the ANS, similar cyclic sedimentation continued through the Triassic and Jurassic, with sandy units alternating with limestone, shale and locally gypsum (Goldberg, 1970; Druckman, 1976). The continuity of the sedimentation was interrupted at system boundaries by exposure, erosion and associated events, e.g., mass extinction at the Permian-Triassic (Eshet et al., 1995) and lateritization at the Triassic-Jurassic transition (Goldbery, 1979). Uplift near the Jurassic-Cretaceous boundary and subsequent erosion resulted in the truncation of most of the Permian and Early Mesozoic formations and the Early Cretaceous directly overlies older Palaeozoic units. The abundant Early Cretaceous exposures, which fringe the shield are built mainly of sandstone with several marine intercalations, which pinch-out southwards (Weissbrod, 2002).

The Permian and Early Mesozoic deposition was partly coeval with extensional tectonics, block faulting and igneous activity along the Arabian plate margins associated with the opening of the Neo-Tethys and the formation of the passive continental margin.

3. PREVIOUS HEAVY MINERAL STUDIES

Most of the heavy mineral studies on the Neoproterozoic-Mesozoic siliciclastic succession were carried out in Egypt, Israel and Jordan, with a qualitative study in

NW Saudi Arabia (Fig. 2). Vroman (1944) was the first to examine the heavy minerals of the so-called 'Nubian Sandstone' in the region and his data, based on a limited number of samples, have subsequently been confirmed throughout the region by later comprehensive studies. Shukri and Said (1945) studied eight sections located in the Eastern Desert of Egypt along the Gulf of Suez and the Red Sea. In the northern examined exposures the sections consist of Carboniferous, Jurassic (?) and Early Cretaceous sandstones, whereas in the southern exposures they are of Early Cretaceous age. Subsequently, Shukri and El Ayouti (1953) examined two horizons within the Early Cretaceous siliciclastic succession (1 m above the igneous basement and tens of meters higher up) in four sections in the vicinity of Aswan, and El-Hinnawi et al. (1973) examined similar levels at Barramyia. Other investigations were made on the Early Cretaceous clastics from boreholes in the Kharga Oasis (El Shazly and Shata, 1960) and in the Dakhla basin (Bisewski, 1982).

A systematic study of heavy minerals in the Cambrian, Ordovician, Silurian and Early Cretaceous siliciclastic sediments in southern Jordan (Quweira-Mudawwara area) was carried out by Bender (1968), who presented a detailed frequency log of the mineral species, whereas Lillich (1969) analysed the Cambrian and Early Cretaceous successions in the central Wadi Araba area. Later, important heavy mineral data were contributed by Amireh (1991, 1992, 1994) who studied the Palaeo-Mesozoic deposits in southern and central Jordan, including analyses of Permian, Triassic and Jurassic clastics from the Dead Sea area but only the range and average values for each of the rock units were shown. Nasir and Sadeddin (1989, 1990) added complementary data on the Early Cretaceous in northern and southern Jordan. Farther south in Saudi Arabia, the Palaeozoic is extensively exposed but only qualitative data from a preliminary heavy mineral study, probably from the north-western part of the country (Tabuk-Jawf area), were reported by Powers et al. (1966).

In Israel, Greenberg (1968) examined several hundred samples from the Early Cretaceous section in the northern Negev (Makhtesh Hatira), and detailed studies were carried out by Weissbrod (1980) and Weissbrod and Nachmias (1986) in the Cambrian and Early Cretaceous sections in the southern Negev (Timna-Elat area), and for several core samples from the Neoproterozoic-Early Cambrian arkose in the central Negev (Fig. 2; Ramon-1 borehole). They also studied the Palaeo-Mesozoic siliciclastic succession in central Jordan (SE Dead Sea area) and SW Sinai (Um Bogma area); in the latter, Carboniferous and Permo-Triassic rock units were also examined. Overall, 400 samples were analysed (Figs. 5–7). Implications on the occurrence of detrital and authigenic apatite (A-apatite) within the Neoproterozoic and Cambrian sediments and its absence in the Late Palaeozoic and onward were discussed by Weissbrod et al. (1987).

Various mineral dating methods were applied to reconstruct the origin and/or provenance of the successions. Harlavan (1991) measured K-Ar and Ar-Ar ages of micas and clay minerals in the Cambrian sandstones of southern Israel. Kohn and Weissbrod (1993) studied fission tracks of authigenic, A-apatite (formed in the Miocene) from Cambrian sandstones in southern Israel, while Becker and Becker (1997) dated detrital zircons from Jurassic and Early Cretaceous sections in the central Negev using Thermal Ion Emission—$^{207}Pb/^{206}Pb$ methods. Ages, obtained by Becker and Becker (1997) correspond to the Pan-African crust as well as older ages (~2000 Ma). However, due to the multigrain analytical procedure these results

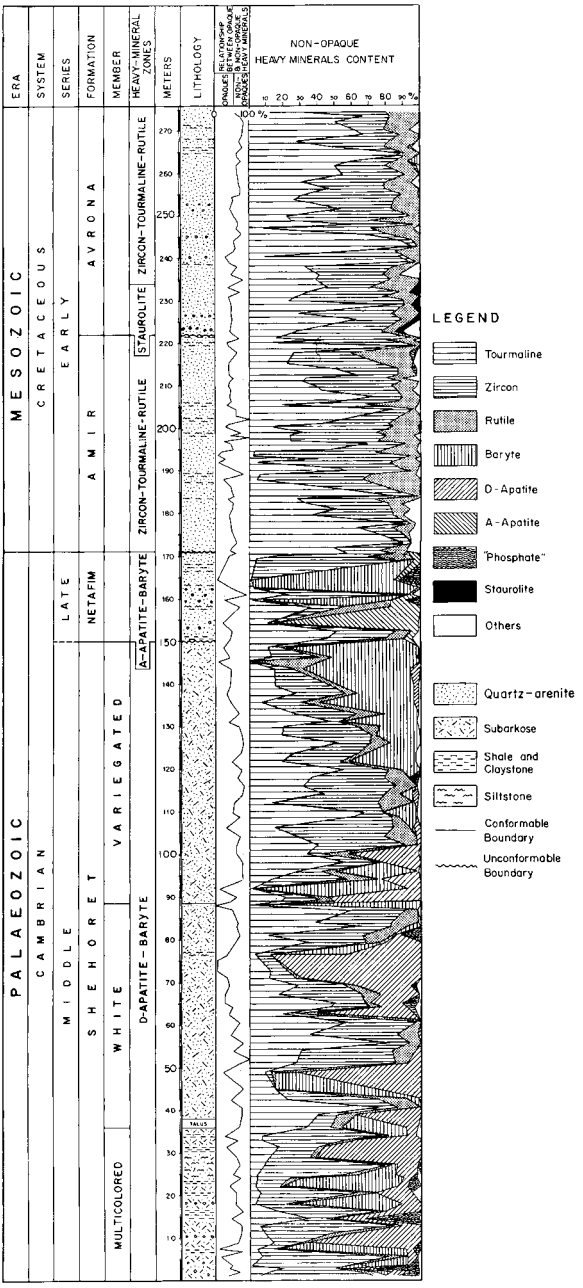

Fig. 5. Heavy mineral contents of the Palaoe-Mesozoic succession in southern Israel. Composite section at Nahal Shehoret, with permission from Elsevier.

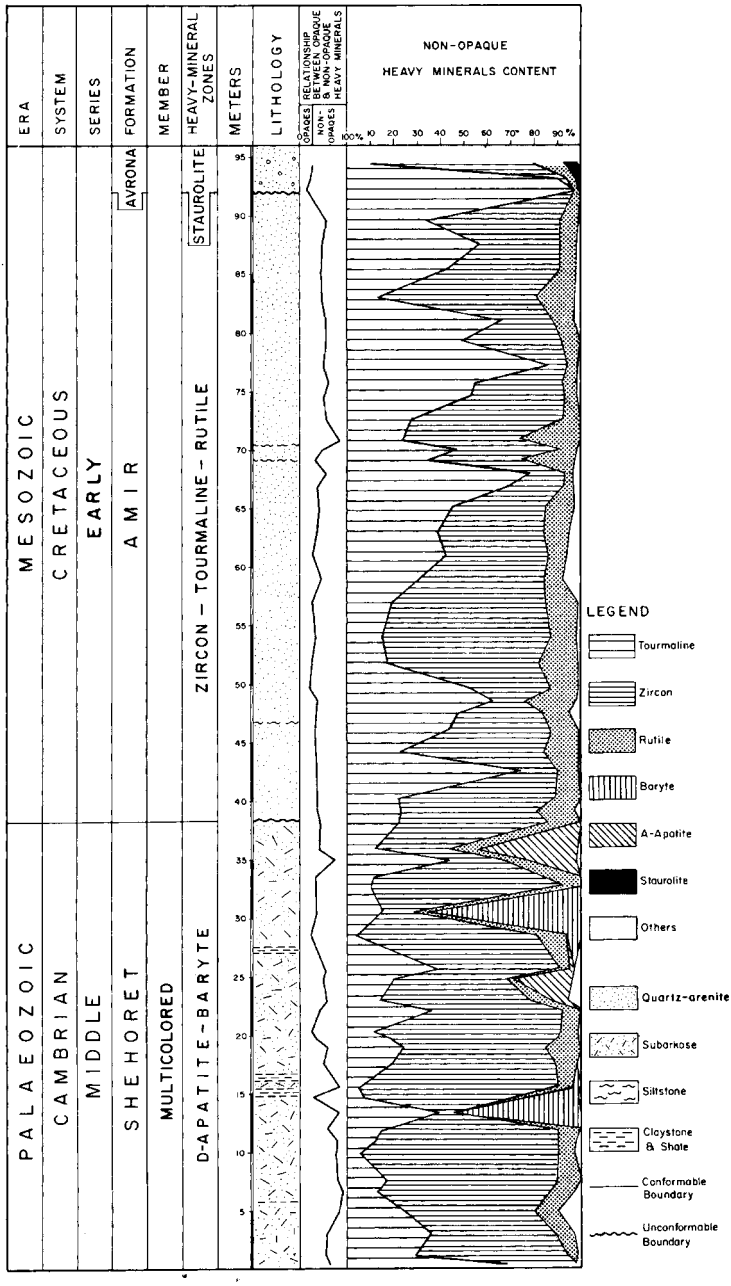

Fig. 6. Heavy mineral contents of the Palaoe-Mesozoic succession in southern Israel. Composite section at Timna Valley, with permission from Elsevier.

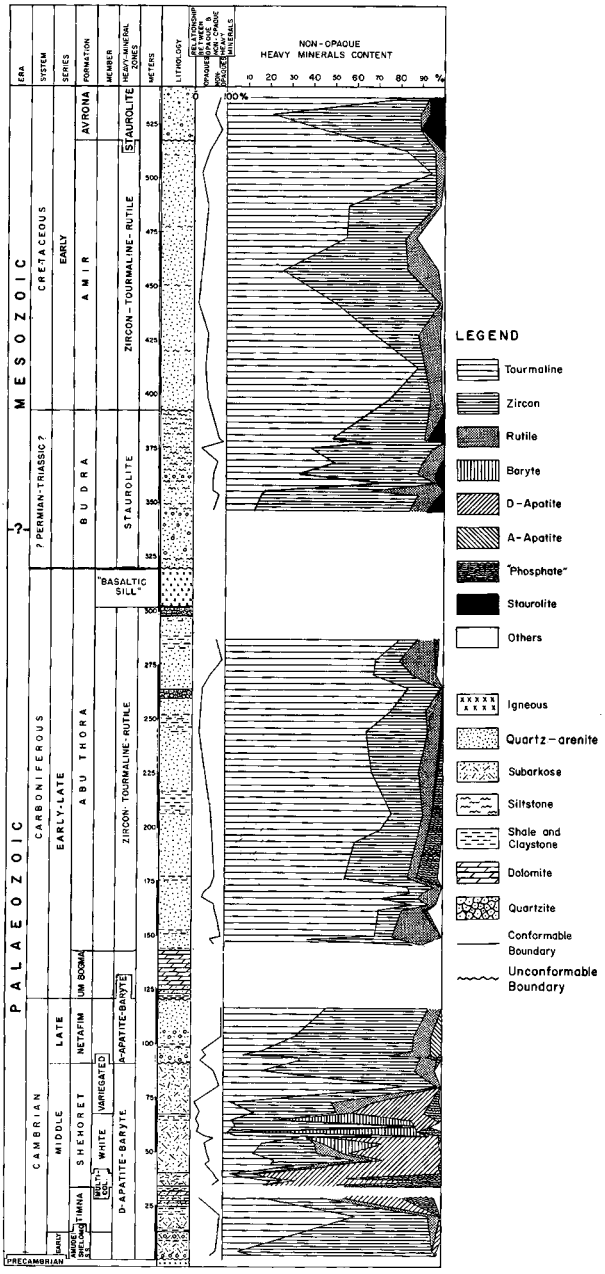

Fig. 7. Heavy mineral contents of the Palaeo-Mesozoic siliciclastic succession in west central Sinai. Composite section of the Um Bogma and Gebel el-Foka areas. [After Weissbrod and Nachmias (1986), with permission from Elsevier.]

are less specific. Wilde and Youssef (2002) analysed detrital zircons in samples from the Neoproterozoic Hammamat Group in the Eastern Desert using the SHRIMP U-Pb dating technique, and Avigad et al. (2003) and K. Kolodner (personal communication, 2004) employed this method to date zircons from several Cambrian and Ordovician sandstones in southern Israel and southern Jordan. These authors found that most of the grains fall within the Pan-African range (~540–900 Ma), with a smaller proportion (30%) showing older ages. Avigad et al. (2003) and K. Kolodner (personal communication, 2004) divided the older zircons (mostly discordant ages) into three age groups: (1) 900–1100 Ma; (2) 1650–1850 Ma and (3) 2450–2700 Ma. They considered that the majority of the zircons were derived from the Pan-African orogenic crust, mainly the ANS, whereas the two oldest groups were considered by them to be derived from remobilised pre-Pan-African crust in the East Saharan Craton (Petters, 1991) and the southern Afif terrain in central Saudi Arabia (Stacey and Hedge, 1984), all ~1000 km to the south of Israel. Rocks of 900–1100 Ma old, and related to the Kibaran orogenic event, are not known in the ANS but are currently exposed in central and southern Africa, at least 3000 km to the south. Avigad et al. (2003) suggested that zircons carrying the Kibaran age signature were initially transported northward by glacial processes during the Neoproterozoic, and later recycled and incorporated into the Early Palaeozoic deposits of the Arabian platform.

4. HEAVY MINERAL CONTENTS

The heavy mineral fraction generally ranges from 0.05 to 0.3 wt.% in the Palaeozoic-Mesozoic siliciclastic successions, but there are enrichments in sporadic laminae. Relatively high amounts (2%) were also recorded in the underlying Neoproterozoic immature arkose and exceptionally high contents (average 5.8%) were reported from sandstone layers overlying the igneous basement in the central Eastern Desert (El-Hinnawi et al., 1973). The heavy and light mineral associations display a parallel tendency of maturation with an upward trend of heavy mineral assemblages and framework constituents, evolving from unstable associations to ultrastable suites and changing from feldspar-rich arkose and subarkose to feldspar-free quartz-arenites.

Opaques form the greater part of the heavy mineral suite ($>80\%$) consist mainly of iron oxides, including ilmenite, magnetite, hematite and "limonite" with minor sulphides (pyrite and pyrrhotite) and chromite. The opaque minerals were not counted individually; however, the ratio between the opaque and transparent heavy minerals is given in certain studies (Figs. 5–7).

The ultrastable, zircon, tourmaline and rutile (ZTR) suite dominates the transparent heavy mineral assemblages, often exceeding 90% or more of the bulk in many successions. Accessory metastable and unstable minerals occur consistently in some intervals, but are mainly randomly distributed and usually average $<3\%$. In places, one or more of these species occur as local "floods" reaching concentrations of up to 15% of the transparent heavy minerals. Hornblende, apatite, garnet and staurolite are abundant in certain rock units. Augite, chlorite, epidote and kyanite are more sporadic, while andalusite, diopside, fluorite, monazite, sphene and zoisite occur as

traces. Also present are authigenic heavy minerals, including baryte, apatite, anatase, brookite and leucoxene, sometimes in large amounts. Generally, they are unevenly distributed but occasionally make up most of the transparent fraction and mask the frequencies of the detrital heavy mineral components. Weissbrod and Nachmias (1986) found a high proportion of authigenic baryte and apatite (average 15–26% and 8–20%, respectively) in certain Cambrian rock units in southern Israel and west-central Sinai (Figs. 5 and 7).

The Neoproterozoic-Early Cambrian immature siliciclastic succession is dominated by an unstable heavy mineral suite, whereas the overlying Palaeozoic and Mesozoic strata consist mostly of the ultrastable ZTR suite and occasionally of some of the less stable and/or authigenic minerals. The ZTR suite persists throughout the Palaeo-Mesozoic clastic succession but the frequencies and the ratios between the individual species vary considerably. The ZTR suite generally exceeds 90% except for certain rock units or intervals in the Palaeo-Mesozoic strata where one or more of the authigenic (baryte, A-apatite, anatase) and metastable (garnet, staurolite) minerals are widespread.

Zircon is the most abundant transparent heavy mineral with an average of 8–87% in the various rock units. It occurs mostly as sub-rounded to rounded grains, but in places as prismatic crystals terminated by double pyramids, or with broken and rounded edges. It is generally colourless with a clear to dusky appearance, but pink to red, greenish yellow, brown and light purple varieties occur as well. Some of the grains are zoned. Opaque, fluid and gas inclusions are common; overgrowths are rare. Most investigators did not differentiate between the various types with the exception of El-Hinnawi et al. (1973) who classified the zircons from the Early Cretaceous of the Eastern Desert according to their colour, shape, inclusions and zoning.

Tourmaline is second in abundance, averaging 10–66%. It occurs in various forms, mostly as prisms with broken and rounded terminations or as rounded, pitted and etched grains, rarely with a flaky habit, and displays a broad range of colours dominated by olive and pale green (orange, yellow-brown, pink, blue and colourless varieties are less common). Corrosion marks and small pyramidal overgrowths are locally present, and opaque inclusions are widespread. El-Hinnawi et al. (1973) distinguished between schorl, indicolite and elbaite varieties and presented their average frequencies.

Rutile is reddish to yellowish, forming irregular and rounded grains (rarely as prisms) with striations and corrosion pits. It is generally third in abundance (up to 15%), but in the Early Cretaceous at Barramyia, El-Hinnawi et al. (1973) reported exceptionally high values (up to 45%) with an average of 32.5%. Other high values for rutile were reported from two Ordovician rock units in southern Jordan (Amireh, 1991).

On the whole, zircon dominates the Cambrian, Ordovician and Silurian successions whereas tourmaline is more abundant in the Carboniferous and in the Mesozoic clastic formations. Weissbrod and Nachmias (1986) illustrated this trend in detailed frequency diagrams of the Palaeo-Mesozoic deposits in southern Israel and west-central Sinai (Figs. 5–7). Vertical differences and the consistent upward enrichment trends of tourmaline are most prominent in the section from Timna (20–43% average) where no authigenic minerals mask the frequencies of the detrital components. The same trend is also evident in the Nahal Shehoret section where the

moderate tourmaline content in the Cambrian succession (23%) increases to nearly double in the overlying Early Cretaceous (Figs. 5 and 6). In the Cambrian of the Sinai tourmaline averages 27%, and increases to much higher amounts in the Carboniferous, Permo-Triassic and Early Cretaceous sandstones. A similar dominance of tourmaline over zircon was reported in Carboniferous, Jurassic and Early Cretaceous sandstone samples from the Eastern Desert of Egypt (Shukri and Said, 1945) and in the Early Cretaceous sandstones from northern (King Talal Dam) and southern (Wadi Quseib) Jordan (Nasir and Sadeddin, 1989). Nevertheless, other studies in the region have demonstrated different frequencies and trends of enrichment for zircon and tourmaline. Amireh (1991) studied the Palaeo-Mesozoic siliciclastic deposits in Jordan, including Ordovician and Silurian sediments that are absent in Israel and Egypt, and also Permian and Triassic strata that have not been examined in these countries. He found that zircon is dominant in the entire section, and is enriched in the Mesozoic formations at the expense of tourmaline. Lillich (1969) also reported on the dominance of zircon (four times that of tourmaline) in the Cambrian and Early Cretaceous sections in the central Wadi Araba area (southern Jordan), and Greenberg (1968) showed a similar enrichment of zircon in the Lower Cretaceous of southern Israel. It should be noted that certain of the mineral frequency studies display marked discrepancies, as shown in differences of data between various investigators who studied the same rock units at proximal localities. Thus, Nasir and Sadeddin (1989) found that within the Early Cretaceous succession in northern and southern Jordan, tourmaline is more abundant than zircon, whereas Amireh (1991, 1992) reported on an opposite trend in nearby localities. These discrepancies and the frequent changes in the distribution of zircon and tourmaline may imply that the use of such minerals for stratigraphic discrimination and evaluation of provenance and sorting is misleading. Moreover, the amounts and proportions of heavy minerals may change in sediments enriched in finer fractions. An analysis of coarse and fine fractions from a Carboniferous sample (Khashm el Galala) has shown that tourmaline and staurolite decrease in the finer material whereas zircon and rutile increase (Shukri and Said, 1945).

Hornblende is significant in the Neoproterozoic-Early Cambrian molasse-type sediments (conglomerates and arkoses) deposited in intramontane depressions and marginal basins on the ANS. Hornblende is a major constituent of the arkose and generally comprises up to 5% of the bulk sediment. In one case, in the lower part of Sinaf-1 borehole (southern Israel, Fig. 2), a 200 m thick interval contains exceptionally large, irregular grains, which together with chlorite, may form >15% of the rock (Weissbrod, 1969). However, only a limited number of arkose core samples were studied for their heavy mineral contents (Weissbrod and Nachmias, 1986).

In the Palaeozoic and Mesozoic successions, hornblende is a minor component, occurring mainly in the Early Cretaceous clastics. The apparent presence of small amounts (1–3%) with local concentrations was reported by Greenberg (1968) in the Early Cretaceous section of southern Israel, and similar figures (0–25%, average 5%) were found in equivalent sections in northern and southern Jordan (Lillich, 1969; Nasir and Sadeddin, 1989). However, Bender (1968) reported high hornblende contents in southern Jordan (Quweira-Mudawwara area) where it persists through the Cambrian, Ordovician, Silurian and Early Cretaceous sections (Fig. 8). According to Bender (1968) the amount of hornblende in the Cambrian section ranges from 3

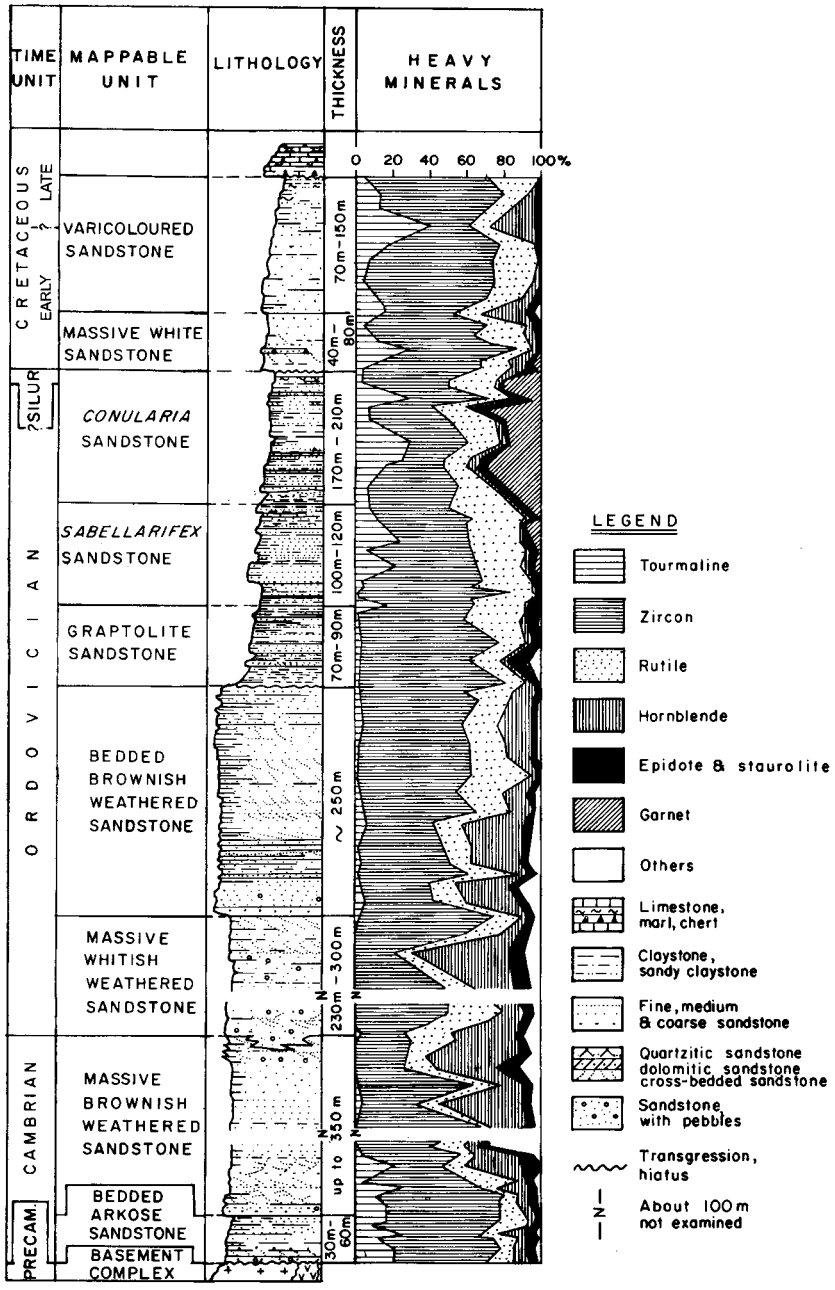

Fig. 8. Heavy mineral contents of the Palaeo-Mesozoic siliciclastic succession in southern Jordan. Composite section at the Quweira-Mudawwara area. [After Bender (1968).]

to 53% with a mean of 18%, and in the Early Cretaceous it ranges from 2 to 32%, averaging 22%. These values are in sharp contrast with its virtual absence in correlative strata from the surrounding areas in Israel, Sinai and Saudi Arabia. This discrepancy, in addition to the incompatible presence of significant amounts of unstable hornblende in the mature sandstones, and the complementary nature of hornblende and tourmaline in Bender's (1968) frequency diagram (one is abundant when the other is absent or rare and vice versa, while the proportions of the other minerals are practically unchanged), led Weissbrod and Nachmias (1986) to question the reliability of these findings. They argued that the presence of a permanent igneous/metamorphic province that supplied the hornblende during such a long time span only to Jordan is not reasonable and postulated that the quandary relates to erroneous identification (optical techniques; perhaps when certain varieties of tourmaline were identified as hornblende). Indeed, later studies in the same area by Amireh (1991, 1992, 1994) found no hornblende in these sediments.

Staurolite occurs as angular to sub-rounded and etched, reddish-yellow to yellow grains, occasionally with 'hacksaw' terminations and opaque inclusions. It was recorded by most investigators and is consistently present in small amounts (2–3%) in most rock units, mainly in the Mesozoic succession, but locally high concentrations were recorded. Shukri and Said (1945) reported on irregular staurolite distribution in the Carboniferous, Jurassic and Early Cretaceous sandstones of the Eastern Desert of Egypt, reaching 20% of the transparent heavy mineral suite in some samples. In Jordan, Bender (1968) and Lillich (1969) described a persistent distribution of staurolite in the Cambrian to Silurian and Early Cretaceous successions (generally 2–3% and locally 10%), and Amireh (1991, 1992) found similar amounts in the Triassic, Jurassic and Early Cretaceous sections. In Israel, Greenberg (1968) and Weissbrod and Nachmias (1986) recorded almost consistent amounts of staurolite (2–5%) in the Early Cretaceous section, and similarly in the Permo-Triassic section of Sinai (Figs. 5–7).

Garnet is mainly distributed in the Neoproterozoic and Early Palaeozoic successions. It varies from colourless to pale pink, and is present as irregular to rounded grains with pitted surfaces and dissolution features. Bender (1968) found a persistent occurrence of garnet in relatively high amounts (up to 30%) in the Middle Ordivician to Early Silurian formations in southern Jordan (Fig. 8). These findings were later confirmed by Amireh (1991) who recorded an average content of 8% garnet in equivalent sections. Moderate amounts of garnet (up to 10%) were found in Neoproterozoic arkose layers and in Middle Cambrian marine intercalations from the Dead Sea area of Jordan (Vroman, 1944), and sporadic amounts were also reported in Triassic rock units in the same area (Amireh, 1991).

Detrital apatite (D-apatite) generally appears as rounded grains with euhedral authigenic overgrowths or, more rarely as prisms with rounded edges and black granular inclusions. It is abundant in the Cambrian succession in southern Israel and west-central Sinai (Weissbrod and Nachmias, 1986). In the Nahal Shehoret section it averages 20%, 18% and 8% in the individual members (Fig. 5), and in the Um Bogma area it is 50%, 27% and 15% (Fig. 7). Studies in Jordan recorded subordinate amounts mainly in the Cambrian deposits (Weissbrod and Nachmias, 1986) with the exception of the basal Cambrian rock unit where the apatite ranges from 0 to 49% (average 16%) (Amireh, 1991). The latter apatite is most probably

authigenic (see below). D-apatite has been also reported from the Palaeozoic and Mesozoic siliciclastic succession in northwestern Saudi Arabia (Powers et al., 1966). Unlike the other studied areas, it occurs within Ordovician to Devonian sections but not in the Cambrian. Low apatite content was also reported from the Neoproterozoic arkose in the subsurface of southern Israel where it averages 2% (Weissbrod et al., 1987).

A-apatite occurs in the Cambrian section of southern Israel and Jordan on both sides of the Dead Sea Rift. It appears as sector-twinned hexagonal platelets or prisms within cement in several horizons of the Late Cambrian succession (Fig. 5) (Weissbrod and Nachmias, 1986), and in two layers of irregular and imbricated platy blocks of apatite- and iron-cemented grit in the Early Cambrian section in southern Israel (Karcz et al., 1971). Amireh (1991) found apatite in an Early Cambrian rock unit in southern Jordan, which is probably related to the same epigenetic event. Other A-apatite was reported by Bar-Matthews (1987) within Middle Cambrian marine siliciclastic facies in southern Israel.

Anatase was formed at the expense of rutile and ilmenite. It occurs in small amounts as euhedral plates with a bluish-grey colour, occasionally together with authigenic brookite. From two intervals within the Early Cretaceous succession near Aswan, Shukri and El Ayouti (1953) reported the presence of 6% anatase in the lower interval and 3.5% higher in the section, and El-Hinnawi et al. (1973), who studied similar intervals in the Barramyia area, found anatase consistently in all samples, with an exceptionally high content (42%) near the basement. Weissbrod and Nachmias (1986) found an average of 2–3% in the lower part of the Early Cretaceous succession in southern Israel and west-central Sinai, whereas Nasir and Sadeddin (1989) detected traces in the Early Cretaceous of northern and southern Jordan. Amireh (1991) reported on a consistent occurrence of anatase and brookite in all Palaeo-Mesozoic siliciclastic formations of Jordan with averages ranging between 3 and 6% and up to 9% in the Middle Cambrian section, and similarly a reconnaissance study in northwestern Saudi Arabia has recorded anatase in all Palaeozoic (Cambrian to Devonian) formations (Powers et al., 1966).

Baryte is authigenic and occurs mainly in the Cambrian deposits as tabular crystals. It is unevenly distributed and is restricted to certain horizons; where present it usually occurs in large amounts (20–90%, Figs. 5 and 6). In west-central Sinai (Um Bogma) it is concentrated in the middle part of the section averaging 18% (Fig. 7), but in a section from Jordan (Dead Sea area) it amounts to only 2.5% (Weissbrod and Nachmias, 1986). In the latter locality it also occurs in the Early Cretaceous sediments (average 3.5%). Similar figures for baryte were reported from the Early Cretaceous in northern Jordan (Nasir and Sadeddin, 1989). Exceptionally high amounts of baryte (87% of the transparent suite) were recorded by Shukri and Said (1945) from several samples of the Early Cretaceous succession in the central Eastern Desert.

5. HEAVY MINERAL ZONES

Although there are discrepancies in data between studies, and occasional 'abnormal' abundances are reported, a general pattern of heavy mineral distribution

can be constructed. The studies enable recognition of two discrete, laterally consistent, suites: (1) a Neoproterozoic-Early Cambrian suite of orogenic, immature sediments dominated by unstable minerals and (2) a Palaeo-Mesozoic suite of platformal, mature deposits containing mainly ultrastable minerals. The latter can be further subdivided into two parts, based on the presence of apatite and metastable minerals (garnet, staurolite) and locally superimposed authigenic minerals that can be applied for zoning. The ultrastable ZTR suite forms most of the transparent fraction and is ubiquitous. The frequencies of the individual ZTR minerals and intermineral ratios vary (irregularly) and cannot be used alone to characterise rock units. However, Amireh (1994) considered the zircon/tourmaline ratio as an unequivocal criterion for distinguishing between the lithologically similar Ordovician Disi Formation and the Early Cretaceous Kurnub Sandstone. The Z/T ratio in the Disi Formation varies between 0.79 and 1.98 (generally less than 1.5; average 1.1), whereas in the Kurnub Sandstone, the Z/T ratio varies between 0.83 and 3.63 (generally exceeding 1.5; average 2.2.).

Properties defining a zone are the presence of one or more accessory mineral species (either stable, metastable, unstable or authigenic) in moderate to high amounts, showing vertical regularities and lateral continuity. The zone boundaries are marked by abrupt changes of the mineral species, generally indicating unconformities accompanied by stratigraphic gaps. Most of the zones are system-wide rather than defining a certain formation. Four zones have been established.

5.1. Hornblende, Chlorite and Staurolite Zone

This zone comprises Neoproterozoic-Early Cambrian immature conglomerate and arkose and is characterised by a dominance of unstable and metastable heavy minerals. It is the only zone where ZTR is subordinate. The abundance of easily altered hornblende and the presence of staurolite and garnet in this suite indicate rapid deposition and limited chemical weathering, even though the position of the ANS at that time was at low latitudes under temperate to tropical conditions.

5.2. Apatite-Baryte Zone

Apatite-baryte zone includes Cambrian subarkoses and quartz-arenites with a dominance of the ZTR suite, and is characterised by abundant apatite (detrital or authigenic) and authigenic baryte, displaying irregular frequencies. Apatite occurs consistently throughout the clastic section from the Neoproterozoic through the Cambrian, sporadically from the Ordovician to the Silurian, but disappears abruptly from Carboniferous and younger units. This is ascribed to warm climatic conditions with the development of well-leached, low pH humic soils with widespread land vegetation in which apatite was dissolved (Weissbrod et al., 1987).

A fission track study of A-apatite from the Late Cambrian section in southern Israel yielded mid-Miocene ages of 13.1–15.4 Ma (Kohn and Weissbrod, 1993). This implies that A-apatite found in the Cambrian of Israel and Jordan is neoformed (i.e., reprecipitation after initial dissolution of D-apatite, possibly related to hydrothermal activity during the early stages of movement along the Tertiary Dead Sea Rift).

5.3. Garnet Zone

This zone includes Middle Ordovician to Early Silurian quartz-arenites and shales, and is characterised by a dominance of ZTR and relatively large amounts of garnet. It has been reported only in southern Jordan (Bender, 1968). Garnet was not detected in the Ordovician-Silurian deposits of Saudi Arabia, perhaps due to the preliminary nature of the study, whereas in Israel, Sinai and the Eastern Desert, the Ordovician-Silurian sections were removed by erosion. The relatively large amounts of garnet and its apparent confinement to the Ordovician-Silurian succession, at the time when the continent had moved to polar and sub-polar latitudes (Konert et al., 2001), may imply a shift of provenance towards more interior parts of Gondwana (now present-day central Africa) where garnet-bearing rocks were exposed, glaciers were present and chemical weathering was limited. The sand-size detritus along with striated boulders and faceted pebbles were transported to the ANS and its margins by a glacial-fluvial drainage system. The garnet could have been partly derived from proximal sources as the channels locally cut down to the crystalline basement.

5.4. Staurolite Zone

This zone comprises the Early Cretaceous super-mature quartz-arenites and is characterised by the dominance of ZTR and small to moderate amounts of staurolite, although an exceptionally high staurolite content was reported from the Eastern Desert (average 18%: Shukri and Said, 1945). It also appears in Permo-Triassic clastic sections in Jordan (Dead Sea area) and west-central Sinai (Um Bogma area) and sporadically in part of the Early Palaeozoic succession. The apparent regular distribution of staurolite in the Late Palaeozoic and Mesozoic siliciclastic sections signals exposed igneous and metamorphic complexes over a large area in Saudi Arabia (Riyadh swell) as a result of Late Palaeozoic uplift, followed by erosion and a subsequent Early Cretaceous uplift in Egypt and Sudan (Aswan swell).

6. DISCUSSION

Numerous studies on the Neoproterozoic to Early Mesozoic siliciclastics along the northern margin of the ANS have indicated that their sediment source area was located to the south of the depositional basin (e.g., McKee, 1962; Karcz and Key, 1966; Soliman and El Fetouh, 1969; Selley, 1972; Amireh, 1991). This was deduced from the distribution of facies belts, isopachs, palaeocurrent pattern and grain size trends. The ANS has long been considered to be an area of permanent detritus supply (Weissbrod and Nachmias, 1986; Amireh, 1991). However, subsequent studies suggested that the source for part of the Palaeozoic clastics in the Arabian Peninsula could have been beyond the ANS. Vaslet (1990) and Konert et al. (2001) postulated that late Early Cambrian basal clastics in the ANS derived from the interior of Gondwana to the south and west, and Stump and Van der Eem (1994) argued that Late Ordovician sediments in Saudi Arabia originated in Central Africa and were carried northwards by a fluvial drainage system.

Lithology, heavy mineral compositions, zircon geochronology, palaeogeographical field data and circumstantial evidence for the presence of Neoproterozoic to Mesozoic clastic deposits over most or all of the ANS permitted the reconstruction of three major depositional successions, their evolution and provenance.

6.1. Neoproterozoic: Early Cambrian Siliciclastic Succession

This succession is characterised by coarse, unsorted first-cycle immature sediments, comprising dominantly unstable and metastable heavy minerals derived from the erosion of the ANS igneous/metamorphic basement. Clasts found in the conglomerates, which form the bulk of the material in the central and southern areas, are petrographically identical to the lithology of the basement, while the arkose, that dominates in the north, contains up to ~50% feldspar and a relatively large amount of hornblende and chlorite, with subordinate staurolite and garnet. These are clear signatures of sediment provenance from the surrounding mountainous terrain that underwent mainly mechanical erosion and, apparently, short-distance transport. Most of the detritus was accumulated and rapidly buried in fault-controlled basins, with the finer material transported further towards the northern passive margin. However, the roundness of the pebbles in part of the conglomerates indicates a somewhat longer transport and testifies that, already at this stage, the drainage system was well developed.

Wilde and Youssef (2002), using the sensitive high-resolution ion microprobe technique (U-Pb SHRIMP), measured zircons from the Hammamat Group in north Eastern Desert of Egypt (equivalent to the Neoproterozoic-Early Cambrian clastic succession of Saudi Arabia, Jordan and Israel). Most measurements yielded ages in the ~600 to ~750 Ma range, although several (mainly discordant) Proterozoic to Archaean ages were also obtained. They considered that the Pan-African zircons originated in the surrounding igneous basement whereas the older (mainly Proterozoic) zircons were derived from an earlier, remobilized, continental crust that was incorporated in the ANS by accretion. Other source areas may include the central or southern Eastern Desert and the Nile craton where sparse anhedral and corroded zircons of this age have previously been recorded. The occurrence of older zircons interpreted as being transported from more distal areas supports the existence of an extensive drainage system even then.

6.2. Early Palaeozoic Siliciclastic Succession

This is a first-cycle, mature, medium- to fine-grained and moderately well-sorted package, derived from igneous and metamorphic complexes, located mostly beyond the ANS. The paucity or absence of feldspar and the less stable heavy mineral species, and the abundance of ZTR and apatite, is attributed primarily to chemical weathering (with the lack of vegetation) at the source. A long-distance fluvial transport is envisaged, including bypass storage stations, which resulted in the elimination of the labile minerals. Feldspars are still prominent in the Cambrian section (subarkose) but form only minor amounts or traces in the Ordovician to Devonian sections (Weissbrod, 1980). The distribution and abundance of apatite is due to its mechanical resistance and durability during long transportation. Exceptionally high

amounts of garnet in the Middle Ordovician to Early Silurian sediments are attributed to provenance and reduced chemical weathering under glacial conditions both at the source area and the depocentre. However, the presence of euhedral and subhedral zircon and tourmaline, with occasional "floods" of other accessory metastable or unstable heavy minerals, may represent a contribution from local sources, since the less stable minerals cannot withstand prolonged chemical weathering and transportation.

In a synthesis of Early Palaeozoic sedimentation processes in the region, Garfunkel (2002) argued for a progressive expansion and migration of the depositional area of the Early Palaeozoic units, initiated by the wedging-out of the older units inland and the onlap of the younger units onto the basement. He postulated that the Early Cambrian sediments covered an ~500 km wide belt in the Arabian Peninsula while Ordovician sediments extended more than 1000 km further southwards where they directly overlie the basement in the most remote outcrops. This suggests that the greater part of the ANS basement was exposed at least during the Early Cambrian to Early Ordovician, while other extensive parts were exposed during the Late Ordovician and Silurian. On the other hand, stratigraphic data from the widespread exposures in the region revealed that wherever Early Palaeozoic sediments overlie the igneous basement, they are always of Cambrian age. Only in SW Egypt was the basal sandstone attributed to the Ordovician based on the presence of a single ichnofossil species (Klitzsch, 1990), although the possibility that the lower part of this section is of Cambrian age cannot be ruled out. Evidence for a basement/Cambrian contact is seen in exposures fringing the northern and eastern margins of the ANS, from the Eastern Desert and Sinai, across Jordan to Saudi Arabia and farther to Yemen (e.g., Powers et al., 1966; Bender, 1968; Weissbrod, 1980; Vaslet, 1990; Abdallah et al., 1992).

The present data explicitly show that the Palaeozoic siliciclastic succession in the southeastern part of the shield (Wajid basin) is time-equivalent and lithologically similar to most of the Palaeozoic successions in the northern part (Evans et al., 1991; Stump and Van der Eem, 1994, 1995). These two large provinces that were already separated in the Late Palaeozoic by uplifting of the Riyadh swell and exposure of the crystalline basement (Gvirtzman et al., 1988) are today separated by the Central Arabian Arch (Powers et al., 1966).

The ANS basement is presently widely exposed caused by uplift during the Tertiary opening of the Red Sea and the resulting erosion of the sedimentary cover. Circumstantial evidence for the extension of the Cambrian sediments over this exposed area can be deduced from the landward edge of their present outcrop in the northern and eastern parts of the shield. The basal Cambrian sediments at most of these localities are usually more than 100 m thick without evidence of wedging-out. Moreover they disappear abruptly, indicating that they may have extended for a considerable distance further inland to the south and west, far from the present exposures, particularly since they probably overlaid the Late Proterozoic-Early Cambrian peneplain surface and onlapping over relief was unlikely. The same considerations are also applicable for the overlying, thick Middle to Late Cambrian, Ordovician and Silurian successions. Indeed, palaeogeographic maps of the Early Palaeozoic sediment distribution suggest that the ANS was mostly or totally covered (Schandelmeier et al., 1997). On the other hand, the basal section in west-central

Sinai and in the northern Eastern Desert wedges out southwards, and at its most southern exposures is only some 20 m thick, implying that the sediments could not have extended far to the south, and that therefore the basement was probably exposed in the Early Cambrian.

Such basement exposures may have acted as a source for part of the clastics, as suggested by the small amounts (and local "floods") of unstable and metastable heavy minerals in the Early Palaeozoic sections. However, these limited outcrops could not have contributed to the huge volume of material incorporated in the sedimentary successions from the Middle Cambrian and onward, when—for the most part—the shield was covered. Removal of such large amounts of detritus would have been expressed by the level of erosion down to deeper parts of the orogen, but evidence for this has not been found. The earliest 'opening' and exhumation of the underlying igneous/metamorphic basement is likely to have occurred in the Late Cambrian, as is indicated by block movements and differential erosion in Sinai and the Eastern Desert (Weissbrod, 2003), but this may have been local and limited. Extensive exposure of the basement occurred later in the Late Devonian and in the Late Carboniferous, following the uplift of the Riyadh swell. Subsequent erosion removed a thick section of Early Palaeozoic siliciclastic sediments then cut down to the igneous/metamorphic basement at the culmination of the structure (see outline of the swell, Fig. 1).

In the late Neoproterozoic-Early Cambrian, a peneplain formed on the igneous/metamorphic basement over most of the ANS and wherever it is presently exposed, it generally displays a flat surface without features of morphological rejuvenation such as a prominent relief or channelling, and the basal sediments above it generally lack pebbles of local derivation. Erosion drastically slowed down as the mature peneplain landscape approached sea level. Although weathering processes continued, the degenerate drainage system was not capable of removing and carrying large amounts of detritus towards the base level. Only near newly formed fault blocks, where morphology was rejuvenated, did the irregular boulders and gravels of scree locally infill the relief (Karcz and Key, 1966; Bender, 1968; Selley, 1972; Vaslet, 1990).

Following uplift in the interior of Gondwana in the Early Cambrian, large amounts of coarse clastic material were carried and deposited by a rejuvenated drainage network. These sediments covered the surface of the peneplain over most of the ANS and its margins, while continuous subsidence during the Early Palaeozoic increased the rate of deposition resulting in the accumulation of a thick platform-type siliciclastic succession over the basal blanket. It is, therefore, obvious that the buried basement could not contribute the large amounts of detritus that constitute the thick Early Palaeozoic deposits, thus the source region for the clastic material should be traced to a Gondwanan hinterland outside the ANS.

Further evidence for more distal igneous/metamorphic provenance is provided by the wide distribution of well-rounded pebbles of vein-quartz ('quartzite'), chert and jasper, occurring either as laterally discontinuous bands with local concentrations, or randomly scattered in the basal Cambrian sandstones. The conglomerates and arkoses of the Neoproterozoic suite known to have been derived from the local basement are devoid of such pebbles. The roundness of the major sand grade components (Weissbrod, 1980) and the general absence of heavy minerals of local

igneous/metamorphic basement signatures in the pebbly beds, even when they directly overlie the crystalline basement, also suggest long-distance transport. Post-depositional modification of the heavy minerals in the Early Palaeozoic siliciclastics was minor, although slight effects of dissolution can be seen in the pitting and corrosion of tourmaline grains.

6.3. Late Palaeozoic and Early Mesozoic Siliciclastic Succession

This is a largely recycled, super-mature, medium- to fine-grained and moderately to well-sorted succession, derived from reworked Palaeozoic sandstones in the ANS. Quartz arenites displaying a high ZTR index, without feldspar or mica, and with occasionally minor admixtures of staurolite, hornblende and epidote from local igneous/metamorphic terrains, are characteristic (Greenberg, 1968; Lillich, 1969; Weissbrod and Nachmias, 1986). The truncations of the Late Palaeozoic swells (up to 2500–3000 m) provided reworked material from the Early Palaeozoic units and where the basement was exposed it became a source of unstable heavy minerals. The quartz grains in the sandstones are well-rounded despite their relatively short transport distance, indicating reworking. A contribution from an igneous source in the interior of Gondwana, that was the main source of the Early Palaeozoic clastics, is unlikely because the Riyadh swell (Fig. 1) and the ANS as a whole, though deeply eroded, remained exposed in a somewhat elevated setting above its surroundings. It thus acted as a barrier from Permian to the Early Cretaceous as shown by the inland thinning of sand units and by the pinching-out of Late Palaeozoic and Early Mesozoic marine intercalations along its margins (e.g., Powers et al., 1966). Other changes in the drainage pattern around the ANS caused by epeirogenic uplift during this time interval were described from the western margin of the shield. Klitzsch and Wycisk (1987) reported on an inversion of the drainage system following the Late Palaeozoic uplift of central and southern Egypt. This inversion resulted in the erosion of large amounts of Palaeozoic strata and underlying igneous rocks from the ANS. The resulting debris was transported southward by braided rivers into a large and shallow east–west elongated basin, situated in northern Sudan, southeastern Libya and northeastern Chad, where continental sediments of Permian to Early Jurassic age were accumulated. This basin contains a succession of texturally and mineralogically immature fluvial arkosic sandstones and conglomerates containing large amounts of unstable and metastable heavy minerals, which reflect an igneous source and short-distance transport (Wycisk, 1990).

The composition of the Late Palaeozoic and Early Mesozoic clastics in the Arabian Platform indicates that the contribution from an igneous source was moderate as expressed by local enrichments of accessory heavy minerals, apparently due to the flat morphology and low elevation of the exposed basement. The denudation of the igneous basement did not reach to a level much deeper in the orogen than that achieved during the Neoproterozoic and Early Palaeozoic, despite a similar time span (250 Ma). Subsequently the ANS was buried for a long time beneath thick calcareous strata and later exhumed following Tertiary tectonics when erosion became intensive.

7. CONCLUSIONS

The transparent heavy mineral spectrum in the Neoproterozoic-Early Mesozoic siliciclastic succession of the ANS consists of ultrastable ZTR (> 90%) together with mainly one of the metastable or unstable accessories in specific individual units (apatite, garnet, staurolite, hornblende), and traces of other minerals. The heavy mineral assemblages generally display an upward trend of "inverted" maturation parallel to that of the major framework components. Their content is largely controlled by the nature of the provenance and chemical weathering either at the source or during transportation. Effects of post-depositional intrastratal dissolution are negligible.

Effective stratigraphic discrimination based on the heavy minerals is limited, although they characterise large depositional cycles and help to define provenance. Sharp changes in the assemblages indicate unconformities and shifts of provenance, whereas the presence or disappearance of certain metastable heavy minerals reflects changes in climate and other environmental conditions (e.g., garnet is preserved due to colder climate, apatite disappeared because of development of soils with humic acids and the spread of land vegetation).

The heavy minerals together with sedimentological and palaeogeographic data, and detrital zircon geochronology allow a division of the Neoproterozoic-Mesozoic siliciclastics into three major depositional successions, reflecting provenance and weathering processes.

(1) The Neoproterozoic-Early Cambrian siliciclastic deposits consist of first-cycle, immature, coarse, unsorted arkose and greywacke successions with a dominance of unstable and metastable heavy minerals (hornblende, chlorite, garnet and staurolite), derived mostly from Pan-African crust within the ANS. They underwent mainly mechanical wear, short-distance transport and rapid burial. A minor contribution from Pan-African crust and older Proterozoic crust beyond the ANS is plausible.
(2) The Early Palaeozoic siliciclastics comprise first-cycle, mature, medium- to fine-grained moderate to well-sorted subarkoses and quartz-arenites with a dominance of resistant ZTR, apatite and metastable staurolite, derived from Pan-African and older crust outside the ANS (interior Gondwana). They underwent chemical weathering and long-distance transportation, with many alluvial storage stations. Sporadic admixtures of metastable minerals point to local sources within the ANS. The presence of relatively large amounts of garnet in the Ordovician-Silurian section is attributed to limited chemical weathering at the source and during transportation under a colder climate, following the wandering of the continent to polar latitudes.
(3) The Late Palaeozoic-Early Mesozoic siliciclastic succession contains recycled, supermature medium- to fine-grained and moderate to well-sorted quartz-arenite with a dominance of ZTR and in places staurolite, derived from reworked sandstones in the ANS, and sporadic admixtures from local exposures of basement rocks.

A change of the fluid regime during the early stages of the Dead Sea Rift led to the formation of A-apatite (at the expense of D-apatite) and the impregnation of baryte within the Cambrian section along this structure.

ACKNOWLEDGEMENTS

We thank K. Kolodner, Y. Druckman, M. Mange and D. Wright for their helpful comments.

REFERENCES

Abdallah, A.M., Darwish, M., El Aref, M., Helba, A.A., 1992. Lithostratigraphy of the pre-Cenomanian clastics of north Wadi Qena, Eastern Desert, Egypt. 1st International Conference on the Geology of the Arab World 2, 255–282.

Abdallah, A.M., El Adindani, A., 1965. Stratigraphy of Upper Palaeozoic rocks, western side of the Gulf of Suez. Egypt Geological Survey Mineral Resources Department, Paper No. 25, 18.

Al-Laboun, A.A., 1986. Stratigraphy and hydrocarbon potential of the Palaeozoic succession in both Tabuk and Widyan basins, Arabia. In: Halbouty, M.T. (Ed.), Future Petroleum Provinces of the World. American Association of Petroleum Geologists Memoir, vol. 40, pp. 373–397.

Al-Laboun, A.A., 1990. The Palaeozoic succession and the influence of the Hercynian equivalent movements in the greater Arabian basin. Bulletin Faculty of Earth Sciences King Abdulaziz University, Jeddah 3, 201–215.

Al Youssef, W., Ayed, H., 1992. Evolution of Upper Palaeozoic sequences and the application of stratigraphy as a tool for hydrocarbons exploration in Syria: Egypt General Petroleum Corporation, 11th Petroleum Production Conference, Cairo, vol. 2, pp. 636–657.

Amireh, B.S., 1991. Mineral composition of the Cambrian-Cretaceous Nubian Series of Jordan: provenance, tectonic setting and climatological implications. Sedimentary Geology 71, 99–119.

Amireh, B.S., 1992. Sedimentology and mineral composition of the Kurnub Sandstone in Wadi Qsieb, SW Jordan. Sedimentary Geology 78, 267–283.

Amireh, B.S., 1994. Heavy and clay minerals as tools in solving stratigraphic problems: a case study from the Disi Sandstone (Early Ordovician) and the Kurnub Sandstone (Early Cretaceous) of Jordan. Neues Jahrbuch Geologie Paläontologie Monatshefte 4, 205–222.

Avigad, D., Kolodner, K., McWilliams, M., Persing, H., Weissbrod, T., 2003. Origin of northern Gondwana Cambrian sandstone revealed by detrital zircon SHRIMP dating. Geology 31, 227–230.

Bar-Matthews, M., 1987. The genesis of uranium in manganese and phosphorite assemblages, Timna basin, Israel. Geological Magazine 124, 211–229.

Becker, N., Becker, A., 1997. Zircon as a tool for stratigraphic correlation and an indicator of source rocks for the Cretaceous sandstones of central Negev, Israel: Results of morphological study and U-Pb isotope spectrometry. Israel Ministry of Energy and Infrastructure, Report ES/14/97, 16.

Bender, F., 1968. Geologie von Jordanien. Gebrueder Borntraeger, Berlin, 230pp.

Bentor, Y.K., 1985. The crustal evolution of the Arabo-Nubian Massif with special reference to the Sinai Peninsula. Precambrian Research 28, 1–74.

Bisewski, H., 1982. Zur Geologie des Dakhla-Beckens (Sudwest Agypten). Berliner Geowissenschaftliche Abhandlungen (A) 40, 1–86.

Dean, W.T., Martin, F., Monod, O., Gunay, Y., Kozlu, H., Bozdogan, N., 1997. Precambrian? and Cambrian stratigraphy of the Penbegli-Tut inlier, southeastern Turkey. Geological Magazine 134, 37–53.

Delfour, J., 1970. Le Group de J'Balah. Bureau de Rècherches Géologiques et Minières Bulletin Section 4, 19–32.

Druckman, Y., 1976. The Triassic in southern Israel and Sinai: a sedimentological model of marginal epicontinental marine environments: Ph.D. thesis. Hebrew University of Jerusalem, 188pp. (in Hebrew).

El-Hinnawi, E.E., Kabesh, M.L., Zahran, I., 1973. Mineralogy and chemistry of Nubian sandstones from the Central Eastern Desert of Egypt. Neues Jahrbuch Mineralogische Abhandlungen 118, 211–234.

El Shazly, M.M., Shata, A., 1960. Contribution to the study of the heavy minerals in the Nubian Sandstone section of the New Valley Project area. Part 1. El Kharga Oasis. Bulletin de l'Institut du Désert d'Egypte 10, 11–25.

Eshet, Y., Rampino, M.R., Visscher, H., 1995. Fungal event and palynological record of ecological crisis and recovery across the Permian-Triassic boundary. Geology 23, 967–970.

Evans, D.S., Lathon, R.B., Senalp, M., Connally, T.C., 1991. Stratigraphy of the Wajid Sandstone of southwestern Saudi Arabia. Proceedings of 7th SPE Middle East Oil Shows Conference, Bahrain, pp. 947–960.

Freund, R., Garfunkel, Z., Zak, I., Goldberg, M., Weissbrod, T., Derin, B., 1970. The shear along the Dead Sea rift. Philosophical Transactions Royal Society London, Series A 267, 107–130.

Garfunkel, Z., 1999. History and palaeogeography during the Pan-African orogen to stable platform transition: reappraisal of the evidence from the Elat area and the northern Arabian-Nubian Shield. Israel Journal of Earth Sciences 48, 135–157.

Garfunkel, Z., 2002. Early Palaeozoic sediments of NE Africa and Arabia. Products of continental-scale erosion, sediment transport, and deposition. Israel Journal of Earth Sciences 51, 135–156.

Goldberg, M., 1970. The Lithostratigraphy of the Arad Group (Jurassic) in the Northern Negev. Ph.D. thesis. Hebrew University of Jerusalem, 178pp. (in Hebrew).

Goldbery, R., 1979. Sedimentology of the Lower Jurassic flint clay-bearing Mishhor Formation, Makhtesh Ramon, Israel. Sedimentology 26, 229–251.

Greenberg, M., 1968. Type section of the Lower Cretaceous Hatira Formation in Hamakhtesh Hagadol Northern Negev. Israel Geological Survey, Stratigraphic Sections, 5, 6pp.

Grothaus, B., Eppler, D., Ehrlich, R., 1979. Depositional environment and structural implications of the Hammamat Formation, Egypt. Annales Egyptian Geological Survey 9, 564–590.

Gvirtzman, G., Weissbrod, T., 1984. The Hercynian geanticline of Helez and the late Palaeozoic history of the Levant. In: Dixon, J.E., Robertson, A.H.F. (Eds.), The Geological Evolution of the Eastern Mediterrainan, vol. 17. Geological Society of London, Special Publication, pp. 177–186.

Gvirtzman, G., Weissbrod, T., Ginzburg, A., 1988. The Palaeozoic Riyadh Geanticline in central Saudi Arabia: a structure similar to the Helez Geanticline: Israel Geological Society Annual Meeting, En Boqeq, pp. 46–47 (Abstract).

Hadley, D.G., Schmidt, D.L., 1980. Sedimentary rocks and basins of the Arabian Shield and their evolution. In: Cooray, P.G., Tahoun, S.A. (Eds.), Evolution and Mineralization of the Arabian-Nubian Shield, vol. 4. Pergamon Press, Jiddah, Saudi Arabia, pp. 26–50.

Harlavan, Y., 1991. Geochronology of the clay minerals in the Palaeozoic section in southern Israel. Israel Geological Survey Report GSI/2/92, 150pp.

Karcz, I., Key, C.A., 1966. Note on the pre-Palaeozoic morphology of the basement in the Timna area (southern Israel). Israel Journal of Earth Sciences 15, 47–56.

Karcz, I., Weiler, Y., Key, C.A., 1971. Lithology and environment of deposition of the "Amudei Shelomo Sandstone" in Nahal Shani, Elat. Israel Journal of Earth Sciences 22, 119–124.

Keeley, M.L., 1989. The Palaeozoic history of the Western Desert of Egypt. Basin Research 2, 35–48.

Ketin, I., 1966. Cambrian outcrops in southeastern Turkey and their comparison with the Cambrian of east Iran. Bulletin Mineral Resources Exploration Institute Turkey 66, 77–89.
Klitzsch, E., 1990. Palaeozoic. In: Said, R. (Ed.), The Geology of Egypt, Chapter 21. Balkema, Rotterdam, pp. 393–406.
Klitzsch, E., Wycisk, P., 1987. Geology of the sedimentary basins of northern Sudan and bordering areas. Berliner Geowissenschaftliche Abhandlungen (A) 75, 97–135.
Kohn, B., Weissbrod, T., 1993. Fission track of authigenic apatite in Cambrian sediments, southern Israel: implications for timing of initiation of the Dead Sea transform. Nuclear Tracks and Radiation Measurements 21, 595.
Konert, G., Al-Afifi, A.M., Al-Hajri, S.A., Droste, H.J., 2001. Palaeozoic stratigraphy and hydrocarbon habitat of the Arabian Plate. GeoArabia 6, 407–442.
Lillich, W., 1969. Sedimentologische Untersuchungen in kambrischen Jordaniens. Geologische Jahrbbuch 81, 13–34.
Lüning, S., Craig, J., Loydell, D.K., Storch, P., Fitches, B., 2000. Lower Silurian hot shale in North Africa and Arabia: regional distribution and depositional model. Earth-Science Reviews 49, 121–200.
McClure, H.A., Hussey, E., Kaill, I., 1988. Permian-Carboniferous glacial deposits in southern Arabia. Geologische Jahrbuch Reihe B 68, 3–31.
McKee, E.D., 1962. Origin of the Nubian and similar sandstones. Geologische Rundschau 52, 551–587.
Nasir, S., Sadeddin, W., 1989. The heavy minerals of the Kurnub Sandstone (Early Cretaceous) of Jordan. Sedimentary Geology 62, 101–107.
Nasir, S., Sadeddin, W., 1990. The heavy minerals of the Kurnub Sandstone (Early Cretaceous) of Jordan—reply to comments by B. Amireh. Sedimentary Geology 68, 315–328.
Petters, S.W., 1991. Regional Geology of Africa. Springer-Verlag, Berlin, 722pp.
Picard, L., 1938. Synopsis of stratigraphic terms in Palestinian geology. Hebrew University, Geological Department Bulletin 2, 24.
Pomeyrol, R., 1968. Nubian Sandstone. American Association Petroleum Geologists Bulletin 52, 589–600.
Powell, J.H., 1989. Stratigraphy and sedimentation of the Phanerozoic rocks in central and south Jordan. Part A: Ram and Khreim groups. National Resources Authority Geological Bulletin 11, 72pp.
Powell, J.H., Mohamed, B.K., Masri, A., 1994. Late Ordovician-Early Silurian glaciofluvial deposits preserved in palaeovalleys in south Jordan. Sedimentary Geology 89, 303–314.
Powers, R.W., Ramirez, L.F., Redmond, C.D., Elberg, E.L., Jr., 1966. Geology of the Arabian Peninsula—Sedimentary geology of Saudi Arabia. U.S. Geological Survey Professional Paper No. 560-D, 147.
Rüssegger, J., 1847. Reisen in Europa, Asien und Afrika, Bd. 3, Reisen in Unter-Egypten, auf der Halbinsel der Sinai und im gelobten Land. E. Schweizerbart, Stuttgart, Germany, 292pp.
Rybakov, M., Goldshmidt, V., Shamir, G., 1996. The use of magnetic patterns for plate reconstruction: an example from the Mediterranean-Red Sea region. Israel Journal of Earth Sciences 45, 147–151.
Schandelmeier, H., Reynolds, P.O., Semtner, A.K. (Eds.), 1997. Palaeogeographic-Palaeotectonic Atlas of North-Eastern Africa, Arabia, and Adjacent Areas. Balkema, Rotterdam.
Selley, R.C., 1972. Diagnosis of marine and non-marine environments from the Cambro-Ordovician sandstones of Jordan. Journal Geological Society, London 128, 135–150.
Shukri, N.M., El Ayouti, 1953. The mineralogy of the Nubian Sandstone in Aswan. Bulletin de l'Institut du Désert d'Egypte 3, 65–88.
Shukri, N.M., Said, R., 1945. Contribution to the geology of the Nubian Sandstone. Bulletin de l'Institut du Désert d'Egypte 27, 229–264.

Soliman, S.M., El Fetouh, M., 1969. Lithostratigraphy of the Carboniferous Nubian-type sandstones in west-central Sinai, Egypt. 6th Arab Science Congress, Damascus, Part 4 (A), pp. 311–377.

Stacey, J.S., Hedge, C.E., 1984. Geochronologic and isotopic evidence for early Proterozoic crust in the eastern Arabian shield. Geology 12, 310–313.

Stern, R.J., 1994. Arc assembly and continental collision in the Neoproterozoic East African orogen: implications for the consolidation of Gondwanaland. Annual Review of Earth Planetary Sciences 22, 319–351.

Stump, T.E., Van der Eem, J.G., 1994. Overview of the stratigraphy, depositional environments and periods of deformation of the Wajid outcrop belt, southwestern Saudi Arabia. In: Al-Husseini, M.I. (Ed.), GEO 94—The Middle East Petroleum Geosciences, vol. 2, pp. 867–876.

Stump, T.E., Van der Eem, J.G., 1995. The stratigraphy, depositional environments and periods of deformation of the Wajid outcrop belt, southwestern Saudi Arabia. Journal of African Earth Sciences 21, 421–441.

Vaslet, D., 1990. Upper Ordovician glacial deposits in Saudi Arabia. Episodes 13, 147–161.

Vroman, A., 1944. The petrology of sandy sediments of Palestine. Bulletin of the Geological Department, Hebrew University of Jerusalem 5, 1–11.

Weissbrod, T., 1969. The Palaeozoic of Israel and adjacent countries: Part I—The subsurface Palaeozoic stratigraphy of southern Israel. Israel Geological Survey, Bulletin 47, 1–23.

Weissbrod, T., 1980. The Palaeozoic of Israel and Adjacent Countries (Lithostratigraphic Study). Ph.D. thesis. Hebrew University, Jerusalem, 275pp. (In Hebrew, with English abstract).

Weissbrod, T., 2002. Stratigraphy and correlation of the Lower Cretaceous exposures across the Dead Sea transform with emphasis on tracing the Amir Formation in Jordan. Israel Journal of Earth Sciences 51, 55–78.

Weissbrod, T., 2003. Middle to Late Cambrian vertical movements in Sinai and the Eastern Desert of Egypt: lithostratigraphic consequence. Israel Journal of Earth Sciences 52, 97–111.

Weissbrod, T., 2004. A reassessment of the Naqus Formation in Sinai and the Eastern Desert of Egypt: stratigraphic and tectonic implications. Israel Journal of Earth Sciences 53, 87–97.

Weissbrod, T., 2005. The Palaeozoic in Israel and environs. In: Hall, J.K., Krasheninnikov, V.A., Hirsch, F., Benjamini, C., Flexer, A. (Eds.), Geological Framework of the Levant, vol. II, The Levantine Basin and Israel, Chapter 18b. Historical Productions-Hall, Jerusalem, pp. 283–316.

Weissbrod, T., Gvirtzman, G., 1988. The Late Devonian event in the Near East. Courier Forschungsinstitut Senckenberg 100, 221–233.

Weissbrod, T., Nachmias, J., 1986. Stratigraphic significance of heavy minerals in the Late Precambrian-Mesozoic clastic sequence (''Nubian Sandstone'') in the Near East. Sedimentary Geology 47, 263–291.

Weissbrod, T., Perath, I., Nachmias, J., 1987. Apatite as a palaeoenvironmental indicator in the Precambrian-Mesozoic clastic sequence of the Near East. Journal of African Earth Sciences 6, 797–805.

Weissbrod, T., Sneh, A., 2002. Sedimentology and palaeogeography of the Late Precambrian-Early Cambrian arkosic and conglomeratic facies in the northern margin of the Arabo-Nubian Shield. Israel Geological Survey Bulletin 87, 44.

Wilde, S., Youssef, 2002. A re-evaluation of the origin and setting of the Late Precambrian Hammamat Group based on SHRIMP U-Pb dating of detrital zircons from Gebel Umm Tawat, North Eastern Desert, Egypt. Journal of the Geological Society, London 159, 595–604.

Wycisk, P., 1990. Aspects of cratonal sedimentation: facies distribution of fluvial and shallow marine sequences in NW Sudan/SW Egypt since Silurian time. Journal of African Earth Sciences 10, 215–228.

Chapter 27

THE USE OF HEAVY MINERALS IN THE RECONSTRUCTION OF ICE-SHEET DRAINAGE PATTERNS: AN EXAMPLE FROM THE EDGE OF THE EAST ANTARCTIC ICE SHEET

SANDRA PASSCHIER

Department of Earth and Environmental Studies, Mallory Hall 252, Montclair State University, Montclair, NJ 07043, USA

ABSTRACT

Heavy-mineral analysis is proven as a powerful tool in reconstructing ice-sheet drainage patterns and has been used in the past in both drift exploration and studies of ice-sheet dynamics. Although ice flow patterns can be extracted from morphological indicators such as striated and grooved bedrock surfaces, clast orientation in tills, or glacial landforms, these properties are not suitable to analyse the sequence of multiple ice-sheet events. Antarctica has been glaciated for the past 34 Myr and has experienced several glacial advances and retreats. Here a case study is presented in which heavy minerals were used to reconstruct East Antarctic glacial events in the Transantarctic Mountains that form an active rift margin. Heavy-mineral analyses demonstrate that the tills in these mountains should be subdivided into at least two end-member petrofacies. The first petrofacies is characterised by tills derived from the highest stratigraphic succession of the Transantarctic Mountains, which were deposited when ice was overriding the mountains. Tills of the second petrofacies originate from erosion and deposition within the glacial troughs that traverse the Transantarctic Mountains, and now form the drainage pathway for the outlet glaciers of the East Antarctic ice sheet. The two petrofacies represent different ice-sheet drainage patterns and the tills were deposited during consecutive stages of denudation of the rift margin.

Keywords: heavy minerals; till; ice-sheet drainage; glacial events; Transantarctic Mountains

1. INTRODUCTION

The heavy-mineral composition of glacial sediments has long been of interest in both ore exploration and glacial studies, the latter including subjects such as till provenance, till stratigraphy, and the processes involving erosion and transport of

Developments in Sedimentology, Vol. 58, 677–699

ISSN: 0070-4571/doi:10.1016/S0070-4571(07)58027-1

glacial debris (Dreimanis and Vagners, 1972; Peuraniemi, 1990; Shilts, 1996). More recently, the heavy-mineral composition of deposits on the margins of large continental ice-sheets has received attention because of its potential in reconstructing ice-sheet drainage patterns and ice-sheet dynamics (e.g., Gravenor, 1979; Gwyn and Dreimanis, 1979; Zandstra, 1983; Rappol and Stoltenberg, 1985; Passchier, 2001). Studies of the behaviour of continental ice-sheets are important because of the global effects of changes in ice-sheet volume.

Knowledge of the location and timing of major ice drainage paths is crucial for the reconstruction of former continental ice-sheets (Stokes and Clark, 2001). The main controls on ice-flow patterns are the position of snow-accumulation areas and subglacial topography. During glaciation of a continent, the main snow-accumulation areas shift in response to climatic and glaciological effects. Glacial lineations and till fabric analyses can be used to reconstruct Quaternary ice-sheet drainage patterns (e.g., Boulton and Clark, 1990). However, these properties alone usually indicate the youngest drainage stage of an ice-sheet and preclude interpretations of changing sediment transport paths during glaciation. Compositional analyses of tills reflect the pathways of glacial dispersal and the sequence of erosional events. Even though bulk geochemical surveys have become common practice in determining till provenance due to the availability of inexpensive analytical techniques (McClenaghan et al., 2000), a study of the sand and gravel-sized fraction of till is necessary to identify all the sediment sources (Shilts, 1996).

Heavy-mineral assemblages can provide unique information on the composition of a given sediment, not available through thin section analysis or bulk chemical techniques. The purpose of this chapter is: (1) to present a review on the value of heavy minerals in reconstructing ice-sheet drainage patterns, and (2) to demonstrate the use of heavy minerals in a case study concerning the drainage history of the East Antarctic ice sheet.

2. BACKGROUND

2.1. Glacial Processes and Glacial Dispersal

Glacial erosion occurs through abrasion and plucking of rigid substrates by debris-laden basal ice and through deformation of unconsolidated (soft) substrates (Alley et al., 1986; Boulton, 1996). The eroded sediment is homogenised in the basal debris zone of a glacier or ice-sheet and the resulting sediment is called a till. As a glacier or ice-sheet erodes a source rock with a distinct mineralogical composition, the basal glacial debris downstream will have a specific composition, which is called a dispersal train by Shilts (1996). Single-flow dispersal trains are narrow ribbon-like bands with abrupt lateral and vertical contacts, which climb gently downstream within the basal debris zone (DiLabio, 1990). However, shifting ice-flow directions through a major continental glaciation may produce fan-shaped dispersal patterns. Continental ice-sheets, in particular, erode many different source rock types along a flow-line, and the composition of tills deposited in the ice-marginal area will reflect the combination of consecutive dispersal trains.

During glacial transport, rock fragments and mineral grains in the basal debris zone are comminuted to their terminal grades, because the effect of crushing and abrasion during glacial transport decreases with particle size (Dreimanis and Vagners, 1972). The terminal grade represents a specific particle size range for each mineral in a till matrix, which depends on the original mineral size in the source rock, and the mechanical stability of each mineral. Resistant minerals, such as garnets, are comminuted to their terminal grades after glacial transport of 80–180 km, whereas mechanically unstable minerals, such as dolomite, reach their terminal grade within 0–3 km of transport. For most minerals the terminal grade is in the sand or silt-size range (Dreimanis and Vagners, 1972; Haldorsen, 1981), but well-crystallised phyllosilicates may be grounded to clay-sized fragments (Shilts, 1996). The difference in the original size and mechanical stability of the minerals leads to partitioning of components in the different size fractions of a till.

2.2. *Use of Heavy Minerals in Determining the Provenance of Tills Derived from Continental Ice-Sheets*

Heavy-mineral assemblages in glacial sediments are controlled by three main factors: (1) the composition of the source rock, (2) the mechanical resistance of minerals to crushing and abrasion during glacial transport, and (3) dissolution caused by diagenesis and chemical weathering at different stages of glacial-interglacial sedimentation (Dreimanis and Vagners, 1972; Gravenor, 1979). Microscopic analyses of heavy-mineral assemblages are usually carried out on the fine-sand size fraction, where the effects of mechanical and chemical processes on the heavy-mineral composition are best identified. However, the partitioning of components in a till during glacial transport causes some minerals, e.g., phyllosilicates, to be underrepresented in the heavy-mineral separates. If necessary, other techniques, such as bulk X-ray diffraction (XRD) or bulk multi-element geochemistry, can be used in combination with the heavy-mineral analyses to assess the provenance and weathering history of tills.

Heavy-mineral studies in glacial sediments have been used to reconstruct ice-flow patterns. For example, Gwyn and Dreimanis (1979) and Rappol and Stoltenberg (1985) showed that source rock composition is the main control on the heavy-mineral composition of the Late Pleistocene tills at the margins of the Canadian and Scandinavian Shields. Along the southern border of the Canadian Shield, the heavy-mineral composition of till samples is representative of source rocks exposed 50–150 km up-glacier. The geographic distribution of heavy-mineral assemblages has revealed the flow paths of Late Pleistocene glacial lobes in the Great Lakes region (Gwyn and Dreimanis, 1979). Tills in the Netherlands can be subdivided into (1) flint-rich, with a dominance of epidote and stable minerals of West Baltic origin, and (2) flint-poor, with a relatively high amount of amphibole and garnet derived from Palaeozoic and Precambrian rocks in the East Central Baltic. The variation in the heavy-mineral assemblages can be attributed to deposition by ice streams from different sources and with a different flow pattern (Rappol and Stoltenberg, 1985; Haldorsen et al., 1989).

Although the Pleistocene ice sheets and their deposits in the Northern hemisphere form good analogues for the study of ancient glaciations, some important differences

need to be kept in mind. The Pleistocene ice sheets were present during a relatively short time and developed in tectonically stable shield and platform settings. When ice sheets are active for much longer periods of time, crustal uplift, subsidence, and chemical weathering between glaciations may affect heavy-mineral assemblages (Gravenor, 1979). Irrespective of the erosional process, the tectonic setting has a strong control on heavy-mineral assemblages on continental margins (Nechaev and Isphording, 1993) that may be masked by effects of chemical weathering, diagenesis, and sediment recycling. Thus, the resulting heavy-mineral suites have lower abundances of unstable minerals and become enriched in the mechanically and chemically resistant species (Morton and Hallsworth, 1999).

3. SIRIUS GROUP: GLACIAL DEPOSITS AT THE MARGIN OF THE EAST ANTARCTIC ICE SHEET

Antarctic glaciation commenced with small ephemeral ice sheets during the Late Eocene (Hambrey and Barrett, 1993; Zachos et al., 2001). Chemical weathering prevailed on the Antarctic continent in the Eocene with a steady decrease in the supply of chemical weathering products from the Late Eocene to the Late Oligocene marking the onset of continental glaciation (Ehrmann and Mackensen, 1992; Robert and Chamley, 1992). Antarctica's Neogene glacial history is poorly known, because of a scarcity of records from drilling on the Antarctic continental margin. The Sirius Group, formerly called the Sirius Formation (Mercer, 1972), comprises glaciogenic strata overlying pre-Tertiary rocks in the Transantarctic Mountains. Outcrops occur from the regions of the Reedy Glacier in the southern Transantarctic Mountains to David Glacier in southern Victoria Land (Fig. 1). The sediments consist mainly of diamictons, with some pebbly sands and muds of terrestrial and shallow marine glacial origin (Mercer, 1972; Mayewski and Goldthwait, 1985; McKelvey et al., 1991; Verbers and Van der Wateren, 1992; Webb et al., 1996; Stroeven and Prentice, 1997). The age of the Sirius Group is a subject of debate because of the uncertainties in transport pathways for Pliocene diatoms in the tills (Harwood and Webb, 1998; Stroeven et al., 1998). Reported ages range from older than Middle Miocene (>14 Ma) to late Pliocene (2.5–3.1 Ma).

The Transantarctic Mountains form the uplifted margin of the Ross Sea rift system separating the East Antarctic craton from the West Antarctic crustal blocks (Fig. 1). Basement rocks in the Transantarctic Mountains are composed of Precambrian and Cambrian meta-sediments, Cambro-Ordovician granites of the Granite Harbour Intrusives, and the Devonian Admiralty Intrusives (Stump, 1995). The Beacon Supergroup unconformably overlies the Precambrian-Lower Palaeozoic basement and consists of glacial, fluvial, and shallow marine sediments (Barrett, 1991). During the Jurassic, the Beacon Supergroup was intruded and capped by tholeiitic basalts of the Ferrar Group, forming dolerite sills and flood basalts (Tingey, 1991). The flood basalts that cap the Beacon Supergroup are referred to as the Kirkpatrick Basalt. In the Neogene, alkaline basalts and tephras of the McMurdo Volcanic Group erupted (Kyle, 1990). Sirius Group deposits unconformably overlie metamorphic basement, deformed Beacon Supergroup, and the striated or grooved Ferrar Dolerite surfaces (Mabin, 1986).

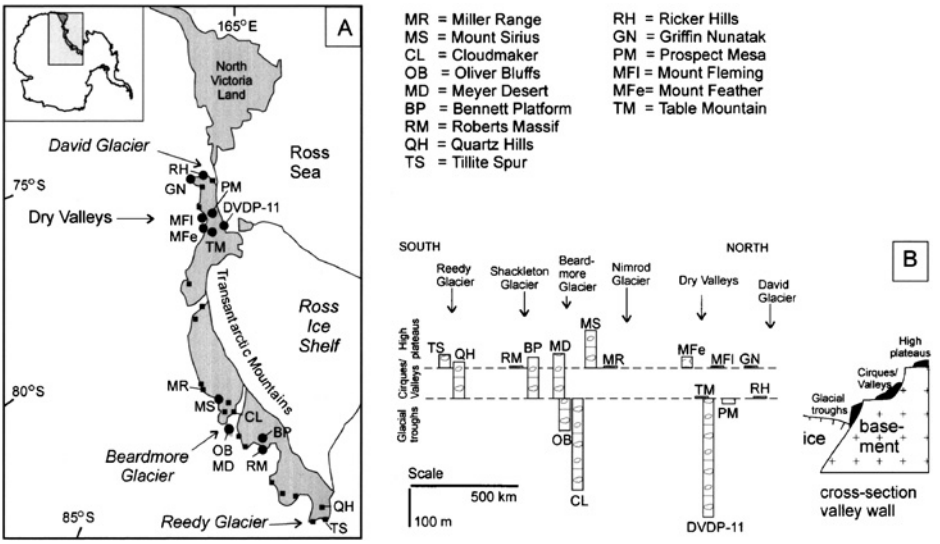

Fig. 1. (A) Location of important Sirius Group outcrops in of the Transantarctic Mountains (small squares) and the outcrops selected for this study (large dots). (B) Stratigraphic thickness, topographic position, and geomorphological setting of the best documented and best preserved Sirius Group and other Late Cenozoic successions.

At present, the East Antarctic ice-sheet drains through several large outlet glaciers flowing perpendicular to the Transantarctic Mountain front. Between 74° and 87° South, the present drainage system is characterised by 32 over-deepened glacial troughs, which dissect the Transantarctic Mountains between the East Antarctic polar plateau and the Ross Sea Basin (Webb, 1994). The Sirius Group is exposed in two typical settings: as thin erosional remnants of tills on flat mountain summits, and in up to over 100 m thick vertical sections along the walls of the glacial troughs (Figs. 1B and 2). In the Dry Valleys, the Sirius Group crops out as relatively thin till sheets on mountain summits at high elevation. In the central and southern Transantarctic Mountains, the deposits are thicker and comprise diamictons and stratified successions. Equivalent glaciomarine sediments of Late Miocene (>5.6 Ma) to Early Pliocene age (Ishman and Rieck, 1992) have been recovered in the Dry Valleys Drilling Project Hole 11 (DVDP-11) in the floor of Taylor Valley and at Prospect Mesa in Wright Valley.

4. METHODS

Heavy minerals of 42 samples were separated by gravity settling in sodium polytungstate (density 2.89). The samples were selected to represent as large geographical and stratigraphic coverage as possible. The weight of the heavy-mineral fraction was determined, and the magnetic minerals were separated from the heavy-mineral fraction and also weighed. Non-magnetic heavy minerals were mounted on glass slides using Norland optical adhesive 61 with a refractive index of 1.6 for

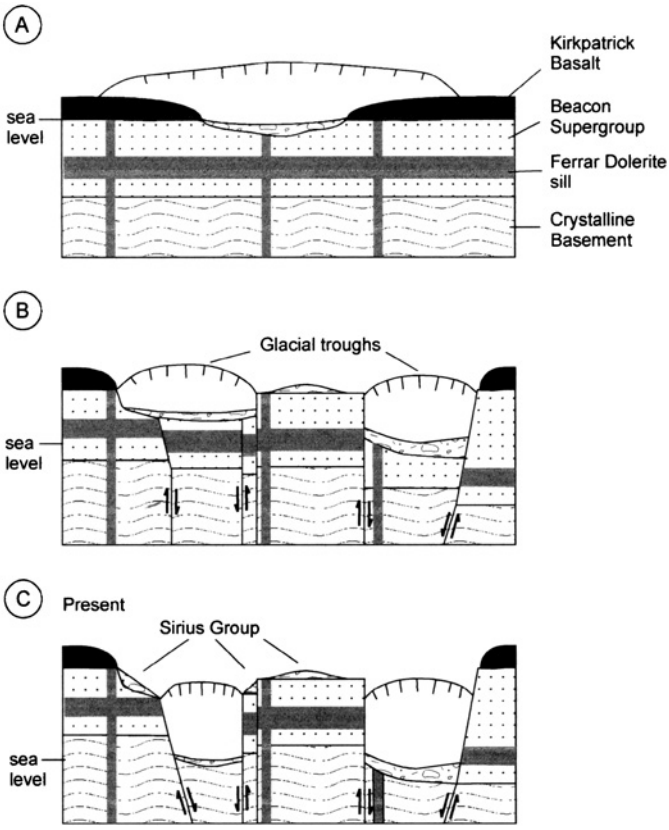

Fig. 2. Geological framework and conceptual model of landscape evolution in the Transantarctic Mountains. (A) Overriding of the Transantarctic Mountains during early stages of glaciation. (B) Development of over-deepened glacial troughs due to uplift and structural segmentation of the Transantarctic Mountains, deposition in terrestrial glacial environments as well as in fjords. (C) Topographic distribution of the Sirius Group in relation to the present morphology of the Transantarctic Mountains.

microscopic identification. The fine-sand fraction (125–250 μm) was used in this study because identification of minerals using optical properties can be more difficult for grains >250 μm, and because the 63–125 μm fraction of some tills from the Transantarctic Mountains is virtually free of heavy minerals (Faure et al., 1995). The latter could be the result of differential chemical weathering (Passchier, 2004) that affects smaller grains more than larger ones. Over 300 grains were counted in each grain mount to estimate the heavy-mineral composition (Fig. 3).

Eight heavy-mineral fractions were examined by XRD. The heavy minerals were crushed with mortar and pestle, and the powder mounts were spiked with alpha-alumina (corundum) for peak calibration purposes. The powders were pressed into aluminium sample holders at random orientation and glycolated (ethylene glycol) for 12 h prior to the analysis. Samples were analysed on a Rigaku Miniflex XRD system with an automated sample changer at the Crary Laboratory in McMurdo

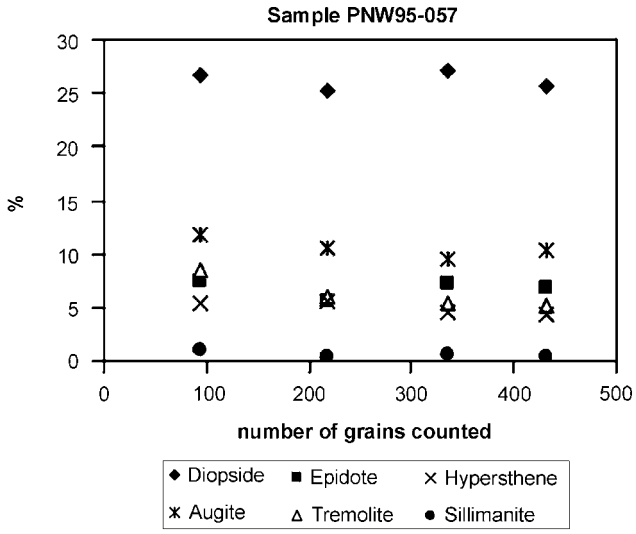

Fig. 3. Test of number of grains to be counted before heavy-mineral grain counts stabilise. Based on this test it was decided that a count of 300 grains per sample was sufficient for this study.

Station, Antarctica. The samples were X-rayed with CuKα radiation (30 kV, 15 mA) with a scan range from 3° to 65° 2α, a step size of 0.02°, and a dwell time of 2 sec per step. The digital data were interpreted using Jade 3.0 software, which comprises a search-match routine based on a Powder Diffraction File (International Center for Diffraction Data). During the Jade 3.0 procedure, background was removed and the diffractograms were calibrated using the peak position of the internal standard (corundum).

5. HEAVY-MINERAL COMPOSITION AND DISTRIBUTION

Clinopyroxenes are the dominant heavy minerals in the Sirius Group and related deposits, which have lithological characteristics similar to those of the Sirius Group but are not officially included in the stratigraphic group identified as Sirius Group (Table 1). Several different varieties occur. Colourless clinopyroxenes with a good cleavage are the most abundant, and colourless, light green, and brown clinopyroxenes without cleavage also occur. Pigeonite was identified by XRD analysis and is a major constituent in most samples from the central Transantarctic Mountains, and in the lowermost part of DVDP-11. Titanaugite and aegerine were optically identified in DVDP-11. Orthopyroxene is a major constituent of some heavy-mineral fractions and most abundant are large grains of pleochroic hypersthene. Olivine was optically identified in the upper part of DVDP-11. Trace amounts of olivine occur in some heavy-mineral fractions of the Sirius Group of the central Transantarctic Mountains. XRD confirmed the presence of ferroan forsterite in samples from DVDP-11 and the Dominion Range.

Table 1. Percentages of minerals in fine-sand heavy-mineral fractions

Sample	cpx1	cpx2	cpx3	opx	am1	am2	am3	gt	stab	ep	bio	ol	ox	op	lith	other	Wt.%
Roberts Massif																	
PNW95–002	1	11	20	2	19	<1	4	0	1	20	0	0	10	1	6	5	14
PNW95–012	11	5	33	8	3	0	4	<1	1	8	0	0	9	1	15	3	17
PNW95–013	5	3	48	6	0	<1	1	<1	1	6	0	0	15	2	8	5	13
PNW95–022	3	3	45	2	3	0	1	1	1	17	0	0	14	4	5	2	5
PNW95–023	3	3	48	6	2	0	1	1	0	7	0	0	16	2	9	2	7
PNW95–032	6	8	37	4	2	0	0	0	<1	18	0	0	12	2	7	3	7
Bennett Platform																	
PNW95–053	6	1	38	10	5	0	2	<1	0	8	0	0	11	1	15	3	22
PNW95–055	13	2	32	5	3	0	1	0	0	8	0	0	15	<1	20	3	25
PNW95–057	10	0	28	5	12	0	6	<1	1	7	0	0	15	1	11	5	14
PNW95–059	15	2	31	5	2	0	2	0	0	6	0	0	19	<1	15	3	13
PNW95–061	7	1	42	7	2	0	3	0	<1	7	0	0	8	2	18	4	21
PNW95–063	15	1	36	3	3	0	1	<1	0	3	0	0	20	1	14	3	21
PNW95–065	5	2	47	5	2	0	2	<1	<1	2	0	0	19	2	10	5	19
PNW95–066	6	0	33	4	12	0	5	1	0	8	0	0	15	2	8	5	12
PNW95–068	23	3	18	10	4	<1	3	0	<1	15	0	3	16	<1	4	3	18
Mount Sirius																	
S-6	7	0	18	9	9	0	3	26	3	1	0	0	11	4	5	4	2
S-4	9	1	22	8	<1	0	6	21	2	3	1	1	9	2	10	7	1
S-9	6	<1	13	7	7	0	6	23	2	5	1	0	8	2	10	10	3
S-12	14	0	7	21	3	<1	0	15	4	4	0	0	2	8	18	3	2
Dominion Range—Meyer Desert Section 13																	
13–8	3	<1	34	5	5	0	6	2	<1	4	0	0	15	1	22	3	4
13–4	25	0	24	8	0	0	0	1	2	9	0	2	18	1	7	4	10
13–2	10	0	29	10	1	0	2	1	<1	12	0	0	14	2	9	9	8

Dominion Range—Oliver Bluffs																	
18-May	9	0	37	7	7	0	<1	2	2	7	0	1	10	3	10	6	13
14-May	8	1	28	7	6	0	2	1	<1	10	0	0	12	1	21	3	27
12-May	4	0	32	2	5	<1	2	1	<1	10	0	<1	19	1	22	3	18
10-May	22	0	11	9	0	0	5	0	<1	7	0	0	13	4	23	6	9
5–8b	5	1	34	2	5	0	1	0	<1	11	0	0	17	1	19	3	7
6-May	7	<1	33	3	6	0	3	2	1	4	0	0	20	2	14	6	7
4-May	27	0	16	8	0	0	2	<1	3	4	0	0	10	0	25	5	26
2-May	6	1	21	2	2	0	<1	0	0	16	0	0	22	1	25	3	17
95DMH051	15	0	24	7	4	0	2	1	1	8	0	1	14	4	17	3	11
Dry Valley Drilling Project Core 11 (DVDP-11)																	
21.3–23.8 mbsf	9	1	16	7	<1	1	1	0	5	1	0	18	16	9	13	3	19
120.06–120.16	7	1	22	13	1	3	13	<1	8	4	2	0	16	3	4	4	8
156.52–156.62	10	0	8	8	0	0	26	0	4	<1	1	0	18	5	8	13	14
170.35–170.45	5	0	16	10	4	5	19	1	6	<1	1	0	18	3	7	6	14
221.94–222.04	7	3	12	8	4	5	19	0	7	2	4	0	8	1	16	3	14
279.90–280.00	2	3	24	6	4	4	10	0	4	2	5	0	19	3	13	2	10
311.62–311.72	3	5	25	25	4	5	12	0	5	2	2	1	3	1	2	5	12
324.95–325.05	1	3	29	24	7	12	5	<1	4	2	1	0	4	<1	6	2	10
Dry Valleys Sirius Group																	
Mt. Feather	0	0	<1	1	0	0	0	54	4	5	1	0	27	2	6	1	<1
Mt. Flem. #2	0	<1	1	<1	0	0	0	20	16	1	0	0	53	<1	7	3	<1
Prospect Mesa	2	1	44	16	15	1	2	0	0	3	0	0	8	1	1	4	23

Notes: The "other" group consists of chlorite, sillimanite, kyanite, staurolite, topaz, beryl, vesuvianite, serpentine, and unidentified species. Stable minerals include apatite, rutile, zircon, tourmaline, monazite, and sphene.

Garnet is the dominant heavy mineral in samples from Mount Sirius, Mount Fleming, and Mount Feather (Fig. 1). Both colourless and pink garnets are present but the former are more abundant. Some garnet grains are well rounded; others have characteristic etch features. XRD of the heavy-mineral fraction of a sample from Mount Sirius revealed that the garnets in this sample were almandines (Fig. 4). A second, colourless variety with numerous inclusions occurs in samples with low overall garnet content.

Amphiboles of the central Transantarctic Mountains are mainly colourless and appear to be tremolite/actinolite and anthophyllite. In DVDP-11, brown-green and blue-green pleochroic hornblende varieties are more abundant. The epidote group is represented by light green to light yellow pleochroic grains in central Transantarctic

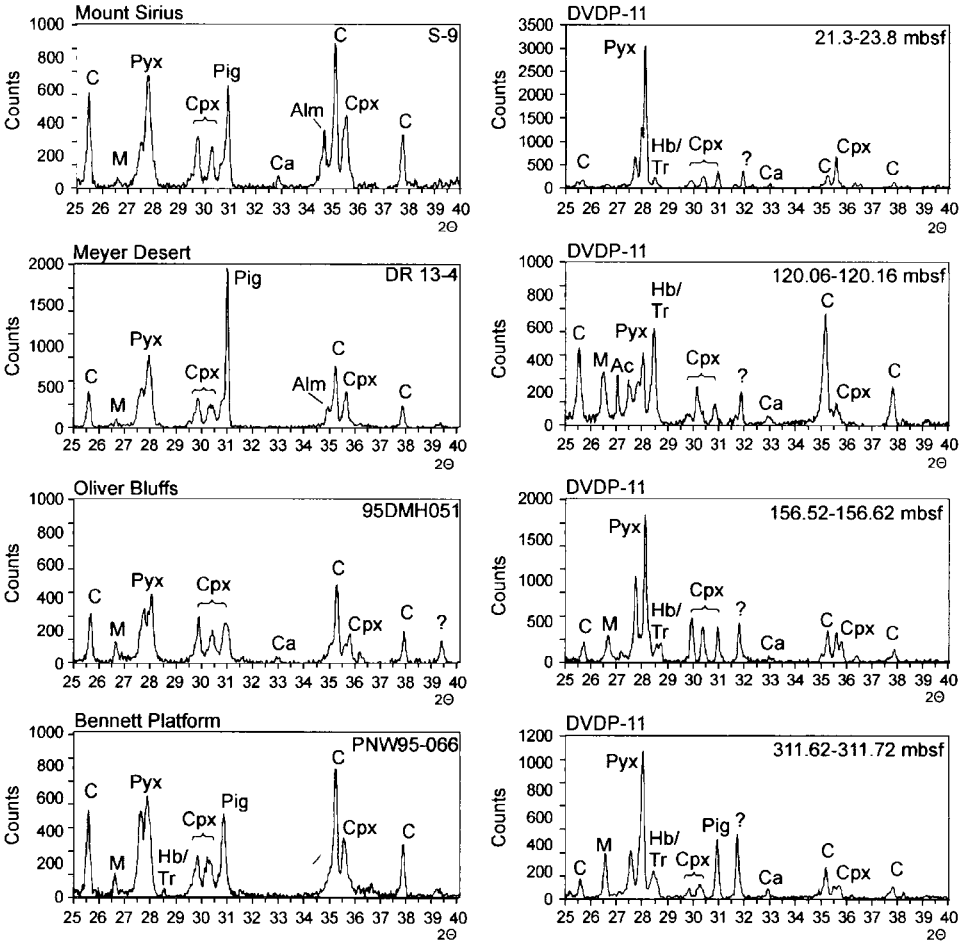

Fig. 4. X-ray diffraction analysis of fine-sand heavy-mineral fractions from four Sirius Group locations in the central Transantarctic Mountains, and from four depths in core from DVDP-11, South Victoria Land. C = corundum (standard); M = mica; Pyx = pyroxene; Cpx = clinopyroxene; Pig = pigeonite; Ca = calcite; Alm = almandine; Hb/Tr = hornblende/tremolite; Ac = actinolite.

Mountains samples. The shapes of these grains are generally irregular. Much stronger coloured lemon-grass-green epidote grains occur in heavy-mineral fractions from the Dry Valleys and some have characteristic blue and yellow anomalous interference colours. Stable minerals include apatite, rutile, zircon, tourmaline, monazite, and sphene. Most of them are rounded, but subhedral apatite, zircon, monazite, and sphene occur in DVDP-11. Biotite is quite abundant in some intervals of DVDP-11, and it was detected by XRD in the heavy-mineral fraction of Mount Sirius (Fig. 4). Other mineral species, such as chlorite, sillimanite, kyanite, staurolite, topaz, beryl, vesuvianite, and serpentine, were encountered in appreciable quantities only in individual samples or appear in trace amounts. For example, large sillimanite grains were observed in the tills at Mount Sirius, but are rare in other tills of the Sirius Group. Non-magnetic opaques, oxidised, highly etched grains, and rock fragments are also present but could not be identified by optical properties alone.

A ternary plot of the relative proportions of clinopyroxenes, amphiboles, and stable minerals, including garnet, illustrates that the heavy-mineral fractions of Mount Fleming and Mount Feather Sirius Group sediments are more enriched in garnet and stable minerals such as apatite, rutile, and zircon. They also contain many oxidised grains (Fig. 5). At Mount Sirius, in most heavy-mineral fractions, garnet is dominant followed by pyroxenes. In contrast, Dominion Range, Bennett Platform, and Roberts Massif deposits are dominated by clinopyroxenes. DVDP-11 samples contain more amphiboles and stable minerals.

Weight percentages of heavy minerals in the fine-sand fraction vary from <1 to 27% (Table 1). The highest percentages of heavy minerals occur in deposits in the glacial valleys at Oliver Bluffs, Bennett Platform, and Prospect Mesa, while the lowest percentages were found at Mount Sirius, Mount Feather, and Mount Fleming in deposits at high elevation. A clear relationship exists between garnet and pyroxene

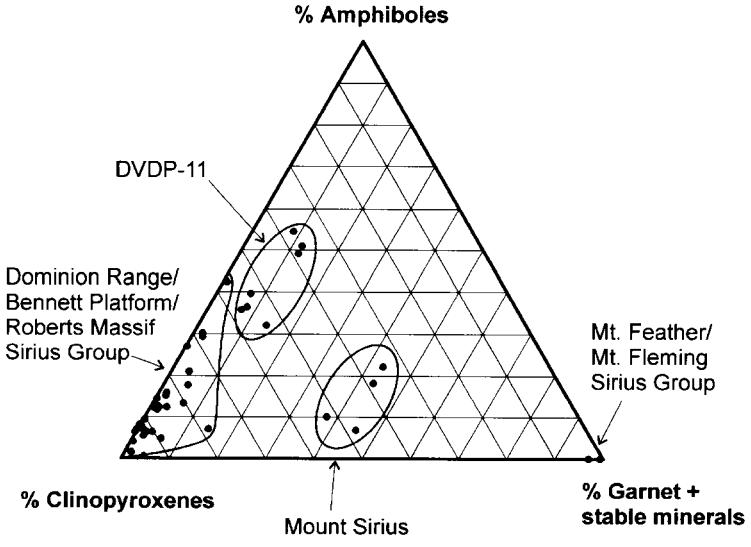

Fig. 5. Relative abundances of clinopyroxenes, amphiboles, and stable minerals plus garnet, for Sirius Group and DVDP-11 sediments.

content and the weight percentage of heavy minerals in a sample. All samples with >10% garnet have <5 weight percent of heavy minerals in the fine-sand fraction contrasting with the dominantly high weight percent of pyroxene-rich samples (Table 1). Percentages of magnetic minerals are generally <1%, except for Bennett Platform deposits, where some samples contain >2% magnetic minerals.

6. PROCESSES INFLUENCING THE HEAVY-MINERAL COMPOSITION OF THE SIRIUS GROUP

6.1. Composition and Distribution of Potential Source Rocks

Brown, Ti-rich clinopyroxenes and olivine are characteristic of rift-type volcanism (Nechaev and Isphording, 1993). Along the Transantarctic rift margin, the Jurassic Ferrar Group consists of dolerite sills and basalts, which have intruded and cap the Palaeozoic-Mesozoic sedimentary basement. Some dolerite sills of the Ferrar Group are reported to contain significant amounts of clinopyroxenes and olivine (Table 2; Grindley, 1963; Elliot et al., 1996). However, the Basement Sill, the lowermost

Table 2. Source rocks of heavy minerals

Mineral	Source rock
Clinopyroxene-brown	Ferrar Group
	McMurdo Volcanics
Clinopyroxene-colourless	Ferrar Group
Orthopyroxene	Ferrar Group
Olivine	McMurdo Volcanics
	Ferrar Group
Opaques	McMurdo Volcanics
	Various other source rocks
Amphibole-brown	Volcanic rocks?
	Beardmore Group
Clinopyroxene-green	Skelton Group
	Beardmore Group
Biotite	Skelton Group
	Beardmore Group
Amphibole-green	Metamorphic basement
Amphibole-colourless	Metamorphic basement
Epidote	Metamorphic basement
	Beacon Supergroup
Garnet, apatite, rutile	Beacon Supergroup
	Granite Harbour Intrusives
Sillimanite	Nimrod Group
Zircon, tourmaline	Beardmore Group
	Skelton Group
	Beacon Supergroup
Sphene	Granite Harbour Intrusives

Ferrar Group sill, is a hypersthene tholeiite that supplies orthopyroxenes (Gunn, 1962). Other potential source rocks contributing olivine and pyroxenes are Cenozoic alkaline volcanics associated with olivine basalts, which are reported from the southern Transantarctic Mountains (Stump et al., 1980). Purple-brown titanaugite is characteristic of alkaline basalts of the McMurdo Volcanic Group, which has its largest known distribution in the Victoria Land Basin (Kyle, 1990).

The Mesozoic portion of the Beacon Supergroup (Figs. 5 and 6) consists mainly of volcaniclastic sandstones, arkoses, and arenites (Barrett, 1972; Barrett and Elliot, 1972). Pink and colourless almandine garnet is a common accessory in these rocks (Barrett, 1966). The percentages of heavy minerals in the Beacon Supergroup are very low. Therefore, the low heavy-mineral percentage and high garnet content in some Sirius Group sediments could be interpreted only by a large supply of Beacon Supergroup materials. Garnet is also derived from some metamorphic basement rocks (Gunner, 1969), but these have a much smaller geographic distribution than the Beacon Supergroup. Metamorphic basement rocks, such as the Beardmore Group and the Skelton Group, are presently exposed within the glacial troughs and contribute amphiboles, tourmaline, and zircon. Apatite and sphene are mainly

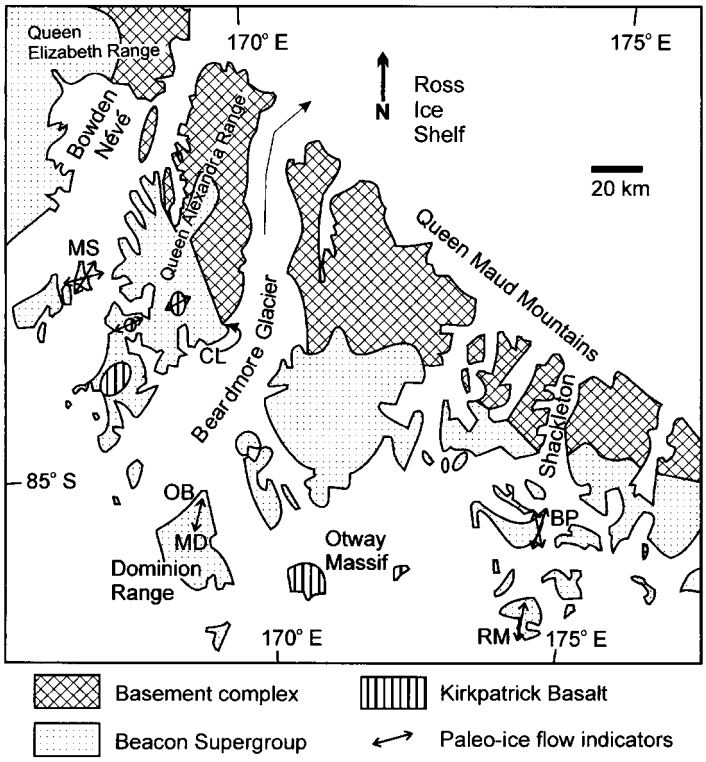

Fig. 6. Simplified geologic map of the central Transantarctic Mountains (after Elliot et al., 1996; Barrett, 1972). Ice-flow indicators from McKelvey et al. (1984), Mayewski and Goldthwait (1985), and McKelvey et al. (1991). Key: see Fig. 1.

sourced from the Granite Harbour Intrusives, which are exposed along the coast of the Transantarctic Mountains.

6.2. Tectonics

Surface uplift, related to rifting, influences the flow direction of glaciers and ice caps. The relation between the development of the East Antarctic ice sheet and the erosional history of the Transantarctic Mountains is, however, not well understood. Today, the development of structural grabens in areas with weak crust has resulted in channelling of the ice-sheet drainage system through large glacial troughs (Salvini and Storti, 1999; Wilson, 1999). Based on morphostratigraphic constraints, several authors pointed out that the Sirius Group has a complex origin and that some deposits predate the erosion of the glacial troughs (e.g., Mercer, 1968, 1972; Brady and McKelvey, 1979, 1983; Barrett and Powell, 1982; Taylor and Faure, 1983; Webb et al., 1986a, b; McKelvey et al., 1991; Van der Wateren et al., 1999).

6.3. Weathering History

The degree of chemical weathering of the materials in the Sirius Group, expressed as the chemical index of alteration (CIA; Nesbitt and Young, 1982), has a wide range (41–70). The sediment sources for the Sirius Group experienced different weathering histories (Passchier, 2004). A low CIA of 41–55 is equivalent to the range of CIAs for different crystalline rock types, and indicates that chemical weathering was unimportant in the source area, or that fresh bedrock was eroded. A high CIA of >60 is characteristic for materials that experienced considerable chemical weathering (e.g., Morton and Hallsworth, 1999) which affected chemically unstable pyroxenes and olivine. Their common presence in many Sirius Group assemblages reflects the low intensity of chemical weathering of their host sediments.

7. GLACIAL EROSION AND DRAINAGE PATTERNS

7.1. Central Transantarctic Mountains

The heavy-mineral fractions of Sirius Group tills from the central Transantarctic Mountains are characterised by high abundances of colourless clinopyroxenes (Table 1) derived from erosion of Ferrar Group source rocks (Table 2). However, the localities show systematic differences in weight percentage of heavy minerals, and in the abundance of garnet (Table 2). Samples from the five localities in the central Transantarctic Mountains (Fig. 6) can be subdivided into three groups with (1) and (3) as end-member petrofacies and (2) as an intermediate group. (1) The Sirius Group at the summit of Mount Sirius, the type locality in the Bowden Névé drainage basin, has a low weight percentage and diversity of heavy minerals, but relatively high garnet contents. (2) Tills at the upper levels of the nearby Dominion Range (Meyer Desert) and Roberts Massif contain slightly higher weight percentages of heavy minerals, with a dominance of colourless clinopyroxenes of Ferrar Group provenance. (3) The Sirius Group deposits of Oliver Bluffs and Bennett Platform

that occur within valleys incised into the Meyer Desert and Roberts Massif base levels also have a dominance of colourless clinopyroxenes but higher weight percentages of heavy minerals. Although source rock was the primary control on heavy-mineral composition, judging from the high percentages of clinopyroxenes and the local presence of olivine, pre-glacial chemical weathering may have played a role. The sediments at Mount Sirius (1) have CIAs of 58–65, those at Meyer Desert and Roberts Massif (2) of 55–62, and those of Bennett Platform and Oliver Bluffs (3) of 47–58 (Passchier, 2004). Low CIAs, indicating minimal chemical weathering, thus coincide with relatively high weight percentages of heavy minerals and a dominance of clinopyroxenes over garnet and stable minerals.

The sediments at Mount Sirius overlie a striated Ferrar Dolerite pavement with directional data indicating a glacial flow direction between 022° and 105° with a predominant direction of 075° (McKelvey et al., 1984; Mabin, 1986). The presence of large sillimanite grains and significant amounts of mica in the Sirius Group at Mount Sirius indicates a supply from mica schists and meta-quartzites of the Nimrod Group. Outcrops of the Nimrod Group are known from the Miller Range (Fig. 1) southwest of Mount Sirius (Gunner, 1969). Palaeo-ice flow direction indicators and heavy minerals, derived from Miller Range, point to a uniform source with a flow direction from the southwest through the Bowden Névé Basin (Fig. 5). The same palaeo-ice flow direction has also been found in the Sirius Group in the Queen Elizabeth and Queen Alexandra Ranges by Prentice et al. (1986). At present, the Bowden Névé is not a major drainage corridor for the East Antarctic ice sheet, but the directional data of the Queen Alexandra and Elizabeth Ranges are consistent with deposition of the Sirius Group in a broad (> 30 km wide) palaeo-valley system at higher base level and at an angle to the present glacial troughs.

In contrast to the palaeo-ice flow directions at Mount Sirius, fabric data and glacial grooves at Meyer Desert, Oliver Bluffs, Roberts Massif, and Bennett Platform have a N-S orientation, which is parallel to the present Beardmore and Shackleton glacial troughs. However, the geomorphology of the erosion surfaces indicates that ice was flowing at different base levels when the diamictons were deposited. The Oliver Bluffs and Bennett Platform successions occur within a valley incised into the Meyer Desert and Roberts Massif base level, and therefore represent younger drainage systems (cf. McKelvey et al., 1991).

The garnet-rich heavy-mineral composition and the low weight percentage of heavy minerals of the Mount Sirius glacial sediments confirm a combined Beacon Supergroup sandstone and Ferrar Group provenance, suggesting that ice was flowing at a higher base level within the Transantarctic Mountains than at present when the pyroxene-rich Sirius Group sediments were deposited. Rock fragments identified in thin sections of samples from Mount Sirius, Meyer Desert, and Roberts Massif also point to an additional source of Kirkpatrick basalt and volcaniclastic rock types of the Beacon Supergroup, which form the upper sections of the central Transantarctic Mountains (Passchier, 2001). Pyroxene enrichment and supply of larger weight percentages of heavy minerals occurred when the outlet glaciers started to erode the deeper segments of the Transantarctic Mountains that are dominated by Ferrar Group dolerite sills, Beacon Supergroup mudrocks (not supplying minerals to the sand fraction) and metamorphic basement. The result is an inverted stratigraphy of Sirius Group sediments with the oldest end-member deposits at mountain

summits and the youngest end-member deposits in the deepest portions of the glacial troughs.

7.2. The Dry Valleys

In the Dry Valleys, the morphostratigraphical relations of the glacial sediments are similar to those of the Transantarctic Mountains. The Mount Feather Diamicton rests within a depression cut by the main glacial troughs of Taylor and Wright Valley (Fig. 7). This morphostratigraphical relation suggested to Barrett and Powell (1982) and Brady and McKelvey (1983) that the deposits predated the carving of Taylor and Wright Valley, where DVDP-11 and Prospect Mesa are situated. Fabric data suggest that the Feather Diamicton was deposited by ice flowing along a southeast to northwest oriented flow-line, which is at an angle to the present orientation of the glacial troughs. The NW-SE orientation is derived from clast-fabric data of the Feather Diamicton and striated pavements at two locations in the Dry Valleys at approximately 2700 m above sea level (Fig. 7). Clast-fabric data and some sedimentary rat-tails point to a more NNE-SSW oriented palaeo-ice flow for the Mount Fleming Upper Till (Stroeven and Prentice, 1997). After the carving of Taylor and Wright Valley, the diamictons penetrated by DVDP-11 and at Prospect Mesa were deposited on the valley floors.

The low abundance of heavy minerals in the Sirius Group at Mount Fleming and Mount Feather in the Dry Valleys (Figs. 1 and 6) suggests that sedimentary rocks were the main sources of the sand-sized components. Garnet and apatite are dominant heavy minerals, but the heavy-mineral fraction on Mount Feather also contains epidote and zircon. Possible sources for these heavy minerals include the Beacon Supergroup, or the Precambrian to Lower Palaeozoic meta-sedimentary and granitic basement (Skinner and Ricker, 1968). However, studies of the bulk chemistry of these

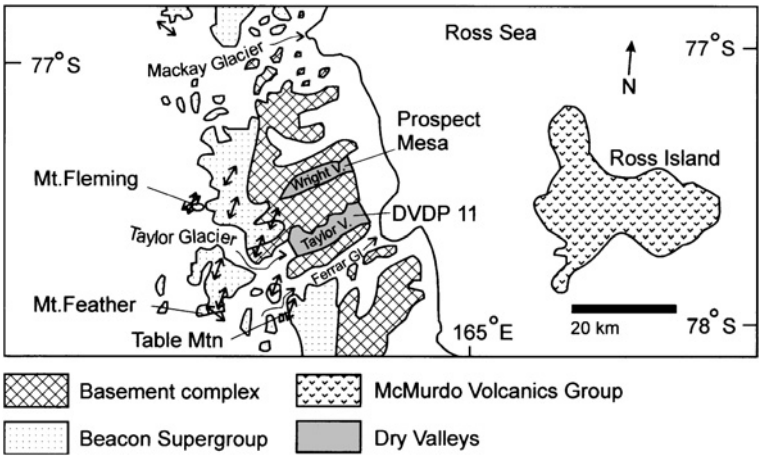

Fig. 7. Simplified geological map of South Victoria Land (after Lopatin, 1972). Palaeo-ice flow indicators are from Brady and McKelvey (1979, 1983), Stroeven and Prentice (1997), and Denton et al. (1984).

deposits (Passchier, 2004) indicate that chemical weathering may have affected the heavy-mineral composition through dissolution of unstable minerals, such as pyroxenes. CIAs are 66 for the sample from Mount Fleming and 63 for the sample from Mount Feather, which is consistent with the large numbers of oxidised grains in the samples at these locations (Table 1).

In Taylor Valley, the DVDP-11 core shows a sharp change in heavy-mineral composition at around 300 m below valley floor, where abundances of biotite, oxidised grains, and rock fragments increase uphole, whereas orthopyroxenes diminish (Fig. 8). The lower part of Unit 8 is dominated by colourless clinopyroxenes, mainly pigeonite (Fig. 4), green pyroxenes, green amphiboles, some garnet, and apatite. The clinopyroxenes and orthopyroxenes are probably derived from Ferrar Dolerite sills, which are exposed at the head of Taylor Valley. The Basement Sill (Gunn, 1962), which extends from Mackay Glacier to the head of Ferrar Glacier, is a hypersthene tholeiite and is the most likely source of the high abundance of orthopyroxenes below 300 m below valley floor. Low-grade metamorphic rocks also contribute to the lower part of the succession in DVDP-11. Biotite schists of the Skelton Group, which form the base of Taylor Valley (Lopatin, 1972; Mudrey, 1975), are the most probable source of the green clinopyroxenes and biotite. Both the upsection increase of brown titanium-rich pyroxenes and opaques, and the decrease in green pyroxenes and amphiboles (Fig. 8), signal an increasing contribution from the McMurdo Volcanic Group towards the top of the succession. The dominance of brown pyroxene and brown amphibole at 156 m below valley floor (Table 1) indicates a large influx of volcanic detritus at this level in the core. A general increase in volcanogenic detritus from the early Pliocene onward is consistent with the heavy-mineral record of the nearby CIROS-2 drillhole beneath the Ferrar Glacier (Ehrmann and Polozek, 1999). These studies and the heavy-mineral results of DVDP-11 indicate an increasing upsection influence of local mountain glaciers and the Ross Ice Shelf, and a decreasing input from the East Antarctic ice sheet in the Dry Valleys.

The heavy-mineral fraction of the Prospect Mesa lower diamicton in Wright Valley consists almost entirely of colourless clinopyroxenes and colourless amphiboles, which suggests a simultaneous erosion of Ferrar Group and metamorphic basement source rocks. Ferrar Dolerite outcrops are more abundant to the west than to the east of Prospect Mesa. In addition, the general absence of granitic material with sources east of Prospect Mesa also suggests that the lower diamicton of Prospect Mesa was deposited by ice flowing from the west, probably from the East Antarctic ice sheet (Prentice et al., 1993).

7.3. *Model of Landscape Evolution and Ice-Sheet Drainage*

It has been noted before that the present glacial troughs that drain the East Antarctic ice sheet follow re-activated Mesozoic fault systems (Mazzarini et al., 1997). Ice-sheet modelling indicates that the structural segmentation of the Transantarctic Mountains allowed ice to enter the Ross Sea Basin through narrow corridors with steep gradients. Reduction of the ice surface gradients is caused by the development of the glacial troughs that inhibited ice from overriding the high mountain ranges (Kerr and Huybrechts, 1999). Pyroxene and amphibole-rich heavy-mineral assemblages of the

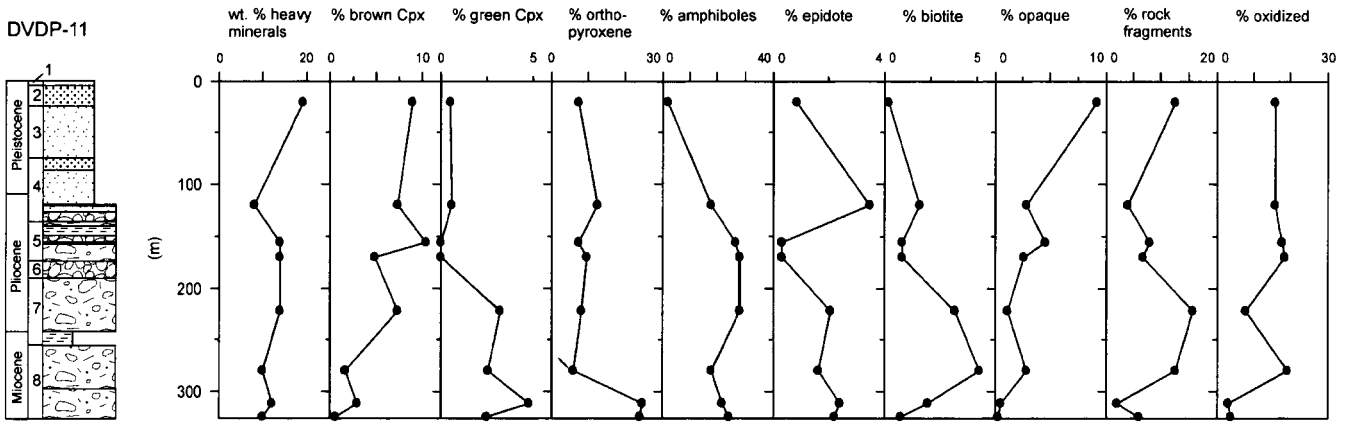

Fig. 8. Percentages of dominant heavy minerals in core from DVDP-11, Dry Valleys. Cpx = clinopyroxene.

deposits within the glacial troughs of the central Transantarctic Mountains and on the valley floors in the Dry Valleys indicate deposition by outlet glaciers of the East Antarctic ice sheet during over-deepening and headward erosion into Ferrar Group and metamorphic basement rocks. The Sirius Group deposits, rich in garnet and stable minerals at Mount Sirius, Mount Fleming, and Mount Feather, originate from an ice sheet or local ice caps that overtopped the Transantarctic Mountains prior to the over-deepening of the glacial troughs. Hence, these deposits are older than the pyroxene-rich glaciogenic sediments in the glacial troughs. The Sirius Group therefore represents deposits of multiple glacial events with considerably different ice-sheet drainage configurations.

8. CONCLUSIONS

In the Transantarctic Mountains, heavy minerals convey information on palaeo-ice flow directions by carrying signatures of their source rocks, outcropping several 100 km upstream, and on the level of dissection of the rift margin during glacial erosion. Heavy-mineral analysis of Cenozoic glaciogenic sediments of the Sirius Group permitted their subdivision into two petrofacies. The first petrofacies is characterised by a low heavy-mineral content, and assemblages that are dominated by garnet and stable-ultrastable minerals, consistent with derivation from sedimentary rocks, meta-sediments, or granitic basement rocks. The second petrofacies contains high weight percentages of heavy minerals, dominated by pyroxenes and amphiboles, as well as lithic fragments, derived from mafic igneous and metamorphic basement lithologies.

Heavy-mineral data, palaeo-ice flow directions, and the geomorphological setting of the deposits suggest that the garnet-rich petrofacies was deposited when ice was overriding the highest stratigraphic succession of the Transantarctic Mountains (Fig. 2A). These deposits occur on mountain summits, which represent the oldest erosional remnants of a widespread glacial landscape. The Mount Sirius, Mount Feather, and Mount Fleming successions belong to this part of the Sirius Group. The second, pyroxene- and amphibole-rich petrofacies, observed at Oliver Bluffs, Bennett Platform and in DVDP-11, shows evidence of active erosion of the unweathered Ferrar Group and basement. The latter suggests that valley erosion was an ongoing process throughout the deposition of the Sirius Group.

Heavy-mineral assemblages demonstrate that the Sirius Group resulted from multiple glacial events. The sediments represent different ice-sheet drainage systems; some deposits are associated with overriding of the Transantarctic Mountains by the ice prior to over-deepening of the glacial troughs, while others are associated with deposition from outlet glaciers in the glacial troughs. Together with geomorphological and directional indicators, the heavy minerals show that the Sirius Group was deposited during stepwise denudation of the rift margin, causing progressively deeper parts of the geological framework of the Transantarctic Mountains to be exposed to glacial erosion. This process produced an inverted stratigraphy with the oldest glacial deposits in the higher regions of the Transantarctic Mountains and the younger deposits within the glacial troughs.

REFERENCES

Alley, R.B., Blankenship, D.D., Bentley, C.R., Rooney, S.T., 1986. Deformation of till beneath ice stream B, West Antarctica. Nature 322, 57–59.

Barrett, P.J., 1966. Petrology of some Beacon rocks between the Axel Heiberg and Shackleton Glaciers, Queen Maud Range, Antarctica. Journal of Sedimentary Petrology 36, 794–805.

Barrett, P.J., 1972. Stratigraphy and petrology of the mainly fluviatile Permian and Triassic part of the Beacon Supergroup, Beardmore Glacier area. Antarctic Geology and Geophysics. Universitetsforlaget, Oslo, pp. 365–372.

Barrett, P.J., 1991. The Devonian to Triassic Beacon Supergroup of the Transantarctic Mountains and correlatives in other parts of Antarctica. In: Tingey, R.J. (Ed.), The Geology of Antarctica. Clarendon Press, Oxford, U.K., pp. 120–152.

Barrett, P.J., Elliot, D.H., 1972. The early Mesozoic volcaniclastic Prebble Formation, Beardmore Glacier area. Antarctic Geology and Geophysics. Universitetsforlaget, Oslo, pp. 403–409.

Barrett, P.J., Powell, R.D., 1982. Middle Cenozoic glacial beds at table Mountain, Southern Victoria Land. Third Symposium on Antarctic Geology and Geophysics. The University of Wisconsin Press, Madison, pp. 1059–1067.

Boulton, G.S., 1996. Theory of glacial erosion, transport and deposition as a consequence of subglacial sediment deformation. Journal of Glaciology 42, 43–62.

Boulton, G.S., Clark, C.D., 1990. A highly mobile Laurentide ice sheet revealed by satellite images of glacial lineations. Nature 346, 813–817.

Brady, H., McKelvey, B., 1979. The interpretation of a Tertiary tillite at Mount Feather, Southern Victoria Land, Antarctica. Journal of Glaciology 22, 189–193.

Brady, H., McKelvey, B., 1983. Some aspects of the Cenozoic glaciation of Southern Victoria Land, Antarctica. Journal of Glaciology 29, 343–349.

Denton, G.H., Prentice, M.L., Kellogg, D.E., Kellogg, T.B., 1984. Late Tertiary history of the Antarctic ice sheet: evidence from the Dry Valleys. Geology 12, 263–267.

DiLabio, R.N.W., 1990. Chapter 7—glacial dispersal trains. In: Kujansuu, R., Saarnisto, M. (Eds.), Glacial indicator tracing. Balkema, Rotterdam, pp. 109–122.

Dreimanis, A., Vagners, U.J., 1972. The effect of lithology upon texture of till. In: Yatsu, E., Falconer, A. (Eds.), Research Methods in Pleistocene Geomorphology, pp. 66–82.

Ehrmann, W., Polozek, K., 1999. The heavy mineral record in the Pliocene to Quaternary sediments of the CIROS-2 drill core, McMurdo Sound, Antarctica. Sedimentary Geology 128, 223–244.

Ehrmann, W.U., Mackensen, A., 1992. Sedimentological evidence for the formation of an East Antarctic ice sheet in Eocene/Oligocene time. Palaeogeography, Palaeoclimatology, Palaeoecology 93, 85–112.

Elliot, D.H., Fleming, T.H., Gero, C.M., 1996. Geologic studies on rocks from the Jurassic Ferrar Group. Antarctic Journal of the United States 31, 37–38.

Faure, G., Hagen, E.H., Johnson, K.S., Strobel, M.L., Whiting, K.S., 1995. Geological exploration of East Antarctica: iron, manganese, and titanium in the heavy mineral fractions of till in the Transantarctic Mountains. In: Elliot, D.H. (Ed.), Contributions to Antarctic Research IV. Antarctic Research Series, Vol. 67. American Geophysical Union, Washington D.C, pp. 19–31.

Gravenor, 1979. The nature of the Late Paleozoic glaciation in Gondwana as determined from an analysis of garnets and other heavy minerals. Canadian Journal of Earth Sciences 16, 1137–1153.

Grindley, G.W., 1963. The geology of the Queen Alexandra Range, Beardmore Glacier, Ross Dependency, Antarctica; with notes on the correlation of Gondwana sequences. New Zealand Journal of Geology and Geophysics 6, 307–360.

Gunn, B.M., 1962. Differentiation in Ferrar Dolerites. New Zealand Journal of Geology and Geophysics 5, 820–863.

Gunner, J.D., 1969. Petrography of metamorphic rocks from the Miller Range, Antarctica. Institute of Polar Studies, Columbus, Ohio, Report 32.

Gwyn, Q.H.J., Dreimanis, A., 1979. Heavy mineral assemblages in tills and their use in distinguishing glacial lobes in the Great Lakes region. Canadian Journal of Earth Sciences 16, 2219–2235.

Haldorsen, S., 1981. Grain-size distribution of subglacial till and its relation to glacial crushing and abrasion. Boreas 10, 91–105.

Haldorsen, S., Jørgensen, P., Rappol, M., Riezebos, P.A., 1989. Composition and source of the clay-sized fraction of Saalian till in The Netherlands. Boreas 18, 89–97.

Hambrey, M.J., Barrett, P.J., 1993. Cenozoic sedimentary and climatic record, Ross Sea region, Antarctica. In: Kennett, J.P., Warnke, D.A. (Eds.), The Antarctic Paleoenvironment: A Perspective on Global Change, Part Two. Antarctic Research Series, vol. 60, American Geophysical Union, Washington D.C., pp. 91–124.

Harwood, D.M., Webb, P.-N., 1998. Glacial transport of diatoms in the Antarctic Sirius Group: Pliocene refrigerator. GSA Today 8, 1–8.

Ishman, S.E., Rieck, H.J., 1992. A late Neogene Antarctic glacio-eustatic record, Victoria Land Basin margin, Antarctica. In: Kennett, J.P., Warnke, D.A. (Eds.), The Antarctic Paleoenvironment: A Perspective on Global Change Part One. Antarctic Research Series, vol. 56. American Geophysical Union, Washington D.C., pp. 327–347.

Kerr, A., Huybrechts, P., 1999. The response of the East Antarctic Ice Sheet to the evolving tectonic configuration of the Transantarctic Mountains. Global and Planetary Change 23, 213–229.

Kyle, P.R., 1990. McMurdo Volcanic Group, western Ross Embayment. In: W. E. LeMasurier, J. W. Thomson (Eds.), Volcanoes of the Antarctic Plate and Southern Oceans. Antarctic Research Series, vol. 48, American Geophysical Union, Washington D.C., pp. 19–25.

Lopatin, B.G., 1972. Basement complex of the McMurdo 'Oasis', South Victoria Land. Antarctic Geology and Geophysics. Universitetsforlaget, Norway, pp. 287–292.

Mabin, M.C.G., 1986. Sirius Formation basal contacts in the Beardmore Glacier region. Antarctic Journal of the United States 21, 32–33.

Mayewski, P.A., Goldthwait, R.P., 1985. Glacial events in the Transantarctic Mountains: a record of the East Antarctic ice sheet. Antarctic Research Series, vol. 36, American Geophysical Union, Washington D.C., pp. 275–324.

Mazzarini, F., DellaVedova, B., Salvini, F., 1997. Crustal segmentation of the Transantarctic Mountains rift shoulder along the David Glacier lineament, Victoria Land (Antarctica). VII International Symposium on Antarctic Earth Sciences. Terra Antarctica Publication, Siena, Italy, pp. 565–569.

McClenaghan, M.B., Thorleifson, L.H., DiLabio, R.N.W., 2000. Till geochemical and indicator mineral methods in mineral exploration. Ore Geology Reviews 16, 145–166.

McKelvey, B.C., Mercer, J.H., Harwood, D.M., Stott, L.D., 1984. The Sirius Formation: further considerations. Antarctic Journal of the United States 19, 42–43.

McKelvey, B.C., Webb, P.-N., Harwood, D.M., Mabin, M.G.C., 1991. The Dominion Range Sirius Group: a record of the late Pliocene—early Pleistocene Beardmore Glacier. Fifth International Symposium on Antarctic Earth Sciences. Cambridge University Press, Cambridge, England, pp. 675–682.

Mercer, J.H., 1968. Glacial geology of the Reedy Glacier area, Antarctica. Geological Society of America Bulletin 79, 471–486.

Mercer, J.H., 1972. Some observations on the glacial geology of the Beardmore Glacier area. Antarctic Geology and Geophysics. Universitetsforlaget, Oslo, pp. 427–433.

Morton, A.C., Hallsworth, C.R., 1999. Processes controlling the composition of heavy mineral assemblages in sandstones. Sedimentary Geology 124, 3–29.

Mudrey, M.G., 1975. Basement rocks in DVDP-12, Lake Leon, Taylor Valley. Bulletin of the Department of Geology at Northern Illinois University in the Kalb IL, Illinois, Report No. 5.

Nechaev, V.P., Isphording, W.C., 1993. Heavy-mineral assemblages of continental margins as indicators of plate-tectonic environments. Journal of Sedimentary Petrology 63, 1110–1117.

Nesbitt, H.W., Young, G.M., 1982. Early Proterozoic climates and plate motions inferred from major element chemistry of lutites. Nature 299, 715–717.

Passchier, S., 2001. Provenance of the Sirius Group and related Upper Cenozoic glacial deposits from the Transantarctic Mountains, Antarctica: relation to landscape evolution and ice-sheet drainage. Sedimentary Geology 144, 263–290.

Passchier, S., 2004. Variability in geochemical provenance and weathering history of Sirius Group strata, Transantarctic Mountains: implications for Antarctic glacial history. Journal of Sedimentary Research 74, 607–619.

Peuraniemi, V., 1990. Chapter 10—heavy minerals in glacial material. In: Kujansuu, R., Saarnisto, M. (Eds.), Glacial indicator tracing. Balkema, Rotterdam, pp. 165–185.

Prentice, M.L., Bockheim, J.G., Wilson, S.C., Burckle, L.H., Hodell, D.A., Schlüchter, C., Kellogg, D.E., 1993. Late Neogene Antarctic glacial history: evidence from Central Wright Valley. In: Kennett J.P., Warnke, D.A. (Eds.), The Antarctic Paleoenvironment: A Perspective on Global Change, Part Two. Antarctic Research Series, vol. 60, American Geophysical Union, Washington D.C., pp. 207–250.

Prentice, M.L., Denton, G.H., Lowell, T.V., Conway, H.C., Heusser, L.E., 1986. Pre-late Quaternary glaciation of the Beardmore Glacier region, Antarctica. Antarctic Journal of the United States 21, 95–98.

Rappol, M., Stoltenberg, H.M.P., 1985. Compositional variability of Saalien till in The Netherlands and its origin. Boreas 14, 33–50.

Robert, C., Chamley, H., 1992. Late Eocene-early Oligocene evolution of climate and marine circulation: deep-sea clay mineral evidence. In: Kennett, J.P., Warnke, D.A. (Eds.), The Antarctic Paleoenvironment: A Perspective on Global Change, Part One. American Geophysical Union, Washington D.C., pp. 97–117.

Salvini, F., Storti, F., 1999. Cenozoic tectonic lineaments of the Terra Nova Bay region, Ross Embayment, Antarctica. Global and Planetary Change 23, 129–144.

Shilts, W.W., 1996. Chapter 15—drift exploration. In: Menzies, J. (Ed.), Past Glacial Environments; Sediments, Forms and Techniques—Glacial Environments, vol. 2. Butterworth-Heinemann, Oxford, pp. 411–439.

Skinner, D.N.B., Ricker, J., 1968. The geology of the region between Mawson and Priestley Glaciers, North Victoria Land, Antarctica. New Zealand Journal of Geology and Geophysics 11, 1009–1076.

Stokes, C.R., Clark, C.D., 2001. Palaeo-ice streams. Quaternary Science Reviews 20, 1437–1457.

Stroeven, A., Burckle, L.H., Kleman, J., Prentice, M.L., 1998. Atmospheric transport of diatoms in the Antarctic Sirius Group: pliocene deep freeze. GSA Today 8, 1–5.

Stroeven, A.P., Prentice, M.L., 1997. A case for Sirius Group alpine glaciation at Mount Fleming, South Victoria Land, Antarctica: a case against Pliocene east Antarctic ice sheet reduction. Geological Society of America Bulletin 109, 825–840.

Stump, E., 1995. The Ross Orogen of the Transantarctic Mountains. Cambridge University Press, Cambridge, U.K.

Stump, E., Sheridan, M.F., Borg, S.G., Sutter, J.F., 1980. Early Miocene subglacial basalts, the East Antarctic ice sheet, and uplift of the Transantarctic Mountains. Science 207, 757–759.

Taylor, K.S., Faure, G., 1983. Provenance dates of feldspar in glacial deposits, southern Victoria Land, Antarctica. In: Oliver, R.L., James, P.R., Jago, J.B. (Eds.), Antarctic Earth Science. Australian Academy of Science, Canberra, pp. 453–457.

Tingey, R.J., 1991. Mesozoic tholeiite igneous rocks in Antarctica: the Ferrar (Super) Group and related rocks. In: Tingey, R.J. (Ed.), The Geology of Antarctica. Clarendon Press, Oxford, pp. 153–174.

Van der Wateren, F.M., Dunai, T.J., van Balen, R.T., Klas, W., Verbers, A.L.L.M., Passchier, S., Herpers, U., 1999. Contrasting denudation histories of different structural regions in the Transantarctic Mountains rift flank constrained by cosmogenic isotope measurements. Global and Planetary Change 23, 145–172.

Verbers, A.L.L.M., Van der Wateren, F.M., 1992. A glacio-geological reconnaissance of the southern Prince Albert Mountains, Victoria Land, Antarctica. In: Yoshida, Y., Kaminuma, K., Shiraishi, K. (Eds.), Recent Progress in Antarctic Earth Science. Terrapub, Tokyo, pp. 715–719.

Webb, P.-N., 1994. Paleo-drainage systems of East Antarctica and sediment supply to west Antarctic rift system basins. Terra Antarctica 1, 457–461.

Webb, P.-N., Harwood, D.M., Mabin, M.G.C., McKelvey, B.C., 1986a. Late Cenozoic tectonic and glacial history of the Transantarctic Mountains. Antarctic Journal of the United States 21, 99–100.

Webb, P.-N., Harwood, D.M., Mabin, M.G.C., McKelvey, B.C., 1996. A marine and terrestrial Sirius Group succession, middle Beardmore Glacier-Queen Alexandra Range, Transantarctic Mountains, Antarctica. Marine Micropalaeontology 27, 273–297.

Webb, P.-N., McKelvey, B.C., Harwood, D.M., Mabin, M.C.G., Mercer, J.H., 1986b. Sirius Formation of the Beardmore Glacier region. Antarctic Journal of the United States 22, 8–13.

Wilson, T.J., 1999. Cenozoic structural segmentation of the Transantarctic Mountains rift flank in southern Victoria Land. Global and Planetary Change 23, 105–127.

Zachos, J., Pagani, M., Sloan, L., Thomas, E., Billups, K., 2001. Trends, rhythms, and aberrations in global climate 65 Ma to present. Science 292, 686–693.

Zandstra, J.G., 1983. Fine gravel, heavy mineral, and grain-size analyses of Pleistocene, mainly glacigenic deposits in The Netherlands. In: Ehlers, J. (Ed.), Glacial deposits in North West Europe. Balkema, Rotterdam, pp. 361–377.

This page intentionally left blank

Chapter 28

HEAVY AND LIGHT MINERAL FRACTIONS INDICATE POLYGENESIS OF EXTENSIVE TERRA ROSSA SOILS IN ISTRIA, CROATIA

GORAN DURN[a], DUNJA ALJINOVIĆ[a], MARTA CRNJAKOVIĆ[b] AND BOŠKO LUGOVIĆ[a]

[a]*University of Zagreb, Faculty of Mining, Geology and Petroleum Engineering, Pierottijeva 6, HR-10000 Zagreb, Croatia*
[b]*Croatian Natural History Museum, Demetrova 1, HR-10000 Zagreb, Croatia*

ABSTRACT

Terra rossa is the most widespread soil type in Istria, Croatia, a region that has been affected by karst processes, (neo)tectonic activity and sediment supply since the Late Tertiary. Analysis of the heavy and light mineral fractions of the terra rossa in Istria reveals a polygenetic origin. For comparative purposes, the heavy and light mineral composition in the insoluble residue of underlying limestones and dolomites, and that in the insoluble residue of other potential source formations such as flysch and loess, have been analysed. The extent of pyroclastic influence on these terra rossa soils was also evaluated.

Amphiboles, zircon, tourmaline, garnet, kyanite, clinopyroxene and orthopyroxene, present in both loess deposits in Istria and in the terra rossa, prove that detritus mineralogically similar to that found in Late Pleistocene loess has been incorporated into the terra rossa. Heavy mineral data indicate that material was also derived from Istrian flysch during terra rossa formation. Air-fall of particles from the Roman-Campanian Volcanic Province may also have contributed, and hypidiomorphic K-feldspars accompanying clinopyroxene and orthopyroxene in some loess and terra rossa samples might be of this volcanic origin. It is difficult to estimate to what extent materials other than the insoluble residue of limestones and dolomites have contributed to terra rossa in Istria, though analytical data available to date suggest that this might have reached 50%. We conclude that the main external contributor is Middle Pleistocene loess, followed by flysch and tephra. Late Pleistocene loess may have become incorporated in the upper parts of already formed terra rossa. In the terra rossa on the island of Korčula, devitrified pumice clasts, sanidine, hyalophane, Ti-andradite, potassic hastingsite, along with orthopyroxene and black mica, clearly represent volcanic input.

Developments in Sedimentology, Vol. 58, 701–737

ISSN: 0070-4571/doi:10.1016/S0070-4571(07)58028-3

Keywords: terra rossa; soil parent materials; heavy mineral fraction; light mineral fraction; polygenesis; Istria (Croatia)

1. INTRODUCTION

Terra rossa is a reddish clayey to silty/clayey soil that is especially widespread in the Mediterranean region, where it overlies limestones and dolomites. Bright red colours are a diagnostic feature of terra rossa and are the result of preferential formation of hematite over goethite (termed rubification). Terra rossa has a slightly alkaline to neutral pH and an almost completely saturated base complex (dominated by calcium and/or magnesium). Terra rossa is well drained because it is well aggregated (high exchangeable Ca and Mg content) and situated on highly permeable carbonate rocks (Torrent, 1995). It is formed as a result of (1) decalcification, (2) rubification and (3) bisiallitisation (formation of 2:1 clay minerals) and/or monosiallitisation (formation of 1:1 clay minerals). However, according to Fedoroff (1997), bisiallitic weathering is not a specific property of red Mediterranean soils. Kaolinites as the main pedogenic clay mineral phases were found in terra rossas from Istria (Durn, 1996; Durn et al., 1999) and NW Morocco (Bronger and Bruhn-Lobin, 1997; Bronger and Sedov, 2002). This may imply that the type of weathering in terra rossas, and the resulting authigenic clay mineral phases, depend on the time of formation, climate and soil parent materials. For example, Boero et al. (1992) found that illite and kaolinite are the main clay mineral phases in terra rossas from xeric sites whereas Al-interlayered vermiculite occurred in cool, moist sites.

In Soil Taxonomy (Soil Survey Staff, 1975), terra rossas are classified as Alfisols (Haploxeralfs or Rhodoxeralfs), Ultisols, Inceptisols (Xerochrepts) and Mollisols (Argixerolls or Haploxerolls). According to the UN Food and Agriculture Organisation system (FAO, 1974) terra rossa is recognised as Luvisols (Chromic Luvisols), Phaeozems (Haplic Phaeozems or Luvic Phaeozems) and Cambisols. In other classification systems using Mediterranean climate as the major soil differentiating criterion, the term terra rossa is used to describe the soil subclass "Modal Fersiallitic Red soil" when situated on limestones (Duchaufour, 1982). Several national soil classifications (e.g., Croatia, Italy, Israel) retain the term "terra rossa" for limestone-derived red soils.

Different authors have considered terra rossa to be a soil, vetusol, relict soil (non-buried-palaeosol), palaeosol or pedo-sedimentary complex. However, most authors today believe that terra rossa is a polygenetic relict soil, formed during the Tertiary and/or hot and humid periods of the Quaternary (e.g., Altay, 1997; Bronger and Bruhn-Lobin, 1997; Durn et al., 1999). For example, Bronger and Bruhn-Lobin (1997) concluded that terra rossa situated on Quaternary calcarenites in NW Morocco is probably of Mid-Pleistocene age and that its formation extended over most parts of the Brunhes epoch, including those of the cool (glacial) stages. Recent investigation in the Atlantic coastal region of Morocco (Bronger and Sedov, 2002) shows that at least some terra rossa soils, previously referred to as polygenetic relict soils, should be regarded as Vetusols (soils that are marked by a continuity of pedogenetic processes) according to the concept of Cremaschi (1987). Bronger and

Sedov (2002) concluded that soil-forming processes were the same during terra rossa formation due to slight climatic fluctuations in the region through the Brunhes epoch and Holocene.

The nature and relationship of terra rossas to underlying carbonates is a long-standing problem that has resulted in contrasting opinions with respect to their parent materials and origins. The most widely accepted theory is that terra rossa has developed from the insoluble residue of carbonate rocks (Kišpatić, 1912; Tućan, 1912; Kubiëna, 1953; Ćirić and Aleksandrović, 1959; Marić, 1964; Plaster and Sherwood, 1971; Škorić, 1979, 1987; Bronger et al., 1983; Moresi and Mongelli, 1988; Bronger and Bruhn-Lobin, 1997). Other authors have emphasised that the addition of various external materials might have masked the influence of limestone and dolomite residues as the primary parent material of terra rossa. Soil geomorphic studies by Olson et al. (1980) in southern Indiana, USA indicate that the terra rossa is mainly debris derived from the erosion of overlying clastic sedimentary rocks, and deposited on pediments cut into underlying limestone. Aeolian contributions to terra rossa have been recognised from the similarities in clay mineralogy (Balagh and Runge, 1970; Durn et al., 1999), heavy mineral composition (Šinkovec, 1974; Durn et al., 1992; Durn and Aljinović, 1995), particle size distribution (MacLeod, 1980), divergence of oxygen isotopic ratios of associated fine quartz (Jackson et al., 1982) and SEM study of the morphology of the quartz grains (Delgado et al., 2003). Yaalon (1997) concluded that practically all terrestrial soils in the Mediterranean region over the past 5 Ma might include a contribution from Saharan aeolian dust, inferring values of up to 50% in limestone-derived soils. Evidence of Saharan dust was found in terra rossas in Italy, Spain, Portugal, Greece, Morocco, Turkey and Israel (e.g., Yaalon and Ganor, 1973; MacLeod, 1980; Jackson et al., 1982; Danin et al., 1983; Rapp, 1984; Jahn et al., 1991; Nihlen and Olsson, 1995; Altay, 1997; Bronger and Bruhn-Lobin, 1997;).

Chiesa et al. (1990) concluded that in the Marche region (Italy), aeolian deposits formed during the Pleistocene were affected by pyroclastic material originating from the Tyrrhenian area, implying that terra rossa soils in that region might also contain material of that parentage. Lippi-Boncampi et al. (1955) and Yaalon and Ganor (1973) mentioned the role of airborne pyroclastics in the surrounding area in the formation of terra rossa, while Šušnjara et al. (1994) found vitric tuff intercalated within terra rossa near Gljev, central Dalmatia (Croatia). Detailed research on two palaeosols of Late Pleistocene (Pedomarker A) and Holocene (Pedomarker B) age in the calcareous Central Apennines showed that they developed from airborne pyroclastic material (Frezzotti and Narcisi, 1996). In some isolated karst terrains, terra rossas may have formed exclusively from limestone and dolomite insoluble residues (i.r.), but they more frequently comprise a variety of added materials, including aeolian dust, volcanic debris or clastic sedimentary particles that were brought to the carbonate terrain via various transport mechanisms (Durn, 2003).

Istria, where terra rossa is the most abundant soil type, is an example of a non-isolated karst terrain that was affected by karst processes, (neo)tectonic activity and external sediment contributions since the Late Tertiary. According to Durn et al. (1999), the rather limited variation of selected Fe-oxide characteristics in 40 terra rossa samples from Istria makes them very similar to those of Boero and Schwertmann (1989). While analyses by Boero and Schwertmann (1989) showed that Fe_d

(dithionite soluble iron-total iron oxide) in 45 terra rossa samples averaged 3.5% [with 0.3 at 0.95 confidence interval (0.95 C.I.)] the Fe_d in 40 samples from Istria averaged 3.68% (with 0.28 at 0.95 C.I.). The arithmetic means of the two sets of data are not significantly different at the 0.05 level (*t*-test). The two populations are indistinguishable at the 0.05 level; that is, two arithmetic means represent two independent estimates of the same population (Fe_d in terra rossa). This supports Boero and Schwertmann's (1989) conclusion that the rather limited extent of variation of selected Fe-oxide characteristics may indicate a specific pedo-environment in which terra rossa is formed. Durn et al. (1999) presented evidence for the polygenetic nature of terra rossa in Istria, based on detailed mineralogical and geochemical investigations. Neither the mineral content and particle size distribution, nor the bulk and clay mineralogy of the insoluble residue of limestone and dolomite support development of terra rossa entirely by dissolution of carbonate rocks. They concluded that both aeolian sediments, older than those of Upper Pleistocene and flysch, contributed to the genesis of terra rossa. According to some ongoing studies, deposition of pyroclastic material, which occurred frequently throughout the Quaternary in the Adriatic region, may also have significantly affected soil development in the region (B. Lugović, personal communication, July 2003).

The aim of the present contribution is to assess to what extent the heavy and light mineral compositions of terra rossa can be used as indices of its polygenetic nature in Istria. Our work includes the study of heavy and light minerals, i.r. of presumed limestone and dolomite source formations, other potential source rocks such as flysch and loess. Results on bulk and clay mineral composition and geochemical "fingerprinting" (e.g., Zr, Nb, Ti and REE) from previous investigations (Durn, 1996, 2003; Durn et al., 1999, 2001, 2003) are summarised, and the influence of pyroclastic material flux to terra rossa is evaluated.

2. STUDY AREA

The Istrian Peninsula represents the north west part of the Adriatic Carbonate Platform and consists predominantly of carbonate rocks ranging in age from Middle Jurassic (Late Dogger) to Eocene, with subordinate Eocene siliciclastic rocks, marly flysch and calcareous breccia, and Quaternary terra rossa and loess (Fig. 1). The most apparent geological structure of the Istrian Peninsula is the Western Istrian anticline (Polšak and Šikić, 1973; Marinčić and Matičec, 1991). The Istrian Middle Jurassic (Late Dogger) to Eocene successions can be divided into four large-scale sequences (Velić et al., 1995). The 1st, 2nd and 3rd of these are composed of carbonates, each terminated by a long-lasting emersion, that represents a type 1 sequence boundary (Tišljar et al., 1998). The 4th large-scale sequence consists of carbonate and clastic rocks, and unconformably overlies palaeo-relief developed on the carbonate rocks. The most widespread sediments in this sequence are flysch deposits which are characterised by an alternation of hemipelagic marls and gravity-flow deposits (Velić et al., 2003).

Since flysch formation in the Eocene, the uplifted rocks have been affected by tectonics, karst processes and weathering, which together have led to the

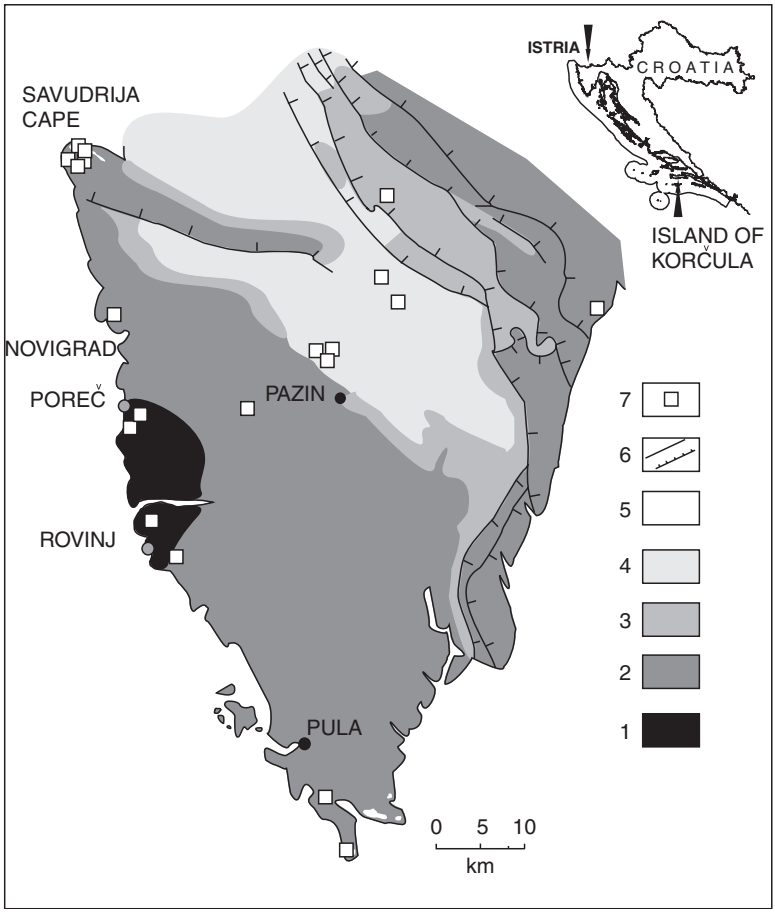

Fig. 1. Simplified geological map of Istria (modified from Geological map of SFRJ 1:500000, 1970). (1) Late Jurassic (limestones and dolomites). (2) Cretaceous (limestones and dolomites). (3) Palaeocene-Eocene (mainly limestones). (4) Eocene (flysch). (5) Quaternary (loess). (6) Faults. (7) Sample locations (limestone, dolomite, loess and flysch). (after Durn et al., 1999, with permission from Elsevier.)

development of a number of surficial and underground features. Various kinds of sediments and soils have been formed. For the most part they irregularly cover all carbonates and flysch. The oldest Quaternary sediments were discovered in Šandalja cave near Pula and are represented by a red breccia with Early Pleistocene faunal remains (Malez, 1981). Climatic and biotic factors have changed during the Late Tertiary and Quaternary but the pedo-environment on hard carbonate rocks of the Jurassic-Cretaceous-Palaeogene carbonate plain of southern and western Istria generally remained suitable for rubification. Terra rossa is found on the Jurassic-Cretaceous-Palaeogene carbonate plain of southern and western Istria (Figs. 1 and 2). It fills cracks and sinkholes, and forms a discontinuous surface layer up to 2.5 m thick that is, in places, covered by Late Pleistocene loess. Thick (up to 14 m) accumulations of terra rossa-like material are found in karst depressions, in the form of

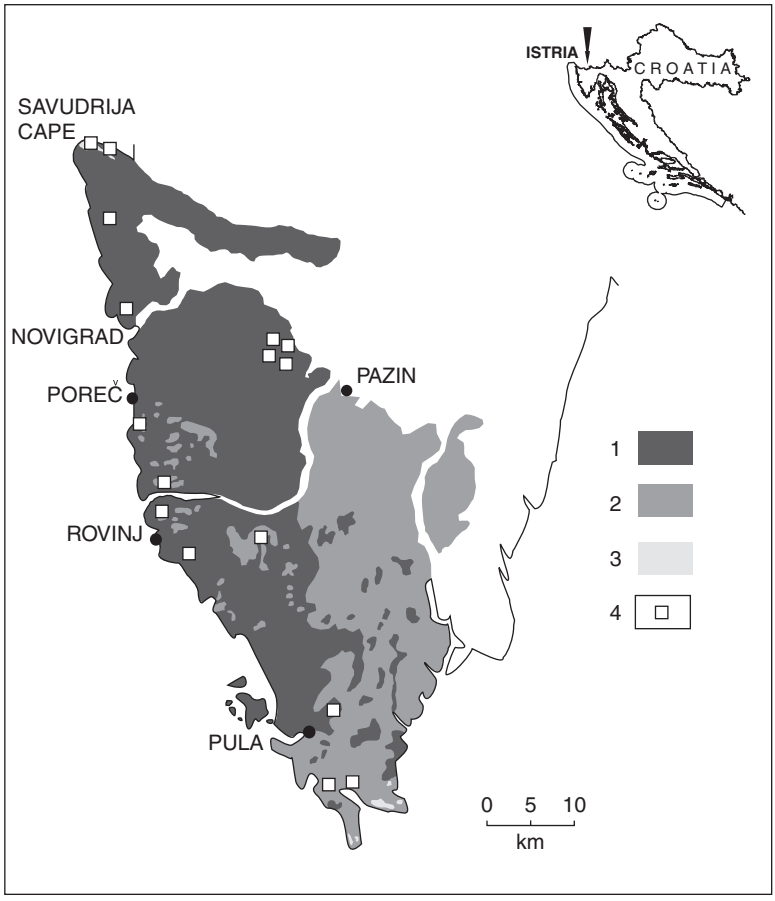

Fig. 2. Distribution of terra rossa in Istria. (modified after Škorić, 1987). (1) Terra rossa, calcaric cambisol, eutric cambisol, regosol from terra rossa (area of terra rossa >70%). (2) Terra rossa, calcaric cambisol, eutric cambisol (area of terra rossa is 50–70%). (3) Eutric cambisol on loess, luvisol on loess, regosol from luvic and eutric cambisol (40:30:30). (4) Locations of terra rossa samples. (after Durn et al., 1999, with permission from Elsevier.)

colluvial pedo-sedimentary complexes. Terra rossa soils in Istria have very important agricultural potential (especially vineyards).

Loess deposition has affected Istria and the Dalmatian Archipelago since the early Middle Pleistocene (Cremaschi, 1990a). Loess is found in the southern part (Premantura and Mrlera) and in the northwestern part of Istria (Savudrija) where it is considered to be Late Pleistocene (Polšak, 1970). The loess is ~4 m thick and overlies a red palaeosol that we regard as a terra rossa (Figs. 1 and 2). The Late Pleistocene loess post-dates terra rossa formation in Istria (Durn et al., 1999). Based on similarities with some loess successions on Susak island (Cremaschi, 1990b), Durn et al. (2003) tentatively proposed that the loess complex in Savudrija was also deposited during the last glacial when the plain of the Po River extended a few hundred kilometres farther to the east as a result of a fall in sea level. Since

rubification and clay illuviation imply Mediterranean-type pedoclimate (Cremaschi, 1990a), we have good reasons to think that the red palaeosol beneath the loess complex was formed in the mild Eemian interglacial period. Its parent material, although of mixed provenance, also contains aeolian sediments, which were deposited during the Middle Pleistocene.

3. MATERIALS AND METHODS

A total of 42 terra rossa samples from the B horizons on Jurassic and Cretaceous limestone were taken at 16 localities in Istria (Fig. 2). The Novigrad profile, situated on the coast of Novigrad Bay NW of Novigrad town (Fig. 2), is used as the type section. It represents a polygenetic terra rossa soil ~1.5 m thick, situated on Early Cretaceous (Late Albian) fine-grained pelletal wackestone. A detailed description of the Novigrad profile is presented in Fig. 3.

Samples of limestone or dolomite were collected from six terra rossa profiles and at three distant sites (Fig. 1). Although terra rossa may no longer be found in its original position, the underlying hard carbonate rocks should have a genetic relationship with the soil that was subjected to rubification (Boero and Schwertmann, 1989). Seven flysch (marl) and five loess samples were also taken for reference (Fig. 1). To evaluate the influence of pyroclastic material, one additional terra rossa soil sample was taken from the island of Korčula where this imprint was recognised (Fig. 1). The island of Korčula is located approximately 300 km SE of Istria. A terra rossa sample was taken at the depth of 2.5 m from a ditch in a vineyard of the polje named Bradat, at the NW cape of the island. The Bradat polje occurs as a relatively deep karst depression in highly karstified palaeo-relief of a Cenomanian-Turonian bedrock succession that is composed of clastics, limestones and dolomites.

Terra rossa samples were air-dried after crushing by hand and passed through a 2 mm sieve. Particle size was determined on the <2 mm fraction after dispersion in water and ultrasonic treatment. Fractions >45 μm were obtained by wet sieving. The <2 μm and 2–10 μm fractions were separated by sedimentation in cylinders and quantitatively obtained after the appropriate settling time. The remaining material in the cylinders was calculated as the 10–45 μm fraction.

Comparative samples of limestone, dolomite and marl were carefully crushed to pass through a 4 mm sieve. To remove carbonates, samples of loess and crushed fragments of limestone, dolomite and marl (2–4 mm) were treated with a 1 M NaOAc solution buffered at pH 5 with HOAc (Jackson, 1979; Tassier et al., 1979). Particle size analysis of i.r. was determined as described above.

The analysis of heavy and light mineral separates was performed on the 45–63 μm size interval of terra rossa and i.r. of flysch and loess. Limestones and dolomites yielded only a small amount of i.r. and from this, the >45 μm fraction was best for the analysis. Heavy and light minerals were separated in bromoform (density 2.87). Both the heavy and light mineral fractions were analysed on glass slides, identifying and counting over 300 grains per slide under a polarising microscope. Point counted mineral proportions were calculated as number percentages. Canada balsam was used as the mounting medium.

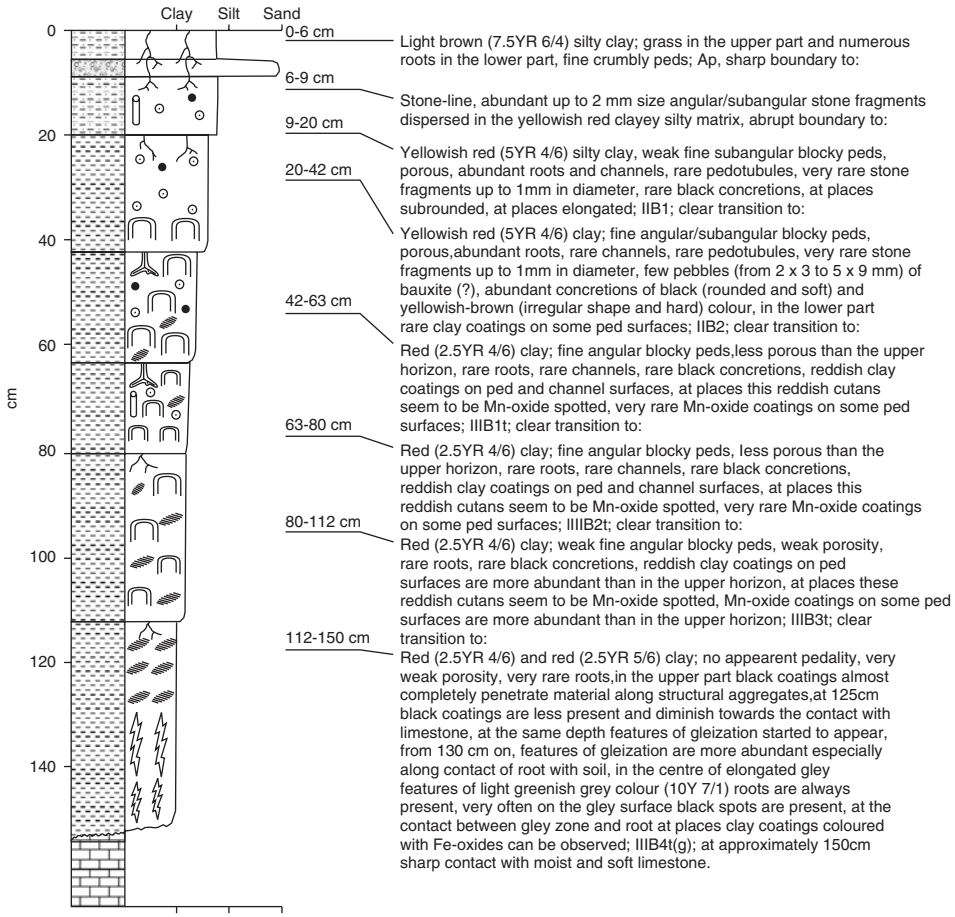

Fig. 3. Lithological log of polygenetic terra rossa soil in the Novigrad profile.

Terra rossa samples from the island of Korčula were analysed using an electron microprobe. The 80–150 μm fraction was extracted following disaggregation in an ultrasonic bath and treatment in diluted HCl. This fraction was selected for the analysis because it includes all virtual mineral species in proportions representative for the bulk sample. Heavy minerals were separated by bromoform and were subjected to magnetic separation in the steeply controlled current range of 0.1–0.7 A to obtain monomineralic concentrates for the microprobe. The light minerals were also analysed to detect light vitric fragments and volcanic feldspars, the dominant constituents of many distal tephras. Mineral grains were mounted in epoxy resin discs, polished and carbon coated, following the standard procedure for electron microprobe analysis. The measurements were obtained at the Mineralogisches Institute, University of Heidelberg with a Camebax SX51 microprobe, equipped with five wavelength-dispersive spectrometers using an accelerating voltage of 15 kV and beam current of 20 nA. A defocused beam of 10 μm was used only for feldspar analyses. Synthetic silicates and oxides were used for calibration.

4. RESULTS

4.1. Particle Size

The i.r. content of limestone and dolomite from Istria averages 0.86%, which indicates that a vast thickness of such rocks had to be dissolved to form terra rossa, and that the preservation rate of that residue through the Quaternary must have been unusually high (Durn et al., 1999). Terra rossa soils are enriched in the silt size fraction compared with the i.r. content of limestone and dolomite (Fig. 4). The average silt/clay ratio in the i.r. of limestone and dolomite (0.25) is lower than that in terra rossa (0.81), indicating a contribution of coarser external material to the terra rossa. Both the i.r. of loess and marl are enriched in silt and sand size fractions, compared with the i.r. of limestone and dolomite (Fig. 4b).

4.2. Bulk and Clay Mineralogy

The differing bulk and clay mineral assemblage in the i.r. of limestones and dolomites is further evidence against the development of terra rossa entirely by the dissolution of carbonate rocks in Istria. According to Durn et al. (1999) the i.r. of limestone and dolomite contain quartz, micaceous clay minerals (illitic material and mica), mixed-layer clay minerals, goethite and amorphous organic and inorganic compounds, while sporadically present are K-feldspar, plagioclase, chlorite and well-crystallised kaolinite which forms intercalation compounds with dimethylsulphoxide (DMSO). The dominant mineral phase of the clay fraction of the i.r. is illitic material. The Istrian terra rossa is composed of quartz, plagioclase, K-feldspar, micaceous clay minerals (illitic material and mica), kaolinites (Kl_{DMSO} and Kl), chlorite, vermiculite, low-charge-vermiculite or high-charge-smectite, mixed-layer clay minerals (other than illitic material), hematite, goethite and XRD-amorphous inorganic compounds. Calcite, dolomite and boehmite are sporadically present and locally important. In all terra rossa samples the content of poorly crystallised kaolinite, which does not form intercalation compounds with DMSO, hereafter referred to as "(Kl)", is higher than that of kaolinite which intercalates with DMSO, hereafter referred to as "(Kl_{DMSO})". (Kl) is the dominant mineral phase in the fine clay and is considered predominantly authigenic (pedogenic) rather than being inherited from parent materials (Durn et al., 1999). Low-charge vermiculite or high-charge smectite was detected only in the fine clay of terra rossa samples, situated below or near the Late Pleistocene loess in the northwestern part of Istria (Savudrija Cape) (Fig. 1).

Flysch (marl) is composed of calcite, quartz, plagioclase, micaceous clay minerals (illitic material and mica), smectite and chlorite, while vermiculite is sporadically present (Durn et al., 1999). The clay fraction of marls is dominated by illitic material and smectite. The Late Pleistocene loess from north-west Istria (Savudrija Cape) contains calcite, dolomite, quartz, plagioclase, K-feldspar, goethite, micaceous clay minerals (illitic material and mica), chlorite, vermiculite, low-charge vermiculite or high-charge smectite, chlorite/vermiculite and both (Kl) and (Kl_{DMSO}). In the coarse grained loess from Premantura, amphibole and epidote were also detected (Durn et al., 1999).

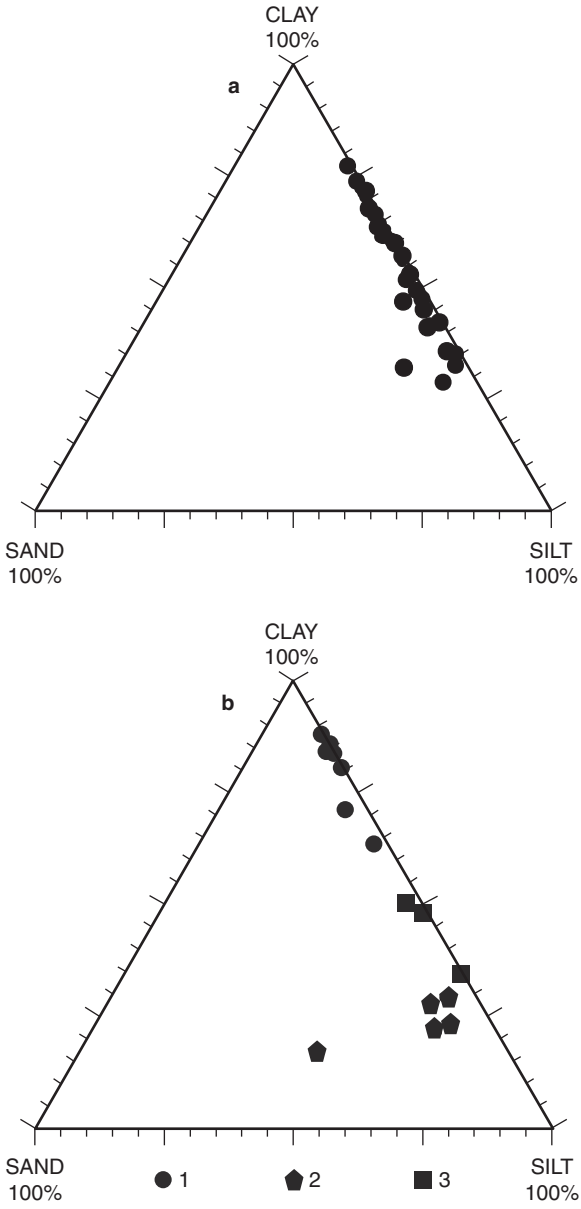

Fig. 4. Ternary plots showing data of particle size analysis. (a) Particle size analysis of terra rossa (after Durn et al., 1999); (b) particle size analysis of: (1) insoluble residues of limestone and dolomite, (2) loess and (3) flysch (marl) (after Durn et al., 1999, with permission from Elsevier).

The i.r. of limestone and dolomite is devoid of vermiculite and kaolinite, neither of which form intercalation compounds with DMSO (Kl). (Kl_{DMSO}) and plagioclase is only sporadically present. By contrast, all terra rossa samples contain vermiculite (Kl_{DMSO}) and plagioclase. Durn et al. (1999) postulated that the appearance of vermiculite and plagioclase in terra rossa from Istria can be related to parent materials other than the i.r. of limestone and dolomite. The presence of low-charge vermiculite or high-charge smectite in the fine clay of terra rossa samples, situated below or near the Late Pleistocene loess, may indicate its aeolian origin, because it was detected as one of the main mineral phases in the fine clay of the Late Pleistocene loess in Savudrija. This loess post-dated terra rossa formation in Istria, but similar external materials might have been introduced into the earlier terra rossa during its formation. This is especially important when we bear in mind that since the early Middle Pleistocene loess deposition affected Istria and the Dalmatian Archipelago (Cremaschi, 1990b).

4.3. Geochemistry

To characterise chemically the i.r. of carbonate rocks and to compare it with terra rossa, flysch (marl) and loess, Durn et al. (1999) used elements with both high ionic potential (considered relatively immobile in soil environments and suitable for geochemical "fingerprinting"; e.g., Muhs et al., 1987, 1990) and low ionic potential (considered relatively mobile in soil environments). The reason for taking into consideration the latter is the direct relationship of these elements to plagioclase (Na), and micaceous clay minerals (illitic material and mica) and K-feldspar (K). Muhs et al. (1987, 1990) found that $(Na_2O/K_2O) \times 100$ and Zr/Nb ratios in the i.r. of limestone and dolomite are significantly lower than ratios in terra rossa, marl and loess. This, together with the results of bulk mineralogy, indicates that terra rossa, loess and marl are enriched in plagioclase compared with the i.r. of limestones and dolomites and adds further evidence to external source contribution during the genesis of terra rossa. Durn et al. (2001, 2003) concluded that the wide range of total REE contents in terra rossa, the difference in LREE/HREE ratios in different grain size fractions, and the significant positive Ce-anomaly observed in some terra rossa samples, all favour a polygenetic origin of terra rossa in Istria. Durn et al. (2003) attributed the difference in REE distribution to the varying REE content of both parent carbonate rocks and different external materials (loess, flysch, bauxite) that have affected the genesis of terra rossa. Weathering processes in the specific pedo-environment in which the terra rossa soils were formed caused further modification and imparted specific individual characteristics.

4.4. Light Mineral Fraction

The light mineral assemblages (fraction 45–63 μm) of selected terra rossa samples and i.r. of limestone and dolomite, flysch (marl) and loess are summarised in Tables 1 and 2. Within the light mineral fraction the following grains were identified: (1) quartz, (2) feldspar, (3) muscovite, (4) biotite, (5) chlorite, (6) glauconite, (7) gibbsite, (8) brucite and (9) opaque and transparent lithic fragments. Quartz and transparent lithic fragments were quantitatively subdivided in detail.

Table 1. Light mineral composition in selected terra rossa samples (TR) situated on limestone and dolomite (45–63 μm fraction)

Sample no.	1	2	9	15	22	25	131	134	136	47	52	234	237	42	97	101
Sample type	TR	TR	TR	TR	TR	TR	TR	TR	TR	TR	TR	TR	TR	TR	TR	TR
Opaque rock particles	2.5	3	16.2	4.8	1.8	2.3	11.6	3.4	3.2	1.7	1.4	2.9	15.9	n.a.	19.9	5.2
Transparent rock particles	5.5	4.8	3.6	5.4	3.6	4.7	5.8	7.3	6.1	20.8	18.1	8.8	5.7		4	4.3
Quartz	82.3	77.3	65	78.4	83.9	85.3	80.4	80.5	87	70.9	74.9	76.1	73.3		65.6	81.5
Feldspar	3.4	2.7	6.4	7.4	6.8	4.3	2.1	3.6	3.2	2	4.8	7.9	3		1.9	2.2
Muscovite	5.6	11	6.7	3.5	3.2	3	0.4	5.0	0.2	4.3	0.7	3.5	1.5		3.7	5.2
Biotite	–	–	–	0.6	0.9	–	–	0.2	0.1	0.3	–	–	0.3		4.2	–
Chlorite	0.6	1.2	1.8	–	–	0.3	–	–	–	–	–	0.6	–		0.8	0.8
Glauconite	–	–	–	–	–	–	–	–	–	–	–	–	–		–	–
Gibbsite	–	–	–	–	–	–	–	–	–	–	–	–	–		–	0.3
Brucite	–	–	–	–	–	–	–	–	–	–	–	–	–		–	0.3
Transparent rock particles (100%)																
Chert	16.4	18.8	41.7	9.1	25	21.3	43.1	37	41	26	40.3	28.4	10.5		32.5	14
Quarzite	10.9	43.8	16.7	50	33.3	42.5	31	26	36.1	61.1	23.2	6.8	21.1		40	28
Pelitic particles	10.9	6.3	8.3	13.6	16.7	21.3	–	6.8	11.5	9.6	11.6	3.4	21.1		12.5	25.6
Other	61.8	31.1	33.3	27.3	25	14.9	25.9	30.2	11.4	3.3	24.9	61.4	47.3		15	32.4
Quartz (100%)																
Idiomorphic, hypidiomorphic, zoned and rosette-shaped quartz	0.4	1.9	2.8	–	0.3	0.4	1.8	1.8	1.6	3.3	0.9	2.1	0.8		0.4	0.4
Polycrystalline quartz	3.4	2.3	2.3	4.1	2.8	3.9	5.9	4.5	4.1	–	5.1	2.9	2.9		4.5	2.4
Clear quartz and shards without inclusions	51.4	46	37.1	40.6	39.7	32.3	32	37	31	2.4	1.4	38.1	36.4		14.2	23.7
Others	44.8	49.8	57.8	55.3	57.2	63.4	60.3	56.7	63.3	94.3	92.6	56.9	59.9		80.9	73.5

Table 2. Light mineral composition in the selected insoluble residues of limestone and dolomite (IRL, >45 μm), flysch (IRF, 45–63 μm) and loess (IRLO, 45–63 μm fraction)

Sample no.	3	9	17	56	63	87	88	89	91	93	94	44	48	46
Sample type	IRL	IRL	IRL	IRL	IRL	IRF	IRF	IRF	IRF	IRF	IRF	IRLO	IRLO	IRLO
Opaque rock particles	17.6	24.9	30*	16.5	19.5	7.8	5.1	6.6	8.2	13.6	2.6	5.2	1.7	0.3
Transparent rock particles	25.6	13.1		16.8	24.6	25.8	24.8	35.5	18.6	13.7	21.1	28.7	25.4	15.9
Quartz	51.4	54.9	36.8	49.3	33.3	58.1	59.4	51.0	66.5	53.2	49.6	50.2	54.9	68.6
Feldspar	2.8	4.1	27.9	1.9	4.2	7.1	6.8	6.8	5.4	6.3	6.3	8.1	6.8	5.3
Muscovite	1.1	1.1	2.0	4.9	0.4	0.5	2.6	–	0.2	2.2	4.1	6.0	8.0	7.2
Biotite	0.9	1.6	–	9.3	0.2	0.3	0.5	–	–	10.0	12.2	0.2	1.7	–
Chlorite	0.2	0.2	3.0	1.5	–	0.5	0.9	–	1.0	1.3	3.7	1.2	1.4	0.5
Glauconite	–	–	–	3.2	19.9	–	–	–	–	–	–	–	–	–
Gibbsite	–	–	–	–	–	–	–	–	–	–	–	–	–	–
Brucite	–	–	–	–	–	–	–	–	–	–	–	–	–	–
Transparent rock particles (100%)														
Chert	6.3	19.1	–	17.9	3.7	12.8	9.3	19.2	25.3	29.2	29.9	32.8	21.6	50.3
Quarzite	3.5	–	–	–	10.6	22.5	16.1	14.1	21.5	20.4	14.2	55.4	53.1	25.2
Pelitic particles	31.6	60.3	–	42.9	74.0	35.3	58.5	42.0	37.6	25.5	30.8	–	11.4	21.4
Others	58.6	20.6	–	39.2	11.7	29.4	16.1	24.7	15.6	24.9	25.1	11.8	13.9	3.1
Quartz (100%)														
Idiomorphic.	0.9	1.2	4.5	2.1	6.6	–	–	–	–	–	–	1.5	–	3.1
Hypidiomorphic, zoned and rosette-shaped quartz crystals														
Polycrystalline quartz	2.6	4.9	–	5.6	6.0	8.3	5.9	12.6	3.4	5.5	6.7	8.4	–	9.3
Clear quartz and shards without inclusions	20.2	11.5	49.5	6.4	14.1	4.7	15.7	6.1	21.7	25.5	13.9	8.8	9.5	14.7
Others	76.3	82.4	46.0	85.9	73.3	87.0	78.4	81.3	74.9	69.0	79.4	81.3	90.5	72.9

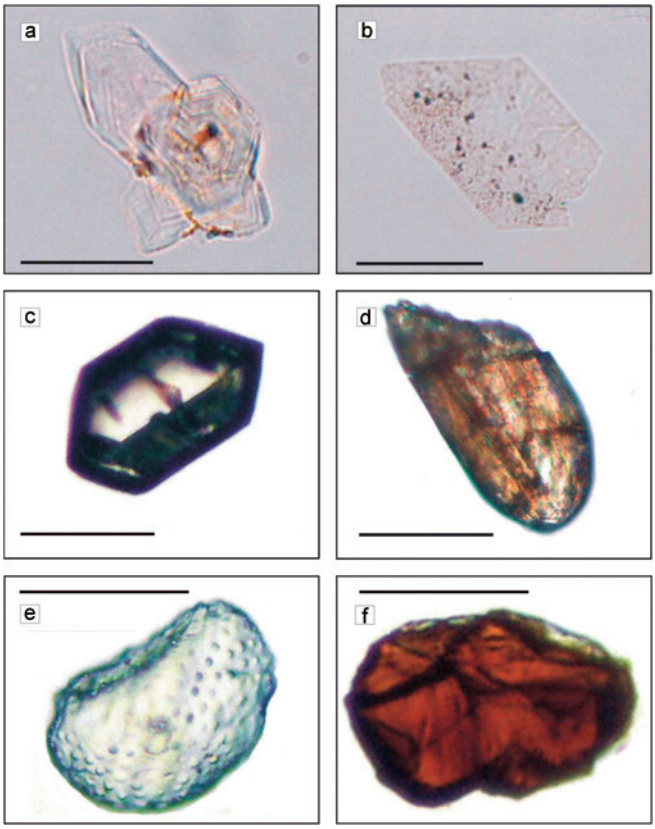

Fig. 5. Characteristic light and heavy mineral grains from terra rossa and loess samples in Istria. (a) Rosette-shaped quartz in terra rossa (sample no. 136); (b) idiomorphic K-feldspar (possibly sanidine) in loess (sample no. 44); (c) sharp euhedral zircon crystal from terra rossa showing bipyramidal terminations (sample no. 2); (d) zircon grain from loess showing grooves and striation developed through abrasion (sample no. 409); (e) well rounded grain of celestite in flysch. Specific surface characteristics suggest its precipitation in a foraminiferal cell (sample no. 89). (f) Chrome spinel grain in terra rossa (sample no. 2). Length of scale bar is 50 μm in all photomicrographs.

4.4.1. Quartz

The following groups were recognised and separately counted: (1) idiomorphic, hypidiomorphic, zoned and rosette-shaped (Fig. 5a) quartz crystals, (2) compound quartz grains (with undulatory extinction or several grains appear in different orientation), (3) clear quartz crystals and shards without inclusions and (4) other quartz types. The average quartz content is lowest in the i.r. of limestone and dolomite, higher in the i.r. of flysch and loess and highest in terra rossa (Tables 1 and 2; Fig. 6). Idiomorphic, hypidiomorphic, zoned and rosette-shaped quartz crystals are most abundant in the i.r. of limestone and dolomite with their content within the quartz population varying from 0.9 to 6.6% (Table 2). In the i.r. of flysch these types were not detected. However, two of three i.r. analysed from loess contain them and they are present in all terra rossa samples, except sample no. 15, ranging from 0.3 to

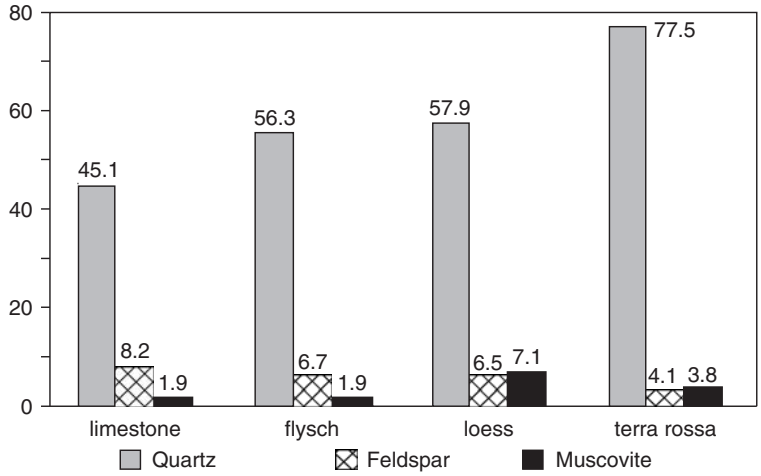

Fig. 6. Average content of quartz, feldspars and muscovite in the light fraction of terra rossa (45–63 μm) and the insoluble residues of flysch, loess (45–63 μm) and limestone and dolomite (>45 μm).

3.3%. Compound quartz grains and clear quartz crystals and shards without inclusions were found in all analysed samples (Tables 1 and 2). Their average content is highest in terra rossa (30.9%), lower in the i.r. of limestone and dolomite (20.34%), while the i.r. of flysch and loess contain them in 14.6 and 11% respectively (Tables 1 and 2).

4.4.2. Feldspars

Feldspars are present in all analysed samples and are dominated by hypidiomorphic and idiomorphic K-feldspar monocrystals. Some hypidiomorphic K-feldspars found in loess and terra rossa were tentatively interpreted as sanidine (Fig. 5b). Plagioclase is present in almost all samples in significantly lower amounts. In a few i.r. of limestone and dolomite, rare microcline grains were also observed. The average feldspar content is highest in the i.r. of limestone and dolomite, lower in the i.r. of loess and flysch and lowest in terra rossa (Tables 1 and 2, Fig. 6).

4.4.3. Other components

Muscovite is the most abundant mineral among the analysed phyllosilicates and was detected in all samples except flysch sample no. 89, while biotite and chlorite are sporadically present in all groups of analysed samples (Tables 1 and 2). It is interesting to note that the terra rossa sample with the highest biotite content (no. 97) was situated close to the flysch exposure from where the two flysch samples (nos. 93, 94), containing the highest amounts of biotite, were taken. Glauconite was observed only in the i.r. of limestone and dolomite and is considered authigenic. Gibbsite and brucite were detected only in a terra rossa sample in the vicinity of a Palaeogene bauxite.

4.4.4. Lithic fragments

Limonitic (iron hydroxide) and red-stained particles were found in all analysed samples and recorded as opaque lithic fragments. They are most abundant in the i.r. of limestone and dolomite (Tables 1 and 2). Within the transparent lithic fragments, the following grains were recognised and counted separately (1) chert, (2) quartzite, (3) pelitic particles and (4) other transparent rock particles. These include: composite grains, comprising quartz and some phyllosilicate, chlorite-schist and quartz spherulites. Most abundant in the i.r. of limestone, dolomite and flysch are the pelitic particles (Table 2). Compared with the i.r. of limestone and dolomite, all flysch samples contain quartzite and chert. Dominant transparent lithic fragments in the i.r. of loess are quartzites, followed by chert (Table 2). Pelitic particles are significantly less abundant in the loess than in the i.r. of limestone, dolomite and flysch. Compared with the i.r. of limestone and dolomite, flysch and loess, the terra rossa samples generally contain significantly fewer transparent lithic fragments (Tables 1 and 2), the most abundant being quartzite. In Fig. 7 the composition of the terra rossa and the i.r. of limestone and dolomite, flysch and loess is plotted in relation to selected transparent lithic fragments (chert, quartzite and pelitic).

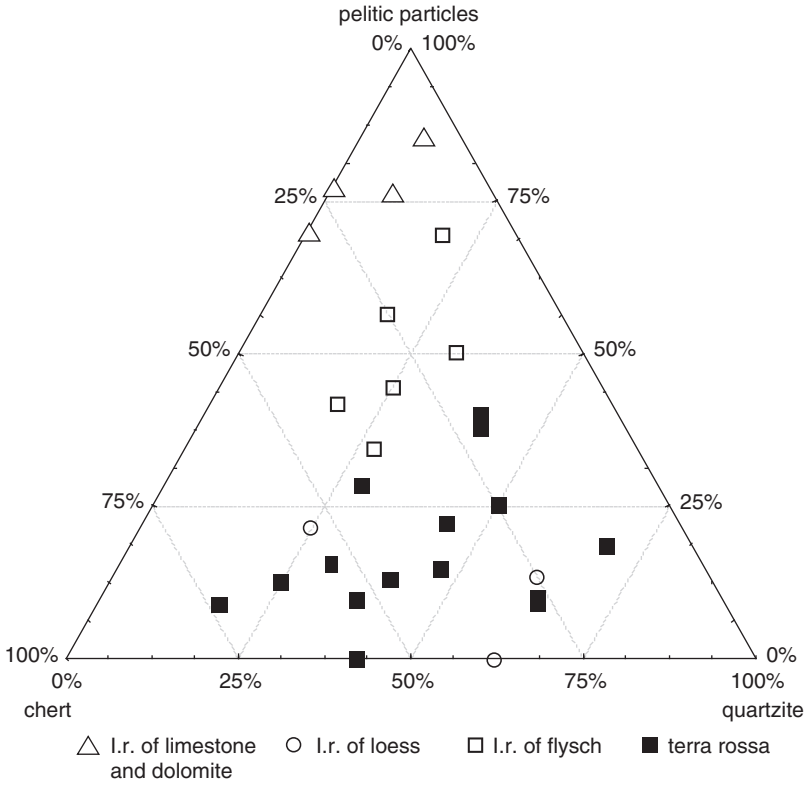

Fig. 7. Ternary diagram showing the relationship between the selected transparent rock particles (chert + quartzite + pelitic particles = 100%) in the terra rossa and insoluble residue of limestone and dolomite, flysch and loess.

Fig. 7 shows that the majority of the terra rossa samples contain significantly fewer pelitic particles and considerably more quartzite and chert than the i.r. of flysch and especially that of limestone and dolomite. Although terra rossa soils have significantly fewer transparent lithic fragments than the i.r. of limestone, dolomite, flysch and loess, their composition (in relation to selected transparent rock particles) mostly matches that of the Late Pleistocene loess. Although the Late Pleistocene loess post-dates terra rossa formation, its composition indicates that during terra rossa formation similar external materials contributed to terra rossa, thus complementing the i.r. of limestone and dolomite that constituted the primary parent material.

4.5. Heavy Mineral Fraction

Heavy mineral assemblages of the 45–63 μm size fraction of selected terra rossa samples and i.r. of limestone and dolomite, flysch (marl) and loess are given in Tables 3 and 4. Within the heavy mineral residue the following mineral grains and lithic fragments were recognised: (1) transparent heavy minerals, (2) opaque grains, (3) phyllosilicates, (4) limonitic particles, (5) various lithic fragments and (6) pyritised foraminifers. Transparent heavy minerals were semi-quantitatively subdivided in detail. Phyllosilicates (muscovite, chlorite, biotite and glauconite) and rock particles were also present in the light fraction and will not be discussed here.

4.5.1. Transparent heavy minerals

Heavy minerals identified and counted separately within the transparent heavy minerals are shown in Tables 3 and 4. Transparent heavy minerals are more abundant in terra rossa samples and in the i.r. of loess than in that of limestone, dolomite and flysch. Their content is similar in terra rossa (15–86%) and in the i.r. of loess (29–87%). In the i.r. of flysch they range from 9 to 37% and in the i.r. of limestone and dolomite from 2 to 34%. Typical transparent heavy minerals in terra rossa samples and i.r. of loess are shown in Figs. 8a, d respectively.

Epidote group minerals. Generally, the most abundant among transparent heavy minerals in all analysed samples is the epidote group (epidote-clinozoisite-zoisite). Epidote grains are usually equidimensional, irregular (Fig. 8a), yellow to greenish-yellow and show weak pleochroism. White to grey or yellowish prismatic grains with lower relief correspond probably to zoisite or clinozoisite. Epidote and presumed clinozoisite and zoisite grain counts were combined together as epidote group minerals (Tables 3 and 4).

Zircon. Zircon abundance in some of the terra rossa samples can reach 26% (Table 4). Grains from terra rossa samples often show sharply angular bipyramidal forms (Fig. 5c) while subangular or rounded grains are subordinate. Irregularly distributed inclusions in zircon grains are a common feature. Completely rounded grains that are occasionally present in the i.r. of loess, show pitted and striated

Table 3. Heavy mineral spectrum in selected terra rossa samples (TR) lying on limestone and dolomite (45–63 μm fraction)

Sample no.	1	2	9	15	22	25	131	134	136	53	55	47	52	234	237	42	97	101
Sample type	TR	TR	TR	TR	TR	TR	TR	TR	TR	TR	TR	TR	TR	TR	TR	TR	TR	TR
Opaque	8	15	24	11	12	21	36	42	36	27	11	23	40	21	18	27	50	8
Phyllosilicates	1	12	4	61	1	2	4	6	2	5	6	4	+	3	2	2	+	—
Limonitised particles	14	6	11	7	2	7	19	11	15	10	14	31	34	4	8	18	34	54
Rock particles	–	1	–	1	–	–	–	–	–	–	–	–	–	–	–	–	–	–
Pyritised foraminifera	–	–	–	–	–	–	–	–	–	–	–	–	–	–	–	–	–	–
Transparent	77	66	71	20	86	70	42	41	48	58	69	43	26	71	72	52	15	37
Epidote group	80	68	73	57	63	63	60	51	45	66	57	31	18	66	63	58	57	61
Zircon	3	+	2	2	4	3	4	7	8	3	7	17	26	4	5	3	5	7
Rutile	1	–	–	–	3	3	3	4	8	3	2	10	13	2	+	3	2	3
Garnet group	5	8	4	2	9	5	6	7	3	1	10	12	5	6	11	6	9	5
Tourmaline	2	1	+	2	2	6	13	15	14	7	7	18	17	6	3	11	8	13
Hornblende	2	–	4	4	3	2	3	1	1	2	3	4	5	3	1	2	2	1
TFSM	4	13	11	24	10	12	3	8	10	12	11	4	1	11	13	8	12	5
Glaucophane	1	+	–	1	1	1	2	1	+	+	1	–	+	+	1	–	1	–
Amphibole (other)	–	5	2	–	1	–	–	–	3	1	–	–	–	–	–	–	–	4
Clinopyroxene	–	1	+	–	–	–	+	–	–	–	–	–	–	–	–	–	–	–
Orthopyroxene	–	1	–	–	–	–	–	2	–	–	–	–	–	–	–	–	–	–
Chrome spinel	–	–	–	–	–	+	+	–	1	+	–	2	3	–	–	2	–	–
Kyanite	–	–	–	+	–	2	1	3	1	1	1	–	2	1	+	1	4	1
Corundum	–	+	+	–	–	+	–	–	–	+	–	–	–	–	–	2	–	–
Anatase	1	–	–	+	–	–	–	–	2	+	–	1	3	–	–	+	–	1
Titanite	–	–	+	–	–	–	+	–	–	–	–	–	2	–	–	–	–	–
Chloritoid	–	+	1	2	1	2	2	–	+	–	–	1	+	–	–	+	–	–
Apatite	–	–	–	5	–	–	+	1	–	–	–	–	–	–	–	–	–	–
Brookite	–	–	–	–	1	+	–	–	–	–	+	1	1	–	–	–	–	1
Andalusite	–	–	–	–	–	–	+	–	–	–	–	–	–	–	–	–	–	–
Staurolite	–	–	–	–	–	–	–	–	1	–	–	–	–	–	–	–	–	–
Gypsum	–	–	–	–	–	–	–	–	–	–	–	–	–	–	–	–	–	–
Celestite	–	–	–	–	–	–	–	–	–	–	–	–	–	–	–	–	–	–
Barite	–	–	–	–	–	–	–	–	–	–	–	–	–	–	–	–	–	–
Volcanic glass fragments	–	–	–	–	–	–	–	–	–	–	–	–	–	–	–	–	–	–
Vesuvianite	–	–	–	–	–	–	–	–	–	–	–	–	–	–	–	–	–	–
Unidentified	+	–	+	+	+	+	2	1	+	+	+	2	3	–	+	+	1	1

Note: TFSM, tremolite-ferroactinolite series minerals.

surfaces (Fig. 5d). In the i.r. of flysch and partly in limestone and dolomite, detrital zircons are generally rounded.

Rutile. Rutile is sporadically present in the majority samples of terra rossa and i.r. of loess and flysch, and was detected in only one limestone i.r. (Tables 3 and 4; Fig. 8a).

Garnet. Garnet was found in nearly all analysed samples, with the terra rossa samples containing it in the lowest amounts (Tables 3 and 4). Only colourless garnet was encountered (Fig. 8d). Grains are rarely euhedral; more commonly they show irregular forms with conchoidal fractures as well as various inclusions. Traces of corrosion on garnet surfaces are common.

Table 4. Heavy mineral spectrum in the selected insoluble residues of limestone and dolomite (IRL, >45 μm), flysch (IRF, 45–63 μm fraction) and loess (IRLO, 45–63 μm fraction)

Sample no.	3	9	17	56	87	88	89	91	92	93	94	18	44	48	409	411
Sample type	IRL	IRL	IRL	IRL	IRF	IRF	IRF	IRF	IRF	IRF	IRF	IRLO	IRLO	IRLO	IRLO	IRLO
Opaque	8.0	7.0	2.0	43.0	2.0	46.0	10.0	19.0	28.0	66.0	64.0	7.0	8.0	11.0	8.0	5.0
Phyllosilicates	10.0	1.0	5.0	10.0	11.0	1.0	4.0	4.0	2.0	9.0	2.0	6.0	2.0	26.0	6.0	4.0
Limonitised particles	50.0	90.0	8.0	9.0	65.0	18.0	58.0	40.0	33.0	20.0	10.0	5.0	34.0	34.0	3.0	4.0
Rock particles	22.0	+	55.0	1.0	10.0	–	8.0	1.0	–	1.0	+	–	2.0	–	–	–
Pyritised foraminifera	8.0	+	–	27.0	–	2.0	1.0	1.0	–	19.0	14.0	–	–	–	–	–
Transparent	9.0	2.0	30.0	10.0	12.0	33.0	19.0	34.0	37.0	9.0	10.0	81.0	53.0	29.0	85.0	87.0
Epidote group	–	7.0	40.0	25.0	53.0	49.0	32.0	38.0	41.0	5.0	9.0	43.0	24.0	32.0	40.0	35.0
Zircon	–	4.0	11.0	9.0	7.0	4.0	9.0	9.0	4.0	1.0	–	4.0	12.0	5.0	3.0	6.0
Rutile	–	–	–	–	3.0	2.0	–	7.0	1.5	–	–	1.0	5.0	1.0	3.0	–
Garnet group	–	7.0	23.0	13.0	17.0	19.0	26.0	21.0	22.0	1.0	2.0	17.0	17.0	18.0	26.0	18.0
Tourmaline	–	–	1.0	1.0	7.0	6.0	3.0	9.0	9.0	–	–	1.0	7.0	11.0	1.0	2.0
Hornblende	–	–	18.0	1.0	1.0	7.0	–	5.0	3.5	3.0	–	14.0	7.0	8.0	6.0	12.0
TFSM	–	–	–	1.0	–	3.0	–	2.0	10.5	–	–	15.0	3.0	17.0	7.0	7.0
Glaucophane	–	–	–	–	–	–	–	–	1.0	–	–	+	–	+	+	–
Amphibole (other)	–	–	–	1.0	–	–	–	–	–	–	–	–	4.0	1.0	4.0	7.0
Clinopyroxene	–	–	1.0	1.0	–	–	–	1.0	–	–	–	–	5.0	–	–	2.0
Orthopyroxene	–	–	2.0	–	–	–	1.0	–	–	–	–	–	+	–	3.0	5.0
Chrome spinel	–	5.0	–	1.0	3.0	5.0	5.0	4.0	5.5	1.0	+	–	9.0	+	–	+
Kyanite	–	–	–	2.0	–	1.0	–	–	–	–	–	1.0	1.0	+	7.0	1.0
Corundum	–	18.0	–	2.0	–	1.0	+	2.0	–	–	–	–	–	–	–	–
Anatase	–	–	–	–	–	–	–	–	1.5	–	–	–	–	+	–	–
Titanite	–	–	–	–	–	1.0	–	–	–	–	–	–	–	–	–	–
Chloritoid	–	–	1.0	–	–	1.0	–	–	–	–	–	+	1.0	+	1.0	1.0
Apatite	–	4.0	–	6.0	+	–	1.0	1.0	–	3.0	2.0	–	–	–	–	–
Brookite	–	–	–	–	–	–	3.0	–	–	–	–	+	3.0	+	–	2.0
Andalusite	–	–	–	–	–	–	–	–	–	–	–	–	–	–	–	–

Table 4 (*Continued*)

Sample no.	3	9	17	56	87	88	89	91	92	93	94	18	44	48	409	411
Sample type	IRL	IRL	IRL	IRL	IRF	IRF	IRF	IRF	IRF	IRF	IRF	IRLO	IRLO	IRLO	IRLO	IRLO
Staurolite	–	–	–	–	–	–	–	–	–	–	–	+	1.0	–	–	–
Gypsum	–	–	+	4.0	–	–	–	–	–	5.0	–	–	–	–	–	–
Celestite	–	54.0	–	32.0	8.0	–	20.0	–	–	77.0	85.0	–	–	–	–	–
Barite	–	–	–	–	–	–	–	–	–	1.0	1.0	–	–	–	–	–
Volcanic glass fragments	–	–	–	–	–	–	–	–	–	–	+	+	–	1.0	–	–
Vesuvianite	–	–	–	–	–	–	–	–	–	–	–	–	1.0	–	–	–
Unidentified	–	–	1.0	1.0	3.0	2.0	2.0	2.0	+	+	–	–	1.0	–	+	1.0

Note: TFSM, tremolite-ferroactinolite series minerals.

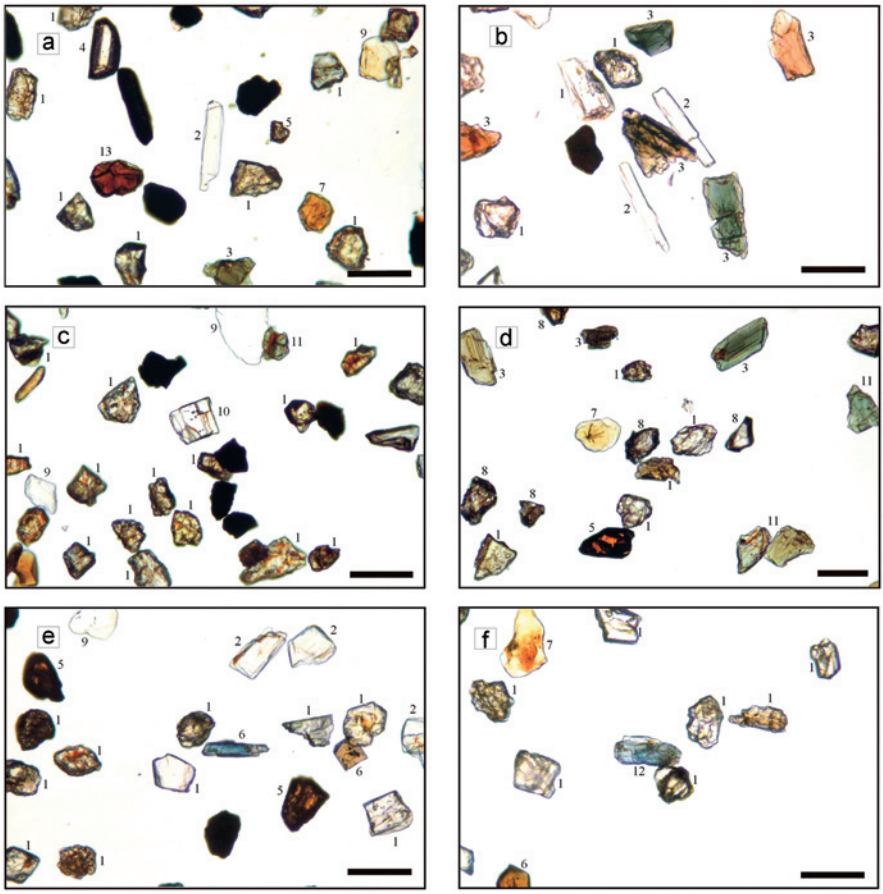

Fig. 8. (a) A typical heavy mineral association in terra rossa (sample no. 2). Transparent minerals dominate but opaque/limonitic grains (dark) are also present. Note that mineral grains of the epidote group are relatively fresh; (b) amphibole-dominated assemblage from loess sample no. 409; (c) kyanite, a significant mineral in loess (sample no. 409). (d) Typical heavy mineral association of loess (sample no. 411). Note the high proportion of transparent grains; (e) brown and blue prismatic tourmaline varieties found in terra rossa sample no. 2; (f) glaucophane grain (blue) in loess sample no. 411. Key: 1, epidote group; 2, tremolite-ferroactinolite series minerals; 3, hornblende; 4, zircon; 5, rutile; 6, tourmaline; 7, chlorite; 8, garnet; 9, muscovite; 10, kyanite; 11, clinopyroxene; 12, glaucophane; 13, chrome spinel. Length of bar is 100 μm.

Tourmaline. Tourmaline grains are prismatic and sometimes exhibit vertical striations or random inclusions and their terminations are generally irregular. Fractured tourmaline grains are not common. They are dominantly brown but a few blue varieties were observed, especially in terra rossa samples (Fig. 8e). Tourmaline is most abundant in terra rossa samples, whereas the lowest contents were observed in the i.r. of limestone and dolomite (Tables 3 and 4).

Amphiboles. Within the amphibole group the following members have been distinguished and counted separately: (1) hornblende group (Fig. 8b), (2) members of tremolite-ferroactinolite series (Fig. 8b), (3) minerals of glaucophane series (Fig. 8f) and (4) other amphiboles (could not be identified positively). Of the amphibole group tremolite-ferroactinolite series minerals are the most abundant in terra rossa (Table 3). The i.r. of loess is also enriched in amphiboles. Compared with terra rossa and i.r. of loess, samples of i.r. of flysch and especially i.r. of limestone and dolomite (except sample 17) contain significantly fewer amphiboles. Using epidote group minerals + amphiboles, zircon + tourmaline and garnets, data from terra rossa and from i.r. of limestone and dolomite, flysch and loess are plotted in a ternary diagram (Fig. 9a). Fig. 9a shows that the majority of terra rossa samples are more enriched in the epidote-zoisite group and amphiboles, compared with the i.r. of loess, flysch, as well as limestone and dolomite. A relatively good correspondence exists between the i.r. of loess and flysch and (in part) that of limestone and dolomite. However, plotting the abundance of amphiboles, zircon + tourmaline and garnet from the terra rossa and that of the i.r. of limestone and dolomite, flysch and loess in a ternary diagram (Fig. 9b), the data cluster of loess falls close to that of terra rossa, suggesting that the nature of external material incorporated into the terra rossa was similar to the composition of Late Pleistocene loess. Apatite and corundum were not found in the i.r. of loess. However, they are present in the i.r. of limestone and dolomite, and flysch.

In many i.r. of flysch, as well as in some i.r. of limestone and dolomite, appreciable amounts of celestite are present (Table 4; Fig. 5e). It is considered authigenic and is completely absent from terra rossa and loess assemblages. Other transparent heavy minerals, e.g., chloritoid, chrome spinel (Fig. 5f) are present in several of the analysed samples in low amounts.

4.5.2. Opaque grains

Opaque grains and limonitic particles were detected in all analysed samples. The i.r. of flysch has the highest average contents of opaque grains (33.6%) while limonitic particles are most abundant in the i.r. of limestone and dolomite (Tables 3 and 4). Pyritised foraminifers were recognised only in the i.r. of limestone and dolomite and flysch. The pyrite is considered authigenic.

4.6. Heavy and Light Mineral Fraction in Terra Rossa from the Island of Korčula

Heavy minerals detected in terra rossa soil from the island of Korčula in significant abundances are garnet, spinel, amphibole, epidote, orthopyroxene and Fe–Ti oxides. Tourmaline, staurolite, black mica, rutile, titanite and fragments of mantle-peridotite, containing olivine and spinel were occasionally found. The light fraction is dominated by quartz and includes abundant sanidine, sparse hyalophane (Ba-sanidine), Na-feldspar and rare K-feldspar. Also observed were pumice fragments of likely rhyolitic or trachytic composition, consisting of microphenocrysts of sanidine and quartz set in a totally altered matrix (Fig. 10).

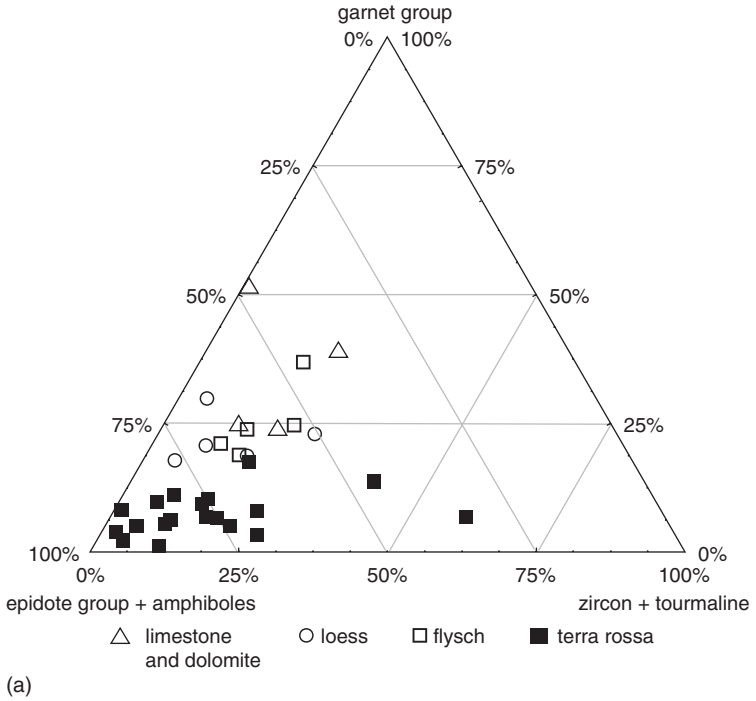

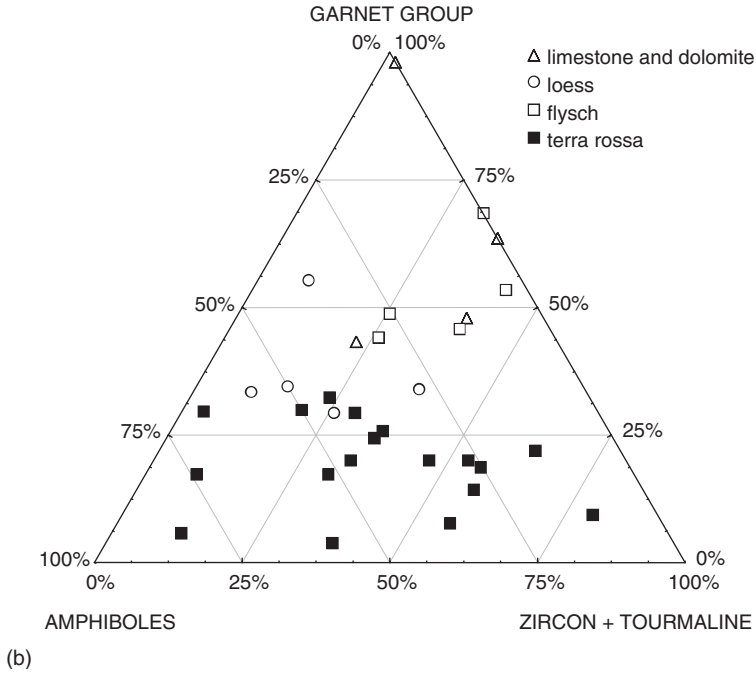

Fig. 9. (a) Ternary diagram showing the relationship between the proportions of garnet group vs. epidote group + amphiboles vs. zircon + tourmaline (= 100%) in terra rossa and insoluble residues of limestone and dolomite, flysch and loess; (b) ternary diagram showing the relationship between the proportions of garnet group vs. amphiboles vs. zircon + tourmaline (= 100%) in terra rossa and insoluble residues of limestone and dolomite, flysch and loess.

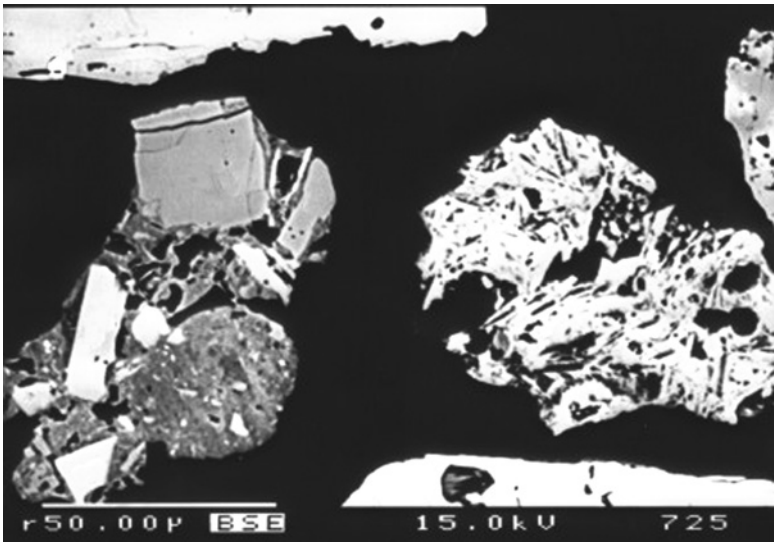

Fig. 10. Backscattered electron photomicrograph of juvenile volcanic clasts of probably rhyolitic/trachytic composition. The fragments contain sanidine and quartz, set in the highly altered matrix.

4.7. Geochemistry of Individual Heavy Minerals

4.7.1. Garnet

Representative garnet analyses are shown in Table 5 and their compositions are plotted in Fig. 11 where three compositional groups are distinguished. Group 1 comprises pyrope-rich garnets (40–60%) with relatively high grossular (10–30%) and less than 2.5% spessartine. These compositions are typical of eclogitic garnets from migmatite-gneiss terraines (e.g., Coleman et al., 1965) and are similar to garnets reported from Austridic eclogites from the Pohorje Mts, Eastern Alps (Fig. 11; Hinterlechner-Ravnik et al., 1991). Garnets of Group 2 are almandines with less then 10% pyrope, 15% grossular and 1.5% spessartine, and are characteristic for schistose metapelitic rocks of amphibolite facies, associated with migmatite-gneiss terraines. Grandites of garnet Group 3 show bimodal compositions: grossular rich compositions (>70%) and andradite-rich compositions (>60%). The latter, containing up to 10% melanite, represent the most abundant garnet population of analysed terra rossa. Melanitic garnet is commonly found in alkaline igneous rocks and was reported from potassic under-saturated lavas of the Colli Albani (Baldridge et al., 1981) and trachytic lavas of Roccamonfina (Gianetti and Luhr, 1983) from the Quaternary Roman volcanic province (RVP) in central Italy. The latter lavas enclose monzonite and syenite nodules which also contain melanitic garnet (Gianetti, 1982).

4.7.2. Chrome spinel

The chemical composition of chrome spinels is given in Table 5. They contain less than 0.21 wt% TiO_2 and are peridotitic according to the subdivision established for detrital spinels occurring in the flysch sandstones of the Late Cretaceous/Middle

Table 5. Microprobe analyses of selected heavy and light minerals from terra rossa in Korčula

Mineral	Grt	Grt	Grt	Grt	Grt	Spl	Spl	Spl	Spl	Amp	Opx	Bt	Na-fsp	K-fsp	Sa	Sa	Sa	Ba-fsp
Analysis no.	2-66	1-90	1-84	1-46	1-48	1-50	18-2	1-35	1-98	1-57	1-33	13-2	1-65	23-1	1-61	1-66a	1-59	6-1
Remarks	gr1	gr1	gr2	gr3	gr3	I	II	III	pleo	vol.c	vol.c	vol.c	eol.c	eol.c	vol.c	pum	vol.c	vol.c
SiO_2	41.2	40.15	37.32	37.85	31.25	0.02	0.04	0.02	0.03	34.99	53.64	36.63	68.38	63.07	62.2	63.57	61.85	54.86
TiO_2	0.04	0.07	0.08	0.08	5.62	0.06	0.15	0.08	0.22	1.38	0.29	4.82	n.d.	n.d.	n.d.	n.d.	n.d.	n.d.
Al_2O_3	22.87	22.28	20.61	16.35	1.99	46.88	24.07	7.4	65.55	13.65	1.05	14.58	20.13	18.6	19.9	19.17	21.19	21.96
Cr_2O_3	0.21	0.09	0.05	0.06	0.12	23.09	44.66	61.38	0	0.02	0.05	0.01	n.d.	n.d.	n.d.	n.d.	n.d.	n.d.
FeO_{tot}	12.62	16.27	35.91	8	25.03	12.76	17.2	21.1	8.76	27.34	17.63	13.37	0.11	2.93	0.19	0.17	0.45	0.25
MnO	0.22	0.4	0.59	0.66	0.7	0.1	0.06	0.11	0.07	1.73	0.57	0.2	n.d.	n.d.	n.d.	n.d.	n.d.	n.d.
MgO	15	12.5	2	0.02	0.64	16.82	12.88	9.03	25.33	2.35	24.94	15.01	n.d.	n.d.	n.d.	n.d.	n.d.	n.d.
CaO	8.35	8.46	4.01	36.09	31.85	0	0	0.02	0.05	10.86	1.45	0.16	0.21	0.46	0.44	0.31	1.63	0.21
BaO	n.d.	n.d.	n.d.	n.d.	n.d.	n.d.	n.d.	n.d.	n.d.	n.d.	1.45	0.78	0.03	0.01	1.91	0.39	1.4	9.16
Na_2O	0	0	0	0	0	0	0	0	0	2.04	0.03	0.45	11.41	0.43	1.51	1.44	5.09	1.86
K_2O	0	0	0	0	0	0	0	0	0	2.45	0	8.76	0.2	13.61	12.8	13.71	6.69	8.7
Total	100.5	100.2	100.6	99.12	97.19	99.72	99.06	99.13	100	96.81	101.1	94.76	100.5	99.11	98.95	98.76	98.31	96.98

Note: Grt, garnet (gr1, gr2 and gr3 refer to the three distinct compositional groups). Formulae were calculated on the basis of 12 oxygens and 8 cations. Spl, spinel (I, II and III indicate type of spinel peridotite; pleo, pleonaste). Cations were calculated on the basis of 3 cations and 4 oxygens. vol.c, volcanic clast; eol.c, aeolian clast; pum, sanidine from pumiceous lithoclast.

Amp, amphibole. Cations were calculated on the basis of 23 oxygens and 13 cations, excluding Ca, Na and K. Bt, biotite/phlogopite. Cations were calculated on the basis of 11 oxygens and $FeO = FeO_{tot}$. Na-fsp, sodic feldspar; K-fsp, potassic feldspar; Sa, sanidine; Ba-fsp, hyalophane (Note: Sr and Rb EDS concentrations were not included in total). n.d., not determined. Feldspar formulae were calculated on the basis of 8 oxygens and total Fe as Fe_2O_3.

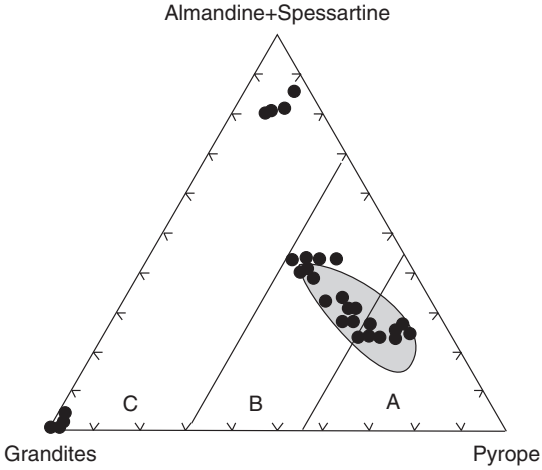

Fig. 11. Ternary diagram of all garnet compositions from the analysed terra rossa. Shaded contour field refers to the garnets from the Pohorje eclogites, Eastern Alps (Hinterlechner-Ravnik et al., 1991). Boundary lines for different rock types are from Coleman et al. (1965). A, eclogites, associated with kimberlite pipes, and eclogites within mantle ultramafic rocks; B, eclogites in gneisses or migmatitic terrain; C, amphibolites, charnokites and granulites.

Eocene sedimentary basins in the SE Alps (Lenaz et al., 2000). In the formula of Mg # [= 100 × Mg/Mg + Fe^{2+}] and Cr # [= (100 × Cr/(Cr + Al)] chemical parameters (Fig. 12), the peridotite-derived chrome spinels from Korčulan terra rossa show a compositional range (Cr # = 25–85) that is typical for all three groups of Alpine-type peridotites (Dick and Bullen, 1984) with the majority spreading within the field of spinels from Type III peridotites (Cr # > 60). Peridotite-derived detrital chrome spinels in the flysch from the Istrian Flysch Basin show a similar compositional span (Lenaz and Princivalle, 2000). The peridotite clast incorporating chrome spinel with Cr # 55.4 (Table 5: analysis 2–18) and olivine ($Fo_{94.2}$, 0.49 wt% NiO) represents a Type II peridotite. Volcanic spinels were not detected. The single pleonaste grain (Table 5; Fig. 12) encountered was probably generated by thermal metamorphism.

4.7.3. Amphiboles

All analysed amphiboles are Ca-amphiboles (Fig. 13); the majority is Mg-rich (Mg # = 72–92) and Al-poor with compositions ranging from magnesio-hornblende (4.1–6.9 wt% Al_2O_3) to actinolite (< 4 wt% Al_2O_3). They are low-pressure amphiboles, typical of retrograde metamorphic rocks or altered mafic igneous rocks. Only one amphibole grain indicated volcanic origin (Table 5: analysis 1–57). In the amphibole classification scheme (Leake et al., 1997) it plots in the potassic hastingsite field (K/Na = 0.93; Mg # = 16.2) with distinctly high Mn content (1.73 wt% MnO). Such amphiboles are typical of alkaline igneous rocks. Similar compositions were reported in association with melanitic garnets from trachytic and foiditic lavas of RVP (Baldridge et al., 1981; Gianetti, 1982; Gianetti and Luhr, 1983).

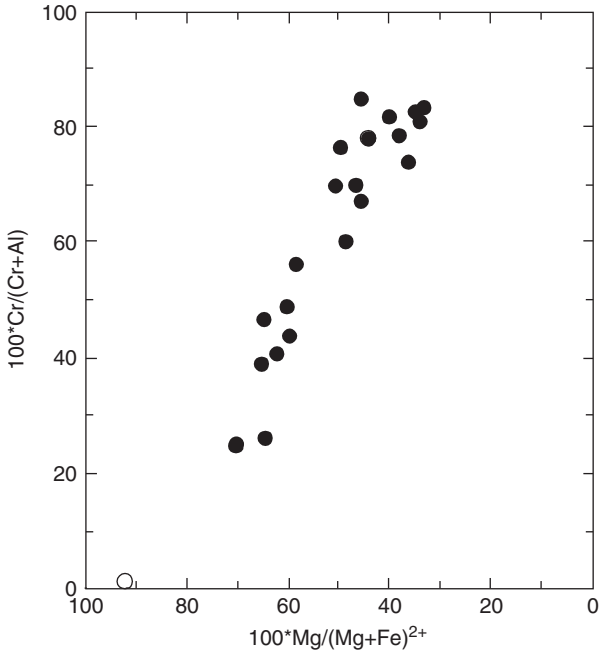

Fig. 12. Compositional relationship in terms of Cr # vs. Mg # for peridotite-derived chrome spinels (<0.2 wt% TiO_2) from Korčulan terra rossa. Note discrete pleonaste grain (open circle, bottom left) unrelated to spinels from peridotites.

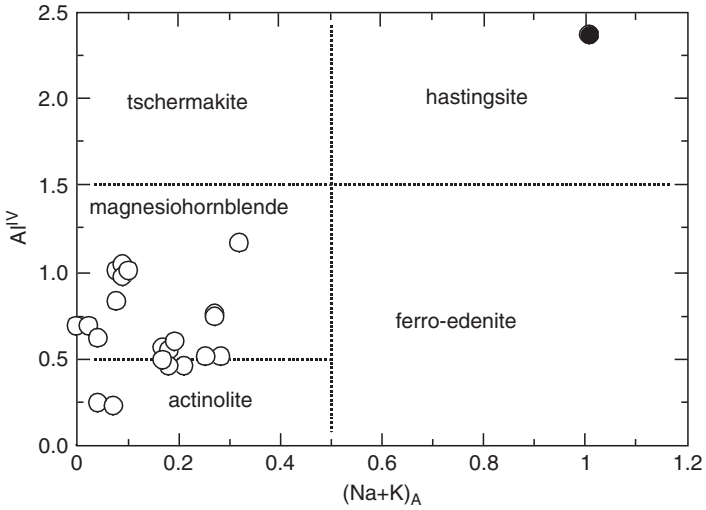

Fig. 13. Compositions of Korčulan terra rossa amphiboles plotted in as $Al^{IV} - (Na+K)_A$ onto the classification diagram of Leake et al. (1997).

4.7.4. Other heavy minerals

Epidote group minerals are very abundant in the Korčulan terra rossa, characterised by a relatively narrow compositional range (0.239–0.157 $Fe^{3+}/(Fe^{3+} + Al)$ ratios) suggesting low-grade metamorphic source complexes. Orthopyroxene grains have a magmatic composition (Mg # = 71.7–81.0, Al_2O_3 1.05–1.46 wt%, CaO 1.12–1.45; Table 5: analysis 1–33) and may have been crystallised from a trachytic melt. Black mica is the fresh Ti-rich biotite/phlogopite (Mg # 66.7; TiO_2 4.82 wt %; Table 5: analysis 2–13) with minor BaO (0.78 wt%) and represents volcanic derivation. Ilmenite grains show variable compositions in terms of end members ($Ilm_{83.5–94.1}Hm_{3.2–10.9}Mg_{0.55–2.73}Mn_{1.8–5.6}$) and cannot be assigned to specific source rocks. Titanite contains 1.82 wt% Al_2O_3 and 3.06 wt% total Fe_2O_3; this titanite variety, termed grothite, is either metamorphic in origin or a product of alteration. Tourmaline grains are always prismatic and zoned, and some discrete grains show an extremely broad compositional range. They belong to the Na-alkali group (1.59–2.68 wt% Na_2O) and are members of the dravite-schorl series (<7.25 wt% MgO; <17.74 wt% FeO). Staurolite shows low Mg # and insignificant $Al–Fe^{3+}$ substitution [18.138 Al atoms per formula unit (apfu)].

4.7.5. Feldspars

Feldspars, dominated by a volcanogenic population, indicate volcanic and aeolian dust origins (Table 5). Volcanic feldspars are represented by sanidine and minor hyalophane (BaO >2 wt%). Na-feldspar and rare K-feldspar may have been derived either from the Cenomanian-Turonian bedrock clastites or by aeolian transport. The majority of volcanic feldspars are sanidine, showing a compositional range of $Or_{58.7–84.2}Ab_{12.8–35.6}An_{0.2–4.4}$ (Fig. 14) and contain up to 1.91 wt% BaO. Sanidine microphenocrysts from pumice clasts (Fig. 10) belong to this compositional group. A discrete sanidine group at $Or_{40–50}$ also exists. Hyalophane crystals contain 2.80–9.16 wt% BaO and have a compositional range of $Or_{54.4–80.3}Ab_{11.6–34.0}An_{1.2–4.1}Cn_{5.6–19.4}$. They are Sr- and Rb-rich with EDS-concentrations of

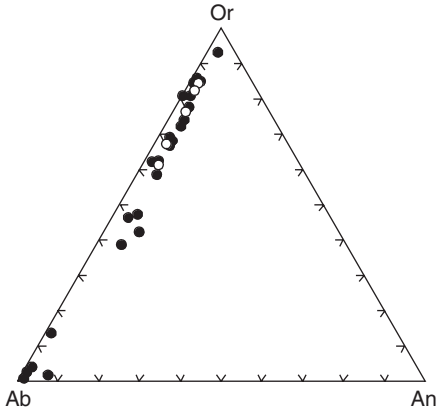

Fig. 14. Ternary plot showing albite (Ab) vs. orthoclase (Or) vs. anorthite (An) feldspar compositions in the terra rossa. Open circles indicate sanidines from pumice lithic clasts.

1–1.5 wt% for each oxide. Hyalophane is common in potassic alkaline igneous rocks, as in foiditic vitric fiammé from the pyroclastic Villa Senni Eruption Unit (VSEU) in the Colli Albani Volcanic District. A Ba- and Sr-bearing sanidine with similar composition to that of the hyalophane in Korčulan terra rossa (11 wt% BaO, 1.0–1.5 wt% SrO) was reported from the Lower Flow Unit of the VSEU (Gaeta, 1998).

5. DISCUSSION AND CONCLUSIONS

5.1. Provenance of External Material

5.1.1. Flysch contribution

Istrian flysch deposits represent only a small part of the elongated Dinaric coastal zone that crop out in the Trieste-Pazin, Labin and Plomin basins, Mt. Učka and partly on Mt. Ćićarija (Fig. 1). They are characterised by the alternation of hemipelagic marls and gravity-flow deposits (Bergant et al., 2003). Their total thickness is estimated as up to 350 m (Velić et al., 2003). Based on the analysis of the middle part of the Istrian flysch deposits, Magdalenić (1972) found that in the marls and sandstones garnets, zircon, tourmaline and rutile predominate. Epidote, chrome spinel and staurolite are less abundant, while titanite, glaucophane, chloritoid, zoisite and brookite occur only in small quantities. In the heavy mineral fraction of flysch basins of the SE Alps and Outer Dinarides (including the Istrian Flysch Basin), Alberti et al. (1999) found chrome spinel, garnet (pyralspite and grandite series), zircon, tourmaline, rutile, pyrite, chloritoid, pyroxene (both ortho- and clinopyroxene), staurolite and amphibole and found that their occurrence varied from basin to basin. In Istrian flysch Lenaz (2000) identified two types of chrome spinels with peridotite affinities, showing an identical compositional range to chrome spinels from peridotites which have recently been recognised in Mt. Medvednica and Mt. Kalnik in the south-western region of the Middle-Transdanubian mountains. Although our findings are similar to those of Magdalenić (1972) and Alberti et al. (1999), our samples contain significantly higher amounts of epidote-zoisite minerals, accompanied by sporadic apatite and corundum. The overall heavy mineral composition of Istrian flysch strongly suggests that a diverse source area was feeding the flysch basin: (1) an area comprising a complex association of volcanic and mantle-derived ophiolitic rocks and (2) an area dominated by high-grade metamorphic rocks. Comparison of the light and heavy mineral fractions of terra rossa and i.r. of flysch (Tables 1–4; Figs. 7, 9a, b) suggests that flysch might have acted as a parent material during terra rossa formation. Further evidence to this assumption is provided by the terra rossa sample with the highest biotite content (sample 97, with 4.2% of biotite, Table 3) that is situated close to the flysch exposure where the two flysch samples with the highest biotite content were taken (sample 93 with 10% and sample 94 with 12.2% of biotite, Table 4). Other analyses either support flysch contribution to terra rossa (particle size analysis; geochemical fingerprinting, REE content and distribution) or at least do not exclude a flysch contribution to terra rossa (e.g., bulk and clay mineralogy).

5.1.2. Aeolian contribution

Loess. Loess is situated in the southern (Premantura and Mrlera) and north-western part of Istria (Savudrija) (Fig. 1) and is considered to be Late Pleistocene in age (Polšak, 1970). Although there are no data supporting the presence of older loess deposits in Istria, they were found on the neighbouring island of Susak, below the Late Pleistocene loess. A reddish alfisol, developed at the top of these deposits, is supposed to have formed in the Riss-Würm interglacial (Cremaschi, 1990b). According to Cremaschi (1990a), loess deposition was a very important recurrent process in Northern and Central Italy from at least the early Middle Pleistocene. It also affected Istria and the Dalmatian Archipelago since the early Middle Pleistocene and was derived from the deflation of the sediments of the Po plain (Cremaschi, 1990b). Dominant transparent heavy minerals in the 63–250 μm fraction of the loess on Susak and Lošinj are epidote-zoisite group and amphiboles (Cremaschi, 1990b). Garnets are less abundant, while zircon, tourmaline, rutile, anatase, brookite, titanite, staurolite, kyanite, chloritoid, glaucophane and silimanite appear in small quantities. Our results for the Late Pleistocene loess in Istria (Table 4, Fig. 9a) are similar to those of Cremaschi (1990b) for the loess in Susak and Lošinj. However, our samples contain larger amounts of zircon, as well as sporadic clinopyroxene, orthopyroxene and Cr-spinel. It is also important to note that we analysed a significantly finer size interval (45–63 μm) than Cremaschi (1990b).

The majority of terra rossa samples are richer in epidote-zoisite minerals and amphiboles than the i.r. of loess (Fig. 9a). However, a considerable overlap exists between the i.r. of loess and flysch. Comparison of our results with those of Cremaschi (1990b) shows a good correspondence between the Late Pleistocene loess in Istria and that of the Po plain. A good superposition exists between the majority of terra rossa samples and those from the sea-floor of the Central Adriatic Basin. Amphiboles, zircon + tourmaline and garnet compositions (Fig. 9b), and the presence of kyanite (Fig. 8c), clinopyroxene and orthopyroxene in loess signal a flux of external detritus to the terra rossa, similar to that deposited in the Late Pleistocene loess. Furthermore, chert, quartzite and pelitic particles in terra rossa resemble strongly those present in the Late Pleistocene loess (Fig. 7).

Other analyses also confirm that aeolian material furnished the terra rossa. For example, the i.r. of limestone and dolomite are devoid of vermiculite, but it was observed in small amounts in the clay fractions of all terra rossa samples and in all samples of the i.r. of loess (Durn et al., 1999). Also, low-charge vermiculite or high-charge smectite was detected in the <0.2 μm fraction of terra rossa samples, situated below (sample no. 47) or near (sample no. 52) outcrops of Late Pleistocene loess (Durn et al., 1999). Their presence in the above samples may indicate its aeolian origin because it was detected as one of the principal mineral phases in the fine clay incorporated in the Late Pleistocene loess in Savudrija. The clay content in the highly weathered loess, analysed by Cremaschi (1990a) from Northern and Central Italy, ranges from 58 to 75 wt% and that in the sand fraction ranges from 1 to 3 wt%, which are similar to those obtained for the Istrian terra rossa (Fig. 4a). Thus, the above data, and the similarity of the clay mineral assemblages, geochemical ratios, REE content and distribution in the Late Pleistocene loess and terra rossa provide evidence that aeolian deposits older than Late Pleistocene contributed significantly to the terra rossa.

Tephra. Devitrified pumice clasts, sanidine, hyalophane, Ti-andradite, potassic hastingsite, along with orthopyroxene and black mica, are all clear signatures of volcanic input to the terra rossa on the island of Korčula. The diversity of residual volcanic material points to two different eruptive events: (1) a potassic undersaturated volcanic event and (2) evolved trachytic-rhyolitic eruption.

The chemical composition of hyalophane and Ti-andradite from Korčulan terra rossa is fairly similar to the analogue minerals in the vitric fiames from the VSEU in Colli Albani Volcanic District (Freda et al., 1997; Gaeta, 1998) suggesting the RVP as a source area. The volcanic activity in the Colli Albani Volcanic District produced more than 280 km^3 of pyroclastic products between 0.7 and 0.3 Ma (De Rita et al., 1992) with VSEU ignimbrite succession, dated at 351 ka (Villa, 1992) as the highest magnitude eruption of this volcanism.

For terra rossas situated along the eastern Adriatic islands and coast, the VSEU is important because of the NE dispersion of air-fall material, producing 1–2 cm thick tephra layers even 900 km from the source region (Pouclet et al., 1999). The second volcanic event is not easy to correlate with any known eruption close to the time of the VSEU. The White Trachytic Tuff of Roccamonfina has initial eruptions dated at 327 ka (Ballini et al., 1989) and appears to be the best candidate as a source, although the low-magnitude eruption(s) of White Trachytic Tuff may not have been capable of producing a distal tephra layer 350 km away from the source.

Terra rossa soils of Istria may have been affected at several sites with air-fall products sourced from the Roman-Campanian Volcanic Province. We postulate that some hypidiomorphic K-feldspars (tentatively identified as sanidines, Fig. 5b), found together with clinopyroxene and orthopyroxene in some loess and terra rossa samples might be of volcanic origin.

Several eruptions appear to be potential sources for volcanic supply to Istrian terra rossa soils:

(1) Two thick volcaniclastic markers, covering an area of 500 km^2 along the Central Adriatic Swell (Tari Kovačić, 1995). The older marker contains phonolite pumices of unknown origin while the younger marker, containing bimodal rhyolitic glasses, correlates with a 1.75 Ma eruption on Palmarola islet of Pontian islands (Lugović et al., 2005).
(2) Piànico-Sèllere trachytic tephra of early Middle Pleistocene (780 ka) archived in the lacustrine succession in the Southern Italian Alps (Pinti et al., 2001).
(3) CI-tephra (approximately 35–40 ka) and NYT-tephra (approximately 12 ka) recorded in the Apennine pedomarkers (Frezzotti and Narcisi, 1996) and within terra rossa near Gljev in southern Croatia (Šušnjara et al., 1994).

5.2. Polygenetic Origin

Discrepancies between granulometric composition, bulk and clay mineralogy and geochemical characteristics of the i.r. of carbonate rocks and terra rossa soils strongly suggest flux of external material during the genesis of terra rossa in Istria (Durn et al., 1999, 2001, 2003; Durn, 2003). Our current study of the heavy and light mineral fractions of terra rossa soils, complemented by analysis of the insoluble residue of underlying limestones and dolomites and other potential source

formations proved to be an efficient and valuable tool that aided the accurate evaluation of diverse parent materials, thus demonstrating the polygenetic origin of terra rossa soils in Istria. Various amphiboles, zircon + tourmaline and garnets, and the presence of kyanite, clinopyroxene and orthopyroxene both in loess deposits in Istria and in the terra rossa, prove that detritus, mineralogically similar to that found in Late Pleistocene loess was incorporated into the terra rossa. Our results indicate that flysch has also acted as a parent material. Terra rossa soils of Istria have probably also received air-fall particles from the Roman-Campanian Volcanic Province. Although it is difficult to estimate accurately the proportions of external materials embedded in the terra rossa soils, we estimate that in such a non-isolated karst terrain like Istria their contribution might have been up to 50%. We agree that, because the average i.r. content of limestone and dolomite being only 0.86%, such a low amount is insufficient to form the thick and widespread terra rossa deposits on Istria. Also, the average silt/clay ratio in terra rossa is more than three times higher than that in the i.r. of limestone and dolomite, so that the substantial contribution of coarser material to the terra rossa had to be external. Both the i.r. of loess and flysch (marl) are enriched in silt and sand size fractions, compared with the i.r. of limestone and dolomite. We propose that the highest amount of external material was Middle Pleistocene loess, followed by flysch and tephra (minor contribution). At later stages, Late Pleistocene loess (e.g., in the southern and north-western part of Istria) may have become intermixed in the upper parts of terra rossa profiles. On the island of Korčula terra rossa comprises devitrified pumice clasts, sanidine, hyalophane, Ti-andradite, potassic hastingsite, along with orthopyroxene and black mica, all are clear signatures of volcanic input.

6. SUMMARY

In some isolated karst terrains, terra rossa may have formed exclusively from the i.r. of limestone and dolomite, but it most commonly comprises a variety of external materials, including aeolian dust, volcanic debris and clastic sedimentary particles that were carried to the carbonate terrain by various transport mechanisms. Because Istria is a non-isolated karst terrain, the most likely additional flux influencing terra rossa formation is aeolian dust, an important and recurrent process in Istria since the early Middle Pleistocene. Flysch successions, which extended much further southward than their present location, may also be contributors. Material from volcanic eruptions was dispersed frequently over the Adriatic region throughout the Quaternary and has significantly affected soil formation.

Terra rossa is the most widespread soil type in Istria, an archetypal example of a non-isolated karst terrain that has been affected by karst processes, (neo)tectonic activity and contributions of external materials since the Late Tertiary. Erosional and depositional processes operating on the karst terrains, induced by climatic changes, tectonics and/or deforestation, might be responsible for both the patchy distribution of terra rossa and the thick colluvial or alluvial terra rossa accumulations in uvala- and dolina-type karst depressions (pedo-sedimentary complexes, soil-sediments) in Istria.

ACKNOWLEDGEMENTS

The authors would like to thank Andrea Mindszenty and especially Richard Bateman for their reviews. Their valuable suggestions and helpful comments have highly improved the quality of the present contribution. We are also thankful to Maria Mange for her encouragement in preparing this publication. Both Maria Mange and David Wright have made important comments and suggestions on the structure, content and the English of this paper.

REFERENCES

Alberti, L., Lenaz, D., Princivalle, F., Tunis, G., 1999. Mineralogical characterization of flysch sequences of the SE Alps and Outer Dinarides (NE Italy, Slovenia, Croatia). Geologica Carpathica, Abstract Volume, Special Issue 50, 9–10.

Altay, I., 1997. Red Mediterranean soils in some karstic regions of Taurus mountains, Turkey. Catena 28, 247–260.

Balagh, T.M., Runge, E.C.A., 1970. Clay-rich horizons over limestone, illuvial or residual? Soil Science Society of America Proceedings 34, 534–536.

Baldridge, W.S., Carmichael, I.S.E., Albee, A.L., 1981. Crystallization path of leucite-bearing lavas: examples from Italy. Contributions to Mineralogy and Petrology 76, 321–335.

Ballini, A., Frullani, A., Mezzetti, F., 1989. La formazione piroclastica del Tufo Trachitico Bianco (''White Trachytic Tuff''-WTT Auctorum) de1 vulcano di Roccamonfina. Bollettino del Gruppo Nazionale per la Vulcanologia 2, 557–574.

Bergant, S., Tišljar, J., Šparica, M., 2003. Eocene carbonates and flysch deposits of the Pazin Basin. In: Vlahović, I., Tišljar, J. (Eds.), Evolution of Depositional Environments from the Palaezoic to the Quaternary in the Karst Dinarides and the Pannonian Basin, 22nd IAS Meeting of Sedimentology-Opatija 2003, Field trip guidebook, pp. 57–63.

Boero, V., Premoli, A., Melis, P., Barberis, E., Arduino, E., 1992. Influence of climate on the iron oxide mineralogy of terra rossa. Clays and Clay Minerals 40, 8–13.

Boero, V., Schwertmann, U., 1989. Iron oxide mineralogy of terra rossa and its genetic implications. Geoderma 44, 319–327.

Bronger, A., Bruhn-Lobin, N., 1997. Paleopedology of Terrae rossae-Rhodoxeralfs from Quaternary calcarenites in NW Morocco. Catena 28, 279–295.

Bronger, A., Ensling, J., Gütlich, P., Spiering, H., 1983. Rubification of terrae rossae in Slovakia: a Mösbauer effect study. Clays and Clay Minerals 31, 269–276.

Bronger, A., Sedov, S.N., 2002. Vetusols and Paleosols: natural versus man-induced environmental change in the Atlantic coastal region of Morocco. 17th World Conference on Soil Science, Paper no. 1530, pp. 1–12.

Chiesa, S., Coltorti, M., Cremaschi, M., Ferraris, N., Floris, B., Prosperi, L., 1990. The loess and Quaternary deposits in the Marche region. In: Cremaschi, M. (Ed.), The loess in Northern and Central Italy. Centro di Studio per la Stratigrafia e Petrografia delle Alpi Centrali. Editrice Gutenberg, Milano, pp. 103–132.

Ćirić, M., Aleksandrović, D., 1959. A view on the genesis of terra rossa. Zbornik radova Poljoprivrednog fakulteta 7, 1–12.

Coleman, R.G., Lee, D.E., Beatty, L.B., Brannock, W.W., 1965. Eclogites and eclogites: their differences and similarities. Geological Society of America Bulletin 76, 483–580.

Cremaschi, M., 1987. Paleosols and Vetusols in the Central Po plain (Northern Italy). Edizioni Unicopli, Milano, 306pp.

Cremaschi, M., 1990a. The loess in Northern and Central Italy: a loess basin between the Alps and the Mediterranean regions. In: Cremaschi, M. (Ed.), The loess in Northern and Central

Italy. Centro di Studio per la Stratigrafia e Petrografia delle Alpi Centrali. Editrice Gutenberg, Milano, pp. 15–19.
Cremaschi, M., 1990b. Stratigraphy and palaeoenvironmental significance of the loess deposits on Susak Island (Dalmatian Archipelago). Quaternary International 5, 97–106.
Danin, A., Gerson, R., Carty, J., 1983. Weathering patterns on hard limestone and dolomite by endolithic lichens and cyanobacteria: supporting evidence for eolian contribution to terra rossa soil. Soil Science 136, 213–217.
Delgado, R., Martín-Garcia, J.M., Oyonarte, C., Delgado, G., 2003. Genesis of the terrae rossae of the Sierra Gádor (Andalusia, Spain). European Journal of Soil Science 54, 1–16.
De Rita, D., Funiciello, R., Rosa, C., 1992. Volcanic activity and drainage network evolution of the Alban Hills area (Rome, Italy). Acta Vulcanologica 2, 185–198.
Dick, H.J.B., Bullen, T., 1984. Chromian spinel as a petrogenetic indicator in abyssal and alpine-type peridotites and spatially associated lavas. Contributions to Mineralogy and Petrology 86, 54–76.
Duchaufour, P., 1982. Pedology: Pedogenesis and Classification. Allen and Unwin, London, 448pp.
Durn, G., 1996. Origin, Composition and Genesis of Terra Rossa in Istria. Ph.D. thesis (in Croatian), University of Zagreb, 204pp.
Durn, G., 2003. Terra rossa in the Mediterranean region: parent materials, composition and origin. Geologia Croatica 56/1, 83–100.
Durn, G., Aljinović, D., 1995. Heavy mineral assemblage in terra rossa from the peninsula of Istria, Croatia. In: Vlahović, I., Velić, I., Šparica, M. (Eds.), 1st Croatian geological congress, Opatija, Abstracts, 31pp.
Durn, G., Marchig, V., Ottner, F., 2001. Distribution of rare earth elements in different grain-size fractions of terra rossa soils in Istria, Croatia: Mid-European Clay Conference '01, September 9–14, Book of abstracts, Stara Lesna, Slovakia, 38pp.
Durn, G., Ottner, F., Slovenec, D., 1999. Mineralogical and geochemical indicators of the polygenetic nature of terra rossa in Istria, Croatia. Geoderma 91, 125–150.
Durn, G., Ottner, F., Tišljar, J., Mindszenty, A., Barudžija, U., 2003. Regional subaerial unconformities in shallow-marine carbonate sequences of Istria: sedimentology, mineralogy, geochemistry and micromorphology of associated bauxites, palaeosols and pedosedimentary complexes. In: Vlahović, I., Tišljar, J. (Eds.), Evolution of Depositional Environments from the Palaezoic to the Quaternary in the Karst Dinarides and the Pannonian Basin, 22nd IAS Meeting of Sedimentology-Opatija 2003, Field trip guidebook, pp. 209–254.
Durn, G., Slovenec, D., Šinkovec, B., 1992. Eolian influence on terra rossa in Istria: 7th International Congress of ICSOBA, Abstracts, Balatonalmádi, 89pp.
FAO, 1974. Soil Map of the World, 1:5,000,000, Vol. 1. Legend, UNESCO, Paris.
Fedoroff, N., 1997. Clay illuviation in Red Mediterranean soils. Catena 28, 171–189.
Freda, C., Gaeta, M., Palladino, D.M., Trigila, R., 1997. The Villa Senni Eruption (Alban Hills, Central Italy): the role of H_2O and CO_2 on magma chamber evolution and on eruptive scenario. Journal of Volcanology and Geothermal Research 78, 103–120.
Frezzotti, M., Narcisi, B., 1996. Late Quaternary tephra-derived paleosols in central Italy's carbonate Appennine range: stratigraphical and paleoclimatological implications. Quaternary International 34–36, 147–153.
Gaeta, M., 1998. Petrogenetic implications of Ba-sanidine in the Lionato Tuff (Colli Albani Volcanic District, Central Italy). Mineralogical Magazine 62, 697–701.
Gianetti, B., 1982. Cumulate inclusion from K-rich magmas, Roccamonfina volcano, Italy. Earth and Planetary Science Letters 57, 313–335.
Gianetti, B., Luhr, J.F., 1983. The white trachytic tuff of Roccamonfina Volcano (Roman Region, Italy). Contributions to Mineralogy and Petrology 84, 235–252.

Hinterlechner-Ravnik, A., Sassi, F.P., Visonà, D., 1991. The Austridic eclogites, metabasites and metaultrabasites from the Pohorje area (Eastern Alps, Yugoslavia): the eclogites and related rocks, Atti della Accademia Nazionale dei Lincei, Rendiconti Lincei, Scienze Fisiche e Naturali, serie 9, vol. 2, pp. 157–173.

Jackson, M.L., 1979. Soil chemical analysis—advanced course. Soil Science Department, University of Wisconsin, Madison, 250pp.

Jackson, M.L., Clayton, R.N., Violante, A., Violante P., 1982. Eolian influence on terra rossa soils of Italy traced by oxygen isotopic ratio. In: van Olphen, H., Veniale, F. (Eds.), 7th International Clay Conference, Pavia, Italy, pp. 293–301.

Jahn, R., Zarei, M., Stahr, K., 1991. Genetic implications of quartz in "Terra Rossa" soils in Portugal. Proceedings of 7th Euroclay Conference, Dresden, pp. 541–546.

Kišpatić, M., 1912. Bauxites des Kroatischen Karstes und ihre Einstehung: Neues Jahrbuch. Mineralogie, Geologie, Paleontologie. 34, 513–552.

Kubiëna, W.L., 1953. The soils of Europe. Thomas Murby and Co., London, 317pp.

Leake, B.E., Woolley, A.R., Birch, W.D., Gilbert, M.C., Grice, J.D., Hawthorne, F.C., Kato, A., Kisch, H.J., Krivovichev, V.G., Linthout, K., Laird, J., Mandarino, J., Maresch, W.V., Nickel, E.H., Rock, N.M.S., Schumacher, J.C., Smith, D.C., Stephenson, N.C.N., Ungaretti, L., Whittaker, E.J.W., Youzhi, G., 1997. Nomenclature of amphiboles. European Journal of Mineralogy 9, 623–651.

Lenaz, D., 2000. Mineralogy of Cretaceous-Tertiary Flysch from South-Eastern Alps and Outer Dinarides with Particular Attention to Cr-spinel: Geodynamic Implications. Ph.D. thesis (in Italian), Trieste University, 165pp.

Lenaz, D., Kamenetsky, V.S., Crawford, A.J., Princivalle, F., 2000. Melt inclusions in detrital spinels from the SE Alps (Italy-Slovenia): a new approach to provenance studies of sedimentary basins. Contributions to Mineralogy and Petrology 139, 748–758.

Lenaz, D., Princivalle, F., 2000. The Julian and Istrian basins (SE Alps and Outer Dinarides): different source areas through Cr-spinel chemical and structural data. In: Karamata, S., Janković, S. (Eds.), Proceeding of the International Symposium: Geology and metalogeny of the Dinarides and the Vardar Zone, Banja Luka-Sarajevo, pp. 85–190.

Lippi-Boncampi, C., Mackenzie, R.C., Mitcheel, W.A., 1955. The mineralogy of some soils from Central Italy. Clay Mineral Bulletin 2, 281–288.

Lugović, B., Tari Kovačić, V., Miletić, D., 2005. Voluminous Lower Pleistocene volcaniclastic deposits from the central and northern Adriatic off-shore (Croatia): where were the edifices? 3rd Croatian Geological Congress, Opatija, September 29–October 1, 2005, Abstract Book, pp. 87–88.

MacLeod, D.A., 1980. The origin of the red Mediterranean soils in Epirus, Greece. Journal of Soil Science 31, 125–136.

Magdalenić, Z., 1972. Sedimentology of central Istria flysch deposits (in Croatian). Acta Geologica 7/2, 34.

Malez, M., 1981. Karst underground in Istria as a place for settling of fossil people (in Croatian). In: Ekl, V. (Ed.), Liburnijske teme, book 4, Opatija, pp. 119–135.

Marić, L., 1964. Terra rossa in the karst of Jugoslavia (in Croatian). Acta Geologica JAZU 4, 19–72.

Marinčić, S., Matičec, D., 1991. Tectonics and kinematics of deformations: an Istrian model. Geološki Vjesnik 44, 257–268.

Moresi, M., Mongelli, G., 1988. The relation between the terra rossa and the carbonate-free residue of the underlying limestones and dolostones in Apulia, Italy. Clay Minerals 23, 439–446.

Muhs, D.R., Bush, C.A., Stewart, K.C., 1990. Geochemical evidence of Saharan dust parent material for soils developed on Quaternary limestone of Caribbean and Western Atlantic Islands. Quaternary Research 33, 157–177.

Muhs, D.R., Crittenden, R.C., Rosholt, J.N., Bush, C.A., Stewart, K.C., 1987. Genesis of marine terrace soils, Barbados, West Indies: evidence from mineralogy and geochemistry. Earth Surface Processes and Landforms 12, 605–618.

Nihlen, T., Olsson, S., 1995. Influence of eolian dust on soil formation in the Aegean area. Zeitschrift für Geomorphologie 39, 341–361.

Olson, C.G., Ruhe, R.V., Mausbach, M.J., 1980. The terra rossa limestone contact phenomena in Karst, Southern Indiana. Soil Science Society of America Journal 44, 1075–1079.

Pinti, D.L., Quidelleur, X., Chiesa, S., Rivazzi, S., Gillot, P.-Y., 2001. K–Ar dating of an early Middle Pleistocene distal tephra in the interglacial varved succession of Piànico-Sèllere (Southern Alps, Italy). Earth and Planetary Science Letters 188, 1–7.

Plaster, R.W., Sherwood, W.C., 1971. Bedrock weathering and residual soil formation in Central Virginia. Geological Society of America Bulletin 82, 2813–2826.

Polšak, A., 1970. Base geological map 1:100.000. Legend for sheet Pula L33-112 (in Croatian). Institute of Geology, Zagreb, State Institute of Geology, Beograd, 44pp.

Polšak, A., Šikić, D., 1973. Osnovna geološka karta SFRJ 1:100.000, Tumač za list Rovinj (Basic Geological Map of SFRY, 1:100000, Geology of the Rovinj sheet): Institut za geološka istraŽivanja, Zagreb, Savezni geološki zavod, Beograd, 51pp.

Pouclet, A., Horvath, E., Gabris, G., Juvigné, E., 1999. The Bag Tephra, a widespread tephrochronological marker in Middle Europe: chemical and mineralogical investigations. Bulletin of Volcanology 60, 265–272.

Rapp, A., 1984. Are terra rossa soils in Europe eolian deposits from Africa? Geologiska Foreningens i Stockholm Forhandlingar 105, 161–168.

Soil Survey Staff, 1975. Soil Taxonomy: A Basic System of Soil Classification for Making and Interpreting Soil Surveys. USDA Handbook No. 436, U.S. Government Printing Office, Washington, DC.

Šinkovec, B., 1974. The origin of terra rossa in Istria (in Croatian). Geološki vjesnik 27, 227–237.

Škorić, A., 1979. Two-layer soil profile on the area of terra rossa in Istria (in Croatian). Zemljište i Biljka 28, 111–131.

Škorić, A., 1987. Pedosphere of Istria (in Croatian): Project Council of Pedological Map of Croatia, Special edition, book 2, Zagreb, 192pp.

Šušnjara, A., Šćavničar, B., Gabrić, A., 1994. The occurrence of vitric tuff in the Quaternary deposits of Gljev in Dalmatia (Southern Croatia). Geologia Croatica 47/2, 193–198.

Tari Kovačić, V., 1995. Development of Pliocene and Pleistocene sediments of Northern and Central Adriatic-logging markers and correlation (in Croatian). Proceedings of 1st Croatian geological congress, Opatija, pp. 609–612.

Tassier, A., Campbell, P.C.G., Bisson, M., 1979. Sequential extraction procedure for the speciation of particulate trace metals. Analytical Chemistry 5, 844–851.

Tišljar, J., Vlahović, I., Velić, I., Matičec, D., Robson, J., 1998. Carbonate facies evolution from the Late Albian to Middle Cenomanian in southern Istria (Croatia): influence of synsedimentary tectonics and extensive organic carbonate production. Facies 38, 137–152.

Torrent, J., 1995. Genesis and properties of the soils of the Mediterranean regions: Dipartimento di Scienze Chimico-Agrarie, Universitá degli Studi di Napoli Federico II, 111pp.

Tućan, F., 1912. Terra Rossa, deren Natur and Entstehung. Neues Jahrbuch Mineralogie, Geologie, Paleontologie 34, 401–430.

Velić, I., Tišljar, J., Matičec, D., Vlahović, I., 1995. Opći prikaz geološke građe Istre (A review of the geology of Istria). In: Vlahović, I., Velić, I. (Eds.), 1st Croatian Geological Congress, Excursion Guide-Book, Zagreb, pp. 5–30.

Velić, I., Tišljar, J., Vlahović, I., Matičec, D., Bergant, S., 2003. Evolution of the Istrian Part of the Adriatic carbonate platform from the Middle Jurassic to the Santonian and formation of the Flysch basin during the Eocene: main events and regional comparison. In:

Vlahović, I., Tišljar, J. (Eds.), Evolution of Depositional Environments from the Palaezoic to the Quaternary in the Karst Dinarides and the Pannonian Basin, 22nd IAS Meeting of Sedimentology, Opatija 2003, Field trip guidebook, pp. 3–17.

Villa, I.M., 1992. Datability of Quaternary volcanic rocks: an $^{40}Ar/^{39}Ar$ perspective on age conflicts in lavas from the Alban Hills, Italy. European Journal of Mineralogy 4, 369–383.

Yaalon, D.H., 1997. Soils in the Mediterranean region: what makes them different? Catena 28, 157–169.

Yaalon, D.H., Ganor, E., 1973. The influence of dust soils during the Quaternary. Soil Science 116, 233–251.

This page intentionally left blank

2.2 Tectonogenic Sediments: The Use of Heavy Minerals in Active Geodynamic Settings

This page intentionally left blank

Chapter 29

PLATE TECTONICS AND HEAVY MINERAL SUITES OF MODERN SANDS

EDUARDO GARZANTI AND SERGIO ANDÒ

Laboratorio di Petrografia del Sedimentario, Dipartimento di Scienze Geologiche e Geotecnologie, Università di Milano-Bicocca, Piazza della Scienza 4, 20126 Milano, Italy

ABSTRACT

This contribution classifies detrital heavy mineral assemblages produced in contrasting geodynamic settings, following the provenance scheme proposed by Dickinson and co-workers in the late 1970s. The vital link with bulk-sediment detrital modes was established by systematically coupling high-resolution heavy mineral and petrographic analyses on the same sample sets, in a series of actualistic provenance studies carried out in key geological areas, characterised by arid to semiarid climate.

Quartzofeldspathic to quartzose sands of "Continental Block Provenance" contain either heavy-mineral-rich, hornblende-dominated assemblages derived from amphibolite-facies basements exposed along rift escarpments and in cratonic shields, or heavy-mineral-poor suites with commonly rounded ultrastable grains recycled from cover strata. Volcanic rifted margins shed lithofeldspathic detritus with clinopyroxene-dominated suites (largely lilac-brown Ti-rich augite) that commonly include olivine. Abundant clinopyroxenes (mostly green augite) and hypersthene, associated with olivine or dark-brown to reddish-brown hornblende (oxyhornblende), characterise feldspatholithic sands of "Magmatic Arc Provenance". The proportion of mainly blue-green hornblende increases progressively with erosion cutting deeper into the batholithic core of the arc massif. Quartzolithic sands of "Orogenic Provenance" include suites dominated by amphiboles, garnet, and epidote. The relative abundance of garnet (associated with subordinate staurolite, kyanite, and sillimanite) and blue-green to green-brown hornblende increases with increasing metamorphic grade of the sedimentary or igneous protoliths, respectively. Oman-type obduction orogens shed abundant heavy minerals, dominated by mafic and ultramafic minerals derived from the obducted ophiolite nappe. Apennine-type thin-skinned thrust belts provide heavy-mineral-poor assemblages recycled from accreted passive-margin successions or foredeep turbidites. Pyroxenes, derived from offscraped ophiolitic sequences, are locally present. The wealth of information heavy minerals provide on the geology of source areas makes their analysis an

Developments in Sedimentology, Vol. 58, 741–763

ISSN: 0070-4571/doi:10.1016/S0070-4571(07)58029-5

extremely powerful complementary tool in provenance studies of sediments not modified by diagenesis.

Keywords: heavy minerals; plate tectonics; continental rifts; cratons; magmatic arcs; orogenic belts

1. INTRODUCTION

The plate-tectonic revolution of the 1960s provided a new conceptual framework in which to interpret the evolution of the Earth's surface, leading to a new classification of sedimentary basins (Dickinson, 1974; Ingersoll and Busby, 1994). Petrologic models relating detrital modes of sands and sandstones to their geodynamic setting could thus be established (Dickinson and Suczek, 1979). Based on tabulated detrital modes of 88 worldwide terrigenous suites of Precambrian to Holocene age, Dickinson and Suczek defined three end-members: "Continental Block Provenance", "Magmatic Arc Provenance", and "Recycled Orogen Provenance", further subdivided into sub-provenances and evolutionary trends (Dickinson, 1985). Such an approach combined insight and simplicity, and represented a major breakthrough in clastic petrology. Subsequent years proved the Dickinson model to be successful in discriminating detrital signatures of contrasting plate-tectonic settings at continental scale (Ingersoll, 1990; Potter, 1994), provided that complexities of natural processes are taken into due account (including transition between tectonic regimes, long-distance transport, and modifications induced by chemical weathering or diagenesis: Mack, 1984; McBride, 1985; Johnsson, 1993).

A similar approach has been attempted for the chemical composition of sandstones (Schwab, 1975; Bathia, 1985), but with more limited success. Bulk-chemistry data in fact show large overlaps (Potter, 1978; Maynard et al., 1982) and are markedly influenced by a variety of processes (including grain size, mixing with intrabasinal grains, and diagenetic cementation, dissolution and replacement; Korsch et al., 1993), which are best recognised and assessed with the aid of the petrographic microscope (Roser and Korsch, 1986; Zuffa, 1987). The attempts made to investigate the relationships between heavy mineral suites and tectonic setting (Stattegger, 1987; Nechaev and Isphording, 1993) meet similar difficulties because of the great sensitiveness of heavy minerals to diagenetic dissolution and hydraulic sorting (Gazzi, 1965; Mange and Maurer, 1992; Morton and Hallsworth, 1999).

The aim of the present work, which follows an exemplary rather than exhaustive approach, is to describe and classify detrital heavy mineral assemblages produced in contrasting geodynamic settings within the same conceptual scheme (Fig. 1) as that proposed by Dickinson and coworkers (Dickinson and Suczek, 1979; Dickinson, 1985; Ingersoll, 1990). In order to establish the link between sediment mineralogy and Dickinson's provenance types, we systematically coupled heavy mineral and petrographic analyses on the same sample sets, drawing from numerous case histories carried out with the same analytical methods in key geologic areas (Fig. 2). The cases considered here are all from modern settings, where tectonic processes and geology of source terranes are known in detail, and principally from the arid tropical

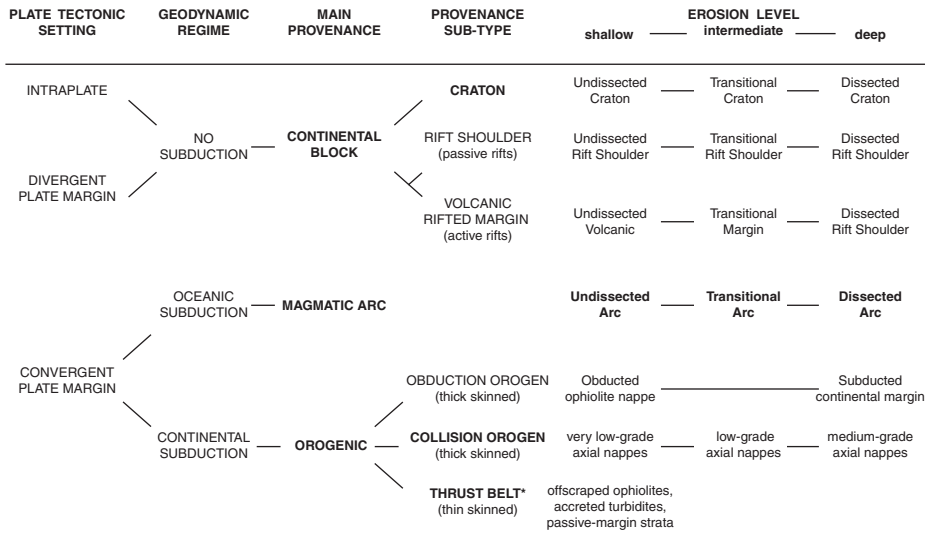

*Thick-skinned external belts of collision orogens (Garzanti et al. 2004 a) are not included in this scheme

Fig. 1. Provenance scheme adopted in the present work. Provenance terms introduced by Dickinson and Suczek (1979) and Dickinson (1985) are in bold.

to semiarid Mediterranean climatic belt, where chemical weathering can be considered to be negligible. Detrital signatures can thus be held as primary and used as a reference for provenance interpretation of ancient clastic suites deposited in comparable geodynamic settings.

2. METHODS

2.1. Analytical Procedures

In all of our provenance studies we adopted the same standard methods for heavy mineral separation and analysis (Parfenoff et al., 1970). Loose sand samples were either dry or wet sieved. The very fine- to fine-grained sand fraction (63–250 μm) was selected and treated with acetic and oxalic acids to eliminate carbonates and iron oxides, respectively. Heavy minerals were separated with sodium metatungstate (density 2.90 g/cm^3). For each sample, at least 200 points were counted in grain mounts according to the ''ribbon-counting'' or ''Fleet'' methods (Mange and Maurer, 1992).

2.2. The Representation of Heavy Mineral Assemblages

The potential of heavy mineral studies owes much to the great number of different species found in sediments (some 50 varieties of frequent occurrence). On the other hand, such numerous detrital species cannot be grouped easily into the few basic parameters that can be plotted in binary or ternary diagrams, and there is no

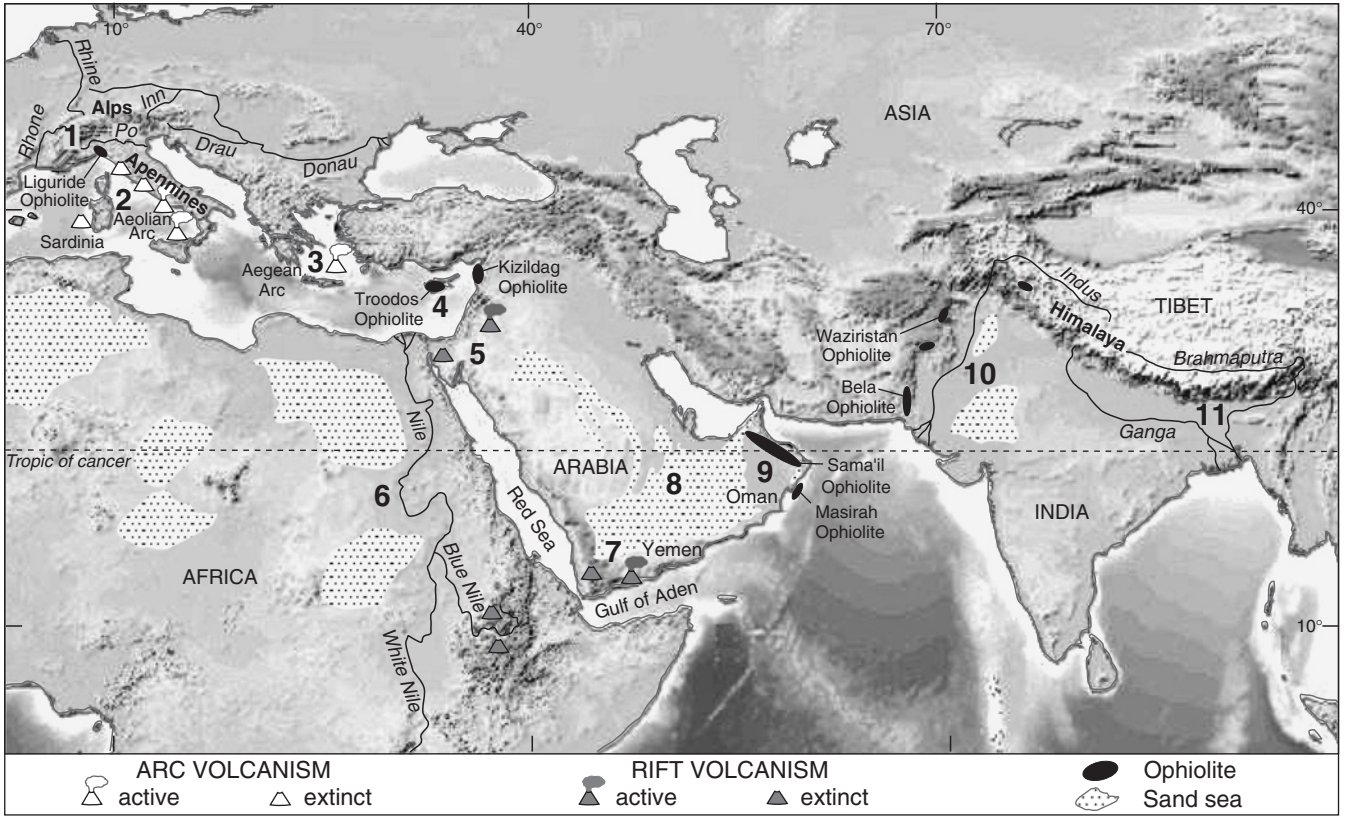

Fig. 2. Map of the key natural laboratories that we used to establish the relationships between plate-tectonic setting and heavy mineral suites of modern sands. For more information on geological framework and full analytical data the reader may refer to the following provenance studies: (1) Western and Central Alps (Garzanti et al., 2004a); (2) Apennines and Tyrrhenian Sea (Garzanti et al., 1998; 2002a); (3) Aegean Arc (Mezzadri and Saccani, 1989); (4) Troodos and Kizildag ophiolites (Garzanti et al., 2000); (5) Levant margin and Northern Red Sea (own unpublished data); (6) Nile river system (Garzanti et al., 2006); (7) Southern Red Sea and Gulf of Aden (Garzanti et al., 2001); (8) Arabian deserts (Garzanti et al., 2003); (9) Sama'il and Masirah ophiolites (Garzanti et al., 2002b); (10) Indus River system (Garzanti et al., 2005); (11) Brahmaputra River system (Garzanti et al., 2004b).

established way to classify heavy minerals for this purpose. Nechaev (1991; see also Nechaev and Isphording, 1993) proposed a three-end-member genetic classification, based on subtle distinctions (e.g., pale-coloured and blue-green amphiboles of the tremolite-actinolite-hornblende series are lumped with epidote and garnet in his MT end-member, diagnostic of mafic metamorphic provenance, whereas green-brown hornblende is grouped with pyroxenes and olivine in his MF end-member, indicative of mafic igneous provenance).

A different approach designed to reduce a great number of species into a limited number of factors is the use of statistical techniques (Imbrie and Van Andel, 1964; Klovan and Imbrie, 1971; Derkachev and Nikolajeva, 2007—this volume; Thamó-Bozsó and Kovács, 2007—this volume). The principal inconvenience of this method is that the identified end-members emerge as artefacts of elusive significance, while the actual direct information provided by the raw data set remains concealed.

2.3. The Ten Key Indices

As a settlement between the need to consider the full spectrum of minerals present in each sample and the ability to compare heavy mineral assemblages of many different samples, we define here 10 relatively homogeneous standard groups of transparent heavy minerals with similar provenance implications (Table 1). These can be either combined further into supergroups (e.g., triangular plots) or split into subgroups, as required by the specific case under scrutiny.

The four most common transparent heavy minerals in modern sands are the amphibole, pyroxene, epidote, and garnet groups. Within the amphibole group, we choose to separate (1) the widely abundant calcic amphiboles (Hb = hornblende) from (2) all of the other species (&A = other amphiboles, including minerals of key significance, such as glaucophane). An obvious distinction, among the pyroxene group, is between (3) clinopyroxenes (CPX, including augite and diopside), and (4) orthopyroxenes (OPX, including enstatite and hypersthene). We group (5) all minerals characterising prehnite-pumpellyite-facies, blueschist-facies, and greenschist-facies metamorphic source rocks as LgM (LgM = "low-grade minerals": epidote, clinozoisite, zoisite, allanite, piemontite, prehnite, pumpellyite, carpholite, lawsonite, chloritoid). (6) Garnet is considered separately (Gt) and (7) species chiefly derived from amphibolite-facies metasediments are categorised as HgM (HgM = "high-grade minerals": staurolite, andalusite, kyanite, and sillimanite). We finally group (8) olivine and spinel, mostly derived from mafic and ultramafic rocks (OS), and (9) the ultrastable minerals zircon, tourmaline, and rutile (ZTR), which tend to form a residual concentrate in both recycled modern sands and ancient sandstones affected by diagenesis (Hubert, 1962); (10) all remaining transparent heavy minerals are combined in the last index (T&, including the titanium minerals sphene, anatase, and brookite, as well as monazite, xenotime, apatite, and barite, found in traces in felsic igneous or sedimentary source rocks).

These 10 indices are conventionally tabulated in the following order that mainly represents petrogenetic suites: ultrastable to relatively stable minerals, mainly derived from sedimentary and felsic igneous source rocks (ZTR, T&), minerals chiefly provided by low- to high-grade metamorphic source rocks (LgM, Gt, HgM), and amphiboles (Hb, &A), pyroxenes (CPX, OPX), olivine and spinel (OS) largely

Table 1. Recalculated key indices for a synthetic representation of heavy mineral assemblages

HMC	Heavy mineral concentration index (Garzanti and Andò, 2007—this volume)
% Transparent	Identified transparent heavy minerals/total heavy minerals
% Opaque	Opaque heavy minerals/total heavy minerals
% Turbid	Altered unidentified heavy minerals/total heavy minerals
ZTR	Ultrastable minerals (Z = zircon; T = tourmaline; R = rutile)
T&	Titanium minerals (sphene, anatase, brookite) + others (e.g., apatite, monazite, barite)
LgM	Low-grade metamorphic minerals (e.g., epidote-group, chloritoid, carpholite, lawsonite)
Gt	Garnet
HgM	High-grade metasedimentary minerals (staurolite, andalusite, kyanite, sillimanite)
Hb	Hornblende
&A	Other amphiboles (including glaucophane, tremolite, actinolite)
CPX	Clinopyroxenes
OPX	Orthopyroxenes
OS	Olivine (O) + spinel (S)
HCI = (1/3 green hornblende + 2/3 green-brown hornblende + brown hornblende)/ hornblende × 100	
MMI = (1/3 staurolite + 2/3 kyanite + sillimanite)/(chloritoid + staurolite + kyanite + sillimanite) × 100	
% Rounded	Rounded transparent heavy minerals/total transparent heavy minerals

supplied by intermediate, mafic, and ultramafic igneous or meta-igneous source rocks. It must be noted that the LgM and HgM categories are not labelled rigorously (e.g., epidote, here included in the LgM pole, may persist well into medium-grade metamorphism: Winkler, 1976). Although high-pressure/low-temperature metamorphic minerals (e.g., carpholite, lawsonite, glaucophane) have a great diagnostic significance in provenance studies (e.g., Mange-Rajetzky and Oberhänsli, 1982), their separation in a distinct group is impractical because it requires distinctions that cannot be done under the microscope (e.g., Mg- vs. Fe-rich chloritoid) and a rather arbitrary split of the "other amphiboles" category.

2.4. Other Useful Indices

The basic string of 10 primary compositional parameters defined above can be supplemented by a set of secondary parameters providing detailed and crucial information. These may include concentration parameters (HMC, tHMC, and SRD parameters defined in Garzanti and Andò, 2007—this volume), as well as ratio parameters based on heavy mineral species either with highest density and chemical stability (in order to reveal the effects of hydraulic sorting and diagenetic dissolution;

% opaque, % ultradense, % ZR defined in Garzanti and Andò, 2007—this volume), or with similar density and chemical stability and therefore characterised by similar behaviour during transport, deposition, and diagenesis (in order to reveal provenance specifically in sandstones modified by diagenesis: Morton and Hallsworth, 1994).

Other parameters, quite helpful in the study of orogenic sediments to estimate the average metamorphic grade of source rocks, are the hornblende colour index (HCI: Garzanti et al., 2004a) and the metasedimentary minerals index (MMI). The latter is defined here as the weighted sum of the relative percentage of the four index minerals most commonly found in low- to high-grade metasediments (chloritoid, staurolite, kyanite, and sillimanite; Table 1). MMI and HCI indices vary from 0 in greenschist-facies to lowermost amphibolite-facies rocks (yielding chloritoid and blue-green amphibole), to 100 in granulite-facies rocks (yielding sillimanite and brown hornblende).

3. CONTINENTAL BLOCK PROVENANCE AND HEAVY MINERAL SUITES

Quartzofeldspathic to quartzose sands of "Continental Block Provenance" ("Uplifted Basement" to "Craton Interior" subprovenances of Dickinson and Suczek, 1979) are deposited along young continental rifts and mature passive continental margins, respectively. The source of detritus is the continental crust, either disrupted by extensional tectonic processes and exposed along rift-shoulder escarpments, or representing the backbone of vast but low-relief cratonic areas.

3.1. Rifted-Margin Provenances

The most spectacular modern example of an active rift is the Dead Sea-Red Sea-Gulf of Aden system. Successive evolutionary stages are documented from north to south, from continental wrenching along the Levant fault, to diffuse extension in the northern Red Sea, to initial spreading in the southern Red Sea, to full spreading along the Sheba Ridge (Cochran, 1981, 1983; Rihm and Henke, 1998).

Heavy mineral suites in volcaniclastic, to sedimentaclastic, to basementaclastic detritus produced along this divergent plate margin from Syria to Oman depend directly and primarily on the intensity of tectonic and magmatic activity in the source terrane (Garzanti et al., 2001, 2003). Three provenance end-members are recognised (Table 2).

Along rift segments associated with prominent volcanic activity, as in the southernmost Red Sea where extensive magmatism controlled by the Afar Plume began in the Oligocene (Davison et al., 1994; Ukstins et al., 2002), heavy mineral suites are invariably dominated by lilac-brown and subordinately green augite, locally associated with olivine and brown hornblende ("Volcanic Rifted Margin Provenance").

Rift segments where volcanic activity is minor are characterised either by continuous exposures of pre-rift sedimentary successions ("Undissected Rift Shoulder subprovenance") or by extensive outcrops of the underlying basement rocks ("Dissected Rift Shoulder subprovenance"), depending on pre-rift stratigraphy as well as on the intensity and duration of uplift associated with tectonic extension. Quartzose

Table 2. Modern heavy mineral suites of "Continental Block Provenance"

	No.	HMC	% t_{HM}	% op_{HM}	% tu_{HM}	ZTR	T&	LgM	Gt	HgM	Hb	&A	CPX	OPX	OS	HCI	MMI	% Rounded
Volcanic rifted margin provenance																		
Levant Margin (Harrat Ash Shams)	3	21	75	16	10	0	0	1	0	0	0	0	79	0	20	n.d.	n.d.	0
Gulf of Aden (Shuqrah)	1	32	91	1	8	0	0	0	0	0	8	0	75	0	17	100	n.d.	0
Southern Red Sea (Ethiopian Traps)	2	36	74	22	4	0	0	11	0	0	3	0	79	1	5	n.d.	n.d.	0
Southern Red Sea (Yemen Traps)	11	15	74	18	9	0	1	8	0	0	6	0	84	1	0	n.d.	n.d.	2
Undissected rift shoulder provenance																		
Levant Margin	2	0.3	40	9	51	80	5	2	1	0	9	0	4	0	0	15	n.d.	19
Northern Red Sea	3	1	32	27	41	30	6	20	3	6	19	1	15	0	0	31	33	22
Gulf of Aden	8	1	52	39	9	24	1	27	15	1	24	1	4	2	1	27	35	23
Dissected rift shoulder provenance																		
Northern Red Sea	11	9	55	27	18	6	9	12	1	1	53	1	16	0	0	11	39	13
Southern Red Sea	4	12	92	5	3	1	2	17	1	0	62	2	14	0	0	9	n.d.	8
Gulf of Aden	10	13	87	8	5	2	2	11	2	1	72	2	5	3	1	11	34	1
Cratonic provenance																		
Northeastern Africa	8	1	35	41	24	30	2	29	9	14	10	0	3	1	0	7	43	39
Arabia	12	0.9	69	18	13	7	0	49	15	1	17	2	5	2	1	38	28	20
Northern India	7	5	75	11	14	14	4	14	11	2	47	2	5	1	0	16	62	5

Note: %Transparent = $\%t_{HM}$, %Opaque = $\%op_{HM}$, %Turbib = $\%tu_{HM}$.

to carbonaticlastic sands of ''Undissected Rift Shoulder subprovenance'' have limited amount and low-diversity heavy mineral suites with commonly rounded ultrastable grains, testifying to extensive recycling of pre-rift strata. Quartzofeldspathic sands of ''Dissected Rift Shoulder subprovenance'' yield, by contrast, abundant heavy minerals with assemblages that are dominated by mainly blue-green to green-brown hornblende grains from amphibolite-facies basement rocks.

As typically occurs in nature, all intermediate cases exist, both between ''Volcanic Rifted Margin'' and ''Rift Shoulder'' Provenances, and between ''Undissected Rift Shoulder'' and ''Dissected Rift Shoulder'' subprovenances (Fig. 3). Because heavy minerals are supplied in much greater abundance by volcanic or basement rocks than by sedimentary successions, sands of ''Transitional Rifted-Margin'' or ''Transitional Rift Shoulder'' subprovenances are typically poor in heavy minerals (with suites dominated by augite or hornblende, respectively), and contain rounded ultrastable minerals only in subordinate quantities. In areas where upper crustal levels are widely preserved within basement complexes, modern sands may include abundant to dominant epidote (e.g., detritus from the shallow roots of ancient magmatic arcs) or garnet and staurolite from lower-amphibolite-facies metasediments.

3.2. Craton Provenance

Heavy minerals of quartzose to quartzofeldspathic sands derived from cratonic shields are comparable with ''Rift Shoulder'' suites (Fig. 3). A low heavy mineral content with commonly rounded ultrastables, epidote, garnet, staurolite, and kyanite characterises areas where upper-crustal basement levels and cover strata are widely preserved (''Undissected Craton subprovenance''). Instead, deeply eroded shield areas where amphibolite-facies middle-crustal levels are extensively exposed (''Dissected Craton subprovenance'') supply abundant heavy minerals, with assemblages dominated by mainly blue-green to green and brown hornblende.

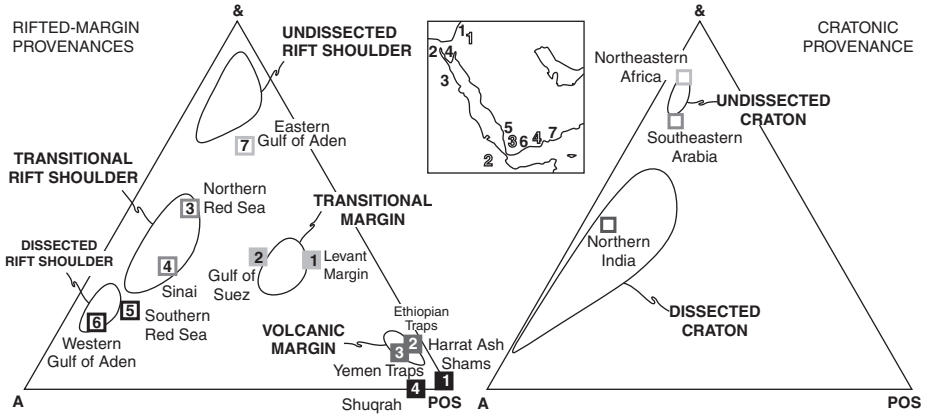

Fig. 3. ''Continental Block Provenance'' and heavy mineral suites. & = all transparent heavy minerals not included in the other two poles. A = Hb + &A = total amphiboles. POS = CPX + OPX + OS = pyroxenes, olivine, and spinel. Parameters defined in Table 1. 90% confidence regions about the mean calculated after Weltje (2002).

4. MAGMATIC ARC PROVENANCE AND HEAVY MINERAL SUITES

Lithofeldspathic detritus derived from volcanic arcs is typified by pyroxene-dominated heavy mineral assemblages (''Undissected Arc subprovenance''). These include only a limited number of diagnostic species, which display the narrow range of chemical compositions typical of orogenic magmatism (Ewart, 1976). The two dominant minerals are augite, found in the vast majority of orogenic lavas, and hypersthene, absent in basalts but widespread in andesites. Olivine, ubiquitous in basalts, is found even in felsic andesites. Hornblende is common in medium- to high-K felsic andesites and dacites, frequently associated with biotite. The ratio of orthopyroxene to clinopyroxene phenocrysts typically increases with increasing silica contents, and orthopyroxene is generally antipathic with both olivine and hornblende (Gill, 1981). Other clinopyroxenes are pigeonite (tholeiitic andesites lacking olivine) and clinoenstatite (boninites). Magnetite (relatively Ti-poor titanomagnetite) is the dominant opaque mineral. Garnet and spinel (locally occurring as inclusions in olivine phenocrysts) are infrequent.

Quartzofeldspathic detritus from calc-alkaline batholiths, representing the remnants of eroded arcs, is hornblende-dominated (Fig. 4; ''Dissected Arc subprovenance''). Mixed assemblages, including augite and hypersthene from volcanic covers, associated in various proportions with hornblende and subordinate epidote from the plutonic roots and metamorphic wallrocks of the arc massif (''Transitional Arc subprovenance'') are frequently found in Circum-Pacific sands. These range from the western Pacific (Murdmaa et al., 1980; Sato, 1981; Nechaev, 1991) to the Bering Sea and Gulf of Alaska (Knebel and Creager, 1974; Slatt and Piper, 1974; Stewart, 1976), to offshore North America (Scheidegger et al., 1973; Nechaev and Isphording, 1993; Zuffa et al., 2000), Middle America (Ross, 1971; Bachman and Leggett, 1982; Enkeboll, 1982; Prasad and Hesse, 1982), South America (Thornburg and Kulm, 1987), and as far as the Antarctic Peninsula (Peters and Hollister, 1976). The correspondence with Dickinson's provenance fields was established on petrographic information either available on the same sample sets (Stewart, 1976; Thornburg and Kulm, 1987; Zuffa et al., 2000) or found in Marsaglia and Ingersoll (1992).

4.1. Modern Sands from Circum-Pacific Volcanic Arcs

Heavy mineral assemblages in Circum-Pacific lithofeldspathic volcaniclastic sands (Dickinson, 1982; Marsaglia and Ingersoll, 1992) have a variable clinopyroxene/orthopyroxene ratio (Table 3). Clinopyroxene dominates in beach placers of the Tonga islands, where olivine is locally present and hornblende invariably absent (Dye and Dickinson, 1996). Augite-olivine and augite-hypersthene assemblages characterise turbidites of the West Philippine Basin and Parece Vela to Mariana basins, respectively (Nechaev, 1991). Turbidites of the Izu-Bonin Arc display a temporal trend from abundant augite with common orthopyroxenes and minor hornblende in the Oligocene, to prevalent orthopyroxenes, augite, and locally olivine in the Pleistocene (Fujioka and Saito, 1992). Orthopyroxene prevails in beach sands of northern Hokkaido (Noda, 2005) and Kamchatcka. Hornblende is common in many Solomons and some Bismarck and Vanuatu (New Hebrides) sands (W.R. Dickinson, Written Communication, 2004).

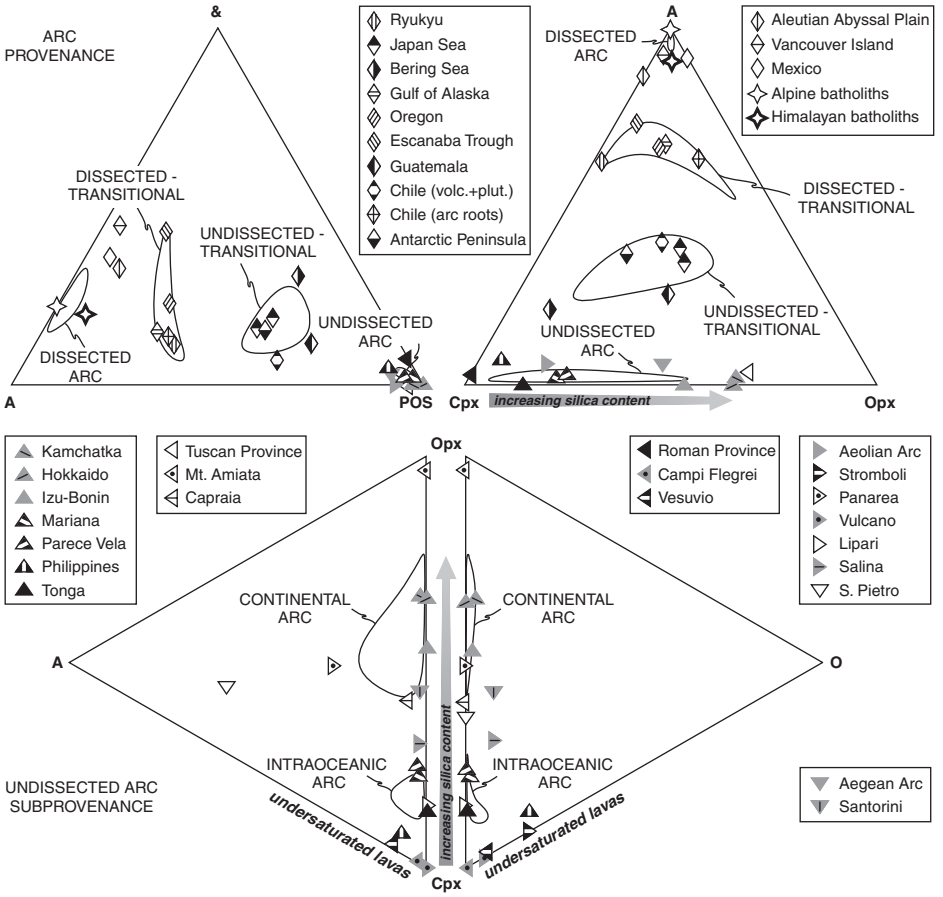

Fig. 4. "Magmatic Arc Provenance" and heavy mineral suites. The double triangle below discriminates between intraoceanic (largely basalts and basaltic andesites) and continental (commonly felsic andesites to rhyolites) "Undissected Arc subprovenance". Modern beach sands from Miocene peralkaline rhyolites of southwestern Sardinia (S. Pietro Island) include sodic amphiboles and pyroxenes (abundant arfvedsonite, minor aegirine). & = all transparent heavy minerals not included in the other two poles. A = Hb + &A = total amphiboles. POS = CPX + OPX + OS = pyroxenes, olivine, and spinel. Parameters defined in Table 1. 90% confidence regions about the mean calculated after Weltje (2002). Data for Roman Province and Aegean Arc mostly from Gandolfi and Paganelli (1984) and Mezzadri and Saccani (1989), respectively. Data for Circum-Pacific arcs after various sources cited in text.

4.2. Modern Sands from Mediterranean Volcanic Arcs

River and beach sands from silica-saturated felsic products of the Tuscan Province (central Italy) are characterised by yellow-green hypersthene (Serri et al., 1993), which is either dominant (Mt. Amiata) or subordinate to green augite and associated with oxyhornblende and biotite (Capraia Island). Detritus from slightly to strongly undersaturated potassic to ultrapotassic lavas of the Roman Province (central and southern Italy) are dominated by green augite, with minor hornblende,

Table 3. Modern heavy mineral suites of "Magmatic Arc Provenance"

	No.	HMC	$\%t_{HM}$	$\%op_{HM}$	$\%tu_{HM}$	ZTR	T&	LgM	Gt	HgM	Hb	&A	CPX	OPX	OS	HCI	MMI	% Rounded
Undissected magmatic arc provenance																		
Mediterranean Arcs																		
Tuscan Province	2	6	86	3	11	0	0	0	1	0	2	0	32	65	0	100	n.d.	0
Roman Province	57	32	90	5	5	0	0	1	3	0	3	0	90	0	2	79	n.d.	0
Aeolian Arc	11	47	86	5	9	0	0	0	0	0	6	0	73	15	6	n.d.	n.d.	0
Aegean Arc	38	22	84	2	13	0	1	2	0	1	2	4	46	43	0	100	n.d.	1
Pacific Arcs																		
Tonga	7	91	n.d.	11	n.d.	0	0	0	0	0	0	0	86	14	Trace	n.d.	n.d.	n.d.
Philippines	9	n.d.	n.d.	25	n.d.	0	1	4	0	0	6	0	69	4	16	n.d.	n.d.	n.d.
Parece Vela	21	n.d.	n.d.	25	n.d.	0	0	2	0	0	3	0	72	23	0	n.d.	n.d.	n.d.
Mariana	47	n.d.	n.d.	18	n.d.	0	0	1	0	0	2	0	75	21	0	n.d.	n.d.	n.d.
Izu-Bonin	99	n.d.	n.d.	n.d.	n.d.	0	0	0	0	0	0	0	46	51	2	n.d.	n.d.	n.d.
Hokkaido	28	20	n.d.	15	n.d.	0	0	0	0	0	0	0	35	65	0	n.d.	n.d.	n.d.
Kamchatka	1	83	67	25	8	0	0	0	0	0	2	0	32	62	3	n.d.	n.d.	1
Dissected magmatic arc provenance																		
Alpine batholiths	5	14	85	12	2	3	4	15	0	0	78	0	0	0	0	7	n.d.	0
Himalayan batholiths	5	25	80	8	12	1	3	16	0	0	69	3	4	4	0	16	n.d.	0

Note: Data for Roman Province and Aegean Arc mostly from Gandolfi and Paganelli (1984) and Mezzadri and Saccani (1989), respectively. Data for Circum-Pacific arcs after various sources cited in text.
%Transparent = $\%t_{HM}$, %Opaque = $\%op_{HM}$, %Turbib = $\%tu_{HM}$.

oxyhornblende, olivine, chrome spinel, and locally significant melanite (Gt up to 15) (Gandolfi and Paganelli, 1984; Peccerillo, 1985; Garzanti et al., 2002a).

Green augite is widespread in the heavy mineral-rich beach sands of the Aeolian Arc. High-K basalts and basaltic andesites of Stromboli Island also supply abundant olivine, whereas felsic andesites, dacites, and rhyodacites of Panarea Island (Calanchi et al., 2002) also contribute abundant yellow-green hypersthene and dark-brown hornblende. Rhyolite-derived sands on Lipari Island contain fewer heavy minerals. Detrital green to pale-green clinopyroxene and hypersthene are largely xenocrysts, derived from more mafic enclaves and pumices within felsic lava domes and pyroclastic deposits (Gioncada et al., 2003). Beach to turbidite sands derived from the Aegean Arc are dominated by augite and hypersthene, with minor oxyhornblende and trace olivine (Mezzadri and Saccani, 1989).

4.3. *Modern Sands from Alpine and Himalayan Batholiths*

The deeply eroded roots of ancient magmatic arcs, representing the Cretaceous-Eocene Asian active margin of Neotethys, are exposed all along the Indus-Tsangpo suture from Pakistan to Burma (Gansser, 1980). Quartzofeldspathic detritus from these Transhimalayan batholiths include dominant blue-green to more rarely green and brown hornblende, associated with epidote, clinopyroxenes, hypersthene, and sphene (Garzanti et al., 2004b, 2005). Abundant epidote and minor actinolite are supplied locally by greenschist-facies metamorphosed arc rocks. Similar signatures, with dominant blue-green to more rarely green and brown hornblende, along with epidote, minor sphene or zircon, and trace monazite, characterise quartzofeldspathic detritus from Tertiary Alpine plutons (Bregaglia, Adamello).

5. OROGENIC PROVENANCE AND HEAVY MINERAL SUITES

Orogenic provenance is a complex subject, difficult to deal with in brief because each thrust belt has its own tectonic style, peculiar rock assemblage, and stacking pattern. Moreover, orogenic belts commonly incorporate remnants of ophiolitic complexes and magmatic arcs, eroded to various levels along the suture zone (the latter contributing detritus of "Magmatic Arc Provenance"), and basement slivers overlain by passive-margin strata along the external flanks (contributing detritus of "Continental Block Provenance").

Different classes of orogens, defined as allochthonous tectonic prisms formed in the hangingwall of subducting continental crust, exist. They include Alpine or Himalayan-type thick-skinned collision orogens, Oman-type ophiolite-capped obduction orogens, and Apennine-type thin-skinned thrust belts (Cawood, 1991; Michard et al., 1991; Doglioni et al., 1999; Garzanti et al., 2002b).

5.1. *Modern Sands from the Alpine Collision Orogen*

The Alps are a double-vergent thick-skinned orogen formed by continental collision (Pfiffner et al., 1997). Alpine calc-alkaline magmatic rocks are confined to tonalite-granodiorite plutons and associated andesite dike-swarms intruded along the

Periadriatic Zone (e.g., Bregaglia, Adamello). The axial metamorphic backbone of the orogen incorporates remnants of the thinned distal edges of collided continental margins and intervening oceanic rocks, which underwent attempted subduction and high-pressure metamorphism in the early orogenic (Late Cretaceous-Eocene) stage (Dal Piaz, 1999; Gebauer, 1999). The external belts on both sides of the orogen (Southalpine and Helvetic-Dauphinois Zones) include inverted listric wedges of European and Adriatic basements along with their covers that experienced negligible to lower-amphibolite-facies Tertiary metamorphism (Frey et al., 1999).

Heavy mineral suites of Alpine-derived modern sediments are primarily related to structural level of source rocks (Garzanti et al., 2004a). Quartzofeldspathic gneissiclastic detritus derived from the amphibolite-facies Lepontine Dome of the Central Alps include abundant hornblende. The abundance of hornblende grains in sands carried by local streams increases from the periphery to the core of the dome, while their most frequent colour changes from exclusively blue-green to green, green-brown, and locally brown, reflecting compositional changes with increasing metamorphic grade (Miyashiro, 1972, p. 254). Epidote-group minerals, actinolite, or garnet are most abundant in sands carried by rivers draining the periphery (or partly outside) of the dome. Pyroxenes, staurolite, kyanite, and sillimanite are invariably subordinate; olivine occurs locally.

Quartzolithic metamorphiclastic detritus derived from the high-pressure metamorphic nappes exposed extensively in the Western Alps, as well as in the Engadine and Tauern windows of the Eastern Alps, contain dominant epidote, largely reflecting extensive retrogression at greenschist facies. High-pressure minerals include carpholite, zoisite, Mg-chloritoid, glaucophane, and Mg- and Ca-rich almandine garnet. Meta-ophiolites supply heavy mineral-rich sediment with amphiboles (actinolite, blue-green barroisitic hornblende, glaucophane), and minor pyroxenes. Continental basements contribute abundant garnet and, locally, even sillimanite, hypersthene, and brown hornblende from pre-Alpine granulite-facies relics (e.g., Dent Blanche Nappe). Metasedimentary covers provide mostly turbid grains and a few ultrastable heavy minerals.

Lithoquartzose sedimentaclastic detritus derived from sedimentary thrust sheets (Liguride remnant-ocean turbidites in the Western Alps, Austroalpine platform carbonates and clastics in the Eastern Alps) are very poor in heavy minerals, which largely consist of recycled grains (ultrastables, garnet, staurolite). Oceanic turbidites also supply amphiboles, pyroxenes, and chrome spinel. Reactivated basement slivers of the external belts contribute heavy mineral suites similar to those contained in the sands of ''Dissected Continental Block'' subprovenances.

5.2. Modern Sands from the Himalayan Collision Orogen

The Himalaya is the paradigm of a thick-skinned belt produced by continent–continent collision (Hodges, 2000). In contrast to the Alps, the Himalaya includes a passive margin on the Indian side (North Himalaya, Tethys Himalaya, Greater Himalaya, and Lesser Himalaya zones; Le Fort, 1996) and a fully developed active margin on the Asian side (Transhimalaya zone), separated by the Indus-Tsangpo suture (Gansser, 1980). Only the two largest fluvial systems, the Indus and the Tsangpo-Brahmaputra, drain the Asian active margin. Their sands contain high

proportions of heavy minerals, dominated by blue-green hornblende associated with epidote, garnet, and kyanite. Such a signature is unique with respect to any other major river sourced in the Himalaya or in the Alps (Fig. 5). Although it partly reflects contributions from Transhimalayan batholiths, it is largely related to another peculiarity of the two systems, that have about a fourth of their sediment load produced by super-fast erosion of the western and eastern Himalayan syntaxes (Garzanti et al., 2004b, 2005). Upper-amphibolite-facies mid-crustal levels are here unroofed at the core of crustal-scale antiforms, at rates up to 5 mm per year (Burg et al., 1998; Rolland et al., 2001). Contributions from ophiolitic mélanges and volcaniclastic suites exposed along oceanic suture zones (pyroxenes, olivine, chrome spinel, glaucophane) are negligible. All of the other major Himalayan rivers, including the Ganga, chiefly drain the Greater and Lesser Himalaya zones along the southern flank of the range. Their load is significantly poorer in heavy minerals, and comprise, in order of abundance, blue-green to green and locally brown hornblende, garnet, epidote, clinopyroxene, kyanite, and sillimanite (Table 4).

5.3. Modern Sands from Oman-Type Obduction Orogens

The best-studied obducted ophiolite belt on Earth is spectacularly exposed in northern Oman, where a thick-skinned thrust belt was generated by attempted subduction of the eastern Arabian continental platform underneath an oceanic plate (Glennie et al., 1974; Searle and Cox, 1999). Modern sands produced in such a geodynamic setting contain abundant mafic and ultramafic minerals, derived from the obducted oceanic lithosphere (Table 4; Garzanti et al., 2000, 2002b).

Mantle harzburgites supply enstatitic orthopyroxene, associated with olivine and minor chrome spinel. Olivine and chrome spinel are subordinate for contrasting

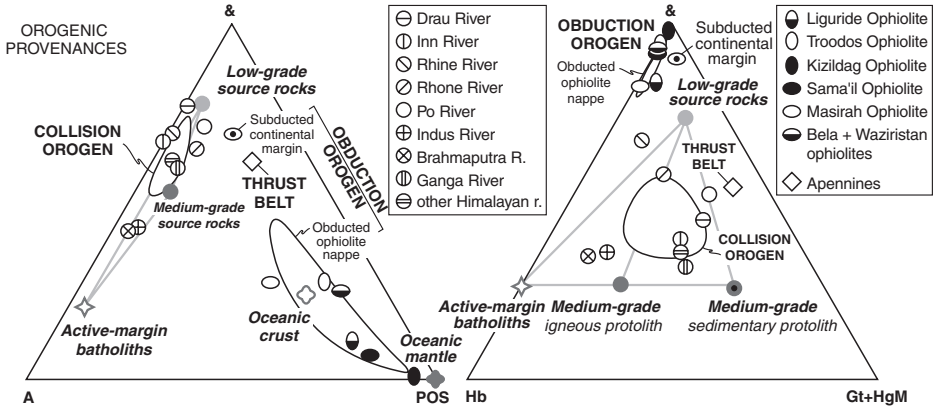

Fig. 5. "Orogenic Provenance" and heavy mineral suites. & = all transparent heavy minerals not included in the other two poles. A = Hb + &A = total amphiboles. POS = CPX + OPX + OS = pyroxenes, olivine, and spinel. Parameters defined in Table 1. 90% confidence regions about the mean calculated after Weltje (2002). Data for Po delta and Internal Liguride units include analyses by Gazzi et al. (1973) and Gandolfi and Paganelli (1975). End-member compositions calculated after selected data from provenance studies listed in Fig. 2.

Table 4. Modern heavy mineral suites of "Orogenic Provenance"

	No.	HMC	$\%t_{HM}$	$\%op_{HM}$	$\%tu_{HM}$	ZTR	T&	LgM	Gt	HgM	Hb	&A	CPX	OPX	OS	HCI	MMI	% Rounded
Collision orogen provenance																		
Himalaya																		
Indus River	12	12	84	7	9	2	2	24	13	3	48	2	3	3	0	12	61	0
Brahmaputra River	8	11	89	6	6	3	2	25	11	1	53	2	3	1	0	8	73	0
Ganga River	12	4	88	5	7	7	2	14	28	9	31	2	6	0	0	9	71	1
Other rivers	18	4	83	8	9	7	2	19	28	6	30	2	5	0	0	13	67	1
Alps																		
Po River	17	11	77	12	11	3	2	33	31	3	15	7	4	3	0	38	47	0
Rhone River	4	4	61	14	25	6	2	39	18	1	23	3	9	0	0	25	61	1
Rhine River	1	3	36	20	44	9	1	51	9	0	24	7	1	0	0	6	n.d.	0
Inn River	3	3	71	12	17	3	1	30	26	6	28	5	0	0	0	3	32	0
Drau River	5	6	78	6	15	3	2	37	33	2	20	1	1	0	0	6	32	0
Obduction orogen provenance																		
Obducted ophiolite nappe																		
Internal Liguride	21	4	67	11	22	1	1	6	4	0	12	3	65	5	4	77	17	0
Troodos	7	20	87	3	9	0	0	27	0	0	6	9	53	5	1	28	n.d.	1
Bela and Waziristan	2	18	65	6	29	1	0	24	0	0	8	3	50	9	6	25	n.d.	0
Masirah	7	24	70	11	19	1	0	24	1	0	17	10	42	2	2	30	n.d.	3
Sama'il	24	32	80	9	11	0	0	6	0	0	8	5	20	47	14	57	n.d.	0
Kizildag	5	30	92	1	6	0	0	1	0	0	2	3	20	42	32	19	n.d.	2
Subducted continental margin units																		
Saih Hatat	4	31	43	26	31	5	0	58	5	0	4	12	10	5	0	n.d.	n.d.	1
Thrust belt provenance																		
Apennines	93	2	59	9	32	5	3	17	35	3	8	6	17	5	2	n.d.	36	n.d.

Note: Data for Po delta and Internal Liguride units include analyses by Gazzi et al. (1973) and Gandolfi and Paganelli (1975).
%Transparent = $\%t_{HM}$, %Opaque = $\%op_{HM}$, %Turbib = $\%tu_{HM}$.

reasons (Garzanti and Andò, 2007—this volume). The former, abundant in the source rocks but chemically very unstable, is selectively destroyed by serpentinization before, during, and after obduction (Wenner and Taylor, 1974) or by weathering in sedimentary environments. The latter, chemically stable but sparse in the source rocks, is concentrated only in detritus derived from very-extensively serpentinised peridotites, or by sedimentary processes including intense weathering in equatorial climates, hydraulic sorting, and recycling.

Lower-crustal gabbroic rocks release not only abundant pyroxenes, including diopside or diallage but also significant green-pink hypersthene from noritic gabbros generated in supra-subduction settings (Lachize et al., 1996). Subordinate hornblende is chiefly derived from isotropic high-level gabbros. Sheeted-dyke complexes, intensely altered during oceanic metamorphism, supply diopsidic clinopyroxenes, actinolitic amphiboles, locally abundant epidote, and significant hypersthene in supra-subduction settings. Lavas contribute dominantly pyroxenes (green to brown augite, along with yellow-green orthopyroxene in supra-subduction settings).

When and where erosion bites into the continental roots of the orogen beneath the ophiolite nappe, detritus displays features similar to "Collision Orogen Provenance". Modern sands derived from blueschist- to eclogite-facies subducted remnants of the Arabian outer continental margin contain epidote-dominated assemblages with carpholite, lawsonite, glaucophane, and garnet, which is comparable with those derived from high-pressure units of the Western Alps (Garzanti et al., 2004a).

5.4. *Modern Sands from Apennine-Type Thrust Belts*

Thin-skinned thrust belts, chiefly consisting of allochtonous passive-continental-margin successions, provide few and largely recycled heavy minerals. Unroofed metamorphic complexes may locally supply a few low-grade or high-pressure minerals (e.g., epidote, chloritoid).

Heavy mineral suites of Apennine-derived sands largely include clinopyroxenes from either offscraped ophiolites (diallage; Northern Apennines) or Quaternary volcanic rocks (green augite; Tyrrhenian coast). Garnet, epidote, and minor staurolite and kyanite are recycled from extensively exposed foredeep turbidites, ultimately fed from the adjacent Alpine thick-skinned orogen (Garzanti et al., 2002a).

6. CONCLUSIONS

High-resolution heavy mineral analysis is an extremely powerful tool in provenance studies. The great number of mineral species and varieties found in modern sediments, not modified by diagenesis, allow us to obtain a wealth of detailed information on source areas, augmenting that provided by the petrographic analysis of bulk sediment.

We follow here the model of Dickinson (1985), which identifies three main provenances of terrigenous sediments. Sources of detritus in "Continental Block Provenance" are variously dissected rifted margins or cratonic shields, located along divergent plate boundaries or in intraplate settings and not associated with subduction zones. Sources of detritus in "Magmatic Arc Provenance" are volcanic and

volcano-plutonic belts, formed in the hanging-wall of an oceanic subduction zone. Sources of detritus in "Orogenic Provenance" are thick-skinned collision or obduction orogens and thin-skinned thrust belts, chiefly consisting of metamorphic complexes, oceanic sequences, and passive-margin successions tectonically stacked in the hanging-wall of a continental subduction zone.

Major provenance types cannot be discriminated just by the simple acritical use of one standardised binary or ternary diagram. All of the evidence provided by detrital assemblages must be given full consideration. Subtle distinctions, such as those based on colour of amphibole and pyroxene grains (Nechaev and Isphording, 1993; Garzanti et al., 2004a), are crucial in differentiating magmatic or metamorphic assemblages exposed along rifted margins, magmatic arcs, and collision or obduction orogens.

Through a series of modern case studies, we highlighted the strict relationships that exist between plate-tectonic setting and both bulk-framework composition and heavy mineral assemblages of terrigenous sediments, and showed how the conceptual models, proposed and refined by Dickinson and co-workers since the 1970s (Dickinson and Suczek, 1979), can be integrated and extended to provenance diagnosis of heavy mineral suites. A precise and accurate discrimination of geodynamic processes, character of magmatic activity, depth of erosion level, metamorphic grade, and original nature of protoliths eroded in the source terrane can thus be achieved.

ACKOWLEDGEMENTS

The manuscript benefited from careful reviews by Bill Dickinson and John Dewey. Ada Ali Abdel Megid, Stefania Canclini, Giovanna Castiglioni, Andrea Coltura, Giulia Erbetta, Elisabetta Mauri, Stefano Monguzzi, Paolo Paparella, and Cristian Vidimari prepared and analysed hundreds of heavy mineral slides through the years. Yani Najman, Christian France-Lanord, Peter Clift, Erich Draganitz, Gavin Foster, Giacomo Ghielmi, Gianluca Groppelli, Filippo Lazzati, Bruno Lombardo, Mike Searle, Hugh Sinclair, Dario Sciunnach, Annalisa Tunesi, and Giovanni Vezzoli collected crucial samples from various parts of the world. Salvatore Critelli, Bill Dickinson, Ray Ingersoll, Renzo Valloni and Gianni Zuffa gave precious help and advice through the years. Financial support by FIRB 2002 and PRIN 2003 to E. Garzanti.

REFERENCES

Bachman, S.B., Leggett, J.K., 1982. Petrology of Middle America trench and trench-slope sands, Guerrero margin, Mexico. In: Initial Report of the Deep Sea Drilling Project, vol. 66, pp. 429–436.

Bathia, M.R., 1985. Plate tectonics and geochemical composition of sandstones. Journal of Geology 91, 611–627.

Burg, J.-P., Nievergelt, P., Oberli, F., Seward, D., Davy, P., Maurin, J.-C., Diao, Z., Meier, M., 1998. The Namche Barwa syntaxis: evidence for exhumation related to compressional crustal folding. Journal of Asian Earth Science 16, 239–252.

Calanchi, N., Peccerillo, A., Tranne, C.A., Lucchini, F., Rossi, P.L., Kempton, P., Barbieri, M., Wu, T.W., 2002. Petrology and geochemistry of volcanic rocks from the island of Panarea: implications for mantle evolution beneath the Aeolian island arc (southern Tyrrhenian sea). Journal of Volcanology and Geothermal Research 115, 367–395.

Cawood, P.A., 1991. Processes of ophiolite emplacement in Oman and Newfoundland. In: Peters, T., Nicolas, A., Coleman, R.G. (Eds.), Ophiolite Genesis and Evolution of Oceanic Lithosphere. Kluwer, Dordrecht, pp. 501–516.

Cochran, J.R., 1981. The Gulf of Aden: structure and evolution of a young ocean basin and continental margin. Journal of Geophysical Research 86, 263–287.

Cochran, J.R., 1983. A model for development of Red Sea. American Association of Petroleum Geologists Bulletin 67, 41–69.

Dal Piaz, G.V., 1999. Austroalpine-Piedmont nappe stack and the puzzle of Alpine Tethys. Memorie della Società Geologica Italiana 51, 155–176.

Davison, I., Al-Kadasi, M., Al-Khirbash, S., Al-Subbary, A., Baker, J., Blakey, S., Bosence, D., Dart, C., Heaton, R., McClay, K., Menzies, M., Nichols, G., Owen, L., Yelland, A., 1994. Geological evolution of the southeastern Red Sea rift margin, Republic of Yemen. Geological Society of America Bulletin 106, 1474–1493.

Derkachev, A.N., Nikolajeva, N.A., 2007. Multivariate analysis of heavy mineral assemblages of sediments from the marginal seas of the Western Pacific. In: Mange, M.A., Wright, D.T. (Eds.), Heavy Minerals in Use. Developments in Sedimentology (this volume).

Dickinson, W.R., 1974. Plate tectonics and sedimentation. In: Dickinson, W.R. (Ed.), Tectonics and Sedimentation, Society of Economic Paleontologists and Mineralogists. Special Publication 22, 1–27.

Dickinson, W.R., 1982. Composition of sandstones in Circum-Pacific subduction complexes and fore-arc basins. American Association of Petroleum Geologists Bulletin 66, 121–137.

Dickinson, W.R., 1985. Interpreting provenance relations from detrital modes of sandstones. In: Zuffa, G.G. (Ed.), Provenance of Arenites, Reidel, Dordrecht, NATO ASI Series 148, pp. 333–361.

Dickinson, W.R., Suczek, C.A., 1979. Plate tectonics and sandstone composition. American Association of Petroleum Geologists Bulletin 63, 2164–2172.

Doglioni, C., Harabaglia, P., Merlini, S., Mongelli, F., Peccerillo, A., Piromallo, C., 1999. Orogens and slabs vs. their direction of subduction. Earth Science Reviews 45, 167–208.

Dye, T.S., Dickinson, W.R., 1996. Sources of sand tempers in Prehistoric Tongan pottery. Geoarchaeology 11, 141–164.

Enkeboll, R.H., 1982. Petrology and provenance of sands and gravels from the Middle America Trench and trench slope, southwestern Mexico and Guatemala. Initial Report of the Deep Sea Drilling Project 66, 521–530.

Ewart, A., 1976. Mineralogy and chemistry of modern orogenic lavas—some statistics and implications. Earth and Planetary Science Letters 31, 417–432.

Frey, M., Desmons, J., Neubauer, F., 1999. The new metamorphic map of the Alps. Schweizerische Mineralogische und Petrographische Mitteilungen 79, 1–209.

Fujioka, K., Saito, S., 1992. Composition of heavy minerals from sands and sandstones of the Izu-Bonin Arc, Leg 126. In: Proceedings of the Ocean Drilling Program, Scientific Results, vol. 126, pp. 155–169.

Gandolfi, G., Paganelli, L., 1975. Il litorale toscano fra Livorno e il promontorio di Piombino (area campione Alto Tirreno): composizione, provenienza e dispersione delle sabbie. Bollettino della Societa Geologica Italiana 94, 1833–1854.

Gandolfi, G., Paganelli, L., 1984. Petrografia delle sabbie del litorale Tirrenico fra i Monti dell' Uccellina e Monte di Procida. Mineralogica et Petrographica Acta 28, 173–191.

Gansser, A., 1980. The Peri-Indian suture zone. In: Auboin, J., Debelmas, J., Latreille, M. (Eds.), Géologie des Châines Alpines Issues de la Téthys, Mémoires du Bureau de Recherches Géologiques et Minières 115, 140–148.

Garzanti, E., Andò, S., 2007. Heavy mineral concentration in modern sands: implications for provenance interpretation. In: Mange, M.A., Wright, D.T. (Eds.), Heavy Minerals in Use. Developments in Sedimentology (this volume).

Garzanti, E., Andò, S., Scutellà, M., 2000. Actualistic ophiolite provenance: the Cyprus Case. Journal of Geology 108, 199–218.

Garzanti, E., Andò, S., Vezzoli, G., Dell'Era, D., 2003. From rifted margins to foreland basins: investigating provenance and sediment dispersal across desert Arabia (Oman, UAE). Journal of Sedimentary Research 73, 572–588.

Garzanti, E., Andò, S., Vezzoli, G., Ali Abdel Megid, A., El Kammar, A., 2006. Petrology of Nile River sands (Ethiopia and Sudan): sediment budgets and erosion patterns. Earth and Planetary Science Letters 252, 327–341.

Garzanti, E., Canclini, S., Moretti Foggia, F., Petrella, N., 2002a. Unraveling magmatic and orogenic provenances in modern sands: the back-arc side of the Apennine thrust-belt (Italy). Journal of Sedimentary Research 72, 2–17.

Garzanti, E., Scutella', M., Vidimari, C., 1998. Provenance from ophiolites and oceanic allochthons: modern beach and river sands from Liguria and the Northern Apennines (Italy). Ofioliti 23, 65–82.

Garzanti, E., Vezzoli, G., Andò, S., 2002b. Modern sand from obducted ophiolite belts (Oman, U.A.E.). Journal of Geology 110, 371–391.

Garzanti, E., Vezzoli, G., Andò, S., Castiglioni, G., 2001. Petrology of rifted-margin sand (Red Sea and Gulf of Aden, Yemen). Journal of Geology 109, 277–297.

Garzanti, E., Vezzoli, G., Lombardo, B., Andò, S., Mauri, E., Monguzzi, S., Russo, M., 2004a. Collision-orogen provenance (Western and Central Alps): detrital signatures and unroofing Trends. Journal of Geology 112, 145–164.

Garzanti, E., Vezzoli, G., Andò, S., France-Lanord, C., Singh, S.K., Foster, G., 2004b. Sediment composition and focused erosion in collision orogens: the Brahmaputra case. Earth and Planetary Science Letters 220, 157–174.

Garzanti, E., Vezzoli, G., Andò, S., Paparella, P., Clift, P.D., 2005. Petrology of Indus River sands: a key to interpret erosion history of the Western Himalayan Syntaxis. Earth and Planetary Science Letters 229, 287–302.

Gazzi, P., 1965. On the heavy mineral zones in the geosyncline series, recent studies in the Northern Apennines, Italy. Journal of Sedimentary Petrology 35, 109–115.

Gazzi, P., Zuffa, G.G., Gandolfi, G., Paganelli, L., 1973. Provenienza e dispersione litoranea delle sabbie delle spiagge adriatiche fra le foci dell' Isonzo e del Foglia: inquadramento regionale. Memorie della Società Geologica Italiana 12, 1–37.

Gebauer, D., 1999. Alpine geochronology of the Central and Western Alps: new constraints for a complex geodynamic evolution. Schweizerische Mineralogische und Petrographische Mitteilungen 79, 191–208.

Gill, J., 1981. Orogenic Andesites and Plate Tectonics. Springer-Verlag, Berlin, 390pp.

Gioncada, A., Mazzuoli, R., Bisson, M., Pareschi, M.T., 2003. Petrology of volcanic products younger than 42 ka on the Lipari-Vulcano complex (Aeolian Islands, Italy): an example of volcanism controlled by tectonics. Journal of Volcanology and Geothermal Research 122, 191–220.

Glennie, K.W., Boeuf, M.G.A., Hughes-Clarke, M.W., Moody-Stuart, M., Pilaar, W.F.H., Reinhardt, B.M., 1974. Geology of the Oman Mountains. The Hague, Verhandelingen van het Koninklijk Nederlands Geologisch Mijnbouwkundig Genootschap Transactions, vol. 31, 423pp.

Hodges, K.V., 2000. Tectonics of the Himalaya and southern Tibet from two perspectives. Geological Society of America Bulletin 112, 324–350.

Hubert, J.F., 1962. A zircon-tourmaline-rutile maturity index and the interdependence of the composition of heavy minerals assemblages with the gross composition and texture of sandstones. Journal of Sedimentary Petrology 32, 440–450.

Imbrie, J., Van Andel, T.H., 1964. Vector analysis of heavy mineral data. Geological Society of America Bulletin 75, 1131–1156.

Ingersoll, R.V., 1990. Actualistic sandstone petrofacies: discriminating modern and ancient source rocks. Geology 18, 733–736.

Ingersoll, R.V., Busby, C.J., 1994. Tectonics of sedimentary basins. In: Busby, C.J., Ingersoll, R.V. (Eds.), Tectonics of Sedimentary Basins. Blackwell, Oxford, pp. 1–51.

Johnsson, M.J., 1993. The system controlling the composition of clastic sediments. In: Johnsson, M.J., Basu, A. (Eds.), Processes Controlling the Composition of Clastic Sediments. Geological Society of America Special Paper 284, 1–19.

Klovan, J.E., Imbrie, J., 1971. An algorithm and FORTRAN-IV program for large scale Q-mode factor analysis and calculation of factor scores. Mathematical Geology 3, 61–77.

Knebel, H.J., Creager, J., 1974. Heavy minerals of the east-central Bering Sea continental shelf. Journal of Sedimentary Petrology 44, 553–561.

Korsch, R.J., Roser, B.P., Kamprad, J.L., 1993. Geochemical, petrographic and grain-size variations within single turbidite beds. Sedimentary Geology 83, 15–35.

Lachize, M., Lorand, J.P., Juteau, T., 1996. Calc-alkaline differentiation trend in the plutonic sequence of the Wadi Haymiliyah section, Haylayn massif, Semail ophiolite, Oman. Lithos 38, 207–232.

Le Fort, P., 1996. Evolution of the Himalaya. In: Yin, A., Harrison, M.T. (Eds.), The Tectonic Evolution of Asia. Cambridge University Press, Cambridge, pp. 95–109.

Mack, G.H., 1984. Exceptions to the relationship between plate tectonics and sandstone composition. Journal of Sedimentary Petrology 54, 212–220.

Mange, M.A., Maurer, H.F.W., 1992. Heavy Minerals in Colour. Chapman and Hall, London, 147pp.

Mange-Rajetzky, M., Oberhänsli, R., 1982. Detrital lawsonite and blue sodic amphibole in the Molasse of Savoy, France and their significance in assessing Alpine evolution. Schweizerische Mineralogische und Petrographische Mitteilungen 62, 415–436.

Marsaglia, K.M., Ingersoll, R.V., 1992. Compositional trends in arc-related, deep-marine sand and sandstone: a reassessment of magmatic-arc provenance. Geological Society of America Bulletin 104, 1637–1649.

Maynard, J.B., Valloni, R., Yu, H.-S., 1982. Composition of modern deep-sea sands from arc-related basins. In: Leggett, J.K. (Ed.), Trench-Forearc Geology: Sedimentation and Tectonics on Modern and Ancient Active Plate Margins, vol. 10. Geological Society of London Special Publication, pp. 107–119.

McBride, E.F., 1985. Diagenetic processes that affect provenance determinations in sandstones. In: Zuffa, G.G. (Ed.), Provenance of Arenites. Reidel, Dordrecht, NATO ASI Series 148, pp. 95–113.

Mezzadri, G., Saccani, E., 1989. Heavy mineral distribution in Late Quaternary sediments of the Southern Aegean Sea: implications for provenance and sediment dispersal in sedimentary basins at active margins. Journal of Sedimentary Petrology 59, 412–422.

Michard, A., Boudier, F., Goffé, B., 1991. Obduction versus subduction and collision in the Oman case and other Tethyan settings. In: Peters, T., Nicolas, A., Coleman, R.G. (Eds.), Ophiolite Genesis and Evolution of Oceanic Lithosphere. Kluwer, Dordrecht, pp. 447–467.

Miyashiro, A., 1972. Metamorphism and Metamorphic Belts. Wiley, New York, NY, 492pp.

Morton, A., Hallsworth, C.R., 1994. Identifying provenance-specific features of detrital heavy mineral assemblages in sandstones. Sedimentary Geology 90, 241–256.

Morton, A.C., Hallsworth, C.R., 1999. Processes controlling the composition of heavy mineral assemblages in sandstones. Sedimentary Geology 124, 3–29.

Murdmaa, I., Kazakova, V., Shirshov, P.P., 1980. Coarse-silt-fraction mineralogy of Japan Trench sediments, Deep Sea Drilling Project Legs 56 and 57. Initial Report of the Deep Sea Drilling Project, 56–57, 1005–1009.

Nechaev, V.P., 1991. Evolution of the Philippine and Japan Seas from the clastic sediment record. Marine Geology 97, 167–190.

Nechaev, V.P., Isphording, W.C., 1993. Heavy mineral assemblages of continental margins as indicators of plate-tectonic environments. Journal of Sedimentary Petrology 63, 1110–1117.

Noda, A., 2005. Texture and petrology of modern river, beach and shelf sands in a volcanic back-arc setting, northeastern Japan. The Island Arc 14, 687–707.

Parfenoff, A., Pomerol, C., Tourenq, J., 1970. Les minéraux en grains—méthodes d' étude et détermination. Masson, Paris, 578pp.

Peccerillo, A., 1985. Roman comagmatic province (central Italy): evidence for subduction-related magma genesis. Geology 13, 103–106.

Peters, C.S., Hollister, C.D., 1976. Heavy mineral characteristics and dispersal patterns from DSDP Leg 35, Southeast Pacific Basin. Initial Report of the Deep Sea Drilling Project 35, 291–300.

Pfiffner, O.A., Lehner, P., Heitzmann, P., Müller, S., Steck, A., 1997. Deep structure of the Swiss Alps. Results of NRP 20. Birkhäuser Verlag, Basel. 460pp.

Potter, P.E., 1978. Petrology and chemistry of modern big river sands. Journal of Geology 86, 423–449.

Potter, P.E., 1994. Modern sands of South America: composition, provenance and global significance. Geologische Rundschau 83, 212–232.

Prasad, S., Hesse, R., 1982. Provenance of detrital sediments from the Middle America trench transect off Guatemala, Deep Sea Drilling Project Leg 67. Initial Report of the Deep Sea Drilling Project, 67, 507–514.

Rihm, R., Henke, C.H., 1998. Geophysical studies on early tectonic controls on Red Sea rifting, opening and segmentation. In: Purser, B.H., Bosence, D.W.J. (Eds.), Sedimentation and Tectonics in Rift Basins: Red Sea-Gulf of Aden. Chapman and Hall, London, pp. 29–49.

Rolland, Y., Mahéo, G., Guillot, S., Pêcher, A., 2001. Tectono-metamorphic evolution of the Karakorum metamorphic complex (Dassu-Askole area, NE Pakistan): exhumation of mid-crustal HT-MP gneisses in a convergent context. Journal of Metamorphic Geology 19, 717–737.

Roser, B.P., Korsch, R.J., 1986. Determination of tectonic setting of sandstone-mudstone suites using SiO_2 content and K_2O/Na_2O ratio. Journal of Geology 94, 635–650.

Ross, D.A., 1971. Sediments of the northern Middle America Trench. Geological Society of America Bulletin 82, 303–322.

Sato, Y., 1981. Heavy mineral composition of Tertiary sediments at Deep Sea Drilling Project Sites 445 and 446, Northeastern Philippine Sea, Deep Sea Drilling Project. Initial Report of the Deep Sea Drilling Project, 58, 661–667.

Scheidegger, K.F., Kulm, L.D., Piper, D.J.W., 1973. Heavy mineralogy of unconsolidated sands in northeastern Pacific sediments, Leg 18, Deep Sea Drilling Project. Initial Report of the Deep Sea Drilling Project, 18, 877–887.

Schwab, F.L., 1975. Framework mineralogy and chemical composition of continental margin-type sandstone. Geology 3, 487–490.

Searle, M.P., Cox, J., 1999. Tectonic setting, origin, and obduction of the Oman ophiolite. Geological Society of America Bulletin 111, 104–122.

Serri, G., Innocenti, F., Manetti, P., 1993. Geochemical and petrological evidence of the subduction of delaminated Adriatic continental lithosphere in the genesis of Neogene-Quaternary magmatism of central Italy. Tectonophysics 223, 117–147.

Slatt, R.M., Piper, D.J.W., 1974. Sand-silt petrology and sediment dispersal in the Gulf of Alaska. Journal of Sedimentary Petrology 44, 1061–1071.

Stattegger, K., 1987. Heavy minerals and provenance of sands: modeling of lithological end members from river sands of Northern Austria and from sandstones of the Austroalpine Gosau Formation (Late Cretaceous). Journal of Sedimentary Petrology 57, 301–310.

Stewart, R.J., 1976. Turbidites of the Aleutian abyssal plain: mineralogy, provenance, and constraints for Cenozoic motion of the Pacific plate. Geological Society of America Bulletin 87, 793–808.

Thamó-Bozsó, E., Kovács, L. Ó., 2007. Evolution of Quaternary to modern fluvial network in the Mid-Hungarian Plain, indicated by heavy mineral distributions and statistical analysis of heavy mineral data. In: Mange, M.A., Wright, D.T. (Eds.), Heavy Minerals in Use. Developments in Sedimentology (this volume).

Thornburg, T.M., Kulm, L.D., 1987. Sedimentation in the Chile Trench: petrofacies and provenance. Journal of Sedimentary Petrology 57, 55–74.

Ukstins, I.A., Renne, P.R., Wolfenden, E., Baker, J., Ayalew, D., Menzies, M., 2002. Matching conjugate volcanic rifted margins: $^{40}Ar/^{39}Ar$ chrono-stratigraphy of pre- and syn-rift bimodal flood volcanism in Ethiopia and Yemen. Earth and Planetary Science Letters 198, 289–306.

Weltje, G.J., 2002. Quantitative analysis of detrital modes: statistically rigorous confidence methods in ternary diagrams and their use in sedimentary petrology. Earth Science Reviews 57, 211–253.

Wenner, D.B., Taylor, H.P., 1974. D/H and O^{18}/O^{16} studies of serpentinization of ultramafic rocks. Geochimica et Cosmochimica Acta 38, 1255–1286.

Winkler, H.G.F., 1976. Petrogenesis of Metamorphic Rocks. Springer-Verlag, Berlin, 334pp.

Zuffa, G.G., 1987. Unravelling hinterland and offshore palaeogeography from deep-water arenites. In: Leggett, J.K., Zuffa, G.G. (Eds.), Marine Clastic Sedimentology—Concept and Case Studies. Graham and Trotman, London, pp. 39–61.

Zuffa, G.G., Normark, W.R., Serra, F., Brunner, C.A., 2000. Turbidite megabeds in an oceanic rift valley recording Jökulhlaups of Late Pleistocene glacial lakes of the Western United States. Journal of Geology 108, 253–274.

This page intentionally left blank

Chapter 30

PROVENANCE OF FLYSCH SEDIMENTS AND THE PALAEOGENE-EARLY MIOCENE GEODYNAMIC EVOLUTION OF THE HELLENIDES: A CONTRIBUTION FROM HEAVY MINERAL INVESTIGATIONS

PETER FAUPL[a], ANDREAS PAVLOPOULOS[b] AND GEORGE MIGIROS[b]

[a]*Department of Geological Sciences, University of Vienna, Althanstrasse 14, A-1090 Vienna, Austria*
[b]*Department of Sciences, Laboratory of Mineralogy-Geology, Agricultural University of Athens, Iera Odos 75, GR-11855 Athens, Greece*

ABSTRACT

The Palaeogene-Early Miocene geodynamic evolution of the Hellenides is characterised by widespread flysch deposition. In the Pelagonian, Parnassos-Ghiona and Pindos Zones, flysch sedimentation commenced during the Maastrichtian-Palaeocene and lasted until the Eocene, but in the northern Pindos Zone it continued until the Oligocene, and in the Ionian and Gavrovo-Tripolitza Zones, flysch deposition lasted from the Late Eocene to the Early Miocene.

During the Maastrichtian-Palaeocene, two source terrains supplied the Pelagonian flysch basin. In the eastern parts the stable heavy mineral group (zircon, tourmaline, rutile and apatite) predominates, while in the western margin a tectonic wedge, generated by the subduction of the Pindos Ocean, shed garnet and glaucophane to western parts of the Pelagonian basin, and also to the Pindos and Parnassos flysch. The appearance of detrital glaucophane (which shows a chemical affinity to Cycladic blue amphiboles) in Palaeocene sediments reveals the exhumation of blueschist facies rocks which underwent metamorphism during the Late Cretaceous. The stratigraphically younger parts of the Pindos flysch (Middle Eocene to Late Oligocene) show a considerable increase in abundance of the stable minerals and ophiolite detritus.

In the Late Eocene, the internal flysch basins were tectonically incorporated into a nappe pile with the Pindos nappe in front. The resulting crustal loading led to the formation of a foreland basin and deposition of sediments in the Gavrovo-Tripolitza and the Ionian Zones. The reworking of Pindos flysch occurred during progradation of the nappe pile. Stable heavy minerals and ophiolite detritus, typical of the higher stratigraphic successions of the Pindos flysch, have been found in the eastern parts of the Gavrovo-Tripolitza Zone, exposed only in the Peloponnese, while

Developments in Sedimentology, Vol. 58, 765–788

ISSN: 0070-4571/doi:10.1016/S0070-4571(07)58030-1

the western parts in the Peloponnese, the mainland and the Ionian Zone are characterised by garnet-dominated assemblages accompanied by glaucophane, derived possibly from lower sections of the Pindos flysch. Heavy mineral assemblages of the meta-flysch in the tectonic windows of Olympos and Ossa are comparable with those from the eastern Gavrovo-Tripolitza Zone.

Keywords: Hellenides; Ionian; Gavrovo-Tripolitza; Pindos; Parnassos-Ghiona and Pelagonian zones; flysch sediments; provenance; detrital blue amphibole; ophiolitic detritus

1. INTRODUCTION

The collision of the Apulian and Eurasian continents (Stampfli et al., 1998) and the contemporaneous destruction of the Tethys Ocean governed the Tertiary orogenic evolution of the Hellenides (among others Mountrakis, 1986; Doutsos et al., 1993). In the evolving Hellenic synorogenic basin terrigenous deep-water clastics of Maastrichtian/Palaeocene to Miocene age became progressively the most important sedimentary facies, deposited as flysch in sub-basins in front of a rising orogenic wedge. The westwards progradation of the deformational front shifted the depocentre of synorogenic sedimentation more and more towards external zones. The terrigenous flysch sediments were derived mainly from the orogenic wedge, in the course of which reworking and redeposition of deep-water clastics seem to have played an important rôle.

Spatial and temporal investigations of the composition, facies development and distribution of the deep-water clastics hold the promise of important insights into the geodynamic evolution of the Tertiary stages of the Hellenic orogen (Richter, 1976a, b; Piper and Pe-Piper, 1980; Alexander et al., 1990; Pe-Piper and Koukouvelas, 1992; Richter, 1993; Richter et al., 1993; Gonzales-Bonorino, 1996; Neumann et al., 1996; Schneider et al., 1998; Avramidis et al., 2000; Ananiadis, 2003; Vakalas, 2003). In this respect, heavy minerals can provide valuable information on the petrological composition of the source terrain, which cannot be fully reconstructed by analysis of the major siliciclastic constituents, e.g., the existence of ophiolitic complexes or blueschist belts in the source terrains can be clearly proved by their diagnostic heavy minerals. Heavy mineral analysis has long been a common method for deciphering the provenance signals of siliciclastic sediments in orogenic belts (e.g., Woletz, 1967; Faupl and Wagreich, 1992; Winkler and Slaczka, 1994; von Eynatten and Gaupp, 1999). The purpose of the present contribution is to synthesize the results of heavy mineral studies conducted on the flysch successions of the different tectonic units of the Hellenides (Faupl et al., 1994, 1998, 1999a, b, 2002), and to incorporate them into a geodynamic model of the Hellenic orogen.

2. GEOLOGICAL SETTING

The Hellenic orogen comprises several tectono-stratigraphic isopic zones (Fig. 1): from west towards the east the Paxos, Ionian, Gavrovo-Tripolitza, Pindos and the

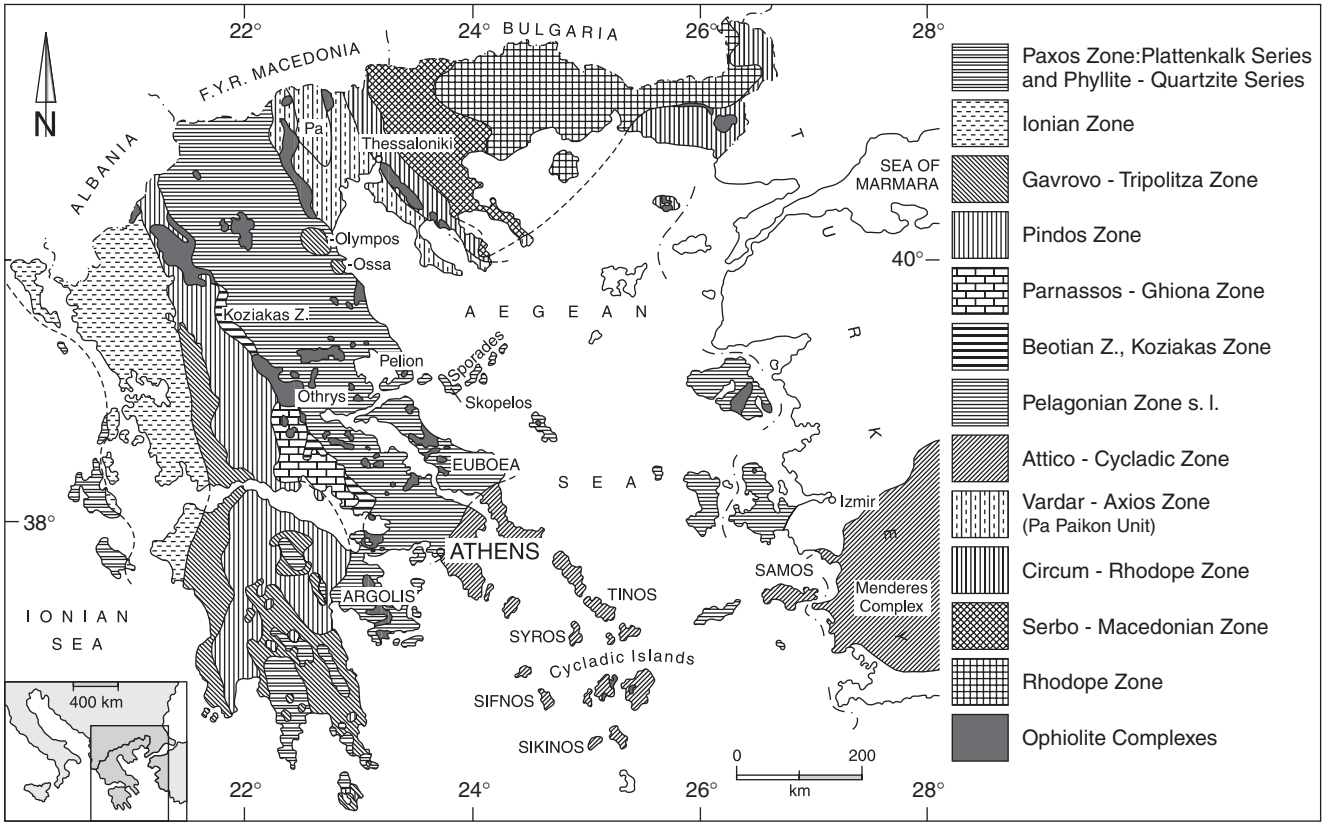

Fig. 1. Map of the geotectonic zones of Greece based on Jacobshagen (1986).

Parnassos-Ghiona Zones, which are considered as the "External Hellenides" (Brunn, 1956), whereas the Pelagonian, Vardar-Axios, Circum-Rhodope, Serbo-Macedonian and Rhodope Zones are referred to as the "Internal Hellenides" (Jacobshagen, 1986; Katsikatsos, 1992). The heavy mineral data presented in the present contribution come from locations ranging from the eastern parts of the Ionian Zone to the eastern parts of the Pelagonian Zone.

The palaeogeographic position of the tectono-stratigraphic isopic zone of the Hellenides within the Tethys realm is depicted in several Tethys reconstructions (among others Robertson et al., 1991; Katsikatsos, 1992; Stampfli et al., 2001; Golonka, 2004). The palaeotectonic situation during the Palaeogene flysch sedimentation is shown in two sketch maps at the end of the present contribution. The sedimentary successions of the Paxos, Ionian, Gavrovo-Tripolitza and Pindos tectono-stratigraphic isopic zones (Fig. 1) are situated palaeogeographically at the Apulian passive continental margin (Robertson et al., 1991). The Parnassos-Ghiona Zone has been thought to be an isolated continental fragment between the Apulian margin and the Pelagonian microcontinent, bordered towards the north and south by two transform faults (among others Skourlis and Doutsos, 2003). The Pelagonian Zone was an extended calcareous platform from middle Late Triassic until the Late Jurassic, after which—until the Early Cretaceous—it was affected by two orogenic episodes resulting in the obduction of ophiolites from the eastern and western oceanic realms. The Pindos and Vardar-Axios Zones represent these separate oceanic domains with long-lasting closure, which commenced in the Jurassic. Obducted oceanic fragments are clearly indicated by the detritus in the flysch sediments. Blueschist complexes are also well documented from the subduction zone of the Pindos Ocean and exhumed in an Aegean forearc setting (Ring and Layer, 2003). The Pindos Ocean separated Apulia and the Pelagonian microcontinent, whereas the Vardar Ocean formed an internal oceanic domain (Bernoulli and Laubscher, 1972; Smith et al., 1979; Jones and Robertson, 1991; Robertson et al., 1991; Robertson and Karamata, 1994).

3. THE OCCURRENCE OF FLYSCH SEDIMENTS IN THE HELLENIDES

The term "flysch" describes deep-water terrigenous clastic sediments deposited during the compressional stage of an orogen. The sediments originate mainly from "sediment gravity flows" among which low-density turbidity currents played an important rôle. The deposits can be described on the basis of turbidite facies models (e.g., Mutti and Ricci Lucchi, 1975; Pickering et al., 1989) as well as deep-sea fan models (e.g., Normark, 1978; Shanmugam and Moiola, 1988; Walker, 1992), which are helpful in interpreting the facies associations.

The stratigraphic range of some characteristic flysch successions of the Hellenides is depicted in Fig. 2. The actual onset of terrigenous flysch sedimentation is often predated by so-called "Transitional Beds" which comprise variegated pelitic rocks and calciturbidites interbedded with the precursors of terrigenous turbidites. In the Ionian and Gavrovo-Tripolitza Zones, flysch sedimentation commenced in the Late Eocene and passed into the Early Miocene, but the major bulk of deposition, of up to 3000 m thickness, occurred in the Oligocene. In the other tectono-stratigraphic zones, the

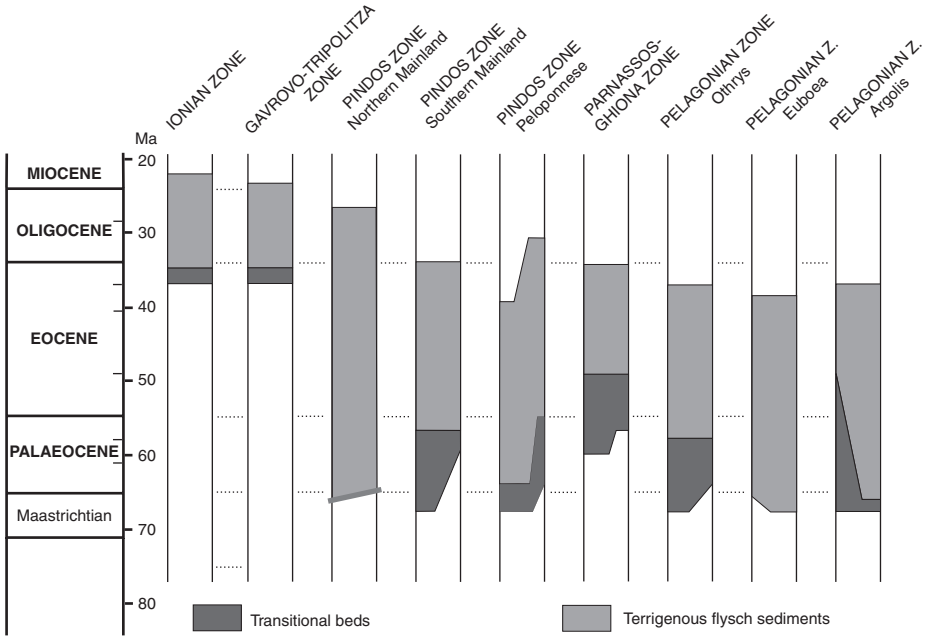

Fig. 2. Stratigraphic chart of the flysch formations in the Hellenides.

Pindos, Parnassos-Ghiona and Pelagonian Zones, flysch sedimentation started, in some parts, in the Late Maastrichtian and passed up into the Eocene. Only in the northern region of the Pindos Zone of the Greek mainland did flysch deposition continue until the Late Oligocene (Richter et al., 1993). Regionally, the base of Pindos flysch is diachronous (Fig. 2), being Maastrichtian in the northern mainland, Palaeocene in the northern Peloponnese (Degnan and Robertson, 1998) and Palaeocene/Eocene in the southern Peloponnese (Neumann et al., 1996). The Early/Middle Eocene onset of terrrigenous flysch sedimentation in the Parnassos-Ghiona Zone, which is underlain by transitional beds of red marls, started relatively late in comparison with flysch deposits of the Pindos and Pelagonian Zones (Richter et al., 1995). Flysch deposits of the Pelagonian Zone, overlying carbonate successions, sometimes with a hiatus, commenced in the Maastrichtian/Palaeocene (Richter et al., 1996). Most of the eastern occurrences of Pelagonian flysch successions are overprinted by anchimetamorphic to greenschist facies metamorphism (Katsikatsos et al., 1986).

Differences in the regional distribution of flysch deposits are clearly visible between the Greek mainland and the Peloponnese (Fig. 1). Whereas the Ionian flysch of the Peloponnese is restricted to the northwestern part of the peninsula, the same zone is very broadly developed farther north on the mainland (Kamberis et al., 2000). The Gavrovo-Tripolitza Zone is much more widely distributed in the Peloponnese than in the mainland. The correlation of the Late Eocene meta-flysch sediments of the Olympos and Ossa tectonic windows (Fig. 1), with other flysch sediments of the Hellenides is an important palaeogeographical problem and our heavy mineral analysis may contribute potentially useful data to its solution (palaeogeographic opinions of Papanikolaou, 1989; Robertson et al., 1991; Doutsos et al., 1993).

4. SAMPLING AND HEAVY MINERAL PREPARATION

Grain size typically decreases upwards in turbidite beds, reflecting waning flow, although exceptions to this trend have been found in massive bedded deep-water sandstones and other types of mass-flow deposits. Reverse grading, for example, has been attributed to rapid deposition by frictional "freezing" of a traction carpet, driven along by shear at the base of the flow (Pickering et al., 1989). Grain size trends and density influence the vertical distribution of heavy minerals within a bed as well as in the transport direction. A sampling protocol should take into consideration the depositional processes involved because heavy minerals, in general, are more enriched at the base of a turbidite sandstone bed than at the top. Species, which commonly appear as coarser grains, like garnet, staurolite and chrome spinel, are more enriched at the base of a bed than the finer grains, such as zircon or apatite. The content of the latter increases relatively towards the top compared with garnet and other coarse minerals. Thin-bedded turbidites (<10 cm) were usually sampled in order to minimise the effect of grain size-controlled selective enrichment or paucity of particular species. In thick-bedded turbidites, samples were taken from the base of the bed (Bouma-interval T_a). To compensate for this weakness in the sampling procedure, a broader range of specimens of different grain size and bed thickness has been taken in each outcrop. A correlation between the maximum grain size of a sample and its heavy mineral content in samples from the Gavrovo flysch of the Greek mainland demonstrates these grain size effects in linear regression lines for garnet, zircon and apatite (Fig. 3).

All analysed samples were subjected to the same laboratory procedure. Hand-sized specimens were crushed to fragments of about 5 mm diameter and subsequently decalcified with diluted acetic acid that avoids destruction of apatite and other less resistant heavy minerals. After wet sieving (retaining 0.4–0.063 mm), the heavy minerals were separated gravitationally using tetrabromoethane (density 2960 kg m^{-3}). The heavy minerals were mounted in Canada balsam and examined under a petrographic microscope (Mange and Maurer, 1991). In some cases of uncertain microscopic mineral identification, additional X-ray diffractometry was used. Blue amphiboles have been separated and analysed by electron microprobe. For calculating the grain

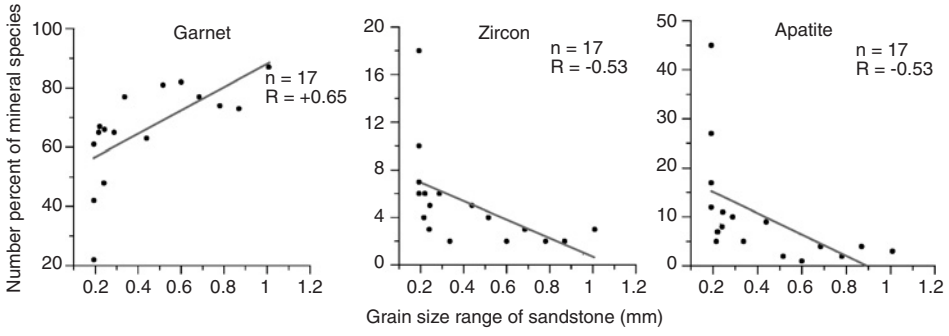

Fig. 3. Correlation diagrams for the Gavrovo-Tripolitza flysch showing the relation between the maximum grain size of sandstone samples and the percentages of garnet, zircon and apatite. R = coefficient of determination.

percentages, more than 200 transparent heavy mineral grains were counted in each sample. Biotite, chlorite and heavy minerals formed during diagenesis, were excluded.

5. HEAVY MINERAL DISTRIBUTION IN THE PALAEOGENE FLYSCH SUCCESSIONS OF THE HELLENIDES

The following heavy minerals have been observed as frequent constituents in the turbiditic sandstones of the Hellenic flysch successions: zircon, tourmaline, rutile, apatite, garnet and chrome spinel. Staurolite, chloritoid, members of the epidote-group, amphiboles and pyroxenes generally occur in minor amounts, sometimes only in traces (1 or 2 grains out of >200). However, a few samples were found to be enriched in epidote, amphiboles and pyroxene. Microscopic identification indicated the presence of green varieties of amphiboles and blue sodic amphiboles.

Average compositions of heavy mineral suites in the various tectonic units of the Hellenides are shown in Table 1. Ternary diagrams (Fig. 4) illustrate the general trends in heavy mineral compositions; the ultrastable group (zircon–tourmaline–rutile), the metamorphic group (garnet, staurolite, chloritoid, blue amphibole) and the ophiolite group (chrome spinel, pyroxene) define the three, provenance-controlled, genetic suites. Although apatite reaches higher abundance in several samples, it is not included in the ternary diagrams because its assignment to one of the groups is equivocal. Apatite occurs as an ubiquitous accessory in a variety of rock types, thus can be derived from granitic rocks, metamorphic complexes and pre-existing sediments. Epidote is generally a metamorphic mineral, but can occur in some mafic rock suites and ophiolite complexes, also as a secondary mineral in several other lithologies and it is also excluded from the plots. The combination of ternary diagrams and average heavy mineral contents aids the discussion below. More details on analytical data can be found in the publications by Faupl et al., cited above.

Diagenetic alterations of the primary heavy mineral assemblages have to be basically assumed, but the degree is hard to estimate in detail. It can be suggested that most of the low-abundance (and chemically unstable or moderately stable) minerals, such as staurolite, chloritoid, epidote, amphibole and pyroxene, suffered intrastratal dissolution to a higher extent than other heavy minerals.

5.1. Pelagonian Zone

An overview of the locations and associations of heavy minerals in the flysch successions of the Pelagonian Zone (stratigraphic range from Maastrichtian to Eocene) has been presented by Faupl et al. (1999a). The results of samples analysed from the Othrys Mountain, Euboea and Argolis locations (Peloponnese) are illustrated here (Fig. 4). Other occurrences (e.g., Pelion, Skopelos) are excluded because they show obvious metamorphic overprints that may have altered the primary heavy mineral assemblages.

Cluster analysis of heavy mineral data (Faupl et al., 1999a) revealed two major groups of heavy mineral associations in the Pelagonian Zone. (1) A garnet-rich group, accompanied by relatively few chrome spinels, is characteristic for the western Othrys (Fig. 4A) and the western Argolis (Fig. 4B). (2) Zircon–tourmaline–rutile and apatite predominate in the second group, where the garnet content is strongly

Table 1. Average heavy mineral composition of flysch sediments in the tectono-stratigraphic zones of the Hellenides

Zrn	Tur	Rt	Ap	Grt	St	Cld	Crspl	Ep	Am	bAm	Px	Oth
Ionian Zone												
Mainland ($n = 53$)												
4.2	2.4	3.1	8.1	60.7	0.4	0.2	14.2	3.9	0.7	0.1	1.3	0.8
Peloponnese ($n = 8$)												
5.7	1.7	4.4	7.2	57.1	0.2	0.2	23.1	0	0	0	0	0.3
Gavrovo Zone												
Mainland ($n = 26$)												
4.7	3.6	3.3	9.3	67.6	0.2	0.1	8	1.2	0	0	0.6	1.3
Peloponnese W ($n = 30$)												
5.8	2.8	4.7	11.1	69.2	0.6	0.3	4.9	0.1	0	0.2	0	0.4
Peloponnese E ($n = 23$)												
21.8	8.9	16.8	29.1	10.7	0.1	0	11.7	0.1	0.1	0	0	0.6
Pindos Zone												
Pre-Middle Eocene: Mainland ($n = 40$)												
5.9	5.7	4.8	15.1	53	0.2	0.2	10.2	3.1	0	0.1	0.5	1.2
Middle Eocene-Oligocene: Mainland ($n = 34$)												
3.9	5.4	6.1	22.7	13.2	0	0.1	16.5	20.8	0.3	0	9.6	1.6
Peloponnese ($n = 29$)												
5.6	4.7	5.4	12.8	55.6	0.6	0.3	6.4	6.3	0.4	0.4	0.4	1.1
Parnassos-Ghiona Zone												
Southeastern region ($n = 6$)												
11.9	9.7	18	9.8	29.9	0.1	0.3	19.7	0	0	0	0.2	0.4
Middle region ($n = 10$)												
6.5	7	9.1	11.6	57.4	0	0.1	2.8	4.2	0.1	0	0.1	0.9
Northwestern region ($n = 5$)												
4.4	0.3	1.6	3.8	51.6	0	0	1.3	34.7	0	0	2.2	0.1
Pelagonian Zone												
Koziakas Unit ($n = 4$)												
2.5	0.1	1	2	12.3	0	0	63.5	16	0.8	0	0.6	1.3
Othrys W ($n = 19$)												
3.4	2.6	2.8	5.3	80.8	1.1	0.4	2	0.2	0	1.2	0	0.1
Othrys NE and E ($n = 19$)												
21.4	12	10.2	37.4	4.7	0	0.2	12.9	0.1	0.2	0	0	0.9
Euboea ($n = 8$)												
24.7	9.1	15.3	44.5	1.1	0	0.1	4.6	0.2	0	0	0.1	0.2
Argolis W: Lighourion ($n = 10$)												
9.1	3.6	5.6	16.7	63.4	0	0.1	1.3	0.1	0.1	0	0	0.2
Argolis E: Methana, Adheres ($n = 16$)												
10.3	16	9.7	46.7	10.5	0	0.2	3.2	0	0	0	0	3.5
Ossa Window ($n = 16$)												
33.6	4.1	4.5	48.1	5.4	0.4	0	0	3.4	0	0	0	0.6
Olympos Window ($n = 6$)												
24.6	2.9	3.1	32.7	3.8	0.3	0	0.2	3.5	28.4	0	0	0.6
Almopias Zone ($n = 16$)												
9.7	13.9	9.7	60.8	2.9	0	0.1	1.1	0.2	0	0	0	1.7

Abbreviations: Zrn, zircon; Tur, tourmaline; Rt, rutile; Ap, apatite; Grt, garnet; St, staurolite; Cld, chloritoid; Crspl, chrome spinel; Ep, epidote group; Am, amphibole, mainly green; bAm, blue amphibole; Px, pyroxene; Oth, other heavy minerals.

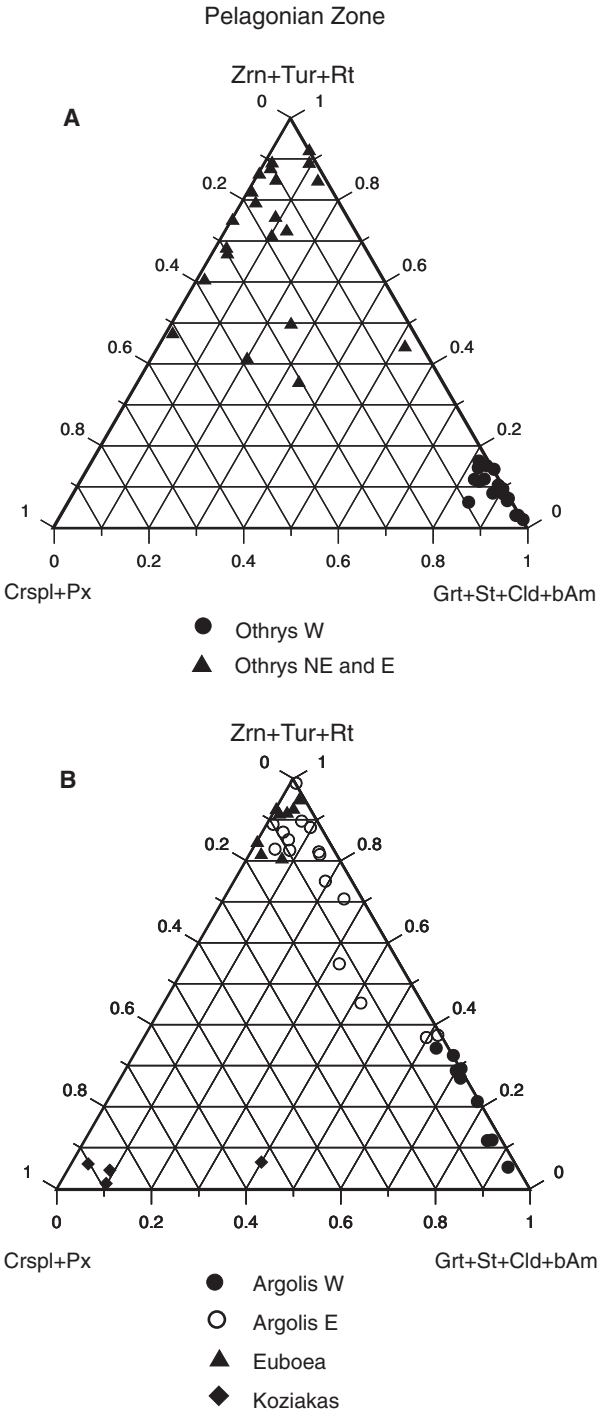

Fig. 4. Heavy mineral distributions in the Palaeogene flysch of the Pelagonian Zone. For abbreviations see Table 1.

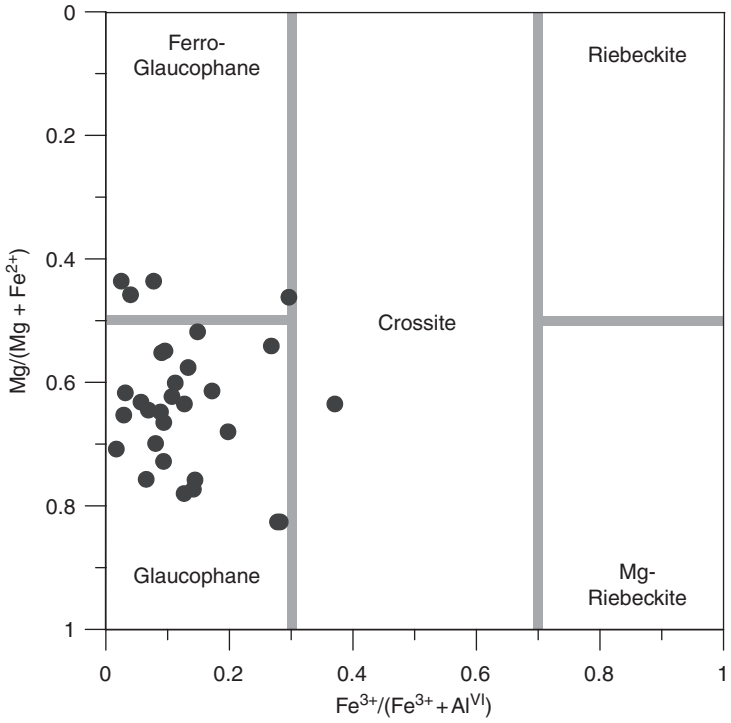

Fig. 5. Chemical analyses of detrital blue amphiboles ($n = 30$) found in the Palaeocene flysch of the western Othrys (Pelagonian Zone). Classification after Leake (1978).

reduced. This second group marks the flysch deposits of the northeastern and eastern Othrys (Fig. 4A) as well as the successions of eastern Argolis and of Euboea (Fig. 4B). Elevated amounts of chrome spinel are restricted to the eastern Othrys but very little is recorded from the Pelagonian flysch from other localities, such as Pelion and Skopelos. The frequent occurrence of minor amounts of detrital blue sodic amphibole in the flysch sediments of the western Othrys are of special interest, because microprobe analyses from single grains indicate a typical glaucophane composition (Fig. 5), indicative of provenance from high pressure-low temperature (HP-LT) metamorphic rocks, originated in subduction zones (Petrakakis et al., 2001; Faupl et al., 2002).

The Palaeogene flysch sediments of the Koziakas unit and the Beotian Zone, situated towards the west of the Pelagonian Zone, differ considerably from all the other Pelagonian locations (Fig. 4B) by their extremely high chrome spinel content which is also typical of the Lower Cretaceous here. Detrital blue amphiboles have not been found in these two zones.

5.2. *Parnassos-Ghiona Zone*

The Parnassos-Ghiona Zone is restricted to the southern part of the Greek mainland and to northernmost parts of the Peloponnese. This zone represents a Triassic to

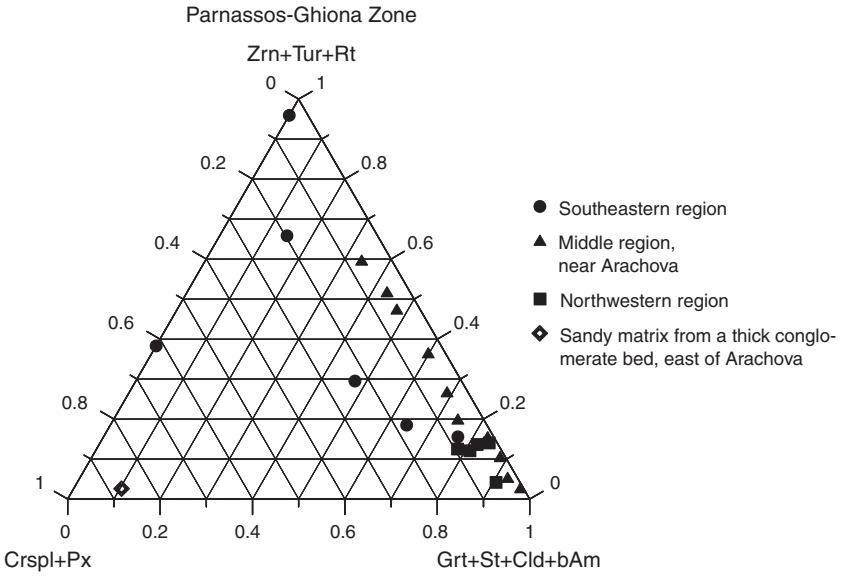

Fig. 6. Heavy mineral distributions in the Palaeogene flysch of the Parnassos-Ghiona Zone. For abbreviations see Table 1.

Cretaceous carbonate platform with several bauxite horizons. In the Maastrichtian, the shallow-water carbonates passed into deep-water limestones, which were then covered by red marls of Palaeocene age, partially with a hiatus. Terrigenous flysch sedimentation started in the Early/Middle Eocene.

The heavy mineral composition varies relatively strongly from east towards the west (Fig. 6). Predominance of the metamorphic group is limited to northwestern regions. These assemblages are also characterised by high amounts of epidote. More to the southeast, ultrastable minerals as well as ophiolitic detritus become more abundant. An exceptional heavy mineral suite has been observed in the sandy matrix of thick deep-water conglomerates exposed along the road near Arachova, comprising extremely high amounts of chrome spinel, and is comparable with those of the Koziakas unit. Schneider et al. (1998) have described traces of blue amphibole in the Parnassos-Ghiona flysch.

5.3. *Pindos Zone*

A succession of Triassic to Cretaceous deep-water pelagic carbonate rocks and radiolarites is indicative for the Pindos Zone, which was deposited on the outer (western) marginal part of the Pindos Ocean domain (among others Robertson et al., 1991). Terrigenous flysch sedimentation started in the Maastrichtian-Palaeocene, lasting until the Late Eocene. In the area to the north of the Kastaniotikos transverse line, an east–west trending structural element in the northern Greek mainland (see Skourlis and Doutsos, 2003), flysch sedimentation continues to the Late

Oligocene (Richter et al., 1993), but in the Peloponnese, only Palaeocene and Eocene flysch formations are recorded.

The heavy minerals of the flysch succession older than Middle Eocene have a relatively uniform distribution (Figs. 7A, B). The predominance of the garnet-rich metamorphic group, sometimes accompanied by frequent blue amphiboles, is characteristic for these formations, whereas chrome spinel plays a subordinate rôle. In a few cases, a higher content of the stable suite has been observed. In samples from the mainland of Middle Eocene to Late Oligocene age, a conspicuous change in the heavy mineral assemblages occurs due to the reduction of metamorphic species and increasing amounts of ophiolitic and stable minerals. In the central parts of the Pindos Zone of the Greek mainland, this change is seen in the elevated epidote and pyroxene abundance rather than in increased chrome spinel content. In the northernmost Pindos Zone (region of Konitsa-Eptachori) chrome spinel is accompanied by pyroxene. Assemblages characterised by stable and ophiolite minerals have not been observed in the Pindos succession of the Peloponnese (Fig. 7B).

5.4. Ionian and Gavrovo-Tripolitza Zones

From Jurassic times until the Palaeogene, the Ionian Zone represented a basinal development, whereas the Gavrovo-Tripolitza Zone, situated to the east of the Ionian Zone, formed a shallow-water carbonate platform. The terrigenous flysch stage commenced in both zones in the Late Eocene. This late onset, in contrast to the palaeogeographically internal zones, such as Pindos, Parnassos-Ghiona and Pelagonian Zones, is seen as the result of the shift of the orogenic front towards the external units. In both zones, garnet-dominated assemblages are most frequent, whereas in particular samples from the Ionian Zone of the mainland, in contrast with the Gavrovo-Tripolitza Zone, an influx of ophiolite minerals can be observed (Figs. 8A, B). Associations enriched in ophiolite-derived minerals are characteristic of sandstones of the stratigraphically higher parts of the Ionian section. The eastern locations of the Gavrovo-Tripolitza Zone of the Peloponnese are typified by elevated amounts of ultrastable heavy minerals from mature sandstones, and differ from the western occurrences, which contain dominantly metamorphics-derived species (Fig. 8B). Such ultrastable mineral assemblages are unknown from the Gavrovo-Tripolitza Zone of the mainland.

5.5. Comparison of Hellenic Flysch Successions Based on Heavy Mineral Assemblages

In order to facilitate comparisons of the flysch successions from different tectonic units, only the averages of heavy mineral compositions have been included in Table 1. The ternary plots in Figs. 9A, B and 10 clearly show a common predominance of the metamorphic mineral group, with garnet as the dominant phase, within the flysch sediments of the Ionian and Gavrovo-Tripolitza Zones (Fig. 10), in Pindos, Parnassos-Ghiona Zones and in the western locations of the Pelagonian Zone such as in western Othrys (Fig. 9B). Associations rich in ultrastable heavy minerals are characteristic of flysch successions of the eastern Pelagonian Zone (Fig. 9b), as well as of Pelagonian flysch successions with low-grade metamorphic overprint such as in Pelion and Skopelos. Such an ultrastable heavy mineral

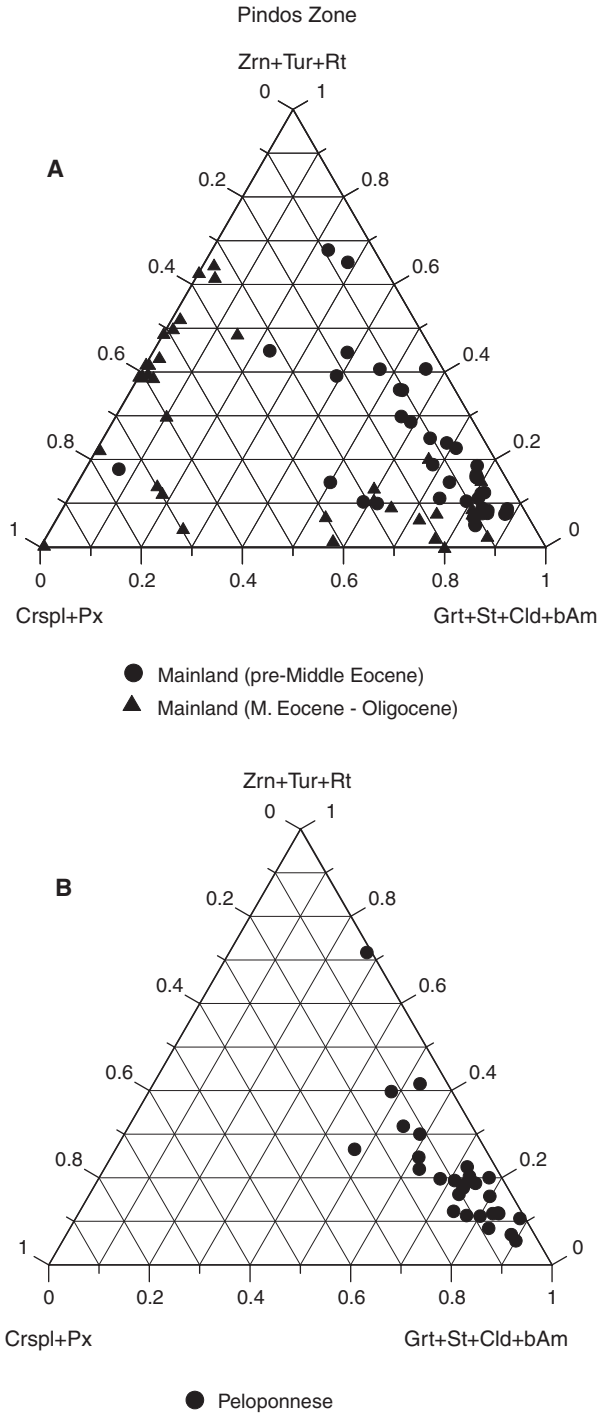

Fig. 7. Heavy mineral distributions in the Palaeogene flysch of Pindos Zone. For abbreviations see Table 1.

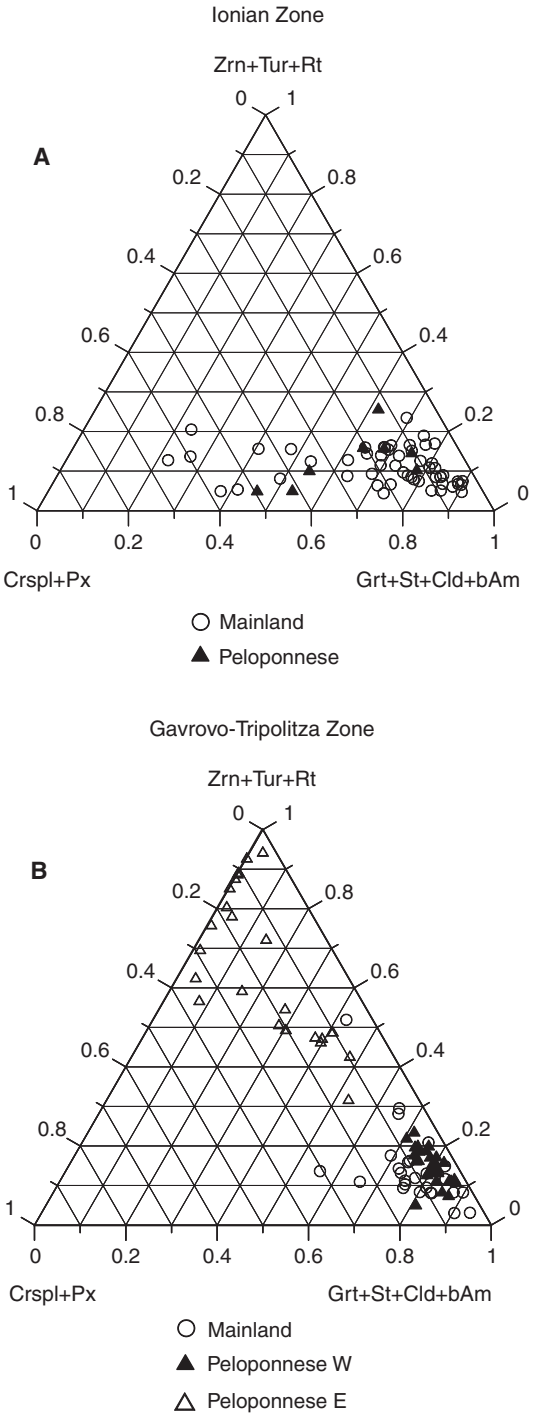

Fig. 8. Heavy mineral distributions in the Palaeogene flysch of the Ionian and Gavrovo-Tripolitza Zones. For abbreviations see Table 1.

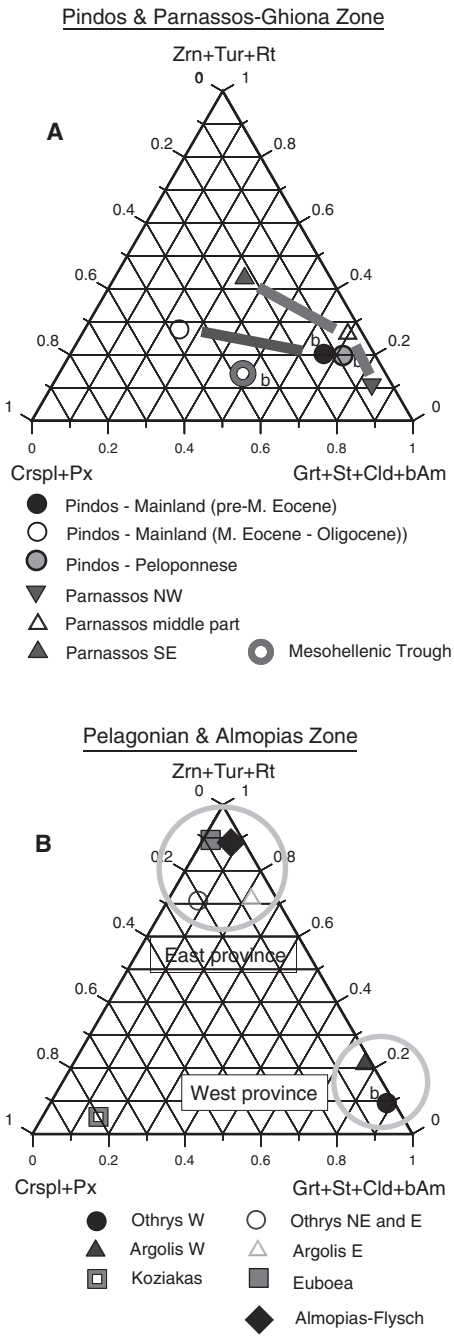

Fig. 9. Ternary plots showing mean heavy mineral compositions in the Palaeogene flysch successions of the Pindos, Parnassos-Ghiona, Pelagonian and Almopias Zones. For abbreviations see Table 1.

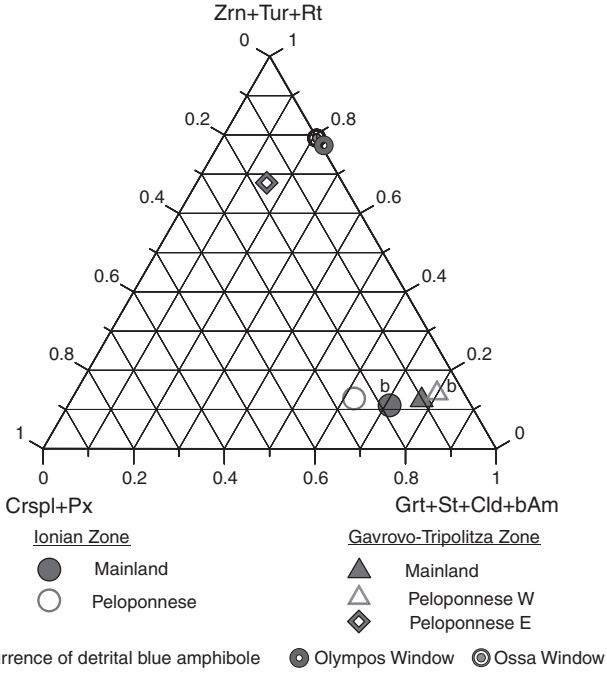

Fig. 10. Ternary plot showing mean heavy mineral composition in the Palaeogene Flysch successions of the Ionian and Gavrovo-Tripolitza Zones. For abbreviations see Table 1.

assemblage is also typical in the eastern flysch occurrences of the Gavrovo-Tripolitza Zone of the Peloponnese (Fig. 10), but this association, with only very few exceptions, has not been observed in the Ionian, Pindos and Parnassos-Ghiona Zones.

A massive predominance of ophiolite detritus, as observed in the whole Koziakas unit, has been occasionally found in the stratigraphically upper formations of the Pindos Zone of the Greek mainland and in sandy matrix of conglomerates from the Parnassos flysch (Figs. 6, 7A and 9B). However, the ophiolite-rich composition of these Pindos samples is relatively non-uniform (Fig. 7A), so that their average values plotted in Fig. 9A are less well constrained.

6. PROVENANCE OF FLYSCH SEDIMENTS AND THE GEODYNAMIC EVOLUTION OF THE HELLENIDES

Increasing compressional deformation of the Hellenides during the Late Cretaceous and the Palaeogene found its expression in the onset of terrigenous flysch sedimentation within the internal parts of the orogen. In time, the deformational belt shifted more and more towards palaeogeographically external zones forming foreland basins by crustal loading, which acted as domains for syndepositional deep-water sedimentation. The shift of the deformation front in the Hellenides was generated by a retreating plate boundary, driven by a slab roll-back mechanism (Thomson et al., 1998). More intensely affected parts of the deformational belt rose

rapidly as a cordillera with high erosional potential, situated in a forearc setting (Ring and Layer, 2003). Heavy minerals eroded from this hinterland reveal the lithological composition and tectonic changes within the source terrain.

The Pelagonian Zone already suffered an intense compressional deformation and experienced high-pressure metamorphism during the Cretaceous (Mountrakis, 1986; Schermer et al., 1990; Doutsos et al., 1993) which led, at the end of the Cretaceous, to the development of two cordilleras along both margins of the Pelagonian basin, with both contributing terrigenous material to the Pelagonian flysch deposited in an intra-wedge basin (Figs. 9B and 11) (Faupl et al., 1999a). During this time, the Pelagonian Zone as a whole, including the cordilleras, became part of an orogenic wedge in a forearc setting. The formation of the orogenic wedge was directly related to the subduction of the Pindos Ocean and the beginning of the collision with the Apulian continent. Heavy mineral signatures indicate that the internal source (eastern province, Fig. 9B) seems to be predominantly built up by granitoid rocks and to a minor extent by garnet-bearing metamorphic rocks and ophiolitic bodies. The term "granitoid" used here includes granitic rocks as well as gneiss and migmatite complexes. It is assumed that this cordillera rose during the Cretaceous development of an Eohellenic nappe complex parallel with the closure of the Vardar Ocean, and supplied the flysch deposits of northeastern and eastern Othrys, Euboea, Skopelos and eastern Argolis. The same source terrain is also believed to have supplied the Palaeogene meta-flysch sediments of the Almopias Zone, a subunit of the Vardar-Axios Zone, as indicated by their comparable heavy mineral associations (Fig. 9B). The flysch basin of the Almopias Zone is interpreted as a slope basin within the Eohellenic tectonic wedge.

The garnet-rich heavy mineral associations of the western locations of the Pelagonian flysch (western province, Fig. 9B), such as western Othrys and western Argolis, point to a source area of medium- to high-grade, garnet-bearing crystalline complexes, whereas granitoid rocks play only a subordinate rôle. Detrital glaucophane accompanying the garnet-rich associations indicate the occurrence of high-pressure metamorphic rocks in the source terrain. The mica schist-dominated lithology of the source as well as the chemical affinity of the blue amphiboles to Cycladic glaucophane (Petrakakis et al., 2001) strongly resemble the tectonic successions of the Cycladic Blueschist unit of the Aegean realm (Ring and Layer, 2003), which contain garnet-mica schists and are intruded by Carboniferous granitoids in the basement nappe. Comparison between the geochemistry of the detrital glaucophanes and those from the blueschist rocks of the Cycladic islands demonstrates that the detrital sodic amphiboles and those from the Cycladic realm were formed under similar high-pressure metamorphic conditions and generated from the same type of protolith. The Cycladic high-pressure event has been dated to range from Late Cretaceous to Eocene (78–50 Ma, Ring et al., 2001). This indicates that subduction along the western Pelagonian margin, as well as high-pressure metamorphism and ensuing exhumation of the blueschist complexes occurred over a long time span beginning in the Late Cretaceous (Schermer, 1993).

The relatively low amounts of chrome spinel in the garnet-rich flysch (western province, Fig. 9B) suggest that the ophiolite bodies, obducted from neighbouring oceanic domains onto the Pelagonian Zone during the Jurassic and Cretaceous, seem to be still largely covered by sediments during Palaeogene times. However, the low

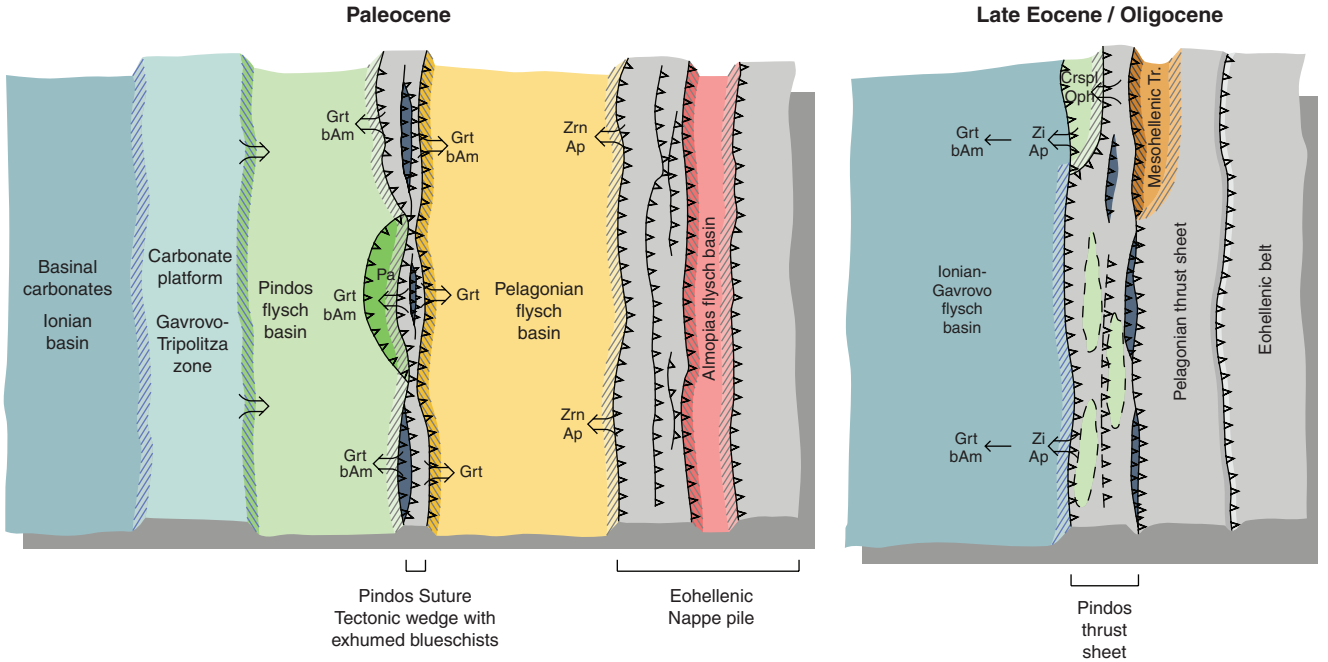

Fig. 11. Simplified palaeogeographic sketch map of the Hellenic flysch basins (not to scale). Pa = Parnassos-Ghiona Zone; Oph = ophiolitic detritus. Light grey = cordilleras composed of crystalline basement, ophiolite bodies and sedimentary rocks; dark blue = exposed high-pressure complexes within the cordilleras; other coloured areas = sedimentary realms. For heavy mineral abbreviations see Table 1.

amount of chrome spinel may indicate derivation from an ophiolitic tectonic slice, which is assumed to be a tectonic equivalent to the Selçuk mélange known from the upper part of the Cycladic Blueschist unit (Ring et al., 1999).

The external source that supplied the western parts of the Pelagonian flysch, also contributed similar, garnet-dominated, heavy mineral associations into the Pindos flysch basin during the Maastrichtian/Palaeocene to the Early Eocene (Fig. 11). The Pindos flysch basin represents a foreland basin in front of the orogenic wedge. Similarly to the western Pelagonian Zone, the heavy mineral associations of the Pindos flysch (Fig. 9A) can be predominantly derived from mica schist-bearing metamorphics and subordinate blueschist and ophiolite complexes. However, during the Middle Eocene prograding tectonic compression further lithologies, especially ophiolite complexes, were tectonically exhumed and contributed to the terrigenous detritus. Therefore, in the younger flysch deposits of the Pindos Zone, the input from ophiolite complexes increased significantly, as deduced from rising amounts of chrome spinel, pyroxene and epidote. A similar development has also been observed in the heavy mineral assemblages of the Eocene flysch sediments of the Parnassos-Ghiona Zone, which commenced in the later Early Eocene. The general increase in ophiolitic components in both zones coincides with the formation of an "ophiolite nappe" (i.e., the "Pindos Ophiolites": Kemp and McCaig, 1984; Jones and Robertson, 1991) and related tectonic units, such as the Koziakas or Beotian unit, which finally covered the Pindos and Parnassos flysch during the Miocene compressional stage. The massive occurrence of ophiolite-derived heavy minerals, known from the Koziakas unit, situated palaeogeographically at the western margin of the Pelagonian Zone (Fig. 9B), could indicate the onset of tectonic activity and ophiolite emplacement, which later formed the extended "ophiolite nappe" of the Pindos Zone. The high amounts of epidote minerals of the Pindos Zone could be derived, among other sources, from greenschist facies rocks in the Loumnitsa unit of the "Pindos Ophiolites", representing a metamorphic sole sequence.

During the Late Eocene, most of the internally sited flysch basins had already been incorporated into a "nappe stack" with the Pindos thrust sheet situated in a frontal position (Fig. 11). Only in the northernmost part of the Pindos flysch basin did sedimentation last until the Late Oligocene (Richter et al., 1993). At the same time an intramontane basin developed within this nappe stack, named Mesohellenic Trough, which represents a piggy-back basin (Ferrière et al., 2004) (Fig. 11). In front of the Eocene nappe stack, a new foreland basin developed due to crustal loading, in which the flysch sediments of the Gavrovo-Tripolitza and the Ionian Zone were deposited. The development of the nappe stack has been indicated by the remarkable change in the heavy mineral assemblages observed in the Pindos Zone during the middle Eocene (Figs. 7 and 9A).

The sedimentary material of the flysch succession of the Gavrovo-Tripolitza and Ionian Zones, deposited in the common Ionian-Gavrovo Flysch basin, was derived to a great extent from erosion of the newly formed nappe complex in the east (Fig. 11). Reworking of the Pindos flysch seems to have been an important process. In general, garnet-rich heavy mineral associations, which are characteristic over large areas of the Pindos flysch, are also typical for the flysch of the Gavrovo-Tripolitza and Ionian Zones (Figs. 8 and 10). Even detrital blue amphiboles, known from the Pindos flysch, are present in trace amounts in the new foreland basin. The obvious

difference seen between the eastern and western locations of the Gavrovo-Tripolitza flysch in the Peloponnese can be largely explained by reworking of Pindos flysch. Firstly, the stratigraphically younger parts of the Pindos flysch, containing more stable heavy mineral components and ophiolitic detritus, were eroded and redeposited in the eastern parts of the axial trough of the Gavrovo-Tripolitza Zone. During continuous progradation of the orogenic front, the trough axis shifted to the more external (western) parts of the Gavrovo-Tripolitza Zone, while at the same time garnet-dominated assemblages from the by then exhumed, stratigraphically lower parts of the Pindos flysch were eroded and redeposited.

The Late Eocene meta-flysch of the tectonic windows of Ossa and Olympos can be correlated with the Gavrovo-Tripolitza Zone, especially from the eastern Peloponnese using stratigraphic criteria besides their correlatable heavy mineral associations (Fig. 10) (Fleury and Godfriaux, 1975; Jacobshagen, 1986; Papanikolaou, 1989; Faupl et al., 2002). The final overthrusting of the internal nappes during the Miocene terminated flysch sedimentation in the Gavrovo-Tripolitza and Ionian foreland basin.

The stratigraphic successions of the Mesohellenic Trough range from Upper Eocene to Middle Miocene. Heavy mineral investigation by Zygojannis and Sidiropoulos (1981) and our own data indicate that the clastic fill of the trough was mainly sourced from metamorphic and ophiolitic complexes (Fig. 9A). This is consistent with the previously presented palaeogeographic reconstruction model, showing that parts of the Pindos wedge and the Pelagonian thrust complexes were emergent and provided clastic material into the Mesohellenic Trough.

7. SUMMARY AND CONCLUSIONS

Our study of heavy mineral assemblages of the flysch successions in mainland Greece and in the Peloponnese constrains the sources of their clastic components and indicates that provenance is largely controlled by the orogenic evolution of the Hellenides. The Palaeocene flysch of the Pelagonian Zone is derived dominantly from metamorphic and granitoid basement rocks. Ophiolitic detritus is less abundant there, except in the Koziakas flysch in the western Pelagonian margin, whereas blue amphiboles have only been found in W. Othrys. Thus, the lithology of the hinterland to the Pelagonian flysch can be reconstructed as being made up of basement rocks and locally exhumed HP-LT and ophiolite complexes.

Palaeocene flysch of the Pindos Zone in the Peloponnese contains heavy minerals dominantly of metamorphic origin, while in the mainland ophiolitic material is also frequent. Blue amphiboles are found in traces both in the Peloponnese and in the lower successions of the mainland. The overall provenance of the Pindos flysch is thus from metamorphic basement, exhumed ophiolitic bodies and rare outcrops of blueschists. Heavy minerals of the Eocene flysch of the Parnassos-Ghiona Zone indicate mainly metamorphic to granitoid derivation with fluctuating participation of ophiolitic material.

The Oligocene-Early Miocene flysch of the Gavrovo-Tripolitza Zone, deposited in the newly developed foreland basin, is divided into eastern and western parts. The eastern area, exposed only in the Peloponnese, contains heavy minerals mostly from granitoids with subordinate ophiolitic material. The meta-flysch exposed in

the Olympos and Ossa windows shows affinities to this eastern flysch succession. The western part of the Gavrovo-Tripolitza flysch is characterised by metamorphics-derived heavy minerals. Blue amphiboles were found only in the western Peloponnese. We conclude that considerable amounts of the clastic components of the Gavrovo-Tripolitza flysch were recycled from the Pindos flysch. The Ionian flysch of Oligocene to Early Miocene age shows similar characteristics to that of the Gavrovo-Tripolitza Zone, but the influence of ophiolite bodies becomes more important towards higher stratigraphic levels.

To summarise, the Mesohellenic Trough, developed between the Late Eocene to Middle Miocene, includes heavy mineral associations ultimately of metamorphic and ophiolitic origin, as well as traces of HP-LT index blue amphiboles. The terrigenous input is considered to be a mixture of Pelagonian and Pindos origin, whereas the ophiolite and high-pressure index assemblages indicate derivation from the east (Zygojannis and Sidiropoulos, 1981).

ACKNOWLEDGEMENTS

The authors express their thanks to the authorities of the University of Vienna and the Agricultural University of Athens as well as to the Hochschuljubiläumsstiftung der Stadt Wien (H24/2001) for financial support. For assistance in preparing some figures we have to thank Norbert Irnberger. The constructive reviews of E.M. Moores and G. Pe-Piper as well as the careful editorial work of M.A. Mange and D.T. Wright, greatly improved the manuscript.

REFERENCES

Alexander, J., Nichols, G.J., Leigh, S., 1990. The origins of marine conglomerates in the Pindus foreland basin, Greece. Sedimentary Geology 66, 243–254.

Ananiadis, E.G., 2003. Systematic analysis of submarine fans in the geotectonic zone of Pindos. Ph.D. thesis. University of Patras, 382pp. (in Greek).

Avramidis, P., Zelilidis, A., Kontopoulos, N., 2000. Thrust dissection control of deep-water clast dispersal patterns in the Klematia-Paramythia foreland basin, western Greece. Geological Magazine 137, 667–685.

Bernoulli, D., Laubscher, H., 1972. The palinspastic problem of the Hellenides. Eclogae Geologicae Helvetiae 65, 107–118.

Brunn, J.H., 1956. Contribution à l' étude géologique du Pinde septentrional et d' une partie de la Macédoine occidentale. Annales géologiques des pays helléniques 7, 1–358.

Degnan, P.J., Robertson, A.H.F., 1998. Mesozoic-early Tertiary passive margin evolution of the Pindos ocean (NW Peloponnese, Greece). Sedimentary Geology 117, 33–70.

Doutsos, T., Pe-Piper, G., Boronkay, K., Koukouvelas, I., 1993. Kinematics of the Central Hellenides. Tectonics 12, 936–953.

Faupl, P., Pavlopoulos, A., Migiros, G., 1998. On the provenance of flysch deposits in the external Hellenides of mainland Greece: results from heavy mineral studies. Geological Magazine 135, 421–442.

Faupl, P., Pavlopoulos, A., Migiros, G., 1999a. The Paleogene history of the Pelagonian Zone s.l. (Hellenides, Greece): heavy mineral study from terrigenous flysch sediments. Geologica Carpathica 50, 449–458.

Faupl, P., Pavlopoulos, A., Migiros, G., 1999b. On the origin of terrigenous flysch meta-sediments exposed in the Olympos-Ossa tectonic window (Central Greece): implications from heavy mineral investigations. Mitteilungen der Österreichischen Geologischen Gesellschaft 90, 57–65.

Faupl, P., Pavlopoulos, A., Migiros, G., 2002. Provenance of Peloponnese (Greece) flysch based on heavy minerals. Geological Magazine 135 (5), 513–524.

Faupl, P., Pavlopoulos, A., Wagreich, M., Migiros, G., 1994. Heavy mineral studies on certain turbiditic sequences in the Greek mainland: preliminary results. Bulletin of the Geological Society of Greece 30, 45–56.

Faupl, P., Wagreich, M., 1992. Cretaceous flysch and pelagic sequences of the Eastern Alps: correlation, heavy minerals, and palaeogeographic implications. Cretaceous Research 13, 387–403.

Ferrière, J., Reynaud, J.-Y., Pavlopoulos, A., Bonneau, M., Migiros, G., Chanier, F., Proust, J.-N., Gardin, S., 2004. Geologic evolution and geodynamic controls of the Tertiary intramontane piggyback Meso-Hellenic basin, Greece. Bulletin de la Société géologique de France 175, 361–381.

Fleury, J., Godfriaux, I., 1975. Arguments pour l'attribution de la série de la fenêtre de l'Olympe (Grèce) à la zone de Gavrovo-Tripolitza présence des fossiles du Maastrichtien et de l'Eocène inférieur (et moyen?). Annales de la Société géologique du Nord 94, 149–156.

Golonka, J., 2004. Plate tectonic evolution of the southern margin of Eurasia in the Mesozoic and Cenozoic. Tectonophysics 381, 235–273.

Gonzales-Bonorino, G., 1996. Foreland sedimentation and plate interaction during closure of the Tethys Ocean (Tertiary; Hellenides; western continental Greece). Journal of Sedimentary Research 66, 1148–1155.

Jacobshagen, V., 1986. Geologie von Griechenland. Gebr. Borntraeger, Berlin, 363pp.

Jones, G., Robertson, A.H.F., 1991. Tectono-stratigraphy and evolution of the Mesozoic Pindos ophiolite and related units, northwestern Greece. Journal of the Geological Society London 148, 267–288.

Kamberis, E., Sotiropoulos, S., Aximniotou, O., Tsaila-Monopoli, S., Ioakim, C., 2000. Late Cenozoic deformation of the Gavrovo and Ionian zones in NW Peloponnesos (Western Greece). Annali di Geofisica 43, 905–919.

Katsikatsos, G.X., 1992. Geology of Greece. Athens (Katsikatsos), 451pp. (in Greek).

Katsikatsos, G., Migiros, G., Triantaphylis, M., Mettos, A., 1986. Geological structure of Internal Hellenides (E. Thessaly–SW Macedonia–Euboe–Attica–Northern Cyclades Islands and Lesvos). Geological and Geophysical Research, Special Issue, Institute of Geological and Mining Exploration, Athens, pp. 191–212.

Kemp, A.E.S., McCaig, A., 1984. Origins and significance of rocks in an imbricate thrust zone beneath the Pindos ophiolite, northwestern Greece. In: Dixon, J.E., Robertson, A.H.F. (Eds.), The Geological Evolution of the Eastern Mediterranean, Geological Society of London Special Publication Book-Series, vol. 17, pp. 569–580.

Leake, B.E., 1978. Nomenclature of amphiboles. The Canadian Mineralogist 16, 501–520.

Mange, M.A., Maurer, H.F.W., 1991. Schwerminerale in Farbe. Ferdinand Enke Verlag, Stuttgart, Publication Book-Series, 148pp.

Mountrakis, D., 1986. The Pelagonian zone in Greece: a polyphase-deformed fragment of the Cimmerian continent and its role in the geotectonic evolution of the Eastern Mediterranean. Journal of Geology 94, 335–347.

Mutti, E., Ricci-Lucchi, F., 1975. Turbidite facies and facies associations. 9th International Congress of Sedimentology, Nice, Field trip A11, 21–36.

Neumann, P., Risch, H., Zacher, W., Fytrolakis, N., 1996. Die stratigraphische und sedimentologische Entwicklung der Olonos-Pindos-Serie zwischen Koroni und Finikounda (SW-Messenien, Griechenland). Neues Jahrbuch für Geologie und Paläontologie Abhandlungen 200, 405–424.

Normark, W.R., 1978. Fan valley, channels and depositional lobes on modern submarine fans: characters for recognition of sandy turbiditic environments. American Association of Petroleum Geologists Bulletin 62, 912–931.

Papanikolaou, D.J., 1989. Are the Medial Crystalline Massifs of the Eastern Mediterranean drifted Gondwanian fragments? Geological Society of Greece Special Publication, vol. 1, pp. 63–90.

Pe-Piper, G., Koukouvelas, I., 1992. Petrology, geochemistry and regional geological significance of igneous clasts in Parnassos flysch, Amphissa area, Greece. Neues Jahrbuch für Mineralogie Abhandlungen 164, 94–112.

Petrakakis, K., Faupl, P., Migiros, G., Pavlopoulos, A., 2001. Pre-Tertiary blueschist facies metamorphism in the Hellenides evidenced by detrital blue amphiboles in the Palaeocene flysch of the Othrys Mountain. Bulletin of the Geological Society of Greece 34, 97–102.

Pickering, K.T., Hiscott, R.N., Hein, F.J., 1989. Deep Marine Environments—Clastic Sedimentation and Tectonics. Unwin Hyman, London, 416pp.

Piper, D.J.W., Pe-Piper, G., 1980. Was there a western (external) source of terrigenous sediment for the Pindos zone of the Peloponnese (Greece)? Neues Jahrbuch für Geologie und Paläontologie Monatshefte 1980, 107–115.

Richter, D., 1976a. Das Flysch-Stadium der Hellendiden—ein Überblick. Zeitschrift der deutschen Geologischen Gesellschaft 127, 467–483.

Richter, D., 1976b. Die Flysch-Zonen Griechenlands III. Flysch, sowie spät- und postorogene Serien in West-Griechenland zwischen Albanien und dem Golf von Patras. Teil 1. Neues Jahrbuch für Geologie und Paläontologie Abhandlungen 151, 73–100.

Richter, D., 1993. Die Flysch-Zonen Griechenlands VII. Sedimentstrukturen, Ablagerungsart und Schüttungsrichtungen im Flysch der Pindos-Zone (Griechenland). Neues Jahrbuch für Geologie und Paläontologie Monatshefte 1993, 513–544.

Richter, D., Müller, C., Hottinger, L., Risch, H., 1995. Die Flysch-Zonen Griechenlands X. Neue Daten zur Stratigraphie und Paläogeographie des Flysches und seiner Unterlage im Giona-Parnass-Elikon-Gebirge (Parnass-Zone, Griechenland). Neues Jahrbuch für Geologie und Paläontologie Abhandlungen 197, 295–329.

Richter, D., Müller, C., Mihm, A., 1993. Die Flysch-Zonen Griechenlands V. Zur Stratigraphie des Flysches der Pindos-Zone im nördlichen Pindos-Gebirge zwischen der albanischen Grenze und der Querzone von Kastaniotikos (Griechenland). Neues Jahrbuch für Geologie und Paläontologie Monatshefte 1993, 257–291.

Richter, D., Müller, C., Risch, H., 1996. Die Flysche der Zonen Griechenlands, XI. Neue Daten zur Stratigraphie und Paläogeographie des Flysches und seiner Unterlage in der Pelagonischen Zone (Griechenland). Neues Jahrbuch für Geologie und Paläontologie Abhandlungen 201, 327–366.

Ring, U., Laws, S., Bernet, M., 1999. Structural analysis of a complex nappe sequence and late-orogenic basins from the Aegean Island of Samos, Greece. Journal of Structural Geology 21, 1575–1601.

Ring, U., Layer, P.W., 2003. High-pressure metamorphism in the Aegean, eastern Mediterranean: underplating and exhumation from Late Cretaceous until the Miocene to Recent above a retreating Hellenic subduction zone. Tectonics 22, 1–23.

Ring, U., Layer, P.W., Reischmann, T., 2001. Miocene high-pressure metamorphism in the Cyclades and Crete, Aegean Sea, Greece: evidence for large-magnitude displacement on the Cretean detachment. Geology 29, 395–398.

Robertson, A.H.F., Clift, P.D., Degnan, P., Jones, G., 1991. Palaeogeography and palaeotectonic evolution of the eastern Mediterranean Neotethys. Palaeogeography Palaeoclimatology Palaeoecology 87, 289–343.

Robertson, A.H.F., Karamata, S., 1994. The role of subduction-accretion processes in the tectonic evolution of the Mesozoic Tethys in Serbia. Tectonophysics 234, 73–94.

Schermer, E.R., 1993. Geometry and kinematics of continental basement deformation during the Alpine orogeny, Mt. Olympos region, Greece. Journal of Structural Geology 15, 571–591.

Schermer, E.R., Lux, D.R., Burchfield, B.C., 1990. Temperature-time history of subducted continental crust, Mount Olympos region, Greece. Tectonics 9, 1165–1195.

Schneider, W., Bode, S., Oppermann, A., 1998. Zusammenhänge zwischen Deckenvorschub, Suturprogradation, Erosion und Flyschzusammensetzung in den Helleniden. Neues Jahrbuch für Geologie und Paläontologie Abhandlungen 209, 349–379.

Shanmugam, G., Moiola, R.J., 1988. Submarine fans: characteristics, models, classification, and reservoir potential. Earth-Science Reviews 24, 383–428.

Skourlis, K., Doutsos, T., 2003. The Pindos Fold-and-thrust belt (Greece): inversion kinematics of a passive continental margin. International Journal of Earth Sciences 92, 891–903.

Smith, A.G., Woodcock, N.H., Naylor, M.A., 1979. The structural evolution of a Mesozoic continental margin, Othris Mountains, Greece. Journal of the Geological Society London 146, 589–603.

Stampfli, G.M., Borel, G., Cavazza, W., Mosar, J., Ziegler, P.A. (Eds.), 2001. The Palaeotectonic Atlas of the PeriTethyan Domain. European Geophysical Society, CD-ROM.

Stampfli, G.M., Mosar, J., Marquer, D., Marchant, R., Baudin, T., Borel, G., 1998. Subduction and obduction processes in the Swiss Alps. Tectonophysics 296, 159–204.

Thomson, S.N., Stockhert, B., Brix, M.R., 1998. Thermochronology of the high-pressure metamorphic rocks of Crete, Greece: implications for the speed of tectonic processes. Geology 26, 259–262.

Vakalas, P.J., 2003. Evolution of foreland basins in western Greece. Ph.D. thesis. University of Patras, 333pp. (in Greek).

von Eynatten, H., Gaupp, R., 1999. Provenance of Cretaceous synorogenic sandstones in the Eastern Alps: constraints from framework petrography, heavy mineral analysis and mineral chemistry. Sedimentary Geology 124, 81–111.

Walker, R.G., 1992. Turbidites and submarine fans. In: Walker, R.G., James, N.P. (Eds.), Facies Models. Response to Sea Level Changes, Geological Association of Canada, pp. 239–263.

Winkler, W., Slaczka, A., 1994. A Late Creatceous to Paleogene geodynamic model for the western Carpathians in Poland. Geologica Carpathica 45, 71–82.

Woletz, G., 1967. Schwermineralvergesellschaftungen aus ostalpinen Sedimentationsbecken der Kreidezeit. Geologische Rundschau 56, 308–320.

Zygojannis, N., Sidiropoulos, D., 1981. Schwermineralverteilungen und paläogeographische Grundzüge der tertiären Molasse in der Mesohellenischen Senke, Nordwest-Griechenland. Neues Jahrbuch für Geologie und Paläontologie Monatshefte 1981, 100–128.

Chapter 31

THE USE OF HEAVY MINERALS IN DETERMINING THE PROVENANCE AND TECTONIC EVOLUTION OF MESOZOIC AND CAENOZOIC SEDIMENTARY BASINS IN THE CONTINENT-PACIFIC OCEAN TRANSITION ZONE: EXAMPLES FROM SIKHOTE-ALIN AND KORYAK-KAMCHATKA REGIONS (RUSSIAN FAR EAST) AND WESTERN PACIFIC

PAVEL V. MARKEVICH[a,†], ALEXANDER I. MALINOVSKY[a], MARIANNA I. TUCHKOVA[b], SERGEI D. SOKOLOV[b] AND VLADIMIR N. GRIGORYEV[b]

[a]*Far East Geological Institute, Far-East Division, Russian Academy of Sciences, 690022, Vladivostok-22, Prospect 100-letyia Vladivostoka, 159, Russia*
[b]*Geological Institute of the Russian Academy of Sciences, 119017, Moskow, Pyzhevsky pereulok 7, Russia*

ABSTRACT

This paper documents the achievements of Russian sedimentologists and mineralogists who have used heavy minerals to reconstruct the provenance and source lithologies of Mesozoic-Caenozoic sedimentary complexes of the Far East and the western Pacific Ocean, and identify their plate tectonic settings. We provide a review of publications, written mostly in Russian, which have not been available or intelligible to non-Russian speakers. Investigations concentrated mainly on the sedimentary and volcano–sedimentary rocks of the Sikhote-Alin fold belt and Koryak-Kamchatka region, but they also included the Pengina Bay and the Vanuatu Trench in the Pacific Ocean.

Caenozoic sediment samples were collected during marine geological expeditions and analysed using traditional microscopy of detrital minerals, bulk sediment chemistry, and electron microprobe analysis. Distinctive heavy mineral associations have been recognised that indicated their deposition in particular plate tectonic settings. Geochemical analysis of individual heavy minerals has revealed their source lithologies in a plate tectonic context.

The Sikhote-Alin sediments were derived from the continental Siberian and Chinese cratons, complemented—at the beginning and the close of the Phanerozoic—by minor input from contemporary oceanic fragments, including volcanics. In the Koryak-Kamchatka region, forearc

Developments in Sedimentology, Vol. 58, 789–822

ISSN: 0070-4571/doi:10.1016/S0070-4571(07)58031-3

basins were fed almost entirely by intermediate and basic rocks amongst which the products of island arc volcanism played a dominant role throughout the Phanerozoic. The principal source of detrital heavy minerals of the Middle Eocene-Pleistocene deep-sea sediments of the Vanuatu Trench was the tholeiitic basalts of the Vanuatu island arc with limited addition from ocean-floor basalts. Only insignificant amounts of terrigenous material reached the depositional area from the Australian continent.

Keywords: heavy mineral associations; Sikhote-Alin; Koryak-Kamchatka Region; plate tectonic settings

1. INTRODUCTION

The aim of this contribution is to provide a brief, informative summary of the achievements of Russian sedimentologists and mineralogists who used heavy mineral analysis in the study of Mesozoic-Caenozoic sedimentary and volcano–sedimentary successions in the Russian Far East and in some parts of the western Pacific Ocean. A review of previous publications, published mostly in Russian that have not been available or intelligible to non-Russian speakers, is presented.

During the last twenty years our group's research focused on the Mesozoic and Caenozoic evolution of the transitional zone between East Asia and the Pacific Ocean. The foci of main interest were the Sikhote-Alin fold belt, the Koryak-Kamchatka region (P.V. Markevich and A.I. Malinovsky) including the Pengina Bay area (M.I. Tuchkova, V.N. Grigoryev, S.D. Sokolov, and P.V. Markevich) and certain areas of the western Pacific (A.I. Malinovsky) (Fig. 1).

Heavy mineral analysis proved a powerful tool in the study of Caenozoic oceanic and marginal sea floor sediments in the Pacific and Indian Oceans, surveyed during numerous marine geological expeditions (Nechaev, 1991; Nechaev and Isphording, 1993; Nechaev et al., 1996), and has achieved the characterisation of different types of environments. Results also served as a reference database for the study of other older settings.

Several hundred samples were obtained from the Sikhote-Alin area between 1980 and 2000. The Olyutorsky Terrane was sampled between 1978 and 1986 (from the Northern Province 277 and Southern Province 118 samples were collected). In 1992–1993, sampling was extended to the Udyl area (189 samples), and between 1997 and 2002 to the Kema Terrane (from the Kema fragment 103, Sovgavansky 62, and Vysokogorsky 55 samples were taken). From the Vanuatu trench, 77 samples were collected in 1988, while between 2000 and 2004, ~100 samples were taken from the Penzhina area. Details of analytical data can be obtained from the authors on request, and data published in English can be found in Nechaev (1991); Nechaev and Isphording (1993); and Nechaev et al. (1996).

Preparation for heavy mineral analysis included conventional crushing (up to 0.25 mm), sieving, washing off the <0.01-mm-size fractions with distilled water, followed by drying and heavy liquid separation. Around 50–100 g dry samples were used from which two size fractions, viz. 0.01–0.10 mm and 0.10–0.25 mm, were retained for the heavy mineral separation, using bromoform (density 2.85). Heavy mineral compositions were studied under the polarising microscope in immersion oil

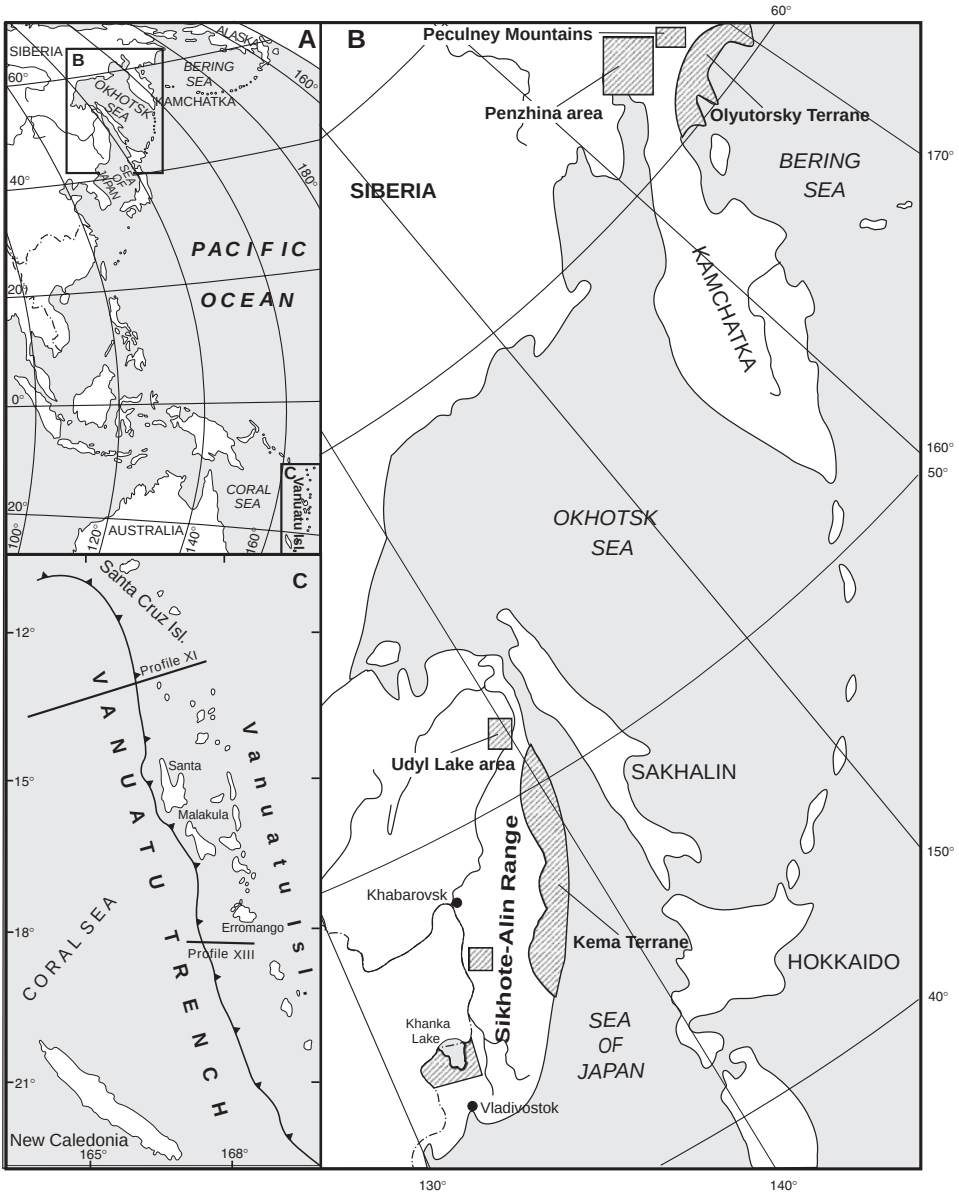

Fig. 1. Investigated areas of the Russian Far East and West Pacific. (A): General map; (B): Russian Far East; (C): Vanuatu area (for profiles XI and XIII: see Fig. 2).

grain mounts, using both size fractions, and point counting at least 200 grains on each grain mount. The average values of their point counts were used for data presentation and plots. In order to unmask the relationship between particular minerals and recognise those that carry the most informative palaeogeographic signatures, only the detrital mineral components were counted.

It proved important to integrate the heavy mineral technique with the analysis of framework components (quartz, feldspars, and rock fragments), bulk chemical compositions and the products of synsedimentary volcanism (lava, tuffs, and tephra). Because an association of heavy minerals can originate from different sources (for example, magnetite and ilmenite may originate from different granites, metamorphic rocks, basalts, and andesites), chemical analysis is essential to link assemblages to their particular source rocks which, in turn, can reveal the plate tectonic setting of the depositional area. For this purpose electron microprobe analysis was conducted on diagnostic heavy minerals, using a JEOL JXA-5A electron microprobe.

2. STUDY AREAS

2.1. Oceanic Volcanic Island Arc Sedimentation: the Vanuatu Region

The Vanuatu region of the south-western Pacific (Fig. 1) is the southernmost of the unique island arc and deep-sea trench system that extends from New Guinea to latitude 23° South, covering a length of 2500 km. The peculiarity of the Vanuatu island arc system is that the trench is situated westward and the Benioff zone is inclined eastward (Vasiliev, 1990; Tanahashi, 1994).

Across the 5500 m isobath, the Vanuatu Trench is ~1600 km long and 40 km wide. Its deepest parts have a slightly inclined floor 0.5–1.5 km wide with a maximum depth of 9174 m. The trench has stepped slopes, and relief is very complex, consisting of a chain of depressions 7000–9000 m deep, separated by barriers that are only 5500–6000 m deep. Friable (non-lithified) sediments in the Vanuatu Trench and on the adjacent Coral Sea floor were collected at profiles XI and XIII by hydrostatic and gravitational samplers and by dredging (Fig. 2). Material taken represents all types of Tertiary and Quaternary sediments in the trench and comprises clay, carbonates, and tephra.

Heavy minerals of the Middle Eocene-Holocene deep-sea sediments of the Vanuatu Trench are homogeneous, and characterised by the predominance (up to 100%) of island arc volcaniclastic clino- and orthopyroxene (Opx), magnetite, olivine, and hornblende (Hb) (Fig. 2). A typical association consists of clinopyroxene (Cpx) (30–92%) and magnetite (10–62%). Orthopyroxene (2–43%), hornblende (0.1–17%), and olivine (up to 10%) are less abundant, while heavy minerals of the sialic association (zircon, sphene, apatite, rutile, garnet, and corundum) are present only in accessory ($<2.5\%$) amounts, attesting to the insignificant occurrence of sialic source rocks in the region.

The MF (total amount of olivine, ortho- and clinopyroxene, green hornblende) component (MF: see caption, Fig. 3) permits identification of detritus from oceanic and island arc volcanics and, within them, differentiation of arcs that have either oceanic or continental basement. The island arc material differs from oceanic basement by the high percentage of orthopyroxenes and the low proportion of olivine. Orthopyroxene strongly prevails over olivine, which bears witness to the domination of island arc material.

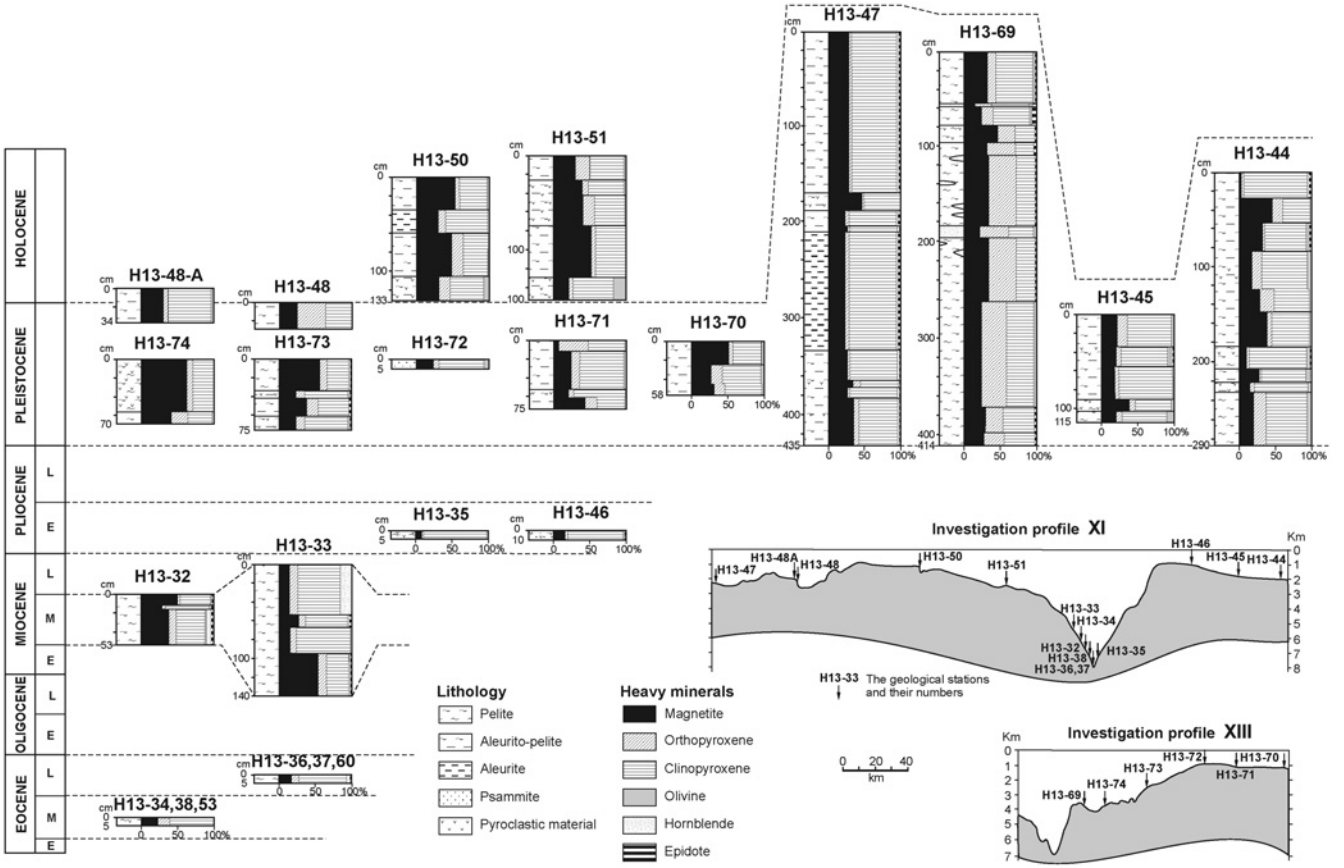

Fig. 2. Heavy mineral distribution in the deposits of the investigated profiles across the Vanuatu deep-water trench, (after Vasiliev, 1990). For locations of profiles XI and XIII: see Fig. 1.

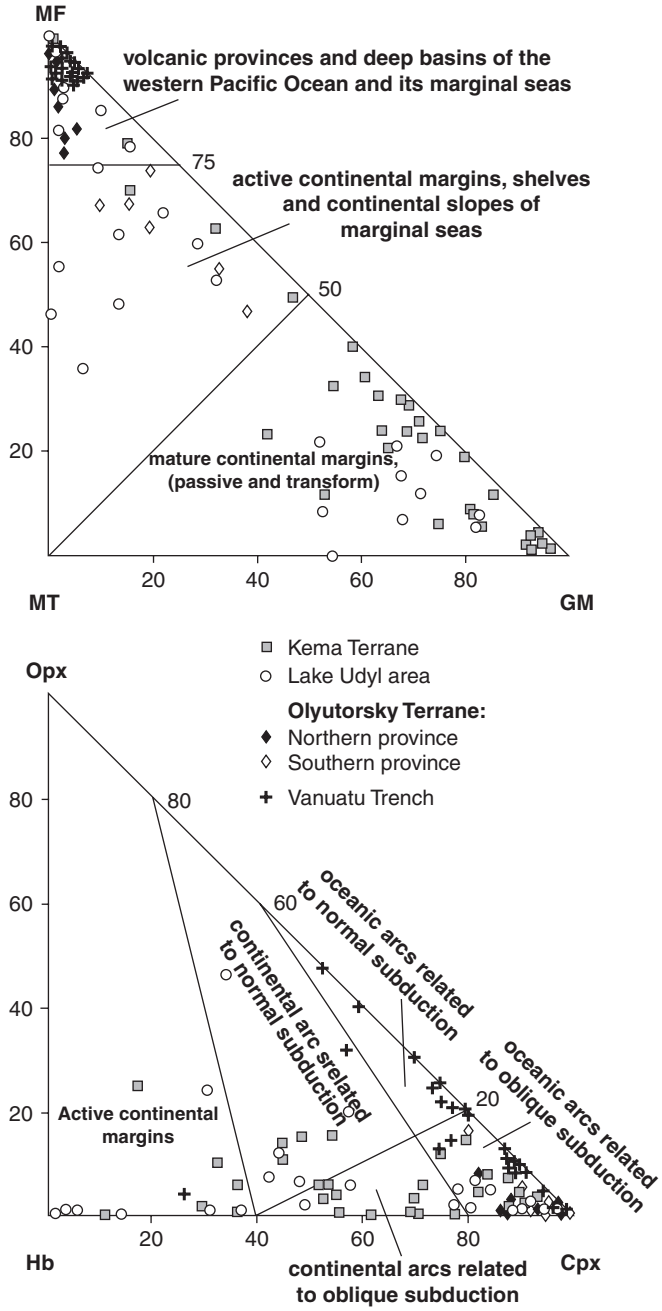

Fig. 3. Correlation of mineral compositions of heavy minerals from sandstones of different ancient rocks and modern sediments from various geodynamic settings on MF-GM-MT and Opx-Hb-Cpx diagrams (after Nechaev and Isphording, 1993). Values on axes are in percentages. MF: total amount of olivine, ortho- and clinopyroxene, green hornblende; MT: total amount of epidote, garnet, blue-green amphibole; GM: total amount of zircon, tourmaline, staurolite, monazite, sillimanite, kyanite, and andalusite. Opx: orthopyroxene; Hb: hornblende; Cpx: clinopyroxene.

Analytical data of heavy minerals, plotted as MF-MT-GM diagrams in Fig. 4 (Nechaev and Isphording, 1993), show the clustering of data points close to the MF apex, indicating their correspondence with assemblages of deep-sea sediments in the depressions of the Pacific Ocean marginal seas.

The Opx-Cpx-Hb ratios (Fig. 3), where the principal heavy mineral is hornblende, allows division of the continental and oceanic arc-derived detritus (Nechaev and Isphording, 1993). In the studied sediments, hornblende abundance is low, and an oceanic island arc source (e.g., in the Vanuatu Islands) is therefore likely (Hanus and Vanek, 1983). A changing ratio of orthopyroxene vs. other components over time allows us to assess the temporal evolution of tectonic plate convergence. Thus increased proportions of orthopyroxenes with sediment younging indicate that the Middle Eocene-Pliocene oblique plate convergence and subduction changed to orthogonal (normal) in the Late Pliocene (Fig. 3).

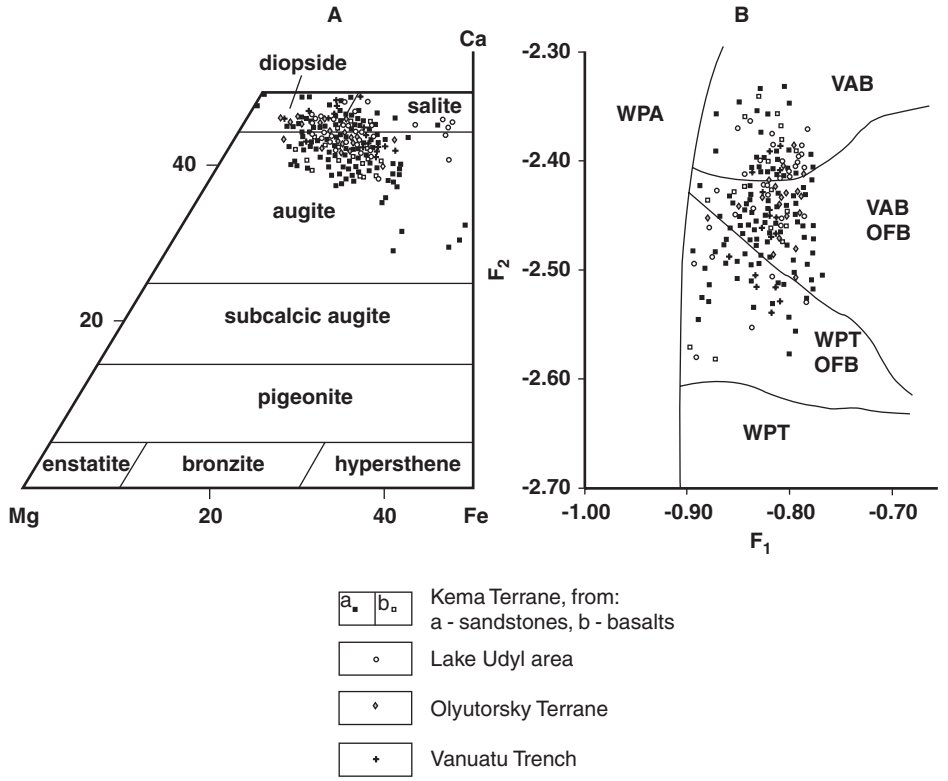

Fig. 4. (A): Comparative diagram showing composition of clinopyroxenes from basalts and sandstones; (B): Discriminant diagram for basalt-hosted clinopyroxenes from different geodynamic settings (after Nisbet and Pearce, 1977). VAB: volcanic arc basalts; OFB: ocean-floor basalts; WPT: within-plate tholeiitic basalts; WPA: within-plate alkaline basalts. $F_1 = -0.012 \times SiO_2 - 0.0807 \times TiO_2 + 0.0026 \times Al_2O_3 - 0.0012 \times FeO - 0.0026 \times MnO + 0.0087 \times MgO - 0.0128 \times CaO - 0.0419 \times Na_2O$;
$F_2 = -0.0496 \times SiO_2 - 0.0818 \times TiO_2 - 0.02126 \times Al_2O_3 - 0.0041 \times FeO - 0.1435 \times MnO - 0.0029 \times MgO - 0.0085 \times CaO + 0.0160 \times Na_2O$.

The character of the volcanic sediment source can be identified by the chemical composition of diagnostic heavy minerals: ortho- and clinopyroxenes, olivine, and hornblende. In this regard clinopyroxene proves to be the most informative. Chemical composition (Fig. 4A) of the Vanuatu Trench clinopyroxenes corresponds to diopside, augite and, to a lesser degree, salite. Their origin can be seen from the discriminant diagrams, permitting us to confirm with more than 80% probability that these pyroxenes are from basalts, and that they were generated in different tectonic settings. Fig. 4B (Nisbet and Pearce, 1977) shows that the majority of pyroxenes correspond to clinopyroxenes of island arc basalts, and in part to those of ocean-floor basalts, originating probably from the island arc's roots. The composition of clinopyroxenes, analysed from sediments collected from the proximity of the island arc, shows a clear link to those of ocean-floor basalt. In the discriminant diagram 1 of Fig. 5 (Leterrier et al., 1982) all pyroxenes from the Vanuatu Trench occupy the fields not far from the line separating clinopyroxenes from alkaline intraplate and oceanic island basalts (A) from non-alkaline basalts (T).

Similar to those of the other analysed terranes, they have low titanium and sodium contents and thus cannot be allocated to the alkaline basalt category. Diagram 2 divides non-alkaline basalts into MORB basalts (D) and calc-alkaline and tholeiitic

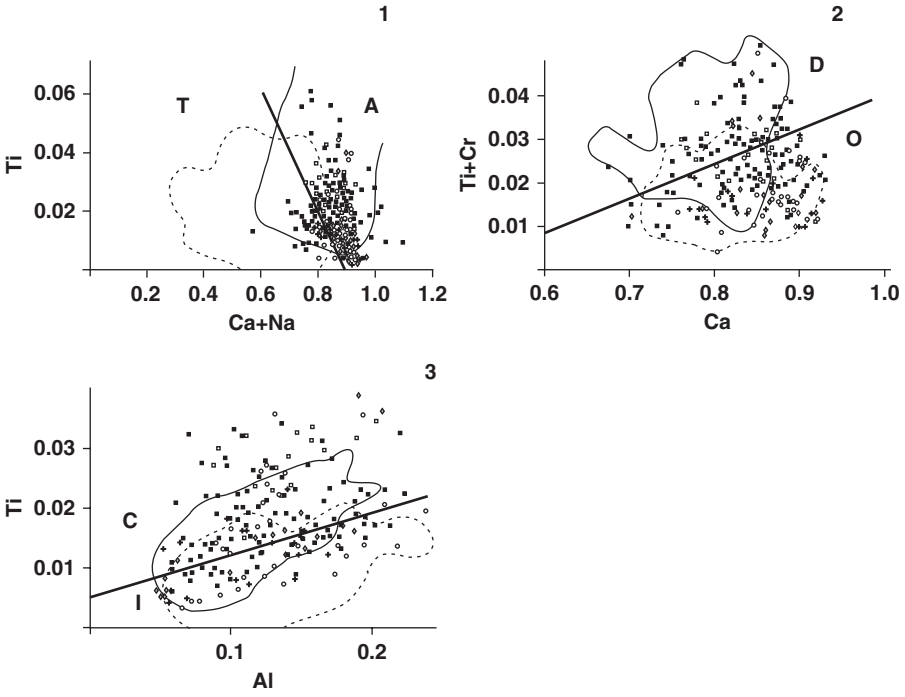

Fig. 5. Discriminant diagrams for clinopyroxenes of basalts from different geodynamic settings (after Leterrier et al., 1982). 1: alkaline intraplate basalts (A) and non-alkaline (T) basalts; 2: non-alkaline basalts distinguishing MORB (D) from calc-alkaline and tholeiitic basalts of epicontinental and island arcs (O); 3: calc-alkaline (C) and tholeiites of epicontinental and island arcs (I). The fields corresponding to different basalts are represented by solid and dashed lines; elements are given in formula units.

basalts of the continental margin and island arcs (O); all detrital clinopyroxenes of the Vanuatu Trench prove to be of island arc origin. Diagram 3 divides island arc clinopyroxenes into calc-alkaline (C) and tholeiitic types, and here the pyroxenes define a tholeiitic basalt source. The island arc character of the hornblendes is demonstrated in the diagram of 10Ti-Al-Fe (Nechaev, 1991), where low total chromium and titanium contents suggest that the amphiboles were derived from basic and intermediate volcanic rocks of the island arcs (Fig. 6B).

Our analyses indicate that the principal source of detrital heavy minerals of the Middle Eocene-Pleistocene deep-sea sediments of the Vanuatu Trench was predominantly the tholeiitic basalts of the island arc with limited addition from ocean-floor basalts. Heavy minerals also reveal that only insignificant amounts of terrigenous material reached the depositional area from the Australian continent.

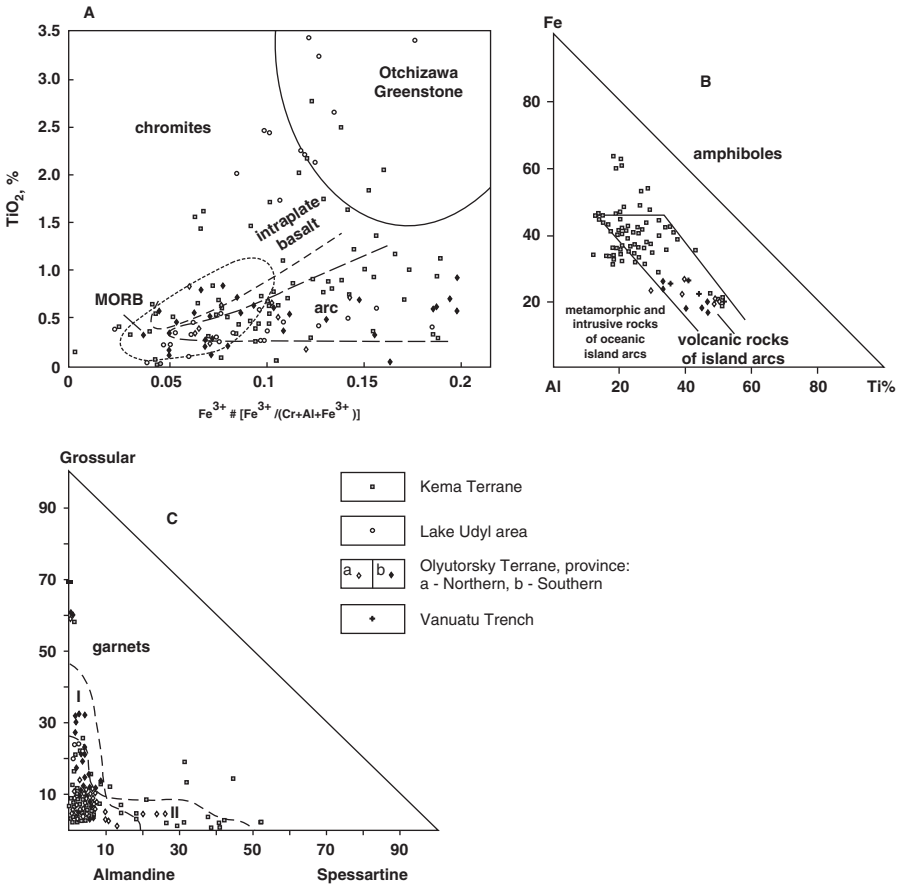

Fig. 6. Diagrams of the composition of heavy minerals of sandstone from different sedimentary successions. Discrimination fields for magma chemistry. (A): For chromites (after Arai, 1992); (B): For amphiboles (after Nechaev, 1991); (C): For garnets—from acidic volcanic rocks (I) and intrusive rocks (II) (after Kazachenko, 2001). All Ti values are multiplied by 10 and recalculated as percentages.

2.2. Sikhote-Alin Range

The main part of this Mesozoic complex consists of marine arkoses, which contain rock-forming and accessory minerals of continental, granitic, and metamorphic provenance. Locally narrow belts of sialic continental and mafic, oceanic volcanic arc systems also occur with fragments of volcano–sedimentary, forearc and backarc basin sediments, intercalated with andesitic and basaltic rocks. Two main types of sediment composition and corresponding sedimentation can be distinguished in the Sikhote-Alin fold system: (1) mixed epiplatformal and (2) epioceanic, arkosic sediments.

2.2.1. Mixed epiplatformal sedimentation.

Mesozoic epiplatformal sedimentation has been identified positively only on the eastern margin of the Khanka crystalline massif, which is postulated to be a fragment of the North China craton (Bersenev, 1969). In the Central Sikhote Alin (Fig. 1) during the Late Triassic, the sediment source province comprised acid volcanics, granites, and sedimentary rocks, as indicated by high amounts of zircon (up to 85%) and by the presence of lithic fragments from these rocks in the analysed sandstones. In adjacent Chinese territory, heavy minerals of the sandstones include 60–78% zircon with minor leucoxene, apatite, magnetite, and hornblende.

In the southern Sikhote-Alin, Mesozoic heavy minerals have been studied only cursorily in Triassic and Late Jurassic to Berriasian sediments, where they are represented chiefly by zircon (40–88%), suggesting a source in the granitic and metamorphic rocks of the Khanka crystalline massif, located to the west. Small quantities of tourmaline, zircon, garnet and magnetite, minor leucoxene, titanite, apatite, glauconite, and rare staurolite grains were also found.

2.2.2. Arkosic and epioceanic sedimentation: accretionary complexes of the Sikhote-Alin range.

In the Sikhote-Alin range (Fig. 1) the majority of the Mesozoic heavy minerals are represented by the sialic association (zircon, apatite, garnet, sphene, tourmaline, and rutile), derived from acid magmatic and metamorphic rocks of continental origin. This association constitutes, on average, 56–82% of all clastic heavy minerals. The major component of this association is zircon (up to 95%) of granitic and acid–volcanic derivation. Less common is the mafic, oceanic (femic) association (18–44%), which includes chromite, ilmenite, and leucoxene, associated with ultrabasic source rocks, together with clinopyroxene, hornblende, and epidote, derived mainly from basic volcanic island arc complexes. The chemical composition of most of the chromites from the upper Aptian-Albian part of the succession is very similar to chromites of the Jurassic meimechite-picrite assemblage (TiO_2-rich ultramafic volcanic rocks, containing high-titanium spinels) of Sikhote-Alin. Other chromites are low in titanium and occupy the field of ultramafic chromites. Some grains are high in alumina and correspond with chromites of dunite-hartzburgite (Alpine-type) peridotites. In the lower part of the succession, there is a limited upward increase in the proportion of mafic mineral associations, which become particularly evident in the upper part. This signature in the lower part of the succession therefore records the onset of pre-orogenic volcanism.

2.2.3. Epicontinental volcanic island arc sedimentation: Kema Terrane.
The Kema Terrane is situated in the eastern part of the Sikhote-Alin range, extending as a band up to 80 km wide along the Japan Sea coast (Figs. 1 and 7). The terrane includes Barremian(?)-Albian deposits, with turbidites, siltstones, and mixtites (unsorted, mixed grain-size sedimentary rocks). Mafic lavas and their pyroclastics are widespread, interpreted as the backarc basin fill of the Early Cretaceous Moneron-Samarga island arc system. Volcanic island arc sources have been identified for the Early Cretaceous deposits of the Kema Terrane (Primorsky region of Russia) (Malinovsky et al., 2002).

Fragments of the Kema Terrane are also exposed in the ''windows'' among the rocks of the Late Cretaceous East Sikhote-Alin volcanic belt. Volcano–sedimentary formations were studied in three fragments: Kemsky (Kema River basin), Sovgavansky (Buta River basin) and Vysokogorsky (Muly River basin) (Figs. 7 and 8). The lithostratigraphy of sections in the studied Kema Terrane fragment is described below (Fig. 8).

In the *Kemsky fragment* the lower turbidite unit (up to 1100 m thick) lies at the base of the type section (Fig. 8), consisting of alternating packages of sandstones and siltstones with typical turbidite characteristics. The alternation is occasionally interrupted by siltstones with thin sandstone horizons, slump deposits, and gravelstones (cemented gravels comprising clasts 2–10 mm in size). The overlying coarse clastic unit (~1500 m) is represented by conglomerate, gravels, sandstones, mixtites, rare packages of rhythmically alternating sandstones and siltstones, slump horizons, tuffs, and isolated basalt flows. Above this is the volcanic unit (up to 770 m) consisting mainly of basalts, tuffs, and tephra; in places there are volcaniclastic sandstones, rhythmical alternations of sandstones and siltstones, horizons of slump deposits and mixtites. The upper turbidite unit (up to 1700 m) is characterised by thick rhythmic alternations of sandstones and siltstones. This monotonous succession is, in places, interrupted by thinner horizons of sandstones, siltstones and mixtites, and is complicated by deformation related to subaquaeous landslides. The uppermost part is a sandstone unit (up to 550 m), containing rare horizons of conglomerates, gravels and siltstones and, in the lower part, andesitic basalt layers.

In the *Sovgavansky fragment* (Fig. 8), the basal sandstone and siltstone unit (up to 800 m) is composed of sandstones with gravels, conglomerates, and packets of rhythmically intercalated sandstones and siltstones, containing mixtite horizons. The overlying turbidite-clayey unit (up to 1600 m) consists mainly of siltstones, passing up into rhythmical intercalations of sandstones and siltstones, occasionally with sandstones and mixtites. A turbidite-sandstone unit (up to 1500 m), representing the upper part of the section, comprises rhythmically alternating sandstones and siltstones, with thick sandstone intervals, containing gravel lenses. Siltstone horizons are comparatively rare in the thick sandstone beds.

The *Vysokogorsky fragment* (Fig. 8) contains a siltstone and sandstone unit (> 1550 m thick) at the base of the lower part of the section, comprising siltstones and sandstones or, occasionally, sandstones with siltstone intercalations. Above this lies the turbidite unit (> 870 m) with sandstone and siltstone rhythmites, sometimes interrupted by siltstones or sandstones. Next is a volcano–sedimentary unit (> 1450 m), which has significant volcanic products—diabases, basalts, and basic tuffs—together with volcaniclastic sandstones, siltstones, conglomerates, mixtites,

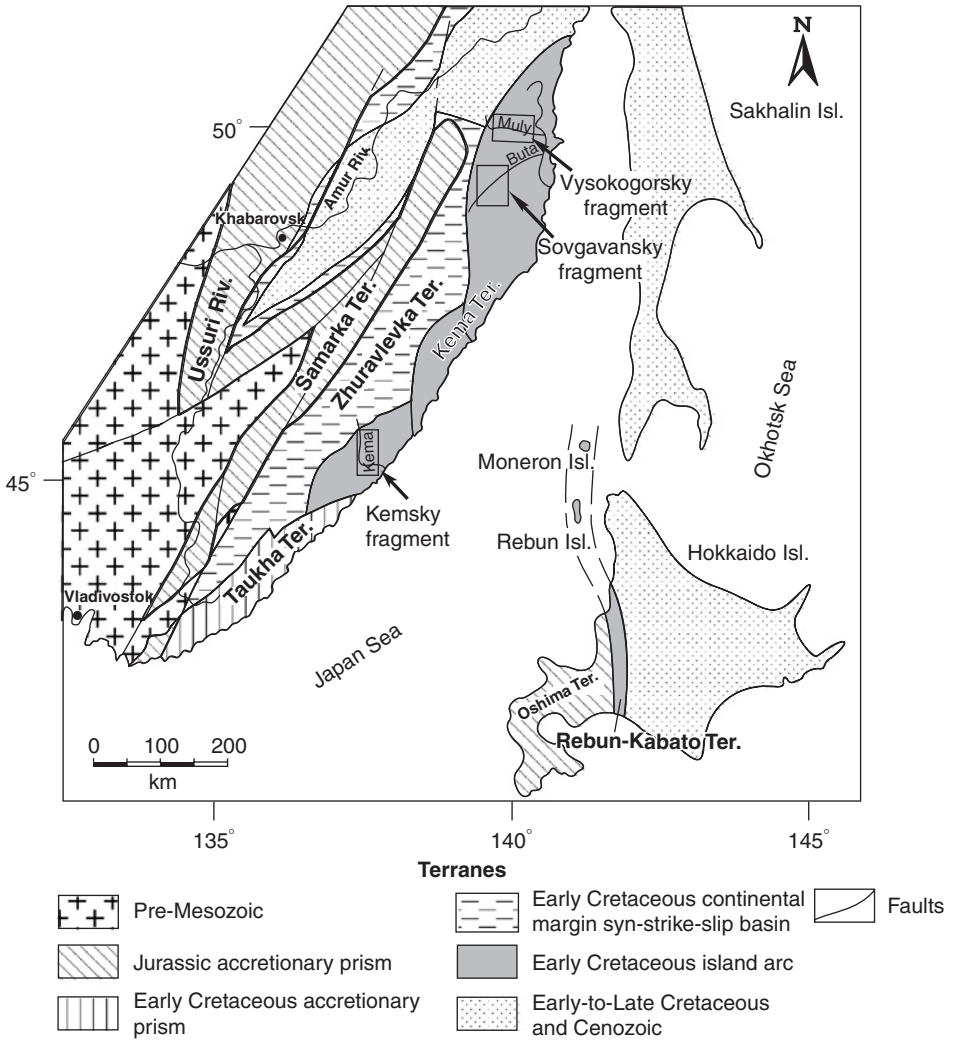

Fig. 7. Major terranes of the Russian Far East and adjacent area (after Malinovsky et al., 2002).

and rhythmically interbedded sandstone/siltstone couplets. The overlying siltstone unit (> 850 m) is made up of massive siltstones with lenses and interlayers of sandstones, conglomerates, and mixtites. The uppermost sandstone unit (~2200 m) consists mainly of sandstones, with siltstones and gravel lenses and thin rhythmical sandstone/siltstone couplets.

Two heavy mineral associations have been distinguished in the Kema Terrane. The first is volcanogenic, constituting ~40% of all heavy minerals, and including typical representatives of island arc volcaniclastics: ortho and clinopyroxenes, hornblende, chromite, and magnetite. Most of these minerals are in the Kema River fragment where some samples contain up to 100% heavy minerals. The dominant

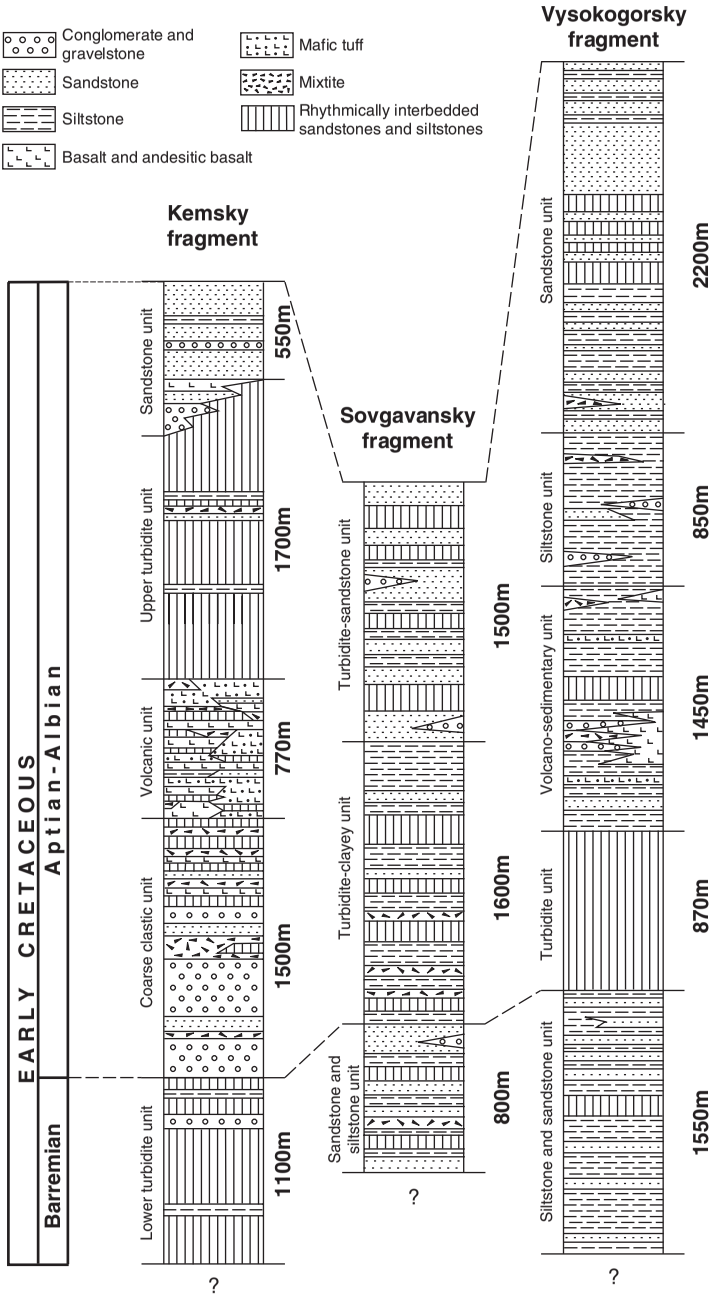

Fig. 8. Correlation of the lithostratigraphic columns of the of the Kema Terrane's different fragments.

mineral of the volcanic association is clinopyroxene (up to 98%), followed by hornblendes (up to 60%), orthopyroxenes (up to 38%), chromites (up to 46%), and magnetite (up to 25%). The second association is sialic and includes on average of 60% of all heavy minerals; it comprises zircon, garnet, tourmaline, epidote, apatite, sphene, and rutile. The principal mineral is zircon (up to 100% in some samples), followed by, in decreasing abundance, garnet (up to 77%), tourmaline (up to 18%), and epidote (up to 11%).

It is well documented for this region that the different tectonic settings have distinctive heavy mineral associations (Nechaev et al., 1996; Markevich et al., 1997). Our analysis of the heavy mineral associations from the Kema Terrane is shown in the MF-MT-GM and Opx-Hb-Cpx diagrams of Nechaev and Isphording (1993). Fig. 3 shows that they originate from two contrasting sources. The volcanogenic association corresponds to a continental volcanic arc and/or an active continental margin at a low plate convergence angle. This association originates, principally, from island arc volcanics, which contribute considerably larger amounts than does the sialic source in the Kema River fragment. The source of the sialic association was probably the continental foundation of the arc. As a possible source a convergent plate boundary without volcanic activity, perhaps like northern Peru, can also be considered.

The nature of the volcanic sediment source (Fig. 4) can be best identified by the chemical composition of clinopyroxenes in the sandstones. In Fig. 4, their compositions are compared with pyroxenes from basalts that are widespread in the Kema Terrane. In the Mg-Ca-Fe plot (Fig. 4A) the composition of the pyroxenes corresponds to augite, diopside, and salite (a rare intermediate member of the diopside-hedenbergite series). The diagrams also allow the discrimination of pyroxenes from different geodynamic settings, with a confidence level of more than 80%. In Fig. 4B (after Nisbet and Pearce, 1977), the majority of the detrital pyroxenes correspond to pyroxenes of volcanic island arc basalts, and partially to pyroxenes of oceanic-floor basalts that probably intruded into the island arc's foundation. The plots of Ti/(Ca + Na), (Ti + Cr)/Ca, and Ti/Al (Fig. 5, after Leterrier et al., 1982) allow the distinction of pyroxenes from different geodynamic settings with probability similar to those shown in Fig. 4. In plot 1 of Fig. 5, clinopyroxenes (including those from basalts) cluster close to the line that demarcates clinopyroxenes of the alkaline intraplate (intracontinental and oceanic islands) basalts (A) from non-alkaline basalts (T). Part of the clinopyroxenes plot in the alkaline basalt field, but their low titanium and sodium content prevent them from being assigned to that group. Fig. 5, diagram 2, divides non-alkaline basalts into MORB basalts (D) and calc-alkaline and tholeiitic basalts with continental margin and island arc signatures (O). This plot shows that the detrital clinopyroxenes are situated in, or close to, the island arc field. Diagram 3 divides island arc pyroxenes into calc-alkaline (C) and tholeiitic (I) origin. This plot shows that the source of the pyroxenes is calc-alkaline basalts, characteristic of a backarc setting.

In Fig. 6A, the composition of the detrital chromite is plotted (Arai, 1992). Most of the data points are located in the field of island arc basalts with a minor part pointing to chromites from high-alkaline intraplate basalts. The compositions of amphiboles (Fig. 6B) from the sandstones are close to those of island arc volcanics, thus indicating a mainly island arc source (Nechaev, 1991). Garnets from sandstones are mainly pure almandine and only incidentally contain grossular or spessartine

components. They originate, most likely, from acid intrusive and effusive volcanic rocks, although metamorphic parageneses cannot be ruled out (Fig. 6C, after Kazachenko, 2001). Garnets were, probably, eroded from blocks of sialic continental crust, which constitutes the foundation of the island arc.

In summary, in the Kema Terrane heavy mineral compositions reveal three sources of the detritus: (1) sub-alkaline and calc-alkaline basalts of a volcanic island arc, (2) island arc foundation, consisting of fragments of continental crust and (3) oceanic crust, accreted to the arc. This indicates that the study sediments accumulated on the active continental margin in a backarc basin of a continental volcanic island arc.

2.2.4. Oceanic volcanic island arc system: the Udyl Lake area.

In the Lower Amur region of the northern Sikhote-Alin, which includes the Udyl Lake area (Markevich et al., 1997), a series of fragments of the oceanic volcanic island arc system have been identified (Figs. 1 and 9). Strata include chert, volcaniclastic greywacke, and arkosic rock complexes (Fig. 10).

The cherty complex (Fig. 10) consists of radiolarian cherts, mudstones, rare alkaline oceanic basalts, and pelagic limestones. In this complex island arc-derived green clinopyroxene predominates in association with orthopyroxene, hornblende, and magnetite from similar sources. Terrigenous zircon, garnet, apatite, and epidote are rare. Although the cherty complex has typical oceanic characteristics, the basin may have formed in a backarc setting of a marginal sea, as suggested by the prevalence of the amphibole–pyroxene association (MF, Fig. 3). As a whole, the MF-MT-GM components ratio is most characteristic of the deep-water parts of the Pacific marginal seas, where the main source of detritus was a volcanic island arc complex, complemented by terrestrial material from the continental margin.

The volcano–sedimentary complex (Fig. 10), representing a forearc basin, consists entirely of alternating tuffs, volcaniclastic sandstones, mixtites, tuffaceous siliceous mudstones ('silicites'), mudstones, and clayey-cherty rocks, including radiolarian cherts, with only rare basalts. Heavy minerals of the lower part of this complex are almost entirely volcanogenic clinopyroxene, magnetite, hornblende, and orthopyroxene (Fig. 3). In the upper part, these components are mixed with abundant epidote, garnet, chromite, zircon, apatite, sphene, and rutile. Such a heavy mineral sequence reflects the evolution of the basin fill that accumulated in forearc and island arc basins. At the initial stage, deposition was paralleled by synsedimentary volcanism. The succeeding volcaniclastic sediments incorporate material from a consumed accretionary prism that contained fragments of the volcanic arc, oceanic islands, and ophiolites.

The greywacke complex (Fig. 10) consists mainly of mudstones and sandstone, with horizons of tuffs and varied gravitational deposits: mixtites, turbidites, and contourites. The proportions of heavy minerals vary (Fig. 3) as shown by the occasionally elevated (50–94%) percentages of chromite, associated sometimes with pyroxene (up to 37%). The principal heavy minerals were sourced from ophiolites. Some beds contain large amounts of zircon and garnet, reflecting input from a granitic and metamorphic continental source. Lastly, in some cases, sediments are enriched in pyroxenes, amphiboles, and epidote with minor chromite content. The greywacke complex reflects derivation from island arc volcanics and their

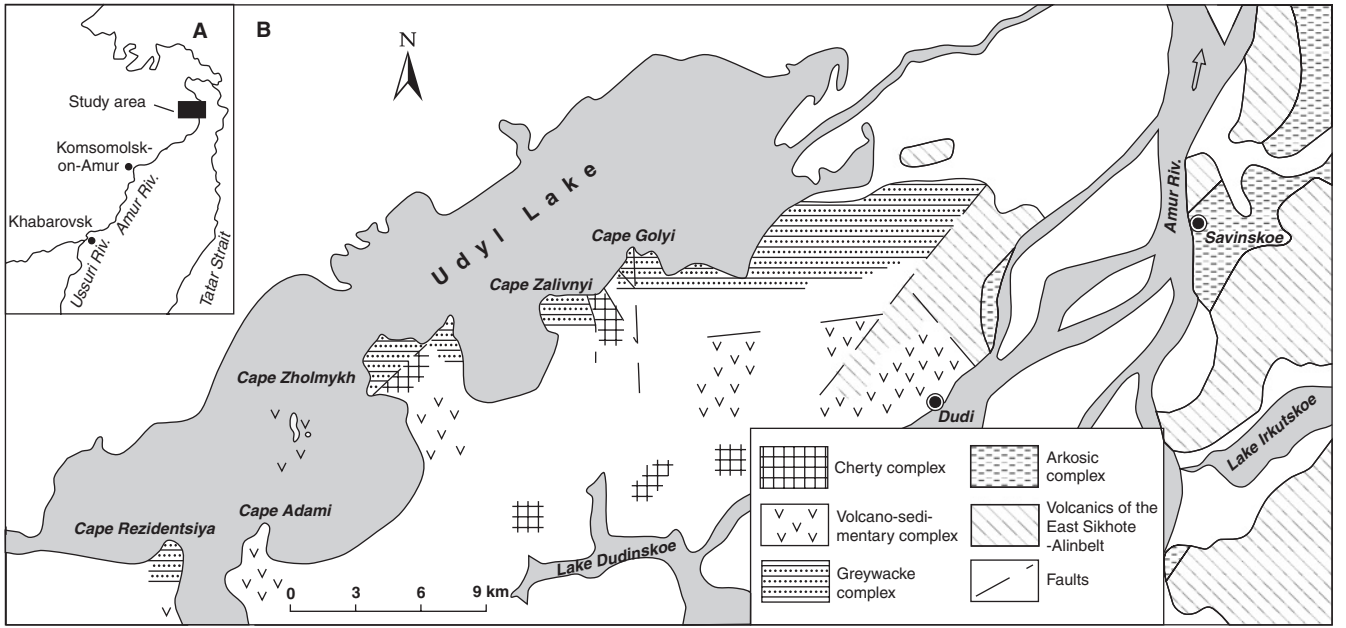

Fig. 9. Location (A) and schematic geologic map (B) of the Udyl Lake area (after Markevich et al., 1997).

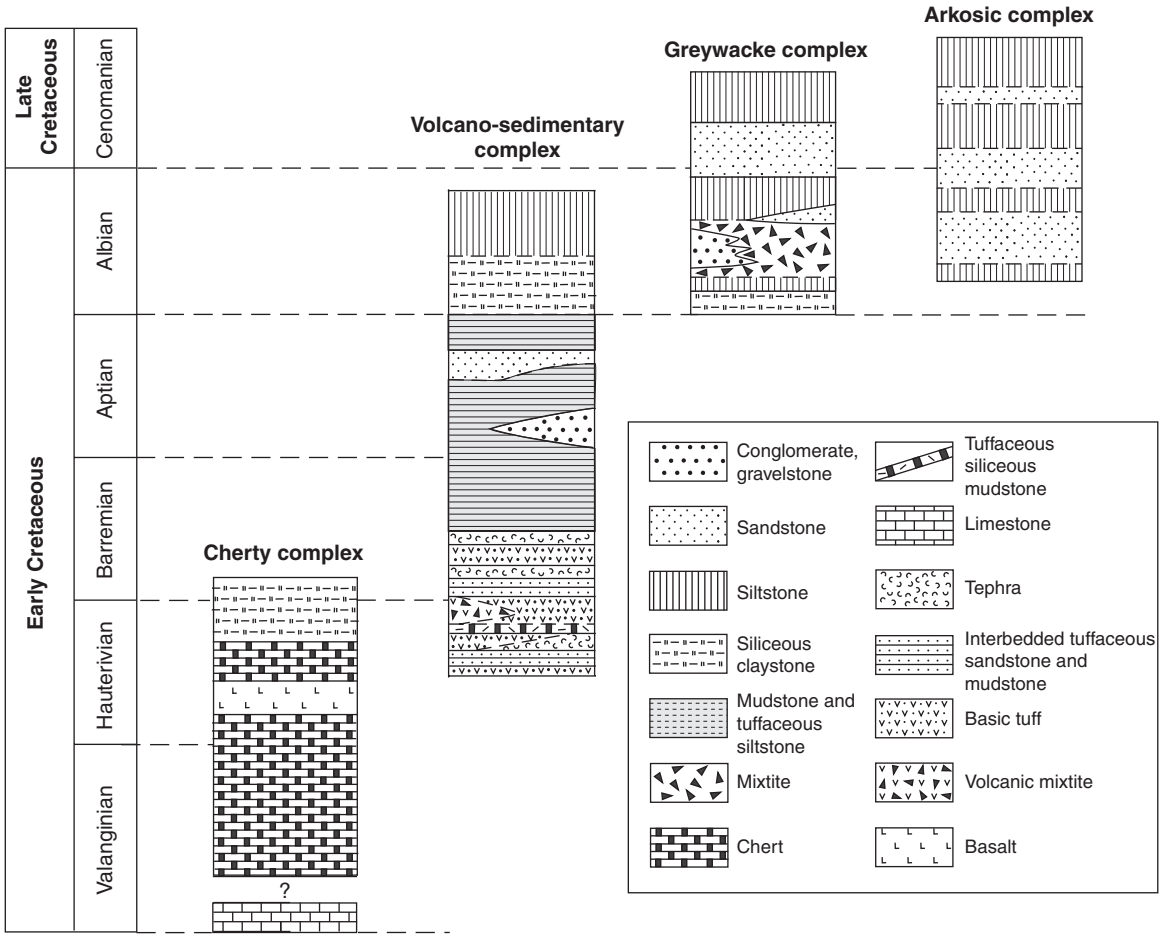

Fig. 10. Stratigraphic position and generalised structure of the lithofacies assemblages (after Markevich et al., 1997).

metamorphic equivalents. Thus, the heavy mineral spectrum indicates that detritus were derived from a heterogeneous source region. The greywackes were, most probably, shed by an accretionary prism, receiving material from oceanic, island arc, and continental parentages.

In the lower part of the arkosic complex (Fig. 10) sandstones are prevalent, whereas mudstones with some sandstone predominate in the upper part. The heavy mineral associations of this complex (Fig. 3) differ sharply from those of the three previous rock complexes with the dominance of zircon, garnet and apatite, accompanied by minor hornblende, chromite, magnetite, rutile, sphene, leucoxene, tourmaline, and pyroxenes. This association is typical of Sikhote-Alin Cretaceous successions and is interpreted as originating from mature continental margin sources without any volcanic input.

Heavy mineral distributions of the analysed successions pinpoint five main source provinces that furnished the fore- and backarc basins of island arcs. The parent rocks include two volcanic arcs of different age and origin (Valanginian-Barremian and Albian-Cenomanian), two continental blocks (northern and southern), and an ophiolite complex (Fig. 11).

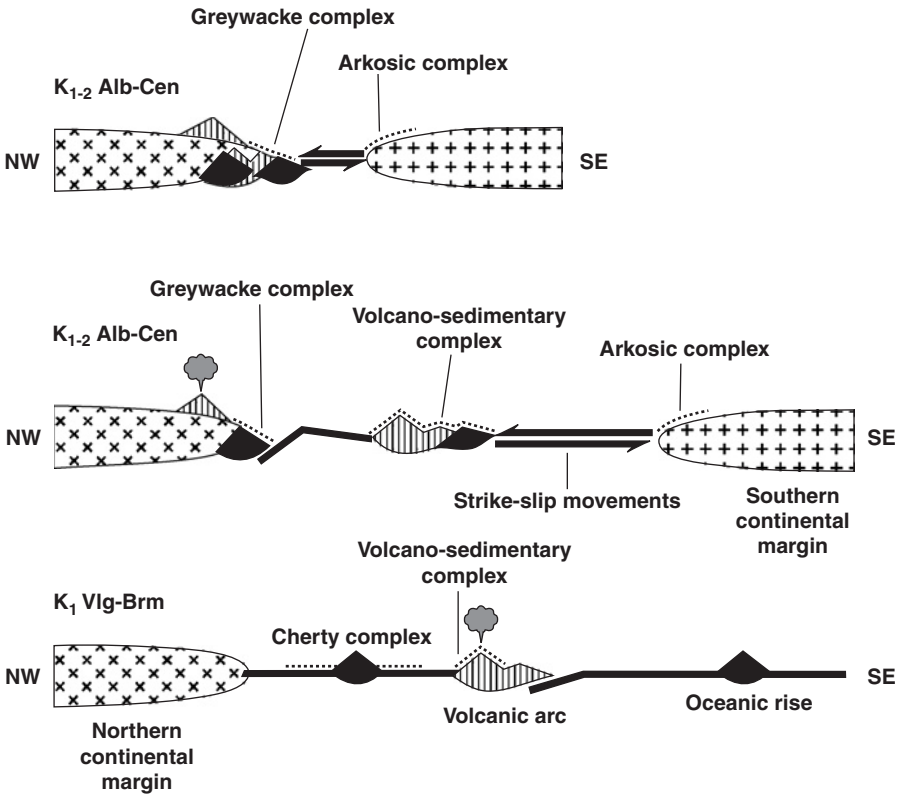

Fig. 11. Early Cretaceous geodynamic settings of the Udyl Lake area (after Markevich et al., 1997).

In summary, in the Udyl Lake area the Valanginian-Barremian volcanic island arc complexes, characterised by volcaniclastic sediments and chert, contain a low-diversity heavy mineral suite in which clinopyroxenes of augite and diopside compositions dominate, indicating a basaltic volcanic arc source (Figs. 4 and 5). The prevalence of clinopyroxenes is typical of obliquely convergent continental margins and volcanic arc (Nechaev et al., 1996) (Fig. 3: Opx-Hb-Cpx diagram), and shows the direct influence of an Izu-Bonin type oceanic arc.

The Albian-Cenomanian volcanic island arc and its foundation served as a source for the greywacke complex, which had been accumulated, most probably, on the inner slope of a deep-water trench. The composition of detrital pyroxenes and chromites attests to their island arc origin (Figs. 4, 5, and 6A). The Opx-Hb-Cpx ratio (Fig. 3) indicates continental volcanic arc and (or) active continental margin with oblique convergence (Fig. 11).

The heavy mineral association of the northern continental margin greywackes consists of zircon, garnet, sphene, apatite, and tourmaline with rare to absent rutile. Heavy mineral proportions are especially high in the middle part of the greywacke complex. These deposits accumulated, perhaps, adjacent to a continental rise at the arc's foundation. Almandine garnets (Fig. 6C) were probably derived from acid intrusive and effusive rocks, although a metamorphic source can also be considered (Kazachenko, 2001).

Lithologies exposed in the region of the southern continental margin provided the heavy mineral association of the arkosic complex. Its major components, zircon, garnet, tourmaline, sphene, apatite and rutile, indicate that a non-volcanic continental margin was eroded at the time of their deposition (Fig. 3).

The ophiolite-derived sedimentary complex was identified by the abundance of chromite in the greywackes, often associated with clinopyroxene, epidote, and hornblende. Electron microprobe analysis of the chromites and clinopyroxenes shows that those with high TiO_2 originate from alkaline magmatic rocks of inner-plate rises and islands (Figs. 4, 5, and 6A). Our proposed generalised sequence of tectonic events, documented by the sediment fill in the study areas, is shown in Fig. 11.

2.3. Koryak-Kamchatka Region

2.3.1. Penzhina area.

The studied region represents the northwest part of the Shelikhov Gulf, Penzhina Bay, and Kamchatka Peninsula (Figs. 1 and 12). It is situated between the western Koryak and Koryak-Kamchatka fold belts (Fig. 12), and is regarded as an active continental margin, consisting of deformed Palaeozoic to Mesozoic oceanic sediments, metamorphics, and volcanic rocks. The heavy mineral associations of the Cretaceous clastic deposits have been investigated from several areas (Fig. 13).

The tectonic development of the Cretaceous basins and the temporal variation of sedimentary environments were reconstructed using the heavy mineral assemblages of the basinal successions. They allowed the unravelling of major stages in the depositional and tectonic history of the sedimentary basins. Although heavy mineral studies are an appropriate tool for such investigations, this technique has not been systematically utilised until now in this region. We document the heavy mineral

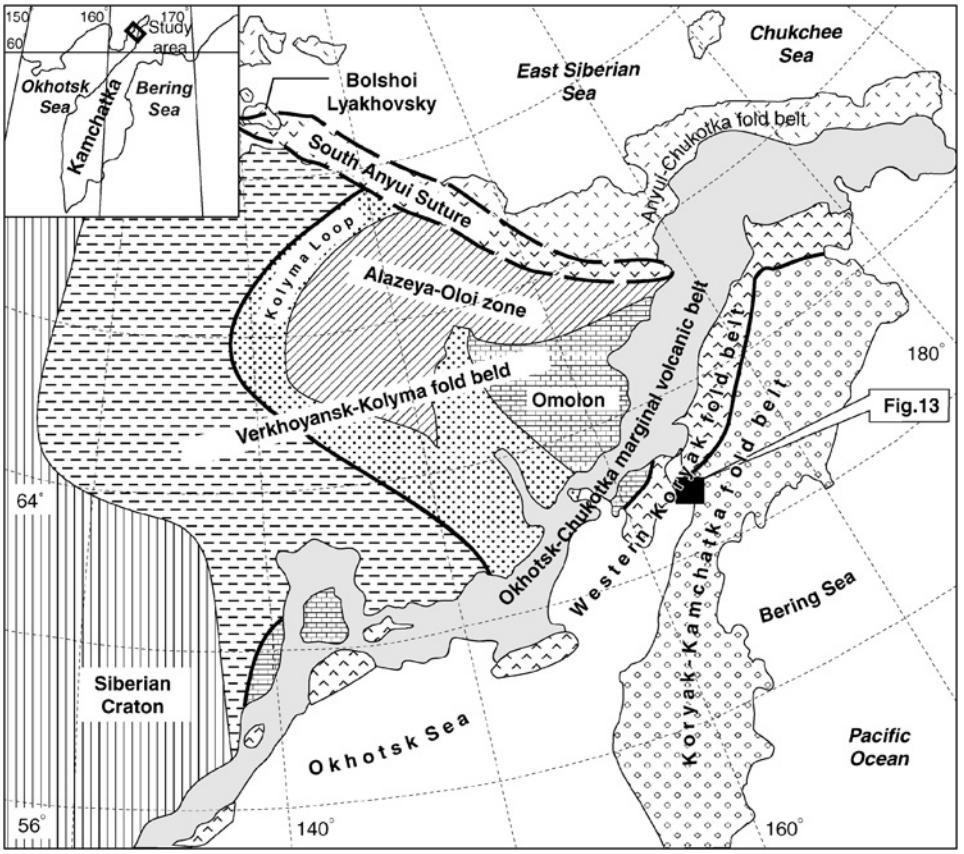

Fig. 12. The major tectonic elements in Northeast Asia (after Sokolov et al., 1999).

distributions in the Cretaceous deposits of Penzhina Bay, and present new data on the heavy mineral associations of Kamchatka's Cretaceous sedimentary basin. Results help reconstruction of the tectonic setting of the basin and its development with time. Heavy mineral associations have been investigated in the Upupkin, Kuyul, and Ainyn terranes (Figs. 12 and 13). The Ainyn Terrane includes the Yelistratov and Mametchinsky peninsulas, which share similar basin development, facies, and heavy mineral compositions.

The stratigraphic charts of Fig. 14 show the geological evolution of the area during the Cretaceous. In Berriasian-Early Albian times, deep-water clastics flysch successions were deposited on the continental slope (Sokolov et al., 1999; Tuchkova, 2003). By the Late Albian, sedimentation had changed from deep to shallow water. The earlier flysch was then deformed by the growth of the accretionary prism and by the accretion of the Kuyul Terrane. From Albian to Santonian times, sedimentation took place on shallow and deep-water shelves and in coastal environments.

Heavy minerals in Berriasian-Valanginian sediments are mainly zircon, tourmaline, apatite and, less abundantly, epidote and garnet, derived from granitic and metamorphic lithologies of the Upupkin and Ainyn terranes (Fig. 15). Metamorphic

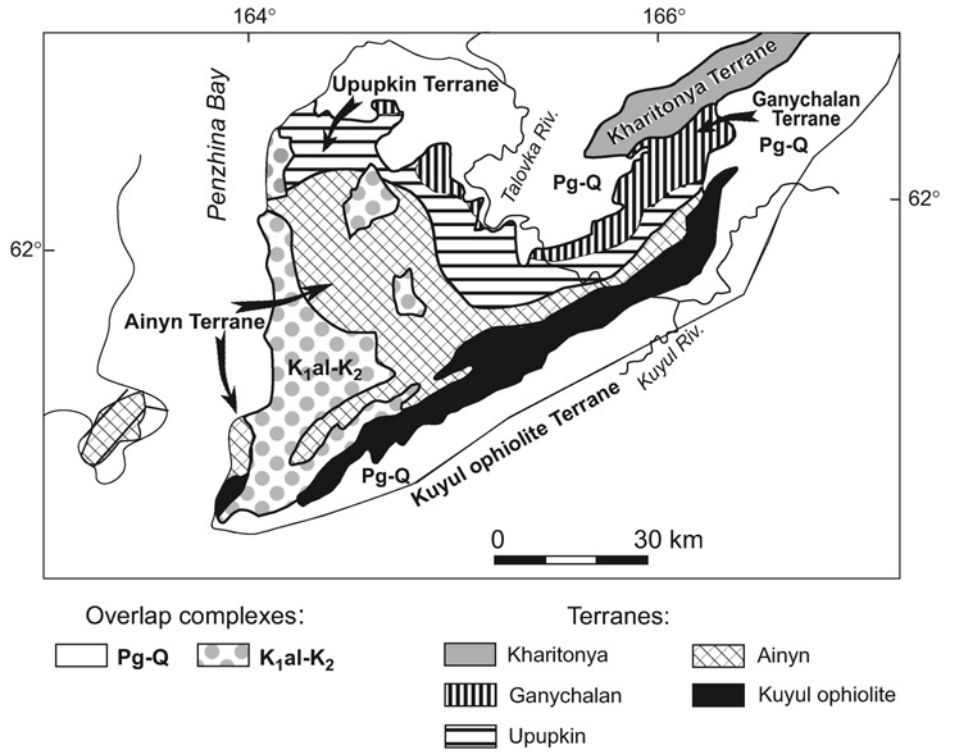

Fig. 13. Generalised terrane map of Penzhina Bay region (after Sokolov et al., 2003).

amphiboles average less than 10%. Magmatic magnetite, ilmenite, and chromite, up to 25–35%, also characterise the sandstones from the eastern part of the region. Magnetite, ilmenite, chromite, and clinopyroxenes predominate in samples from the Kuyul Terrane, but zircon, garnet, apatite, and epidote are also present (Fig. 15).

Heavy minerals from the Hauterivian-Albian sediments are very similar in the different sections (Fig. 16). Magmatic magnetite, ilmenite, clinopyroxenes and occasionally chromite dominate the deep-marine deposits of the three terranes. They are almost free of garnet and the stable/ultrastable group. Amphibole is present only in a few samples in the western part of Penzhina Bay (Yelistratov and southern part of Mametchinsky peninsulas). Epidote is, in most cases, a major constituent.

The Late Cretaceous shallow-marine deposits contain high percentages of zircon, apatite, ilmenite, epidote, tourmaline, and magnetite (Fig. 17). These suites are similar to those of Berriasian-Valanginian sediments, but in the Albian-Cenomanian and Turonian-Campanian part of the succession, abundances of magnetite, ilmenite, and clinopyroxenes increase in the western part of the region (Fig. 17).

The geochemical composition of the heavy minerals, shown in MF-MT-GM plots (Fig. 18), distinguishes, in general, two major heavy mineral suites: one is composed of stable minerals, whereas the second encompasses unstable, volcanogenic species. Complementing the two major groups, evidence of a minor, "exotic", suite is shown

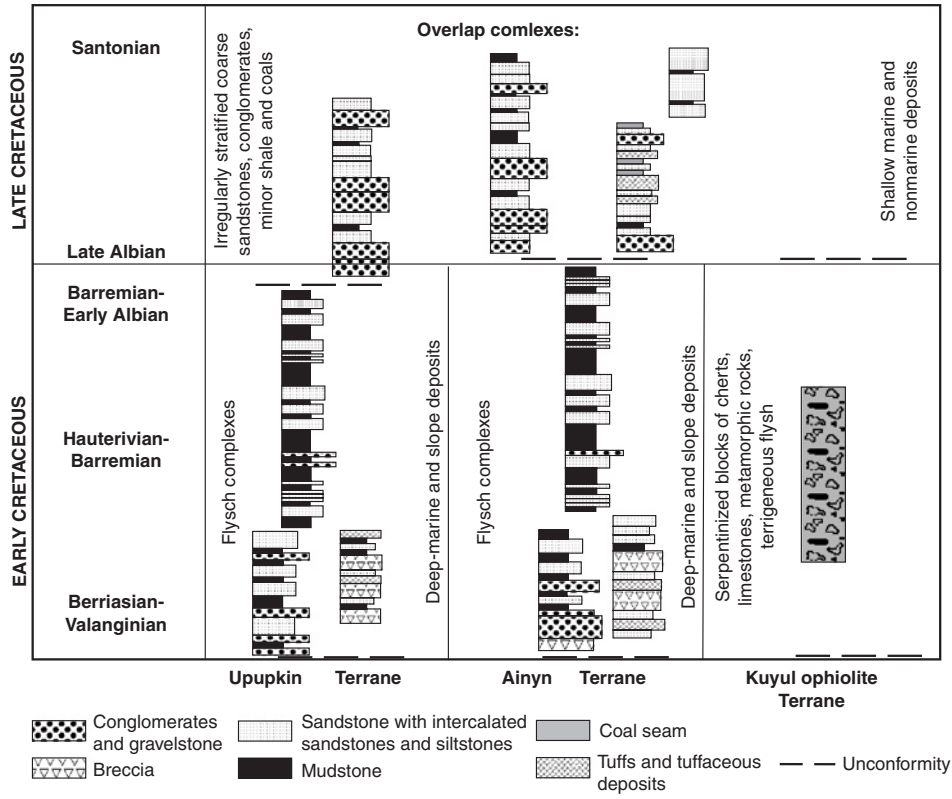

Fig. 14. Generalised lithostratigrapy of the Upupkin, Ainyn, and Kuyul ophiolite terranes.

by serpentinite-bearing sandstones, situated in the northeastern part of the Upupkin Terrane. Another suite, near the western part of the Kuyul Terrane, is distinguished by high abundances of chromite, magnetite, and ilmenite.

Analyses of two sections have enabled reconstruction of sediment provenance and tectonic evolution of the Penzhina area: (1) in the northern region, in the Dlinnaya Mountain of the Upupkin Terrane, ophiolite-derived serpentinite-bearing assemblages have been identified from Hauterivian sandstones (Fig. 16); (2) in the eastern part, chromite-dominated Barremian-Albian sandstones occur, derived from the northern Kuyul ophiolitic rocks (Ainyn Terrane, Vesyolaya river). Epidote is magmatic and is shed by the ophiolites.

Heavy mineral signatures point to two major source provinces for the sediments of the Penzhina area. The zircon, garnet, amphibole and epidote-bearing assemblages, found in Berriasian-Valanginian and Late Cretaceous deposits, were probably derived from the crystalline, medium grade metamorphic basement of the Upupkin and Ainyn terranes. A granitoid or granite-gneiss source, signalled by the abundance of zircon, sphene, and apatite, seems to have played an important role. The second province, associated with island arc volcanics, is indicated by magnetite, ilmenite, and clinopyroxenes in the Hauterivian-Albian formations. A high percentage of detrital chromite records the erosion of the ultramafic unit of an ophiolite body.

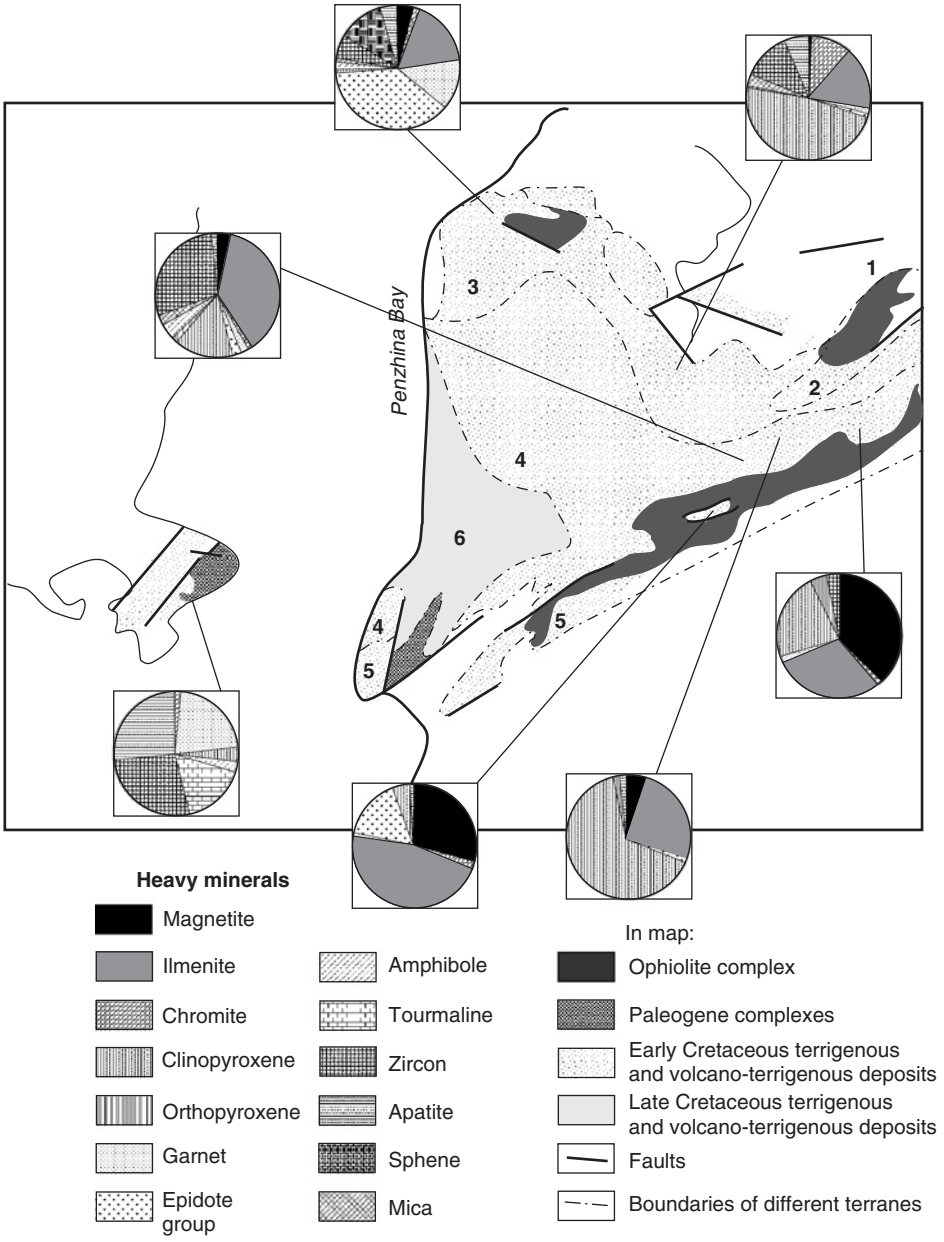

Fig. 15. Average heavy mineral associations in the Berriasian-Valanginian deposits. Numbers in map are the main terranes 1: Kharitonia; 2: Ganychalan; 3: Upupkin; 4: Ainyn; 5: Kuyul ophiolite; 6: Albian-Upper Cretaceous overlap complexes.

According to Sokolov et al. (1999) and Sokolov (2000) the accretionary prism of the Penzhina-Anadyr Terrane consists of Berriasian-Valanginian sediments, accumulated in the deep-seated zone of a forearc, bordered by the Uda-Murgal island arc to the west, and by the accretionary uplift of the Kuyul ophiolites to

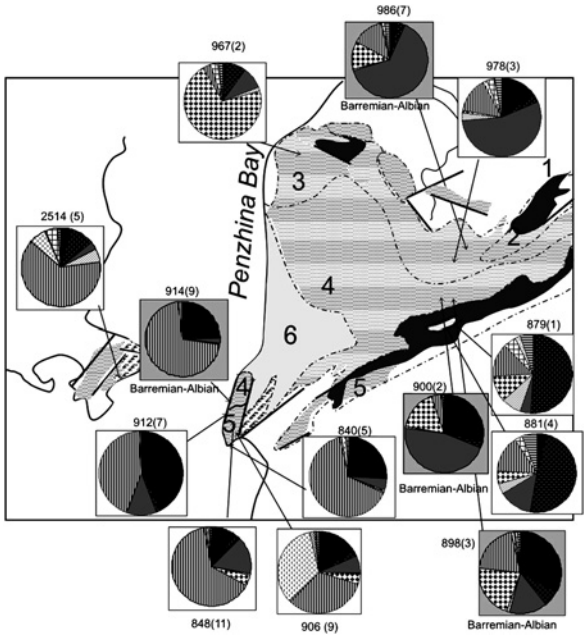

Fig. 16. Average heavy mineral associations in the Hauterivian-Albian deposits. Numbers in parentheses indicate the number of samples used at each location for calculating average heavy mineral compositions. Legend same as in Fig. 15.

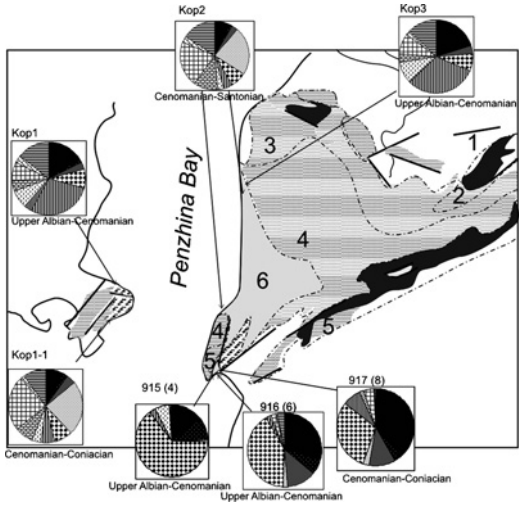

Fig. 17. Average heavy mineral associations in the Albian-Late Cretaceous deposits. Legend same as in Fig. 15.

the east. In the forearc segment of the Uda-Murgal arc, deep-water flysch-type sediments accumulated. They incorporate recycled detritus from the Ainyn and Upupkin terranes, which contain associations of metamorphic origin. In some areas of the Kuyul Terrane sediments predominantly from ophiolitic sources were

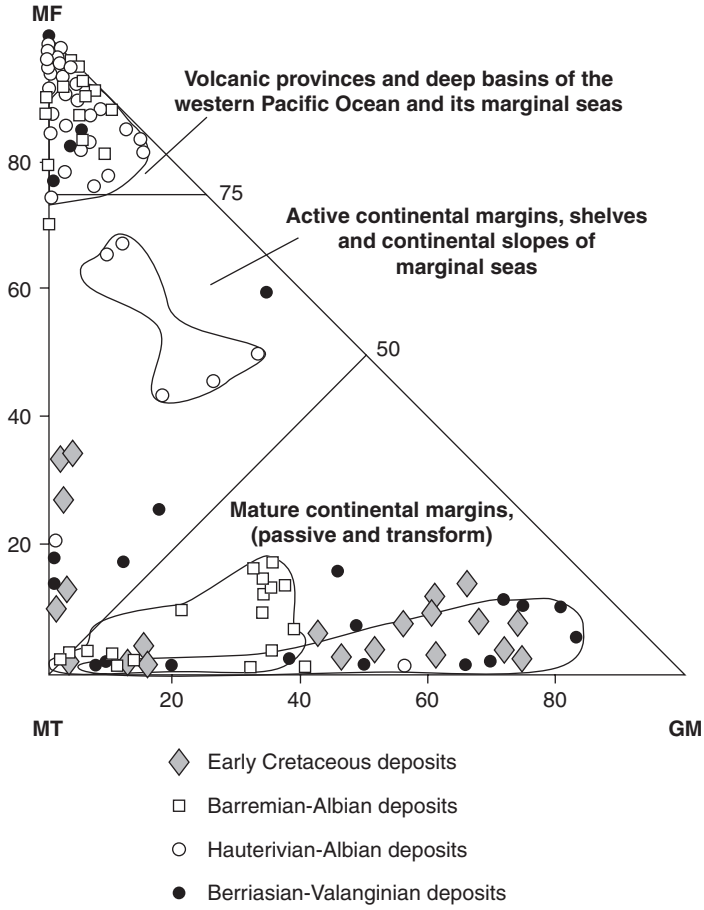

Fig. 18. Correlation of heavy mineral associations from the Penzhina area (sandstones from Upupkin, Ainyn, and Kuyul terranes) and modern sediments from various geodynamic setting on MF-GM-MT diagram (after Nechaev and Isphording, 1993). Legend same as in Fig. 3.

deposited. Hauterivian and Barremian-Albian successions accumulated in similar basins (Fig. 19).

During Albian accretion, Cretaceous sedimentation of the Penzhina Basin changed from deep-marine flysch to a shallow-marine facies. Parallel with the shift in the depositional environment, heavy mineral associations also changed, denoting provenance from continental granitic–metamorphic and basic rocks; one or the other of these lithologies became dominant at different times during the Cretaceous.

Systematic variations in the heavy mineral associations through time reflect the *tectonic evolution* of the region. Tectonic development of the Asian continental margin and of the West Koryak fold belt, which includes the studied region, was related to the sequential accretion of various lithotectonic units to the Asian continent (Sokolov, 2003). Terranes of the Penzhina segment accreted in two stages: (1) pre-Late Albian and (2) during the Late Albian. In the earlier stages (Berriasian-Valanginian), the continental margin acted as the main sediment source. Metamorphic complexes were

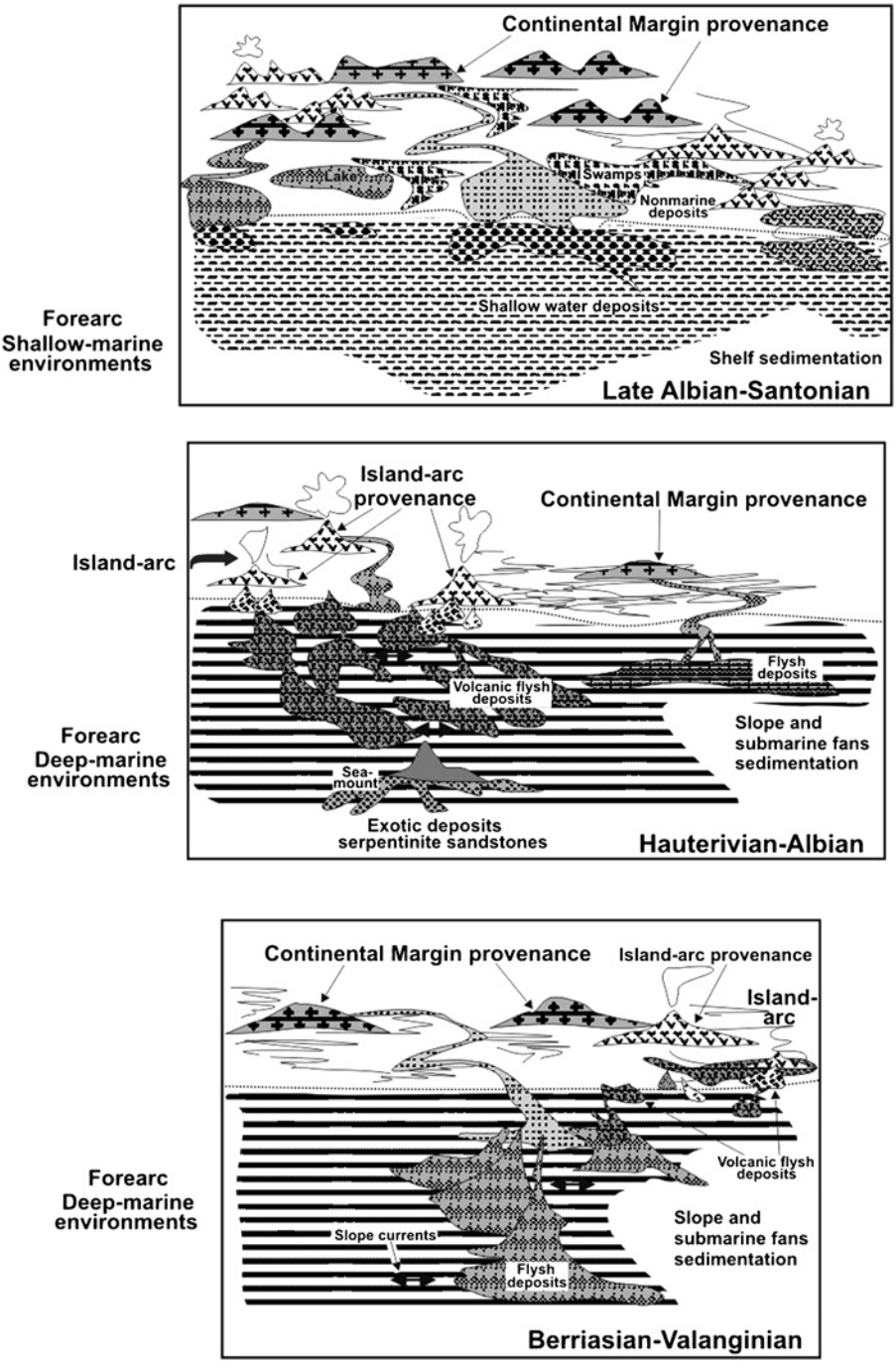

Fig. 19. Model of the Cretaceous sedimentary evolution of the Penzhina Basin, from deep-marine deposits during the Berriasian-Valanginian and Hauterivian-Barremian to shallow-marine—during the Late Albian-Santonian.

eroded and their detritus were delivered to the sedimentary basin by gravity flows and deposited in submarine fans. The low abundance of magnetite and ilmenite indicates a minor influence of island arc volcanism. This was ascertained by the associated volcanic rock fragments and by bulk chemical composition. The dramatic enhancement of volcanism in the Uda-Murgal island arc in the Hauterivian and the erosion of adjacent volcanic edifices resulted in a change of provenance. Heavy mineral associations from volcanics became predominant, whereas the supply of stable minerals from the continental margin declined. The influence of volcanic sources continued in the Barremian and Albian. Following the first stage of accretion, before the Late Albian, the Kharitonia, Ganychalan, and Upupkin terranes had been accreted to the Asian continental margin (Fig. 19). This Middle Cretaceous tectonic rearrangement, caused by the disappearance of the Uda-Murgal island-arc system, changed the environment of sedimentation in the Penzhina Basin. Subsequently, a new subduction zone developed which governed the evolution of the Okhotsk-Chukotka volcanic belt and related sedimentation. During the Late Albian, the second stage of accretion resulted in the accretion of Ainyn and Kuyul Terranes to the Asian continental margin. After the Late Albian, following the disappearance of the Uda-Murgal island-arc, the Okhotsk-Chukotka volcanic belt became the source of volcanogenic detritus to the forearc basins. Following the second stage of accretion, Albian-Cenomanian marine, terrigenous, and Turonian-Early Senonian coal-bearing sequences were deposited in the Penzhina forearc trench of the Okhotsk-Chukotka volcanic belt via numerous fan deltas. Heavy mineral associations from the Upper Cretaceous deposits contain both stable and unstable minerals. Local volcanism of the Okhotsk-Chukotka volcanic belt was active in Albian-Cenomanian and Turonian-Campanian times, reflected by the increasing proportions of volcanic minerals in the Early Albian-Cenomanian deposits.

2.3.2. Olyutorsky Terrane.

The Olyutorsky Terrane is a constituent of the Mesozoic-Caenozoic Olyutorsky-Kamchatka fold belt (Malinovsky, 1993, 1996). The Terrane is situated in the southern part of the Koryak upland region (Figs. 1 and 19), extending toward the northeast along the Bering Sea coast. In the north, it is separated from the Anadyr-Koryak fold belt by the Vatyn Thrust. The Olyutorsky Terrane (Figs. 20 and 21) is a composite of juxtaposed sedimentary units that were once deposited in different environments, probably some considerable distance from their present position. The successions include: Aptian (?)-Turonian volcano–cherty, Coniacian-Palaeocene volcano–sedimentary, Eocene-turbidite, and Oligocene-Pliocene molasse complexes.

The volcano–cherty complex consists of basalts, lava-breccia, tuffs, radiolarian jaspers, and cherts and their clayey alteration products. Mudstones, sandstones, and limestones are rare. The *volcano–sedimentary complex* contains intercalated basalts, tuffs, tephra, volcaniclastic sandstones, cherts, siliceous tuffs and mudstones, mudstones, and cherty-clay. In the upper part of the succession, gravels and conglomerates occur. The turbidite complex encompasses thick, rhythmically alternating sandstones and siltstones, sometimes interrupted by horizons of siltstones, sandstones, gravelstones, basalts, tuffs, tuffaceous-breccia, and mixtites. The molasse complex includes mudstones, sandstones, gravelstones, and conglomerates.

In the Olyutorsky Terrane, detrital heavy mineral signatures define two heavy mineral provinces: Northern and Southern (Fig. 20) (Malinovsky, 1993, 1996).

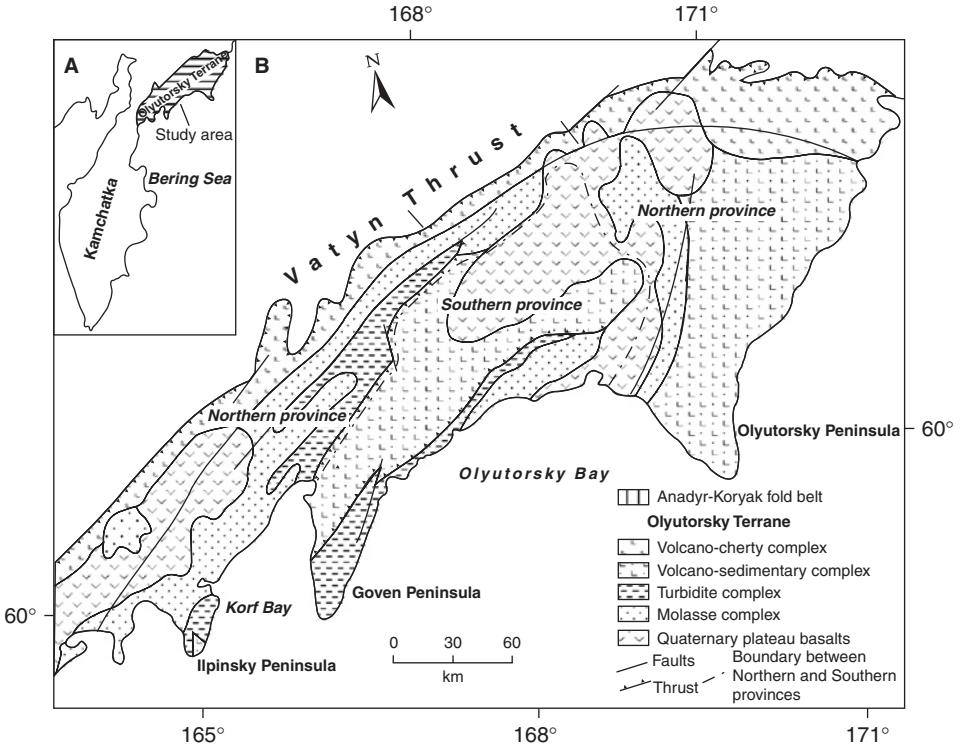

Fig. 20. The location (A) and schematic geologic map (B) of the Olyutorsky Terrane (after Malinovsky, 1996).

In the Northern Province, volcaniclastic, island arc type minerals, such as clino- and orthopyroxenes, magnetite and hornblendes predominate, forming not less than 90% of the total detrital assemblage. Minerals with island arc affinities are dominantly clinopyroxene (with an average of 40–70%, but in one individual case it contains 100% of the heavy mineral suite). Magnetite is less common (average contents in the analysed samples range between 15 and 55%), hornblende makes up 2–30%, and orthopyroxene 1–7%. The high proportion of minerals of the volcanic association, present in the Northern Province, testifies to the erosion of a prominent volcanic hinterland that also contributed synchronous pyroclastic material.

In the Southern Province, the role of the volcanic island arc association was also important. Similarly to the Northern Province, clinopyroxene dominates, although with much lower percentages, viz. ranging from 24 to 40%. Magnetite varies from 10 to 35% and chromite from 6 to 14%, but the content of hornblendes and orthopyroxenes is distinctly lower in *the Southern Province* (3% and 5%, respectively). Sialic minerals (10–39%) are, however, more significant; these include zircon, tourmaline, sphene, apatite, rutile, and garnet, the source of which could be sialic magmatic and older sedimentary rocks. Metamorphic and metasomatic corundum, vesuvianite, anatase, allanite, brookite, sillimanite, staurolite, andalusite, kyanite, and fluorite (as aggregates—up to 8%) are also found. These are absent in the

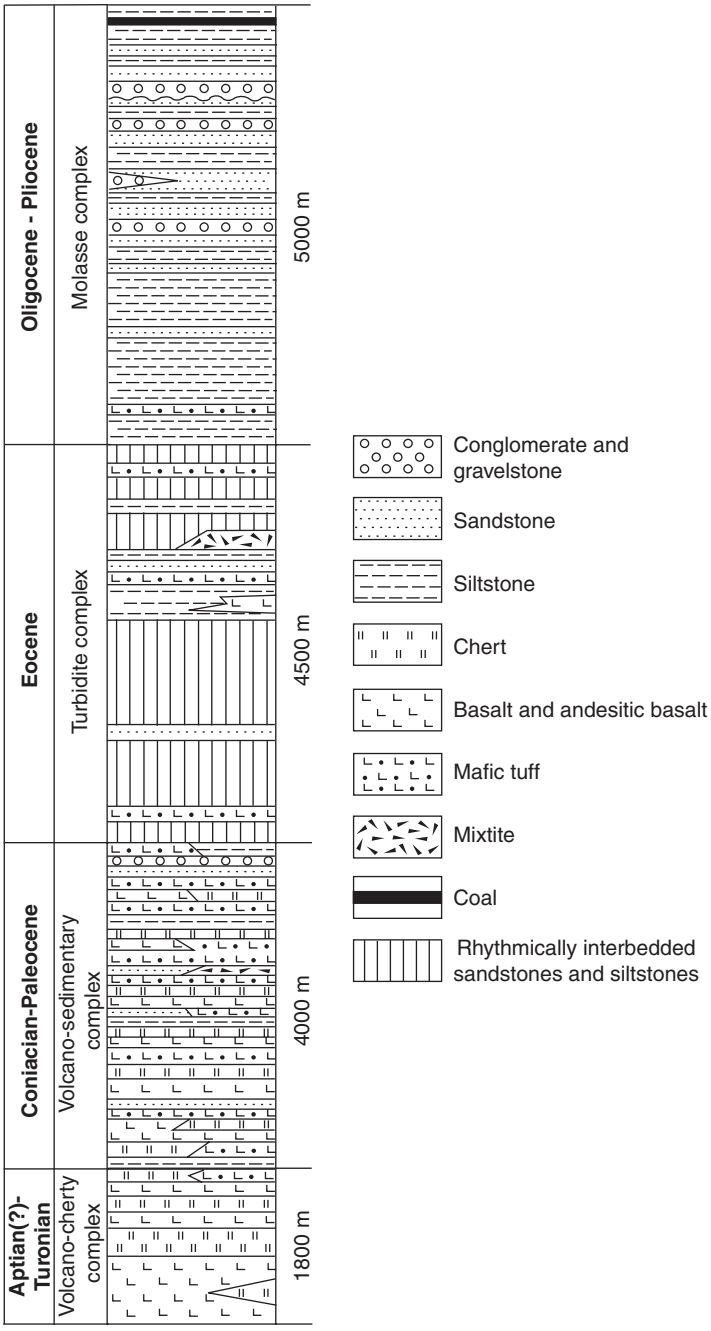

Fig. 21. Generalised lithostratigraphic column of the Olyutorsky Terrane.

Northern Province. The main silicic heavy mineral is zircon (5–25%, occasionally reaching 73%). Apatite (up to 22%), garnet (up to 13%), and rutile (up to 5%) are also present. Other minerals are much rarer. Relatively abundant silicic heavy minerals in the Southern Province suggest granitic–metamorphic continental sources, which made a small but noticeable contribution to the sedimentation.

The evaluation of geochemical data of detrital heavy minerals on the MF-MT-GM and Cpx-Opx-Hb plots (Fig. 3) (Nechaev and Isphording, 1993) allows us to distinguish heavy mineral provenances of both oceanic and island arc origin. The latter resulted from the destruction of an island arc with either an oceanic or a continental foundation. On the MF-MT-GM diagram, all data points of the Olyutorsky Terrane are close to the MF apex, corresponding with sediments of the deep-water depressions of the West-Pacific marginal seas whose main sources of detritus were the island arc volcanics. In the basins of the Southern province, the latter were mixed with continental detritus. The Cpx-Opx-Hb ratios for all points of the Olyutorsky Terrane correspond with an oceanic arc with a small convergence angle of the plates, as suggested by the low content of Opx and Hb (Nechaev and Isphording, 1993).

The nature of the volcanic source of the Olyutorsky Terrane sediments can be identified by the chemical composition of diagnostic detrital heavy minerals. Fig. 4A shows that clinopyroxenes from both provinces of this terrane are diopside and augite. Their origin can be determined on the discriminant diagrams, thus allowing us to distinguish between pyroxenes of basalts from different tectonic settings. In Fig. 4B (after Nisbet and Pearce, 1977), most of the clinopyroxenes correspond with those of island arc basalts but, in part, also with clinopyroxenes from ocean-floor basalts, constituting, probably, some portion of the island arc foundation. This interpretation is supported by the close chemical composition of the Olyutorsky Terrane clinopyroxenes to those from the Vanuatu Trench, which were sourced from the Vanuatu oceanic island arc volcanics. On discrimination diagram 1 in Fig. 5, all pyroxenes cluster near the line demarcating the pyroxenes of alkaline intercontinental basalts and the basalts of the oceanic islands (A) from all other non-alkaline basalts (T). Formally, they would be alkaline basalts, but their low titanium and sodium content prevent them to be confidently related to that group. Diagram 2, which divides non-alkaline basalts into MORB (D) from calc-alkaline and tholeiitic basalts of continental margins and of volcanic island arcs (O), the majority of the Olyutorsky Terrane pyroxenes cluster in the island arc area. In diagram 3, which differentiates island arc pyroxenes into calc-alkaline (C) and tholeiitic types (I), it is apparent that the pyroxenes were derived from tholeiitic basalts.

In Fig. 6 the majority of detrital chromite data points are in the field of volcanic island arcs, whereas the remainder correspond with chromites of intraplate and MORB basalts. The island arc character of the hornblendes is demonstrated by the Ti-Al-Fe diagram (Nechaev, 1991). Their low titanium content suggests they are amphiboles of basic and intermediate island arc volcanics (Fig. 6B). All detrital garnets are almandine (19.49–22.36% Al_2O_3; 22.10–37.27% $FeO + Fe_2O_3$). The garnets (Fig. 6C) most probably originated from acid plutonic and effusive rocks (Kazachenko, 2001) and/or metamorphic sources. This is most likely for the garnets of the Southern Province, which are noticeably different in composition from garnets of the Northern Province, and are associated with sialic minerals.

Heavy mineral associations and the chemical composition of individual heavy minerals identify two principal source regions for the forearc basin sediments of both provinces of the Olyutorsky Terrane. Their lithologies persisted from the Late Cretaceous to the Neogene, throughout the geological history of the terrane. The prominent source for both provinces of the Olyutorsky Terrane was the Cretaceous-Palaeogene oceanic island arc and products of associated synsedimentary volcanism. The second source included an external continental, silicic complex that played a subordinate role, sourcing mainly the Southern province. Concluding from granitic–metamorphic heavy mineral signatures in the Southern province, the continental source formed a significant high that was exposed south of the Olyutorsky Terrane in the current Bering Sea.

2.3.3. Peculney Mountains.
From the Peculney Mountains Ordovician to Early Cretaceous sandstones have been studied. Ordovician sandstones are highly tuffaceous and contain almost exclusively pyroxenes, originating from synsedimentary volcanism. In Silurian and younger sandstones, there are two heavy mineral associations: (1) a dominant mafic suite, including chromite, magnetite, ilmenite, leucoxene, pyroxenes, hornblendes, and epidote and (2) a sialic suite, comprising zircon, sphene, tourmaline, apatite, rutile, and garnet. In the Lower Silurian and Carboniferous sections of the succession, abundant chromite indicates a typical ultramafic source, postulated as an ultramafic, ophiolitic oceanic rise. The Permian and, especially, the Lower Cretaceous sections, have low abundances of chromite, coinciding with increased amounts of ilmenite and magnetite. This may indicate mainly gabbroic source rocks. In the upper part of the Lower Cretaceous, the quantity of the heavy minerals with ultrabasic and mafic signatures diminished. The remaining part of the heavy mineral spectra is occupied by the mafic suite, with abundant pyroxenes, resembling the Ordovician associations. Parallel with temporal changes in the distribution of the mafic associations, a clear trend with a progressive decrease of the sialic component can be detected from the Silurian to Permian. In the upper part of the Lower Cretaceous the sialic continental influence is virtually absent. The chemical composition of chromites from the Silurian sediments shows affinities with the ultrabasic and basic pre-Silurian rocks of the Kuyul ophiolite Terrane (Fig. 13), and therefore, it can be considered as the source of the detritus.

3. SUMMARY OF SEDIMENTATION AND TECTONIC RECONSTRUCTIONS

The north-western part of the Circum-Pacific orogenic belt, spanning the Phanerozoic of the Russian Far East, incorporates a series of lithologies from a lower, ophiolitic pile, through flysch to molasse. These constitute, as a whole, two main zones within this belt: an inner one, situated to the east of volcanic island arcs, and an outer zone which is sialic and rests on Precambrian continental crust. Marine sedimentary basins were situated in different settings adjacent to an active continental margin. These include foreland, borderland, and backarc basins. The inner zone is oceanic, and developed as an island arc, with prolonged intensive volcanic

activity. It supplied large amounts of juvenile mafic material to the sedimentary basins, with sediments accumulating as a series of volcaniclastic greywackes.

The Circum-Pacific orogenic belt comprises two principal sedimentary complexes: arkosic and greywacke. The arkosic complex is characteristic of the outer zone of the north-western part, situated between the Siberian and Chinese cratons. It also occurs as isolated fragments, the Bureya and Khanka massifs, and extends into the Late Cretaceous–Caenozoic East Asia volcanic belt. This complex constitutes the Mesozoic orogenic fold belts and includes the Sikhote-Alin system. It consists mainly of arkosic terrigenous and volcaniclastic rocks, intruded by granitoids of different dimensions, extending to thousands of kilometres. This zone becomes young progressively toward the east from the Palaeozoic to late Early Cretaceous. The mineralogy of the arkosic sediments indicates that the provenance of material in the Mesozoic sedimentary basins was the continental (granitic and metamorphic) crust of the Siberian and Chinese cratons. These contributed sialic heavy mineral associations comprising mainly zircon, sphene, apatite, tourmaline, garnet, sillimanite, rutile, anatase, and brookite.

The greywacke complex is peculiar to the inner zone, situated to the east of the East Asia volcanic belt. Its detrital heavy mineral assemblage is in stark contrast to that of the arkosic complex, and contains associations derived mainly from basic and ultrabasic plutonic and volcanic crustal rocks. The greywackes also incorporate products of volcanic island arc activity. During the initial stages of development, ultrabasic, ophiolite-derived material was the primary sediment constituent. Typical heavy minerals are pyroxenes, chromite, olivine, ilmenite, leucoxene, and hornblendes. Common in both the arkosic and greywacke rocks are magnetite, various garnets, and epidote.

The provenance of the Sikhote-Alin sediments has been interpreted as being the continental Siberian and Chinese cratons, complemented, at the beginning and the close of the Phanerozoic, by minor input from contemporary volcanics. In the Koryak-Kamchatka region sedimentary forearc basins were fed almost entirely by basic rocks amongst which the products of island arc volcanism played a dominant role throughout the Phanerozoic.

Distinctive heavy mineral suites characterise particular plate tectonic settings and indicate provenances, whereas geochemical analysis of individual heavy mineral species serves as a useful tool to define source lithologies and their settings in a plate tectonic context. For example, in our research we used magnetite and chromite compositions to identify, and differentiate between, associations sourced from different types of ophiolites, while the chemistry of detrital pyroxenes identified the main types of volcanic arc sources.

ACKNOWLEDGMENTS

Our work was supported by the Russian Foundation for Basic Research, projects Nos. 02-05-65222, 02-05-64217 and 01-05-64602. We thank K.A. Krylov and D.I. Kudryavtsev for their critical remarks, consultancy, and support in preparing this paper. Dr. Andrew Hanson's careful review and useful suggestions are greatly

appreciated. We thank Professor John F. Dewey for his valuable comments on the revised manuscript. We gratefully acknowledge the editorial help of the editors and their efforts for correcting the English.

REFERENCES

Arai, S., 1992. Chemistry of chromian spinel in volcanic rocks as a potential guide to magma chemistry. Mineralogical Magazine 56, 173–184.

Bersenev, I.I. (Ed.), 1969. Geology of the U.S.S.R. Nedra, Moscow, Vol. 23, 695pp (in Russian).

Hanus, V., Vanek, J., 1983. Deep structure of the Vanuatu (New Hebrides) island arc: intermediate depth collision of subducted lithospheric plates. New Zealand Journal of Geology and Geophysics 26, 133–154.

Kazachenko, V.T., 2001. Petrology and Mineralogy of Hydrothermal Manganese Rocks of the Russian East. Vladivostok, Dal'nauka, 250pp (in Russian).

Leterrier, J., Maury, R.C., Thonon, P., 1982. Clinopyroxene composition as a method of identification of the magmatic affinities of palaeo-volcanic series. Earth and Planetary Science Letters 59, 139–154.

Malinovsky, A.I., 1993. Cenozoic molasses of the Southern Koryak Highland. Vladivostok, Dal'nauka, 228pp (in Russian).

Malinovsky, A.I., 1996. Molasse of the Southern Koryak Highland. structure, lithology, depositional environment, and geologic history. Geology of the Pacific Ocean (Amsterdam) 12, 251–274.

Malinovsky, A.I., Philippov, A.N., Golozoubov, V.V., Simanenko, B.P., Markevich, V.S., 2002. Lower Cretaceous deposits of the Kema River area (Eastern Sikhote-Alin): sedimentary filling of a back-arc basin. Tikhookeanskaya Geologiya 21 (1), 52–66 (in Russian).

Markevich, P.V., Zyabrev, S.V., Filippov, A.N., Malinovsky, A.I., 1997. East flank of the Kiselevka-Manoma terrane: an island arc fragment in the accretionary prism. Geology of the Pacific Ocean 13, 295–338.

Nechaev, V.P., 1991. Evolution of the Philippine and Japan Seas from the clastic sediment record. Marine Geology 97, 167–190.

Nechaev, V.P., Isphording, W.C., 1993. Heavy-mineral assemblages of continental margins as indicators of plate-tectonic environments. Journal of Sedimentary Petrology 63, 1110–1117.

Nechaev, V.P., Markevich, P.V., Malinovsky, A.I., Philippov, A.N., Vysotskiy, S.V., 1996. Tectonic settings of deposition of the Cretaceous sediments from the Lower Amur region, Russian Far East. Journal of the Sedimentological Society of Japan 43, 69–81.

Nisbet, E.G., Pearce, J.A., 1977. Clinopyroxene composition in mafic lavas from different tectonic settings. Contributions to Mineralogy and Petrology 63, 149–160.

Sokolov, S.D., Bondarenko, G.E., Morozov, O.L., Grigoriev, V.N., 1999. The Asian continent-Northwestern Pacific transition zone in the Late Jurassic—Early Cretaceous: theoretical and regional problems of geodynamics. Nauka, Moscow, vol. 515, pp. 30–84 (in Russian).

Sokolov, S.D., 2000. Position of ultramafic rocks in the mount Dlinnaya Section (Penzhina region, Northeastern Russia) and their tectonic interpretation. Byulleten' Moskovskogo Obshchestva Ispytatelei Prirody Otdel Geologichesky 75 (6), 50–55 (in Russian).

Sokolov, S.D., 2003. Accretionary structure of the Penzhina Range in Northeast Russia. Geotectonica 5, 3–10 (in Russian).

Tanahashi, M., 1994. Tectonics of the spreading center in the North Fiji Basin. Bulletin of the Geological Survey of Japan 45 (4), 173–234.

Tuchkova, M.I., 2003. Framing of the Penzhina Bay and Yelistratov and Mametchinskii peninsulas. Tikhookeanskaya Geologia 22 (3), 93–106 (in Russian).

Vasiliev, B.I. (Ed.), 1990. Geological and Geophysical investigations in the Vanuatu region. Vladivostok, Dal'nauka, 268pp (in Russian).

Chapter 32

HEAVY MINERAL CONSTRAINTS ON THE PROVENANCE OF CENOZOIC SEDIMENTS FROM THE FORELAND BASINS OF ASSAM AND BANGLADESH: EROSIONAL HISTORY OF THE EASTERN HIMALAYAS AND THE INDO-BURMAN RANGES

ASHRAF UDDIN[a], PRANAV KUMAR[a], JOGEN N. SARMA[b] AND SYED H. AKHTER[c]

[a]*Himalayan Research Laboratory, Department of Geology and Geography, Auburn University, Auburn, AL 36849, USA*
[b]*Department of Applied Geology, Dibrugarh University, Dibrugarh, Assam, India*
[c]*Department of Geology, Dhaka University, Dhaka-1000, Bangladesh*

ABSTRACT

The Assam-Bengal Basin system, located near the eastern syntaxis of the Himalayas and the northern end of the Indo-Burman Ranges, has received synorogenic sediments of several kilometres thick from these orogenic belts. These deposits provide valuable information on tectonic events, palaeogeography, and evolution of the sedimentary basin. Studies of heavy minerals document temporal variations in detrital compositions reflecting changes in the hinterland.

Heavy mineral weight percentages in the Palaeogene and Neogene samples from the Assam Basin vary from negligible to ~1.5%, and from <1 to 3.5%, respectively. In the complete Cenozoic succession of Assam opaque minerals dominate. Non-opaque heavy minerals in the Assam Palaeogene are zircon, rutile, tourmaline, biotite, chloritoid, epidote, garnet, hornblende, kyanite, staurolite, zoisite, apatite, pumpellyite, and spinel; whereas in the Neogene formations of Assam, these are garnet, chloritoid, topaz, zircon, tourmaline, apatite, kyanite, zoisite, rutile, pyroxenes, and amphiboles. The assemblages become more diverse in Miocene and younger formations. The relatively low diversity and high chemical stability of assemblages in the Palaeogene sediments indicate a homogenous and localised source and, possibly, the effects of intense post-depositional weathering. By contrast, the Neogene successions in Assam show marked variations in heavy mineral distribution.

In the Bengal Basin, Oligocene heavy mineral weight percentages are low (0.2%), and most of the grains are opaque; non-opaque minerals are zircon, tourmaline, and rutile, suggesting intense weathering of the Oligocene sediments. Miocene and younger heavy minerals are much more diverse and include garnet, aluminosilicates, epidote group minerals, pyroxenes, chlorite,

Developments in Sedimentology, Vol. 58, 823–847

ISSN: 0070-4571/doi:10.1016/S0070-4571(07)58032-5

hornblende, tremolite-actinolite, micas, prehnite, pumpellyite, and opaques. In contrast to the Assam Basin, provenance-diagnostic minerals from the Cenozoic successions of the Bengal Basin show a distinctive pattern in their distribution, indicating gradual unroofing of the contributing orogenic belts. The presence of blue-green amphiboles in Mio-Pliocene strata from Pakistan, the Assam Basin, the Bengal Basin, and Bengal Fan signal orogen-wide unroofing of arc-type rocks.

Modal analysis of framework components and heavy mineral analysis indicate that the sediments in both the Assam and Bengal Basins were derived from discrete sources during the Oligocene. Source areas were the incipient uplifted orogenic belts in the Himalayas for Assam, and the Indian craton for the Bengal Basin. Heavy mineral contents in Miocene and younger successions suggest that both the Bengal and Assam Basins received detritus from orogenic hinterlands, i.e., the Himalayas in the north and the Indo-Burman Ranges to the east. Overall, the Assam Basin appears to represent an earlier and more proximal repository of detritus, shed from the Himalayan convergence, whereas the Bengal Basin was a downstream and somewhat younger depocentre.

Keywords: Assam; Bengal Basin; Himalayas; Eastern Himalayan syntaxis; Indo-Burman Ranges; Cenozoic; Himalayan orogeny; Bengal fan; provenance; Himalayan unroofing

1. INTRODUCTION

The east-west trending Alpine-Himalayan mountain belts document important Cenozoic orogenic events as a result of continent/continent collision. Our study area lies in the eastern segment of the Himalayas. The junction of the easternmost Himalayas and the northern tip of the north-south trending Indo-Burman Ranges forms the eastern syntaxis (Fig. 1). To the southwest of this syntaxis is the Assam-Bengal Basin, which records the orogenic and unroofing events of the mountain belts in the synorogenic sediments of the evolving foreland basins.

The Assam Basin is located in close proximity to the eastern syntaxis of the Himalayas, whereas the Bengal Basin is situated farther southwest. Several imbricate thrust faults of the Schuppen Belt of the Assam Basin strongly influenced the evolution of this important basin (Fig. 2). The Bengal Basin is bounded by the Precambrian Indian craton to the west and the Indo-Burman Ranges to the east, and opens to the south into the Bay of Bengal and the Bengal deep-sea fan (Figs. 1 and 2). Kilometres of Tertiary sediments are present in the Assam and Bengal Basins, both as exposures and explored by drillings. The stratigraphic successions of these large foreland basins have not been studied well compared with those of the western Himalayas. Synorogenic Cenozoic sediments filled the Assam and Bengal Basins, which were probably, in part, remnants of an ocean basin during early development (Graham et al., 1975). The sediment in both basins preserves a more or less continuous record of the orogenic events. As a result of collision and sedimentation in the basins, tectonic events, such as flexural loading and basement faulting, led to the formation of complex foreland basins of dramatic topographic relief and geometry (Evans, 1964; Uddin and Lundberg, 2004). The topographic relief is clearly attributed to under-thrusting of India beneath Asia, resulting in buoyant doubly crustal thickness at the base of the Himalayas.

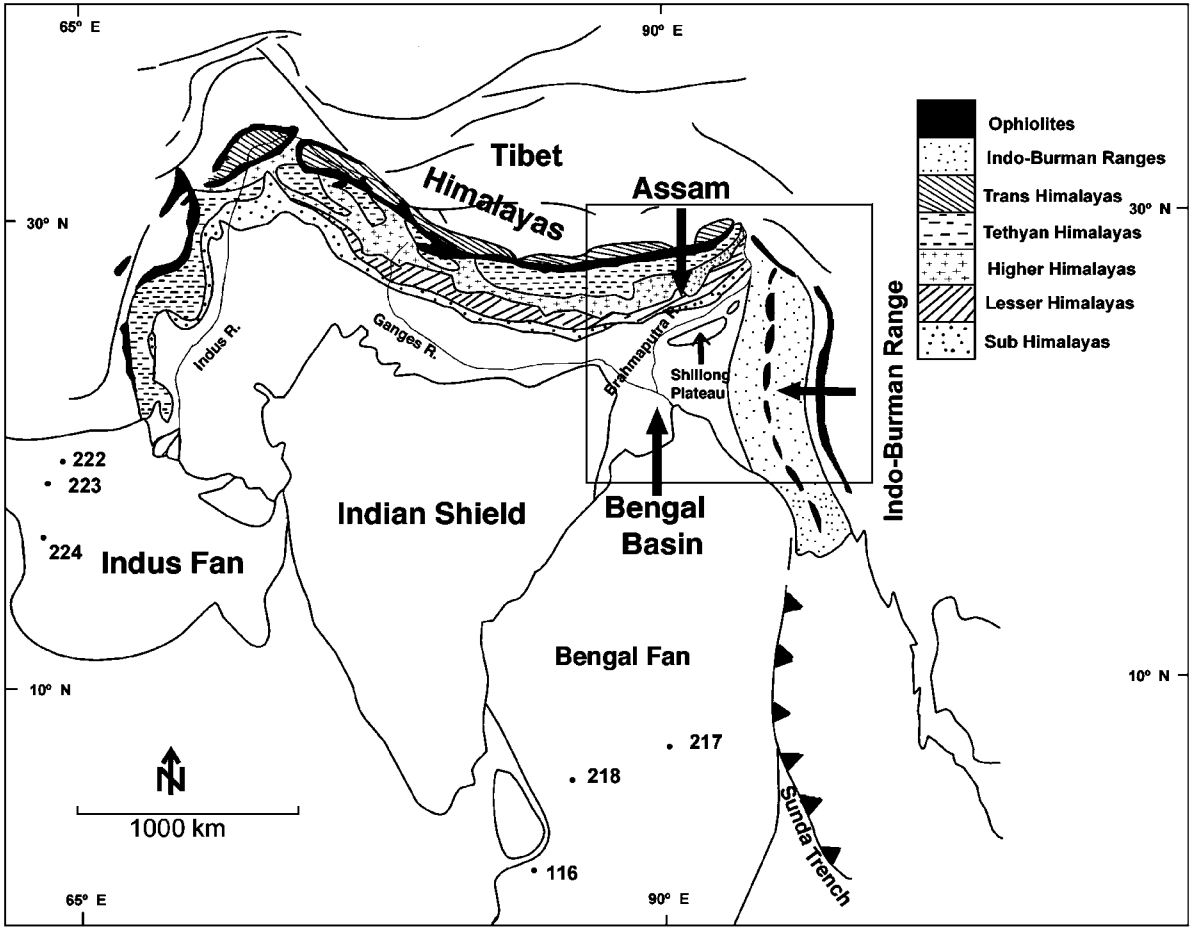

Fig. 1. Map showing the major tectonic framework of the study area, including the Assam and Bengal Basins. Also shown are locations of the DSDP and ODP sites in the northern Indian Ocean (modified after Uddin and Lundberg, 1998b).

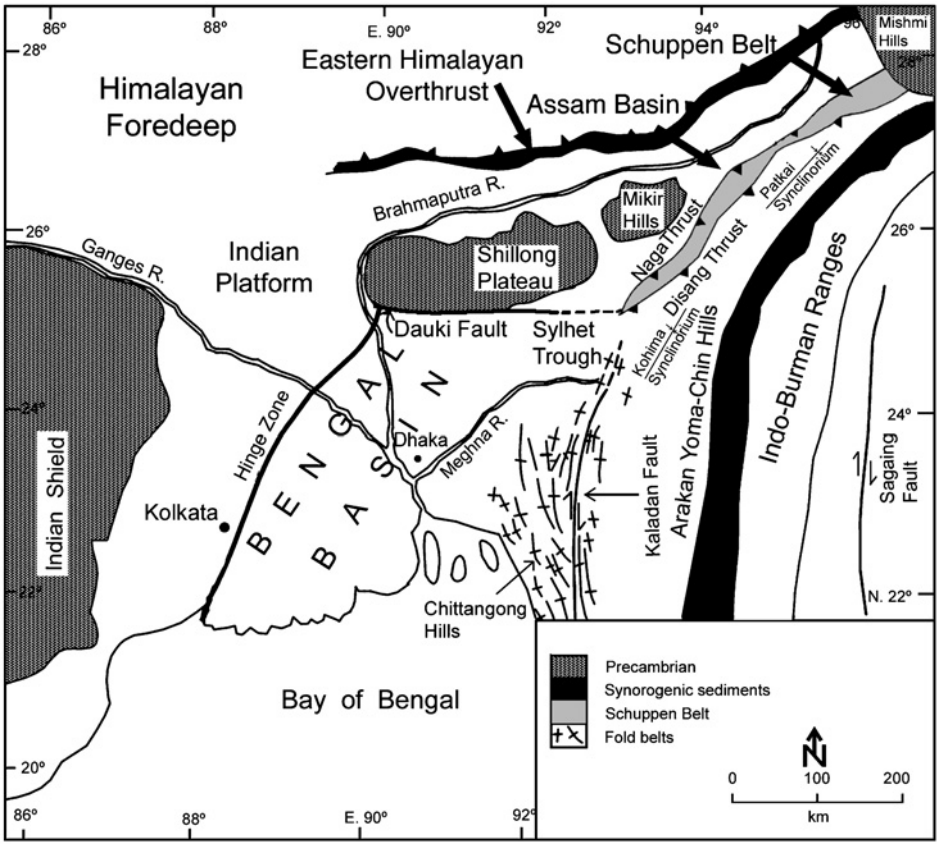

Fig. 2. Map showing the Assam and Bengal Basins and their tectonic elements such as the Eastern Himalayas and Indo-Burman Ranges. Areas enclosed by the Naga and Disang thrusts form the Schuppen Belt. Samples for this study were collected from the northeastern part of the Schuppen Belt of the Assam Basin and from outcrops in the eastern hills (Sylhet Trough and Chittagong Hills), and from cores from petroleum exploration drill holes in the Bengal Basin. The Shillong Plateau, Mikir Hills, and Mishmi Hills are uplifted blocks of Precambrian massifs. The Naga Thrust is also known as Naga Hills. The Dauki Fault demarcates the Shillong Plateau from the Sylhet Trough of the Bengal Basin. The Kaladan Fault, located east of the Bengal Basin, separates the Burmese side from the Bengal Basin (modified after Hutchison, 1989).

Detrital heavy minerals can provide important provenance information by complementing overall modal analysis of sandstones (Morton, 1985; Najman and Garzanti, 2000). In the case of relatively proximal synorogenic sediments, which are typically eroded prior to extensive weathering, transported over relatively brief intervals, and deposited rapidly, heavy mineral assemblages may closely reflect the petrology of source area complexes. In previous studies, heavy mineral analysis has proven to be effective in provenance reconstruction of sediments in the Himalayan foredeep in the east (e.g., Sinha and Sastri, 1973; Uddin and Lundberg, 1998a) and the west (e.g., Chaudhri, 1972; Cerveny et al., 1989), and in deep-sea cores of the

Bengal Fan (Yokoyama et al., 1990; Amano and Taira, 1992). Their analysis has been instrumental in determining the nature of source rocks, in reconstructing the paths of ancestral fluvial systems, and in establishing relationships of source rocks to unroofing of the Himalayas.

In this study, we report semi-quantitative analyses of heavy mineral assemblages in representative sandstones from Oligocene through Pleistocene strata of the Assam Basin, and compare these with existing heavy mineral data from coeval Cenozoic successions from the Bengal Basin (Uddin and Lundberg, 1998a), in order to help constrain the erosional history of the eastern Himalayas and the Indo-Burman orogens. This was accomplished by determining the relative abundance of all important heavy mineral species preserved in each stratigraphic unit, by recognising dominant members of mineral groups, identifying the first stratigraphic appearances of key minerals, evaluating associations or parageneses of specific heavy minerals, and establishing diagnostic minerals for stratigraphic levels in selected sections. Our further aim was to evaluate progressive changes in the rock types exposed to erosion through the history of the mountain belt. We also compared the results with existing data sets on equivalent sediments in the Siwalik deposits of Pakistan (Cerveny et al., 1989), northwest India (Chaudhri, 1972) and northeast India, including Assam (Sinha and Sastri, 1973). Data are compared with available information on regional source rock lithologies in the Indian craton and adjacent orogens (Fig. 1). One of the prime objectives of our project was to gain an insight into the pre-Miocene unroofing history of the eastern Himalayas and the Indo-Burman Ranges, as preserved in the successions of the Assam and Bengal Basins which predate the oldest (17 Ma) strata recovered by deep-sea drilling in the Bengal Fan (Yokoyama et al., 1990).

2. GEOLOGICAL FRAMEWORK OF THE ASSAM-BENGAL SYSTEM

The Assam-Bengal system is bounded to the west by the Indian craton. Crystalline rocks, predominantly of gneisses of Precambrian age make up the bulk of the Indian craton that is sporadically overlain by Permian Gondwana deposits and Cretaceous flood basalts of the Rajmahal trap (Hutchison, 1989). The Himalayan mountain ranges are located to the north of the mammoth Assam-Bengal system. The Himalayas have six longitudinal lithotectonic units juxtaposed along generally north-dipping thrust faults (Le Fort, 1996). From north to south, these are: (1) Trans-Himalayas consisting of calc-alkaline plutons; (2) Indus suture zone, exposing ophiolitic bands representing the zone of collision between India and Eurasia; (3) Tibetan Himalayas, represented by fossiliferous Cambrian to Eocene sediments; (4) Higher Himalayas, located north of the Main Central Thrust, composed of schists, gneisses, and leucogranites; (5) Lower or Lesser Himalayas, composed of unfossiliferous Precambrian and Palaeozoic sedimentary rocks, and crystalline rocks; and (6) Sub-Himalayas, representing Miocene to Pleistocene molasse-type deposits of the Siwaliks. The north-south trending Indo-Burman Ranges, toward the east and south of the Assam-Bengal system consist of early Tertiary synorogenic sediments, with turbidites and schists including also ophiolitic belts.

The Assam Basin, located in northeastern India, is bounded by the eastern Himalayas in the north, the Mishmi Hills in the northeast, the Indo-Burman Ranges

in the east and southeast, the Bengal Basin in the southwest, and the Shillong Plateau in the west (Fig. 2). Crustal material of a pre-Gondwana landmass outcrops in the Mikir Hills, the Shillong Plateau, and the Mishmi Hills, most of which lie outside Assam. Geomorphologically, the Assam and Bengal Basins are separated by the Mikir Hills, the Shillong Plateau, and the Schuppen Belt. These crustal rocks form the basement upon which Cretaceous to Holocene sediments were deposited. The Brahmaputra River has been a major geomorphic feature and has influenced the sedimentological characters of the Assam and Bengal Basins.

The study area in Assam is in Digboi-Margherita, located in the northeastern part of India, in the northeastern part of the Schuppen belt, which consists of a series of imbricate thrust faults located between the Naga Thrust in the northwest and the Disang thrust in the southeast (Fig. 2; Rangarao, 1983). The Digboi-Margherita area is geologically important, as it is located in close proximity to both the Himalayan and Indo-Burman Ranges. Similar to the Himalayas, the Indo-Burman Ranges have experienced geological events resulting from multiple convergence of the Indian plate with the Eurasian plate and the Burmese platelet (Curray et al., 1979). Several kilometres of sediment have been deposited in the Digboi-Margherita area since the Eocene as a direct response to the collision-induced uplift of the Himalayas and the Indo-Burman Ranges.

The tectonics of northeastern India and northwestern Myanmar are controlled by north-south plate convergence along the Himalayas and east-west plate convergence along the Indo-Burman Ranges. A 230 km-wide active orogenic belt associated with eastward subduction of the Indian plate beneath the Burma plate developed as a result (Fig. 1) (Brunnschweiler, 1966; Le Dain et al., 1984; Sengupta et al., 1990; Johnson and Nur Alam, 1991). The northernmost extension of the Indo-Burman Ranges merges with the east-west-trending Himalayas at the eastern Himalayan syntaxis. The eastern Himalayan overthrust, initiated in the late Miocene or Pliocene (Le Fort, 1996), forms the northern margin of the Indo-Gangetic foredeep (Figs. 1 and 2). The continental crust of India forms the basement of the sediments in the Assam and Bengal Basins. In the Assam Basin, the continental crust is exposed in the Shillong Plateau, Mikir Hills, and various other small isolated outcrops (Fig. 2). These are the northeastern extension of the Indian Peninsular complex. The Shillong Plateau, which is a major geomorphic feature in the region, was uplifted to its present height in the Pliocene (Johnson and Nur Alam, 1991). The southern edge of the plateau is bounded by the Dauki Fault (Fig. 2) (Johnson and Nur Alam, 1991).

The Bengal Basin, further downstream of the River Brahmaputra, has two broad tectonic provinces: the shallower Precambrian Indian platform (adjacent to the Indian Shield) to the northwest and west, and the deeper part to the south and east (Uddin and Lundberg, 1998a, b). A northeast-trending hinge zone separates these two provinces (Fig. 2). The Bengal foredeep is a zone of extremely thick sedimentary successions overlying deeply subsided basement (Paul and Lian, 1975). Thick successions of the foredeep basin fill have been uplifted strongly along the northern and eastern margins of the Sylhet Trough, in northeastern Bangladesh, and also along the Chittagong fold belts of eastern Bangladesh. The Sylhet Trough, also known as the Surma Basin, is an important tectonic element that holds abundant hydrocarbon reserves (Johnson and Nur Alam, 1991). The Chittagong fold belts comprise tight NNW-trending folds along the eastern edge of the foredeep. The Kohima-Patkai

synclinorium is developed in the southern and southeastern parts of the Schuppen Belt and includes the folded belt of the Sylhet Trough and Chittagong Hills (Fig. 2) (Dasgupta, 1984). The fold belts of the Chittagong Hills and Sylhet Trough represent a series of north-south trending anticlinal ridges and synclinal valleys, an arcuate belt that is convex towards the west. The fold belt shows an increase in structural complexity towards the east, into the Arakan Yoma Chin Hill and the Indo-Burman Ranges (Fig. 2). The Indo-Burman Ranges are bounded by two north-south trending right lateral faults, Sagaing to the east and Kaladan to the west, adjacent to the Bengal Basin (Uddin and Lundberg, 2004). These large-scale, regional folds of the eastern Bengal Basin and the imbricate thrust belt of the Naga Thrust developed through compression during subduction (Fig. 2) (Saikia, 1999).

3. STRATIGRAPHY

The stratigraphy of the Assam and Bengal Basins was established initially by work on outcrops, augmenting it with the results of exploratory drilling in the 1890s in Assam, and in the 1930s in the Bengal Basin (Khan and Muminullah, 1980). The Cenozoic stratigraphy of the Bengal Basin has long been based on lithostratigraphic correlations to previously studied strata in Assam (Evans, 1964; Holtrop and Keizer, 1970; Khan and Muminullah, 1980). Lithofacies and petrologic research, however, questions the similarity of these neighbouring foreland basin successions in the eastern Himalayas. The present stratigraphic framework of these basins has been refined by subsequent studies of palynology (e.g., Baksi, 1972; Reimann, 1993), micropalaeontology (Rangarao, 1983; Banerji, 1984) and seismic stratigraphy (Salt et al., 1986; Lindsay et al., 1991).

Palaeogene successions are much thicker in Assam (Table 1). The Eocene Disang strata (> 3 km thick) in the Assam Basin are almost non-existent in the Bengal Basin. The Disang Group is considered as the deep-marine facies in upper Assam, equivalent to the Sylhet and Kopili Formations of Eocene age to the south in the lower Assam and the Bengal Basin (Table 2) (Rangarao, 1983). The Disang sediments are fine-grained, much indurated, and represents deep marine deposits in an arc-trench system (Uddin et al., 1999). The thick Oligocene Barail strata are more prominent in the Assam Basin compared to the Bengal Basin. The predominantly arenaceous Barail unit is subdivided into three formations (Naogaon, Baragolai, and Tikak Parbat Formations) in Assam, with abundant coaly material in the youngest, Tikak Parbat Formation. The Barail unit of the Bengal Basin is also predominantly arenaceous, consisting mostly of quartzose sandstones (Uddin and Lundberg, 1998b). The Palaeogene sediments are highly deformed and weakly metamorphosed in Assam, whereas deformation is very limited in the Bengal Basin. Depositional successions in Assam suffered syn- and post-tectonic deformation resulting in NW-verging thrusts that resulted in migration of depositional lobes (Rangarao, 1983). An important widespread unconformity occurs at the top of the Barail unit in the Assam-Bengal Basin (Evans, 1964). The unconformity is identified by an abrupt change in bed thickness and the presence of a conglomerate between the Barail and Surma units in Assam, and by a laterite bed in the Bengal Basin. This widespread unconformity is marked as the Oligocene/Miocene boundary (Rangarao, 1983). The

Table 1. General stratigraphy of the Assam Basin (modified after Bhandari et al., 1973; Rangarao, 1983)

Chronostratigraphy		Unit	Thickness (m)	Brief lithology
Pleistocene	Moran Group	Dihing Formation	> 500	Sandstones with coarse carbonaceous shale
Pliocene		Namsang Formation	> 1000	Sandstones and clays with thin bands of coal seam
Unconformity				
Mio-Pliocene	Tipam Group	Girujan Clay	2300	Clay with siltstone and sandstone "alterations"
		Tipam Sandstone	2300	Sandstones with a few thin clay bands
	Surma Group	Boka Bil Formation	400	Grey shale, associated with sandstone
		Upper Bhuban Formation	400	Fine-grained sandstone, silt, shale, and mudstone
		Lower Bhuban Formation	> 450	Sandy shale, mudstone, and siltstone
Unconformity				
Oligocene to Eocene	Barail Group	Tikak Parbat Formation	700	Sandstones, thin-bedded grey sandy siltstone
		Baragolai Formation	2700	Predominantly shale with subordinate thin sandstone beds and prominent coal seams
		Naogaon Formation	1040	Thinly bedded sandstone, thin subordinate shale
Eocene	Disang	Upper Disang Formation	> 1000	Dark-grey splintery shale rich in carbonaceous matter and massive siltstone with concretions
		Lower Disang Formation (not exposed)	> 1000	Fine-grained sandstone with subordinate shale
Unconformity				
Pre-Eocene	Deragaon Formation (not exposed)		~250	Inferred to be fine grained sandstones and argillites

Table 2. Generalised Cenozoic stratigraphic units of the Bengal Basin (modified after Uddin and Lundberg, 1998a)

Chronostratigraphy	Unit		Thickness (m)	Brief lithology
Pliocene to Pleistocene	Dupi Tila Sandstone		300–500	Medium to coarse grained, massive to cross-bedded, variously coloured sand(stone) with pebbles and clay galls
Late Miocene to Pliocene	Tipam Group	Girujan Clay	70–1000	Brown to blue mottled clay with calcareous nodules
		Tipam Sandstone	80–1100	Yellow-brown to orange, medium to coarse grained, massive and cross-bedded, sand(stone) with pebbles and coal fragments
Unconformity				
Middle to Late Miocene	Surma Group	Boka Bil Formation	300–1400	Alternation of bedded and rippled mudstone, siltstone and sandstone with calcareous concretions; top is marked by the "upper marine shale"
Early to Middle Miocene		Bhuban Formation	250–1700	Light grey to light yellow bedded siltstone, sandstone and sandy mud in top unit; blue to yellowish grey silty and sandy mudstone in the middle unit; bedded siltstone, sandstone and sandy mud in the lower unit
Unconformity				
Oligocene	Barail Formation		45–1600	Pink, massive, medium- to coarse-grained sand(stone)
Late Eocene	Kopili Formation		7–150	Thinly bedded, fossiliferous mudstone
Middle Eocene	Sylhet Limestone		90–240	Nummulitic limestone

magnitude of this unconformity decreases basinward to the south, in step with the presence of successive formations of the Surma Group (Rangarao, 1983).

Neogene strata, deposited in both the Assam and the Bengal Basin, are relatively similar in composition compared to the compositional difference in the Palaeogene deposits between the two basins. Depocentres shifted throughout the early Miocene in Assam, mostly toward the south thus resulting in deposition of thicker units (Surma Group, including the Bhuban and Boka Bil Formations) in the Bengal Basin. In the late Miocene to Pliocene, the units (Tipam Group, including Tipam Sandstone and Girujan Clay) deposited in the Schuppen Belt are thicker, however, compared to the Bengal Basin. This is due to channel shifting in the locally under-filled Assam Basin, resulting from tectonics within the thrust belts (Fig. 2). Depocentres shifted again (Pliocene-Pleistocene) toward the south as a result of encroaching mountain fronts close to the Assam Basin, resulting in the deposition of the Moran sediments. The Moran-equivalent unit in the Bengal Basin is known as the Dupi Tila Formation (Table 2). Compositionally, Neogene sediments in both the Assam and Bengal Basins are quartzolithic to quartzofeldspathic, presumably because of provenance from the approaching orogenic fronts (Uddin and Lundberg, 1998b; Kumar, 2004).

4. METHODS

Approximately 150 g of each sample were crushed to disaggregate the sandstone into discrete mineral grains. In order to evaluate the general grain-size distribution of heavy minerals and to assess the optimum size fractions for analyses, sediments were sieved at 1 phi intervals from 0 to 4 phi (1 to 0.063 mm). Resulting analysis showed that the 2–3 phi (0.250–0.125 mm) and 3–4 phi (0.125–0.063 mm) fractions of Assam Basin sediments generally contain the highest concentration of heavy minerals. For heavy-mineral grain counting the 2–3 phi fractions were used because the grains were easier to identify under the petrographic microscope. The 2–3 phi fractions were separated using a magnetic separator into 0.4, 0.8, and 1.2-A magnetic fractions based on mass magnetic susceptibility. By grouping the heavy minerals into different fractions based on magnetic susceptibility, their identification was facilitated. The 0.4-A magnetic group at slide slope 20° separates out ilmenite, garnet, olivine, chromite, and chloritoid. The 0.8-A group at slide slope 20° separates out hornblende, hypersthene, augite, actinolite, staurolite, epidote, biotite, chlorite, and tourmaline (dark). The 1.2-A group at slide slope 20° separates out diopside, tremolite, enstatite, spinel, staurolite (light), muscovite, zoisite, clinozoisite, and tourmaline (light). At the slide slope of 5°, the magnetic fraction at 1.2-A separates out sphene, leucoxene, apatite, andalusite, monazite, and xenotime. The non-magnetic fraction includes zircon, rutile, anatase, brookite, pyrite, corundum, topaz, fluorite, kyanite, sillimanite, anhydrite, and beryl (Hess, 1966).

Slide mounts were then made of each magnetically defined heavy mineral subfraction by sprinkling mineral grains (usually more than 300) onto a slide in a drop of mineral oil with a refractive index of 1.550. Mineral identification was carried out with a petrographic microscope using a modification of the Fleet method (Fleet, 1926), in which nearly all identifiable grains (more than 300) on each microscope

slide were counted. Grains identified from each magnetically separated fraction were then added together to calculate the frequency percentage of heavy minerals present in 2–3 phi size fraction of a sample. Twenty-five different heavy-mineral species were identified, including opaque minerals as a single group.

5. RESULTS

5.1. Assam Basin

Semi-quantitative point-counting results for heavy minerals from the Assam Basin sediments are presented in Table 3. Total heavy mineral contents in the Oligocene sandstone from Assam range from 1.5 weight percent, to sometimes as low as 0.1%. Heavy mineral weight percentages in various units in the study area in Assam, from old to young, are 1.55 (Barail Group), 0.73 (Surma Group), 1.86 (Tipam Group), and 2.47% (Moran Group) (Fig. 3). Heavy mineral assemblages show variations through time and are most diverse in the Miocene and younger formations.

The most common particle size for the Assam Basin heavy minerals is 2–3 phi (fine sand), with 41–66% of the heavy fraction falling into this interval. Most of the remaining heavy fraction is roughly evenly spread between the 1–2 and 3–4 phi intervals. The 0–1 phi fraction comprises generally less than 1% of total heavy minerals. Heavy mineral weight percentages in the Oligocene and post-Oligocene samples from Assam range from negligible to ~1.5%, and from <1 to 3.5%, respectively. Opaque minerals dominate over the non-opaque varieties in the whole Cenozoic succession of Assam (Fig. 3).

The non-opaque minerals identified in the Oligocene succession of Assam are zircon, rutile, tourmaline, biotite, chloritoid, epidote, garnet, hornblende, kyanite, staurolite, zoisite, apatite, pumpellyite, and spinel (Fig. 4). Heavy minerals present in the Neogene formations are garnet, chloritoid, topaz, zircon, tourmaline, apatite, zoisite, epidote, staurolite, rutile, pyroxenes, tremolite-actinolite, chlorite, and aluminosilicates (Table 3; Fig. 4). The assemblages are generally dominated by opaque minerals (88%). The ZTR (zircon-tourmaline-rutile; Hubert, 1962) index decreases from the Oligocene to the younger units (Table 3). The ZTR in the Barail, Surma, Tipam, and Moran groups is 32.52, 14.22, 13.10, and 10.47%, respectively. Miocene and younger sands and sandstones have lower amounts of opaque minerals (~25% of the total heavy minerals), and correspondingly higher percentages of diverse non-opaque assemblages (Table 3; Fig. 4).

Of the ultra-stable heavy minerals, tourmaline is much more abundant than zircon and rutile throughout the succession. Tourmaline grains are mainly iron- and magnesium-bearing, assessed from their strong pleochroism and absorption (Mange and Maurer, 1992). Although garnets are present in Oligocene samples, they are more abundant in the younger units (Fig. 4). Heavy mineral assemblages of Miocene sands and sandstones are dominated by chlorite/chloritoid and garnets. All other groups are less dominant. Most garnets are almandine, with some compositions approaching grossular; pyrope contents rarely exceed 35% (Kumar, 2004). Aluminosilicate minerals as a group (i.e., sillimanite, kyanite, and andalusite) are sparse

Table 3. Normalised abundances of heavy minerals, Assam Basin, India

Number of samples	Oligocene	Miocene	Miocene-Pliocene	Pliocene-Pleistocene
	Barail Group	Surma Group	Tipam Group	Moran Group
	$N = 4$	$N = 5$	$N = 3$	$N = 4$
Total heavy minerals (wt% of total framework grains)	1.55	0.73	1.86	2.47
Total opaque minerals (as % of total heavy minerals)	68.0	35.0	24.0	22.0
Zircon	6.3	1.9	2.4	1.4
Tourmaline	14.6	7.2	6.4	5.8
Rutile	17.5	5.1	4.3	3.3
ZTR index*	38.6	14.2	13.1	10.5
Sillimanite	0.0	3.8	1.0	1.9
Kyanite	3.3	3.5	4.0	3.6
Andalusite	1.6	1.4	1.0	1.7
Staurolite	8.1	3.7	6.4	4.7
Epidote	2.0	1.4	2.9	3.3
Zoisite and clinozoisite	1.2	3.5	1.0	1.1
Pyroxene	6.5	2.8	5.5	2.2
Garnet	18.7	11.4	36.1	43.0
Chlorite and chloritoid	1.6	28.9	23.3	18.5
Hornblende	3.3	5.6	1.3	6.9
Tremolite and actinolite	4.8	7.0	1.1	0.6
Glaucophane	0.0	1.4	0.0	0.0
Biotite and muscovite	2.0	5.6	2.1	0.6
Prehnite and pumpellyite	2.4	2.8	0.5	0.0
Apatite	5.7	6.3	1.3	1.7

*ZTR = zircon + tourmaline + rutile.

in Oligocene sandstones, comprising only 4.3% of the non-opaque heavy minerals, but are relatively common in younger units, making up 5–6% of the heavy minerals in the Miocene to Pleistocene formations (Fig. 4). Sillimanite appears in appreciable amounts only in the Miocene sediments, with persistent appearance in the Girujan Clay of the Tipam Group. Minerals of the epidote group (epidote, zoisite, and clinozoisite) do not show any perceptible changes and are relatively low in abundance throughout the stratigraphic section in the Assam Basin sands and

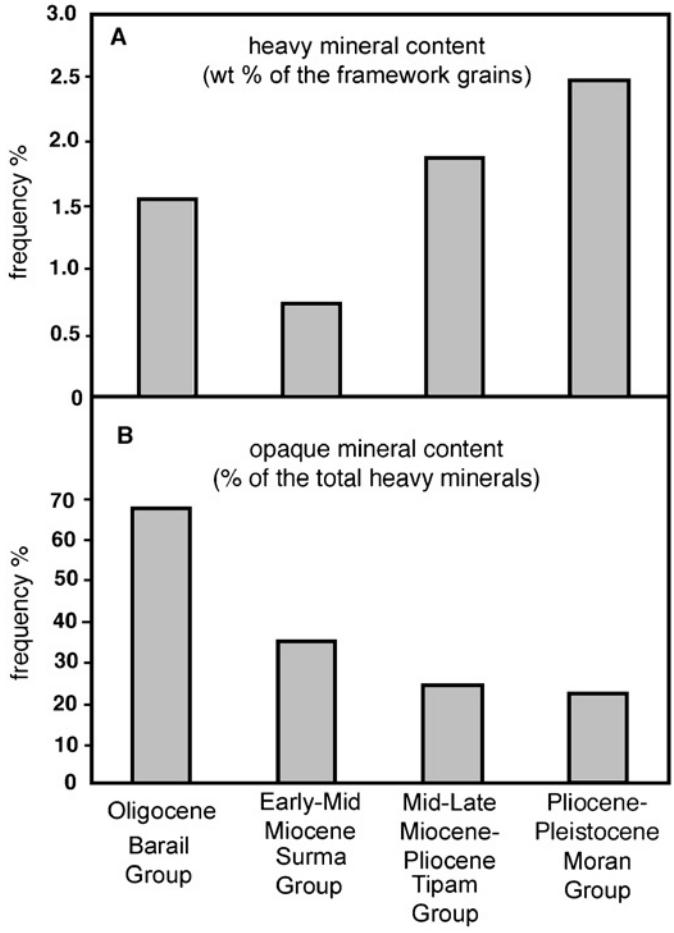

Fig. 3. Total heavy mineral content of Cenozoic successions from Assam, shown as weight percentage of total framework grains (A), and opaque mineral content, indicated as percentage of total heavy minerals (B). Note that the Oligocene Barail unit contains more opaque minerals than the younger units.

sandstones (Table 3). The abundance of blue-green hornblende is generally low but varies irregularly with stratigraphy. Significant amounts of blue-green hornblende appear in the Surma and Tipam Group sandstones. Tremolite and actinolite are present in Oligocene but are less abundant in the Miocene and younger successions. Mica is present in small amounts throughout the sequence, but is more abundant in the Neogene sediments. Although relatively uncommon, orthopyroxene is most common in the Oligocene Barail Group sediments (5%) and constitutes less than 1% of the non-opaque heavy minerals in the younger sediments (Fig. 4). The opaque fraction includes magnetite, pyrite, ilmenite, and hematite. Chromite is present in traces. In the Pliocene-Pleistocene Moran Group, the heavy mineral suites include garnet, staurolite, chlorite-chloritoid, epidote, kyanite, as well as

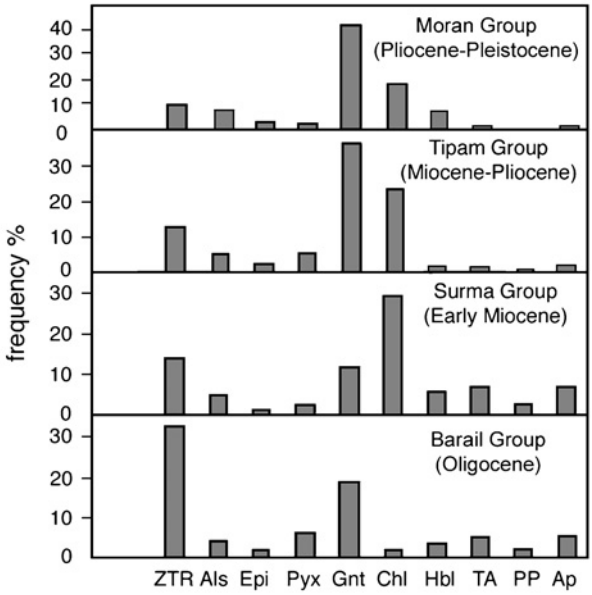

Fig. 4. Abundance of heavy minerals in four groups of different age in the Cenozoic successions of the Digboi-Mergherita area of Assam, shown as percentages of non-opaque heavy minerals. ZTR = sum of zircon, tourmaline, and rutile; Als = aluminosilicate minerals (andalusite, kyanite, and sillimanite); Epi = epidote group; Pyx = pyroxene group; Gnt = garnet group; Chl = chlorite and chloritoid; Hbl = hornblendes; TA = tremolite and actinolite; PP = prehnite and pumpellyite; Ap = apatite.
Note: ZTR percentages decrease through time, whereas garnet increases in the upper sections.

sillimanite, andalusite, zircon, tourmaline, rutile, monazite, hornblende, tremolite, and actinolite.

5.2. *Bengal Basin*

Similar to the Assam successions, the 2–3 phi size fractions contain most of the heavy minerals in the Bengal Basin sediments (Table 4) (Uddin and Lundberg, 1998a). Quartzose sandstones of the Palaeogene from the Bengal Basin contain only 0.2% heavy minerals, comprising abundant opaque and only stable minerals such as tourmaline, garnet, rutile, and zircon (Figs. 5 and 6) (Uddin and Lundberg, 1998a). By contrast, the Neogene sandstones contain more abundant and more diverse heavy mineral assemblages. These include, in addition to abundant opaque grains, garnet (mostly almandine), and moderate to minor amounts of tourmaline, kyanite, zircon, tremolite, rutile, chlorite, zoisite, staurolite, epidote, sillimanite, and clinopyroxene. The Mio-Pliocene successions along with the above minerals also contain abundant blue-green hornblende, orthopyroxene, and sparse chromite. Heavy mineral assemblages of the sands and sandstones of the Plio-Pleistocene units are similar to those of the underlying Miocene sandstones, but they comprise larger amounts of high-grade mineral phases.

Table 4. Normalised abundances of heavy minerals, Bengal Basin (modified after Uddin and Lundberg, 1998a)

Number of samples	Eo-Oligocene	Early-Mid Miocene	Mid-Late Miocene	Late Miocene-Pliocene	Pliocene-Pleistocene
	Kopili & Barail Fms	Bhuban Formation	Boka Bil Formation	Tipam Group	Dupi Tila Sandstone
	$N = 4$	$N = 7$	$N = 8$	$N = 9$	$N = 6$
Total heavy minerals (wt% of total framework grains)	0.21	0.50	0.98	1.92	2.90
Total opaque minerals (as % of total heavy minerals)	54.0	17.2	14.8	13.6	11.4
Non-opaque heavy minerals: (as % of non-opaque heavy minerals)					
Zircon	5.0	7.0	2.0	3.0	5.0
Tourmaline	41.2	11.9	13.4	12.6	11.7
Rutile	5.0	7.0	4.0	3.0	5.0
ZTR index*	51.2	25.9	19.4	18.6	21.7
Sillimanite	0.0	1.0	1.0	1.6	8.1
Kyanite	1.5	4.7	3.3	11.3	10.0
Andalusite	2.6	1.3	3.0	2.1	2.7
Staurolite	0.3	2.2	2.9	3.0	3.1
Epidote	1.0	6.8	8.7	10.0	11.1
Zoisite and clinozoisite	0.3	1.6	1.8	2.1	3.7
Orthopyroxene	0.0	0.6	0.7	1.3	3.9
Clinopyroxene	1.4	1.0	1.0	1.0	1.5
Garnet	6.0	31.0	27.0	12.0	9.0
Chlorite and chloritoid	0.0	4.1	5.8	6.9	2.2
Hornblende	0.9	3.3	4.0	14.8	4.6
Tremolite and actinolite	2.0	1.3	1.0	2.3	2.1
Glaucophane	0.0	1.5	0.3	0.1	1.4
Biotite and muscovite	5.5	7.4	11.1	6.0	3.2
Prehnite and pumpellyite	0.0	0.0	0.1	0.0	0.1
Apatite	3.4	2.5	1.9	1.2	2.9

*ZTR = zircon + tourmaline + rutile.

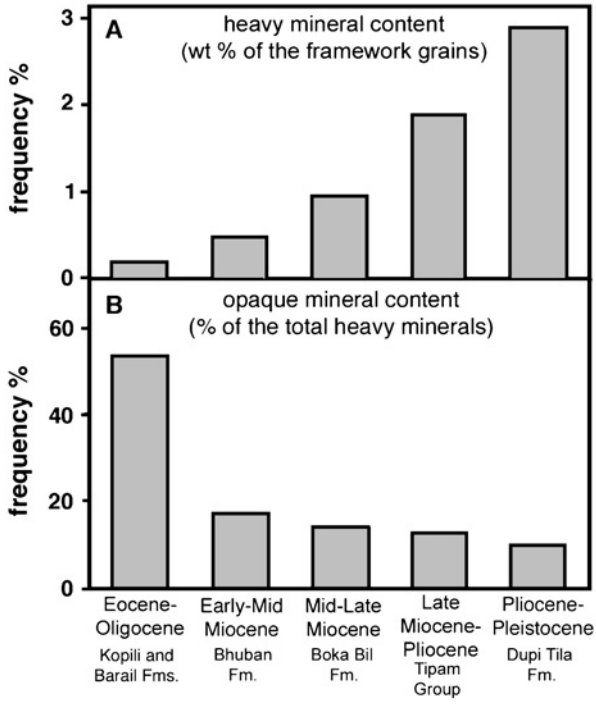

Fig. 5. Total heavy mineral content of Cenozoic successions studied from the Bengal Basin, expressed as weight percentage of total framework grains (A), and opaque mineral content, shown as percentage of total heavy minerals (B). Note that the Eocene-Oligocene Kopili and Barail Formations have the least amount of heavy minerals, and that most of them are opaque (modified after Uddin and Lundberg, 1998b).

6. PROVENANCE HISTORY

6.1. Assam Basin

Semi-quantitative grain counts of heavy mineral assemblages from the Assam Basin sediments illustrate relationships between individual mineral species, and the assemblages in which they are found as detrital grains, and provide information on the source rocks from which they are derived. In the Oligocene Barail Group, abundant opaque grains, low-diversity heavy mineral assemblages, a relatively high ZTR index, poor preservation, and moderate grain rounding indicate intense weathering in the source areas and/or diagenetic dissolution of the unstable components.

Sinha and Sastri (1973) studied heavy minerals from the Eocene Disang Group of sediments further south of the study area, which show an impoverished suite dominated by very abundant opaque minerals (nearly 88%; mostly pyrite) and traces of garnet, tourmaline, zircon, rutile, and monazite. The heavy mineral suites of the Disang and Oligocene Barail are similar and differ only quantitatively (Sinha and Sastri, 1973; Kumar, 2004). The Disang Group consists of shale, siltstone, and fine-grained sandstone, whereas the Barail Group is mostly represented by fine- to

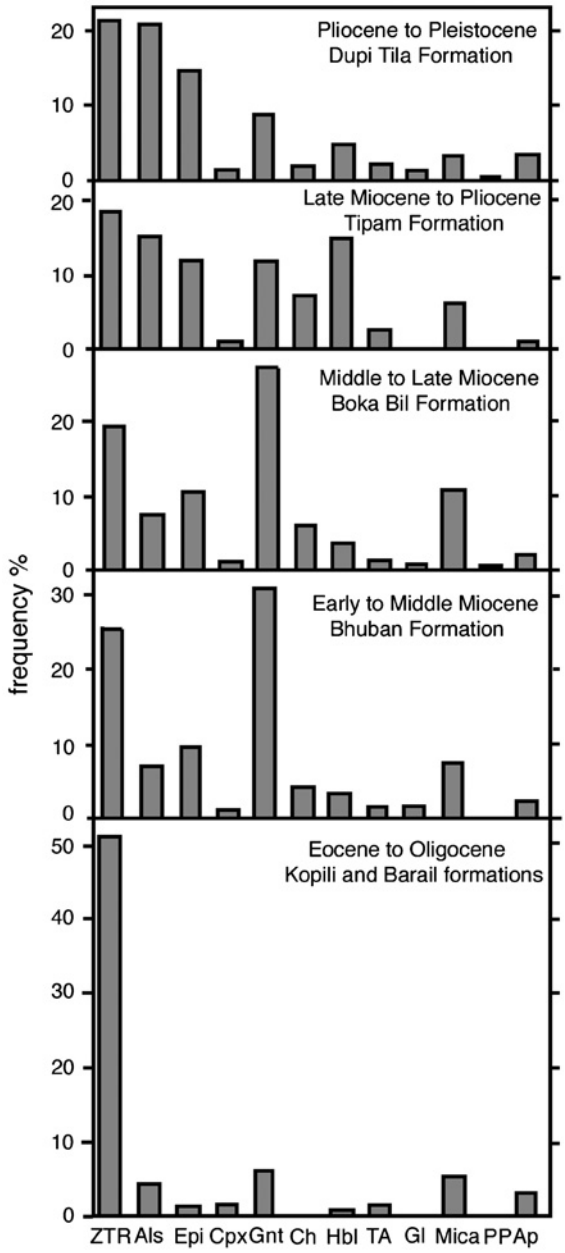

Fig. 6. Content of key heavy minerals in five formations of different age in the Cenozoic successions of the Bengal Basin, shown as percentages of non-opaque heavy minerals. Key as in Fig. 4.

Note: ZTR percentages decrease through time, whereas garnet increases in the Miocene (modified after Uddin and Lundberg, 1998a).

medium-grained sandstones. The Palaeogene sandstones from the Assam Basin (Disang and Barail Groups) are quartzolithic in composition and the heavy mineral assemblages show very little variation. The Disang sediments were deposited in deep-marine environments close to an arc-trench system during the Eocene (Kumar, 2004). During the Cretaceous-Eocene, ophiolites of the ophiolite belts were obducted onto the continent close to the Assam Basin in the Indo-Burman Ranges (Saikia, 1999). Thus, the occurrence of a few mafic rock fragments such as those present in the Disang sandstone (Saikia, 1999) may have derived from the ophiolite belts in the Indo-Burman orogen (Fig. 2). These ophiolites are thrust over the Disang rocks at a high-angle reverse fault, suggesting tectonic contacts.

During the initial deposition of the Oligocene Barail Group sediments, the depositional environment changed from deep marine to deltaic. With delta progradation, the growing delta plains were incised by a number of distributary channels in which coal-bearing sediments were deposited (Rangarao, 1983). The presence of radiolarian chert fragments in the basal conglomerates may indicate a contribution from the eastern ophiolite belt of the Indo-Burman Ranges.

The Neogene Surma Group sediments that unconformably overly the Oligocene sandstones comprise diverse heavy mineral assemblages, and are in stark contrast with the Oligocene Barail Group. They contain a very high percentage of chlorite, chloritoid, and epidote, and are also enriched in garnet and ZTR compared to the underlying Barail Group, indicating derivation from low- to medium-grade metamorphic terranes.

The Tipam Group bulk suite is very diverse, consisting of almost all the heavy mineral species found in the underlying Surma Group, but also contains enstatite, sillimanite, and andalusite. Opaque minerals are less abundant than in the underlying Barail and Surma groups. All these heavy mineral species suggest an orogenic source, with input from additional source terranes of diverse lithologies, ranging from high-grade contact metamorphic rocks to igneous rocks. Blue-green amphiboles in Miocene sediments have been reported from the Bengal Basin (Uddin and Lundberg, 1998a) and further south from the Bengal Fan (Amano and Taira, 1992). Cerveny et al. (1989) also found similar mineral species in the Siwaliks from the western Himalayas. The blue-green amphiboles present in the Tipam Group of the study area suggest simultaneous unroofing along the complete strike of the Himalayas. The Girujan Clay contains thin arenaceous bands that also yield diverse heavy mineral assemblages. The suite is similar to that of the Tipam Group, except that it contains more abundant enstatite, sillimanite, and andalusite.

The Pliocene-Pleistocene Moran Group sediments (Namsang and Dihing Formations) are characterised by diverse heavy minerals. They suggest derivation from different rock complexes in the adjacent orogenic belts similar to those in the eastern Himalayas and Indo-Burman Ranges.

6.2. *Bengal Basin*

The record of the Himalayan collisional orogen in the Himalayan foreland basin sediments reveals that the Eocene to Oligocene pre-collisional to syn-collisional sediments in the Bengal Basin are overwhelmingly quartzose and contain only small amounts of heavy minerals (mainly ultra-stable species of ZTR) of which about 60%

are opaque varieties (Table 4; Figs. 5 and 6) (Uddin and Lundberg, 1998a). The low diversity of heavy minerals indicates intense weathering during deposition of the Palaeogene sandstones of the Bengal Basin, because the basin was located close to the equator (Lindsay et al., 1991). The subangular nature of the Palaeogene detrital grains suggests a short transport distance along a pathway of low relief. Compositional and textural characteristics of these pre-Miocene sandstones signal that these were derived from the Indian craton immediately to the west. Streams currently draining the Himalayan and Indo-Burman orogenic fronts were a long distance away during that time, and their depocentres were farther upstream, possibly more proximal to the orogenic fronts, as in the basins preserved in Assam. Garnets are not abundant in the Oligocene sandstones of the Bengal Basin (6%) compared with the much higher garnet quantities in the Assam Basin (with 18.7% garnets).

Contrasting with the Oligocene, the Neogene strata from the Bengal Basin contain abundant and diverse heavy mineral assemblages (Figs. 5 and 6) and suggest derivation from orogenic fronts that may have moved by then close to the Bengal Basin. Modal analysis of sandstones from these successions reveals that significant amounts of feldspars and lithic fragments first appeared at about the same time, roughly at the Oligocene/Miocene boundary (Uddin and Lundberg, 1998b), providing further evidence for the dramatic shift to an orogenic sediment source for Bengal Basin detritus. The youngest stratigraphic units, the Tipam Sandstone and the Dupi Tila Formation, contain heavy mineral assemblages that are even more abundant and more diverse than those of the underlying strata (Figs. 5 and 6). These observations suggest the emergence of additional source terranes with complex lithologies, ranging from high-grade contact metamorphic rocks to various igneous bodies. Aluminosilicates and related minerals throughout the Bengal Basin successions also reflect systematic exhumation of progressively deeper crustal levels in the eastern Himalayas (Uddin and Lundberg, 1998a). Similar trends have been observed in heavy mineral assemblages of Siwalik successions in the western Himalayas (e.g., Chaudhri, 1972; Gill, 1984). Modal analysis also indicates unroofing of progressively deeper crustal levels in the source area through the Neogene, as revealed by the appearance of systematically higher grade metamorphic lithic fragments in the sandstones (Johnson and Nur Alam, 1991; Uddin and Lundberg, 1998b). Mineralogical evidence shows that orogenic activity in the eastern Himalayas and the Indo-Burman Ranges was significant during the Neogene and Pleistocene, and that modern drainage patterns were well developed by then.

Blue-green amphiboles appear first in the late Miocene Boka Bil Formation and are found abundantly in the Mio-Pliocene Tipam Sandstone (Uddin and Lundberg, 1998b). The presence of blue-green amphiboles and the initial appearance of sparse chromites signal unroofing of arc and ophiolitic rocks from suture zones of the Himalayas and/or the Indo-Burman Ranges (Fig. 1). Blue-green amphiboles are also present in strata of similar ages in the Siwalik sandstones on the Potwar Plateau of the Pakistan Himalaya (Johnson et al., 1985; Cerveny et al., 1989); successions in Assam (Kumar, 2004) and in cores from Ocean drilling programme (ODP) Leg 116 sites on the distal Bengal Fan (Yokoyama et al., 1990; Amano and Taira, 1992) suggest sediment dispersal to the southern Himalayan basins from erosion of similar rocks from the entire Himalayas. Similarly, orthopyroxenes, particularly

hypersthene, first appear in the Bengal Basin in the early to middle Miocene Bhuban Formation, and become relatively abundant in the Plio-Pleistocene Dupi Tila Sandstone. This increase in orthopyroxene content provides further evidence for continued orogenic unroofing, and along with the small amounts of chromites, also indicates erosion of ophiolitic rocks (Uddin and Lundberg, 1998a).

It is probable during the Miocene that a major fluvial system, similar to the present-day Brahmaputra River, developed or migrated toward the remnant ocean basin, represented by the Bengal Basin of that time. This paleo-Brahmaputra system apparently drained through the upper Assam valley and reached the eastern part of the Sylhet Trough to enter the Bengal Basin (Uddin and Lundberg, 1999), and—with its distributaries—may have formed the first major delta in the Bengal Basin. This major drainage, caught between the southward-advancing Himalayan belt and the westward-advancing Indo-Burman Ranges, shifted westward in the northern part of the Bengal Basin during the Pliocene, because of uplift of the Shillong Plateau (Johnson and Nur Alam, 1991). The Arakan-Yoma hills of the Indo-Burman Ranges probably contributed sediment to the Chittagong area via a second sediment plume (*palaeo-Karnafuli?*), most probably a submarine one. However, the major sediment source for Miocene sediments of the Bengal Basin was the early uplifted range of the eastern Himalayas (Uddin and Lundberg, 1999). This suggestion is also supported by the existence of a third major stream (*palaeo-Ganges?*) in the northwestern Bengal Basin, where long-term sediment accumulation was restricted by very limited subsidence in the Indian Platform (Uddin and Lundberg, 2004). These Miocene deltas in Bangladesh migrated from east to west and from north to south, toward the Bay of Bengal, as under-thrusting of India beneath southeast Asia along the Sunda Trench and its northern extension continued during the post-Palaeogene (Uddin and Lundberg, 2004). Subsidence of the deltaic deposits continued from at least the Miocene, with subsidence near the mountain belts accelerated by loading of the advancing orogens.

Although the Assam Basin sediments signal orogenic provenance, compared with the Bengal Basin their heavy mineral compositions do not show the obvious trend observed in the Bengal Basin. There is no evidence for a systematic and progressive unroofing of an orogenic belt, and medium- and low-grade minerals are equally distributed in all Cenozoic sections. Several regional and local thrust faults and the close proximity to the eastern syntaxis of the Himalayas have apparently resulted in homogenisation of the heavy mineral distribution in the Cenozoic successions of Assam.

7. REGIONAL TECTONIC IMPLICATIONS

The Oligocene heavy mineral assemblages from Assam contrast strongly with coeval units from the Bengal Basin, indicating distinct provenance histories for these two eastern Himalayan foreland basins. The presence of chrome-spinel in Oligocene sediments of Assam suggests provenance from ophiolitic rocks from the orogenic belts (Kumar, 2004). This finding is consistent with the modal analysis from Assam (Uddin et al., 1999; Kumar, 2004). Palaeogene sandstones from the Digboi-Mergherita area of northeastern Assam show a strongly orogenic derivation,

being compositionally and texturally immature with quartz (both mono- and polycrystalline), plagioclase and lithic fragments of both sedimentary and low-grade metamorphic origin. Late Oligocene units in this area also show significant amounts of volcanic and higher grade metamorphic detritus.

Pre-Miocene strata of the Bengal Basin are, however, apparently not orogenic, in accord with their mature heavy mineral suites. Temporal variations between heavy mineral assemblages in the Bengal Basin and the coeval western Himalayan strata, e.g., the Murree redbeds and the Chulung La Formation near the western Himalayan syntaxis in Pakistan (Critelli and Garzanti, 1994), suggest that orogenic detritus appeared in the eastern Himalayan Basin (Bengal Basin) much later (early Miocene) than in the western Himalayan basins (Eocene) (Uddin and Lundberg, 1998b). However, the Palaeogene successions in Assam (further northeast of the Bengal Basin) suggest an orogenic source. Thus, the Himalayan convergence cannot have been as diachronous as previously assumed (Uddin and Lundberg, 1998b), with convergence in both syntaxial parts in pre-Miocene time. The Bengal Basin may have been more distant from the Assam Basin and/or was protected by a barrier from orogenic sedimentation from the Himalayas and the Indo-Burman Ranges (Uddin et al., 2002). If "distance" was the cause, then the part of the Indian continent represented by the Bengal Basin was far to the south of Asia until the Early Miocene. Movement of this part of the Indian plate relative to Southeast Asia (Indochina) was most likely along right-lateral faults, as in the north-south trending Kaladan fault, located east of the Bengal Basin (Fig. 2) (Uddin et al., 2002).

By Miocene times, major fluvial systems had developed and debouched sediments into both the Assam and the Bengal Basins (Uddin and Lundberg, 1999). Other than changes in stratigraphic thickness, Miocene and younger heavy mineral assemblages are similar in both the Assam and Bengal Basins. Study of framework components corroborates this observation where feldspars, polycrystalline quartz and sedimentary, volcanic and metamorphic lithic fragments are found in sandstones of both the Assam and Bengal Basin (Uddin and Lundberg, 1998b; Kumar, 2004). The appearance of blue-green amphiboles in both basins toward the end of the Miocene is significant, and indicates orogen-wide unroofing of arc-type material. Cerveny et al. (1989) suggest the Kohistan island arc as the source of the blue-green amphiboles in the Siwalik successions of Pakistan. Blue-green amphiboles in the Assam and Bengal basins may have derived from coeval arcs in the eastern Himalayas, Tibet, and the Indo-Burman Ranges (Srimal, 2005). The Linzizhong Formation of Tibet and the Abor Volcanics of the eastern syntaxis of the Himalayas are considered to be contemporary to the Kohistan arc of the western Himalayas (Srimal, 2005). A source of these blue-green amphiboles in the amphibolites, granites, and gneisses in the Higher Himalayas cannot be ruled out either (Amano and Taira, 1992). The Assam Basin at this time records the presence of abundant plagioclase feldspars, suggesting erosion of thrusted crystalline basement rocks and dissected magmatic arcs from the orogenic belts (Kumar, 2004). Alternatively, plagiogranite-bearing lithotectonic belt may have since been eroded from the eastern Himalayas or the Indo-Burman Ranges. While continental convergence was active in the Schuppen Belt area of Assam, subduction-related processes deposited the early Miocene Surma trench slope turbidites in the southeastern Bengal Basin (Uddin and Lundberg, 2004). These

are now exposed in several sections in and around the Chittagong Hills (Fig. 2) (Akhter et al., 1998). Although the last Miocene marine transgression covered most of the Bengal Basin during the late Miocene, Assam successions were deposited mostly in fluvial and transitional environments. The younger units are much thicker in the Bengal Basin as a result of orogenic encroachment toward the basin from both north and east.

8. CONCLUSIONS

The Assam Basin strata show a marked variation in their heavy mineral compositions through time. The moderate to low diversity of heavy mineral assemblages in the Palaeogene sediments indicates that the source rocks were uniform and localised, and may have experienced intense weathering. In contrast, marked variations in heavy mineral distributions in Neogene sediments reflect diverse sources, including low- to medium-grade metamorphics. This also suggests unroofing of the orogenic belts in the higher areas, such as the Himalayas in the north and in the Indo-Burman Ranges to the east. Heavy mineral compositions in Assam, however, do not show a characteristic trend of progressive unroofing of an orogenic belt throughout the Cenozoic.

Palaeogene sandstones from the Bengal Basin also contain relatively few mineral species. Opaque minerals are dominant in these sandstones, with most of the non-opaque suite comprising stable minerals, and assemblages showing a high degree of compositional maturity (Uddin and Lundberg, 1998b), possibly related to intense weathering. The moderate textural maturity (e.g., moderate rounding, poor sorting) suggests relatively short transport. These assemblages indicate a cratonic source, most probably the Indian craton immediately to the west, and maybe the more distant orogenic belts in the north and east from the Bengal Basin.

Palaeogene sediments from the Assam Basin are derived from an orogenic source. Although the heavy mineral suites of the Palaeogene in the Assam and Bengal Basins are both relatively rich in ZTR, the Assam successions contain a more diverse heavy mineral assemblage than those in the Bengal Basin. Assam was more proximal to the orogenic fronts during the Palaeogene, and sedimentation most probably occurred in a trench-slope setting. This suggests input of orogenic detritus from the eastern Himalayas and the Indo-Burman Ranges.

Diagnostic and diverse minerals in the younger sediments in the Bengal Basin signal erosion from complex source lithologies, including high-grade to contact-metamorphic rocks, and silicic to ultra-mafic igneous rocks. Similar conclusions can also be drawn from coeval strata in the Assam Basin. Blue-green amphiboles are widespread, occurring in Assam, the Siwaliks in both Pakistan and northwest India, and in the Bengal Fan. They signal orogen-wide unroofing of arc-type material and/or derivation from amphibolites, granites, and gneisses of the Higher Himalayas. The upward increase in aluminosilicates in both the Assam and Bengal Basins suggests that Miocene and younger deposits of both basins were derived from orogenic terranes. Local and regional tectonism has, however, contributed toward subtle differences in composition between these younger units.

ACKNOWLEDGMENTS

We thank the US National Science Foundation (INT 0117405 and EAR 0310306) for supporting this project. PK acknowledges support from the Geological Society of America. Several students from Dibrugarh University (Assam) and Dhaka University (Bangladesh) helped during fieldwork and sample collection for the project. Bangladesh Petroleum Exploration helped with petroleum core samples. M. Shamsudduha helped improve the figures and tables. This manuscript has been greatly improved by thoughtful reviews and editing by Steve Graham, Ray Ingersoll, Maria Mange and David Wright.

REFERENCES

Akhter, S.H., Bhuiyan, M.A.H., Hussain, M., Imam, M.B., 1998. Turbidite sequence located in SE Bangladesh. Oil and Gas Journal, Exploration 96 (51), 109–111.

Amano, K., Taira, A., 1992. Two-phase uplift of Higher Himalayas since 17 Ma. Geology 20, 391–394.

Baksi, S.K., 1972. On the palynological biostratigraphy of the Bengal Basin. In: Chanda, S., Ghosh, T.K., Bakshi, S.K., Banerjee, E. (Eds.), Proceedings of the Seminar on Paleopalynology and Indian Stratigraphy. Department of Botany, University of Calcutta, Calcutta, pp. 188–206.

Banerji, R.K., 1984. Post-Eocene biofacies, palaeoenvironments, and palaeogeography of the Bengal Basin, India. Palaeogeography, Palaeoclimatology, Palaeoecology 45, 49–73.

Bhandari, L.L., Fuloria, R.C., Sastri, V.V., 1973. Stratigraphy of Assam Valley, India. American Association of Petroleum Geologists Bulletin 57, 642–654.

Brunnschweiler, R.O., 1966. On the geology of the Indo-Burman ranges (Arakan coast and Yoma, Chin Hills, Naga Hills). Geological Society of Australia Bulletin 13, 137–194.

Cerveny, P.F., Johnson, N.M., Tahirkheli, R.A.K., Bonis, N.R., 1989. Tectonic and geomorphic implications of Siwalik Group heavy minerals, Tectonics of western Himalayas. Geological Society of America Special Paper 232, 129–136.

Chaudhri, R.S., 1972. Heavy minerals from Siwalik formations of the northwestern Himalayas. Sedimentary Geology 8, 77–82.

Critelli, S., Garzanti, E., 1994. Provenance of the lower Tertiary Murree redbeds (Hazara-Kashmir syntaxis, Pakistan) and initial rising of the Himalayas. Sedimentary Geology 89, 265–284.

Curray, J.R., Moore, D.G., Lawyer, L.A., Emmel, F.J., Raitt, R.W., Henry, M., Kieckhefer, R., 1979. Tectonics of the Andaman Sea and Burma, geological and geophysical investigations of continental margins. In: Watkins, J.S., Montadert, J., Dickerson, P.W. (Eds.), American Association of Petroleum Geologists Memoir, vol. 29, pp. 189–198.

Dasgupta, S., 1984. Tectonic trends in Surma basin and possible genesis of folded belt. Geological Survey of India, Memoir 113, 58–61.

Evans, P., 1964. The tectonic framework of Assam. Journal of Geological Society of India 5, 80–96.

Fleet, W.F., 1926. Petrological notes on the old red sandstones of the West Midlands. Geological Magazine 63, 505–516.

Gill, G.T.S., 1984. Heavy mineral assemblage of the Siwalik Group exposed between the rivers Ghaggar and Markanda, northwestern Himalaya. In: Srivastava, R.A.K. (Ed.), Sedimentary Geology of the Himalaya: Current Trends in Geology, vol. 5. Today and Tomorrow's Publishers and Printers, New Delhi, pp. 223–234.

Graham, S.A., Dickinson, W.R., Ingersoll, R.V., 1975. Himalayan-Bengal model for flysch dispersal in the Appalachian-Ouachita system. Geological Society of America Bulletin 86, 273–286.

Hess, H.H., 1966. Notes on operation of Frantz isodynamic magnetic separator. Princeton University, Princeton NJ User manual guide, pp. 1–6.

Holtrop, J.F., Keizer, J., 1970. Some aspects of the stratigraphy and correlation of the Surma Basin wells, East Pakistan. ECAFE Mineral Resources Development Series (United Nations, N.Y.) 36, 143–155.

Hubert, J.F., 1962. A zircon-tourmaline-rutile maturity index and the interdependence of the composition of heavy mineral assemblages with the gross composition and texture of sandstones. Journal of Sedimentary Petrology 32, 440–450.

Hutchison, C.S., 1989. Geological Evolution of Southeast Asia. Oxford Science Publications, Oxford, 368pp.

Johnson, S.Y., Nur Alam, A.M., 1991. Sedimentation and tectonics of the Sylhet trough, Bangladesh. Geological Society of America Bulletin 103, 1513–1527.

Johnson, N.M., Stix, J., Tauxe, L., Cerveny, P.F., Tahirkheli, R.A.K., 1985. Paleomagnetic chronology, fluvial processes, and tectonic implications of the Siwalik deposits near Chinji Village, Pakistan. Journal of Geology 93, 27–40.

Khan, M.R., Muminullah, M., 1980. Stratigraphy of Bangladesh. In: Petroleum and Mineral Resources of Bangladesh, Seminar and Exhibition. Government of the People's Republic of Bangladesh, Dhaka, pp. 35–40.

Kumar, P., 2004. Provenance history of the Cenozoic sediments near Digboi-Margherita area, eastern syntaxis of the Himalayas, Assam, northeast India. Unpublished M.Sc. thesis. Auburn University, Auburn, 131pp.

Le Dain, A.Y., Tapponnier, P., Molnar, P., 1984. Active faulting and tectonics of Burma and surrounding regions. Journal of Geophysical Research 89, 453–472.

Le Fort, P., 1996. Evolution of the Himalaya. In: Yin, A., Harrison, M. (Eds.), The Tectonic Evolution of Asia: World and Regional Geology Series. Cambridge University Press, New York, pp. 95–109.

Lindsay, J.F., Holliday, D.W., Hulbert, A.G., 1991. Sequence stratigraphy and the evolution of the Ganges-Brahmaputra Delta complex. American Association of Petroleum Geologists, Bulletin 75, 1233–1254.

Mange, M.A., Maurer, H.F.W., 1992. Heavy Minerals in Colour. Chapman and Hall, London, 147pp..

Morton, A.C., 1985. Heavy minerals in provenance studies: In: Zuffa, G.G., (Ed.), Provenance of Arenites, NATO ASI Series. Series C: Mathematical and Physical Sciences, vol. 148. Reidel Publishing Company, Dordrecht, pp. 249–277.

Najman, Y., Garzanti, E., 2000. Reconstructing early Himalayan tectonic evolution and paleogeography from Tertiary foreland basin sedimentary rocks, northern India. Geological Society of America Bulletin 112, 435–449.

Paul, D.D., Lian, H.M., 1975. Offshore Tertiary Basins of South-east Asia, Bay of Bengal to South China Sea. Proceedings of the 9th World Petroleum Congress, London, Applied Science Publishers, Limited, vol. 3, pp. 107–121.

Rangarao, A., 1983. Geology and hydrocarbon potential of a part of Assam-Arakan Basin and its adjacent area. Petroleum Asia Journal 6, 127–158.

Reimann, K.-U., 1993. Geology of Bangladesh. Gebrüder Borntraeger, Berlin, 160pp..

Saikia, M.M., 1999. Indo-Burman orogenic belt, its plate tectonic evolution. In: Verma, P.K. (Ed.), Geological Studies in the Eastern Himalayas. Pilgrims Book (Pvt.), Delhi, pp. 19–39.

Salt, C.A., Alam, M.M., Hossain, M.M., 1986. Bengal Basin: current exploration of the hinge zone of southwestern Bangladesh. In: Proceedings of 6th Offshore Southeast Asia Conference, Singapore, pp. 55–67.

Sengupta, S., Ray, K.K., Acharyya, S.K., De Smith, J.B., 1990. Nature of ophiolite occurrence along the eastern margin of the Indian plate and their tectonic significance. Geology 18, 439–442.

Sinha, R.N., Sastri, V.V., 1973. Correlation of the Tertiary geosynclinal sediments of the Surma valley, Assam, and Tripura state (India). Sedimentary Geology 10, 107–134.

Srimal, N., 2005. Abor volcanics: slab window volcanism at the India-Asia collision zone: Abstracts with Programs. Geological Society of America 37, 57.

Uddin, A., Lundberg, N., 1998a. Unroofing history of the eastern Himalaya and the Indo-Burman ranges; heavy mineral study of Cenozoic sediments from the Bengal Basin, Bangladesh. Journal of Sedimentary Research 68, 465–472.

Uddin, A., Lundberg, N., 1998b. Cenozoic history of the Himalayan-Bengal system; sand composition in the Bengal Basin, Bangladesh. Geological Society of America Bulletin 110, 497–511.

Uddin, A., Lundberg, N., 1999. A paleo-Brahmaputra? Subsurface lithofacies analysis of Miocene deltaic sediments in the Himalayan-Bengal system, Bangladesh. Sedimentary Geology 123, 227–242.

Uddin, A., Lundberg, N., 2004. Miocene sedimentation and subsidence during continent–continent collision, Bengal Basin, Bangladesh. Sedimentary Geology 164, 131–146.

Uddin, A., Burchfiel, B.C., Geissman, J.W., Lundberg, N., 2002. Tectonic configuration of the Bengal Basin: Miocene juxtaposition with Assam, India: Abstracts with Programs. Geological Society of America 34, 509.

Uddin, A., Sarma, J.N., Kher, S., Lundberg, N., Odom, L.A., 1999. Pre-Miocene orogenic history of the eastern Himalayas: compositional studies of sandstones from Assam, India (abstract). Eos Transaction AGU, Spring Meeting Supplementary 80 (17), S313.

Yokoyama, K., Taira, A., Saito, Y., 1990. Mineralogy of silts from the Bengal Fan. Proceedings of Ocean Drilling Programs, Scientific Results, vol. 116, pp. 59–73.

This page intentionally left blank

PART III: INTEGRATED AND INTERDISCIPLINARY HEAVY MINERAL APPLICATIONS

3.1 Heavy Mineral Studies Integrated with Other Geoanalytical Techniques

This page intentionally left blank

Chapter 33

HEAVY MINERALS AND DETRITAL FISSION-TRACK THERMOCHRONOLOGY

ANDREW CARTER

Research School of Earth Sciences, University and Birkbeck College, London WC1E 6 BT, UK

ABSTRACT

Heavy minerals provide key constraints on sediment provenance by describing the composition of a source terrain, documenting changes in source or deeper levels of exhumation. Fission-track analysis of detrital apatite and zircon provides complementary information on timing and rates of source exhumation that helps place heavy mineral evidence within a temporal framework. While combined heavy mineral—fission-track analyses strengthen provenance studies, the effects of lithological bias, small datasets and non-uniqueness of fission-track ages (and thermochronometric ages in general) can limit or hinder interpretation. Using examples these issues are discussed and new approaches are presented that link high precision geochemical data from single detrital grains with sediment composition and detrital age structure. Combined geochemical and isotopic signatures extracted from single grains permit more detailed resolution of source composition and evolution that strengthen the role of heavy mineral studies and fission-track thermochronometry.

Keywords: fission-track; provenance; exhumation; thermochronology

1. INTRODUCTION

Sedimentary provenance studies rely on diagnostic minerals to determine where component grains have come from in terms of their source lithology. Taking into account any affects from weathering, change in detrital mineralogy reflects either exhumation of rock from progressively deeper levels within the crust or changes in the sediment routing system. To help explain such changes, detrital thermochronometry can be used to provide a more quantitative description of the source terrain in terms of age structure, composition and timing and rates of uplift and exhumation. Detrital thermochronometry is based on extracting records of isotopic decay from parent atoms contained within single detrital grains using mass spectrometry

Developments in Sedimentology, Vol. 58, 851–868

ISSN: 0070-4571/doi:10.1016/S0070-4571(07)58033-7

(^{40}Ar-^{39}Ar, U-Pb, Rb/Sr), ion probe (U-Pb) or neutron activation techniques (fission-track, FT). Advances in technology (principally laser ablation mass spectrometry: LA-ICP-MS) have increased analytical sensitivity and precision to levels that permit routine detailed investigation of grain age and compositional structure providing larger, statistically more robust datasets and thus an improved image of sediment source. Commonly used thermochronometric methods include zircon U-Pb dating (Gehrels et al., 1995; Carter and Bristow, 2000), FT analysis (Cerveny et al., 1988; Hurford and Carter, 1991; Carter, 1999; Garver et al., 1999) and more recently detrital mica argon dating (Von Eynatten et al., 1996; Sherlock et al., 2002; Hodges et al., 2005). Zircon U-Pb dating records crystal formation and growth history due to isotopic closure at high temperatures, typically >700 °C, which is ideal for identifying formation age of source terrain lithologies (e.g., DeCelles et al., 2004), provided the dated zircon has not been through crustal recycling events as is often the case in orogens. With recycling the durability of zircon and resistance of the U-Pb system to thermal, resetting can result in detrital zircon U-Pb ages unconnected to the immediate source terrain. Although knowledge about hinterland rock formation age is useful for identifying where sediment may have come from, it provides little insight into the geodynamic development of a source region and the processes driving erosion and producing stratigraphic changes in heavy minerals. Constraints on erosion processes can be retrieved using detrital zircon and apatite FT analysis, a low temperature method that records cooling history from ~300 °C down to ~50 °C, temperatures that correspond to parts of the upper crust most sensitive to earth surface/climate/tectonic interactions. This chapter examines the role of detrital FT analysis in heavy mineral and provenance studies and considers how it can be best used to understand source evolution and trends in sediment composition and accumulation.

2. PRINCIPLES OF FT ANALYSIS

FT thermochronometry, based on uranium decay, is dependant on data obtained from single grains (Fig. 1) and is therefore ideally suited to provenance studies. It was first used as a provenance tool by Gleadow and Lovering (1974) and a succession of provenance-related FT studies have since followed (see reviews by Hurford and Carter, 1991; Carter, 1999; Garver et al., 1999; Bernet and Garver, 2005). FT analysis is based on quantifying the amount of natural decay of uranium (^{238}U) by spontaneous fission, a process that creates zones of linear damage (fission tracks) in the host crystal lattice. There are two components of FT dataset: the measured age and track-length distribution. An age derives from an observable density of natural spontaneous tracks that is controlled by uranium concentration, rate of uranium decay by spontaneous fission, duration of track accumulation and length of tracks, which governs the probability of intersecting an observation surface. Tracks all form at the same length, but observed lengths can subsequently vary since a fission track damaged crystal lattice has the ability to self-repair when exposed to elevated temperatures over time. This process of track annealing is progressive and causes length shortening. The eventual measured length of a track is a product of the maximum temperature experienced by the sample for a given period of time. Above a certain threshold temperature–time combination fission tracks will disappear completely

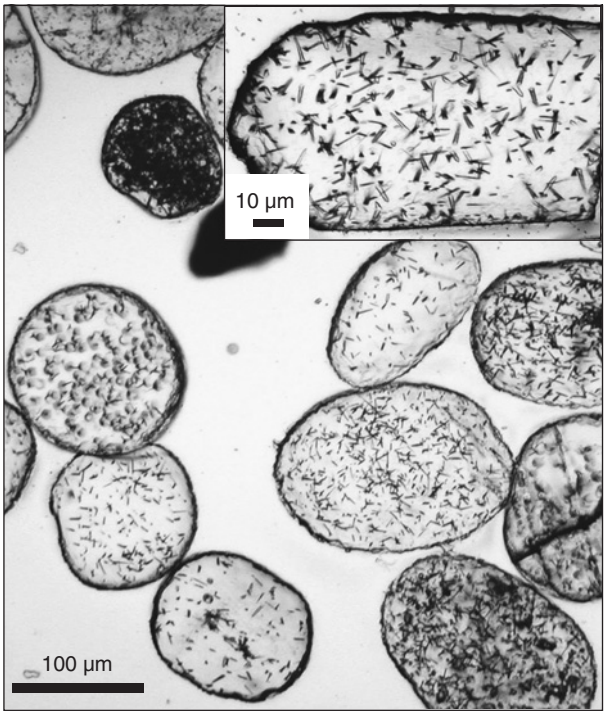

Fig. 1. Randomly orientated detrital apatites that have been polished and etched to reveal spontaneous fission tracks. Unique amongst thermochronometric techniques, etched fission tracks provide an image of accumulated isotopic decay and hence geological time.

from a crystal lattice causing age resetting. Tracks will continue to form but are not retained within the crystal lattice until cooling below the threshold occurs. Since all newly formed tracks start with the same initial length (~16 µm in apatite and ~11 µm in zircon) and form continuously, individual tracks, created during cooling, will experience differing proportions of a sample's overall thermal history, the summation of which is recorded by the track length distribution.

Deciphering a set of FT data to extract the thermal history, which produced the observed age and track-length distribution is dependant on understanding the behaviour of tracks at elevated temperatures. Laboratory based annealing experiments (Tagami et al., 1998; Carlson et al., 1999; Barbarand et al., 2003) and geological observations for the two minerals in most common use (apatite and zircon) have produced quantitative annealing models (for certain grain compositions) that have been incorporated into data-driven modelling programs used to extract probable thermal histories (Gallagher, 1995; Ketcham, 2005). Published apatite annealing models (Laslett et al., 1987; Laslett and Galbraith, 1996; Ketcham et al., 1999) and zircon annealing models (Yamada et al., 1995; Tagami et al., 1998) show that for durations of heating lasting 10^6–10^8 years, progressive track shortening occurs between ~60 and 110 °C for common fluorapatites and between ~200 and 320 °C for non-metamict zircon. These temperature ranges, often referred to as partial annealing zones or PAZ, define the boundary isotherms below which tracks are

effectively stable (minimal length reduction) and above which tracks are totally annealed (a zero, totally reset age). A track length distribution is therefore a measure of the time spent within the PAZ and/or below the lowest PAZ temperatures. Well-defined track length distributions can be measured on samples that comprise a single age population but multi-age component samples are more problematic as they generally lack sufficient grains to produce statistically robust length distributions for each age mode (Lonergan and Johnson, 1998). For this reason, track length distributions are generally absent from FT provenance datasets. More detailed summaries of FT methodology can be found in Wagner and Van den Haute (1992) and Gallagher et al. (1998).

3. UNDERSTANDING THE SIGNIFICANCE OF DETRITAL FT AGES

Providing that detrital apatite or zircon FT ages have not been reset by heating, resulting from post-depositional burial, measured ages will relate either to the formation age of a source lithology or its exhumation history defined as movement of rock towards the surface (Fig. 2). Apatites are more sensitive than zircon to resetting since post-depositional burial to temperatures >80–100 °C will degrade or reset an

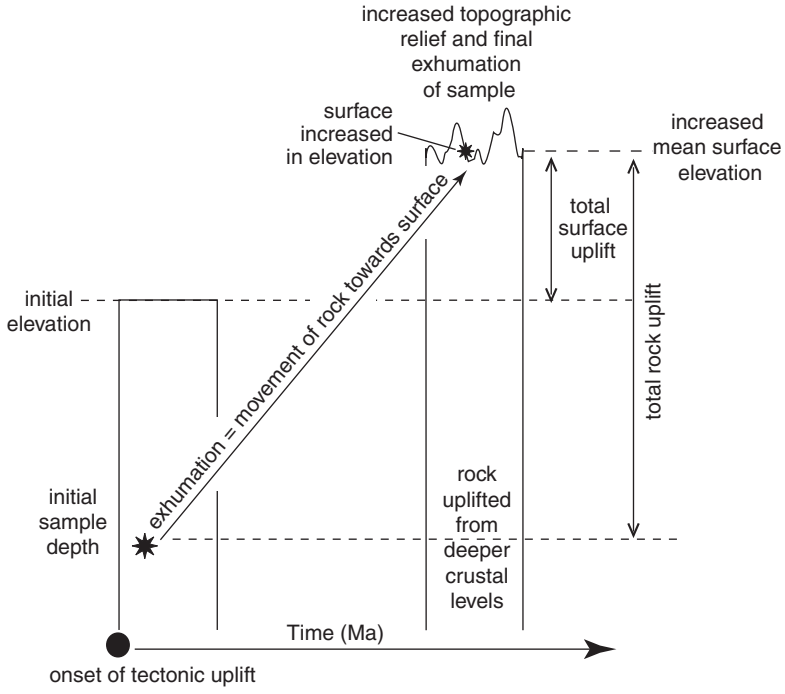

Fig. 2. An episode of tectonic uplift coupled with erosion will drive rock uplift and exhumation. Generalised use of the term 'uplift' should not be confused with 'surface uplift' that describes a change in mean surface elevation. Thermochronometric data record sample cooling history, generally assumed to correlate with sample exhumation.

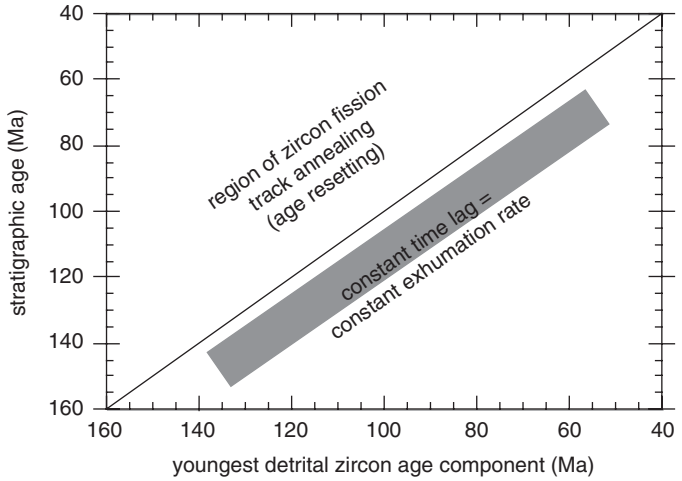

Fig. 3. Relationship between the youngest sample exhumation age and sediment depositional age provides a measure of how a source region developed over time as tectonic forces wax and wane.

apatite's FT provenance record, the precise temperature depending on grain composition and relationship between provenance history and depositional age (Carter and Gallagher, 2004). Zircon has greater resistance to thermal resetting (typically heating >250 °C for $>10^6$ years is required) which enables a more complete interrogation of a stratigraphic record. As a tool for dating sediments, both apatite (Mitchell, 1997) and zircon (Kowallis et al., 1986) have been used to record the age of contemporaneous volcanism. More commonly apatite and zircon grains record source cooling during exhumation and hence provenance studies generally use FT analysis to understand the tectonic/erosion history of a source region, relying on heavy mineral assemblages to identify sources(s).

A useful concept in detrital exhumation studies is lag-time (Brandon and Vance, 1992), the time difference between sample stratigraphic or depositional age and the time a mineral grain cooled through the relevant FT partial annealing zone or, for other dating methods, closure temperature (Fig. 3). Decreasing lag-times are diagnostic of increasing exhumation rates and vice versa. Studies of time lags on samples collected through a stratigraphic succession inform about source region behaviour in terms of whether it is in exhumation steady-state (Willet and Brandon, 2002), or in a growing (decreasing lag times) or decaying stage (increasing lag times). Examples of studies testing for the exhumation state of an orogen include Bernet et al. (2001), Carrapa et al. (2003), Spiegel et al. (2004) and Ruiz et al. (2007, this volume) whilst a review by Bernet and Garver (2005) provides good examples of time lag applications based on detrital zircon FT data.

3.1. Size of Dataset

Provenance studies require gathering of sufficient data to represent the sources contained within the sample under study. For age dating this means gathering

data from an adequate number of grains to detect the constituent age components. What constitutes an appropriate number of grains has been the subject of discussion for some time. Dodson et al. (1988) used

$$p = (1 - f)^k$$

to show that at least 60 grain ages ($k = 60$) are needed to achieve a 95% probability (p) of detecting population fractions (f) where $f = 0.05$. More recently Vermeesch (2004) argued that the Dodson equation has been misused and that at least 117 grains are needed to achieve 95% confidence that any fraction $f \geq 0.05$ of the population has not been missed. For detrital FT datasets >100 grains may not be needed, however, partly because of the size of uncertainty attached to FT ages (typically ~15–20% at 2σ) that limits the resolvable age structure in a dataset, and (for subaerial erosion) partly because of the tectonic/geomorphic factors that govern erosion and exhumation within river catchments. The latter was the subject of a detailed study by Ruhl and Hodges (2005), investigating the distribution of detrital mineral cooling ages in modern river sediments. Using rivers in the Nepalese Himalaya they compared catchment hypsometry with the distribution of detrital mica argon exhumation ages. For catchments with simple erosion histories they found that ~50 grain ages were sufficient to detect the underlying catchment age structure but that in regions affected by active deformation 70–85 single-grain ages were required. Importantly Ruhl and Hodges (2005) were also able to show that in some catchments the distribution of ages varied from year to year, linked to short-term events such as seismic shaking and landsliding. For localised sediments and small basins the possibility that sediment production can be skewed to certain areas during short-lived events can ultimately lead to a misleading image of source. In large drainages where multiple catchments combine to feed large rivers or fan systems the combined effects of long distance transport and short-term storage will tend to smooth out such effects to the extent that even large datasets (>100 single grain ages) are no longer able to capture the behaviour of an entire drainage system. Understanding what single sediment samples from large delta/fan systems actually tell us about source erosion and exhumation history is an area of ongoing investigation, aided by systematic/sequential analysis of heavy minerals.

3.2. Visualising and Extracting Age Components from a Dataset

A dataset comprising 50–100 mixed single grain ages requires deconvolution into principal component ages. Conventional histogram plots require individual data to be placed into groups or bins of similar values but fail to take into account the uncertainties attached to single-grain ages and in consequence researchers have resorted to using probability plots, a type of continuous histogram that plots each grain age error as a Gaussian density function (Hurford et al., 1984). All of the data are combined into a single continuous curve that has a shape comprising peaks and troughs according to the different age components and errors inherent to the component grain ages. Thus, high precision age modes have narrow curves and less precise ages have broader curves (Fig. 4a). Ar-Ar mica and U-Pb ages generally have smaller errors with the result that probability plots provide an easy way of visibly

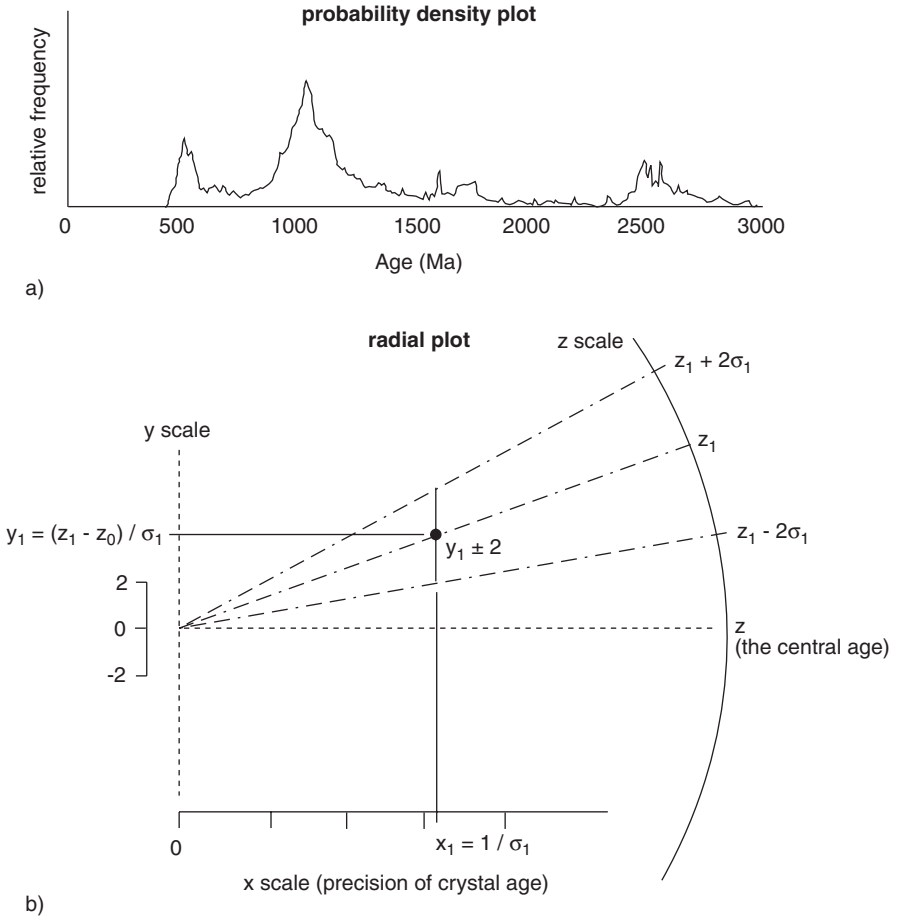

Fig. 4. Probability density diagrams (a) are widely used to show the distribution of single grain detrital ages but are only suited to datasets with uniform small age uncertainties. For data with a heterogeneous mix of uncertainties such as detrital FT ages the radial plot (b) is a more useful way of plotting results (see text for details).

comparing relative abundances of age modes (fingerprinting) between samples. However, there are several problems with this type of approach when applying it to FT data or any dataset with a large heterogeneous mix of uncertainties. The effect of such datasets is to obscure useful information by inappropriately weighting curves with poor information, i.e., an overlap effect associated with broad, imprecise peaks, resulting in apparent age modes that do not necessarily correspond with the true age components. Further, detailed discussion of probability density plots and their limitations can be found in Galbraith (1988, 1990). Because probability density plots are inherently flawed Galbraith (1988) designed and proposed the use of radial plots (Fig. 4b), for visualising the distribution of populations of FT grain ages. Single ages are plotted with standard error σ according to their precision ($1/\sigma$ on the 'x' axis, and standard estimate ($(z-z_0)/\sigma$ where $z_0 =$ the central age) on the 'y' axis). The error

attached to each plotted point is standardised on the y scale. The value of the age and the 2σ uncertainty can be read off the z scale by extrapolating lines from point 0,0 through the plotted age providing an easy way of distinguishing more precise ages.

Graphical display of single-grain ages provides a simple visual means of identifying and comparing sample age components but more rigorous statistical treatment is needed to extract ages and errors. Methods for deconvolving mixed age datasets include decomposing grain age distributions into component Gaussian distributions (Brandon, 1992) or Poissonian models and goodness of fit (Galbraith and Green, 1990). The binomial peak-fitting algorithm of Galbraith and Green (1990) has been incorporated into a software program (BINOMFIT) widely used amongst the FT community (see Stewart and Brandon, 2004, for a discussion of the use of BINOMFIT to decompose mixed FT grain-age distributions). Several statistical methods have been adapted to form a statistical approach for the analysis of U-Pb and FT data (Sambridge and Compston, 1994). Based on mixture modelling this approach uses several competing methods to derive most likely ages, their proportions and number of distinct components.

4. COMBINED HEAVY MINERAL: DETRITAL FT STUDIES

FT analysis has a relatively long record of use in provenance studies (Hurford and Carter, 1991; Carter, 1999; Garver et al., 1999, and references therein), principally because it was one of the first mineral dating techniques based on data extracted from single grains. A wide range of FT provenance applications can be found in the literature, covering topics as diverse as dating stone tools and fossil beds to detect movements of *Homo erectus* (Moorwood et al., 1998), to constrain when India and Asia first came into contact (Najman et al., 2005). Many of these studies combine heavy mineral data with FT ages to understand how changes in source or source lithology relate to long-term exhumation as tectonic processes wax and wane. In the Andean Amazon Basin in Ecuador heavy minerals extracted from Tertiary and Cretaceous sandstones collected along the western exhumed margin of the Ecuadorian Amazonian Basin (Fig. 5) show clear evidence for changes in source or source composition (Ruiz et al., 2004, 2007—this volume). Prior to ~80 Ma sediment provenance is dominated by granitic sources reflected in a near 100% ZTR assemblage. This changes in the Santonian with a switch to increasing proportions of metamorphic minerals that—by the Eocene—include kyanite and sillimanite, and—from the late Miocene—augite, olivine and hypersthene. Although such data record change, it is unclear whether this reflects different sources or tectonic activity, and increased rates of uplift and exhumation, revealing different lithologies from greater crustal depths. To understand how the source region was behaving Ruiz et al. (2004) used detrital zircon FT data to monitor source exhumation behaviour. Results revealed a correlation between lag-time (exhumation rate) of the youngest detrital age modes with changes in heavy mineral suites. From ~90 Ma, lag-times progressively decrease until ~85 Ma when lag-times are near zero. Allowing for analytical uncertainties this requires rock at depths of ~7–8 km being exhumed, eroded and deposited within <5 Ma. Such extreme high rates of exhumation are consistent with a major phase of tectonism. From ~60 Ma metamorphic minerals start appearing in progressively

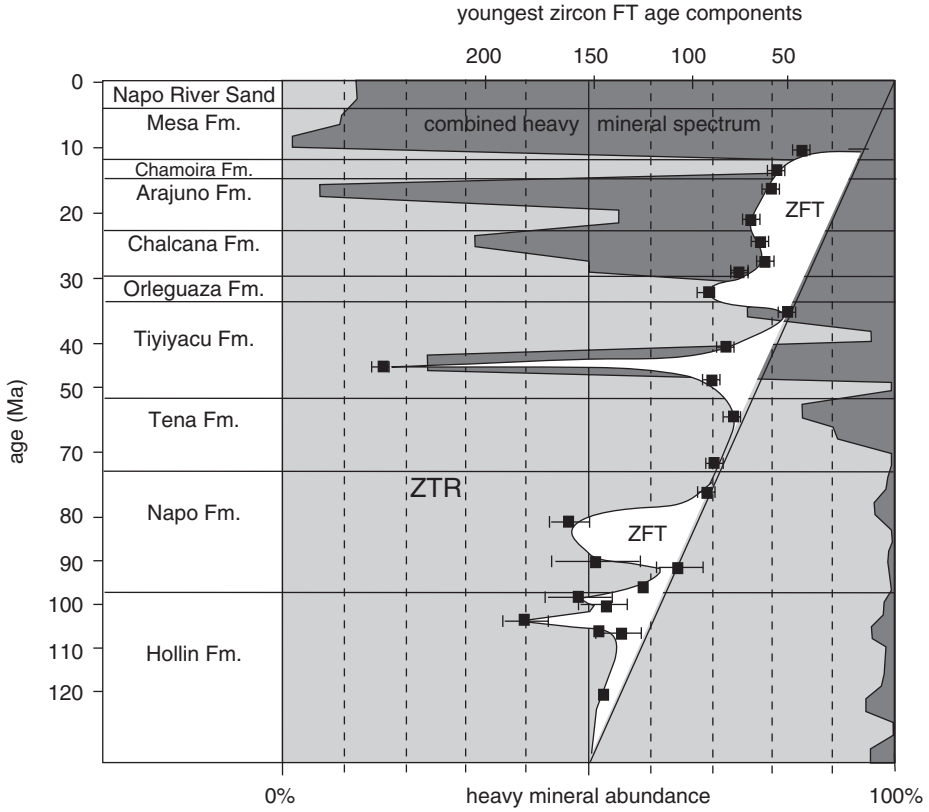

Fig. 5. Plot showing stratigraphic change in heavy minerals from sandstones on the western exhumed margin of the Ecuadorian Amazonian Basin (Ruiz et al., 2004). Pale grey shading records ZTR (resistant minerals, zircon, tourmaline, rutile, etc.). Dark grey is the combined heavy mineral spectrum for pumpellyite, garnet, epidote, chloritoid, staurolite, kyanite, sillimanite, hornblende, tremolite, augite, hypersthene, diopside, olivine, chromite and cassiterite. Overlain are the youngest zircon FT (ZFT) age components relative to depositional age. The closer FT ages plot to the diagonal line, recording depositional age, the faster were exhumation/erosion rates.

larger proportions as the rising Cordilleras were more deeply eroded while the ZFT data continue to show high but more variable rates of exhumation, linked to pulses of tectonism associated with terrane accretion events. From ~37 Ma lag-times reduce to maintain a broadly constant rate to the present, reflecting near tectonic stability.

4.1. Potential for Bias

Heavy minerals can play a major part in helping to understand the composition of a source region and whether thermochronometric data are biased to certain lithologies. In a study of foreland basin sediments from the Central Alps of Europe, Spiegel et al. (2004) showed examples of zircon FT lag plots from the molasse basin that, at face value, could be taken to represent exhumation signatures. However, consideration of

possible sources opened the possibility that some of the grains may not be reset and thus not related directly to hinterland exhumation at the time of molasse sedimentation. That ages relate to local exhumation signatures is a common type of assumption and is not often questioned. Recycling of grains from a sedimentary cover containing partially reset grains can have little value in terms of constraining the most recent source exhumation history.

Lithological bias is another important aspect touched on by Spiegel et al. (2004). Thermochronometric studies are inherently biased to lithologies that bear zircon and mica, minerals generally not associated with more basic rock types. In the Alps, the potential for lithological bias could be important since epidote is present in the foreland sediments. Spiegel et al. (2004) studied the Nd compositions of epidote from the Early Miocene sandstone in the Molasse basin and found two distinct signatures consistent with erosion of Penninic ophiolites and Austroalpine metagranitoids. Zircon is unlikely to be derived from these specific sources hence two important sources could be missed. A combination of heavy mineral study, single grain geochemical data and thermochronometric evidence provide a more robust approach to provenance studies.

5. INTEGRATING MINERAL GEOCHEMISTRY WITH THERMOCHRONOMETRY

Use of heavy mineral assemblages to track changes in source or hinterland exhumation and thermochronometric data to record timing and rates of exhumation provide an image of the sediment source with a resolution that largely depends on the size of a given drainage system. In the case of large orogens such as the ~2000 km Himalayan arc, a single sample collected from either the Bengal or Indus fan is unlikely to be diagnostic of a discrete part of the orogen due to the effects of mixing during long-distance transport. Viewed at the large scale, the Himalayas each have a relatively simple geology comprising four main tectonostratigraphic units (Fig. 6), each with a characteristic heavy mineral assemblage (Garzanti et al., 2004). Heavy minerals sampled from Bengal or Indus sands might show a sediment sample dominated by grains from a particular tectonostratigraphic unit, but this could represent a small part of a catchment undergoing high rates of erosion or a much larger area, spread over several catchments and many tens of thousands of square kilometres. Similarly, apatite FT data from the same sample might yield a single population of grain ages, but whether these represent the same tectonostratigraphic unit as the heavy mineral assemblage and whether they come from a small or large drainage area cannot be known without some additional constraint. In the case of the Himalayas, being able to tie a FT-dated grain to a particular tectonostratigraphic unit would be a major step forward since bedrock ages show that along strike, a tectonostratigraphic unit can display a variable exhumation history linked to out-of-sequence thrusting or climate influences on precipitation–erosion rate.

5.1. Arsenic Poisoning in the West Bengal Bain

Uncertainty as to the tectonostratigraphic origin of single detrital grains reduces the provenance value of detrital thermochronometric data. An example of the need to

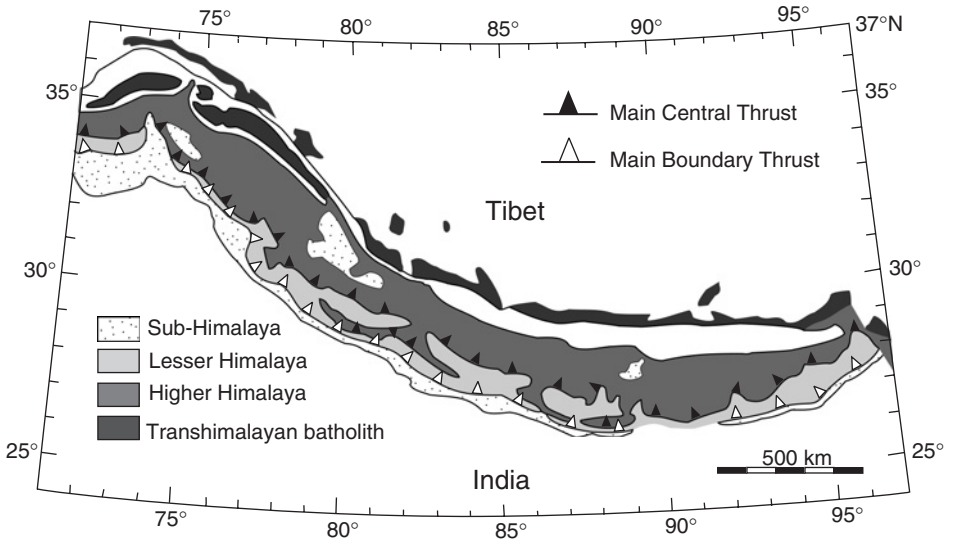

Fig. 6. The Himalayan arc has a relatively simple outcrop geology based on distinct tectonostratigraphic units bounded by major sutures and thrusts.

determine a sediment source can be found in sandstone samples from West Bengal where some Bengal Basin groundwaters contain levels of arsenic well above recommended drinking water limits. Contamination typically occurs in a thick aquifer of unconsolidated sands at shallow depths between ~10 and 30 m. A lower confining clay aquitard separates a deeper sand aquifer that is free of arsenic-polluted waters. The polluted sands are Holocene whereas the deeper unpolluted sands are Late Pleistocene. Numerous models have been put forward to account for As-enrichment, including oxidation of As-bearing pyrite (Mandal et al., 1998), reduction of As-bearing Mn oxides (Smedley and Kinniburgh, 2002) and exchange of sorbed As with HCO_3 (Appelo et al., 2002) or PO_4-bearing fertilizer (Acharyya et al., 2000). There is ongoing debate about the wider applicability of these and other models but it is apparent that depositional environment and provenance are key controls on the distribution of the arsenic-polluted groundwaters. Depositional environment governs production and preservation of organic matter that is broken down by microbial action to produce a redox environment (aqueous-As is derived principally from the reductive dissolution of FeOOH, and As-bearing micas) and sediment provenance governs the abundance of arsenic-bearing minerals.

The modern bed load and suspended sediment in the River Ganga and surface floodplain sediments in the Bengal Delta region are derived mostly from the Higher Himalayan crystalline units, comprising staurolite-sillimanite-bearing schists and gneisses, diopside-bearing banded marbles and amphibolites (Wasson, 2003; Garzanti et al., 2004). The aquifer sands are rich in quartz, biotite, muscovite and chlorite with subordinate (<5 vol.%) ferro-hornblende, calcite, dolomite, K-feldspar, albite, smectite, illite and minor (<1 vol.%) monazite, zircon, ilmenite, garnet and rutile. Although aquifer mineralogy and present-day drainage are consistent with High Himalayan crystalline sources, it is not clear whether all the grains came from this

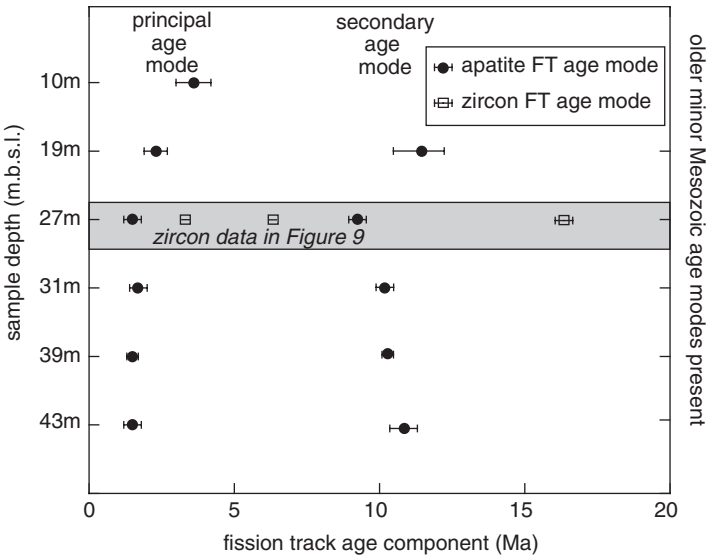

Fig. 7. Apatite and zircon FT age modes from the polluted aquifer sands in the West Bengal basin near Calcutta.

unit or the source region had a long or short exhumation history that might influence mineral weathering, making certain key minerals more prone to releasing arsenic. Apatite FT analysis of the aquifer sediments (Fig. 7) records ages <5 Ma, consistent with the high rates of exhumation measured on bedrock samples from either Lesser or Higher Himalayan units in the region of the Main Central Thrust. The FT data are useful for showing that the source area was undergoing high rates of rock uplift and fast exhumation, leaving little time for weathering, but the data do not constrain source in terms of which tectonostratigraphic unit the measured grains came from. Heavy mineral data suggest High Himalayan crystalline sources, but both apatite and zircon are ubiquitous to most Himalayan units.

5.2. *Identifying Grain Recycling*

The Bengal study highlights a major problem of studying large orogens, namely how to identify and track exhumation of individual tectonostratigraphic units. Such information is crucial to understanding orogen architecture and the role of major tectonic boundaries in their development and subsequent erosion. Non-uniqueness of thermochronometric signatures is an issue that faces all detrital thermochronometric systems. Another issue is grain recycling. A major problem for detrital-zircon U-Pb ages is the inherent resistance of zircon to weathering. Where there has been crustal recycling, this could result in a measured zircon U-Pb age unconnected to the most recent host rock. Thus, a zircon with an Archean U-Pb age can be found in metamorphosed Triassic sandstone derived from a Caledonian orogen. Here a post-metamorphic cooling age would be the more useful indicator of source. Recognising this, Carter and Moss (1999) demonstrated how, by combining U-Pb and FT dating, it is possible to extract both formation and post-metamorphic history

from single zircon grains to provide a more robust image of source. This combined-dating approach has now been extended to include (U-Th)/He dating (Reiners et al., 2005) making it possible to undertake triple dating of zircon grains.

5.3. Identifying Different Sources with Similar Grain Ages

Application of combined dating methods on single grains can help pin down source, but some data remain ambiguous because in some tectonic settings, high rates of rock uplift and erosion combine to produce spatially uniform exhumation ages across large areas that span different tectonostratigraphic domains. An illustration of problems associated with identifying different sources that possess similar grain ages is provided by samples from a Palaeogene forearc-accretionary succession exposed on the Andaman Islands (Bay of Bengal, India). The Eocene Namunagargh Grit contains abundant juvenile andesitic material, including well-preserved delicate glass shards and pumice fragments consistent with direct volcanic input during sedimentation. Euhedral volcanic apatites yield FT ages of 40 ± 3 Ma. Similar apatite ages are also found within overlying Oligocene turbidite sandstones of the Andaman Flysch Formation. These quartz-rich turbidites are considered to have been sourced from either Burma or the Himalayas in contrast to the locally derived quartz-poor Namunagargh Grit. The question arises as to whether circa 40 Ma apatites detected in both units are from the same source.

Morphologically the turbidite apatites are subhedral rather than euhedral but this might simply reflect abrasion of volcanic apatites during later reworking of the Namunargargh Grit. The answer as to whether these grains are derived from the same source can be found in their grain compositions. Apatite composition is complex and variable, but the main substitutions concern replacement of fluorine by chlorine. Volcanic apatites typically display a range of chlorine contents in grains from the same source. Microprobe analyses of apatites from the two Andaman units show major differences in grain fluorine–chlorine and uranium contents (Fig. 8). Arc volcanic apatites are characteristically low in uranium and have variable amounts of chlorine whereas non-volcanic apatites have little to no chlorine and variable amounts of uranium. Based on these differences it is clear that, although similar grain ages are found in the Namunagargh Grit and Andaman Flysch Formation, they do not share the same source.

The example from Andaman demonstrates how grain composition can be used to identify different sources from within a population of apatites with the same FT age. Grain composition has been widely used in heavy mineral studies for many years but until recently has been largely ignored by detrital thermochronological studies. The benefits of combining grain age data with composition are only now being realised. Along with their uranium and fluorine–chlorine contents apatite grains can be interrogated for their Sm-Nd-Rb-Sr signatures (Carter and Foster, 2004; Richards et al., 2005). Nd model ages ($^{143}Nd/^{144}Nd$ ratios) provide constraints as to when source region protoliths were first extracted from the mantle and can therefore be used to detect differences in crustal sources. Conventional Nd studies are based on whole-rock samples that provide an averaged image of source. Technological advances mean that it is now practical to overcome this limitation by measuring Nd in single grains. For a single detrital apatite grain $^{143}Nd/^{144}Nd$ ratios yield internal

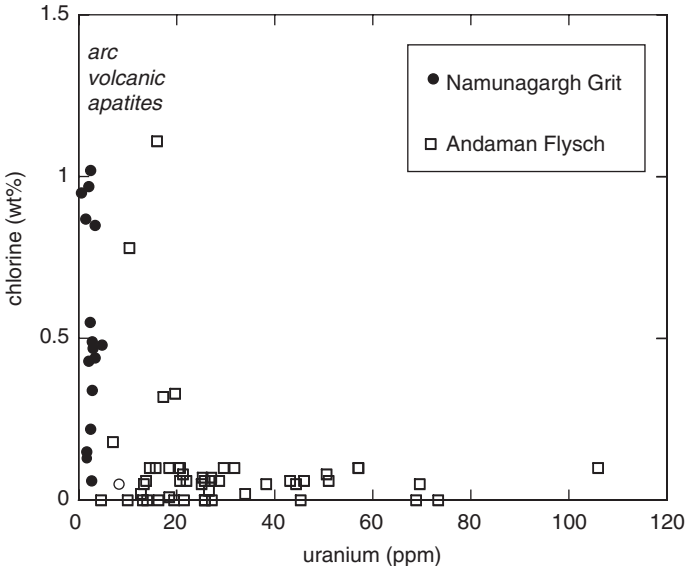

Fig. 8. Plot comparing apatites of the Namunagargh Grit and Andaman Flysch Formation from the Tertiary accretionary-forearc succession exposed on the Andaman Islands. Both samples share similar detrital apatite FT ages at ~40 Ma. Comparison of grain uranium and chlorine contents shows the two samples do not share the same source.

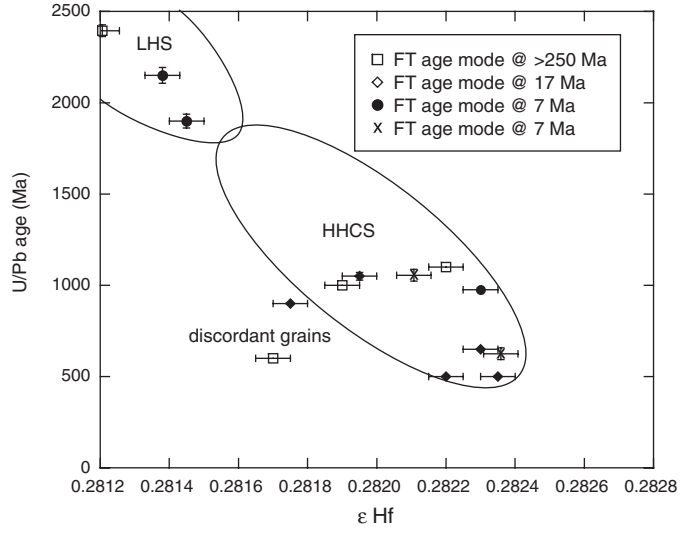

Fig. 9. Zircon U-Pb ages plotted against grain εHf units (epsilon units represent data normalised to chondritic uniform reservoir) for sample TL3 from West Bengal (Fig. 7). Most grains plot within the High Himalayan sequence confirming that this tectonostratigraphic unit was the main source for the polluted aquifer sands in the sampled part of the West Bengal basin. LHS, Lower Himalayan sequence; HHCS, High Himalayan sequence.

precisions to within 1–2 ε units sufficient to discriminate sources (epsilon units represent data normalised to chondritic uniform reservoir). Similarly for zircon the Lu-Hf isotopic system can be combined with U-Pb dating on single grains to provide more robust constraint on crustal residence age (Richards et al., 2005). Fig. 9 plots the result of zircon taken from the polluted aquifer sands in Bangladesh and illustrates the potential for this approach. The plot shows that most of the FT dated zircons plot within the field of the Higher Himalayan unit tying specific FT grain ages to a specific tectonostratigraphic unit.

6. CONCLUSIONS

Detrital FT analysis remains an essential tool in provenance research, especially for studies that seek to use the sediment record to reconstruct source exhumation history. Robust interpretation of detrital thermochronometric data requires understanding the composition of the source terrain in terms of its formation, age, structure and component tectonostratigraphic units, as obtained from complementary heavy mineral data. Although the heavy mineral community have long recognised the benefit of using mineral compositional data to better understand sediment source, the thermochronometric community has generally ignored the utility of such data. This is changing as technological advances permit the routine generation of high-precision age and compositional data from single detrital grains that, when combined with heavy mineral evidence, provide increasingly detailed images of source and extend understanding of controls on sediment production and accumulation.

ACKNOWLEDGEMENTS

The author thanks Tony Hurford and Mathias Bernet for their careful reviews and helpful suggestions.

REFERENCES

Acharyya, S.K., Lahiri, S., Raymahashay, B.C., Bhowmik, A., 2000. Arsenic toxicity of groundwater in parts of the Bengal basin in India and Bangladesh: the role of Quaternary stratigraphy and Holocene sea-level fluctuations. Environmental Geology 39, 1127–1137.

Appelo, C.A.J., Van der Weiden, M.J.J., Tournassat, C., Charlet, L., 2002. Carbonate ions and arsenic dissolution by groundwater. Environmental Science and Technology 36, 3096–3103.

Barbarand, J., Carter, A., Wood, I., Hurford, T., 2003. Compositional and structural control of fission-track annealing in apatite. Chemical Geology 198, 107–137.

Bernet, M., Garver, J.I., 2005. Fission-track analysis of detrital zircon. Reviews in Mineralogy and Geochemistry 58, 205–238.

Bernet, M., Zattin, M., Garver, J.I., Brandon, M.T., Vance, J.A., 2001. Steady-state exhumation of the European Alps. Geology 29, 35–38.

Brandon, M.T., 1992. Decomposition of fission track grain age distributions. American Journal of Science 292, 535–564.

Brandon, M.T., Vance, J.A., 1992. New Statistical methods for analysis of FT grain age distributions with applications to detrital zircon ages from the Olympic subduction complex, western Washington State. American Journal of Science 292, 565–636.

Carlson, W.D., Donelick, R., Ketcham, R.A., 1999. Variability of apatite fission-track annealing experiments: I. Experimental results. American Mineralogist 84, 1213–1223.

Carrapa, B., Wijbrans, J., Bertotti, J.G., 2003. Episodic exhumation in the Western Alps. Geology 31, 601–604.

Carter, A., 1999. Present status and future avenues of source region discrimination and characterisation using fission track analysis. Sedimentary Geology 124, 31–45.

Carter, A., Bristow, C.S., 2000. Detrital zircon geochronology: enhancing the quality of sedimentary source information through improved methodology and combined U-Pb and fission track techniques. Basin Research 12, 47–57.

Carter, A., Foster, G., 2004. Strategies to overcome non-uniqueness of detrital age data from Himalayan sediments. Eos Transaction AGU, Fall Meeting Supplementary, 85 (47), Abstract T52A-01.

Carter, A., Gallagher, K., 2004. Characterising the significance of provenance on the inference of thermal history models from apatite fission track data—a synthetic data study. In: M. Bernet, C. Spiegel (Eds.), Detrital Thermochronology—Provenance Analysis, Exhumation, and Landscape Evolution of Mountain Belts, GSA Special Paper 378, 7–23.

Carter, A., Moss, S.J., 1999. Combined detrital-zircon fission-track and U-Pb dating: a new approach to understanding hinterland evolution. Geology 27, 235–238.

Cerveny, P.F., Naeser, N.D., Zeitler, P.K., Naeser, C.W., Johnson, N.M., 1988. History of uplift and relief of the Himalaya during the past 18 million years: evidence from FT ages of detrital zircons from sandstones of the Siwalik Group. In: Kleinspehn, K., Paola, C. (Eds.), New Perspectives in Basin Analysis. Springer Verlag, New York, pp. 43–61.

DeCelles, P.G., Gehrels, G.E., Najman, Y., Martin, A.J., Carter, A., Garzanti, E., 2004. Detrital geochronology and geochemistry of Cretaceous—early Miocene strata of Nepal: implications for timing and diachroneity of initial Himalayan orogenesis. Earth and Planetary Science Letters 227, 313–330.

Dodson, M.H., Compston, W., Williams, I.S., Wilson, J.F., 1988. A search for ancient detrital zircons in Zimbabwean sediments. Journal of the Geological Society, London 145, 977–983.

Galbraith, R.F., 1988. Graphical display of estimates having differing standard errors. Technometrics 30, 271–281.

Galbraith, R.F., 1990. The radial plot: graphical assessment of spread in ages. Nuclear Tracks and Radiation Measurement 17, 207–214.

Galbraith, R.F., Green, P.F., 1990. Estimating the component ages in a finite mixture. Nuclear Tracks and Radiation Measurement 17, 197–206.

Gallagher, K., 1995. Evolving temperature histories from apatite FT data. Earth and Planetary Science Letters 136, 421–435.

Gallagher, K., Brown, R., Johnson, C., 1998. Fission track analysis and its application to geological problems. Annual Reviews in Earth and Planetary Science 26, 519–572.

Garver, J.I., Brandon, M.T., Rice, M.T., Kamp, P.J., 1999. Exhumation history of orogenic highlands determined by detrital fission-track thermochronology. In: Ring, U., Brandon, M.T., Lister, G.S., Willet, S.D. (Eds.), Exhumation Processes: Normal Faulting, Ductile Flow and Erosion, vol. 154. Geological Society of London Special Publication, pp. 283–304.

Garzanti, E., Vezzoli, G., Ando, S., France-Lanord, C., Sing, S.K., Foster, G., 2004. Sand petrology and focused erosion in collision orogens: the Brahmaputra case. Earth and Planetary Science Letters 220, 157–174.

Gehrels, G.E., Dickinson, W.R., Ross, M.G., Stewart, J.H., Howell, D.G., 1995. Detrital zircon reference for Cambrian to Triassic miogeoclinal strata of western North America. Geology 23, 831–834.

Gleadow, A.J.W., Lovering, J.F., 1974. The effect of weathering on FT dating. Earth and Planetary Science Letters 22, 163–168.

Hodges, K.V., Ruhl, K.W., Wobus, C.W., Pringle, M.S., 2005. $^{40}Ar/^{39}Ar$ thermochronology of detrital minerals. Reviews in Mineralogy and Geochemistry 58, 239–257.

Hurford, A.J., Carter, A., 1991. The role of FT dating in discrimination of provenance. In: Morton, A.C., Todd, S.P., Haughton, P.D.W. (Eds.), Developments in Sedimentary Provenance Studies, vol. 57. Geological Society of London Special Publication, pp. 67–78.

Hurford, A.J., Fitch, F.J., Clarke, A., 1984. Resolution of the age structure of the detrital zircon populations of two Lower Cetaceous sandstones from the Weald of England by fission-track dating. Geology Magazine 121, 269–277.

Ketcham, R.A., 2005. Forward and inverse modelling of low temperature thermochronometry data. Reviews in Mineralogy and Geochemistry 58, 275–311.

Ketcham, R.A., Donelick, R.A., Carlson, W.D., 1999. Variability of apatite fission-track annealing kinetics: III extrapolation to geological time-scales. American Mineralogist 84, 1235–1255.

Kowallis, B.J., Heaton, J.S., Bringhurst, K., 1986. Fission-track dating of volcanically derived sedimentary rocks. Geology 14, 19–22.

Laslett, G.M., Galbraith, R.F., 1996. Statistical modelling of FTs in apatite. Geochimica Cosmochimica Acta 60, 5117–5131.

Laslett, G.M., Green, P.F., Duddy, I.R., Gleadow, A.J.W., 1987. Thermal annealing of fission tracks in apatite 2. A quantitative analysis. Chemical Geology (Isotope Geoscience Section v.) 65, 1–13.

Lonergan, L., Johnson, C., 1998. A novel approach for reconstructing the denudation histories of mountain belts: with an example from the Betic Cordillera (S. Spain). Basin Research 10, 353–364.

Mandal, B.K., Chowdhury, T.R., Samanta, S., Mukherjee, D., Chanda, C.R., Saha, K.C., Chakraborti, D., 1998. Impact of safe water for drinking on five families for 2 years in West Bengal, India. Science of the Total Environment 218, 185–201.

Mitchell, M., 1997. Identification of multiple detrital sources for Otway Supergroup sedimentary rocks: implications for basin models and chronostratigraphic correlations. Australian Journal of Earth Sciences 44, 743–750.

Moorwood, M.J., O'Sullivan, P.B., Aziz, F., Raza, A., 1998. Fission track ages of stone tools and fossils on the east Indonesian Island of Flores. Nature 392, 173–176.

Najman, Y., Carter, A., Oliver, G., Garzanti., E., 2005. Provenance of early foreland basin sediments, Nepal: constraints to the timing and diachroneity of early Himalayan orogenesis. Geology 33, 309–312.

Reiners, P.W., Campbell, I.H., Nicolescu, S., Allen, C.A., Hourigan, J.K., Garver, J.I., Mattinson, J.M., Cowan, D.S., 2005. (U-Th)/(He-Pb) "double dating" of detrital zircons. American Journal of Science 305, 259–311.

Richards, A., Argles, T., Harris, N., Parrish, R., Ahmad, T., Darbyshire, F., Dragantis, E., 2005. Himalayan architecture constrained by isotopic tracers from clastic sediments. Earth and Planetary Science Letters 236, 773–796.

Ruhl, K.W., Hodges, K.V., 2005. The use of detrital mineral cooling ages to evaluate steady state assumptions in active orogens: an example from central Nepalese Himalaya. Tectonics, vol. 24, TC4015, doi 10.1029/2004TC001712.

Ruiz, G.M.H., Seward, D., Winkler, W., 2004. Detrital thermochronology—a new perspective on hinterland tectonics, an example from the Andean Amazon Basin, Ecuador. Basin Research 16, 413–430.

Ruiz, G.M.H., Seward, D., Winkler, W., 2007. Evolution of the Amazon Basin in Ecuador with special reference to hinterland tectonics: data from zircon fission-track and heavy

mineral analysis. In: M. Mange, D.K. Wright (Eds.), Heavy Minerals in Use. Developments in Sedimentology (this volume).
Sambridge, M.S., Compston, W., 1994. Mixture modelling of multi-component data sets with application to ion-probe zircon ages. Earth and Planetary Science Letters 128, 373–390.
Sherlock, S.C., Jones, K.A., Kelley, S.P., 2002. Fingerprinting polyorogenic detritus using the $^{40}Ar/^{39}Ar$ ultraviolet laser microprobe. Geology 30, 515–518.
Smedley, P.L., Kinniburgh, D.G., 2002. A review of the source, behaviour and distribution of arsenic in natural waters. Applied Geochemistry 17, 517–568.
Spiegel, C., Siebel, W., Kuhlemann, J., Frisch, W., 2004. Toward a comprehensive provenance analysis: A multi-method approach and its implications for the evolution of the Central Alps. In: Bernet, M., Spiegel, C. (Eds.), Detrital Thermochronology—Provenance Analysis, Exhumation, and Landscape Evolution of Mountain Belts. Geological Society of America Special Paper 378, 37–50.
Stewart, R.J., Brandon, M.T., 2004. Detrital zircon fission-track ages for the ''Hoh Formation'': implications for late Cenozoic evolution of the Cascadia subduction wedge. Geological Society of American Bulletin, 116, 60–75.
Tagami, T., Galbraith, R.F., Yamada, G.M., Laslett, G.M., 1998. Revised annealing kinetics of fission-tracks in zircon and geological implications. In: Van den Haute, P., De Corte, F. (Eds.), Advances in Fission-Track Geochronology. Kluwer Academic Press, Amsterdam, pp. 99–112.
Vermeesch, P., 2004. How many grains are needed for a provenance study? Earth and Planetary Science Letters 224, 441–451.
Von Eynatten, H., Gaup, R., Wijbrans, J.R., 1996. (super 40) Ar/(super 39) Ar laser-probe dating of detrital white micas from Cretaceous sedimentary rocks of Eastern Alps: evidence for Variscan high-pressure metamorphism and implications for Alpine orogeny. Geology 24, 691–694.
Wagner, G., Van den Haute, P., 1992. Fission Track Dating. Solid Earth Sciences Library. Kluwer Academic Publishers, Amsterdam.
Wasson, R.J., 2003. Sediment budget for the Ganga-Brahmaputra catchment. Current Science 84, 1041–1047.
Willet, S.D., Brandon, M.T., 2002. On steady-state in mountain belts. Geology 30, 175–178.
Yamada, R., Tagami, T., Nishimura, S., Ito, H., 1995. Annealing kinetics of FTs in zircon: an experimental study. Chemical Geology (Isotope Geoscience Section) 122, 249–258.

Chapter 34

HEAVY MINERALS IN THE SUBSURFACE: TRACKING SEDIMENT SOURCES IN THREE DIMENSIONS

D. JOHANNES HUISMAN[a] AND GERARD TH. KLAVER[b]

[a]*National Service for Archaeological Heritage, P.O. Box 1600 3800 Amersfoort, The Netherlands*
[b]*TNO-NITG/National Geological Survey, P.O. Box 80015, 3508 TA, Utrecht, The Netherlands*

ABSTRACT

The former Dutch Geological Survey from 1950 to 2000 used heavy-mineral compositions to systematically distinguish lithostratigraphic units in single boreholes or borehole transects. This large-scale work has produced an extensive database, with 25,000 heavy-mineral analyses from ~800 boreholes to a depth of 100 m, together with ~15,000 from quarries, giving a total number of around 40,000 analyses across the Netherlands, providing a unique opportunity to visualise the 3-D build-up of the subsurface. The greatest challenge in this kind of approach is the visualisation of 3-D variation in 2-D figures. The construction of multiple contour maps of heavy-mineral concentrations, with stacked threshold maps and colouring codes for depths gives an effective overview of the temporal and spatial distributions of sediments derived from various sources to the area.

The spatial variation of single minerals, as opposed to mineral assemblages, is used here to illustrate the geometry of sediments on a countrywide scale. The zircon distribution maps reveal the pre-Pleistocene margins of the major Caenozoic depositional basins and reflect tectonic influences. The geometry of the distribution of hornblende- and augite-rich sediments shows not only two depositional phases of Pleistocene Rhine sediments, but also reveals the ancient floodplain of the proto-Weser. Moreover, main channel directions, depositional basins, and delta-like features can thus be identified. By tracking the occurrence of Vosges-derived hornblende and Meuse-specific garnet, the domain of the Meuse sediments in different periods can be documented. It has also been shown that the Scheldt system appears to contain minerals from a source similar to that of the Meuse. The distribution of topaz reflects the influence and extent of sediments delivered by the Baltic system and reveals that the most likely transport mechanism was glacial and not fluvial.

The examples are intended to exploit the opportunities provided by the extensive databases in visualising the distribution of sediments with differing provenance in the Netherlands. Re-analysis of old datasets and employing relatively simple methods provides new insights into the geometry of sediment bodies and the sedimentation history of subsurface deposits.

Developments in Sedimentology, Vol. 58, 869–885

ISSN: 0070-4571/doi:10.1016/S0070-4571(07)58034-9

Keywords: GIS; Rhine; Meuse; Scheldt; Proto-Weser; Eridanos; spatial modelling; sediment source; Netherlands; stratigraphy

1. INTRODUCTION

The use of heavy minerals for research into the provenance of sediments has a long tradition in the Netherlands. In the first comprehensive study, Edelman (1933) distinguished different sediment sources in the Netherlands on the basis of their heavy-mineral content. Later, the heavy-mineral compositions of the sediments of the modern rivers Meuse and Rhine were determined in order to trace the source areas of the minerals in these sediments (Edelman, 1938; Van Andel, 1950). Since the pioneering work of Edelman, and especially after the 1950s, heavy-mineral compositional diagrams were used profusely as a stratigraphic tool (Zonneveld, 1958). This culminated in the stratigraphic nomenclator, established in 1975, where each Quaternary formation was not only characterised by its lithology and stratigraphic position, but also by the composition of its heavy-mineral suite (Zagwijn and Van Staalduinen, 1975). To achieve this, heavy-mineral analyses were conducted on a routine basis as an integral part of the geological mapping of the subsurface of the Netherlands. However, in 2003, a revised nomenclator of the Dutch lithostratigraphy was issued in which the heavy-mineral contents of the lithostratigraphical units were no longer used as a diagnostic stratigraphical criterion (De Mulder et al., 2003; Ebbing et al., 2003). By that time, a total of 40,000 samples had been analysed for their heavy-mineral content; some 25,000 from boreholes and some 15,000 from quarries.

Until recently, heavy-mineral studies in the Netherlands mainly entailed the study of single boreholes or transects with multiple boreholes. This logical approach is probably the best for using heavy-mineral data to obtain stratigraphical support for the interpretation of lithostratigraphical units in a borehole. Subsequently, large-scale spatial geological maps were constructed. However, these were based on lithostratigraphical interpretations of the borehole data rather than on the spatial distribution of their heavy-mineral content.

The available extensive heavy-mineral database of the subsurface sediments provides a unique opportunity to study:

- 3-D variations in heavy-mineral compositions that facilitates a deeper insight into the build-up of the subsurface of the Netherlands;
- the distribution of sediments from various sources, deposited by fluvial and marine processes;
- the effects of ice and tectonic movements on the displacement or redistribution of sediments.

The successful application of such studies shows the potential of a substantial heavy-mineral database from local to national scale. Results of pilot studies to examine the spatial distribution of the heavy minerals on larger scales have been presented by Huisman (1998) and Huisman et al. (2000). Heavy-mineral variations within one geological unit (Kedichem Formation) were evaluated using a multivariate statistical technique (i.e., factor analysis). Variations in sediment provenance were identified by factor loadings interpreted as sediment source indicators. Maps of these factor

loadings were constructed to show the 3-D spatial variations in heavy-mineral composition within the test formation.

In this contribution we demonstrate how the availability of an extensive database in the Netherlands has enabled the study of subsurface sediments in three dimensions. Huisman (1999) tested first the applicability of this method on the complete, nation-wide, heavy-mineral database. Factor analysis yielded five interpretable factors, but when these were compared with the interpretation of the heavy-mineral counts in core samples, it became apparent that too much information is lost when all the variation is combined and limited to a small number of factors. Moreover, the factor scores of more than half of the minerals were so low that they could not be assigned to any factor. There are probably a number of reasons why the method that Imbrie and Van Andel (1964) used successfully, and proved informative for one single formation from our database, did not succeed for larger datasets. The most plausible explanation is that there are too many factors (i.e., sediments sources) and that many of them are too similar. As a result, the major factors represent only general mineral groups. An additional problem is that several of the most source-specific minerals are rare; in most samples they are not detected at all, and where they do occur, usually only a few grains are found. The resulting non-normal discrete distribution for part of the dataset is difficult to deal with in multivariate statistics. In this study, as an alternative, we decided to focus on specific minerals that are well-established signatures of sediment sources and use them as indicators.

In order to demonstrate how easily the potential of the available heavy-mineral database can be exploited, we used only simple programs that are widely available for personal computers for data handling and presentation. These programs do not require special computer hardware, complex Geographical Information Systems or large, complex statistical packages.

2. GEOLOGICAL SETTING

The subsurface of the Netherlands consists of a series of basins that are filled with Caenozoic sediments. The thicknesses of these fills vary considerably due to differential tectonics (see Fig. 1A and B). Most of the (Caenozoic) deeper, older deposits have a marine origin, but especially during the Pleistocene extensive sediment bodies were deposited in a fluvial environment by four distinct river systems. The most important river systems are the Rhine, Meuse, and Scheldt and a river system—usually known as the Baltic river or Eridanos—that entered the country from the northeast and drained Fennoscandia and northern and central Germany up to the Thüringer Wald (Zagwijn, 1974, 1978, 1979; Tebbens et al., 1995; De Mulder et al., 2003). This river's influence diminished during the Early Pleistocene, and in the Middle-Pleistocene one of its tributaries—that drained the German Variscan Massifs—took over. From then on, this river is referred to as the proto-Weser River. However, the proto-Weser should not be seen as a river system that is completely different from the Eridanos, but rather as a continuation with a more limited drainage area. The River Scheldt, draining the Brabant Massif, had significant influence in the southwest of the country (Fig. 1A).

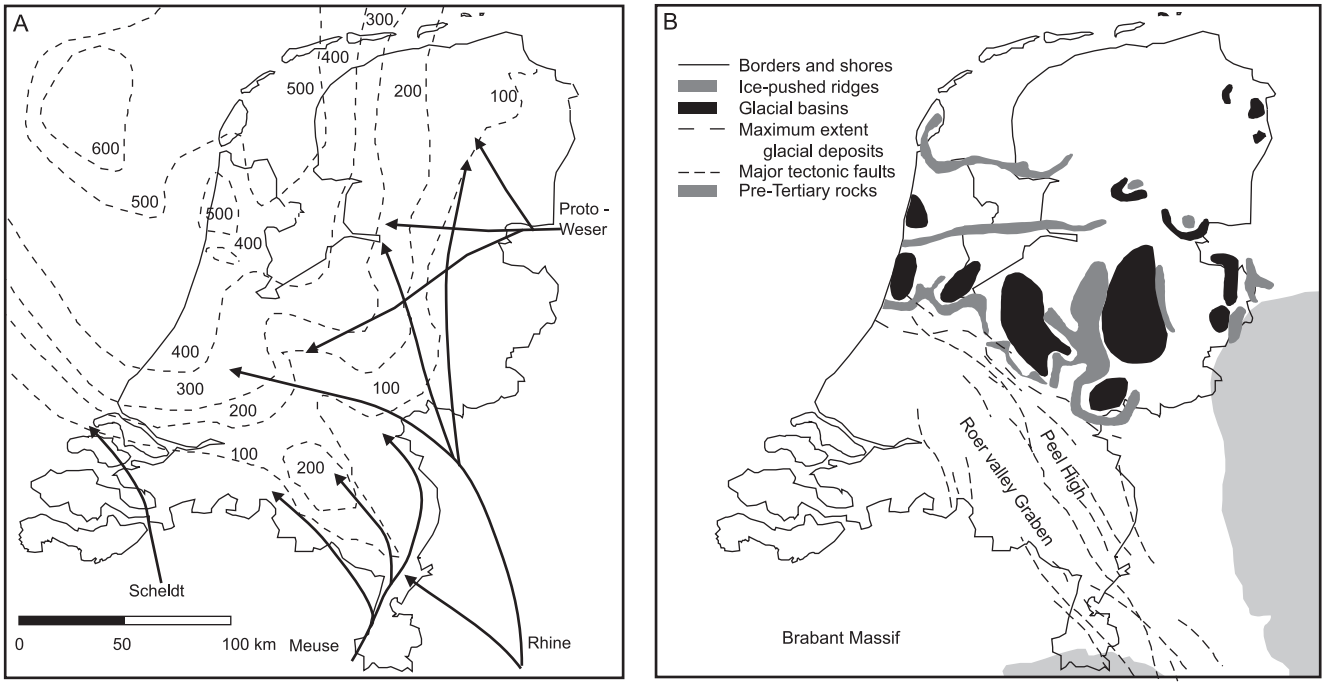

Fig. 1. Maps of the Netherlands. (A) Major river systems and depth-contours of the base Pleistocene. The major basins, filled with Pleistocene sediment, can be seen in the west of the country (after Zagwijn, 1974, 1978). (B) Tectonic and glacial features (after Zagwijn, 1974, 1978; Zagwijn and Van Staalduinen, 1975).

Ice-flow from the Scandinavian ice sheet advanced into the north of the Netherlands at least twice during the Pleistocene (Elsterian and Saalian glaciations). The Saalian glaciation produced a series of ice-pushed ridges and deep glacial basins that form a band running more or less E–W through the centre of the country (see Fig. 1B).

Differentiation between Pleistocene sediments and older deposits on the basis of distinctive heavy-mineral assemblages is well documented in the literature (e.g., Zonneveld, 1958; Boenigk, 1970; Zagwijn and Van Staalduinen, 1975). Throughout the Pleistocene deposits of each of the larger fluvial sources (Rhine, Meuse, Eridanos/proto-Weser) can be differentiated from each other. In addition, the Rhine and Meuse show variations in their heavy-mineral composition through time due to changes in their respective hinterlands. We selected particular heavy-minerals that appeared to be most suitable for mapping to illustrate the temporal and spatial distribution of the four main systems.

2.1. Zircon

Together with tourmaline, zircon is the most common mineral in the silt and fine sand fractions of strongly weathered sediments. In the Netherlands, zircon *grosso modo* is considered typical of polycyclic and strongly weathered sediments that were deposited during the Tertiary by various fluvial systems. Around the Pliocene-Pleistocene transition, both the Eridanos and the Rhine system began to deposit sediments that contained a wider spectrum of heavy minerals, including garnet, epidote, and hornblende (Boenigk, 1970; Zagwijn and Van Staalduinen, 1975). As a result, the proportion of zircon in the heavy-mineral counts decreases. Modern sediments (mostly the sand and silt fraction) of the Rhine and Meuse have low zircon contents (Van Andel, 1950).

2.2. Green Hornblende

Green hornblende is a common heavy mineral in the Pleistocene Baltic, and Rhine deposits. The foothills of the Alps provided ample green hornblende to a Rhine system that carries Alpine heavy-mineral suites to the Netherlands even today (Van Andel, 1950).

2.3. Augite

Following the onset of volcanic activity in the Eiffel Mountains (~750 ka BP; Van den Berg, 1996), the heavy-mineral fraction of Rhine-derived sediments is dominated by volcanic minerals. The most common mineral of the volcanic suite is augite (Zagwijn and Van Staalduinen, 1975).

2.4. Vosges-Type Hornblende

Brown-green hornblende is considered to be a typical signature of sediments derived from the Vosges area (Zonneveld, 1958). In the heavy-mineral database it is therefore recorded as Vosges-type hornblende. The Vosges formed part of the hinterland of the Meuse system until the Elsterian or Saalian glaciation, when the Upper Meuse

was captured by the Moselle near Toul (Bustamante, 1976; Tebbens et al., 1995). Therefore the Vosges-type hornblende is a unique index mineral of the pre-Elsterian Meuse River system. The abundance of Vosges-type hornblende is usually very low.

2.5. Meuse-Type Garnet

Garnets of the Meuse sediments are generally turbid and colourless and are distinguished as Meuse-type garnets. They are considered to be typical of the Cambrian metamorphic massifs of Libramont-Bastogne in the Ardennes present in the hinterland of the Meuse (Zonneveld, 1947; Tebbens et al., 1995). Meuse-type garnets when present are represented only by a few grains in the heavy-mineral slides.

2.6. Topaz

Topaz is a rare mineral that is considered to be typical of Baltic sediment sources. It is thought to be transported by the Eridanos and/or the proto-Weser system, originating either from Scandinavia (De Mulder et al., 2003) or possibly from the Thüringer Wald.

3. MATERIALS AND METHODS

Samples selected for heavy-mineral analysis were treated with HCl and HNO_3 to remove carbonates, Fe (hydr)oxides, and organic matter followed by sieving to extract the 63–500 μm grain-size fraction. The heavy minerals were separated from 63 to 500 μm fraction by heavy-liquid separation (bromoform or sodium polytungstate). The density of the liquid was set at 2.78 kg/l. The heavy-mineral fraction was mounted on microscope slides, and 100 or (in most cases) 200 transparent minerals were identified and counted. The opaque grains were usually not included in the grain counts.

It is important to note that the percentage of heavy-mineral content given in this study is the percentage of a specific mineral in the two hundred or hundred counts and *not* a percentage of the total sediment. The percentage cannot be linked to the sediment sample as the initial amount of sediments used in the sample processing, the 63–500 μm fraction and the heavy-mineral fraction were not weighted. The consequences of this is that a high amount of e.g., zircons in a certain area does not necessarily mean that the concentration of zircons in the sediments is high, but that of the 200 or 100 counted grains a high percentage of these grains consists of zircons.

Our total database was obtained from the analyses of ~40,000 samples. We limited the sample base to borehole samples from cores where the sampled interval was less than 5 m, excluding those from quarries. A total of slightly over 25,000 analyses remained and were stored in an ACCESS database. Subsets were extracted from this database, each representing a 5 m thick horizontal zone. The 10 m depth zone for instance contains all samples with either top or bottom depth between 7.5 and 12.5 m (10 ± 2.5) below Dutch Ordnance Level. As the sampled interval was required to be 5 m maximum, any sample can be present in only two of the subsets. Each subset was stored in a separate spreadsheet (MICROSOFT EXCEL) for further work.

We first made draft sheets with post maps of the 16 available depths, dot size representing mineral contents, using the Golden Software SURFER package (versions 6–8). These were then used for a first screening and to select depth ranges that were most useful to demonstrate the effects of different visualisation techniques. This was continued by making, what we named, "*stacked threshold maps*" for the selected minerals that involved first the choosing of a range of depths suitable for displaying the variation in mineral contents. In this selection, depths were confined between 0 and 70 m below Dutch Ordinance Level. Below 70 m, the availability of data was too limited. Above sea level (0 m) the maps would become unintelligible because of the interference of topography—in the study region roughly half of the land surface is within 5 m above sea level. We used the interpolation module in Surfer to construct grid files, applying inverse distance to power 2, with grid density of 500 m and averaging duplicate data. The resulting grids were cut off at 5000 m from the borders and the seashore.

Finally, from the grid files contour maps were made, on which the area above a certain concentration ("threshold") was coloured, whereas the rest of the map was left blank. Several such maps were stacked into one figure and each of the maps given a different colour or grey tone, according to the depth it represented.

The major advantage of this type of map is that it gives a quick overview of the pattern of distribution of a particular mineral in three dimensions. There are, however, drawbacks. One disadvantage is that a coloured area at a shallow depth completely blanks out any information below it because of the stacking. Another disadvantage is that only one threshold value can be chosen. The spatial characteristics of variations in concentration—as could be seen in a 'true' contour map—cannot be made visible. In this study, if analysis of the stacked threshold maps proved it to be necessary, we have made additional sets of contour maps to show variations for an informative mineral in more detail.

4. RESULTS AND EVALUATION

4.1. Tectonic Setting as Demonstrated by Zircon

A combined threshold map of zircon is illustrated in Fig. 2. It shows clearly delineated zones with continuous high zircon values in the east and southeast. They represent the areas where pre-Pleistocene, highly weathered sediments occur at relatively shallow depths. Outside this zone, patchy locations with high zircon values appear in the south of the country. They probably reflect reworking of the same, strongly weathered Tertiary sediments from the Brabant Massif to the south, intermixing with less weathered material, especially from the Rhine system during the Early Pleistocene (Kasse, 1988). In the rest of the country, zircon values are generally low.

Since the depth differences in zircon distribution patterns cannot be seen from Fig. 2, we have made a series of contour maps at different depths (Fig. 3). By changing the threshold from 20 to 5%, Fig. 3 reveals that the areas of continuous high zircon values extend further towards the west. Moreover, both the southwest of the country and the very northeast can also be included in the zircon-dominated areas. The zircon-dominated areas coincide with the general contours that delineate

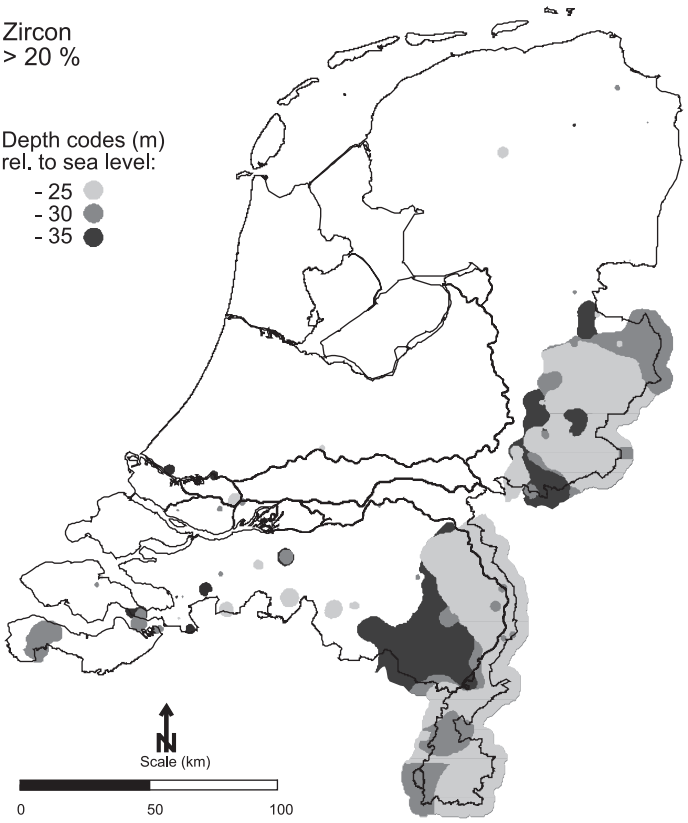

Fig. 2. Combined threshold map of zircon. The threshold is set at 20% zircon grains in the transparent heavy-mineral fraction. The high values of zircon reflect the areas where pre-Pleistocene sediments are close to the surface.

the eastern and southern rim of major Pleistocene deposition. The basins in the west show lower zircon values. It is remarkable that the areas with high zircon values are nearly identical in shape, size, and position at all depths shown here, indicating that the boundary between zircon-rich and zircon-poor sediments is sharp. Moreover, this boundary coincides with tectonic fault lines in several places (see Fig. 1B). The only area where the zircon content frequently varies with depth is the Roer Valley Graben, which is inside the 1–5% zircon concentration areas at the –30 m depths, but falls (totally or partially) outside the −45 and −65 m depth. This reflects the local reworking and mixing of zircon-rich sediments with Rhine- and Meuse-supplied, zircon-poor material during the Middle and Late Pleistocene.

4.2. Reconstruction of Rhine and proto-Weser Depositional Belts from Green Hornblende and Augite

4.2.1. Green hornblende

The map of green hornblende distribution (Fig. 4) shows that two zones with high values of green hornblende can be distinguished:

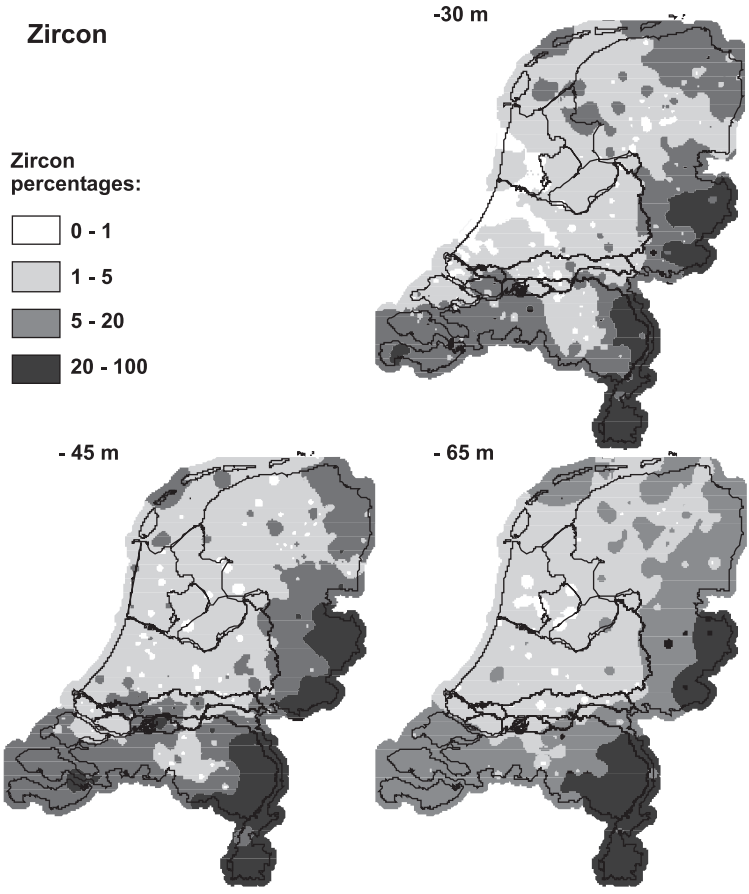

Fig. 3. Zircon contour maps at various depths.

(1) A funnel-shaped area runs east–west through the centre of the country directly underneath the present-day Rhine system. This zone probably represents a Rhine course during the Early Pleistocene. The westward-widening shape of the funnel may outline an ancient estuary, but it could represent a valley in the east with an associated floodplain in the west. The zone dips towards the north, caused probably by the post-sedimentary tectonic subsidence in the north while the more or less stable Brabant Massif is present in the south (Van den Berg, 1996). In the centre of the map, the top of the green hornblende dominated zone lies lower than in the east and west as a result of subsidence in the Roer Valley Graben. Here we do not detect the Early Pleistocene Rhine sediments that are present further to the south in the Roer Valley Graben at depths >100 m, due to strong local subsidence. Consequently, they were not included in the dataset. It is striking to see the almost perfect match of the Early Pleistocene and the present-day Rhine floodplains.
(2) A smaller area with high values (over 22%) of green hornblende appears in the northwest of the country. Although this zone is less clearly delineated, it appears to run southeast–northwest and dips slightly seaward; it may represent a

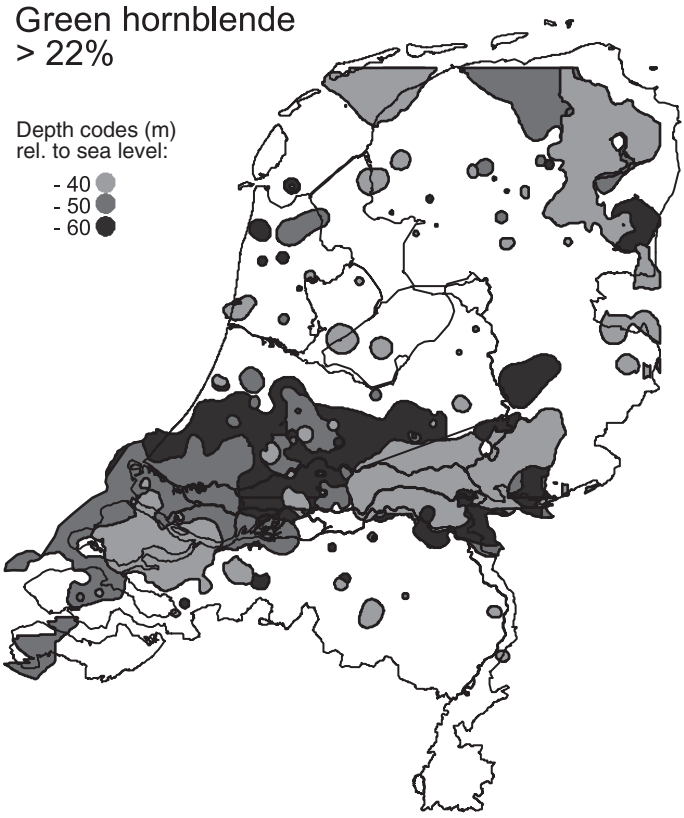

Fig. 4. Combined threshold map of green hornblende. The threshold is set at 22% green hornblende grains in the transparent heavy-mineral fraction. The zone in the centre, running east–west, coincides with a former floodplain of the Rhine. In the north, a floodplain of the proto-Weser runs southeast–northwest.

floodplain of the proto-Weser. In earlier studies (e.g., Zagwijn, 1974, 1978) sediments of this system were interpreted as being Rhine-derived: on maps of ancient river courses (including Fig. 1A), a Rhine channel is shown in the east of the country running north which is not confirmed by our green hornblende map. This has also been recognised in the present lithostratigraphical classification used in The Netherlands (De Mulder et al., 2003).

At shallower depths than those used in this map (between −40 and 0 m below sea level), the Rhine sediments are dominated by Eiffel-derived volcanogenic minerals, such as augite. As a result, augite rather than green hornblende becomes a diagnostic mineral for the younger part of the Rhine sediments (see below).

4.2.2. Augite

The combined threshold map (> 5%) of augite distribution (Fig. 5) shows high values in most parts of the Netherlands. In fact, all the major sedimentary basins are filled with augite-bearing sediments at some depths (Fig. 1A). The augite seems to form a nearly continuous layer with a downward slope towards the northeast. The layer appears to be partially interrupted only by the ice-pushed ridge in the centre of

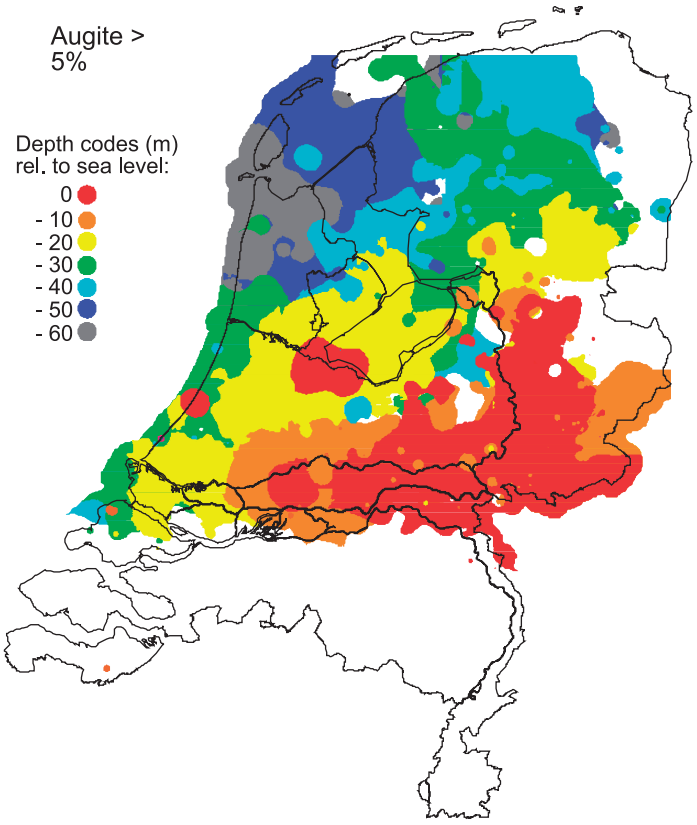

Fig. 5. Combined threshold map of augite. The threshold is set at 5% augite grains in the transparent heavy-mineral fraction. An extensive, continuous layer with high values of augite can be seen extending from the present-day Rhine floodplain to the north, sloping towards the northwest.

the country (Fig. 1B). At first glance, the overall picture is that of a large sedimentation area that has been filled by the Rhine.

A closer inspection of the area in the extreme north shows that the proto-Weser also deposited there. This is revealed by the contour maps of augite values at 0, 30, and 40 m below NAP (Fig. 6). At the 30 m depth, a clear elongate lobe is visible that is interpreted as a former floodplain of the proto-Weser system. Its position is just south of the proto-Weser floodplain identified on the map of green hornblende (Fig. 4).

The map showing the augite distribution at the 40 m depth also reveals an interesting, triangular-shaped feature in the centre of the country which probably represents a former valley or estuary. This shape has been identified earlier by Zonneveld (1947) as a Rhine floodplain.

4.3. Identifying the Meuse Dispersal Pattern from two Rare Minerals

4.3.1. Vosges-type hornblende

The combined threshold map in Fig. 7 shows the occurrence of Vosges-type hornblende. This hornblende variety occurs in an area that is mostly restricted to the east

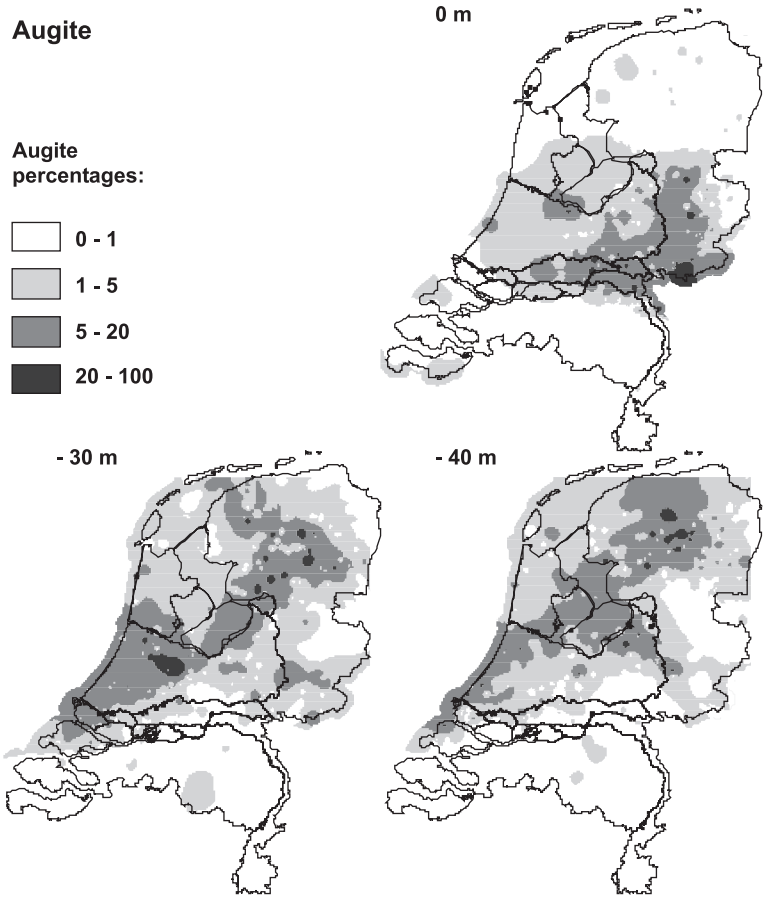

Fig. 6. Augite contour maps at various depths.

side of the Roer Valley Graben that had been the Meuse floodplain before the Elsterian or Saalian capture of the Upper Meuse by the Moselle (Bustamante, 1976). A small area with a high abundance of Vosges-type hornblende can be seen on top of the Peel High. This is probably a mini-graben within the (strongly fragmented) Peel High, where remnants of Meuse deposits are still present. On the rest of the high they have probably been eroded, or never have been deposited. Vosges-type hornblende occurrences in the far west of the country could be a small remaining part of a Meuse floodplain, but the number of samples there is too small to draw a more meaningful interpretation. The layer with high concentrations in the eastern Roer Valley Graben dips towards the north as a result of faster subsidence rates in its central part (Van den Berg, 1996).

4.3.2. Meuse-type garnet

Fig. 8 is a combined threshold map for Meuse-type garnet. The threshold is chosen at $>0.45\%$ so that all samples in which at least one garnet grain was found could be included. It must be noted that problems may arise from the fact that in some

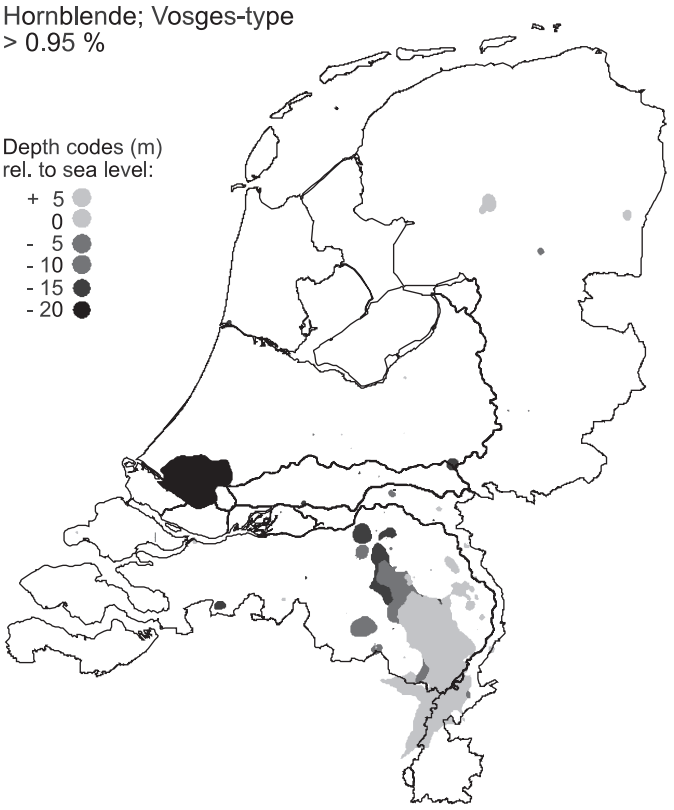

Fig. 7. Combined threshold map of Vosges-type hornblende. The threshold is set at 0.95% Vosges-type hornblende grains in the transparent heavy-mineral fraction. The occurrence of this mineral is restricted to an area in the southeast, reflecting a Meuse floodplain before the Elsterian or Saalian capture of the upper Meuse by the Moselle at Toul.

samples the point counting was limited to 100 grains instead of 200. Because the threshold was set at a value below the detection limit for part of the samples (1 grain in 100), anomalies can be expected and the very patchy occurrence, seen especially in the southeast on the map, may be related to this problem. Despite these anomalies, the overall distribution shows two discrete areas where Meuse-type garnet occurs: one in the southeast and the other in the southwest.

In the southeast, Meuse-type garnet can be found in the Roer Valley Graben from -35 to -10 m. From -5 to $+15$ m it occurs mostly in the present-day Meuse valley. This can be attributed to a shift of the Meuse floodplain from the Roer Valley towards its present position, and by the relatively fast subsidence rates in the Roer Valley Graben (Van den Berg, 1996). Though the map gives no clear spatial delineation of the sediment body that originates form the River Meuse (especially compared to the map of Vosges-type hornblende; Fig. 7), it provides an insight into the position of the Meuse floodplain during larger parts of its existence.

In the southwest an area with high garnet content is clearly delineated. It lies outside the drainage basin of the River Meuse and seems to coincide with a former

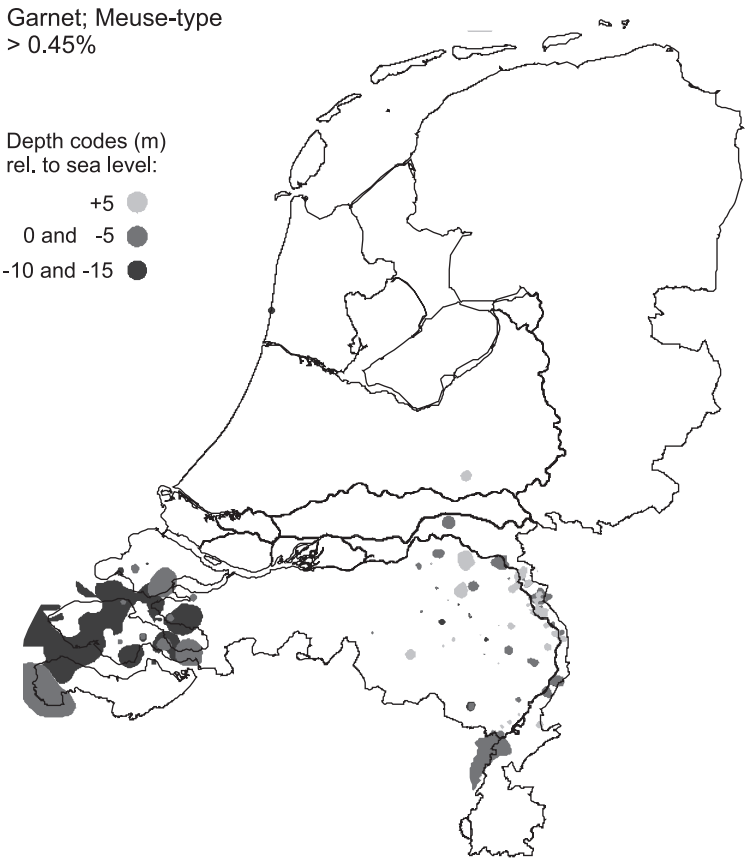

Fig. 8. Combined threshold map of Meuse-type garnet. With a threshold of 0.45% Meuse-type garnet grains in the transparent heavy-mineral fraction, all areas where this mineral was identified are shown. Apart from a patchy occurrence in the Meuse depositional area in the southeast, Meuse-type garnet is also found in the depositional area of the Scheldt river in the southwest.

valley of the River Scheldt. From the Meuse-type garnet pattern a SE–NW-running belt can be envisaged that would indicate a former Scheldt floodplain, continuing in a NE–SW zone, parallel to the present coastline. This area would outline the depositional belt or the shoreline where Scheldt-derived sediments were once deposited. We presume that the Scheldt and Meuse had transported sediments from the same source region and same rock types.

4.4. The Effects of Glaciation, Deduced from the Distribution of Topaz

In order to obtain an interpretable pattern for topaz, its threshold has been set at 0.45 in the combined topaz threshold map (Fig. 9), so that, as in the Meuse-type garnet map (Fig. 8), all recorded topaz grains are plotted. Compared with the zonal maps of zircon, green hornblende, or augite (Figs. 4 and 5), the areas of topaz-bearing sediments are far less continuous, making it difficult to detect spatial

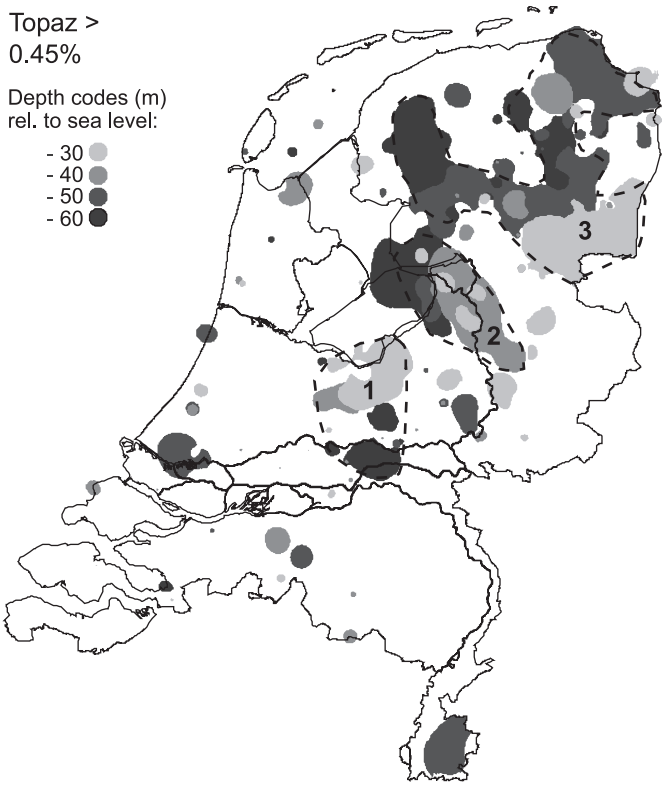

Fig. 9. Combined threshold map of topaz. With a threshold of 0.45% topaz grains in the transparent heavy-mineral fraction, all areas where this mineral was identified are shown. In the centre of the country, the topaz mainly occurs in two glacial basins (1: Gelderse vallei and 2: IJssel vallei) and on the outwash plains of ice-pushed ridges. This might indicate glacial action transporting the mineral from Scandinavia. In a large area in the north (3) the mineral is probably derived from the proto-Weser, although glacial transport and deposition cannot be excluded.

variations. Moreover, there are isolated occurrences of the mineral scattered over the country, hinting at the presence of this mineral in very low amounts in all sediments. Overall, two major areas containing topaz-bearing sediments can be distinguished.

In the centre of the country, topaz occurs at multiple depths. Close inspection and comparison with Fig. 1B reveals that topaz here is concentrated in the glacial basins and on outwash planes bordering the Saalian ice-pushed ridges (1 and 2 in Fig. 9). It is likely that their distribution reflects the transport paths of topaz-bearing sand from Scandinavia by the Saalian glaciers, and their deposition in kame terraces, outwash plains and in small basins. The relatively minor amounts of topaz in the ice-pushed ridges—which consist mainly of deformed and displaced Rhine, Meuse, Eridanos, and proto-Weser sediments—may indicate that the topaz-bearing sediments were transported primarily by the glacial ice, and not by fluvial systems. However, selective concentration of topaz grains in the coarse-grained periglacial deposits in the glacial basins may also have played a role.

A rather extensive area in the north (identified with 3 in Fig. 9) that seems to dip northeastward most probably comprises a series of sediments that were either deposited by the proto-Weser, or were derived from the Fennoscandian hinterland of the Baltic system through glacial action. In contrast to augite and green hornblende (Figs. 4 and 5), the distribution of topaz-bearing sediments does not permit the identification of floodplains or other interpretable sediment forms.

5. SYNTHESIS: FUTURE APPLICATIONS FOR OLD HEAVY-MINERAL DATASETS

The heavy-mineral maps introduced in this paper demonstrate that large heavy-mineral databases hold a remarkable potential for the 3-D study of sedimentary successions derived from a variety of sources. Former floodplains, sedimentary basins, glacial features, and tectonic framework can be discerned from these maps. Some of our findings have been identified earlier, such as the augite-dominated valley (Fig. 6) that had already been described by Zonneveld (1947). Others are unexpected new findings that were not apparent from the study of whole borehole successions; for example, the maps of augite and green hornblende reveal the buried floodplains of the proto-Weser, whereas the map of Meuse-type garnet gives new information on the Scheldt's floodplain and its sediment source area. The map of topaz, surprisingly, indicates both a different transport mechanism (glacial instead of fluvial) and thus a different source area for the topaz-bearing sediments in the centre of the country.

Visualisation of the 3-D variation presented the greatest challenge in this study. We applied simple tools, and basic functions from widely available PC-based databases and spreadsheets were used for the handling and selection of all data. The different types of 2-D maps used to approach the 3-D variation were all made by user-friendly and low-cost PC programs. In short, our study demonstrates that potentially useful and informative results can be achieved by means of widely available, relatively simple computing tools.

The present study has focused solely on the distribution patterns of heavy minerals in the subsurface sediments, and on their interpretation. We did not compare our results to known lithostratigraphic formations, and only general reference was made to known tectonic framework and sediment build-up. We feel that our results have advanced understanding of the geology of the subsurface in the Netherlands and have provided a larger picture of interchanging systems and their depocentres. In addition, they have demonstrated that renewed analysis of data from old databases by using advanced visualisation techniques is a viable and powerful tool that can be applied to regions wherever adequate subsurface data are available. It has potential applicability in prospecting for economic minerals, in the provenance determination of reservoir sediments and for correlation or differentiation of sediment packages.

ACKNOWLEDGEMENTS

Results presented in this study were originally obtained as part of the GEMSTRAT project at TNO-NITG/National Geological Survey. DJH wishes to thank the ROB/

National Service for Archaeological Heritage for allocating time to work on this publication. We acknowledge the valuable comments of H.J.T. Weerts and an anonymous reviewer.

REFERENCES

Boenigk, W., 1970. Zur Kenntnis des Altquartärs bei Brüggen, Köln. Geologisches Institute der Universität Köln, Germany, 143pp.

Bustamante, S.C.L., 1976. L'évolution Plio-Pléistocène du basin Mosa d'après ses minéraux lourds. Revue de Géographie Physique et de Géologie Dynamique 18, 291–300.

De Mulder, E.F.J., Geluk, M.C., Ritsema, I., Westerhoff, W.E., Wong, Th.E., 2003. De ondergrond van Nederland. Utrecht, TNO-NITG, 380pp.

Ebbing, J.H.J., Weerts, H.J.T., Westerhoff, W.E., 2003. Towards an integrated land-sea stratigraphy of the Netherlands. Quaternary Science Reviews 22, 1579–1587.

Edelman, C.H., 1933. Petrologische Provincies in het Nederlandsche Kwartair. Ph.D. thesis. D.B. Centen's Uitgevers Maatschappij, Amsterdam, 104pp.

Edelman, C.H., 1938. Petrology of recent sands of the Rhine and the Meuse in the Netherlands. Journal of Sedimentary Petrology 8, 59–66.

Huisman, D.J., 1998. Geochemical characterization of subsurface-sediments in the Netherlands. Ph.D. thesis. Wageningen University, Wageningen, 175pp.

Huisman, D.J., 1999. Bulk geochemie als karteringsgereedschap. TNO-NITG report 99-1-B (in Dutch).

Huisman, D.J., Weijers, J.P., Dijkshoorn, L., Veldkamp, A., 2000. Spatial prediction of variability of Early Pleistocene subsurface sediments in the Netherlands. Part 1: Heavy minerals. Netherlands Journal of Geosciences 79, 373–381.

Imbrie, J., Van Andel, T.H., 1964. Vector analysis of heavy-mineral data. Geological Society of America Bulletin 75, 1131–1156.

Kasse, C., 1988. Early Pleistocene Tidal and Fluviatile Environments in the Southern Netherlands and Northern Belgium. Free University Press, Amsterdam, 190pp.

Tebbens, L.A., Kroonenberg, S.B., Van den Berg, M.W., 1995. Compositional variation of detrital garnets in Quaternary Rhine, Meuse and Baltic River sediments in the Netherlands. Geologie en Mijnbouw 74, 213–224.

Van Andel, Tj.H., 1950. Provenance, Transport and Deposition of Rhine Sediments. Ph.D. thesis. Groningen University, Groningen, 129pp.

Van den Berg, M.V., 1996. Fluvial Sequences of the Maas. Ph.D. thesis. Wageningen University, Wageningen, 181pp.

Zagwijn, W.H., 1974. The paleogeographic evolution of the Netherlands during the Quarternary. Geologie en Mijnbouw 53, 369–385.

Zagwijn, W.H., 1978. Upper Cenozoic of the southern North Sea Basin: paleoclimatic and paleogeographic evolution. Geologie en Mijnbouw 57, 577–588.

Zagwijn, W.H., 1979. Early and Middle Pleistocene coastlines in the southern North Sea Basin. In: Oele, E., Schütenhelm, R.T.E., Wiggers, A.J. (Eds.), The Quaternary History of the North Sea. Acta Univ. Upps. Symp., Univ. Upps. Annum Quingentesium Celebrantis, 2, Uppsala, pp. 31–42.

Zagwijn, W.H., Van Staalduinen, C.J., 1975. Toelichting bij geologische overzichtskaarten van Nederland. Geological Survey of the Netherlands, Haarlem, 134pp.

Zonneveld, J.I.S., 1947. Het kwartair van het Peelgebied en de naaste omgeving (een sediment petrologische studie). Mededelingen van de Geologische Stichting C-VI-3, 223.

Zonneveld, J.I.S., 1958. Litho-stratigrafische eenheden in het Nederlandse Pleistoceen, Mededelingen van de Geologische Stichting. Nieuwe Serie 12, 31–64.

This page intentionally left blank

Chapter 35

HEAVY MINERALS IN THE SWISS MOLASSE BASIN: OCCURRENCE, FREQUENCY, CHEMISTRY AND THERMOCHRONOLOGY

HILMAR VON EYNATTEN

Geowissenschaftliches Zentrum der Universität Göttingen, Abteilung Sedimentologie und Umweltgeologie, Goldschmidtstrasse 3, D-37077 Göttingen, Germany

ABSTRACT

The Swiss Molasse Basin represents an ideal setting to study the sedimentary response to orogenic processes, because (1) the sediments of the Swiss Molasse Basin are chronostratigraphically well-calibrated and (2) the orogenic hinterland, the Central Alps, has been extensively studied. Heavy minerals are sensitive recorders of both tectonic and exogenic processes, and have been widely used to constrain the stratigraphy, transport, provenance and diagenesis of Swiss Molasse Basin sediments. After a brief review of almost a century of heavy mineral research in the Swiss Molasse Basin, this contribution focuses on modern analytical techniques including high-resolution single-grain chemistry and thermochronological studies ($^{40}Ar/^{39}Ar$ laser-probe dating of white mica, fission-track dating of zircon). These techniques have been applied to Rupelian to Serravallian (~31 to ~13 Ma) sandstones from two composite sections of the Swiss Molasse Basin, one in the east (Honegg-Kronberg-Hörnli) and one in the central part (Honegg-Napf). In the east, the data reflect a normal unroofing sequence of the Austroalpine-Penninic nappe stack, lacking any signal of rapid exhumation in the hinterland at any time. In the central part, erosion of basement rocks started significantly earlier, and sediments younger than ~20 Ma document increasing cooling rates of their source rocks, reflecting accelerated exhumation in the hinterland. The timing of maximum cooling as well as the cooling rates (up to ~40 °C/Ma) correspond exactly with $^{40}Ar/^{39}Ar$ data obtained from the presently exposed Lepontine metamorphic dome.

Keywords: heavy minerals; Swiss Molasse Basin; Central Alps; mineral chemistry; $^{40}Ar/^{39}Ar$ dating; zircon fission-track dating

Developments in Sedimentology, Vol. 58, 887–905

ISSN: 0070-4571/doi:10.1016/S0070-4571(07)58035-0

1. INTRODUCTION

The Swiss Molasse Basin provides an ideal example for studying the interaction of sedimentation in the basin and late orogenic processes in the Central Alps. This is because (1) the chronostratigraphy of the sedimentary basin fill is precisely calibrated to the global geomagnetic polarity time scale (GPTS) of Cande and Kent (1992, 1995) by a combination of detailed magnetostratigraphy and mammal biostratigraphy (Schlunegger et al., 1996; Kempf et al., 1997, 1999; Strunck and Matter, 2002), and (2) the Alpine orogenic hinterland, the principal source area of the sediments, still exists and belongs to one of the best-known orogens in the world (Schmid et al., 1996; Frey and Ferrero Mählmann, 1999). The sedimentary response to the orogenic evolution of the Central Alps, as documented in the Swiss Molasse Basin deposits, was reconstructed in several ways using, among other approaches, facies analysis and stratigraphy (Homewood et al., 1986; Schlunegger et al., 1997), stratigraphic modelling (Sinclair et al., 1991), sediment budget calculations (Kuhlemann et al., 2001) and sediment framework composition or other detrital signatures such as heavy mineral analysis or single-grain varietal studies (cf. Morton, 1991) to identify source-rock evolution in time and space (Füchtbauer, 1964; von Eynatten, 2003).

In several case studies, heavy minerals have been proven to faithfully record geological conditions such as source area lithology, physiography, climate, sediment recycling, transport and diagenetic overprint (Morton and Johnsson, 1993; Lonergan and Mange-Rajetzky, 1994). However, studies based on conventional heavy mineral analysis (frequency distribution based on grain counting) alone may lead to ambiguous or even misleading results as outlined by, among others, Morton (1991). This may be circumvented by multi-method approaches that relate heavy mineral distribution to data on framework composition, whole-rock geochemistry, and/or specific single-grain characteristics. With respect to provenance analysis, single-grain techniques have proven to be most promising for precise characterisation of source rock petrology and thermal history (e.g., von Eynatten and Gaupp, 1999; Rahl et al., 2003). However, the full potential of single-grain techniques for quantitative provenance studies will be only completely realised if results are firmly connected to the bulk mass transfer from the source area to the sedimentary basin (Weltje and von Eynatten, 2004).

The objectives of this contribution are first to provide a brief review of heavy mineral research on the Swiss Molasse Basin and to summarise the results of recent studies (von Eynatten et al., 1999; Spiegel et al., 2000, 2002; von Eynatten, 2003; von Eynatten and Wijbrans, 2003) and secondly to discuss the advantages of integrating heavy mineral analysis with single-grain geochemical and geochronological techniques.

2. GEOLOGICAL OUTLINE

The Alpine orogeny, in general, is driven by Cretaceous to Neogene convergence between the African and European plates. The Helvetic units in the Alps represent the former southern margin of the European plate, whereas the Austroalpine and

Southalpine units are part of the former northern margin of the Adriatic plate (northern Africa; Frisch, 1979). The Penninic units are remnants of the oceanic realms formerly located between the two plates. During Tertiary continent/continent collision, European lithosphere was subducted beneath the Adriatic plate, leading to strong crustal shortening and formation of the present-day Alpine nappe stack (Schmid et al., 1996, and references therein).

The Central Alps in Switzerland, the source area for most of the Swiss Molasse Basin deposits, form a doubly vergent orogen with high-grade metamorphic rocks of the Lepontine Dome (Fig. 1a) in its core (Schmid et al., 1996). The southern flank, the Southalpine realm, is not considered here because it never acted as a source for Swiss Molasse Basin deposits (Schlunegger et al., 1998). The northern flank consists of a north-vergent nappe stack of low-grade metamorphic to unmetamorphosed rocks representing Helvetic, Penninic and Austroalpine basement and cover nappes (Fig. 1a). Emplacement of these nappes occurred contemporaneously with the peak of Alpine metamorphism in the Central Alps (40–32 Ma; Steck and Hunziker, 1994; Gebauer, 1999) and prior to the onset of molasse sedimentation in the Swiss Molasse Basin. The exhumation of the Lepontine Dome was initiated at ~30 Ma, with the highest rates of hanging-wall displacement and exhumation being observed between 18 and 15 Ma (Grasemann and Manktelow, 1993). The Late Oligocene to Recent orogen-parallel extension was largely accommodated by slip along the SW-dipping Simplon low-angle detachment fault to the West of the Lepontine (Fig. 1a). In the east, the Lepontine Dome is bordered by steeply dipping normal faults (Turba, Forcola).

The Swiss Molasse Basin represents a typical foreland basin formed on European continental crust by flexural bending in response to the tectonic loading caused by the northward-prograding Alpine orogen (Homewood et al., 1986; Sinclair et al., 1991). The southern part of the Oligocene to Miocene Swiss Molasse Basin deposits close to the main Alpine thrust front forms a stack of south-dipping thrust sheets (Subalpine Molasse: Fig. 1a), whereas the sediments further north are essentially undeformed (Plateau Molasse). The basin fill consists of two regressive megacycles (Berger, 1996). The first megacycle lasted from the Rupelian Lower Marine Molasse (UMM: the German term "Untere Meeresmolasse" is traditionally adopted in the literature) up to the Chattian—Aquitanian Lower Freshwater Molasse (USM = "Untere Süsswassermolasse"). The second megacycle started with a marine ingression and deposition of the Early Burdigalian Upper Marine Molasse (OMM = "Obere Meeresmolasse") followed by the Late Burdigalian to Serravallian Upper Freshwater Molasse (OSM = "Obere Süsswassermolasse"). Close to the Alpine thrust front, however, proximal coarse-grained alluvial fans prevailed and the marine deposits are only poorly represented (Fig. 1b).

3. ANALYTICAL METHODS

Heavy mineral frequency data were obtained by ribbon counting of generally 200 non-opaque non-micaceous non-carbonate mineral grains, following careful sample crushing, disaggregation in warm 10% acetic acid, sieving (63–125 μm fraction), centrifuge-aided settling of the heavy fraction in sodium metatungstate (density 2.8),

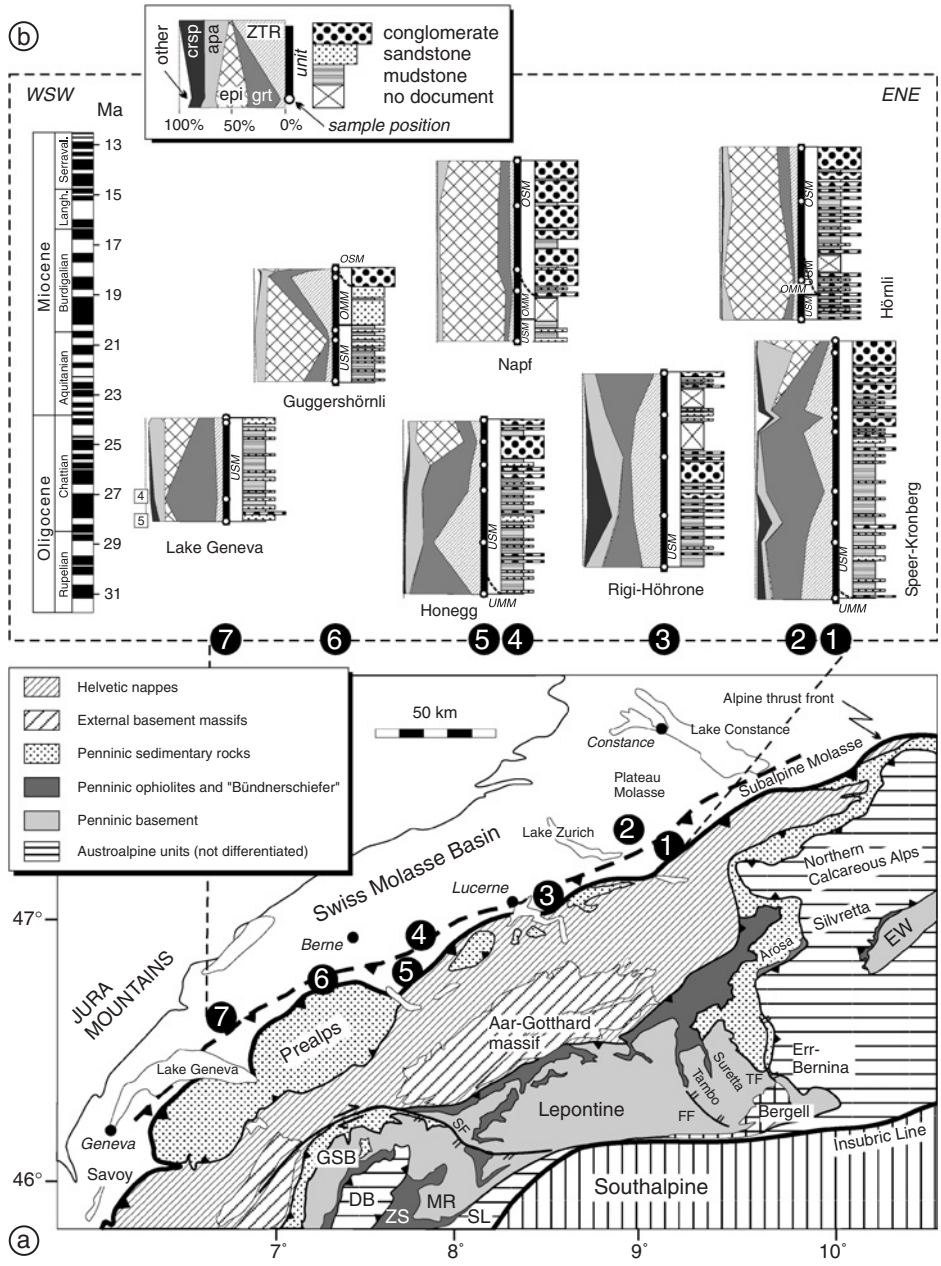

Fig. 1. (a) Geological sketch map of the Central Alps with the major Alpine structural units and the Swiss Molasse Basin located north of the Alpine thrust front. [Modified after Frey and Ferrero Mählmann (1999).] Stippled line indicates transition between Subalpine Molasse and Plateau Molasse. DB = Dent Blanche; EW = Engadine window; FF = Forcola Fault; SF = Simplon Fault zone; TF = Turba Fault zone. Numbers 1–7 indicate locations of composite sections, each representing a major dispersal system. (b) Chronostratigraphic display of composite sections (1–7) showing a strongly simplified lithology (right) and heavy mineral composition (left) for each dispersal system. UMM = Lower Marine Molasse; USM = Lower Freshwater Molasse; OMM = Upper Marine Molasse; OSM = Upper Freshwater Molasse. ZTR = zircon + tourmaline + rutile, grt = garnet, epi = epidote-group minerals, apa = apatite, crsp = chrome spinel; "other" includes staurolite, titanite, kyanite, chloritoid, monazite/xenotime, and blue sodic amphibole. The latter occurs exclusively in the Lower Chattian of the westernmost section (numbers in open boxes give percentages).

and subsequent mounting on glass slides (Meltmount 1.66). Mineral chemistry was determined on polished mineral separates in the electron microprobe laboratory at the Geoscience Centre Göttingen (Jeol JXA 8900 RL) using WDS technique and synthetic as well as natural mineral standards. The current grain-size interval selected differs from previous studies where broader size ranges were used (usually 63–350 μm), because the smaller grain-size interval is especially suitable for garnet-rich samples (von Eynatten, 2003).

$^{40}Ar/^{39}Ar$ dating of single detrital white mica grains was performed in the VULKAAN Ar/Ar laserprobe laboratory at the Vrije Universiteit Amsterdam. Total fusion as well as incremental heating experiments were carried out on hand-picked white mica of the 250–500 and 500–1000 μm grain-size fractions. For more details, see von Eynatten and Wijbrans (2003). Fission-track (FT) dating of detrital zircon was performed at the FT-laboratory of the University of Tübingen. The resulting complex zircon FT age spectra were modelled to distinguish individual age groups that follow a log-normal distribution. For more details, see Spiegel et al. (2000).

4. HEAVY MINERAL BACKGROUND: A BRIEF REVIEW

The first systematic and comprehensive study of heavy minerals in the Swiss Molasse Basin was performed by Armin von Moos (1935). He recognised the alternating dominance of garnet and epidote and their systematic variation both in space and time. He was also the first to record the occurrence of blue amphiboles, especially in Chattian and Burdigalian deposits of the western part of the basin. Previous petrographical studies of the Swiss Molasse have largely concentrated on the conglomerates (for review, see von Moos, 1935) and are not considered here. A second—even more extensive—study, covering the whole North Alpine Foreland Basin in Germany and Switzerland except for its westernmost parts, was published by Füchtbauer (1964). Based on these fundamental research, covering large areas of the basin, several regional sediment petrographical studies, including heavy mineral analysis, were performed in the 1960s and 1970s (e.g., Matter, 1964; Gasser, 1968; Schlanke, 1974; Maurer et al., 1978, 1982; Maurer, 1983). In these works, further constraints on lithostratigrapic correlation, palaeoenvironment, sediment provenance and sediment dispersal were identified. The various transverse (alluvial fans/fan deltas) and longitudinal drainage systems were also recognised, including some local perturbations of the major dispersal pattern. Furthermore, the tectonic style of the Subalpine Molasse and its various thrust slices was clarified in some detail.

Heavy mineral data were also used to evaluate sedimentary processes in the basin and their interplay with denudation processes in the hinterland. Heavy mineral distributions assisted in the identification of sediment pathways, for example in the OMM of the Burdigalian seaway (Allen et al., 1985), and the relationships between changes in petrographic composition and facies and orogenic processes in the Central Alps (Schlunegger et al., 1993). The first chemical investigation of heavy minerals from the westernmost Swiss Molasse Basin was carried out by Mange-Rajetzky and Oberhänsli (1982), proving the high-pressure origin of blue amphiboles and

lawsonite in Swiss Molasse Basin strata, and the onset of erosion of high-pressure rocks as early as Early Chattian.

In the 1990s three Ph.D. theses, completed at the University of Berne, covered almost the entire Swiss Molasse Basin, focusing on a detailed magnetostratigraphic calibration of the Molasse deposits (Schlunegger, 1995; Kempf, 1998; Strunck, 2001). Intensive sampling of the whole area included sandstones for heavy mineral analysis, thus providing a dense set of heavy mineral data with well-constrained chronostratigraphic information.

The results presented in this contribution are based on a careful selection from the exceptionally large data set of the afore-mentioned studies, focusing on temporally well-calibrated proximal molasse deposits that provide representative images of the exposed source rocks in the hinterland for certain time slices. These samples were used to determine the sequential evolution of heavy mineral assemblages in the proximal deposits of the Swiss Molasse Basin, ranging from the Lake Geneva dispersal system in the west to the Speer-Kronberg alluvial fan system in the east (Fig. 1a). The most prominent features of this evolution in space and time can be summarised as follows (Fig. 1b):

(1) a major shift from garnet and/or ZTR (zircon + tourmaline + rutile) to epidote-dominated assemblages occurred at ~21 Ma in the eastern sections (Speer-Kronberg system) and ~4 Ma earlier at ~25 Ma in the central and western sections (Honnegg, Guggershörnli and Lake Geneva systems);
(2) a high contribution of chrome spinel (up to 31%) is present in the older (>21–22 Ma) sediments of the eastern sections (Speer-Kronberg and Rigi-Höhrone) that appear to be associated with relatively high ZTR contents; and
(3) lower but still significant quantities of chrome spinel occur in the younger (<21 Ma) sediments of the eastern basin (Hörnli; maximum 2%) and in the older sediments (>27 Ma) of the western part (Lake Geneva; maximum 9%). The latter are associated with significant amounts of blue sodic amphibole, which form up to 5% of the translucent heavy mineral spectra.

5. HEAVY MINERAL CHEMISTRY AND GEOCHRONOLOGY

Complementing the results of conventional heavy mineral analysis with recently obtained single-grain geochemical and geochronological data provides further constraints on, and a more precise reconstruction of, hinterland evolution. The clear advantage of these combined techniques, compared with conventional heavy mineral analysis, can be best demonstrated by examining the evolution of two almost continuous composite sections of two relatively stationary alluvial fan systems: the deposits of the Speer-Kronberg-Hörnli alluvial fan system, situated east of Lake Zürich, and those of the Honegg-Napf alluvial fan system, exposed ~100 km to the southeast in the area NE of Lake Thun (Fig. 1).

5.1. Speer-Kronberg-Hörnli Alluvial Fan System

The entire Speer-Kronberg-Hörnli alluvial fan system was active from the Rupelian to the Serravallian (~31 to ~13 Ma: Kempf et al., 1999), draining the present-day

boundary area between the Central and the Eastern Alps (i.e., around the western termination of the main Austroalpine nappes at ~9°30′E; Fig. 1a). The lower (Speer) and middle (Kronberg) deposits are best exposed (Kempf et al., 1999) in the Necker section (no. 1 in Fig. 1a), and represent the almost complete coarsening-upward sequence of the USM (~31–20 Ma). The upper part (Hörnli) represents the prograding and generally coarsening upward deposits of the uppermost USM and the OSM (20–13 Ma), and are best exposed (Kempf et al., 1999) in the Jona and Hörnli sections (no. 2 in Fig. 1a).

The most prominent characteristic of the heavy mineral spectra of the Speer-Kronberg-Hörnli system is the abrupt increase in epidote quantities in parallel with a decrease of garnet concentration in the Late Aquitanian at ~21 Ma (Fig. 1b; see also Füchtbauer, 1964; Kempf et al., 1999; von Eynatten, 2003). In sediments older than 21 Ma (Speer, Kronberg), epidote is almost completely absent whereas in the younger sediments (uppermost Kronberg and Hörnli) epidote abundance consistently exceeds 60%. The older sediments are dominated by garnet and/or the ultrastable heavy minerals (ZTR). At certain stratigraphic levels, apatite and staurolite are significant. Chrome spinel may range up to almost 20% and is most frequent in the lower part (Speer) but rare (<3%) in the upper part (Hörnli).

A significant change in garnet composition precedes the marked decrease in garnet frequency between 29 and 24 Ma (Fig. 2). Garnets in a ~29 Ma old sandstone show generally low concentrations of the grossular end-member (<15%) while pyrope end-member ranges up to >40%. Younger garnets from 24, 21 and 13 Ma old sandstones are characterised by a generally low content of pyrope end-member (<15%), and a significant proportion of garnet grains (36–48%) contain relatively high concentrations of the grossular end-member (>15 to ~50%). The change in garnet composition at ~24 Ma may correlate with the onset of the Kronberg alluvial fan, which incorporates a significant contribution from felsic crystalline rocks. It is characterised by a change in the heavy mineral spectra towards higher apatite and, locally, elevated staurolite concentrations (Kempf et al., 1999; see also Fig. 1b).

Chrome spinel, present in relatively high abundance in the lower part of the Speer-Kronberg-Hörnli alluvial fan system, differs in composition from that in the upper part, where its overall quantities are very low (Fig. 2). In the ~29 Ma old sandstone, it is low in TiO_2 and $Fe^{III}\#$ [$Fe^{III}/(Cr + Al + Fe^{III})$] and plots generally outside the fields of chrome spinel of basaltic rocks (Arai, 1992). Such chrome spinel is typically derived from ultrabasic rocks (Lenaz et al., 2000). In the youngest sandstone sample at ~13 Ma, chrome spinels are generally higher in both TiO_2 and $Fe^{III}\#$ suggesting their derivation from mid-ocean ridge and intra-plate basalts (Fig. 2). Chrome spinel is both mechanically and chemically a highly stable mineral (Morton and Hallsworth, 2007—this volume) making it a possible candidate for recycling from older strata. This can be crosschecked by comparing heavy-mineral frequencies with the frequencies of volcanic lithoclasts or serpentinite fragments in the thin sections of the sandstones. Chrome spinel in the younger samples is accompanied by significant amounts of basic and ultrabasic framework components (up to 12%, Fig. 3), whereas the much higher chrome spinel contents in the older sandstones lack any lithoclasts that are petrogenetically related to chrome spinel within the framework grains. This is best explained by the recycling of chrome spinels from older sediments in which the more labile lithoclasts were entirely destroyed or diminished.

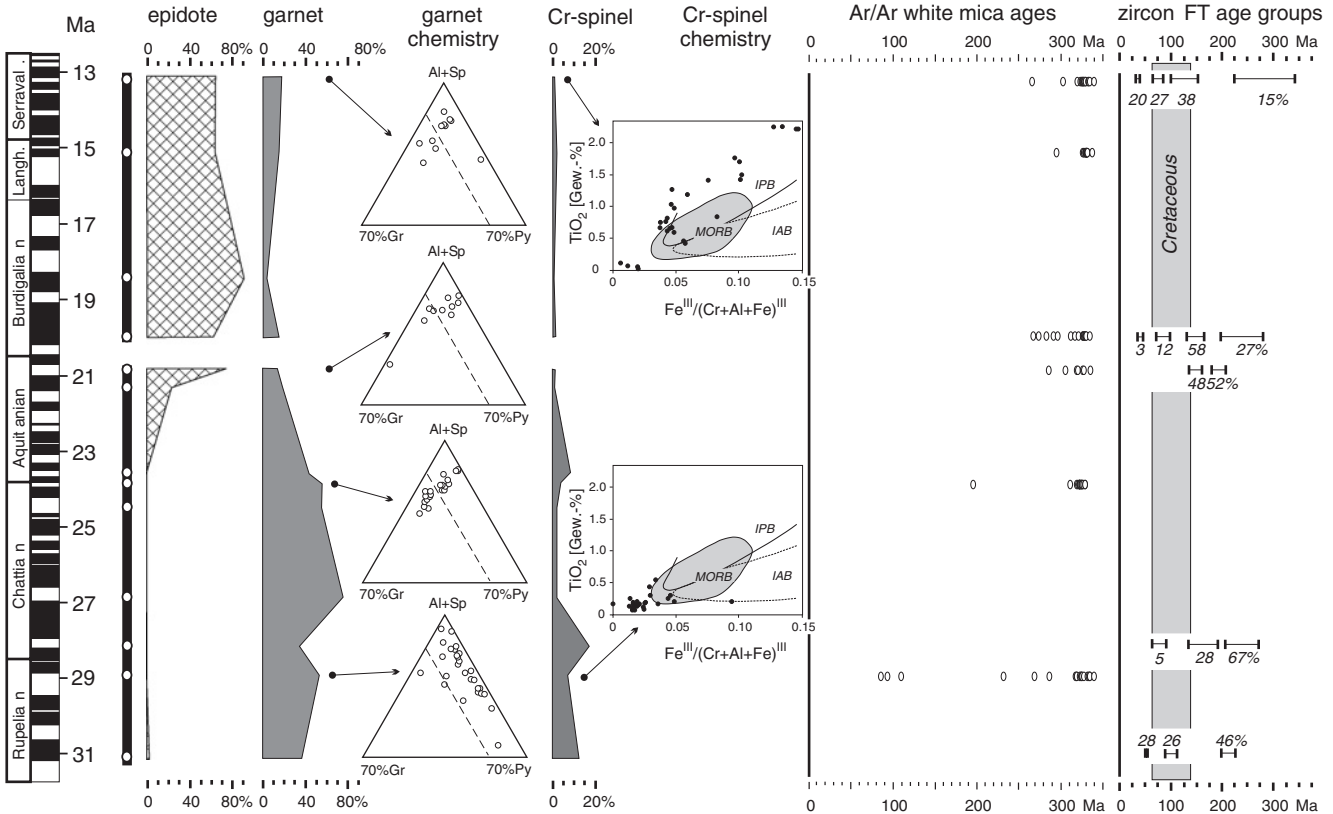

Fig. 2. Composite section of the Speer-Kronberg-Hörnli alluvial fan system showing epidote, garnet and chrome spinel percentages in 13 samples, covering the chronostratigraphic range from 31.1 to 13.2 Ma. Garnet chemistry of selected samples is displayed in almandine + spessartine—grossular—pyrope ternary diagrams with stippled line indicating 15% grossular component. Chrome spinel chemistry from two samples is displayed in bivariate diagrams after Arai (1992) showing compositional fields for chrome spinel in basaltic rocks with mid-ocean ridge (MORB), intra-plate (IPB) and island-arc (IAB) affinities. $^{40}Ar/^{39}Ar$ white mica single-grain ages are shown by ellipsoids, each representing an individual mica cooling age with errors less than the symbol size (von Eynatten and Wijbrans, 2003). Zircon fission-track data are illustrated by modelled age groups with corresponding error bars ($\pm 1\sigma$); percentages give the size of an age group relative to all measured crystals (~60 grains; Spiegel et al., 2000).

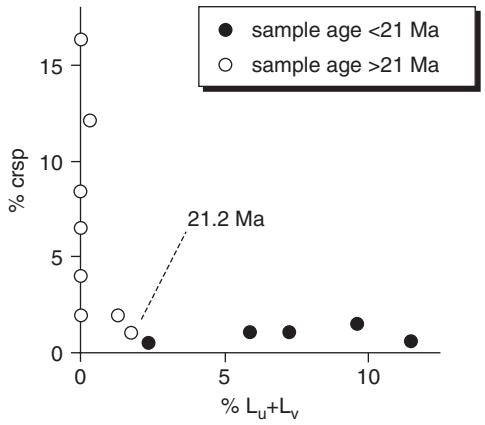

Fig. 3. Bivariate plot of chrome spinel percentages in heavy mineral spectra vs. basic/intermediate (L_v) plus ultrabasic (L_u) lithoclast content within framework composition of sandstone samples from the Speer-Kronberg-Hörnli alluvial fan system. [Data from von Eynatten (2003).] The two age groups are perfectly separated, with the transitional sample (21.2 Ma) plotting directly between the two groups.

The fact that chrome spinel composition from the lower part is similar to detrital chrome spinel from Cretaceous flysch deposits of the Eastern Alps (Pober and Faupl, 1988; von Eynatten, 1996, 2003) strongly supports this interpretation.

The fundamental change in the abundances of chrome spinel and basic to ultrabasic lithoclasts occurred quite abruptly at ~21 Ma (Fig. 3), contemporaneously with the first appearance of basic 'greenstone' pebbles in associated conglomerates (Kempf et al., 1999) and with the dramatic increase in epidote proportions (Figs. 1b and 2). Therefore, chrome spinel in the upper part (younger than ~21 Ma) is considered to be derived from Penninic (meta)basaltic rocks that also supplied most of the epidote. Chrome spinel is rare in such rocks, whereas epidote, replacing former plagioclase crystals, may become a major constituent. This interpretation is consistent with the results of a recent study on trace-element geochemistry and Sr and Nd isotopic compositions of epidote concentrates from molasse sandstones, suggesting that epidotes from the 20 to 13 Ma old sandstones of the Hörnli alluvial fan were derived from Penninic ophiolites (Spiegel et al., 2002).

$^{40}Ar/^{39}Ar$ dating of detrital white mica from the Speer-Kronberg-Hörnli alluvial fan system showed predominantly Variscan ages between 300 and 340 Ma (Fig. 4). This distribution is more or less constant throughout the section. Some scattered Permian ages, concentrating at ~20 Ma in the younger sandstones, and a few Cretaceous ages in the ~29 Ma old sandstone sample were also observed (Fig. 2). In contrast, zircon fission-track data reveal mostly Mesozoic ages (Spiegel et al., 2000) throughout the section ($\geq$70%, Fig. 2). In addition, there is a significant Palaeocene/Eocene age group (54 $\pm$ 4 Ma, 28%) in the oldest sandstone at ~31 Ma, and an Eocene/Oligocene age group (32 $\pm$ 2 Ma, 20%) in the youngest sandstone. Although there is some scatter in the thermochronological data, the overall picture suggests a temporally consistent hinterland with respect to the thermal history of the Central Alpine rock complexes that were exposed in Oligocene to Miocene time. The slight

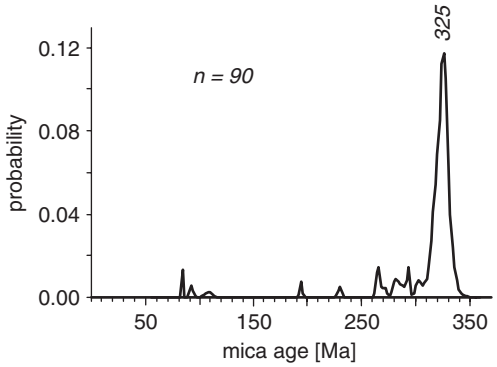

Fig. 4. Probability distribution plot of $^{40}Ar/^{39}Ar$ single-grain ages of white mica from the Speer-Kronberg-Hörnli alluvial fan system. 83% of the grains range between 300 and 340 Ma with a peak age of 325 Ma (von Eynatten and Wijbrans, 2003).

younging of the zircon FT ages in the youngest sandstone sample reflects erosional unroofing of a continuously emerging hinterland, but cannot be interpreted as a pronounced exhumation event as it is observed in the Honegg-Napf alluvial fan system (see below).

5.2. *Honegg-Napf Alluvial Fan System*

The activity of the Honegg-Napf alluvial fan system covers approximately the same time span as the Speer-Kronberg-Hörnli system (~31 to ~13.6 Ma: Schlunegger et al., 1996; Kempf et al., 1997), draining large parts of the present-day Central Alps including the northern Lepontine area (von Eynatten et al., 1999). The external Helvetic massifs (Aar and Gotthard: Fig. 1a) were not exhumed at that time. The lower part (Honegg) represents most of the large-scale coarsening-upward sequence of the USM. Its deposits are located in the area NE of Lake Thun, and are best exposed in the Marbach, Honegg and Prässerebach sections (Schlunegger et al., 1993, 1996). The upper part (Napf) represents the prograding successions of the OSM, outcropping at 25 km NE from the Honegg area, with best exposures being in the Fontannen and Schwändigraben sections (Schlunegger et al., 1996). In order to present an almost complete Rupelian to Serravallian composite section of the Honegg-Napf area, upper Aquitanian USM deposits, exposed in the Fischenbach section located ~15 km E of the Napf area, are included (see base of Napf composite section in Fig. 1b, ~21 Ma: Schlunegger et al., 1996), although significant proportions of the detrital material of the Fischenbach section may have been deposited by the Rigi-Höhrone dispersal system (Fig. 1; see also Schlunegger et al., 1997).

The most striking characteristic of the heavy mineral spectra of the entire Honegg-Napf section is the abrupt increase of epidote and the parallel decrease of garnet quantities in the Late Chattian (Matter, 1964; Schlunegger et al., 1993, 1997; von Eynatten, 2003) at ~25 Ma (Figs. 1b and 5). In sediments older than 25 Ma, epidote is almost completely absent whereas in the younger sediments epidote is dominant, with values usually exceeding 60%. The older sediments are enriched in garnet and at

some stratigraphic levels also by ZTR and/or apatite. A further characteristic is the minor occurrence of chrome spinel (up to 5%) in the lower Chattian and Rupelian samples, which is in contrast with the younger sandstones.

Garnet composition shows a clear separation between the upper (Napf) and the lower (Honegg) part of the section (Fig. 5). In the lower part the majority of garnet grains (~80%) contain the grossular and pyrope end-members in low proportions (<15%), although the latter may range up to ~33%. In the upper part, the grossular end-member is higher (>15% to ~60%) in the majority of grains (60–70%) and, on average, the pyrope end-member is slightly lower (<10%). Garnet composition is, again, decoupled from garnet frequency, as the two samples from the lower part contain both low and high garnet quantities (in ~25 and ~27 Ma old sandstones, respectively) without any significant change in garnet composition. The upsection shift in garnet composition is not accompanied by significant changes in the heavy mineral spectra, but appears to be related to processes that can be identified by further chemical and radiometric single-grain analyses, as discussed below.

The chemistry of single white mica grains from seven individual sandstone levels was investigated to further constrain source rocks and to substantiate the interpretation of the radiometric data obtained from these micas. Mica composition is displayed in bivariate Si vs. Mg plots [atoms per formula unit (p.f.u.), calculated for 11 cations] (Fig. 5). In the lower part of the section, white micas are exclusively muscovite in composition ranging from 3.06 to 3.20 Si p.f.u. and 0.06 to 0.13 Mg p.f.u. At ~21 Ma, the first phengitic mica appears, with Si content ~3.45 p.f.u. and Mg contents ranging between 0.28 and 0.40 atoms p.f.u. Upsection, the proportion of phengitic micas, clustering between 3.3 and 3.5 Si p.f.u. and 0.25 and 0.40 Mg p.f.u., continuously increase to more than 80% of the measured white mica at 15.4 and 13.6 Ma sedimentation age (Fig. 5). The change in mica composition somewhere between 25 and 21 Ma appears to coincide with that in garnet composition towards higher grossular contents that happened, as our data indicate, sometime between 25 and 19 Ma. Generally, the switch from muscovite to phengite in samples younger than 21 Ma can be interpreted as reflecting the change in the exposed source lithologies. The former hinterland, comprising predominantly granitic and/or sedimentary rocks (the latter containing detrital muscovite), began to incorporate increasingly higher proportions of metamorphics, formed under low temperature and most probably medium to high pressure (von Eynatten et al., 1999; von Eynatten and Wijbrans, 2003). A shift in garnet composition towards a higher grossular component supports this interpretation.

Epidote concentrates from the Honegg-Napf alluvial fan system reveal considerably different isotopic and trace element signatures compared with epidotes from the Hörnli alluvial fan (see above and Spiegel et al., 2002). At ~25 Ma (i.e., the onset of epidote predominance in the Honegg composite section), relatively high contents of incompatible trace elements and low εNd values suggest that epidotes were derived from differentiated crustal sources (i.e., granitic rocks). Higher up in the succession, this clear chemical and isotopic signal from detrital epidotes is somewhat obscured in samples between 21 and 15 Ma sedimentation age, and may indicate the exposure of Penninic ophiolites in the hinterland by that time (Spiegel et al., 2002). However, whole-rock petrographic and chemical data, and the disappearance of

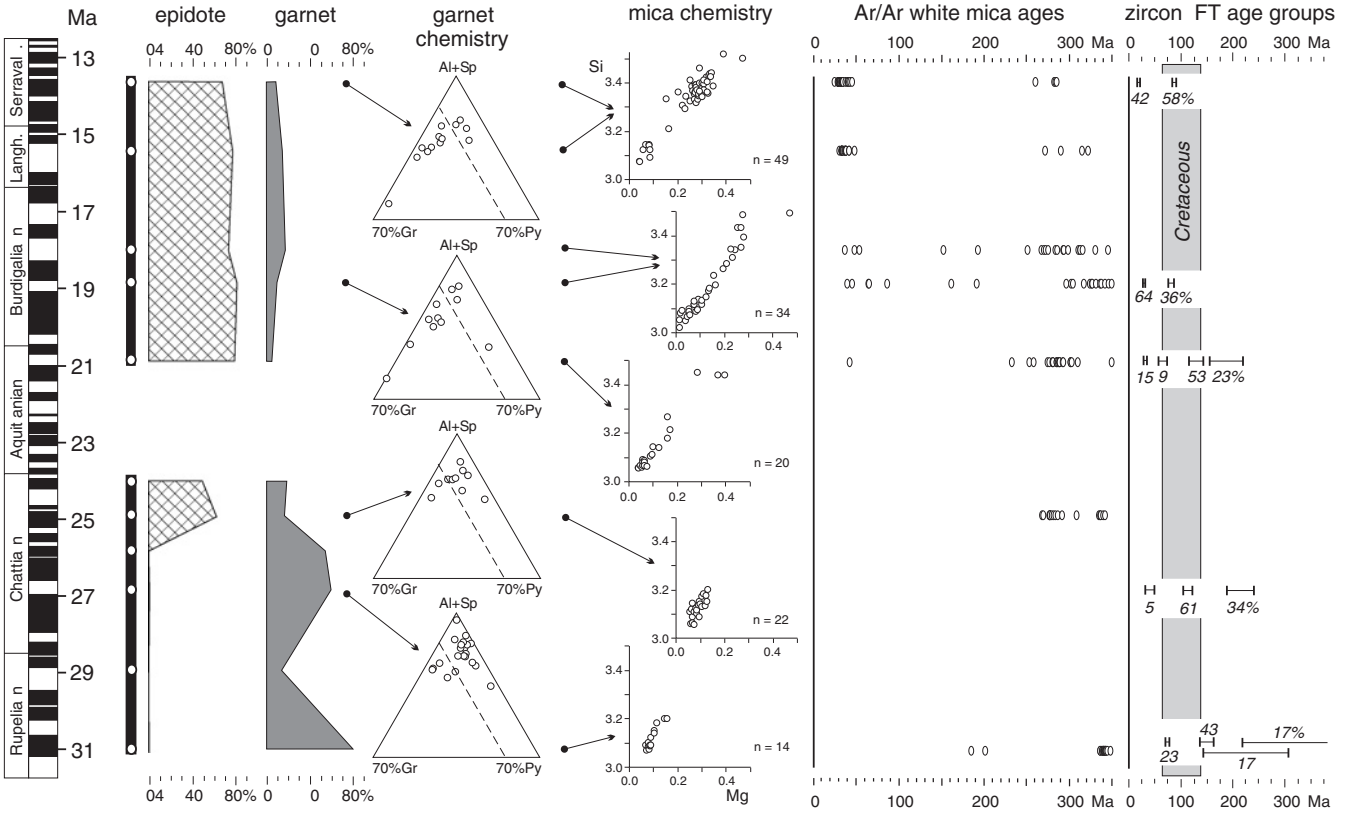

Fig. 5. Composite section of the Honegg-Napf alluvial fan system showing epidote and garnet percentages in 11 samples, covering the chronostratigraphic range from 31.0 to 13.6 Ma. Garnet chemistry from selected samples is displayed in almandine + spessartine—grossular—pyrope ternary diagrams with stippled line indicating 15% grossular component. Mica chemistry is displayed on bivariate Si vs. Mg (11 cations) diagrams; samples with similar compositional distributions were plotted in a single diagram. $^{40}Ar/^{39}Ar$ white mica single-grain ages are shown by ellipsoids, each representing an individual mica cooling age with errors less than the symbol size (von Eynatten and Wijbrans, 2003). Zircon fission-track data are illustrated by modelled age groups with corresponding error bars ($\pm 1\sigma$); percentages give the size of an age group relative to all measured crystals (~60 grains; Spiegel et al., 2000).

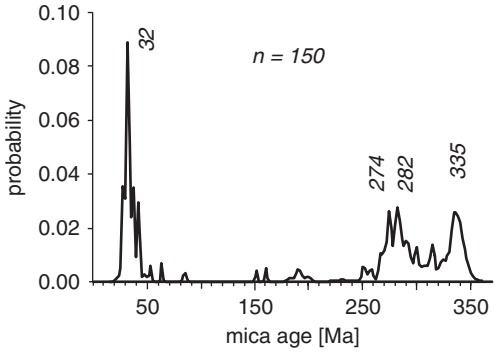

Fig. 6. Probability distribution plot of $^{40}Ar/^{39}Ar$ single-grain ages of white mica from the Honegg-Napf alluvial fan system (von Eynatten and Wijbrans, 2003). See text for discussion.

chrome spinel in the upper part of the Honegg-Napf alluvial fan system are not consistent with detritus sourced from mafic to ultramafic rocks (von Eynatten, 2003).

$^{40}Ar/^{39}Ar$ data of detrital white micas from the Honegg-Napf alluvial fan system show three prominent age groups (Fig. 6). The first group ranges from 320 to 350 Ma with a 335 Ma peak age (Early Carboniferous), while the second ranges from 265 to 295 Ma with two peaks at 274 and 282 Ma (Early Permian). The Tertiary age group is most prominent with a peak at ~32 Ma. This distribution strongly differs from the Speer-Kronberg-Hörnli system to the east (Fig. 4), although the Early Carboniferous age group of the Honegg-Napf system shows considerable overlap with the predominantly Variscan ages of the Speer-Kronberg-Hörnli system. The three age groups of the Honegg-Napf composite section show a marked chronostratigraphic distribution within the section (Fig. 5). Early Carboniferous ages are most prominent in the oldest sandstone sample at ~31 Ma but are absent in the youngest samples. The dominance of Early Permian ages starts at ~25 Ma sedimentation age, concurrent with the onset of epidote dominance, and ends at ~18 Ma. Tertiary ages first appear at ~21 Ma, paralleled by the first occurrence of phengitic micas, which become predominant and continuously younger toward the uppermost sandstone samples at 15.4 and 13.6 Ma. At 13.6 Ma, 87% of the dated grains have Tertiary cooling ages, and the youngest grains yield a 23.8 Ma plateau age (von Eynatten and Wijbrans, 2003).

Zircon fission-track data indicate mostly (>75%) Mesozoic ages for samples between 31 and 21 Ma sedimentation age (Fig. 5; Spiegel et al., 2000). The first small Tertiary age group (32 +/−2 Ma, 15% of the dated Zircon grains) appears in sandstones at 21 Ma sedimentation age, but further upsection at 15.4 and 13.6 MA sedimentation age Tertiary age groups became prominent (Fig. 5; 28 +/−1.2 Ma and 19.5 +/−0.9 Ma, respectively). Results of zircon fission-track analysis thus strongly support the $^{40}Ar/^{39}Ar$ data with respect to (1) an overall younging trend of ages with decreasing sedimentation age for the entire section and (2) the upsection increasing proportion of Tertiary ages and continuous younging of these ages for sediments younger than ~21 Ma (upper part, Napf). The latter implies rapid exhumation in the hinterland with cooling rates up to 40 °C/Ma (von Eynatten and Wijbrans, 2003).

6. DISCUSSION AND CONCLUSIONS

Petrographic data including clast composition, conventional heavy mineral analysis and geochemical and geochronological single-grain techniques all suggest a normal, erosional, unroofing trend in the hinterland of the Speer-Kronberg-Hörnli alluvial fan system. Erosion cut down from Austroalpine sedimentary cover nappes into Austroalpine basement rocks at 24–22 Ma and, at ~21 Ma, into Penninic units that included (meta)basaltic rocks (ophiolites). However, a contribution from Austroalpine cover nappes (mostly dolomites plus chrome spinel-bearing siliciclastics) continued to be significant to the youngest deposits (von Eynatten, 2003), suggesting a deeply incised hinterland, driven by ongoing orogeny, with rivers draining a series of tectonically stacked structural units.

The Honegg-Napf alluvial fan system reflects a strongly contrasting tectonic evolution of its hinterland compared with the Speer-Kronberg-Hörnli system. Erosion of crystalline rocks occurred significantly earlier, at ~25 Ma, and the removal of the sedimentary cover nappes became much more advanced (von Eynatten, 2003). The earlier exhumation of basement rocks in the hinterland is interpreted as the earliest indication of doming in the Lepontine area (von Eynatten et al., 1999). Penninic low-grade metamorphic rocks from the footwall of the Simplon fault became exposed at ~20 Ma, as documented by phengitic micas with Tertiary cooling ages. Upsection, the proportion of these micas increases while cooling ages decrease, reflecting continuous exhumation with increasing cooling rates of the Lepontine metamorphic dome up to, at least, ~13 Ma sedimentation age (Fig. 5; von Eynatten and Wijbrans, 2003). The timing of maximum cooling, as well as the cooling rates, coincide perfectly with thermochronological data obtained from the presently exposed Central Alps (Hammerschmidt and Frank, 1991; Seward and Mancktelow, 1994; Steck and Hunziker, 1994; Markley et al., 1998).

Augmenting conventional heavy mineral analysis by varietal studies and/or advanced heavy mineral techniques (e.g., single-grain geochemical and geochronological methods) significantly enhances the potential of provenance studies (Morton, 1991; von Eynatten et al., 1996; Rahl et al., 2003). In the Swiss Molasse Basin, heavy mineral spectra from alluvial fan deposits of the proximal basin close to the Alpine thrust front, show distinct changes in space and time. However, interpretations based on species and frequency analysis alone can be misleading, largely because (1) ultrastable ZTR and chrome spinel, and mineral species that crystallise under wide petrogenetic conditions, such as epidote, garnet and white mica may derive from highly contrasting source rocks and from different regions, (2) originally similar source rocks may have experienced different thermal histories. Combining heavy mineral analysis with single-grain geochemical and geochronological techniques, information on source rock evolution and erosion through time can be deciphered that cannot be achieved by conventional heavy mineral analysis alone. Results obtained from this integrated study can be summarised as follows.

(i) Chrome spinel in the lower part of the molasse sections was recycled from Cretaceous flysch sediments, and can be differentiated from first cycle chrome spinel, eroded directly from Penninic (meta)basites. When erosion cut down into basement lithologies, chrome spinel either disappeared from the heavy

mineral spectra (Honegg-Napf system, ~25 Ma; provenance from felsic crystalline basement source rocks) or differed in composition, indicating erosion of mafic crystalline rocks (Speer-Kronberg-Hörnli system, ~21 Ma; sourced from Penninic ophiolites). This result is supported by whole-rock petrographic and geochemical data (von Eynatten, 2003).

(ii) The interpretation above is supported by isotopic and trace element data of epidote concentrates from molasse sandstones, which suggest that epidotes in the eastern Speer-Kronberg-Hörnli system, dated between ~21 and ~13 Ma, were derived from metabasic rocks, while those in the Honegg-Napf system, occurring at ~25 Ma, were derived from metagranitic complexes (Spiegel et al., 2002). However, single-grain analysis of epidote is not yet available, and these statements may need refining, especially in respect to intermixing of grains from different sources.

(iii) Significant changes in garnet composition observed at ~24 Ma in the Speer-Kronberg-Hörnli system, and at ~20 Ma in the Honegg-Napf system, are decoupled from the major changes of garnet frequency in the heavy mineral spectra. The former compositional change is thought to be related to the onset of the Kronberg alluvial fan along with the first contribution from felsic crystalline rocks, as indicated by conglomerate clast data (Kempf et al., 1999). However, the change in the Honegg-Napf system cannot be interpreted accurately without obtaining further information on mica chemistry.

(iv) White micas from the Honegg-Napf system display a distinct shift in chemistry from the oldest to the youngest deposits. In the lower part, up to ~25 Ma sedimentation age, the mica is exclusively muscovite, implying that the major change from garnet-dominated to epidote-rich heavy mineral compositions did not influence the delivery of micas to the basin. This is in line with the derivation of these micas from polycyclic sediments and metagranitic rocks as indicated by chrome spinel and epidote chemistry. At ~21 Ma, the first phengitic micas appear and then increase upsection to become the predominant white mica variety in the youngest sandstones at 15.4 and 13.6 Ma sedimentation age. This systematic change of white mica composition indicates an increasing contribution of mica from low-grade metamorphic rocks (von Eynatten et al., 1999; von Eynatten and Wijbrans, 2003). The more or less contemporaneous change in garnet chemistry can be best explained by derivation of, or at least parts of, the garnet from low-grade metamorphics.

(v) The progressive change in mica chemistry, starting at ~21 Ma in the Honegg-Napf system, correlates well with a continuous shift towards increasingly younger Tertiary $^{40}Ar/^{39}Ar$ ages (Fig. 5). While mica in sediments older than 21 Ma is exclusively Palaeozoic in age, the younger sediments record an increasing contribution of phengitic micas that yield Tertiary cooling ages.

(vi) Cooling rates of up to 40 °C/Ma can be calculated for the youngest (phengitic) mica ages and, accordingly, for the youngest zircon FT age group (von Eynatten et al., 1999; Spiegel et al., 2000). Such high cooling rates in the Central Alpine hinterland must be related to the exhumation of the Lepontine metamorphic dome, because other potential source areas in the hinterland have cooling rates of 10–20 °C/Ma (Markley et al., 1998; Schlunegger and Willett,

1999). The Miocene exposure of footwall rocks (with respect to the Simplon detachment fault; Fig. 1a), related to exhumation of the Lepontine, was not detected previously by conventional heavy mineral analysis. This is due to the fact that low-grade metamorphics are usually devoid of distinct index minerals, thus optical microscopy alone proves inconclusive for such rocks.

(vii) In contrast to the Honegg-Napf system, single-grain dating of mica and zircon from the Speer-Kronberg-Hörnli system does not reveal such a pronounced younging of ages in the upper part of the section. $^{40}Ar/^{39}Ar$ mica ages are Palaeozoic throughout, and zircon FT ages remain mostly Mesozoic but also include some Palaeozoic ages. Although there is a small Tertiary zircon age group in the youngest sandstone, calculated cooling rates for this group are as low as 10–15 °C/Ma, implying that no pronounced exhumation was taking place in the hinterland at that time. Consequently, the catchment area of the Speer-Kronberg-Hörnli system was never linked to the exhuming Lepontine dome.

The contrast between the dominance of Variscan Ar/Ar mica and Mesozoic zircon fission-track ages throughout most of the sections (except for the uppermost part of the Honegg-Napf section) can be best explained by a thermal overprint during Jurassic rifting (von Eynatten, 1996) and/or Cretaceous ('Eoalpine') metamorphic overprint that led to the resetting of most of the zircon ages but did not significantly affect the Ar distribution in white mica. This interpretation would constrain the maximum temperature reached during Jurassic/Cretaceous events from 250 to 300 °C in the rock complexes that later formed the Oligocene—Miocene Central Alpine hinterland.

Finally, the reconstruction of sediment provenance in the Swiss Molasse Basin is complicated by the accretion of molasse successions on to the orogenic wedge (Kempf et al., 1999). Uplift and erosion of the wedge initiated the recycling of detritus from older Molasse strata to the younger Molasse and this process can often neither be detected unambiguously nor quantified by bulk sediment or by heavy mineral analysis. Single-grain analysis can be a viable technique in addressing this problem, although results may still remain ambiguous. For example, the few muscovite grains among the white micas of predominantly phengitic composition in the uppermost part of the Honegg-Napf system (Fig. 5) may have been sourced either from still exposed remnants of the primary metagranitic source rocks, or could have been recycled from older, muscovite-rich Molasse strata.

ACKNOWLEDGEMENTS

The Swiss Molasse Basin project was supported by *Deutsche Forschungsgemeinschaft* and *Friedrich-Schiller-Universität Jena*. Field work and sampling strongly benefited from guidance and advice by Oliver Kempf, Fritz Schlunegger and Peter Strunck. Stimulating discussions with István Dunkl, Reinhard Gaupp, Andreas Kronz, Conny Spiegel and Jan Wijbrans are greatly appreciated. I am indebted to Oliver Kempf and Fritz Schlunegger for constructive reviews as well as to Maria Mange and David Wright for careful editorial handling of the manuscript.

REFERENCES

Allen, P.A., Mange-Rajetzky, M., Matter, A., Homewood, P., 1985. Dynamic paleogeography of the open Burdigalian seaway, Swiss Molasse basin. Eclogae Geologicae Helvetiae 78, 351–381.

Arai, S., 1992. Chemisty of chromian spinel in volcanic rocks as a potential guide to magma chemistry. Mineralogical Magazine 56, 173–184.

Berger, J.-P., 1996. Cartes paléogeographiques-palinspastiques du bassin molassique suisse (Oligocène inférieur—Miocéne moyen), Neues Jahrbuch für Geologie und Paläontologie, Abhandlungen, pp. 1–44.

Cande, S.C., Kent, D.V., 1992. A new geomagnetic polarity timescale for the late Cretaceous and Cenozoic. Journal of Geophysical Research 97, 13917–13951.

Cande, S.C., Kent, D.V., 1995. Revised calibration of the geomagnetic polarity timescale for the late Cretaceous and Cenozoic. Journal of Geophysical Research 100, 6093–6095.

Frey, M., Ferrero Mählmann, R., 1999. Alpine metamorphism of the Central Alps. Schweizerische Mineralogische und Petrographische Mitteilungen 79, 135–154.

Frisch, W., 1979. Tectonic progradation and plate tectonic evolution of the Alps. Tectonophysics 60, 121–139.

Füchtbauer, H., 1964. Sedimentpetrographische Untersuchungen in der älteren Molasse nördlich der Alpen. Eclogae Geologicae Helvetiae 57, 157–298.

Gasser, U., 1968. Die innere Zone der Subalpinen Molasse des Entlebuchs (Kt. Luzern). Geologie und Sedimentologie. Eclogae Geologicae Helvetiae 61, 229–313.

Gebauer, D., 1999. Alpine geochronology of the Central and Western Alps: new constraints for a complex geodynamic evolution. Schweizerische Mineralogische und Petrographische Mitteilungen 79, 191–208.

Grasemann, B., Manktelow, N.S., 1993. Two-dimensional thermal modelling of normal faulting: the Simplon Fault Zone, Central Alps, Switzerland. Tectonophysics 225, 155–165.

Hammerschmidt, K., Frank, E., 1991. Relics of high pressure metamorphism in the Lepontine Alps (Switzerland): $^{40}Ar/^{39}Ar$ and microprobe analyses on white K-micas. Schweizerische Mineralogische und Petrogrographische Mitteilungen 71, 261–274.

Homewood, P., Allen, P.A., Williams, G.D., 1986. Dynamics of the Molasse basin of western Switzerland. In: Allen, P.A., Homewood, P. (Eds.), Foreland Basins. International Association of Sedimentologists Special Publications, vol. 8, pp. 199–217.

Kempf, O., 1998. Magnetostratigraphy and facies evolution of the Lower Freshwater Molasse (USM) of eastern Switzerland. Doctoral thesis. University of Berne, 138pp.

Kempf, O., Bolliger, T., Kälin, D., Engesser, B., Matter, A., 1997. Magnetostratigraphic calibration of Early to Middle Miocene mammal biozones of the North Alpine foreland basin. In: Actes du Congrès BiochroM'97, Mém. Trav. E.P.H.E. Institute of Montpellier, pp. 547–561.

Kempf, O., Matter, A., Burbank, D.W., Mange, M., 1999. Depositional and structural evolution of a foreland basin margin in a magnetostratigraphic framework: the eastern Swiss Molasse Basin. International Journal of Earth Sciences 88, 253–275.

Kuhlemann, J., Frisch, W., Dunkl, I., Székely, B., 2001. Quantifying tectonic versus erosive denudation by the sediment budget: the Miocene core complexes of the Alps. Tectonophysics 330, 1–23.

Lenaz, D., Kamenetsky, V.S., Crawford, A.J., Princivalle, F., 2000. Melt inclusions in detrital spinel from the SE Alps (Italy-Slovenia): a new approach to provenance studies of sedimentary basins. Contributions to Mineralogy and Petrology 139, 748–758.

Lonergan, L., Mange-Rajetzky, M.A., 1994. Evidence for Internal Zone unroofing from foreland basin sediments, Betic Cordillera, SE Spain. Journal of the Geological Society London 151, 515–529.

Mange-Rajetzky, M., Oberhänsli, R., 1982. Detrital lawsonite and blue sodic amphibole in the Molasse of Savoy, France, and their significance in assessing Alpine evolution. Schweizerische Mineralogische und Petrographische Mitteilungen 62, 415–436.

Markley, M.J., Teyssier, C., Cosca, M.A., Caby, R., Hunziker, J.C., Sartori, M., 1998. Alpine deformation and $^{40}Ar/^{39}Ar$ geochronology of synkinematic white mica in the Siviez-Mischabel nappe, western Pennine Alps, Switzerland. Tectonics 17, 407–425.

Matter, A., 1964. Sedimentologische Untersuchungen im östlichen Napfgebiet. Eclogae Geologicae Helvetiae 57, 315–428.

Maurer, H., 1983. Sedimentpetrographische Analysen an Molasseabfolgen der Westschweiz. Jahrbuch der Geologischen Bundesanstalt Wien 126, 23–69.

Maurer, H., Funk, H., Nabholz, W., 1978. Sedimentpetrographische Untersuchungen an Molasse-Abfolgen der Bohrung Linden 1 und ihrer Umgebung (Kt. Bern). Eclogae Geologicae Helvetiae 71, 497–515.

Maurer, H., Gerber, M.E., Nabholz, W., 1982. Sedimentpetrographie und Lithostratigraphie der Molasse im Einzugsgebite der Langete (Aarwangen-Napf, Oberaargau). Eclogae Geologicae Helvetiae 75, 381–413.

Morton, A.C., 1991. Geochemical studies of detrital heavy minerals and their application to provenance research. In: Morton, A.C., Todd, S.P., Haughton, P.D.W. (Eds.), Developments in Sedimentary Provenance Studies. Geological Society of London, Special Publication, vol. 57, pp. 31–45.

Morton, A.C., Hallsworth, C.R., 2007. Stability of detrital heavy minerals during burial diagenesis. In: Mange, M.A., Wright, D.T. (Eds.), Heavy Minerals in Use. Developments in Sedimentology (this volume).

Morton, A.C., Johnsson, M.J., 1993. Factors influencing the composition of detrital heavy mineral suites in Holocene sands of the Apure River drainage basin, Venezuela. Geological Society of America, Special Paper 284, 171–185.

Pober, E., Faupl, P., 1988. The chemistry of detrital chromian spinels and its implications for the geodynamic evolution of the Eastern Alps. Geologische Rundschau 77, 641–670.

Rahl, J.M., Reiners, P.W., Campbell, I.H., Nicolescu, S., Allen, C.M., 2003. Combined single-grain (U-Th)/He and U/Pb dating of detrital zircons from the Navajo Sandstone, Utah. Geology 31, 761–764.

Schlanke, S., 1974. Geologie der Subalpinen Molasse zwischen Biberbrugg SZ, Hütten ZH und Ägerisee ZG. Eclogae Geologicae Helvetiae 67, 243–331.

Schlunegger, F., 1995. Magnetostratigraphische und fazielle Entwicklung der Unteren Süßwassermolasse zwischen Aare und Limmat. Doctoral thesis. University of Berne, 185pp.

Schlunegger, F., Burbank, D.W., Matter, A., Engesser, B., Mödden, C., 1996. Magnetostratigraphic calibration of the Oligocene to Middle Miocene (30–15 Ma) mammal biozones and depositional sequences of the Swiss Molasse Basin. Eclogae Geologicae Helvetiae 89, 753–788.

Schlunegger, F., Matter, A., Burbank, D.W., Klaper, E.M., 1997. Magnetostratigraphic constraints on relationships between evolution of the central Swiss Molasse basin and Alpine orogenic events. Geological Society of American Bulletin 109, 225–241.

Schlunegger, F., Matter, A., Mange, M.A., 1993. Alluvial fan sedimentation and structure of the southern Molasse basin margin, Lake Thun area, Switzerland. Eclogae Geologicae Helvetiae 86, 717–750.

Schlunegger, F., Slingerland, R., Matter, A., 1998. Crustal thickening and crustal extension as controls on the evolution of the drainage network of the central Swiss Alps between 30 Ma and the present: constraints from the stratigraphy of the North Alpine Foreland Basin and the structural evolution of the Alps. Basin Research 10, 197–212.

Schlunegger, F., Willett, S., 1999. Spatial and temoral variations in exhumation of the Swiss Alps and implications for exhumation mechanisms. In: Geological Society of London Special Publication, vol. 154, pp. 157–179.

Schmid, S.M., Pfiffner, O.A., Froitzheim, N., Schönborn, G., Kissling, E., 1996. Geophysical-geological transect and tectonic evolution of the Swiss-Italian Alps. Tectonics 15, 1036–1064.

Seward, D., Mancktelow, N., 1994. Neogene kinematics of the central and western Alps: evidence from fission-track dating. Geology 22, 803–806.

Sinclair, H.D., Coakley, B.J., Allen, P.A., Watts, A.B., 1991. Simulation of foreland basin stratigraphy using a diffusion model of mountain belt uplift and erosion: an example from the Central Alps, Switzerland. Tectonics 10, 599–620.

Spiegel, C., Kuhlemann, J., Dunkl, I., Frisch, W., von Eynatten, H., Balogh, K., 2000. Erosion history of the Central Alps: evidence from zircon fission track data of the foreland basin sediments. Terra Nova 12, 163–170.

Spiegel, C., Siebel, W., Frisch, W., Zsolt, B., 2002. Nd and Sr isotopic ratios and trace element geochemistry of epidote from the Swiss Molasse Basin as provenance indicators: implications for the reconstruction of the exhumation history of the Central Alps. Chemical Geology 189, 231–250.

Steck, A., Hunziker, J., 1994. The Tertiary structural and thermal evolution of the Central Alps: compressional and extensional structures in an orogenic belt. Tectonophysics 238, 229–254.

Strunck, P., 2001. The Molasse of western Switzerland. Doctoral thesis. University of Berne, 246pp.

Strunck, P., Matter, A., 2002. Depositional evolution of the western Swiss Molasse. Eclogae Geologicae Helvetiae 95, 197–222.

von Eynatten, H., 1996. Provenanzanalyse kretazischer Siliziklastika aus den Nördlichen Kalkalpen: Petrographie, Mineralchemie und Geochronologie des frühalpidisch umgelagerten Detritus. Doctoral thesis. University of Mainz, 145pp.

von Eynatten, H., 2003. Petrography and chemistry of sandstones from the Swiss Molasse Basin: an archive of the Oligo/Miocene evolution of the Central Alps. Sedimentology 50, 703–725.

von Eynatten, H., Gaupp, R., 1999. Provenance of Cretaceous synorogenic sandstones in the Eastern Alps: constraints from framework petrography, heavy mineral analysis, and mineral chemistry. Sedimentary Geology 124, 81–111.

von Eynatten, H., Gaupp, R., Wijbrans, J.R., 1996. $^{40}Ar/^{39}Ar$ laser-probe dating of detrital white micas from Cretaceous sedimentary rocks of the Eastern Alps: evidence for Variscan high-pressure metamorphism and implications for Alpine orogeny. Geology 24, 691–694.

von Eynatten, H., Schlunegger, F., Gaupp, R., Wijbrans, J.R., 1999. Exhumation of the Central Alps: evidence from $^{40}Ar/^{39}Ar$ laserprobe dating of detrital white micas from the Swiss Molasse Basin. Terra Nova 11, 284–289.

von Eynatten, H., Wijbrans, J.R., 2003. Precise tracing of exhumation and provenance using Ar/Ar-geochronology of detrital white mica: the example of the Central Alps. In: McCann, T., Saintot, A. (Eds.), Tracing Tectonic Deformation Using the Sedimentary Record. Geological Society of London Special Publication, vol. 208, pp. 289–305.

von Moos, A., 1935. Sedimentpetrographische Untersuchungen an Molassesandsteinen. Schweizerische Mineralogische und Petrographische Mitteilungen 15, 169–265.

Weltje, G.J., von Eynatten, H., 2004. Quantitative provenance analysis of sediments: an introduction. In: Weltje, G.J., von Eynatten, H. (Eds.), Quantitative Provenance Analysis of Sediments. Sedimentary Geology, vol. 171, pp. 1–11.

This page intentionally left blank

Chapter 36

EVOLUTION OF THE AMAZON BASIN IN ECUADOR WITH SPECIAL REFERENCE TO HINTERLAND TECTONICS: DATA FROM ZIRCON FISSION-TRACK AND HEAVY MINERAL ANALYSIS

GEOFFREY M.H. RUIZ[1], DIANE SEWARD AND WILFRIED WINKLER

Geological Institute, Department of Earth Sciences, ETH-Zentrum, 8092 Zürich, Switzerland

ABSTRACT

The retro-arc Andean Amazon Basin (AAB), a foreland basin located east of the evolving Andes, has been an active sediment depocentre since the late Early Cretaceous (Aptian-Albian). Heavy mineral analysis of the proximal shallow marine and continental deposits in the Sub-Andean Zone reveals an overall trend from ultrastable zircon, tourmaline and rutile (ZTR) dominated assemblages, to more complex heavy-mineral suites with metamorphic and mafic volcanic signatures. This reflects successive derivation from shallow to deep crustal rocks and, subsequently, from accreted oceanic terranes during formation of the proto-Andes.

In parallel with heavy mineral analysis, detrital zircons were dated using fission-track methodology. The measured lag times of the zircons range from 400 to 0 Ma. Approximately zero lag times generally represent fast cooling events in the source region, while long lag times are the result of slow cooling or recycling in the source regions. In the present study, zero lag times combined with lithological and mineralogical data sets have also been used to identify volcanic events in the hinterland which, in turn, establishes the stratigraphic age of the enclosing sediments more precisely. Changes in source areas are identified by changes in lag times, which coincide with variations in the composition of the heavy mineral suites.

During early stages of basin evolution (Aptian-Campanian), lag times of detrital zircons, occurring in the dominantly ultrastable ZTR mineral suite, allow the discrimination of sediment input from two different continental basement sources. Zircons, with very long lag times ($\approx$400 Ma), indicate input from the Amazonian Craton regions at the eastern margin of the basin, while comparatively short lag times (0–60 Ma) in zircons infer coeval sediment flux from

[1]*Present address: Geological Institute, University of Neuchâtel, Rue Emile-Argand 11, 2009 Neuchâtel, Switzerland*

Developments in Sedimentology, Vol. 58, 907–934

ISSN: 0070-4571/doi:10.1016/S0070-4571(07)58036-2

the primordial Cordillera Real to the west. Higher up in the succession, a switch in provenance to dominantly westerly sources to the evolving Cordillera Real occurred, where progressively higher grade metamorphics were eroded. In the uppermost, Miocene to Pliocene sections, the appearance of mafic minerals documents new sources associated with the uplift of accreted basement terranes of the Cordillera Occidental and the reworking of arc volcanics.

Keywords: provenance analysis; heavy minerals; zircon fission-track ages; exhumation; geodynamics; Andes; Ecuador

1. INTRODUCTION

Six discrete topographic and tectono-stratigraphic regions can be identified in northern Ecuador (Fig. 1). These are from west to east: (1) the coastal lowlands (Costa), consisting of accreted oceanic plateau and arc series together with their Late Cretaceous to Neogene sedimentary cover; (2) the Cordillera Occidental, assembled as a tectonic patchwork of accreted Cretaceous oceanic basement, volcanic arcs and sedimentary successions; (3) the Inter-Andean Depression, formed during the last 6–5 Ma due to differential uplift and thrusting of the cordilleras; (4) the Cordillera Real comprising a tight tectonic stack of Palaeozoic and Mesozoic, medium- to high-grade metamorphosed plutonic, volcanic and sedimentary rocks; (5) the Sub-Andean Zone comprising a Jurassic volcanic arc basement and Cretaceous to Palaeogene cover rocks; (6) the Oriente, which is part of the upper Amazon Basin where the Proterozoic basement of the South American plate is overlain by fragmentary Palaeozoic and Mesozoic rocks. These include sedimentary and volcanic successions with mid-Cretaceous to Neogene, dominantly siliciclastic, cover (e.g., Baldock, 1982; Balkwill et al., 1995; Rivadeneira and Baby, 1999). The mid-Cretaceous to Neogene sedimentary series is common to both the Sub-Andean Zone and the Oriente and here is referred to as the AAB, which formed in a retro-arc foreland basin system (Fig. 1B) (Willett et al., 1993; DeCelles and Giles, 1996).

The Sub-Andean Zone is subdivided into a proximal, highly deformed stack of tectonic slivers between the Sub-Andean Fault to the west and the Cosanga Fault to the east, referred to as the Sub-Andean Thrust Belt, (Figs. 1B and 2) and an outer, less deformed push-up, commonly called the Napo Uplift, in the north and the Cutucú Uplift in the south (Figs. 1 and 2). Both units form the transition between the over 4000 m high Cordillera Real and the Oriente in front of the Andean Front Fault with an elevation of less than 400 m (Fig. 2). The observed stratigraphic relationships imply that the Sub-Andean Zone and the Oriente originally represented a composite basin system that was initiated during the Middle Cretaceous. Since then and until recent times, the basin received clastic material from both the Amazon Craton (i.e., the Guyana Shield) and the Andean cordilleras. However, proximal parts of the basin were successively eliminated as sedimentation sites and became tectonically integrated into the orogenic wedge by eastward-directed thrust propagation (see below).

The Northern Andes in Ecuador and Colombia are thought to be the product of repeated accretion of oceanic terranes, and continental compression (e.g., Jaillard et al., 1995). During the Early Cretaceous (approximately 140–120 Ma) possibly

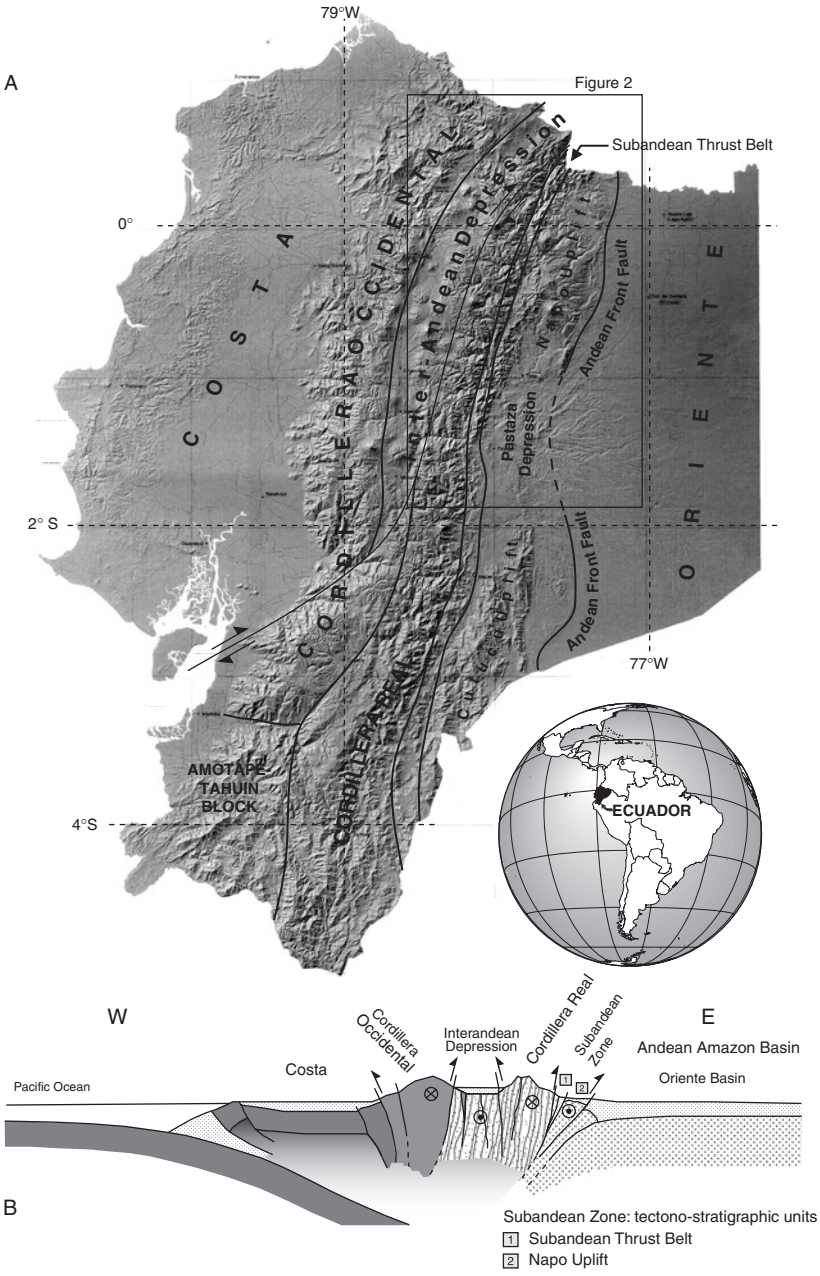

Fig. 1. Andean tectono-morphologic provinces in Ecuador (A) and a schematic tectonic section (B) across northern Ecuador. Note also the composite, dextral transpressive fault system consisting of the Pallatanga Fault (south), the Pisayambo Fault (centre) and the Chingual-La Sofia Fault (north) that separates the southern tip of the North Andean Block in the west from the South American plate in the east.

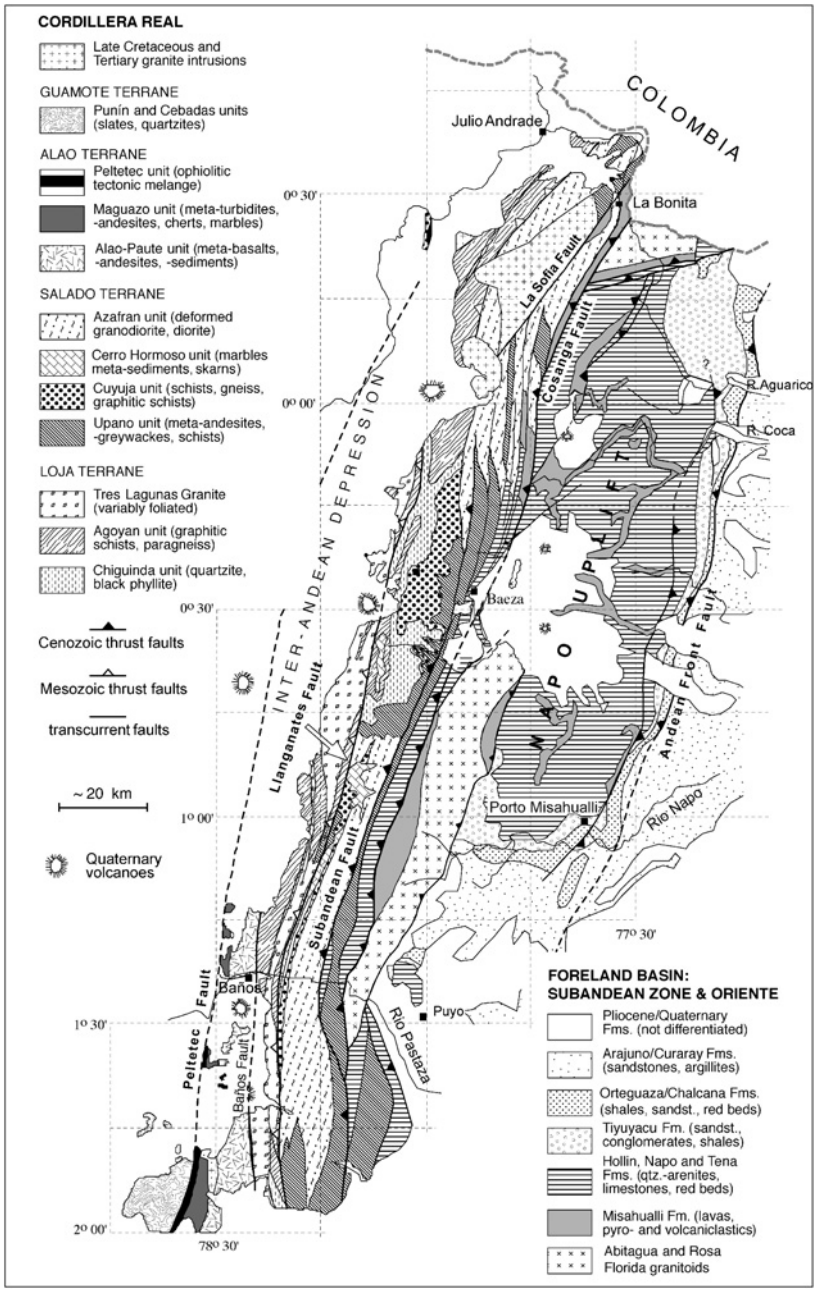

Fig. 2. Geological map of the Sub-Andean Zone and Cordillera Real in northern Ecuador (terrane terminology after Litherland et al., 1994).

various small continental and oceanic plates were accreted during the tectono-metamorphic Peltetec event in the Cordillera Real (Litherland et al., 1994). The Pallatanga and Piñon terranes of the Cordillera Occidental and Costa are assumed to have been accreted during the latest Cretaceous and Eocene, respectively (e.g., Egüez, 1986; Hughes and Pilatasig, 2002; Kerr et al., 2002). The younger history of the Ecuadorian Andes is related to the NNE movement of the Northern Andean Block after about 15 Ma (Hungerbühler et al., 2002; Winkler et al., 2004). Displacement of the block is accompanied by approximately E–W oriented shortening and right-lateral displacement along regional scale strike-slip faults (e.g., Ego et al., 1996; Winkler et al., 2004).

With this regional setting in mind, the main goal of the present study was to carry out integrated heavy mineral and fission-track analysis (FTA) of detrital zircon and apatite to determine the source of the sediments of the AAB, and to reveal stages of hinterland exhumation.

2. THE EVOLUTION OF THE ANDEAN AMAZON BASIN

The sediments of the AAB lie unconformably on a basement composed of Proterozoic metamorphic and plutonic rocks, Palaeozoic-Early Jurassic sediments and arc volcanics. The Misahualli volcanic arc series spans from Early Jurassic to Early Cretaceous (approximately 190–130 Ma) (Romeuf et al., 1995; Spikings et al., 2001; Ruiz, 2002). The Abitagua granite and the equivalent Zamora granite in the southern Sub-Andean Zone are considered to represent arc-related intrusions (Litherland et al., 1994; Spikings et al., 2001; Ruiz, 2002).

An angular unconformity exists between the oldest AAB sediments, the Hollin Formation and the basement (Fig. 3) (Tschopp, 1953; White et al., 1995; Shanmugam et al., 2000). The Aptian-Albian succession, up to 170 m thick, comprises coarse, porous, often tabular cross-bedded quartz-arenites characterised by the presence of blue quartz. The facies trend shows a transgressive sequence from alluvial braid plain to tidal plain and shallow marine conditions (White et al., 1995; Shanmugam et al., 2000).

The Middle Albian to Campanian Napo Group (Fig. 3) consists of organic-rich shales, limestones and sandstones, which were deposited in a restricted paralic-neritic sea (Mello et al., 1995; Jaillard, 1997; Vallejo et al., 2002). The many stratigraphic gaps that exist in the Turonian to Campanian section of the Sub-Andean Zone were the result of tectonic movements and wedge-top erosion (Vallejo et al., 2002). The analysis of seismic lines in the Oriente reveals that large-scale, basement-involving transpressive tectonic inversions affected the area since the Turonian (Balkwill et al., 1995; Rivadeneira and Baby, 1999).

The deposition of redbeds in the Maastrichtian-Paleocene Tena Fm. (Fig. 3) marks an extreme change towards prevailing continental conditions in a fluvial environment. During this time-span, the AAB developed a typical triangular retro-arc foreland profile with a maximum thickness (approximately 1000 m) in the west (i.e., in the Sub-Andean Zone) wedging out to ~150 m toward the easternmost Ecuadorian Oriente (Dashwood and Abbotts, 1990).

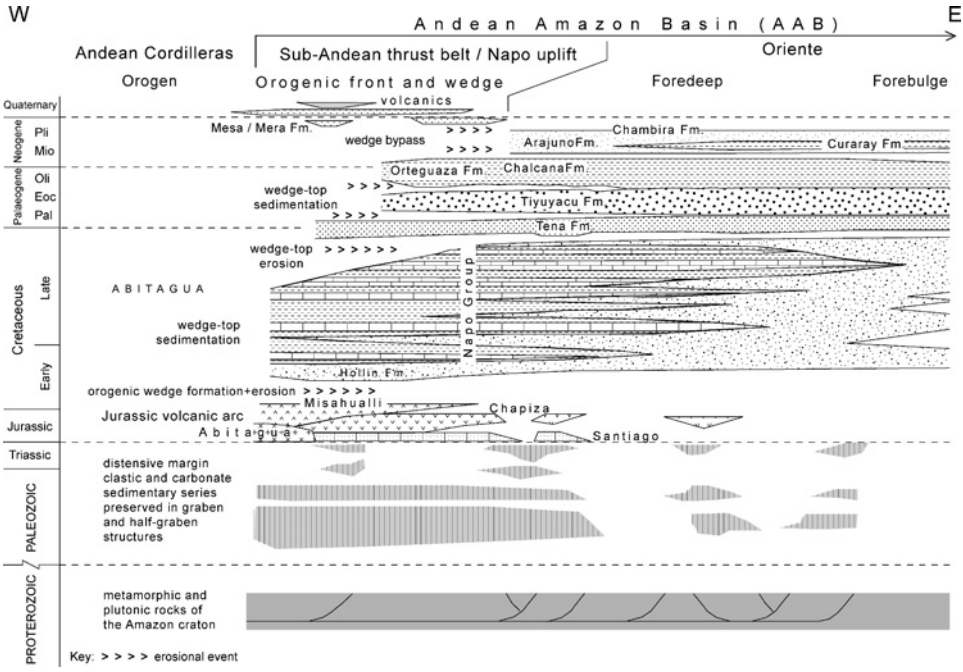

Fig. 3. Simplified chronostratigraphy of the Andean Amazon Basin series as observed in the Sub-Andean Zone and Oriente (modified from Balkwill et al., 1995). The definition of depo-zones (wedge, foredeep and forebulge) follows DeCelles and Giles (1996). The incomplete sedimentary record in the orogenic wedge depo-zone depicts changing periods of sedimentation, erosion and non-deposition.

A major erosional unconformity separates the Tena Fm. from the conglomeratic, Eocene Tiyuyacu Fm. (Fig. 3). A shift of the depocentre towards the east is described by Christophoul et al. (2002a). This succession was deposited in fluvial (lower member) and alluvial-fan (upper member) systems—both sourced from the west in the Andean Cordillera. The marginal marine deposits of the ~250 m thick Oligocene Orteguaza Fm. paraconformably overlap the Tiyuyacu Fm. (Christophoul et al., 2002a), and pass up into the 250–450 m thick continental sediments of the Chalcana Fm. The overlying Neogene fluvial-alluvial Arajuno and Chambira formations (Fig. 3) are separated by a minor erosional unconformity (Christophoul et al., 2002b; Ruiz, 2002). The sandy and silty Curaray Fm. is considered to represent the contemporaneous estuarine system toward the east (e.g., Baldock, 1982). The Neogene series had a clear western source with transport directions turning parallel to the Andean Cordillera in distal position in the Oriente foredeep (Christophoul et al., 2002b) and the shifting of the depocentres towards the east. The Late Pliocene alluvial fan deposits of the Mesa/Mera formations are restricted to the Pastaza Depression, the most important outlet draining the Cordillera Real and the Inter-Andean Depression.

Notably, in the Sub-Andean Thrust Belt (Litherland et al., 1994) (Fig. 1), the older horizons of the AAB series, the Hollin Fm., the Napo Group and the Tena Fm. together with the arc basement (Misahualli Fm. and Abitagua granite) are present as

a steeply westward-dipping tectonic slice (Fig. 1B). This indicates that, by the end of the Palaeocene, proximal parts of the AAB had already been eliminated through shortening, i.e., were integrated into the orogenic wedge (DeCelles and Giles, 1996). From the Miocene onward (Arajuno Fm.), sedimentation was directed towards the Pastaza Depression between the Napo and Cutucú uplifts on which sediment bypass occurred (Christophoul et al., 2004). This suggests the emergence of these highs since that time. Due to prevailing transpressive shortening, this uplift was probably driven in positive flower structures (Rivadeneira and Baby, 1999).

3. METHODS—THEORY AND PRACTICE

Heavy mineral analysis and detrital zircon fission-track (ZFT) analysis were performed on the same samples, ranging from sandstones to fine conglomerates and minor siltstones. Details on samples including universal transverse mercator (UTM) coordinates are given in Table 1. Both methods were also conducted on a sand sample from the modern Napo River near to Puerto Misahualli, as a control. The known drainage area of this river provides a reliable assessment of the sand composition derived from ancient sedimentary and magmatic source rocks. Stratigraphic ages based on previous work in the AAB (Tschopp, 1953; Faucher and Savoyat, 1973; Bristow and Hoffstetter, 1977; Baldock, 1982; Balkwill et al., 1995; White et al., 1995; Jaillard, 1997; Rivadeneira and Baby, 1999; Zambrano et al., 1999; Christophoul et al., 2002a, 2002b; Barragán et al., 2005) were augmented by the dating of syn-depositional volcanic events during the present study.

3.1. Heavy Mineral Analysis

The heavy mineral preparation procedure followed the standard methods described by Mange and Maurer (1992). Rocks were crushed and the carbonate fraction was dissolved in 10% acetic acid, while organic material and carbonate acetates were removed by the repeated addition of hydrogen peroxide. The heavy minerals were separated from the 0.063 to 0.4 mm sieve fraction using bromoform (density 2.88–2.9), and the residues were mounted in piperine (refraction index 1.67). Ideally, a minimum of 200 grains were counted under the petrographic microscope, using the mid-point ribbon counting method (Van der Plas, 1962) to provide grain-size independent frequency percentage distributions. Where one particular mineral species was dominant, up to 300 grains were counted in order to encounter the rare components. Special attention was also paid to the presence of idiomorphic zircons, prismatic and inclusion-rich apatite and pseudo-hexagonal biotite, as these are potential indicators of contemporaneous volcanic influx (Weaver, 1963; Winkler et al., 1985), critical for the correct interpretation of the meaning of lag times of the detrital ZFT ages.

3.2. Detrital Zircon Age Studies

The detrital zircons were separated from 24 horizons for fission-track analysis. Technical details are reported in Ruiz (2002) and Ruiz et al. (2004).

Table 1. Geographic and stratigraphic location of the samples from the northern Sub-Andean Zone and Pastaza Depression of Ecuador investigated in the present study

Sample no.	UTM	UTM	Altitude (m)	Map sheet	Location	Formation/ Group	Rock type
00GR05	21091	9884500	357	Puerto Misahualli	Porto Misahualli: Rio Napo	Quaternary	River sand
00GR01	154600	9837582	1084	Mera	Mera	Mesa/Mera	Sandmatrix of conglomerate
00GR06	184083	9820200	1018	Vera Cruz	Road Puyo-Macas	Mesa/Mera	Sandstone
98GR16	176850	9883480	590	Puerto Napo	Talag	Chambira	Conglomerate with quartz pebbles
98GR28	183856	9822555	700	Vera Cruz	Road Puyo-Macas	Arajuno	Coarse sandstone
00GR04	216517	9882580	364	Puerto Misahualli	Porto Misahualli: Rio Napo	Arajuno	Arkosic sandstone
00GR03	212561	9886172	374	Puerto Misahualli	Porto Misahualli: Rio Napo	Chalcana	Sandstone
00GR02	189475	9879828	571	Puerto Napo	Road Tena-Puyo	Chalcana	Fine sandstone
99GR81	246500	N0009350	400	Lumbaqui	Rio Aguarico	Orteguaza	Conglomerate
99GR44	189343	9880298	500	Puerto Napo	Road Tena-Puyo	Tiyuayacu	Fine sandstone
98GR81	185967	9896510	600	Tena	Tena	Tiyuyacu	Conglomerate with quartz pebbles
99GR52	242139	N0004314	840	Lumbaqui	Cerro Lumbaqui	Tiyuyacu	Sandstone with white mica
99GR36	244995	N0003650	560	Lumbaqui	Cerro lumbaqui	Tiyuyacu	Conglomerate
98GR83	185967	9896510	600	Tena	Tena	Tena	Green spotted red sandstone
98GR37	232689	9999867	500	Atenas	La Delicia	Tena	Red siltstone

99GR67	150510	9936429	1320	Mera	Rio Gringo	Tena	Fine green sandstone
98RS06	160050	9842950	1240	Mera	Puyo: Mirador Anticline	Napo	Fine conglomerate
98GR41	224435	9998965	1100	Atenas	Road San Francisco-La Delicia	Napo	Arkosic sandstone
98GR57	196101	9973320	1800	Las Palmas	Road Baeza-Lumbaqui	Napo	Glauconitic sandstone
98GR02	191210	9968100	1600	Santa Rosa de Quijos	El Chaco	Napo	Immature glauconitic sandstone
98GR48	211061	9991009	1700	Atenas	Rio Azuela	Napo	Glauconitic sandstone
99GR73	144450	9844850	1280	Mera	Rio Topo	Hollin	Blue qtz-bearing sandstone
99GR22	223150	9918125	610	Loreto	Rio Tucsi	Hollin	Sandstone
98GR69	193292	9919767	1150	Sardinas	Narupa	Hollin	Coarse blue qtz-bearing sandstone
98GR09	192702	9919713	1150	Sardinas	Road Narupa-Avila-Loreto	Hollin	Conglomerate
98GR50	212376	9989981	1400	Volcan El Reventador	Road Baeza-Lumbaqui	Hollin	Quartz sandstone
98GR05	187585	9921730	1150	Sardinas	Road Cosanga-Tena	Hollin	Quartz sandstone
99GR65	149450	9936250	1370	Mera	Rio Gringo	Hollin	Blue qtz-bearing sandstone
99GR71	150700	9937050	1220	Mera	Rio Gringo	Pumbuiza	Muscovite-rich sandstone

3.2.1. The concept of lag time

Zeitler et al. (1986) first used the concept of lag time with fission-track ages of detrital zircons in a study of the Neogene molasse-type sediments from northern Pakistan. The lag time (L_g) is defined as the difference between the time of closure of a geochronological system in the source region and the time of sedimentation in the basin (Fig. 4). The closure temperature is variable and dependent on the cooling/exhumation rates but for this study a closure temperature of 260°C for ZFT (Brandon et al., 1998) has been used throughout.

In applying detrital thermochronology with emphasis on the concept of lag time, several points should first be noted (Ruiz et al., 2004). Generally, in an exhuming single tectonic block, the first material eroded contains the oldest signature. This implies that ages derived from such a block are younger as the pile is eroded and deposited into the basin (Garver et al., 1999) (Fig. 4). Long lag times may represent either a slowly exhuming source region or reworking of older sediments. The distinction between these two can often be clarified by identifying the heavy minerals associated with the zircons. Short lag times, on the other hand, clearly indicate rapid exhumation of the source rocks, and as they approach a zero value, they become positive markers of active tectonics in the hinterland. Zero lag times are also indicative of input from contemporaneous volcanics into a basin, which may be confirmed by mineral and lithological associations.

Thus, by tracking the variation in lag time in clastic sediments overtime, the observed changes can be linked to events in the hinterland. During a phase of exhumation, the first erosional products will yield inherited thermochronological ages from an earlier phase—these ages cannot constrain the exhumation rates associated with the new phase. The new phase is recorded only when the rocks at depth (10 km?) pass through the closure temperature. Once the newly recorded tectonic phase is at the surface, it is possible to estimate the exhumation rate in the hinterland by dividing the estimated depth of closure (Z_c) by the lag time (L_g): $\mathrm{Exh} = Z_c/L_g$ in $\mathrm{mm} \cdot \mathrm{a}^{-1}$ (Garver et al., 1999) on the assumption that the time of transport (t_e) from erosion site to basin is negligible (Fig. 4). The rock cover above the temperature of closure T_c before this new phase is termed the thermochronological "dead zone".

3.2.2. Detrital age curves

In the present study, the majority of sample ages failed the $P\chi^2$-test (Green, 1981), a value that is suggestive of the presence of multiple populations (Table 2). Statistical separation of the grains (Brandon, 1992, 1996) revealed three to five populations (P_n) at some horizons. In order to visualise the change in the lag time upwards in the section, populations (P_1–P_n) were then joined according to their rank forming the detrital, D_1–D_n curves (Fig. 5). Their change of gradient upwards within the stratigraphic column is a gauge of different events in the source regions. Ruiz (2002) and Ruiz et al. (2004) presented a series of five theoretical paths illustrating the possible trends that may occur in any sequence (Fig. 6). Inflection points along a D_n curve, depicting increases or decreases in lag times, indicate changes in the exhumation of the source regions and/or flipping of source regions. The D_1 curve is the easiest and safest to interpret because it hosts the population with the shortest lag time and, consequently, the most probable record of rapid cooling events in the nearby hinterland. The five paths are briefly described below with reference to Fig. 6.

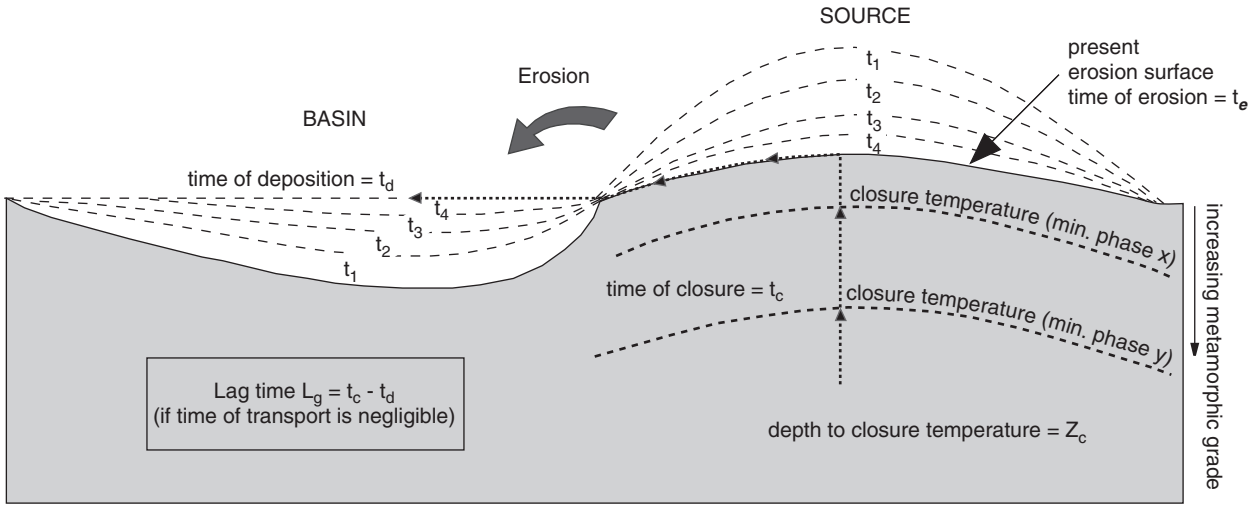

Fig. 4. The lag time concept for detrital grains (adapted from Garver et al., 1999).

Table 2. Zircon fission-track ages from the Aptian to Recent basin fill series of the northern Ecuadorian Sub-Andean Zone

Formation	N	$P\chi^2$	Central age	P_1	P_2	P_3	P_4	P_5	Stratigraphic age	Lag time P_1 (Ma)
Sample no.		%	±1s (Ma)	±1s (Ma)	±1s (Ma)	±1s (Ma)	±1s (Ma)	±1s (Ma)	(Ma)	±1s
Others										
00GR05 (Recent)	37	0	59±5	30±5 (4)	50±3 (23)	142±13 (10)	–	–	0	30±5
00GR01 (Mesa/ Mera)	25	0	49±7	43±2 (16)	57±6 (8)	255±84 (1)	–	–	4	39±2
98GR16 (Chambira)	46	0	61±3	45±4 (14)	60±7 (18)	80±7 (13)	242±49 (1)	–	9	36±4
Arajuno Fm.										
98GR28	40	0	63±4	56±3 (38)	198±33 (2)	–	–	–	16	40±3
00GR04	55	0	57±5	23±1 (6)	49±3 (26)	70±5 (10)	115±9 (8)	330±48 (5)	22	0±1
Chalcana Fm.										
00GR03	56	0.3	55±5	50±3 (38)	70±6 (18)	–	–	–	24	26±3
00GR02	29	17	60±3	60±3 (29)	–	–	–	–	27	33±3
Orteguaza Fm.										
99GR81	23	0	98±7	77±5 (12)	123±8 (11)	–	–	–	32	45±5
Tiyuyacu Fm.										
99GR44	51	0	56±5	36±4 (4)	53±3 (30)	70±5 (17)	–	–	37	0±3
98GR81	25	0	69±5	67±3 (24)	269±46 (1)	–	–	–	44	23±3

99GR52	10	57	234±31	234±31 (10)	–	–	–	–	50	184±31
99GR36	24	0	57±7	51±5 (4)	72.7±6.0 (8)		–	–	52	1±5
Tena Fm.										
99GR67	30	0	106±13	72±3 (20)	232±40 (1)	494±44 (9)	–	–	70	2±3
98GR83	35	13.7	65±07	63±3 (34)	242±72 (1)	–	–	–	59	0±3
Napo Group										
98RS06	54	0	189±20	86±6 (16)	224±20 (18)	481±35 (20)	–	–	86	0±6
98GR41	49	0.4	247±18	153±13 (16)	335±23 (33)	–	–	–	90	63±13
98GR57	16	2.1	188±26	139±18 (9)	323±69 (7)	–	–	–	99	30±18
98GR02	57	0	263±24	101±11 (6)	267±22 (36)	516±43 (15)	–	–	101	0±11
Hollin Fm.										
99GR73	29	0	227±30	118±11 (10)	301±45 (10)	579±65 (9)	–	–	105	13±11
99GR22	50	0	284±22	150±16 (10)	355±23 (40)	–	–	–	107	43±16
98GR69	45	0	298±29	134±16 (7)	227±33 (11)	518±32 (27)	–	–	110	24±16
98GR50	33	0	258±25	174±11 (15)	359±48 (11)	569±85 (7)	–	–	112	62±11
98GR05	61	0	285±26	139±8 (16)	426±24 (45)	–	–	–	113	26±8
99GR65	31	0	316±40	128±10 (6)	309±44 (6)	506±45 (19)	–	–	115	13±10

Notes: Total number of zircon grains counted in sample. The samples with a $P\chi^2 < 5$ are considered to represent multiple populations (Galbraith, 1981). Such populations were discriminated using different statistical techniques (Brandon, 1992, 1996) and labeled as P_1 to P_n with increasing age. Numbers in parentheses indicate the number of counted grains for each population. Lag time 1 indicates the time difference between the stratigraphic age and the age of zircon population 1 (P_1). All ages were determined using the zeta approach (Hurford and Green, 1983), with a ζ value of 121±3 for CN1 (GR). They are reported as central ages (Galbraith and Laslett, 1993) with a 1-sigma error. The magnification used was × 1600 (oil). Samples were irradiated at the ANSTO Facility Lucas Heights, Australia.

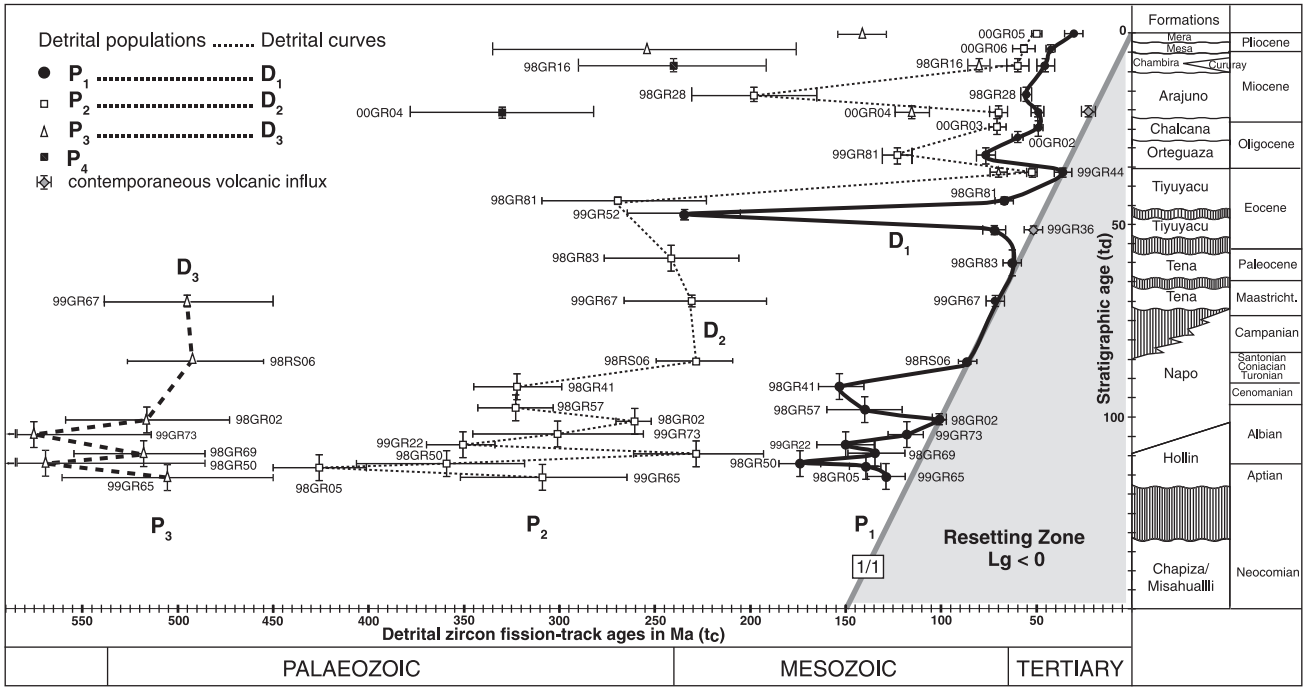

Fig. 5. Detrital zircon fission-track age populations versus stratigraphic age of their host sediments (modified from Ruiz, 2002).

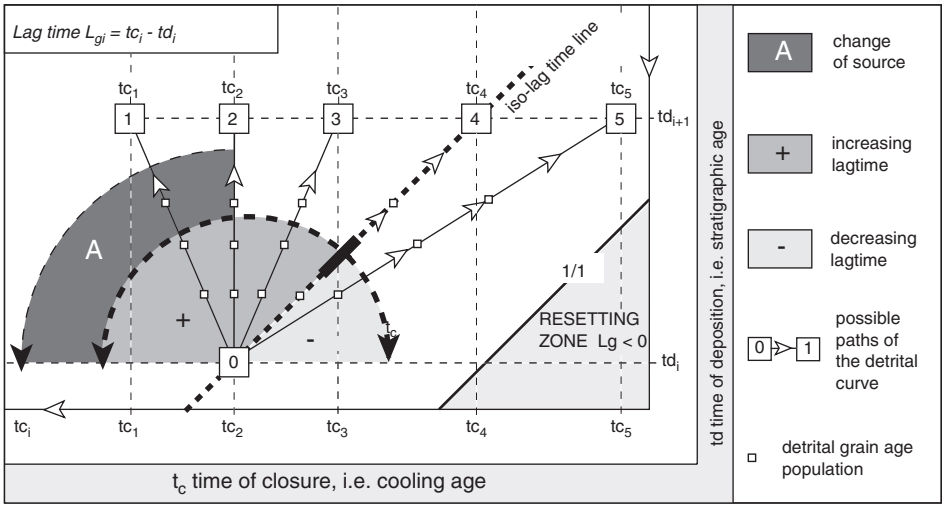

Fig. 6. Detrital age path concept (modified from Ruiz, 2002).

The type 1 path most likely occurs in connection with a change of source region. The older ages may also be those derived from the upper thermochronological "dead zone" of a newly exhuming block in the hinterland where rocks from a renewed event have not yet reached the surface as explained above. Such examples can be identified and/or verified through the combination of heavy mineral studies. A type 2 path may suggest the erosion of a thick pile of volcanic rocks that were extruded over a short period of time as, for example, plateau basalts, or the erosion of a succession that underwent extremely rapid exhumation. Ages decrease upwards, but with increasing lag time the characteristic pattern of a type 3 path appears. Such a path represents waning of the exhumation assuming a constant depth of closure, and might follow the slowing down of an orogenic phase. The type 4 path describes a constant lag time through the stratigraphic record along an iso-lag time line parallel to the stratigraphic correlation line 1/1 (Fig. 6). This path characterises "steady-state cooling" within the source region. The type 5 path is characterised by a decreasing lag time up-section, which implies increasing cooling/exhumation in the source region. This is typically associated with orogenic growth phases (e.g., Garver et al., 1999).

4. RESULTS OF HEAVY MINERAL PROVENANCE ANALYSIS

Our data set represents the first integrated application of heavy mineral analysis for tracing the provenance of the detrital material in the Ecuadorian Andean domain. The results are summarised in Fig. 7 and Table 3. The highly variable heavy mineral suites indicate a complex provenance from changing lithologies with time (see Mange and Maurer, 1992, for a compilation of diagnostic minerals of specific rock types).

With regard to the preservation potential of the heavy minerals in the sediments, we have positive arguments for excluding high-level diagenetic or metamorphic

overprint. According to apatite fission-track (AFT) modelling in rocks of the Napo uplift (Ruiz, 2002), from where the majority of our samples is derived, the volcanic basement (Misahualli Fm.) and, consequently, the sedimentary cover series were—since the start of deposition in the middle Cretaceous—never buried to a depth greater than the temperature-equivalent of 110°C (i.e., approximately 3–4 km at an assumed geothermal gradient of 30°C/km). Obviously, the sediments remained in a middle-grade diagenetic stage inferring only minor diagenetic modification of the heavy mineral assemblages. On the other hand, due to the high mineralogical and textural maturation stage of the quartz-arenites of the mid-Cretaceous Hollin Fm., a possible enrichment of stable minerals, i.e., the zircon/tourmaline/rutile (ZTR) association, may be invoked (Hubert, 1962). However, the striking similarity with the mineral assemblages observed in the immature sandstones of the Napo Group suggests a primary source rock-induced signal for both formations.

4.1. Stratigraphic Trends of Heavy Minerals

The Hollin Fm. and the Napo Group are dominated by the ZTR group, accompanied by other Ti-bearing minerals (brookite, anatase and sphene) as well as by minor amounts of monazite (rarely xenotime), and few clinopyroxenes of diopsidic composition (simply referred to as diopside) (Fig. 7). In addition, the Hollin Fm. and the lower Napo Group are characterised by the abundance of pink and remarkably dark-brownish, often zoned, zircons. The dark-brownish colour of these zircons suggests long-lasting radioactive damage, i.e., they may represent "old" grains as confirmed by the fission-track measurements (see below). Rounded and rounded zoned zircons make up more than 94%, often 98–100% of the zircon population. Muscovite is abundant. The marine Napo Group also contains many diagenetic phosphatic and glauconite grains (not quantified in Fig. 7 and Table 3). With the strong dominance of the ZTR group, this assemblage indicates derivation of the clastic material primarily from shallow granitic continental crust comprising pegmatites (cassiterite), with minor additions from basic rocks or skarns (signalled by diopside), and polycyclic sediments. In the uppermost Napo Group and in the Tena Fm., apatite becomes common. In sample 98GR37 (Tena Fm., Fig. 7), the presence of inclusion-rich apatites suggests a volcanic source. However, no fission-track dating of associated zircons was obtained from this sample.

Significantly, the first occurrence of metamorphic grains (garnet and chloritoid, most likely derived from medium-grade metamorphic shales) is observed in the Tena Fm. Up-section an increasing number of other metamorphic grains (epidote group, kyanite, sillimanite) is obvious (Fig. 7). These generally medium- to high-grade metamorphics-derived associations commonly contain muscovite and chlorite. The metamorphic grains are accompanied by variable proportions of the ZTR group, representing associated granitic and reworked sedimentary rocks in the source areas. Several abrupt changes in the stratigraphic succession, depicted in Fig. 7, suggest repeated switching of source terranes, i.e., variable activation or abandonment of sources and/or associated palaeodrainage systems. A quantitative increase from low/medium- to high-grade metamorphic assemblages in the stratigraphic column (e.g., samples 98GR81—99GR44 and 99GR81—00GR02—00GR03) points to accelerated exhumation of deeper, metamorphic crustal levels in the source areas.

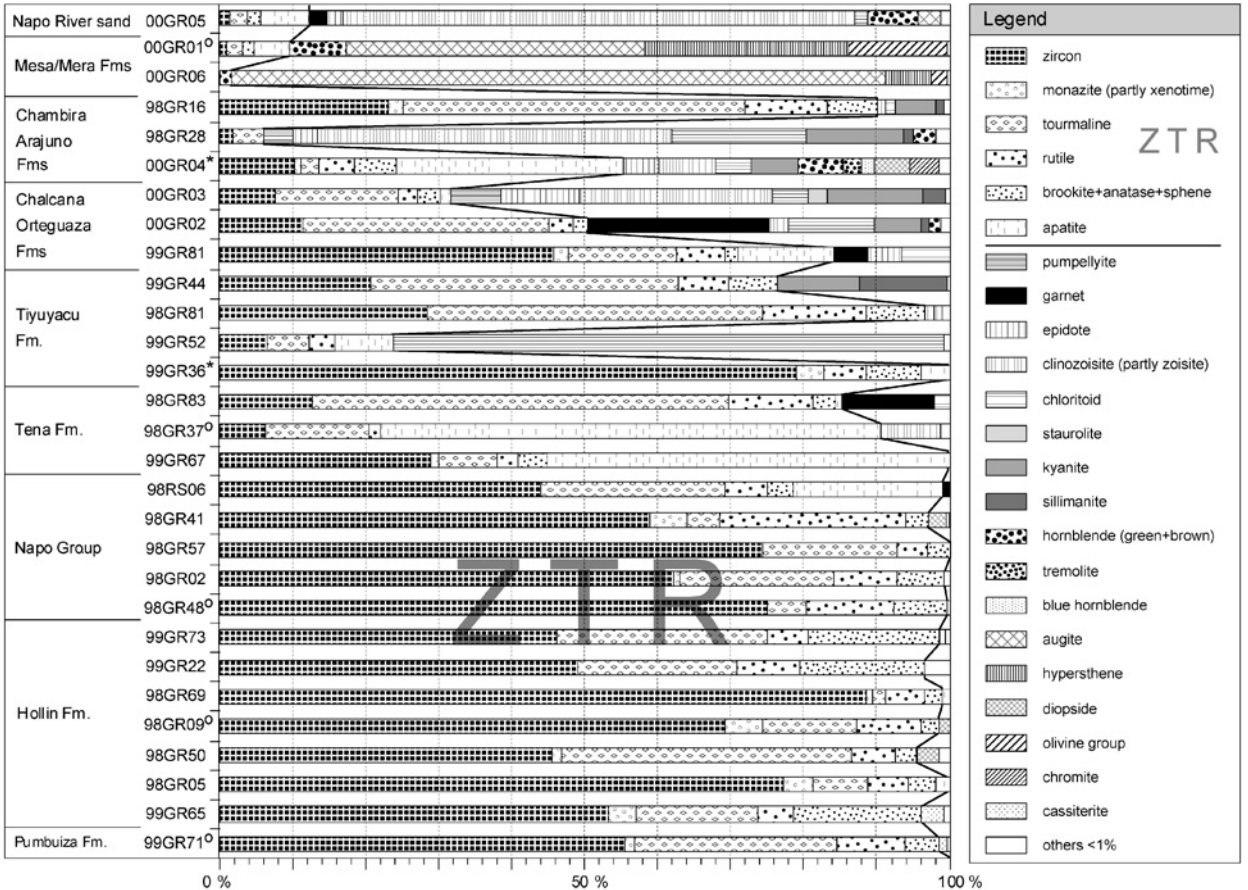

Fig. 7. Bar diagrams depicting heavy mineral frequencies in the Ecuadorian Andean Amazon Basin series in stratigraphic order. See also Table 3. ZTR refers to the stable zircon/tourmaline/rutile association. Note the diversification of heavy mineral suites up-section (modified from Ruiz, 2002). Samples marked with open circle: no detrital fission-track ages are available. Samples marked with an asterisk indicate evidence for contemporaneous volcanic influx.

Table 3. Heavy mineral percentages in sandstones from the northern Sub-Andean Zone and Pastaza Depression of Ecuador

Formation/Group	Zircon	Monazite (p.p. xenotime)	Tourmaline	Rutile	Branti	Apatite	Pumpellyite	Garnet	Epidote	Clinozoisite (p.p. zoisite)	Chloritoid	Staurolite	Kyanite	Sillimanite
Napo River sand	1.3	0	2.6	0	1.8	6.5	0	2.6	2.2	70	1.8	0	0	0
Mesa/Mera	1	0	2.1	0	1.7	4.8	0	0	0	0	0	0	0	0
Mesa/Mera	0	0	0	0	0	0	0	0	0	0	0	0	0	0
Chambira	23	2	47	11	6.8	0	0	0	0	1.2	1.2	0	5.7	1
Arajuno	1.8	0	4.2	0	0	0	4.1	0	3.3	49	18	0	13	1.4
Arajuno (base)	10	1	2.4	4.8	5.8	31	0	0	4.9	7.8	4.9	0	6.3	0
Chalcana	7.6	0	17	2.7	3.2	1.6	0	6.5	11	27	4.9	2.7	13	3.2
Chalcana	11	0	34	3.3	2	0	0	25	0	2.8	12	0	6.2	1.2
Orteguaza	46	2	15	6.5	1.8	13	0	4.7	4.7	0	6.5	0	0	0
Tiyuyacu (top)	21	0	42	6.8	6.8	0	0	0	0	0	0	0	11	12
Tiyuyacu	28	0	46	14	8	0	0	0	1.3	1.3	0	0	0	0
Tiyuyacu	6.5	0	5.8	3.6	0	7.9	0	0	0	0	76	0	0	0
Tiyuyacu (base)	79	3.8	0	5.7	7.7	3.8	0	0	0	0	0	0	0	0
Upper Tena	13	0	57	12	3.1	1	0	13	0	0	2.1	0	0	0
Tena	6.3	0	14	1.6	0	69	0	0	0	8.2	0	0	0	0
Lower Tena	29	1	8	3	4	55	0	0	0	0	0	0	0	0
Napo	44	0	26	5.7	3.5	20	0	1	0	0	0	0	0	0
Napo	74	0	18	4.4	2.9	0	0	0	0	0	0	0	0	0
Napo	59	5.1	4.6	25	3.2	0	0	0	0	0	0	0	0	0
Napo	62	1	21	8.6	6.5	0	0	0	0	0	0	0	0	0
Napo	75	0	5.4	12	7.2	0	0	0	0	0	0	0	0	0
Hollin	46	0	29	5.4	18	0	0	0	1	0	0	0	0	0
Hollin	49	0	22	8.6	17	0	0	0	0	0	0	0	0	0
Hollin	89	1	1.8	5.2	2.5	1	0	0	0	0	0	0	0	0
Hollin	69	4.9	13	9	2.3	0	0	0	0	0	0	0	0	0
Hollin	46	1.5	40	6	3	0	0	0	0	0	0	0	0	0
Hollin	77	4	7.4	5.7	3.6	2	0	0	0	0	0	0	0	0
Hollin	53	3.6	17	4.9	17	0	0	0	0	0	0	0	0	0
Pumbuiza?	56	1.3	28	9.3	4.8	0	0	0	0	0	0	0	0	0

Abbreviation key: branti = brookite + anatase + sphene; r = rare; p = present; f = frequent; vf = very frequent.

Hornblende (gr + br)	Tremolite	Blue hornblende	Augite	Hypersthene	Diopside	Olivine group	Chromite	Cassiterite	Others <1%	Muscovite	Chlorite	Biotite	Glauconite
6.9	0	0	3.1	0	0	0	0	0	1.2	r	p	p	
7.8	0	0	41	28	0	13	0	0	0.4	f	p	r	
1.7	0	0	90	6.2	0	2.1	0	0	0.4				
0	0	0	0	0	0	0	0	0	0.8	f			
3.2	0	0	0	0	0	0	0	0	1.8	p	r		p
6.3	2.4	1.9	0	0	4.8	0	3.9	0	1.5	p		r	
0	0	0	0	0	0	0	0	0	0.5	f	p		
1.6	0	0	0	0	0	0	0	0	1.2	p	r	p	r
0	0	0	0	0	0	0	0	0	0	f	p		
0	0	0	0	0	0	0	0	0	0.4	vf	r		
0	0	0	0	0	0	0	0	0	0.9	f			
0	0	0	0	0	0	0	0	0	0.7	vf	vf	r	
0	0	0	0	0	0	0	0	0	0	r			
0	0	0	0	0	0	0	0	0	0	f	p		
0	0	0	0	0	0	0	0	0	1.2				
0	0	0	0	0	0	0	0	0	0				
0	0	0	0	0	0	0	0	0	0	f	p	p	vf
0	0	0	0	0	0	0	0	0	0	p	p		f
0	0	0	0	0	2.3	0	0	0	0.4				
0	0	0	0	0	0	0	0	0	0.8				vf
0	0	0	0	0	0	0	0	0	0.4	p			f
0	0	0	0	0	0	0	0	0	0.5	f		p	
0	0	0	0	0	0	0	0	0	3.5	f			f
0	0	0	0	0	0	0	0	0	0	p			
0	0	0	0	0	1.5	0	0	0	0	r			
0	0	0	0	0	3	0	0	0	1.5	p			
0	0	0	0	0	0	0	0	0	0				
0	0	0	0	0	0	0	0	3.3	0.7	p			r
0	0	0	0	0	0	0	0	1	0.4	f	r		

Increasingly diverse heavy mineral associations occur up-section from the Miocene Chalcana Fm. (00GR02) and the Miocene Arajuno Fm. (00GR04). The additional but variable appearance of augite, hypersthene, olivine, diopside, chromite and (green and brown) hornblendes points to the presence of basic to intermediate as well as ultrabasic source rocks.

In the lower Tiyuyacu Fm. (99GR36) and Arajuno Fm. (00GR04) prismatic apatites and apatites with abundant strings of inclusions are present. They occur together with many volcanic rock fragments (in 99GR36) and pseudo-hexagonal biotite (in 00GR04). The inferred, contemporaneous volcanic influx is corroborated by the ZFT analysis revealing 0 Ma lag times (see below).

The modern Napo River's main catchment area lies in the Cordillera Real between latitudes 1°S and 30°S. Its sand is rich in medium-grade metamorphic minerals (approximately 60% clinozoisite and minor zoisite, Fig. 7) and granitic rock fragments. Associated hornblende and augite may be derived either from minor intermediate to basic volcanic rocks or from reworking of the Miocene-Pliocene series, drained by its tributary, the Rio Arajuno, flowing along the Pastaza Depression towards the Rio Napo. Hence, the observed mineral association mirrors the rocks encountered in the drainage basin.

In summary, the provenance of detrital material reflects an overall trend from shallow continental granitic crustal (Hollin Fm. and Napo Group) to medium- to high-grade metamorphic continental sources, with signatures from the latter appearing first in the Maastrichtian Tena Fm. This trend mirrors the tectonic evolution of the Cordillera Real, where increasingly deeper metamorphic levels of the nascent orogen were exhumed by differential uplift and unroofing. Furthermore, transport from a discrete, important source region, the Amazon Craton (i.e., the Guyana Shield), providing detritus during the Cretaceous, is suggested tentatively by the presence of "old" zircon grains. The relatively high abundance of rounded brookite, anatase and sphene, and the minor but continuous presence of monazite/xenotime, diopside and cassiterite in these sediments, could also be indicative of a cratonic source.

In the Miocene sequences, the appearance of minerals from ultrabasic and basic volcanics indicates exposure of mafic rocks in the Cordillera Occidental that accreted in the Maastrichtian (Vallejo et al., 2006). Alternatively, a part of these minerals also may have been reworked from arc volcanics in the cordilleras. This new supply into the basin coincides with the eastward shift of the depocentre in Arajuno Formation time (Miocene), and the opening of a fluvial conduit from the Cordillera Occidental across the Cordillera Real into the Pastaza Depression, as it exists today.

5. RESULTS OF DETRITAL ZIRCON FISSION-TRACK STUDY

The ages of the analysed zircon populations from the full succession range from 579 ± 65 Ma to 22.9 ± 1.2 Ma (Table 2), and a general younging trend of the P_1 and P_2 populations is observed upwards (Fig. 8). Lag times vary erratically throughout the section but it is interesting to note that the D_1 and D_2 curves are often parallel. This implies the possibility of a large-scale regional pattern overprinting the

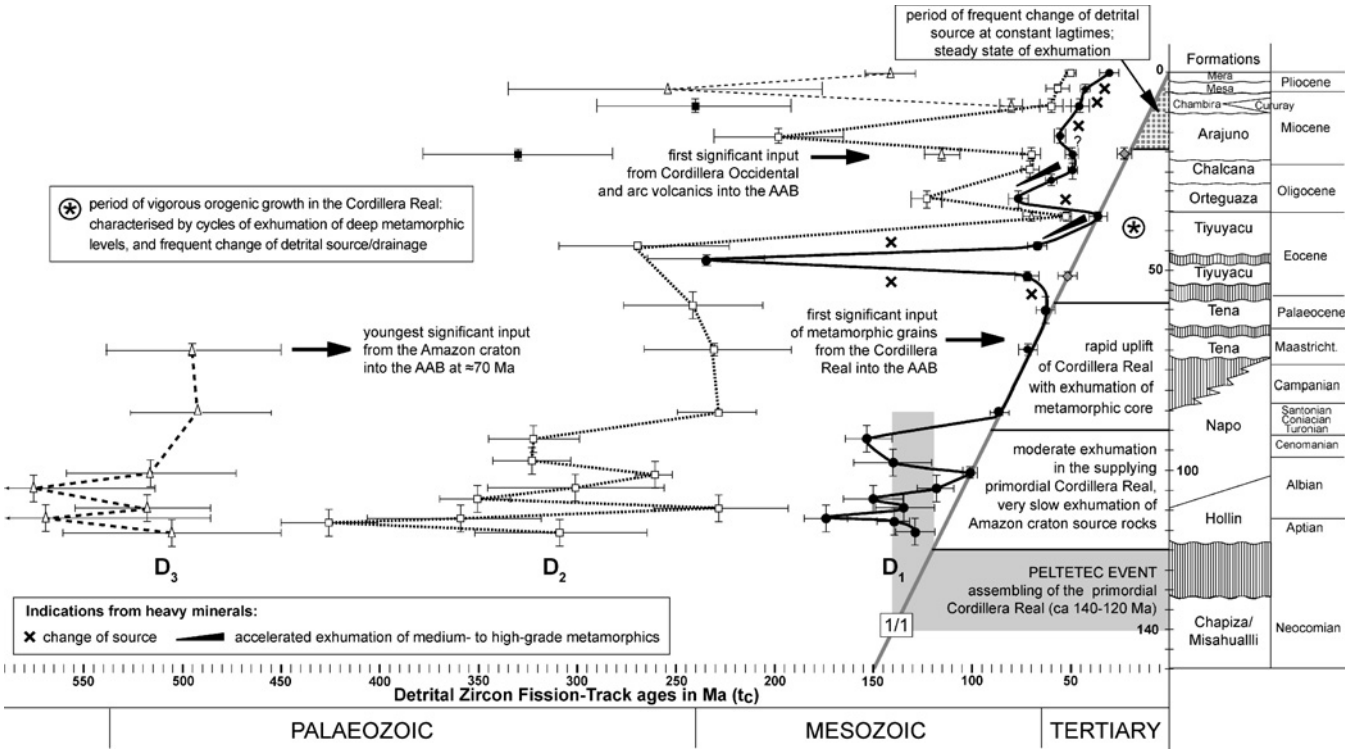

Fig. 8. Detrital zircon fission-track age populations correlated with heavy mineral variations, including the interpretation of the source areas and geodynamic implications for the Ecuadorian Andean Cordilleras.

differently cooling/exhuming regions. The third population, P_3 in Fig. 8, in sediments older than Maastrichtian, has ages older than 450 Ma. Many rounded and zoned pink zircons from the Hollin Fm. and Napo Group often had strong radiation damage and are un-datable because they are too old (track density too high to count). This leads to an immediate bias in this data set, but was not considered important for the present study because the identification of new proximal tectonic phases was the immediate goal of the project. The extremely long lag time is indicative of long, slow exhumation in the range of $0.02\,\mathrm{mm}\cdot\mathrm{a}^{-1}$, typical of cratonic regions in Brazil (Harman et al., 1998). The abundance of the associated ZTR group in the Late Cretaceous succession points to a probable source in the Guyana Shield and its Palaeozoic cover-rocks to the east of the basin. The old zircon-age population declines abruptly at the end of the Cretaceous when a major switch to prevailing supply from the Cordillera Real is inferred.

In the Hollin Fm. and lower Napo Group, lag times measured in population P_1 range from 63 to 0 Ma, suggesting exhumation in the source regions in the order of $0.1–1\,\mathrm{mm}\cdot\mathrm{a}^{-1}$. Such exhumation rates—an order faster—are not compatible with a derivation of the detrital material from the Amazon Craton, but rather suggest the initiation of a primordial Cordillera Real to the west of the basin. This is corroborated by the exhumation ages of the P_1 zircons, which correlate with the previous Peltetec tectonic event (Fig. 8), when the northern South American continental margin was deformed (Litherland et al., 1994). Our observation stands in clear contrast with sedimentary facies reconstructions in oil exploration boreholes (e.g., White et al., 1995; Barragán et al., 2004) in the Oriente whereby a sole supply to the early AAB from the Amazon Craton is interpreted.

From Late Cenomanian to Coniacian, a strong type 5 path is evident in the D_1 and D_2 paths (Fig. 8), implying an increase in exhumation in the source region that is interpreted as the initiation of a tectonic event. A minimum exhumation rate of $1\,\mathrm{mm}\cdot\mathrm{a}^{-1}$ using a maximum lag time of 6 Ma (error on 98RS06, Table 2) is estimated (Garver et al., 1999). A very short lag time is evident in the D_1 path through to the middle Palaeocene (a type 4 path) and is correlated with the incoming of low- to medium-grade metamorphic minerals (Figs. 7 and 8) in the Tena Fm. This detrital record most likely reflects the initiation and closure of the Pallatanga event, associated with the accretion of the oceanic Pallatanga Terrane in the Ecuadorian forearc (Cosma et al., 1998; Lapierre et al., 2000; Hughes and Pilatasig, 2002, Vallejo et al., 2006), and coincides also with the disappearance of the presumably Guyana Shield derived old zircons. The short lag time, the loss of older ages and the incoming of metamorphic minerals are strong indications that the new source is to the west of the AAB, i.e., in the growing Cordillera Real. This is confirmed by (1) a switch in palaeocurrent direction from an easterly to a dominant westerly source for the Tena Fm. (e.g., Tschopp, 1953; Balkwill et al., 1995), resulting in lower input from the eastern basin margins; (2) a major change in the depositional environment from shallow marine (Napo Group) to continental (Tena Fm.); and (3) increased tectonic subsidence (Thomas et al., 1995), suggesting an increase in orogenic load to the west of the basin.

Evidence for the first volcanic input in the Lower Eocene sediments is provided by sharp, idiomorphic zircons and a tuffaceous cement in the conglomerate sample 99GR36 (Figs. 5 and 7). The clast lithology at this horizon 99GR36 is unique,

comprising dominantly sub-rounded radiolarian black cherts of 10–12 cm in diameter, which may have been derived from the earlier accreted (Maastrichtian) Pallatanga Terrane (Ruiz, 2002). The zircons in the matrix yield a zero lag time for the P_1 population with an age of 51 ± 5 Ma (Table 1) and hence record the age of the host sediment. Because of the contemporaneous volcanic origin of the P_1 population, it is not considered in the detrital curves, and at this horizon P_2 becomes P_1. This leads into an extreme type 1 path (Fig. 8), implying a switch to a new hinterland. This path coincides with a dramatic change in the heavy mineral suite as evidenced by sample 99GR52, which contains a chloritoid-dominated group and less than 25% ZTR (Fig. 7). The long lag time implies that the new metamorphic source terrane experienced an early exhumation at the end of the Palaeozoic but was eroded only during the Eocene.

From Middle to Late Eocene, a major type 5 path defines the change in lag time from 184 Ma to approximately zero (Fig. 3). This is recorded in both the D_1 and D_2 paths. During the Middle to Late Eocene, rates of exhumation in the source region were probably $> 1\,\mathrm{mm} \cdot \mathrm{a}^{-1}$, assessed from the approximately zero lag time in 99GR44 (Table 3). The two sub-parallel D_1 and D_2 curves suggest that two different hinterland blocks were rapidly and contemporaneously denuded at this time. The continuous period of exhumation is supported by the appearance of higher grade metamorphic minerals, e.g., kyanite and sillimanite (99GR44) in increasing proportions (Figs. 7 and 8), sourced from deeper crustal levels.

Two main events are revealed in the evolution of the source terranes during deposition of the Tiyuyacu Fm.: (1) during the Early Eocene, a change of source terrane occurred, caused most probably by a radical tectonic rearrangement of the hinterland; (2) higher in the section, during the Middle-Late Eocene (44–36 Ma), exhumation of high-grade metamorphic terranes was dominant. We interpret this as a response to Middle to Late Eocene compression and unroofing of the metamorphic core in the Cordillera Real.

The Oligocene detrital curves (Orteguaza and Chalcana Fms) begin with a type 1 path and represent a further change in source. The heavy mineral input changed from ZTR and high-grade index kyanite and sillimanite (99GR44) to one with dominantly medium-grade metamorphic suites, such as garnets, epidote and chloritoid (99GR81). The subsequent reappearance of kyanite and sillimanite-containing assemblages in 00GR02 and 00GR03 (Fig. 7) parallels a clear shortening of lag times and is indicative of the re-activation of high-grade metamorphic rock source regions (Fig. 8).

A second period of volcanic activity is recorded in the Early Miocene (00GR04; Table 2). Pseudo-hexagonal biotites, hornblende, euhedral, inclusion-rich apatites and idiomorphic zircons in the basal Arajuno Fm., combined with indistinguishable ZFT and AFT ages of 23 Ma (Ruiz, 2002), suggest supply from contemporaneous volcanics. Because of the volcanic components, the D_1 and D_2 paths, spanning the upper Chalcana and lower Arajuno Fms., depict two type 2 paths. These contain identical ZFT populations in both levels that are attributed to (1) the presence of similar zircon assemblages in both formations (Fig. 7), and (2) the unconformable contact between the Chalcana and Arajuno Fms. This supports the interpretation of Christophoul et al. (2002a), who suggested reworking of the Chalcana Fm. into the Arajuno Fm.

The pattern of the detrital zircon ages for the Miocene to Pliocene Chambira and Mesa/Mera Fms and those from the modern Napo River sand follow a simple type 4 path for D_1 with constant lag time values of ~30–40 Ma (Fig. 8; Table 2). This lag time persisted, despite the dramatic change in the source region during the Pliocene, as evidenced by the flux of mafic minerals from the Cordillera Occidental in the Mesa/Mera Fms, and by the dominance of medium-grade metamorphic grains from the Cordillera Real in the modern Napo River sand (Fig. 7). The constant lag time suggests that the entire hinterland had already been brought through the partial zircon-annealing zone by Oligocene times. Smaller, young events, recorded by AFT analysis at 15 Ma and younger (Spikings et al., 2001), did not achieve sufficient erosion to bring lithologies with associated zircon ages to the surface. The young events included (1) thrust propagation involving the Napo and Cutucú Uplift areas, causing Neogene sedimentation to become localised in the Pastaza Depression and in front to the east of the uplifted areas, (2) enhanced exhumation in the northern Cordillera Real since 15 Ma (Spikings et al., 2001), and (3) the formation of the Inter-Andean Depression since 6–5 Ma (Winkler et al., 2004).

6. CONCLUSIONS

Integrated heavy mineral and detrital ZFT analysis has proved instrumental in the reconstruction of the evolution of the mid-Cretaceous to Recent retro-arc AAB foreland basin and adjacent source terranes (Fig. 8). Major events identified are:

(1) Aptian to Turonian sediment supply to the nascent marginal and shallow marine AAB from both the Amazon Craton to the east and the primordial Cordillera Real to the west. The latter source area was established during the preceding Peltetec event that also caused deep erosion of the volcanic basement (Misahualli Fm.) before initiation of the AAB. Exhumation in the primordial Cordillera Real occurred at a rate of 0.1–1 mm $\cdot$ a^{-1}, which contrasts with the exhumation rates of at least one order lower in the Amazon Craton.

(2) Exhumation rates increased in the Cordillera Real from Turonian to Paleocene ($\geqslant$1 mm $\cdot$ a^{-1}), but supply continued from the Amazon Craton until the Maastrichtian. Turonian and younger inversion caused transpressive deformation in the Oriente Basin. Rapid exhumation and unroofing of the Cordillera Real is indicated by the first appearance of metamorphic minerals in the basin since the Maastrichtian, simultaneously with the termination of supply from the Amazon Craton. This development was related to the accretion of the oceanic plateau Pallatanga Terrane along the Ecuadorian forearc during the Maastrichtian-Palaeocene (Luzieux et al., 2006; Vallejo et al., 2006), dated thermochronologically from the Cordillera Real at approximately 75–60 Ma (Spikings et al., 2001), indicating that the rapid exhumation of the Cordillera Real was driven by the collision of the oceanic terranes with the forearc.

(3) The Eocene to Oligocene history of detrital supply to the basin is characterised by intervals of repeatedly switching palaeotransport paths carrying material from different source regions and progressive exhumation of deeper metamorphic levels (Fig. 8). We ascribe this to a main phase of orogenic growth by vigorous tectonic uplift and unroofing in the Cordillera Real.

(4) Following a pronounced Oligocene exhumation of high-grade metamorphic complexes in the Cordillera Real at 33–25 Ma (Fig. 7 and 8), the Mio-Pliocene detrital path is characterised by approximately constant lag times of some 30–40 Ma (a path 4 iso-lag time), along with frequent changes of source complexes and drainage patterns. The activation of a new Cordillera Occidental source occurred during this time. The relatively long lag time, seen also in the zircons from the modern river sediments, is connected with a regional exhumation during the Eocene-Early Oligocene orogenic growth (Fig. 8). Although younger events have been identified through AFT analysis (Spikings et al., 2001), young zircon ages associated with them are not apparent because they have not yet been exhumed to the surface.

ACKNOWLEDGEMENTS

This work was supported by the Swiss Science Foundation Grants No. 21-050844.97 and 20-056794-99. The reviewers John Aspden and Roberto Barragán are thanked for their constructive comments on an earlier version of the manuscript.

REFERENCES

Baldock, J.W., 1982. Geología del Ecuador: Boletín de Explicación del Mapa geológico de la Républica del Ecuador. Dirección General de Geología y Minas, Quito, Ecuador, 70pp.

Balkwill, H.R., Rodrigue, G., Paredes, F.I., Almeida, J.P., 1995. Northern part of the Oriente Basin, Ecuador: reflexion seismic expression of structures. American Association of Petroleum Geologists Memoir 62, 559–571.

Barragán, R., Baby, P., Duncan, R., 2005. Cretaceous alkaline intra-plate magmatism in the Ecuadorian Oriente Basin: geochemical, geochronological and tectonic evidence. Earth and Planetary Science Letters 236, 670–690.

Barragán, R., Christophoul, F., White, H., Baby, P., Rivadeneira, M., Ramírez, F., Rodas, J., 2004. Estratigrafia secuencial del Cretacio de la Cuenca Oriente del Ecuador. In: Baby, P., Rivadeneira, M., Barragan, R. (Eds.), La Cuenca Oriente: Geologia y Petroléo, vol. 144. Traveaux de l'Institut Français d'Etudes Andines, pp. 45–68.

Brandon, M.T., 1992. Decomposition of fission-track grain-age distributions. American Journal of Science 292, 535–564.

Brandon, M.T., 1996. Probability density plot for fission-track grain-age samples. Radiation Measurements 26, 663–676.

Brandon, M.T., Roden-Tice, M.K., Garver, J.I., 1998. Late Cenozoic exhumation of the Cascadia accretionary wedge in the Olympic Mountains, NW Washington State. Geological Society of America Bulletin 110, 985–1009.

Bristow, C.R., Hoffstetter, R., 1977. Ecuador. In: Hoffstetter, R. (Ed.), Lexique Stratigraphique International (2e éd.), vol. 5. Centre national de la recherche scientifique (CNRS), Paris, 410pp.

Christophoul, F., Baby, P., Dávila, C., 2002a. Stratigraphic response to a major tectonic event in a foreland basin: the Ecuadorian Oriente basin from Eocene to Oligocene times. Tectonophysics 345, 281–298.

Christophoul, F., Baby, P., Soula, J.-C., Rosero, M., Burgos, J., 2002b. Les ensembles fluviatiles néogènes du bassin subandine d'Equateur et implications dynamiques. Comptes Rendus Geoscience 334, 1029–1037.

Christophoul, F., Burgos, J.D., Baby, P., Soula, J.-C., Bès de Berc, S., Dàvila, C., Rosero, M., Rivadeneira, M., 2004. Dinàmica de la Cuenca de antepaìs Oriente desde el Paleògeno. In: Baby, P., Rivadeneira, M.,Barragán, R. (Eds.), La Cuenca Oriente. Geología y Petróleo. Petroecuador, Quito-Ecuador, 295pp, ISBN 9978-43-859-9.

Cosma, L., Lapierre, H., Jaillard, E., Laubacher, G., Bosch, D., Desmet, A., Mamberti, M., Gabriele, P., 1998. Pétrographie et géochimie des unités magmatiques de la Cordillère occidentale d'Equateur (0°30′S): implications tectoniques. Bulletin de la Société Géologique de France 169, 739–751.

Dashwood, M.F., Abbotts, I.L., 1990. Aspects of the petroleum geology of the Oriente Basin, Ecuador. In: Brooks, J. (Ed.), Classic Petroleum Provinces, vol. 50. Geological Society of London Special Publication, pp. 89–117.

DeCelles, P.G., Giles, K.A., 1996. Foreland basin systems. Basin Research 8, 105–123.

Ego, F., Sébrier, M., Lavenu, A., Yepes, H., Egüez, A., 1996. Quaternary state of stress in the Northern Andes and the restraining bend model for the Ecuadorian Andes. Tectonophysics 259, 101–116.

Egüez, A., 1986. Evolution Cénozoique de la Cordillère Septentrionale d'Equateur: les minéralisations associées. Unpublished Ph.D. thesis. Université Pierre et Marie Curie, Paris, 116pp.

Faucher, B., Savoyat, E., 1973. Esquisse géologique des Andes de l'Equateur. Revue de Géographie Physique et de Géologie Dynamique 15, 115–142.

Galbraith, R.F., 1981. On statistical models for fission-track counts. Mathematical Geology 13, 471–478; reply, pp. 485–488.

Galbraith, R.F., Laslett, G.M., 1993. Statistical models for mixed fission-track ages. Nuclear Tracks Radiation Measurements 21, 459–470.

Garver, J.I., Brandon, M.T., Roden-Tice, M., Kamp, P.J.J., 1999. Erosional denudation determined by fission-track ages of detrital apatite and zircon. In: Ring, U., Brandon, M.T., Willett, S., Lister, G. (Eds.), Normal Faulting, Ductile Flow, and Erosion, Exhumation Processes, vol. 154. Geological Society of London Special Publication, pp. 283–304.

Green, P.F., 1981. A new look at statistics in fission-track dating. Nuclear Tracks and Radiation Measures 5, 77–86.

Harman, R., Gallagher, K., Brown, R., Raza, A., 1998. Accelerated denudation and tectonic/geomorphic reactivation of the cratons of northeastern Brazil in the Late Cretaceous. Journal of Geophysical Research 103, 27091–27105.

Hubert, J.F., 1962. A zircon-tourmaline-rutile maturity index and the interdependence of the composition of heavy mineral assemblages with the gross composition and texture of sandstones. Journal of Sedimentary Petrology 32, 440–450.

Hughes, R.A., Pilatasig, L.F., 2002. Cretaceous and Tertiary terrane accretion in the Cordillera Occidental of the Andes of Ecuador. Tectonophysics 35, 29–48.

Hungerbühler, D., Steinmann, M., Winkler, W., Seward, D., Egüez, A., Peterson, D.E., Helg, U., Hammer, C., 2002. Neogene stratigraphy and Andean geodynamics of southern Ecuador. Earth-Science Reviews 57, 75–124.

Hurford, A.J., Green, P.F., 1983. The zeta calibration of fission-track dating. Chemical Geology 1, 285–317.

Jaillard, E., 1997. Sintesis Estratigrafica del Cretaceo y Paleogeno de la Cuenca Oriental del Ecuador. Convenio ORSTOM-Petroproduccion, Quito, 164pp.

Jaillard, E., Ordoñez, M., Benítez, S., Berrones, G., Jiménez, N., Montenegro, G., Zambrano, I., 1995. Basin development in an accretionary, oceanic-floored forearc setting: southern coastal Ecuador during late Cretaceous to late Eocene times. In: Tankhard, A.J., Suárez, R., Welsink, H.J. (Eds.), Petroleum Basins of South America, vol. 62. American Association of Petroleum Geologists Memoir, pp. 615–631.

Kerr, A.C., Aspden, J.A., Tarney, J., Pilatasig, L.F., 2002. The nature and provenance of accreted oceanic terranes in western Ecuador: geochemical and tectonic constraints. Journal of the Geological Society of London 159, 577–594.

Lapierre, H., Bosch, D., Dupuis, V., Polvé, M., Maury, R.C., Hernandez, J., Monié, P., Yeghicheyan, D., Jaillard, E., Tardy, M., Mercier De Lépinay, B., Mamberti, M., Desmet, A., Keller, F., Sénebier, F., 2000. Multiple plume events in the genesis of the peri-Caribbean Cretaceous oceanic plateau province. Journal of Geophysical Research 105, 8403–8421.

Litherland, M., Aspden, J.A., Jemielita, R.A., 1994. The metamorphic belts of Ecuador. British Geological Survey, Overseas Memoir 11, 147.

Luzieux, L.D.A., Heller, F., Spikings, R., Vallejo, C.F., Winkler, W., 2006. Origin and Cretaceous tectonic history of the coastal Ecuadorian forearc between 1°S–4°S: paleomagnetic, radiometric and fossil evidence. Earth and Planetary Science Letters 249, 400–414.

Mange, M.A., Maurer, H.F.W., 1992. Heavy Minerals in Colour. Chapman and Hall, London, 147pp.

Mello, M.R., Koutsoukos, E.A.M., Erazo, W.Z., 1995. The Napo Formation, Oriente Basin, Ecuador: hydrocarbon source potential and paleoenvironmental assessment. In: Katz, B.J. (Ed.), Petroleum Source Rocks. Springer-Verlag, New York, pp. 167–181.

Rivadeneira, M., Baby, P., 1999. La Cuenca Oriente: Estilo Tectónico, Etapas de Deformación y Caracteristicas Geológicas de los Principales Campos de Petroproducción. Convenio ORSTOM-Petroproducción, Quito, 88pp.

Romeuf, N., Aguirre, L., Soler, P., Féraud, G., Jaillard, E., Ruffet, G., 1995. Middle Jurassic volcanism in the Northern and Central Andes. Revista Geológica de Chile 22, 245–259.

Ruiz, G., 2002. Exhumation of the northern Sub-Andean Zone of Ecuador and its Source Region: A Combined Thermochronological and Heavy Mineral Approach. Unpublished Ph.D. thesis. ETH-Zurich, 260pp (http://e-collection.ethbib.ethz.ch/)

Ruiz, G.M.H., Seward, D., Winkler, W., 2004. Enhancing detrital radiogenic provenance studies towards understanding geodynamic development of hinterland orogens: an example using zircon fission-track analysis from the northern Ecuadorian Sub-Andean Zone. Basin Research 16, 413–430.

Shanmugam, G., Poffenberger, M., Toro Alava, J., 2000. Tide-dominated estuarine facies in the Hollin and Napo (''T'' and ''U'') formations (Cretaceous), Sacha Field, Oriente Basin, Ecuador. American Association of Petroleum Geologists Bulletin 84, 652–682.

Spikings, R.A., Winkler, W., Seward, D., Handler, R., 2001. Along-strike variations in the thermal and tectonic response of the continental Ecuadorian Andes to the collision with heterogeneous oceanic crust. Earth and Planetary Science Letters 186, 57–73.

Thomas, G., Lavenu, A., Berrones, G., 1995. Evolution de la subsidence dans le Nord du bassin de l'Oriente équatorien (Crétacé supérieur à Actuel). Comptes Rendu Géodynamique 320, 617–624.

Tschopp, H.J., 1953. Oil exploration in the Oriente of Ecuador. American Association of Petroleum Geologists Bulletin 37, 2303–2347.

Vallejo, C., Hochuli, P.A., Winkler, W., Von Salis, K., 2002. Palynological and sequence stratigraphic analysis of the Napo Group in the Pungarayacu 30 well, Sub-Andean Zone, Ecuador. Cretaceous Research 23, 845–859.

Vallejo, C.F., Spikings, R., Luzieux, L., Winkler, W., Chew, D., Page, L., 2006. The early interaction between the Caribbean Plateau and the NW South American Plate. Terra Nova 18, 264–269.

Van der Plas, L., 1962. Preliminary note on the granulometric analysis of sedimentary rocks. Sedimentology 1, 145–157.

Weaver, C.E., 1963. Interpretative value of heavy minerals from bentonites. Journal of Sedimentary Petrology 33, 343–349.

White, H.J., Skopec, R.A., Ramirez, F.A., Rodas, J.A., Bonilla, G., 1995. Reservoir characterization of the Hollin and Napo Formations, Western Oriente Basin, Ecuador. In: Tankard, A.J., Suárez, S.R., Welsink, H.J. (Eds.), Petroleum Basins of South America, vol. 62. American Association of Petroleum Geologists Memoir, pp. 573–596.

Willett, S., Beaumont, C., Fullsack, Ph., 1993. Mechanical models for the tectonics of doubly vergent compressional orogens. Geology 21, 371–374.

Winkler, W., Galetti, G., Maggetti, M., 1985. Bentonite im Gurnigel-, Schlieren- u. Wägital-Flysch: Mineralogie, Chemismus, Herkunft. Eclogae geologicae Helveticae 78, 545–564.

Winkler, W., Villagómez, D., Spikings, R.A., Abegglen, P., Tobler, St., Egüez, A., 2004. The Chota Basin and its significance for the inception and tectonic setting of the Inter-Andean Depression in Ecuador. Journal of South American Earth Sciences 19, 5–19.

Zambrano, I., Ordoñez, M., Jiménez, N., 1999. Micropaleontología de 63 Muestras de Afloramientos de la Cuenca Oriental Ecuatoriana. Informe Tecnico No. 016-PPG-99, LABOGEO, Petroproducción, Guayaquil, 67pp.

Zeitler, P.K., Johnson, N.M., Briggs, N.D., Naeser, C.W., 1986. Uplift history of the NW Himalaya as recorded by fission-track ages on detrital Siwalik zircons. In: Huang, J. (Ed.), Proceedings of the Symposium on Mesozoic and Cenozoic Geology in Connection of the 60th Anniversary of the Geological Society of China. Geological Publishing House, Beijing, pp. 481–496.

3.2 The Use of Heavy Minerals in Interdisciplinary Research

3.2.1 Forensic Science—Evidence from Heavy Minerals in Criminal Investigation

This page intentionally left blank

Chapter 37

HEAVY MINERALS IN FORENSIC SCIENCE

SKIP PALENIK

Microtrace, 1750 Grandstand Place, Elgin, IL 60123, USA

ABSTRACT

The study of heavy minerals can provide information of significance in forensic investigations involving microscopic trace evidence derived from sand, soil and dust. Special techniques are frequently necessary to recover the minute quantities of accessory minerals that are typical of such evidence and these are described along with the precautions that must be observed when working under legal scrutiny. Identification of the minerals themselves follows well-established petrographic methods. Several examples show the use of heavy mineral evidence in actual cases.

Keywords: forensic geology; trace evidence; mineralogy; geographic sourcing; polarized light microscopy; heavy minerals

1. INTRODUCTION

Forensic science, simply stated, is the application of science to the law, and it follows from this that forensic geology deals with geological disciplines and techniques as they apply in legal matters (Murray, 2004). In this contribution it will be defined more narrowly still and confined to criminal investigations, court proceedings and to studies undertaken for the purpose of gathering intelligence. In these instances heavy minerals can be regarded as another type of microscopic trace evidence (i.e., particulate evidence), the identification and comparison of which may be helpful in forensic matters.

Locard's Exchange Principle provides the fundamental basis for collecting, analysing and comparing particles of microscopic evidence. It was described, in principle, by Edmond Locard of Lyon, France in the 1920s and formally stated in its present form by Nickolls (1956) as follows: "*Whenever two objects come into contact there is always a transfer of material*".

Developments in Sedimentology, Vol. 58, 937–961

ISSN: 0070-4571/doi:10.1016/S0070-4571(07)58037-4

The quantity of material transferred may be so small as to escape detection, or the decay rate may be such that all evidence of transfer is lost before the objects carrying the transferred matter are subjected to examination, but nevertheless the transfer will have occurred. The validity of this principle has been confirmed by numerous experiments (primarily with fibres) carried out during the last 50 years. Based on this principle, present-day forensic scientists collect, isolate, identify and compare microscopic trace evidence for the purpose of establishing connections between victims and suspects, between persons and locations, between persons and vehicles, etc.

This evidence may be used in one of two ways, although the myriad ramifications arising from these are too varied to be discussed here in specific cases. Most often the results of positive associations of this type are used at trial. This constitutes the most common forensic use of microscopic trace evidence. For example, the soil on a suspect's shoe might be compared with the soil from the scene of the crime. A correspondence of the components of both soils would indicate that the suspect had been at the crime scene or another location that had exactly the same type of soil. In this regard it is helpful if the suspect can provide an explanation of the source of the soil. Such *alibi samples* are particularly helpful in comparative examinations of this type. If the soil from the site, indicated by the suspect as the source, has the same type of soil as that found on his shoe, then it is likely he is telling the truth. If the soil is different from that found at the alibi site and is essentially identical to that from the crime scene, then it indicates that he/she may not have been straightforward and could well have been at the scene as suspected.

Forensic examinations conducted for the purpose of aiding in an investigation (i.e., developing investigative leads) are more rarely undertaken than comparative ones. These investigations are typically more difficult since the purpose is to describe an unknown location based only on the internal evidence that the sediment itself (and usually a very small sample) can provide. In the most favourable cases it may be possible to achieve the ultimate goal of naming the location or at least several likely ones (Palenik, 1979). Balancing the difficulty, however, is the knowledge that the conclusions drawn do not necessarily have to withstand the scientific and legal rigour necessary when providing evidence in court at a trial. The purpose here is to help provide direction in an active investigation. As an example, we might consider the case of a kidnap victim, still missing. We can imagine the police intercepting the vehicle of a suspect who turns up to collect the ransom. If an examination of the wheel wells show a buildup of dirt, it may be possible to arrive at conclusions as to the off road location where the soil originated by subjecting it to a thorough separation and analysis of the soil components. If the clumps of soil are stratified, these may be separated and it may be possible to construct a route based on the composition of these strata and their relative locations with respect to the order in which they were deposited. In all these investigations it must be possible to perform the separations and analyses with the small samples typically available for study.

This contribution is intended (1) to illustrate the role of heavy minerals in forensic investigations involving sediments and dust, (2) to describe the techniques developed to perform these examinations on the small samples typically available, (3) to define the criteria for acceptance of the results of heavy mineral analyses in court and (4) to provide examples of such analyses in practice.

2. HEAVY MINERALS AS EVIDENCE

2.1. General Principles and Commonly Used Techniques of Forensic Soil Analysis

Heavy minerals are normally studied for forensic purposes when they occur as components of earth or building materials. They can provide useful evidence for both comparative purposes and as a source of information when trying to develop investigative leads. Forensic scientists have been slow to exploit heavy minerals, however, since laboratory personnel, even those assigned to work on geological evidence, are more likely than not to have been trained as chemists rather than in mineralogy or sedimentary petrology. As a result, techniques such as density gradient, trace element analysis and particle size distribution are more likely to be used in some laboratories than methods that rely on mineralogy.

The density gradient technique is still used in some jurisdictions in the United States because of its ease in use, visual appeal and its association with Kirk (1951), who introduced it into criminalistics. Chaperlin and Howarth (1983) have critically reviewed this technique and concluded that it should not be used as proof that two soils could have originated from the same source. The present author prepared and used a large number of density gradient tubes as part of a science fair project to compare soils in the 1960s. The coloured, high refractive index minerals that were recovered from the bottoms of these tubes first awakened his interest in using the polarising microscope for the examination of soils for forensic purposes. Although the density gradient has been discredited as a definitive technique for soil comparison, it can be useful in separating fractions on the basis of their densities from small quantities of fine sands and soils and in the analysis of dust traces. McCrone and Hudson (1969) described a useful and easy to use apparatus for this purpose.

Trace element analysis of soils and sands is used to conduct comparisons in a number of laboratories. These analyses are typically performed using atomic absorption (AA) spectroscopy or Inductively Coupled Plasma/Mass Spectrometry (ICM/MS). Trace element analysis is occasionally helpful in this field (Pye and Blott, 2004) but it can be difficult to interpret the results for comparative purposes without extensive sampling and analysis of surrounding sediments. As a technique for developing investigative leads it is almost entirely useless, unless the area indicated is one that has been extensively studied in the past or contains unusual elements, elemental concentrations or unusual combinations of elements. If these techniques are performed on evidence without preliminary microscopical or X-ray analysis there is a very strong possibility (bordering on inevitability) that important evidence will be lost when the sediment is dissolved.

One of the attractions of particle size distribution analysis is its relative simplicity. Although sophisticated instrumentation is available (Blott et al., 2004), simple sieving and/or elutriation are often adequate to obtain sufficiently accurate and precise size distribution data for forensic purposes. While particle size is often an important and useful tool in general soil science, its value is more limited when applied to forensic evidence samples that are more often than not far from ideal in both quantity and purity. Separation of a sediment sample into size fractions for the purpose of concentrating specific components is, in most cases, a more valuable forensic exercise than obtaining a highly accurate particle size distribution.

There is growing awareness in forensic laboratories throughout North America, Europe and Japan that a particle-by-particle approach to soil comparison and analysis holds more promise than bulk analytical methods such as those just described (Graves, 1979). The value of this approach lies in the fact that soil is a mixture of natural (geological, floral, faunal) and anthropogenic components that are unique (or nearly so) to a particular location. The size of a location that shares all of the individual components that determine such units is variable. It may encompass tens or hundreds of square kilometres in rural areas (e.g., the Badlands of the western U.S.) or vary over distances of less than 1 m or even a few centimetres at a construction site in a city.

2.2. Sources of Geological Evidence

Evidence of a geological nature may be obtained from an almost unlimited variety of sources. Evidence received by the author includes the following examples.

Soil stains on clothing
These are typically concentrated on the knees of trousers and elbows of shirts and jackets, although such stains can be found almost anywhere. Sampling of these stains must be carefully considered before diving in blindly to isolate specimens for analysis. It is always helpful to examine these stains under a stereomicroscope before taking samples. Thick crusts may sometimes be detached intact. In other instances a good sample might be obtained by scraping and sometimes it is helpful to simply tie a rubber band around the stain and immerse it in a beaker placed in an ultrasonic bath.

Mud clumps on shoes
These are normally located on the soles but samples have included crusts on the surfaces of shoes and clumps stuck between the sole and upper portions of the shoes that corresponded, in one case, with toe holes in the grass where a victim had been raped and murdered. Soil stuck to shoes may often be found in the region between the heel and the sole or stuck in the crevices of soles with treads. The analyst must be especially careful when recovering specimens from locations such as these because they are often stratified and potentially valuable information may be lost if the sediment is simply scraped away. Mixed sediments that cannot be confidently separated are normally unsuitable for analysis for any forensic purpose.

Mud on vehicles
Soil from floor mats is normally of little value for either comparison or for developing investigative leads. The reason, of course, is that the soil from these almost always originates from a variety of sources. In some circumstances it may be necessary to pick out and examine distinctive clumps of dried mud. Helpful information may be obtained in this way but a high degree of caution must be exercised in drawing conclusions from the analysis of such samples. The circumstances of the particular case will determine if such an analysis should even be attempted.

More promising are individual clumps of dried mud found on door thresholds, bumpers, the undercarriage and the wheel wells. Such samples, especially those from

the undercarriage and wheel wells, are often stratified and may often yield valuable information when properly sampled and carefully examined.

Dried clumps of mud whether from shoes, vehicles or other sources must be carefully handled and given a thorough preliminary examination before beginning the analysis. Special attention must be taken first of all to determine the presence of layers or mixing. Frei-Sulzer (1949) has described a practical method that has been adopted by the present author for softening and sectioning layered clumps. Mixed clumps can frequently be separated as well when the various components are recognised by differences in their colour, texture or admixtures of discrete particles. After recognising and determining the locations and extent of the individual layers, they must be carefully separated. This should always be done while examining under a stereomicroscope or illuminated magnifier by gently teasing the layers apart after softening them with drops of water. In this way delicate plant tissues such as fragile leaf fragments may be softened and separated intact for study. Simply cutting through the layers while dry would cause the loss of brittle plant tissues by breaking them into little pieces.

Bags or containers of sand or building materials

These have included bags of sand substituted for a container of cigarettes shipped to South America from the U.S., substitution of sand for recovered silver flake shipped across the U.S. from Denver to the East Coast, cement blocks substituted for computers manufactured in Texas and sent to Argentina and brick particles recovered from the shirt of a suspect believed to have chipped out security bars from a brick wall before entering a building to murder a young woman. Each of these samples presented particular challenges in terms of sampling and analysis. The methods used in sampling and studying some of these are described in the examples given at the end of this contribution.

While this list is not complete, it is illustrative of the types of geological samples that the forensic scientist can expect to be called upon to investigate. Since each case presents its own special challenges, the analyst can normally assume little and must keep an open and inquiring mind. Sample poverty and impurity will be about the only things one can count on in the majority of cases.

2.3. Legal Requirements

Although requirements vary widely depending on local laws, samples taken as evidence, whether they be questioned material or exemplars for comparison, must be collected in such a way that they can be traced back to their sampling origin. This relates back to the universal legal requirement of *chain-of-custody*. If evidence cannot be traced back to its point of collection, and if its security since it was collected cannot be vouched for, it is almost certain that it will be challenged and disallowed in court. Minimum requirements are that the sample be sealed after packaging and clearly labelled with the location where the sample was taken (this must be clear and unambiguous), the name of the collector, the time and date of collection and a case number and/or name. Packages should be sealed (after drying, if necessary) and the tape should be initialled to prevent (or more accurately, in most cases, to prevent the appearance of) tampering.

In the laboratory, the examiner opening the evidence for the first time will note the fact that the seals were intact when received and the information from the label. Whenever possible packages are opened (cutting if necessary) at locations other than the seals so that the seal integrity may be preserved. All subsets of the evidence (beakers, slides, filters, etc.) must be carefully labelled to prevent mix-ups and a clear and careful record kept in the laboratory notebook. Unless express directions are received from the authorities with overall responsibility for the investigation, none of the evidence must be destroyed or discarded after the laboratory investigation is completed. Scientific evidence is almost always subject to review by the opposing side in a criminal case and it is expected that all evidence will be available to their experts for review should they decide to do so. The condition of the evidence will be noted and, as might be expected, will be commented upon. Evidence that is well prepared (clean slides in good condition and well and legibly labelled vials of cleaned mineral separates, etc.) will make a good impression and reflect on the general quality of work performed by the laboratory that first analysed the evidence. Poorly labelled and prepared slides, notes, etc. will produce the opposite effect.

Documentation is essential in all forensic work. Insofar as possible the analyst will be asked to provide proof of the statements that are proffered. While laboratory notes will be subject to review, it is often helpful, and in many cases essential, to obtain documentary proof in the form of photomicrographs, spectra, etc. Photomicrographs can dramatically aid in the presentation of microscopical evidence; both to a judge and jury in the courtroom and also to a prosecutor or defence attorney prior to trial. An easel with a display of high quality photomicrographs (with, e.g., grains from the questioned evidence on one side and corresponding minerals from the suspected source on the other) provides a helpful visual aid for explaining a difficult concept to a lay jury. In this way the members of the jury can see for themselves what the microscopist has seen through the lens that led to his/her conclusion even if they must rely on the expert to interpret the results for them.

Before leaving the topic of sediments as evidence, it is important to address the issue of exemplar samples. Since the majority of soil examinations are comparative, it follows that the analyst must have samples to compare the questioned sample (i.e., the evidence in question) to. It is rare that the forensic scientist will collect these samples. This is almost always done by crime scene specialists or investigators. One of the biggest mistakes made by investigators, who typically collect both questioned and known evidence, is to collect poor soil standards for comparison. Since soil changes both laterally and vertically, improper collection may have profound consequences on the results of such a comparison. It is important that the crime scene technician or investigator understands both the importance and implications of sample collection in each particular case. For example, he or she must understand that if a soil stain on the knees of a pair of trousers is to be compared with the soil at the location where the suspect is believed to have kneeled on the ground, the known sample must be taken from the suspected location by gently scraping only the surface at that spot. If, on the other hand, the suspect dug a hole and buried something and the soil is to be compared with mud clumps on a shovel found in his garage then sampling must be adjusted accordingly. It is most important, though often neglected, that known samples should always be obtained, whenever possible, to provide the *alibi* sample mentioned earlier. This is a sample taken from the location that the

suspect has volunteered as the source of the mud on his shoes, clothing, car, motorcycle, etc. The workup and comparison of the questioned soil to this sample is almost always extremely helpful in interpreting the results of any comparative soil examination.

To conclude this section, a few words about the role of the forensic scientist as expert witness might be of value. In the United States, law expert witnesses are given permission to offer opinions on the witness stand, an option not open to other witnesses who may only testify about facts. For scientists, the test is that the opinion must be held "*to a reasonable degree of scientific certainty.*" This gives the testifying scientist a serious responsibility and it is essential that expert scientific witnesses realise that their role is not to help prosecution or defence but to inform the court in an honest manner about the results of their scientific examinations and their interpretation of those results to the best of their ability. The experts will often be asked by opposing counsel if the facts may not suggest more than one interpretation. They should listen carefully to the question and weigh it in the light of the facts known to them before answering in a thoughtful and honest manner. In this way they will be performing their duty to the court and setting an example for the role of science in the criminal justice system.

3. LABORATORY STUDY OF MINERALOGICAL EVIDENCE FOR FORENSIC PURPOSES

Once received in the laboratory, the evidence must be processed to separate and concentrate the various fractions. It will be assumed for the remainder of this contribution that the forensic scientist has chosen to pursue a petrographic approach to the investigation. Because one never knows at the outset which characteristics of the soil or sediment may be most useful in characterising it for comparison or attempting to determine its origin so as to provide an investigative lead, and since the evidential sample will almost always be smaller than one would like, it is essential to have a plan for conducting the preliminary separations that will meet all of the—sometimes conflicting—requirements associated with the various components of a typical soil.

Petrographers have their own tested methods for isolating the light and heavy mineral fractions of sediments. Palynologists have their own techniques for isolating palynomorphs from a soil and archaeologists have yet their own procedures to separate opal phytoliths (tiny, three-dimensional copies of plant cells created by a plant as a product of taking in water with dissolved silica) from samples taken from study sites. Most of these specialist methods permit isolation of the particles of interest by destroying particles of no interest to them, or begin with an unrealistically large quantity of starting material. Thus petrographers often recommend beginning with a kilogram of starting sample that is riffle-split into a smaller sample that is washed, sieved and fractionated in a separation funnel. Other fractions may be saved for particle size analysis but the organic fraction is of little or no interest. The palynologist, on the other hand, is content to employ hydrochloric acid to dissolve the calcareous minerals and hydrofluoric acid to dissolve the siliceous ones to isolate and concentrate the pollen and spores that constitute his/her specimens of study.

The forensic microscopist cannot afford to loose any of the particles that typically constitute the entire sample available for analysis; let alone dissolve or destroy one component to concentrate another. With this in mind the author developed, some years ago (Palenik, 1984), a scheme of analysis for forensic soil samples that concentrates various components by class and can be applied to the small samples typically encountered in actual casework. The procedures have been continually modified since that time, as study, research and real-life casework suggested useful changes. The technique was not devised as a rigorous method that must be adhered to in all cases, but a model for teaching the subject of forensic soil examination by microscopy. By applying this method, as one learns to conduct such investigations, the student is exposed to the variety of components that together characterise a soil or sediment from a particular location. Having developed an appreciation for these components during their education, forensic soil examiners should be able to tackle not only the routine but the most difficult samples as a scientist, who can make changes in procedures as circumstances warrant, and not as a technician who merely follows the flow-charts. It is fully expected that the forensic microscopist, who has learned to separate the various fractions of a minute sample of geological evidence and to isolate and identify the various components therein, will make deviations from the scheme suggested here, as well as completely ignore certain fractions that do not apply to the case in hand or will not provide information that will further the investigation. It is the author's belief, however, that this approach provides a useful starting point for the forensic scientist faced with characterising a small and irreplaceable sample of geological evidence, for the young forensic microscopist who is just learning to compare soil samples, and for the advanced worker who may intend to perform certain instrumental examinations outside the scope of this chapter on particular fractions of a soil for casework as well as pure research. Discussions with former students and other scientists who have adopted the approach outlined here have confirmed this latter point.

3.1. Preliminary Observations

The technique described here is intended to isolate soil fractions, no matter what the quantity of original sample, in a sequence that best preserves the features of each component, so that they will be in the best possible condition for subsequent analysis and identification (and, if necessary, at least relative quantification). A sequential scheme almost always requires compromises. This is recognised and the order of the separations has been arranged to minimise the effects on fraction yields and condition for most soils and sediments. As stated above, it is expected that the experienced examiner will use the procedures as a general guide, making whatever changes thought necessary based on the nature of the sample itself and the question(s) to be answered.

Fig. 1 illustrates the procedure for the preliminary separation of the sample into concentrated fractions in tabular form. As shown, the examination begins with the observation of colour and texture. Colour is best observed on the dry soil with daylight or good fluorescent lighting without the aid of magnification unless the sample size is very small. Texture is observed both with the unaided eye and with a stereomicroscope. Colour and texture are considered together because, to some

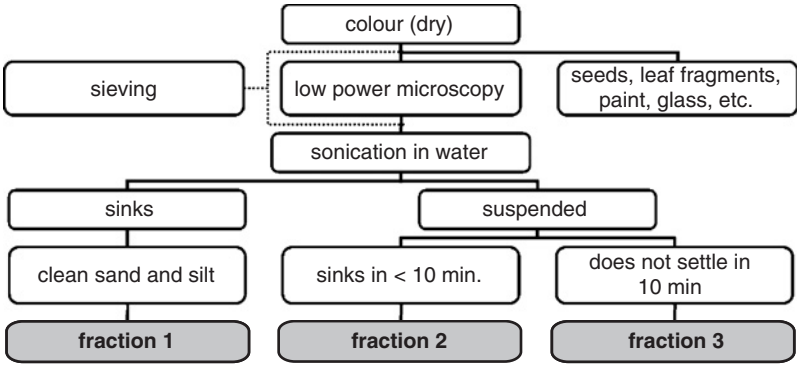

Fig. 1. Schematic flow chart of soil separation process (after Palenik, 1984).

extent, they affect each other and they are both simple to observe during the initial examination. As a general rule it can be stated that if two samples (typically, the questioned and known soils) do not have the same colour they can be excluded from sharing a common origin. In comparative soil examinations, a side-by-side comparison of colour and texture, taking the necessary precautions that the questioned and known samples cannot be mixed or contaminated, is the necessary first step. When the purpose of the examination is to develop an investigative lead in an attempt to determine the origin of an unknown soil or to describe a location from which the soil could have originated, it may be helpful to match the colour to a colour scale such as the Munsell® Soil Colour Charts or determine the colour coordinates with a spectrometer or colorimeter. Such instruments are easy to use and provide objective colour coordinates with relatively little difficulty as long as an instrument having a small measurement area is available.

Following the evaluation and comparison of colours, the sample is placed in a Petri dish or watch glass of the appropriate size and transferred to the stage of a stereomicroscope. An instrument capable of providing both darkfield (oblique) reflected and transmitted light is preferred. Clumps of soil, particularly those removed from the wheel wells of vehicles and between the heel and sole of shoes should always be inspected carefully to determine if they are composed of layers. If so, the layers must not be disturbed but exposed and then carefully separated. Gentle misting with distilled water from an atomiser, repeated over time in a closed container, can be used to soften the clump so that it can be cut with a sharp knife or razor to reveal the edges of the layers. The individual layers must then be separated by cutting, if possible, or by gentle layer by layer removal as described earlier.

If no layers are apparent, the sample is gently picked apart with needles while observing through the stereomicroscope and softening and dispersing the clump with small drops of distilled water. The water loosens the soil and delicate particles such as leaf fragments and seeds can be removed without destroying them. Rock particles, glass, paint chips, seeds, leaf fragments, shingle stones, in short, anything of potential analytical value that is larger than the mass of the soil as a whole, should be removed and transferred to the edge of the dish or to separate well slides where they can be stored until they are ready to be analysed. Some of these particles, such as

paint chips (particularly if layered) may have significant evidential value and may greatly strengthen one's conclusion. Seeds, leaves and other (relatively) larger botanical particles can provide significant environmental information when one is attempting to describe the location from which a clump of soil could have originated. Rock particles, of course, point directly to parent rock sources. If the microscopist has sufficient training, experience and reference materials in the form of books, atlases and/or physical reference specimens, he/she may undertake the identification of these materials themselves; if not, specialists must be consulted.

3.2. The Concentration of Heavy Minerals and Other Fractions from Forensic Soil Samples

A few drops of alcohol are added to the now dispersed clump of soil in the watch glass to reduce the surface tension and the suspension is then washed into a beaker with a stream of distilled water from a wash bottle. Alcohol is used in preference to surfactants since we typically analyse the aqueous extract when attempting to determine the geographic location of a sample. A detergent would interfere with that analysis. The beaker should be chosen so as to be appropriate for the size of the sample. A mud clump from a shoe may require a 250 ml beaker while a 10 ml one may be more appropriate for a mud stain recovered from the knee of a pair of trousers. The beaker is then placed in an ultrasonic bath for 2 minutes. Time in the ultrasonic bath is kept at a minimum to reduce the potential for damage to the mineral surfaces if it is anticipated that SEM study of the grain surface textures might be performed. At the end of this time the suspension is allowed to settle for approximately 1 min and the supernatant is poured off into a larger beaker. These fines are designated Fraction 2 (Fig. 2). More water is delivered into the beaker with the original sample and it is swirled and allowed to settle for a minute and again poured off into the larger beaker. This is repeated until no more fines are suspended and then a few drops of alcohol are added and the original sample is placed in the sonic bath again for 1 or 2 minutes. The settling and washing procedures are repeated and the process is continued until the sample in the original beaker consists of clean fine sand or silt: this is designated Fraction 1 (Fig. 3). A few drops of acetone are added to this fraction. If the acetone becomes coloured it indicates the presence of soluble organic compounds (typically man-made ones) and the grains are extracted sequentially with hexane and then chloroform (to extract non-polar and polar components, respectively); the extracts are saved for potential analysis by gas chromatography/mass spectroscopy or infrared microspectroscopy. In most cases the acetone will remain colourless and the sample is washed a few times to remove the remaining water and speed up drying. The beaker with Fraction 1 is then placed in a warm oven to dry.

While Fraction 1 is drying it is helpful to pipette a few drops of the sediment from the bottom of the large beaker containing Fraction 2 onto a microscope slide, cover it with a coverslip and make a brief examination with the polarising microscope. The proportions and types of minerals (calcareous, micaceous, siliceous) in the fine silt size range, presence of plant opal (phytoliths), diatoms, pollen grains, tyre rubber, etc. are noted and this information is used to determine how Fraction 2 will be treated to separate and concentrate these fractions most effectively.

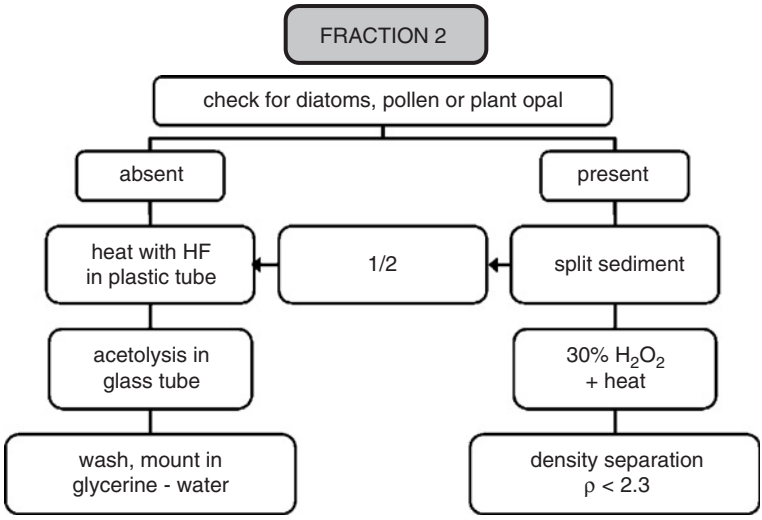

Fig. 2. Flow chart for the processing of the pollen fraction—Fraction 2.

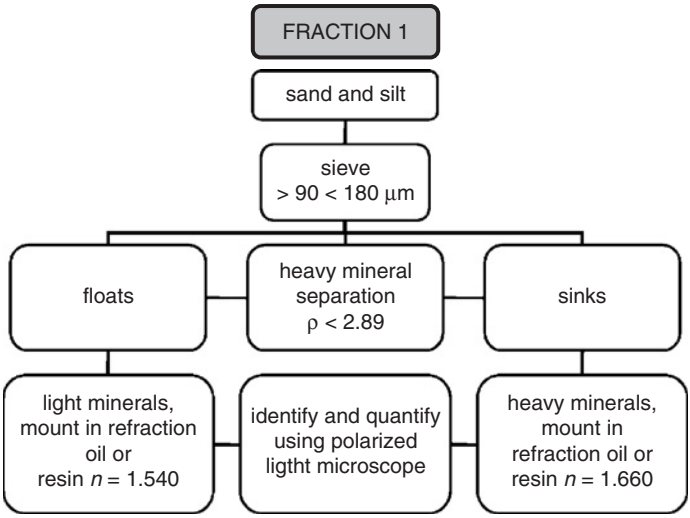

Fig. 3. Flow chart for the processing of sand and silt—Fraction 1.

Since Fraction 2 rarely contains a significant proportion of heavy minerals, its further separation and treatment will be described only briefly. The large volume of water in the beaker is poured off into large centrifuge tubes (this may require many tubes depending on the final volume of washings) and centrifuged for approximately 5 minutes in a benchtop centrifuge at ~6500 rpm. The clear supernatant (which will very likely still exhibit a Tyndall beam) is poured through a membrane filter (we typically use 0.8 or 1.2 μm pore size filters) in a filter apparatus and filtered under vacuum. The filtrate is saved, evaporated to dryness with moderate heat under a stream of nitrogen or filtered air and qualitatively analysed for soluble cations and

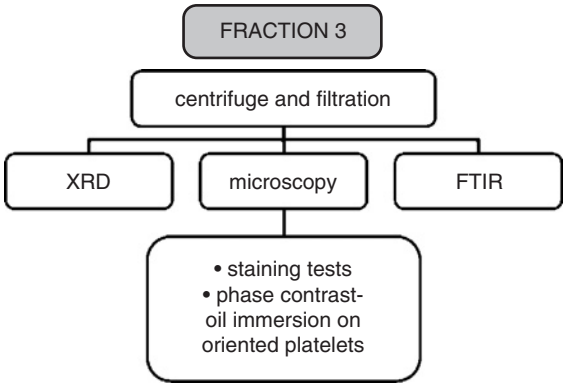

Fig. 4. Flow chart for the processing of the clay fraction—Fraction 3.

anions using microchemical tests, energy dispersive X-ray (EDS) spectroscopy (or X-ray fluorescence) and infrared spectroscopy. The clay fraction (Fraction 3) on the filter(s) is dried at room temperature or in a warm oven and examined directly by X-ray diffraction (Fig. 4). It is often useful also for forensic purposes to prepare samples of the clay for elemental analysis by EDS and to obtain the infrared spectrum on some of this fraction as a potassium bromide pellet.

The sediments in the bottom of the beaker and from the centrifuge tubes (containing Fraction 2) are combined and concentrated. Based on the reconnaissance examination, this residue is processed to either destroy most of the organic components (with concentrated hydrogen peroxide or sulphuric and/or perchloric acids) or the inorganic ones (hydrofluoric acid followed by acetolysis). If the purpose of the investigation is to geosource the sample, all—or at least a major portion—of Fraction 2, is always processed for pollen and spores. This follows the normal sequence described originally by Erdtman (1969) and consists of dissolution of the carbonates and silicates in hydrochloric and hydrofluoric acids followed by destruction of most of the organic matter by acetolysis with sulphuric acid and acetic anhydride. In addition to pollen grains and spores some other organic and anthropogenic particles such as tyre wear rubber are concentrated by this process. If the preliminary microscopical examination revealed the presence of significant or interesting diatoms, opal phytoliths, etc., one half of the residue is processed to destroy the organic matter and the remaining inorganic particles are separated and concentrated in a specially prepared density liquid or in a density gradient tube such as that described by McCrone and Hudson (1969). The preparation, identification and interpretation of these particles are outside the scope of this chapter.

Once dried, the fine sand and silt comprising Fraction 1 are passed through a set of small sieves if at all possible (Fig. 5a) unless the sample is too small. Dry sieving is performed first over a pan followed by wet sieving with water (to which a few drops of acetone or alcohol are added) over a small Hirsch funnel which holds a 1.5 mm filter on a filter flask connected to an aspirator. Each sieve, starting with the coarsest, is sequentially removed as it is examined and washed with acetone to help the grains pass through the fine mesh openings which are otherwise plugged with water held in place by surface tension. After all the sieves are removed, the 90 μm size fraction on

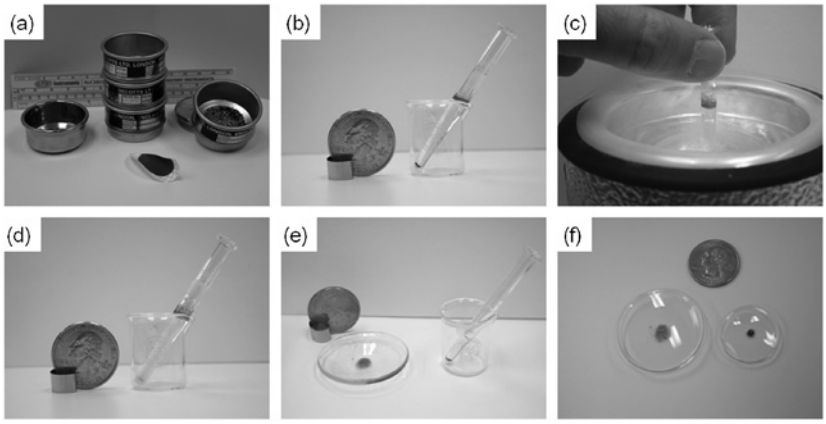

Fig. 5. One inch (2.5 cm) diameter sieves and filter with the size fractions separated (a), and heavy mineral separation of a small sieve fraction with bromoform in a 0.5 ml microcentrifuge tube (b–f).

the filter is gently washed with acetone as well and then the sieves and filter are placed in a warm oven to dry.

The coarser fractions may be examined under the stereomicroscope, thin section grain mounts may be prepared and larger quartz grains might be picked out and studied with the SEM. Experience has shown that evidence-sized samples are generally confined to the smaller size ranges. Our "routine" size fractions for mineralogical analysis are the 90–180 μm and <90 μm fractions. Fortunately, not only do these fractions normally contain the majority of the heavy mineral suite, they typically constitute the majority of the soil or sediment fraction that sticks to clothing in the form of mud stains. Minerals in this size range are also most convenient to study as grain mounts with the polarising microscope and are readily isolated should further analysis by instrumental techniques become necessary for identification.

Fraction 1 is now ready to be separated into heavy and light fractions. Because the amount of material available from an evidence sample is almost always too small to use either conventional separating funnels or standard centrifuge tubes for the heavy mineral separation, we use small glass centrifuge tubes of 12, 3, 2 or 0.5 ml capacity; the size chosen depending on the size of the fraction we wish to separate.

Figs. 5b–f illustrate an actual heavy mineral separation performed in a 0.5 ml microcentrifuge tube. Two tubes are filled approximately half way with bromoform, being careful not to wet the sides when doing so (operations with bromoform, which is toxic and a known carcinogen, should be performed in a fume cupboard). The free flowing Fraction 1 minerals are then poured into one of the tubes from a sheet of glassine weighing paper which has been creased on one side to form a trough. The weighing paper is just touched with a tuning fork (which has just been struck) to quantitatively transfer all of the grains into the tube. The tube is then stirred with a stout stainless steel wire (a straightened paper clip will do) and any grains adhering to the sides are pushed down with the others. The tube is then transferred to an

ultrasonic bath for 1/2–1 min.The tube is then centrifuged (using the other tube with bromoform to balance it) for a minute or two. After removal from the centrifuge it is then gently stirred with the wire again, and the process is repeated as necessary until the analyst is satisfied that the separation is as complete as possible. The bromoform may become deeply coloured by asphalt if this substance is present and was not removed during the washing process. The presence of asphalt may be confirmed by exposing the tube to long-wave ultraviolet light in a dark room. The appearance of a bright orange fluorescence serves to confirm asphalt. If asphalt is present the bromoform may be saved and the asphalt extracted and compared with potential source material by thin layer chromatography.

The grains should now be cleanly separated into heavy and light fractions. If the examination is of a comparative nature the fractions should have been weighed at each stage of separation. This includes the light and heavy fractions of the size ranges that were separated. A microbalance is sometimes necessary to perform the weighing because of the small quantities of heavies involved. The separation procedure begins with immersing the conical tip of the tube into a small dewar filled with liquid nitrogen and the bottom one-third of the tube is frozen solid. The light minerals are poured off into a white porcelain crucible of appropriate size and the tube is washed out with acetone making certain that the walls of the tube are washed clean. In the diluted bromoform the minerals now sink to the bottom and the crucible is swirled and the bromoform is pipetted off to another container. The light mineral fraction is washed and swirled a few more times with acetone and the washings poured into the bromoform waste. The crucible is carefully labelled and placed in a warm oven to dry. When the bromoform in the bottom of the tube melts the heavies are poured or pipetted (a 1.5 mm diameter capillary tube is used when working in a 0.5 ml centrifuge tube) out into a small white porcelain crucible and washed and swirled with acetone until free of bromoform and then labelled and dried. Both of the smallest fractions are separated in this manner. Based on the results of these operations, the analyst can choose which separations to complete on the known comparison samples.

3.3. Petrographic Examination, Characterisation, Identification and Comparison of the Heavy Mineral Suite

The heavy and light mineral suites from the two smallest size fractions are now ready for analysis. Specimen slides are prepared by transferring grains to microscope slides and applying a mounting medium. Since the quantity of light minerals is almost always many times greater than the heavies, we typically prepare two slides of these. Unless the quantity is very small, a microspatula is used to transfer grains to a slide which is covered with a circular No. $1^{1/2}$ coverslip. The circular coverslip permits easy dispersal of the grains in the mounting medium if a pencil eraser is brought into contact with it and gently rubbed out in a circular motion. No. 11/2 coverslips are chosen because their nominal thickness (0.17 mm) will prevent spherical aberration when using high dry objectives; a necessity for the petrographic examination of grains in the $<90\,\mu m$ size fraction.

The heavy mineral fraction from questioned samples will almost always be quite small in forensic work. In some cases there are barely enough grains to make one

slide; in others it might be possible to prepare two or three slides from this fraction. We have found the use of small artists brushes composed of synthetic fibres to be most useful for transferring grains from the crucible onto the microscope slide. This operation is best performed under a stereomicroscope. The grains are brushed out onto the slide which is sitting over a piece of glazed white paper so that any grains that fall off the slide can be recovered and mounted. When enough grains have been transferred to make the preparation, the brush is pressed down on the slide and splayed out. A tungsten needle is used to recover any grains that stuck among the bristles of the brush. Needless to say this operation is performed under a stereomicroscope. When all the grains are in place a coverslip is applied.

Either temporary or permanent mounts are made depending on whether or not permanence or ease of grain removal is most important. If a large number of grains are available both types of preparations may be made up. For temporary mounts we use the Cargille index of refraction oils with refractive indices of 1.540 and 1.662. For permanent mounts we use Cargille Melt Mounts®. These latter are permanently thermoplastic and grains can be removed from them at any time by warming up the slide on a hot plate and sliding off the coverslip. Either the index oils or the Melt Mount is allowed to flow under the coverslip (the latter with the slide on a hot plate) and the grains are dispersed with a pencil eraser. They are then ready for study with the polarising microscope.

In a departure from petrographic tradition we have found it helpful to mount the light and heavy mineral fractions in media of different refractive indices. The light fraction is mounted in a medium with $n = 1.540$. This has all the advantages associated with traditional mounting in Canada balsam for quartz (and its polymorphs) as well as the alkali and plagioclase feldspars. We also often prepare a slide in a medium with $n = 1.662$, since the light minerals show high contrast in this medium and details of surface texture are accentuated. This preparation often makes an SEM examination unnecessary. Another preparation method proves sometimes valuable, viz. if the sediment originates from a desert: one can then stain the grains first in an aqueous solution of methylene blue (a basic dye) for a minute or two, wash them in water and then in alcohol and finally mount them in a liquid with $n = 1.662$ or in Melt Mount. The basic dye stains the silica (in the form of silicic acid) on the grain surfaces showing the extent and thickness of the silica pellicle on the grain surfaces. The dye also stains feldspar decomposition products although other dyes are better for this purpose.

We mount the heavy mineral fraction in 1.662 Cargille oil or Melt Mount of the same refractive index. Unlike Canada balsam, in which all the heavy minerals show high contrast, minerals mounted in this high-index medium show optical effects which give immediate clues to their identification. The three principal ones are the following.

Refractive index higher or lower than the medium. Some minerals have indices less than 1.662, unlike Canada balsam which has a refractive index less than all of the heavy minerals. For example, olivine (forsterite and intermediate types) and sillimanite have one refractive index lower than 1.662 and one higher. By rotating to two adjacent extinction positions and checking Becke lines it will be found that these minerals have a higher index than the medium in one position and a lower one in the other.

Degree of contrast. Some minerals are, in a specific orientation, close to the refractive index of the mounting medium, whereas they may be far away from it in another orientation; this affects the contrast of the grain in the medium. For example, calcite crystals, whether macro- or microcrystalline, show one index slightly less than 1.662 ($\omega = 1.658$) and in this orientation exhibit very low relief (the crystals practically disappear in this orientation). In the adjacent extinction position where the index is some value of ε', the contrast will be very high and the index less than 1.662. Magnesium-containing rhombohedral carbonates (e.g., dolomite, magnesite) have $\omega > 1.662$ and exhibit low contrast but this time their refractive index is greater than that of the medium.

Dispersion. Higher refractive index minerals and immersion media both typically exhibit a greater dispersion of the refractive index, resulting in strong dispersion colours that are distinctly visible without special apparatus (e.g., a dispersion staining objective). For minerals with normal dispersion curves this means that grains close to but less than the refractive index of the mounting medium will exhibit yellow dispersion colours and minerals with a refractive index greater than but close to the index of the medium will show a blue colour around its edge. For example, apatite grains will be outlined in yellow, whereas xenotime grains will show blue edges for their lower refractive index. Zircon grains have refractive indices too high to show dispersion colours in 1.662 and will have a normal black outline. Calcite, when its ω refractive index is aligned with the polar, will be yellow but dolomite and magnesite (and siderite and rhodochrosite as well) will have blue edges since their ω refractive indices are greater than 1.662. Olivine and sillimanite have yellow outlines when their low refractive indices are aligned with the polariser and blue ones when the stage is rotated 90° to the high index position.

The microscopical examination of the heavy mineral suite is first conducted to determine its qualitative composition. Minerals are either identified or classified (characterised) at this point based on their optical properties: morphology, colour, pleochroism, relative refractive index, dispersion of refractive index, birefringence, interference figure (and estimated optic axial angle if biaxial) and optic sign. If the purpose of the examination is comparative, it may not be necessary to identify all of the minerals, for if they are well characterised it may be sufficient to prepare a list of mineral *types*. This list may be used to compare the qualitative composition of the soils to be compared or to make up *bins* if mineral counts are to be performed. It should be stated here that there will rarely be enough gains in the heavy mineral suite from a questioned evidence sample to perform a statistically significant mineral count. The quantity of minerals in the light fraction is almost always overly abundant in this respect and significant counts can always be performed on this fraction if necessary. We have found that the best we can do with the heavy minerals in most cases is to determine whether each of the minerals (i.e., each mineral and variety) in the heavy mineral suite can be found in the known sample, which should—if a sufficient sample was taken—have the full association of minerals of minerals which characterises that suite.

We have come to place perhaps more than ordinary importance on the concept of mineral variety when comparing samples by means of their heavy minerals. Thus

varieties of tourmaline, hornblende (and other amphiboles), rutile, hypersthene, etc. are each noted and carefully characterised optically. It is possible, utilising microspectrophotometry (a technique increasingly common in the forensic laboratory for comparing the colours of fibres and paints), to obtain spectrophotometric curves of the pleochroic colours of a mineral which can lend further confidence to a comparison of these minerals. Of course a simple microspectroscopic ocular will serve as well but these are no longer manufactured and unless one is already available in the laboratory the microscopist must build his/her own. We have found, however, that a modern microspectrophotometer is far more sensitive for this purpose than a microspectroscopic ocular. Microspectrophotometry is also valuable for looking at visible absorption spectra obtained from rare earth elements such as those in monazite. The identification and interpretation of the absorption bands is much easier and unequivocal with a microspectrophotometer than with a spectroscopic ocular.

Bloss (personal communication, 1999) has suggested that the spindle stage could be used to characterise the varieties of pyroxenes and amphiboles in a sediment as a means of comparison. When we feel it is necessary, particular grains are isolated by removing them from the grain mount using a tungsten needle while observing with a stereomicroscope. The isolated and washed grains can be mounted on a polished beryllium plate for EDS analysis, mounted on a needle for characterisation with the spindle stage, mounted on a polished aluminum slide for Raman microspectroscopy or for cathodoluminescence study (Palenik and Buscaglia, 2007) or on a microscope slide for fluorescence microscopy.

If the purpose of the examination is to attempt to determine the geographic origin of the sample, it is almost always necessary to identify all the minerals in the suite. In this case it is frequently necessary to pick out grains for identification and determine their actual optical properties supplemented, as necessary, with elemental and chemical information from the techniques noted in the previous paragraphs. For identification we rely on an extensive collection of known minerals that we have crushed and sieved, or personally picked out from mineral suites, characterised and identified, and books and atlases especially those by Krumbein and Pettijohn (1938), Hutton (1950), Mange and Maurer (1992) and Milner (1962). In addition to the natural minerals, the forensic microscopist expects to encounter man-made minerals as well. Thus, it is necessary that the microscopist be able to recognise and identify crystals of artificial minerals such as carborundum® and steel slag among the non-opaques and such products as welding and grinding spheres among the opaques. Naturally occurring opaque minerals are characterised optically by darkfield reflected illumination and then, if required, picked out and mounted on a beryllium for elemental analysis with EDS in the SEM.

The interpretation of the results of a microscopical comparison of a questioned and known soil(s) is a complex subject and beyond the scope of this contribution since it depends not only on the heavy mineral suites but also on all the other components of the soil, including the light minerals and the biological and anthropogenic components. It is hoped that the examples which follow will help to explain this aspect to some degree.

4. EXAMPLES

4.1. Japanese Balloon Bombs

In the fall of 1944 the Japanese military launched the first of approximately 10,000 balloon bombs (*fusen bakudan*) into the newly discovered *jet stream* towards the West Coast of the U.S. To control the elevation of the bombs (i.e., to keep them within the altitude of the jet stream) during the approximately 3-day voyage, a system was devised to release ballast bags filled with sand or to release hydrogen from the balloon envelope as necessary to raise or lower the balloon. Although the ballast bags were missing from most of the balloons that reached North America, some bags still containing the sand were recovered. Samples of this sand were brought to the Military Geology Unit of the U.S. Geological Survey in an attempt to determine the origin of the sand and thus the launching site of the bombs.

Geologists examined the mineralogy and size distribution of the sand and isolated diatoms, foraminifera and small molluscs. Each of these fractions was studied by specialists. It has proven impossible for the present author to track down any of the original reports of this project through the USGS and all of the information below comes from the open literature. One report by the mineralogist and petrographer who analysed and identified the minerals in the sand, was published in the American Mineralogist (Ross, 1950). His list of minerals shows a very unusual mineral suite that consists almost entirely of heavy minerals:

Hypersthene	52%
Augite	7%
Hornblende	8%
Garnet	1%
Magnetite	10%
Quartz phenocrysts	8%
Quartz, detrital	8%
Plagioclase (the types were also determined)	6%
Zircon	$<1\%$
Sphene	Sparse
Biotite	Rare
Hornblende schist (rock fragment)	Present
Shell material	Not included
Volcanic glass	Rare

These minerals were all in the beach sand size range, and the texture and narrow particle size distribution left no doubt that the sand originated from a beach. Based upon this mineralogy the scientists were able to determine that this could not have originated from the U.S. The military believed that the balloons might have been launched from Japanese relocation camps, German prisoner of war camps, nearby islands in the Pacific or even submarines. They had not even considered the possibility that they could have been launched from Japan.

The diatoms were studied by Ken Lohman who claimed, many years later, to have identified more than 100 species of both recent and fossil forms from the various

samples of the sand submitted (McPhee, 1997). However, the specific value of the diatoms in sourcing the sand was never specifically stated. Kathryn Lohman found foraminifers in the sand that had been described from localities north of Tokyo and from the east coast of the Japanese mainland. There is no mention in any of these accounts of the value of the molluscs, if any, in this study. The absence of coral in the samples placed the source above the 35th parallel (about that of Tokyo) since coral does not occur above that latitude. This effectively eliminated the lower third of Japan from consideration. There is also a report that a Canadian group also analysed sand from balloons that had come down in Canada (Mikesh, 1973). Their samples contained blast furnace slag which indicated that their sand came from a source near a steel mill blast furnace.

The source of the sand was eventually narrowed down to the beach at Ichinomiya which is ~65 km southeast of Tokyo. This was later confirmed (by some accounts aerial photography showed gas production apparatus and partially filled balloons on this beach) as one of three launch sites by investigators after the conclusion of the war. Fig. 6A shows a sample of the sand from Ichinomiya beach, recently collected, as it appears in *n* 1.662 Cargille index of refraction oil.

4.2. Rainbow Warrior Explosion

On 10 July 1985 two explosions ripped a hole in the hull of the Greenpeace ship *Rainbow Warrior* as it lay moored in harbour in Auckland, New Zealand (Anonymous, 1985). One person died in the explosion (trapped below the water level when the ship sank) and the ship was destroyed. The ship and crew had been attempting to foil French plans for nuclear weapons tests in the South Pacific. Eventually French intelligence agents were arrested and tried for setting the bombs. During the course of the investigation, the police recovered the camper van that had been rented by the agents as they travelled around New Zealand establishing their cover; and it was from this van that the inflatable boat, 'Zodiac', from which the raid was conducted had been launched. Geologists at the DSIR (Department of Scientific and Industrial Research New Zealand) were asked to see if they could determine the route taken by the van (and agents) as they travelled about New Zealand up to the time they launched their attack in Auckland harbour and the escape route they took afterwards.

Scientists recovered soil and debris from the wheel wells, behind the license plate and the floor of the van. A wide variety of material was obtained from these locations and all of them were carefully analysed using primarily petrographic microscopy and stereomicroscopy (Skinner, 1988). The samples obtained from the wheel wells contained chips of quartzose greywacke, fragments of white argillaceous (clayey) limestone, coiled segmented insect shells and a significant amount of quartz and feldspar grains. This composition was consistent with a road metal dump site in a small forest locality at which a witness thought he had observed the van a few days before the bombing. The road metal dumpsite was the only local occurrence of Oligocene argillaceous limestone, whereas the end of the forest road where the second possible sighting (of the van) was made over weathered early Miocene quartzose and feldspathic siltstones and sandstones. The rock from which the road metal was produced came from a single quarry and was particularly identifiable

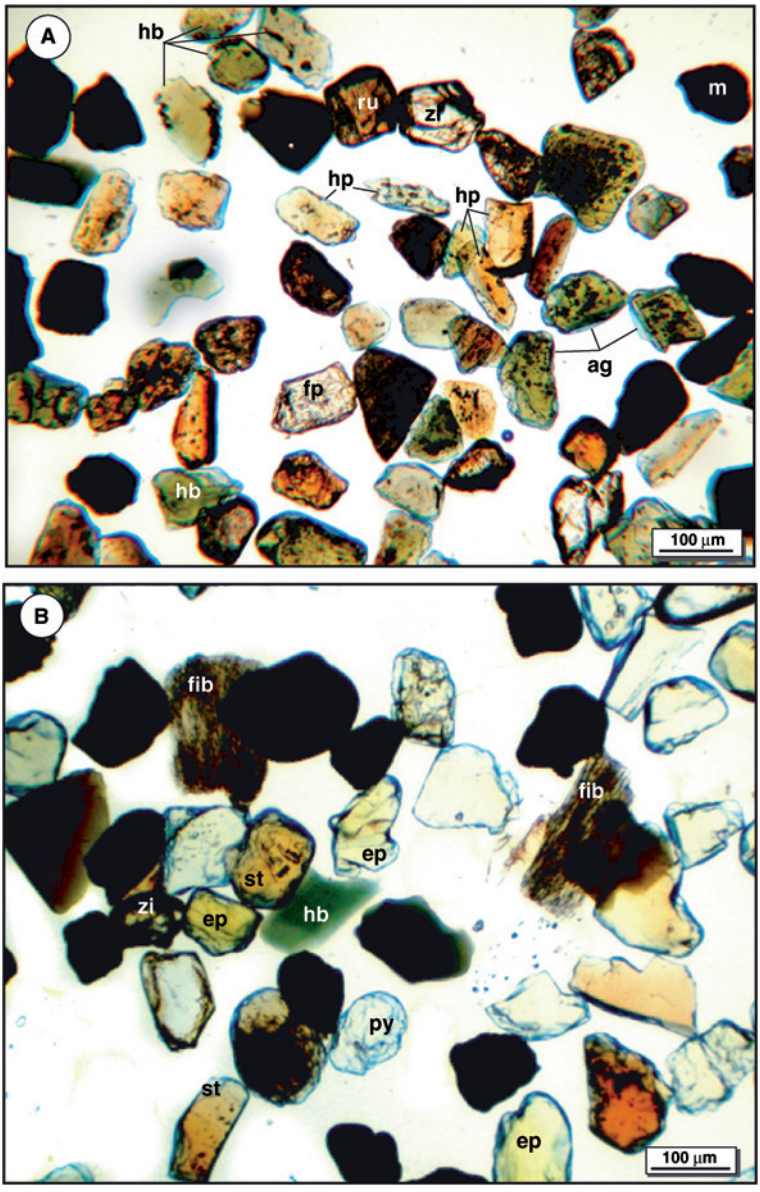

Fig. 6. Heavy mineral assemblages of key samples providing clues to forensic investigation. (A) Heavy minerals from the beach at Ichinomiya. In *n* 1.662 Cargille oil. Hb, hornblende; hp, hypersthene; ag, augite; ru, rutile; m, magnetite; fp, feldspar (showing negative relief). (B) Heavy minerals from cement blocks substituted for computers. In *n* 1.662 Cargille oil. ep, epidote; hb, hornblende; py, pyroxene; st, staurolite; zi, zircon; fib, fibrous sillimanite (fibrolite).

hard, dark and grey Mesozoic quartzose greywacke to quartzite. This location also contained the same type of cast-off coiled insect shells as those found in the soil from the wheel wells.

The samples from inside the campervan and the wheel wells contained other materials including significant amounts of magnetite, black volcanic glass, glassy and feldspathic volcanic rock fragments and angular red chert chips. In addition to these particles, the sample from behind the rear license plate also contained black sand containing quartz grains coated with magnetite, a few magnetite grains and minor hypersthene.

The license plate sand could be identified as beach sand off the west to northwest coast of Auckland and the relative mineral percentages could be related to a relatively short region of beach based on previously published studies of the sand mineralogy. This was a very popular surf beach and indicated that the French agents had taken time to visit this tourist area before carrying out their mission. The other mineral sources were located as well, once again, based on good geological mapping available for virtually all of the island. Of special interest were the red chips of chert. These were used as "sealing chip" on the Auckland waterfront road footpaths, adjacent to where the Zodiac boat had been abandoned. Thus the campervan driven by the two French agents was positively known to have driven along this road. The results of this investigation helped significantly in the investigation, preparation for trial and in the trial itself.

4.3. Substitution of Sand for Silver Flake

In 1984 we were approached by a large photographic film manufacturer in New York State to inquire if it might be possible to determine the source of a sand sample they provided (Palenik, unpublished report). The story behind this was as follows: for years they evaporated spent developing solutions from their film developing operations in Rochester, NY and sent them to a precious metals refinery in Denver, CO. The recovered silver was in the form of fine flakes and these were shipped back to New York in unguarded freight cars by rail. The silver flake itself was packaged in ordinary steel milk cans. When the most recent shipment was unloaded from the freight car, they were surprised to find that when the cans were opened they contained not silver but sand. The sand we received was from one of those cans.

A preliminary examination of this sand under a stereomicroscope showed that some pieces of silver flake were present among the mineral grains. This was interpreted as indicating that the milk can had probably contained silver before most of it was removed and sand substituted in its place. The sand exhibited a wide particle size distribution and the grains were coated. It was characteristic of alluvium from a dry, open plain.

The sand was placed in an ultrasonic bath and the recovered fines were acetolysed to concentrate any pollen grains that might be present, although from the appearance we did not expect to find many, if any present. A small quantity of pollen grains was recovered, however, and most of the grains were identified as *Artemisia* spp. (sage brush). These plants are rare in the Midwest or Eastern United States; their normal habitat is in the dry Western plains.

The heavy minerals were recovered and examined with the polarising microscope. One of the most common minerals in this suite was euhedral zircon with oscillatory zoning. By pure chance we had recently prepared and examined a sample of sand from the top of Pike's Peak, Colorado, that had originally been received some years earlier and added to our reference collection. This sand also contained zoned zircons with nearly identical morphology, indicating that they may originate from Colorado.

Based on these findings we requested samples of any sand that could be found in the vicinity of the train station where the freight had been loaded, and also around the precious metals treatment plant. The sand sample taken from the train station was nearly identical to the unknown sample we had received from our client. The investigation was then directed towards individuals handling freight at the train station from which the silver has been shipped. Although we never heard of the outcome directly from the company, we did hear from a scientist friend employed in their research laboratories that the information had been helpful in bringing the investigation to a successful conclusion.

4.4. Stolen Computers

When a shipment of computers, manufactured in Texas, was uncrated at the company that had purchased them in Buenos Aires, they were found to contain cement blocks instead. After several months the investigation hit a dead end and we were consulted to see if we might be able to redirect the investigation by determining the source of the bricks (Palenik, 1997). We had at first hoped to wash off the dust, from what we were originally told were bricks, to collect and isolate the pollen in an attempt to determine if they were consistent with a northern or southern hemisphere pollen flora. As it turned out, the contents of the crate were not bricks but porous cement blocks that had been tossed out in the back lot where they lay exposed to the air for several months.

Several pieces of the cement blocks were submitted for study. Weak acids were used to dissolve the cement and release the aggregate. After washing and drying the aggregate was recovered and sieved. The sieving showed that the sand had a very narrow particle size distribution and there were no fines. Microscopical analysis of this sand by polarising microscope and SEM indicated that quartz was the major component and that surface texture of the quartz was indicative of water immersion. The narrow particle size distribution, absence of fine minerals and the quartz grain surface texture all pointed to beach sand as the source of the aggregate.

A heavy mineral separation was performed using the techniques described earlier. The heavy mineral fraction (Fig. 6B) contained abundant zircon along with a suite of metamorphic minerals that included sillimanite, kyanite and staurolite. This combination of minerals is characteristic of the south eastern coast of the U.S. and especially Florida down to about Miami, where the beach sand contains increasing amounts of coral fragments. The mineral varieties were quite similar to those from various beaches in Florida from our reference collection that we compared them with. Based on this heavy mineral assemblage it was postulated that the cement blocks had originated in Florida and that the substitution had occurred there. When investigators concentrated their attention on Miami International Airport, they found a building in a remote location that was being constructed using similar

cement blocks. A petrographic analysis of one of these blocks using the same procedure showed a mineralogical composition nearly identical to that of the blocks that were shipped in the original computer crates. We were informed that this led investigators to uncover a theft ring composed of airline freight and baggage handlers at Miami airport.

4.5. *Murder in California*

The body of a young woman was discovered just off the road at the base of a berm off a busy road near Disneyland in California. A woman driving onto the road from the adjacent cross road, the night before the body was found, thought she saw a man kneeling next to a motorcycle at this spot as her headlights swept across the location as she made her turn. A suspect was located who had been seen with the victim at a nearby bar the night of the murder. He drove a motorcycle and when it was taken into evidence the next day was found to contain numerous mud spots. These were individually removed and submitted for analysis along with samples of the soil from the site where the victim's body was found and from surrounding areas. An aerial photograph was helpful in selecting samples for comparison. We also received a sample of soil from the ground under the overhang where the suspect parked his motorcycle and from where he maintained the soil spots had originated (alibi sample).

The mud samples were the typical small spots and were processed as described earlier. Three of the mud stains could not be distinguished from the soil from the spot where the body was found. None of the soil was consistent with the soil from the alibi sample, and the soil surrounding the location where the body was found, both up and down the road and in adjacent fields exhibited mineralogy that differed from the three spots and the murder site. Tables were prepared to show the mineralogy of each of the samples. The jury found the suspect guilty of the murder and in a retrial a few years later the verdict was upheld.

5. CONCLUSIONS

The role of heavy minerals in forensic science is yet to be fully exploited. At present it is, as are many specialist fields, underutilised because most forensic scientists are not prepared by training or experience to use them to advantage. An attempt has been made in this contribution to show, at least some ways, in which heavy mineral analysis may be helpful in forensic science. Some of the techniques that have been developed for dealing with the small samples, typical of most forensic evidence, are also described. The microscopical techniques shown here (particularly the mounting of heavy mineral suites in a single high refractive index medium of 1.662) are believed to have a wider applicability to heavy mineral identification with the polarising microscope. It might be of interest to the reader that, as the polarising microscope has declined in prestige in the geological sciences, it has ascended to a pre-eminent role in the forensic examination of physical evidence where it is not only used, but is essential in almost every type of trace evidence analysis.

Although it is only hinted at here, the study of heavy minerals for provenance interpretation (contemporary, not historical) has become an important tool in certain aspects of intelligence collection, when it is desired to know where a person or object has been. We have successfully undertaken a number of investigations of this kind and, although a vast amount of research would be required to make the technique routine, it is clear that the study of heavy minerals, combined with other microscopic components of soil, dust and other sediments, holds a great potential in the infant field of geosourcing. In the meantime it is hoped that professional petrographers will be inspired to carry out research to tackle problems involving contemporary provenance of sediment particles. The potential rewards are not only intellectual but also of practical importance in the war on terrorism.

REFERENCES

Anonymous, 1985. Uncovering a French Connection. Time 19 August, 28pp.

Blott, S.J., Croft, D.J., Pye, K., Saye, S.E., Wilson, H.E., 2004. Particle size analysis by laser diffraction. In: Pye, K., Croft, D.J. (Eds.), Forensic Geoscience: Principles, Techniques and Applications. Geological Society of London, vol. 232, pp. 63–74.

Chaperlin, K., Howarth, P.S., 1983. Soil comparison by the density gradient method: a review and evaluation. Forensic Science International 23, 161–177.

Erdtman, G., 1969. Handbook of Palynology: Morphology, Taxonomy, Ecology. Hafner Publishing Co., New York, pp. 213–216.

Frei-Sulzer, M., 1949. Mikroskopische Analyse von Verbrecherspuren. Mikroskopie 3, 176–181, 355–360.

Graves, W.J., 1979. A mineralogical soil classification technique for the forensic scientist. Journal of Forensic Sciences 24, 323–338.

Hutton, C.O., 1950. Studies of heavy detrital minerals. Bulletin of the Geological Society of America 81, 635–716.

Kirk, P.L., 1951. Density and Refractive Index: Their Application in Criminal Identification. Charles C. Thomas Co., Springfield, IL.

Krumbein, W.C., Pettijohn, F.J., 1938. Manual of Sedimentary Petrography. D. Appleton-Century-Croft Company, Inc., New York, 549pp.

Mange, M.A., Maurer, H.F.W., 1992. Heavy Minerals in Colour. Chapman & Hall, London, 147pp.

McCrone, W.C., Hudson, W., 1969. The analytical use of density gradient separations. Journal of Forensic Sciences 14, 370–384.

McPhee, J.A., 1997. Irons in the Fire. Farrar, Straus and Giroux, New York.

Mikesh, R.C., 1973. Japan's World War II Balloon Bomb Attacks on North America. Smithsonian Institution Press, Washington DC.

Milner, H.B., 1962. Sedimentary Petrography. George Allen & Unwin Ltd., London, 715pp.

Murray, R.C., 2004. Evidence form the Earth. Forensic Geology and Criminal Investigation. Mountain Press Publishing Co., Missoula, 226pp.

Nickolls, L.C., 1956. The Scientific Investigation of Crime,. Butterworth & Co. Ltd., London, 39pp.

Palenik, S.J., 1979. The determination of geographical origin of dust samples. In: McCrone, W.C., Delly, J.G., Palenik, S.J. (Eds.), The Particle Atlas. Ann Arbor Science Publishers Inc., Ann Arbor, MI, pp. 1347–1361.

Palenik, S.J., 1984. Microscopical techniques for the examination of soil in criminal cases. In: Proceedings 10th Triennial Meeting of the International Association of Forensic Scientists (on microfiche), Oxford.

Palenik, S.J., 1997. Forensic Microscopy. Microscopy and Analysis, November 1996, pp. 7–9.

Palenik, C.S., Buscaglia, J., 2007. Cathodoluminescence in forensic science. In: Blackledge, R. (Ed.), Forensic Analysis on the Cutting Edge: New Methods for Trace Evidence Analysis. Wiley, New York. (in press)

Pye, K., Blott, S.J., 2004. Comparison of soils and sediments using major and trace element data. In: Pye, K., Croft, D.J. (Eds.), Forensic Geoscience: Principles, Techniques and Applications. Geological Society of London, vol. 232. Special Publication, pp. 183–196.

Ross, C.S., 1950. The darkfield stereoscopic microscope for mineralogical studies. American Mineralogist 35, 907–908.

Skinner, D.N.B., 1988. Sampling Procedures in Forensic Earth Science. New Zealand Geological Survey, Lower Hutt, 18pp.

This page intentionally left blank

Chapter 38

FORENSIC USE OF HEAVY MINERALS IN CIVIL AND CRIMINAL INVESTIGATIONS

WAYNE C. ISPHORDING

Department of Earth Sciences, University of South Alabama, Mobile, AL 36688, USA

ABSTRACT

Extensive historic use has been made of heavy minerals in sedimentological and stratigraphic studies. More recently, heavy minerals have been utilised in a wide variety of forensic applications. Five examples are presented to show how heavy minerals have been used in a murder investigation, identify the source of groundwater contamination, quantify the volume of sediment deposited in a wetland area as a result of improper erosion control in an adjacent subdivision, identify the source and cause of the premature aircraft engine failure and in a case involving industrial sabotage. These examples illustrate well how a mineral component, which often comprises less than 1% of a typical sample, can provide the geoscientist with information that is critical in a wide variety of forensic investigations.

Keywords: forensic; sabotage; groundwater contamination

1. PRE-TRIAL RESPONSIBILITIES AND CONSIDERATIONS OF AN EXPERT WITNESS

Webster's Dictionary (Guralnik and Friend, 1964, p. 566) defines forensics as "characteristic of, or suitable for a law court or public debate". While none would argue the economic value of heavy minerals or their use in stratigraphic and sedimentological investigations, only a sparse literature exists documenting heavy mineral use in various forms of litigation. This is unfortunate because a sample's heavy mineral signature can be quite diagnostic and can be employed in a wide variety of applications. To do so effectively, however, the geoscientist must not only be knowledgeable of variations in both local and regional stratigraphic units, and the provenance of these units, but also be familiar with basic legal procedures. For example, it must be kept in mind that under current rules of discovery the scientist does not simply present

Developments in Sedimentology, Vol. 58, 963–982

ISSN: 0070-4571/doi:10.1016/S0070-4571(07)58038-6

evidence to a jury. Prior to any opportunity of doing so the opposing side will certainly insist on deposing the expert witness. At this time they will have the opportunity of reviewing the witnesses' credentials and may well use any apparent lack of the same to later challenge the admission of a witnesses' report(s) or to prevent actual testimony in court. It is therefore critical during the deposition process for the witness to clearly demonstrate not only qualifications, but also that the "science" being used has precedent, or is widely accepted by the scientific community in his/her field. With respect to the former, potential witnesses who consider themselves "qualified" may find their testimony ruled in-admissible because they lack either: (1) demonstrable experience of employment wherein the particular skill area has been used in the preparation of reports for a client, (2) prior court testimony as an acknowledged expert witness on a subject, (3) refereed publications or presentations at meetings of professional societies that treat the subject, (4) education substantiated from a college transcript or (5) evidence of having taught a particular subject.

The present author knows of several instances where academicians and individuals associated with consulting firms were prevented from testifying simply because they could not produce such evidence. Because of the breadth of material covered under the subject of geology, the mere possession of an advanced degree in the field does not necessarily qualify one as an expert in all areas. In a recent case, for example, an expert witness (a metamorphic petrologist) offered by the opposing side as an expert "mineralogist" was ruled unqualified to offer testimony. Heavy mineral evidence was critical in connecting a defendant with a specific contamination problem. It was quickly shown that: (1) the defendant's expert had no knowledge of the mineralogy of local and regional clastic sedimentary units, (2) had never carried out a single heavy mineral analysis, (3) had no publications on the general subject of heavy mineral interpretation and (4) had never even visited the area. In another instance, a potential witness whose expertise was in clay mineralogy was disqualified because, even though he had taught sedimentary petrology for several years, he was forced to admit that he was unfamiliar with the local geology, had never performed a heavy mineral analysis and did not include such instruction in his course, was not knowledgeable about procedures applicable to the sampling of unconsolidated clastic sedimentary units and had no knowledge regarding constraints imposed by the use of parametric versus non-parametric statistical methods for analysis of heavy mineral data. For individuals to represent themselves to a client as "experts" when they lack such qualifications is not only a disservice to the client, but also a glaring violation of basic ethics in our profession! Unfortunately, our field is not exempt from such instances.

As noted above, it is not solely an expert witness' credentials that may be attacked by the opposing side, but also the scientific basis for any reports or testimony that is to be offered. It is therefore incumbent on the witness to provide a basis for such testimony. This may be in the form of reference(s) to prior cases where the specific type of evidence was accepted by the court, or by citation of refereed articles in scientific journals considered creditable by the scientific community. An abundant literature, for example, can be cited to document the use of heavy minerals for stratigraphic analysis and correlation (Rosen, 1969; Isphording, 1976; Isphording and Flowers, 1980; Isphording et al., 1984; Morton et al., 2007: this volume), identification of depositional environments (Suzuki, 1975; Lee et al., 1988; Nechaev,

1991), provenance investigations (Van Andel and Poole, 1960; Isphording, 1971; Isphording and Flowers, 1983; Morton, 1985; Smale and Horton, 1987; Morton et al., 1992), tectonic settings (Nechaev and Isphording, 1993) and as palaeoclimate indicators (Isphording, 1970; Schneiderman, 1997; Egger et al., 2002). Other applications are also described in Mange and Maurer (1992).

While use of such references is not generally made during the trial phase of litigation, the ability to cite and to produce such references will be demanded by the opposing side at the time of deposition. Consequently, a witness whose deposition is to be taken is generally served with a subpoena duces tecum. The subpoena will not only include the time and place where the deposition is to be taken but also demand, but not be limited to, the following:

1. the deponent's current curriculum vitae;
2. a list of all cases in which the deponent has been tendered as an expert in the last 5 years;
3. all documents provided to the deponent by his client (i.e. attorney) or those represented by the attorney(s);
4. the deponent's entire case file, including, but not limited to, all correspondence, notes, field notes, raw data, records, computations, digital images, audio and/or video tapes;
5. *all documents, texts, journals, articles, publications etc., deponent reviewed or relies upon as authoritative, which were used in formulating his opinions in this matter* (author's italics).

Because a judge is not present at the time a deposition is taken, the witness has somewhat more freedom to elaborate and render opinions in order to convince the opposing legal team of not only his/her expertise, but also the significance and interpretation of the results of any studies that were carried out. This freedom may not be present during actual trial when opposing attorneys can demand simple "yes–no" answers to questions that have been prepared to limit testimony that they consider damaging to their client. Thus, the deposition takes on even greater significance because the opinions and reports rendered by the expert may well convince the opposing attorneys that their case either is unwinnable or might result in a significant damage award against their client at the time of trial and that a pre-trial settlement is the best course of action.

One final word of caution and advice is offered by the author, based on ~40 years of work as an expert witness. In all but the most exceptional instances the expert witness should never be apprised of the "case facts" by either a plaintiff or defendant, prior to being contacted by an attorney (and retained by the attorney). During deposition (and trial) the witness will be invariably asked when contact about the case was first made, and *who* made the contact. It is critical to be able to answer that the witness was first contacted by the attorney and asked to carry out an investigation to obtain case facts. As such, the perception of an unbiased scientist is maintained and any work produced has been, therefore, objectively generated by the scientist who will serve as an "expert witness" on the matter. If the report is prepared at the request of the plaintiff (or defendant), the jury will often perceive the expert witness as an "advocate" for the client and that any report has been "cleansed" of any damaging information. The distinction is critically important at the time of trial.

2. PRESENTATION OF HEAVY MINERAL EVIDENCE IN COURT: JURY INSTRUCTION

To use heavy minerals at the trial stage of litigation it is necessary to first "educate" the jury as to what heavy minerals are and what they represent. Years of experience has shown that the easiest way of showing "what" they are, can be most easily accomplished by first telling the jury that sediments are simply the weathered debris remaining from erosion of rocks in upland areas. They are told that most of the sediment consists of the mineral quartz (a specimen of beach sand is helpful at this point) and that heavy minerals are always a minor fraction of the sediment (usually less than 1%). The debris is then carried by rivers and streams and may be deposited on the flood plain of rivers, during time of high water, or may be carried all the way to the ocean where it forms beaches. Then, using a magnet covered by a white piece of paper, the magnet is passed over a sand sample containing magnetite. The magnetite is readily apparent to the jury adhering to the paper. It is then pointed out that magnetite is only one of a number of heavy minerals and that, in fact, any mineral that has a specific gravity greater than quartz (technically, greater than 2.85) is considered as a heavy mineral. The same sample can then be used to show the jury that the magnetite will sink in a heavy liquid, such as bromoform or tetrabromoethane, while the quartz will "float". The jury is then advised that each mineral can be identified by its specific optical properties and that strata deposited during a restricted time period within the same general area will all contain approximately the same relative percentages of various heavy minerals. It is also pointed out that if there is a significant "time gap" in the depositional process, erosion will likely have exposed older rocks and that these may well provide either some different heavy minerals or, at the very least, different percentages of mineral species than were formerly seen. It can then be emphasised that the relative percentages of the various heavy mineral species can thus serve as a "fingerprint" for various stratigraphic units and that these percentages do not vary greatly within a given area.

3. EXAMPLES FROM CASE HISTORIES

3.1. Michael Macdonald Murder Case

This case received nation-wide publication in the United States by virtue of the fact that it was one of the last in the country to involve the notorious Ku Klux Clan.

On March 21, 1981 a young, black, 19-year-old male was abducted from a street in downtown Mobile, Alabama, and taken across Mobile Bay to a site where he was brutally murdered. The crime was in apparent revenge for a mistrial granted in a case involving the murder of a white Birmingham, Alabama police officer. Two members of the Ku Klux Clan were arrested and a third was subsequently arrested and charged as an accessory. Ultimately, one of the defendants was executed for the crime and the other two are now serving life sentences. Evidence gathered and presented by the prosecution, however, was nearly compromised by the lack of expertise of the prosecution's expert on chemistry. Inappropriate statistical tests were

used in an attempt to associate the defendant with the victim at the crime scene, and mineralogical evidence that could have been used to accomplish this was not presented. Fortunately, for the sake of justice, two of the defendants opted to plea bargain and implicated the third as the actual murderer, in exchange for life sentences.

All defendants were clearly guilty, however, and each had been present at the crime scene. Mineralogical evidence was present on the soil in the truck, on the defendant's clothes and shoes and on the victim that categorically proved this. The defendants had stated (prior to the plea bargain) that they were "innocent" and had spent the evening the murder took place at the principal defendant's home and had not ventured elsewhere in the City of Mobile. Fig. 1 shows a geological map of the south Alabama area and it is seen that the defendant's home is located in an area of Mobile adjacent to Mobile Bay that is underlain by Quaternary terrace deposits. The crime, in contrast, was committed across the bay at a site underlain by sediments of the Plio-Pleistocene Citronelle Formation. These stratigraphic units are distinctively different in their mineralogy (see Isphording, 2004a) and can be differentiated by clay mineral analysis and heavy mineral content. The floodplain deposits contain both smectite clay and calcite (as fine grained shell material) whereas the Citronelle sediments are devoid of both of these minerals. The heavy mineral suite is similarly different (see Table 1). The terrace deposits are consistently lower in ilmenite, zircon and kyanite and higher in leucoxene and staurolite. Further, the terrace deposits invariably contain small percentages of the less resistant heavy minerals

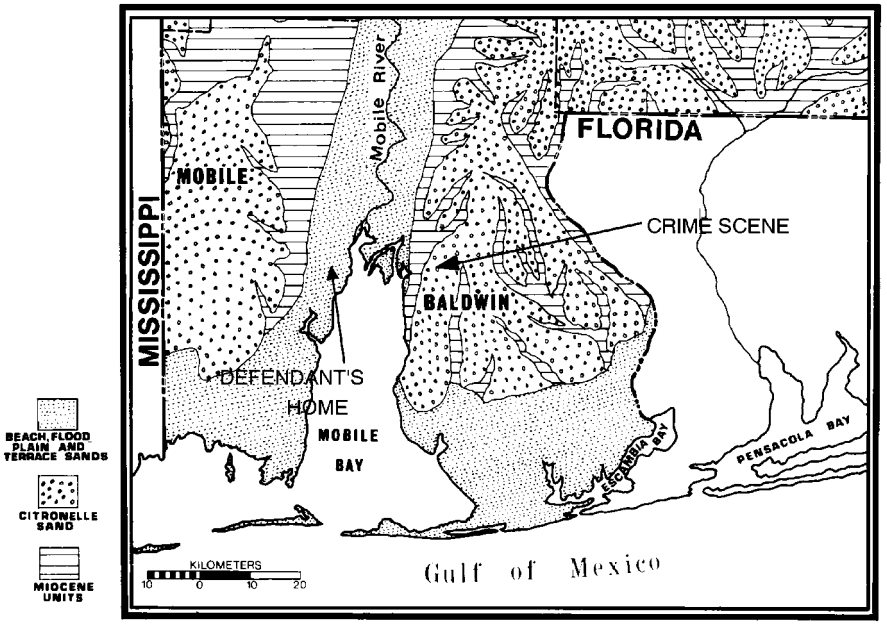

Fig. 1. Location map showing principal geological units exposed in Mobile and Baldwin counties with crime scene and defendant's homes noted.

Table 1. Heavy mineral content of Citronelle, Miocene and Terrace deposits and their ZTR index

	Citronelle Fm. (Crime scene)			Miocene sediments			Terrace deposits		
	Sample 1	Sample 2	Sample 3	Sample 1	Sample 2	Sample 3	Sample 1	Sample 2	Sample 3
Black opaques	36	34	30	30	22	30	27	22	21
Leucoxene	6	7	4	12	21	15	13	13	14
Zircon	4	7	4	2	1	1	5	6	7
Tourmaline	6	7	6	13	15	16	8	8	10
Staurolite	14	11	13	14	16	11	16	19	15
Rutile	7	8	10	5	5	4	5	6	7
Kyanite	15	15	14	20	16	19	12	10	8
Garnet	0	0	0	1	Tr	Tr	0	0	Tr
Tan opaques/others*	12	11	19	3	4	4	14	16	18
$\sum$	100	100	100	100	100	100	100	100	100
ZTR index	1.4	1.8	1.0	3.0	3.2	4.3	2.6	2.3	2.4

*Others = sillimanite, andalusite, epidote, sphene, hornblende, pyrite etc., depending on stratigraphic unit.

hornblende and garnet. The [zircon + tourmaline + rutile (ZTR)] index is also clearly different. Soil samples from the defendant's automobile, shoes and clothes possessed a typical Citronelle mineralogy, as did samples collected from the victim. This information also could have been presented to the jury as evidence that the defendants had lied and had, at the very least, been to some site underlain by the Citronelle Formation.

3.2. Alabama State Docks Industrial Vandalism Case

In 1978 the author was contacted by an official at the State Docks and asked to assist in a legal matter. A large Caterpillar bulldozer, model D-9, had been vandalised and its engine destroyed by someone who had placed sand in the engine's crankcase. The replacement value of the engine was nearly US$ 100,000. The situation was such, however, that the bulldozer was owned not by the State of Alabama, but rather by a private contractor. Further, though the State Docks acknowledged that it was responsible for the equipment's security, the insurance carrier demanded proof that the sand had been introduced while the bulldozer was on State property (the owner had admitted that the unit had been used the previous week at a quarry in northern Mobile County).

The contents of the crankcase were examined by first removing all organic material by treatment with methyl ethyl ketone and, subsequently, hydrogen peroxide. All metal fragments were removed by passing a strong magnet over the remaining sample. Several samples were also obtained from the quarry in northern Mobile County where sand and gravel from Miocene age sediments were being mined and from indigenous sediments at the State Docks site. All samples were then sieved on a one-phi interval to obtain the size frequency distributions and to obtain size fractions

for heavy mineral separations. Tetrabromoethane (density 2.96) was then used to carry out heavy mineral (and light mineral) separations on the 1.0–2.0 phi fraction (250–500 μm), the 2.0–3.0 phi fraction (125–250 μm) and the 3.0–4.0 phi fraction (62.5–125 μm), and the mineralogy of each fraction determined by standard petrographic examination. The results of these analyses are shown in Table 2.

Examination of the data in Table 2 would likely lead an experienced geologist to conclude, on the basis of the size analysis alone, that the material found in the bulldozer's crankcase was indigenous material from the State Docks facility. This is strongly indicated by the paucity of granule size [particles > -2 phi, (4mm) in size], the lower percentages of particles in the very fine sand category (3.0–4.0 phi) and higher quantities of sediment in the <4.5 phi (44 μm) size category. An argument could be raised, however, that a comparison of the size of particles would not be

Table 2. Mineralogical and particle size analyses for samples from State Docks, quarry site, and bulldozer crankcase

	Alabama State Docks		Quarry samples		Bulldozer sample
	Sample 1	Sample 2	Sample 1	Sample 2	
Size analysis (%)					
Phi value					
−2.0 to −1.0	0	0.7	2.41	2.13	0
−1.0 to 0.0	0.55	1.04	1.55	1.63	0.64
0.0 to 1.0	3.08	2.56	2.14	1.66	2.88
1.0 to 2.0	9.58	11.31	7.44	8.32	8.57
2.0 to 3.0	21.82	20.64	16.07	18.28	22.72
3.0 to 4.0	36.06	39.52	47.08	43.97	38.50
4.0 to 4.5	17.04	13.11	18.55	21.78	16.62
< 4.5	11.87	11.12	4.76	2.23	10.07
	100	100	100	100	100
Mineral analysis (%)					
Muscovite	0.2	Tr	0	0	0
Feldspar	Tr	0.4	0	0	Tr
Garnet	0.4	0.2	0	Tr	0.1
Epidote	0.6	0.2	0	0	0.2
Hornblende	0.5	0.2	0	0	0.3
Kyanite	19.7	23.3	15.3	16.4	17.9
Rutile	7.0	6.4	2.3	6.6	7.7
Sillimanite	0.5	0.3	1.0	0.7	0.3
Staurolite	17.9	20.6	9.9	13.3	20.8
Tourmaline	8.5	9.4	16.5	15.8	10.1
Zircon	2.7	3.1	9.5	6.2	1.9
Ilmenite	32.2	29.8	19.5	23.6	30.4
Leucoxene	4.6	2.1	12.1	7.7	3.9
Tan opaques	5.1	3.9	11.5	8.0	4.1

Note: Trace amounts of other minerals (andalusite, mica, sphene, spinel, pyrite etc.) were also present in the samples.

valid because of "abrasion" that took place when particles were carried upward in the oil and crushed by the piston rings. Although this point was never raised by the State Docks insurance carrier, it is a valid point and could have obfuscated the result. Not arguable, however, were the results of the mineral analyses. Samples from the sediments at the State Docks were very similar in mineral content to that found in the bulldozer crankcase and patently dissimilar to minerals found in the quarry samples. Epidote, garnet and feldspar are totally lacking in Miocene sediments in the south Alabama area but are common in modern river sediments and beach sands in Alabama. These minerals also occur in the recent sediments that comprise flood plain materials on which the State Docks are located. Hence, presentation of this information by State Docks personnel to the insurance carrier resulted in the State Docks insurance company compensating the contractor for damage to his equipment without any attempt to avoid responsibility for liability.

3.3. Teledyne Continental "Mystery"

The author was involved in a somewhat similar case in 1979 when he was approached by the senior metallurgist of the Teledyne Continental Aircraft Company. This company operates a facility in Mobile, Alabama, building and overhauling commercial aircraft and aircraft engines. A problem had developed in a particular engine model that was being supplied to the Piper Aircraft Company, in California. Piper reported that a number of incidents of compression loss and premature engine failure had been reported by users. Bench testing of the engine by Teledyne engineers, however, did not show any anomalous failure of the engine, and although a number of engines were torn down, following different periods of sustained operating times, all failed to show anything other than expected wear. Hundreds of man-hours were spent on this problem with no results, except that engines returned to the Mobile, Alabama plant did have elevated levels of fine particulate material in the crankcases. In desperation, this material was sent to the author for identification. Again, standard laboratory methodology was used to "clean" the organic component from the sediment and to isolate both the light mineral and heavy mineral fractions. The results of petrographic examination of the light mineral and heavy mineral fraction are shown in Table 3.

Even the most cursory examination of the sample by one familiar with mineralogy would have led to an immediate conclusion that the crankcase material was non-indigenous sediment. The Teledyne facility is located not far from Mobile Bay and lies on terrace sediments deposited during higher stands of the sea during the Pleistocene. While some orthoclase feldspar has been observed in terrace sediments, the presence of plagioclase in the crankcase sample was irrefutable proof that the material was not of a local nature. This was further confirmed by the similar presence of orthopyroxene, clinopyroxene, epidote, apatite and magnetite. With the exception of the very rare occurrence of epidote and apatite, the other minerals are totally lacking in all south Alabama Neogene sediments. The crankcase sample possessed a mineral suite that strongly resembled one associated with volcanic rocks (e.g., andesites).

The Teledyne engineer was advised that the contaminants definitely were *not* introduced during the manufacturing process in Mobile, Alabama. He was asked if

Table 3. Results of mineralogical analysis of particulate material present in aircraft engine crankcase

Mineral	Per cent
Quartz	32.1
Feldspar (Pl + Or)	12.1
Clinopyroxene	2.4
Orthopyroxene	0.6
Amphibole	14.6
Epidote	2.1
Garnet	0.6
Zircon	1.2
Rutile	0.3
Apatite	0.7
Sphene	0.3
Ilmenite/magnetite	32.1

there was any post-manufacturing assembly that was carried out at Piper's California facility and was told that a special oil filter was installed by Piper. A request was then made for Teledyne to obtain a sample of the sediment at the Piper plant. A company jet was used to immediately fly to California, acquire the sample and then return it to Mobile. Examination of the sample showed that the mineral suite was nearly identical to that found in the crankcase sample. The problem was finally traced to failure of a gasket on the oil filter to produce an air-tight seal. Consequently, when the planes were tested in California, dust and other sediments on the runway were being aspirated into the engine. This problem persisted after sale of the aircraft and eventually caused premature failure of the engine.

3.4. *Conoco–Agrico Groundwater Contamination Case*

This case documents a classical example of the use of heavy minerals in forensic investigations. The study was centred in Pensacola, Florida (Fig. 2) and involved the source of contamination of municipal drinking water wells in the Pensacola area.

Unlike most other cities located around the margin of the northern Gulf of Mexico, Pensacola is wholly dependent on deep wells to supply its drinking water. Beginning in the late 1950s, concern began to be raised about the pH and high levels of sulphate and fluorine in some of the wells. Subsequently, in 1959, the first of 16 major wells on which the city was dependent was ordered shut down. The likely source of the contaminants was traced to a massive groundwater plume emanating from a large phosphate manufacturing facility that had been operating at the site since the 1890s. Initially, the plant simply produced sulphuric acid from pyrite. Beginning in the 1920s, however, superphosphate became the main product and was derived from treatment of phosphate ores shipped from peninsular Florida. The plant was sold to Conoco by American Agricultural Chemical Company in 1963 and Conoco continued to produce phosphate until 1972 when the Williams Company purchased the operation and formed the Agrico Division. Agrico manufactured

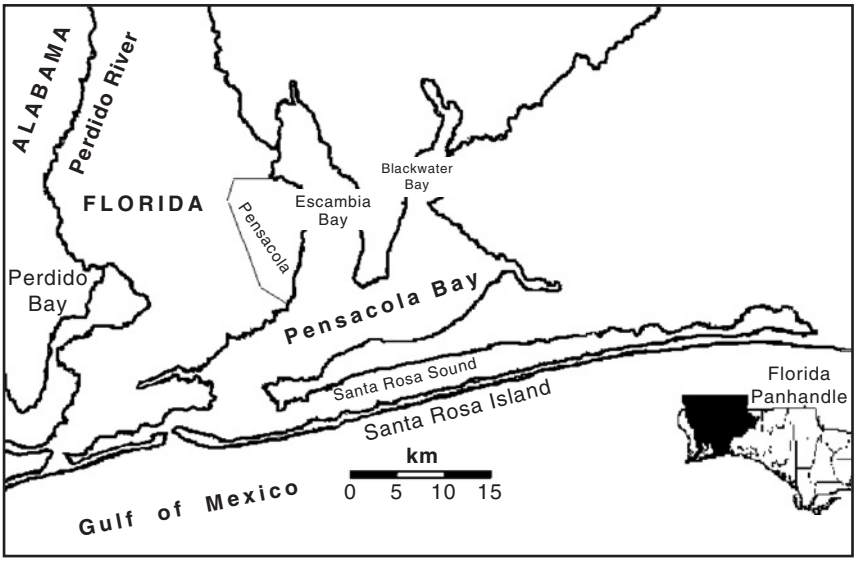

Fig. 2. Pensacola, Florida location map.

superphosphate until 1975, at which time the facility was shut down and the site abandoned. All buildings were removed in 1979. During the 1980s, the Florida Department of Environmental Regulation continued to address concern to the Escambia County Utilities Authority (ECUA) about high levels of a number of contaminants in water wells. In 1987, the facility was declared a Superfund site. In 1992, a second drinking water well was ordered shut down because of low pH and high levels of aluminium, sulphate and fluorine. It was during this time that first mention of high levels of radium (Ra), up to 20.8 picocuries per litre (pCi/l), were first noted in monitoring wells by Conoco personnel but this was not passed on to state or local agencies. In 1996, however, radium was included on the Environmental Protection Agency's (EPA) contaminant list that permits no more than 5 pCi/l in drinking water wells. As a result, one additional well was shut down in 1998 due to high radium and nitrate levels and a fourth well was ordered abandoned in 2000 because of unacceptable radium, nitrate and aluminium levels. Late in 2000, a class action suit was filed against the former owners on behalf of property owners.

The defendants did not strongly contest that the elevated aluminium, sulphate and fluorine, values observed in the groundwater plume, and the low pH, might have originated "in part" from the unlined ponds on the property to which manufacturing effluent had long been pumped. They did strongly contest, however, the allegation that they were similarly responsible for the elevated $^{226+228}$Ra levels that had forced recent closure of two of the wells. They argued that only ^{226}Ra is associated with fertiliser manufacturing and that any ^{228}Ra present must be from "natural sources" and, therefore, not the result of treatment of ores at the site. ^{226}Ra, the defendants argued, is an acknowledged daughter isotope formed by radioactive decay of ^{238}U. Uranium (U) is a ubiquitous substitutional impurity for calcium in phosphate (apatite) ores from around the world. ^{228}Ra is not a daughter isotope in this series and originates only by decay of ^{232}Th (thorium). The source of the ^{228}Ra was thus

critical to both sides involved in the litigation and, to a large degree, the major part of any damage award would hinge on the plaintiffs being able to show that this isotope, also, was associated with the manufacture of superphosphate fertiliser.

To anyone familiar with the heavy mineral content of Florida Miocene age sediments, the source of the radium was no mystery. Miocene sediments throughout peninsular Florida are known to possess the mineral monazite as part of the heavy mineral suite (see Pirkle et al., 1965; Lewis, 1978; Garner, 1980; Scholten and Timmermans, 1996; Isphording, 2004b). In fact, the mineral was mined for an extended period of time at a site near Green Cove Springs, Florida. Monazite, chemically, is $(Ce,La,Th,Y)PO_4$. ^{228}Ra is a daughter isotope of ^{232}Th. The ultimate source of the mineral can be traced to erosion of crystalline rocks in the Piedmont and Blue Ridge Mountains of Georgia, South Carolina and North Carolina. Even though present only in trace quantities in the ores, the amounts that were processed at the site over a period of some 50 years are more than sufficient to explain the levels of ^{228}Ra now seen in groundwater in the down-gradient plume (see Table 4). Unlike the ^{226}Ra isotope derived from uranium in the ores, and which typically remains with the superphosphate after the ore is processed into fertiliser, the ^{228}Ra isotope is largely discharged into the waste stream that was sent to the unlined ponds. Treatment of the ores with sulphuric acid during the manufacture of superphosphate dissolved the monazite and thereby liberated the thorium (and radium).

One final argument raised by the defence that was necessary to address involved their contention that the ^{228}Ra might well have been derived from thorium present in monazite in the Pensacola area indigenous sediments. The author was able to produce over 100 heavy mineral analyses from his own personal files documenting the fact that monazite, other than a few rare grains, is essentially absent as a heavy mineral component in the Miocene sediments and the Plio-Pleistocene Citronelle Formation sediments that crop out in the Pensacola area (see also, Coe, 1979). The mineral is found in trace amounts in recent sediments and in Pleistocene age beach deposits but these units are restricted to the near-coastal zone.

As a result of this testimony, and that by the plaintiff's hydrologists, a pre-trial settlement was reached with the defendants. On April 22, 2004, the Pensacola News

Table 4. Radium activity associated with monazite occurring as a heavy mineral constituent of Florida phosphate deposits

Calculation of radium activity per unit mass of ore
(1) Florida phosphate ores have a heavy mineral content of ~0.17% (Isphording, 2004b). One percent of this is monazite (thus the average monazite content is ~0.002%).
(2) Monazite contains 5% thorium; 87.88% of ThO_2 is thorium.
(3) One pound (0.45 kg) of ore therefore contains: (1 lb)(% heavy mineral in ore)(% monazite in ore)(% ThO_2 in monazite) (% thorium in ThO_2)(100) = 7.47×10^{-7} lb of thorium (3.39×10^{-7} kg of thorium).
(4) The specific activity of ^{232}thorium is 0.0041 disintegrations per second (dps) per microgram and 1 Curie = 3.7×10^{10} dps.
(5) Hence, 7.47×10^{-7} lb of thorium/1 lb ore × 453.59 g/lb × 1.1×10^{9} pCi/g = 37.3 pCi/g = the activity of radium in 1 g of ore.

Journal printed a story stating that Conoco had agreed to a US$ 70,000,000 settlement with Pensacola residents whose property was potentially contaminated by the toxic plume that had spread down gradient from the manufacturing site. While still alleging that the plume posed no risk to the residents, Conoco thereby avoided inclusion of an even larger area of the city in the litigation. As such, this settlement amounted to the largest ever reached in a case involving groundwater contamination in the United States.

3.5. *Lake Forest Estates: D'Olive Bay Habitat Destruction Case*

It is a well-known fact that large-scale urban or industrial development projects may profoundly alter rates of erosion (see Fig. 3). The magnitude of such changes is generally ignored because of a general belief that no reliable means exists that allows the identification in core samples of "pre" versus "post" impact sediments (impact referring to the time at which the accelerated erosion began as a consequence of land clearing and construction activities). The geologist, more and more frequently, is involved in such types of litigation and heavy mineral analysis may often be used to aid in "quantifying" the magnitude of changes that have taken place.

An example illustrating this involved a case where improper erosion controls associated with development of a large subdivision (1500 acres ~625 hectares) caused an extensive amount of sediment to be deposited in an adjacent wetland area—D'Olive Bay. This bay is located in the northeastern corner of Mobile Bay, Alabama (Fig. 4) and, over a period of some 15 years during which development of the subdivision took place, suffered an average depth loss of over some 70 cm as a result of sediment runoff from the subdivision.

Studies carried out by the Alabama Water Improvement Commission (Carlton and Gail, 1980) and the Soil Conservation Service (Crisler, 1981) clearly showed that

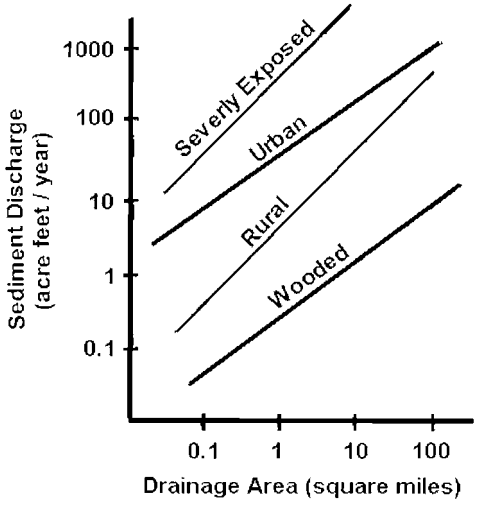

Fig. 3. Expected sediment discharge (annual) for various size Watershed areas (U.S.G.S. Open File Report, 1972, compiled by Weld et al., 1973).

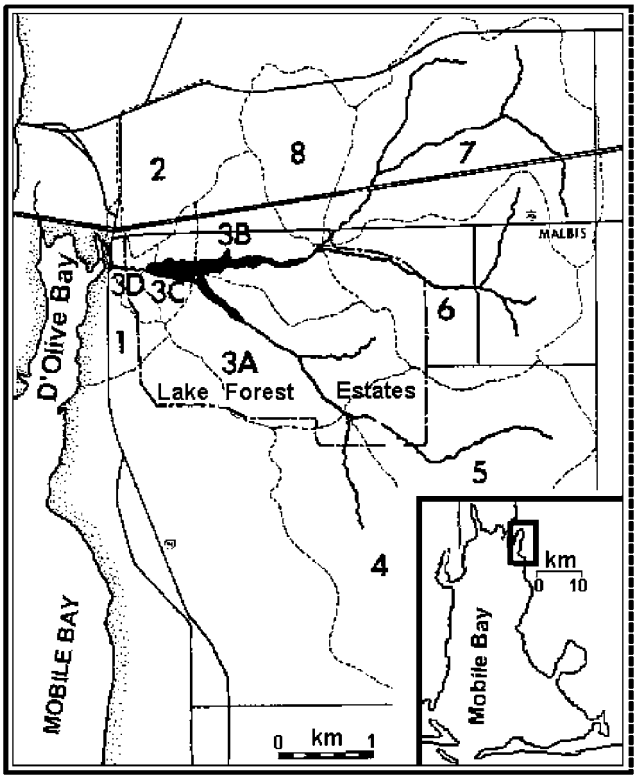

Fig. 4. Location map showing areas draining into D'Olive Bay. Lake Forest Estates subdivision includes 3A, 3B, 3C and 3D. Area shown in black is Lake Forest.

erosion in the D'Olive Bay drainage area had increased by an amount estimated at six times as great as those previously occurring when the area was largely farm and pasture land. Land development by Lake Forest developers, however, was done in a manner that even more greatly exacerbated erosion because over 48 km of streets were created in the subdivision and many of these remained unpaved for long periods of time (see Table 5 and Figs. 5 and 6). Similarly, check dams designed to attenuate runoff were poorly maintained (Fig. 7) and failed to prevent large amounts of sediment from being deposited initially in Lake Forest, but ultimately in D'Olive Bay.

Efforts by local and state agencies to force the developers to address the erosion problem met with only limited success and extensive erosion continued to cause large amounts of sediment to be deposited in the bay. Threats by property owners to file suit against the developers were countered by their contention that, because the bay is connected by its south entrance to Mobile Bay and because dredging had earlier taken place just to the north of D'Olive Bay during construction of Interstate Highway 10, no way existed to determine the degree to which erosion from the subdivision had impacted the bay. The U.S. Army Corps of Engineers, who had become involved in the controversy, contacted the author and asked if he thought that there might be a way of identifying the source(s) of sediment in the bay, and the

Table 5. Lengths of paved versus unpaved roads in Lake Forest Subdivision (Modified after Crisler, 1981)

Year	Miles of unpaved roads	Miles of paved roads
1971	35	3
1974	27	11
1975	17	21
1976	10	28
1980	6.6	31.4

Fig. 5. Oakland Drive, Lake Forest Subdivision (Photo: John Carlton, June 10, 1979).

degree to which the bay had been affected by construction activities in the subdivision. The author advised the Corps that any significant change in the sediment regimen of a drainage area must leave its record, in some form, in the deposited sediments (unless these sediments were later removed by erosion). This record might be in the form of: (1) an abrupt change in the particle size distribution of sediments analysed from cores, (2) possible changes in the mineralogy of core samples as new units are exposed by erosion, (3) changes in the carbon and sulphur content of the sediments as a result of increased (or decreased) oxidation rates and (4) changes in sediment chemistry, similarly brought about by erosion as new units are exposed. In the D'Olive Bay situation (1) and (2) above offered the strongest likelihood of allowing the depth in cores at which "impact" began to be recognised. This arose from the fact that, prior to development of the subdivision, most of the sediments in D'Olive Bay would have been derived from the periodic tidal currents that brought material from Mobile Bay into D'Olive Bay. Mobile Bay sediments originate from materials being brought into the bay by the Alabama-Mobile, the nation's fourth largest river system (exceeded, in discharge, only by the Mississippi, Columbia and

Fig. 6. Aerial view showing unpaved road in Lake Forest Subdivision (Photo: S. Coleman, June 22, 1979).

Fig. 7. Collapsed check dam in Lake Forest Subdivision (Photo: J. Carlton, August 31, 1979).

Yukon rivers) that brings sediment from the Piedmont, Ridge and Valley, Cumberland Plateau and Coastal Plain Provinces of southeastern United States. This produces a clay mineral suite dominated by smectite, and to a lesser extent, kaolinite and illite. The location on which the subdivision is developed, in contrast, is underlain by sediments belonging to the Miocene Ecor Rouge Formation and the

Plio-Pleistocene Citronelle Formation. Both of these units lack smectite and are composed chiefly of kaolinite, with lesser amounts of illite. The heavy mineral populations differ similarly. Sediments carried into Mobile Bay from northern and central Alabama contain a mineral suite that is rich in igneous and metamorphic minerals derived from crystalline rocks in the Ridge and Valley and Piedmont Provinces. The Miocene and Plio-Pleistocene sediments on which the subdivision is built were derived largely from reworking of older Coastal Plain Province sediments. Consequently, even though pre-impact and post-impact sediments might be made up largely of the same minerals, the percentages of these minerals would be expected to differ significantly. Given this information, the author was asked to collect necessary cores and samples to see if these conclusions could be substantiated.

The result came as no surprise to anyone familiar with geological processes. The expected abrupt change in clay mineral percentages was clearly evident in core samples taken throughout D'Olive Bay (see Isphording et al., 1984), as was also a marked change in the heavy mineral population. Core samples collected below the impact boundary were made up of particles whose grain size ranged from fine to medium sand (50–225 μm); those from above the boundary varied from clay size to medium silt (4–50 μm). The finer grain size of material from above the boundary was a simple consequence of the fact that larger particles were trapped behind the dam that was constructed to form Lake Forest. Consequently, only smaller particles were deposited in the bay from material washed over the spillway. Mineralogically the boundary was also apparent. Samples from below the boundary invariably contained less than 20% kaolinite (i.e. were very rich in smectite); those from above the boundary typically contained up to 40% (or more) kaolinite.

Analysis of the heavy minerals from samples from above and below the impact horizon provided further strong evidence that the boundary was a real entity. Even though the same minerals were used in the analysis of samples from above and below the boundary, the powerful statistical analytical procedure known as Discriminant Analysis clearly indicated that a different mineral population exists in samples from above versus below the boundary. The mathematical objective of a discriminant analysis is to "weigh" and compare variables from two (or more) groups and to then linearly combine the weighting in a manner such that the groups are forced to be as statistically different as possible (see Isphording and Flowers, 1980). This operation thus acts to transform the measured values obtained for all variables in a given sample into a single discriminant score that can be plotted on the resulting discriminant line. The transformation can therefore be envisioned as a search for an orientation in multivariate space where the two (or more) groups show the greatest separation, and the least dispersion. For the D'Olive Bay problem, each discriminant score plotted on the discriminant function (discriminant line) represents a weighting of the percentage of all the minerals in a single sample. When all samples from above and below the impact boundary are plotted (see Fig. 8) a clear separation is seen. From a statistical standpoint this would indicate that there is little doubt as to the presence of a distinct boundary, and the position identified for the boundary.

Table 6 shows the results of the discriminant analysis and identifies the discriminating variables that were most effective in separating the two groups, i.e. "pre-impact" and "post-impact" samples. Samples from above the impact boundary were statistically higher in tourmaline, rutile, kyanite and leucoxene; those from below the

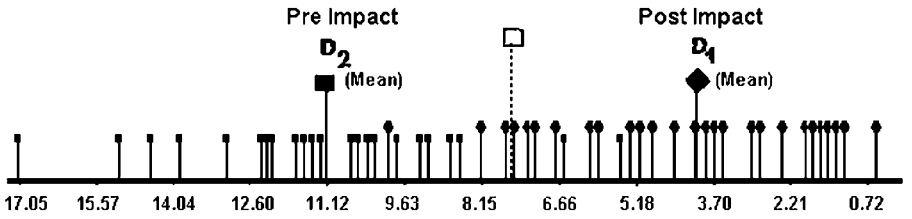

Fig. 8. Plot of discriminant scores (D) from heavy mineral analyses for "pre-impact" and "post-impact" D'Olive Bay core samples. D_1: average discriminant score for Group 1 (post-impact samples); D_2: average discriminant score for "pre-impact" samples. Open square is average value for all samples from both groups.

Table 6. Results of discriminant analysis for "pre-impact" versus "post-impact" samples

Variable	Mineral	Constant*	Per cent**
1	Epidote	−3.292	−28.67
2	Garnet	−4.532	−1.38
3	Hornblende	−5.202	−59.37
4	Kyanite	−5.416	227.37
5	Pyrite	−5.291	42.44
6	Rutile	−5.581	220.76
7	Sillimanite	−5.013	13.35
8	Staurolite	−5.188	5.89
9	Tourmaline	−5.760	144.87
10	Zircon	−5.471	89.15
11	Ilmenite	−5.170	−556.46
12	Leucoxene	−5.431	226.00
13	Tan Opaques	−4.743	−263.95

Notes: F-Test results: $F_{(13,42,.05)} = 2.00$ (value from F tables); $F_{(\text{calculated})} = 2.64$. Conclusion: Reject null hypothesis H_0: $D_1 = D_2$. The two groups are statistically different at the 0.05 level of significance.
*Predictive coefficients used in the discriminant equation.
**Variables preceded by negative sign are "associating" variables; those with a positive sign are "discriminating" variables that best serve to separate the two groups.

boundary were statistically lower in these minerals. Samples for comparison were chosen from each group by using a random number generator in order to not introduce bias into the analysis. A total of 32 samples were used from above the boundary and 23 from below the boundary. In all cases, at least 300 heavy mineral grains were counted for each sample.

The information obtained from heavy mineral analysis, combined with the clay mineral percentages and the size analysis data, was mutually supportive and allowed the impact horizon to be identified in core samples from a series of traverses taken across the bay. It was clear from the results that erosion from the subdivision had, over the period of 15 years, caused the bay to lose an average depth of slightly over 60 cm. When apprised of the results of this investigation, no further attempt was made by the developers to contest responsibility for in-filling of the bay.

While the technique (discriminant analysis) used in this example may be foreign to some geologists, it is included to demonstrate that even when the same minerals are analysed from two groups, statistical procedures exist that may permit their differentiation. Further, discriminant analysis can be applied to other types of investigations involving heavy minerals and was successfully used to identify an apparent conformable relationship between two adjacent stratigraphic units in the New Jersey Coastal Plain (the Miocene Kirkwood Formation and overlying late Miocene-Pliocene Cohansey Sand) and an unconformable relationship between the Late Miocene Ecor Rouge Sand and overlying Plio-Pleistocene Citronelle Sand in south Alabama (see Isphording and Flowers, 1980). The failure of a discriminant analysis to find a significant difference between the percentages of minerals present in overlying and underlying units would be interpreted, statistically, as indicating that all samples were drawn from the same ''population''. Geologically, this would indicate not only that both units were derived from the same provenance area, but also that no significant time gap(s) had taken place during the depositional process (i.e. a ''conformable'' relationship exists). Where a major diastem exists between two units, however (i.e. an ''unconformable'' relationship), and even if the two formations were derived from the same provenance area, it is unlikely that the same ratios and percentages of heavy minerals would be present in sediments from the two stratigraphic horizons.

4. SUMMARY

The five cases described illustrate just some of the ways that heavy minerals can be used to aid in the solution of geological problems and social controversies. Heavy minerals not only are indicators of provenance, but also serve as an important ''fingerprint'' for the stratigraphic unit from which they are obtained. Unlike particle size analyses, which can vary widely within the same formation as a result of facies changes, and unlike clay mineral analyses that necessitate a sample possessing a clay fraction, the heavy minerals in a sample from a given unit generally do not vary greatly, as long as the same size fraction is examined. As such, they are a valuable tool in the geologist's arsenal of useful analytical methods.

ACKNOWLEDGEMENTS

I express my sincere thanks to Richard Munroe and Raymond C. Murray for reviewing the manuscript and for their excellent suggestions to improve the final draft. Special thanks are also extended to Dr. James H. C. Martens and Dr. Earl C. Pirkle who first demonstrated to me, many years ago, the value of heavy minerals in geological investigations.

REFERENCES

Carlton, J., Gail, T., 1980. Special study—D'Olive Creek: Tiawassee Creek and D'Olive Bay in Baldwin County. Alabama Water Improvement Commission, Mobile Field Office, Alabama, 94pp.

Coe, C., 1979. Geology of the Plio-Pleistocene sediments in Escambia and Santa Rosa counties, Florida. Unpublished M.Sc. thesis, Florida State University, Tallahassee, Florida, 76pp.

Crisler, R., 1981. Report on erosion in the area draining to D'Olive Bay in Baldwin County, Alabama, for the years 1967 and 1980. Prepared for Mobile District, U.S. Army Corps of Engineers, by U.S. Department of Agriculture, Soil Conservation Service, 14pp.

Egger, H., Homayoun, M., Schnabel, W., 2002. Tectonic and climatic control of Paleogene sedimentation in the Rhenodanubian flysch basin (Eastern Alps, Austria). Sedimentary Geology 152, 247–262.

Garner, T., 1980. Heavy minerals industry of North America. Proceedings of the 4th Industrial Minerals International Congress, Atlanta, Georgia, pp. 1–13.

Guralnik, D.B., Friend, J.H. (Eds.), 1964. Webster's New Dictionary. World Publishing Company, New York, 1724pp.

Isphording, W.C., 1970. Upper Tertiary paleoclimate of eastern United States. American Association of Petroleum Geologists Bulletin 54, 334–343.

Isphording, W.C., 1971. Provenance and petrography of Gulf Coast Miocene sediments. 15th Field Conference Guidebook, Southeastern Geological Society, pp. 43–55.

Isphording, W.C., 1976. Multivariate mineral analysis of Miocene–Pliocene Coastal Plain sediments. Transactions: Gulf Coast Association of Geological Societies 26, 326–331.

Isphording, W.C., 2004a. The right way and the wrong way of presenting statistical and geological evidence in a court of law (a little knowledge is a dangerous thing!). In: Pye, K., Croft, D. (Eds.), Forensic Geoscience: Principles, Techniques and Applications. Geological Society of London, Special publications, vol. 232, pp. 281–288. [Note: order of Isphording's works changed.]

Isphording, W.C., 2004b. Origin, fate, and transport of ^{228}Ra and ^{226}Ra in groundwater and public drinking water, Pensacola, Florida, USA. In: Wanty, R.B., Seals, R.R. (Eds.), Water-Rock Interaction, Proceedings of the 11th International Symposium on Water-Rock Interaction (WR-11), vol. 2, A. Balkema, Leiden, pp. 1535–1538.

Isphording, W.C., Flowers, G.C., 1980. Use of classification procedures and discriminant analysis in differentiating Tertiary coarse clastics in the Alabama Coastal Plain. Journal of Sedimentary Petrology 50, 31–41.

Isphording, W.C., Flowers, G.C., 1983. Differentiation of unfossiliferous clastic sediments: solutions from the southern portion of the Alabama–Mississippi Coastal Plain. Tulane Studies in Geology and Paleontology 17, 59–73.

Isphording, W.C., Imsand, F.D., Isphording, G.W., 1984. Identification of short-term changes in sediment depositional rates: importance in environmental analysis and impact investigations. Transactions: Gulf Coast Association of Geological Societies 34, 69–84.

Lee, H.J., Jeong, K.S., Han, S.J., Bahk, K.S., 1988. Heavy minerals indicative of Holocene transgression in the southeastern Yellow Sea. Continental Shelf Research 8, 255–266.

Lewis, R., 1978. Possible recovery of heavy minerals from phosphate tailings. American Institute of Mining Engineering Preprint 78-B-300.

Mange, M.A., Maurer, H.F.W., 1992. Heavy Minerals in Color. Chapman and Hall, New York, 147pp.

Morton, A.C., 1985. Heavy minerals in provenance studies. In: Zuffa, G.G. (Ed.), Provenance of Arenites. Riedel, Dordrecht, pp. 249–277.

Morton, A.C., Davies, J.R., Waters, R.A., 1992. Heavy minerals as a guide to turbidite provenance in the Lower Palaeozoic Southern Welsh Basin: a pilot study. Geological Magazine 129, 573–580.

Morton, A., Herries, R., Fanning, M., 2007. Correlation of Triassic sandstones in the Strathmore Field, west of Shetland, using heavy mineral provenance signatures (this volume).

Nechaev, V.P., 1991. Evolution of the Philippine and Japan seas from the clastic sediment record. Marine Geology 97, 167–190.

Nechaev, V.P., Isphording, W.C., 1993. Heavy mineral assemblages of continental margins as indicators of plate tectonic environments. Journal of Sedimentary Petrology 63, 1110–1117.

Pirkle, E., Yoho, W., Allen, A., 1965. Hawthorn, Bone Valley and Citronelle sediments of Florida. Journal of the Florida Academy of Sciences 28, 7–58.

Rosen, N.C., 1969. Heavy minerals and size analysis of the Citronelle Formation of the Gulf Coastal Plain. Journal of Sedimentary Petrology 39, 1552–1565.

Schneiderman, J.S., 1997. Potential paleoclimate indicators: composition of detrital pyroxene and ilmenite in River Nile delta sediments. In: Baojun, L. (Ed.), Basin Analysis, Global Sedimentary Geology and Sedimentology. Proceedings of the 30th International Geological Congress, vol. 8. VSP International Science Publishers, The Netherlands, pp. 81–106.

Scholten, L., Timmermans, C., 1996. Natural radioactivity in phosphate fertilizers. Fertilizer Research 43, 103–107.

Smale, D., Horton, A.C., 1987. Heavy mineral suites of core samples from the McKee Formation (Eocene-Lower Oligocene), Taranaki: implications for provenance and diagenesis. New Zealand Journal of Geology and Geophysics 30, 299–306.

Suzuki, T., 1975. Heavy mineral composition of recent marine sediments in three different environments. Geological Survey of Japan, Cruise Reports 255, 1–48.

Van Andel, T.J., Poole, D.M., 1960. Sources of recent sediments in the northern Gulf of Mexico. Journal of Sedimentary Petrology 30, 91–122.

Weld, B.A., Iseri, K.T., Millgate, M.L., 1973. Reports and maps of the Geological Survey released only in the open files, 1972.

3.2.2 Geoarchaeology

This page intentionally left blank

Chapter 39

DISCRIMINATING AMONG VOLCANIC TEMPER SANDS IN PREHISTORIC POTSHERDS OF PACIFIC OCEANIA USING HEAVY MINERALS

WILLIAM R. DICKINSON

Department of Geosciences, University of Arizona, Box 210077, Tucson, AZ 85721, USA

ABSTRACT

Many volcanic sand tempers used for the fabrication of prehistoric ceramics in Pacific Oceania are beach placer sands with heavy mineral contents that reflect the phenocryst mineralogy of bedrock on the islands where pottery was made. Island groups within the region of ceramic cultures extending from western Micronesia to western Polynesia include hotspot, arc, postarc, and backarc geotectonic settings. The abundance of opaque minerals is governed by intensity of placering and is not diagnostic of geotectonic temper class, but differing proportions of ferromagnesian silicate mineral grains faithfully reflect island provenance. Clinopyroxene is the most abundant non-opaque heavy mineral in nearly all tempers of volcanic derivation. Hotspot tempers are marked by relative abundance of olivine (>25%), which also occurs in subordinate amounts in selected arc and postarc tempers. Hornblende accompanies clinopyroxene in varying proportions in other arc and postarc tempers, and orthopyroxene accompanies clinopyroxene in arc tempers from New Britain and Tonga. Relative proportions of heavy mineral species in Oceanian placer tempers correlate with the nature of restricted bedrock sources on individual islands, and serve as diagnostic evidence for temper origins wherever pottery was transported between islands.

Keywords: Heavy minerals; Oceania; Pacific; Potsherds; Temper; Volcanic sand

1. INTRODUCTION

Earthenware potsherds (broken pottery) are the most abundant and durable artifacts recovered from many archaeological sites on islands of Pacific Oceania within the region of prehistoric ceramic cultures embracing much of Micronesia, all of island Melanesia, and the western fringe of Polynesia (Fig. 1). The span of the

Developments in Sedimentology, Vol. 58, 985–1005

ISSN: 0070-4571/doi:10.1016/S0070-4571(07)58039-8

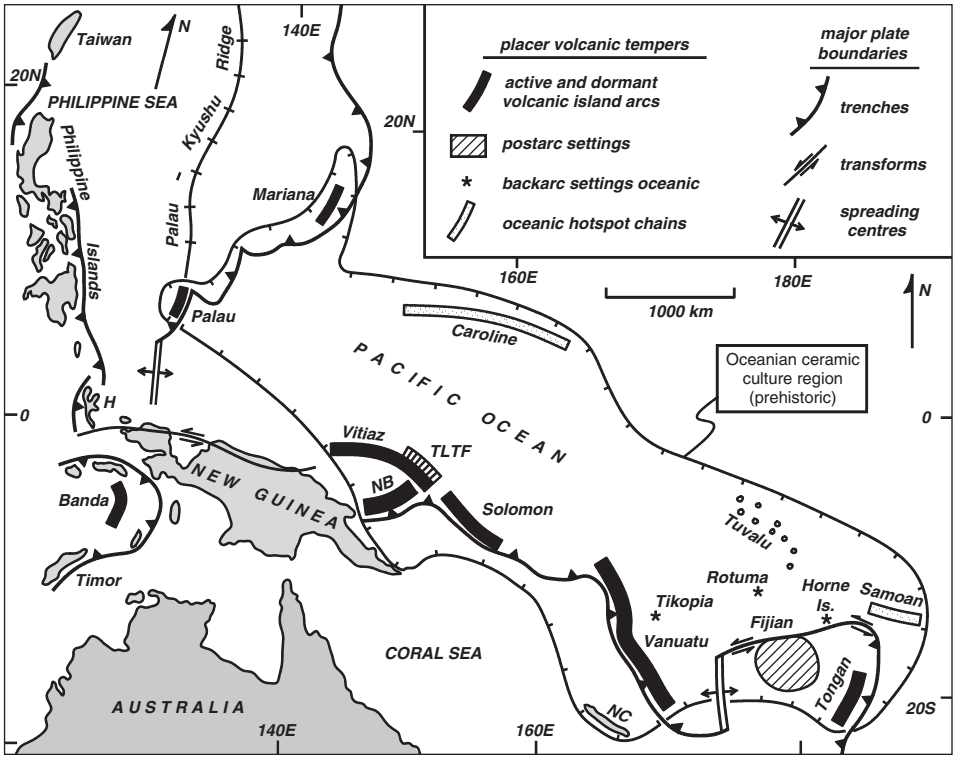

Fig. 1. Tectonic settings of mafic volcanic placer tempers within the region of prehistoric ceramic cultures in Pacific Oceania (plate boundaries schematic); abbreviations: H, Halmahera; NB, New Britain; NC, New Caledonia; TLTF, Tabar-Lihir-Tanga-Feni chain.

ceramic culture region was ~6000 km from northwest to southeast. The oldest Oceanian pottery traditions, dating to ~1500 BC in both cases, are pre-Latte ware of the Mariana Islands east of the Philippine Sea (Dickinson et al., 2001) and Lapita ware of the Bismarck Archipelago (Vitiaz-NB-TLTF of Fig. 1) lying northeast of New Guinea to the northwest of the Solomon Islands (Kirch, 1997; Spriggs, 1997). Pre-Latte ware was restricted to the Mariana Islands, but Lapita ware spread during the interval 1200–800 BC through multiple island groups as far southeast as Tonga and Samoa ~4000 km from the Bismarck Archipelago. The makers of Lapita pottery were the first occupants of all the island groups southeast of the Solomon Islands.

2. TEMPER SANDS

Ancient Oceanian potters added non-plastic temper sands to clay bodies to improve workability during ceramic fabrication, and to impart strength to finished ceramic vessels by binding clay pastes and retarding shrinkage of fired clay. The temperatures of 600–900°C attained during firing of earthenware vessels in open bonfires (Intoh, 1990; Clough, 1992) were sufficient to dewater and harden clay into

ceramic ware, but not to alter the silicate mineralogy of terrigenous temper sands. Oceanian tempers can accordingly be studied by standard petrographic methods of sedimentary petrology in thin sections of Oceanian potsherds.

Oceanian tempers fall into generic classes governed by the geotectonic settings of the various islands where prehistoric pottery occurs (Dickinson, 1998). As no sediment is dispersed between islands, all terrigenous temper sands from a given island were derived from bedrock exposures on that island. Small islands exposing a restricted assemblage of bedrock types serve as virtual point sources of sandy detritus. On a given island, tempers in Lapita and post-Lapita or pre-Latte and Latte wares are generically indistinguishable (Dickinson and Shutler, 2000; Dickinson, 2001; Dickinson et al., 2001), although sedimentologically varied sources of sand were tapped for temper from time to time during cultural evolution.

Prehistoric island potters commonly used placer sands as ceramic temper (Dickinson, 1994). The placer tempers are natural heavy mineral concentrates preserved in ceramic mounts. Most Oceanian placer tempers are well-sorted beach sand, although more poorly sorted alluvial placers from the channels of local island streams also occur among the varied sedimentological spectrum of temper sands. High contents of heavy mineral grains in beach and alluvial placers allow reproducible and statistically significant proportions of heavy mineral types to be determined by frequency counts of grain types in thin section. Associated non-placer tempers from the same islands contain the same heavy mineral species in less uniform proportions, but emphasis in this paper is placed on the placer sands for which relative frequencies of different types of heavy mineral grains are more consistent.

Transport of ceramic wares or raw materials from one island to another can be detected by temper analysis unless different islands are composed of indistinguishable bedrock assemblages (Dickinson and Shutler, 2000). On the basis of petrography, most tempers can be identified as indigenous or exotic (off-island). This distinction applies to natural tempers present as sandy impurities in clay bodies as well as to manually added tempers. Many island temper sands are broadly comparable volcanic sands of oceanic hotspot chains and intraoceanic island arcs (Fig. 1). In many cases, different populations of ferromagnesian silicate mineral grains are the most reliable criteria for discriminating among volcanic temper sands from different islands or island groups. Other criteria for discrimination based on different types of volcanic lithic fragments are generally not as clearcut as the contrasting suites of heavy minerals.

Some Oceanian tempers are exclusively calcareous sands composed of reef detritus not diagnostic of island of origin, for offshore reefs throughout the tropical Pacific Ocean yield similar calcareous sediment. The terrigenous fractions of hybrid beach sands (Zuffa, 1979) composed of mixed calcareous and terrigenous grains are suitable, however, for heavy mineral analysis, particularly if the terrigenous grain fraction is placer sand. Non-calcareous volcanic sands and the terrigenous fractions of hybrid sands containing volcanic detritus are treated jointly in this report.

3. GEOTECTONIC TEMPER CLASSES

Regionally, non-calcareous or hybrid Oceanian temper sands are grouped into regional temper classes (Dickinson, 1998; Dickinson and Shutler, 2000). Volcanic

sand tempers include *oceanic basalt* tempers from hotspot chains lying within the Pacific Ocean basin, *andesitic arc* tempers from active intraoceanic island arcs and related remnant arcs, *postarc* tempers derived from eruptive suites that postdate subduction along dormant island arcs, and *backarc* tempers derived from the eruptive suites of backarc basins. In this contribution, these volcanic sand tempers are designated as *hotspot, arc, postarc*, and *backarc* tempers, respectively (Fig. 1). The volcanic sand tempers were derived dominantly from mafic (basaltic to andesitic) source rocks. Subordinate silicic (dacitic to rhyolitic) variants of arc or backarc tempers and rare trachytic variants of hotspot tempers are also known.

The mafic volcanic temper sands are quartz-free or quartz-poor, but commonly rich in ferromagnesian silicate mineral grains. Plagioclase feldspar grains, volcanic lithic fragments, and opaque grains are the only other abundant grain types in the mafic volcanic sands. Arc and backarc tempers derived from more silicic volcanic source rocks can be identified from the presence of abundant quartz grains, but contain only sparse ferromagnesian mineral grains and are not discussed further here. Non-volcanic Oceanian temper classes not discussed here include *dissected orogen* tempers derived from deeply dissected magmatic arcs where plutonic roots of volcanic edifices are exposed, and varied *tectonic highland* tempers derived from the erosion of exposed subduction complexes thrust above either oceanic or continental crust. These non-volcanic temper sands are typically quartz-rich and contain only minor heavy minerals except where ultramafic detritus from ophiolitic source rocks is abundant. Broken-pottery (“grog”) and crushed-rock tempers used in selected island groups (Dickinson and Shutler, 2000), and composite tempers (Fitzpatrick et al., 2003) composed of mixed grog and sand, also contain few heavy mineral grains.

4. MAFIC VOLCANIC TEMPERS

Mafic volcanic sands containing varied heavy mineral grains of volcanic derivation are the most abundant of Oceanian temper types. Of ~1900 prehistoric Oceanian potsherds containing non-calcareous and non-grog sand tempers examined to date in thin section (Dickinson, 2006), more than three-quarters (~77%) contain mafic volcanic sand as temper, among which more than two-thirds (~68%) represent arc tempers, with postarc (~19%), hotspot (~12%), and backarc (~1%) tempers less abundant among sherds that have been examined in thin section. Quartzose arc and backarc tempers lacking any heavy mineral grains in significant amounts account for an additional 7% of the studied sherds. The cited proportions of temper types observed in thin section are not necessarily reflective of the proportions of temper types in unstudied sherds, but provide a general indication of the relative abundances of volcanic temper types within Pacific Oceania. The mafic volcanic sands contain the following ferromagnesian silicate mineral species in approximate order of overall abundance in Oceanian tempers: clinopyroxene (dominantly common augite but including titanaugite and aegirine-augite in selected temper types), dominantly green but also brown or green-brown hornblende, olivine, orthopyroxene (dominantly hypersthene), and rare oxyhornblende (lamprobolite). The latter is grouped with commonly associated hornblende in this report. Ferromagnesian silicate sand grains in volcanic tempers are derived from phenocrysts of sand size or larger in the volcanic

source rocks. Biotite flakes are a common minor constituent of many silicic arc and backarc temper sands, but are rare in the more mafic volcanic sands. Heavy mineral fractions of the mafic sands also include opaque iron oxide grains, dominantly magnetite but including ilmenite, in widely varying proportions that are largely governed by the intensity of sedimentological placering at the sites of sand collection. Opaque mineral grains are more abundant in arc-related tempers than in hotspot tempers because phenocrysts of opaque oxides are less common in the lavas of hotspot chains than in the lavas of island arcs. In general, however, proportions of opaque grains provide no reliable guide to the bedrock sources of temper aggregates because of the placering influence.

Proportions of ferromagnesian silicate mineral grains of different species in the mafic temper sands are reported as frequency percentages determined from areal or traverse counts of numbers of sand grains observed in thin section. Except for sherds in which temper grains are too sparse or for which sherd slices are too small, 400 total sand grains were counted in each thin section of Oceanian sherds from all temper classes (Dickinson, 2006). Relative abundances of heavy mineral species are tabulated in this contribution only for placered sands containing $>25\%$ ferromagnesian silicate mineral grains. This convention is arbitrary but restricts the reported database to temper variants for which >100 heavy mineral grains were counted in each thin section, omitting less placered sands or opaque-rich placer sands where the counting statistics for transparent heavy mineral grains are less reliable. Many of the 360 tabulated placer temper sands (Table 1) contain 25–75% ferromagnesian mineral grains, and a significant proportion contain $>90\%$. Plates 1 and 2 are photomicrographs of typical placer tempers displaying sand grains of the various ferromagnesian minerals present in Oceanian sherd tempers.

5. OLIVINE-BEARING TEMPERS

Olivine is the most abundant heavy mineral in Oceanian placer tempers in hotspot tempers from western Upolu in Samoa (Table 1, H1 and H2; Fig. 2A). Olivine is also more abundant in placer tempers from farther east along the Samoan hotspot chain (Fig. 1) on eastern Upolu (Table 1, H3) and Ofu (Table 1, H4) than in non-Samoan placer tempers, but is subordinate to clinopyroxene (Fig. 2A) which is commonly pleochroic titanaugite in Samoan tempers. The abundance of olivine reflects the dominance of olivine basalt (or basanite) in all eruptive assemblages of Samoa and American Samoa (Natland, 1980). The greater abundance of olivine in tempers from western Upolu than in tempers from eastern Upolu and Ofu reflects derivation of the former from post-shield lavas in which olivine is commonly the only abundant phenocrystic mineral, whereas the latter are derived from lavas of the shield phase in which clinopyroxene as well as olivine is a prominent phenocrystic mineral (Kear and Wood, 1959; Stice, 1968; Natland and Turner, 1985).

Non-placer tempers from the backarc islands of Rotuma and Tikopia (Fig. 1) contain olivine in an abundance, relative to clinopyroxene, comparable to Samoan tempers (Ladefoged et al., 1998; Dickinson and Shutler, 2000). Olivine is also prominent in hybrid and composite tempers (Intoh and Dickinson, 2002) from the

Table 1. Relative frequency percentages of ferromagnesian silicate grain types in 360 mafic volcanic placer sand tempers of Pacific Oceania

Temper	*N*	Hornblende	Clinopyroxene	Orthopyroxene	Olivine
A. Micronesian and Moluccan arc tempers					
1. Tarague Beach (north Guam)	2	0	99±0	1±0	0
2. Fouha-Nomna Bays (south Guam)	5	0	92±4	1±1	7±5
3. Palau (origins on Babeldaob)	20	2±2	98±2	0	0
4. Banda (anomalous hornblende-rich)	2	79±2	21±2	0	0
B. Bismarck arc tempers					
1. Manus (Admiralty Gp) hornblendic	7	56±10	44±10	0	0
2. Manus (Admiralty Gp) pyroxenic	3	16±4	84±4	0	0
3. Fissoa (east coast of New Ireland)	4	15±5	85±5	0	0
4. Arawe Islands (off west New Britain)	8	1±1	91±1	7±2	1±1
5. Boduna Island (off north New Britain)	2	6±2	59±1	32±1	3±1
6. Watom Island (off east New Britain)	3	0	88±4	12±4	0
C. TLTF postarc and NMB backarc tempers					
1. Kamgot Lapita site (Babase Island)	5	3±1	96±1	1±1	0
2. Balbalankin Lapita site (Anir Island)	3	2±1	98±1	0	0
3. Malekolon Lapita site (Anir Island)	4	46±15	54±15	0	0
4. Tanga Islands (exotic Anir ware)	5	34±8	66±8	0	0
5. Tanga Islands (indigenous ware)	16	0	100	0	0
6. Futuna-Alofi (Horne Islands)	18	0	100	0	0
D. Solomon arc tempers					
1. Paubake site (south Bougainville)	7	54±10	46±10	0	0
2. Kieta sites (east Bougainville)	11	94±3	6±3	0	0
3. Roviana Lagoon, New Georgia	8	2±2	75±5	0	23±5
E. Vanuatu arc tempers					
1. Taumako (Duff Islands)	9	1±1	99±1	0	0

Table 1. (*Continued*)

Temper	*N*	Hornblende	Clinopyroxene	Orthopyroxene	Olivine
2. Nendö (Santa Cruz Group) Lapita	10	0	95±4	0	5±4
3. Reef Islands (Santa Cruz Gp) Lapita	12	0	92±3	0	8±3
4. Reef Islands (Santa Cruz Gp) post-Lapita	16	0	90±2	0	10±2
5. Santo (including offshore Malo)	5	10±3	90±3	0	0
6. Malakula (offshore islets)	2	32±4	68±4	0	0
7. Ponamla-Ifo sites (Erromango)	10	0	98±1	0	2±1
F. Fiji postarc tempers					
1. Yasawa Islands (off Viti Levu)	8	1±1	97±2	2±1	0
2. Kulu-Vaga Bays, Beqa Island	7	40±10	60±10	0	0
3. Natunuku site (Vatia temper)	5	19±5	75±6	0	7±4
4. Natunuku site (Tavua temper)	15	1±1	92±4	0	7±4
5. Navatu site (northeast Viti Levu)	15	27±3	62±4	0	11±3
6. Moturiki (indigenous or Ovalau)	23	21±7	79±7	0	0
7. Naigani (from Moturiki or Ovalau)	7	24±3	76±3	0	0
8. Votua site (Mago Island) in Lau	3	0	95±3	0	5±3
9. "Kedekede Temper" (origin in Lau)	9	0	96±2	0	4±2
G. Tongan arc tempers					
1. Tongatapu Island Lapita sites	15	0	86±2	14±2	0
2. Ha'apai Group Lapita sites	9	0	84±2	16±2	0
3. Ha'apai Group post-Lapita sites	9	0	87±2	13±2	0
4. Vava'u Group sites	100	0	93±1	7±1	0
5. Exotic Nendö-Nukuleka temper	2	3±1	97±1	0	0
H. Samoan hotspot tempers					
1. Mulifanua Lapita (west Upolu)	9	0	19±3	0	81±3
2. Vailele post-Lapita (west Upolu)	8	0	20±3	0	80±3

Table 1. (*Continued*)

Temper	*N*	Hornblende	Clinopyroxene	Orthopyroxene	Olivine
3. Sasoa'a, Falefa Valley (east Upolu)	3	0	63±4	0	37±4
4. To'aga-Vaota, Ofu (Manu'a Gp)	8	0	71±2	0	29±2

Notes: Statistics: *N*, number of thin sections counted (±indicates standard deviation for *N* grain frequency counts).Grain types: Hornblende is pleochroic in green tints except for brown hornblende at Paubake (near Buin on Bougainville); clinopyroxene is augite except for aegirine-augite along TLTF postarc chain and titanaugite in Samoan hotspot tempers; orthopyroxene is generally hypersthene; olivine compositions not determined.Geographic–geologic locales (see Fig. 1): Micronesian arcs (A) include Mariana forearc islands and Palau east of the Philippine Sea, and the Banda arc of the Banda Sea (included for comparison); Bismarck Archipelago (B) includes islands surrounding the Bismarck Sea off New Guinea (ancestral Vitiaz arc assemblage of Manus and New Ireland, and active New Britain arc); TLTF (C) is Tabar-Lihir-Tanga-Feni chain off New Ireland and NMB (C) is northern Melanesian borderland (Horne Islands) between Fiji and Samoa; Solomon arc (D) includes Bougainville (politically part of Papua New Guinea) and New Georgia; Vanuatu arc (E) includes eastern political outliers of Solomon Islands along New Hebrides island arc; Fiji (F) includes the Lau Archipelago (Yasawa Islands are an extinct segment of the ancestral Vitiaz island arc); Tongan arc (G) includes only central forearc island groups; Samoan chain (H) includes American Samoa.

Caroline hotspot chain (Fig. 1). Placer tempers discovered by future work in those tectonic settings could be expected to contain as much olivine as Samoan tempers.

Selected arc (Fig. 2B) and postarc (Fig. 2C) placer tempers contain subordinate olivine in addition to dominant clinopyroxene, and in some cases minor hornblende or orthopyroxene. Proportions of olivine in these non-hotspot placer tempers are distinctly lower than in Samoan tempers except for a placer temper from Roviana Lagoon (Felgate and Dickinson, 2001) in the New Georgia Group of the Solomon Islands in which the olivine content is almost as high as in selected Samoan tempers (Table 1, D3). The New Georgia volcanic assemblage was erupted along an anomalous segment of the Solomon magmatic arc where the Woodlark spreading system is subducted at the trench axis (Crook and Taylor, 1994), and is more picritic (magnesian) than other Oceanian arc assemblages (Stanton and Bell, 1969; Ramsay et al., 1984). The composition of the Roviana placer temper reflects a phenocryst ratio of olivine to clinopyroxene in New Georgia volcanic rocks almost as high as in hotspot lavas.

Other olivine-bearing arc and postarc placer tempers are distributed in almost random fashion on various islands of the Mariana (Table 1, A), New Britain (Table 1, B), and New Hebrides or Vanuatu (Table 1, E) island arcs and the postarc Fiji platform (Table 1, F). These tempers containing olivine in consistently minor proportions reflect local variations in the phenocrystic olivine content of eruptive suites, and their distribution allows recognition of ceramic assemblages derived from specific islands. Origins of the olivine-bearing arc and postarc tempers can be understood from known variations in island geology (Dickinson, 2000, 2001; Dickinson et al., 2001):

(1) Along the Eocene-Oligocene paleovolcanic chain exposed within the forearc belt of the Mariana arc, pillow basalt and basaltic andesite rich in olivine are exposed only on southern Guam (Reagan and Meijer, 1984) where the olivine-bearing

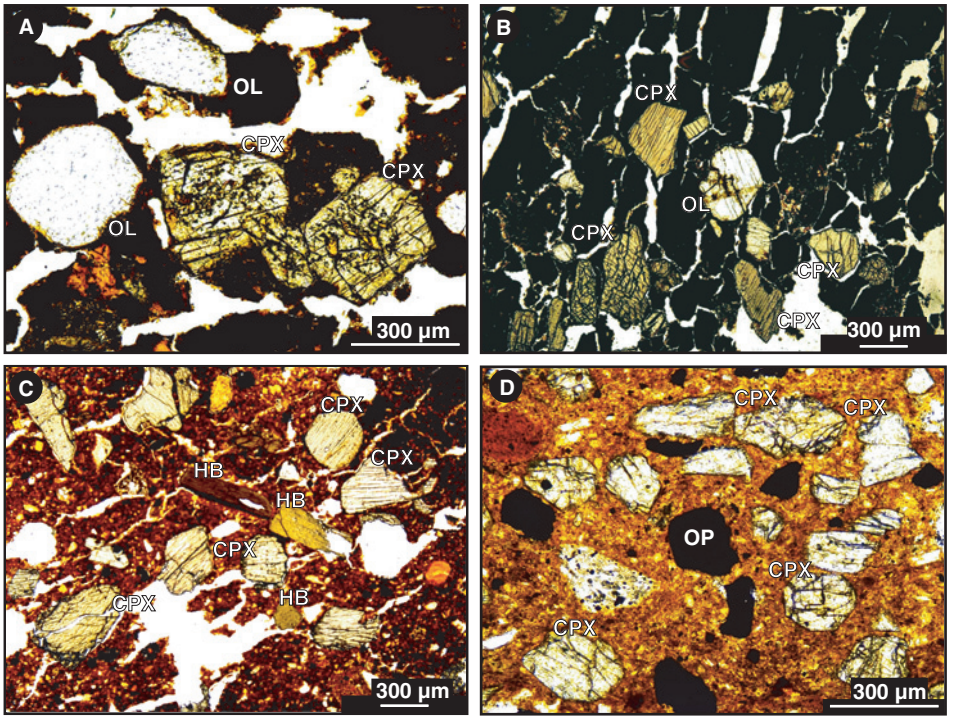

Plate 1. Photomicrographs in plane light prepared from sherd thin sections by editor Maria Mange of selected Oceanian placer sand tempers (hotspot and postarc) containing clinopyroxene (A–D) and olivine (A–C) mineral grains (dark or reddish backgrounds are clay pastes in which diverse temper grains are embedded): (A) olivine-bearing hotspot temper (Fig. 2A, Table 1, H2) with more olivine (OL, pale grains) than clinopyroxene (CPX, green grains) in sherd 26-6 from the Vailele site on the north coast of Upolu in Samoa; (B) olivine-bearing hotspot temper (Fig. 2A; Table 1, H3) with more clinopyroxene (CPX, green grains) than olivine (OL, pale grain in center tinged by reddish iddingsite produced by deuteric alteration) in sherd 25-8 from the Sasoa'a site in Falefa Valley of inland Upolu in Samoa; (C) olivine-bearing postarc temper (Fig. 2B; Table 1, F3) containing olivine (one pale grain near top left), clinopyroxene (CPX, multiple weakly coloured grains), and hornblende (HB, multiple strongly coloured grains) in slide 22-7 (containing Vatia temper) from the Natunuku site on the north coast of Viti Levu in Fiji; (D) clinopyroxene (CPX)-dominated postarc temper (Fig. 3B; Table 1, E5) in sherd ETZ-15 from the Ampuli site on the islet of Malendok in the Tanga Islands of the TLTF chain northeast of New Ireland in the Bismarck Archipelago of Papua New Guinea containing multiple opaque iron oxide grains (OP) in addition to clinopyroxene.

Fouha-Nomna placer tempers (Table 1, A2) are unique for the Mariana ceramic suite. Early arc lavas were erupted while the Mariana arc was still attached to the Palau-Kyushu Ridge (Fig. 1) before seafloor spreading had opened the eastern Philippine Sea as an interarc basin (Meijer et al., 1983).

(2) Along the New Hebrides arc, basalt and basaltic andesite assemblages yielding olivine to derivative detritus are widespread to the north on Nendö (Table 1, E2) of the eastern Solomon outliers (Hughes et al., 1981), and to the south on Erromango (Table 1, E7) in southern Vanuatu (Colley and Ash, 1971), but are less common on

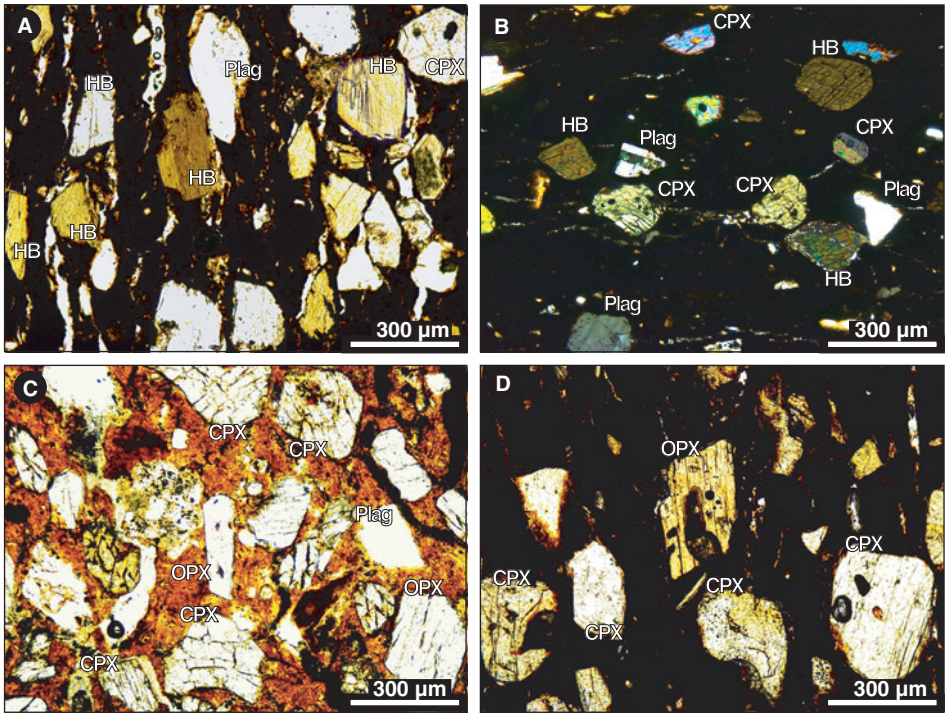

Plate 2. Photomicrographs in plane light (except for B under crossed polars) prepared from sherd thin sections by editor Maria Mange of Oceanian placer sand tempers of arc derivation containing pyroxene (A–D) and hornblende (A–B) mineral grains (dark or reddish backgrounds are clay pastes in which diverse temper grains are embedded): (A) both clinopyroxene (CPX, weak colouration) and hornblende (HB, strong colouration), with pale plagioclase feldspar grains (Plag) also visible, in sherd 59-5 from M'Buke islet south of Manus in the Admiralty Group of the Bismarck Archipelago (Papua New Guinea); (B) clinopyroxene (CPX, weak colouration) and hornblende (HB, strong colouration), with pale plagioclase feldspar grains (Plag) also visible (twinned at center left), in sherd 4473-BS-6 from the Paubake site near the south end of Bougainville (Solomon chain) in Papua New Guinea; (C) clinopyroxene (CPX) and orthopyroxene (OPX), with plagioclase feldspar mineral grains (Plag) also visible, in sherd To6-1475 from the Tufu Mahina site on Tongatapu in Tonga; (D) clinopyroxene (CPX) and orthopyroxene (OPX) in sherd 58 from the Faleloa site on Foa in the Ha'apai Group of central Tonga.

the larger islands (Santo, Malakula) of central Vanuatu where less mafic andesitic assemblages are dominant (Carney et al., 1985; MacFarlane et al., 1988). Olivine-bearing Nendö tempers in exotic sherds from the calcareous Reef Islands (Table 1, E3 and E4), where no volcanic sand is present, document systematic transfer of ceramic products on a large scale across the intervening waters (~50 km) between Nendö and the Reef Islands (Green, 1996).

(3) On the Fiji platform, postarc volcanic edifices of subalkalic Pliocene basalt with shoshonitic affinities lie along the north coast of Viti Levu (Rodda and Lum, 1990; Rodda, 1994), and contributed olivine-bearing detritus to several local temper types (Table 1, F3–F5). Farther east on the Lau Ridge, which is the remnant arc of

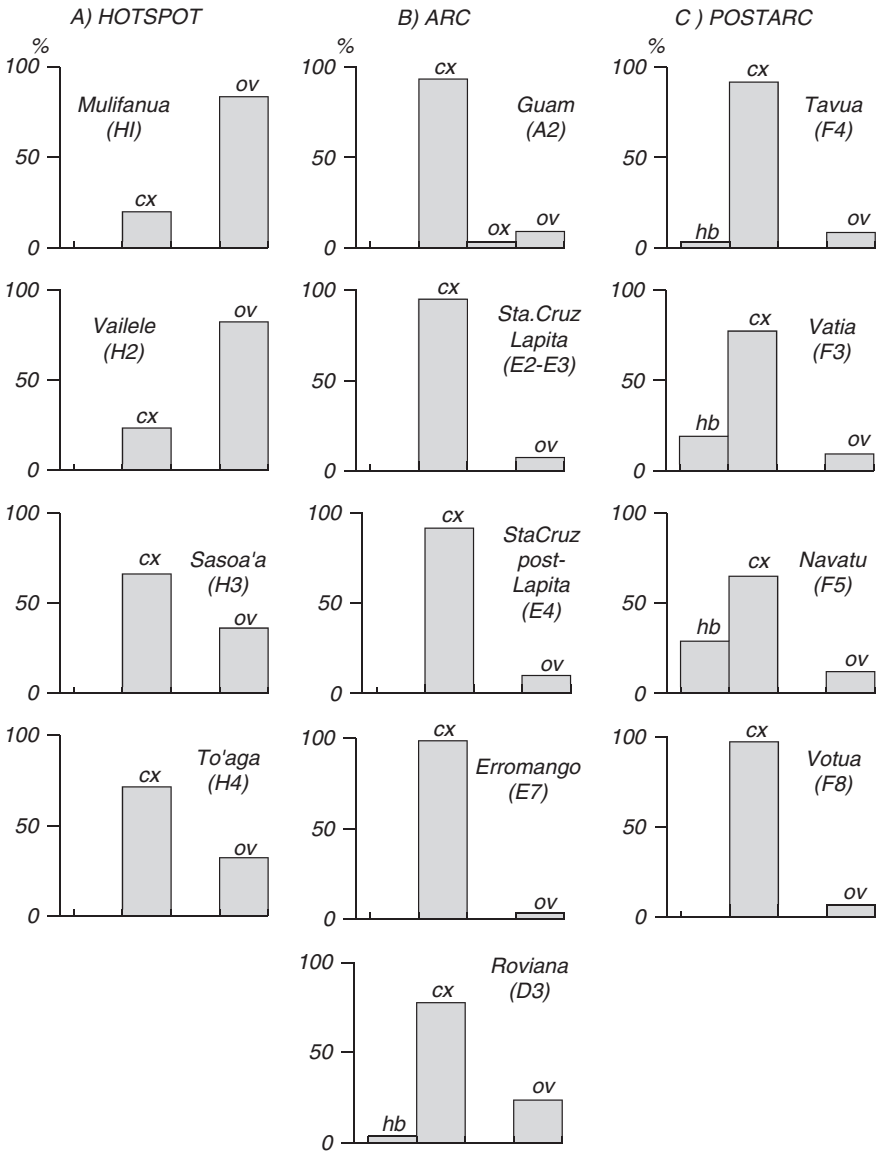

Fig. 2. Relative proportions of different ferromagnesian silicate mineral grains in olivine-bearing placer temper types of Pacific Oceania (A, hotspot; B, arc; C, postarc); all contain abundant clinopyroxene and some also contain subordinate hornblende or orthopyroxene (letter–numeral designations of temper types keyed to Table 1). Frequency percentages plotted are mean values from Table 1. ov, olivine; ox, orthopyroxene; cx, clinopyroxene; hb, hornblende.

the Tongan arc-trench system, alkalic Quaternary postarc basalt (Cole et al., 1985; Woodhall, 1985), erupted on selected islands after opening of the interarc Lau Basin, contributed olivine to local temper sand at the Votua site on Mago (Table 1, F8). Olivine-bearing "kedekede temper" (Table 1, F9), present in sherds from multiple

sites on several islands in Lau and elsewhere in Fiji, was probably derived from subalkalic Pliocene postarc basalt that is widespread on the Lau Ridge (Cole et al., 1985; Woodhall, 1985), but its exact origin remains uncertain (Dickinson and Shutler, 2000).

6. CLINOPYROXENE-RICH TEMPERS

Placer tempers composed exclusively, or nearly so, of clinopyroxene (Fig. 3) are dominant along the Mariana and Palau arcs fringing the Philippine Sea, in the postarc Tabar-Lihir-Tanga-Feni (TLTF) chain of Neogene alkalic volcanic edifices (Johnson et al., 1976; Wallace et al., 1983) bordering the Bismarck Archipelago northeast of New Ireland, and on the backarc Horne Islands (Futuna and Alofi) of the northern Melanesian borderland (Fig. 1). In alkalic TLTF placer tempers, clinopyroxene is weakly pleochroic (green to yellowish green) aegirine-augite with high optic axial angle ($2V > 75^\circ$), whereas other Oceanian placer tempers contain varieties of normal augite ($2V \sim 60^\circ$) displaying little or no pleochroism except for the titanaugite common in Samoan hotspot tempers. Accessory ferromagnesian silicate mineral grains allow some distinctions to be drawn among clinopyroxene-rich placer tempers (Dickinson, 2000, 2001; Dickinson et al., 2001; Fitzpatrick et al., 2003): (a) minor orthopyroxene but no hornblende on Guam (Table 1, A1), (b) minor hornblende but no orthopyroxene in Palau (Table 1, A3) and Vanuatu (Table 1, E1 and E5), and (c) both hornblende and orthopyroxene on Babase in the TLTF Feni Islands (Table 1, C1). Other clinopyroxene-rich placer tempers from Anir in the TLTF Feni Islands (Table 1, C2), the TLTF Tanga Islands (Table 1, C5), and Futuna-Alofi in the Horne Islands (Table 1, C6) contain no ferromagnesian silicate mineral grains other than clinopyroxene in more than trace amounts.

Clinopyroxene-rich arc (Fig. 3A) and postarc (Fig. 3B) tempers lacking appreciable amounts of hornblende or orthopyroxene are broadly similar, whether olivine-bearing (Fig. 2) or olivine-free (Fig. 3), throughout the ceramic culture region of Pacific Oceania. There are accordingly close generic resemblances among selected temper types from a wide geographic range in the Mariana Islands, Palau, Banda, the TLTF chain, Vanuatu, and Fiji. As clinopyroxene is ubiquitous in all Oceanian placer tempers (Table 1), reliable distinctions among most of the local temper types are dependent upon the presence of other ferromagnesian silicate mineral grains in diagnostic proportions. The challenge for discrimination is exacerbated for non-placer tempers because thin sections of sherds may fail to transect any grains of the minor accessory minerals. Attention to placer variants of local temper suites is the most effective strategy for recognition of different temper types from various islands and island groups.

7. HORNBLENDE-BEARING TEMPERS

Hornblende-bearing temper types, some quite rich in hornblende, are characteristic of particular segments of selected island arcs (Fig. 4A) and of specific postarc settings (Fig. 4B). Their occurrence provides a valuable means to discriminate local tempers.

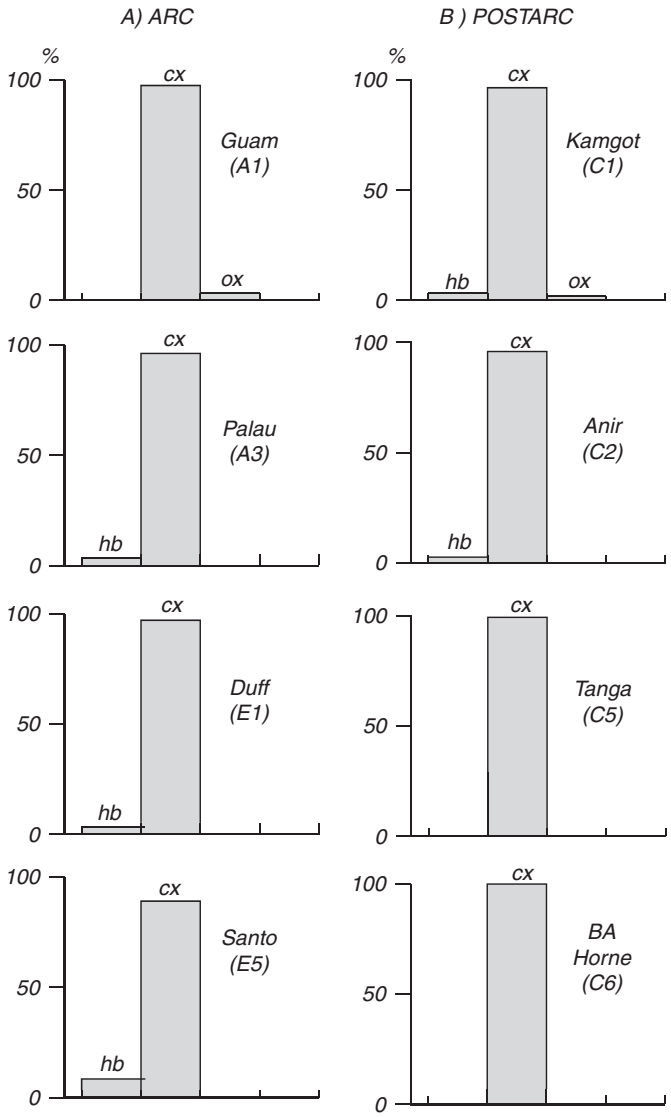

Fig. 3. Relative proportions of different ferromagnesian silicate mineral grains in arc (A) and postarc (B) placer temper types of Pacific Oceania composed dominantly of clinopyroxene mineral grains (letter–numeral designations of temper types keyed to Table 1). Frequency percentages plotted are mean values from Table 1. BA denotes backarc Futuna-Alofi tempers (Table 1, C6). ov, olivine; ox, orthopyroxene; cx, clinopyroxene; hb, hornblende.

Absence of hornblende is also a useful regional discriminant because some island arcs, notably the Mariana and Tonga arcs, erupt no lavas or ejecta containing hydrous phases. An unresolved problem for temper analysis is the occurrence in the Banda arc (Fig. 1) of a hornblende-rich placer temper (Table 1, A4) in two sherds interpreted as exotic to Banda because indigenous sherds with non-placer tempers

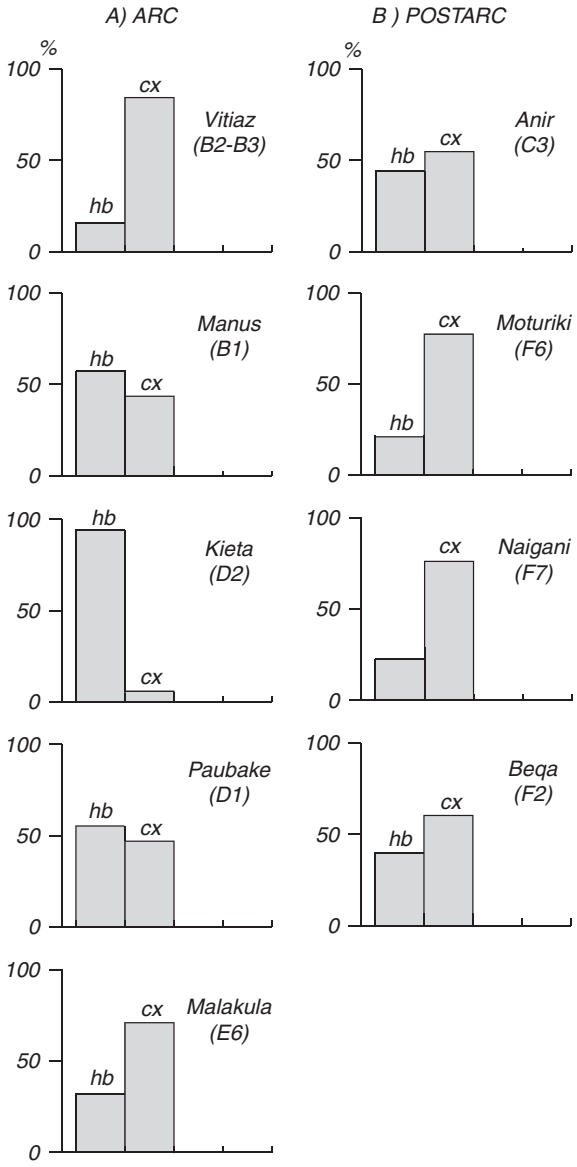

Fig. 4. Relative proportions of different ferromagnesian silicate mineral grains in arc (A) and postarc (B) placer temper types of Pacific Oceania containing significant proportions of clinopyroxene and hornblende but not orthopyroxene or olivine (letter–numeral designations of temper types keyed to Table 1). Frequency percentages plotted are mean values from Table 1. In A (arcs), Manus (B2) and New Ireland (B3) are segments of the ancestral Vitiaz island arc. ov, olivine; ox, orthopyroxene; cx, clinopyroxene; hb, hornblende.

contain clinopyroxene as their only ferromagnesian silicate grain type. The origin of the exotic sherds is still unknown.

In the Bismarck Archipelago, placer tempers derived from a Palaeogene volcanogenic assemblage that forms the basement of all the larger islands (Manus, New

Hanover, New Ireland, New Britain), contain hornblende and clinopyroxene in variable proportions (Table 1, B1–B3). The Palaeogene volcanic rocks were erupted along the ancestral Vitiaz island arc, subducting Pacific seafloor downward to the southwest before reversal in arc polarity gave rise to the modern New Britain and Solomon arcs subducting seafloor of marginal seas downward to the northeast, and before Neogene seafloor spreading in the Bismarck Sea had dispersed the various islands of the Bismarck Archipelago to their present positions (Dickinson, 2000).

Along the alkalic Neogene TLTF chain northeast of New Ireland, a placer temper type from Anir in the Feni Islands (Table 1, C3) is rich in hornblende and contrasts in that respect with other Feni placer tempers (Table 1, C1 and C2). Transport of pottery from Anir to the nearby Tanga Islands has been detected from the occurrence of exotic sherds with hornblende-bearing temper (Table 1, C4) among more abundant indigenous sherds that contain placer temper composed exclusively of clinopyroxene and opaque grains (Table 1, C5). The Anir hornblende-bearing placer temper, anomalous for the TLTF chain, is inferred to reflect the complex volcanic geology of Anir as compared with other TLTF islands (Wallace et al., 1983).

In the Solomon chain, Bougainville placer tempers uniformly contain hornblende, which is locally dominant over clinopyroxene (Table 1, D1 and D2), reflecting the prevalence of hornblende in Bougainville volcanic assemblages (Blake and Miezitis, 1967; Rogerson et al., 1989). Analogous hornblende-rich placer tempers are characteristic of Malakula in central Vanuatu (Table 1, E6). The ubiquity of hornblende in Malakula and Santo temper sands of central Vanuatu serves to distinguish them from the hornblende-free tempers known farther north and south along the New Hebrides island arc (Dickinson and Shutler, 2000; Dickinson, 2001).

Hornblende-bearing placer tempers also occur in sherd suites from small volcanic islands offshore from Viti Levu, the largest island on the Fiji platform (Fig. 1). Beqa sherds (Table 1, F2) are inferred to be indigenous, made using temper sand derived from the postarc Pliocene Beqa volcano, whereas sherds from the small islets of Moturiki (Table 1, F6) and Naigani (Table 1, F7) are inferred to derive from the nearby larger island of Ovalau, formed by a postarc Pliocene volcano similar in geotectonic origin to the Beqa volcano (Dickinson, 2001).

The Navatu temper type of northeast Viti Levu contains a comparable proportion of hornblende (Table 1, F5), but also olivine which is lacking in Beqa and Ovalau tempers. The hornblende in Navatu temper was derived from subvolcanic plugs exposed in the eroded core of the postarc Pliocene Rakiraki volcano (Seeley and Searle, 1970), and Navatu temper is especially notable because it occurs in exotic sherds transported north to Tuvalu ~1000 km away (Dickinson et al., 1990). Farther west on northern Viti Levu, indigenous sherds from Natunuku, located near the sulcus between two postarc Pliocene volcanic edifices (Setterfield et al., 1991), contain two different olivine-bearing placer temper types. A nearly hornblende-free temper sand was derived from the slopes of the Tavua volcano (Table 1, F4) and a hornblende-bearing temper sand was derived from the slopes of the Vatia volcano (Table 1, F3).

8. ORTHOPYROXENE-BEARING TEMPERS

Orthopyroxene-bearing placer tempers (Fig. 5) are characteristic of the New Britain and Tongan island arcs, but orthopyroxene is rare in other Oceanian tempers. The

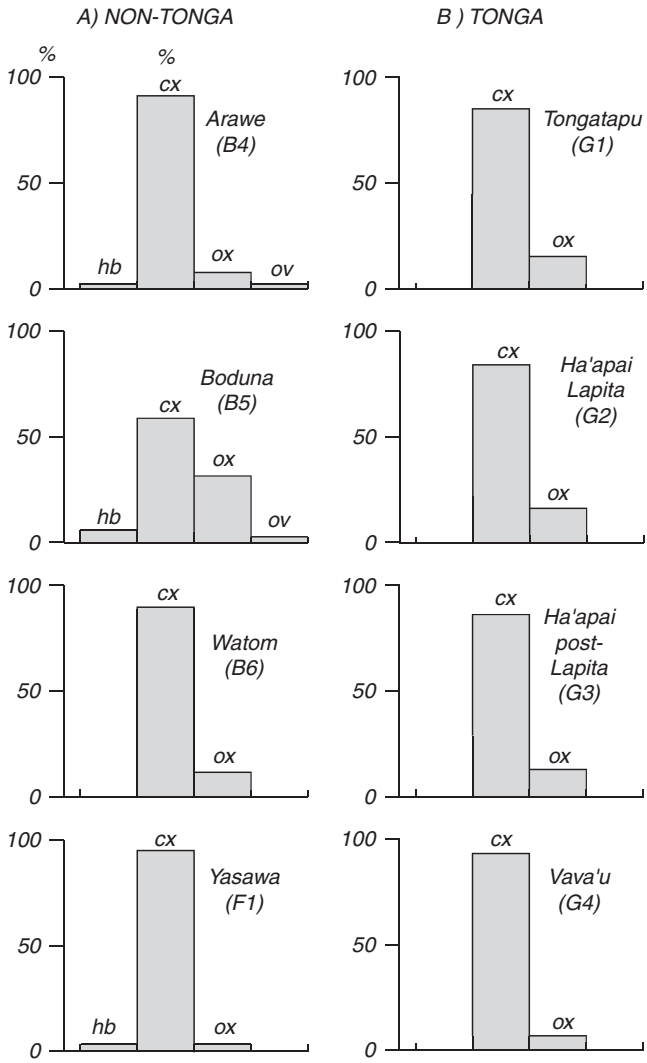

Fig. 5. Relative proportions of different ferromagnesian silicate mineral grains in arc placer temper types (A, non-Tongan; B, Tongan) of Pacific Oceania containing both clinopyroxene and orthopyroxene but only minor proportions of either hornblende or olivine (letter–numeral designations of temper types keyed to Table 1). Frequency percentages plotted are mean values from Table 1. ov, olivine; ox, orthopyroxene; cx, clinopyroxene; hb, hornblende.

most orthopyroxene-rich placer temper type occurs on Boduna (Table 1, B5) off the north coast of New Britain where two-pyroxene andesite is the dominant eruptive product (Lowder and Carmichael, 1970; Blake and Ewart, 1974). Lesser proportions of orthopyroxene accompany clinopyroxene in sherds from offshore islands to the west and east where eruptive assemblages on the nearby New Britain mainland have reduced orthopyroxene contents (Heming, 1974, 1977). The correlation of placer temper variations with variations in volcanic geology along the trend of nearby New

Britain implies that the sherds from tiny Arawe (Table 1, B4) and Boduna (Table 1, B5) islets were derived from segments of the adjacent New Britain coast. Sherds containing Watom placer temper (Table 1, B6) are indigenous to Watom island (Dickinson, 2000), which exposes the outermost margin of the Rabaul caldera complex (Walker et al., 1981). Watom was the place where the first known Lapita pottery was discovered in 1909 by a German missionary (Green, 2000).

Minor orthopyroxene is present in placer tempers from the Yasawa Islands (Table 1, F1) west of Viti Levu in Fiji where volcanic rocks of an extinct Late Miocene arc assemblage are exposed, and orthopyroxene occurs sparingly in poorly studied non-placer tempers from the large island of Vanua Levu lying to the north of Viti Levu (Dickinson, 2001). Orthopyroxene-bearing arc tempers of Fiji were derived from Miocene components of the ancestral Vitiaz island arc that underpins the Fiji platform, but was active before polarity reversal of the Vitiaz arc, tectonic rotation of the Fiji platform adjacent to the North Fiji Fracture Zone (Fig. 1), and opening of the North Fiji Basin to the west by backarc seafloor spreading behind the New Hebrides (Vanuatu) island arc. All postarc tempers of Fiji lack orthopyroxene (Table 1, F2–F9).

Tongan placer tempers (Table 1, G1–G4) were derived from blankets of airfall tephra deposited over the surfaces of uplifted limestone islands in the forearc belt by pyroclastic eruptions along the volcanic chain to the west (Dye and Dickinson, 1996; Dickinson et al., 1996). The placer sands used as temper occur as pockets of black sand on modern beach faces composed dominantly of calcareous sand washed onshore from offshore reef tracts. The compositions of placer tempers in sherds from Tongatapu and the Ha'apai Group are statistically indistinguishable, but sherds from the Vava'u Group farther north contain tempers with consistently less orthopyroxene (Table 1, G4 vs. Table 1, G1–G3). The contrast in temper mineralogy suggests a systematic difference in the orthopyroxene content of the tephra blanket in Vava'u as opposed to the tephra blankets on Tongatapu and in Ha'apai. The lack of hornblende in any Tongan tempers accords with the absence of hydrous phases from all Tongan eruptive assemblages (Bryan et al., 1972; Ewart and Bryan, 1973; Ewart et al., 1973; Ewart, 1976).

In the Mariana Islands, non-placer tempers derived from andesitic sources on Saipan contain significantly more orthopyroxene than tempers derived from andesitic sources on Guam (Dickinson et al., 2001), but no placer tempers derived from mafic volcanic rocks are yet known from Saipan where many temper sands were derived from dacitic sources. If present in unstudied sherds, Saipan placer tempers would be expected to contain as much orthopyroxene, relative to clinopyroxene, as Tongan placer tempers.

9. SUMMARY RELATIONS

Fig. 6 displays the compositions of all known Oceanian placer temper types of volcanic derivation in graphical format. Except for one hornblende-rich arc temper from Bougainville and two olivine-rich hotspot tempers from Samoa, clinopyroxene is the most abundant species of ferromagnesian mineral grain in all temper types. Olivine forms $>25\%$ of the placer temper grains only in Samoan hotspot tempers ($n = 4$). Except for one postarc TLTF temper, orthopyroxene occurs only in selected

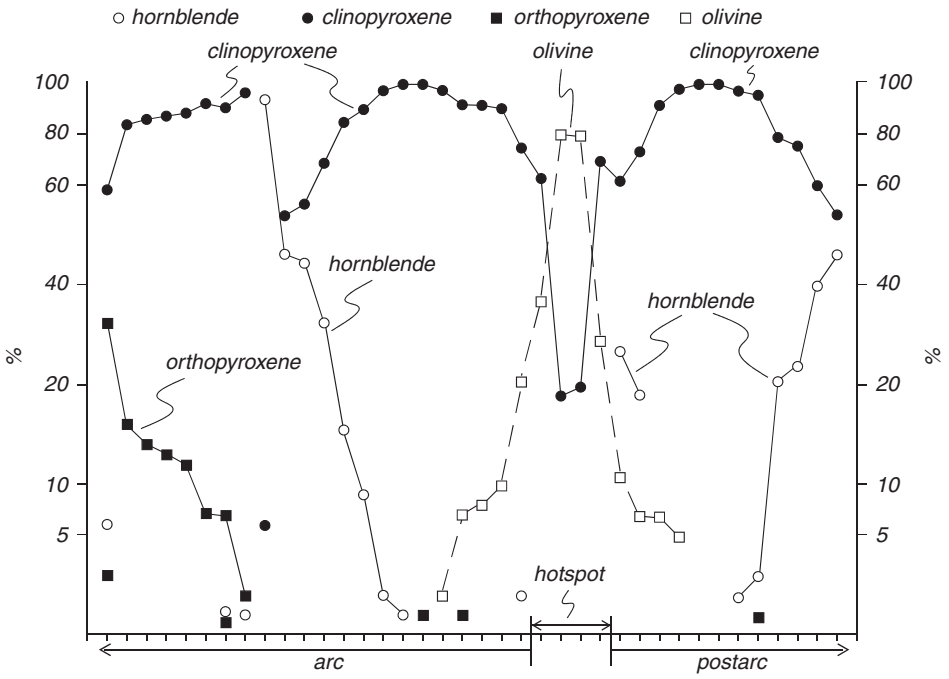

Fig. 6. Plot of Oceanian placer temper compositions ($n = 38$). Note scale changes at 5, 20, and 60% (data from Table 1 and Figs. 2–5). Placement of temper types along abscissa arbitrary within each temper class (arc, hotspot, postarc).

arc tempers ($n = 10$), mainly from New Britain and Tonga. Hornblende and olivine occur in selected placer tempers from both arc and postarc geotectonic settings, and in similar numbers of temper types in each case (arc: $n = 9$ for hornblende and $n = 5$ for olivine; postarc: $n = 8$ for hornblende and $n = 4$ for olivine). Hornblende and olivine occur in combination, however, only in selected postarc tempers of Fiji ($n = 3$) and selected arc tempers ($n = 2$) of New Britain. In general, distinctions between arc and postarc tempers on the basis of heavy mineral content alone are not feasible except where aegirine-augite derived from alkalic volcanic assemblages is present in TLTF postarc temper types. Despite overlaps between the heavy mineral populations of arc and postarc tempers, the compositions of all the placer tempers are explicable in terms of known geologic relations on the islands where the tempers are present in indigenous sherds. Placer tempers of anomalous composition occur only in exotic sherds derived from other islands.

ACKNOWLEDGEMENTS

Preparation of this contribution was encouraged by Maria Mange. Sherds containing placer tempers were provided for petrographic study by archaeologists Wallace R. Ambrose, Simon Best, David V. Burley, Geoffrey Clark, Janet Davidson, Matthew Felgate, Stephanie Garling, Chris Gosden, Roger C. Green, Elizabeth

Hinds (née Shaw), Terry L. Hunt, Jesse D. Jennings, Jean Kennedy, Patrick V. Kirch, Peter Lape, B. Foss Leach, Patrick C. McCoy, Patrick D. Nunn, Sue O'Connor, Douglas Osborne, Edwin R. Ray, Fred M. Reinman, Richard Shutler, Jr., Matthew Spriggs, Glenn Summerhayes, and John Terrell. Thin sections of potsherds were prepared expertly by Ruperto Laniz and Ray Lund. Figures were prepared by Jim Abbott of SciGraphics (Tucson). Photomicrographs of sherd thin sections were kindly prepared by Maria Mange. Reviews by Peter F. Ballance, Richard Shutler, Jr., and Maria Mange improved the presentation of data.

REFERENCES

Blake, D.H., Ewart, A., 1974. Petrography and geochemistry of the Cape Hoskins volcanoes, New Britain, Papua New Guinea. Geological Society of Australia Journal 21, 319–331.

Blake, D.H., Miezitis, Y., 1967. Geology of Bougainville and Buka Islands, New Guinea. Australian Bureau of Mineral Resources, Geology, and Geophysics Bulletin 93 (Bulletin PNG 1), 56.

Bryan, W.B., Stice, G.D., Ewart, A., 1972. Geology, petrography, and geochemistry of the volcanic islands of Tonga. Journal of Geophysical Research 77, 1566–1585.

Carney, J.N., MacFarlane, A., Mallick, D.I.J., 1985. The Vanuatu island arc: an outline of the stratigraphy, structure, and petrology. In: Nairn, A.E.M., Stehli, F.G., Uyeda, S. (Eds.), The Ocean Basins and Margins, vol. 7A, The Pacific Ocean. Plenum Press, New York, pp. 683–718.

Clough, R., 1992. Firing temperatures and the analysis of oceanic ceramics: a study of Lapita ceramics from Reef/Santa Cruz, Solomon Islands. In: Galipaud, J.-C. (Ed.), Poterie Lapita et Peuplement. ORSTOM (Office de Recherche Scientifique et Technologique Outre-Mer), Noumea, pp. 177–192.

Cole, J.W., Gill, J.B., Woodhall, D., 1985. Petrologic history of the Lau Ridge, Fiji. In: Scholl, D.W., Vallier, T.L. (Eds.), Geology and Offshore Resources of Pacific Island Arcs—Tonga Region. Circum-Pacific Council for Energy and Mineral Resources Earth Science Series, vol. 2, pp. 379–409.

Colley, H., Ash, R.P., 1971. The Geology of Erromango: New Hebrides Condominium Geological Survey Regional Report Series, 111pp.

Crook, K.A.W., Taylor, B., 1994. Structure and Quaternary tectonic history of the Woodlark triple junction region. Solomon Islands: Marine Geophysical Researches 16, 65–89.

Dickinson, W.R., 1994. Natural beach placer analogous to prehistoric island tempers. Journal of the Polynesian Society 103, 217–219.

Dickinson, W.R., 1998. Petrographic temper provinces of prehistoric pottery in Oceania. Australian Museum Records 50, 263–276.

Dickinson, W.R., 2000. Petrography of temper sands in prehistoric Watom sherds and comparison with other temper suites of the Bismarck Archipelago. New Zealand Journal of Archaeology 20 (1998), 261–282.

Dickinson, W.R., 2001. Petrography and geologic provenance of sand tempers in prehistoric potsherds from Fiji and Vanuatu. Geoarchaeology 16, 275–322.

Dickinson, W.R., 2006. Temper sands in prehistoric Oceanian pottery: geotectonics, sedimentology, petrography, provenance. Geological Society Special Paper, vol. 406, 164pp.

Dickinson, W.R., Butler, B.M., Moore, D.R., Swift, M., 2001. Geologic sources and geographic distribution of sand tempers in prehistoric potsherds from the Mariana Islands. Geoarchaeology 16, 827–854.

Dickinson, W.R., Shutler, R. Jr., 2000. Implications of petrographic temper analysis for Oceanian prehistory. Journal of World Prehistoryn 14, 203–266.

Dickinson, W.R., Shutler, R. Jr., Shortland, R., Burley, D.V., Dye, T.S., 1996. Sand tempers in indigenous Lapita and Lapitoid Polynesian Plainware and imported protohistoric Fijian pottery of Ha'apai (Tonga) and the question of Lapita tradeware. Archaeology in Oceania 31, 87–98.

Dickinson, W.R., Takayama, J., Snow, E.A., Shutler, R. Jr., 1990. Sand temper of probable Fijian origin in prehistoric potsherds from Tuvalu. Antiquity 64, 307–312.

Dye, T.S., Dickinson, W.R., 1996. Sources of sand tempers in prehistoric Tongan pottery. Geoarchaeology 11, 141–164.

Ewart, A., 1976. A petrological study of the younger Tongan andesites and dacites, and the olivine tholeiites of Niaufo'ou Island, S.W. Pacific. Contributions to Mineralogy and Petrology 58, 1–21.

Ewart, A., Bryan, W.B., 1973. The petrology and geochemistry of the Tongan islands. In: Coleman, P.J. (Ed.), The Western Pacific: Island Arcs, Marginal Seas, Geochemistry. Crane Russak and Company, New York, pp. 503–522.

Ewart, A., Bryan, W.B., Gill, J.B., 1973. Mineralogy and geochemistry of the younger volcanic islands of Tonga. Journal of Petrology 14, 429–465.

Felgate, M.W., Dickinson, W.R., 2001. Late-Lapita and post-Lapita pottery transfers: evidence from intertidal-zone sites of Roviana Lagoon, Western Province, Solomon Islands. In: Jones, M., Sheppard, P. (Eds.), Australasian Connections and New Directions. University of Auckland Research in Anthropology and Linguistics No. 5, pp. 105–122.

Fitzpatrick, S.M., Dickinson, W.R., Clark, G., 2003. Ceramic petrography and cultural interaction in Palau, Micronesia. Journal of Archaeological Science 30, 1175–1184.

Green, R.C., 1996. Prehistoric transfers of portable items during the Lapita horizon in Remote Oceania: a review. Indo-Pacific Prehistory Association Bulletin 15, 119–130.

Green, R.C., 2000. An introduction to investigations on Watom Island, Papua New Guinea. New Zealand Journal of Archaeology 20 (1998), 5–27.

Heming, R.F., 1974. Geology and petrology of the Rabaul Caldera, Papua New Guinea. Geological Society of America Bulletin 85, 1253–1264.

Heming, R.F., 1977. Mineralogy and proposed *P-T* paths of basaltic lavas from Rabaul Caldera, Papua New Guinea. Contributions to Mineralogy and Petrology 61, 15–33.

Hughes, G.W., Craig, P.M., Dennis, R.S., 1981. Geology of the eastern outer islands. Solomon Islands Geological Survey Division Bulletin 4, 108.

Intoh, M., 1990. Ceramic environment and technology: a case study in the Yap Islands in Micronesia. Man and Culture in Oceania 6, 35–52.

Intoh, M., Dickinson, W.R. (2002). Prehistoric pottery movements in western Micronesia: technological study of potsherds from Fais Island. In: Bedford, S., Sand, C., Burley, D. (Eds.), Fifty Years in the Field: Essays in Honour and Celebration of Richard Shutler, Jr.'s Archaeological Career. New Zealand Archaeological Association Monograph, vol. 25, pp. 123–134.

Johnson, R.W., Wallace, D.A., Ellis, D.J., 1976. Feldspathoid-bearing potassic rocks and associated types from volcanic islands off the coast of New Ireland, Papua New Guinea: a preliminary account of geology and petrology. In: Johnson, R.W. (Ed.), Volcanism in Australasia. Elsevier, Amsterdam, pp. 297–316.

Kear, D., Wood, B.L., 1959. The geology and hydrology of Western Samoa. New Zealand Geological Survey Bulletin n.s. 63, 90pp.

Kirch, P.V., 1997. The Lapita Peoples: Ancestors of the Oceanic World. Blackwell Publishers, Cambridge, 353 pp.

Ladefoged, T.N., Wall, J., Black, P., Dickinson, W.R., 1998. Exotic and indigenous ceramic sherds from the island of Rotuma. Journal of the Polynesian Society 107, 301–311.

Lowder, G.G., Carmichael, I.S.E., 1970. The volcanoes and caldera of Talasea, New Britain: geology and petrology. Geological Society of America Bulletin 81, 17–38.

MacFarlane, A., Carney, J.N., Crawford, A.J., Greene, H.G., 1988. Vanuatu—a review of the onshore geology. In: Greene, H.G., Wong, F.L. (Eds.), Geology and Offshore Resources of Pacific Island Arcs—Vanuatu Region. Circum-Pacific Council for Energy and Mineral Resources Earth Science Series, vol. 8, pp. 45–91.

Meijer, A., Reagan, M., Ellis, H., Shafiqullah, M., Suter, J., Damon, P., Kling, S., 1983. Chronology of events in the eastern Philippine Sea. In: Hayes, D.E. (Ed.), The Tectonic and Geologic Evolution of Southeast Asian Seas and Islands; Part 2. American Geophysical Union Geophysical Monograph, vol. 27, pp. 349–359.

Natland, J.H., 1980. The progression of volcanism in the Samoan linear volcanic chain. American Journal of Science 280-A, 709–735.

Natland, J.H., Turner, D.L., 1985. Age progression and petrological development of Samoan shield volcanoes: evidence from K-Ar ages, lava composition, and mineral studies. In: Brocher, T.M. (Ed.), Investigations of the Northern Melanesian Borderland, vol. 3. Circum-Pacific Council for Energy and Mineral Resources Earth Science Series, pp. 139–171.

Ramsay, W.R.H., Crawford, A.J., Foden, J.D., 1984. Field setting, mineralogy, chemistry, and genesis of arc picrites, New Georgia, Solomon Islands. Contributions to Mineralogy and Petrology 88, 386–402.

Reagan, M., Meijer, A., 1984. Geology and geochemistry of early arc-volcanic rocks from Guam. Geological Society of America Bulletin 95, 701–713.

Rodda, P., 1994. Geology of Fiji. In: Stevenson, A.J., Herzer, R.H., Ballance, P.F. (Eds.), Geology and Submarine Resources of the Tonga-Lau-Fiji Region. South Pacific Council (SOPAC) Technical Bulletin 8, 131–151.

Rodda, P., Lum, J., 1990. Geological evolution and mineral deposits of Fiji. Geologisches Jahrbuch D92, 37–66.

Rogerson, R.J., Hilyard, D.B., Finlayson, E.J., Johnson, R.W., McKee, C.O., 1989. The geology and mineral resources of Bougainville and Buka Islands, Papua New Guinea. Geological Survey of Papua New Guinea Memoir 16, 217.

Seeley, J.B., Searle, E.J., 1970. Geology of the Rakiraki district, Viti Levu. New Zealand Journal of Geology and Geophysics 13, 52–71.

Setterfield, T.N., Eaton, P.C., Rose, W.J., Sparks, R.S.J., 1991. The Tavua caldera, Fiji: a complex shoshonitic caldera formed by concurrent faulting and sagging. Geological Society of London Journal 148, 115–127.

Spriggs, M., 1997. The Island Melanesians. Blackwell Publishers, Oxford, 326pp.

Stanton, R.L., Bell, J.D., 1969. Volcanic and associated rocks of the New Georgia Group, British Solomon Islands Protectorate. Overseas Geology and Mineral Resources 10, 113–145.

Stice, G.D., 1968. Petrography of the Manu'a Islands, Samoa. Contributions to Mineralogy and Petrology 19, 343–357.

Walker, G.P.L., Heming, R.F., Speed, T.J., Walker, R.F., 1981. Latest major eruption of Rabaul volcano. In: Johnson, R.W. (Ed.), Cooke-Ravian Volume of Volcanological Papers. Geological Survey of Papua New Guinea Memoir 10, 181–193.

Wallace, D.A., Johnson, R.W., Chappell, B.W., Arculus, R.J., Perfit, M.R., Crick, I.H., 1983. Cainozoic volcanism of the Tabar, Lihir, Tanga, and Feni Islands, Papua New Guinea: geology, whole-rock analyses, and rock-forming mineral compositions. Australian Bureau of Mineral Resources, Geology, and Geophysics Report 243 [BMR Microfilm MF197], 62.

Woodhall, D., 1985. Geology of the Lau Ridge. In: Scholl, D.W., Vallier, T.L. (Eds.), Geology and Offshore Resources of Pacific Island Arcs—Tonga Region. Circum-Pacific Council for Energy and Mineral Resources Earth Science Series, vol. 2, pp. 351–378.

Zuffa, G.G., 1979. Hybrid arenites: their composition and classification. Journal of Sedimentary Petrology 50, 21–29.

This page intentionally left blank

Chapter 40

THE PROVENANCE OF PASTE AND TEMPER IN ROMAN AMPHORAE FROM THE ISTRIAN PENINSULA, CROATIA

MARIA A. MANGE[a] AND TAMÁS BEZECZKY[b]

[a]*Department of Geology, UC Davis, One Shields Avenue, Davis, CA 95616, USA*
[b]*Institute for Studies of Ancient Culture, Austrian Academy of Sciences, Bäckerstrasse 13, PF 8 1010 Vienna, Austria*

ABSTRACT

Roman amphorae, manufactured in the Laecanius workshop in Istria, Croatia, between 10-5 B.C. and 78 A.D, were analysed by integrating archaeological and geological laboratory methods, including thin section petrography, X-ray diffractometry (XRD) and, for the first time, heavy mineral analysis. Characteristics of the fabric allow categorisation of the amphora sherds into fabric groups. Petrography shows that quartz is the dominant clastic component in the sherds while carbonate is common as temper; XRD provided information on firing temperatures that ranged between 750 and 900°C. The amphora sherds contain diverse detrital heavy minerals with generally high epidote and garnet quantities. Occasionally zircon is also important. Garnet/epidote ratios and the presence of diagnostic species (pyroxene, hornblende) show systematic variations that coincide with similar variations in fabric characteristics. Heavy mineral signatures in amphorae produced in other workshops facilitated their distinction from the Laecanius sherds. Comparative heavy mineral analysis of terra rossa found close to the workshop indicate that terra rossa was the major source of the paste. Differences observed in the heavy mineral composition of the amphora sherds and terra rossa are interpreted by the polygenetic nature and spatial heterogeneity of the latter and the mixing of the paste with sandy temper. Modern Adriatic sponge spicules present in the majority of Laecanius amphora sherds and the temper-derived, generally immature, heavy mineral assemblages suggest that the sandy material for the temper was obtained from Adriatic deposits. The heavy mineral technique, as a powerful archaeometric tool, is demonstrated by revealing the provenance of raw materials, and by recognising the compositional difference between the Laecanius amphorae and the sherds from other workshops and the spica sample.

Keywords: Laecanius workshop; Dressel 6B amphora; amphora sherds; terra rossa; firing temperatures; raw material provenance; sponge spicules

Developments in Sedimentology, Vol. 58, 1007–1033

ISSN: 0070-4571/doi:10.1016/S0070-4571(07)58040-4

1. INTRODUCTION

Archaeology and geology have long enjoyed a mutual interdependence because archaeological raw materials have predominantly geological origin. Artefacts made of stone or clay, the principal inorganic raw material of ancient times, can be best analysed by techniques used in geological laboratories. Pottery sherds are amongst the most abundant artefacts at archaeological sites, amongst which the study of Roman amphorae has established a distinguished place in ceramics research. Amphorae were the two-handled large pottery containers of the Greek and Roman world, used for the storage and transportation of liquids, especially wine, olive oil and other foodstuffs.

We have conducted an interdisciplinary study of Roman amphorae manufactured during the first century A.D. (10-5 B.C. and 78 A.D.) on the western coast of the Istrian peninsula in the northern Adriatic region. We attempted to integrate archaeological and geological methods to increase precision in characterisation and grouping of amphorae and to determine the provenance of the material used for the paste and temper. Geological methods included heavy mineral analysis, thin section petrography and XRD. Knowledge of the source of raw material can also provide an insight into ancient transport, trade routes and manufacturing practices, indicating improvements or decline in technology. Variations in output are controlled principally by the strength of the economy; therefore, new information on the production, distribution and dating of amphorae from any Roman period may advance our understanding of contemporary economy. The prolonged existence of pottery workshops in Istria, supported by the high output of agricultural products, has long been the focus of archaeological research (Baldacci, 1967–1968; Buchi, 1973; Carre, 1985; Manacorda, 1994; Mazzocchin and Pastore, 1996–1997; Bezeczky, 1998; Cipriano and Mazzocchin, 1998; Martin-Kilcher, 2000; Pesavento Mattioli et al., 2000; Tassaux, 2001). In this study we concentrate on previously unexplored aspects of ceramics research in Istria.

1.1. The Istrian Peninsula, Physiography and Geology

The Istrian Peninsula in northwestern Croatia occupies an area of 2820 km^2, rising from sea level to approximately 1400 m in the Cicarija Mountains in the northeast (Fig. 1, inset). The southwestern part of the Peninsula is a 300 m high plateau with a typical karstic landscape, characterised by 5–10 m deep dolines (sinkholes) and karren (limestone pavements). The soil here is the conspicuous terra rossa, a red clay to silty-clay soil widespread throughout the Mediterranean. Terra rossa is intimately linked to carbonate rocks and is thus typically associated with karstic features, filling in cracks and sinkholes (Durn et al., 1999; Miko et al., 1999). This area is commonly referred to as ''Red Istria'' because of the intense red colour of the soil. The Trieste-Pazin belt in central and north-western Istria, with its greyish marly or sandy soil, is called ''Grey Istria''. The Cicarija Mountains to the north, with their bare white cliffs (''White Istria''), form a prominent landscape feature.

As part of the northwestern region of the Adriatic Carbonate Platform (Velić et al., 1995), Istria comprises three principal geological units (Fig. 1): (1) the Upper Jurassic to Cretaceous carbonate plain of southern and western Istria; (2) Cretaceous-Palaeogene

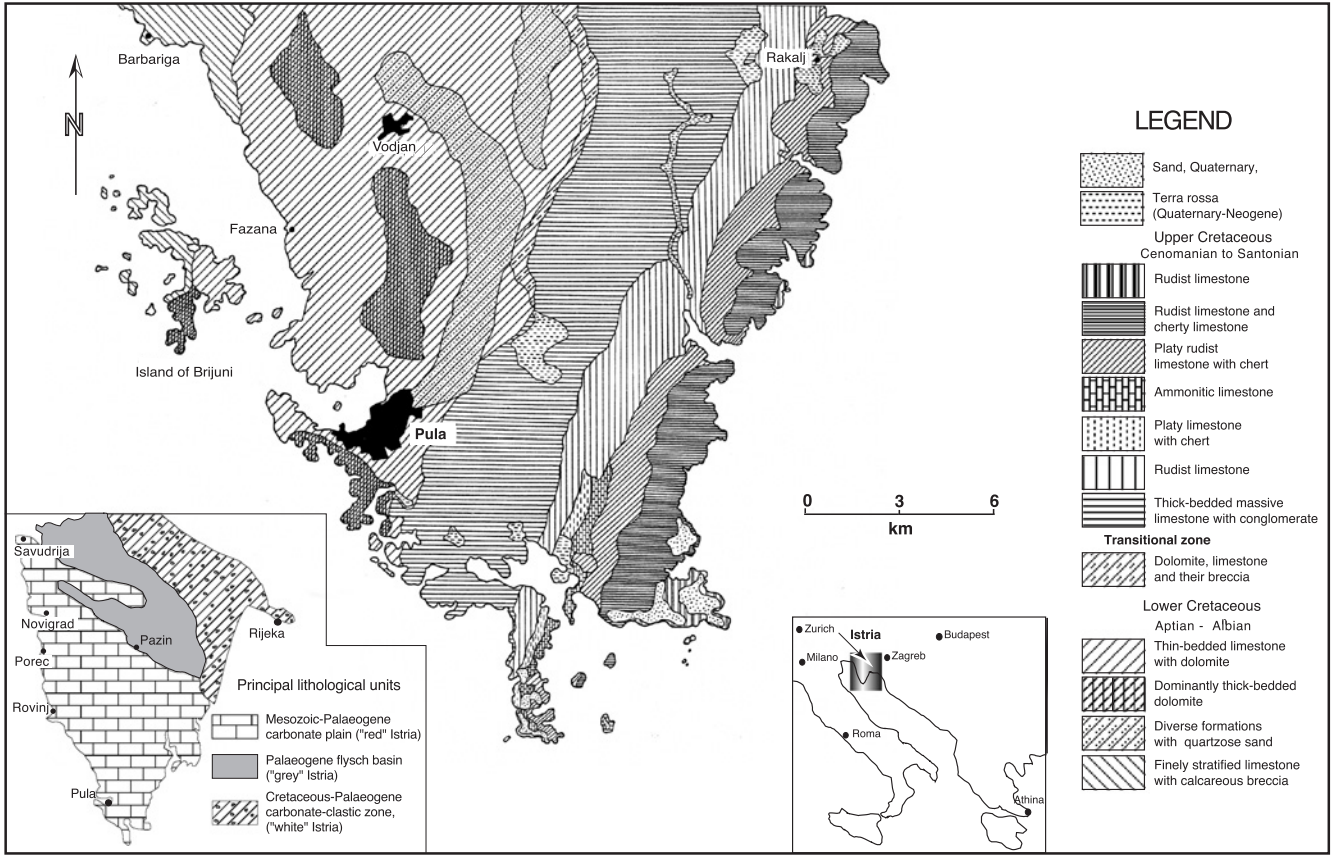

Fig. 1. Simplified geological map of the southern part of Istria. [After Polšac (1964).] Inset shows the three principal geological regions of the island.

carbonate-clastic successions occupying the eastern and north-eastern part of Istria and (3) a Palaeogene flysch basin in central Istria. Late Pleistocene loess occurs only in the southern and north-eastern regions (Durn et al., 1999, 2007—this volume).

1.2. Historical Background

The Romans showed interest in the Istrian region already at the time of the Roman Republic (second century B.C.) with the establishment of the colony of Aquileia in the vicinity in 181 B.C. This served as a centre for military, economical and commercial activities after the founding of the colonies at Pola and Tergeste (Fig. 2) in the middle of the first century. A number of Roman settlers and merchants colonised the fertile western coastal region. After the end of the Roman Republic and the chaos of civil war from which Augustus emerged victoriously in 31 B.C., the Roman Empire entered into a phase of peace and security that spread

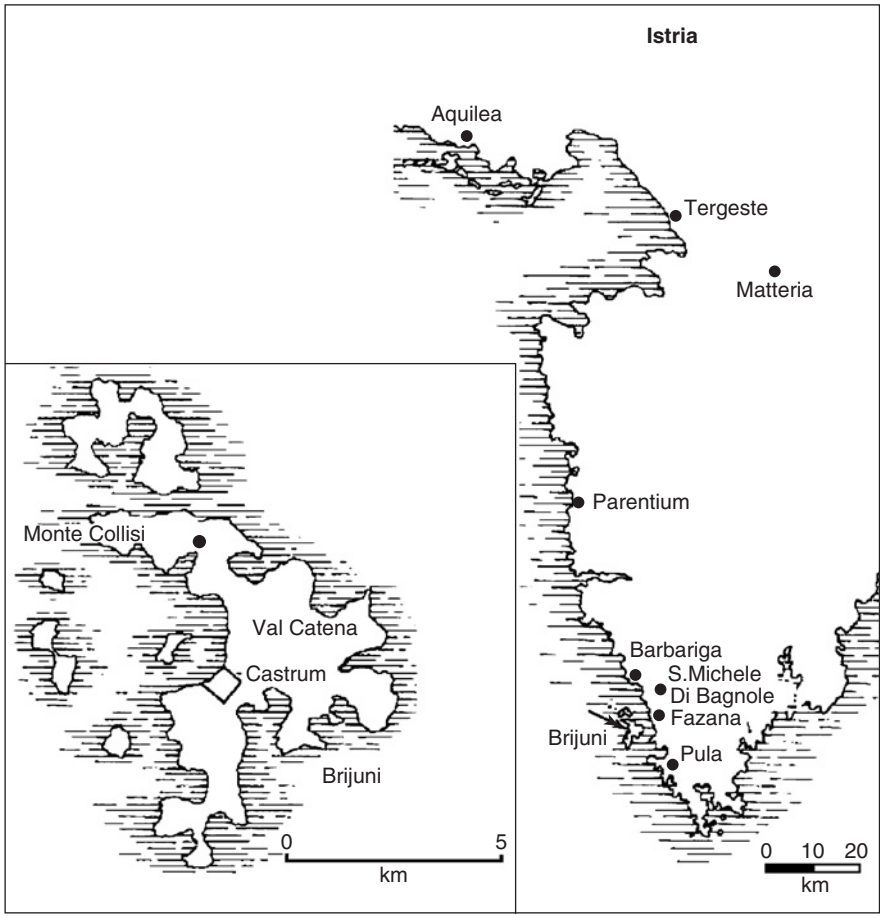

Fig. 2. Historical map of Istria, showing Roman names of ancient towns, and map of the Island of Brijuni.

throughout the Empire and influenced, for a long period, the life and economy of the provinces. Political stability resulted in prosperity with thriving trade and cultural vitality throughout the Mediterranean. The ties between Italy proper and Istria developed quickly, and between 18 and 12 B.C. the peninsula became part of Regio X (Venetia et Histria). Augustus himself, senators and the ruling elite showed increasing interest in the Istrian peninsula and purchased estates in the region (Tassaux, 2001).

In the Mediterranean climate a thriving agriculture developed and produced large quantities of wine and olives. The ancient textural sources (Pliny the Elder: Natural History 15.9; see translation in Pliny the Elder, 1952) regarded Istrian olive oil among the best on the market. The Istrian wine reached the emperor's table, and Pliny the Elder (Natural History 2.127; 16.60; 17.31; see translation in Pliny the Elder, 1952) tells us that Empress Livia enjoyed the wine produced in Pucinum, near Tergeste. The Roman landowners cultivated, harvested and processed the olives, had their own oil presses, storage cellars and ceramic workshops. The olive oil produced by the Istrian estates (villas) fulfilled the needs of the northern Roman provinces (Raetia, Noricum and Pannonia) and the rest of northern Italy for more than a century. Excavations in these regions have brought to light large quantities of amphorae, both in civil settlements and in military camps. The production of olive oil in Istria, from the end of the first century B.C. and the beginning of the second century A.D., is well-documented. Near the end of the reign of Emperor Hadrian (A.D. 117–138), the Istrian olive oil suddenly disappeared from the market. Istrian oil production by the villas satisfied only local demand afterwards (Baldacci, 1967–1968; Bezeczky, 1998; Tassaux, 2001).

1.3. The Istrian Villas

Traces of several villas with olive-producing facilities (Matijašić, 1993) have been discovered between Pula and Tergeste (Fig. 2). Their owners were mainly senators and members of the Roman elite. Among the best-known landowners the Laecanius Family owned a villa at Fazana, 9 km north of Pula, location of a well-known amphora workshop in Istria (Fig. 2). The villa was excavated at by Gnirs (1910), who also found the amphora kiln of the workshop. Between the late first century B.C. and early second century A.D. the amphorae produced in this workshop were shipped to northern Italy and provinces beyond the Alps. They were found in over 50 ancient sites in Italy, Austria, Switzerland, Hungary, Slovenia and Croatia (Mazzocchin and Pastore, 1996–1997; Bezeczky, 1998; Cipriano and Mazzocchin, 1998; Pesavento Mattioli et al., 2000). Initially the members of the Laecanius Family were ordinary landowners. The first well-known member was Caius Laecanius Bassus. He and his son by the same name were consuls in 40 and 64 A.D. (Tassaux, 1982). In a very short time the family attained great wealth by producing and trading olive oil, then held various offices, became members of the equestrian aristocracy and the Senate. Other Istrians had similarly meteoric careers. Amphorae were found at a villa near the hill of Loron (Fig. 2) outside Parentium (modern Poreč), that initiated Croatian and French archaeologists to search for additional workshops. The Loron amphorae suggest that this

villa was, probably, first owned by T. Statilius Taurus Sisenna, and later by Calvia Crispinilla (Tassaux et al., 2001).

1.4. The Laecanius Villas, Workshops and Amphorae

Further to the villa and workshop (figlina) in Fazana (Fig. 2), the remains of three other villas were discovered on the Island of Brijuni where amphorae, marked with Laecanius stamps, were also identified. Although no owner stamps were found on the amphorae, these villas were identified as probably owned by the Laecanius Family (Bezeczky, 1998; Tassaux, et al., 2001). The Val Catena villa was a luxurious maritime-villa (Fig. 3a) with elegant peristyles and colonnades, developed atria, bathrooms and an industrial area with presses and a cellar (Fig. 3b). Gnirs found a villa rustica on Monte Collisi (Kolci Hill: Fig. 3c), on the northwestern part of the island (Gnirs, 1908; Bezeczky, 1998). The three wings of the villa were built around a central courtyard. The living quarters were in the southwestern wing. The kitchen, presses and the large cellar were east of them. There is another villa in Dobrika Bay (Fig. 3d), in the western part of the island of Brijuni (Girardi Jurkić, 1985; Matijašić, 1993; Bezeczky, 1998). This villa was later surrounded by a late Roman/Byzantine fortress (Castrum). The excavations unearthed a central courtyard, a cistern, presses, millstones and two storage cellars among the early Imperial buildings. A pottery kiln (Fig. 3e) was also located in the workshop of the Fazana villa. The storage capacity in the cellars of the three villas was 10,000–12,000 amphorae annually. The products of the figlina include amphorae, stoppers, dolia, (dolium: big clay container/barrel, capacity ~1500 l) tiles, clay lamps, heating pipes and spicae (spica: small brick).

Traditionally, the Laecanius amphorae are regarded as of Dressel 6B type (Fig. 4), a typical product of Istria (Baldacci, 1967–1968; Buchi, 1973; Carre, 1985). This form is characteristic for all the Laecanian amphorae, although there may be some variations between the individual pieces. Unfortunately, very few complete amphorae were found, the overwhelming majority of the pieces are only fragments. Each amphora had two stamps on the rim, with the Laecanius stamp in the centre and the second stamp, the vilicus's (estate manager) stamp, above the handle (Fig. 5A). The names of more than 40 successive vilici are preserved in these stamps (e.g. Amicus, Amethystus, Clarus, Clymenus, Datus, Eucharistus, Felix, Hermes, Ialysus, Martius, Optatus, Paganus, Pierus, Speratus, Urbanus, Viator and others), providing a relative chronology of the workshop's history. These names also allow dating of the various historic phases (Bezeczky, 1998).

There are three known phases of the figlina at Fazana, and its complete history can be read from the stamps, from the stone inscriptions and from ancient written sources (Bezeczky, 1998; Tassaux, 2001): (1) from the end of the first century B.C. until A.D. 78 it belonged to the Laecanius Family; (2) during the reign of Emperor Vespasian (A.D. 69–79) the last Laecanius died without an heir and the ownership was taken over by the Emperor Vespasian, but there is also record of its use during Hadrian; (3) it is presumed that M. Aurelius Iustus rented the workshop around the last third of the second century A.D.

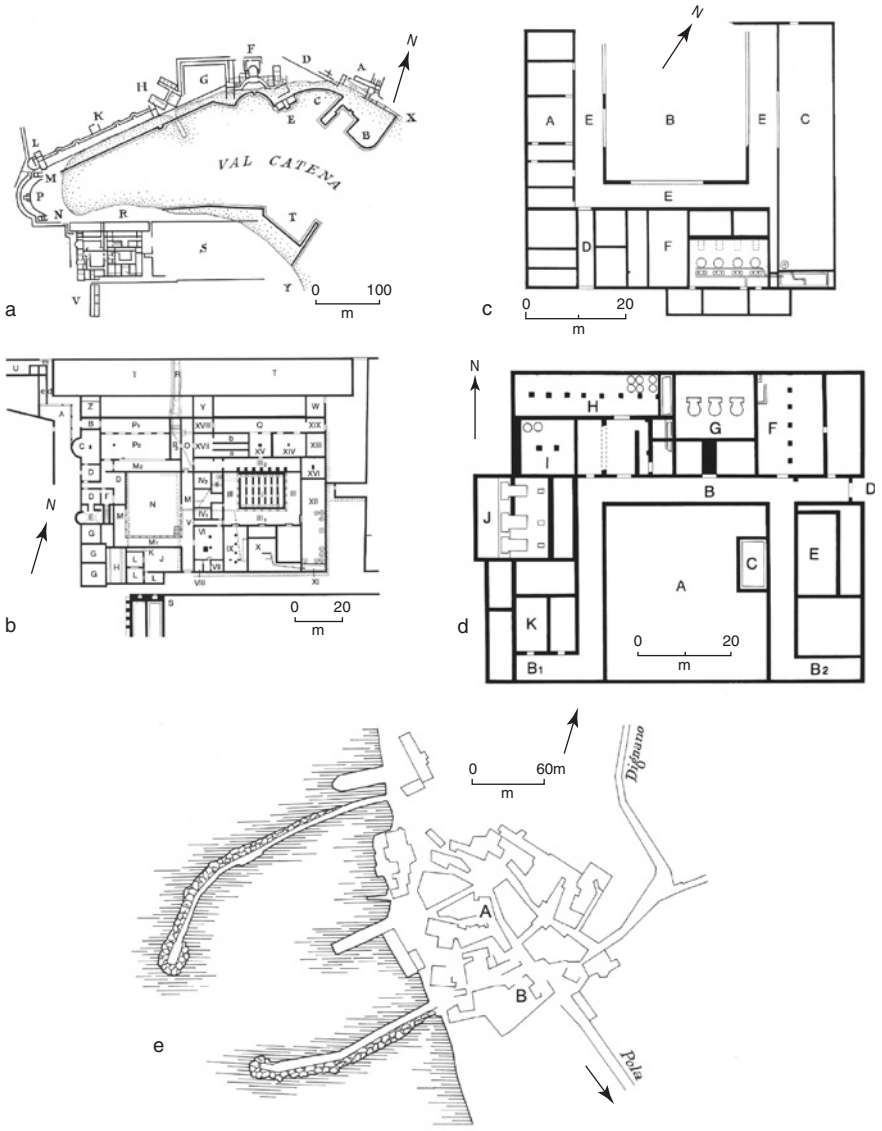

Fig. 3. Istrian villas. (a) Verige (Val Catena) maritime villa; (b) Verige villa, living quarters and industrial unit (X = press room, XII = *cella olearia* with *dolia*); (c) Kolci Hill (Monte Collisi) *villa rustica* (F = preparation room and press room, C = *cella olearia* with *dolia*); (d) Castrum *villa rustica* (G and J = press rooms, H and I = *cella olearia* with *dolia*); (e) Fazana modern village (A = pottery kiln, B = *villa rustica*).

2. METHODS

Fabric analysis is generally the first archaeological method in the description of ceramics. Fabric is important for the characterisation of the raw material and for

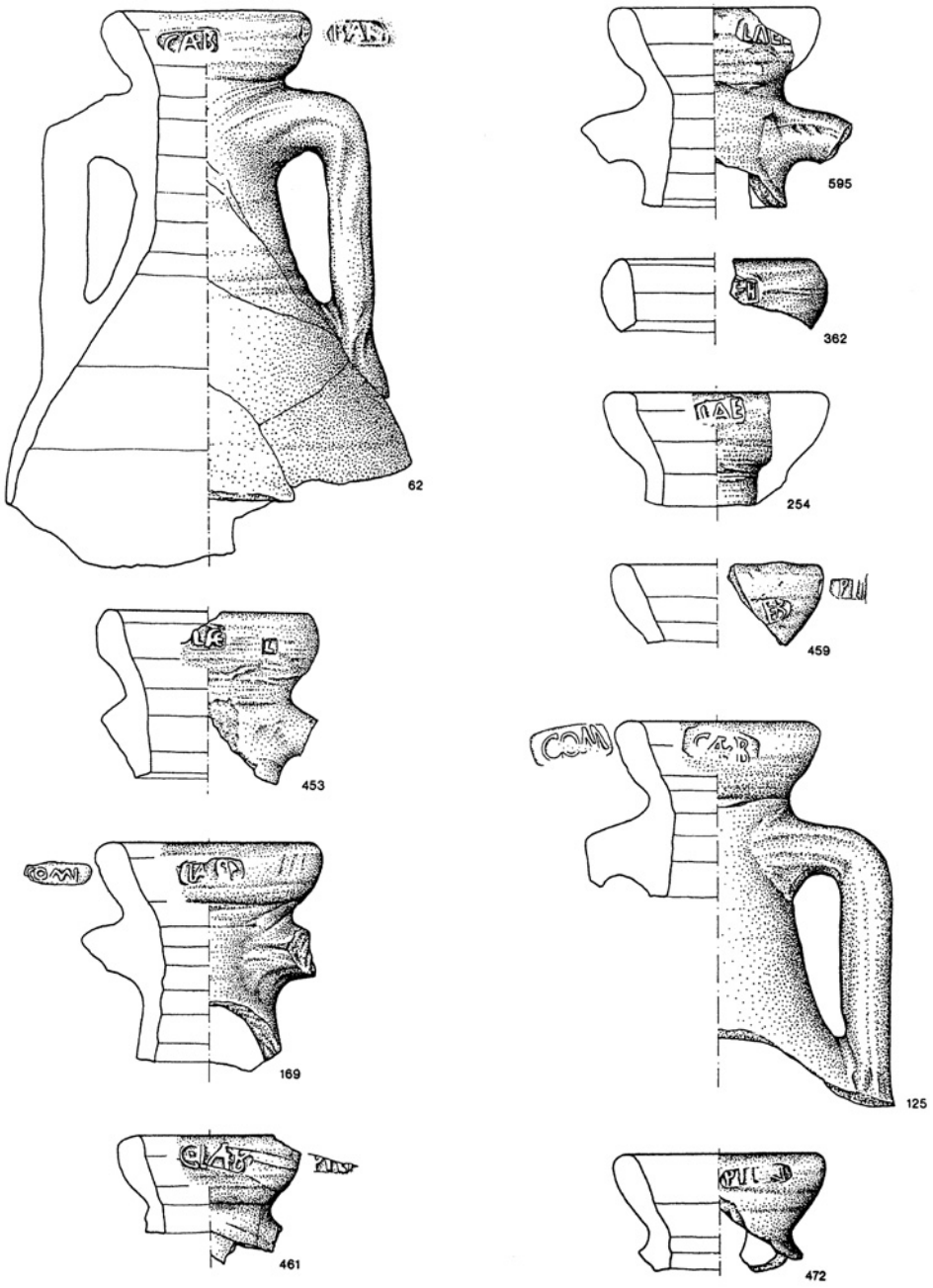

Fig. 4. Examples of Dressel 6B type amphorae. Catalogue numbers correspond with heavy mineral sample numbers.

Fig. 5. (A) Amphora stamps showing the stamp of Laecanius, C(aius) Laec(anii) Bassi (L_1) and Vicillus Felix ser(vus) (V_1), L-A-E in ligature; C(aius) Laek(anii) B(assi) (L_2) and Vicillus Barb (V_2), L-A-E-K in ligature. In 99% of the cases, the name was written as LAEK(ani). Literary sources and stone inscriptions always have the name as LAEC. (In our own text, we will consistently use the Laecanius form). (B) Stereomicroscope photographs of the surface of representative sherds from each fabric group. Scale 0.5 cm in all photomicrographs.

providing an insight into processes used in the manufacture of pottery. Distinguishing signatures include colour, physical properties, texture and inclusions. These vary between sherds and those with similar characteristics are allocated into discrete fabric groups. Consequently, sherds with corresponding fabrics indicate similar raw material and production technology.

Because ceramics are anthropogenically prepared and high-temperature-fired products, derived from naturally occurring, predominantly "soft" rocks, geological laboratory techniques developed for the analysis of their source materials are equally

suitable for ceramic analysis. Peacock (1967, 1970) was one of the first to recommend heavy mineral analysis as an archaeometric tool, especially for ceramics. He emphasised its potential for locating the source of raw material and aiding accuracy in classification and grouping. Identification of the temper added to the paste is important for the reconstruction of methods used by different workshops. Heavy mineral analysis is an effective tool for temper characterisation (Dickinson, 2007—this volume). Numerous researchers have used heavy mineral analysis successfully in the study of ceramics, especially amphorae (Williams, 1977; Peacock and Williams, 1986). This technique has been frequently used in recent years for comparative investigation and provenance evaluation of ceramics in Austria (Sauer, 1989, 1997; Zabehlicky-Scheffenegger et al., 1996).

In an earlier study (Mange and Bezeczky, 2006) Laecanius amphorae sherds were analysed using XRD and thin section petrography and in the present contribution we report on the heavy mineral study of Laecanius amphorae, manufactured in the Fazana workshop in Istria. Sherds were collected in Fazana, other locations on the island or at more distant sites, such as Magdalensberg (Austria) and Aquincum (Hungary). Our objectives were (i) to trace the sources of raw material that was, until now, poorly understood and (ii) to compare and differentiate the products of various coeval workshops in the region. Study material included 50 Laecanius amphora sherds, one spica sample, five sherds from other workshops in the region and six surface samples that were collected for comparison from quarries near Pula and Rovinj (Fig. 1).

Neck, rim or handle fragments proved most suitable for the analyses, because their larger size (rarely larger than 2×2 cm) provides sufficient amounts of heavy minerals. Sample preparation and heavy mineral separation followed the technique described by Mange and Maurer (1992). Sherds were gently crushed, using a mortar and pestle and sieved frequently through a 300 μm diameter sieve to prevent over-grinding and breakage of the grains. The fine substances were removed by wet-sieving, using a sieve of 40 μm diameter. The dry material was sieved, retaining the finer than 210 μm fraction for the heavy mineral separation. This relatively "coarse" size was chosen for the upper grain size limit to avoid overlooking any informative mineral species that may occur in the coarser grades. Separation was performed in bromoform (density 2.85), using the centrifuge and partial freezing method. Of the 50 sherds prepared and separated, only 31 yielded sufficient amounts of heavy residue that enabled counting 150–200 grains per sample, excluding micas. Heavy mineral residues were mounted in liquid Canada balsam on microscope slides, identified and counted under the polarizing microscope. All non-opaque grains were counted, including micas. The latter were counted separately and used for general information or comparison.

3. RESULTS

3.1. Fabric Analysis

Fabric analysis was carried out under the stereo microscope at magnification $20 \times$, focusing on physical properties and microscopic contents. Examination and

Table 1. Fabric groups of the Laecanius amphorae sherds and their percentage distribution in each group

Fabric	A	B	C	D	E	F	G	H	I	Total
%	40.9	26.6	2.7	9.8	8.2	1.6	2.3	7.0	0.9	100

variations of these properties permitted the allocation of the amphora sherds into fabric groups A–I, within which four main groups, A, B, E, H proved dominant (Table 1). Some amphora sherds have the characteristics of both types A and B but, because they were fired at higher temperatures, discrete groups (C and D) were created for them. Some enigmatic pieces were allocated to groups G and I. Approximately 80% of the amphorae belong to fabric groups A–D (Table 1). Stereomicroscopic photographs in Figs. 5B (a–i) portray representative specimens form each fabric group.

Colour of the fresh breaks and surfaces was recorded as Munsell Soil colour. The amphorae generally are light red (2.5YR 6/6–6/8), red (2.5YR 5/6–5/8) or reddish yellow (5YR 7/6–6/8). These are typical colours of the Istrian amphorae (Figs. 5B: a, b, f, h). By contrast, the colour of group E is pink with a porcellaneous groundmass (Fig. 5B: e). Sherds in groups C, D and G are light red and pink (2.5 YR 6/6 and 5YR 7/4) and enclose pieces of carbonate rocks and fine calcareous matter, dispersed in the fabric (Fig. 5B: c, d, g). Many sherds in group I contain inclusions comprising ground up ceramic pieces (Fig. 5B: i).

Regarding the physical characteristics, hardness, feel and fracture of the clay, as well as the frequency, sorting, size, rounding and the composition of the inclusions in the clay matrix were described according to Peacock (1977, 1984). The feel of all studied amphorae appeared ''smooth'', a texture caused by the small size range of the sand inclusions. Fracture was defined as: conchoidal, smooth, hackly or laminated. The fracture of the Fazana amphorae is 'hackly' with jagged, irregular surfaces and sharp edges.

Inclusions are embedded particles (Fig. 5B: i) and can be a natural part of the raw clay material or may have been intentionally added by the potter as temper to improve cohesion of the clay during working and firing and to increase durability in use. Our description and categorisation of the inclusions followed the criteria defined by Peacock (1977, 1984) such as (1) frequency (sparse $<5\%$, moderate 5–10%, common 10–30%, abundant $>30\%$); (2) sorting (well-sorted and poorly sorted; in the majority of the Fazana amphorae the inclusions are poorly sorted, with a moderate alignment of the grains); (3) size of the inclusions; (4) rounding grade (angular, sub-rounded, rounded; the inclusions were only slightly rounded in most of the products of the Fazana workshop); (5) composition (a measure for the percentage distribution of individual inclusions (Table A3.1, p. 379 in Whitbread, 1995): predominant $>70\%$, dominant 50–70%, frequent 30–50%, common 15–30%, few 5–15%, very few 2–5%, rare 0.5–2%, very rare $<0.5\%$). Details on inclusions in the Fazana workshop's amphorae are shown in the Appendix of Mange and Bezeczky (2006).

Even in amphorae marked with the same stamps, differences in both the groundmass and in clast content can be detected by microscopy. It is possible that such

amphorae were produced in different years with the raw material coming from a different bed of the same clay outcrop or from another location. The individual analysis of the rim, neck, body and handle of one particular amphora revealed that the handle was made of a stronger material. This suggests that either the phases of the manufacturing were well-coordinated (i.e. different paste was used for different parts of the amphorae according to their functions) or reflects the potter's skill (Bezeczky, 1987; Manacorda, 1994).

XRD analysis of the Dressel 6B amphora sherds from the Fazana workshop identified quartz as the dominant mineral phase in all samples. Plagioclase feldspars, illite and other micas were found only in low proportions. XRD provided the key for the reconstruction of firing-temperatures that varied between 750 and 900 °C. The range of the firing temperature was constrained by the stability of carbonate components and by neoformed calcium silicates. Three temperature brackets were recognised: (i) at "low" temperatures carbonate (added to the clay as temper, indicated by the study of inclusions) is present but pyroxene and gehlenite are absent; (ii) "moderate" firing temperature initiates the transformation of carbonate, though it is still recognizable, and pyroxene and gehlenite also appear; (iii) at "high" temperatures carbonate is no longer present, whereas calcium silicates (pyroxene and gehlenite) can be clearly identified. The distribution of the analysed samples according to firing temperature reveals that firing temperatures were dominantly in the "low" range (Weiszburg and Papp, 1987; Józsa et al., 1994; Mange and Bezeczky, 2006).

3.2. Heavy Mineral Analysis

The amphora sherds contain diverse, well-preserved heavy mineral suites enriched in epidote-group minerals and garnet (Fig. 6: Ep, G). Zircon, tourmaline, and brown hornblende (Fig. 6: Z, T, Hb.br) are present in moderately high proportions. Apatite, rutile (Fig. 6, A, Ru) and sphene are fairly common. Other species, occurring frequently but in low number include green and brown spinel, several amphibole varieties, pyroxenes, staurolite, kyanite and, rarely, anatase, brookite, allanite, corundum, blue sodic amphibole, serpentine and sillimanite. Point counting data, recalculated as number percentages, are shown in Table 2. Of the mica group, biotite is the most common: chlorite was occasionally found in small amounts, and white mica is rare. The original grain shapes may have been modified during manufacturing, but because euhedral or prismatic forms are common (Fig. 6: Z, Bi, T) and typical dissolution features on some pyroxenes, staurolite and kyanite—produced during diagenesis in their host sediments—are preserved (Fig. 6: St, G, Ky), the intensity of grinding cannot have been severe. This is also shown by the limited rounding of the inclusions observed during fabric analysis.

When low sample numbers preclude numerical analysis, presentation and evaluation of data is best achieved by graphical means. Histograms were created (Fig. 7) using principal heavy mineral content from representative Laecanius amphora sherds, amphorae sherds from other workshops, and our current terra rossa analyses from Istria.

The compositional trends of each group, especially the abundance variations of their major heavy mineral components, are clearly discernible in the histograms and

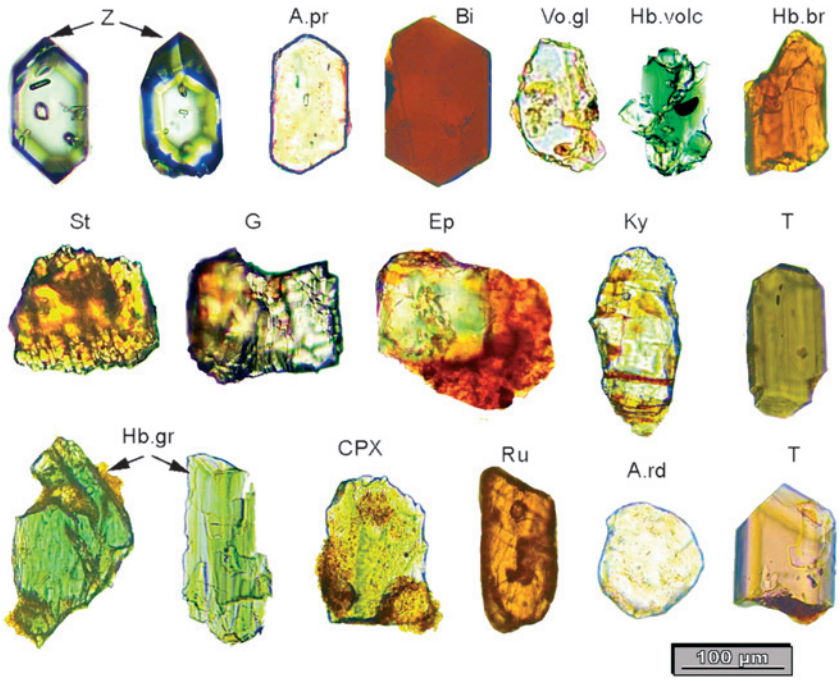

Fig. 6. Heavy minerals from the sherds. Z: zircon (euhedral, volcanogenic); Apr: apatite, gently rounded euhedral prism of volcanic derivation; Bi: hexagonal volcanogenic biotite; Vo.gl: volcanic glass shard (note the very low relief of the grain); Hb.volc: fresh blue-green hornblende, presumably volcanogenic; Hb.br: brown hornblende, presumably volcanogenic; St staurolite (etched); G: garnet (etched); Ep: epidote (note adhering clay matrix); Ky: kyanite; T: tourmaline, sharp euhedral; Hb.gr. blue-green hornblende; CPX: clinopyroxene; Ru: rutile; A.rd: rouded apatite grain.

are summarised in Table 3. The power of the method is demonstrated by the difference between Laecanius amphora sherds and those manufactured elsewhere. Workshops which produced Dressel 6B amphorae include amphora sherds from Costini, Apici, Vari Pacci and Calvia Crispinilla. The location of the workshop of the latter is known only, excavated in Loron near Parentium, others originated probably in northern Italy. The use of a different raw material is shown by the high garnet ratios (garnet/epidote >1; Table 3), variable—often high—zircon and apatite abundance and clinopyroxene frequency. Their distinctive signature is the presence of clinopyroxene in appreciable amounts. Costini contains fairly coarse heavy minerals (average 150 µm with several coarser epidote and garnet grains), and many fine botryoidal pyrites. The Apici heavy mineral suite is characterised by an unusually high quantity of sphene and a few grains of andalusite (the latter is absent in the Laecanius amphora sherds), an elevated amount of chlorite that is rare in the Laecanius samples, and some white mica. The two Vari Pacci amphora sherds are coarse-grained and enriched in either zircon or apatite. The single Calvia Crispinilla sherd yielded a small amount of fine grained heavy mineral residue with high zircon and tourmaline proportions. The distinctly coarser grained (150–200 µm) spica sample, found in a

Table 2. Heavy mineral composition of the Laecanius amphorae sherds, products of other workshops and terra rossa

	Zircon	Tourmaline	Apatite	Rutile	Staurolite	Kyanite	Epidote group	Sphene	Hornblende	Pyroxene	Spinel, brown	Garnet	Others	Remarks; other species
Amphora sherds														
A 62	11	14	9	4	0	1	29	1	7	0	1	23	0	Anthophyllite tr.
A 75	11	14	8	5	0	0	29	3	8	0	0	22	0	
A 336	18	7	5	10	0	0	27	0	9	0	0	24	0	
A 388	4	13	15	3	0	1	31	2	20	0	0	12	0	
A 414	6	9	7	5	1	1	30	1	25	0	1	12	2	Anthophyllite, tremolite
A 433	8	12	4	8	0	1	30	1	15	1	1	19	2	Tremolite
A 656	4	12	4	2	0	0	38	3	11	1	0	25	0	
B 151	8	18	6	1	0	0	26	4	1	3	0	28	3	Sillimanite, orthopyroxene
B 453	7	9	20	2	0	2	29	1	10	0	0	21	0	
B 339	1	3	7	6	0	1	38	2	15	0	0	28	0	Volcanic glass shards
C 169	21	17	5	8	0	1	17	2	8	0	1	20	2	Allanite, tremolite, kyanite tr.
D 461	4	4	7	3	1	0	33	5	4	1	1	36	2	Allanite
D 595	4	5	12	1	1	1	23	3	4	0	1	43	1	Allanite
E 71	10	12	4	8	2	0	23	0	12	0	0	29	0	
E 362	16	1	13	7	0	1	15	4	12	1	2	28	0	Orthopyroxene tr.
F 161	17	10	10	2	0	0	27	0	8	0	0	25	0	
F 254	16	11	6	2	0	0	32	3	13	1	0	16	1	Pale blue amphibole
G 459	11	3	13	2	0	0	38	1	12	5	1	12	3	Corundum, green spinel
H 467	3	2	10	1	0	1	43	2	19	0	0	16	4	Glaucophane, serpentine, tremolite

H 125	2	5	9	0	0	0	36	3	11	0	1	32	1	Sillimanite
I 370	6	6	9	4	0	0	46	1	15	0	0	12	1	Tremolite, sillimanite tr.
I 472	9	5	5	2	0	1	48	3	9	1	0	17	0	Orthopyroxene tr.
I 611	2	7	2	3	0	1	47	3	18	0	0	12	4	Tremolite
Spica, found at Verige Bay	19	5	5	11	0	6	9	1	20	18	0	3	2	Orthopyroxene, baryte, other amphiboles
Different workshops														
29 Costini	2	3	10	1	0	2	19	1	14	1	0	45	0	Allanite
17 Apici	2	1	22	1	0	0	21	7	13	3	0	28	3	Andalusite
116 Vari Pacci	27	2	5	2	0	0	20	0	5	7	0	30	2	Allanite
118 Vari Pacci	3	3	23	1	0	1	23	4	12	2	0	29	0	Orthopyroxene tr.
822 Calvia-Crispinilla	17	21	3	3	0	0	21	0	0	0	0	34	0	
Terra rossa														
Pula 1	1	5	5	3	3	1	34	3	17	1	3	21	3	Pale blue amphibole
Pula 2	7	7	1	2	2	1	41	2	17	0	1	9	11	Glaucophane, chloritoid
Pula region 03/1	15	23	2	10	2	1	12	4	6	2	4	19	0	
Pula region 03/2	11	26	5	11	2	1	8	9	2	0	10	16	0	
Pula quarry 03/1	10	34	9	4	1	1	9	8	5	0	5	12	1	Glaucophane
Rovijn quarry 03	7	5	1	4	3	1	46	1	7	0	1	10	13	Glaucophane, green spinel, tremolite

Note: tr. = in trace amounts.

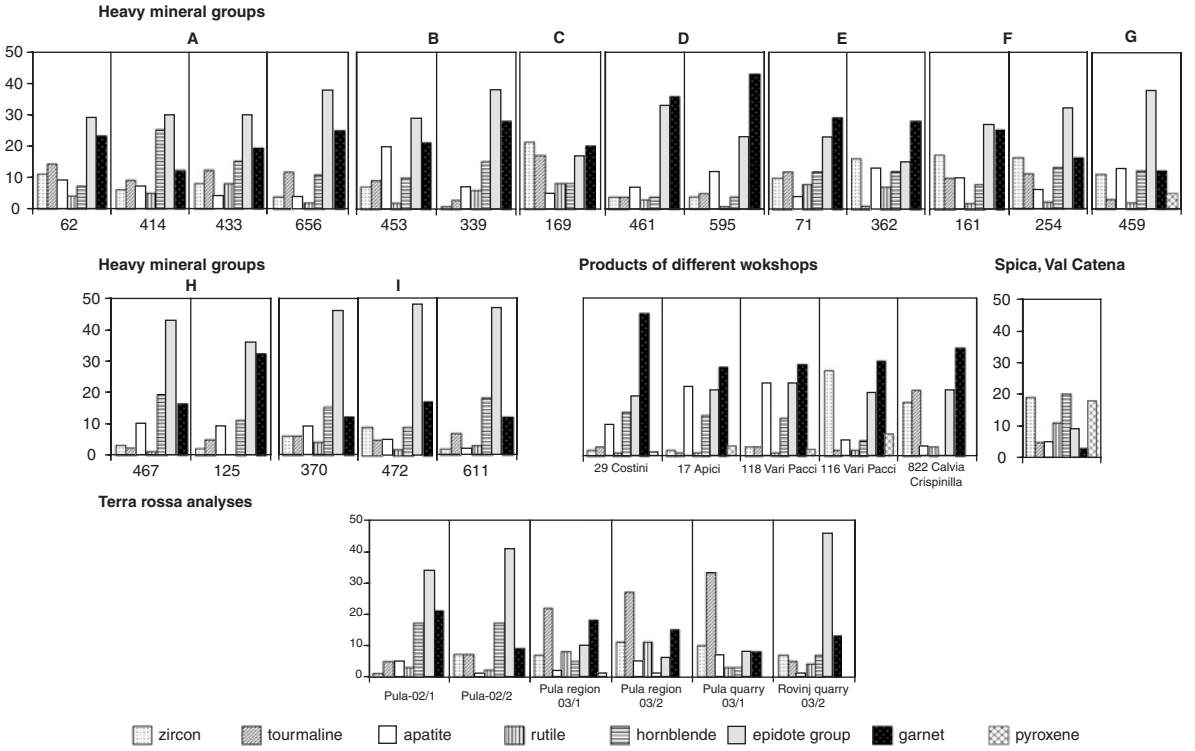

Fig. 7. Histograms, showing the abundance of heavy minerals (zircon, tourmaline, apatite, rutile, hornblende, epidote-group, garnet and pyroxene) in representative samples from the combined fabric and heavy mineral groups of Laecanius amphorae sherds, in sherds from other workshops and in terra rossa samples.

Table 3. Fabric groups of the Laecanius amphorae sherds, and sherds from other workshops with the abundance variations of their major heavy mineral components

Groups	Garnet and epidote	Zircon	Tourmaline	Pyroxene
	Ratios or quantity (%)		Quantity (%)	
A and B	<1	Varying, <1	5–10	Trace
C	>1	>20	>10	0
D	>1	<5	<5	Trace
E	>1	10–16	Varying %	Trace
F	<1	>15	~10	Trace
G	High epidote %	~10	<5	~5
H	High epidote %	<5	<5	Trace
I	Epidote >45%	2–9	5–7	Trace
Various other workshops	Very high garnet %	Variable, often high	<5	1–7
Calvia Crispinilla	Very high garnet %	High	>20	0
Spica, Verige Bay	<1	>15	~5	18

press room in Verige Bay (Val Catena), can also be distinguished by its unique heavy mineral suite, comprising abundant pyroxene and having low garnet and epidote content.

Epidote, garnet and zircon percentages were plotted in a ternary diagram to gain further constraints on the grouping (Fig. 8). It depicts the clustering of data from groups A and B, with E and I forming a cluster close to them. The separation of groups C and D from the former and the wide scatter of data points in samples of other workshops also proves informative.

In order to augment information from heavy mineral and thin section data, the loose light fractions were mounted in clove oil and inspected under the polarizing microscope. This allows observation of a larger bulk of material, and the rolling of particles in the clove oil facilitates a 3-D view of grain morphology. The chance of finding identifiable microfauna is also enhanced. Relatively thick clayey fragments comprise the bulk, which appear opaque under the polarizing microscope. However, the thin platelets represented by clay aggregates are translucent and show incorporation of "rock flour" (5–20 μm) made up of sub-angular to sub-rounded, occasionally rounded quartz grains. Faunal remains are embryonic planktonic foraminifera and a variety of sponge spicules. This qualitative approach added further information to categorisation. Groups A and B share many similarities with low quantities of quartz, few feldspars, relatively abundant chert and a small amount of chalcedony. Sponge spicules are fairly common in each sample. Also, sherd B 339 incorporates hexagonal biotite, volcanic glass shards (Fig. 6: Bi, Vo.gl) and hexagonal apatite of 80–120 μm size, originating probably from volcanic ash. Group C is unusual with the presence of metamorphic lithic fragments in higher proportions, in addition to abundant polycrystalline quartz, chert and chalcedony. Sponge spicules are also present. Group D amphora sherds are variable; sherd D 461 yielded relatively abundant heavy minerals but the amount of quartz is low. It contains volcanic glass shards, botryoidal pyrite and some microfauna. Sherd D 595, one of the high-temperature fired dark pieces, is also low in quartz, includes a few

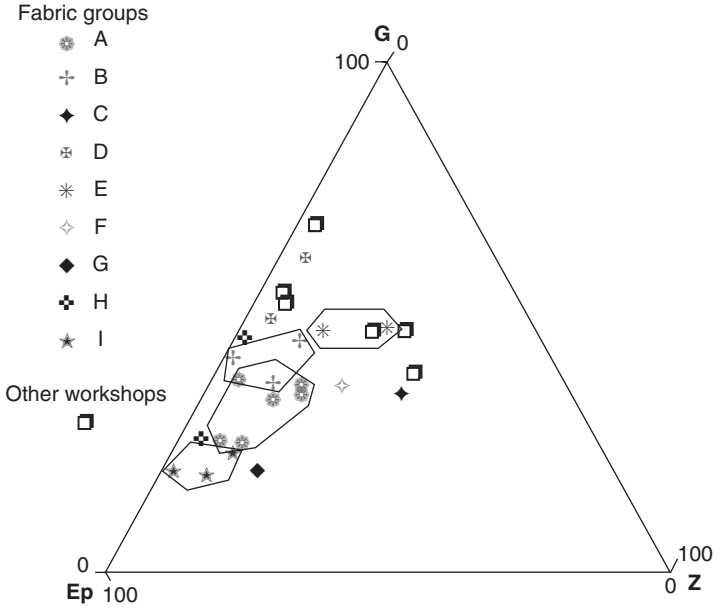

Fig. 8. Ternary plot illustrating the mineralogical relationship of the heavy mineral groups of the Laecanius amphorae sherds, and the different heavy mineral proportions in sherds of other workshops. Ep: epidote; G: garnet; Z: zircon.

botryoidal pyrites, shows abundant neo-formed calcite (Fig. 9), and is free of microfauna. Chert is absent from both samples. Groups E and F are "sandy": their quartz content is high while chert and microfauna are common. Sherd G 459 is markedly different due to its abundant polycrystalline quartz, chalcedony, volcanic grains (clinopyroxene, hexagonal biotite and volcanic glass shards) and traces of microfauna. Groups H and I have a low quartz content, siliceous or schistose fragments are more prominent than in the other samples; chert, chalcedony and microfossils are rare.

All amphora sherds from the other workshops contain varying proportions of quartz and some feldspars. The Costini workshop sample is quartz-rich with common potash feldspar, many fine botryoidal pyrites, formed probably as foraminifer-infill, and contain relatively abundant planktonic foraminifers. It is important to note that these are all fossil forms and the shells are recrystallised. The Apici amphora sherd is also rich in quartz. The two Vari Pacci amphora sherds are coarse-grained but have low amounts of quartz. Few botryoidal pyrites were detected, but no microfauna. The amount of clastic particles in the Calvia Crispinilla sherd is low, very fine grained and no microfauna was encountered.

4. DISCUSSION

The close proximity and continuous supply of raw material over time was essential to the operation of a cost-effective ceramic workshop under the Roman

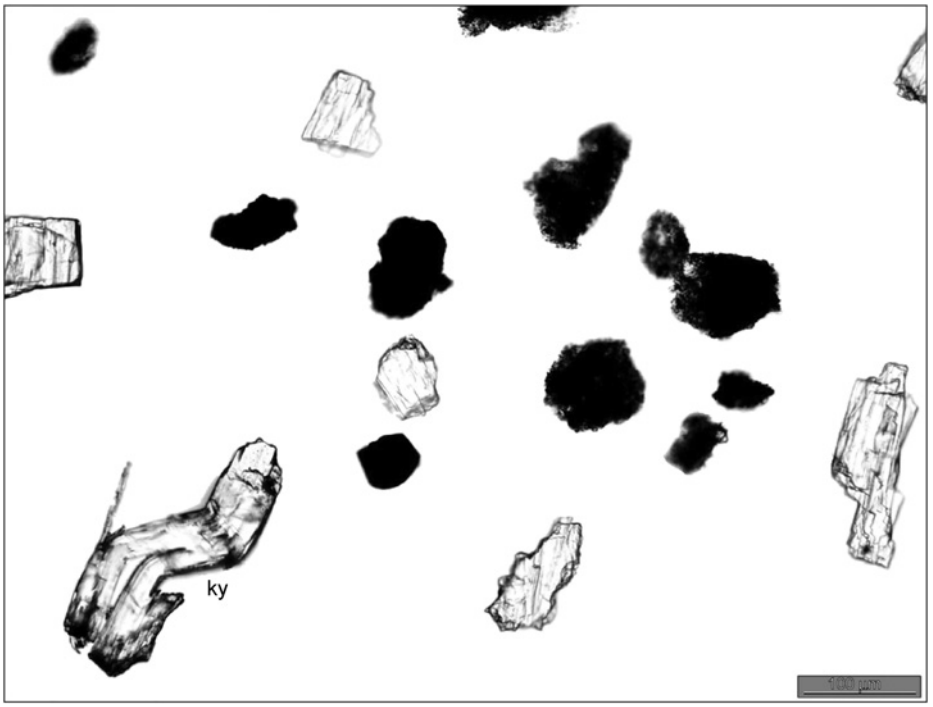

Fig. 9. Grain mount of a high-temperature fired specimen containing neo-formed calcite crystals and a bent, etched kyanite (ky) grain.

infrastructure. The Laecanius-owned villas that produced 10,000 or 12,000 amphorae yearly were evidently able to fulfil these prerequisites. Their success, first under management of the Laecanius family (80–90 years) then for 50 years under imperial ownership, reflects a well-organised enterprise with continued access to raw material, skilled managers and workers. By integrating the results of archaeological and geological analyses, we have obtained sufficient information to constrain the provenance of clay and temper used for paste.

The first step in the search of raw material is a geological reconnaissance survey of the potential source region: Istria is dominated by Mesozoic carbonates, while Palaeocene-Eocene carbonate-clastic successions of variable thickness are confined to the narrow central zone. Both sediment types are unsuitable for pottery and can be excluded. Late Neogene to Quaternary deposits include loess and terra rossa. Terra rossa, with its high clay mineral content, is a suitable raw material for ceramics and until fairly recently it was quarried and used for brick and cement manufacturing. It is widespread as a red soil in the southern and western parts of the peninsula, where it reaches a maximum thickness of 14 m (Durn et al., 1999).

The origin, chemistry and environmental implications of Istrian terra rossa have been investigated in detail in recent years. Their results provide valuable information to reconstruct the provenance of raw material used by ancient Istrian potters (Šinkovec, 1974; Škorić, 1987; Durn and Aljinović, 1995; Durn, 1996; Prohić et al., 1997; Durn et al., 1999, 2001, 2007—this volume; Miko et al., 1999). The studies of

Šinkovec (1974) and Durn (1996) are especially relevant because they included heavy mineral analyses.

The histograms in which heavy mineral proportions in the amphora sherds and in six terra rossa samples were plotted in Fig. 7 indicate similarities in overall heavy mineral composition between the terra rossa and the Laecanius amphora sherds but there is a visible difference between the two. Terra rossa, as a polygenetic soil (Durn, 1996; Durn et al., 1999, 2007—this volume), is highly heterogeneous and variations in mineral proportions are common. Such variations are detectable between localities or even between different layers of the same outcrop. For example, some of the currently analysed terra rossa samples from the Pula region are rich in unusually coarse tourmaline and also contain fossils. Both components were probably reworked from adjacent Mesozoic beds. Variations can also be ascribed to the availability of different outcrops in Roman times.

Percentages of epidote, garnet and zircon from all available data (including those from Durn, 1996; Šinkovec, 1974) were plotted on a ternary diagram (Fig. 10) that permits evaluation of the mineralogical linkage between the analysed terra rossa and amphora sherds. Heavy minerals of the Laecanius amphora sherds cluster in a well-defined field, whereas those originated in other workshops are more scattered. Our terra rossa analyses appear within the Laecanius field in the plot while Durn's (1996) epidote-rich samples form a tight cluster, close to and somewhat overlapping with data points of the Laecanius amphora sherds. The zircon-dominant terra rossa samples of Šinkovec (1974) fall in a separate area, coinciding only with the spica sample. The overlapping or adjacent clustering of amphora sherds with terra rossa samples indicates a linkage between the principal heavy minerals of the two data sets,

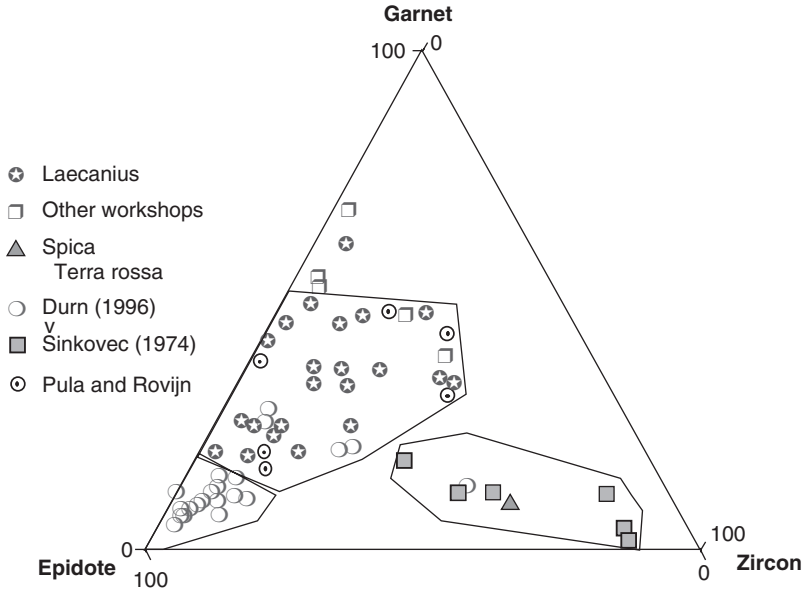

Fig. 10. Comparative ternary plot based on epidote, zircon and garnet proportions, using data from Laecanius amphorae sherds, other workshops and terra rossa.

suggesting that the clay used for the paste was terra rossa. It is widespread in the region (Durn, 1996), and ancient overgrown quarries are known within the Pula area, indicating that it was available locally. The workers presumably selected and quarried outcrops of suitable quality. Clayey bauxite, occurring mostly in central Istria as thick deposits, is rejected as a clay source, because neither bauxite-specific minerals nor anatase—common in Istrian bauxites (Šinkovec, 1973)—were found in the ceramics.

The cause for the differences in heavy mineral abundance between our data and Durn's (1996) is attributed to grain size. Durn (1996) used a narrower and finer (45–63 μm) size range than we did (45–250 μm), therefore, the difference between the two data sets can be ascribed to grain size-controlled fluctuations. For example, garnet usually appears in the coarser size grades and is reflected in the generally high garnet abundance in our data. No such details are available for Šinkovec's (1974) data. All the above emphasises that analytical methods and operating conditions used by various authors need to be stringently assessed before comparisons are attempted.

Both Figs. 7 and 10 show that there is an appreciable mineralogical difference between the amphora sherds and the terra rossa. We suggest that this reflects the diluting effect of added temper. Temper petrography is a highly important source of information in geoarchaeology as demonstrated by Dickinson (2001, 2007—this volume), Dickinson et al. (1990) and Dorais et al. (2004). Thin section and fabric analyses have indicated that, in addition to carbonate fragments (either dolomite or limestone), fine sand is invariably present in the amphora sherds. The carbonate material, taken presumably from local outcrops, was ground to a fine size and added to the clay but dolomite and limestone are inherently free of clastic grains.

This raises the question where the other, ''sandy-silty'', temper came from. Two lines of evidence, one mineralogical and the second microfaunal, indicate that its source was the silty, sandy deposit of the Adriatic Sea. First, the majority of the amphora sherds contain fresh brown hornblende and abundant brown biotite, some with a hexagonal shape (Fig. 6: Bi, Hb.volc), indicating a volcanogenic (tephra) origin. The presence of sharp euhedral volcanic zircon (Fig. 6: Z), euhedral pyroxene and apatite in the amphora sherds is another proof for volcanic derivation. Previous studies in the Adriatic region have also documented volcanogenic heavy minerals in modern sediments. Durn (personal communication, 2001) found abundant volcaniclastic grains in deep paleosol profiles on the Island of Hvar, Croatia and interpreted them as products of Mediterranean volcanic eruptions. Šinkovec (1974) analysed the heavy mineral composition of one modern sand sample from the northern Adriatic Sea and one aeolian sand sample from the Island of Susak. He reported a high hornblende content ($>30\%$) associated with pyroxenes in Adriatic sand and found apatite both in the modern Adriatic and in the aeolian sediments. By contrast, terra rossa contains only small amounts of brown hornblende; only 1–5% hornblende was present in samples analysed by Durn (1996) and apatite content was minor. Although two of the terra rossa samples in Table 2 (Pula 1 and 2) have high percentages of hornblende, it is predominantly the blue-green variety with different chemistry, formed under different petrogenetic conditions. Brown hornblende that characterises the ash-fall suite and is also common in the amphora sherds, is rare in the analysed terra rossa samples. The presence or absence of apatite is also meaningful. Apatite content is maximum 20% in the amphora sherds, but is rare in the

terra rossa. All these characteristics suggest that the potters used clastic temper which contained diverse and well-preserved heavy mineral assemblages, different from those in the terra rossa. This clearly explains the bimodality of heavy mineral assemblages in the amphora sherds. Our interpretation for the dominantly Adriatic provenance of the temper is further supported by the particular microfauna in the amphora sherds. This issue will be addressed after we consider another provenance effect.

Because Adriatic sediments, loess and terra rossa incorporate some detritus from a common source, from the fine sandy and silty alluvium of the Po River, their heavy mineral suites share similar characteristics. The Po River carries diverse Alpine assemblages to the Adriatic, and deposits them on its floodplain (Van Straaten, 1970; Rizzini, 1974; Gandolfi et al., 1982; Marchesini et al., 2000). During the Pleistocene, fine grained sediment from the floodplain was carried by wind and dispersed over a wide area (Durn and Aljinović, 1995), and probably became intermixed with the terra rossa (Durn et al., 1999, 2007—this volume). Thus, traces of diagnostic Alpine-derived mineral species, e.g. glaucophane and chrome spinel, appear in the terra rossa. These minerals are common in Adriatic sediments and occasionally were also encountered in the amphora sherds (Table 2).

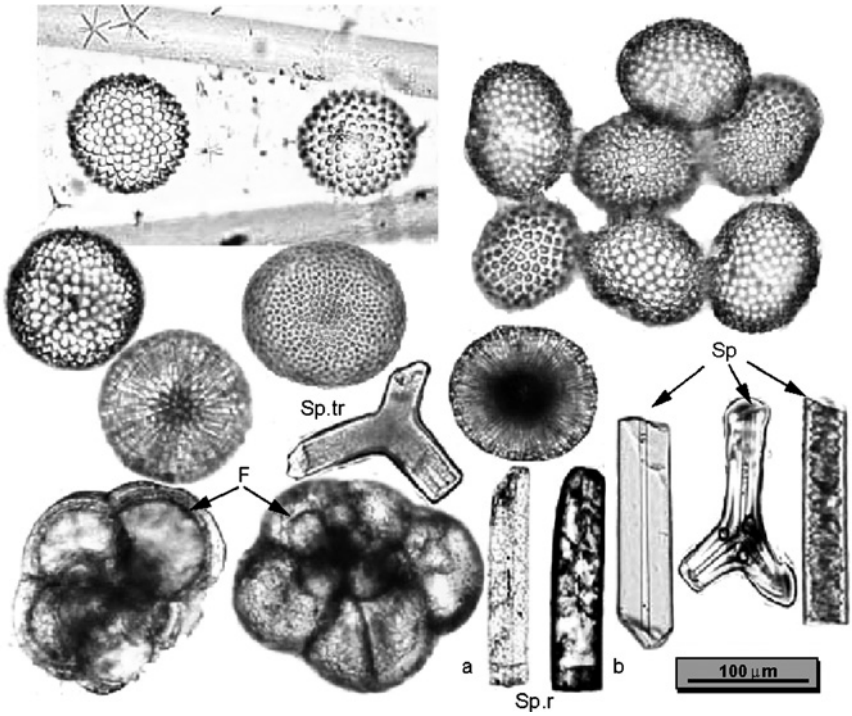

Fig. 11. *Geodia* sponge spicules (sterrasters) from *Geodia* sp. Belize (top row) sterrasters (middle) and sponge spicules (bottom right) from the Laecanius amphorae sherds, and planktonic foraminifers (bottom left); F: planktonic foraminifers: Sp.tr: trilete spicules and Sp: mono spicules; Sp.r: recrystallised fossil sponge spicule (a: plane polarized light, b: crossed polars). Note the worn appearance of this spicule.

Second, fresh and unusually small, planktonic foraminifers and sponge spicules are present in the majority of the amphora sherds. Although the dominantly embryonic or fragmentary nature of the foraminifers precluded precise identification, the well-preserved, fresh sponge spicules have provided definitive evidence for the source of the temper. The globular sponge spicules (Fig. 11) were identified by Prof. Jean Vacelet and Dr. Klaus Rützler (personal communication, 2003) as spicules from the cortex of the modern sponge *Geodia cydonium* (Jam.) (order Tetractinellida). These almost spherical spicules are sterrasters which are microsclere spicules forming a dense cortex at the surface of the Geodiidae. Megasclere spicules with triactine and monactine types are frequent (Fig. 11: sp) and, most probably, belong to the same Geodiidae.

The mineralogy and microfauna found in the ceramics, therefore, constrain the source of the temper added to the paste. It was probably dredged from the Adriatic Sea. Microfauna is markedly more common in amphora sherds with a relatively high detrital grain content, suggesting that the fine clastic temper and not the clay contributed the microfauna. The modern origin of the sponge spicules is suggested by their excellent preservation. It supports our conclusion on temper provenance: (1) if they were reworked and redeposited in the terra rossa they should show signs of abrasion and (2) were they Mesozoic or Palaeocene in age, recrystallisation of the opaline silica to chalcedony should have taken place (as seen in almost all fossilized sponge spicules, e.g. Fig. 11: Sp.r). Recrystallization, however, has not been observed in any of the samples.

5. CONCLUSIONS

Our interdisciplinary study, which integrated traditional fabric analysis with petrography, XRD and heavy mineral analysis has added new dimensions to the study of Roman Dressel 6B type amphora sherds, manufactured in the Laecanius workshop in Istria between 10-5 B.C. and 78 A.D. Fabric analysis has established nine fabric groups, A–I, with the majority of the amphora sherds belonging to groups A and B. This consistency suggests that the bulk raw material used for the paste and temper, and the manufacturing methods remained relatively unchanged throughout the operation of the workshop.

The firing temperature of the amphorae, estimated by XRD, ranges between 750 and 900°C. This wide variation indicates that the nature of the initial material may have been taken into account during the firing process. Alternatively, based on the availability of the firing substances, the pottery workers may have adjusted the paste composition.

Heavy mineral analyses have pinpointed the sources of raw material used for the paste and temper that, despite numerous studies on the Laecanius amphorae, have not been identified previously. Our comparative study of the heavy mineral composition of Istrian terra rossa and the Laecanius amphora sherds shows appreciable similarities, indicating that the workshops used the widely available terra rossa for the clay base, mixed with either carbonate or clastic temper or both. The difference in the principal heavy mineral compositions between the amphora sherds and terra rossa, is interpreted as the result of the polygenetic origin of terra rossa which is known to have temporal and spatial heterogeneity.

The abundance and local availability of Istrian terra rossa, a cost-effective base material, explains the success and prolonged existence of the workshop. Further evidence for its efficient operation is shown by our finding that much of the temper was taken from a local, Adriatic, source. Fresh, modern sponge spicules in the amphora sherds, similar to those in the Adriatic Sea, and specific heavy mineral assemblages of Alpine provenance, transported to the Adriatic by the Po River, constrain the Adriatic derivation of the sandy temper. Different material was used for light-coloured, relatively silty/sandy amphorae. The presence of microfauna in them points to an Adriatic origin. The material was probably mixed with local loess. The finely dispersed carbonate in the matrix may also suggest the use of loess because most loess contains poorly crystallised carbonate.

Heavy mineral characteristics of amphora sherds manufactured in other workshops are different from those in the traditional Laecanius amphorae. The difference recognised between the Laecanius amphorae and those of other workshops, including the spica sample, demonstrated the potential of the heavy mineral technique as a useful archaeometric tool.

ACKNOWLEDGMENTS

The second author wishes to express his gratitude to Professor David Peacock for his invitation to the Archaeology Department of Southampton University and for stimulating discussions and his useful comments on the manuscript. We are indebted to Professor Goran Durn for providing heavy mineral data of Istrian terra rossa and for valuable information on Istrian geology. Sincere thanks are extended to Professor Jean Vacelet and Dr. Klaus Rützler for identifying the sponge spicules and for the comparative material sent by Dr. Klaus Rützler. We are grateful to Professors David Jones and Howie Spero whose suggestions finally led us to the specialists who have identified the sponge spicules. We thank Professors John F. Dewey and David F. Williams, and Dr. David T. Wright for their useful comments on earlier versions of the manuscript. Thanks are also extended to Dr. Ervin Otvos whose suggestions have greatly improved the final manuscript. The technical assistance of Jill Phillips, Andy Vowles and Barry Marsch of Southampton University, UK is very much appreciated. Professor Friedrich Krinzinger has made it possible to complete the Laecanius study. Financial support to T.B. was provided by the Soros Foundation and the Archaeology Department of Southampton University, UK.

REFERENCES

Baldacci, P., 1967–1968. Alcuni aspetti dei commerci nei territorii cisalpini. In: Atti del Centro Studi e Documentazione sull Italia Romana, I. 7–50, Milano–Varese.

Bezeczky, T., 1987. Roman amphorae from the Amber Route in Western Pannonia. BAR International Series, No. 386, Oxford, 286p.

Bezeczky, T., 1998. The Laecanius Amphora Stamps and the Villas of Brijuni. Österreichische Akademie der Wissenschaften, Philosophische-Historische Klasse Denkschriften, 261, Wien, 286pp.

Buchi, E., 1973. Banchi di anfore romane a Verona. Note sui commerci cisalpini. In Il territorio veronese in eta romana. Atti del convegno tenuto a Verona 1971, 531–637.

Carre, M.B., 1985. Les amphores de la Cisalpine et de l'Adriatique au début de l'émpire. Mélanges de L'école Française de Rome Antiquité 97, 207–245.

Cipriano, S., Mazzocchin, S., 1998. I bolli di C. Laecanius Bassus: un aggiornamento alla luce di nuovi dati da Patavium. Aquileia Nostra 69, 361–378.

Dickinson, W.R., 2001. Petrography and geologic provenance of sand tempers in prehistoric potsherds from Fiji and Vanuatu, South Pacific. Geoarchaeology. An International Journal 16, 275–322.

Dickinson, W.R., 2007. Discriminating among volcanic temper sands in prehistoric potsherds of Pacific Oceania using heavy minerals (this volume).

Dickinson, W.R., Takayama, J., Snow, E.S., Shutler, R. Jr., 1990. Sand temper of probable Fijian origin in prehistoric potsherds from Tuvalu. Antiquity 64, 307–312.

Dorais, M.J., Lindblom, M., Shriner, C.M., 2004. Evidence for a single clay/temper source for the manufacture of Middle and Late Helladic Aeginetan pottery from Asine, Greece. Geoarchaeology. An International Journal 19, 657–684.

Durn, G., 1996. Origin, composition and genesis of terra rossa in Istria. Unpublished doctoral dissertation. University of Zagreb, Zagreb.

Durn, G., Aljinović, D., 1995. Heavy mineral assemblage in terra rossa from the peninsula of Istria, Croatia. Abstracts 1st Croatian Geological Congress, Opatija, 31pp.

Durn, G., Aljinović, D., Crnjakovic, M., Bocko Lugovic, B., 2007. Heavy and light fractions indicate polygenesis of extensive terra rossa soil in Istria, Croatia (this volume).

Durn, G., Ottner, F., Slovenec, D., 1999. Mineralogical and geochemical indicators of the polygenetic nature of terra rossa in Istria, Croatia. Geoderma 91, 125–150.

Durn, G., Slovenec, D., Covic, M., 2001. Distribution of iron and manganese in terra rossa from Istria and its genetic implications. Geologica Croatia 54, 27–36.

Gandolfi, G., Mordenti, A., Paganelli, L., 1982. Composition and longshore dispersal of sands from the Po and Adige rivers since the pre-Etruscan age. Journal of Sedimentary Petrology 52, 797–805.

Girardi Jurkić, V., 1985. Brioni, Castrum Bizantino. In: Archeologia e Arte dell'Istria. Pula, pp. 91–94.

Gnirs, A., 1908. Istrische Beispiele für Formen der antik-römischen villa rustica. Jahrbuch für Altertumskunde 2, 124–143.

Gnirs, A., 1910. Eine römische Tonwarenfabrik in Fasana bei Pola. Jahrbuch für Altertumskunde 4, 35–39.

Józsa, S., Sauer, R. Szakmány, Gy., Weiszburg, T., 1994. Mineralogisch-petrographische Untersuchungen. In: Bezeczky, T. (Ed.), Amphorenfunde vom Magdalensberg und aus Pannonien, ein Vergleich. Archäologische Forschungen zu den Grabungen auf dem Magdalensberg, vol. 12, pp. 143–166, Klagenfurt.

Manacorda, D., 1994. A proposito delle anfore della Pannonia romana: appunti e riflessioni. In: La Pannonia el'Impero Romano. Annuario dell'Accademia d'Ungheria, Roma, pp. 177–191.

Mange, M.A., Bezeczky, T., 2006. Petrography and provenance of Laecanius amphorae from Istria, northern Adriatic region, Croatia. Geoarchaeology: An International Journal 21, 427–458.

Mange, M.A., Maurer, H.F.W., 1992. Heavy Minerals in Color. Chapman and Hall, London, 147pp.

Marchesini, L., Amorosi, A., Cibin, U., Zuffa, G.G., Spadafora, E., Preti, G., 2000. Sand composition and sedimentary evolution of a Late Quaternary depositional sequence, northwestern Adriatic coast, Italy. Journal of Sedimentary Research 70, 829–838.

Martin-Kilcher, S., 2000. Les Laecanii et les amphores à huile d′Istrie. Journal of Roman Archaeology 13, 506–509.

Matijašić, R., 1993. Oil and wine production in Istria and Dalmatia. In: Amouretti, M.C., Brun, J.P. (Eds.), Classical Antiquity and the Early Middle Ages. Bulletin de corresponance hellénique. Supplement 26, 247–261.

Mazzocchin, S., Pastore, P., 1996–1997. Nuove testimonianze epigrafiche sul commercio dell′olio Istriano a Padova. Archeologia Veneta 19–20, 151–176.

Miko, S., Durn, G., Prohic, E., 1999. Evaluation of the terra rossa geochemical baselines from Croatian karst regions. Journal of Geochemical Exploration 66, 173–182.

Peacock, D.P.S., 1967. The heavy mineral analysis of pottery; a preliminary report. Archaeometry 10, 97–100.

Peacock, D.P.S., 1970. The scientific analysis of ancient ceramics: a review. World Archaeology 1, 375–389.

Peacock, D.P.S., 1977. Ceramics in Roman and Medieval archaeology. In: Peacock, D.P.S. (Ed.), Pottery and Early Commerce: Characterization and Trade in Roman and Later Ceramics, pp. 21–34.

Peacock, D.P.S., 1984. Petrology and origins, 6–8, In: Fulford, M.G., Peacock, D.P.S. (Eds.), Excavations at Carthage: The British Mission. The Avenue du President Habib Bourguiba, Salammbo: The pottery and other ceramic objects from the site 1, 2: Sheffield, 284p.

Peacock, D.P.S., Williams, D.F., 1986. Amphorae and the Roman Economy, an Introductory Guide. Longman, London, 239p.

Pesavento Mattioli, S., Mazzocchin, S., Pavoni, M.G., 2000. I ritrovamenti di anfore presso l'anfiteatro romano di Padova. Bolletino del Museo Civico di Padova 88 (1999), 7–44.

Pliny the Elder (1952). Olive and other fruit trees. Natural History, vol. 4, books 12–16. (English translation in ten volumes by Raackham, H.) The Loeb Classical Library. Harvard University Press, Cambridge, MA, pp. 1952–1960.

Polšac, A., 1964. Géologie de I'Istrie méridionale spécielment par rapport à la biostratigraphie des couches crétacées. Geoloski vjesnik 18, 490–509.

Prohić, E., Hausberger, G., Davis, J.C., 1997. Geochemical patterns in soils of the karst region, Croatia. Journal of Geochemical Exploration 60, 139–155.

Rizzini, A., 1974. Holocene sedimentary cycle and heavy mineral distribution, Romagna-Marche Coastal Plain, Italy. Sedimentary Geology 11, 17–37.

Sauer, R., 1989. Die Anwendung der Schwemineralanalyse für die Herkunftsbestimmung von antiker Keramik anhand von Beispielen aus Carnuntum und St. Pölten. Wiener Berichte über Naturwissenschaft in der Kunst 6/7/8(1989–1991), 121–141.

Sauer, R., 1997. Naturwissenschaftliche Untersuchungen an Keramikproben aus dem Töpferofen im Auxiliarkastell, Petronell. In: Stiglitz, H. (Ed.), Das Auxiliarkastell von Carnuntum 1, Forschungen 1977–1988. Österreichisches Archäologisches Institut, Sonderschriften 29, pp. 245–268.

Šinkovec, B., 1973. The origin of Early Palaeogene bauxites of Istria, Yugoslavia. 3rd International Symposium ICSOBA, Nice, pp. 151–164.

Šinkovec, B., 1974. The origin of terra rossa in Istria. Geoloski vjesnik 27, 227–237.

Škorić, A., 1987. Pedosphere of Istria. Project Council of Pedological Map of Croatia, Special Edition, Book 2, Zagreb, 192p.

Tassaux, F., 1982. Laecanii, Recherches sur une famille sénatoriale d'Istrie. Mélanges de l'Ecole Française de Rome Antiquité 94, 227–269.

Tassaux, F., 2001. Production et diffusion des amphores à huile Istriennes. In: Strutture portuali e rotte marittime nell' Adriatico di età romana, Antichità Altoadriatiche, 46, Trieste-Roma, pp. 501–543.

Tassaux, F., Matijašić, R., Kovačić, V., 2001. Loron (Croatie), Un grand centre de production d'amphores à huille istriennes (I^{er}-IV^{e} S.P.C.). Institut Ausonius Publications, Mémoires 6, 365p.

Van Straaten, L.M.J.U., 1970. Holocene and Late Pleistocene sedimentation in the Adriatic Sea. Geologische Rundschau 60, 106–131.

Velić, I., Tišljar, J., Matičec, D., Vlahović, I., 1995. A review of the geology of Istria. In: Vlahovic, I., Velic, I. (Eds.), Excursion Guidebook 1st Croatian Geological Congress, pp. 21–30.

Weiszburg, T., Papp, G., 1987. X-ray powder diffraction analyses. In: Bezeczky, T. (Ed.), Roman Amphorae from the Amber Route in Western Pannonia BAR International Series, vol. 386, 128–133.

Whitbread, I.K., 1995. Greek transport amphorae. A petrological and archaeological study. The British School at Athens, Fitch Laboratory Occasional Papers 4, Oxford, 453p.

Williams, D.F., 1977. The Romano-British black-burnished industry: an essay on characterization by heavy mineral analysis. In: Peacock, D.P.S. (Ed.), Pottery and Early Commerce: Characterization and Trade in Roman and Later Ceramics, pp. 163–220.

Zabehlicky-Scheffenegger, S., Sauer, R., Schneider, G., 1996. Graue Platten aus Ephesos und vom Magdalensberg. In: Herford-Koch, M., Mandel, U., Schädler, U. (Eds.), Hellenistische und römische Keramik des östlichen Mittelmeergebietes. Kolloquium, Frankfurt. Archäologisches Institut der Johann Wolfgang Goethe-Universität Frankfurt, pp. 41–59.

This page intentionally left blank

PART IV: INDUSTRIAL APPLICATIONS: RESERVOIR CHARACTERISATION, ECONOMIC HEAVY MINERAL DEPOSITS, DIAMOND PROSPECTING

4.1 Reservoir Characterisation

This page intentionally left blank

Chapter 41

CORRELATION OF TRIASSIC SANDSTONES IN THE STRATHMORE FIELD, WEST OF SHETLAND, USING HEAVY MINERAL PROVENANCE SIGNATURES

ANDREW C. MORTON[a,b], ROB HERRIES[c] AND MARK FANNING[d]

[a]*HM Research Associates, 2 Clive Road, Balsall Common, West Midlands CV7 7DW, UK*
[b]*CASP, University of Cambridge, 181a Huntingdon Road, Cambridge CB3 0DH, UK*
[c]*Amerada Hess Malaysia, Level 9, Menara Tan and Tan, 207 Jalan Tun Razak, Kuala Lumpur 50400, Malaysia*
[d]*Research School of Earth Sciences, The Australian National University, Canberra, ACT 0200, Australia*

ABSTRACT

Integrated heavy mineral, mineral–chemical and zircon age data show that Triassic sandstones in the Strathmore Field result from the interplay of sediment derived from eastern and western sources. The Early Triassic Otter Bank Formation is interpreted as having a source on the British margin of the Faeroe-Shetland rift. Two main provenance components (recycled Devonian-Carboniferous Upper Clair Group in conjunction with Lewisian orthogneiss) were involved. The overlying Foula Formation (Middle-Late Triassic) was derived from high-grade metasedimentary/charnockitic basement rocks, interpreted as lying in the Nagssuqtoqidian belt of southern East Greenland on the opposite side of the rift. Zircon age data from the Foula Formation also provide evidence for an important Permian igneous event along the proto-northeast Atlantic rift.

The switch in sediment supply from easterly-sourced to westerly-sourced detritus is the most clearly defined correlative event in the Triassic succession of the Strathmore Field. Variable supply from a subordinate zircon-rich component (probably of granitic origin) provides a basis for intra-Foula subdivision and correlation. The upper part of the Otter Bank Formation is characterised by a relatively high apatite/tourmaline ratio, believed to indicate the initial appearance of sediment from East Greenland.

The construction of the correlation framework for the Triassic succession in the Strathmore Field depends crucially on identification and quantification of parameters that are sensitive to changes in provenance and insensitive to other processes that operate during the sedimentation cycle.

Developments in Sedimentology, Vol. 58, 1037–1072

ISSN: 0070-4571/doi:10.1016/S0070-4571(07)58041-6

This study demonstrates that ditch cuttings and core samples yield closely comparable heavy mineral data, indicating that construction of correlation frameworks can be readily achieved using ditch cuttings samples, although ideally cuttings data would benefit from calibration with core material.

Keywords: Correlation; heavy minerals; provenance; Triassic; NE Atlantic; Strathmore Field

1. INTRODUCTION

The provenance-sensitive nature of heavy mineral assemblages makes heavy mineral analysis one of the leading non-biostratigraphic methods for correlation of sandstones (Dunay and Hailwood, 1995). Traditionally, correlation is achieved using biostratigraphic methods, but this may be difficult if biostratigraphic control is poor or absent. This is frequently the case for sandstones deposited in non-marine or paralic environments, particularly in red-bed settings, but may also occur in marine depositional environments, if sedimentation rates are so rapid that biostratigraphic events lack sufficient resolution for detailed sand body correlation. In such circumstances, it is important that other methods of correlation are used, either in isolation or to complement biostratigraphic data.

There are a number of non-biostratigraphic approaches that can be used for correlation, including sequence stratigraphic methods, direct or indirect dating and provenance studies (Dunay and Hailwood, 1995; Morton et al., 2002). Heavy mineral analysis belongs to the group of provenance-based methods, together with approaches such as clay mineral analysis (Jeans, 1995), whole-rock geochemistry (Pearce et al., 1999) and Sm-Nd isotope geochemistry (Dalland et al., 1995). Successful application of any provenance-based correlation method depends first on the existence of changes in sediment provenance or transport history during deposition, and second on the recognition of such events. Heavy mineral analysis is ideally suited for establishing a non-biostratigraphic correlation framework, since heavy minerals are sensitive indicators of provenance and because the mineralogical manifestation of changing provenance can be readily distinguished from the effects of other processes that operate during the sedimentation cycle.

Heavy mineral analysis has been successfully applied to the correlation of sedimentary successions since the early part of the last century. The principles behind application of heavy mineral analysis in correlation were first laid out by Milner (1923), and although new approaches have been developed and analytical methods have become more sophisticated, the same principles still apply today. Heavy mineral correlation studies have been used to help map and delineate sedimentary units, for example in the Permian Karroo system of South Africa (Koen, 1955), the Tertiary of southern England (Blondeau and Pomerol, 1969) and the Tertiary of California (Tieh, 1973). More commonly, however, heavy minerals have been used to aid correlation of hydrocarbon-bearing sandstones, driven by the economic need to develop reservoir correlation schemes. One of the earliest studies in this context was that of Reed and Bailey (1927) in the San Joaquim Valley of California; other key

publications are those of Feo-Codecido (1956) on Venezuela, Rahmani and Lerbekmo (1975) on Alberta, Hurst and Morton (1988) on the North Sea, and Allen and Mange-Rajetzky (1992) on the Clair Field, west of Shetland. Heavy mineral correlation has been applied across a wide range of clastic reservoir facies, from aeolian, through fluvial, deltaic and shallow marine, to deep water, and from Palaeozoic to Mesozoic (Morton et al., 2002).

2. CORRELATION USING HEAVY MINERALS

Although heavy minerals are generally volumetrically minor constituents of sandstones, assemblages are potentially diverse; Mange and Maurer (1992) illustrate around 50 minerals of relatively common occurrence, many of which have restricted parageneses that are diagnostic of particular source lithologies. Heavy mineral data therefore readily identify the changes in provenance required to construct a correlation framework. Changes in sand provenance may be relatively gradual, due to unroofing of fresh lithologies in a single source area through continued erosion. Such changes are manifested by evolutionary trends in heavy mineral parameters. By contrast, sudden changes in heavy mineral assemblages indicate switching of source lithologies, suggesting either tectonic evolution of the hinterland or changes in basin configuration.

Provenance, however, is not the only factor that controls sediment composition. The processes that have the potential to overprint the provenance signal during the sedimentary cycle include: weathering at source, prior to incorporation in the transport system; mechanical breakdown during transport; weathering during periods of alluvial storage on the floodplain; hydraulic processes during transport and final deposition; diagenesis during deep burial; and weathering at outcrop (Morton and Hallsworth, 1999).

It is crucial for reliable correlation that the parameters used to construct the correlation framework are sensitive to provenance but not to the other processes that operate during the sedimentary cycle. In this regard, heavy mineral analysis has one major advantage over other provenance-based correlation methods; the technique has a long history, and consequently there has been a considerable amount of research into the response of heavy mineral suites to the processes that act during the sedimentation cycle (Hubert, 1971; Morton, 1985; Mange and Maurer, 1992; Morton and Hallsworth, 1999). The knowledge gained during this research has made it possible to generate parameters that filter out overprinting effects and can be used for correlation because they accurately reflect changes in sediment provenance and transport history.

As discussed by Morton and Hallsworth (1999), the most important of the overprinting processes are (1) hydrodynamics, which fractionate abundances of minerals with contrasting hydraulic behaviour during transport, and (2) diagenesis, which leads to dissolution of unstable minerals by pore fluids. Two complementary methods are used to counteract the effects of hydrodynamic and diagenetic processes on heavy mineral suites. One is to use ratios of the abundance of stable minerals with similar hydraulic behaviour (Morton and Hallsworth, 1994). Since hydraulic behaviour is controlled mostly by grain size and grain density, these

provenance-sensitive ratios compare the abundances of minerals with similar densities, with the analysis confined to a limited size range (63–125 μm). Suitable ratios include apatite/tourmaline, rutile/zircon, monazite/zircon and chrome-spinel/zircon. Garnet/zircon is also a valid discriminator of provenance provided there is no evidence for garnet dissolution.

The alternative approach is to undertake varietal studies, which concentrate on variations seen within one mineral group. This strongly diminishes the range of density and stability within the data set, resulting in data that reflect provenance characteristics without significant hydrodynamic or diagenetic modification. The classical approach to varietal studies is to distinguish types on the basis of their optical properties. Optically determined varietal data include tourmaline colour and morphology (Krynine, 1946; Mange-Rajetzky, 1995), zircon morphology (Poldervaart, 1955; Lihou and Mange-Rajetzky, 1996), apatite roundness (Allen and Mange-Rajetzky, 1992; Morton et al., 2003) and garnet and staurolite morphology (Van Loon and Mange, 2007—this volume). With the widespread availability of electron microprobe facilities, it has become commonplace to constrain provenance on the basis of the geochemical characteristics of a mineral population. Geochemical data from a wide variety of minerals have been successfully used to infer provenance, but many of these, such as pyroxene (Styles et al., 1989), amphibole (Von Eynatten and Gaupp, 1999) and epidote (Spiegel et al., 2002), are unstable during diagenesis, and therefore have limited application, especially in correlation of deeply buried sandstones.

Of all mineral groups used in mineral–chemical studies, garnet has proved the most useful to date. This is because garnet has a wide potential compositional range, with solid solution between seven principal end-members, shows significant differences in composition between different types of garnet-bearing lithology (Wright, 1938; Sobolev, 1964; Rub et al., 1977), and is relatively stable during burial diagenesis (Morton and Hallsworth, 1999). In consequence, garnet geochemical studies have proved particularly useful in characterising, distinguishing and correlating sand bodies on the basis of their provenance (e.g. Morton, 1985; Haughton and Farrow, 1988; Tebbens et al., 1995; Hutchison and Oliver, 1998; Hallsworth and Chisholm, 2000). Tourmaline is also stable during diagenesis, but although it shows provenance-related geochemical variations (Henry and Guidotti, 1985), comparatively few studies have used tourmaline geochemistry for differentiation and correlation of sandstones (Jeans et al., 1993; Morton et al., 2005a).

Although heavy mineral and mineral–chemical data provide important constraints on the lithological and mineralogical characteristics of the sediment sources, they do not supply information on the age of the source regions. Information on provenance age can be acquired by isotopic methods, including whole-rock methods such as Sm-Nd (Mearns et al., 1989), and single grain methods, such as U-Pb dating of zircon (e.g. Sircombe, 1999) or monazite (Evans et al., 2001). The rationale adopted in this paper follows that of Morton and Grant (1998), who used heavy mineral and mineral–chemical data to distinguish sandstones with different provenances, and then undertook a limited programme of single-grain U-Pb zircon age dating using the sensitive high-resolution ion microprobe (SHRIMP) to constrain the location of their respective sources.

3. TRIASSIC OF THE STRATHMORE FIELD

Triassic sandstones in and around the British Isles almost invariably occur in red-bed facies, deposited in broadly fluvial environments under arid to semi-arid conditions (Fisher and Mudge, 1998). Biostratigraphic controls are therefore scarce, and alternative approaches to correlation are required. Correlation is an especially important issue since Triassic sandstones are major hydrocarbon reservoirs across the entire region, including Wytch Farm in the Wessex Basin of southern Britain, Hewett in the southern North Sea, Marnock in the central North Sea, Beryl, Tern and Cormorant in the northern North Sea, Morecambe Bay in the Irish Sea, Corrib to the west of Ireland and Strathmore west of Shetland. Provenance-based correlation methods have been applied in several of these oil and gas fields. Heavy minerals (including tourmaline and apatite varieties) have been used to correlate Triassic reservoir sandstones in the Irish Sea area (Mange et al., 1999), tourmaline varieties in the Marnock Field and adjacent areas of the central North Sea (Mange-Rajetzky, 1995), and whole-rock geochemistry integrated with heavy minerals in the Beryl Field in the northern North Sea (Preston et al., 1998) and the Wessex Basin of southern Britain (Svendsen and Hartley, 2002).

This contribution extends the application of heavy mineral methods in hydrocarbon reservoir correlation into the basins to the west of Britain. The Strathmore Field lies in the East Solan Basin, UK continental shelf Blocks 204/30 and 205/26 (Fig. 1), and contains hydrocarbons in the Triassic (Herries et al., 1999). As a result, the Triassic succession in the area has been drilled by several boreholes and extensively sampled by both core and ditch cuttings, providing a unique opportunity to characterise the provenance of Triassic sandstones in the rift systems to the northwest of Britain.

The East Solan Basin is a Permo-Triassic rift basin that lies on the eastern edge of the Faeroe-Shetland Basin (Swiecicki et al., 1995). The Faeroe-Shetland Basin is contiguous with the Møre Basin to the northeast and the Rockall Trough to the southwest, all of which have a prolonged Mesozoic to Early Tertiary rift history that culminated with the separation of East Greenland from northwest Europe in the early Eocene (Roberts et al., 1999). The ultimate line of separation lies close to the East Greenland margin, as shown in Fig. 1. The sediment fill in the Permo-Triassic rift system to the northwest of Britain is interpreted as being entirely continental (Ziegler, 1990), but a narrow seaway was present further north along the rift system between northeast Greenland and mid-Norway (Seidler et al., 2004). Prospective source areas therefore occur on the Orkney-Shetland Platform (to the east), in central east and southeast Greenland (to the west), and the Rockall Plateau (to the southwest), as shown in Fig. 1. It should be borne in mind that Fig. 1 shows the reconstruction at end Palaeocene (immediately prior to the opening of the northeast Atlantic), and does not take into account the substantial stretching that occurred during the Mesozoic. Prospective sources to the west of Britain are therefore likely to have been considerably closer to the Strathmore area than the reconstruction in Fig. 1 suggests.

The Triassic succession in the Strathmore Field (Fig. 2) is nearly 1000 m thick, as proved by well 204/30a-2, and comprises two sand-rich formations: the Otter Bank Fm. and the overlying Foula Fm. (Fig. 3). The Otter Bank Fm. is underlain by the

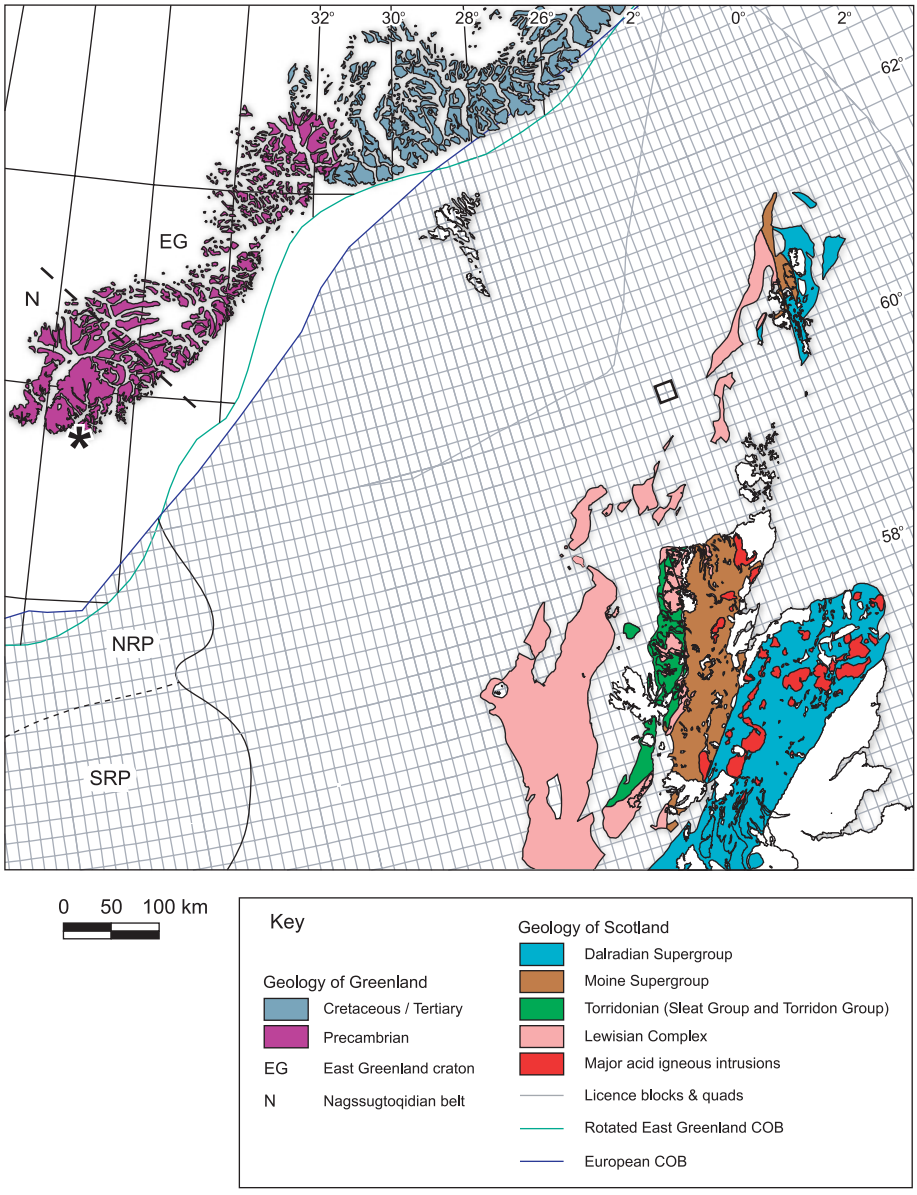

Fig. 1. Best-fit pre-rift reconstruction of the northeast Atlantic (pre-magnetic anomaly 24), showing distribution of basement terrains on the British and Greenland margins, adapted from Scott (2000). Boundary between northern Rockall Plateau (NRP) and southern Rockall Plateau (SRP) is the inferred suture between Archaean crust in the north and Palaeoproterozoic crust, similar to the Ketilidian of south Greenland, in the south (Dickin, 1992). Box shows location of the map in Fig. 2. COB = continent-ocean boundary. ∗ = location of Kulusuk sample described by Sørensen and Kalvig (2002).

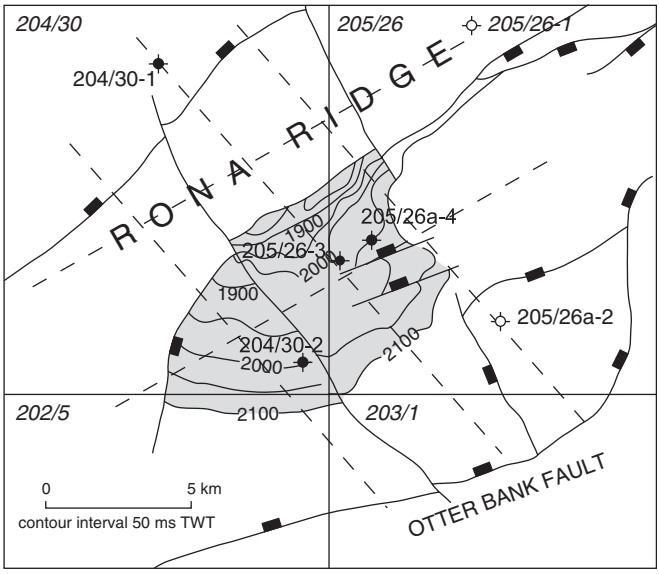

Fig. 2. Location of the Strathmore Field wells discussed in this contribution. See Fig. 1 for regional location. Contours are on the base Cretaceous. Dashed lines show the 2D seismic grid used to define the prospect (Herries et al., 1999).

Otter Bank Shale Fm., dated as Griensbachian (basal Scythian) on the basis of a distinctive palynological assemblage (Swiecicki et al., 1995; Herries et al., 1999).

The Otter Bank Fm. contains a very sparse palynological assemblage, most likely indicating a Scythian (Early Triassic) age (Swiecicki et al., 1995). Palaeomagnetic data (Swiecicki et al., 1995) indicate that the Otter Bank Fm. has predominantly reversed polarity, suggesting that it was deposited in the Diererian-Smithian (mid-Scythian). The lower part of the Otter Bank Fm. comprises braided sandy fluvial deposits, with the upper part containing interbedded fluvial and aeolian sabkha deposits.

Palynological constraints on the age of the Foula Fm. are also poor, but suggest that deposition began in the Ladinian and extended into the Carnian (Swiecicki et al., 1995). The Foula Fm. has also predominantly reversed polarity, consistent with a Ladinian age (Swiecicki et al., 1995). The lower part of the Foula Fm. also comprises interbedded fluvial and aeolian sabkha deposits, replaced by wholly fluvial deposits higher in the succession.

4. ANALYTICAL METHODS

Core samples were gently disaggregated by use of a pestle and mortar, avoiding grinding action. Ditch cuttings samples were already disaggregated through the action of the drill bit. No chemical pretreatment was used, thus avoiding the possibility of modifying assemblages in the laboratory. Following disaggregation, the samples

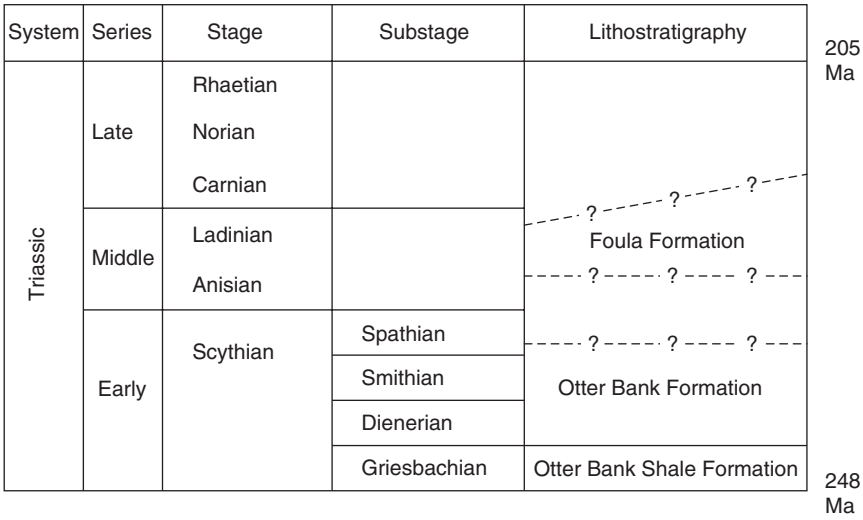

Fig. 3. Triassic stratigraphy in the Strathmore Field area (from Swiecicki et al., 1995, and Herries et al., 1999).

were immersed in water and cleaned by ultrasonic probe to remove and disperse any clay that might have been adhering to grain surfaces. The 63–125 μm (very fine sand) fraction was separated by sieving, and placed in bromoform with a measured specific gravity of 2.8 to enable separation of heavy minerals by gravity settling. The heavy mineral residues were mounted under Canada balsam for optical study using a polarising microscope, with a split retained for microprobe study. Relative abundances of the non-opaque detrital component were estimated using a grain count of 200 (Table 1).

Provenance-sensitive heavy mineral ratios (Table 2) were determined during the conventional petrographic analysis, using a count of at least 200 grains per mineral pair (where recovery allowed). The parameters used are as follows:

- ATi (apatite/tourmaline index) = % apatite in total apatite plus tourmaline
- GZi (garnet/zircon index) = % garnet in total garnet plus zircon
- RuZi (rutile/zircon index) = % rutile in total rutile plus zircon
- MZi (monazite/zircon index) = % monazite in total monazite plus zircon
- CZi (chrome-spinel/zircon index) = % chrome spinel in total chrome spinel plus zircon

Mineral–chemical data were acquired from garnet using an AN10000 energy-dispersive X-ray analyser attached to a Cambridge Instruments Microscan V electron microprobe. Data reduction used the ZAF-4 programme. Garnet populations are plotted on ternary diagrams using molecular proportions of Fe + Mn, Mg and Ca as poles, as recommended by Droop and Harte (1995).

The U-Pb analyses were undertaken using SHRIMP I at The Australian National University in Canberra. Zircon separates were obtained by standard density and magnetic separation techniques, avoiding further splitting on the basis of size or paramagnetic behaviour. An arbitrary, and presumed representative, fraction for

Table 1. Detrital non-opaque heavy mineral abundances (frequency %) in the 63–125 μm fraction of Triassic sandstones from the Strathmore Field, on counts of 200 grains per sample

Well	Depth (m)	Sample	Formation	At	Ap	Ca	Cr	Ep	Gt	Ky	Mo	Ru	St	To	Zr	Other (R)
205/26a-3	2454.0	Core	Foula	R	15.0				84.0		R	0.5		R	0.5	
	2485.1	Core	Otter Bank	0.5	82.0				2.5		0.5	2.0		4.0	8.5	Gh
	2513.9	Core	Otter Bank	R	11.5				82.5		R	1.5		1.0	3.5	
	2544.3	Core	Otter Bank	0.5	36.0				52.5		0.5	2.0		3.0	5.5	Gh
	2574.1	Core	Otter Bank	1.0	15.5				68.0		0.5	3.0		2.5	9.5	
	2610.0	Core	Otter Bank	0.5	38.5				34.0		R	3.0		6.0	18.0	
	2629.6	Core	Otter Bank	0.5	13.0		R	0.5	78.0		R	1.5	0.5	1.5	4.5	Sp
	2630.8	Core	Otter Bank	R	8.0		R	0.5	83.5		R	1.5		0.5	5.0	
	2638.1	Core	Otter Bank	R	3.0		R	R	93.0		R	1.0		2.0	1.0	
	2648.4	Core	Otter Bank	0.5	21.5				66.0		R	1.5		4.0	6.5	
	2661.8	Core	Otter Bank	R	11.5				81.5		R	1.0		5.5	0.5	
	2671.6	Core	Otter Bank	0.5	27.5			R	46.0		1.5	3.5		4.0	17.0	
205/26a-4	2470.8	Core	Foula	R	14.5				83.0		R	2.0		R	0.5	
	2488.8	Core	Foula	R	16.0				80.0		R	1.5		0.5	2.0	
	2500.6	Core	Foula	R	17.5				75.5		R	3.0		R	4.0	
	2534.4	Core	Foula	R	4.5				93.5		R	1.0		0.5	0.5	
	2548.8	Core	Foula	R	9.5				87.0		R	2.0	R	R	1.5	
	2563.5	Core	Foula	R	6.5				91.5		R	1.0		R	1.0	
	2582.2	Core	Foula	R	11.5				86.0		R	1.0		R	1.5	
	2596.5	Core	Foula	R	6.0				90.0		R	1.0		0.5	2.5	
	2606.0	Core	Foula	R	7.5				89.5		R	1.5		0.5	1.0	
	2619.5	Core	Foula	0.5	14.0				81.0		0.5	1.0		0.5	2.5	
	2632.0	Core	Foula	R	5.0				92.0		0.5	1.5		R	1.0	
	2647.5	Core	Foula	R	4.0				94.5		R	0.5		R	1.0	
	2661.2	Core	Foula	R	11.0				86.0		R	1.0		R	2.0	
	2702.5	Core	Otter Bank	0.5	15.5				79.0		R	1.0		R	4.0	
	2723.1	Core	Otter Bank	1.0	15.5				74.5		R	0.5		1.5	7.0	Br
	2739.0	Core	Otter Bank	R	12.0				78.5		R	2.0		4.0	3.5	Br, Cp
	2762.1	Core	Otter Bank	0.5	10.0				78.0		0.5	2.5		2.5	6.0	
	2778.7	Core	Otter Bank	R	5.5		R		85.5		R	1.0		R	8.0	
	2794.9	Core	Otter Bank	0.5	3.5				89.5		R	1.5		1.5	3.5	
	2809.9	Core	Otter Bank	1.0	8.0				84.0		R	1.5		0.5	5.0	
204/30a-2	2444.1	Core	Foula	0.5	42.0				53.5		R	2.5		0.5	1.0	
	2464.0	Core	Foula	R	9.0				90.0		R	1.0		R	R	
	2497.6	Core	Foula	R	12.5				85.0		R	1.0	R	R	1.5	
	2530	uwc	Foula	R	4.0	R		R	93.5		R	1.0	R	R	1.5	Sp
	2557	uwc	Foula	0.5	23.0	2.5		1.0	66.0			0.5	R	2.0	4.5	Cp
	2591	uwc	Foula	0.5	6.0	R		2.0	88.5		R	2.0		R	1.0	
	2605.9	Core	Foula	R	7.5			4.0	85.0			1.5		0.5	1.5	
	2635.9	Core	Foula	R	6.0			1.0	88.5		R	2.0		0.5	2.0	
	2679	uwc	Foula	R	1.0	R		0.5	96.0		R	1.0		R	1.5	
	2713	uwc	Foula	R	1.0			0.5	93.5			2.5		R	2.5	
	2743	uwc	Foula	R	3.5	R	R	3.5	89.5			2.0		R	1.0	
	2774	uwc	Foula	R	6.0	0.5		R	91.0			1.0		R	1.5	
	2804	uwc	Foula	R	3.5	R		R	93.0	R	R	1.5		0.5	1.5	
	2835	uwc	Foula	R	10.0	R	R	1.0	86.0			1.0	R	0.5	1.5	
	2865	uwc	Foula	R	7.5	R	0.5	2.0	81.5			2.5			5.5	
	2896	uwc	Foula	R	16.0	R		0.5	75.0		R	0.5		0.5	7.5	
	2926	uwc	Foula	R	4.5			0.5	91.0			1.0		R	3.0	
	2957	uwc	Foula	R	3.0			R	92.0	0.5		1.0		R	3.5	Cp
	2987	uwc	Foula	R	3.5	R		R	93.0		0.5	1.5	R	R	1.5	
	3018	uwc	Foula	R	R	R		R	97.5			2.0		R	0.5	
	3045	uwc	Foula	1.0	2.0	R		0.5	91.0	R		4.5		R	1.0	Cp
	3079	uwc	Foula	R	5.0	R		R	92.5		R	1.5		R	1.0	Cp

Table 1 (*Continued*)

Well	Depth (m)	Sample	Formation	At	Ap	Ca	Cr	Ep	Gt	Ky	Mo	Ru	St	To	Zr	Other (R)
	3109	uwc	Foula	R	0.5	R	R	R	96.5	R		1.5	R	R	1.5	Cp
	3139	uwc	Foula	R	2.0	0.5		R	94.0		R	3.0		R	0.5	Cp
	3170	uwc	Foula	R	4.0	R		R	93.5		R	1.5	R	R	1.0	
	3209.8	Core	Otter Bank	R	11.0				85.5		R	0.5		1.0	2.0	
	3228.7	Core	Otter Bank	0.5	15.0				77.0		0.5	2.0		1.0	4.0	
	3261	uwc	Otter Bank	0.5	6.0	R		0.5	82.5			2.5		4.0	4.0	Cp
	3292	uwc	Otter Bank	0.5	3.0	R	R	1.0	86.0		R	1.5	R	2.5	5.5	Cp
	3322	uwc	Otter Bank	R	1.5	R			85.0		R	3.0		2.0	8.5	
	3353	uwc	Otter Bank	R	5.0			1.0	84.5	R	R	2.0		1.5	6.0	

Note: At = anatase, Ap = apatite, Br = brookite, Ca = calcic amphibole, Cp = clinopyroxene, Cr = chrome spinel, Ep = epidote, Gh = gahnite, Gt = garnet, Ky = kyanite, Mo = monazite, Ru = rutile, Sp = titanite, St = staurolite, To = – tourmaline, Zr = zircon, R = rare (<0.5%), uwc = unwashed cuttings.

each sample was poured onto double-sided tape, cast into an epoxy disk, sectioned and polished. Transmitted and reflected light photomicrographs, and cathodoluminescence (CL) images were prepared for all grains. The procedures employed for zircon U-Pb dating followed Williams (1998) and references therein. The number of scans through the mass stations was limited to four, thereby achieving rapid data acquisition at the expense of some counting precision per analysis. In the first instance, an arbitrary group of 60 zircons were analysed from each sample, to ensure a 95% probability of identifying a component comprising 5% of the entire population (Dodson et al., 1988). Subjectivity in zircon dating was avoided by analysing all zircons encountered during the traverse of the mount, unless the grain showed evidence of being metamict or otherwise structurally compromised as determined from examination of the reflected and transmitted light photomicrographs and CL images. Normalisation of Pb/U isotopic ratios was achieved by reference to analyses of the AS3 reference zircon (1099 Ma; $^{206}Pb/^{238}U = 0.1589$; Paces and Miller, 1993). The raw SHRIMP data were processed using SQUID (Ludwig, 2001), with plots generated using Isoplot/Ex (Ludwig, 1999). For zircon areas that are older than approximately 800 Ma, the measured $^{206}Pb/^{204}Pb$ ratios have been used to correct for common Pb and the radiogenic $^{207}Pb/^{206}Pb$ ratio used to calculate the preferred age. For zircon areas that are younger than approximately 800 Ma, correction for common Pb was made using the measured $^{207}Pb/^{206}Pb$ and $^{238}U/^{206}Pb$ ratios, giving a radiogenic $^{206}Pb/^{238}U$ ratio and age following Tera and Wasserburg (1972) as described in Williams (1998, and references therein). When an analysis of Neoproterozoic and older zircons was 20% discordant, it was excluded from the relative probability plots. For the younger analyses, the validity of the radiogenic $^{206}Pb/^{238}U$ age has been determined on the basis of a number of factors, including the amount of common Pb (that is, if the total $^{207}Pb/^{206}Pb$ ratio deviates significantly from concordance on the Tera and Wasserburg plot), the relative concentrations of U and Th, the nature of the area analysed when examined post analysis and the abundance of a particular age grouping. The data from the two samples are given in Tables 3 and 4.

Table 2. Provenance-sensitive heavy mineral ratios from Triassic sandstones of the Strathmore Field

Well	Depth (m)	sample	Formation	ATi	Total	GZi	Total	RuZi	Total	MZi	Total	CZi	Total
205/26a-3	2454.0	Core	Foula	98.5	200	99.5	203	69.7	66	4.7	21	0.0	20
	2485.1	Core	Otter Bank	95.5	200	24.1	108	24.8	109	2.4	84	0.0	82
	2513.9	Core	Otter Bank	88.5	200	95.7	209	25.5	106	1.3	80	0.0	79
	2544.3	Core	Otter Bank	92.0	200	90.5	221	20.3	251	2.0	204	0.5	201
	2574.1	Core	Otter Bank	84.5	200	87.7	228	27.8	277	2.0	204	0.0	200
	2610.0	Core	Otter Bank	83.0	200	59.5	247	18.4	245	1.5	203	0.0	200
	2629.6	Core	Otter Bank	82.5	200	94.8	211	27.4	197	3.4	148	0.7	144
	2630.8	Core	Otter Bank	88.5	200	94.8	211	28.3	258	2.1	189	0.5	186
	2638.1	Core	Otter Bank	64.0	200	98.5	203	26.5	272	5.7	212	0.5	201
	2648.4	Core	Otter Bank	83.5	200	90.9	220	25.1	267	0.5	201	0.0	200
	2661.8	Core	Otter Bank	65.6	186	98.0	204	38.5	39	4.0	25	0.0	24
	2671.6	Core	Otter Bank	89.0	200	70.7	283	18.0	244	5.7	212	0.0	200
205/26a-4	2470.8	Core	Foula	98.0	200	99.5	201	52.8	212	3.4	207	0.0	200
	2488.8	Core	Foula	98.0	200	97.1	206	43.6	266	4.3	209	0.0	200
	2500.6	Core	Foula	99.5	200	96.2	208	42.1	259	5.2	211	0.0	200
	2534.4	Core	Foula	97.0	200	99.5	201	61.5	260	9.2	206	0.0	187
	2548.8	Core	Foula	99.5	200	98.0	204	58.7	242	7.0	215	0.0	200
	2563.5	Core	Foula	99.0	200	99.0	202	62.1	264	6.5	214	0.0	200
	2582.2	Core	Foula	99.5	200	98.5	203	59.7	248	9.0	158	0.0	145
	2596.5	Core	Foula	98.5	200	97.6	205	59.5	247	3.4	207	0.0	200
	2606.0	Core	Foula	97.0	200	99.0	202	63.5	274	7.1	127	0.0	118
	2619.5	Core	Foula	98.0	200	97.1	206	60.2	251	8.3	109	0.0	100
	2632.0	Core	Foula	96.5	200	99.0	202	60.0	250	11.7	197	0.0	174
	2647.5	Core	Foula	95.5	200	99.0	202	60.8	255	6.4	109	0.0	102
	2661.2	Core	Foula	99.5	200	98.0	204	57.8	237	1.5	203	0.0	200
	2702.5	Core	Otter Bank	97.5	200	95.2	210	17.0	241	2.0	204	0.0	200
	2723.1	Core	Otter Bank	93.0	200	89.7	223	30.1	286	5.7	212	0.0	200
	2739.0	Core	Otter Bank	81.5	200	96.2	208	30.8	289	3.8	208	0.0	200
	2762.1	Core	Otter Bank	85.0	200	93.5	214	27.5	276	3.8	208	0.0	200
	2778.7	Core	Otter Bank	91.0	200	91.3	219	14.9	235	3.8	208	1.0	202
	2794.9	Core	Otter Bank	72.5	200	96.2	208	21.3	254	2.9	206	0.0	200
	2809.9	Core	Otter Bank	82.5	200	94.3	212	24.5	265	2.9	206	0.0	200
204/30a-2	2444.1	Core	Foula	99.0	200	97.6	205	56.1	228	6.7	195	0.0	180
	2464.0	Core	Foula	97.5	200	99.5	201	58.9	243	9.5	221	0.0	200
	2497.6	Core	Foula	97.0	200	98.0	204	64.0	278	9.9	222	0.0	200
	2530	uwc	Foula	92.0	200	98.5	203	51.0	204	3.3	182	0.0	176
	2557	uwc	Foula	96.5	200	93.5	214	18.6	43	0.0	35	0.0	35
	2591	uwc	Foula	97.8	185	99.0	202	54.4	90	4.7	43	0.0	41
	2605.9	Core	Foula	95.5	200	98.5	203	66.9	163	0.0	54	0.0	54
	2635.9	Core	Foula	98.0	200	97.6	205	58.2	146	1.6	62	0.0	61
	2679	uwc	Foula	95.0	179	99.5	201	48.9	235	1.5	134	0.0	132
	2713	uwc	Foula	98.1	107	96.2	208	51.2	215	0.0	105	0.0	105
	2743	uwc	Foula	99.5	200	99.0	202	64.3	176	0.0	62	1.6	63
	2774	uwc	Foula	98.3	59	98.5	203	48.0	50	0.0	26	0.0	26
	2804	uwc	Foula	98.0	200	98.5	203	52.4	210	0.6	178	0.0	177
	2835	uwc	Foula	98.0	200	99.0	202	40.3	124	0.0	74	1.3	75
	2865	uwc	Foula	100.0	73	94.3	212	27.2	62	0.0	45	2.2	46
	2896	uwc	Foula	98.0	200	91.3	219	13.4	172	0.7	150	0.0	149
	2926	uwc	Foula	97.2	179	97.1	206	38.9	175	0.0	107	0.0	107
	2957	uwc	Foula	97.4	116	96.6	207	64.8	196	0.0	69	0.0	69
	2987	uwc	Foula	96.9	128	97.6	205	57.3	96	2.7	37	0.0	36
	3018	uwc	Foula	94.9	79	99.5	201	69.7	188	0.0	57	0.0	57
	3045	uwc	Foula	89.6	48	99.0	202	68.0	147	0.0	47	0.0	47
	3079	uwc	Foula	96.0	200	97.6	205	59.2	245	0.7	137	0.0	136

Table 2 (*Continued*)

Well	Depth (m)	sample	Formation	ATi	Total	GZi	Total	RuZi	Total	MZi	Total	CZi	Total
	3109	uwc	Foula	93.2	117	98.5	203	69.4	327	0.0	106	0.9	107
	3139	uwc	Foula	96.8	156	99.0	202	58.3	240	1.5	137	0.0	135
	3170	uwc	Foula	91.4	186	99.0	202	48.0	244	0.8	128	0.0	127
	3209.8	Core	Otter Bank	88.5	200	98.0	204	23.5	238	2.2	186	0.0	182
	3228.7	Core	Otter Bank	91.0	200	93.5	214	26.4	148	5.2	115	0.0	109
	3261	uwc	Otter Bank	60.0	200	93.0	215	29.5	190	0.0	134	0.0	134
	3292	uwc	Otter Bank	60.5	200	92.2	217	26.8	205	1.1	191	0.0	189
	3322	uwc	Otter Bank	54.0	100	90.9	220	25.9	270	1.0	202	0.0	200
	3353	uwc	Otter Bank	66.7	117	92.6	216	26.4	208	0.7	154	0.0	153

Note: ATi = apatite/tourmaline index (% apatite in total apatite plus tourmaline); GZi = garnet/zircon index (% garnet in total garnet plus zircon); RuZi = rutile/zircon index (% rutile in total rutile plus zircon); MZi = monazite/zircon index (% monazite in total monazite plus zircon); CZi = chrome-spinel/zircon index (% chrome-spinel in total chrome-spinel plus zircon). See Morton and Hallsworth (1994) for further information.

5. HEAVY MINERAL STRATIGRAPHY

Three wells were used in the study: 204/30a-2, 205/26a-3 and 205/26a-4 (Fig. 2). The sandstones in 205/26a-3 and 205/26a-4 were characterised exclusively using core material. By contrast, only three short cores were taken in the Triassic succession in 204/30a-2, and thus comprehensive coverage of this well was achieved using ditch cuttings, which were taken at 9 m intervals.

5.1. Provenance-Sensitive Ratio Data

Of the provenance-sensitive mineral parameters determined in the study, the rutile/zircon (RuZi), garnet/zircon (GZi) and apatite/tourmaline (ATi) indices show marked variations. Downhole variations in these parameters for the three wells are shown in Figs. 4–6. By contrast, variations in monazite/zircon (MZi) appear to lack stratigraphic significance. Finally, the chrome-spinel/zircon (CZi) values are low to very low throughout, and have no value in discriminating the formations in this example.

The most dramatic feature shown by the downhole plots is the sudden increase in RuZi in all three wells, from a baseline value of approximately 20–30 in the lower part of each well, to a baseline value of approximately 60 in the upper part. The increase in RuZi occurs at the boundary between the Otter Bank and Foula Fms, coincident with an increase in gamma ray measurements (Figs. 4–6). The ATi and GZi also show changes across the Otter Bank-Foula Boundary. GZi is consistently extremely high in the Foula Fm., but is slightly lower and more variable in the Otter Bank Fm. ATi is also consistently high in the Foula Fm. and generally lower in the Otter Bank Fm. However, variations in ATi appear to define a two-fold subdivision of the Otter Bank Fm., with the upper part of the Otter Bank Fm. (subunit O2) having higher ATi than the lower part (subunit O1).

Within the Foula Fm., GZi and ATi values remain uniformly high, but there are distinct variations in RuZi. These are best developed in the thickest Foula Fm.

Table 3. U-Pb ages of detrital zircons in the Foula Fm. (well 205/26a-3, 2454.0 m) as determined by SHRIMP

Grain spot	U (ppm)	Th (ppm)	Th/U	Pb* (ppm)	$^{204}Pb/^{206}Pb$	f_{206}%	Total ratios				Radiogenic ratios							Age (Ma)				
							$^{238}U/^{206}Pb$	±	$^{207}Pb/^{206}Pb$	±	$^{206}Pb/^{238}U$	±	$^{207}Pb/^{235}U$	±	$^{207}Pb/^{206}Pb$	±	ρ	$^{206}Pb/^{238}U$	±	$^{207}Pb/^{206}Pb$	±	% Disc.
1.1	159	162	1.02	45.5	0.0000	<0.01	2.9974	0.0400	0.1164	0.0010	0.3336	0.0044	5.351	0.084	0.1163	0.0010	0.8509	1856.0	22.0	1901	15	2
2.1	267	216	0.81	69.4	0.0002	0.29	3.3087	0.0406	0.1244	0.0008	0.3013	0.0037	5.065	0.086	0.1219	0.0014	0.7288	1698.0	18.0	1984	21	14
3.1	9	17	1.79	0.4	0.0076	12.85	22.3772	1.3152	0.1541	0.0146	0.0389	0.0026						246.3	15.8			
4.1	65	59	0.90	18.7	0.0009	1.34	2.9783	0.0519	0.1172	0.0029	0.3400	0.0059	5.956	0.179	0.1271	0.0031	0.5787	1887.0	32.0	2058	43	8
5.1	348	170	0.49	14.3	0.0006	0.15	20.9445	0.2834	0.0535	0.0011	0.0477	0.0007						300.2	4.0			
6.1	21	11	0.55	6.4	0.0004	0.54	2.7941	0.0757	0.1435	0.0030	0.3560	0.0099	6.817	0.345	0.1389	0.0059	0.5467	1963.0	47.0	2213	74	11
7.1	62	61	0.99	29.5	0.0002	0.26	1.8039	0.0283	0.1967	0.0015	0.5529	0.0087	14.814	0.286	0.1943	0.0022	0.8174	2837.0	36.0	2779	18	−2
8.1	187	55	0.30	79.0	0.0001	0.13	2.0308	0.0249	0.1884	0.0009	0.4918	0.0060	12.697	0.176	0.1873	0.0012	0.8868	2578.0	26.0	2718	11	5
9.1	715	85	0.12	274.3	0.0001	0.12	2.2382	0.0239	0.1834	0.0005	0.4462	0.0048	11.221	0.125	0.1824	0.0006	0.9608	2379.0	21.0	2675	5	11
10.1	137	215	1.57	4.9	0.0015	0.27	24.0399	0.3999	0.0536	0.0017	0.0415	0.0007						262.0	4.3			
11.1	126	85	0.67	5.0	–	0.56	21.6772	0.3618	0.0566	0.0019	0.0459	0.0008						289.1	4.8			
12.1	255	163	0.64	130.7	0.0000	0.05	1.6748	0.0195	0.2318	0.0008	0.5968	0.0070	19.042	0.233	0.2314	0.0009	0.9511	3017.0	28.0	3062	6	1
13.1	140	42	0.30	41.2	0.0001	0.16	2.9112	0.0361	0.1158	0.0008	0.3443	0.0043	5.590	0.080	0.1177	0.0008	0.8654	1908.0	21.0	1922	13	1
14.1	159	131	0.82	46.1	0.0001	0.10	2.9640	0.0376	0.1162	0.0008	0.3370	0.0043	5.358	0.078	0.1153	0.0008	0.8758	1872.0	21.0	1885	13	1
15.1	155	40	0.26	69.8	0.0001	0.08	1.9063	0.0241	0.1870	0.0010	0.5242	0.0066	13.466	0.190	0.1863	0.0012	0.8977	2717.0	28.0	2710	10	0
16.1	110	107	0.98	3.9	0.0003	0.34	24.1461	0.4235	0.0541	0.0019	0.0413	0.0007						260.7	4.6			
17.1	161	97	0.60	42.9	0.0006	0.87	3.2218	0.0410	0.1197	0.0009	0.3077	0.0040	4.760	0.111	0.1122	0.0022	0.5523	1729.0	20.0	1835	35	6
18.1	149	87	0.58	45.2	0.0000	0.04	2.8261	0.0359	0.1167	0.0009	0.3542	0.0045	5.738	0.084	0.1175	0.0009	0.8647	1955.0	23.0	1918	13	−2
19.1	129	51	0.40	64.2	0.0001	0.13	1.7230	0.0222	0.1938	0.0014	0.5806	0.0075	15.540	0.229	0.1941	0.0014	0.8740	2951.0	32.0	2777	12	−6
20.1	65	40	0.61	30.7	0.0002	0.21	1.8303	0.0273	0.1897	0.0014	0.5452	0.0082	14.118	0.259	0.1878	0.0020	0.8165	2805.0	34.0	2723	17	−3
21.1	482	34	0.07	133.1	0.0000	0.06	3.1104	0.0340	0.1174	0.0005	0.3213	0.0035	5.177	0.063	0.1169	0.0006	0.8998	1796.0	17.0	1909	10	6
22.1	49	77	1.58	14.5	0.0003	0.42	2.8794	0.0550	0.1174	0.0015	0.3458	0.0067	5.421	0.198	0.1137	0.0035	0.5315	1915.0	32.0	1859	56	−3
23.1	28	24	0.87	8.8	0.0001	0.13	2.7318	0.0548	0.1165	0.0019	0.3656	0.0074	5.814	0.174	0.1153	0.0026	0.6721	2009.0	35.0	1885	40	−7
24.1	201	165	0.82	56.7	0.0000	0.07	3.0417	0.0361	0.1159	0.0007	0.3285	0.0039	5.224	0.075	0.1153	0.0009	0.8247	1831.0	19.0	1885	15	3
25.1	178	43	0.24	79.7	–	<0.01	1.9182	0.0230	0.1876	0.0009	0.5216	0.0063	13.525	0.175	0.1881	0.0009	0.9289	2706.0	27.0	2725	8	1
26.1	451	414	0.92	18.5	0.0001	0.11	20.9096	0.2483	0.0532	0.0008	0.0478	0.0006						300.8	3.5			
27.1	532	252	0.47	100.5	0.0002	0.38	4.5478	0.0495	0.1807	0.0010	0.2190	0.0024	5.370	0.070	0.1778	0.0012	0.8419	1277.0	13.0	2633	12	51
28.1	82	97	1.18	21.6	0.0006	0.92	3.2380	0.0483	0.1231	0.0013	0.3060	0.0046	4.860	0.146	0.1152	0.0030	0.5058	1721.0	23.0	1883	47	9
29.1	138	84	0.61	63.7	0.0001	0.07	1.8604	0.0236	0.1846	0.0010	0.5371	0.0068	13.628	0.195	0.1840	0.0012	0.8876	2772.0	29.0	2689	11	−3
30.1	495	432	0.87	19.0	0.0011	1.82	22.3273	0.2691	0.0664	0.0066	0.0440	0.0007						277.4	4.1			
31.1	407	80	0.20	187.5	0.0000	0.03	1.8647	0.0205	0.1860	0.0006	0.5361	0.0059	13.732	0.158	0.1858	0.0006	0.9580	2767.0	25.0	2705	5	−2
32.1	240	253	1.06	64.1	0.0001	0.19	3.2119	0.0383	0.1152	0.0007	0.3108	0.0037	4.864	0.072	0.1135	0.0010	0.8035	1744.0	18.0	1856	16	6
33.1	78	69	0.88	37.4	–	<0.01	1.8009	0.0273	0.1879	0.0014	0.5554	0.0084	14.404	0.242	0.1881	0.0014	0.9014	2848.0	35.0	2726	12	−4
34.1	689	589	0.85	24.0	0.0002	0.45	24.6586	0.2965	0.0549	0.0009	0.0404	0.0005						255.1	3.0			
35.1	366	157	0.43	158.9	0.0000	0.05	1.9800	0.0218	0.1869	0.0006	0.5048	0.0056	12.979	0.149	0.1865	0.0006	0.9553	2634.0	24.0	2711	6	3
36.1	120	140	1.17	57.3	0.0001	0.07	1.8002	0.0220	0.1956	0.0009	0.5551	0.0068	14.924	0.196	0.1950	0.0009	0.9319	2846.0	28.0	2785	8	−2
37.1	94	66	0.69	3.6	0.0010	0.68	22.5232	0.3956	0.0573	0.0019	0.0441	0.0008						278.2	4.9			

Table 3 (*Continued*)

Grain spot	U (ppm)	Th (ppm)	Th/U	Pb* (ppm)	$^{204}Pb/^{206}Pb$	f_{206}%	Total ratios				Radiogenic ratios							Age (Ma)				
							$^{238}U/^{206}Pb$	±	$^{207}Pb/^{206}Pb$	±	$^{206}Pb/^{238}U$	±	$^{207}Pb/^{235}U$	±	$^{207}Pb/^{206}Pb$	±	ρ	$^{206}Pb/^{238}U$	±	$^{207}Pb/^{206}Pb$	±	% Disc.
38.1	295	71	0.24	83.8	0.0000	0.03	3.0222	0.0340	0.1151	0.0006	0.3308	0.0037	5.239	0.066	0.1149	0.0007	0.8895	1842.0	18.0	1878	10	2
39.1	35	17	0.50	17.3	–	<0.01	1.7404	0.0310	0.1942	0.0018	0.5749	0.0102	15.429	0.314	0.1946	0.0019	0.8759	2928.0	42.0	2782	16	−5
40.1	279	99	0.36	63.1	0.0002	0.32	3.7973	0.0457	0.1186	0.0009	0.2625	0.0032	4.195	0.083	0.1159	0.0018	0.6172	1503.0	16.0	1894	28	21
41.1	183	98	0.54	77.1	0.0000	0.05	2.0347	0.0238	0.1915	0.0006	0.4912	0.0058	12.942	0.158	0.1911	0.0007	0.9589	2576.0	25.0	2752	6	6
42.1	171	114	0.66	51.5	0.0000	0.02	2.8529	0.0345	0.1160	0.0007	0.3505	0.0042	5.600	0.077	0.1159	0.0007	0.8818	1937.0	20.0	1894	12	−2
43.1	6	2	0.30	2.8	–	<0.01	1.7951	0.0654	0.2047	0.0045	0.5584	0.0204	15.923	0.690	0.2068	0.0048	0.8413	2860.0	84.0	2881	38	1
44.1	232	326	1.40	9.0	0.0005	0.70	22.0705	0.2917	0.0576	0.0011	0.0450	0.0006						283.7	3.7			
45.1	465	149	0.32	38.3	–	<0.01	10.4405	0.1163	0.0587	0.0006	0.0959	0.0011						590.3	6.4			
46.1	498	240	0.48	53.8	0.0038	6.69	7.9513	0.0910	0.1680	0.0257	0.1174	0.0058	1.885	0.760	0.1165	0.0466	0.1224	715.0	33.0	1903	719	62
47.1	300	155	0.52	136.7	0.0000	0.02	1.8832	0.0209	0.1862	0.0006	0.5309	0.0059	13.612	0.158	0.1860	0.0006	0.9547	2745.0	25.0	2707	6	−1
48.1	1280	1407	1.10	50.6	0.0001	0.07	21.7134	0.2320	0.0527	0.0005	0.0460	0.0005						290.0	3.1			
49.1	73	62	0.85	34.4	0.0001	0.16	1.8254	0.0256	0.1909	0.0012	0.5469	0.0077	14.284	0.224	0.1894	0.0013	0.8954	2812.0	32.0	2737	12	−3
50.1	80	117	1.46	24.7	0.0004	0.60	2.7793	0.0399	0.1164	0.0011	0.3579	0.0051	5.537	0.100	0.1122	0.0012	0.7941	1972.0	30.0	1835	20	−7

Note: Uncertainties given at the 1σ level. Error in AS3 reference zircon calibration was 0.75% for the analytical session. f_{206}% denotes the percentage of ^{206}Pb that is common Pb. For zircon areas older than ~800 Ma, correction for common Pb made using the measured $^{204}Pb/^{206}Pb$ ratio. For zircon areas younger than ~800 Ma correction for common Pb made using the measured $^{238}U/^{206}Pb$ and $^{207}Pb/^{206}Pb$ ratios, following Tera and Wasserburg (1972) as outlined in Williams (1998). For % Disc., 0% denotes a concordant analysis.

Table 4. U-Pb ages of detrital zircons in the Otter Bank Fm. (well 205/26a-3, 2648.4 m) as determined by SHRIMP

Grain spot	U (ppm)	Th (ppm)	Th/U	Pb* (ppm)	$^{204}Pb/^{206}Pb$	f_{206}%	Total ratios				Radiogenic ratios							Age (Ma)				
							$^{238}U/^{206}Pb$	±	$^{207}Pb/^{206}Pb$	±	$^{206}Pb/^{238}U$	±	$^{207}Pb/^{235}U$	±	$^{207}Pb/^{206}Pb$	±	ρ	$^{206}Pb/^{238}U$	±	$^{207}Pb/^{206}Pb$	±	% Disc.
1.1	101	53	0.52	52.3	0.0003	0.36	1.6551	0.0272	0.2170	0.0017	0.6022	0.0099	17.820	0.325	0.2146	0.0017	0.9016	3039	42	2941	13	−3
2.1	164	130	0.79	63.5	0.0001	0.14	2.2168	0.0324	0.2003	0.0014	0.4505	0.0066	12.367	0.208	0.1991	0.0016	0.8703	2397	29	2819	14	15
3.1	950	142	0.15	62.7	0.0000	0.43	13.0168	0.1508	0.0601	0.0007	0.0765	0.0009						475.1	5.4			
4.1	105	29	0.28	27.3	0.0002	0.25	3.2964	0.0643	0.0993	0.0025	0.3030	0.0059	4.101	0.131	0.0982	0.0025	0.6112	1706	30	1590	47	−7
5.1	409	120	0.29	122.0	0.0000	0.04	2.8802	0.0352	0.1163	0.0007	0.3471	0.0042	5.546	0.078	0.1159	0.0008	0.8683	1921	20	1894	13	−1
6.1	167	68	0.41	26.4	0.0002	0.37	5.4343	0.0842	0.0794	0.0013	0.1833	0.0028	1.927	0.053	0.0762	0.0017	0.5615	1085	16	1101	46	1
7.1	316	68	0.22	146.9	0.0001	0.07	1.8474	0.0250	0.2013	0.0009	0.5409	0.0073	14.967	0.215	0.2007	0.0009	0.9444	2787	31	2832	8	2
8.1	310	247	0.80	66.0	0.0002	0.37	4.0308	0.0573	0.0963	0.0016	0.2472	0.0035	3.174	0.081	0.0931	0.0020	0.5595	1424	18	1491	40	4
9.1	109	130	1.19	50.9	0.0001	0.14	1.8381	0.0301	0.1918	0.0016	0.5433	0.0089	14.278	0.275	0.1906	0.0019	0.8521	2797	37	2747	17	−2
10.1	115	65	0.56	28.6	0.0004	0.67	3.4671	0.0585	0.1104	0.0015	0.2865	0.0049	4.133	0.144	0.1046	0.0032	0.4926	1624	25	1708	56	5
11.1	82	23	0.28	40.2	0.0000	0.05	1.7503	0.0311	0.2061	0.0019	0.5710	0.0101	16.189	0.324	0.2056	0.0019	0.8862	2912	42	2871	15	−1
12.1	293	140	0.48	137.1	0.0000	0.04	1.8367	0.0237	0.1998	0.0010	0.5442	0.0070	14.965	0.209	0.1994	0.0011	0.9241	2801	29	2822	9	1
13.1	285	226	0.79	122.8	0.0000	0.02	1.9971	0.0268	0.1945	0.0012	0.5006	0.0067	13.411	0.198	0.1943	0.0012	0.9096	2616	29	2779	10	6
14.1	211	81	0.39	103.4	0.0001	0.08	1.7494	0.0252	0.2051	0.0013	0.5712	0.0082	16.101	0.256	0.2045	0.0014	0.9064	2913	34	2862	11	−2
15.1	272	325	1.19	61.5	0.0006	0.98	3.8049	0.0547	0.1897	0.0016	0.2603	0.0038	6.538	0.132	0.1822	0.0025	0.7227	1491	19	2673	23	44
16.1	66	53	0.80	30.1	0.0002	0.26	1.8779	0.0398	0.1940	0.0024	0.5311	0.0113	14.037	0.355	0.1917	0.0026	0.8402	2746	48	2757	23	0
17.1	346	109	0.32	95.7	0.0000	0.04	3.1046	0.0398	0.1126	0.0009	0.3220	0.0041	4.981	0.076	0.1122	0.0009	0.8360	1799	20	1835	15	2
18.1	269	188	0.70	113.8	0.0001	0.12	2.0338	0.0280	0.1934	0.0012	0.4911	0.0068	13.019	0.201	0.1923	0.0014	0.8908	2575	29	2762	12	7
19.1	237	241	1.02	114.1	0.0001	0.10	1.7866	0.0252	0.2015	0.0012	0.5591	0.0079	15.462	0.242	0.2006	0.0013	0.9035	2863	33	2831	11	−1
20.1	101	31	0.31	30.6	0.0002	0.26	2.8444	0.0536	0.1257	0.0018	0.3506	0.0067	5.968	0.178	0.1235	0.0028	0.6380	1938	32	2007	41	3
21.1	725	6	0.01	108.2	0.0001	0.14	5.7539	0.0749	0.0750	0.0007	0.1736	0.0023	1.767	0.035	0.0739	0.0011	0.6528	1032	12	1037	31	1
22.1	47	48	1.02	15.8	0.0006	0.90	2.5817	0.0653	0.1821	0.0031	0.3838	0.0099	9.236	0.381	0.1745	0.0056	0.6270	2094	46	2601	54	19
23.1	207	103	0.50	98.8	0.0002	0.28	1.7978	0.0284	0.2064	0.0015	0.5547	0.0088	15.597	0.285	0.2039	0.0019	0.8648	2845	36	2858	15	0
24.1	97	88	0.91	44.3	–	<0.01	1.8806	0.0467	0.2079	0.0031	0.5319	0.0132	15.260	0.440	0.2081	0.0031	0.8608	2749	56	2891	24	5
25.1	653	176	0.27	180.9	0.0002	0.25	3.1002	0.0391	0.1126	0.0008	0.3218	0.0041	4.899	0.079	0.1104	0.0011	0.7881	1798	20	1806	18	0
26.1	74	30	0.41	19.3	0.0011	1.78	3.2811	0.0776	0.1047	0.0036	0.3023	0.0071	4.085	0.184	0.0980	0.0038	0.5240	1703	38	1587	72	−7
27.1	140	107	0.77	56.2	0.0004	0.57	2.1397	0.0383	0.1896	0.0019	0.4647	0.0084	11.830	0.289	0.1846	0.0030	0.7394	2460	37	2695	27	9
28.1	324	129	0.40	70.6	0.0001	0.09	3.9497	0.0572	0.0919	0.0011	0.2530	0.0037	3.180	0.062	0.0912	0.0012	0.7403	1454	19	1450	25	0
29.1	113	153	1.36	50.1	0.0001	0.11	1.9394	0.0381	0.1961	0.0021	0.5151	0.0101	13.858	0.315	0.1951	0.0022	0.8653	2678	43	2786	19	4
30.1	107	85	0.79	16.7	0.0002	0.36	5.5005	0.1193	0.0848	0.0022	0.1800	0.0039	1.901	0.073	0.0766	0.0024	0.5664	1067	25	1111	63	4
31.1	105	72	0.69	26.5	0.0003	0.50	3.4080	0.0702	0.1112	0.0021	0.2920	0.0061	4.305	0.154	0.1069	0.0031	0.5818	1651	30	1748	53	6
32.1	113	57	0.50	51.3	0.0002	0.31	1.8875	0.0370	0.2016	0.0037	0.5282	0.0104	14.485	0.406	0.1989	0.0040	0.7012	2734	44	2817	33	3
33.1	668	566	0.85	81.6	0.0003	0.57	7.0268	0.0867	0.1927	0.0011	0.1415	0.0018	3.680	0.056	0.1886	0.0016	0.8228	853	10	2730	14	69
34.1	160	83	0.52	43.3	–	<0.01	3.1713	0.0481	0.1105	0.0012	0.3148	0.0048	4.742	0.089	0.1092	0.0012	0.8086	1764	25	1787	20	1
35.1	75	145	1.94	34.9	0.0003	0.38	1.8421	0.0341	0.1929	0.0019	0.5412	0.0100	14.232	0.300	0.1907	0.0019	0.8793	2789	54	2748	17	−1

Table 4 (*Continued*)

Grain spot	U (ppm)	Th (ppm)	Th/U	Pb* (ppm)	$^{204}Pb/^{206}Pb$	f_{206}%	Total ratios				Radiogenic ratios							Age (Ma)				
							$^{238}U/^{206}Pb$	±	$^{207}Pb/^{206}Pb$	±	$^{206}Pb/^{238}U$	±	$^{207}Pb/^{235}U$	±	$^{207}Pb/^{206}Pb$	±	ρ	$^{206}Pb/^{238}U$	±	$^{207}Pb/^{206}Pb$	±	% Disc.
36.1	103	106	1.03	45.1	0.0002	0.25	1.9579	0.0327	0.1841	0.0016	0.5095	0.0085	12.777	0.253	0.1819	0.0019	0.8458	2654	36	2670	17	1
37.1	159	130	0.82	53.8	0.0000	0.01	2.5334	0.0376	0.1864	0.0015	0.3947	0.0059	10.143	0.176	0.1864	0.0017	0.8587	2145	27	2710	15	21
38.1	562	161	0.29	253.3	0.0001	0.07	1.9071	0.0223	0.1974	0.0007	0.5240	0.0061	14.219	0.176	0.1968	0.0008	0.9472	2716	26	2800	6	3
39.1	635	338	0.53	133.5	0.0003	0.43	4.0852	0.0485	0.1861	0.0010	0.2437	0.0029	6.144	0.088	0.1828	0.0014	0.8363	1406	15	2679	13	48
40.1	320	276	0.86	84.7	0.0003	0.51	3.2499	0.0428	0.1916	0.0012	0.3061	0.0041	7.920	0.129	0.1876	0.0018	0.8108	1722	20	2722	16	37
41.1	405	114	0.28	77.0	0.0004	0.63	4.5177	0.0578	0.1160	0.0010	0.2200	0.0028	3.360	0.071	0.1108	0.0018	0.6141	1282	15	1812	30	29
42.1	294	95	0.32	123.6	0.0001	0.17	2.0461	0.0270	0.1895	0.0010	0.4879	0.0064	12.652	0.184	0.1881	0.0011	0.9088	2562	28	2725	10	6
43.1	282	134	0.47	130.9	0.0001	0.13	1.8525	0.0247	0.2068	0.0011	0.5391	0.0072	15.285	0.223	0.2056	0.0012	0.9171	2780	30	2871	9	3
44.1	178	405	2.28	81.2	0.0003	0.40	1.8829	0.0277	0.1923	0.0013	0.5290	0.0078	13.765	0.239	0.1887	0.0017	0.8494	2737	33	2731	15	0
45.1	119	38	0.32	55.1	0.0004	0.49	1.8522	0.0309	0.1939	0.0016	0.5373	0.0090	14.038	0.283	0.1895	0.0021	0.8302	2772	38	2738	18	−1
46.1	643	141	0.22	241.5	0.0002	0.27	2.2883	0.0282	0.1951	0.0011	0.4358	0.0054	11.588	0.161	0.1928	0.0012	0.8861	2332	24	2767	11	16
47.1	610	21	0.03	297.5	0.0001	0.11	1.7613	0.0207	0.2188	0.0009	0.5672	0.0067	17.035	0.213	0.2178	0.0010	0.9371	2896	27	2965	7	2
48.1	761	69	0.09	86.0	0.0003	0.48	7.6013	0.0903	0.0718	0.0007	0.1309	0.0016	1.223	0.032	0.0678	0.0016	0.4524	793	9	862	49	8
49.1	904	66	0.07	276.7	0.0001	0.18	2.8065	0.0319	0.1625	0.0007	0.3557	0.0040	7.897	0.098	0.1610	0.0008	0.9174	1962	19	2466	8	20
50.1	579	237	0.41	251.4	0.0000	0.06	1.9787	0.0252	0.1820	0.0007	0.5051	0.0064	12.635	0.170	0.1814	0.0008	0.9459	2636	28	2666	7	1

Note: Justification of columns (according to decimal point) everywhere correct! Uncertainties given at the 1σ level. Error in AS3 reference zircon calibration was 0.73% for the analytical session. f_{206}% denotes the percentage of ^{206}Pb that is common Pb. For zircon areas older than ~800 Ma, correction for common Pb made using the measured $^{204}Pb/^{206}Pb$ ratio. For zircon areas younger than ~800 Ma correction for common Pb made using the measured $^{238}U/^{206}Pb$ and $^{207}Pb/^{206}Pb$ ratios, following Tera and Wasserburg (1972) as outlined in Williams (1998). For % Disc., 0% denotes a concordant analysis.

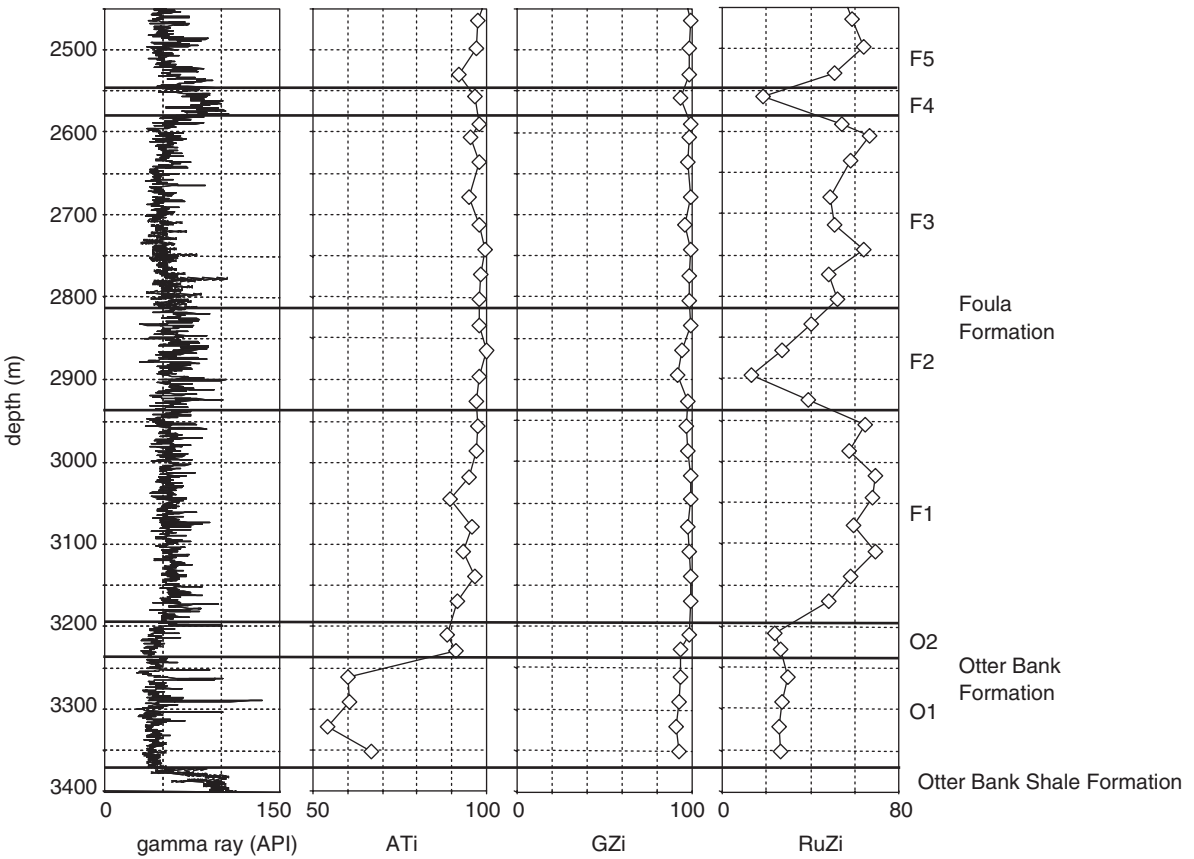

Fig. 4. Downhole variations in key heavy mineral ratio parameters for well 204/30a-2, showing subdivision into heavy mineral units O1-O2 and F1-F5. ATi = apatite/tourmaline index, GZi = garnet/zircon index, RuZi = rutile/zircon index (for definitions, see text).

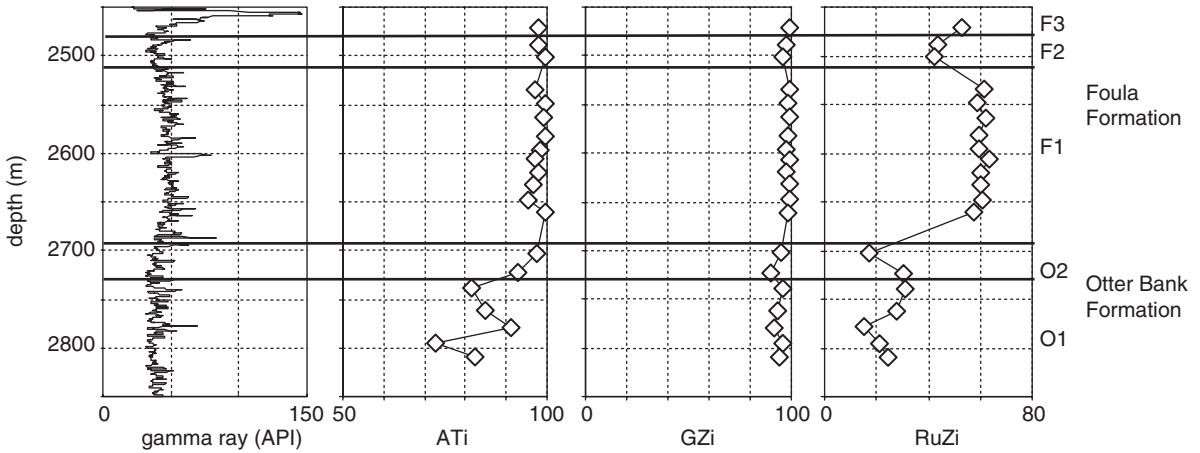

Fig. 5. Downhole variations in key heavy mineral ratio parameters for well 205/26a-4, showing subdivision into heavy mineral units O1-O2 and F1-F3. ATi = apatite/tourmaline index, GZi = garnet/zircon index, RuZi = rutile/zircon index (for definitions, see text).

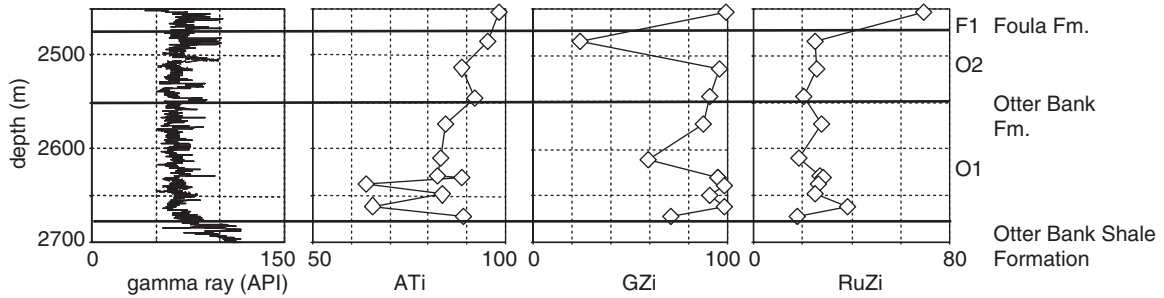

Fig. 6. Downhole variations in key heavy mineral ratio parameters for well 205/26a-3, showing subdivision into heavy mineral units O1-O2 and F1. ATi = apatite/tourmaline index, GZi = garnet/zircon index, RuZi = rutile/zircon index (for definitions, see text).

succession, present in 204/30a-2 (Fig. 4), but are also manifested by the cored succession in 205/26a-4 (Fig. 5). The variations in RuZi enable subdivision of the Foula Fm. into five subunits, three with high RuZi (F1, F3 and F5) and two with low RuZi (F2 and F4). The two subunits with low RuZi are also characterised by a slight lowering of GZi.

The clear distinction between the Foula and Otter Bank assemblages is also manifested by cross-plots of the ratio parameters (Fig. 7). Foula Fm. samples show well-defined clustering, with very high ATi and GZi and generally high RuZi. Otter Bank samples show greater variation, but display little overlap with the Foula Fm. data. They have uniformly low RuZi, and generally lower ATi and GZi than the Foula samples. The only area of overlap is between the Otter Bank and the low-RuZi subunits in the Foula Fm. (subunits F2 and F4), which have similar RuZi, GZi and ATi values.

The Foula and Otter Bank assemblages have been characterised using both core and ditch cuttings samples. Data from core samples are reliable since their position within the well is accurately known and they cannot be contaminated or otherwise altered during the drilling process. Ditch cuttings, however, represent a range of depths (dependent on the sampling frequency), may be contaminated by downhole caving, and may have been modified by the mechanical action of the drill bit.

The conventional heavy mineral data (Table 1) show evidence for contamination of cuttings samples. In core samples, the unstable minerals epidote, calcic amphibole and clinopyroxene are extremely scarce (epidote) or entirely absent (calcic amphibole, clinopyroxene), but occur in small amounts in most of the cuttings samples. The almost complete absence of these minerals in the core samples indicates that minor contamination of the cuttings has occurred. This is most likely to be related to caving of lithologies from higher in the well bore, although it is possible that the unstable minerals have been present in low-porosity siltstone and mudstone intercalations within the Triassic succession.

Use of provenance-sensitive ratios helps to eliminate the problems caused by caving or other forms of contamination. Plots of ratio data from core and ditch cuttings (Fig. 8) show that there is remarkable consistency between the two types of sample, with little deviation between the ratios determined from core and cuttings. GZi and ATi values in core and cuttings are virtually identical, the only slight deviation being that some cuttings samples in the Otter Bank of 204/30a-2 have marginally lower ATi than Otter Bank core samples. A more pronounced deviation in ATi between core and cuttings was identified in the Clair Field, west of Shetland (Morton et al., 2003), where it was ascribed to loss of apatite by the mechanical action of the drill bit. Apatite is more susceptible to mechanical loss than the other heavy minerals because of its lower hardness, and is preferentially lost through the grinding action of the drill bit. However, in the Otter Bank case, it is possible that the slight difference in ATi values between core and cuttings is due to provenance heterogeneity.

RuZi values in core and cuttings samples from the Otter Bank Fm. are closely comparable, but some cuttings samples from the Foula Fm. have distinctly lower RuZi than the core. These occur in 204/30a-2, and represent the samples defining subunits F2 and F4. The deviation in this case is ascribed to genuine differences in sediment provenance, since mechanical abrasion would cause cuttings values to be

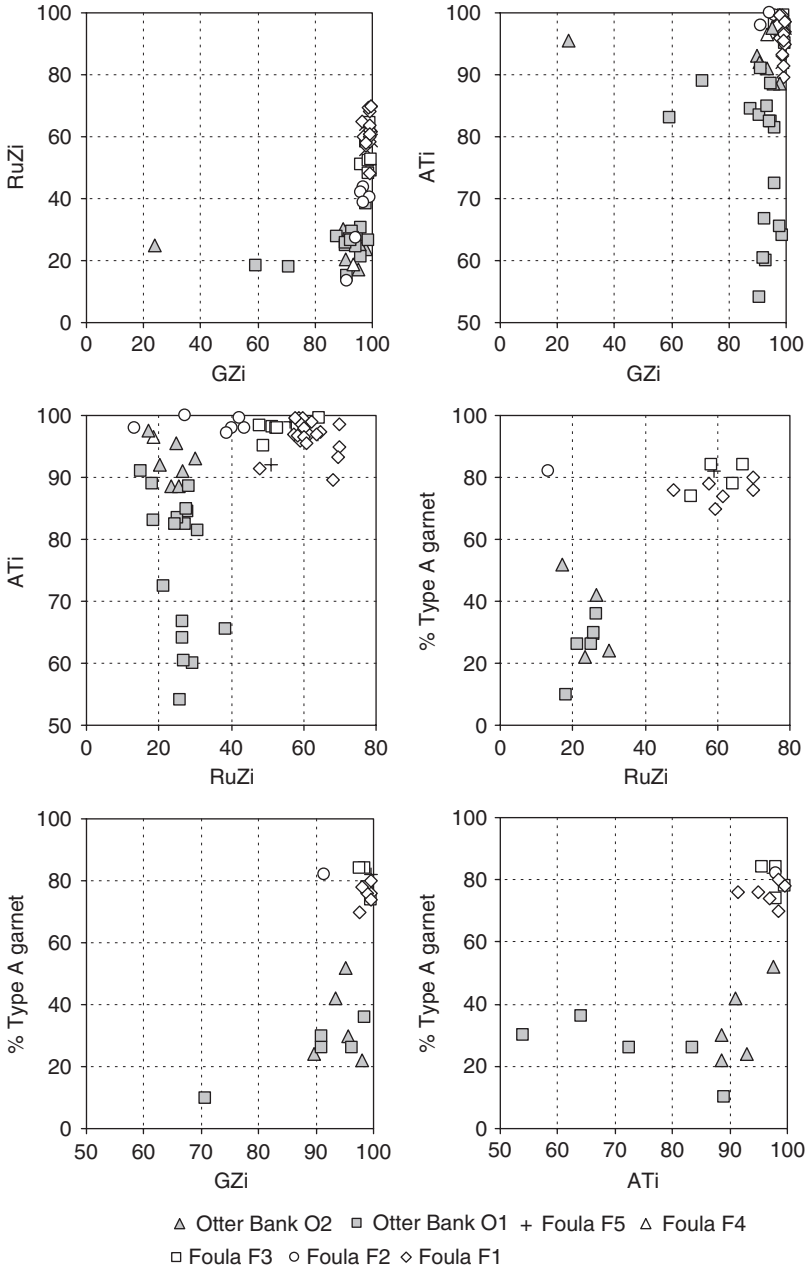

Fig. 7. Binary plots of key heavy ratio and garnet geochemical parameters, displaying the marked difference in provenance characteristics between the Foula and Otter Bank Fms and the intraformational variations enabling the distinction of subunits O1-O2 and F1-F5.

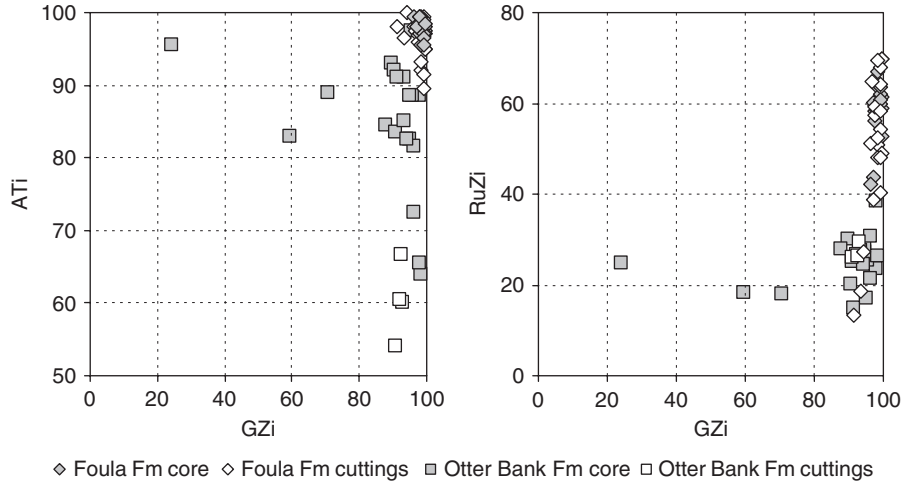

Fig. 8. Comparison of ratio parameters acquired from different sample types (core and ditch cuttings) in all three wells.

uniformly lower than core, rather than confining the effect to distinct zones, and because core data in 205/26a-4 also show the presence of a low-RuZi excursion. In the case of the Strathmore Field Triassic, therefore, ratio data from cuttings are considered reliable, their only disadvantage being the imprecision associated with their depth in the drilled succession. Greater care is required when interpreting conventional data, since assemblages in cuttings contain minerals that are absent from core, and have therefore been contaminated during the drilling process.

5.2. *Garnet Geochemical Data*

Garnet compositions also show marked stratigraphic variations (Fig. 9). The Foula Fm. is characterised by garnet assemblages dominated by high-Mg, low-Ca types, termed Type A (Morton et al., 2004). Low-Mg types (Type B) and high-Mg, high-Ca types (Type C) are scarce. By contrast, the Otter Bank Fm. has fewer Type A garnets, being dominated by low-Mg types (Type B) with small amounts of high-Mg, high-Ca garnets (Type C). The abundance of Type A garnets is therefore another effective discriminant of the Foula and Otter Bank Fms. As shown in Fig. 7, plots of Type A garnet vs. GZi, ATi and RuZi show the clear distinction between the two formations. The garnet data also enable discrimination between the low-RuZi units in the Foula Fm. (subunits F2 and F4) and the Otter Bank Fm., which show a degree of overlap on the ratio cross-plots. This is because the garnets in the low-RuZi parts of the Foula Fm. are identical to those in the high-RuZi parts, both having approximately 70–90% Type A garnet, whereas Type A garnet abundances in the Otter Bank samples reach only a maximum of approximately 50%.

It appears from the cross-plots (Fig. 7) that Otter Bank subunit O2 has slightly higher proportions of Type A garnet compared with O1, and therefore plots slightly closer to the Foula Fm. data cluster. This is especially noticeable on the cross-plot of Type A garnet and ATi.

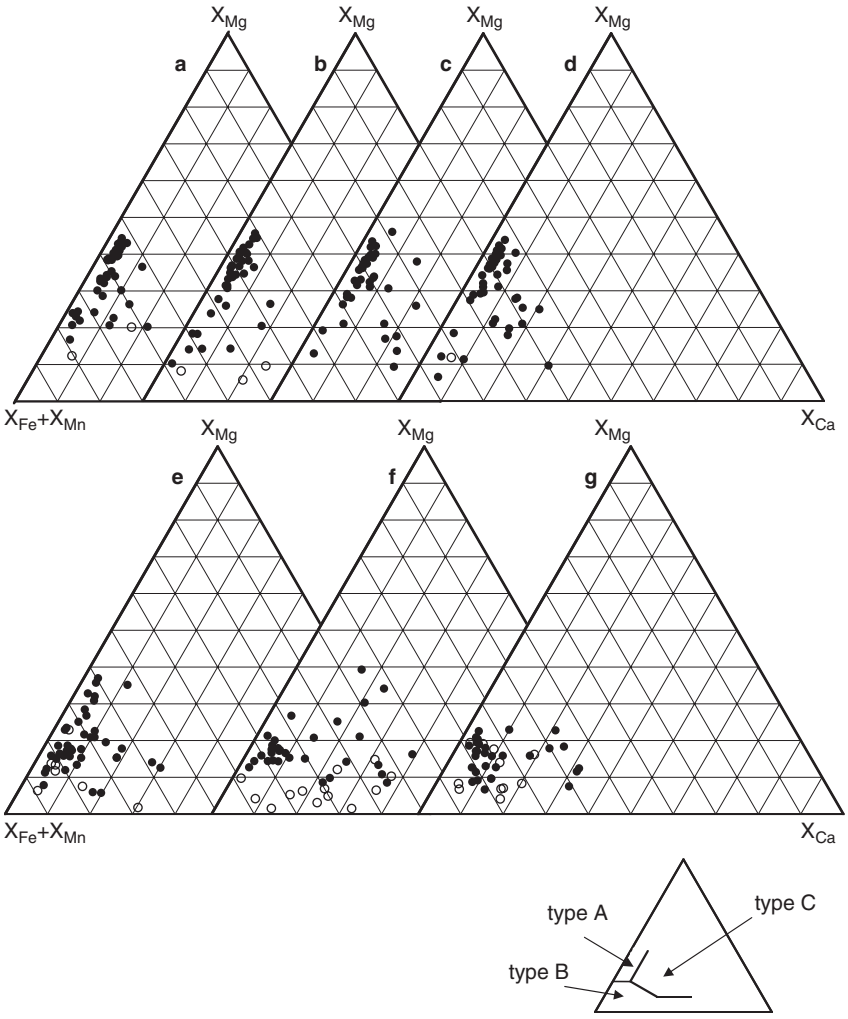

Fig. 9. Garnet compositions in selected samples from Foula and Otter Bank sandstones in the Strathmore Field. X_{Fe}, X_{Mg}, X_{Ca}, X_{Mn} = molecular proportion of Fe, Mg, Ca and Mn respectively, calculated on the basis of 24 oxygens, and normalised to total Fe + Mg + Ca + Mn, as recommended by Droop and Harte (1995). All Fe calculated as Fe^{2+}. Small plot shows the differentiation into fields A, B and C (from Morton et al., 2004). ●, $X_{Mn} < 5\%$; ○, $X_{Mn} > 5\%$; (a) 204/30a-2, 2464.0 m, Foula Fm., subunit F5 (core); (b) 204/30a-2, 2743 m, Foula Fm., subunit F3 (ditch cuttings); (c) 205/26a-3, 2454.0 m, Foula Fm., subunit F1 (core); (d) 205/26a-4, 2596.5 m, Foula Fm., subunit F1 (core); (e) 204/30a-2, 3322 m, Otter Bank Fm., subunit O1 (ditch cuttings), (f) 205/26a-3, 2671.6 m, Otter Bank Fm., subunit O1 (core); (g) 205/26a-4, 2723.1 m, Otter Bank Fm., subunit O2 (core).

5.3. Correlation

The heavy mineral correlation of the three wells is shown in Fig. 10. The correlation is ultimately constrained by the top Triassic unconformity (marked by a major rise in gamma-ray readings) and by the underlying Griesbachian Otter Bank Shale Fm. (not penetrated in 205/26a-4). A particular feature of note is the coincidence of boundaries between the heavy mineral units and events on the gamma-ray log. The most notable of these is the boundary between units O2 and F1, which coincides with a small but distinct upward increase in gamma intensity in all three wells. In 204/30a-2, the mineralogically defined subunits F2 and F4 coincide with intervals of elevated gamma-ray values. In 205/26a-4, subunit F2 is also characterised by a change in gamma-ray readings but in this case the subunit has slightly lower gamma activity than the underlying and overlying sediment. The change in gamma-ray readings suggests a difference in facies between the two wells, demonstrating the value of using an independent approach to correlation. The boundary between O1 and O2 does not appear to have any obvious manifestation on the gamma-ray log, again

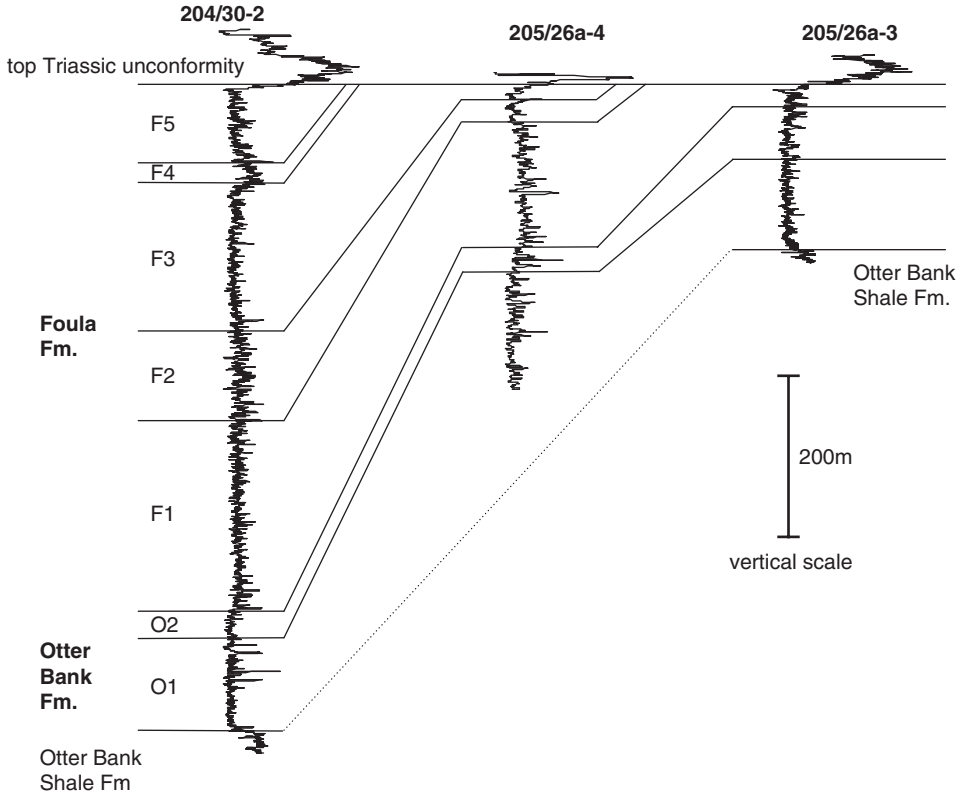

Fig. 10. Correlation of the Triassic succession in Strathmore Field wells 204/30a-2, 205/26a-3 and 205/26a-4, showing the heavy mineral units defined in Figs. 4–6. Location of wells shown in Fig. 2. Well 205/26a-4 was terminated before penetration of the Otter Bank Shale Formation.

showing that the use of heavy mineral data provides an added level of sophistication to the correlation.

The most obvious feature of the correlation is the marked thinning of the Foula Fm. from 204/30a-2, through 206/26a-4, to 205/26a-3. Despite the overall thinning, the individual subunits F1 and F2 appear to have relatively similar thicknesses, suggesting that the thinning is largely due to erosion at the top Triassic unconformity, rather than to differences in subsidence during the Triassic. Consequently, a considerable amount of sediment must have been stripped off prior to deposition of the overlying Jurassic.

6. PROVENANCE

The marked difference in heavy mineral characteristics between the Foula and Otter Bank Fms indicates that there was a pronounced shift in the nature of the sediment source. The relatively wide spread of ratio values and garnet compositions within the Otter Bank sandstones indicates that the Otter Bank source was relatively heterogeneous. By contrast, the Foula Fm. source appears to have been more homogeneous, given the strong clustering of ratio parameters and the consistent nature of the garnet assemblages. The only exception to the overall homogeneity of the Foula sediment source is the lower RuZi in subunits F2 and F4.

The heavy mineral data indicate that the ultimate sources of both the Foula and Otter Bank sandstones were predominantly metamorphic, as indicated by the high abundance of garnet. The higher abundance of zircon in the Otter Bank Fm. suggests a greater involvement of granitic or other intermediate-acidic igneous rocks, although recycling from pre-existing sandstones may also have played a role, especially since ATi is generally lower in the Otter Bank Fm. than in the Foula Fm. Other metamorphic indicator minerals, such as kyanite and staurolite, are scarce, owing to dissolution during burial diagenesis. The Foula Fm. is characterised by high rutile contents (high RuZi), suggesting a high-grade metamorphic source (Force, 1980).

Garnet data provide the most important mineralogical constraints on the provenance of the Foula and Otter Bank sandstones. Garnet assemblages in the Foula Fm. are dominated by Type A (high-Mg, low-Ca) garnet. Garnets of this type are believed to be derived from high-grade (granulite facies) metasedimentary or charnockitic rocks (Sabeen et al., 2002). As shown in the summary ternary diagram (Fig. 11), such garnets are exceptionally scarce in the basement rocks of Scotland. Garnets from metasedimentary rocks of northern Scotland, such as the Moine of the Northern Highlands, the Dalradian of the Grampian Highlands, the Moine/Dalradian of Shetland and the supracrustal rocks of the Loch Maree Group (Lewisian), fall almost exclusively into the low-Mg group, Type B (Morton et al., 2004). Garnets from typical Lewisian orthogneisses are also rich in Type B, but also contain some Type C (high-Mg, high-Ca). The only region providing Type A garnets is South Harris (Outer Hebrides), but even there they are overwhelmed by Type C garnets derived from the metabasic rocks of the South Harris Igneous Complex. The small numbers of Type A garnets derived from the South Harris region are believed

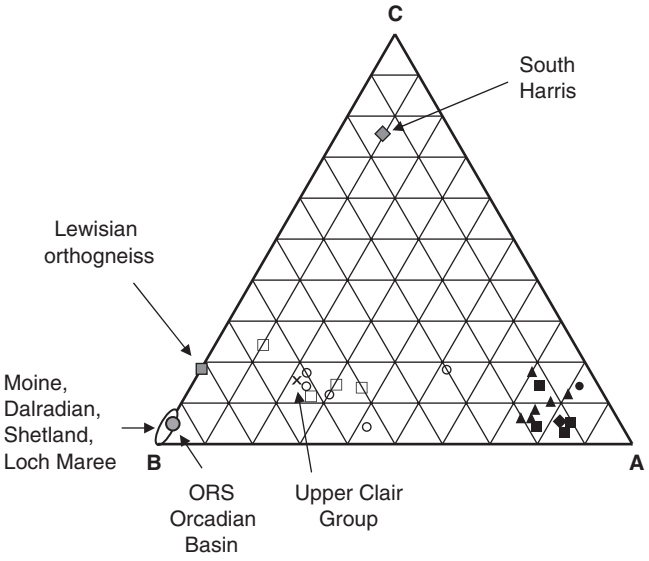

Fig. 11. Ternary diagram showing the marked differences between Foula and Otter Bank garnet assemblages in the Strathmore Field. Garnet compositions from Scottish basement terrains and the Old Red Sandstone of the Orcadian Basin (Morton et al., 2004) and from the Upper Clair Group (unpublished data) are shown for comparison. The diagram plots the relative abundances of Type A, Type B and Type C garnets, the compositional ranges of which are shown in the inset for Fig. 9. □, Otter Bank Fm. subunit O1; ○, Otter Bank Fm. subunit O2; ▲, Foula Fm. subunit F1; ◆, Foula Fm. subunit F2; ■, Foula Fm. subunit F3; ●, Foula Fm. subunit F5.

to represent sediment sourced from high-grade metasediments of the Leverburgh and Langavat belts (Morton et al., 2004).

The scarcity of Type A garnets in the basement terrains of northern Scotland suggest that the sandstones of the Foula Fm. had an exotic source, which, given the location of the Strathmore Field, is likely to have lain to the west of Britain. The heavy mineral and garnet geochemical data indicate that the source terrain comprised high-grade (granulite facies) metasediments and/or charnockites. Analysis of garnets from modern beach sediments from Kulusuk, located in the eastern Nagssugtoqidian belt of East Greenland (Fig. 1), have revealed the presence of closely comparable assemblages rich in the Type A component (Sørensen and Kalvig, 2002), suggesting one possible source of the Foula sediments lay on the conjugate margin of the Faeroe-Shetland rift. Support for a source to the west is given independently by palaeocurrent evidence acquired from borehole imaging log data (Swiecicki et al., 1995), which shows that the Foula Fm. was primarily deposited by easterly-flowing currents.

Zircon age data provide the most definitive evidence for the source of the Foula Fm. As shown by the relative probability plot (Fig. 12), the zircon age spectrum in the Foula Fm. has three clearly defined components (Archaean, Early Proterozoic and Permian). The Archaean group forms 32% of the zircon population, most of the

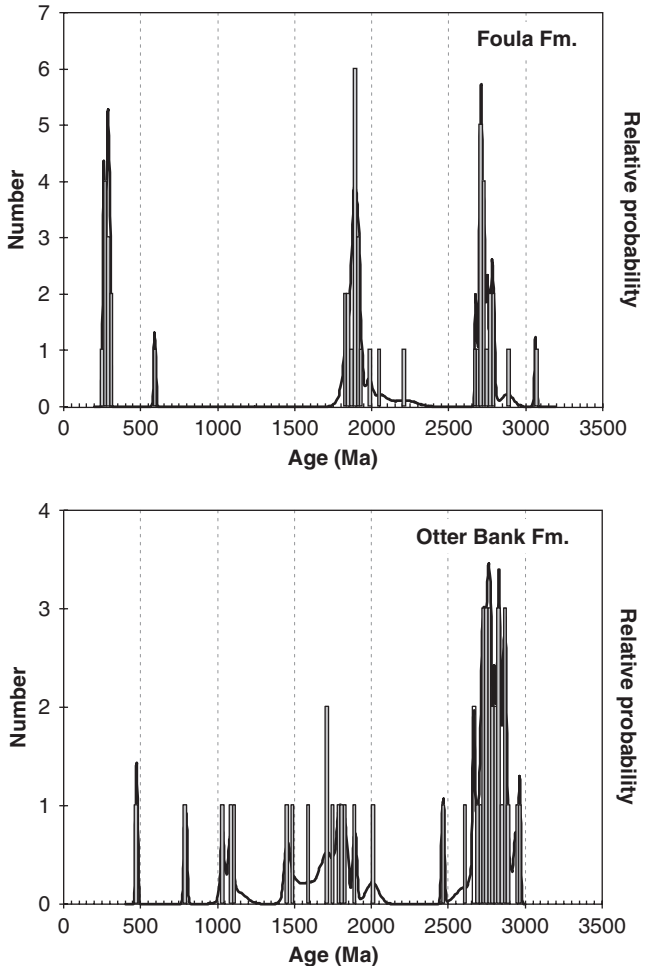

Fig. 12. Detrital zircon ages from the Foula Fm., subunit F1 (205/26a-3, 2454.0 m) and the Otter Bank Fm., subunit O1 (205/26a-3, 2648.4 m), displayed on combined relative probability/histogram plots.

Archaean grains being dated between approximately 2650 and 2800 Ma, with two slightly older grains (2910, 3070 Ma). The Early Proterozoic group, which comprises 30% of the zircon population, has a relatively narrow age range (approximately 1800–1900 Ma), peaking at 1880 Ma. Permian zircons are dated between approximately 250 and 300 Ma, and form 26% of the population. The Archaean group could have been derived from Lewisian basement rocks of Scotland, although similar age basement rocks also occur on the Greenland margin. By contrast, the 1880 Ma event cannot be related to any basement terrain in Scotland. The main phase of Laxfordian granite magmatism, which affects the southern part of the Lewisian complex, is some 180 Ma younger at approximately 1700 Ma (Park et al., 1994). Moine and Dalradian metasediments have a range of Proterozoic zircons, but grains around 1880 Ma are scarce (Cawood et al., 2003, 2004; Friend et al., 2003).

The combination of an Archaean group at 2650–2800 Ma and an Early Proterozoic group peaking at 1880 Ma can be matched with geological events in the Nagssugtoqidian belt of Greenland (Fig. 1). Most geochronological studies of the Nagssugtoqidian belt have been undertaken on its western part, but it extends under the inland ice to be continuous with the eastern Nagssugtoqidian belt (also known as the Ammassalik belt). Early Proterozoic zircon-forming events in the Nagssugtoqidian comprise a phase of arc magmatism at 1920–1870 Ma followed by granulite-facies peak metamorphism at 1860–1840 Ma (Van Gool et al., 2002). The belt also includes Archaean gneisses that were reworked during the early Proterozoic metamorphic event (Kalsbeek et al., 1984, 1993).

The origin of the Permian group of zircons is more enigmatic. The zircons are clearly of igneous origin, as they have high Th/U ratios (Table 3), are euhedral, and show intricate zoning under cathodoluminescence. They cannot be interpreted as Caledonian zircons that have leaked Pb, since they are concordant, and there are no undoubted Caledonian grains in the sample. Consequently, they are most likely to represent Permian intermediate-acidic igneous activity. There is scant record of Permian volcanism in East Greenland, the only published evidence being that by Stemmerik and Sørensen (1980) who identified Permian lamprophyre dykes in Scoresby Land. However, Cretaceous sandstones in the vicinity of Geographical Society Ø, northern East Greenland, also contain common Permian zircons (Morton et al., 2005b), providing further evidence for igneous activity of this age in East Greenland. Speculatively, the Permian zircons found in the Foula Fm. (and those from the Cretaceous of northern East Greenland) may be related to igneous activity associated with Permian rifting along the proto-northeast Atlantic. Elsewhere in northwest Europe, Permian rifting is widely associated with volcanism (Ziegler, 1990; Glennie, 2002), although this is generally basic (and hence zircon-poor) in character.

The only other possible source for the Foula Fm. is the Rockall Plateau, a large submerged fragment of continental crust that lies between southeast Greenland and the British Isles (Fig. 1). The only published information on the nature of the Rockall Plateau crust comes from a small number of samples acquired by drilling, dredging, and diving on Rockall Bank (Hitchen, 2004), which show that the basement comprises high-grade basic to acidic gneisses and granites. On the basis of whole-rock Rb-Sr, Sm-Nd and U-Pb data (Morton and Taylor, 1991), Dickin (1992) argued that the Rockall Bank crust is equivalent to the Ketilidian metamorphic belt of southern Greenland and to the Islay-Inistrahull terrane of Scotland and Ireland. U-Pb zircon crystallisation ages from the Ketilidian belt and the Islay-Inistrahull terrane are younger than the 1880 Ma peak in the Foula Fm. sample. There were two main phases of granitoid emplacement in the Ketilidian belt (Garde et al., 2002), the first phase comprising intrusion of the calc-alkaline Julienehåb batholith at 1795–1854 Ma, closely followed by high-temperature/low-pressure metamorphism and intrusion of I-type granites at 1785–1795 Ma. Subsequent emplacement of rapakivi granite sheets occurred between 1732 and 1755 Ma. Daly et al. (1995) reported a U-Pb zircon crystallisation age of approximately 1750 Ma for the Annagh Gneiss of north Mayo (Ireland), and imply that samples from Rockall Bank yielded similar U-Pb zircon ages. It therefore appears that the Rockall Plateau and the Inishtrahull-Islay block share a common geological history with the Ketilidian belt, as proposed by Dickin (1992).

The available evidence therefore precludes derivation of the Foula Fm. from the southern part of the Rockall Plateau. However, isotopic data from Tertiary basalts (Hitchen et al., 1997) indicate that the northern part of the Rockall Plateau region (George Bligh Bank region) is underlain by Archaean rocks. In view of the juxtaposition of the northern Rockall Plateau with the Nagssugtoqidian belt and the adjacent Archaean craton in southern East Greenland (Fig. 1), it may be that the northern part of the Rockall Plateau is a suitable hinterland to supply sediment with Foula Fm. characteristics. It is impossible to test this hypothesis at present, however, because of the absence of basement samples from George Bligh Bank and adjacent areas.

The garnet assemblages in the Otter Bank Fm. are much richer in Type B than those in the Foula Fm. However, although they plot close to typical Lewisian orthogneiss on the summary ternary diagram (Fig. 11), they contain significantly more Type A garnets than the Lewisian orthogneiss end-member. There are two possible explanations for this: they could represent mixing between a Lewisian component and a Foula-type component, but alternatively they could have been derived entirely from a different source. The most likely alternatives are the Devonian Old Red Sandstone (ORS) of the Orcadian Basin and the Devonian-Carboniferous Clair Group that forms the reservoir for the Clair Field to the northeast (Allen and Mange-Rajetzky, 1992). The only published garnet data from ORS of the Orcadian Basin (Morton et al., 2004) indicates that assemblages are directly comparable to those from the Moine and Dalradian (Fig. 11). Recycling from the ORS therefore seems unlikely, although the ORS garnet database is very small, and this conclusion may require re-evaluation should further data become available. By contrast, the close match between garnet data from the Upper Clair Group and Otter Bank sandstones (Fig. 11) suggests that recycling of the Upper Clair Group is a viable model for generation of the Otter Bank garnet suites.

Zircon age data from an Otter Bank sandstone sample (Table 4) further emphasises the strong contrast in provenance between the Otter Bank and Foula Fms. The Otter Bank zircon population is dominated by Archaean zircons (64% of the assemblage falling between approximately 2500 and 3000 Ma), with a subordinate Proterozoic group, most of which lie between approximately 1050 and 1850 Ma), and a single Early Palaeozoic grain. There is no evidence for either the major Early Proterozoic (1880 Ma) or Permian zircon groups found in the Foula Fm., and although both formations contain Archaean zircons, there is a distinct difference in the age of the main peak on the two spectra (Fig. 12). The Archaean zircons can be matched with the local Lewisian basement, which is believed to have originated between 2900 and 2700 Ma (Hamilton et al., 1979; Whitehouse, 1988, 1989) with a prolonged period of subsequent metamorphic reworking (Park et al., 1994). The Proterozoic zircons are broadly comparable to those seen in the Moine and Dalradian (Cawood et al., 2003, 2004; Friend et al., 2003). Although post-Grampian Group Dalradian metasediments include some Archaean zircons (Cawood et al., 2003), they are less abundant than in the Otter Bank Fm., indicating that recycled Dalradian cannot be invoked as the sole source of the Otter Bank. The single Palaeozoic zircon (473 Ma) corresponds to the Grampian orogenic event of northern Scotland, but the high Th/U ratio indicates it is of igneous, rather than metamorphic origin. Migmatites within the Moine, which have been dated as

between 460 and 470 Ma (Kinny et al., 1999; Rogers et al., 2001), may therefore have sourced this zircon.

Zircon age data are therefore consistent with derivation of the Otter Bank sandstones from local Scottish basement rocks, although they do not rule out recycling from either the ORS or the Clair Group, since published data on zircon ages in both are lacking. The most likely scenario is that Otter Bank sandstones were derived from a combination of Upper Clair Group and Lewisian basement, with possible additional supply from the ORS. Garnet data suggest that reworking of the Upper Clair Group played an important role in the deposition of the Otter Bank Fm. However, GZi values in the Upper Clair Group are much higher than in the Otter Bank Fm. (mean GZi in the Upper Clair group being approximately 96, compared with approximately 85 in the Otter Bank Fm.). A significant proportion of zircon-rich sediment must therefore have diluted the Upper Clair Group in order to generate the lower GZi values present in the Otter Bank Fm. Given the large numbers of Archaean zircons in the Otter Bank Fm., the most likely source of the zircon-rich component is Lewisian orthogneiss. The extent of the role of the ORS cannot be readily determined given the scarcity of data on garnet compositions and detrital zircon ages; however, Sm-Nd data (Knudsen, 2000) suggests that Archaean sources played a minor role in ORS provenance, and therefore it is unlikely that there was extensive recycling of ORS into the Otter Bank Fm.

The upper part of the Otter Bank Fm. (subunit O2) has characteristics that are intermediate between subunit O1 and the overlying Foula Fm., suggesting that minor amounts of sediment from the Greenland margin reached the Strathmore area during the later phase of Otter Bank deposition. The parameter that shows the strongest deviation from the typical Otter Bank character is ATi. One possible explanation for this phenomenon is that apatite and tourmaline, being the least dense of the heavy minerals, were transported more rapidly from the distal East Greenland source than the denser garnet, rutile and zircon. As a result, changes in ATi provide the earliest manifestation of supply from the East Greenland source, with changes in RuZi and GZi following subsequently.

7. CONCLUDING REMARKS

This case study has provided further evidence for the value of heavy mineral analysis as a non-biostratigraphic method for correlation of sand-rich successions. The careful selection of parameters that are sensitive to changes in provenance and insensitive to other processes that operate during the sedimentation cycle is a key part of the development of a reliable heavy mineral correlation framework. Suitable parameters are (i) ratios of abundance of minerals with similar hydraulic and diagenetic behaviour and (ii) varietal data, both petrographic and geochemical.

The heavy mineral correlation framework for the Triassic of the Strathmore Field relies on the interplay between inputs from two distinct sand source regions. The two sand types can be identified using conventional heavy mineral data, heavy mineral ratio data and garnet geochemical data. Integration of this information with detrital zircon age data has given powerful constraints on the location and lithological composition of the source regions.

The Early Triassic Otter Bank Fm. is interpreted as having a source on the British margin of the Faeroe-Shetland rift. A two-component provenance, comprising recycled Devonian-Carboniferous Upper Clair Group in conjunction with Lewisian orthogneiss, is envisaged. By contrast, the Middle-Late Triassic Foula Fm. was derived from a high-grade metasedimentary/charnockitic basement source area, most likely to lie in the eastern Nagssuqtoqidian belt (also known as Ammassalik belt) of southern East Greenland, on the opposite side of the rift. Derivation from the northern part of the Rockall Plateau, a submerged continental crustal fragment between Greenland and the British Isles, cannot be entirely ruled out, since the age and nature of this region is poorly constrained. However, derivation from the southern part of the Rockall Plateau is precluded, since this region is characterised by younger Palaeoproterozoic U-Pb zircon ages (<1800 Ma). Zircon age data from the Foula Fm. also provide evidence for an important Permian igneous event along the proto-northeast Atlantic rift, confirming previous indications of Permian volcanism found during SHRIMP zircon age dating of Cretaceous sandstones in northern East Greenland (Morton et al., 2005b).

The switch in sediment supply from easterly-sourced to westerly-sourced detritus is the most clearly defined correlative event in the Triassic succession of the Strathmore Field. Variable supply from a subordinate zircon-rich component (probably of granitic origin) resulted in changes in heavy mineral ratios within the Foula Fm., providing the basis for intra-Foula subdivision and correlation. The Otter Bank Fm. is subdivided on the basis of an upward increase in ATi, believed to indicate the initial appearance of sediment from East Greenland.

ACKNOWLEDGEMENTS

We are grateful to Jon Gluyas, Todd Greene and Maria Mange for their constructive comments on an earlier version of this manuscript.

REFERENCES

Allen, P.A., Mange-Rajetzky, M.A., 1992. Devonian-Carboniferous sedimentary evolution of the Clair Area, offshore northwestern UK: impact of changing provenance. Marine and Petroleum Geology 9, 29–52.

Blondeau, A., Pomerol, C.H., 1969. A contribution to the sedimentological study of the Palaeogene of England. Proceedings of the Geologists Association 79, 441–455.

Cawood, P.A., Nemchin, A.A., Smith, M., Loewy, S., 2003. Source of the Dalradian Supergroup constrained by U-Pb dating of detrital zircon and implications for the East Laurentian margin. Journal of the Geological Society, London 160, 231–246.

Cawood, P.A., Nemchin, A.A., Strachan, M., Kinny, P.D., Loewy, S., 2004. Laurentian provenance and intracratonic setting for the Moine Supergroup, Scotland, constrained by detrital zircons from the Loch Eil and Glen Urquhart successions. Journal of the Geological Society, London 161, 861–874.

Dalland, A., Mearns, E.W., McBride, J.J., 1995. The application of samarium-neodymium (Sm-Nd) provenance ages to correlation of biostratigraphically barren strata: a case study of the Statfjord Formation in the Gullfaks oilfield, Norwegian North Sea. In: Dunay, R.E.,

Hailwood, E.A. (Eds.), Non-Biostratigraphical Methods of Dating and Correlation. Geological Society of London Special Publication, vol. 89, pp. 201–222.

Daly, J.S., Heaman, L.M., Fitzgerald, R.C., Menuge, J.F., Brewer, T.S., Morton, A.C., 1995. Age and crustal evolution of crystalline basement in western Ireland and Rockall. In: Croker, P.F., Shannon, P.M. (Eds.) The Petroleum Geology of Ireland's Offshore Basins. Geological Society of London Special Publication, vol. 93, pp. 433–434.

Dickin, A.P., 1992. Evidence for an Early Proterozoic crustal province in the North Atlantic region. Journal of the Geological Society, London 149, 483–486.

Dodson, M.H., Compston, W., Williams, I.S., Wilson, J.F., 1988. A search for ancient detrital zircons in Zimbabwean sediments. Journal of the Geological Society, London 145, 977–983.

Droop, G.T.R., Harte, B., 1995. The effect of Mn on the phase relations of medium grade pelites: constraints from natural assemblages on petrogenetic grid topology. Journal of Petrology 36, 1549–1578.

Dunay, R.E., Hailwood, E.A. (Eds.), 1995. Non-Biostratigraphical Methods of Dating and Correlation. Geological Society of London Special Publication, vol. 89.

Evans, J.A., Chisholm, J.I., Leng, M.J., 2001. How U-Pb detrital monazite ages contribute to the interpretation of the Pennine Basin infill. Journal of the Geological Society, London 158, 741–744.

Feo-Codecido, G., 1956. Heavy mineral techniques and their application to Venezuelan stratigraphy. Bulletin of the American Association of Petroleum Geologists 40, 984–1000.

Fisher, M.J., Mudge, D.C., 1998. Triassic. In: Glennie, K.W. (Ed.), Petroleum Geology of the North Sea: Basic Concepts and Recent Advances. Blackwell Science Ltd., Oxford, pp. 212–244.

Force, E.R., 1980. The provenance of rutile. Journal of Sedimentary Petrology 50, 485–488.

Friend, C.R.L., Strachan, R.A., Kinny, P.D., Watt, G.R., 2003. Provenance of the Moine Supergroup of NW Scotland: evidence from geochronology of detrital and inherited zircons from (meta)sedimentary rocks, granites and migmatites. Journal of the Geological Society, London 160, 247–257.

Garde, A.A., Hamilton, M.A., Chadwick, B., Grocott, J., McCaffrey, K.J.W., 2002. The Ketilidian orogen of South Greenland: geochronology, tectonics, magmatism, and fore-arc accretion during Palaeoproterozoic oblique convergence. Canadian Journal of Earth Sciences 39, 765–793.

Glennie, K.W., 2002. Permian and Triassic. In: Trewin, N.H. (Ed.), The Geology of Scotland. Geological Society, London, pp. 301–321.

Hallsworth, C.R., Chisholm, J.I., 2000. Stratigraphic evolution of provenance characteristics in Westphalian sandstones of the Yorkshire coalfield. Proceedings of the Yorkshire Geological Society 53, 43–72.

Hamilton, P.J., Evensen, N.M., O'Nions, R.K., Tarney, J., 1979. Sm-Nd systematics of Lewisian gneisses: implications for the origin of granulites. Nature 277, 705–708.

Haughton, P.D.W., Farrow, C.M., 1988. Compositional variation in Lower Old Red Sandstone detrital garnets from the Midland Valley of Scotland and the Anglo-Welsh Basin. Geological Magazine 126, 373–396.

Henry, D.J., Guidotti, C.V., 1985. Tourmaline as a petrogenetic indicator mineral: an example from the staurolite-grade metapelites of NW Maine. American Mineralogist 70, 1–15.

Herries, R., Poddubiuk, R., Wilcockson, P., 1999. Solan, Strathmore and the back basin play, west of Shetland. In: Fleet, A.J., Boldy, S.A.R. (Eds.), Petroleum Geology of Northwest Europe: Proceedings of the 5th Conference. Geological Society, London, pp. 693–712.

Hitchen, K., 2004. The geology of the UK Hatton-Rockall margin. Marine and Petroleum Geology 21, 993–1012.

Hitchen, K., Morton, A.C., Mearns, E.W., Whitehouse, M., Stoker, M.S., 1997. Geological implications from geochemical and isotopic studies of Late Cretaceous and early Tertiary igneous rocks around the northern Rockall Trough. Journal of the Geological Society, London 154, 517–521.

Hubert, J.F., 1971. Analysis of heavy mineral assemblages. In: Carver, R.E. (Ed.), Procedures in Sedimentary Petrology. Wiley, New York, pp. 453–478.

Hurst, A.R., Morton, A.C., 1988. An application of heavy-mineral analysis to lithostratigraphy and reservoir modelling in the Oseberg Field, northern North Sea. Marine and Petroleum Geology 5, 157–169.

Hutchison, A.R., Oliver, G.J.H., 1998. Garnet provenance studies, juxtaposition of Laurentian marginal terranes and timing of the Grampian Orogeny in Scotland. Journal of the Geological Society, London 155, 541–550.

Jeans, C.V., 1995. Clay mineral stratigraphy in Palaeozoic and Mesozoic red bed facies, onshore and offshore UK. In: Dunay, R.E., Hailwood, E.A. (Eds.), Non-Biostratigraphical Methods of Dating and Correlation. Geological Society of London Special Publication, vol. 89, pp. 31–55.

Jeans, C.V., Reed, S.J.B., Xing, M., 1993. Heavy mineral stratigraphy in the UK Trias of the North Sea Basin. In: Parker, J.R. (Ed.), Petroleum Geology of NW Europe: Proceedings of the 4th Conference. Geological Society, London, pp. 609–624.

Kalsbeek, F., Austrheim, H., Bridgwater, D., Hansen, B.T., Pedersen, S., Taylor, P.N., 1993. Geochronology of the Ammassalik area, South-East Greenland, and comparisons with the Lewisian of Scotland and the Nagssugtoqidian of West Greenland. Precambrian Research 62, 239–270.

Kalsbeek, F., Taylor, P.N., Henricksen, N., 1984. Age of rocks, structures, and metamorphism in the Nagssugtoqidian mobile belt, West Greenland—field and Pb-isotope evidence. Canadian Journal of Earth Sciences 21, 1126–1131.

Kinny, P.D., Friend, C.R.L., Strachan, R.A., Watt, G.R., Burns, I.M., 1999. U-Pb geochronology of regional migmatites, East Sutherland, Scotland: evidence for crustal melting during the Caledonian orogeny. Journal of the Geological Society, London 156, 1143–1152.

Knudsen, T.-L., 2000. The provenance of Devonian sandstones from Shetland: a Sm-Nd and trace element study. Scottish Journal of Geology 36, 61–72.

Koen, G.M., 1955. Heavy minerals as an aid to correlation of sediments of the Karroo system in the northern part of the Union of South Africa. Transactions of the Geological Society of South Africa 58, 281–366.

Krynine, P.D., 1946. The tourmaline group in sediments. Journal of Geology 54, 65–87.

Lihou, J.C., Mange-Rajetzky, M.A., 1996. Provenance of the Sardona Flysch, eastern Swiss Alps: example of high resolution heavy mineral analysis applied to an ultrastable assemblage. Sedimentary Geology 105, 141–157.

Ludwig, K.R., 1999. Isoplot, a Geochronological Toolkit for Microsoft Excel. Berkeley Geochronology Center, Berkeley, CA, Special Publication 1a.

Ludwig, K.R., 2001. SQUID 1.00, A User's Manual. Berkeley Geochronology Center, Berkeley, CA, Special Publication, vol. 2, 17pp.

Mange, M.A., Maurer, H.F.W., 1992. Heavy Minerals in Colour. Chapman and Hall, London, 147pp.

Mange, M., Turner, P., Ince, D., Pugh, J., Wright, D., 1999. A new perspective on the zonation and correlation of barren strata: an integrated heavy mineral and palaeomagnetic study of the Sherwood Sandstone Group, East Irish Sea Basin and surrounding areas. Journal of Petroleum Geology 22, 325–348.

Mange-Rajetzky, M.A., 1995. Subdivision and correlation of monotonous sandstone sequences using high resolution heavy mineral analysis, a case study: the Triassic of the

Central Graben. In: Dunay, R.E., Hailwood, E.A. (Eds.), Non-Biostratigraphical Methods of Dating and Correlation. Geological Society of London Special Publication, vol. 89, pp. 23–30.

Mearns, E.W., Knarud, R., Raestad, N., Stanley, K.O., Stockbridge, C.P., 1989. Samarium-neodymium isotope stratigraphy of the Lunde and Statfjord Formations of Snorre oil field, northern North Sea. Journal of the Geological Society, London 146, 217–228.

Milner, H.B., 1923. The study and correlation of sediments by petrographic methods. Mining Magazine (London) 28, 80–92.

Morton, A.C., 1985. Heavy minerals in provenance studies. In: Zuffa, G.G. (Ed.), Provenance of Arenites. Reidel, Dordrecht, pp. 249–277.

Morton, A.C., Grant, S., 1998. Cretaceous depositional systems in the Norwegian Sea: heavy mineral constraints. Bulletin of the American Association of Petroleum Geologists 82, 274–290.

Morton, A.C., Hallsworth, C.R., 1994. Identifying provenance-specific features of detrital heavy mineral assemblages in sandstones. Sedimentary Geology 90, 241–256.

Morton, A.C., Hallsworth, C.R., 1999. Processes controlling the composition of heavy mineral assemblages in sandstones. Sedimentary Geology 124, 3–29.

Morton, A.C., Hallsworth, C.R., Chalton, B., 2004. Garnet compositions in Scottish and Norwegian basement terrains: a framework for interpretation of North Sea sandstone provenance. Marine and Petroleum Geology 21, 393–410.

Morton, A.C., Hallsworth, C.R., Moscariello, A., 2005a. Interplay between northern and southern sediment sources during Westphalian deposition in the Silverpit Basin, southern North Sea. Yorkshire Geological Society Special Issue 7, 135–146.

Morton, A.C., Knox, R.W.O'B., Hallsworth, C.R., 2002. Correlation of hydrocarbon reservoirs using quantitative heavy mineral analysis. Petroleum Geoscience 8, 251–262.

Morton, A.C., Spicer, P.J., Ewen, D.F., 2003. Geosteering of high-angle wells using heavy mineral analysis: the Clair Field, West of Shetland. In: Carr, T.R., Mason, E.P., Feazel, C.T. (Eds.), Horizontal Wells: Focus on the Reservoir. American Association of Petroleum Geologists, Methods in Exploration, vol. 14, pp. 249–260.

Morton, A.C., Taylor, P.N., 1991. Geochemical and isotopic constraints on the nature and age of basement rocks from Rockall Bank, NE Atlantic. Journal of the Geological Society, London 147, 631–634.

Morton, A.C., Whitham, A.G., Fanning, C.M., Claoué-Long, J.C., 2005b. The role of East Greenland as a source of sediment to the Vøring Basin during the Late Cretaceous. In: Wandås, B.T.G., Eide, E.A., Gradstein, F., Nystuen, J.P. (Eds.), Onshore-Offshore Relationships on the North Atlantic Margin. NPF (Norsk Petroleumsforening) Special Publication, vol. 12. Elsevier, Amsterdam, pp. 83–110.

Paces, J.B., Miller, J.D., 1993. Precise U-Pb ages of Duluth Complex and related mafic intrusions, northeastern Minnesota: geochronological insights to physical, petrogenetic, paleomagnetic, and tectonomagmatic process associated with the 1.1 Ga midcontinent rift system. Journal of Geophysical Research 98, 13997–14013.

Park, R.G., Cliff, R.A., Fettes, D.J., Stewart, A.D., 1994. Precambrian rocks in northwest Scotland west of the Moine Thrust: the Lewisian complex and the Torridonian. In: Gibbons, W., Harris, A.L. (Eds.), A Revised Correlation of Precambrian Rocks in the British Isles. Geological Society of London Special Report, vol. 22, pp. 6–22.

Pearce, T.J., Besly, B.M., Wray, D.S., Wright, D.K., 1999. Chemostratigraphy: a method to improve interwell correlation in barren sequences—a case study using onshore Duckmantian/Stephanian sequences (West Midlands, U.K.). Sedimentary Geology 124, 197–220.

Poldervaart, A., 1955. Zircon in rocks, 1: sedimentary rocks. American Journal of Science 253, 433–461.

Preston, J., Hartley, A., Hole, M., Buck, S., Bond, J., Mange, M., Still, J., 1998. Integrated whole-rock trace element geochemistry and heavy mineral chemistry studies: aids to the correlation of continental red-bed reservoirs in the Beryl Field, UK North Sea. Petroleum Geoscience 4, 7–16.

Rahmani, R.A., Lerbekmo, J.F., 1975. Heavy-mineral analysis of Upper Cretaceous and Paleocene sandstones of Alberta and adjacent areas of Saskatchewan. Geological Association of Canada Special Paper 13, 607–632.

Reed, R.D., Bailey, J.P., 1927. Surface correlation by means of heavy minerals. Bulletin of the American Association of Petroleum Geologists 11, 359–368.

Roberts, D.G., Thompson, M., Mitchener, B., Hossack, J., Carmichael, S., Bjørnseth, H.M., 1999. Paleozoic to Tertiary rift and basin dynamics: mid-Norway to the Bay of Biscay—a new context for hydrocarbon prospectivity in the deep water frontier. In: Fleet, A.J., Boldy, S.A.R. (Eds.), Petroleum Geology of Northwest Europe: Proceedings of the 5th Conference. Geological Society, London, pp. 7–40.

Rogers, G., Kinny, P.D., Strachan, R.A., Friend, C.R.L., Paterson, B., 2001. U-Pb chronology of the Fort Augustus granite gneiss: constraints on the timing of Neoproterozoic and Palaeozoic tectonothermal events in the NW Highlands of Scotland. Journal of the Geological Society, London 158, 7–14.

Rub, M.G., Palov, V.A., Gladkov, N.G., Grishina, N.V., 1977. Accessory garnet as an indicator of the genesis of ore-bearing granitoid rocks. Doklady Akademii Nauk SSSR 235, 1397–1400.

Sabeen, H.M., Ramanujam, N., Morton, A.C., 2002. The provenance of garnet: constraints provided by studies of coastal sediments from southern India. Sedimentary Geology 152, 279–287.

Scott, R.A., 2000. Mesozoic-Cenozoic evolution of East Greenland: implications of a reinterpreted continent-ocean boundary location. Polarforschung 68, 83–91.

Seidler, L., Steel, R.J., Stemmerik, L., Surlyk, F., 2004. North Atlantic marine rifting in the Early Triassic: new evidence from East Greenland. Journal of the Geological Society, London 161, 583–592.

Sircombe, K.N., 1999. Tracing provenance through the isotopic ages of littoral and sedimentary detrital zircon, eastern Australia. Sedimentary Geology 124, 47–67.

Sobolev, N.V., 1964. Classification of rock-forming garnets. Doklady Akademii Nauk SSSR 157, 353–356.

Sørensen, J.B., Kalvig, P., 2002. Garnet sand in Greenland: examples from Tuttoqqortooq, Taslilaq area and Sisimiut area. Danmarks og Grønlands Geologiske Undersøgelse Rapport, 2002/12.

Spiegel, C., Siebel, W., Frisch, W., Berner, Z., 2002. Nd and Sr isotopic ratios and trace element geochemistry of detrital epidote from the Swiss Molasse Basin as provenance indicators: implications for the reconstruction of the exhumation history of the Central Alps. Chemical Geology 189, 231–250.

Stemmerik, L., Sørensen, M., 1980. Upper Permian dykes in southern Scoresby Land. East Greenland. Grønlands Geologiske Undersøgelse Rapport 100, 108pp.

Styles, M.T., Stone, P., Floyd, J.D., 1989. Arc detritus in the Southern Uplands: mineralogical characterisation of a 'missing' terrain. Journal of the Geological Society, London 146, 397–400.

Svendsen, J.B., Hartley, N.R., 2002. Synthetic heavy mineral stratigraphy: applications and limitations. Marine and Petroleum Geology 19, 389–405.

Swiecicki, T., Wilcockson, P., Canham, A., Whelan, G., Homann, H., 1995. Dating, correlation and stratigraphy of the Triassic sediments in the West Shetlands area. In: Boldy, S.A.R. (Ed.), Permian and Triassic Rifting in Northwest Europe. Geological Society of London Special Publication, vol. 91, pp. 57–85.

Tebbens, L.A., Kroonenberg, S.B., Vandenbergh, M.W., 1995. Compositional variation of detrital garnets in Quaternary Rhine, Meuse and Baltic river sediments in the Netherlands. Geologie en Mijnbouw 74, 213–224.

Tera, F., Wasserburg, G., 1972. U-Th-Pb systematics in three Apollo 14 basalts and the problem of initial Pb in lunar rocks. Earth and Planetary Science Letters 14, 281–304.

Tieh, T.T., 1973. Heavy mineral assemblages in some Tertiary sediments in San Mateo County, California. Journal of Sedimentary Petrology 43, 408–417.

Van Gool, J.A.M., Connelly, J.N., Marker, M., Mengel, F.C., 2002. The Nagssugtoqidian orogen of West Greenland: tectonic evolution and regional correlations from a West Greenland perspective. Canadian Journal of Earth Sciences 39, 665–686.

Van Loon, A.J., Mange, M.A., 2007. 'In situ' dissolution of heavy minerals through extreme weathering, and the application of the surviving assemblages and their dissolution characteristics to correlation of Dutch and German silver sands. In: Mange, M.A., Wright, D.T. (Eds.), Heavy Minerals in Use. Developments in Sedimentology (this volume).

Von Eynatten, H., Gaupp, R., 1999. Provenance of Cretaceous synorogenic sandstones in the Eastern Alps: constraints from framework petrography, heavy mineral analysis and mineral chemistry. Sedimentary Geology 124, 81–111.

Whitehouse, M.J., 1988. Granulite facies Nd-isotopic homogenisation in the Lewisian complex of NW Scotland. Nature 331, 705–707.

Whitehouse, M.J., 1989. Sm-Nd evidence for diachronous crustal accretion in the Lewisian complex of NW Scotland. Tectonophysics 161, 245–256.

Williams, I.S., 1998. U-Th-Pb geochronology by ion microprobe. In: McKibben, M.A., Shanks, W.C. III, Ridley, W.I. (Eds.), Applications of Microanalytical Techniques to Understanding Mineralising Processes. Society of Economic Geologists, Reviews in Economic Geology, vol. 7, pp. 1–35.

Wright, W.I., 1938. The composition and occurrence of garnets. American Mineralogist 23, 436–449.

Ziegler, P.A., 1990. Geological Atlas of Western and Central Europe (2nd ed.). Shell Internationale Petroleum Maatschappij, The Hague.

Chapter 42

HIGH-RESOLUTION HEAVY MINERAL- AND MAGNETOSTRATIGRAPHY; A POWERFUL TOOL FOR SUBDIVISION AND CORRELATION OF BARREN SUCCESSIONS: AN EXAMPLE FROM THE SHERWOOD SANDSTONE GROUP (TRIASSIC) OF THE EAST IRISH SEA BASIN AND SURROUNDING AREAS

MARIA A. MANGE[a], PETER TURNER[b], DAVID INCE[c] AND DAVID T. WRIGHT[d]

[a]*Department of Geology, UC Davis, One Shields Avenue, Davis, CA 95616, USA*
[b]*School of Geography, Earth and Environmental Sciences, The University of Birmingham, Birmingham B15 2TT, UK*
[c]*Technical Geoscience Department, PCSB (Petronas Carigali Sdn Bhd) Level 16, Tower 2, Petronas Twin Towers KLCC 50088, Kuala Lumpur, Malaysia*
[d]*Department of Geology, University of Leicester, University Road, Leicester LE1 7RH, UK*

ABSTRACT

High resolution heavy mineral analysis was carried out on sandstones from the Triassic Sherwood Sandstone Group and results were integrated with palaeomagnetic data from interbedded mudstone samples. This has generated a heavy mineral-magnetostratigraphy and achieved regional correlation of nine wells in the Irish Sea. All well successions showed a consistent threefold zonation (locally with subzones). Heavy mineral zones were defined by systematic changes in characteristic heavy mineral suites, reflecting the influence of tectonic events and climatic controls. Palaeomagnetic results indicate that the characteristic remanent magnetization (ChRM) of the analysed samples was acquired as a post-detrital remanent magnetization (PDRM) or chemical remanent magnetization (CRM) as the sediments were reddened during and shortly after deposition.

A reference section has been constructed from onshore sections and cored wells using magnetopolarities, with heavy mineral zones tied to specific magnetostratigraphic chrons. Heavy mineral Zone A coincides with a period of dominantly normal polarity, fixed by a 244 Ma chron of Middle Scythian age. Comparison with other areas shows that our Zone A can be correlated on a global scale. A change in polarity from normal to reversed at >243 Ma coincides with the boundary of Zones A/B. Zone B is Middle to Late Scythian and shows a dominantly reversed polarity.

Developments in Sedimentology, Vol. 58, 1073–1097

ISSN: 0070-4571/doi:10.1016/S0070-4571(07)58042-8

A well-defined chron of 242.7 Ma has been detected close to the boundary of Zones B/C. Zone C is Anisian in age and is characterized by a dominantly normal polarity. Interpolation of well-constrained zones within coeval onshore successions and cored wells proves that the combined application of the two techniques is an effective tool for subdivision and correlation of uncored wells.

Keywords: high resolution heavy mineral analysis; correlation; zonation; magnetostratigraphy; magnetopolarity; red beds

1. INTRODUCTION

The Triassic Sherwood Sandstone Group (SSG) of the Irish Sea Basin (Jackson et al., 1995) comprises thick, early Triassic, predominantly fluviatile and aeolian continental successions (Fig. 1). The nomenclature used initially to divide the SSG of the Irish Sea and adjacent areas has become complicated through ongoing research and oil exploration (Thompson, 1970; Colter and Barr, 1975; Warrington et al., 1980). Synthesis is difficult because different lithostratigraphies are used for the SSG in various geographic areas. The most recent attempts to revise and update this nomenclature were published by Jackson et al. (1995, 1997). Fig. 2 shows a summary of the lithostratigraphy of the East Irish Sea Basin (EISB) and the Cheshire Basin as used in this paper, which is a simplification of the schemes of Jackson et al. (1995, 1997).

Ongoing exploration activities have highlighted the need for improved correlation techniques to better predict the distribution of potentially higher quality, particularly aeolian, reservoir sections. The effective and reliable zonation and correlation of economically important hydrocarbon reservoirs in thick, palaeontologically barren

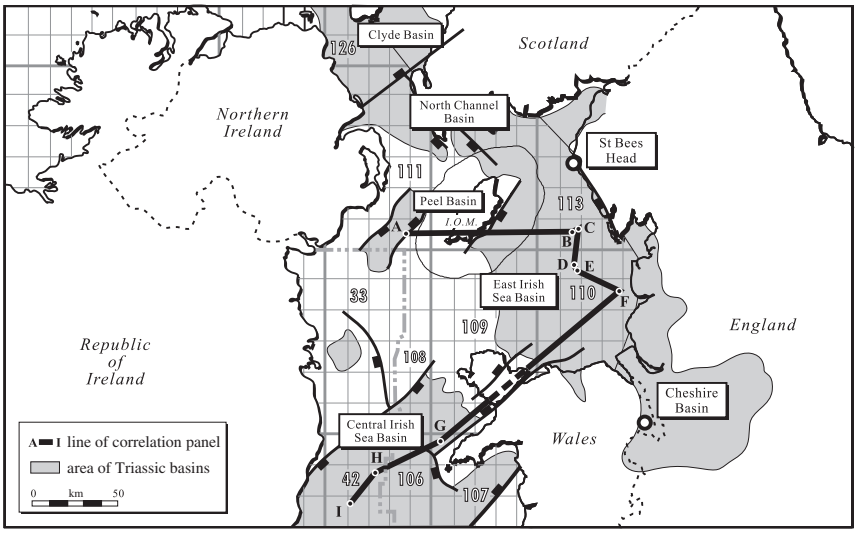

Fig. 1. Outline map of the Irish Sea Basin and surrounding areas, showing main faults and location of study wells and onshore sections. Adapted from Mange et al. (1999) with permission from Journal of Petroleum Geology.

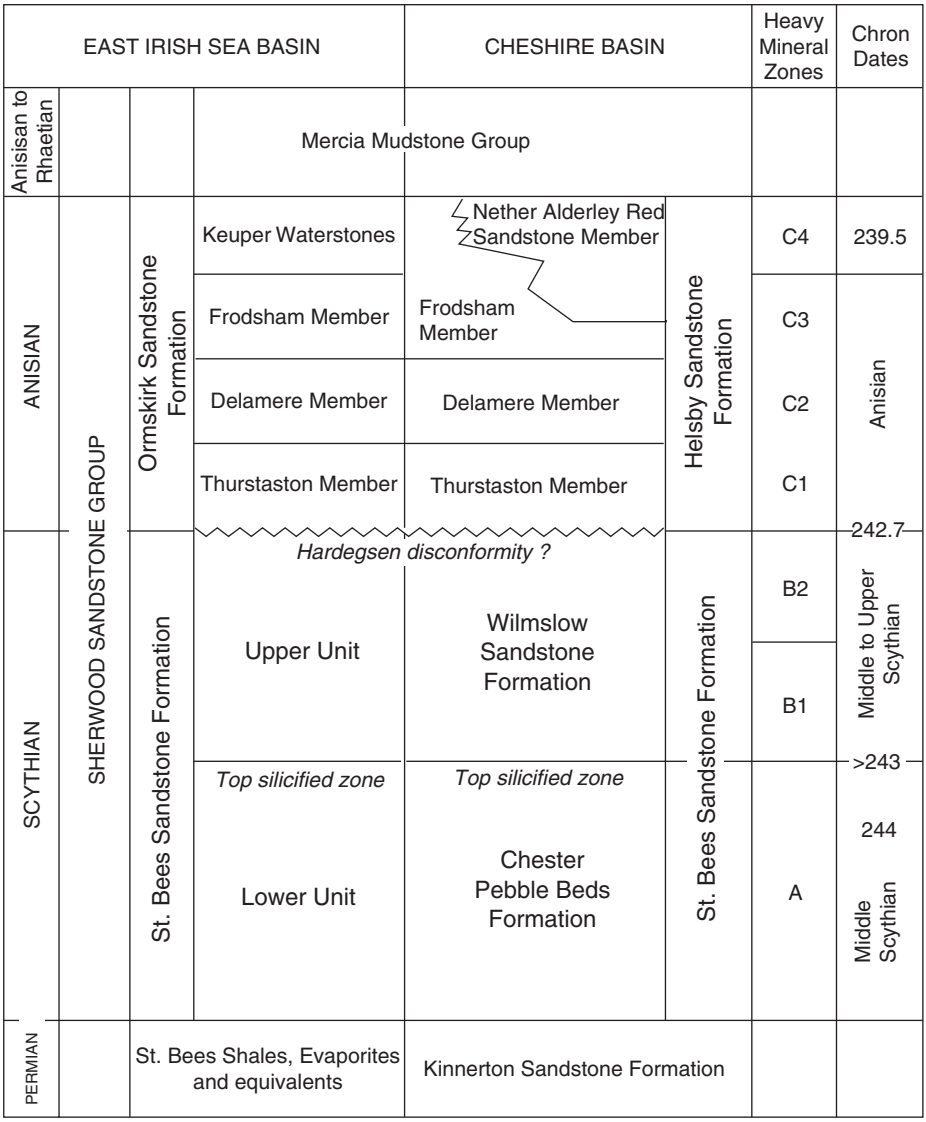

Fig. 2. Comparative lithostratigraphy of the East Irish Sea Basin and Cheshire Basin with heavy mineral zonation and chron dates. Modified after Jackson et al. (1995). Adapted from Mange et al. (1999) with permission from Journal of Petroleum Geology.

and lithologically monotonous continental redbed successions is a serious shortcoming that has been exacerbated by the lack of suitable core samples (Dunay and Hailwood, 1995). However, high resolution heavy mineral analysis (HRHMA) can provide a stratigraphy, based on genetically related heavy mineral zones that can be correlated, and is one of the few techniques suitable for outcrop, core and cuttings samples. It does not, however, establish a temporal framework for the interpretation of the structural and depositional history of a basin.

Magnetostratigraphy uses samples from core and/or outcrop and relies on changes in geomagnetic polarity, recorded in sedimentary successions and revealed as magnetic polarity zones or magnetozones. Because polarity reversals occur essentially simultaneously over the whole surface of the Earth, the magnetozones are considered to represent absolute time planes (Hailwood, 1989; Turner et al., 1996). Under favourable circumstances, magnetozones can be correlated, thereby achieving the correlation of absolute time zones.

Combined heavy mineral-magnetostratigraphy of Triassic red beds can also be related to high-resolution studies which use gamma logs or detailed sedimentological analysis. Such studies (e.g., Kent and Olsen, 1999; Szurlies et al., 2003) show that the zonations in red beds may reflect Milankovitch eccentricity cycles with a potential stratigraphic resolution of ~100 ka. Furthermore, stratigraphies of this type, based on orbital tuning provide a basis for refinement of Phanerozoic stratigraphy (Gradstein et al., 2004). The integration of HRHMA and magnetostratigraphy has been carried out on sandstone and mudstone samples from well-cores and field outcrops from the Triassic SSG to determine its potential for refinement of zonation and correlation. The identification of specific magnetozones within the study intervals has allowed the assignment of absolute ages to the identified heavy mineral zones, and provided a time-stratigraphic framework for the Triassic of the EISB and adjacent areas, within which basin evolution may be better reconstructed.

2. GEOLOGICAL SETTING

Remnants of an extensive sedimentary basin, developed during the Permian and Triassic, are preserved in the Irish Sea (Fig. 1). The largest of these, the EISB, lies between North Wales, the Isle of Man and north-west England and is bounded to the north and west by basement ridges and to the south and east by Palaeozoic rocks of the U.K. onshore. These boundaries are partially faulted and partially dip-controlled, while the smaller Peel and Central Irish Sea basins are also partially fault-bounded. Local thickening of the Permo-Triassic section with the presence, in places, of locally derived conglomerate beds, may indicate syndepositional growth on at least some of the more significant basement controlled faults (Jackson and Mulholland, 1993).

The SSG was deposited in a continental setting, associated with a semi-arid climate at a palaeolatitude of around N 20° (Jackson et al., 1995). Clastic material was transported by rivers from the Hercynian massifs of SW England and northern France, through interconnected internal basins to depocentres in the Cheshire and Irish Sea Basins (Fitch et al., 1966; Audley-Charles, 1970; Wills, 1970; Colter and Barr, 1975; Bushell, 1986); the main entry point to the Irish Sea being an outlet NW of the Cheshire Basin (Jackson and Mulholland, 1993; Thompson and Meadows, 1997).

In the EISB, five facies associations have been identified in the SSG, consisting of fluvial channel sandstones together with ephemeral stream, sheetflood, playa and aeolian deposits (Cowan, 1993; Meadows and Beach, 1993). Although fluvial deposits account for up to 90% of the SSG, aeolian sedimentation was widespread and resulted in the episodic deposition of dunes and aeolian sand flats. Aeolian

sandstones rarely form intervals more than a metre thick, but their high permeabilities make them important reservoir rocks (Cowan et al., 1993). The SSG is overlain by the Anisian to Rhaetian Mercia Mudstone Group, within which the Tarporley Siltstone Formation represents the first marine incursion into the Cheshire Basin (Jackson et al., 1995).

3. RATIONALE, MATERIALS AND METHODS

3.1. Palaeomagnetism

Core and field samples for palaeomagnetic analysis were taken at an optimum spacing of 3 m, and preference was given to horizons that were either reddened and/or fine-grained, because pilot studies showed that these rocks had the most suitable palaeomagnetic character. Samples were selected from five unorientated cores from wells in the EISB, (Quadrant 111, Well A, Quadrant 110, Wells D, E, Quadrant 107 Well G) and from outcrops in the Cheshire Basin and the Cumbrian coast (Fig. 1).

Sample locations included: Burton Point (SJ 302735), where the Chester Pebble Beds Formation sits unconformably on the Kinnerton Sandstone Formation; Thurstaston Road Cutting (SJ 242849), mainly in the Thurstaston Member of the Helsby Sandstone Formation (Thompson, 1970; Warrington et al., 1980); Grinshill (SJ 519238), near the top of the SSG close to the overlying Tarporley Siltstone Formation; and The Dungeon (SJ 251831), a section in the lower part of the Tarporley Siltstone Formation.

Samples from the St Bees Sandstone Formation were collected from a number of sections on the Cumbrian coast between Saltom Bay and St Bees South Head (St Bees North Head: NX 940143; St Bees South Head: NX 955154; Fleswick Bay: NX 946133), where the more or less continuous exposure provided a nearly complete section through the lower part of the SSG.

A total of 291 samples were processed using standard laboratory techniques (see Hailwood, 1989; Hailwood and Ding, 1995, for a discussion). In continental red beds the characteristic remanent magnetization (ChRM) can be isolated only using partial thermal demagnetization because hematite is the main magnetic carrier. Selected specimens were heated in 50 °C steps, allowed to cool in magnetic 'field free' space, and remeasured. In addition, at each temperature step the initial magnetic susceptibility was measured in order to monitor any temperature-dependent changes in the magneto-mineralogy. The vectorial data collected were then analysed using orthogonal vector plots and principal components analysis (Dunlop, 1979; Kirschvink, 1980). This method enables the isolation of the ChRM which is used as the basis for determining the magnetopolarity.

3.2. High Resolution Heavy Mineral Analysis

The barren red beds of the SSG are a perfect problem for testing the potential of HRHMA. The strength of the technique is that, in addition to species-level identification and point counting of the heavy mineral assemblages, it categorizes the diagnostic varieties of chemically and mechanically resistant, and generally abundant

zircon, tourmaline and apatite. Varietal differentiation is based on the recognition that virtually all mineral species comprise several optical, chemical, morphological and structural varieties controlled by specific conditions during crystallization in their parent rocks, with further diversification caused by sedimentary processes (Mange-Rajetzky, 1995).

A given depocentre receives clastic detritus from a wide range of lithologies, and therefore the heavy mineral assemblages of sands are complex with many individual species being represented by several varieties, each bearing the signatures of their respective petrogenetic and/or sedimentary histories. Zircon, tourmaline and, when suitable, apatite are the most useful to study, since they are ubiquitous and are largely unaffected by burial diagenesis (Figs. 3A–H and J–L). Focusing on individual species eliminates the influence of hydraulic and diagenetic factors (Morton, 1985).

Heavy mineral varieties can be either (i) provenance-diagnostic, facies-independent, or (ii) facies-sensitive. Provenance-index signatures (e.g., colour, inclusions and internal structure) remain unchanged in any facies during sedimentation and after

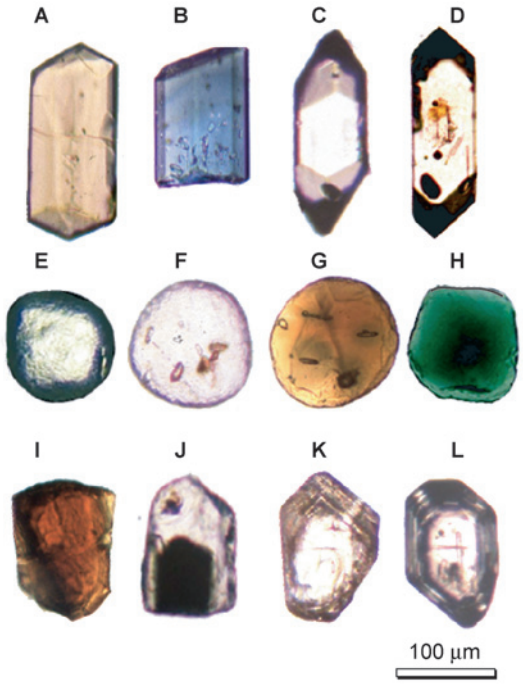

Fig. 3. Representative heavy mineral varieties. A–D: First cycle grains. (A) Doubly terminated, euhedral tourmaline; (B) broken prismatic tourmaline with well-developed, sharp crystal faces; (C) doubly terminated euhedral zircon; (D) doubly terminated sharp euhedral volcanic zircon. E–H: Very well rounded to spherical morphologies. (E) Zircon; (F) apatite; (G) brown tourmaline; (H) green tourmaline. I–L: Provenance-diagnostic species or varieties. (I) Chrome spinel; (J) cored apatite; (K) zircon with zoned overgrowth around a pre-existing rounded core; (L) euhedral zircon with concentrically zoned overgrowth around a pre-existing rounded core. Adapted from Mange et al. (1999) with permission from Journal of Petroleum Geology.

burial, and are instrumental for provenance reconstructions. Facies-sensitive varieties include morphology, grain size and surface textures. These carry the imprint of, for instance, fluvial or aeolian transport and recycling, and may display diagenetic dissolution effects.

A total of 323 samples were selected from the EISB, Peel Basin and from the Central Irish Sea Basin. Sandstones were collected also from St Bees Head and several locations in the North Cheshire Basin. Preparation and separation for heavy mineral analysis followed the methods described by Mange and Maurer (1992). The 0.063−0.250 mm size fractions were sieved out for the heavy mineral separation in bromoform (density 2.89). Heavy minerals were analysed in liquid Canada balsam mounts. The non-opaque suite was counted, excluding micas, using the "ribbon counting" method (Galehouse, 1971). For the species-level analysis 200 grains were point counted, which yields an estimate of individual heavy mineral proportions, whereas 75–100 grains each of zircon, tourmaline and apatite were recorded for varietal differentiation. The varieties distinguished are:

- zircon: euhedral, subhedral, anhedral, rounded colourless and purple; structural types were recorded as zoned and with overgrowth;
- tourmaline: angular, prismatic, rounded prism, subrounded rounded and well rounded to spherical forms; green, brown and blue tourmaline colour varieties were also distinguished, and the types of inclusions (e.g., mineral, fluid, graphite) were recorded;
- apatite: prismatic, rounded prism, subrounded, rounded and spherical grains.

4. RESULTS

4.1. Palaeomagnetism

4.1.1. Classification of magnetization types

During partial thermal demagnetization, the NRM vectors show a variety of directional and intensity changes which can be sub-divided into six magnetization types (A–F) as follows:

- Type A: Characterized by a single ChRM component of magnetization with an inclination of approximately $+30$ to -30° and unblocking temperatures of up to 650 °C. The ChRM is interpreted as Triassic normal or reversed polarity.
- Type B: These are more complex magnetizations which comprise two distinct components of magnetization: a low unblocking temperature component of variable direction and commonly steep positive inclination overprinted upon a higher unblocking temperature component of magnetization with an inclination of $\sim+30$ to -30°. The higher unblocking temperature component is regarded as Triassic.
- Type C: hese components have variable declinations and constant inclinations with relatively low inclinations of $\sim+30$ to -30°. They are interpreted as Triassic in age.
- Type D: These are magnetizations consisting of a single low unblocking temperature component. In the majority of cases Type D magnetizations have steep positive inclinations consistent with the ambient geomagnetic field. This magnetization type

is interpreted as a viscous magnetization associated with burial. The absence of significant ChRM is due to diagenetic interaction between hydrocarbons and the host rocks.
- Type E: These magnetizations are best described as "unstable" in that no significant components can be isolated.
- Type F: In these samples, the inclination of a single component is often too shallow to confidently define either a normal or reversed polarity. Although such magnetizations might conceivably be Triassic in age, the absence of declination data means that the polarity is impossible to determine. In this study, the magnetization Types A, B and C have been used to construct a polarity-based magnetostratigraphy for each of the study wells and for the onshore Cheshire Basin section.

4.1.2. *Offshore wells*

Examples of the behaviour of samples during partial thermal demagnetization and their characteristic polarities from well D are shown in Figs. 4A–C.

Well D. The initial NRM directions in this well are of both normal and reversed polarity and show a range of inclinations from shallow to steep. The intensity ranges from 0.04 to 16.41 mA/m with a mean of 1.08 mA/m. Values of the initial magnetic susceptibility range from 30 to 2833 with a mean of 700 SI units. Samples from Well D display 19 Type A magnetizations (24.1%), 2 Type B magnetizations (2.5%), 8 Type C magnetizations (10.1%), 9 Type D magnetizations (11.4%), 39 Type E magnetization (49.4%) and 2 Type F magnetizations (2.5%). It was, therefore, possible to define a primary magnetic polarity in ~37% of the samples from this well.

Well E. The initial NRM directions in this well are of both normal and reversed polarity and show a range of inclinations from shallow to steep. The intensity ranges from 0.04 to 16.13 mA/m with a mean of 1.63 mA/m. Values of the initial magnetic susceptibility range from 95 to 2314 with a mean of 352 SI units. Samples from Well E display 14 Type A magnetizations (20.3%), 12 Type B magnetizations (17.4%), 5 Type C magnetizations (7.2%), 4 Type D magnetizations (5.8%), 30 Type E magnetization (43.5%) and 4 Type F magnetizations (5.8%). It was, therefore, possible to define a primary magnetic polarity in ~45% of the samples from this well.

Well G. The initial NRM directions in this well are of both normal and reversed polarity and show a range of inclinations from shallow to steep. The intensity ranges from 3.00 to 10.98 mA/m with a mean of 5.19 mA/m. Values of the initial magnetic susceptibility range from 921 to 4223 with a mean of 2668 units. Samples from Well G display 3 Type A magnetizations (33.3%), a single Type B magnetizations (11.1%), 3 Type C magnetizations (33.3%), a single Type D magnetizations (11.1%), a single Type E magnetization (11.1%) and no Type F magnetizations. It was, therefore, possible to define a primary magnetic polarity in ~78% of the samples from this well.

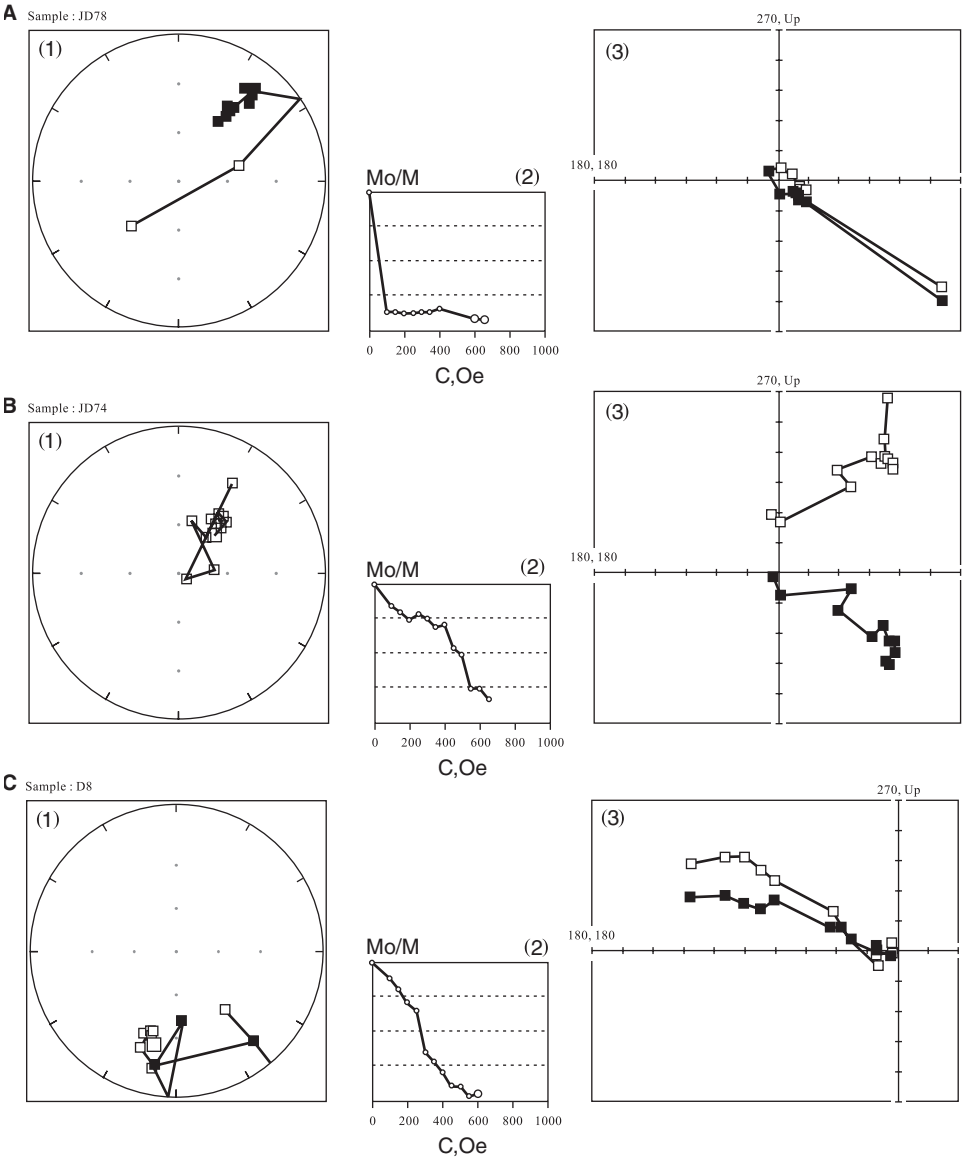

Fig. 4. Palaeomagnetic results. (A) Ormskirk Sandstone Formation (Type B) from well D. The sharp unblocking temperature at 100 °C is associated with the removal of a viscous component of magnetization. In subpart (3) there is little intensity change between 100 and 650 °C. The ChRM is of normal polarity. (B) Ormskirk Sandstone Formation (Type A) from well D. There is a constant loss of remanence with temperature indicating a thermally distributed ChRM. Subpart (3) shows little internal variability. The ChRM is of reversed polarity. (C) Tarporley Siltstone Formation (Type A) from the Cheshire Basin. Note the smooth demagnetization trend with a maximum unblocking temperature of ~575 °C. The ChRM is of reversed polarity. (1) Stereographic projection of directional changes with arbitrary declination; open symbols, upward inclination; closed symbols, downward inclination. (2) Normalized intensity decay curves. (3) Orthogonal vector plots. Adapted from Mange et al. (1999) with permission from Journal of Petroleum Geology.

Well A. The initial NRM directions in this well are of both normal and reversed polarity and show a range of inclinations from shallow to steep. The intensity ranges from 0.25 to 1.59 mA/m with a mean intensity of 0.73 mA/m. Values of the initial magnetic susceptibility range from 223.07 to 40.39.14 SI with a mean of 1060.30 SI. Samples from Well A display 3 Type A magnetizations (27.3%), 3 Type B magnetizations (27.3%), a single Type C magnetization (9.1%), 4 Type D magnetizations (36.4%), no Type E magnetizations and no Type F magnetizations. It was, therefore, possible to define a primary magnetic polarity in ~64% of the samples from this well.

4.1.3. Cheshire Basin

The vector directions of the initial NRM in this region are of both normal and reversed polarity and show a range of inclinations from shallow to steep. Examples of the behaviour of a sample during partial thermal demagnetization from the Tarporley Siltstone Formation is shown in Fig. 4C.

The intensity of the initial NRM for samples from the Cheshire Basin ranges from 0.59 to 10.74 mA/m, with mean intensity of 2.59 mA/m. Values of the initial magnetic susceptibility range from 86 to 593 with a mean of 507 SI units.

Samples from the Cheshire Basin display 9 Type A magnetizations (42.9%), 9 Type B magnetizations (42.9%), no Type C magnetizations, 3 Type D magnetizations (14.3%), no Type E magnetizations and no Type F magnetizations. It was, therefore, possible to define a primary magnetic polarity in ~86% of the outcrop samples examined in this area.

4.1.4. Cumbrian coast

Because of a nearly complete section through the lower part of the SSG, the magnetostratigraphy on the Cumbrian coast is the most complete of any of the studied sections. The St Bees Sandstone shows the most consistent palaeomagnetic results of all of the studied sections. They are predominantly Type A and Type B magnetizations, and the ChRM indicates a mixture of normal and reversed polarities. Examples of the behaviour during partial thermal demagnetization of samples with reversed and normal polarities are illustrated in Fig. 5. The quality of the data from this section results from the generally fine-grained nature of the rocks and from the absence of iron reduction processes by gas or oil emplacement.

4.1.5. Remanence acquisition and composite magnetostratigraphy

Both detrital hematite/ilmenohematite and authigenic hematite are present in the offshore study wells and the Cheshire Basin. In the former, the hematite probably comprises oxidized magnetite, whereas the authigenesis of ultrafine pigmentary hematite was formed from the alteration of Fe-bearing oxides and silicates under oxidizing conditions at or near the depositional surface. In several wells, hematite authigenesis appears to have been enhanced over intervals where soil-forming processes were active. This suggests that the original magnetization of these samples was acquired as a detrital remanent magnetization (DRM) with an additional post-depositional remanent magnetization (PDRM/CRM) within an ambient Triassic field direction. Detrital hematite grains and their authigenic overgrowths have been documented by Turner and Ixer (1977) and Ixer et al. (1979). In combination with the palaeomagnetic data that show mixed normal and reversed polarities and

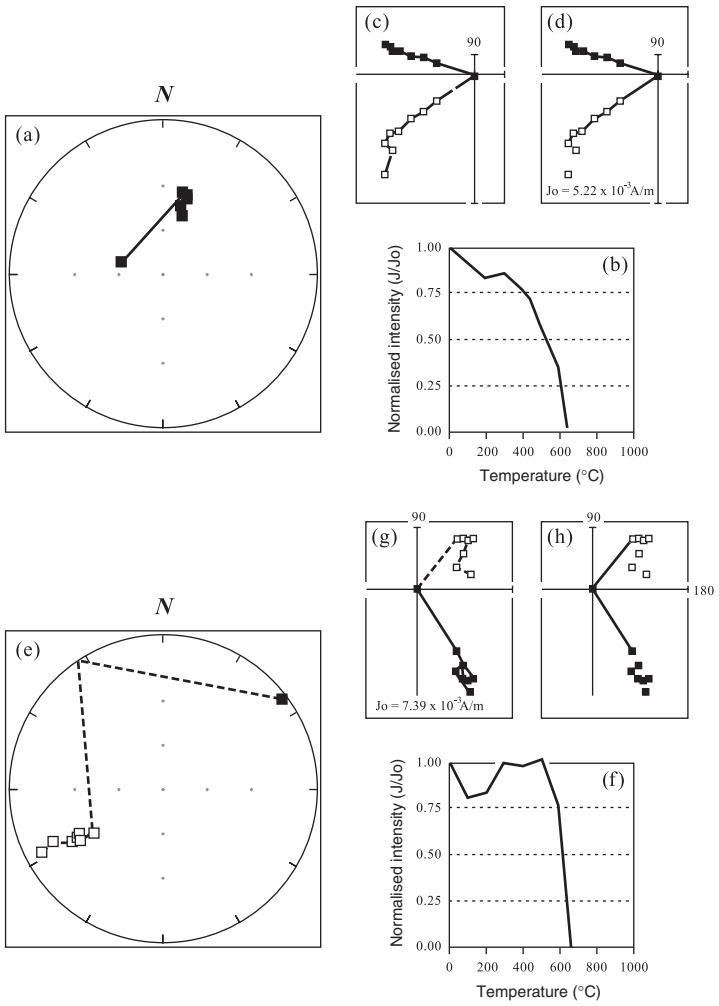

Fig. 5. Palaeomagnetic results from the St Bees Sandstone on the Cumbrian Coast. The sample above (a–d) shows normal polarity and the sample below (e–h) reversed polarity. (a, e) Stereographic projections (details as in the other figures). (b, f) Normalized intensity decay curves. (c, g) Orthogonal vector plots. (d, h) Orthogonal vector plots showing ChRM component isolated by principal components analysis.

Triassic palaeo-directions, this hematite strongly suggests that the ChRM in the Triassic red beds was acquired during and shortly after deposition.

The magnetic properties of drab-coloured sediments (buff or grey in colour), particularly in the upper parts of Wells D and E are quite different. The NRM intensities are very weak and it is commonly not possible to isolate any characteristic remanence. This is interpreted as resulting from the large-scale removal of the primary magnetic mineralogy from these sandy intervals by bleaching as a consequence of reducing diagenetic conditions following burial. Because the reduction appears to be independent of facies, it is probably associated with hydrocarbon emplacement in the

EISB. The magnetizations in these intervals are generally steeply inclined and have low unblocking temperature components. Mostly they probably represent either a present-day viscous overprint approximating to the Earth ambient geomagnetic field direction or a component induced during coring or laboratory drilling.

The magnetostratigraphies shown here have been constructed on the basis of polarity determinations in Type A, B or C magnetizations. Because of the diagenetic problems highlighted above, it has proved difficult to assign polarities to some sections, so that magnetopolarities have been interpolated using all the available data. The main features of the Triassic magnetostratigraphy are described below.

The St Bees Sandstone Formation comprises a zone of predominantly normal polarity (N1–N3) separated by two thin reversed magnetozones (R1–R2) overlain by a thick reversed magnetozone (R3). The Burton Point section (in part at least, stratigraphically equivalent to the St Bees section) shows mixed polarity magnetozones in the Kinnerton Sandstone Formation and predominantly normal polarity in the lower part of the Chester Pebble Beds. The normal magnetozone is considered to be the time equivalent of the N1–N2 magnetozone identified in the St Bees Sandstone. The magnetostratigraphy of the Ormskirk Sandstone Formation, investigated in Wells D and E, is poorly defined because many of the magnetizations are so weak and the ChRM is difficult to define. However, a number of relatively thick normal zones with thin reversed zones are considered to dominate the Ormskirk Sandstone Formation.

4.1.6. Results of HRHMA

The transparent heavy mineral suite of the SSG comprises principally zircon, tourmaline and apatite, accompanied by low quantities of rutile and, occasionally, monazite-xenotime, garnet and staurolite. Green and brown hornblende, fibrous amphiboles, ortho- and clinopyroxenes, epidote, kyanite and chrome spinel occur in trace amounts. Authigenic minerals include various carbonates, baryte, anhydrite and anatase, while organogenic phosphatic particles, collophane and francolite, represent various faunal remains. Well-rounded detrital opaque grains are common throughout. The cumulative percentages of transparent, detrital heavy minerals, and those of the informative tourmaline and apatite varieties, were each plotted against depth and gamma ray logs (Figs. 6–8). These plots allow comparison of the mineralogical trends with the wire-line logs and permit recognition of corresponding changes. In this contribution, for simplicity, the species-level heavy mineral compositions and the patterns of apatite varieties are shown for the type wells, which comprise the most fully developed successions (Figs. 6–8). The distribution of tourmaline varieties is illustrated by the trends of representative tourmaline–apatite varietal pairs.

4.2. Heavy Mineral Stratigraphy

Distinctive vertical changes in heavy mineral and varietal trends have been used both to constrain heavy mineral zones and to construct a heavy mineral stratigraphy. Zone boundaries generally coincide with changes in the electric log motifs. Heavy mineral zones have been defined on the basis of the coinciding, systematic changes in the trends of both individual mineral species, and their varieties, within the studied successions. Each heavy mineral zone can be defined in terms of a set of mineralogically

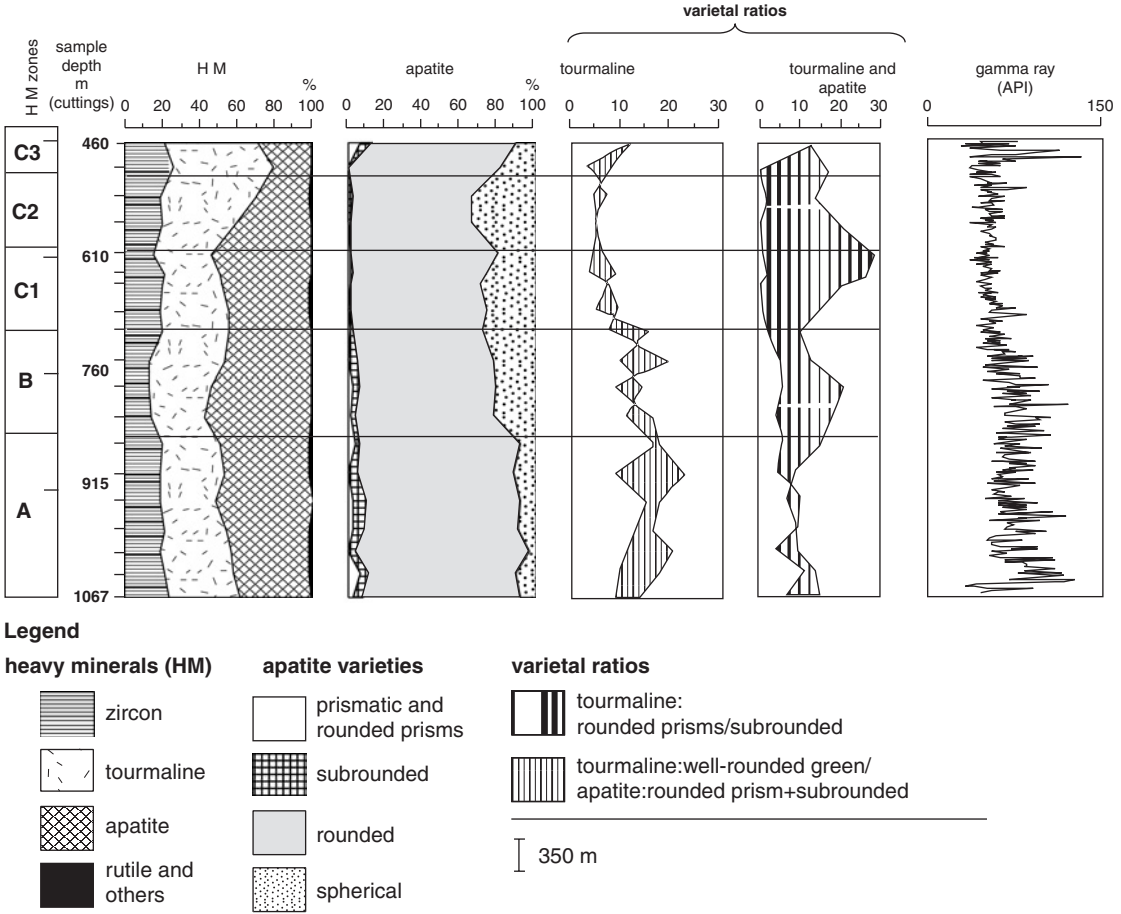

Fig. 6. Well A (Quadrant 111, Peel Basin). Heavy mineral composition, distribution of apatite morphological varieties, trends of tourmaline and apatite varietal pairs, and gamma-ray log. Adapted from Mange et al. (1999) with permission from Journal of Petroleum Geology.

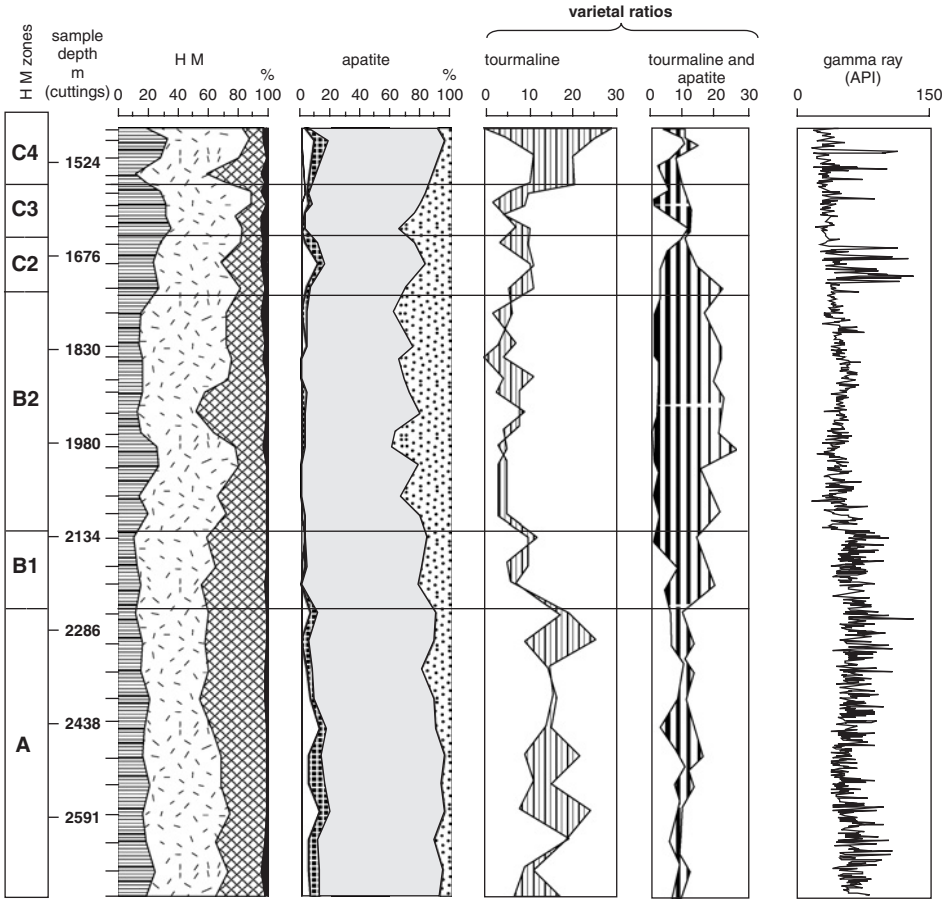

Fig. 7. Well B (Quadrant 113). Heavy mineral composition, distribution of apatite morphological varieties, trends of tourmaline and apatite varietal pairs, and gamma-ray log. For legend see Fig. 6.

conformable strata, related by similar provenance and depositional setting. Zone boundaries are placed at horizons recognized by a change in mineralogical signatures that reflects a shift either in depositional processes or in provenance.

Three principal heavy mineral Zones, A, B and C, have been recognized, while more subtle mineralogical variations suggest further subdivisions of Zones B and C. In Well H, Zone A is underlain by an interval which shows markedly different heavy mineral and varietal proportions. This is labelled Zone P and is considered to be Permian in age.

4.2.1. Main characteristics of the heavy mineral zones

Zone A is distinguished by a relatively high grain angularity and by the frequency of euhedral and subhedral zircons. These signatures have been recognized in all wells and indicate the wide lateral extent of Zone A (Figs. 6–8). In Zone B, the number of euhedral–subhedral zircons decreases, as does the angularity of tourmaline and

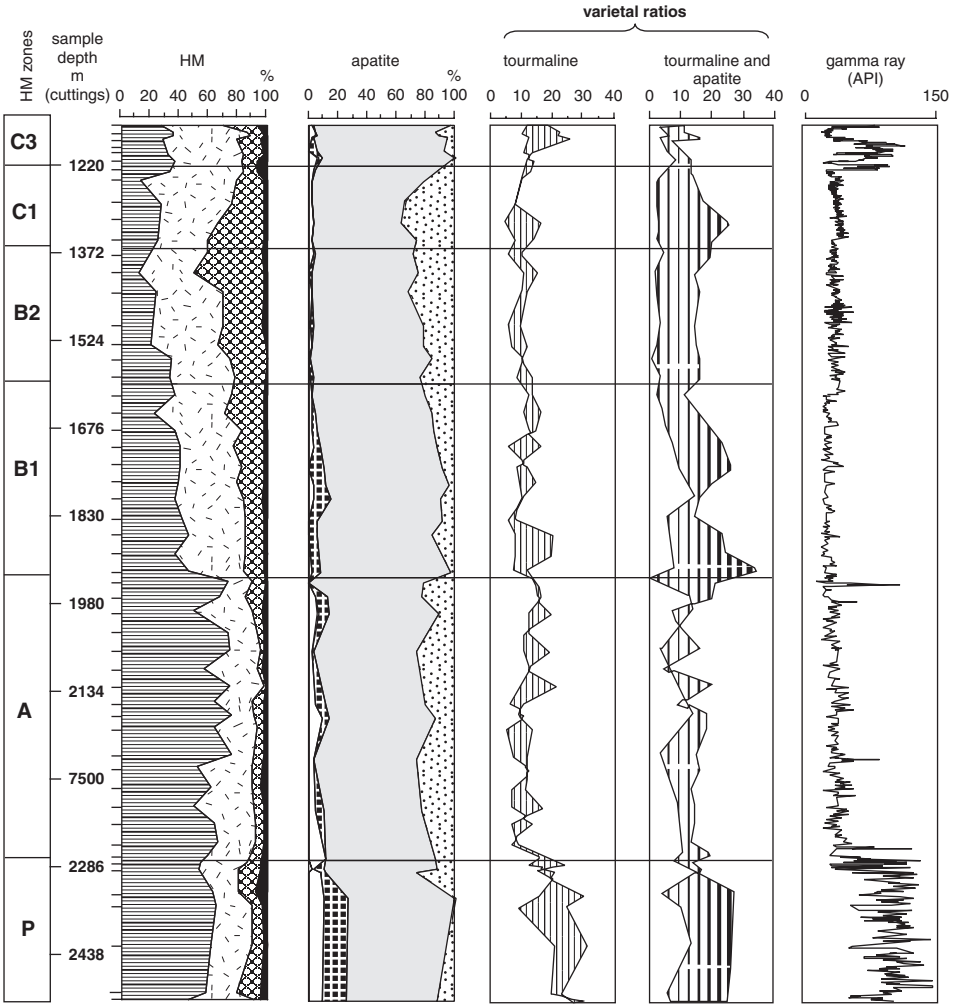

Fig. 8. Well H (Quadrant 42, Central Irish Sea). Heavy mineral composition, distribution of apatite morphological varieties, trends of tourmaline and apatite varietal pairs, and gamma-ray log. For legend see Fig. 6.

apatite, whereas spherical apatites become abundant. The proportions of brown and green tourmaline also change at this boundary, with a considerable increase in green tourmaline quantities. Zone B has been divided into subzones B_1 and B_2, based on a further advance in the degree of rounding of all grains and by the decline of euhedral–subhedral zircons in subzone B_2.

Zone C is not fully developed in all study wells. Analysis of core from Wells D and E in Quadrant 110 has resulted in the delineation of four subzones ($C_{1–4}$) within it. All four subzones have been identified from cuttings in Well F in Quadrant 113. Subzone C_1 is characterized by relatively high amounts of zircon showing complex overgrowth (Figs. 3K, L) and abundant spherical apatite (Fig. 3F) allowing its confident recognition in both cored and uncored wells. Subzone C_2 is differentiated

from C_1 by the absence or considerably smaller proportions of the diagnostic zircon variety and by higher apatite angularity. There is a further increase in tourmaline and apatite angularity in subzone C_3, whereas subzone C_4 is fairly similar to subzone C_3 but it contains differing proportions of tourmaline colour varieties and shows a more intensive variation in tourmaline and apatite angularity/sphericity.

5. THE REFERENCE SECTION: INTEGRATION OF HEAVY MINERAL AND MAGNETOSTRATIGRAPHY

Good quality data from the St Bees Sandstone Formation at St Bees Head and from cores of the overlying Ormskirk Sandstone Formation (from wells D and E) was integrated and used in the construction of a composite HRHMA-magnetostratigraphic reference section (Fig. 9), that is key to the understanding of the litho- and chronostratigraphy of the SSG in offshore areas. By comparing the wells in different basins with the reference section, local versus regional variations in depositional style and provenance can also be assessed.

5.1. Heavy Mineral and Magnetozones of the Reference Section

The apatite-rich lower interval of the composite reference section corresponds to the St Bees Sandstone Formation (Fig. 9), where heavy mineral zones A (Chester Pebble Beds Formation equivalent) and B (Wilmslow Sandstone Formation equivalent) have been delineated. Based on apatite and tourmaline signatures, Zone B was subdivided further into B_1 and B_2 subzones. The overlying strata, cored in Wells D and E, represent the Ormskirk Sandstone Formation, labelled as Heavy Mineral Zone C. As discussed earlier, this zone was subdivided into subzones C_1–C_4.

Integration of magnetostratigraphy with heavy mineral stratigraphy places the heavy mineral zones into the global chronostratigraphy for the Early to Early-Mid Triassic (Gradstein et al., 1994). Zone A coincides with a dominantly normal polarity defined by chron (N2) at 244 Ma, and is Middle Scythian in age (Fig. 9). Normal polarity changes to reversed (R2) at the boundary of Zones A/B which is older than 243 Ma. Zone B has a dominantly reversed polarity and is Middle to Upper Scythian, indicated by a chron of 242.7 Ma close to the boundary of Zones B/C. Zone C is Anisian in age and is characterized by a dominantly normal polarity including several short-term reversals which increase in frequency and duration upwards. A horizon near to the top of the study sequence yielded a chron of 239.5 Ma.

5.2. Heavy Mineral and Magnetostratigraphic Regional Correlation Scheme for the EISB

Extrapolation of the integrated heavy mineral-magnetostratigraphic framework from the reference section to the offshore wells is illustrated in Fig. 10. Correlatable zones or subzones are indicated by similar letters and zone boundaries are correlated by tie-lines. The regional extent of the facies-independent zonation is tied to chrons at key boundaries and demonstrates the isochroneity of the depositional system across the basin.

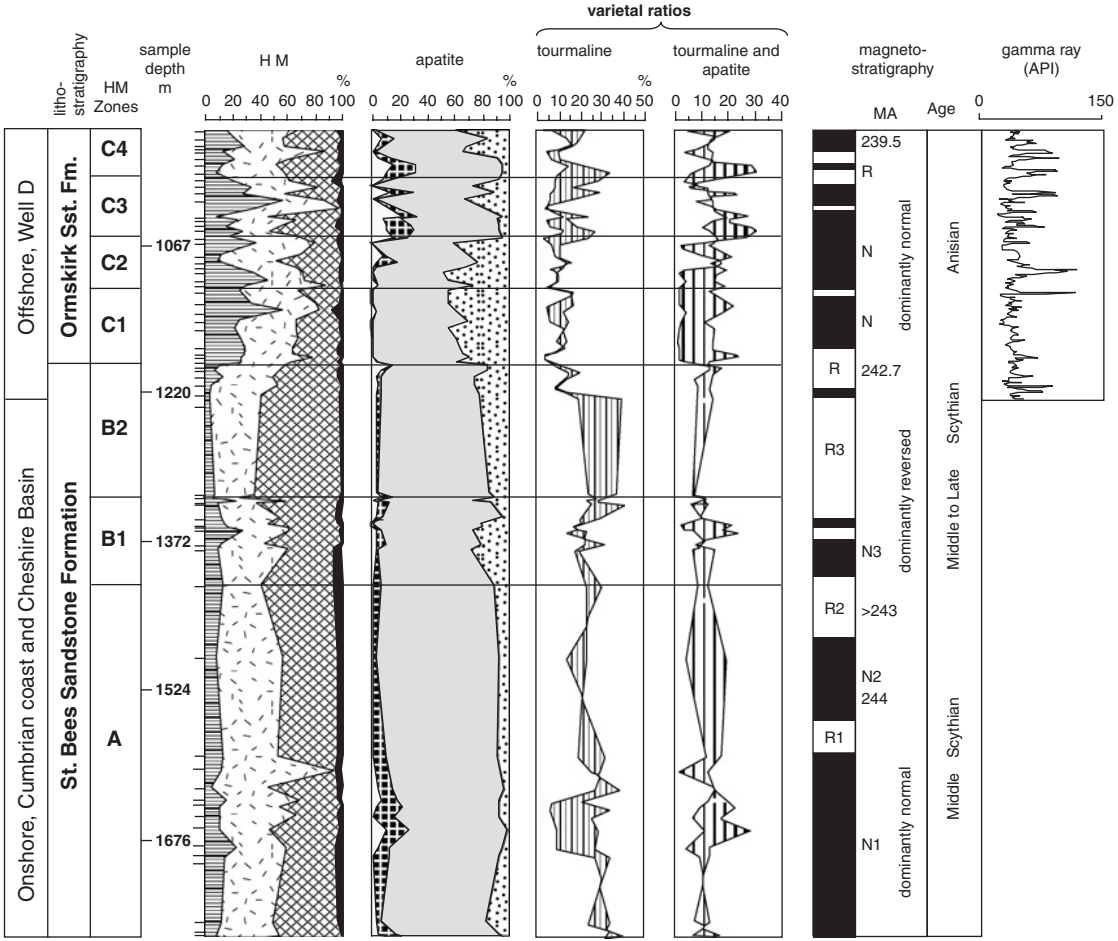

Fig. 9. Integrated reference section compiled from data onshore sections and Well D. This figure shows heavy mineral composition, distribution of apatite morphological varieties, trends of tourmaline and apatite varietal pairs, and gamma-ray log from Well D (Quadrant 110) together with the composite magnetozones. For legend see Fig. 6. Adapted from Mange et al. (1999) with permission from Journal of Petroleum Geology.

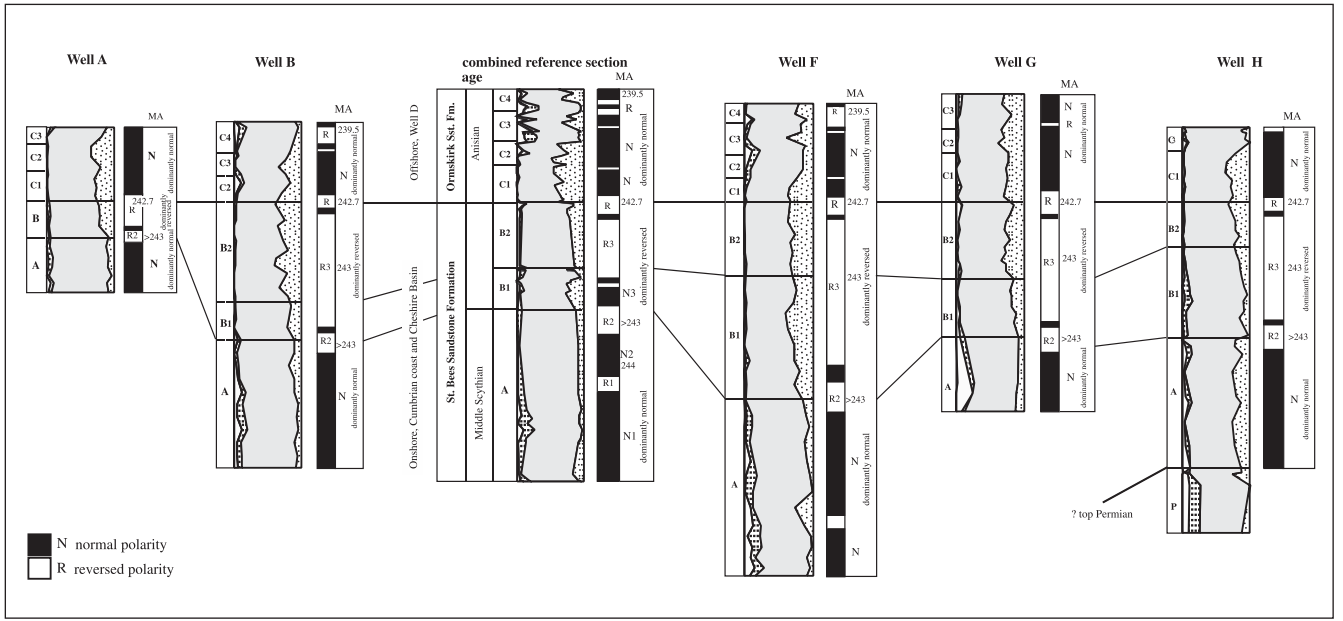

Fig. 10. Heavy mineral- and magnetostratigraphy: regional zonation and correlation, exemplified by the patterns of apatite. For legend see Fig. 6. Adapted from Mange et al. (1999) with permission from Journal of Petroleum Geology.

Regionally significant changes at the boundary of Zones A/B both in the reference section and in the type wells permit extrapolation of the thin reversed magnetozone R2 (>243 Ma), obtained for the St Bees section. Consequently, heavy mineral zone A coincides with the dominantly normal-polarity lower magnetozone. The boundary of Zones B/C is marked by chron 242.7 Ma, where the underlying dominantly reversed polarity passes up to an interval of dominantly normal polarity. Chron 239.5 in subzone C_4, close to the top of the analysed section in Wells D and E, has been extrapolated to Well F.

The robust nature of this zonation scheme is demonstrated by the fact that it compares well with magnetostratigraphies developed in central Germany and the Boreal and Tethyan Triassic (Hounslow et al., 1996; Scholger et al., 2000; Szurlies et al., 2000, 2003; Nawrocki, 1997). In Fig. 11, the Cheshire Basin zonation scheme is shown compared with magnetostratigraphies from these areas.

6. DISCUSSION

New palaeomagnetic and heavy mineral data from the cored and uncored successions allows a refined model of Sherwood Sandstone sedimentation in the EISB and adjacent areas. Basin configuration during the deposition of the SSG, constrained by a northward-dipping regional palaeoslope (Wills 1948, 1956; Fitch et al., 1966; Audley-Charles, 1970; Burley, 1987), determined that the major drainage pattern was axial, with sediment transported from the Variscan highlands to the south. Lateral drainage from marginal ridges and structural highs also contributed detritus to the major system and to local depocentres. The abundance of polycyclic detritus points to the widespread erosion of older sediments and metasediments that formed the cover to granitic intrusions (Groves, 1931), marginal ridges and structural highs, including the Ramsey-Whitehaven Ridge, Isle of Man and the Welsh-Brabant Massif. Local prominence of provenance-index species, e.g., ultramafics-derived chrome spinel (Fig. 3I) and varieties (volcanogenic sharp euhedral zircons, Figs. 3C, D, and pleochroic apatites), detected in the SSG sediments, may indicate derivation from ophiolitic and volcanic terranes in the North Wales area. Cored apatites (Fig. 3J) were reported from the Leinster Massif of Ireland (Fleet and Smithson, 1928) and these are frequently found in wells H and I in the Central Irish Sea Basin, again indicating a more localized derivation. Generally, high grain angularity is in accord with the dominantly fluvial processes operating during Zone A deposition before 243 Ma.

Axial (S–N) versus lateral (E–W) sand derivation and transport is reflected by the provinciality of the heavy mineral assemblages. Pairs of provenance-diagnostic varieties (e.g., zircon with simple overgrowth against tourmaline spherical brown, and blue tourmaline against spherical apatite) plotted as bivariate plots for Zones A and B (Fig. 12) highlight the source-controlled mineralogical differences between the eastern and western part of the basin, which are especially pronounced in Zone A (Figs. 12a, b). Wells in the Central Irish Sea Basin (I, G, H) to the west can be distinguished readily from wells in the EISB to the east (Wells B, F) (Figs. 12a–c). The relationship appears closer between wells in the Central Irish Sea Basin and the Peel Basin (Fig. 12d). The tight cluster of Well G (Fig. 12b) suggests some localized sediment input, whereas data points of Wells B and F appear within a common cluster, indicating their similar provenance.

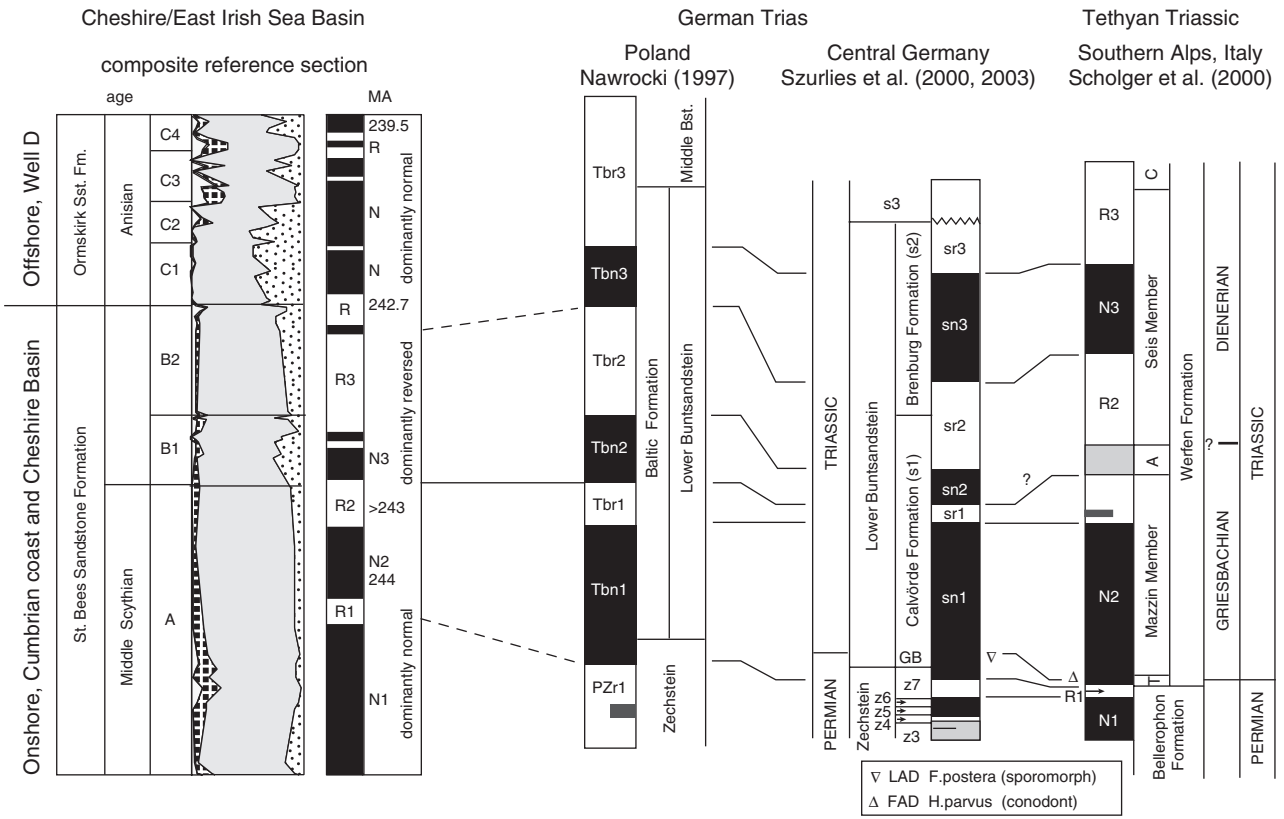

Fig. 11. Cheshire Basin zonation scheme compared with magnetostratigraphies from other Triassic sections (modified from Szurlies et al., 2003).

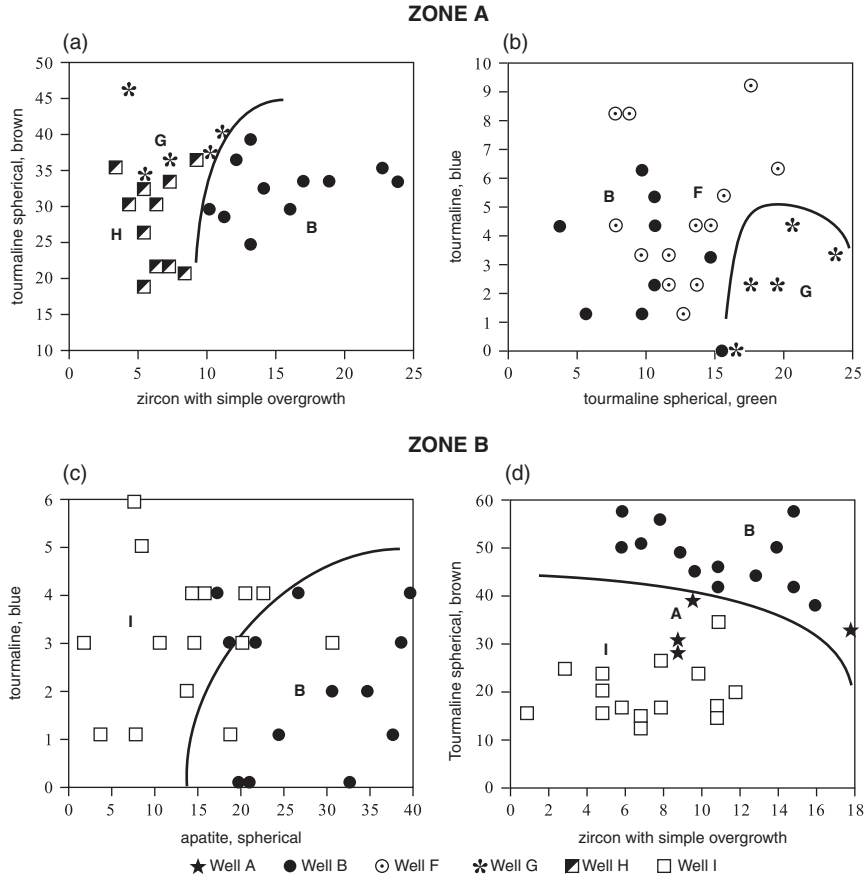

Fig. 12. Bivariate plots of varietal pairs, illustrating the provinciality of heavy mineral suites, for legend, see Fig. 6. Adapted from Mange et al. (1999) with permission from Journal of Petroleum Geology.

The marked change in the varietal trends at the Zone A/B boundary is broadly coincident with the "Top Silicified Zone" (Fig. 2) of Colter and Barr (1975) in all study wells, and records a prominent change both in sand provenance and palaeoenvironment. This silicified zone, interpreted as a result of burial diagenesis (Burley, 1984, 1987), can be identified from a well-documented sonic-velocity decrease in the logs (see also Jackson and Mulholland, 1993). It has a laterally uniform thickness and extends from the Cheshire Basin through the EISB to the Ulster-Larne-North Channel Basin. The striking coincidence of the regional change in detrital mineralogy and subsequent diagenetic silicification is an important discovery which may have implications for the interpretation of the origin of silica cements in this zone.

In Zone B, which has a dominantly reversed magnetic polarity, homogenization of mineral assemblages occurs, and is particularly noticeable in the adjacent sub-basins (e.g., between the Central Irish Sea and Peel Basin), suggesting more extensive intrabasinal reworking. This process may have been initiated by the denudation of the

distal hinterland (Kent, 1975) so that the resulting low topographic relief limited sediment supply to local sources. Easterly and northeasterly trade winds were prominent during the Early Triassic (Clemmensen, 1985; Cowan et al., 1993) and could have transported sand westwards from alluvial fans or dry floodplains. The increase in the number of green tourmalines at the boundary of Zones A and B signals sand contribution from different regions which, as it is paralleled by an abrupt increase in the rounding grade of the majority of the grains, can be ascribed to aeolian processes.

In the Central Irish Sea Basin (wells H and I), higher grain angularity and the common presence of first cycle euhedral zircon, tourmaline and apatite in Zone B suggest that, as opposed to the EISB, localized sources continued to supply detritus to Zone A. Zone B/C boundary coincides with chron 242.7 Ma and, as shown in Fig. 2, separates the St Bees and the Ormskirk Sandstone Formations. The base of Zone C coincides with the Hardegsen disconformity, a major tectonic event well documented throughout Europe (Geiger and Hopping, 1968; Fisher and Mudge, 1998). Although it has not so far been recognized as an angular unconformity in the EISB and adjacent areas (e.g., Cowan et al., 1993), this episode triggered a general uplift of the footwalls of basin-bounding faults and massifs (Jackson et al., 1995), exhumed new source complexes and modified basin configuration and transport paths. Consequently, the abrupt appearance of provenance-diagnostic varieties (e.g., zircon with complex overgrowth in subzone C_1, Figs. 3K, L) may well be consistent with the presence of an hiatal surface, correlative with the Hardegsen disconformity.

7. CONCLUSIONS

Results of a heavy mineral and magnetostratigraphic study of the Triassic SSG have demonstrated that the integration of these techniques provides an effective means for subdividing, correlating and dating barren successions in uncored wells with increased levels of confidence. A reference section compiled from cored wells and/or onshore equivalents of offshore successions, where heavy mineral stratigraphy is tied to specific magnetostratigraphic chrons, provides a temporal framework within which the structural and sedimentary history of a basin can be interpreted. With continuing demand to find potential tools for subdivision and correlation of productive successions that are barren of fossils and lacking persistent lithological markers, this case study offers a model of the techniques that can be applied. The combination of HRHMA and magnetostratigraphy has two advantages: (1) zones, defined on the basis of polarity changes, are chronostratigraphic and can potentially be correlated on a global scale; (2) the combination with HRHMA shows the potential for further zonation refinement and also yields vital information on sediment provenance and dispersal within the basin. Furthermore, this integrated approach provides key information for cyclic analysis of sedimentary successions and can readily be interpreted in terms of orbital tuning.

ACKNOWLEDGEMENTS

The authors wish to thank Mobil North Sea Limited for permission to publish and for support through this work. We are grateful to Professor John F. Dewey for

critically reading the manuscript. The manuscript benefited from the constructive reviews by Ken W. Glennie, Stuart D. Burley and David G. Quirk. We thank Steve Wyatt, Department of Earth Sciences University of Oxford, U.K. for his help with the laboratory techniques. We gratefully acknowledge the permission of Journal of Petroleum Geology to use some of the figures from a paper published earlier in the journal.

REFERENCES

Audley-Charles, M.G., 1970. Triassic palaeogeography of the British Isles. Journal of the Geological Society, London 126, 19–47.

Burley, S.D., 1984. Patterns of diagenesis in the Sherwood Sandstone Group (Triassic), United Kingdom. Clay Minerals 19, 403–440.

Burley, S.D., 1987. Diagenetic modelling of the Triassic Sherwood Group of England and its offshore equivalents, U.K. Continental Shelf. Unpublished Ph.D. thesis, Hull University.

Bushell, T.P., 1986. Reservoir geology of the Morecambe field. In: Brooks, J., Goff, J.C., Van Hoorn, B. (Eds.), Habitat of Palaeozoic Gas in NW Europe. Geological Society of London, Special Publication, vol. 23, pp. 189–208.

Clemmensen, L.B., 1985. Desert sand plain and sabhka deposits from the Bunter Sandstone Formation (L. Triassic) at the northern margin of the German Basin. Geologische Rundschau 74, 519–536.

Colter, V.S., Barr, K.W., 1975. Recent developments in the geology of the Irish Sea and Cheshire Basins. In: Woodland, A.W. (Ed.), Petroleum and the Continental Shelf of North-West Europe. Applied Sciences Publishers, London, pp. 61–75.

Cowan, G., 1993. The identification and significance of aeolian deposits in the dominantly fluvial Sherwood Sandstone Group of the EISB, UK. In: North, C.P., Prosser, D.J. (Eds.), Characterization of Fluvial and Aeolian Reservoirs. Geological Society of London, Special Publication, vol. 73, pp. 231–245.

Cowan, G., Ottesen, C., Stuart, I.A., 1993. The use of dipmeter logs in the structural interpretation and palaeocurrent analysis of Morecambe Fields, East Irish Sea Basin. In: Parker, J.R. (Ed.), Petroleum Geology of Northwest Europe: Proceedings of the 4th Conference, London. Geological Society of London, pp. 867–882.

Dunay, R.E., Hailwood, E.A., 1995. Non-biostratigraphical methods of dating and correlation. Geological Society of London, Special Publication, vol. 89, 265pp.

Dunlop, D.J., 1979. On the use of Zijderveld diagrams in multicomponent paleomagnetic studies. Physics of the Earth and Planetary Interiors 20, 12–24.

Fisher, M.J., Mudge, D.C., 1998. Triassic. In: Glennie, K.W. (Ed.), Petroleum Geology of the North Sea (4th ed.). Blackwell Science, Oxford, pp. 212–244.

Fitch, F.J., Miller, J.A., Thompson, D.B., 1966. The palaeogeographic significance of isotopic age determinations on detrital micas from the Triassic of the Stockport-Macclesfield district, Cheshire. Palaeogeography Palaeoclimatology Palaeoecology 2, 281–313.

Fleet, W.F., Smithson, F., 1928. On the occurrence of dark apatite in some British rocks. Geological Magazine 65, 6–8.

Galehouse, J.S., 1971. Point counting. In: Carver, R.E. (Ed.), Procedures in Sedimentary Petrology. Wiley, New York, pp. 385–407.

Geiger, M.E., Hopping, C.A., 1968. Triassic stratigraphy of the southern North Sea. Philosophical Transactions of the Royal Society of London 254B, 1–36.

Gradstein, F.M., Agterberg, F.P., Ogg, J.G., Hardenbol, J., van Veen, P., Thierry, J., Huang, Z., 1994. A Mesozoic time scale. Journal of Geophysical Research 99 (B12), 24051–24074.

Gradstein, F.M., Ogg, J.G., Smith, A.G., 2004. A Geologic Time Scale 2004. Cambridge University Press, Cambridge, 610pp.

Groves, A.W., 1931. The unroofing of the Dartmoor Granite and the distribution of its detritus in the sediments of southern England. Journal of the Geological Society, London 87, 62–96.

Hailwood, E.A., 1989. Magnetostratigraphy. Special Report of the Geological Society of London 19, 84pp.

Hailwood, E.A., Ding, F., 1995. Palaeomagnetic reorientation of cores and the magnetic fabric of hydrocarbon reservoir sands. In: Turner, P., Turner, A. (Eds.), Palaeomagnetic Applications in Hydrocarbon Exploration and Production. Geological Society of London, Special Publication, vol. 98, pp. 245–258.

Hounslow, M.W., Merk, A., Peters, C., Weitschat, W., 1996. Boreal Lower Triassic magnetostratigraphy from Deltadalen, Central Svalbard. Albertiana 17, 3–10.

Ixer, R.A., Turner, P., Waugh, B., 1979. Authigenic iron and titanium oxides in Triassic red beds: St Bees Sandstone, Cumbria, Northern England. Geological Journal 14, 179–192.

Jackson, D.I., Mulholland, P., 1993. Tectonic and stratigraphic aspects of the East Irish Sea Basin and adjacent areas: contrasts in their post-Carboniferous structural styles. In: Parker, J.R. (Ed.), Petroleum Geology of Northwest Europe: Proceedings of the 4th Conference, London. Geological Society of London, pp. 791–808.

Jackson, D.I., Jackson, A.A., Evans, D., Wingfield, R.T.R., Barnes, R.P., Arthur, M.J., 1995. United Kingdom offshore regional report: the geology of the Irish Sea. British Geological Survey, HMSO, London.

Jackson, D.I., Johnson, H., Smith, N.J.P., 1997. Stratigraphical relationships and a revised lithostratigraphical nomenclature for the Carboniferous, Permian and Triassic rocks of the offshore East Irish Sea Basin. In: Meadows, N.S., Trueblood, S.P., Hardman, M., Cowan, G. (Eds.), Petroleum Geology of the Irish Sea and Adjacent Areas. Geological Society of London, Special Publication, vol. 124, pp. 11–32.

Kent, P.E., 1975. The tectonic development of Great Britain and the surrounding seas. In: Woodland, A.W. (Ed.), Petroleum and the Continental Shelf of North-West Europe. Geology Applied Sciences Publishers, Barking, pp. 3–28.

Kent, D.V., Olsen, P.E., 1999. Astronomically tuned geomagnetic polarity timescale for the late Triassic. Journal of Geophysical Research B 104, 12831–12841.

Kirschvink, J.L., 1980. The least-squares line and planes and the analysis of palaeomagnetic data. Geophysical Journal of the Royal Astronomical Society 62, 699–718.

Mange, M.A., Maurer, H.F.W., 1992. Heavy minerals in colour. Chapman and Hall, London, 147pp.

Mange-Rajetzky, M.A., 1995. Subdivision and correlation of monotonous sandstone sequences using high-resolution heavy mineral analysis, a case study: the Triassic of the Central Graben. In: Dunay, R.E., Hailwood, E.A. (Eds.), Non-Biostratigraphical Methods of Dating and Correlation. Geological Society of London, Special Publication, vol. 89, pp. 23–30.

Mange, M.A., Turner, P., Ince, D.M., Pugh, J.M., Wright, D.T., 1999. A new perspective on the zonation and correlation of barren strata: an integrated heavy mineral and palaeomagnetic study of the Sherwood Sandstone Group, East Irish Sea Basin and surrounding areas. Journal of Petroleum Geology 22, 325–348.

Meadows, N.S., Beach, A., 1993. Controls on reservoir quality in the Triassic Sherwood Sandstone of the Irish Sea. In: Parker, J.R. (Ed.), Petroleum Geology of Northwest Europe: Proceedings of the 4th Conference, London. Geological Society of London, pp. 823–833.

Morton, A.C., 1985. Heavy minerals in provenance studies. In: Zuffa, G.G. (Ed.), Provenance of Arenites. Reidel, Dordrecht, pp. 249–277.

Nawrocki, J., 1997. Permian to Early Triassic magnetostratigraphy from the central European basin in Poland: implications on regional and worldwide correlations. Earth and Planetary Science Letters 152, 37–58.

Scholger, R., Mauritsch, H.J., Brandner, R., 2000. Permian-Triassic boundary magnetostratigraphy from the southern Alps (Italy). Earth and Planetary Science Letters 176, 495–508.

Szurlies, M., Menning, M., Nowaczyk, N. R., Bachmann, G. H., 2000. Magnetostratigraphy and cyclic stratigraphy of the Lower Buntsandstein (Central Germany), from secular variation to paleomagnetism – a new view of the dynamic geomagnetic field. Workshop (Potsdam 2000), pp. 105–107.

Szurlies, M., Bachmann, G.H., Menning, M., Nowaczyk, N.R., Kading, K.-C., 2003. Magnetostratigraphy and high-resolution lithostratigraphy of the Permian-Triassic boundary interval in Central Germany. Earth and Planetary Science Letters 212, 263–278.

Thompson, D.B., 1970. Sedimentation of the Triassic (Scythian) red pebbly sandstones in the Cheshire Basin and its margins. Geological Journal 7, 183–216.

Thompson, J., Meadows, N.S., 1997. Clastic sabhkas and diachroneity at the top of the Sherwood Sandstone Group: East Irish Sea. In: Meadows, N.S., Trueblood, S.P., Hardman, M., Cowan, G. (Eds.), Petroleum Geology of the Irish Sea and Adjacent Areas. Geological Society of London, Special Publication, vol. 124, pp. 237–251.

Turner, P., Ixer, R.A., 1977. Diagenetic development of unstable and stable magnetization in the St Bees Sandstone (Triassic) of Northern England. Earth and Planetary Science Letters 34, 113–124.

Turner, P., Heywood, M.L., Bird, D.J., Chandler, P., 1996. Magnetostratigraphy and depositional sequence analysis of Triassic fluvial sediments: UK Central North Sea. Cuadernos de Geología Ibérica 21, 117–147.

Warrington, G., Audley-Charles, M.G., Elliott, R.E., Evans, W.B., Ivimey-Cook, H.C., Kent, P.E., Robinson, P.L., Shotton, F.W., Taylor, F.M., 1980. A correlation of Triassic rocks in the British Isles. Special Report of the Geological Society of London, vol. 13, 78 pp.

Wills, L.J., 1948. The Palaeogeography of the Midlands. University Press of Liverpool, Liverpool, 144pp.

Wills, L.J., 1956. Concealed Coalfields. Blackie, Glasgow, 208pp.

Wills, L.J., 1970. The Triassic succession in the central Midlands in its regional setting. Journal of the Geological Society London 126, 225–285.

This page intentionally left blank

Chapter 43

THE APPLICATION OF BULK ROCK GEOCHEMISTRY TO REVEAL HEAVY MINERAL SORTING AND FLOW UNITS IN THICK, MASSIVE GRAVITY FLOW DEPOSITS, SIRI CANYON PALAEOCENE SANDSTONES, DANISH NORTH SEA

METTE LISE K. POULSEN[a,1], HENRIK FRIIS[a], JOHAN B. SVENDSEN[b], CHRISTIAN B. JENSEN[a] AND RIKKE BRUHN[c]

[a]*Department of Earth Sciences, Aarhus University, DK-8000 Århus C, Denmark*
[b]*Altinex Oil Denmark A/S, Kongevejen 100C, DK-2840 Holte, Denmark*
[c]*Dong energy, Exploration and Production, Agern Allé 24-26, DK-2970 Hørsholm, Denmark*

ABSTRACT

The Palaeocene reservoirs in the Siri Canyon consist of laterally limited gravity flow deposits of glauconite-rich quartzose sand. The sands, which occasionally form up to 40 m thick massive units, are interbedded with deep marine muds, and although they are mainly in-situ deposits, post depositional remobilisation and/or injection have affected certain intervals.

This contribution presents a geochemical study of the Siri Canyon Palaeocene sandstones based mainly on whole rock X-ray fluorescence analysis, complemented by thin section petrography. Data presented here is from the Cecilie Field, generally focusing on the type well, Cecilie-1A. Massive sand units of the penetrated succession cannot be subdivided by means of macroscopic core description, overall grain size data, glauconite content or biostratigraphy. However, they can be subdivided into a series of flow units by interpreting the trends of Zr, Th and TiO_2 on the geochemical logs and heavy mineral grain size sorting. In the Cecilie-1A well, four distinct cycles have been recognised in a 41 m section of homogenous, massive sand on the basis of elemental trends, gamma ray and grain density logs, and in factor score depth plots, calculated by Principal Component Analysis (PCA). These trends are interpreted as reflecting systematic heavy mineral variations.

A strong correlation is observed between zircon percentages from thin section point counting data and the Zr log, calculated as percentages of whole rock volume. Within one cycle, the

[1]*Present address: Dong energy, Exploration and Production, Agern Allé 24-26, DK-2970 Hørsholm, Denmark*

Developments in Sedimentology, Vol. 58, 1099–1121

ISSN: 0070-4571/doi:10.1016/S0070-4571(07)58043-X

upwards decrease in zircon volume percentage within the unit reflects a decrease in zircon grain size and frequency and results from detrital zircon grain sorting through suspension fall-out; this conclusion is supported by PCA.

We argue, therefore, that each well-defined cycle represents a single surge within a larger flow event, and that the sediments were sorted by suspension fallout during deposition. Our study demonstrates that heavy mineral grain size sorting may be reliably inferred from petrophysical log patterns. Chemical and petrophysical cyclicity is observed in several wells in the Siri Canyon area, suggesting that suspension fallout sorting of heavy mineral grains may be a common feature in concentrated density flow deposits, allowing the recognition of individual flow units within thick massive sands.

Keywords: Gravity flows; heavy mineral sorting; remobilisation; Siri Canyon; Palaeocene; injected sand

1. INTRODUCTION

Interpretation of thick, massive sandstones, deposited by gravity flows that are barren in biostratigraphical components and often lacking primary sedimentary structures, presents a particular challenge. The lack of biological markers hampers stratigraphical correlation of, and between, massive sand bodies, while the absence of sedimentary structures makes reconstruction of sand transport processes, deposition and sand-body geometry difficult (e.g., Stow and Johansson, 2000).

A number of non-biostratigraphical tools have been developed for dating and correlating barren successions, including heavy mineral (HM) analysis (Basu and Molinaroli, 1989; Morton, 1991; Mange-Rajetzky, 1995; Morton and Hurst, 1995) and bulk rock geochemistry (Pearce and Jarvis, 1995; Svendsen et al., 2003). Further to conventional grain counting, HM analysis has often focused on provenance and provenance-related correlation, based on single grain chemical analysis of minerals such as Fe-Ti oxides (Basu and Molinaroli, 1989), garnet (Morton et al., 1993) and zircon (Owen, 1987), while the application of bulk geochemistry may also provide information on HM sorting within stratigraphic units (Svendsen and Hartley, 2002).

Facies analysis, hydraulic calculations and computational modelling, often as a multidisciplinary approach, are the main methods used for interpreting massive gravity flow deposits (Kneller and Branney, 1995; Coussot et al., 1998; Johansson et al., 1998; Mulder and Alexander, 2001; Van den Berg et al., 2002; Kneller and McAffrey, 2003; Baas, 2004). A number of different flow types have been proposed for the deposition of massive sands (for a review, see Mulder and Alexander, 2001). The pattern of grain or clast sorting in gravity flow deposits, in general, is a critical parameter in the interpretation of flow properties (e.g., Mulder and Alexander, 2001), yet studies of differential sorting between HM grains and framework components are rare (Sallenger, 1979). Different sorting mechanisms in depositional systems may result in highly variable HM distributions in sediment bodies both laterally and vertically because of HM density variations (for a review, see Morton and Hallsworth, 1999). In relation to sorting by suspension settling, a hydraulic equivalence exists between HMs and quartz grains, resulting in a comparable sorting pattern for HMs and quartz, but within a significantly finer grade for the HMs

(Rubey, 1933; Hand, 1967; Sallenger, 1979). In some cases, sorting patterns can be revealed by gamma ray (GR) logs due to the incorporation of radiogenic elements (U and Th) in some HMs, dominantly zircon and monazite (e.g., Svendsen and Hartley, 2002).

In this study, we apply whole rock geochemistry to a 40 m thick massive sand succession in the Cecilie Field, Danish North Sea, as a tool for recognition of, and differentiation between, individual submarine gravity flow units, and as a means for interpreting flow type and depositional properties. The recognition of flow units is based on the relative immobility of certain elements (e.g., REE, Ti, Th, Zr, Y: Preston et al., 1998) and the detrital geochemical signature imposed on the sand by the HM content. Observed variations in trace elements provide information on HM sorting patterns in the flow deposits.

The results presented here are part of the "Geochemistry of the Siri Canyon Sand" project, an ongoing study in which 21 wells from 4 oil-producing fields in the Danish North Sea have been investigated, primarily by bulk geochemistry of sandstones using X-ray fluorescence spectrometry (XRF). This contribution focuses on data from four cored exploration wells of the Cecilie Field, including comparisons between sedimentological, geochemical and petrophysical logs of the Cecilie-1A well. Analytical data were also obtained from thin section analysis, scanning electron microscopy (SEM) and principal component analysis (PCA) with the purpose of identifying and predicting grain size variations in the vertical distribution of HMs and obtaining new information on the depositional processes of these gravity flow deposits.

A geochemical approach to the problem of HM sorting has some important limitations. Except in HM placers, significant variations can only be expected in trace and minor elements, which are mainly carried by HMs. Therefore, many HM species will be camouflaged by minerals in the bulk sediment. The concentration of very mobile elements may also be unrelated to detrital mineralogy and only relate to a diagenetic overprint. In this study, we found a strong correlation between Zr, TiO_2, U, Th, Nb, La and Y. These elements are characteristic for a large number of HMs such as zircon, Fe-Ti oxides, rutile, anatase, sphene, monazite and xenotime. Because zircon is the main contributor of Zr and it is very stable during diagenesis, we expect that large variations in the content of Zr reflect a detrital signal, carried by identical variations in zircon content. Other elements may also be carried by zircon and therefore reflect a parallel variation to Zr, or they may be carried by other minerals with hydraulic behaviour similar to that of zircon. Some of these minerals are less stable and dissolve during diagenesis. Immobile elements from such minerals will be incorporated in in-situ diagenetic minerals and will still reflect the overall detrital signal, whereas other mobile elements may redistribute and obliterate the detrital signal. Although some TiO_2 minerals are very stable (rutile, anatase), others may easily dissolve during diagenesis (ilmenite, magnetite, hematite). But Ti is rather immobile and will generally reprecipitate "immediately" as leucoxene or anatase (Weibel and Friis, 2007). Therefore, the content of TiO_2 will still reflect the overall detrital signal, although the original detrital mineralogy may not be reliably estimated. The selection of elements that correlate with the content of detrital HMs may vary, caused by different solubility of HMs under different conditions, and because of different mobility of elements in different diagenetic environments. In this study,

we consider the variation of Zr and TiO_2 as a proxy for the variation of HMs with similar hydraulic behaviour as zircon and the heavy Ti-minerals. All elements may occur in other minerals, either as substitutions or as mineral inclusions. Here, they may contribute to the "base-level" content.

2. GEOLOGICAL SETTING

The Siri Canyon stretches over 150 km along and across the present day Danish-Norwegian North Sea border, terminating at the Coffee Soil Fault (Fig. 1) (Clausen and Huuse, 1999; Huuse, 1999; Hamberg et al., 2005). It forms part of a larger system of submarine canyons in the Palaeogene Norwegian-Danish Basin, running in an E–W to NE–SW direction towards the Central Graben. The Siri Canyon is 15–20 km wide. Canyon formation took place in Danian times and has been attributed to major submarine mass failure in the chalk succession, caused by uplift of the Scandinavian hinterlands (Hamberg et al., 2005). The narrow confinement of the canyon may be at least partially controlled by salt structure growth (Hamberg et al., 2005).

The canyon in-fill consists of Palaeocene to Early Eocene deep marine pelagic and hemi-pelagic marls and shales of the Rogaland Group embedding a series of sandstone intervals (Fig. 2). The sands were shed from glauconite-producing shelf areas of the Stavanger Platform and transported as gravity flows through the submarine canyon to their present day location 20–75 km up, dip from the Central Graben (Danielsen et al., 1995; Hamberg et al., 2005). They comprise glauconite-rich (18–35%), well-sorted, fine- to medium-grained quartzose sand and can be recognised by their high background value on GR logs (Danielsen et al., 1995). The deposits vary from thin (5–20 cm) upwards fining turbidite units to thick (0.5–13 m) structureless massive sand units, constituting up to 40 m thick successions, often lacking sedimentary structures. The massive sand deposits of the Siri Canyon have been interpreted by Cecchi et al. (2001) as debris-flows, deposited by en-masse freezing, and as high-density turbidites in which primary sedimentary structures have been obliterated through post depositional fluidisation (Hamberg et al., 2005). Apart from glauconitic pellets, the sandstones are remarkably clean, with minor detrital clay (<0.1%, Hamberg et al., 2005) and up to 30% porosity; however, in places extensive authigenic chlorite and calcite may influence the porosity and permeability.

3. SAMPLES AND METHODS

Geochemical data presented here are from the Cecilie-1, Cecilie-1A, Cecilie-1B and Cecilie-2 exploration wells, drilled by DONG E&P and its partners in license 16/98, Danish North Sea sector. All Palaeocene sand units from the four Cecilie Field cores have been sampled with an approximate sampling distance of 1 m; thin units (0.02–1 m) are represented by at least one sample. The core in focus of this contribution, the Cecilie-1A core, comprises 120 m of Palaeocene sediments, primarily consisting of sand with only minor shale and marl intervals (Fig. 3). The upper part of the core includes a 70 m thick sand succession, with very few and thin shale

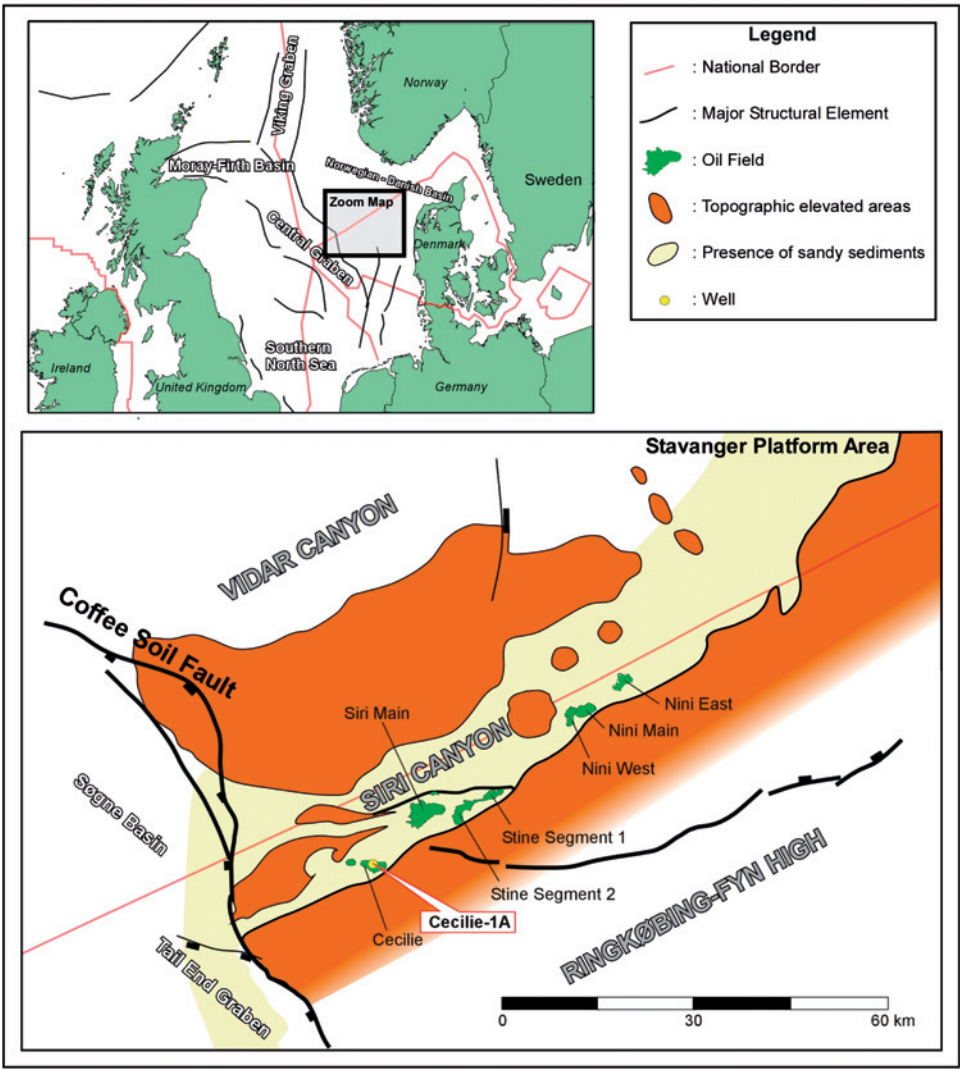

Fig. 1. Location map of the Siri Canyon. Modified from Hamberg et al. (2005).

intervals, of which the lower 40 m are massive, while the upper 30 m displays remobilisation features such as soft sediment folding and water escape pipes. A 15 m section in the lower part of the Cecilie-1A core (2319–2334 m) has been subject to detailed sampling, with a sample density of five samples per metre.

A total of 415 samples, covering 454 core metres and three stratigraphical members (Bor, Gerd and Rind Members) (Fig. 2), have been subject to XRF analysis, determining 10 major elements measured in oxides (SiO_2, TiO_2, Al_2O_3, Fe_2O_3, Mn_3O_4, MgO, CaO, Na_2O, K_2O and P_2O_5) and 16 trace elements (Ni, Cu, Zn, Rb, Sr, Y, Zr, Nb, Pb, Th, U, Ba, La, Ce, V and Cr). In addition, a calculation of the volatile content was made. Geochemical data are too extensive to be included here;

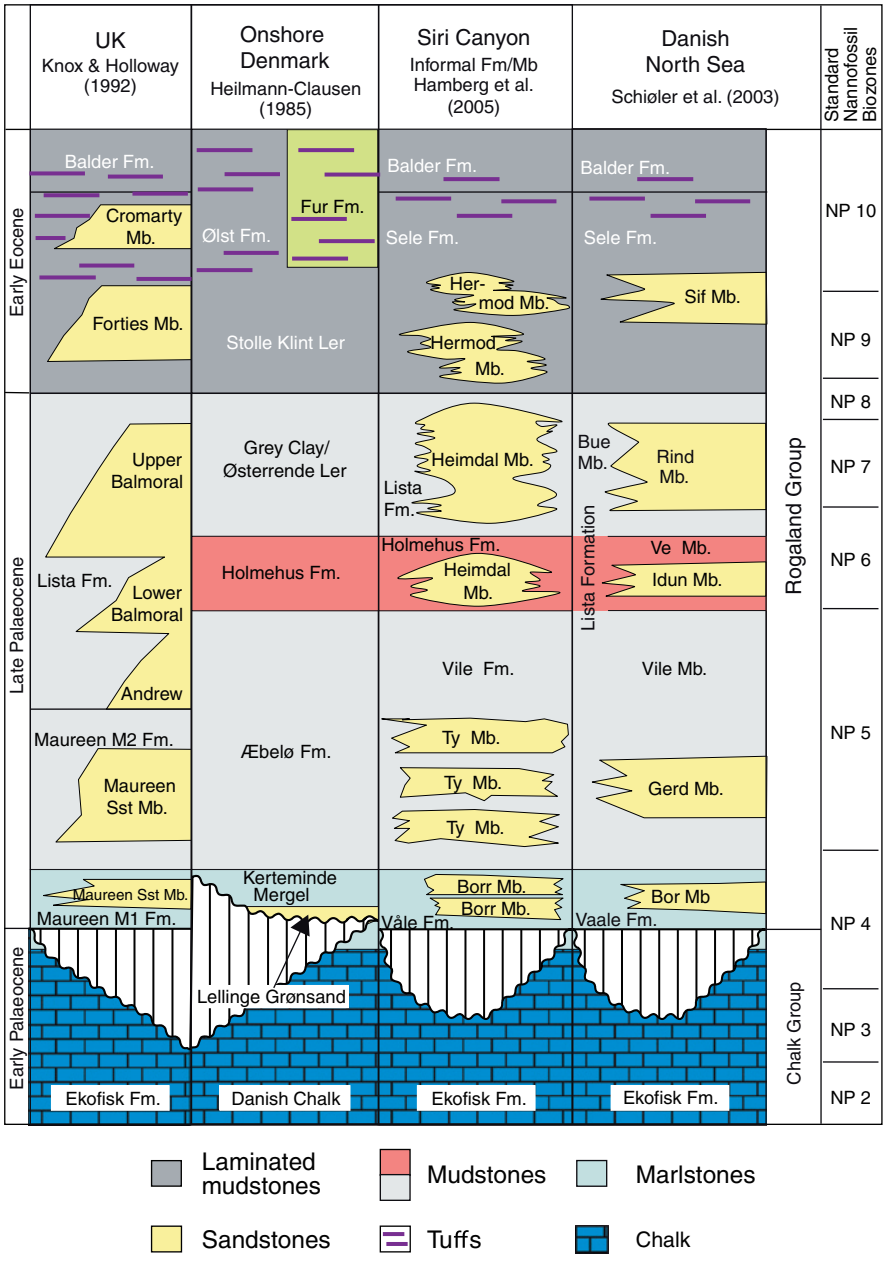

Fig. 2. Late Palaeocene to Early Eocene stratigraphy of the Danish North Sea and Siri Canyon. Modified from Heilmann-Clausen (1985); Knox and Holloway (1992); Schiøler et al. (2003) and Hamberg et al. (2005).

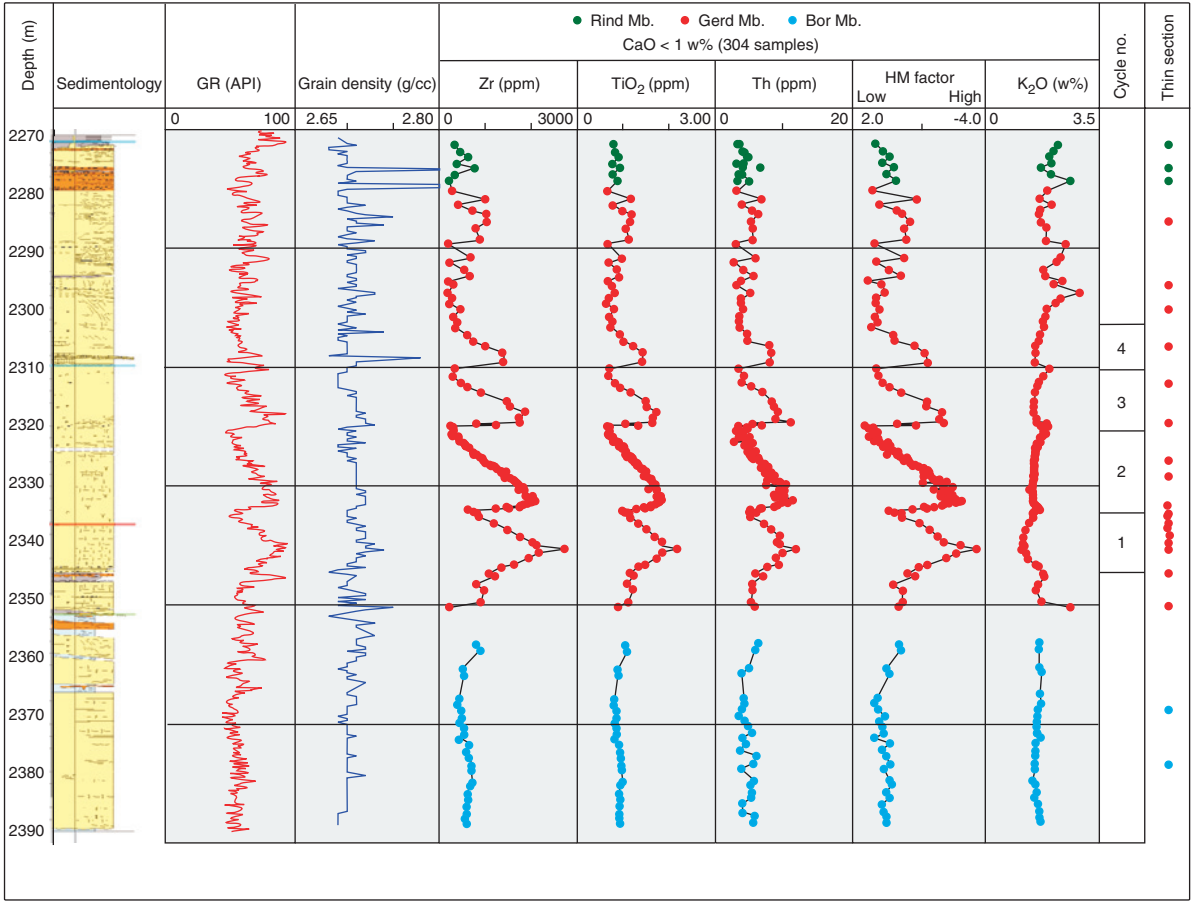

Fig. 3. Log panel of the Cecilie-1A well, including sedimentological, integrated GR log, grain density log, Zr, TiO_2, Th and K_2O logs (XRF) and HM factor log (PCA). Four cyclic units (2303–2344 m) are displayed in all geochemical and petrophysical logs.

they are available from Elsevier's data depository upon request. Fifty-four thin sections have been examined by the petrological microscope and SEM using backscattered electron (BSE) images. Differentiation of detrital and authigenic minerals is of crucial importance to obtain meaningful information from a sedimentary geochemical data set because diagenetic alterations may significantly blur or overprint the original, detrital geochemical signal of a sample, thus severely limiting interpretations of depositional processes.

Diagenetic overprint can be eliminated either by data screening (removal of overprinted data points from the data set) or by subtracting diagenetic components from the data points. The Palaeocene sands of the Siri Canyon are, in certain intervals, heavily cemented by calcite, leading to dilution of the detrital components. Large variations in calcite compositions due to Fe, Mg and Mn substitution (common elements in many of the minerals contained in the Siri sands, e.g., glauconite, chlorite, Fe-Ti oxides) make simple subtraction of the diagenetic components impossible. The data set presented here has therefore been CaO-screened to exclude all calcite-cemented samples (where $CaO > 1$ wt.%).

The NCSS® (Number Cruncher Statistical System) software was used for PCA. PCA is a mathematical procedure, reducing the dimensionality (number of variables) of a large number of possibly correlated variables into a smaller number of uncorrelated variables, termed *factors* or *principal components*, while retaining as much information as possible. Thus, each principal component (PC), calculated from a geochemical data set, contains a number of associated (correlating) elements, which call for mineralogical explanations (Pearce and Jarvis, 1995; Swan and Sandilands, 1995; Hartley, 2000). Hence, individual minerals or mineral groups can be recognised directly through PCA results. When supported by thin section analysis, PCA offers a powerful tool in the interpretation of a geochemical data set. PCA also includes a calculation of factor scores in which each data point is given an arbitrary number, describing how much that particular data point is influenced by the minerals indicated by the PCs. By plotting the factor scores against depth, a log describing the relative mineralogical variations will appear. PCA was conducted on the CaO-screened data set to enhance information on detrital mineralogy from the analytical data.

Variations in Zr content are believed to be primarily (if not exclusively) a result of variations in zircon proportions. To support geochemical Zr variations identified by XRF, zircon abundance and size (length of long axis) 28 samples from Cecilie-1A in a selected 2340.60–2319.20 m depth interval were determined from backscattered electron (BSE) images (25 mm^2 per sample) retrieved from SEM, and analysed in MapInfo®. Subsequently, correlations between point counted and whole rock geochemical data were made. Because ~60% of the sand samples consist of quartz, point counting was also carried out on quartz grains in order to compare the grain size distribution of the bulk sediment with the zircon size distribution. Interpretation of integrated GR logs generally depends on the differentiation between sand and shale intervals and the sand/shale ratio of the sediment (Rider, 2002), but the GR log may also pinpoint fluctuations in HM content (Svendsen and Hartley, 2001). The studied sands are practically free of detrital clay and no K-bearing diagenetic clay has been documented; the GR borehole log of Cecilie-1A is therefore suitable for comparison with the grain density log and the vertical geochemical plots (Fig. 3).

4. DATA AND RESULTS

4.1. Principal Component Analysis

Table 1 presents the PCA loading scores of the CaO-screened data set. Scores of +1 or −1 indicate perfect positive and inverse correlation, respectively, whereas a score of 0 is an indication of non-correlation. A level of ±0.4, which is well within the 99% confidence interval (Sachs, 1984), is arbitrarily chosen to show very significant relationships.

Table 1. PCA loading scores of CaO-screened Cecilie Field data (304 data points)

Variables	Factor 1	Factor 2	Factor 3
Ni	*−0.89*	0.08	−0.02
Cu	*−0.77*	−0.14	0.06
Zn	*−0.66*	−0.08	0.00
Rb	*−0.71*	**0.43**	0.07
Sr	*−0.40*	−0.05	−0.23
Y	−0.14	*−0.93*	0.00
Zr	0.28	*−0.92*	−0.03
Nb	0.13	*−0.96*	−0.07
Pb	−0.39	−0.19	0.02
Th	−0.09	*−0.93*	0.00
U	0.13	*−0.66*	0.01
Ba	0.21	−0.10	*−0.91*
La	−0.07	*−0.55*	−0.01
Ce	0.05	−0.25	−0.31
V	*−0.85*	0.00	0.06
Cr	0.07	−0.30	0.06
SiO_2	**0.89**	−0.10	−0.05
TiO_2	0.18	*−0.96*	−0.06
Al_2O_3	*−0.87*	0.13	0.09
Mn_3O_4	−0.38	−0.12	0.06
MgO	*−0.91*	0.26	0.11
CaO	−0.35	0.08	0.09
Na_2O	*−0.45*	0.09	0.06
K_2O	*−0.61*	**0.51**	0.06
P_2O_5	*−0.56*	−0.24	−0.02
Norm__Fe	*−0.88*	0.02	0.07
Norm__Vol_	−0.31	0.26	0.01
Percent	29.55	22.53	3.86
Cumulative	29.55	52.08	55.94
Interpretation	Glauconite (quartz and apatite)	Heavy minerals (glauconite/feldspar)	Barite

Note: Table for CD-ROM and/or data depository. Geochemical data of the Cecilie Field (304 samples). Factor 1 represents essential, substitutional and adsorbed elements in clay minerals, primarily glauconite (see text), P_2O_5 probably representing apatite and inversely correlating SiO_2 corresponding to quartz. Factor 2 is a heavy mineral factor also including inversely correlating K_2O and Rb, mainly corresponding to glauconite. Factor 3 includes Ba (barite).Level of significance: >0.40 (bold); $[-0.39; 0.39]$; <-0.40 (italic).

PC1 accounts for 29.55% of the variance within the data set. It primarily represents clay mineral components, including essential (Al, Mg, Fe, K) and substitutional and adsorbed elements (Rb, Ni, Cu, Zn, V, Sr). Since the Siri Canyon sands contain abundant glauconite, but are otherwise practically free of detrital clay, PC1 is interpreted to primarily describe the glauconite components with minor contributions from authigenic chlorite. Si, representing quartz, is seen to correlate inversely with all other elements of PC1. This inverse relationship is a consequence of "dilution"; the more glauconite is present in the sediment, the lower the quartz percentage and vice versa. Also, a small input to PC1 may be added by feldspar and phosphate minerals, such as apatite and monazite.

PC2 is responsible for 22.53% of the variation of the data set and includes Zr, TiO_2, Th, Nb and Y, all showing very high negative loadings (<-0.8), as well as U and La with loadings between -0.4 and -0.8. These elements are typical for HMs. Zircon is the most important source for Zr and may also contain some U, Th, Nb and Y. PC2-elements other than Zr are carried by a large number of different HMs, such as Fe-Ti oxides, rutile, anatase, sphene, monazite and xenotime. The HMs may occur as single-mineral detrital grains, but they may also be present as mineral inclusions in light minerals and in other HMs. Anatase, apatite and monazite are also formed diagenetically in the sands. Due to the large degree of immobility of elements such as Zr, Ti, Nb and Th (Preston et al., 1998), the trace elements included in PC2 are considered to reflect a depositional geochemical signature and the strong correlation between the individual PC2 elements thus indicates that HM sorting is responsible for their variation. As the PC2 elements are characteristic for some of the more dense HMs, such as zircon and Fe-Ti oxides, with comparable hydraulic properties they can be expected to have similar sorting patterns. The obvious correlation in the simple Zr vs. TiO_2 raw data plot of all Cecilie Field data points (Fig. 4) exemplifies the common source of Zr and TiO_2, that reside in zircon and titanium minerals. Monazite also has high density (4.7 g/cm^3), and it might be expected that both Ce and La would have the same depositional distribution as Zr. However, monazite appears as both detrital grains and as authigenic phases in microporosity in glauconite and also in open pore space. Within the Siri sands, Ce (and partly also La) may have significant detrital sources other than HMs and the expected correlation with Zr may have been camouflaged by variation within these sources. Diagenetic remobilisation may have blurred the correlation further.

A large group of common HMs such as tourmaline, garnet, epidote, amphibole and apatite are not detected in PC2. Such minerals are largely composed of the major elements, which are common constituents in the bulk sediment as detrital and/or diagenetic minerals. They may have carried PC2-trace elements and therefore partly contribute to correlation between these elements, but this would depend on efficiency of density sorting.

K is inversely correlated with a loading of $+0.51$. The variation of K is mainly described by its correlation with clay mineral elements (glauconite) in PC1 and its representation in PC2 is caused by a strong negative correlation with the HM elements in the interval 2303–2344 m in the Cecilie-1A well (Fig. 3). Point count data indicate the variation in K-content to be caused by variations in the amount of glauconite.

PC3 describes 3.86% of the variance, and contains only one significant component, Ba, representing barite. Barite cement is a common feature in the Siri Canyon

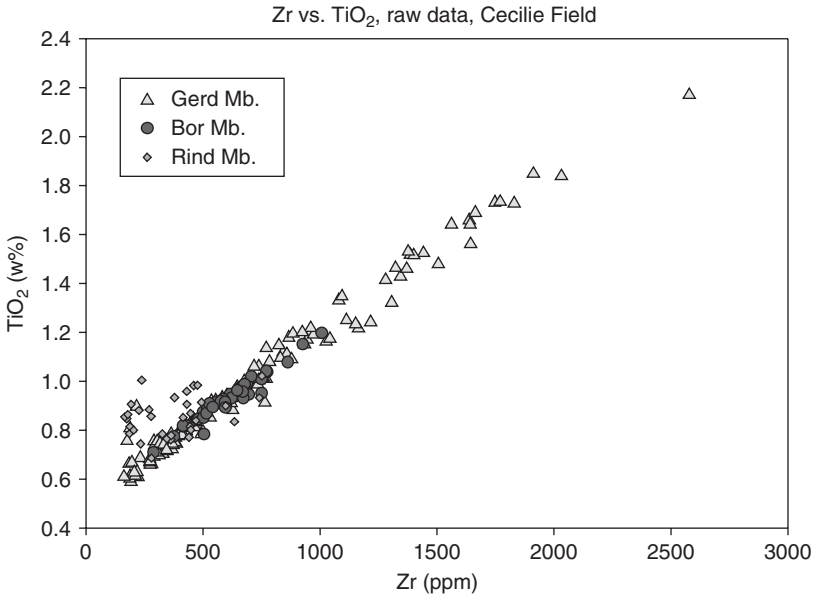

Fig. 4. Zr vs. TiO_2 raw data plot. Obvious correlation illustrates common detrital source of zircon and Fe-Ti oxides.

sands. Dissolution of feldspar may have been responsible for releasing the Ba ions needed for barite precipitation.

4.2. Geochemical and Petrophysical Logs of Cecilie-1A

A log panel of Cecilie-1A, including the sedimentological log, petrophysical GR and grain density logs and the geochemical Zr, TiO_2, Th and K logs, is depicted in Fig. 3, along with the PC2 factor (HM Factor) score plot, expected to represent variations in HM content. Since all HM components of PC2 have negative factor loadings (Table 1), a large negative factor score number will reflect large HM contents.

A distinct cyclicity in the 2303–2344 m depth interval is displayed. The cycles (numbered 1–4) are recognised by four relatively abrupt increases in the log traces, each followed by a gradual upwards decrease. These trends appear with a large degree of regularity throughout the units. The decreasing trends within the individual cycles are accompanied by an overall upward fall in log values through the cycles. A general upwards decrease in cycle maximum (peak) and minimum levels is also evident. Above 2303 m, the log traces become more irregular and assume a jagged appearance. (However, despite the jaggedness, a general overall tendency of upwards increase in log values is detectable in the upper 20 m of the Gerd Member (2303–2280 m)).

Cycle thickness varies from 7 to 13 m. The Zr log displays decreases from >2500 to $\sim$700 ppm in cycle 1 and from 1300 to 300 ppm in cycle 4, resulting in a Zr fall of 75–87% within each cycle interval and of $\sim$50% in maximum and minimum values from cycles 1 to 4. The Zr and TiO_2 logs, believed to represent zircon and Fe-Ti

oxides, exhibit practically perfect correlation between Zr and TiO_2. This is also shown in the Zr vs. TiO_2 plot in Fig. 4 and the PCA results in Table 1.

A positive correlation between the petrophysical and the geochemical logs is obvious throughout the Cecilie-1A core, except in 2308–2310 m (in cycle 4) where the GR and the grain density logs display a distinct low and high, respectively. On the sedimentological log, it is seen that this 2 m interval of non-correlation coincides with a zone of heavy calcite cementation (CaO > 20 wt.%) causing a general density increase and a relative fall in radioactivity (low GR). The corresponding unscreened geochemical dataset exhibits a similar, sudden low caused by the dilution effect, but as a result of CaO-screening these data points are removed from the geochemical logs of Fig. 3. The distinct cyclicity is also seen in the K-log, although increasing–decreasing trends do not mirror the trends in HM elements precisely.

Cycle 2 (2319–2334 m) has been subjected to a detailed XRF study. Five samples per metre were selected, resulting in a resolution of geochemical data close to that of the GR log. The results are shown in Fig. 5 where the Zr log is compared with the integrated GR and the Th and U logs from the spectral GR log. The logs display a relatively abrupt, yet sequential, increase to maximum values in the lower 1.7 m (~600–2100 ppm Zr) after which they fall gradually to a minimum (corresponding to 250 ppm Zr) over the next 12.5 m. Thus, the bottom of a cycle does not coincide with the maximum log values, but to the depth at which the increasing trend starts. A close inspection of the Zr log may indicate a higher order of cyclicity, since approximately every fourth sample exhibits a small increase in Zr level compared to the underlying sample. A possible sub-cyclicity is also illustrated in Fig. 5 by the tentatively exaggerated schematic HM log. However, demonstration of a higher order of cyclicity would require an even closer sampling interval than presented here that is beyond the scope of this study.

4.3. Microscopic Study of the 2340–2319 m Depth Interval

Fifteen samples from cycle 1 and twelve samples from cycle 2 have been studied in closer detail by point counting of thin sections or polished samples to compare zircon abundance and size distribution with the geochemical logs as well as with the quartz distribution. As seen in Figs. 6 and 7, there is a clear fall in zircon abundance and size from 2340.60 to 2332.60 m (upper part of cycle 1). Fig. 7 also demonstrates a very uniform distribution of quartz mean grain size throughout each cycle. This suggests a sorting of the HMs, but limited or no sorting of the quartz component. The total number of counted zircon grains is low; thus, the statistical significance may not be too strong; however, the data show a remarkably stable trend with depth and coincide well with the Zr content of the XRF dataset, which lends confidence to our interpretation. An estimation of the total zircon volume has been calculated from the point counted zircon data (% of total rock volume; Fig. 7) and it is seen how the point counted data reveal a gradual fall in total zircon content within cycle 1 from a maximum of 0.2 to 0.05% in the uppermost cycle 1 data point. This corresponds closely to an estimated zircon volume based on XRF data (1000 ppm Zr equals 0.13 vol.% zircon), although a direct recalculation cannot be made due to the unknown grain density of the particular glauconite.

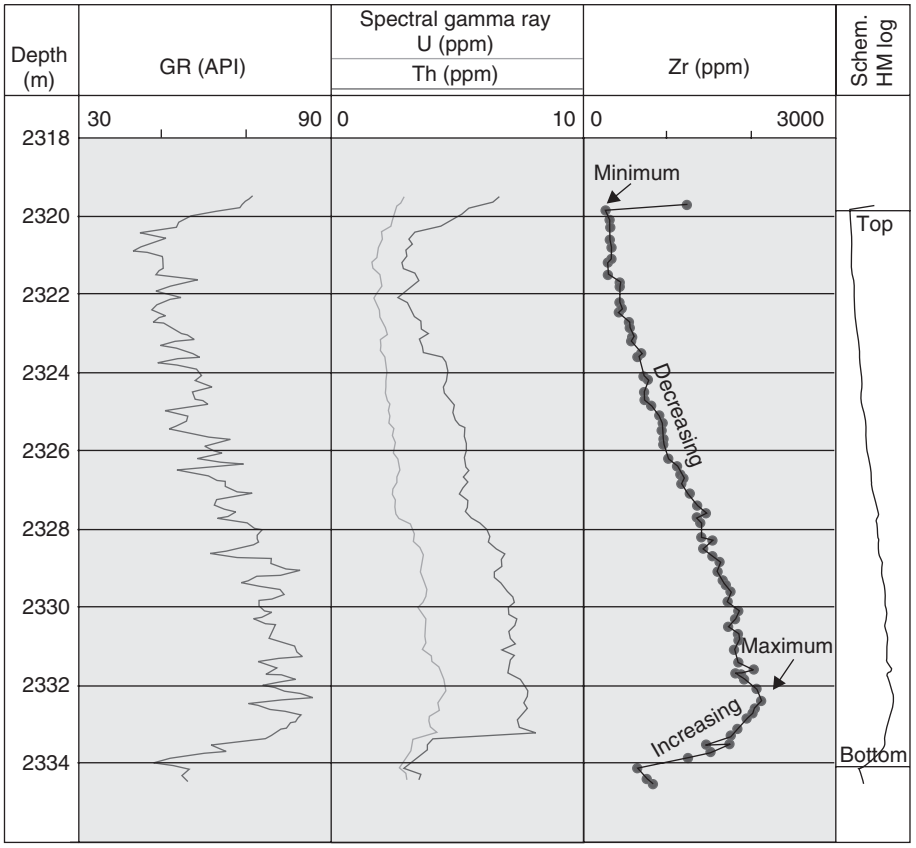

Fig. 5. Log panel of cycle 2, including integrated GR log, U and Th logs (spectral GR), Zr log (XRF) and schematic HM log based on the detailed Zr log. Increasing log-trend marks the initiation of cycle 2, while minimum log values mark the top of this cycle. Correlation between the XRF Zr log and the spectral GR, U and Th logs illustrates that U and Th are mainly carried by heavy minerals.

The amount of HMs in the sediments influences its bulk density. Small variations in the amount of higher density HMs such as zircon, rutile and Fe-Ti oxides have large influence on the bulk density compared to similar variations in the lighter HMs such as epidote and tourmaline. The grain density variation within a cycle is $\sim$0.03 g/cm^3 (Fig. 3). If only the very heavy minerals are considered, and the average density is taken to be 4.7 g/cm^3, a grain density variation of 0.03 g/cm^3 would correspond to a HM variation of 1.5 wt.%. The decrease in point counted zircon content is 0.15 vol.% from the bottom to the top of cycle 1 (Fig. 7). With a presumed porosity of 30%, the zircon content alone accounts for a density fall of approximately 0.20 wt.%. Adding an average TiO_2 fall of $\sim$1 wt.% (Fig. 3) and an unknown contribution from minerals such as xenotime and monazite, the variations in grain density within the cycles can easily be explained as the result of variation in the proportions of the heavier HM components in the sands although the lighter HMs are also expected to contribute to the variation.

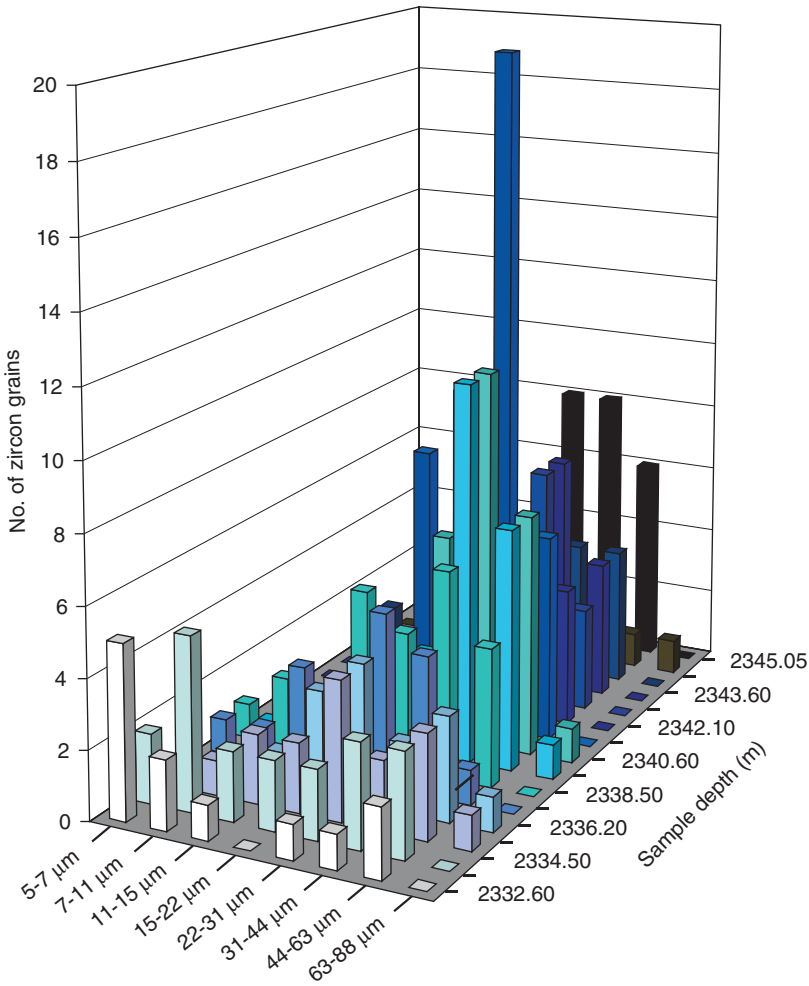

Fig. 6. Zircon grain size distribution (frequency) in cycle 1, from point counting data. The upward decrease in amount and size of detrital zircon grains is interpreted as a result of differential settling of heavy minerals through the flow.

5. DISCUSSION

The systematic cyclicity and regularity exhibited by the geochemical and petrophysical logs of the Cecilie-1A well (Fig. 3) lead to the interpretation that the massive sand in this interval (2303–2344 m) is in-situ, reflecting a primary, detrital signature of the HM components, and has not been subject to remobilisation by fluidisation. The HM distribution in remobilised sand is, instead, likely to be homogenous, resulting in a more uniform geochemical log pattern with unpredicted distribution, giving the logs a "jagged" look, as displayed in the 2280–2303 m interval. Considering the depositional environment and the gravity flow origin of the sediments in the Siri Canyon (Cecchi et al., 2001; Hamberg et al., 2005), the geochemical cyclicity is

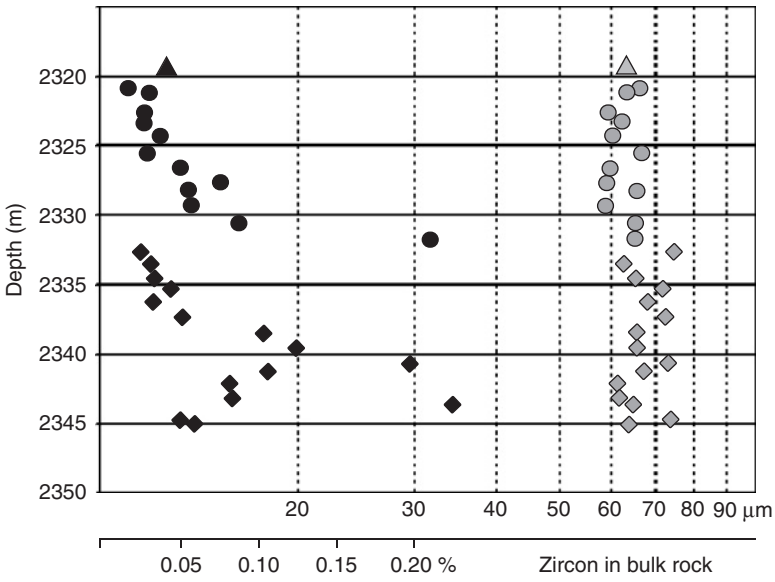

Fig. 7. Zircon volume of bulk rock (vol.%) calculated from point count data (black symbols) plotted with mean grain size of quartz (measured from thin sections: grey symbols). Diamonds are cycle 1; circles are cycle 2; triangle is cycle 3. Zircon volume reflects the cyclic pattern, whereas quartz mean grain size appears constant within each cycle. A subtle shift in quartz mean grain size is seen from cycles 2 to 3.

interpreted to mirror HM sorting within four distinct stacked flow units, and thus reflects an upwards diminishing capacity to transport HM grains within the flows.

Sedimentological evidence suggests that specific hydraulic conditions of the flows depositing the cyclic sands of Cecilie-1A resulted in a selective downwards sorting of the heavier grains such as zircon and Fe-Ti oxides (Fig. 6) and an upwards sorting of glauconite (Fig. 3). Due to a high intragranular microporosity in glauconite, its density may have been considerably lower than that of quartz at the time of deposition. Considering the thickness and the massive nature of the flow units, this would require a flow type transitional between a hyperconcentrated and a concentrated density flow, according to the classification of flow types presented by Mulder and Alexander (2001). Grain-to-grain collisions dominate in such a flow, allowing only the sorting of heavy and/or large grains during transportation. The density contrast between the main constituents in the flow and the 'heavier' HMs was sufficient to allow sorting by suspension settling, whereas quartz was kept in suspension. No upwards trend in sorting is seen within individual cycles, but a slight decrease from cycle to cycle is indicated (Fig. 7). Sorting processes may therefore be predominantly related to transportation within a flow rather than to deposition. The depositional process is mainly frictional freezing of the bottom layer, resulting in the accretion of successive small-scale flow surges (Kneller and Branney, 1995; Mulder and Alexander, 2001). Therefore, the thickness of the flow units does not reflect the thickness of the flow as it moves through the canyon. A higher order of possible cyclicity can be observed in the densely sampled cycle 2 (Fig. 5), and each

0.5–1 m sub-cycle may then reflect the aggradational deposition of individual bottom layers, but the chemical data to support the sub-cyclicity are insufficient.

The detailed geochemical study of cycle 2 (Fig. 5) reveals a gradual, but rather rapid, rise in Zr level within the lower 1.7 m of the unit; a feature which is repeated in cycles 1, 3 and 4 (Fig. 3). The upward increase in values is followed by a slower gradual upward decrease.

Fluidisation is a common phenomenon in the Siri Canyon sands (Hamberg et al., 2005) and it has been suggested that dewatering could result in the settling of HMs (Lowe, 1975). The examples by Lowe (1975) indicate that settling took place over a very short distance. In the Cecilie-1A cycles, settling distances of several metres for HMs should occur within the short period of fluidisation and, further, successive cycles should represent separate events. This is considered to be highly unlikely.

We advocate a scenario in which the HM profile represents time-related differential sorting from a concentrated (to hyperconcentrated?) density flow. The first sand deposit reflects the initial HM distribution of the sand. As the flow evolves, large HM grains fall out of suspension and sink down through the sediment/water column so that there is an increase of HM (size and abundance) in the lower part of the cycle, reflected by the successive deposition of sand enriched in (large) HM grains. Alternatively, the basal increase may be a reverse grading in zircon caused by the laminar flow regime of a hyperconcentrated flow (Lowe, 1982; Ballance, 1984; Smith, 1986; Mulder and Alexander, 2001).

Although deposition took place from a highly concentrated laminar flow in the lower part, a less concentrated turbulent flow in the upper part may have facilitated settling of HMs. When the sorting profile within the flow was well developed, a maximum level of HM content was reached at the flow base and deposited as the depositional front moved upwards. Subsequently, HM-depleted sediments were deposited in the upper interval.

Based on the zircon sorting in cycle 1 and 2 deduced from thin section analysis (Fig. 6), it is concluded that the variation in Zr within cycles 1–4 is related not only to the amount of zircon, but also to size and that the overall zircon grain size and frequency decreases from cycle 1 up-section to cycle 4. This sorting within and between the decreasing units is believed to create the cyclic log patterns as well as the falling maximum and minimum values of the individual cycles as depicted in Fig. 8. The gradients of the total HM content have been schematically illustrated. They depend on flow properties such as velocity, concentration and initial HM content, and include HM species not detected by this geochemical study.

The progressive decrease of maximum and minimum values from cycles 1 to 4 (Fig. 3) suggests that the flows evolved from the same initial sediment (single source) with a systematic evolution in HM sorting. Major (1997) described a series of debris flow experiments in which saturated sediment was abruptly released from a single source down a ramp with a slope of 31°. Invariably, the flows developed waves that surged down the ramp as a result of mechanical instability within the flows. During deposition, each surge would override the previous one and the resulting deposit accumulated as a series of stacked surge units. Although the slope, the flow regime and hydraulic properties of the flows produced by Major (1997) are different from those of the gravity flows in the Siri Canyon, the idea of a flow developing into a series of surges may be a viable analogue to the creation of the stacked flow units

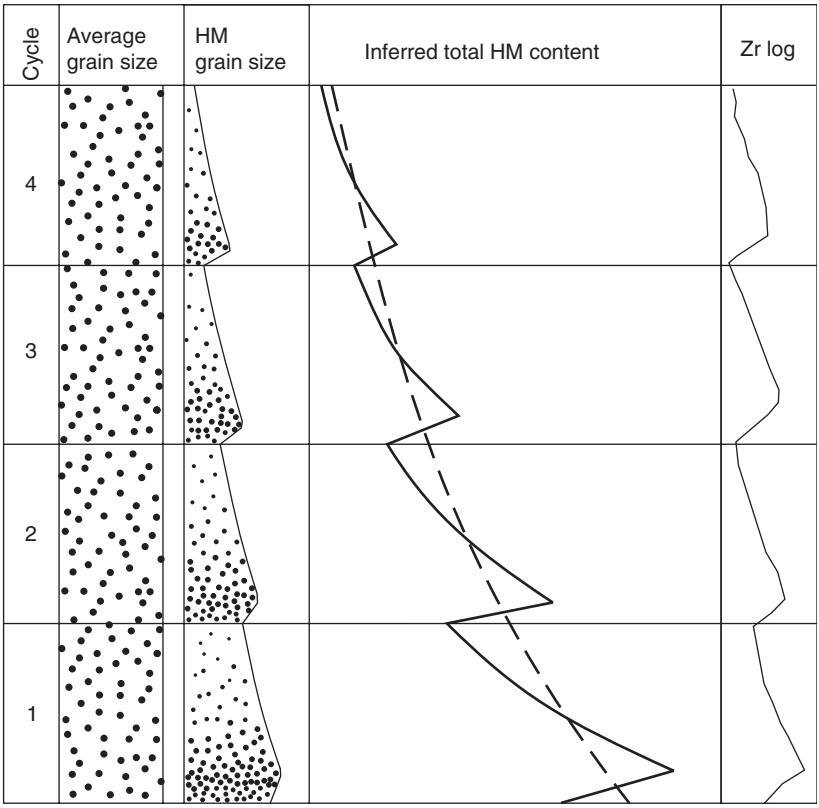

Fig. 8. Schematic model of differential sorting of HM throughout four flow surge units. Full line: inferred total HM-content. Dotted line: inferred total HM-content within initial flow before establishment of surges. Thin line: smoothed Zr log (XRF).

observed in the Cecilie-1A succession (Fig. 9). If a flow, in which a certain initial HM sorting profile is developed during the early transport (dotted line, Fig. 8), evolves into a series of surges or pulses, each surge would have a systematic and specific initial HM distribution. During continued transport, new sorting profiles would be established within each surge, creating a number of sorted units, corresponding to the number of surges (thick black line, Fig. 8).

The possibility that the flow units were derived from four different slumping events on the shelf also exists. Due to the decreasing trend in log values in cycles 1–4, slumping events could not be randomly distributed over the shelf area but must be rather confined so that a primary lateral or vertical systematic HM sorting can be imposed. Retrogradational slumping would in that case involve a landwards decrease in HM grain size (systematic lateral variation). In most geological settings, the opposite is what is expected from the grain size distribution when moving from a more distal to a proximal location. If the slumps cut successively downwards into the shelf the HM grain size distribution would be an upwards-increasing succession (systematic vertical variation). Both models, invoking slumping, would imply a very regular organisation of the HM distribution on the shelf as well as very regular and orientated slumps.

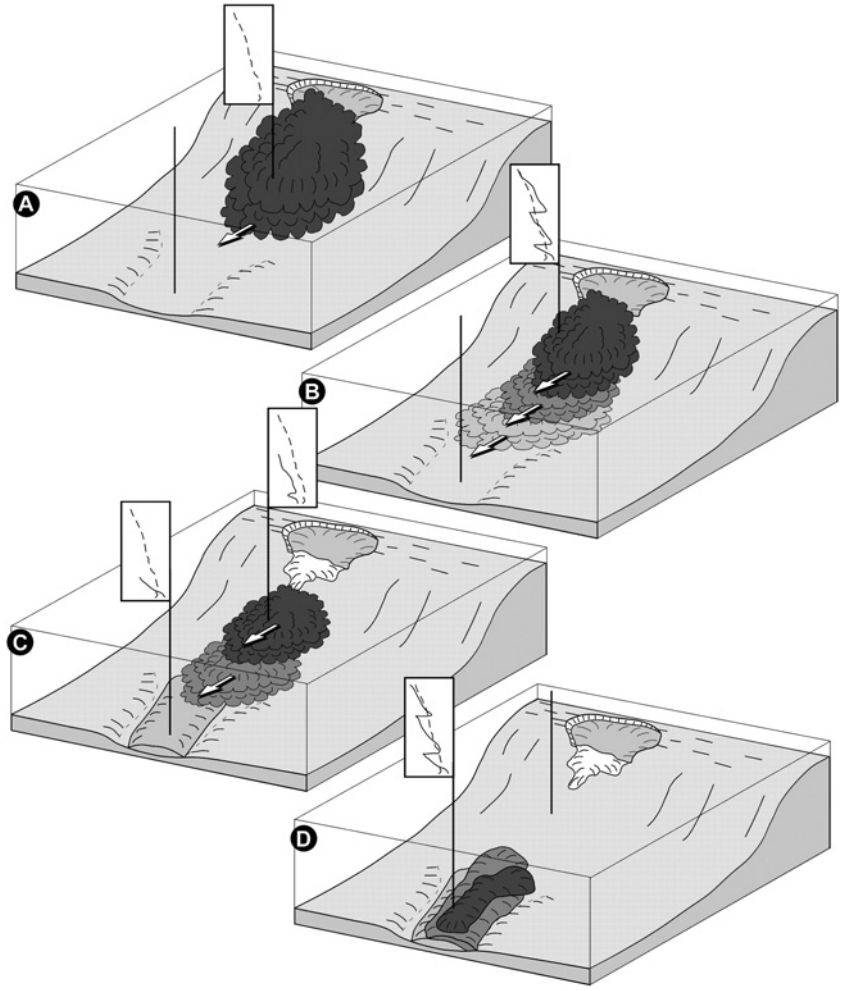

Fig. 9. Proposed sedimentological model invoking mechanical instability of original flow and generation of sub-surges. Parts A–D show the evolution from an original flow over generation of sub-surges to final deposition. Original HM profile (dashed line) and resulting HM profile (full line) is shown in two locations.

Correlation within the Cecilie Field (Fig. 10) shows that flow units thin away from 1A well. A cyclic pattern in Zr-content can be observed also in neighbouring wells, but the cycles are less distinct because they are found in thinner intervals, represented by fewer samples, and the obtained maximum values are considerably lower. Correlation between wells indicates that flow was rather confined with its flow axis close to Cecilie-1A.

A series of cyclic log patterns within thick massive sand units, similar to that seen in Cecilie-1A, have been observed in other wells in analyses from the ''Geochemistry of the Siri Canyon Sand'' project. In one case, an almost identical scenario of cyclic units with an upward decrease in maximum and minimum values was observed.

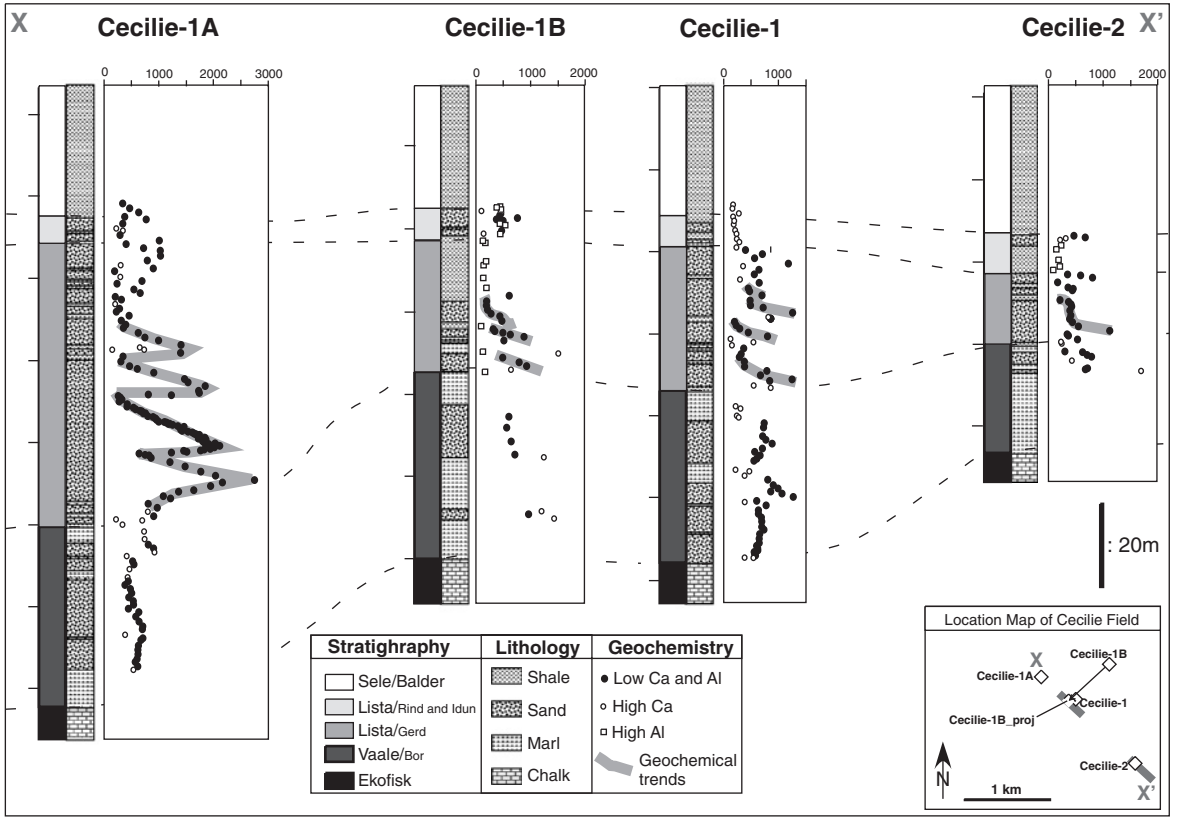

Fig. 10. Correlation between wells in the Cecilie Field. Well-developed stacked cycles are only seen in the thick Gerd Member sandstones in Cecilie-1A, but they may partly correlate to much thinner and less distinct cycles in neighbouring wells.

Units of 3–10 m, with relatively abrupt increases in values and then gradual upward decreases in values, can be seen in most of the geochemical logs from the areas covered by the project.

This regularity indicates that geochemical differentiation may be applied more widely to the identification and characterisation of individual flow units within massive sands. Although geochemical log patterns of in-situ massive sands may not always reveal cyclicity, the recognition of cycles is believed to be a unique proof of the in-situ nature of massive sand units. Remobilisation caused by fluidisation is a pervasive phenomenon in the Siri Canyon sands (Hamberg et al., 2005). Although the remobilisation may have caused loss of primary sedimentary structures, we believe that the movement of sand was strongly limited (few centimetres at maximum) in cases where well-preserved HM sorting can be detected.

6. CONCLUSIONS

In Cecilie-1A well, a remarkable correlation between the GR log and the geochemical HM logs is observed (Figs. 3 and 5). This correlation is promoted by the ability of some HMs (e.g., zircon) to incorporate the radioactive elements Th and U. PC2 (Table 1) illustrates this association between essential and substitutional elements of HMs since Zr, TiO_2, U, Th, Nb, La and Y all display negative correlation. Although the glauconitic sands of the Siri Canyon have high GR reading because of a high K-content, the large fluctuations are alone caused by HM sorting, and the sorting and subdivision in flow units might be concluded directly on the basis of the GR-log.

Whole rock geochemical analysis of a 40 m thick massive sand succession of the Cecilie-1A well has permitted the identification of four sequential cyclic flow units. The units are recognised in the Zr, TiO_2 and Th logs, showing a relatively abrupt increase in values, followed by a gradual decrease. Such patterns are interpreted as the result of differential sorting mechanisms within the flows depositing the sand. The geochemical logs correlate perfectly with the integrated GR log and the U and Th spectral GR logs, reflecting the incorporation of radiogenic elements (U and Th) into HMs.

Each cycle is the result of differential HM sorting within a stratified flow with highly concentrated laminar flow behaviour in the lower part and less concentrated turbulent flow regime in the upper parts. The four cyclic units are a stacked succession of flow deposits with a general upward decrease in HM content. The flow units are believed to originate from a single slump event, creating a large flow which developed into a series of four surges caused by the mechanical instability in the initial flow. Within the initial flow an incomplete HM sorting profile developed which, when the flow separated into surges, resulted in systematic and specific HM distributions in each surge. Subsequently, each surge attained its own individual HM sorting profile.

This contribution demonstrates the use of a geochemical tool for the recognition and differentiation of flow units in massive sand successions, and for the identification of in-situ sand as opposed to remobilised sand. The striking correlation between spectral GR log and geochemical logs permits HM sorting and individual

flow units to be inferred from petrophysical log patterns alone. Differential sorting of HMs may be a common feature in massive flow deposits, facilitating the identification of individual flow units within thick homogeneous sands.

ACKNOWLEDGEMENTS

The project "Geochemistry of the Siri Canyon sands" was carried out at Aarhus University in co-operation with DONG E & P A/S, representing the companies participating in the licences 4/95, 6/95 and 16/98 in the Danish North Sea. We acknowledge the financial support and the enthusiastic co-operation from the companies. We express our gratitude to DONG E&P A/S and the companies participating in the licence 16/98 for the permission to publish confidential data from the Cecilie Field. We are grateful to the reviewers Lars Hamberg and Mads Huuse and editors Maria Mange and Dave Wright for their very careful and constructive reviews, which improved the manuscript considerably.

REFERENCES

Baas, J.H., 2004. Conditions for formation of massive turbiditic sandstones by primary depositional processes. Sedimentary Geology 166, 293–310.

Ballance, P.F., 1984. Sheet-flow-dominated gravel fans of the non-marine middle Cenozoic Simmler Formation, Central California. Sedimentary Geology 38, 337–359.

Basu, A., Molinaroli, E., 1989. Provenance characteristics of detrital opaque Fe-Ti oxide minerals. Journal of Sedimentary Petrology 59, 922–934.

Cecchi, M., Guargena, C., Hansen, L., Rhodes, D., Roberts, A., 2001. Use of integrated 3D seismic technology and sedimentology core analysis to resolve the sedimentary architecture of the Palaeocene succession of the North Sea. In: Martinsen, O.J., Dreyer, T., (Eds.), Sedimentary Environments Offshore Norway—Palaeozoic to Recent, NPF Special Publication, Elsevier Science, Amsterdam, pp. 407–419.

Clausen, O.R., Huuse, M., 1999. Topography of the top Chalk surface on- and offshore Denmark. Marine and Petroleum Geology 16, 677–691.

Coussot, P., Laigle, D., Arattano, M., Deganutti, A., Marchi, L., 1998. Direct determination of rheological characteristics of debris flows. Journal of Hydraulic Engineering—ASCE 124, 865–868.

Danielsen, M., Clausen, O.R., Michelsen, O., 1995. Stratigraphic correlation of late Palaeocene sand deposits in the Søgne Basin area of the Danish and Norwegian central North Sea. Terra Nova 7, 516–527.

Hamberg, L., Dam, G., Wilhelmson, C., Ottesen, T., 2005. Palaeocene deep-marine sandstone plays in the Siri Canyon, offshore Denmark–southern Norway. In: Doré, A.G., Vining, B.A. (Eds.), Petroleum Geology: North-West Europe and Global Perspectives, Proceedings of the 6th Petroleum Geology Conference. Geological Society of London, pp. 1185–1198.

Hand, B.M., 1967. Differentiation of beach and dune sands using settling velocities of light and heavy minerals. Journal of Sedimentary Petrology 37, 514–520.

Hartley, N.R., 2000. The geochemistry of barren Triassic sequences: implications for chemostratigraphic correlation and reservoir characterisation. Unpublished Ph.D. thesis. Royal Holloway University of London, London, 457pp.

Heilmann-Clausen, C., 1985. Lithostratigraphy and depositional evnironments in the Upper Palaeocene and Eocene of Denmark. Bulletin of the Geological Society of Denmark 33, 287–323.

Huuse, M., 1999. Detailed morphology of the top Chalk surface in the eastern Danish North Sea. Petroleum Geoscience 5, 303–314.

Johansson, M., Braakenburg, N.E., Stow, D.A.W., Faugères, J.-C., 1998. Deep-water massive sands: facies, processes and channel geometry in Numidian flysch, Sicily. Sedimentary Geology 115, 233–265.

Kneller, B.C., Branney, M.J., 1995. Sustained high-density turbidity currents and the deposition of thick massive sands. Sedimentology 42, 607–616.

Kneller, B.C., McAffrey, W.D., 2003. The interpretation of vertical sequences in turbidite beds: the influence of longitudinal flow structure. Journal of Sedimentary Research 73, 706–713.

Knox, R.W.O'B., Holloway, S., 1992. Paleogene of the Central and Northern North Sea. In: Knox, R.W.O'B., Cordey, W.G. (Eds.), Lithostratigraphic nomenclature of the UK North Sea. British Geological Survey, Nottingham.

Lowe, D.R., 1975. Water escape structures in coarse-grained sediments. Sedimentology 22, 157–204.

Lowe, D.R., 1982. Sediment gravity flows: II. Depositional models with special reference to the deposits of high-density turbidity currents. Journal of Sedimentary Petrology 52, 279–297.

Major, J.J., 1997. Depositional processes in large-scale debris-flow experiments. Journal of Geology 105, 345–366.

Mange-Rajetzky, M.A., 1995. Subdivision and correlation of monotonous sandstone sequences using high-resolution heavy mineral analysis, a case study: the Triassic of the Central Graben. In: Dunay, R.E., Hailwood, E.A. (Eds.), Non-Biostratigraphical Methods of Dating and Correlation, vol. 89. Geological Society of London Special Publication, pp. 23–30.

Morton, A.C., 1991. Geochemical studies of detrital heavy minerals and their application to provenance studies. In: Morton, A.C., Todd, S.P., Haughton, P.D.W. (Eds.), Developments in Sedimentary Provenance Studies, vol. 57. Geological Society of London Special Publication, pp. 31–45.

Morton, A.C., Hallsworth, C.R., 1999. Processes controlling the composition of heavy mineral assemblages in sandstones. Sedimentary Geology 124, 3–29.

Morton, A.C., Hallsworth, C.R., Wilkinson, G.C., 1993. Stratigraphic evolution of sand provenance during Palaeocene deposition in the Northern North Sea region. In: Parker, J.R. (Ed.), Petroleum Geology of Northwest Europe, Proceedings of the 4th Conference. Geological Society of London.

Morton, A.C., Hurst, A., 1995. Correlation of sandstones using heavy minerals: an example from the Stratfjord Formation of the Snorre Field, northern North Sea. In: Dunay, R.E., Hailwood, E.A. (Eds.), Non-Biostratigraphical Methods of Dating and Correlation, vol. 89. Geological Society of London Special Publication, pp. 3–22.

Mulder, T., Alexander, J., 2001. The physical character of subaqueous sedimentary density flows and their deposits. Sedimentology 48, 269–299.

Owen, M.R., 1987. Hafnium content of detrital zircons, a new tool for provenance study. Journal of Sedimentary Petrology 57, 824–830.

Pearce, T.J., Jarvis, I., 1995. High-resolution chemostratigraphy of Quaternary distal turbidites: a case study of new methods for the analysis and correlation of barren sequences. In: Dunay, R.E., Hailwood, E.A. (Eds.), Non-Biostratigraphical Methods of Dating and Correlation. Geological Society Special Publications. vol. 89. Geological Society of London Special Publication, pp. 107–143.

Preston, J., Hartley, A., Hole, M., Buch, S., Bond, J., Mange, M., Still, J., 1998. Integrated whole-rock trace element geochemistry and heavy mineral studies: aids to the correlation of continental red-bed reservoirs in the Beryl Field, UK North Sea. Petroleum Geoscience 4, 7–16.

Rider, M., 2002. The geological interpretation of well logs. Rider-French Consulting Ltd., Sutherland, Scotland, 280pp.

Rubey, W.W., 1933. The size-distribution of heavy minerals within a water-laid sandstone. Journal of Sedimentary Petrology 3, 3–29.

Sachs, L., 1984. Applied Statistics: A Handbook of Techniques. Springer-Verlag, New York.

Sallenger, A.H., 1979. Inverse grading and hydraulic equivalence in grain-flow deposits. Journal of Sedimentary Petrology 49, 553–562.

Schiøler, P., Andsbjerg, J., Dybkjær, K., Kristensen, L.E., Rasmussen, J.A., 2003. A stratigraphic study of the Palaeogene succession East of the Central Graben in the Danish North Sea sector: executive summary. Danmarks og Grønlands Geologiske Undersøgelse Rapport 2003/71, 12pp.

Smith, G.A., 1986. Coarse-grained nonmarine volcaniclastic sediment: terminology and depositional processes. Geological Society of America Bulletin 97, 1–10.

Stow, D.A.V., Johansson, M., 2000. Deep-water massive sands: nature, origin and hydrocarbon implications. Marine and Petroleum Geology 17, 145–174.

Svendsen, J.B., Hartley, N.R., 2001. Comparison between outcrop-spectral gamma ray logging and whole rock geochemistry: implications for quantitative reservoir characterisation in continental sequences. Marine and Petroleum Geology 18, 657–670.

Svendsen, J.B., Hartley, N.R., 2002. Synthetic heavy mineral stratigraphy: applications and limitations. Marine and Petroleum Geology 19, 389–405.

Svendsen, J.B., Stollhofen, H., Krapf, C.B.E., Stanistreet, I.G., 2003. Mass and hyperconcentrated flow deposits record dune damming and catastrophic breakthrough of ephemeral rivers, Skeleton Coast Erg, Namibia. Sedimentary Geology 160, 7–31.

Swan, A.R.H., Sandilands, M., 1995. Introduction to Geological Data Analysis. Blackwell Science, New York, 446pp.

Van den Berg, J.H., Van Gelder, A., Mastbergen, D.R., 2002. The importance of breaching as a mechanism of subaqueous slope failure in fine sand. Sedimentology 49, 81–95.

Weibel, R., Friis, H., 2007. Alteration of opaque heavy minerals as a reflection of the geochemical conditions in depositional and diagenetic environments. In: Mange, M., Wright, D. (Eds.), Heavy Minerals in Use. Developments in Sedimentology. Elsevier, Amsterdam (this volume).

This page intentionally left blank

Chapter 44

THE ROLE OF HEAVY MINERAL ANALYSIS AS A GEOSTEERING TOOL DURING DRILLING OF HIGH-ANGLE WELLS

ANDREW C. MORTON[a,b]

[a]*HM Research Associates, 2 Clive Road, Balsall Common, West Midlands CV7 7DW, UK*
[b]*CASP, University of Cambridge, 181a Huntingdon Road, Cambridge CB3 0DH, UK*

ABSTRACT

The use of heavy mineral analysis on a 'real-time' basis at well site is a logical extension of the application of the method as a non-biostratigraphic correlation tool. To date, the method has been used to monitor the stratigraphy during drilling of horizontal wells in three fields on the UK continental shelf (Clair, Ross and Hannay), and in several cases heavy mineral data have been integral in deciding to amend well bore trajectories in order to remain within hydrocarbon-bearing zones, a process known as 'geosteering'. Heavy mineral analysis now has a positive track record for geosteering horizontal wells in a variety of depositional environments, from fluvial/aeolian to shallow and deep marine, and can therefore be genuinely considered as an alternative geosteering tool in circumstances where biostratigraphic methods have inadequate resolution. Heavy mineral data have been used in the decision-making process in a variety of situations, including whether to maintain angle, to steer up or to steer down, to sidetrack and to terminate drilling. Application of heavy mineral analysis at the well site requires establishment of a robust correlation scheme prior to drilling horizontal wells, using samples from offset wells adjacent to the proposed well track. Parameters used to monitor the geology during horizontal drilling include those conventionally used for reservoir correlation (principally, ratios of stable minerals with similar hydrodynamic behaviour), but other parameters have also proved useful in the particular circumstance associated with individual fields. For example, the abundance of unstable minerals is locally useful in the Clair Field, and ratios of minerals with contrasting hydrodynamic behaviour are useful in the Ross and Hannay Fields.

Keywords: heavy minerals; stratigraphy; correlation; geosteering; North Sea

Developments in Sedimentology, Vol. 58, 1123–1142

ISSN: 0070-4571/doi:10.1016/S0070-4571(07)58044-1

1. INTRODUCTION

Heavy mineral analysis is one of the most widely used of the various non-biostratigraphic methods available for sandstone correlation (Dunay and Hailwood, 1995), especially in the hydrocarbon industry. Correlation by heavy mineral means is crucially dependent on the existence of stratigraphically significant variations in provenance and/or transport history during deposition of the succession under investigation, a prerequisite to the successful application of any provenance-based correlation method (Morton et al., 2002). Heavy minerals are especially well suited for sandstone correlation since they are highly sensitive indicators of provenance and sediment transport history (Mange and Maurer, 1992; Morton and Hallsworth, 1999). The first applications date back to the early part of the last century, the work of Milner (1923) being of seminal importance in establishing the value of the technique. Since then, heavy minerals have been used for correlation purposes in many sedimentary basins worldwide, examples including the Pliocene of the San Joaquim Valley, California (Reed and Bailey, 1927), the Cretaceous-Tertiary of Venezuela (Feo-Codecido, 1956) and the Paleozoic-Mesozoic of the Middle East (Weissbrod and Nachmias, 1986). The technique has proved especially useful in the hydrocarbon basins of the UK and Norway, with a wide range of applications through a wide range of depositional environments, from fluvial and aeolian through paralic, shallow marine and deep marine settings, and across a large part of the geological column, from Devonian to Tertiary (Allen and Mange-Rajetzky, 1992; Morton and Berge, 1995; Mange et al., 1999; Morton et al., 2002).

In recent years, the correlative value of heavy mineral analysis has been taken a step further, with the technique being used 'real-time' at the well site to monitor the stratigraphy encountered during drilling of high-angle wells. High-angle (horizontal or near-horizontal) wells are increasingly being used to facilitate economic exploitation of hydrocarbon reserves, since a large number of high-angle wells can be drilled from a single production facility. In many cases, successful exploitation depends on ensuring the well bore remains in the productive parts of the reservoir (the so-called 'pay' zone). The use of geological parameters to alter the trajectory of wells during drilling, thereby ensuring the well bore remains within the pay zone, is known as geosteering. Geosteering therefore requires continual monitoring of the geology during drilling operations. In most cases, this is achieved using a combination of cuttings description by the well site geologist, geophysical logging while drilling (LWD) and high-resolution biostratigraphy. However, in some reservoirs, the biostratigraphic component of this 'geosteering suite' may not be available, for example, when biostratigraphic events lack sufficient resolution, or when the succession is entirely biostratigraphically barren. Under such circumstances, heavy mineral analysis can play an important role.

To date, applications of heavy mineral analysis at well site to monitor the geology encountered in high-angle wells have been confined to the UK continental shelf. This probably reflects the widespread application of heavy mineral analysis as a correlation tool in the hydrocarbon basins of the UK. Heavy mineral analysis at well site was pioneered on appraisal wells in the Clair Field, west of Shetland, in 1996–1997, but its first application in a field development programme was on the Ross Field in the North Sea. It has subsequently been applied in a number of other field developments, including Hannay, Clyde and Murchison.

2. PRINCIPLES AND PRACTICE

In order for heavy mineral analysis to be successfully applied at well site, the pay zone must be mineralogically different to the overlying and underlying units. Ideally, the zones underlying and overlying the pay zone should also differ from one another. If such mineralogical differences exist, it should be possible to establish whether the drill bit is drilling productive reservoir, and if not, how the hole trajectory should be altered in order to return to the pay zone.

Prior to application of heavy mineral analysis at well site, it is therefore necessary to establish whether the productive stratigraphic unit has a distinctive mineralogical signature that distinguishes it from the overlying and underlying units. This is achieved by undertaking heavy mineral analysis of the reservoir succession in previously drilled wells adjacent to the proposed well trajectory. Ideally, this template should be established using core material, since—although the well site analysis is conducted on ditch cuttings—cores have greater integrity, being significantly less subject to contamination and other forms of alteration that may occur during the drilling process.

Although heavy mineral templates are best established using core data, it is important to recognise that there may be differences in mineral parameter measurements made on core and ditch cuttings samples from the same succession, caused by the drilling process and by downhole contamination. Abundances of mechanically unstable heavy minerals may be depleted in ditch cuttings compared with core, owing to the action of the drill bit. This problem is likely to be exacerbated in wells drilled with polycrystalline diamond compact (PDC) bits, which essentially grind through the formation, compared with tricone bits, which have a cutting action. Identification of stratigraphic events at well site should therefore be based on the along-hole patterns shown by the mineral parameters, rather than on their actual measured values.

The range of heavy mineral parameters that can be analysed at well site is more limited than that in conventional laboratory-based correlation studies. The establishment of a valid correlation framework critically depends on acquisition of provenance-sensitive parameters. These parameters reflect changes in sediment provenance and transport history, but are unaffected by other processes that operate during the sedimentary cycle (Morton et al., 2002), such as hydraulic fractionation and diagenesis. Provenance-sensitive criteria fall into two categories: ratio data and varietal data (Morton and Hallsworth, 1994). Ratio data determine the relative abundance of minerals with similar hydraulic and diagenetic behaviour, such as apatite and tourmaline, and can be readily acquired at well site using conventional optical microscopy. By contrast, varietal data, which quantify differences shown by individual mineral populations, are routinely acquired by single-grain electron microprobe analysis, for instance on garnet (Morton, 1985) or tourmaline (Henry and Guidotti, 1985), but this approach is not applicable at the well site since the technology is not available offshore. However, it is possible to undertake varietal studies using conventional optical microscopy, subdividing mineral populations on the basis of properties such as colour, habit or internal structure (Mange-Rajetzky, 1995), and such data can be readily acquired at well site.

The application of heavy mineral analysis at well site is illustrated using three examples, all from the UK continental shelf, covering a range of ages and depositional settings. Example 1 is from the fluvial/aeolian/lacustrine Devonian-Carboniferous Clair Group in the Clair Field, west of Shetland; example 2 is from the shallow marine Jurassic Ross Formation of the Ross Field, outer Moray Firth; and example 3 is from the deep marine Cretaceous Britannia Formation of the Hannay Field, central North Sea.

3. CLAIR FIELD

The Devonian-Carboniferous non-marine clastic succession that forms the reservoir in the Clair Field (Fig. 1) is essentially devoid of biostratigraphic markers. A combination of heavy mineral and sedimentological data enabled the establishment of a stratigraphic breakdown of the succession into 10 units, labelled I–X from base to top (Allen and Mange-Rajetzky, 1992). Units I–VI comprise the Lower Clair Group, and VII–X comprise the Upper Clair Group (Fig. 2).

Fluid flow from the main part of the Clair Field reservoir is dependent on the combined presence of permeable sandstones and open fractures (Coney et al., 1993). In the Core Area of the Clair Field, these requirements are met by Unit V, which has the best reservoir quality and is the locus for an open fracture system. Successful exploitation of the Clair Field is therefore dependent on drilling horizontal wells targeted on Unit V, in order to optimise hydrocarbon production. In view of the variations in mineralogy recognised by Allen and Mange-Rajetzky (1992), heavy mineral analysis was considered a possible option to assist with geosteering of these high-angle wells (Morton et al., 2003).

The possible application of heavy mineral analysis for geosteering high-angle wells in the Clair Field was tested by undertaking a high-resolution study of the Units IV–VI interval in the key well 206/8-8 (Fig. 3). Within this interval, important variations in several parameters were recognised, enabling identification of three heavy mineral units, Units VIm, Vm and IVm (Morton et al., 2003). The VIm–Vm boundary is close to the boundary between lithostratigraphic Units VI and V, but the Vm–IVm boundary occurs some 20 m below the boundary between lithostratigraphic Units V and IV. The parameters that are useful for discrimination of Units VIm, Vm and IVm are as follows:

(1) apatite/tourmaline ratio (ATi): ATi is high (> 90) in both Units VIm and IVm, but generally lower in Unit Vm;
(2) garnet/zircon ratio (GZi): the GZi pattern is similar to that of ATi, high (> 90) in both Units VIm and IVm, but generally lower in Unit Vm;
(3) abundance of unstable minerals: Unit VIm is characterised by common unstable minerals throughout (principally epidote and titanite); by contrast, these minerals are generally absent in Units Vm and IVm, although occasional samples contain amounts similar to Unit VIm; the abundance of unstable minerals is measured in two ways, first as a frequency % determination and second as a ratio against tourmaline (denoted as UTi);
(4) apatite roundness (ARi): apatite morphology was recognised as a key parameter for Clair Field correlation by Allen and Mange-Rajetzky (1992). Apatite tends to

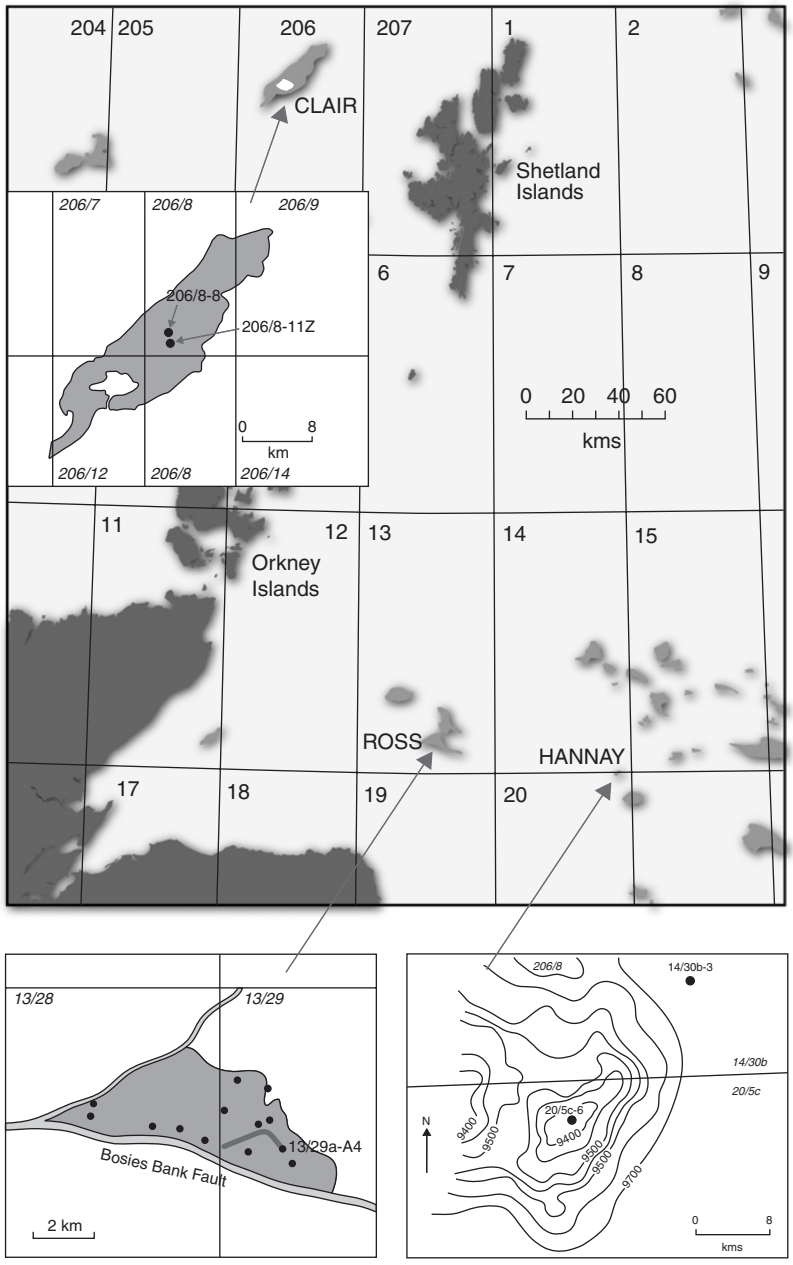

Fig. 1. Location of Clair, Ross and Hannay Fields on the UK continental shelf. Inset maps show relevant well locations (adapted from Coney et al., 1993; Law et al., 1999; Morton et al., 2001). Contours on the Hannay inset map are depth to top Britannia sandstone (in feet).

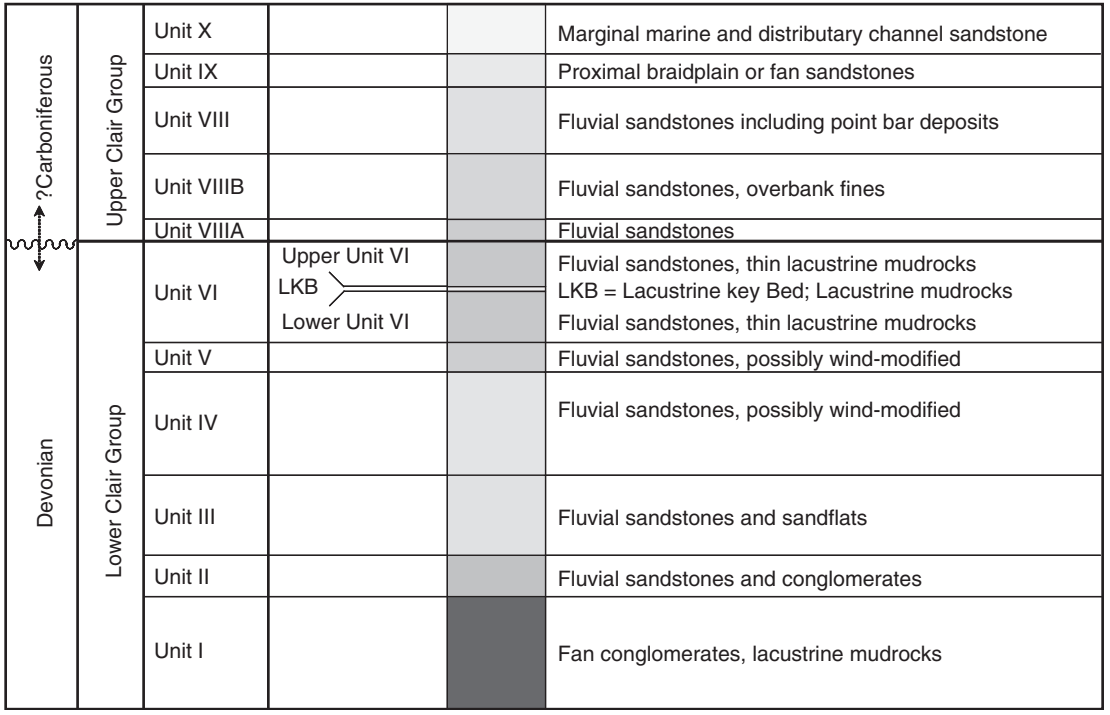

Fig. 2. Clair Field stratigraphy (after Allen and Mange-Rajetzky, 1992; Morton et al., 2003).

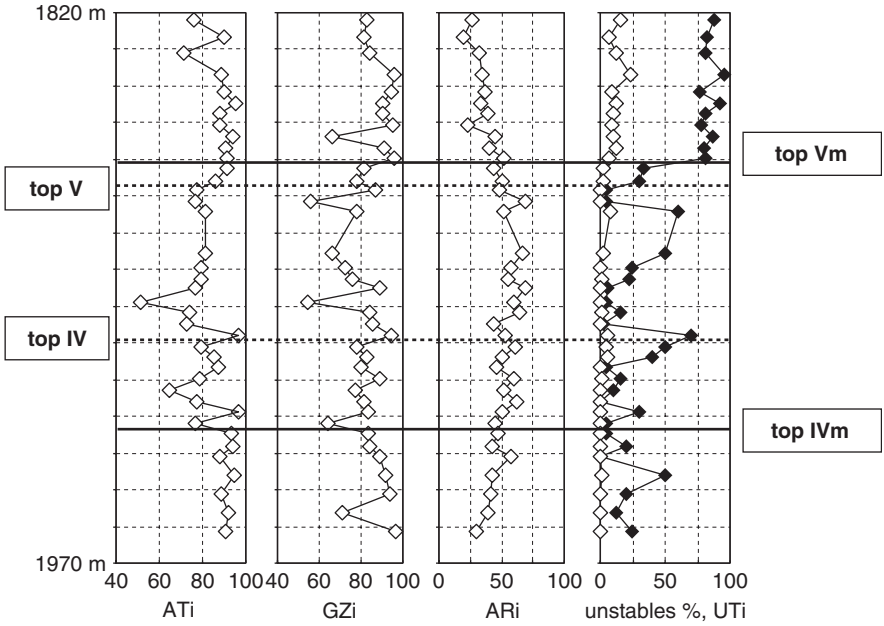

Fig. 3. Downhole heavy mineral profile across the lower part of Unit VI, Unit V and into top Unit IV in the cored well 206/8-8. VIm, Vm and IVm are the mineralogical zones that approximately equate to lithostratigraphic Units VI, V and IV (from Morton et al., 2003). ATi = apatite/tourmaline index; GZi = garnet/zircon index; ARi = apatite roundness index (% rounded apatite in apatite population); unstables (open diamonds) = % epidote + titanite; UTi (filled diamonds) = unstables-tourmaline index (% unstables in total unstables + tourmaline).

become rounded more rapidly than many of the other clastic components due to its relatively low hardness, and apatite roundness is therefore a sensitive indicator of prolonged transport, including the extent of aeolian activity. In 206/8-8 (Fig. 3), ARi values are low in Units VIm and IVm, and high in Unit Vm. However, the pattern is gradational, and unit boundaries cannot be specified on the basis of this parameter alone.

In addition, changes in RuZi (rutile/zircon ratio) are useful for discrimination of the Upper Clair Group from the Lower Clair Group, with the former having high RuZi and the latter low RuZi. This change reflects a significant change in provenance across the Lower Clair/Upper Clair boundary (Allen and Mange-Rajetzky, 1992).

The variations in heavy mineral parameters over the Units IVm–VIm interval result from the interplay of provenance, transport history and diagenesis. Differences in ATi and GZi are ascribed to provenance, and the greater apatite roundness in Unit Vm reflects more prolonged transport. Since variations in ATi, GZi and apatite roundness reflect changes in provenance and transport history, they are likely to be correlatable on a field-wide basis. By contrast, the presence of unstable minerals in Unit VIm is due to lower porosity in this part of the succession (McKie and Garden, 1996), inhibiting pore fluid movement and leading to the preservation of relatively unstable minerals. The abundance of epidote- and titanite-bearing sandstones at specific levels in Unit Vm (Fig. 3) reflects the presence of similar low

porosity/permeability sandstones lower in the succession. Since the distribution of unstable minerals is controlled by diagenesis, this parameter is unlikely to be a reliable discriminator between Unit VIm and Unit Vm over the field as a whole, although it appears to be laterally consistent in the Core Area.

The pilot study on 206/8-8 established that heavy mineral analysis provides a sound basis for distinguishing the good quality reservoir Unit Vm from the poorer quality Units VIm and IVm. Additional studies, using both core and cuttings, showed that similar heavy mineral events could be identified in adjacent wells (Morton et al., 2003), thereby establishing that the events can be traced across the Core Area of the field and that they could be identified in cuttings as well as core samples. Given these encouraging results, it was decided that the technique would be used at well site during drilling of subsequent horizontal wells.

3.1. *Clair Field Example: Well 206/8-11Z*

One of the horizontal wells where well site heavy mineral analysis was pioneered is 206/8-11Z (Morton et al., 2003). The well track for 206/8-11Z is shown in Fig. 4, with the heavy mineral parameters acquired at well site shown in Fig. 5. Four key heavy mineral events (nos. 1–4) were identified during drilling. The upper part of the drilled Clair Group succession (down to point no. 1) is characterised by extremely high GZi, low ATi, low ARi, relatively high RuZi, moderate abundances of unstable minerals and high ratios of unstable minerals to tourmaline (UTi). These features are typical of the Upper Clair Group. At point no. 1, there is a marked change in mineralogy, with ATi values becoming consistently high, GZi and RuZi showing marked decreases, and unstable minerals showing a significant increase. This marks a fundamental change in provenance within the Clair Group, and indicates penetration of Unit VIm. The increased abundance of unstable minerals in Unit VIm

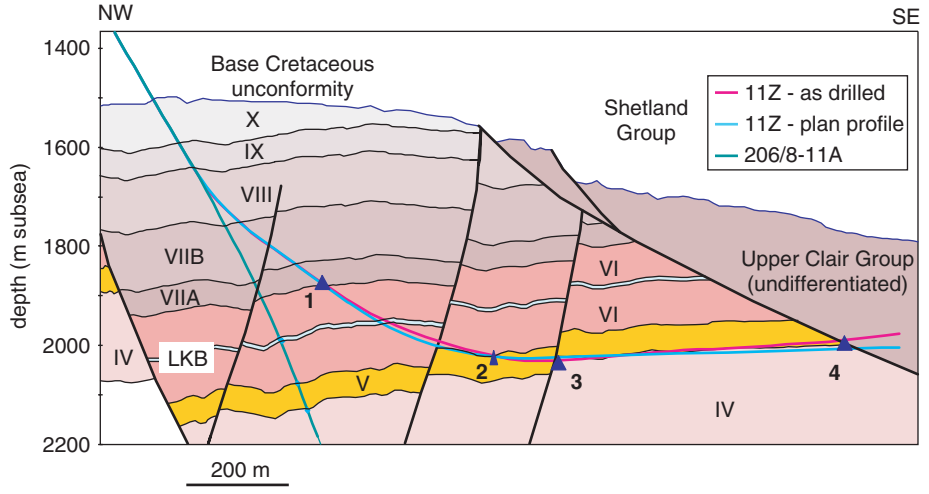

Fig. 4. Interpreted cross-section along trace of wells 206/8-11A and -11Z, showing locations of heavy mineral events nos. 1–4 (from Morton et al., 2003). LKB = lacustrine key bed (an important stratigraphic marker horizon in mid Unit VI).

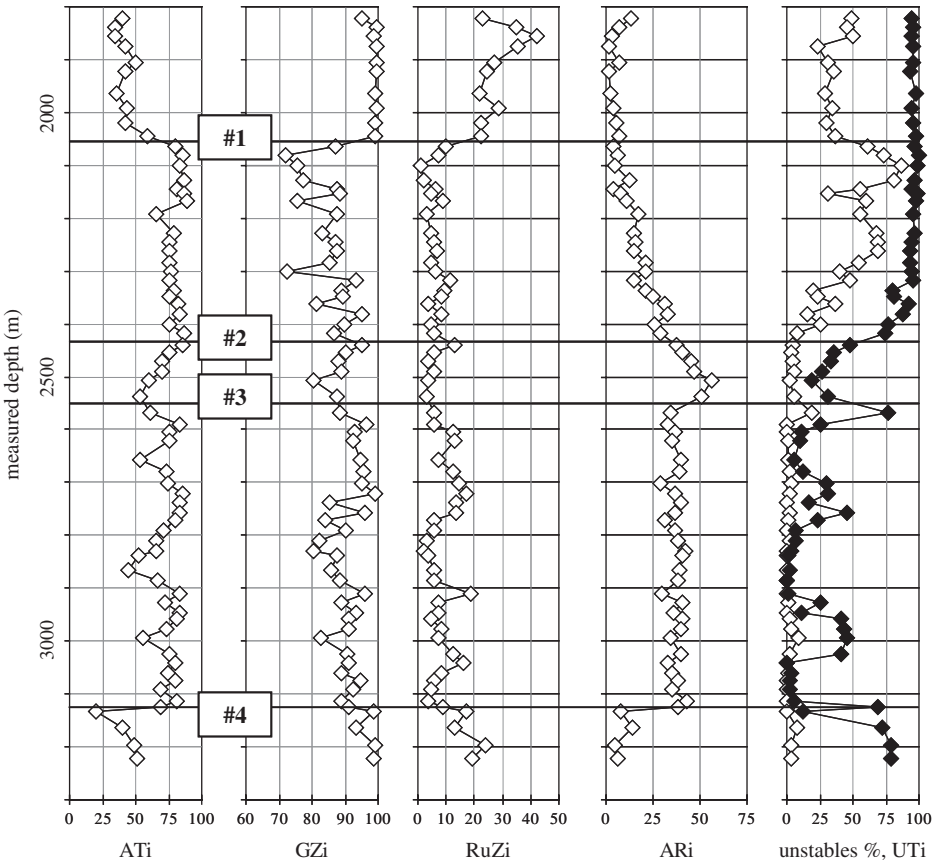

Fig. 5. Variations in heavy mineral parameters in 206/8-11Z, showing heavy mineral events nos. 1–4. ATi = apatite/tourmaline index; GZi = garnet/zircon index; RuZi = rutile/zircon index; ARi = apatite roundness index (% rounded apatite in apatite population); unstables (open diamonds) = % epidote + titanite; UTi (filled diamonds) = unstables-tourmaline index (% unstables in total unstables + tourmaline).

compared with the Upper Clair Group may be due to the change in provenance, but could also result from greater preservation in the poor-quality Unit VIm succession. Unit VIm characteristics persist as far as point no. 2, where there is a decrease in UTi, an increase in ARi and a decrease in ATi. This combination of parameters indicates entry into the good-quality reservoir Unit Vm.

Unit Vm characteristics continue to point no. 3 (Fig. 5), where there is a change to lower ARi, higher ATi and higher GZi, suggesting penetration of Unit IVm. This was unexpected, since the well trajectory was essentially horizontal and nearly parallel to bedding (Fig. 4), and the normal full vertical thickness of Unit Vm had not been penetrated. The original well prognosis was therefore reviewed in the light of these changes in heavy mineral data. Morton et al. (2003) considered that at this point, the well bore crossed a subseismic fault, thereby crossing from the main part of Unit Vm into sediments belonging to Unit IVm.

Between points nos. 3 and 4, the succession alternates between two mineralogical types, one with relatively low ARi, high ATi and high GZi (similar to Unit IVm), the other with higher ARi, lower ATi and lower GZi (similar to Unit Vm type). Morton et al. (2003) suggested that the well bore was tracking close to the Unit Vm/Unit IVm boundary. Since this position was sub-optimal, it was decided to steer the well up-section to try to regain a position nearer to the mid-point of Unit Vm. This demonstrated the value of the HM data, since this conclusion could not have been made on the basis of the cuttings and LWD data alone.

There is a major change in mineralogy at point no. 4 (Fig. 5), with ATi and ARi dropping dramatically, GZi rising to nearly 100, and RuZi also showing a significant increase. These features all indicate renewed penetration of the Upper Clair Group, implying that the well trajectory had intersected a major fault (Fig. 4). Unstable mineral abundances are slightly lower than previously seen in the Upper Clair Group, probably because of dilution by material from the stables-dominated high-angle section. This is probably also the reason why the UTi value levels out at ~80, compared with >90 for the equivalent section penetrated prior to point no. 1. The well was terminated shortly after this event was recognised.

4. ROSS FIELD

The main reservoir in the Ross Field (Moray Firth, North Sea, Fig. 1) consists of shoreface sandstones of the Ross Formation, with significant reserves in the underlying alluvial/fluvial Parry Formation (both Late Jurassic). The Ross Formation, which was deposited during a progressive marine transgression, is informally subdivided into four units, termed R1, R2, R3 and R4, in ascending order (Morton et al., 2001). Each unit is approximately 6 m thick, and represents a basal transgressive event followed by shoreface progradation. Reservoir quality in the Ross Formation is strongly dependent on depositional facies, the best quality being associated with the more proximal marine facies (middle/upper shoreface) and the poorest quality with the most distal (offshore) facies. The distribution of good-quality reservoir across the field is therefore dependent on both stratigraphy and paleogeographic setting. Exploitation of the Ross Field requires drilling horizontal wells that target the relatively thin R1–R4 pay zones. Since biostratigraphy lacks sufficient resolution to distinguish R1, R2, R3 and R4, heavy mineral analysis was considered as an alternative geosteering tool.

As with the Clair Field case study, prior to drilling horizontal wells, the potential value of heavy mineral analysis as a geosteering tool in the Ross Field was investigated by analysing cores of the Ross Formation from adjacent offset wells. These studies showed the existence of stratigraphic variations in a number of heavy mineral parameters of various types, including overall detrital heavy mineral recovery, mineral ratios and mineral grain attributes. The most useful parameters in the Ross Field proved to be:

(1) Heavy mineral recovery (relative abundance of detrital non-opaque heavy minerals compared with other components of the heavy mineral residues), which is very low in distal offshore sediments, but increases with proximity to the paleoshoreline; the poor recovery in the more distal facies is related to the reduction in

clastic sediment supply, with authigenic pyrite being the main phase; recovery also tends to be relatively low in paralic sediments (Parry Formation and R1 coastal plain facies);
(2) Zircon/tourmaline ratio (ZTi), which varies on a high-frequency basis throughout both Ross and Parry due to a combination of changes in sediment provenance and hydrodynamic conditions during deposition;
(3) Apatite/tourmaline ratio (ATi), which reflects the extent to which sediment has been weathered during the sedimentation cycle; ATi is high throughout in the marine parts of the Ross Formation (R1–R4) but very low in paralic sediments (Parry Formation and R1 coastal plain facies);
(4) Abundance of euhedral and brown zoned zircons, which are indicators of sediment derived directly from the Ross granite of the adjacent hinterland. Such zircons are scarce in the Ross Formation but are common in the underlying Parry Formation.

An example of the stratigraphic variations in these parameters is shown for well 13/29a-A3 (Fig. 6). The existence of stratigraphic variations in heavy mineral data provided confidence that the method would have sufficient resolution to identify and distinguish the various stratigraphic units during drilling of horizontal wells. Consequently, the technique was used at well site during drilling of nine horizontal wells on the Ross Field (13/29a-A3Y, 13/29a-A4, 13/28a-B2, 13/28a-B3, 13/28a-C1Z, 13/28a-C2, 13/29a-D1, 13/29a-D2 and 13/29a-E1). Heavy mineral analysis is particularly effective in the Ross Field because of the relatively slow penetration rates (typically 3–6 m/h) and because the logging tools are placed at considerable distance behind the drill bit. For example, the gamma ray tool is approximately 16 m behind the bit, and with a typical rate of penetration of 5 m/h, a change in formation can be identified by heavy mineral analysis around 2 h before the gamma ray log, taking into account cuttings lag time and heavy mineral extraction.

4.1. Ross Field Example: Well 13/29a-A4

Well 13/29a-A4 (Fig. 1) targeted the R3 unit, which has the best reservoir quality in this part of the Ross Field. In this well, heavy mineral data provide a clear distinction between R3 and the overlying non-reservoir R4 unit, and also differentiate the better-quality upper R3 from the poorer-quality lower R3 (Fig. 7). R4 is distinctive in having a combination of very low detrital heavy mineral recovery and low ZTi. Detrital heavy mineral recovery and ZTi are both high in upper R3, but lower R3 has high recovery in conjunction with low ZTi. Consequently, when heavy mineral analysis indicated that the well track had penetrated lower R3, for example at 4337 m and subsequently at 4788 m, it was decided to build angle, thus enabling the well track to re-enter better-quality upper R3. Similarly, when heavy mineral analysis indicated that the well track had penetrated R4 at 4615 m and subsequently at 4996 m, decisions to drop angle were taken. This was successfully achieved after the first penetration of R4 between 4615 and 4706 m. However, after the second R4 section between 4996 and 5029 m, R3 sediment was encountered only until 5052 m, at which point penetration of R4 was renewed. This indicated that it was no longer possible to steer the well, and since the target of drilling 760 m of high-quality reservoir had already been achieved, the decision to terminate drilling was made.

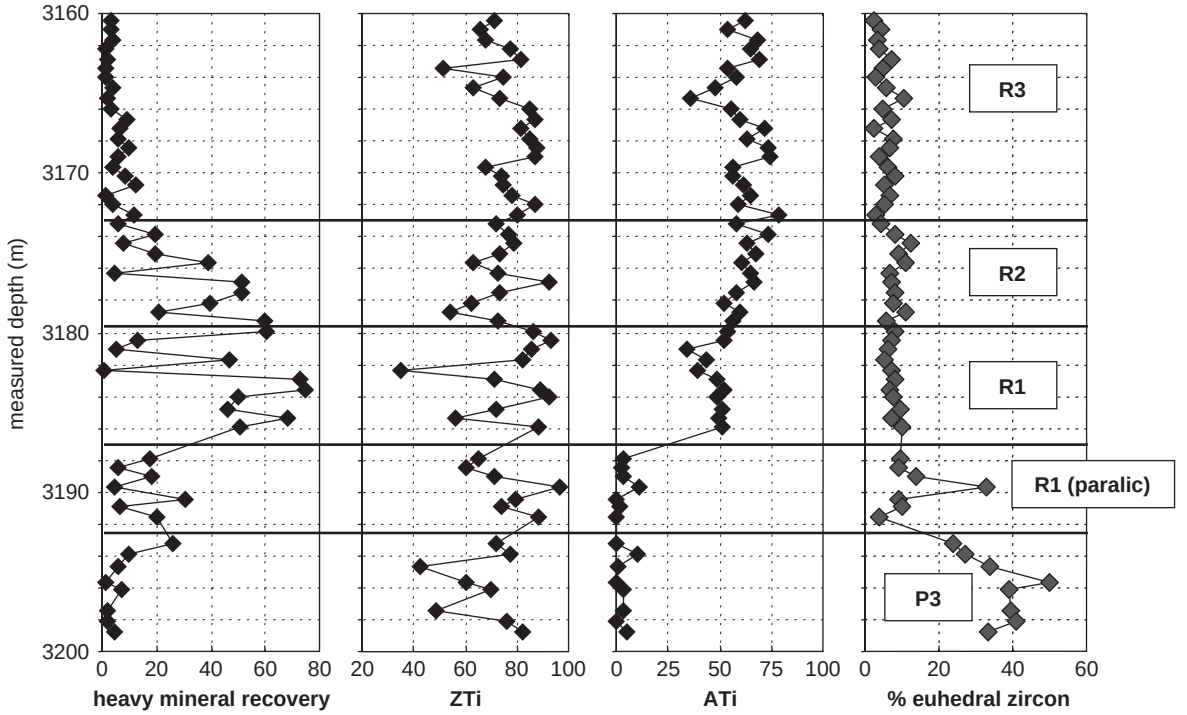

Fig. 6. Variations in key heavy mineral parameters from part of the core in Ross Field well 13/29a-A3. These parameters were used to build up a template of mineralogical characteristics of the Ross and Parry Formations across the field to help calibrate and interpret the parameters determined subsequently at well site (adapted from Morton et al., 2001).

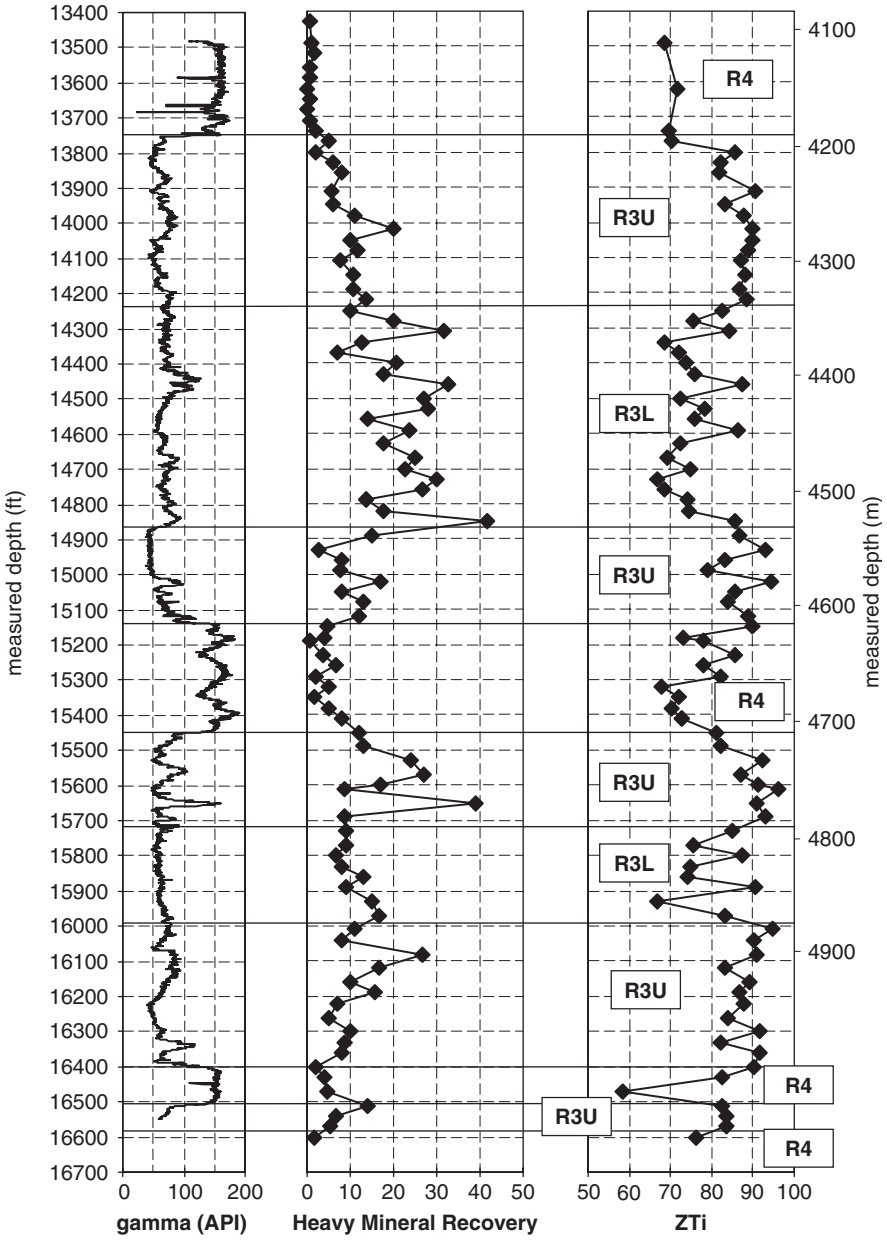

Fig. 7. Along-hole variations in two key parameters determined at well site during drilling of Ross Field well 13/29a-A4, shown against the LWD gamma ray log. The mineralogy clearly identifies penetrations of R4, upper R3 (R3U) and lower R3 (R3L), on the basis of variations in heavy mineral recovery (detrital heavy minerals/detrital heavy minerals plus opaques) and ZTi (zircon/tourmaline index) (adapted from Morton et al., 2001).

5. HANNAY FIELD

Deep-water Aptian-Albian sandstones form reservoirs for a number of hydrocarbon accumulations in the Moray Firth and central North Sea, including the Captain and Britannia Fields (Garrett et al., 2000). One area of particular interest in recent years has been the so-called 'Kopervik fairway', lying to the south of the Halibut Horst in the Moray Firth, UK (Law et al., 2000). Several accumulations have been found along this trend, notably Atlantic, Blake, Cromarty, Goldeneye and Hannay (Garrett et al., 2000; Law et al., 2000).

The Hannay Field (Fig. 1), which was discovered in 1996 by well 20/5c-6 (Law et al., 2000), has an oil column of approximately 30 m, with exploitation achieved by a horizontal well, 20/5c-8, drilled in 2001–2002. The sandstones that comprise the reservoir belong to the Britannia Sandstone Formation (Johnson and Lott, 1993), and underlie mudstones of the Carrack Formation. Owing to the sand-rich nature of the reservoir succession in the Hannay Field, heavy mineral analysis was considered as a potential geosteering tool.

Core from the discovery well 20/5c-6 was used to establish a heavy mineral template for the subsequent horizontal well. The results of the core study were promising, showing the presence of variations in a number of heavy mineral parameters that established the existence of four heavy minerals units, H1–H4 (Fig. 8). The key parameters used in the subdivision of the 20/5c-6 succession are:

(1) Heavy mineral recovery (relative abundance of detrital non-opaque heavy minerals compared with other components of the heavy mineral residues), which distinguishes good-quality, sand-rich intervals from poor-quality, sand-poor units;
(2) Garnet/zircon (GZi), apatite/tourmaline (ATi) and to a lesser extent rutile/zircon (RuZi), all of which reflect changes in sand provenance;
(3) Zircon/apatite (ZAi) and zircon/tourmaline (ZTi), which reflect a combination of changes in provenance and hydraulic conditions at the time of deposition;
(4) TiO_2 minerals/zircon (RZi), which responds mainly to local diagenetic conditions, variations being due to the extent of authigenic anatase development.

The most distinctive unit in the 20/5c-6 succession is H2 (Fig. 8), which has lower heavy mineral recovery, lower ZAi and lower ZTi, together with higher ATi, higher GZi and slightly higher RuZi than the rest of the Britannia Sand. The other units (H1, H3 and H4) all have relatively high recovery, ZAi and ZTi values, in conjunction with low ATi and GZi. There are subtle differences in these parameters between Units H1, H3 and H4, with H3 having lower recovery, lower ZTi and lower ZAi than H1 and H4. The most well defined variations in zones H1, H3 and H4, however, are shown by the RZi value, which varies from ~20 to ~60 (Fig. 8). These variations are essentially due to differences in abundance of authigenic anatase, which is scarce in H1, moderately abundant in H3 and very abundant in H4, especially at the top of the unit.

The heavy mineral variations within the succession are due to a combination of differences in provenance, depositional facies and diagenetic history. The markedly higher GZi, ATi and slightly higher RuZi in Unit H2 indicate that this unit has a different provenance than the rest of the succession. The difference in provenance is also associated with a facies change, H2 being less sandy, as manifested by the higher gamma ray response and lower heavy mineral recovery (Fig. 8). The lower ZTi and

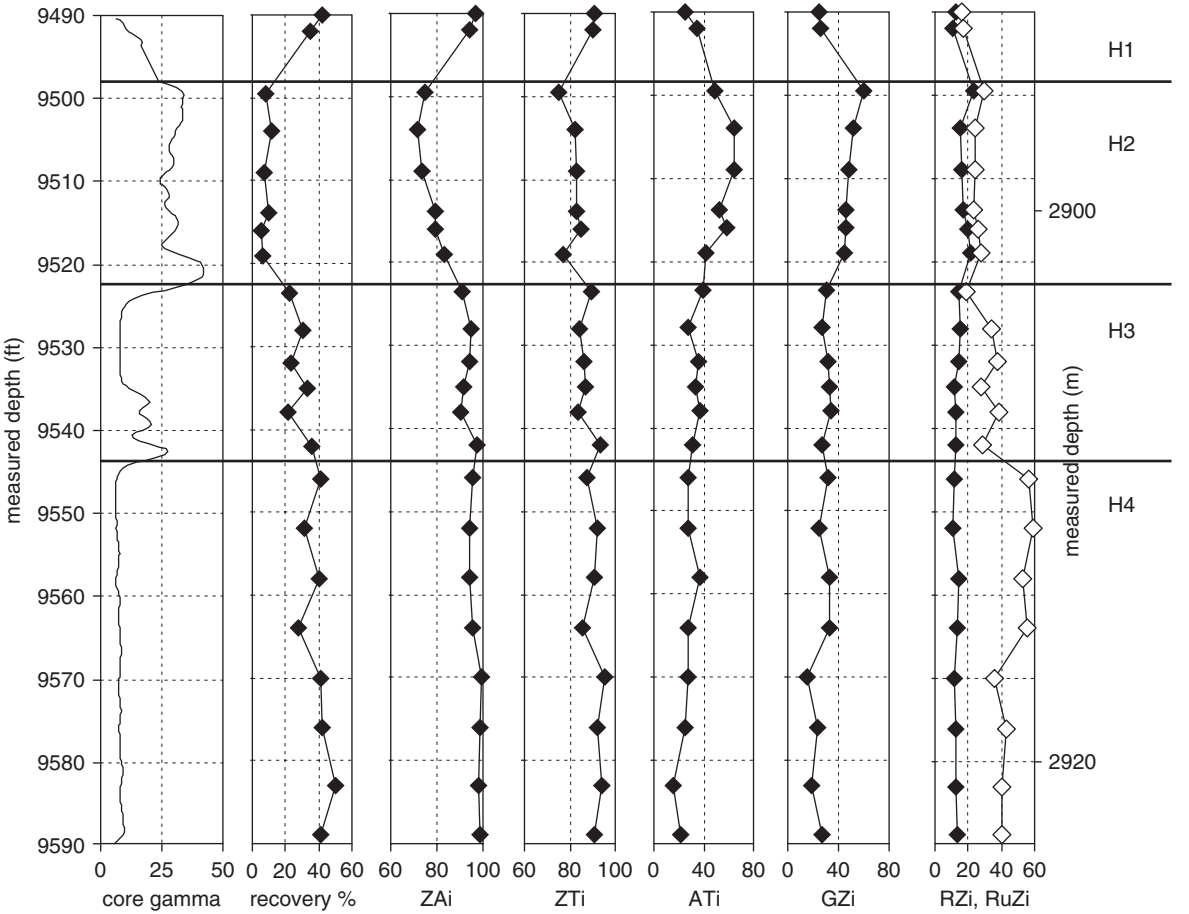

Fig. 8. Heavy mineral profile in the cored Britannia Sand of Hannay Field well 20/5c-6, showing definition of Units H1–H4. Recovery = % detrital heavy minerals in the heavy mineral residue; ZAi = zircon/apatite index; ZTi = zircon/tourmaline index; ATi = apatite/tourmaline index; GZi = garnet/zircon index; RZi = TiO_2 minerals/zircon index (filled diamonds); RuZi = rutile/zircon index (open diamonds).

ZAi values in Unit H2 could be due to hydraulic conditions, but might also be due, at least in part, to the different provenance. The more subtle variations in ZAi and ZTi between Unit H3 and Units H1 and H4 reflect different hydraulic conditions, since other parameters (GZi, ATi and RuZi) show no variation, indicating a uniform provenance. The variations in abundance of authigenic anatase are a diagenetic effect, and it is therefore questionable whether the RZi value is correlatable on a field-wide basis.

5.1. Hannay Field Example: Wells 20/5c-8Z and 20/5c-8Y

Development of the Hannay Field reservoir was achieved by the horizontal well 20/5c-8. The first penetration of the Britannia Sand was made by well 20/5c-8Z (Fig. 9). Four heavy mineral units (Z1–Z4) were identified in this well.

(1) Unit Z1 is characterised by good heavy mineral recovery, extremely high ZAi (close to 100), high ZTi (c. 90), very low ATi (<4) and low GZi (~20). These parameters are consistent with penetration of the upper part of the Britannia Sand, equivalent to Unit H1 in the template well 20/5c-6. One sample within Unit Z1 has relatively low recovery, but other parameters remain unchanged, and the low recovery is therefore ascribed to the presence of mud-rich lithologies rather than penetration of sandstones equivalent to Unit H2.
(2) Unit Z2 is characterised by relatively poor heavy mineral recovery, a decrease in ZAi and ZTi, an increase in ATi and GZi, and a slight increase in RuZi. These parameters indicate penetration of strata equivalent to Unit H2.
(3) Unit Z3 is marked by a return to parameters closely comparable to those in Z1 (Fig. 9), with an increase in heavy mineral recovery, ZAi and ZTi, together with a decrease in ATi, GZi, RuZi and mica abundance. Unit Z3 represents renewed penetration of sandstones equivalent to Unit H1 in 20/5c-6.
(4) Unit Z4 has an unusual mineralogical composition, with very low heavy mineral recovery and a high abundance of carbonate. These parameters cannot be matched with any previously seen, higher either in 20/5c-8Z or in the template well 20/5c-6. Unit Z4 is therefore interpreted as indicating penetration of the overlying stratigraphic unit, the Carrack Formation.

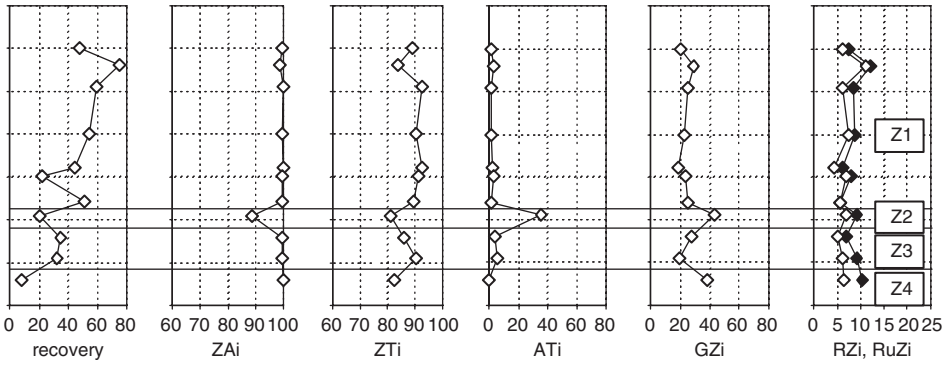

Fig. 9. Along-hole variations in key heavy mineral parameters from Hannay Field well 20/8c-8Z, showing definition of four units, Z1–Z4. Legend same as in Fig. 8, except 'recovery' (= % detrital heavy minerals/detrital heavy minerals plus opaques).

Penetration of the Carrack Formation indicated that the well trajectory required major amendment. This could have been achieved by altering the angle to enable downcutting back into the Britannia Sand reservoir. However, this was not considered feasible, and therefore a decision was taken to sidetrack the well within Unit Z2.

Four heavy mineral units (Y1–Y4) were recognised in the sidetrack well 20/5c-8Y (Fig. 10):

(1) The first of these, Unit Y1, is identical to Unit Z1, having been drilled in 20/8c-Z.
(2) Unit Y2 is characterised by relatively low recovery, relatively low ZAi (~70–90), relatively low ZTi (~70–80), relatively high ATi (> 20) relatively high GZi (> 40) and increased RuZi. This combination of parameters indicates penetration of strata equivalent to Unit H2.
(3) Unit Y3 has increased heavy mineral recovery, higher ZAi and ZTi, and lower ATi, GZi and RuZi. ZAi and ZTi values are intermediate between those seen in Y2 and the subsequent Unit Y4, suggesting that Unit Y3 is equivalent to H3 in 20/5c-6.
(4) Unit Y4 is characterised by good heavy mineral recovery, very high ZAi, high ZTi, low ATi low GZi and low RuZi. These parameters indicate penetration of strata equivalent to Unit H4 in 20/5c-6. The decision to terminate drilling was made after the well had penetrated sufficient good-quality Britannia Sand reservoir for production purposes.

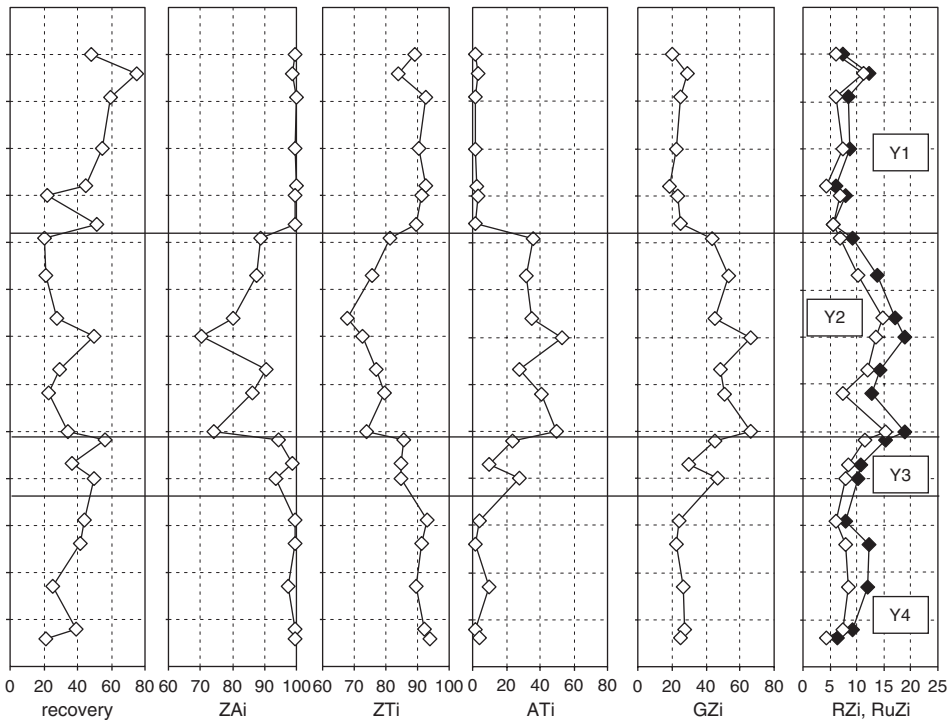

Fig. 10. Along-hole variations in key heavy mineral parameters from Hannay Field well 20/8c-8Y, showing definition of four units, Y1–Y4. Legend same as in Figs. 8 and 9.

All the parameters that established the reservoir breakdown in the Hannay Field template well 20/5c-6 proved to be useful in the horizontal well, with the notable exception of the RZi value. Consequently, parameters that reflect differences in provenance and hydrodynamic conditions appear to be laterally consistent across the Hannay Field. By contrast, the parameter most strongly affected by diagenetic conditions is laterally variable, with no increase seen in Units Y3 and Y4.

6. CONCLUSIONS

As a result of its application in the Clair, Ross and Hannay Fields, heavy mineral analysis now has a positive track record for geosteering horizontal wells during field appraisal and development programmes in a variety of depositional environments, including fluvial/aeolian, shallow marine and deep marine. The technique can therefore be genuinely considered as an alternative geosteering tool in circumstances where biostratigraphic methods have inadequate resolution. Heavy mineral data have been used in the decision-making process in a variety of situations, including whether to maintain angle, to steer up or to steer down, to sidetrack, and to decide when to terminate drilling.

Parameters used to monitor the geology during horizontal drilling include those conventionally used for reservoir correlation (Morton et al., 2002), but other parameters have also proved useful in the particular circumstance associated with individual fields. For example, the abundance of unstable minerals in the Clair Field is an important parameter for distinguishing Unit VIm from Vm and IVm, whereas detrital heavy mineral recovery proved useful in both the Ross and Hannay Fields. Hydrodynamically controlled parameters such as zircon/apatite and zircon/tourmaline ratios also proved useful in Ross and Hannay. Consequently, a wide variety of parameters should be considered when undertaking feasibility studies prior to application at well site. Caution is always required, however, when using parameters that are not only controlled by provenance, since lateral variations in hydrodynamic and diagenetic conditions are likely to occur across individual fields. This is exemplified by the RZi parameter in the Hannay Field. Authigenic anatase is abundant in certain zones in the template well 20/5c-6, causing marked variations in RZi. However, this feature is absent from the horizontal wells 20/5c-8Z and 20/5c-8Y, indicating that authigenic anatase development is highly localised and that variations in RZi cannot be used for correlation purposes in the Hannay Field.

Application of heavy mineral analysis at well site requires establishment of a robust correlation scheme prior to drilling horizontal wells, using samples from offset wells adjacent to the proposed well track. Each individual field must be considered as a separate case, since there is no guarantee that correlatable variations exist, and there is no consistency to the parameters that permit stratigraphic subdivision in different reservoir successions.

In several cases, there are differences in absolute values between data acquired from core and cuttings, due to the mechanical action of the drill bit, and emphasis should therefore be placed on trends rather than absolute values when undertaking analysis at well site. Despite the potential for discrepancy between core and cuttings data, the technique has advantages over other non-biostratigraphic well site

methods, notably 'chemostratigraphic' methods, since the method deals with samples in terms of their constituent components rather than in bulk, enabling contamination from drilling additives and caving to be filtered out.

Limitations of the application of heavy mineral analysis at well site are threefold. First, the method is applicable only to clastic reservoir successions. Second, for the technique to be successful at well site, the succession under evaluation must show stratigraphically significant variations in heavy mineralogy. This requires investigation of the heavy mineral signatures of existing offset wells prior to drilling horizontal wells. Finally, data production takes approximately 2 h from receipt of sample, and thus the rate of penetration is a limiting factor. In formations that can be drilled rapidly, heavy mineral data production may be too slow to allow decision-making. Nevertheless, there are many fields in which the technique may prove to be a valuable component of the geosteering suite, and with the increasing emphasis on field development using horizontal wells, heavy mineral analysis has an important potential role to play in the future.

ACKNOWLEDGEMENTS

I am grateful to BP and the Clair Field partners for permission to present the Clair Field example, and to Talisman for permission to use the Ross and Hannay examples.

REFERENCES

Allen, P.A., Mange-Rajetzky, M.A., 1992. Sedimentary evolution of the Devonian-Carboniferous Clair Field, offshore northwestern UK: impact of changing provenance. Marine and Petroleum Geology 9, 29–52.

Coney, D., Fyfe, T.B., Retail, P., Smith, P.J., 1993. Clair appraisal: the benefits of a co-operative approach. In: Parker, J.R. (Ed.), Petroleum Geology of Northwest Europe. Proceedings of the 4th Conference. Geological Society, London, pp. 1409–1420.

Dunay, R.E., Hailwood, E.A. (Eds.), 1995. Dating and Correlating Biostratigraphically-Barren Strata. Geological Society of London Special Publication, vol. 89.

Feo-Codecido, G., 1956. Heavy mineral techniques and their application to Venezuelan stratigraphy. Bulletin of the American Association of Petroleum Geologists 40, 984–1000.

Garrett, S.W., Atherton, T., Hurst, A., 2000. Lower Cretaceous deep-water sandstone reservoirs of the UK central North Sea. Petroleum Geoscience 6, 231–240.

Henry, D.J., Guidotti, C.V., 1985. Tourmaline as a petrogenetic indicator mineral: an example from the staurolite-grade metapelites of NW Maine. American Mineralogist 70, 1–15.

Johnson, H., Lott, G.K., 1993. Cretaceous of the central and northern North Sea. In: Knox, R.W.O'B., Cordey, W.G. (Eds.), Lithostratigraphic Nomenclature of the UK North Sea. British Geological Survey, Nottingham.

Law, A., Raymond, A., White, G., Atkinson, A., Clifton, M., Atherton, T., Dawes, I., Robertson, E., Melvin, A., Brayley, S., 2000. The Kopervik fairway, Moray Firth, UK. Petroleum Geoscience 6, 265–274.

Mange, M.A., Maurer, H.F.W., 1992. Heavy Minerals in Colour. Chapman and Hall, London, 147pp.

Mange, M.A., Turner, P., Ince, D., Pugh, J., Wright, D., 1999. A new perspective on the zonation and correlation of barren strata: an integrated heavy mineral and palaeomagnetic

study of the Sherwood Sandstone Group, East Irish Sea Basin and surrounding areas. Journal of Petroleum Geology 22, 325–348.

Mange-Rajetzky, M.A., 1995. Subdivision and correlation of monotonous sandstone sequences using high resolution heavy mineral analysis, a case study: the Triassic of the Central Graben. In: Dunay, R.E., Hailwood, E.A. (Eds.), Dating and Correlating Biostratigraphically-Barren Strata, Geological Society of London Special Publication, vol. 89, pp. 23–30.

McKie, T., Garden, I.R., 1996. Hierarchical cycles in the non-marine Clair Group (Devonian), UKCS. In: Howell, J.A., Aitken, J.F. (Eds.), High Resolution Sequence Stratigraphy: Innovations and Applications, Geological Society of London Special Publication, vol. 104, pp. 139–157.

Milner, H.B., 1923. The study and correlation of sediments by petrographic methods. Mining Magazine (London) 28, 80–92.

Morton, A.C., 1985. A new approach to provenance studies: electron microprobe analysis of detrital garnets from Middle Jurassic sandstones of the northern North Sea. Sedimentology 32, 553–566.

Morton, A.C., Berge, C., 1995. Heavy mineral suites in the Statfjord and Nansen Formations of the Brent Field, North Sea: a new tool for reservoir subdivision and correlation. Petroleum Geoscience 1, 355–364.

Morton, A.C., Hallsworth, C.R., 1994. Identifying provenance-specific features of detrital heavy mineral assemblages in sandstones. Sedimentary Geology 90, 241–256.

Morton, A.C., Hallsworth, C.R., 1999. Processes controlling the composition of heavy mineral assemblages in sandstones. Sedimentary Geology 124, 3–29.

Morton, A.C., Knox, R.W.O'B., Hallsworth, C.R., 2002. Correlation of hydrocarbon reservoirs using quantitative heavy mineral analysis. Petroleum Geoscience 8, 251–262.

Morton, A.C., Safton, K., Mundy, D.J.C., Passingham, B., Sargent, M., 2001. Geosteering high-angle wells in the Ross Field, North Sea: the application of heavy mineral analysis. Offshore Magazine, April Issue, 64–66.

Morton, A.C., Spicer, P.J., Ewen, D.F., 2003. Geosteering of high-angle wells using heavy mineral analysis: the Clair Field, West of Shetland. In: Carr, T.R., Mason, E.P., Feazel, C.T. (Eds.), Horizontal Wells: Focus on the Reservoir. American Association of Petroleum Geologists, Methods in Exploration, vol. 14, pp. 249–260.

Reed, R.D., Bailey, J.P., 1927. Surface correlation by means of heavy minerals. Bulletin of the American Association of Petroleum Geologists 11, 359–368.

Weissbrod, T., Nachmias, J., 1986. Stratigraphic significance of heavy minerals in the late Precambrian-Mesozoic clastic sequence ('Nubian Sandstone') in the Near East. Sedimentary Geology 47, 263–291.

4.2 Mineral Exploration and Mining

Frontispiece A. Henry Buckman (left) and George A. Pritchard examining heavy-mineral stringers in 3 m (30 ft) high sand dunes on the site of what was to become Mineral City, ca. 1915. Photograph courtesy of the Beaches Area Historical Society, Jacksonville Beach, FL.

Frontispiece B. Mining in 1919 on the beach at Mineral City, site of the current Ponte Vedra Beach ~24 km southeast of Jacksonville, FL. This is the first heavy-mineral sand mining operation for titanium minerals in the USA. Mining was done by the clam-shell at the end of the train. The locomotive transported the ore in the cars to a wet mill over a narrow gage wooden track. The mill was adjacent to the beach. Photograph courtesy of the Beaches Area Historical Society, Jacksonville Beach, FL.

Chapter 45

HEAVY-MINERAL SANDS OF THE ATLANTIC AND GULF COASTAL PLAINS, USA

FREDRIC L. PIRKLE[a], WILLIAM A. PIRKLE[b] AND E.C. PIRKLE[c,1]

[a]*Gannett Fleming, Inc., 10751 Deerwood Park Blvd., Suite 140, Jacksonville, FL 32256, USA*
[b]*Department of Biology and Geology, University of South Carolina Aiken, Aiken, SC 29801, USA*
[c]*Emeritus, Department of Geology, University of Florida, Gainesville, FL 32611, USA*
[1]*Present Address: 211 Boxwood Rd., Aiken, SC 29803, USA*

ABSTRACT

The Eastern North American Titanium Province extends from Labrador to Florida and westward toward the Mississippi River. In the United States, this province covers the Atlantic Coastal Plain and a substantial portion of the Gulf Coastal Plain. Heavy minerals were first mined from surface and near-surface sands of the Atlantic Coastal Plain in 1916, when Buckman and Pritchard opened a mine on a beach near Mineral City, Florida, to recover ilmenite. Numerous heavy-mineral deposits have since been identified within the surface sands of the Atlantic and Gulf coastal plains. Although some of the deposits are now being mined, others are no longer active, or have been lost to mining because of cultural developments. Some are likely to be mined in the future. Significant heavy-mineral deposits have been or are being exploited in New Jersey, Virginia, South Carolina, Georgia, and Florida. Some important heavy-mineral deposits formed in beach ridges at the height of major marine transgressions, e.g., the Trail Ridge and Highland (Maxville) deposits along Trail Ridge, and the Yulee, Cabin Bluff, Altama, Aurora, and Chowan deposits along the Pamlico shoreline. Other deposits developed in beach ridges formed at times of temporary halts or during minor transgressions in periods of general regression, e.g., the Green Cove Springs, Boulougne, Folkston, and Lulaton deposits. Those formed in alluvial environments include Manchester, Lakehurst, and Camden, as well as those of the Virginia and North Carolina Fall Zone. The most significant heavy-mineral deposits of the onshore Atlantic and Gulf coastal plains, as far west as the Louisiana–Texas border, are reviewed.

Keywords: heavy minerals; heavy-mineral orebodies; Atlantic coastal plain; Gulf coastal plain; heavy-mineral sands

Developments in Sedimentology, Vol. 58, 1145–1232

ISSN: 0070-4571/doi:10.1016/S0070-4571(07)58045-3

1. GENERAL GEOLOGICAL SETTING

The Eastern North American Titanium Province (Stanaway, 1996) extends 3500 km from Labrador south to Florida, and westward some 200–800 km toward the Mississippi River (Fig. 1). The western limit of this province in Canada is the Grenville Front, and in the United States, the Appalachian Orogen in the north, and towards the Mississippi River in the south (Stanaway, 1996). In the United States, this province covers the Atlantic Coastal Plain and much of the Gulf Coastal Plain, where numerous heavy-mineral deposits have been identified within the surface sands (Fig. 1). Some of these deposits are currently being mined, some have been mined in the past and are no longer active, some have been lost to mining because of cultural developments, and some probably will be mined in the future.

The heavy-mineral assemblages of the Atlantic and Gulf coastal plains generally contain ~40–60% ilmenite, 2–5% rutile, and 8–15% zircon, with the remaining heavy minerals being mainly staurolite, kyanite, sillimanite, and tourmaline (Cannon, 1950; Stanaway, 1996). Mineral assemblage maturity decreases as titanium content of the ilmenite declines. Younger sands may include locally up to 50% pyroxene, amphibole, epidote, and garnet. For example, epidote and hornblende are rare in the sands of Trail Ridge in Florida but are abundant in the younger sands of deposits, located to the east near Jacksonville (Cannon, 1950; Pirkle et al., 2005). Maturity also decreases generally northward (Anonymous, 1976; Stanaway, 1996).

The heavy-mineral deposits of the Atlantic and Gulf coastal plains occur in beach, bar, dune, and stream sands throughout the region, concentrated by gravity segregation of the chemically and physically resistant grains (Lynd and Lefond, 1983). Moving water sorts clastic grains according to size in gravels and sands, and according to size and shape in silts, and also sorts grains according to their density (Garnar and Stanaway, 1994, p. 1075; Komar, 2007, this volume). Placer deposits can form in nearly all clastic sedimentary environments (Garnar and Stanaway, 1994), dependent on appropriate source rocks, weathering, erosion, and flow regimes.

Garnar and Stanaway (1994) suggest that significant shoreline heavy-mineral placer formation requires marine regression and seaward transport. Accumulation of heavy minerals is favoured in the foreshore but can also occur in the upper shoreface or surf zone where hydrodynamics and sediment supply are favourable. Sediment reworking during marine transgression also results in high heavy-mineral accumulations but these rarely reach economic size. Formation of significant bed placers during transgression requires either the transportation of winnowed heavy-mineral lags to onshore, where they are stored in aeolian dunes, or multiple transgressions, with each succeeding transgression leaving a portion of the previous deposits intact (Garnar and Stanaway, 1994). An example of placer formation during marine transgression is Trail Ridge, Florida. An origin incorporating temporary stillstands or slight transgressions during an overall regressive trend may help explain the accumulation of the Green Cove Springs deposits in Florida.

Despite the economic dominance of shoreline, beach, and dune placers, river placers are also important. Evidence from drill holes suggests that heavy-mineral deposits in New Jersey are alluvial (Stanaway, 1992). Other deposits in North Carolina, Virginia, and Tennessee also might be, at least in part, alluvial (Pirkle et al., 1994; Newton and Romeo, 2006).

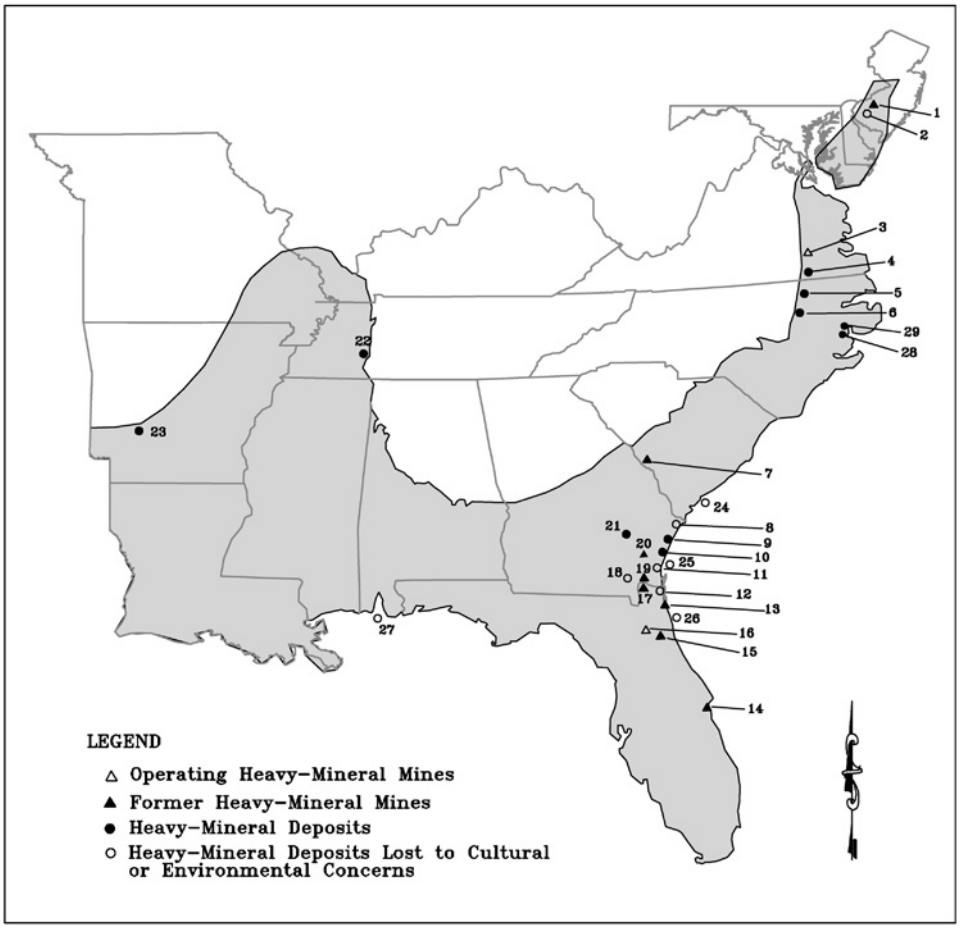

Fig. 1. Approximate locations of heavy-mineral deposits of the Atlantic and Gulf Coastal plains (New York to the Texas–Louisiana border): (1) New Jersey orebodies (Lakehurst and Manchester mines); (2) Pine Barrens deposits such as Pemberton; (3) Old Hickory orebody; (4) Virginia B (Brink) deposits; (5) Halifax (Aurelian Springs) deposits; (6) Bailey deposit; (7) Horse Creek orebody; (8) Oak Level deposit; (9) Darien deposit; (10) Altama deposit; (11) Cabin Bluff deposits; (12) Yulee deposits; (13) Arlington/Jacksonville and Mineral City deposits; (14) Vero Beach/Melbourne deposits (Central Florida); (15) Green Cove Springs orebody; (16) Trail Ridge and Highland (Maxville) orebodies; (17) Boulougne deposit; (18) Folkston West, Toledo, and Saunders Tract deposits; (19) Folkston orebody; (20) Lulaton orebody; (21) Amelia A, B, and C deposits; (22) West Tennessee deposits; (23) Arkansas Tokio Formation deposits; (24) South Carolina Sea Islands (Hilton Head, St. Helena, St. Phillips, Hunting, Wadmalaw, Johns, Capers, Bull, Isle of Palms, Edisto, and Dewees islands); (25) Georgia Sea Islands (Cumberland, Jekyll, St. Simon, St. Catherine, Ossabaw, and Skidaway islands); (26) Florida Sea Islands (Little Talbot and Amelia islands); (27) Gulf Coast Islands (Cat, Ship, Horn, Petit Bois, and Dauphin islands); (28) Aurora deposit; and (29) Chowan deposit.

Important heavy-mineral deposits in northern Florida and southeastern Georgia, formed in beach ridges, developed at the height of major marine transgressions. Others developed in beach ridges formed during stillstands or at times of minor transgressions during periods of general marine regression. Heavy-mineral concentrations found along the Fall Zone of Virginia and North Carolina are more problematic in their origin, as are those found in Tennessee and Arkansas. Other deposits in North Carolina were formed at the height of major marine transgressions.

In 1956, the New Jersey Geological Survey identified the late Tertiary sediments in the northern part of New Jersey's Coastal Plain as an ilmenite province (Markewicz, 1969). The main heavy-mineral accumulations are found in the Miocene Kirkwood Formation, the Pliocene (?) Cohansey Formation, and the Pleistocene Cape May sands and gravels. The Cape May accumulations were derived from the Kirkwood and Cohansey formations and from sediments farther inland. Heavy-mineral placers hosted in the sands of the Miocene Kirkwood Formation of New Jersey are probably of shoreline origin, while the sands of the overlying Cohansey Formation are, in part, alluvial placers.

2. USES OF HEAVY MINERALS

Cannon (1950) identifies ilmenite, leucoxene, rutile, zircon, monazite, sillimanite, kyanite, epidote, staurolite, tourmaline, hornblende, pyroxene, garnet, andalusite, spinel, corundum, collophane, and limonite along the coastal plain throughout the southeastern United States. Garnar (1980) provides guidance for the naming of the titanium minerals ilmenite, leucoxene, and rutile. He suggests that titanium minerals containing 45–65% TiO_2 be termed ilmenite, those containing 68–92% TiO_2 leucoxene, and those containing 94–98% TiO_2 rutile. Garnar (1980) reports the most common heavy minerals as ilmenite [$FeTiO_3$], leucoxene, rutile [TiO_2], staurolite [$FeAl_4Si_2O_{10}(OH)_2$], monazite [$(Ce,La,Y,Th)PO_4$], xenotime [YPO_4], zircon [$ZrSiO_4$], and the aluminium silicates kyanite and sillimanite [Al_2SiO_3]. Almandine garnet [$Fe_3Al_2(SiO_4)_3$] and epidote [$Ca_2(Al,Fe)_3Si_3O_{12}(OH)$] are less common but are present in many deposits. With one exception, all heavy-mineral deposits of the Atlantic and Gulf coastal plains in the United States have been developed for the purpose of obtaining titanium minerals, but their economic viability commonly depends on the recovery of additional economically valuable minerals.

2.1. Titanium Minerals

A majority of the titanium minerals produced in the United States today are used to manufacture TiO_2 pigments. This industry, started in 1918, traditionally used two processes (sulphate and chloride routes) to make TiO_2 pigment. The sulphate-route process uses ilmenite (43–65% TiO_2) or slag (70–72% TiO_2) as a feedstock. Leucoxene and rutile cannot be used as feedstock because they are relatively insoluble in sulphuric acid. The ilmenite or slag is converted to water-soluble sulphates, and the TiO_2 is recovered by hydrolysis of high TiO_2 solutions. Rutile (95% TiO_2) or high-TiO_2 ilmenite and rutile substitutes (60–95% TiO_2) are used as feedstock in the chloride process. These ores are converted to volatile chlorides, and the TiO_2 is

recovered by vapour phase oxidation of titanium tetrachloride (Lynd and Lefond, 1975). The last sulphate-route TiO_2-pigment manufacturing facility in the United States was Kerr McGee's Savannah, Georgia, facility, which closed in September 2004 (TZ Minerals International, 2005). In addition to pigment manufacturing, minor amounts of ilmenite have been used for non-pigment applications such as foundry sand filter-bed sand, and for heavy concrete in the oil drilling industry. Titanium minerals also have been used in the manufacture of tracer bullets. This application prompted the mining of titanium bearing beach sands in 1916 near Mineral City, Florida. Rutile has been used in the manufacturing of welding rods and in the manufacture of titanium metal.

2.2. Other Heavy Minerals

Zircon is used as specialty foundry sand, and in the manufacture of refractories, ceramics opacifiers, zirconium metal, and chemicals. In the 1920s, the refractory uses for zircon were recognised, and patents were granted for refractory uses. In the late 1940s, zircon began to be widely used in the steel industry. In 2004, approximately 51% of the zircon produced was consumed in the ceramics industry, 14% in refractories, 14% in foundry applications, 11% in the production of zirconia and zirconium chemicals, 8% in television glass, and 2% in other applications (Gilman, 2005). Warland (2006) reports only slight changes in the uses of zircon. He reports that 57% of the zircon produced is consumed in the ceramics industry, 12% in refractories, 10% in foundry applications, 9% in the production of zirconia chemicals, 6% in television glass, and 6% in investment casting.

Staurolite was first recovered on a commercial scale in 1952 from DuPont's Trail Ridge deposit. It is used as a source of aluminium in Portland cement, as premium-grade foundry sand, and as a sandblasting agent.

The *aluminium silicate minerals* (sillimanite, kyanite, andalusite, and corundum) have low coefficients of thermal expansion, and their high corrosion resistance makes them desirable for refractory applications, especially in the steel and foundry industries.

Garnet is separated from placer and beach sand deposits and sold for use as an abrasive. In 2004, the major uses for garnet and their estimated market share were abrasive blasting media (35%), waterjet cutting (30%), water filtration (15%), abrasive powders (10%), and other end uses (10%) (Olson, 2005). In general, higher quality industrial garnet is used as a loose-grain abrasive because of its hardness, whereas lower quality industrial garnet is used as a filtration medium because it is relatively inert and resists chemical degradation.

The most common *rare earth minerals* in beach sand and placer deposits are monazite [$(Ce,La,Y,Th)PO_4$] and xenotime [YPO_4] (Garnar, 1985a). Major uses for the cerium group rare earths are automotive catalytic converters, petroleum fluid-cracking catalysts, permanent magnets, glass polishing compounds, ceramics, metal-alloying additives, phosphors, and rechargeable batteries (Hedrick, 2005). The yttrium-group rare earths are used for special high-temperature lenses, infrared windows, lasers, and high-intensity lamps (Garnar, 1985a). Monazite is also a source of thorium, which is used in the nuclear energy industry. Thorium (Th) is bombarded with slow neutrons in breeder reactors to create fissionable ^{233}Th for nuclear fuel

cells. The primary non-energy use for thorium is the manufacture of Welsbach incandescent gas mantles (Shannon, 1983).

No commercial applications are known for *epidote*. Its chemical composition is not suitable for the cement industry and its low refractoriness and unfavourable expansion characteristics make it unsuitable as a candidate for refractory or foundry use.

No market has been developed for *tourmaline* that would justify creating a separation process for recovering this mineral by itself from placer and/or beach sand deposits.

3. HISTORY OF HEAVY-MINERAL MINING

Heavy minerals have been mined from the sands of the Atlantic Coastal Plain since the early part of the twentieth century. In 1916, Henry H. Buckman and George A. Pritchard noticed the occurrence of ilmenite in commercial quantities on the beach near Mineral City, Florida (Figs. 1 and 2; Frontispiece A), and began production of ilmenite in 1916. This first mining development was for war purposes: to supply titanium minerals for the manufacture of titanium tetrachloride, a fuming liquid which was used in tracer bullets, flares, and smoke screens. The first-reported production of zircon from the Mineral City deposit was in 1922, the same year that the Titanium Pigment Co., Inc., a subsidiary of the National Lead Company (now NL Industries, Inc.), purchased Buckman and Pritchard's mining and milling operations (Gunter, 1924; Calver, 1957; Elsner, 1997). These operations ceased in 1929. Rutile contains less iron than ilmenite, and is more suitable for the titanium metals industry than for pigments. The first-reported exploitation of rutile in Florida was at Mineral City in 1925 (Gunter, 1927).

From 1929 to 1939, no companies mined heavy minerals in Florida. In 1940, the Riz Mineral Company was formed and produced a small quantity of ilmenite, rutile, and zircon (Calver, 1957), exploiting heavy minerals from beach sands near Melbourne, Florida, and later from sands in an area near Vero Beach, Florida. In general, this operation mined natural concentrations of heavy minerals found in areas along the coastal beach from Cape Canaveral southward to the vicinity of Eau Gallie Beach. The concentrates were trucked several miles to a mineral separation plant located at Palm Bay. Production was mostly continuous until 1946 and intermittent until 1948, when the operation was sold and operated under the name Florida Ore Processing Company, Inc. Improvements were made to the Palm Bay mineral separation plant, and five products were sold: ilmenite, rutile, zircon, garnet, and monazite.

The Hobart Brothers, Inc. organised a mining company under the name Florida Minerals Company to dredge and concentrate heavy minerals from deposits located south of Vero Beach. The concentrates were processed at Florida Ore Processing Company, Inc.'s Palm Bay mineral separation plant. Florida Minerals Company later mined a Florida deposit west of Winter Beach, Indian River County. In March 1955, the Florida Ore Processing Company ceased mining activities but continued to process heavy-mineral concentrates supplied by Florida Minerals Company. After a fire at the Palm Bay mineral separation plant on October 17, 1955 (Calver, 1957), a new processing plant constructed by Hobart Brothers, Inc. near the Winter Beach mine operated from February 1956 until 1963.

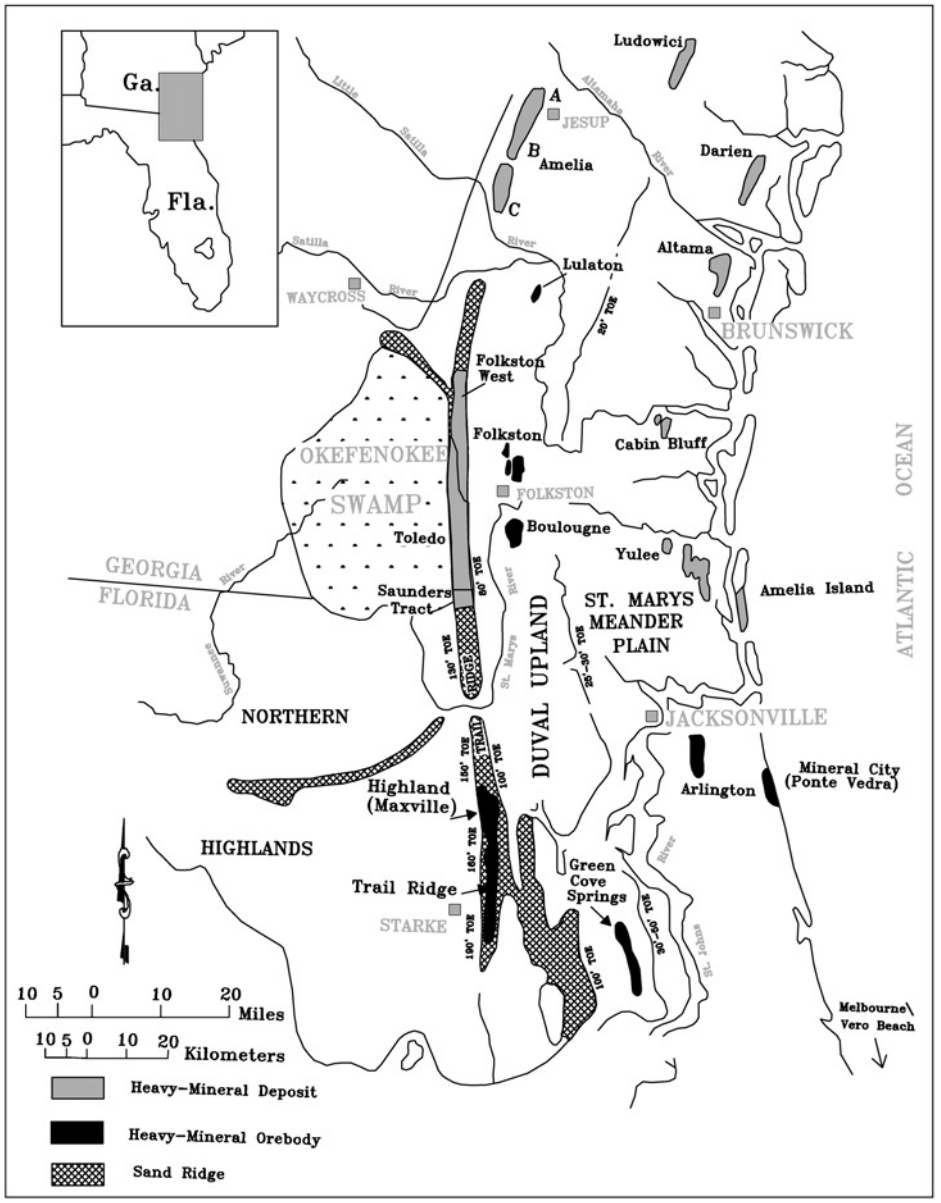

Fig. 2. Heavy-mineral deposits located in southeastern Georgia and northeastern Florida. The Lulaton, Folkston, Boulougne, Green Cove Springs, Arlington, and Mineral City (Ponte Vedre) orebodies have been exploited. The Trail Ridge and Highland (Maxville) orebodies are being mined at the present time (February 2007). The other heavy-mineral concentrations have not been developed. The Amelia concentrations near the top of the figure actually occur in two separate tracts as shown in Fig. 11. Modified from Pirkle et al. (1993b).

In 1942, heavy-mineral mining operations were established by the Rutile Mining Company of Florida, a subsidiary of the Titanium Alloy Manufacturing Company, on a 2-km^2 tract situated in Duval County, Florida some 16 km east of the centre of Jacksonville, Florida, in an area now known as Arlington (Fig. 2). Titanium Alloy Manufacturing Company was a subsidiary of National Lead Company (NL Industries, Inc.). In 1944, the Humphreys Gold Corporation, later known as Humphreys Mining Company, took over the operation under leases from National Lead Company and Rutile Mining Company of Florida (Detweiler, 1952). They operated the mine and mineral separation plant until operations ended in 1964.

The large Trail Ridge heavy-mineral deposit of northern Florida was discovered by E.I. du Pont de Nemours & Co. (DuPont) geologists in cooperation with the U.S. Bureau of Mines and the Florida Geological Survey, and was developed by DuPont (Garnar, 1980). In December 1947, DuPont entered into a lease with the State of Florida's Armory Board to mine a titanium-mineral-bearing property located on the Trail Ridge landform within the boundary of Camp Blanding in Clay County, Florida. In January 1948, DuPont engaged Humphreys Gold Corporation to design, construct, and operate a mine and associated mineral separation plants to exploit this reserve. Construction on the Trail Ridge Plant commenced in April 1948 and production began in April 1949 (Carpenter et al., 1953). DuPont developed a second mining complex on the Trail Ridge landform known as DuPont's Highland Plant, operated again by Humphreys Gold Corporation; production began in April 1955 (Roberts, 1955). DuPont took over operations of both the Trail Ridge and Highland plants in 1958 when the contract with Humphreys Gold Corporation expired. When DuPont opened their Maxville mine on Trail Ridge in 1992, the Highland mine closed, although the Highland mineral separation plant continues to operate and to process the Maxville heavy-mineral concentrate. The Trail Ridge mine and mineral separation plants are still in operation (Fig. 3) but the mine is nearing the end of its reserves. The Trail Ridge mine is expected to cease operation in the spring of 2007.

In the summer of 1951, Owen H. Perry discovered a fluvial placer in the lower valley of Horse Creek in Aiken County, South Carolina (Fig. 1). Mining of this deposit began in the spring of 1955 near Clearwater, South Carolina. Marine Minerals, Division of Heavy Minerals Co., Inc., operated a dredge on the property for recovery of heavy minerals from June 1955 to July 1958, though gravel operations continued (Williams, 1967). O.H. Perry first controlled the deposit and mining equipment with financial backing of the Callahan Lead and Zinc Co. Later, ownership passed to the Crane Co., the Vitro Corporation of America, the French Pechiney organisation, and finally the Heavy Minerals Co. (Mertie, 1975).

In 1962, the Glidden-Durkee Division of SCM Corporation began exploiting a deposit at Legler, Jackson Township, Ocean County, New Jersey, ~3 km north of Lakehurst. This operation lasted until 1978 when the recovery of heavy minerals ceased, although sand is still produced from this mine by the current owner, Clayton Companies.

Asarco, Inc. opened their Manchester mine in 1973. This deposit is ~96 km south of New York City near Lakehurst, New Jersey in Manchester Township, Ocean County. Mining ceased in 1982. Heritage Minerals, Inc. continued to reprocess tailings for zircon and monazite until 1990 when all mining-related activities ended.

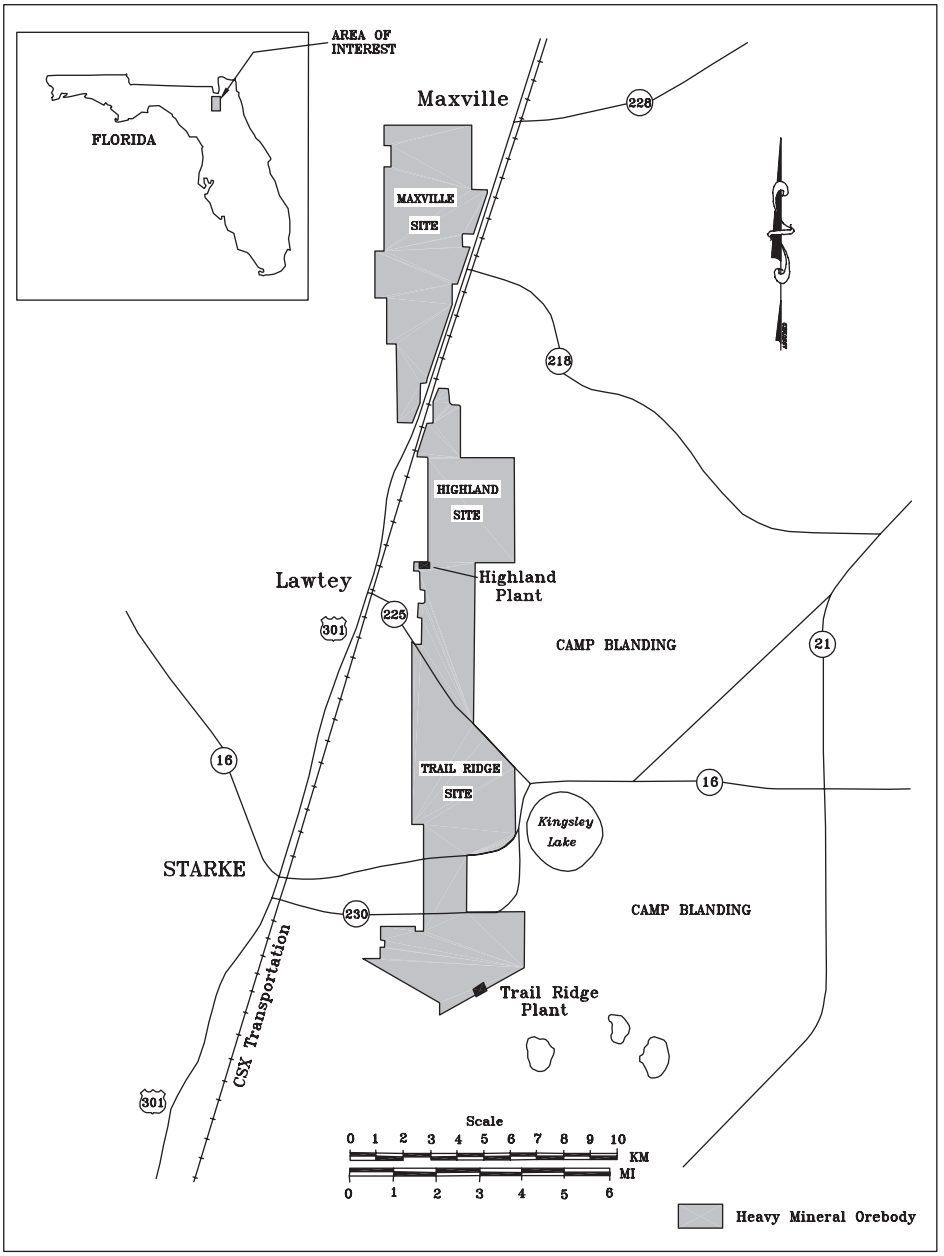

Fig. 3. Relationship of DuPont's Trail Ridge, Highland, and Maxville orebodies and mineral processing plants along Trail Ridge in northern Florida.

In 1964, Humphreys Gold Corporation finished mining in Duval County, Florida, and moved their equipment to an area on the north side of Folkston, Georgia (Fig. 2). Humphreys mined an orebody there, owned by DuPont, until it was exhausted in 1974. Humphreys then moved their mining equipment to Boulougne,

Florida, where they continued to mine under contract to DuPont. The mineral separation plant that had been built to process the Folkston orebody concentrates received Boulougne concentrates until the operation ceased in 1979.

In 1972, Titanium Enterprises, a Union Camp Corporation and American Cyanamid Company joint venture, began exploiting a heavy-mineral deposit located near the town of Green Cove Springs in Clay County, Florida (Fig. 2). On July 1, 1978, Titanium Enterprises ended mining operations and began processing tailings. In late April 1980, Associated Minerals Consolidated, Ltd., a subsidiary of Consolidated Gold Fields, purchased the entire operation. In 1981, Associated Minerals Consolidated Ltd. became a unit of Renison Goldfields Consolidated Limited (RGC). In 1992, the name was changed to RGC (USA) Mineral Sands, Inc. In 1998, RGC and Westrailian Sands, Ltd. merged and, in 1999, the name was changed to Iluka Resources, Limited (Iluka). Iluka ceased mining operations in February 2006, although the reprocessing of tailings through the mineral processing plant continues. In 1997, Iluka Resources, Inc., a subsidiary of Iluka Resources Ltd., opened a mine near Stony Creek, Virginia. Known as the Old Hickory orebody, this deposit occurs along the Fall Zone (Figs. 1 and 4), and is the first mine to be opened in this new heavy-mineral mining district.

In January 2004, TE Consolidated, Inc., a wholly owned subsidiary of Iluka Resources, Ltd., began exploiting the Lulaton orebody, a heavy-mineral deposit located west of Lulaton in Brantley County, Georgia (Figs. 2 and 5). This is the most recent heavy-mineral mine to be opened within the Atlantic and Gulf coastal plains of the United States. Mining ceased June 30, 2006 (Csar, Iluka Exploration Manager, USA, Personal Communication, 2006).

4. HEAVY-MINERAL EXPLORATION IN THE ATLANTIC AND GULF COASTAL PLAINS

The coastal plain lies along the Atlantic Coast of the United States from Long Island, New York, south to Florida and west along the Gulf of Mexico to Mexico. In the Mississippi Embayment, it extends north to southern Illinois. Heavy minerals have been extracted from coastal plain sediments in New Jersey, Virginia, South Carolina, Georgia, and Florida. Also, heavy-mineral deposits have been discovered and evaluated in Atlantic or Gulf coastal plain sediments in North Carolina, South Carolina, Georgia, Tennessee, Arkansas, the barrier islands of the Gulf Coast and the South Carolina, Georgia, and Florida coasts (Fig. 1). Exploration has also been conducted throughout the coastal plain sediments of Delaware, Maryland, Alabama, Mississippi, and Louisiana.

In the early days of heavy-mineral exploration, prospectors searched creeks for traces of dark-coloured minerals that might indicate the possible presence of alluvial placer deposits. Prospectors also searched beaches for surface expressions of dark coloured beach sands. H.H. Buckman and G.A. Pritchard conducted one of the first, if not the first, systematic exploration program for heavy minerals. They examined more than 1250 km of coast, stretching from Charleston, South Carolina to the Straits of Florida, a portion of the Gulf Coast of Florida, and both sides of the Indian River in Florida (Martens, 1928).

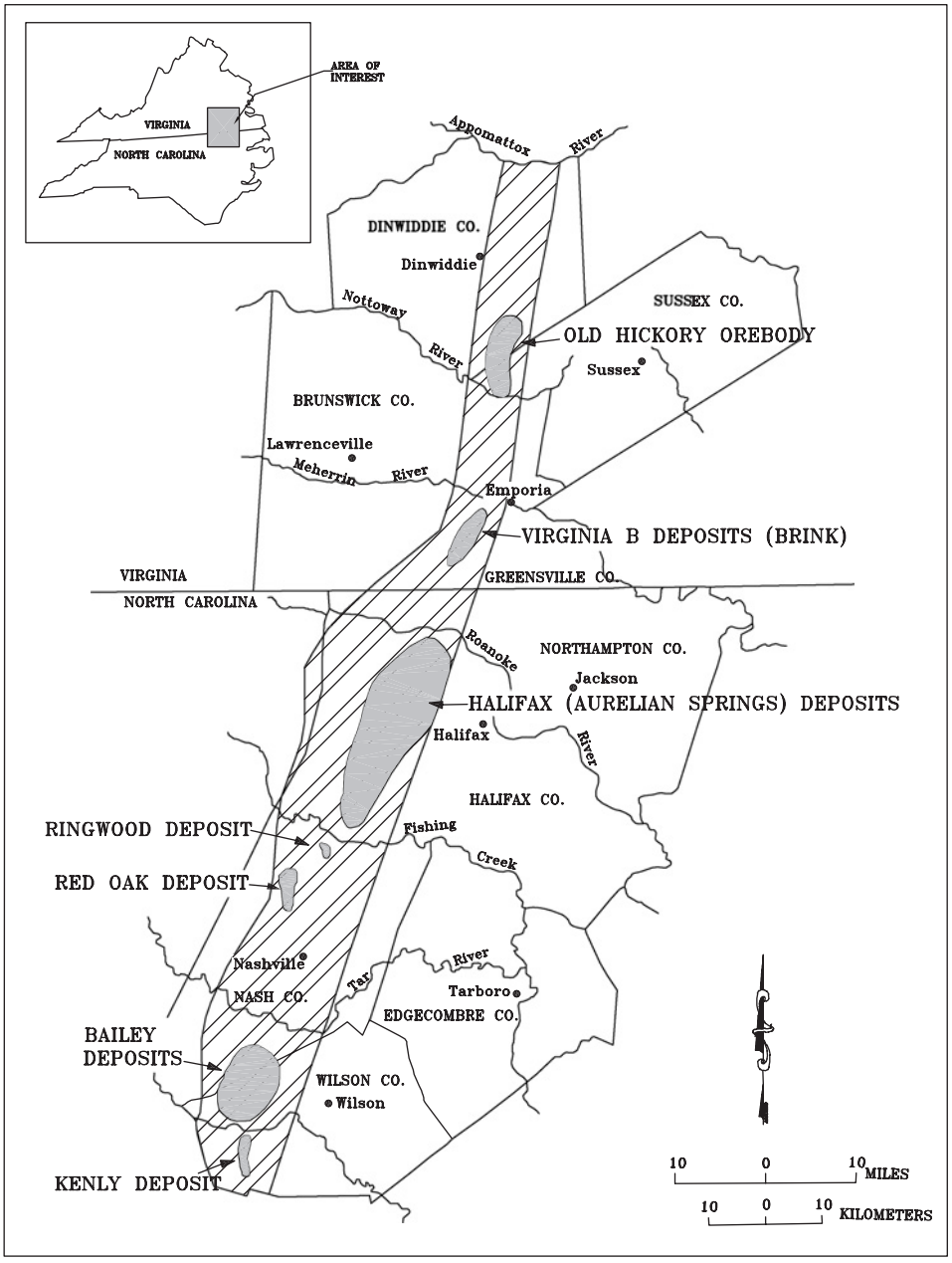

Fig. 4. Areas along the Fall Zone in Virginia and North Carolina in which heavy-mineral concentrations are present. The various areas shown in the figure by parallel lines are not underlain throughout by heavy-mineral concentrations. However, there are heavy-mineral deposits within the lined areas. The Old Hickory orebody is being mined at the present time. The Virginia B (Brink) deposits are being developed. None of the other heavy-mineral concentrations has been developed. Modified from Pirkle et al. (1991b) and Carpenter and Carpenter (1991).

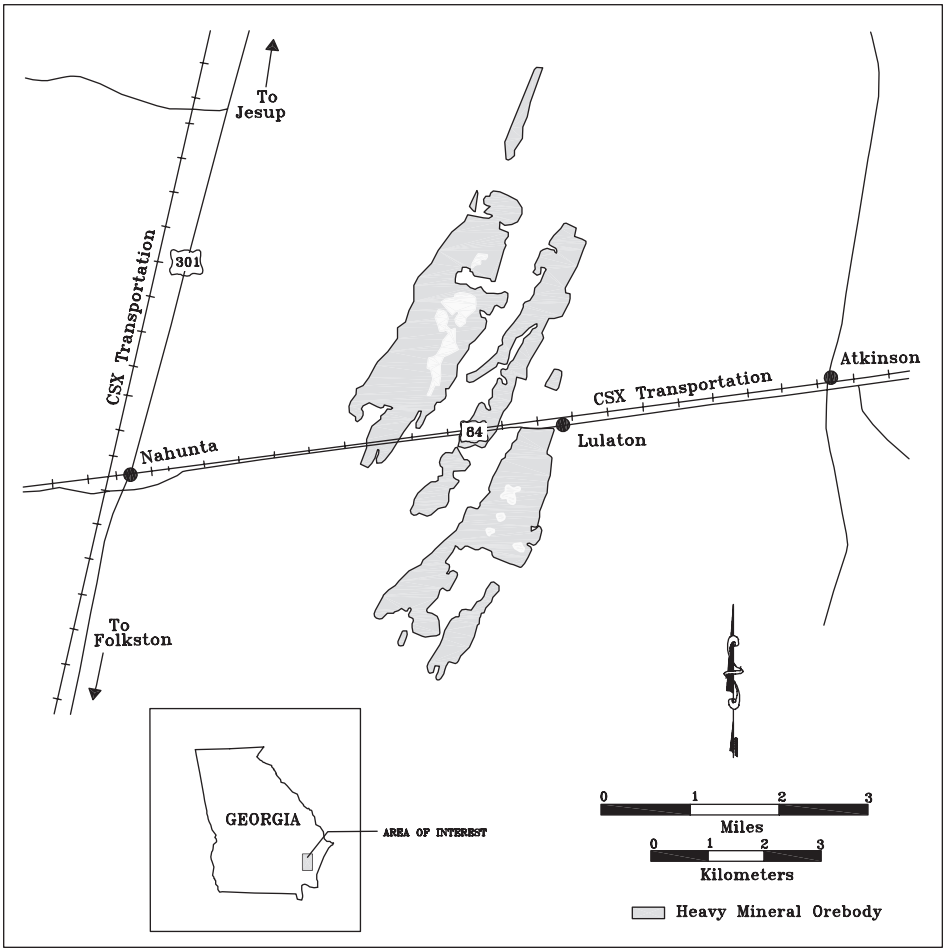

Fig. 5. Location of the Lulaton heavy-mineral orebody in southeastern Georgia. Modified from Iluka Resources, Ltd. (2004).

Martens (1928) performed his own evaluation of the heavy-mineral potential of beach deposits from numerous samples, collected from Florida and some from Georgia. He concluded, that "in case the amount of material at any one place does not justify the erection of a mill, it might be possible to use a portable outfit for separating the heavy minerals from the quartz on the beach and transport the concentrates to the mill for the final separation of the different minerals" (Martens, 1928, p. 154).

Prior to initiating his study, Martens investigated the heavy-mineral deposits at Mineral City and developed an exploration strategy, based on his understanding of the origin of the deposits. He noted that the heavy minerals and quartz, found in the beach sands of the Florida east coast, originated from an ultimate source and, because the only associated grains in the sands on the coastal plain were shell fragments and collophane, the other minerals in the sands had to be originated by the

disintegration of hard rocks such as schist, gneiss, and granite. He reasoned that the "relative proportions" of the various minerals in the sand are different than in their host rocks, therefore, a long series of intervening processes must have occurred to account for what is observed in the beach deposits. Finally, he concluded that the heavy minerals were transported from an ultimate source to an ultimate deposit and were subjected to a series of concentrating processes. Also, he argued that some of the heavy minerals have not come from the Piedmont by a direct path but were delayed in various sediments, later re-entrained and their transport continued to the coast. He concluded that the formation of heavy-mineral deposits, like those at Mineral City, is limited to beaches of either lakes or oceans. Martens also realised the need of preservation, and this led him to conclude that there was not much chance of a large deposit preserved in ancient formations. Using that model, Martens explored modern beaches and collected spot samples for evaluation.

Vernon (1943, p. 145) stated "The difficulty in locating deposits of these heavy minerals has limited the production and the estimation of reserves, upon which the expansions of any plant should be based. The occurrence of these materials along present strand lines should promote the search for concentrations along former strand lines." He suggested that, when a "fossil" strand line is discovered, it should be evaluated by drilling or geophysical methods. In particular, he suggested that a magnetometer might be useful, which is a method, he reported, as recently being used in Oregon. More recently, magnetometer surveys have been used successfully in Australia to locate buried titanium-bearing heavy-mineral deposits in the Murray Basin. The U.S.G.S. (Wynn et al., 1985) suggested that a geophysical method, induced polarisation, be used in exploring for heavy-mineral deposits that lack a surface expression.

In 1948, McKelvey and Balsley published "Distribution of coastal black sands in North Carolina, South Carolina, and Georgia as mapped from an airplane." Geologists examining shorelines from planes have found many heavy-mineral deposits throughout the world. Uranium exploration led to a method of heavy-mineral exploration that would allow large areas to be surveyed quickly by plane. Geiger counters and, later, total-count scintillometers were flown over areas to locate radiometric anomalies that might reflect the presence of monazite and associated heavy minerals. Monazite is the major contributor to the radioactivity of the anomalies because it contains the correct proportions of uranium and thorium to account for the observed anomalies. Generally, zircon is present but its abundance and typical ratio of thorium to uranium is too low to account for much of the radioactivity of the anomalies (Force et al., 1982). Moxham (1954) reported geophysical work with practical application to heavy-mineral exploration, describing an airborne radiometric survey conducted in southeastern Georgia and northeastern Florida.

The use of radiometric surveys to explore for heavy minerals, whether by aerial or ground methods, is based upon the assumption that radioactive minerals such as monazite and zircon are concentrated with non-radioactive minerals such as ilmenite, rutile, leucoxene, and staurolite. (Grosz et al., 1989). Numerous "false" anomalies were detected initially with this method, while some deposits, such as Richard's Bay, South Africa, remained undetected. As the sophistication of radiometric analyses and instrumentation increased, so did the ability of the geologists to eliminate some of the "false" anomalies. Multi-channel gamma-ray spectrometers, for

instance, were used so that explorers were better able to determine the character of the anomaly. By coupling the radiometric character with additional data from sources such as regional geological maps, soil maps, land-use/land-cover maps, and shoreline and terrace maps, explorers could better distinguish anomalies caused by heavy minerals from those caused by phosphate deposits or cultural activities (Force et al., 1982; Grosz et al., 1989; Pirkle et al., 1994). Radiometric anomalies associated with placer heavy-mineral deposits are dominated by thorium radiation, while those associated with phosphate deposits are dominated by uranium radiation. Anomalies associated with cultural activities are characterised by the radioelement spectra of potassium or uranium radiation or both (Robson and Sampath, 1977; Force et al., 1982; Grosz et al., 1989).

In 1988, a major heavy-mineral district was discovered along the Fall Zone of Virginia and North Carolina (Fig. 4). Initially, geochemistry was used to help locate some of these deposits. Analyses of stream sediment samples that had been collected as part of the U.S. Department of Energy's National Uranium Resource Evaluation program were obtained by explorers and evaluated for titanium dioxide. An area along the North Carolina Fall Zone emerged as having anomalously high titanium dioxide values within stream sediments, and an investigation led to the discovery of deposits bearing large quantities of ilmenite.

Many of the tools discussed above depend upon heavy-mineral deposits having a surficial expression (e.g., a modern beach with visible heavy-mineral concentrations, a geomorphic feature with beach line features, a deposit associated with surface radioactive minerals, or a deposit associated with high titanium dioxide values in stream sediments). Recent advances in heavy-mineral exploration involve remote sensing, integrated with other Geographical Information System (GIS) databases to help identify and prioritise exploration targets. Ultimately, however, the modern beaches or the geomorphic features, interpreted as fossil beaches, must be drilled to verify the existence of heavy-mineral concentrations.

The explorer is facing diminishing opportunities of finding large heavy-mineral deposits on modern beaches anywhere in the world, and it is almost impossible to find a deposit that can be mined along the Atlantic and Gulf Coastal plains of the United States. Large deposits, yet to be discovered, will be more difficult to find and may occur in areas where little or no exploration for heavy-mineral concentrations has been undertaken. Procedures (models) must be developed to allow for the screening of large areas that have the best potential for containing heavy-mineral deposits. Pirkle et al. (1994) have described models that may be applicable to future heavy-mineral exploration and have shown how they may be applied to exploration for mineral sands in the coastal plains of the southeastern United States.

Within the Atlantic and Gulf coastal plains, it is becoming necessary for producers to change their economic models and concepts for a commercial heavy-mineral deposit. Martens (1928) was very prophetic when he predicted that portable mining systems might be required if the deposits of the Atlantic and Gulf coastal plains were to be fully exploited. Deposits that are being discovered, evaluated, and exploited are smaller and lower grade than those mined in the past. In January 2004, a subsidiary of Iluka Resources, Ltd., an Australian mining company, began production at a new deposit near Lulaton in southeastern Georgia (Figs. 2 and 5)

that a few years ago would have been considered uneconomic. As times change, exploration techniques must evolve so that smaller and lower grade deposits can be found and evaluated efficiently and cost-effectively, and exploited.

5. HISTORICAL OREBODIES OF THE COASTAL PLAINS

5.1. Atlantic Coastal Plain

Concentrations of heavy minerals in the coastal areas of the southeast are related to both recent and ancient marine shorelines (Lynd and Lefond, 1975). Lyell (1845) recognised a series of ancient shoreline scarps in Georgia, McGee (1887) investigated the Chesapeake Bay region, and Shattuck (1901, 1906) made detailed studies of the terraces in Maryland. Johnson (1907) considered terraces of North Carolina, Veatch and Stephenson (1911) described the Coastal Plain terraces of Georgia, and Stephenson (1912) studied terraces in North Carolina. Many other studies followed the investigations of these earlier workers. Some of the contributions include those by Prettyman and Cave (1923), Cooke (1925, 1931, 1932, 1936, 1941, 1943, 1945, 1966), Flint (1940, 1942, 1947), MacNeil (1950), Price (1951), Richards (1954), Doering (1960), Johnson and DuBar (1964), Herrick (1965), Thom (1967), Hoyt and Hails (1967, 1971, 1974), Colquhoun (1969, 1974), Colquhoun and Pierce (1971), Oaks and Coch (1973), DuBar et al. (1974), Oaks and DuBar (1974), Winker and Howard (1977), Howard and Scott (1983), Kussel and Jones (1986), Markewich (1987), and Huddlestun (1988).

There was, and still is, much dispute as to the total number and ages of terraces present in the Atlantic Coastal Plain. Workers such as Cooke (1941, 1945), Flint (1940, 1942, 1947), MacNeil (1950), and Parker and Cooke (1944) have identified as many as seven old shorelines with which the heavy-mineral deposits can be associated. The four most widely recognised of the shorelines are Okefenokee (46 m above sea level), Wicomico (+31 m), Pamlico (+8 to 11 m) and Silver Bluff (+2 to 3 m). All are regarded as lines of farthest marine transgression during interglacial and postglacial periods, and all have produced commercial heavy-mineral deposits (Lynd and Lefond, 1975).

Winker and Howard (1977) correlated three major shoreline successions on the Atlantic Coastal Plain and found that the highest and innermost succession follows the line of maximum transgression in the Pliocene. The oldest and highest succession hosts the Trail Ridge, Highland, and Maxville orebodies that occur along the Trail Ridge physiographic feature in northern Florida (Figs. 2 and 3). Orebodies currently being mined and developed in Virginia (Fig. 4) might also lie on this same shoreline (Carpenter and Carpenter, 1991; Garnar and Stanaway, 1994). The shoreline is not everywhere at the same elevation; some workers believe that this is a result of subsequent relative uplift in northern Florida and even greater uplift on the Cape Fear Arch around the border between North Carolina and South Carolina. In central Florida, the base of the shore and dune sands is around 45 m above sea level, dropping gradually northward to a minimum of 30 m above sea level in the Southeast Georgia Embayment. From Georgia, it rises gradually until, in North Carolina

and Virginia, a closely spaced series of parallel-stepped shoreline packages sits on bases 60–75 m above sea level (Stanaway, 1996).

The Folkston, Boulougne, and Green Cove Springs orebodies of Georgia and Florida (Fig. 2) are located on Winker and Howard's Effingham shoreline succession of Pleistocene age. The lowest and youngest regressional beach ridge sand accumulations are termed the Chatham Sequence by Winker and Howard (1977) and may be separable into two units in Georgia and the Carolinas (Garnar and Stanaway, 1994). Heavy-mineral concentrations in the inland beach ridges of the Chatham Sequence in Florida include the Jacksonville (Arlington) orebody and Yulee deposits, the Cabin Bluff and Altama deposits in Georgia (Fig. 2), and the Aurora and Chowan deposits in North Carolina (Fig. 1). The deposits on or near the present-day coast of the outer edge of the Chatham Sequence include the Mineral City (Ponte Vedra) orebody (Fig. 2).

There seems to be a general absence of heavy-mineral deposits in the Central Atlantic Coastal Plain in the Carolinas. Garnar and Stanaway (1994) suggest that this may be the result of the rivers eroding only the low-grade metamorphic rocks of the Carolina Slate Belt, which are poor sources of titanium minerals. Earlier, Puffer and Cousminer (1982) concluded that the concentrations of titanium along the beaches of South Carolina and Georgia are caused mainly by climatic factors that allow for the development of thick, well-drained saprolites over granitic and gneissic rocks. They further stated that the lack of modern titanium beach placers along the beaches of North Carolina cannot be ascribed to differences in source rocks. They contended that the granulite-facies metamorphic rocks of the Appalachians from Maine to Georgia, described by Force (1976), are important source rocks of the southeastern placers in most northeastern Atlantic Coast states.

The Atlantic Coastal Plain deposits are economic because of the presence of altered ilmenite, called leucoxene. Ilmenite grains have undergone leaching of their iron content to yield titanium upgrades from 50% to around 60–70% or higher (Cannon, 1957). Dimanche and Bartholome (1976) and Mucke and Chaudhri (1991) describe the process of natural alteration. The greatest amount of ilmenite leaching has occurred in the older deposits, whether alluvial or fluvial, for which Stanaway (1996) proposes three possible causes. First, the source rock for the older deposits may have been metamorphic, and more completely weathered during the Cretaceous to mid-Tertiary. Second, these older deposits are generally within a few metres of the surface and have been undergoing prolonged leaching. Thirdly, older shoreline sediments may have been reworked from older inner coastal plain Cretaceous and Palaeogene sediments, whose rates of erosion are now much slower.

5.1.1. New Jersey

Markewicz and Parrillo (1957) outlined four potentially economic ilmenite-sand type heavy-mineral orebodies within the New Jersey Coastal Plain. The resulting exploration conducted by private companies, as well as studies by the New Jersey Geological Survey, resulted in the exploitation of two heavy-mineral deposits from the 1960s to the 1980s. Markewicz (1969) outlined six large deposits in New Jersey, and Stanaway (1992) reported that the aggregate reserve of these deposits could be more than 700 million metric tons of sand, grading 3–5% heavy minerals.

Approximately 75% of the heavy-mineral suite is ilmenite, with zircon being the next most abundant. Markewicz (1969) believed that the Cape May, Cohansey, and Kirkwood Formations had the greatest potential for hosting economic heavy-mineral deposits.

Geological formations. The Kirkwood Formation is of Miocene age and underlies the Cohansey Formation. Markewicz (1969) describes the former as a marine micaceous sand, silt, and clay. Its greatest heavy-mineral potential is in the northeastern portion of the outcrop area and is 6–15 m thick. The heavy-mineral suite is fine-grained and comprised of zircon, kyanite, sillimanite, and rutile with lower percentages of ilmenite than the overlying Cohansey sands. The Miocene Cohansey Formation is a fluvial, poorly sorted fine- to coarse-grained quartz sand (Markewicz, 1969). Its thickness varies from 30 m in its outcrop area to more than 75 m in the lower southeast counties of New Jersey. After the withdrawal of the Kirkwood Sea, the deposition of the Cohansey Formation began in the inland region with deltaic and shallow estuarine deposits occurring toward the coast with local swampy areas. A thin clay veneer coats the sand and heavy minerals in some areas, and pebbles occur locally. Clay beds from <10 cm to 3 m thick are present, but there are no continuous sand members or clay lenses that can be recognised over large distances. The unit containing the ilmenite consists of a fairly clean quartz sand with some gravel and limited clay (Markewicz, 1969).

Puffer and Cousminer (1982) believe that the ore-bearing sands of the Cohansey Formation represent backshore and dune facies that were preceded by sublittoral Kirkwood Formation sand deposition, rather than being part of a fluvial system. According to Stanaway (1992), who studied drill core samples collected from these deposits, there is a clear evidence that the deposits are fluvial.

The Pleistocene Cape May Formation consists of sands and gravels, recycled from the Kirkwood and Cohansey Formations and from sediments further inland. It is limited in areal extent in the ilmenite province in New Jersey, but it may be important because, locally, it contains higher quantities of heavy minerals. The Cape May Formation is interpreted as being deposited along low-elevation inland drainage basins as estuarine deposits, and along the margin of the coast. It varies from clean, fine- to coarse-quartz sand with lenses and pockets of fine to coarse, clean to dirty gravel, commonly occurring as channel-fill deposits (Markewicz, 1969).

Heavy-mineral provenance. Dryden and Dryden (1940), Isphording (1966), Markewicz (1969), and Puffer and Cousminer (1982) suggested that a major percentage of the ilmenite came from Precambrian gneisses and granites, with some contributions from Triassic rocks. These include southern New York and Northern New Jersey granites, gneisses, pegmatites, schists, syenites, diorites, and the central New Jersey Triassic diabases and sandstones. Markewicz (1969) thought that the mineral suite observed in the Cohansey Formation could have been derived from these sources, with the transportation mechanism available. He stated that the low percentages of rutile and monazite in the mineral suite suggests a Precambrian origin because Precambrian rocks in the region generally contain only small quantities of these minerals but contain moderate to locally substantial amounts of ilmenite. Ilmenite also occurs in the Wissahickan Schist and Baltimore Gneiss, which crop out from

southwest of Philadelphia to north of Trenton, New Jersey. Zircon could come from both the northern New Jersey rocks and metasediments and gneisses present between Trenton and Philadelphia. Kyanite, sillimanite, staurolite, rutile, and monazite could have been derived from the Wissahickon Schist and Baltimore Gneiss (Markewicz, 1969).

The path of heavy-mineral transport and concentration probably included several stages, starting with the erosion of heavy-mineral grains from the host rocks by Late Cretaceous to Tertiary tributary streams and subsequent deposition along the ancient coasts. Some of the more stable minerals may have originated in areas far from New Jersey and were added to the Late Cretaceous and Tertiary sediments by longshore currents. Substantial portions of the ilmenite grains are sub-angular, suggesting that they may not have been transported for long distances (Markewicz, 1969). A large percentage of the minerals may have been removed from their original host rocks during the middle or later part of the Tertiary. During transit and alluvial storage, attrition and leaching may have eliminated the less-stable grains and leached iron from the ilmenite (Markewicz, 1969).

The Lakehurst orebody. From late 1962 until the cessation of operations in 1978, the Glidden Company (later known as the Glidden-Durkee Division of SCM Corporation and now owned by Imperial Chemical Industries PLC) produced approximately 81,650 metric tons per year of 61.5% TiO_2 ilmenite/leucoxene concentrate for its own consumption from a property located at Legler, Jackson Township, Ocean County, New Jersey. This location is approximately 3 km north of Lakehurst, New Jersey, on Route 571.

Markewicz (1969) described the ore-bearing sediments at this site as Cohansey sediments varying in thickness from <6 m to >12 m, with an average ore zone thickness of 8 m. The stratigraphy is described as Pensauken (Pleistocene) sand and gravel from 0.3 to 3.0 m thick, overlying the Cohansey orebody. Below the orebody, lies a 6–12 m thick barren red sand zone. Beneath this sand is the Kirkwood Formation, more than 12 m thick. This unit averages 4.5% heavy minerals but only the Cohansey ore was mined. Markewicz (1969) reports a black, silty, lignite/charcoal band up to 5 m thick within the ore in the northwestern portion of the deposit. He interpreted this band as possibly the remains of a partially burned wooded swamp.

The heavy-mineral content of the ore averages 5%, but varies from 3 to >15% over distances of a few metres. An average heavy-mineral grain count for this deposit (Markewicz, 1969) is:

Mineral species	% of heavy-mineral fraction
Ilmenite/leucoxene	85–90
Zircon	2–4
Kyanite/sillimanite	1–2
Staurolite	Trace: 1
Rutile, anatase	Trace: 1
Tourmaline	Trace: >2
Garnet, monazite, epidote, andalusite, hypersthene	Trace

The Manchester orebody. Between 1973 until its closing in March 1982, Asarco, Inc. extracted heavy minerals from the Manchester mine on approximately 4–5 km^2 of land located ~100 km south of New York City, on Route 70 near Lakehurst, Manchester Township, Ocean County, New Jersey. The geology is very similar to that at the Lakehurst mine and the ore-bearing unit is the Cohansey Formation. Reserves were reported to be 163 million metric tons of sand averaging ~4% heavy minerals (Anonymous, 1974) and 1.95% TiO_2 (Li, 1973). The plan was for the mine to begin producing 140,000 metric tons per year of 63% TiO_2 ilmenite, and to eventually increase production to 168,000 metric tons of ilmenite per year. Under this scenario, the operation should have lasted between 20 and 22 years from 1973. All ilmenite production was under a sales contract to DuPont. The mine was closed in March 1982 because of escalating cost and market conditions. At this site, the heavy minerals were pumped as slurry from the dredge pond to a fixed wet mill, where they were separated from the gangue minerals (mainly quartz). The rejects were pumped back to the dredge pond.

Between the time operations ceased and 1986, evaluation of residual materials by private companies for commercial use continued. In 1986, Heritage Minerals, Inc. purchased the property from Asarco, Inc. and leased it to Mineral Recovery, Inc., who performed operational testing for titanium recovery until 1987. Heritage Minerals, Inc. assumed property control, and began recovering and selling ilmenite/leucoxene, rutile, and zircon using the old Asarco dry-mill tailings as feed stock. In early 1990, Heritage Minerals, Inc. began using the tailings from the Mineral Recovery, Inc. operations as feed but, because of economic conditions, ceased all operations in August 1990. Now, the property is the centre of a controversy between land developers and environmentalists. Developers are proposing to build 2450 homes on the 4 km^2 of land originally mined by Asarco (Anonymous, 2003, 2004; Lettman, 2004).

5.1.2. South Carolina

South Carolina consists of three physiographic regions: the mountainous Blue Ridge, the rolling Piedmont; and the relatively flat Coastal Plain.

The Piedmont and the Coastal Plain dominate South Carolina with the Blue Ridge Province as a narrow strip 16 km to some 50 km wide and ~80 km long in the northwest corner of the state. The Fall Line, separating the Piedmont from the Coastal Plain, extends across the state from the vicinity of North Augusta, South Carolina on the Savannah River to the crossing of the North Carolina–South Carolina state border by the Great Pee Dee River.

The Blue Ridge and the Piedmont consists of Late Precambrian to Early Palaeozoic low- to high-rank metamorphic rocks, schists and gneisses, intruded by felsic and mafic igneous masses of Early to Middle Palaeozoic age. The low-grade metamorphic rocks are predominantly pyroclastic volcanics, whereas most of the larger igneous bodies are granitic. The smaller igneous bodies tend to be dioritic or gabbroic in composition. The Coastal Plain is a belt ~160 km wide between the Fall Line and the coast, composed of non-metamorphosed sands, clays, and limestones of Cretaceous to Recent age. The Coastal Plain beds are thinnest at the Piedmont edge and thicken as they dip gently toward the southeast at a steeper angle than the

surface (Heron and Johnson, 1969). A belt of Quaternary sands and clays overlies the older deposits near the coast.

Small fluvial placer deposits of monazite were mined in North and South Carolina from 1887 to 1911 and, sporadically, from 1915 to 1917. The Carolina deposits were located in the headwaters of streams that drained monazite-bearing rocks in the western Piedmont. The richer and more-extensive deposits of Brazil and India, discovered in 1905 and 1909, respectively, rendered the American mining unprofitable.

During the summer of 1951, Owen H. Perry discovered a fluvial placer in the lower valley of Horse Creek in Aiken County, South Carolina. Horse Creek's headwater is in Edgefield County, South Carolina, from where it flows in a general southwesterly direction until it joins the Savannah River at a point southwest of Aiken, South Carolina. This deposit is different from other placers in the Atlantic Coastal Plain, mined mainly for ilmenite, because monazite is its primary ore mineral with subsidiary rutile, ilmenite, and zircon. This is the only heavy-mineral orebody to be exploited within the South Carolina Coastal Plain. The deposit is underlain and surrounded by the Late Cretaceous Middendorf Formation. Reworking and concentrating of heavy minerals from Cretaceous and Tertiary sediments and from monazite-bearing old granitic rocks at the Fall Line probably formed this deposit (Mertie, 1975).

Initially, the ore zone was reported to be 11–13 km in length and 550 m in width. However, mining did not verify the length, and whereas the width started out at ~550 m at the upper end of the mineable portion of the deposit its width was reported to have narrowed to ~250 m or less. The alluvium at the start of mining was ~6 m thick and consisted of silt, sand, and gravel. At the base of the section, an approximately 1.2 m thick fine quartz-gravel stratum rests upon the Middendorf Formation. This gravel was sold for use as concrete aggregate and helped to make the deposit economic (Mertie, 1975).

According to Mertie (1975), the heavy-mineral content ranged from 1 to 2% but usually ran from 1 to 1.5%. Estimates of the proportions of mineral species recovered from the jigs at the plant are as follows (Mertie, 1975):

Mineral species	% of recovered heavy minerals
Ilmenite	23
Zircon	19
Rutile	15
Monazite and xenotime	8
Staurolite	7
Quartz and other minerals	28

The ratio of xenotime to monazite has been reported from 1:12 to 1:32 with the most probable value between 1:15 and 1:20 (Mertie, 1975). Ilmenite, zircon, rutile, monazite, and xenotime were the main heavy minerals of value, although some staurolite was also sold for sand blasting. Monazite and xenotime comprised ~12% of the saleable minerals. Heavy-mineral mining ceased in 1958.

5.1.3. Georgia and Florida

Heavy minerals have been mined from surface sands and near surface sands of the Atlantic Coastal Plain in Florida and Georgia for decades. These heavy-mineral concentrations occur mostly in beach ridges of quartz sand that formed along ancient shorelines during the late Cenozoic. However, not all of the ore-grade concentrations have the same origin or the same heavy-mineral suite (Table 1).

Important heavy-mineral deposits in northern Florida and southeastern Georgia (Fig. 2) have been described earlier. Many investigators have studied the deposits on which the heavy-mineral orebody ridges rest. Fenneman (1938) described the materials underlying the terrace surfaces as consisting of poorly stratified, sometimes cross-bedded, sheets of sand, gravel, and clay. Herrick (1965) described these sediments in Georgia as composed of interbedded sands and clays with clays becoming more predominant in down-dip coastal areas. Herrick (1965, p. 2) further stated that many investigators treated the deposits as "physiographic forms, classifying them as marine terraces consisting of marine and fluvial sediments." Huddlestun (1988) points out that the terraces are geomorphic features, not stratigraphic units.

In general, the sediments on which the ridges rest are mostly sand and clayey sand with the clay content usually increasing in the lower parts of the sediments. At some sites, thin stringers and small lenses of massive clay are common and become more abundant with depth. In some areas, granules and small pebble size particles of quartz are common, especially in the lower portions of the sediments. Deltaic materials constitute an important part of the surface sediment blanket at the sites where major rivers emptied into the seas as the sediments were accumulating (Pirkle et al., 1991a). Winker and Howard (1977) recognised some areas where the formation of deltas was significant.

Folkston orebody. DuPont discovered the Folkston deposit in September 1952 during the exploration of elevated sand bars and ancient shorelines lying along the Atlantic and Gulf coasts. Gillson (1955) reported that the Folkston deposit comprised three units: the Main Area, the West Extension, and the North Extension. The Main Area covers 7.8 km^2, the West Extension 1.3 km^2, and the North Extension 1.7 km^2. Of the 10.8 km^2 of the three areas, ore underlays some 9.3 km^2. Gillson estimated the total in ground titanium mineral reserve at 998,685 metric tons (Table 2).

Folkston is in the southeastern corner of Georgia, in Charlton County, approximately 18 km north of the Florida line and ~55 km inland from the Atlantic Ocean. Gillson (1955, pp. 3–4) describes the topography of the area north and east of Folkston where the titanium-bearing sand was found as "remarkably flat, lying (except for some swampy areas) between the 85' and 95' contours." East of the main orebody is a creek called Gibbs Branch. The northern limit of the ore zone in the Main Area is the valley of May's Bluff Branch, an eastward-flowing tributary of the Satilla River. A total of 0.33 km^2 of the swampy areas occur within the mining area. According to Gillson (1955), these depressions, which had no outlets, were neither erosion channels nor sinkholes but were original, and were formed at the time of sand-terrace deposition. Many were elongated in a north–south direction, and he identified them as lagoons or depressions that were never filled. These areas, even when occurring within the ore deposit, carry no ore and contain dense growths of cypress trees.

Table 1. Weight percent of total heavy minerals*

Mineral species	Heavy mineral deposit													
	Trail Ridge		Highland (Maxville)	Folkston	Boulougne	Green Cove Springs		Jacksonville	Yulee	Cabin Bluff	Altama	Little Talbot Island	Amelia Island	Mineral City
Ilmenite	34.7	36.8	32.8	31	35.2	47.0	33.8	38–40	52.7	62.0	54.6	31.0	37.0	ca. 47
Leucoxene	7.9	14.3	10.1	27	19.8	6.4	2.2	4–10	2.2	3.0	1.7	4.8	9.7	ca. 3
Rutile	3.4	1.7	1.8	7	6.8	4.6	7.4	7–10	7.4	5.6	6.9	3.4	4.6	5.4
Zircon	20.6	15.0	16.2	9	13.0	15.1	16.0	10–15	16.0	14.1	10.5	4.9	11.2	11.1
Kyanite/ sillimanite	17.5		12.3			6.7			6.7	5.1	8.4			
Staurolite	11.0		19.5			9.4			5.2	3.7	6.0			
Spinel	0.0		0.1			0.1					0.0			
Corundum	0.6		0.4			0.3				0.1	0.1			
Tourmaline	4.2		6.7			6.2			1.7	1.4	2.7			
Monazite/ xenotime	0.1	0.03	0.1	1	0.5	0.7	0.2	0.5–0.7		1.7	0.9	0.1	0.2	0.8
Garnet	0.0		0.0			0.5			0.4	0.8	0.3			
Epidote	0.0		0.0			3.1			6.6	1.8	7.3			
Hornblende	0.0		0.0			0.1			0.8	0.8	0.6			

*From Pirkle et al. (1991a) and Elsner (1997).

Table 2. Summary of areas and tonnages, Folkston, Georgia*

Area	Depth (m/ft)	Km^2/acres	Wt.% heavy mineral	Tons heavy mineral metric/long	% TiO_2 in heavy mineral	Tons TiO_2 metric/long
Main area	2.70/8.89	7.1/1748.9	4.36	1,339,559/1,318,399	41.9	560,621/551,765
West extension	2.15/7.05	0.9/230.5	3.45	110,710/108,961	42.9	47,496/46,746
North extension	2.20/7.23	1.2/299.4	4.23	178,908/178,082	43.6	78,844/77,599
Total or average	2.58/8.48	9.3/2278.8	4.27	1,631,209/1,605,442	42.1	686,962/676,110

*From Gillson (1955).

Gillson (1955) suggested that, because the deposit at Folkston is a wide bar with a flat top, it is better described as a marine terrace and not a sand bar or old shoreline. A little north of Folkston, the terrace is 6 km wide and over 30 km long. Gillson (1955, p. 13) stated: "After the Illinoian glacier withdrew and the ice melted and the water ran to the sea, the level of the sea rose to the 100-foot stage. This stage is now called the Wicomico—and it was during this time that the clays of the marine terrace of the Folkston area were covered with sand, partly mineral-bearing." Elsner (1997) believed the Main Area formed as part of a barrier island that can be correlated with one of the maxima of the Penholoway transgression, and the Folkston North and West extensions are presumed to have formed as nearshore bars during the same transgression. It is possible, however, that the deposit formed during a stillstand of the sea during a period of general regression over a regressional beach ridge plain (Pirkle et al., 1991a).

The deposit was evaluated by drilling and collecting samples from each 1.5 m of drill hole. The scintillation counter, used in uranium exploration at the time, proved helpful, although somewhat limited as a prospecting tool. The discovery of the North Extension orebody was achieved sooner than would have happened through systematic exploration by drilling, and the scintillation counter proved useful in eliminating areas of no importance. It permitted rapid screening of large areas and revealed that monazite and zircon in the sand caused the scintillation counter to react (Gillson, 1955).

Titanium minerals comprise 57–65% of the heavy-mineral suite in the Main Area (Table 3) and in the West and North extensions (Table 4). A single titanium product, averaging 72% TiO_2 (Gillson, 1955) containing ilmenite, leucoxene, and rutile, was produced from this deposit and sold to DuPont. DuPont also purchased the zircon concentrate that was produced as a by-product of the operation. A second by-product, a monazite concentrate, was also produced and was sold to W.R. Grace & Co. To increase the rare earth-content in the monazite concentrate, xenotime was separated from the heavy-mineral concentrate and mixed with the monazite. This procedure increased the rare earth-content from ~56–57% to >60%, which allowed the monazite product to sell for a higher price.

Table 3. Mineral analyses of samples from the Main Area of the Folkston, Georgia, heavy-mineral deposit

Mineral species*	Gillson (1955)	Anonymous (1959)†	Folkston—ore sand; Elsner (1997)
Total heavy mineral content (%)	4.66	3.81	4.22
Average ore thickness (m/ft)	2.85/9.38	NR	NR
Ilmenite	43.9	59.6	31
Leucoxene	10.25	In ilmenite	27
Rutile	5.13	In ilmenite	7
Total titanium minerals	59.28	59.6	65
Zircon	16.44	16.5	9
Kyanite	7.80	7.9	2
Sillimanite	In kyanite	In kyanite	5
Andalusite	In kyanite	In kyanite	<0.5
Staurolite	11.49	11.5	9
Tourmaline	In staurolite	In staurolite	3
Epidote	3.64	3.7	3
Garnet	In epidote	In epidote	1
Hornblende	NR	0.0	<0.5
Monazite	0.74	0.8	1
Xenotime	NR	In monazite	<0.5
Topaz	NR	0.0	1
Corundum	NR	0.0	0
Spinel	NR	0.0	0
Anatase	NR	0.0	<0.5
Sphene	NR	0.0	<0.5
Chloritoid	NR	0.0	<0.5

Note: NR = not reported.
*The abundance of each mineral species is reported in weight percent as is the total heavy mineral content.
†As reported in Elsner (1997).

The Folkston titanium deposit is a thin mantle of sand over clay. The clay has the same heavy-mineral suite as the overlying sands but in quantities too low (<1%) to be economically mined. Gillson (1955) provided sieve analyses of heavy minerals from all three areas (Table 5).

Only the Main Area of the Folkston deposit was mined. The heavy-mineral production, which began in August 1965, ceased in July 1974, and Humphreys Mining Company moved its mining equipment across the Florida state line and began mining near Boulougne, Florida. The reclamation that took place at the end of mining the Folkston deposit left behind "eye-pleasing green pastures enhanced by two lakes for recreation and water storage" (Anonymous, 1970, p. 36). The state of Georgia gave Humphreys Mining Company an "outstanding reclamation of surface mined land" award for their efforts.

Table 4. Mineral analyses of composite samples at the Folkston, Georgia, heavy-mineral deposit*

Mineral species	West extension	North extension
Total heavy mineral content (%)	3.4	4.12
Average ore thickness (m/ft)	2.02/6.65	2.15/7.07
Ilmenite	39.08	42.56
Leucoxene	12.82	10.44
Rutile	5.34	6.07
Total titanium minerals	57.24	59.07
Zircon	21.66	21.61
Kyanite	7.53	6.75
Sillimanite	In kyanite	In kyanite
Andalusite	In kyanite	In kyanite
Staurolite	11.68	10.41
Tourmaline	In staurolite	In staurolite
Epidote	0.42	0.88
Garnet	In epidote	In epidote
Hornblende	NR	NR
Monazite	0.545	0.51
Xenotime	NR	NR
Topaz	NR	NR
Corundum	NR	NR
Spinel	NR	NR
Anatase	NR	NR
Sphene	NR	NR
Chloritoid	NR	NR

Notes: NR = not reported. The abundance of each mineral species is reported in weight percent as is the total heavy mineral content.
*From Gillson (1955).

Boulougne orebody. The Boulougne deposit is located in a ridge area on the Duval Upland in extreme northeastern Florida, between the towns of Boulougne and Hilliard (Fig. 2). In the general area of the deposit, the Duval Upland has an elevation of ~23–27 m. The highest elevation of the ridge, in which the heavy-mineral orebody occurs, is approximately 32.5 m (Elsner, 1997). According to Lynd and Lefond (1983), the orebody trends in a north–south direction and is ~4–5 km long, 0.8–1.2 km wide, and 2–8 m thick. Its northern boundary is the St. Marys River, which is actively eroding the deposit.

The ore-bearing quartz sands are loose to slightly consolidated, well-sorted, and fine-grained containing an average of 3–4% heavy minerals (Pirkle et al., 1974). The principal ore minerals are ilmenite, leucoxene, zircon, and monazite (Table 6). The ore-bearing sands are underlain by sands with diminishing heavy-mineral content that, in turn, are underlain by a clayey sand of various colours, then by a thin shell bed, and finally by Miocene sediments of the Hawthorne Formation.

The ilmenite is highly altered, with a TiO_2 content commonly exceeding 63%. There is a distinct weathering profile (Pirkle et al., 1974; Table 7) near the surface

Table 5. Size analyses (weight percent) of heavy minerals in composite samples from the Folkston heavy-mineral deposits*

Mesh	Main area				West extension			North extension		
	Spl. 1	Spl. 2	Spl. 3	Spl. 4	Spl. 5	Spl. 6	Spl. 7	Spl. 8	Spl. 9	Spl.10
+48	–	–	–	–	–	–	–	–	–	–
−48 to +60	–	–	–	–	–	–	–	–	–	–
−60 to +80	–	0.6	0.4	–	–	–	–	–	–	–
−80 to +100	–	3.2	2.6	3.1	3.2	3.8	5.0	6.3	4.9	4.7
−100 to +140	33.5	25.4	33.5	32.7	34.6	38.3	42.9	46.9	43.0	44.2
−140 to +200	63.3	71.3	63.0	64.1	62.2	57.9	52.1	52.1	52.1	51.1
−200 to +270	–	–	–	–	–	–	–	–	–	–
−270 to +325	–	–	–	–	–	–	–	–	–	–

*Modified from Gillson (1955).

that has elevated TiO_2 levels in the ilmenite and leucoxene (Rose, Written Communication, 2004).

Pirkle et al. (1974) suggested that the Duval Upland is a regressional beach ridge plain that formed when the regressing seas underwent periodic stillstands of relatively long durations and even slight transgressions. During these intervals, more prominent ridges formed and greater concentrations of heavy minerals accumulated. Elsner (1997) stated that the placer accumulated in a nearshore bar environment at the maximum of the Penholoway transgression. He believed that, during the regression of the sea, barrier islands formed a little farther east allowing heavy minerals to be concentrated in dunes, leading to placer deposits similar to those in Folkston's Main Area. Rose (Written Communication, 2004) stated that the deposit may have formed as a regressive barrier island along the Penholoway shoreline, and was flooded during a subsequent Pleistocene transgression. A period of sea level stasis followed by a regressing sea stranded the Boulougne sand body at its present location. Rose thought that the sands that underlie the deposit are fluvial and the clays were deposited in backbarrier lagoons.

Humphreys Mining Company mined the deposit from 1974 to 1979 for DuPont and, according to Elsner (1997), during that period produced 193,137 metric tons of titanium product, 50,046 metric tons of zircon, and 2834 metric tons of monazite. As at Folkston, the Humphreys Mining Company made a single titanium product that contained ilmenite, leucoxene, and rutile. This product was sold to DuPont and assayed 71.7% TiO_2. A zircon concentrate was made and sold to DuPont, and a monazite concentrate was made and sold to W.R. Grace & Company.

The northern portion of this deposit, mined by Humphreys Mining Company, now has houses built upon the tailings, whereas the unmined portion of the deposit is in timber. Over the last several years, there has been renewed interest in possibly mining additional portions of the deposit. Large parts of the deposit remain unmined because the cutterhead dredge used by Humphreys Mining Company was unable to mine the shallow portions (Rose, Written Communication, 2004), which has an average depth of 3.6 m.

Table 6. Heavy-mineral suite of the Boulougne heavy-mineral deposit*

Mineral species	%
Ilmenite	35.2
Leucoxene	19.8
Rutile	6.8
Zircon	13.0
Monazite/xenotime	0.5
Garnet	0.4
Epidote	2.4
Hornblende	0.6
Sillimanite	6.5
Andalusite	0.3
Kyanite	1.6
Staurolite	8.9
Tourmaline	1.9
Spinel	0.1
Corundum	0.6
Topaz	1.2
Anatase	0.1
Brookite	0.0
Sphene	0.1
Chloritoid	<0.1

*From Elsner (1997).

Table 7. Percentages of selected heavy minerals in 1/8–1/16 mm heavy-mineral fraction, Boulougne Deposit*

Surface sands [ore zone from land surface to depth of 7.6 m (25 ft)]				
Depth (m/ft)	% Leucoxene	% Ilmenite	% Epidote	% Garnet
0–1.4/0–4.5	32.93	24.17	0.00	0.00
1.4–1.8/4.5–6	23.03	37.17	0.00	0.00
1.8–3.0/6–10	1.56	57.01	0.00	0.00
3.0–4.6/10–15	0.33	62.42	0.00	0.00
4.6–5.3/15–17.5	3.16	64.87	0.00	0.00
5.3–5.9/17.5–19.5	2.17	55.59	0.31	1.25
5.9–7.6/19.5–25	1.71	58.55	4.27	1.24
7.6–9.1/25–30	3.10	32.56	22.22	0.82
9.1–10.7/30–35	1.9	18.99	31.01	0.37
10.7–12.2/35–40	2.63	23.22	25.33	0.77
12.2–12.6/40–41.5	2.44	26.56	21.95	0.20

*Modified from Pirkle et al. (1974).

Arlington/Jacksonville orebody. The Jacksonville plant of Humphreys Gold Corporation (Humphreys Mining Company) operated under leases from National Lead Company (now NL Industries, Inc.) and Rutile Mining Company of Florida between 1944 and 1964. During this time, rutile, ilmenite, zircon, and monazite were recovered from a beach deposit located approximately 16 km east of downtown Jacksonville, Florida (Fig. 2). This location is ~4.4 km S80°E of Arlington, Duval County, Florida. In the early 1950s, the deposit was surrounded by the expansion of Arlington, a thriving suburb of Jacksonville (Detweiler, 1952). The main part of the deposit lies north of Atlantic Boulevard, which is a major east–west highway, and extends south of the highway. The main portion of the orebody had maximum dimensions of ~1.5 km by 6.5 km and trended N35°E (Mertie, 1975). The average width of the main deposit was approximately 0.6 km with a north–south length of 10 km (Detweiller, 1952).

The elevation of the plant site is approximately 15 m above sea level (Detweiler, 1952). The elevation of the orebody ranges from 12 to 20 m and averages 16 m above sea level (Mertie, 1975). According to Mertie (1975), the sands mined extend from the surface to a depth of 6–9 m. Based on elevation of the orebody, Mertie (1975) stated that it belongs to the Penholoway terrace. However, he cited evidence of aeolian action and thus leaves open the possibility that the deposit is a dune that lies on the Talbot terrace. Elsner (1997) believed that it was associated with the Pamlico complex and suggested, that during the last interglacial (Sangamonian), the Pamlico-sediment complex developed along the Atlantic coastal plain and a barrier island, which he terms ''Jacksonville Island,'' formed in the area east of Jacksonville. The dimensions of this island are similar to those of Amelia Island to the northeast. West of ''Jacksonville Island'' there was an extensive salt marsh, and large sand dune ridges developed on ''Jacksonville Island'' in which heavy minerals were concentrated. With the onset of the Wisconsinian glacial, a slow regression of sea level began and the former salt marsh, west of ''Jacksonville Island,'' fell dry. Because sea level was falling slowly, an environment favourable to the formation of an extensive beach ridge plain existed. Elsner (1997, p. 31) stated that this plain is ''… clearly visible to the east on air photos and satellite images.''

The Titanium Alloy Manufacturing Company, a division of National Lead Company (NL Industries, Inc.) and its subsidiary, Rutile Mining Company of Florida, founded in December 1942, originally operated the deposit. Rutile Mining Company of Florida began mining the deposit using a bucket wheel dredge, also referred to as a slack dragline dredge. The ore was transported a short distance to a wet plant that used several wet-concentration baffle tables to treat part of the feed, and used flotation to treat the balance. The bulk concentrate was then sent to a dry mill containing electrostatic and electromagnetic equipment for the separation of various heavy minerals from the concentrate (Detweiller, 1952; Mertie, 1975; Elsner, 1997). According to Elsner (1997), National Lead Co. used the ilmenite in their St. Louis pigment plant, and Titanium Alloy Manufacturing Company used the rutile. Neither the dredge nor the wet plant produced a satisfactory rate or yield.

In 1944, Humphreys Gold Corporation took over the operation and installed a plant using, for the first time in Florida, Humphreys Spiral Concentrators for bulk concentrate production. During 1944 and 1945, Humphreys Gold Corporation installed a unit to recover zircon from the bulk heavy-mineral concentrate. When

Humphreys took over total responsibility for the Jacksonville operation on April 1, 1944, they replaced the bucket wheel dredge with a cutterhead suction dredge capable of mining ~363 metric tons/h of sand. The sand was pumped to the concentrator through a 46-cm pipeline.

Detweiler (1952) states that ore begins at the surface over most of the deposit and terminates at a layer of clay that forms the base of the deposit. To the south, the ore zone plunges beneath the surface and is covered by ~6 m of overburden. Detweiler lists the following heavy minerals that make up 4% of the sand:

Mineral species	% of heavy-mineral fraction
Ilmenite	40
Leucoxene	4
Rutile	7
Zircon	11
Monazite	<0.5

Note: Remainder—various silicate minerals including sillimanite, kyanite, staurolite, tourmaline, and garnet

Others, including Calver (1957) and Elsner (1997), have repeated this analysis. Elsner obtained additional analyses from unpublished reports of Humphreys Gold Corp. and reproduced these analyses in his 1997 work. His table is reproduced here as Table 8. Using all available data, Elsner (1997) derived an average heavy-mineral composition of the Arlington/Jacksonville deposit, which appears as the last column in Table 8.

Approximately 4 km south of the main orebody is another deposit, the Skinner Tract, mined between October 2, 1958 and December 31, 1964. This deposit is approximately 5 km in length, 0.8 km in width, and its ore thickness is 2.4–3 m. The ore zone was reported by Mertie (1975) to contain 4–5% heavy minerals, but Elsner (1997) determined the value as 5.5%. This deposit differs from the northern (main) deposit in that the mineral-bearing sands do not begin at the surface but at a depth of 6–9 m above sea level.

An ilmenite concentrate containing 59.9% TiO_2 and a rutile concentrate containing 92.4% TiO_2 were produced (Elsner, 1997). In August 1945, Humphreys began extracting a zircon concentrate from the main deposit, and in 1949 they began producing and selling a monazite concentrate from the main deposit. Small quantities of garnet reportedly were sold to individual customers. Carpco Engineering Company returned to the site after mining had ended and reprocessed the tailings from the operation to recover monazite and xenotime during 1966 and 1967 (Elsner, 1997).

According to Elsner (1997), 7.628 km^2 was mined, containing an average ore thickness of 4.1 m, with an average heavy-mineral content of 5.55%. A total of 2,752,000 metric tons of heavy minerals were produced from the Arlington/Jacksonville orebody. Elsner also lists the TiO_2 content of 10 samples reported in the literature as having an average TiO_2 content of 61.4%, ranging from a high of 64.0% to a low of 59.3%. When the mining on the Skinner tract ceased in 1964, Humphreys

Table 8. Heavy-mineral composition of ore sand of wet mill concentrate* Arlington/Jacksonville orebody

Mineral species	Sample 1 (ore sand) (%)	Sample 2 (ore sand) (%)	Sample 3 (ore sand) (%)	Sample 4 (wet mill concentrate) (%)	Average heavy-mineral composition of the deposit (%)
Ilmenite	40	38	39.2	16	38–40
Leucoxene	4				4–10
Rutile	7	12	10.5	5	7–10
Zircon	11	15	15	3	10–15
Kyanite	Present	10	10	3	3
Staurolite	Present	6	Present	21	6–10
Sillimanite	Present				10–15
(Enstatite)†				24	
Garnet	Present	1	Present	1	1
Monazite/ xenotime	<0.	0.5	0.5	<0.5	0.5–0.7
Tourmaline	Present	Present	Present	6	3–6
Magnetite		4	Present	<0.5	
Epidote		Present	Present	11	10–15
Hornblende		Present	Present	1	1–5
Sphene				1	0.1
Topaz					1–2
Corundum					<1
Andalusite					<1
Anatase					<1
Spinel					0.1
Chloritoid					0.1

*From various authors, as reproduced by Elsner (1997).
†In the fourth sample, the investigator took sillimanite to be enstatite.

moved all plants to Folkston, Georgia, where mining started under a contract from DuPont. While mining the Jacksonville deposit, between 115 and 150 persons were employed by Humphreys Gold Corporation (Elsner, 1997).

Mineral city orebody. Henry H. Buckman and George A. Pritchard, after examining the coast from Charleston, South Carolina, to the Straits of Florida, decided that the only place where ilmenite was found in commercial quantities was along the coast between the St. Johns River and St. Augustine in northeastern Florida (Fig. 2). They formed a mining company, Buckman and Pritchard, Inc., bought property near where the deposit was richest, and erected plants and administration buildings. This settlement became known as Mineral City (Martens, 1928; Elsner, 1997).

Martens (1928) describes the beaches as ~150 m wide at low tide with a line of dunes a few hundred metres wide and heights up to or slightly more than 9 m at the back. Immediately behind the dunes from Mineral City south to St. Augustine were marshes. The heavy-mineral ore occurred in "beds" with width exceeding thickness and length greatly exceeding width. The greatest extent was parallel to the shore

(Martens, 1928). The principal beds occurred on the back part of the beach at the foot of the dunes and extended out a short distance in front of them.

Initially, the foot of the dunes were the richest zones of ore, and contained 60% heavy minerals for a thickness of 0.6–0.8 m with a width of 7.6–10.7 m, but the average sand worked had an average of 20% heavy minerals over smaller dimensions. Beside the beds on the back part of the beach some of the adjoining dunes that appeared richest in dark minerals also were worked. The workings extended almost 5 km north of the mill at Mineral City and 13 km south. To the north, deposits continued, but mining was prevented because the beach was being developed as a pleasure resort (Martens, 1928; Foley, 1992). A floating dredge had limited success because the ore did not, in general, extend below the water table. Most of the heavy minerals in the beach sands were loaded onto trucks and hauled to the wet mill in Mineral City. For part of the beach, a narrow-gauge tramway was used (Martens, 1928) (Frontispiece B).

Mr. W.M. Phillips furnished Martens (1928) the following composition of a wet mill concentrate in percent by number of grains, which is different from weight percent:

Mineral species	Composition of wet mill concentrate (% by number of grains)
Ilmenite	55
Zircon	20
Rutile	6
Monazite	2
Greenspar	14
Quartz	3

Greenspar includes various silicate minerals but the principals are staurolite and epidote. Table 9 provides several more analyses based on percent by number of grains.

When the mine opened in 1916, only ilmenite was produced, but in 1922, for the first time in Florida, zircon was separated on a large scale. All of the zircon concentrate was used in the refractory industry, for which National Lead Company held U.S. patents. National Lead Company purchased Buckman and Pritchard, Inc. in 1922 and made them a subsidiary. In 1925, rutile was separated for the first time (Martens, 1928). Because initially only ilmenite was extracted from the sands, the tailings became important and were reprocessed for their zircon and rutile content. Production reached a peak in 1927. The ilmenite produced had a TiO_2 content of 53.66% and the rutile contained 90.80% TiO_2 (Martens, 1928). Mining activities ceased in 1929 (Martens, 1928; Elsner, 1997).

After mining ended, Buckman and Pritchard, Inc., still a subsidiary of National Lead Company, was renamed the Ponte Vedra Company. This company developed the property residentially and sold it in 1942 (Calver, 1957; Elsner, 1997). Today, the Ponte Vedra Country Club and Golf Course is situated near the centre of the former mining site.

Table 9. Mineralogical analyses of heavy-mineral concentrates from the Mineral City, Florida heavy-mineral deposit*

Sample	Natural heavy concentrate 5 km (3 miles) north of Mineral City	Wet mill concentrate Buckman and Pritchard, Inc.	Natural heavy concentrate 5 km (3 miles) north of Mineral City (corrected for quartz and feldspar)
Total grains counted	1586	3220	1400
	Percent by number of grains		
Quartz and feldspar	11.9	1.5	–
Ilmenite	49.6	45.9	56.2
Zircon	17.2	32.0	19.4
Rutile	6.6	9.7	7.5
Monazite	2.1	3.6	2.4
Staurolite	3.0	2.2	3.4
Epidote	4.8	2.8	5.4
Garnet	1.2	0.9	1.3
Disthene	0.6	0.2	0.6
Sillimanite	0.9	0.2	1.1
Tourmaline	0.3	0.1	0.3
Hornblende	0.2	0.2	0.2
Leucoxene	0.6	0.5	0.6
Titanite	0.1	0.1	0.1
Spinel	Tr	0.1	Tr
Corundum	0.1	Tr	0.1
Andalusite	–	–	–
Collophane	0.9	0.2	1.1
Anatase	Tr	Tr	Tr
Shell (calcite)	Tr	–	Tr

Note: Tr = indicates presence of mineral in amount so small that it did not appear among the grains counted.
*From Martens (1928).

Vero Beach/Melbourne orebodies (Central Florida). The Riz Mineral Company was formed in 1940 to mine the narrow and thin, rich natural heavy-mineral concentrations found along the beaches near Melbourne, Florida from Cape Canaveral southward to the vicinity of Eau Gallie Beach (Fig. 1). According to Vernon (1943), most of the mining occurred along the beach between low and high tide, though some concentrates were mined in the dunes and in shallow water at low tide. The ore concentrates were shovelled by hand into wheelbarrows and dumped onto barges, and were barged to the separation plant located at Palm Bay ~4 km south of Melbourne, Florida, for further processing.

Vernon (1943, p. 142) states: "The raw ore is a dark grey, fine to coarse, cross-bedded, quartz sand containing approximately 28 per cent heavy minerals ...." Using values provided by Vernon, the following composition of the heavy-mineral suite can be calculated:

Mineral species	Heavy-mineral suite composition %
Ilmenite	36
Rutile	36
Zircon	11
Garnet, epidote, staurolite, sillimanite, allanite, and others	18

Vernon (1943) reports that the rutile concentrate produced in 1940 averaged 96% TiO_2, whereas that produced in 1941 averaged 93.5% TiO_2. He further reported that the ilmenite concentrate produced in 1940 averaged 55.0% TiO_2 and the 1941 ilmenite concentrate averaged 54.0% TiO_2.

The placers originally mined by the Riz mining Company on both sides of the Indian River in Brevard and Indian River counties were depleted in 1943. Starting in September 1943, Riz Mineral Company began mining dune placers located 5 km onshore. The ore was still transported to the Palm Bay mill south of Melbourne. The Riz Mineral Company was sold in 1948 and began operating under the name Florida Ore Processing Company, Inc. At this time, a garnet concentrate was produced and the company moved its mining operations to dune placers south of Vero Beach. Mining of these deposits continued until 1954 (Calver, 1957). In 1954, these placers were depleted and mining shifted to areas west of Winter Beach, south of Wabasso and northwest of Vero Beach where, before the end of World War II, George A. Pritchard had discovered a dune placer deposit averaging 1.5–2% by weight heavy minerals (Mertie, 1975; Elsner, 1977). In March 1955, Florida Minerals Company, a subsidiary of Hobart Brothers Welding Company, took over mining the deposit. The heavy minerals were still shipped to Florida Ore Processing Company's mill at Palm Bay for processing. This arrangement continued until the Palm Bay plant burned on October 17, 1955. With the destruction of the mill all Florida Ore Processing Company activities ceased (Calver, 1957; Elsner, 1997). Hobart Brothers Company decided to continue the mining operation in central Florida, and built a new mill near the Winter Beach deposit. From February 1956 to the end of all heavy-mineral mining in central Florida in 1963, ilmenite, rutile, zircon, monazite, and garnet were produced (Calver, 1957; Garnar, 1980; Elsner, 1997).

5.2. *Gulf Coastal Plain*

The host sediments for heavy-mineral deposits in western Tennessee are the Cretaceous McNairy sands, which outcrop within the Mississippi Embayment of the Gulf Coastal Plain. Also, heavy-mineral concentrations have been evaluated in the southwestern part of Arkansas, where they occur in the Late Cretaceous Tokio Formation. Concentrations of heavy minerals have been studied from the Recent barrier islands located along the Gulf Coast from the Florida Panhandle to Louisiana. These occurrences, though none have been exploited, will be examined in more detail later in this contribution.

6. RECENT HEAVY-MINERAL MINES OF THE COASTAL PLAIN

There recently have been four active heavy-mineral operations in the Atlantic Coastal Plain. Two of these ceased mining operations during the winter and summer of 2006, and one is scheduled to cease mining during the spring of 2007.

6.1. Trail Ridge and Highland (Maxville) Orebodies

The largest deposit in the Coastal Plain of Florida and Georgia is the Trail Ridge orebody, currently being mined by DuPont east of Starke, Florida (Figs. 2 and 3). The deposit occurs in the southern part of Trail Ridge, which is one of the most conspicuous topographic features in northern Florida and southeastern Georgia. The elevation of the ridge crest varies from more than 75 m above mean sea level in northern Florida to ~43–46 m above mean sea level near the Altamaha River in Georgia.

Most of the quartz sand composing the Trail Ridge landform is medium (1–2 ϕ) to fine (2–3 ϕ) in size. The medium sand fraction typically constitutes 50–70% of the total sand, and the fine sand fraction usually constitutes 20–40% of the sand (Pirkle and Yoho, 1970). The heavy-mineral suite of Trail Ridge sands consists of ilmenite, leucoxene, rutile, zircon, kyanite, sillimanite, staurolite, spinel, corundum, and tourmaline (Cannon, 1950; Garnar, 1972). Of these heavy minerals, 46% by weight are the titanium minerals ilmenite, leucoxene, and rutile (Table 1). These titanium minerals plus zircon are the main economic minerals of the deposit. Other economic minerals include kyanite, sillimanite, and staurolite.

In 1955, National Lead Company purchased 27.5 km^2 along Trail Ridge immediately north and adjacent to DuPont's mining operations (Miller, 1958) and named the heavy-mineral deposit on this land the Highland Deposit. DuPont purchased the property from National Lead Company in the late 1980s. Because DuPont already had an operating mine and mill complex on Trail Ridge, called the Highland Plant, in an effort to reduce confusion DuPont renamed the Highland orebody the Maxville orebody after the community of Maxville, Florida. On January 26, 1993, DuPont began exploiting the Maxville orebody. The Maxville orebody is a continuation of the Trail Ridge deposit and the grain sizes of the quartz particles are the same as those of the Trail Ridge deposit. As shown in Table 1, the heavy-mineral suite is also very similar.

Holes have been drilled through both the Trail Ridge and Highland (Maxville) orebodies on Trail Ridge to determine the nature of the sediments on which the ridge sands rest. In the Trail Ridge #1 drill hole, which was drilled through the Trail Ridge orebody, ore sands were encountered from the crestal area of the Trail Ridge landform to a depth of ~19 m. These ore-grade sands (mainly medium to fine sands) are separated by an unconformity from an underlying 7-m zone consisting of intercalated layers of peaty or sapropelic sediments and quartz sand. The quartz sand in this underlying unit is primarily medium, fine, and very fine size. Approximately 92% by weight of the upper 1.5 m of this 7-m zone is woody or peaty material. Pirkle and Yoho (1970) and Pirkle et al. (1970) provide sediment characteristics and heavy-mineral data for these sediments.

In the Highland #1 drill hole (Pirkle et al., 1977), drilled through the Highland (Maxville) orebody, Trail Ridge size quartz sand was encountered from the land surface to a depth of ~16.3 m. Of this interval, the upper 10.6–12 m contain ore-grade concentrations of heavy minerals. The sediments beginning at 16.3 m consist of intercalated lenses or layers of quartz sand, clayey sand, sandy clay, and massive clay. The quartz sand in this underlying unit ranges from very fine to coarse, but most of the sand is very fine. As at Trail Ridge #1 drill hole, brown woody (peaty) material occurs in sediments underlying the Trail Ridge sands (Pirkle et al., 1991a). Pirkle et al. (1977) describe the sediments and heavy minerals.

The Florida Geological Survey originally outlined the Trail Ridge deposit. It was proven commercial during a cooperative study completed in April 1947, with the U.S. Bureau of Mines (Calver, 1957). Mining at the southern end of Trail Ridge by Humphreys Gold Corporation for DuPont started in April 1949 (Trail Ridge Plant) with the separation of ilmenite and residue (a mixture of rutile, ilmenite, and leucoxene). Zircon was marketed starting in 1950 (Garnar, 1983), and staurolite in June 1952 (Evans, 1955; Fulton, 1975, 1983). Approximately 16 km north, a second plant (Highland) was opened in April 1955, and in January 1958 DuPont took over both mining operations. In 1993, DuPont started operations at Maxville (Fig. 3). Mining of the Trail Ridge orebody is scheduled to end during spring 2007, but mining of the Maxville orebody will continue.

In 1952, the Trail Ridge plant employed a staff of 225 (Anonymous, 1952). In 1988, ~260 people worked for DuPont in Florida (Pirkle and Reynolds, 1988) and in 1999 ~245 people were employed with payroll and benefits of $17 million per year, purchases of goods and services of $29 million per year, and state and county taxes of $3 million per year (Anonymous, 1999a).

Elsner (1997) recalculated the heavy-mineral content of the deposit, calculating the total area of the Trail Ridge deposit, plus the original Highland deposit, and the Maxville deposit to be 77.6 km^2. Numerous investigators have provided the average thickness of the deposit and average heavy-mineral concentration. Elsner (1997), after reviewing the available data, used an area of 77.6 km^2, an average thickness of 10.7 m, a weight of 1.60 metric tons/m^3, and an average heavy-mineral content of 3.9 wt.% to calculate the original heavy-mineral content as 51.8 million metric tons of available heavy minerals (as titanium minerals 27.4, zircon 7.8, staurolite 8.9 million metric tons, and monazite 15,500 metric tons). Elsner then removed areas that could not be mined for various reasons and determined that the deposit had original reserves of 40.1 million metric tons of heavy minerals.

6.2. *Green Cove Springs Orebody*

The Green Cove Springs heavy-mineral orebody is in Florida to the west of Highway 17 between the towns of Green Cove Springs in Clay County and Palatka in Putnam County (Fig. 2). Iluka Resources, Inc. is currently processing tailings, although mining ceased in February 2006. The deposit was named after the town of Green Cove Springs, along the western shore of the St. Johns River. The deposit is 28 km long and up to 7 km wide, with a thickness of 1.5–13.7 m. Its entire area is in pine timber production. Erosion created by Black Creek restricts the northern extension

of the deposit and a karst depression and erosion by the St. Johns River restricts the southern extension (Rose, Written Communication, 2004; 2005).

In 1966, an exploration geologist working for Union Camp Corporation (now International Paper Company) discovered the main orebody of the Green Cove Springs deposit. He was evaluating all Union Camp-owned forest areas in the southeastern United States. The deposit consists of three separate orebodies. The main orebody stretches from southeast of Green Cove Springs for approximately 25 km to south of the community of Bostwick, in Putnam County, Florida, covering 23.218 km^2. The average width of the main orebody is 1.4 km, forming the eastern and central portion of a weakly delineated ridge (Elsner, 1997). Approximately 2.5 km west of the main deposit is a small orebody that is a few hundred metres wide and approximately 7 km long, covering 1.811 km^2. To the west of this small deposit is the westernmost deposit, which is also ~7 km long and ~1.3 km wide, covering 6 km^2. This deposit is in a ridge that is better defined than the one containing the main deposit. The western deposit reaches a maximum elevation of 39.3 m above mean sea level (Elsner, 1997). Rose (2005) provides descriptions of the deposits that comprise the Green Cove Springs orebody.

The heavy-mineral concentrations are present in ridges of quartz sand that occur in the Duval Upland. Generally, 90% or more of the quartz sand composing the ridges falls into the fine (2–3 ϕ) and very fine (3–4 ϕ) sand fractions (Pirkle et al., 1974, 1991a). The heavy-mineral suite, though similar to that of the Trail Ridge deposit, contains minor amounts of epidote and garnet, which are not commonly found in the Trail Ridge sediments (Table 10). Titanium minerals constitute ~58–62% by weight of the total heavy minerals of the Green Cove Springs deposits (Tables 10 and 11). The ilmenite is highly altered, typically above 63% TiO_2. There is a distinct weathering profile near the surface that has elevated TiO_2 levels in the ilmenite and leucoxene. The heavy-mineral assemblage across the orebodies is highly variable and can result in mineral values in the heavy-mineral concentrate changing by up to 50% (Rose, Written Communication, 2004).

Pirkle et al. (1974) have described the sediments beneath the ridges containing the Green Cove Springs orebody. In one drill hole (U.C. #3, Pirkle et al., 1974), 7.6 m of grey and moderate brown quartz sand with black organic zones overlie ~5.8 m of brown sand. Over 90% of the quartz sand in the top 7.6-m zone is fine to very fine (Table 12). Also, over 90% of the sand in the upper part of the underlying 5.8-m zone is fine to very fine (Pirkle et al., 1974). However, the sand in the lower part of the 5.8-m zone becomes somewhat coarser.

The sediments and the heavy-mineral suites in the areas of the Boulougne and Folkston orebodies are similar in grain size and composition to the Green Cove Springs deposits. Elsner (1992, 1997) believes that the geologic history of the Green Cove Springs deposit is very similar to that of the Folkston and Boulougne orebodies (discussed earlier in this contribution, and in detail by Elsner, 1992). He postulates that the main orebody was formed in a nearshore bar environment during the Penholoway transgression (1.3 ± 0.1 Ma) and speculates that the Western orebody must have been formed as a coastal dune containing a different heavy-mineral suite with less economic minerals than the main deposit (Table 12).

According to (Rose, Written Communication, 2004; 2005), the deposit represents a series of regressive barrier island sequences formed during the Pleistocene. An

Table 10. Average heavy-mineral composition of the Green Cove Springs Main Orebody*

Mineral species	Pirkle et al. (1991a)	Elsner (1992)
Ilmenite	47.0	33.8
Leucoxene	6.4	19.7
Rutile	4.6	8.8
Zircon	15.1	15.1
Kyanite	6.7	1.1
Sillimanite	In kyanite	5.2
Staurolite	9.4	10.3
Spinel	0.1	<0.1
Corundum	0.3	0.3
Tourmaline	6.2	2.7
Monazite/xenotime	0.7	0.7
Garnet	0.5	0.3
Epidote	3.1	0.1
Hornblende	0.1	0.5
Topaz		0.7
Anatase		0.4
Andalusite		0.2
Sphene		0.1

Note: All data are in weight percent.
*Modified from Pirkle et al. (1991a) and Elsner (1992).

initial transgression of the sea, up to the Western orebody location, culminated in an extensive sea level stillstand. Intermittent regression with periodic stillstands, progressing eastward, followed the phase of the previous extensive stillstand, stranding the sand bodies that make up the other orebodies (including the main orebody). Rose believes that predominantly unmineralised fluvial sands and occasional backshore lagoonal clays lacking heavy-mineral concentrations underlie the orebodies.

Pirkle et al. (1974, 1991a) believe that the Duval Upland, upon which these deposits lie, is a regressional beach ridge plain. As the seas regressed, lengthy stillstands and possibly slight transgressions took place. During these intervals beach ridges, some containing heavy-mineral concentrations, were formed.

As noted by Elsner (1997), the ridges containing the Green Cove Springs heavy-mineral deposits are not as well-defined as Trail Ridge and the ridges in the crestal areas of the Pamlico transgression. White (1970) believes that the presence of shells in sediments that accumulate to form ridges along shorelines may play a role in their preservation. Some ridges, formed at the crest of eroding transgressing seas, are distinct and well defined, partly because of the lack of fossils in the original sediments that accumulated to form the ridges. In these cases, the transgressing seas eroded into sediments from which fossil shells, if originally present, had been leached out or dissolved over long periods of time. White concludes that landward sediments are the main suppliers of sand for beach ridges, developed in crestal regions of eroding, transgressing seas. The ridges would not become diminished with age as a result of removal of fossils through solution. In contrast, ridges formed along shorelines of regressing seas or along prograding shorelines are built of sediments

Table 11. Average heavy-mineral composition of the Green Cove Springs deposits*

Mineral species	Union Camp 1	Union Camp 2	Western orebody
Ilmenite	33.9	33.6	26
Leucoxene	20.3	19.1	17
Rutile	8.1	9.4	7
Zircon	16.9	13.4	7
Monazite/xenotime	1.0	0.3	0
Garnet	0.7	0.0	2
Epidote	0.2	<0.1	13
Hornblende	0.8	0.3	2
Sillimanite	4.5	5.9	4
Andalusite	0.3	0.2	1
Kyanite	1.2	1.1	
Staurolite	8.5	12.1	15
Tourmaline	2.0	3.4	4
Spinel	<0.1	0.0	
Corundum	0.2	0.3	
Topaz	0.6	0.8	1
Anatase	0.5	0.0	0
Brookite	<0.1	0.0	0
Sphene	0.2	0.1	0
Chloritoid	0.0	0.0	0

Note: All data are in weight percent.
*From Elsner (1997).

Table 12. U.C. Drill Hole No. 3—mechanical analyses of quartz sand extracted from sediments SE 1/4, SE1/4, Sec. 6, T. 7 S., R. 26 E., Clay County Florida; approximately 9.6 km (6 miles) southwest of Green Cove Springs; surface elevation, 36 m (118 ft)*

Depth (m)	Percent of sand in various size fractions					Mean grain size (mm)
	Very coarse (2–1 mm)	Coarse (1–1/2 mm)	Medium (1/2–1/4 mm)	Fine (1/4–1/8 mm)	Very fine (1/8–1/16 mm) mean grain size (mm)	
Grey sand with black organic zones and moderate brown sand (elev. 36 m; 118 ft)						
0–1.5		0.13	7.00	67.12	25.75	0.18
1.5–3.0	0.02	0.04	5.08	69.44	25.42	0.17
3.0–4.5		0.04	4.46	68.41	27.08	0.17
4.5–6.1		0.04	4.32	73.39	22.25	0.17
6.1–7.6		0.11	4.96	73.51	21.42	0.18
Brown sand (elev. 28 m; 93 ft)						
7.6–9.1	0.04	0.13	5.53	72.78	21.51	0.18
9.1–10.7	0.02	0.13	5.28	69.08	25.49	0.17
10.7–12.2	0.12	1.42	22.68	61.70	14.07	0.23
12.2–13.3	0.08	0.78	23.82	27.27	48.04	0.19

*Modified from Pirkle et al. (1974).

brought by longshore drift or shoreward-transport across the fore-beach. Sediments from the sea contain a relatively high percentage of shells. During later weathering under warm and humid climate, the shells would dissolve and the ridges, having lost a considerable amount of their original bulk, would become less well defined and less distinct.

The Green Cove Springs deposits are in the more interior part of the Duval Upland, rather than along the eastern or seaward edge and the ridges do not appear to lie atop erosional scarps. Of most importance, perhaps, is the fact that no physiographic features in a landward direction appear to be truncated by the shorelines along which mineral-bearing ridges formed.

Titanium Enterprises was established to mine the Green Cove Springs deposit. The company was 50% owned by Union Camp Corporation as the landowner and 50% owned by American Cyanamid Corporation as the mineral purchaser (Pirkle et al., 1974; Lynd and Lefond, 1975, 1983; Elsner, 1997). Mining started in 1972 from the north, proceeding southward, using a cutterhead dredge. Titanium minerals, zircon, and monazite were separated in the early years of mining and the average mining rate was ~1000 metric tons/h (Anonymous, 1979; Elsner, 1997). On July 1, 1978, mining ceased (Anonymous, 1978); while sale negotiations were taking place, tailings were processed for staurolite, zircon, and monazite. In late April 1980, Associated Minerals Consolidated Ltd., a subsidiary of Consolidated Gold Fields Australia, bought the whole operation and mining permits of the Green Cove Springs deposit. The dredge was changed from a cutterhead to a bucketwheel cutter when Associated Minerals purchased the operation. Associated Minerals Consolidated Ltd. established a subsidiary, Associated Minerals (USA) Inc., to operate the mining and milling facilities. In 1981, Renison Goldfields Consolidated Ltd. (RGC), 49% owned by Consolidated Gold Fields and 51% public holding, was established and Associated Minerals Consolidated was one of the four units comprising the new company (Johnson, 1987). In 1992, the name of the operator at the Green Cove Springs deposit was changed from Associated Minerals to RGC Mineral Sands. In 1998, RGC and Westrailian Sands merged and, in 1999, the company name was changed to Iluka Resources Limited, the current name of the Green Cove Springs operator. Elsner (1997) reports that in 1990 the Green Cove Springs operation employed 125 workers at the Green Cove Springs operation.

6.3. Lulaton Orebody

The Lulaton heavy-mineral deposit is in southeastern Georgia about halfway between Nahunta and Atkinson and just west of Lulaton (Fig. 2). U.S. Highway 82 runs east–west and bisects the deposit (Fig. 5). The deposit trends north–northeast and some workers believe it is located along the Penholoway terrace. It is truncated on the north by erosion from the Satilla River and on the south by erosion from Buffalo Creek. Buffalo Creek separates the Lulaton deposit from the Mission deposit south of Buffalo creek.

In 1976, DuPont made several exploration borings in the area now known as the Lulaton deposit. They encountered mineralisation that reached 3 m in thickness, starting at the surface, and averaging 2% heavy minerals. At that time, a minimum of 3 m in thickness averaging 2.5% heavy minerals was required for a deposit to be of

interest, and DuPont did not pursue the property further. It should be noted that the term "mineralisation" is traditionally used in the heavy-mineral mining industry, and refers to economically significant or substantial concentration of heavy minerals within sand bodies. In this contribution, this term is adopted but should not be confused with the process of mineralisation by which minerals are introduced into a rock, forming potential ore deposits.

Iluka Resources, Inc. reassessed the deposit in 2001 and began commercial mining in January 2004, making Lulaton the most recent mine to be opened in the Atlantic Coastal Plain. The Lulaton concentrator had a nameplate feet-rate capacity of 1000 metric tons/h (Folwell, 2004). The heavy-mineral concentrate was trucked from the Lulaton mine to Iluka's dry mill at the Green Cove Springs deposit in Florida for further mineral processing. Mining at Lulaton ceased on June 30, 2006.

Rose (Written Communication, 2004) states that drilling identified five ore zones. A western zone is approximately 5500 m long and 1200 m wide, and contains the best ore grades, of up to 30% heavy minerals. A central zone is 5500 m long with a width from 244 to 850 m, averaging 500 m. The central zone contains concentrations of up to 10% heavy minerals that are consistent along strike. An eastern zone has a length of 5200 m and widths up to 1000 m. A southern zone is 1200 m long and up to 370 m wide, and contains a few high-grade zones of up to 5% heavy minerals. A southeastern zone is separated by river drainage into northern and southern sections. The northern is 1200 m long and 300 m wide. The southern is 3500 m long and 60–250 m wide. Heavy-mineral grades range between 2 and 4% in the southeastern zone. The heavy-mineral assemblage at Lulaton is 15% rutile, 14% zircon, 38% ilmenite and 8% leucoxene (Rose, Written Communication, 2004).

Three distinct facies foreshore, backbarrier, and tidal inlet exist in the deposit. The foreshore facies contains the highest percentage of ore minerals—rutile, zircon, and ilmenite—and has a medium- to fine- heavy-mineral grain size. The backbarrier facies has a lower concentration of economic heavy minerals and a more variable heavy-mineral grain size that overall is generally fine. The tidal inlet facies also has a lower percentage of ore minerals than the foreshore facies, with a fine- to very-fine heavy-mineral grain size. In the coarser channel lag portions, the heavy-mineral grain size is medium to coarse and contains moderately high percentages of non-economic heavy minerals (Rose, Written Communication, 2004).

6.4. Old Hickory Orebody

Berquist (1987) reported heavy-mineral concentrations within the Fall Zone between Petersburg and Emporia, Virginia. As a result, RGC (USA) Minerals, Inc., now Iluka Resources, Ltd., E.I. du Pont de Nemours & Co., and South East TiSand, a joint venture between Becker Minerals, Inc. and Consolidated Rutile, Ltd., now controlled by Iluka Resources, Ltd., began exploring the region and evaluating heavy-mineral concentrations in 1988.

By the end of 1991, RGC (USA) Minerals, Inc. had acquired 72 mining leases. A pilot mine was operated for 6 months in 1994. In 1995, a purchaser for the ilmenite was found and a contract signed. In 1996, RGC (USA) Minerals, Inc. announced that the Old Hickory deposit was economically viable; in July 1997 mining commenced. Reserves were calculated to consist of 73 million metric tons of ore

averaging 8.1% heavy minerals. Proven reserves were calculated to be 27 million metric tons of ore averaging 10% heavy minerals. A mine life of 17 years was forecast (Skillen, 1996).

The dry mining rate was 330 metric tons/h with a spiral feed rate of 240–250 metric tons/h after clay and oversize material was removed prior to the spirals. The dry mill feed rate is 50 metric tons/h of heavy-mineral concentrate (Iluka Resources, Ltd., 2004). In 2001, Iluka decided to increase production. A second concentrator and mining unit was constructed, the Concord Unit, and modifications were made to the dry mill. The construction was completed in 2002, and final commissioning was completed in the first quarter of 2003. Like the original Old Hickory Unit, the mining rate is 330 metric tons/h and the spiral feed rate is 240–250 metric tons/h after removing clay and oversize material (Iluka Resources, Ltd., 2004). Iluka's Virginia Operation now consists of two mining units (Old Hickory and Concord), two concentrators (Old Hickory and Concord) and a single dry mill. The operation, employing more than 100 people, is located in a forestry and row-cropping (tobacco, cotton, peanuts, soybeans, and corn) district.

The Old Hickory orebody is located in Dinwiddie and Sussex counties in southeastern Virginia (Fig. 4) ~80 km south of Richmond and 15 km west of Stony Creek along Highway 40. The deposit strikes north–south and is 12 km long and up to 4 km wide. It is situated along the Fall Zone where Miocene-Pliocene coastal plain sediments overlap onto Palaeozoic basement rocks. The host sediments are feldspathic quartz sands, probably fluvial deposits that have been reworked in marine beach/back-barrier environments (Rose, Written Communication, 2004; Romeo, 2005; Newton and Romeo, 2006).

The Old Hickory deposit consists of two distinct zones of high mineral concentrations, an older western zone, possibly 5–10 Ma old, and a 3–5 Ma eastern zone (Berquist, 1987). The western zone was deposited on a rolling surface of metamorphic basement rocks, then exposed and weathered in Miocene-Early Pliocene time. In a subsequent Pliocene regression, the eastern zone, overlapping and adjacent to the earlier mineralisation, was derived largely by reworking material from the western zone (Rose, Written Communication, 2004).

Both the older and the younger zones were faulted, folded, and uplifted along low-angle and high-angle reverse faults. This tectonism was episodic throughout the depositional history of the deposits and may have helped localise mineral-enrichment by producing coastal barriers and traps (Berquist and Bailey, 1999; Romeo, 2005; Newton and Romeo, 2006). Uplift of linear ridges of the early zone locally accelerated erosion, liberating heavy minerals to the younger deposit.

The orebodies were subjected to prolonged intense weathering from the Tertiary to present. Where it has not been eroded away, a strong weathering profile is evident where supergene clay commonly comprises more than 40% of the upper few metres of the deposit. Titanium dioxide is also enriched in the weathered top 3 m of section. Hard laterite from iron cementation is locally abundant at depths of 1–3 m. The average clay/fines content for the entire deposit is 33%. There is generally no overburden, and mining depths range from 2 to 12 m.

The Old Hickory mineral assemblage consists of 63% ilmenite averaging 59% TiO_2, 19% zircon, 3% rutile plus leucoxene, and 25% gangue minerals. The average grain size of the heavy minerals coarser than 75 μm, is 138 μm. Uranium and thorium

contents are low, averaging around 110 ppm U plus Th in ilmenite, and 200 ppm U plus Th in zircon (Rose, Written Communication, 2004; Newton and Romeo, 2006).

7. DEPOSITS LOST TO CULTURAL AND ENVIRONMENTAL CONCERNS

Along both the Atlantic and Gulf coastal plains, the mining of heavy minerals competes with a variety of other land uses such as forestry, residential development, and resort development. In the southeastern United States, the competition is particularly strong because of the Sea Islands off the Atlantic Coast and a barrier island chain off the Gulf Coast mainland.

Mathieson and Wall (1982, p. 120) state: "As the intensity of tourist development has increased and competition for resources has intensified, resorts have been forced to expand and new ones have been established on the fringes of existing resorts." The expansion may be either radial or linear depending on transportation networks, topography, and planning regulations. They suggest that most seaside resorts display a pattern of linear expansion along the oceanfront.

As island property that can be developed becomes limited, developments appear on the mainland where they radiate from the major access routes. Thus, not only are the heavy-mineral deposits on the Sea Islands lost by preservation and development but deposits on the mainland near the coast also are vulnerable to residential and resort development as development spreads from the island along mainland access routes. Deposits have also been lost as a result of environmental concerns or regulations associated with mining activities, particularly in southeast Georgia and in New Jersey.

7.1. Sea Islands Deposits

"Sea Islands" refer to the barrier islands from the mouth of the St. Johns River in Florida to the Santee River in South Carolina (White, 1970; Fillman-Richards, 1982). From south to the north, commercial heavy-mineral deposits have been evaluated from Amelia Island, Hilton Head Island, and Isle of Palms. Teas (1921) reported on the black sands of the coastal islands, with a brief description of samples collected from St. Simons Island and Sapelo Island off the Georgia coast, and chemical analyses of a sample from each island. Parker (1948) evaluated other Georgia Sea Islands such as Little Talbot, Cumberland, Jekyll, St. Catherine, Ossabaw, Skidaway, St. Simon, and Sapelo islands. He also reported on the islands of St. Helena, St. Phillips, Hunting, Wadmalaw, Johns, Capers, and Bull off the coast of South Carolina. He noted that most of the islands contained heavy-mineral concentrations but the deposits were too small and low grade to be of commercial interest.

Neiheisel (1958) reported that, along the coast of South Carolina, heavy-mineral deposits other than those on Hilton Head Island might be more significant economically, particularly on Bull, Capers, Isle of Palms, Edisto, and Dewees islands. Williams (1967) described a Pawleys Island sample averaging 9.8% heavy-mineral concentrate and containing 33% ilmenite, and described samples collected from Isle of Palms, and Folly Beach.

St. Simons Island in Glynn County, Georgia, and Cumberland Island in Camden County, Georgia, had been prospected for heavy minerals with two or more large companies prospecting Cumberland Island extensively and a large paint company acquiring the mineral rights to the mineral deposits (Mertie, 1975). According to Mertie, the heavy-mineral deposits on Cumberland Island lie at the centre of the island, trending nearly north, at a maximum elevation of ~12 m, which suggests their association with the Talbot terrace.

Amelia and Hilton Head islands, and Isle of Palms appear to have the deposits with the best chance to be exploited but, because of cultural and environmental restrictions, they could not be developed. Other deposits and properties such as Yulee in northeastern Florida, Cabin Bluff in southeastern Georgia, and Oak Level near Savannah, Georgia, have been or could be lost to residential and resort development.

7.1.1. Amelia Island

Martens (1928) reported the presence of ilmenite in small amounts and thin streaks of dark, heavy concentrates in the beach and dune sands of Amelia Island, located in the extreme northeastern corner of Florida. However, he did not believe that the concentrates were rich enough to be commercial. He analysed a sample collected three miles south of the St. Marys River jetty; its mineral suite is shown in Table 13.

Elsner (1997), using values from the literature determined that the deposit contained 900,000 metric tons of heavy minerals. Union Carbide planned to produce 27,215 metric tons of ilmenite and 4535 metric tons of rutile per year. The average TiO_2 content of the Amelia Island ilmenite was 58.4%, while the leucoxene

Table 13. Petrographic analyses of heavy-mineral concentrates from Amelia Island

Mineral species	Garnar's Personal Communication with Elsner (Elsner, 1997) (%)	Peyton as reported by Elsner (1997) (%)	Martens (1928) (%)
Ilmenite	37.0	49.2	54.4
Leucoxene	9.7		0.8
Rutile	4.6	5.3	4.2
Zircon	11.2	10.7	23.8
Monazite/xenotime	0.2	0.7	4.0
Staurolite	6.9	5.5	2.8
Tourmaline		2.7	0.8
Kyanite	6.4	1.7	Included in sillimanite
Sillimanite		3.8	1.5
Garnet	0.6	2.2	1.1
Epidote	20.3	16.4	3.2
Hornblende		0.3	0.6
Mica	1.8		
Collophane		1.5	1.3
Others	1.3		0.8

contained 74% TiO_2, and rutile contained 98% TiO_2 (Elsner, 1997). Parker (1948) reported exploring the southern portion of the island where samples ran as high as 45% heavy minerals. Titaniferous minerals averaged 53.6% with zircon averaging 14.8%.

Because of economic conditions, a proposed mining project was postponed and the property was developed into a luxury resort, Amelia Island Plantation (Garnar, 1978; Elsner, 1997).

7.1.2. Hilton Head Island

Hilton Head Island is one of the larger Sea Islands and is located in Beaufort County, South Carolina. It is ~19 km long and averages almost 5 km wide. Parker (1948) investigated one region that was almost 10 km long and 1.6 km wide. The average water depth (a limiting factor in sampling) was ~2 m and the average grade of 5.7% heavy mineral. The heavy-mineral suite was composed of 45–50% titanium minerals. This results in a deposit containing 2,540,104 metric tons of heavy minerals and ~1,156,655 metric tons of titanium bearing minerals (Parker, 1948).

In 1954 and 1955, the U.S. Bureau of Mines and the National Lead Company (NL Industries, Inc.) performed independent investigations to evaluate the deposits of heavy minerals on Hilton Head Island. The U.S. Bureau of Mines drilled 265 holes, while the National Lead Company drilled 545 holes (McCauley, 1960). Table 14 shows the mineralogical analyses made by the U.S. Bureau of Mines on composite samples concentrated from Hilton Head Island as reported by McCauley (1960). The TiO_2 of the ilmenite in the mineral suite is 54.7%.

The U.S. Bureau of Mines had determined an average heavy-mineral content of 2.19% to an average mineable depth of 3.4 m within the deposit boundaries. National Lead Company's data provided an average mining depth of 3 m with an average heavy-mineral content of 2.14%. The richest deposits appeared along the beach and adjacent foredune on the northern part of the island. The average heavy-mineral

Table 14. Petrographic analyses of samples from Hilton Head Island*

Mineral species	Minimum (%)	Maximum (%)	Average (%)
Ilmenite	28.20	42.7	35.00
Epidote	16.20	17.6	16.70
Celopaq (?)	8.60	17.9	12.60
Zircon	8.40	20.0	11.70
Quartz	5.90	14.9	10.80
Ferromagnesian minerals	5.20	6.90	6.00
Rutile	4.00	8.10	5.50
Garnet	1.00	1.60	1.30
Monazite	0.64	2.30	1.15
Magnetite	0.20	0.70	0.37
Tourmaline	Tr	0.80	0.37
Xenotime	0.03	0.10	0.07

*Taken from McCauley (1960).

content in this portion of the deposit was 7.87% with a maximum of 18.44% (McCauley, 1960). Using the 3-m depth, McCauley calculated that the deposit covered approximately 73 km^2. Thus it could contain at least 7,462,463 metric tons of heavy minerals. Williams (1967) used the same data as McCauley and recalculated the potential reserves after removing portions of the island that had been developed for restricted residential plots. The Hilton Head deposit, similarly to that on Amelia Island, was never exploited and is now covered by residential and resort development.

7.1.3. *Isle of Palms*

The Isle of Palms is a coastal island ~25 km northeast of Charleston, South Carolina. There is little information available on the potential deposit on the island. Williams (1967) reported on samples taken from Isle of Palms, and based on 1952 field observations, he calculated a resource of 59,422 metric tons of heavy minerals containing 19,312 metric tons of ilmenite, 1604 metric tons of rutile, and 178 metric tons of monazite. Even in 1967 Williams stated: "The 2,000,000 cubic yard resource material available, …, based on field observation in 1952, probably needs continued re-adjustment due to expansion of real estate development" (Williams, 1967, p. 22). The evaluation was based on eight bulk samples taken by Neiheisel (1958) and on one drill hole.

When Neiheisel performed his fieldwork, the eastern portion of the island contained a series of dunes that are generally parallel to the coast representing former positions of the coastline. He studied a series of dunes on the southeastern portion of the island and divided the dunes into three categories according to approximate height: 2 m, 3.5 m, and 10.5 m. The first set of dunes averaged 12%, the second set 8%, and the third set 5% heavy minerals, respectively. Table 15 provides the mineral suites of the heavy minerals found in the various dunes.

Table 15. Petrographic analyses of heavy-mineral concentrates collected from the Isle of Palms*

Mineral species	2.1 m dunes (%)	3.66 m dunes (%)	10.67 m dunes (%)
Ilmenite	40	35	31
Epidote	32	30	22
Hornblende	4	9	20
Zircon	8	6	6
Staurolite	4	6	5
Rutile	3	4	3
Leucoxene	4	5	4
Kyanite	2	2	4
Garnet	1	1	1
Tourmaline	1	1	1
Other†	1	1	2

*Taken from Neiheisel (1958).
†Others include trace amounts of monazite, sillimanite, magnetite, and hypersthene.

7.2. Gulf Coast Island Deposits

Along the Gulf coast, heavy-mineral concentrations on islands such as Cat, Ship, Horn, Petit Bois, and Dauphin have been studied. According to Foxworth et al. (1962), 26 different species of heavy minerals, most of which are metamorphic, have been identified from these islands (Table 16). Foxworth et al. (1962) concluded that the original source was the metamorphosed-intruded rocks of the southern Appalachians. Intermediate sources are possibly the overlapping Palaeozoic rocks of Alabama and Tennessee and the Cretaceous and Eocene sediments of the Coastal Plain of Mississippi, Alabama, and western Georgia. The rivers that drain the Coastal Plain are still active transporting agents. They believe, however, that the immediate source of most of the heavy minerals is Pleistocene and Recent sediments which are being reworked by wave action.

In the late 1980s and early 1990s, a major company re-evaluated the heavy-mineral potential of the islands, even though they are part of the Gulf Islands National Seashore that extends along the northeastern Gulf of Mexico from west of Ship Island, Mississippi, to the far end of Santa Rosa Island in Florida. The evaluation suggested a probable average heavy-mineral content of 8%, with a 10% chance that it could be as high as 12%, and a 90% chance that the concentration was higher than 3%. This evaluation indicated that there probably was 15% ilmenite, 6% rutile, and 6% zircon in the heavy-mineral suite. Further, the evaluation suggested that there was little chance that the TiO_2 content of the ilmenite was less than 64%, and there was a 50% chance that the TiO_2 content in the ilmenite was as high as 68%. The calculated reserves suggested 650,272 metric tons of recoverable TiO_2, which would allow for a production rate of 123,958 metric tons of TiO_2 per year. In addition, it was believed that 68,000 metric tons of zircon could be produced each year. However, since the islands are part of a National Seashore, this resource probably will not be exploited.

7.3. Mainland Deposits

Further to losing the barrier island deposits along the Atlantic and Gulf coasts, four inland deposits and numerous inland prospects have been lost. These include the Yulee deposit in northeast Florida, the Cabin Bluff deposit in Camden County, Southeastern Georgia, to residential and/or resort developments, and the Folkston West deposit because of environmental concerns over potential mining effects on the Okefenokee Swamp. In New Jersey, a deposit evaluated near Pemberton is no longer of significant interest due to environmental restrictions.

7.3.1. Yulee heavy-mineral deposits

The Yulee heavy-mineral sand deposits are located a few kilometres east, northeast and north of the town of Yulee in northeastern peninsular Florida (Fig. 2). It is believed that these heavy-mineral sand deposits were discovered by Joseph L. Gillson during his heavy-mineral studies of the Coastal Plain (Pirkle et al., 1984). Lynd and Lefond (1975, p. 1170) provide the first published description of the deposits, although Gillson (1959) showed the deposits on his map of all known heavy-mineral deposits of the southeastern United States. Pirkle et al. (1984, 1993a) and Elsner

Table 16. Average heavy-mineral composition of major mineral species of the beach of each area and the total area* (Northern Gulf of Mexico coastal area)

Mineral species	Average frequency for total area	Mainland	Deer Island	Round Island	Cat Island	Ship Island	Horn Island	Petit Bois Island
Epidote								
Garnet								
Hornblende	0.1	0.1				0.2	0.2	
Ilmenite	13.4	13.1	3.1	6.1	8.9	24.8	10.8	11.4
Kyanite	27.4	26.3	25.5	32.9	30.5	22.1	31.3	26.7
Leucoxene	2.5	3.5	3.5	2.2	3.3	1.7	1.5	0.1
Rutile	1.8	1.4	2.2	0.4	1.2	6.0	0.2	0.3
Sillimanite	1.2	1.5	0.5	0.7	1.2	0.3	1.6	1.5
Staurolite	26.2	24.6	20.5	22.5	28.7	25.2	31.0	30.8
Tourmaline	20.4	20.2	29.1	31.2	21.0	9.6	19.3	26.2
Zircon	1.6	1.6	0.9	0.2	0.5	6.3	0.1	0.4
Other	5.4	7.7	14.7	3.8	4.7	3.8	4.0	2.6

*Modified from Mellen (1959).

(1997) have described these deposits in more detail, and several companies have performed detailed drilling at various times from the 1950s to the present.

The heavy-mineral deposits are in low, north-south trending ridges that are irregular in shape with a general surface elevation ranging from ~7.5 m to slightly more than 18 m above mean sea level. Even though the individual ridges are not wide, their combined width is a little over 7 km (Fig. 6). White (1970) considers these ridges as part of the Atlantic Coastal Ridge, which he describes as extending, with occasional interruptions, along the mainland coast of the Florida Peninsula from the south shore of the St. Marys River to the vicinity of Homestead, Florida, ~50 km southwest of Miami. A plains region, with surface elevations generally from ~9 to 10.7 m above mean sea level, extends westward from the Yulee ridges for ~25–30 km to the eastern edge of the Duval Upland. This plain is crossed by rivers and streams flowing eastward and southeastward and is called the "St. Marys meander plain" by White (1970). Surface elevations east of the Yulee ridges are lower than those west of the ridges. These lower surfaces pass into salt marshes, which extend to Amelia Island along the Atlantic Coast.

Hoyt and Hails (1974) consider the regions in which the Yulee ridges are present to be parts of a Pamlico barrier island complex of Pleistocene age. White (1970, p. 34) points out areas in eastern Florida where the Pamlico shoreline, along which these Yulee ridges occur, truncates older relict beach ridges. From such studies of the Pamlico shoreline and from elevations of fossil burrows of a marine decapod, *Ophiomorpha*, the ridges containing the Yulee heavy-mineral concentrations can be correlated with the crestal area of the Pamlico transgression.

The Yulee ridges have a counterpart on Amelia Island, a modern barrier island discussed above (see also Pirkle et al., 1984). Amelia Island is positioned just south (downdrift) and a little east of the mouth of the modern St. Marys River. The Pamlico barrier islands containing the Yulee deposits were formed just south (downdrift) and a little east of the mouth of the ancestral St. Marys River. Where large rivers enter oceans, coastal current patterns may be locally interrupted, and river sediments added to the ocean waters. At such localities, heavy minerals may be concentrated in favourable environments in a downdrift direction from the river mouths. Amelia Island, in a downdraft direction from the mouth of the St. Marys River, contains substantial heavy-mineral deposits already discussed.

Sediments consisting of fine quartz sand and clayey sand underlie the Yulee ridges. At some sites, these sediments contain stringers and thin lenses of coarse quartz sand and clay. Howard and Scott (1983), Kussel and Jones (1986), Pirkle et al. (1991a), and Rich and Pirkle (1993) provide more detailed descriptions of the sediments that underlie the Yulee ridges.

Table 17 provides reserves that result from the different studies conducted over the years. The heavy-mineral suite is composed of ilmenite with moderate amounts of zircon, rutile, and leucoxene. The TiO_2 content in the ilmenite exceeds 60% according to Rose (Written Communication, 2004). Pirkle et al. (1984) report that the ilmenite of the Yulee heavy-mineral sand deposits contains 59% TiO_2, and DuPont reports that it contains 61% TiO_2. Epidote occurs in quantities up to 6% (Rose, Written Communication, 2004). Table 18 shows petrographic data for the heavy minerals in these deposits. Sand grain sizes are mostly very fine.

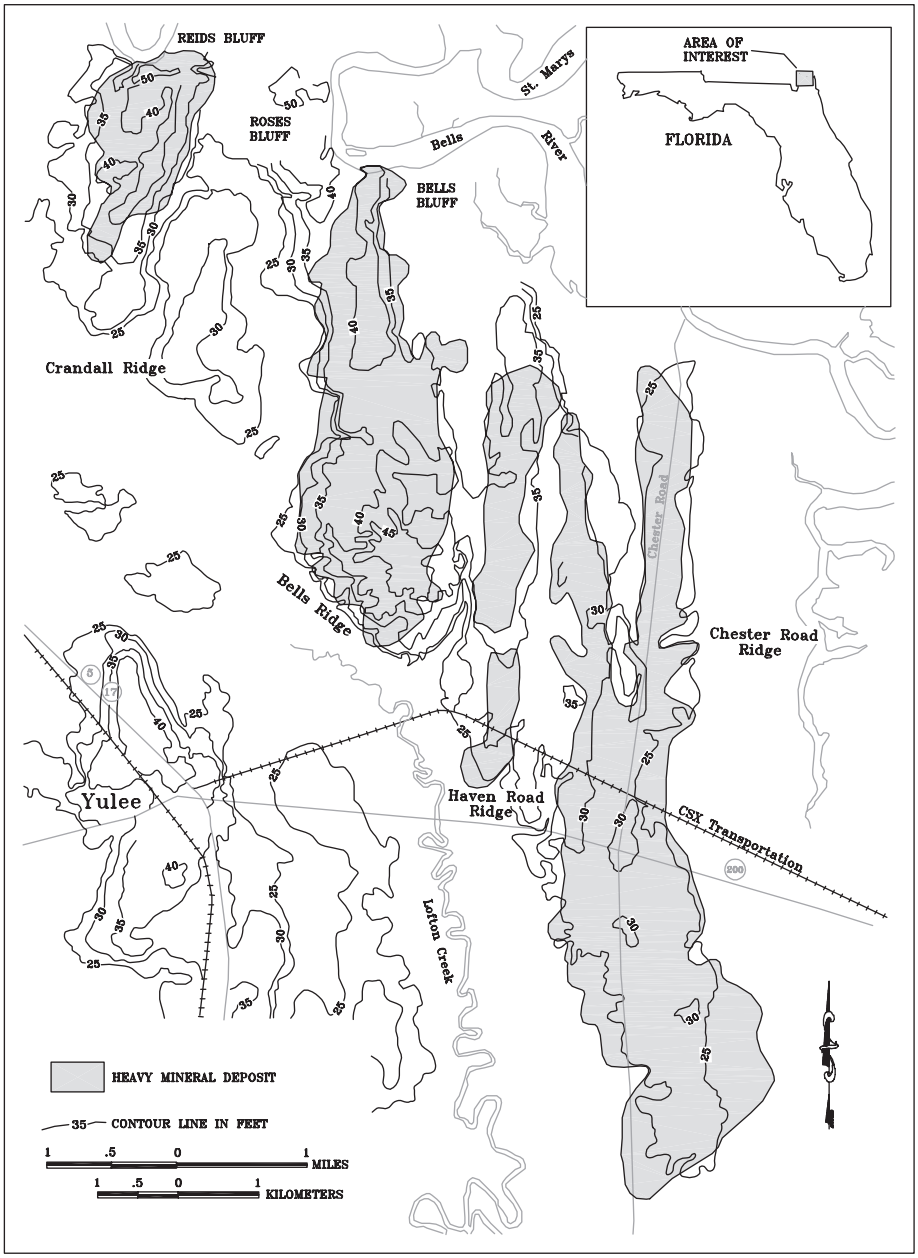

Fig. 6. Yulee heavy-mineral concentrations. The deposits (shaded) have a minimum thickness of 1.8 m (6 ft) from the land's surface and a minimum TiO_2 content of 1%. A few contour lines (in feet) are shown in the areas of the ridges. No contour lines were drawn on the plains regions to the west or to the east of the ridges. Modified from Pirkle et al. (1984).

Table 17. Yulee heavy-mineral deposits reserve estimates

Parameter	Crandall Ridge*				Bells Ridge*				Haven Road Ridge*				Chester Road Ridge*				Total			
	1	2	3	4	1	2	3	4	1	2	3	4	1	2	3	4	1	2	3	4
Area (km^2)			4.63	0.97			8.98	6.5			2.38	0.067			13.733	1.127	20.234	24.285	29.729	8.635
Thickness (m)			3.55	3.60			2.97	3.5			2.44	–			2.94	3.5	2.75	2.47	3.00	3.51
Weight (metric tons/m^3)			1.60	1.60			1.60	1.6			1.60	1.6			1.60	1.6		1.60	1.60	1.6
Weight percent heavy mineral			3.34	3.00			3.37	3.0			2.96	–			2.92	3	3–4	3.72	3.12	3
Million metric tons heavy mineral.			0.88				1.44				0.28				1.886		3	3.57	4.479	3.148

Notes: (1) Pirkle et al. (1984). Individual ridges were not evaluated. Elsner made the calculation based on numbers from Pirkle et al. (1984). They provided a reserve in terms of TiO_2. Elsner calculated a conversion factor from the Humphreys Mining Company data. (2) 1986 evaluation conducted by E.I. du Pont de Nemours & Co. Individual ridges were not evaluated. (3) Elsner (1997) based on Humphreys Mining Company's 1970–1971 drill data. (4) 2002 evaluation conducted by Iluka Resources, Inc. No weight percent heavy mineral was given, so a value of 3% was assumed.

*Ridge locations are shown in Fig. 6.

Table 18. Heavy-mineral composition of the Yulee placer deposits

Mineral species	Pirkle et al. (1991a) (%)	Grosz et al. (1989) (%)	Elsner (1997) (%)
Ilmenite	52.7	31.2	28.7
Leucoxene	2.2	4.6	8.7
Rutile	7.4	10.2	2.7
Zircon	16.0	8.3	5.5
Epidote	6.6	7.5	26.2
Sillimanite	5.4	10.3	10.7
Kyanite	1.3		2.5
Staurolite	5.2	12.2	7.2
Tourmaline	2.3	5.7	2.5
Hornblende	0.8	0.4	3.0
Garnet	0.4		1.0
Others	0.3		
Monazite		2.0	<0.1
Xenotime			<0.1
Andalusite			0.2
Topaz			0.5
Corundum			0.2
Sphene			0.1
Chloritoid			<0.1
Anatase			0.2

7.3.2. *Cabin Bluff deposits*

The Cabin Bluff heavy-mineral deposits are located in Camden County, Georgia, just south of the Satilla River. Pirkle et al. (1991b) describe these deposits: they are approximately 8 km east of the town of Woodbine and ~11 km inland from the Atlantic Ocean (Fig. 2). The heavy-mineral deposits genetically are related to a series of parallel-trending beach ridges composed for the most part of fine to very fine quartz sand. The ore-grade sediments underlie an area of ~12.5 km^2 and reserves have been estimated to range between 1.15 and 2.34 million metric tons of heavy minerals. Table 19 gives representative estimates of the heavy-mineral tonnage. Heavy-mineral concentrations begin at the land surface and extend downward to an average depth of ~2 m.

The heavy-mineral concentrations are found in five distinct ridges (Fig. 7). Most of the ore is concentrated in the main deposit (labelled B on Fig. 7), which comprises approximately 59% of the total surface area, 63% of the total ore, and 73% of the total heavy minerals (Table 19). A cemetery is located within the Ceylon pod (labelled A on Fig. 7), which will most likely exclude this pod from being mined.

According to Hoyt and Hails (1974) and Goodman (1989), the main deposit and the Ceylon deposit are parts of a barrier island complex formed during the Pleistocene along the 7.6-m Pamlico shoreline. These workers correlate the ridges east of the main deposit with the lower Princess Anne shoreline. Beach ridge sands of the Cabin Bluff area rest on sediments consisting primarily of fine to very fine quartz sand and clayey sand. The sands of the Cabin Bluff deposits contain an average of 3–3.5% heavy minerals by weight. These heavy minerals include ilmenite, zircon,

Table 19. Summary of ore reserves of the Cabin Bluff property

Areas of ore-grade sediments†	Humphreys-Brunswick (1957)*		Pirkle et al. (1991b)		DuPont (late 1980s)	
	km^2/acres	Metric tons of heavy minerals	Km^2/acres	Metric tons of heavy minerals	km^2/acres	Metric tons of heavy minerals
Ceylon			0.38/95	71,175		
Main deposit	6.0/1480	1,168,450	8.90/2200	1,294,080	8.90/2200	1,194,534
Ocean Pond			1.74/430	68,850	2.24/554	149,980
Pine Barren			0.60/150	62,680	1.02/253	796,635
Copeland			0.93/230	117,240	2.96/732	202,518
Total	6.0/1480	1,168,450	12.55/3105	1,614,025	15.13/3739	2,343,667

*From Czel (1977).
†Locations are shown in Fig. 7.

rutile, kyanite, sillimanite, staurolite, leucoxene, epidote, monazite, tourmaline, hornblende, garnet, and corundum (Table 20). The ilmenite contains an average of 61% TiO_2 (Pirkle et al., 1991b).

During 1957, Scott Paper Company working with Humphrey's Gold Corp. and Brunswick Pulp Land Company (a joint venture of Scott Timber Company and Mead Timber Company) evaluated the heavy-mineral potential of the Cabin Bluff tract. DuPont evaluated the property in 1977 and again in the late 1980s, acquiring a mineral lease that subsequently expired. Ore reserve estimates from these evaluations along with estimates from Pirkle et al. (1991b) are given in Table 19. No mining was ever commenced on the property largely due to the economic climates in existence when these studies were completed. In 2002, Iluka Resources, Inc. approached the Cabin Bluff owners about mining the deposits. There was little interest expressed by the current owners because they want to develop it as residential property, and do not wish to do anything that might jeopardise those plans.

7.3.3. Folkston West, Toledo, and Saunders Tract deposits

The deposits discussed previously in this section were lost to exploitation because of residential and resort development. The Folkston West, Toledo, and Saunders Tract deposits were lost to exploitation due to environmental concerns. These deposits are located on Trail Ridge near the eastern edge of the Okefenokee Swamp and extend from near Race Pond, Georgia on the north to state road 94 on the south (Fig. 2). An extensive exploration program in the mid- to late-1970s resulted in the recognition of the Folkston West deposits as a potential heavy-mineral orebody. The Toledo deposits, immediately south of the Folkston West deposits, were recognised in the early 1990s. Pirkle et al. (1993b) describe the Folkston West deposits.

The elevation of Trail Ridge in the area of the Folkston West and Toledo deposits ranges from ~43 to 47 m above mean sea level. These deposits contain a typical Trail Ridge heavy-mineral suite (Table 21), with the most abundant heavy minerals being ilmenite, staurolite, zircon, kyanite/sillimanite, tourmaline, rutile, and leucoxene.

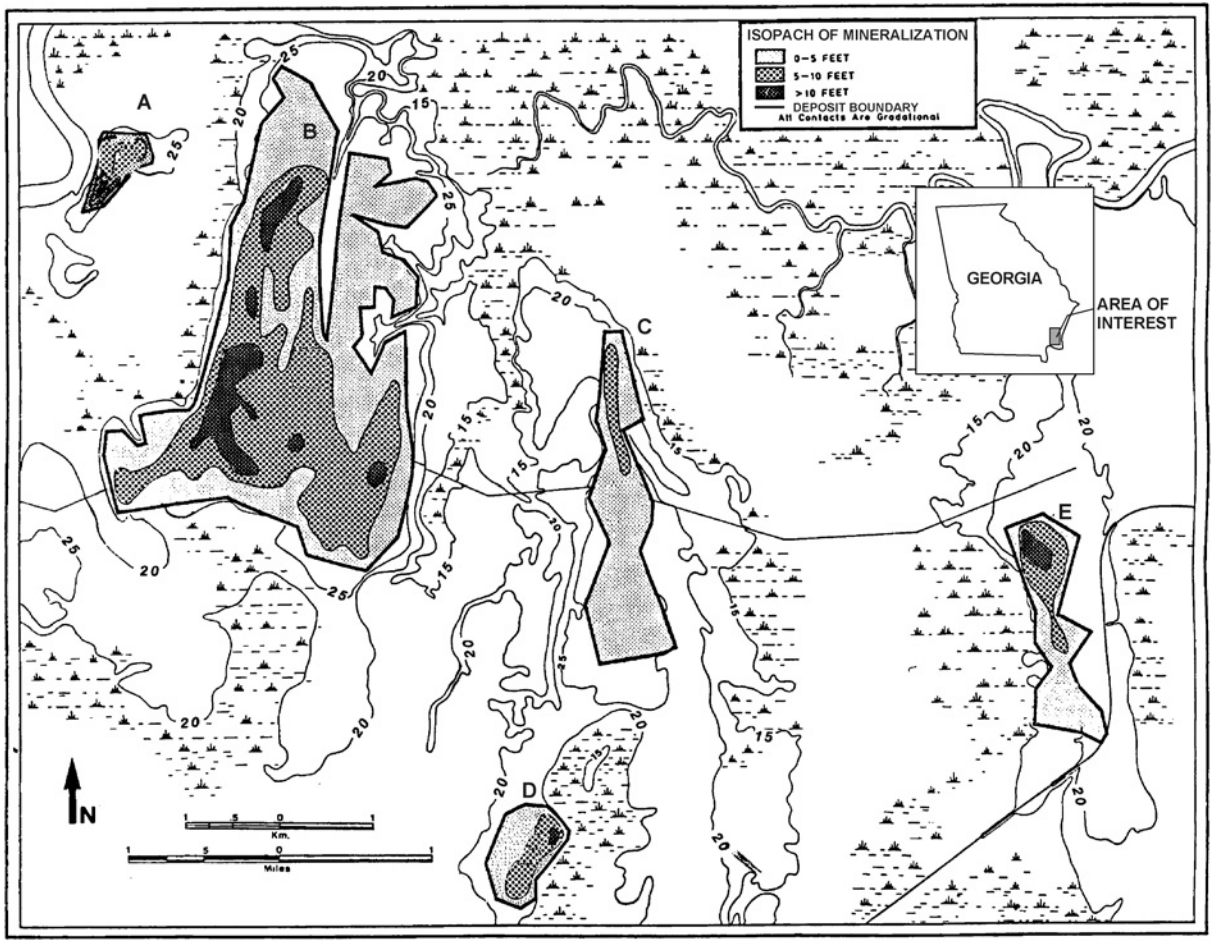

Fig. 7. Cabin Bluff heavy-mineral deposits. The areas of heavy-minerals are named or referred to as follows: (A) Ceylon, (B) Main deposit, (C) Ocean Pond, (D) Pine Barrens, and (E) Copeland. A few contour lines (in feet) are shown in the areas of the ridges. The thickness of mineralised sediments is also shown. Modified from Pirkle et al. (1991b).

Table 20. Weight percent of heavy minerals extracted from composite samples from various areas of the Cabin Bluff heavy-mineral concentrations*

Mineral species	Weight percent of total heavy minerals			
	Main deposit†	Ocean Pond†	Pine Barren†	Copeland†
Ilmenite	62.0	63.8	59.8	53.1
Zircon	14.1	17.9	10.0	16.1
Rutile	5.6	5.0	6.0	8.8
Kyanite/sillimanite	5.1	5.8	5.7	6.2
Staurolite	3.7	3.3	4.2	6.2
Leucoxene	2.9	1.0	2.2	3.3
Epidote	1.8		5.6	1.3
Monazite	1.7	2.2	2.7	2.3
Tourmaline	1.4	0.5	1.3	2.2
Hornblende	0.8	0.5	1.4	0.3
Garnet	0.8		1.0	0.1
Corundum	0.1		0.1	0.1

*Modified from Pirkle et al. (1991b).
†Locations are shown in Fig. 7.

Table 21. Petrographic analysis of heavy minerals from the Folkston West and Toledo heavy-mineral deposits

Mineral species	Weight percent of total heavy minerals	
	Folkston West*	Toledo†
Ilmenite	45.6	33.64
Staurolite	18.4	16.57
Zircon	12.9	16.31
Kyanite/sillimanite	11.3	13.01
Tourmaline	4.8	
Rutile	2.9	3.71
Leucoxene	2.8	8.55
Monazite	0.3	0.09
Garnet	0.2	
Epidote	0.1	
Others	0.7	8.12

*From Pirkle et al. (1993b).
†Average of samples from 17 drill holes.

The TiO_2 content of the ilmenite averages ~65%. The Folkston West deposits contain ~9.4 million metric tons of heavy minerals.

The Toledo orebody is located on the eastern flank of Trail Ridge, rather than on its crestal area. It contains approximately 19.2 million metric tons of heavy minerals. The TiO_2 content of the ilmenite averages ~66%, and the average heavy-mineral content is 1.9 wt.%. The Toledo heavy-mineral suite is given in Table 21.

Whereas the coastal heavy-mineral concentrations are shallow deposits, the Folkston West deposit has an average ore thickness of ~10.7 m, and the Toledo deposits average ~9.4 m. The mineralisation starts at the surface. The present authors are not aware of any published information on the Toledo deposit.

Immediately south of the Toledo deposit, a small deposit, known as the Saunders Tract, extends to State Highway 94 (Fig. 8). At one time this deposit was under a single ownership (Gilman Paper Company), but during the past few years it has been divided and sold to multiple owners. This probably will make its exploitation difficult, if not impossible. DuPont first explored the Saunders Tract deposit in 1977, and re-evaluated it in 1994. This deposit covers 51.3 km^2 located west of the town of St. George, and is situated primarily on Trail Ridge. Crestal elevations of Trail Ridge in this vicinity are slightly more than 53 m. Pirkle and Czel (1983) describe the sediments of this small deposit in more detail, and report the occurrence of marine fossils in the upper sands of the Saunders Tract along the western side of Trail Ridge. Teas (1921, p. 377) reports on a sample containing heavy minerals collected 3 miles west of St. George along the Georgia and Florida Railway, now the Norfolk Southern Railroad, which runs parallel to and immediately south of Georgia State Highway 94 (Fig. 8).

Using a 1.5% heavy-mineral cut-off and a 4.6-m minimum ore thickness, 8.4 km^2 of land containing an indicated 112,395,493 metric tons of sand averaging 2.17 wt.% heavy minerals were identified. These sediments contain an indicated resource of 2,654,520 metric tons of heavy minerals. The mineralised zone has an average thickness of 8.6 m, starting at the land surface.

Preliminary mineral processing tests indicate that an ilmenite product averaging 65.4% TiO_2 and a high titanium product averaging 90.4% TiO_2 can be made from the heavy minerals in the Saunders Tract deposit. Calculations made from petrographic data and analytical data suggest that the ilmenite in the Saunders Tract deposit contains an average TiO_2 content of 66.7% and that the high titanium product averages 91.0% TiO_2. These "theoretical" values compare very well with the preliminary mineral processing results.

The Saunders Tract deposit's mineral suite is compared with that of the Trail Ridge and Maxville deposits in Table 22. Much of the sand in the sediments penetrated has typical Trail Ridge sand-size distribution. It should be noted, however, that the sands, especially in the upper parts of the sequence, tend to be somewhat finer than typical Trail Ridge sands. Pirkle and Czel (1983) examined several possible origins for the fossiliferous sands they reported, and concluded that these sands most likely accumulated in inlets or in a shallow embayment as seas encroaching from the east breached Trail Ridge in post-Trail Ridge time.

The Trail Ridge sand sequence is underlain by a unit consisting of fine quartz sand and clayey sand. In general, the clay content in this underlying unit increases with depth. Locally, granules and small pebbles of quartz are common. These sediments might be the equivalent of the Citronelle sediments of peninsular Florida. Beneath these Citronelle-like sediments, stringers and small lenses of massive clay are present at some sites, especially in the lower parts of the sediments, and some of them contain attapulgite clay. The presence of attapulgite indicates that the sediments are probably Miocene in age. Some of the attapulgite-bearing sediments contain dolomite or calcite and may be equivalent to those considered to be part of the Hawthorne Group in Florida.

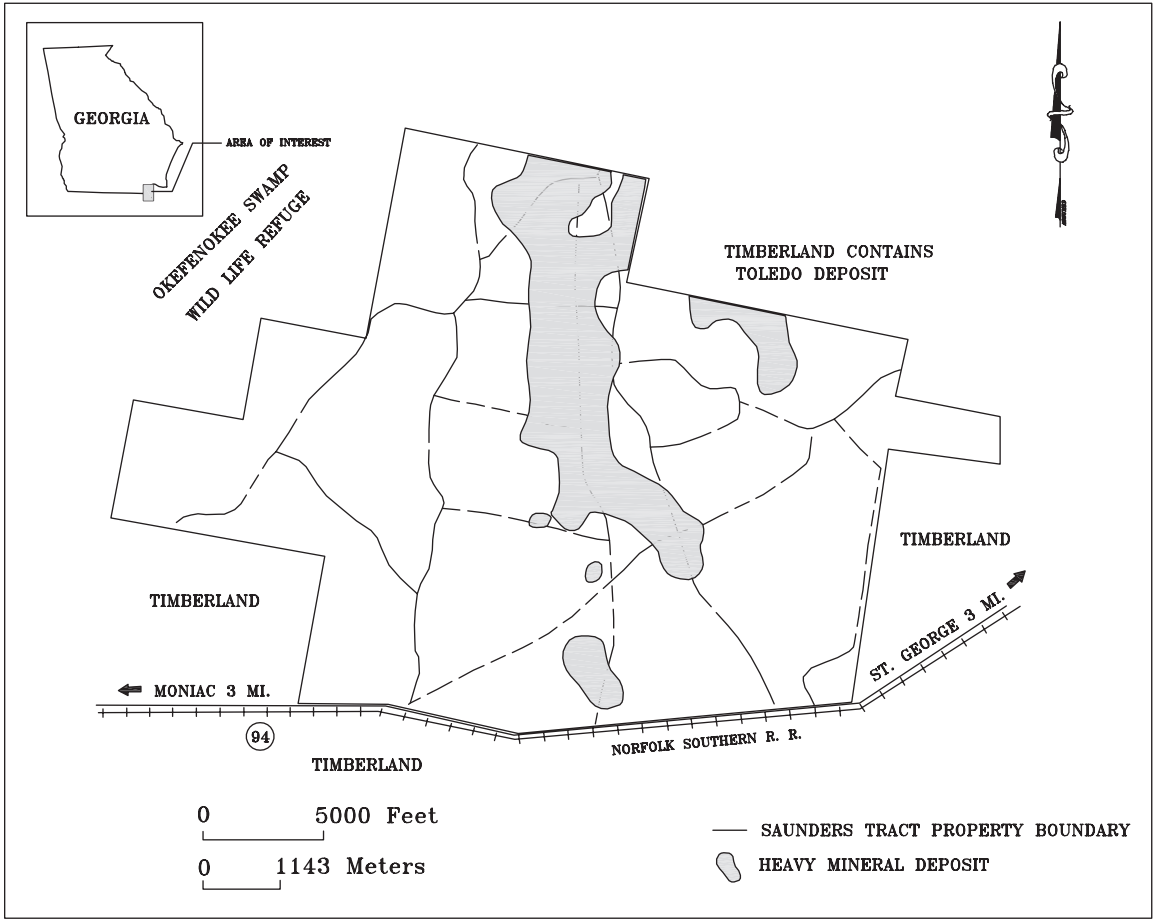

Fig. 8. Location of heavy-mineral concentration on the Saunders Tract in southeastern Georgia. Heavy-mineral cut-off used is 1.5 wt.% and the required minimum thickness is 4.6 m (15 ft) starting at the land's surface.

Table 22. Comparison of selected species of Saunders Tract heavy-mineral species with Trail Ridge and Maxville heavy-mineral species

Property	Weight percent of heavy-mineral species			
	Rutile	Ilmenite	Leucoxene	Zircon
Saunders*	4.20	46.90	8.20	16.10
Saunders†	3.09	30.88	12.26	16.61
Trail Ridge**	1.21	45.17	4.59	14.79
Maxville‡	1.86	40.70	0.86	16.95

*Average of 22 samples derived from 1977 drilling.
**From Garnar (1981).
†Average of 81 samples derived from 1994 drilling.
‡Average of 124 samples.

The sequence of the Saunders Tract deposit consists of four units: (1) non-typical Trail Ridge sands (mostly finer) that overlie typical Trail Ridge sands; (2) fine- to-medium-grained quartz sand (typical Trail Ridge sand); (3) very fine- to coarse-grained sand to clayey sand (kaolinite) that contains granules and small discoid pebbles (possibly Citronelle equivalent); and (4) fine-grained sand with clay (attapulgite and montmorillonite) and silt stringers (possibly Miocene Hawthorne Group sediments).

The Folkston West, Toledo, and Saunders Tract deposits contain more than 31 million metric tons of heavy minerals. Because of environmental concerns, DuPont donated 65 km^2 of the Folkston West deposit to The Conservation Fund, which has permanently retired the mining rights on the area (Seabrook, 2003).

7.3.4. Pemberton deposit, New Jersey

The southeastern United States is not the only area where heavy-mineral deposits have been lost to cultural and environmental activities. The Pemberton deposit is located in the Pine Barrens of New Jersey near the town of Pemberton. It was evaluated in the mid-1980s and was determined to contain enough ilmenite to produce ~162,000 metric tons of ilmenite per year for ~10.5 years. The TiO_2 content of the ilmenite was determined to be ~63%.

Mining is an allowed activity in the Pine Barrens. The company, conducting the evaluation, met with interested parties and after that single meeting decided not to pursue the project. Very little if any exploration for heavy-mineral deposits in New Jersey has occurred since the mid-1980s, even though there are several prospects.

8. FUTURE OPERATIONS

8.1. Florida and Georgia

In Florida and Georgia, eight deposits are under evaluation for future exploitation. There are several other prospects also that have not been evaluated but, based on limited geologic information, are potential deposits provided that cultural and

environmental activities do not prevent their development. An example is the Oak Level prospect, south of Savannah near Richmond Hill in Bryan County, Georgia. It covers ~45 km^2 and lies north of the Medway River, east of the Bear River, and south of the Ogeechee River. It is ~11 km long, 5.6 km wide and is associated with the Pamlico transgression. A broad low ridge, trending N 11° E, occupies much of the area. It reaches a height of ~9 m and is similar in cross-section to existing coastal barrier islands, which are known to contain concentrations of heavy minerals.

Using the above information and field reconnaissance, one company modelled the potential of this prospect and estimated that it contained 3.42 million metric tons of heavy minerals and 2.19 million metric tons of TiO_2. An offer to lease the mineral and mining rights was made to the owners in the mid-1980s but they showed little interest. A possible explanation is the length of time the property would be under lease, which would prohibit other types of development. Considering the prospect's location, residential development was a real possibility.

There are other deposits in northern Florida and southeastern Georgia that might be exploited in the future. These deposits are of sufficient interest to the industry, so that during the past several years detailed exploration and feasibility studies have been conducted on each of them. In Florida, these deposits include areas along Trail Ridge from DuPont's Trail Ridge and Maxville operations north to Interstate 10, plus an extensive area of the Boulougne deposit not mined earlier by the Humphreys Mining Company. In southeastern Georgia, the potential deposits are Mission, Buffalo Ridge, Altama, Darien, Amelia, and Ludowici. Each is discussed briefly below.

8.1.1. North of Maxville deposit

DuPont's Trail Ridge and Maxville operations are scheduled to shut down in 2007 if no additional reserves are added. North of the Maxville operation lies approximately 15 km^2 of land containing 4,888,000 metric tons of heavy minerals. The ore averages 2.3% heavy minerals with an average thickness of 9.0 m. The mineral suite and grain size are the same as in the Maxville deposit. With these reserves added to their current reserve base, DuPont should be able to operate until 2016 (McMahill, Personal Communication, 2004).

8.1.2. Boulougne deposit

In the 1970s, the Humphreys Mining Company used a cutterhead dredge under contract to DuPont to mine the northern portion of the Boulougne deposit (Fig. 9). However, large portions of the deposit remain unmined because the dredge was not able to access the shallow portions of the remaining deposit (average depth of 3.6 m). The deposit is 8.5 km long and up to 1.12 km wide with a thickness of 1.5–7.6 m. The mined-out northern portion has houses built upon the tailings and the unmined southern portion is in timber production (Rose, Written Communication, 2004).

According to Rose, the morphology indicates that the deposit formed as a regressive barrier island sequence. During the Pleistocene, there was a transgression across the present deposit. A period of sea level stillstand, followed by a regressing sea stranded the Boulougne sand body. There is a predominance of wetlands on the southern extents of the zone as the surface elevations decrease and the relict topographic expression becomes more subdued.

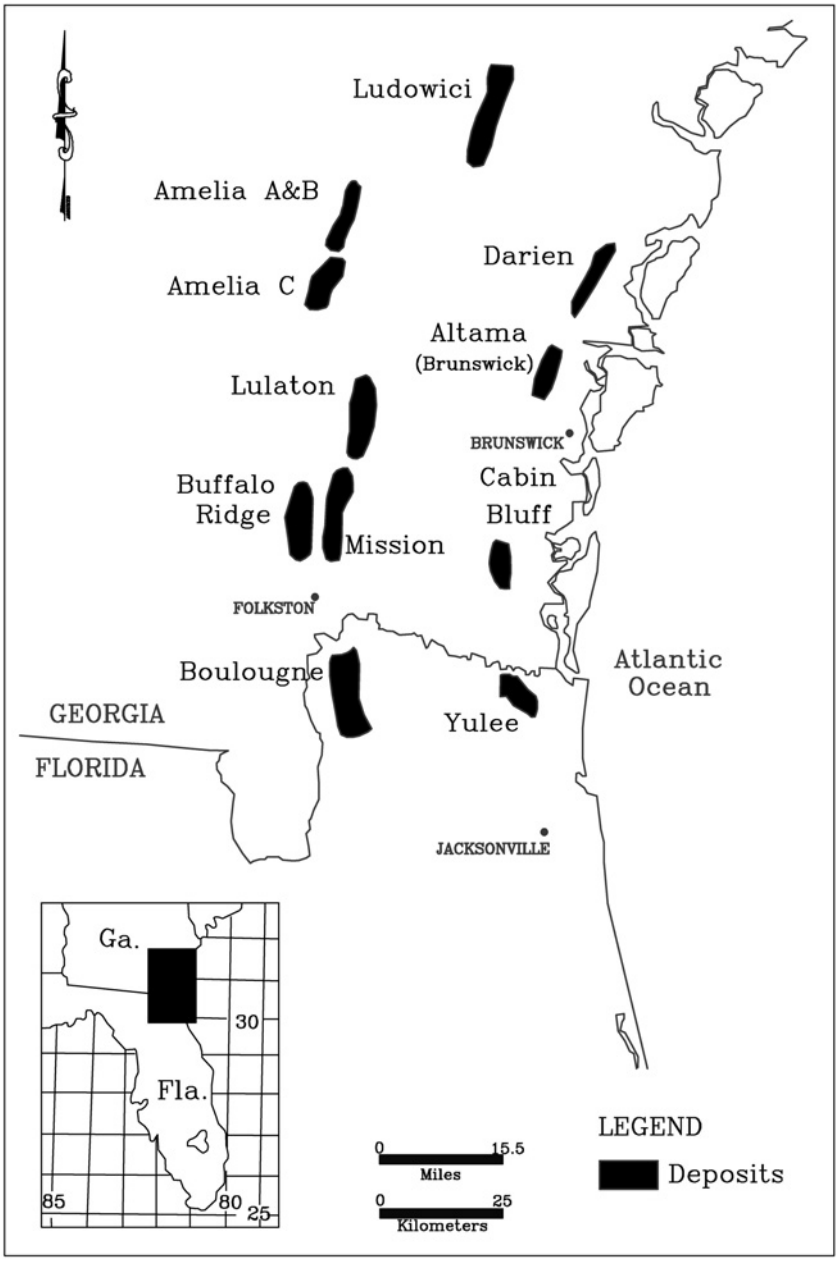

Fig. 9. Prospective heavy-mineral sand deposits in northeastern Florida and southeastern Georgia. Boulougne and Lulaton have partially been mined. Yulee and Cabin Bluff may be lost to cultural development.

The deposit's grain-size distribution and heavy-mineral assemblage is similar to the Green Cove Springs deposit and contains ilmenite with moderate amounts of zircon, rutile, and leucoxene. The ilmenite is highly altered, typically above 63% TiO_2. There is a distinct weathering profile near the surface that has elevated TiO_2

levels in the ilmenite and leucoxene. The mineralised zones are well-sorted, fine-grained sands and the deposit is underlain predominantly by sands and clays with low heavy mineral content.

8.1.3. Mission deposit

The Mission resource is located northeast of Folkston, Georgia (Fig. 9), immediately east of, and parallel with, Highway 301. The deposit is situated along the Penholoway shoreline (Rose, Written Communication, 2004). Drilling intersected three major zones of mineralisation, all of which trend north–northeast. Several smaller zones have been identified but not described. To the north, the Penholoway Terrace is eroded by Buffalo Creek, which separates the Mission and Lulaton deposits. To the south, the terrace is eroded by Baileys Branch, which separates the Mission from the mined-out Folkston orebody.

The western zone is 3690 m long and averages 400 m wide with an average thickness of 3.6 m. Mineralisation occurs primarily on the landward side of the Penholoway Terrace. The central part of the zone contains no overburden, but overburden increases to 1.5 m on the northern and southern ends of the zone. The northern zone lies on the eastern margin of the Penholoway Terrace and is 3440 m long, averages 610 m in width, and has an average ore zone thickness of 2.7 m. Low-grade overburden (HM < 2%) is less than 0.75 m thick. The northern zone appears to have several heavy-mineral strands. The southern zone extends to the southwest of the northern zone and consists of several distinguishable strands. It is 5.74 km long, has an average width of 450 m, and a mean thickness of 4.9 m.

The geological information obtained from drilling indicates that the Mission deposit was formed in a beach environment, predominantly in a foreshore facies but, within some areas of the southern zone, mineralisation extends into an intertidal backbarrier facies (Rose, Written Communication, 2004). The highest heavy-mineral grades are found close to the boundary between backbarrier and foreshore sands. The contact boundary between these facies is not distinct within some areas of the deposit. The depth to the top of the backbarrier facies is highly variable, and high grades are often found in areas where there is a drop in elevation of the contact. The highest grades within the southern zone occur within the westernmost of three identifiable strands (Rose, Written Communication, 2004).

The deposit's grain-size distribution and heavy-mineral assemblage are similar to those of the Green Cove Springs deposit. The heavy minerals are predominately ilmenite, with moderate amounts of zircon, rutile, and leucoxene. The ilmenite is highly altered, typically above 63% TiO_2. There is a distinct weathering profile in the surficial 3 m of sands that contains elevated TiO_2 levels in ilmenite and leucoxene. The minerals have been highly weathered, converting ilmenite to leucoxene and altering the leucoxene to near-rutile in property and makeup. The suite is relatively low in non-economic minerals as a result, in part, of in situ weathering and erosion of the less resistant gangue minerals, resulting in higher percentages of rutile, zircon, and ilmenite.

The foreshore facies, having undergone higher-energy sorting processes, is lower in gangue minerals than the backbarrier facies and has higher percentages of valuable heavy minerals (rutile, leucoxene, zircon and ilmenite). The higher-grade

heavy-mineral intervals (> 5%) appear to have very little gangue minerals. The heavy-mineral grain size is predominantly fine.

The backbarrier facies contains heavy minerals derived from the sediments of the adjacent barrier system of the time, and from those transported down the fluvial/inter-tidal system. The mineral suite is a mixture of the two sources, with elevated levels of epidote, pyrite, garnet, staurolite, tourmaline, kyanite, and sillimanite. The heavy-mineral grain size is fine to silt size.

8.1.4. Buffalo Ridge deposit

The Buffalo Ridge deposit is approximately 18 km south and 3 km west of the intersection of U.S. Highway 82 and U.S. Highway 301 in Charlton County, Georgia (Fig. 9). It is situated on the eastern flank of the Wicomico Terrace, 2.5 km west of the Mission Deposit (Rose, Written Communication, 2004). An unnamed tributary of Little Buffalo Creek flows through the area.

The Buffalo Ridge deposit consists of five separate mineralised zones along three roughly parallel strike lines, separated by zones of lower-grade heavy-mineral content. The mineralised zones range in length from 945 to 2195 m and in width from 125 to over 300 m. A 520-m wide zone of lower-grade heavy minerals, probably the result of erosion, interrupts the north–south continuity of the mineral-rich zones. Overburden of probable aeolian origin is present across most of the resource, and ranges in thickness up to 2.3 m. The Buffalo Ridge resource ranges in thickness from 0.8 to 4.5 m. The depth to the base of the mineral-rich zone ranges from 1.5 to 4.5 m. Mineralisation occurs within a foreshore beach facies and is underlain by an upper shoreface facies. The westernmost zones with mineral enrichment were accumulated and concentrated during a transgressive sea level phase. Those along the two eastern strike lines were deposited during sea level stillstands within an overall regressive phase (Rose, Written Communication, 2004). The foreshore facies has undergone high-energy sorting processes, which is reflected in the mineral suite. The surficial 1.5–3 m of sands have been highly weathered, converting ilmenite to leucoxene and altering the leucoxene to near-rutile in property and makeup. The suite is relatively low in non-economic minerals resulting, in part, from in situ weathering and erosion of the less-resistant gangue minerals, and hence contains higher percentages of rutile, zircon, and ilmenite. The heavy-mineral assemblage of the Buffalo Ridge deposit is 14% rutile, 12% zircon, and 44% ilmenite plus leucoxene.

8.1.5. Altama deposits

The Altama heavy-mineral deposits (referred to as the "Brunswick deposits" by Iluka Resources, Inc.) are located in eastern Glynn County, Georgia, northwest of Brunswick, in north–south-trending dune ridges of quartz sand that accumulated along a Pamlico shoreline during the Pleistocene (Fig. 9). The deposit strikes north–northeast immediately west of, and parallel with, Interstate 95 (Figs. 2, 9, and 10), and has been described in detail by Pirkle et al. (1989).

In 1960–1961, Scott Paper Company drilled 44 holes on the Altama prospect (Mateer, 1961). Data gathered from this drilling program indicated the presence of ~2.99 million metric tons of heavy minerals over an area of approximately 12 km^2. The delineated mineralised area is approximately 9.5 km long averaging 1 km in width. The average thickness of the mineralised zone is 3.6 m and the average

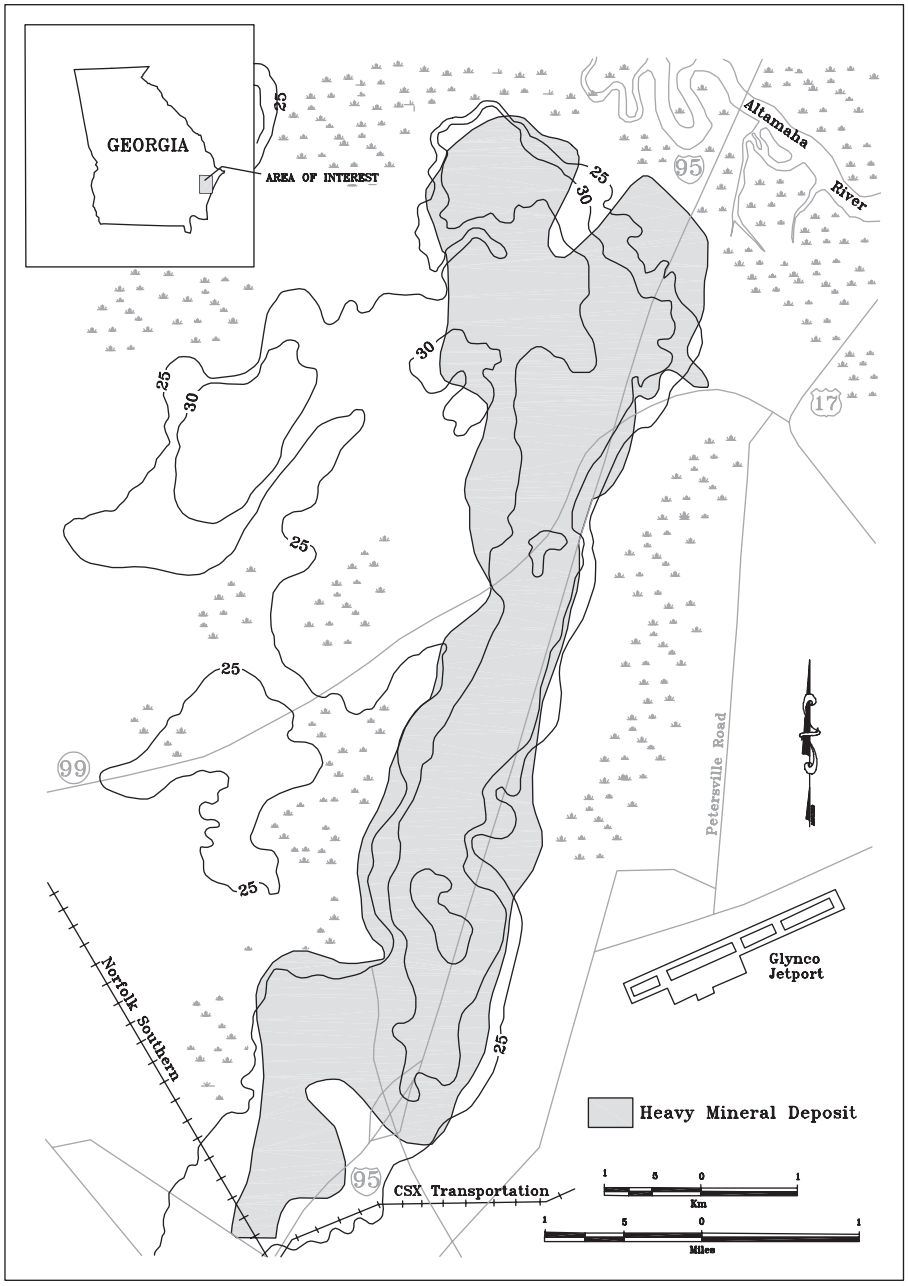

Fig. 10. Main deposit of the Altama heavy-mineral concentrations. The deposit trends essentially north–south. A few contour lines (in feet) are drawn in the areas of the ridges. Modified from Pirkle et al. (1989).

Table 23. Petrographic analysis of heavy minerals from the Altama Orebody. Counts were made of heavy minerals extracted from samples of ore sediments collected throughout the area of the orebody

Minerals	Total heavy minerals (weight percent) from Mateer (1961)	Total heavy minerals* (weight percent) from Pirkle et al. (1989)
Ilmenite	47.0	54.65
Zircon	10.8	10.51
Kyanite/sillimanite	12.5	8.39
Epidote		7.29
Rutile	3.8	6.89
Staurolite	5.2	5.97
Tourmaline		2.69
Leucoxene	8.4	1.70
Monazite	0.9	0.87
Hornblende		0.61
Garnet		0.33
Corundum		0.09
Spinel		0.01
Other gangue	11.4	
Total	100.0	100.00

*Weight percent converted from volume percent using method described by Wahlstrom (1947) and Garnar (1985b).

heavy-mineral content of the mineralised sands is 4.6%. Table 23 gives the average composition of the heavy-mineral suite as reported by Mateer (1961). Pirkle et al. (1989) described the main deposit as covering approximately 15 km^2 extending northward from Brunswick to the valley of the Altamaha River, a distance of ~11 km. Its width varies from a little more than 0.4 km to ~2.8 km. Ore-grade sands begin at the surface and extend downward to an average depth of 2.7–3.0 m. The main deposit has an average heavy-mineral content of approximately 3.5%.

Pirkle et al. (1989) state that the surface elevations of the Altama ridges range from some 7.5 m to more than 10 m above mean sea level (Fig. 10). The most extensive summit areas have elevations between 9 and 11 m. Fine to very fine sands and clayey sands are present beneath the Pleistocene sands that compose the ridges. These underlying sediments contain stringers and thin lenses of massive clay. X-ray diffraction reveals that the dominant clay minerals are smectite and kaolinite. In some areas, especially in the northern parts of the region, these underlying sands and clayey sands contain a high content of granule to small pebble-size angular quartz.

Pirkle et al. (1989) report that the dominant heavy minerals of the Altama deposits are ilmenite, zircon, kyanite, sillimanite, epidote, rutile, staurolite, tourmaline, and leucoxene, with lesser amounts of monazite, hornblende, and garnet (Table 23). Smaller amounts of other heavy minerals include corundum and spinel. The titanium minerals ilmenite (average 60% TiO_2), rutile, and leucoxene constitute ~63% of the total heavy minerals, and zircon accounts for almost 11%. According to Pirkle et al. (1989), most of the heavy minerals occur in thin stringers, disseminated throughout the dune sands, and not as thick ribbons of black sands such as those that

characterise many storm-line deposits. Some storm-line deposits, containing heavy-mineral concentrations, are present in the Altama deposit. Those that developed along the seaward side of dune ridges, and concentrations that formed in the backshore environment of the upper beach, would be covered by dunes as seas regressed and dunes built seaward. Pirkle et al. (1989) concluded that the Altama heavy-mineral deposits are beach ridges (dune ridges) that developed on the landward side of ancient beaches on a Pamlico barrier island during the Pleistocene.

In 1985, DuPont conducted a detailed evaluation of the main Altama deposit and several ancillary, smaller deposits, surveying over 41 km^2 and determining 18.6 km^2 of potential interest. This area contained approximately 2.34 million metric tons of heavy minerals including approximately 227,000 metric tons of zircon. More recently, Iluka Resources, Inc. re-evaluated the Altama deposit and purchased acreage that they planned to mine. However, in December 2006, Iluka sold the property and thus the orebody may be lost to exploitation. Rose (Written Communication, 2004) provides the following description of the Altama deposit from their recent investigation: ''The mineralisation has been identified along a strike length of 8200 m (27,000 ft) and width varying from 2700 m (9000 ft) in the north narrowing to 900 m (3000 ft) in the south. Depths of mineralisation are up to 6 m (20 ft) with the average being 3.6 m (12 ft). Sand, silt, and clay interbeds underlie the mineralisation. Surficial ridge elevations are generally at 10–11 m (32–37 ft) above sea level. The northern end of the deposit has three regressive barrier island strandlines to form the 2750-m (9000 ft) width whereas to the south a single mineralised strandline is present. The Altamaha River erodes the deposit to the north while the mineralisation continues to the south into commercially-developed land.''

The paleo-Altamaha River carried the sediment and heavy minerals for the Altama deposit, which was formed in a nearshore beach environment at the height of the marine transgression that formed the Pamlico shoreline. The morphology indicates that the deposit formed a regressive barrier island sequence with intervals of sea level stillstands creating distinct mineralised ridges. The surface mineralisation is underlain by very fine-grained quartz sand containing silt and clay interbeds representing backbarrier deposition. The paleo-beach placers possess moderate to high heavy-mineral grades with areas of aeolian dune-sands of lower heavy-mineral grade sitting above and landward of the placers. The deposit is composed mostly of ilmenite, with moderate amounts of zircon, rutile, and leucoxene. The ilmenite is less altered than that in the Green Cove Springs deposit but the TiO_2 content remains above 60%. Also, sand grain sizes are finer than in the Green Cove Springs orebody and are mainly very fine-grained.

8.1.6. Darien deposit

The Darien deposit is located in southeast Georgia, approximately 8 km north of the Altama deposit, and approximately 21 km inland from the present-day coastline (Fig. 9). It is eroded by the Sapelo River to the north and by the Altamaha River to the south. This deposit was described in detail in a Mineral Development International, Inc. report (Popp, 1975) and was reviewed briefly in 1976 in another report prepared by Mineral Development International, Inc. (Anonymous, 1976). The latter states that the prospect encompasses an area of approximately 28 km^2 of which approximately 16 km^2 are considered mineralised sufficiently to warrant

Table 24. Petrographic analysis of selected heavy-mineral species, Darien deposit

Minerals	Total heavy minerals (%) Popp (1975) as reported by Mineral Development International, Inc. (Anonymous, 1976)	Total heavy minerals (%) from Rose (Written Communication)
Ilmenite + leucoxene	43.5	38
Rutile	9.7	7
Zircon	10.3	8

exploitation. The underlying sands contain an average of 3.5% heavy minerals. Table 24 provides the average composition of the heavy-mineral suite by Popp (1975) as reported by Mineral Development International, Inc. (Anonymous, 1976).

The Darien deposit exhibits a classic transgressive barrier sequence. A backbarrier environment was eroded into, and overlain by, a nearshore beach sequence during a transgression. As sea level subsequently fell during a regression, the beach prograded seaward. A series of transgressions and regressions reworked the pre-existing beach sediments during transgression, and stranded them during regression. This led to the development of multiple mineralised zones within the Darien deposit. A significant sea level drop stranded the deposit (Rose, Written Communication, 2004).

The beach facies consists of very fine- to medium-grained, well- to very well-sorted sands. The majority of the mineralisation (> 2% HM) occurs within the beach facies although it extends into the backbarrier facies in some areas. Backbarrier sands, silts, and clays in the western part of the deposit, and upper shore face sands and clays in its eastern part underlie the beach facies. The nearshore beach facies is overlain by an aeolian facies consisting of very fine- to fine-grained, very well-sorted sands. The aeolian facies occurs primarily above the northwestern and western mineralised zones. In general, the aeolian facies has marginal heavy-mineral grades (1.5–2% heavy minerals), although there is a higher-grade (up to 4.5%) aeolian sequence that occurs as part of the western mineralised zone.

There are at least six mineralised zones that are separated by marginal-grade material. The heavy-mineral assemblage of the Darien deposit contains 7% rutile, 8% zircon, and 38% ilmenite plus leucoxene (Rose, Written Communication, 2004). Rutile percentages increase near the surface because increased weathering intensity near the surface has leached iron from the ilmenite and leucoxene. Zircon and ilmenite/leucoxene percentages increase with increasing grade, as does the uranium and thorium content (an indicator of monazite). Thus, zircon and monazite have the highest concentrations within the eastern zone, where the heavy-mineral grades are highest. The highest concentrations of ilmenite are in the southern end of the western zone.

8.1.7. Amelia deposits

The existence of the Amelia deposits (Fig. 9) was first suspected during the summer of 1973 as a result of the study of topographic maps and surface sands. The surface sand data were generated from samples collected along east-west traverses that extended from the Atlantic coast deep into the interior of the Atlantic Coastal Plain. These traverses were part of a systematic survey, initiated in the 1960s, of surface

sediments of the Coastal Plain of Florida and southeastern Georgia. In 1976, areas of the Amelia deposits outlined in 1973 were tested and determined to contain concentrations of heavy minerals. Pirkle et al. (1993b) provide a detailed description of these deposits. From Fig. 2 it can be seen that the Amelia heavy-mineral deposits are near the northern end of Trail Ridge. The deposits consist of two separate tracts of heavy-mineral concentrations, a northern tract west and southwest of Jesup, Wayne County, Georgia, and a southern tract south and southeast of Screven and U.S. Highway 84 (Fig. 11). The part of the northern tract north of the Holmesville Road is Amelia A; the part south of the road is Amelia B. According to Pirkle et al. (1993b) the mineable sediments containing heavy-mineral concentrations in the Amelia A and B tract average ~5.2 m in thickness. They contain an average of approximately 2.5% heavy minerals by weight. The southern tract is called Amelia

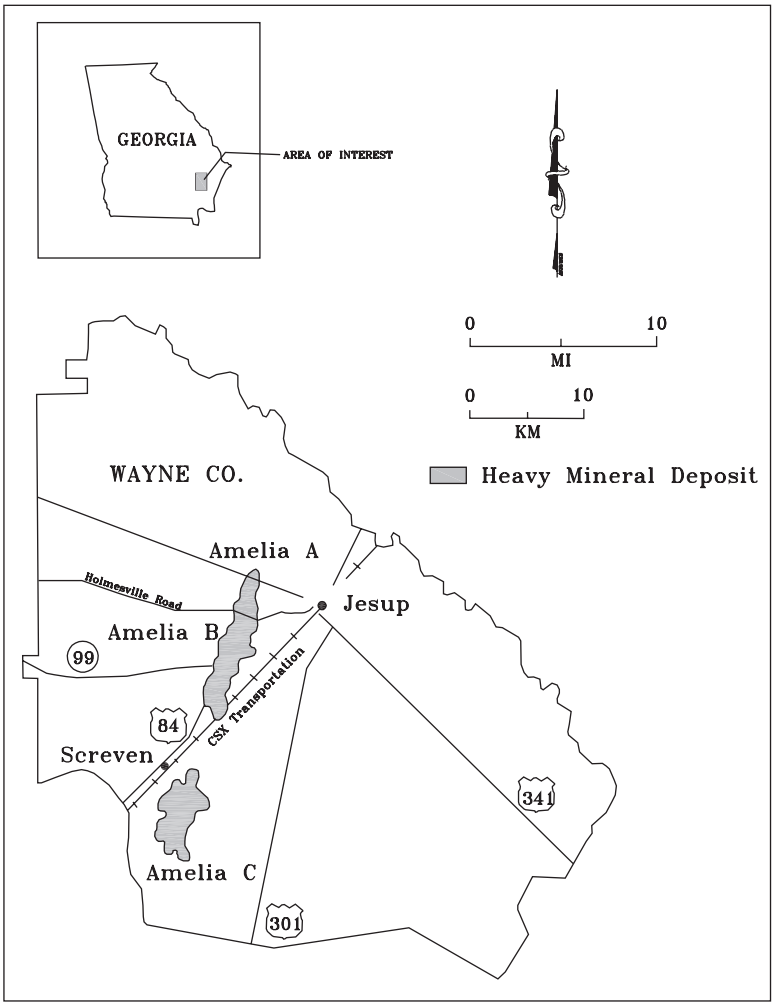

Fig. 11. Amelia A, B, and C heavy-mineral deposits located west and southwest of Jesup, Georgia. Modified from Pirkle et al. (1993b).

C. Mineable sediments with heavy-mineral concentrations in this tract average almost 6.7 m in thickness and contain an average of ~2.3% heavy minerals. The ore-grade sediments of the Amelia A, B, and C deposits contain a total of slightly more than 4.1 million metric tons of heavy minerals. Of these, ~60% by weight are titanium minerals (ilmenite, leucoxene, and rutile) and more than 13% by weight is zircon. The TiO_2 content of the ilmenite averages almost 66% (Pirkle et al., 1993b).

The Amelia heavy-mineral deposits occur in two different types of ore-bearing sands, differing from other Trail Ridge heavy-mineral deposits in this respect. Mallard (1988) points out the differences in the two types of heavy-mineral-bearing sands in the Amelia C tract. The upper sedimentary sequence, containing heavy-mineral concentrations, consists of mainly medium- to fine-grained typical Trail Ridge sands. The ore-bearing sands of the second type locally underlie the typical Trail Ridge sands and are mainly coarse- to medium-grained. Because of their colour, these underlying coarser sands are referred to locally as golden-brown sands.

It appears from the geological information obtained from drilling that the Amelia deposit was formed as two sequences: deltaic channel fill, and beach and dune. The surface sands are underlain by a terrestrial basal clay and a deltaic channel facies. The deltaic sediments were deposited during a phase of marine regression. During a subsequent transgression, beach sediments were deposited on top of the deltaic sediments. Most of the mineralisation occurs within the aeolian, foreshore, and deltaic facies, although some heavy-mineral concentrations extend into the underlying basal clay. Heavy minerals in the foreshore deposits have been concentrated by high wave energies in a beach environment and have been preserved in aeolian dunes above and behind the foreshore deposits. The heavy minerals have been further concentrated by reworking that has occurred during multiple transgressions and regressions. Within the deltaic sediments, heavy minerals occur as channel lags (Rose, Written Communication, 2004).

The Amelia deposit is coarser grained than the Penholoway or Pamlico, and is typical of Trail Ridge deposits. The heavy-mineral assemblage is predominately ilmenite with moderate amounts of zircon and leucoxene. The ilmenite is highly altered, typically above 63% TiO_2. There is a distinct weathering profile in the surficial 3 m of sands, with elevated TiO_2 levels in ilmenite and leucoxene. The minerals have been highly weathered, converting ilmenite to leucoxene and altering the leucoxene to near-rutile. The suite is relatively low in trash minerals because of, in part, in situ weathering and erosion of the less-resistant gangue minerals, resulting in higher percentages of rutile, zircon, and ilmenite. Table 25 provides petrographic analyses of the Amelia heavy minerals.

8.1.8. Ludowici deposit

The Ludowici deposit is located in Long and Liberty counties in Georgia, between Ludowici and Hinesville (Fig. 9) along the Penholoway shoreline (Rose, Written Communication, 2004). In general, the mineralised zones trend north–northeast and are long and linear. The surficial sands are well sorted, fine to medium-grained, and contain 5–15% slimes (<53 μm materials). Drilling data indicate that the mineralised zones were formed in a beach environment. Most are located within the foreshore facies, although some occur within a backbarrier facies. The western zone was formed at the height of the initial transgression. As the sea regressed, the sand body

Table 25. Petrographic analyses of heavy minerals from ore grade sediments of the Amelia deposits*

Mineral species	Weight percent of total heavy minerals		
	Trail Ridge Sands Amelia A and B	Trail Ridge Sands Amelia C	Golden Brown† Sands Amelia C
Ilmenite	45.7	44.8	35.5
Staurolite	6.6	9.5	12.9
Zircon	13.6	14.0	12.1
Kyanite/sillimanite	11.1	9.5	16.2
Tourmaline	3.7	4.5	6.7
Rutile	5.9	5.9	5.6
Leucoxene	13.0	10.1	3.0
Monazite	0.2	0.5	0.3
Epidote	0.1	0.7	6.7
Garnet	Tr	0.1	0.2
Corundum	Tr	0.2	0.7
Spinel	0.1	Tr	0.1
Hornblende	0.0	0.1	0.1

*From Pirkle et al. (1993b).
†Values for the various heavy minerals of the golden brown sands may vary considerably from one locality to another; such variation, however, is not characteristic of the heavy minerals of the Trail Ridge sands.

was stranded at its present location. It has undergone significant erosion and replacement of mineralised portions of sands resulting in its small size. A later transgression followed by sea level stillstand formed the middle zone. This transgressive/regressive barrier sequence did not overtake the western zone. The sea level stillstand lasted for a substantial time interval, as evidenced by the 7.6 m thickness at the core of the zone. Several smaller transgressive/regressive cycles eroded and re-deposited high-grade zones within the mineralised package. After the sea regressed, stranding the middle zone, a later transgression and sea level stillstand formed the eastern zone. This transgressive/regressive barrier sequence did not overtake the previous two stranded sand bodies. The resultant stillstand built a 6-m thick package of sand but with a lower grade than that in the other ridges, because of either lower storm activities at the time of deposition or the lack of sediments from reworked high-grade strands of previously transgressed barrier sequences. The Cypress Head (Citronelle) Formation, an open sound depositional succession of interbedded silty micaceous sands and clays, underlies the surficial foreshore mineralisation (Rose, Written Communication, 2004).

The foreshore facies sediments have undergone high-energy sorting processes, which is reflected in the mineral suite. The heavy-mineral suite in the surficial 3 m of sands has been highly weathered (with alteration of ilmenite to leucoxene, then to near rutile), and therefore contains relatively low percentages of gangue minerals and higher percentages of rutile and zircon. The higher-grade heavy-mineral intervals ($> 5\%$) appear to have fewer gangue minerals, which may be a result of the higher-grade lenses/areas being deposited during times of elevated storm activity and,

therefore, undergoing a number of very high-energy sorting process. The heavy-mineral grain size is predominantly fine.

8.2. Eastern North Carolina

Exploration for heavy minerals has been conducted in eastern North Carolina for many years. Much of this exploration has concentrated on modern beaches, the Suffolk Scarp, and the more westerly Surry Scarp. Williams (1964) reported that, in 1942, DuPont obtained a non-exclusive lease from the State of North Carolina to prospect for ilmenite in and along Albermarle Sound. The Federal Bureau of Mines drilled four holes in Perquimans County (Williams, 1964), and National Lead Company (now known as NL Industries, Inc.) secured leases to explore for ilmenite on 1.3 km^2 in Chowan County. National Lead Company also secured leases for titanium exploration in Beaufort County (1951) and in Pamlico County. Allied-Kennecott Titanium Corporation registered deeds for property during the years of 1957 and 1958 for 7.0 km^2 in New Hanover County fronting on the Cape Fear River ~8 km south of Wilmington, North Carolina. Williams (1964) reports that the erection of a titanium processing plant was originally indicated but that no development was in evidence at the end of 1960.

There are several prospects that have been long identified along the Suffolk Scarp, such as the Aurora and Chowan deposits, but no prospects have been identified along the Surry Scarp. Cannon (1957) reported the TiO_2 content of the ilmenite in the Aurora deposit as 57.6%. In the 1990s, a company looked at the possibility of combining the deposits of the Suffolk Scarp into a single mine concept. One prospect contains an estimated 377 million metric tons of sand averaging 2.69% heavy minerals or 10 million metric tons of heavy minerals. The mineralised sands in this deposit covered approximately 48.8 km^2. These numbers were obtained using a heavy-mineral cut-off of 1.5% and a minimum mining thickness of 3 m. Some smaller prospects were added to this prospect. A review of the data led the evaluators to believe that, most likely, sands for the single mine operation would average 3% heavy minerals with a 10% chance for averaging as low as 1.5% and a 10% chance for averaging as high as 5%. They further estimated that the heavy-mineral suite consisted of 70% ilmenite that averaged 60% TiO_2, 3% rutile, and 10% zircon. It was recognised that the TiO_2 content in the ilmenite could be as low as 54% or as high as 64%. Because of changes in the economy, neither the prospect nor the single mine concept was pursued further.

8.3. Fall Zone of North Carolina and Virginia

The Fall Zone is a 16–32 km wide area where the wedge of sediments of the Coastal Plain Province overlaps and pinches out on the crystalline rocks of the Piedmont Province (Gallagher and Hoffman, 1990). In 1988, a program began to evaluate titanium anomalies along the Fall Zone in North Carolina. These anomalies had been reported for stream sediment samples taken as part of the National Uranium Resource Evaluation (NURE) program. At about the same time, Berquist (1987) recognised heavy-mineral concentrations in the high-level gravels of the Fall Zone in southeastern Virginia. Evaluation of the titanium anomalies led to the discovery of

several areas in Wilson, Nash, Northampton, and Halifax counties, North Carolina, that contained more than 3 wt.% heavy minerals (Fig. 4). The dominant heavy minerals are ilmenite and zircon.

Pirkle et al. (1991b) published the locations of these deposits. Carpenter and Carpenter (1991) proposed that the sediments containing the heavy-mineral deposits are up-dip equivalents of the Yorktown Formation (Early Pliocene) and relate the depositional history to the phases of transgression and regression described by Bailey (1987). Carpenter and Carpenter (1991) discuss two sedimentary units that are present throughout the upper Coastal Plain as the lower unit and the upper unit. The heavy-mineral deposits occur within the upper unit. They reported that a collective total of 22.7 million metric tons of heavy minerals at an average grade of 6 wt.% in 377.8 million metric tons of sand has been delineated from numerous heavy-mineral deposits in the upper Coastal Plain of North Carolina and Virginia, and suggested that the deposits formed during a worldwide, Pliocene, transgressive/regressive event between 3.5 and 3.0 Ma. The deposits formed in beach or dune sands during the regressive phase over an elevation range of 96–53 m. They concluded that the Trail Ridge deposits in Florida and Georgia are related to this event. Other workers, however, contend that these Fall Zone deposits are the result of Fall Zone deltas and that the concentrating mechanism for the heavy-mineral deposits within the Fall Zone deltas was a combination of fluvial processes, allied with basement highs and lows. Little or no tidal/wave action is thought to have been influential, although this would not exclude local tombolo effects (Pirkle et al., 2007).

The largest of the Fall Zone heavy-mineral deposits are Old Hickory (a deposit located in Virginia that is currently exploited), the Halifax deposit in northern North Carolina (Pirkle et al., 1991b), renamed ''Aurelian Springs'' by Carpenter and Carpenter (1991), and the Bailey deposit south of Bailey, North Carolina. Smaller deposits are the Kenley, Ringwood, Red Oak and Virginia B (Pirkle et al., 1991b) renamed ''Brink'' by Carpenter and Carpenter (1991). Table 26 provides petrographic information for the heavy-mineral suite of the North Carolina–Virginia

Table 26. Averages and ranges in percentages of heavy minerals in deposits containing > 3% heavy minerals, North Carolina–Virginia heavy minerals belt*

Mineral	Average %	Range in average % for individual deposits
Ilmenite + leucoxene	60.0	53.0–71.0
Rutile	2.5	1.6–4.5
Zircon	12.5	7.0–19.1
Subtotal	75.0	70.0
Staurolite	8.5	92.6
Tourmaline	0.7	3.7–18.0
Kyanite	3.0	0.3–1.1
Sillimanite	1.3	1.2–6.0
Other†	11.5	0.6–2.5

*From Carpenter and Carpenter (1991).
†Other minerals include certain ferromagnesians, limonite, monazite (<0.4%), and traces of other minerals.

heavy-mineral deposits containing more than 3% heavy minerals. The TiO_2 content of the ilmenite in these deposits averages 57.6%.

8.3.1. Bailey deposit

The Bailey deposit is located south of Bailey in Nash and Wilson counties, North Carolina (Fig. 4). The mineralised area covers 12.9 km^2, with mineralised sand averaging 6.2 m. The deposit contains 5.72 million metric tons of heavy minerals. The sediments comprising this deposit average 4.72 wt.% heavy minerals (McMahill, Written Communication, 2004). Mallard (1992) reports an indicated resource of 50 million metric tons of sand with an average heavy-mineral content of 6.1 wt.%. Local concentrations exceed 20% heavy minerals. The thickness of the deposit ranges between 6.1 and 7.6 m. Valuable heavy minerals contained in the deposit are ilmenite, zircon, rutile, and leucoxene, which comprise 65–70% of the heavy-mineral suite (Mallard, 1992).

Hoffman and Carpenter (1992) described two sedimentary units that occur consistently throughout the heavy-mineral belt of North Carolina and Virginia. The lower unit, where present, lies directly on the crystalline basement rocks and ranges in thickness from 0 to 12 m. Gravel-rich (pebble- to boulder-size clasts), micaceous, quartz sand typically characterises the lowermost several metres of this unit. Arkosic sand is present locally in areas of granitic basement. Poorly sorted, medium to coarse, sub-angular to angular quartz sands with dispersed sparse granules and fine gravel are typical of the lower unit above the basal gravel-rich zone. Thin clayey and silty beds are locally present within the lower unit. Dispersed clay is ubiquitous and often comprises over 25 wt.% of the sediment (Hoffman and Carpenter, 1992).

The upper unit is much finer and is better sorted than the lower unit. Its thickness near the Bailey deposit ranges from 0 to 17 m, and is mainly a fine-grained, well-sorted and rounded, clayey quartz sand that contains abundant heavy minerals. Dispersed clay, mostly sub-micron size kaolinite, generally comprises >25 wt.% of the upper unit (Hoffman and Carpenter, 1992). The upper unit usually overlies the lower unit but, in a few areas, rests on crystalline basement, and hosts the heavy-mineral deposits of the Fall Zone such as the Bailey deposit. Although heavy minerals locally comprise up to 50 wt.% of some beds, concentrations in the Bailey area average 4–6 wt.% (Hoffman and Carpenter, 1992). Carpenter and Carpenter (1991) report the weighted average concentrations of heavy minerals in the upper unit for deposits of the entire Fall Zone belt containing >3 wt.% heavy minerals as follows:

Mineral species	% of heavy-mineral fraction
Ilmenite/leucoxene	60.0
Rutile	2.5
Zircon	12.5
Staurolite	8.5
Tourmaline	0.7
Kyanite	3.0
Sillimanite	1.3
Others	11.5

Hoffman and Carpenter (1992) state that the suite of heavy minerals in the Bailey area is slightly more enriched in kyanite, sillimanite, staurolite and rutile, and carries less zircon than the above averages. According to Hoffman and Carpenter (1992), the upper unit becomes less sorted and the grains are less rounded below an elevation of 53 m. Also, silt content increases and the heavy minerals are finer-grained and less abundant. Within the North Carolina–Virginia Fall Zone, all known deposits containing > 3 wt.% heavy minerals occur above elevations of 53 m.

Mallard (1992) described the deposit as being represented by a heavy-mineral-bearing clayey sand, at the surface when present, underlain by an unmineralised clayey sand and a basement of granite (Sims Pluton) or metamorphosed rocks. According to Mallard (1992), there are three distinct strands in the Bailey area that contain significant thicknesses of mineralised sands. The bases of these are at 82, 76, and 55 m, with the higher grades being in the 82- and 76-m strands. Mallard (1992) believes deposition of these strands occurred as a result of stillstands or slight transgressions during a regressive period. The high-grade portion of the Bailey deposit overlies the Sims Pluton. The heavy-mineral-bearing unit is generally a fine- to medium-grained, well-sorted, feldspathic clayey sand that contains primarily kaolinite, and reaches thicknesses of up to 12 m. It is underlain by an unconformity characterised by a transgressive lag (gravel, pebble) layer. The unmineralised sand is generally a fine- to coarse-grained, poorly sorted, clayey sand that contains silt/clay and gravel/pebble layers. Sands of this unit contain heavy minerals that are finer than those above it, but are gangue (Mallard, 1992).

8.3.2. Virginia B (Brink) deposit

The Brink resource is located in Greensville County, Virginia, 9 km southwest of Emporia on state road 627 (Fig. 4). The deposit consists of southwest (Brink West) and northeast (Brink East) zones with a combined strike-length of 6 km in a north–northeast direction. Significant stream dissection has occurred and the two deposits were probably originally contiguous. The deposit is geologically similar to Old Hickory, 30 km to the north. Both are in the Fall Zone where Miocene-Pliocene coastal plain sediments overlap onto Palaeozoic basement rocks. The host sediments are feldspathic quartz sands, which are probably fluvial deposits that have been reworked in marine beach/backbarrier environments (Rose, Written Communication, 2004).

The Brink West mineral assemblage consists of 70% ilmenite averaging 60% TiO_2, 15% zircon, 3% rutile plus leucoxene, and 10% gangue minerals. The average grain size of heavy minerals larger than 75 μm is 115 μm. The Brink East mineral assemblage consists of 65% ilmenite averaging nearly 60% TiO_2, 14% zircon, 5% rutile plus leucoxene, and 15% gangue minerals. Like Old Hickory, both Brink deposits have pronounced weathering profiles and TiO_2 commonly is enriched in the weathered top 3 m of the section (Rose, Written Communication, 2004).

8.4. Gulf Coastal Plain

The Gulf Coastal Plain in the U.S. extends westward along the Gulf of Mexico from Florida to the Texas border with Mexico. This section describes heavy-mineral occurrences located within the Gulf Coastal Plain as far west as the Texas/Louisiana

border. Private companies have performed exploration within the Texas Gulf Coastal Plain between the Louisiana and Mexican borders, but most of their results are unavailable. Some workers place an arbitrary boundary between the Gulf Coastal Plain and the Atlantic Coastal plain at the Alabama/Georgia state border and extend the boundary southward along the Apalachicola River through Florida to the Gulf of Mexico. In the Mississippi Embayment, the Gulf Coastal Plain extends north to southern Illinois. The Gulf Coastal Plain covers the western panhandle of Florida, the southwestern two-thirds of Alabama, some of western Tennessee and Kentucky, southernmost Illinois, most of Mississippi, Louisiana, southwest Arkansas, the southeast corner of Oklahoma, and easternmost Texas. Although considerable exploration has been conducted and several heavy-mineral deposits have been identified, no significant commercial exploitation of heavy-mineral deposits has occurred in the Gulf Coastal Plain (Fig. 1).

Anderson (2000) and McGrain (2001) both note that heavy minerals in the Cretaceous and Tertiary sediments of western Kentucky (the Mississippi Embayment) have been examined and have potential as an economic resource. Landowners in Calloway County, Kentucky, have reported that Ethyl Corporation performed exploration within their county. According to the landowners, some holes were drilled and heavy minerals were encountered but very little information is available.

The Cretaceous sands of extreme southern Illinois (McNairy Sand) contain heavy minerals that are economically valuable if they occur in sufficiently large concentrations and in deposits of sufficiently large size (Lamar and Grim, 1937). Shrode and Lamar (1953) and Pryor (1960) have described the mineralogy of the Cretaceous sands, and Hunter (1968) reports that the heavy-mineral fraction of the McNairy Formation has the following average heavy-mineral composition:

Mineral species	% of heavy-mineral fraction
Ilmenite + leucoxene	60.3
Rutile	5.5
Zircon	12.6
Monazite + xenotime	1.1
Staurolite	6.5
Kyanite	8.0
Sillimanite	1.4
Tourmaline	4.5

8.4.1. Western Tennessee deposits

E.I. du Pont de Nemours & Co. conducted a reconnaissance exploration program during 1957–1958 to investigate reported surface heavy-minerals in western Tennessee. The exploration program led to the discovery of ore-grade occurrences of titanium minerals in the Cretaceous McNairy Formation. The McNairy Formation is a poorly consolidated, clay-bearing fine-grained sandstone ~90 m thick, outcropping in a north–south belt starting just west of Kentucky Lake in Henry County, Tennessee, and continuing south through McNairy County, Tennessee, at the Tennessee–Mississippi border (Miller et al., 1966). The formation dips very gently to the west.

Ethyl Corporation and Kerr-McGee Corporation conducted exploration programs during 1970–1972, and both companies outlined several potential orebodies. Production plans were deferred because of environmental concerns and changing market conditions (Lynd and Lefond, 1975, 1983). During this period, Wilcox (1971) performed a preliminary investigation into the occurrence of heavy minerals in the McNairy Sands of western Tennessee for the Tennessee Department of Conservation, Division of Geology.

Data from these programs indicate that the western Tennessee deposits range in grade from 1.5 to 3% TiO_2 in the ground and may contain approximately 1–6 million metric tons of TiO_2. The mineralised sediments are fine-grained, with most of the heavy-mineral content being in the −170-mesh (88 μm) fraction (Wilcox, 1971; Costin and Lloyd, Written Communication, 2004). Wilcox (1971, p. 6) reported that ilmenite comprised 46.6–64.4 wt.% of the heavy-mineral suite. He reported that the other major heavy-mineral species in approximate order of decreasing abundance are zircon, leucoxene, staurolite, kyanite, tourmaline, monazite, and rutile, with a few grains of spinel and garnet. He calculated that the TiO_2 content of the titanium product from the Manleyville deposit should be ~58% and argued that the TiO_2 content from some of the other deposits, such as Buchanan and Lexington, are higher because of a higher leucoxene and rutile content in the titanium product.

In western Tennessee, mineralisation occurs in every formation from the Cretaceous Tuscaloosa Formation to Quaternary/Tertiary fluvial deposits. However, exploration has been confined to the lower portion of the Cretaceous McNairy Sand, which was mapped sometimes in combination with the Tertiary Clayton Formation. The McNairy Sand has a thickness of up to 137–152 m throughout the states of Tennessee, Kentucky, and Illinois. Heavy-mineral deposits have been identified near Camden, Bruceton, Buchanan, Lexington, Manleyville, and Oak Grove in Tennessee. Some of these deposits are close together and may be continuous or, at least, may be mined as a continuous orebody.

In the early 1990s, the western Tennessee deposits were evaluated again, confirming the previous high values for rutile and zircon in the heavy-mineral suite but also indicating high values for ilmenite. The presumed average heavy-mineral content of the sands is 5.4%, with the heavy-mineral suite most likely containing 64% ilmenite, 8% rutile, and 24% zircon. Ilmenite contains 64% TiO_2. This evaluation was based on the assumption of mining the deposits as a single mine. Fantel et al. (1986) reported a large resource of fine-grained ilmenite and zircon in the Cretaceous sediments of western Tennessee containing an estimated 8 million metric tons of TiO_2. Garnar and Stanaway (1994) suggested that the stratigraphy implies a submarine origin, some distance offshore, for the western Tennessee heavy-mineral deposits.

A mineralised area ~8 km northwest of Camden, covering approximately 34 km^2, was evaluated in the mid- to late-1990s by Altair International, Inc. (now Altair Nanotechnologies, Inc.). The economically important heavy-mineral concentrations occur near the base of the late Cretaceous McNairy Sand Formation between elevations of ~128 and 150 m above sea level (Lloyd and Costin, Written Communication, 2004). According to Lloyd and Costin (Written Communication, 2004), the deposits have a very regular, shallow dipping form that has been dissected into three discrete bodies by recent stream erosion. Two sand bodies east of the Big Sandy River are the Camden deposit, and the single sand body west of the Big Sandy River

is the Little Benton deposit (Fig. 12). The Camden deposit covers approximately 20 km^2 and the Little Benton deposit ~14 km^2.

Thiers (1999) and Anonymous (1999b) report that the Camden deposit has an indicated reserve of 400 million metric tons of mineralised sand containing an average of 3.3% heavy minerals, and that the Little Benton Deposit contains an additional 236 million metric tons of sand averaging 3.5% heavy minerals. Together, these deposits should contain approximately 21.46 million metric tons of heavy minerals. Hedrick (2001) reported that the Camden deposits contain an estimated 490 million metric tons of sand averaging 3.6% heavy minerals. Based on 167 auger drill holes and using a 2% heavy-mineral cut-off, Lloyd and Costin (Written Communication, 2004) report that the Camden deposit contains approximately 275.8 million metric tons of sand averaging 3.66% heavy minerals, and that the Little Benton deposit contains somewhat over 214 million metric tons of sand with an average of 3.63% heavy minerals (heavy minerals reported are between 50 and 325 mesh—25–170 μm; coarser and finer heavy minerals are not reported). Together the deposits contain approximately 490 million metric tons of sand containing almost 18 million metric tons of heavy minerals. Anonymous (1998, p. 2) describes the Camden deposit as consisting of "Two discrete mineralised bodies, each exhibiting continuity in terms of bed thickness and heavy-mineral grade. Certain zones exist within the mineralised boundaries which could provide higher than average grade material in early production years …." Using a 2% total heavy-mineral cut-off, Anonymous (1998) reports the following indicated reserve:

Unit	Tonnage (metric tons/short tons)	Grade (% total heavy minerals)
Strand (Bed 2)	275 million/304 million	3.66
Dune (Bed 1)	82 million/91 million	1.23
Overburden	50 million/55 million	

The heavy-mineral suite of the Camden deposits is fairly fine-grained (Table 27). Ilmenite alteration to leucoxene is pronounced. Ilmenite/leucoxene, rutile, and zircon comprise 50.3, 12.6, and 13.2% of the heavy-mineral suite respectively (Table 28), with staurolite, kyanite, and sillimanite making up much of the remainder. Bulk ilmenite/leucoxene grades vary from 64 to 74% TiO_2 (Lloyd and Costin, Written Communication, 2004). The heavy-mineral bearing sands of the Camden deposits contain an average of 27% slimes (<44 μm). However, less than 2% of the mineralised sands is smaller than 2 μm. The bulk of the 2–44 μm slime fraction is composed of fine silica (Lloyd and Costin, Written Communication, 2004). The Camden deposits occur in a thin package of well-sorted, very fine-grained deltaic sediments. *Ophiomorpha* are commonly found proximate to mineral sheets, indicating a nearshore environment that might be a transitional fresh-water/salt-water depositional environment (Lloyd and Costin, Written Communication, 2004).

8.4.2. Arkansas

Titanium-bearing minerals in Arkansas occur in Pulaski, Saline, Hot Springs, Garland, Pike, Howard, Sevier, Little River counties, and in the alluvial sands of the

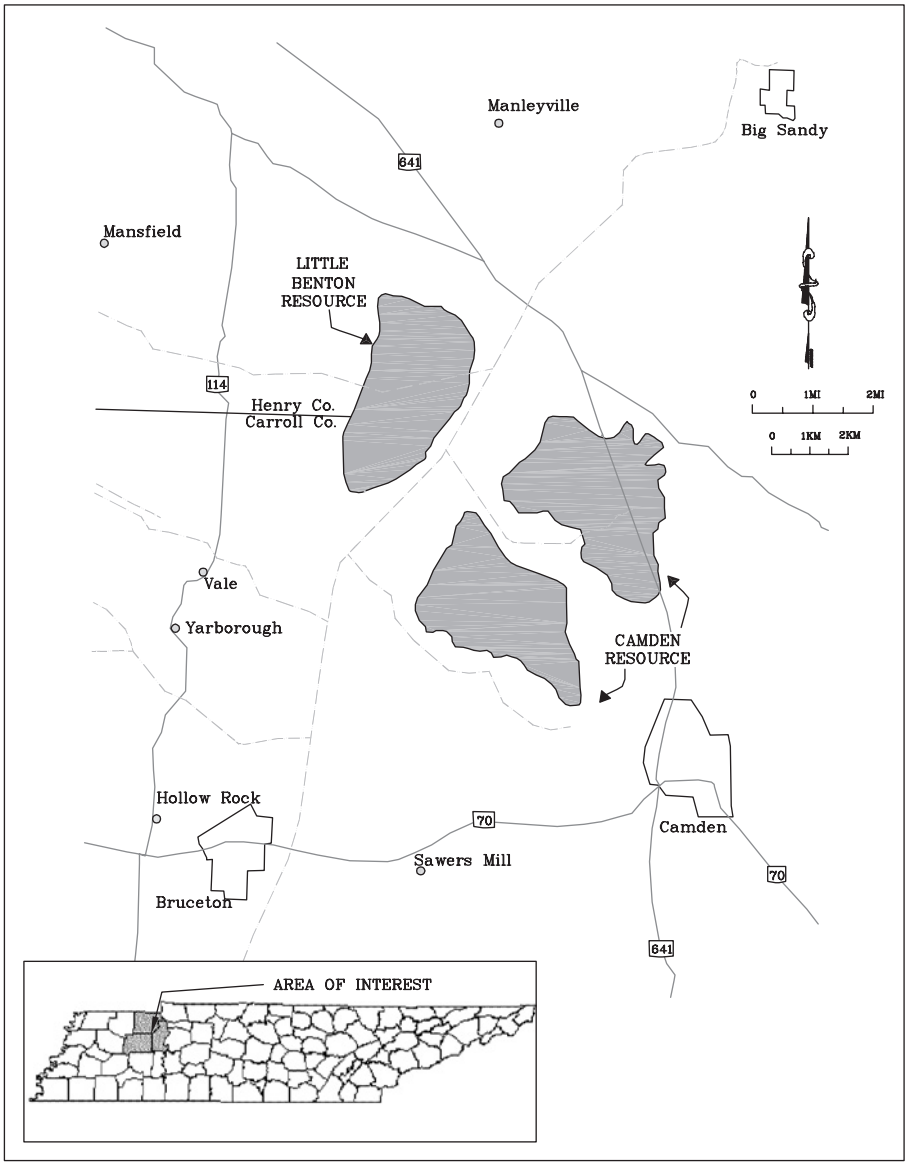

Fig. 12. Location of the Camden and Little Benton heavy-mineral deposits, which are within the Cretaceous McNairy Formation of western Tennessee.

Arkansas River (Arkansas Geological Commission, 2006). The titanium-bearing minerals in Pulaski and Saline counties are in intrusive bodies of nepheline syenite and bauxite deposits. Rutile, brookite, and perovskite occur at Magnet Cove, Hot Springs County. In Garland County, sporadic titanium values were noted during vanadium mining at Potash Sulphur Springs but none was recovered.

Occurrences of interest to this review occur in Pike, Howard, Siever, and Little River counties as well as the Arkansas River (Fig. 13). In Pike, Howard, Siever, and

Table 27. Sieve analysis of heavy minerals in the Camden deposits*

Mesh	Ilmenite (weight percent)	Rutile (weight percent)	Zircon (weight percent)
+20	0.52	0.62	0.03
120–140	4.05	5.09	0.12
140–170	25.04	22.89	3.06
170–200	33.42	29.97	12.94
200–230	30.19	31.75	38.67
230–270	5.08	7.40	21.85
270–325	1.43	2.10	19.58
325–400	0.22	0.16	3.30
>400	0.05	0.02	0.45

*From Lloyd and Costin (Written Communication, 2004).

Table 28. Camden heavy-mineral deposits heavy-mineral suite*

Mineral species	% Heavy minerals	
	Lloyd and Costin	Anonymous (1998)
Ilmenite/leucoxene	50.3	60
Rutile	12.6	5
Zircon	13.2	15
Other heavy minerals	10.7	20

*From Lloyd and Costin (Written Communication, 2004).

Little River counties, ilmenite is in the upper sandy part of the Cretaceous Tokio Formation. The Tokio Formation crops out near Arkadelphia, Clark County, and extends westward to the Arkansas state line, north of Arkinda, Little River County. The largest known deposits of ilmenite sands are located near Mineral Springs, Howard County (Fig. 13). One deposit was surface mined, but minimal ilmenite was recovered. During 1939 and 1940, 12.8 short tons of ilmenite were recovered by processing sand from the Arkansas River, Yell County. No ilmenite is being mined in Arkansas (Arkansas Geological Commission, 2006).

According to Holbrook (1948) and Hanson (1997), King Rankin discovered, in 1938, heavy-mineral sands in the Late Cretaceous Tokio Formation near Mineral Springs in southern Howard County, Arkansas, while prospecting for the State Mineral Survey. Holbrook (1948) published the first report on the ilmenite-bearing sands of the Tokio Formation. Thorsen (1959, pp. 6–7) states "The Tokio formation (sic) is represented in the western part of its outcrop in southwest Arkansas by 350–375 ft of grey, micaceous, lignitic clay with several beds of red, brown, and white quartz sand and a basal bed of gravel …. The sands are both massive and bedded and consist of fine to medium, angular to subrounded, grains of quartz with a large percentage of heavy minerals." In discussing the origin of the Tokio Formation, Thorsen (1959, p. 21) states "That portion of the Tokio formation (sic) exposed at

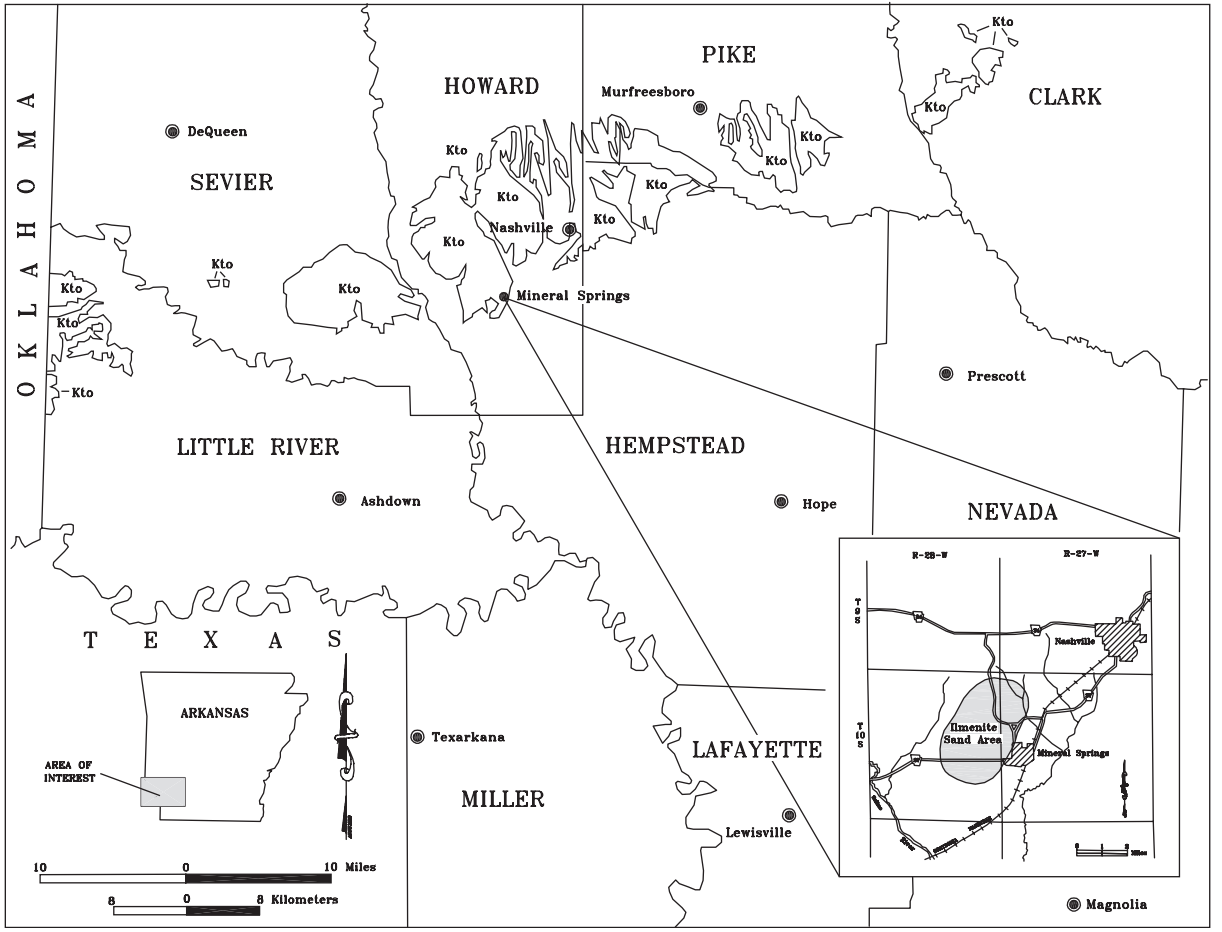

Fig. 13. Outcrop of the Tokio Formation (Kto) in southwest Arkansas and the location of the Howard County ilmenite sand area. Modified from Holbrook (1948) and Hanson (1997).

the outcrop in southwest Arkansas was deposited in a shallow water, near shore, marine environment. The proximity of the shore line is suggested by the coarseness of the basal Tokio clastics, the abundance of cross-bedded sands, and the presence of carbonised plant material. The marine origin of the outcropping Tokio is shown by the fauna which it contains.''

Holbrook (1948) reported small amounts of ilmenite disseminated throughout the sand members of the upper part of the Tokio formation in an area of ~15.5 km^2 located northwest of Mineral Springs, Arkansas. State Highway 27 crosses the southern end of the ilmenite sand area. Within this area, Holbrook reports small local concentrations of ilmenite designated as the Pink Green deposit and the Beulah Green deposit. The Pink Green deposit is located ~2.4 km northwest of Mineral Springs (Secs. 12, T. 10 S., R. 28 W.) and the Beulah Green deposit is 1.6 km west of Mineral Springs (Secs. 23 and 24, T. 10 S., R. 28 W.). In 1943, the U.S. Bureau of Mines collected samples from auger holes, domestic wells, and road cuts on the Pink Green and Beulah Green deposits. According to Holbrook (1948), the Bureau of Mines reported that one 4–8-ft sample interval from the Pink Green deposit contained 4.75% TiO_2. Holbrook resampled the road cut from which the Bureau of Mines' sample had been collected and obtained a TiO_2 value of 4.5%. Holbrook believes the Beulah Green deposit is the better of the two deposits. He provides chemical analyses on samples from six hand auger holes drilled by the Bureau of Mines. Each hole was 1.8 m deep and the average TiO_2 content of the holes ranged from 1.06 to 12.63%. Holbrook (1948) took the following samples:

Depth (m)	Sample descriptions, Beulah Green Deposit	TiO_2 (%)
0.0–0.45	Buff topsoil (15 cm) and red clayey sand	5.2
0.45–0.91	Red clayey sand with red clay seams	5.5
0.91–1.22	Red clay and red and brown sand	10.9
1.22–1.52	Brown, red, and white clayey sand	12.3
1.52–1.83	Hard yellow sand and sandy red clay	9.8
1.83–2.13	Brown and red clayey sand	4.0

Note: Hole was bottomed in a very fine-grained grey clay.

Holbrook (1948) suggests that the ilmenite sand concentrations represent the reworking of sands along ancient beaches. If this is the case, the ilmenite deposits might be scattered over a large area, but the individual deposits probably would be discontinuous. Holbrook (1948) reports that the ilmenite from these ilmenite-bearing sands contains 54.8% TiO_2. In the early 1990s, private companies became interested in the ilmenite sands of Howard County and drilling programs were conducted. However, it was concluded that the deposits were too small under current economic conditions for exploitation.

Hanson (1997) summarised the ilmenite sands of Howard County. The heavy-mineral assemblage, northwest of Mineral Springs, consists of 66.1% ilmenite, 19.4% iron oxide, 2.5% leucoxene, 0.8% zircon, 0.3% staurolite, 0.2% undifferentiated pyroxene and amphibole, 0.2% tourmaline, 0.1% kyanite/sillimanite, 0.1% rutile, 8.9% others, and traces of monazite and corundum. The titanium-bearing minerals

average 47% TiO_2 and make up 68.7% of the heavy-mineral fraction. The titanium mineral distribution is ilmenite 96.25%, leucoxene 3.6%, and rutile 0.14%. The highest 60 cm concentration of heavy minerals encountered is 20.64%. The suite consists predominantly of medium-grained sand-size particles. He reported that 229,000 metric tons of titanium-bearing minerals are contained within the sediments located in part of the south half of Sec. 12, T. 10 S., R. 28 W. The lack of radioactive heavy minerals, the grain size of the heavy minerals, and the high concentration of heavy-mineral sands in a relatively small area favour commercial development. Unfavourable economic factors are the small size of the deposits, the low TiO_2 content of the ilmenite, and the amount of clay (approximately 30%) in the heavy-mineral-bearing sands.

9. HEAVY-MINERAL TRENDS IN THE ATLANTIC COASTAL PLAIN

Proceeding up the coast from Florida to Virginia, the heavy-mineral suite gradually changes. Generally rutile, zircon, and monazite are present with an abundance of ilmenite in economic quantities in Florida and Georgia. In South Carolina, rutile percentage declines steadily, dropping from 6–8 to 1–3%, near the North Carolina border. Zircon also declines from 11–15% in Florida and southern Georgia to 6–8% in northern South Carolina. Monazite, present in only small quantities of 0.5–2.0% in coastal Florida and Georgia, declines in South Carolina and is virtually absent in North Carolina and states further north.

As the above economic minerals decline, ilmenite becomes the predominant economic mineral present in North Carolina, Virginia, and New Jersey. As an example, the percentage of ilmenite and leucoxene is 30–50 in Florida and Georgia, 50–65 in South Carolina, and 80 in New Jersey (Anonymous, 1976).

ACKNOWLEDGEMENTS

The authors are indebted to Mr. Ron Rose of the Exploration Division of Iluka (USA) Resources, Inc., Jacksonville, Florida; Mr. Gary McMahill of E.I. du Pont de Nemours & Co., Starke, Florida; Mr. Dave Lloyd of Mineral Recovery Systems, Inc., Reno, Nevada; and Mr. Pat Costin of Mineral Recovery Systems, Inc., Reno, Nevada. These individuals gave freely of their knowledge of the heavy-mineral industry and the deposits of the Atlantic and Gulf coastal plains of the United States. This review is greatly improved by information provided by these individuals. We extend our thanks to The Beaches Area Historical Society, Jacksonville Beach, FL, who kindly provided the two historical photographs for the frontispiece.

REFERENCES

Anderson, W.H., 2000. Industrial minerals resources of the Jackson Purchase Region. Kentucky Geological Survey, http://www.uky.edu/KGS/coal/webindmn/pages/minera/jackson.htm.

Anonymous, 1952. Florida sands boost supply of titanium mineral. Engineering & Mining Journal 153 (5), 82–87.

Anonymous, 1959. Folkston heavy mineral project. Humphreys Mining Corporation, Unpublished Company Report, 30pp.
Anonymous, 1970. Lakes and green fields win friends for Humphreys Mining. Mining Engineering 22 (7), 36.
Anonymous, 1974. U.S. TiO_2 mine on stream. Mining Magazine 130 (1), 7.
Anonymous, 1976. Heavy mineral prospects of the coastal plain of Georgia and South Carolina. Mineral Development International, Inc., Unpublished Company Report, 44pp.
Anonymous, 1978. Green Cove Springs up for sale. Industrial Minerals 208 (10), 17.
Anonymous, 1979. Rare earths—industry profile and market review. Industrial Minerals 209 (3), 1–59.
Anonymous, 1998. Pre-feasibility assessment of the potential for development of a heavy mineral sand deposit located near Camden, Tennessee. TZ Minerals International Pty Ltd., Unpublished Executive Summary, 9pp.
Anonymous, 1999a. Key Facts About DuPont's Florida Plant. E.I. du Pont de Nemours & Co., Starke, Florida.
Anonymous, 1999b. Altair's titanium deposit doubled. Altair International Inc., News Release, January 19.
Anonymous, 2003. DEP negotiates smart growth settlement for Heritage Minerals property. New Jersey Department of Environmental Protection News Release, September 4.
Anonymous, 2004. Manchester update. January 27, accessed at http://www.OceanCountyPOLITICS.com.
Arkansas Geological Commission, Resource Report on Titanium 2006. Arkansas Geological Commission website, http://www.state.ar.us/agc/titanium.htm. Site accessed July 30, 2006.
Bailey, R.H., 1987. Stratigraphy and depositional history of the Yorktown Formation in northeastern North Carolina. Southeastern Geology 28, 1–19.
Berquist, C.R. Jr., 1987. Minerals in high-level gravel deposits along the Fall Zone of Virginia. Virginia Minerals 33, 37–40.
Berquist, C.R. Jr., Bailey, C.M., 1999. Late Cenozoic reverse faulting in the Fall Zone, southeastern Virginia. Journal of Geology 107, 727–732.
Calver, J.L., 1957. Mining and mineral resources. Florida Geological Survey Bulletin 39, 132.
Cannon, H.B., 1950. Economic minerals in the beach sands of the southeastern United States. In: Symposium on Mineral Resources of the Southeastern United States. University of Tennessee Press, Knoxville, (pp. 202–210).
Cannon, H.B., 1957. Sand Ilmenites of the Eastern United States. American Institute of Mining, Metallurgical, and Petroleum Engineers Mining Conference, Tampa, FL.
Carpenter, R.H., Carpenter, S.F., 1991. Heavy mineral deposits in the upper coastal plain of North Carolina and Virginia. Economic Geology 86, 1657–1671.
Carpenter, J.H., Detweiler, J.C., Gillson, J.L., Weichel, E.C., Wood Jr., J.P., 1953. Mining and concentration of ilmenite and associated minerals at Trail Ridge, Fla. Mining Engineering Bulletin 18, 8.
Colquhoun, D.J., 1969. Geomorphology of the lower coastal plain of South Carolina. In: South Carolina Division of Geology Publication MS-15, 36pp.
Colquhoun, D.J., 1974. Cyclic surficial stratigraphic units of the middle and lower coastal plains, central South Carolina. In: Oaks, R.Q. Jr., DuBar, J.R. (Eds.), Post-Miocene Stratigraphy Central and Southern Atlantic Coastal Plain. Utah State University Press, Logan, pp. 179–190.
Colquhoun, D.J., Pierce, W., 1971. Pleistocene transgressive-regressive sequences on the Atlantic Coastal Plain. Quaternaria XV, Roma, pp. 35–50.
Cooke, C.W., 1925. Physical geography of Georgia: the coastal plain. Georgia Geological Survey Bulletin 42, 19–54.

Cooke, C.W., 1931. Seven coastal terraces in the southeastern states. Washington Academy of Sciences Journal 21, 503–513.
Cooke, C.W., 1932. Tentative correlation of American glacial chronology with the marine time scale. Washington Academy of Sciences Journal 22, 310–313.
Cooke, C.W., 1936. Geology of the coastal plain of South Carolina. U.S. Geological Survey Bulletin 867, 196.
Cooke, C.W., 1941. Two shore lines or seven? American Journal of Science 239, 457–458.
Cooke, C.W., 1943. Geology of the coastal Plain of Georgia. U.S. Geological Survey Bulletin 941, 121.
Cooke, C.W., 1945. Geology of Florida. Florida Geological Survey Bulletin 29, 339.
Cooke, C.W., 1966. Emerged Quaternary shorelines in the Mississippi Embayment. Smithsonian Miscellaneous Collection 149 (10), 41.
Czel, L.J., 1977. Cabin Bluff reserve estimate. E.I. du Pont de Nemours & Co., Unpublished Report, 9pp.
Detweiler, J.C., 1952. Jacksonville plant produces titanium from beach deposit. Mining Engineering Bulletin 16, 4.
Dimanche, F., Bartholome, P., 1976. The alteration of ilmenite in sediments. Minerals, Science and Engineering 8 (3), 187–201.
Doering, J.A., 1960. Quaternary surface formations of southern part of Atlantic coastal Plain. Journal of Geology 68, 182–202.
Dryden, A.L., Dryden, C., 1940. Heavy minerals and the history of the Coastal Plain. Geological Society of America Bulletin 51, 1993–1994.
DuBar, J.R., Johnson, H.S. Jr., Thom, B.G., Hatchell, W.O., 1974. Neogene stratigraphy and morphology, south flank of the Cape Fear Arch, North and South Carolina. In: Oaks, R.Q. Jr., DuBar, J.R. (Eds.), Post-Miocene Stratigraphy Central and Southern Atlantic Coastal Plain. Utah State University Press, Logan, pp. 139–173.
Elsner, H., 1992. Granulometry and mineralogy of some northeastern Florida placers: a consequence of heavy mineral concentration in nearshore bars. Sedimentary Geology 76, 233–255.
Elsner, H., 1997. Economic geology of the heavy mineral placer deposits in northeastern Florida. Florida Geological Survey Open-file Report No. 71, 98pp.
Evans, C.H., 1955. Staurolite—new industrial mineral. Presented at American Institute of Mining, Metallurgical, and Petroleum Engineers Annual Meeting, February 14–17, 14pp.
Fantel, R.J., Buckingham, D.A., Sullivan, D.E., 1986. Titanium minerals availability—market economy countries. U.S. Bureau of Mines Information Circular 9061, 28pp.
Fenneman, N.M., 1938. Physiography of Eastern United States. McGraw-Hill, New York, 691pp.
Fillman-Richards, J., 1982. Colour infrared techniques in archeological site location: shell rings along the South Carolina coastlands. MA thesis. University of Florida, Gainesville, Florida.
Flint, R.F., 1940. Pleistocene features of the Atlantic coastal plain. American Journal of Science 238, 757–787.
Flint, R.F., 1942. Atlantic coastal terraces. Washington Academy of Sciences Journal 32, 235–237.
Flint, R.F., 1947. Glacial Geology and the Pleistocene Epoch. John Wiley, New York, 589pp.
Foley, B., 1992. Beach glitters in tribute to those who stood against tide of mining. Florida Times Union, Sunday, May 3, p. E-1.
Folwell, M., 2004. Iluka USA operations update. Iluka Notice to the Australian Stock Exchange, February 10.
Force, E.R., 1976. Metamorphic source rocks of titanium placer deposits, a geochemical cycle. U.S. Geological Survey Professional Paper 959B, B1–B16.

Force, E.R., Grosz, A.E., Loferski, P.J., Maybin, A.H., 1982. Aeroadioactivity maps in heavy-mineral exploration—Charleston, South Carolina, area. United States Geological Survey Professional Paper 1218, 19.

Foxworth, R.D., Priddy, R.R., Johnson, W.B., Moore, W.S., 1962. Heavy minerals of sand from Recent beaches of the Gulf coast of Mississippi and associated islands. Mississippi Geological Survey Bulletin 93, 92.

Fulton, R.B. III, 1975. Staurolite. In: Lefond, S.J. (Ed.), Industrial Minerals and Rocks, fourth edition. New York, Society of Mining Engineers of the American Institute of Mining, Metallurgical, and Petroleum Engineers, Inc., pp. 1095–1097.

Fulton, R.B. III, 1983. Staurolite. In: Lefond, S.J. (Ed.), Industrial Minerals and Rocks, fifth edition. New York, Society of Mining Engineers of the American Institute of Mining, Metallurgical, and Petroleum Engineers, vol. 2, pp. 1225–1227.

Gallagher, P.E., Hoffman, C.W., 1990. Geology and heavy-mineral exploration of sedimentary deposits along the Fall Zone of Northampton, Halifax, Nash, and Wilson counties, North Carolina. North Carolina Geological Survey Division of Land Resources Open-File Report 90-4, 17pp.

Garnar, T.E., 1972. Economic geology of Florida heavy mineral deposits. In: Puri, H.S. (Ed.), Proceedings of the 7th Forum on Geology of Industrial Minerals, Vol. 17. Florida Bureau of Geology Special Publication, pp. 17–21.

Garnar, T.E., 1978. Geological classification and evaluation of heavy mineral deposits: Twelfth Forum on the Geology of Industrial Minerals. Georgia Geological Survey Information Circular 49, 25–36.

Garnar, T.E., 1980. Heavy minerals industry of North America. Presented at 4th International Minerals International Congress, Atlanta, GA, 13pp.

Garnar, T.E., 1981. Florida wet material balances. DuPont Unpublished Company Report.

Garnar, T.E., 1983. Zirconium and hafnium minerals. In: S.J. Lefond (Ed.), Industrial Minerals and Rocks, 5th ed., Vol. 2. New York Society of Mining Engineers of the American Institute of Mining, Metallurgical, and Petroleum Engineers, pp. 1433–1446.

Garnar, T.E., 1985a. Mineral sand products and their uses. Presented at the Society of Mining, Metallurgy, and Exploration, Inc., Fall Meeting and Exhibit, October 16, Albuquerque Convention Centre, Albuquerque, New Mexico.

Garnar, T.E., 1985b. Mineralogical methods used in the heavy minerals industry. In: W.C. Park, D.M. Hausen, R.D. Hagni (Eds.), Proceedings of the Second International Congress on Applied Mineralogy in the Minerals Industry, Los Angeles, CA, February 22–25, 1984, New York. The Metallurgical Society of the American Institute of Mining, Metallurgical and Petroleum Engineers, pp. 297–317.

Garnar, T.E., Stanaway, K.J., 1994. Titanium minerals. In: Carr, D.D. (Ed.), Industrial Minerals and Rocks, 6th Edn. Society for Mining, Metallurgy, and Exploration, Inc, Littleton, CO, pp. 1071–1089.

Gilman, S.K., 2005. Zirconium. Mining Engineering 57 (6), 62–63.

Gillson, J.L., 1955. Titanium mineral deposit, Folkston, Georgia. E.I. du Pont de Nemours & Co. Unpublished Company Report, 20pp; plus Appendices.

Gillson, J.L., 1959. Sand deposits of titanium minerals. Mining Engineering 11, 421–429.

Goodman, T.A., 1989. The stratigraphy and depositional history of a Pleistocene barrier island complex near Woodbine, Camden County, Georgia. Unpublished MS thesis. University of Florida, Gainesville, 105pp.

Grosz, A.E., Cathcart, J.B., Macke, D.L., Knapp, M.S., Schmidt, W., Scott, T.M., 1989. Geologic interpretations of gamma-ray aeroradiometric maps of central and northern Florida. U.S. Geological Survey Professional Paper 1461, 48pp.

Gunter, H., 1924. Statistics on mineral production in Florida during 1921 and 1922. Florida State Geological Survey, Fifteenth Annual Report, pp. 14–23.

Gunter, H., 1927. Statistics of mineral production. Florida State Geological Survey, Eighteenth Annual Report, 16pp.
Hanson, W.D., 1997. Heavy-mineral sands of the Tokio Formation in southwest Arkansas. Arkansas Geological Commission Information Circular 34, 9pp; 2 Appendices.
Hedrick, J.B., 2001. Zirconium and Hafnium. U.S. Geological Survey Minerals Yearbook, pp. 86.1–86.6.
Hedrick, J.B., 2005. Rare earths, the lanthanides, yttrium and scandium. Mining Engineering 57 (6), 50–52.
Heron, S.D., Jr., Johnson, H.S., 1969. Radioactive mineral resources of South Carolina. Division of Geology, State Development Board MR-4, 4pp.
Herrick, S.M., 1965. A subsurface study of Pleistocene deposits in coastal Georgia. Georgia Geological Survey Information Circular 31, 8pp.
Hoffman, C.W., Carpenter, R.H., 1992. Heavy-mineral deposits in the Bailey area, Nash and Wilson counties, North Carolina. In: Dennison, J.M., Stewart, K.G. (Eds.), Geologic Field Guides to North Carolina and Vicinity. Geologic Guidebook No. 1, Southeastern Section, Geological Society of America Annual Meeting Field Trip Number 5. University of North Carolina, Chapel Hill, pp. 49–63.
Holbrook, D.F., 1948. Titanium in southern Howard County, Arkansas. Arkansas Resources and Development Commission Division of Geology Bulletin 13, 16.
Howard, J.D., Scott, R.M., 1983. Comparison of Pleistocene and Holocene barrier island beach-to-offshore sequences, Georgia and northeast Florida coasts, U.S.A. Sedimentary Geology, 34, 167–183.
Hoyt, J.H., Hails, J.R., 1967. Pleistocene shoreline sediments in coastal Georgia: deposition and modification. Science 155, 1541–1543.
Hoyt, J.H., Hails, J.R., 1971. Regional distortions along the southern United States Coast Quaternaria 15, 51–63.
Hoyt, J.H., Hails, J.R., 1974. Pleistocene stratigraphy of southeastern Georgia. In: Oaks, R.Q., DuBar, J.R. (Eds.), Post-Miocene Stratigraphy: central and southern Atlantic Coastal Plain. Utah State University Press, Logan, pp. 191–205.
Huddlestun, P.F., 1988. A revision of the lithostratigraphic units of the coastal plain of Georgia—the Miocene through Holocene. Georgia Geological Survey Bulletin 104, 162.
Hunter, R.E., 1968. Heavy minerals of the Cretaceous and Tertiary sands of extreme southern Illinois. Illinois State Geological Survey Circular 428, 22.
Iluka Resources, Ltd., 2004. Iluka USA operations—investor site visit. http://www.iluka.com.
Isphording, W.C., 1966. Petrology and stratigraphy of the Kirkwood Formation. Ph.D. dissertation. Rutgers University, New Brunswick pp 181.
Johnson, B.L., 1907. Pleistocene terracing in the North Carolina coastal plain. Science 26, 640–642.
Johnson, H.S. Jr., DuBar, J.R., 1964. Geomorphic elements of the area between the Cape Fear and Pee Dee rivers, North and South Carolina. Southeastern Geology 6, 37–48.
Johnson, P., 1987. Gold Fields a Centenary Portrait. St. Martin's Press, New York, 256pp.
Komar, P.D., 2007. The entrainment, transport and sorting of heavy minerals by waves and currents. In: Mange, M.A., Wright, D.T. (Eds.), Heavy Minerals in Use. Developments in Sedimentology (this volume).
Kussel, C.M., Jones, D.S., 1986. Depositional history of three Pleistocene bluffs in northeastern Florida. Florida Scientist 49, 242–254.
Lamar, J.E., Grim, R.E., 1937. Heavy minerals in Illinois sands and gravels of various ages. Journal of Sedimentary Petrology 7, 78–83.
Lettman, T., 2004. Hearing set on settlement of Heritage Mineral case. Inside the Pinelands Newsletter 11 (2), accessed at http://www.pinelandsalliance.org.

Li, T.M., 1973. Startup of Manchester mine and mill. Engineering & Mining Journal December, 71–75.
Lyell, C., 1845. Travels in North America, Vol. 1. Wiley and Putnam, New York, 231pp.
Lynd, L.E., Lefond, S.J., 1975. Titanium minerals. In: Lefond, S.J. (Ed.), Industrial Minerals and Rocks, Fourth ed.,. American Institute of Mining, Metallurgical, and Petroleum Engineers, Inc, New York, pp. 1149–1208.
Lynd, L.E., Lefond, S.J., 1983. Titanium minerals. In: Lefond, S.J. (Ed.), Industrial Minerals and Rocks, Fifth ed., Vol. 2. Society of Mining Engineers of the American Institute of Mining, Metallurgical, and Petroleum Engineers, Inc, pp. 1303–1362.
MacNeil, F.S., 1950. Pleistocene shorelines in Florida and Georgia. U.S. Geol. Survey Professional Paper 221-F, pp. 95–107.
Mallard, E.A., 1988. The differentiation and classification of a sand underlying typical Trail Ridge sands near Screven, Wayne County, Georgia. Unpublished MS thesis. University of Florida, Gainesville, 75pp.
Mallard, E.A., 1992. An overview of RGC (USA) minerals bailey deposit. In: Dennison, J.M., Stewart, K.G. (Eds.), Geologic Field Guides to North Carolina and Vicinity. Geologic Guidebook No. 1, Southeastern Section, Geological Society of America Annual Meeting Field Trip Number 5. University of North Carolina, Chapel Hill, pp. 60–61.
Markewicz, F.J., 1969. Ilmenite deposits of the New Jersey Coastal Plain. In: Subitzky, S. (Ed.), Geology of Selected Areas in New Jersey and Eastern Pennsylvania. Rutgers University Press, New Brunswick, pp. 363–382.
Markewich, H.W., 1987. The Orangeburg Scarp and other paleo-shoreline features of Southeastern Georgia. In: Geological Society of America Abstracts with Programs vol. 19 (2), 96.
Markewicz, F.J., Parrillo, D.G., 1957. Preliminary report on ilmenite-bearing sands from the Coastal Plain of New Jersey (abstracts). Geological Society of America Annual Meeting, 92pp.
Martens, J.H.C., 1928. Beach deposits of ilmenite, zircon and rutile in Florida. Florida Geological Survey Nineteenth Annual Report 1926–1927, pp. 124–154.
Mateer, R.G., 1961. Geologic report on the Altama heavy mineral deposit Glynn, County, Georgia. Georgia Geological Survey, Unpublished Report.
Mathieson, A., Wall, G., 1982. Tourism: economic, physical, and social impacts. Longman Group Ltd, London, 216pp.
McCauley, C.K., 1960. Exploration for heavy minerals on Hilton Head Island, South Carolina. Division of Geology, South Carolina State Development Board Bulletin 26, 13.
McGee, W.J., 1887. The Columbia formation. In: Proceedings of the American Association for the Advancement of Science 36, 221–222.
McGrain, P., 2001. Contributions to the Geology of Kentucky—Economic Geology. U.S. Geological Survey Professional Paper 1151-H, http://pubs.usgs.gov/pp/p1151h/economic.html.
McKelvey, V.E., Balsley, J.R. Jr., 1948. Distribution of coastal black sands in North Carolina, South Carolina, and Georgia as mapped from an airplane. Economic Geology 43 (6), 518–524.
Mellen, F.F., 1959. Mississippi mineral resources. Mississippi State Geological Survey Bulletin 86, 86–87.
Mertie, J.B., 1975. Monazite placers in the southeastern Atlantic states. U.S. Geological Survey Bulletin 1390, 41.
Miller, J.A., 1958. Minerals yearbook metals and minerals (except fuels) 1955. Titanium: U.S. Bureau of Mines, pp. 1171–1193.
Miller, R.A., Hardeman, W.D., Fullerton, D.S., 1966. West sheet, geologic map of Tennessee. State of Tennessee, Department of Conservation, Division of Geology, scale 1:250,000.

Moxham, R.M., 1954. Airborne radioactivity survey in the Folkston area, Charlton County, Georgia, and Nassau County, Florida. U.S.G.S. Geophysical Investigation Map GP 119.
Mucke, A., Chaudhri, J.N.B., 1991. The continuous alteration of ilmenite through pseudorutile to leucoxene. Ore Geology Review 6, 25–44.
Neiheisel, J., 1958. Origin of the dune system on the Isle of Palms, South Carolina: Division of Geology, South Carolina State Development Board Mineral Industries Laboratory. Monthly Bulletin 2 (7), 46–51.
Newton, M.C., Romeo, A.J., 2006. Geology of the Old Hickory heavy mineral sand deposit, Dinwiddie and Sussex counties, Virginia in Reid. In: C. Jeffrey (Ed.), Proceedings of the 42nd Forum on the Geology of Industrial Minerals. Information Circular 34, North Carolina Geological Survey, pp. 464–480.
Oaks, R.Q., Coch, N.K. Jr., 1973. Post-Miocene stratigraphy and morphology, southeastern Virginia. Virginia Division of Mineral Resources Bulletin 82, 135.
Oaks, R.Q. Jr., DuBar, J.R., 1974. Tentative correlation of post-Miocene units, central and southern Atlantic coastal Plain. In: Oaks, R.Q. Jr., DuBar, J.R. (Eds.), Post-Miocene Stratigraphy Central and Southern Atlantic Coastal Plain. Utah State University Press, Logan, pp. 232–245.
Olson, D.W., 2005. Industrial garnet. Mining Engineering 57 (6), 37.
Parker, G.G., Cooke, C.W., 1944. Late Cenozoic geology of southern Florida. Florida Geological Survey Bulletin 27, 119.
Parker, N.A., 1948. Ilmenite exploration southeastern United States interim report #2. DuPont Company Report, Unpublished, 22pp.
Pirkle, E.C., Pirkle, F.L., Pirkle, W.A., Stayert, P.R., 1984. The Yulee heavy mineral sand deposits of northeastern Florida. Economic Geology 79, 725–737.
Pirkle, E.C., Pirkle, W.A., Yoho, W.H., 1974. The Green Cove Springs and Boulougne heavy-mineral sand deposits of Florida. Economic Geology 69 (7), 1129–1137.
Pirkle, E.C., Pirkle, W.A., Yoho, W.H., 1977. The Highland heavy-mineral sand deposit on Trail Ridge in northern peninsular Florida. Florida Bureau of Geology Report of Investigation 84, 50.
Pirkle, E.C., Yoho, W.H., 1970. The heavy-mineral orebody of Trail Ridge, Florida. Economic Geology 65, 17–30.
Pirkle, E.C., Yoho, W.H., Hendry, C.W., 1970. Ancient sea level stands of Florida. Florida Bureau of Geology Bulletin 52, 61.
Pirkle, F.L., Czel, L.J., 1983. Marine fossils from region of Trail Ridge, a Georgia-Florida landform. Southeastern Geology 24, 31–38.
Pirkle, F.L., Pirkle, E.C., Pirkle, W.A., Dicks, E.E., Jones, D.S., Mallard, E.A., 1989. Altama heavy mineral deposits in southeastern Georgia. Economic Geology 84, 425–433.
Pirkle, F.L., Pirkle, W.A., Pirkle, E.C., Pirkle, D.L., Spangler, D.P., 2007. Heavy-mineral deposits of Bailey, North Carolina. Southeastern Section, Geological Society of America 56th Annual meeting, Abstracts with Programs, vol. 39 (2), 77.
Pirkle, F.L., Pirkle, E.C., Reynolds, J.G., 1991a. Heavy mineral deposits of the southeastern Atlantic Coastal Plain. In: Pickering, S.J. (Ed.), Proceedings of the Symposium on the Economic Geology of the Southeastern Industrial Minerals. Georgia Geological Survey Bulletin, 120, 15–41.
Pirkle, F.L., Pirkle, E.C., Reynolds, J.G., 1993a. Yulee heavy-mineral deposits. In: K.M. Farrell, C.E. Hoffman, V.J. Henry (Eds.), Geomorphology and Facies Relationships of Quaternary Barrier Island Complexes Near St. Marys, Georgia. Georgia Geological Society Guidebook, vol. 13, no. 1, pp. 68–73.
Pirkle, F.L., Pirkle, E.C., Reynolds, J.G., Pirkle, W.A., Henry, J.A., Rice, W.J., 1993b. The Folkston West and Amelia heavy mineral deposits of Trail Ridge, southeastern Georgia. Economic Geology 88, 961–971.

Pirkle, F.L., Pirkle, E.C., Reynolds, J.G., Pirkle, W.A., Jones, D.S., Spangler, D.P., Goodman, T.A., 1991b. Cabin Bluff heavy mineral deposits of southeastern Georgia. Economic Geology 86 (2), 436–443.

Pirkle, F.L., Reynolds, J.G., 1988. Field trip log. In: F.L. Pirkle, J.G. Reynolds (Eds.), Southeastern Geological Society Annual Field Trip Guidebook, February 19 and 20, pp. 3–9.

Pirkle, F.L., Reynolds, J.G., Akser, M., Spangler, D.P., 1994. Models for exploration and evaluation of heavy-mineral sand deposits as applied to the western Black Sea coast of Turkey. In: Demerial, H., Ersayin, S. (Eds.), Proceedings of 5th International Mineral Processing Symposium, Cappadocia Turkey, 6–8 September 1994, Progress in Mineral Technology. A.A. Balkema, Rotterdam, pp. 251–263.

Pirkle, F.L., Pirkle, W.A., Pirkle, E.C., Pirkle, D.L., 2005. Heavy mineral mining in the Atlantic Coastal Plain of Florida and Georgia and the chemical and physical characteristics of the deposits. In: Akser, M., Elder, J. (Eds.), 2005 Heavy Minerals Conference Proceedings: Society for Mining, Metallurgy, and Exploration, Inc., pp. 7–18.

Popp, A.W., 1975. McIntosh County, Georgia heavy mineral prospect. Mineral Development International, Inc., Company Report.

Prettyman, T.M., Cave, H.S., 1923. Petroleum and natural gas possibilities in Georgia. Georgia Geological Survey Bulletin 40, 164.

Price, W.A., 1951. Barrier island not off-shore bar. Science 113, 487–488.

Pryor, W.A., 1960. Cretaceous sedimentation in upper Mississippi Embayment. American Association of Petroleum Geologists Bulletin 44, 1473–1504.

Puffer, J.H., Cousminer, H.L., 1982. Factors controlling the accumulation of titanium-iron oxide-rich sands in the Cohansey Formation, Lakehurst area, New Jersey. Economic Geology 77, 379–391.

Rich, F.J., Pirkle, F.L., 1993. Palynology and paleoecology of Reids Bluff. In: Farrell, K.M., Hoffman, C.E., Henry, V.J. (Eds.), Geomorphology and Facies Relationships of Quaternary Barrier Island Complexes Near St. Marys, Georgia. Georgia Geological Society Guidebook, vol. 13, no. 1, pp. 74–81.

Richards, H.G., 1954. The Pleistocene of Georgia. Georgia Geological Survey Mineral Newsletter 7 (3), 110–114.

Roberts, A.E., 1955. How new $3,000,000 Highland Plant recovers titanium minerals. Mining World, Bulletin No. 21, 9pp.

Robson, D.F., Sampath, N., 1977. Geophysical response of heavy-mineral sand deposits at Jerusalem Creek, New South Wales. Bureau of Mineral Resources Journal of Australian Geology and Geophysics 2, 149–154.

Romeo, A.J., 2005. Grade control in mineral sands—the unique conditions at Old Hickory, Virginia. In: Akser, M., Elder, J. (Eds.), 2005 Heavy Minerals Conference Proceedings, Ponte Vedra, FL. Society of Mining, Metallurgy, and Exploration, Inc, pp. 235–239.

Rose, R. Jr., 2005. Green Cove Springs deposit geology. In: Akser, M., Elder, J. (Eds.), 2005 Heavy Minerals Conference Proceedings, Ponte Vedra, FL. Society of Mining, Metallurgy, and Exploration, Inc, Littleton, CO, pp. 1–6.

Seabrook, C., 2003. 16,000-acre gift to Okefenokee Swamp DuPont donation "retires" mining rights. The Atlanta Journal-Constitution, August 27.

Shannon, S.S. Jr., 1983. Rare earths and thorium. In: Lefond, S.J. (Ed.), Industrial Minerals and Rocks, 5 Edn.. Vol. 2. Society of Mining Engineers, American Institute of Mining, Metallurgical, and Petroleum Engineers, Inc, New York, pp. 1109–1118.

Shattuck, G.B., 1901. The Pleistocene problem of the North Atlantic Coastal Plain. American Geologist 28, 78–107.

Shattuck, G.B., 1906. The Pliocene and Pleistocene deposits of Maryland. In: G.B. Shattuck, W.B. Clark, A. Hollick, F.A. Lucas (Eds.), Maryland Geological Survey, Pliocene and Pleistocene, pp. 21–137.

Shrode, R.S., Lamar, J.E., 1953. Sands and silts of extreme southern Illinois. Illinois Geological Survey Circular 184, 28.
Skillen, A., 1996. Titaniferous feedstocks: Industrial Minerals, July, pp. 25–35.
Stanaway, K.J., 1992. Heavy mineral placers. Mining Engineering 44 (4), 352–358.
Stanaway, K.J., 1996. The Eastern North America Titanium Province—a review. Lithology and Mineral Resources 31 (6), 509–517.
Stephenson, L.W., 1912. The coastal plain of North Carolina: the Cretaceous, Lafayette, and Quaternary formations. North Carolina Geological Survey Bulletin 3, 73–171.
Teas, L.P., 1921. Preliminary report on the sand and gravel of Georgia. Geological Survey of Georgia Bulletin 37, 376–377.
Thiers, E.A., 1999. Pre-feasibility assessment of the Camden deposit. SRI Consulting, Unpublished Report, 2pp.
Thom, B.G., 1967. Coastal and fluvial landforms—Horry and Marion counties South Carolina. Louisiana State University Coastal Studies Series 19, Technical Report 44, 75pp.
Thorsen, C.P.E., 1959. Stratigraphy and Ostracoda of the Brownstown and Tokio Formations southwest Arkansas. Ph.D. dissertation. Louisiana State University, Baton Rouge, 121pp.
TZ Minerals, 2005. Titanium. Mining Engineering 57 (6), 59–60.
Veatch, J.O., Stephenson, L.W., 1911. Preliminary report on the geology of the coastal plain of Georgia. Georgia Geological Survey Bulletin 26, 466.
Vernon, R.O., 1943. Florida mineral industry with summaries of production for 1940 and 1941. Florida Geological Survey Geological Bulletin No. 24, pp. 139–146.
Wahlstrom, E.E., 1947. Igneous Minerals and Rocks. Wiley, New York, 367pp.
Warland, I., 2006. The Eucla Basin—The new zircon province. Presented at the South Australian Resources and Energy Conference, Adelaide, South Australia, May. Presentation located on Iluka Resources Limited website, http://www.iluka.com/news. Site accessed July 30, 2006.
White, W.A., 1970. The geomorphology of the Florida peninsula. Florida Bureau of Geology Bulletin 51, 164.
Wilcox, J.T., 1971. Preliminary investigations of heavy minerals in the McNairy sand of west Tennessee. State of Tennessee Department of Conservation, Division of Geology Report of Investigation, 31, 11pp.
Williams, L., 1964. Titanium deposits in North Carolina. U.S. Department of the Interior, Bureau of Mines, Information Circular 19, 51pp.
Williams, L., 1967. Heavy minerals in South Carolina. Division of Geology, South Carolina State Development Board, Bulletin 35, 35pp.
Winker, C.D., Howard, J.D., 1977. Correlation of tectonically deformed shorelines on the southern Atlantic coastal plain. Geology 5, 123–127.
Wynn, J.C., Grosz, A.E., Foscz, V.M., 1985. Induced polarization response of titanium-bearing placer deposits in the southeastern United States. U.S. Geological Survey Open-file Report 85-756, 25.

4.3 The Role of Upper Mantle Derived Heavy Minerals in Diamond Exploration

This page intentionally left blank

Chapter 46

DIAMONDS AND ASSOCIATED HEAVY MINERALS IN KIMBERLITE: A REVIEW OF KEY CONCEPTS AND APPLICATIONS

TOM E. NOWICKI[a], RORY O. MOORE[a], JOHN J. GURNEY[b] AND MIKE C. BAUMGARTNER[a]

[a]*Mineral Services Canada, 205-930 Harbourside Drive, North Vancouver, B.C., Canada*
[b]*Mineral Services South Africa, 42 Morningside, N'Dabeni, Cape Town, South Africa*

ABSTRACT

Kimberlite, a variety of ultramafic volcanic and sub-volcanic rock, is the dominant source of diamonds worldwide. It is widely accepted that the majority of diamonds are not formed within the kimberlite and much evidence points towards an ancient origin for most diamond in the deep lithospheric keels of Archaean cratons. The kimberlites, therefore, are transporting agents that ''sample'' deep, occasionally diamond-bearing, mantle material and rapidly convey it to surface. The dominant source rocks for diamond are highly depleted peridotite (harzburgite or dunite) and high-pressure eclogite. These are minor components of the mantle lithosphere, which is dominated by less-depleted peridotite (primarily lherzolite) and lesser amounts of non-diamondiferous eclogite. While other diamond sources are known, these rarely contribute significantly to diamond populations in kimberlite. Despite the limited range of source lithologies, diamond population characteristics in any given kimberlite are typically highly complex and indicative of several distinct populations, most likely formed in discrete events occurring at different times, ranging from the Archaean to the age of kimberlite emplacement.

In addition to rare diamond, disaggregation of mantle rocks sampled by kimberlite yields relatively large quantities of other mantle minerals, commonly referred to as kimberlitic indicator minerals. From an exploration point of view, the most important indicator minerals are garnet, chromite, ilmenite, Cr-diopside and olivine. Several of these minerals display diagnostic visual and compositional characteristics, making them ideal pathfinders for kimberlite. The more chemically resistant minerals (garnet, ilmenite and chromite) are particularly useful due to their greater ability to survive weathering in the surface environment. Thus, sampling of surface materials to recover kimberlitic indicator minerals and tracing these back to their source is a key component of most diamond exploration programs.

Developments in Sedimentology, Vol. 58, 1235–1267

ISSN: 0070-4571/doi:10.1016/S0070-4571(07)58046-5

Studies of diamond inclusions and diamond-bearing xenoliths permit geochemical characterisation of diamond source materials and have led to major advances in the understanding of the relationship between diamond and its host rock in the mantle.

Keywords: indicator-mineral; exploration; geochemistry; peridotite; eclogite; garnet; chromite; ilmenite; clinopyroxene

1. INTRODUCTION

Kimberlite is an ultramafic, alkaline igneous rock of deep-seated origin that can contain significant quantities of diamond (Mitchell, 1986). It is by far the most important primary source of these gems, accounting for more than 70% of world diamond production by value in 2003 (based on data in Willmott, 2004). The only other commercially significant primary diamond source is olivine lamproite, an ultramafic, ultrapotassic rock similar in certain respects to kimberlite (Mitchell, 1995). This rock type currently provides ~5% by value (~20% by weight) of world diamond production, with the balance of production deriving from secondary deposits in alluvial and marine sediments. The development of laboratory processes to produce diamonds (Bundy et al., 1973), and subsequent refinements that enable the mass manufacture of a superior product for industrial purposes, has had a major effect on the world market for natural diamonds which is now predominantly reliant for revenue on the global jewellery market.

It has been apparent for some years that kimberlite and lamproite are merely transporting agents carrying diamond from its source region in the upper mantle to the crust. Whether diamond remains at the end of the journey depends on whether it was present in the mantle rocks sampled and disaggregated by the kimberlite and on whether or not the diamonds were preserved (Gurney, 1984). A very high-grade kimberlite or lamproite might contain 5 carats (1 carat = 0.2 g) of diamonds per tonne of host rock, translating to a concentration of 1 part per million.

The proven diamond source rocks in the mantle are various types of peridotite (Dawson and Smith, 1975; McCallum and Eggler, 1976; Pokhilenko et al., 1977; Shee et al., 1982), certain high pressure eclogite assemblages (e.g., Rickwood et al., 1969; Sobolev, 1974; Reid et al., 1976; Robinson et al., 1984) and closely associated websterites (e.g., Gurney, 1989), and the ultra-high pressure mineral majorite (Moore and Gurney, 1985). With the exception of majorite (a very rare association believed to be sourced from the asthenosphere), these diamond-bearing sources occur only in the deep portions of the thick lithosphere developed under Archaean cratons. Thus, all known significantly diamondiferous kimberlites occur within regions underlain by Archaean crust and/or mantle.

Minerals derived from the diamond source rocks described above are present in all kimberlites with significant concentrations of diamond. However, even in highly diamondiferous kimberlite, they are typically subordinate to ubiquitous mantle-derived minerals from rock types that do not have a clear association with diamond. In addition, most kimberlite intrusions do not contain significant concentrations of diamond, indicating that diamond is rare and sporadically distributed even in its original source region within the mantle.

Mantle-derived minerals sampled and brought to surface by kimberlite (and other similar rock types) are typically referred to as kimberlitic indicator minerals. The most important of these are garnet, ilmenite, chromite, Cr-diopside and olivine. Orthopyroxene (enstatite) is a key component of the lithospheric mantle but is highly reactive with the kimberlite magma and is, therefore, commonly absent or only preserved in trace amounts (Seifert and Schreyer, 1968). Similarly, omphacitic clinopyroxene, which makes up a significant proportion of mantle eclogite, is highly unstable at low pressure and it typically breaks down on ascent to the surface. Thus enstatite and omphacite are rarely useful as kimberlitic indicator minerals. The other mantle-derived minerals are commonly present in significant concentrations in most kimberlites and, even in highly diamondiferous bodies, are typically three or four orders of magnitude more abundant than diamond. As a result, indicator minerals provide an invaluable exploration tool, firstly as pathfinder minerals for locating kimberlites and, secondly, as indicators of the diamond potential of their host intrusion.

In this contribution, we review some important concepts relating to the origin of diamond and its association with other mantle minerals. These concepts form the basis for a tried and tested approach to the application of indicator mineral geochemistry in kimberlite exploration.

2. DIAMOND: PETROLOGICAL ASSOCIATIONS AND GENESIS

2.1. Multiple Diamond Populations

In both kimberlites and lamproites, diamonds range in size from microcrystals smaller than 50 μm to macrocrystals occasionally over 1 cm in size. It is clear that the full diamond suite in any given deposit incorporates several overlapping populations with diverse origins. Evidence for more than one population of eclogitic or peridotitic diamonds has been presented for several localities (Moore and Gurney, 1985, 1989; Deines et al., 1987; Otter and Gurney, 1989). In a study of diamonds from the low-grade Letseng La Terai locality in northern Lesotho, McDade and Harris (1999) detected 10 different diamond parageneses. Developing the same theme, Gurney et al. (2004) have described widely disparate diamonds recovered from various kimberlites on the Slave Craton (Fig. 1). These include flat-faced sharp-edged octahedra, fibrous cubes, coated stones, diamonds of various colours, cloudy stones, deformed crystals and extensively resorbed diamonds. It has been suggested that these also have been produced by a number of different diamond-forming processes in the mantle. It is apparent, therefore, that diamonds recovered from kimberlite generally reflect a variety of processes and most likely represent several different diamond sources.

2.2. Peridotite and Eclogite: Key Diamond Sources

Every diamond-bearing locality, for which a reasonable body of data exists, has diamonds of eclogitic and peridotitic paragenesis, as judged by mineral inclusions in the diamonds and often confirmed by the finding of diamond-bearing xenoliths

Fig. 1. Diamonds from kimberlites in the Ekati property, Slave province, Canada. These diamonds were recovered from geographically closely associated kimberlites in the Slave craton but are also broadly representative of diamonds from kimberlite worldwide. Examples of most of these diamond types can be found in any given kimberlite of the Ekati property. (A) Colourless, flat-faced octahedra from Fox. (B) Colourless, flat-faced octahedron from Fox, showing a characteristic imperfectly developed crystal termination. (C) Light brown octahedra from Grizzly. (D) Colourless, step-faced octahedron from Koala. (E) Colourless contact-twinned octahedral (macles) from Fox. (F) Brown, step-faced octahedron from Misery. (G) Dark brown octahedron from Koala. (H) Fibrous-coated, flat-faced octahedron from Panda. (I) Remnant fibrous coat on surface of a flat-faced octahedron from Panda; the coat has been sufficiently resorbed at the edges and corners to reveal a colourless, gem-quality interior. (J) Translucent lemon yellow cube from Sable. (K) Opaque, fibrous cubes from Grizzly. (L) Colourless cubo-octahedra from Piranha; the diamonds have a translucent core and transparent rims. (M) Light brown, rounded resorbed diamond from Fox with relict octahedral surfaces. (N) Colourless dodecahedron from Koala. (O) Light brown, rounded resorbed dodecahedron from Misery with well-developed curvilinear faces acquired during resorption. (P) Dark brown rutted and rounded dodecahedron from Misery. Diamonds in (A) through (G) have primary shapes and are expected to be old by analogy to other studies; (H) and (I) are primary old diamonds coated with young fibrous diamond; (J) may be a Type Ib, very young diamond; (K) are young fibrous cubes; (L) are intermediate between (A) through (G) and (K); (L) through (O) are all resorbed forms of diamonds anticipated to be old. [Reproduced from Gurney et al., (2004), Fig. 2, p. 29; permission by Elsevier, 2007.]

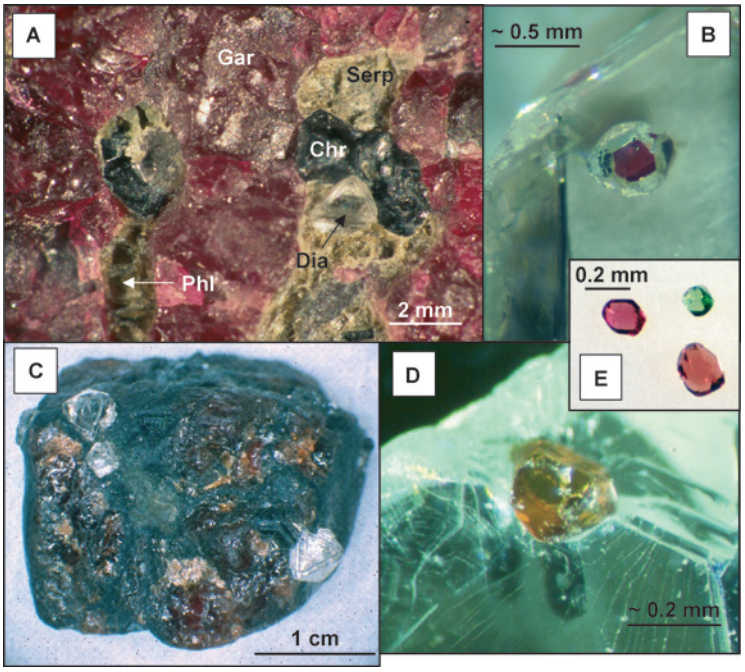

Fig. 2. (A) Diamondiferous sub-calcic garnet harzburgite xenolith from Newlands kimberlite, South Africa. Minerals present: garnet (Gar), chromite (Chr), phlogopite (Phl), serpentinized orthopyroxene and olivine (Serp), diamond (Dia). (B) Peridotitic garnet inclusion in diamond. (C) Diamondiferous eclogite xenolith from the Ardo kimberlite, South Africa; three colourless diamonds feature prominently on the surface; careful visual inspection of the hand specimen reveals three more diamonds on that surface and, taking all surfaces into account, 12 diamonds can be seen in this xenolith; other minerals are fresh garnet and partially altered clinopyroxene; prominent diamonds at lower right weighs ~0.3 carat. (D) Eclogitic garnet inclusion in diamond. (E) Comparison of harzburgitic G10 garnet (purple, upper left), lherzolitic G9 garnet (red, lower right) and diopside (green) inclusions liberated from two generations of peridotitic diamonds from the 1.2 Ga Premier kimberlite, Kaapvaal craton. [Photographs A, C and E reproduced from Gurney et al., (2005), Fig. 4, p. 158 with permission from the Society of Economic Geologists.]

(Fig. 2). Eclogite is a high-pressure rock type of broadly basaltic composition that is dominated by magnesium-rich but relatively chrome-poor garnet (pyrope) and sodic clinopyroxene (omphacite). Diamond-bearing eclogites are relatively common in diamondiferous kimberlite, particularly at some of the localities where eclogitic diamonds are common such as Orapa in Botswana. These xenoliths are not cognate to the host volcanic rock, but have clearly been sampled in the upper mantle and transported to the earth's surface fairly rapidly. This diamond source is also commonly represented as xenocrysts of low-Cr garnet with compositions similar to those of garnets in diamond-bearing eclogite and eclogitic garnet inclusions in diamond (see below).

Peridotites are a group of ultramafic rocks that are characterised by significant amounts of olivine (forsterite) in combination with varying quantities of

orthopyroxene (enstatite) and clinopyroxene (Cr-diopside). Chrome-rich pyrope garnet and/or chromite are important minor phases in many mantle-derived peridotites. Diamond-bearing peridotite xenoliths are much scarcer than diamond eclogites. It is clear from studies of inclusions in diamonds, however, that peridotitic diamonds are as abundant as those formed in eclogite. Compensating for the lack of xenoliths, xenocrysts of disaggregated peridotites are always found in diamondiferous kimberlite. Some of these xenocrysts have compositions consistent with derivation from diamond-bearing garnet harzburgites (Gurney, 1984). This rock is considered to be preferentially disaggregated on sampling and transport to the surface because of the presence of a carbonate-rich phase that dissociates in response to pressure reduction while temperature remains relatively high (Boyd and Gurney, 1982; Wyllie et al., 1983). The constituent minerals of the diamond peridotites are, therefore, mostly introduced as dispersed phases into the host volcanic magma. Other peridotitic diamonds are derived from garnet lherzolites, but such source rocks appear to be much less significant than the harzburgites, and their constituent minerals have not been shown to have diamond diagnostic compositions.

Lithospheric harzburgite is a highly depleted ultramafic rock type that forms initially as the residue after extraction of large amounts of partial melt from fertile mantle peridotite. Eclogite is a high-pressure rock of broadly basaltic composition and the mantle eclogite sampled by kimberlite is generally interpreted to represent subducted mafic oceanic crust (Helmstaedt and Schulze, 1989; Helmstaedt and Gurney, 1995). Although eclogite could be generated by partial melting of mantle leaving a depleted peridotitic residuum, it is clear that the eclogitic minerals associated with diamonds cannot be derived by the partial melting processes that produce diamond-bearing harzburgite residue. For instance, high rare earth element (REE) concentration and light-REE enrichment patterns in harzburgite garnets (Shimizu and Richardson, 1987) are quite irreconcilable with the low-garnet REE concentrations and heavy-REE enrichment patterns in eclogitic diamonds at Finsch (Shimizu, unpublished data). Harzburgitic and eclogitic diamonds, therefore, are quite clearly unrelated populations; this is confirmed by different model ages and carbon isotope characteristics. Therefore, at least two unrelated source rocks (eclogitic and peridotitic) for diamond are sampled by all well-studied primary occurrences.

The diamond content of these host rocks appears to vary widely, as indicated by the disparate abundances of diamond in eclogite xenoliths found at mines such as Orapa and Roberts Victor (Hatton and Gurney, 1979; Shee and Gurney, 1979). Eclogites also show large disparities in diamond content even within different portions of the same xenolith (Hatton and Gurney, 1979; Fig. 2). Furthermore, the diamond-bearing rocks may form minor lenses and pods in the mantle, as suggested by evidence from the Beni Bouchera high temperature peridotite (Slodkevich, 1983). Here, octahedral graphite (formerly diamond) is irregularly distributed in lenses of igneous garnet pyroxene cumulate rocks of minor extent. Locally the original diamond content could have been as high as 15–20%. Only small amounts of such rocks need be disaggregated to provide the total diamond content of a typical diamondiferous kimberlite, usually <1 ppm.

Based on diamond inclusion studies, the relative proportions of eclogitic to peridotitic diamonds in one locality can vary widely, from at least 90% eclogitic (Orapa,

Botswana: Gurney et al., 1984) to at least 99% peridotitic (Mir, U.S.S.R.: Yefimova and Sobolev, 1977). Worldwide, peridotitic and eclogitic diamonds are the dominant recognisable parageneses and appear to have a similar overall abundance to each other.

2.3. Isotopic Composition of Diamond

Eclogitic diamonds display a wide range of carbon isotope compositions ($-34 < \delta^{13}C < +3$: Sobolev et al., 1979). This range could be derived from an upper mantle that has retained a primary heterogeneity (Deines et al., 1987), or from crustal sources subducted into the mantle (Helmstaedt and Gurney, 1984; Helmstaedt and Schulze, 1989; Kirkley et al., 1991). Most of the eclogitic range can be found at a single locality (Sloan: Otter et al., 1989), which is difficult to explain unless at least some eclogitic diamonds are related to recycling processes active during subduction, such as those associated with ophiolite formation (Taylor and Anand, 2004). In contrast, peridotitic diamonds have a more restricted range in carbon isotope composition ($-9 < \delta^{13}C < -2$), which is thought to be derived from a more homogeneous asthenospheric source for the carbon. However, most peridotitic diamonds appear to be of Archaean age (see below) and it is possible that the smaller range of carbon isotope ratios result from the lack of advanced life forms at that time and that the carbon is also subduction related (Westerlund, 2005).

2.4. Age-Constraints on Diamond Formation

There is abundant evidence of the old age of both eclogitic and peridotitic diamonds. Some of the more persuasive observations are radiogenic isotope measurements on diamond inclusions (Kramers, 1977, 1979; Richardson et al., 1984, 1990; Richardson, 1986, 1989; Smith et al., 1989; Menzies et al., 1999; Westerlund, 2005). These studies point to harzburgitic diamonds being Archaean, and eclogitic diamonds being younger and spanning an age range from the Archaean through at least most of the Proterozoic.

Since isotope studies can be controversial to interpret, evidence supporting an old age for diamond is important. Diamonds are found in xenoliths of peridotite and eclogite where they are in general well preserved, showing predominantly growth forms. This indicates that the diamonds were formed in their original host rock prior to incorporation by the kimberlite. Many diamonds show direct evidence that they have been deformed under mantle conditions in a plastic manner, reflecting stress under conditions of grain boundary contact (Robinson, 1979) and, again, indicating residence in the mantle for a significant period prior to incorporation into the kimberlite. Finally, most diamonds show complex nitrogen aggregation patterns that would appear to need more than 10^9 years to develop at mantle temperatures and pressures (Evans and Harris, 1989). Thus all these lines of evidence point towards an ancient origin for the majority of diamonds. The reason that diamonds are associated with ancient continental cratons may be because they are predominantly formed and preserved in very old rocks.

The processes by which diamonds form are a subject of much debate (Bulanova, 1995; Harte et al., 1999; Taylor and Anand, 2004; Westerlund et al., 2004). However,

in general, available information suggests formation of most peridotitic diamonds by a major worldwide event at $\sim 3.3 \pm 0.3$ Ga that produced diamonds in a metasomatised garnet/chromite bearing harzburgite (Gurney et al., 2005). The metasomatising fluids are likely to have been generated by subduction processes (Westerlund, 2005). Eclogitic diamond formation has also been documented to be related to metasomatic activity associated with subduction (Westerlund et al., 2004). This has been identified to occur at various times in the Proterozoic and Archaean (~1–2.9 Ga), on a more localised basis than the widespread 3.3 Ga harzburgitic event, in mafic oceanic crust recycled into the upper mantle during ancient subduction events (Richardson et al., 2001).

2.5. Other Diamond Associations

In addition to the dominant harzburgitic and eclogitic diamond associations described above, other upper mantle lithologies that can contain diamond include lherzolite and websterite. The former is a common variety of peridotite (in fact the dominant rock type in the upper mantle) whereas the latter is a pyroxene-rich rock similar to eclogite but with a higher Cr and Mg content. In rare cases, diamonds have been found with inclusions of majorite, a very high-pressure mineral with a garnet structure but containing pyroxene in solid solution. Majorite is stable only at great depths (~200–450 km) indicating that at least some diamonds originate in the asthenospheric mantle. Websteritic, lherzolitic and majoritic diamonds are very subordinate in abundance overall, but may be locally significant, such as lherzolitic diamonds at Premier Mine, South Africa (Gurney et al., 1985; Richardson et al., 1993), the majoritic diamonds at Monastery (Moore and Gurney, 1985) and Jagersfontein mines (Deines et al., 1991), South Africa, and the websteritic association at Victor kimberlite project, Canada (Armstrong et al., 2004).

All the above associations are older than and non-cognate to their host magma. At some localities, fast-grown younger diamonds, at most only slightly older than the host magma, have been noted. These occur as low value fibrous cubes, fibrous coats on older diamonds or unusual diamond distinguished by complex crystal forms, a distinctive amber colour and single nitrogen atom substitution for carbon in the diamond lattice (1b diamonds). The fibrous diamonds may be abundant (e.g., Mbuji Mayi, Democratic Republic of Congo) but are of very low commercial value. The 1b diamonds are very rare and have shapes that are not amenable to manufacturing of cut gemstones. The paragenesis of these younger diamonds is not well-established. Both varieties have been found to be associated with eclogite (Hills and Haggerty, 1989; McKenna et al., 2003), whereas only the slenderest of evidence associates fibrous diamond with peridotitic minerals (Talnikova, 1995). No diamond deposits worldwide are known to have a commercially significant population of 1b diamonds and, although fibrous diamonds are abundant at a few locations, they are of very low value (per carat) and do not sustain mining operations on a commercial basis. These younger diamonds have, like majorite, academic rather than economic significance. Relatively little is known about the processes that produce them and tracing them receives little or no attention in prospecting for diamond deposits.

2.6. Diamond Resorption and the Relationship Between Macrodiamonds and Microdiamonds

It has been comprehensively proven that many diamonds are partially resorbed en route to the earth's surface from the upper mantle (Robinson, 1979; Robinson et al., 1989), primarily by oxidation. This process is sufficiently common and significant to deduce that many diamonds assume a round-dodecahedral morphology from their original octahedral shape, implying a weight loss of the order of at least 45%. Under such oxidising conditions it is considered probable that many microdiamonds (>0.5 mm) would be completely resorbed and therefore disappear. This, in turn, has led to the proposal that the microdiamonds that do occur in kimberlite may be mainly a separate population, crystallising just prior to kimberlite emplacement and unrelated to macrodiamond populations, which appear to be much older (Haggerty, 1986). However, microdiamonds appear to carry similar inclusions to macrodiamonds and have similar nitrogen aggregation characteristics (Trautman et al., 1997) indicating that they have the same ancient origins. Nonetheless, resorption may well affect the size distribution of the overall diamond population in a particular deposit, which is in any case, a composite of diamonds formed by several mantle processes.

2.7. Significance to Diamond Exploration

In terms of diamond exploration, the important factors known about diamond genesis can be summarised as follows.

(1) The macrodiamonds in economic deposits are derived from pre-existing, sometimes highly diamondiferous, ultrabasic and basic rocks that formed in the lithospheric upper mantle.
(2) Both peridotitic and eclogitic diamonds occur in every known diamond deposit worldwide.
(3) Peridotitic diamonds can be subdivided into harzburgitic and lherzolitic types. Harzburgitic diamonds are common to all diamondiferous kimberlites and are interpreted to be of Archaean age (~3.3 Ga). Lherzolitic diamonds are subordinate to harzburgitic diamonds and represent another, somewhat younger population, which at the Premier Mine is 1.9–2.0 Ga in age (Richardson et al., 1993).
(4) Eclogitic diamonds show a range of ages from 0.99 to 2.9 Ga, except for the rare instances of younger diamonds described above.
(5) As diamonds are released into the host magma by disaggregation of pre-existing diamond-bearing mantle rocks, other constituent minerals of those rocks are incorporated with the diamonds. Quite small volumes of these, sometimes richly diamondiferous, mantle rocks can provide the concentrations of diamond (generally <1 ppm) found in economic kimberlites.
(6) In a single kimberlite intrusion, it is reasonable to expect a roughly linear relationship between the amount of diamond present and the abundance of fragments of the host diamondiferous rocks from the mantle.
(7) In different kimberlites, such comparisons can never be expected to be as quantitative because of variations in the diamond grade of the eclogite and peridotite sources, the superimposed reductions in diamond content by

resorption, and more speculatively because of assimilation of the diamond source rock in the magma, which may be particularly relevant in lamproites.

(8) Microdiamond counts in a kimberlite or lamproite are, in general expected to correlate broadly with macrodiamond abundance, but in certain cases may not give good correlations with the grade of commercially sized stones (>1 mm) because of the decoupling effects of resorption followed by subsequent growth of another population of microdiamonds.

(9) The relationship described in (6) can be used to predict the presence of diamond with a high degree of certainty and can give a semi-quantitative estimate of diamond abundance with some success.

(10) The heavy mineral geochemistry approach can give the first signal about the diamond potential of the source in an exploration program.

(11) The approach is perhaps more likely to go wrong in terms of predicting the presence of diamonds that are not there, than to miss out on predicting their presence when they are there.

(12) Macrodiamonds are likely to be found in regions of the earth with thick cool lithospheric keels where old rocks are preserved. Consequently, continental cratons may be prime targets if they are thick enough. Complex structural settings where over-thrusting will allow old keels to survive underneath younger rocks are not ruled out of contention (Gurney et al., 2005).

(13) In order to provide diamonds in appropriate size ranges and abundance for economic exploitation, transport to the surface from depths of diamond stability must be rapid and thus far has proven to involve volatile-rich, ultrabasic volcanics, with only minor exceptions (Gurney et al., 2005).

3. KIMBERLITIC INDICATOR MINERALS AS A TOOL FOR DIAMOND EXPLORATION

3.1. Mantle Minerals as Indicators of the Presence of Kimberlite

From the above discussion, it is clear that kimberlites (and certain related rock types) generally contain significant amounts of high-pressure minerals (including diamond) derived by sampling of mantle rock types. The presence of such minerals as xenocrysts in kimberlite or lamproite is the product of disaggregation of these mantle rocks sampled at depth and transported into the crust by the host magma. Processes contributing towards the disaggregation of mantle material include: precursor intrusive and/or metasomatic activity which locally weakens the lithospheric mantle prior to kimberlite emplacement; physical stoping and partial melting/assimilation during the early stages of kimberlite emplacement; attrition associated with ascent of the kimberlite through the lithosphere via narrow conduits and explosive eruption of the kimberlite or lamproite at surface. Field evidence indicates that the emplacement of volcanic kimberlite or lamproite pipes occurs as a series of highly explosive eruptions, whereas the magmatic feeders are thin (often <1 m wide) dykes. In accordance with the latter observation, upper mantle xenoliths in kimberlite have been observed to occasionally approach but never exceed a meter in largest dimension. The above-described intrusion and eruption processes are an efficient mechanism for

the disaggregation of mantle rocks such as peridotite, eclogite, websterite and megacryst assemblages (see below), causing the release of numerous individual mineral grains into the host magma.

These mantle-derived minerals commonly display visual and compositional characteristics that permit their distinction from minerals of crustal derivation. In addition, several of the key mantle minerals are relatively resistant to chemical weathering and are commonly dispersed into the secondary environment by sedimentary processes. Thus, they provide ideal pathfinders for kimberlite and are typically referred to as kimberlitic indicator minerals.

As mentioned previously, the most important indicator minerals for kimberlite exploration are garnet, chromite, ilmenite, Cr-diopside and olivine (Fig. 3). Cr-diopside and olivine break down rapidly in most surface environments and, other than in frigid arctic or sub-arctic conditions, are generally not transported significant distances from their source kimberlite. In contrast, garnet, chromite and ilmenite are resistant and may be dispersed considerable distances away from their

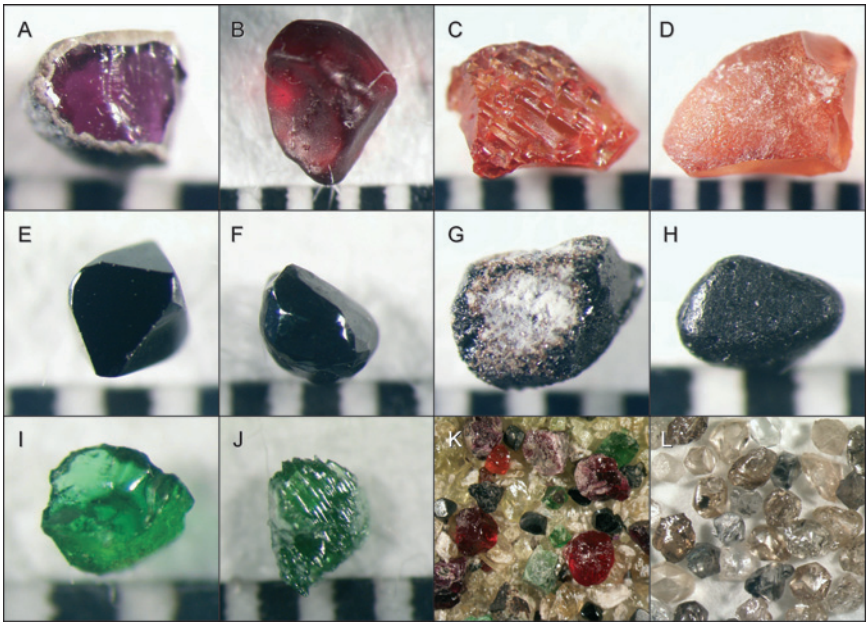

Fig. 3. Photomicrographs of typical kimberlitic indicator minerals and microdiamonds recovered from kimberlite. Scale bar division in A to J = 1 mm. (A) Mauve peridotitic garnet with primary alteration rim (kelyphite). (B) Red peridotitic garnet with finely frosted (sub-kelyphitic) surface. (C) Orange low-Cr garnet displaying "sculpted" surface due to crystallographically controlled dissolution of grain in kimberlite. (D) Orange low-Cr garnet displaying sub-kelyphitic surface texture. (E) Euhedral chromite. (F) Subhedral chromite. (G) Ilmenite with primary alteration rim (mostly perovskite). (H) Unaltered ilmenite. (I) Cr-diopside with conchoidal fracture. (J) Cr-diopside with "sculpted" surface. (K) Typical kimberlite concentrate showing abundant pale yellowish-green olivine plus garnet, Cr-diopside, chromite and ilmenite (grain size ranges to ~1.5 mm). (L) Microdiamonds derived by dissolution of kimberlite and visual sorting of residue (grains size ranges to ~0.5 mm).

point of origin. Thus these minerals typically form the focus of stream-sediment and soil sampling programs aimed at detecting kimberlites. The indicator minerals in kimberlite show a very wide range of sizes, from less than 0.5 mm to in excess of 20 mm. However, most grains are less than 2 mm in size and, in surface sediments, by far the majority of them are recovered in the fine and medium sand fractions.

Techniques for sampling and recovery of these indicator minerals rely largely on their relatively high density (Gregory and White, 1989; Muggeridge, 1995). In environments that are rich in heavy minerals of crustal origin, magnetic separation methods can be used to help concentrate the kimberlitic indicator minerals. The latter are then extracted from the concentrate by visual sorting processes, typically undertaken with binocular microscopes. Mantle-derived garnet, Cr-diopside, ilmenite and chromite have visual characteristics that permit their distinction, with varying degrees of confidence, from similar minerals of crustal origin. However, with the exception of peridotitic garnet, there is a considerable amount of overlap, and confirmation of visual classifications by compositional analysis is usually advisable.

In general, kimberlitic indicator minerals are characterised by Mg- and commonly Cr-rich compositions. Garnets from peridotite are Cr-pyropes with compositions that do not overlap with crustal garnet types. Eclogitic garnets are also typically Mg-rich pyropes, but they are poor in Cr and range to relatively Fe-rich and Ca-rich compositions that overlap with certain crustal almandines and grossulars. Nonetheless, eclogitic garnet from kimberlite is generally compositionally distinguishable from most crustal varieties with a reasonable degree of confidence. Ilmenite (commonly of megacrystic origin, see below) from kimberlite is diagnostically Mg-rich (picroilmenite) and is reliably distinguished from non-kimberlitic varieties using a combination of Mg and Ti content (Wyatt et al., 2004). Mantle-derived chromites (from chromite peridotite) show near complete compositional overlap with those from a variety of crustal sources and reliable identification of grains from kimberlitic sources generally requires careful study of population trends (Gurney and Zweistra, 1995). Fortunately, chromite also occurs as a phenocryst phase in kimberlite and this variety (commonly recovered in prospecting samples) displays diagnostic Cr–Ti relationships (Grütter and Apter, 1998). ''Kimberlitic'' Cr-diopside and olivine, derived from mantle peridotite, show compositional ranges similar to those of equivalent minerals from ultramafic crustal sources. While portions of the compositional spectrum seen in kimberlitic olivine and Cr-diopside are unique, in certain cases, unequivocal confirmation of a kimberlitic origin may not be possible.

Numerous approaches based on chemical composition have been proposed for the classification of kimberlitic indicator minerals (Dawson and Stephens, 1975; Danchin and Wyatt, 1979; Jago and Mitchell, 1989; Schulze, 2003; Grütter et al., 2004). For the most part, these focus on distinguishing different varieties of mantle-derived garnet. The most recent classification scheme by Grütter et al. (2004) provides a relatively simple, practical scheme for application by diamond explorers.

The use of kimberlitic indicator minerals to provide evidence for the proximity of potentially diamondiferous source rocks has been in practice for more than 100 years, virtually since kimberlite was first recognised as a host for diamond in South Africa (Draper and Frames, 1898). In the past three decades, application of indicator mineral techniques has progressed considerably, particularly through advent of electron microprobe technology. This has led to significant improvements

in the recognition of kimberlite-derived minerals and, perhaps more importantly, to the development of advanced indicator-mineral-based techniques for the assessment of diamond potential in kimberlite source rocks (Gurney et al., 1993; Griffin and Ryan, 1995).

3.2. Assessing Diamond Potential Based on Indicator Minerals: Principles

In this contribution we present an overview of the use of indicator mineral geochemistry in the evaluation of the diamond potential of kimberlites. This approach was developed primarily on the basis of studies of kimberlites and has been successfully applied to all major kimberlite provinces worldwide. The principles are nonetheless applicable to lamproites and other magma types that have sampled the upper mantle, although the precise relationship between kimberlitic indicator mineral criteria and diamond content in these rock types may vary.

The model on which the method is based considers that macrodiamonds are xenocrysts in the volcanic kimberlites from which they are recovered, and that they are derived from disaggregated mantle-equilibrated rocks that pre-date the age of emplacement of the volcanic intrusion. This is consistent with evidence reviewed earlier.

The validity for this approach rests on the fact that some diamonds contain mineral inclusions that can clearly be assigned to an eclogitic or peridotitic source and, as discussed above, diamonds are occasionally found in xenoliths of eclogite, or more rarely peridotite. The unequivocal assignation of the paragenesis of most diamonds is, however, not possible because they are recovered as single crystals and are commonly without any definitive inclusions. It is assumed that these diamonds have similar origins to the minority that can be defined. On the basis of carbon isotope measurements in inclusion-free diamonds compared to those of known paragenesis, this seems reasonable (Jaques et al., 1989; Gurney, 1990).

The amount of diamond the volcanic host-rock contains will depend on at least six variables:

(a) the quantity of diamond peridotite that it sampled;
(b) the average grade of the diamond peridotite;
(c) the quantity of diamond eclogite that it sampled;
(d) the grade of the diamond eclogite;
(e) the degree of preservation of diamonds during transportation and
(f) the efficiency with which the diamonds were transported to the earth's surface.

The amount of diamond peridotite or diamond eclogite that has been sampled (a and c) should be reflected in the amount of disaggregated mineral grains and/or xenoliths in the kimberlite. If these can be identified, it should be possible to forecast whether diamond could be present or not. Identification of garnets and chromites that have specific compositions has indeed turned out to be a useful diamond indicator (Gurney, 1989; Gurney et al., 1993; Lee, 1993; Fipke et al., 1995; see also below).

Forecasting accurately the diamond content of a rock that is in the mantle and cannot be directly sampled is unfortunately impossible, so that variations in source-rock grade (b and d) cannot be quantified in any rigorous way. Fortunately, the diamond indicator minerals can be identified by certain compositional parameters

and the higher the abundance of these minerals in kimberlites, the better the diamond content of the body usually is. However, there are exceptions to this, as must be expected from considerations (a–e) above.

3.3. Geochemical Criteria for Recognition of Diamond-Associated Minerals

Recognition of diamond-associated indicator minerals is based largely on relatively simple compositional criteria derived from studies of diamond inclusions and mineral compositions in diamond-bearing xenoliths. Fortunately for the diamond explorer, these minerals define characteristic compositional fields that show only limited overlap with mineral compositions from non-diamondiferous mantle lithologies. This simple empirical approach has been refined over the last decade or so to incorporate recent developments in geothermobarometry and an improved understanding of the pressure–temperature–composition (P–T–X) relationships in specific diamond source rocks. These refinements have to a large extent been incorporated into the recent garnet classification scheme of Grütter et al. (2004).

3.3.1. Peridotitic minerals associated with diamond

In the peridotitic diamond paragenesis three sub-groupings are apparent: garnet harzburgite/dunite, chromite harzburgite and garnet lherzolite. The harzburgites and dunites are depleted in calcium relative to the lherzolites in three ways: the absence of a Ca-saturated phase (diopside); a low bulk-rock Ca content and a low mineral content of Ca (i.e., sub-calcic garnet). As with most classification schemes, there is overlap between categories. For example, chromite and garnet can occur in the same harzburgite and chromite can be present in a lherzolite. Other features are incompatible: a sub-calcic garnet, for instance, cannot be in equilibrium with diopside and is, therefore, never found in a lherzolite. It has been established that the relative importance with respect to diamonds is: garnet harzburgite/dunite > chromite harzburgite ≫ garnet lherzolite, i.e., diamonds are highly preferentially associated with peridotite of depleted composition. Garnet lherzolite is not a major component of the diamond inclusion suite at any locality yet described. This is fortunate since garnet lherzolite is the most common mantle rock type found in kimberlite, and there is no simple way to differentiate between a diamond-bearing and a barren garnet lherzolite (Gurney, 1984). The preferential association of diamond with depleted peridotite is highlighted by comparison of peridotitic garnets found as inclusions in diamonds or in diamond-bearing xenoliths with those present in "average" lithospheric mantle sampled by kimberlite (i.e., as reflected in the xenolith and xenocryst suites of large numbers of kimberlites). Approximately 85% of peridotitic garnets directly associated with diamond are sub-calcic in composition (e.g., Gurney, 1984), indicating derivation from depleted mantle harzburgite or dunite. In contrast, studies of xenoliths and garnet xenocryst populations from kimberlites indicates that the peridotitic mantle is dominated by relatively "fertile" (i.e., undepleted) lherzolite, which yields garnets with more calcium-rich compositions. For example, sub-calcic garnets make up only ~15% of the peridotitic component of kimberlite xenocryst suites in the Kaapvaal craton (Herman Grütter, personal Communication, 2003).

This indicates an approximately 32-fold preferential association of carbon with depleted harzburgite or dunite. Therefore garnets of lherzolitic composition have to

be discriminated against in an exploration program, and the method described by Gurney (1984) has repeatedly proved to be useful in exploration programs on several continents. In addition, it needs to be emphasised that, by definition, Cr-diopside does not occur in depleted harzburgite and, therefore, is not useful as a diamond indicator mineral. Under certain circumstances, however, it can yield very useful pressure and temperature information. This is discussed further below.

The minerals closely associated with diamonds have well-defined ranges in composition (Meyer, 1987). For harzburgitic diamonds, the garnets are high in Mg and Cr and low in Ca (Gurney and Switzer, 1973; Sobolev, 1974; Gurney, 1984). The component of diamonds derived from garnet harzburgite is assessed by considering both the number of sub-calcic garnets found in a kimberlite and their degree of calcium depletion. While not strictly in accord with the Dawson and Stephens (1975) classification, these garnets have been referred to as "G10" garnets, while lherzolitic garnets have been referred to as "G9". The compositional fields for these garnet types are defined in Fig. 4. More recently, the field designated G10 has been called the "diamond in" field and the G9 field "diamond out" for reasons developed by Gurney and Zweistra (1995). In the case of G10 garnets it has been noticed

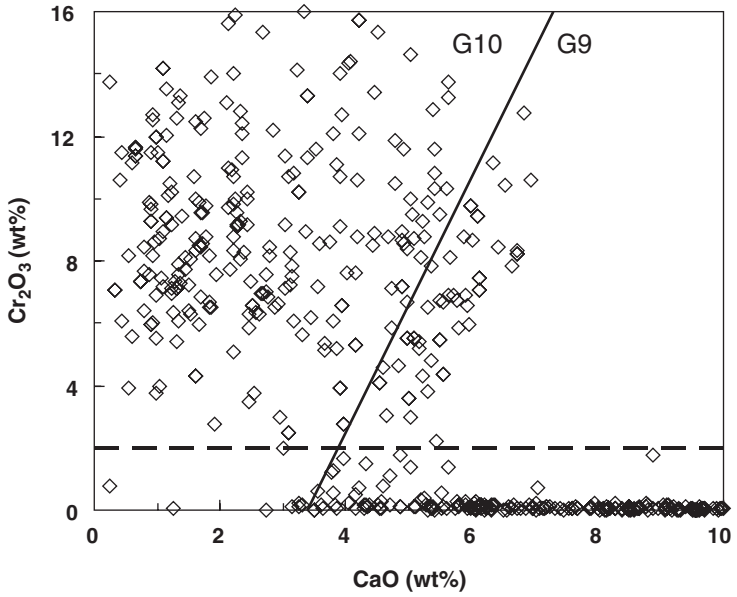

Fig. 4. Plot of Cr_2O_3 versus CaO for diamond inclusion garnets from worldwide localities. The diagonal line distinguishing sub-calcic "G10" garnets from calcium saturated "G9" garnets was defined by Gurney (1984) on the basis that 85% of peridotitic garnets associated with diamond plot in the G10 field. The horizontal line drawn at 2 wt.% Cr_2O_3 is used as an arbitrary division between eclogitic (<2 wt.% Cr_2O_3) and peridotitic (>2 wt.% Cr_2O_3) garnets. Diamond inclusion data represent 49 kimberlite, lamproite and alluvial localities in southern Africa, West Africa, Russia, Australia, South America, North America and China. [Sourced from the KRG Database, Department of Geology, University of Cape Town, South Africa.]

empirically that richer kimberlites with abundant harzburgitic diamonds tend to have more sub-calcic and chromiferous G10 garnets.

Chromites associated with diamond show a high average Cr_2O_3 content, characteristically in excess of 62.5 wt.% (Lawless, 1974; Sobolev, 1974; Dong and Zhou, 1980; Fig. 5). Chromite is used in a manner similar to garnet to provide an indication of the amount of diamond in the kimberlite derived from disaggregated chromite harzburgite.

Over the last two decades, it has become apparent that not all garnets falling in the G10 "diamond in" field are indicators of the presence of diamond. This stems from the fact that, although they have a very strong association with mantle carbon, garnets of this compositional range do not necessarily equilibrate within the diamond stability field.

3.3.2. Pressure, temperature and diamond stability

There are several approaches to determine whether G10 garnets are associated with graphite or diamond. The basis for all of these methods is a clear understanding of the relationship between geothermal gradient and diamond stability in the lithosphere. Diamond stability is dependent on oxygen fugacity, pressure and temperature. Typical cratonic lithosphere is relatively reducing (McCammon et al., 2001) and thus, in the absence of oxidizing events (e.g., metasomatism), carbon will occur

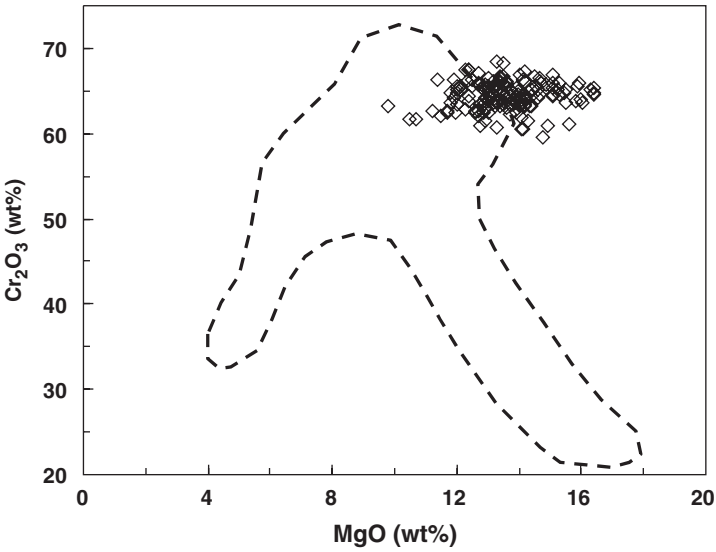

Fig. 5. Plot of Cr_2O_3 versus MgO for chromite diamond inclusions from worldwide localities shown in relation to the compositional range observed for chromites from samples of kimberlite concentrate (dashed line). Note the highly restricted Cr- and Mg-rich character of the inclusions. Diamond inclusion data represent 22 kimberlite localities in southern Africa, West Africa, Russia, South America and China. [Sourced from the KRG Database, Department of Geology, University of Cape Town, South Africa.] The concentrate chromite composition field is based on data for 28 kimberlite localities in southern Africa, Russia and North America (Mineral Services, internal database).

in the form of diamond or graphite (as opposed to carbonate). The boundary between the stability fields of these two carbon polymorphs is illustrated in Fig. 6 relative to a series of reference geothermal gradients (“geotherms”). The latter represent the change in temperature with depth in the lithosphere and the curves shown in Fig. 6 illustrate conductive models (Pollack and Chapman, 1977) applicable to surface heat flows of 35, 40, 45 and 50 mW/m^2. Old, thick, stable cratonic regions have low geothermal gradients, equivalent to models for surface heat flows of ~35–41 mW/m^2. Under these conditions, diamond is stable in the deep lithosphere over a relatively wide range of pressure and temperature. Under hotter geothermal conditions associated with younger, thinner lithosphere or a thermal perturbation of old lithosphere, the upper boundary of the diamond stability field shifts to greater pressures and temperatures, thereby substantially reducing the size of the diamond window. Depending on the thickness of the lithosphere, geotherms exceeding

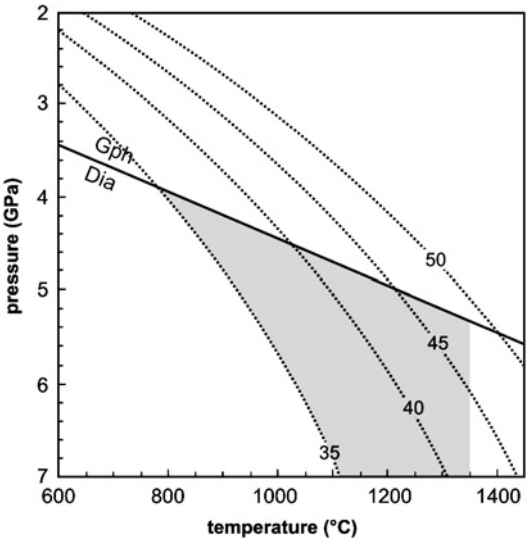

Fig. 6. Plot of pressure against temperature illustrating the concept of geothermal gradients (geotherms), diamond stability and the diamond window. The boundary between the stability fields of diamond and graphite (Kennedy and Kennedy, 1976) is shown as a solid line. Curved dotted lines represent model conductive geotherms for surface heat-flows of 35, 40, 45 and 50 mW/m^2 (Pollack and Chapman, 1977). Pressure is directly proportional to depth (e.g., 40 kb $\approx$ 130 km), thus the geotherms represent the change in temperature with depth in the lithosphere. Undisturbed Archean cratons typically have geothermal gradients that correspond with geotherm models of 35–41 mW/m^2. For any given section of lithosphere, the “diamond window” (the zone within which diamond can form and be preserved) is represented by the portion of the geotherm that lies below (i.e., at greater pressure than) the graphite/diamond phase boundary and above the base of the lithosphere. The latter typically occurs at temperatures of between 1250 and 1400 °C. The shaded region on the plot illustrates the potential extent of the diamond window for geotherms exceeding 35 mWm^2 and assuming a temperature at the base of the lithosphere of 1350 °C. It is evident that, as the geotherm increases, the potential depth range for diamond stability within the lithosphere is substantially reduced.

~44 mW/m^2 may not intersect the diamond stability field at all, because diamond cannot be formed and/or preserved in the lithosphere in this case.

Geothermal conditions at the time of kimberlite emplacement can be determined using mineral geothermometers and geobarometers applied to fragments of mantle rocks (Rudnick and Nyblade, 1999). Most of these require analysis of equilibrated mineral pairs and, therefore, are only applicable to mantle xenoliths with appropriate mineralogy. However, Nimis and Taylor (2000) developed a method for determining pressure and temperature from single grains of Cr-diopside, thereby permitting determination of the geotherm based on concentrate grains derived from kimberlite (i.e., without the occurrence of xenoliths being required).

In order to determine whether a garnet is derived from the diamond stability field, it is necessary to determine its pressure and temperature of equilibration. The temperature of equilibration can be determined based on the Ni content of individual peridotitic garnet grains using the Ni-in-garnet geothermometer (Griffin et al., 1989; Canil, 1994; Ryan et al., 1996). An alternative approach allows temperature information to be derived from the Mn content of peridotitic garnet (Grütter et al., 1999, 2004). This has the advantage of being applicable to electron microprobe data (Ni content occurs in trace amounts and typically requires analysis by laser ablation mass spectrometry or proton probe) but is susceptible to analytical error and is significantly less precise than the Ni thermometer. Consequently, Mn thermometry is best applied to garnet populations rather than individual grains.

There is no direct method available for determining the equilibration pressure of a single garnet grain. However, if the geotherm at the time of kimberlite emplacement is known, the pressure or depth of origin of the garnet grain can be determined by projecting the Ni-temperature onto this geotherm. Alternatively, because the cut-off temperature of diamond stability is fixed and known for any given geotherm, the calculated equilibration temperature allows one to directly determine whether a garnet grain equilibrated in the diamond or graphite stability field.

Graphite-associated G10 garnets can occur in regions with cool geotherms as a result of sampling of relatively shallow, low-temperature harzburgite (e.g., Fig. 7), or in cases where the kimberlite has sampled mantle that equilibrated on a hot geotherm (Shee et al., 1989). Clearly, a high proportion of such garnets will substantially downgrade or eliminate the potential for peridotitic diamonds in a kimberlite or lamproite.

3.3.3. The "graphite–diamond constraint" and the Cr/Ca barometer

Although it is not possible to reliably determine the depth of equilibration of single grains of garnet, the Cr/Ca content of garnet in garnet-chromite peridotite is sensitive to pressure, i.e., increased Cr/Ca concentration correlates with increased pressure. This relationship has been used to determine lines of equal pressure (isobars) based on the Cr_2O_3 and CaO content of peridotitic garnets that coexist with chromite (Grütter et al., 2006). The isobars are fixed for a given geothermal gradient and Grütter et al. (2006) show that, for common cratonic geothermal conditions, the graphite–diamond transition occurs at 4.3 GPa and is represented on a garnet Cr–Ca plot by the relationship $Cr_2O_3 = 5.0 + 0.94 \times CaO$ (Fig. 8). This is referred to as the graphite–diamond constraint (GDC), and it forms a convenient reference with which to characterise Cr-pyrope garnets that occur in heavy mineral concentrates. An important proviso is that the relationship between Cr/Ca in peridotitic garnet and

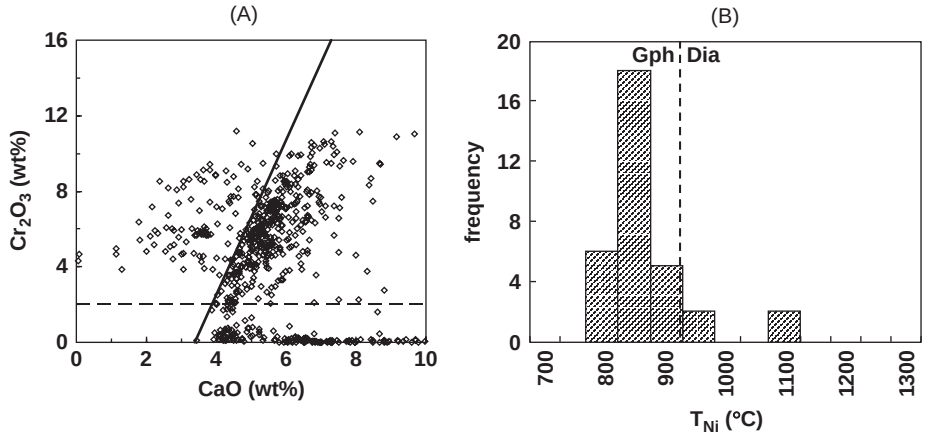

Fig. 7. Plot of Cr_2O_3 versus CaO (A) and T_{Ni} histogram (B) for garnets from a kimberlite locality in the central Slave Province, Northwest Territories, Canada. The Cr–Ca plot shows all garnet grains recovered from the kimberlite sample and indicates a relatively high proportion of G10 grains. The T_{Ni} histogram illustrates the distribution of equilibration temperatures (determined using the nickel thermometer of Ryan et al., 1996) for a compositionally representative selection of 33 G10 garnets. The majority of these grains equilibrated at temperatures of $<900\,^{\circ}C$. This places them in the graphite (Gph) stability field (for the $\sim$38 mW/m^2 geotherm applicable to this locality) signifying that, for this kimberlite, the majority of G10 garnets are not indicative of a diamond association.

pressure assumes equilibrium with chromite. Where chromite is not present, the Cr/Ca content provides a minimum pressure estimate. Thus, in the case of garnet grains from kimberlite heavy mineral concentrates where coexistence with chromite cannot be confirmed, the Cr-pyrope compositions yield minimum-pressure estimates. Where a minimum-pressure estimate exceeds 4.3 GPa (i.e., the garnet compositions have higher Cr than the GDC), the grain is clearly derived from within the diamond stability field. Garnet compositions with lower Cr indicate minimum-pressures of less than 4.3 GPa, i.e., they cannot be unequivocally assigned to the diamond or graphite stability field. For these garnets, it is necessary to determine temperature of equilibration (as described above) in order to establish whether they are associated with diamond or graphite (see Grütter et al., 2004).

The P–T–X relationships for garnet $\pm$ chromite peridotite are evaluated in more detail by Grütter et al. (2006), who develop the concept of a garnet Cr/Ca barometer and demonstrate its use to estimate pressure and lithospheric thickness based on the Cr–Ca compositions represented in peridotitic garnet populations. These concepts are illustrated with numerous examples from kimberlite and related-rock localities worldwide.

3.3.4. Eclogitic minerals associated with diamond

As for peridotite, studies of eclogitic mineral inclusions in diamond and minerals from diamond-bearing eclogite reveal distinctive compositional features that are useful for distinguishing diamond-associated minerals from those derived from

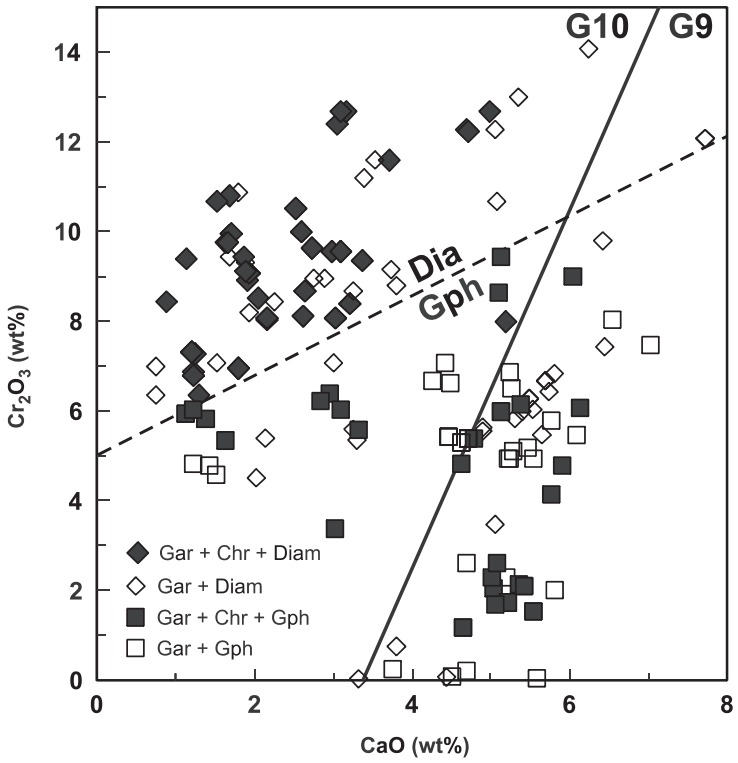

Fig. 8. Cr_2O_3–CaO compositions of garnets in graphite-bearing (Gph, square symbols) or diamond-bearing (Dia, diamond symbols) peridotite xenoliths, with coexisting chromite (Chr, filled symbols), or lacking coexisting chromite (unfilled symbols). Under Cr-saturated conditions the graphite–diamond constraint (GDC, dashed line) of Grütter et al. (2004, 2006) separates graphite-facies from diamond-facies conditions for common cratonic geotherms. Garnets with Cr content higher than the GDC are derived from pressures within the diamond stablity field (i.e., filled and unfilled diamond symbols). Garnets with lower Cr than the GDC are derived from graphite-facies pressures if they are known to coexist with chromite (i.e., filled square symbols), or potentially from higher pressures if chromite coexistence is indeterminate (e.g., unfilled diamond symbols). [Diagram modified after Grütter et al. (2006).]

non-diamondiferous eclogite. Eclogitic garnet is particularly important because it is a resistant mineral commonly recovered in kimberlitic concentrate and shows diagnostic compositions. It can be readily distinguished from peridotitic garnet by its orange to orange-brown colour and significantly lower Cr content (Grütter et al., 2004). The most diagnostic feature of eclogite garnets associated with diamonds are elevated trace amounts of Na ($Na_2O > 0.07$ wt.%), first noted by Sobolev and Lavrent'yev (1971) and expanded on by McCandless and Gurney (1989). These garnets also show slightly higher Ti levels relative to non-diamondiferous eclogite (Danchin and Wyatt, 1979). The composition of eclogitic garnets associated with diamonds worldwide with respect to these two key oxides is presented in Fig. 9. These compositional features are characteristic of a texturally distinct, coarse-grained variety of eclogite classified as Group 1 (McCandless and Gurney, 1989).

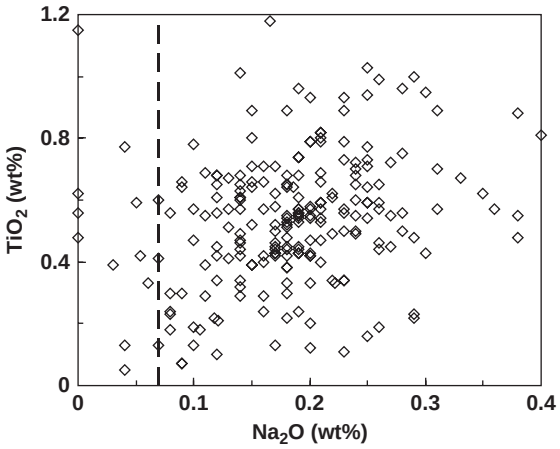

Fig. 9. Plot of TiO_2 versus Na_2O for eclogitic diamond inclusion garnets from worldwide localities. Note that the elevated levels of both of these elements is characteristic of eclogitic garnets associated with diamonds. In exploration applications, garnets with $Na_2O > 0.07$ wt.% (dashed line) are generally considered significant (see text for further discussion). Diamond inclusion data represent 45 kimberlite, lamproite and alluvial localities in southern Africa, West Africa, Russia, Australia, South America, North America and China. [Sourced from the KRG Database, Department of Geology, University of Cape Town, South Africa.]

Group 2 eclogites are finer-grained, do not show elevated Na or Ti contents, and do not appear to be associated with diamond.

In contrast to the peridotite association in which the presence of diamond or graphite is strongly related to the bulk composition of the host rock, diamonds (and graphite) occur within the full compositional range displayed by mantle eclogite (Grütter and Quadling, 1999) and the diagnostic elevated trace Na contents reflect high pressures of equilibration appropriate for diamond formation. However, Na concentration in garnet is also dependent on the bulk composition of the host eclogite (Grütter and Quadling, 1999). Thus, while the empirically determined value of 0.07 wt.% Na_2O provides a useful threshold for identifying the majority of diamond-associated eclogitic garnets, predictions of eclogitic diamond potential may be improved by allowing for a variable Na_2O threshold value, dependent on the bulk composition of the host eclogite, as reflected in the garnet composition.

The clinopyroxene (omphacite) in diamond-eclogite has been shown to have elevated concentrations of K_2O (McCandless and Gurney, 1989) relative to that in non-diamondiferous eclogite. However, due to the instability of omphacite at low pressure, it is rarely preserved in kimberlitic concentrate (unlike Cr-diopside which is common in unaltered kimberlite) and hence, is not commonly used to assess diamond potential.

3.3.5. The megacryst suite of minerals

Many kimberlites contain a suite of closely related very coarse-grained (often >2 cm, occasionally >20 cm) mantle-derived minerals, commonly referred to as megacrysts. These include olivine, orthopyroxene, garnet and clinopyroxene, all

commonly occurring together with megacryst ilmenite. Ilmenite can also occur on its own and in various combinations with phlogopite, zircon and possibly carbonate. The megacryst minerals are not genetically related to diamond. Geochemical and isotopic data show that the entire megacryst suite recovered from any given kimberlite locality can form in one magmatic event. Radiogenic isotopic evidence shows that the megacrysts remain an open system until the host kimberlite event, and their formation is interpreted to be closely related to that intrusion. Geothermobarometry indicates an association between megacrysts and a layer of highly deformed, high-temperature garnet lherzolite at the base of the cratonic lithosphere, below the primary diamond bearing strata. In fact, the megacrysts are thought to represent pegmatitic vein systems within these deformed garnet lherzolite host rocks. Megacrysts can be identified compositionally and are useful indicators of the presence of kimberlite. The vast majority of ilmenite recovered in exploration programs are megacrystic in origin. Megacryst phlogopite and zircons are excellent and reliable minerals for dating of kimberlite intrusive events.

Megacryst garnets are visually similar to garnet from eclogite. They also show similar low-Cr compositions and commonly contain trace levels of Na_2O that overlap with those of garnet from potentially diamondiferous (Group 1) eclogite. The Na content of megacryst garnets is sensitive to pressure and they can be used to monitor craton thickness. However, since megacryst garnets are not related to diamond, they must be discriminated against when assessing the diamond potential of a kimberlite. This can be very effectively done using geochemical parameters such as TiO_2, CaO, MgO and FeO contents (Grütter et al., 2004).

At each locality the contribution of each of the garnet harzburgite, chromite harzburgite and eclogite parageneses is assessed by establishing the abundance of the garnets and chromites derived from disaggregation of the mantle host rock. These three diamond sources are additive and a really good contribution from any one of them could be sufficient to provide an economic grade in a kimberlite. Clearly, it is necessary to establish both the compositions of the indicator minerals and their relative abundances.

3.4. Geochemical Criteria Related to Diamond Preservation

Having sampled diamondiferous rocks in the mantle, an igneous intrusion must carry them to the surface. En route, conditions within the magma must eventually be outside the diamond stability field. Providing that reaction kinetics are sufficiently rapid, diamond may be converted to graphite or, more frequently, to CO_2. The latter will happen more rapidly as a result of higher oxygen activity in the magma. The effect of this resorption on the diamond content of an intrusion can be large.

In the model developed for southern Africa, it appears that ilmenite compositions give some measure of these redox conditions. Ilmenites with low Fe^{3+}/Fe^{2+} ratios are associated with higher diamond contents than those with more ferric iron (Fe^{3+}). In kimberlitic ilmenites, high Fe^{3+} is associated with low MgO. High Cr^{3+} can be found in either association but is only a positive factor when it occurs with high Mg. Favourable and unfavourable trends can be seen readily on simple MgO/Cr_2O_3 plots or ternary diagrams, such as that presented by Haggerty and Tompkins (1983). This is illustrated in Fig. 10, taken from Horwood (1998). Young, fast-grown fibrous

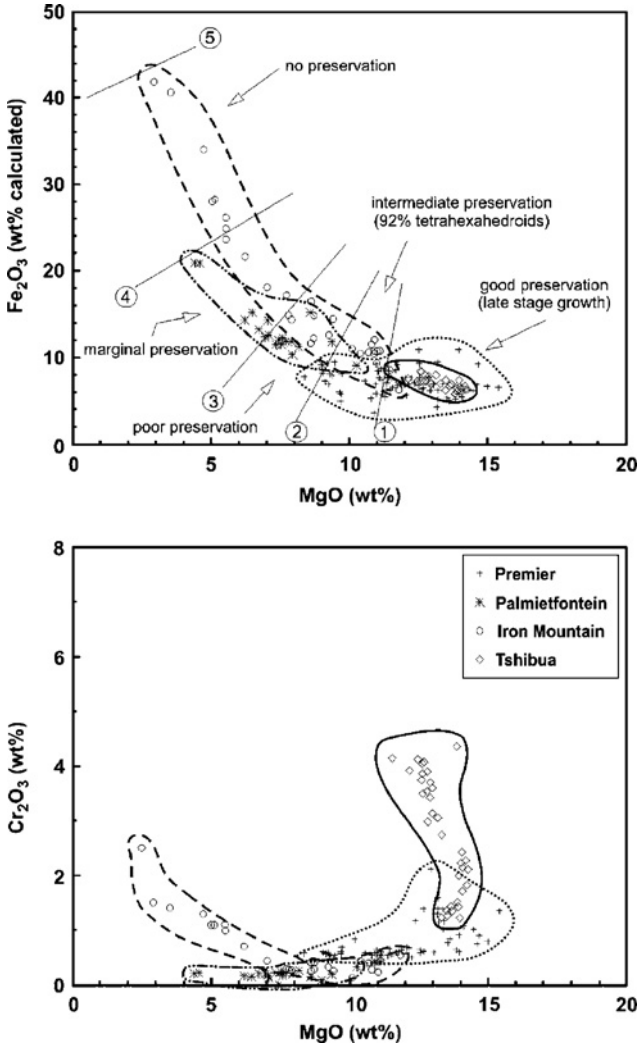

Fig. 10. Plots of Fe_2O_3 versus MgO and Cr_2O_3 versus MgO illustrating the composition of ilmenites from four kimberlite localities. [Reproduced from Horwood, 1998.] The ilmenites define a trend from MgO-rich and Fe_2O_3-poor to Fe_2O_3-rich and MgO-poor compositions. This trend corresponds with a gradual increase in oxygen fugacity and associated reduction in diamond preservation potential. Compositional fields 1–5 are from Horwood (1998) and illustrate the interpreted correlation between ilmenite composition and the extent of diamond preservation.

diamond is associated with ilmenite of very high Mg, high Cr, and very low Fe^{3+} content. Very resorbed diamonds, on the other hand, are found in kimberlites that have megacryst ilmenites high in Fe^{3+} and lower in Mg. Hence, megacryst ilmenite composition appears to provide an index of diamond preservation potential.

In addition to resorption processes taking place in the host magma, it has been suggested that metasomatism of the mantle lithosphere, at some time prior to

kimberlite emplacement, may be detrimental to diamond preservation (Griffin and Ryan, 1995). Such processes are reflected in the composition of peridotitic garnet and in certain instances appear to be associated with significant increases in oxygen fugacity, suggesting increased potential for diamond resorption (McCammon et al., 2001). In general, the effects of these metasomatic processes on the diamond potential of a kimberlite are likely to be accounted for by the compositional criteria described above. For example, metasomatism generally increases the Ca content and will reduce the proportion of G10's present in any given peridotitic garnet population. Similarly, peridotite that has been subjected to significant melt metasomatism (Griffin and Ryan, 1995) will manifest as Ca-saturated, Ti-rich garnet that is discounted when determining the potential diamond budget of a kimberlite. Nonetheless, understanding the "signatures" associated with metasomatic processes as well as the potential effect of such processes on diamond preservation helps to constrain the history of the lithosphere sampled by a kimberlite or lamproite and, therefore, is an important aspect of indicator mineral geochemistry.

4. APPLICATION OF INDICATOR MINERAL METHODS IN DIAMOND EXPLORATION AND EVALUATION

Flow charts summarising how indicator minerals and diamonds are used in exploring for and evaluating primary diamond deposits are provided in Figures 11 and 12.

Different diamond provinces appear to obey different sets of rules particularly with respect to preservation. For instance, at most kimberlite localities on the Kalahari Craton, resorption of diamonds is a very significant process (Robinson, 1979). In the Malo-Botuoba and Daldyn-Alakhit regions of the Siberian Platform, which include the Mir, Udachnaya and Jubilee kimberlites, resorption is of minor significance. In Zaire and Sierra Leone, late stage fibrous coats on numerous diamonds suggest that the last event in the diamond history in those regions was a period of diamond growth. Variations in the eclogitic to peridotitic ratio of the diamonds may also be regional. The three kimberlite mines in Botswana for instance show higher than average proportions of eclogitic diamonds, which is also the case for the described primary diamond resources in Australia (Hall and Smith, 1984; Jaques et al., 1989). In contrast, diamonds from kimberlites in the Kimberley region of South Africa have a preponderance of peridotitic inclusions and minimal eclogitic minerals. As with most geochemical approaches to mineral exploration, an orientation survey within a prospective area is a necessary prerequisite and the interpretations must be continuously adapted to the database compiled.

A vital question is how much reliance to place on diamond potential forecasts based on the geochemistry of indicator minerals. To reach its full potential, the method needs to be rigorously applied, taking into consideration all of the factors described above. If that is done, most "anomalies" can be accounted for, and it is clear that the system can be a major aid to exploration programs. In Botswana, where an early version was applied by Falconbridge Exploration to several tens of kimberlites discovered under Kalahari cover in the early 1980s, the heavy mineral

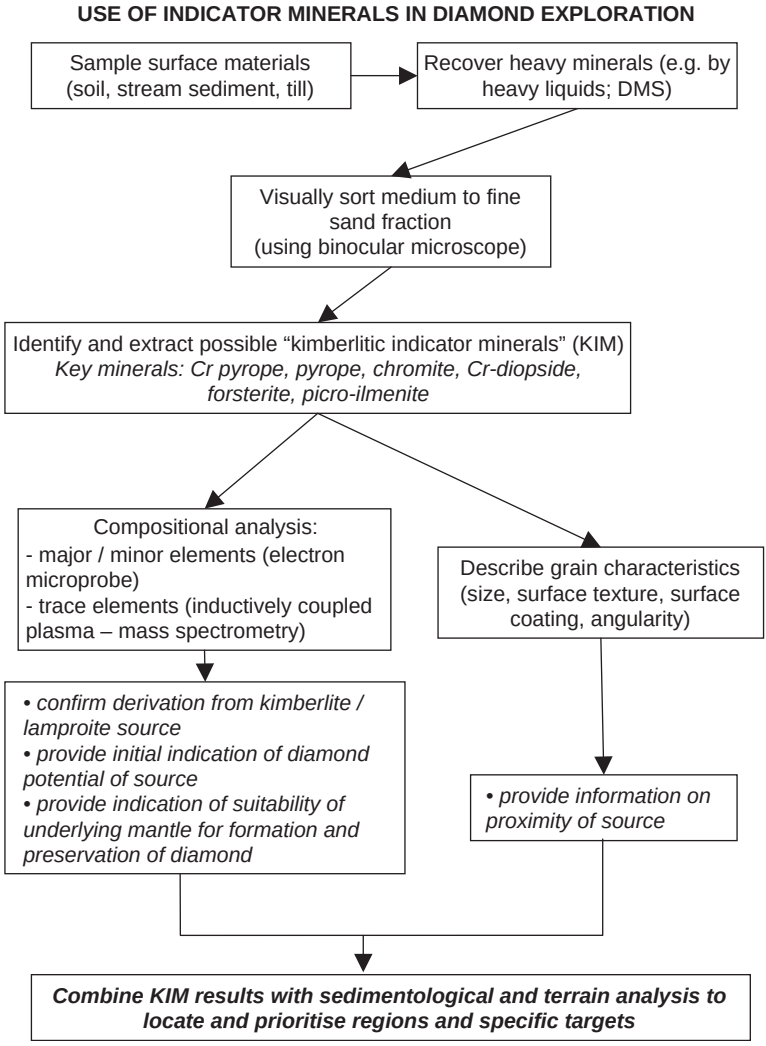

Fig. 11. Flow-chart summarising key aspects of the application of indicator mineral studies in diamond exploration.

analyses correctly identified all the barren kimberlites and all the diamond-bearing kimberlites. Notably, the method flagged the best ore-bearing body found (GO25) as soon as the first batch of heavy minerals from that source passed in front of the microprobe. In this environment of hidden ore bodies, it was an unqualified success (Lee, 1993). Subsequently the method was a major factor in the early stages of prospecting for the Ekati kimberlites by DiaMet and in the subsequent evaluation and development of the Ekati diamond mine by the BHP/DiaMet/Fipke/Blusson consortium (Fig. 12) (Fipke et al., 1995).

In a Venezuelan stream sampling program in 1975, the presence of G10 garnets from a nearby diamond source was picked up in the Guaniamo region where the

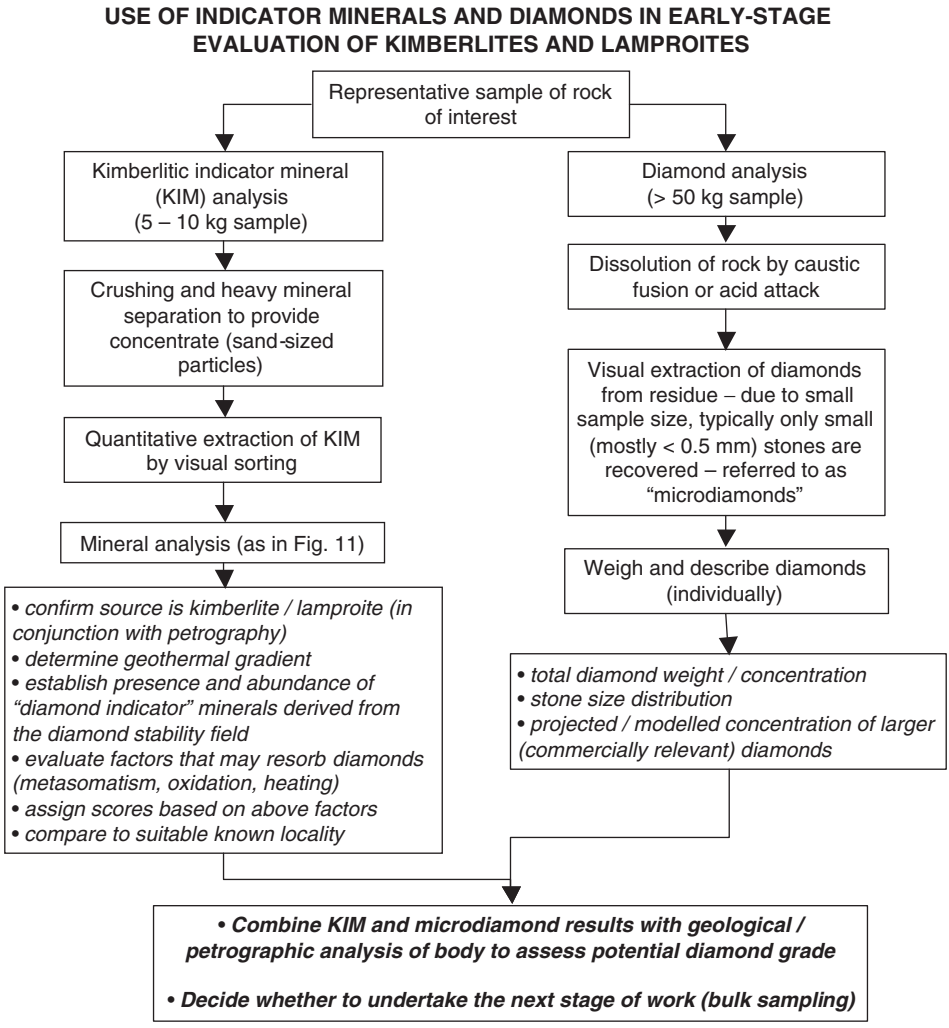

Fig. 12. Flow-chart summarising key aspects of the application of indicator mineral and microdiamond studies in the early-stage evaluation of kimberlite or lamproite deposits.

primary source of some of the alluvial diamonds has now been found (Nixon et al., 1989). Earlier, the system demonstrated the proximity of a then unknown primary source (Dokolwayo) to the Hlane alluvial diamonds in Swaziland.

Accurate forecasts about the presence or absence of diamonds have also been made for Brazilian kimberlites and for numerous localities in southern Africa, both barren and diamond-bearing. The method has been successfully applied in the Banankoro region in Guinea, West Africa. In North America, it was used to prioritise the sampling of the Georges Creek dyke in the Colorado/Wyoming State Line District (Carlson and Marsh, 1989). It provided acceptable forecasts for the nearby Schaffer and Sloan 2/5 intrusions, predicted the absence of diamonds at Iron Mountain, Garnet Ridge, Moses Rock and Green Knobs, and was successfully

applied to diamond exploration in the North American Cordillera (Dummett et al., 1986). The heavy mineral assessment of the kimberlites in the Upper Peninsula, Michigan is again in good accord with the known facts in that area (McGee, 1988). Even the Twin Knobs lamproite in Arkansas conforms to the general pattern (Waldman et al., 1987). The fact that diamonds are being (or can be) traced by association with fragments of the mantle rocks from which they have been originally released by disaggregation is such a fundamental association that whatever geological vehicle has been used to convey them to the surface, there is a chance that semi-quantitative relationships may hold. Where they do not, further geochemical or petrological detective work may reveal relevant clues. The diamonds may not have been preserved en route to surface, the lithosphere may not have been thick enough or the geothermal gradient sufficiently low to permit diamond formation and/or storage to have occurred. The apparently necessary metasomatic activity that may have a particularly important role in the formation of peridotitic diamonds may never have occurred and a suitable carbon source may, therefore, not be available. Clues may come from the major and trace element contents of other mantle minerals that occur in the intrusion under investigation. Given the wide range of uncertainties, a balanced view has to be permissive of exceptions to the rules since these are certain to occur.

ACKNOWLEDGEMENTS

The development of this geochemical approach to assessing the diamond potential of volcanic ore bodies has taken more than three decades of research and practical experience. The project profited greatly from the enthusiastic support of Hugo T. Dummett while he was employed by Superior Oil Company and BHP. A key early input was made by Dr. George Switzer from the Smithsonian Institution and by J. Barry Hawthorne, of De Beers Consolidated Mines in Kimberley. The method has been refined and greatly improved by the contributions of numerous scientists around the world whom we have hopefully correctly referenced in the text. Financial support during various phases of this period of time is gratefully acknowledged from De Beers Consolidated Mines, Falconbridge Explorations, Superior Oil and BHP Billiton Diamonds, Inc. The authors would also like to acknowledge Jon Carlson of BHP Billiton for supporting application and ongoing research of the methods described in this paper. Thanks to Herman Grütter for valuable input to aspects of the manuscript and to Meilanie Zamora for drafting several of the figures. Finally, we would like to thank Laurence Robb, John Dewey and Maria Mange for efficient and constructive reviews that have improved this manuscript.

REFERENCES

Armstrong, K.A., Nowicki, T.E., Read, G.H., 2004. Kimberlite AT-56: A mantle sample from north central Superior craton Canada. Lithos 77, 695–704.

Boyd, F.R., Gurney, J.J., 1982. Low-Calcium Garnets: Keys to Craton Structure and Diamond Crystallisation. Carnegie Institute of Washington Yearbook, vol. 81, Washington DC, U.S., pp. 261–267.

Bulanova, G.P., 1995. The formation of diamond. Journal of Geochemical Exploration 53, 1–24.

Bundy, F.P., Strong, H.M., Wentorf, R.H., 1973. In: Walker, P.L., Thrower, P.A. (Eds.), Chemistry and Physics of Carbon. Marcel Dekker, New York, pp. 213–263.

Canil, D., 1994. An experimental calibration of the "Ni-in-garnet" geothermometer with applications. Contributions to Mineralogy and Petrology 117, 410–420.

Carlson, J.A., Marsh, S.W., 1989. Discovery of the George Creek, Colorado kimberlite dykes. In: Ross, J. (Ed.), Kimberlites and Related Rocks, vol. 2. Geological Society of Australia, Special Publication, vol. 14. Blackwell Scientific Publications, Perth, pp. 1169–1178.

Danchin, R., Wyatt, B.A., 1979. Statistical cluster analyses of garnets from kimberlites and their xenoliths. Kimberlite Symposium II, Cambridge, U.K., pp. 22–27.

Dawson, J.B., Smith, J., 1975. Occurrence of diamond in a mica-garnet lherzolite xenolith from kimberlite. Nature 254, 580–581.

Dawson, J.B., Stephens, W.E., 1975. Statistical classification of garnets from kimberlite and associated xenoliths. Journal of Geology 83, 589–607.

Deines, P., Harris, J.W., Gurney, J.J., 1987. Carbon isotopic composition, nitrogen content and inclusion composition of diamonds from Roberts Victor kimberlite, South Africa: evidence for ^{13}C depletion in the mantle. Geochimica et Cosmochimica Acta 51, 1227–1243.

Deines, P., Harris, J.W., Gurney, J.J., 1991. The carbon and nitrogen content of lithospheric and asthenospheric diamonds from the Jagersfontein and Koffiefontein kimberlites, South Africa. Geochimica et Cosmochimica Acta 55, 2615–2625.

Dong, Z., Zhou, J., 1980. The typomorphic characteristics of chromites from kimberlites in China, and the significance in exploration of diamond deposits. Acta Geologica Sinica 4, 299–309.

Draper, D., Frames, M.E., 1898. The Diamond, with Hints to Prospectors in Search of these Gems. Mathews and Walker, Johannesburg, 44pp.

Dummett, H.T., Fipke, C.E., Blusson, S.L., 1986. Diamond exploration in the North American Cordillera. In: Elliot, I.L., Smee, B.W. (Eds.), Joint Publication of the Association of Exploration Geochemists and the Geological Association of Canada, pp. 168–176.

Evans, T., Harris, J.W., 1989. Nitrogen aggregation, inclusion equilibration temperatures and the age of diamonds. In: Ross, J. (Ed.), Kimberlites and Related Rocks, vol. 2. Geological Society of Australia, Special Publication, vol. 14. Blackwell Scientific Publications, Perth, pp. 1001–1006.

Fipke, C.E., Gurney, J.J., Moore, R.O., 1995. Diamond exploration techniques emphasising indicator mineral geochemistry and Canadian examples. Geological Survey of Canada, Bulletin 423, 86.

Gregory, G.P., White, D.R., 1989. Collection and treatment of diamond exploration samples. In: Ross, J. (Ed.), Kimberlites and Related Rocks, vol. 2. Geological Society of Australia, Special Publication, vol. 14. Blackwell Scientific Publications, Perth, pp. 1123–1134.

Griffin, W.L., Gurney, J.J., Ryan, C.G., Cousens, D.R., Sie, S.H., Suter, G.F., 1989. Trapping temperatures and trace elements in P-type garnets in diamonds: a proton microprobe study. Extended Abstracts, Workshop on Diamonds, 28th International Geological Congress, Washington, DC, pp. 23–25.

Griffin, W.L., Ryan, C.G., 1995. Trace elements in indicator minerals: area selection and target evaluation in diamond exploration. Journal of Geochemical Exploration 53, 311–337.

Grütter, H.S., Apter, D.B., 1998. Kimberlite- and lamproite-borne chromite phenocrysts with "diamond-inclusion"-type chemistries. Extended Abstracts, 7th International Kimberlite Conference, Cape Town, South Africa, pp. 280–282.

Grütter, H.S., Apter, D.B., Kong, J., 1999. Crust-mantle coupling: evidence from mantle-derived xenocryst garnets. In: Gurney, J.J., Gurney, J.L., Pascoe, M.D., Richardson, S.H.

(Eds.), Proceedings of 7th International Kimberlite Conference, vol. 1 (J.B. Dawson Volume). Red Roof Design, Cape Town, pp. 307–313.
Grütter, H.S., Gurney, J.J., Menzies, A.H., Winter, F., 2004. An updated classification scheme for mantle-derived garnet, for use by diamond explorers. Lithos 77, 841–857.
Grütter, H.S., Latti, D., Menzies, A.H., 2006. Cr-saturation arrays in concentrate garnet compositions from kimberlite and their use in mantle barometry. Journal of Petrology 47, 801–820.
Grütter, H.S., Quadling, K.E., 1999. Can sodium in garnet be used to monitor eclogitic diamond potential? In: Gurney, J.J., Gurney, J.L., Pascoe, M.D., Richardson, S.H. (Eds.), Proceedings of 7th International Kimberlite Conference, vol. 1 (J.B. Dawson Volume), Red Roof Design, Cape Town, pp. 314–320.
Gurney, J.J., 1984. A correlation between garnets and diamonds in kimberlites. In: Glover, J.E., Harris, P.G. (Eds.), Kimberlite Occurrence and Origin: A Basis for Conceptual Models in Exploration. Geology Department and University Extension, University of Western Australia, Publication, vol. 8. Blackwell Scientific Publications, Perth, pp. 143–166.
Gurney, J.J., 1989. Diamonds. In: Ross, J. (Ed.), Kimberlites and Related Rocks, vol. 1. Geological Society of Australia, Special Publication, vol. 14. Blackwell Scientific Publications, Perth, pp. 935–965.
Gurney, J.J., 1990. The diamondiferous root zones of our wandering continents. South African Journal of Geology 93, 423–437.
Gurney, J.J., Harris, J.W., Rickard, R.S., 1984. Silicate and oxide inclusions in diamonds from the Orapa mine, Botswana. In: Kornprobst, J. (Ed.), Kimberlites II: The Mantle and Crust-Mantle Relationships. Elsevier, Amsterdam, pp. 3–9.
Gurney, J.J., Harris, J.W., Rickard, R.S., Moore, R.O., 1985. Premier mine diamond inclusions. Transactions of the Geological Society of South Africa 88, 301–310.
Gurney, J.J., Helmstaedt, H.H., le Roex, A.P., Nowicki, T.E., Richardson, S.H., Westerlund, K.J., 2005. Diamonds: crustal distribution and formation processes in time and space and an integrated deposit model. Society of Economic Geologists, 100th Anniversary Volume 143–177.
Gurney, J.J., Helmstaedt, H., Moore, R.O., 1993. A review of the use and application of mantle mineral geochemistry in diamond exploration. Pure and Applied Chemistry 65, 2423–2442.
Gurney, J.J., Hildebrand, P.R., Carlson, J.A., Fedortchouk, Y., Dyck, D.R., 2004. The morphological characteristics of diamonds from the Ekati Property, Northwest Territories, Canada. Lithos 77, 21–38.
Gurney, J.J., Switzer, G.S., 1973. The discovery of garnets closely related to diamonds in the Finsch Pipe, South Africa. Contributions to Mineralogy and Petrology 39, 103–116.
Gurney, J.J., Zweistra, P., 1995. The interpretation of the major element compositions of mantle minerals in diamond exploration. Journal of Geochemical Exploration 53, 293–309.
Haggerty, S.E., 1986. Diamond genesis in a multiply-constrained model. Nature 320, 34–38.
Haggerty, S.E., Tompkins, L.A., 1983. Redox state of the earth's upper mantle from kimberlitic ilmenites. Nature 303, 295–300.
Hall, A.E., Smith, C.B., 1984. Lamproite diamonds—are they different? In: Glover, J.E., Hams, G. (Eds.), Kimberlite Occurrence and Origin: A Basis for Conceptual Models in Exploration. Geology Department and University Extension, University of Western Australia, Publication, vol. 8, Blackwell Scientific Publications, Perth.
Harte, B., Harris, J.W., Hutchison, M.T., Watt, G.R., Wilding, M.C., 1999. Lower mantle mineral associations in diamonds from Sao Luiz, Brazil. In: Fei, Y., Bertka, C.M., Myson, B.O. (Eds.), Mantle Petrology: Field Observations and High-Pressure Experimentation: A Tribute to Francis R. (Joe) Boyd, Chemical Society, Special Publication, vol. 6, pp. 125–154.

Hatton, C.J., Gurney, J.J., 1979. A diamond-graphite eclogite from the Roberts Victor mine. In: Boyd, F.R., Meyer, H.O.A. (Eds.), The Mantle Sample. American Geophysical Union, Washington, DC, pp. 29–36.

Helmstaedt, H., Gurney, J.J., 1984. Kimberlites of southern Africa—are they related to subduction processes? In: Kornprobst, J. (Ed.), Kimberlites I: Kimberlites and Related Rocks. Elsevier, Amsterdam, pp. 425–434.

Helmstaedt, H.H., Gurney, J.J., 1995. Geotectonic controls of primary diamond deposits: implications for area selection. Journal of Geochemical Exploration 53, 125–144.

Helmstaedt, H., Schulze, D.J., 1989. Southern African kimberlites and their mantle sample—implication for Archean tectonics and lithosphere evolution. In: Ross, J. (Ed.), Kimberlites and Related Rocks, vol. 1. Geological Society of Australia, Special Publication, vol. 14. Blackwell Scientific Publications, Perth, pp. 358–368.

Hills, D.V., Haggerty, S.E., 1989. Petrochemistry of eclogites from the Koidu kimberlite complex, Sierra Leone. Contributions to Mineralogy and Petrology 103, 397–422.

Horwood, S.J., 1998. The use of upper mantle derived ilmenite to predict preservation of diamond parcels in kimberlite. Unpublished M.Sc. thesis. University of Cape Town, 154 pp.

Jago, B.C., Mitchell, R.H., 1989. A new garnet classification technique: devisive cluster analysis applied to garnet populations from Somerset kimberlites. In: Ross, J. (Ed.), Kimberlites and Related Rocks, vol. 1. Geological Society of Australia, Special Publication, vol. 14. Blackwell Scientific Publications, Perth, pp. 298–310.

Jaques, A.L., Hall, A.E., Sheraton, J.W., Smith, C.B., Sun, S.-S., Drew, R.M., Foudoulis, C., Ellingsen, K., 1989. Composition of crystalline inclusions and C isotopic composition of Argyle and Ellendale diamonds. In: Ross, J. (Ed.), Kimberlites and Related Rocks, vol. 2. Geological Society of Australia, Special Publication, vol. 14. Blackwell Scientific Publications, Perth, pp. 966–989.

Kennedy, C.S., Kennedy, G.C., 1976. The equilibrium boundary between graphite and diamond. Journal of Geophysical Research 81, 2467–2470.

Kirkley, M.B., Gurney, J.J., Otter, M.L., Hill, S.J., Daniels, L.R., 1991. The application of C isotope measurements to the identification of the sources of C in diamonds: a review. Applied Geochemistry 6, 477–494.

Kramers, J.D., 1977. Lead and strontium isotopes in Cretaceous kimberlites and mantle-derived xenoliths from southern Africa. Earth and Planetary Science Letters 34, 419–431.

Kramers, J.D., 1979. Lead, uranium, strontium, potassium and rubidium in inclusion bearing diamonds and mantle-derived xenoliths from southern Africa. Earth and Planetary Science Letters 42, 58–70.

Lawless, J., 1974. Some aspects of the geochemistry of kimberlite xenocrysts. Unpublished Ph.D. thesis. University of Cape Town, South Africa, 193 pp.

Lee, J.E., 1993. Indicator mineral techniques in a diamond exploration program at Kokong, Botswana. In: Diamond: Exploration, Sampling and Evaluation. Prospectors and Developers Association, Diamond Exploration Short Course Notes, pp. 1–21.

McCallum, M.E., Eggler, D.H., 1976. Diamonds in an upper mantle peridotite nodule from kimberlite in southern Wyoming. Science 192, 253–256.

McCammon, C.A., Griffin, W.L., Shee, S.R., O'Neill, H.S.C., 2001. Oxidation state during metasomatism in ultramafic xenoliths from the Wesselton kimberlite, South Africa: implications for the survival of diamond. Contributions to Mineralogy and Petrology 141, 287–296.

McCandless, T.E., Gurney, J.J., 1989. Sodium in garnet and potassium in clinopyroxene: criteria for classifying mantle xenoliths. In: Ross, J. (Ed.), Kimberlites and Related Rocks, vol. 2. Geological Society of Australia, Special Publication, vol. 14. Blackwell Scientific Publications, Perth, pp. 827–832.

McDade, P., Harris, J.W., 1999. Syngenetic inclusion bearing diamonds from Letseng-la-Terai, Lesotho. In: Gurney, J.J., Gurney, J.L., Pascoe, M.D., Richardson, S.H. (Eds.), Proceedings of 7th International Kimberlite Conference, vol. 2 (P.H. Nixon Volume). Red Roof Design, Cape Town, pp. 557–565.

McGee, E.S., 1988. Potential for diamond in kimberlites from Michigan and Montana as indicated by garnet xenocryst compositions. Economic Geology 83, 428–432.

McKenna, N., Gurney, J.J., Davidson, J.M., 2003. A study of the diamonds, diamond inclusion minerals and other mantle minerals from the Swartruggens kimberlite dyke swarm. Extended Abstracts, 8th International Kimberlite Conference, Victoria, BC, abstract 0054 (CD-ROM).

Menzies, A.H., Carlson, R.W., Shirey, S.B., Gurney, J.J., 1999. Re-Os systematics of Newlands peridotite xenoliths: Implications for diamond and lithosphere formation. In: Gurney, J.J., Gurney, J.L., Pascoe, M.D., Richardson, S.H. (Eds.), Proceedings of 7th International Kimberlite Conference, vol. 2 (P.H. Nixon Volume). Red Roof Design, Cape Town, pp. 566–573.

Meyer, H.O.A., 1987. Inclusions in diamond. In: Nixon, P.H. (Ed.), Mantle Xenoliths. Wiley, Chichester, pp. 501–522.

Mitchell, R.H., 1986. Kimberlites: Mineralogy, Geochemistry and Pertrology. Plenum Press, New York, 442pp.

Mitchell, R.H., 1995. Kimberlites, Orangeites, and Related Rocks. Plenum Press, New York, 410pp.

Moore, R.O., Gurney, J.J., 1985. Pyroxene solid solution in garnets included in diamond. Nature 318, 553–555.

Moore, R.O., Gurney, J.J., 1989. Mineral inclusions in diamond from the Monastery kimberlite, South Africa. In: Ross, J. (Ed.), Kimberlites and Related Rocks, vol. 2. Geological Society of Australia, Special Publication, vol. 14. Blackwell Scientific Publications, Perth, pp. 1029–1041.

Muggeridge, M.T., 1995. Pathfinder sampling techniques for locating primary sources of diamond: recovery of indicator minerals, diamonds and geochemical signatures. Journal of Geochemical Exploration 53, 183–204.

Nimis, P., Taylor, W.R., 2000. Single clinopyroxene thermobarometry for garnet peridotites: Part 1. Calibration and testing of a Cr-in-Cpx barometer and an enstatite-in-Cpx thermometer. Contributions to Mineralogy and Petrology 139, 541–554.

Nixon, P.H., Davies, G.R., Condliffe, E., Baker, R., Baxter Brown, R., 1989. Discovery of ancient source rocks of Venezuela diamonds. Extended Abstracts, Workshop on Diamonds, 28th International Geological Congress, Washington, DC, pp. 73–75.

Otter, M.L., Gurney, J.J., 1989 Mineral inclusions in diamonds from the Sloan diatremes, Colorado-Wyoming State Line kimberlite district, North America. In: Ross, J. (Ed.), Kimberlites and Related Rocks, vol. 2. Geological Society of Australia, Special Publication, vol. 14. Blackwell Scientific Publications, Perth, pp. 1042–1053.

Otter, M.L., Gurney, J.J., McCandless, T.E., 1989. The carbon isotope composition of Sloan diamonds. Extended Abstracts, Workshop on Diamonds, 28th International Geological Congress, Washington, DC, pp. 76–79.

Pokhilenko, N.P., Sobolev, N., Lavrent'yev, Y.G., 1977. Xenoliths of diamondiferous ultramafic rocks from Yakutian kimberlites. Extended Abstracts, 2nd International Kimberlite Conference, Sante Fe, American Geophysical Union (unpaged).

Pollack, H.N., Chapman, D.S., 1977. On the regional variation of heat flow, geotherms, and lithosphere thickness. Tectonophysics 38, 279–296.

Reid, A.M., Brown, R.W., Dawson, J.B., Whitfield, G.C., Siebert, J.C., 1976. Garnet and pyroxene compositions in some diamondiferous eclogites. Contributions to Mineralogy and Petrology 58, 203–220.

Richardson, S.H., 1986. Latter-day origin of diamonds of eclogitic paragenesis. Nature 322, 623–626.

Richardson, S.H., 1989. Radiogenic isotope studies of diamond inclusions. Extended Abstracts, Workshop on Diamonds, 28th International Geological Congress, Washington, DC, pp. 87–90.

Richardson, S.H., Erlank, A.J., Harris, J.W., Hart, S.R., 1990. Eclogitic diamonds of Proterozoic age from Cretaceous kimberlites. Nature 346, 54–56.

Richardson, S.H., Gurney, J.J., Erlank, A.J., Harris, J.W., 1984. Origin of diamonds in old enriched mantle. Nature 310, 198–202.

Richardson, S.H., Harris, J.W., Gurney, J.J., 1993. Three generations of diamonds from old continental mantle. Nature 366, 256–258.

Richardson, S.H., Shirey, S.B., Harris, J.W., Carlson, R.W., 2001. Archean subduction recorded by Re-Os isotopes in eclogitic sulfide inclusions in Kimberley diamonds. Earth and Planetary Science Letters 191, 257–266.

Rickwood, C., Gurney, J.J., White-Cooper, D.R., 1969. The nature and occurrence of eclogite xenoliths in the kimberlites of southern Africa. Geological Society of South Africa, Special Publication, vol. 2, pp. 371–393.

Robinson, D.N., 1979. Surface textures and other features of diamonds. Unpublished Ph.D. thesis. University of Cape Town, South Africa, 221pp.

Robinson, D.N., Gurney, J.J., Shee, S.R., 1984. Diamond eclogite and graphite eclogite xenoliths from Orapa, Botswana. In: Kornprobst, J. (Ed.), Kimberlites II: The Mantle and Crust-Mantle Relationships. Elsevier, Amsterdam, pp. 11–24.

Robinson, D.N., Scott, J.A., Van Niekerk, A., Anderson, G., 1989. The sequence of events reflected in the diamonds of some southern African kimberlites. In: Ross, J. (Ed.), Kimberlites and Related Rocks, vol. 2. Geological Society of Australia, Special Publication, vol. 14. Blackwell Scientific Publications, Perth, pp. 980–990.

Rudnick, R.L., Nyblade, A.A., 1999. The thickness and heat production of Archean lithosphere: constraints from xenolith thermobarometry and surface heat flow. In: Fei, Y., Bertka, C.M., Myson, B.O. (Eds.), Mantle Petrology: Field Observations and High-Pressure Experimentation: A Tribute to Francis R. (Joe) Boyd, Chemical Society, Special Publication, vol. 6, pp. 3–12.

Ryan, C.G., Griffin, W.L., Pearson, N.J., 1996. Garnet geotherms: pressure–temperature data from Cr-pyrope garnet xenocrysts in volcanic rocks. Journal of Geophysical Research B3, 5611–5625.

Schulze, D.J., 2003. A classification scheme for mantle-derived garnet in kimberlite: a tool for investigating the mantle and exploring for diamonds. Lithos 71, 195–213.

Seifert, F., Schreyer, W., 1968. Die Möglichkeit der Entstehung ultrabasischer Magmen bei Gegenwart geringer Alkalimengen. Geologische Rundschau 57, 349–362.

Shee, S.R., Bristow, J.W., Bell, D.R., Smith, C.B., Alsopp, H.L., Shee, P.B., 1989. The petrology of kimberlites, related rocks and associated mantle xenoliths from the Kuruman province, South Africa. In: Ross, J. (Ed.), Kimberlites and Related Rocks, vol. 1. Geological Society of Australia, Special Publication, vol. 14. Blackwell Scientific Publications, Perth, pp. 60–82.

Shee, S.R., Gurney, J.J., 1979. The mineralogy of xenoliths from Orapa, Botswana. In: Boyd, F.R., Meyer, H.O.A. (Eds.), The Mantle Sample. American Geophysical Union, Washington, DC, pp. 37–49.

Shee, S.R., Gurney, J.J., Robinson, D.N., 1982. Two diamond-bearing peridotite xenoliths from the Finsch kimberlite, South Africa. Contributions to Mineralogy and Petrology 81, 79–87.

Shimizu, N., Richardson, S.H., 1987. Trace element abundance patterns of garnet inclusions in peridotite-suite diamonds. Geochimica et Cosmochimica Acta 51, 755–758.

Slodkevich, V.V., 1983. Graphite paramorphs after diamond. International Geology Review 23, 497–514.

Smith, C.B., Gurney, J.J., Harris, J.W., Robinson, D.N., Shee, S.R., Jagoutz, E., 1989. Sr and Nd isotopic systematics of diamond-bearing eclogite xenoliths and eclogitic inclusions in diamond from southern Africa. In: Ross, J. (Ed.), Kimberlites and Related Rocks, vol. 2. Geological Society of Australia, Special Publication, vol. 14. Blackwell Scientific Publications, Perth, pp. 853–863.

Sobolev, N., 1974. Deep seated inclusions in kimberlites and the problem of the composition of the upper mantle. English Translation by Brown, D.A., 1977, American Geophysical Union, Washington, DC.

Sobolev, N., Galimov, E.M., Ivanovskaya, I.N., Yefimova, E.S., 1979. Isotope composition of carbon of diamonds containing crystalline inclusions. Doklady Akademii Nauk SSSR 249, 1217–1220 (in Russian).

Sobolev, N., Lavrent'yev, Y.G., 1971. Isomorphic sodium admixture in garnets formed at high pressures. Contributions to Mineralogy and Petrology 31, 1–12.

Talnikova, S.B., 1995. Inclusions in diamonds of different habits. Extended Abstracts, 6th International Kimberlite Conference, Novosibirsk, Russia, pp. 603–605.

Taylor, L.A., Anand, A., 2004. Diamonds: time capsules from the Siberian mantles. Chemie der Erde 64, 1–74.

Trautman, R.L., Griffin, B.J., Taylor, W.R., Spetsius, Z.V., Smith, C.B., Lee, D.C., 1997. A comparison of the microdiamonds from kimberlite and lamproite of Yakutia and Australia. 6th International Kimberlite Conference, Novosbirsk, Russia, Russian Geology and Geophysics 38, 341–355.

Waldman, M.A., McCandless, T.E., Dummett, H.T., 1987. Geology and petrography of the Twin Knobbs #1 lamproite, Pike County, Arkansas. In: Morris, E.M., Pasteris, J.D. (Eds.), Mantle Metasomatism and Alkaline Magmatism. Geological Society of America, Special Publication, vol. 215, pp. 205–216.

Westerlund, K.J., 2005. A Geochemical Study of Diamonds, Mineral Inclusions in Diamonds and Mantle Xenoliths from the Panda Kimberlite, Slave Craton. Unpublished Ph.D. thesis. University of Cape Town. 170pp.

Westerlund, K.J., Gurney, J.J., Carlson, R.W., Shirey, S.B., Hauri, E.H., Richardson, S.H., 2004. A metasomatic origin for late Archean eclogitic diamonds: implications from internal morphology of Klipspringer diamonds and Re-Os and S isotope characteristics of their sulfide inclusions. South African Journal of Geology 107, 119–130.

Willmott, E., 2004. World diamond production. Rough Diamond Review 7, 28–30.

Wyatt, B.A., Baumgartner, M., Anckar, E., Grütter, H.S., 2004. Compositional classification of "kimberlitic" and "non-kimberlitic" ilmenite. Lithos 77, 819–840.

Wyllie, J., Huang, W.-L., Otto, J., Byrnes, A.P., 1983. Carbonation of peridotites and decarbonation of siliceous dolomites represented in the system CaO-MgO-SiO_2-CO_2 to 30 kbar. Tectonophysics 100, 359–388.

Yefimova, E.S., Sobolev, N., 1977. Abundance of crystalline inclusions in diamonds of Yakutia. Doklady Akademii Nauk SSSR 237, 1475–1478 (in Russian).

This page intentionally left blank

CONCLUDING REMARKS

The 46 contributions in this volume consist of a representative selection of heavy mineral uses from various parts of the world, covering a broad range of geological research, multidisciplinary and interdisciplinary works and applied uses. They demonstrate how heavy minerals are used to address a variety of problems that cannot be satisfactorily solved by other geoanalytical techniques.

The clear lesson imparted by these papers is that a holistic approach to heavy mineral studies is necessary, and that full and unbiased information can be obtained only from the study of the entire assemblage. Analysing one or two single species while ignoring the rest of the assemblage will inevitably lead to partial and misleading, or dubious interpretations. Consequently, single-grain geochemical and geochronological techniques should be always carried out in conjunction with full-spectrum heavy mineral analysis.

A very important message is that the varieties of a mineral species must be distinguished and recorded, at least optically, in different categories, especially for mature sediments. The simple approach of using single-species is inherently biased because it combines grains with different petrogenesis, sedimentary and provenance history into a single category. The varietal heterogeneity of an individual mineral species (in most sediments and hard rocks) is well illustrated by studies of zircon geochronology or garnet, chrome spinel and other heavy mineral geochemistry. Zircon concordia diagrams commonly exhibit bi- or multimodal age clustering; probability density zircon age plots also depict clearly the presence of multiple zircon populations in most assemblages. Similarly, separate clusters of garnet compositions in ternary plots reflect the inherent complexity of a heavy mineral species. In higher diversity suites, mineral species related by similar petrogenesis should be allocated in genetic categories (e.g., high-grade metamorphic, volcanic, ophiolite-derived) that closely reflect source area lithology and provide a valuable provenance signal. Larger datasets needed to be assessed through rigorous numerical analysis.

The broad range of studies and investigative techniques presented here demonstrate that heavy minerals have a proven record in serving geological curiosity, problem-solving, academic research and the needs of industry. We believe that the information they encode will continue to stimulate scientific enquiry, technological innovation and the pursuit of knowledge long into the future.

Maria A. Mange and David T. Wright

This page intentionally left blank

SUBJECT INDEX

D

H

I

N

O

S

This page intentionally left blank